frontiers | Research Topics

Women in cytokines and soluble mediators in immunity

Edited by
Diana Boraschi, Giselle Penton-Rol, Marita Troye Blomberg and Olukemi Amodu

Published in
Frontiers in Immunology

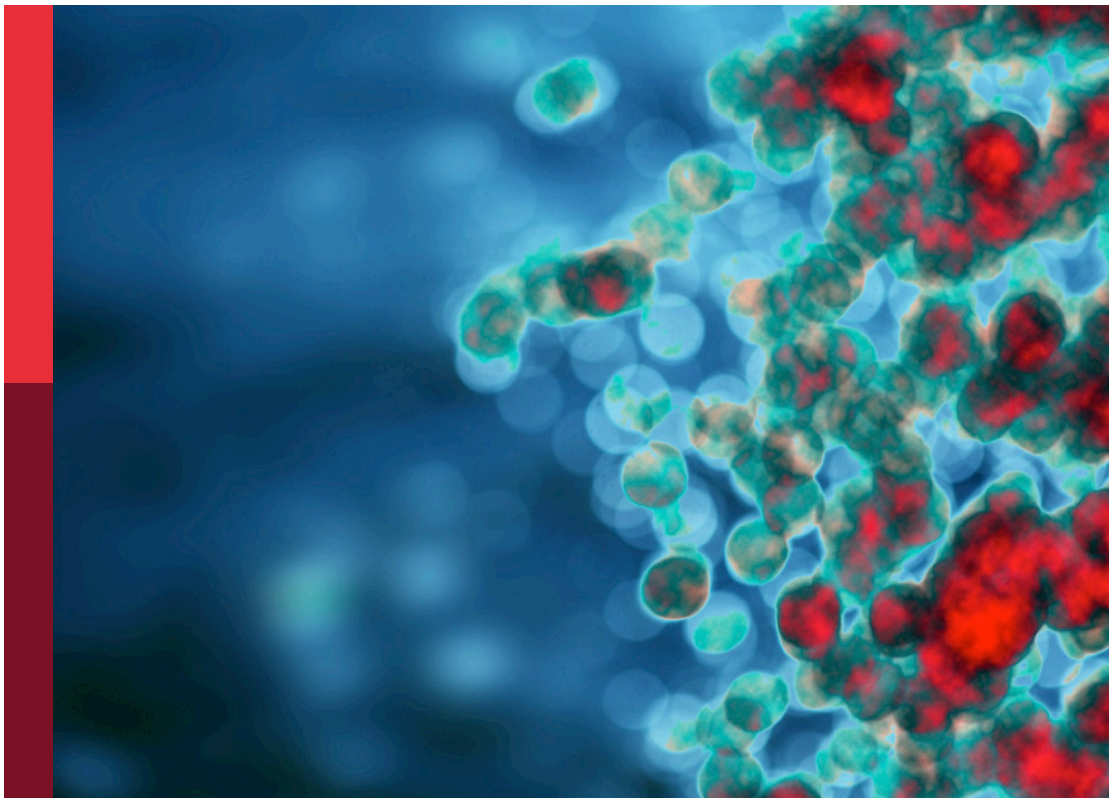

ISSN 1664-8714
ISBN 978-2-8325-4434-1
DOI 10.3389/978-2-8325-4434-1

About Frontiers

Frontiers is more than just an open access publisher of scholarly articles: it is a pioneering approach to the world of academia, radically improving the way scholarly research is managed. The grand vision of Frontiers is a world where all people have an equal opportunity to seek, share and generate knowledge. Frontiers provides immediate and permanent online open access to all its publications, but this alone is not enough to realize our grand goals.

Frontiers journal series

The Frontiers journal series is a multi-tier and interdisciplinary set of open-access, online journals, promising a paradigm shift from the current review, selection and dissemination processes in academic publishing. All Frontiers journals are driven by researchers for researchers; therefore, they constitute a service to the scholarly community. At the same time, the *Frontiers journal series* operates on a revolutionary invention, the tiered publishing system, initially addressing specific communities of scholars, and gradually climbing up to broader public understanding, thus serving the interests of the lay society, too.

Dedication to quality

Each Frontiers article is a landmark of the highest quality, thanks to genuinely collaborative interactions between authors and review editors, who include some of the world's best academicians. Research must be certified by peers before entering a stream of knowledge that may eventually reach the public - and shape society; therefore, Frontiers only applies the most rigorous and unbiased reviews. Frontiers revolutionizes research publishing by freely delivering the most outstanding research, evaluated with no bias from both the academic and social point of view. By applying the most advanced information technologies, Frontiers is catapulting scholarly publishing into a new generation.

What are Frontiers Research Topics?

Frontiers Research Topics are very popular trademarks of the *Frontiers journals series*: they are collections of at least ten articles, all centered on a particular subject. With their unique mix of varied contributions from Original Research to Review Articles, Frontiers Research Topics unify the most influential researchers, the latest key findings and historical advances in a hot research area.

Find out more on how to host your own Frontiers Research Topic or contribute to one as an author by contacting the Frontiers editorial office: frontiersin.org/about/contact

Women in cytokines and soluble mediators in immunity

Topic editors

Diana Boraschi — Shenzhen Institute of Advanced Technology, Chinese Academy of Sciences (CAS), China

Giselle Penton-Rol — Center for Genetic Engineering and Biotechnology (CIGB), Cuba

Marita Troye Blomberg — Stockholm University, Sweden

Olukemi Amodu — University of Ibadan, Nigeria

Citation

Boraschi, D., Penton-Rol, G., Troye Blomberg, M., Amodu, O., eds. (2024). *Women in cytokines and soluble mediators in immunity*. Lausanne: Frontiers Media SA. doi: 10.3389/978-2-8325-4434-1

Dr. Penton-Rol was employed by Center for Genetic Engineering and Biotechnology.

Table of contents

C. CYTOKINES/SOLUBLE FACTORS' PROFILE IN DISEASES AS DIAGNOSTIC/PROGNOSTIC MARKERS

1. INFECTIONS

2. PREGNANCY

3. OTHER CONDITIONS

D. CYTOKINES/SOLUBLE FACTORS IN PATHOGENIC MECHANISMS

E. CYTOKINES AND CYTOKINE MODULATION IN THERAPY

frontiers | Frontiers in Immunology

TYPE Editorial
PUBLISHED 14 March 2024
DOI 10.3389/fimmu.2024.1395165

OPEN ACCESS

EDITED BY
Silvano Sozzani,
Sapienza University of Rome, Italy

*CORRESPONDENCE
Diana Boraschi
diana.boraschi@itb.cnr.it

RECEIVED 03 March 2024
ACCEPTED 08 March 2024
PUBLISHED 14 March 2024

CITATION
Boraschi D, Penton-Rol G, Amodu O and Blomberg MT (2024) Editorial: Women in cytokines and soluble mediators in immunity. *Front. Immunol.* 15:1395165.
doi: 10.3389/fimmu.2024.1395165

Editorial: Women in cytokines and soluble mediators in immunity

Diana Boraschi[1,2,3]*, Giselle Penton-Rol[4,5], Olukemi Amodu[6] and Marita Troye Blomberg[7]

[1]Laboratory Inflammation and Vaccines, Shenzhen Institute of Advanced Technology (SIAT), Chinese Academy of Sciences (CAS), and China-Italy Joint Laboratory of Pharmacobiotechnology for Medical Immunomodulation, Shenzhen, China, [2]Institute of Biomolecular Chemistry, National Research Council (CNR), Pozzuoli, Italy, [3]Stazione Zoologica Anton Dohrn, Napoli, Italy, [4]Center for Genetic Engineering and Biotechnology (CIGB), Playa, Cuba, [5]Department of Physiological Sciences, Professor of Immunology at the Latin American School of Medicine (ELAM), Havana, Cuba, [6]Genetics and Molecular Sciences Unit, Institute of Child Health, College of Medicine, University of Ibadan, Ibadan, Nigeria, [7]Department Molecular Biosciences, the Wenner-Gren Institute, Stockholm University, Stockholm, Sweden

KEYWORDS

women, cytokines, soluble mediators, immunity, pathology, diagnosis, therapy

Editorial on the Research Topic
Women in cytokines and soluble mediators in immunity

The Research Topic dedicated to "*Women in Cytokines and Soluble Factors in Immunity*" was launched in March 2022 by two experienced and two younger female scientists, active in four different continents. In 24 months, we have collected over 60 contributions from female scientists around the World. Most of the papers are original research studies and deal with human diseases (tumors, infections), evaluating the pathological or predictive role of cytokines, but also the importance of cytokines in invertebrate immune defense. Most of the papers list young PhD students as first author, but many very experienced female scientists have also contributed. Most of the papers come from Europe, but significant contributions were received from Asia, Americas and Africa. Impressively, almost one third of the papers are cross-continental collaborations. While much still must be done for promoting female participation to scientific research, in particular in developing countries, this Research Topic underlines an encouraging scenario of commitment and dedication to science, desire of collaboration, capacity to coach, train and support younger female scientists to engage in a scientific career.

1 Cytokines and soluble factors in immunity

The field of cytokines and other soluble factors in immunity encompasses many different scientific areas, from evolution of immunity to clinical diagnostic studies. This Research Topic includes several important contributions in different areas of basic and clinical research on soluble immune factors, as briefly summarized below.

1.1 Invertebrate immunity

Soluble immune factors are essential elements in the defensive system of invertebrate metazoans, and include enzymes such as lysozyme and phenoloxidase, complement and inflammatory cytokines such as IL-17 and TNF (1–6). A comprehensive analysis of soluble factors-mediated immunity in two different invertebrate phyla, annelids and bivalve mollusks, is reported by an excellent group of four women scientists active in two different European countries (Canesi et al.). Two studies from Italy and Italy-China analyzed the immune response of tunicates to biotic or abiotic challenges and showed that the modulation of several immune factors, including complement, cytokines, enzymes and variable chitin-binding and LPS-binding proteins, is the basis of primary and memory responses in *Ciona robusta* (Marino et al., Liberti et al.).

1.2 Mammalian immunity

In mammalian immunity, soluble factors have a major importance both for innate and adaptive immune response. As for invertebrates, complement is one of the key anti-bacterial effector systems (4, 7, 8). For adaptive immunity, antibodies are the highly specific and effective neutralizing tools (8). Cytokines and chemokines are soluble factors that participate to both innate and adaptive immunity, representing the natural bridge between the two systems (8). The role of soluble factors in the T cell development has been extensively examined, including at the level of intrathymic differentiation (8, 9). A very interesting study addresses the role of two such factors, IL-2 and IL-15, in driving the differentiation of distinct Treg cells in the thymus (Apert et al.). It is notable that such study is the result of a collaboration between three different European countries, France, Switzerland and UK. A comprehensive assessment of the multifaceted role of chemokines in immunity is provided by a young researcher active in one of the groups that discovered chemokines, in Switzerland (Cecchinato et al.). The ability of innate cells such as macrophages to produce cytokines and other soluble factors in response to challenges is generally assessed *in vitro* in culture systems that may not reproduce accurately the *in vivo* conditions (10, 11). This is a shortcoming that may lead to misleading results and inaccurate prediction of immune reactivities. A joint collaboration between Dutch, UK and German researchers pointed out how variations in cell density in culture can influence the function and cytokine production by human macrophages, which warrants a particular attention in the reliable design of our cell culture systems (Ruder et al.).

1.3 Cytokines/soluble factors' profile in diseases as diagnostic/prognostic markers

The role of cytokines and other immune soluble factors in diseases has gained increasing importance, and many studies have pointed at the possibility of using them as diagnostic markers, able to identify the type and stage of multiple different diseases, and as prognostic tools for predicting future susceptibility or resistance to disease development.

1.3.1 Infections

The recent COVID-19 pandemic has produced numerous studies of cytokines as markers of disease and disease severity. Association with mortality, as well as other immune and vascular biomarkers, is reported in two studies, one in Spain (Sanchez-de Prada et al.) and one in South Africa in collaboration with UK (Shaw et al.). The soluble immune factors' profile in COVID-19 convalescent pregnant women was examined in an extensive Brazilian study encompassing ten different institutions (Fernandes et al.). The lung inflammatory conditions and the infection-dependent epithelial to mesenchymal transition was examined at the single cell level in a collaborative study between China and USA (Zhang et al.). The importance of the viral nucleoprotein in inducing anti-inflammatory innate memory was examined in a joint study between the European Commission JRC, Italy and China (Urban et al.). A very interesting study in Cameroon in collaboration with Italy highlighted the presence of antibodies reactive to SARS-CoV-2 in archive samples of HIV patients dating back to before the COVID-19 pandemic (Aissatou et al.). Inflammation-related soluble factors were examined in HIV patients both for optimizing treatment in Cameroonian adolescents in a collaborative study between Cameroon, Italy, France and South Africa (Ka'e et al.) and for predicting hematological complications and, again, optimize treatment, in a Danish study (Grønbæk et al.). Response to viruses has been further examined in a collaborative Brazil-Germany study in terms of systems biology dynamical evaluation of interferon-related signatures in Dengue infection (Usuda et al.) and single cell-based identification of the chemokine CCL5 as biomarker of macrophage response to DNA sensing in a USA work (McCarty et al.).

Several studies focused on parasitic diseases, in particular malaria. A comprehensive immunogenomic study was performed in a collaboration between USA, Mali and Portugal to identify an immune profile predictive of susceptibility to clinical malaria (Mbambo et al.). Another study from Nigeria explored the possible pathogenic role of TNF-α in malaria patients with type 2 diabetes (Ademola et al.). In a study from the Côte d'Ivoire, another inflammatory cytokine, IL-1β, and other members of the IL-1 family, were examined in sickle cell disease in Sub-Saharan Africa, in the attempt to design a better management of the disease (Siransy et al.). The immunological aspects of clinical forms of cutaneous leishmaniasis in North Africa and French Guiana were addressed in a collaborative study between France, Tunisia and French Guiana (Saidi et al.).

Focus on bacterial infections encompasses a study examining the profile of cytokines and chemokines in people recently infected with *Mycobacterium tuberculosis*, within a collaboration between Colombia and Canada (Herrera et al.), a Canadian-Swedish study reported on correlates of protection in *Francisella tularensis* infection (Lindgren et al.), a very interesting evaluation of the osteoblast

secretome in osteomyelitis induced by *Streptococcus aureus* was contributed by an Italian group (Granata et al.), and an Italian-UK collaboration provided an excellent review of the value of PTX3 as prognostic marker of mortality in sepsis (Davoudian et al.).

1.3.2 Pregnancy

The involvement of soluble immune factors in some pathological aspects associated with pregnancy has been the focus of a number of manuscripts. The levels of cytokines in patients undergoing procedures for *in vitro* fertilization were examined in a study from Poland (Piekarska et al.). The cytokine levels in first trimester-pregnant women developing hypertension after assisted reproductive technology were examined in a Chinese study (Lan et al.), while another Chinese study addressed the association between circulating inflammatory cytokines and pregnancy-associated hypertension (Guan et al.). Pregnancy-associated immunomodulation through extracellular vesicles and soluble factors released by amniotic mesenchymal stromal cells was investigated for possible translational applications by an Italian study (Papait et al.). The correlation between immune parameters, including cytokines, and cervical insufficiency and preterm births was addressed by a Korean study (Jeong et al.). Eventually, the association between monocyte signatures and the risk of developing chronic lung disease in preterm infants was shown in a German study (Windhorst et al.).

1.3.3 Other conditions

Cytokines and soluble factors can act as markers of disease, disease progression and disease severity in several diseases in which inflammation is involved. A collaborative study between Germany and Austria addressed the presence of systemic inflammation-related markers in polyneuropathies (Garcia-Fernandez et al.), while a study from Qatar has investigated the cellular sources of anomalous cytokine levels in autism (Nour-Eldine et al.). In a Finnish/USA study, circulating IL-21 was found to correlated with disease progression in type 1 diabetes (Schroderus et al.), whereas a Polish study suggested adipokines could be disease biomarkers in type 2 diabetes, demonstrated in a cat model (Sierawska and Niedźwiedzka-Rystwej et al.). Soluble prognostic and diagnostic biomarkers of osteoporosis were investigated in a Chinese study (Wang et al.). In an Italian study, soluble biomarkers of disease mechanisms and phenotypes of systemic sclerosis were identified with an aptamer-based proteomic approach (Motta et al.). The distribution of IL-22BP in Crohn's disease was the focus of a French investigation (Fantou et al.). Eventually, the contribution of mast cell proteases and IL-33 processing in the development of allergic lung inflammation was examined in a mouse model in a collaborative study between Belgium, Austria, Russia, Germany and China (Krysko et al.).

1.4 Cytokines and soluble factors in pathogenic mechanisms

Whether anomalies in cytokine production is a consequence of disease or may be part of the pathogenesis is still an open question. Several studies included in this collection tackle the issue in the attempt to identify the involvement of cytokines in pathogenesis vs. pathology. Several of the studies focused on cytokines of the IL-1 family, which include highly inflammatory factors, such as IL-1β, that have a well-known role in many chronic inflammatory and degenerative diseases (12, 13). A manuscript from Italy and China examined the role of IL-1 family cytokines in neuroinflammatory and neurodegenerative diseases and concluded that most likely these cytokines are involved in both pathogenesis and downstream pathological symptoms (Boraschi et al.). That IL-1β, the best-known inflammatory cytokine of the family, can be involved in tumorigenesis is known (14, 15), but a study from Singapore and Switzerland further identified AIM2 activation as one of the factors contributing to the production of IL-1β in the tumor microenvironment (Chew et al.). IL-1α, a cytokine mostly present as membrane bound molecule thereby acting through cell-to-cell contact (16, 17), was found responsible for activating leukocyte adhesion during atherogenesis in a German study (Maeder et al.). Another German study found that IL-36γ, a less known inflammatory cytokine of the IL-1 family mostly active at the tissue level, is responsible for interferon-independent liver injury caused by the Rift Valley virus (Anzaghe et al.). Other specific cases were examined: the role of IL-11 in fibrosis in interstitial lung disease, studied using human organoids by a German group (Kastlmeier et al.); the dysregulation of LIF in endometriosis, proposed by a Canadian-USA collaboration (Zutautas et al.); the role of GAS6/TAM in regulating NK cell recognition of multiple myeloma cells and degranulation studied by an Italian-USA group (Kosta et al.); and the involvement of the complement terminal complex in the inflammatory activation of retinal pigment epithelium and the associated development of age-related macular degeneration proposed by a German collaboration study (Busch et al.). Eventually, a group of studies examined the entire spectrum of cytokines and soluble factors associated with initiation *vs.* maintenance of different pathologies. A collaborative study between Switzerland and Spain reviewed the contribution of cytokines to the hyperinflammatory spectrum (Planas et al.). A USA group reviewed the contribution of oncostatin M, a cytokine of the IL-6 family, in inflammatory diseases (Wolf et al.). In cancer, the contribution of tumor-associated macrophages and their soluble factors in lung metastatic melanoma was addressed in a China-Germany collaborative study (Xiong et al.). Eventually, an informative review on the role of cytokines in Acute Myeloid Leukemia was contributed by an Austrian group (Luciano et al.).

1.5 Cytokines and cytokine modulation in therapy

Targeting cytokines for curing diseases is an approach that has turned out to be successful in several instances, see as an example the TNF-α or IL-1β inhibitory biologicals currently used in several chronic inflammatory diseases (18–21), although the efficacy is not complete and side effects can be observed [such as the tuberculosis activation in patients with latent tuberculosis treated with anti-

TNF-α drugs; (22)]. An historical excursus describing how several of these cytokine inhibitors were originally identified is provided by Daniela Novick, a pioneer woman scientist who accelerated substantially the development of anti-cytokine drugs (Novick et al.). Inflammation, including induction of inflammatory cytokines, has been for decades the core of cancer immunotherapy, with the use of bacteria and bacterial-derived molecules (23). The use of BCG is currently the golden standard treatment for non-invasive bladder cancer, and its effect includes the activation of an anti-tumor innate and inflammatory response (24, 25). Based on the notion that innate immunity is non-specific, a large collaborative study (involving researchers from Austria, The Netherlands, France, Italy, Russia, Poland and Hong Kong) showed that treatment of bladder cancer patients with BCG induced a systemic innate response able to counteract the SARS-CoV-2 infection (Pichler et al.). On the same line, a very interesting study from an Iranian and Canadian collaboration shows that the use of molecules that induce innate/inflammatory activation can substantially increase the therapeutic immune response against colon cancer in a preclinical model and also downregulates the pathological presence of fibroblasts in the tumor microenvironment (Haijabadi et al.). A review of the innate immunity in the airways, contributed by an Icelandic/Swedish group, comes to similar conclusions, *i.e.*, that activation of innate immune/inflammatory epigenetic mechanisms by bacterial products may contribute to effective response and disease resolution (Myszor and Gudmundsson).

Anti-inflammatory strategies are the most common approaches to cytokine inhibition in different diseases. In liver transplantation from brain dead donors, inflammation is largely dependent on increased IL-1β production and was shown, in a study from a Mexico-Spain-Uruguay collaboration, to be the main cause of rejection, as it could be mitigated by treatment with the IL-1 antagonist IL-1Ra (Casillas-Ramirez et al.). Interestingly, a German-UK study on IL-37, an anti-inflammatory cytokine of the IL-1 family that is active in the gut, showed that the IL-37 role at the level of the mucosal epithelium is minimal, suggesting an anatomically distinct and localized anti-inflammatory activity (Krohn et al.). Among anti-inflammatory strategies, the use of phycocyanobilin, a tetrapyrrole chromophore from microalgae, displays substantial anti-inflammatory properties and was found able to inhibit leukocyte infiltration and cytokine production in a rheumatoid arthritis model (Marin-Prida et al.) and in a multiple sclerosis model (Marin-Prida et al.), as reported by two Cuban studies, one in collaboration with Brazil, China, Mexico, and the other one with Brazil and Germany. A French study explored the use of a synthetic histamine analogue that binds to CXCR4 (a chemokine receptor important for leukocyte mobilization) for inhibiting inflammation in juvenile arthritis cells *in vitro* and in a mouse model *in vivo*. Using this model, they observed substantial reduction of inflammatory cytokines, immune cell infiltration and joint and bone erosion (Bekaddour et al.). Anti-inflammatory effects were also observed in a Cuban study using a modified peptide derived from HSP60 both in animal models of RA and in human patients The treatment inhibited inflammatory cytokine production, including IL-17, and ameliorated the cytokine storm in COVID-19 patients (Dominguez-Horta et al.). Anti-inflammatory strategies targeting T cells included the above-mentioned study, which identified an increase in Treg cells, and a collaborative study between Cuba, Korea and Portugal on a mutant of IL-2, which showed that the antitumor activity of the mutein is based on the change of the balance between $CD8^+$ and Treg cells (Carmenate et al.). Eventually, an Italian study showed that a synthetic sulfolipid can decrease IL-12 production by dendritic cells and promote T cell differentiation towards Treg (Barra et al.).

2 Women in cytokines and soluble factors in immunity

This Research Topic provides much more than a number of good scientific papers on the general topic of cytokines and soluble factors in immunity. Being dedicated to women immunologists active in the area of cytokines, the Research Topic aimed to be as inclusive as possible, having expert scientists who could set an inspiring example for the young students who are just approaching science, and encouraging female researchers to engage in a scientific career in every country, in particular those where research conditions are more difficult in general and for women in particular. To reflect our intention, the four editors of the Research Topic are two old and two young female immunologists, active in four different continents. We have collected 62 contributions, in which the first or the senior author are female scientists. Many are young PhD students, while others are very experienced researchers. Authors of these papers come from 40 countries across four continents (Europe, Asia and Middle East, Africa, Americas). Impressively, over 77% of the studies are collaborative studies, and 44% of these collaborations are intercontinental, as we did underline in the previous paragraphs. This reflects a very encouraging trend, *i.e.*, that scientists (and women in particular) strongly believe that progress means collaboration without borders and without any type of bias (Figure 1).

We had in 2023 two important examples of successful women, whom are worth mentioning for their life-long commitment. Claudia Goldin, an American economist, has been awarded the Nobel Prize in Economic Sciences for her relentless engagement in understanding and making known the gap between women and man in the labor market (26). Her work and her analysis of the reasons why the majority of undergraduates in USA are women are impacting substantially on the general understanding of the female working and social conditions, well beyond her country. Another inspiring example is Katalin Karicó, a Hungarian biochemist who moved to USA when she was 30, after she lost her lab position due to lack of funding. Katalin is an expert in RNA, and in 1989, soon after having moved to the USA, she started working on mRNA and focused on mRNA-based therapeutic approaches. In the following years, she encountered huge difficulties in obtaining funding and in developing her academic career but she never abandoned her focus on therapeutic mRNA, and eventually she succeeded in dumping the RNA inflammatory activity and devising an effective delivery system. This was the basis for the first widespread human application of mRNA, as vaccine for SARS-CoV-2. She was awarded the Nobel Prize in Physiology and Medicine in October 2023. Few months earlier, her biography was published as an illustrated children book, with the compelling title “Never give up” (27).

FIGURE 1
Worldwide distribution of the contributions to "Women in Cytokines and Soluble Factors in Immunity" with their collaborative interconnections. Artwork by Denise Ruiz Castro and Maykel Pedro Penton Martinez (Design project InDi productions, Havana, Cuba) and Sheila Delgado-Lora.

The contribution of women to science is substantial, but the gaps and inequalities are still outstanding in many countries and institutions. Although there are many initiatives aiming at raising awareness and encourage women's participation in science (for instance the International Day of Women and Girls in Science, celebrated every February 11), we, as women scientists, are those who should "never give up", both in pursuing advancement of knowledge and in closing gaps and eliminating inequalities.

Author contributions

DB: Writing – review & editing, Writing – original draft. GP-R: Writing – review & editing. OA: Writing – review & editing. MB: Writing – review & editing.

Funding

The author(s) declare financial support was received for the research, authorship, and/or publication of this article. DB was supported by the EU H2020 project PANDORA (GA 671881), the China-Italy NSFC-MAECI bilateral project 82261138630, the Key Collaborative Research Program of the Alliance of International Science Organizations ANSO-CR-KP-2022-01, and the Bill & Melinda Gates Foundation grant INV-059115.

Acknowledgments

The authors are grateful for the active collaboration and support of many colleagues, who helped in making this endeavor a success. Of the people of Frontiers in Immunology, we thank in particular the editor-in-chief Gigi Notarangelo and the section editor Silvano Sozzani, who always patiently answered all our queries and requests of help, Jonathan Paul, who relentlessly followed the editorial work, and Madeleine Metcalf, who has concretely supported the participation of young female scientists from developing countries. We are very grateful to Denise Ruiz Castro and Maykel Pedro Penton Martinez (Design project InDi productions, Havana, Cuba), who conceived a compelling figure for illustrating the worldwide collaboration of women immunologists, and Sheyla Delgado-Lora, a young Cuban scientist who completed the design with great sensibility. Lastly, we are happy to acknowledge many fruitful collaborations with our male colleagues and the feeling that gender is slowly becoming a non-issue in an increasing number of research labs in several countries.

Conflict of interest

The authors declare that the research was conducted in the absence of any commercial or financial relationships that could be construed as a potential conflict of interest.

Publisher's note

References

1. Gerdol M, Venier P. An updated molecular basis for mussel immunity. *Fish Shellfish Immunol.* (2010) 46:17–30. doi: 10.1016/j.fsi.2015.02.013

2. Bachali S, Jager M, Hassanin A, Schoentgen F, Jolles P, Fiala-Medioni A, et al. Phylogenetic analysis of invertebrate lysozymes and the evolution of lysozyme function. *J Mol Evol.* (2002) 54:652–64. doi: 10.1007/s00239-001-0061-6

3. Soderhall K, Cerenius L. Role of the prophenoloxidase-activating system in invertebrate immunity. *Curr Opin Immunol.* (1998) 10:23–8. doi: 10.1016/S0952-7915(98)80026-5

4. Nonaka M. Evolution of the complement system. *Subcell Biochem.* (2014) 80:31–43. doi: 10.1007/978-94-017-8881-6_3

5. Saco A, Rey-Campos M, Rosani U, Novoa B, Figueras A. The evolution and diversity of Interleukin-17 highlight an expansion in marine invertebrates and its conserved role in mucosal immunity. *Front Immunol.* (2021) 12:692997. doi: 10.3389/fimmu.2021.692997

6. Quistad SD, Traylor-Knowles N. Precambian origins of the TNFR superfamily. *Cell Death Discovery.* (2016) 2:16058. doi: 10.1038/cddiscovery.2016.58

7. Dunkelberger JR, Song W-C. Complement and its role in innate and adaptive immune responses. *Cell Res.* (2010) 20:34–50. doi: 10.1038/cr.2009.13

8. Murphy KM, Weaver C, Berg LJ. *Janeway's immunobiology. 10th edition*. New York, NY, USA: W.W. Norton & Company (2022).

9. Shah DK, Zuniga-Pflucker JC. An overview of the intrathymic intricacies of T cell development. *J Immunol.* (2014) 192:4017–23. doi: 10.4049/jimmunol.1302259

10. Swartzwelter BJ, Verde A, Rehak L, Madej M, Puntes VF, De Luca AC, et al. Interaction between macrophages and nanoparticles: *in vitro* 3D cultures for the realistic assessment of inflammatory activation and modulation of innate memory. *Nanomaterials.* (2021) 11:207. doi: 10.3390/nano11010207

11. Linde N, Gutschalk CM, Hoffmann C, Yilmaz D, Mueller MM. Integrating macrophages into organotypic co-ultures: a 3D *in vitro* model to study tumor-associated macrophages. *PLoSONE.* (2012) 7:e40058. doi: 10.1371/journal.pone.0040058

12. Dinarello CA. A clinical perspective of IL-1β as the gatekeeper of inflammation. *Eur J Immunol.* (2011) 41:1203–17. doi: 10.1002/eji.201141550

13. Dinarello CA. The IL-1 family of cytokines and receptors in rheumatic diseases. *Nat Rev Rheumatol.* (2019) 15:612–32. doi: 10.1038/s41584-019-0277-8

14. Mantovani A, Barajon I, Garlanda C. IL-1 and IL-1 regulatory pathways in cancer progression and therapy. *Immunol Rev.* (2018) 281:57–61. doi: 10.1111/imr.12614

15. Garlanda C, Mantovani A. Interleukin-1 in tumor progression, therapy and prevention. *Cancer Cell.* (2021) 39:1023–7. doi: 10.1016/j.ccell.2021.04.011

16. Rider P, Carmi Y, Voronov E. Apte RN. *Interleukin-1α. Semin Immunol.* (2013) 25:430–8. doi: 10.1016/j.smim.2013.10.005

17. Cavalli G, ColaFrancesco S, Emmi G, Imazio M, Lopalco G, Maggio MC, et al. Interleukin-1α: a comprehensive review on the role of IL-1α in the pathogenesis and treatment of autoimmune and inflammatory diseases. *Autoimmun Rev.* (2021) 20:102763. doi: 10.1016/j.autrev.2021.102763

18. Feldmann M, Maini RN. Lasker Clinical Medical Research Award. TNF defined as a therapeutic target for rheumatoid arthritis and other autoimmune diseases. *Nat Med.* (2003) 9:1245–50. doi: 10.1038/nm939

19. Croft M, Benedict CA, Ware CF. Clinical targeting of the TNF and TNFR superfamilies. *Nat Rev Drug Discovery.* (2013) 12:147–68. doi: 10.1038/nrd3930

20. Dinarello CA. Therapeutic strategies to reduce IL-1 activity in treating local and systemic inflammation. *Curr Opin Pharmacol.* (2004) 4:378–85. doi: 10.1016/j.coph.2004.03.010

21. Dinarello CA, Simon A, van der Meer J. Treating inflammation by blocking interleukin-1 in a broad spectrum of diseases. *Nat Rev Drug Discovery.* (2012) 11:633–52. doi: 10.1038/nrd3800

22. Harris J, Keane J. How tumor necrosis factor blockers interfere with tuberculosis immunity. *Clin Exp Immunol.* (2010) 161:1–9. doi: 10.1111/j.1365-2249.2010.04146.x

23. Boraschi D, Tagliabue A. Harnessing the power of inflammation in immunoprevention and immunotherapy. *Innovation Life.* (2023) 1:100025. doi: 10.59717/j.xinn-life.2023.100025

24. Pettenati C, Ingersoll MA. Mechanisms of BCG immunotherapy and its outlook for bladder cancer. *Nat Rev Urol.* (2018) 15:615–25. doi: 10.1038/s41585-018-0055-4

25. Kowalewicz-Kulbat M, Locht C. Recombinant BCG to enhance its immunomodulatory activities. *Vaccines.* (2022) 10:827. doi: 10.3390/vaccines10050827

26. *Bio for Claudia Goldin – Scholars at Harvard.* Available online at: https://scholar.harvard.edu/goldin/biocv (Accessed January 30, 2024).

27. Dadey D, Oakley J. *Never Give Up. Dr. Kati Karikó and the Race for the Future of Vaccines.* Brookfield, CT, USA: Millbrook Press (2023).

CYTOKINES IN INVERTEBRATES

frontiers | Frontiers in Immunology

TYPE Mini Review
PUBLISHED 02 December 2022
DOI 10.3389/fimmu.2022.1051155

OPEN ACCESS

EDITED BY
Giselle Penton-Rol,
Center for Genetic Engineering and Biotechnology (CIGB), Cuba

REVIEWED BY
Peter Engelmann,
University of Pécs, Hungary

*CORRESPONDENCE
Petra Prochazkova
kohler@biomed.cas.cz

SPECIALTY SECTION
This article was submitted to Cytokines and Soluble Mediators in Immunity, a section of the journal Frontiers in Immunology

RECEIVED 22 September 2022
ACCEPTED 14 November 2022
PUBLISHED 02 December 2022

CITATION
Canesi L, Auguste M, Balbi T and Prochazkova P (2022) Soluble mediators of innate immunity in annelids and bivalve mollusks: A mini-review.
Front. Immunol. 13:1051155.
doi: 10.3389/fimmu.2022.1051155

Soluble mediators of innate immunity in annelids and bivalve mollusks: A mini-review

Laura Canesi[1], Manon Auguste[1], Teresa Balbi[1] and Petra Prochazkova[2]*

[1]Department of Earth Environment & Life Sciences, University of Genoa, Genoa, Italy, [2]Laboratory of Cellular and Molecular Immunology, Institute of Microbiology of the Czech Academy of Sciences, Prague, Czechia

Annelids and mollusks, both in the superphylum of Lophotrochozoa (Bilateria), are important ecological groups, widespread in soil, freshwater, estuarine, and marine ecosystems. Like all invertebrates, they lack adaptive immunity; however, they are endowed with an effective and complex innate immune system (humoral and cellular defenses) similar to vertebrates. The lack of acquired immunity and the capacity to form antibodies does not mean a lack of specificity: invertebrates have evolved genetic mechanisms capable of producing thousands of different proteins from a small number of genes, providing high variability and diversity of immune effector molecules just like their vertebrate counterparts. This diversity allows annelids and mollusks to recognize and eliminate a wide range of pathogens and respond to environmental stressors. Effector molecules can kill invading microbes, reduce their pathogenicity, or regulate the immune response at cellular and systemic levels. Annelids and mollusks are "typical" lophotrochozoan protostome since both groups include aquatic species with trochophore larvae, which unite both taxa in a common ancestry. Moreover, despite their extensive utilization in immunological research, no model systems are available as there are with other invertebrate groups, such as *Caenorhabditis elegans* or *Drosophila melanogaster*, and thus, their immune potential is largely unexplored. In this work, we focus on two classes of key soluble mediators of immunity, i.e., antimicrobial peptides (AMPs) and cytokines, in annelids and bivalves, which are the most studied mollusks. The mediators have been of interest from their first identification to recent advances in molecular studies that clarified their role in the immune response.

KEYWORDS

Innate immunity, invertebrate, earthworm, bivalves, antimicrobial peptides, cytokines

10.3389/fimmu.2022.1051155

Annelids

Annelids, or segmented worms, are invertebrates with a true coelom filled with coelomic fluid containing several coelomocyte populations. Annelids include polychaetes (marine worms), oligochaetes (earthworms), and leeches. All members of this group are, to some extent, segmented, i.e., they consist of segments that are made up of sub-segments partially intersecting with the body cavity. Since their body is open to the environment, the coelomic cavity is not aseptic, and therefore they had to evolve extremely effective weapons against unwanted enemies. Effector immunocytes called amoebocytes are involved in a broad range of defense functions, including phagocytosis modulated by humoral components, opsonins, which are complement-like molecules, and lectins. The coelomic fluid of annelids contains various antimicrobial factors like lysozyme, hemolytic factors that bind sphingomyelin (fetidin, lysenin, lysenin-related proteins), antimicrobial peptides (AMPs), proteases (lumbrokinase, catalase, superoxide dismutases), cytolytic proteins (coelomic cytolytic factor (CCF)), clotting and coagulation factors, and enzyme-activation-based cascades (prophenoloxidase cascade) (1). Bioactive agents in the coelomic fluid also include several metabolites, like drilodefensins, responsible for the inhibitory effects of polyphenols in the earthworm digestive tract (2), and metallothioneins, small metal-binding proteins responsible for the detoxification and regulation of heavy metals (3). Notably, the humoral defense also includes pattern recognition receptors (PRRs) (such as Toll-like receptors (TLRs) and CCF) that are frequently based on lectin-saccharide interactions designed to recognize highly conserved structures present in different microorganisms (pathogen-associated molecular patterns (PAMPs)). Consequently, cellular and humoral pathways of the innate defense are orchestrated by cytokine-like factors (4).

AMPs

AMPs are evolutionarily ancient molecules produced by all living organisms, including annelids. They represent the first line of defense against microbes but also regulate commensal symbionts at various anatomical sites. Although more than 2,000 AMPs have been described in a wide range of organisms, the number of AMPs described in annelids is very small (Table 1).

The first discovered AMP in annelids was lumbricin-1 from the earthworm *Lumbricus rubellus* (5). Related peptides were subsequently identified in several annelids: Hm-lumbricin from the leech *Hirudo medicinalis* (6), peptide PP-1 from the Asian earthworm *Metaphire tschiliensis* (7), lumbricin-PG from the earthworm *Pheretima guillelmi* (8), and lumbricin and lumbricin-related peptide from the earthworm *Eisenia andrei* (9). These AMPs are enriched with prolines and display a broad spectrum of antibacterial activities. However, they are not inordinately abundant and probably do not represent their primary biological function. Their mechanism of action on microorganisms remains unknown.

Macins are quite long cationic cysteine-rich AMPs with an α-helix/β-sheet structure. In leeches, the group includes theromacin from *Theromyzon tessulatum* (6) and Hm-neuromacin and Hm-theromacin from *H. medicinalis* (10). In addition to their antimicrobial activity, these AMPs are associated with regenerating damaged nerve cords. Their

TABLE 1 Antimicrobial peptides in annelids.

AMP family	Name	Structure	Annelida group	Species	Habitat	Ref.
	lumbricin-1		oligochaetes	*L. rubellus*	terrestrial	
	Hm-lumbicin		leeches	*H. medicinalis*	freshwater	
Lumbricins	PP-1	proline-rich	oligochaetes	*P. tschiliensis*	terrestrial	(5)
	lumbricin-PG		oligochaetes	*P.guillelmi*	terrestrial	(6–9)
	lumbricin, LuRP		oligochaetes	*E. andrei*	terrestrial	
	theromacin			*T. tessulatum*		
Macins	Hm-neuromacin	α-helix/	leeches	*H. medicinalis*	freshwater	(6, 10)
	Hm-theromacin	β-sheet		*H. medicinalis*		
	arenicin-1			A. marina		
	arenicin-2			*A. marina*		
	arenicin-3			*A. marina*		
BRICHOS-AMPs	alvinellacin	β-sheet	polychaetes	*A. pompejana*	marine	(11–15)
	capitellacin			*C. teleta*		
	nicomicin-1			*N. minor*		
	nicomicin-2			*N. minor*		
	hedistin	α-helix	polychaetes	*H. diversicolor*	marine	(16)
	perinerin	UN	polychaetes	*P. aibuhitensis*	marine	(17)
	Ms-hemerycin	α-helix	polychaetes	*M. sanguinea*	marine	(18)

A. marina, Arenicola marina; A. pompejana, Alvinella pompejana; C. teleta, Capitella teleta; E. andrei, Eisenia andrei; H. diversicolor, Hediste diversicolor; H. medicinalis, Hirudo medicinalis; L. rubellus, Lumbricus rubellus; LuRP, lumbricin-related peptide; M. sanguinea, Marphysa sanguinea; N. minor, Nicomache minor; P. aibuhitensis, Perinereis aibuhitensis; P. guillelmi, Pheretima guillelmi; P. tschiliensis, Pheretima tschiliensis; T. tessulatum, Theromyzon tessulatum; UN, unknown.

mechanism of action consists of the induction of bacteria aggregation followed by membrane permeabilization (19).

The BRICHOS-AMPs (Bri2 chondromodulin and prosurfactant protein C) are cysteine-rich AMPs only found in polychaetes. They arise from a precursor containing the BRICHOS domain, a hydrophobic region, and a cysteine-rich C-terminal region folding into a double-stranded β-sheet. Interestingly, the BRICHOS domain is linked to amyloid formations occurring in several major human diseases like Parkinson's and Alzheimer's (20). The first described members of the BRICHOS family were arenicin 1 and 2 in the polychaete *Arenicola marina* (11). The subsequently identified arenicin 3 differs in its primary sequence and contains an extra disulfide bond (12). A similar AMP, alvinellacin, was identified in the hydrothermal Pompeii worm *Alvinella pompejana*, a deep ocean polychaete associated with hydrothermal vents (13). By genome screening of *Capitella teleta*, another member of the BRICHOS-AMPs family called capitellacin was described (14). Nicomicin-1 and-2 were discovered in the artic polychaete *Nicomache minor*, which lives in frigid waters (15). Except for Nicomicin-2, all BRICHOS-AMPs exhibit a broad spectrum of antimicrobial activities against Gram-negative and Gram-positive bacteria, including multi-resistant species and fungi. These AMPs have membranolytic activity, causing membrane permeabilization of microbes within minutes. Arenicins are also hemolytic and cytotoxic to mammalian cells (21).

Hedistin, characterized by a linear α-helix structure, has only been described in the marine polychaete *Hediste diversicolor* (16). Hedistin contains bromotryptophan residues, making it stereochemically less susceptible to proteolysis. It is expressed by NK-like cells, suggesting its involvement in innate immune responses, which is confirmed by its comprehensive antimicrobial activity (16). Perinerin from the Asian marine clamworm *Perinereis aibuhitensis* is a hydrophobic and highly basic peptide with antimicrobial and bactericidal activity (17). It contains four cysteine residues forming disulfide bonds and acts through its pore-forming activity. Ms-hemerycin was identified in the marine lugworm *Marphysa sanguinea*, which lives in a swamp (18). This small peptide forms an unordered structure with a partial helical region. It has strong antimicrobial activity, but its mode of action is unconventional (Table 1).

Cytokines

Most of our understanding of cytokines and their receptors in invertebrates relies on functional assays and similarities at the physicochemical level. The existence of cytokines in annelids, specifically IL-1-α, TNF-α) and POMC-derived peptide-like molecules, is indicated by work using immunohistochemical methods for their detection (22). Flow cytometry using monoclonal antibodies against human or mouse cytokines detected TNF-α and tumor growth factor-α (TGF-α) in earthworm coelomocytes (23).

Several genomic sequence analyses suggest that the innate immune system of invertebrates and vertebrates evolved independently and that invertebrate cytokine-like molecules and vertebrate cytokines do not have the same evolutionary ancestry. One of the molecules that can be considered a cytokine is coelomic cytolytic factor (CCF), which was first found in the earthworm *E. fetida* and later in other earthworm species (24, 25). CCF exists in both membrane and soluble forms and functions primarily as a PRR (4). However, some of its properties indicate that it also functions as a cytokine. Based on similar lectin-like activities, CCF shares functional analogies with mammalian tumor necrosis factor (TNF-α). They both lyse the TNF-sensitive tumor cell line L929, and in African and American trypanosomes, they are secreted after LPS stimulation, have opsonizing properties, bind antigens *via* lectin-like interactions, and increase membrane conductance in mammalian cells by interacting with ion-channels or ion-channel-coupled molecules. Despite the functional analogies of CCF and TNF-α, they do not display any gene or amino acid sequence homology, which indicates distinct evolutionary origins and convergence of invertebrate and vertebrate cytokine molecules (26–28) (Table 2).

Endothelial monocyte-activating polypeptide II (p43/EMAP-II), a chemokine, has been described in earthworms and leeches (46, 47). Endothelial monocyte-activating polypeptide II (p43/EMAP-II), a chemokine, has been described in earthworms and leeches (46, 47). In mammals, EMAP-II is released after processing the p43 precursor and functions as a pro-inflammatory cytokine chemotactic for monocytes and granulocytes and as a marker of microglial cell reactivity induced by brain tissue inflammation or neurodegeneration, but it has more pleiotropic biological activities (48). Similarly, the medicinal leech *Hm*EMAP-II is processed from the *Hm*p43 precursor, which is released by apoptotic cells and serves as a monocyte chemo-attractant (49). The *Hm*EMAP-II has a chemo-attractant effect on microglial cells, *e.g.*, the effect of mammalian EMAP-II on monocytes. Further, gene expression of HmEMAP-II, which can recruit phagocytic cells at lesion sites, is controlled by *Hm*TLR (46). In earthworms, greater expression of EMAP-II is accompanied by a greater abundance of mccEaTLR in seminal vesicles, suggesting its involvement in signal transduction (50) (Table 2).

Interleukin 17 (IL-17), the most conserved cytokine across animal phyla, is an essential factor in innate immunity. In humans, it is produced by activated T lymphocytes and cells participating in innate immunity, *e.g.*, mucosal epithelial cells (51). IL-17 has also been described in some annelids, including the segmented worm *C. teleta*, whose genome screening identified seven genes for IL-17. However, the function of IL-17 molecules has not been identified (31). Although the innate immunity signaling pathways involving cytokine action are not well described in annelids, several pathways have been identified by analysis of the coelomic fluid transcriptome of two

10.3389/fimmu.2022.1051155

TABLE 2 Cytokines in annelids and bivalve mollusks.

Cytokines

Type	Annelids	Bivalve mollusks
TNF-α	**CCF**: found in earthworms; a functional analog of mammalian TNF-α (27)	**AbTNF-α**: homolog of TNF-α in abalone *Haliotis discus discus*; expressed in both immune and non-immune tissues; activation by pathogenic bacteria, viruses, LPS (29) **CgTNF-1, CgTNF-2** in *C. gigas* hemocytes, activated by bacterial stimuli (30)
IL-17	**IL-17**: 7 genes for IL-17 in polychaete *C. teleta*; function was not identified (31)	**IL-17**: 15 genes for IL-17 in *P. fucatamartensii* (**PmIL-17**), 10 in *C. gigas* (**CgIL-17**), 6 in *M. galloprovincialis*, 10 in scallop *Mizuhopecten yessoensis;* mucosal immunity; upregulation after bacterial stimulation; inflammatory response; NF-κB signaling pathway (32–35)
AIF-1	**AIF-1**: detected in leech *H. medicinalis*; chemo-attractant for macrophages that induces their migration towards an inflammation site (36)	**CgAIF-1**: identified in *C. gigas;* calcium-binding cytokine associated with immune cell activation and inflammatory response; activated by multiple PAMPS; enhances mRNA levels of MIF, TNF-α, and IL-17 (37)
EMAP-II	**EMAP-II**: chemokine for microglial cells, found in earthworms and leeches (3, 4)	n/i
MIF	n/i	**MgMIF**: identified in *M. galloprovincialis*; downregulated following a challenge by bacteria and fungi (38); **CfMIF**: identified in scallop *Chlamys farreri*; upregulated by LPS, PGN, and β-glucans; rCfMIF promotes migration of sheep fibroblast into scraped spaces *in vitro* (39) **PoMIF**: identified in oyster *Pinctada fucata*; upregulation upon bacterial stimulation (40)
IFN-γ	n/i	**CgIFNLP**: identified in oyster *C. gigas* has an IFN domain; shares low sequence identities with vertebrate IFNs, but displays a similar three-dimensional structure with class II helical cytokines; promotes the apoptosis and phagocytosis of hemocytes; responds to poly (I:C) stimulation; several components of the **IFN-like system**, activation by virus, poly (I:C), LPS; antiviral immunity (41–44)
Prokineticins	n/i	**Astakins:** homologs of vertebrate prokineticins; regulates hematopoiesis and the function of immune cells; lack of the essential sequence for proper signaling and binding of the G-protein coupled receptors; different receptor-mediated mechanisms; characterized in oyster *C. gigas* with a CgATP synthase β subunit protein involved in signaling in hemocytes (45)

AbTNF-α, tumor necrosis factor alpha homolog in Haliotis; AIF-1, allograft inflammatory factor- 1; CCF, coelomic cytolytic factor; CfMIF, macrophage migration inhibitory factor in Chlamys; C. gigas, Crassostrea gigas; CgAIF-1, allograft inflammatory factor-1 in Crassostrea; CgIFNLP, interferon gamma like protein in Crassostrea; CgIL-17, interleukin 17 in Crassostrea; CgTNF-1/2, tumor necrosis factor alpha in Crassostrea; C. teleta, Capitella teleta; EMAP-II, endothelial monocyte-activating polypeptide II; IL-17, interleukin 17; IFN-γ, interferon gamma; n/i, not identified; LPS, lipopolysaccharide; MgMIF, macrophage migration inhibitory factor in Mytilus; MIF, macrophage migration inhibitory factor; NF-κB, nuclear factor kappa B; PAMPs, pathogen-associated molecular patterns; PGN, peptidoglycan; P. fucata martensii, Pinctada fucata martensii; PmIL-17, interleukin 17 homolog in Pinctada; PoMIF, macrophage migration inhibitory factor in Pinctada; rCfMIF, recombinant CfMIF; TNF-α, tumor necrosis factor alpha.

earthworm species, *E. andrei* and *fetida*. In doing so, specific innate immune pathways were identified, such as the complement cascade, regulation of autophagy, NK-mediated cytotoxicity, chemokine-, MAPK-, mTOR-, NOD-like receptor-, and TLR- and Jak-STAT signaling (52). This suggests that many hidden molecules functioning as cytokines have not been discovered yet, and establishing their ability to build molecular networks is needed (Table 2).

Allograft inflammatory factor-1 (AIF-1) is a calcium-binding protein induced by cytokines participating in the allograft immune and inflammatory response of humans. It is expressed by monocytes/macrophages, the homolog of which was detected in the medicinal leech *H. medicinalis*, where it serves as a potent chemo-attractant for macrophages, and it induces their migration towards sites of inflammation (36) (Table 2).

Bivalves

Among *Mollusca*, bivalves, including edible and aquacultured species (oysters, mussels, clams, etc.), are the most widely studied relative to their immune defenses. Bivalve hemocytes are responsible for cell-mediated immunity through the combined action of phagocytic processes and humoral defense factors such as agglutinins (*e.g.*, lectins), lysosomal enzymes (*e.g.*, acid phosphatase, lysozyme), reactive oxygen intermediates, and cytokines and various AMPs (53). Bivalve hemolymph serum contains a wide range of secreted components that participate in agglutination, opsonization, degradation, and encapsulation of microorganisms, as well as clotting and wound healing. In general, non-self recognition (in the form of PAMP) by soluble lectins and other PRRs and opsonins in hemolymph and hemocytes, which are present in the circulation and tissues, triggers signaling transduction cascades that release several effectors from tissues and hemocytes that lead to humoral and cellular immune responses, depending on the nature and location of the immune stimuli. An overview of the most recent accomplishments in the fields of recognition, agglutination, and opsonization (lectins, fibrinogen-related domain-containing proteins, C1q domain-containing proteins, lysozymes, bactericidal/permeability-increasing proteins, and other pore-forming molecules, proteases, and protease inhibitors, cathepsins, phenoloxidase cascade) is provided by Gerdol et al. (54).

AMPs

From the first identification (20 years ago), in the hemolymph of the mussel *Mytilus galloprovincialis*, of a peptide sharing sequence similarity with the arthropod defensin, and therefore named *Mytilus galloprovincialis* Defensin-1 (MGD-1) (55), research on bivalve AMPs has steadily increased. With advances in molecular technologies, different AMPs have been identified in several bivalve species (mussels, oysters, clams, scallops), which are generally characterized by structural differences, different activities, differential tissue/cell expression, accessory functions, and often species-specific biological properties (reviewed in (54, 56, 57).

Resilience to pollution, pathogens, and changing environmental conditions means that some bivalve species are important models for studying the role of AMPs in adaptation and immunity. The Mediterranean mussel, *M. galloprovincialis*, which is not subjected to the same massive pathogen-associated mortalities as other bivalves, represents a unique model for studying AMPs. In this species, a remarkable abundance of AMPs has been reported, with antimicrobial activity against various bivalve and vertebrate pathogens, with different AMPs (including defensins, mytilins, and myticins) sharing antibacterial and antifungal properties; mytimycin appears to be a strictly antifungal protein. *Mytilus* AMPs are highly polymorphic and have high genetic variability: the recent assembly of the *M. galloprovincialis* genome showed that, although dozens of different sequence variants were identified for each AMP family, each individual possessed a unique combination of a small number of variants (58).

Myticin C (MytC), the most expressed AMP in adult mussels, has the highest RNA polymorphism relative to other mussel AMPs (59). MytC has been shown to inhibit the replication of bacteria, fish viruses, and human herpesvirus (56) and to have chemotactic and wound healing properties (59, 60). In oyster hemocytes, treatment with mussel hemolymph, or synthetic MytC peptides, inhibits replication of OsHV-1. In addition, *in vivo* studies suggested that overexpression of MytC in hemocytes could alter the transcription of other immune-related genes (AMPs, complement proteins, lysozyme). These data suggested that MytC may also play a role as an immune system modulator with chemokine-like activities (56, 59). In *M. galloprovincialis*, the extensive repertoire of AMPs, endowed with a broad spectrum of immune functions, might have significantly contributed to the evolutionary advantage of mussels in adapting to extremely changing environments (56, 58).

Among AMPs, Big defensins (BD), the ancestors of β-Defensins, essential components of innate immunity in vertebrates and invertebrates, are a large family of AMPs characterized by a highly hydrophobic globular N-terminal domain, which is present in different phylogenetically distant species, including both marine and freshwater bivalves (61). Bivalves often display an expanded repertoire of BD sequences and thus represent an excellent case for investigating the processes behind the remarkable diversity of the primary sequence, both between and within species. In contrast with human β-defensins, BDs are characterized by antimicrobial activities over a wide range of osmolarity. Studies in bivalves showed that the presence of the conserved hydrophobic domain confers bactericidal activity even at high salt concentrations (62). Moreover, bivalve BD displays a characteristic mechanism of action, i.e., the N-terminal domain drives bacteria-triggered peptide assembly into antimicrobial aggregates termed "nanonets," which entrap microbes and prevent invasive pathogens from entering host cells (63). This effect has been described for the Cg-BigDef1 in *C. gigas* (62) and the ApBD1 in the scallop *Argopecten purpuratus* (64).

An exhaustive list of AMPs isolated from marine bivalves and their main characteristics (peptide sequence, length, net charge, percent hydrophobic residues, structure, antimicrobial activity), updated to 2017, is provided in an article by Zannella C, et al. Microbial diseases of bivalve mollusks: infections, immunology, and antimicrobial defense (57). As mentioned above, most data refer to *Mytilus* sp. and *Crassostrea gigas* (57). More recently, other AMPs have also been characterized, *i.e.*, Myticusin-beta in *Mytilus coruscus* (65), Myticalin in *M. galloprovincialis* (66), and hemoglobin-derived polypeptides in *Tegillarca granosa* (67).

Cytokines

Recent developments in the study of bivalves are based on studies first carried out on Pacific oyster *C. gigas*, one of the most widely cultivated marine species. Partly because of its commercial importance, Guofan Z. et al., using genetic and genomic techniques, sequenced the genome in 2012 (68). The sequencing led to a significant increase in studies on bivalve cytokines (roughly 70% of all publications on the subject have occurred in the last decade, according to PubMed).

Pioneering work in the early '90s shed the first light on the conservation of cytokine-like molecules in mollusks (69, 70). Subsequent studies indicated that host defense mechanisms in different invertebrate groups, including bivalves, can be modulated by a cytokine-like network like that in vertebrates (71–73). However, until the identification of the first molecules with a cytokine-like activity (24, 74), most information relied on functional assays, using heterologous cytokines and antibodies directed towards vertebrate cytokines and their receptors.

The first studies were limited to evolutionarily conserved factors identifiable by sequence similarities, such as IL-17 (32), MIF (38), AIF-1 (37), and TNF-α (29, 30). The functional role of these conserved cytokines was indicated by their increased expression in response to bacterial stimuli. Most current information for IL-17 comes from phylogenetic studies, identification of related signaling pathways, and effector mechanisms in models of *M.*

galloprovincialis and *C. gigas* (33–35). IL-17 plays a crucial role in mucosal immunity in mussels, just like in vertebrates (35), which was first identified in *C. gigas* (32) and later on in *Pinctada fucata* (75). Further genomic searching found that there were fifteen IL-17 genes in *P. fucata martensii*, ten in *C. gigas*, six in *M. galloprovincialis*, and ten in scallop *Mizuhopecten yessoensis* (31) (Table 2). At least some of these IL-17 molecules, *e.g.*, PmIL-17-2 from *P. fucata martensii and CgIL-17-5* from *C. gigas*, were found to be involved in the innate immune response after bacterial stimulation (31, 34). The inflammatory IL-17 cytokines are encoded by a diverse gene family leading to expanded IL-17 repertoires in various marine invertebrates. This can be seen, for example, in the study of 16 mussel genomes, which revealed 379 unique IL-17 sequences and 96 unique IL-17 receptor variants (35). Phylogenetic analysis revealed that all detected invertebrate IL-17 genes, from both annelids and mollusks, are clustered into one group, suggesting a common ancestral gene of these invertebrate IL-17s (31) (Table 2).

However, for many other divergent cytokines, their presence and function in bivalves remained elusive and can only be demonstrated indirectly; interferon-γ is a good example. In *M. galloprovincialis* hemocytes, human recombinant IFN-γ was shown to activate members of a STAT-like pathway; moreover, hemocyte pretreatment with IFN-γ increased bacteria-induced STAT1-like phosphorylation, indicating that the function of mussel hemocytes may be physiologically regulated *in vivo* by endogenous IFN-γ-like cytokines (76). Since the release of the genome of *C. gigas* and other species, several components of the IFN-like system (IFN-like molecules, IFN-like receptors, and components of related signaling pathways) have been identified (41–43). Interestingly, the IFN system of bivalves can be activated by virus or poly (I:C) challenges and further regulate the antiviral response of hemocytes; however, some components also showed a positive response to other immunostimulants, such as lipopolysaccharide (LPS) and bacteria. Unlike vertebrate IFN systems, the bivalve IFN-like system may participate in multiple biological activities, such as antibacterial immunity (reviewed in (44) (Table 2).

Other cytokines that developed independently in different invertebrate groups are now being identified. For example, Astakines, considered homologous of vertebrate prokineticins, regulate hematopoiesis and immune cell function. Astakines lack the AVITGA sequence in the N-terminus essential for proper signaling and binding of G-protein coupled receptors, indicating the presence of distinct receptor-mediated mechanisms in invertebrates. Recently, a *C. gigas* astakine was identified and characterized using a CgATP synthase β subunit protein, which is involved in hemocyte signaling (45).

Whatever the role of the various bivalve cytokines, transcriptomic data indicate modulation within different species in response to environmental stressors ((77) and refs. therein). However, little is known about how cytokine expression is physiologically regulated. Recent studies underlined the role of different miRNAs in the expression of TNF-α and IL-17 in oyster hemocytes (78, 79).

Conclusions and perspectives

Annelids and bivalve mollusks represent important invertebrate groups for investigating innate immunity, particularly for the wide range of soluble immune mediators, which show a large diversity in structure and functions.

With regards to AMPs in annelids, three main classes have been identified so far in oligochaetes (lumbricins), polychaetes (BRICHOS-AMPs), and leeches (macines). Bivalves, in particular marine species, display a much wider repertoire of different AMPs (55), with some of them (*i.e.*, myticins, big defensins) also showing immune-related functions other than direct antibacterial activity.

Several soluble factors endowed with cytokine-like activity have been described in annelids and bivalves; however, few are structurally conserved in both groups relative to their vertebrate counterparts (*i.e.*, IL-17), which underlies their distinct evolutionary origin. From this perspective, research on invertebrate cytokines still represents an open and promising field for the identification of new immunoactive molecules.

Moreover, the properties of AMPs and cytokines in both groups of invertebrates suggest they have application potential in human health and the environment, especially given the global problem of antibiotic resistance. The increasing appearance of bacterial strains resistant to antibiotics has promoted an intense search for new anti-infective drugs that can be an effective alternative to conventional antibiotics. Invertebrate AMPs are in the spotlight as innovative drug candidates not only for the treatment of infectious diseases but also for their immunomodulatory potential.

To develop AMPs as efficient and safe new drugs, their mode of action needs to be fully understood. Despite their advantages, selecting suitable AMPs for clinical use is progressing very slowly. Pharmaceutical companies have had little interest in developing new antibiotics over the last 30 years because of high production costs and short efficacy periods (since bacterial resistance to new drugs develops rapidly). Although microorganisms can develop resistance to AMPs as a consequence of continuous selection pressure, AMPs still present several important advantages over antibiotics, e.g., they are much less stable in the environment and thus much reduced environmental impact. It was shown that cationic AMPs do not induce bacterial stress pathways and thus do not increase bacterial mutagenesis, which is not the case with antibiotics (80). Further, AMPs often use different mechanisms of action, including disruption of bacterial membranes, inhibition of metabolic pathways, and recruitment and activation of various immune cells (81).

Few annelid AMPs are currently being evaluated in clinical trials as treatments against various bacterial and fungal infections. An analog of Arenicin-3 was selected for preclinical trial by

Adenium Biotech Ltd. for its effective action in treating urinary tract infections (82), but the trial was unfortunately stopped due to the company's bankruptcy. The only molecule derived from the earthworm *L. rubellus* and successfully used in therapy, although not an AMP, is the enzyme lumbrokinase, used for its fibrinolytic properties to treat thrombus-related diseases. Similarly, since leech saliva contains large amounts of various enzymes with thrombolytic, anticoagulant, anti-inflammatory, and analgetic activity, leeches have been used to treat various diseases such as vascular disorders, cardiovascular disease, skin disorders, diabetic foot ulcers, migraine, knee osteoarthritis, and even in cosmetic surgery (83). The best-known enzyme from leeches is hirudin, which was discovered in 1884 when an extract from *H. medicinalis* was found to have anticoagulant properties (84). Recently, hirudin derivatives (*e.g.*, lepirudin, desirudin) and hirudin analogs (*e.g.*, bivalirudin) have been used clinically as direct bivalent thrombin inhibitors. However, despite its effectiveness, safety, and few complications, leech treatment is still controversial.

Despite the enormous potential of marine biodiversity for discovering AMPs, no bivalve AMPs have been tested in clinical trials. If, on the one hand, their resistance to high salt concentrations may represent potential advantages in medical applications (57), on the other hand, development has been hampered by many issues, such as discrepancies between *in vitro* and *in vivo* tests and susceptibility to proteases and pH, which affects AMP half-life *in vivo* (85).

Annelids and bivalves represent a vast source of AMPs that could serve as potential candidates for antibacterial drug development in human and veterinary medicine. Due to their broad spectrum of antimicrobial activities and emerging new immune modulation functions, AMPs have great potential for biotechnological applications and continue to be the subject of many molecular and functional studies. Antimicrobial peptides (AMPs) have been successfully applied in various areas of human health, including clinical medicine and drugs. However, as with AMPs from humans and other sources, high cost, poor stability, and toxicity are disadvantages that limit the clinical development of AMPs (86). In this light, a promising biotechnology field is genetically engineered microorganisms, where natural AMPs can be expressed or modified to create improved antibacterial abilities and increased stability while reducing toxicity (86).

The same applies to their cytokines, which act as natural immunomodulators with potential new biomedical applications. However, our understanding of invertebrate cytokines is still limited compared to AMPs and hampers the development of biotechnological products. The multiple and complex immunoregulatory roles of annelid and bivalve cytokines represent a still largely unexplored field of research with substantial innovative potential. This particularly applies to those cytokines that are not structurally conserved and whose role and molecular machinery are still elusive. The application of multiple molecular and functional approaches will help to better define their biological role in immune homeostasis in health and disease.

Author contributions

PP, MA, TB, and LC contributed to the writing of the manuscript. PP and LC provided critical review and input. All authors read and approved the final manuscript.

Funding

This project has received funding from the European Union's Horizon 2020 research and innovation program under the Marie Skłodowska-Curie grant agreement No 671881.

Conflict of interest

The authors declare that the research was conducted in the absence of any commercial or financial relationships that could be construed as a potential conflict of interest.

Publisher's note

References

1. Bilej M, Prochazkova P, Silerova M, Joskova R. Earthworm immunity. *Adv Exp Med Biol* (2010) 708:66–79. doi: 10.1007/978-1-4419-8059-5_4

2. Liebeke M, Strittmatter N, Fearn S, Morgan AJ, Kille P, Fuchser J, et al. Unique metabolites protect earthworms against plant polyphenols. *Nat Commun* (2015) 6:7869. doi: 10.1038/ncomms8869

3. Schenk S, Hoeger U. Annelid coelomic fluid proteins. In: Schenk S, Hoeger U, editors. *Vertebrate and invertebrate respiratory proteins, lipoproteins and other body fluid proteins subcellular biochemistry*, vol. 94 . Cham: Springer (2020).

4. Prochazkova P, Roubalova R, Dvorak J, Navarro Pacheco NI, Bilej M. Pattern recognition receptors in annelids. *Dev Comp Immunol* (2020) 102:103493. doi: 10.1016/j.dci.2019.103493

5. Cho JH, Park CB, Yoon YG, Kim SC. Lumbricin I, a novel proline-rich antimicrobial peptide from the earthworm: purification, cDNA cloning and molecular characterization. *Biochim Biophys Acta* (1998) 1408(1):67–76. doi: 10.1016/S0925-4439(98)00058-1

6. Schikorski D, Cuvillier-Hot V, Leippe M, Boidin-Wichlacz C, Slomianny C, Macagno E, et al. Microbial challenge promotes the regenerative process of the

injured central nervous system of the medicinal leech by inducing the synthesis of antimicrobial peptides in neurons and microglia. *J Immunol* (2008) 181(2):1083–95. doi: 10.4049/jimmunol.181.2.1083

7. Wang X, Wang X, Zhang Y, Qu X, Yang S. An antimicrobial peptide of the earthworm pheretima tschiliensis: cDNA cloning, expression and immunolocalization. *Biotechnol Lett* (2003) 25(16):1317–23. doi: 10.1023/A:1024999206117

8. Li W, Li S, Zhong J, Zhu Z, Liu J, Wang W. A novel antimicrobial peptide from skin secretions of the earthworm, pheretima guillelmi (Michaelsen). *Peptides* (2011) 32(6):1146–50. doi: 10.1016/j.peptides.2011.04.015

9. Bodo K, Boros A, Rumpler E, Molnar L, Borocz K, Nemeth P, et al. Identification of novel lumbricin homologues in eisenia andrei earthworms. *Dev Comp Immunol* (2019) 90:41–6. doi: 10.1016/j.dci.2018.09.001

10. Tasiemski A, Vandenbulcke F, Mitta G, Lemoine J, Lefebvre C, Sautiere PE, et al. Molecular characterization of two novel antibacterial peptides inducible upon bacterial challenge in an annelid, the leech theromyzon tessulatum. *J Biol Chem* (2004) 279(30):30973–82. doi: 10.1074/jbc.M312156200

11. Ovchinnikova TV, Aleshina GM, Balandin SV, Krasnosdembskaya AD, Markelov ML, Frolova EI, et al. Purification and primary structure of two isoforms of arenicin, a novel antimicrobial peptide from marine polychaeta arenicola marina. *FEBS Lett* (2004) 577(1-2):209–14. doi: 10.1016/j.febslet.2004.10.012

12. Sandvang D, Kristensen HH, Neve S. Arenicin-3: A novel antimicrobial peptide showing potent in vitro activity against gram-negative multiresistant clinical isolates. Proceedings of the 46th Annual Meeting, Idsa. (2008) Washington, DC, USA. p. F1-3986.

13. Tasiemski A, Jung S, Boidin-Wichlacz C, Jollivet D, Cuvillier-Hot V, Pradillon F, et al. Characterization and function of the first antibiotic isolated from a vent organism: the extremophile metazoan alvinella pompejana. *PloS One* (2014) 9(4):e95737. doi: 10.1074/jbc.M312156200

14. Safronova VN, Panteleev PV, Sukhanov SV, Toropygin IY, Bolosov IA, Ovchinnikova TV. Mechanism of action and therapeutic potential of the beta-hairpin antimicrobial peptide capitellacin from the marine polychaeta capitella teleta. *Mar Drugs* (2022) 20(3):167. doi: 10.3390/md20030167

15. Panteleev PV, Tsarev AV, Bolosov IA, Paramonov AS, Marggraf MB, Sychev SV, et al. Novel antimicrobial peptides from the arctic polychaeta nicomache minor provide new molecular insight into biological role of the BRICHOS domain. *Mar Drugs* (2018) 16(11):401. doi: 10.3390/md16110401

16. Tasiemski A, Schikorski D, Le Marrec-Croq F, Pontoire-Van Camp C, Boidin-Wichlacz C, Sautiere PE. Hedistin: A novel antimicrobial peptide containing bromotryptophan constitutively expressed in the NK cells-like of the marine annelid, nereis diversicolor. *Dev Comp Immunol* (2007) 31(8):749–62. doi: 10.1016/j.dci.2006.11.003

17. Pan W, Liu X, Ge F, Han J, Zheng T. Perinerin, a novel antimicrobial peptide purified from the clamworm perinereis aibuhitensis grube and its partial characterization. *J Biochem* (2004) 135(3):297–304. doi: 10.1093/jb/mvh036

18. Seo JK, Nam BH, Go HJ, Jeong M, Lee KY, Cho SM, et al. Hemerythrin-related antimicrobial peptide, msHemerycin, purified from the body of the lugworm, marphysa sanguinea. *Fish Shellfish Immunol* (2016) 57:49–59. doi: 10.1016/j.fsi.2016.08.018

19. Jung S, Sonnichsen FD, Hung CW, Tholey A, Boidin-Wichlacz C, Haeusgen W, et al. Macin family of antimicrobial proteins combines antimicrobial and nerve repair activities. *J Biol Chem* (2012) 287(17):14246–58. doi: 10.1074/jbc.M111.336495

20. Gharibyan AL, Wasana Jayaweera S, Lehmann M, Anan I, Olofsson A. Endogenous human proteins interfering with amyloid formation. *Biomolecules* (2022) 12(3):446. doi: 10.3390/biom12030446

21. Edwards IA, Elliott AG, Kavanagh AM, Zuegg J, Blaskovich MA, Cooper MA. Contribution of amphipathicity and hydrophobicity to the antimicrobial activity and cytotoxicity of beta-hairpin peptides. *ACS Infect Dis* (2016) 2(6):442–50. doi: 10.1021/acsinfecdis.6b00045

22. Cooper E, Franchini A, Ottaviani E. Earthworm coelomocytes possess immunoreactive cytokines and POMC-derived peptides. *Anim Biol* (1995) 4 (1):25–9.

23. Engelmann P, Pal J, Berki T, Cooper EL, Nemeth P. Earthworm leukocytes react with different mammalian antigen-specific monoclonal antibodies. *Zool (Jena)* (2002) 105(3):257–65. doi: 10.1078/0944-2006-00068

24. Beschin A, Bilej M, Torreele E, De Baetselier P. On the existence of cytokines in invertebrates. *Cell Mol Life Sci* (2001) 58(5-6):801–14. doi: 10.1007/PL00000901

25. Silerova M, Prochazkova P, Joskova R, Josens G, Beschin A, De Baetselier P, et al. Comparative study of the CCF-like pattern recognition protein in different lumbricid species. *Dev Comp Immunol* (2006) 30(9):765–71. doi: 10.1016/j.dci.2005.11.002

26. Beschin A, Bilej M, Brys L, Torreele E, Lucas R, Magez S, et al. Convergent evolution of cytokines. *Nature* (1999) 400(6745):627–8. doi: 10.1038/23164

27. Beschin A, Bilej M, Magez S, Lucas R, De Baetselier P. Functional convergence of invertebrate and vertebrate cytokine-like molecules based on a similar lectin-like activity. *Prog Mol Subcell Biol* (2004) 34:145–63. doi: 10.1007/978-3-642-18670-7_6

28. Bilej M, Joskova R, Van den Bergh R, Prochazkova P, Silerova M, Ameloot P, et al. An invertebrate TNF functional analogue activates macrophages *via* lectin-saccharide interaction with ion channels. *Int Immunol* (2006) 18(12):1663–70. doi: 10.1093/intimm/dxl100

29. De Zoysa M, Jung S, Lee J. First molluscan TNF-alpha homologue of the TNF superfamily in disk abalone: molecular characterization and expression analysis. *Fish Shellfish Immunol* (2009) 26(4):625–31. doi: 10.1016/j.fsi.2008.10.004

30. Zheng Y, Liu Z, Wang L, Li M, Zhang Y, Zong Y, et al. A novel tumor necrosis factor in the pacific oyster crassostrea gigas mediates the antibacterial response by triggering the synthesis of lysozyme and nitric oxide. *Fish Shellfish Immunol* (2020) 98:334–41. doi: 10.1016/j.fsi.2019.12.073

31. Cao Y, Yang S, Feng C, Zhan W, Zheng Z, Wang Q, et al. Evolution and function analysis of interleukin-17 gene from pinctada fucata martensii. *Fish Shellfish Immunol* (2019) 88:102–10. doi: 10.1016/j.fsi.2019.02.044

32. Roberts S, Gueguen Y, de Lorgeril J, Goetz F. Rapid accumulation of an interleukin 17 homolog transcript in crassostrea gigas hemocytes following bacterial exposure. *Dev Comp Immunol* (2008) 32(9):1099–104. doi: 10.1016/j.dci.2008.02.006

33. Cao W, Wang W, Fan S, Li J, Li Q, Wu S, et al. The receptor CgIL-17R1 expressed in granulocytes mediates the CgIL-17 induced haemocytes proliferation in crassostrea gigas. *Dev Comp Immunol* (2022) 131:104376. doi: 10.1016/j.dci.2022.104376

34. Lv X, Sun J, Li Y, Yang W, Wang L, Leng J, et al. CgIL17-5 regulates the mRNA expressions of immune effectors through inducing the phosphorylation of CgMAPKs and the nuclear translocation of CgRel and CgAP-1 in the pacific oyster crassostrea gigas. *Dev Comp Immunol* (2022) 127:104263. doi: 10.1016/j.dci.2021.104263

35. Saco A, Rey-Campos M, Rosani U, Novoa B, Figueras A. The evolution and diversity of interleukin-17 highlight an expansion in marine invertebrates and its conserved role in mucosal immunity. *Front Immunol* (2021) 12:692997. doi: 10.3389/fimmu.2021.692997

36. Schorn T, Drago F, Tettamanti G, Valvassori R, de Eguileor M, Vizioli J, et al. Homolog of allograft inflammatory factor-1 induces macrophage migration during innate immune response in leech. *Cell Tissue Res* (2015) 359(3):853–64. doi: 10.1007/s00441-014-2058-7

37. Zhang Y, Li J, Yu F, He X, Yu Z. Allograft inflammatory factor-1 stimulates hemocyte immune activation by enhancing phagocytosis and expression of inflammatory cytokines in crassostrea gigas. *Fish Shellfish Immunol* (2013) 34 (5):1071–7. doi: 10.1016/j.fsi.2013.01.014

38. Parisi MG, Toubiana M, Mangano V, Parrinello N, Cammarata M, Roch P. MIF from mussel: coding sequence, phylogeny, polymorphism, 3D model and regulation of expression. *Dev Comp Immunol* (2012) 36(4):688–96. doi: 10.1016/j.dci.2011.10.014

39. Li F, Huang S, Wang L, Yang J, Zhang H, Qiu L, et al. A macrophage migration inhibitory factor like gene from scallop chlamys farreri: Involvement in immune response and wound healing. *Dev Comp Immunol* (2011) 35(1):62–71. doi: 10.1016/j.dci.2010.08.009

40. Cui S, Zhang D, Jiang S, Pu H, Hu Y, Guo H, et al. A macrophage migration inhibitory factor like oxidoreductase from pearl oyster pinctada fucata involved in innate immune responses. *Fish Shellfish Immunol* (2011) 31(2):173–81. doi: 10.1016/j.fsi.2011.03.009

41. Qiao X, Zong Y, Liu Z, Wu Z, Li Y, Wang L, et al. The cGAS/STING-TBK1-IRF regulatory axis orchestrates a primitive interferon-like antiviral mechanism in oyster. *Front Immunol* (2021) 12:689783. doi: 10.3389/fimmu.2021.689783

42. Zhang R, Liu R, Wang W, Xin L, Wang L, Li C, et al. Identification and functional analysis of a novel IFN-like protein (CgIFNLP) in crassostrea gigas. *Fish Shellfish Immunol* (2015) 44(2):547–54. doi: 10.1016/j.fsi.2015.03.015

43. Zhang R, Liu R, Xin L, Chen H, Li C, Wang L, et al. A CgIFNLP receptor from crassostrea gigas and its activation of the related genes in human JAK/STAT signaling pathway. *Dev Comp Immunol* (2016) 65:98–106. doi: 10.1016/j.dci.2016.06.010

44. Qiao X, Wang L, Song L. The primitive interferon-like system and its antiviral function in molluscs. *Dev Comp Immunol* (2021) 118:103997. doi: 10.1016/j.dci.2021.103997

45. Yang Y, Qiao X, Song X, Zhang D, Yu S, Dong M, et al. CgATP synthase beta subunit involved in the regulation of haemocytes proliferation as a CgAstakine receptor in crassostrea gigas. *Fish Shellfish Immunol* (2022) 123:85–93. doi: 10.1016/j.fsi.2022.02.054

46. Schikorski D, Cuvillier-Hot V, Boidin-Wichlacz C, Slomianny C, Salzet M, Tasiemski A. Deciphering the immune function and regulation by a TLR of the

cytokine EMAPII in the lesioned central nervous system using a leech model. *J Immunol* (2009) 183(11):7119–28. doi: 10.4049/jimmunol.0900538

47. Pacheco NIN, Roubalova R, Dvorak J, Benada O, Pinkas D, Kofronova O, et al. Understanding the toxicity mechanism of CuO nanoparticles: the intracellular view of exposed earthworm cells. *Environ Science-Nano* (2021) 8(9):2464–77. doi: 10.1039/D1EN00080B

48. Shalak V, Kaminska M, Mitnacht-Kraus R, Vandenabeele P, Clauss M, Mirande M. The EMAPII cytokine is released from the mammalian multisynthetase complex after cleavage of its p43/proEMAPII component. *J Biol Chem* (2001) 276(26):23769–76. doi: 10.1074/jbc.M100489200

49. Knies UE, Behrensdorf HA, Mitchell CA, Deutsch U, Risau W, Drexler HC, et al. Regulation of endothelial monocyte-activating polypeptide II release by apoptosis. *Proc Natl Acad Sci USA* (1998) 95(21):12322–7. doi: 10.1073/pnas.95.21.12322

50. Prochazkova P, Roubalova R, Skanta F, Dvorak J, Pacheco NIN, Kolarik M, et al. Developmental and immune role of a novel multiple cysteine cluster TLR from eisenia andrei earthworms. *Front Immunol* (2019) 10:1277. doi: 10.3389/fimmu.2019.01277

51. Cua DJ, Tato CM. Innate IL-17-producing cells: the sentinels of the immune system. *Nat Rev Immunol* (2010) 10(7):479–89. doi: 10.1038/nri2800

52. Hernadi SB. *Earthworm system immunity and its modulation by nanoparticles*. Cardiff: Cardiff University (2020).

53. Canesi L, Pruzzo C. Specificity of innate immunity in bivalves: A lesson from bacteria. In: Ballarin L, Cammarata M, editors. *Lessons in immunity: from single-cell organisms to mammals*. London, UK: Academic Press, Elsevier Inc (2016).

54. Gerdol M, Gomez-Chiari M, Castillo MG, Figueras A, Fiorito G, Moreira R, et al. Immunity in molluscs: recognition and effector mechanisms, with a focus on bivalvia. In: Cooper E, editor. *Advances in comparative immunology*. Cham, Switzerland: Springer (2018). p. 225–342.

55. Hubert F, Noel T, Roch P. A member of the arthropod defensin family from edible Mediterranean mussels (Mytilus galloprovincialis). *Eur J Biochem* (1996) 240(1):302–6. doi: 10.1111/j.1432-1033.1996.0302h.x

56. Figueras A, Moreira R, Sendra M, Novoa B. Genomics and immunity of the Mediterranean mussel mytilus galloprovincialis in a changing environment. *Fish Shellfish Immunol* (2019) 90:440–5. doi: 10.1016/j.fsi.2019.04.064

57. Zannella C, Mosca F, Mariani F, Franci G, Folliero V, Galdiero M, et al. Microbial diseases of bivalve mollusks: infections, immunology and antimicrobial defense. *Mar Drugs* (2017) 15(6):182. doi: 10.3390/md15060182

58. Gerdol M, Moreira R, Cruz F, Gomez-Garrido J, Vlasova A, Rosani U, et al. Massive gene presence-absence variation shapes an open pan-genome in the Mediterranean mussel. *Genome Biol* (2020) 21(1):275. doi: 10.1186/s13059-020-02180-3

59. Balseiro P, Falco A, Romero A, Dios S, Martinez-Lopez A, Figueras A, et al. Mytilus galloprovincialis myticin c: a chemotactic molecule with antiviral activity and immunoregulatory properties. *PloS One* (2011) 6(8):e23140. doi: 10.1371/journal.pone.0023140

60. Rey-Campos M, Moreira R, Romero A, Medina-Gali RM, Novoa B, Gasset M, et al. Transcriptomic analysis reveals the wound healing activity of mussel myticin c. *Biomolecules* (2020) 10(1):133. doi: 10.3390/biom10010133

61. Gerdol M, Schmitt P, Venier P, Rocha G, Rosa RD, Destoumieux-Garzon D. Functional insights from the evolutionary diversification of big defensins. *Front Immunol* (2020) 11:758. doi: 10.3389/fimmu.2020.00758

62. Loth K, Vergnes A, Barreto C, Voisin SN, Meudal H, Da Silva J, et al. The ancestral n-terminal domain of big defensins drives bacterially triggered assembly into antimicrobial nanonets. *mBio* (2019) 10(5):e01821-19. doi: 10.1128/mBio.01821-19

63. Ouellette AJ, Selsted ME. Immunology. HD6 defensin nanonets. *Science* (2012) 337(6093):420–1. doi: 10.1126/science.1225906

64. Stambuk F, Ojeda C, Machado Matos G, Rosa RD, Mercado L, Schmitt P. Big defensin from the scallop argopecten purpuratus ApBD1 is an antimicrobial peptide which entraps bacteria through nanonets formation. *Fish Shellfish Immunol* (2021) 119:456–61. doi: 10.1016/j.fsi.2021.10.037

65. Oh R, Lee MJ, Kim YO, Nam BH, Kong HJ, Kim JW, et al. Myticusin-beta, antimicrobial peptide from the marine bivalve, mytilus coruscus. *Fish Shellfish Immunol* (2020) 99:342–52. doi: 10.1016/j.fsi.2020.02.020

66. Pacor S, Benincasa M, Musso MV, Krce L, Aviani I, Pallavicini A, et al. The proline-rich myticalins from mytilus galloprovincialis display a membrane-permeabilizing antimicrobial mode of action. *Peptides* (2021) 143:170594. doi: 10.1016/j.peptides.2021.170594

67. Zheng X, Yuan C, Zhang Y, Zha S, Mao F, Bao Y. Prediction and characterization of a novel hemoglobin-derived mutant peptide (mTgHbP7) from tegillarca granosa. *Fish Shellfish Immunol* (2022) 125:84–9. doi: 10.1016/j.fsi.2022.05.007

68. Zhang G, Fang X, Guo X, Li L, Luo R, Xu F, et al. The oyster genome reveals stress adaptation and complexity of shell formation. *Nature* (2012) 490(7418):49–54. doi: 10.1038/nature11413

69. Hughes TK, Smith EM, Leung MK, Stefano GB. Immunoreactive cytokines in mytilus edulis nervous and immune interactions. *Acta Biol Hung* (1992) 43(1-4):269–73.

70. Ottaviani E, Franchini A. Immune and neuroendocrine responses in molluscs: the role of cytokines. *Acta Biol Hung* (1995) 46(2-4):341–9.

71. Ottaviani E, Malagoli D, Franchini A. Invertebrate humoral factors: cytokines as mediators of cell survival. *Prog Mol Subcell Biol* (2004) 34:1–25. doi: 10.1007/978-3-642-18670-7_1

72. Beschin A, Muller WEG. *Invertebrate cytokines and the phylogeny of immunity: facts and paradoxes*. Berlin Heidelberg New York: Springer-Verlag (2004).

73. Betti M, Ciacci C, Lorusso LC, Canonico B, Falcioni T, Gallo G, et al. Effects of tumour necrosis factor alpha (TNFalpha) on mytilus haemocytes: role of stress-activated mitogen-activated protein kinases (MAPKs). *Biol Cell* (2006) 98(4):233–44. doi: 10.1042/BC20050049

74. Herpin A, Lelong C, Favrel P. Transforming growth factor-beta-related proteins: an ancestral and widespread superfamily of cytokines in metazoans. *Dev Comp Immunol* (2004) 28(5):461–85. doi: 10.1016/j.dci.2003.09.007

75. Wu SZ, Huang XD, Li Q, He MX. Interleukin-17 in pearl oyster (Pinctada fucata): molecular cloning and functional characterization. *Fish Shellfish Immunol* (2013) 34(5):1050–6. doi: 10.1016/j.fsi.2013.01.005

76. Canesi L, Betti M, Ciacci C, Citterio B, Pruzzo C, Gallo G. Tyrosine kinase-mediated cell signalling in the activation of mytilus hemocytes: possible role of STAT-like proteins. *Biol Cell* (2003) 95(9):603–13. doi: 10.1016/j.biolcel.2003.09.006

77. Balbi T, Auguste M, Ciacci C, Canesi L. Immunological responses of marine bivalves to contaminant exposure: contribution of the -omics approach. *Front Immunol* (2021) 12:618726. doi: 10.3389/fimmu.2021.618726

78. Han Z, Li J, Wang W, Li J, Zhao Q, Li M, et al. A calmodulin targeted by miRNA scaffold659_26519 regulates IL-17 expression in the early immune response of oyster crassostrea gigas. *Dev Comp Immunol* (2021) 124:104180. doi: 10.1016/j.dci.2021.104180

79. Chen H, Zhou Z, Wang H, Wang L, Wang W, Liu R, et al. An invertebrate-specific and immune-responsive microRNA augments oyster haemocyte phagocytosis by targeting CgIkappaB2. *Sci Rep* (2016) 6:29591. doi: 10.1038/srep29591

80. Rodriguez-Rojas A, Makarova O, Rolff J. Antimicrobials, stress and mutagenesis. *PloS Pathog* (2014) 10(10):e1004445. doi: 10.1371/journal.ppat.1004445

81. Kumar P, Kizhakkedathu JN, Straus SK. Antimicrobial peptides: Diversity, mechanism of action and strategies to improve the activity and biocompatibility *In vivo*. *Biomolecules* (2018) 8(1):4. doi: 10.3390/biom8010004

82. Elliott AG, Huang JX, Neve S, Zuegg J, Edwards IA, Cain AK, et al. An amphipathic peptide with antibiotic activity against multidrug-resistant gram-negative bacteria. *Nat Commun* (2020) 11(1):3184. doi: 10.1038/s41467-020-16950-x

83. Abdualkader AM, Ghawi AM, Alaama M, Awang M, Merzouk A. Leech therapeutic applications. *Indian J Pharm Sci* (2013) 75(2):127–37.

84. Markwardt F. Past, present and future of hirudin. *Haemostasis* (1991) 21 Suppl 1:11–26. doi: 10.1159/000216258

85. Fernandez Robledo JA, Yadavalli R, Allam B, Pales Espinosa E, Gerdol M, Greco S, et al. From the raw bar to the bench: Bivalves as models for human health. *Dev Comp Immunol* (2019) 92:260–82. doi: 10.1016/j.dci.2018.11.020

86. Wei D, Zhang X. Biosynthesis, bioactivity, biotoxicity and applications of antimicrobialpeptides for human health. *Biosafety Health* (2022) 4:118–34. doi: 10.1016/j.bsheal.2022.02.003

frontiers | Frontiers in Immunology

TYPE Original Research
PUBLISHED 29 May 2023
DOI 10.3389/fimmu.2023.1176982

OPEN ACCESS

EDITED BY
Annalisa Del Prete,
University of Brescia, Italy

REVIEWED BY
Gallo Carmela,
National Research Council (CNR), Italy
Loriano Ballarin,
University of Padua, Italy
Tiziana Musso,
University of Turin, Italy

*CORRESPONDENCE
Diana Boraschi
diana.boraschi@itb.cnr.it

RECEIVED 01 March 2023
ACCEPTED 19 May 2023
PUBLISHED 29 May 2023

CITATION
Marino R, Melillo D, Italiani P and Boraschi D (2023) Environmental stress and nanoplastics' effects on *Ciona robusta*: regulation of immune/stress-related genes and induction of innate memory in pharynx and gut.
Front. Immunol. 14:1176982.
doi: 10.3389/fimmu.2023.1176982

Environmental stress and nanoplastics' effects on *Ciona robusta*: regulation of immune/stress-related genes and induction of innate memory in pharynx and gut

Rita Marino[1,2], Daniela Melillo[2], Paola Italiani[1,2,3] and Diana Boraschi[1,2,3,4]*

[1]Biology and Evolution of Marine Organisms, Stazione Zoologica Anton Dohrn (SZN), Napoli, Italy, [2]Institute of Biochemistry and Cell Biology, National Research Council (CNR), Napoli, Italy, [3]China-Italy Joint Laboratory of Pharmacobiotechnology for Medical Immunomodulation (CNR, SZN, SIAT), Shenzhen, China, [4]Laboratory of Inflammation and Vaccines, Shenzhen Institute of Advanced Technology (SIAT), Chinese Academy of Sciences, Shenzhen, China

In addition to circulating haemocytes, the immune system of the solitary ascidian *Ciona robusta* relies on two organs, the pharynx and the gut, and encompasses a wide array of immune and stress-related genes. How the pharynx and the gut of *C. robusta* react and adapt to environmental stress was assessed upon short or long exposure to hypoxia/starvation in the absence or in the presence of polystyrene nanoplastics. We show that the immune response to stress is very different between the two organs, suggesting an organ-specific immune adaptation to the environmental changes. Notably, the presence of nanoplastics appears to alter the gene modulation induced by hypoxia/starvation in both organs, resulting in a partial increase in gene up-regulation in the pharynx and a less evident response to stress in the gut. We have also assessed whether the hypoxia/starvation stress could induce innate memory, measured as gene expression in response to a subsequent challenge with the bacterial agent LPS. Exposure to stress one week before challenge induced a substantial change in the response to LPS, with a general decrease of gene expression in the pharynx and a strong increase in the gut. Co-exposure with nanoplastics only partially modulated the stress-induced memory response to LPS, without substantially changing the stress-dependent gene expression profile in either organ. Overall, the presence of nanoplastics in the marine environment seems able to decrease the immune response of *C. robusta* to stressful conditions, hypothetically implying a reduced capacity to adapt to environmental changes, but only partially affects the stress-dependent induction of innate memory and subsequent responses to infectious challenges.

KEYWORDS

nanoplastics, *Ciona robusta*, innate immunity, innate memory, stress

1 Introduction

It is well known that marine organisms ingest plastic particles, including fish (1, 2) and several invertebrate species (3–5). The major threat of plastics released into the environment is related to the degradation of these materials into micro- and nano-sized particulates that can more easily bioaccumulate (6). Across marine filter-feeding invertebrate organisms, the solitary ascidian *Ciona robusta* represents an optimal model to study the impact of sub-micron particle bioaccumulation on fundamental physiological functions (7, 8). In fact, unlike bivalves (9), *C. robusta* does not have the ability to sort particles and reject the unsuitable material (10). The impact of nanoplastics accumulation on the immune defensive functions is of particular interest because of the importance of such functions for optimal adaptation to environmental changes. To fully understand the possible impact of nanoplastics on *C. robusta* it is therefore important to assess it in conditions of environmental stress.

Major stressful environmental conditions for ascidians are starvation and hypoxia. Starvation is known to affect the ascidian metabolic profile and induce autophagy-related genes. In a metabolomic study on *Halocynthia roretzi*, a strong upregulation of defence and energy metabolites was observed in response to starvation, largely mediated by the impact on the gut associated microbiota (11).

Hypoxia is a decrease in dissolved oxygen that causes significant physiological disturbances in many marine organisms (12, 13), including increased vulnerability to diseases and parasites (14). Hypoxia threshold is species- and stage-specific (13), and its effects depend on the presence of other environmental challenges (warming, acidification, pollution). Hypoxia causes a decrease of energy supply from mitochondrial metabolism, which cells seek to compensate by undergoing a metabolic reprogramming (*i.e.*, enhanced glycolysis, glutaminolysis, fatty acid synthesis and decreased gluconeogenesis, nucleotide synthesis, fatty acids β-oxidation) that mostly involves the family of hypoxia-inducible transcription factors (HIFs) (15). In mammalian immune cells, hypoxia and HIF signalling influence immune cell functions in a cell-type specific manner (16). Of special interest is the cross-talk between hypoxia and inflammation. Inflammation plays a key role in the physiological response to hypoxic stress, as shown for instance by the increase of circulating inflammatory cytokines in individuals with mountain sickness (17). Conversely, tissue sites where an inflammatory reaction takes place undergo significant shifts in metabolic activity leading to O_2 deficiency, defined as "inflammatory hypoxia" (16, 18). In addition, HIF transcription/stabilisation can be activated by a variety of inflammation-related extracellular factors, such as bacterial products (*e.g.*, lipopolysaccharide or LPS), TNF-α, IL-1, reactive oxygen and nitrogen species (ROS, RNS), even in normoxic conditions.

In the present study, we have evaluated the primary response of *C. robusta* in terms of expression of immune and oxidative stress-related genes induced by exposure to a combined hypoxic and starvation stress, and how the presence of nanoplastics in the environment can interfere with the stress-induced immune adaptation response. We focused on two organs involved in immune defence, namely the pharynx and the gut, as these organs, involved in respiration and digestion, are directly exposed to environmental stresses. We have also evaluated how a previous exposure to such combined stresses could influence the ability of the *C. robusta* immune organs to react to a subsequent bacterial challenge.

2 Materials and methods

2.1 Animals and treatments

Adults of *C. robusta* were collected in the small sea of Taranto, Italy, and maintained at the SZN in tanks with circulating aerated seawater at 18°C with proper feeding. Hypoxia/starvation (H/S) treatment was performed by starving animals in tanks for 12 h, then transferring individual animals in 200 mL millifiltered sea water (MFSW) within a 250 mL glass beaker at 18°C for 2 or 18 h (starvation plus hypoxia). Treatments with polystyrene beads (MPs) of either 0.1 µm or 0.35 µm (cat. 00876 and 07306; Polysciences, Inc., Warrington, PA, USA) was conducted by diluting nanoplastic beads in MFSW at the concentration of $9.1x10^8$ particles/mL and $7.4x10^7$ particles/mL, respectively, and adding them to individual animals in beaker for 2 or 18 h. The concentration of 0.1 µm nanoplastics was selected based on previous dose-response experiments as the concentration causing the highest bioaccumulation after 2 h of exposure (8, and data not shown). The concentration of 0.35 µm nanoplastics was selected in order to correspond to that of 0.1 µm particles in terms of surface area. Endotoxin treatment was carried out by inoculation of 50 µg of lipopolysaccharide (LPS, from *Escherichia coli*, serotype O55:B5; Merck Sigma-Aldrich®, St. Louis, MO, USA). LPS was inoculated in 50 µL of marine solution (MS: NaCl 0.45 M, $MgCl_2$ 26 mM, KCl 11 mM, $CaCl_2$ 12 mM, pH 7.4), through the tunic between the two siphons.

For memory experiments, animals were first exposed to H/S stress alone or in the presence of nanoplastics for 2 or 18 h as described above, then were transferred to the aquarium, where they were kept in large aerated tanks and properly fed for additional 7 days (resting or extinction period). After the resting period, animals were injected with 50 µL of LPS, as described above. After 24 h, animals were sacrificed and exanguinated, and gut and pharynx fragments were collected for gene expression analysis. For each condition, three animals were included.

2.2 RNA extraction and real-time PCR

Tissue samples were weighed and immediately homogenised with an Ultra-Turrax T25 at 0°C with 3 cycles of 30 s, then processed for total RNA extraction with commercially available kits (miRNeasy Kit; Qiagen, Hilden, Germany), according to the manufacturer's instructions. A mix of Oligo (dT) and random-primed single stranded cDNA were synthetised from 2 µg of pharynx RNA using the QuantiTect Reverse Trascription Kit (Qiagen).

Real-time PCR experiments were carried out with a RotorGene instrument (Qiagen) with RealAmp qPCR Master mix chemistry (GeneAll Biotechnology Co., Ltd., Seoul, South Korea). Specific primers were designed, according to the nucleotide sequence, for genes encoding the *C. robusta* homologues of the complement component C3-1 (*C3-1*), the C3 receptor C3aR (*C3ar*), the two isoforms of interkeukin-17 *Il17-1*, *Il17-2*, the IL-17 receptor *Il17r*, the tumour necrosis factor *Tnf*, the transforming growth factor beta *Tgfb*, the LPS binding protein *Lbp*, the Toll-like receptors *Tlr-2* and *Tlr13*, the cluster of differentiation 36 *Cd36*, the variable chitin-binding proteins *VCBP-B* and *VCBP-C*, the superoxide dismutase A *SodA*, the glutathione-S transferase *GST* and the glutathione reductase *GR* (Table 1). Gene nomenclature is designed according to previous publications (19–27) and includes the indication of the *C. robusta* gene isoforms as a number after a dash. Other isoforms of C3 (*C3-2*), IL-17 (*Il17-3*), and TLR (*Tlr-1*) could not be evaluated because their expression resulted undetectable in every condition in both gut and pharynx. Likewise, expression of the gene encoding the precursor of the enzyme phenoloxidase was not detectable. After preliminary evaluation of different housekeeping genes (*Actin*, *S27*, *Gapdh*), the glyceraldehyde 3-phosphate dehydrogenase gene *Gapdh* was selected for its consistent expression stability, and used as reference gene in all experiments. All primers produced single-band amplicons of the expected size, which were verified by DNA sequencing. Reactions were performed in triplicate, and the PCR programme included a denaturation step (95°C for 15 min) followed by 40 cycles of amplification (94°C for 15 s, 60°C for 30 s, and 72°C for 30 s), and a final extension step (72°C for 10 min). PCR amplification efficiencies, calculated for primer pairs of the reference and target genes, were both 2. All data were normalised against *Gapdh* using the Pfaffl method (28). Real-time PCR results are reported as relative gene expression towards *Gapdh* or as the ratio between treated and control animals.

2.3 Statistical analysis

All values were expressed as mean ± SEM of samples from 3 animals with the same treatment. Statistical significance of differences between treatments was assessed by using the one sample Student's *t* test followed by non-parametric Mann-Whitney U-test correction for PCR data of primary effects, and ordinary one-way ANOVA of one sample *t* test for PCR data of memory experiments, using the GraphPad Prism 6 software. *p* values <0.05 were considered statistically significant.

3 Results

3.1 Induction of immune response by hypoxia/starvation stress

The basal expression of sixteen genes was examined in *C. robusta*. Genes were selected based on three criteria, immune-related genes that are already known to be involved in the *Ciona* immune responses (*C3-1*, *C3ar*, *Il17-1*, *Il17-2*, *Il17r*, *Tnf*, *Tgfb*, *Lbp*, *Tlr-2*, *Tlr13*, *Cd36*) (19–26), pharynx- and gut-specific genes involved in mucosal immunity (*VCBP-B* and *VCPB-C*) (27) and

TABLE 1 List of primers used for evaluating gene expression in *C. robusta*.

GENE	FORWARD	REVERSE	Genbank acc. No.
C3-1	5′ -acagacgtggcgtgtgcaag-3	5′-tactttgcctaggaggccggt-3′	AJ320542
C3ar	5′ -ttgccccgccatgcgagga-3′	5′-aggtacgactccatacaacacc-3′	AJ966353
Il17-1	5'-ccgggaacgtgacagaaaac-3'	5'-tcgtggaagcaccataggga-3'	NM_001129875.1
Il17-2	5′-cgggtgcattgcttctagt-3′	5′-cacgcaggtacagcctattg-3′	NM_001129874.1
Il17r	5′-gtgacccgtggcaatcaatgg-3′	5′-caagttaggcattttgctccgt-3′	AY261862
Tnf	5′-catctccccaccctactacac-3′	5′-atttgcgcaaacgtctggca-3′	AM982527
Tgfb	5′-ctcgttcaaatgtgtctcaaaccg-3′	5′-cgttgccagattttacgacg-3′	AB210727
Lbp	5′-ggtttcgggaagctgggatt-3′	5′-gaaggggcctgtttcttcca-3′	XM_002126995.2
Tlr-2	5′-acgcaagaaacaagagagacg-3′	5′-gcttttcttccatttcctccagc-3′	AB495262.1
Tlr13	5′-cggaagcattgtgctggaaa-3′	5′-acgcaagacaaatacgcctg-3′	XM_002120484.4
Cd36	5′-ggttcgcttttatttcttggacct-3′	5′-ctgcaccgtttggtttacgg-3′	XM_009860510.1
VCBP-B	5'- ttcacccacacggagattgg-3'	5'-cggcgcttgatctggatact-3'	HQ324165
VCBP-C	5'-gcaacactcagtggcaaca-3'	5'-ccgcatttctcatctcgcac-3'	NM_001204050
SodA	5'- ccacaaaatatagacgaaggcgac-3'	5'-gacaacgcactattcaacggg-3'	XM_002121064
GST	5'-ccaagcgatgctaatgcgag-3'	5'- cggcgggattgaggtatgt-3'	XM_002121841
GR	5'- agcacttcttacaccagttgc-3'	5'-cccaatgggtggatgactga-3'	XM_002119519
Gapdh	5′-cattttcgacgcaggagctg-3′	5′-ctgcgtggtgtttaactggc-3′	XM_002131188.4

oxidative stress-related genes (*Sod-A*, *GST*, *GR*) (29). Gene expression was measured in the two organs that display immune reactivity, namely the pharynx and the gut. The relative contribution of haemocytes, the main circulating immune cells of *C. robusta*, was not specifically assessed, as the number of recovered cells was insufficient for RNA extraction.

Results in Table 2 show the basal expression of immune/stress-related genes in both organs in unexposed animals kept in optimal conditions of oxygenation and nutrition. Gene expression was also measured in animals treated with the bacterial agent LPS, to mimic exposure to an infectious challenge. Substantial variations in gene expression could be observed, which differ between the two organs. In the pharynx, reaction to LPS resulted in a general upregulation of the majority of the immune/stress-related genes, with a very high increase in the expression of *Tnf*, *Tgfb*, *VCBP-B* and *VCBP-C* and a significant but less substantial increase of *Il17-2* and *Tlr-2* expression. Only one gene, *GST*, was significantly down-regulated in the pharynx in response to LPS. The scenario in the gut is very different, with only one gene, *C3ar*, significantly up-regulated in response to LPS. The expression of most genes is either unchanged or down-regulated by LPS in the gut, although a statistically significant decrease was only observed for *Il17r*, *VCBP-B* and *GR*. Notably, expression of *VCBP-B*, which was increased over 4000x in the pharynx, was completely inhibited by LPS in the gut (Table 2).

We analysed whether stress conditions could induce an immune reaction similar to exposure to an infectious agent. Stress was obtained by keeping animals in a small volume of millifiltered seawater (MFSW) for 2 or 18 hr, without oxygenation and feeding. The expression of the selected immune/stress-related genes was examined in the stressed animals as compared to control animals kept in oxygenated tanks with food. The results in Figure 1 show that the stress induced by hypoxia/starvation (H/S) has a significant effect on the expression of immune/stress-related genes, and that this effect is different depending on the organ and the duration of stress. In the pharynx, a short H/S stress induced a significant upregulation of *C3-1*, *Tnf*, *Tgfb*, *Lbp*, *VCBP-B*, *VCBP-C* and *GR* (Figure 1A). An H/S stress of 18 h induced expression of the *Il17r* gene and further increased *Tnf* expression, while upregulation of *C3-1*, *Tgfb* and *Lbp* remained sustained at the same level, and that of *VCBP-B* and *VCBP-C* returned to baseline (Figure 1B). The response of the gut to H/S stress was substantially different. The short 2 h stress induced a strong up-regulation of the *C3ar* and *VCBP-C* genes, and a significant increase of *Il17-2*, *Tgfb*, *Lbp*, *Trl-2*, *VCBP-B* and *SodA*, while other genes were only marginally affected (Figure 1C). After 18 h of H/S stress, expression of *C3-1*, *Il17r*, *Tnf* and *Cd36* was up-regulated, up-regulation of the *C3ar*, *VCBP-B* and *VCBP-C* was sustained at the same level, while that of *Tgfb* was further increased, and that of the other genes decreased towards basal expression levels (Figure 1D). Full data (mean levels of gene expression with SEM and statistical analysis) are reported in the Supplementary Table S1. Thus, H/S stress could induce substantial variations in immune/stress gene expression both in the pharynx and in the gut, suggesting an active

TABLE 2 Immune/stress-related gene expression levels in the pharynx and gut of *C. robusta*.

Gene	Gene expression level [a] (mean ± SEM)			
	Pharynx		Gut	
	Control	LPS	Control	LPS
C3-1	2.52 ± 1.49	4.54 ± 1.22	1.22 ± 0.50	0.10 ± 0.05
C3ar	2.29 ± 1.73	2.18 ± 0.59	1.04 ± 0.21	6.55 ± 1.08*
Il17-1	1.16 ± 0.47	1.28 ± 0.38	1.08 ± 0.29	0.53 ± 0.21
Il17-2	1.76 ± 1.16	10.02 ± 3.67**	1.49 ± 0.94	1.30 ± 0.19
Il17r	1.36 ± 0.61	1.37 ± 0.49	1.09 ± 0.33	0.03 ± 0.01*
Tnf	1.19 ± 0.40	62.3 ± 5.7**	1.18 ± 0.51	0.08 ± 0.02
Tgfb	1.06 ± 0.24	80.9 ± 9.5**	2.12 ± 1.37	0.52 ± 0.24
Lbp	1.05 ± 0.23	1.90 ± 0.17	1.10 ± 0.35	0.31 ± 0.09
Tlr-2	1.31 ± 0.53	11.37 ± 1.41*	1.08 ± 0.26	0.62 ± 0.01
Tlr13	1.04 ± 0.20	0.45 ± 0.14	1.35 ± 0.74	0.28 ± 0.04
Cd36	1.06 ± 0.24	0.59 ± 0.08	1.17 ± 0.49	0.15 ± 0.05
VCBP-B	1.11 ± 0.36	4129.5 ± 1042.5**	1.25 ± 0.61	0.00 ± 0.00*
VCBP-C	1.09 ± 0.27	30.24 ± 6.35*	1.13 ± 0.40	0.63 ± 0.09
SodA	1.04 ± 0.20	0.82 ± 0.59	1.43 ± 0.79	0.50 ± 0.15
GST	1.06 ± 0.26	0.03 ± 0.00**	2.43 ± 1.93	0.17 ± 0.02
GR	1.09 ± 0.33	3.05 ± 1.38	1.26 ± 0.51	0.06 ± 0.00*

[a]relative to Gapdh.
*p<0.05, **p<0.01, LPS vs. controls.

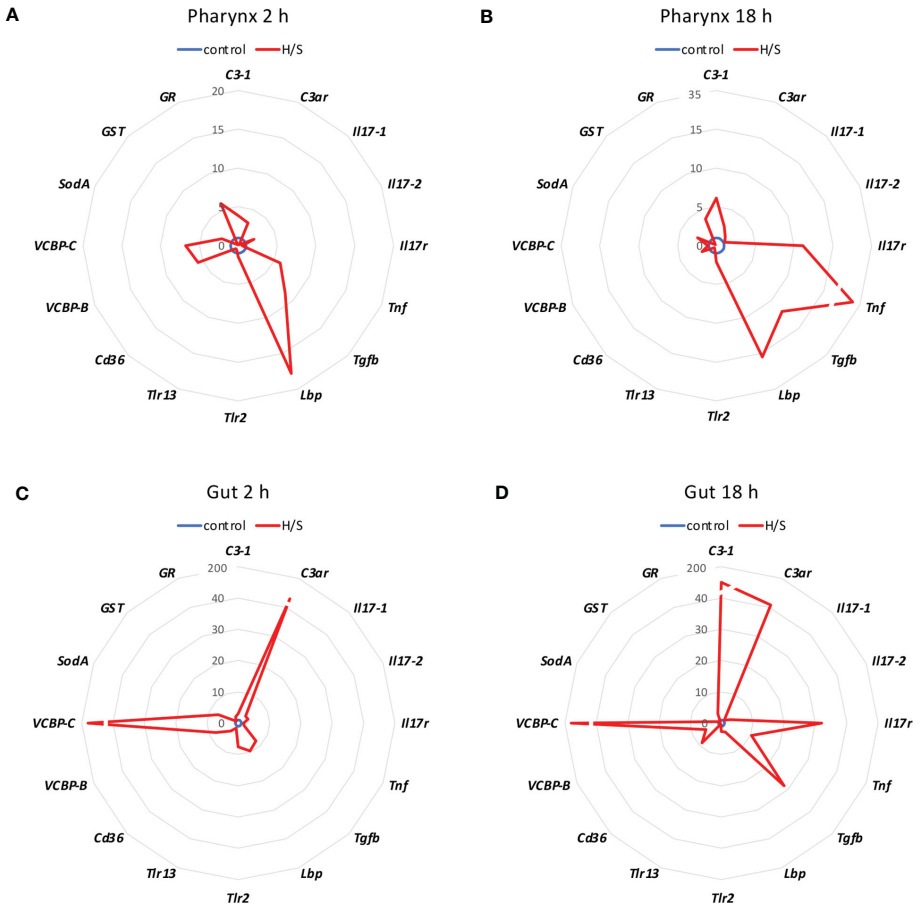

FIGURE 1
Hypoxia/starvation stress-induced gene expression in the pharynx and gut of *Ciona robusta*. Gene expression was measured in the pharynx and in the gut of animals exposed to hypoxia/starvation (H/S) stress (red line) for 2 h or 18 h. **(A, B)** gene expression in the pharynx; **(C, D)** gene expression in the gut. **(A, C)** gene expression at 2 h; **(B, D)** gene expression at 18 h. Data are the mean of values from 3 animals and are expressed relative to gene expression in control naïve animals (blue line). The mean values of gene expression relative to the housekeeping gene *Gapdh*, the SEM values and the statistical analysis are reported in the Supplementary Table S1.

immune adaptation to the environmental changes. The kinetic differences in the expression profiles underline the evolution of the adaptive changes, while the difference between the two immune organs strongly support their distinct roles in immune responses.

3.2 Modulation of stress-induced immune response by nanoplastics

To assess whether concomitant exposure to nanoplastics could affect the stress-induced response, animals were exposed to polystyrene beads of two different sizes (diameter 0.1 and 0.35 μm) in H/S conditions. After 2 or 18 h, the gene expression was assessed. As shown in Figures 2 and 3, the presence of nanoplastics could affect the gene expression changes induced by H/S both in the pharynx and in the gut. In the pharynx, the presence of nanoplastics induced some significant changes in the gene expression induced by a 2 h exposure to H/S stress alone, *i.e.*, further up-regulation of H/S stress-induced *Tgfb* gene expression, and down-regulation of H/S stress-induced *C3-1* and *Lbp* gene expression (Figure 2A). Other changes (*e.g.*, up-regulation of the stress-induced decrease of *Il17-1* and *Cd36* genes) were not statistically significant. After 18 h, the presence of nanoplastics induced several changes compared to H/S alone, in particular a decrease in *C3-1*, *Il17r* and *Tnf* expression and an increase of *Il17-2* (Figure 2B). In the pharynx, differences were also noted between nanoplastics of different size, with the larger particles in combination with H/S for 18 h able to up-regulate the expression of *C3ar*, *Tgfb*, *Tlr13*, *Cd36*, *VCBP-B* and *VCBP-C* (not induced by the combination of H/S and small nanoplastics).

In the gut, no substantial size-dependent effect of nanoplastics was noted on the gene modulation induced by H/S stress (Figures 2C, D). After 2 h of exposure to H/S stress in the presence of nanoplastics, gene expression was either unaffected or decreased, with a significant inhibition of *C3-1*, *C3ar*, *Tgfb*, *Lbp*, *Tlr-2*, and *VCBP-C* (Figure 2C). After 18 h of combined exposure to H/S stress and nanoplastics, gene expression changes were more evident than with the shorter exposure, showing a significant decrease in the expression of *C3-1*, *C3ar*, *Il17r*, *Tnf*, *Tgfb*, *Cd36*, *VCBP-B* and *VCBP-C* (Figure 2D). The increased expression of *Il17-1*, *SodA* and *GR* genes in the presence of nanoplastics was not statistically different from H/S stress alone.

Notably, the comparison of the gene expression profiles induced by H/S stress and by H/S stress plus nanoplastics with those of naïve

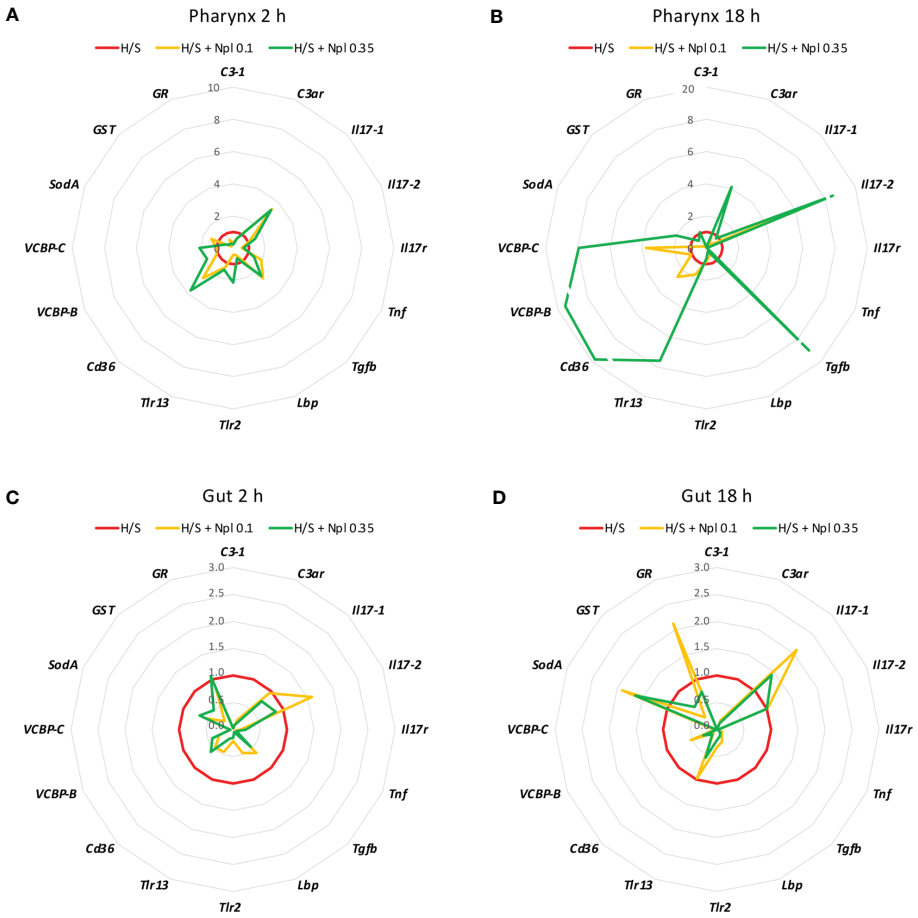

FIGURE 2
Effect of nanoplastics on the hypoxia/starvation stress-induced gene expression in the pharynx and gut of *Ciona robusta*. Gene expression was measured in the pharynx and in the gut of animals exposed to hypoxia/starvation (H/S) stress alone (red line) or combined with nanoplastics for 2 or 18 h. **(A, B)** gene expression in the pharynx; **(C, D)** gene expression in the gut. **(A, C)** gene expression at 2 h; **(B, D)** gene expression at 18 h. Nanoplastics of two different sizes were used, 0.1 µm (yellow line) and 0.35 µm (green line). Data are the mean of values from 3 animals and are expressed relative to gene expression in H/S-exposed animals. The mean values of gene expression relative to the housekeeping gene *Gapdh*, the SEM values and the statistical analysis are reported in the Supplementary Table S2.

animals shows that the presence of nanoplastics may reduce some of the gene expression changes induced by H/S stress (Figure 3). This is particularly evident in the gut, both after a short or long exposure to stress, where exposure to nanoplastics substantially limited the up-regulation of several of the immune/stress genes induced by H/S (Figures 3C, D). Full data (mean levels of gene expression with SEM and statistical analysis) are reported in the Supplementary Tables S2 and S3.

Thus, the presence of nanoplastics may dampen some of the stressful effects induced by H/S, which however may result in inadequate adaptation to the environmental changes.

3.3 Organ-specific modulation of immune/stress-related gene expression by stress-induced innate memory

We assessed the response to the prototypical bacterial agent LPS in the pharynx and gut of animals that were previously primed by H/S in comparison to unprimed controls. As described above for the primary response, the "memory" response was measured as expression of immune/stress-related genes. As already mentioned, the response of naïve animals to LPS encompasses a general up-regulation of immune/stress-related genes in the pharynx, opposite to a general down-regulation in the gut (Table 2). In animals previously exposed to H/S stress (either 2 or 18 h, followed by one week in tank with proper oxygenation and nutrition) the response to LPS was significantly different, implying the establishment of a stress-induced innate memory, able to modulate the response to an infectious challenge. In the pharynx, pre-exposure to H/S stress induce a substantial decrease in the expression of several genes and the up-regulation of the *GST* gene (Figure 4A, Table S4). Notably, down-regulation exclusively occurred for genes that were up-regulated in response to LPS in naïve animals, while up-regulation occurred for the only gene that was strongly down-regulated by LPS in naïve animals. This implies that animals exposed to H/S stress have developed "tolerance" to LPS in the pharynx, as their expression profile of immune/stress-related genes is similar to the basal expression profile of untreated animals (Table S4). A similar induction of "tolerance" to LPS was observed in the gut of animals

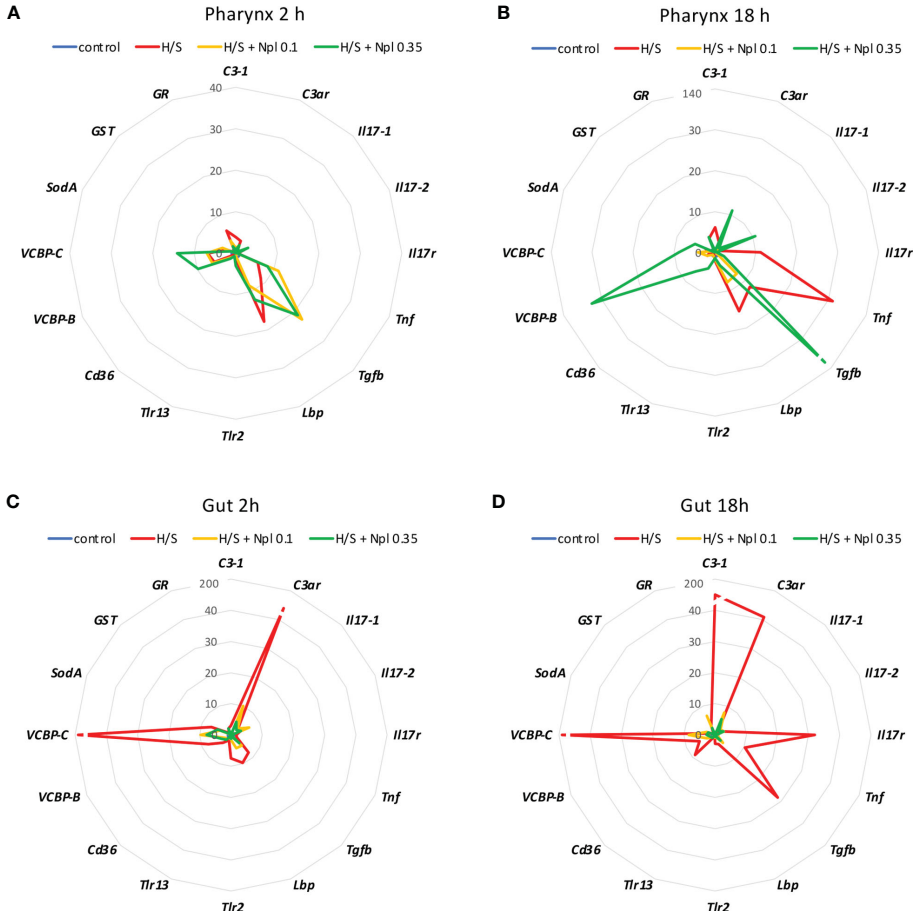

FIGURE 3
Effect of the combined exposure to hypoxia/starvation and nanoplastics on the immune/stress-related gene expression in the pharynx and gut of *Ciona robusta*. Gene expression was measured in the pharynx and in the gut of animals exposed to hypoxia/starvation (H/S) stress alone (red line) or combined with nanoplastics for 2 or 18 h. **(A, B)** gene expression in the pharynx; **(C, D)** gene expression in the gut. **(A, C)** gene expression at 2 h; **(B,D)** gene expression at 18 h. Nanoplastics of two different sizes were used, 0.1 µm (yellow line) and 0.35 µm (green line). Data are the mean of values from 3 animals and are expressed relative to gene expression in control naïve animals (kept in tank in optimal oxygenation and nutrition conditions; blue line). The mean values of gene expression relative to the housekeeping gene *Gapdh*, the SEM values and the statistical analysis are reported in the Supplementary Tables S2 (pharynx) and S3 (gut).

pre-exposed to H/S stress. While the response to LPS in the gut is a general down-regulation of immune/stress gene-expression, expression of these genes in response to LPS was higher in animals pre-exposed to H/S stress (Figure 4B, Table S5). Thus, as in the pharynx, pre-exposure to H/S stress induced a state of unresponsiveness to LPS in the gut, with the gene expression profile of H/S-primed animals challenge with LPS similar to that of naïve unchallenged animals (Table S5). No substantial differences were observed between 2 *vs.* 18 h of pre-exposure to H/S stress (Figures 4A, B).

3.4 Effect of nanoplastics on the organ-specific stress-induced innate memory

We examined whether the combined exposure to H/S stress and nanoplastics could affect the tolerance type of innate memory response to LPS induced by H/S stress alone. Data in Figure 4 show the innate memory response to LPS of animals pre-exposed to H/S stress alone (H/S) or in the presence of small 0.1 µm nanoplastics (H/S + Nlp 0.1) or 0.35 µm particles (H/S + Npl 0.35), compared to unexposed animals (no priming). Notably, nanoplastics appear to reverse in some cases the gene down-regulation caused by pre-exposure to H/S stress in the pharynx (*e.g.*, *Tnf*, *Tgfb*, *VCBP-B*) and increase the expression of genes that were either up-regulated (*GST*) or not affected (*Lbp*, *SodA*) by H/S stress (Figure 4A, Table S4). Some changes were common to nanoplastics of both sizes, *e.g.*, upregulation of *Tnf* and *Lbp* gene expression, while other were size-specific, with larger particles able to significantly upregulate *SodA* and *GST*, while small particles were inactive (Figure 4A, Table S4). After 18 h, the nanoplastics effects on H/S-induced changes were essentially maintained, except for the loss of effects for small particles on H/S-induced down-regulation of *Tgfb* and the up-regulation of *GR* by large particles. Notably, up-regulation of *C3ar* was observed with larger particles (inactive at 2 h), while the effect of small particles (active at 2 h) was lost (Figure 4A, Table S4). In the gut, both common and size-dependent effects of nanoplastics were observed on the gene modulation

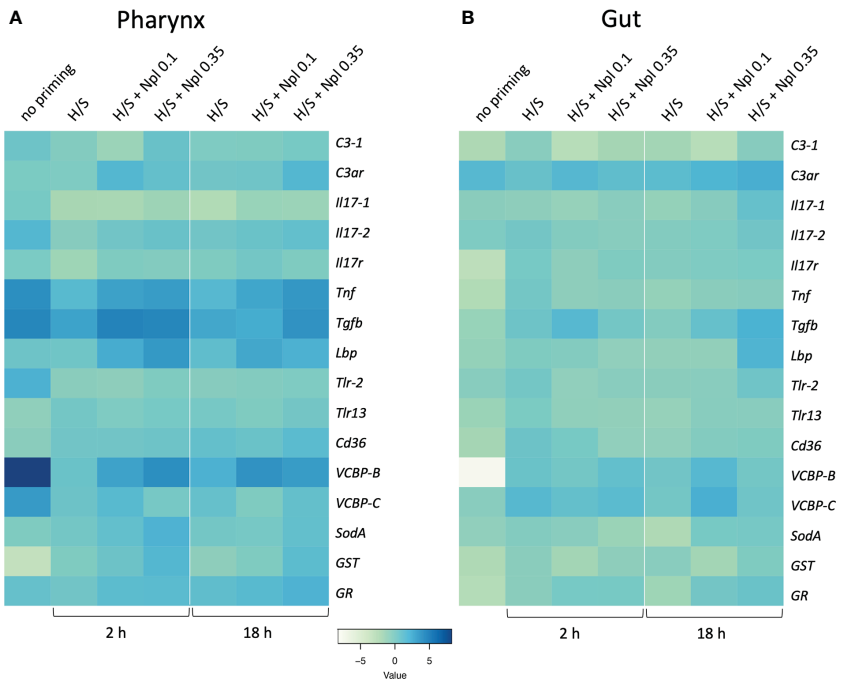

FIGURE 4
Stress-induced memory response to LPS in *Ciona robusta*. The response to LPS was measured in naïve animals (no priming) and animals pre-exposed to H/S stress alone (H/S) or with nanoplastics of 0.1 µm (H/S + Npl 0.1) and 0.35 µm (H/S + Npl 0.35) for 2 or 18 h. After pre-exposure, animals were then transferred in tanks and kept in optimal oxygenation and nutrition conditions for one week, before receiving 50 µg LPS intratunically. Gene expression in response to the LPS challenge was measured 24 h later. **(A)** gene expression in the pharynx; **(B)** gene expression in the gut. The heatmaps report the results of gene expression (mean values from 3 animals relative to gene expression in unchallenged control animals). The SEM values and the statistical analysis are reported in Supplementary Tables S4 (pharynx) and S5 (gut).

induced by H/S stress (Figure 4B, Table S5). After 2 h of pre-exposure to H/S stress in the presence of nanoplastics, small particles could induce a statistically significant increase of the expression of the *Tgfb* gene compared to H/S alone, an effect not shared by larger particles (Figure 4B, Table S5), while after 18 h both types of particles were active (Figure 4B, Table S5). After 18 h, smaller particles were able to further increase the H/S-induced expression of the *VCBP-B* and *VCBP-C* genes, as opposed to the lack of effect by larger particles (Figure 4B, Table S5).

4 Discussion

Studies of inflammatory responses to LPS in tunicates have demonstrated an up-regulation of cytokine-like genes such as *Tnf* (25) and *Il17* (22), as well as complement components (30, 31), mostly evident in haemocytes and in the pharynx. On the other hand, data concerning the stress-induced response are poorly represented. Several invertebrate species, such as oysters, are remarkably resilient to fluctuating environmental conditions, and this adaptation is based on a large repertoire of immune-related genes, many of which are greatly expanded in the genome (32). Rather than on the main circulating immune cells, the haemocytes, in our study we focused on the pharynx and the gut, two organs involved in respiration and digestion and therefore directly exposed to environmental stresses, to assess the organ-specific immune adaptation. We found that an environmental stress, represented by hypoxia and starvation (H/S), up-regulates the expression of a variety of immune/stress-related genes, both in the pharynx and in the gut of *C. robusta*. Interestingly, beyond the up-regulation in both organs of the complement gene *C3-1*, the cytokine/cytokine receptor genes *Il17r*, *Tnf*, *Tgfb* and *Lbp*, the chitin-binding protein genes *VCBP-B* and *VCBP-C* and the stress-related gene *GR*, we could observe a gut-specific up-regulation of *C3ar*, *Tlr-2* and *CD36*. We also examined how the additional presence of another environmental stress, *i.e.*, nanoplastics, may affect the adaptation reaction to H/S. In the pharynx, co-exposure to H/S and nanoplastics induces an enhanced up-regulation of the *Il17-2*, *Tgfb*, *VCBP-B* and *VCBP-C* genes, a substantial down-regulation of *Tnf*, and no change in the other genes. On the contrary, the effect of nanoplastics co-exposure in the gut is a general down-regulation of all the immune/stress-related genes. These data suggest two scenarios. First, while the H/S stress strongly affects the expression of immune/stress-related genes, in line with the expected adaptation to the changing environmental conditions, such effects are different between the two immune organs, stressing their different immune protective role. The second observation is that the presence of nanoplastics interferes with the stress-induced immune response, which may therefore affect the adaptation capacity of the animals.

It is interesting to examine the regulation of the *Lbp* gene in response to LPS (used as positive control) *vs.* stress. In mammals, LBP is induced by LPS stimulation and displays a concentration-dependent modulation of LPS activity: at low concentrations, LBP shuttles LPS to monocytes or other immune cells, whereas at high

concentration it inhibits the endotoxic activity of LPS by facilitating its elimination (33–35). Unexpectedly, in the present study we found that the *Lbp* gene in *C. robusta* is unresponsive to LPS stimulation in both organs, while it is up-regulated by H/S stress in particular in the pharynx. These results seem to suggest that *Lbp* activation is independent of LPS, but necessary in the adaptive immune reaction initiated by H/S stress. Notably, this protective effect is partially abolished in presence of nanoplastics, supporting the hypothesis that animals exposed to nanoplastics may be less able to adapt to environmental changes.

The induction of innate memory was examined in the pharynx and in the gut of animals previously exposed to H/S stress alone or together with nanoplastics. Pre-exposed animals were administered with LPS, and the expression of immune/stress-related genes was compared to that of naïve animals. Upon previous H/S and H/S nanoparticles experience, haemocytes and/or pharynx cells react to a systemic LPS challenge by turning off most immune/inflammatory response as compared to unprimed animals, a response that compatible with a tolerance type of innate memory, while only transcription of *GST* is increased in animals pre-exposed to H/S and nanoplastics. GSTs are a multigene family of isozymes that catalyse the conjugation of glutathione (GSH) to several molecules. In our animal model, we could hypothesise that immune memory in the pharynx is linked to the oxidative stress generated by hypoxic conditions, which may be exacerbated in the presence of nanoplastics. In fact, nanoplastics may amplify the oxidative and inflammatory effects of H/S by reducing the filtration rate of the animals and related O_2 supply, by clotting mucus and clogging the pharynx stigmata. Upon challenge with LPS, known to lower the GSH levels in vertebrate models (36), there is a strong upregulation of the *GST* gene in animals pre-exposed to H/S and nanoplastics, likely underlying a memory-dependent protective response aiming at restoring the tissue GSH pool and its detoxification effects.

In order to appropriately assess the innate memory induced by H/S and nanoplastics in the gut, it is important to keep in mind some organ-related effects. The role of starvation in the gut is twofold. As in all tissues and organs, together with hypoxia, starvation contributes in eliciting oxidative and inflammatory stress. More specifically in the gut, starvation impairs mucus production/transport to the post-branchial digestive tract, and this makes the gut epithelium more vulnerable to microorganism colonisation. Regarding the effect of size and time of exposure to nanoplastics, we expect bigger particles to accumulate more easily in the gut after being trapped by mucus in the pharynx (8), thereby depleting the external nanoplastics concentration with time. In the memory experiments, the gut from primed animals reacts to an LPS challenge by increasing the expression of *VCBP* genes. This upregulation likely occurs in newly differentiating cells of the stomach. Since the stomach is the tract of the gut system with the fastest cell-renewing rate (about 14 days from stem cells to fully mature cells) (37), we can hypothesise that the stem cells primed by H/S and nanoplastics start expressing *VCBP* genes during the LPS-induced differentiation. Previous studies on *VCBP* expression in adult animals showed that *VCBP-C* is expressed in crypts, the stem cells reservoir, and in mucous cells, located at the junction between stomach and intestine, whereas *VCBP-B* is detected in folds, with a scattered pattern (38). Therefore, the potentiation of *VCBP-B* seems to represent a true memory-induced protective response, while the upregulation of *VCBP-C* may represent a sustained response, *i.e.*, a re-stimulation of a response already ongoing in developing stem cells.

The most striking findings in this study regard the regulation of the *VCBP* genes. Chitin-binding peptides/proteins and chitinase-like proteins are involved in constitutive and induced resistance to fungal colonisation, and are found in a number of organisms (39), including bacteria (40), plants (41), invertebrates (42, 43) and humans (44). The antifungal activity of these proteins is likely the result of their binding to nascent fungal cell wall chitin, through their chitin-binding lectin-like domain (CBD), resulting in disrupted fungal cell polarity with concomitant inhibition of growth (39). The variable region-containing chitin-binding domain proteins (VCBPs), thus far identified in two protochordates, the amphioxus *Branchiostoma floridae* (45) and the ascidian *Ciona robusta* (28), are secreted molecules expressed in stomach and gut lumen and in blood (28, 38). These proteins are thought to actively contribute to gut microbiota homeostasis *via* their IgV domains (46), while the Ig domains apparently have a structural role that allows for optimal binding to the cell walls, sporangia (spore-forming bodies) and spores of a diverse set of filamentous fungi isolated from the *Ciona* gut (47). The function of VCBPs secreted in the blood has been ascribed to their opsonising activity towards bacteria, mediated by the Ig domains with the contribution of CBD (27, 48). Since most studies focused on *VCBP* expression in the stomach and gut, there is no information about their expression and possible role in the pharynx, the filter feeding organ of the animal from which food particles entangled in mucus, secreted by the endostyle, are moved to the alimentary canal to be digested.

In our study, we have assessed the expression of *VCBP-B* and *VCBP-C* in the gut and in the pharynx of *C. robusta* in response to various stimuli, both as primary immune reaction and in immune memory responses. The *VCBP-B* gene product, expressed in the stomach of adults and in blood cells of *Ciona*, is a protein displaying one IgV domain, one Ig-like domain and one CBD. Conversely, the *VCBP-C* gene product, expressed in the stomach and gut of juvenile and adult animals and in blood cells, displays two Ig-like domains (no IgV domain) and a CBD. The differences in their expected functions are however not known (48). We observed that these genes are sensitive to every stimulus administered to animals, but in an organ-specific way. In response to systemic LPS, both genes were strongly up-regulated in the pharynx (over 4000-fold for *VCBP-B*), while in the gut the basal *VCBP-B* expression was decreased to zero in response to LPS and that of *VCBP-C* was not affected. Examining the gene expression in response to H/S stress, we observed a significant up-regulation of both genes (about 5-8-fold for *VCBP-B* and 200-fold for *VCBP-C*) upon both short and long stress. We could hypothesise that H/S stress decreases the mucus production and/or mucus transport (10) from the endostyle to the gut, and consequently the gut epithelium is less protected, resulting in an inflammatory condition similar to the experimental colitis in the mouse, which also displays a significant functional/physical impairment of the gut

barrier (49). In the mouse colitis model, the disease is associated with an overgrowth of *Candida albicans* (50). Fungal overgrowth in the gut is in turn associated with dysbiotic changes in the gut microbiota and alterations of the digestive mucosa that promote *C. albicans* translocation across the digestive intestinal barrier and its haematogenous dissemination and invasive fungal infections (51, 52). Therefore, we can hypothesise that, following a stressful event compromising the mucus production/transport, the strong up-regulation of *VCBP* genes (mostly *VCBP-C* whose tissue expression pattern involves the majority of stomach outer folds and gut) could be due to the urgency of fighting epithelium colonisation by microorganisms. When animals are exposed to nanoplastics in the same H/S conditions, the up-regulation of *VCBP-C* was lost, similar to other genes, probably because of a higher toxicity of particles for the gut cells, poorly protected by mucus.

In the pharynx, LPS was extremely potent in up-regulating the expression of *VCBP-B*. So far, this gene was known to be expressed in the stomach of adult individuals and in granular amoebocytes (28, 38), but our qPCR data could also show an expression in the pharynx. However, the systemic LPS administration implies the stimulus reaching the blood, thus it is possible that granular amoebocytes contribute to the gene up-regulation observed in the pharynx. From our previous study (27), we know that the intratunical LPS administration in *Ciona* triggers an inflammatory response, which entails blood cell composition changes as well as a transcriptomic modulation of several genes. The strong induction of *VCBP-B* expression in the pharynx of LPS-treated animals is consistent with a close relationship between *VCBP*s and inflammatory environments and bacterial burden. Such correlation is supported by data in different systems. For instance, the human chitinase-3-like protein 1 (YKL-40) is highly expressed in serum from healthy volunteers inoculated with *Escherichia coli* endotoxin (53). In *S. pneumoniae*-infected mice, the Chi3l1 protein is up-regulated and plays central roles in promoting bacterial clearance and mediating host tolerance through inhibition of macrophage pyroptosis (54).

Although the exact functions of different VCBP proteins are still unknown (48), our data support the hypothesis that VCBPs exhibits a tissue-specific protective function, with VCBP-B mainly involved in patrolling the pharynx/blood district, whereas VCBP-C is mainly involved in the control of gut homeostasis.

In conclusion, our study demonstrates that *C. robusta* mounts a potent organ-specific adaptation response to environmental changes (the combination of hypoxia and starvation) and that such response depends on the duration of stress. The adaptation response is different in the pharynx and the gut or H/S-exposed animals, underlining the different protective role of the two organs. The presence of nanoplastics, in combination with H/S stress, changes gene expression as compared to H/S alone, resulting in an anomalous expression profile in the pharynx after 18 h of exposure and in a general inhibition of the H/S-induced changes in the gut. This may result in a hampered capacity of the animals to adapt to the environmental changes. When assessing the immune response to a bacterial challenge (LPS) in animals pre-exposed to H/S with or without nanoplastics, we could observe that the strong reaction to LPS in the pharynx was substantially decreased in animals that had previously experienced an H/S stress, whereas the low/down-regulated gene expression in the gut in response to LPS was generally abolished in previously stressed animals. Thus, animals experiencing environmental stress mount a robust adaptation response, based on changes in the expression of several immune/stress-related genes. Such adaptation (immune memory) strongly influences the immune reaction to a subsequent infectious challenge, which is less strong both in the gut and in the pharynx. We can hypothesise that the mitigation of the response to LPS (decrease in gene up-regulation in the pharynx and increase of gene down-regulation in the gut) may have a double effect, less protective capacity against infections but also less self-damage caused by an exceedingly strong reaction. It is notable that the presence of nanoplastics, which has effects on the primary adaptation response, does not have substantial effects on the H/S stress-induced memory reaction to ensuing challenges. This may be interpreted as an interference (likely due to particle accumulation in tissues) with the tissue homeostasis and functionality, *i.e.*, with adaptation to the environmental changes, which however does not substantially affect the defensive capacity (measured as memory response to an infectious challenge).

Data availability statement

The original contributions presented in the study are included in the article/Supplementary Material. Further inquiries can be directed to the corresponding author.

Ethics statement

Studies on *Ciona robusta* do not need ethical review and approval, in accordance with the national and international legislation regulating animal experimentation. All activities were performed according to the Italian DLgs 26/2014, the European Directive 2010/63/EU and the associated "A working document on Animal Welfare Bodies and National Committees to fulfil the requirements under the Directive". Ethical clearance was confirmed by the Animal Welfare Committee of the Stazione Zoologica Anton Dohrn (Ethical Clearance Waive request 01/2023).

Author contributions

RM and DM planned and performed the experiments. PI and DB contributed to the experimental design. All authors contributed to writing the manuscript. PI and DB critically revised the manuscript. All authors contributed to the article and approved the submitted version.

Funding

This work was supported by the EU Commission H2020 projects PANDORA (GA671881) and ENDONANO (GA 812661) (PI, DB), the project MIUR/PRIN-20173ZECCM of the Italian Ministry of Research (PI), the China-Italy NSFC-MAECI bilateral project 82261138630 (DB) and the Key Collaborative Research Program of the Alliance of International Science Organizations ANSO-CR-KP-2022-01 (DB).

Conflict of interest

The authors declare that the research was conducted in the absence of any commercial or financial relationships that could be construed as a potential conflict of interest.

Publisher's note

Supplementary material

The Supplementary Material for this article can be found online at: https://www.frontiersin.org/articles/10.3389/fimmu.2023.1176982/full#supplementary-material

References

1. Boerger CM, Lattin GL, Moore SL, Moore CJ. Plastic ingestion by planktivorous fishes in the north pacific central gyre. *Mar pollut Bull* (2010) 60:2275–8. doi: 10.1016/j.marpolbul.2010.08.007

2. Lusher A, McHugh M, Thompson R. Occurrence of microplastics in the gastrointestinal tract of pelagic and demersal fish from the English channel. *Mar pollut Bull* (2013) 67:94–9. doi: 10.1016/j.marpolbul.2012.11.028

3. Thompson RC, Olsen Y, Mitchell RP, Davis A, Rowland SJ, John AWG, et al. Lost at sea: where is all the plastic? *Science* (2004) 304:838. doi: 10.1126/science.1094559

4. Browne MA, Dissanayake A, Galloway TS, Lowe DM, Thompson RC. Ingested microscopic plastic translocate to the circulatory system of the mussel, *Mytilus edulis* (L.). *Environ Sci Technol* (2008) 42:5026–31. doi: 10.1021/es800249a

5. Murray F, Cowie PR. Plastic contamination in the decapod crustacean *Nephrops norvegicus* (Linnaeus, 1758). *Mar pollut Bull* (2011) 62:1207–17. doi: 10.1016/j.marpolbul.2011.03.032

6. Wright SL, Kelly FJ. Plastic and human health: a micro issue? environ. *Sci Technol* (2017) 51:6634–47. doi: 10.1021/acs.est.7b00423

7. Hamann L, Blanke A. Suspension feeders: diversity, principles of particle separation and biomimetic potential. *J R Soc Interface* (2022) 19:0210741. doi: 10.1098/rsif.2021.0741

8. Valsesia A, Parot J, Ponti J, Mehn D, Marino R, Melillo D, et al. Detection, counting and characterization of nanoplastics in marine bioindicators: a proof of principle study. *Micropl Nanopl* (2021) 1:5. doi: 10.1186/s43591-021-00005-z

9. Jones J, Allam B. Pales espinosa e. particle selection in suspension-feeding bivalves: does one model fit all? *Biol Bull* (2020) 238:41–53. doi: 10.1086/707718

10. Petersen JK. Ascidian suspension feeding. *J Exp Mar Biol Ecol* (2007) 342:127–37. doi: 10.1016/j.jembe.2006.10.023

11. Wei J, Gao H, Yang Y, Liu H, Yu H, Chen Z, et al. Seasonal dynamics and starvation impact on the gut microbiome of urochordate ascidian. *Halocynthia roretzi Anim Microb* (2020) 2:30. doi: 10.1186/s42523-020-00048-2

12. Spicer JI. What can an ecophysiological approach tell us about the physiological responses of marine invertebrates to hypoxia? J. *Exp Biol* (2014) 217:46–56. doi: 10.1242/jeb.090365

13. Yoann T, Flye Sainte Marie J, Chabot D, Aguirre-Velarde A, Marques Gonçalo M, Pecquerie L. Effects of hypoxia on metabolic functions in marine organisms: observed patterns and modelling assumptions within the context of dynamic energy budget (DEB) theory. *J Sea Res* (2019) 143:231–42. doi: 10.1016/j.seares.2018.05.001

14. Breitburg DL, Hondorp D, Audemard C, Carnegie RB, Burrell RB, Trice M, et al. Landscape-level variation in disease susceptibility related to shallow-water hypoxia. *PloS One* (2015) 10:e0116223. doi: 10.1371/journal.pone.0116223

15. Chen Y, Gaber T. Hypoxia/HIF modulates immune responses. *Biomedicines* (2021) 9:260. doi: 10.3390/biomedicines9030260

16. Eltzschig HK, Carmeliet P. Hypoxia and inflammation. *New Eng J Med* (2011) 364:656–65. doi: 10.1056/NEJMra0910283

17. Pham K, Parikh K, Heinrich EC. Hypoxia and inflammation: insights from high-altitude physiology. *Front Physiol* (2021) 12:676782. doi: 10.3389/fphys.2021.676782

18. Colgan SP, Campbell EL, Kominsky DJ. Hypoxia and mucosal inflammation. *Annu Rev Pathol* (2016) 11:77–100. doi: 10.1146/annurev-pathol-012615-044231

19. Marino R, Kimura Y, De Santis R, Lambris JD, Pinto M. Complement in urochordates: cloning and characterization of two C3-like genes in the ascidian. *Ciona intest Immunogen* (2002) 53:1055–64. doi: 10.1007/s00251-001-0421-9

20. Melillo D, Sfyroera G, De Santis R, Graziano R, Marino R, Lambris JD, et al. First identification of a chemotactic receptor in an invertebrate species: structural and functional characterization of *Ciona intestinalis* C3a receptor. *J Immunol* (2006) 177:4132–40. doi: 10.4049/jimmunol.177.6.4132

21. Vizzini A, Di Falco F, Parrinello D, Sanfratello MA, Mazzarella C, Parrinello N, et al. *Ciona intestinalis* interleukin 17-like genes expression is upregulated by LPS challenge. *Dev Comp Immunol* (2015) 48:129–37. doi: 10.1016/j.dci.2014.09.014

22. Terajima D, Yamada S, Uchino R, Ikawa S, Ikeda M, Shida K, et al. Identification and sequence of seventy-nine new transcripts expressed in hemocytes of *Ciona intestinalis*, three of which may be involved in characteristic cell-cell communication. *DNA Res* (2003) 10:203–12. doi: 10.1093/dnares/10.5.203

23. Vizzini A, Di Falco F, Parrinello D, Sanfratello MA, Cammarata M. Transforming growth factor β (*CiTGF-β*) gene expression is induced in the inflammatory reaction of. *Ciona intest Dev Comp Immunol* (2016) 55:102–10. doi: 10.1016/j.dci.2015.10.013

24. Parrinello N, Vizzini A, Arizza V, Salerno G, Parrinello D, Cammarata M, et al. Enhanced expression of a cloned and sequenced *Ciona intestinalis* TNFα-like (*CiTNFα*) gene during the LPS-induced inflammatory response. *Cell Tissue Res* (2008) 334:305–17. doi: 10.1007/s00441-008-0695-4

25. Sasaki N, Ogasawara M, Sekiguchi T, Kusumoto S, Satake H. Toll-like receptors of the ascidian. *Ciona intest J Biol Chem* (2009) 284:27336–43. doi: 10.1074/jbc.M109.032433

26. Melillo D, Marino R, Della Camera G, Italiani P, Boraschi D. Assessing immunological memory in the solitary ascidian. *Ciona robusta Front Immunol* (2019) 10:1977. doi: 10.3389/fimmu.2019.01977

27. Dishaw LJ, Giacomelli S, Melillo D, Zucchetti I, Hair RN, Natale L, et al. A role for variable region-containing chitin-binding proteins (VCBPs) in host gut-bacteria interactions. *Proc Natl Acad Sci USA* (2011) 108:16747–52. doi: 10.1073/pnas.1109687108

28. Pfaffl MW. A new mathematical model for relative quantification in real-time RT-PCR. *Nucleic Acids Res* (2001) 29:45. doi: 10.1093/nar/29.9e45

29. Liberti A, Bertocci I, Pollet A, Musco L, Locascio A, Ristoratore F, et al. An indoor study of the combined effect of industrial pollution and turbulence events on the gut environment in a marine invertebrate. *Mar Environ Res* (2020) 158:104950. doi: 10.1016/j.marenvres.2020.104950

30. Giacomelli S, Melillo D, Lambris JD, Pinto MR. Immune competence of the *Ciona intestinalis* pharynx: complement system-mediated activity. *Fish Shellfish Immunol* (2012) 33:946–52. doi: 10.1016/j.fsi.2012.08.003

31. Franchi N, Ballarin L. Preliminary characterization of complement in a colonial tunicate: C3, bf and inhibition of C3 opsonic activity by compstatin. *Dev Comp Immunol* (2014) 46:430–8. doi: 10.1016/j.dci.2014.05.014

32. Guo X, He Y, Zhang L, Lelong C, Jouaux A. Immune and stress responses in oysters with insights on adaptation. *Fish Shellfish Immunol* (2015) 46:107–19. doi: 10.1016/j.fsi.2015.05.018

33. Weiss J. Bactericidal/permeability-increasing protein (BPI) and lipopolysaccharide-binding protein (LBP): structure, function and regulation in host

defence against gram-negative bacteria biochem. *Soc Trans* (2003) 31:785–90. doi: 10.1042/bst030785

34. Hamann L, Alexander C, Stamme C, Zahringer U, Schumann RR. Acute-phase concentrations of lipopolysaccharide (LPS)-binding protein inhibit innate immune cell activation by different LPS chemotypes via different mechanisms. *Infect Immun* (2005) 73:193–200. doi: 10.1128/IAI.73.1.193-200.2005

35. Canny G, Levy O, Furuta GT, Narravula-Alipati S, Sisson RB, Serhan CN, et al. Lipid mediator-induced expression of bactericidal/permeability-increasing protein (BPI) in human mucosal epithelia. *Proc Natl Acad Sci USA* (2002) 99:3902–7. doi: 10.1073/pnas.052533799

36. Lu SC. Regulation of glutathione synthesis. *Mol Aspects Med* (2009) 30:42–59. doi: 10.1016/j.mam.2008.05.005

37. Ermak TH. The renewing cell populations of ascidians. *Am Zool* (1982) 22:795–805. doi: 10.1093/icb/22.4.795

38. Liberti A, Melillo D, Zucchetti I, Natale L, Dishaw LJ, Litman GW, et al. Expression of *Ciona intestinalis* variable region-containing chitin-binding proteins during development of the gastrointestinal tract and their role in host-microbe interactions. *PloS One* (2014) 9:e94984. doi: 10.1371/journal.pone.0094984

39. Selitrennikoff CP. Antifungal proteins. *Appl Environ Microbiol* (2001) 67:2883–94. doi: 10.1128/AEM.67.7.2883-2894.2001

40. Bormann C, Baier D, Hörr I, Raps C, Berger J, Jung G, et al. Characterization of a novel, antifungal, chitin-binding protein from *Streptomyces tendae* Tü901 that interferes with growth polarity. *J Bacteriol* (1999) 181:7421–9. doi: 10.1128/JB.181.24.7421-7429.1999

41. Berthelot K, Peruch F, Lecomte S. Highlights on *Hevea brasiliensis* (pro)hevein proteins. *Biochimie* (2016) 127:258–70. doi: 10.1016/j.biochi.2016.06.006

42. Destoumieux D, Muñoz M, Cosseau C, Rodriguez J, Bulet P, Comps M, et al. Penaeidins, antimicrobial peptides with chitin-binding activity, are produced and stored in shrimp granulocytes and released after microbial challenge. *J Cell Sci* (2000) 113:461–9. doi: 10.1242/jcs.113.3.461

43. Osaki T, Omotezako M, Nagayama R, Hirata M, Iwanaga S, Kasahara J, et al. Horseshoe crab hemocyte-derived antimicrobial polypeptides, tachystatins, with sequence similarity to spider neurotoxins. *J Biol Chem* (1999) 274:26172–8. doi: 10.1074/jbc.274.37.26172

44. Kzhyshkowska J, Gratchev A, Goerdt S. Human chitinases and chitinase-like proteins as indicators for inflammation and cancer. *biomark Insights* (2007) 2:128–46. doi: 10.1177/117727190700200023

45. Dishaw LJ, Mueller MG, Gwatney N, Cannon JP, Haire RN, Litman RT, et al. Genomic complexity of the variable region-containing chitin-binding proteins in amphioxus. *BMC Genet* (2008) 9:78. doi: 10.1186/1471-2156-9-78

46. Dishaw LJ, Cannon JP, Litman GW, Parker W. Immune-directed support of rich microbial communities in the gut has ancient roots. *Dev Comp Immunol* (2014) 47:36–51. doi: 10.1016/j.dci.2014.06.011

47. Liberti A, Cannon JP, Litman GW, Dishaw LJ. A soluble immune effector binds both fungi and bacteria via separate functional domains. *Front Immunol* (2019) 10:369. doi: 10.3389/fimmu.2019.00369

48. Dishaw LJ, Leigh B, Cannon JP, Liberti A, Mueller MG, Skapura DP, et al. Gut immunity in a protochordate involves a secreted immunoglobulin-type mediator binding host chitin and bacteria. *Nat Commun* (2016) 7:10617. doi: 10.1038/ncomms10617

49. Zhao T, Su Z, Li Y, Zhang X, You Q. Chitinase-3 like-protein-1 function and its role in diseases. *Signal Transduction Targeting Ther* (2020) 5:201. doi: 10.1038/s41392-020-00303-7

50. Liberti A, Zucchetti I, Melillo D, Skapura D, Shibata Y, De Santis R, et al. Chitin protects the gut epithelial barrier in a protochordate model of DSS-induced colitis. *Biol Open* (2018) 7:bio029355. doi: 10.1242/bio.029355

51. Jawhara S, Thuru X, Standaert-Vitse A, Jouault T, Mordon S, Sendid B, et al. Colonization of mice by *Candida albicans* is promoted by chemically induced colitis and augments inflammatory responses through galectin-3. *J Infect Dis* (2008) 197:972–80. doi: 10.1086/528990

52. Jawhara S. How gut bacterial dysbiosis can promote *Candida albicans* overgrowth during colonic inflammation. *Microorganisms* (2002) 10:1014. doi: 10.3390/microorganisms10051014

53. Johansen JS, Krabbe KS, Møller K, Pedersen BK. Circulating YKL-40 levels during human endotoxaemia. *Clin Exp Immunol* (2005) 140:43–348. doi: 10.1111/j.1365-2249.2005.02763x

54. Dela Cruz CS, Liu W, He CH, Jacoby A, Gornitzky A, Ma B, et al. Chitinase 3-like-1 promotes *Streptococcus pneumoniae* killing and augments host tolerance to lung antibacterial responses. *Cell Host Microbe* (2012) 12:34–46. doi: 10.1016/j.chom.2012.05.017

frontiers | Frontiers in Immunology

TYPE Original Research
PUBLISHED 02 August 2023
DOI 10.3389/fimmu.2023.1217077

OPEN ACCESS

EDITED BY
Andrew Rowley,
Swansea University, United Kingdom

REVIEWED BY
Zhao Lv,
Hunan Agricultural University, China
Valentina Valenzuela-Muñoz,
University of Concepcion, Chile

*CORRESPONDENCE
Assunta Liberti
assunta.liberti@szn.it;
assusy.liberti@gmail.com
Paolo Sordino
paolo.sordino@szn.it

†PRESENT ADDRESS
Carla Pollastro,
Cell Biology and Disease Mechanisms Unit, Telethon Institute of Genetics and Medicine, Pozzuoli, Italy

‡These authors have contributed equally to this work

RECEIVED 04 May 2023
ACCEPTED 13 July 2023
PUBLISHED 02 August 2023

CITATION
Liberti A, Pollastro C, Pinto G, Illiano A, Marino R, Amoresano A, Spagnuolo A and Sordino P (2023) Transcriptional and proteomic analysis of the innate immune response to microbial stimuli in a model invertebrate chordate.
Front. Immunol. 14:1217077.
doi: 10.3389/fimmu.2023.1217077

Transcriptional and proteomic analysis of the innate immune response to microbial stimuli in a model invertebrate chordate

Assunta Liberti[1*‡], Carla Pollastro[1†‡], Gabriella Pinto[2,3], Anna Illiano[2,3], Rita Marino[1], Angela Amoresano[2,3], Antonietta Spagnuolo[1] and Paolo Sordino[4*]

[1]Biology and Evolution of Marine Organisms (BEOM), Stazione Zoologica Anton Dohrn, Naples, Italy, [2]Department of Chemical Sciences, University of Naples Federico II, Naples, Italy, [3]Istituto Nazionale Biostrutture e Biosistemi-Consorzio Interuniversitario, Rome, Italy, [4]Biology and Evolution of Marine Organisms (BEOM), Stazione Zoologica Anton Dohrn, Sicily Marine Centre, Messina, Italy

Inflammatory response triggered by innate immunity can act to protect against microorganisms that behave as pathogens, with the aim to restore the homeostatic state between host and beneficial microbes. As a filter-feeder organism, the ascidian *Ciona robusta* is continuously exposed to external microbes that may be harmful under some conditions. In this work, we used transcriptional and proteomic approaches to investigate the inflammatory response induced by stimuli of bacterial (lipopolysaccharide -LPS- and diacylated lipopeptide - Pam2CSK4) and fungal (zymosan) origin, in *Ciona* juveniles at stage 4 of metamorphosis. We focused on receptors, co-interactors, transcription factors and cytokines belonging to the TLR and Dectin-1 pathways and on immune factors identified by homology approach (*i.e.* immunoglobulin (Ig) or C-type lectin domain containing molecules). While LPS did not induce a significant response in juvenile ascidians, Pam2CSK4 and zymosan exposure triggered the activation of specific inflammatory mechanisms. In particular, Pam2CSK4-induced inflammation was characterized by modulation of TLR and Dectin-1 pathway molecules, including receptors, transcription factors, and cytokines, while immune response to zymosan primarily involved C-type lectin receptors, co-interactors, Ig-containing molecules, and cytokines. A targeted proteomic analysis enabled to confirm transcriptional data, also highlighting a temporal delay between transcriptional induction and protein level changes. Finally, a protein-protein interaction network of *Ciona* immune molecules was rendered to provide a wide visualization and analysis platform of innate immunity. The *in vivo* inflammatory model described here reveals interconnections of innate immune pathways in specific responses to selected microbial stimuli. It also represents the starting point for studying ontogeny and regulation of inflammatory disorders in different physiological conditions.

KEYWORDS

inflammatory response, innate immunity, *Ciona robusta*, marine invertebrates, microbial stimuli, transcriptional analysis, proteomic analysis, protein-protein interactome

1 Introduction

The ascidian *Ciona robusta* is a filter-feeding marine species belonging to Tunicata, the sub-phylum most closely related to Vertebrata within the phylum Chordata (1). This species commonly thrives in polluted habitats highly enriched in pathogenic and nonpathogenic bacteria, fungi and viruses, sensing either potentially infectious ones or establishing homeostatic relationships, respectively. *C. robusta* is a consolidated experimental system in a wide array of biological fields (2–5) including immunology since, like all invertebrates, it possesses only innate immunity as a defense strategy against infections (6). The absence of the adaptive immune system facilitates studies of the innate immune crosstalk with the environment and of the establishment and maintenance of homeostasis with nonpathogenic and "foreign" microorganisms. In recent years, this marine species has been exploited for studies of host-microbiome interactions within the digestive tract in relation to microbial settlement and mucus colonization, leading to the characterization of different elements of the gut environment, such as chitin-rich mucus and a subset of secreted immune effectors (7, 8). *Ciona* has also been used in the context of identifying and defining immunological memory as a consequence of sophisticated responses mediated by trained immunity after inflammatory challenges (9).

The study of inflammatory mechanisms is essential to understanding the role of the immune system in the interaction with microbiota (10), and as a sentinel in cellular and tissue homeostasis (11–13). When these conditions deviate from homeostasis, activation of inflammatory pathways can help to restore the physiological equilibrium (11). In *Ciona*, several genomic and transcriptional studies have focused on the role of the innate immune system in the inflammatory response after challenges mainly with lipopolysaccharide (LPS) (reviewed in (14)), a component of Gram-negative bacterial membrane that belongs to the category of pathogen-associated molecular patterns (PAMPs). The knowledge of the immune repertoire of *C. robusta* is based on domain sequence similarities and phylogenetic relationships with their vertebrate counterparts (14), while the immunological role was functionally confirmed at the protein level in only few cases (15–17).

Several classes of immune factors have been recognized in *C. robusta*, such as *i*) pathogen recognition receptors (PRRs) like the Toll-like receptors (TLRs) TLR1 and TLR2 (17, 18) and C-type lectin receptors (CLRs) like CD94 (19); *ii*) cytosolic lectins like galectins, collectins (i.e. mannose-binding lectins) and intelectins (14, 20–24); *iii*) molecules of the complement system like C3 and its receptor C3aR (15, 16, 25, 26); *iv*) cytokines like the three interleukin-17 family members IL17-1, IL17-2 and IL17-3, the interleukin receptor IL17-R (27), the tumor necrosis factor α (TNFα) (28), the transforming growth factor beta (TGF-β) (29) and the macrophage migration inhibitory factor (MIF) (30), *v*) defensins like the molecule against microbes A precursor (mamA) (31); and *vi*) cytokine induction mediators like the gene coding for the transcription factor nuclear factor kappa B (NF-κB) (17, 32). All these immune molecules are transcriptionally, and sometimes translationally, upregulated in hemocytes and pharynx following subtunical injection of LPS in the pharyngeal wall, the first portion of the digestive tract of adult individuals of *C. robusta* (14). Moreover, C3 and C3aR have been proven to exert a chemotactic activity on ascidian hemocytes (15, 16). Here, our analyses of mRNA and protein expression patterns included most of these molecules, as well as additional genes putatively involved in the inflammatory response that were identified by homology search analysis in the current study.

An important experimental advantage of adopting *C. robusta* in comparative immunology is the capacity to perform *in vitro* fertilization and rear thousands of transparent filter-feeding juveniles. Metamorphic stage 4 of juvenile development (1st ascidian stage) is the first filter-feeding stage in the life cycle of *Ciona* (33), and can be used for investigating the inflammatory response to environmental microbial components at the early phase of immune system development and maturation. While the inflammatory response in adult ascidians usually involves stimulus injection in the body wall, stage 4 *C. robusta* juveniles can be exposed to resuspended, exogenous, and sometimes harmful compounds that can be ingested by filtration, thus reproducing a more natural physiological condition. In this work, this juvenile stage was used to explore the activation of key components of the innate immune response in the whole animal after exposure to different PAMPs.

The inflammatory molecules used in this study include components of bacterial [i.e., LPS and diacylated lipopeptide (Pam2CSK4)] and fungal (*i.e.*, zymosan, an insoluble preparation of *Saccharomyces cerevisiae* cell wall, consisting of β-glucans, mannans, mannoproteins and chitin) cell walls. Of note, the effect of Pam2CSK4 [present in both Gram-positive and Gram-negative bacteria (34, 35)] on *Ciona* immune response has not been previously investigated. In mammals, these stimuli are described to be agonists of TLRs and Dectin-1. Specifically, LPS is an agonist of human TLR4 (36, 37), Pam2CSK4 is an activator of TLR2/TLR6 heterodimer (38), and zymosan is an agonist of human TLR2 and Dectin-1 (39). In a previous study conducted by Sasaki and coworkers using *Ciona* adults, activation of TLRs was induced by zymosan and not by another lipopeptide, Pam3CSK4 (17).

Here, we gathered evidence in support of specific transcriptional and translational changes induced by PAMPs, and of possible interactions between molecules and pathways involved in the immune response, specifically TLRs and Dectin-1 pathways. In summary, this study depicts *C. robusta* as a unique chordate organism for studying factors and mechanisms that modulate immune activation and homeostasis, thus supporting its use as a viable experimental system in translational research and biotechnological approaches.

2 Materials and methods

2.1 Ethics statement and animal sampling

The research described herein was performed by using *Ciona* specimens collected in the Mar Piccolo of Taranto (Taranto, Italy, ~40° 29'29"N, 17°17'55"E) and in the Fusaro lagoon (Naples, Italy, ~40° 49'10"N, 14°03'28"E), in locations that are not privately-owned nor

protected in any way, according to the authorization of Marina Mercantile (Decree of the President of the Republic (DPR) 1639/68, Sep. 19, 1980, confirmed on Jan. 10, 2000). The study did not involve mammalian or vertebrate subjects, or endangered or protected species, and was carried out in strict accordance with European (Directive 2010/63/EU) and Italian (Legislative Decree n. 26/2014) legislation for the care and use of animals for scientific purposes. *C. robusta* is considered an introduced species and is not regulated or protected by environmental agencies in Italy. The animal collection services contracted in this study maintain current permits and licenses for collection and distribution of marine invertebrates to academic institutions. No special permission was required to collect ascidians, and animal handling was in accordance with the guidelines of our academic institutions. Animals were recovered and brought to the laboratory alive and maintained in clean water with aeration, temperature control and properly fed. In accordance with general animal protocols, the least number of specimens required per experiment were utilized. Animal waste products were disposed appropriately.

2.2 Juvenile treatment and sample preparation for gene expression and proteomic analyses

To obtain stage 4 *Ciona* juveniles, *in vitro* fertilization was performed using eggs and spermatozoa surgically collected from the gonoducts of different animals that had been exposed to constant light to elicit gamete maturation. *In vitro* egg fertilization follows the procedure described previously (40), with the exception that 0.22 µM filtered seawater (FSW) was used and no sterilization step was performed. After the time required for egg fertilization (about 10 minutes), fertilized eggs were diluted in FSW in 150 mm Petri dishes and raised at 18°C. Eighteen hours (hr) later, when animal have reached the non-feeding swimming tadpole larval stage, batches containing at least 90% normally developed larvae were selected for inflammatory treatments. Then, larvae were gently transferred to 6-well plates containing 4 ml FSW and 600-700 larvae per well. Animals were let to grow O/N at 18°C, and the day after the FSW was replaced with fresh one to eliminate post-metamorphic stages not attached to the dish, or unsettled larvae not properly developed. When juveniles have reached stage 4 (33), 3-4 days post fertilization, they were ready to be treated with different inflammatory stimuli, such as LPS (Sigma #L2880), Pam2CSK4 (InvivoGen #tlrl-pm2s-1) and zymosan (InvivoGen #tlrl-zyn). We referred to literature for the concentration of each inflammatory agent that best suits the activation of the immune system. LPS is usually injected in adults in the quantity of 100 µg dissolved in marine solution (27–29), or resuspended in a cell line-based heterologous system at the concentration of 2.5 and 5 µg/ml (17). Here, we used LPS at an intermediate concentration of 10 µg/ml. The triacylated form Pam3CSK4 was tested on cell lines in a heterologous system at the concentration of 0.5 and 2 µg/ml (17). Here, we used Pam2CSK4 at 1 and 10 µg/ml concentrations. The third inflammatory agent, zymosan, was reported in *Ciona* as a modulator of TLR activation in an *in vitro* heterologous system at the concentration of 100 µg/ml (17). Here, we used it at 10 and 100 ug/ml concentration. Each compound was resuspended at the appropriate concentration in 4 ml of 0.22 µm FSW, and animals were treated with these solutions for 30 minutes (min), 2 hr and 4 hr, while control animals were exposed to normal FSW. At the end of each time treatment, samples for gene expression analysis were collected in RNA*later* by replacing the FSW supplemented with the microbial stimulus with 1 ml RNA*later* solution in each well. Sample storage followed the manufacturer's instruction; briefly, after O/N incubation in RNA*later* at room temperature (RT), RNA*later* solution was removed and samples (whole animals still attached to the bottom of 6-well plates) were frozen at -20°C for long term storage until RNA extraction. In turn, samples for proteomic analyses were processed by removing FSW supplemented with the microbial stimulus followed by fast freezing in dry ice and storage at -80°C until protein extraction.

2.3 Gene expression analysis

2.3.1 The identification of immune molecules

To search for new immunocompetent molecules, we used orthologous gene search and homology domain approaches to explore the *C. robusta* genome annotation databases ANISEED (v.2019) (41), NCBI (42) and UCSC Genome Browser (assembly ID: ci3 (43)). A combination of tools (e.g., PSI-BLAST (44), BLAST v.2.13.0 (45) and Jalview v.2.11.2.0 (46)) and resources (e.g., UniProt (47), InterPro (48) and SMART (49)) was used to compare protein functional and structural domains and to analyze the percentage of sequence identity of molecules of interest between *Ciona robusta* and *Homo sapiens*. The following protein domains were used as queries: *i*) C-type lectin (CTL) or carbohydrate-recognition domain (CRD) (CLECT); *ii*) interferon regulatory factor (IRF) domain (also known as tryptophan pentad repeat); and *iii*) immunoglobulin (Ig) and immunoglobulin-like (Ig-like) domains.

2.3.2 RNA extraction

Total RNA was extracted from whole-body *Ciona* juveniles using RNAqueous™-Micro Total RNA Isolation Kit (Invitrogen #AM193) following manufacturer's instructions. Briefly, juvenile samples collected in 6-well plates as described in the previous section, were allowed to thaw slowly before proceeding to RNA extraction. After adding lysis buffer, samples were detached by scraping using flat blade cell lifter, collected, and transferred to 1.5 ml microtube, and mechanically broken using an ultra sonicator (Branson) for 15 seconds (sec) at 20% of maximum power. RNA extracted was eluted in 20 µl elution buffer, and subsequently DNA contamination was eliminated by performing DNase step as described in the manufacturer's procedure. RNA quality and quantity were evaluated through agar gel electrophoresis and NanoDrop spectrophotometer (ThemoFisher) reading, respectively.

2.3.3 Quantitative reverse transcription PCR analysis

Single-stranded cDNA was synthesized from 1 µg of total RNA employing QuantiTect Reverse Transcription kit (Qiagen #205311). Gene expression was analyzed by quantitative reverse transcription PCR (RT-qPCR) on cDNA from control juvenile

samples and juvenile samples exposed to the different microbial stimuli. Primer sequences for the genes to be examined are listed in Supplementary Tables 1A, B. Actin gene was used as reference for internal standardization.

The amplification efficiency of each RT-qPCR primer set was assessed employing 10-fold serial dilution of juvenile cDNA or it was already tested in a previous work, employing 10-fold serial dilution of cDNA synthetized from *Ciona* digestive tract (50) (Supplementary Tables 1A, B). RT-qPCR was performed according to the manufacturer's recommendation with the Fast SYBR Green MasterMix (Applied Biosystems #4385612), 0.28 µM of each primer and 5 ng of cDNA per reaction. A denaturation step at 95°C for 20 sec, 40 amplification cycles (95°C for 1 sec and 60°C for 20 sec) and a Melt Curve step (95°C for 15 sec, 60°C for 1 min and 95°C for 15 sec) were employed. Reactions for each sample were performed in triplicate on five or six biological replicates. In order to calculate mRNA expression level (mRNA RQ) relative to the control sample of each fertilization, data were analyzed with Vii^{TM} 7 Real-Time PCR software (Life Technologies) and quantified with the comparative C_t method ($2^{-\Delta\Delta Ct}$) based on Ct values. Expression level of the selected genes is indicated as fold change. Results are represented as violin plots, showing the full distribution of the data, reported as value of the fold change of each sample (biological replicate), and the median for each condition analyzed. Significance of the relative $2^{-\Delta\Delta Ct}$ of each group (biological replicates n = 5 or 6), compared to the controls, was determined using 'paired parametric t-test'. One-way ANOVA analysis, according to normality test results, performed on each gene, was employed to determine statistically significant differences between the three time points for each microbial stimulus treatment. The statistical analyses were performed using GraphPad PRISM software, version 9.3.1.

2.4 Targeted proteomics analysis

2.4.1 Protein extraction and samples preparation for mass spectrometry analysis

Total protein extraction from whole-body *C. robusta* juveniles followed the same procedure used for RNA extraction (*paragraph 2.3.2*) with the exception that the juveniles were lysed in 2% CHAPS buffer (100 µl per well, Sigma #C9426) and mechanically broken using an ultra sonicator (Branson) for 30 sec at 20% of maximum power. Sample lysates were then centrifuged at 13,000 rpm for 15 min at 4°C, supernatants were collected in 1.5 ml microtubes and stored at -80°C. An aliquot of 30 µl of each protein lysate was subjected to the *in-solution* digestion protocol by reducing with 100 mM dithiothreitol (dissolved in 50 mM ammonium bicarbonate) to a final concentration of 20 mM and incubated for 60 min at 60°C. After cooling the protein solution at RT, the protein cysteines were alkylated by adding iodoacetamide to a final concentration of 40 mM, followed by incubation in the dark for 45 min at RT. A solution of formic acid was added at a final concentration of 1% to block the alkylation reaction and proteins precipitated by a chloroform/methanol/water precipitation protocol (51). Supernatants were removed and the pellets dried. Digestion of protein mixtures was carried out in 10 mM ammonium bicarbonate by using trypsin at 50:1 protein:enzyme mass ratio. The samples were incubated at 37°C for 16 hr, and the trypsin digestion stopped by acidification of the peptide's mixture.

The peptides were dried under vacuum and finally resuspended in 50 µl of 0.1% HCOOH for a further desalting step using manually equipped tips with three Empore disc C18 (Merck, #66883-U) before the liquid chromatography-mass spectrometry tandem (LC-MS/MS) analysis in Multiple Reaction Monitoring ion mode (MRM).

2.4.2 LC-MS/MS analysis

The peptide mixture was analyzed by LC-MS/MS analysis using a Xevo TQ-S (Waters, Milford, MA, USA) equipped with an ionkey coupled to an Acquity UPLC system (Waters, Milford, MA, USA). For each run, the peptide mixture (2 µl) was injected and separated on a BEH C18 peptide separation device (130Å, 1.7 µm, 150 µm X 50 mm) at 45°C with a flow rate of 3 µl/min using an aqueous solution (LC-MS grade) containing 2% ACN as a mobile phase A and 98% ACN of an aqueous solution as a mobile phase B, both acidified with 0.2% HCOOH. The gradient for the MRM method started with 7% buffer B for 5 min, from 5 to 40 min reached 50% buffer B to 95% buffer B during the next 2 min. The column was finally re-equilibrated to initial conditions for 4 min. The parameters of the MS source were as follow: 3900 V as ion spray voltage, 150°C interface heater temperature, 150 l/h gas flow with 7 bar nebulizer pressure.

MRM mass spectrometric analyses were performed in positive ion mode for the run time with 5 points per peak and 3 min dwell times. The cone voltage was set to 35 V. A range of 300-1000 m/z was preferentially selected as precursor or product ions.

2.4.3 Informatics tools

The latest version of Skyline software (22.2 - 64 bit version MacCossLab Software, University of Washington, USA) (52) was used for *in silico* selection of peptides with proteotypic sequences for each selected protein. For each peptide, m/z precursor ion, m/z product ion, and relative collision energy were provided by Skyline (Supplementary Table 2). Seven and thirty amino acid-long tryptic proteotypic peptides, preferably without missed cleavages and devoid of methionine and cysteine residues, were chosen for the development of MRM assays. Sequences with a proline (P) on the C-terminal side of arginine (R) or lysine (K) or showing the NXT or NXS glycosidic consensus motif were also excluded. The six transitions of proteotypic peptides were selected for method development based on the y-fragment ions.

2.4.4 Statistical analysis

The areas of extracted ion chromatograms of all proteotypic peptides for each protein were averaged to get a value representative of a specific protein. Such values were uploaded on Perseus software (53) used for the statistical analysis. Expression values of each protein were log2 transformed to obtain a Perseus matrix. Finally, heatmap of cluster analysis and principal component analysis (PCA) were performed by using the obtained Perseus matrix.

2.5 *In silico* analysis of potential interactions

To increase knowledge about the landscape of molecular dynamics triggered by inflammation, a protein-protein interaction map was generated using the STRING database (54). Multiple sequence queries were followed by evaluation of protein sequence identity by means of Multiple Sequence Alignment (MSA) in Jalview (46) and BlastP (44, 45). The resulting interaction networks were modified and merged with the Cytoscape v.3.9.0 software (55) in order to build a complete protein-protein interactome in which to connect all molecules whose gene expression was analyzed in this study. Among the applications available in Cytoscape "App Manager" for functional analyses of immune-related pathways, we installed and used the STRING Enrichment application, that is based mainly on KEGG (56), SMART, COMPARTMENTS (57), Panther (58, 59), AmiGO 2 (60) and QuickGO (61), Pfam (62), InterPRO and Reactome (63) databases. This application was used to retrieve annotations about compartmentation, Gene Ontology (GO), pathway analysis and domain analysis of the selected nodes of the map. The main findings are reported in the protein-protein interaction network.

3 Results

3.1 Experimental setup: concentration and exposure time to microbial stimuli

In this study, the effect of 30 min, 2 hr and 4 hr exposure to microbial stimuli in *C. robusta* juveniles has been investigated by evaluating changes in the expression levels of immune genes and proteins in the whole-body animal (Figure 1A). Also, juveniles were exposed for 4 hr at all selected concentrations (10 µg/ml LPS, 1 and 10 µg/ml Pam2CSK4, 10 and 100 µg/ml zymosan), raised in FSW for 24 hr, and then analyzed for survival and altered gross phenotypes. In all experimental conditions, juveniles were alive and morphologically normal, suggesting that the concentrations of the microbial stimuli did not trigger a strong immune response that could be lethal for the animals (Figure 1B).

3.2 Immune gene mining and expression

Previous studies have identified the main molecular actors of the innate immune system of *C. robusta*, revealing high-rate conservation of PRRs, cytokines and complement system molecules, to name a few. In our work, to widen the spectrum of molecules that could be responsive to the inflammatory stimuli here tested, more counterparts of genes involved in the inflammatory response of vertebrates were included. The genes encoding the tyrosine-protein kinase SYK and Nuclear factor of activated T-cells 5 (NFAT5), respectively co-interactor and transcription factor of PRR pathways, were identified by orthologous gene search and had already been annotated (http://www.aniseed.cnrs.fr). Then, more immune genes were uncovered by homology search analysis of *C. robusta* genome and proteome (Table 1). Specifically, we searched for molecules containing the CLECT and the Ig domains, since they are present in proteins with immune functions (64–67), and the IRF domain contained in the homonymous transcription factor involved in PRR pathways (68).

The CLECT domain allowed to identify the Dectin-1 CLR family 4 members M (CLEC4M) and F (CLEC4F), and Macrophage mannose receptor 1-like (MR). Ig- or Ig-like domains were found in FAM187A, fibronectin (FN), fibronectin like (FN-like), and tyrosine-protein kinase receptor 3 (TYRO3). TYRO3 is a receptor which is also characterized by FN and Tyrosine kinase catalytic domains and is involved in inflammation resolution (69, 70). FAM187A (Cirobu.g00001161) groups together with the ascidian *Botryllus schlosseri* Triggering receptor expressed on myeloid cells (TREM)-like 2 gene (TREML2) (Boschl.g00005277) in the "Gene Phylogeny" section of the ANISEED database. In human, the TREM2 pathway is expressed in various tissue macrophages, such as the microglia of the central nervous system, and increasing evidence suggests that TREM2 is involved in neuroinflammatory responses and neurodegenerative diseases like Alzheimer and Parkinson (71, 72) and contributes to mucosal inflammation in the digestive tract during the development of colitis in mice (73). The IRF domain was present in IRF-like gene. Furthermore, search for *C. robusta* NFAT5 led to the identification of FAM136A, a mitochondrial protein conserved across metazoans (74) whose human orthologue shows a correlation with Meniere's disease, an inner ear problem with an autoimmune condition (75).

In detail, the effect of LPS, Pam2CSK4 and zymosan has been tested on the activity of the following *Ciona* factors: *i*) immune receptors such as TLR1, TLR2, CLEC4M, CLEC4F and MR; *ii*) Ig-like V-type domain-containing proteins as FAM187A, FN, FN-like and TYRO3; *iii*) the co-interactor SYK; *iv*) transcription factor coding genes NF-κB, IRF-like and NFAT5; *v*) FAM136A; *vi*) cytokines IL17-1, IL17-2, IL17-3, and their receptor IL17R, TNFα, TGFβ and MIF; *vii*) defensins like mamA and *viii*) complement system genes C3 and C3aR. The results obtained for each stimulus are described below. For sake of simplicity in the presentation, FAM136A and IL17R were included in the categories of transcription factors and cytokine signaling, respectively, besides their different roles.

3.2.1 LPS: effects on TLR2 and TYRO3 genes

LPS is the inflammatory agent more widely used in *Ciona* adults (by injection). Here, 10 µg/ml LPS did not induce a significant immune response in stage 4 juveniles, as shown by lack of changes in the expression of most genes (Supplementary Figure 1) apart from the upregulation of *TLR2* and *TYRO3* after 30 min treatment (Figure 2). Thus, the modest activation of an immune response following LPS infection is rapidly resolved.

3.2.2 Pam2CSK4: effects on genes encoding for PRRs, transcriptional factors, and cytokines

Unlike LPS, the inflammatory stimulus Pam2CSK4 was seen to induce transcriptional modulation of several molecules and

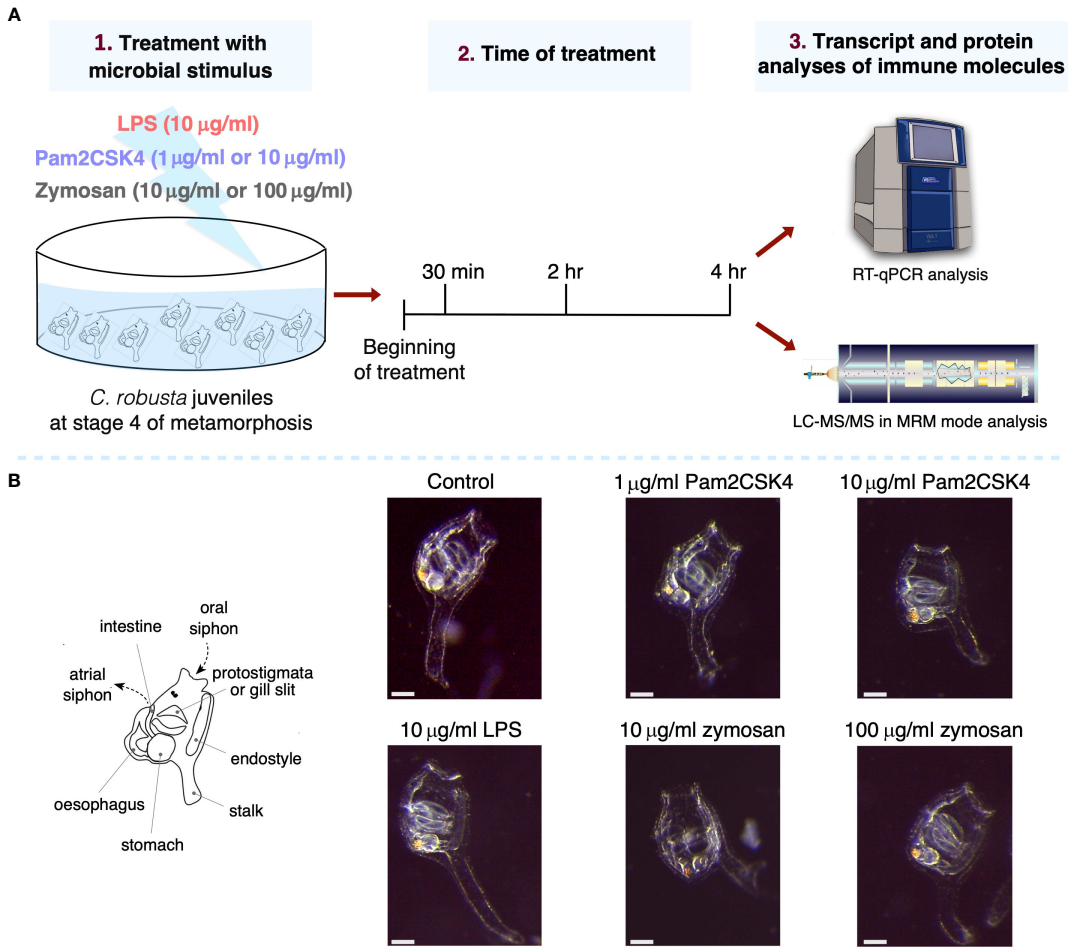

FIGURE 1
Experimental setup and effect on morphology of *.C. robusta* juveniles after 24 hours from the treatment. **(A)** Scheme of *C. robusta* juveniles' treatment with different microbial stimuli, concentrations and duration, followed by quantification of immune molecules through gene expression (RT-qPCR technique) and protein level (LC-MRM/MC technique). **(B)** On the left, schematic representation of *C. robusta* juveniles at stage 4 showing the main anatomical features observed at this metamorphic stage. On the right, after 24 hours juveniles (exposed for 4 hours to diverse concentration of microbial stimuli) appear morphologically normal. Scale bar, 100 µm.

pathways at all concentrations and time points. Following 1 µg/ml Pam2CSK4 treatment, *TLR1* was upregulated after 30 min treatment, *TLR2* after 30 min and 2 hr, and *CLEC4F* receptor after 4 hr treatment (Figure 3). While the expression of the genes encoding the receptor, *CLEC4M*, the Ig-domain containing proteins *FAM187A*, *FN*, *FN-like* and *TYRO3*, the cofactor *SYK*, was not regulated by Pam2CSK4 exposure, the expression of *FN*, *FN-like* and *TYRO3* was significantly modulated between 30 min and 4 hr treatments (Supplementary Figure 2). The expression of the transcription factor coding gene *NF-κB* was affected at all time points analyzed, with upregulation at 30 min and down-regulation at 2 hr and 4 hr; *IRF-like* was upregulated at both 30 min and 2 hr, whereas *NFAT5* was downregulated at 4 hr (Figure 3). Significant upregulation of *FAM136A* was observed after 30 min exposure (Figure 3). Concerning cytokines, *IL17-3* and *TGFβ* were significantly upregulated at 30 min and 2 hr treatment, respectively (Figure 3). Upregulation of *IL17R* was also observed at both 30 min and 2 hr time points (Figure 3). Conversely, cytokines *IL17-1*, *IL17-2*, *TNFα* and *MIF*, defensin *mamA*, and molecules of the complement system *C3* and *C3aR* were not affected in their transcriptional levels (Supplementary Figure 2). Statistical analysis by using one-way ANOVA test revealed that 1 µg/ml Pam2CSK4 had a significant effect on the modulation of genes coding for receptors (*TLR2*, *CLEC4F* and *MR*), transcription factors (*NF-κB*, *IRF-like* and *NFAT5*) and cytokines (*IL17-3* and *TGFβ*) (Figure 3).

Pam2CSK4 at the concentration of 10 µg/ml induced downregulation of *CLEC4M* and *CLEC4F* after both 2 and 4 hr treatment. TLR receptor coding genes were only affected after 4 hr, with downregulation of *TLR1* and upregulation of *TLR2* (Figure 4). Cytokines were upregulated following 30 min and 4 hr treatment (*IL17-1*), at all-time points (*IL17-3*) and 2 and 4 hr (*TGFβ*), while a downregulation of *MIF* was observed at 2 and 4 hr treatment (Figure 4). The highest concentration of Pam2CSK4 also induced upregulation of both defensin *mamA* and molecules of the complement system *C3* and *C3aR* after 4 hr treatment (Figure 4).

10.3389/fimmu.2023.1217077

TABLE 1 *Ciona robusta* immune-related molecules identified by *in silico* analysis.

	Protein Name	NCBI Protein Acc. Number *C. robusta*	UniProtKB Acc. Number *C. robusta*	PSI-BLAST % identity	MSA % identity	Human Protein
CLECT domain	CLEC4M	XP_026689560.1	F7BDF2	34	23.40	CLEC4E
				33	21.40	CLEC4M
	CLEC4F	XP_002121230.2	H2XYQ6	23	18.40	CLEC4F
				23	20.73	CLEC4K
	MR	XP_026691626.1	F6TDB0	31	27.74	Macrophage mannose receptor 1 (MRC1)
				28	24.18	C-type mannose receptor 2 (MRC2)
Ig-domain	FAM187A (A/B)	XP_002120037.3	F6RE92	27	19.83	FAM187B
				25	19.60	FAM187A
	FN	AOO95899.1	F6TTH0 F6UFX8	24	21.30	Fibronectin
				21	20.77	Tenascin x
	FN-like	XP_002120276	F6TWX3	24	21.51	Fibronectin
				20	22.14	Tenascin x
	TYRO3	XP_002124888.2	F6U7K8	35	27.01	Tyro3
				33	26.02	Tyrosine-protein kinase receptor UFO
IRF domain	IRF4-like	NP_001071743.1	Q4H3B3	32	28.92	IRF4
				28	26.54	IRF5
	SYK	XP_002123000.1	F6QTW3	35	35.25	Syk
				33	33.33	Zap70
	NFAT5	XP_018666864.1	H2Y0S5	31	24.19	NFATC3
				29	26.07	Nfat5
	FAM136A	XP_002129880.1	A0A1W2WJY0	36	33.82	Fam136A
				24	17.99	NOP56

Protein names, accession numbers in NCBI and UniProtKB databases of C. robusta immune-related molecules are reported, together with the percentage of identity respect to human orthologs, investigated with both Protein Similarity Search (PSI-BLAST) database and Multiple Sequence Alignment Viewer application (MSA).

No change in gene expression was observed for *MR*, *FAM187A*, *FN*, *FN-like*, *TYRO3*, *SYK*, *NF-κB*, *IRF-like* and *NFAT5*, protein coding gene *FAM136A*, and cytokines *TNFα*, *IL17-2* and the receptor *IL17R* (Supplementary Figure 3). Statistical analysis by using one-way ANOVA test revealed that 10 µg/ml Pam2CSK4 induces a significant modulation in the expression of *CLEC4F*, *IL17-1*, *IL17-3* and *TGFβ* (Figure 4).

Taken together, these data show that Pam2CSK4 is able to trigger the activation of both PRR pathways investigated, modulating the transcription of receptors (*TLRs* and *CLEC4M*) and transcription factors (*NF-κB*, *IRF-like* and *NFAT5*) with concentration-dependent timing of activation. The inflammatory state induced by this bacterial stimulus is demonstrated by the activation of pro-inflammatory cytokines like *IL17-1* and *IL17-3*. Finally, the upregulation of *TGFβ* cytokine at late time point indicates a resolution of the inflammatory response.

3.2.3 Zymosan: effects on genes encoding for CLRs, Ig-containing molecules, cofactors, transcriptional factors, and cytokines

Ciona juveniles exposed for 4 hr to the lower concentration of zymosan, 10 µg/ml, showed a significant downregulation of the receptors *CLEC4M*, *MR*, *FN*, *FN-like* and the cofactor *SYK* (Figure 5). A similar effect was observed on the transcription factor coding genes *NFAT5* and *IRF-like*, the last one being downregulated also at 2 hr (Figure 5). Downregulation of the cytokine *IL17-2* (2 and 4 hr) and of the complement component *C3* (30 min and 4 hr) was also observed (Figure 5). The other genes analyzed, such as receptors (*TLR1*, *TLR2*, *CLEC4F*), Ig domain-containing proteins (*FAM187A* and *TYRO3*), transcription factor coding genes (*NF-κB*), *FAM136A*, cytokines (*IL17-1*, *IL17-3*, *IL17R*, *TGFβ*, *TNFα* and *MIF*), defensins (*mamA*) and complement system components (*C3aR*) were not affected by this inflammatory stimulus (Supplementary Figure 4).

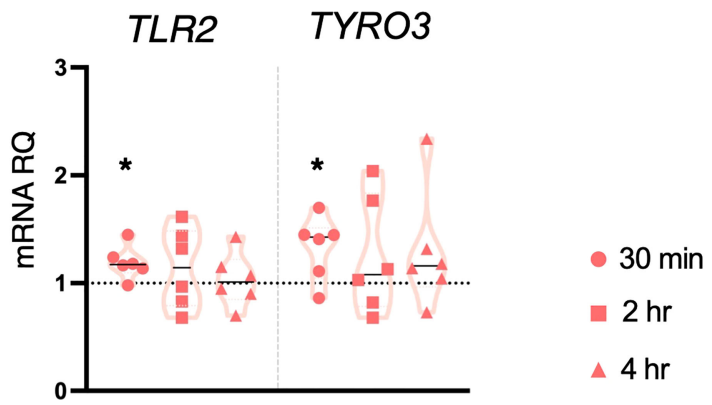

FIGURE 2
Effect of 10 µg/ml LPS treatment on gene expression. *C. robusta* juveniles at stage 4 of metamorphosis treated with 10 µg/ml LPS show significant changes in gene expression of *TLR2* and *TYRO3*, detected by RT-qPCR, after 30 min treatment. Truncated violin plots represent the distribution and the density of numerical data of gene expression reported as fold changes ($2^{-\Delta\Delta Ct}$) of mRNA Relative Quantification (mRNA RQ) compared to the corresponding control samples (no treated juveniles), that are reported as dotted black line. The black lines in each violin plots indicate the median of data set (n = 6, biological replicates). Statistical methods: paired samples t-test, significance indicated by black asterisk. (*p. value < 0.05).

One-way ANOVA analysis revealed a modulation in *IRF-like*, *IL17-2* and *C3* expression (Figure 5).

Zymosan at the concentration of 100 µg/ml induced significant upregulation in the expression of genes coding for the Ig-domain containing proteins *FAM187A* (4 hr) and *TYRO3* (2 hr), cofactor *SYK* (2 hr), cytokines *IL17-3* (30 min and 4 hr), *TGFβ* (2 and 4 hr), *MIF* (30 min) and complement component *C3aR* (2 hr) (Figure 6). No effect was observed on the expression of the genes coding for receptors and Ig-domain containing proteins (*TLRs*, *CLE4M*, *CLEC4F*, *MR*, *FN* and *FN-like*), transcription factors (*NF-κB*, *IRF-like* and *NFAT5*), *FAM136A*, cytokines (*IL17-1*, *IL17-2*, *IL17R*, *TNFα*), defensins (*mamA*) and complement system molecules (*C3*) (Supplementary Figure 5). One-way ANOVA analysis showed a significant modulation of *IL17-3* expression during the analyzed time points, and a significant shift in the transcriptional response of *FAM187A* between 30 min and 4 hr treatments (Figure 6).

Collectively, the immune response induced by zymosan involves CLRs (*CLEC4M* and *MR*), cofactors (*SYK*) and transcription factors (*IRF-like* and *NFAT5*), suggesting an interplay of distinct PRR pathways. Among immune stimuli tested in this study, zymosan was the only one that affected the expression of Ig-containing molecules (*FAM187A*, *FN*, *FN-like* and *TYRO3*). Moreover, the activation of the inflammatory state following exposure to the higher concentration is highlighted by the modulation of the cytokine's transcripts, pro-inflammatory (*IL17-3*), and consequently anti-inflammatory (*TGFβ*), indicating again a resolution of the inflammation.

3.3 Targeted proteomics

To explore the effect of each stimulus treatment at protein level, the targeted proteomic approach has been conceived for detecting changes in protein amount of the immune molecules here investigated. Indeed, A LC-MRM/MS method was developed for the detection of changes in protein abundance for the immune molecules. We first selected a panel of 1-3 proteotypic peptides for each protein and then recorded from 3 to 6 transitions (a combination of each precursor ion to several fragment ions) for each peptide. A total number of 32 peptides belonging to 16 proteins (listed in the Supplementary Table 1 and in the Figure 7B) was selected by monitoring 139 transitions displaying a good instrumental response (the same retention time for all transitions and a peak area higher than 1,000). An example of MRM chromatogram was reported for one peptide of the NFAT5 protein (Supplementary Figure 6). After selecting the best instrumental response (see instrumental parameters in Supplementary Table 2), the relative quantification was performed by comparing the areas underlying the extracted ion chromatogram (EIC) peaks reflecting the differential expression of selected 16 proteins following the various stimulation *versus* the control sample. As an example, the EIC peak areas of two proteins, e.g. FAM136A and FN, were reported in a histogram representation (Supplementary Figure 7), displaying a similar trend in the samples. A significant downregulation was observed for the FAM136A and fibronectin protein along the Pam2CSK4 and zymosan treatment (independently from the stimulus kinetics) in comparison to the other samples, included the control.

The EIC peak areas were then uploaded on Perseus software to discover the response of *C. robusta* juveniles to stimulation with 10 µg/ml LPS, 1 µg/ml Pam2CSK4 and 100 µg/ml zymosan at 30 min, 2 hr and 4 hr of treatment compared to the control samples. The PCA analysis allowed to summarize and visualize the overall protein response to the microbial stimulation within a biplot where the control and treated samples were graphically

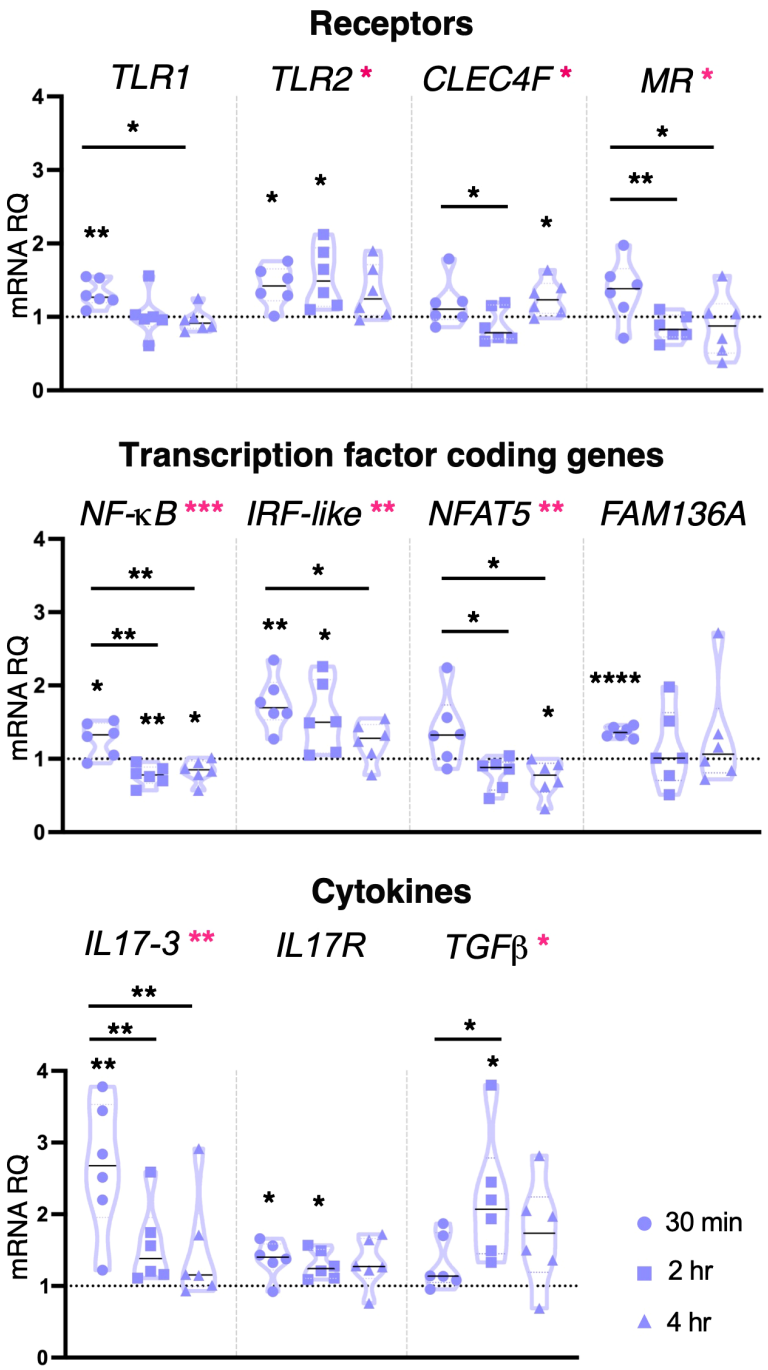

FIGURE 3
Effect of 1 µg/ml Pam2CSK4 treatment on gene expression. *C. robusta* juveniles at stage 4 of metamorphosis, treated with Pam2CSK4 at the concentration of 1 µg/ml, show significant changes in gene expression of *TLR1*, *TLR2*, *CLEC4F*, *MR*, *NF-κB*, *IRF-like*, *NFAT5*, *FAM136A*, *IL17-3*, *IL17R* and *TGFβ*, detected by RT-qPCR, after 30 min, 2 hr and 4 hr of treatment. Truncated violin plots represent the distribution and the density of numerical data of gene expression reported as fold changes ($2^{-\Delta\Delta Ct}$) of mRNA Relative Quantification (mRNA RQ) compared to the corresponding control samples of juveniles (not treated) and reported as dotted black line. The black lines in violin plots indicate the median of data set (n = 6, biological replicates). Graphics shows also significant expression changes between two different time points of the treatment, indicated by horizontal black lines. Statistical methods: paired samples t-test, significance indicated by black asterisks; one-way ANOVA test, significance indicated by magenta asterisks. (*p. value < 0.05, **p. value < 0.01, ***p. value < 0.001, and ****p. value < 0.0001).

represented. Among all revealed components, the first two (Supplementary Table 3) resulted in a two-dimensional PCA biplot (Figure 7A). PCA reduced the dimensionality of the multivariate data to two principal components explaining almost 90% variance (79.6% for Component 1 and 9.7% for Component 2) with minimal loss of information. The statistical analysis revealed a clear separation between a large cluster that included control, LPS (30 min, 2 hr, 4 hr), Pam2CSK4 (30 min) and zymosan (30 min, 2 hr) treatments, a small cluster consisting of 2 hr Pam2CSK4 and 4 hr zymosan treatments, and the 4 hr Pam2CSK4 treatment that was

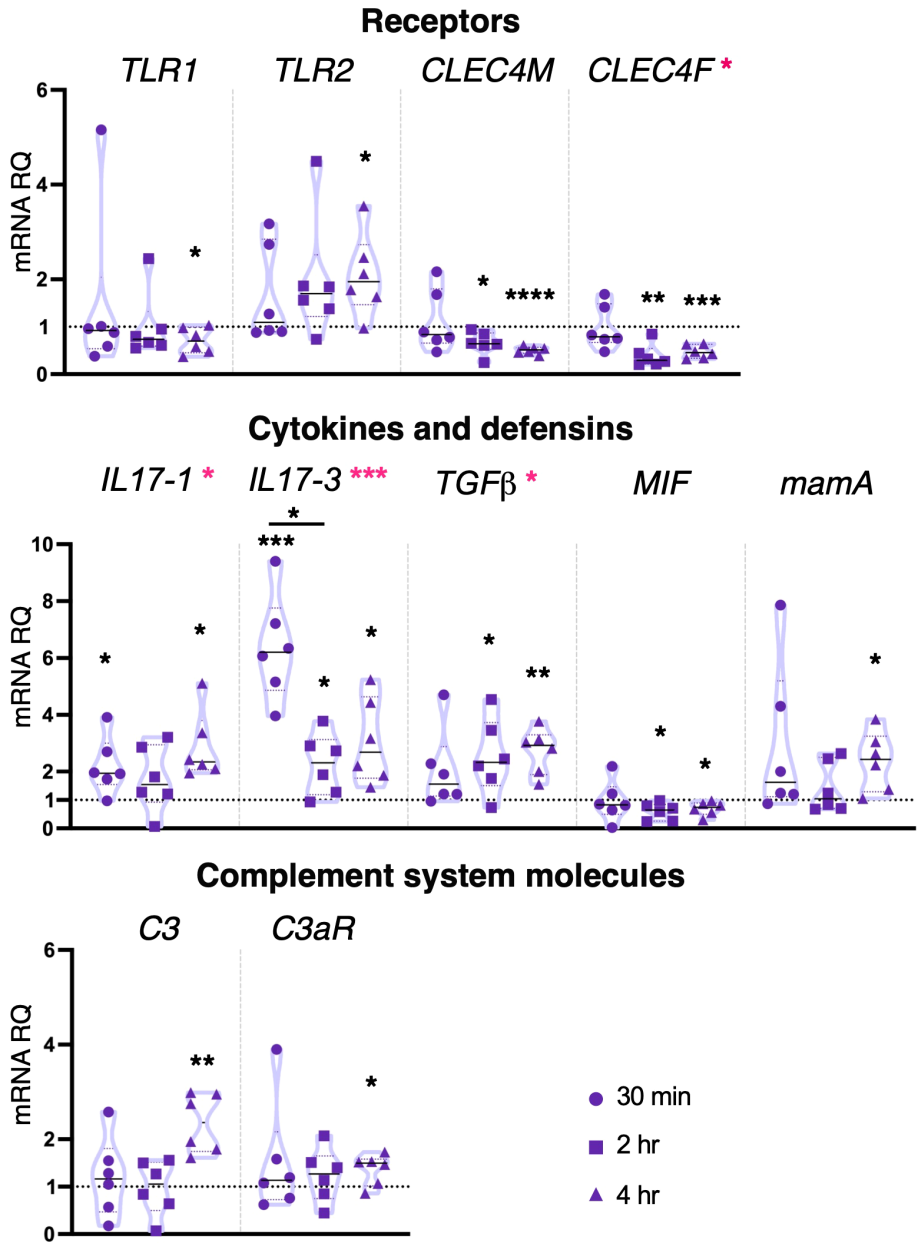

FIGURE 4
Effect of 10 µg/ml Pam2CSK4 treatment on gene expression. *C. robusta* juveniles at stage 4 of metamorphosis, treated with Pam2CSK4 at the concentration of 10 µg/ml, show significant changes in gene expression, detected by RT-qPCR, of *TLR1*, *TLR2*, *CLEC4M*, *CLEC4F*, *IL17-1*, *IL17-3*, *TGFβ*, *MIF*, *mamA*, *C3* and *C3aR*, after 30 min, 2 hr and 4 hr. Truncated violin plots represent the distribution and the density of numerical data of gene expression reported as fold changes ($2^{-\Delta\Delta Ct}$) of mRNA Relative Quantification (mRNA RQ) compared to the corresponding control samples of juveniles (not treated) and reported as dotted black line. The black lines in each violin plots indicate the median of data set (n = 6, biological replicates). Graphics shows also significant expression changes between two different treatment time points, indicated by black lines. Statistical methods: paired samples t-test, significance indicated by black asterisks; one-way ANOVA test, significance indicated by magenta asterisks. (*p. value < 0.05, **p. value < 0.01, ***p. value < 0.001 and ****p. value < 0.0001).

different from all other analyzed conditions (Figure 7A). This finding suggested that the stimulation of *C. robusta* juveniles with zymosan for 4 hr and Pam2CSK4 for 2 hr, and with Pam2CSK4 for 4hr induced a significant dysregulation of protein abundance as a consequence of microbial treatment response. Even the heatmap representation enabled the visualization of *hierarchical clustering* where the aforementioned microbial stimuli displayed the greatest response of immune molecules (Figure 7B).

3.4 Interactome of immune molecules

A protein-protein interaction network, based on STRING output and then modified and merged in Cytoscape, has been constructed to include all the immune molecules whose gene expression has been investigated in this study (Figure 8). The interactome shows that both receptors TLR1 and TLR2 are connected with the three transcription factors NF-κB, IRF-like,

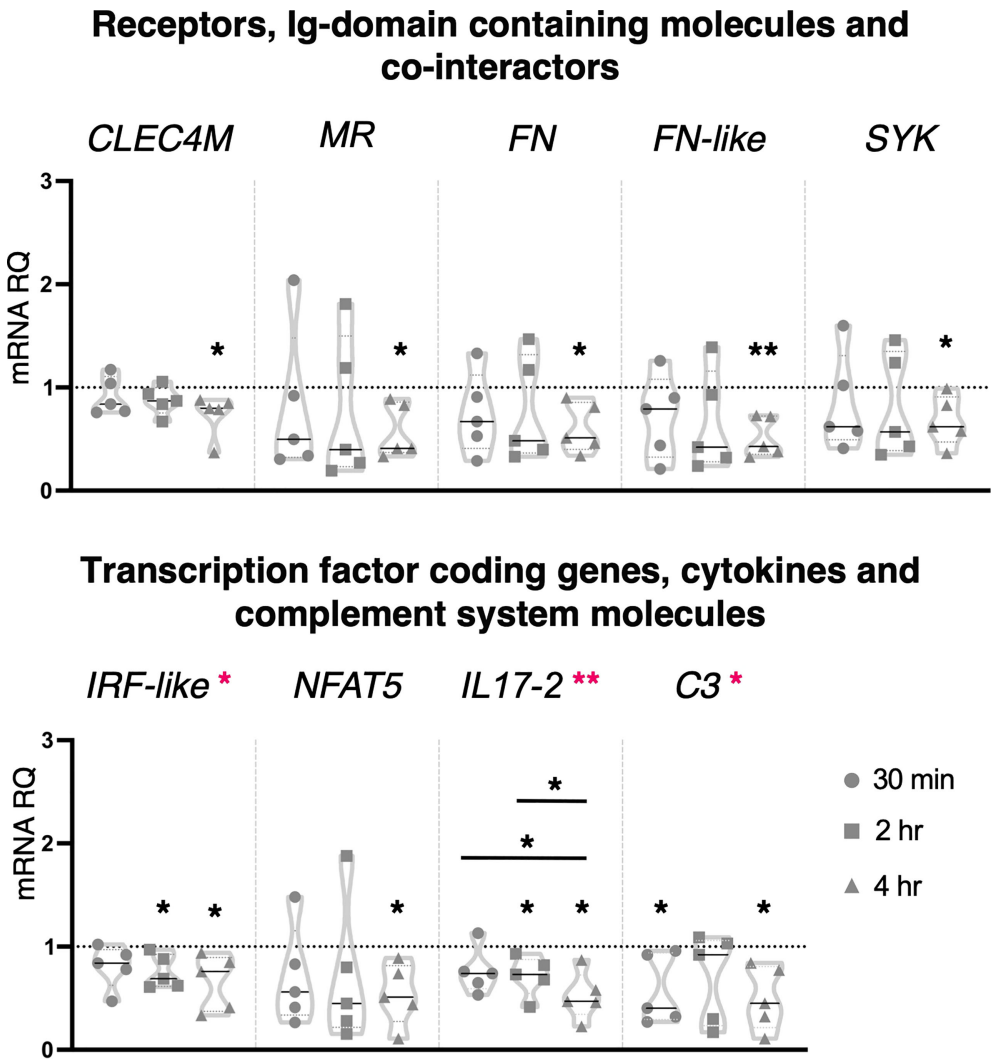

FIGURE 5
Effect of 10 µg/ml zymosan treatment on gene expression. *C. robusta* juveniles at stage 4 of metamorphosis, treated with zymosan at the concentration of 10 µg/ml, show significant changes in gene expression, detected by RT-qPCR, of *CLEC4M*, *MR*, *FN*, *FN-like*, *SYK*, *IRF-like*, *NFAT5*, *IL17-2* and *C3* after 30 min, 2 hr and 4 hr. Truncated violin plots represent the distribution and the density of numerical data of gene expression reported as fold changes ($2^{-\Delta\Delta Ct}$) of mRNA Relative Quantification (mRNA RQ) compared to the corresponding control samples of juveniles (not treated) and reported as dotted black line. The black lines in each violin plots indicate the median of data set (n = 5, biological replicates). Graphics shows also significant expression changes between two different treatment time points, indicated by horizontal black lines. Statistical methods: paired samples t-test, significance indicated by black asterisks; one-way ANOVA test, significance indicated by magenta asterisks. (*p. value < 0.05, **p. value < 0.01).

NFAT5, and with the interleukin receptor IL17R. Notably, TLR2 is also connected with cofactor SYK, receptors MR and TYRO3, complement molecule C3, cytokine MIF and the molecule FAM136A. Although the lack of STRING annotations for IL17 gene products, possibly due to difficulties in investigating such proteins in C. *robusta*, the presence of connections with the receptor, IL17R, could provide clues about the interactions of these interleukins (Figure 8).

As reported for IL17s, lack of annotation information also affects other proteins, such as CLEC4M, CLEC4F, C3aR, mamA and TNFα. However, we found connection of similar domains belonging to other proteins, as in the case of CLEC17A-like that reveals a connection with the protein SYK (Figure 8). The interaction map shows that other main players of TLR signaling are connected, including MyD88, IRAK4, IKK, TAK1, p38, TRAF3 (13, 76, 77) and MAPKs. The genes coding for these proteins were not investigated in this work but should be future objects of similar studies. All the molecules included in the interaction map that were not investigated by transcriptional and proteomics analyses in this study, are listed in the Supplementary Table 4.

The enrichment analysis has been performed through STRING Enrichment app in Cytoscape to depict the Biological Processes, Molecular Functions and Cellular Components in which these molecules are involved. Some of the results are represented as Split Donut Chart (chosen option in the Network specific settings

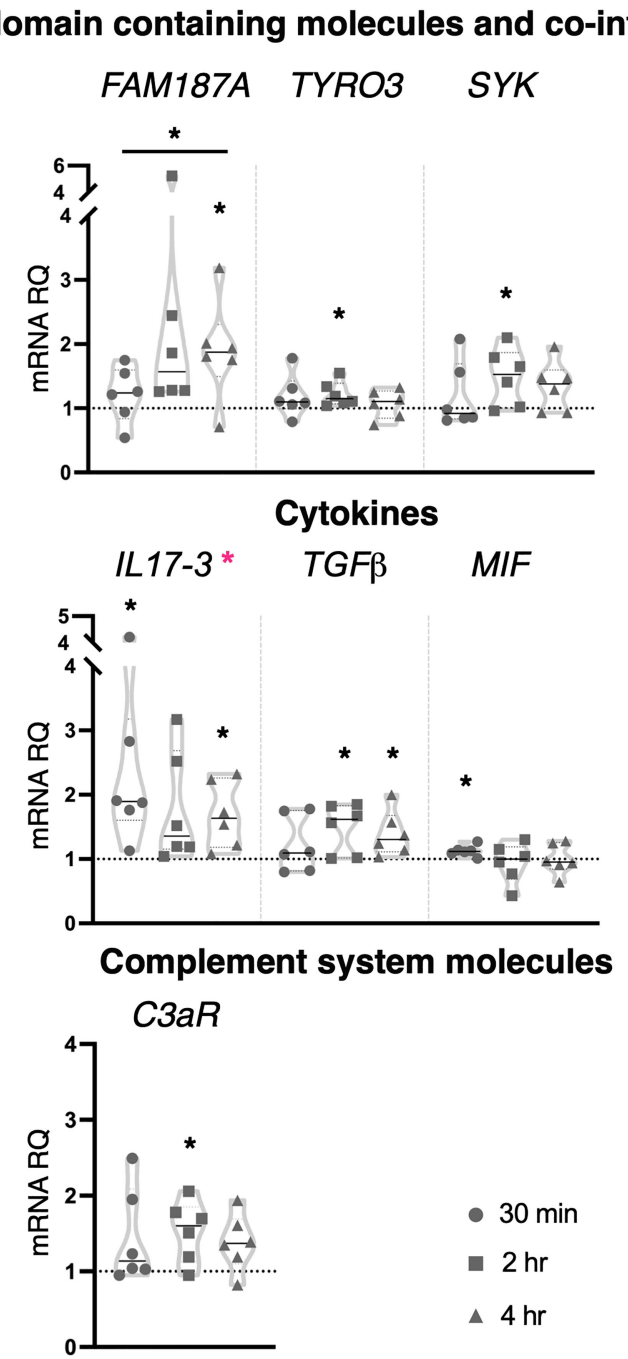

FIGURE 6
Effect of 100 µg/ml zymosan treatment on gene expression. *C. robusta* juveniles at stage 4 of metamorphosis, treated with zymosan at the concentration of 100 µg/ml, show significant changes in gene expression, detected by RT-qPCR, of *FAM187A*, *TYRO3*, *SYK*, *IL17-3*, *TGFβ*, *MIF* and *C3aR* after 30 min, 2 hr and 4 hr. Truncated violin plots represent the distribution and the density of numerical data of gene expression reported as fold changes ($2^{-\Delta\Delta Ct}$) of mRNA Relative Quantification (mRNA RQ) compared to the corresponding control samples of juveniles (not treated) and reported as dotted black line. The black lines in each violin plots indicate the median of data set (n = 6, biological replicates). Graphics shows also significant expression changes between two different time points of the treatment, indicated by horizontal black lines. Statistical methods: paired samples t-test, significance indicated by black asterisks; one-way ANOVA test, significance indicated by magenta asterisks. (*p. value < 0.05).

for STRING Enrichment table) in the protein-protein interaction network, using certain colors from the Enrichment color palette to underline specific outputs. To generate a map easier to understand, we have highlighted the biological processes that are more significant for this study. These comprise TLR signaling pathways (GO:0002224), innate immunity including inflammation and response to external stimulus (GO:0050896, GO:0002682, GO:0050794, GO:0050778), regulation and response to cytokine production (GO:0034097, GO:0001817, GO:0001818, GO:0001819), CTL or CRD domains (SM00034), and leukocyte-mediated immunity and adhesion to endothelial cells (GO:0045785, GO:0050900, GO:0002443) (Figure 8).

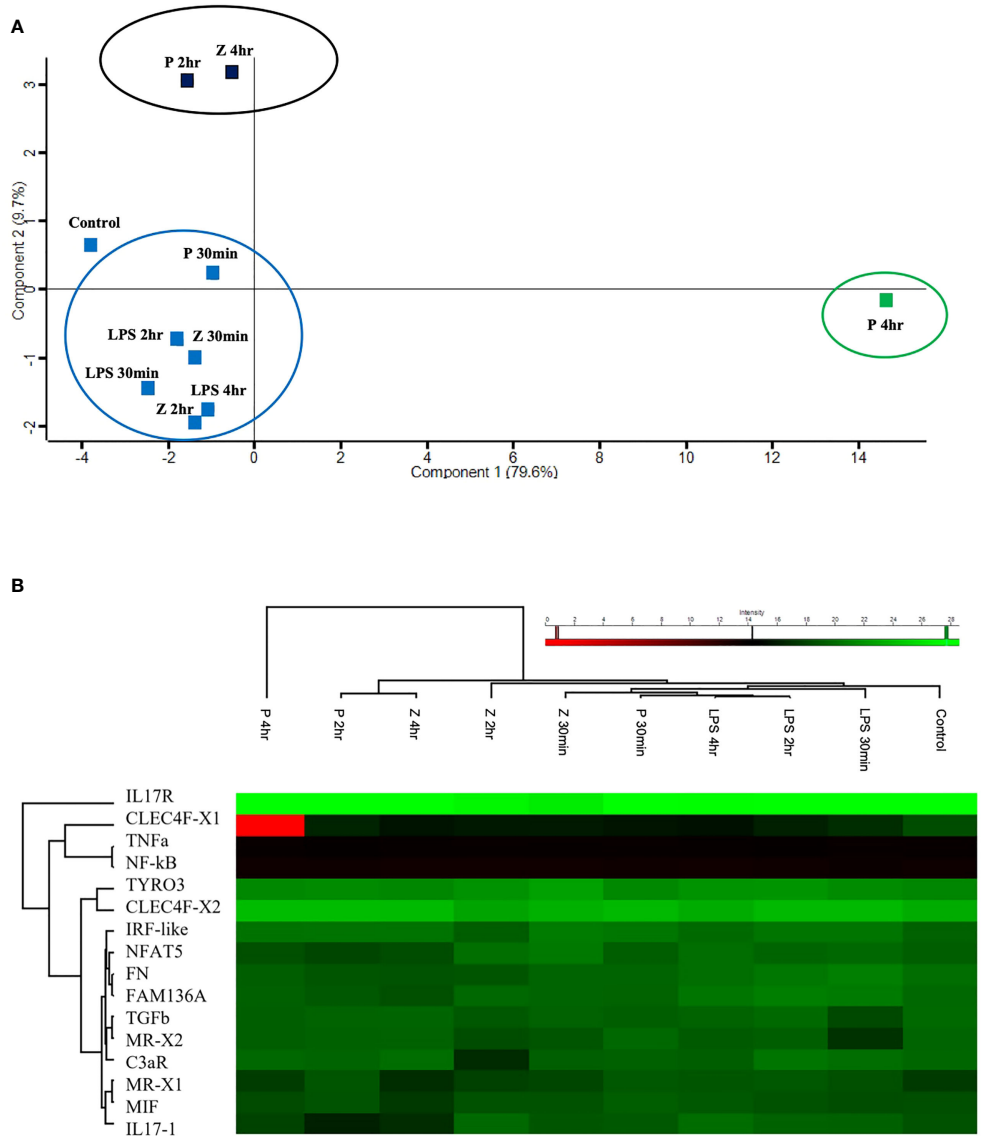

FIGURE 7
Targeted proteomic analysis of *C. robusta* juveniles expose to 10 µg/ml LPS, 1 µg/ml Pam2CSK4 and 100 µg/ml zymosan. **(A)** PCA analysis, clustering overall protein level variations at each time point of animals treated with microbial stimuli, shows similar protein level among control, LPS treated-, 2 hr and 4 hr zymosan treated-, and 30 min Pam2CSK4 treated- samples. 4 hr zymosan treated- and 2 hr Pam2CSK4 treated- samples have protein levels that cluster together and differs from control samples; whereas 4 hr Pam2CSK4 treated samples have protein level that highly differ from all the other treatment conditions. **(B)** Heatmap shows both hierarchical clustering of the treatment conditions and protein levels of the analyzed immune molecules, extracted from *C. robusta* juveniles expose to 10 µg/ml LPS, 1 µg/ml Pam2CSK4 and 100 µg/ml zymosan for 30 min, 2 hr and 4 hr and detected through LC-MRM/MS method. "P" and "Z" indicate Pam2CSK4 and zymosan treatments, respectively.

4 Discussion

The marine invertebrate *C. robusta* has recently become an excellent experimental organism for studying gut mucosal immunity, including processes mediating host mucosal-microbial associations (7, 8, 40, 78–82). In this work we used *Ciona* for investigating the inflammatory response activated by three PAMPs (LPS, Pam2CSK4 and zymosan) and for developing an invertebrate inflammatory model to use in research fields, from comparative immunology to translational biology and drug discovery.

4.1 Inflammation and the "patterns of pathogenesis" hypothesis

To interpret the inflammatory response in ascidian juveniles, it is important to recall some basic immunological concepts, such as the definition of inflammation and which factors/conditions activate it. The term "inflammation" defines the process triggered by innate immune cells when the homeostatic state is altered due to microbial infection or tissue injury (11–13). Marine organisms are continuously exposed to, and challenged by, a multitude of

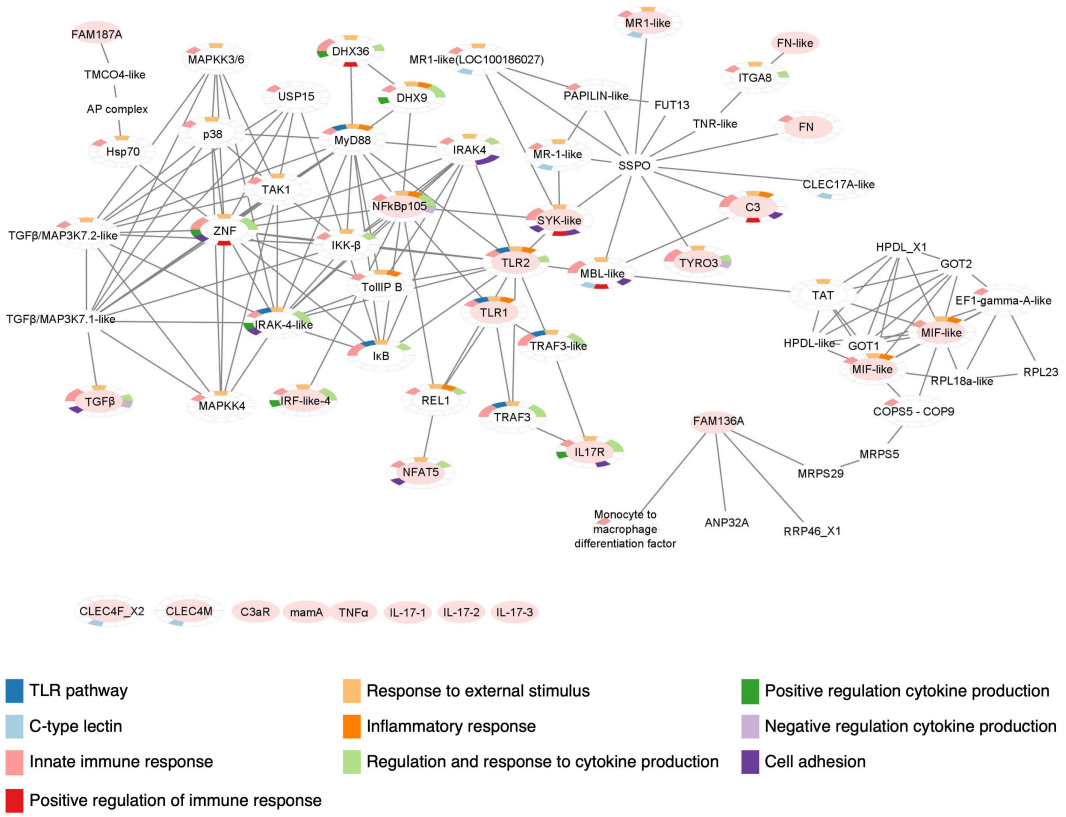

FIGURE 8
Protein-protein interaction network of *Ciona robusta* immune molecules. Protein-protein interaction map constructed with the STRING database and modified with Cytoscape, reveals the interaction between *C. robusta* immune molecules investigated through gene expression. Here, these molecules are indicated with an oval filled with light red color and those that are still not connected in the map are reported below. GO enrichment analysis is also indicated, highlighting in the color-legend some of the Biological Processes, related with immunological features, in which the molecules present in the map are involved.

microorganisms (e.g., bacteria, archaea, fungi, viruses, protozoans) inhabiting the surrounding environment (83). These microbes may be beneficial for the host by helping to shape the immune system and influencing developmental and physiological processes (84). The superorganism theory emphasizes how the concept of *self* and *non-self* has changed over time by incorporating host microbiota in the definition of *self* (84–86). During early development, the crosstalk between host and microbes is crucial to shape immune system maturation, that will allow to discriminate between *self* and *non-self*, and to establish a homeostatic state with beneficial components (86). These processes are mostly studied within the gastrointestinal tract where the symbiotic interactions mostly take place (87, 88). This equilibrium is broken when pathogenic microbes, or their components (as PAMPs), invade the host epithelial barrier and induce infection. Colonization and invasion by pathogens activate an inflammatory response that primarily involves PRRs (and their signaling pathways), the main players of the innate immune system (13, 68, 89, 90), with the aim to eliminate the infectious agents and to restore homeostasis (11, 12). PRRs have broad specificity and can recognize many PAMPs, which have a common structural motifs or patterns, thus representing a sort of pathogenicity markers (89, 91). In 2009, Vance and coauthors have proposed the "patterns of pathogenesis", or POP hypothesis, according to which the immune system recognizes pathogens not only by virtue of the presence of PAMPs but also by their pathogenic behaviors (92). These include growth upon host invasion, cytosolic invasion and disruption of the normal functions in the host cell cytoskeleton (92). On these grounds, a microbe can be considered pathogenic or nonpathogenic depending on the site of infection and on the immune state of the host. Hence, POP do not define a pathogen, rather a pathogenic behavior (86, 92). These new concepts may help to better understand the effect of PAMPs on the immune response, and thus on the onset of the inflammation, in different organisms and physiological states.

Based on the POP hypothesis, it is important to consider the physiological conditions at which the immune challenge is encountered. *Ciona* stage 4 juveniles are immunological naïve and probably they still do not have a stable microbiota. As they start interacting with the surrounding environment by seawater filtration, ascidian juveniles are here exposed to resuspended microbial components (8, 33, 40) and an immune response is observed if microbial components interact with the epithelial barrier. In line with *Ciona* LPS injection-based studies (14, 25, 93), the resuspension approach used herein may act differently in terms of immune activation patterns on older juveniles, like stage 8 (2^{nd} ascidian stage) (33).

4.2 Stimulus-specific response of innate immunity in *C. robusta* juveniles

In this work we found that LPS, the most common inflammatory stimulus used in vertebrates (13, 68, 94, 95), ascidians and other marine invertebrates (96–99), does not significantly alter gene expression in the adopted experimental setup, that are naïve metamorphic stage 4 juveniles. In line with the transcriptional results, targeted proteomics data show that LPS treatment does not elicit protein level variations. The POP hypothesis may help to explain the lack of an immune response to LPS in *C. robusta* juveniles treated by LPS resuspension. Since these organisms inhabit a habitat rich in LPS-containing Gram-negative bacteria (78) that are continuously filtered by the organism and interact with host mucosal sites, ascidian juveniles may not recognize LPS as a PAMP and/or LPS may not cross the epithelial barrier of their gastrointestinal tract. Instead, the other two microbial components that we used as inflammatory stimuli, the bacterial Pam2CSK4 and the fungal zymosan, are apparently able to interact with the epithelial barrier and then be sensed by host immune surveillance as PAMPs, thus triggering an immune response.

Pam2CSK4, which is not commonly used as a microbial stimulus in vertebrates as well as marine organisms, has been shown to bind the heterodimer TLR1/TLR6 (38) and, in monocytes, to enhance expression and function of Fcγ, a receptor involved in phagocytosis and inflammatory cytokine production (100). In mice, *in vitro* and *in vivo* stimulation of macrophages induces the activation of MAP kinase and NK-κB pathways upon TLR2 binding (101). Also, Pam2CSK4 treatment of human platelets *in vitro* activates TLR2/TLR6 complex and initiates signaling events that stimulate increase of NF-kB protein level and interactions between platelets and endothelial cells (ECs). This event increases inflammatory cytokine production and reduces EC permeability (102). In our experiments, Pam2CSK4 was the most effective inflammatory stimulus in ascidian juveniles, featuring a concentration-dependent influence on both TLR and Dectin-1 pathways. Also, it is worth mentioning that 1 µg/ml is lower than the concentration of Pam2CSK4 used on human cell lines (10 ug/ml) (100, 102), suggesting that ascidian juveniles are highly responsive to this microbial stimulus. The immune response to Pam2CSK4 observed in *Ciona* juveniles at stage 4 include the modulation of the PRRs expression, TLRs and CLECs, and of the transcription factors just at the lower concentration tested. While expression data show that Pam2CSK4 exposure modulates both TLR and Dectin-1 pathways, the protein-protein interaction network could not confirm it, as long as CLEC4M and CLEC4F receptors are concerned.

The time of activation of each pathway depends on the amount of microbial component that interacts with host mucosal barrier. We may hypothesize a stronger, but vital, immune response induced by 10 µg/ml Pam2CSK4 that can penetrate mucus barrier (due to the higher amount of Pam2CSK4 molecules), interact with epithelial layer and affect gene expression of *Ciona* complement system components C3 and C3aR, that consequently can activate cell adhesion, chemotaxis and phagocytosis processes in order to fight the invading microbial molecules (103, 104). Moreover, as in human platelets (102), Pam2CSK4 is able to alter transcriptional levels of cytokines (e.g., *IL17-3* and *TGFβ*) in *Ciona*. The activation of *TGFβ* following *IL17-3* modulation could be explained as a possible resolution of the inflammation induced by this microbial stimulus (105), in agreement with the observation that juveniles after 24 hr treatment are healthy (Figure 1B). That 10 µg/ml Pam2CSK4 can induce a strong inflammatory response is corroborated by the evidence of expression changes of other cytokine coding genes like *IL17-1* and *MIF*. In mammals, *MIF* has pro-inflammatory and immunoregulatory properties, and upregulates *TLR4* expression (106). In LPS-injected *Ciona* adults, a major role of MIF signaling pathway has been described in regulating *IL17s* and TGF*β* expression (93). A similar effect is observed also here in the inflammatory state induced by Pam2CSK4 treatment, where a downregulation of *MIF* expression is concurrent with the upregulation of *IL17s* and *TGFβ* (after 2 and 4 hr treatment with 10 µg/ml Pam2CSK4).

Compared to Pam2CSK4 infection, zymosan modulates a smaller and diverse set of molecules and pathways in *Ciona* juveniles (Figure 9). As a cell wall preparation of yeast *S. cerevisiae*, zymosan is a mix of glucans, mannans, mannoproteins and chitin (107). These components are implicated in yeast recognition by innate immune cells, stimulating phagocytosis by macrophages (108) and cytokine production (i.e. TNFα, IL1β, IL-10 and TGFβ) by monocytes, macrophages and dendritic cells (39, 109–111). In vertebrates, zymosan activates both TLR and Dectin-1 pathways (39). Moreover, a cell signaling cascade activated by the binding of β-glucan to Dectin-1 receptor can initiate both Syk-dependent and Syk-independent cascades (68, 112). In mammals, Syk is involved in cytokine transcription upon recruitment by Dectin-1 (113). However, Syk factor is involved in both PRR pathways (68, 114).

In *Ciona*, the protein-protein interaction network here generated highlights a potential connection among TLR2, SYK and MR molecules. Although activation of *Ciona* TLRs was induced by zymosan in a heterologous cellular system (17), here we did not observe changes in the expression of the two *TLR* genes investigated, but we found an alteration of *SYK* expression that does not permit us to rule out the hypothesis of an involvement of TLR pathway. The high zymosan concentration seems to induce a stronger inflammatory response that affect mainly gene transcription of cofactors involved in both TLR and Dectin-1 pathways, highlighting again an interconnection between the two pathways as observed in juveniles exposed to Pam2CSK4, although we did not observe a direct effect on the expression of the PRRs investigated. The finding that high concentration induces upregulation of the gene coding for TYRO3, a coreceptor involved in the resolution of inflammation, is in line with the upregulation of *TGFβ* observed after the increase of the expression of the two pro-inflammatory cytokines *IL17-3* and *MIF*. The role of TYRO3 in the negative regulation of cytokine production has been depicted also by GO analysis of the biological process of *Ciona* protein-protein interaction map.

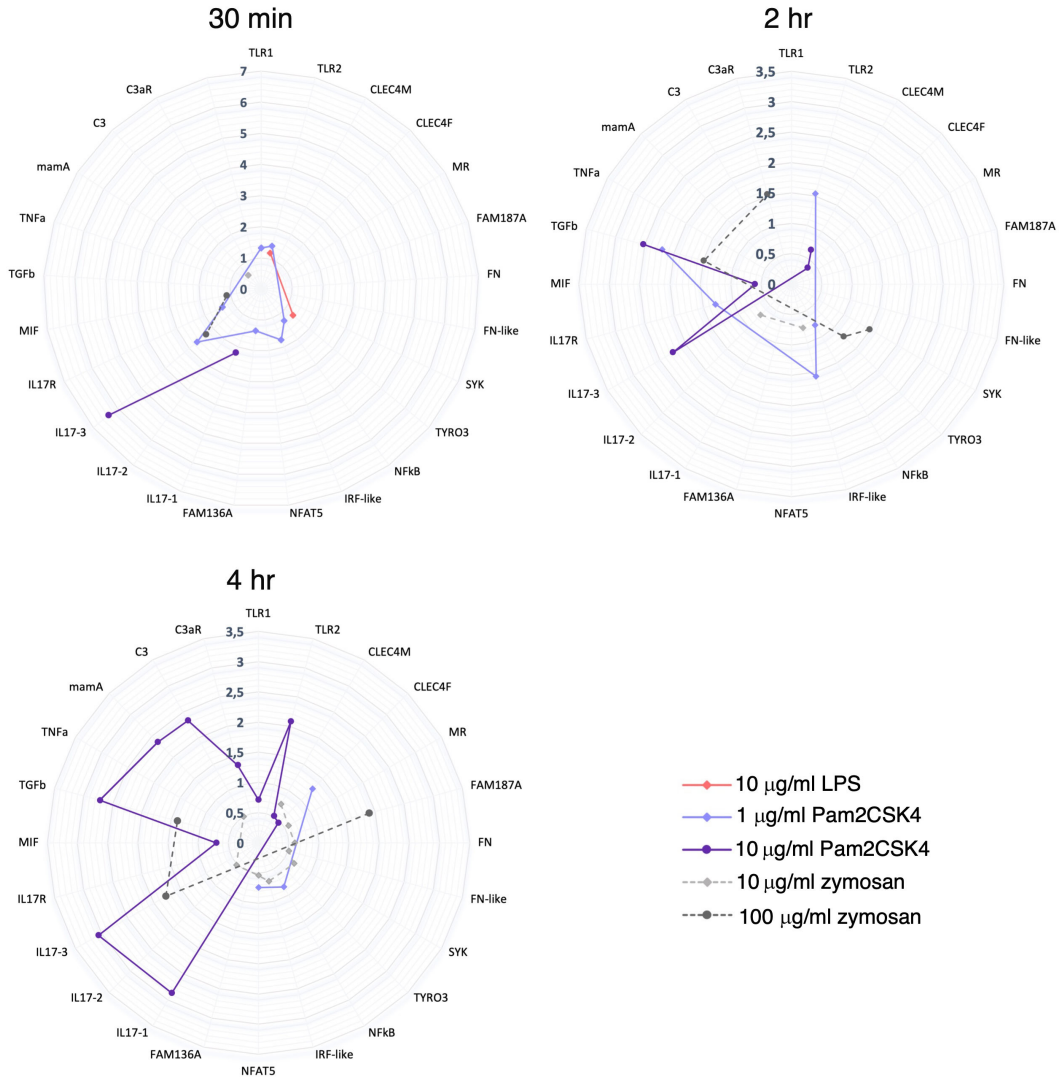

FIGURE 9
Summary of gene expression modulation at 30 min, 2 hr and 4 hr treatment. Radar plots show a summary of the genes that are (significantly) modulated at each time point treatment (30 min, 2 hr and 4 hr) by 10 µg/ml LPS, 1 and 10 µg/ml Pam2CSK4 and 10 and 100 µg/ml zymosan. 10 µg/ml LPS modulated just 2 genes at 30 min treatment. 1 µg/ml Pam2CSK4 modulate a higher number of genes at 30 min (7 genes) and 2 hr (4 genes) respect to 4 hr (3 genes) treatment. On the contrary, 10 µg/ml Pam2CSK4 has a major effect at late time points, 2 hr (5 genes) and 4 hr (11 genes), respect to the 30 min (2 genes) treatment. zymosan treatment, at both concentrations used, has an effect at the late time points, 2 hr (10 µg/ml, 2 genes; 100 µg/ml, 4 genes) and 4 hr (10 µg/ml, 9 genes; 100µg/ml, 3 genes) respect to the 30 min treatment (10 µg/ml, 1 genes; 100µg/ml, 2 genes).

In this study, we have observed an effect on the transcriptional levels of Ig-domain containing molecules (*FAM187A*, *FN* and *FN-like*) at both zymosan concentrations. Of note, the connection of these molecules with the Dectin-1 and TLR immune pathways was confirmed by the protein-protein interaction network. The immune role of these Ig-domain containing molecules represents an interesting starting point for future investigation in deciphering their role in the inflammatory response to fungal wall components. Moreover, the finding that *Ciona FAM187A* is phylogenetically related to *B. schlosseri TREML2* gene and that homology search analysis of *C. robusta* genome and proteome revealed the presence of genes coding for SYK (a downstream effector of the TREM2 pathway) and TYRO3, the latter binding in mammals TYRO protein tyrosine kinase binding protein (TYROBP), also known as DNAX-activating protein of 12 kDa (DAP12) whose putative receptor is TREM2 (115), induce to hypothesize that the existence of the TREM2 signaling is an ancient trait whose origin dates back to the common chordate ancestor. It also prompts for a better understanding of the evolution of this pathway in immune function, and in particular in the response to molecules of fungal origin.

Finally, we report that zymosan affect the transcription of the *Ciona* complement system, suggesting the activation of a phagocytosis process. This has been observed also in mammals, where zymosan is phagocytosed by macrophages with or without opsonization and can activate alternative pathway of complement system (116–118).

4.3 Targeted proteomics supports transcriptional data and show time delay between mRNA and protein expression

Proteomic data reveal an effect on protein level modulation after 2 hr Pam2CSK4 and 4 hr zymosan treatments, and a major effect after 4 hr treatment with Pam2CSK4. Here, the targeted proteomic analysis performed on a small subset of proteins (encoded by the genes analyzed at the transcriptional level) and experimental conditions highlights that *i*) Pam2CSK4 has a major effect in the immune regulation respect to zymosan, and that *ii*) the immune response to these two PAMPs differs in the time of activation. As to the latter aspect, low concentration of Pam2CSK4 is sufficient to induce early expression changes (30 min and 2 hr) as suggested by the transcriptional modulation of a higher number of genes at these time points (Figure 9). This evidence corresponds to a significant effect in a general protein modulation at 2 hr and 4 hr of treatment (Figure 7). A similar delay is observed also in the case of zymosan, which induces a significant modulation of protein levels only at 4 hr, compared to the transcriptional response observed at 2 and 4 hr (Figures 7, 9). These analyses help draw a first consideration concerning the temporal delay observed in the synthesis of proteins with respect to mRNA expression. The initiation of protein translation occurs within minutes after mRNA export into the cytoplasm, thus justifying the lag between transcription and translation. However, we cannot exclude the involvement of mechanisms, such as translational control through RNA binding proteins, that tightly regulate the production of specific proteins, thereby helping to resolve the inflammatory response (119). In mouse dendritic cells treated with LPS, time delay between transcriptional induction and protein level increases was described, with rapid expression of immune response genes (5 hr post LPS treatment) followed by the best quantitative correlation of protein levels to the mRNA levels at 12 hr (120).

4.4 Concluding remarks

In our study, we have added a further tile in the use of the ascidian *C. robusta* as an experimental system in comparative immunology field. Specifically, we have *i*) developed *Ciona* as an *in vivo* inflammatory model for studying the activation of the immune response to selected microbial stimuli, showing an interconnection between different PRR pathways and indicating the upregulation of cytokines gene expression (*IL17-3* and *TGFβ*) as markers of inflammation, *ii*) constructed a first protein-protein interaction map that can help to predict potential molecular interactions, and *iii*) correlated changes observed at transcriptional and translational levels. This new marine invertebrate inflammatory model represents the starting point for future studies, that include either large-scale sequencing or other "-omics" approaches for better defining the cellular pathways or biological processes affected by microbial treatments, but also for investigating host response to PAMPs in different physiological conditions and at different stages of maturation of the immune system. These advancements will contribute to our understanding of the crosstalk between host and microbiota and to test the POP hypothesis. As suggested by Newton and Dixit (2012), it is important to understand how, in a whole organism, innate immune cells exposed to multiple inflammatory stimuli can integrate signaling triggered by different receptors to identify critical components that can be targeted for therapeutic benefit in inflammatory disorder (13). In this framework we believe that, based on the results obtained in this study, this marine model organism could represent a proficient experimental system. Future studies can lead to the use of *C. robusta* experimental system in translation research or in any kind of approach (i.e., biotechnological or ecotoxicological) where the effect of molecules, either drugs or pollutants, on the activation and regulation of the innate immune system has to be investigated, like in large-scale screening of inflammatory modulators.

Data availability statement

The original contributions presented in the study are included in the article/Supplementary Material. Further inquiries can be directed to the corresponding authors.

Ethics statement

Ethical review and approval was not required for the study on animals in accordance with the local legislation and institutional requirements.

Author contributions

AL, CP, RM, AS and PS contributed to conception and design of the study. AL and CP performed *in vivo* treatments and gene expression analysis. CP executed *in silico* analysis and wrote the corresponding sections of the manuscript. GP, AI and AA performed proteomic analysis, its data curation and wrote the corresponding sections of the manuscript. AL performed interpretation and curation of data and wrote the first full version of the manuscript. RM, AS and PS reviewed and edited the manuscript, and contributed to the discussion. AL and PS supervised the project. All authors contributed to the article and approved the submitted version.

Funding

This work was supported by "Antitumor drugs and vaccines from the sea (ADViSE)" funded by the Regione Campania POR Campania FESR 2014/2020 Asse I. to AL, CP, PS and AS. The funders had no role in study design, data collection and analysis, decision to publish, or preparation of the manuscript.

Acknowledgments

The authors thank Dr. Angelo Fontana for the meaningful discussion on the project and Dr. Larry J. Dishaw for helpful comments and valuable suggestions to improve the manuscript. The authors also wish to thank the Service of Marine Biological Resources (SZN) for providing technical assistance.

Conflict of interest

The authors declare that the research was conducted in the absence of any commercial or financial relationships that could be construed as a potential conflict of interest.

Publisher's note

Supplementary material

The Supplementary Material for this article can be found online at: https://www.frontiersin.org/articles/10.3389/fimmu.2023.1217077/full#supplementary-material

References

1. Satoh N. The ascidian tadpole larva: comparative molecular development and genomics. *Nat Rev Genet* (2003) 4(4):285–95. doi: 10.1038/nrg1042

2. Christiaen L, Wagner E, Shi W, Levine M. Isolation of individual cells and tissues from electroporated sea squirt (Ciona) embryos by fluorescence-activated cell sorting (FACS). *Cold Spring Harb Protoc* (2009) 2009(12):pdb prot5349. doi: 10.1101/pdb.prot5349

3. Davidson B. Ciona intestinalis as a model for cardiac development. *Semin Cell Dev Biol* (2007) 18(1):16–26. doi: 10.1016/j.semcdb.2006.12.007

4. Lemaire P, Smith WC, Nishida H. Ascidians and the plasticity of the chordate developmental program. *Curr Biol* (2008) 18(14):R620–31. doi: 10.1016/j.cub.2008.05.039

5. Satoh N, Levine M. Surfing with the tunicates into the post-genome era. *Genes Dev* (2005) 19(20):2407–11. doi: 10.1101/gad.1365805

6. Azumi K, De Santis R, De Tomaso A, Rigoutsos I, Yoshizaki F, Pinto MR, et al. Genomic analysis of immunity in a Urochordate and the emergence of the vertebrate immune system: "waiting for Godot". *Immunogenetics* (2003) 55(8):570–81. doi: 10.1007/s00251-003-0606-5

7. Dishaw LJ, Flores-Torres JA, Mueller MG, Karrer CR, Skapura DP, Melillo D, et al. A Basal chordate model for studies of gut microbial immune interactions. *Front Immunol* (2012) 3:96. doi: 10.3389/fimmu.2012.00096

8. Liberti A, Natarajan O, Atkinson CGF, Sordino P, Dishaw LJ. Reflections on the use of an invertebrate chordate model system for studies of gut microbial immune interactions. *Front Immunol* (2021) 12:642687. doi: 10.3389/fimmu.2021.642687

9. Melillo D, Marino R, Della Camera G, Italiani P, Boraschi D. Assessing immunological memory in the solitary ascidian ciona robusta. *Front Immunol* (2019) 10:1977. doi: 10.3389/fimmu.2019.01977

10. Garrett WS, Gordon JI, Glimcher LH. Homeostasis and inflammation in the intestine. *Cell* (2010) 140(6):859–70. doi: 10.1016/j.cell.2010.01.023

11. Meizlish ML, Franklin RA, Zhou X, Medzhitov R. Tissue homeostasis and inflammation. *Annu Rev Immunol* (2021) 39:557–81. doi: 10.1146/annurev-immunol-061020-053734

12. Medzhitov R. Origin and physiological roles of inflammation. *Nature* (2008) 454 (7203):428–35. doi: 10.1038/nature07201

13. Newton K, Dixit VM. Signaling in innate immunity and inflammation. *Cold Spring Harb Perspect Biol* (2012) 4(3). doi: 10.1101/cshperspect.a006049

14. Longo V, Parrinello D, Longo A, Parisi MG, Parrinello N, Colombo P, et al. The conservation and diversity of ascidian cells and molecules involved in the inflammatory reaction: The Ciona robusta model. *Fish Shellfish Immunol* (2021) 119:384–96. doi: 10.1016/j.fsi.2021.10.022

15. Melillo D, Sfyroera G, De Santis R, Graziano R, Marino R, Lambris JD, et al. First identification of a chemotactic receptor in an invertebrate species: structural and functional characterization of Ciona intestinalis C3a receptor. *J Immunol* (2006) 177 (6):4132–40. doi: 10.4049/jimmunol.177.6.4132

16. Pinto MR, Chinnici CM, Kimura Y, Melillo D, Marino R, Spruce LA, et al. CiC3-1a-mediated chemotaxis in the deuterostome invertebrate Ciona intestinalis (Urochordata). *J Immunol* (2003) 171(10):5521–8. doi: 10.4049/jimmunol.171.10.5521

17. Sasaki N, Ogasawara M, Sekiguchi T, Kusumoto S, Satake H. Toll-like receptors of the ascidian Ciona intestinalis: prototypes with hybrid functionalities of vertebrate Toll-like receptors. *J Biol Chem* (2009) 284(40):27336–43. doi: 10.1074/jbc.M109.032433

18. Satake H, Sekiguchi T. Toll-like receptors of deuterostome invertebrates. *Front Immunol* (2012) 3:34. doi: 10.3389/fimmu.2012.00034

19. Zucchetti I, Marino R, Pinto MR, Lambris JD, Du Pasquier L, De Santis R. ciCD94-1, an ascidian multipurpose C-type lectin-like receptor expressed in Ciona intestinalis hemocytes and larval neural structures. *Differentiation* (2008) 76(3):267–82. doi: 10.1111/j.1432-0436.2007.00214.x

20. Bonura A, Vizzini A, Salerno G, Parrinello N, Longo V, Colombo P. Isolation and expression of a novel MBL-like collectin cDNA enhanced by LPS injection in the body wall of the ascidian Ciona intestinalis. *Mol Immunol* (2009) 46(11-12):2389–94. doi: 10.1016/j.molimm.2009.04.035

21. Hayashibe M, Nakayama S, Ogasawara M. Shared hemocyte- and intestine-dominant expression profiles of intelectin genes in ascidian Ciona intestinalis: insight into the evolution of the innate immune system in chordates. *Cell Tissue Res* (2017) 370 (1):129–42. doi: 10.1007/s00441-017-2647-3

22. Skjoedt MO, Palarasah Y, Rasmussen K, Vitved L, Salomonsen J, Kliem A, et al. Two mannose-binding lectin homologues and an MBL-associated serine protease are expressed in the gut epithelia of the urochordate species Ciona intestinalis. *Dev Comp Immunol* (2010) 34(1):59–68. doi: 10.1016/j.dci.2009.08.004

23. Vizzini A, Parrinello D, Sanfratello MA, Salerno G, Cammarata M, Parrinello N. Inducible galectins are expressed in the inflamed pharynx of the ascidian Ciona intestinalis. *Fish Shellfish Immunol* (2012) 32(1):101–9. doi: 10.1016/j.fsi.2011.10.028

24. Parrinello N, Cammarata M, Parrinello D, Vizzini A. Inflammatory response of the ascidian ciona intestinalis. In: *Book: Lessons in Immunity, From Single-Cell Organisms to Mammals*. London, UK: Academic Press (2016). p. 177–92. doi: 10.1016/B978-0-12-803252-7.00013-8

25. Giacomelli S, Melillo D, Lambris JD, Pinto MR. Immune competence of the Ciona intestinalis pharynx: complement system-mediated activity. *Fish Shellfish Immunol* (2012) 33(4):946–52. doi: 10.1016/j.fsi.2012.08.003

26. Marino R, Kimura Y, De Santis R, Lambris JD, Pinto MR. Complement in urochordates: cloning and characterization of two C3-like genes in the ascidian Ciona intestinalis. *Immunogenetics* (2002) 53(12):1055–64. doi: 10.1007/s00251-001-0421-9

27. Vizzini A, Di Falco F, Parrinello D, Sanfratello MA, Mazzarella C, Parrinello N, et al. Ciona intestinalis interleukin 17-like genes expression is upregulated by LPS challenge. *Dev Comp Immunol* (2015) 48(1):129–37. doi: 10.1016/j.dci.2014.09.014

28. Parrinello N, Vizzini A, Arizza V, Salerno G, Parrinello D, Cammarata M, et al. Enhanced expression of a cloned and sequenced Ciona intestinalis TNFalpha-like (CiTNF alpha) gene during the LPS-induced inflammatory response. *Cell Tissue Res* (2008) 334(2):305–17. doi: 10.1007/s00441-008-0695-4

29. Vizzini A, Di Falco F, Parrinello D, Sanfratello MA, Cammarata M. Transforming growth factor beta (CiTGF-beta) gene expression is induced in the inflammatory reaction of Ciona intestinalis. *Dev Comp Immunol* (2016) 55:102–10. doi: 10.1016/j.dci.2015.10.013

30. Vizzini A, Parisi MG, Di Falco F, Cardinale L, Cammarata M, Arizza V. Identification of CPE and GAIT elements in 3'UTR of macrophage migration inhibitory factor (MIF) involved in inflammatory response induced by LPS in Ciona robusta. *Mol Immunol* (2018) 99:66–74. doi: 10.1016/j.molimm.2018.04.009

31. Fedders H, Michalek M, Grotzinger J, Leippe M. An exceptional salt-tolerant antimicrobial peptide derived from a novel gene family of haemocytes of the marine invertebrate Ciona intestinalis. *Biochem J* (2008) 416(1):65–75. doi: 10.1042/BJ20080398

32. Yagi K, Satou Y, Mazet F, Shimeld SM, Degnan B, Rokhsar D, et al. A genomewide survey of developmentally relevant genes in Ciona intestinalis. III. Genes for Fox, ETS, nuclear receptors and NFkappaB. *Dev Genes Evol* (2003) 213(5-6):235–44. doi: 10.1007/s00427-003-0322-z

33. Chiba S, Sasaki A, Nakayama A, Takamura K, Satoh N. Development of Ciona intestinalis juveniles (through 2nd ascidian stage). *Zoolog Sci* (2004) 21(3):285–98. doi: 10.2108/zsj.21.285

34. Kurokawa K, Kim MS, Ichikawa R, Ryu KH, Dohmae N, Nakayama H, et al. Environment-mediated accumulation of diacyl lipoproteins over their triacyl counterparts in *Staphylococcus aureus*. *J Bacteriol* (2012) 194(13):3299–306. doi: 10.1128/JB.00314-12

35. Tokuda H. Biogenesis of outer membranes in Gram-negative bacteria. *Biosci Biotechnol Biochem* (2009) 73(3):465–73. doi: 10.1271/bbb.80778

36. Chow JC, Young DW, Golenbock DT, Christ WJ, Gusovsky F. Toll-like receptor-4 mediates lipopolysaccharide-induced signal transduction. *J Biol Chem* (1999) 274(16):10689–92. doi: 10.1074/jbc.274.16.10689

37. Hirschfeld M, Ma Y, Weis JH, Vogel SN, Weis JJ. Cutting edge: repurification of lipopolysaccharide eliminates signaling through both human and murine toll-like receptor 2. *J Immunol* (2000) 165(2):618–22. doi: 10.4049/jimmunol.165.2.618

38. Kang JY, Nan X, Jin MS, Youn SJ, Ryu YH, Mah S, et al. Recognition of lipopeptide patterns by Toll-like receptor 2-Toll-like receptor 6 heterodimer. *Immunity* (2009) 31(6):873–84. doi: 10.1016/j.immuni.2009.09.018

39. Gantner BN, Simmons RM, Canavera SJ, Akira S, Underhill DM. Collaborative induction of inflammatory responses by dectin-1 and Toll-like receptor 2. *J Exp Med* (2003) 197(9):1107–17. doi: 10.1084/jem.20021787

40. Leigh BA, Liberti A, Dishaw LJ. Generation of germ-free ciona intestinalis for studies of gut-microbe interactions. *Front Microbiol* (2016) 7:2092. doi: 10.3389/fmicb.2016.02092

41. Dardaillon J, Dauga D, Simion P, Faure E, Onuma TA, DeBiasse MB, et al. ANISEED 2019: 4D exploration of genetic data for an extended range of tunicates. *Nucleic Acids Res* (2020) 48(D1):D668–D75. doi: 10.1093/nar/gkz955

42. Coordinators NR. Database resources of the national center for biotechnology information. *Nucleic Acids Res* (2016) 44(D1):D7–19. doi: 10.1093/nar/gkv1290

43. Dehal P, Satou Y, Campbell RK, Chapman J, Degnan B, De Tomaso A, et al. The draft genome of Ciona intestinalis: insights into chordate and vertebrate origins. *Science* (2002) 298(5601):2157–67. doi: 10.1126/science.1080049

44. Altschul SF, Madden TL, Schaffer AA, Zhang J, Zhang Z, Miller W, et al. Gapped BLAST and PSI-BLAST: a new generation of protein database search programs. *Nucleic Acids Res* (1997) 25(17):3389–402. doi: 10.1093/nar/25.17.3389

45. Altschul SF, Gish W, Miller W, Myers EW, Lipman DJ. Basic local alignment search tool. *J Mol Biol* (1990) 215(3):403–10. doi: 10.1016/S0022-2836(05)80360-2

46. Waterhouse AM, Procter JB, Martin DM, Clamp M, Barton GJ. Jalview Version 2–a multiple sequence alignment editor and analysis workbench. *Bioinformatics* (2009) 25(9):1189–91. doi: 10.1093/bioinformatics/btp033

47. UniProt C. UniProt: the universal protein knowledgebase in 2021. *Nucleic Acids Res* (2021) 49(D1):D480–D9. doi: 10.1093/nar/gkaa1100

48. Blum M, Chang HY, Chuguransky S, Grego T, Kandasaamy S, Mitchell A, et al. The InterPro protein families and domains database: 20 years on. *Nucleic Acids Res* (2021) 49(D1):D344–D54. doi: 10.1093/nar/gkaa977

49. Letunic I, Khedkar S, Bork P. SMART: recent updates, new developments and status in 2020. *Nucleic Acids Res* (2021) 49(D1):D458–D60. doi: 10.1093/nar/gkaa937

50. Liberti A, Bertocci I, Pollet A, Musco L, Locascio A, Ristoratore F, et al. An indoor study of the combined effect of industrial pollution and turbulence events on the gut environment in a marine invertebrate. *Mar Environ Res* (2020) 158:104950. doi: 10.1016/j.marenvres.2020.104950

51. Wessel D, Flugge UI. A method for the quantitative recovery of protein in dilute solution in the presence of detergents and lipids. *Anal Biochem* (1984) 138(1):141–3. doi: 10.1016/0003-2697(84)90782-6

52. Pino LK, Searle BC, Bollinger JG, Nunn B, MacLean B, MacCoss MJ. The Skyline ecosystem: Informatics for quantitative mass spectrometry proteomics. *Mass Spectrom Rev* (2020) 39(3):229–44. doi: 10.1002/mas.21540

53. Tyanova S, Temu T, Sinitcyn P, Carlson A, Hein MY, Geiger T, et al. The Perseus computational platform for comprehensive analysis of (prote)omics data. *Nat Methods* (2016) 13(9):731–40. doi: 10.1038/nmeth.3901

54. Szklarczyk D, Gable AL, Nastou KC, Lyon D, Kirsch R, Pyysalo S, et al. Correction to 'The STRING database in 2021: customizable protein-protein networks, and functional characterization of user-uploaded gene/measurement sets'. *Nucleic Acids Res* (2021) 49(18):10800. doi: 10.1093/nar/gkab835

55. Shannon P, Markiel A, Ozier O, Baliga NS, Wang JT, Ramage D, et al. Cytoscape: a software environment for integrated models of biomolecular interaction networks. *Genome Res* (2003) 13(11):2498–504. doi: 10.1101/gr.1239303

56. Kanehisa M, Goto S. KEGG: kyoto encyclopedia of genes and genomes. *Nucleic Acids Res* (2000) 28(1):27–30. doi: 10.1093/nar/28.1.27

57. Binder JX, Pletscher-Frankild S, Tsafou K, Stolte C, O'Donoghue SI, Schneider R, et al. COMPARTMENTS: unification and visualization of protein subcellular localization evidence. *Database (Oxford)* (2014) 2014:bau012. doi: 10.1093/database/bau012

58. Mi H, Thomas P. PANTHER pathway: an ontology-based pathway database coupled with data analysis tools. *Methods Mol Biol* (2009) 563:123–40. doi: 10.1007/978-1-60761-175-2_7

59. Mi H, Ebert D, Muruganujan A, Mills C, Albou LP, Mushayamaha T, et al. PANTHER version 16: a revised family classification, tree-based classification tool, enhancer regions and extensive API. *Nucleic Acids Res* (2021) 49(D1):D394–403. doi: 10.1093/nar/gkaa1106

60. Carbon S, Ireland A, Mungall CJ, Shu S, Marshall B, Lewis S, et al. AmiGO: online access to ontology and annotation data. *Bioinformatics* (2009) 25(2):288–9. doi: 10.1093/bioinformatics/btn615

61. Binns D, Dimmer E, Huntley R, Barrell D, O'Donovan C, Apweiler R. QuickGO: a web-based tool for Gene Ontology searching. *Bioinformatics* (2009) 25(22):3045–6. doi: 10.1093/bioinformatics/btp536

62. Finn RD, Bateman A, Clements J, Coggill P, Eberhardt RY, Eddy SR, et al. Pfam: the protein families database. *Nucleic Acids Res* (2014) 42(Database issue):D222–30. doi: 10.1093/nar/gkt1223

63. Gillespie M, Jassal B, Stephan R, Milacic M, Rothfels K, Senff-Ribeiro A, et al. The reactome pathway knowledgebase 2022. *Nucleic Acids Res* (2022) 50(D1):D687–D92. doi: 10.1093/nar/gkab1028

64. Cannon JP, Dishaw LJ, Haire RN, Litman RT, Ostrov DA, Litman GW. Recognition of additional roles for immunoglobulin domains in immune function. *Semin Immunol* (2010) 22(1):17–24. doi: 10.1016/j.smim.2009.11.006

65. Liberti A, Natarajan O, Atkinson CGF, Dishaw LJ. Secreted immunoglobulin domain effector molecules of invertebrates and management of gut microbial ecology. *Immunogenetics* (2022) 74(1):99–109. doi: 10.1007/s00251-021-01237-2

66. Oreste U, Ametrano A, Coscia MR. On origin and evolution of the antibody molecule. *Biol (Basel)* (2021) 10(2). doi: 10.3390/biology10020140

67. Brown GD, Willment JA, Whitehead L. C-type lectins in immunity and homeostasis. *Nat Rev Immunol* (2018) 18(6):374–89. doi: 10.1038/s41577-018-0004-8

68. Brubaker SW, Bonham KS, Zanoni I, Kagan JC. Innate immune pattern recognition: a cell biological perspective. *Annu Rev Immunol* (2015) 33:257–90. doi: 10.1146/annurev-immunol-032414-112240

69. Rothlin CV, Ghosh S, Zuniga EI, Oldstone MB, Lemke G. TAM receptors are pleiotropic inhibitors of the innate immune response. *Cell* (2007) 131(6):1124–36. doi: 10.1016/j.cell.2007.10.034

70. Vago JP, Amaral FA, van de Loo FAJ. Resolving inflammation by TAM receptor activation. *Pharmacol Ther* (2021) 227:107893. doi: 10.1016/j.pharmthera.2021.107893

71. Colonna M, Wang Y. TREM2 variants: new keys to decipher Alzheimer disease pathogenesis. *Nat Rev Neurosci* (2016) 17(4):201–7. doi: 10.1038/nrn.2016.7

72. Painter MM, Atagi Y, Liu CC, Rademakers R, Xu H, Fryer JD, et al. TREM2 in CNS homeostasis and neurodegenerative disease. *Mol Neurodegener* (2015) 10:43. doi: 10.1186/s13024-015-0040-9

73. Correale C, Genua M, Vetrano S, Mazzini E, Martinoli C, Spinelli A, et al. Bacterial sensor triggering receptor expressed on myeloid cells-2 regulates the mucosal inflammatory response. *Gastroenterology* (2013) 144(2):346–56 e3. doi: 10.1053/j.gastro.2012.10.040

74. Blakeley P, Siepen JA, Lawless C, Hubbard SJ. Investigating protein isoforms *via* proteomics: a feasibility study. *Proteomics* (2010) 10(6):1127–40. doi: 10.1002/pmic.200900445

75. Requena T, Cabrera S, Martin-Sierra C, Price SD, Lysakowski A, Lopez-Escamez JA. Identification of two novel mutations in FAM136A and DTNA genes in autosomal-dominant familial Meniere's disease. *Hum Mol Genet* (2015) 24(4):1119–26. doi: 10.1093/hmg/ddu524

76. Deguine J, Barton GM. MyD88: a central player in innate immune signaling. *F1000Prime Rep* (2014) 6:97. doi: 10.12703/P6-97

77. Federico S, Pozzetti L, Papa A, Carullo G, Gemma S, Butini S, et al. Modulation of the innate immune response by targeting toll-like receptors: A perspective on their agonists and antagonists. *J Med Chem* (2020) 63(22):13466–513. doi: 10.1021/acs.jmedchem.0c01049

78. Dishaw LJ, Flores-Torres J, Lax S, Gemayel K, Leigh B, Melillo D, et al. The gut of geographically disparate Ciona intestinalis harbors a core microbiota. *PLoS One* (2014) 9(4):e93386. doi: 10.1371/journal.pone.0093386

79. Dishaw LJ, Giacomelli S, Melillo D, Zucchetti I, Haire RN, Natale L, et al. A role for variable region-containing chitin-binding proteins (VCBPs) in host gut-bacteria interactions. *Proc Natl Acad Sci U S A* (2011) 108(40):16747–52. doi: 10.1073/pnas.1109687108

80. Dishaw LJ, Leigh B, Cannon JP, Liberti A, Mueller MG, Skapura DP, et al. Gut immunity in a protochordate involves a secreted immunoglobulin-type mediator binding host chitin and bacteria. *Nat Commun* (2016) 7:10617. doi: 10.1038/ncomms10617

81. Liberti A, Cannon JP, Litman GW, Dishaw LJ. A soluble immune effector binds both fungi and bacteria *via* separate functional domains. *Front Immunol* (2019) 10:369. doi: 10.3389/fimmu.2019.00369

82. Liberti A, Leigh B, De Santis R, Pinto MR, Cannon JP, Dishaw LJ, et al. An immune effector system in the protochordate gut sheds light on fundamental aspects of vertebrate immunity. *Results Probl Cell Differ* (2015) 57:159–73. doi: 10.1007/978-3-319-20819-0_7

83. McFall-Ngai M, Hadfield MG, Bosch TC, Carey HV, Domazet-Loso T, Douglas AE, et al. Animals in a bacterial world, a new imperative for the life sciences. *Proc Natl Acad Sci U S A* (2013) 110(9):3229–36. doi: 10.1073/pnas.1218525110

84. Sommer F, Backhed F. The gut microbiota–masters of host development and physiology. *Nat Rev Microbiol* (2013) 11(4):227–38. doi: 10.1038/nrmicro2974

85. Lederberg J. Infectious history. *Science* (2000) 288(5464):287–93. doi: 10.1126/science.288.5464.287

86. Eberl G. A new vision of immunity: homeostasis of the superorganism. *Mucosal Immunol* (2010) 3(5):450–60. doi: 10.1038/mi.2010.20

87. Hooper LV, Littman DR, Macpherson AJ. Interactions between the microbiota and the immune system. *Science* (2012) 336(6086):1268–73. doi: 10.1126/science.1223490

88. Okumura R, Takeda K. Maintenance of gut homeostasis by the mucosal immune system. *Proc Jpn Acad Ser B Phys Biol Sci* (2016) 92(9):423–35. doi: 10.2183/pjab.92.423

89. Janeway CA Jr. Approaching the asymptote? Evolution and revolution in immunology. *Cold Spring Harb Symp Quant Biol* (1989) 54 Pt 1:1–13. doi: 10.1101/sqb.1989.054.01.003

90. Medzhitov R. Recognition of microorganisms and activation of the immune response. *Nature* (2007) 449(7164):819–26. doi: 10.1038/nature06246

91. Medzhitov R. Approaching the asymptote: 20 years later. *Immunity* (2009) 30 (6):766–75. doi: 10.1016/j.immuni.2009.06.004

92. Vance RE, Isberg RR, Portnoy DA. Patterns of pathogenesis: discrimination of pathogenic and nonpathogenic microbes by the innate immune system. *Cell Host Microbe* (2009) 6(1):10–21. doi: 10.1016/j.chom.2009.06.007

93. Arizza V, Bonura A, La Paglia L, Urso A, Pinsino A, Vizzini A. Transcriptional and *in silico* analyses of MIF cytokine and TLR signalling interplay in the LPS inflammatory response of Ciona robusta. *Sci Rep* (2020) 10(1):11339. doi: 10.1038/s41598-020-68339-x

94. Palsson-McDermott EM, O'Neill LA. Signal transduction by the lipopolysaccharide receptor, Toll-like receptor-4. *Immunology* (2004) 113(2):153–62. doi: 10.1111/j.1365-2567.2004.01976.x

95. Lu YC, Yeh WC, Ohashi PS. LPS/TLR4 signal transduction pathway. *Cytokine* (2008) 42(2):145–51. doi: 10.1016/j.cyto.2008.01.006

96. Moreira R, Romero A, Rey-Campos M, Pereiro P, Rosani U, Novoa B, et al. Stimulation of Mytilus galloprovincialis Hemocytes With Different Immune Challenges Induces Differential Transcriptomic, miRNomic, and Functional Responses. *Front Immunol* (2020) 11:606102. doi: 10.3389/fimmu.2020.606102

97. Chiaramonte M, Inguglia L, Vazzana M, Deidun A, Arizza V. Stress and immune response to bacterial LPS in the sea urchin Paracentrotus lividus (Lamarck, 1816). *Fish Shellfish Immunol* (2019) 92:384–94. doi: 10.1016/j.fsi.2019.06.017

98. Costa MM, Prado-Alvarez M, Gestal C, Li H, Roch P, Novoa B, et al. Functional and molecular immune response of Mediterranean mussel (*Mytilus galloprovincialis*) haemocytes against pathogen-associated molecular patterns and bacteria. *Fish Shellfish Immunol* (2009) 26(3):515–23. doi: 10.1016/j.fsi.2009.02.001

99. Prado-Alvarez M, Lynch SA, Kane A, Darmody G, Pardo BG, Martinez P, et al. Oral immunostimulation of the oyster Ostrea edulis: Impacts on the parasite Bonamia ostreae. *Fish Shellfish Immunol* (2015) 45(1):43–51. doi: 10.1016/j.fsi.2015.01.019

100. Shah P, Fatehchand K, Patel H, Fang H, Justiniano SE, Mo X, et al. Toll-like receptor 2 ligands regulate monocyte Fcgamma receptor expression and function. *J Biol Chem* (2013) 288(17):12345–52. doi: 10.1074/jbc.M113.449983

101. Long EM, Millen B, Kubes P, Robbins SM. Lipoteichoic acid induces unique inflammatory responses when compared to other toll-like receptor 2 ligands. *PLoS One* (2009) 4(5):e5601. doi: 10.1371/journal.pone.0005601

102. Parra-Izquierdo I, Lakshmanan HHS, Melrose AR, Pang J, Zheng TJ, Jordan KR, et al. The toll-like receptor 2 ligand Pam2CSK4 activates platelet nuclear factor-kappaB and bruton's tyrosine kinase signaling to promote platelet-endothelial cell interactions. *Front Immunol* (2021) 12:729951. doi: 10.3389/fimmu.2021.729951

103. Dunkelberger JR, Song WC. Complement and its role in innate and adaptive immune responses. *Cell Res* (2010) 20(1):34–50. doi: 10.1038/cr.2009.139

104. Kumar V. The complement system, toll-like receptors and inflammasomes in host defense: three musketeers' one target. *Int Rev Immunol* (2019) 38(4):131–56. doi: 10.1080/08830185.2019.1609962

105. Li MO, Wan YY, Sanjabi S, Robertson AK, Flavell RA. Transforming growth factor-beta regulation of immune responses. *Annu Rev Immunol* (2006) 24:99–146. doi: 10.1146/annurev.immunol.24.021605.090737

106. Calandra T, Roger T. Macrophage migration inhibitory factor: a regulator of innate immunity. *Nat Rev Immunol* (2003) 3(10):791–800. doi: 10.1038/nri1200

107. Di Carlo FJ, Fiore JV. On the composition of zymosan. *Science* (1958) 127 (3301):756–7. doi: 10.1126/science.127.3301.756-a

108. Underhill DM. Macrophage recognition of zymosan particles. *J Endotoxin Res* (2003) 9(3):176–80. doi: 10.1179/096805103125001586

109. Dillon S, Agrawal S, Banerjee K, Letterio J, Denning TL, Oswald-Richter K, et al. Yeast zymosan, a stimulus for TLR2 and dectin-1, induces regulatory antigen-presenting cells and immunological tolerance. *J Clin Invest* (2006) 116(4):916–28. doi: 10.1172/JCI27203

110. Nohmi K, Tokuhara D, Tachibana D, Saito M, Sakashita Y, Nakano A, et al. Zymosan induces immune responses comparable with those of adults in monocytes, dendritic cells, and monocyte-derived dendritic cells from cord blood. *J Pediatr* (2015) 167(1):155–62.e1-2. doi: 10.1016/j.jpeds.2015.03.035

111. Sato M, Sano H, Iwaki D, Kudo K, Konishi M, Takahashi H, et al. Direct binding of Toll-like receptor 2 to zymosan, and zymosan-induced NF-kappa B activation and TNF-alpha secretion are down-regulated by lung collectin surfactant protein A. *J Immunol* (2003) 171(1):417–25. doi: 10.4049/jimmunol.171.1.417

112. Brown GD. Dectin-1: a signalling non-TLR pattern-recognition receptor. *Nat Rev Immunol* (2006) 6(1):33–43. doi: 10.1038/nri1745

113. Rogers NC, Slack EC, Edwards AD, Nolte MA, Schulz O, Schweighoffer E, et al. Syk-dependent cytokine induction by Dectin-1 reveals a novel pattern recognition pathway for C type lectins. *Immunity* (2005) 22(4):507–17. doi: 10.1016/j.immuni.2005.03.004

114. Miller YI, Choi SH, Wiesner P, Bae YS. The SYK side of TLR4: signalling mechanisms in response to LPS and minimally oxidized LDL. *Br J Pharmacol* (2012) 167(5):990–9. doi: 10.1111/j.1476-5381.2012.02097.x

115. Deczkowska A, Weiner A, Amit I. The physiology, pathology, and potential therapeutic applications of the TREM2 signaling pathway. *Cell* (2020) 181(6):1207–17. doi: 10.1016/j.cell.2020.05.003

116. Ara Y, Saito T, Takagi T, Hagiwara E, Miyagi Y, Sugiyama M, et al. Zymosan enhances the immune response to DNA vaccine for human immunodeficiency virus type-1 through the activation of complement system. *Immunology* (2001) 103(1):98–105. doi: 10.1046/j.1365-2567.2001.01201.x

117. Czop JK, Fearon DT, Austen KF. Opsonin-independent phagocytosis of activators of the alternative complement pathway by human monocytes. *J Immunol* (1978) 120(4):1132–8. doi: 10.4049/jimmunol.120.4.1132

118. Ezekowitz RA, Sim RB, Hill M, Gordon S. Local opsonization by secreted macrophage complement components. Role of receptors for complement in uptake of zymosan. *J Exp Med* (1984) 159(1):244–60. doi: 10.1084/jem.159.1.244

119. Zhang X, Chen X, Liu Q, Zhang S, Hu W. Translation repression *via* modulation of the cytoplasmic poly(A)-binding protein in the inflammatory response. *Elife* (2017) 6. doi: 10.7554/eLife.27786

120. Jovanovic M, Rooney MS, Mertins P, Przybylski D, Chevrier N, Satija R, et al. Immunogenetics. Dynamic profiling of the protein life cycle in response to pathogens. *Science* (2015) 347(6226):1259038. doi: 10.1126/science.1259038

MAMMALIAN IMMUNITY

frontiers | Frontiers in Immunology

TYPE Original Research
PUBLISHED 08 September 2022
DOI 10.3389/fimmu.2022.965303

OPEN ACCESS

EDITED BY
Yousuke Takahama,
National Cancer Institute (NIH),
United States

REVIEWED BY
Xuguang Tai,
National Cancer Institute (NIH),
United States
Jennifer Elizabeth Cowan,
University College London,
United Kingdom

*CORRESPONDENCE
Joost P. M. van Meerwijk
Joost.van-Meerwijk@inserm.fr

SPECIALTY SECTION
This article was submitted to Immunological Tolerance and Regulation, a section of the journal Frontiers in Immunology

RECEIVED 09 June 2022
ACCEPTED 09 August 2022
PUBLISHED 08 September 2022

CITATION
Apert C, Galindo-Albarrán AO, Castan S, Detraves C, Michaud H, McJannett N, Haegeman B, Fillatreau S, Malissen B, Holländer G, Žuklys S, Santamaria JC, Joffre OP, Romagnoli P and van Meerwijk JPM (2022) IL-2 and IL-15 drive intrathymic development of distinct periphery-seeding CD4$^+$Foxp3$^+$ regulatory T lymphocytes.
Front. Immunol. 13:965303.
doi: 10.3389/fimmu.2022.965303

IL-2 and IL-15 drive intrathymic development of distinct periphery-seeding CD4$^+$Foxp3$^+$ regulatory T lymphocytes

Cécile Apert[1], Ariel O. Galindo-Albarrán[1,2], Sarah Castan[1], Claire Detraves[1], Héloise Michaud[1], Nicola McJannett[1], Bart Haegeman[2], Simon Fillatreau[3,4,5], Bernard Malissen[6], Georg Holländer[7,8,9], Saulius Žuklys[7], Jérémy C. Santamaria[1], Olivier P. Joffre[1], Paola Romagnoli[1] and Joost P. M. van Meerwijk[1*]

[1]Toulouse Institute for Infectious and Inflammatory Diseases (Infinity), INSERM UMR1291 – CNRS UMR5051 – University Toulouse III, Toulouse, France, [2]Station d'Ecologie Théorique et Expérimentale, CNRS, Moulis, France, [3]Institut Necker Enfants Malades, Inserm U1151, CNRS UMR8253, Paris, France, [4]Université de Paris Descartes, Faculté de Médecine, Paris, France, [5]AP-HP, Hôpital Necker-Enfants Malades, Paris, France, [6]Centre d'Immunophénomique (CIPHE), Aix Marseille Université, INSERM, CNRS, Marseille, France, [7]Paediatric Immunology, Department of Biomedicine, University of Basel and University Children's Hospital Basel, Basel, Switzerland, [8]Department of Paediatrics and the Weatherall Institute of Molecular Medicine, University of Oxford, Oxford, United Kingdom, [9]Department of Biosystems Science and Engineering, ETH Zurich, Basel, Switzerland

Development of Foxp3-expressing regulatory T-lymphocytes (Treg) in the thymus is controlled by signals delivered in T-cell precursors *via* the TCR, co-stimulatory receptors, and cytokine receptors. In absence of IL-2, IL-15 or their receptors, fewer Treg apparently develop in the thymus. However, it was recently shown that a substantial part of thymic Treg are cells that had recirculated from the periphery back to the thymus, troubling interpretation of these results. We therefore reassessed the involvement of IL-2 and IL-15 in the development of Treg, taking into account Treg-recirculation. At the age of three weeks, when in wt and IL-15-deficient (but not in IL-2-deficient) mice substantial amounts of recirculating Treg are present in the thymus, we found similarly reduced proportions of newly developed Treg in absence of IL-2 or IL-15, and in absence of both cytokines even less Treg developed. In neonates, when practically no recirculating Treg were found in the thymus, the absence of IL-2 led to substantially more reduced Treg-development than deficiency in IL-15. IL-2 but not IL-15 modulated the CD25, GITR, OX40, and CD73-phenotypes of the thymus-egress-competent and periphery-seeding Treg-population. Interestingly, IL-2 and IL-15 also modulated the TCR-repertoire expressed by developing Treg. Upon transfer into Treg-less *Foxp3*^{sf} mice, newly developed Treg from IL-2- (and to a much lesser extent IL-15-) deficient mice suppressed immunopathology less efficiently than wt Treg. Taken together, our results firmly establish important non-redundant

10.3389/fimmu.2022.965303

quantitative and qualitative roles for IL-2 and, to a lesser extent, IL-15 in intrathymic Treg-development.

KEYWORDS

thymus, T lymphocyte, regulatory T cell (T reg), immunopathology, cytokines

Introduction

Regulatory T lymphocytes expressing the forkhead/winged helix transcription factor Foxp3 (Treg) play a central role in the control of innate and adaptive immune responses (1). This is best illustrated by the observation that the absence of Treg in individuals and animals carrying mutations in the gene encoding Foxp3 leads to a rapidly lethal inflammatory autoimmune syndrome (2, 3). The thymus is the major organ where Treg development occurs, even if Treg can also differentiate from conventional T cells (Tconv) in the periphery (4). In the thymus, development of T cell precursors into either Treg or Tconv is governed by several parameters including signals transmitted by the TCR, co-stimulatory receptors, and cytokine receptors. Thus, it was shown that high affinity interactions between the precursor's TCR and MHC/peptide complexes expressed by thymic stromal cells are required for Treg development (5–7), which results in a Treg population enriched in autospecific cells (as compared to the Tconv-population) (8, 9). Several co-stimulatory molecules are selectively implicated in the development of Treg, including CD28, LFA-1, and CD27 (10–13). Finally, also cytokines appear important for Treg development (14).

Previous reports indicated roles for the cytokines IL-2 and IL-15 in the intrathymic development of Treg (15–23). Mice deficient in IL-2, IL-15, the IL-2-receptor α chain CD25, the β chain shared between the receptors for IL-2 and IL-15 (CD122), or the "common" cytokine-receptor γ chain (γ_c, CD132), all have reduced proportions of Treg in the thymus. *In vitro*, these cytokines drive differentiation of $CD25^+Foxp3^-$ Treg precursors to fully mature Treg (21). IL-2 was reported to prevent apoptotic cell death of autospecific Treg-precursors and appears to induce Foxp3-expression (22, 24). IL-15 was shown to be involved in the development of $CD25^-Foxp3^+$ (but not $CD25^+Foxp3^-$) Treg precursors (19). Similar mechanisms apparently also operate in the human thymus (25, 26). However, in at least one report unaltered numbers of TCR-transgenic Treg developed in absence of IL-2 (27). Moreover, a large fraction of thymic Treg are cells that had recirculated from the periphery back to the thymus (28). Since IL-2 is required for peripheral survival of Treg (29), this recirculation-process would be expected to be strongly reduced in mice deficient in IL-2, which would, at least in part, explain reduced Treg levels in mice carrying a null-mutation of the *Il2* locus (*Il2*°). Therefore, the roles of IL-2 and IL-15 in development of Treg remain unclear.

In the thymus, IL-2 and IL-15 appear to be produced by stromal cell-types involved in selection of the TCR-repertoire expressed by Treg, including dendritic cells (DC) and medullary epithelial cells (mTEC), as well as by T lymphocytes, but this issue remains controversial (19, 30–34). Through trans-presentation by their respective high affinity receptor α-chains, IL-2 and IL-15 can have very local effects (19, 31, 35). Distinct thymic stromal cell-types have distinct phenotypes and thus apparently convey distinct signals to developing T cells (36). It is therefore conceivable that Treg developing in an IL-2 vs. IL-15-dependent manner are phenotypically and/or functionally distinct.

Mice deficient in IL-2 or its receptor develop a severe and rapidly lethal autoimmune pathology (37–40), which is at least in large part due to the requirement of this cytokine for peripheral survival and function of Treg (29). Also mice deficient in IL-15 or its trans-presenting receptor α-chain develop symptoms of autoimmune-disease, though much later and much less severely. Defects in thymic negative selection of autospecific precursors of $CD4^+$ T cells may be involved in the development of these symptoms (32). It remains to be investigated if IL-2 and IL-15 modulate the selection of the TCR-repertoire expressed by Treg developing in the thymus and/or their functional potential, both of which may be involved in the development of symptoms of autoimmune-pathology.

We reassessed the involvement of IL-2 and IL-15 in Treg-development using mice in which we could distinguish newly developed from recirculating Treg. Thus, we firmly confirm that in IL-2- and, to a lesser extent, in IL-15-deficient mice substantially less Treg develop in the thymus. Our data also reveal that these cytokines drive development of thymus-egress and periphery-seeding competent Treg that are phenotypically distinct and that express partly distinct TCR-repertoires. Upon adoptive transfer into new-born Treg-deficient mice, thymus-exit-competent Treg that had developed in IL-2-deficient mice protected less efficiently from immune-pathology than Treg from wt or IL-15-deficient mice. Finally, we found that whereas the IL-2 involved in Treg development is non-redundantly produced by T cells and by DC, the IL-15

appears, at least in part, derived from DC. Based on our and previously reported data, we discuss mechanisms potentially involved in our finding that IL-2 and IL-15 apparently drive development of different Tregs.

Materials and methods

Mice

Rag2-Gfp mice (41, 42) were kindly provided by Drs. A. Liston and P. Fink; *Foxp3-Thy1*^{a} mice (43) by Dr. A. Liston; *Il15*° mice (44) by Dr. Y. Tanriver; and CD4-Cre (45) and CD11c-Cre mice (46) by Dr. J.-C. Guéry. Kaa *Tcrb*-transgenic mice (7) and β5t-Cre mice (47) were previously described. *Il2*° (B6.129P2-*Il2*^{tm1Hor}/J) mice, *Tcra*° mice, and *Foxp3*^{sf} mice were purchased from JAX laboratories, *Il15*^{fl} (C57BL/6N-*Il15*$^{tm1c(EUCOMM)Hmgu}$/H) mice (48) from MRC Harwell Institute/Mary Lyon Centre, Oxfordshire, UK. *Il2*^{fl} mice were generated as described in the Supplementary Materials and Methods section. All animals were on a C57BL/6 genetic background.

Rare sick animals, identified based on abnormally high proportions of CD4SP cells (>10% of total thymocytes), were excluded from analysis. *Il2*^{fl} or *Il15*^{fl} mice with germline recombination (as determined by PCR on tail biopsies) were excluded from analysis. Because mice were analysed before sexual maturity, we have not observed any differences between male and female mice, and all data are pools of both sexes.

Generation of *Il2*^{flox} knock-in mice

The mouse *Il2* gene (ENSMUSG00000027720) was edited using a double-stranded homology-directed repair (HDR) template (targeting vector) with 3.5 and 3.3 kb-long 5' and 3' homology arms, respectively. It included a first loxP site located 173 bp upstream of exon 3, a second loxP site located 150 bp downstream of exon 3, and a frt-neo^{r}-frt cassette. The final targeting vector was abutted to a cassette coding for the diphtheria toxin fragment A (49). JM8.F6 C57BL/6N ES cells (50) were electroporated with 20 mg of targeting vector. After selection in G418, ES cell clones were screened for proper homologous recombination by Southern blot and PCR analysis. A neomycin specific probe was used to ensure that adventitious non-homologous recombination events had not occurred in the selected ES clones. Mutant ES cells were injected into BalbC/N blastocysts. Following germline transmission, excision of the frt-neo^{r}-frt cassette was achieved through genetic cross with transgenic mice expressing a FLP recombinase under the control of the actin promoter (51). A pair of primers (sense 5'-GCCACAGAATTGAAAGATCTTC-3' and antisense 5'-TCTTGTGGAATTCTACTCCG-3') amplified a 418 bp-long band in the case of the wild-type *Il2* allele and a 500 bp-long band in the case of the mutant LoxP-flanked *Il2*^{flox} allele.

The resulting *Il2*^{flox} knock-in mice (official name B6-*Il2*^{Tm1Ciphe} mice) have been established on a C57BL/6N background. When bred to mice that express tissue-specific Cre recombinase, the resulting offspring will have exon 3 removed in Cre-expressing cells, preventing them to produce IL-2. Germline-recombination was tested by tail DNA genotyping using 5'-AGATTGGAACA ATAGTCTGAACTTGTGCT-3', 5'-TTGCAGGTGATGGTA GGTGGAAAT-3', and 5'-TCAAATCCAGAACATGCCGCA-3' primers, allowing to detect 633bp, 755bp, and 245bp bands corresponding to wt, *Il2*^{flox} and recombined *Il2*^{flox} alleles, respectively. Requests for *Il2*^{flox} mice should be addressed to BM.

Flow cytometry

Sample preparation and staining were performed using standard procedures. S1P1 staining was performed on ice as follows: after blocking non-specific labelling with mouse IgG (100µg/ml), cells were stained with unlabelled anti-S1P1 (50µg/ml, 90'), then stained with donkey-anti-rat IgG-biotin (1/100 diluted) in presence of mouse IgG (100 µg/ml, 30'), then blocked with rat anti-mouse FcγR antibody 2.4G2 (10 µg/ml, 15') and then incubated with streptavidin-PE (30'). Finally, staining with antibodies to indicated surface markers was performed in presence of 2.4G2 (10 µg/ml, 30'). Antibodies are listed in Table S1A. For MOG (35–55)/I-A^{b} tetramer (NIH tetramer facility) staining, after organ digestion, cells were washed, resuspended in RPMI medium, and incubated 15min on ice with an Fc block mix (2.4G2 at 10µg/ml; mouse and rat IgG at 25µg/ml) and 100nM dasatinib (Sigma-Aldrich). 6x10^{6} cells were then incubated for 2 hours at 25°C with 1.5 µl tetramer in 100 µl RPMI medium. Labelled cells were acquired using an LSRII or a Fortessa flow cytometer (BD Biosciences, San Jose, CA) and the data analysed using FlowJo software (Tree Star, Ashland, OR). Doublets and dead cells were excluded from the analysis by using appropriate FSC/SSC gates.

Generation of TCRseq libraries

CD4^{+}CD8^{-}Thy1.1^{+}GFP^{+} thymic Treg (105) were FACS sorted from individual three-week-old wt (n=4), *Il2*° (n=4), or *Il15*° (n=4) *Rag2-Gfp Foxp3-Thy1a Tcra*$^{+/o}$ Kaa TCRβ-transgenic B6 mice. RNA was extracted by Nucleospin RNA XS (Macherey-Nagel) according to the manufacturer´s instructions, and was quality controlled (RIN > 8) using Agilent 2100 BioAnalyzer (Agilent technology). cDNA synthesis and library preparation were performed as previously described (52), and was adjusted to our

different conditions. In brief, cDNA synthesis was performed in a thermocycler using 1 µM of reverse transcription oligonucleotides mixture corresponding to the TCRα constant region (Table S1B: TRAC_RT_1-9), a DNA-RNA hybrid template-switch oligonucleotide with 12 random nucleotides serving as unique molecular identifier (UMI) to tag individual mRNA molecules (Table S1B: UNIV5_TSv2), 5 U/µl of SMART Scribe reverse transcriptase (Clontech), 2 U/µl of Recombinant RNase inhibitor (Clontech), 0.5 mM of each dNTP, Ultra low fast first strand buffer, 5mM of DTT, 1M of Betaine, 6 mM of $MgCl_2$, incubated during 45' at 42°C, 10' at 70°C. After removal of hybrid oligonucleotide with 1U of Uracil-DNA Glycosylase (Biolabs) incubated during 40' at 37°C, the cDNA was purified using Agenecourt AMPure XP beads (Beckman Coulter) according to the manufacturer´s instructions. The first PCR reaction was performed with 0.2 µM of the oligonucleotides UNIV5_P12v2 and TRAC3_P1v2 (Table S1B), in the PCR-mix-solution (manufacturer's buffer with 1.5 mM $MgSO_4$, 0.2 mM of each dNTP, and 0.02 U/µL Hot Start DNA Polymerase (Millipore)), with the parameters 2' at 95°C; 10 cycles of 20" at 95°C, 15" at 59°C, 45" at 70°C; and a final incubation of 3.5' at 70°C. The amplicons were then purified using Agenecourt AMPure XP beads. The second, semi-nested PCR was done using 2' at 95°C followed by 20 cycles of 20" at 95°C, 15" at 59°C, 45" at 70°C; and a final incubation of 3.5' at 70°C with UNIV5_P12v2 and TRAC3_P2v2 (Table S1B). In the third PCR a 3' index, P5 and P7 Illumina sequences, and read1, read2, and index sequencing sequences were added. It was performed using UNIV5_P3v2 and TRAC3_P3v2-index (Table S1B), as follows: 2' at 95°C, 1 cycle of 20" at 95°C, 15" at 59°C, 45" at 70°C; 5 cycles of 20" at 95°C, 15" at 75°C, 45" at 70°C; and a final incubation of 3.5' at 70°C. For the fourth amplification PCR, primers UNIV5_P4v2 and UNIV3_P4v2 (Table S1B) and thermocycler parameters 2' at 95°C, 5 cycles of 20" at 95°C, 15" at 60°C, 45" at 70°C; and a final incubation of 3.5' at 70°C, were used. The quality of each library was checked by using Agilent 2100 BioAnalyzer with a 640pb mean peak size. The samples were indexed and sequenced with 300pb paired end on Illumina MiSeq sequencer (Illumina).

Processing of TCRseq data

Initially, reads were processed with the toolkit pRESTO (53) as follows. Using FilterSeq, reads with a quality higher than 20 were selected. Using MaskPrimers and PairSeq algorithms, the sequences corresponding to the *Tcra* constant region (AGCAGGTTCTGGGTTCTGGA) and indicating location of the UMI (CTTGGGGG) were searched for and indexed to the head of the paired reads. Using BuildConsensus, consensus-sequences of the reads with the same UMI were constructed. Next, the forward and reverse reads were aligned to assemble the *Tcra* sequences (AssemblePairs) and the UMI groups containing at least two reads were selected. The sequenced fragments from each selected UMI were aligned to the *Tcra* genomic region using the toolkit MiXCR (54), with the tools "align" and "assemble". The aligned fragments were exported as data tables "clonotype-tables" using the tool "exportClones". Using VDJtools (55) these clonotype-tables were then processed to graph with customized scripts in R. For all graphics described below, the "clonotypes" were selected according to their differences in the amino-acid sequences of the V segments, CDR3, and J segments. The Chao1 and Shannon-Wiener diversity-measures of the total *Tcra* repertoires were calculated using the command CalcDiversityStats from VDJtools. The Morisita-Horn similarity measure of clonotypes represented at ≥ 5 UMIs in individual samples was determined using the R package "divo". "Public repertoires" were defined as the clonotypes present in all four replicates for each condition. Custom scripts used are available at https://github.com/arielgalindoalbarran/IL2_IL15_Tregdependents.

In vivo Treg-assays

New-born (*Foxp3^{sf}Rag2°* x *Foxp3^{sf}Tcra°*)F1 mice were i.v. injected into the temporal vein (56) with $4x10^5$ $GFP^+CD4^+CD8^-Thy1.1^+$ Treg cells FACS-sorted from *Rag2-Gfp Foxp3-Thy1^a* thymi. At three weeks of age, mice were euthanized, macroscopically analysed, and blood and organs collected for analysis.

Determination of antibody titres and of autoantibodies

Serum antibody titres were determined using LegendPlex (BioLegend), according to the manufacturer's instructions. For tissue-immunoblots, organs/tissues were harvested from RAG2-deficient B6 mice, rinsed in PBS, and lysed with a Dounce homogenizer in RIPA buffer containing a protease inhibitor cocktail. The crude tissue extracts were centrifuged (10^4G, 12 min) and the soluble protein extracts were aliquoted and stored at -80°C. The protein concentration was determined using standard Bradford Protein Assay. 35 µg of total soluble protein-extract was run on SDS-PAGE, then blotted on a nitrocellulose membrane. Membranes were incubated in Odyssey blocking buffer (Li-Cor) for 30' at RT, then incubated o/n at 4°C with 800-fold-diluted sera from *scurfy* mice injected or not with Treg. Bound immunoglobulin was detected using IRDye® 800CW-labeled Goat-anti-Mouse IgG(1/2a/2b/3) (LiCor, 1h at RT). This antibody also reacts with Igκ and Igλ. Fluorescence was visualized and quantified using the Odyssey Classic Imaging System and ImageStudio software (Li-Cor).

Data and materials availability

The TCRseq data reported in this study are available from Gene Expression Omnibus with accession code GSE153484. Mice are available upon request.

Statistical analysis

The statistical significance of differences between groups of data was analysed using the two-tailed Mann-Whitney test or the Wilcoxon matched pairs signed rank test, as indicated.

Results

IL-2 and IL-15 play major non-redundant quantitative roles in intrathymic Treg development

We and others recently showed that a substantial proportion of the thymic Treg-pool is composed of cells that had recirculated from the periphery back to the thymus (28, 57–60). Thus, in young B6 adults, typically analysed in reports, 40 to 80% of thymic Treg are recirculating cells (28). This issue was not taken into account in the studies demonstrating reduced numbers of Treg in the thymus of mice deficient for IL-2, IL-15, or their receptors, and may dramatically impinge on interpretation of results. We therefore first reassessed the respective roles of IL-2 and IL-15 in intrathymic differentiation of Treg strictly focusing on newly developed Treg. To do so, we used mutant mice expressing green-fluorescent-protein (GFP) under control of the *Rag2* promoter and the allelic cell-surface marker Thy1.1 under control of the *Foxp3* promoter (*Rag2-Gfp Foxp3-Thy1*^{a}). In the thymi of such mice, GFP^{+}Thy1.1^{+} and GFP^{-}Thy1.1^{+} cells are newly developed and recirculating/thymus-resident Treg, respectively (28). Initial analyses were conducted on thymi of three-week-old mice to avoid any potential confounding effects due to the thymic involution resulting from the immune-pathology developing later-on in IL-2-deficient mice. Importantly, Treg developing early in life play a central role in the prevention of lethal immunopathology (61), validating this choice. We compared IL-2- and/or IL-15-deficient (*Il2° and Il15°*, respectively), *Rag2-Gfp Foxp3-Thy1a* mice with *Il2*$^{wt/wt}$ or *Il15*$^{wt/wt}$ ("wt") littermates. The absolute numbers of total thymocytes recovered from wt, *Il2°*, and *Il15°* mice were similar (Figure S1A). We determined the percentages of Foxp3^{+} Treg among newly developed (GFP^{+}) CD4^{+}CD8^{-}TCR^{high} (CD4SP) thymocytes (Figures S1B, 1A) and thus observed that in the absence of IL-2 substantially (39 ± 14%) less Foxp3^{+} Treg developed in the thymus (Figure 1B). Remarkably, a similar analysis revealed that, as compared to wt littermates, also in *Il15°* mice substantially (25 ± 12%) less Treg newly developed. Mice lacking both IL-2 and IL-15 (*Il2°Il15°* mice) displayed the strongest decrease in newly developed Treg among CD4SP cells (reduction of 74 ± 11%). These effects were specific to Treg as the development of CD4SP Tconv was not much affected (Figure S1C). Further analysis of the absolute numbers of newly developed Treg in the thymi of wt and mutant mice confirmed that IL-2 and IL-15 play quantitatively non-redundant roles in intrathymic Treg development (Figure S1D).

Negative selection through induction of apoptosis can happen up to late stages of T cell development (62). To assess the involvement of IL-2 and IL-15 in Treg development up to late stages of this process, we therefore first quantified developing Treg expressing the sphingosine 1-phosphate receptor (S1P1), sufficient for thymic egress of T lymphocytes (63). As expected, a large proportion of Treg expressed S1P1 (Figure S1E). Analyses of thymocytes from wt and cytokine-mutant mice revealed substantially lower levels of Treg among newly developed GFP^{+}S1P1^{+}CD4^{+}CD8^{-} thymocytes in *Il2°* and in *Il15°* mice, as compared to wt littermates (reductions of 20 ± 11% and 31 ± 9%, respectively), with a defect that was most pronounced in *Il2°Il15°* mice (reduction of 70 ± 6%, Figure 1C). To assess involvement of IL-2 and IL-15 up to the very last stage of intrathymic Treg development, we also assessed the influx of recent thymic emigrants (RTE) Treg into the spleen of the various mutant mice. In *Rag2-Gfp* transgenic mice, these cells can be identified by their remaining low but detectable levels of GFP (Figure S1F). We found substantially less Foxp3^{+} Treg among CD4^{+} RTE in spleens of *Il2°*, *Il15°*, and *Il2°Il15°* mice than in wt controls (Figure 1D). Taken together, these data indicate that IL-2 and IL-15 non-redundantly and to similar extents control the thymic production of Treg that egress into the periphery.

These data suggest that IL-2 and IL-15 play quantitatively similar roles in Treg development in the thymus. However, we previously showed that Treg recirculating from the periphery inhibit *de novo* development of Treg (28). Since IL-2 plays a crucial role in the survival of Treg in the periphery (29), it would be expected that in *Il2°* mice much less recirculating Treg recirculate to the thymus. We indeed found much less recirculating Treg in thymi of *Il2°* and of *Il2°Il15°* (but not of *Il15°*) mice as compared to wt animals (reduction of 87 ± 5% and 90 ± 6%, respectively, Figures 1E, S1G). To assess the implication of IL-2 and IL-15 in Treg-development independently of their effect on recirculation of peripheral Treg to the thymus, we quantified Treg in four-day-old mice, in which the thymus only just started to produce Treg and inhibition of Treg development by recirculating cells is minimal (28). Given the consistent results we obtained when analysing Treg-proportions among

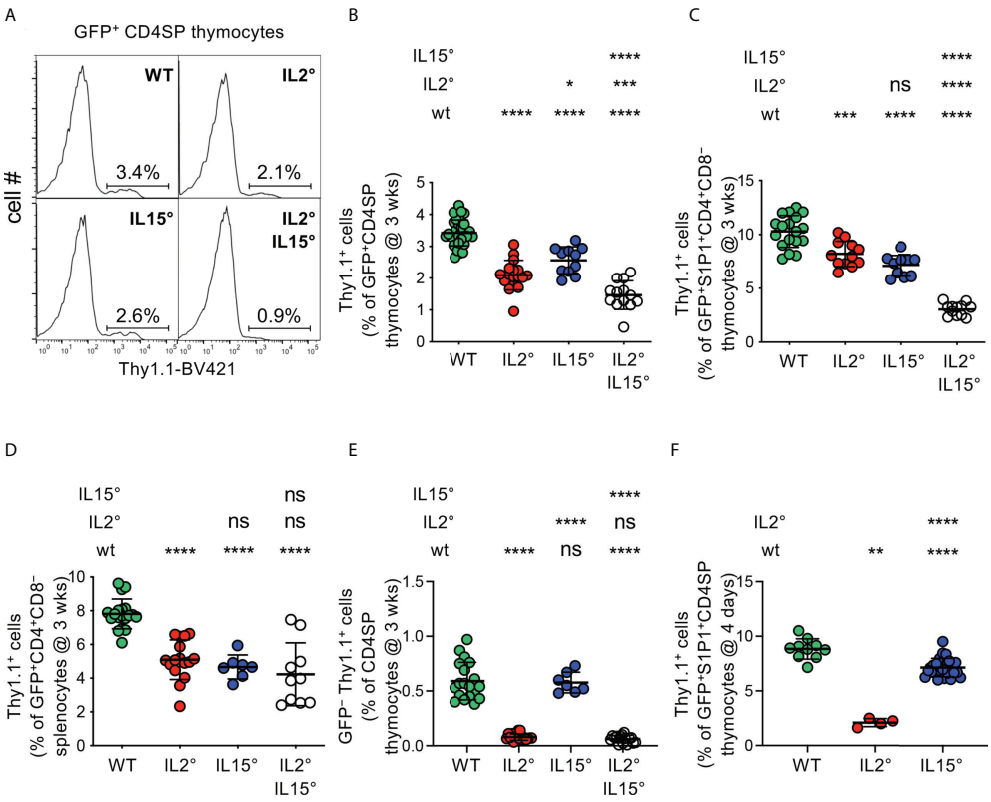

FIGURE 1
IL-2 and IL-15 quantitatively regulate intrathymic Treg-development. Thymocytes from **(A–E)** three-week-old or **(F)** four-day-old *Rag-Gfp Foxp3-Thy1*^{a} mutant, *Il2°* and/or *Il15°* mice, and *Il2*$^{wt/wt}$ and *Il15*$^{wt/wt}$ littermates (for absolute numbers see Figure S1A), were stained with fluorescent antibodies against indicated markers and analysed by flow cytometry. **(A)** Representative histograms of Thy1.1 expression (indicating Foxp3-expression) on GFP^{+} (*i.e.* newly developed) CD4^{+}CD8^{-}TCR^{high} (CD4SP) thymocytes (gated as in Figure S1B). Indicated gates were used for the quantification of Thy1.1^{+} Treg. **(B)** Percentages of Treg among GFP^{+} CD4SP thymocytes from indicated mice (n=31, 17, 11, and 13 wt, *Il2°*, *Il15°*, and *Il2°Il15°* mice, respectively). **(C)** Percentages of Treg among GFP^{+} S1P1^{+} CD4^{+}CD8^{-} thymocytes (n=18, 12, 10, and 12 mice). For S1P1 gates see Figure S1E. **(D)** Percentages of Treg among RTE in the spleen (n=19, 16, 7, 10 mice). For RTE gates see Figure S1F. **(E)** Percentages of GFP^{-} (recirculating) Treg among CD4SP thymocytes (n=19, 17, 7, and 15 mice). For recirculating Treg-gates see Figure S1G. **(F)** Percentages of Treg among GFP^{+} S1P1^{+} CD4SP thymocytes from four-day-old mice (n=10, 4, and 25 mice) For absolute numbers see Figure S1H. Dots indicate individual mice. ns, not significant; *$p < 0.05$; **$p < 0.01$; ***$p < 0.001$; ****$p < 0.0001$ (Mann-Whitney test). Bars indicate mean values ± SD.

GFP^{+}CD4SP and among GFP^{+} S1P1^{+} CD4^{+}CD8^{-} thymocytes in three-week-old mice (*cf.* Figures 1B, C), and the observation that Treg only start to leave the thymus at four days of age and are therefore quite rare in the spleen (64), we limited these analyses to GFP^{+} S1P1^{+} CD4SP thymus egress-competent cells. We found substantially (76 ± 4%) less Treg among GFP^{+} S1P1^{+} CD4SP thymocytes in *Il2°* as compared to wt mice (Figure 1F). Absence of IL-15 led to a more modest (19 ± 10%) reduction in Treg-development. Analysis of absolute numbers of S1P1^{+} Treg newly developed in four-day-old mice confirmed the major role for IL-2 in Treg-development (Figure S1H).

Taken together, our data unequivocally demonstrate that IL-15 and, more prominently, IL-2 play substantial and non-redundant quantitative roles in intrathymic Treg development, which directly impacts the influx of newly developed Treg into peripheral secondary lymphoid organs.

IL-2 and IL-15 differentially drive development of thymus-exit-competent and periphery-seeding CD25^{+} and CD25^{-} Treg subsets.

The peripheral Treg pool consists of cells expressing or not the IL-2Rα-chain CD25, and CD25^{+} vs. CD25^{-} Treg have distinct properties (65). The observation that IL-2 and IL-15 quantitatively controlled intrathymic Treg development in a non-redundant manner led us therefore to assess expression of CD25 by newly developed Treg.

In *Il2°* and *Il2°Il15°* mice, we found an almost complete lack of newly developed CD25^{high} Treg, while a deficiency in IL-15 did not have a statistically significant impact on the development of this population (Figure S2A). Consistently, we found strongly reduced proportions of CD25^{high} cells among newly developed

10.3389/fimmu.2022.965303

S1P1-expressing Treg in the thymus of *Il2*° and *Il2*°*Il15*° mice (reductions of 92 ± 9% and 100 ± 0%, respectively) but unaltered percentages in *Il15*° mice (Figures 2A, B). Whereas *Il2*° and *Il2*° *Il15*° mice also displayed a nearly complete (93 ± 5% and 97 ± 6%, respectively) loss of $CD25^{high}$ RTE Treg in the spleen, in *Il15*° mice, we found a smaller decrease of this population (28 ± 9%, Figure 2C). We obtained similar results in thymi of four-day-old mice, indicating that they are due to absence of IL-2 or IL-15 and not to differences in accumulation of Treg that had recirculated back from the periphery (Figure 2D).

The total absence of newly-developed $CD25^{high}$ Treg in the thymus of *Il2*° mice suggested that development of $CD25^{-/low}$ Treg might be much less affected by the deficiency in IL-2. Importantly, in wt animals, thymus-exit-competent $S1P1^{+}CD25^{-/low}$ Treg were even more abundant than $S1P1^{+}CD25^{high}$ Treg (Figure S2B) and we obtained similar results for RTE in the spleen (Figure S2C). Since S1P1-expression is sufficient for thymus-egress (63), these observations indicate that $Foxp3^{+}CD25^{-/low}$ $CD4^{+}CD8^{-}$ thymocytes can leave the thymus and are not, or at least not exclusively, precursors for $Foxp3^{+}CD25^{high}$ newly developing thymic Treg. As compared to three-week-old wt animals, newly developed $CD25^{-/low}$ Treg were abundant and even somewhat increased in the thymus of *Il2*° mice (Figure S2D). We also observed unaltered proportions of exit-competent ($S1P1^{+}$) $CD25^{-/low}$ Treg among $CD4^{+}CD8^{-}$ cells in the thymus and increased percentages among RTE in the spleen (Figures 2E, F). The increase in $CD25^{-/low}$ Treg in the thymus (Figure S2D) and among RTE (Figure 2F) in *Il2*° mice may be due to (an expected) failure in CD25-expression and/or absence of recirculating Treg. To study the implication of recirculating Treg, we analysed four-day-old *Il2*° mice. As compared to wt animals, we observed strongly (63 ± 6%) reduced levels of newly developed $CD25^{-/low}$ Treg in the thymus of *Il2*° mice (Figure 2G). In absence of IL-15, we consistently found substantial reductions in the proportions of $CD25^{-/low}$ Treg among $S1P1^{+}$ Treg in the thymus (reduction of 41 ± 13%) and among RTE in the spleen (reduction of 57 ± 14%) of three-week-old mice, as well as in the thymi of four-day-old animals (reduction of 24 ± 11%, Figures 2E, F, G, S2D). In thymi of *Il2*°*Il15*° mice, we found even more reduced proportions of $CD25^{-/low}$ Treg among exit-competent $S1P1^{+}$ $CD4^{+}CD8^{-}$ cells than in *Il15*° mice (54 ± 8% vs. 41 ± 13%), indicating non-redundant roles of IL-2 and IL-15 in the development of these cells (Figure 2E).

Combined, these data indicate that IL-2 is strictly required for the development of thymus-exit-competent $CD25^{high}$ Treg and, to a lesser extent, also drives that of $CD25^{-/low}$ Treg. By contrast, IL-15 modestly drives development of $CD25^{high}$ as well as of $CD25^{-/low}$ Treg. Since peripheral $CD25^{-}$ vs. $CD25^{+}$ Treg have distinct *in vivo* functional properties (65)(*cf.* discussion-section), these data suggest that IL-2 and IL-15 drive development of functionally distinct Treg.

IL-2 but not IL-15 modulates expression of GITR, OX40 and CD73 by the newly developed Treg-population

We then searched for further phenotypic differences of Treg developing in wt, *Il2*° and *Il15*° mice. It was previously reported that GITR is expressed at distinct levels on newly developed Treg-subsets (66) and, among several markers studied, we found that OX40 and CD73 are expressed in a bi-modal manner in wt animals (Figure S3A). Moreover, in wt animals, GITR, OX40 and CD73 are expressed at higher levels on $CD25^{high}$ than on $CD25^{-/low}$ Treg (Figures S3A, B). As a consequence of reduced development of $CD25^{high}$ Treg in *Il2*° mice, average expression levels of these three markers were lower on Treg from *Il2*° than from wt and *Il15*° animals (Figures 2H, I, J, S3A). Expression of these cell-surface molecules by Treg developing in *Il15*° mice was similar to that on wt Treg (Figures 2H, I, J, S3A). Together with the data on CD25, these results indicate that IL-2 (but not IL-15) modulates the phenotype of the Treg population newly developing in the thymus and suggest that it may thus affect the functional potential of these cells.

The TCR-repertoires expressed by Treg that developed in an IL-2 vs. IL-15-dependent manner are distinct

Very localized activity of the IL-2 vs. IL-15 produced by in part distinct thymic (stromal) cell-populations appears involved in Treg development (19, 31). Different thymic stromal cells present distinct self-peptides and thus select Treg with different specificities (33). We therefore hypothesized that the TCR-repertoires expressed by Treg that developed in an IL-2 vs. IL-15-dependent manner are dissimilar. To address this possibility, we bred *Rag2-Gfp Foxp3-Thy1*^{a} mice expressing a transgene encoding the public TCRβ clonotype ("Kaa") of the MOG-reactive $CD4^{+}$ T cell response during EAE in C57BL/6 mice (7, 67), and that were either *Il2*°, *Il15*°, or wt littermates. We analysed the development of MOG (35–55)/I-A^{b}-specific Treg by flow-cytometry. A quite substantial proportion (26 ± 6%) of newly developed Treg stained positive with the MOG (35–55)/I-A^{b}-tetramer in Kaa TCRβ-transgenic mice, but not in non-transgenic littermates used as controls (Figures 3A, B). We did not observe a significant difference between wt and *Il2*° mice. By contrast, we found 22 ± 8% less MOG (35–55)/I-A^{b}-specific cells among newly developed Treg in *Il15*° than in wt mice. We conclude that IL-15 plays a significant quantitative role in the development of MOG (35–55)/I-A^{b} -specific Treg while IL-2 appears not involved. These data therefore show different contributions of IL-2 and IL-15 to the development of Treg specific for a self-antigen.

10.3389/fimmu.2022.965303

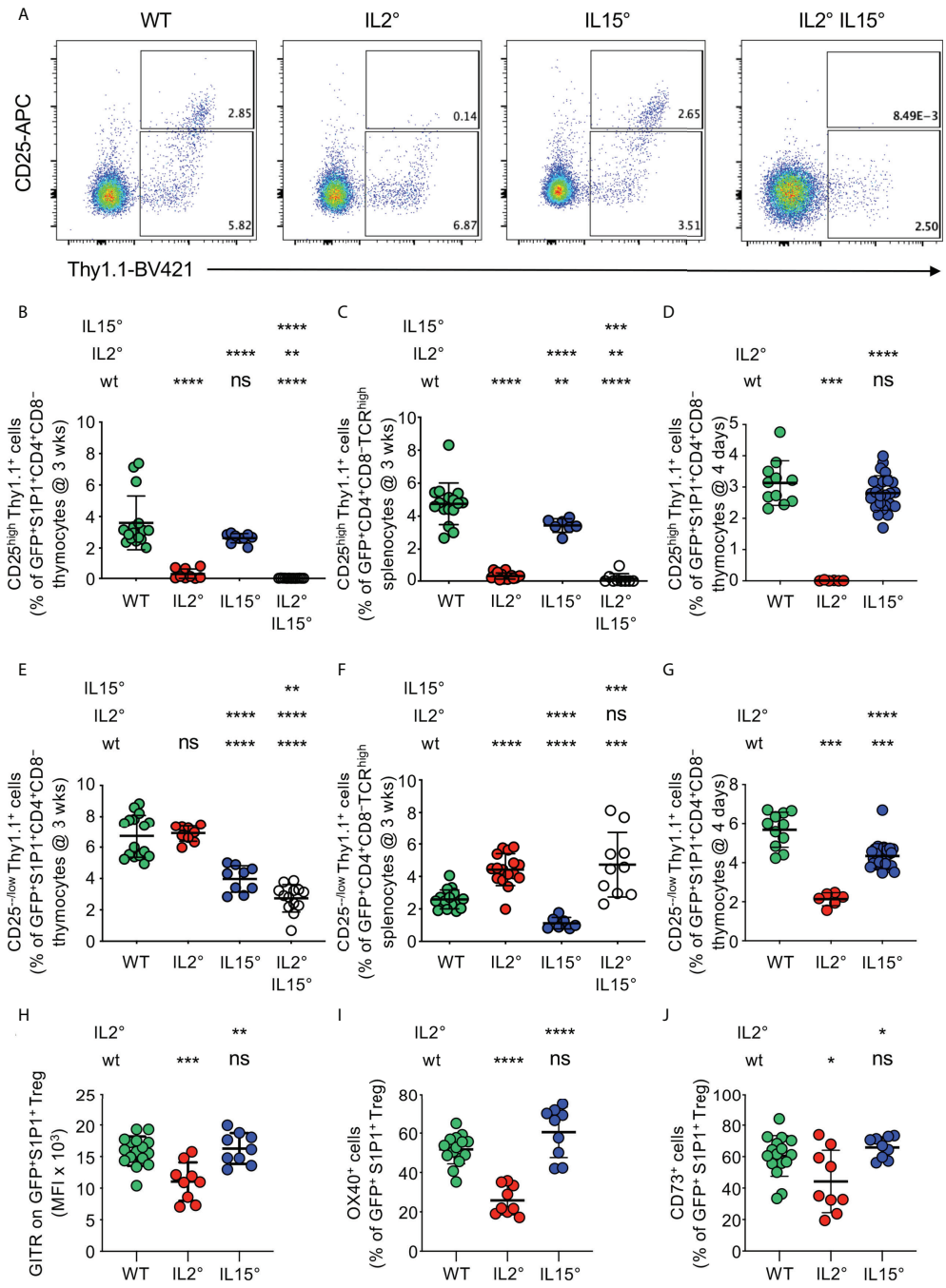

FIGURE 2
IL-2 and IL-15 differentially affect the phenotype of thymus exit-competent Treg. Thymocytes from *Rag-Gfp Foxp3-Thy1*^{a} mutant, *Il2°* and/or *Il15°* mice, and *Il2*$^{wt/wt}$ and *Il15*$^{wt/wt}$ littermates, were stained with fluorescent antibodies against the indicated markers and analysed by flow cytometry. **(A)** Foxp3 vs. CD25 expression by GFP^{+} S1P1^{+} CD4^{+}CD8^{-} thymocytes from indicated mice. Depicted gates were used to quantify CD25$^{-/low}$ and CD25^{high} Treg. Percentages of **(B–D)** CD25^{high} or **(E–G)** CD25$^{-/low}$ Treg among **(B, E)** newly developed S1P1^{+} CD4^{+}CD8^{-} thymocytes (n=16, 9, 9, and 13 wt, *Il2°*, *Il15°*, and *Il2°Il15°* mice, respectively) and **(C, F)** CD4^{+}CD8^{-}TCR^{high} RTE in the spleen from three-week-old animals (n=16, 16, 7, and 9 mice), and **(D, G)** newly developed S1P1^{+} CD4^{+}CD8^{-} thymocytes from four-day-old animals (n=11, 6, and 25 mice). **(H–J)** Expression (MFI, % positive cells, as indicated) of indicated markers on GFP^{+}S1P1^{+}CD69^{low} CD4^{+}CD8^{-} thymic Treg from indicated mice (n=16, 9, and 9 mice). Typical cytometry-plots are shown in Figure S3. ns, not significant; *$p < 0.05$; **$p < 0.01$; ***$p < 0.001$; ****$p < 0.0001$ (Mann-Whitney test). Dots indicate individual mice. Bars indicate mean values ± SD.

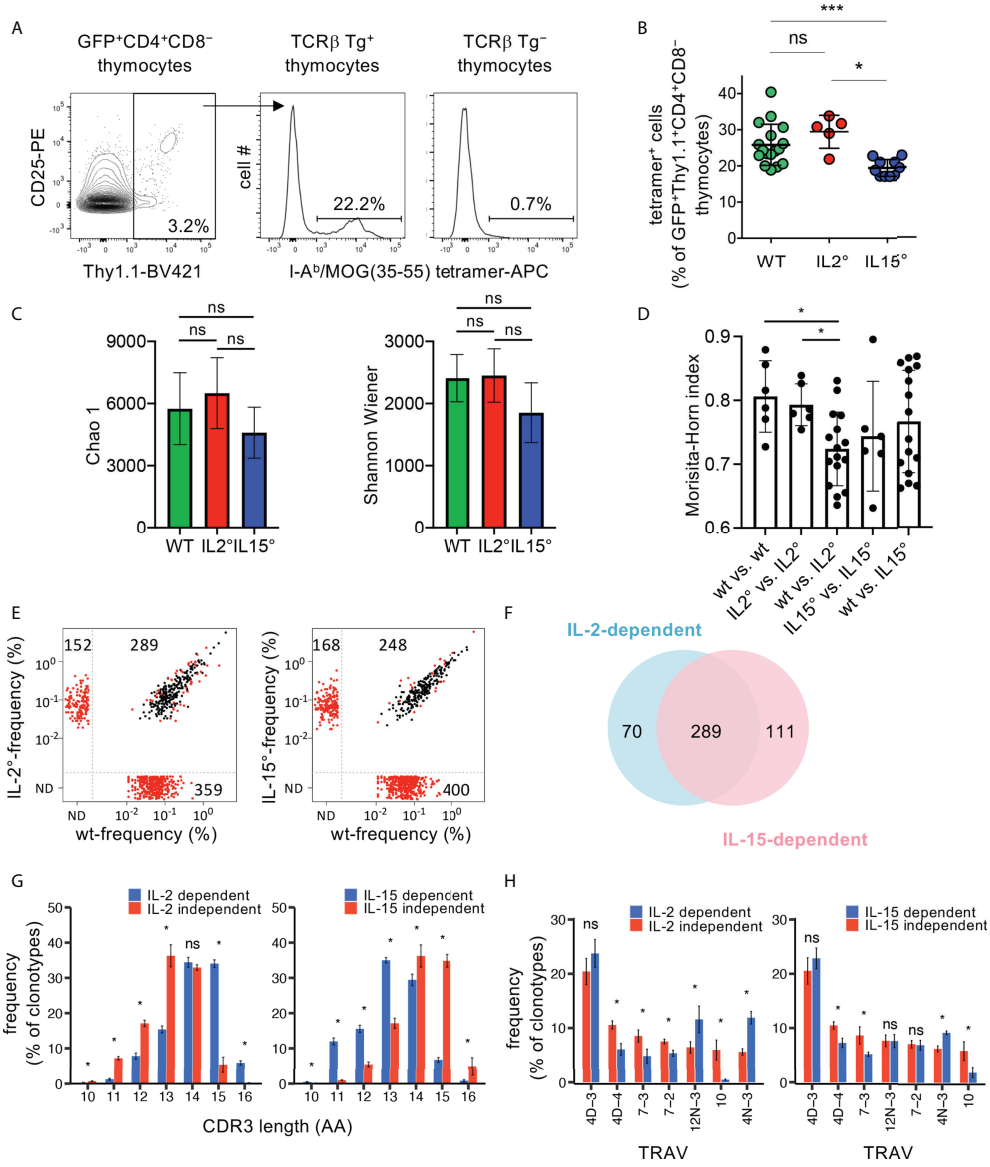

FIGURE 3
The TCR-repertoires expressed by Treg developing in an IL-2 and IL-15-dependent manner are partially distinct. **(A)** Flow-cytometry analysis of thymocytes from Rag2-Gfp Foxp3-Thy1^a Kaa TCRβ-transgenic (Tg$^+$) or non-transgenic (Tg$^-$) mice. Representative I-A^b/MOG (35–55) tetramer-stainings on GFP$^+$Thy1.1$^+$CD4$^+$CD8$^-$ wt thymocytes (i.e. newly developed Treg) are shown. **(B)** Proportions of tetramer positive cells, gated as in **(A)**, in wt (n=17), Il2° (n=5), and Il15° (n=10) mice. Dots indicate individual mice. **(C–H)** TCRseq analysis of TCRα repertoires expressed by newly developed Treg from Rag2-Gfp Foxp3-Thy1^a Tcra$^{+/o}$ Kaa TCRβ-transgenic wt (n=4), Il2° (n=4) and Il15° (n=4) mice. **(C)** Chao1 and Shannon-Wiener diversity of the TCR-repertoires. **(D)** Morisita-Horn similarity between all individual samples from indicated mice based on clonotypes with ≥ 5 UMIs. Dots indicate distinct comparisons. **(E)** Frequency of individual clonotypes in the public TCR-repertoire expressed by Treg from indicated mice. Red dots indicate clonotypes differentially expressed between wt and mutant Treg (p< 0.05, LIMMA test). N.D., not detected. **(F)** Venn diagram showing the partial overlap of the IL-2 and the IL-15-dependent public clonotypes (i.e. those within the lower-right quadrants in **(E)**. **(G)** Distribution of the TCRα CDR3-lengths of IL-2 and the IL-15-dependent and -independent public clonotypes (lower-right vs. upper-right quadrants in E, respectively). CDR3α start with conserved Cys and Ala and end with conserved Phe. See Figure S4 for average CDR3-lengths. **(H)** TRAV- (TCR Vα-segment-) usage in the indicated groups of TCRα clonotypes. Only TRAV represented at ≥5% in at least one indicated group are shown. See Figures S5, S6 for clonotypes found only in cytokine-deficient mice (upper-left quadrants in **(E)**. ns, not significant; *p < 0.05; ***p < 0.001 (Mann-Whitney test). Bars indicate mean values ± SD.

10.3389/fimmu.2022.965303

To investigate the involvement of IL-2 and IL-15 in shaping of the TCR-repertoire expressed by Treg in a broader manner, we next bred *Rag2-Gfp Foxp3-Thy1*^{a} mice that expressed the Kaa transgenic TCRβ chain, that were heterozygous for a *Tcra* null-mutation, and that were either *Il2*°, *Il15*°, or homozygous wt littermates. We analysed the TCRα-repertoires expressed by newly developed Treg in the thymus by high-throughput sequencing of *Tcra* mRNAs. The diversity (*i.e.* the number of clonotypes and their abundance) of the TCRα-repertoires expressed by Treg populations developing in wt and mutant animals appeared similar (Figure 3C). Comparison of the TCR-repertoires demonstrated higher similarities within the four wt and the four *Il2*° replicates than between the four wt and the four *Il2*° samples (Figure 3D). We did not find significant differences in the similarities between TCR-repertoires expressed by Treg from wt and *Il15*° mice (Figure 3D). These results demonstrate that IL-2 modulates the TCR-repertoire expressed by newly developing Treg. We argued that the principal differences in the TCR-repertoires are the ones reproducibly found in all mice of the same genotype, *i.e.*, the "public" TCR-repertoires. *Il2*° mice lacked a substantial part (55%) of the public TCR clonotypes we detected in wt animals (Figure 3E). Wt animals lacked 34% of the public TCRs we detected in *Il2*° mice. Similarly, *Il15*° mice lacked 62% of the public TCRs detected in wt animals and wt animals lacked 40% of the public TCRs we detected in *Il15*° mice. A quite large proportion (61%) of the public clonotypes lacking in *Il2*° or *Il15*° mice were identical, and therefore appeared to require both IL-2 and IL-15 for their development (Figure 3F). However, 19% of the IL-2-dependent and 28% of the IL-15-dependent public clonotypes appeared to specifically require these respective cytokines. Given that these data concern TCR-clonotypes reproducibly found in wt vs. *Il2*° vs. *Il15*° mice, they strongly suggest that IL-2 and IL-15 contribute to shaping of the TCR-repertoire expressed by newly developing Treg.

To obtain insight into the potentially different characteristics of the public TCRα-clonotypes expressed by Treg developing in an IL-2- vs. IL-15-dependent manner, we next compared their CDR3-lengths and TCR-Vα (TRAV)-usages. The distributions of the CDR3-lengths were different between IL-2- or IL-15-dependent vs. independent clonotypes (Figure 3G). The average CDR3-sizes of the public IL-2-dependent clonotypes were somewhat greater than those of the IL-2-independent ones (Figure S4). By contrast, the average CDR3-sizes of the public IL-15-dependent clonotypes were slightly smaller than those of the IL-15-independent ones (Figure S4). Also clonotypes found in *Il2*° or *Il15*° but not in wt animals had average CDR3-size and distribution of CDR3-lengths that were significantly different from those that were cytokine-independent (Figures S5A, B). Analysis of the TRAV-usage revealed substantial differences between cytokine-dependent vs. -independent clonotypes (Figure 3H). Also clonotypes found in *Il2*° or *Il15*° but not in wt animals had TRAV-usages that were significantly different from those that were cytokine-independent (Figure S6). Taken together, these observations indicate distinct characteristics of the public TCRα-chain clonotypes expressed by Treg requiring the presence or absence of IL-2 or IL-15 for their development. The reproducibility of these results in the four biological replicates for each genotype also indicated that the differences were not due to sampling randomness.

Origins of the IL-2 and IL-15 involved in Treg development

Probably through trans-presentation by their respective high affinity receptor α-chains, IL-2 and IL-15 can have very local effects (19, 31, 35, 68). Distinct thymic stromal cell-types have distinct phenotypes and thus apparently convey distinct signals to developing T cells (36). Our observation that IL-2 and IL-15 appear to qualitatively modulate Treg development may therefore be due to interactions of developing Treg with distinct stromal cell-types. We therefore sought to identify the stromal cells producing the IL-2 and IL-15 involved in Treg-development, which remains a controversial issue (19, 30–34).

In the thymus, TEC and DC appear to produce IL-15 and to express the IL-15Rα chain required for its trans-presentation to responder cells (19, 32, 34). To assess the role of the IL-15 produced by these cells in Treg-development, we generated *Rag2-Gfp Foxp3-Thy1*^{a} mice in which one *Il15* allele was constitutively and the other conditionally invalidated (*Il15*$^{o/fl}$). The Cre recombinase required for invalidation of the *Il15* locus was expressed under control of the promoter of the gene encoding the thymus-proteasome β5t-subunit, active during early stages of TEC-development (47), or that of the gene encoding CD11c, expressed by DC (46). The development of iNKT cells depends on IL-15 (69). *Il15*-invalidation in TEC or in DC led to reduced accumulation of CD4SP iNKT cells (Figures S7A, B). Interestingly, *Il15*-invalidation in TEC, but not in DC, led to reduced accumulation of CD4^{+}CD8^{-} iNKT cells (Figure S7C). These data thus confirm conditional invalidation of the *Il15* locus in the mice. They also suggest distinct origins of the IL-15 involved in the development of CD4^{-}CD8^{-}vs. CD4^{+}CD8^{-} iNKT cells. Unexpectedly, in β5t-Cre *Il15*$^{o/fl}$ mice we found unaltered proportions of Treg among CD4SP thymocytes (Figure 4A). By contrast, in CD11c-Cre *Il15*$^{o/fl}$ mice (16.8 ± 24.3%) less Treg developed than in control mice not expressing the Cre-recombinase (Figure 4A). These results suggest that the IL-15 involved in Treg-development is, at least in part, produced by DC.

Whereas T cells appear to produce IL-2 involved in Treg-development in the thymus, the role of dendritic cells (DC) remains controversial (19, 30, 31, 68). As compared to in their Cre^{-} littermates, in CD4-Cre^{+} *Il2*$^{o/fl}$ mice, in which T cells do not produce IL-2, we found very strongly (90.7 ± 4.4%) reduced proportions of CD25^{high} Treg among CD4SP (Figure 4B), which

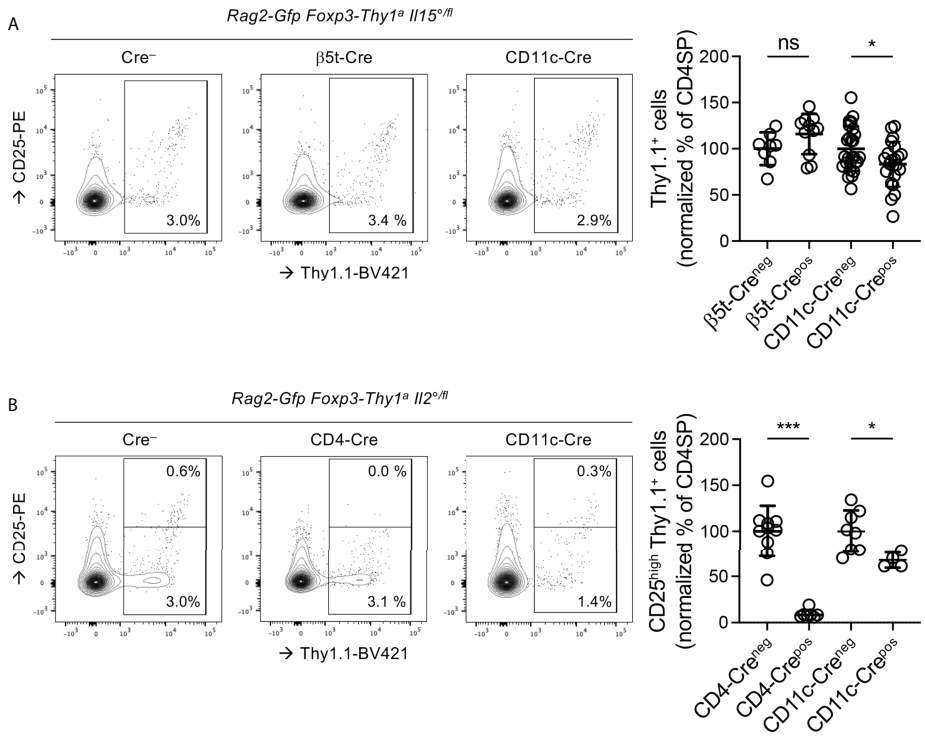

FIGURE 4
The IL15 involved in Treg development is produced by DC and the IL-2 by T cells and, to a lesser extent, by DC. Thymocytes from three-week-old Rag-Gfp Foxp3-Thy1^a mutant, **(A)** Il15$^{°/fl}$ or **(B)** Il2$^{°/fl}$ mice, expressing or not the indicated Cre-transgenes, were stained with fluorescent antibodies against indicated markers and analysed by flow cytometry. (left hand panels) Representative histograms of Thy1.1 (indicating Foxp3-expression) vs. CD25 expression on GFP$^+$ (i.e. newly developed) CD4SP thymocytes (gated as in Figure S1B). Indicated gates were used for the quantification of (CD25$^{-/low}$ and CD25^{high}) Thy1.1$^+$ Treg among CD4SP cells. (right-hand panels) Quantification of **(A)** total or **(B)** CD25^{high} Treg among GFP$^+$ CD4SP thymocytes. Dots indicate individual mice and values were normalized to the average percentages found in Foxp3$^{Thy1a/Y}$ male and Foxp3$^{Thy1a/wt}$ female, Cre$^-$ littermates ((**A**) n=8 β5t-Cre$^-$, 11 β5t-Cre$^+$, 27 CD11c-Cre$^-$, 22 CD11c-Cre$^+$, **(B)** 10 CD4-Cre$^-$,7 CD4-Cre$^+$, 8CD11c-Cre$^-$, and 4 CD11c-Cre$^+$ mice). ns, not significant; *p < 0.05; ***p < 0.001 (Mann-Whitney test). Dots indicate individual mice. Bars indicate mean values ± SD.

confirms that T-cell-derived IL-2 plays an important role in Treg development. Also in CD11c-Cre *Il2*$^{°/fl}$ mice, in which DC do not produce IL-2, we found substantially (32.2 ± 8.4%) less newly developed CD25^{high} Treg (Figure 4B). These data therefore indicate that IL-2 derived from both T and dendritic cells is involved in Treg-development.

Thymic Treg from Il2° and from Il15° mice have distinct capacities to prevent autoimmune pathology

Our results reveal that Treg developing in the thymi of wt, *Il2*° and *Il15*° mice are phenotypically distinct and that the TCR-repertoires they express are, in part, distinct. We therefore postulated that Treg from wt vs. *Il2*°vs. *Il15*° mice may have distinct capacities to prevent autoimmune pathology. To assess this possibility, we adoptively transferred (by i.v. injection) identical numbers of GFP$^+$Thy1.1$^+$CD4$^+$CD8$^-$ thymic Treg, sorted from three-week-old wt, *Il2*° or *Il15*°, *Rag2-Gfp Foxp3-Thy1*^{a} mice, into new-born Treg-deficient *Foxp3*^{sf} mice and analysed lymphocyte-activation, cytokine production, (auto) antibody production, and development of immunopathology three weeks later (Figures 5, S8, S9).

Injection of newly developed wt thymic Treg into *Foxp3*^{sf} mice reconstituted Treg levels to 11 ± 3% and strongly reduced the symptoms of the autoimmune-pathology observed in sham-treated animals: Skin desquamation; hunched posture; spleno- and lymphadeno-megaly (Figures 5A, B, S8); activation of splenic CD4$^+$ or CD8$^+$ T cells (as indicated by a CD44^{high}CD62L^{low} phenotype, Figure 5C); IFN-γ or IL-13 production by splenic CD4$^+$ Tconv (Figure 5D); circulation of serum antibodies of IgM, IgG1, IgG2a, IgG3, and IgA isotypes (Figure 5E); production of circulating antibodies directed against a large array of autoantigens of all organs assessed (Figure 5F), and infiltration by mononuclear cells in pancreas, skin, and lungs, and associated bronchial- and ear-thickening (Figure S9). Newly developed Treg isolated from *Il2*° and from *Il15*° thymi

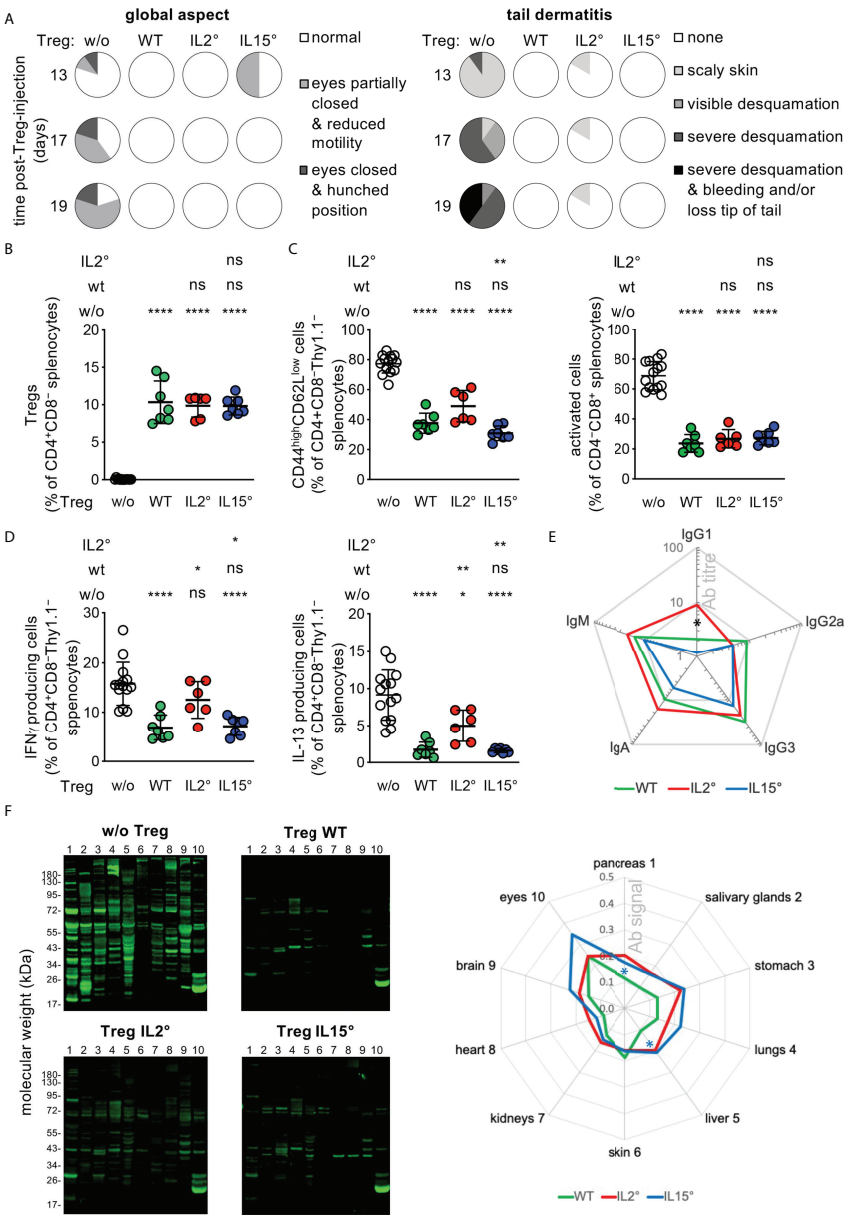

FIGURE 5
Treg developing in Il2° vs. Il15° mice have distinct in vivo functions. Newborn *Foxp3*^{sf} mice were i.v. injected with electronically sorted newly developed thymic Treg from three-week-old *Rag2-Gfp Foxp3-Thy1*^{a} wt, *Il2°*, or *Il15°* mice, or sham PBS-treated, and analysed three weeks later. **(A)** Eye pathology, reduced motility, hunched posture, and tail-skin-pathology in control *scurfy* mice, and its prevention upon neonatal injection of thymic Treg from wt, *Il2°* and *Il15°* mice. See Figure S8 for representative pictures of mice, tail close-ups, and lymphadeno- and spleno-megaly. **(B)** Reconstitution of Treg levels in the spleen of *Foxp3*^{sf} mice upon injection of wt, *Il2°*, or *Il15°* Treg. **(C)** Proportions of activated (*i.e.* CD44^{high}CD62L^{low}) CD4 (left) or CD8 (right) Tconv in spleens. **(D)** IFN-γ (left) and IL-13 (right) producing CD4^{+} Tconv in spleens (as determined by flow-cytometry). **(E)** Titres of serum-antibodies of indicated isotypes. "Ab titre" is expressed as mean % of that found in sham-treated *Foxp3*^{sf} mice (IgG1, 73.1 ± 35.9; IgG2a, 2.4 ± 2.4; IgG3, 1.2 ± 0.4; IgG2b, 0.0 ± 0.0; IgA, 38.0 ± 6.9; IgM, 137.1 ± 40.6 pg/ml). Mice injected with Treg from wt, *Il2°* or *Il15°* mice had lower titres of all detected antibody-isotypes than sham-treated animals ($p \leq 0.01$, Mann-Whitney test). **(F)** Autoantibodies in sera from indicated mice (as determined by incubating Western blots carrying total extracts from indicated *Rag2°* tissues with sera). Representative blots (left panels) and semi-quantification of total signals on indicated tissues (right panel, mean ratios Treg-injected/sham-injected mice) are shown. Numbers on the left side correspond to the tissues indicated on the right side. Statistical significance concern differences between mice that had received IL2°vs. IL15° Treg (black asterisk in **(E)** and IL15° Treg vs. wt Treg (blue asterisks in **(F)**. Sham-treated *Foxp3*^{sf} mice, n=14, 8 independent experiments; *Foxp3*^{sf} mice injected with thymic Treg from wt mice, n=7, 3 experiments; from IL-2° mice, n=6, 3 experiments; from IL-15° mice, n=7, 4 experiments. ns, not significant; *$p < 0.05$; **$p < 0.01$; ****$p < 0.0001$ (Mann-Whitney test). Dots indicate individual mice. Bars indicate mean values ± SD.

populated *Foxp3*^{sf} mice as efficiently as wt Treg (Figure 5B). They also inhibited development of all of the symptoms, but to distinct degrees (Figures 5A, C–F, S8, S9). Thus, despite similar reconstitution, Treg from *Il2*° (but not those from *Il15°)* mice inhibited to a lesser extent than Treg from wt mice IFN-γ and IL-13 production by CD4 Tconv (Figure 5D). Treg from *Il2*° mice prevented the production of IgG1 less efficiently than Treg from *Il15*° mice (Figure 5E). Quantification of the tissue blots hybridized with sera from *Foxp3*^{sf} mice injected with Treg from wt, *Il2*° or *Il15*° thymi, revealed some minor differences, but all three quite efficiently prevented autoantibody production (Figure 5F). We did not find significant differences between the capacity of wt vs. *Il2*° or *Il15*° Treg to prevent infiltration by mononuclear cells in the pancreas, lungs and ears, or thickening of bronchus-walls or ears (Figure S9). Combined, these data indicate that the intrathymic availability of IL-2 is essential for the development of a fully functional Treg population. The role of IL-15 in this process appears more subtle.

Discussion

In the study reported here, we investigated the quantitative and qualitative roles of IL-2 and IL-15 in the intrathymic generation of Treg. By focusing on newly developed Treg and by analysing young mice in which Treg development is practically uninhibited by recirculating Treg, we showed important quantitative roles of IL-2 and, to a lesser extent, IL-15 in Treg development. IL-2 and IL-15 drive the development of phenotypically distinct, thymus egress-competent and periphery-seeding Treg, and differently modulate the selection of the TCR-repertoire they express. Treg developing in absence of IL-2 (but not of IL-15) had clearly detectable, though limited, defects in the control of immune-responses *in vivo*. Combined, these data consolidate and extend the suspected quantitative roles of IL-2 and IL-15 in Treg-development in the thymus and indicate that these cytokines also play important qualitative roles in this process.

The thymi of mice deficient in the IL-2Rα or β chains, in IL-2 or in IL-15 contain fewer Treg (16, 18–20, 23, 70–72). However, among thymic Treg, the proportion of cells that had recirculated from the periphery back to the thymus is very large in wt animals (28). These data therefore mostly failed to formally demonstrate a role for IL-2 and IL-15 in Treg development in the thymus. In our experimental mouse model, we could unambiguously identify newly developed Treg and found substantially less Treg in IL-2- or IL-15-deficient mice than in wt animals. Using an elegant experimental model in which T cell-development was induced through induction of ZAP70-expression, Marshall et al. showed that antibody-mediated IL-2-blockade reduced *de novo* development of Treg, which is consistent with our results (19). It now therefore appears clearly demonstrated that IL-2 affects Treg development in the thymus.

IL-2 and IL-15 do not only act on Treg-precursors but also on other cell-types (potentially) involved in Treg development in the thymus. Thus, IL-2 plays a crucial role in the peripheral survival of Treg (29). Accordingly, in IL-2-deficient mice we found almost no Treg that had recirculated from the periphery back to the thymus. Therefore, as compared to wt mice, in IL-2-deficient mice at least two parameters affecting Treg development had changed: availability of IL-2 and inhibition of Treg development by recirculating cells. To exclude this additional parameter, we analysed Treg-development four days after birth, *i.e.* when Treg just start to develop and leave the thymus, the proportion of recirculating Treg in the thymus is very low, and inhibition of Treg-development is minimal (28). We observed that in absence of IL-2 substantially fewer Treg developed than in absence of IL-15. Our results thus confirm and substantially extend an earlier report in which *de novo* development of Treg was studied through induction of ZAP70-expression (19). Interestingly, we observed a more robust decrease in Treg development in neonate than in three-week-old IL-2-deficient mice (as compared to wt animals). A hypothesis that may explain this observation is that in three-week-old (but not in neonatal) mice, Treg development is substantially inhibited by recirculating Treg, in part through limitation of the availability of IL-2 (28). Further limiting IL-2-availability through genetic invalidation of the gene encoding it would affect Treg development to a lesser extent in three-week-old mice than in neonates, in which recirculating-Treg-mediated inhibition of Treg-development is minimal. Assessing this hypothesis will require the generation of mice in which recirculating Treg do not accumulate in the thymus.

Also iNKT cells may, through production of IL-4, modulate Treg development (73). As we here confirmed, in absence of IL-15 substantially fewer iNKT cells accumulated in the thymus. It remains therefore unclear if the reduced Treg development we observed in IL-15-deficient mice was due to a direct effect on Treg precursors or on iNKT cells. It will be important to study the effect of IL-15 deficiency on Treg development in iNKT cell-deficient mice.

Deficiency in IL-2 or IL-15 will also affect differentiation and/or maintenance of other cell-types known to modulate T cell-development in the thymus but not addressed in this study. For example, IL-15 drives differentiation of CD8 memory T cells (74), reported to reduce negative selection of autospecific thymocytes through deletion of DC and mTEC (75). Therefore, it will now be important to address the involvement of other cell types potentially involved in the effects of IL-2 or IL-15-deficiency on Treg-development.

Combined, our results thus firmly demonstrate quantitatively substantial and non-redundant (direct and/or indirect) roles for IL-2 and, to a lesser extent, IL-15 in Treg development. We also found that the phenotypes of Treg developing in an IL-2- vs. IL-15-dependent manner are distinct: Whereas IL-2 is strictly required for the differentiation of CD25^{+} Treg, IL-15 only plays a modest role,

and both cytokines play a role in the development of $CD25^{-/low}$ Treg. Our results thus support and extend an earlier report on the distinct roles of IL-2 and IL-15 in Treg development in the thymus (19). Importantly, in wt animals, the egress-competent phenotype of the thymic $CD25^{-/low}$ Treg subset and the fact that these cells were abundant among RTE in the spleen indicated that it is not (only) a precursor population for newly developing thymic $CD25^{+}$ Treg. The fact that we readily detected these cells among splenic RTE in IL-2-deficient mice supports our conclusion that they do not need to go through a $CD25^{+}$ phase to leave the thymus. Komatsu and colleagues showed that $CD25^{-}$ Treg have a less stable phenotype than $CD25^{+}$ Treg and can lose Foxp3-expression and suppressive activity and acquire the capacity to produce IL-2, IFN-γ, IL-4, and IL-17 (65). *In vitro*, IL-2 did not stabilize Foxp3-expression of peripheral $CD25^{-}$ Treg, suggesting that availabilities of IL-2 in the thymus and in the periphery play non redundant roles. Our results indicate that this apparently functionally distinct $CD25^{-/low}$ Treg subset may, in part, have a thymic origin. Also the GITR, OX-40 and CD73-phenotypes were differentially affected by absence of IL-2 or Il-15. Together, these observations suggest that IL-2 and IL-15 may drive the development of potentially *in vivo* functionally distinct Treg populations.

We hypothesized that IL-2 and IL-15 may drive development of Treg expressing distinct TCR-repertoires. We found that 73% of the public clonotypes observed in wt animals required IL-2 and/or IL-15 for their development. Much smaller proportions of the public clonotypes observed in wt animals specifically required IL-2 (but not IL-15: 11%) or IL-15 (but not IL-2: 17%) for their development. Since distinct proportions of $CD25^{-}$ vs. $CD25^{+}$ Treg developed in *Il2°* vs. wt and *Il15°* mice, these observations are consistent with a recent report showing that intrathymic $CD25^{-}$ vs. $CD25^{+}$ Treg express distinct TCR-repertoires (73). The non-redundant roles of IL-2 and IL-15 may in part be due to an anti-apoptotic action of IL-2 (22) which would allow selection of Treg expressing TCRs recognizing self-MHC/peptide complexes with higher affinity. The public TCRα-repertoires expressed by Treg developing in an IL-2- or IL-15-dependent manner have different CDR3-lengths and TRAV-usages than those developing in wt mice. Previous work demonstrated shortening of the CDR3α during T cell selection in the thymus (76). Interestingly, whereas IL-2-dependent TCRα-chains have larger CDR3 than IL-2-independent ones, IL-15-dependent TCRα-chains have smaller CDR3 than IL-15-independent ones. Distinct CDR3α-lengths and TRAV usages will probably have an influence on the affinities of the TCRs for peptide/MHC complexes expressed by thymic stromal cells, suggesting an interplay between cytokine-receptors and TCR in driving development of the Treg-subsets. Whatever the precise origin(s) of these distinct characteristics may be, they also indicate that the differences in the TCRα-repertoires we observed are not due to sampling biases.

Intriguingly, some Treg newly developing in the thymus of *Il2°* and of *Il15°* mice expressed public TCR-clonotypes that we did not observe in wt animals. Limiting our analysis to clonotypes found in all four replicates will constrain but not entirely avoid effects of sampling randomness, which may therefore be involved in the detection of clonotypes exclusively in *Il2°* or *Il15°* mice. However, small but statistically significant differences in CDR3 lengths and in TRAV-usage of public TCRα found in IL-2° *but not* in wt mice vs. those found in wt *and* in IL-2° mice, indicated that a substantial proportion of Treg-clonotypes found exclusively in *Il2°* or *Il15°* mice is not due to sampling biases. By contrast, they suggested that these cells have distinct peptide/MHC-recognition characteristics. A hypothesis that may explain this observation is, again, that signals through the TCR synergize with signals through the receptors for IL-2 and IL-15 to drive differentiation and selection of Treg-precursors, *i.e.* the cytokines would act as a rheostat.

The differences in the TCR-repertoires expressed by Treg from wt, IL-2- and IL-15-deficient mice may be due to the distinct sources of these cytokines in the thymus. Consistent with this postulate, it was previously shown that Treg specific for a model-antigen expressed by mTEC do not require IL-2 for their development (27). IL-2-deficient DC supported the development of Treg less efficiently than wt cells in an *in vitro* thymus culture system (31). In agreement with this observation, we observed a reduction in newly developed Treg in mice with an IL-2-ablation targeted to DC. DC trans-presenting IL-2 *via* the IL-2Rα-chain (35) may favour differentiation of Treg specific for ligands expressed by these stromal cells, as previously suggested (68). Whereas *Il2*-mRNA was detected in thymic DC (31), using an experimental model in which *Il2*-expression-history could be traced, Hemmers et al. did not find evidence for expression in $CD90^{-}CD19^{-}Ly6G^{-}Ly6C^{-}$ thymic DC (30). Together with our data, these observations suggest that IL-2 expression by thymic DC is limited to a particular subset of these cells (or of other $CD11c^{+}$ cells). It appears rather unlikely that the reduced Treg development we observed in the $Il2^{o/fl}$ CD11c-Cre mice was due to the previously reported very limited activity of the transgenic construct in T lymphocyte-progenitors (<10%) (46). In mice with an IL-15-ablation targeted to DC, we found fewer newly developed Treg, and DC are known to express the IL-15Rα-chain (32). It remains to be investigated if the IL-2Rα and IL-15Rα chains are expressed by the same or by distinct DC and if these DC present the same repertoires of MHC/peptide complexes. Similarly, mTEC trans-presenting IL-15 *via* the IL-15Rα-chain (32) might favour differentiation of Treg specific for ligands expressed by these stromal cells. It was indeed shown that radioresistant stromal cells play an important role in the trans-presentation of the IL-15 involved in Treg development (19). However, even if the abridged development of iNKT cells indicated reduced IL-15 production in our mice with an IL-

15-deficiency targeted to TEC, we have not observed a reduction in Treg development. The precise stromal origin of the IL-15 involved in Treg development will therefore require further work.

A non-mutually exclusive explanation for the differences in TCR-repertoires expressed by Treg that had newly developed in wt, IL-2 or IL-15-deficient mice is related to the indirect effects of these cytokines. Both recirculating Treg and iNKT cells (and potentially other cell-types), the presence of which is controlled by IL-2 and IL-15, respectively, appear to modulate Treg development in the thymus (28, 73), and these cells may also modulate selection of the TCR-repertoire, *e.g.* through affecting thymic stromal cells. This postulate would imply that also the TCR-repertoires of Tconv developing in wt vs. *Il2*° vs. *Il15*° animals may be distinct. Assessing these possibilities will require analysis of TCR-repertoires expressed by Tconv and Treg developing in mice lacking recirculating Treg and iNKT cells.

Treg developing in absence of IL-2 or IL-15 therefore are phenotypically (and potentially functionally) distinct and they express distinct TCR-repertoires. We postulated that these cells may have distinct capacities to prevent (auto)immune pathology *in vivo*. To distinguish between roles of these cytokines in the thymus vs. the periphery, we transferred Treg isolated from wt, IL-2 or IL-15-deficient thymi into *Foxp3*^{sf} hosts sufficient for these cytokines. Upon transfer into neonatal *scurfy* mice, newly developed thymic Treg from wt, *Il2*° and *Il15*° mice equally efficiently reconstituted adoptive hosts. However, Treg from *Il2*° mice less efficiently inhibited IFN-γ and IL-13 production by CD4 T cells than wt Treg. Consistent with their reduced capacity to inhibit production of a Th2 cytokine, they also less efficiently inhibited serum accumulation of antibodies of IgG1 isotype. Treg from *Il15*° mice had a slightly lower capacity to inhibit formation of autoantibodies to pancreas and liver. However, we did not observe differences in the capacity of newly developed Treg from wt, *Il2*° and *Il15*° mice to prevent the histological lesions observed in Treg-deficient *Foxp3*^{sf} mice. These results indicate that IL-2 (and potentially IL-15) plays a qualitative role in the intrathymic development of Treg, a role that cannot be replaced by exposure to this cytokine in the periphery. Redundancy of Treg with distinct antigen-specificities and/or effector-functions may explain the modest nature of the defects we observed.

The reduced capacity of Treg from IL-2-deficient mice to inhibit cytokine production by T cells *in vivo* may be due to reduced stability of Foxp3-expression by these cells. In absence of IL-2, Treg precursors failed to express high levels of CD25. Komatsu and colleagues showed that CD25^{-} Treg have a less stable phenotype than CD25^{+} Treg: They lose Foxp3-expression and suppressive activity, and even acquire the capacity to produce IL-2, IFN-γ, IL-4, and IL-17 (65). Taken together, these two observations suggest that, upon adoptive transfer into IL-2-sufficient mice, (CD25^{-}) thymic Treg from IL-2-deficient animals will have a defect in Foxp3-stability and therefore less efficiently control T cell-activation *in vivo*. Extensive (*e.g.* single cell transcriptomic) analysis of the similarity of the CD25$^{-/low}$ Treg-populations developing in wt vs. *Il2*° mice and assessment of their differentiation upon adoptive transfer into neonatal *Foxp3*^{sf} mice will be required to assess this hypothesis. Whatever the precise explanation, IL-2 in the thymus and in the periphery apparently has non redundant effects on Treg.

The data presented here indicate a more complex role for the cytokines IL-2 and IL-15 in the intrathymic differentiation of Treg than what was previously appreciated. Rather than only quantitatively controlling this process, they appear to also qualitatively do so by guiding differentiation of Treg with distinct phenotypes and by shaping the antigen-specificity of Treg emerging from the thymus. This is, in part, potentially due to the distinct thymic cell-types known to produce and to respond to these cytokines. The relative availability of IL-2 and IL-15 in the thymus may change during life. We thus previously described that Treg recirculating from the periphery back to the thymus limit the availability of IL-2 and thus inhibit Treg development (28). It will now be important to assess how such potential changes influence the development of Treg in the thymus and the immunosuppressive activity of these cells in the periphery.

Data availability statement

The datasets presented in this study can be found in online repositories. The names of the repository/repositories and accession number(s) can be found below: https://www.ncbi.nlm.nih.gov/geo/, GSE153484.

Ethics statement

The animal study was reviewed and approved by the "Comité d'éthique en matière d'expérimentation animale" UMS006 CEEA-122, authorisation number APAFIS#4151-201602171 0481496.v6.

Author contributions

Conceptualization: CA, OJ, PR, and JM. Methodology: SC and CD. Formal analysis: AG-A and BH. Investigation: CA, NM, SC, CD, HM, JS. Mouse model: BM. Resources: SF, GH, SZ. Writing – original draft: CA, JM; Writing – review & editing: OJ. Supervision: JM. All authors contributed to the article and approved the submitted version.

Funding

This work was financially supported by the Fondation pour la Recherche Médicale (to JvM, DEQ20160334920); the IdEx Toulouse (to PR); the Région Midi Pyrénées (to JvM, 15/06/12.05); the Agence Nationale pour la Recherche (to PR, ANR-16-CE15-0015-01), and the Fondation ARC pour la Recherche sur le Cancer (to CA, DOC20180507201). Il2fl knock-in mice were generated by the Centre d'Immunophénomique (CIPHE, Marseille, France). CIPHE is supported by the Investissement d'Avenir program PHENOMIN (French National Infrastructure for Mouse Phenogenomics; ANR-10-INBS-07 to BM).

Acknowledgements

We thank Adrian Liston and Pamela Fink for providing *Rag-Gfp Foxp3-Thy1*^{a} mutant mice and the NIH tetramer-facility for MOG (35–55)/I-A^{b} tetramers. We are very grateful to the following persons for excellent technical assistance: Fatima L'Faqihi, Valérie Duplan-Eche, Anne-Laure Iscache, Lidia De la Fuente, Paul Menu of the INFINITy Cytometry platform; Adrien Castinel of the GeT-PlaGE Genotoul; and the personnel of the Inserm US006 ANEXPLO/Creffre animal and experimental histopathology facilities. We thank F. Fiore for supervising the construction of the *Il2*^{fl} mice and the members of the 'Integrative T cell Immunobiology team' and Sylvie Guerder for discussions and input in the project. JPMvM is grateful to the staff of the Biochemistry Institute of the Lausanne University, Epalinges, Switzerland, for its hospitality. CA, AGA, SC, NM, JS, OJ, and JvM dedicate this work to the memory of their late, much respected and regretted colleague PR.

Conflict of interest

The authors declare that the research was conducted in the absence of any commercial or financial relationships that could be construed as a potential conflict of interest.

Publisher's note

Supplementary material

The Supplementary Material for this article can be found online at: https://www.frontiersin.org/articles/10.3389/fimmu.2022.965303/full#supplementary-material

References

1. Sakaguchi S. Regulatory T cells: Key controllers of immunologic self-tolerance. *Cell* (2000) 101(5):455–8. doi: 10.1016/S0092-8674(00)80856-9

2. Brunkow ME, Jeffery EW, Hjerrild KA, Paeper B, Clark LB, Yasayko SA, et al. Disruption of a new Forkhead/Winged-helix protein, scurfin, results in the fatal lymphoproliferative disorder of the scurfy mouse. *Nat Genet* (2001) 27(1):68–73. doi: 10.1038/83784

3. Wildin RS, Ramsdell F, Peake J, Faravelli F, Casanova JL, Buist N, et al. X-Linked neonatal diabetes mellitus, enteropathy and endocrinopathy syndrome is the human equivalent of mouse scurfy. *Nat Genet* (2001) 27(1):18–20. doi: 10.1038/83707

4. Sakaguchi S, Ono M, Setoguchi R, Yagi H, Hori S, Fehervari Z, et al. Foxp3+ CD25+ CD4+ natural regulatory T cells in dominant self-tolerance and autoimmune disease. *Immunol Rev* (2006) 212:8–27. doi: 10.1111/j.0105-2896.2006.00427.x

5. Jordan MS, Boesteanu A, Reed AJ, Petrone AL, Holenbeck AE, Lerman MA, et al. Thymic selection of CD4+CD25+ regulatory T cells induced by an agonist self-peptide. *Nat Immunol* (2001) 2(4):301–6. doi: 10.1038/86302

6. Picca CC, Larkin J3rd, Boesteanu A, Lerman MA, Rankin AL, Caton AJ. Role of TCR specificity in CD4+ CD25+ regulatory T-cell selection. *Immunol Rev* (2006) 212:74–85. doi: 10.1111/j.0105-2896.2006.00416.x

7. Kieback E, Hilgenberg E, Stervbo U, Lampropoulou V, Shen P, Bunse M, et al. Thymus-derived regulatory T cells are positively selected on natural self-antigen through cognate interactions of high functional avidity. *Immunity* (2016) 44 (5):1114–26. doi: 10.1016/j.immuni.2016.04.018

8. Romagnoli P, Hudrisier D, van Meerwijk JPM. Preferential recognition of self-antigens despite normal thymic deletion of CD4+CD25+ regulatory T cells. *J Immunol* (2002) 168:1644–8. doi: 10.4049/jimmunol.168.4.1644

9. Hsieh CS, Liang Y, Tyznik AJ, Self SG, Liggitt D, Rudensky AY. Recognition of the peripheral self by naturally arising CD25+ CD4+ T cell receptors. *Immunity* (2004) 21(2):267–77. doi: 10.1016/j.immuni.2004.07.009

10. Tang Q, Henriksen KJ, Boden EK, Tooley AJ, Ye J, Subudhi SK, et al. Cutting edge: CD28 controls peripheral homeostasis of CD4+CD25+ regulatory T cells. *J Immunol* (2003) 171(7):3348–52. doi: 10.4049/jimmunol.171.7.3348

11. Salomon B, Lenschow DJ, Rhee L, Ashourian N, Singh B, Sharpe A, et al. B7/CD28 costimulation is essential for the homeostasis of the CD4+CD25+ immunoregulatory T cells that control autoimmune diabetes. *Immunity* (2000) 12(4):431–40. doi: 10.1016/S1074-7613(00)80195-8

12. Marski M, Kandula S, Turner JR, Abraham C. CD18 is required for optimal development and function of CD4+CD25+ T regulatory cells. *J Immunol* (2005) 175(12):7889–97. doi: 10.4049/jimmunol.175.12.7889

13. Coquet JM, Ribot JC, Babala N, Middendorp S, van der Horst G, Xiao Y, et al. Epithelial and dendritic cells in the thymic medulla promote CD4+Foxp3+ regulatory T cell development *via* the CD27-Cd70 pathway. *J Exp Med* (2013) 210 (4):715–28. doi: 10.1084/jem.20112061

14. Apert C, Romagnoli P, van Meerwijk JPM. IL-2 and IL-15 dependent thymic development of Foxp3-expressing regulatory T lymphocytes. *Protein Cell* (2018) 9(4):322–32. doi: 10.1007/s13238-017-0425-3

15. Bayer AL, Yu A, Adeegbe D, Malek TR. Essential role for interleukin-2 for CD4(+)CD25(+) T regulatory cell development during the neonatal period. *J Exp Med* (2005) 201(5):769–77. doi: 10.1084/jem.20041179

16. Burchill MA, Yang J, Vogtenhuber C, Blazar BR, Farrar MA. IL-2 receptor beta-dependent STAT5 activation is required for the development of Foxp3+ regulatory T cells. *J Immunol* (2007) 178(1):280–90. doi: 10.4049/jimmunol.178.1.280

17. Malek TR. The biology of interleukin-2. *Annu Rev Immunol* (2008) 26:453–79. doi: 10.1146/annurev.immunol.26.021607.090357

18. Vang KB, Yang J, Mahmud SA, Burchill MA, Vegoe AL, Farrar MA. IL-2, -7, and -15, but not thymic stromal lymphopoeitin, redundantly govern CD4+Foxp3+ regulatory T cell development. *J Immunol* (2008) 181(5):3285–90. doi: 10.4049/jimmunol.181.5.3285

19. Marshall D, Sinclair C, Tung S, Seddon B. Differential requirement for IL-2 and IL-15 during bifurcated development of thymic regulatory T cells. *J Immunol* (2014) 193(11):5525–33. doi: 10.4049/jimmunol.1402144

20. Toomer KH, Lui JB, Altman NH, Ban Y, Chen X, Malek TR. Essential and non-overlapping IL-2Ralpha-Dependent processes for thymic development and peripheral homeostasis of regulatory T cells. *Nat Commun* (2019) 10(1):1037. doi: 10.1038/s41467-019-08960-1

21. Lio CW, Hsieh CS. A two-step process for thymic regulatory T cell development. *Immunity* (2008) 28(1):100–11. doi: 10.1016/j.immuni.2007.11.021

22. Tai X, Erman B, Alag A, Mu J, Kimura M, Katz G, et al. Foxp3 transcription factor is proapoptotic and lethal to developing regulatory T cells unless counterbalanced by cytokine survival signals. *Immunity* (2013) 38(6):1116–28. doi: 10.1016/j.immuni.2013.02.022

23. Fontenot JD, Rasmussen JP, Gavin MA, Rudensky AY. A function for interleukin 2 in Foxp3-expressing regulatory T cells. *Nat Immunol* (2005) 6 (11):1142–51. doi: 10.1038/ni1263

24. Dikiy S, Li J, Bai L, Jiang M, Janke L, Zong X, et al. A distal Foxp3 enhancer enables interleukin-2 dependent thymic treg cell lineage commitment for robust immune tolerance. *Immunity* (2021) 54(5):931–46.e11. doi: 10.1016/j.immuni.2021.03.020

25. Nazzal D, Gradolatto A, Truffault F, Bismuth J, Berrih-Aknin S. Human thymus medullary epithelial cells promote regulatory T-cell generation by stimulating interleukin-2 production *via* ICOS ligand. *Cell Death Dis* (2014) 5: e1420. doi: 10.1038/cddis.2014.377

26. Caramalho I, Nunes-Silva V, Pires AR, Mota C, Pinto AI, Nunes-Cabaco H, et al. Human regulatory T-cell development is dictated by interleukin-2 and -15 expressed in a non-overlapping pattern in the thymus. *J Autoimmun* (2015) 56:98–110. doi: 10.1016/j.jaut.2014.11.002

27. D'Cruz LM, Klein L. Development and function of agonist-induced CD25 +Foxp3+ regulatory T cells in the absence of interleukin 2 signaling. *Nat Immunol* (2005) 6(11):1152–9. doi: 10.1038/ni1264

28. Thiault N, Darrigues J, Adoue V, Gros M, Binet B, Perals C, et al. Peripheral regulatory T lymphocytes recirculating to the thymus suppress the development of their precursors. *Nat Immunol* (2015) 16:628–34. doi: 10.1038/ni.3150

29. Setoguchi R, Hori S, Takahashi T, Sakaguchi S. Homeostatic maintenance of natural Foxp3(+) CD25(+) CD4(+) regulatory T cells by interleukin (Il)-2 and induction of autoimmune disease by IL-2 neutralization. *J Exp Med* (2005) 201 (5):723–35. doi: 10.1084/jem.20041982

30. Hemmers S, Schizas M, Azizi E, Dikiy S, Zhong Y, Feng Y, et al. IL-2 production by self-reactive CD4 thymocytes scales regulatory T cell generation in the thymus. *J Exp Med* (2019) 216(11):2466–78. doi: 10.1084/jem.20190993

31. Weist BM, Kurd N, Boussier J, Chan SW, Robey EA. Thymic regulatory T cell niche size is dictated by limiting IL-2 from antigen-bearing dendritic cells and feedback competition. *Nat Immunol* (2015) 16(6):635–41. doi: 10.1038/ni.3171

32. Hou MS, Huang ST, Tsai MH, Yen CC, Lai YG, Liou YH, et al. The interleukin-15 system suppresses T cell-mediated autoimmunity by regulating negative selection and nT(H)17 cell homeostasis in the thymus. *J Autoimmun* (2015) 56:118–29. doi: 10.1016/j.jaut.2014.11.003

33. Perry JS, Lio CW, Kau AL, Nutsch K, Yang Z, Gordon JI, et al. Distinct contributions of aire and antigen-Presenting-Cell subsets to the generation of self-tolerance in the thymus. *Immunity* (2014) 41(3):414–26. doi: 10.1016/j.immuni.2014.08.007

34. Cui G, Hara T, Simmons S, Wagatsuma K, Abe A, Miyachi H, et al. Characterization of the IL-15 niche in primary and secondary lymphoid organs *in vivo*. *Proc Natl Acad Sci USA* (2014) 111(5):1915–20. doi: 10.1073/pnas.1318281111

35. Wuest SC, Edwan JH, Martin JF, Han S, Perry JS, Cartagena CM, et al. A role for interleukin-2 trans-presentation in dendritic cell-mediated T cell activation in humans, as revealed by daclizumab therapy. *Nat Med* (2011) 17(5):604–9. doi: 10.1038/nm.2365

36. Irla M. Instructive cues of thymic T cell selection. *Annu Rev Immunol* (2022) 40:95–119. doi: 10.1146/annurev-immunol-101320-022432

37. Sadlack B, Lohler J, Schorle H, Klebb G, Haber H, Sickel E, et al. Generalized autoimmune disease in interleukin-2-Deficient mice is triggered by an uncontrolled activation and proliferation of CD4+ T cells. *Eur J Immunol* (1995) 25:3053–9. doi: 10.1002/eji.1830251111

38. Suzuki H, Kundig TM, Furlonger C, Wakeham A, Timms E, Matsuyama T, et al. Deregulated T cell activation and autoimmunity in mice lacking interleukin-2 receptor beta. *Science* (1995) 268(5216):1472–6. doi: 10.1126/science.7770771

39. Willerford DM, Chen J, Ferry JA, Davidson L, Ma A, Alt FW. Interleukin-2 receptor alpha chain regulates the size and content of the peripheral lymphoid compartment. *Immunity* (1995) 3(4):521–30. doi: 10.1016/1074-7613(95)90180-9

40. Cheng G, Yu A, Malek TR. T-Cell tolerance and the multi-functional role of IL-2R signaling in T-regulatory cells. *Immunol Rev* (2011) 241(1):63–76. doi: 10.1111/j.1600-065X.2011.01004.x

41. Yu W, Nagaoka H, Jankovic M, Misulovin Z, Suh H, Rolink A, et al. Continued RAG expression in late stages of b cell development and no apparent re-induction after immunization. *Nature* (1999) 400(6745):682–7. doi: 10.1038/23287

42. Boursalian TE, Golob J, Soper DM, Cooper CJ, Fink PJ. Continued maturation of thymic emigrants in the periphery. *Nat Immunol* (2004) 5(4):418–25. doi: 10.1038/ni1049

43. Liston A, Nutsch KM, Farr AG, Lund JM, Rasmussen JP, Koni PA, et al. Differentiation of regulatory Foxp3+ T cells in the thymic cortex. *Proc Natl Acad Sci USA* (2008) 105(33):11903–8. doi: 10.1073/pnas.0801506105

44. Kennedy MK, Glaccum M, Brown SN, Butz EA, Viney JL, Embers M, et al. Reversible defects in natural killer and memory CD8 T cell lineages in interleukin 15-deficient mice. *J Exp Med* (2000) 191(5):771–80. doi: 10.1084/jem.191.5.771

45. Lee PP, Fitzpatrick DR, Beard C, Jessup HK, Lehar S, Makar KW, et al. A critical role for Dnmt1 and DNA methylation in T cell development, function, and survival. *Immunity* (2001) 15(5):763–74. doi: 10.1016/S1074-7613(01)00227-8

46. Caton ML, Smith-Raska MR, Reizis B. Notch-RBP-J signaling controls the homeostasis of CD8- dendritic cells in the spleen. *J Exp Med* (2007) 204(7):1653–64. doi: 10.1084/jem.20062648

47. Ohigashi I, Zuklys S, Sakata M, Mayer CE, Zhanybekova S, Murata S, et al. Aire-expressing thymic medullary epithelial cells originate from Beta5t-expressing progenitor cells. *Proc Natl Acad Sci USA* (2013) 110(24):9885–90. doi: 10.1073/pnas.1301799110

48. Skarnes WC, Rosen B, West AP, Koutsourakis M, Bushell W, Iyer V, et al. A conditional knockout resource for the genome-wide study of mouse gene function. *Nature* (2011) 474(7351):337–42. doi: 10.1038/nature10163

49. Soriano P. The PDGF alpha receptor is required for neural crest cell development and for normal patterning of the somites. *Development* (1997) 124 (14):2691–700. doi: 10.1242/dev.124.14.2691

50. Pettitt SJ, Liang Q, Rairdan XY, Moran JL, Prosser HM, Beier DR, et al. Agouti C57BL/6N embryonic stem cells for mouse genetic resources. *Nat Methods* (2009) 6(7):493–5. doi: 10.1038/nmeth.1342

51. Rodriguez CI, Buchholz F, Galloway J, Sequerra R, Kasper J, Ayala R, et al. High-efficiency deleter mice show that FLPe is an alternative to cre-loxP. *Nat Genet* (2000) 25(2):139–40. doi: 10.1038/75973

52. Feng Y, van der Veeken J, Shugay M, Putintseva EV, Osmanbeyoglu HU, Dikiy S, et al. A mechanism for expansion of regulatory T-cell repertoire and its role in self-tolerance. *Nature* (2015) 528(7580):132–6. doi: 10.1038/nature16141

53. Vander Heiden JA, Yaari G, Uduman M, Stern JN, O'Connor KC, Hafler DA, et al. pRESTO: A toolkit for processing high-throughput sequencing raw reads of lymphocyte receptor repertoires. *Bioinformatics* (2014) 30(13):1930–2. doi: 10.1093/bioinformatics/btu138

54. Bolotin DA, Shugay M, Mamedov IZ, Putintseva EV, Turchaninova MA, Zvyagin IV, et al. MiTCR: Software for T-cell receptor sequencing data analysis. *Nat Methods* (2013) 10(9):813–4. doi: 10.1038/nmeth.2555

55. Shugay M, Bagaev DV, Turchaninova MA, Bolotin DA, Britanova OV, Putintseva EV, et al. VDJtools: Unifying post-analysis of T cell receptor repertoires. *PLoS Comput Biol* (2015) 11(11):e1004503. doi: 10.1371/journal.pcbi.1004503

56. Gombash Lampe SE, Kaspar BK, Foust KD. Intravenous injections in neonatal mice. *J Vis Exp* (2014) 93):e52037. doi: 10.3791/52037

57. Darrigues J, Santamaria JC, Galindo-Albarran A, Robey EA, Joffre OP, van Meerwijk JPM, et al. Robust intrathymic development of regulatory T cells in young NOD mice is rapidly restrained by recirculating cells. *Eur J Immunol* (2021) 51(3):580–93. doi: 10.1002/eji.202048743

58. Peligero-Cruz C, Givony T, Sebe-Pedros A, Dobes J, Kadouri N, Nevo S, et al. IL18 signaling promotes homing of mature tregs into the thymus. *Elife* (2020) 9. doi: 10.7554/eLife.58213

59. Cowan JE, McCarthy NI, Anderson G. CCR7 controls thymus recirculation, but not production and emigration, of Foxp3(+) T cells. *Cell Rep* (2016) 14 (5):1041–8. doi: 10.1016/j.celrep.2016.01.003

60. Yang E, Zou T, Leichner TM, Zhang SL, Kambayashi T. Both retention and recirculation contribute to long-lived regulatory T-cell accumulation in the thymus. *Eur J Immunol* (2014) 44(9):2712–20. doi: 10.1002/eji.201444529

61. Yang S, Fujikado N, Kolodin D, Benoist C, Mathis D. Regulatory T cells generated early in life play a distinct role in maintaining self-tolerance. *Science* (2015) 348(6234):589–94. doi: 10.1126/science.aaa7017

62. Kishimoto H, Sprent J. Negative selection in the thymus includes semimature T cells. *J Exp Med* (1997) 185(2):263–71. doi: 10.1084/jem.185.2.263

63. Zachariah MA, Cyster JG. Neural crest-derived pericytes promote egress of mature thymocytes at the corticomedullary junction. *Science* (2010) 328 (5982):1129–35. doi: 10.1126/science.1188222

64. Asano M, Toda M, Sakaguchi N, Sakaguchi S. Autoimmune disease as a consequence of developmental abnormality of a T cell subpopulation. *J Exp Med* (1996) 184(2):387–96. doi: 10.1084/jem.184.2.387

65. Komatsu N, Mariotti-Ferrandiz ME, Wang Y, Malissen B, Waldmann H, Hori S. Heterogeneity of natural Foxp3+ T cells: A committed regulatory T-cell lineage and an uncommitted minor population retaining plasticity. *Proc Natl Acad Sci USA* (2009) 106(6):1903–8. doi: 10.1073/pnas.0811556106

66. Wyss L, Stadinski BD, King CG, Schallenberg S, McCarthy NI, Lee JY, et al. Affinity for self antigen selects treg cells with distinct functional properties. *Nat Immunol* (2016) 17(9):1093–101. doi: 10.1038/ni.3522

67. Fazilleau N, Delarasse C, Sweenie CH, Anderton SM, Fillatreau S, Lemonnier FA, et al. Persistence of autoreactive myelin oligodendrocyte glycoprotein (MOG)-specific T cell repertoires in MOG-expressing mice. *Eur J Immunol* (2006) 36(3):533–43. doi: 10.1002/eji.200535021

68. Owen DL, Mahmud SA, Vang KB, Kelly RM, Blazar BR, Smith KA, et al. Identification of cellular sources of IL-2 needed for regulatory T cell development and homeostasis. *J Immunol* (2018) 200(12):3926–33. doi: 10.4049/jimmunol.1800097

69. Matsuda JL, Gapin L, Sidobre S, Kieper WC, Tan JT, Ceredig R, et al. Homeostasis of V alpha 14 iNKT cells. *Nat Immunol* (2002) 3(10):966–74. doi: 10.1038/ni837

70. Malek TR, Yu A, Vincek V, Scibelli P, Kong L. CD4 regulatory T cells prevent lethal autoimmunity in IL-2Rbeta-Deficient mice. Implications for the nonredundant function of IL-2. *Immunity* (2002) 17(2):167–78. doi: 10.1016/s1074-7613(02)00367-9

71. Cheng G, Yu A, Dee MJ, Malek TR. IL-2R signaling is essential for functional maturation of regulatory T cells during thymic development. *J Immunol* (2013) 190(4):1567–75. doi: 10.4049/jimmunol.1201218

72. Soper DM, Kasprowicz DJ, Ziegler SF. IL-2Rbeta links IL-2R signaling with Foxp3 expression. *Eur J Immunol* (2007) 37(7):1817–26. doi: 10.1002/eji.200737101

73. Owen DL, Mahmud SA, Sjaastad LE, Williams JB, Spanier JA, Simeonov DR, et al. Thymic regulatory T cells arise *via* two distinct developmental programs. *Nat Immunol* (2019) 20(2):195–205. doi: 10.1038/s41590-018-0289-6

74. Steel JC, Waldmann TA, Morris JC. Interleukin-15 biology and its therapeutic implications in cancer. *Trends Pharmacol Sci* (2012) 33(1):35–41. doi: 10.1016/j.tips.2011.09.004

75. Edelmann SL, Marconi P, Brocker T. Peripheral T cells re-enter the thymus and interfere with central tolerance induction. *J Immunol* (2011) 186(10):5612–9. doi: 10.4049/jimmunol.1004010

76. Matsutani T, Ogata M, Fujii Y, Kitaura K, Nishimoto N, Suzuki R, et al. Shortening of complementarity determining region 3 of the T cell receptor alpha chain during thymocyte development. *Mol Immunol* (2011) 48(4):623–9. doi: 10.1016/j.molimm.2010.11.003

frontiers | Frontiers in Immunology

TYPE Review
PUBLISHED 11 May 2023
DOI 10.3389/fimmu.2023.1176619

OPEN ACCESS

EDITED BY
Diana Boraschi,
Chinese Academy of Science (CAS), China

REVIEWED BY
Raffaella Bonecchi,
Humanitas University, Italy
Sofie Struyf,
KU Leuven, Belgium

*CORRESPONDENCE
Valentina Cecchinato
valentina.cecchinato@irb.usi.ch
Veronica Martini
veronica.martini@irb.usi.ch

RECEIVED 28 February 2023
ACCEPTED 19 April 2023
PUBLISHED 11 May 2023

CITATION
Cecchinato V, Martini V, Pirani E, Ghovehoud E and Uguccioni M (2023) The chemokine landscape: one system multiple shades.
Front. Immunol. 14:1176619.
doi: 10.3389/fimmu.2023.1176619

The chemokine landscape: one system multiple shades

Valentina Cecchinato*, Veronica Martini*, Edisa Pirani, Elaheh Ghovehoud and Mariagrazia Uguccioni

Institute for Research in Biomedicine, Università della Svizzera italiana, Bellinzona, Switzerland

Leukocyte trafficking is mainly governed by chemokines, chemotactic cytokines, which can be concomitantly produced in tissues during homeostatic conditions or inflammation. After the discovery and characterization of the individual chemokines, we and others have shown that they present additional properties. The first discoveries demonstrated that some chemokines act as natural antagonists on chemokine receptors, and prevent infiltration of leukocyte subsets in tissues. Later on it was shown that they can exert a repulsive effect on selective cell types, or synergize with other chemokines and inflammatory mediators to enhance chemokine receptors activities. The relevance of the fine-tuning modulation has been demonstrated *in vivo* in a multitude of processes, spanning from chronic inflammation to tissue regeneration, while its role in the tumor microenvironment needs further investigation. Moreover, naturally occurring autoantibodies targeting chemokines were found in tumors and autoimmune diseases. More recently in SARS-CoV-2 infection, the presence of several autoantibodies neutralizing chemokine activities distinguished disease severity, and they were shown to be beneficial, protecting from long-term sequelae. Here, we review the additional properties of chemokines that influence cell recruitment and activities. We believe these features need to be taken into account when designing novel therapeutic strategies targeting immunological disorders.

KEYWORDS

Chemokines, Antagonism, Repulsion, Synergism, CXCL12/HMGB1 heterocomplex, Autoantibodies

Introduction

Chemokines, chemotactic cytokines, engage in a promiscuous fashion a panel of over 20 chemokine receptors, key regulators of leukocyte migrations and functions. The chemokine system includes approximately 50 ligands, which play a fundamental role both in physiological and pathological immune responses (1).

10.3389/fimmu.2023.1176619

The three-dimensional structures of all chemokines, as determined by nuclear magnetic resonance (NMR) spectroscopy or by X-ray crystallography, reveal remarkably similar protein backbones, tied together by two disulfide bonds formed among the four cysteines conserved in almost all chemokines. In all known structures, the N-terminal domain is unordered and contains two of the four cysteines. The loop region after the second cysteine, often referred to as "the N-loop", is followed by three antiparallel β–strands and a C-terminal α–helix, all of which are connected by short, random-coiled loops. The proximity of the cysteines in the N-loop has been used to classify chemokines in subfamilies: CC, where the cysteines are adjacent, CXC, in which one amino acid is interposed between the cysteines and CX_3C, where three amino acids are present in between, while XC chemokines lack the first and the third conserved cysteine (2–4).

To mediate their activity, chemokines bind to cell surface receptors, which belong to the largest branch of the γ subfamily of rhodopsin-like G protein-coupled receptors (GPCRs). Today, 19 signaling receptors have been identified: 6 CXCRs, (CXCR1-6), 10 CCRs (CCR1-10), CX3CR1 and XCR1 (5). In addition, there are four "atypical" receptors (ACKR1-4) that use β-arrestins to elicit their functions. Atypical chemokine receptors impacts chemokine availability by scavenging and degrading the chemokine in the lysosomes, or by transporting the chemokines across different barriers *via* transcytosis (6).

Initial studies on structure-function relationships of chemokines were performed with CXCL8, using N-terminal truncations and amino acid substitutions. NMR–studies of CXCL8 in complex with peptides derived from the N-terminus of CXCR1, together with single-site mutagenesis, led to the identification of the major receptor-binding region: a positively charged groove between the N-loop and the third β–strand, into which the N–terminus of the receptor binds (7). Further studies of other chemokine receptor-peptide complexes corroborated this model (2).

Despite the apparent redundancy within the chemokine system, characterized by multiple chemokines binding to a single receptor and one receptor being activated by multiple chemokines, the system has been demonstrated to exhibit a high degree of specificity and complexity. Chemokine receptors are selectively expressed on specific subsets of cells, which contributes to their functional characteristics and homing abilities. Their ligands, on the other hand, can be expressed either individually or in combination within a particular tissue, both under normal and pathological conditions (8).

Studies investigating expression of chemokines in human samples from different diseases have revealed that many chemokines can be produced during the disease process (9). *In vivo* models and *in vitro* studies have highlighted the importance of chemokine binding to extracellular matrix components, and their activities as complexes (10). However, in pathological conditions, chemokine production does not always entirely account for the disease characteristics. This discrepancy might be partially explained by the additional chemokine activities and their natural regulation that we, and others, have described in the last three decades (Table 1). This review aims to summarize these findings and their relevance to disease progress and treatment.

TABLE 1 Modulators of chemokine activities.

Activity	Receptor	Modulator	Reference
Antagonism	CCR1	CCL4 CCL26	(11) (12)
	CCR2	CCL2 (9–76) CCL11	(13) (14)
	CCR3	CCL18 CXCL9 CXCL10 CXCL11	(15–17)
	CCR5	CCL7 CCL26 CXCL11	(18) (12) (19)
Repulsion	CCR2	CCL26	(20, 21)
	CXCR4	CXCL12	(22–24)
Synergism	CCR2	CCL19 CCL21	(25)
	CCR4	CXCL10	(26)
	CCR5	CXCL4	(27)
	CCR7	CXCL13	(28)
	CXCR3	CXCL12	(29, 30)
	CXCR4	CXCL9 HNP1 Galectins HMGB1	(31) (32) (33) (34, 35)

Natural chemokine antagonists

The concomitant expression of several chemokines in inflamed tissues led us to explore the possibility that leukocyte infiltration may occur stepwise in response to gradients of different chemokines, and that chemokines can modulate, as natural antagonists, the activity of receptors that are different from their "traditional" target ones.

Chemokine receptor antagonism by unmodified naturally occurring ligands, therefore, constitutes a potentially important regulatory principle of chemokine-driven reactions.

Several reports have described that natural chemokine antagonists block the migration of inflammatory cells or provide an additional mechanism for selecting the leukocyte sub-type to be recruited at site of inflammation (Figure 1A).

A thorough pharmacological characterization of CCR5 revealed CCL7, a promiscuous agonist for CCR1, CCR2, and CCR3, as a highly potent, complete antagonist (18). An extensive study by Loetscher et al. showed CXCL11, an agonist of CXCR3, to be a highly selective and potent antagonist for CCR3, while CXCL9 and CXCL10, the other two agonists of CXCR3, were less efficient inhibitors (15). CCL18 and CXCL11 have independently been

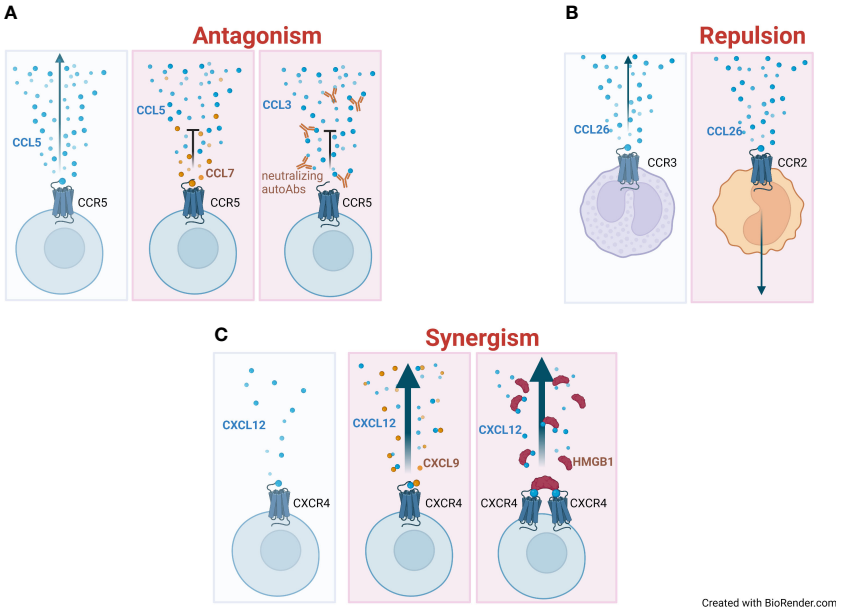

FIGURE 1
Mechanisms of regulation of chemokine activities. **(A)** Directional migration (indicated with an arrow) of a chemokine (blue circles) on its respective receptor, and the gradient formation (left panel). Antagonistic effect and impairment of migration elicited by the co-presence of high levels of a non-agonist chemokine (CCL7, orange circles) (middle panel) or by neutralizing autoantibodies (autoAbs) targeting the chemokine (right panel). **(B)** Repulsive effect of CCL26 on monocytes that move away from the chemokine gradient (right panel) compared to eosinophils, which are attracted by it (left panel). **(C)** Absence of migration at low concentrations of the agonist (blue circles) (left panel). Enhanced migration (represented as a thick arrow) in the presence of an heterocomplex formed at low concentration of the agonist (CXCL12) and concomitant high concentration of a non-agonist chemokine (CXCL9, orange circles) (middle panel) or the alarmin High Mobility Group Box 1 (HMGB1) (red half-circles) (right panel).

confirmed as CCR3 antagonists (16, 17). We have reported on the antagonistic effects of CCL11 on CCR2 (14), while another report characterized CCL11 as a partial antagonist of CCR2 (36). Similarly, CCL4 has been described as an antagonist (11) or partial agonist (37) for CCR1, possibly depending on the cellular background. Furthermore, we have characterized CCL26 as a natural antagonist for CCR1 and CCR5 (12), and CXCL11 for CCR5 (19).

In addition, naturally occurring post-translational modifications of chemokines, such as proteolytic processing of the N-terminus domain (38), as well as synthetic N–terminal truncated forms (13) have been shown to have antagonist activity. As an example, a truncated variant of CCL2 (MCP- 1 (9–76)) prevents the onset of arthritis, and reduces symptoms and cellular infiltrates in the MRL-*lpr* mouse model. Despite this important finding, clinical trials aimed at blocking CCL2/CCR2 interaction in Rheumatoid Arthritis (RA) failed to reach phase III (5), most likely due to the complexity of the disease in humans (*e.g.*: synovial infiltrate with predominant follicle like structure, monocyte/macrophages, or fibroblasts) and the different chemokines produced.

The unmodified natural antagonists act similarly to the truncated variants, which lack the N-terminal motif, and bind to the receptors *via* the structurally conserved N–loop and third β–strand, but then present the receptor with an N-terminal motif that is incapable of activating it. This notion is supported by experiments showing that a CCL11 variant, featuring the N–terminal motif of CXCL11 instead of its native one, acted as a highly potent CCR3 antagonist (39).

Repulsive chemokines

A second feature of chemokines is their potential to exert a repulsive effect on selected cell types (Figure 1B). This feature was first described in 2000 by Poznansky and colleagues: high concentrations of CXCL12 exert a repulsive rather than an attractive effect on mature T cells (22).

While low concentrations of the chemokine attract a variety of leukocyte subpopulations, high concentrations of CXCL12 induce a repulsive effect on both naïve and memory $CD4^+$ and $CD8^+$ T cells, which move away from the source of the stimulus. The repulsive effect of CXCL12 on T cells is mediated by distinct signaling pathways as compared to those involved in chemotaxis: while the first is inhibited by cAMP agonists, the second requires tyrosine kinase activity, and they both depend on CXCR4, Gαi protein and phosphatidylinositol 3-kinase activities. Differences in i) receptor dimerization and internalization, ii) signal transduction pathways elicited by surface or endocytosed receptor/ligand complexes, and iii) ratio between GAG-bound and free CXCL12, have been theorized as mechanisms involved in the different activity exerted by low or high chemokine concentrations, but no definitive experimental evidence has been provided to support these possibilities (40). It has been speculated that the repulsive effect exerted by CXCL12 on T cells prevents their infiltration in organs that produce abundant amounts of the chemokine, such as the bone marrow or the thymus, or can act as a limiting mechanism to avoid excessive accumulation of lymphocytes at site of inflammation to avoid self-perpetuating immune responses.

The relevance of the repulsive effect of CXCL12 on T cells in physiology has been later proven in the setting of mature thymocytes emigration from the thymus (23). Mature single positive $CD4^+$ and $CD8^+$ thymocytes, but not immature triple negative or double positive thymocytes, migrate away from thymic fragments through a *Bordetella Pertussis* toxin sensitive process, indicating that Gαi protein-coupled receptors are responsible for the active movement of cells away from the tissue. Lack of a negative CXCL12 gradient and/or inhibition of CXCR4 prevent thymocytes emigration from thymic fragments, thus demonstrating that the repulsive effect is dependent on the presence of CXCR4 on mature thymocytes and on the high concentrations of CXCL12 produced by the thymic stroma.

Elevated levels of CXCL12 are also found in dysplastic tissues, such as primary brain tumors, melanomas, and ovarian carcinomas. Despite high concentrations of the chemokine, these tumors are rarely infiltrated by T cells. In 2006, Vianello and colleagues provided evidence that melanomas expressing elevated levels of CXCL12 can repel T cells, thereby abrogating Antigen (Ag)-specific T cell infiltration into the tumor and allowing it to escape immune control (24). Melanomas engineered to express low or high concentrations of CXCL12 display distinct levels of tumor infiltrating lymphocytes. Ag-specific T cells infiltrate tumors expressing low levels of CXCL12, but not those expressing elevated levels of the chemokine. The infiltration of Ag-specific T cells into these tumors is therefore affected by the concentration of CXCL12, with low concentrations leading to chemotactic effects and high concentrations to repulsion. These activities are mediated by CXCR4, as Ag-specific T cell pre-treatment with the antagonist AMD3100 results in decreased infiltration of low CXCL12 expressing tumors, but abrogates the repulsive effect, and restores infiltration in tumors expressing high levels of CXCL12, possibly *via* different chemokine receptors.

The ability to induce migration away from the stimulus is not an exclusive feature of CXCL12. Indeed, we showed that CCL26 actively repulses monocytes (20), a finding that was later confirmed in an independent study (21). While both the chemotactic and repulsive effects exerted by different CXCL12 concentrations are mediated by CXCR4, the repulsive effect of CCL26 does not require the expression of its cognate receptor CCR3. This repulsive effect on monocytes depends on CCR2 availability, and requires Gαi protein and tyrosine kinase activities. Moreover, monocyte migration along a CCL2 gradient is significantly increased in the presence of an opposite CCL26 gradient, indicating that the concomitant presence of two opposite gradients in the microenvironment could enhance monocyte responses to CCL2. This effect could be relevant *in vivo* to direct monocytes from the blood stream to the site of inflammation, with CCL26 being expressed by vascular endothelial cells, during allergic reactions (41), and CCL2 by the inflamed tissue.

Synergy-inducing chemokines

A third level of modulation in chemokine activity is their ability to interact with other chemokines or molecules in the microenvironment, leading to synergistic effects on leukocyte functions in response to chemoattractants (Figure 1C). This can occur through direct interactions between molecules or through engagement of different receptors on the same cell. The first description of this mechanism dates to 2002 when the bovine chemokine regakine−1 was discovered to induce an enhanced neutrophil migration when combined with CXCL7, CXCL8 and C5a (42). The receptor or the mechanism of regakine-1 induced synergism were not identified. Competition with labelled C5a for binding to neutrophils or receptor transfected cell lines demonstrated that regakine−1 does not alter receptor recognition. The protein kinase inhibitors 2'−amino−3'−methoxyflavone (PD98059), wortmannin and staurosporin had no effect on the synergy between C5a and regakine−1. This first observation was followed by the description that migration of natural type I IFN−producing cells, a subpopulation of murine and human lymphocytes, to the CXCR3 agonists requires stimulation of CXCR4 by CXCL12 (29). The mechanism by which CXCL12 induces enhanced migration in response to CXCR3 agonists remains unknown. CXCL12 does not upregulate the expression of CXCR3 and does not increase the affinity of CXCR3 for its agonists. Apart from chemotaxis, the authors did not investigate other cell functions, and did not assess the signaling pathways involved. Similarly, the same enhanced migration in response to CXCR3 agonists, induced by stimulation with CXCL12, was observed by Vanbervliet et al. on human plasmacytoid dendritic cells (30). These reports undoubtedly indicated, as for natural antagonist chemokines, the necessity to further investigate the mechanisms governing concomitant expression of chemokines and cell functions, fostering research in this area.

Assessing the activity of chemokine heterocomplexes, von Hundelshausen et al. demonstrated that the complex between two chemokines, CCL5 and CXCL4, triggers the arrest of monocytes on activated endothelium (27), while concomitantly we demonstrated that the heterocomplex between CXCL13 and CCL21 or CCL19 modulates CCR7-expressing cell activities (28). Likewise, $CCR4^+$ lymphocytes migrate toward low concentrations of CCL22 in the presence of CXCL10 (26), monocytes migrate toward low concentrations of CCL7 in the presence of CCL19 or CCL21 (25), and lymphoma cells respond to the heterocomplex formed by CXCL12 and CXCL9 *via* CXCR4 (31).

Von Hundelshausen et al. extensively studied how human chemokines interact with each other and demonstrated their relevance in enhancing receptor triggering or inhibiting receptor activities (43). Several studied performed *in vivo* highlighted the importance of disrupting the heterocomplex formation to ameliorate inflammation (44–46).

Recently, a non-dissociating CXCL4–CXCL12 heterodimer was used as a new tool to further study chemokine-chemokine and chemokine heterodimer-receptor interactions in breast cancer cells (47).

Chemokine heterocomplexes might provide an amplification system, when the concentration of the agonist is too low to trigger a proper receptor response (48). On the other hand, when synergy-inducing molecules are present in an environment rich of the agonist, they could possibly dampen cellular responses, as indicated by *in vitro* migration (26, 28, 34).

Chemokine activity can also be modulated by their interaction with other molecules such as the alarmin High Mobility Group Box 1 (HMGB1) (34), as described in the next section, the α-defensin HNP1 (32), or galectins (33), further supporting the relevance of the tissue microenvironment in modulating cellular recruitment and responses in inflammation.

CXCL12/HMGB1 heterocomplex

Damage-associated molecular patterns, also known as alarmins, are danger signals released upon tissue damage to activate the inflammatory response. The alarmin HMGB1 has been shown to form a heterocomplex with CXCL12, favoring cell migration *via* CXCR4 both *in vitro* and *in vivo*. This synergistic activity, demonstrated *in vitro* using mouse fibroblasts and monocytes, was further assessed in an *in vivo* model of sterile inflammation. Moreover, this effect is blocked by glycyrrhizin, which prevents the formation of the heterocomplex, by anti-CXCL12 antibodies, or by AMD3100, inhibiting CXCR4 activation (34).

HMGB1 is characterized by two DNA binding domains, Box A and Box B, connected by a flexible linker region, and a long acidic C-terminal tail. In the tissue microenvironment, HMGB1 can be present in two different redox isoforms: reduced-HMGB1 in which the two conserved cysteines at position 23 and 45 within Box A are reduced, and oxidized-HMGB1 in which these two cysteines form a disulfide bond. Only reduced-HMGB1 synergises on CXCL12 activities (49). Results from NMR and Surface Plasmon Resonance experiments revealed that CXCL12 interacts separately with each of the HMGB1 boxes (34). Molecular dynamics simulations and protein-protein docking calculations showed that reduced-HMGB1 can accommodate two CXCL12 molecules, while oxidized-HMGB1 tends to be more compact and displays a lower accessible surface for the chemokine. Furthermore, only when the two CXCL12 bind to the reduced-HMGB1, their N-terminal domains are oriented in the best conformation to trigger CXCR4 dimers (Figure 2A) (50). Fluorescence Resonance Energy Transfer studies investigating CXCR4 dimer formation showed that the CXCL12/HMGB1 heterocomplex induces different rearrangements of CXCR4 homodimers on the cell surface, compared to CXCL12 alone, without altering the overall number of CXCR4 homodimers formed (34). Triggering of CXCR4 by the heterocomplex, in comparison to CXCL12 alone, results in a distinctive engagement of the β-arrestin proteins: β-arrestin1 for actin polymerization and β-arrestin2 for directional migration. In addition, CXCR4 is preserved on the cell surface and this results in an enhanced response to the chemotactic signal (51).

CXCL12/HMGB1 heterocomplex in inflammation

The early recruitment of mononuclear cells at the site of inflammation, also driven by the CXCL12/HMGB1 heterocomplex, is an essential step to mount a proper immune response. In such cases, it is essential that HMGB1 is maintained reduced in the microenvironment.

The heterocomplex mediated migration was first assessed in an *in vivo* model of sterile inflammation, achieved by the injection of

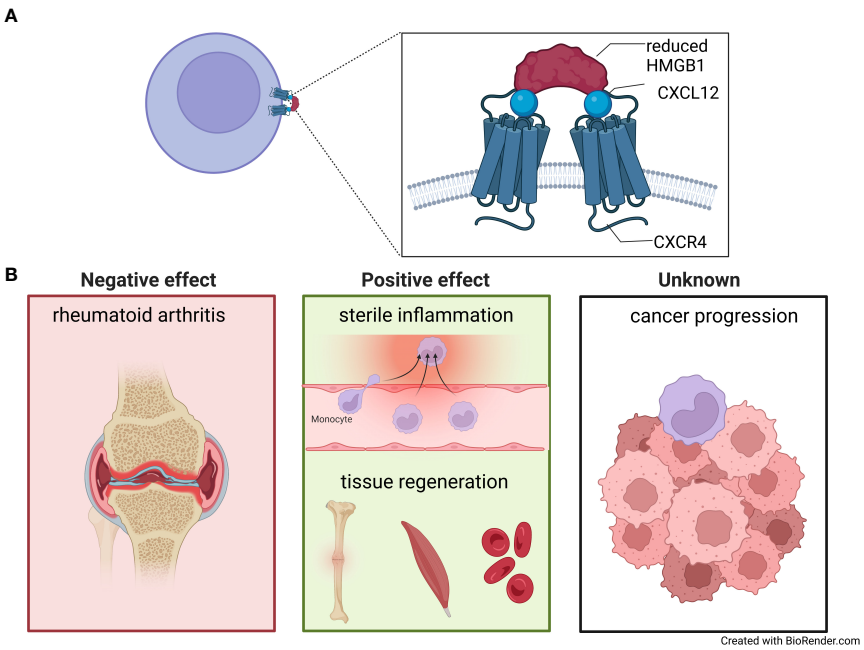

FIGURE 2
The CXCL12/HMGB1 heterocomplex. **(A)** Model of two molecules of CXCL12 (blue circle) complexed with reduced High Mobility Group Box 1 (HMGB1) (red half-circles), binding and triggering CXCR4 homodimers on the cell surfaces. **(B)** CXCL12/HMGB1 heterocomplex is present in rheumatoid arthritis, where it sustains inflammation in the synovial membrane (left panel). A positive effect of the CXCL12/HMGB1 heterocomplex has been shown in models of sterile inflammation, fracture healing, muscle repair and hematopoiesis after chemotherapeutic myeloablation (middle panel). The role of the heterocomplex in cancer has yet to be fully understood (right panel).

cardiotoxin into the muscle. Endogenous production of HMGB1, and subsequent heterocomplex formation with the CXCL12 expressed on endothelial cells, promotes a fast recruitment of $CD11b^+$ mononuclear cells (34). In this model, pre-treatment with glycyrrhizin, completely abolishes leukocyte infiltration.

More recently, Ferrara and colleagues, monitored HMGB1 redox status and leukocyte infiltration in tissues, demonstrating that in early inflammation HMGB1 is mainly reduced, while oxidized-HMGB1 is prevalent at later stages, possibly due to the production of Reactive Oxygen Species by infiltrating leukocytes (52).

Despite its beneficial role in early leukocyte recruitment during acute inflammation, persistent expression of the heterocomplex might be detrimental and delay resolution of inflammation.

In patients with RA, an autoimmune condition affecting the joints, monocytes are known to be recruited *via* CXCL12 (53), and HMGB1 is found overexpressed in the synovial fluid (54), where the heterocomplex can be detected (35). Monocytes from RA patients with active disease migrate towards the CXCL12/HMGB1 heterocomplex formed at lower HMGB1 concentration, compared to monocytes obtained from healthy individuals, due to the production of thioredoxin and thioredoxin reductase, enzymes implicated in maintaining HMGB1 in its reduced form (35). *In vitro* treatment of monocytes from healthy individuals with prostaglandin E2, found at high concentration in the sera of RA patients, recapitulates the response to the heterocomplex of monocytes from active RA. This effect is abolished by celecoxib, a COX2 inhibitor used in RA treatment, which restores migration patterns to normal levels. Together, this study demonstrated the pathological role of CXCL12/HMGB1 heterocomplex in the recruitment of monocytes during active disease status, where they promote tissue damage (Figure 2B).

Indirect evidence points to a role for the CXCL12/HMGB1 heterocomplex in autoimmune disorders affecting the eyes. In a model of autoimmune uveitis, adoptive transfer of uveitogenic Ag–specific T cells promotes the active secretion of HMGB1 by retinal cells, a process mediated by Fas-FasL interaction (55, 56). Yun and colleagues demonstrated that, early after adoptive transfer, retinal cells actively secrete HMGB1 and subsequently produce CXCL12 (57). In addition, CXCR4 inhibition significantly reduces ocular leukocyte infiltration and improves clinical score. Although this represents the first indication of HMGB1 and CXCL12 pathological expression in uveitis, redox status of HMGB1 and therefore heterocomplex formation remains to be proven. Local upregulation of HMGB1 has been shown in vitreous samples of diabetic patients with ongoing retinopathy, and in the retinas of diabetic rat and mice models (58–60). The presence of CXCL12/HMGB1 heterocomplex has been demonstrated after intravitreal HMGB1 injection in diabetic mice, which upregulates CXCL12 (61). Future studies should investigate heterocomplex mediated leukocytes recruitment in the retina and how best to pharmacologically impair this migration.

A potential pathological role of CXCL12/HMGB1 has also been suggested for infectious diseases.

HMGB1 is secreted locally in response to *Pseudomonas aeruginosa* lung infection (62). De Leo and colleagues have recently demonstrated, in an *in vivo* model, that a newly discovered CXCL12/HMGB1 heterocomplex inhibitor, pamoic acid, can reduce lung neutrophil load during the acute and chronic phase of the infection (63). This is the first report highlighting neutrophil recruitment *via* the heterocomplex, and future studies are needed to validate its activity in other pathological conditions driven by this cell type.

The research on inhibitors of the CXCL12/HMGB1 heterocomplex was boosted by the results obtained in patients with RA and *in vivo* models of inflammation, in view of developing additional treatments for several pathological conditions fueled by monocyte infiltration (63–66). Currently, small molecules and computationally identified peptides have been tested for their ability to inhibit the heterocomplex *in vitro* and *in vivo*.

CXCL12/HMGB1 heterocomplex in tissue repair

Two independent works have demonstrated that the CXCL12/HMGB1 heterocomplex enhances tissue regeneration *in vivo* after muscle injury or bone fracture, acting *via* CXCR4 (Figure 2B) (67, 68). Tirone and colleagues showed that HMGB1 accelerates tissue regeneration by acting on resident stem cells. This process requires the presence of both CXCL12 and CXCR4, indicating a role for the CXCL12/HMGB1 heterocomplex (67).

Systemically administrated exogenous HMGB1 in C57BL6/J mice accelerates hematopoietic recovery after myeloablation induced by chemotherapy (68). On the other hand, genetic deletion of HMGB1 delays fracture healing. The regenerative process is inhibited by adding glycyrrhizin or AMD3100, suggesting that HMGB1 exerted these regenerative effects by forming the heterocomplex with CXCL12 and acting *via* CXCR4. By investigating the cell cycle rate, cell dimensions, ATP concentrations, mitochondrial DNA, and mTORC1 dependence, Lee and colleagues showed that HMGB1 drives hematopoietic stem cells into the dynamic GAlert phase, defined as an intermediate active state between G0 and G1 (68).

Both groups proposed 3S-HMGB1, a synthetic non-oxidizable form of HMGB1 in which the cysteines are replaced by serines, as a potential new pharmacological tool with a broad range of medical uses, including hematopoietic recovery after chemotherapy, healing after injury or elective surgery.

CXCL12/HMGB1 heterocomplex in cancer

While the multiple activities orchestrated by CXCL12 in the tumor microenvironment have been well documented, as well as the presence of HMGB1, little is known on the relevance of the CXCL12/HMGB1 heterocomplex in mediating tumor growth and metastasis.

CXCL12 promotes cancer development by two main mechanisms: i) directly activating signaling pathways involved in cancer cell growth, metastasis, and angiogenesis, and ii) indirectly promoting metastasis by recruitment of $CXCR4^+$ cancer cells to CXCL12-expressing organs (69).

On the other hand, HMGB1 plays paradoxical roles in cancer, depending on its localization. While nuclear HMGB1 acts as a tumor suppressor for its roles in chromosome stability and induction of tumor cell death, high extracellular HMGB1 expression has been associated with poor prognosis in patients with various type of cancers (70). Although tumor cells mainly express reduced-HMGB1, infiltrating leukocytes are responsible for the presence of oxidized-HMGB1 in tumor microenvironment (52).

Whether tumor cell migration, metastasis formation, and immune cell recruitment can be modulated by the heterocomplex is yet to be demonstrated.

Naturally arising antibodies against chemokines

A further mechanism by which chemokine activities can be modulated is through the development of autoantibodies targeting their binding or triggering sites (Figure 1A).

Arise of anti-cytokines antibodies is well documented in pathology, where they prolong the half-life of circulating cytokines, as observed for interleukin (IL)3, IL4, IL6 and IL7 (71, 72). In addition they trigger Fcγ receptors and stimulate pro-inflammatory responses (73) or promote complement mediated cytotoxicity (74). Similar mechanisms of action could be envisioned for anti-chemokine autoantibodies.

Few reports described the role and functions of anti-chemokine autoantibodies. They can promote or prolong chemokine activities, or be beneficial to the host, through dampening excessive inflammation, thanks to their neutralizing properties (Table 2) (78, 79).

Anti-chemokine antibodies sustaining pathology

Acute respiratory distress syndrome (ARDS) is a life threatening pulmonary condition characterized by pulmonary infiltrates, hypoxemia and edema. Bronchoalveolar lavage fluid (BAL) of ARDS patients presents elevated levels of autoantibodies complexed with CXCL8 (82). In a study aimed at investigating the relationship between the presence of these complexes and development stages of acute lung injury, Kurdowska and colleagues demonstrated an association between elevated levels of autoantibodies bound to CXCL8 and an adverse outcome (75). CXCL8-autoantibodies complexes, isolated from BAL after acute lung injury, maintain the CXCL8 chemotactic activity on neutrophils and, in addition, can trigger superoxide release by

TABLE 2 Naturally arising antibodies against chemokines.

Anti-chemokine antibodies sustaining pathology			
Disease	Autoantibody specificity	Mode of action	Reference
Acute respiratory distress syndrome	CXCL8 (immune-complexes)	Associated to adverse outcome Chemotactic activity on neutrophil maintained Superoxide release *via* FcγRIIa	(75) (73)
Asthma	CXCL8 (immune-complexes)	Proinflammatory	(76)
Rheumatoid Arthritis	CXCL8	Proinflammatory;	(77)
	CCL4, CCL19, CCL25, CXCL7, CXCL8, CXCL9	Increased in patients with advanced extra-articular and clinical manifestations	(78)
Anti-chemokine antibodies preventing adverse outcome			
Disease	Autoantibody specificity	Mode of action	Reference
Type1 Diabetes Mellitus	CCL3	Neutralizing activity; Counteract disease progression	(79)
Atopic Dermatitis	CCL3	Neutralizing activity; Counteract disease progression	(80)
Prostate Cancer	CCL2	Neutralizing activity; Limit tumor growth	(81)
COVID-19	CCL19, CCL22, CXCL17	Unknown; Increased in COVID-19 convalescents	(78)
	CXCL8, CCL25, CXCL5	Unknown; Increased in COVID-19 convalescents with mild disease	
	CCL21, CXCL13, CXCL16	Neutralizing activity (CXCL13, CXCL16); Increased in COVID-19 convalescents without long COVID	

binding to FcγRIIa (73). Elevated levels of both IgG and IgA autoantibodies complexes with CXCL8 are also found in circulation, as well as in BAL of asthmatic patients, confirming their proinflammatory role (76). Anti-CXCL8 autoantibodies were also identified in RA patients, with high levels of IgA anti-CXCL8 present in patients with advanced extra-articular and clinical manifestations (77). The authors hypothesize that prolonged CXCL8 production leads to the arising of anti-CXCL8 antibodies, aiming at limiting the persistent inflammation; however, the presence of such antibodies complexed with CXCL8, instead, promotes Fc mediated activities, contributing to the persistent chronic inflammation. We recently confirmed elevated levels of circulating anti-CXCL8 IgG autoantibodies in RA patients together with other autoantibodies targeting CCL4, CCL19, CCL25, CXCL7 and CXCL9 (78).

Anti-chemokine antibodies preventing adverse outcome

Type 1 (insulin-dependent) diabetes mellitus (T1DM) is a chronic autoimmune disease in which insulin-secreting cells within Langerhans islets in pancreas are eliminated by the immune system (83). Patients with T1DM develop autoantibodies against several antigens, which include insulin and islet cells, before symptoms onset. Of note, the majority of T1DM patients selectively develop anti-CCL3 antibodies, with neutralizing properties (79). Anti-CCL3 antibodies production might be specific of T1DM, since the authors did not find them in other autoimmune diseases. Interestingly, anti-CCL3 antibodies are also found in 95% of first-degree relatives of T1DM patients. Cameron and colleagues showed that in CCL3-deficient NOD mice about 60% of the pancreas islets display a normal histology. In contrast, in NOD mice expressing CCL3, 40% of pancreatic islets showed sign of moderate to severe insulitis (84). Indeed, when NOD mice were treated with an anti-CCL3 antibody, a reduction in incidence of diabetes was observed (84). Collectively, these data suggest that, these antibodies might counteract disease progression.

Higher level of autoantibodies against CCL3 were shown in atopic dermatitis (AD), a chronic skin inflammation which leads to skin lesions (80). This is in line with previous studies on AD patients in which CCL3 was shown to be produced by PBMCs (85). The presence of these autoantibodies, if proven to neutralize CCL3 activities, might play a role in suppressing disease progression, similarly to T1DM.

In cancer, several studies highlighted the importance of CCL2 in promoting monocyte migration from the bone marrow to the circulation and ultimately to the tumor site, where they elicit immune suppressive activity and stimulate tumor growth (81, 86–89). Prostate cancer patients present high expression of CCL2 in the tumor, and elevated levels of anti-CCL2 neutralizing autoantibodies (81). Importantly, the presence of anti-CCL2 autoantibodies was exclusive in patients bearing malignant, but not benign tumors. Nevertheless, in a mouse model, CCL2 overexpression induced a sustained autoantibody production and significantly limited tumor growth, suggesting a potential beneficial role of these autoantibodies (81). The authors speculated that a therapeutic strategy aiming at enhancing the pre-existing anti-CCL2 antibodies might be beneficial as the sera concentration of these antibodies might not be elevated enough to completely suppress monocyte infiltration and tumor cell migration.

A novel coronavirus, severe acute respiratory syndrome coronavirus 2 (SARS-CoV-2), emerged in December 2019, causing pneumonia outbreaks worldwide (90). Autoantibodies targeting cytokines and several immune factors have been described in patients with coronavirus disease 2019 (COVID-19) (91). In particular, autoantibodies targeting type I IFN have been found in ~ 10% of life-threatening pneumonia and in ~ 20% of deaths due to COVID-19. We have recently demonstrated that autoantibodies targeting several chemokines, including CCL19, CCL22 and CXCL17, are developed post-SARS-CoV-2 infection. Convalescent individuals who experienced mild COVID-19 have higher levels of autoantibodies targeting CXCL8, CCL25 and CXCL5 compared to those that required hospitalization. We showed that these autoantibodies have neutralizing properties, and therefore could be beneficial in dampening the inflammatory response, preventing hyper-activation of the immune system and tissue damage associated to severe COVID-19. Long-term sequelae (long COVID), spanning from neurological, to respiratory and systemic/inflammatory symptoms, have been reported after SARS-CoV-2 infection (92). We found that autoantibodies to CCL21, CXCL13 and CXCL16 are present in individuals that do not develop long COVID (78). All together these data point to a beneficial role of anti-chemokine antibodies in COVID-19, with their presence correlating with better outcome and lack of long COVID.

Conclusions

Even though, in modern pharmacology, the γ subfamily of GPCR represents the most successful target of small molecule inhibitors for treating diseases affecting different systems, inhibitors of chemokines and chemokine receptors were unsuccessful for the treatment of inflammatory diseases, where the involvement of the chemokine system plays a key role. The extensive characterization of chemokine expression in tissues, both in physiological and pathological conditions, fostered researchers to look at the chemokine system from a distinct perspective, leading to the identification of additional functions. The complexity of the tissue microenvironment influences chemokine receptor mediated cell recruitment and activities. Natural chemokine antagonism modulates cell recruitment in response to different chemokine gradients. Chemokines can exert a repulsive effect either at different chemokine concentrations or acting on different receptors, contributing to tumor immune evasion or tissue egress. Chemokines and inflammatory molecules, concomitantly expressed, can also synergistically act on cell migration and activities. The presence of autoantibodies targeting chemokines, either neutralizing their activities or promoting Fc-mediated functions, sustain pathology or prevent adverse outcome. Therefore, we believe that all these features should be taken into account for future drug development studies and novel approaches into personalized medicine.

Author contributions

All authors listed, have made substantial, direct and intellectual contribution to the work, and approved it for publication.

Funding

The authors would like to thank, for the support received over the years: the Swiss National Science Foundation (3100A0-143718/1 and 141773-RM3); Innosuisse (46411.1 IP-LS); the European Union's Programs for research technological development and demonstration (INNOCHEM - LSHB-CT-2005-518167 (FP6), DEC-VAC - LSHP-CT-2005-018685 (FP6), ADITEC – 280873 (FP7), and TIMER – 281608 (FP7)); the San Salvatore Foundation; the Novartis Foundation; the Helmut Horten Foundation; the Institute for Arthritis Research; the Gottfried and Julia Bangerter-Rhyner-Foundation; the Ceschina Foundation and the Fratelli Agostino Enrico Rocca Foundation.

Conflict of interest

VC and MU have filed a provisional patent application in connection with the work on autoantibodies targeting chemokines. MU is inventor in the patent # PCT/EP2019/057125 on peptides inhibitors of the CXCL12/HMGB1 heterocomplex.

The remaining authors declare that the research was conducted in the absence of any commercial or financial relationships that could be construed as a potential conflict of interest.

Publisher's note

References

1. Charo IF, Ransohoff RM. The many roles of chemokines and chemokine receptors in inflammation. *N Engl J Med* (2006) 354(6):610–21. doi: 10.1056/NEJMra052723

2. Crump MP, Gong JH, Loetscher P, Rajarathnam K, Amara A, Arenzana-Seisdedos F, et al. Solution structure and basis for functional activity of stromal cell-derived factor-1; dissociation of Cxcr4 activation from binding and inhibition of hiv-1. *EMBO J* (1997) 16(23):6996–7007. doi: 10.1093/emboj/16.23.6996

3. Bacon K, Baggiolini M, Broxmeyer H, Horuk R, Lindley I, Mantovani A, et al. Chemokine/Chemokine receptor nomenclature. *J Interferon Cytokine Res* (2002) 22 (10):1067–8. doi: 10.1089/107999002760624305

4. Allen SJ, Crown SE, Handel TM. Chemokine: receptor structure, interactions, and antagonism. *Annu Rev Immunol* (2007) 25:787–820. doi: 10.1146/annurev.immunol.24.021605.090529

5. Bachelerie F, Ben-Baruch A, Burkhardt AM, Combadiere C, Farber JM, Graham GJ, et al. International union of basic and clinical pharmacology. [Corrected]. lxxxix. update on the extended family of chemokine receptors and introducing a new nomenclature for atypical chemokine receptors. *Pharmacol Rev* (2014) 66(1):1–79. doi: 10.1124/pr.113.007724

6. Vacchini A, Locati M, Borroni EM. Overview and potential unifying themes of the atypical chemokine receptor family. *J Leukoc Biol* (2016) 99(6):883–92. doi: 10.1189/jlb.2MR1015-477R

7. Rajarathnam K, Clark-Lewis I, Sykes BD. 1h nmr studies of interleukin 8 analogs: characterization of the domains essential for function. *Biochemistry* (1994) 33 (21):6623–30. doi: 10.1021/bi00187a032

8. Griffith JW, Sokol CL, Luster AD. Chemokines and chemokine receptors: positioning cells for host defense and immunity. *Annu Rev Immunol* (2014) 32:659–702. doi: 10.1146/annurev-immunol-032713-120145

9. Uguccioni M, Gionchetti P, Robbiani DF, Rizzello F, Peruzzo S, Campieri M, et al. Increased expression of ip-10, il-8, mcp-1, and mcp-3 in ulcerative colitis. *Am J Pathol* (1999) 155(2):331–6. doi: 10.1016/S0002-9440(10)65128-0

10. Lau EK, Paavola CD, Johnson Z, Gaudry JP, Geretti E, Borlat F, et al. Identification of the glycosaminoglycan binding site of the cc chemokine, mcp-1: implications for structure and function in vivo. *J Biol Chem* (2004) 279(21):22294–305. doi: 10.1074/jbc.M311224200

11. Chou CC, Fine JS, Pugliese-Sivo C, Gonsiorek W, Davies L, Deno G, et al. Pharmacological characterization of the chemokine receptor, Hccr1 in a stable transfectant and differentiated hl-60 cells: antagonism of Hccr1 activation by mip-1beta. *Br J Pharmacol* (2002) 137(5):663–75. doi: 10.1038/sj.bjp.0704907

12. Petkovic V, Moghini C, Paoletti S, Uguccioni M, Gerber B. Eotaxin-3/Ccl26 is a natural antagonist for cc chemokine receptors 1 and 5. a human chemokine with a regulatory role. *J Biol Chem* (2004) 279(22):23357–63. doi: 10.1074/jbc.M309283200

13. Gong JH, Ratkay LG, Waterfield JD, Clark-Lewis I. An antagonist of monocyte chemoattractant protein 1 (Mcp-1) inhibits arthritis in the mrl-lpr mouse model. *J Exp Med* (1997) 186(1):131–7. doi: 10.1084/jem.186.1.131

14. Ogilvie P, Bardi G, Clark-Lewis I, Baggiolini M, Uguccioni M. Eotaxin is a natural antagonist for Ccr2 and an agonist for Ccr5. *Blood* (2001) 97(7):1920–4. doi: 10.1182/blood.v97.7.1920

15. Loetscher P, Pellegrino A, Gong JH, Mattioli I, Loetscher M, Bardi G, et al. The ligands of cxc chemokine receptor 3, I-tac, mig, and Ip10, are natural antagonists for Ccr3. *J Biol Chem* (2001) 276(5):2986–91. doi: 10.1074/jbc.M005652200

16. Fulkerson PC, Zimmermann N, Brandt EB, Muntel EE, Doepker MP, Kavanaugh JL, et al. Negative regulation of eosinophil recruitment to the lung by the chemokine monokine induced by ifn-gamma (Mig, Cxcl9). *Proc Natl Acad Sci U.S.A.* (2004) 101(7):1987–92. doi: 10.1073/pnas.0308544100

17. Nibbs RJ, Salcedo TW, Campbell JD, Yao XT, Li Y, Nardelli B, et al. C-c chemokine receptor 3 antagonism by the beta-chemokine macrophage inflammatory protein 4, a property strongly enhanced by an amino-terminal alanine-methionine swap. *J Immunol* (2000) 164(3):1488–97. doi: 10.4049/jimmunol.164.3.1488

18. Blanpain C, Migeotte I, Lee B, Vakili J, Doranz BJ, Govaerts C, et al. Ccr5 binds multiple cc-chemokines: mcp-3 acts as a natural antagonist. *Blood* (1999) 94(6):1899–905. doi: 10.1182/blood.V94.6.1899

19. Petkovic V, Moghini C, Paoletti S, Uguccioni M, Gerber B. I-Tac/Cxcl11 is a natural antagonist for Ccr5. *J Leukoc Biol* (2004) 76(3):701–8. doi: 10.1189/jlb.1103570

20. Ogilvie P, Paoletti S, Clark-Lewis I, Uguccioni M. Eotaxin-3 is a natural antagonist for Ccr2 and exerts a repulsive effect on human monocytes. *Blood* (2003) 102(3):789–94. doi: 10.1182/blood-2002-09-2773

21. Hummitzsch L, Berndt R, Kott M, Rusch R, Faendrich F, Gruenewald M, et al. Hypoxia directed migration of human naive monocytes is associated with an attenuation of cytokine release: indications for a key role of Ccl26. *J Transl Med* (2020) 18(1):404. doi: 10.1186/s12967-020-02567-7

22. Poznansky MC, Olszak IT, Foxall R, Evans RH, Luster AD, Scadden DT. Active movement of T cells away from a chemokine. *Nat Med* (2000) 6(5):543–8. doi: 10.1038/75022

23. Poznansky MC, Olszak IT, Evans RH, Wang Z, Foxall RB, Olson DP, et al. Thymocyte emigration is mediated by active movement away from stroma-derived factors. *J Clin Invest* (2002) 109(8):1101–10. doi: 10.1172/JCI13853

24. Vianello F, Papeta N, Chen T, Kraft P, White N, Hart WK, et al. Murine B16 melanomas expressing high levels of the chemokine stromal-derived factor-1/Cxcl12 induce tumor-specific T cell chemorepulsion and escape from immune control. *J Immunol* (2006) 176(5):2902–14. doi: 10.4049/jimmunol.176.5.2902

25. Kuscher K, Danelon G, Paoletti S, Stefano L, Schiraldi M, Petkovic V, et al. Synergy-inducing chemokines enhance Ccr2 ligand activities on monocytes. *Eur J Immunol* (2009) 39(4):1118–28. doi: 10.1002/eji.200838906

26. Sebastiani S, Danelon G, Gerber B, Uguccioni M. Ccl22-induced responses are powerfully enhanced by synergy inducing chemokines *Via* Ccr4: evidence for the involvement of first beta-strand of chemokine. *Eur J Immunol* (2005) 35(3):746–56. doi: 10.1002/eji.200525800

27. von Hundelshausen P, Koenen RR, Sack M, Mause SF, Adriaens W, Proudfoot AE, et al. Heterophilic interactions of platelet factor 4 and rantes promote monocyte arrest on endothelium. *Blood* (2005) 105(3):924–30. doi: 10.1182/blood-2004-06-2475

28. Paoletti S, Petkovic V, Sebastiani S, Danelon MG, Uguccioni M, Gerber BO. A rich chemokine environment strongly enhances leukocyte migration and activities. *Blood* (2005) 105(9):3405–12. doi: 10.1182/blood-2004-04-1648

29. Krug A, Uppaluri R, Facchetti F, Dorner BG, Sheehan KC, Schreiber RD, et al. Ifn-producing cells respond to Cxcr3 ligands in the presence of Cxcl12 and secrete inflammatory chemokines upon activation. *J Immunol* (2002) 169(11):6079–83. doi: 10.4049/jimmunol.169.11.6079

30. Vanbervliet B, Bendriss-Vermare N, Massacrier C, Homey B, de Bouteiller O, Briere F, et al. The inducible Cxcr3 ligands control plasmacytoid dendritic cell responsiveness to the constitutive chemokine stromal cell-derived factor 1 (Sdf-1)/Cxcl12. *J Exp Med* (2003) 198(5):823–30. doi: 10.1084/jem.20020437

31. Venetz D, Ponzoni M, Schiraldi M, Ferreri AJ, Bertoni F, Doglioni C, et al. Perivascular expression of Cxcl9 and Cxcl12 in primary central nervous system lymphoma: T-cell infiltration and positioning of malignant b cells. *Int J Cancer* (2010) 127(10):2300–12. doi: 10.1002/ijc.25236

32. Alard JE, Ortega-Gomez A, Wichapong K, Bongiovanni D, Horckmans M, Megens RT, et al. Recruitment of classical monocytes can be inhibited by disturbing heteromers of neutrophil Hnp1 and platelet Ccl5. *Sci Transl Med* (2015) 7 (317):317ra196. doi: 10.1126/scitranslmed.aad5330

33. Eckardt V, Miller MC, Blanchet X, Duan R, Leberzammer J, Duchene J, et al. Chemokines and galectins form heterodimers to modulate inflammation. *EMBO Rep* (2020) 21(4):e47852. doi: 10.15252/embr.201947852

34. Schiraldi M, Raucci A, Munoz LM, Livoti E, Celona B, Venereau E, et al. Hmgb1 promotes recruitment of inflammatory cells to damaged tissues by forming a complex with Cxcl12 and signaling *Via* Cxcr4. *J Exp Med* (2012) 209(3):551–63. doi: 10.1084/jem.20111739

35. Cecchinato V, D'Agostino G, Raeli L, Nerviani A, Schiraldi M, Danelon G, et al. Redox-mediated mechanisms fuel monocyte responses to Cxcl12/Hmgb1 in active rheumatoid arthritis. *Front Immunol* (2018) 9:2118. doi: 10.3389/fimmu.2018.02118

36. Martinelli R, Sabroe I, LaRosa G, Williams TJ, Pease JE. The cc chemokine eotaxin (Ccl11) is a partial agonist of cc chemokine receptor 2b. *J Biol Chem* (2001) 276 (46):42957–64. doi: 10.1074/jbc.M103933200

37. Neote K, DiGregorio D, Mak JY, Horuk R, Schall TJ. Molecular cloning, functional expression, and signaling characteristics of a c-c chemokine receptor. *Cell* (1993) 72(3):415–25. doi: 10.1016/0092-8674(93)90118-a

38. Metzemaekers M, Van Damme J, Mortier A, Proost P. Regulation of chemokine activity - a focus on the role of dipeptidyl peptidase Iv/Cd26. *Front Immunol* (2016) 7:483. doi: 10.3389/fimmu.2016.00483

39. Loetscher P, Clark-Lewis I. Agonistic and antagonistic activities of chemokines. *J Leukoc Biol* (2001) 69(6):881–4. doi: 10.1189/jlb.69.6.881

40. Zlatopolskiy A, Laurence J. 'Reverse gear' cellular movement mediated by chemokines. *Immunol Cell Biol* (2001) 79(4):340–4. doi: 10.1046/j.1440-1711.2001.01015.x

41. Shinkai A, Yoshisue H, Koike M, Shoji E, Nakagawa S, Saito A, et al. A novel human cc chemokine, eotaxin-3, which is expressed in il-4-Stimulated vascular endothelial cells, exhibits potent activity toward eosinophils. *J Immunol* (1999) 163 (3):1602–10. doi: 10.4049/jimmunol.163.3.1602

42. Gouwy M, Struyf S, Mahieu F, Put W, Proost P, Van Damme J. The unique property of the cc chemokine regakine-1 to synergize with other plasma-derived inflammatory mediators in neutrophil chemotaxis does not reside in its Nh2-terminal structure. *Mol Pharmacol* (2002) 62(1):173–80. doi: 10.1124/mol.62.1.173

43. von Hundelshausen P, Agten SM, Eckardt V, Blanchet X, Schmitt MM, Ippel H, et al. Chemokine interactome mapping enables tailored intervention in acute and chronic inflammation. *Sci Transl Med* (2017) 9(384). doi: 10.1126/scitranslmed.aah6650

44. Koenen RR, von Hundelshausen P, Nesmelova IV, Zernecke A, Liehn EA, Sarabi A, et al. Disrupting functional interactions between platelet chemokines inhibits atherosclerosis in hyperlipidemic mice. *Nat Med* (2009) 15(1):97–103. doi: 10.1038/nm.1898

45. Brandhofer M, Hoffmann A, Blanchet X, Siminkovitch E, Rohlfing AK, El Bounkari O, et al. Heterocomplexes between the atypical chemokine mif and the cxc-motif chemokine Cxcl4l1 regulate inflammation and thrombus formation. *Cell Mol Life Sci* (2022) 79(10):512. doi: 10.1007/s00018-022-04539-0

46. Grommes J, Alard JE, Drechsler M, Wantha S, Morgelin M, Kuebler WM, et al. Disruption of platelet-derived chemokine heteromers prevents neutrophil extravasation in acute lung injury. *Am J Respir Crit Care Med* (2012) 185(6):628–36. doi: 10.1164/rccm.201108-1533OC

47. Nguyen KTP, Volkman B, Dreau D, Nesmelova IV. A new obligate Cxcl4-Cxcl12 heterodimer for studying chemokine heterodimer activities and mechanisms. *Sci Rep* (2022) 12(1):17204. doi: 10.1038/s41598-022-21651-0

48. Cecchinato V, D'Agostino G, Raeli L, Uguccioni M. Chemokine interaction with synergy-inducing molecules: fine tuning modulation of cell trafficking. *J Leukoc Biol* (2016) 99(6):851–5. doi: 10.1189/jlb.1MR1015-457R

49. Venereau E, Casalgrandi M, Schiraldi M, Antoine DJ, Cattaneo A, De Marchis F, et al. Mutually exclusive redox forms of Hmgb1 promote cell recruitment or proinflammatory cytokine release. *J Exp Med* (2012) 209(9):1519–28. doi: 10.1084/jem.20120189

50. Fassi EMA, Sgrignani J, D'Agostino G, Cecchinato V, Garofalo M, Grazioso G, et al. Oxidation state dependent conformational changes of Hmgb1 regulate the formation of the Cxcl12/Hmgb1 heterocomplex. *Comput Struct Biotechnol J* (2019) 17:886–94. doi: 10.1016/j.csbj.2019.06.020

51. D'Agostino G, Artinger M, Locati M, Perez L, Legler DF, Bianchi ME, et al. Beta-Arrestin1 and beta-Arrestin2 are required to support the activity of the Cxcl12/Hmgb1 heterocomplex on Cxcr4. *Front Immunol* (2020) 11:550824. doi: 10.3389/fimmu.2020.550824

52. Ferrara M, Chialli G, Ferreira LM, Ruggieri E, Careccia G, Preti A, et al. Oxidation of Hmgb1 is a dynamically regulated process in physiological and pathological conditions. *Front Immunol* (2020) 11:1122. doi: 10.3389/fimmu.2020.01122

53. Blades MC, Ingegnoli F, Wheller SK, Manzo A, Wahid S, Panayi GS, et al. Stromal cell-derived factor 1 (Cxcl12) induces monocyte migration into human synovium transplanted onto scid mice. *Arthritis Rheum* (2002) 46(3):824–36. doi: 10.1002/art.10102

54. Andersson U, Erlandsson-Harris H. Hmgb1 is a potent trigger of arthritis. *J Intern Med* (2004) 255(3):344–50. doi: 10.1111/j.1365-2796.2003.01303.x

55. Jiang G, Sun D, Yang H, Lu Q, Kaplan HJ, Shao H. Hmgb1 is an early and critical mediator in an animal model of uveitis induced by irbp-specific T cells. *J Leukoc Biol* (2014) 95(4):599–607. doi: 10.1189/jlb.0613337

56. Jiang G, Wang Y, Yun J, Hajrasouliha AR, Zhao Y, Sun D, et al. Hmgb1 release triggered by the interaction of live retinal cells and uveitogenic T cells is Fas/Fasl activation-dependent. *J Neuroinflamm* (2015) 12:179. doi: 10.1186/s12974-015-0389-2

57. Yun J, Jiang G, Wang Y, Xiao T, Zhao Y, Sun D, et al. The Hmgb1-Cxcl12 complex promotes inflammatory cell infiltration in uveitogenic T cell-induced chronic experimental autoimmune uveitis. *Front Immunol* (2017) 8:142. doi: 10.3389/fimmu.2017.00142

58. El-Asrar AM, Nawaz MI, Kangave D, Geboes K, Ola MS, Ahmad S, et al. High-mobility group box-1 and biomarkers of inflammation in the vitreous from patients with proliferative diabetic retinopathy. *Mol Vis* (2011) 17:1829–38.

59. Mohammad G, Siddiquei MM, Othman A, Al-Shabrawey M, Abu El-Asrar AM. High-mobility group box-1 protein activates inflammatory signaling pathway components and disrupts retinal vascular-barrier in the diabetic retina. *Exp Eye Res* (2013) 107:101–9. doi: 10.1016/j.exer.2012.12.009

60. Abu El-Asrar AM, Siddiquei MM, Nawaz MI, Geboes K, Mohammad G. The proinflammatory cytokine high-mobility group box-1 mediates retinal neuropathy induced by diabetes. *Mediators Inflammation* (2014) 2014:746415. doi: 10.1155/2014/746415

61. Abu El-Asrar AM, Mohammad G, Nawaz MI, Siddiquei MM. High-mobility group box-1 modulates the expression of inflammatory and angiogenic signaling pathways in diabetic retina. *Curr Eye Res* (2015) 40(11):1141–52. doi: 10.3109/02713683.2014.982829

62. Entezari M, Weiss DJ, Sitapara R, Whittaker L, Wargo MJ, Li J, et al. Inhibition of high-mobility group box 1 protein (Hmgb1) enhances bacterial clearance and protects against pseudomonas aeruginosa pneumonia in cystic fibrosis. *Mol Med* (2012) 18(1):477–85. doi: 10.2119/molmed.2012.00024

63. De Leo F, Rossi A, De Marchis F, Cigana C, Melessike M, Quilici G, et al. Pamoic acid is an inhibitor of Hmgb1.Cxcl12 elicited chemotaxis and reduces inflammation in murine models of pseudomonas aeruginosa pneumonia. *Mol Med* (2022) 28(1):108. doi: 10.1186/s10020-022-00535-z

64. Sgrignani J, Cecchinato V, Fassi EMA, D'Agostino G, Garofalo M, Danelon G, et al. Systematic development of peptide inhibitors targeting the Cxcl12/Hmgb1 interaction. *J Med Chem* (2021) 64(18):13439–50. doi: 10.1021/acs.jmedchem.1c00852

65. De Leo F, Quilici G, Tirone M, De Marchis F, Mannella V, Zucchelli C, et al. Diflunisal targets the Hmgb1/Cxcl12 heterocomplex and blocks immune cell recruitment. *EMBO Rep* (2019) 20(10):e47788. doi: 10.15252/embr.201947788

66. Mollica L, De Marchis F, Spitaleri A, Dallacosta C, Pennacchini D, Zamai M, et al. Glycyrrhizin binds to high-mobility group box 1 protein and inhibits its cytokine activities. *Chem Biol* (2007) 14(4):431–41. doi: 10.1016/j.chembiol.2007.03.007

67. Tirone M, Tran NL, Ceriotti C, Gorzanelli A, Canepari M, Bottinelli R, et al. High mobility group box 1 orchestrates tissue regeneration *Via* Cxcr4. *J Exp Med* (2018) 215(1):303–18. doi: 10.1084/jem.20160217

68. Lee G, Espirito Santo AI, Zwingenberger S, Cai L, Vogl T, Feldmann M, et al. Fully reduced Hmgb1 accelerates the regeneration of multiple tissues by transitioning stem cells to G(Alert). *Proc Natl Acad Sci U.S.A.* (2018) 115(19):E4463–E72. doi: 10.1073/pnas.1802893115

69. Duda DG, Kozin SV, Kirkpatrick ND, Xu L, Fukumura D, Jain RK. Cxcl12 (Sdf1alpha)-Cxcr4/Cxcr7 pathway inhibition: an emerging sensitizer for anticancer therapies? *Clin Cancer Res* (2011) 17(8):2074–80. doi: 10.1158/1078-0432.CCR-10-2636

70. Wu T, Zhang W, Yang G, Li H, Chen Q, Song R, et al. Hmgb1 overexpression as a prognostic factor for survival in cancer: a meta-analysis and systematic review. *Oncotarget* (2016) 7(31):50417–27. doi: 10.18632/oncotarget.10413

71. Finkelman FD, Madden KB, Morris SC, Holmes JM, Boiani N, Katona IM, et al. Anti-cytokine antibodies as carrier proteins. prolongation of in vivo effects of exogenous cytokines by injection of cytokine-Anti-Cytokine antibody complexes. *J Immunol* (1993) 151(3):1235–44. doi: 10.4049/jimmunol.151.3.1235

72. May LT, Neta R, Moldawer LL, Kenney JS, Patel K, Sehgal PB. Antibodies chaperone circulating il-6. paradoxical effects of anti-Il-6 "Neutralizing" antibodies in vivo. *J Immunol* (1993) 151(6):3225–36. doi: 10.4049/jimmunol.151.6.3225

73. Krupa A, Kato H, Matthay MA, Kurdowska AK. Proinflammatory activity of anti-Il-8 Autoantibody:Il-8 complexes in alveolar edema fluid from patients with acute lung injury. *Am J Physiol Lung Cell Mol Physiol* (2004) 286(6):L1105–13. doi: 10.1152/ajplung.00277.2003

74. van der Meide PH, Schellekens H. Anti-cytokine autoantibodies: epiphenomenon or critical modulators of cytokine action. *Biotherapy* (1997) 10 (1):39–48. doi: 10.1007/BF02678216

75. Kurdowska A, Noble JM, Steinberg KP, Ruzinski JT, Hudson LD, Martin TR. Anti-interleukin 8 autoantibody: interleukin 8 complexes in the acute respiratory distress syndrome. relationship between the complexes and clinical disease activity. *Am J Respir Crit Care Med* (2001) 163(2):463–8. doi: 10.1164/ajrccm.163.2.2005109

76. Shute JK, Vrugt B, Lindley IJ, Holgate ST, Bron A, Aalbers R, et al. Free and complexed interleukin-8 in blood and bronchial mucosa in asthma. *Am J Respir Crit Care Med* (1997) 155(6):1877–83. doi: 10.1164/ajrccm.155.6.9196089

77. Kraan MC, Patel DD, Haringman JJ, Smith MD, Weedon H, Ahern MJ, et al. The development of clinical signs of rheumatoid synovial inflammation is associated with increased synthesis of the chemokine Cxcl8 (Interleukin-8). *Arthritis Res* (2001) 3 (1):65–71. doi: 10.1186/ar141

78. Muri J, Cecchinato V, Cavalli A, Shanbhag AA, Matkovic M, Biggiogero M, et al. Autoantibodies against chemokines post-Sars-Cov-2 infection correlate with disease course. *Nat Immunol* (2023) 24(4):604–11. doi: 10.1038/s41590-023-01445-w

79. Shehadeh N, Pollack S, Wildbaum G, Zohar Y, Shafat I, Makhoul R, et al. Selective autoantibody production against Ccl3 is associated with human type 1 diabetes mellitus and serves as a novel biomarker for its diagnosis. *J Immunol* (2009) 182(12):8104–9. doi: 10.4049/jimmunol.0803348

80. Bergman R, Ramon M, Wildbaum G, Avitan-Hersh E, Mayer E, Shemer A, et al. Psoriasis patients generate increased serum levels of autoantibodies to tumor necrosis factor-alpha and interferon-alpha. *J Dermatol Sci* (2009) 56(3):163–7. doi: 10.1016/j.jdermsci.2009.08.006

81. Izhak L, Wildbaum G, Weinberg U, Shaked Y, Alami J, Dumont D, et al. Predominant expression of Ccl2 at the tumor site of prostate cancer patients directs a selective loss of immunological tolerance to Ccl2 that could be amplified in a beneficial manner. *J Immunol* (2010) 184(2):1092–101. doi: 10.4049/jimmunol.0902725

82. Kurdowska A, Miller EJ, Noble JM, Baughman RP, Matthay MA, Brelsford WG, et al. Anti-Il-8 autoantibodies in alveolar fluid from patients with the adult respiratory distress syndrome. *J Immunol* (1996) 157(6):2699–706. doi: 10.4049/jimmunol.157.6.2699

83. Katsarou A, Gudbjornsdottir S, Rawshani A, Dabelea D, Bonifacio E, Anderson BJ, et al. Type 1 diabetes mellitus. *Nat Rev Dis Primers* (2017) 3:17016. doi: 10.1038/nrdp.2017.16

84. Cameron MJ, Arreaza GA, Grattan M, Meagher C, Sharif S, Burdick MD, et al. Differential expression of cc chemokines and the Ccr5 receptor in the pancreas is associated with progression to type I diabetes. *J Immunol* (2000) 165(2):1102–10. doi: 10.4049/jimmunol.165.2.1102

85. Kaburagi Y, Shimada Y, Nagaoka T, Hasegawa M, Takehara K, Sato S. Enhanced production of cc-chemokines (Rantes, mcp-1, mip-1alpha, mip-1beta, and eotaxin) in patients with atopic dermatitis. *Arch Dermatol Res* (2001) 293(7):350–5. doi: 10.1007/s004030100230

86. Muller A, Homey B, Soto H, Ge N, Catron D, Buchanan ME, et al. Involvement of chemokine receptors in breast cancer metastasis. *Nature* (2001) 410(6824):50–6. doi: 10.1038/35065016

87. Loberg RD, Day LL, Harwood J, Ying C, St John LN, Giles R, et al. Ccl2 is a potent regulator of prostate cancer cell migration and proliferation. *Neoplasia* (2006) 8 (7):578–86. doi: 10.1593/neo.06280

88. Loberg RD, Ying C, Craig M, Day LL, Sargent E, Neeley C, et al. Targeting Ccl2 with systemic delivery of neutralizing antibodies induces prostate cancer tumor regression in vivo. *Cancer Res* (2007) 67(19):9417–24. doi: 10.1158/0008-5472.CAN-07-1286

89. Izhak L, Wildbaum G, Jung S, Stein A, Shaked Y, Karin N. Dissecting the autocrine and paracrine roles of the Ccr2-Ccl2 axis in tumor survival and angiogenesis. *PloS One* (2012) 7(1):e28305. doi: 10.1371/journal.pone.0028305

90. Huang C, Wang Y, Li X, Ren L, Zhao J, Hu Y, et al. Clinical features of patients infected with 2019 novel coronavirus in wuhan, China. *Lancet* (2020) 395(10223):497–506. doi: 10.1016/S0140-6736(20)30183-5

91. Zhang Q, Bastard P, Liu Z, Le Pen J, Moncada-Velez M, Chen J, et al. Inborn errors of type I ifn immunity in patients with life-threatening covid-19. *Science* (2020) 370(6515). doi: 10.1126/science.abd4570

92. Mehandru S, Merad M. Pathological sequelae of long-haul covid. *Nat Immunol* (2022) 23(2):194–202. doi: 10.1038/s41590-021-01104-y

frontiers | Frontiers in Immunology

TYPE Original Research
PUBLISHED 10 March 2023
DOI 10.3389/fimmu.2023.1078591

OPEN ACCESS

EDITED BY
Nicole Horwood,
University of East Anglia,
United Kingdom

REVIEWED BY
Chenyang Zhao,
Ocean University of China, China
Elise Laura Kessler,
University Medical Center Utrecht,
Netherlands
Ricardo Pujol Borrell,
Autonomous University of Barcelona, Spain

*CORRESPONDENCE
Erik A.L. Biessen
erik.biessen@mumc.nl

†These authors share last authorship

SPECIALTY SECTION
This article was submitted to Inflammation, a section of the journal Frontiers in Immunology

RECEIVED 24 October 2022
ACCEPTED 28 February 2023
PUBLISHED 10 March 2023

CITATION
Ruder AV, Temmerman L, van Dommelen JMA, Nagenborg J, Lu C, Sluimer JC, Goossens P and Biessen EAL (2023) Culture density influences the functional phenotype of human macrophages.
Front. Immunol. 14:1078591.
doi: 10.3389/fimmu.2023.1078591

Culture density influences the functional phenotype of human macrophages

Adele V. Ruder[1], Lieve Temmerman[1], Joep M.A. van Dommelen[1], Jan Nagenborg[1], Chang Lu[1], Judith C. Sluimer[1,2], Pieter Goossens[1†] and Erik A.L. Biessen[1,3*†]

[1]Cardiovascular Research Institute Maastricht (CARIM), Department of Pathology, Maastricht University Medical Center (UMC), Maastricht, Netherlands, [2]BHF Centre for Cardiovascular Science, University of Edinburgh, Edinburgh, United Kingdom, [3]Institute for Molecular Cardiovascular Research, RWTH Aachen University, Aachen, Germany

Macrophages (MΦ) are commonly cultured *in vitro* as a model of their biology and functions in tissues. Recent evidence suggests MΦ to engage in quorum sensing, adapting their functions in response to cues about the proximity of neighboring cells. However, culture density is frequently overlooked in the standardization of culture protocols as well as the interpretation of results obtained *in vitro*. In this study, we investigated how the functional phenotype of MΦ was influenced by culture density. We assessed 10 core functions of human MΦ derived from the THP-1 cell line as well as primary monocyte-derived MΦ. THP-1 MΦ showed increasing phagocytic activity and proliferation with increasing density but decreasing lipid uptake, inflammasome activation, mitochondrial stress, and secretion of cytokines IL-10, IL-6, IL-1β, IL-8, and TNF-α. For THP-1 MΦ, the functional profile displayed a consistent trajectory with increasing density when exceeding a threshold (of 0.2 x 10^3 cells/mm^2), as visualized by principal component analysis. Culture density was also found to affect monocyte-derived MΦ, with functional implications that were distinct from those observed in THP-1 MΦ, suggesting particular relevance of density effects for cell lines. With increasing density, monocyte-derived MΦ exhibited progressively increased phagocytosis, increased inflammasome activation, and decreased mitochondrial stress, whereas lipid uptake was unaffected. These different findings in THP-1 MΦ and monocyte-derived MΦ could be attributed to the colony-forming growth pattern of THP-1 MΦ. At the lowest density, the distance to the closest neighboring cells showed greater influence on THP-1 MΦ than monocyte-derived MΦ. In addition, functional differences between monocyte-derived MΦ from different donors could at least partly be attributed to differences in culture density. Our findings demonstrate the importance of culture density for MΦ function and demand for awareness of culture density when conducting and interpreting *in vitro* experiments.

KEYWORDS

macrophage, quorum sensing, culture density, *in vitro*, macrophage function

1 Introduction

Macrophages (MΦ) have attracted growing interest as a therapeutic target due to their dynamic role in various pathologies, including inflammatory diseases and cancer (1–3). Cell lines like THP-1, J774 or RAW264.7, or primary MΦ derived from bone marrow cells or blood monocytes are commonly used as models of human MΦ in biological assays or screening tools *in vitro* (1). To ensure reproducibility and comparability of results obtained from MΦ cultured *in vitro*, standardized cultivation protocols optimized for each cell type and assay are essential (4, 5). However, culture density at point of observation is an often-overlooked factor and either not specified at all or insufficiently substantiated by experimental data. Even though seeding density is usually mentioned and cells are often seeded at similar densities, differences in growing protocols, experimenters, and experimental conditions may result in density differences during experimentation. This is particularly worrisome in view of the reported importance of local contact and context for MΦ viability (6) and recent growing evidence of quorum sensing by MΦ (7).

Quorum sensing, a term adopted from bacteriology, refers to the modulation of gene expression by diffusible molecular cues (autoinducers) which convey information about density between cells (8–10). Quorum sensing had originally been established for biofilm formation of bacteria (8) but has recently also been observed in MΦ (7, 9, 11). In RAW264.7 MΦ, gelsolin was identified as autoinducer of programmed cell death 4 (PDCD4) expression which increased at higher cell density (11). Moreover, a quorum sensing mechanism has been observed in mice where the inflammation-resolving effect of nitric oxide (NO) was found to be dependent on the density of NO-producing MΦ (7).

Along with quorum sensing, cell density is vital for MΦ proliferation and viability. Indeed, MΦ were found to resume exponential growth faster (12), and to exhibit a more mature phenotype (13) and improved viability (12) at lower density. At higher density on the other hand, more MΦ adopted a high activation state (9). Moreover, culture density has been shown to influence several key functions of MΦ, including cytokine secretion (9, 13), polarization (13), phagocytosis (14), accumulation of esterified cholesterol (15), formation of multinucleated giant cells (16), and inhibition of mycobacterial growth (17). However, previous studies mostly compared two densities ("high" versus "low") for only a single function, and either focused on murine MΦ cell lines or on bone marrow-derived MΦ (BMDM). So far, a comprehensive study of the functional implications of density in human MΦ models is lacking. Failure to account for density differences may introduce bias as it remains unclear whether observed effects of a treatment agent are merely attributable to its effect on culture density, either by promoting proliferation and cell survival, or by inducing cell death.

The aim of this study was to investigate the influence of culture density on human MΦ function. Using high-throughput measurement of 10 functional parameters, we studied the phenotype of THP-1 MΦ as well as human primary monocyte-derived MΦ (MDM). Moreover, we considered the colony-forming growth pattern of THP-1 cells, and donor-specific differences in MDM as additional modulators of culture density-related functional changes.

2 Materials and methods

2.1 THP-1 cell culture and differentiation to MΦ

THP-1 cells were seeded at increasing densities in 96-well black clear-bottom imaging microplates (Corning #353219) in RPMI medium with HEPES and GlutaMAX (Gibco #72400-021) supplemented with 10% heat-inactivated (30 minutes at 56°C) fetal bovine serum (FBS; SERANA #S-FBS-SA-015) and 1% penicillin-streptomycin (Gibco #15070-063). Seeding densities were 5,000, 12,000, 21,000, 37,000, 53,000, 69,000, or 87,000 cells/well, denoted as x 10^3 cells/mm^2 (0.16, 0.38, 0.66, 1.16, 1.66, 2.16, or 2.72 x 10^3 cells/mm^2, respectively) that were rounded to one decimal digit to improve readability (0.2, 0.4, 0.7, 1.2, 1.7, 2.2, or 2.7 x 10^3 cells/mm^2, respectively). THP-1 cells were differentiated into MΦ by exposure to 2000 nM phorbol 12-myristate 13-acetate (PMA; Sigma #P1585) for 48 hours at 37°C, 5% CO_2 after which they were rested for 24 hours in fresh culture medium before performing the functional assays.

2.2 PBMC isolation, monocyte isolation, and differentiation to MΦ

Peripheral blood mononuclear cells (PBMCs) were isolated from leukocyte reduction system cones, a by-product of thrombopheresis of routine blood donations from healthy volunteers collected at the University Hospital RWTH Aachen, Germany, by density centrifugation with Lymphoprep™ (STEMCELL Technologies #07861). Isolated PBMCs were cryopreserved for later use in one-third freezing medium containing 75% FBS and 25% dimethyl sulfoxide (DMSO; Merck #102950). CD14 MicroBeads (Miltenyi #130-096-052) were used to positively select CD14+ monocytes, following the manufacturer's protocol. Monocytes of 6 donors were pooled before seeding at the respective densities in 96-well black clear-bottom imaging microplates, or kept separate and seeded in 384-well plates (Greiner Bio-One #781866) in culture medium containing RPMI medium with HEPES and GlutaMAX supplemented with 10% heat-inactivated FBS and 1% penicillin-streptomycin. Seeding densities were 30,000, 64,000, 98,000, 132,000, 166,000, or 200,000 cells/well, denoted as x 10^3 cells/mm^2 (0.94, 2.0, 3.06, 4.13, 5.19, or 6.25 x 10^3 cells/mm^2, respectively) that were rounded to integers to improve readability (1, 2, 3, 4, 5, or 6 x 10^3 cells/mm^2, respectively). At 384-well format, cells were plated at 13,000 cells/well. Monocytes were differentiated into MΦ with 100 ng/ml recombinant human macrophage colony-stimulating factor (M-CSF) (ImmunoTools #11343113) for 7 days at 37°C, 5% CO_2 with one medium change.

2.3 Functional high-throughput measurements

MΦ functions were assessed using the "MacroScreen" high-content analysis (HCA) platform developed in-house, a semi-automated microscale (96- to 384-well format) assay platform to perform an expanding range of fluorescence-based functional assays (18). All MacroScreen assays have been benchmarked against conventional mesoscale assays. Images were taken using the BD Pathway 855 automated fluorescent microscope (BD Biosciences) by taking 9 images per well with a 10x Olympus 0.40 NA objective (96-well format) or 20x Olympus 0.75 NA objective (384-well format). All experiments were performed in n=3-6 replicates. Images were analyzed with CellProfiler software version 4.0.4 (19) by creating a digital segmentation mask for each cell based on its nuclear staining signal using the IdentifyPrimaryObjects module followed by the ExpandOrShrinkObject module. Percentage of positive cells was measured using the MeasureObjectIntensity module followed by the ClassifyObjects module, which determines the amount of positive cells relative to the total number of segmented objects in the image. Distance to the closest neighboring cell was measured per image, for each cell, using the MeasureObjectNeighbors module in CellProfiler 4.0.4 (19).

2.4 Phagocytosis

Cells were incubated with 25 µl/ml pHrodo™ Red Zymosan Bioparticles™ (ThermoFisher Scientific #P35364) per well in culture medium for 1 hour at 37°C, 5% CO_2. Zymosan particles taken up by cells are reflected by tetramethyl rhodamine isothicyanate (TRITC) fluorescence signal. Nuclei were stained with Hoechst 33342 (Sigma #B2261) in culture medium for 10 minutes at 37°C, 5% CO_2 which was replaced by PBS before imaging.

2.5 Lipid uptake

Low-density lipoprotein (LDL) was isolated from serum of healthy volunteers *via* density centrifugation and oxidized using $CuSO_4$ as described previously (20). Cells were incubated with 8 µg/ml oxidized LDL (oxLDL) pre-mixed with 2 µg/ml TopFluor® Cholesterol (Avanti Polar Lipid #810255P) in culture medium for 3 hours at 37°C, 5% CO_2, reflected by fluorescein isothiocyanate (FITC) fluorescence signal. Nuclei were stained with Hoechst 33342 in culture medium for 10 minutes at 37°C, 5% CO_2 which was replaced by PBS before imaging.

2.6 Inflammasome

Cells were primed with 50 ng/ml LPS from E. coli (Invivogen #tlrl-eblps) for 3 hours at 37°C, 5% CO_2. 10 µM nigericin (Invivogen #tlrl-nig) for 1 hour at 37°C, 5% CO_2 served as second signal for inflammasome activation. Fc receptor was blocked with Fc receptor binding inhibitor antibody (Invitrogen #14-9161-73) before cells were fixed using 2% PFA with 5 mM EDTA in PBS and permeabilized using 5% FBS and 0.5% Triton X-100 in PBS for 20 minutes on ice. Next, the intracellular adapter protein apoptosis associated speck-like protein containing a CARD (ASC) was stained using PE-conjugated anti-ASC antibody (clone HASC-71; BioLegend #653904) overnight at 4°C. Nuclei were stained with Hoechst 33342 in PBS for 10 minutes on ice, and cells were washed with and imaged in PBS afterwards.

2.7 Mitochondrial stress

Mitochondrial stress was induced using 1200 nM staurosporine (Sigma #S4400) for 1 hour at 37°C, 5% CO_2. Mitochondria and nuclei were stained simultaneously with 250 nM MitoTracker™ Deep Red FM (ThermoFisher Scientific #M22426) and Hoechst 33342, respectively, in culture medium for 30 minutes at 37°C, 5% CO_2 before imaging in PBS. Alexa 594 fluorescence signal reflects mitochondrial staining dependent on membrane potential.

2.8 Proliferation

Cells were incubated with 10 µM 5'ethynyl-2'-deoxyuridine (EdU; ThermoFisher Scientific #A10044) for 2 hours at 37°C, 5% CO_2. Next, cells were fixated with 3.7% PFA in PBS for 15 minutes and washed twice with PBS before permeabilization with 0.1% Triton X-100 in PBS for 15 minutes. After another wash with PBS, Click-iT reaction cocktail (ThermoFisher Scientific #C10269) including Alexa Fluor 594 azide (ThermoFisher Scientific, #A10270) prepared according to the manufacturer's instructions was added. After 30 minutes, cells were washed with PBS and nuclei stained with Hoechst 33342 for 15 minutes. Cells were imaged in 1:5 KI quencher (1M KI in 10 mM KH_2PO_4) in PBS.

2.9 Multiplex ELISA

THP-1-derived MΦ were stimulated with 50 ng/ml LPS from E. coli for 6 hours at 37°C, 5% CO_2. Supernatant was collected and cytokine levels of IL-1β, IL-6, IL-8, IL-10, IL-12p70, and TNF-α were measured in a custom V-plex human cytokine ELISA (MSD Meso Scale Diagnostics) according to the manufacturer's protocol. Measured levels of IL-12p70 were close to or below the standard curve (0.1169 pg/ml), thus these data are not presented here.

2.10 Dimensionality reduction and visualization

We calculated the mean of the replicates for each feature of HCA functional data and cytokine data at the same density, resulting in a density-feature matrix with 7 rows (densities) and 10 columns (features/functions). The functional profile of THP-1 MΦ for the 7 different densities was analyzed in an integrated manner by two-dimensional Principal Component Analysis (PCA), where the relative contribution

of each individual function to the first (PC1) and second principal component (PC2) axes was visualized outside the X and Y axes.

2.11 Statistical analysis

Data are expressed as mean ± SEM, unless stated otherwise. Normal distribution was assessed by Shapiro-Wilkes normality test, and equality of variances by Brown-Forsythe test. For normally distributed data with equal variance, significance was assessed by one-way ANOVA followed by Tukey's multiple comparisons test at a significance level of $p < 0.05$. For normally distributed data with unequal variance, significance was assessed by Brown-Forsythe ANOVA and Dunnett's T3 multiple comparisons test, and Kruskal-Wallis test with Dunn's multiple comparisons test was used for not normally distributed data. All statistical analyses were performed using GraphPad Prism 8 software.

3 Results

3.1 Density influences the functional phenotype of MΦ

We assessed the functional phenotype of THP-1-derived MΦ seeded at 7 different densities ranging from 0.2 to 2.7 x 10^3 cells/mm^2 using the MacroScreen platform, an HCA platform based on several fluorescent imaging-based functional assays. For clarity's sake, we presented the p-values of all group comparisons for all assays in a significance matrix (Supplementary Table 1). As expected, the number of nuclei per fluorescent image increased with density in all high-content functional assays (Supplementary Figures 1A–E). No changes in the pH of the culture medium were observed. Whereas the phagocytic activity of THP-1 MΦ was found to increase with higher density (Figure 1A), uptake of oxLDL decreased (Figure 1B). MΦ seeded at 0.2 x 10^3 cells/mm^2, the lowest density in the tested density range, showed the highest inflammasome activation in response to LPS and nigericin (Figure 1C). Moreover, at lower densities, MΦ were found to be more resistant to staurosporine-induced mitochondrial stress (Figure 1D). Proliferation measured by EdU incorporation increased with density (Figure 1E). Secretion of the cytokines IL-10, IL-1β, IL-6, IL-8, and TNF-α in response to LPS stimulation was measured using multiplex ELISA, and was found to decrease with density, after an initial sharp increase between the two lowest densities included in the density range (0.2 and 0.4 x 10^3 cells/mm^2) (Figures 1F–J). PCA allowed separation of THP-1 MΦ seeded at different densities based on their functional profiles (Figure 1K). A large proportion of variation (61.27%) could be explained by PC1 which loadings included mitochondrial stress, lipid uptake, proliferation and phagocytosis, suggesting these functions to be mostly influenced by density. Variation along PC2 (largely attributable to inflammasome activation and cytokine secretion) almost exclusively manifested at the lowest density (0.2 x 10^3 cells/mm^2). Together, these data demonstrate the profound and variable impact of culture density on several THP-1 MΦ functions. Execution of certain functions may depend on exceeding a lower density threshold.

3.2 Density influences the functional phenotype of primary MΦ

We also investigated whether culture density influences the functional phenotype of human MDM, pooled from 6 healthy donors. A significance matrix with the p-values of all group comparisons can be found in Supplementary Table 2. As seen in THP-1 MΦ, the number of detected nuclei increased with increasing seeding density (Supplementary Figures 1F–I). Phagocytic activity increased in the lower densities but decreased again at seeding densities exceeding 3 x 10^3 cells/mm^2, possibly reflecting limited substrate (Figure 2A). Using a constant substrate-to-cell ratio, increased phagocytosis also at higher densities could be observed (Supplementary Figure 2). OxLDL uptake between MDM seeded at different densities was similar, contrary to THP-1 MΦ (Figure 2B). With increasing density, MDM demonstrated more inflammasome activation (Figure 2C) and were more susceptible to mitochondrial stress (Figure 2D). Overall, our findings show that density also affects primary MΦ and leads to changes in several functions. In MDM, these changes were less pronounced and less consistent compared to THP-1 MΦ, suggesting that the observed impact of density on MΦ function may be particularly relevant for cell lines.

3.3 Colony formation may contribute to density-dependent functional effects

We observed that THP-1 MΦ formed colonies in culture, especially if cultured at higher densities. Thus, we set out to study if at least part of the density-dependent functional changes may be attributed to changes in the colony-forming growth pattern of THP-1 cells. We assessed the association between the functional outcome of an index cell with its distance to the closest neighboring cell. Index cells that were close to neighboring cells had higher proliferation rates compared to MΦ in more scarcely populated niches (Figure 3A). However, at very low seeding density (0.2 x 10^3 cells/mm^2), MΦ proliferation was low regardless of the index cell's distance to neighboring cells, suggesting proliferation to be linked to colony formation. Similarly, we found that at a seeding density of 0.2 x 10^3 cells/mm^2, MΦ with neighboring cells in close proximity had taken up fewer fluorescent beads compared to equally dense MΦ seeded at higher densities (Figure 3B), a finding that was less pronounced for the uptake of oxLDL (Figure 3C). Interestingly, a similar proximity effect on phagocytosis and lipid uptake in MDM (Figures 3D, E), in which we did not observe colony formation in culture, was not apparent. These findings suggest that MΦ only exert certain functions beyond a local cell density threshold.

3.4 Functional differences between MDM of different donors may arise from density differences

Inter-donor variability has previously been proposed to compromise reproducibility of *in vitro* experiments with MDM (21, 22). Therefore, we looked at functions of MDM from 6 healthy

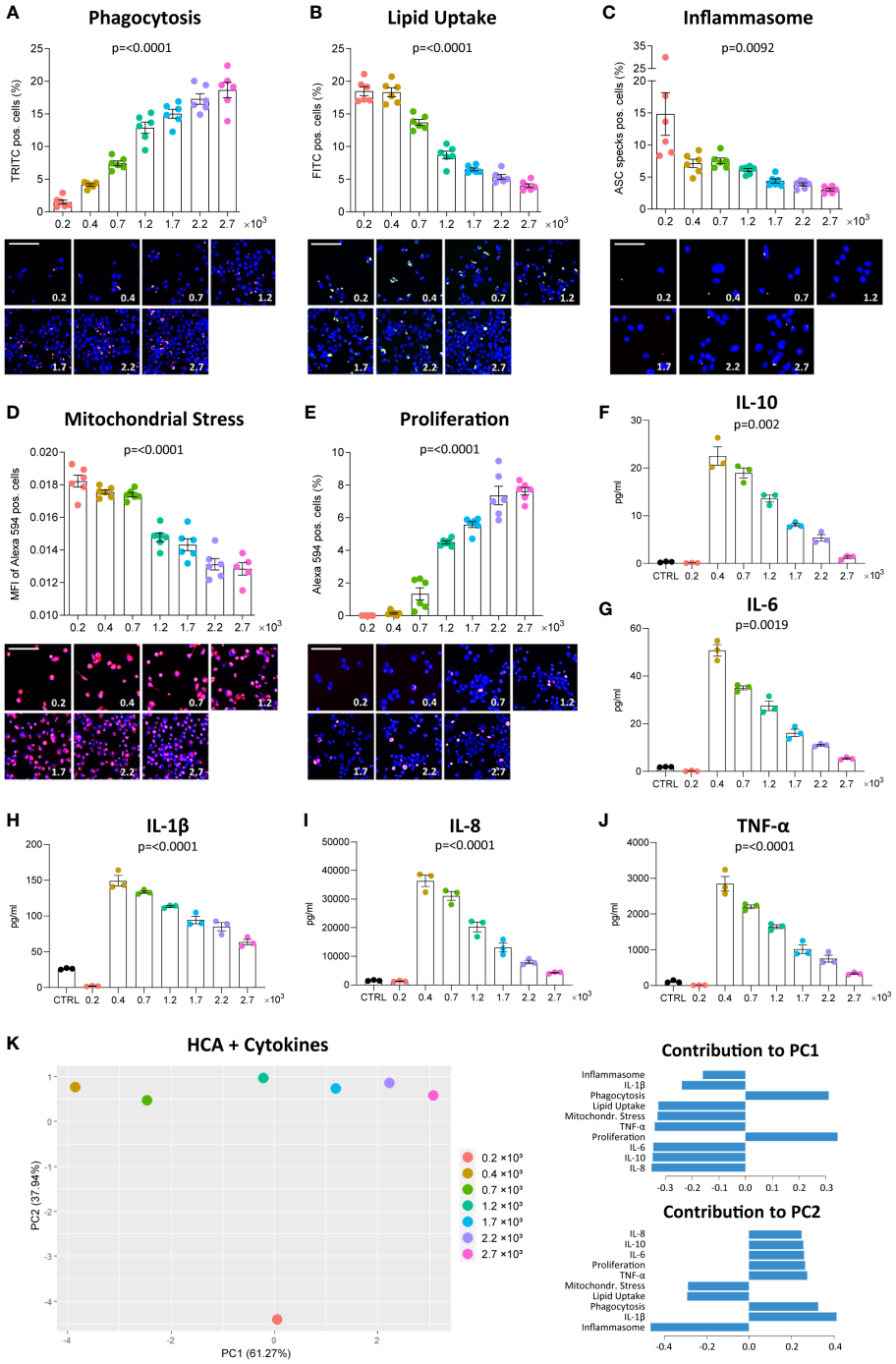

FIGURE 1
Density affects MΦ function. THP-1 cells were seeded at the respective densities (0.2-2.7 x 10^3 cells/mm^2) and differentiated with 2000 nM PMA for 48 hours followed by a resting period of 24 hours. Phagocytosis of zymosan-coated beads **(A**, red**)**, uptake of fluorescently-labelled oxLDL **(B**, green**)**, inflammasome activation **(C**, red**)**, mitochondrial stress in response to staurosporine **(D**, red**)** and EdU incorporation in proliferating cells **(E**, red**)** were assessed using the fluorescent imaging MacroScreen platform. Hoechst was used for nuclear labelling (blue). In the representative fluorescent images, the scale bar refers to 50 µM. In the representative images for the inflammasome assay, the scale bar refers to 25 µM. Secretion of IL-10 **(F)**, IL-6 **(G)**, IL-1β **(H)**, IL-8 **(I)**, and TNF-α **(J)** in response to 6-hour stimulation with 50 ng/ml LPS were measured by multiplex ELISA. Cells in the control (CTRL) condition were seeded at 1.7 x 10^3 cells/mm^2 and not stimulated with LPS. The indicated p-values refer to overall significance, p-values of all group comparisons can be found in Supplementary Table 1. **(K)** PCA plot of the high-content analysis (HCA) data and cytokine measurements with the factor loadings for PC1 and PC2. MFI: Mean fluorescence intensity.

donors (A-F) plated at the same density (13,000 cells/well). A significance matrix with the p-values of all group comparisons can be found in Supplementary Table 3. Differences in the number of nuclei (Figure 4A), phagocytosis (Figure 4B), oxLDL uptake (Figure 4C), inflammasome activation (Figure 4D) and mitochondrial stress (Figure 4E) between donors were apparent. Interestingly, MDM from donors A and B, which showed higher phagocytic activity and oxLDL uptake, also had a higher number of

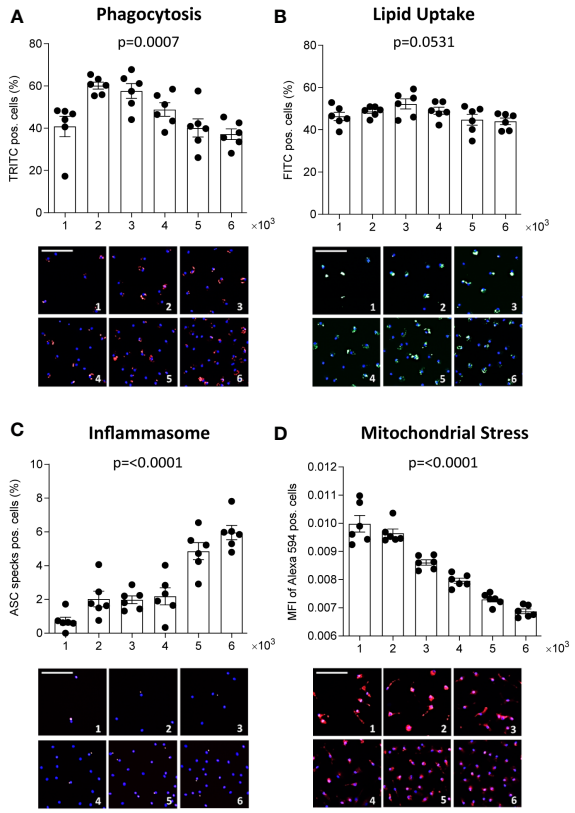

FIGURE 2
Density affects human primary MΦ function. CD14-positive monocytes were isolated from PBMCs of 6 healthy donors, pooled and seeded at the respective densities (1-6 x 10^3 cells/mm^2) and differentiated to MΦ using 100 ng/ml macrophage colony-stimulating factor (M-CSF) for 7 days. Phagocytic activity **(A**, red**)**, oxLDL uptake **(B**, green**)**, inflammasome activation **(C**, red**)**, and mitochondrial stress **(D**, red**)** were assessed using the MacroScreen platform. Hoechst was used for nuclear labelling (blue). The scale bar in the representative fluorescent images refers to 50 µM. The indicated p-values refer to overall significance, multiple comparison significance can be found in Supplementary Table 2. MFI: Mean fluorescence intensity.

nuclei compared to the other donors. This suggests that functional differences between MDM obtained from different donors may well be related to inter-donor differences in density, possibly resulting from differences in adherence and survival capacity.

4 Discussion

In vitro studies are an indispensable step in the screening of genes or drugs and the safety testing of compounds, before costly and time-consuming pre-clinical *in vivo* studies may commence (23). Parameters that should be considered for robust *in vitro* testing include the culture medium and supplements such as growth factors or antibiotics, the culture dish and its coating, and culture maintenance (24). In this study, we have shown that culture density, a frequently overlooked factor, is an at least equally important parameter with major impact on MΦ assay outcome. As we show, density affects the functional phenotype of both THP-1 MΦ and primary MDM, with individual functions showing distinct density responses. Moreover, our data suggest the distance of index cells to their neighbor cells to influence functionality of THP-1 MΦ but less so of MDM, and the functional profiles and density response to vary considerably between donors.

The effect of low and high culture density on individual MΦ functions has been studied previously. In BMDM, secretion of TNF-α and other cytokines (MCP-1, RANTES, MIP-1α and MIP-1β) was found to increase with cell density (9). However, another study found BMDM at higher density to secrete less pro-inflammatory cytokines, including IL-6 and TNF-α (13). These contradicting results may be explained by differences in applied seeding densities in the two studies, as these were approximately 10 times higher in the latter study. Although our study did not look at BMDM, our THP-1 MΦ results do support a decrease of cytokine secretion with increasing density. However, at the lowest density, cytokine secretion by THP-1 MΦ was at most marginal, suggesting a defective response of sparsely seeded MΦ to toll-like receptor (TLR) activation, potentially due to quiescence or compromised viability.

Although phagocytosis and lipid uptake are both clearance mechanisms, they showed a divergent density response pattern in both THP-1 MΦ and MDM. Previously, THP-1 MΦ seeded at a lower density were found to show a 5-fold higher accumulation of esterified cholesterol after exposure to acetylated LDL (acLDL), which the authors attributed to increased scavenger receptor activity and acLDL degradation (15). Moreover, murine peritoneal IC-21 MΦ showed decreased phagocytosis of latex beads when seeded at a higher density (14), which partly concurs with our findings in human primary MDM and can be attributed to the limited availability of beads per cell. Bead concentration should be increased if cells are cultured at higher density to ensure sufficient bead availability for all actively phagocytosing cells.

Primary cells or cell lines are frequently and often interchangeably used in MΦ *in vitro* studies; the latter offering the advantages of easier availability and culture maintenance, and a uniform genetic background which may increase reproducibility (21). A serious disadvantage of cell lines is that compared to primary cells, they are to a certain degree de-differentiated and show clear transcriptional and functional differences. For example, the murine J774A.1 MΦ cell line and BMDM were found to respond differently to mycobacterial infection (25). Often myeloma-derived or immortalized cell lines have aberrant contact inhibition and growth patterns (26); indeed, we found the proximity of neighboring cells to have a greater impact on THP-1 MΦ than MDM function. In THP-1 MΦ, this may be attributed to increased proliferation at closer proximity which is absent at lower density, and suggests quorum sensing to induce functional changes locally at sites of colony formation. Comparing primary human monocytes with the monocytic cell lines U-937, HL-60, and THP-1, the latter were found to most closely resemble primary monocytes (27). Nevertheless, in contrast to primary MDM, cell line-derived MΦ do not capture inter-donor variability. This might be evaded by iPSC-derived MΦ, although Vaughan-Jackson et al. recently demonstrated density-related effects also in iPSC, including a more rounded and less elongated morphology, decreased cytokine secretion, and altered surface marker expression at higher density (28). However, it could be argued that also primary MΦ in monocultures *in vitro* do

10.3389/fimmu.2023.1078591

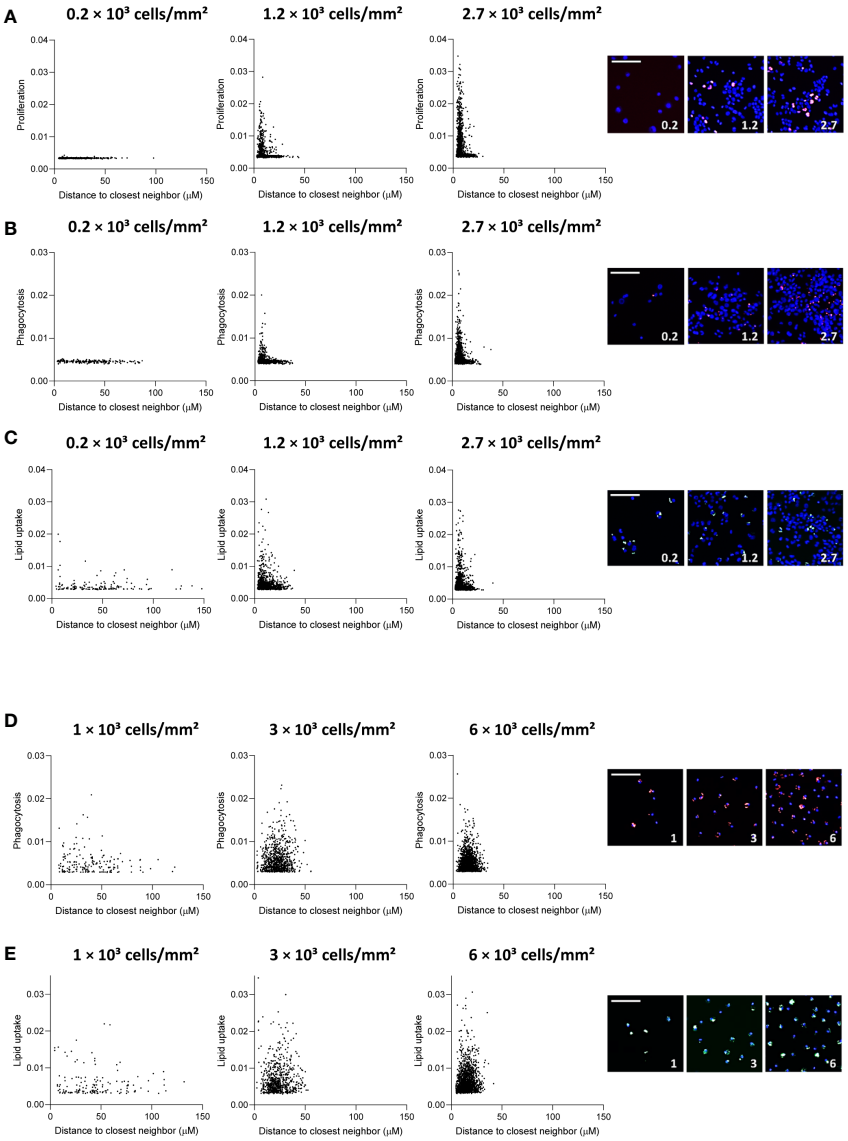

FIGURE 3
Distance to neighboring cells influences THP-1 function. Distance to closest neighbor was plotted against mean fluorescence intensity (MFI) per cell for proliferation **(A)**, phagocytosis **(B)** and lipid uptake **(C)** assays in THP-1 MΦ, and **(D)** phagocytosis and **(E)** lipid uptake assay in primary MDM, for 3 plating densities each. The scale bar corresponds to 50 µm.

not mirror the *in vivo* conditions, where MΦ are embedded in a local heterogenous tissue microenvironment with implications for cell function (21). The complex cellular and molecular microenvironment tissue MΦ are exposed to *in vivo* cannot be mimicked by exposure to a single or a few selected stimuli such as LPS and IFN-γ, or IL-4 and IL-10, as commonly done (29, 30).

Of note, we did not observe any indications for increased acidification of the culture medium which could explain the observed density effects and even at the highest density, the total cell number was most likely too low to deplete key nutrients. However, the comparability of our results on THP-1 MΦ and MDM may be impeded because different seeding densities had to be used due to the proliferating nature of the THP-1 cell line. In addition, the culturing process of MDM (7 days) and THP-1 MΦ (2 days PMA stimulation and 1 day resting) differs considerably. An extended resting period (5 days after 3 days PMA stimulation) has been shown to yield THP-1 MΦ with a phenotype closer to MDM (31). Moreover, the functional profile we provide here is not comprehensive as it only includes measurements of 5 cellular readouts and 5 cytokines. Future studies could reveal if the observed culture density effects also apply to other functions such as efferocytosis, susceptibility to apoptosis, production of reactive oxygen species (ROS), and metabolic differences.

In conclusion, our study highlights the importance of culture density for *in vitro* MΦ assay outcome and pleads for more awareness and closer monitoring of differences in cell density between conditions. This is particularly important for the THP-1 cell line which demonstrated more pronounced density effects compared to primary MDM, and when treatments are suspected to act pro-apoptotic or favor cell detachment or proliferation, which in turn impacts cell density. Moreover, a sufficiently large donor pool should be

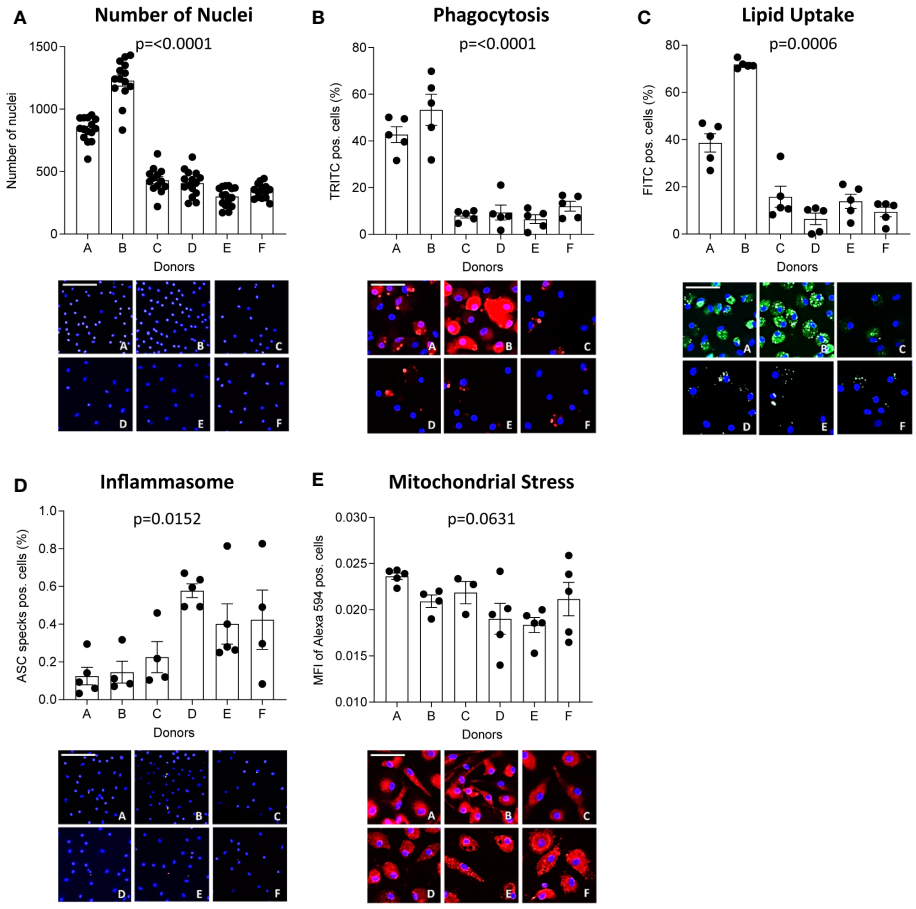

FIGURE 4
MΦ function differs between donors. CD14-positive monocytes of 6 healthy donors were seeded at 13,000 cells/well and differentiated into MΦ for 7 days using 100 ng/ml macrophage colony-stimulating factor (M-CSF). The number of nuclei per donor at experimentation **(A)** is given. Their functional phenotype was assessed using the MacroScreen platform: phagocytosis **(B**, red**)**, lipid uptake **(C**, green**)**, inflammasome activation **(D**, red**)**, and mitochondrial stress **(E**, red**)**. The scale bar corresponds to 25 μM. The indicated p-values refer to overall significance, multiple comparison significance can be found in Supplementary Table 3. MFI: Mean fluorescence intensity.

used in experiments with primary MDM to account for inter-donor variability, as the number of cells after differentiation and culture differed between donors despite seeding at the same density. Disregarding density differences may lead to secondary effects on MΦ functions, and thus misinterpretation of findings.

Data availability statement

The raw data supporting the conclusions of this article will be made available by the authors, without undue reservation.

Author contributions

AR, JN, LT, PG and EB contributed to the conception and design of the study. AR, JD and JN carried out the experiments. CL performed the bioinformatic analyses. PG, LT, JS and EB contributed to the interpretation of results. AR wrote the manuscript with input from all authors. All authors contributed to the article and approved the submitted version.

Funding

This work was supported by the European Research Area Network Joint Transnational Call for Cardiovascular Disease (ERA-CVD; JTC-2017t100 AtheroMacHete to P.G. and E.A.L.B.), the Netherlands Organisation for Scientific Research (NWO)/São Paulo Research Foundation (FAPESP; DNAMoving to L.T. and E.A.L.B.), NWO-STW (#13568 Barcoding the Obese to E.A.L.B., L.T, and A.V.R.), NWO-VIDI (#91718364 to J.C.S.) and ASPASIA grant (#015.013.064 to J.S.C.), the Dutch Heart Foundation (Dekker 2020T042 to P.G.) and the Chinese Scholarship Council (CSC, #201706990018 to C.L.).

Conflict of interest

The authors declare that the research was conducted in the absence of any commercial or financial relationships that could be construed as a potential conflict of interest.

Publisher's note

All claims expressed in this article are solely those of the authors and do not necessarily represent those of their affiliated organizations, or those of the publisher, the editors and the reviewers. Any product that may be evaluated in this article, or claim that may be made by its manufacturer, is not guaranteed or endorsed by the publisher.

Supplementary material

The Supplementary Material for this article can be found online at: https://www.frontiersin.org/articles/10.3389/fimmu.2023.1078591/full#supplementary-material

References

1. Rodell CB, Koch PD, Weissleder R. Screening for new macrophage therapeutics. *Theranostics* (2019) 9(25):7714–29. doi: 10.7150/thno.34421

2. Wynn TA, Chawla A, Pollard JW. Macrophage biology in development, homeostasis and disease. *Nature* (2013) 496(7446):445–55. doi: 10.1038/nature12034

3. Zhang C, Yang M, Ericsson AC. Function of macrophages in disease: Current understanding on molecular mechanisms. *Front Immunol* (2021) 12:620510. doi: 10.3389/fimmu.2021.620510

4. Baker M. Reproducibility: Respect your cells! *Nature* (2016) 537(7620):433–5. doi: 10.1038/537433a

5. Hirsch C, Schildknecht S. *In vitro* research reproducibility: Keeping up high standards. *Front Pharmacol* (2019) 10:1484. doi: 10.3389/fphar.2019.01484

6. Guilliams M, Scott CL. Does niche competition determine the origin of tissue-resident macrophages? *Nat Rev Immunol* (2017) 17(7):451–60. doi: 10.1038/nri.2017.42

7. Postat J, Olekhnovitch R, Lemaître F, Bousso P. A metabolism-based quorum sensing mechanism contributes to termination of inflammatory responses. *Immunity* (2018) 49(4):654 65.e5. doi: 10.1016/j.immuni.2018.07.014

8. Miller MB, Bassler BL. Quorum sensing in bacteria. *Annu Rev Microbiol* (2001) 55(1):165–99. doi: 10.1146/annurev.micro.55.1.165

9. Muldoon JJ, Chuang Y, Bagheri N, Leonard JN. Macrophages employ quorum licensing to regulate collective activation. *Nat Commun* (2020) 11(1):878. doi: 10.1038/s41467-020-14547-y

10. Chen C-C, Wang L, Plikus Maksim V, Jiang Ting X, Murray Philip J, Ramos R, et al. Organ-level quorum sensing directs regeneration in hair stem cell populations. *Cell* (2015) 161(2):277–90. doi: 10.1016/j.cell.2015.02.016

11. Sharma RK, Goswami B, Das Mandal S, Guha A, Willard B, Ray PS. Quorum sensing by gelsolin regulates programmed cell death 4 expression and a density-dependent phenotype in macrophages. *J Immunol* (2021) 207(5):1250–64. doi: 10.4049/jimmunol.2001392

12. Zhuang JC, Wogan GN. Growth and viability of macrophages continuously stimulated to produce nitric oxide. *Proc Natl Acad Sci U.S.A.* (1997) 94(22):11875–80. doi: 10.1073/pnas.94.22.11875

13. Lee CM, Hu J. Cell density during differentiation can alter the phenotype of bone marrow-derived macrophages. *Cell Biosci* (2013) 3:30. doi: 10.1186/2045-3701-3-30

14. Vishniakova KS, Kireev II, Dunina-Barkovskaya AY. Effects of cell culture density on phagocytosis parameters in ic-21 macrophages. *Biochem (Moscow) Supplement Ser A: Membrane Cell Biol* (2011) 5(4):355–63. doi: 10.1134/S1990747811050138

15. Rodriguez A, Kafonek SD, Georgopoulos A, Bachorik PS. Cell density can affect cholesteryl ester accumulation in the human thp-1 macrophage. *J Lipid Res* (1994) 35 (11):1909–17. doi: 10.1016/S0022-2275(20)39937-5

16. Trout KL, Holian A. Factors influencing multinucleated giant cell formation in vitro. *Immunobiology* (2019) 224(6):834–42. doi: 10.1016/j.imbio.2019.08.002

17. Boechat N, Bouchonnet F, Bonay M, Grodet A, Pelicic V, Gicquel B, et al. Culture at high density improves the ability of human macrophages to control mycobacterial growth. *J Immunol* (2001) 166(10):6203–11. doi: 10.4049/jimmunol.166.10.6203

18. Fontaine MAC, Jin H, Gagliardi M, Rousch M, Wijnands E, Stoll M, et al. Blood milieu in acute myocardial infarction reprograms human macrophages for trauma repair. *Advanced Sci* (2023) 10(5):2203053. doi: 10.1002/advs.202203053

19. Lamprecht MR, Sabatini DM, Carpenter AE. Cellprofiler: Free, versatile software for automated biological image analysis. *Biotechniques* (2007) 42(1):71–5. doi: 10.2144/000112257

20. Redgrave TG, Roberts DC, West CE. Separation of plasma lipoproteins by density-gradient ultracentrifugation. *Anal Biochem* (1975) 65(1-2):42–9. doi: 10.1016/0003-2697(75)90488-1

21. Chanput W, Mes JJ, Wichers HJ. Thp-1 cell line: An in vitro cell model for immune modulation approach. *Int Immunopharmacol* (2014) 23(1):37–45. doi: 10.1016/j.intimp.2014.08.002

22. Rey-Giraud F, Hafner M, Ries CH. *In vitro* generation of monocyte-derived macrophages under serum-free conditions improves their tumor promoting functions. *PLoS One* (2012) 7(8):e42656. doi: 10.1371/journal.pone.0042656

23. Sivinski SE, Mamedova LK, Rusk RA, Elrod CC, Swartz TH, McGill JM, et al. Development of an in vitro macrophage screening system on the immunomodulating effects of feed components. *J Anim Sci Biotechnol* (2020) 11(1):89. doi: 10.1186/s40104-020-00497-4

24. Riss TL, Moravec RA, Duellman SJ, Niles AL. Treating cells as reagents to design reproducible assays. *SLAS DISCOVERY: Advancing Sci Drug Discovery* (2021) 26 (10):1256–67. doi: 10.1177/24725552211039754

25. Andreu N, Phelan J, de Sessions PF, Cliff JM, Clark TG, Hibberd ML. Primary macrophages and J774 cells respond differently to infection with mycobacterium tuberculosis. *Sci Rep* (2017) 7(1):42225. doi: 10.1038/srep42225

26. Rennert K, Nitschke M, Wallert M, Keune N, Raasch M, Lorkowski S, et al. Thermo-responsive cell culture carrier: Effects on macrophage functionality and detachment efficiency. *J Tissue Eng* (2017) 8:2041731417726428. doi: 10.1177/2041731417726428

27. Riddy DM, Goy E, Delerive P, Summers RJ, Sexton PM, Langmead CJ. Comparative genotypic and phenotypic analysis of human peripheral blood monocytes and surrogate monocyte-like cell lines commonly used in metabolic disease research. *PLoS One* (2018) 13(5):e0197177. doi: 10.1371/journal.pone.0197177

28. Vaughan-Jackson A, Stodolak S, Ebrahimi KH, Johnson E, Reardon PK, Dupont M, et al. Density dependent regulation of inflammatory responses in macrophages. *Front Immunol* (2022) 13. doi: 10.3389/fimmu.2022.895488

29. Chen H-J, Li Yim AYF, Griffith GR, de Jonge WJ, Mannens MMAM, Ferrero E, et al. Meta-analysis of in vitro-differentiated macrophages identifies transcriptomic signatures that classify disease macrophages in vivo. *Front Immunol* (2019) 10:2887. doi: 10.3389/fimmu.2019.02887

30. Luque-Martin R, Mander PK, Leenen PJM, Winther MPJ. Classic and new mediators for in vitro modelling of human macrophages. *J Leukoc Biol* (2021) 109 (3):549–60. doi: 10.1002/JLB.1RU0620-018R

31. Daigneault M, Preston JA, Marriott HM, Whyte MKB, Dockrell DH. The identification of markers of macrophage differentiation in PMA-stimulated THP-1 cells and monocyte-derived macrophages. *PLoS One* (2010) 5(1):e8668. doi: 10.1371/journal.pone.0008668

CYTOKINES/SOLUBLE FACTORS' PROFILE IN DISEASES AS DIAGNOSTIC/PROGNOSTIC MARKERS

frontiers | Frontiers in Immunology

TYPE Original Research
PUBLISHED 27 September 2022
DOI 10.3389/fimmu.2022.946730

OPEN ACCESS

EDITED BY
Diana Boraschi,
Shenzhen Institute of Advanced Technology (SIAT), (CAS), China

REVIEWED BY
Federico Pratesi,
University of Pisa, Italy
Hanlet Camacho,
Center for Genetic Engineering and Biotechnology (CIGB), Cuba

*CORRESPONDENCE
Esther Gómez-Sánchez,
esther.gomez.sanchez@uva.es

†These authors have contributed equally to this work and share senior authorship

SPECIALTY SECTION
This article was submitted to Cytokines and Soluble Mediators in Immunity, a section of the journal Frontiers in Immunology

RECEIVED 17 May 2022
ACCEPTED 13 September 2022
PUBLISHED 27 September 2022

CITATION
Sánchez-de Prada L, Gorgojo-Galindo Ó, Fierro I, Martínez-García AM, de Quintana GS-L, Gutiérrez-Bustillo R, Pelaez-Jareño MT, Álvarez-Fuente E, Gómez-Sánchez E, Tamayo E, Tamayo-Velasco Á and Martín-Fernández M (2022) Time evolution of cytokine profiles associated with mortality in COVID-19 hospitalized patients.
Front. Immunol. 13:946730.
doi: 10.3389/fimmu.2022.946730

Time evolution of cytokine profiles associated with mortality in COVID-19 hospitalized patients

Laura Sánchez-de Prada[1,2], Óscar Gorgojo-Galindo[1,3], Inmaculada Fierro[4], Ana María Martínez-García[2], Guillermo Sarmentero-López de Quintana[5], Rocío Gutiérrez-Bustillo[1,5], María Teresa Pelaez-Jareño[5], Elisa Álvarez-Fuente[5], Esther Gómez-Sánchez[1,3,5*], Eduardo Tamayo[1,3,5,6†], Álvaro Tamayo-Velasco[1,6,7†] and Marta Martín-Fernández[1,6,8†]

[1]BioCritic, Group for Biomedical Research in Critical Care Medicine, Valladolid, Spain, [2]Microbiology and Immunology Department, Hospital Clínico Universitario de Valladolid, Valladolid, Spain, [3]Department of Surgery, Faculty of Medicine, Universidad de Valladolid, Valladolid, Spain, [4]Faculty of Health Science, Universidad Europea Miguel de Cervantes, Valladolid, Spain, [5]Anesthesiology and Critical Care Department, Hospital Clínico Universitario de Valladolid, Valladolid, Spain, [6]Centro de Investigación Biomédica en Red de Enfermedades Infecciosas (CIBERINFEC), Instituto de Salud Carlos III, Madrid, Spain, [7]Haematology and Hemotherapy Department, Hospital Clínico Universitario de Valladolid, Valladolid, Spain, [8]Department of Medicine, Faculty of Medicine, Universidad de Valladolid, Valladolid, Spain

Background: High cytokine levels have been associated with severe COVID-19 disease. Although many cytokine studies have been performed, not many of them include combinatorial analysis of cytokine profiles through time. In this study we investigate the association of certain cytokine profiles and its evolution, and mortality in SARS-CoV2 infection in hospitalized patients.

Methods: Serum concentration of 45 cytokines was determined in 28 controls at day of admission and in 108 patients with COVID-19 disease at first, third and sixth day of admission. A principal component analysis (PCA) was performed to characterize cytokine profiles through time associated with mortality and survival in hospitalized patients.

Results: At day of admission non-survivors present significantly higher levels of IL-1α and VEGFA (PC3) but not through follow up. However, the combination of HGF, MCP-1, IL-18, eotaxine, and SCF (PC2) are significantly higher in non-survivors at all three time-points presenting an increased trend in this group through time. On the other hand, BDNF, IL-12 and IL-15 (PC1) are significantly reduced in non-survivors at all time points with a decreasing trend through time, though a protective factor. The combined mortality prediction accuracy of PC3 at day 1 and PC1 and PC2 at day 6 is 89.00% ($p<0.001$).

10.3389/fimmu.2022.946730

Conclusions: Hypercytokinemia is a hallmark of COVID-19 but relevant differences between survivors and non-survivors can be early observed. Combinatorial analysis of serum cytokines and chemokines can contribute to mortality risk assessment and optimize therapeutic strategies. Three clusters of cytokines have been identified as independent markers or risk factors of COVID mortality.

KEYWORDS

COVID-19, cytokines, mortality, principal component analysis - PCA, hospitalized patients

Introduction

Coronavirus disease 2019 (COVID-19) has emerged as a global infectious respiratory disease caused by a novel betacoronavirus: the SARS- CoV-2 (severe acute respiratory syndrome coronavirus 2) (1, 2). Since its emergence in December 2019 until December 2021, it has infected nearly 300 million people and killed more than 5 million people across the world (3). COVID-19 infection displays a wide clinical presentation ranging from asymptomatic or mild symptoms to severe pneumonia and critical respiratory failure (4). Due to its complex physiopathology, prognosis at hospital admission remains a challenge.

Severe COVID-19 has been associated with an acute hyperimmune response known as "cytokine storm" or "cytokine release syndrome" (CRS) contributing to multiorgan failure (5). Recent studies suggest its relation to an impaired type I IFN immunity (6, 7). That hypercytokinemia, has been correlated with respiratory failure, ARDS and adverse clinical outcomes (8–10). Cytokines released by immune cells in case of uncontrolled inflammation, have been studied as markers and profiles of severity to predict outcomes (11–16). Although individual cytokine analysis can shed some light on COVID-19 pathology, the immune responses are complex, and a combinatorial analysis could better explain the relations between cytokine levels. Previous studies with principal component analysis (PCA) and transcriptomic have determined the cytokine profiles regarding COVID-19 severity and mortality (7, 17–19). However, differences between the different cytokine profiles and how they evolve through time in hospitalized patients, comparing mortality and survival has not been performed yet.

In this study, we aimed to establish the timeline of different cytokine profiles that help to predict patient outcome in order to anticipate, adapt treatment and improve survival.

Materials and methods

Study design

We performed a prospective study at Hospital Clínico of Valladolid (Spain). A total of 108 patients with RT-PCR-confirmed SARS-CoV2 infection and were recruited from late March to 11th April of 2020. Patients with other active infections or a terminal chronic disease were excluded. Patients were divided into two groups according to the occurrence of mortality. In addition, 28 age and gender matched healthy volunteers with a negative RT-PCR test for SARS-CoV2 infection were also recruited during routine pre-anesthetic evaluation for scheduled surgery. The present study was approved by the Valladolid Hospital's Clinical Ethics Committee (CEIm) (cod: PI 20-1717) and all subjects provided a written informed consent.

Plasma samples were collected the first, third and sixth day of hospital admission in 3.2% sodium citrate tubes and centrifuged at 2000 g for 20 minutes at room temperature. Plasma was aliquoted and stored at -80°C until used.

Cytokine analysis

Concentration of 45 cytokines in plasma was determined by 45-plex Human XL Cytokine Luminex Performance Panel (R&D), following manufacturer instructions. The cytokines analyzed are the following ones: BDNF, EGF, eotaxin (also known as CCL11), FGF-2, GM-CSF, GRO-α (CXCL1), HGF, IFN-α, IFN-γ, IL-1α, IL-1 β, IL-10, IL-12 p70, IL-13, IL-15, IL-17a (CTLA-18), IL-18, IL-1RA, IL-2, IL-21, IL-22, IL-23, IL-27, IL-31, IL-4, IL-5, IL-6, IL-7, IL-8 (also known as CXCL8), IL-9, IP-1 beta (CCL4), IP-10 (CXCL10), LIF, MCP-1 (CCL2), MIP-1α (CCL3), NGF-β, PDGF-BB, PIGF-1, RANTES (CCL5), SCF, SDF-1α, TNF-α, TNF- β, VEGF-A, and VEGF-D.

Statistical analysis

Since most of the cytokine data did not follow a normal distribution, continuous variables were presented in terms of median (interquartile range, IQR) and compared among groups using the Mann-Whitney U-test or T-test. Categorical variables were described as count and percentages, which were compared using the $\chi 2$ test or Fisher exact test, when appropriate.

Distributions of the cytokine values were assessed and log2 transformed to render the principal component analysis (PCA). PCA was carried out with all variables related to cytokine concentrations that showed significant differences between survivors and non-survivors in the univariate analysis, on at least one of the three analyzed days. All participants for whom the variables of interest were available were included in the final analysis and no assumptions were made for missing data. Prior to extraction of factors, Kaiser-Meyer-Olkin (KMO) measure of sampling adequacy and the Bartlett test of sphericity were checked to evaluate the fitness of the data for factor analysis. The factor solution was formed based on the eigenvalues, which represent the amount of variance captured by given components. Factors with eigenvalues >1.0 were retained, according to the Kaiser-Guttman criterion and the Scree Plot. Then we optimized the factor solution using varimax rotation. A factor-based-score was calculated for each component, and we estimated the factor scores on all COVID-19 patients at the first, third and sixth day of admission.

To assess changes over time in outcome measures within each group, Friedman's repeated measures test with Dunn's multiple comparison test was used for non-parametric data and a repeated-measures analysis of variance (RM-ANOVA) with Tukey's multiple comparison test for parametric data.

A multivariable logistic regression analysis was performed to estimate the relevance of each factor obtained in the PCA analysis, differentiating the profile of the patients who survived versus those who did not survive 28 days after admission. The logistic regression model was internally validated by performing bootstrap resampling (1000 resamples). The area under the receiver operating characteristic curves (AUC ROC) shows the accuracy for the final logistic regression model and individual predictors. All statistical analyses were performed using SPSS version 28.0 for Windows (SPSS, Inc, Chicago, Ill). A p-value of less than 0.05 was regarded as statistically significant.

Results

Characteristics of the patients

A total of 108 hospitalized subjects admitted with clinical SARS-CoV-2 pneumonia were enrolled, of whom 20 died within 28 days after admission and composed the non-survivors' group. The other 88 patients were included in the survivors' group. Baseline characteristics of patients are reported in Table 1. The group of non-survivors was significantly older than the other group. There were no differences in terms of gender and comorbidities between groups. Considering the analytical variables, non-survivors presented higher levels of glycaemia, creatinine, leukocytes, neutrophils, procalcitonin, CRP, D-dimer and LDH. There were no significant differences in clinical outcomes referring to the percentage of patients with invasive mechanical ventilation and length of stay in hospital and intensive care unit.

Cytokine profile

In bivariate analysis, the levels of 10 cytokines were different ($p< 0.05$), at least in one of the three moments (1, 3 and 6 days) between survivors and non-survivors (Tables S1-3). On the first day of admission (Table S1), significant differences were observed regarding HGF, IL-2, IL-1α, IL-15 and VEGFA levels. IL-15 and IL-2 were the only cytokines whose levels were significantly reduced by half in the group of non-survivors at 28 days. The rest of cytokines were significantly increased in this group. Specifically, IL-1α and VEGFA quadrupled and doubled their levels, respectively. On the third day of admission (Table S2), differences between groups were found in the case of BDNF, eotaxin, IL-18 and again HGF and IL-15 levels. In non-survivors, levels of HGF and IL-18 were significantly higher, where HGF tripled the levels compared to survivors. On the other hand, levels of BDNF, eotaxin and IL-15 were significantly lower in this group. Finally, on the sixth day of admission (Table S3), cytokines significantly elevated in non-survivors were SCF, MCP-1, IL-18, VEGFA and HGF. The exception became again IL-15, which barely showed variation over time, and whose levels in non-survivors remained the half of those in survivors. IL-18 increased its levels compared to day 3 of admission; and VEGFA, which significantly doubled the level on the first day of admission, tripled the levels in non-survivors on the sixth day. However, HGF stands out as the only cytokine that remained significantly elevated in the group of non-survivors through all three measurement times, reaching its maximum peak and difference compared to survivors, on the sixth day of admission.

Some of these 10 cytokines and chemokines (IL-1a, IL-2, IL-15, IL-18, eotaxin, HGF, MCP-1, SCF and VEGFA) have been linked to different aspects of COVID-19 disease, its severity and even mortality but a combinatorial analysis can help us to understand its complex interaction. Principal component analysis (PCA) is a technique for reducing the dimensionality of such datasets, increasing interpretability but at the same time minimizing information loss.

10.3389/fimmu.2022.946730

TABLE 1 Clinical characteristics of the patients. Data are represented as [median (IQR)] and as [% (n)].

	Non-survivors at 28 days (N=20)	Survivors (N=88)	p-value
Age in years [median (IQR)]	73.5 (14)	67 (17)	0.017
Male [n (%)]	12 (60)	47 (53.4)	0.593
Comorbidities [n (%)]			
Smoking	4 (20)	5 (5.7)	0.059
Coronary disease	2 (10)	8 (9.1)	1.000
Atrial fibrillation	4 (20)	8 (9.1)	0.229
Diabetes	5 (25)	14 (15.9)	0.340
Neurological disease	1 (5)	1 (1.1)	0.337
Stroke	0 (0)	1 (1.1)	1.000
Hypertension	11 (55)	39 (44.3)	0.460
Liver disease	1 (5)	1 (1.1)	0.337
Obesity	2 (10)	8 (9.1)	1.000
COPD	2 (10)	5 (5.7)	0.611
Kidney disease	2 (10)	1 (1.1)	0.087
Laboratory. [median (IQR)]			
Glycaemia (mg/dL)	198 (227)	106 (67.25)	<0.001
Creatinine (mg/dL)	0.995 (0.86)	0.815 (0.23)	0.007
Total bilirubin (mg/dL)	0.5 (0.58)	0.5 (0.39)	0.482
Leukocytes ($x10^9$/L)	8.16 (10.23)	6.41 (3.72)	0.042
Lymphocytes ($x10^9$/L)	0.72 (0.74)	1 (0.56)	0.185
Neutrophil ($x10^9$/L)	7125 (9590)	4725 (3272.5)	0.016
Procalcitonin (ng/ml)	0.3 (0.57)	0.09 (0.195)	<0.001
Platelet ($x10^9$/L)	195 (95.25)	208 (117)	0.512
CRP (mg/L)	160 (190)	76 (95.5)	0.003
Ferritin (μg/L)	1024.5 (113.25)	671 (1107)	0.126
D-dimer (mg/L)	2029 (23629.25)	711 (769.5)	0.015
LDH (mmol/L)	385 (183.25)	306 (96.25)	0.002
Clinical outcomes			
Invasive mechanical ventilation [n (%)]	12 (60)	21 (23.9)	0.122
Length of hospital stay [days.median (IQR)]	15.5 (11.75)	11 (13.5)	0.153
Length of ICU stay [days. median (IQR)]	17.5 (8.75)	20 (19.5)	0.253

IQR, interquartile range; COPD, chronic obstructive pulmonary disease; CRP, C-Reactive protein; ICU, intensive care unit.

Principal component analysis

The Kaiser-Meyer-Olkin measure of sampling adequacy (0.7) and the Bartlett test of sphericity ($p < 0.001$) indicated that the factor matrix was adequate for data (Table S4).

PCA resulted in three components with eigenvalues greater than one that describe relationships between cytokines' levels in patients with COVID-19. The three components accounted for 66.09% of the total variance. PC1, PC2, and PC3 accounted for 32.63%, 19.14%, and 14.32% of the variance, respectively. PC1 is composed by IL-15, IL-2 and BDNF; PC2 by HGF, MCP-1, IL-18, eotaxin and SCF; and PC3 by IL-1α and VEGFA. Figure 1 show three-dimensional score plot illustrating how cytokines were distributed on PCs.

The algorithms of the principal components were applied to all patients and calculated scores were saved as new variables PC1, PC2 and PC3 at the first, third and sixth day of admission.

Principal components score in COVID patients vs control group

In addition, the algorithms of the principal components were applied to the control group and the PCA scores (PC1, PC2 y PC3) were compared between COVID-19 and healthy SARS-CoV-2-negative control subjects on the day of admission. The calculated scores were higher in COVID-19 patients than in controls: PC1 ($t_{(52.26)}= 3.53$; p=0.001); PC2 (U= 988.00; p=

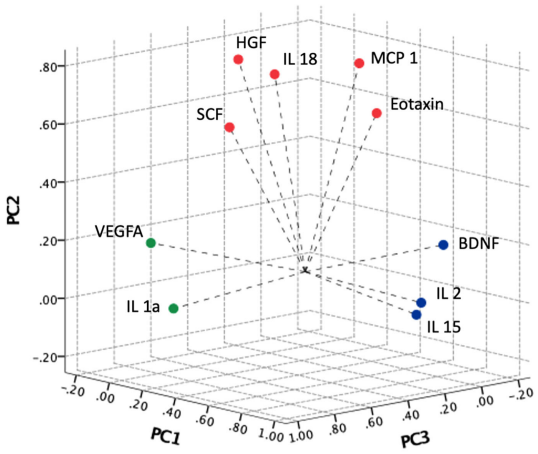

Rotated Component Matrix

	Component 1	2	3
IL15	.888	-.008	.194
IL2	.866	.025	.148
BDNF	.749	.182	-.078
HGF	-.126	.744	.251
MCP1	.206	.732	-.109
IL18	-.010	.697	.157
Eotaxin	.420	.600	-.011
SCF	.091	.568	.494
IL1a	.183	.002	.882
VEGFA	.005	.200	.845

FIGURE 1
Component plot in rotated space. Results of principal component analysis (PCA) and Varimax rotation method with Kaiser normalization. The three components accounted for 66.09% of the total variance.

0.005); PC3 (U= 1111.00; p= 0.031). These values let us confirm that those cytokines are different between infected and healthy subjects, emphasizing the importance of these cytokines in COVID-19 infection.

Principal components score in survivors *vs* non-survivors

Figure 2 shows PC1, PC2 and PC3 scores at the first, third and sixth day of admission for survivors and non-survivors. In Figure 2A, significant differences are observed between both groups. Mortality was associated with lower scores of PC1 and higher scores of PC2 and PC3. This indicates that higher scores in PC1 are protective while PC2 and PC3 represent risk factors. In contrast to PC3, which is only significantly elevated in non-survivors at day one; the differences between survivors and non-survivors in the cytokines of PC1 and PC2 intensified through time. Figure 2B shows that in the first 6 days of hospitalization, the mean score is stable and significantly lower for patients who survived than for those who died. In addition, a growing trend is observed for this marker in patients who did not survive.

Multivariate analysis of principal components associated with mortality at 28 days

Sex and age between both groups were not significant variables in the final adjusted model. Logistic regression analysis (Table S5) showed that on the day of admission, only the combination of cytokines defined by PC3 was significant [OR: 2.35, 95%CI: 1.09-5.06, p=0.029]. In contrast, PC1 and PC2 were significant on the sixth day of admission, where PC1 cytokines represented a protective factor relative to mortality at 28 days [OR: 0.273, 95%CI: 0.12-0.64, p=0.003] while PC2 was pointed out as the major risk factor [OR: 5.24, 95%CI: 2.03-13.48, p=0.001]. ROC curves of significant factors and predicted probability for final logistic regression model are shown in Figure 3. The area under the curve (AUC= 0.89, 95%CI= 0.81-0.96, p <0.001) shows a good discrimination ability of the model.

Discussion

Several studies have been carried out comparing cytokine profiles in severe and moderate COVID-19 (20–23). However, there are fewer studies comparing differences in cytokine profiles between survivors and non-survivors or analyzing the relationship between the evolution of cytokines profile in COVID-19 hospitalized patients and mortality (17, 24). Severe disease is characterized by acute lung injury (ALI) that can eventually lead to highly lethal acute respiratory distress syndrome (ARDS) and a cytokine storm (25, 26). Previous studies have associated the significant elevation of many cytokines such as IL-2, IL-7, IL-10, GSCF, IP-10, MCP-1, MIP-1a and TNF-α in the blood of patients with severity of the disease. Particularly the level of IL-6 and IL-10 (27–30). However, we found three cytokine clusters (PC1, PC2 and PC3) that could be considered as independent risk factors. Their different contribution would be associated to a higher or lower mortality risk. On one hand, IL-2, IL-15 and BDNF levels (PC1) are significantly reduced in the group of non-survivors, which

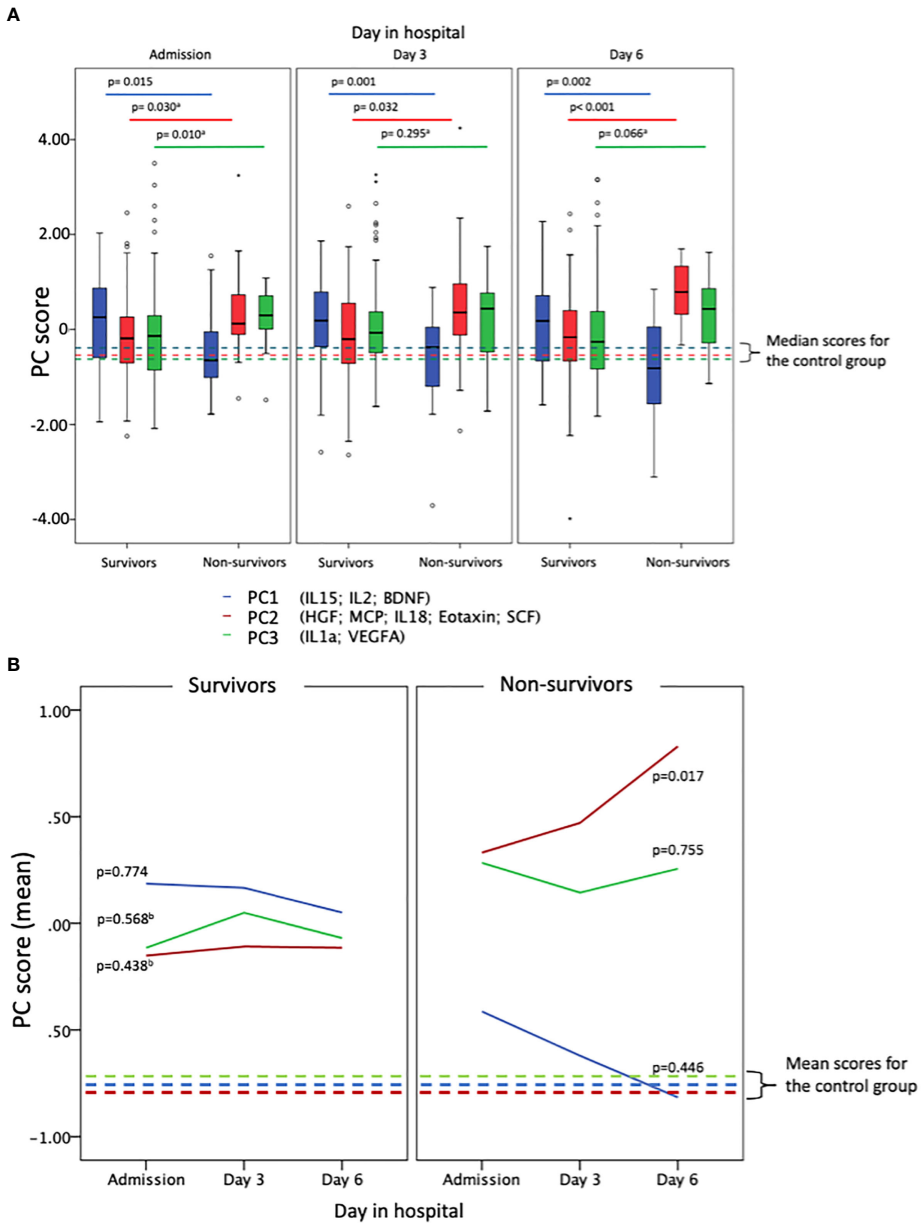

FIGURE 2
PC scores for COVID patients (survivors and non-survivors) and controls when applying PC estimators. In blue PC1 groups IL-15; IL-2 and BDNF. In red PC2 groups HGF; MCP1; IL-18; eotaxin and SCF. In green PC3 groups IL-1a and VEGFA. **(A)** Box-plots shows the different contribution of each of the factors obtained in the analysis of principal components for survivors and non-survivors, showing, in addition, three moments in the evolution of the disease (first, third and sixth days of admission of the patients). **(B)** Shows that in the first 6 days of hospitalization, the mean score is stable and significantly lower for patients who survived than for those who died. In addition, a growing trend is observed for this marker in patients who did not survive. Trends over time of the PC scores for survivors and non-survivors were calculated separately by using RM-ANOVA or Friedman test.

suggests they constitute a protective factor. In contrast, cytokines included in PC2 (HGF, SCF, IL-18, MCP-1 and eotaxin) together with the combination of PC3 (IL-1α and VEGFA) are significantly increased in non-survivors representing a risk factor for mortality at 28 days. It is interesting that, while PC1 and PC2 are significantly reduced and increased, respectively, at the three stages evaluated; PC3 only showed to be significantly increased in non-survivors at the day of admission. In addition, whereas no trend is observed in PC1 or PC3, PC2 seems to display an increasing trend through time.

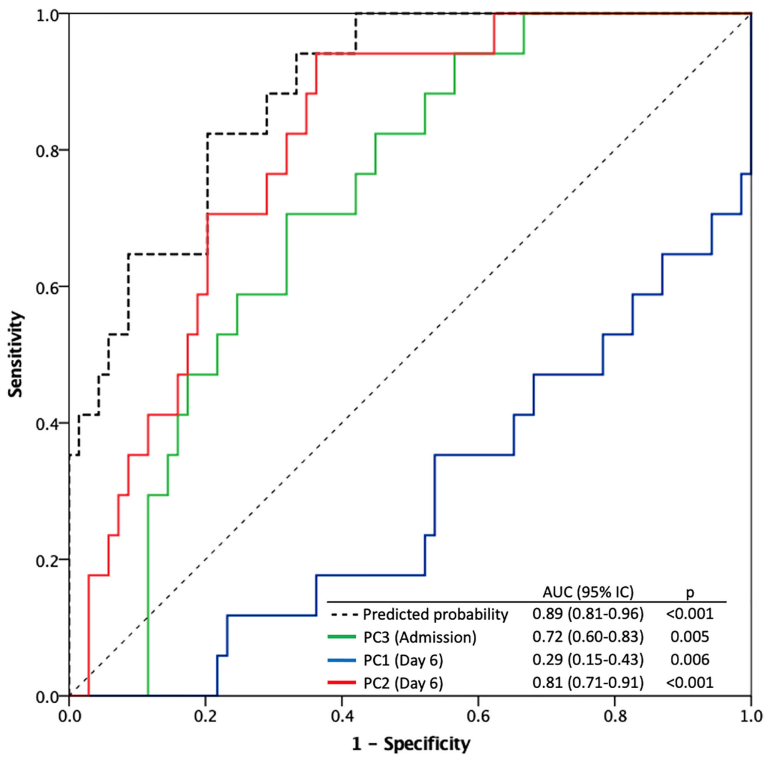

FIGURE 3
Receiver operating characteristic (ROC) curves for the predicted probability of the logistic regression model and significant predictors for 28-day mortality (PC3 at the day of admission, PC1 and PC2 at the sixth day after admission).

PC3, constituted by the combination of IL-1α and VEGFA is only significantly increased at day of admission. The importance of this set at day 0 may be explained by its implication in the initial response to COVID-19 severe infection. Initial COVID-19 studies revealed higher levels of IL-1α, which is a cytokine of initial states of the innate immune response (31). Actually, IL-1α has recently been described as an early marker to predict a bad outcome in COVID-19 severe patients (23). This could be explained by the fact that the precursor of IL-1α, in contrast to IL-1β or IL-1ra, does not need to be activated and is capable of triggering a powerful inflammatory response when it is released by damaged cells (32). Its main biological activities are activation of T lymphocytes, and B cell proliferation along with synthesis of immunoglobulins (31). On the other hand, VEGFA has a key role in lung development resulting in an appropriate organization of the pulmonary vascular network (33). VEGFA can be released during hypoxia, in inflammatory situations where there is damage to the endothelium. Its effect is mediated by VEGFR-1 and VEFGR-2 that contribute to hematopoiesis and monocyte chemotaxis and increased permeability, respectively. PC3 component could be interpreted as the initial expression of the existence of a severe cell damage in lungs due to macrophage infiltration produced by SARS-CoV-2 virus (34), which would initiate the subsequent fatal pathogenesis and exacerbate the immune response observed in following stages of disease. As a matter of fact, our results support previous studies that prove the early use in severe disease of treatments with IL-1 antagonists such as anakinra, improves outcome by blocking progression of the cytokine storm (35).

Our results showed that despite cytokine levels were increased in both survivors and non-survivors, in the first group levels remain similar through time. However, there is a significant upward trend in PC2 in non-survivors through time, which could remark their importance as mortality markers, as they are particularly elevated at day 6. The cytokines of PC2 are HGF, SCF, IL-18, MCP-1 and eotaxin. The importance of PC2 is that, altogether, represent the intense and probably irretrievable damage in lung tissue due to the virus itself as well as the extreme immune response. First, IL-18, a cytokine belonging to the IL-1 family and intervening in cellular immune response it is secreted upon macrophage activation in viral infections and courses with endothelial damage in lung tissue (32). IL-18 binds in its mature form to specific receptor IL-1 receptor 5 (IL-1R5, known as IL-18 receptor alpha chain), leading to the recruitment of the coreceptor, IL-1 receptor 7 (IL-1R7, known as IL-18 receptor

beta chain). IL-18BP, a natural inhibitor of IL-18, circulates maintaining a balance between both of them. Severe COVID-19 patients have been shown to have an imbalance of IL-18/IL-18BP (36, 37). Actually, an antibody against IL-1R7 has been proposed to reduce inflammatory signalling of IL-18 in COVID-19 patients (38). SCF, HGF and eotaxin are upregulated by inflammatory processes and secreted by mast cells upon cytokine stimulation including IL-18. All of them have also been related to severe lung injury. Eotaxin and SCF play a central role in mast cell and eosinophilic infiltration and, SCF promotes the expression and release of MCP-1 from lung mast cells (39–41). In addition, HGF can promote the development of different cell lineages, including thrombocytes, as to contribute to tissue repair and modulate the adaptive immune response to control inflammation (15, 42). Worthy of remark is that HGF and eotaxin were found to be elevated in patients with severe influenza A (H1N1) virus and other viral infections and in patients with inflammatory lung injury (43–46).. Finally, we have MCP-1, which has been previously described as a factor to predict severity in COVID-19 patients due to its activity in monocyte recruitment to arterial wall (47). More than 70% of the deaths related to COVID-19 are associated with deregulation of the mechanisms that control blood clotting, as a part of the innate immune response to limit pathogen spread in a process known as immunothrombosis (48, 49). Moreover, hypoxic environment due to pulmonary affection activates pro-coagulation factors that may promote thrombosis (50). In our work, both MCP-1 and D-dimer are elevated in non-survivors indicating thrombotic events were taking place. Taking together PC2, has a potential as a marker of bad prognosis due to extreme inflammation and lung injury.

According to the logistic regression model, the most contributing factor to survival in this case is a protective factor for mortality that involves high plasma levels of the cytokines IL-2, IL-15 and BDNF in survivors compared to those determined in deceased patients. The elevation of the plasmatic levels of some of these three cytokines would, therefore, increase this protective factor. BNDF has a pivotal role in neuroplasticity that is considerably affected by inflammatory states. The most common pro-inflammatory cytokines are IL-1β, IL-6, TNF-α and IFN-γ cause a significant reduction of BDNF gene expression (51). In fact, low serum BDNF levels were correlated with severe SARS-CoV-2 infection in a recent study where BDNF levels were restored during patients´ recovery. This has been linked to the lymphopenia observed in critical COVID-19 patients as lymphocytes contribute to peripheral BNDF secretion (52). IL-2 and IL-15 have several similar functions. Both cytokines stimulate the proliferation of T cells; induce the generation of cytotoxic T lymphocytes; facilitate the proliferation of B cells as well as immunoglobulin secretion; and induce generation and persistence of natural killer cells (53). On one hand, IL-15 has a pivotal role in viral clearance by long-lasting, high avidity T-cell responses to invading pathogens by ensuring survival of memory cells. Actually, influenza and other respiratory viruses induce peripheral and local expression of IL-15, which is critical for anti-viral responses by different lymphocyte populations. Low levels of circulating IL-15 have been associated with high viremia and poor disease outcome (54). On the other hand, IL-2 is involved in maintenance of peripheral regulatory T cells and elimination of self-reactive ones (53). What is more important, both IL-2 and IL-15 can regulate cell proliferation, thus controlling excessive response (31).The progressive decrease of BDNF, IL-15 and IL-2 in plasma may be a warning factor of disease deterioration in severe patients with COVID-19 pneumonia. For that matter, IL-2 and IL-15 supplementation have been proposed as to improve the immune disorder and reduce mortality (55, 56).

The independence of the three factors suggests three possible independent therapeutic pathways of intervention. One aimed at stopping the initial proinflammatory response by blocking IL-1 and VEGFA. Other aimed at regulating the immune response by increasing IL-15 levels, IL-2 and BDNF. And other aimed at limiting lung tissue by interfering with HGF, SCF, IL-18, MCP-1 or eotaxin. As a multiphasic disease, immune monitoring and multiple targets would be a great approach to improve outcomes.

The main limitations of the study are that we only performed a plasma analysis including 45 cytokines. This means some relevant cytokines in severity of COVID-19, might not be included. However, we selected this panel as it was the most complete available for cytokine analysis and eligible for clinical implementation. As future directions, we considered it would be interesting to confirm our results, especially in relevant cytokines by a classic ELISA analysis. In addition, we consider it would be interesting to evaluate cytokine profiles in healthy population and how these levels correlate with clinical parameters and outcomes. Also, a further multicentric corroboration of our findings would be of interest.

Conclusions

In summary our findings unravel the cytokine evolution in relation to mortality caused by COVID-19 disease. We propose the use of PC2 associated with clinical data as a marker of strong lung damage, and evolution of values of PC1 and PC3 to predict outcome thus personalize treatment. In addition, we consider early target of the markers of dysregulation of immune responses and therapies to promote tissue repair could be a better approach in severe patients as antiviral therapy could not be useful at that point.

Data availability statement

The raw data supporting the conclusions of this article will be made available by the authors, without undue reservation.

Ethics statement

This study was reviewed and approved by Valladolid Hospital's Clinical Ethics Committee (CEIm) (cod: PI 20-1717). The patients/participants provided their written informed consent to participate in this study.

Author contributions

All authors contributed to the article and approved the submitted version. EG-S, ET, AT-V and MM-F designed the methodology of the study. AM-G, GQ, RG-B, MP-J and EA-F collected the samples and clinical data. AT-V and LSP supervised the laboratory work. IF-L performed the statistical analysis and prepared the figures with the help of ET and MM-F. LSP and OG-G prepared the original draft. All authors contributed to the article and approved the submitted version.

Funding

This work was supported by Instituto de Salud Carlos III (COV20/00491, PI18/01238, CIBERINFEC CB21/13/00051), Junta de Castilla y León (VA321P18, GRS 1922/A/19, GRS 2057/A/19), Consejería de Educación de Castilla y León (VA256P20) and Fundación Ramón Areces (CIVP19A5953). LSP received a Río Hortega grant (CM20/00138) from Instituto Carlos III (Co-funded by European Regional Development Fund/European Social Fund "A way to make Europe"/"Investing in your future").

Conflict of interest

The authors declare that the research was conducted in the absence of any commercial or financial relationships that could be construed as a potential conflict of interest.

Publisher's note

All claims expressed in this article are solely those of the authors and do not necessarily represent those of their affiliated organizations, or those of the publisher, the editors and the reviewers. Any product that may be evaluated in this article, or claim that may be made by its manufacturer, is not guaranteed or endorsed by the publisher.

Supplementary material

The Supplementary Material for this article can be found online at: https://www.frontiersin.org/articles/10.3389/fimmu.2022.946730/full#supplementary-material

References

1. Zhu N, Zhang D, Wang W, Li X, Yang B, Song J, et al. A novel coronavirus from patients with pneumonia in China, 2019. *New Engl J Med* (2020) 382:727–33. doi: 10.1056/NEJMoa2001017

2. Wang Q, Zhang Y, Wu L, Niu S, Song C, Zhang Z, et al. Structural and functional basis of SARS-CoV-2 entry by using human ACE2. *Cell* (2020) 181:894–904.e9. doi: 10.1016/j.cell.2020.03.045

3. World Health Organisation (WHO). *WHO coronavirus (COVID-19) dashboard* (2021). Available at: https://covid19.who.int/ (Accessed July 27, 2022).

4. Huang C, Wang Y, Li X, Ren L, Zhao J, Hu Y, et al. Clinical features of patients infected with 2019 novel coronavirus in wuhan, China. *Lancet* (2020) 395:497–506. doi: 10.1016/S0140-6736(20)30183-5

5. Azkur AK, Akdis M, Azkur D, Sokolowska M, van de Veen W, Brüggen M-C, et al. Immune response to SARS-CoV-2 and mechanisms of immunopathological changes in COVID-19. *Allergy* (2020) 75:1564–81. doi: 10.1111/all.14364

6. Galani I-E, Rovina N, Lampropoulou V, Triantafyllia V, Manioudaki M, Pavlos E, et al. Untuned antiviral immunity in COVID-19 revealed by temporal type I/III interferon patterns and flu comparison. *Nat Immunol* (2021) 22(1):32–40. doi. doi: 10.1038/s41590-020-00840-x

7. Hadjadj J, Yatim N, Barnabei L, Corneau A, Boussier J, Smith N, et al. *Impaired type I interferon activity and inflammatory responses in severe COVID-19 patients* . Available at: https://www.science.org (Accessed May 17, 2022).

8. Moore JB, June CH. Cytokine release syndrome in severe COVID-19. *Sci (1979)* (2020) 368:473–4. doi: 10.1126/science.abb8925

9. Pedersen SF, Ho Y-C. SARS-CoV-2: A storm is raging. *J Clin Invest* (2020) 130:2202–5. doi: 10.1172/JCI137647

10. Quartuccio L, Fabris M, Sonaglia A, Peghin M, Domenis R, Cifù A, et al. Interleukin 6, soluble interleukin 2 receptor alpha (CD25), monocyte colony-stimulating factor, and hepatocyte growth factor linked with systemic hyperinflammation, innate immunity hyperactivation, and organ damage in COVID-19 pneumonia. *Cytokine* (2021) 140:155438. doi: 10.1016/j.cyto.2021.155438

11. Meizlish ML, Pine AB, Bishai JD, Goshua G, Nadelmann ER, Simonov M, et al. A neutrophil activation signature predicts critical illness and mortality in COVID-19. *Blood Adv* (2021) 5:1164–77. doi: 10.1182/bloodadvances.2020003568

12. Hafezi B, Chan L, Knapp JP, Karimi N, Alizadeh K, Mehrani Y, et al. Cytokine storm syndrome in SARS-CoV-2 infections: A functional role of mast cells. *Cells* (2021) 10:1761. doi: 10.3390/cells10071761

13. Soy M, Keser G, Atagündüz P, Tabak F, Atagündüz I, Kayhan S. Cytokine storm in COVID-19: pathogenesis and overview of anti-inflammatory agents used in treatment. *Clin Rheumatol* (2020) 39:2085–94. doi: 10.1007/s10067-020-05190-5

14. Wang J, Jiang M, Chen X, Montaner LJ. Cytokine storm and leukocyte changes in mild versus severe SARS-CoV-2 infection: Review of 3939 COVID-19 patients in China and emerging pathogenesis and therapy concepts. *J Leukocyte Biol* (2020) 108:17–41. doi: 10.1002/JLB.3COVR0520-272R

15. Perreau M, Suffiotti M, Marques-Vidal P, Wiedemann A, Levy Y, Laouénan C, et al. The cytokines HGF and CXCL13 predict the severity and the mortality in COVID-19 patients. *Nat Commun* (2021) 12:4888. doi: 10.1038/s41467-021-25191-5

16. Gao R, Cao B, Hu Y, Feng Z, Wang D, Hu W, et al. Human infection with a novel avian-origin. *New Engl J Med* (2013) 368:1888–97. doi: 10.1056/NEJMoa1304459

17. Dorgham K, Quentric P, Gökkaya M, Marot S, Parizot C, Sauce D, et al. Distinct cytokine profiles associated with COVID-19 severity and mortality. *J Allergy Clin Immunol* (2021) 147:2098–107. doi: 10.1016/j.jaci.2021.03.047

18. Lucas C, Wong P, Klein J, Castro TBR, Silva J, Sundaram M, et al. Longitudinal analyses reveal immunological misfiring in severe COVID-19. *Nature* (2020) 584:463. doi: 10.1038/s41586-020-2588-y

19. Van der Wijst MGP, Vazquez SE, Hartoularos GC, Bastard P, Grant T, Bueno R, et al. Type I interferon autoantibodies are associated with systemic immune alterations in patients with COVID-19. *Sci Transl Med* (2021) 13(612): eabh2624. doi: 10.1126/SCITRANSLMED.ABH2624

20. Zhang X, Tan Y, Ling Y, Lu G, Liu F, Yi Z, et al. Viral and host factors related to the clinical outcome of COVID-19. *Nature* (2020) 583:437–40. doi: 10.1038/s41586-020-2355-0

21. Liu J, Li S, Liu J, Liang B, Wang X, Wang H, et al. Longitudinal characteristics of lymphocyte responses and cytokine profiles in the peripheral blood of SARS-CoV-2 infected patients. *EBioMedicine* (2020) 55:102763. doi: 10.1016/j.ebiom.2020.102763

22. Bindoli S, Felicetti M, Sfriso P, Doria A. The amount of cytokine-release defines different shades of sars-Cov2 infection. *Exp Biol Med* (2020) 245:970–6. doi: 10.1177/1535370220928964

23. Tamayo-Velasco Á, Martínez-Paz P, Peñarrubia-Ponce MJ, de la Fuente I, Pérez-González S, Fernández I, et al. HGF, IL-1α, and IL-27 are robust biomarkers in early severity stratification of COVID-19 patients. *J Clin Med* (2021) 10(9):2017. doi: 10.3390/jcm10092017

24. Zhang L, Han C, Zhang S, Duan C, Shang H, Bai T, et al. Diarrhea and altered inflammatory cytokine pattern in severe coronavirus disease 2019: Impact on disease course and in-hospital mortality. *J Gastroenterol Hepatol (Australia)* (2021) 36:421–9. doi: 10.1111/jgh.15166

25. Qin C, Zhou L, Hu Z, Zhang S, Yang S, Tao Y, et al. Dysregulation of immune response in patients with coronavirus 2019 (COVID-19) in wuhan, China. *Clin Infect Dis* (2020) 71:762–8. doi: 10.1093/cid/ciaa248

26. Ragab D, Salah Eldin H, Taeimah M, Khattab R, Salem R. The COVID-19 cytokine storm; what we know so far. *Front Immunol* (2020) 11:1446. doi: 10.3389/fimmu.2020.01446

27. Han H, Ma Q, Li C, Liu R, Zhao L, Wang W, et al. Profiling serum cytokines in COVID-19 patients reveals IL-6 and IL-10 are disease severity predictors. *Emerging Microbes Infections* (2020) 9:1123–30. doi: 10.1080/22221751.2020.1770129

28. Tsang K, Zhong NS. SARS: Pharmacotherapy. *Respirology* (2003) 8:S25–30. doi: 10.1046/j.1440-1843.2003.00525.x

29. Sun X, Wang T, Cai D, Hu Z, Chen J, Liao H, et al. Cytokine storm intervention in the early stages of COVID-19 pneumonia. *Cytokine Growth Factor Rev* (2020) 53:38–42. doi: 10.1016/j.cytogfr.2020.04.002

30. Chen G, Wu D, Guo W, Cao Y, Huang D, Wang H, et al. Clinical and immunological features of severe and moderate coronavirus disease 2019. *J Clin Invest* (2020) 130:2620–9. doi: 10.1172/JCI137244

31. Borish LC, Steinke JW. 2. cytokines and chemokines. *J Allergy Clin Immunol* (2003) 111:S460–75. doi: 10.1067/mai.2003.108

32. Slaats J, ten Oever J, van de Veerdonk FL, Netea MG. IL-1β/IL-6/CRP and IL-18/ferritin: Distinct inflammatory programs in infections. *PloS Pathog* (2016) 12:1–13. doi: 10.1371/journal.ppat.1005973

33. Shannon JM, Wikenheiser-Brokamp KA, Greenberg JM. 2 - lung growth and development. In: Broaddus VC, Mason RJ, Ernst JD, King TE, Lazarus SC, Murray JF, Nadel JA, Slutsky AS, Gotway MB, editors. *Murray And nadel's textbook of respiratory medicine (Sixth edition)*. Philadelphia: W.B. Saunders: Elsevier (2016). p. 22–31.e4. doi: 10.1016/B978-1-4557-3383-5.00002-6

34. Wang C, Xie J, Zhao L, Fei X, Zhang H, Tan Y, et al. Alveolar macrophage dysfunction and cytokine storm in the pathogenesis of two severe COVID-19 patients. *EBioMedicine* (2020) 57:102833. doi: 10.1016/j.ebiom.2020.102833

35. Cauchois R, Koubi M, Delarbre D, Manet C, Carvelli J, Blasco VB, et al. Early IL-1 receptor blockade in severe inflammatory respiratory failure complicating COVID-19. *Proc Natl Acad Sci U.S.A.* (2020) 117:18951–3. doi: 10.1073/pnas.2009017117

36. Dinarello CA, Novick D, Kim S, Kaplanski G. Interleukin-18 and IL-18 binding protein. *Front Immunol* (2013) 4:289. doi: 10.3389/fimmu.2013.00289

37. Kerget B, Kerget F, Aksakal A, Aşkın S, Sağlam L, Akgün M. Evaluation of alpha defensin, IL-1 receptor antagonist, and IL-18 levels in COVID-19 patients with macrophage activation syndrome and acute respiratory distress syndrome. *J Med Virol* (2021) 93:2090–8. doi: 10.1002/jmv.26589

38. Li S, Jiang L, Beckmann K, Højen JF, Pessara U, Powers NE, et al. A novel anti-human IL-1R7 antibody reduces IL-18-mediated inflammatory signaling. *J Biol Chem* (2021) 296:100630. doi: 10.1016/J.JBC.2021.100630

39. Huaux F, Gharaee-Kermani M, Liu T, Morel V, McGarry B, Ullenbruch M, et al. Role of eotaxin-1 (CCL11) and CC chemokine receptor 3 (CCR3) in bleomycin-induced lung injury and fibrosis. *Am J Pathol* (2005) 167:1485–96. doi: 10.1016/S0002-9440(10)61235-7

40. Hemelaers L, Louis R. Eotaxin: an important chemokine in asthma. *Rev medicale Liege* (2006) 61:223–6.

41. Reber L, da Silva CA, Frossard N. Stem cell factor and its receptor c-kit as targets for inflammatory diseases. *Eur J Pharmacol* (2006) 533:327–40. doi: 10.1016/j.ejphar.2005.12.067

42. Ilangumaran S, Villalobos-Hernandez A, Bobbala D, Ramanathan S. The hepatocyte growth factor (HGF)-MET receptor tyrosine kinase signaling pathway: Diverse roles in modulating immune cell functions. *Cytokine* (2016) 82:125–39. doi: 10.1016/j.cyto.2015.12.013

43. Bradley-Stewart A, Jolly L, Adamson W, Gunson R, Frew-Gillespie C, Templeton K, et al. Cytokine responses in patients with mild or severe influenza A(H1N1)pdm09. *J Clin virology : Off Publ Pan Am Soc Clin Virol* (2013) 58:100–7. doi: 10.1016/j.jcv.2013.05.011

44. Takigawa N, Segawa Y, Maeda Y, Takata I, Fujimoto N. Serum hepatocyte growth factor/scatter factor levels in small cell lung cancer patients. *Lung Cancer* (1997) 17:211—218. doi: 10.1016/s0169-5002(97)00651-x

45. Higa F, Akamine M, Furugen M, Hibiya K, Koide M, Tamayose M, et al. Hepatocyte growth factor levels in legionella pneumonia: A retrospective study. *BMC Infect Dis* (2011) 11:74. doi: 10.1186/1471-2334-11-74

46. Kawaguchi M, Kokubu F, Kuga H, Tomita T, Matsukura S, Suzaki H, et al. Influenza virus a stimulates expression of eotaxin by nasal epithelial cells. *Clin Exp Allergy* (2001) 31:873–80. doi: 10.1046/j.1365-2222.2001.01103.x

47. Chen Y, Wang J, Liu C, Su L, Zhang D, Fan J, et al. IP-10 and MCP-1 as biomarkers associated with disease severity of COVID-19. *Mol Med* (2020) 26:97. doi: 10.1186/s10020-020-00230-x

48. Wichmann D, Sperhake J-P, Lütgehetmann M, Steurer S, Edler C, Heinemann A, et al. Autopsy findings and venous thromboembolism in patients with COVID-19. *Ann Internal Med* (2020) 173:268–77. doi: 10.7326/M20-2003

49. Nicolai L, Leunig A, Brambs S, Kaiser R, Joppich M, Hoffknecht ML, et al. Vascular neutrophilic inflammation and immunothrombosis distinguish severe COVID-19 from influenza pneumonia. *J Thromb Haemostasis* (2021) 19:574–81. doi: 10.1111/jth.15179

50. Pujhari S, Paul S, Ahluwalia J, Rasgon JL. Clotting disorder in severe acute respiratory syndrome coronavirus 2. *Rev Med Virol* (2021) 31:1–5. doi: 10.1002/rmv.2177

51. Calabrese F, Rossetti AC, Racagni G, Gass P, Riva MA, Molteni R. Brain-derived neurotrophic factor: A bridge between inflammation and neuroplasticity. *Front Cell Neurosci* (2014) 8:430. doi: 10.3389/fncel.2014.00430

52. Azoulay D, Shehadeh M, Chepa S, Shaoul E, Baroum M, Horowitz NA, et al. Recovery from SARS-CoV-2 infection is associated with serum BDNF restoration. *J Infection* (2020) 81:e79–81. doi: 10.1016/j.jinf.2020.06.038

53. Waldmann TA. The biology of interleukin-2 and interleukin-15: Implications for cancer therapy and vaccine design. *Nat Rev Immunol* (2006) 6:595–601. doi: 10.1038/nri1901

54. Verbist KC, Klonowski KD. Functions of IL-15 in anti-viral immunity: Multiplicity and variety. *Cytokine* (2012) 59:467–78. doi: 10.1016/j.cyto.2012.05.020

55. Kandikattu HK, Venkateshaiah SU, Kumar S, Mishra A. IL-15 immunotherapy is a viable strategy for COVID-19. *Cytokine Growth Factor Rev* (2020) 54:24–31. doi: 10.1016/j.cytogfr.2020.06.008

56. Shi H, Wang W, Yin J, Ouyang Y, Pang L, Feng Y, et al. The inhibition of IL-2/IL-2R gives rise to CD8+ T cell and lymphocyte decrease through JAK1-STAT5 in critical patients with COVID-19 pneumonia. *Cell Death Dis* (2020) 11:429. doi: 10.1038/s41419-020-2636-4

frontiers | Frontiers in Immunology

TYPE Original Research
PUBLISHED 03 July 2023
DOI 10.3389/fimmu.2023.1219097

OPEN ACCESS

EDITED BY
Etel Rocha-Vieira,
Universidade Federal dos Vales do Jequitinhonha e Mucuri, Brazil

REVIEWED BY
Andreas Ronit,
University of Copenhagen, Denmark
Martin Zacharias,
Medical University of Graz, Austria

*CORRESPONDENCE
Peter S. Nyasulu
pnyasulu@sun.ac.za

†These authors share last authorship

RECEIVED 08 May 2023
ACCEPTED 12 June 2023
PUBLISHED 03 July 2023

CITATION
Shaw JA, Meiring M, Snyders C, Everson F, Sigwadhi LN, Ngah V, Tromp G, Allwood B, Koegelenberg CFN, Irusen EM, Lalla U, Baines N, Zemlin AE, Erasmus RT, Chapanduka ZC, Matsha TE, Walzl G, Strijdom H, du Plessis N, Zumla A, Chegou N, Malherbe ST and Nyasulu PS (2023) Immunologic and vascular biomarkers of mortality in critical COVID-19 in a South African cohort. *Front. Immunol.* 14:1219097. doi: 10.3389/fimmu.2023.1219097

Immunologic and vascular biomarkers of mortality in critical COVID-19 in a South African cohort

Jane Alexandra Shaw[1], Maynard Meiring[1], Candice Snyders[1], Frans Everson[2], Lovemore Nyasha Sigwadhi[3], Veranyay Ngah[3], Gerard Tromp[1,4,5], Brian Allwood[6], Coenraad F. N. Koegelenberg[6], Elvis M. Irusen[6], Usha Lalla[6], Nicola Baines[6], Annalise E. Zemlin[7], Rajiv T. Erasmus[7], Zivanai C. Chapanduka[8], Tandi E. Matsha[9], Gerhard Walzl[1], Hans Strijdom[2], Nelita du Plessis[1], Alimuddin Zumla[10,11], Novel Chegou[1], Stephanus T. Malherbe[1†] and Peter S. Nyasulu[3,12*†] for the COVID-19 Research Response Collaboration

[1]Department of Science and Technology/National Research Foundation (DST-NRF) Centre of Excellence for Biomedical Tuberculosis Research, South African Medical Research Council Centre for Tuberculosis Research, Biomedical Research Institute, Division of Molecular Biology and Human Genetics, Faculty of Medicine and Health Sciences, Stellenbosch University, Cape Town, South Africa, [2]Centre for Cardiometabolic Research in Africa, Division of Medical Physiology, Faculty of Medicine and Health Sciences, Stellenbosch University, Cape Town, South Africa, [3]Division of Epidemiology and Biostatistics, Department of Global Health, Faculty of Medicine and Health Sciences, Stellenbosch University, Cape Town, South Africa, [4]South African Tuberculosis Bioinformatics Initiative, Stellenbosch University, Cape Town, South Africa, [5]Centre for Bioinformatics and Computational Biology, Stellenbosch University, Stellenbosch, South Africa, [6]Division of Pulmonology, Department of Medicine, Stellenbosch University and Tygerberg Hospital, Cape Town, South Africa, [7]Division of Chemical Pathology, Department of Pathology, Faculty of Medicine and Health Sciences, Stellenbosch University and National Health Laboratory Service, Tygerberg Hospital, Cape Town, South Africa, [8]Division of Haematological Pathology, Department of Pathology, Faculty of Medicine and Health Sciences, Stellenbosch University and National Health Laboratory Service (NHLS) Tygerberg Hospital, Cape Town, South Africa, [9]Sefako Makgatho University of Health Sciences, Ga-Rankuwa, South Africa, [10]Division of Infection and Immunity, Centre for Clinical Microbiology, University College London, London, United Kingdom, [11]National Institute for Health Care Research (NIHR) Biomedical Research Centre, University College London (UCL) Hospitals National Health Service (NHS) Foundation Trust, London, United Kingdom, [12]Division of Epidemiology and Biostatistics, School of Public Health, Faculty of Health Sciences, University of the Witwatersrand, Johannesburg, South Africa

Introduction: Biomarkers predicting mortality among critical Coronavirus disease 2019 (COVID-19) patients provide insight into the underlying pathophysiology of fatal disease and assist with triaging of cases in overburdened settings. However, data describing these biomarkers in Sub-Saharan African populations are sparse.

Methods: We collected serum samples and corresponding clinical data from 87 patients with critical COVID-19 on day 1 of admission to the intensive care unit (ICU) of a tertiary hospital in Cape Town, South Africa, during the second wave of the COVID-19 pandemic. A second sample from the same patients was collected on day 7 of ICU admission. Patients were followed up until in-hospital death or hospital discharge. A custom-designed 52 biomarker panel was performed on the Luminex® platform. Data were analyzed for any association between biomarkers and mortality based on pre-determined functional groups, and individual analytes.

Results: Of 87 patients, 55 (63.2%) died and 32 (36.8%) survived. We found a dysregulated cytokine response in patients who died, with elevated levels of type-1 and type-2 cytokines, chemokines, and acute phase reactants, as well as reduced levels of regulatory T cell cytokines. Interleukin (IL)-15 and IL-18 were elevated in those who died, and levels reduced over time in those who survived. Procalcitonin (PCT), C-reactive protein, Endothelin-1 and vascular cell adhesion molecule-1 were elevated in those who died.

Discussion: These results show the pattern of dysregulation in critical COVID-19 in a Sub-Saharan African cohort. They suggest that fatal COVID-19 involved excessive activation of cytotoxic cells and the NLRP3 (nucleotide-binding domain, leucine-rich–containing family, pyrin domain–containing-3) inflammasome. Furthermore, superinfection and endothelial dysfunction with thrombosis might have contributed to mortality. HIV infection did not affect the outcome. A clinically relevant biosignature including PCT, pH and lymphocyte percentage on differential count, had an 84.8% sensitivity for mortality, and outperformed the Luminex-derived biosignature.

KEYWORDS

biomarkers, cytokines, COVID-19, SARS-CoV-2, prognostic, mortality

1 Introduction

Understanding the mechanisms driving severe disease and causing mortality or recovery among Coronavirus disease 2019 (COVID-19) patients is crucial for developing future clinical decision support systems, planning disease control strategies, and developing host-directed therapies. Older age, obesity, diabetes, hypertension, lymphopenia, and neutrophilia have been consistently identified in many studies as predictors of mortality (1, 2). HIV has also been associated with poor outcomes from COVID-19 in multi-center prospective studies, especially in people with a low CD4 cell count (3, 4). Many immunological biomarkers of mortality have been reported, such as interleukin-1α (IL-1α), IL-1β, IL-6, IL-10, IL-18, and tumor necrosis factor (TNF) (5, 6). Along with ferritin, D-dimer, C-reactive protein (CRP), and procalcitonin (PCT), these immunologic biomarkers are found in the group of people infected with Severe Acute Respiratory Syndrome coronavirus-2 (SARS-CoV-2) who develop hyperinflammation, known as a 'cytokine storm' (2). Excessive cytokine production from inflammatory cell death is associated with acute organ damage which is life-threatening. This is mediated in part by synergism between TNF and interferon gamma (IFNγ), which triggers the PANoptosis (pyroptosis, apoptosis, and necroptosis), a mechanistic compendium of programmed cell death pathways (7). In addition to hyperinflammation, endothelial markers such as intercellular adhesion molecule-1 (ICAM-1), vascular cell adhesion molecule-1 (VCAM-1), and E-selectin have been associated with disease severity and death. This highlights the important role of vascular endothelial cells as targets of SARS-CoV-2, and of endothelial activation with dysfunction in the pathogenesis of severe COVID-19 (8, 9).

Despite the extraordinary number of publications on this topic during the pandemic, few data from African countries are available in the public domain. Furthermore, Sub-Saharan African populations have a low vaccination coverage to mitigate the effects of future waves or variants which escape immunity acquired from previous infection (10). Therefore, data on the predictors of mortality in Sub-Saharan African populations are greatly needed. The second wave of COVID-19 in South Africa, which occurred between October 2020 and February 2021, was dominated by the B.1.351 Beta variant of SARS-CoV-2 (10). The rapid spread of infection in the population resulted in a high rate of admission of critically ill patients that overwhelmed the health care services. The B.1.351 Beta variant was associated with a high mortality rate among patients admitted in the Intensive Care Unit (ICU) and other healthcare environments (10).

In this study, our team examined the serum of critical COVID-19 patients in Cape Town, South Africa, for key immunological and endothelial cell biomarkers of mortality. The aim was to gain insight into the immune mechanisms underlying fatal COVID-19 and identify the biomarkers with the best predictive potential.

2 Materials and methods

This investigation was a sub-study of a large prospective cohort spanning the whole COVID-19 pandemic, performed in the ICU of Tygerberg Hospital, Cape Town, South Africa. Participants for this sub-study were admitted during the second wave of the COVID-19 pandemic from 9 October 2020 to 10 February 2021. All adult patients admitted to the ICU during this timeframe with laboratory-confirmed SARS-CoV-2 infection on quantitative real-time reverse transcription polymerase chain reaction (RT-qPCR) from nasopharyngeal swab testing, and COVID-19 acute respiratory distress syndrome (ARDS) according to the Berlin definition (11),

were recruited on the day of admission to ICU. They were followed until the primary endpoint of death or survival to hospital discharge. Eligibility for ICU admission was predetermined by the provincial Department of Health guidelines, based on the severity of illness, likely prognosis, and ICU bed availability (12).

Baseline demographic characteristics, comorbidities, medication history, and indicators of the severity of illness (i.e., type and intensity of respiratory support, arterial blood gas values, and evidence of other organ dysfunction) were collected and transferred by authorized study staff to an access-controlled Research Electronic Data Capture (REDCap®) database hosted by Stellenbosch University (13). Baseline laboratory measurements were retrieved from the National Health Laboratory Service (NHLS) Laboratory Information System (TrakCare® Lab Enterprise). Only results from blood taken on the day of ICU admission were used. In cases where a full panel blood test was not performed on the day of ICU admission, the results from blood taken within 48 hours of the date and time of ICU admission were used. The first arterial blood gas performed after admission to ICU was selected for the analysis, irrespective of the type of respiratory support at that time. Further data on the patient's clinical progress during admission were collected, including the primary outcome of death or discharge from the hospital, progression to mechanical ventilation, and initiation of new medications. Data were verified remotely using electronic hospital records and the TrakCare® system. Serum samples were collected from all patients on day 1 (the day of ICU admission), and a second sample was collected from those who survived to day 7, to capture the trajectory of key analytes at a time point when they were likely to differentiate between survivors and non-survivors (5).

2.1 Laboratory procedures

The baseline blood tests and SARS-CoV-2 RT-qPCR were performed according to the protocols of the NHLS at Tygerberg Hospital, accredited as ISO15189 compliant by the South African National Accreditation Services (SANAS), and all methods are subjected to both internal and external quality control schemes. These methods have been described in a previous publication (14).

Day 1 and day 7 serum samples were aliquoted and frozen at -80° C on the day of sampling. After a single freeze-thaw cycle, a magnetic Luminex® assay with a Luminex® MAGPIX® CCD Imager [xPONENT® software; Research and Diagnostics Systems Inc.® a Bio-techne® brand (Catalog number LXSAHM); Minneapolis, NE, USA] was used to determine the levels of a custom-designed 52-analyte panel of immune and vascular/endothelial cell biomarkers including: Arginase-1, CRP, D-dimer, Endothelin-1 (ET-1), E-Selectin, ferritin, growth differentiation factor-15 (GDF-15), granulocyte macrophage colony stimulating factor (GMCSF), granulysin, hypoxia inducible factor 1-α (HIF1α), High mobility group box 1 (HMGB1), I-309/chemokine ligand 1(I-309/CCL1), ICAM-1, Indoleamine-2,3-dioxygenase 1 (IDO-1), IFNβ, IFNγ, IL-1a, IL-1b, IL-1Ra, IL-2, IL-4, IL-5, IL-6, IL-8, IL-10, IL-13, IL-15, IL-17, IL-18, IL-21, IL-22, IL-23, IL-33, Interferon gamma-induced protein 10/Chemokine (C-X-C motif) ligand 10 (IP-10/CXCL10), monocyte chemoattractant protein 1/chemokine (C-C motif) ligand 2 (MCP-1/CCL2), MCP-3/CCL7), MCP-4/CCL13, monokine induced by gamma interferon/Chemokine (C-X-C motif) ligand 9 (MIG/CXCL9), myeloperoxidase (MPO), plasminogen activator inhibitor-1 (PAI-1), PCT, P-selectin, S100 calcium-binding protein A8/migration inhibitory factor-related protein 8 (S100A8/MRP-8), S100 calcium-binding protein A9/migration inhibitory factor-related protein 14 (S100A9/MRP-14), growth stimulation gene-2/Interleukin-1 receptor-like-1 (ST2/IL-1RL1), transforming growth factor β1 (TGFβ1), TGFβ2, TGFβ3, TNFα, VCAM-1, vascular endothelial growth factor (VEGF), Von Willebrand Factor A2 (vWF A2). Analyte kits were supplied by Whitehead Scientific (Pty) Ltd, Cape Town, South Africa, and Merck (Pty) Ltd, Gauteng, South Africa.

2.2 Statistical analysis

Data were analyzed using R suite® statistical software (R version 4.2.3) (15). Selected clinical variables, NHLS-derived laboratory variables, and all Luminex®-derived variables were assessed for their effect on the primary outcome of death, or survival to hospital discharge. Pairwise comparisons were done using robust t-tests for the continuous variables, and Cochran-Armitage tests for the trends of the categorical variables. Analytes where all measured values were lower than the limit of detection were excluded from this analysis. For patients with values on both days 1 and 7, a paired Yuen's t-test with standardized winsorization was used to assess the effect of both values on the outcome. Analytes for which most of the results were lower than the limit of detection but had at least five valid entries (IL-1a, IL-4, IL-5, IL-21, IL-22, IL-23, and HMGB-1) were converted into categorical variables for the specific sample day using the minimum, maximum, and median of the measurable values, as shown in Supplementary Table 1. The minimum value indicated the lowest concentration (including those extrapolated downwards), while the maximum value was the highest concentration and any values which were extrapolated upwards, and the median was simply the standard median value. The analytes were then stratified by the outcome status of death or survival, and a Cochran-Armitage test for trend was applied.

Variables with the highest impact on the outcome from day 1 and day 7 separately, as well as the difference between day 1 and day 7 values in patients who had both day 1 and day 7 values measured (hereafter the trajectory analysis), were identified using a Boruta algorithm. Boruta is an all-relevant feature-selection algorithm that makes use of a permuted random forest selection process. It was chosen for this analysis because of the rigorous method by which it identifies variables with a real impact on the outcome, without relying on assumptions about the distribution of the data or excluding all variables with incomplete data in the way that other tools would. Through multiple iterations, it provides a ranking of variables' importance to the outcome as well as a statistical interpretation of the performance based on the binomial distribution, i.e., a score of the feature importance (16). On day 1 analysis, all Luminex® analytes and the baseline clinical variables were included in the Boruta. On the day 7 analysis, and the trajectory analysis only the Luminex® analytes were included.

The variables thus identified were further subjected to correlation-based filtering, and the remaining variables were then used as predictors in two independent classification models (logistic regression and a random forest model). V-fold cross-validation (stratified by outcome, with five repeats) was applied to obtain measures of performance. A second analysis was done using predetermined 'functional groups' of cytokines and vascular/endothelial biomarkers (Table 1). These were analyzed together to assess their combined effect, using a robust t-test on a pooled average value for that group, obtained by scaling and centering each analyte separately (independent of the outcome state), then calculating the mean for each patient. A $p < 0.05$ was considered significant. However, to minimize the impact of multiple testing and forgo *post-hoc* correction, those interactions which remained significant at $p < 0.005$ are highlighted.

3 Results

Table 2 presents the baseline characteristics of the 87 critically ill COVID-19 patients included in the analysis, of whom 55 (63.2%) died in ICU, and 32 (36.8%) survived to hospital discharge (median 3 days after ICU discharge, range 1–48 days). All patients were receiving 8mg of intravenous dexamethasone daily, and therapeutic dose subcutaneous enoxaparin sodium from admission to ICU. None of the patients received any antiviral treatment or immunomodulatory drugs for COVID-19.

3.1 Clinical variables

On admission to ICU, all patients had clinically diagnosed ARDS with hypoxemia: 68 (78.2%) had a ratio of partial pressure of oxygen in arterial blood (PaO_2) to the fraction of inspired oxygen (FIO_2), hereafter PaO_2/FIO_2, of < 100 (severe hypoxemia); 16 (18.4%) had a PaO_2/FIO_2 of 100 – 200 (moderate hypoxemia); and 3 (3.4%) had a $PaO_2/FIO_2 > 200$ (mild hypoxemia) (11). Most patients (59, 67.8%) required invasive mechanical ventilation during their admission. The remaining 28 (32.2%) were supported with non-invasive ventilation or high-flow nasal cannula oxygen.

All patients had at least one comorbidity, of which hypertension (51, 58.6%) was the most common. Nineteen (21.8%) patients were known to have diabetes mellitus, but 49 (56.3%) patients had an

TABLE 1 List of predetermined functional groups of analytes.

Group number	Group name	Analytes
1	Clinical markers of inflammation or infection	CRP; Ferritin; PCT; D-dimer
2	Th1	IFNγ, TNFα, IL-2, IL-12, IL-15
3	Th2	IL-4, IL-13, IL-5, IL-33, ST2, IL-21
4	Treg	IL-10, TGFβ
5	Th17	IL-17, IL-22, IL-23
6	Th1 activation	TNFα; IL-6, IL-1b, IL-1a, IL-18; IL-15
7	Th2 activation	IL-4; IL-13; IL-5; IL-10
8	Myeloid derived suppressor cells	Arginase-1; S100A8; S100A9; TFGβ; IL-10; IDO-1; IL-1Ra
9	Anti-inflammatory myeloid cells	IL-1Ra
10	Antiviral	IFNβ
11	Chemokines	IL-8; MCP-1, MCP-3, MCP-4, MIG, IP-10; i309
12	Vascular/endothelial adhesion molecules	VCAM-1, ICAM-1
13	Growth factors	GMCSF; VEGF
14	NK and CTL cytolytic activity	Granulysin
15*	Expanded vascular/endothelial adhesion markers	ICAM-1, E-selectin, P-selectin, VCAM-1
16*	Inflammation	MPO, TNFα, CRP
17*	Hemostatic factors	PAI-1, vWFA2
18*	Cell growth/death factors	GDF-15, VEGF
19*	Vascular tone	Endothelin-1

*These groups were designed to focus on markers of relevance to the vascular endothelium.
CRP, C-reactive protein; CTL, cytotoxic T lymphocyte GDF-15, growth differentiation factor-15; GM-CSF, granulocyte macrophage colony stimulating factor; I-309, chemokine ligand 1(CCL1); ICAM-1, intercellular adhesion molecule-1; IDO-1, Indoleamine-2,3-dioxygenase 1; IFNβ, interferon β; IFNγ, interferon γ; IL, interleukin; IL-1Ra, Interleukin-1 receptor antagonist; IP-10, interferon γ-induced protein 10/Chemokine (C-X-C motif) ligand 10 (CXCL10); MCP, monocyte chemoattractant protein; MIG, monokine induced by interferon γ/Chemokine (C-X-C motif) ligand 9 (CXCL9); MPO, myeloperoxidase; NK, natural killer cell PAI-1, plasminogen activator inhibitor-1; PCT, procalcitonin; S100A8, S100 calcium-binding protein A8/migration inhibitory factor-related protein 8 (MRP-8); S100A9, S100 calcium-binding protein A9/MRP-14; ST2, growth stimulation gene-2/Interleukin-1 receptor-like-1 (IL-1RL1); TGFβ, transforming growth factor β; TNFα, tumour necrosis factor α; VCAM-1, vascular cell adhesion molecule-1; VEGF, vascular endothelial growth factor; vWF A2, Von Willebrand Factor A2.

TABLE 2 Baseline demographic characteristics and laboratory parameters of the study population.

	Pooled (n=87)	Died (n=55)	Survived (n=32)	P value[+]
Female	58 (66.7%)	36 (65.5%)	22 (68.8%)	0.817
Age (years)	55.0 (15.5)	55.0 (14.5)	51.5 (18.5)	0.550
Length of hospital stay (days)	12.0 (9.0)	11.0 (8.5)	13.5 (10.2)	–
Length of ICU stay (days)	10 (8.0)	10 (8.0)	9 (8.0)	–
Type of respiratory support on day of ICU admission:				
Invasive mechanical ventilation	32 (36.8%)	31 (56.4%)	1 (3.1%)	-
Non-invasive mechanical ventilation	4 (4.6%)	4 (7.3%)	0 (0.0%)	-
High-flow nasal oxygen	50 (57.5%)	20 (36.4%)	30 (93.8%)	-
Face mask oxygen	1 (1.1%)	0 (0.0%)	1 (3.1%)	-
Required invasive mechanical ventilation during ICU admission	59 (67.8%)	54 (98.2%)	5 (15.6%)	-
Comorbidities:				
Diabetes mellitus	19 (21.8%)	10 (18.2%)	9 (28.1%)	0.295
HbA1c >6.5% in ICU[$]	49 (56.3%)	33 (60.0%)	16 (50.0%)	0.380
Hypertension	51 (58.6%)	32 (58.2%)	19 (59.4%)	0.999
HIV infection	13 (15.5%)	9 (17.0%)	4 (12.9%)	0.759
Raised BMI[€]	55 (63.2%)	36 (65.5%)	19 (59.4%)	0.796
Baseline arterial blood gas[#]:				
pH	7.4 (0.1)	7.4 (0.1)	7.5 (0.0)	**0.000**
$PaCO_2$ (kPa)	5.5 (1.4)	6.0 (1.4)	5.0 (0.5)	**0.001**
PaO_2 (kPa)	8.0 (2.2)	8.0 (2.4)	8.2 (2.1)	0.539
PaO_2/FIO_2 (mm Hg)*	75.0 (36.4)	71.0 (35.4)	84.2 (42.2)	**0.041**
Lactate	1.6 (0.8)	1.6 (1.0)	1.4 (0.8)	0.377
Baseline laboratory results:				
Creatinine (µmol/L)	76.0 (33.5)	77.0 (41.5)	76.0 (18.0)	0.593
eGFR (mL/min)	79.0 (35.0)	76.0 (37.5)	87.0 (28.5)	0.201
Alanine transferase (U/L)	37.5 (27.2)	36.0 (27.0)	41.0 (42.0)	0.183
Hemoglobin (g/dL)	12.5 (1.6)	12.2 (1.8)	12.7 (1.2)	0.129
White cell count	11.9 (6.8)	12.8 (7.3)	10.5 (5.4)	0.052
Lymphocytes %	8.2 (5.5)	6.8 (5.7)	9.8 (5.3)	**0.017**
Neutrophil %	86.4 (10.2)	88.7 (9.2)	84.2 (6.8)	0.101
C reactive protein (mg/L)	154.0 (152.5)	162.0 (138.0)	106.5 (124.0)	**0.025**
Procalcitonin (ng/mL)	0.3 (0.9)	0.3 (1.5)	0.1 (0.3)	**0.027**
Troponin T (ng/L)	13.0 (19.2)	15.0 (19.0)	6.0 (11.0)	0.061
NT-proBNP (pg/mL)	189.5 (577.0)	284.0 (987.0)	111.0 (196.0)	0.133
Ferritin (µg/L)	737.0 (853.5)	718.0 (881.5)	895.0 (763.0)	0.612
D-dimer (µg/mL)	0.9 (2.1)	1.1 (3.0)	0.4 (1.3)	0.095

Categorical variables are expressed as a number followed by a percentage and the continuous variables are expressed as a median followed by the interquartile range. Laboratory values refer to those obtained on the day of admission to the ICU (day 1). [$]Indicates an elevated glycated hemoglobin fraction, noted independent of an established diabetes diagnosis. [€]A subjective opinion of the treating clinician rather than objective measurement, and as such should be interpreted with caution. [#]The first arterial blood gas done on admission to ICU, whilst receiving oxygen therapy or ventilatory support. *PaO_2/FIO_2 is the ratio of arterial oxygen partial pressure (PaO_2 in mmHg) to fractional inspired oxygen (FIO_2 expressed as a fraction), where a value <300 indicates mild hypoxaemia, <200 moderate hypoxaemia, <100 severe hypoxaemia. [+]p values not corrected for multiple testing effect. In this case, variables with a p-value < 0.005 may be considered most likely to have post-test significance using the modified one-step M-estimator. ICU, intensive care unit; HIV, human immunodeficiency virus; $PaCO_2$, partial pressure of arterial carbon dioxide; PaO_2, partial pressure of arterial oxygen; eGFR, estimated glomerular filtration rate (calculated using Chronic Kidney Disease Epidemiology Collaboration (CKD-EPI) formula uncorrected for ethnicity); NT-proBNP, N-terminal pro-brain natriuretic peptide. Bold values means P values which are statistically significant.

HbA1c >6.5% on admission to the ICU (including all but one of the confirmed diabetics). There were 13 people living with HIV (PLWH), with a median CD4 cell count of 238 cells/mm^3, and all had suppressed viral loads on antiretroviral therapy except for three who had no data available. Four (4.6%) patients had previous tuberculosis, and four had chronic obstructive pulmonary disease. Nine (10.3%) patients reported hyperlipidemia and two (2.3%) reported ischaemic heart disease, two asthma, two hypothyroidism, previous malignancy, and chronic kidney disease, respectively. Three patients (3.4%) were pregnant on admission. Variables associated with mortality are detailed in Table 2. In addition to these, patients receiving antibiotics at any time during their ICU stay had significantly higher odds of death (Odds ratio 10.1, 99.5% C.I. 2.9–55, $p < 0.001$).

3.2 Biomarkers

The Boruta algorithm identified the following combination of clinical and Luminex® variables measured on day 1 as most influential in predicting the outcome: pH, partial pressure of carbon dioxide in arterial blood (PaCO2), lymphocytes percentage on the differential count, PCT, GDF-15, IL-15, ST2, IL-1Ra, and MPO. Only Luminex® data were considered for day 7, as all clinical data were captured on day 1. The most important day 7 variables identified by the Boruta were: IL-15, ET-1, GDF-15, IL-1a, IP-10, MCP-1, MCP-3, PCT, ST2, TGFβ2, VCAM-1, I309, and S100A8. The following variables were the most important in trajectory analysis: IL-15, GDF-15, VCAM-1, MCP-1, IL-18, and MCP-3. Several of these variables were highly correlated with each other (Figure 1).

On day 1 two selections were tested: Group 1 included variables that are readily available in a clinical setting: pH, lymphocyte percentage on the differential count, and PCT. Group 2 included IL-15, MPO, GDF-15, ST-2, and IL-1Ra. Other combinations with randomly selected day 1 variables were also tested, as well as all variables combined. The day 1 clinical biomarker group achieved a diagnostic accuracy of 72.7% on logistic regression and 73.5% on random forest, with an area under the receiver operating curve (AUC) of 85.8% and 82.8%, respectively (Figure 2). Day 1 clinical biomarkers had higher sensitivity (84.8% and 82.8%) than specificity (60.7% and 64.1%). The day 1 Luminex® biomarker group achieved a diagnostic accuracy of 65.1% on logistic regression and 66.7% on random forest, with an AUC of 77.3% and 80.2% respectively. The sensitivities of this group were 78.0% and 80.4%, and specificities were 52.3% and 52.9%. When all the day 1 clinical and Luminex® biomarkers were included without filtering, the diagnostic accuracy was 78.1% and 75.1% on logistic regression and random forest models respectively; the AUCs were 86.2% and 88.6%; sensitivities were 83.2% and 88.8%; and specificities were 73.1% and 61.3%. The following day 7 variables were included in the

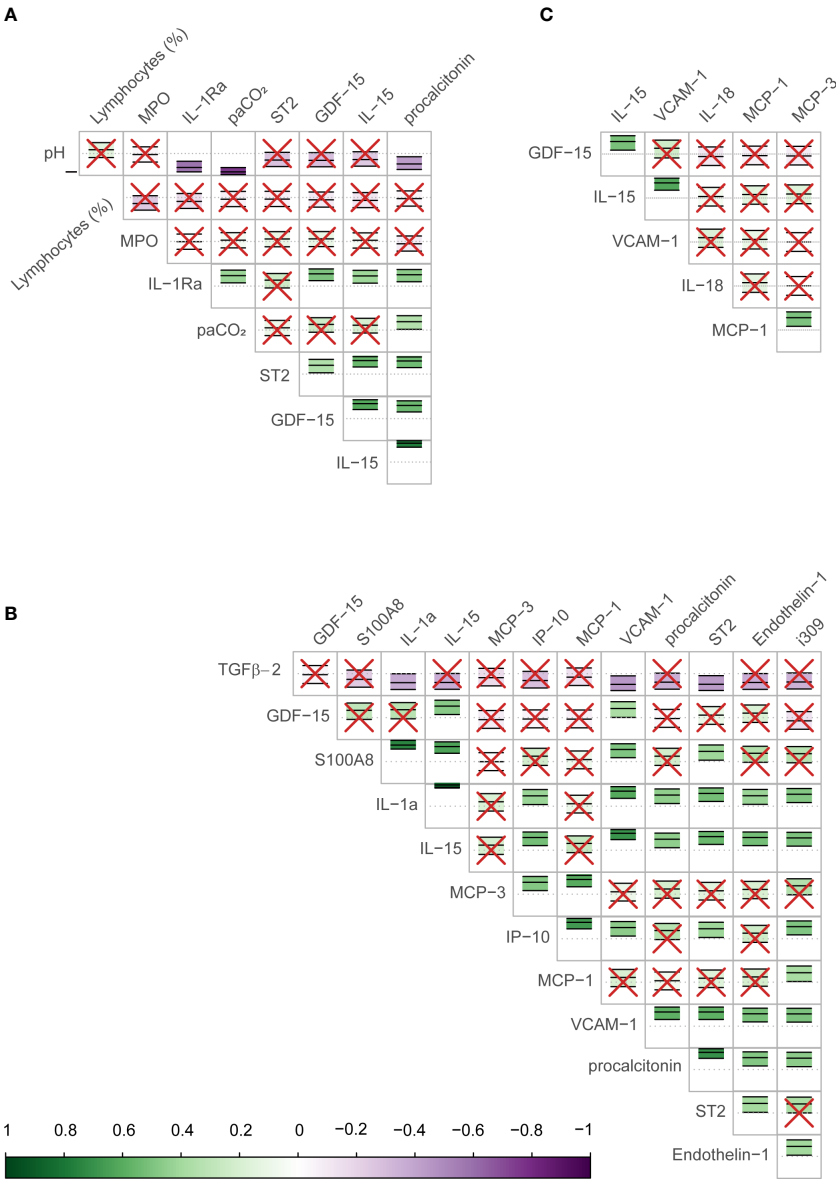

FIGURE 1
Correlation between biomarkers identified as important in predicting COVID-19 mortality in the study sample. The figure shows the correlation (Pearson) between biomarkers identified by the Boruta algorithm as important in determining the outcome (mortality) for day 1 **(A)**, day 7 **(B)**, and the longitudinal trajectory between days 1 and 7 **(C)**. The scale bar on the bottom of the figure shows the strength of the correlation (closer to 1 or -1 are strongly positive or negative respectively) with a corresponding color scale. Within each cell is a central dotted line representing 0, and the green or purple annotation represents the correlation coefficient and confidence intervals for the two biomarkers interacting in that cell, as well as the direction of the interaction. The biomarker names are shown on the labels of the rows and columns. In cells with red crosses, the confidence interval crosses the 0 line and these interactions are non-significant. Those without crosses represent the significant correlations between the biomarkers, the strength of association may be judged by their color.

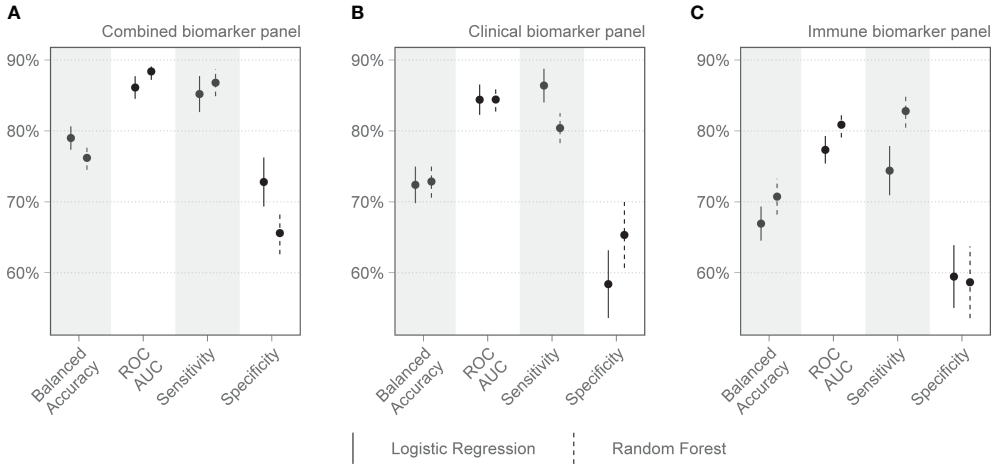

FIGURE 2
Performance metrics for models of clinical and immunologic biomarkers in predicting COVID-19 mortality on admission to the Intensive Care Unit (Day 1). **(A)** shows the combined performance of both clinical and immunologic biomarkers identified by the Boruta algorithm. **(B)** shows the performance of a clinical biomarker panel including pH, procalcitonin (PCT), and lymphocyte percentage on the differential count. **(C)** shows the performance of an immunologic biomarker panel including IL-15, MPO, GDF-15, ST-2, and IL-1Ra. Each dot represents the mean, with the line extending from it representing the standard error. A solid line is the logistic regression model, and a dashed line is the random forest model, both tuned to balanced accuracy. ROC, receiver operating curve; AUC, area under the curve.

modeling: IL-15, VCAM-1, and PCT. The performance metrics for the day 7 biomarkers were: diagnostic accuracy of 85.2% and 82.6% (logistic regression and random forest respectively); AUC of 91.1% and 93.0%; sensitivity of 80.1% and 86.5%; and specificity of 90.2% and 78.8% (Figure 3). When all the day 7 variables were included in the model without filtering, the metrics improved further (accuracy: 90.7% and 88.1%; AUC: 96.7% and 95.1%; sensitivity: 91.6% and 90.2%; specificity: 89.8% and 86.0%). Variables modeled from the trajectory analysis included IL-15, IL-18, and MCP-1. The biomarker trajectory analysis from day 1 to 7 performed less well than the day 7 panel, but performed well in comparison with the other models (Supplementary Figure 1). To test whether there was a confounding effect of HIV, we ran the same analysis excluding the 13 PLWH and compared the resultant performance metrics to the results of the whole cohort using Welch's t-test. There was no difference between the whole cohort and the cohort with PLWH filtered out in the day 1 performance metrics, or in the day 7 metrics from the random forest models. The day 7 logistic regression metrics were better in the cohort without the PLWH, but this is likely because of the tendency of logistic regression to overfit in small datasets (Supplementary Figure 3).

Analysis of predetermined functional groups identified an increase in biomarkers of a pro-inflammatory/T helper cell type 1 (Th1) activating response (IL-1α, p = 0.008; IL-1β, IL-6, IL-15, IL-

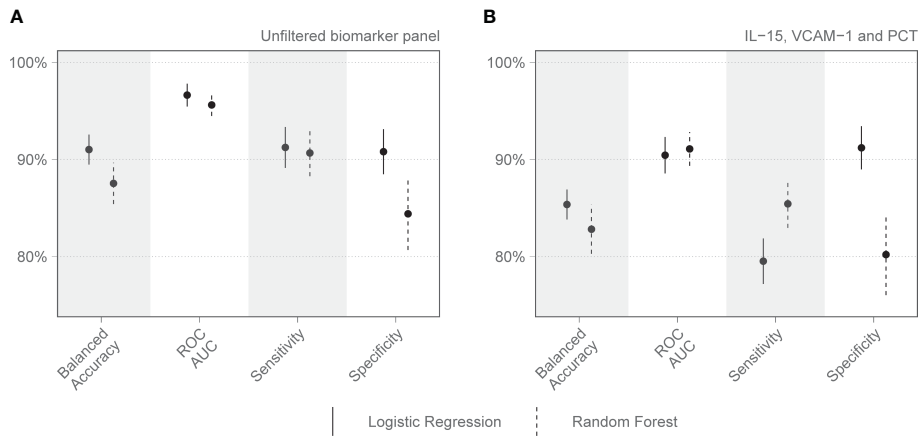

FIGURE 3
Performance metrics for models of immunologic biomarkers in predicting COVID-19 mortality on day 7 of admission to the Intensive Care Unit. **(A)** shows the performance of all day 7 analytes identified by the Boruta algorithm, without filtering. **(B)** shows the performance of the combination of analytes selected after correlation-based filtering, including IL-15, VCAM-1, and PCT. Each dot represents the mean, with the line extending from it representing the standard error. A solid line is the logistic regression model, and a dashed line is the random forest model. Models are tuned to balanced accuracy. ROC receiver operating curve, AUC area under the curve.

18, and TNFα, p = 0.018, 95% C.I. 0.06-0.65) and the chemoattractants/leukocyte trafficking chemokines for both T helper cell type 2 (Th2) and Th1 (I309, IL-8, IP-10, MCP-1, MCP-3, MCP-4, and MIG, p = 0.034, 95% C.I. 0.02–0.57) on day 1 among patients who died. The anti-inflammatory IL-1Ra was also higher in these patients on day 1 (p = 0.003, 95% C.I. 0.04–0.45). On day 7, the inflammatory response on day 1 persisted, and Th2 cytokines (IL-13, IL-21, IL-33, and ST2, p = 0.002, 95% C.I. 0.23–0.89; IL4, p = 0.017) and acute phase pro-inflammatory markers (D-dimer, ferritin, PCT, p = 0.024, 95% C.I. 0.06–0.65) were significantly increased in those who died. Markers of an anti-inflammatory/Treg response were reduced on day 7 in those who died (IL-10, TGFβ1, and TGFβ2, p = 0.005, 95% C.I. -0.65, -0.12). Endothelin-1 (p < 0.001, 95% C.I. 0.61–1.61) and vascular endothelial adhesion markers (ICAM-1 and VCAM-1, p = 0.003, 95% C.I. 0.30–1.15) were increased in those who died. Using a 99.5% confidence interval and assuming significance at a p-value < 0.005, those interactions which remained significant included higher IL-1Ra values on day 1 in those who died (p = 0.004, 99.5% C.I. 0.00–0.52), and higher Th2 cytokines (IL-13, IL-21, IL-33, ST2, p = 0.001, 99.5% C.I. 0.08–1.04), Endothelin-1 (p <0.001, 99.5% C.I. 0.44–1.82) and ICAM-1 and VCAM-1 (p = 0.003, 99.5% C.I. 0.13–1.44) on day 7 in those who died (Figure 4). The results of all functional groups are shown in Supplementary Figure 2. The longitudinal trajectory analysis was significant for three variables: a reduction in the value of IL-18 and VCAM-1 from day 1 to day 7 was associated with survival (p = 0.002 and p = 0.004 respectively), and an increase in IL-15 from day 1 to day 7 was associated with death (p = 0.002) (Figure 5).

A comparison between the results of the biomarkers performed on both the Luminex® and NHLS assay platforms (CRP and PCT) is included in the Supplementary Material (Supplementary Figures 4, 5).

4 Discussion

In this study, we present the immunologic and vascular biomarkers of mortality in 87 patients with critical COVID-19 who were admitted during the second wave of the pandemic in South Africa. Our results show that hyperinflammation was associated with death from COVID-19, as shown by the increased levels of Th1 and Th2 cytokines, Th1/Th2-related chemokines, and acute phase inflammatory proteins in those who died.

Cytokines related to hyperinflammation have been strongly associated with severe COVID-19 in other studies (5, 6). Similar to our findings, Lucas et al. (5) reported that patients with higher incidences of coagulopathy and mortality had a baseline immune signature driven by a combination of Th1 and Th2 responses, however, our study, unlike Lucas et al., did not identify Th17 responses as part of this signature. Moreover, Lucas et al. showed that patients with severe COVID-19 maintained elevated Th1 and Th17 cytokine levels throughout the course of their disease compared to patients with moderate disease and that severe disease was also associated with a rise in Th2 responses. In line with this, elevations in Th1 cytokines were associated with mortality at days 1 and 7 in our cohort of patients with severe COVID-19, and at the later time point, the Th2 cytokines also became significant. In Abers et al., elevated levels of IL-15, soluble ST2, and MCP-1, amongst others, were independently associated with mortality (6). Similar to our findings, the longitudinal trajectory of both IL-15 and MCP-1 in Abers et al. were significantly associated with the outcome (6). IL-1Ra is a competitive antagonist of the potent Th1 cytokine IL-1β. It rises in response to IL-1 and modulates its inductive effects on IL-6 and Th17 responses. In this study, IL-1Ra was strongly associated with mortality, providing further evidence of the presence of hyperinflammation and the body's attempt at immune regulation (17). Many of the cytokines and chemokines reported in this study

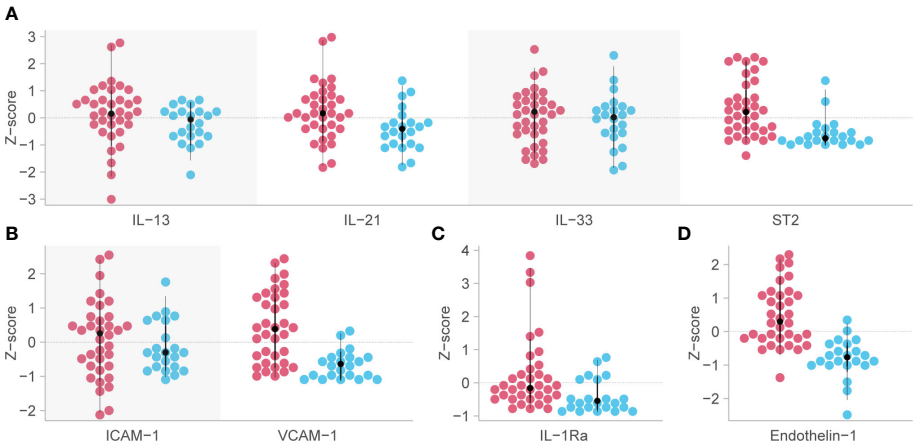

FIGURE 4
Biomarkers associated with mortality in critical COVID-19 which remained significant at the p<0.005 level. Red dots indicate the analyte levels in patients who died and blue dots are those who survived. **(A)** functional group 3, representing Th2 responses [except for Interleukin (IL)-4 and IL-5] on day 7 post-admission. **(B)** functional group 12, representing intercellular adhesion molecule-1 (ICAM-1) and vascular cell adhesion molecule-1 (VCAM-1) on day 7 post-admission. **(C)** IL-1Ra or functional group 9, representing anti-inflammatory myeloid cells on day 1. **(D)** Endothelin-1 (ET-1) or functional group 19, representing vascular tone and endothelial dysfunction on day 7 post-admission. Analyte levels have been scaled and transformed to Z-scores for comparability, and the means were compared with a robust t-test. ST2, growth stimulation gene-2.

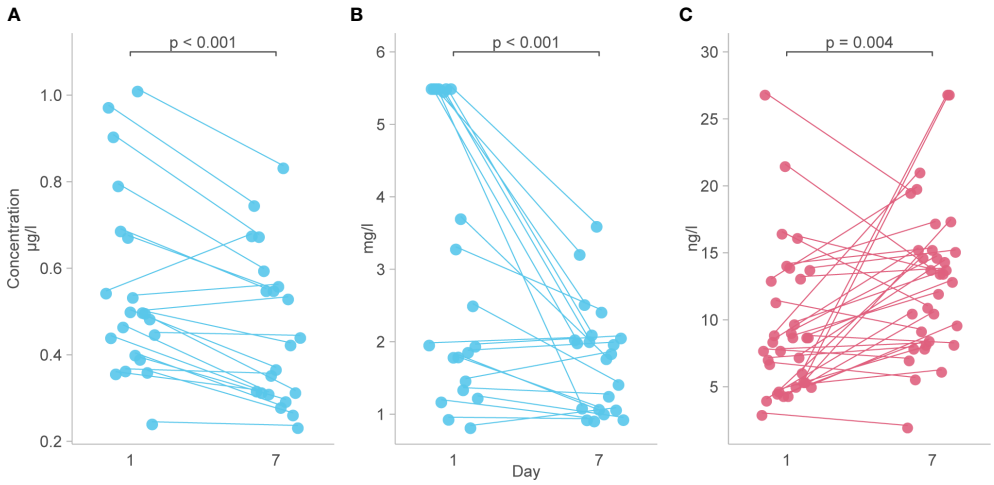

FIGURE 5
Biomarkers with a longitudinal trajectory associated with survival or death. **(A)** Levels of IL-18 between day 1 and day 7 in survivors. **(B)** Levels of VCAM-1 from day 1 to day 7 in survivors. **(C)** Levels of IL-15 from day 1 to day 7 in those who died. Analyte levels have been scaled and transformed to Z-scores for comparability and the means were compared with a robust t-test.

are also known to be elevated and predict mortality in other forms of ARDS and sepsis, particularly IL-6, IL-8, IL-18, TNFα, and IFNγ (18–20). However, this may not represent the cytokine milieu in the lung. In one report from Saris et al., IL-6, IP-10, MCP-1, IL-10, and IFN-α were all elevated in the plasma of critically ill COVID-19 patients (21). In the bronchoalveolar lavage fluid (BALF), however, IL-6, MCP-1, and IL-10 were significantly higher than plasma, but IP-10 was not and IFN-α was undetectable. This demonstrates that while circulating biomarkers are useful for predicting severity, they do not reveal the full picture.

IL-15 is a pro-inflammatory cytokine with important effects on the activation and cytolytic activity of cytotoxic CD8 T lymphocytes and NK cells, particularly in short-term hypoxia (22). IL-15 was significantly associated with mortality in our panel overall. IL-18 is also pro-inflammatory, activated by the NLRP3 (nucleotide-binding domain, leucine-rich–containing family, pyrin domain–containing-3) inflammasome along with IL-1β and, in combination with IL-12, acts on CD4 T cells, CD8 T cells, and NK cells to induce IFN-γ production. Higher levels of IL-18 have been associated with increased severity of COVID-19 (23). In ARDS from avian influenza virus (H5N1 and H7N9), the prolonged activation of the NLRP3 inflammasome and consequently Caspase 1, results in excess IL-18 and IL-1β production. This in turn causes an IFN-γ–biased cytokine storm, pyroptosis, and lung damage (24). In the absence of IL-15, IL-18 does not induce IFN-γ production but rather plays an important role in the differentiation of naive T cells into Th2 cells and stimulates the production of IL-4 and IL-13. In this study, we found that the survivors of COVID-19 ARDS had reduced levels of IL-15 and IL-18 over the period of ICU admission to day 7 and that the levels of these cytokines were consistently higher in those who died than those who survived. Continuous stimulation with IL-15 has been shown to cause exhaustion in certain immune cells, including NK cells (25). Together, this suggests that these pathways are involved in excessive inflammatory cell death and lung damage, and reflects the development of reduced inflammatory processes in those who survived. This may have been perpetuated by the failure of the regulatory responses which was identified at day 7 in those who died.

The chemokines as a functional group, as well as the levels and trajectory of individual chemokines such as IP-10, MCP-1, and MCP-3, featured prominently in predicting the poor outcome in our study and also shown in other studies. This highlights the role of leukocyte chemoattractants in severe disease progression (26, 27). IP-10 and MCP-1 have also been associated with thrombosis, and it is hypothesized that this may be the underlying mechanism that precipitates an increased risk of mortality (27). Both IL-15 and IP-10 (along with IL-6 and IL-10) were shown to be raised in the serum of severe COVID-19 patients as compared to severe non-COVID-19 acute respiratory illness from another cohort in the Sub-Saharan Africa region (28).

Bacterial superinfection and venous thromboembolism are known complications of critical COVID-19 (29). Our patients who died had significantly higher routine PCT values on day 1, and higher Luminex®-derived PCT, ferritin, and D-dimer values on day 7, than those who survived. We also found that receiving antibiotics during admission was associated with mortality. In addition, there was considerable overlap between the markers identified in our study and those known to be associated with mortality from bacterial sepsis (30). In combination, these findings suggest that bacterial superinfection and venous thromboembolism played a role in mortality, although neither condition was verifiable with imaging or autopsy because of the COVID-19-related restrictions and resource constraints. Theoretically, a dysregulated immune response combined with the corticosteroids that were used to treat the hyperinflammation could have resulted in an individual patient's susceptibility to secondary infection. Bacterial superinfections occur in up to 50% of critical COVID-19 patients (29, 31). They prolong ventilation, and along with fungi are common causes of mortality in critical COVID-19 (31, 32). They generally occur later in the ICU admission than our samples were taken, but it may be that some of our patients presented late in the

evolution of their disease (29, 31). An elevated D-dimer, however, may be indicative of more than a complication of critical COVID-19. Endotheliitis and a progressive endothelial thrombo-inflammatory syndrome have been suggested as the main pathological mechanism of organ injury in severe disease, rather than hyperinflammation (30, 33). This is partly because cytokine levels in COVID-19 hyperinflammation are profoundly lower than in non-COVID-19 ARDS and associated bacterial sepsis (30).

In addition to the hypothesized role of IP-10 and MCP-1 in thrombosis discussed earlier, the prominence of vascular/endothelial markers in all our analyses supports the endotheliitis theory. ET-1 is a potent vasoconstrictor released from endothelial and smooth muscle cells, which stimulates interleukin and TNFα expression in monocytes, leukocyte adherence, platelet aggregation, expression of adhesion molecules including ICAM-1 and VCAM-1, production and action of growth factors, DNA and protein synthesis, and cell cycle progression (34). It is a marker of endothelial dysfunction and is higher in patients with severe COVID-19, those with respiratory failure, and those who died in hospital (35, 36). The endothelium-derived vascular adhesion molecules ICAM-1 and VCAM-1 are markers of endothelial activation, have been reported as elevated in severe COVID-19, and are associated with death among patients admitted to the ICU (9, 26, 37). In addition to this, they are critical for the recruitment of inflammatory cells from circulation into the lungs, and in this way may be mediators of lung injury in ARDS (38). Indeed, VCAM-1 has been shown to be elevated in the BALF of patients with COVID-19 ARDS (39). In our study, ET-1, ICAM-1, and VCAM-1 were significantly associated with the outcome, particularly in the day 7 analysis and the trajectory analysis, where a reduction in the level of VCAM-1 from day 1 to 7 predicted survival. ET-1 and the adhesion molecules play a critical role in the pro-atherosclerotic pathway, and it is not clear in this study whether the derangements we observed were because of pre-existing vascular disease, a new onset COVID-19 endotheliitis, or some combination of the two. GDF-15 is a stress-responsive member of the TGFβ cytokine superfamily which is produced by many cell types including activated macrophages, cardiomyocytes, adipocytes, endothelial cells, and vascular smooth muscle cells. It increases during states of tissue injury and inflammation and has a tissue-protective role in sepsis, including the regulation of injury-mediated responses in the lungs (40). GDF-15 levels have been associated with cardiovascular risk and disease, including endothelial dysfunction and atherosclerosis (41). In this particular study, a high GDF-15 was strongly associated with COVID-19 mortality. A study by Ahmed et al. found that GDF-15 was a significant marker of disease severity that correlated with IL-6 as a predictor of ICU and hospital outcomes (42). Taken together these data suggest a prominent role for endothelial dysfunction and inflammation in the pathogenesis of fatal COVID-19, possibly in the context of pre-existing vascular disease.

Our models created a clinically relevant biosignature for predicting mortality on day 1 of admission to the ICU. It only included results which should be made available within a few hours of admission: lymphocyte percentage on the differential count, pH, and PCT. With sensitivities of 82.8% and 84.8%, this signature might be worth further investigation for use as a triaging tool in the overburdened ICU settings during pandemic times. The combination of clinical and Luminex®-derived biomarkers from day 1 performed even better, and our Luminex®-alone signature from day 7 did better on performance metrics than most other reported scoring systems. However, this finding should be regarded with caution. Our sample was from a highly selected population of critically ill COVID-19 ARDS patients from a specific geographic region. Other scoring systems may suffer the same limitations as documented in a critical appraisal of 39 prognostic models for mortality risk in COVID-19, only one model did not show a high risk of bias (1). This model, the 4C mortality score, predicted in-hospital mortality using patient age, sex, number of comorbidities, respiratory rate, peripheral oxygen saturation, level of consciousness, urea level, and CRP. The AUC was 0.79 for the derivation cohort and 0.77 for the validation cohort (43). Our clinical model for use on day 1 in the ICU has fewer variables than the 4C score and our results suggest that if there was a point-of-care assay for some of the Luminex® analytes we could provide critical care clinicians with a highly sensitive and specific prediction score which is easily available at the bedside. The biosignature we found may also be valid in ARDS of other causes considering the similarity between the biomarkers that we have shown and ARDS of other causes, and the significant association between ARDS severity (the PaO_2/FIO_2) and mortality.

Two of the strongest clinical markers of prognosis in this study were the pH and $PaCO_2$ on arterial blood gas. COVID-19 ARDS usually presents as a Type 1 respiratory failure with severe hypoxemia, rather than Type 2 where hypercapnia is the dominant feature. In our patients who all had severe hypoxemia, a rising $PaCO_2$ and drop in pH likely indicated a severe ventilation-perfusion mismatch (from either lung or vascular pathology), where both the transfer of O_2 into the alveolar capillaries and the clearance of CO_2 were impaired. Consistent with this, a rising $PaCO_2$ trajectory has been associated with mortality from COVID-19 in mechanically ventilated patients in a large population-based cohort study (44). The complex relationship between pH and $PaCO_2$ was further explored in the larger cohort, which included the patients in this sub-study of biomarkers of mortality (14).

PLWH made up 15.5% of the study population. Even though the proportion of PLWH was higher among those who died, the data was insufficient to determine an exposure-outcome relationship. In addition, there could have been inherent selection bias due to the fact that the PLWH who were selected for admission to the ICU, based on the local eligibility criteria, were virologically suppressed on ART. Epidemiologic evidence from South Africa has shown a significant association between HIV infection and in-hospital mortality among critical COVID-19 patients (3). In this study patients who were not on ART or virologically suppressed were more likely to die in hospital than their counterparts (3). The mechanism underlying this increased risk remains unknown. A histopathology study found no difference in the lungs, liver, heart, or rate of bacterial co-infection (other than *Mycobacterium tuberculosis*) of PLWH who died of COVID-19 and the HIV-uninfected COVID-19 deceased (45). Another study done within the African continent found no significant difference in serum or nasal lining fluid cytokine responses to moderate-severe COVID-19

between PLWH and HIV-uninfected counterparts (28). However, the study was not sufficiently powered to detect statistically significant differences.

Our study was limited by the small sample size which might have underpowered its ability to detect significant differences. Other key variables such as markers of cardiac dysfunction (Troponin T and NT-proBNP) and hypercoagulability (D-dimer) were seen to be higher in patients who died, but the observed differences were not statistically significant. Other data reported from South Africa have, however, shown these biomarkers of critical illness in COVID-19 in our population to be relevant (46). Selection bias also seems to have played a role in the study as there was no significant difference between groups in age or comorbidity, despite the fact that these have been reported to be among the most common factors associated with mortality. This may be because all our patients had already developed critical illness at the time of admission such that our study sample overall was older with a high rate of comorbidity and therefore a higher risk of death. Lastly, our analysis was limited by the inclusion of only two time points, which may not provide a true reflection of the trajectory over time. Biomarker levels may have fluctuated between the two measured time points or changed significantly after day 7.

In summary, this study has added much-needed data to the pool of biomarkers of severe COVID-19 ARDS in sub-Saharan African populations. We have shown that hyperinflammation, or a severely dysregulated cytokine response, is associated with mortality in the ICU. Our results also suggest that fatal COVID-19 ARDS involves excessive activation of cytotoxic cells and the NLRP3 inflammasome. Bacterial superinfection from immune dysregulation or treatment-induced suppression, and thrombosis from underlying endothelial dysfunction, likely contributed to death in these patients. Our models have made a biosignature of fatal COVID-19 on admission to the ICU which warrants further testing.

Data availability statement

The datasets presented in this study can be found in online repositories. The names of the repository/repositories and accession number(s) can be found below: https://figshare.com/projects/COVID19_ICU_immune_and_vascular_biomarkers_of_mortality/163708.

Ethics statement

The studies involving human participants were reviewed and approved by Stellenbosch University Health Research Ethics Committee. Written informed consent for participation was not required for this study in accordance with the national legislation and the institutional requirements.

Author contributions

AEZ, PN, GW, HS, BA, RE, ZC, TM, AZ and NC conceived and designed the study. CS performed the assays. CK, UL, EI, NB, LS, JS, and VN collected or contributed to the data. MM and GT performed the analysis. GW, NdP, HS, AZ, BA, FE, JS, and SM informed the interpretation of the data. JS wrote the paper, which was critically reviewed and approved in the final draft by all authors. All authors contributed to the article and approved the submitted version.

Funding

This work was conducted under the COVID-19 Africa Rapid Grant Fund supported under the auspices of the Science Granting Councils Initiative in Sub-Saharan Africa (SGCI) and administered by South Africa's National Research Foundation (NRF) in collaboration with Canada's International Development Research Centre (IDRC), the Swedish International Development Cooperation Agency (Sida), South Africa's Department of Science and Innovation (DSI), the Fonds de Recherche du Québec (FRQ), the United Kingdom's Department of International Development (DFID), United Kingdom Research and Innovation (UKRI) through the Newton Fund, and the SGCI participating councils across 15 countries in sub-Saharan countries. JAS is funded by the South African Medical Research Council through its Division of Research Capacity Development under the Bongani Mayosi National Health Scholars Programme for funding received from the Public Health Enhancement Fund/South African National Department of Health. The content hereof is the sole responsibility of the authors and does not necessarily represent the official views of the SGCI/NRF and the SAMRC.

Acknowledgments

The authors wish to acknowledge Chanelle Rinkwest and Soraya Chalklen who diligently collected the data and samples for this study under exceptionally difficult circumstances.

Conflict of interest

The authors declare that the research was conducted in the absence of any commercial or financial relationships that could be construed as a potential conflict of interest.

Publisher's note

Supplementary material

The Supplementary Material for this article can be found online at: https://www.frontiersin.org/articles/10.3389/fimmu.2023.1219097/full#supplementary-material

References

1. Wynants L, Van Calster B, Collins GS, Riley RD, Heinze G, Schuit E, et al. Prediction models for diagnosis and prognosis of COVID-19: systematic review and critical appraisal. *BMJ* (2020) 369:m1328. doi: 10.1136/bmj.m1328

2. Gallo Marin B, Aghagoli G, Lavine K, Yang L, Siff EJ, Chiang SS, et al. Predictors of COVID-19 severity: A literature review. *Rev Med Virol* (2021) 31(1):1–10. doi: 10.1002/rmv.2146

3. Jassat W, Cohen C, Tempia S, Masha M, Goldstein S, Kufa T, et al. Risk factors for COVID-19-related in-hospital mortality in a high HIV and tuberculosis prevalence setting in South Africa: a cohort study. *Lancet HIV*. (2021) 8(9):e554–67. doi: 10.1016/S2352-3018(21)00151-X

4. Parker A, Boloko L, Moolla MS, Ebrahim N, Ayele BT, Broadhurst AGB, et al. Clinical features and outcomes of COVID-19 admissions in a population with a high prevalence of HIV and tuberculosis: a multicentre cohort study. *BMC Infect Dis* (2022) 22(1):559. doi: 10.1186/s12879-022-07519-8

5. Lucas C, Wong P, Klein J, Castro TBR, Silva J, Sundaram M, et al. Longitudinal analyses reveal immunological misfiring in severe COVID-19. *Nature* (2020) 584 (7821):463–9. doi: 10.1038/s41586-020-2588-y

6. Abers MS, Delmonte OM, Ricotta EE, Fintzi J, Fink DL, de Jesus AAA, et al. An immune-based biomarker signature is associated with mortality in COVID-19 patients. *JCI Insight* (2021) 6(1):e144455. doi: 10.1172/jci.insight.144455

7. Diamond MS, Kanneganti T-D. Innate immunity: the first line of defense against SARS-CoV-2. *Nat Immunol* (2022) 23(2):165–76. doi: 10.1038/s41590-021-01091-0

8. Shi H, Zuo Y, Navaz S, Harbaugh A, Hoy CK, Gandhi AA, et al. Endothelial cell-activating antibodies in COVID-19. *Arthritis Rheumatol (Hoboken NJ).* (2022) 74 (7):1132–8. doi: 10.1002/art.42094

9. Tong M, Jiang Y, Xia D, Xiong Y, Zheng Q, Chen F, et al. Elevated expression of serum endothelial cell adhesion molecules in COVID-19 patients. *J Infect Dis* (2020) 222(6):894–8. doi: 10.1093/infdis/jiaa349

10. Madhi SA, Kwatra G, Myers JE, Jassat W, Dhar N, Mukendi CK, et al. Population immunity and COVID-19 severity with omicron variant in South Africa. *N Engl J Med* (2022) 386(14):1314–26. doi: 10.1056/NEJMoa2119658

11. Definition Task Force ARDS, Ranieri VM, Rubenfeld GD, Thompson BT, Ferguson ND, Caldwell E, et al. Acute respiratory distress syndrome: the Berlin definition. *JAMA* (2012) 307(23):22526–33. doi: 10.1001/jama.2012.5669

12. Gopalan PD, Joubert IA, Paruk F, et al. The Critical Care Society of Southern Africa guidelines on the allocation of scarce critical care resources during the COVID-19 public health emergency in South Africa. *S Afr Med J*. 2020;110(8):700-703.

13. Harris PA, Taylor R, Minor BL, Elliott V, Fernandez M, O'Neal L, et al. The REDCap consortium: building an international community of software platform partners. *J BioMed Inform.* (2019) 95:103208. doi: 10.1016/j.jbi.2019.103208

14. Zemlin AE, Sigwadhi LN, Wiese OJ, Jalavu TP, Chapanduka ZC, Allwood BW, et al. The association between acid-base status and clinical outcome in critically ill COVID-19 patients admitted to intensive care unit with an emphasis on high anion gap metabolic acidosis. *Ann Clin Biochem* (2023) 60(2):86-91. doi: 10.1177/00045632221134687.

15. R Core Team. *A language and environment for statistical computing*. Vienna, Austria: R Found Stat Comput (2016).

16. Kursa MB, Rudnicki WR. Feature selection with the boruta package. *J Stat Softw* (2010) 36(11), 1–13. doi: 10.18637/jss.v036.i11

17. Schett G, Dayer J-M, Manger B. Interleukin-1 function and role in rheumatic disease. *Nat Rev Rheumatol* (2016) 12(1):14–24. doi: 10.1038/nrrheum.2016.166

18. Spadaro S, Park M, Turrini C, Tunstall T, Thwaites R, Mauri T, et al. Biomarkers for acute respiratory distress syndrome and prospects for personalised medicine. *J Inflamm* (2019) 16(1):1. doi: 10.1186/s12950-018-0202-y

19. Calfee CS, Ware LB, Glidden DV, Eisner MD, Parsons PE, Thompson BT, et al. Use of risk reclassification with multiple biomarkers improves mortality prediction in acute lung injury. *Crit Care Med* (2011) 39(4):711–7. doi: 10.1097/CCM.0b013e318207ec3c

20. Dolinay T, Kim YS, Howrylak J, Hunninghake GM, An CH, Fredenburgh L, et al. Inflammasome-regulated cytokines are critical mediators of acute lung injury. *Am J Respir Crit Care Med* (2012) 185(11):1225–34. doi: 10.1164/rccm.201201-0003OC

21. Saris A, Reijnders TDY, Nossent EJ, Schuurman AR, Verhoeff J, Asten S v, et al. Distinct cellular immune profiles in the airways and blood of critically ill patients with COVID-19. *Thorax* (2021) 76(10):1010–9. doi: 10.1136/thoraxjnl-2020-216256

22. Velásquez SY, Killian D, Schulte J, Sticht C, Thiel M, Lindner HA. Short term hypoxia synergizes with interleukin 15 priming in driving glycolytic gene transcription and supports human natural killer cell activities*. *J Biol Chem* (2016) 291(25):12960–77. doi: 10.1074/jbc.M116.721753

23. Tjan LH, Furukawa K, Nagano T, Kiriu T, Nishimura M, Arii J, et al. Early differences in cytokine production by severity of coronavirus disease 2019. *J Infect Dis* (2021) 223(7):1145–9. doi: 10.1093/infdis/jiab005

24. Gu Y, Zuo X, Zhang S, Ouyang Z, Jiang S, Wang F, et al. The mechanism behind influenza virus cytokine storm. *Viruses* (2021) 13(7):1362 doi: 10.3390/v13071362

25. Felices M, Lenvik AJ, McElmurry R, Chu S, Hinderlie P, Bendzick L, et al. Continuous treatment with IL-15 exhausts human NK cells via a metabolic defect. *JCI Insight* (2018) 3(3):e96219. doi: 10.1172/jci.insight.96219

26. de Bruin S, Bos LD, van Roon MA, Tuip-de Boer AM, Schuurman AR, Koel-Simmelinck MJA, et al. Clinical features and prognostic factors in COVID-19: a prospective cohort study. *EBioMedicine* (2021) 67:103378. doi: 10.1016/j.ebiom.2021.103378

27. Chen Y, Wang J, Liu C, Su L, Zhang D, Fan J, et al. IP-10 and MCP-1 as biomarkers associated with disease severity of COVID-19. *Mol Med* (2020) 26(1):97. doi: 10.1186/s10020-020-00230-x

28. Morton B, Barnes KG, Anscombe C, Jere K, Matambo P, Mandolo J, et al. Distinct clinical and immunological profiles of patients with evidence of SARS-CoV-2 infection in Sub-Saharan Africa. *Nat Commun* (2021) 12(1):3554. doi: 10.1038/s41467-021-23267-w

29. Maslove DM, Sibley S, Boyd JG, Goligher EC, Munshi L, Bogoch II, et al. Complications of critical COVID-19: diagnostic and therapeutic considerations for the mechanically ventilated patient. *Chest* (2022) 161(4):989–98. doi: 10.1016/j.chest.2021.10.011

30. Leisman DE, Ronner L, Pinotti R, Taylor MD, Sinha P, Calfee CS, et al. Cytokine elevation in severe and critical COVID-19: a rapid systematic review, meta-analysis, and comparison with other inflammatory syndromes. *Lancet Respir Med* (2020) 8 (12):1233–44. doi: 10.1016/S2213-2600(20)30404-5

31. Buehler PK, Zinkernagel AS, Hofmaenner DA, Wendel Garcia PD, Acevedo CT, Gómez-Mejia A, et al. Bacterial pulmonary superinfections are associated with longer duration of ventilation in critically ill COVID-19 patients. *Cell Rep Med* (2021) 2 (4):100229. doi: 10.1016/j.xcrm.2021.100229

32. Zacharias M, Kashofer K, Wurm P, Regitnig P, Schütte M, Neger M, et al. Host and microbiome features of secondary infections in lethal COVID-19. *iScience* (2022) 25(9):104926. doi: 10.1016/j.isci.2022.104926

33. Ciceri F, Beretta L, Scandroglio AM, Colombo S, Landoni G, Ruggeri A, et al. Microvascular COVID-19 lung vessels obstructive thromboinflammatory syndrome (MicroCLOTS): an atypical acute respiratory distress syndrome working hypothesis. *Crit Care Resusc J Australas Acad Crit Care Med* (2020) 22(2):95–7. doi: 10.51893/2020.2.pov2

34. Lüscher TF, Barton M. Endothelins and endothelin receptor antagonists. *Circulation* (2000) 102(19):2434–40. doi: 10.1161/01.CIR.102.19.2434

35. Khodabakhsh P, Asgari Taei A, Mohseni M, Bahrami Zanjanbar D, Khalili H, Masoumi K, et al. Vasoactive peptides: role in COVID-19 pathogenesis and potential use as biomarkers and therapeutic targets. *Arch Med Res* (2021) 52(8):777–87. doi: 10.1016/j.arcmed.2021.05.007

36. Abraham GR, Kuc RE, Althage M, Greasley PJ, Ambery P, Maguire JJ, et al. Endothelin-1 is increased in the plasma of patients hospitalised with COVID-19. *J Mol Cell Cardiol* (2022) 167:92–6. doi: 10.1016/j.yjmcc.2022.03.007

37. Liu N, Long H, Sun J, Li H, He Y, Wang Q, et al. New laboratory evidence for the association between endothelial dysfunction and COVID-19 disease progression. *J Med Virol* (2022) 94(7):3112–20. doi: 10.1002/jmv.27693

38. Vassiliou AG, Vrettou CS, Keskinidou C, Dimopoulou I, Kotanidou A, Orfanos SE. Endotheliopathy in acute COVID-19 and long COVID. *Int J Mol Sci* (2023) 24 (9):8237. doi: 10.3390/ijms24098237

39. Kristensen MK, Plovsing RR, Berg RMG, Krogh-Madsen R, Ronit A. Cell adhesion molecules and vascular endothelial growth factor at the systemic and alveolar level in coronavirus disease 2019 acute respiratory distress syndrome. *J Infect Dis* (2021) 224(6):1101–3. doi: 10.1093/infdis/jiab347

40. Wischhusen J, Melero I, Fridman WH. Growth/Differentiation factor-15 (GDF-15): from biomarker to novel targetable immune checkpoint. *Front Immunol* (2020) 11. doi: 10.3389/fimmu.2020.00951

41. Adela R, Banerjee SK. GDF-15 as a target and biomarker for diabetes and cardiovascular diseases: a translational prospective. *J Diabetes Res* (2015) 2015:490842. doi: 10.1155/2015/490842

42. Ahmed DS, Isnard S, Berini C, Lin J, Routy J-P, Royston L. Coping with stress: the mitokine GDF-15 as a biomarker of COVID-19 severity. *Front Immunol* (2022) 13:820350. doi: 10.3389/fimmu.2022.820350

43. Knight SR, Ho A, Pius R, Buchan I, Carson G, Drake TM, et al. Risk stratification of patients admitted to hospital with covid-19 using the ISARIC WHO clinical characterisation protocol: development and validation of the 4C mortality score. *BMJ* (2020) 370:m3339. doi: 10.1136/bmj.m3339

44. Berg RMG, Ronit A, Haase N, Møller MH, Kristiansen KT, Jonassen T, et al. PaCO2 trajectories in mechanically ventilated patients with COVID-19: a population-based cohort study. *Acta Anaesthesiol Scand* (2023). 67(6):779-787. doi: 10.1111/aas.14233

45. Nunes MC, Hale MJ, Mahtab S, Mabena FC, Dludlu N, Baillie VL, et al. Clinical characteristics and histopathology of COVID-19 related deaths in South African adults. *PloS One* (2022) 17(1):e0262179. doi: 10.1371/journal.pone.0262179

46. Hesse R, van der Westhuizen DJ, George JA. COVID-19-Related laboratory analyte changes and the relationship between SARS-CoV-2 and HIV, TB, and HbA1c in South Africa. *Adv Exp Med Biol* (2021) 1321:183–97. doi: 10.1007/978-3-030-59261-5_16

frontiers | Frontiers in Immunology

TYPE Original Research
PUBLISHED 12 April 2023
DOI 10.3389/fimmu.2023.1176898

OPEN ACCESS

EDITED BY
Diana Boraschi,
Chinese Academy of Science (CAS), China

REVIEWED BY
Olukemi Amodu,
University of Ibadan, Nigeria
Marcelo Cavalcante,
University of Fortaleza, Brazil

*CORRESPONDENCE
Geraldo Magela Fernandes
geraldomafer@gmail.com
Olindo Assis Martins-Filho
olindo.filho@fiocruz.br

†These authors have contributed equally to this work

‡These authors share senior authorship

SPECIALTY SECTION
This article was submitted to Cytokines and Soluble Mediators in Immunity, a section of the journal Frontiers in Immunology

RECEIVED 01 March 2023
ACCEPTED 30 March 2023
PUBLISHED 12 April 2023

CITATION
Fernandes GM, Sasaki LMP, Jardim-Santos GP, Schulte HL, Motta F, da Silva ÂP, de Carvalho AO, Pereira YR, Alves CdO, de Araújo Júnior DA, Mendonça-Silva DL, Costa KN, de Castro MEC, Lauand L, Nery RdR, Tristão R, Kurizky PS, Nóbrega OdT, Espindola LS, de Castro LCG, Alpoim PN, Godoi LC, Dusse LMSA, Coelho-dos-Reis JGA, Amaral LRd, Gomes MdS, Bertarini PLL, Brito-de-Sousa JP, Costa-Rocha IAd, Campi-Azevedo AC, Peruhype-Magalhães V, Teixeira-Carvalho A, Zaconeta AM, Soares AAdSM, Valim V, Gomes CM, de Albuquerque CP, Martins-Filho OA and da Mota LMH (2023) Panoramic snapshot of serum soluble mediator interplay in pregnant women with convalescent COVID-19: an exploratory study. *Front. Immunol.* 14:1176898. doi: 10.3389/fimmu.2023.1176898

Panoramic snapshot of serum soluble mediator interplay in pregnant women with convalescent COVID-19: an exploratory study

Geraldo Magela Fernandes[1*†], Lizandra Moura Paravidine Sasaki[1,2†], Gabriela Profírio Jardim-Santos[1], Heidi Luise Schulte[1], Felipe Motta[1], Ângelo Pereira da Silva[2], Aleida Oliveira de Carvalho[2], Yacara Ribeiro Pereira[2], Caroline de Oliveira Alves[3], David Alves de Araújo Júnior[2], Dayde Lane Mendonça-Silva[2], Karina Nascimento Costa[3], Maria Eduarda Canellas de Castro[1,2], Lucas Lauand[3], Rodrigo de Resende Nery[3], Rosana Tristão[3], Patricia Shu Kurizky[1,2], Otávio de Toledo Nóbrega[1], Laila Salmen Espindola[1], Luiz Cláudio Gonçalves de Castro[1,3], Patrícia Nessralla Alpoim[4], Lara Carvalho Godoi[4], Luci Maria Sant Ana Dusse[4], Jordana Grazziela Alves Coelho-dos-Reis[5], Laurence Rodrigues do Amaral[6], Matheus de Souza Gomes[6], Pedro Luiz Lima Bertarini[6], Joaquim Pedro Brito-de-Sousa[7], Ismael Artur da Costa-Rocha[7], Ana Carolina Campi-Azevedo[7], Vanessa Peruhype-Magalhães[7], Andrea Teixeira-Carvalho[7], Alberto Moreno Zaconeta[3‡], Alexandre Anderson de Sousa Munhoz Soares[1,3], Valéria Valim[8,9], Ciro Martins Gomes[1,3,10], Cleandro Pires de Albuquerque[1,2], Olindo Assis Martins-Filho[7*‡] and Licia Maria Henrique da Mota[1,2,10‡]

[1]Programa de Pós-Graduação em Ciências Médicas, Universidade de Brasília (UnB), Brasília, Brazil, [2]Hospital Universitário de Brasília, Universidade de Brasília (UnB), Brasília, Brazil, [3]Faculdade de Medicina, Universidade de Brasília (UnB), Brasília, Brazil, [4]Faculdade de Farmácia, Universidade Federal de Minas Gerais, Belo Horizonte, Brazil, [5]Laboratório de Virologia Básica e Aplicada, Instituto de Ciências Biológicas, Universidade Federal de Minas Gerais, Belo Horizonte, Brazil, [6]Laboratório de Bioinformática e Análises Moleculares, Universidade Federal de Uberlândia, Patos de Minas, Brazil, [7]Instituto René Rachou, Fundação Oswaldo Cruz (FIOCRUZ-Minas), Belo Horizonte, Brazil, [8]Hospital Universitário Cassiano Antônio Moraes, Universidade Federal do Espírito Santo (HUCAM-UFES), Vitória, Brazil, [9]Programa de Pós-Graduação em Saúde Coletiva (PPGSC), Centro de Ciências Médicas, Universidade Federal do Espírito Santo, Vitória, Brazil, [10]Programa de Pós-Graduação em Patologia Molecular, Universidade de Brasília (UnB), Brasília, Brazil

Introduction: SARS-CoV-2 infection during pregnancy can induce changes in the maternal immune response, with effects on pregnancy outcome and offspring. This is a cross-sectional observational study designed to characterize the immunological status of pregnant women with convalescent COVID-19 at distinct pregnancy trimesters. The study focused on providing a clear snapshot of the interplay among serum soluble mediators.

Methods: A sample of 141 pregnant women from all prenatal periods (1st, 2nd and 3rd trimesters) comprised patients with convalescent SARS-CoV-2 infection at 3-20 weeks after symptoms onset (COVID, n=89) and a control group of pre-pandemic non-infected pregnant women (HC, n=52). Chemokine, pro-inflammatory/regulatory cytokine and growth factor levels were quantified by a high-throughput microbeads array.

Results: In the HC group, most serum soluble mediators progressively decreased towards the 2nd and 3rd trimesters of pregnancy, while higher chemokine, cytokine and growth factor levels were observed in the COVID patient group. Serum soluble mediator signatures and heatmap analysis pointed out that the major increase observed in the COVID group related to pro-inflammatory cytokines (IL-6, TNF-α, IL-12, IFN-γ and IL-17). A larger set of biomarkers displayed an increased COVID/HC ratio towards the 2nd (3x increase) and the 3rd (3x to 15x increase) trimesters. Integrative network analysis demonstrated that HC pregnancy evolves with decreasing connectivity between pairs of serum soluble mediators towards the 3rd trimester. Although the COVID group exhibited a similar profile, the number of connections was remarkably lower throughout the pregnancy. Meanwhile, IL-1Ra, IL-10 and GM-CSF presented a preserved number of correlations (≥5 strong correlations in HC and COVID), IL-17, FGF-basic and VEGF lost connectivity throughout the pregnancy. IL-6 and CXCL8 were included in a set of acquired attributes, named COVID-selective (≥5 strong correlations in COVID and <5 in HC) observed at the 3rd pregnancy trimester.

Discussion and conclusion: From an overall perspective, a pronounced increase in serum levels of soluble mediators with decreased network interplay between them demonstrated an imbalanced immune response in convalescent COVID-19 infection during pregnancy that may contribute to the management of, or indeed recovery from, late complications in the post-symptomatic phase of the SARS-CoV-2 infection in pregnant women.

KEYWORDS

chemokines, cytokines, growth factors, COVID-19, pregnancy

1 Introduction

In March 2020, the World Health Organization (WHO) characterized the outbreak of the Severe Acute Respiratory Syndrome Coronavirus 2 (SARS-CoV-2) disease (COVID-19) as a pandemic, having since confirmed more than 655 million COVID-19 cases, 6.6 million of which resulted in death (1). SARS-CoV-2 is transmitted through airborne droplets, respiratory secretions, and direct contact. The clinical symptoms relating to the COVID-19 disease were primarily respiratory, and later reported as multisystemic effects. COVID-19 illness symptoms can be asymptomatic, mild, moderate, severe, or critical (2–4). Fever, cough, dyspnea, and myalgia were the most common mild symptoms. The pathogenesis of COVID-19 has been strongly associated with an unbalanced immune response; however, the pathophysiology of the disease remains under investigation (5–7).

Multiple studies concluded that pregnant women are a high-risk population for the COVID-19 disease. Infectious diseases in pregnancy are regularly considered a critical condition. Physiological changes during pregnancy have significant effects on the immune system, cardiopulmonary system and coagulation, and these changes may result in an altered response to COVID-19

infection (3, 8–11). Cytokine levels during pregnancy could be responsible for metabolic imprinting as cytokines are transferable from maternal to fetal circulation and are capable of modulating placental nutrient transfer. Maternal inflammation may induce metabolic reprogramming at several levels, from the periconceptional period onwards. Such processes and their consequences on the maternal and perinatal periods have not been extensively studied to date. Moreover, the maternal immune activation triggered by COVID-19 can have impacts for the mother, pregnancy outcome and offspring (12, 13). The understanding such phenomena should contribute to the proper management of children born to SARS-CoV-2-infected mothers (14).

The aim of the present study was to conduct a prospective observational study designed to characterize the immunological status of pregnant women with convalescent COVID-19, focusing on an overall snapshot of the interplay between serum soluble mediators.

2 Materials and methods

2.1 Study population

This cross-sectional observational study was conducted between July 2020 and December 2021 during the COVID-19 pandemic in the Federal District of Brazil during circulation of the SARS-CoV-2 B.1.1.28 and B.1.1.33 strains. A total of 141 participants were enrolled as non-probability convenience sampling, including pregnant women with convalescent SARS-CoV-2 infection (COVID, n=89) at 3-20 weeks after symptoms onset during the prenatal period (1st, 2nd and 3rd trimesters), together with a healthy control group composed of age-matched pre-pandemic non-infected pregnant women (HC, n=52).

The COVID-19 pregnant women were recruited at two public hospitals - the University Hospital of Brasília and the Asa Norte Regional Hospital, both public reference centers for COVID-19 in the Federal District of Brazil and participants of a large research project named PROUDEST (15). The COVID group comprised pregnant women aged 18-44 years, with a median age of 31 years. This group was further categorized into subgroups according to the pregnancy trimester, referred to as: 1st (n=7), 2nd (n=34) and 3rd (n=48). COVID-19 diagnosis was confirmed by a documented positive RT-PCR test using a nasopharyngeal swab or rapid test (Biomanguinhos, FIOCRUZ, Brazil) for IgM or IgG, during pregnancy. Most of the COVID-19 group (97%, 86 out of 89) presented the non-severe form of the disease. The most common symptoms were: Anosmia (68%), runny nose and/or nasal congestion (68%), headache (67%), ageusia (63%), myalgia (57%), cough (43%), fever (43%), dyspnea (31%), sore throat (31%), asthenia (22%), diarrhea (17%), nausea and vomiting (11%), joint pain (5%), dizziness (4%) and skin diseases (2%). SARS-CoV-2 infection during pregnancy was associated with important adverse maternal and neonatal outcomes, including gestational diabetes mellitus (37%), Apgar score at first minute ≤ 7 (22%), systemic arterial hypertension (18%), fetal restriction growth (11%), preterm labor (11%), acute fetal distress (8%), Apgar score at fifth minute ≤ 7 (5%) and preeclampsia (3%).

The HC group comprised a selected non-probability convenience sampling from a biorepository maintained at Grupo Integrado de Pesquisas em Biomarcadores, Instituto René Rachou, Fundação Oswaldo Cruz (FIOCRUZ-Minas), Belo Horizonte, Brazil. The HC group comprised pregnant women, aged 18- 42 years, with a median age of 28 years. The healthy control group was composed by primiparous with no previous history or current status of obesity, systemic arterial hypertension, diabetes mellitus and without records of pre-eclampsia. The HC group was further categorized into subgroups according to pregnancy trimester, referred to as: 1st (n=21), 2nd (n=10) and 3rd (n=21).

The Table 1 summarize the major demographic and clinical features of the study population.

TABLE 1 Demographic and clinical features of the study population.

Characteristics	GROUPS	
	Healthy Controls – HC (n=52)	COVID-19 – COVID (n=89)
Age, median (min-max)	28 (18-42)	31 (18-44)
Obstetric History		
Previous Pregnancies, median (min-max)	0% (0)	2 (0-6)
Abortions, median (min-max)	0% (0)	0 (0-2)
Complications* % (n)	0% (0)	24% (21)
Current Study		
Obesity % (n)	0% (0)	11% (10)
SAH % (n)	0% (0)	18% (16)
Diabetes % (n)	0% (0)	37% (33)
Pre-eclampsia % (n)	0% (0)	3% (3)

SAH, systemic arterial hypertension. *Obesity, SAH, diabetes, pre-eclampsia.

All study participants provided written informed consent prior to inclusion in accordance with the Helsinki Declaration and Resolution 466/2012 from the Brazilian National Health Council for research involving human subjects. This study was recorded on the Brazilian Registry of Clinical Trials Platform (ReBEC, RBR-65qxs2) and approved by the National Commission for Ethics in Research in Brazil (CONEP, CAAE 32359620.0.0000.5558). The anonymization strategy to protect the identity of participants was achieved by replacing the direct identifiers by standardized alphanumeric codes (*PRAxxxPNy and PRBxxxPNy*), where "*PR*" refer to the PROUDEST project name (15), "*A*" and "*B*" refers to the hospital unit, the "*xxx*" represent the sequential number of patient inclusion, "*PN*" refer to prenatal period and "*y*" the trimester of sample collection.

2.2 Biological samples

Whole blood sample (10 mL) were collected from each participant in vacuum tubes without anticoagulant by venipuncture at the first prenatal appointment or upon enrolment in the study. Serum samples were obtained by centrifugation (1400 x g, 10 min, 4°C) of original samples within 6 h after blood collection. The serum specimens were aliquoted and stored at -80°C until quantification of serum soluble mediators.

2.3 Quantification of serum soluble mediators

Serum soluble mediators were quantified by a high-throughput Luminex microbead multiplex assay (Bio-Plex Pro™ Human Cytokine 27-plex Assay, Bio-Rad Laboratories, Hercules, CA, USA). The manufacturer's instructions were followed to determine the concentrations of chemokines (CXCL8; CCL11; CCL3; CCL4; CCL2; CCL5; CXCL10), pro-inflammatory cytokines (IL-1β; IL-6; TNF-α; IL-12; IFN-γ; IL-15; IL-17), regulatory cytokines (IL-1Ra; IL-4; IL-5; IL-9; IL-10; IL-13) and growth factors (FGF-basic; VEGF; PDGF; G-CSF; GM-CSF; IL-2; IL-7). The assays were conducted in parallel batches by a trained technician at the flow cytometry facility at FIOCRUZ-Minas. The concentrations of serum soluble mediators (pg/mL) were obtained according to a 5-parameter logistic curve fit regression of standard curves.

2.4 Statistical analysis

Descriptive statistics were carried out using the Prism 8.0.2 software (GraphPad Software, San Diego, USA). Data normality was assessed using the Shapiro-Wilk test. Considering the nonparametric distribution of all data sets, multiple comparisons amongst HC and COVID subgroups were carried out using the Kruskal-Wallis followed by Dunn's post-test. Additionally, comparative analysis between HC and COVID at matching trimesters was performed using the Mann-Whitney test. In all cases, statistical significance was considered at $p<0.05$.

The serum soluble mediator signatures were calculated as the proportion (%) of pregnant women with serum levels above the reference values (cut-off) defined as the median Z-score of each soluble mediator detected for all HC along the 1st, 2nd and 3rd trimesters (CXCL8=-0.3; CCL11=-0.3; CCL3=-0.3; CCL4=-0.3; CCL2=-0.4; CCL5=-0.2; CXCL10=-0.2; IL-1β=-0.3; IL-6=-0.3; TNF-α=-0.3; IL-12=-0.3; IFN-γ=-0.4; IL-15=-0.5; IL-17=-0.4; IL-1Ra=-0.4; IL-4=-0.3; IL-5=-0.2; IL-9=-0.2; IL-10=-0.2; IL-13=-0.4; FGF-basic=-0.5; PDGF=-0.4; VEGF=-0.4; G-CSF=-0.2; GM-CSF=-0.4; IL-2=-0.4; IL-7=-0.3). Additionally, trimester-matching signatures were assembled, considering the reference values (cut-off) defined as the median Z-score of each soluble mediator detected for HC trimester subgroups at 1st (CXCL8 = 0.2; CCL11 = 0.1; CCL3 = 0; CCL4=-0.6; CCL2 = 0.4; CCL5=-0.2; CXCL10=-0.7; IL-1β=-0.2; IL-6 = 1.6; TNF-α=-0.1; IL-12=-0.2; IFN-γ=0.1; IL-15=-0.5; IL-17 = 0.1; IL-1Ra=0.1; IL-4=-0.5; IL-5=-0.1; IL-9 = 0.5; IL-10=-0.2; IL-13 = 0.2; FGF-basic=0.3; PDGF=0.2; VEGF=0.1; G-CSF=-0.2; GM-CSF=0.1; IL-2=-0.4; IL-7=-0.2), 2nd (CXCL8=-0.3; CCL11=-0.2; CCL3=-0.3; CCL4=-0.2; CCL2=-0.5; CCL5=-0.1; CXCL10=-0.6; IL-1β=-0.3; IL-6=-0.4; TNF-α=-0.3; IL-12=-0.3; IFN-γ=-0.4; IL-15 = 0.2; IL-17=-0.2; IL-1Ra=-0.5; IL-4 = 0.2; IL-5=-0.2; IL-9=-0.6; IL-10=-0.2; IL-13=-0.4; FGF-basic=-0.6; PDGF=-0.6; VEGF=-0.2; G-CSF=-0.1; GM-CSF=-0.6; IL-2=-0.1; IL-7=-0.2) and 3rd trimesters (CXCL8=-0.4; CCL11=-0.4; CCL3=-0.3; CCL4 = 0.3; CCL2=-0.5; CCL5 = 0.1; CXCL10 = 0.6; IL-1β=-0.4; IL-6=-0.3; TNF-α=-0.3; IL-12=-0.3; IFN-γ=-0.4; IL-15=-0.5; IL-17=-0.4; IL-1Ra=-0.6; IL-4=-0.3; IL-5=-0.2; IL-9=-0.8; IL-10=-0.3; IL-13=-0.4; FGF-basic=-0.6; PDGF=-0.7; VEGF=-0.4; G-CSF=-0.2; GM-CSF=-0.7; IL-2=-0.5; IL-7=-0.3). The serum soluble mediators displaying a proportion above 50% in pregnant women were included in the set of biomarkers with increased levels.

Heatmap constructs were assembled using conditional formatting in Microsoft Excel to illustrate the overall profile of serum soluble mediator signatures of the COVID and HC subgroups along the pregnancy trimesters. The ratio between the proportion of pregnant women with serum levels above the reference values in the COVID group in relation to HC (% COVID/%HC) was also assessed by comparative analysis.

Serum-soluble mediator networks were built based on correlation analysis (Pearson and Spearman rank tests) between pairs of serum-soluble mediators. Only significant strong correlations ($p<0.05$ and "r" scores $\geq |0.67|$) were employed to construct the comprehensive networks. The open-source Cytoscape software (available at https://cytoscape.org) was used to create cluster network layouts comprising the 4 categories of serum soluble mediators - chemokines, pro-inflammatory cytokines, regulatory cytokines, and growth factors. Descriptive analysis of

serum soluble mediator networks was performed by considering the ascendant number of strong correlations to identify the set of biomarkers with five or more strong correlations (≥ 5). Venn Diagram analysis (available at (http://bioinformatics.psb.ugent.be/webtools/Venn/) was performed to assess the preserved (common), lost or acquired (selective) serum soluble mediators with ≥ 5 strong correlations in COVID subgroups compared to trimester-matching HC.

The MATLAB software was employed for Principal Component Analysis (PCA). The PCA data was assembled to verify the ability of serum soluble mediators to cluster convalescent COVID-19 pregnant women from HC, as well as subgroups of COVID-19 as compared to trimester-matching HC. The PCA analysis enabled data dimensionality reduction.

3 Results

3.1 Levels of serum soluble mediators in convalescent COVID-19 at distinct pregnancy trimesters

The levels of chemokines, pro-inflammatory cytokines, regulatory cytokines and growth factors were measured in serum samples from pregnant women with convalescent COVID-19 at 3-20 weeks after symptoms onset (COVID) and compared with those detected in trimester-matching pre-pandemic non-infected pregnant women as a healthy control (HC). The results are presented in Figures 1 and 2.

In general, healthy pregnant women presented a progressive decrease in most serum soluble mediators towards the 2nd and 3rd pregnancy trimester, including: chemokines (CXCL8, CCL11, CCL3 and CCL2); pro-inflammatory cytokines (IL-1β, IL-6, TNF-α, IL-12, IFN-γ, and IL-17); regulatory cytokines (IL-1Ra, IL-4, IL-5, IL-9, IL-10 and IL-13), and growth factors (FGF-basic, VEGF, PDGF, GM-CSF and IL-7). Conversely, progressive increases in CCL4, CCL5, CXCL10 and G-CSF were observed in the HC group. No difference was observed in the HC group for IL-15 and IL-2 (Figures 1, 2).

Overall, higher levels of the most soluble mediators were observed in convalescent COVID-19 pregnant women compared to the healthy controls, especially at the 2nd and 3rd trimesters, including higher levels of CXCL8; CCL11; CCL2; CCL3; IL-1β; IL-6; TNF-α; IL-12; IFN-γ; IL-17; IL-1Ra; IL-5; IL-9; IL-10; IL-13; FGF-basic; VEGF, and GM-CSF. Conversely, lower levels of CCL4, CCL5, CXCL10, G-CSF and IL-7 were observed towards the 2nd and 3rd trimesters in the COVID group compared to the HC group (Figures 1, 2).

Additional analysis amongst the COVID subgroups along the pregnancy trimesters demonstrated an inverted profile of CCL3, IL-1Ra and FGF-basic towards higher levels in the 3rd trimester (Figures 1, 2).

Supplementary Figure 1 summarizes the major changes observed in serum soluble mediators along the trimesters of healthy and convalescent COVID-19 pregnancy.

3.2 Serum soluble mediator signatures in convalescent COVID-19 at distinct pregnancy trimesters

Serum soluble mediator signatures were assembled as the percentage of pregnant women with serum levels above the reference values defined as the median Z-score of each soluble mediator detected in all healthy controls along the pregnancy. The results are presented in Figure 3.

Data analysis demonstrated that the proportion of healthy pregnant women with high levels of serum soluble mediators progressively decreased towards the 2nd and 3rd pregnancy trimesters. These data further corroborated that a healthy pregnancy course has a progressive decrease in most serum soluble mediators towards the 2nd and 3rd trimesters, except for CCL4, CCL5 and CXCL10 (Figure 3A).

On the other hand, the proportion of pregnant women with convalescent COVID-19 presenting high serum soluble mediator levels progressively increased from the 1st to the 3rd pregnancy trimester (Figure 3A). Heatmap constructs further illustrated that the major increase in serum soluble mediators observed in pregnant women with convalescent COVID-19 occurred in pro-inflammatory cytokines, namely IL-6, TNF-α, IL-12, IFN-γ and IL-17 (Figure 3B).

The profile of serum soluble mediators was further characterized as the ratio (%COVID/%HC), assessed by dividing the percentage of pregnant women with soluble mediator levels above the reference values observed in the COVID group by the percentage of trimester-matching HC patients. Using this strategy, the results confirmed that a larger set of biomarkers presented a high ratio (%COVID/%HC) towards the 2nd and 3rd trimester. In the 2nd pregnancy trimester, increased ratios were observed for IL-6, IFN-γ, IL-5 and GM-CSF (3x increase) in the COVID-19 group. A larger set of serum soluble mediators with increased ratios was identified for COVID-19 groups at the 3rd pregnancy trimester, including CXCL8, CCL11, IL-5 and PDGF (3x increase), CCL3, IL-1β, IFN-γ, IL-17 and IL-13 (4x increase), CCL2, TNF-α (7x) along with IL-1Ra, IL-9, GM-CSF and FGF-basic (5x, 9x, 9x, and 15x increase, respectively) (Figure 3C).

The signatures of serum soluble mediators were also assessed considering the reference values of trimester-matching healthy controls. The results are presented in the Supplementary Figure 2. Data reinforce that larger sets of serum soluble mediators with increased ratios were identified for the 2nd and 3rd pregnancy trimesters as compared with trimester-matching controls (Supplementary Figure 2).

3.3 Serum soluble mediator networks in convalescent COVID-19 at distinct pregnancy trimesers

Aimed at assessing a panoramic snapshot of serum soluble mediator interplay in pregnant women with convalescent COVID-19 and healthy controls, integrative networks were constructed

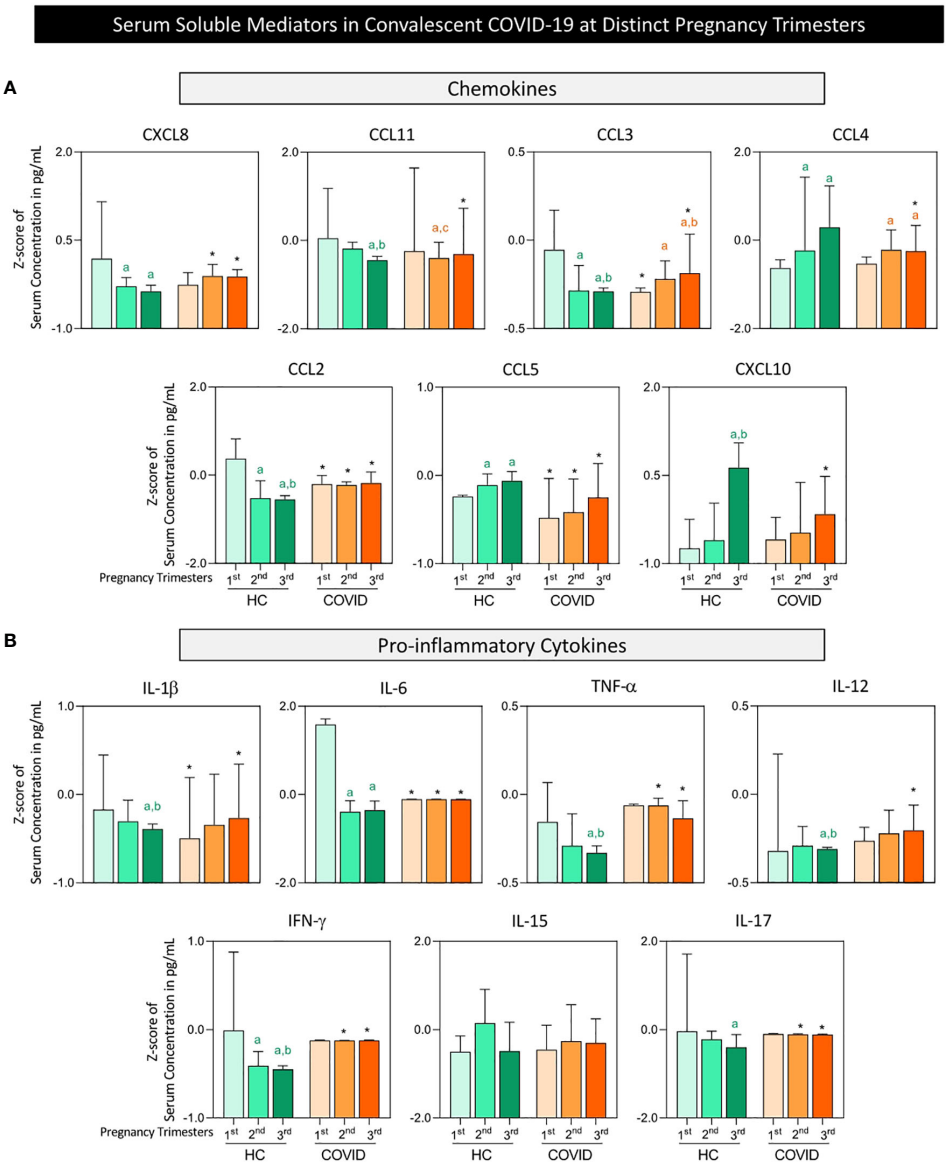

FIGURE 1
Serum and pro-inflammatory cytokines in convalescent COVID-19 patients at distinct pregnancy trimesters. The levels of: **(A)** chemokines (CXCL8, CCL11, CCL3, CCL4, CCL2, CCL5, CXCL10), and **(B)** pro-inflammatory cytokines (IL-1β, IL-6, TNF-α, IL-12, IFN-γ, IL-15, IL -17) were measured in serum samples from pregnant women with convalescent COVID-19 at 3-20 weeks after symptoms onset (COVID, n=89), with pre-pandemic non-infected pregnant women as a Healthy Control (HC, n=52). The HC and COVID-19 groups were further categorized into subgroups according to pregnancy trimester, referred to as: HC 1st (, n=21), HC 2nd (, n=10), HC 3rd (, n=21), and COVID 1st (, n=7), COVID 2nd (, n=34), COVID 3rd (, n=48). The measurements were taken by high-throughput multiplex bead array as described in Material and Methods. The results are presented in bar charts of median values and interquartile ranges for Z-score of serum concentration (pg/mL). Multiple comparative analysis was performed by Kruskal-Wallis followed by Dunn's post-test and comparisons between COVID-19 and HC at matching pregnancy trimesters assessed using the Mann-Whitney test. In all cases, significance was considered at $p<0.05$. Intragroup differences were underscored by the letters "a", "b" and "c" for comparisons with the 1st, 2nd and 3rd trimesters, respectively. Inter-group differences at matching pregnancy trimesters were highlighted denoted by an asterisk (*).

based on the overall correlation between pairs of molecules. The results are presented in Figure 4.

Data analysis demonstrated that healthy pregnancy evolves towards the 3rd trimester with an overall decrease in network connectivity (1st = 336; 2nd = 300 and 3rd = 112 strong correlations). Although pregnant women with convalescent COVID-19 exhibited a similar continuous decrease in network connectivity towards the 3rd trimester (1st = 146; 2nd = 78 and 3rd = 70 strong correlations), the number of connections was remarkably lower in the COVID group compared to HC group (Figure 4).

Overall, the analysis of cluster connectivity during healthy pregnancy showed that pro-inflammatory cytokines presented more connections at the 1st and 2nd trimesters (96 and 92 strong

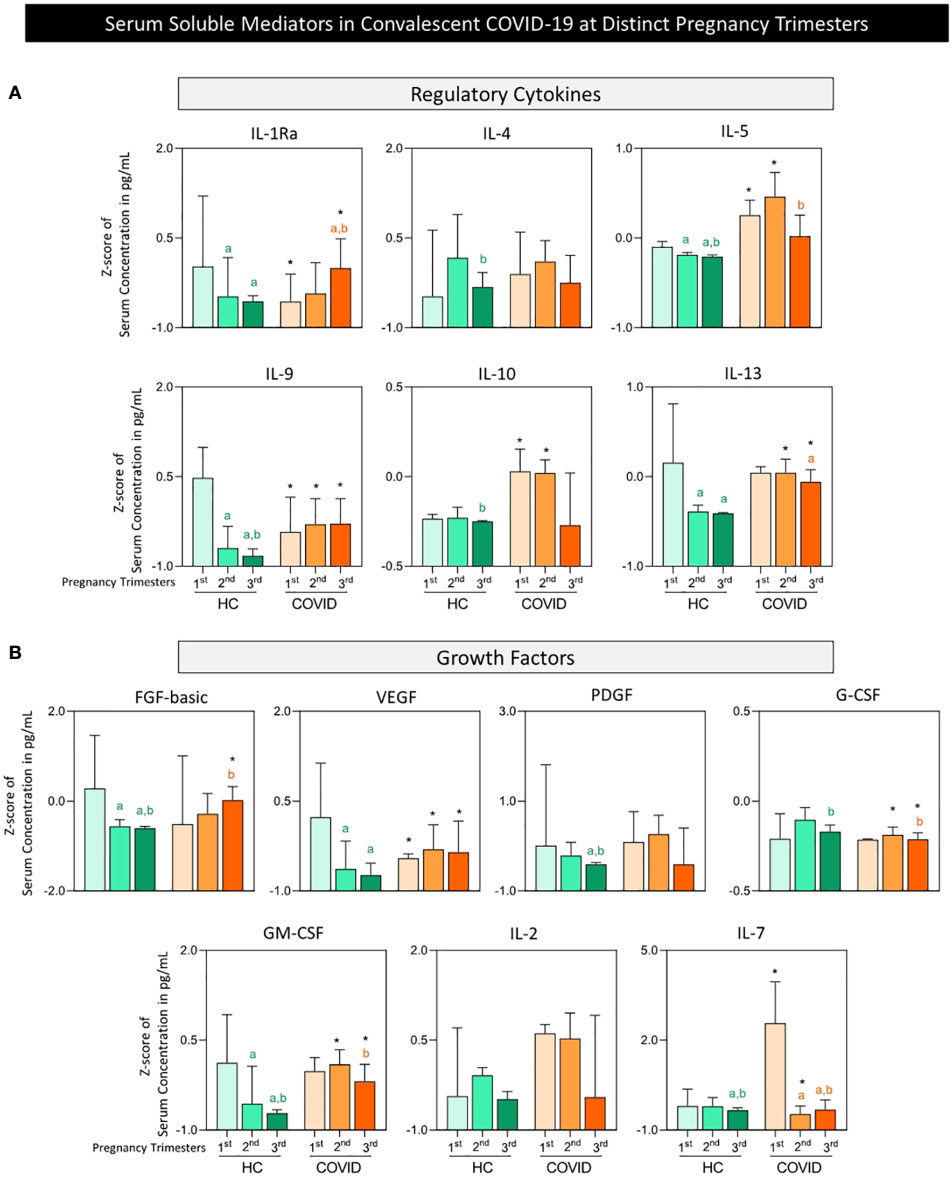

FIGURE 2
Serum regulatory cytokines and growth factors in convalescent COVID-19 patients at distinct pregnancy trimesters. The levels of: **(A)** regulatory cytokines (IL-1Ra, IL- 4, IL-5, IL-9, IL-10, IL-13), and **(B)** growth factors (FGF-basic, PDGF, VEGF, G-CSF, GM- CSF, IL-2, IL-7) were measured in serum samples from pregnant women with convalescent COVID-19 at 3-20 weeks after symptoms onset (COVID, n=89), with pre-pandemic non-infected pregnant women as a Healthy Control (HC, n=52). The HC and COVID-19 groups were further categorized into subgroups according to pregnancy trimester, referred to as: HC 1st (, n=21), HC 2nd (, n=10), HC 3rd (, n=21), and COVID 1st (, n=7), COVID 2nd (, n=34), COVID 3rd (, n=48). The measurements were taken by high-throughput multiplex bead array as described in Material and Methods. The results are presented in bar charts of median values and interquartile ranges for Z-score of serum concentration (pg/mL). Multiple comparative analysis was performed by Kruskal-Wallis followed by Dunn's post-test, and comparisons between COVID-19 and HC at matching pregnancy trimesters assessed by the Mann-Whitney test. In all cases, significance was considered at $p<0.05$. Intragroup differences were underscored by the letters "a" and "b" for comparisons with the 1st and 2nd trimesters, respectively. Inter-group differences at matching pregnancy trimesters were denoted by an asterisk (*).

correlations, respectively), with growth factor predominance at the 3rd trimester (42 strong correlations). Conversely, the COVID group displayed a predominance of regulatory cytokines in the 1st trimester (47 strong correlations) with growth factor predominance in the 2nd and 3rd trimesters (24 and 21, respectively) (Figure 4).

In general, convalescent COVID-19 infection during pregnancy leads to a loss of network connectivity, with fewer strong correlations and changes in the predominance of connectivity amongst the categories of serum soluble mediators (Figure 4).

3.4 Descriptive analysis of serum soluble mediator networks in convalescent COVID-19 patients at distinct pregnancy trimesters

In order to provide a more comprehensive overview of the network connectivity between serum soluble mediators in pregnant women with convalescent COVID-19 and healthy controls along the pregnancy trimesters, a descriptive Venn diagram analysis was

10.3389/fimmu.2023.1176898

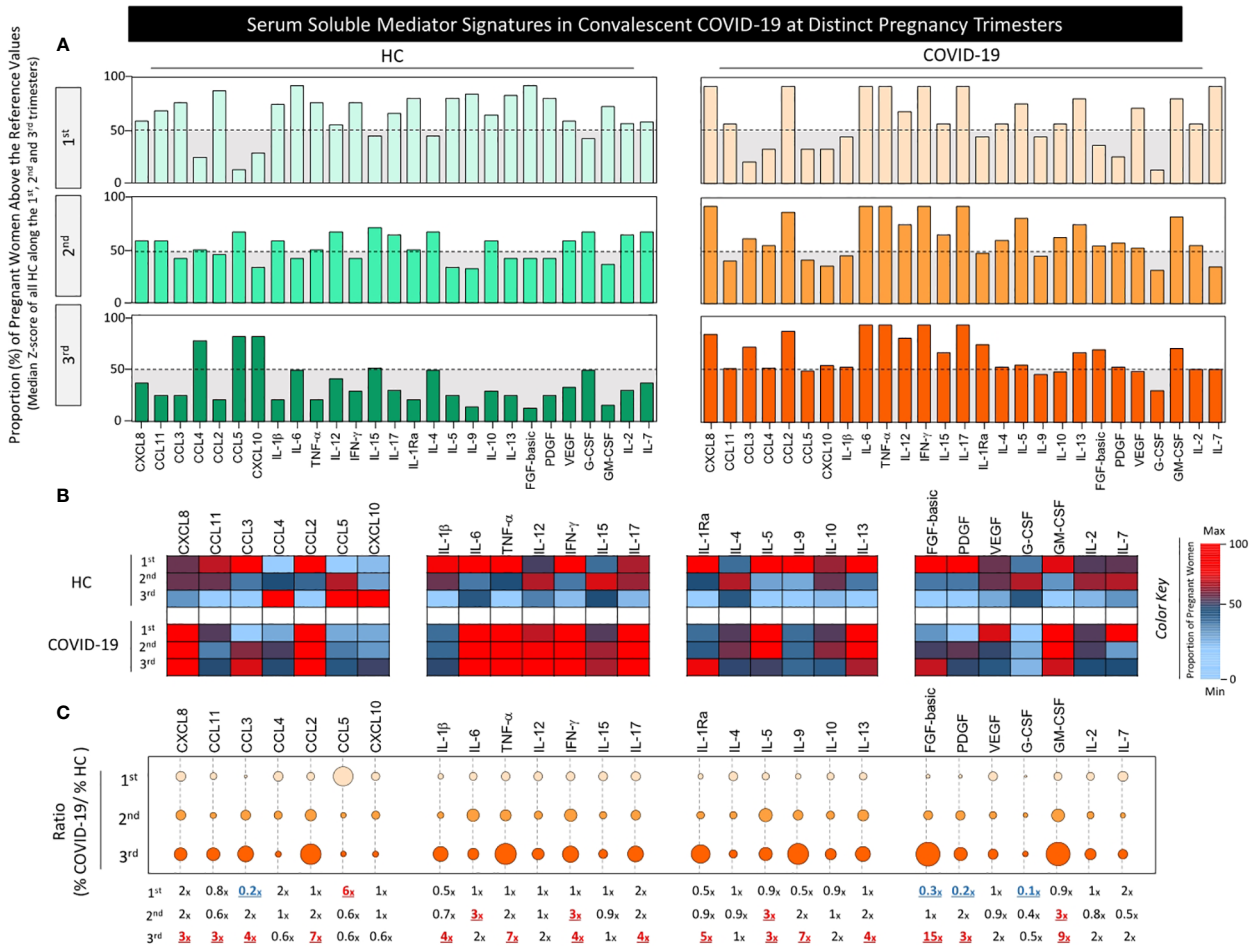

FIGURE 3
Serum soluble mediator signatures in convalescent COVID-19 patients at distinct pregnancy trimesters. Signatures of: serum chemokines (CXCL8, CCL11, CCL3, CCL4, CCL2, CCL5, and CXCL10), pro-inflammatory cytokines (IL-1β, IL-6, TNF-α, IL-12, IFN-γ, IL-15, and IL-17), regulatory cytokines (IL-1Ra, IL-4, IL-5, IL-9, IL-10, and IL-13), and growth factors (FGF-basic, PDGF, VEGF, G-CSF, GM-CSF, IL-2, and IL-7) were assembled for pregnant women with convalescent COVID-19 at 3-20 weeks after symptoms onset (COVID, n=89) and for pre-pandemic non-infected pregnant women as a Healthy Control (HC, n=52). The HC and COVID-19 groups were further categorized into subgroups according to pregnancy trimester, referred to as: HC 1st (□, n=21), HC 2nd (□, n=10), HC 3rd (□, n=21) and COVID 1st (□, n=7), COVID 2nd (□, n=34), COVID 3rd (□, n=48). The measurements were taken by high-throughput multiplex bead array as described in Material and Methods. **(A)** The results are presented in bar charts showing the proportion (%) of pregnant women with serum levels above the reference values (cut-off) defined as the median Z-score of each soluble mediator detected for all HC along the 1st, 2nd and 3rd trimesters, as described in Material and Methods. The serum soluble mediators displaying a proportion of pregnant women above 50% (grey zone, dashed line) were included in the set of biomarkers with increased levels. **(B)** Heatmap constructs were further assembled to illustrate the overall profile of serum soluble mediator signatures of COVID and HC subgroups along the pregnancy trimesters. A color key was used to underscore the serum soluble mediators with decreased (proportion <50%, towards light blue), unaltered (proportion =50%, black) or increased levels (proportion>50%, towards red). **(C)** The ratio between the proportion of pregnant women with serum levels above the reference values in the COVID group in relation to HC (%COVID/%HC) was further calculated and presented in orbital graphs. The ratios of each serum soluble mediator along the 1st, 2nd and 3rd trimesters are provided in the figure, underscored as decreased (≤0.3x, blue), unaltered (0.4-2x, black) or increased (≥3x, red).

performed to identify the set of biomarkers with preserved (common), lost or acquired (selective) attributes with five or more (≥ 5) strong correlations in COVID subgroups as compared to the trimester-matching HC group. The results are presented in the Figure 5.

Heatmap constructs were assembled to organize the serum soluble mediators with an ascending order of strong correlations and identify the set of biomarkers with five or more (≥ 5) strong correlations at each pregnancy trimester in the COVID and HC groups (Figure 5A).

Data analysis demonstrated that the number of preserved attributes referred to as common in HC and COVID (≥5 strong correlations in HC and COVID) with five or more correlations progressively decreased from the 1st (n=12) to the 2nd (n=6) and 3rd trimesters (n=4). In detail: 1st: CCL11, CCL3, CCL2, IL-1β, IL-12, IL-15, IL-1Ra, IL-5, IL-9, IL-10, GM-CSF, and IL-2; 2nd: IL-6, TNF-α, IL-1Ra, IL-5, IL-10, GM-CSF and 3rd:IFN-γ, IL-1Ra, G-CSF, and GM-CSF.

The number of lost attributes referred to as HC-selective (≥5 strong correlations in HC and <5 strong correlations in COVID)

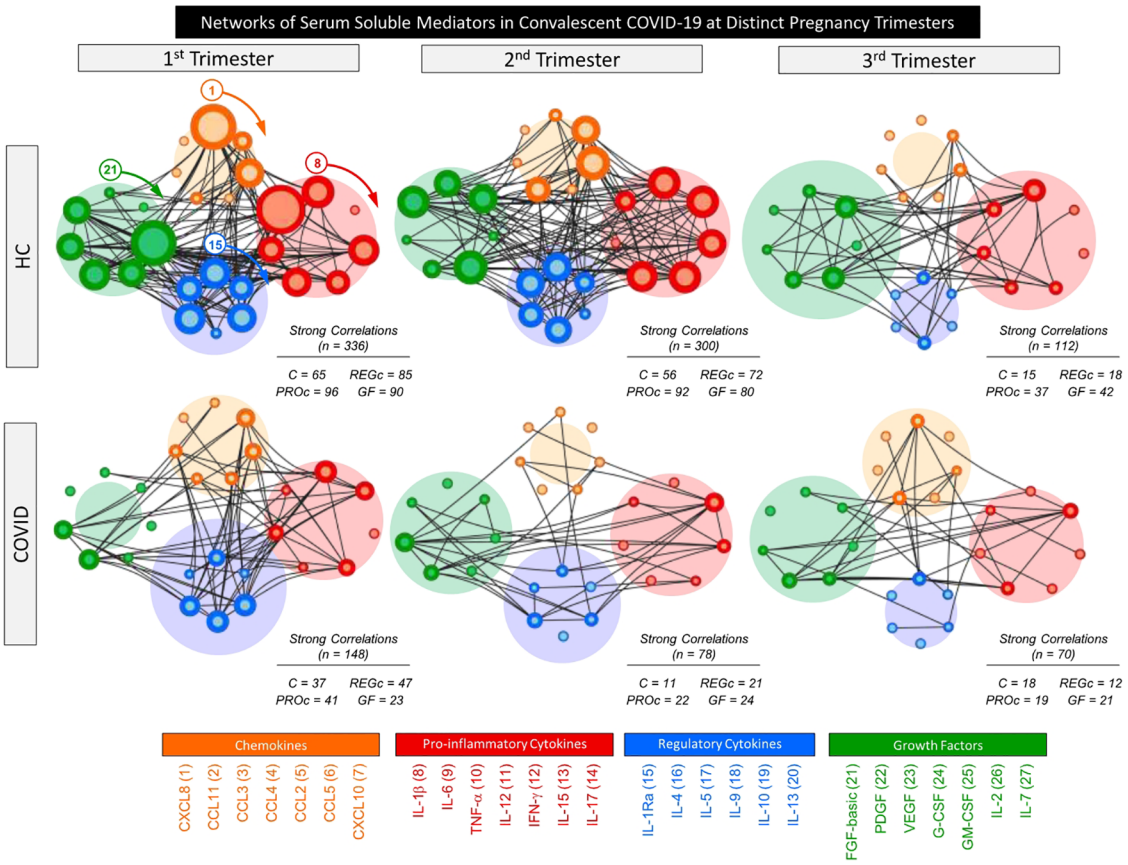

FIGURE 4
Networks of serum soluble mediators in convalescent COVID-19 patients at distinct pregnancy trimesters. Comprehensive networks were assembled for serum chemokines, pro-inflammatory cytokines, regulatory cytokines, and growth factors observed in pregnant women with convalescent COVID-19 at 3-20 weeks after symptoms onset (COVID, n=89), with pre-pandemic non-infected pregnant women as a Healthy Control (HC, n=52). The HC and COVID-19 groups were further categorized into subgroups according to pregnancy trimester, referred to as: 1st (HC=21 and COVID=7), 2nd (HC=18 and COVID=34) and 3rd (HC=21 and COVID=48). The measurements were taken by high-throughput multiplex bead array as described in Material and Methods. Data analyses were carried out by Pearson and Spearman rank tests with only significant strong correlations ($p<0.05$ and "r" scores $\geq |0.67|$) employed to construct the comprehensive networks. Cluster layout networks were assembled, comprising 4 categories of serum soluble mediators as follows: - Chemokines – C (orange nodes – 1=CXCL8; 2=CCL11; 3=CCL3; 4=CCL4; 5=CCL2, 6=CCL5 and 7=CXCL10); Pro-inflammatory – PROc (red nodes – 8= IL-1β; 9=IL-6; 10= TNF-α; 11=IL-12; 12= IFN-γ; 13=IL-15 and 14=IL-17); Regulatory cytokines – REGc (blue nodes – 15=IL-1Ra; 16=IL-4; 17=IL-5; 18=IL-9; 19=IL-10 and 20=IL-13), and Growth Factors – GF (green nodes – 21=FGF-basic; 22=PDGF; 23=VEGF; 24=GCSF; 25=GM-CSF; 26=IL-2 and 27=IL-7). Node border thickness is proportional to the number of strong correlations. Connecting edges (black lines) are used to link pairs of serum soluble mediators presenting significant correlations. The number of strong correlations (C, PROc, REGc and GF) observed for each network is provided in the figure and used for comparative analysis between COVID and HC, as well as amongst subgroups. The circular background area is proportional to the number of strong correlations of each cluster within the respective network.

was higher in the 2nd trimester (n=15) compared to 1st (n=10) and 3rd (n=9). In detail: 1st: CXCL8, TNF-α, IFN-γ, IL-17, IL-4, IL-13, FGF-basic, VEGF, G-CSF, and IL-7; 2nd: CXCL8, CCL11, CCL3, CCL2, IL-1β, IL-12, IFN-γ, IL-17, IL-4, IL-9, IL-13, FGF-basic, VEGF, G-CSF, and IL-7; 3rd: CCL11, CCL3, IL-1β, IL-12, IL-15, IL-17, IL-9, FGF-basic, and VEGF. A set of acquired attributes, named COVID-selective (<5 strong correlations in HC and ≥5 strong correlations in COVID) were identified in each trimester: 1st (n=3): CCL4, CCL5, and IL-6, 2nd: (n=1) IL-2, and 3rd (n=3) CXCL8, CCL2 and IL-6 (Figure 5B).

From an overall perspective, a pronounced decrease in network connectivity between serum soluble mediators was observed in convalescent COVID-19 infection during pregnancy as demonstrated by the fewer number of molecules establishing strong correlations driven by an imbalance between preserved, lost and acquired attributes in the COVID group. While IL-1Ra, IL-10 and GM-CSF presented a preserved number of correlations (≥5 strong correlations in HC and COVID), IL-17, FGF-basic and VEGF lost connectivity throughout pregnancy. IL-6 (at 1st and 3rd trimesters) and CXCL8 (at 3rd trimester) were included in a set of acquired

10.3389/fimmu.2023.1176898

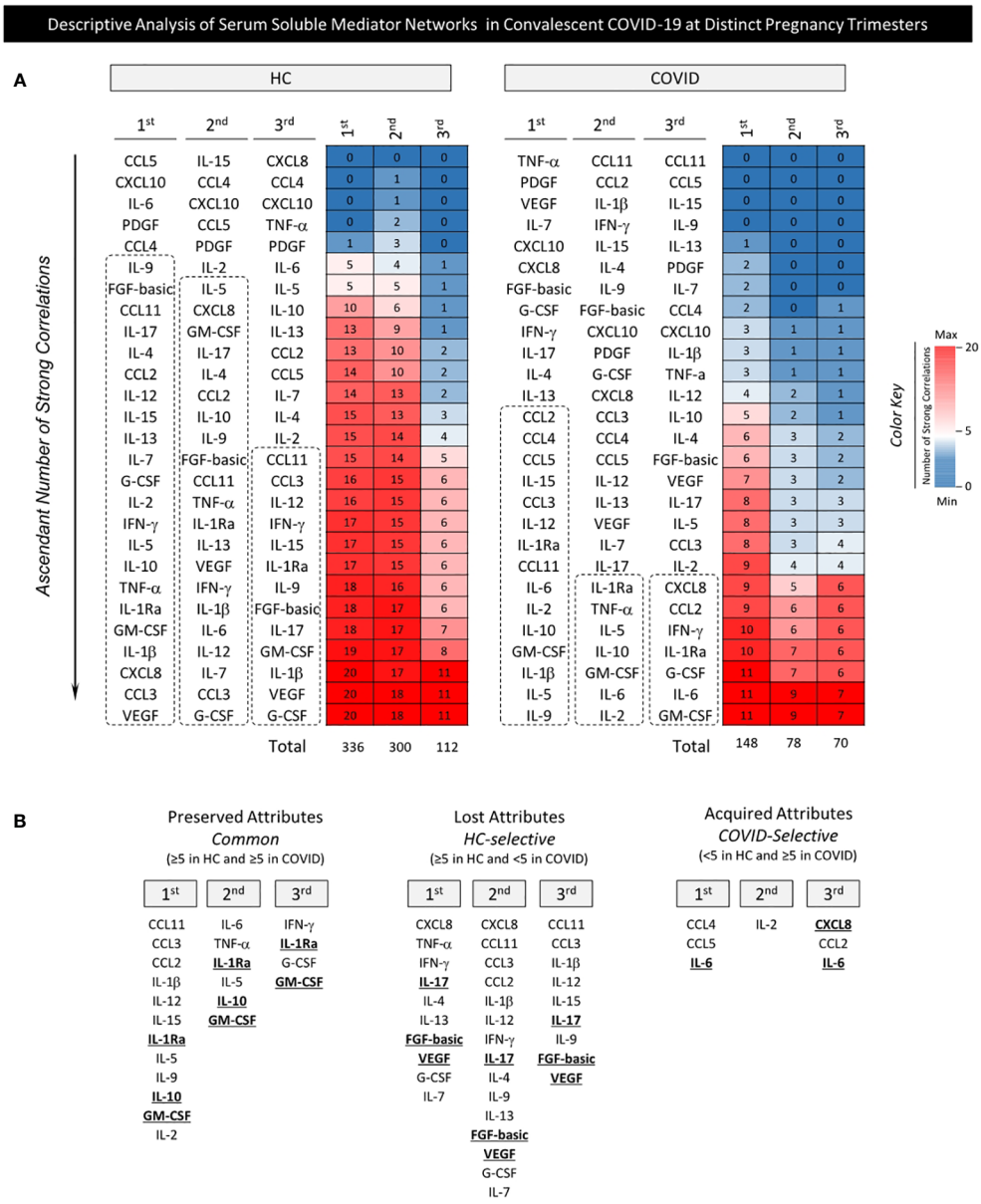

FIGURE 5
Descriptive analysis of serum soluble mediator networks in convalescent COVID-19 patients at distinct pregnancy trimesters. The overall profile of serum soluble mediator networks was assessed in pregnant women with convalescent COVID-19 at 3-20 weeks after symptoms onset (COVID, n=89) with pre-pandemic non-infected pregnant women as a Healthy Control (HC, n=52). The HC and COVID-19 groups were further categorized into subgroups according to pregnancy trimester, referred to as: 1st (HC=21 and COVID=7), 2nd (HC=10 and COVID=34), and 3rd (HC=21 and COVID=48). **(A)** The ascendant number of strong correlations was arranged to identify the set of biomarkers with five or more (≥ 5) strong correlations with other molecules at each pregnancy trimester in HC and COVID subgroups. Heatmap constructs were assembled to illustrate the overall profile of serum soluble mediator networks of COVID and HC subgroups along the pregnancy trimesters. A color key was used to underscore the serum soluble mediators with ≥ 5 strong correlations (towards red). **(B)** A summary of preserved (≥5 in HC and ≥5 in COVID), lost (≥5 in HC and <5 in COVID) or acquired (<5 in HC and ≥5 in COVID) attributes were identified by Venn diagram analysis. Attributes identified along the trimesters are highlighted by bold underline format.

attributes, named COVID-selective (≥5 strong correlations in COVID and <5 in HC) (Figure 5B, bold underline attributes).

3.5 Multivariate analysis of serum soluble mediators in convalescent COVID-19 patients at distinct pregnancy trimesters

Multivariate analysis of chemokines, pro-inflammatory cytokines, regulatory cytokines and growth factors was performed using PCA to verify the ability of serum mediators to cluster convalescent COVID-19 pregnant women apart from trimester-matching pre-pandemic non-infected pregnant women as a healthy control (HC). The results are presented in Figure 6. The PCA coordinates (2nd and 3rd principal components) demonstrated that although convalescent COVID pregnant women could be clustered apart from the HC when considering all trimesters together, the segregation profile was more evident when the COVID and HC

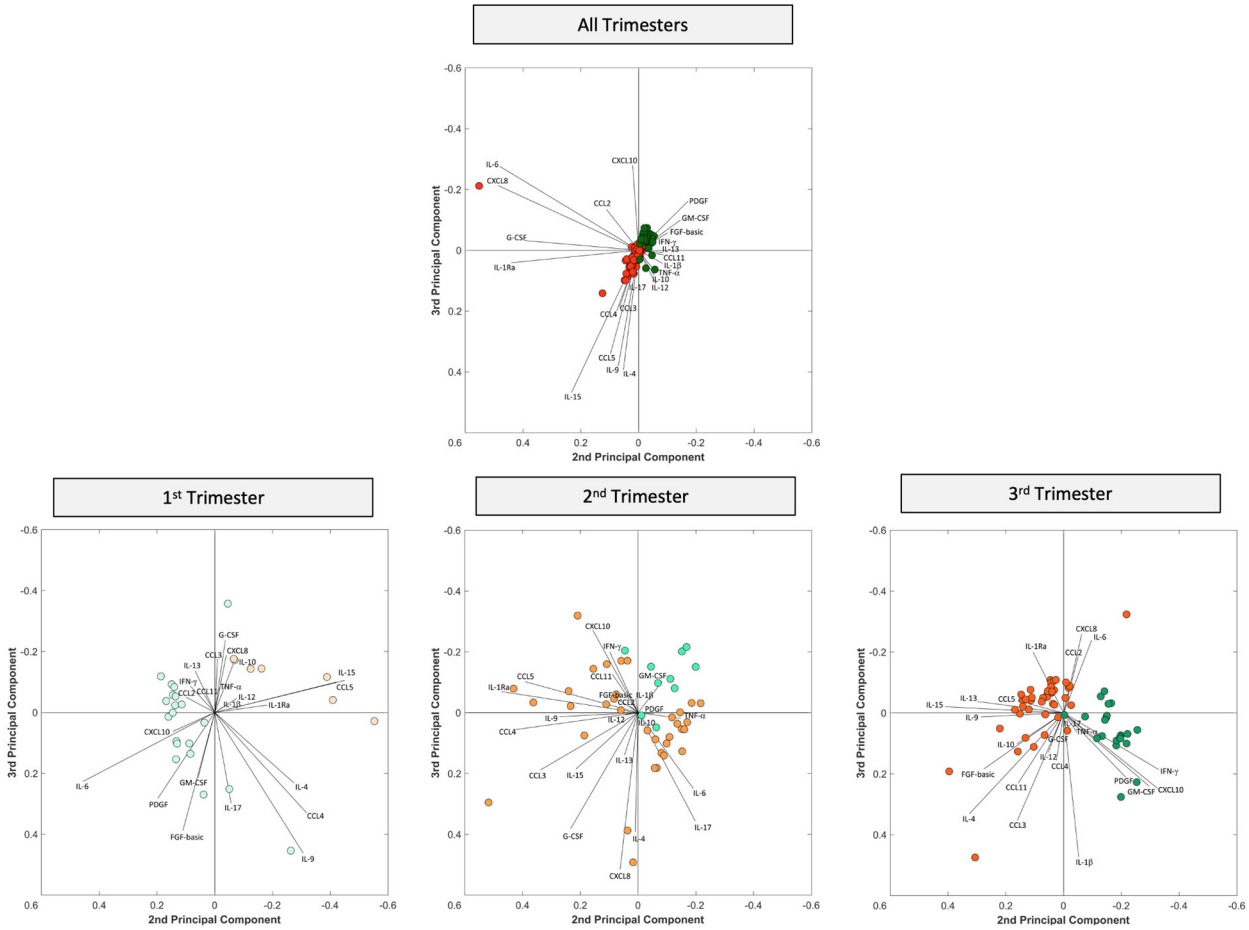

FIGURE 6
Multivariate analysis of serum soluble mediator networks in convalescent COVID-19 patients at distinct pregnancy trimesters. Multivariate analysis of serum chemokines, pro-inflammatory cytokines, regulatory cytokines and growth factors were performed to verify the ability of soluble mediators to cluster convalescent COVID-19 pregnant women at 3-20 weeks after symptoms onset (COVID, n=89), with pre-pandemic non-infected pregnant women as a Healthy Control (HC, n=52) as well as subgroups of COVID-19 and HC categorized according to pregnancy trimester, referred to as: HC 1st (, n=21), HC 2nd (, n=10), HC 3rd (, n=21) and COVID 1st (, n=7), COVID 2nd (, n=34), COVID 3rd (, n=48). The measurements were taken by high-throughput multiplex bead array as described in Material and Methods. Principal Component Analysis (PCA) was carried out by MATLAB software as described in Material and Methods. PCA coordinates (2nd and 3rd principal components) were used to compare and visualize the grouping of convalescent COVID-19 *vs* HC and subgroups according to pregnancy trimesters.

subgroups were compared at matching gestational trimesters (Figure 6). Vector analysis conducted in the 1st trimester indicated that CXCL8, CCL3, CCL5, IL-1β, TNF-α, IL-12, IL-15, IL-1Ra, IL-10, and G-CSF were associated with convalescent COVID-19 in pregnant women. Data from the 2nd trimester showed that most soluble mediators were vectors associated with differential distribution of convalescent COVID-19 in pregnant women, except for GM-CSF. Additionally, the PCA coordinates obtained from the 3rd trimester demonstrated that several soluble mediators were vectors related to convalescent COVID-19 in pregnant women, except for CXCL10, IL-1β, TNF-α, IFN-γ, PDGF and GM-CSF (Figure 6).

4 Discussion

Pregnancy triggers a unique immunological status, aiming to protect the fetus from maternal rejection and guarantee fetal development until birth. Several studies have reported that the immune system plays a balancing role during pregnancy with constant changes according to maternal and fetal demands (16, 17). Physiological changes in immune status during pregnancy are often characterized by alterations in cell-mediated immunity and humoral responses, from the 1st to 3rd pregnancy trimesters. Previous studies have demonstrated that successful implantation is associated with a transient increase in systemic proinflammatory

profile followed by a switch toward an anti-inflammatory profile after blastocyst transfer when pregnancy is confirmed (18). Pregnant women are particularly susceptible to COVID-19 due to physiological changes in the immune system, which may result in an altered response to SARS-CoV-2 infection in pregnancy. Furthermore, SARS-CoV-2 infection during pregnancy can disrupt the immune response homeostasis, impacting the maternal immune activation, with effects on pregnancy outcome and offspring (12, 13, 19, 20). It has already been reported that the adverse impacts of the COVID-19 pandemic on maternal health are not limited to morbidity and mortality caused by the disease itself, but are also associated with adverse pregnancy outcomes, including preeclampsia, preterm birth and stillbirth (19).

Most of the information on the impact of SARS-CoV-2 infection in pregnancy has been derived from reports concerning acute symptomatic infection (21). However, little data is available regarding the long-term impact of SARS-CoV-2 infection on pregnancy during the convalescent phase of the disease. In view of this, we designed this study as a pioneer exploratory investigation to perform descriptive and panoramic analysis of serum soluble mediator interplay in pregnant women during the convalescent phase of SARS-CoV-2 infection throughout prenatal care. This study comprises an innovative investigation of the long-lasting impact of SARS-CoV-2 infection during pregnancy focusing on the analysis of the immune response during the convalescent phase comprising 3-20 weeks after symptoms onset.

Our results demonstrate that, in general, serum soluble mediators have different trajectories during healthy pregnancy and are disturbed in pregnant women with convalescent SARS-CoV-2 infection. Herein, healthy pregnant women presented a progressive decrease in most serum soluble mediators towards the 2nd and 3rd pregnancy trimester, including chemokines, pro-inflammatory and regulatory cytokines, in addition to growth factors. Previous studies corroborate our findings in healthy pregnancies. The levels of chemokines and pro-inflammatory cytokines usually peak in the first trimester of pregnancy and decline in the 2nd and 3rd trimesters, while regulatory cytokines and growth factors have diverse trajectories (22, 23). Our findings highlighted that higher levels of most soluble mediators were observed in the COVID group compared to HC control group. The major increase occurred in pro-inflammatory cytokines, including IL-6, TNF-α and IFN-γ, a larger set of biomarkers with elevated COVID/HC ratios observed towards the 2nd (3x increase) and 3rd (3-15x increase) pregnancy trimesters. Studies of immune mediators in SARS-CoV-2 infection during pregnancy remain scarce. It has been proposed that the immunomodulation observed during pregnancy may protect pregnant COVID-19 patients from suffering from a cytokine storm (15, 24). However, no studies focusing on comparative analysis of immunological profiles of COVID-19 and healthy pregnant women at matching pregnancy trimesters have been reported. It is noteworthy that due to physiological changes in the immune response during pregnancy, the inclusion of trimester-matching healthy controls is essential to enable conclusive analysis. Therefore, our study is pioneering in terms of providing a detailed profile of long-lasting changes during convalescent COVID-19 infection in pregnancy as it made direct comparison to trimester-matching healthy controls. Our findings did not support that an immunomodulatory profile is triggered by SARS-CoV-2 infection during pregnancy. In fact, the lower levels of soluble mediators previously reported in convalescent COVID-19 pregnant women were compared with those observed in non-pregnant women and did not consider the physiological changes triggered by pregnancy or alterations in soluble mediators inherent in trimesters (24). Moreover, other studies proposing the immunomodulatory state for acute COVID-19 infection during pregnancy in comparison to healthy pregnant women did not consider stratification by gestational trimesters (15). According to our findings, higher levels of serum soluble mediators were observed for convalescent COVID-19 infection during pregnancy, especially IL-6, TNF-α and IFN-γ in comparison to healthy pregnant women at matching pregnancy trimesters.

Successful pregnancy requires finely coordinated communication between the maternal and fetal microenvironments. Cytokine signaling pathways participate as mediators of these communications to guarantee healthy pregnancy. From the existing data available, there is no consensus trend for the changes observed for IL-6, TNF-α and IFN-γ during pregnancy (16). Several studies have demonstrated that IL-6, TNF-α and IFN-γ concentrations significantly increased between the 1st, 2nd and 3rd trimesters of healthy pregnancy (25–30). However, corroborating our findings, other authors detected significant reductions in IL-6, TNF-α and IFN-γ in maternal serum concentrations between the 1st and 3rd trimesters (31–33).

Infections or inflammatory conditions, such as COVID-19 during pregnancy, can have a detrimental impact on fetal development and also contribute to pregnancy-associated pathological conditions (34). Despite the conflicting data regarding the overall profile of IL-6, TNF-α and IFN-γ during healthy pregnancy, there is a consensus that the establishment of a pro-inflammatory microenvironment is associated with the risk of developing pregnancy-associated pathological conditions, including pregnancy loss, preeclampsia, and gestational diabetes mellitus (35). In this sense, the upregulation of pro-inflammatory cytokines in pregnant women with convalescent COVID-19 may suggest that these patients are more vulnerable to developing adverse pregnancy outcomes.

Integrative network analysis demonstrated that both HC and convalescent COVID-19 pregnancies evolve with decreasing connectivity between serum soluble mediators towards the 3rd trimester. However, the COVID group exhibited a remarkably lower number of connections. Overall, IL-1Ra, IL-10 and GM-CSF presented a preserved number of correlations throughout the pregnancy.

Further research is warranted to determine the precise IL-10 profile during healthy pregnancy (14). A few studies have reported that IL-10 significantly increases from the 1st to the 2nd and 3rd trimesters in healthy pregnancy (30, 36). However, corroborating our findings, other studies have detected that IL-10 decreases between the 1st and 3rd trimesters (31, 37). Considering the critical role of IL-10 as a chief anti-inflammatory cytokine, the preserved IL-10 connectivity axis observed during the 1st and 2nd trimesters may represent a mechanism to protect the fetus from

maternal pro-inflammatory rejection and guarantee fetal development until birth.

Our data demonstrated that IL-1Ra decreased in convalescent COVID-19 pregnant women in the 1st trimester but increased in the 3rd trimester. Previous studies reported that IL-1Ra levels increased during the inflammatory response to control acute inflammation and prevent immunopathological events (38). The IL-1 receptor antagonist (IL-1Ra) is an anti-inflammatory cytokine that blocks IL-1α and IL-1β functions and modulates their biological effects (39). It has been previously demonstrated in experimental models that high IL-1Ra levels at the beginning of pregnancy may lead to miscarriage due to impaired embryonic adhesion (40), and data from human studies showed that higher levels of circulating IL-1Ra have been reported in adverse pregnancy outcomes, including preeclampsia (41). Regarding the changes in IL-1Ra levels observed in convalescent COVID-19 along the pregnancy trimesters, our findings of preserved correlation profile between IL-1Ra and other soluble mediators throughout the pregnancy may suggest that an intricate microenvironment of soluble mediators is relevant to guarantee fetal development until birth.

Our data also demonstrated that GM-CSF presented preserved correlation with other soluble mediators throughout pregnancy. It was previously reported that after embryo implantation, GM-CSF participates in a network of cytokines and growth factors that regulate morphological and functional development of the placenta (42).

Conversely, despite increases in IL-17, FGF-basic and VEGF, loss of connectivity was observed throughout pregnancy. IL-17 up-regulates the expression of a variety of biological molecules with angiogenic properties including VEGF (43–47). VEGF plays a central role in vasculogenesis and angiogenesis, which augments vascular endothelial cell proliferation, migration, and survival. Moreover, data from previous studies have shown that IL-17 can induce placental oxidative stress and vascular dysfunction, resulting in hypertension and increased risk of preeclampsia (48). The loss of network connection of IL-17 and VEGF with other soluble mediators throughout the pregnancy may lead to intrinsic vascular dysfunction that results in impaired neonatal development. Post-natal follow-up studies may contribute to identifying impaired new-born growth and development related to altered angiogenesis.

Our data also demonstrated that IL-6 and CXCL8 were included in the set of attributes acquiring strong correlation in the 3rd pregnancy trimester, named COVID-selective correlations. Implications of IL-6 and CXCL8 in pregnancy-associated pathological conditions, such as pregnancy loss, preeclampsia, gestational diabetes mellitus, and infection/inflammation have been reported (35). These two soluble mediators are abundantly produced at the feto-maternal interface throughout pregnancy and have been shown to participate in several pregnancy-related events. Unbalanced expression/secretion of IL-6 and CXCL8 at the feto-maternal interface has been indicated in unexplained pregnancy loss (35). A study of the dynamic connections of the soluble mediator network in pre-eclampsia identified positive correlation between IL-6 and CXCL8, suggesting that these molecules are implicated in the pathophysiology of this pregnancy-associated disease (35, 49). Moreover, a meta-analysis and systematic review suggested a role of CXCL8 in shaping the immune microenvironment in gestational diabetes mellitus (50).

The present study has some limitations. The low number of pregnant women enrolled in each pregnancy trimester re-enforce the need to further validate our findings. This work was performed during circulation of the B.1.1.28 and B.1.1.33 SARS-CoV-2 strains and therefore, the impact of other variants on the immunological profiles remains to be addressed. Despite the pioneering approach of this exploratory investigation, the observational design with multiple comparisons without corrections for co-morbidities or other confounding variables also constitutes a study limitation that may interfere in the levels of systemic soluble mediators. Moreover, regardless the relevance of nutritional aspects ant the dietary inflammatory indices interfering in the immune response during pregnancy (51), we did not have the opportunity to address this issue in the present investigation.

In conclusion, the main finding of this study, a pronounced increase in serum levels of soluble mediators with decreased network interplay between them, portrayed an imbalanced immune response in convalescent COVID-19 infection during pregnancy that may contribute to the prevention or management of clinical course pregnancy complications.

Data availability statement

The original contributions presented in the study are included in the article/Supplementary Material. Further inquiries can be directed to the corresponding authors.

Ethics statement

The studies involving human participants were reviewed and approved by National Commission for Ethics in Research in Brazil (CONEP, CAAE 32359620.0.0000.5558). The patients/participants provided their written informed consent to participate in this study.

Author contributions

Study design: GF, LS, FM, CA, KC, MC, RT, ON, AS, CPA, AZ and LM. Advisory committee: CG, DM-S, PK, ON, LC, COA, and AZ. Funding acquisition: LE, OM-F and LM. Sample collection, experimental procedures, and data acquisition: ÂS, AC, YP, DA, LL, RN, PA, LG, LD, and JCdR. Data analysis: GF, LS, GJ-S, HS, LA, MG, PB, JBdS, IC-R, AC-A, VP-M, AC, and OM-F. Writing and reviewing the manuscript: GF, LS, GJ-S, HS, OM-F and LM. All authors contributed to the article and approved the submitted version.

Funding

This work was supported by the Conselho Nacional de Desenvolvimento Tecnológico (CNPq), Fundação de Amparo à Pesquisa do Estado de Minas Gerais (FAPEMIG) and the University of Brasilia (Grant # 7155, "Fundo COVID-19 UnB em Ação: Ações emergenciais para combate à COVID-19 e mitigação das consequências da pandemia", "Eficácia de um protocolo de testagem RT-PCR para SARS-CoV-2 sobre a preservação da força de trabalho em saúde durante a pandemia COVID-19 no Brasil: ensaio clínico randomizado" and Grant # 7110, "Amamentar em tempos de pandemia de COVID-19: um protocolo para avaliação do impacto do SARS-COV-2 no sucesso do aleitamento materno").

Acknowledgments

This study was performed by students and professors enrolled in Postgraduate Programs: Programa de Pós-graduação em Ciências Médicas da Universidade de Brasília (UnB), supported by Coordenação de Aperfeiçoamento de Pessoal de Nível Superior (CAPES). The authors thank the Program for Technological Development in Tools for Health-RPT-FIOCRUZ for use of the flow cytometry facilities. The authors also express their gratitude to Dayane Andriotti Otta for technical support. ON, MG, JCdR, LA, AC and OM-F received PQ fellowships from CNPq. AC and OM-F are research fellows from FAPEAM (PVN-II, PRÓ-ESTADO Program #005/2019).

Conflict of interest

The authors declare that the research was conducted in the absence of any commercial or financial relationships that could be construed as a potential conflict of interest.

Publisher's note

All claims expressed in this article are solely those of the authors and do not necessarily represent those of their affiliated organizations, or those of the publisher, the editors and the reviewers. Any product that may be evaluated in this article, or claim that may be made by its manufacturer, is not guaranteed or endorsed by the publisher.

Supplementary material

The Supplementary Material for this article can be found online at: https://www.frontiersin.org/articles/10.3389/fimmu.2023.1176898/full#supplementary-material

References

1. World Health Organization. *WHO coronavirus (COVID-19) dashboard data* (2022). Available at: https://covid19.who.int/ (Accessed January 25, 2022).

2. Brandt JS, Hill J, Reddy A, Schuster M, Patrick HS, Rosen T, et al. Epidemiology of coronavirus disease 2019 in pregnancy: risk factors and associations with adverse maternal and neonatal outcomes. *Am J Obstet Gynecol* (2021) 224(4):e1–9. doi: 10.1016/j.ajog.2020.09.043

3. Khoury R, Bernstein PS, Debolt C, Stone J, Sutton DM, Simpson LL, et al. Characteristics and outcomes of 241 births to women with severe acute respiratory syndrome coronavirus 2 (SARS-CoV-2) infection at five new York city medical centers. *Obstetrics Gynecol* (2020) 136(2):273–82. doi: 10.1097/AOG.0000000000004025

4. Metz TD, Clifton RG, Hughes BL, Sandoval G, Saade GR, Grobman WA, et al. Disease severity and perinatal outcomes of pregnant patients with coronavirus disease 2019 (COVID-19). *Obstetrics Gynecol* (2021) 137(4):571–80. doi: 10.1097/AOG.0000000000004339

5. Darif D, Hammi I, Kihel A, Idrissi Saik I, Guessous F, Akarid K. The pro-inflammatory cytokines in COVID-19 pathogenesis: What goes wrong? *Microb Pathog* (2021) 153:104799. doi: 10.1016/j.micpath.2021.104799

6. Asakura H, Ogawa H. COVID-19-associated coagulopathy and disseminated intravascular coagulation. *Int J Hematol* (2021) 113(1):45–57. doi: 10.1007/s12185-020-03029-y

7. Chen R, Lan Z, Ye J, Pang L, Liu Y, Wu W, et al. Cytokine storm: The primary determinant for the pathophysiological evolution of COVID-19 deterioration. *Front Immunol* (2021) 12. doi: 10.3389/fimmu.2021.589095

8. Allotey J, Fernandez S, Bonet M, Stallings E, Yap M, Kew T, et al. Clinical manifestations, risk factors, and maternal and perinatal outcomes of coronavirus disease 2019 in pregnancy: living systematic review and meta-analysis. *BMJ* (2020), 370:m3320. doi: 10.1136/bmj.m3320

9. Villar J, Ariff S, Gunier RB, Thiruvengadam R, Rauch S, Kholin A, et al. Maternal and neonatal morbidity and mortality among pregnant women with and without COVID-19 infection. *JAMA Pediatr* (2021) 175(8):817. doi: 10.1001/jamapediatrics.2021.1050

10. Huntley BJF, Huntley ES, di Mascio D, Chen T, Berghella V, Chauhan SP. Rates of maternal and perinatal mortality and vertical transmission in pregnancies complicated by severe acute respiratory syndrome coronavirus 2 (SARS-Co-V-2) infection. *Obstetrics Gynecol* (2020) 136(2):303–12. doi: 10.1097/AOG.0000000000004010

11. Savasi VM, Parisi F, Patanè L, Ferrazzi E, Frigerio L, Pellegrino A, et al. Clinical findings and disease severity in hospitalized pregnant women with coronavirus disease 2019 (COVID-19). *Obstetrics Gynecol* (2020) 136(2):252–8. doi: 10.1097/AOG.0000000000003979

12. Cavalcante MB, Cavalcante CTMB, Sarno M, Barini R, Kwak-Kim J. Maternal immune responses and obstetrical outcomes of pregnant women with COVID-19 and possible health risks of offspring. *J Reprod Immunol* (2021) 143:103250. doi: 10.1016/j.jri.2020.103250

13. Cavalcante MB, de Melo Bezerra Cavalcante CT, Cavalcante ANM, Sarno M, Barini R, Kwak-Kim J. COVID-19 and miscarriage: From immunopathological mechanisms to actual clinical evidence. *J Reprod Immunol* (2021) 148:103382. doi: 10.1016/j.jri.2021.103382

14. Parisi F, Milazzo R, Savasi VM, Cetin I. Maternal low-grade chronic inflammation and intrauterine programming of health and disease. *Int J Mol Sci* (2021) 22(4):1732. doi: 10.3390/ijms22041732

15. Fernandes GM, Motta F, Sasaki LMP, da Silva ÂP, Miranda AM, de Carvalho AO, et al. Pregnancy outcomes and child development effects of SARS-CoV-2 infection (PROUDEST trial): Protocol for a multicenter, prospective cohort study. *JMIR Res Protoc* (2021) 10(4):e26477. doi: 10.2196/26477

16. Spence T, Allsopp PJ, Yeates AJ, Mulhern MS, Strain JJ, McSorley EM. Maternal serum cytokine concentrations in healthy pregnancy and preeclampsia. *J Pregnancy* (2021) 2021:1–33. doi: 10.1155/2021/6649608

17. Chen G, Liao Q, Ai J, Yang B, Bai H, Chen J, et al. Immune response to COVID-19 during pregnancy. *Front Immunol* (2021) 12. doi: 10.3389/fimmu.2021.675476

18. Zhao Y, Zhang T, Guo X, Wong CK, Chen X, Chan YL, et al. Successful implantation is associated with a transient increase in serum pro-inflammatory cytokine profile followed by a switch to anti-inflammatory cytokine profile prior to confirmation of pregnancy. *Fertile Sterile* (2021) 115(4):1044–53. doi: 10.1016/j.fertnstert.2020.10.031

19. Wei SQ, Bilodeau-Bertrand M, Liu S, Auger N. The impact of COVID-19 on pregnancy outcomes: a systematic review and meta-analysis. *Can Med Assoc J* (2021) 193(16):E540–8. doi: 10.1503/cmaj.202604

20. Chen G, Zhang Y, Zhang Y, Ai J, Yang B, Cui M, et al. Differential immune responses in pregnant patients recovered from COVID-19. *Signal Transduct Target Ther* (2021) 6(1):289. doi: 10.1038/s41392-021-00703-3

21. Mullins E, Perry A, Banerjee J, Townson J, Grozeva D, Milton R, et al. Pregnancy and neonatal outcomes of COVID-19: The PAN-COVID study. *Eur J Obstetrics Gynecol Reprod Biol* (2022) 276:161–7. doi: 10.1016/j.ejogrb.2022.07.010

22. Jarmund AH, Giskeødegård GF, Ryssdal M, Steinkjer B, Stokkeland LMT, Madssen TS, et al. Cytokine patterns in maternal serum from first trimester to term and beyond. *Front Immunol* (2021) 12. doi: 10.3389/fimmu.2021.752660

23. Azizieh F, Dingle K, Raghupathy R, Johnson K, VanderPlas J, Ansari A. Multivariate analysis of cytokine profiles in pregnancy complications. *Am J Reprod Immunol* (2018) 79(3):e12818. doi: 10.1111/aji.12818

24. Tartaglia E, Bordoni V, Oliva A, Vergori A, Girardi E, Antinori A, et al. T Helper profile in pregnant women recovered from COVID-19. *J Reprod Immunol* (2022) 153:103661. doi: 10.1016/j.jri.2022.103661

25. Subha M, Pal P, Pal GK, Habeebullah S, Adithan C, Sridhar MG. Decreased baroreflex sensitivity is linked to sympathovagal imbalance, low-grade inflammation, and oxidative stress in pregnancy-induced hypertension. *Clin Exp Hypertens* (2016) 38 (8):666–72. doi: 10.1080/10641963.2016.1200596

26. Blackmore ER, Moynihan JA, Rubinow DR, Pressman EK, Gilchrist M, O'Connor TG. Psychiatric symptoms and proinflammatory cytokines in pregnancy. *Psychosom Med* (2011) 73(8):656–63. doi: 10.1097/PSY.0b013e31822fc277

27. Simavli S, Derbent AU, Uysal S, Turhan NÖ. Hepcidin, iron status, and inflammation variables among healthy pregnant women in the Turkish population. *J Maternal-Fetal Neonatal Med* (2014) 27(1):75–9. doi: 10.3109/14767058.2013.804054

28. Björkander S, Bremme K, Persson JO, van Vollenhoven RF, Sverremark-Ekström E, Holmlund U. Pregnancy-associated inflammatory markers are elevated in pregnant women with systemic lupus erythematosus. *Cytokine* (2012) 59(2):392–9. doi: 10.1016/j.cyto.2012.04.046

29. Lindsay K, Buss C, Wadhwa P, Entringer S. Maternal stress potentiates the effect of an inflammatory diet in pregnancy on maternal concentrations of tumor necrosis factor alpha. *Nutrients* (2018) 10(9):1252. doi: 10.3390/nu10091252

30. Olimpia SS, Magdalena P, Tomasz P, Piotr W, Elzbieta RW. Changes in the concentration of sHLA-I and selected cytokines in pregnancy complicated by antiphospholipid syndrome. *Ginekol Pol* (2011) 82(5):354–8. doi: 10.3390/nu10091252

31. Stokkeland LMT, Giskeødegård GF, Stridsklev S, Ryan L, Steinkjer B, Tangerås LH, et al. Serum cytokine patterns in first half of pregnancy. *Cytokine* (2019) 119:188–96. doi: 10.1016/j.cyto.2019.03.013

32. Doria A, Cutolo M, Ghirardello A, Zen M, Villalta D, Tincani A, et al. Effect of pregnancy on serum cytokines in SLE patients. *Arthritis Res Ther* (2012) 14(2):R66. doi: 10.1186/ar3782

33. Iaccarino L, Ghirardello A, Zen M, Villalta D, Tincani A, Punzi L, et al. Polarization of TH2 response is decreased during pregnancy in systemic lupus erythematosus. *Reumatismo* (2012) 64(5):314–20. doi: 10.4081/reumatismo.2012.314

34. Yockey LJ, Iwasaki A. Interferons and proinflammatory cytokines in pregnancy and fetal development. *Immunity* (2018) 49(3):397–412. doi: 10.1016/j.immuni.2018.07.017

35. Vilotić A, Nacka-Aleksić M, Pirković A, Bojić-Trbojević Ž, Dekanski D, Jovanović Krivokuća M. IL-6 and IL-8: An overview of their roles in healthy and pathological pregnancies. *Int J Mol Sci* (2022) 23(23):14574. doi: 10.3390/ijms232314574

36. Nayak M, Peinhaupt M, Heinemann A, Eekhoff MEW, van Mechelen W, Desoye G, et al. Sedentary behavior in obese pregnant women is associated with inflammatory markers and lipid profile but not with glucose metabolism. *Cytokine* (2016) 88:91–8. doi: 10.1016/j.cyto.2016.08.031

37. Ross KM, Miller G, Culhane J, Grobman W, Simhan HN, Wadhwa PD, et al. Patterns of peripheral cytokine expression during pregnancy in two cohorts and associations with inflammatory markers in cord blood. *Am J Reprod Immunol* (2016) 76(5):406–14. doi: 10.1111/aji.12563

38. Witkin SS, Gerber S, Ledger WJ. Influence of interleukin-1 receptor antagonist gene polymorphism on disease. *Clin Infect Diseases* (2002) 34(2):204–9. doi: 10.1086/338261

39. Steinkasserer A, Spurr NK, Cox S, Jeggo P, Sim RB. The human IL-1 receptor antagonist gene (IL1RN) maps to chromosome 2q14-q21, in the region of the IL-1 alpha and IL-1 beta loci. *Genomics* (1992) 13(3):654–7. doi: 10.1016/0888-7543(92)90137-H

40. Simón C, Valbuena D, Krüssel J, Bernal A, Murphy CR, Shaw T, et al. Interleukin-1 receptor antagonist prevents embryonic implantation by a direct effect on the endometrial epithelium. *Fertil Steril* (1998) 70(5):896–906. doi: 10.1016/S0015-0282(98)00275-1

41. Kimya Y, Akdiş C, Cengiz C, Ozan H, Tatlikazan S, Uncu G, et al. Plasma interleukin-1alpha, interleukin-1beta and interleukin-1 receptor antagonist levels in pre-eclampsia. *Eur J Obstet Gynecol Reprod Biol* (1997) 73(1):17–21. doi: 10.1016/S0301-2115(97)02698-5

42. Bowen JM, Chamley L, Mitchell MD, Keelan JA. Cytokines of the placenta and extra-placental membranes: biosynthesis, secretion and roles in establishment of pregnancy in women. *Placenta* (2002) 23(4):239–56. doi: 10.1053/plac.2001.0781

43. Numasaki M, Lotze MT, Sasaki H. Interleukin-17 augments tumor necrosis factor-alpha-induced elaboration of proangiogenic factors from fibroblasts. *Immunol Lett* (2004) 93(1):39–43. doi: 10.1016/j.imlet.2004.01.014

44. Numasaki M, Takahashi H, Tomioka Y, Sasaki H. Regulatory roles of IL-17 and IL-17F in G-CSF production by lung microvascular endothelial cells stimulated with IL-1beta and/or TNF-alpha. *Immunol Lett* (2004) 95(1):97–104. doi: 10.1016/j.imlet.2004.06.010

45. Numasaki M. Interleukin-17 promotes angiogenesis and tumor growth. *Blood* (2003) 101(7):2620–7. doi: 10.1182/blood-2002-05-1461

46. Takahashi H, Numasaki M, Lotze MT, Sasaki H. Interleukin-17 enhances bFGF-, HGF- and VEGF-induced growth of vascular endothelial cells. *Immunol Lett* (2005) 98(2):189–93. doi: 10.1016/j.imlet.2004.11.012

47. Numasaki M, Watanabe M, Suzuki T, Takahashi H, Nakamura A, McAllister F, et al. IL-17 enhances the net angiogenic activity and *In vivo* growth of human non-small cell lung cancer in SCID mice through promoting CXCR-2-Dependent angiogenesis. *J Immunol* (2005) 175(9):6177–89. doi: 10.4049/jimmunol.175.9.6177

48. Cornelius DC, Lamarca B. TH17- and IL-17- mediated autoantibodies and placental oxidative stress play a role in the pathophysiology of pre-eclampsia. *Minerva Ginecol* (2014) 66(3):243–9. doi: 10.4049/jimmunol.175.9.6177

49. Pinheiro MB, Martins-Filho OA, Mota APL, Alpoim PN, Godoi LC, Silveira ACO, et al. Severe preeclampsia goes along with a cytokine network disturbance towards a systemic inflammatory state. *Cytokine* (2013) 62(1):165–73. doi: 10.1016/j.cyto.2013.02.027

50. Liu H, Liu A, Kaminga AC, McDonald J, Wen SW, Pan X. Chemokines in gestational diabetes mellitus. *Front Immunol* (2022) 13. doi: 10.3389/fimmu.2022.705852

51. de Freitas NPA, Carvalho TR, Gonçalves CCRA, da Silva PHA, de Melo Romão LG, Kwak-Kim J, et al. The dietary inflammatory index as a predictor of pregnancy outcomes: Systematic review and meta-analysis. *J Reprod Immunol* (2022) 152:103651. doi: 10.1016/j.jri.2022.103651

frontiers | Frontiers in Immunology

TYPE Original Research
PUBLISHED 29 September 2022
DOI 10.3389/fimmu.2022.976512

OPEN ACCESS

EDITED BY
Diana Boraschi,
Shenzhen Institute of Advanced Technology (SIAT) (CAS), China

REVIEWED BY
Sukhwinder Singh Sohal,
University of Tasmania, Australia
Shixue Gou,
Guangzhou Institutes of Biomedicine and Health (CAS), China

*CORRESPONDENCE
Dan Liu
liudan10965@wchscu.cn
Lanlan Zhang
llzhang@scu.edu.cn
Xin Zhang
xinzhang201618@gmail.com

SPECIALTY SECTION
This article was submitted to Cytokines and Soluble Mediators in Immunity, a section of the journal Frontiers in Immunology

RECEIVED 23 June 2022
ACCEPTED 24 August 2022
PUBLISHED 29 September 2022

CITATION
Zhang L, Tang C, Zhang M, Tong X, Xie Y, Yan R, Wang X, Zhang X, Liu D and Li S (2022) Single cell meta-analysis of EndMT and EMT state in COVID-19. *Front. Immunol.* 13:976512. doi: 10.3389/fimmu.2022.976512

Single cell meta-analysis of EndMT and EMT state in COVID-19

Lanlan Zhang[1*], Chuang Tang[2], Min Zhang[3], Xia Tong[2,4], Yingying Xie[5], Ruitong Yan[6], Xiangjun Wang[7], Xin Zhang[2,4*], Dan Liu[1*] and Shasha Li[8,9]

[1]Division of Pulmonary Diseases, State Key Laboratory of Biotherapy, And Department of Respiratory and Critical Care Medicine, West China Hospital of Sichuan University, Chengdu, China, [2]Department of Gastroenterology, West China (Airport) Hospital, Sichuan University, Chengdu, China, [3]Oncology Bussiness Department, Novogene Co., Ltd, Beijing, China, [4]Department of Gastroenterology, West China Hospital of Sichuan University, Chengdu, China, [5]Department of Nephrology, Seventh Affiliated Hospital Sun Yat-sen University, Shenzhen, China, [6]Sichuan University, Chengdu, China, [7]First Affiliated Hospital of Sun Yat-Sen University, Guangzhou, China, [8]Athinoula A. Martinos Center for Biomedical Imaging, Department of Radiology, Massachusetts General Hospital, Charlestown, MA, United States, [9]Harvard Medical School, Boston, MA, United States

COVID-19 prognoses suggests that a proportion of patients develop fibrosis, but there is no evidence to indicate whether patients have progression of mesenchymal transition (MT) in the lungs. The role of MT during the COVID-19 pandemic remains poorly understood. Using single-cell RNA sequencing, we profiled the transcriptomes of cells from the lungs of healthy individuals (n = 45), COVID-19 patients (n = 58), and idiopathic pulmonary fibrosis (IPF) patients (n = 64) human lungs to map the entire MT change. This analysis enabled us to map all high-resolution matrix-producing cells and identify distinct subpopulations of endothelial cells (ECs) and epithelial cells as the primary cellular sources of MT clusters during COVID-19. For the first time, we have identied early and late subgroups of endothelial mesenchymal transition (EndMT) and epithelial-mesenchymal transition (EMT) using analysis of public databases for single-cell sequencing. We assessed epithelial subgroups by age, smoking status, and gender, and the data suggest that the proportional changes in EMT in COVID-19 are statistically significant. Further enumeration of early and late EMT suggests a correlation between invasive genes and COVID-19. Finally, EndMT is upregulated in COVID-19 patients and enriched for more inflammatory cytokines. Further, by classifying EndMT as early or late stages, we found that early EndMT was positively correlated with entry factors but this was not true for late EndMT. Exploring the MT state of may help to mitigate the fibrosis impact of SARS-CoV-2 infection.

KEYWORDS

COVID-19, endothelial-mesenchymal transition (EndMT), epithelial-mesenchymal transition (EMT), single cell RNA sequencing, endothelial cells (ECs)

Abbreviations: COVID-19, Coronavirus disease 2019; MT, Mesenchymal transition; EndMT, Endothelial-mesenchymal transition; EMT, Epithelial-mesenchymal transition; IPF, Idiopathic pulmonary fibrosis.

Introduction

Alveolar epithelial type II cells (AEC2s) produce surfactants and serve as progenitors (1). Type II alveolar epithelium is reduced due to massive necrosis with SARS-COV-2 infection in patients (2). This leads to decreased barrier permeability and accumulation of proteinaceous edema fluid in the alveolar cavity, resulting in hypoxemia and even acute respiratory distress syndrome (ARDS), with a prognosis including fibrosis formation (3). Epithelial-mesenchymal transition (EMT) is the process by which epithelial cells differentiate into mesenchymal (fibroblast-like) cells expressing mesenchymal biomarkers such as α-Smooth Muscle Actin (α-SMA), and N-cadherin (4, 5). Therefore, we speculated that EMT might underlie the mechanism of lung fibrosis observed with ARDS in COVID-19 patients.

Early-stage and late-stage mesenchymal transition (MT) processes are considered the most critical pathogenic mechanisms of fibrosis in diseases like idiopathic pulmonary fibrosis (IPF), pulmonary hypertension, coronary artery disease, and other vascular-related disorders (6). Once endothelial cells (ECs) are damaged and the collagen and matrix are exposed, in addition to activation of the coagulation system, immune cells are recruited, leading to the release of large amounts of inflammatory factors are then released (7). Endothelial-mesenchymal transition (EndMT) occurs when ECs respond to chronic inflammation, transforming themselves into a more aggressive mesenchymal state (8, 9). In the early stages, irreversible vascular damage or EndMT, mainly presents more robust endothelial markers (e.g., vascular endothelial cadherins (VE-cadherins), *CD31* and Tie1/2) and expresses weaker mesenchymal markers (e.g., *N-cadherin*, *fibroblast specific protein-1* or *S100A4*, *fibronectin*, *vimentin*, *SM22-α*, *calponi*n, and *α-smooth muscle actin*) (10, 11). Otherwise, late-stage EndMT presents weaker endothelial markers but with more robust mesenchymal markers.

EMT also has a similar process with the presence of EndMT as well as MT markers in the early stages (12, 13). However, in the late stage, epithelial markers are lost, and fibroblast markers are predominant (12, 13). Therefore, we hypothesized that EMT and EndMT may underlie factors implicated in the prolonged ventilator dependence and high mortality rates observed in hospitalized COVID-19 patients.

Herein, we draft EndMT and EMT by integrated analysis of 167 single-cell and single-nucleus RNA-sequencing (scRNA-seq and snRNA-seq, respectively) samples. We performed the first single-cell RNA sequencing meta-analysis associating COVID-19 with underlying contributor genes for MT. We have also identified specific gene programs enriched in MT-associated genes with fibrosis and highlight other entry factors that are significantly expressed in the lungs, which may play a role in SARS-CoV-2 infection.

Materials and methods

Data collection

We obtained scRNA/snRNA sequencing data from Gene Expression Omnibus database (GEO) database (https://www.ncbi.nlm.nih.gov/geo/). The majority of the data used in this manuscript is publicly available from previously published studies: COVID-19:GEO accession GSE171524, GSE171668, GSE149878, GSE161382 and GSE163919 (14–17). IPF: GEO accession GSE136831 and GSE135893 (18, 19). The Bulk RNA data is also available in the GEO database (accession number GSE47460) (20).

scRNA/snRNA-seq data processing

We analyzed the scRNA and snRNA sequencing data using R(version 4.1.3) and Seurat v 4.0.2 (21). To eliminate low quality/dead cells or empty droplets, any single cells containing less than 200 genes or greater than 5,000 genes, or cells with more than 10% mitochondrial genes were removed. We next removed doublet contamination. As a result. We detected 49,795 genes in a total of 612,151 cells. Next, we performed LogNormalize() to normalize the gene expression data, used the FindVariableFeatures() function to identify genes whose expression was highly variable between cells, and used ScaleData() to scale the data. The •"RunPCA•" function was used for principal component analysis (PCA). Using the default parameters, Harmony package (22) was utilized to combine data and eliminate batch effect, Using the default parameters, Harmony performs de-batching by single patients. Subsequently, the top 20 statistically significant principal components were used in the "•FindNeighbors•" function. Cells were clustered (Cluster resolution = 0.6) by using the •FindClusters• function and visualized with the UMAP method.

Cell type identification and data visualization

Cell type identification was mostly accomplished with the use of "FindAllMarkers," classical cell marker genes, R-packages (clustermole, singscore), and cell type annotation using a mixture of known cell marker genes. *EPCAM*$^+$ epithelial cells, *CLDN5*$^+$ endothelial cells, *PTPRC*$^+$ immune cells, and *COL1A2*$^+$ (mesenchymal cells). Cell clustering was performed using the Seurat "FindNeighbors" and "FindClusters" functions, and the final Seurat objects were created after UMAP downscaling. The pheatmap was created using the R package ggplot2 in Seurat, and umap maps, violin maps, bar maps, heat maps, and point maps were created.

Enrichment analysis

Enriched gene ontology biological (http://geneontology.org/) processes with a false discovery rate less than 5 percent were identified using the Gene Ontology Resource. KEGG (http://www.kegg.jp) enrichment analyses were carried out with the Fisher's exact test, and FDR correction for multiple testing was also performed. Gene Set Enrichment Analysis (GSEA) were performed with clusterProfile. The three methods determine whether a set of genes has statistically significant differences between two biological states (23).

Trajectory analysis

The R package monocle3 v1.0.0 was used to construct single cell trajectory analysis. Cells marked as EndMT/EMT and their subsets information were input and constructed into a monocle object (24). The left side of the heat map, created with the R package monocle2, shows the signaling pathways enriched to the gene set. Each row of the heat map (ranging from red to blue) represents a gene; each column represents a proposed time point; and the color represents the average expression value of the gene at the current time point (from high to low expression, respectively) (25).

Bulk RNA data

Univariate analysis was performed by using the Pearson's correlation coefficient of gene expression data and diffusing capacity of the lung for carbon monoxide (DLCO). The data is available in the Gene Expression Omnibus database (accession number GSE47460).

Statistical analysis of functional data

The R language or the GraphPad Prism software, version 9 (San Diego, California USA, www.graphpad.com) were used to perform all computations and analyses. T-tests were used for comparisons between groups, and one-way ANOVA was used for comparisons between multiple groups. A statistically significant difference was defined as a p value <0.05. The Wilcoxon rank sum statistical test was used to examine differentially expressed genes in each cluster. The meta package was used to perform the meta-analysis in R.

Results

Single-cell transcriptome sequencing reveals the presence of fibrosis-associated cell subpopulations

To investigate the contribution of EndMT in SARS-CoV-2 infection in the lungs, we analyzed existing scRNA/snRNA-seq datasets to assess which clusters express EndMT markers. In a previously unpublished dataset consisting of COVID-19 and IPF lung tissue (n=167), we recovered at least 14 distinct major cell types, including macrophages, monocytes, neutrophils, T cells, B cells, DCs, granulocytes, endothelial cells, fibroblasts, SMC/pericytes, goblet cells, alveolar type 1 epithelial cells (AT1), alveolar type 2 epithelial cells(AT2), ciliated cell populations, and proportional analysis of subpopulations, of whole lung tissue (Figures 1A, B). After analyzing their differentially expressed genes (DEGs), compared to controls, we found that the DEGs in COVID-19 patients were mainly concentrated in macrophages and monocytes, and the DEGs in IPF patients were mainly concentrated in the epithelium (Figure 1C). Further, we analyzed the ratio of cell subpopulations and found that the ratio of ECs and epithelial was upregulated in COVID-19 patients, while higher than in pulmonary fibrosis (Figure 1D). Using correlation analysis, we found that lymphatic ECs, SMC/pericytes, myofibroblasts, rest ECs, late EMT, proliferative fibroblast, rest fibroblasts, late EndMT, *DKK2*+ ECs, and activated ECs cells had a strong correlation. This phenomenon prompted us to question why fibroblasts and correlate strongly with ECs (Figure 1E). Therefore, we analyzed fibroblasts, and based on a literature search, we analyzed fibroblast subpopulations such as rest fibroblasts, myofibroblasts, and proliferative fibroblasts (Figures 1F, H). A comparison of COVID-19 and IPF samples revealed that the, myofibroblast proportion was significantly higher in patients with IPF compared to COVID-19 patients (Figure 1G). Interestingly, we also found that myofibroblast expression was much higher in male COVID-19 patients than male patients, but the opposite was true for rest fibroblasts (Figure 1I). We also analyzed the expression of entry factors in whole lung cells, and consistent with previous literature reports, *ACE2* was mainly concentrated in respiratory epithelium cells such as AT1 and AT2. However, BSG, CTSL, and FURIN were also abundantly expressed in macrophages and fibroblasts (Figure 1J). TMPRSS2 and ACE2 expression were upregulated in COVID-19 patients but BSG, CTSL, FURIN expression was higher in IPF patients, suggesting their role in increased myofibroblast expression in COVID-19 (Figure 1K). We also analyzed correlation analysis of entry factors and lung function test (%predicted DLCO) and found that lung function was negatively correlated with the normalized bulk RNA-seq gene expression of the entry factors (*CTSL*, *BSG*, *ACE2*) (Figure 1L).

Single-cell transcriptome sequencing Atlas of EMT stage

EMT is a common type of transition, and we divided the epithelium into goblet, ciliated, EMT, AT1, and AT2 cell subgroups, in which the EMT proportion was significantly upregulated in COVID-19 and IPF patients, but there were no significant

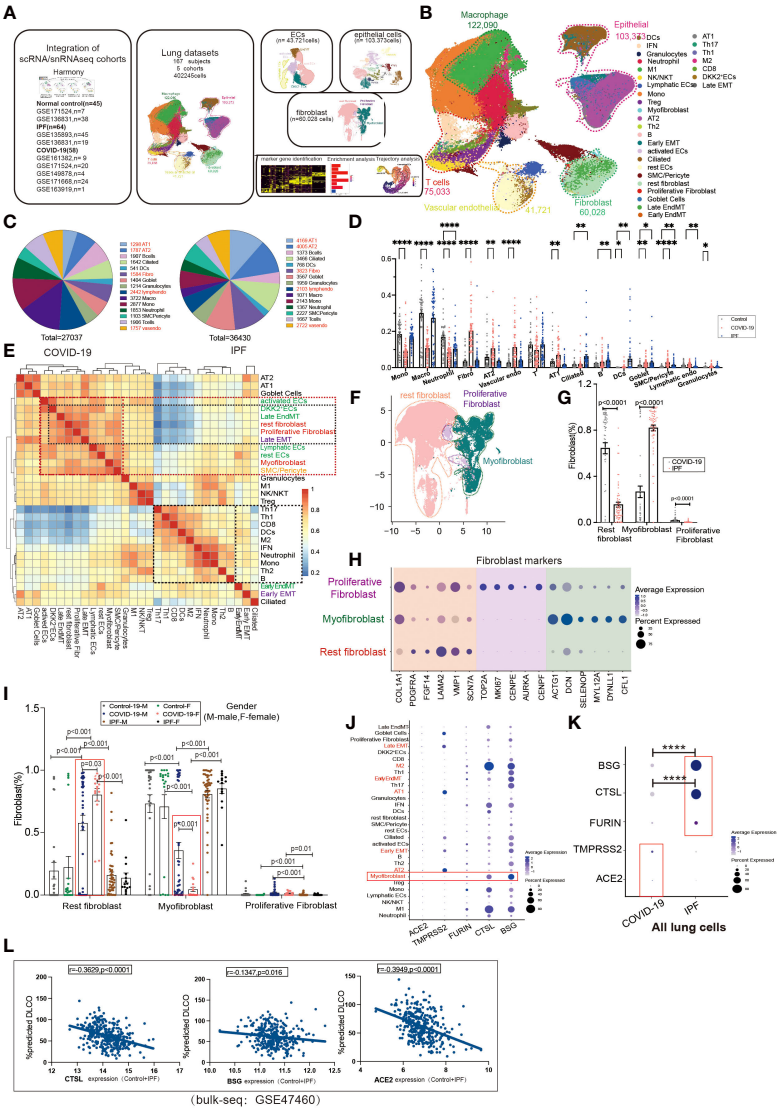

FIGURE 1
Subpopulation correlation analysis suggested a strong correlation between MT subpopulation and fibroblast subpopulation. **(A)** Scheme of this study. **(B)** Demonstration of HC, COVID-19, and IPF subgroups using UMAP, including Endothelial (vascular endothelial: rest ECs, EndMT, DKK2+ ECs, activated ECs; Lymphatic ECs); Epithelial (AT2, AT1, Goblet Cell, EMT, Ciliated); Fibroblast (Proliferative Fibroblast, Myofibroblast, Rest fibroblast, Late EndMT, Late EMT); SMC/Pericyte; T cells (Th1, Th17, Th2, Treg, NK/NKT, CD8, IFN); Macrophage (M2, M1); Granulocytes; DCs; Mono; Neutrophil. And the proportion of cell subpopulations in HC, COVID-19, IPF. Marker genes: Endothelial cells:PECAM1, VWF, CLDN5; Macrophages: MARCO, MSR1, MRC1;T cells:CD3E, CD3D, GZMH; Granulocytes:MS4A2, CPA3, TPSAB1; B cells:MS4A1, BANK1, CD79A;Monocytes:CD14, FCN1; Neutrophil:S100A8, S100A9; Epithelial cells:EPCAM; Fibroblast:COL1A1, PDGFRA, ELN;SMC:SCGB1A1, RPL26). **(C)** Pie charts show the number of differentially expressed genes per cell type in COVID-19/IPF compared to controls. The DEGs of COVID-19 were mainly concentrated in macrophages and monocytes, and the DEGs of IPF were mainly concentrated in epithelium. **(D)** The proportion of cell subpopulations in HC, COVID-19, IPF. **(E)** The heat-map shows the correlation analysis for each cell subpopulation. The correlation between late-stage EMT, late-stage EndMT and fibroblast subpopulation was higher. **(F)** UMAP suggests a subpopulation distribution of fibroblasts, including Myofibroblas,Proliferative fibroblas and Rest fibroblast. **(G)** Ratio of fibroblast subpopulations in patients with COVID-19, IPF, showing myofibroblast ratio in IPF is higher than that in COVID-19, but Rest fibroblast ratio in IPF is lower than that in COVID-19. **(H)** Markers of fibroblast subpopulations, including Myofibroblast (ACTG1, DCN, SELENOP, MYL12A, DYNLL1, CFL1), Proliferative fibroblast (TOP2A, MKI67, CENPE, AUPKA, CENPF) and Rest fibroblast (COL1A1, PDGFRA, FGF14, LAMA2, VMP1, SCN7A). **(I)** The proportion of fibroblast subpopulations in COVID-19, IPF by female and male, showing Myofibroblast ratio in females is lower than that in males with COVID-19. **(J)** The DOT plot shows the expression of entry factors in subgroups of control, COVID-19, IPF. Subgroups including Rest fibroblast, Myofibroblast, Proliferative Fibroblast, Late EndMT, Late EMT, SMC/Pericyte; rest ECs, DKK2^{+} ECs, activated ECs, Lymphatic ECs, EndMT-early; AT1, AT2, Ciliated, Early EMT, Goblet Cell; Granulocytes; B, Th2, Th1, Th17, Treg, CD8, Mono, M1, M2, Neutrophil, DCs, NK/NKT. **(K)** The DOT plot shows the expression of entry factors in COVID-19, IPF. **(L)** Correlation analysis of entry factors (CTSL, BSG, ACE2) and lung function test (%predicted DLCO) showed that lung function was negatively correlated with the normalized bulk RNA-seq gene expression of the entry factors. *P < 0.05, **P < 0.01,**** P< 0.0001

differences between COVID-19 and IPF (Figures 2A, B). After excluding datasets with significant heterogeneity, we performed a meta-analysis using 3 GEO datasets with a pooled SMD of 0.99 and 95% CI (0.49; 1.49) (Figure 2C). Surprisingly, the EMT rate was much more significant in the middle-aged group than in the aged group. The middle-aged group was mainly enriched for inflammation-related signaling pathways, and then the aging adult group was enriched for more fibrosis-related signaling pathways (Figures 2D, E). Whether classified by smoking or not, we observed that EMT was higher in both COVID-19 patients than in controls, and then IPF was higher in the non-smoking group compared to samples. In COVID-19, smoking is enriched for more interferon-related signaling pathways compared to samples from non-smoking individuals (Figures 2F, G). We found that the proportion of EMT was higher in patients who smoked, while in COVID-19 patients, the proportion of EMT was more significant in non-smoking males than in females (Figures 2H, I). This phenomenon indicates that males contribute more to EMT progression. EMT is positively correlated with myofibroblasts in COVID-19 patients, and IPF patients also have the same expression trend. Males upregulated inflammation-related signaling pathways, however females were enriched for downregulated inflammatory signaling pathways (Figure 2J).

Trajectory analysis mentions early and late mesenchymal transitions, and its marker also suggests its transition status (Figure 3A). *EPCAM* expression was significantly decreased from early to late stages. TAGLN expression was increased in the early stages but decreased in the late stages. *COL3A1* expression was somewhat lower during the early stages but increased significantly during the late stages (Figures 3C, D, G). From early to late stages, Monocel2 displayed the primary enhanced signaling pathways concurrently (Figure 3B). *TAGLN* is a typical EMT marker gene that is elevated in COVID-19 patients. A meta-analysis of a dataset of five GEO resulted in a pooled SMD of 0.73, 95 CI% (0.30; 1.15) (Figures 3D–F). *COL3A1* is a well-characterized marker of late MT that is increased in COVID-19 patients. The dataset of five GEOs was analyzed using meta-analysis, resulting in a pooled SMD of 1.77, 95 CI% (0.82; 2.72) (Figures 3G–I). Further analysis of the correlation between invasion genes showed that the epithelial entry factor genes (*BSG*, *FURIN*, *CTSL*) were positively correlated with the ratio of early EMT in COVID-19, *TMPRSS2* was negatively correlated with the ratio of early EMT in COVID-19, and FURIN was positively correlated with the ratio of early EMT in IPF (Figure 3J). *TMPRSS2* was positively correlated with the ratio of late EMT in COVID-19 and *BSG* was negatively correlated with the ratio of late EMT in COVID-19 (Figure 3K).

Single-cell transcriptome sequencing Atlas of EndMT stage

A further exploration of the potential cause of elevated fibroblast expression in COVID-19, revealed subpopulations of endothelium cells based on the high correlation between fibroblasts and endothelial cells (Figure 1D), and we found a subpopulation of endothelial cells with EndMT as in IPF (Figure 4A), which highly expresses the marker gene for subpopulations (Figure 4B). We divided the subgroups of endothelial cells into lymphatic ECs, EndMT, *DKK2*+ ECs, activated ECs, and rest ECs. Comparing the endothelium subgroup ratios in ECs, we found that the ratio of EndMT was increased in COVID-19 and higher in IPF than in the controls (Figure 4C). We showed common inflammation-associated cytokines through different subpopulations, implying an abundant expression of EndMT(Figure 4D). To exclude the effect of smoking, we selected nonsmoking patients for comparison, and the results suggested that the proportion of EndMT was also higher in males than in females in COVID-19 patients (Figure 4E). We compared the proportion of entry factor genes in Lymphatic ECs, EndMT, *DKK2*+ ECs, activated ECs, and rest ECs in COVID-19 and IPF (Figures 4F, G). The findings suggest that EndMT plays a unique function in COVID-19, and meta-analysis of data from several GEO databases indicates that the EndMT proportion in COVID-19 vs. control pooled SMD was 0.64, 95% CI [0.16; 1.12] (Figure 4H). After dividing the data into two groups, $EndMT^{low}$ and $EndMT^{high}$, the latter group was found to have a higher proportion of myofibroblasts (Figure 4I). A hypothesis was then raised about whether EndMT led to the increase in fibroblasts. Enrichment analysis of cytokine expression in the EndMT subpopulation revealed high expression of cytokines associated with fibrosis in COVID-19 and IPF (Figure 4J). The EndMT ratio was positively correlated with myofibroblast cells and negatively correlated with rest fibroblast (Figure 4K).

We then tried to determine whether EndMT has a series of genes that can affect COVID-19 and IPF MT by trajectory analysis and classified EndMT into early, intermediate, and late stages (Figure 5A). The enrichment of genes in early and late stages demonstrates that the interferon-gamma signaling pathway is upregulated in early stages. Simultaneously, late stages exhibit increased expression of the ECM-receptor interaction signaling pathway (Figure 5B). The expression of marker genes associated with EndMT also suggested early, intermediate, and late stages (Figure 5C). *ACTA2* expression was low in the intermediate stage but rapidly increased in the late stage (Figure 5D). Calculating the fraction of *ACTA2* present throughout the early stages of the disease reveals that the expression in COIVD-19 is more significant than in controls (Figure 5E). By screening the marker genes of early stage EndMT, the marker gene at the early stage was finally identified as *ACTA2* with an SMD of 0.87,95% CI (0.23,1.51) for COVID-19 vs. control in 5 GEO datasets following meta-analysis (Figure 5F). Subsequently, MMP2 and COL3A1 were used to identify the late-stage marker gene (Figure 5G, J). COL3A1 expression was increased in COVID-19 compared to controls (Figure 5K), and although all GSE statistics of MMP2-

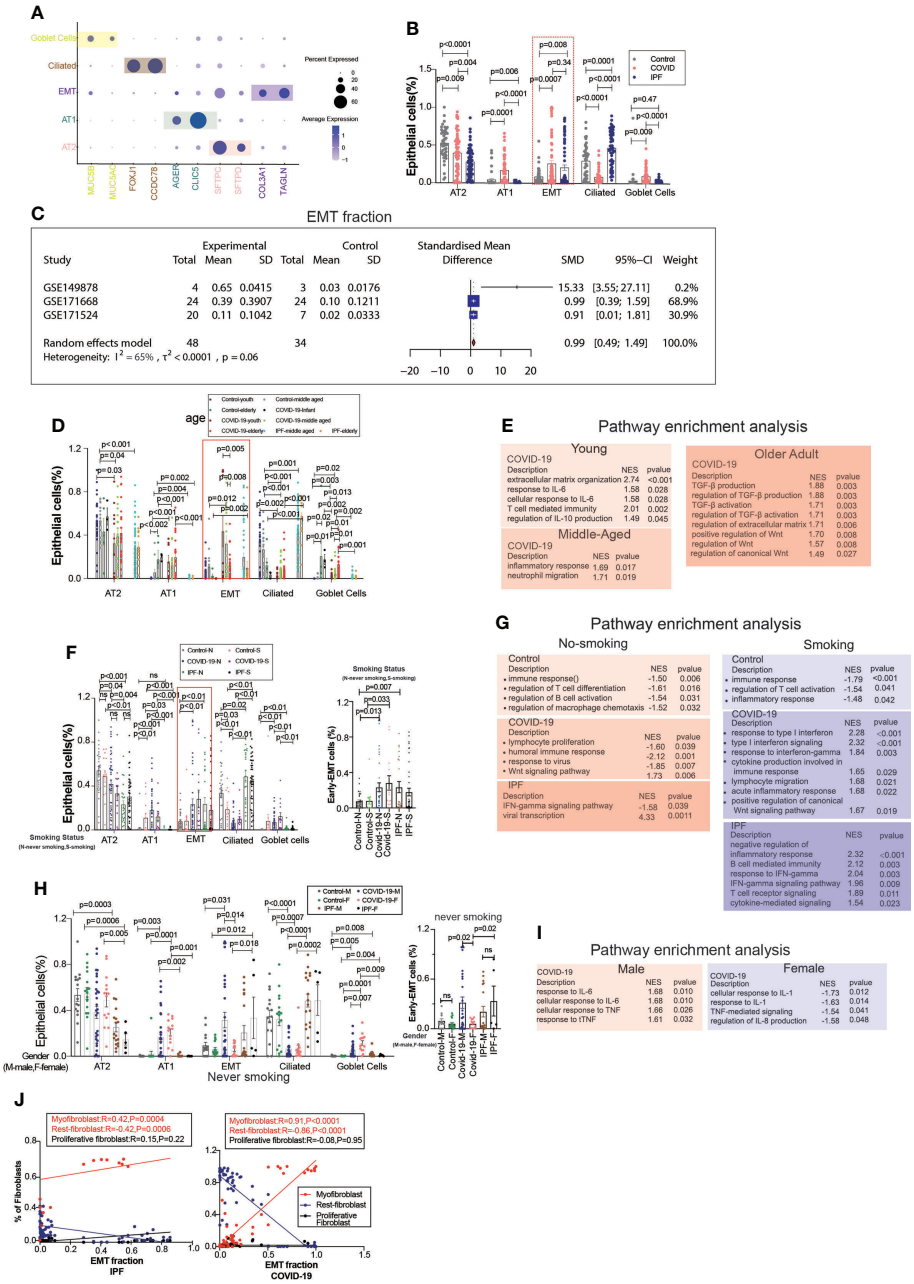

FIGURE 2
EMT by age, smoking status, and gender. **(A)** Dot chart shows the marker of epithelial subpopulations, including AT1(AGER, CLIC5), AT2(SFTPC, SFTPD), Ciliated (FOXJ1, CCDC78), Goblet cells (MUC5B, MUC5AC), EMT(TAGLN, COL3A1). **(B)** Comparison of the ratios of HC, COVID-19, IPF subpopulations of epithelium. EMT proportion was significantly upregulated in COVID-19 and IPF. **(C)** Forest plot of studies with EMT ratio on the COVID-19 and HC, after excluding a study with only one case and a high heterogeneity study. The analysis included data from 3 studies with a total of 48 COVID-19 and 34 controls. p value for heterogeneity was 0.06, I^2 was 65%. (SD, Standard deviation). **(D)** Comparison of the ratios of HC, COVID-19, IPF subpopulations of epithelium by age. **(E)** GO (Gene ontology) enrichment analysis was performed on the genes highly expressed in EMT in normal control, COVID-19 and IPF groups in patients of different ages, respectively, and the graphs show the signaling pathways enriched to EMT cell populations in different groups. **(F)** Comparison of the ratios of HC, COVID-19, IPF subpopulations of epithelium by smoking. **(G)** GO enrichment analysis was performed to enrich for genes that were highly expressed in EMT of smoking and non-smoking patients in normal control, COVID-19 and IPF groups, respectively, and the graphs show the signaling pathways enriched in EMT cell populations of different groups. **(H)** Comparison of the ratios of HC, COVID-19, IPF subpopulations of epithelium by sex. **(I)** GO enrichment analysis of the genes highly expressed in EMT in normal control, COVID-19 and IPF groups by sex, respectively. **(J)** Correlation analysis of EMT with myofibroblast, rest fibroblast and proliferative fibroblast in COVID-19 and IPF patients (Pearson test), showing EMT is positively correlated with myofibroblasts.

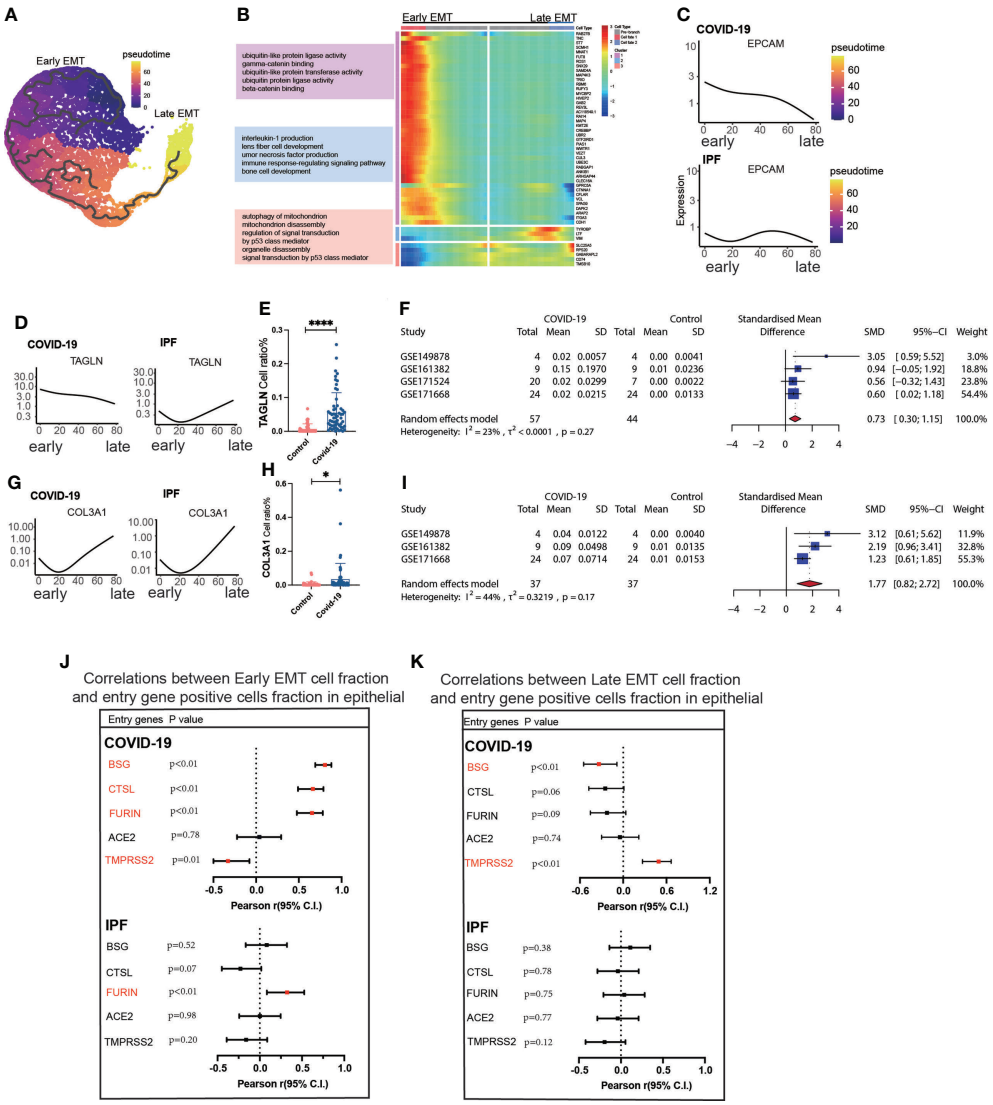

FIGURE 3
Characteristics of early late-stage EMT. **(A)** Pseudotime projection analysis showing early-stage EMT could evolve to late-stage EMT. **(B)** Single cell proposed time branch point analysis showing genes with progressively lower and higher expression from Early EMT to Late EMT. Each row of the heat map on the right represents a gene, each column is a proposed time point, and the color represents the average expression value of the gene at the current time point, with the color decreasing from red to blue. The left side shows the signaling pathways that the gene set is enriched. **(C)** Proposed time traces of individual genes, showing the change in gene expression from the beginning to the end of the proposed time course for epithelial cell marker genes (EPCAM) in COVID-19 and IPF patients, respectively. **(D)** Time-sensitive trajectories of individual genes, showing the change of Early EMT marker gene (TAGLN) expression from the beginning to the end of the proposed time course in COVID-19 and IPF patients, respectively. **(E)** TAGLN gene positive epithelial cell ratio is higher in COVID-19 than that in HC. **(F)** Forest plot of studies with TAGLN gene positive epithelial cell ratio on the COVID-19 and HC, after excluding a study with only one case. the analysis included data from 4 studies with a total of 57 COVID-19 and 44 controls. p value for heterogeneity was 0.27, I2 was 23%.**(G)** Temporal trajectories of individual genes, showing changes in gene expression of Late EMT marker gene (COL3A1) in COVID-19 and IPF patients by the start to the end of the proposed time course, respectively. **(H)** COL3A1 gene positive epithelial cell ratio is higher in COVID-19 than that in HC. **(I)** Forest plot of studies with COL3A1 gene positive epithelial ratio on the COVID-19 and HC, after excluding a study with only one case and a high heterogeneity study. The analysis included data from 3 studies with a total of 37 COVID-19 and37 controls. p value for heterogeneity was 0.17, I^2 was 44%. **(J)** Forest plot showing the correlation between Early EMT cell fraction and entry gene positive cells fraction in epithelial cells. And entry factors (BSG, FURIN, CTSL) were positively correlated with the expression of Early EMT in COVID-19 ($p < 0.05$, Pearson's $r > 0$). TMPRSS2 was negatively correlated with the expression of Early EMT in COVID-19 ($p < 0.05$, Pearson's $r < 0$). FURIN was positively correlated with the expression of Early EMT in IPF ($p < 0.05$, Pearson's $r > 0$). **(K)** Forest plot showing the correlation between Late EMT cell fraction and entry gene positive cells fraction in epithelial cells. And entry factor (TMPRSS2) was positively correlated with the expression of Late EMT in COVID-19 ($p < 0.05$, Pearson's $r > 0$). BSG was negatively correlated with the expression of Late EMT in COVID-19 ($p < 0.05$, Pearson's $r < 0$) *P < 0.05,**** P< 0.0001.

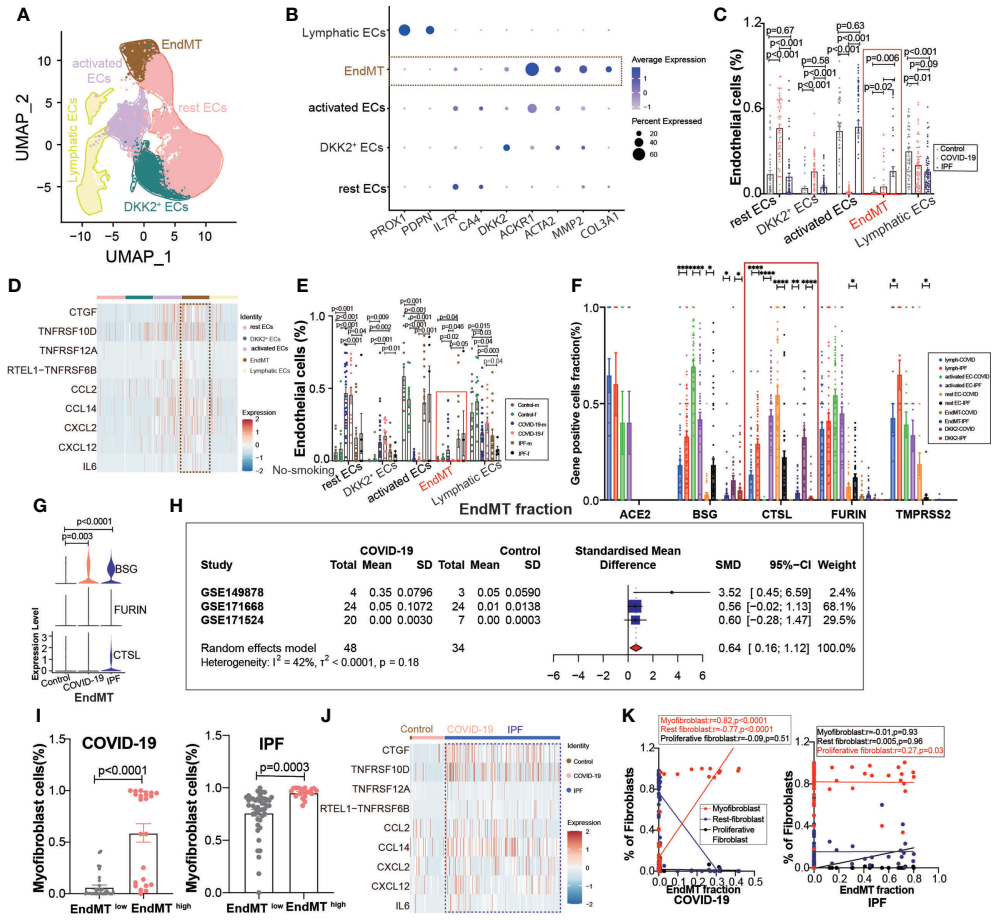

FIGURE 4
EndMT proportion is upregulated in COVID-19. **(A)** The expression of pulmonary ECs in patients with health control, COVID-19, IPF was demonstrated using UMAP plots with subpopulations marked by a color code. ECs subpopulations including rest ECs, EndMT, *DKK2*$^{+}$ ECs, activated ECs; Lymphatic ECs. **(B)** Dot chart shows the marker of EndMT, mainly focusing on ACTA2, MMP2, COL3A1; rest ECs (IL7R, CA4), *DKK2*$^{+}$ ECs (DKK2), activated ECs (ACKR1); Lymphatic ECs(PROX1,PDPN). **(C)** Proportion of ECs among normal control group, COVID-19 group and IPF group, the ratio of EndMT was increased in COVID-19 and IPF than controls. One-way ANOVA was used to compare multiple groups ($p<0.05$). **(D)** Heatmap shows a comparison of the expression of major cytokines in the cell subpopulations of ECs shows that EndMT is enriched in more cytokines compared to the other groups. **(E)** Comparison of the ratios of HC, COVID-19, IPF subpopulations of ECs by gender in nonsmokers. EndMT ratio in females is lower than that in males with COVID-19. **(F)** Comparison of entry factors (ACE2, BSG, FURIN, CTSL, TMPRSS2) positive cell fraction in ECs subtype of COVID-19 and IPF. **(G)** Comparison of EndMT proportion of entry factors (BSG, FURIN, CTSL) in HC, COVID-19, IPF. **(H)** Forest plot of studies with lung scRNA data on the COVID-19, after excluding a study with only one case and a high heterogeneity study. The analysis included data from 3 studies with a total of 48 COVID-19 and 34 controls. p value for heterogeneity was 0.18, I^2 was 42%. (SD: Standard deviation). **(I)** Ratio of myofibroblasts in COVID-19 and IPF for EndMT ^{low} versus EndMT ^{high}, showing myofibroblast ratio in EndMT ^{high} is higher than that in EndMT ^{low}. **(J)** A comparison of the expression of major cytokines in the EndMT shows that COVID-19 and IPF are enriched in more profibrotic cytokines compared to HC group. **(K)** Correlation analysis of EndMT with myofibroblast, rest fibroblast and profilerative fibroblast in COVID-19 and IPF patients (Pearson test), showing EndMT is positively correlated with myofibroblasts in COVID-19 patients. *$P < 0.05$, **$P < 0.01$, ***$P < 0.001$,****$P < 0.0001$.

positive cells were not significant (Figure 5H), MMP2-positive cells were statistically differentially upregulated in late stage of EndMT by meta-analysis of GSE data. Using meta-analysis, we demonstrated that the MMP2 pooled SMD in 5 distinct GEO datasets was 0.54, 95% CI (0.13.0.96) (Figure 5I), and ultimately, meta-analysis revealed that the COL3A1 pooled SMD of late stages of COVID-19 was 0.84, 95% CI (0.24,1.44) when compared to controls (Figure 5L). Further analysis of the correlation with invasion genes showed that the entry factor genes (*BSG, FURIN, and CTSL*) were positively correlated with the ratio of early EndMT in COVID-19, and *CTSL* was positively correlated with the ratio of early EndMT in IPF (Figure 5M). *ACE2* was positively correlated with the ratio of late EndMT in IPF (Figure 5N).

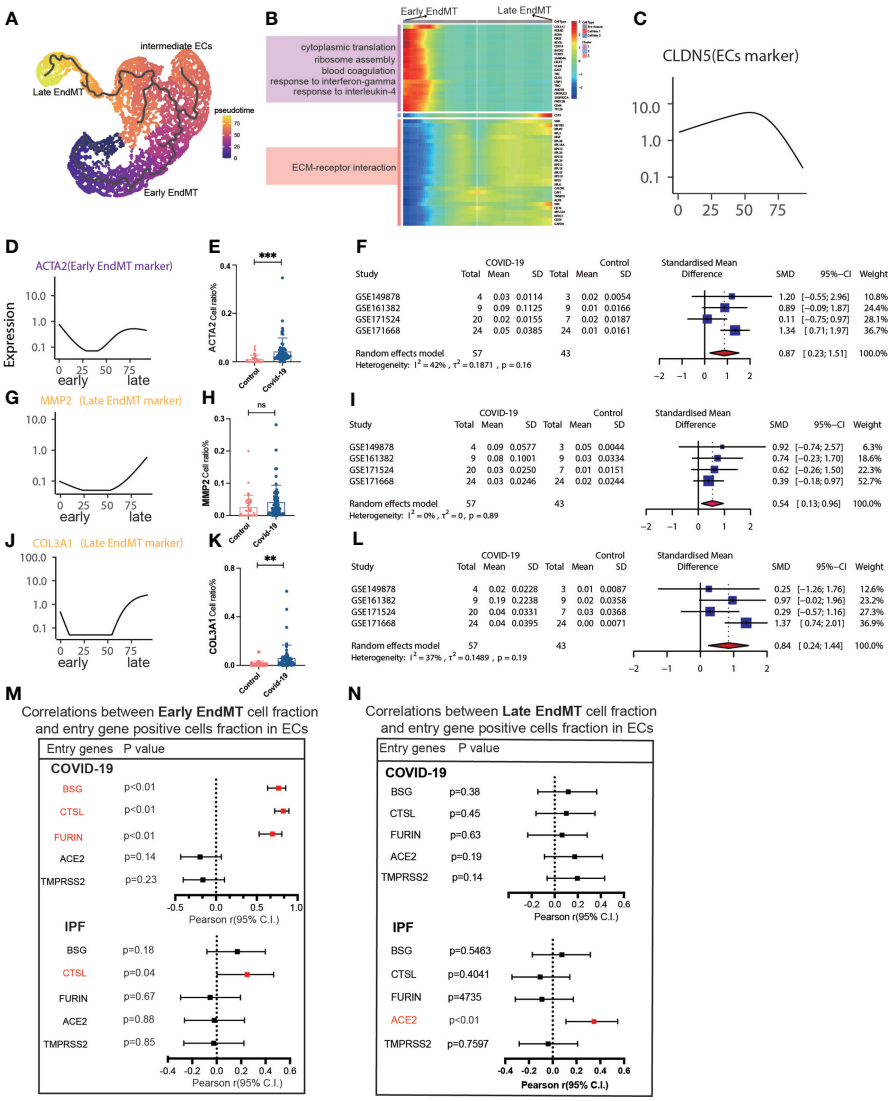

FIGURE 5
Characteristics of early and late stage EndMT. **(A)** Pseudotime projection analysis showing early-stage EndMT could evolve to late-stage EndMT. **(B)** Single cell proposed time branch point analysis showing genes with progressively lower and higher expression from Early EndMT to Late EndMT. Each row of the heat map on the right represents a gene, each column is a proposed time point, and the color represents the average expression value of the gene at the current time point, with the color decreasing from red to blue. The left side shows the signaling pathways that the gene set is enriched to. **(C)** The proposed time trajectory of a single gene, showing the change in gene expression of the ECs marker gene (CLDN5) from the beginning to the end of the proposed time course. **(D)** Trajectories of individual genes, showing changes in gene expression of Early EndMT marker genes (ACTA2) from the beginning to the end of the proposed time course. **(E)** ACTA2 gene positive ECs ratio is higher in COVID-19 than that in HC. **(F)** Forest plot of studies with ACTA2 gene positive ECs ratio on the COVID-19 and HC, after excluding a study with only one case. The analysis included data from 4 studies with a total of 57 COVID-19 and 43 controls. p value for heterogeneity was 0.16, I2 was 42%. **(G)** Temporal trajectories of individual genes showing changes in gene expression of Late EndMT marker gene (MMP2) from the beginning to the end of the proposed time course. **(H)** MMP2 gene positive ECs ratio is higher in COVID-19 than that in HC. **(I)** Forest plot of studies with MMP2 gene positive ECs ratio on the COVID-19 and HC, after excluding a study with only one case. The analysis included data from 4 studies with a total of 57 COVID-19 and 43 controls. p value for heterogeneity was 0.89, I2 was 0%. **(J)** Trajectories of individual genes showing changes in gene expression of the Late EndMT marker gene (COL3A1) from the beginning to the end of the proposed time course. **(K)** COL3A1 gene positive ECs ratio is higher in COVID-19 than that in HC. **(L)** Forest plot of studies with COL3A1 gene positive ECs ratio on the COVID-19 and HC, after excluding a study with only one case. The analysis included data from 4 studies with a total of 57 COVID-19 and 43 controls. p value for heterogeneity was 0.19, I^2 was 37%. **(M)** Forest plot showing the correlation between Early EndMT cell fraction and entry gene positive cells fraction in ECs. Entry factors (BSG, FURIN, CTSL) was positively correlated with the expression of Early EndMT in COVID-19 ($p < 0.05$, Pearson's $r > 0$). CTSL was positively correlated with the expression of Early EndMT in IPF ($p < 0.05$, Pearson's $r > 0$). **(N)** Forest plot showing the correlation between Late EndMT cell fraction and entry gene positive cells fraction in ECs. Entry factors (ACE2) was positively correlated with the expression of Late EndMT in COVID-19 ($p < 0.05$, Pearson's $r > 0$). **P < 0.01, ***P < 0.001; NS, P > 0.05.

Discussion

To our knowledge, this first single-cell meta-analysis that describes MT-related clusters in COVID-19 patients. When we examined the MT transition state in COVID-19 using IPF with MT and a high number of fibroblasts as a control, we identified a substantial link between fibroblasts and MT across all subpopulations. By analyzing the correlation of each subgroup, we screened the relevant subgroups of MT (i.e., EndMT and EMT). COVID-19 patients exhibited a increased MT than healthy controls, but less than IPF patients. We further found that male patients had a higher proportion of cells in EMT and EndMT. Several studies have shown a higher prevalence of pulmonary fibrosis after COVID-19 in males. This is likely because males are more exposed to fibrotic triggers, such as occupational agents (26–28).

In EMT, young people are more enriched in inflammation such as *IL-6* signaling pathways, aging adults are enriched with more fibrosis-promoting signaling pathways such as TGF-b. Increased levels of TGF-b, an anti-inflammatory but profibrotic cytokine, might be the leading cause of EMT in aging adults (29). Smoking COVID-19 patients showed a higher percentage of EMT, but were more enriched in the interferon signaling pathway, compared to non-smoking COVID-19 patients. Despite early reports to the opposite, there is mounting evidence that individuals with severe COVID-19 have a strong type I interferon response, as opposed to the delayed, potentially suppressed response observed early in infection (30). Through various pathways, a potent type I interferon response might increase hyperinflammation in the progression to severe COVID-19 (31). Insights into the therapeutic use of type I interferon in patients with MT will come from an improved knowledge of the functions of type I interferon at various stages of the disease and in patients who are non-smokers vs. smokers.

MT is involved in pulmonary fibrosis and vascular remodeling in the pathogenesis of IPF. Several triggers and pathways are associated with the EMT and EndMT (32). Archana et al. have shown that EndMT markers(N-cadherin, S100A4, and vimentin) are increased in the arterial layers (intima, media, and adventitia) of IPF patients (33). Similarly, during the EndMT process, active ECs express adhesion molecules, such as intercellular adhesion molecule-1 (*ICAM-1*) and vascular cell adhesion molecule-1 (*VCAM-1*), which enhance EndMT formation in our results. Moreover, ICAM-1 is also an adhesion molecule for another virus, such as human rhinovirus (34), influenza virus (35), and HIV (36). It is reasonable to speculate that with the activation of ICAM-1, the risk of associated secondary infection may also increase.

The mesenchymal cells we identified are divided into early and late stage. Compared to IPF, these cells are related to the expression of entry factors such as *BSG*, *CTSL*, and *FURIN*. Sohal et al. indicate that ILDs, especially IPF, have a higher risk of developing severe COVID-19 infection and post-COVID-19 interstitial pulmonary fibrosis. They found TGF-β1 and α-smooth muscle actin (myofibroblast marker) are in similar areas as COVID-19 markers. They suggest that myofibroblasts and surrounding tissue secrete growth factors which could further affect COVID-19 adhesion proteins/cofactors and post-COVID-19 interstitial pulmonary fibrosis (37). Our study confirms that entry factors are negatively correlated with early EndMT cell fraction and are positively correlated with fibroblasts. This suggests that the conversion of activated ECs to EndMT is linked to mesenchymal conversion of ECs in the early phases. Therefore, this provides a strategy for the early prevention of pulmonary fibrosis in COVID-19 patients.

Improvements in patient stratification and therapeutic approaches for lung fibrosis will be contingent on the capacity to reprogram EMT (38). EMT has been hypothesized as a source of myofibroblast also in SSc (39) and EMT-related pathways (40). Early EMT leads to activation fibrosis as a result of the downregulation and/or destruction of junctional components like *TAGLN*. The late EMT mesenchymal marker *COL3A1* increases along with the slow loss of *EPCAM*, a marker of epithelial cells (41). Late EMT has been classically associated with fibrosis in organs such as the kidneys, liver, and lungs. It is interesting to note that, in consistent with our data, the EMT status of primary tumors was not consistently associated with poor patient survival (38). Our study suggests that late EMT and invasive genes are almost independent, and early EMT is associated with invasive genes. The process of EndMT can also represent a therapeutic target in the early stages of the disease (42). Early, immature stress fibers are present in the early stages of EndMT. Late stages of EndMT, however, may be identified by matured stress fibers formed by microfilaments (43). The inflammatory leukocytes engaged in the early stages of the illness trigger the EndMT, which has also been discovered in lung fibrosis (44). Therefore, late EndMT could contribute to aggravating the pro-fibrotic signaling in lung fibrosis. Late EndMT, then, could contribute to exacerbating the pro-fibrotic TGF-β signaling in lung fibrosis. According to this principle, we chose *ACTA2* as the early marker and also MMP2 and *COL3A1* as the late markers. *ACTA2* was only transiently displayed in the early EndMT, but *MMP2* and *COL3A1* were subsequently upregulated through further remodeling (45).

It is important to note that our study has some limitations:1. First, we not count whole organ MT because this included all the up-regulation of the entry factor. This data will be included in our subsequent studies. Second, no in vitro or in vivo animal experiments were performed to validate the key genes. Third, we did not validate COVID-19 patient samples. Fourth, no SARS-CoV-2 positive cells were extracted for further analysis. Finally, the correlation between MT and entry factor was inadequate and required further exploration.

Conclusion

In conclusion, for the first time, we have analyzed ECs as well as epithelial MT subpopulations in COVID-19 patients, establishing the correlation between their MT subpopulations with irreversible myofibroblasts. However, although entry factors are also highly expressed in IFP, it is not associated with the MT of IPF. Thus, we further explored the mesenchymal-associated cluster's genes and found that some genes are expressed both in COVID-19 patients and IPF patients. This suggests potent targets that could reverse MT in COVID-19 and IPF.

Data availability statement

The original contributions presented in the study are included in the article/Supplementary Material. Further inquiries can be directed to the corresponding authors.

Author contributions

LZ, XZ, and DL conceived the topic for this study. LZ, XZ, MZ, and XT performed single-cell RNA sequencing. LZ, XZ, XW, SL, RY, MZ, YX, XT, CT, and DL contributed to the writing and revising of the manuscript. DL, and CT critically revised the manuscript. All authors listed have read and approved the manuscript before submission.

Funding

Postdoctoral Funding of the Personnel Office-Special Fund for Postdoctoral New Crown Epidemic Prevention and Control (0040204153344), National Science Foundation for Young Scientists of China (81900065), Project supported by the Natural Science Foundation of Sichuan province (2022NSFSC1394), the Youth Innovation Project of Sichuan Medical Association (Q21018), and Chengdu Medical Research Projects (2022516).

Acknowledgments

The authors thank Dr. Jianming Zeng (University of Macau), and all the members of his bioinformatics team, biotrainee, for generously sharing their experience and codes.

Conflict of interest

Author MZ is employed by the Oncology Bussiness Department, Novogene Co., Ltd, Beijing, China.

The remaining authors declare that the research was conducted in the absence of any commercial or financial relationships that could be construed as a potential conflict of interest.

Publisher's note

Supplementary material

The Supplementary Material for this article can be found online at: https://www.frontiersin.org/articles/10.3389/fimmu.2022.976512/full#supplementary-material

References

1. Jacob A, Vedaie M, Roberts DA, Thomas DC, Villacorta-Martin C, Alysandratos KD, et al. Derivation of self-renewing lung alveolar epithelial type ii cells from human pluripotent stem cells. *Nat Protoc* (2019) 14(12):3303–32. doi: 10.1038/s41596-019-0220-0

2. Merad M, Martin JC. Pathological inflammation in patients with covid-19: A key role for monocytes and macrophages. *Nat Rev Immunol* (2020) 20(6):355–62. doi: 10.1038/s41577-020-0331-4

3. Bost P, Giladi A, Liu Y, Bendjelal Y, Xu G, David E, et al. Host-viral infection maps reveal signatures of severe covid-19 patients. *Cell* (2020) 181(7):1475–88.e12. doi: 10.1016/j.cell.2020.05.006

4. Kim KK, Kugler MC, Wolters PJ, Robillard L, Galvez MG, Brumwell AN, et al. Alveolar epithelial cell mesenchymal transition develops in vivo during pulmonary fibrosis and is regulated by the extracellular matrix. *Proc Natl Acad Sci United States America* (2006) 103(35):13180–5. doi: 10.1073/pnas.0605669103

5. Willis BC, Liebler JM, Luby-Phelps K, Nicholson AG, Crandall ED, Du Bois RM, et al. Induction of epithelial-mesenchymal transition in alveolar epithelial cells by transforming growth factor-B1: Potential role in idiopathic pulmonary fibrosis. *Am J Pathol* (2005) 166(5):1321–32. doi: 10.1016/S0002-9440(10)62351-6

6. Lamouille S, Xu J, Derynck R. Molecular mechanisms of epithelial–mesenchymal transition. *Nat Rev Mol Cell Biol* (2014) 15(3):178–96. doi: 10.1038/nrm3758

7. Legein B, Temmerman L, Biessen EA, Lutgens E. Inflammation and immune system interactions in atherosclerosis. *Cell Mol Life Sci* (2013) 70(20):3847–69. doi: 10.1007/s00018-013-1289-1

8. Fang S, Guo H, Cheng Y, Zhou Z, Zhang W, Han B, et al. Circhectd1 promotes the silica-induced pulmonary endothelial–mesenchymal transition *via* Hectd1. *Cell Death Dis* (2018) 9(3):1–16. doi: 10.1038/s41419-018-0432-1

9. Hashimoto N, Phan SH, Imaizumi K, Matsuo M, Nakashima H, Kawabe T, et al. Endothelial–mesenchymal transition in bleomycin-induced pulmonary fibrosis. *Am J Respir Cell Mol Biol* (2010) 43(2):161–72. doi: 10.1165/rcmb.2009-0031OC

10. Dejana E, Hirschi KK, Simons M. The molecular basis of endothelial cell plasticity. *Nat Commun* (2017) 8(1):1–11. doi: 10.1038/ncomms14361

11. Eapen MS, Lu W, Gaikwad AV, Bhattarai P, Chia C, Hardikar A, et al. Endothelial to mesenchymal transition: A precursor to post-Covid-19 interstitial pulmonary fibrosis and vascular obliteration? *Eur Respir J* (2020) 56(4):2003167. doi: 10.1183/13993003.03167-2020

12. Kong D, Li Y, Wang Z, Sarkar FH. Cancer stem cells and epithelial-to-Mesenchymal transition (Emt)-phenotypic cells: Are they cousins or twins? *Cancers* (2011) 3(1):716–29. doi: 10.3390/cancers30100716

13. Singh M, Yelle N, Venugopal C, Singh SK. Emt: Mechanisms and therapeutic implications. *Pharmacol Ther* (2018) 182:80–94. doi: 10.1016/j.pharmthera.2017.08.009

14. Melms JC, Biermann J, Huang H, Wang Y, Nair A, Tagore S, et al. A molecular single-cell lung atlas of lethal covid-19. *Nature* (2021) 595(7865):114–9. doi: 10.1038/s41586-021-03569-1

15. Delorey TM, Ziegler CGK, Heimberg G, Normand R, Yang Y, Segerstolpe Å, et al. Covid-19 tissue atlases reveal sars-Cov-2 pathology and cellular targets. *Nature* (2021) 595(7865):107–13. doi: 10.1038/s41586-021-03570-8

16. Xu G, Liu Y, Liao M, Gou J, Wang X, Yuan J, et al. Persistent viral activity, cytokine storm, and lung fibrosis in a case of severe covid-19. *Clin Transl Med* (2020) 10(7):e224. doi: 10.1002/ctm2.224

17. Wang A, Chiou J, Poirion OB, Buchanan J, Valdez MJ, Verheyden JM, et al. Single-cell multiomic profiling of human lungs reveals cell-Type-Specific and age-dynamic control of sars-Cov2 host genes. *Elife* (2020) 9:e62522. doi: 10.7554/eLife.62522

18. Adams TS, Schupp JC, Poli S, Ayaub EA, Neumark N, Ahangari F, et al. Single-cell rna-seq reveals ectopic and aberrant lung-resident cell populations in idiopathic pulmonary fibrosis. *Sci Adv* (2020) 6(28):eaba1983. doi: 10.1126/sciadv.aba1983

19. Habermann AC, Gutierrez AJ, Bui LT, Yahn SL, Winters NI, Calvi CL, et al. Single-cell rna sequencing reveals profibrotic roles of distinct epithelial and mesenchymal lineages in pulmonary fibrosis. *Sci Adv* (2020) 6(28):eaba1972. doi: 10.1126/sciadv.aba1972

20. Kim S, Herazo-Maya JD, Kang DD, Juan-Guardela BM, Tedrow J, Martinez FJ, et al. Integrative phenotyping framework (Ipf): Integrative clustering of multiple omics data identifies novel lung disease subphenotypes. *BMC Genomics* (2015) 16:924. doi: 10.1186/s12864-015-2170-4

21. Stuart T, Butler A, Hoffman P, Hafemeister C, Papalexi E, Mauck WM, et al. Comprehensive integration of single-cell data. *Cell* (2019) 177(7):1888–1902.e21. doi: 10.1016/j.cell.2019.05.031

22. Korsunsky I, Millard N, Fan J, Slowikowski K, Zhang F, Wei K, et al. Fast, sensitive and accurate integration of single-cell data with harmony. *Nat Methods* (2019) 16(12):1289–96. doi: 10.1038/s41592-019-0619-0

23. Yu G, Wang L-G, Han Y, He Q-Y. Clusterprofiler: An r package for comparing biological themes among gene clusters. *OMICS* (2012) 16(5):284–7. doi: 10.1089/omi.2011.0118

24. Cao J, Spielmann M, Qiu X, Huang X, Ibrahim DM, Hill AJ, et al. The single-cell transcriptional landscape of mammalian organogenesis. *Nature* (2019) 566(7745):496–502. doi: 10.1038/s41586-019-0969-x

25. Qiu X, Mao Q, Tang Y, Wang L, Chawla R, Pliner HA, et al. Reversed graph embedding resolves complex single-cell trajectories. *Nat Methods* (2017) 14 (10):979–82. doi: 10.1038/nmeth.4402

26. Aul DR, Gates DJ, Draper DA, Dunleavy DA, Ruickbie DS, Meredith DH, et al. Complications after discharge with covid-19 infection and risk factors associated with development of post-covid pulmonary fibrosis. *Respir Med* (2021) 188:106602. doi: 10.1016/j.rmed.2021.106602

27. Marvisi M, Ferrozzi F, Balzarini L, Mancini C, Ramponi S, Uccelli M. First report on clinical and radiological features of covid-19 pneumonitis in a Caucasian population: Factors predicting fibrotic evolution. *Int J Infect Dis* (2020) 99:485–8. doi: 10.1016/j.ijid.2020.08.054

28. McGroder CF, Zhang D, Choudhury MA, Salvatore MM, D'Souza BM, Hoffman EA, et al. Pulmonary fibrosis 4 months after covid-19 is associated with severity of illness and blood leucocyte telomere length. *Thorax* (2021) 76(12):1242–5. doi: 10.1136/thoraxjnl-2021-217031

29. Pawelec G. Aging as an inflammatory disease and possible reversal strategies. *J Allergy Clin Immunol* (2020) 145(5):1355–6. doi: 10.1016/j.jaci.2020.02.022

30. Lee JS, Shin EC. The type I interferon response in covid-19: Implications for treatment. *Nat Rev Immunol* (2020) 20(10):585–6. doi: 10.1038/s41577-020-00429-3

31. Kim YM, Shin EC. Type I and iii interferon responses in sars-Cov-2 infection. *Exp Mol Med* (2021) 53(5):750–60. doi: 10.1038/s12276-021-00592-0

32. Gaikwad AV, Eapen MS, McAlinden KD, Chia C, Larby J, Myers S, et al. Endothelial to mesenchymal transition (Endmt) and vascular remodeling in pulmonary hypertension and idiopathic pulmonary fibrosis. *Expert Rev Respir Med* (2020) 14(10):1027–43. doi: 10.1080/17476348.2020.1795832

33. Gaikwad AV, Lu W, Dey S, Bhattarai P, Chia C, Larby J, et al. Vascular remodelling in idiopathic pulmonary fibrosis patients and its detrimental effect on lung physiology: Potential role of endothelial-to-Mesenchymal transition. *ERJ Open Res* (2022) 8(1):00571–2021. doi: 10.1183/23120541.00571-2021

34. Atto B, Eapen MS, Sharma P, Frey U, Ammit AJ, Markos J, et al. New therapeutic targets for the prevention of infectious acute exacerbations of copd: Role of epithelial adhesion molecules and inflammatory pathways. *Clin Sci (Lond)* (2019) 133(14):1663–703. doi: 10.1042/CS20181009

35. Othumpangat S, Noti JD, McMillen CM, Beezhold DH. Icam-1 regulates the survival of influenza virus in lung epithelial cells during the early stages of infection. *Virology* (2016) 487:85–94. doi: 10.1016/j.virol.2015.10.005

36. Yu X, Shang H, Jiang Y. Icam-1 in hiv infection and underlying mechanisms. *Cytokine* (2020) 125:154830. doi: 10.1016/j.cyto.2019.154830

37. Lu W, Eapen MS, Singhera GK, Markos J, Haug G, Chia C, et al. Angiotensin-converting enzyme 2 (Ace2), transmembrane peptidase serine 2 (Tmprss2), and furin expression increases in the lungs of patients with idiopathic pulmonary fibrosis (Ipf) and lymphangioleiomyomatosis (Lam): Implications for sars-Cov-2 (Covid-19) infections. *J Clin Med* (2022) 11(3):777. doi: 10.3390/jcm11030777

38. Mandal S, Tejaswi T, Janivara R, Srikrishnan S, Thakur P, Sahoo S, et al. Transcriptomic-based quantification of the epithelial-Hybrid-Mesenchymal spectrum across biological contexts. *Biomolecules* (2021) 12(1). doi: 10.3390/biom12010029

39. Nikitorowicz-Buniak J, Denton CP, Abraham D. Stratton r. partially evoked epithelial-mesenchymal transition (Emt) is associated with increased tgfβ signaling within lesional scleroderma skin. *PloS One* (2015) 10(7):e0134092. doi: 10.1371/journal.pone.0134092

40. Lee DW, Lee WJ, Cho J, Yun CO, Roh H, Chang HP, et al. Inhibition of wnt signaling pathway suppresses radiation-induced dermal fibrosis. *Sci Rep* (2020) 10 (1):13594. doi: 10.1038/s41598-020-70243-3

41. Zeisberg M, Neilson EG. Biomarkers for epithelial-mesenchymal transitions. *J Clin Invest* (2009) 119(6):1429–37. doi: 10.1172/jci36183

42. Mendoza FA, Piera-Velazquez S, Farber JL, Feghali-Bostwick C, Jiménez SA. Endothelial cells expressing endothelial and mesenchymal cell gene products in lung tissue from patients with systemic sclerosis-associated interstitial lung disease. *Arthritis Rheumatol* (2016) 68(1):210–7. doi: 10.1002/art.39421

43. Ciszewski WM, Wawro ME, Sacewicz-Hofman I, Sobierajska K. Cytoskeleton reorganization in endmt-the role in cancer and fibrotic diseases. *Int J Mol Sci* (2021) 22(21). doi: 10.3390/ijms222111607

44. Thuan DTB, Zayed H, Eid AH, Abou-Saleh H, Nasrallah GK, Mangoni AA, et al. A potential link between oxidative stress and endothelial-to-Mesenchymal transition in systemic sclerosis. *Front Immunol* (2018) 9:1985. doi: 10.3389/fimmu.2018.01985

45. Zhang S, Li Y, Huang X, Liu K, Wang QD, Chen AF, et al. Seamless genetic recording of transiently activated mesenchymal gene expression in endothelial cells during cardiac fibrosis. *Circulation* (2021) 144(25):2004–20. doi: 10.1161/circulationaha.121.055417

frontiers | Frontiers in Immunology

ORIGINAL RESEARCH
published: 19 July 2022
doi: 10.3389/fimmu.2022.963627

The SARS-CoV-2 Nucleoprotein Induces Innate Memory in Human Monocytes

Patricia Urbán[1], *Paola Italiani*[2,3], *Diana Boraschi*[2,3,4] *and Sabrina Gioria*[1]*

[1] European Commission, Joint Research Centre (JRC), Ispra, Italy, [2] Institute of Protein Biochemistry and Cell Biology (IBBC), National Research Council (CNR), Napoli, Italy, [3] Stazione Zoologica Anton Dohrn, Napoli, Italy, [4] Shenzhen Institute of Advanced Technologies (SIAT), Chinese Academy of Sciences (CAS), Shenzhen, China

The interaction of SARS-CoV-2 with the human immune system is at the basis of the positive or negative outcome of the infection. Monocytes and macrophages, which are major innate immune/inflammatory effector cells, are not directly infected by SARS-CoV-2, however they can react to the virus and mount a strong reaction. Whether this first interaction and reaction may bias innate reactivity to re-challenge, a phenomenon known as innate memory, is currently unexplored and may be part of the long-term sequelae of COVID-19. Here, we have tested the capacity of SARS-CoV-2 and some of its proteins to induce innate memory in human monocytes *in vitro*. Our preliminary results show that the Spike protein subunits S1 and S2 and the entire heat-inactivated virus have no substantial effect. Conversely, monocytes pre-exposed to the nucleocapsid N protein react to subsequent viral or bacterial challenges with an increased production of anti-inflammatory IL-1Ra, a response profile suggesting a milder response to new infections.

Keywords: SARS-CoV-2, nucleoprotein, innate immunity, innate memory, monocytes, cytokines

OPEN ACCESS

Edited by:
Cinzia Fionda,
Sapienza University of Rome, Italy

Reviewed by:
Shanze Chen,
Jinan University, China
Detlef Neumann,
Hannover Medical School, Germany

***Correspondence:**
Sabrina Gioria
sabrina.gioria@ec.europa.eu

Specialty section:
This article was submitted to Cytokines and Soluble Mediators in Immunity, a section of the journal Frontiers in Immunology

Received: *07 June 2022*
Accepted: *15 June 2022*
Published: *19 July 2022*

Citation:
Urbán P, Italiani P, Boraschi D and Gioria S (2022) The SARS-CoV-2 Nucleoprotein Induces Innate Memory in Human Monocytes. Front. Immunol. 13:963627. doi: 10.3389/fimmu.2022.963627

INTRODUCTION

The novel coronavirus SARS-CoV-2, which suddenly emerged in December 2019, is still haunting mankind and has affected not only the healthcare systems but also the global socio-economic balances (1–3). COVID-19, the disease caused by the virus, was designated as a global pandemic by the World Health Organization, with more than 534 million confirmed cases and over 6.3 million confirmed deaths, as of June 2022 (4). Taking advantage of the recent progress in virology, molecular biology and pharmacology, and thanks to an amazing effort of the international scientific community, both in academia and industry, and a huge resource allocation, we were rapidly able to dissect and understand the SARS-CoV-2 structure, functions, lifecycle, and pathological characteristics (5–9). This led in a very short time to vaccine development and to several pharmacological approaches to treat or reduce the severity of patients' symptoms (2, 10, 11).

Despite the rapid and huge progress in understanding the interactions between the virus and the human immune system, much is still unknown to explain/predict the variability of immune responses that determines different susceptibility to severe effects, reactivity to re-infection, or response to vaccination.

Specific antiviral immunity is mainly based on the development of neutralizing antibodies and cytotoxic CD8+ T cells, while innate immune reactions encompass the activation of inflammatory

protective responses triggered by recognition of viral patterns by membrane and cytoplasmic pattern-recognition receptors (12). While vaccination strategies are currently based on the generation of specific anti-viral immune memory, much less emphasis has been dedicated to harnessing the protective potential of innate immunity and its memory capacity.

The concept of innate immune memory, i.e., a change in the non-specific reactivity to challenges of innate immune cells previously exposed to various stimuli, is well known in plants, invertebrates and also in vertebrates (13–15). Thus, it can be hypothesized that innate memory, induced by previous exposure to infections or other challenges (including vaccination), may participate to the effectiveness of subsequent defensive innate responses in a personalized fashion, which is dependent on individual history of pathogen/antigen exposure: the "immunobiography" (16).

While abundant information is available on the specific functions and kinetics of the adaptive immune response to SARS-CoV-2 (17–19), less is established regarding the balance between protective and detrimental effects of innate immune responses in COVID-19. A general increase in the circulating levels of inflammatory cytokines has been observed (possibly secondary to barrier disruption and release of bacterial products) in parallel to downregulation of myeloid cells' markers and function (20). There is clear evidence that the variability in innate immune system components is a main contributor to the heterogeneous disease course observed for COVID-19 (20–22) and in the response to vaccination (23). Thus, it is fundamental to understand if and how interaction of innate cells with SARS-CoV-2 induces an innate memory, and whether such memory may contribute to future protection or to post-infection pathologies, as suggested by epigenetic studies (24).

Here, we provide preliminary evidence that the SARS-CoV-2 nucleocapsid protein N, as opposed to other viral components, can induce innate memory in human primary monocytes in culture. This memory is limited to a significant increase in the production of the anti-inflammatory cytokine IL-1Ra in response challenges, suggesting a less inflammatory secondary reactivity. On this basis, we hypothesize that innate memory to viral components may contribute to the overall response to subsequent challenges (viral or bacterial infections or re-infections), including response to vaccination. The large inter-individual variability suggests the needs for a personalized assessment, in order to predict the features of innate/inflammatory reactivity to future challenges in previously infected individuals.

MATERIALS AND METHODS

Selection of Stimuli

The human recombinant coronavirus SARS-CoV-2 nucleocapsid protein (N; ab272107) was expressed in *E. coli* with a C-terminal His tag. Expression in *E. coli* produces a non-glycosylated protein, similar to the "natural" protein. Human recombinant Spike glycoprotein subunit 1 (S1; ab 272105) and subunit 2 (S2; ab272106) were expressed in HEK 293 cells as chimeras with a C-terminal Fc tag. Recombinant proteins were purchased from Abcam (Milan, Italy). LPS contamination was checked in-house with the chromo-genic LAL assay Pyros Kinetix® Flex (Associates of Cape Cod, Inc., East Falmouth, MA, USA). The endotoxin contamination was 353 EU/mg for N, 26 EU/mg for S1 and 7 EU/mg for S2. Heat-inactivated SARS-CoV-2 (ATCC VR-1986HK) was obtained from LGC standards (Milan, Italy); LPS from E. coli O55:B5 was from Sigma Aldrich® (Merck KGaA, St. Louis, MO, USA); the TLR7/8 agonist Resiquimod (R848; cat. tlrl-rR848, purity ≥ 95% by UHPLC) was purchased from InvivoGen (San Diego, CA, USA). R848 was devoid of TLR2 (lipoproteins) and TLR4 agonist activity, tested on HEK-Blue TLR2 and TLR4 cells.

Concentration of viral stimuli to be used in culture was based on preliminary dose-response experiments, viability assessment and LAL results, while concentrations of reference stimuli (LPS and R848) were selected based on previous experience and *ad hoc* dose-response assessment (data not shown). Thus, the same concentration of 1 μg/mL was selected for N, S1 and S2, which corresponded to an endotoxin contamination of 0.35, 0.03 and 0.01 EU/mL. Since 1 EU roughly corresponds to 100 pg of LPS, the LPS contamination of N was estimated around 35 pg/mL in the assay, a concentration unable to induce monocyte activation in our hands. For the whole heat-inactivated virus, $5x10^5$ RNA genome copies were used as stimulus in culture, based on preliminary dose-response experiments (data not shown).

Human Monocyte Isolation

Blood was obtained from anonymized healthy SARS-CoV-2 negative non-vaccinated donors, upon informed consent and in agreement with the Declaration of Helsinki. The protocol was approved by the Regional Ethics Committee for Clinical Experimentation of the Tuscany Region (Ethics Committee Register n. 14,914 of May 16, 2019). Monocytes were isolated by CD14 positive selection with magnetic microbeads (Miltenyi Biotec, Bergisch Gladbach, Germany) from peripheral blood mononuclear cells (PBMC), obtained by Ficoll-Paque gradient density separation (GE Healthcare, Bio-Sciences AB, Uppsala, Sweden). Monocyte preparations used in the experiments were > 95% viable and > 95% pure (assessed by trypan blue exclusion and cytosmears).

Monocytes were cultured in culture medium (RPMI 1640 + Glutamax-I; GIBCO by Life Technologies, Paisley, UK) supplemented with 50 μg/mL gentamicin sulfate (GIBCO) and 5% heat-inactivated human AB serum (Sigma-Aldrich). Cells ($1x10^5$) were seeded in a final volume of 100 μL in 96-wells flat bottom plates (Corning® Costar®; Corning Inc. Life Sciences, Oneonta, NY, USA) at 37°C in moist air with 5% CO_2. Monocyte stimulation was performed after overnight resting.

Human Monocyte Activation and Induction of Innate Memory

For assessing the primary response to stimulation, monocytes were exposed for 24 h to culture medium alone (medium/negative control) or containing LPS (positive bacterial control, 1 ng/mL), R848 (positive viral control, 0.5 μg/mL),

heat-inactivated SARS-CoV-2 virus (5x10^5 RNA copies), N (1 μg/mL), S1 (1 μg/mL) or S2 (1 μg/mL). Cell viability, measured both as lack of LDH release (LDH-Cytotoxicity Colorimetric Assay Kit; BioVision, Inc., Milpitas, CA, USA) and as metabolic activity (reduction of MTT to formazan) (25) was unaffected by treatment (data not shown). At the end of the exposure time, all supernatants were collected. For memory experiments, cells were then washed and cultured with fresh culture medium for 7 additional days (one medium change after 4 days). During this period, after the activation induced by previous stimulation subsides, cells return to their baseline status (as determined by evaluation of inflammation-related cytokines in the supernatant; data not shown). At the end of the resting phase, the supernatant was collected and cells were challenged for 24 h with fresh medium alone or containing 5 ng/mL LPS, 2.5 μg/mL R848, or 5 μg/mL N (i.e., a 5x higher concentration than in the primary stimulation), according to the standard protocols for *in vitro* innate memory assessment (14, 15). All supernatants (after the first stimulation, after the resting phase and after the challenge phase) were frozen at -80°C for subsequent cytokine analysis. By visual inspection, cell viability and cell number did not substantially change in response to the different treatments.

Cytokine Analysis by Multiplex ELISA

Samples were tested for the presence of cytokines and chemokines by commercial ELISA-based microarrays that simultaneously measure multiple proteins in a single sample aliquot. Multiplex Bio-Plex Pro™ Human Cytokine 8-plex Assay (cat. M50000007A) was used for assessing the production of IL-2, IL-4, IL-6, IL-8, IL-10, TNFα, IFN-γ, and GM-CSF. Singleplex for IL-1β (cat. 171B5001M) and IL-1Ra (cat. 171B5002M) were also included. Samples were run according to the manufacturer's instructions. Cytokines were analyzed with the Bio-Plex200 System using the Bio-Plex Manager™ software, and data were analyzed by the Bio-Plex Data Pro™ software, using five-parametric curve fitting. For each cytokine, assay ranges and LOD were provided by the manufacturer. All reagents and instruments, including Washing Station and Shaker Incubator, were from BIO-RAD Laboratories, Inc. (Hercules, CA, USA). Two repeated measurements were made for each marker for each donor. The symbols reported in the figures are the averages of such repeated measurements.

Statistical Analysis

Data were analyzed using the GraphPad Prism 6.01 software (GraphPad Inc., La Jolla, CA, USA). For cytokine production, results are presented as ng produced cytokine/10^6 plated monocytes. Results from individual donors are reported as mean values of 2-3 replicates (each tested with technical duplicates in ELISA). Average values of individual donors' data are reported as light grey columns. Statistical significance of differences is indicated by *p* values, calculated using one way ANOVA and Dunnett's Multiple Comparison.

RESULTS

Primary Response of Human Monocytes to Inactivated SARS-CoV-2 or Its Components

The primary response of human monocytes to different SARS-CoV-2 stimuli was assessed after exposure *in vitro* for 24 h. Monocytes are key innate immune cells responsible of inflammatory defensive responses, and their activation was evaluated in terms of production of four innate cytokines, the inflammatory factors TNFα and IL-6, and the anti-inflammatory cytokines IL-10 and IL-1Ra (**Figure 1**). As positive control, cells were exposed to LPS or R848, potent activators of human monocyte innate/inflammatory responses that mimic bacterial and viral challenges, respectively. The concentrations of LPS (1 ng/mL) and R848 (0.5 μg/mL) were selected in order to induce a measurable but not maximal response (data not shown). The viral agents used were the heat-inactivated SARS-CoV-2 virus (5x10^5 RNA genomic copies/well; 5:1 vs. monocytes), the nucleocapsid protein N (1 μg/mL), the S1 subunit of the Spike protein (responsible for viral binding to target cells; 1 μg/mL) and the S2 subunit of the Spike protein (responsible for viral entry in target cells; 1 μg/mL). The endotoxin contamination of the recombinant viral proteins was below monocyte activation

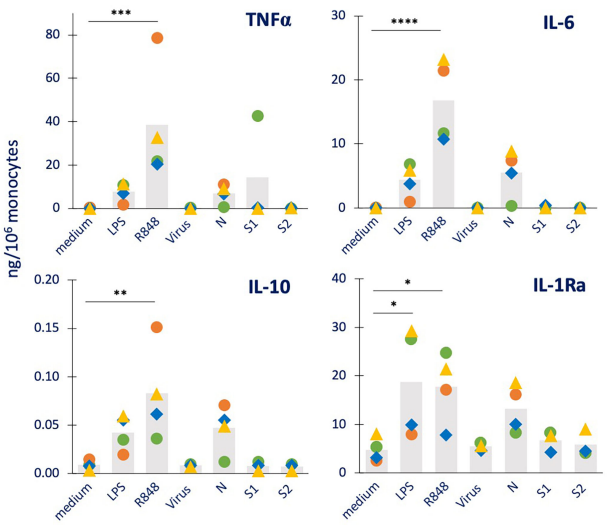

FIGURE 1 | Primary innate immune primary response to inactivated SARS-CoV-2 or its proteins in human monocytes. Human monocytes isolated from blood of four individual donors (green, red, blue, and yellow symbols) were cultured for 24 h in culture medium alone or containing the inactivated SARS-CoV-2 virus (5 x10^5 copies), or the viral proteins N, S1, S2 (all at 1 μg/mL). The production of TNFα (upper left), IL-6 (upper right), IL-10 (lower left) and IL-1Ra (lower right) was measured in the 24 h supernatants by ELISA. Medium alone was used as baseline value, LPS (1 ng/mL) and R848 (0.5 μg/mL) were used as positive controls. Data are presented as individual donors' values (colored symbols) and as mean of the individual values (gray columns). Statistical significance: * p <0.05; ** p <0.01; *** p <0.01; **** p <0.0001.

threshold (see Materials and Methods). Monocytes from four SARS-CoV-2 negative non-vaccinated donors were tested.

As shown in **Figure 1**, both LPS and R848 were able to induce a substantial production of the inflammatory factors TNFα and IL-6 and of the anti-inflammatory cytokine IL-10, although with a high inter-individual variability (which in some cases did not allow for reaching statistical significance). For the other anti-inflammatory cytokine IL-1Ra, as expected, a measurable constitutive production was evident in unstimulated cells, which was increased by exposure to LPS or R848. Among the viral agents, only N showed the capacity to stimulate monocytes (in 2/3 of 4 donors), whereas the inactivated whole virus and the two Spike proteins were essentially inactive.

The production by monocytes of other inflammation-related factors was also examined. Data for the inflammatory cytokine IL-1β, the chemokine IL-8, the immune interferon IFN-γ and the growth factor GM-CSF are reported in **Supplementary Figure S1**, while the production of the T cell cytokines IL-2 and IL-4 was undetectable (data not shown). Again, N was the only viral factor able to activate monocyte responses (evident for IL-8 and GM-CSF production in 3 out of 4 donors), which were in the same range as those induced by the positive controls LPS and R848. These results partially confirm a previous report, showing that N could induce the production of IL-6 and IL-10 in human monocytes, but not TNFα and IL-1β (26). At variance with the same study, here we could not see any effect by S1. The differences in the recombinant protein constructs and in the exposure time (1 *vs.* 3-5 days), and the fact that the endotoxin contamination was not assessed in the other study may explain the different result.

Secondary Memory Response of Human Monocytes Primed With Inactivated SARS-CoV-2 or Its Components

After the primary response (**Figures 1** and **S1**), cells were washed and cultured for 7 additional days in fresh culture medium to allow extinction of activation and return to baseline. The culture medium was refreshed after 4 days. The extinction of cell activation was confirmed by examining the production of cytokines released in the culture medium at the end of the resting period (representing the cytokine release in the last 3 days of resting) (data not shown). After the extinction period, cells were either exposed to medium alone (control) or challenged with 5x higher concentration of LPS (representing a bacterial challenge) or R848 (representing a viral challenge), in order to assess the development of a memory response able to react to more severe challenges. LPS priming was used as control of LPS challenge, while R848 priming was used as control of R848 challenge. As for the primary response, the memory response was assessed in terms of production of inflammatory and anti-inflammatory cytokines, and the results are reported in **Figures 2** and **3** for the major inflammatory (TNFα, IL-6) and anti-inflammatory (IL-10, IL-1Ra) cytokines.

As expected, LPS challenge of medium-primed cells showed a general induction of TNFα, IL-6 and IL-10 production, but no increase over the substantial baseline production of IL-1Ra (columns "medium" vs. "Control" in **Figure 2**). Although the

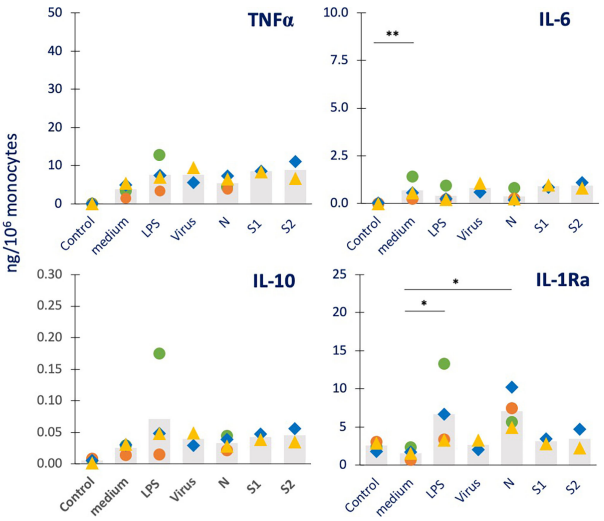

FIGURE 2 | Innate immune memory response to a bacterial challenge in human monocytes primed with inactivated SARS-CoV-2 or its proteins. Human monocytes isolated from blood of four individual donors (green, red, blue, and yellow symbols) were cultured for 24 h in culture medium alone (column "medium") or containing LPS (1 ng/mL, positive bacterial control, column "LPS"), the inactivated SARS-CoV-2 virus (5 x10^5 copies, column "virus"), N, S1, or S2 (all at 1 μg/mL; columns "N", "S1" and "S2"). Cells were then washed and rested for 7 days in the absence of stimuli, then challenged for 24 h in fresh medium alone (column "control") or containing 5 ng/mL LPS. The column "control" values from cells that received no challenge are included in each panel as "control" and encompasses the values from primed and unprimed cells that received no challenge, i.e., fresh medium alone. These values did not differ between primed and unprimed cells, confirming the return to baseline after the resting period. The production of TNFα (upper left), IL-6 (upper right), IL-10 (lower left) and IL-1Ra (lower right) was measured in the 24 h supernatants by ELISA. Data are presented as individual donors' values (colored symbols) and as mean of the individual values (grey columns). Statistical significance: * p <0.05; ** p <0.01.

increase did not always reach statistical significance on average, this was evident at the individual donor's level. LPS-primed cells did not show the development of a tolerance memory response (columns "LPS" *vs.* "medium") relative to the inflammatory cytokine TNFα, while this was small but detectable in 2/4 donors for IL-6, confirming the variability in the development of LPS tolerance already observed in other subjects (15, 27, 28). A tendency to a potentiated response could be observed in LPS-primed cells in terms of production of the anti-inflammatory factor IL-10 (although not reaching statistical significance), while a significant increase in IL-1Ra was evident. Priming with the inactivated virus did not have substantial effects on the response to the LPS challenge (columns "Virus" *vs.* "medium"). When examining the memory-inducing capacity of viral proteins, it was observed that the S1 and S2 subunits of the Spike protein had no memory-inducing activity (columns "S1" and "S2" *vs.* "medium"), similar to the inactivated virus. Priming with the nucleocapsid protein N, on the other hand, induced a significant and considerable potentiation of IL-1Ra production (columns "N" *vs.* "medium"). When examining the memory effects of virus or viral components on other innate immune factors induced by

the bacterial challenge LPS (**Supplementary Figure S2**), we observed that neither LPS nor virus/viral components had clear effects on the production of the inflammatory cytokine IL-1β, the chemokine IL-8, the immune interferon IFN-γ and the growth factor GM-CSF, again with inter-individual variability of response.

We also assessed the capacity of SARS-CoV-2 and its components to induce innate memory to a viral challenge, using R848 as prototypical viral agent (**Figure 3**). As a control, priming with R848 was included. The results show that unprimed monocytes respond to R848 challenge with a potent production of TNFα, IL-6 and IL-10 (in 3/4 donors), generally higher than that induced by the bacterial challenge. Conversely, the R848 challenge was completely inactive in modulating the constitutive production of IL-1Ra (columns "medium" *vs.* "Control"). Priming with R848 potentiated the secondary response to the R848 (columns "R848" *vs.* "medium") in all donors for TNFα, IL-6 and IL-1Ra, and in 2/4 donors for IL-10 (although the average increase reached statistical significance only for TNFα and IL-1Ra). Priming with the inactivated virus had little/no effect on the secondary response to the R848 virus-like challenge (columns "virus" *vs.* "medium"). Priming with the nucleocapsid protein N showed potentiation of the memory response to R848 in terms of IL-1Ra production (in all 4 donors), while having limited/no effect of the secondary production of TNFα, IL-6 and IL-10 (columns "N" *vs.* "medium"). The priming with the Spike protein subunits S1 and S2 showed no substantial variations relative to controls (columns "S1" and "S2" *vs.* "medium"). We have additionally examined other four cytokines (IL-1β, IL-8, IFN-γ, GM-CSF; **Supplementary Figure S3**). All four factors are produced by medium-primed cells in response to R848 (columns "medium" *vs.* "Control"). While the production of IL-8 was never significantly modified by priming with any agent (upper right panel), priming with R848 potentiates the production of IL-1β, IFN-γ and GM-CSF (columns "R848" *vs.* "medium" in the left and lower right panels). As in other cases, priming with the inactivated virus had no memory effect (columns "Virus" *vs.* "medium"). Priming with N showed a potentiation of the response to R848 in terms of IL-1β production in all donors and GM-CSF in 3/4 donors (columns "N" *vs.* "medium").

Eventually, we investigated the possibility that exposure to N could induce a memory response in previously primed cells. Thus, we have measured the production of cytokines in response to N (5 μg/mL) in monocytes previously primed with medium alone or containing LPS (1 ng/mL), R848 (0.5 μg/mL) or N (1 μg/mL). The data in **Figure 4** show that challenge with N could induce a significant production of TNFα, and measurable levels of IL-6, IL-10, IL-1β, IL-8 and GM-CSF in unprimed cells (of 3/4 donors), while unable to increase the constitutive production of IL-1Ra and IFN-γ (columns "medium"). None of the priming agents used (LPS, R848, N) was able to induce a memory that substantially changed the secondary response (although with strong inter-individual variability), except in the case of IL-1Ra, whose production in response to challenge with N was significantly increased in cells primed with LPS, R848 or N.

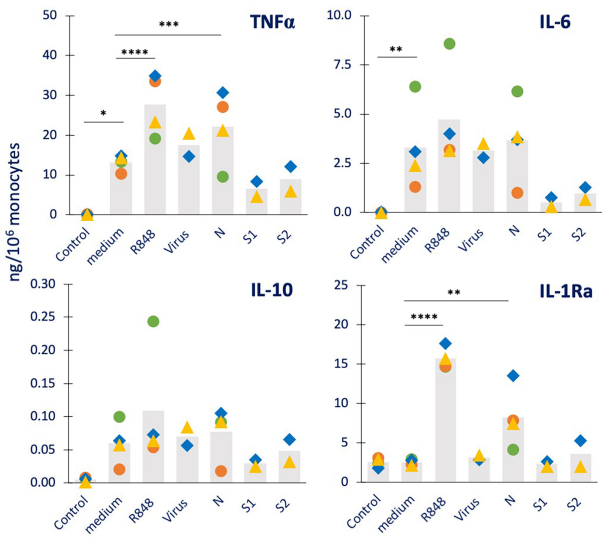

FIGURE 3 | Innate immune memory response to a viral challenge in human monocytes primed with inactivated SARS-CoV-2 or its proteins. Human monocytes isolated from blood of four individual donors (green, red, blue, and yellow symbols) were cultured for 24 h in culture medium alone or containing R848 (0.5 μg/mL, positive viral control), the inactivated SARS-CoV-2 virus (5 x10^5 copies), or the viral proteins N, S1, and S2 (all at 1 μg/mL). Cells were then washed and rested for 7 days in the absence of stimuli, then challenged for 24 h in fresh medium alone or containing 2.5 μg/mL R848. The production of TNFα (upper left), IL-6 (upper right), IL-10 (lower left) and IL-1Ra (lower right) was measured in the 24 h supernatants by ELISA. The values from cells that received no challenge are included in each panel as "control" and encompass the values obtained from primed and unprimed cells (which did not differ, confirming the return to baseline after the resting period). Data are presented as individual donors' values (colored symbols) and as mean of the individual values (gray columns). Statistical significance: * p <0.05; ** p <0.01; *** p < 0.001; **** p <0.0001.

DISCUSSION AND CONCLUSIONS

This study provides initial evidence that the major SARS-CoV-2 structural nucleocapsid (N) protein has the ability to induce an innate memory that changes the monocyte response profile upon re-challenge. It should be noted that these results are preliminary, since only cytokine production was examined, and their interpretation is likewise limited, since only four non-vaccinated donors are included.

Several studies have pointed to a possible role of innate memory, induced by live attenuated vaccines such as BCG, for preventing the severe effects of SARS-CoV-2 infection (29, 30). On the other hand, the innate immune/memory profile of monocytes/macrophages from convalescent or vaccinated subjects revealed that both the whole infective virus and the Spike protein encoding vaccine are able to induce a transcriptional and epigenetic reprogramming suggestive of establishment of innate memory (19, 23, 24). Notably, *in vitro* challenge of blood leukocytes from convalescent individuals showed an increased production of the inflammatory/activating cytokines IL-1β and IL-6, based on an extensive

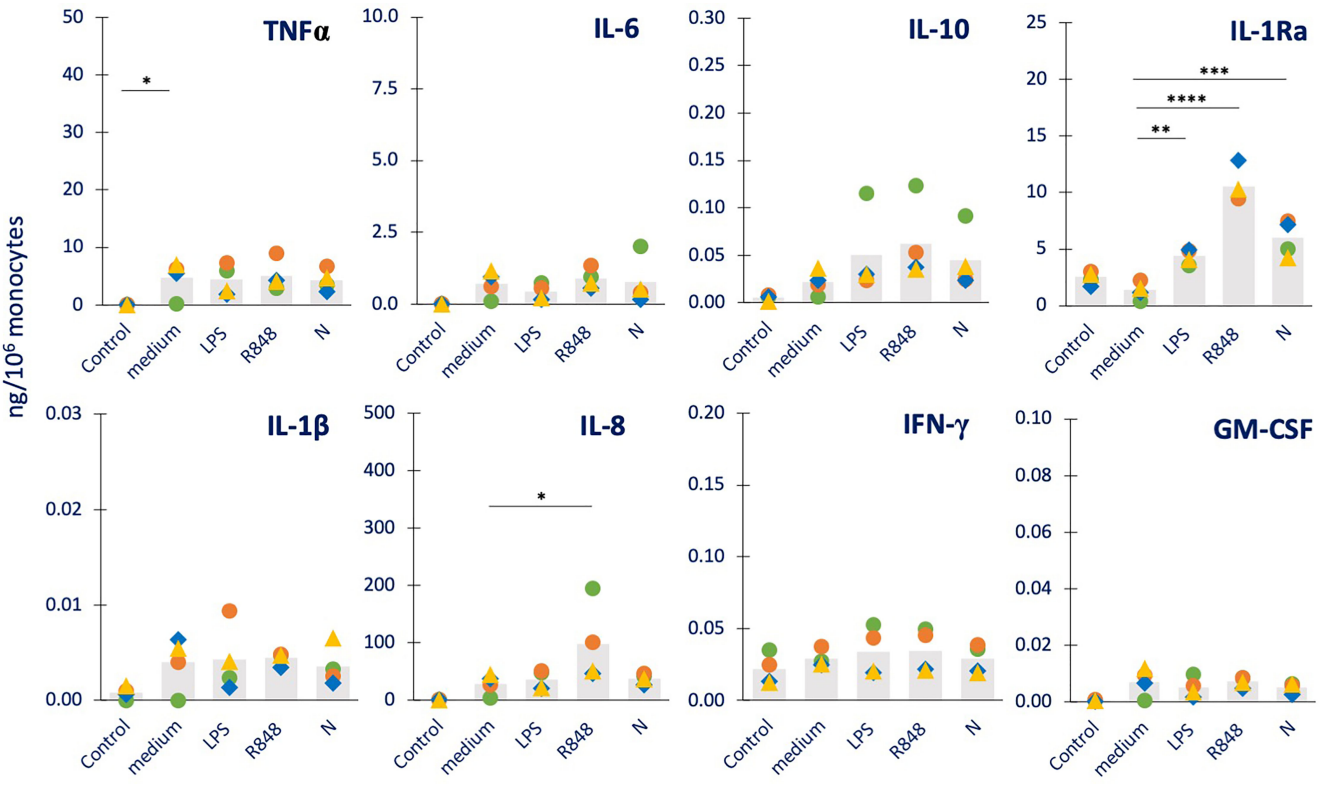

FIGURE 4 | Innate immune memory response to a challenge with the N protein in human monocytes primed with bacterial or viral agents. Human monocytes isolated from blood of four individual donors (green, red, blue, and yellow symbols) were cultured for 24 h in culture medium alone (column "medium") or containing LPS (1 ng/mL, column "LPS", control bacterial agent), R848 (0.5 μg/mL, column "R848", control virus-like agent) or N (1 μg/mL, column "N"). Cells were then washed and rested for 7 days in the absence of stimuli, then challenged for 24 h in fresh medium alone or containing 5 μg/mL N. The production of TNFα, IL-6, IL-10, IL-1Ra (upper panel from right to left) and IL-1β, IL-8, IFN-γ, GM-CSF (lower panel from right to left) was measured in the 24 h supernatants by ELISA. The values from cells that received no challenge are included in each panel as "Control" and encompass the values obtained from primed and unprimed cells (which did not differ, confirming the return to baseline after the resting period). Data are presented as individual donors' values (colored symbols) and as mean of the individual values (gray columns). Statistical significance: * p <0.05; ** p <0.01; *** p < 0.001; **** p <0.0001.

epigenetic reprogramming of both CD14+ and CD16+ monocytes (24). Indeed, inhibitors of IL-6 (e.g., the anti-IL-6 receptor Tocilizumab) and of IL-1β (Anakinra) have been used in the therapy of COVID-19. While the treatment with Tocilizumab showed contradictory results regarding its efficacy (31–33), the use of the recombinant form of the IL-1 receptor antagonist IL-1Ra Anakinra showed encouraging results in decreasing clinical parameters and reducing overall mortality (34–36).

Bearing in mind that these results are preliminary, the major finding of our study is that one of the SARS-CoV-2 proteins, the nucleocapsid protein N, can induce innate memory in human monocytes (from subjects that were not previously infected by SARS-CoV-2 or vaccinated), and that this memory was almost exclusively represented by an increased capacity to produce the IL-1 inhibitor IL-1Ra. While confirming that innate memory is non-specific (the same memory response in terms of increased IL-1Ra production is triggered by challenge with LPS, R848 or N), this finding points to the importance of the N protein in stimulating an anti-inflammatory compensatory mechanism to control the cytokine storm and the tissue inflammation caused by the infection. Only in response to a strong viral-like challenge (R848), priming with N could also result in enhanced production of IL-1β. This suggests that the memory induced by N is preferentially active in anti-viral responses and includes the potentiation of a very important defensive effector molecule while, at the same time, being able to control unwanted inflammation through the enhanced production of anti-inflammatory IL-1Ra. Upregulation of IL-1Ra is expected to inhibit IL-1-dependent inflammation but also the entire inflammatory cascade initiated by IL-1β (37, 38). Conversely, a tendency of decreased production of the inflammatory cytokines TNFα and IL-6 was observed in cells primed with the two spike protein subunits S1 and S2 and challenged with the R848. Since only two donors could be examined for S1 and S2 priming, this tendency cannot be considered reliable. However, it may suggest that different parts of the virus can prime the innate immune system towards a milder secondary reaction by using different mechanisms (increase of anti-inflammatory reactions induced by N protein priming and a concomitant decrease of inflammatory responses induced by

TABLE 1 | Summary of the capacity of SARS-CoV-2 and its proteins to induce innate memory in human monocytes.

Priming and challenge/memory stimuli		Cytokine production*							
		TNFα	IL-6	IL-10	IL-1Ra	IL-1β	IL-8	IFN-γ	GM-CSF
Priming with	*Memory response to*								
SARS-CoV-2	LPS (bacteria)	no	no	no	no	no	no	no	no
	R848 (viruses)	no	no	no	no	no	no	no	no
N	LPS (bacteria)	no	no	no	↑↑	no	no	no	no
	R848 (viruses)	(↑)	no	no	↑↑	↑	no	no	(↑)
	N (SARS-CoV-2)	no	no	no	↑↑	no	no	no	no
S1	LPS (bacteria)	(↑)	no	no	no	no	no	no	no
	R848 (viruses)	(↓)	(↓)	no	no	no	no	no	(↓)
S2	LPS (bacteria)	no	no	no	no	no	no	no	no
	R848 (viruses)	(↓)	(↓)	no	no	no	no	no	(↓)
R848	R848 (viruses)	↑	↑	no	↑↑	↑	no	↑	↑
	N (SARS-CoV-2)	no	no	no	↑↑	no	↑	no	no

**Cytokine production is expressed as increase (↑ or ↑↑), indicating increase and strong increase, respectively), decrease (↓) or no change (no) compared to medium-exposed cells. Symbols within parentheses indicate dubious results, i.e., those in which the trend was observed in 3/4 donors (for N priming) and in which only two donors could be examined (for S1 and S2 priming).*

Spike protein priming). The fact that the whole virus could not induce any memory response may be explained by the cross-regulating effects of the different viral components or by changes induced by the inactivation process.

Table 1 summarizes the findings reported in this study and highlight the strong and consistent potentiation effect of priming with the N protein on IL-1Ra production, which may underlie a less severe response to secondary infections, with a better control of innate/inflammatory effector mechanisms.

DATA AVAILABILITY STATEMENT

The original contributions presented in the study are included in the article/**Supplementary Material**. Further inquiries can be directed to the corresponding author.

ETHICS STATEMENT

Institutional Review Board Statement: The study was conducted according to the guidelines of the Declaration of Helsinki. The protocol was approved by the Regional Ethics Committee for Clinical Experimentation of the Tuscany Region (Ethics Committee Register n. 14,914 of May 16, 2019). Informed Consent Statement: Informed consent was obtained from all subjects involved in the study.

AUTHOR CONTRIBUTIONS

PU, SG, DB and PI planned the work. PU and SG performed the experiments and prepared the figures. PI and DB supervised the study. PI performed statistical analysis. DB critically assessed the results; all authors contributed to writing the manuscript and have read and agreed to the published version of the manuscript. All authors contributed to the article and approved the submitted version.

FUNDING

This research work was supported by the European Commission's Joint Research Centre (JRC) within the Consumer Products Safety of the Directorate of Health, Consumers and Reference Materials and partly funded the Horizon 2020 Framework Programme under the project ATAC-H2020-SC1-PHE-CORONAVIRUS-2020 (GA 101003650). Additional support was provided by the President's International Fellowship Programme (PIFI) of CAS (to DB) and by the Italian project MIUR/PRIN-20173ZECCM (to PI).

ACKNOWLEDGMENTS

We are very thankful to Prof. Paola Migliorini (University of Pisa, Italy) for her help in the coordination and ethical monitoring of the study, and to Dr. Giacomo Della Camera for his technical and methodological support. The authors gratefully acknowledge Dr. Arnd Hoeveler and Dr. Luigi Calzolai (JRC) for insightful discussions.

SUPPLEMENTARY MATERIAL

The Supplementary Material for this article can be found online at: https://www.frontiersin.org/articles/10.3389/fimmu.2022.963627/full#supplementary-material

REFERENCES

1. Vilcek S. SARS-CoV-2: Zoonotic Origin of Pandemic Coronavirus. *Acta Virol* (2020) 64:281–7. doi: 10.4149/av_2020_302c
2. Chilamakuri R, Agarwal S. COVID-19: Characteristics and Therapeutics. *Cells* (2021) 10:1–29. doi: 10.3390/cells10020206
3. Khan M, Adil SF, Alkhathlan HZ, Tahir MN, Saif S, Khan M, et al. COVID-19: A Global Challenge With Old History, Epidemiology and Progress So Far. *Molecules* (2021) 26:39. doi: 10.3390/molecules26010039
4. *WHO Coronavirus (COVID-19) Dashboard With Vaccination Data* (2022). Available at: https://covid19.who.int/ (Accessed June 15, 2022).
5. Hu B, Guo H, Zhou P, Shi ZL. Characteristics of SARS-CoV-2 and COVID-19. *Nat Rev Microbiol* (2021) 19:141–54. doi: 10.1038/s41579-020-00459-7
6. Wang MY, Zhao R, Gao LJ, Gao XF, Wang DP, Cao JM. SARS-CoV-2: Structure, Biology, and Structure-Based Therapeutics Development. *Front Cell Infect Microbiol* (2020) 10:587269. doi: 10.3389/fcimb.2020.587269
7. Wu F, Zhao S, Yu B, Chen YM, Wang W, Song ZG, et al. A New Coronavirus Associated With Human Respiratory Disease in China. *Nature* (2020) 579:265–9. doi: 10.1038/s41586-020-2008-3
8. Newman JA, Douangamath A, Yadzani S, Yosaatmadja Y, Aimon A, Brandão-Neto J, et al. Structure, Mechanism and Crystallographic Fragment Screening of the SARS-CoV-2 NSP13 Helicase. *Nat Commun* (2021) 12:4848. doi: 10.1038/s41467-021-25166-6
9. Naqvi AAT, Kisa F, Taj M, Urooj F, Singh IK, Singh A, et al. Insights Into SARS-CoV-2 Genome, Structure, Evolution, Pathogenesis and Therapies: Structural Genomics Approach. *BBA - Mol Basis Dis* (2020) 1866:165878. doi: 10.1016/j.bbadis.2020.165878
10. Artese A, Svicher V, Costa G, Salpini R, Di Maio VC, Alkhatib M, et al. Current Status of Antivirals and Druggable Targets of SARS CoV-2 and Other Human Pathogenic Corona-Viruses. *Drug Resist Updat* (2020) 53:100721. doi: 10.1016/j.drup.2020.100721
11. Le TT, Cramer JP, Chen R, Mayhew S. Evolution of the COVID-19 Vaccine Development Landscape. *Nat Rev Drug Discov* (2020) 19:667–8. doi: 10.1038/d41573-020-00151-8
12. Murphy KM, Weaver C. Janeway's Immunobiology. *9th edition*. New York: WW Norton & Company (2016). p. 904.
13. Boraschi D, Italiani P. Innate Immune Memory: Time for Adopting a Correct Terminology. *Front Immunol* (2018) 9:799. doi: 10.3389/fimmu.2018.00799
14. Netea MG, Quintin J, van der Meer JWM. Trained Immunity: A Memory for Innate Host Defense. *Cell Host Microbe* (2011) 9:355–61. doi: 10.1016/j.chom.2011.04.006
15. Italiani P, Boraschi D. Induction of Innate Immune Memory by Engineered Nanoparticles: A Hypothesis That may Become True. *Front Immunol* (2017) 8:734. doi: 10.3389/fimmu.2017.00734
16. Franceschi C, Salvioli S, Garagnani P, de Eguileor M, Monti D, Capri M. Immunobiography and the Heterogeneity of Immune Responses in the Elderly: A Focus on Inflammaging and Trained Immunity. *Front Immunol* (2017) 8:982. doi: 10.3389/fimmu.2017.00982
17. Sette A, Crotty S. Adaptive Immunity to SARS-CoV-2 and COVID-19. *Cell* (2021) 184:861–80. doi: 10.1016/j.cell.2021.01.007
18. Grifoni A, Weiskopf D, Ramirez SI, Mateus J, Dan JM, Moderbacher CR, et al. Targets of T Cell Responses to SARS-CoV-2 Coronavirus in Humans With COVID-19 Disease and Un-Exposed Individuals. *Cell* (2020) 181:1489–1501.e15. doi: 10.1016/j.cell.2020.05.015
19. Krammer F. SARS-CoV-2 Vaccines in Development. *Nature* (2020) 586:516–27. doi: 10.1038/s41586-020-2798-3
20. Arunachalam PS, Wimmers F, Mok CKP, Perera RAPM, Scott M, Hagan T, et al. Systems Biological Assessment of Immunity to Mild Versus Severe COVID-19 Infection in Humans. *Science* (2020) 369:1210–20. doi: 10.1126/science.abc6261
21. Schultze JL, Aschenbrenner AC. COVID-19 and the Human Innate Immune System. *Cell* (2021) 184:1671–92. doi: 10.1016/j.cell.2021.02.029
22. Loske J, Röhmel J, Lukassen S, Stricker S, Magalhães VG, Liebig J, et al. Pre-Activated Antiviral Innate Immunity in the Upper Airways Controls Early SARS-CoV-2 Infection in Children. *Nat Biotechnol* (2022) 40:319–24. doi: 10.1038/s41587-021-01037-9
23. Arunachalam PS, Scott MKD, Hagan T, Li C, Feng Y, Wimmers F, et al. Systems Vaccinology of the BNT162b2 mRNA Vaccine in Humans. *Nature* (2021) 596:410–6. doi: 10.1038/s41586-021-03791-x
24. You M, Chen L, Zhang D, Zhao P, Chen Z, Qin EQ, et al. Single-Cell Epigenomic Landscape of Peripheral Immune Cells Reveals Establishment of Trained Immunity in Individuals Convalescing From COVID-19. *Nat Cell Biol* (2021) 23:620–30. doi: 10.1038/s41556-021-00690-1
25. Della Camera G, Lipsa D, Mehn D, Italiani P, Boraschi D, Gioria S. A Step-by-Step Approach to Improve Clinical Translation of Liposome-Based Nanomaterials, a Focus on Innate Immune and Inflammatory Responses. *Int J Mol Sci* (2021) 22:820. doi: 10.3390/ijms22020820
26. Karwaciak I, Sałkowska A, Karaś K, Dastych J, Ratajewski M. Nucleocapsid and Spike Proteins of the Coronavirus SARS-CoV-2 Induce IL6 in Monocytes and Macrophages—Potential Implications for Cytokine Storm Syndrome. *Vaccines* (2021) 9:54. doi: 10.3390/vaccines9010054
27. Madej MP, Töpfer E, Boraschi D, Italiani P. Different Regulation of Interleukin-1 Production and Activity in Monocytes and Macrophages: Innate Memory as an Endogenous Mechanism of IL-1 Inhibition. *Front Pharmacol* (2017) 8:335. doi: 10.3389/fphar.2017.00335
28. Della Camera G, Madej M, Ferretti AM, La Spina R, Li Y, Corteggio A, et al. Personalised Profiling of Innate Immune Memory Induced by Nano-Imaging Particles in Human Monocytes. *Front Immunol* (2021) 12:692165. doi: 10.3389/fimmu.2021.692165
29. O'Neill LAJ, Netea MG. BCG-Induced Trained Immunity: Can it Offer Protection Against COVID-19? *Nat Rev Immunol* (2020) 20:335–7. doi: 10.1038/s41577-020-0337-y
30. Mantovani A, Netea MG. Trained Innate Immunity, Epigenetics, and Covid-19. *N Eng J Med* (2020) 383:1078–80. doi: 10.1056/NEJMcibr2011679
31. Rubin EJ, Longo DL, Baden LR. Interleukin-6 Receptor Inhibition in Covid-19 — Cooling the Inflammatory Soup. *N Engl J Med* (2021) 384:1564–5. doi: 10.1056/NEJMe2103108
32. The REMAP-CAP Investigators. Interleukin-6 Receptor Antagonists in Critically Ill Patients With Covid-19. *N Engl J Med* (2021) 384:1491–502. doi: 10.1056/NEJMoa2100433
33. Rosas IO, Bräu N, Waters M, Go RC, Hunter BD, Bhagani S, et al. Tocilizumab in Hospitalized Patients With Severe Covid-19 Pneumonia. *N Engl J Med* (2021) 384:1503–16. doi: 10.1056/NEJMoa2028700
34. Kooistra EJ, Waalders NJB, Grondman I, Janssen NAF, de Nooijer AH, Netea MG, et al. Anakinra Treatment in Critically Ill COVID-19 Patients: A Prospective Cohort Study. *Crit Care* (2020) 24:688. doi: 10.1186/s13054-020-03364-w
35. Kyriazopoulou E, Huet T, Cavalli G, Gori A, Kyprianou M, Pickkers P, et al. Effect of Anakinra on Mortality in Patients With COVID-19: A Systematic Review and Patient-Level Meta-Analysis. *Lancet Rheumatol* (2021) 3:e690–697. doi: 10.1016/S2665-9913(21)00216-2
36. Geng J, Wang F, Huang Z, Chen X, Wang Y. Perspectives on Anti-IL-1 Inhibitors as Potential Therapeutic Interventions for Severe COVID-19. *Cytokine* (2021) 143:155544. doi: 10.1016/j.cyto.2021.155544
37. Oppenheim JJ, Matsushima K, Yoshimura T, Leonard EJ, Neta R. Relationship Between Interleukin 1 (IL1), Tumor Necrosis Factor (TNF) and a Neutrophil Attracting Peptide (NAP-1). *Agents Actions* (1989) 26:134–40. doi: 10.1007/BF02126586
38. Bethea JR, Gillespie GY, Benveniste EN. Interleukin-1 Beta Induction of TNF-Alpha Gene Expression: Involvement of Protein Kinase C. *Cell Physiol* (1992) 152:264–73. doi: 10.1002/jcp.104152020

Conflict of Interest: The authors declare that the research was conducted in the absence of any commercial or financial relationships that could be construed as a potential conflict of interest.

frontiers | Frontiers in Immunology

TYPE Original Research
PUBLISHED 08 March 2023
DOI 10.3389/fimmu.2023.1155855

OPEN ACCESS

EDITED BY
Diana Boraschi,
Shenzhen Institute of Advanced Technology (SIAT), CAS, China

REVIEWED BY
Olukemi Amodu,
University of Ibadan, Nigeria
Marita Troye Blomberg,
Stockholm University, Sweden
Giselle Penton-Rol,
Center for Genetic Engineering and Biotechnology (CIGB), Cuba

*CORRESPONDENCE
Abba Aissatou
aichabba@ymail.com
Joseph Fokam
josephfokam@gmail.com

†These authors have contributed equally to this work and share first authorship

SPECIALTY SECTION
This article was submitted to Cytokines and Soluble Mediators in Immunity, a section of the journal Frontiers in Immunology

RECEIVED 31 January 2023
ACCEPTED 27 February 2023
PUBLISHED 08 March 2023

CITATION
Aissatou A, Fokam J, Semengue ENJ, Takou D, Ka'e AC, Ambe CC, Nka AD, Djupsa SC, Beloumou G, Ciaffi L, Tchouaket MCT, Nayang ARM, Pabo WLT, Essomba RG, Halle EGE, Okomo M-C, Bissek A-CZK, Leke R, Boum Y II, Mballa GAE, Montesano C, Perno C-F, Colizzi V and Ndjolo A (2023) Pre-existing immunity to SARS-CoV-2 before the COVID-19 pandemic era in Cameroon: A comparative analysis according to HIV-status.
Front. Immunol. 14:1155855.
doi: 10.3389/fimmu.2023.1155855

Pre-existing immunity to SARS-CoV-2 before the COVID-19 pandemic era in Cameroon: A comparative analysis according to HIV-status

Abba Aissatou[1,2*†], Joseph Fokam[1,3,4,5*†], Ezechiel Ngoufack Jagni Semengue[1,6,7], Désiré Takou[1], Aude Christelle Ka'e[1,6], Collins Chenwi Ambe[1,8], Alex Durand Nka[1,6,7], Sandrine Claire Djupsa[1], Grâce Beloumou[1], Laura Ciaffi[9], Michel Carlos Tommo Tchouaket[1,10], Audrey Rachel Mundo Nayang[1], Willy Leroi Togna Pabo[1], René Ghislain Essomba[4,5,11], Edie G. E. Halle[3], Marie-Claire Okomo[4,5,11], Anne-Cecile ZK. Bissek[12], Rose Leke[1,13], Yap Boum II[4], Georges Alain Etoundi Mballa[4,14], Carla Montesano[6], Carlo-Federico Perno[15], Vittorio Colizzi[1,6,7] and Alexis Ndjolo[1,5]

[1]Laboratory of virology, Chantal BIYA International Reference Center for Research HIV/AIDS Prevention and Management, Yaoundé, Cameroon, [2]Serology Unit, Garoua Regional Health Centre, Garoua, Cameroon, [3]Faculty of Health Sciences, University of Buea, Buea, Cameroon, [4]Laboratory Unit, Operations sections, National Public Health Emergency Operations Coordination Centre, Yaounde, Cameroon, [5]Faculty of Medicine and Biomedical Sciences, University of Yaounde I, Yaounde, Cameroon, [6]Department of Biology, University of Rome *"Tor Vergata"*, Rome, Italy, [7]Department of Science and Technology, Evangelical University of Cameroon, Bandjoun, Cameroon, [8]Department of General Medicine, Mvangan District Hospital, Mvangan, Cameroon, [9]Project Coordinator, National Agency for Research on AIDS and Viral Hepatitis, Yaounde, Cameroon, [10]School of Health Sciences, Catholic University of Central Africa, Yaounde, Cameroon, [11]National Public Health Laboratory, Ministry of Public Health, Yaounde, Cameroon, [12]Division of Health Operational Research, Ministry of Public Health, Yaounde, Cameroon, [13]The Biotechnology Center of the University of Yaounde I and the Ministry of Scientific Research, Yaounde, Cameroon, [14]Division of Disease, Epidemic and Pandemic Control, Ministry of Public Health, Yaounde, Cameroon, [15]Department of Microbiology, Bambino Gesu Pediatric Hospital, Rome, Italy

Background: The lower burden of COVID-19 in tropical settings may be due to preexisting cross-immunity, which might vary according to geographical locations and potential exposure to other pathogens. We sought to assess the overall prevalence of SARS-CoV-2 antibodies and determine SARS-CoV-2 seropositivity according to HIV-status before the COVID-19 pandemic era.

Methods: A cross-sectional and comparative study was conducted at the Chantal BIYA International Reference Centre (CIRCB) on 288 stored plasma samples (163 HIV-positive versus 125 HIV-negative); all collected in 2017-2018, before the COVID-19 pandemic era. Abbott Panbio™ COVID-19 IgG/IgM assay was used for detecting SARS-CoV-2 immunoglobulin G (IgG) and M (IgM). Among people living with HIV (PLHIV), HIV-1 viral load and TCD4 cell count

(LTCD4) were measured using Abbott Real Time PCR and BD FACSCalibur respectively. Statistical analyses were performed, with p<0.05 considered statistically significant.

Results: The median [IQR] age was 25 [15-38] years. Overall seropositivity to SARS-CoV-2 antibodies was 13.5% (39/288) of which 7.3% (21) was IgG, 7.3% (21) IgM and 1.0% (3) IgG/IgM. According to HIV-status in the study population, SARS-CoV-2 seropositivity was 11.0% (18/163) among HIV-positive versus 16.8% (21/125) among HIV-negative respectively, p=0.21. Specifically, IgG was 6.1% (10/163) versus 8.8% (11/125), p=0.26; IgM was 5.5% (9/163) versus 9.6%, (12/125), p=0.13 and IgG/IgM was 0.6% (1/163) versus 1.6% (2/125) respectively. Among PLHIV, SARS-CoV-2 seropositivity according to CD4 count was 9.2% (≥500 cells/µL) versus 1.8% (200-499 cells/µL), (OR=3.5; p=0.04) and 0.6% (<200 cells/µL), (OR=17.7; p<0.01). According to viral load, SARS-CoV-2 seropositivity was 6.7% (≥40 copies/mL) versus 4.9% (<40 copies/mL), (OR= 3.8; p<0.01).

Conclusion: Before COVID-19 in Cameroon, cross-reactive antibodies to SARS-CoV-2 were in circulation, indicating COVID-19 preexisting immunity. This preexisting immunity may contribute in attenuating disease severity in tropical settings like Cameroon. Of relevance, COVID-19 preexisting immunity is lower with HIV-infection, specifically with viral replication and poor CD4-cell count. As poor CD4-count leads to lower cross-reactive antibodies (regardless of viral load), people living with HIV appear more vulnerable to COVID-19 and should be prioritized for vaccination.

KEYWORDS

HIV, SARS-CoV-2, immunoglobulin G/M, T-CD4 lymphocytes, HIV viral load

Introduction

December 2019 was marked by the appearance of the new coronavirus 2019 disease (COVID-19) in the city of Wuhan in China, which quickly became a pandemic resulting on January 30th 2020 in a Public Health Emergency of International Concern (PHEIC) (1–4). As of November 22nd 2022, 643,620,075 cases had been diagnosed worldwide with 6,628,090 deaths reported, giving a fatality rate of 1.03% three years after the beginning of the pandemic (5). Seven coronaviruses can lead to infection, but the causal agent of COVID-19 was identified as the novel severe acute respiratory syndrome coronavirus-2 (SARS-CoV-2) (3, 6, 7). Of note, SARS-CoV-2 is an enveloped virus with a linear and unsegmented positive-sense RNA genome, coding for four main structural proteins, namely: the spike (S), nucleocapsid (N), envelope (E) and membrane (M) (8). The S protein contains, the S1 subunit which is divided into an N-terminal domain (NTD) and a receptor binding domain (RBD) responsible for binding the virus to the host cell Angiotensin-Converting Enzyme 2 (ACE2) receptor binding domain (8). The N protein on the other hand is involved in the externalization of viral particles from the infected cell. Additionally, the spike glycoprotein polymer (specifically S1) mediates viral attachment, followed by membrane fusion. This glycoprotein is immunogenic and hence ideal for serosurveys (targeting IgM and IgG humoral circulating antibodies) (3, 7, 9–11), which are one of the best approaches to appraise the extent of COVID-19 infection and disease circulation within a given community.

Surprisingly, from the overall global burden of COVID-19, a small proportion of cases were reported in Africa. On November 22nd 2022, 12,697,321 cases were reported indicating 1.97% of the global burden (5) and suggesting a much lower severity of the disease (12). Several hypotheses have been proposed to explain this low incidence of COVID-19 in Africa among which were: (i) the young population in Sub-Saharan Africa as compared to Caucasians; (ii) SARS-CoV-2 persistence and spread disadvantaged by climatic and environmental factors; (iii) social distancing favored by the lifestyle in rural/less developed areas, which limits the spread of the disease; (iv) underestimation of morbidity and mortality counts due to poor testing coverage, reflecting weak health systems; (v) a rapid activation of the natural innate non-specific immunity due to an overexposure to pathogens; and (vi) specific immune response following a previous contact with viruses sharing common antigenic profiles with SARS-CoV-2 (4, 6, 8). The potential low circulation of SARS-CoV-2 in Africa may be justified by the existence of specific pre-pandemic antibodies, responsible for cross-immunity during the pandemic (8). Furthermore, with the emergence in 2019 of SARS-CoV-2, the

world now has to face two pandemics: COVID-19 and HIV/AIDS (13). As COVID-19 pandemic continues to cause much uncertainty around the world, and especially among people living with and affected by HIV (>67% of whom residing in sub-Saharan Africa), understanding its extent as well as the determinants of induced immunogenicity is crucial to frame the response strategy within national programs and better prepare for future pandemics. We therefore sought to assess the overall prevalence of SARS-CoV-2 antibodies and determine SARS-CoV-2 seropositivity according to HIV-status during the COVID-19 pre-pandemic era in Cameroon.

Methods

Study design

We carried out a case-control study on archived plasma samples collected between 2017 and 2018, before the outbreak of COVID-19 in Cameroon.

Study site

As a COVID-19 reference center for diagnostic and genomic surveillance, the "Chantal BIYA" International Reference Centre for research on HIV/AIDS prevention and management (CIRCB) is a government institution of the Cameroonian Ministry of Public Health committed to research on HIV/AIDS prevention and management. Additionally, CIRCB covers: (a) HIV early infant diagnosis in the frame of the national PMTCT program; (b) diagnosis of co-infections with HIV; (c) viral load measurement; (d) CD4 and CD8 T lymphocytes counts; (e) biochemical and hematological tests for drug follow-up; (f) genotypic HIVDR testing (GRT) at subsidized costs; with quality control programs conducted in partnership with Quality Assessment and Standardization of Indicators (QASI) and other international organizations (http://www.circb.cm/btc_circb/web/).

Sampling and eligibility criteria

We enrolled archived plasma samples previously anonymized and codified as per institutional biobanking procedures (from both HIV-positive and negative individuals). Socio-demographic and clinical data were obtained from the CIRCB database. Samples were from people residing in the Centre region of Cameroon. For HIV-positive individuals, only those with CD4-cell count, HIV-1 viral load measurements and with a complete treatment history were included; those with any co-infection or related co-morbidity were excluded.

Clinical and laboratory procedures

Serological assays

SARS-CoV-2 antibodies were tested using the Abbott Panbio™ COVID-19 IgG/IgM Rapid Test Device as per manufacturer's instructions. Assay performance as reported by the manufacturer was as follows: sensitivity (97.8%); specificity (92.8%); precision (>99% both for intra-assay and inter-assay assessments) (14). Briefly, plasma samples were mixed by low-speed vortex after which 10µL of supernatant was applied to the specimen well (S) of the test device. Two drops (approximately 60 µL) of buffer were added and a timer was started for 10 minutes. At the end of the 10 minutes the test device was read. A valid result consisted of the appearance of a red line in the Control (C) area of the reading window. A negative result consisted of the presence of the red line only in the C area whereas the presence of a red line on both C and G (IgG) areas indicated a reactivity to IgG; a red line on both C and M (IgM) areas, reactivity to IgM and a red line in C and both G and M areas of the reading window indicated a positive result for both IgG and IgM.

T-CD4 lymphocytes phenotyping

Before storage in the biobank, CD4 cells count of PLHIV had also been performed using the BD FACSCalibur™ Flow Cytometer as per the manufacturer's instructions with results reported as the number of cells per microliter of blood (15). We therefore classified CD4 results as follows: no immunodeficiency (above or equal to 500 cell/µL); mild immunodeficiency (between 350 and 499 cell/µL); advanced immunodeficiency (between 200 and 349 cell/µL) and severe immunodeficiency (below 200 cell/µL).

Viral load measurements

Before storage in the biobank, HIV-1 viral load measurement had also been performed using the Abbott™ *m2000rt* instrument for Real Time PCR as-per the manufacturer's instructions (16), with a lower detection threshold of 40 HIV-1 RNA copies/mL and an upper detection threshold of 10,000,000 copies/mL.

Statistical analysis

Data collected were entered on Microsoft Excel 2021. The software IBM.SPSS® Statistics V.20 was used for statistical analysis. Association analyses were performed using Pearson Chi-Square Test with statistical significance considered at $p<0.05$. All variables with $p<0.2$ during bivariate analyses were retained for multivariable analysis.

Results

Clinical characteristics of the study population

Out of a total of 288 selected samples, 163 were HIV positive (56.6%) and 125 HIV negative (43.4%). Median age [interquartile range; IQR] in the study population was 25 [15-38] years; 18 [13-41] years among HIV-positive versus 28 [23-35] years among HIV negative. Majority of our study population was of the male gender, 58.0% (159/288), with similar distribution according to HIV-status. The rest of socio-demographic and clinical parameters are summarized in Table 1.

TABLE 1 Clinical characteristics of the study population.

Variables		Effective n (%)
Gender		
	Female	121 (42.0)
	Male	167 (58.0)
Age		
	Median age	25 years
	0-19	108 (37.5)
	20-39	118 (40.9)
	40-59	54 (18.8)
	>60	8 (2,8)
HIV status		
	HIV positive	163 (56.6)
	HIV negative	125 (43.4)
*WHO clinical stages (for HIV positive) **		
	I	114 (75.5)
	II	21 (13.9)
	III	14 (9.3)
	IV	2 (1.3)
	Median ART-duration (months)	24 [7-66]
ART line		
	First line	139 (85.3)
	Second line	24 (14.7)
Most prescribed regimen		
	TDF+3TC+EFV (in first line)	56 (40.3)
	TDF+3TC+ATV/r (in second line)	9 (37.5)
T-CD4 counts (cells/µL)		
	≥ 500	65 (39.9)
	[350-499]	12 (7.4)
	[200-349]	26 (15.9)
	< 200	60 (36.8)
HIV Viral Load (copies/mL)		
	< 40	50 (30.7)
	≥ 40	113 (69.3)

*Data regarding WHO clinical stages were obtained for 151 participants only.

Overall seroprevalence of SARS-CoV-2 antibodies

The global prevalence of SARS-CoV-2 antibodies was 13.5% (39/288) in the study population; 7.3% (21/288) IgG, 7.3% (21/288) IgM and 1.04% (3/288) IgG/IgM. Distribution of SARS-CoV-2 antibodies was similar according to age and HIV-status (p=0.07 and p=0.21 respectively); but statistically higher in men (aOR=2.54; [95%CI: 1.15-5.64]; p=0.02), as presented in Tables 2, 3 below.

Seroprevalence of SARS-CoV-2 antibodies among HIV-infected participants

Concerning HIV-infected participants, virological control (VL<40copies/mL), high CD4 cells count (>350cells/µL) and ART duration >23 months were all significantly associated to SARS CoV-2 seropositivity in bi-variables analyses (p=0.005; p=0.01; p<0.001 respectively) but not in multivariable analysis (p=0.14; p=0.19; p=0.96 respectively) as presented in Table 4 below.

TABLE 2 Overall prevalence of SARS-CoV-2 antibodies (IgG and IgM) using the rapid diagnostic assay.

Variables	Overall prevalence of Ig		Prevalence of IgG		Prevalence of IgM	
	n (%)	p-value	n (%)	p-value	n (%)	p-value
Gender						
Male	29 (17.37)	0.04	17 (10.18)	0.03	14 (8.38)	0.54
Female	10 (8.26)		4 (3.31)		7 (5.79)	
Age						
<25 years	25 (17.36)	0.08	14 (9.72)	0.17	13 (9.03)	0.36
>25years	14 (9.72)		7 (4.86)		8 (5.56)	
HIV-status						
HIV+	18 (11.04)	0.21	10 (6.13)	0.53	9 (5.52)	0.27
HIV-	21 (16.80)		11 (8.80)		12 (9.60)	

TABLE 3 Determinants of a high SARS-CoV-seroprevalence (multivariable analysis).

Variables	Adjusted odds ratio	95% C.I.	p-value
Age (>25/<25)	0.51	[0.25-1.06]	0.07
Gender (M/F)	2.54	[1.15-5.64]	0.02

Discussion

To the best of our knowledge, no evidence clearly explains the low severity of COVID-19 in Africa, a continent that has the weakest health system and infrastructures. Indeed, the limited number of healthcare infrastructures, the poor access to specialized health services (present only in some urban areas), and the limited number of professionals trained in critical care have already been widely documented across the continent (3, 17–21); thus calling for further investigations to clarify on this low incidence of COVID-19 in Africa (12). The objective of this study was to assess the circulation of SARS-CoV-2 antibodies in a pre-pandemic era according to HIV-infection in Cameroon.

First and foremost, our findings effectively demonstrated the circulation of SARS-CoV-2 antibodies in Cameroon before the disease outbreak in 2019. This pre-existence of specific SARS-CoV-2 antibodies strongly supports the hypothesis of potential cross-immunity during the pandemic. The later could also be justified by a previous contact with other coronaviruses sharing common antigenic profiles (4, 8), which could be either HKU1, NL63, OC43 or 229E. Moreover, the circulation of these specific coronaviruses within Central Africa had never been described before the COVID-19 outbreak (22, 23).. Assessing the titer and immunogenicity of these specific pre-pandemic SARS-CoV-2 antibodies through broadly neutralizing assays will help confirm this hypothesis and further characterize this cross-immunity to understand its effect on SARS-CoV-2 variants and sub-lineages circulating nowadays (24). On one hand, we observed a higher sero-positivity SARS-CoV-2 antibodies among males as compared to females, likely driven by the differential level of ACE-2 receptors among men as compared to women (8, 25). On the other hand, knowing that estrogens decrease plasma renin activity while androgens increase plasma renin activity and the expression of angiotensinogen messenger RNA, it is therefore predicted that the latter hormone would up-regulate ACE2 expression (25). In effect, the human angiotensin-converting enzyme 2 (ACE2) has been described as the functional receptor for the severe acute respiratory syndrome caused by coronaviruses (8, 26), thus facilitating recognition and infection by coronaviruses (26). Therefore, the protective role of ACE2 in chronic pathologies like hypertension, cardiovascular diseases, and acute respiratory distress syndrome (25), would be reversed in the advent of COVID-19.

With respect to HIV-status, we observed here a similar distribution of SARS-CoV-2 antibodies between HIV-infected and uninfected participants. This observation is in line with several studies conducted early in the pandemic, indicating that the clinical presentation of COVID-19 is similar in people with and without HIV, particularly if they are on ART and have achieved HIV viral suppression (13, 27–29). However, among sera of HIV-infected participants, high CD4 counts, virological control (>40copies/mL) and ART duration, seemed individually associated to the presence of SARS-CoV-2 antibodies; suggesting that people with a highly compromised immune system, an uncontrolled viral replication and/or the absence of an effective ART-regimen stand a high risk of not controlling SARS-CoV-2 replication or developing severe symptoms of COVID-19 (13). This observation therefore suggests that a closer monitoring of HIV/SARS-CoV-2 co-infection would be beneficial in order to preserve the benefits of vaccine-induced immunogenicity in this key population. Importantly, the pathogenicity associated to each virus separately and subsequent

TABLE 4 Predictors of SARS-CoV-2 seroprevalence among HIV-infected participants.

Variables	Prevalence of Ig		
	n (%)	OR [95%CI] (p-value)	aOR [95%CI] (p-value)
CD4 (cells/µL)			
≥350	14 (18.18)	4.55 [1.42-14.51] (0.01)	2.65 [0.62-11.26] (0.19)
<350	4 (4.65)		
Viral load (copies/mL)			
<40	10 (20.41)	3.39 [1.25-9.23] (0.026)	0.58 [0.16-2.12] (0.41)
≥40	8 (7.02)		
ART-duration (months)			
< 23	0 (0.00)	/(<0.001)	/(0.96)
>23	18 (22.78)		
Treatment line			
1st line	13 (9.35)	0.39 [0.12-1.22] (0.19)	2.87 [0.85-9.66] (0.08)
2nd line	5 (20.83)		

impairments to the immune system have been described; and even though vaccination of HIV-infected is essential to uphold an already weak immune system, it is important to emphasize that our findings primarily suggest there is a greater risk of COVID-19 severity among the severely immune-compromised and in those with an uncontrolled viral replication.

Conclusion

In summary, cross-reactive antibodies to SARS-CoV-2 were in circulation in Cameroon before COVID-19, suggesting preexisting immunity, which may have contributed in limiting the spread of COVID-19 and attenuating the severity of new variants within this tropical setting. This preexisting immunity appears similar among HIV-infected versus uninfected participants. As poor CD4-count leads to lower cross-reactive antibodies (regardless of viral load), people living with HIV (especially those with poor clinical status) appear more vulnerable to COVID-19 and should be prioritized for vaccination.

Data availability statement

The raw data supporting the conclusions of this article will be made available by the authors, without undue reservation.

Ethics statement

The studies involving human participants were reviewed and approved by National Ethics Committee for Research on Human Health, Cameroon. Written informed consent to participate in this study was provided by the participants' legal guardian/next of kin.

Author contributions

JF and DT, conceptualization. AA, EN, DT, CC, ADN, AK'E, SD, and GB, formal analysis and investigation. AA, JF, EN, DT, CC, ADN, AK'E, MT, AM, and WT, data curation and methodology. AA, EN, DT, and JF, writing the original draft preparation. DT, SD, GB, LC, RE, EH, M-CO, A-CB, RL, YB, GE, CM, C-FP, VC, AN, AM, and WT, resources, supervision, and funding acquisition. AA, JF, EN, DT, CC, ADN, C-FP, VC, and AN, writing-review and editing. All authors contributed to the article and approved the submitted version.

Funding

The study was sponsored by the Chantal BIYA International Reference Centre (CIRCB) and the EDCTP (RIA2020-EF3000) for the sponsorship and the CIRCB COVID for all the efforts for this work.

Conflict of interest

The authors declare that the research was conducted in the absence of any commercial or financial relationships that could be construed as a potential conflict of interest.

Publisher's note

References

1. WHO. *Origin of SARS-CoV-2* (2020). Available at: https://www.who.int/publications/i/item/origin-of-sars-cov-2.

2. WHO. *WHO timeline - COVID-19* (2022). Available at: https://www.who.int/news-room/detail/27-04-2020-who-timeline—covid-19.

3. Nwosu K, Fokam J, Wanda F, Mama L, Orel E, Ray N, et al. SARS-CoV-2 antibody seroprevalence and associated risk factors in an urban district in Cameroon. *Nat Commun* (2021) 12(1):1–9. doi: 10.1038/s41467-021-25946-0

4. Zhu N, Zhang D, Wang W, Li X, Yang B, Song J, et al. A novel coronavirus from patients with pneumonia in China, 2019. *N Engl J Med* (2020) 382(8):727–33. doi: 10.1056/NEJMoa2001017

5. Worldometer. *COVID live - coronavirus statistics - worldometer* (2022). Available at: https://www.worldometers.info/coronavirus/.

6. WHO. *Middle East respiratory syndrome coronavirus (MERS-CoV)* (2022). Available at: https://www.who.int/health-topics/middle-east-respiratory-syndrome-coronavirus-mers#tab=tab_1.

7. *True extent of SARS-CoV-2 infection through seroprevalence studies* (2022). Available at: https://www.who.int/news/item/03-02-2022-true-extent-of-sars-cov-2-infection-through-seroprevalence-studies.

8. Souris M, Tshilolo L, Parzy D, Lobaloba Ingoba L, Ntoumi F, Kamgaing R, et al. Pre-pandemic cross-reactive immunity against SARS-CoV-2 among central and West African populations. *Viruses.* (2022) 14(10):1–11. doi: 10.3390/v14102259

9. Mansuy J-M, Kenfack MT, Burel S, Pollani C, Bidzogo Lebobo M, Ekaé CO, et al. High SARS-CoV-2 IgG seroprevalence among pregnant cameroun women 14 months after the beginning of the pandemic. *Public Health* (2022) 2020–2. doi: 10.1016/j.puhe.2022.09.005

10. Lobaloba Ingoba L, Djontu JC, Mfoutou Mapanguy CC, Mouzinga F, Diafouka Kietela S, Vouvoungui C, et al. Seroprevalence of anti-SARS-CoV-2 antibodies in a population living in bomassa village, republic of Congo. *IJID Reg* (2022) 2:130–6. doi: 10.1016/j.ijregi.2022.01.002

11. Ndongo FA, Guichet E, Mimbé ED, Ndié J, Pelloquin R, Varloteaux M, et al. Rapid increase of community SARS-CoV-2 seroprevalence during second wave of COVID-19, yaoundé, Cameroon. *Emerg Infect Dis* (2022) 28(6):1233–6. doi: 10.3201/eid2806.212580

12. Tcheutchoua DN, Tankeu AT, Angong DLW, Agoons BB, Nguemnang NYY, Djeunga HCN, et al. Unexpected low burden of coronavirus disease 2019 (Covid-19) in sub-saharan africa region despite disastrous predictions: Reasons and perspectives. *Pan Afr Med J* (2020) 37(352):1–15. doi: 10.11604/pamj.2020.37.352.25254

13. Nkengasong J. HIV And COVID-19: juxtaposition of two pandemics. In: *The lancet HIV*, vol. Vol. 9. Elsevier Ltd (2022). p. p.e300–1. doi: 10.1016/S2352-3018(22)00095-9.

14. Abbott. *Panbio COVID-19 IgG/IgM rapid test | Abbott point of care* (2022). Available at: https://www.globalpointofcare.abbott/en/product-details/panbio-covid-19-igg-igm-antibody-test.html.

15. BD Biosciences. BD FACSCalibur instructions for use. In: *User's guide* (2007). Available from: https://www.manualslib.com/manual/1260537/Bd-Facscalibur.html.

16. Abbott. (2022). Available at: www.abbottmolecular.com/products/infectious-diseases/realtime-pcr/hiv-1-assay.

17. Tessema GA, Kinfu Y, Dachew BA, Tesema AG, Assefa Y, Alene KA, et al. The COVID-19 pandemic and healthcare systems in Africa: A scoping review of preparedness, impact and response. *BMJ Glob Heal* (2021) 6(12):1–14. doi: 10.1136/bmjgh-2021-00717

18. Hogan AB, Jewell B, Sherrard-Smith E, Vesga J, Watson OJ, Whittaker C, et al. Report 19: The potential impact of the COVID-19 epidemic on HIV, TB and malaria in low- and middle-income countries. *Lancet Global Health* (2020) 8(9):e1132–41. doi: 10.1016/S2214-109X(20)30288-6.

19. Abraham SA, Berchie GO, Doe PF, Agyare E, Addo SA, Obiri-Yeboah D. Effects of COVID-19 pandemic on ART service delivery: perspectives of healthcare workers in a teaching hospital in Ghana. *BMC Health Serv Res* (2021) 21(1):1–10. doi: 10.1186/s12913-021-07330-2

20. Health policy Watch. *Universal health coverage: Only half of africans have access to health care - health policy watch* (2021). Available at: https://healthpolicy-watch.news/only-half-of-africans-have-access-to-health-care/.

21. Raizes E, Hader S, Birx D. The US president's emergency plan for AIDS relief (PEPFAR) and HIV drug resistance: Mitigating risk, monitoring impact. *J Infect Dis* (2017) 216:S805–7. doi: 10.1093/infdis/jix432

22. Lau SKP, Woo PCY, Yip CCY, Tse H, Tsoi HW, Cheng VCC, et al. Coronavirus HKU1 and other coronavirus infections in Hong Kong. *J Clin Microbiol* (2006) 44(6):2063–71. doi: 10.1128/JCM.02614-05

23. Sechan F, Grobben M, Edridge AWD, Jebbink MF, Loens K, Ieven M, et al. Atypical antibody dynamics during human coronavirus HKU1 infections. *Front Microbiol* (2022) 13:1–9. doi: 10.3389/fmicb.2022.853410

24. Goh YS, Rouers A, Fong S-W, Zhuo NZ, Hor PX, Loh CY, et al. Waning of specific antibodies against delta and omicron variants five months after a third dose of BNT162b2 SARS-CoV-2 vaccine in elderly individuals. *Front Immunol* (2022) 13:1031852/full. doi: 10.3389/fimmu.2022.1031852/full

25. Majdic G. Could Sex/Gender differences in ACE2 expression in the lungs contribute to the Large gender disparity in the morbidity and mortality of patients infected with the SARS-CoV-2 virus? *Front Cell Infect Microbiol* (2020) 10. doi: 10.3389/fcimb.2020.00327

26. Yan R, Zhang Y, Li Y, Xia L, Guo Y, Zhou Q. Structural basis for the recognition of SARS-CoV-2 by full-length human ACE2. *Sci (80-)* (2020) 367(6485):1444–8. doi: 10.1126/science.abb2762

27. WHO. *HIV* (2022). Available at: https://www.who.int/data/gho/data/themes/hiv-aids.

28. The Lancet HIV. Lockdown fears for key populations. In: *The lancet HIV*, vol. Vol. 7. Elsevier Ltd (2020). p. p.e373. doi: 10.1016/S2352-3018(20)30143-0

29. IAS. *COVID-19 & HIV | international AIDS society (IAS)* (2022). Available at: https://www.iasociety.org/covid-19-hiv.

frontiers | Frontiers in Immunology

TYPE Original Research
PUBLISHED 14 August 2023
DOI 10.3389/fimmu.2023.1239877

OPEN ACCESS

EDITED BY
Diana Boraschi,
Chinese Academy of Science (CAS), China

REVIEWED BY
Marita Troye Blomberg,
Stockholm University, Sweden
Giselle Penton-Rol,
Center for Genetic Engineering and Biotechnology (CIGB), Cuba
Maria Rosaria Coscia,
National Research Council (CNR), Italy

*CORRESPONDENCE
Aude Christelle Ka'e
kae.audechristelle@gmail.com
Aubin Joseph Nanfack
a_nanfack@yahoo.fr
Joseph Fokam
josephfokam@gmail.com

†These authors have contributed equally to this work and share first authorship

‡These authors have contributed equally to this work as second authors

RECEIVED 14 June 2023
ACCEPTED 21 July 2023
PUBLISHED 14 August 2023

CITATION
Ka'e AC, Nanfack AJ, Ambada G, Santoro MM, Takou D, Semengue ENJ, Nka AD, Bala MLM, Endougou ON, Elong E, Beloumou G, Djupsa S, Gouissi DH, Fainguem N, Tchouaket MCT, Sosso SM, Kesseng D, Ndongo FA, Sonela N, Kamta ACL, Tchidjou HK, Ndomgue T, Ndiang STM, Nlend AEN, Nkenfou CN, Montesano C, Halle-Ekane GE, Cappelli G, Tiemessen CT, Colizzi V, Ceccherini-Silberstein F, Perno C-F and Fokam J (2023) Inflammatory profile of vertically HIV-1 infected adolescents receiving ART in Cameroon: a contribution toward optimal pediatric HIV control strategies. *Front. Immunol.* 14:1239877. doi: 10.3389/fimmu.2023.1239877

Inflammatory profile of vertically HIV-1 infected adolescents receiving ART in Cameroon: a contribution toward optimal pediatric HIV control strategies

Aude Christelle Ka'e[1,2*†], Aubin Joseph Nanfack[1*†], Georgia Ambada[1,3‡], Maria Mercedes Santoro[2‡], Desire Takou[1], Ezechiel Ngoufack Jagni Semengue[1], Alex Durand Nka[1], Marie Laure Mpouel Bala[1,4], Orphelie Ndoh Endougou[1,5], Elise Elong[1], Grace Beloumou[1], Sandrine Djupsa[1], Davy Hyacinthe Gouissi[1], Nadine Fainguem[1], Michel Carlos Tommo Tchouaket[1,5], Samuel Martin Sosso[1], Daniel Kesseng[6], Francis Ateba Ndongo[6,7,8], Nelson Sonela[1], Arnaud Cedric Lacmago Kamta[9,10], Hyppolite K. Tchidjou[11], Therese Ndomgue[1,4], Suzie Tetang Moyo Ndiang[12], Anne Esther Njom Nlend[13], Celine Nguefeu Nkenfou[1], Carla Montesano[2], Gregory Edie Halle-Ekane[14], Giulia Cappelli[1,15], Caroline T. Tiemessen[16], Vittorio Colizzi[1,2,17], Francesca Ceccherini-Silberstein[2], Carlo-Federico Perno[1,18] and Joseph Fokam[1,4,14*]

[1]Chantal BIYA International Reference Centre for Research on HIV/AIDS Prevention and Management (CIRCB), Yaounde, Cameroon, [2]Department of Experimental Medicine, University of Rome Tor Vergata, Rome, Italy, [3]Faculty of Science, University of Yaounde 1, Yaounde, Cameroon, [4]Faculty of Medicine and Biomedical Sciences, University of Yaoundé 1, Yaoundé, Cameroon, [5]School of Health Sciences, Catholic University of Central Africa, Yaounde, Cameroon, [6]Mother and Child Centre, Chantal BIYA Foundation, Yaounde, Cameroon, [7]Division of Operational Health Research, Ministry of Public Health, Yaounde, Cameroon, [8]Faculty of Medicine and Biomedical Sciences, University of Garoua, Garoua, Cameroon, [9]Elisabeth Glaser Pediatric AIDS Foundation (EGPAF), Country-office, Yaoundé, Cameroon, [10]HIV Management Unit, Mfou District Hospital, Mfou, Cameroon, [11]Amiens University Hospital, Amiens, France, [12]National Social Welfare Hospital, Yaounde, Cameroon, [13]Higher Institute of Medical Technology, Yaounde, Cameroon, [14]Faculty of Health Sciences, University of Buea, Buea, Cameroon, [15]National Research Council, Rome, Italy, [16]National Institute for Communicable Diseases and Faculty of Health Sciences, University of the Witwatersrand, Johannesburg, South Africa, [17]Faculty of Science and Technology, Evangelic University of Cameroon, Bandjoun, Cameroon, [18]Bambino Gesu Pediactric Hospital, Rome, Italy

Antiretroviral therapy (ART) has improved the lifespan of people living with HIV. However, their immune system remains in a state of sustained activation/inflammation, which favors viral replication and depletion of helper T-cells with varying profiles according to ART-response. We herein sought to ascertain the inflammatory profile of adolescents living with perinatal HIV-1 infection (ALPHI) receiving ART in an African context. In this cross-sectional and comparative study among ART-experienced ALPHI in Yaoundé-Cameroon, HIV-1 RNA was measured by Abbott Real-time PCR; CD4 cells were enumerated using flow cytometry;

serum cytokines were measured by ELISA; HIV-1 proviral DNA was genotyped by Sanger-sequencing; and archived drug resistance mutations (ADRMs) were interpreted using Stanford HIVdb.v9.0.1. Overall, 73 adolescents were enrolled (60 ALPHI and 13 HIV-1 negative peers) aged 15 (13-18) years; 60.00% were female. ART median duration was 92 (46-123) months; median viral load was 3.99 (3.17-4.66) RNA Log_{10} (copies)/mL and median CD4 count was 326 (201-654) cells/mm^3. As compared to HIV-negative adolescents, TNFα was highly expressed among ALPHI ($p<0.01$). Following a virological response, inflammatory cytokines (IFNγ and IL-12), anti-inflammatory cytokines (IL-4 and IL-10) and inflammation-related cytokines (IL-6 and IL-1β) were highly expressed with viral suppression (VS) vs. virological failure (VF), while the chemokine CCL3 was highly expressed with VF ($p<0.01$). Regarding the immune response, the inflammatory cytokine TNFα was highly expressed in those that are immunocompetent (CD4≥500 cell/mm^3) vs. immunocompromised (CD4<500 cell/mm^3), $p \leq 0.01$; while chemokine CCL2 was highly expressed in the immunocompromised ($p<0.05$). In the presence of ADRMs, IL-4 and CCL3 were highly expressed ($p=0.027$ and $p=0.043$ respectively). Among ART-experienced ALPHI in Cameroon, the TNFα cytokine was found to be an inflammatory marker of HIV infection; IFNγ, IL-1β, IL-6, and IL-12 are potential immunological markers of VS and targeting these cytokines in addition to antiretroviral drugs may improve management. Moreover, CCL3 and CCL2 are possible predictors of VF and/or being immunocompromised and could serve as surrogates of poor ART response.

KEYWORDS

HIV-1, inflammation, antiretroviral therapy, adolescents, cytokines, viral load, CD4

Introduction

Children and adolescents constitute a growing population of people living with HIV in developing countries, mainly due to ongoing mother to child transmission of HIV-1 (MTCT) and the benefits of antiretroviral therapy (ART) in sustaining the lifespan of infected children (1). Of note, sub-Saharan Africa (SSA) is paying the heaviest toll of pediatric HIV as ~85% of worldwide new pediatric infections occur in this region (2). Even though ART has substantially contributed to reducing HIV-1 MTCT (3), women in SSA settings (Cameroon included) (4) still face delayed HIV-1 diagnosis during pregnancy/breastfeeding, which leads to limited coverage in prevention of MTCT (PMTCT) and occurrence of new pediatric HIV-1 infections (5),

With more than 160,000 new cases of HIV-infection reported among children in 2021, pediatric HIV remains a major public health concern, thus calling for novel strategies to ensure optimal management of such a lifelong condition from childhood (1, 2). As in HIV-infected adults, ART increases the life expectancy of HIV-infected infants and children, allowing them to grow toward adulthood. However, the differential features in HIV pathogenesis between adults and children (i.e., faster disease progression and lower control of viral replication) require innovative approaches to optimize the outcomes with current pediatric ART in this underserved population (6–9). Moreover, the inability of antiretrovirals to access latent reservoirs, characterized by infected long-lived memory $CD4^+$ T lymphocytes and macrophages, results in the persistent immune activation and inflammation observed in the course of HIV-1 infection (6–8).

Several cytokines have been associated with HIV-1 infection and pathogenesis (10–14). Of note, inflammatory cytokines, including interleukins (IL)-2, IL-6, IL-12, interferon gamma (IFNγ), and tumor necrosis factor-α (TNFα), were reported to be essential for the clearance of HIV infection (10). Furthermore, IL-4, IL-5, IL-10, and IL-13 are known to be associated with disease progression (13, 15). However, such knowledge gaps still exist in the frame of pediatric HIV-infection, and specifically within sub-Saharan Africa (SSA) clinical settings.

An effective immune response against HIV must strike a balance between inflammatory and anti-inflammatory cytokines. Even though ART acts by trying to restore this equilibrium, it is still unclear how immunologic and virologic parameters of adolescents living with perinatal HIV-1 infection (ALPHI) influence circulating cytokine levels. In view of optimizing immunotherapeutic strategies toward HIV pediatric control, the objective of this study was to determine the cytokine profile of ALPHI in Cameroon and to assess the relationship between cytokine levels and the virologic or immunologic responses.

10.3389/fimmu.2023.1239877

Materials and methods

Study design

A cross-sectional observational and comparative study was conducted among 73 adolescents (60 HIV-positive and 13 HIV-negative, ratio 5:1) aged 13-18 years at the Chantal BIYA International Reference Centre for research on HIV/AIDS prevention and management (CIRCB) in Yaoundé-Cameroon for the period ranging from March to July 2019.

Briefly, 60 ART-experienced ALPHI (60.00% were female) were enrolled from reference pediatric health facilities in the city of Yaoundé-Cameroon (Essos Health Centre and the Mother-Child Centre of the Chantal BIYA Foundation), as previously described within the frame of the EDCTP READY-Study cohort (16). Additionally, 13 age-matched HIV-negative adolescents, without malaria and hepatitis B/C infections, were enrolled as a control group.

Sampling and data collection

From each participating ALPHI, the following parameters were collected: date of HIV diagnosis, age, gender, date of ART initiation, and complete ART history (duration/regimen). Then, 8 mL of whole blood was collected in EDTA tubes for immunological (CD4 count and cytokine testing) and virological (HIV-1 viral load, HIV-1 proviral DNA amplification, and sequencing) analyses.

HIV-1 RNA measurement

A reverse transcription-polymerase chain reaction (RT-PCR) assay was performed on 700µL of plasma samples using the Abbott RealTime (Abbott Park, IL, USA), an in vitro platform with a lower and upper detection limit of 40 and 10,000,000 copies/mL respectively. RT-PCR was then performed to quantify the HIV-1 viral RNA (plasma viral load, PVL) of each participant by RNA extraction from plasma followed by reverse-transcription/amplification of RNA extracts and simultaneous revelation as per the manufacturer's instructions (www.molecular.abbott/int/en/products/infectious-disease/realtime-hiv-1-viral-load). For the purpose of the study, the PVL results of each ALPHI were classified as either viral suppression (PVL<1000 copies/mL) or virological failure (PVL≥1,000 copies/mL).

Helper CD4+ T cells count

CD4+ T cells were enumerated by flow cytometry with a counter cytometer, using the CD4 easy count kit as per the manufacturer's instructions (Sysmex Partec GmbH) as previously described (17). For the purpose of the study, ALHPI were then classified as either immunocompetent (CD4 ≥ 500 cells/µL) or immunocompromised (CD4 < 500 cells/µL).

Cytokine measurement

Inflammatory (IL-1β, IL-6, IL-12, CCL2, CCL3, CCL4, IFNγ, IL-17A, and TNFα), anti-inflammatory (IL-4 and IL-10), and inflammation-related cytokine (IL-6 and TGFβ1) measurement was performed on plasma using the sandwich-based enzyme-linked immunosorbent assay (ELISA) with Multi-Analyte ELISArray (Qiagen, Frederick, Maryland, 21704, USA) following the manufacturer's recommendations (https://www.qiagen.com/us/products/discovery-and-translational research/functional-and-cell-analysis/elisa-assays/multi-analyte-elisarray-kits) (18). The optical density was measured at 450nm (OD_{450}), and the concentration in pg/mL was calculated based on the logarithmic function y=a ln(x) +b obtained through the standard curves of samples with known concentrations. OD_{450} reads between 0 and 2.5 were considered to be within the linear range for all of the analytes as instructed (https://www.qiagen.com/dk/resources/faq?id=c9815b21-393e-4cef-8968-5d4e67801aa1&lang=en).

HIV-1 DNA extraction and genotyping

HIV-1 DNA extraction was done from 200 µL of buffy coat following the protocol of the QIAamp DNA Mini Kit (Qiagen, Maryland, USA). Viral DNA extracts were directly amplified using a two-round PCR according to an in-house genotyping protocol as previously described (9). Sanger-sequencing was performed by capillary electrophoresis on ABI 3500 (Applied Biosystems) using the dye deoxy-termination chain with a set of eight sequencing primers. HIV-1 sequences were assembled and edited using Recall v.2.28 software. Edited sequences were then analyzed for the interpretation of HIV-1 archived drug resistance mutations (ADRMs) using the Stanford HIV Drug Resistance Database algorithm v.9.0.1 (https://hivdb.stanford.edu/). Sequences with more than three mutations in the reverse transcriptase (RT) and/or two mutations in the protease (PR) known to be associated with APOBEC3G/F activity were excluded due to event of hypermutation (19).

Statistical and phylogenetic analysis

Data were coded and recorded in an excel spreadsheet, cleaned, and double checked. The parameters of central tendency (median) and dispersion (interquartile range) were used to describe discontinuous variables. Categorical variables were described in terms of proportions and frequencies. A Mann-Whitney test was used to compare the mean of continuous variables between the following groups: i) ALPHI vs. uninfected adolescents; ii) ALPHI on viral suppression vs. virological failure; iii) immune-competent vs. immunocompromised ALPHI; iv) ALPHI with vs. without ADRMs. A Spearman correlation test was performed between the PVL/CD4 T cell and each cytokine. Any p-value<0.05 was considered statistically significant.

Ethical and regulatory considerations

As per the Declaration of Helsinki adopted by the 18th World Medical Assembly in 1964 with respect to international regulations for ethics and good clinical practices, ethical clearance for the present study was obtained from the National Ethics Committee for research on human health (reference N° 2021/12/CE/CNERSH/SP). Administrative authorisations were obtained from the Directorate General of CIRCB and the Directors of clinical sites. Confidentiality was ensured by the use of de-identified and anonymised datasets. Written informed consent was obtained from parents or legal guardians, and written assent was provided by each participating adolescent. For the purpose of beneficence, all laboratory results (HBV, Malaria, CD4, PVL, genotypic drug resistance testing) related to the clinical management of the study participants were provided free of charge for personalized case management toward optimal HIV treatment or treatment of any reported co-infection or comorbidity.

Results

Socio-demographic, immuno-virological, and treatment characteristics of HIV-1 infected adolescents

Out of the 60 ALPHI, 36 (60%) were female, and the median [interquartile range, IQR] age was 15 [13-18] years. All were receiving ART and the median [IQR] duration on treatment was 92 [46-123] months; 80% were on non-nucleoside reverse transcriptase inhibitor (NNRTI)-based first-line regimens. Regarding the WHO clinical staging, the majority (70%) were categorized as clinical stage I, and 16.7% were categorized as clinical stage II. Regarding virological response, the median PVL was 3.99 [3.17-4.66] log_{10}(copies/mL), of whom about three quarters (n=47) of participating ALPHI were experiencing virological failure (VL≥1000 copies/mL) as defined by WHO in our context. See detailed description in Table 1.

TABLE 1 Socio-demographic, immuno-virological, clinical, and therapeutic features of ALPHI.

Gender	Female, n (%)	36 (60.00)
	Male, n (%)	24 (40.00)
Age at enrollment, years	Median [IQR]	15 [13-18]
ART duration, months	Median [IQR]	92 [46-123]
	<60 months, n (%)	17 (28.33)
	≥60 months, n (%)	36 (60.00)
	Unknown, n (%)	7 (11.67)
ART exposition	First-line (NNRTI based regimen)	48 (80.00)
	Second line (PI based regimen)	12 (20.00)
WHO Clinical stages	I, n (%)	42 (70.00)
	II, n (%)	10 (16.67)
	III, n (%)	6 (10.00)
	IV, n (%)	2 (3.33)
	Median [IQR] (log_{10}(copies/mL))	3.99 [3.17-4.66]
Viral load, copies/mL	<1000, n (%)	13 (21.67)
	≥1000, n (%)	47 (78.33)
CD4+ T cells	Median [IQR]	326 [201-654]
	<500, n (%)	20 (62.5%)
	≥500, n (%)	12 (37.5%)

ART, Antiretroviral therapy; NNRTI, non-nucleoside reverse-transcriptase inhibitors; PI/r, ritonavir-boosted protease inhibitor; CD4, cluster of differentiation.

Profile of cytokines and HIV-1 status

Out of all cytokines measured, only the concentration of the inflammatory cytokine TNFα was significantly higher in HIV-1 infected participants compared to their HIV-negative peers ($p<0.01$), indicating its role as a marker of inflammation or immune activation (Table 2).

Profile of cytokines and virological response

The concentration of inflammatory cytokines IL-1β, IL-12, and IFNγ; anti-inflammatory cytokine IL-4; and inflammation-related cytokine IL-6 were significantly higher in ALPHI with viral suppression compared to those with virological failure; $p<0.05$ (Figure 1). Additionally, the anti-inflammatory cytokine IL-10 was also highly expressed among ALPHI experiencing viral suppression, while the chemokine CCL3 was significantly expressed among ALPHI experiencing virological failure as compared to those on viral suppression; $p<0.01$ (Figure 1) However, only cytokines IL-1β and IL-4 were negatively correlated with PVL (r= -0.44; $p<0.01$ and r= -0.27; p=0.04 respectively; Figure 2), suggesting that lower levels of IL-1β and IL-4 are associated with increased severity of PVL, while chemokine CCL2 alone was positively correlated with PVL; r= 0.36; $p<0.01$.

Profile of cytokines and immune response

According to the distribution of CD4 cells count in the study population, the median value [IQR] was 326 [201-654] cells/mm^3, of which 20 (62.5%) participants were immunocompromised (CD4<500 cells/mm^3) and 12 (37.5%) were immunocompetent (CD4≥500 cells/mm^3) as per the classification of the World Health Organization (Table 1).

One inflammatory cytokine (TNFα) was highly expressed in immunocompetent ALPHI ($p \leq 0.01$), while one anti-inflammatory

10.3389/fimmu.2023.1239877

TABLE 2 Profile of cytokines according to HIV-1 status of adolescents.

Cytokines/ Chemokines	Distribution according to HIV-1 status		*p*-value
	Negative (13) (Median [IQR] in pg/mL)	Positive (60) (Median [IQR] in pg/mL)	
IL-1β	13.8 [11.1-16.6]	10.0 [10.0 – 10.3]	0.26
IL-4	10.1 [10.0-10.2]	10.1 [10.0-10.8]	0.21
IL-6	13.9 [11.1-19.0]	10.5 [10.0-11.8]	0.08
IL-10	10.6 [10.0-12.0]	11.3 [10.0-14.0]	0.39
IL-12	13.1 [10.0-42.0]	10.2 [10.0-11.7]	0.20
IL-17A	14.8 [10.4– 19.6]	13.2 [11.3-18.0]	0.49
IFNγ	10.6 [10.0-11.0]	11.2 [10.2-14.9]	0.42
TNFα	**16.8 [14.5-18.0]**	**78.3 [55.1-112.1]**	**<0.01**
TGF-β1	234.7 [10.0-240.5]	225.4 [203.25-258.8]	0.09
CCL2	11.5 [10.0-22.4]	12.9 [10.1-90.1]	0.97
CCL3	18.1 [15.2-39.5]	10.9 [10.0-15.4]	0.24
CCL4	15.4 [10.6-20.0]	10.0 [10.0-12.1]	0.19

IL, interleukin; TGF, transformative growth factor; TNF, tumor necrosis factor.
Bold: statistical significant.

chemokine CCL2 was highly expressed in immunocompromised ALPHI ($p<0.05$), as shown in Figure 3. Interestingly, both biomarkers (TNFα and CCL2) correlated significantly with the CD4 T cell count (r= 0.42, p=0.01 and r= -0.43, p=0.01 respectively), thus confirming their clinical significance in pediatric HIV infection.

Profile of cytokines and antiretroviral therapy regimen

No significant association was found between the ART regimen (NNRTI-based versus PI/r) and the profile of studied cytokines/ chemokines (data not shown), suggesting minimal (if any) effect of

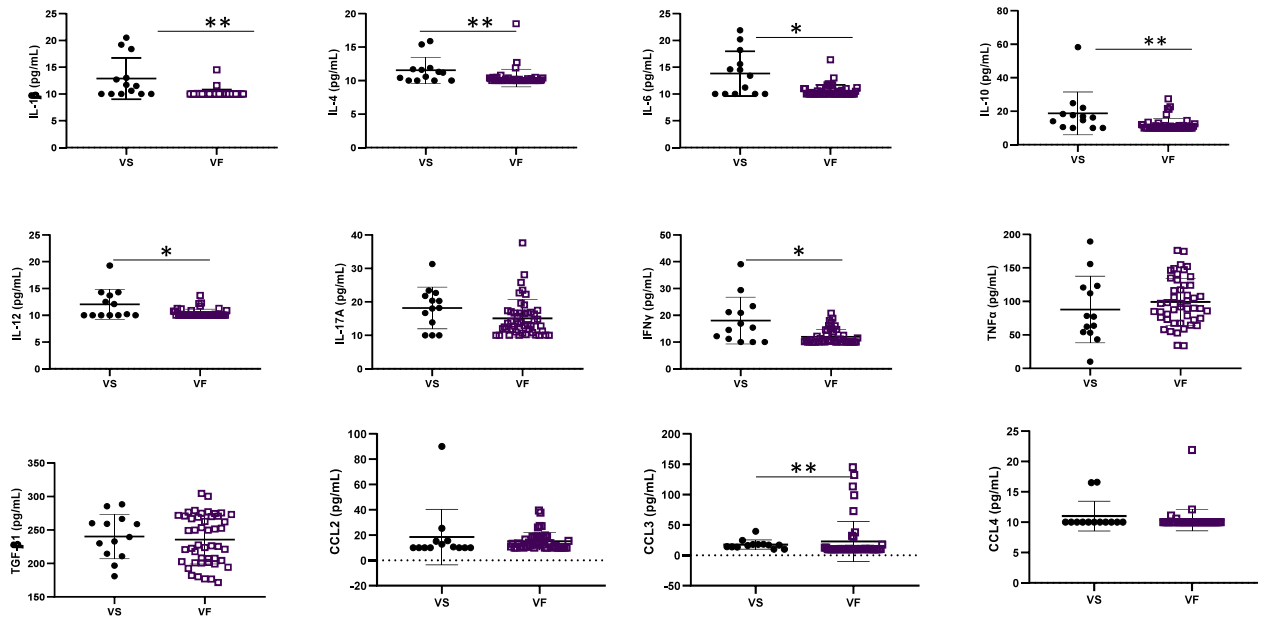

FIGURE 1
Cytokine profile according to virological response. VF, Virological failure (viral load ≥3 Log_{10}(copies/mL)); VS, Viral suppression (viral load <3 Log_{10} (copies/mL)); IL, interleukin; TGF, transformative growth factor; TNF, tumor necrosis factor; (p<0.05), ** (p<0.01). This graph shows the significant low level of inflammatory cytokines IL-12 and IFNy; anti-inflammatory cytokines IL-4 and IL-10 and the inflammation related cytokines IL-1β, IL-6 while the level of chemokine CCL3 was high in adolescents with VF as compared to those with VS.

10.3389/fimmu.2023.1239877

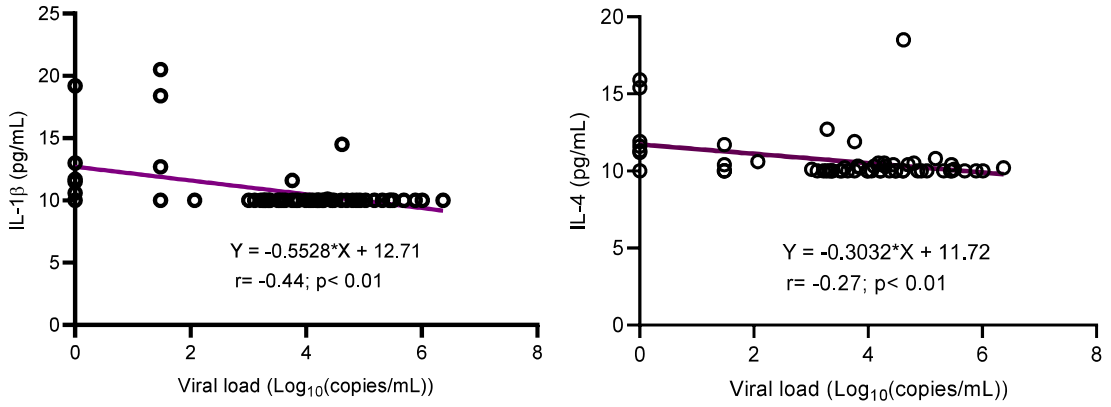

FIGURE 2
Correlation between cytokines (IL-1β and IL-4) and viral load. IL, interleukin. This graph shows the negative correlation between cytokines IL-1β/IL-4 and the plasmatic viral load highlighting the decrease of such interleukins with increasing levels of viral load.

the ART regimen on the profiling and dynamics of cytokines/chemokines during the course of HIV pediatric infection.

Profile of cytokines, HIV-1 clades, and archived drug resistance mutations

Out of 32 adolescents from whom HIV-1 genotyping was successful in proviral DNA, 22 (68.75%) were infected with CRF02_AG, 04 (12.50%) with subtype G, 01 (3.13%) with each of the following: recombinant A1/G/K, A1/G, CRF11_cpx, CRF13_cpx, CRF18_cpx, CRF37_cpx, and subtype H. There was no preferential pattern in cytokine profiling according to HIV-1 clade distribution (data not shown).

According to HIV-1 mutational profile in proviral DNA, 10 participants (31.25%) harbored archived drug resistance mutations (ARDMs), including 10/32 (31.25%) with NNRTI resistance-associated mutations, 8 (25.00%) with NRTI resistance-associated mutations, and only 1 (3.12%) with a ritonavir-boosted protease inhibitor (PI/r) resistance-associated mutation. The profile of cytokines according to the presence of ADRMs revealed that the levels of Il-4 cytokines and CCL3 were significantly higher in

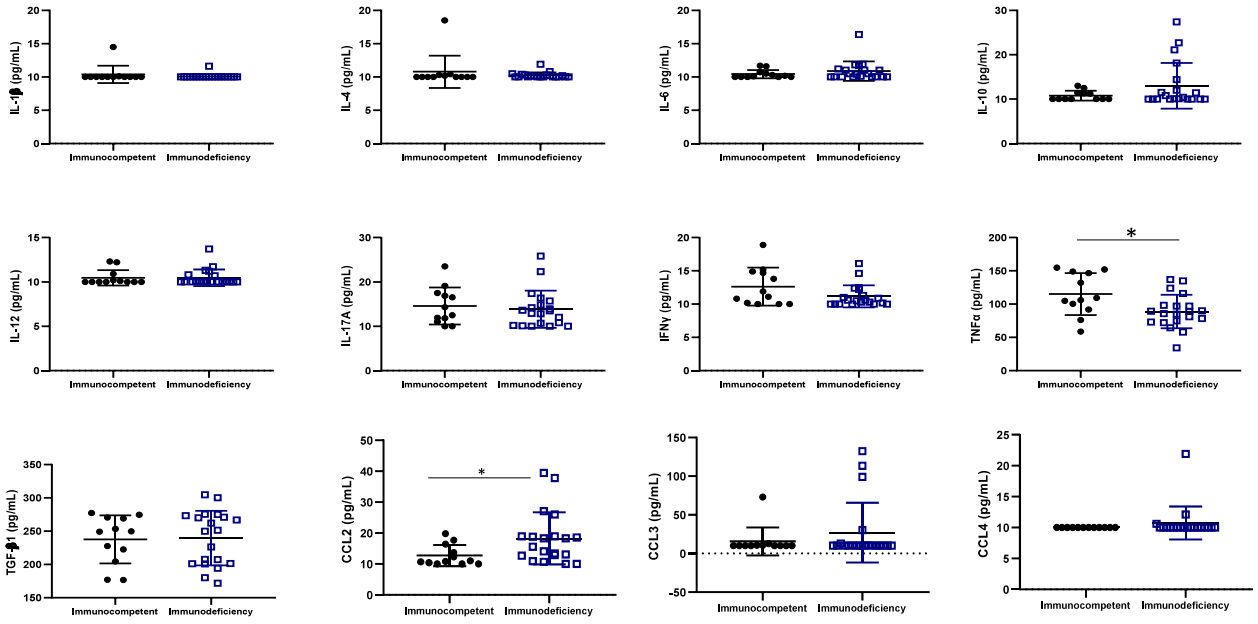

FIGURE 3
Cytokine profile according to immunocompetence. IL, interleukin; TGF, transformative growth factor; TNF, tumor necrosis factor; Immunocompetent: CD4≥500 cells/mm^3; immunodeficiency: CD4<500 cells/mm^3; * (p<0.05); N=32. This graph shows the significant high level of the inflammatory cytokine TNFα in immunocompetent adolescents as compared to those with immunodeficiency while, the level of the chemokine CCL2 was high in adolescents with immunodeficiency as compared to those with good immune response.

adolescents with ADRMs; p<0.05 (Figure 4). The other cytokines/chemokines (IL-1β, IL-6, IL-10, IL-12, MCP1, CCL4, IFNγ, IL-17A, TNFα, and TGF-β1) were not significantly associated to the presence of ADRMs (p=0.19, p= 0.85, p=0.44, p=0.57, p=0.92, p=0.14, p=0.11, p=0.71, p=0.33, p=0.81 respectively).

Discussion

With the goal to contribute to the control of pediatric HIV-infection in the era of ART and to further support the UNAIDS agenda for research into a functional HIV cure in SSA, the present study has provided new insights on the expression of inflammatory (IL-1β, IL-6, IL-12, CCL2, CCL3, CCL4, IFNγ, IL-17A and TNFα), anti-inflammatory (IL-4 and IL-10), and inflammation-related (Il-6 and TGF-β1) cytokines/chemokines in APHI in a typical SSA setting like Cameroon. Taking into consideration the ART paradigm and the high burden of pediatric HIV-infection in SSA settings like Cameroon (4, 9), this setting represents an ideal avenue for setting up baseline investigations that could pave the way for pediatric HIV cure research in this sub-region.

Among participants, the gender distribution was similar among APHI, suggesting an even distribution of the studied parameters. Moreover, the majority (4/5) of APHI were on an NNRTI-first-line ART regimen (in accordance with the proportion of national ART regimens at the time of the study implementation), and a majority (3/4) were also on a virological failure regimen. Despite the fact that the observed rate of virological response was primarily related to sampling for the purpose of our study objectives, poor ART responses among these APHI has been previously reported, driven by poor adherence and the low-genetic barrier to HIV resistance of first-generation NNRTIs that were commonly used, hence supporting transition to newer regimens (20, 21).

Regarding the profile of inflammatory cytokines, only TNFα was highly expressed among HIV-1-infected adolescents compared to their HIV-negative peers. This underscores the fact that TNFα is highly produced during HIV infection to increase antiviral immunity (22, 23) but also to induce NF-kB, which in turn drives proviral transcription and HIV replication (24). Although previous studies have indicated that TNF-α stimulates HIV-1 replication in cultured PBMC (25, 26), recent studies have found no correlation between levels of TNF-α and HIV-1 replication in lymphoid tissue (26). Further, one group has demonstrated that TNF-α suppresses HIV-1 production in peripheral blood monocytes (PBM) (27, 28). These studies indicate that TNF-α may have distinct effects on the pathogenesis of HIV.

Regarding virological response, our findings underscore a decrease in inflammation-related cytokines Il-1β and the anti-inflammatory cytokine IL-4 with increasing levels of plasmatic viral load being observed. Although during the course of HIV-1 infection the level of Il-1β is increased in different anatomical compartments, particularly in lymphatic tissues, and this elevation is associated with disease progression off-ART (29), a consequence of immune depletion and chronic immune activation following HIV replication could be the progressive decrease of the cytokines over time with antiretroviral treatment. On the other hand, HIV can directly infect and deplete specific immune cells that are responsible for producing IL-4, further contributing to its reduced levels (30) as observed in Brazilian adolescents with long ART experience (31). Inflammatory cytokines such as IL-12 and IFNγ as well as the inflammation-related cytokines IL-6 and IL-1β were lowly expressed among viral failure adolescents, while the expression of inflammatory cytokine CCL3 was higher among those experiencing virological failure. In fact the low level of IFNγ observed in a context of sub-optimal virological response was similar to what have been observed in studies conducted in Brazil and Kenya where a low concentration of IFNγ was observed in adolescents with a detectable viral load (31) and ART non-adherent people living HIV with active viral replication (32). Even though there was not significance association between TNFα and viral load, we have noticed a low level of this inflammation cytokine in adolescents with virological suppression, similarly to what observed in a USA children cohort where low levels of TNFα correlated with low levels of viral load (33). The fact that higher levels of IL-12 was observed in virally suppressed adolescents stresses the immune-stimulatory properties of this cytokine that enhances antiviral activity, thereby contributing in the control of viral replication (34). Furthermore, IL-12 is critical for promoting

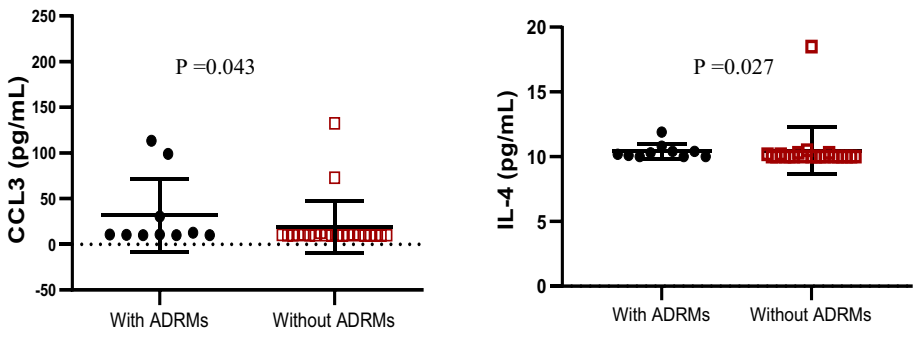

FIGURE 4
Profile of IL-4 and CCL3 according to the occurrence of ADRMs. ADRMs, Archived Drug Resistance Mutations; IL,interleukin. This graph shows the significant high level of the chemokine CCL3 as well as the cytokine IL-4 among adolescents with ADRMs.

the differentiation of CD4+ T cells into Th1 cells, which in turn restrains HIV-1 replication and disease progression. As IL-12 is also known to stimulate IFNγ (35), it might be relevant to consider this biomarker in pediatric HIV control or functional cure research strategies. Although IL-10 is generally considered to be an immunosuppressive cytokine that can inhibit antiviral immune responses and promote viral replication (34, 36), we rather observed its expression in a context of viral suppression in this subset of ALPHI and correspondingly with a study conducted in Brazil (31). Thus, IL-10 might have a complex role in HIV pathogenesis, which may be either context- or age-dependent; thereby requiring further investigations to delineate the underpinning mechanism(s).

TNFα and CCL2 are two important cytokines that play a critical role in the immune response during HIV infection. A higher expression level of TNFα was found in immune-competent compared immunocompromised ALPHI, indicating its role in controlling HIV-1 replication (37). In contrast, the high expression of CCL2 in immunocompromised APHI highlights its role in the recruitment of monocytes and other cells to sites of viral replication, leading to possible immune dysfunction (38). Thus, strategies to minimize the expression of CCL2 may strengthen the pediatric immune response, which in turn would support immune normalization and better control of HIV replication.

Looking at the profile of cytokines according to ADRMs, only IL-4 and CCL3 were highly expressed in the presence of ADRMs. To the best of our knowledge, there is currently no evidence to suggest that these biomarkers (IL-4 and CCL3) can influence archiving of HIV-1 drug resistance mutations (39). While calling for further investigations, IL-4 is known to promoting survival of CD4+ T cells (i.e., primary targets for HIV-1 infection) (39), either by impairing HIV-1 replication/transcription in infected cells or by limiting the viral cytopathic effect, which consequently favors viral archiving in cellular reservoirs (40). Inversely, IL-4 may also increase the expression of certain proteins (Tat) involved in HIV-1 replication, thereby enhancing the transcription of viral genes under sub-optimal ART (41). Thus, in the frame of a fully functional ART, exploring the role of IL-4 as a possible adjuvant to sustained viral control may contribute to future off-ART strategies investigational approaches in pediatrics.

Conclusion

Among ALPHI on ART, evidence of the expression level of cytokines and chemokines shows that TNFα is a specific inflammatory marker contributing to chronic immune activation in the course of pediatric HIV-infection. Regarding the response to ART, IFNγ, IL-1β, IL-6, and IL-12 appear as biomarkers of viral suppression, which highlights their roles as potential adjuvants (in the frame of ART success) toward the development of an optimal pediatric HIV control or functional cure strategy. Furthermore, as CCL2 and CCL3 are associated with virological failure and poor immunity, downregulating these markers may contribute to viral control strategies.

Data availability statement

The original contributions presented in the study are included in the article/supplementary material. Further inquiries can be directed to the corresponding authors.

Ethics statement

The studies involving humans were approved by National Ethics Committee for research on human health. The studies were conducted in accordance with the local legislation and institutional requirements. Written informed consent for participation in this study was provided by the participants' legal guardians/next of kin.

Author contributions

AJN, JF, and GA conceived the study. ACK, MM, GB, and SD enrolled participants. DT, MM, ON, GB, and SD analyzed samples. ACK, AJN, EN, and ON performed the statistical analysis. JF, C-FP, VC, TN, FC, MS, CN, GH-E, and CT interpreted the data; ACK, JF, AJN, and GA drafted the manuscript. AJN, ADN, EN, NF, MT, SS, DK, FA, NS, AL, TN, ST, AEN, CN, CM, GH-E, CT, VC, MS, FC, C-FP, and JF revised the manuscript. AJN and JF supervised the work. All authors contributed to the article and approved the submitted version.

Funding

This work was supported by the Chantal Biya International Reference Centre for Research on HIV/AIDS Prevention and Management (CIRCB) and the European and Developing Countries Clinical Trials Partnerships, through the following grant agreements: READY-Study (TMA2015-CDF1027); and AVIR-Study (TMA2020-CDF3228).

Conflict of interest

The authors declare that the research was conducted in the absence of any commercial or financial relationships that could be construed as a potential conflict of interest.

Publisher's note

References

1. UNICEF. *HIV and AIDS in Adolescents*. New York City, New York, USA: UNICEF Data. Unicef (2021). Available at: https://data.unicef.org/topic/adolescents/hiv-aids/.

2. UNAIDS. *Global HIV Statistics*. Geneva, Switzerland: Fact Sheet 2021 (2022) p. 1–3. Available at: https://www.unaids.org/sites/default/files/media_asset/UNAIDS_FactSheet_en.pdf.

3. Astawesegn FH, Stulz V, Conroy E, Mannan H. Trends and effects of antiretroviral therapy coverage during pregnancy on mother – to – child transmission of HIV in Sub – Saharan Africa . Evidence from panel data analysis. *BMC Infect Dis* (2022) 22:1–13. doi: 10.1186/s12879-022-07119-6

4. Ka'e AC, Nka AD, Yagai B, Kammogne ID, Ngoufack Jagni Semengue E, Nanfack AJ, et al. The mother-to-child transmission of HIV-1 and profile of viral reservoirs in pediatric population: A systematic review with meta-analysis of the Cameroonian studies. *PloS One* (2023) 18:1–19. doi: 10.1371/journal.pone.0278670

5. Endalamaw A, Demsie A, Eshetie S, Habtewold TD. A systematic review and meta-analysis of vertical transmission route of HIV in Ethiopia. *BMC Infect Dis* (2018) 18:1–11. doi: 10.1186/s12879-018-3189-3

6. Brenchley JM. Mucosal immunity in human and simian immunodeficiency lentivirus infections. *Mucosal Immunol* (2013) 6:657–65. doi: 10.1038/mi.2013.15

7. Khaitan A, Unutmaz D. Revisiting immune exhaustion during HIV infection. *Curr HIV/AIDS Rep* (2011) 8:4–11. doi: 10.1007/s11904-010-0066-0

8. Paiardini M, Müller-Trutwin M. HIV-associated chronic immune activation. *Immunol Rev* (2013) 254:78–101. doi: 10.1111/imr.12079

9. Fokam J, Mpouel Bala ML, Santoro MM, Takou D, Tala V, Beloumou G, et al. Archiving of mutations in HIV-1 cellular reservoirs among vertically infected adolescents is contingent with clinical stages and plasma viral load: Evidence from the EDCTP-READY study. *HIV Med* (2021) 00:1–10. doi: 10.1111/hiv.13220

10. Chavan V R, Ahir S, Kerkar S, Ansari Z, Samant-Mavani P, Nanavati R, et al. Th1 cytokine gene polymorphism and the corresponding plasma cytokine levels: A comparative study in HIV-1 positive and exposed uninfected infants. *J Med Virol* (2022) 94:625–33. doi: 10.1002/jmv.27408

11. Naicker DD, Werner L, Kormuth E, Passmore JA, Mlisana K, Karim SA, et al. Interleukin-10 promoter polymorphisms influence HIV-1 susceptibility and primary HIV-1 pathogenesis. *J Infect Dis* (2009) 200:448–52. doi: 10.1086/600072

12. Shrestha S, Wiener HW, Aissani B, Song W, Shendre A, Wilson CM, et al. Interleukin-10 (IL-10) pathway: Genetic variants and outcomes of HIV-1 infection in African American adolescents. *PloS One* (2010) 5:1–8. doi: 10.1371/journal.pone.0013384

13. Clerici M, Shearer GM. A THI- T . 2 switch is a critical step in the etiology of HIV infection. *Immunol Today* (1993) 14:107–11. doi: 10.1016/0167-5699(93)90208-3

14. Graziosi C, Pantaleo G, Gantt KR, Fortin J, James F, Cohen OJ, et al. Lack of evidence for the dichotomy of th1 and th2 predominance in hiv-infected individuals. *Science* (1994) 265:248–52. doi: 10.1126/science.8023143

15. Clerici M, Wynn TA, Berzofsky JA, Blatt SP, Hendrix CW, Sher A, et al. Role of interleukin-10 in T helper cell dysfunction in asymptomatic individuals infected with the human immunodeficiency virus. *J Clin Invest* (1994) 93:768–75. doi: 10.1172/JCI117031

16. Fokam J, Santoro MM, Takou D, Njom-Nlend AE, Ndombo PK, Kamgaing N, et al. Evaluation of treatment response, drug resistance and HIV-1 variability among adolescents on first- And second-line antiretroviral therapy: A study protocol for a prospective observational study in the centre region of Cameroon (EDCTP READY-study). *BMC Pediatr* (2019) 19:1–11. doi: 10.1186/s12887-019-1599-z

17. Abba A, Fokam J, Kamgaing RS, Yimga JF, Kae AC, Nka AD, et al. Correlation between the immuno-virological response and the nutritional profile of treatment-experienced HIV-infected patients in the East region of Cameroon. *PloS One* (2021) 16:1–15. doi: 10.1371/journal.pone.0229550

18. Profile P. Multi-Analyte ELISArray Kits For analysis of multiple cytokines or chemokines Sample & Assay Technologies Sample & Assay Technologies., 2–3.

19. Tzou PL, Kosakovsky Pond SL, Avila-Rios S, Holmes SP, Kantor R, Shafer RW. Analysis of unusual and signature APOBEC-mutations in HIV-1 pol next-generation sequences. *PloS One* (2020) 15:1–16. doi: 10.1371/journal.pone.0225352

20. Ding H, Wilson CM, Modjarrad K, McGwin G, Tang J, Vermund SH. Predictors of suboptimal virologic response to highly active antiretroviral therapy among human immunodeficiency virus-infected adolescents: Analyses of the Reaching for Excellence in Adolescent Care and Health (REACH) Project. *Arch Pediatr Adolesc Med* (2009) 163:1100–5. doi: 10.1001/archpediatrics.2009.204

21. Eshleman SH, Krogstad P, Jackson JB, Wang YG, Lee S, Wei LJ, et al. Analysis of human immunodeficiency virus type 1 drug resistance in children receiving nucleoside analogue reverse-transcriptase inhibitors plus nevirapine, nelfinavir, or ritonavir (Pediatric AIDS Clinical Trials Group 377). *J Infect Dis* (2001) 183:1732–8. doi: 10.1086/320728

22. Stacey AR, Norris PJ, Qin L, Haygreen EA, Taylor E, Heitman J, et al. Induction of a striking systemic cytokine cascade prior to peak viremia in acute human immunodeficiency virus type 1 infection, in contrast to more modest and delayed responses in acute hepatitis B and C virus infections. *J Virol* (2009) 83:3719–33. doi: 10.1128/jvi.01844-08

23. Abel K, Rocke DM, Chohan B, Fritts L, Miller CJ. Temporal and Anatomic Relationship between Virus Replication and Cytokine Gene Expression after Vaginal Simian Immunodeficiency Virus Infection. *J Virol* (2005) 79:12164–72. doi: 10.1128/jvi.79.19.12164-12172.2005

24. Katsikis PD, Mueller YM, Villinger F. The cytokine network of acute hiv infection: A promising target for vaccines and therapy to reduce viral set-point? *PloS Pathog* (2011) 7:1–6. doi: 10.1371/journal.ppat.1002055

25. Mellors JW, Griffith BP, Ortiz MA, Landry ML, Ryan JL, The S, et al. Tumor necrosis factor-α / cachectin enhances human immunodeficiency virus type 1 replication in primary macrophages. *J Infect Dis* (1991) 163:78-82. doi: 10.1093/infdis/163.1.78

26. Li Q, Gebhard K, Schacker T, Henry K, Haase AT. The relationship between tumor necrosis factor and human immunodeficiency virus gene expression in lymphoid tissue. *J Virol* (1997) 71:7080–2. doi: 10.1128/jvi.71.9.7080-7082.1997

27. Herbein G, Montaner LJ, Gordon S. Tumor necrosis factor alpha inhibits entry of human immunodeficiency virus type 1 into primary human macrophages: a selective role for the 75-kilodalton receptor. *J Virol* (1996) 70:7388–97. doi: 10.1128/jvi.70.11.7388-7397.1996

28. Herbein G, Gordon S. 55- and 75-kilodalton tumor necrosis factor receptors mediate distinct actions in regard to human immunodeficiency virus type 1 replication in primary human macrophages. *J Virol* (1997) 71:4150–6. doi: 10.1128/jvi.71.5.4150-4156.1997

29. Yaseen MM NMA. H D. The role of IL-1β during human immunodeficiency virus type 1 infection. *Rev Med Virol* (2023) 33. doi: 10.1002/rmv.2400

30. Vijayan KV, Karthigeyan KP, Tripathi SP, Hanna LE. Pathophysiology of CD4+ T-Cell depletion in HIV-1 and HIV-2 infections. *Front Immunol* (2017) 8:580. doi: 10.3389/fimmu.2017.00580

31. Gustavo L, Munhoz C, Spina FG, MaChado DM. Prolonged antiretroviral therapy in adolescents with vertical HIV infection leads to different cytokine profiles depending on viremia persistence. *Pediatr Infect Dis J* (2019) 38:1115–20. doi: 10.1097/INF.0000000000002446

32. Musa F, Shaviya N, Mambo F, Abonyo C, Barasa E, Wafula P, et al. Cytokine profiles in highly active antiretroviral treatment non-adherent, adherent and naive HIV-1 infected patients in Western Kenya. *Afr Health Sci* (2021) 21:1584–92. doi: 10.4314/ahs.v21i4.12

33. Than S, Hu R, Oyaizu N, ROmano J. Cytokine pattern in relation to disease progression in human immunodeficiency virus- infected children. *J Infect Dis* (1997) 175:47-56. doi: 10.1093/infdis/175.1.47.

34. Liu J, Zhan W, Kim CJ, Clayton K, Zhao H, Lee E, et al. IL-10-producing B cells are induced early in HIV-1 infection and suppress HIV-1-specific T cell responses. *PloS One* (2014) 9:1–13. doi: 10.1371/journal.pone.0089236

35. Kano SI, Sato K, Morishita Y, Vollstedt S, Kim S, Bishop K, et al. The contribution of transcription factor IRF1 to the interferon-γ-interleukin 12 signaling axis and TH1 versus TH-17 differentiation of CD4+ T cells. *Nat Immunol* (2008) 9:34–41. doi: 10.1038/ni1538

36. Jiang Y, Yang M, Sun X, Chen X, Ma M, Yin X, et al. IL-10+ NK and TGF-β+ NK cells play negative regulatory roles in HIV infection. *BMC Infect Dis* (2018) 18:80. doi: 10.1186/s12879-018-2991-2

37. Vaidya SA, Korner C, Sirignano MN, Amero M, Bazner S, Rychert J, et al. Tumor necrosis factor α is associated with viral control and early disease progression in patients with HIV type 1 infection. *J Infect Dis* (2014) 210:1042–6. doi: 10.1093/infdis/jiu206

38. Deshmane SL, Kremlev S, Amini S, Sawaya BE. Monocyte chemoattractant protein-1 (MCP-1): An overview. *J Interf Cytokine Res* (2009) 29:313–25. doi: 10.1089/jir.2008.0027

39. Silva-Filho JL, Caruso-Neves C, Pinheiro AAS. IL-4: An important cytokine in determining the fate of T cells. *Biophys Rev* (2014) 6:111–8. doi: 10.1007/s12551-013-0133-z

40. Valentin A, Lu W, Rosati M, Schneider R, Albert J, Karlsson A, et al. Dual effect of interleukin 4 on HIV-1 expression: Implications for viral phenotypic switch and disease progression *Proc Natl Acad Sci USA* (1998) 95:8886-91. doi: 10.1073/pnas.95.15.8886.

41. Rafat Husain S, Leland P, Aggarwal BB, Puri1 RK. Transcriptional up-regulation of interleukin 4 receptors by human immunodeficiency virus type 1 tat gene. *AIDS Res Hum Retroviruses* (1996) 12:1349–59. doi: 10.1089/aid.1996.12.1349

frontiers | Frontiers in Immunology

TYPE Original Research
PUBLISHED 02 February 2023
DOI 10.3389/fimmu.2023.1115894

OPEN ACCESS

EDITED BY
Diana Boraschi,
Shenzhen Institute of Advanced Technology (SIAT) (CAS), China

REVIEWED BY
Maria Laura Manca,
University of Pisa, Italy
Enzo Iuliano,
eCampus University, Italy

*CORRESPONDENCE
Susanne Dam Nielsen
susanne.dam.poulsen@regionh.dk
Sylvester Klöcker Grønbæk
sylvester.kloecker.groenbaek@regionh.dk

SPECIALTY SECTION
This article was submitted to Cytokines and Soluble Mediators in Immunity, a section of the journal Frontiers in Immunology

RECEIVED 04 December 2022
ACCEPTED 23 January 2023
PUBLISHED 02 February 2023

CITATION
Grønbæk SK, Høgh J, Knudsen AD, Pham MHC, Sigvardsen PE, Fuchs A, Kühl JT, Køber L, Gerstoft J, Benfield T, Ostrowski SR, Kofoed KF and Nielsen SD (2023) Aortic aneurysms and markers of platelet activation, hemostasis, and endothelial disruption in people living with HIV.
Front. Immunol. 14:1115894.
doi: 10.3389/fimmu.2023.1115894

Aortic aneurysms and markers of platelet activation, hemostasis, and endothelial disruption in people living with HIV

Sylvester Klöcker Grønbæk[1]*, Julie Høgh[1], Andreas Dehlbæk Knudsen[1], Michael Huy Cuong Pham[2], Per Ejlstrup Sigvardsen[2], Andreas Fuchs[2], Jørgen Tobias Kühl[2], Lars Køber[2,3], Jan Gerstoft[1,3], Thomas Benfield[4], Sisse Rye Ostrowski[3,5], Klaus Fuglsang Kofoed[2,3,6] and Susanne Dam Nielsen[1,3]*

[1]Department of Infectious Diseases, Copenhagen University Hospital, Rigshospitalet, Copenhagen, Denmark, [2]Department of Cardiology, The Heart Center, Copenhagen University Hospital, Rigshospitalet, Copenhagen, Denmark, [3]Department of Clinical Medicine, University of Copenhagen, Copenhagen, Denmark, [4]Center of Research and Disruption of Infectious Diseases, Department of Infectious Diseases, Copenhagen University Hospital, Amager and Hvidovre, Hvidovre, Denmark, [5]Department of Clinical Immunology, Copenhagen University Hospital, Rigshospitalet, Copenhagen, Denmark, [6]Department of Radiology, Copenhagen University Hospital, Rigshospitalet, Copenhagen, Denmark

Introduction: People living with HIV (PLWH) are at twice the risk of developing cardiovascular diseases and have more than four times higher odds of aortic aneurysm (AA) than the uninfected population. However, biomarkers of AA in PLWH are yet to be discovered. We aimed to investigate whether circulating biomarkers reflecting platelet activation, hemostasis and endothelial disruption, i.e. sCD40L, D-dimer, syndecan-1, and thrombomodulin, were associated with AA in PLWH.

Methods: Five hundred seventy one PLWH from the Copenhagen Comorbidity in HIV Infection (COCOMO) study ≥40 years of age with an available contrast-enhanced CT scan as well as available biomarker analyses were included. The biomarkers were analyzed on thawed plasma. For each biomarker, we defined high level as a concentration in the upper quartile and low level as a concentration below the upper quartile. For D-dimer, the cut-off was defined as the lower limit of detection. Using unadjusted and adjusted logistic and linear regression models, we analyzed associations between AA and sCD40L, D-dimer, syndecan-1, and thrombomodulin, respectively in PLWH.

Results: PLWH had median (IQR) age 52 years (47-60), 88% were male, median (IQR) time since HIV diagnosis was 15 years (8-23), and 565 (99%) were currently on antiretroviral treatment. High level of sCD40L was associated with lower odds of AA in both unadjusted (odds ratio, OR, 0.23 (95% CI 0.07-0.77; *P*=0.017)) and adjusted models (adjusted OR, aOR, 0.23 (95% CI 0.07-0.78; *P*=0.019)). Detectable level of D-dimer was associated with higher odds of AA in both unadjusted (OR 2.76 (95% CI 1.34-5.67; *P*=0.006)) and adjusted models (aOR 2.22 (95% CI 1.02-4.85; *P*=0.045)).

Conclusions: SCD40L was associated with lower odds of AA whereas D-dimer was independently associated with higher odds of AA in PLWH. This calls for further investigations into specific biomarkers to aid early diagnosis of AA in PLWH.

KEYWORDS

HIV, PLWH, aortic aneurysm, sCD40L, D-dimer (DD), syndecan-1, thrombomodulin (TM)

1 Introduction

As the median age of people living with HIV (PLWH) increases (1), so does the burden of age-related comorbidities (2). The risk of incident cardiovascular diseases (CVD) in PLWH is twice that of uninfected individuals (3), with myocardial infarction, stroke, and coronary artery disease being the most frequent manifestations (4). In a previous study by our group, HIV infection was associated with a 4.5 increased odds ratio (OR) of having aortic aneurysms (AA) compared to uninfected controls (5). AA is a rare but potentially severe manifestation of CVD, as the mortality rate of a ruptured abdominal AA may be as high as 80% (6). The European Society of Cardiology recommends screening of populations with a high risk of abdominal AA (7), because most AA are asymptomatic and diagnosed incidentally (8).

The initial phase of the pathogenesis of AA is not fully understood, but studies have suggested endothelial cell injury to contribute (9, 10). Associations have been found between AA, in the majority of studies in patients undergoing surgery for AA, and a marker of platelet activation, soluble CD40L (sCD40L) (11, 12), a marker of hemostasis, D-dimer (13–17), and the markers of endothelial disruption, syndecan-1 (18–20) and soluble thrombomodulin (21, 22), respectively. Importantly, all of these biomarkers have been reported to be elevated in PLWH compared to uninfected controls (23–28).

Possible associations between these biomarkers and AA have yet to be established but could aid in the early identification of high-risk patients. So far, no studies on the association between AA and markers of platelet activation, hemostasis, and endothelial disruption, respectively, in PLWH have been published. Thus, we investigated whether sCD40L, D-dimer, syndecan-1, and thrombomodulin (the biomarkers) are associated with AA in a large cohort of well-treated PLWH. We hypothesized that each of the biomarkers would be independently associated with AA in PLWH.

2 Materials and methods

2.1 Study design and population

The Copenhagen Comorbidity in HIV Infection (COCOMO) study is a non-interventional cohort study that aims to assess non-AIDS comorbidities in PLWH. Inclusion criteria were age above 18 years and a positive HIV test. Between March 2015 and December 2016, 1099 PLWH living in the greater Copenhagen area were included. Procedures for recruitment and collection of data have previously been described elsewhere (29). A combined thoracic and abdominal contrast-enhanced computed tomography (CT) scan was offered to all COCOMO participants. In this study, we included COCOMO participants who were ≥40 years of age, had a contrast-enhanced CT performed, and had biomarkers measured in plasma.

Written informed consent was obtained from all participants. Ethical approval was obtained by the Regional Ethical Committee of Copenhagen (COCOMO: H-8-2014-004). The study was carried out in accordance with the Declaration of Helsinki.

2.2 Clinical characteristics and self-reported outcome

A physical examination including measurement of blood pressure and anthropometrics was performed by trained clinical staff. Venous blood was collected non-fasting. Blood for plasma samples (EDTA anti-coagulated) was stored on ice until centrifugation in a cold centrifuge at 4°C, and cryovials were transferred to liquid nitrogen within 72 hours (29). Extensive questionnaires included questions regarding medication, medical history, and smoking. From medical records, HIV-specific data such as transmission mode, duration of HIV infection, type of antiretroviral therapy, and hepatitis B and C status were obtained. Hepatitis B virus co-infection was defined as positive hepatitis B virus surface-antigen and hepatitis C virus co-infection as positive hepatitis C virus RNA. Hypertension was defined as systolic blood pressure ≥140 mmHg and/or diastolic blood pressure ≥90 mmHg and/or current use of antihypertensive medication according to Joint National Committee guidelines (30).

2.3 CT examinations and aortic analyses

Contrast-enhanced thoracic and abdominal CT examinations including contrast-enhanced CT angiography were performed using a 320-detector CT scanner (Aquilion ONE, ViSION Edition, Canon Medical Systems, Otawara, Japan) at Rigshospitalet University Hospital, Copenhagen, Denmark.

Aortic analyses were performed by two trained examiners on contrast-enhanced CT images. Maximal and minimal inner aortic diameter was measured at seven anatomical points of the aorta, in four of which maximal outer diameter of the aorta was measured as

Abbreviations: PLWH, People living with HIV; CVD, Cardiovascular diseases; AA, Aortic aneurysms; sCD40L, Soluble CD40 ligand; FEU, Fibrin Equivalent Units; ET-1, Endothelin-1; OR, Odds ratio; aOR, Adjusted odds ratio; CI, Confidence interval; SD, Standard deviation.

well (5). According to the European Society of Cardiology guidelines, aortic aneurysms were defined as ≥50% increase in aortic diameter compared to the expected normal diameter or an infrarenal diameter of ≥30 mm (7). This resulted in the definition of AA as diameter of ascending aorta ≥45 mm and/or diameter of descending aorta ≥35 mm and/or diameter of suprarenal aorta ≥30 mm and/or diameter of the infrarenal aorta ≥30 mm (31).

2.4 Markers of platelet activation, hemostasis, and endothelial disruption

Plasma concentrations of sCD40L, soluble syndecan-1, and thrombomodulin, were analyzed on thawed plasma using Luminex® Human Discovery Assays (R&D Systems, UK, Europe) in a 1:2 dilution, according to the manufacturer's instructions, at the Department of Clinical Immunology, Copenhagen University Hospital, Rigshospitalet, Copenhagen, Denmark. Plasma concentrations of D-dimer were measured as routine biochemistry on fresh blood samples at Department of Clinical Biochemistry, Copenhagen University Hospital, Herlev, Copenhagen, Denmark (29).

2.5 Statistics

Continuous data were reported using means and standard deviations for normal deviates and medians with interquartile ranges for variables not normally distributed, as appropriate. For categorical data, frequency counts and percentages of subjects within each category were reported. Logistic regression analyses were applied where the dependent variable was binary and linear regression where the dependent variable was continuous.

As the primary outcome, we investigated the association between AA and high levels of sCD40L, syndecan-1, and thrombomodulin and detectable level of D-dimer one at a time using simple and multivariable logistic regression. For each biomarker, we created a dichotomous variable defining high level of the biomarker as a concentration in the upper quartile and low level as a concentration below the upper quartile. We used the third quartile as cut-off in the dichotomous variables for sCD40L, syndecan-1 and thrombomodulin to make the effect estimates more easily interpretable. For D-dimer, the cut-off was defined as the lower limit of detection (290 ng/mL (Fibrin Equivalent Units, FEU)), creating a dichotomous variable with detectable versus undetectable as most of the measurements were below the lower limit of detection. We created two predefined models; model 1 adjusted for age (per decade) and sex and model 2 adjusted for traditional risk factors that were significant in previous analyses on AA in PLWH (5) (age, sex, BMI category, hypertension, and smoking (current/previous/never)). Furthermore, in sensitivity analyses, we investigated the associations between AA, sCD40L, and (one at a time) use of aspirin, use of statins, weekly alcohol intake, and hypertension. As a sensitivity analysis, we included all four biomarkers into a single analysis with AA.

Additionally, continuous variables were used in pre-specified, secondary analyses to make sure any linear associations between exposure and outcome would not be overlooked. We adjusted for the same predefined models 1 and 2. Moreover, in sensitivity analyses, we investigated associations between aortic diameter (maximum outer diameter of ascending, descending, suprarenal, and infrarenal aorta) and high versus low levels of the biomarkers. Lastly, in sensitivity analyses, we examined associations between aortic wall thickness (maximal outer minus maximal inner diameter of ascending, descending, suprarenal, and infrarenal aorta) and high versus low levels of the biomarkers.

P-values <0.05 were considered statistically significant, and all P-values were two-sided. R (version 4.1.0 (2021-05-18)) was used for all statistical analyses (32).

3 Results

We included 571 participants aged 40 years or older with available contrast-enhanced CT and biomarker measurements. As reported previously, 43 aneurysms were found in 39 PLWH (6.8%). The median (IQR) age of PLWH was 52 years (47-60) and 88% were male (Table 1). The median (IQR) time since HIV diagnosis was 15 years (8-23) and 565 (99%) were currently on antiretroviral therapy (Table 1). Participant characteristics, HIV-specific variables, and biomarkers are listed in Table 1.

TABLE 1 Participant characteristics, HIV-specific risk factors, and concentrations of the biomarkers.

Variable	PLWH (N=571)
Characteristics	
Age, median [IQR]	51.6 [47.0-59.8]
Male sex, n (%)	503 (88.1%)
BMI, mean (SD)	24.8 (3.5)
BMI classification, n (%)	
Underweight	14 (2.5%)
Normal weight	301 (52.7%)
Pre-obesity	211 (37.0%)
Obesity	43 (7.5%)
Smoking status, n (%)	
Never smoker	188 (32.9%)
Current smoker	152 (26.6%)
Previous smoker	219 (38.4%)
Hypertension, n (%)	263 (46.1%)
Platelets, $\times 10^9$/L, mean (SD)	226.8 (57.5)
HIV-specific risk factors	

(Continued)

10.3389/fimmu.2023.1115894

TABLE 1 Continued

Variable	PLWH (N=571)
Transmission mode, n (%)	
MSM	415 (72.7%)
Heterosexual	116 (20.3%)
IDU	6 (1.1%)
Other	28 (5%)
Current $CD4^+$, cells/μL, median [IQR]	680 [520-870]
<200	7 (1.2%)
200-349	34 (6.0%)
350-499	79 (13.8%)
≥500	446 (78.1%)
$CD4^+$ nadir <200, n (%)	235 (41.2%)
$CD4^+/CD8^+$-ratio, median [IQR]	0.813 [0.578-1.13]
Time since HIV diagnosis, median [IQR]	15.1 [7.74-22.6]
Time on ART, median [IQR]	12.8 [5.94-17.8]
Currently on ART, n (%)	565 (98.9%)
Viral load >50	23 (4.0%)
Hepatitis B-virus co-infection, n (%)	18 (3.2%)
Hepatitis C-virus co-infection, n (%)	33 (5.8%)
Concentrations of the biomarkers	
Syndecan-1, pg/mL, median [IQR]	2070 [1801-2413]
Thrombomodulin, pg/mL, median [IQR]	6598 [5541-7823]
sCD40L, pg/mL, median [IQR]	184 [118-243]
D-dimer, ng/mL (FEU), median [IQR]	290 [290-290]

ART, antiretroviral therapy; IDU, injecting drug use; MSM, men who have sex with men; FEU, fibrin equivalent units.

3.1 Aortic aneurysms and the association with markers of platelet activation, hemostasis, and endothelial disruption

We found high levels of sCD40L to be associated with lower odds of AA; univariably with OR 0.23 (95% CI 0.07-0.77; *P*=0.017) and adjusted odds ratio, aOR, 0.23 (95% CI 0.07-0.78; *P*=0.019) adjusted in model 2 (Table 2). In a sensitivity analysis, further adjustment of model 2 for use of aspirin did not significantly alter the association between high level of sCD40L and AA (aOR 0.25 (95% CI 0.07-0.87); *P*=0.029). In other sensitivity analyses, use of statins, weekly alcohol intake, and hypertension were not associated with AA and sCD40L.

Detectable level of D-dimer was associated with higher odds of AA, both univariably (OR 2.76 (95% CI 1.34-5.67; *P*=0.006)) and adjusted in model 1 (aOR 2.22 (95% CI 1.02-4.85; *P*=0.045)). Adjusting for traditional risk factors in model 2 did not change the parameter estimate, (aOR 2.24 (95% CI 0.99-5.04; *P*=0.052). There were aortic aneurysms among PLWH with undetectable D-dimer.

Syndecan-1 and thrombomodulin were not associated with AA (Table 2).

Including all four biomarkers into a single analysis did not significantly alter the associations compared to the individual associations between the biomarkers and AA.

In exploratory analyses with the biomarkers as continuous variables, a doubling in sCD40L concentration was associated with lower odds of AA; univariably with OR 0.81 (95% CI 0.66,0.98; *P*=0.028) and aOR 0.76 (95% CI 0.62-0.95; *P*=0.014) adjusted in model 2. A twofold increase in D-dimer concentration was associated with higher odds of AA; univariably with OR 1.51 (95% CI 1.22-1.86; *P*<0.001) and aOR 1.41 (95% CI 1.08-1.84; *P*=0.010) adjusted in model 2. Syndecan-1 was not significantly associated with AA. A twofold increase in thrombomodulin concentration was univariably associated with higher odds of AA (OR 1.82 (95% CI 1.02-3.26; *P*=0.043) but not in adjusted models (Table 3). Analyses of high versus low levels and with continuous variables are shown in Figure 1.

3.2 Aortic diameter and the association with markers of platelet activation, hemostasis, and endothelial disruption

The mean (SD) aortic diameters are presented in Figure 2 and Table 4. Diameter in ascending aorta 34.54 mm (4.30); in descending aorta 26.36 mm (2.70); in suprarenal aorta 24.97 mm (2.82); and in infrarenal aorta 21.65 mm (3.17). In sensitivity analyses, high level of sCD40L was associated with smaller suprarenal aortic diameter (0.46 mm (95% CI 0.01-0.91; *P*=0.045)) adjusted in model 2 but not univariably (0.40 mm (95% CI 0.14-0.93; *P*=0.144)). Detectable level of D-dimer was associated with larger infrarenal aortic diameter; univariably 1.11 mm (95% CI 0.38-1.84; *P*=0.003) and 0.97 mm (95% CI 0.30-1.63; *P*=0.004) adjusted in model 2. High level of syndecan-1 was univariably associated with larger diameter of the ascending aorta (1.04 mm (95% CI 0.23-1.85; *P*=0.012)) and with larger infrarenal aortic diameter (0.95 mm (95% CI 0.36-1.55; *P*=0.002)). High level of thrombomodulin was associated with larger infrarenal aortic diameter; univariably 1.41 mm (95% CI 0.82-2.00; *P*<0.0001) and 0.89 mm (95% CI 0.38-1.41; *P*<0.001) adjusted in model 2. Furthermore, high level of thrombomodulin was univariably associated with larger diameter of the ascending aorta (1.12 mm (95% CI 0.30-1.92; *P*=0.007)) and with larger suprarenal aortic diameter (0.68 mm (95% CI 0.14-1.21; *P*=0.024)) (Table 4 and Figure 2).

3.3 Aortic wall thickness and the association with markers of platelet activation, hemostasis, and endothelial disruption

The mean (SD) aortic wall thickness was: in ascending aorta 2.28 mm (0.59); in descending aorta 2.32 mm (0.60); in suprarenal aorta 2.22 mm (0.76); and in infrarenal aorta 2.09 mm (0.81). In sensitivity analyses, high level of sCD40L was not associated with aortic wall thickness. Detectable level of D-dimer was associated with greater infrarenal aortic wall thickness; univariably 0.46 mm (95% CI 0.36-0.56; *P*<0.001) and 0.41 mm (95% CI 0.30-0.51; *P*<0.001) adjusted in model 2. High level of syndecan-1 was univariably associated with greater infrarenal aortic wall thickness (0.16 mm

TABLE 2 Associations between AA and high levels of the biomarkers.

Variable	OR (95% CI), P-value	aOR[a] (95% CI), P-value	aOR[b] (95% CI), P-value
sCD40L (high vs. low)	0.23 (0.07,0.77), ***P*=0.017**	0.24 (0.07,0.81), ***P*=0.022**	0.23 (0.07,0.78), ***P*=0.019**
D-dimer (detectable vs. undetectable)	2.76 (1.34,5.67), ***P*=0.006**	2.22 (1.02,4.85), ***P*=0.045**	2.24 (0.99,5.04), *P*=0.052
Syndecan-1 (high vs. low)	1.55 (0.77,3.10), *P*=0.219	1.27 (0.61,2.64), *P*=0.515	0.89 (0.40,1.98), *P*=0.767
Thrombomodulin (high vs. low)	1.75 (0.88,3.47), *P*=0.109	1.31 (0.63,2.74), *P*=0.466	1.06 (0.48,2.36), *P*=0.877

[a]Model 1 and [b]model 2.
Bold values: significant associations.

TABLE 3 Associations between AA and the biomarkers as continuous variables.

Variable	OR (95% CI), P-value	aOR[a] (95% CI), P-value	aOR[b] (95% CI), P-value
sCD40L	0.81 (0.66,0.98), ***P*=0.028**	0.80 (0.65,0.98), ***P*=0.029**	0.76 (0.62,0.95), ***P*=0.014**
D-dimer	1.51 (1.22,1.86), ***P*<0.001**	1.44 (1.13,1.85), ***P*=0.004**	1.41 (1.08,1.84), ***P*=0.010**
Syndecan-1	1.66 (0.85,3.26), *P*=0.139	1.34 (0.66,2.72), *P*=0.417	0.90 (0.41,1.97), *P*=0.787
Thrombomodulin	1.82 (1.02,3.26), ***P*=0.043**	1.40 (0.77,2.56), *P*=0.273	1.15 (0.62,2.12), *P*=0.655

[a]Model 1 and [b]model 2. OR and aOR of AA per doubling in concentration.
Bold values: significant associations.

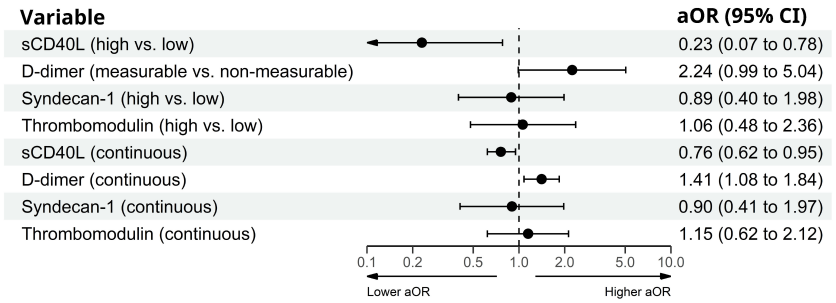

FIGURE 1
Primary (high vs. low variable) and exploratory (continuous variable, aOR associated with doubling of biomarker) analyses of the association between AA and the biomarkers in PLWH adjusted for age, sex, hypertension, smoking status, and BMI category.

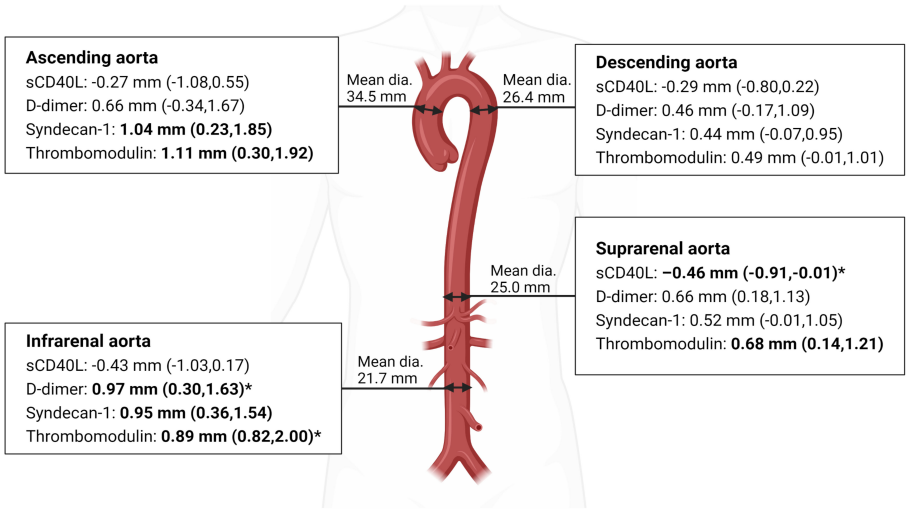

FIGURE 2
Aortic diameter measured as maximum outer diameter. Mean diameter and larger or smaller diameter in mm (95% CI) associated with high level of the biomarker. Bold text: significant associations. *Adjusted for age, sex, hypertension, smoking status, and BMI category. (Made with biorender.com).

TABLE 4 Associations between aortic diameter and the biomarkers.

Variable	Larger or smaller diameter in mm if high level (95% CI), P-value	Larger or smaller diameter in mm if high level[a] (95% CI), P-value	Larger or smaller diameter in mm if high level[b] (95% CI), P-value
Ascending aorta			
sCD40L	-0.27 (-1.08,0.55), *P*=0.519	-0.18 (-0.92,0.57), *P*=0.643	-0.47 (-1.20,0.27), *P*=0.215
D-dimer	0.66 (-0.34,1.67), *P*=0.196	0.29 (-0.63,1-21), *P*=0.538	0.33 (-0.62,1.27), *P*=0.494
Syndecan-1	1.04 (0.23,1.85), ***P*=0.012**	0.51 (-0.24,1.26), *P*=0.182	0.54 (-0.22,1.29), *P*=0.167
Thrombomodulin	1.11 (0.30,1.92), ***P*=0.007**	0.68 (-0.06,1.43), *P*=0.073	0.59 (-0.16,1.34), *P*=0.121
Descending aorta			
sCD40L	-0.29 (-0.80,0.22), *P*=0.266	-0.17 (-0.59,0.24), *P*=0.408	-0.37 (-0.76,0.03), *P*=0.069
D-dimer	0.46 (-0.17,1.09), *P*=0.154	0.16 (-0.35,0.67), *P*=0.535	0.21 (-0.29,0.71), *P*=0.415
Syndecan-1	0.44 (-0.07,0.95), *P*=0.094	-0.08 (-0.50,0.34), *P*=0.723	-0.05 (-0.45,0.36), *P*=0.821
Thrombomodulin	0.49 (-0.01,1.01), *P*=0.057	0.12 (-0.29,0.54), *P*=0.573	0.10 (-0.30,0.50), *P*=0.636
Suprarenal aorta			
sCD40L	-0.40 (-0.93,0.14), *P*=0.144	-0.33 (-0.77,0.11), *P*=0.150	-0.46 (-0.91,-0.01), ***P*=0.045**
D-dimer	0.66 (0.18,1.13), *P*=0.056	0.35 (-0.23,0.92), *P*=0.235	0.38 (-0.21,0.97), *P*=0.213
Syndecan-1	0.52 (-0.01,1.05), *P*=0.057	0.04 (-0.41,0.49), *P*=0.860	0.01 (-0.46,0.47), *P*=0.980
Thrombomodulin	0.68 (0.14,1.21), ***P*=0.024**	0.29 (-0.15,0.74), *P*=0.203	0.26 (-0.19,0.72), *P*=0.1259
Infrarenal aorta			
sCD40L	-0.43 (-1.03,0.17), *P*=0.158	-0.32 (-0.85,0.21), *P*=0.239	-0.40 (-0.91,0.11), *P*=0.122
D-dimer	1.11 (0.38,1.84), ***P*=0.003**	0.88 (0.24,1.53), ***P*=0.008**	0.97 (0.30,1.63), ***P*=0.004**
Syndecan-1	0.95 (0.36,1.54), ***P*=0.002**	0.46 (-0.08,0.99), *P*=0.095	0.32 (-0.20,0.84), *P*=0.232
Thrombomodulin	1.41 (0.82,2.00), ***P*<0.0001**	1.06 (0.54,1.59), ***P*<0.0001**	0.89 (0.38,1.41), ***P*<0.001**

[a]Model 1 and [b]model 2. Larger or smaller diameter in mm associated with high levels of the biomarkers.
Bold values: significant associations.

(95% CI 0.01-0.31; *P*<0.040)). High level of thrombomodulin was associated with greater infrarenal aortic wall thickness; univariably 0.27 mm (95% CI 0.12-0.42; *P*<0.001) and 0.18 mm (95% CI 0.03-0.33; *P*=0.018) adjusted in model 2.

4 Discussion

In a large cohort of well-treated PLWH, we found high level of sCD40L to be associated with lower odds of AA and D-dimer above 290 ng/mL (FEU) to be associated with higher odds of AA. The same associations were found in analyses with biomarkers treated as continuous analyses.

4.1 sCD40L

The primary source of sCD40L is activated platelets (33). A study reported decreased platelet counts in HIV-negative AA patients compared to controls (34), and it is possible that lower platelet count in the PLWH with AA may contribute to the inverse association between AA and sCD40L, since platelets are critical for vascular endothelial integrity and health (35). Other studies have reported aspirin to suppress (36) or block (37) the release of sCD40L from platelets. Furthermore, hypertension is associated with higher concentration of sCD40L (26), statins reduce sCD40L in CVD patients (38, 39), and alcohol is proposed to partially activate platelets (40) resulting in decreased sCD40L production. However, our analyses showed no such associations, so this cannot explain the contrast to previous reports of sCD40L being increased in plasma from HIV-negative patients with abdominal AA compared to matched controls (11) and the lacking finding of associations between sCD40L and AA (41).

In line with the emerging focus on the role of endothelial cells in AA pathogenesis (9, 10), we hypothesized that the biomarkers may be involved in the pathogenesis prior to the aortic diameter exceeding the aneurysmal limit. Therefore, we performed sensitivity analyses regarding associations between aortic diameter and the biomarkers. We found sCD40L to be negatively associated with suprarenal aortic diameter, while, at present, studies regarding associations between aortic diameter and sCD40L have not been published. Another measurement of interest is the aortic wall thickness, which studies have suggested the incorporation of into the risk analysis of AA (42, 43). Therefore, we investigated associations between wall thickness and the biomarkers but found no association with sCD40L.

4.2 D-dimer

D-dimer, an important marker of hemostasis, has been reported elevated in HIV-negative patients with abdominal AA compared to controls without abdominal AA (13–17). Furthermore, a study reported D-dimer to be 49% higher in PLWH on ART aged 45-76 years than in population controls (adjusted percent difference) (27). In line with these findings, our results highlight D-dimer as a possible biomarker, not only associated with abdominal AA, but all AA in PLWH. However, adjusting for known risk factors resulted in an only borderline significant parameter estimate, perhaps caused by an insufficient sample size, as plasma from 83 patients lacked measurement of D-dimer. The reported association between D-dimer and larger infrarenal aortic diameter is consistent with a previous study (44) and suggests a possible role of D-dimer as an indicator of larger infrarenal aortic diameter. Additionally, the reported associations between D-dimer and greater infrarenal aortic wall thickness may indicate increased fibrinolytic activity in the infrarenal aorta. However, as D-dimer is a general marker of fibrinolysis and not disease-specific, combination with other biomarkers may increase the specificity.

4.3 Syndecan-1

A previous study reported concentrations of syndecan-1, a key constituent of the endothelial glycocalyx and a regulator of inflammation, to be elevated in aortic tissue, though not in plasma, from patients with ascending AA compared to matched controls (18). Additionally, a study reported elevated syndecan-1 in PLWH compared to uninfected controls (23). Syndecan-1 is a key constituent of glycocalyx on most endothelial cells in the body, and its soluble form is generated by shedding from the endothelial glycocalyx indicative of damage to endothelial cells (45). As suggested by a previous study (18), it is possible that increased local shedding of syndecan-1 from the aneurysm is masked by the total pool of the biomarker, resulting in non-significant associations with AA in this study. Furthermore, since we only measured syndecan-1 in plasma and not aortic tissue, this may altogether explain why we do not reproduce the previously found association. Syndecan-1 being univariably associated with larger diameter in ascending and infrarenal aorta suggests an association between larger aortic diameter and endothelial disruption.

4.4 Thrombomodulin

Another biomarker shed from endothelial cells indicating endothelial cell injury (46), is soluble thrombomodulin, which has been reported elevated in serum from HIV-negative patients with abdominal AA compared to healthy controls (21, 22). Moreover, several studies have reported thrombomodulin to be elevated in PLWH compared to uninfected controls (24, 25). We found thrombomodulin to be univariably associated with AA when kept as a continuous variable, but not when used as a dichotomous variable. However, this finding was not significant when adjusted for known risk factors in our predefined models and we considered it to be an incidental finding. A potential reason why we found no independent association between thrombomodulin and AA in PLWH is the above-mentioned possible masking of shedding from the aneurysm by the shedding from all endothelial cells. The reported association between thrombomodulin and larger infrarenal aortic diameter suggests thrombomodulin as a possible marker of aortic diameter, though at present, no studies regarding this association have been published. Moreover, as with syndecan-1, the association between thrombomodulin and greater infrarenal aortic diameter indicates an association between larger aortic diameter and endothelial disruption. However, further studies into these associations are required.

4.5 Diameter of aneurysms

The patients in the majority of the previous studies were undergoing surgery for AA, meaning that the diameters of the aneurysms were larger than those in our study, in which the vast majority of aneurysms had diameters below the surgical threshold. A study reported the size of abdominal AA to be associated with concentration of D-dimer (47), while another study suggested endothelin-1 (ET-1), which is released from endothelial cells in response to among other factors vascular injury, as a marker of aneurysm diameter (48). Though such associations have not presently been reported regarding the other biomarkers, it is possible that the smaller diameters of the aneurysms in our study precluded the use of these biomarker concentrations to identify AA, and may, thus, partly explain the negative inverse association between sCD40L and AA and the lack of associations between AA and high levels of syndecan-1 and thrombomodulin, respectively.

4.6 Strengths and limitations

A limitation of this study is its cross-sectional design, making it difficult to investigate causal relationships between the biomarkers and AA. Moreover, the cohort is predominantly male and in fact, all AA were found in men. Strengths include a large cohort of well-treated PLWH and the opportunity to adjust for known risk factors for AA. Lastly, the prevalence of AA is high, making it possible to investigate associations with AA.

5 Conclusions

In conclusion, in this large cohort of well-treated PLWH, we found high sCD40L to be associated with lower odds of AA, and we confirmed previous findings of the association between high D-dimer and higher odds of AA. Furthermore, thrombomodulin and D-dimer were associated with larger aortic diameter and sCD40L with smaller aortic diameter. These findings regarding sCD40L and AA call for further investigation into its utilization as a biomarker of AA in PLWH. D-dimer holds promise as a possible marker, though not specific of AA, why further examinations of specific biomarkers remain necessary to aid in the early diagnosis of AA in PLWH.

Data availability statement

The raw data supporting the conclusions of this article will be made available by the authors, without undue reservation.

Ethics statement

The studies involving human participants were reviewed and approved by Regional Ethical Committee of Copenhagen. The patients/participants provided their written informed consent to participate in this study.

Author contributions

Design of the COCOMO study was carried out by SN et.al (29). and data collection was performed by the COCOMO-team from the Viro-Immunology Research Group. SO contributed to the Luminex® analysis and interpretation of the analysed biomarkers. Statistical analysis plan and design of this sub study was written by SG under supervision by SN and JH. Statistical analyses, interpretation of data, and writing of the manuscript was performed by SKG under supervision by SN, JH and AK. Review of the manuscript was performed by MP, PS, AF, JK, LK, JG, TB, SO, and KK. All authors contributed to the article and approved the submitted version.

Funding

This work was supported by Rigshospitalet Research Council, Region Hovedstaden, Novo Nordisk Foundation, Augustinus Foundation, Gilead Sciences and Lundbeck Foundation. The study was designed, conducted, analyzed, and written by the authors without involvement of any commercial party.

Acknowledgments

We acknowledge the contribution from all patients enrolled in the COCOMO study and the work of the COCOMO-team.

Conflict of interest

SG has received a grant from Rigshospitalet Research Council; AK has received a grant from The Danish Heart Foundation and a grant from the European Commission EU 7th Framework Grant ID no. 603266; LK has received speakers honorarium form AstraZeneca, Bayer, Boehringer, Novartis and Novo; TB reports grants from Novo Nordisk Foundation, Lundbeck Foundation, Simonsen Foundation, GSK, Pfizer, Gilead, Kai Hansen Foundation and Erik and Susanna Olesen's Charitable Fund, personal fees from GSK, Pfizer, Boehringer Ingelheim, Gilead, MSD, Pentabase ApS, Becton Dickinson, Janssen and Astra Zeneca all outside the submitted work; SN has received unrestricted research grants from Novo Nordisk Foundation, Lundbeck Foundation, Augustinus Foundation, Rigshospitalet Research Council and advisory board activity for Gilead and GSK/ViiV. All unrelated to this manuscript.

The remaining authors declare that the research was conducted in the absence of any commercial or financial relationships that could be construed as a potential conflict of interest.

Publisher's note

References

1. Smit M, Brinkman K, Geerlings S, Smit C, Thyagarajan K, van Sighem AV, et al. Future challenges for clinical care of an ageing population infected with HIV: a modelling study. *Lancet Infect Dis* (2015) 15(7):810–8. doi: 10.1016/S1473-3099(15)00056-0

2. Gebo KA. Epidemiology of HIV and response to antiretroviral therapy in the middle aged and elderly. *Aging Health* (2008) 4(6):615. doi: 10.2217/1745509X.4.6.615

3. Shah ASV, Stelzle D, Ken Lee K, Beck EJ, Alam S, Clifford S, et al. Global burden of atherosclerotic cardiovascular disease in people living with HIV: Systematic review and meta-analysis. *Circulation* (2018) 138(11):1100–12. doi: 10.1161/CIRCULATIONAHA.117.033369

4. Neuhaus J, Angus B, Kowalska JD, La Rosa A, Sampson J, Wentworth D, et al. Risk of all-cause mortality associated with non-fatal AIDS and serious non-AIDS events among adults infected with HIV. *AIDS* (2010) 24(5):697. doi: 10.1097/QAD.0b013e3283365356

5. Høgh J, Pham MHC, Knudsen AD, Thudium RF, Gelpi M, Sigvardsen PE, et al. HIV Infection is associated with thoracic and abdominal aortic aneurysms: a prospective matched cohort study. *Eur Heart J* (2021) 42(30):2924–31. doi: 10.1093/eurheartj/ehab348

6. Kent KC. Clinical practice. abdominal aortic aneurysms. *N Engl J Med* (2014) 371 (22):2101–8. doi: 10.1056/NEJMcp1401430

7. Erbel R, Aboyans V, Boileau C, Bossone E, Bartolomeo RD, Eggebrecht H, et al. 2014 ESC guidelines on the diagnosis and treatment of aortic diseases: Document covering acute and chronic aortic diseases of the thoracic and abdominal aorta of the adult. *Eur Heart J* (2014) 35(41):2873–926. doi: 10.1093/eurheartj/ehu281

8. Mathur A, Mohan V, Ameta D, Gaurav B, Haranahalli P. Aortic aneurysm. *J Transl Intern Med* (2016) 4(1):35–41. doi: 10.1515/jtim-2016-0008

9. Franck G, Dai J, Fifre A, Ngo S, Justine C, Michineau S, et al. Reestablishment of the endothelial lining by endothelial cell therapy stabilizes experimental abdominal aortic aneurysms. *Circulation* (2013) 127(18):1877–87. doi: 10.1161/CIRCULATIONAHA.113.001677

10. Siasos G, Mourouzis K, Oikonomou E, Tsalamandris S, Tsigkou V, Vlasis K, et al. The role of endothelial dysfunction in aortic aneurysms. *Curr Pharm Des* (2015) 21 (28):4016–34. doi: 10.2174/1381612821666150826094156

11. Touat Z, Ollivier V, Dai J, Huisse MG, Bezeaud A, Sebbag U, et al. Renewal of mural thrombus releases plasma markers and is involved in aortic abdominal aneurysm evolution. *Am J Pathol* (2006) 168(3):1022–30. doi: 10.2353/ajpath.2006.050868

12. Kusters PJH, Seijkens TTP, Beckers L, Lievens D, Winkels H, De Waard V, et al. CD40L deficiency protects against aneurysm formation. *Arterioscler Thromb Vasc Biol* (2018) 38:1076–85. doi: 10.1161/ATVBAHA.117.310640

13. Golledge J, Tsao PS, Dalman RL, Norman PE. Circulating markers of abdominal aortic aneurysm presence and progression. *Circulation* (2008) 118(23):2382–92. doi: 10.1161/CIRCULATIONAHA.108.802074

14. Sidloff DA, Stather PW, Choke E, Bown MJ, Sayers RD. A systematic review and meta-analysis of the association between markers of hemostasis and abdominal aortic aneurysm presence and size. *J Vasc Surg* (2014) 59(2):528–35. doi: 10.1016/j.jvs.2013.10.088

15. Golledge J, Muller R, Clancy P, McCann M, Norman PE. Evaluation of the diagnostic and prognostic value of plasma d-dimer for abdominal aortic aneurysm. *Eur Heart J* (2011) 32(3):354–64. doi: 10.1093/eurheartj/ehq171

16. Takagi H, Manabe H, Kawai N, Goto S, Umemoto T. Plasma fibrinogen and d-dimer concentrations are associated with the presence of abdominal aortic aneurysm: a systematic review and meta-analysis. *Eur J Vasc Endovasc Surg* (2009) 38(3):273–7. doi: 10.1016/j.ejvs.2009.05.013

17. Vega De Ceniga M, Esteban M, Barba A, Estallo L, Blanco-Colio LM, Martin-Ventura JL. Assessment of biomarkers and predictive model for short-term prospective abdominal aortic aneurysm growth-a pilot study. *Ann Vasc Surg* (2014) 28(7):1642–8. doi: 10.1016/j.avsg.2014.02.025

18. Ntika S, Tracy LM, Franco-Cereceda A, Björck HM, Krizhanovskii C. Syndecan-1 expression is increased in the aortic wall of patients with type 2 diabetes but is unrelated to elevated fasting plasma glucagon-like peptide-1. *Biomedicines* (2021) 9(6):697. doi: 10.3390/biomedicines9060697

19. Wen J, Wang P, Smith SV, Haller CA, Chaikof EL. Syndecans are differentially expressed during the course of aortic aneurysm formation. *J Vasc Surg* (2007) 46(5):1014–25. doi: 10.1016/j.jvs.2007.06.022

20. Xiao J, Angsana J, Wen J, Smith SV, Park PW, Ford ML, et al. Syndecan-1 displays a protective role in aortic aneurysm formation by modulating T cell-mediated responses. *Arterioscler Thromb Vasc Biol* (2012) 32(2):386–96. doi: 10.1161/ATVBAHA.111.242198

21. Budzyń M, Gryszczyńska B, Majewski W, Krasiński Z, Kasprzak MP, Formanowicz D, et al. The association of serum thrombomodulin with endothelial injuring factors in abdominal aortic aneurysm. *BioMed Res Int* (2017) 2017:2791082. doi: 10.1155/2017/2791082

22. Brunelli T, Prisco D, Fedi S, Rogolino A, Farsi A, Marcucci R, et al. High prevalence of mild hyperhomocysteinemia in patients with abdominal aortic aneurysm. *J Vasc Surg* (2000) 32(3):531–6. doi: 10.1067/mva.2000.107563

23. Meneses GC, Cavalcante MG, Da Silva Junior GB, Martins AMC, Da Justa Pires Neto R, Libório AB, et al. Endothelial glycocalyx damage and renal dysfunction in HIV patients receiving combined antiretroviral therapy. *AIDS Res Hum Retroviruses* (2017) 33 (7):703–10. doi: 10.1089/aid.2016.0284

24. Leucker TM, Weiss RG, Schär M, Bonanno G, Mathews L, Jones SR, et al. Coronary endothelial dysfunction is associated with elevated serum PCSK9 levels in people with HIV independent of low-density lipoprotein cholesterol. *J Am Heart Assoc* (2018) 7(19):e009996. doi: 10.1161/JAHA.118.009996

25. De Larrañaga GF, Bocassi AR, Puga LM, Alonso BS, Benetucci JA. Endothelial markers and HIV infection in the era of highly active antiretroviral treatment. *Thromb Res* (2003) 110(2–3):93–8. doi: 10.1016/S0049-3848(03)00291-3

26. Falasca K, Reale M, Di Nicola M, Ucciferri C, Zecca IA, Santilli F, et al. Circulating CD40 ligand, dickkopf-1 and p-selectin in HIV-infected patients. *HIV Med* (2019) 20 (10):681–90. doi: 10.1111/hiv.12789

27. Neuhaus J, Jacobs DR, Baker JV, Calmy A, Duprez D, La Rosa A, et al. Markers of inflammation, coagulation and renal function are elevated in adults with HIV infection. *J Infect Dis* (2010) 201(12):1788. doi: 10.1086/652749

28. Haugaard AK, Lund TT, Birch C, Rönsholt F, Trøseid M, Ullum H, et al. Discrepant coagulation profile in HIV infection: elevated d-dimer but impaired platelet aggregation and clot initiation. *AIDS* (2013) 27(17):2749–58. doi: 10.1097/01.aids.0000432462.21723.ed

29. Ronit A, Haissman J, Kirkegaard-Klitbo DM, Kristensen TS, Lebech AM. Benfield T, et al. Copenhagen comorbidity in HIV infection (COCOMO) study: a study protocol for a longitudinal, non-interventional assessment of non-AIDS comorbidity in HIV infection in Denmark. *BMC Infect Dis* (2016) 16(1):713. doi: 10.1186/s12879-016-2026-9

30. James PA, Oparil S, Carter BL, Cushman WC, Dennison-Himmelfarb C, Handler J, et al. 2014 Evidence-based guideline for the management of high blood pressure in adults: report from the panel members appointed to the eighth joint national committee (JNC 8). *JAMA* (2014) 311(5):507–20. doi: 10.1001/jama.2013.284427

31. Lindholt JS, Rasmussen LM, Søgaard R, Lambrechtsen J, Steffensen FH, Frost L, et al. Baseline findings of the population-based, randomized, multifaceted Danish cardiovascular screening trial (DANCAVAS) of men aged 65-74 years. *Br J Surg* (2019) 106(7):862–71. doi: 10.1002/bjs.11135

32. R Studio Team. *R stud*. Boston, MA: R Studio Team (2015).

33. Aloui C, Prigent A, Sut C, Tariket S, Hamzeh-Cognasse H, Pozzetto B, et al. The signaling role of cd40 ligand in platelet biology and in platelet component transfusion. *Int J Mol Sci* (2014) 15(12):22342–64. doi: 10.3390/ijms151222342

34. Milne AA, Adam DJ, Murphy WG, Ruckley CV. Effects of asymptomatic abdominal aortic aneurysm on the soluble coagulation system, platelet count and platelet activation. *Eur J Vasc Endovasc Surg* (1999) 17(5):434–7. doi: 10.1053/ejvs.1998.0790

35. Nachman RL, Rafii S. Platelets, petechiae, and preservation of the vascular wall. *N Engl J Med* (2008) 359(12):1261. doi: 10.1056/NEJMra0800887

36. Enomoto Y, Adachi S, Matsushima-Nishiwaki R, Doi T, Niwa M, Akamatsu S, et al. Thromboxane A(2) promotes soluble CD40 ligand release from human platelets. *Atherosclerosis*. (2010) 209(2):415–21. doi: 10.1016/j.atherosclerosis.2009.10.024

37. Nannizzi-Alaimo L, Alves VL, Phillips DR. Inhibitory effects of glycoprotein IIb/IIIa antagonists and aspirin on the release of soluble CD40 ligand during platelet stimulation. *Circulation* (2003) 107(8):1123–8. doi: 10.1161/01.CIR.0000053559.46158.AD

38. Li J, Zhao SP, Peng DQ, Xu ZM, Zhou H. Early effect of pravastatin on serum soluble CD40L, matrix metalloproteinase-9, and c-reactive protein in patients with acute myocardial infarction. *Clin Chem* (2004) 50(9):1696–9. doi: 10.1373/clinchem.2003.030940

39. Schönbeck U, Gerdes N, Varo N, Reynolds RS, Horton DB, Bavendiek U, et al. Oxidized low-density lipoprotein augments and 3-hydroxy-3-methylglutaryl coenzyme a reductase inhibitors limit CD40 and CD40L expression in human vascular cells. *Circulation* (2002) 106(23):2888–93. doi: 10.1161/01.CIR.0000043029.52803.7B

40. Salem RO, Laposata M. Effects of alcohol on hemostasis. *Am J Clin Pathol* (2005) 123(Suppl 1):S96–105. doi: 10.1309/113N8EUFXYUECCNA

41. Flondell-Sité D, Lindblad B, Kölbel T, Gottsäter A. Cytokines and systemic biomarkers are related to the size of abdominal aortic aneurysms. *Cytokine* (2009) 46:211–5. doi: 10.1016/j.cyto.2009.01.007

42. Shang EK, Nathan DP, Woo EY, Fairman RM, Wang GJ, Gorman RC, et al. Local wall thickness in finite element models improves prediction of abdominal aortic aneurysm growth. *J Vasc Surg* (2015) 61(1):217–23. doi: 10.1016/j.jvs.2013.08.032

43. Shang EK, Nathan DP, Sprinkle SR, Fairman RM, Bavaria JE, Gorman RC, et al. Impact of wall thickness and saccular geometry on the computational wall stress of descending thoracic aortic aneurysms. *Circulation* (2013) 128(11 Suppl 1):S157–62. doi: 10.1161/CIRCULATIONAHA.112.000200

44. Laughlin GA, Allison MA, Jensky NE, Aboyans V, Wong ND, Detrano R, et al. Abdominal aortic diameter and vascular atherosclerosis: the multi-ethnic study of atherosclerosis. *Eur J Vasc Endovasc Surg* (2011) 41(4):481–7. doi: 10.1016/j.ejvs.2010.12.015

45. Bartlett AH, Hayashida K, Park PW. Molecular and cellular mechanisms of syndecans in tissue injury and inflammation. *Mol Cells* (2007) 24(2):153–66.

46. Martin FA, Murphy RP, Cummins PM. Thrombomodulin and the vascular endothelium: insights into functional, regulatory, and therapeutic aspects. *Am J Physiol Heart Circ Physiol* (2013) 304(12):H1585–97. doi: 10.1152/ajpheart.00096.2013

47. Yamazumi K, Ojiro M, Okumura H, Aikou T. An activated state of blood coagulation and fibrinolysis in patients with abdominal aortic aneurysm. *Am J Surg* (1998) 175(4):297–301. doi: 10.1016/S0002-9610(98)00014-2

48. Třeška V, Wenham PW, Valenta J, Topolčan O, Pecen L. Plasma endothelin levels in patients with abdominal aortic aneurysms. *Eur J Vasc Endovasc Surg* (1999) 17(5):424–8. doi: 10.1053/ejvs.1998.0800

frontiers | Frontiers in Immunology

TYPE Original Research
PUBLISHED 10 August 2023
DOI 10.3389/fimmu.2023.1243516

OPEN ACCESS

EDITED BY
Guido Poli,
Vita-Salute San Raffaele University, Italy

REVIEWED BY
Tesfaye Gelanew,
Armauer Hansen Research Institute (AHRI), Ethiopia
Marco Sgarbanti,
National Institute of Health (ISS), Italy

*CORRESPONDENCE
Júlia Nakanishi Usuda
julia.usuda@usp.br
Desirée Rodrigues Plaça
desiree.placa@usp.br
Otavio Cabral-Marques
otavio.cmarques@usp.br

†These authors have contributed equally to this work

RECEIVED 20 June 2023
ACCEPTED 24 July 2023
PUBLISHED 10 August 2023

CITATION
Usuda JN, Plaça DR, Fonseca DLM, Marques AHC, Filgueiras IS, Chaves VGB, Adri AS, Torrentes-Carvalho A, Hirata MH, Freire PP, Catar R, Cabral-Miranda G, Schimke LF, Moll G and Cabral-Marques O (2023) Interferome signature dynamics during the anti-dengue immune response: a systems biology characterization. *Front. Immunol.* 14:1243516. doi: 10.3389/fimmu.2023.1243516

Interferome signature dynamics during the anti-dengue immune response: a systems biology characterization

Júlia Nakanishi Usuda[1*†], Desirée Rodrigues Plaça[1*†], Dennyson Leandro M. Fonseca[2], Alexandre H. C. Marques[3], Igor Salerno Filgueiras[3], Victor Gabriel Bastos Chaves[1], Anny Silva Adri[1], Amanda Torrentes-Carvalho[4], Mario Hiroyuki Hirata[1], Paula Paccielli Freire[1,3], Rusan Catar[5], Gustavo Cabral-Miranda[3], Lena F. Schimke[3,6,7], Guido Moll[5] and Otavio Cabral-Marques[1,2,3,6,7,8*]

[1]Department of Clinical and Toxicological Analyses, School of Pharmaceutical Sciences, University of São Paulo, São Paulo, Brazil, [2]Interunit PostGraduate Program on Bioinformatics, Institute of Mathematics and Statistics, University of São Paulo, São Paulo, Brazil, [3]Departament of Immunology, Institute of Biomedical Sciences, University of São Paulo, São Paulo, Brazil, [4]Departament of Immunobiology, Institute of Biology, Federal Fluminense University, Niterói, Brazil, [5]Departament of Nephrology and Internal Intensive Care Medicine, Charité University Hospital, Berlin, Germany, [6]Department of Medicine, Division of Molecular Medicine, University of São Paulo School of Medicine, São Paulo, Brazil, [7]Laboratory of Medical Investigation 29, University of São Paulo School of Medicine, São Paulo, Brazil, [8]Network of Immunity in Infection, Malignancy, Autoimmunity (NIIMA), Universal Scientific Education and Research Network (USERN), São Paulo, SP, Brazil

Dengue virus (DENV) infection manifests as a febrile illness with three distinct phases: early acute, late acute, and convalescent. Dengue can result in clinical manifestations with different degrees of severity, dengue fever, dengue hemorrhagic fever, and dengue shock syndrome. Interferons (IFNs) are antiviral cytokines central to the anti-DENV immune response. Notably, the distinct global signature of type I, II, and III interferon-regulated genes (the interferome) remains uncharacterized in dengue patients to date. Therefore, we performed an in-depth cross-study for the integrative analysis of transcriptome data related to DENV infection. Our systems biology analysis shows that the anti-dengue immune response is characterized by the modulation of numerous interferon-regulated genes (IRGs) enriching, for instance, cytokine-mediated signaling (e.g., type I and II IFNs) and chemotaxis, which is then followed by a transcriptional wave of genes associated with cell cycle, also regulated by the IFN cascade. The adjunct analysis of disease stratification potential, followed by a transcriptional meta-analysis of the interferome, indicated genes such as *IFI27*, *ISG15*, and *CYBRD1* as potential suitable biomarkers of disease severity. Thus, this study characterizes the landscape of the interferome signature in DENV infection, indicating that interferome dynamics are a crucial and central part of the anti-dengue immune response.

KEYWORDS

DENV, interferon, transcriptome, interferome, dengue

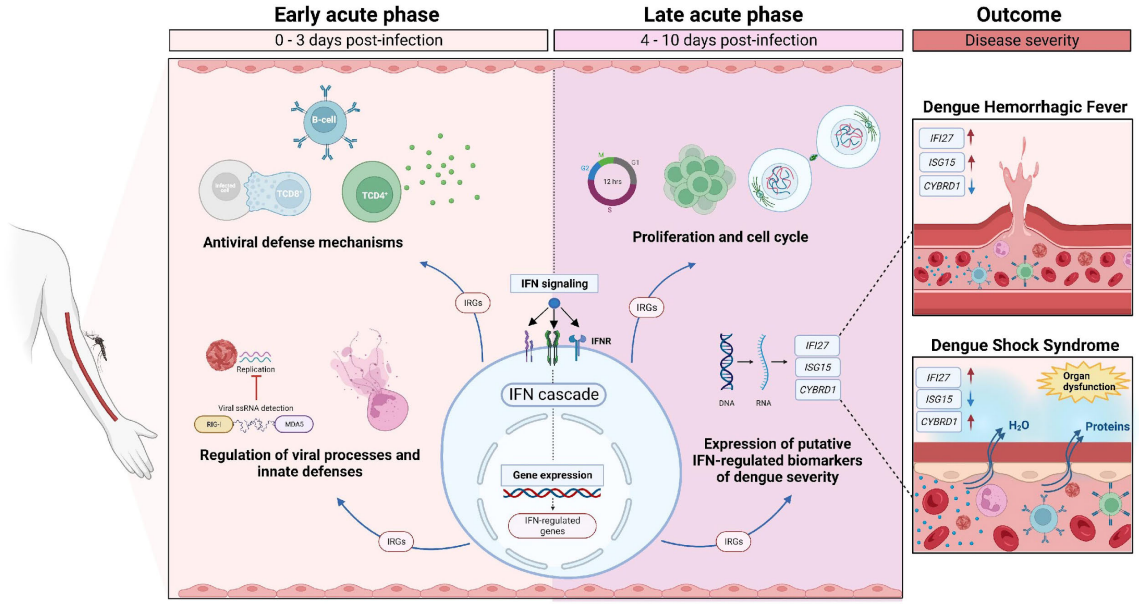

GRAPHICAL ABSTRACT

1 Introduction

Human arboviruses, such as the dengue, Zika, and chikungunya viruses, have frequently emerged or re-emerged worldwide in recent decades, and they are among the most epidemiologically essential viruses (1). Dengue virus (DENV) is the most prevalent among these (it affects a stunning 390 million individuals annually), and DENV is considered endemic in more than 100 countries (2). Surprisingly, despite its high prevalence and substantial global health impact, it is still characterized as a neglected tropical disease.

Four different DENV serotypes (DENV1-4) are transmitted by the vector *Aedes aegypti* and *Aedes albopictus* mosquitoes (3). The course of dengue infection can be divided into phases. The acute phase is characterized by high fever with abrupt onset, lasting between 2 to 7 days, which is characterized by multiple symptoms, such as malaise, myalgia, arthralgia, rash, retro-orbital pain, and headache (3, 4).

The acute phase can be classified into two stages: 1) Early acute (day 0 to 3 from symptom onset) and 2) Late acute or defervescence (day 4 to end of acute phase) (5). The critical stage during defervescence is characterized by increased capillary permeability and plasma leakage. This event may lead to severe shock, organ impairment, and bleeding. If the patient survives, the convalescent phase follows, where leaked fluids are reabsorbed and homeostasis is reestablished (4).

Moreover, dengue can be clinically classified by disease severity: 1) dengue fever (DF), characterized by fever and two or more dengue symptoms; 2) dengue hemorrhagic fever (DHF), marked by increased vascular permeability, plasma leakage, bleeding, and thrombocytopenia (3, 4); and 3) dengue shock syndrome (DSS), when DHF symptoms are aggravated with severe plasma leakage and circulatory compromise (6).

The DENV infection typically presents as a self-limiting febrile disease, indicating a central role of the immune system in controlling disease (7). Antigen-presenting cells can recognize viruses via pattern recognition receptors (PRRs), triggering the production of pro-inflammatory cytokines and phagocytic/microbicidal activity (8). This represents an initial step in controlling the virus spreading, followed by activation of the adaptive immune response (8, 9).

One key mechanism of the anti-viral immune response is the production of interferons (IFNs) by various cell types. IFNs are rapidly induced cytokines that respond strongly to DENV (10, 11). There are three families of IFNs: type I (mainly represented by IFN-α and IFN-β), type II (IFN-γ), and type III (IFN-λ1-4). IFNs are central mediators of innate and adaptive immunity as well as immune homeostasis.

For instance, interferon-alpha/beta (IFN-α/β)-binding to their receptor (IFNAR) triggers the activation of multiple downstream signaling pathways, including the canonical STAT1–STAT2–IFN-regulatory factor 9 (IRF9) signaling complex (12), which then binds to the IFN-stimulated response elements (ISREs) in gene

Abbreviations: AUC, area under the curve; BP, biological process; DEA, differential expression analysis; DENV, dengue virus; DF, dengue fever; DEG, differentially expressed gene; DHF, dengue hemorrhagic fever; DSS, dengue shock syndrome; FC, fold change; GO, gene ontology; IFN, interferon; IFNAR, Interferon-α/β receptor; IL-27, interleukin-27; IRF9, transcription 1 (STAT1)–STAT2–IFN-regulatory factor 9; IRG, interferon-regulated gene; ISRE, IFN-stimulated response elements; MDA5, melanoma differentiation-associated protein 5; OOB, out-of-bag; PCA, principal component analysis; PRR, pattern recognition receptor; RF, random forest; ROC, receiver operating characteristic; RLR, RIG-I-like receptor; RIG-I, retinoic acid-inducible gene I; TAM, Tyro3, AXL, and MerTK; TIM, T cell/transmembrane, immunoglobulin, and mucin.

promoters, leading to the induction of a large number of IFN-stimulated genes (ISGs).

Individual transcriptome studies of DENV-infected patients revealed that different IFN-associated genes are elicited in response to DENV infection (5, 6, 13–15) and that several of them are essential to promote a protective anti-viral reaction (5, 6), corroborated by linear and mechanistic approaches (16–18). In turn, DENV proteins antagonize IFN signaling (19, 20), underscoring the importance of these molecules in the response to DENV.

A comprehensive analysis of the IFN signature in the context of dengue infection has not been conducted yet. Here, we performed an integrative analysis of multiple studies of dengue patients' transcriptomes, considering the disease phases and severities, to characterize the dengue interferome [i.e., types I, II, and III interferon-regulated genes (IRGs)] (Figure 1).

2 Materials and methods

2.1 Data curation

We systematically searched the GEO database to collect publicly available gene expression data (https://www.ncbi.nlm.nih.gov/gds). Our search query *("dengue virus"[MeSH Terms] OR "dengue virus"[All Fields] OR "DENV"[All Fields] OR "dengue"[MeSH Terms] OR "dengue"[All Fields]) AND "Homo sapiens"[Organism] AND (Expression profiling by high throughput sequencing[DataSet Type] OR Expression profiling by array[DataSet Type])* resulted in 93 series as of 17th of August of 2021 (Figure 2A; All results in Table S1).

The inclusion criteria included: (1) *Homo sapiens* microarray or RNAseq expression data, (2) natural dengue infection, (3) blood or PBMC samples, (4) availability of convalescent-phase samples, and (5) at least one group with ten or more samples. The exclusion criteria included (1) *in vitro* samples, (2) cohorts with only infants and/or children, and (3) results from vaccine or drug trials. We included in our analysis seven datasets: GSE25001 (6, 21), GSE28405 (14, 22), GSE28988 (23), GSE28991 (24), GSE43777 (5, 25), GSE40628 (13, 26), and GSE51808 (15, 27).

The samples were categorized into three groups according to time after symptom onset: 1) Early acute (0-3 days), 2) Late acute (4-8 days), and 3) Convalescent (≥14 days). For dataset GSE43777, the late acute phase comprised days 4-10 from disease onset. When applicable, samples were also classified according to disease severity as: 1) Dengue fever (DF), 2) Dengue hemorrhagic fever (DHF), and 3) Dengue shock syndrome (DSS), as determined by the authors when samples were collected. Information about the included series is provided in Table 1.

2.2 Differential expression analysis

The identification of differentially expressed genes (DEGs) was performed with the GEO2R web tool (https://www.ncbi.nlm.nih.gov/geo/geo2r/) (28), applying statistical tests from the *limma* R package (29). All groups were compared to the convalescent. The DEGs were determined following the cutoffs of log2 fold-change (FC) > 1 (upregulated) or < -1 (downregulated) and adjusted p-value < 0.05, using R 4.0.5. DEGs and respective log2 FC are displayed in Table S2.

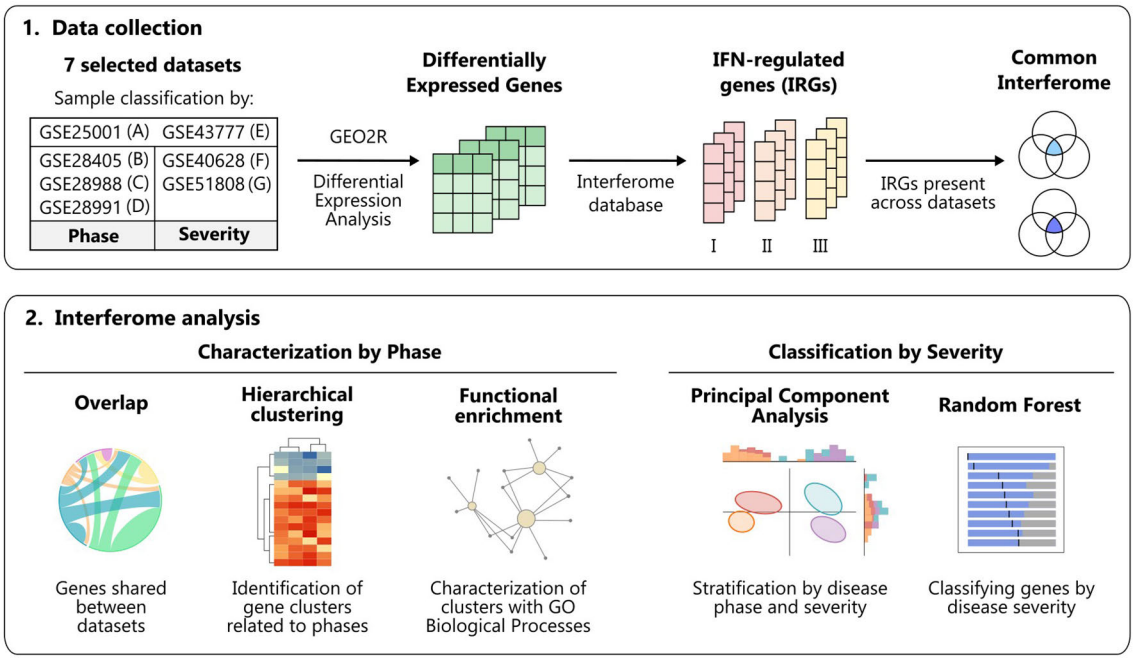

FIGURE 1
Workflow summary. Schematic overview of the data collection and analyses performed to characterize the interferome in dengue infection across disease phases and severity degrees. Figure created with Inkscape. *IFN, interferon; GO, Gene Ontology.*

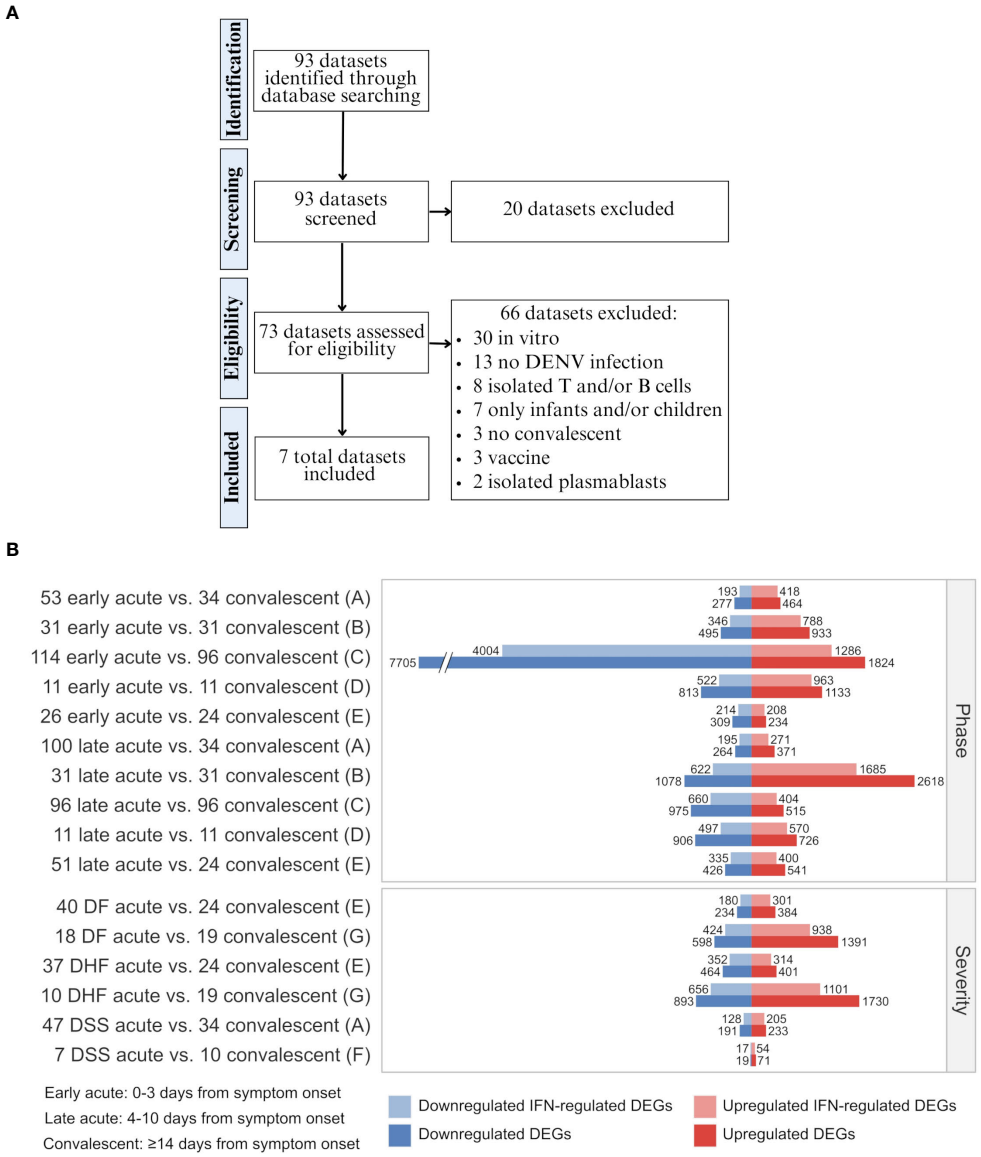

FIGURE 2
Data curation flow chart and differential expression of total genes and interferon-regulated genes across disease phases and disease severity degrees of dengue infection. **(A)** Steps of systematic search and assessment of datasets. Details of datasets and applied inclusion/exclusion criteria are available in Table S1. **(B)** Barplot showing the number of up- and downregulated DEGs and IFN-regulated DEGs for each cohort comparison and dataset as denoted by letters (A, GSE25001; B, GSE28405; C, GSE28988; D, GSE28991; E, GSE43777; F, GSE40628; F, GSE51808) (Table S3). The sample size of each cohort is indicated by a whole number in front of the group name. *DF, Dengue fever; DHF, Dengue hemorrhagic fever; DSS, Dengue shock syndrome; DEG, differentially expressed gene; IFN, interferon.*

2.3 Interferome analysis

To specifically analyze the IFN network, we employed the Interferome database V2.01 (http://www.interferome.org/interferome/home.jspx) (30), which holds information about IFN-regulated genes (IRGs) expression after treatment with IFNs in various experimental systems. The DEGs were submitted to the database to identify IRGs and the specific regulating IFN type. The results summary and IRGs list are in Tables S3, S4.

2.4 Data integration and hierarchical clustering

The overlap of the IFN-regulated DEGs between datasets both by IFN type and disease phase were retrieved and represented with Circos (http://circos.ca/) (31) and UpSet plots generated with the web tool Intervene (https://asntech.shinyapps.io/intervene/) (32). The data used to create the plots are provided in Tables S5, S6. For each combination of IFN type and disease phase or severity, the

TABLE 1 Study and sample information of included series.

Study	GEO accession	Sample size						Sample origin	Platform	Country	DENV serotypes	Ref.
		Early acute (0-3 days)	Late acute (4-8 days)*	Acute DF	Acute DHF	Acute DSS	Convalescent (≥ 14 days)					
A	GSE25001	53	100	–	–	47	34	Whole blood	Illumina HumanRef-8 v2 BeadChip	Vietnam	1, 2, unknown	(6, 21)
B	GSE28405	31	31	–	–	–	31	Whole blood	Sentrix HumanRef-8 Expression BeadChip	Singapore	1, 2, 3	(14, 22)
C	GSE28988	114	96	–	–	–	96	Whole blood	Illumina HumanRef-8 v3.0 expression BeadChip	Unknown	Unknown	(23)
D	GSE28991	11	11	–	–	–	11	Whole blood	Illumina HumanHT-12 V4.0 expression BeadChip	Unknown	Unknown	(24)
E	GSE43777	26	51	40	37	–	24	Whole blood	Affymetrix Human Genome U133 Plus 2.0 Array	Venezuela	1, 2, 3, 4	(5, 25)
F	GSE40628	–	–	–	–	7	10	Blood, PBMCs	SMD Print_980 LC-46	Vietnam	1, 2, unknown	(13, 26)
G	GSE51808	–	–	18	10	–	19	Whole blood	Affymetrix HT HG-U133+ PM Array Plate	Thailand	1, 2, 3, unknown	(15, 27)

Datasets, sample origin, and number of samples by disease phase and/or severity. Annotations: * 4-10 days in GSE43777. DF, Dengue fever; DHF, Dengue hemorrhagic fever; DSS, Dengue shock syndrome; DEG, differentially expressed gene; DENV, dengue virus; IFN, interferon.

10.3389/fimmu.2023.1243516

genes shared by all the datasets considered were selected (Table S7). The heatmaps of the log2 fold-change of these shared genes across disease phases or severities were generated with the web tool Morpheus (https://software.broadinstitute.org/morpheus/) (33). The hierarchical clustering method utilized was Euclidean distance complete linkage. The data used to create the heatmaps are provided in Tables S8, S9.

2.5 Functional enrichment

Functional enrichment analysis based on the clusters of common genes was performed with the web tool EnrichR (https://maayanlab.cloud/Enrichr/) (34). The resulting enriched Gene Ontology (GO) Biological Processes (BPs) were filtered by adjusted p-value < 0.05, as well as combined scores and categories befitting the analyzed cell types. When many results from EnrichR were redundant or closely related terms, these were also filtered with Revigo (http://revigo.irb.hr/) (35). The most relevant BPs were represented with an alluvial plot generated with R package ggalluvial (36). The functional enrichment analysis according to disease phase and IFN type was conducted with R 4.0.5 and the ClusterProfiler (37) R package. The results were filtered by adjusted p-value < 0.05 and presented as dot plots and networks. The results from the functional enrichment analysis by cluster are available in Table S10 and by disease phase and IFN type in Table S11.

2.6 Principal component analysis

Datasets A and E, which had the largest number of samples per phase and severity group (i.e., DSS and DHF, respectively), were selected to analyze the power of the interferome to discriminate the disease severities. The expression values were processed on the ExpressAnalyst web tool (https://www.expressanalyst.ca/) (38), and log2 normalized when applicable. For each disease phase, the IRGs previously identified as commonalities were selected. As of dataset E, four samples (GSM1071100, GSM1071104, GSM1071105, GSM1071108) identified as outliers in the PCA were removed from further analyses. Principal Component Analyses (PCA) by singular value decomposition (39, 40) were performed with the log2-transformed expression values of the intersection genes (Table S12) utilizing R 4.0.5 and packages factoextra (41), ggplot2 (42), and ggExtra (43).

2.7 Ranking of severity-classifying genes

The samples from datasets A and E were grouped by disease severity for each phase. The log2-transformed expression values of the commonalities used in the respective PCAs were applied in the random forest (RF), a machine learning algorithm, which uses the combination of multiple tree classifiers (44) to identify classifiers of dengue severity, using R 4.1.3 and package randomForest (45) (data used in RF available in Table S13). For cross-validation, 75% of the data was set for training and 25% for testing. A heatmap for each dataset depicting the fold change of the top 10 severity-classifying genes across disease phases was plotted using Morpheus (33) (data available in Table S14).

2.8 Transcriptional meta-analysis and gene annotation

The meta-significant genes were obtained by the Fisher p-value combination method using the ExpressAnalyst web tool (https://www.expressanalyst.ca/) (38) (results in Table S15). We used the late acute phase samples from datasets A and E to perform a meta-analysis. Briefly, the log2-transformed expression values were adjusted for batch effect with the combat function from R package sva (46) with R 4.1.3, and the differential expression analyses compared the severe dengue (DSS and DHF) samples with the non-severe dengue (non-DSS and DF) samples. We used Fisher's method to obtain combined p-values for information integration, as recently described (47). A box plot was generated using the Robust Multi-array Average (RMA)-normalized and mean-summarized expression of the putative biomarkers for predicting severe dengue clinical outcome (*IFI27*, *ISG15*, and *CYBRD1)* genes from dataset G (GSE51808) (data available in Table S16). Wilcoxon's test was applied to evaluate the statistical significance between acute DF or acute DHF and convalescent groups. The gene functions were retrieved from the NCBI Gene database (https://www.ncbi.nlm.nih.gov/gene/) (48) and UniProt Knowledgebase (https://www.uniprot.org/) (49) (Table S17).

3 Results

3.1 The interferome signature is a hallmark feature of the anti-dengue immune response

We performed a comprehensive multi-study analysis of dengue cohorts to characterize the interferome signature induced by DENV infection according to the disease phase. We obtained seven datasets of dengue fever transcriptomes according to our inclusion criteria of (1) *Homo sapiens* microarray or RNAseq expression data, (2) natural dengue infection, (3) blood or PBMC samples, (4) availability of convalescent-phase samples, and (5) at least one group with ten or more samples; and exclusion criteria of (1) *in vitro* samples, (2) cohorts with only infants and/or children, and (3) results from vaccine or drug trials. All these datasets were generated through microarray technology (GSE25001 (6, 21) (A), GSE28405 (14, 22) (B), GSE28988 (23) (C), GSE28991 (24) (D), GSE43777 (5, 25) (E), GSE40628 (13, 26) (F), and GSE51808 (15, 27) (G) (Table 1).

We compared the gene expression profiles of the different disease phases (early or late acute phases in contrast with the convalescent phase; datasets A-E) and severities (DF, DHF, or DSS acute phase in contrast with the convalescent phase; datasets A, E-G) through differential expression analyses (DEAs). Following, we identified the interferon-regulated genes (IRGs), as summarized in Figure 2B and Table S3. These results show that most DEGs induced by DENV are regulated by IFNs (On average 72% [minimum: 55%, maximum: 82%]), including a mix of downregulated and upregulated genes. These data confirm the well-established pivotal role of IFNs and the cascade of IFN-associated genes transcribed during the anti-dengue immune response.

3.2 Consistent IFN type I and II interferome signature during different dengue phases

We next analyzed the overlap between dengue's early and late acute phases, identifying the transcriptional intersections between studies A to E. The investigation of common IRGs found 173 common DEGs between the datasets during early and late acute phases (Figures 3A, C, respectively, Table S5), thus revealing a substantial overlap between genes regulated by IFN type I and type II. In contrast, only a few IFN type III-regulated genes were identified. Intriguingly, the distinct difference in the number of IFN type III-regulated genes may be attributed to the limited

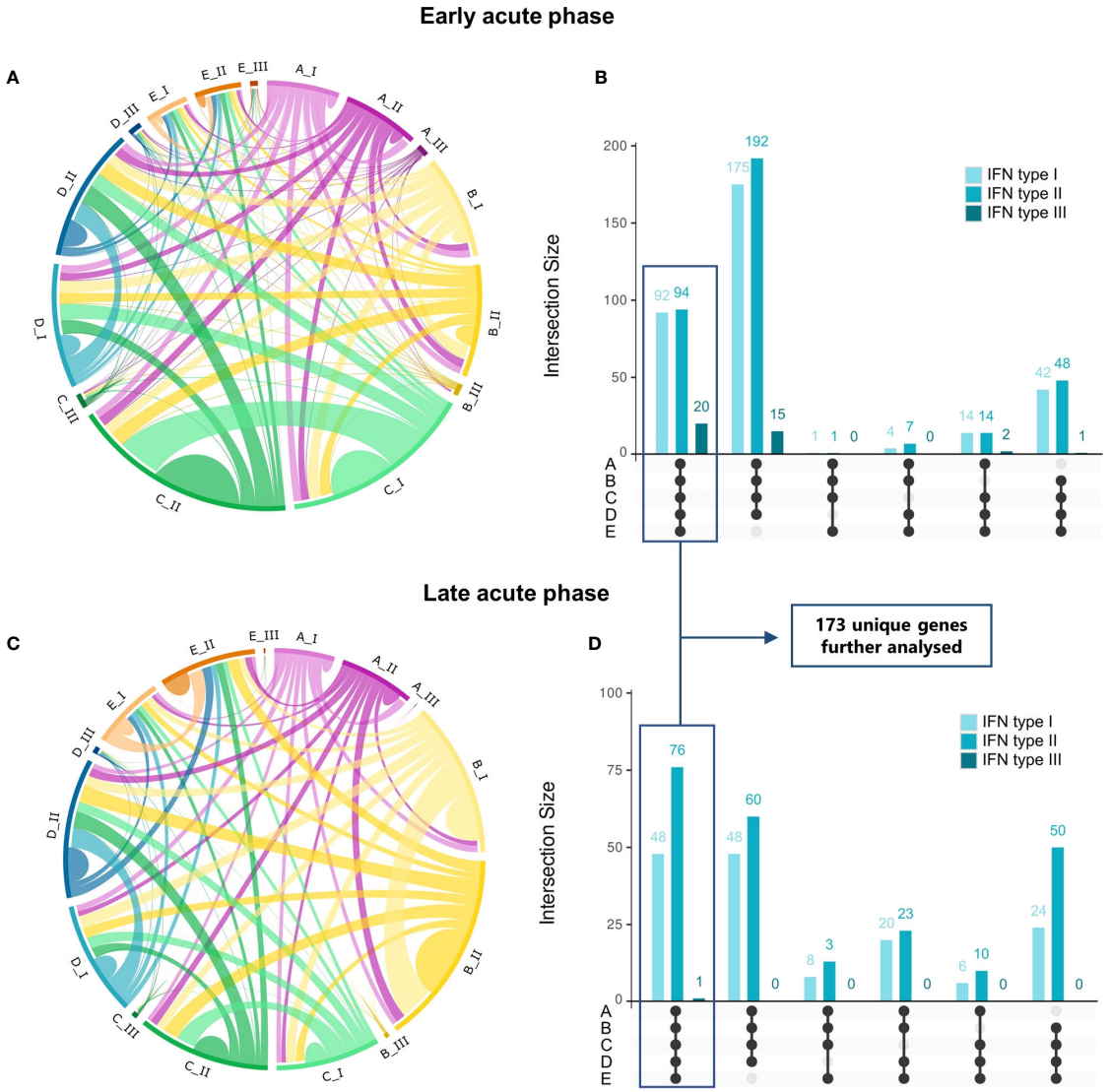

FIGURE 3
Commonalities and uniquenesses of interferon-regulated genes across studies by disease phase and IFN type. **(A, C)**, Circos plots representing IRGs regulated by IFN types I, II, or III that are shared across datasets in the early acute **(A)** or late acute **(C)** disease phases (Table S5). Colors represent the dataset [magenta, dataset A (GSE25001); yellow, dataset B (GSE28405); green, dataset C (GSE28988); blue, dataset D (GSE28991); orange, dataset E (GSE43777)], from lighter to darker indicating genes regulated by IFN types I, II or III, respectively. **(B, D)**, UpSet plots of the number of IRGs shared between datasets in the early acute **(B)** or late acute **(D)** disease phases. Bars are colored according to the regulating IFN type and indicate the number of genes shared in the dataset intersections denoted by connected black dots. Boxes highlight genes common to all datasets (commonalities), totalizing 173 unique genes after duplicate removal, which are further analyzed. A list of genes and complete intersections is available in Tables S6, S7, respectively. *IRG, interferon-regulated gene; IFN, interferon.*

experimental data available for IFN type III, which has been only recently characterized (50), resulting in fewer annotated genes on the database. In contrast, types I and II IFNs have been studied extensively (51).

We found a distinct interferome signature across the datasets during early and late acute phases (Figures 3B, D). This indicates that several IRGs are consistently modulated during the anti-DENV immune response. In the early acute phase, 92, 94, and 20 genes were found to be regulated by type I, II, and III IFNs, respectively, across the five datasets (commonalities). Likewise, in the late acute phase, 48, 76, and 1 gene(s) were found to be regulated by type I, II, and III IFNs, respectively. These commonalities in interferome signatures across datasets suggest a conserved response to DENV infection. A comprehensive list of these genes is provided in Table S6, and their intersection in Table S7.

3.3 Interferome clusterization at the early and late acute dengue phases

We characterized the interferome expression patterns across the transcriptome datasets from dengue patients at acute phases (datasets A-E) with an unsupervised hierarchical clustering analysis (Figure 4 and Table S8). The IRG expression pattern segregated patients at early acute from those at late acute phases. To further investigate whether the IRG expression pattern could also stratify the patients by disease severity, we analyzed samples from DF, DHF, and DSS patients. However, we found that the differences in the expression pattern of IRGs were not strong enough to segregate by disease severity (Figure S1 and Table S9).

Next, we characterized the clusters through gene ontology (GO) analysis to identify distinct biological processes (BPs) that are enriched by the differential expression signatures found in our gene sets (Figure 4 and Table S10). Namely, cluster 1, composed of strongly upregulated genes CCL8 and CCL2 during the early acute phase; cluster 2, comprising downregulated genes at early and late acute phases; cluster 3, including genes more upregulated in the early acute phase; and cluster 4, consisting of genes more upregulated in the late acute phase. Cluster 1 enriched BPs were related to the migration and chemotaxis of lymphocytes, granulocytes, and mononuclear cells. Cluster 2 included genes involved in phagocytosis, cellular response to catecholamine stimulus, and anion homeostasis. Cluster 3 exhibited genes enriching several processes related to the response to the virus (e.g., positive regulation of RIG-I signaling pathway, regulation of viral genome replication) and IFN-related processes (e.g., ISG15-protein conjugation, regulation of type I IFN production). Cluster 4 comprises genes enriching several cell cycle-associated processes such as phase transition, checkpoint, and DNA replication.

To assess whether GO differences depended on the particular IFN type, we further conducted a functional enrichment analysis of the 173 common IRGs by IFN type and disease phase (Table S11). In the early acute phase (Figure 5), genes regulated by IFN types I and II robustly overlapped (86 in 100 genes). Hence, we joined these genes and carried out the enrichment analysis. For the three IFN types, we found a predominance of BPs related to host regulation and defense against the virus, analogous to the enrichment results of cluster 3. In the late acute phase (Figure 6), considering that only one common gene was regulated by IFN type III, we performed the enrichment analysis only for types I and II. We found several cell cycle-associated BPs during the late acute phase, as seen in cluster 4 (Figure 4). Hence, these findings indicate a phase-specific interferome signature.

3.4 Anti-DENV interferome stratifies patients according to disease phase and severity

We further examined a possible stratification power of the anti-DENV interferome with principal component analysis (PCA), considering disease phases and severities. The PCA of IRGs indicated that they stratify DF, DHF, non-DSS, and DSS dengue patients at early and late acute phases from their counterparts in convalescence (Figures 7A–D and Table S12). In the late acute phase, the interferome signature could differentiate DF patients from DHF patients and partially distinguish non-DSS from DSS patients. However, for the IRGs identified in the early acute phase, there was only minimal differentiation power based on disease severity. This fact implies that the interferome signature at the later stage of DENV infection may play a distinct role compared to early dengue stages.

To better understand the interferome's stratification power for dengue patients according to disease severity, we next applied random forest (RF), a machine learning algorithm, to identify classifiers of dengue severity (Table S13). In agreement with the PCA results, RF analysis of DF versus DHF late acute groups indicated an out-of-bag (OOB) error rate of 27.78% and area under the curve (AUC) of the receiver operating characteristic (ROC) curves of 0.952 (Figures 8A, B). Thus, IRGs are strong classifiers of DHF at the late phase. However, we did not find solid classifiers for DSS or the early acute phase. For dataset A, comparing non-DSS and DSS late acute groups, the OOB error rate was high for the non-DSS group (group 1), and the AUC of the ROC curves was 0.833 (Figures S2). When we performed RF with early acute samples from dataset E and dataset A, the OOB error rate was 31.58% and 33.33%, with AUC of 0.583 and 0.622, respectively (Figure S3).

The top ten IRGs classifying dengue severity (DF and DHF; Figure 8C) were *SULF2*, *ISG15*, *NME1*, *CYBRD1*, *GINS2*, *GAS6*, *UBE2T*, *RNASE1*, and *MKI67*, in decrescent order. We evaluated the expression patterns of these top 10 genes through DEAs within each disease phase, comparing disease severities (Figure 8D and Table S14). Only *IFI27* and *ISG15* were significantly differentially expressed between DHF and DF samples in the late acute phase. To further investigate whether these ten genes could also classify by disease

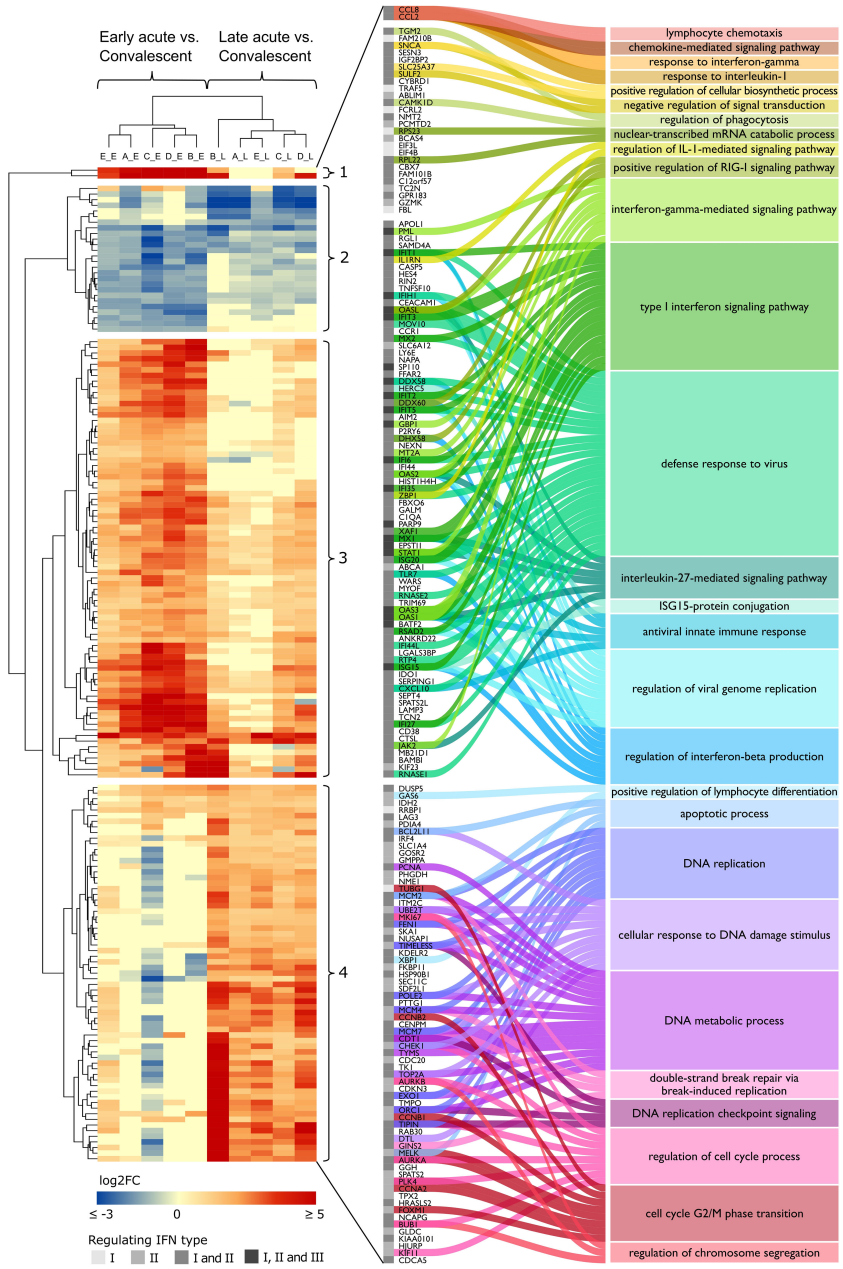

FIGURE 4
DENV infection acute phase interferome landscape. Heatmap of log2 FC of the common IRGs across the acute phases in datasets A to E (Table S8). The red color scale denotes up-regulated genes; the blue color scale denotes down-regulated genes, yellow color denotes genes not differentially expressed (FC close to zero or missing). Hierarchical clustering by Euclidean distance complete linkage metric discriminated cohorts (columns) by disease phase (early acute, late acute) and IRGs (rows) into four distinct clusters (1–4). The amplified view and alluvial plot represent the IRGs of each cluster and the main BPs associated with each cluster. The IFN types that regulate the IRGs are indicated by a grayscale column, from lighter to darker, representing IFN types I and II alone or I and II, as well as I, II, and III together. Complete functional enrichment results by cluster are available in Table S10. Heatmap columns legend: First letter indicates dataset (A, GSE25001; B, GSE28405; C, GSE28988; D, GSE28991; E, GSE43777), while second letter indicates disease phase comparisons (E, early acute vs. convalescent; L, late acute vs. convalescent). *DENV, dengue virus; FC, fold change; IRG, interferon-regulated gene; BP, biological process; IFN, interferon; IL-1, interleukin-1; RIG-I, retinoic acid-inducible gene I; ISG15, ISG15 ubiquitin-like modifier.*

severity, including DSS, we performed a meta-analysis with the late acute samples of datasets A and E. We found 872 meta-significant genes (Table S15). Of the top ten ranked genes, *IFI27*, *ISG15*, and *CYBRD1* were also identified among the meta-significant genes. To further validate these genes as putative biomarkers for predicting severe dengue clinical outcome classification across disease phases, we analyzed their expression on an independent cohort (dataset G). The acute and convalescent phases were significantly different, while there was no difference between the convalescent and healthy control samples (Figure S4 and Table S16).

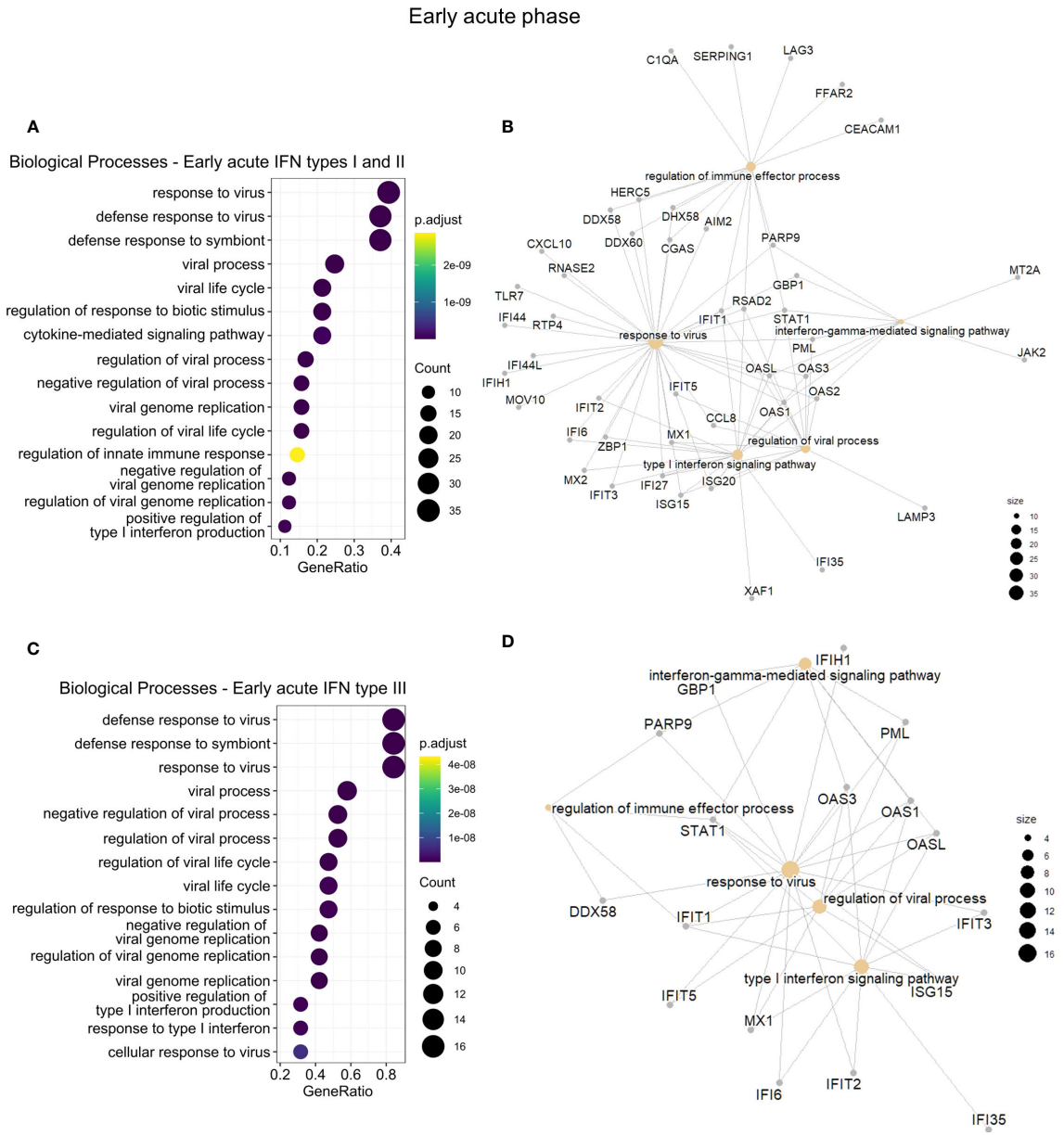

FIGURE 5
Functional gene enrichment characterization of the early acute phase interferome. **(A, C)**, Dot plots of the top 15 BPs enriched by the early acute IRGs regulated by IFN types I and II **(A)** or regulated by IFN type III **(C)**. The color scale indicates the adjusted p-value, and the dot size represents the number of input genes associated with the BP. **(B, D)**, Networks of the main enriched BPs (khaki nodes) and respective genes (gray nodes) for the early acute IRGs regulated by IFN types I and II **(B)** or regulated by IFN type III **(D)**. Node size represents the number of input genes associated with the BP. Complete functional enrichment results available in Table S11. *BP, biological process; IRG, interferon-regulated gene; IFN, interferon.*

4 Discussion

The interferome is a highly complex ancient molecular system (already present in jawed vertebrates) (52), which plays a crucial and central part in the anti-DENV immune response and many other viral infections. Upon virus recognition by PRRs, the IFN system is rapidly triggered within hours from infection, initiating IFN production and a cascade of signaling pathways (53), and as shown here, the transcription of an array of IRGs. In this context, this study comprehensively characterizes the dengue interferome signature in patients, encompassing different datasets, disease phases, and severities. The IFNs are among the oldest known cytokines (51) and the results presented here indicate that the interferome can still be explored in more detail in DENV-infected patients to provide new contextual information that may benefit these patients and result in improved treatment strategies. Our findings align with previous studies highlighting the significant role of IFN responses in the immune response to DENV infection (54–56). Indeed, we consistently observed a functional enrichment of several IFN-related functions during the acute disease phase. Thus, our integrative systems biology analysis based on seven independent datasets confirms the consistency of prior individual

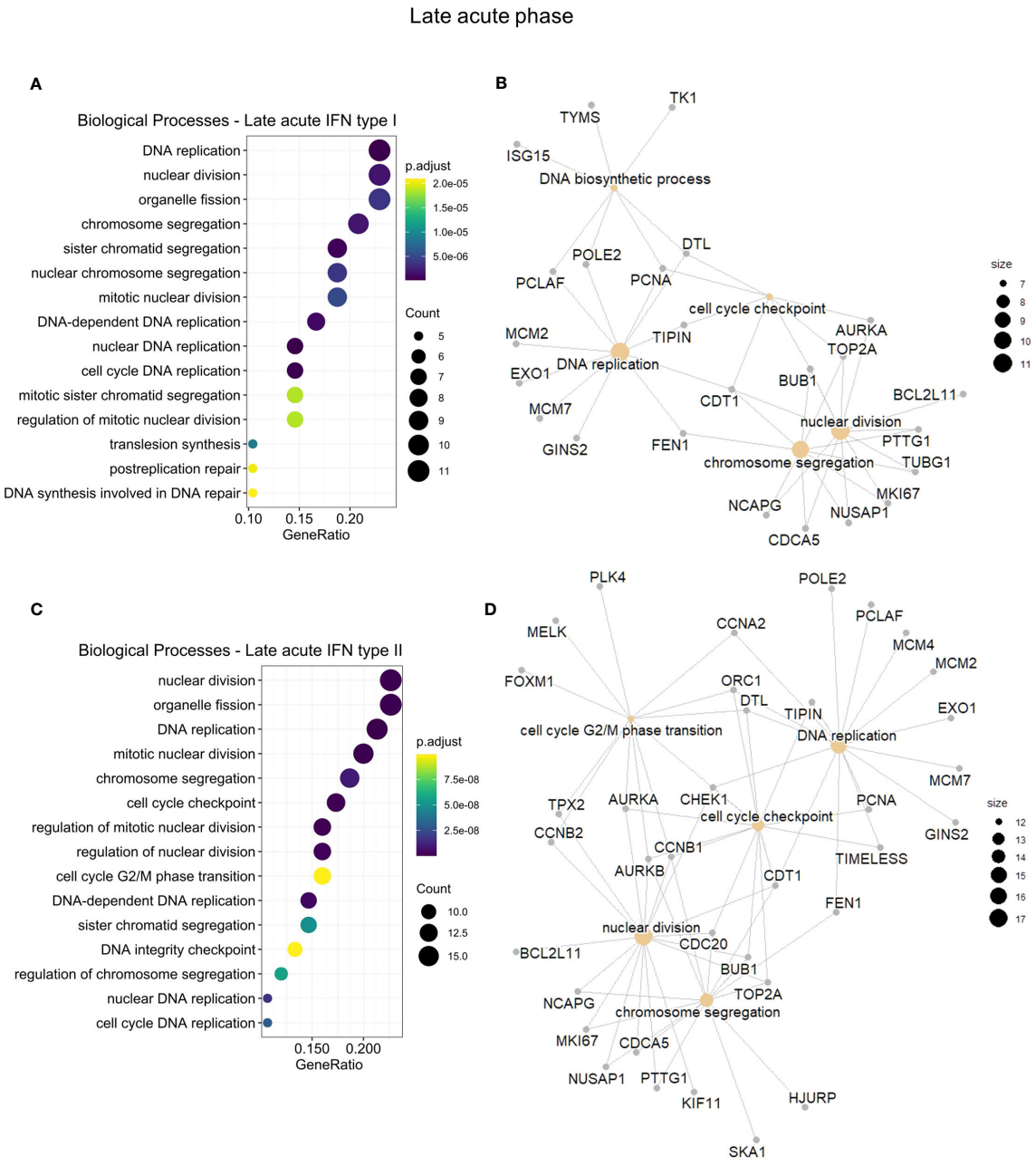

FIGURE 6
Functional gene enrichment characterization of the late acute phase interferome. **(A, C)**, dot plots of the top 15 BPs by gene ratio enriched by the late acute IRGs regulated by IFN types I **(A)** or regulated by IFN type II **(C)**. The dot color indicates the adjusted p-value, dot size represents the number of input genes associated with the BP. **(B, D)**, Networks of the main enriched BPs (khaki nodes) and respective genes (gray nodes) for the early acute IRGs regulated by IFN types I **(B)** or regulated by IFN type II **(D)**. Node size represents the number of input genes associated with the BP. Complete functional enrichment results available in Table S11. *BP, biological process; IRG, interferon-regulated gene; IFN, interferon.*

studies, such as those reported by Sun et al. (5), characterized by cytokine-mediated signaling (e.g., type I IFN) and chemotaxis, which is followed by a transcriptional wave of genes associated with the cell cycle.

Our current study emphasizes the predominance of IFN-regulated genes among DEGs, characterizing the interferome signature as an evident hallmark of the acute response to DENV. This finding agrees with the observation of high levels of type I IFN during acute dengue infection with concomitant CD4+ and CD8+ T cell activation at symptom onset (57). It is already well established that the first powerful wave of type I IFNs may be an early attempt of the host to protect itself against the initiation and development of more advanced disease by employing an early acute phase. Meanwhile, the enrichment of cycle-associated BPs at the late acute phase might represent the simultaneous occurrence of leukocyte proliferation to fight against the infection, together with the manipulation of the cell cycle by the DENV (58, 59) through distinct mechanisms that remain to be explored further in future

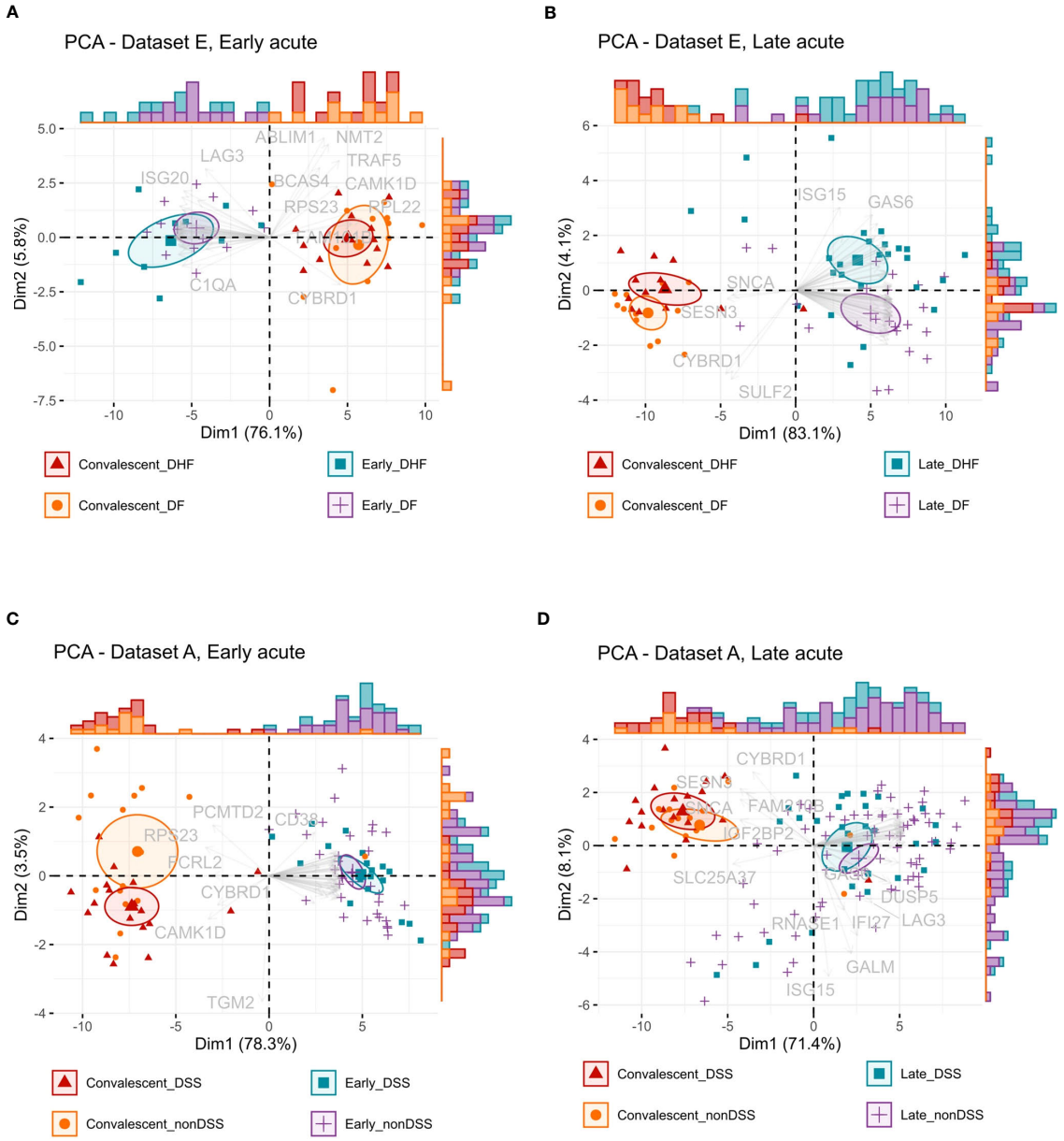

FIGURE 7
Interferon-regulated genes stratification capacity by disease phase and severity. **(A, B)**, Principal component analysis (PCA) biplots of the log2-transformed gene expression values from dataset E of the early acute phase **(A)** or late acute phase **(B)** IRGs common across all studies. **(C, D)**, PCA biplots of the log2-transformed gene expression values from dataset A of the early acute phase **(C)** or late acute phase **(D)** IRGs common across all studies. Data is available in Table S12. Ellipses represent the concentration of samples. Vectors represent the loadings, individual contributions of the genes. Histograms represent the distribution of samples across the biplot. Color and shape identify the groups: red color and triangles represent the convalescent more severe samples (DHF or DSS), orange color and dots represent the convalescent less severe samples (DF or nonDSS), blue color and squares represent the acute phase more severe samples (DHF or DSS), purple color and positive signs represent the acute phase less severe samples (DF or nonDSS). *IRG, interferon-regulated gene. DSS, Dengue shock syndrome DF; nonDSS, non-Dengue shock syndrome; Dengue fever; DHF: Dengue hemorrhagic fever.*

studies. Moreover, our work demonstrates that IRGs are still differentially expressed in the late acute phase. As a result, as IFNs may still be detected, they may also play a regulatory role in this phase of the disease. Genes upregulated at the late acute phase enriched BPs mostly related to mitosis and cell cycle, which was also reported by Sun et al. (5), suggesting this may represent a recovery of the immune cells after viremia has decreased. Thus, indicating a long-lasting cascade effect of the interferome in the anti-DENV immune response.

Clinical investigations of dengue patients have assessed varying timeframes of IFN kinetics and levels during infection, e.g., higher IFN-α levels were identified in the period comprising the early acute phase (0 to 3 days after fever onset) (54, 60), but also throughout the acute phase (57). IFN-γ was also reported to be elevated in the early

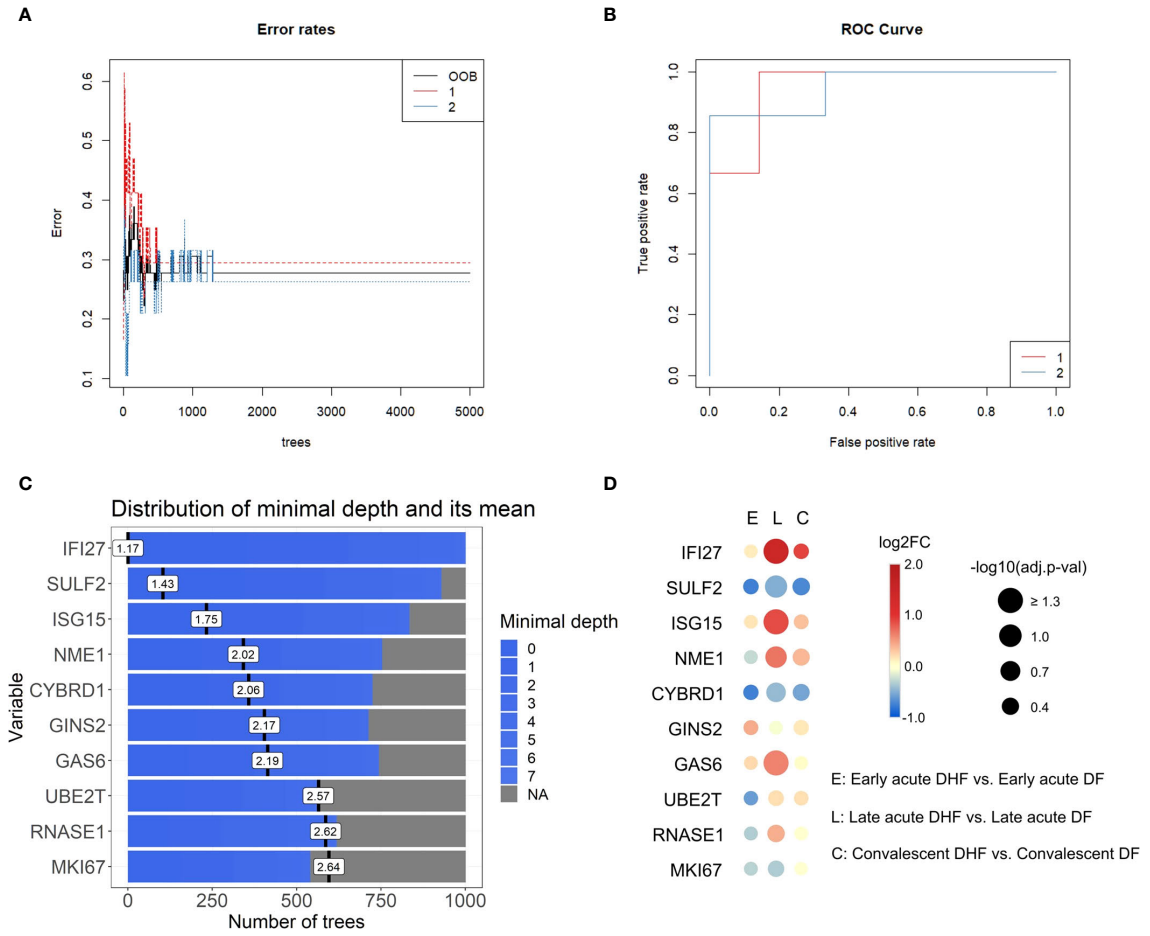

FIGURE 8
Top interferon-regulated genes for severity classification in the late acute phase ranked by random forest (Dataset E). **(A)**, Error rates of random forest models by number of trees. **(B)**, Receiver operating characteristic (ROC) curve of the generated classifying models. The red line corresponds to group 1 (late acute DF), blue line corresponds to group 2 (late acute DHF). **(C)**, Bar plot of the top ten severity classifying genes ranked by the random forest model, number of trees, and distribution of the minimal depth. Blue bars represent the minimum and maximum minimal depth, and black vertical lines represent the mean minimal depth for each classifying gene. Data input of log2-transformed expression values of IRGs common across datasets A to E in the late acute phase are available in Table S13. **(D)**, Bubble heatmap of the log2FC of IRGs resulting from the DHF vs. DF comparison for each disease phase (early acute, late acute, convalescent). The red scale indicates positive FC (up-regulated genes), blue scale indicates negative FC (down-regulated genes). Bubble size represents -log10-transformed adjusted p-value. Data is available in Table S14. *IRG, interferon-regulated gene; DHF, dengue hemorrhagic fever; DF, dengue fever; FC, fold change, OOB: out-of-bag.*

acute phase (57), although peaking around defervescence (61). Likewise, in the early acute phase, we observed the enrichment of BPs primarily related to antiviral defense mechanisms. These BPs included regulating typical viral processes, replication, life cycle, and signaling pathways of RLRs, as well as inflammatory cytokines. These results are consistent with the well-established functions of IFNs in innate immunity. Therefore, our integrative findings from different patient datasets confirm the consistency of the molecular dynamics of the early acute phase of dengue infection, when the viremia, innate immune responses, and IFN responses peak (52).

The observed cell-cycle-related effects of the distinct anti-DENV interferome signature should be investigated further. They may be explained by the fact that IFNs have been reported to negatively regulate the proliferation and differentiation of cell types, such as innate lymphoid type 2 cells and dendritic cells (53), as means of controlling the infection by hampering the viral replication and enhancing the elimination of infected cells (52). On the other hand, both IFN-α and IFN-γ have also been reported to enhance immune proliferation (62, 63). These apparently contradicting effects illustrate how the IFN system is highly pleiotropic, presenting extensive functions and effects (62, 64).

The stratification and classification analyses (PCA and random forest) results demonstrate effective discrimination between disease severities based on the interferome signature only in the late acute phase, indicating that the interferome has a more prominent role at this stage. The late acute phase is critical, wherein the disease course is defined as severe or non-severe dengue (4). So far, identifying early-stage biomarkers to classify which patients will progress to severe dengue is still an unsolved challenge. The random forest algorithm identified the top ten ranking genes (*IFI27*, *SULF2*, *ISG15*, *NME1*, *CYBRD1*, *GINS2*, *GAS6*, *UBE2T*, *RNASE1*, *MKI67*) for differentiation of DHF and DF in the late acute phase. Among them, *IFI27*, *ISG15*, and *CYBRD1* were also meta-significant genes. We confirmed in an independent dataset that these putative

biomarkers are differentially expressed during acute infection for both DF and DHF and return to baseline expression upon disease resolution. Further, *IFI27* and *ISG15* were significantly upregulated in the DHF late acute phase and have previously been associated with dengue severity by Zanini et al. (65).

Mechanistically, *IFI27* (interferon alpha inducible protein 27) is involved in type-I interferon-induced apoptosis (49) and was recently identified as a key ISG in DENV infection, using similar approaches (66). In addition, *IFI27* was predominantly upregulated across disease phases in DHF and DSS, being a putative late-stage biological indicator for severe dengue. In turn, *ISG15* encodes a ubiquitin-like protein with an antiviral activity that can induce NK cell proliferation, act as a chemotactic factor for neutrophils, and induce IFN-γ (49). *ISG15* was upregulated in DHF but downregulated in DSS, representing a potential molecule differentiating patients between the two severities in the late acute phase. On the other hand, *CYBRD1* encodes a plasma membrane reductase that reduces extracellular Fe^{3+} into Fe^{2+}, expressed in monocytes and neutrophils (49, 67). It is a meta-significant gene, downregulated in DHF but upregulated in DSS. *CYBRD1* can potentially be a classifier between DHF and DSS in the late acute phase, and to the best of our knowledge, it has not been previously associated with dengue. *GAS6* encodes a ligand for tyrosine-protein kinase receptors, which has been shown to bind to TAM receptors, inhibiting inflammatory innate immune response. DENV exploits the apoptotic clearance function of TIM and TAM receptors, mediated by Gas6, to gain entry into cells (68). This fact highlights the interplay between *GAS6* and DENV infection, emphasizing the involvement of *GAS6* in modulating immune responses and facilitating viral entry. As this gene was upregulated in the DHF group, this enhanced viral entry may be related to the increased disease severity.

Our work has some limitations. For instance, the molecular signatures identified in this study must be investigated in longitudinal studies and verified further at the protein level. As with all transcriptomic data, it does not necessarily reflect in expressed proteins or functional effects, and possible biomarkers are only putative, with further clinical studies necessary to evaluate their applicability. Another limitation is that some samples included children and infants, whose immune response differs from that of adults (69). As expected, most severe dengue (DHF and DSS) samples were secondary infection cases (70). However, no information allowed us to consistently identify the samples regarding either reinfection or DENV serotype, which can affect the response to infection (71). Other populational factors affecting the response to DENV that could not be considered in this study are ethnicity, geographic location, nutritional status, and comorbidities (72, 73), as that information were unavailable and/or not comparable. Despite these limitations and the cohort heterogeneity, we found consistent molecular signatures across the studies, indicating our results are robust and characteristic of the overall DENV infection.

5 Conclusions

Our study underscores the significant involvement of IFN-regulated genes in the acute dengue response, as reflected by the distinct interferome signature during different phases of DENV infection. Summarily, our approach focused on the expression patterns of IRGs across disease phases and severities in dengue patients. Of note, most DEGs induced by dengue infection were also regulated by IFN, which corroborates the broad modulation of the immune response by the IFN system. Moreover, this study provides valuable insights into the qualitative and quantitative aspects of the dengue interferome, highlighting the dynamic interplay between IFN signaling and gene expression modulation in the context of dengue infection. Hence, our study indicates consistent molecular signatures of disease severity in the late acute stage that can help the development of better classificatory methods and treatment to reduce morbidity and mortality of dengue patients.

Data availability statement

Publicly available datasets were analyzed in this study. This data can be found here: GEO Datasets (https://www.ncbi.nlm.nih.gov/gds), accession numbers GSE25001, GSE28405, GSE28988, GSE28991, GSE43777, GSE40628, GSE51808. Codes utilized in this manuscript are available at the following link: https://github.com/JNUsuda/dengue_interferome.

Ethics statement

Ethical approval was not required for the study involving human samples in accordance with the local legislation and institutional requirements. Written informed consent for participation in this study was provided by the participants' legal guardians/next of kin. Ethical approval was not required for the study involving animals in accordance with the local legislation and institutional requirements because publicly available datasets were used in this study.

Author contributions

JU, DP, and OC-M conceived this study. JU performed the data analysis. DF, AM, IF, VC, AA, AT-C, MH, PF, RC, GM, GC, LS, DP, and OC-M provided scientific insights. JU, RC, GM, DP, and OC-M wrote and revised the final version of the manuscript. DP and OC-M supervised the work. All authors contributed to the article and approved the submitted version.

Funding

We thank the São Paulo Research Foundation (FAPESP) (grants: 2021/03675-5 to JU; 2020/16246-2 to DF; 2023/03841-8 to VC; 2020/11710-2 to DP; and 2018/18886-9 to OC-M) for financial support. We acknowledge the Brazilian Federal Agency for Support and Evaluation of Graduate Education (CAPES/PROEX) (grant 88887.848413/2023-00 to AA) and the National Council for Scientific and Technological Development (CNPq) Brazil (grants: 102430/2022-5 to LS; 309482/2022-4 to OC-M). The contributions by GM were made possible by

funding from the German Federal Ministry for Education and Research (BMBF) and the German Research Foundation (DFG; project EXPAND-PD; CA2816/1-1) through the Berlin Institute of Health (BIH)-Center for Regenerative Therapies (BCRT) and the Berlin-Brandenburg School for Regenerative Therapies (BSRT, GSC203), respectively, and in part by the European Union's Horizon 2020 Research and Innovation Program under grant agreements No 733006 (PACE) and 779293 (HIPGEN) and 754995 (EU-TRAIN).

Conflict of interest

The authors declare that the research was conducted in the absence of any commercial or financial relationships that could be construed as a potential conflict of interest.

Publisher's note

Supplementary material

The Supplementary Material for this article can be found online at: https://www.frontiersin.org/articles/10.3389/fimmu.2023.1243516/full#supplementary-material

References

1. Harapan H, Michie A, Sasmono RT, Imrie A. Dengue: A minireview. *Viruses* (2020) 12. doi: 10.3390/v12080829

2. World Health Organization. *Ending the neglect to attain the Sustainable Development Goals: A road map for neglected tropical diseases 2021–2030. Overview* (2021). Available at: https://www.who.int/publications-detail-redirect/WHO-UCN-NTD-2020.01 (Accessed July 1, 2021).

3. Guzman MG, Gubler DJ, Izquierdo A, Martinez E, Halstead SB. Dengue infection. *Nat Rev Dis Primers* (2016) 2:16055. doi: 10.1038/nrdp.2016.55

4. World Health Organization, Special Programme for Research and Training in Tropical Diseases. *Dengue: guidelines for diagnosis, treatment, prevention, and control*. New. Geneva: World Health Organization (2009). 147 p.

5. Sun P, García J, Comach G, Vahey MT, Wang Z, Forshey BM, et al. Sequential waves of gene expression in patients with clinically defined dengue illnesses reveal subtle disease phases and predict disease severity. *PloS Negl Trop Dis* (2013) 7:e2298. doi: 10.1371/journal.pntd.0002298

6. Hoang LT, Lynn DJ, Henn M, Birren BW, Lennon NJ, Le PT, et al. The early whole-blood transcriptional signature of dengue virus and features associated with progression to dengue shock syndrome in Vietnamese children and young adults. *J Virol* (2010) 84:12982–94. doi: 10.1128/JVI.01224-10

7. Simmons CP, Farrar JJ, van Vinh Chau N, Wills B. Dengue. *New Engl J Med* (2012) 366:1423–32. doi: 10.1056/NEJMra1110265

8. Kawai T, Akira S. Innate immune recognition of viral infection. *Nat Immunol* (2006) 7:131–7. doi: 10.1038/ni1303

9. Mesev EV, LeDesma RA, Ploss A. Decoding type I and III interferon signalling during viral infection. *Nat Microbiol* (2019) 4:914–24. doi: 10.1038/s41564-019-0421-x

10. Ngono AE, Shresta S. Immune response to dengue and zika. *Annu Rev Immunol* (2018) 36:279–308. doi: 10.1146/annurev-immunol-042617-053142

11. Levy DE, Marié IJ, Durbin JE. Induction and function of type I and III interferon in response to viral infection. *Curr Opin Virol* (2011) 1:476–86. doi: 10.1016/j.coviro.2011.11.001

12. Katze MG, He Y, Gale M. Viruses and interferon: a fight for supremacy. *Nat Rev Immunol* (2002) 2:675–87. doi: 10.1038/nri888

13. Simmons CP, Popper S, Dolocek C, Chau TNB, Griffiths M, Dung NTP, et al. Patterns of host genome—Wide gene transcript abundance in the peripheral blood of patients with acute dengue hemorrhagic fever. *J Infect Dis* (2007) 195:1097–107. doi: 10.1086/512162

14. Tolfvenstam T, Lindblom A, Schreiber MJ, Ling L, Chow A, Ooi EE, et al. Characterization of early host responses in adults with dengue disease. *BMC Infect Dis* (2011) 11:209. doi: 10.1186/1471-2334-11-209

15. Kwissa M, Nakaya HI, Onlamoon N, Wrammert J, Villinger F, Perng GC, et al. Dengue virus infection induces expansion of a CD14+CD16+ Monocyte population that stimulates plasmablast differentiation. *Cell Host Microbe* (2014) 16:115–27. doi: 10.1016/j.chom.2014.06.001

16. Elong Ngono A, Chen H-W, Tang WW, Joo Y, King K, Weiskopf D, et al. Protective role of cross-reactive CD8 T cells against dengue virus infection. *EBioMedicine* (2016) 13:284–93. doi: 10.1016/j.ebiom.2016.10.006

17. Hsu Y-L, Shi S-F, Wu W-L, Ho L-J, Lai J-H. Protective roles of interferon-induced protein with tetratricopeptide repeats 3 (IFIT3) in dengue virus infection of human lung epithelial cells. *PloS One* (2013) 8:e79518. doi: 10.1371/journal.pone.0079518

18. Perry ST, Buck MD, Lada SM, Schindler C, Shresta S. STAT2 mediates innate immunity to dengue virus in the absence of STAT1 via the type I interferon receptor. *PloS Pathog* (2011) 7:e1001297. doi: 10.1371/journal.ppat.1001297

19. Jones M, Davidson A, Hibbert L, Gruenwald P, Schlaak J, Ball S, et al. Dengue virus inhibits alpha interferon signaling by reducing STAT2 expression. *J Virol* (2005) 79:5414–20. doi: 10.1128/JVI.79.9.5414-5420.2005

20. Muñoz-Jordán JL, Sánchez-Burgos GG, Laurent-Rolle M, García-Sastre A. Inhibition of interferon signaling by dengue virus. *Proc Natl Acad Sci U.S.A.* (2003) 100:14333–8. doi: 10.1073/pnas.2335168100

21. Hoang LT, Lynn DJ, Henn M, Birren BW, Lennon NJ, Le PT, et al. *Whole blood gene expression in Vietnamese dengue patients. GEO accession GSE25001* (2010). GEO Accession Display. Available at: https://www.ncbi.nlm.nih.gov/geo/query/acc.cgi?acc=GSE25001 (Accessed March 22, 2023).

22. Ling L, Tolfvenstam T, Lindblom A, Hibberd ML. *Genome-wide gene expression analysis of human whole-blood samples in in response to dengue disease. GEO accession GSE28405* (2011). GEO Accession Display. Available at: https://www.ncbi.nlm.nih.gov/geo/query/acc.cgi (Accessed March 22, 2023).

23. Naim AN, Tolfvenstam T, Lindblom A, Hibberd ML. *Global transcriptional assessment of consecutive samples from patients with dengue infection with association to dengue virus IgG serostatus. GEO accession GSE28988* (2014). GEO Accession Display. Available at: https://www.ncbi.nlm.nih.gov/geo/query/acc.cgi?acc=GSE28988 (Accessed March 22, 2023).

24. Naim AN, Tolfvenstam T, Fink K, Hibberd ML. *Genome-wide gene expression analysis of human whole-blood samples during acute dengue disease and early convalescence. GEO accession GSE28991* (2014). GEO Accession Display. Available at: https://www.ncbi.nlm.nih.gov/geo/query/acc.cgi?acc=GSE28991 (Accessed March 22, 2023).

25. Sun P, García J, Comach G, Vahey MT, Wang Z, Forshey BM, et al. *Sequential waves of gene expression in patients with clinically defined Dengue illnesses reveal subtle disease phases and predict disease severity. GEO accession GSE43777* (2013). GEO Accession Display. Available at: https://www.ncbi.nlm.nih.gov/geo/query/acc.cgi?acc=GSE43777 (Accessed March 22, 2023).

26. Popper S. *Dengue patients whole blood. GEO accession GSE40628* (2012). GEO Accession Display. Available at: https://www.ncbi.nlm.nih.gov/geo/query/acc.cgi?acc=GSE40628 (Accessed March 22, 2023).

27. Nakaya HI, Kwissa M, Pulendran B. *Systems biological analysis of immunity to dengue. GEO accession GSE51808* (2014). GEO Accession Display. Available at: https://www.ncbi.nlm.nih.gov/geo/query/acc.cgi?acc=GSE51808 (Accessed March 22, 2023).

28. Barrett T, Wilhite SE, Ledoux P, Evangelista C, Kim IF, Tomashevsky M, et al. NCBI GEO: archive for functional genomics data sets—update. *Nucleic Acids Res* (2013) 41:D991–5. doi: 10.1093/nar/gks1193

29. Ritchie ME, Phipson B, Wu D, Hu Y, Law CW, Shi W, et al. limma powers differential expression analyses for RNA-sequencing and microarray studies. *Nucleic Acids Res* (2015) 43:e47. doi: 10.1093/nar/gkv007

30. Rusinova I, Forster S, Yu S, Kannan A, Masse M, Cumming H, et al. INTERFEROME v2.0: an updated database of annotated interferon-regulated genes. *Nucleic Acids Res* (2013) 41:D1040–6. doi: 10.1093/nar/gks1215

31. Krzywinski MI, Schein JE, Birol I, Connors J, Gascoyne R, Horsman D, et al. Circos: An information aesthetic for comparative genomics. *Genome Res* (2009) 19, 1639–1645. doi: 10.1101/gr.092759.109

32. Khan A, Mathelier A. Intervene: a tool for intersection and visualization of multiple gene or genomic region sets. *BMC Bioinf* (2017) 18:287. doi: 10.1186/s12859-017-1708-7

33. Gould J. *Morpheus* (2022). Available at: https://software.broadinstitute.org/morpheus.

34. Chen EY, Tan CM, Kou Y, Duan Q, Wang Z, Meirelles GV, et al. Enrichr: interactive and collaborative HTML5 gene list enrichment analysis tool. *BMC Bioinf* (2013) 14:128. doi: 10.1186/1471-2105-14-128

35. Supek F, Bošnjak M, Škunca N, Šmuc T. REVIGO summarizes and visualizes long lists of gene ontology terms. *PloS One* (2011) 6:e21800. doi: 10.1371/journal.pone.0021800

36. Brunson JC. ggalluvial: layered grammar for alluvial plots. *J Open Source Softw* (2020) 5:2017. doi: 10.21105/joss.02017

37. Yu G, Wang L-G, Han Y, He Q-Y. clusterProfiler: an R package for comparing biological themes among gene clusters. *OMICS: A J Integr Biol* (2012) 16:284–7. doi: 10.1089/omi.2011.0118

38. Zhou G, Soufan O, Ewald J, Hancock REW, Basu N, Xia J. NetworkAnalyst 3.0: a visual analytics platform for comprehensive gene expression profiling and meta-analysis. *Nucleic Acids Res* (2019) 47:W234–41. doi: 10.1093/nar/gkz240

39. Ringnér M. What is principal component analysis? *Nat Biotechnol* (2008) 26:303–4. doi: 10.1038/nbt0308-303

40. Trendafilov N, Gallo M. PCA and other dimensionality-reduction techniques. In: Tierney RJ, Rizvi F, Ercikan K, editors. *International Encyclopedia of Education (Fourth Edition)*. Oxford: Elsevier (2023). p. 590–9. doi: 10.1016/B978-0-12-818630-5.10014-4

41. Kassambara A, Mundt F. *factoextra: Extract and Visualize the Results of Multivariate Data Analyses* (2020). Available at: https://CRAN.R-project.org/package=factoextra.

42. Wickham H. *ggplot2: Elegant Graphics for Data Analysis*. New York: Springer-Verlag (2016). Available at: https://ggplot2.tidyverse.org.

43. Attali D, Baker C. *ggExtra: Add Marginal Histograms to "ggplot2", and More "ggplot2" Enhancements* (2022). Available at: https://CRAN.R-project.org/package=ggExtra.

44. Breiman L. Random forests. *Mach Learn* (2001) 45:5–32. doi: 10.1023/A:1010933404324

45. Liaw A, Wiener M. Classification and regression by randomForest. *R News* (2002) 2:18–22.

46. Leek JT, Johnson WE, Parker HS, Jaffe AE, Storey JD. The sva package for removing batch effects and other unwanted variation in high-throughput experiments. *Bioinformatics* (2012) 28:882–3. doi: 10.1093/bioinformatics/bts034

47. Prado CA de S, Fonseca DLM, Singh Y, Filgueiras IS, Baiocchi GC, Plaça DR, et al. Integrative systems immunology uncovers molecular networks of the cell cycle that stratify COVID-19 severity. *J Med Virol* (2023) 95:e28450. doi: 10.1002/jmv.28450

48. Sayers EW, Bolton EE, Brister JR, Canese K, Chan J, Comeau DC, et al. Database resources of the national center for biotechnology information. *Nucleic Acids Res* (2021) 50:D20–6. doi: 10.1093/nar/gkab1112

49. The UniProt Consortium. UniProt: the universal protein knowledgebase in 2021. *Nucleic Acids Res* (2021) 49:D480–9. doi: 10.1093/nar/gkaa1100

50. Ank N, West H, Bartholdy C, Eriksson K, Thomsen AR, Paludan SR. Lambda Interferon (IFN-λ), a type III IFN, is induced by viruses and IFNs and displays potent antiviral activity against select virus infections *in vivo*. *J Virol* (2006) 80:4501–9. doi: 10.1128/JVI.80.9.4501-4509.2006

51. Vilcek J. Novel interferons. *Nat Immunol* (2003) 4:8–9. doi: 10.1038/ni0103-8

52. Stetson DB, Medzhitov R. Type I interferons in host defense. *Immunity* (2006) 25:373–81. doi: 10.1016/j.immuni.2006.08.007

53. Lee AJ, Ashkar AA. The dual nature of type I and type II interferons. *Front Immunol* (2018) 9:2061. doi: 10.3389/fimmu.2018.02061

54. De La Cruz Hernández SI, Puerta-Guardo H, Flores-Aguilar H, González-Mateos S, López-Martinez I, Ortiz-Navarrete V, et al. A strong interferon response correlates with a milder dengue clinical condition. *J Clin Virol* (2014) 60:196–9. doi: 10.1016/j.jcv.2014.04.002

55. Shresta S, Kyle JL, Snider HM, Basavapatna M, Beatty PR, Harris E. Interferon-dependent immunity is essential for resistance to primary dengue virus infection in mice, whereas T- and B-cell-dependent immunity are less critical. *J Virol* (2004) 78:2701–10. doi: 10.1128/JVI.78.6.2701-2710.2004

56. Muñoz-Jordán JL. Subversion of interferon by dengue virus. *Curr Top Microbiol Immunol* (2010) 338:35–44. doi: 10.1007/978-3-642-02215-9_3

57. Becquart P, Wauquier N, Nkoghe D, Ndjoyi-Mbiguino A, Padilla C, Souris M, et al. Acute dengue virus 2 infection in Gabonese patients is associated with an early innate immune response, including strong interferon alpha production. *BMC Infect Dis* (2010) 10:356. doi: 10.1186/1471-2334-10-356

58. Chong MK, Ng ML. Significance of cell cycle manipulation in the establishment of dengue virus and west Nile virus infection. *Int J Infect Dis* (2008) 12:e168. doi: 10.1016/j.ijid.2008.05.418

59. Murgue B, Cassar O, Guigon M, Chungue E. Dengue virus inhibits human hematopoietic progenitor growth *in vitro*. *J Infect Dis* (1997) 175:1497–501. doi: 10.1086/516486

60. Kurane I, Innis BL, Nimmannitya S, Nisalak A, Meager A, Ennis FA. High levels of interferon alpha in the sera of children with dengue virus infection. *Am J Trop Med Hyg* (1993) 48:222–9. doi: 10.4269/ajtmh.1993.48.222

61. Green S, Vaughn DW, Kalayanarooj S, Nimmannitya S, Suntayakorn S, Nisalak A, et al. Early immune activation in acute dengue illness is related to development of plasma leakage and disease severity. *J Infect Dis* (1999) 179:755–62. doi: 10.1086/314680

62. Sun S, Zhang X, Tough D, Sprent J. Multiple effects of immunostimulatory DNA on T cells and the role of type I interferons. *Springer Semin Immunopathol* (2000) 22:77–84. doi: 10.1007/s002810000028

63. Becker S. Interferon-γ accelerates immune proliferation via its effect on monocyte HLA-DR expression. *Cell Immunol* (1985) 91:301–7. doi: 10.1016/0008-8749(85)90053-X

64. Schoggins JW, Wilson SJ, Panis M, Murphy MY, Jones CT, Bieniasz P, et al. A diverse range of gene products are effectors of the type I interferon antiviral response. *Nature* (2011) 472:481–5. doi: 10.1038/nature09907

65. Zanini F, Robinson ML, Croote D, Sahoo MK, Sanz AM, Ortiz-Lasso E, et al. Virus-inclusive single-cell RNA sequencing reveals the molecular signature of progression to severe dengue. *Proc Natl Acad Sci U.S.A.* (2018) 115:E12363–9. doi: 10.1073/pnas.1813819115

66. Jiang C, He C, Kan J, Guan H, Zhou T, Yang Y. Integrative bulk and single-cell transcriptome profiling analysis reveals IFI27 as a novel interferon-stimulated gene in dengue. *J Med Virol* (2023) 95:e28706. doi: 10.1002/jmv.28706

67. Monaco G, Lee B, Xu W, Mustafah S, Hwang YY, Carré C, et al. RNA-seq signatures NorMalized by mRNA abundance allow absolute deconvolution of human immune cell types. *Cell Rep* (2019) 26:1627–1640.e7. doi: 10.1016/j.celrep.2019.01.041

68. Meertens L, Carnec X, Lecoin MP, Ramdasi R, Guivel-Benhassine F, Lew E, et al. The TIM and TAM families of phosphatidylserine receptors mediate dengue virus entry. *Cell Host Microbe* (2012) 12:544–57. doi: 10.1016/j.chom.2012.08.009

69. Jain A, Chaturvedi UC. Dengue in infants: an overview. *FEMS Immunol Med Microbiol* (2010) 59:119–30. doi: 10.1111/j.1574-695X.2010.00670.x

70. Soo K-M, Khalid B, Ching S-M, Chee H-Y. Meta-analysis of dengue severity during infection by different dengue virus serotypes in primary and secondary infections. *PloS One* (2016) 11:e0154760. doi: 10.1371/journal.pone.0154760

71. Fialho LG, Torrentes-Carvalho A, Cunha RV, Faria N, Gandini M, Cipitelli M, et al. Induced nitric oxide synthase (iNOS) and indoleamine 2,3-dioxygenase (IDO) detection in circulating monocyte subsets from Brazilian patients with Dengue-4 virus. *Virol Rep* (2017) 7:9–19. doi: 10.1016/j.virep.2017.02.001

72. Carabali M, Hernandez LM, Arauz MJ, Villar LA, Ridde V. Why are people with dengue dying? A scoping review of determinants for dengue mortality. *BMC Infect Dis* (2015) 15:301. doi: 10.1186/s12879-015-1058-x

73. Te H, Sriburin P, Rattanamahaphoom J, Sittikul P, Hattasingh W, Chatchen S, et al. Association between nutritional status and dengue severity in Thai children and adolescents. *PloS Negl Trop Dis* (2022) 16:e0010398. doi: 10.1371/journal.pntd.0010398

frontiers | Frontiers in Immunology

TYPE Original Research
PUBLISHED 18 May 2023
DOI 10.3389/fimmu.2023.1199730

OPEN ACCESS

EDITED BY
Soren Skov,
University of Copenhagen, Denmark

REVIEWED BY
Kai Wang,
The affiliated Huaian No.1 People's Hospital of Nanjing Medical University, China
Lars Andresen,
University of Copenhagen, Denmark

*CORRESPONDENCE
Kevin R. King
krking@ucsd.edu

†These authors have contributed equally to this work

RECEIVED 03 April 2023
ACCEPTED 02 May 2023
PUBLISHED 18 May 2023

CITATION
McCarty E, Yu J, Ninh VK, Calcagno DM, Lee J and King KR (2023) Single cell transcriptomics of bone marrow derived macrophages reveals Ccl5 as a biomarker of direct IFNAR-independent responses to DNA sensing.
Front. Immunol. 14:1199730.
doi: 10.3389/fimmu.2023.1199730

Single cell transcriptomics of bone marrow derived macrophages reveals Ccl5 as a biomarker of direct IFNAR-independent responses to DNA sensing

Emily McCarty[1†], Justin Yu[1†], Van K. Ninh[1†], David M. Calcagno[1], Jodi Lee[1] and Kevin R. King[1,2*]

[1]Department of Bioengineering, Jacobs School of Engineering, University of California San Diego, La Jolla, CA, United States, [2]Division of Cardiovascular Medicine, Department of Medicine, University of California San Diego, La Jolla, CA, United States

Introduction: The type I interferon (IFN) response is an innate immune program that mediates anti-viral, anti-cancer, auto-immune, auto-inflammatory, and sterile injury responses. Bone marrow derived macrophages (BMDMs) are commonly used to model macrophage type I IFN responses, but the use of bulk measurement techniques obscures underlying cellular heterogeneity. This is particularly important for the IFN response to immune stimulatory double-stranded DNA (dsDNA) because it elicits overlapping direct and indirect responses, the latter of which depend on type I IFN cytokines signaling *via* the IFN alpha receptor (IFNAR) to upregulate expression of interferon stimulated genes (ISGs). Single cell transcriptomics has emerged as a powerful tool for revealing functional variability within cell populations.

Methods: Here, we use single cell RNA-Seq to examine BMDM heterogeneity at steady state and after immune-stimulatory DNA stimulation, with or without IFNAR-dependent amplification.

Results: We find that many macrophages express ISGs after DNA stimulation. We also find that a subset of macrophages express ISGs even if IFNAR is inhibited, suggesting that they are direct responders. Analysis of this subset reveals *Ccl5* to be an IFNAR-independent marker gene of direct DNA sensing cells.

Discussion: Our studies provide a method for studying direct responders to IFN-inducing stimuli and demonstrate the importance of characterizing BMDM models of innate immune responses with single cell resolution.

KEYWORDS

dsDNA, Irf3, Ifnar, interferon stimulated genes, single cell RNA-Seq, transcriptomics, macrophages, Ccl5

Introduction

The type I interferon (IFN) response is an innate immune program that fuels inflammation during diverse pathologic processes including infections, malignancies, sterile tissue injury, autoimmunity, and autoinflammatory diseases (1–9). In the setting of viral infections, this response is adaptive; however, in the context of sterile injuries and autoimmune diseases, this response is often overly exuberant and maladaptive. IFNs are thought to mediate pathology by signaling *via* their cell surface IFN alpha receptor (IFNAR) as detailed below. As a result, therapies based on inhibition of type I IFN signaling using neutralizing antibodies against the IFN alpha receptor (INFAR) have been developed and were recently FDA approved for treatment of lupus (10).

The type I IFN response is shown schematically in Figure 1. It begins when molecularly conserved pathogen- and damage-associated molecular patterns (DAMPs and PAMPs) are detected by genome encoded pattern recognition receptors (PRRs), for example, when immune stimulatory double-stranded DNA (dsDNA) is sensed by the cytosolic DNA sensor intracellular cyclic GMP-AMP synthase (cGAS) or Toll Like Receptor 9 (TLR9) (7, 11, 12). Receptor engagement leads to intracellular signaling that culminates in activation of the master transcriptional regulator interferon response factor 3 (IRF3) which, once phosphorylated, dimerizes, and translocates into the nucleus where it induces expression of target genes such as type I IFN secreted cytokines (Ifnα/β) (7, 11, 12). Beyond the cGAS, other cytosolic DNA sensors have been described but they are not known to induce type I IFN responses (13–15).

Type I IFNs are diffusible extracellular cytokines that spread responses from directly-stimulated cells to neighboring cells by binding to cell surface interferon alpha receptors (IFNAR1 and IFNAR2, hereafter IFNAR) (Figure 1). Autocrine signaling is also possible if the directly-stimulated cells express IFNAR. Ligand binding of IFNAR leads to intracellular signaling that activates a heterotrimeric transcriptional regulatory complex composed of STAT1, STAT2, and IRF9, called ISGF3. Within the nucleus, ISGF3 upregulates hundreds of genes that are collectively referred to as interferon stimulated genes (ISGs). Some ISGs are thought to be directly inducible by IRF3, independent of IFNAR, while others are IFNAR-dependent, but it is challenging to separate and quantify direct and indirect effects using bulk measurement techniques (16–18). Most experimental studies of the type I IFN response to immune stimulatory DNA rely on bulk measurement techniques that average responses over large numbers of cells. It is therefore difficult to separate, characterize, and quantify the responses of direct DNA-sensing cells amidst secondary IFNAR-dependent cells. Even when IFNAR Abs are used to block secondary signaling, the primary response is averaged across all cells and is thus severely diluted.

Here, we utilize single cell RNA-Seq to characterize bone marrow derived macrophages (BMDMs), a commonly used *in vitro* model of tissue macrophages, at steady state and after exposure to immune stimulatory dsDNA with or without simultaneous IFNAR Ab treatment or genetic deficiency of IFNAR (19). This enables dissection of IFNAR-dependent and IFNAR-independent responses with single cell resolution, even when cells derive from the same culture well and thus share a

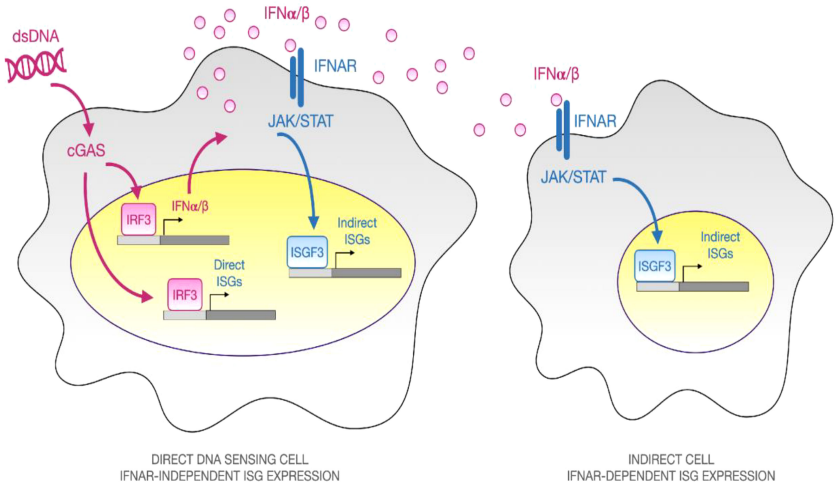

FIGURE 1
Overview of Direct and Secondary Type I IFN response to Immune-stimulatory dsDNA. When double-stranded DNA (dsDNA) is complexed with a polyelectrolyte transfection reagent and added to cells in culture, it activates an innate immune response. Some cells internalize the particulate material, allowing dsDNA to be sensed by the cytosolic pattern recognition receptor cGAS, which catalyzes synthesis of the second messenger, cGAMP that signals *via* the adaptor STING and the TBK1 kinase to promote phosphorylation, dimerization, and nuclear translocation of the master transcriptional regulator IRF3. Once inside the nucleus, IRF3 binds to the promoters of IRF3-dependent genes such as the type I interferon cytokines, IFNα and IFNβ. Secreted type I IFN cytokines can diffuse to neighboring cells and bind to their cognate surface receptor, interferon alpha receptor (IFNAR), leading to JAK/STAT signaling and assembly of a heterotrimeric transcriptional regulatory complex known as ISGF3, composed of Stat1, Stat2, and Irf9. ISGF3 binds to ISRE consensus sequences and upregulates hundreds of effector genes, which are collectively known as interferon stimulated genes (ISGs). By performing experiments in the presence or absence of an IFNAR neutralizing antibody, one can dissect the "Direct" IFNAR-independent and "Indirect" IFNAR-dependent elements of the type I IFN response.

microenvironment. Our results point to *Ccl5*, a proinflammatory chemokine, as a marker of direct DNA sensing cells which is inducible independent of IFNAR-mediated amplification.

Results

Single cell analysis of bone marrow derived macrophage subsets

To dissect direct and indirect responses to transfected immunogenic DNA stimulation with single cell resolution, we designed the following experiment. We used single cell RNA-Seq to define the heterogeneity of cultured BMDMs (i) at steady state, (ii) in response to dsDNA alone, or (iii) in response to dsDNA + IFNAR Ab inhibition of secondary signaling, or (iv) in dsDNA-treated IFNAR KO (Figure 2A). BMDMs were derived by flushing hematopoietic cells from the femurs of adult C57BL6 mice and differentiating them into macrophages in culture using monocyte colony stimulating factor (m-CSF) as we previously described (20). We then subjected the cultures to 24 hours of stimulation with the conditions above, after which BMDMs were collected, stained with DAPI, purified by flow cytometry, and subjected to droplet-based microfluidic single cell barcoding (Chromium, 10X Genomics), library preparation, and next generation sequencing (NovaSeq, Illumina). After demultiplexing and mapping to a reference murine genome, we performed shared nearest neighbor (SNN) clustering on the integrated data from all three treatment groups to define a universal embedding of shared BMDM subtypes (Figure 2B). Unbiased clustering revealed 6 coarse BMDM clusters, 2 of which were interpreted to be proliferating based on expression of canonical cell replication marker genes and labeled them Repl(G2/G1) and Repl(S/G1) (Supplementary Figure S1). Proliferating BMDMs were stratified by cell cycle phase cell based on their expression of *Mcm6* and *Mcm5* (S phase), *Top2a* and *Cenpa* (G1 phase), *Birc5* and *Nusap1* (G2 phase) (Figures 2C, D). Non-proliferating BMDMs were also readily stratified into 3 clusters based on their expression of *Fabp4* and *Fabp5* and MHCII genes such as *H2-Aa* and *H2-Ab1* (Figures 2C, D). We labeled the non-proliferating BMDM subsets (*Fabp4-,MHCII-)*, (*Fabp4+, MHCII-)*, and (*Fabp4+, MHCII+)*. The final cluster was defined as a monocyte-like BMDM Progenitor characterized by expression of *S100a4* and *S100a6*.

Single cell analysis of cytosolic DNA-induced ISG expression in BMDMs

Having defined the BMDM subtypes at steady state, we turned our attention to the response to dsDNA. Experiments based on bulk measurement techniques (e.g., qPCR) have firmly established that dsDNA complexed with a transfection reagent, when delivered to macrophages in culture, induces expression of type I IFNs and ISGs (21). However, underlying single cell heterogeneity remains incompletely defined. Consistent with results from bulk experiments, single cell RNA-Seq profiling of dsDNA-stimulated BMDMs markedly induced expression of ISGs (Irf7, *Ifit2, Oasl2, Rsad2, Isg15*) compared to unstimulated controls as well as compared to dsDNA in the context of IFNAR Ab, thus demonstrating successful inhibition of secondary amplification (Figure 3A). Violin plots confirmed dsDNA-dependent and IFNAR-dependent induction of ISGs at the single gene level while broader macrophage marker genes such as Ms4a7 remained highly expressed across all three conditions (Figure 3B). To evaluate dsDNA responses independent of clustering, we created an ISG Score based on the summed expression of a collection of ISGs derived from previously published studies (Table 1). dsDNA-treated BMDMs had the highest ISG Scores, which were almost completely abrogated by IFNAR Ab inhibition (Figure 3C). Interestingly, we did not find that dsDNA induced ISGs preferentially expressed by one or more of the BMDM subtypes. Instead, they were uniformly elevated across all proliferative and non-proliferative subsets compared to control (Figure 3D). Although we included IFNAR KO BMDMs, they were found to have significant ISG expression in scattered cells with or without DNA stimulation, which limited their utility for identifying direct DNA-stimulated cells (Supplementary Figure S2). Taken together, these data demonstrated that dsDNA stimulation induces ISG expression in both proliferating and non-proliferating BMDMs, and that secondary amplification of the response *via* type I IFN secretion plays a dominant role in the ISG response since it is markedly abrogated by simultaneous blockade with a neutralizing IFNAR Ab.

Direct IFNAR-independent responses to immune stimulatory DNA

Since IFNAR Ab treatment markedly inhibited secondary amplification of DNA-induced IFN responses, we reasoned that any residual ISG expression must result from IFNAR-independent responses to DNA. To identify direct DNA-sensing cells, we bioinformatically combined BMDMs from control and IFNAR Ab treated cells and reclustered (Figure 4A, Supplementary Figure S3). This revealed a small group of BMDMs with high ISG scores despite inhibition of IFNAR-dependent amplification (Figure 4B). We interpreted these ISG-expressing BMDMs to be direct responders to dsDNA stimulation. Unbiased clustering of IFNAR Ab-treated Condition 3 cells revealed 8 distinct clusters including one expressing ISGs embedded within the broader Fabp4+MHCII- cluster, as illustrated in a feature plot (Figure 4C) and heatmap of top marker genes expressed by each cluster (Figure 4C). The top marker genes for directly DNA-stimulated BMDMs were *Ccl5, Irf7, Ifit1, Isg15, Rsad2, Oasl2, Bst2*, and *Ifi204* (Figure 4D). To confirm the result independent of clustering, we plotted the ISG Score for each DNA- and IFNAR-Ab-treated BMDM of Condition 3 and identified the same small population of Fabp4+MHCII-ISG+ cells (Figure 4E). Together, these results suggest that direct DNA-sensing BMDMs are preferentially Fabp4+MHCII- macrophages.

10.3389/fimmu.2023.1199730

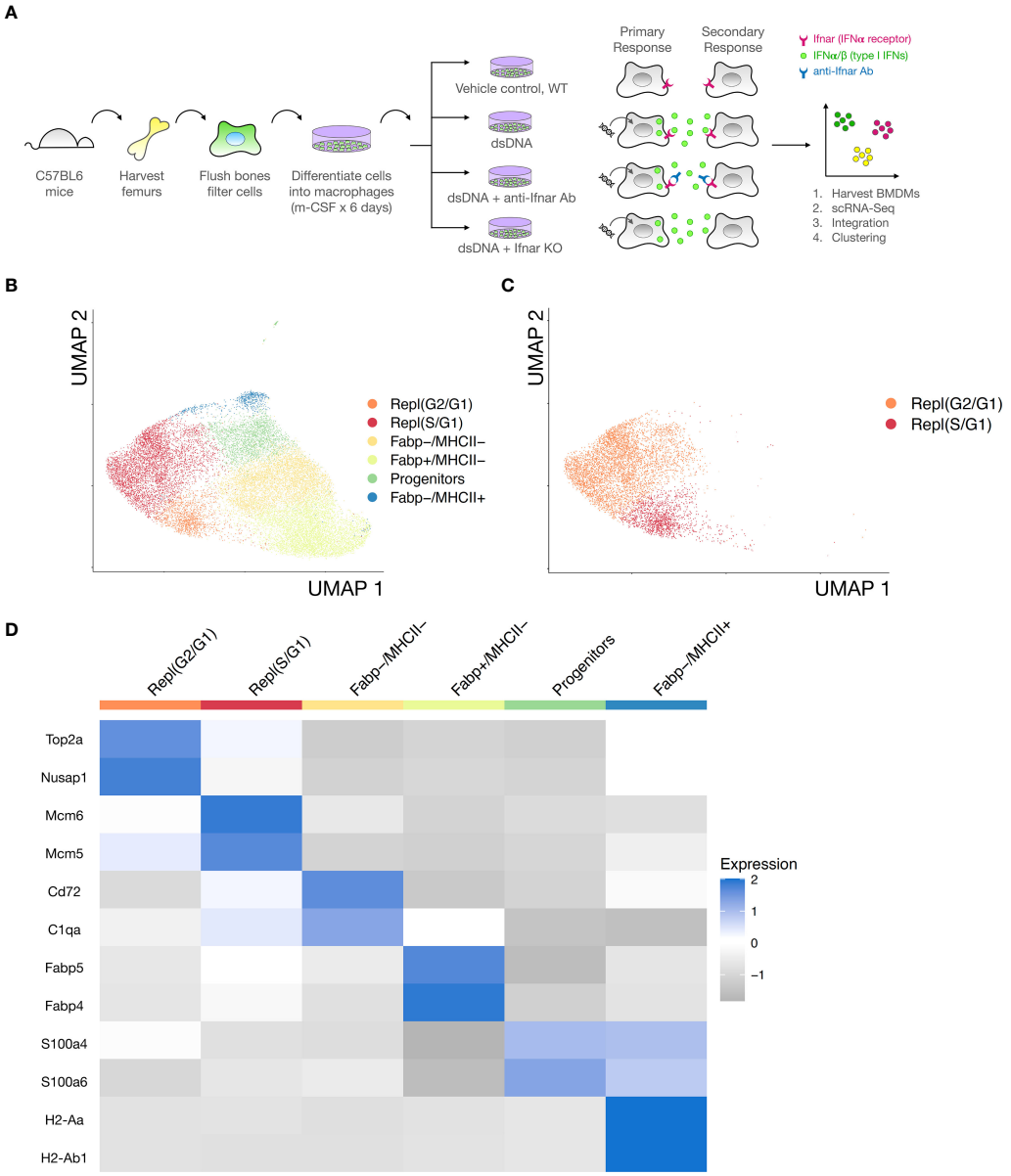

FIGURE 2
Integrated single cell transcriptomes reveal cell-cycling and non-cycling BMDM subsets. **(A)** Bone marrow derived macrophages (BMDMs) were isolated from adult male C57BL6 and IFNAR KO mice and differentiated in culture with m-CSF. BMDM were stimulated for 24 hours with one of the following i) vehicle control, ii) dsDNA complexed to LTX transfection reagent, or iii) dsDNA + IFNAR Ab, or iv) dsDNA-transfected IFNAR KO. Cells were then collected, stained with DAPI, FACS sorted to isolate live single cells, and processed for single cell RNA-Seq barcoding and sequencing using established 10X Genomics protocols. Condition 1 was designed to define the transcriptional heterogeneity and BMDM subsets in the unstimulated state. Condition 2 was designed to define the transcriptional response of BMDM subsets to dsDNA, an inducer of primary and secondary type I IFN responses. Condition 3 was designed to block IFN-dependent secondary responses and isolate the direct effects of dsDNA. **(B)** Data from all three experimental conditions, excluding the IFNAR KO due to strain differences, was integrated and clustered. Unsupervised clustering of integrated data (n= 19,343cells) revealed at least 6 distinct BMDM subsets. Data is dimensionally reduced using UMAP and displayed on a 2D plot to communicate relative similarities in transcriptional profiles between BMDM subsets. **(C)** Identification of replicating BMDMs from clusters based on cell cycle phase (color-coded legend) using cell cycle sorting. **(D)** Heatmap of biological replicates averaged, scaled expression defining differentially expressed genes for each BMDM subset. Cell cycling subsets (clusters 1-2, red & orange) and non-cycling subsets (clusters 3-6, yellow, green, and blue) are annotated.

Gene expression signatures of direct Ifnar-independent DNA-induced macrophages

Bulk measurement techniques do not allow separation of direct DNA-sensing cells from the more abundant secondary IFNAR-dependent cells. This limits separation of cell-specific roles in initiation and amplification of IFN responses *in vivo*. To identify genes that may discriminate direct and indirect cells, we identified the most highly differentially expressed genes between direct DNA responsive cells and secondary IFNAR-dependent cells. First, we isolated Fabp4+MHCII- macrophages, which contained the majority of directly responding cells. We

10.3389/fimmu.2023.1199730

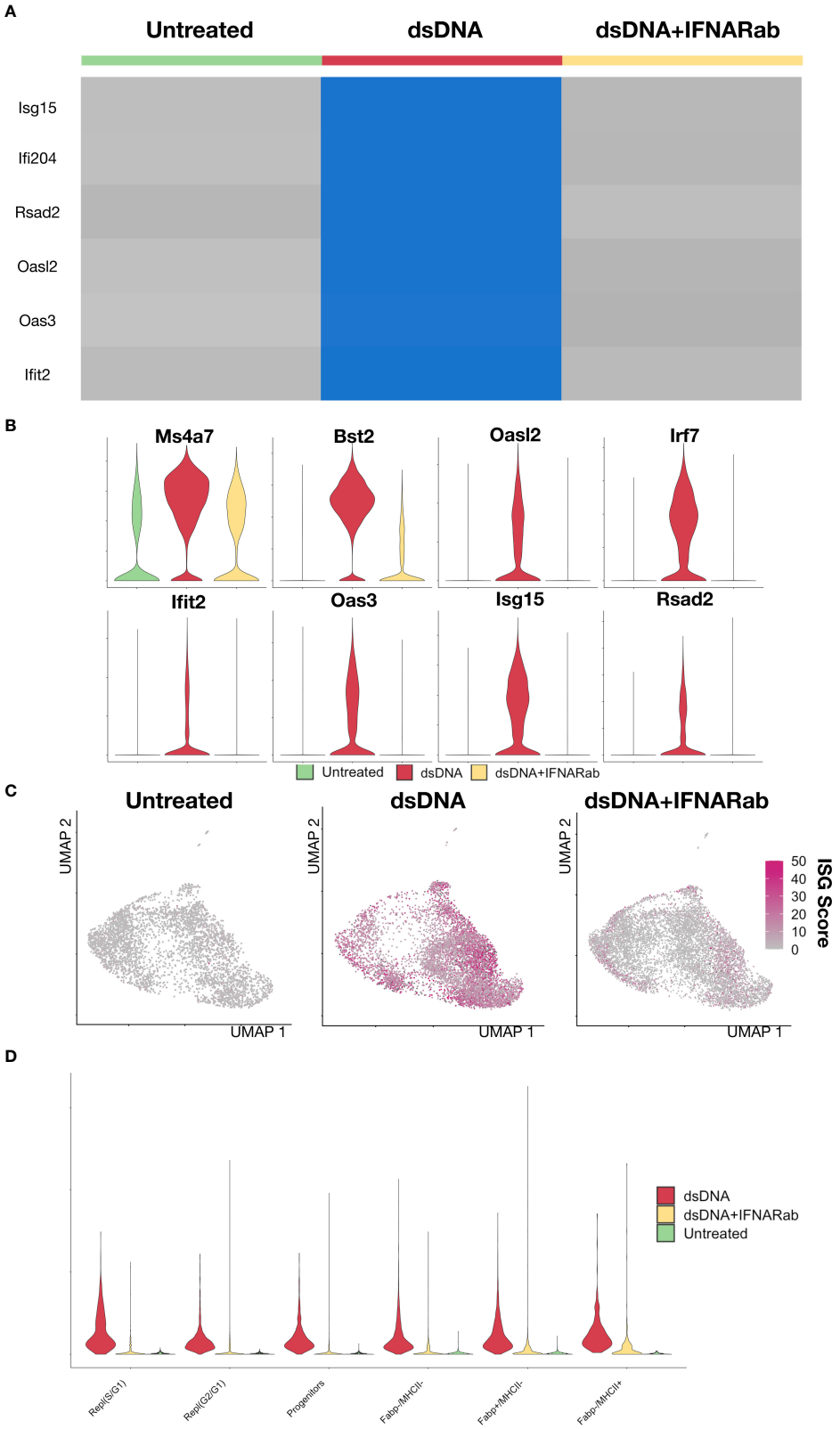

FIGURE 3
Immune stimulatory DNA induces a type I IFN response that can be partially blocked by IFNAR Ab **(A)** Heatmap of of biological replicates averaged, scaled expression of ISG genes sorted by experimental condition (1: control, 2: dsDNA, 3: dsDNA+IFNAR Ab). **(B)** Violin plot of *Ms4a7*, a macrophage marker gene, and several ISGs (*Bst2, Oasl2, Irf7, Ifit2, Oas3, Isg15, Rsad2*). **(C)** An ISG Score defined as the summed expression of canonical ISGs was calculated for each cell and displayed as magenta intensity on a UMAP feature plot for each condition. **(D)** A violin plot of ISG Score was plotted across BMDM subsets and split by experimental condition.

TABLE 1 ISGs used in ISG score.

ISG
Ifi204
Isg15
Irf7
Ifit1
Rsad2
Oasl2
Oas3
Gpb5
Bst2
Ifit2
Ifit3
Oas2
Isg20
Cxcl10
Oasl1
Gpb2
Ccl5
Ccl3

reclustered them, which revealed an ISG+ and ISG- population. Next, we combined the direct macrophages from condition 3 (dsDNA + IFNAR Ab) with the Fabp4+MHCII- macrophages from condition 2 (dsDNA Alone) and reclustered (Figure 5A, Supplementary Figure S4). We displayed expression of 45 ISGs as a heatmap. This revealed *Ccl5* to be the most differentially expressed between the direct cells from condition 3 and combined indirect and direct cells from condition 2 (Figure 5B). Feature plots show the cells colored by ISG Score compared to the more stringent by Direct DNA-sensing Score (Figure 5C). We selected the top 4 genes and created a Direct Score (Ccl5, Cdk8, Cxcl2, and Cd74) (Figure 5D). Based on these results, we propose that the top gene, *Ccl5*, may represent a useful marker gene for identifying direct DNA sensing cells.

Discussion

BMDMs are a widely used experimental tool used across diverse innate immune studies, but they are typically analyzed using bulk measurement techniques that obscure population heterogeneity (19). In this study we applied single cell RNA-seq to reveal functional heterogeneity within cultured BMDMs. Using single cell RNA-Seq, we show that immune stimulatory DNA induces ISG expression across all proliferating and non-proliferating BMDM subsets; however, in the context of anti-IFNAR Ab blockade, DNA was only able to induce a small non-proliferative Fabp4+MHCII- population of macrophages. These cells, which do not benefit from secondary signaling *via* IFNAR, were interpreted as directly-stimulated cells. Using this population, we identified *Ccl5*, also known as RANTES, as a transcriptional biomarker that discriminates directly from indirectly DNA-stimulated cells. Ccl5 is a secreted proinflammatory chemokine capable of recruiting diverse immune cell types (17, 22, 23). However, independent of its functional role, we propose that *Ccl5* may be useful transcriptional biomarker for identifying direct DNA-stimulated cells *in vivo* using single cell RNA-Seq.

BMDMs are a ubiquitous part of an innate immunologist's experimental toolkit, owing to the ease of harvesting and differentiating them in cell culture. However, an often-overlooked assumption of this model is that all cells in the culture are assumed to represent the response of a prototypical macrophage (19). Single cell transcriptomics has emerged as a powerful tool for revealing cellular heterogeneity *in vitro* and *in vivo* within population previously assumed to be homogeneous. *In vivo*, this technology is informing the growing appreciation of macrophage diversity within the bone marrow and at sites of tissue injury (3, 24). Here, we apply single cell transcriptomics to the commonly used BMDM model experimental system. At baseline, transcriptional profiling of BMDMs divides cultured macrophages into proliferative and non-proliferative subsets, each with additional substructure. Our data suggests that when BMDMs are stimulated with immune stimulatory DNA, it is the non-proliferating BMDMs that are directly stimulated, which then broadly recruit both proliferative and non-proliferative cells *via* secreted type I IFN cytokines signaling *via* the IFNAR cell surface receptor to express secondary ISGs (25, 26).

Limitations of our study include the small biological sample size; however, this is somewhat mitigated by the large number of total single cell transcriptomes analyzed (20,000+). An alternative explanation for the directly stimulated cells that we observed is that there is a population of cells that are resistant to IFNAR Ab blockade. While this cannot be disproven, it seems unlikely since the resistant population would have to also have to uniquely respond to DNA stimulation with overexpression of *Ccl5* compared to other ISGs when compared to all IFN-induced cells.

Conclusion

In summary, we have used single cell RNA-Seq to define the heterogeneity of macrophages in culture, both at steady state and in response to immune stimulatory DNA, with and without blockade of secondary IFNAR-dependent amplification, revealing *Ccl5* as an IFNAR-independent marker of direct DNA-sensing cells.

Methods

Animals and tissue processing

Mouse experiments were approved and conducted under the oversight of University of California San Diego Institutional

10.3389/fimmu.2023.1199730

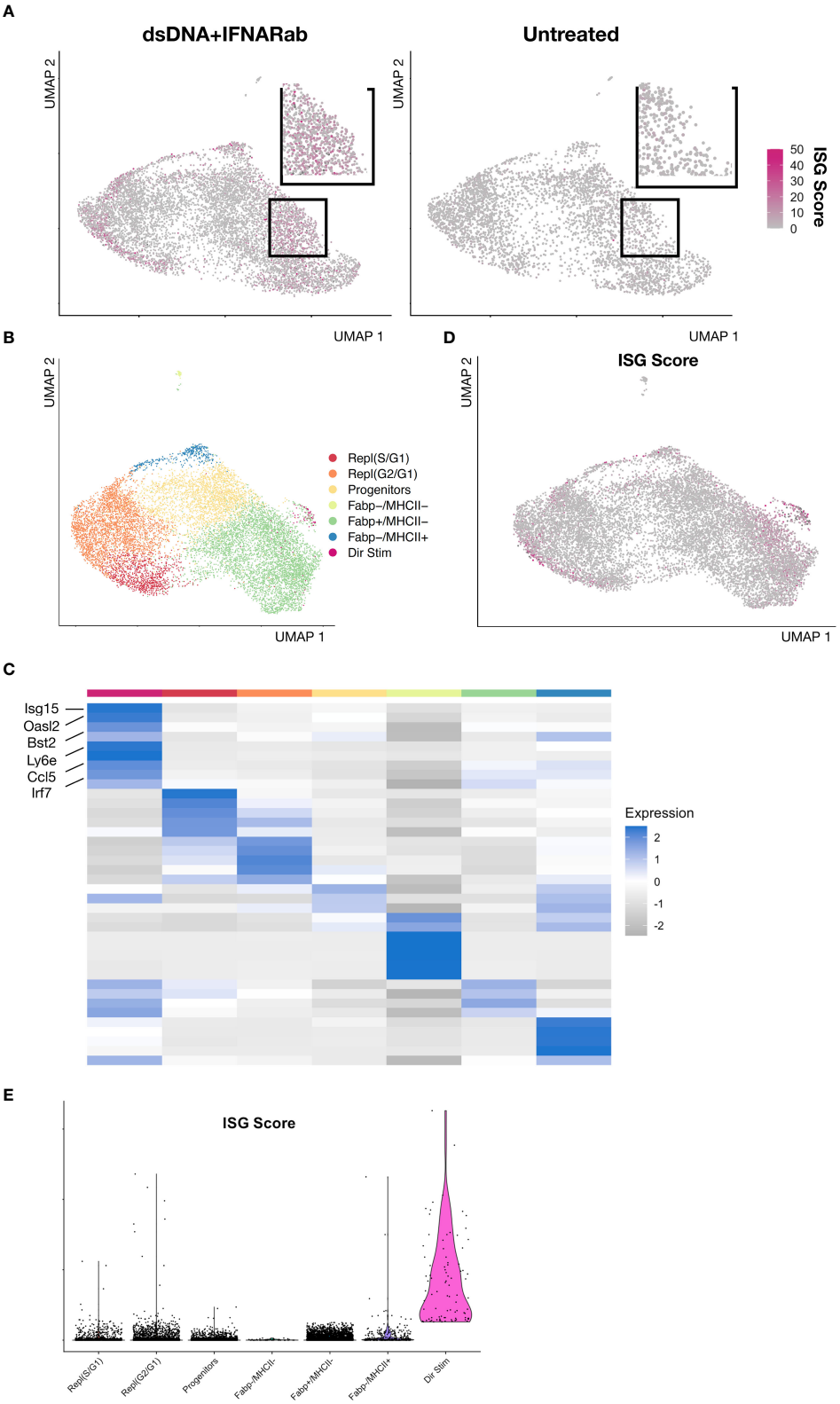

FIGURE 4
IFNAR-independent BMDM responses to immune stimulatory DNA **(A)** Feature plot of dsDNA+IFNAR Ab and untreated experimental conditions colored magenta based on ISG Score. **(B)** Feature plot of integrated and clustered data from dsDNA+IFNAR Ab and Untreated conditions, demonstrating BMDM subsets. **(C)** Heatmap of biological replicates averaged, scaled expression displaying marker genes for each subset. **(D)** Feature plot of ISG Score reveals a small cluster expressing ISGs amidst a larger cluster of Fabp4+MHCII- cluster. **(E)** Violin plot of ISG Score for each BMDM subset from the integration of control and dsDNA+IFNAR Ab conditions.

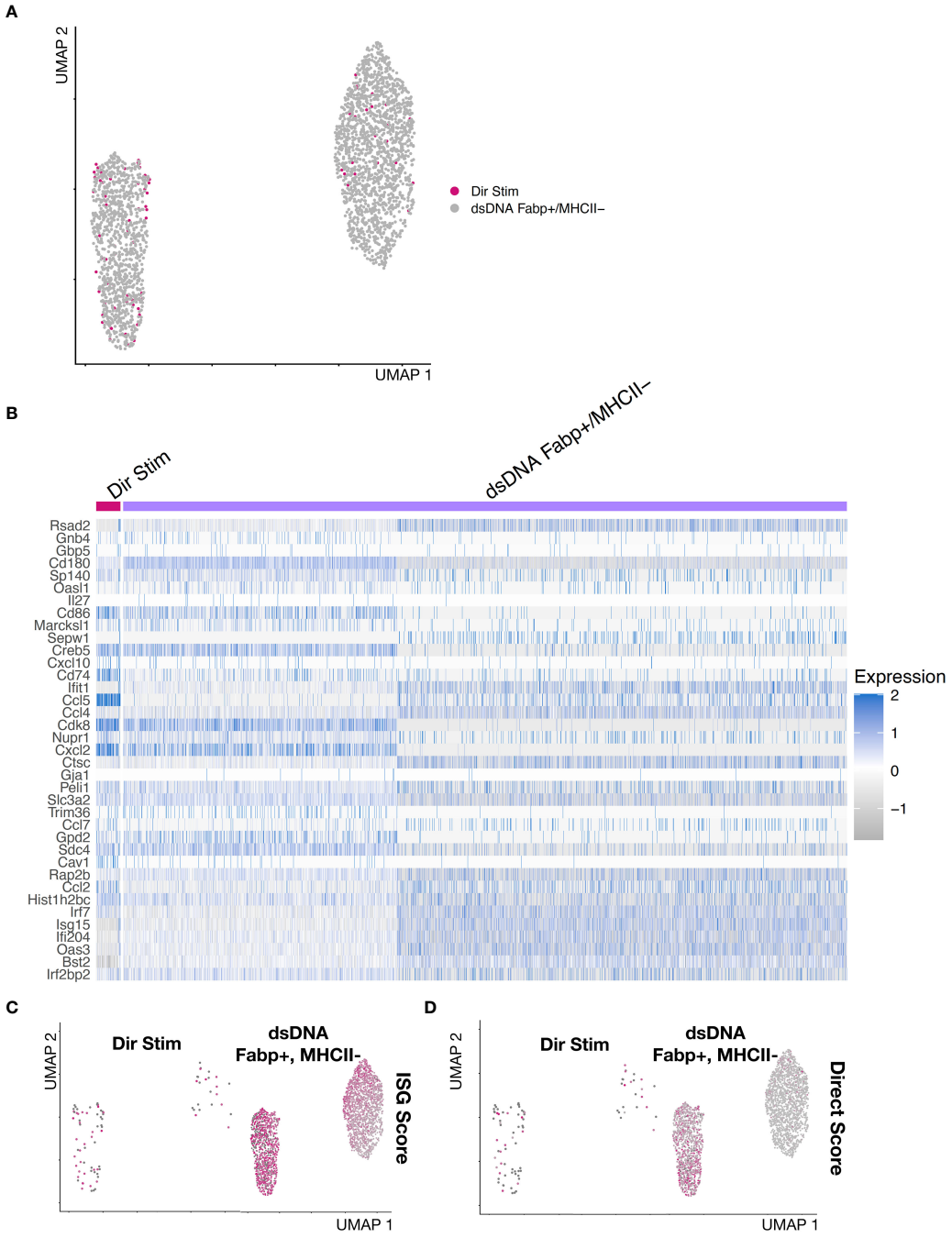

FIGURE 5
Gene expression signature of direct dsDNA-sensing IFNAR-independent BMDMs. **(A)** Reclustering of Direct Stimulated cells from dsDNA + IFNAR Ab condition integrated with Fabp4+MHCII- BMDMs subset from the dsDNA stimulated experimental condition. **(B)** Heatmap of Fabp4+MHCII- BMDMs reveals ISG+ and ISG- subsets. The ISG+ subset are the putative direct dsDNA-stimulated macrophages. Differentially expressed genes between ISG + and ISG- subsets include *Ccl5,Cdk8, Cxcl2, and Cd74*. **(C, D)** Feature plots comparing **(C)** ISG Score compared to a **(D)** DirStim Score (*Ccl5, Cdk8, Cxcl2, and Cd74*).

Animal Care and Use Committee (IACUC #17144) using Adult C57BL/6J (3 *WT mice*, stock 000664, and 2 IFNAR -/- mice, stock 028288). All experiments were performed with 10 to 14-week-old animals and were carried out using age and gender matched groups without randomization. All mice were maintained in a pathogen-free environment of UC San Diego.

Cell culture

Bone marrow derived macrophages (BMDMs) were isolated by flushing femurs of adult mice and culturing the resulting cells in 10% FBS 1% Pen/Strep-containing DMEM supplemented with 10ng/mL recombinant m-CSF (Peprotech) for 7 days. 5μg of immunogenic HT

DNA (*In vivo*gen) was complexed with a Lipofectamine transfection agent (ThermoFisher) at a ratio of 1:1.5 in serum free-media and added to 1 million BMDMs in a 6-well multi-well plate with serum- and mCSF-containing media for each experiment. Two independent experiments were performed, yielding n = 5 for each condition. For inhibition of secondary signaling *via* the IFNAR receptor, cells were treated with 20μg/ml of MAR1-5A3 IFNAR neutralizing antibody or isotype control (BioXCell).

Flow cytometry

Isolated cells were stained at 4°C in FACS buffer (PBS supplemented with 2.5% bovine serum albumin). Cell suspensions were labeled with DAPI just prior to flow cytometric analysis to allow exclusion of dead cells. Doublets and dead cells were excluded by forward scatter and Dapi. Data was acquired by Sony sorter MA900 at UCSD and analyzed with FlowJo software.

Single cell RNA-seq

Single cell RNA-Seq was performed by microfluidic droplet-based encapsulation, barcoding, and library preparation (10X Genomics) as previously described (27). Paired end sequencing was performed on an Illumina NovaSeq instrument. Low level analysis, including demultiplexing, mapping to a reference transcriptome (Ensembl Release 85 - GRCm38.p5), and eliminating redundant UMIs, was performed with the CellRanger pipeline.

Single-cell RNA-seq data quality control, normalization and integration

To account for variations in sequencing depth, total transcript count for each cell was scaled to 10,000 molecules, and raw counts for each gene were normalized to the total transcript count associated with that cell and then natural log transformed. Cells with between 200 and 2,000 uniquely expressed genes and < 1% mitochondrial counts were retained for further analysis. Highly variable genes across individual datasets were identified with the *FindVariableFeatures* method from the Seurat R package (version 3.0) by selecting 3,000 genes with the highest feature variance after variance-stabilizing transformation. Integration of multiple single-cell RNA-seq datasets was performed in Seurat to enable harmonized clustering and downstream comparative analyses across conditions (28–30). Anchoring cell pairs between datasets were identified by Canonical Correlation Analysis (CCA) and the mutual nearest neighbors (MNN) method using the Seurat *FindIntegrationAnchors* function.

Dimensional reduction, unsupervised clustering, sub-clustering

After scaling and centering expression values for each variable gene, linear dimensionality reduction was performed on integrated data using principal component analysis (PCA). Clustering was performed using the shared nearest neighbor (SNN) clustering algorithm with the Louvain method for modularity optimization, as implemented in the Seurat *FindNeighbors* and *FindClusters* functions. To visualize data in two-dimensional space, Uniform Manifold Approximation and Projection (UMAP) dimensional reduction was performed. Differentially expressed genes (DEGs) between clusters were determined using a Wilcoxon Rank Sum test. Where specified, subsets of cells were isolated and reclustered to identify new DEGs.

Quantification of ISG score and direct score

ISG Scores were measured as the sum of the raw reads for the ISGS: Ifi204, Isg15, Irf7, Ifit1, Rsad2, Oasl2, Oas3, Gpb5, Bst2, Ifit2, Ifit3, Oas2, Isg20, Cxcl10, Oasl1, Gpb2, Ccl5, Ccl3. Direct Scores were measured as the sum of the raw reads for: Ccl5, Cdk8, Cxcl2, and Cd74. ISG and Direct Scores were normalized to reads per cell and scaled by 10^4.

Statistics

Statistical analysis was performed using GraphPad Prism software. All data are represented as mean values +/- standard error of mean (S.E.M.) unless indicated otherwise. A statistical method was not used to predetermine sample size. All analyses were unpaired. *P* values are indicated by *P* values less than 0.05 were considered significant and are indicated by asterisks as follows: *p<0.05, **p<0.01, ***p<0.001, ****p<0.0001.

Data availability statement

The single cell RNA-Seq datasets presented in this study have been deposited to the Gene Expression Omnibus under accession no. GSE229311 (GEO). The code used to process this data is publicly available at Zenodo (https://zenodo.org/record/7874451).

Ethics statement

The animal study was reviewed and approved by University of California San Diego Institutional Animal Care and Use Committee (IACUC #17144).

Author contributions

EM, JY, VN, and KK designed the study, performed analysis, and wrote the initial manuscript. VN conducted experiments. EM, JY, and DC performed analysis. KK directed the project. All authors contributed to the article and approved the submitted version.

Funding

The work was funded by the following National Institutes of Health (NIH) grants, NIH T32HL007444 (VN), NIH T32HL105373 (DC), NIH R00HL129168 (KK), and NIH DP2AR075321 (KK).

Acknowledgments

We thank Richard Ng, Avinash Toomu, and Nika Taghdiri for technical assistance. This publication includes data generated at the UC San Diego IGM Genomics Center utilizing an Illumina NovaSeq 6000 that was purchased with funding from a National Institutes of Health SIG grant (#S10 OD026929).

Conflict of interest

The authors declare that the research was conducted in the absence of any commercial or financial relationships that could be construed as a potential conflict of interest.

Publisher's note

All claims expressed in this article are solely those of the authors and do not necessarily represent those of their affiliated organizations, or those of the publisher, the editors and the reviewers. Any product that may be evaluated in this article, or claim that may be made by its manufacturer, is not guaranteed or endorsed by the publisher.

Supplementary material

The Supplementary Material for this article can be found online at: https://www.frontiersin.org/articles/10.3389/fimmu.2023.1199730/full#supplementary-material

SUPPLEMENTARY FIGURE 1
Integrated single cell transcriptomes reveal cell-cycling and non-cycling BMDM subsets. **(A)** Data from all experimental conditions was integrated and clustered. Unsupervised clustering of integrated data (n= 24,377 cells) revealed at least 6 distinct BMDM subsets. Data is dimensionally reduced using UMAP and displayed on a 2D plot to communicate relative similarities in transcriptional profiles between BMDM subsets. **(B)** Identification of replicating BMDMs from clusters based on cell cycle phase (color-coded legend) using cell cycle sorting. **(C)** Heatmap of biological replicates averaged, scaled expression of defining 1065 differentially expressed genes for each BMDM subset. Cell cycling subsets (clusters 1-2, red & orange) and non-cycling subsets (clusters 3-6, yellow, green, and blue) are annotated.

SUPPLEMENTARY FIGURE 2
Immune stimulatory DNA induces a type I IFN response that can be partially blocked by IFNAR Ab. **(A)** Heatmap of of biological replicates averaged, scaled expression of ISG genes sorted by experimental condition (1: control, 2: IFNAR KO control, 3: dsDNA, 4: dsDNA+IFNAR Ab, 5: dsDNA+IFNAR KO). **(B)** Violin plot of Ms4a7, a macrophage marker gene, and several ISGs (Bst2, Oasl2, Irf7, Ifit2, Oas3, Isg15, Rsad2). **(C)** An ISG Score defined as the summed expression of canonical ISGs was calculated for each cell and displayed as magenta intensity on a UMAP feature plot for each condition. **(D)** A violin plot of ISG Score was plotted across BMDM subsets and split by experimental condition.

SUPPLEMENTARY FIGURE 3
IFNAR-independent BMDM responses to immune stimulatory DNA. **(A)** Feature plot of dsDNA+IFNAR Ab, dsDNA+IFNAR KO, and untreated experimental conditions colored magenta based on ISG Score. **(B)** Feature plot of integrated and clustered data from dsDNA+IFNAR Ab, dsDNA+IFNAR KO, and Untreated conditions, demonstrating BMDM subsets. **(C)** Heatmap of biological replicates averaged, scaled expression displaying marker genes for each subset. **(D)** Feature plot of ISG Score reveals a small cluster expressing ISGs amidst a larger cluster of Fabp4+MHCII- cluster.**(E)** Violin plot of ISG Score for each BMDM subset from the integration of control and dsDNA +IFNAR Ab conditions.

SUPPLEMENTARY FIGURE 4
Gene expression signature of direct dsDNA-sensing IFNAR-independent BMDMs. **(A)** Reclustering of Direct Stimulated cells from dsDNA + IFNAR Ab and dsDNA+IFNAR KO conditions integrated with Fabp4+MHCII- BMDMs subset from the dsDNA stimulated experimental condition. **(B)** Heatmap of Fabp4+MHCII- BMDMs reveals ISG+ and ISG- subsets. The ISG+ subset are the putative direct dsDNA-stimulated macrophages. Differentially expressed genes between ISG+ and ISG- subsets include Ccl5, Cdk8, Cxcl2, and Cd74. C-D) Feature plots comparing **(C)** ISG Score compared to a **(D)** DirStim Score (Ccl5, Cdk8, Cxcl2, and Cd74).

References

1. Liu Y, Jesus AA, Marrero B, Yang D, Ramsey SE, Montealegre Sanchez GA, et al. Activated STING in a vascular and pulmonary syndrome. *N Engl J Med* (2014) 371 (6):507–18. doi: 10.1056/NEJMoa1312625

2. Davidson S, Steiner A, Harapas CR, Masters SL. An update on autoinflammatory diseases: interferonopathies. *Curr Rheumatol Rep* (2018) 20(7):38. doi: 10.1007/s11926-018-0748-y

3. King KR, Aguirre AD, Ye YX, Sun Y, Roh JD, Ng RPJr., et al. IRF3 and type I interferons fuel a fatal response to myocardial infarction. *Nat Med* (2017) 23(12):1481–7. doi: 10.1038/nm.4428

4. Biacchesi S, Merour E, Lamoureux A, Bernard J, Bremont M. Both STING and MAVS fish orthologs contribute to the induction of interferon mediated by RIG-I. *PloS One* (2012) 7(10):e47737. doi: 10.1371/journal.pone.0047737

5. Harding SM, Benci JL, Irianto J, Discher DE, Minn AJ, Greenberg RA. Mitotic progression following DNA damage enables pattern recognition within micronuclei. *Nature* (2017) 548(7668):466–70. doi: 10.1038/nature23470

6. Woo SR, Fuertes MB, Corrales L, Spranger S, Furdyna MJ, Leung MY, et al. STING-dependent cytosolic DNA sensing mediates innate immune recognition of immunogenic tumors. *Immunity* (2014) 41(5):830–42. doi: 10.1016/j.immuni.2014.10.017

7. Dhanwani R, Takahashi M, Sharma S. Cytosolic sensing of immuno-stimulatory DNA, the enemy within. *Curr Opin Immunol* (2018) 50:82–7. doi: 10.1016/j.coi.2017.11.004

8. Furie R, Khamashta M, Merrill JT, Werth VP, Kalunian K, Brohawn P, et al. Anifrolumab, an anti-interferon-alpha receptor monoclonal antibody, in moderate-to-Severe systemic lupus erythematosus. *Arthritis Rheumatol* (2017) 69(2):376–86. doi: 10.1002/art.39962

9. Gray EE, Treuting PM, Woodward JJ, Stetson DB. Cutting edge: cGAS is required for lethal autoimmune disease in the Trex1-deficient mouse model of aicardi-goutieres syndrome. *J Immunol* (2015) 195(5):1939–43. doi: 10.4049/jimmunol.1500969

10. Morand EF, Furie R, Tanaka Y, Bruce IN, Askanase AD, Richez C, et al. Trial of anifrolumab in active systemic lupus erythematosus. *N Engl J Med* (2020) 382(3):211–21. doi: 10.1056/NEJMoa1912196

11. Barrat FJ, Meeker T, Gregorio J, Chan JH, Uematsu S, Akira S, et al. Nucleic acids of mammalian origin can act as endogenous ligands for toll-like receptors and may promote systemic lupus erythematosus. *J Exp Med* (2005) 202(8):1131–9. doi: 10.1084/jem.20050914

12. Barton GM, Kagan JC, Medzhitov R. Intracellular localization of toll-like receptor 9 prevents recognition of self DNA but facilitates access to viral DNA. *Nat Immunol* (2006) 7(1):49–56. doi: 10.1038/ni1280

13. Brunette RL, Young JM, Whitley DG, Brodsky IE, Malik HS, Stetson DB. Extensive evolutionary and functional diversity among mammalian AIM2-like receptors. *J Exp Med* (2012) 209(11):1969–83. doi: 10.1084/jem.20121960

14. Hornung V, Ablasser A, Charrel-Dennis M, Bauernfeind F, Horvath G, Caffrey DR, et al. AIM2 recognizes cytosolic dsDNA and forms a caspase-1-activating inflammasome with ASC. *Nature* (2009) 458(7237):514–8. doi: 10.1038/nature07725

15. Unterholzner L. The interferon response to intracellular DNA: why so many receptors? *Immunobiology* (2013) 218(11):1312–21. doi: 10.1016/j.imbio.2013.07.007

16. Au-Yeung N, Horvath CM. Transcriptional and chromatin regulation in interferon and innate antiviral gene expression. *Cytokine Growth factor Rev* (2018) 44:11–7. doi: 10.1016/j.cytogfr.2018.10.003

17. Lin R, Heylbroeck C, Genin P, Pitha PM, Hiscott J. Essential role of interferon regulatory factor 3 in direct activation of RANTES chemokine transcription. *Mol Cell Biol* (1999) 19(2):959–66. doi: 10.1128/MCB.19.2.959

18. Grandvaux N, Servant MJ, tenOever B, Sen GC, Balachandran S, Barber GN, et al. Transcriptional profiling of interferon regulatory factor 3 target genes: direct involvement in the regulation of interferon-stimulated genes. *J Virol* (2002) 76 (11):5532–9. doi: 10.1128/JVI.76.11.5532-5539.2002

19. Link VM, Duttke SH, Chun HB, Holtman IR, Westin E, Hoeksema MA, et al. Analysis of genetically diverse macrophages reveals local and domain-wide mechanisms that control transcription factor binding and function. *Cell* (2018) 173 (7):1796–809 e17. doi: 10.1016/j.cell.2018.04.018

20. Taghdiri N, Calcagno DM, Fu Z, Huang K, Kohler RH, Weissleder R, et al. Macrophage calcium reporter mice reveal immune cell communication in vitro and *in vivo*. *Cell Rep Methods* (2021) 1(8). doi: 10.1016/j.crmeth.2021.100132

21. Stetson DB, Medzhitov R. Recognition of cytosolic DNA activates an IRF3-dependent innate immune response. *Immunity* (2006) 24(1):93–103. doi: 10.1016/j.immuni.2005.12.003

22. Appay V, Rowland-Jones SL. RANTES: a versatile and controversial chemokine. *Trends Immunol* (2001) 22(2):83–7. doi: 10.1016/s1471-4906(00)01812-3

23. Donlon TA, Krensky AM, Wallace MR, Collins FS, Lovett M, Clayberger C. Localization of a human T-cell-specific gene, RANTES (D17S136E), to chromosome 17q11. *2-q12. Genomics* (1990) 6(3):548–53. doi: 10.1016/0888-7543(90)90485-d

24. Calcagno DM, Ng RP, Toomu A, Zhang C, Huang K, Aguirre AD, et al. Type I interferon responses to ischemic injury begin in the bone marrow of mice and humans and depend on Tet2, Nrf2, and Irf3. *bioRxiv* (2020) 765404. doi: 10.1101/765404

25. Calcagno DM, Ng RPJr., Toomu A, Zhang C, Huang K, Aguirre AD, et al. The myeloid type I interferon response to myocardial infarction begins in bone marrow and is regulated by Nrf2-activated macrophages. *Sci Immunol* (2020) 5(51). doi: 10.1126/sciimmunol.aaz1974

26. Patel SJ, Milwid JM, King KR, Bohr S, Iracheta-Velle A, Li M, et al. Gap junction inhibition prevents drug-induced liver toxicity and fulminant hepatic failure. *Nat Biotechnol* (2012) 30(2):179–83. doi: 10.1038/nbt.2089

27. Calcagno DM, Taghdiri N, Ninh VK, Mesfin JM, Toomu A, Sehgal R, et al. Single-cell and spatial transcriptomics of the infarcted heart define the dynamic onset of the border zone in response to mechanical destabilization. *Nat Cardiovasc Res* (2022) 1:1039–55. doi: 10.1038/s44161-022-00160-3

28. Stuart T, Butler A, Hoffman P, Hafemeister C, Papalexi E, Mauck WM3rd, et al. Comprehensive integration of single-cell data. *Cell* (2019) 177(7):1888–902 e21. doi: 10.1016/j.cell.2019.05.031

29. Qiu X, Mao Q, Tang Y, Wang L, Chawla R, Pliner HA, et al. Reversed graph embedding resolves complex single-cell trajectories. *Nat Methods* (2017) 14(10):979–82. doi: 10.1038/nmeth.4402

30. Butler A, Hoffman P, Smibert P, Papalexi E, Satija R. Integrating single-cell transcriptomic data across different conditions, technologies, and species. *Nat Biotechnol* (2018) 36(5):411–20. doi: 10.1038/nbt.4096

frontiers | Frontiers in Immunology

TYPE Original Research
PUBLISHED 03 July 2023
DOI 10.3389/fimmu.2023.1179314

OPEN ACCESS

EDITED BY
Irene S. Soares,
University of São Paulo, Brazil

REVIEWED BY
Katherine Rose Dobbs,
Case Western Reserve University, United States
Isaac Ssewanyana,
Infectious Diseases Research Collaboration, Uganda

*CORRESPONDENCE
Joana C. Silva
jcsilva@som.umaryland.edu
Kirsten E. Lyke
klyke@som.umaryland.edu

†These authors have contributed equally to this work and share senior authorship

RECEIVED 03 March 2023
ACCEPTED 19 June 2023
PUBLISHED 03 July 2023

CITATION
Mbambo G, Dwivedi A, Ifeonu OO, Munro JB, Shrestha B, Bromley RE, Hodges T, Adkins RS, Kouriba B, Diarra I, Niangaly A, Kone AK, Coulibaly D, Traore K, Dolo A, Thera MA, Laurens MB, Doumbo OK, Plowe CV, Berry AA, Travassos M, Lyke KE and Silva JC (2023) Immunogenomic profile at baseline predicts host susceptibility to clinical malaria.
Front. Immunol. 14:1179314.
doi: 10.3389/fimmu.2023.1179314

Immunogenomic profile at baseline predicts host susceptibility to clinical malaria

Gillian Mbambo[1], Ankit Dwivedi[1], Olukemi O. Ifeonu[1], James B. Munro[1], Biraj Shrestha[2], Robin E. Bromley[1], Theresa Hodges[1], Ricky S. Adkins[1], Bourema Kouriba[3], Issa Diarra[3], Amadou Niangaly[3], Abdoulaye K. Kone[3], Drissa Coulibaly[3], Karim Traore[3], Amagana Dolo[3], Mahamadou A. Thera[3], Matthew B. Laurens[2], Ogobara K. Doumbo[3], Christopher V. Plowe[2], Andrea A. Berry[2], Mark Travassos[2], Kirsten E. Lyke[2*†] and Joana C. Silva[1,4,5*†]

[1]Institute for Genome Sciences, University of Maryland School of Medicine, Baltimore, MD, United States, [2]Center for Vaccine Development and Global Health, University of Maryland School of Medicine, Baltimore, MD, United States, [3]Malaria Research and Training Center, International Centers for Excellence in Research (NIH), University of Science Techniques and Technologies of Bamako, Bamako, Mali, [4]Department of Microbiology and Immunology, University of Maryland School of Medicine, Baltimore, MD, United States, [5]Global Health and Tropical Medicine, Instituto deHigiene e Medicina Tropical, Universidade Nova de Lisboa (GHTM, IHMT, UNL), Lisboa, Portugal

Introduction: Host gene and protein expression impact susceptibility to clinical malaria, but the balance of immune cell populations, cytokines and genes that contributes to protection, remains incompletely understood. Little is known about the determinants of host susceptibility to clinical malaria at a time when acquired immunity is developing.

Methods: We analyzed peripheral blood mononuclear cells (PBMCs) collected from children who differed in susceptibility to clinical malaria, all from a small town in Mali. PBMCs were collected from children aged 4-6 years at the start, peak and end of the malaria season. We characterized the immune cell composition and cytokine secretion for a subset of 20 children per timepoint (10 children with no symptomatic malaria age-matched to 10 children with >2 symptomatic malarial illnesses), and gene expression patterns for six children (three per cohort) per timepoint.

Results: We observed differences between the two groups of children in the expression of genes related to cell death and inflammation; in particular, inflammatory genes such as CXCL10 and STAT1 and apoptotic genes such as XAF1 were upregulated in susceptible children before the transmission season began. We also noted higher frequency of HLA-DR+ CD4 T cells in protected children during the peak of the malaria season and comparable levels cytokine secretion after stimulation with malaria schizonts across all three time points.

Conclusion: This study highlights the importance of baseline immune signatures in determining disease outcome. Our data suggests that differences in apoptotic and inflammatory gene expression patterns can serve as predictive markers of susceptibility to clinical malaria.

KEYWORDS

RNA sequencing, mass cytometry, immunoinformatic analysis, baseline immunity, malaria susceptibility, malaria immunity, human parasite immunology

Introduction

Malaria remains a major global health concern that impacts over 200 million people annually, causing an estimated 619,000 deaths in 2021 (1). Despite its global distribution throughout the tropical and subtropical regions, 95% of malaria cases occur in sub-Saharan Africa, and are caused primarily by *Plasmodium falciparum* (1). Individuals in malaria-endemic regions with high transmission are repeatedly exposed to diverse *P. falciparum* strains and their associated antigens; these successive exposures can lead to acquired immunity to clinical malaria (2). However, children with similar levels of malaria exposure can vary in susceptibility to clinical disease. Several host factors, including those related to red blood cell disorders (HbS, HbC, G6PD and alpha-thalassemia), are known to be associated with protection, while some HLA alleles are associated with increased susceptibility to malaria infection (3, 4). Nevertheless, much remains to be understood, particularly regarding differences in the host response to infection (5).

Previous studies have implicated the activation of the type 1 interferon pathway in mitigating severe disease to mild malaria and interferon-gamma (IFNg) secretion with protection from clinical disease (6). However, other studies suggest a role for IFNg in exacerbating severe malaria episodes (cerebral malaria), implying that a delicate balance of inflammatory cytokines is critical to regulate malarial disease and pathogenesis (7). T cell-mediated immune responses play an important role in controlling pro- and anti-inflammatory immune responses during blood stage malaria (8). Type 1 helper CD4 T cells (Th1) produce inflammatory cytokines such as IFNg and TNFa that shape the early adaptive immune response to *Plasmodium* infection. These inflammatory responses are controlled by regulatory T cells (Tregs) that produce cytokines such as IL-10 and TGFb (9). Later in infection, Type 2 helper CD4 T cells (Th2) dominate and aid in antibody production, which is characteristic of a protective response to blood stage *Plasmodium* infection (10).

Transcriptomic analysis from whole blood cells has shown that naïve individuals >13 years old have a higher pro-inflammatory cytokine response when compared to their malaria-experienced counterparts upon infection with *P. falciparum* (11). This may indicate a dampened immune response in individuals with pre-existing immunity to malaria, which could impact the clinical presentation of the disease. Some studies suggest exhausted B and T cells play a role in the lack of robust immune responses in individuals with recurrent exposure to *P. falciparum* (12). However, it remains to be determined how molecular pathways correlate with malaria exposure history in children with distinct levels of susceptibility to clinical malaria, and which immunoprofiles characterize a protective response. Gene expression studies are increasingly used to decipher molecular mechanisms and pathways associated with malaria infection using either peripheral blood mononuclear cells (PBMCs) or whole blood (11, 13), and to analyze gene expression patterns in immune cells during malaria infection only (11, 14). Here, we compare the longitudinal transcriptional profiles of two cohorts of location and age-matched children, ages 4 to 6 years old, who differ in the degree of malaria susceptibility, to better understand the protective immune response to malaria at a time when acquired immunity is developing. We hypothesize that in an area of high malaria transmission, children who do not manifest clinical disease throughout an entire transmission season can control infection better than those who experience two or more symptomatic malaria episodes during the same period (either by preventing erythrocytic infection or by controlling symptoms), and that this difference is reflected in their PBMC transcriptomic profiles. To address this hypothesis, we compared PBMC gene expression profiles derived from a subset of children categorized as "susceptible" versus "non-susceptible/protected" to malaria, and who were part of the control arm of a malaria vaccine trial in Mali (15). An improved understanding of the host immune response to malaria, and in particular the identification of immune cell subpopulations that may play a role in a protective immune response, may identify those at increased risk and inform preventative treatment.

Methods and sample collection

Ethics

Sample processing was conducted with review and oversight by the University of Maryland, Baltimore's Human Research Protection Office. The primary study was reviewed and approved by the Institutional Review Boards of the University of Maryland, Baltimore and the University of Bamako, Mali. Village permission to conduct research was obtained from village chiefs, government

officials, and traditional healers prior to study initiation. Individual written informed consent was obtained from the parent or legal guardian of each child prior to screening and enrollment in accordance with the Declaration of Helsinki. Child assent was also obtained prior to study conduct.

Study design

After obtaining informed parental consent, PBMCs from children who were part of a randomized, controlled, double-blind Apical Membrane Antigen 1 (AMA1) malaria vaccine trial in Bandiagara, Mali, West Africa, were cryopreserved on site using standardized procedures and transported to the University of Maryland, Baltimore (UMB), utilizing a tightly controlled cold chain. Registration on ClinicalTrials.gov (NCT00460525) and full study details have been previously described (15). Bandiagara, Mali, is a Sahelian town of approximately 14,000 inhabitants with highly prevalent and seasonal malaria transmission (June to December) (16, 17). There is no significant variability in the socio-economic state in this remote community. The prevalence of HIV is extremely low, and previous screening of children aged 3 months to 14 years revealed no concomitant infections with filaria. While *S. haematobium* is endemic, prevalence is typically low for children aged 2-6 years. At the time of the study conduct, children under 6 years of age routinely acquired 1-4 symptomatic malaria infections per season. All children were provided government-issued, insecticide-treated bed nets with 61% of control participants reporting use (15). Participants were continuously monitored through passive case detection and the rate of loss to follow-up was less than 7%. The Bandiagara research center served as the primary source of western medical care for most children in the village, and few had access to pharmaceuticals for intermittent malarial therapy. A subset of children (n = 25) ages 4-6 was selected from the control arm (three doses of human diploid-cell rabies vaccine (RabAvert, Chiron Vaccines)) based on age, number of clinical malaria episodes, and availability of sample across all three timepoints (15). We examined PBMCs from this cohort (Supplementary Table 1). The original study followed children during a single malaria transmission season (6 months) and PBMCs were collected at day 0 (beginning of transmission season), day 90 (peak transmission season), and day 150 (end of transmission season) (Supplementary Figure 1A). For this analysis, children with at least two clinical malaria episodes throughout the transmission season were classified as "susceptible" and were age-matched to children with no clinical malaria episodes throughout the same transmission season; the latter were classified as "protected" (Supplementary Figure 1B). Malaria episodes were acquired by susceptible participants between day 8 and 146. The timing of illness varied among participants, with the majority experiencing their first episode before the day 90 timepoint, except for one participant (Supplementary Figure 1C). Clinical malaria was defined as a symptomatic infection consistent with malaria (e.g., fever, headache, malaise) and evidence of parasitemia in the absence of an alternative clinical diagnosis. None of the children met the definition of severe malaria. Only children with PBMC available at all three time points were eligible for analysis. Serum samples were collected for each child at the same timepoints and kept at -80°C.

Peripheral blood mononuclear cells stimulation

Cryopreserved PBMCs were thawed with fetal bovine serum (FBS) enriched media (RPMI, Gibco, Grand Island, New York) and incubated at 37°C/5% CO_2 overnight. After incubation, PBMCs were washed and partitioned into three $1x10^6$ cell aliquots. One aliquot was stimulated with *P. falciparum* schizonts (Pfsz; derived from a Malawian source and cultured *in vitro* at UMB) at a 3:1 ratio (3 schizonts/cell) and incubated at 37°C/5% CO_2 for 4 hours. The other two aliquots served as negative (media) and positive (stimulation with 10 mg/ml *Staphylococcus* enterotoxin B (SEB); Sigma, St. Louis, MO) controls and incubated at 37°C/5% CO_2 for 2 hours. Golgi blockade (BD Pharmingen) was added at 0.5 mL/tube and incubated overnight (16 hours) at 37°C/5% CO_2. As the addition of Golgi blockade compromised RNA integrity, a finding not previously noted in the literature, samples from 6 unique randomly selected children that met the age and malaria episode criteria were immediately extracted after stimulation for RNA sequencing without the addition of Golgi blockade.

Regulatory T cell (Tregs) depletion

PBMCs were thawed as described above. A portion of the cells were partitioned to serve as negative and positive controls. The remaining PBMCs were split into two aliquots that were either mock depleted or depleted of CD25 cells using Dynabeads Pan Mouse IgG or CD25 magnetic beads, respectively (Invitrogen, Carlsbad, California) at a bead to PBMC ratio of 5:1 as described (18). PBMCS were stimulated with media, schizonts and SEB as described above.

Staining protocol

PBMCs were stained with viability marker, Cisplatin ($Pb^{194/195}$) (Sigma Aldrich, Indianapolis) at 1.25 mL per 500 mL for a final concentration of 25 mM. After a 1-minute incubation, PBMCs were washed with PBS supplemented with 10% fetal calf serum (FCS) then incubated with one of two optimized (13-21 cell surface markers) panels (Supplementary Tables 2, 3) for 20 minutes. Cells were then fixed using IC fixation buffer (eBioscience) and permeabilized using Caltag Reagent B (Invitrogen, Oregon) along with an intracellular staining cocktail (Supplemental Tables 2, 3), followed by the addition of DNA intercalator Iridium 191 (Ir-191 intercalator, NA). Cells were then washed 2x with cell staining media (0.2 mg/mL sodium azide in low-barium PBS supplemented with 2% FCS) and resuspended in Milli-Q water for assessment by

mass cytometry. Before analysis, a viability dye, Cisplatin (19) and the DNA metalointercalator $^{191/193}$Ir to identify individual cells, was used to complete the panel.

Generation of RNAseq data

Immediately after PBMC stimulation, Roche Protector RNase inhibitor (3335399001; MilliporeSigma, Burlington, Massachusetts, USA) was added to each sample. RNA was isolated using QIAzol (Qiagen 79306; Hilden, Germany) and the Direct-zol RNA Mini Prep Plus Kit (Zymo Research, Irvine, California, USA) per manufacturer's instructions. RNA quality was assessed using the Agilent Bioanalyzer 2100, and only samples with RNA integrity numbers (RIN) greater than 7 or total RNA concentration greater than 100 ng were selected for RNA sequencing (Supplementary Table 4). PolyA-enriched, strand-specific RNA libraries were constructed and 100bp paired-end reads were sequenced on an Illumina NovaSeq 6000 platform. Reads were assessed for quality, trimmed if PHRED scores fell below 20, and any remaining adapter sequences were removed. These processed paired-end reads were aligned to human reference genome GRCh38 using HISAT2, and counts were generated using the HTseq analysis package (20–22). Reads that successfully mapped to the reference genome were used for downstream analyses. The data are available under bio-project ID (PRJNA603324).

Differential gene expression analyses

To perform differential gene expression analyses, we used DEseq, EdgeR and Cuffdiff R packages (21, 23). Any genes with counts per million (CPM) values of less than 10 in 86% of the samples (or 45 of all 53 samples analyzed) were excluded from the analyses. Hemoglobin genes (the most expressed genes after those encoding rRNAs) were removed to improve power. This cutoff was selected to account for the low sample size and to ensure that each group had at least two samples present for differential expression analyses. For visualization of differentially expressed genes, normalized read counts generated by DEseq were input for the software gEAR (https://umgear.org/multigene_curator.html) to create volcano plots, implemented using the Dash Bio suite of bioinformatics components (v0.6.1 - https://github.com/plotly/dash-bio). Welch's t-test was used to determine significance (24), and was computed using the python package diffxpy (v0.7.4 - https://github.com/theislab/diffxpy).

Pathway and functional analysis

Pathway enrichment analysis was conducted with the output from deseq2. Differentially expressed genes with a false discovery rate (FDR) <0.05, and a log fold change (LFC) >1, were used. Genes that passed these cutoffs were submitted to DAVID web-based tool (https://david.ncifcrf.gov/tools.jsp) (25, 26). Bar plots were created with GraphPad Prism v9. Further functional analyses were performed using GSEA (27), using normalized expression values from all genes as the input.

Mass cytometry data processing

FlowJo v.10.8.0 Software (BD Life sciences, Ashland, Oregon, USA) was used to select intact ($Ir191^+$, $Ir193^+$), live ($PT195^-$), singlet, $CD14/CD19^-$ and $CD3^+$ cells. Specimens were included in the analysis if (*i*) the cell viability was >80% after thawing and (*ii*) cells were shown to be functionally active as determined by the production of IFNg by at least 0.2% $CD3^+$ cells after stimulation with SEB. A response was considered specific if (*i*) the differential in the number of positive events in the stimulant pool compared to the media control was significantly increased by Chi-square analyses; and (*ii*) the net percentage of cytokine producing cells was >0.1% in stimulant pool as compared to the media control. A response was considered positive if the production of one or more cytokines, meeting the pre-defined criteria, was measured in response to antigen stimulation of PBMCs. A mean of ~200,000 cells per sample were analyzed by the CyTOF® Mass Cytometer, with 71%-98% of the cells intact. After gating, $CD3^+$ populations were exported *via* FlowJo to create new FCS files containing only the intact, live, $CD3^+$ cell populations. FCS files were further analyzed in R version 2021.09.2 + 384 using flowCore (28) and CATALYST (29, 30) packages. FlowCore package was used to read the FCS files into R and CATALYST package was used to create a single cell experiment and transform the data with arcsinh cofactor 5. FlowSOM (31) and ConsensusClusterPlus (32) packages were used to perform high dimension clustering and generate 20 clusters using the cell surface marker panel (Supplementary Table 2). UMAP was used to perform high dimension reduction to visualize the clusters generated. Clusters were manually annotated based on cell surface marker expression.

Differential analysis of mass cytometry data

Differential analysis was performed using *diffcyt* (https://bioconductor.org/packages/3.15/bioc/html/diffcyt.html), an R package that utilizes *edgeR*, *limma* and *voom* methods as part of the workflow (33). We used the *diffcyt* differential abundance (DA) method to test for differences in cell type abundance between our two study groups and the *diffcyt* differential states (DS) method to test for differences in intracellular marker expression within each identified cell population between protected and susceptible individuals. We used an FDR cutoff of <0.05 to identify differentially expressed cell types and cytokines.

Differential antibody responses to PfEMP1 microarray

A protein microarray featuring 257 PfEMP1 protein fragments from reference and clinical infections was probed with sera collected before the malaria transmission season (day 0), from 19

children in the same cohort. Samples were randomly selected to include children whose PBMCs were processed *via* RNA sequencing and mass cytometry. Nine serum samples were from protected children while 10 serum samples were from susceptible children. Sera from a pool of North American malaria-naïve adults was used as a negative control while sera from Malian adults from the same study site collected under a different study protocol were used as positive control (34). Slide preparation and serum probing were performed as described elsewhere (35–37). Fluorescence intensity was defined as the raw signal intensity reduced by the mean for the no-DNA negative controls for each serum sample. For each protein fragment, we compared the distribution of fluorescence intensities between sera of susceptible and protected children with a two-tailed Wilcoxon rank-sum test.

Results

Quality control of data and experimental samples

PBMCs were processed from 26 Malian children. Cells from 6 individuals were processed through RNA sequencing and cells from 20 distinct children were profiled *via* mass cytometry. Study groups were assigned based on the number of clinical malaria episodes experienced during a single malaria transmission season.

RNAseq data was generated for six children for each of the three timepoints, and for each of the three stimulation conditions (media, schizonts and SEB), for a total of 54 samples. One SEB stimulated sample from day 150 did not pass QC and was not included in the analyses. For each sample, an average of 30 million Illumina reads were generated (Supplementary Table 5).

Mass cytometry data was generated for 20 different children from the same cohort. For each of the three time points, and each of the three conditions, an average of 200,000 cells were processed. Samples were functionally active if SEB stimulated controls had at least a 0.2% increase in IFNg production relative to unstimulated cells.

Gene expression differences exist between susceptible and protected groups at baseline

To assess if gene expression differences are present between malaria-protected and malaria-susceptible children, we performed a pair-wise comparison of bulk RNA sequence data to identify genes that were either significantly up-regulated or down-regulated at day 0 (start of malaria transmission season) before and after PBMC stimulation with malaria antigen. At baseline, we observed 78 genes significantly differentially expressed based on our analysis parameters (Figure 1A). We observed 74 downregulated and 4 upregulated genes in protected relative to susceptible children. Baseline differences in gene expression at the beginning of the malaria season suggest that differences already exist between children who later develop clinical malaria episodes and those who do not. Of interest, genes upregulated in susceptible children compared to protected children included CXCL10, STAT1, STAT2, IRF1, XAF1 and GZMB. CXCL10, STAT1 and STAT2, all genes that are downstream of interferon signaling, and IRF1, XAF1 and GZMB, which participate in apoptotic processes. Next, we evaluated gene expression patterns in Pfsz-stimulated PBMCs and observed 11 differentially expressed genes, of which 9 were downregulated and 2 upregulated in protected children relative to susceptible children. We observed some overlap in upregulated genes in susceptible children before and after antigen stimulation (Figure 1B and Supplementary Figure 2A). One gene, DDX11, was upregulated in protected children before and after Pfsz stimulation (Figures 1A, B and Supplementary Figure 2B). DDX11 encodes a helicase and plays a role in DNA repair (38). However, the direct role of this gene in regulating immune responses is not known.

To determine if the expression patterns observed were restricted to individual genes or whether, instead, they reflect broader differences at the pathway level, we searched for enriched biological, functional, and immunological pathways at day 0, with DAVID, using genes upregulated in susceptible children (FDR < 0.05; LFC >1) as input. Relative to protected children, we observed enrichment in "Type I interferon signaling," "interferon-gamma signaling," and "apoptotic" pathways in susceptible children (Figures 1C, D). Further analysis using gene set enrichment analysis (GSEA) showed enrichment in IFNg and apoptotic pathways (Supplementary Figure 3).

To determine whether the observed differences in gene and pathway expression were based on different levels of pre-existing immunity to malaria between the susceptible and protected groups, we probed a protein microarray populated with 257 fragments of *P. falciparum* erythrocyte membrane protein-1s (PfEMP1s) with sera from day 0 timepoint. Increased responses to PfEMP1 have been associated with recent malaria exposure (39–41). We compared the PfEMP1 serologic responses between the two groups and observed no differences in antibody responses to 99.2% of the fragments (255/257 PfEMP1 fragments; Supplementary Figure 4B). Additionally, we compared the proportion of individuals within each group with serorecognition of each protein fragment (defined as a fluorescence intensity greater than the mean plus two standard deviations for a serum panel from 10 malaria-naïve North American adults probed on the microarray). We observed that across extracellular PfEMP1 fragments, there was a trend towards greater proportions of protected children with serorecognition of these fragments than susceptible children [68.1% of extracellular PfEMP1 fragments(65/204)]. Interestingly, for 19 of the 20 intracellular PfEMP1 fragments on the microarray, a higher proportion of the susceptible group had serorecognition of the intracellular PfEMP1 fragment than the protected group (Supplementary Figure 4C). Our group previously found that serologic responses to the intracellular region of PfEMP1s is associated with greater malaria exposure (40), suggesting that the susceptible group may have had more malaria exposure than the protected group. In addition, we analyzed previously published ELISA data for Apical Membrane Antigen 1 (AMA1), another

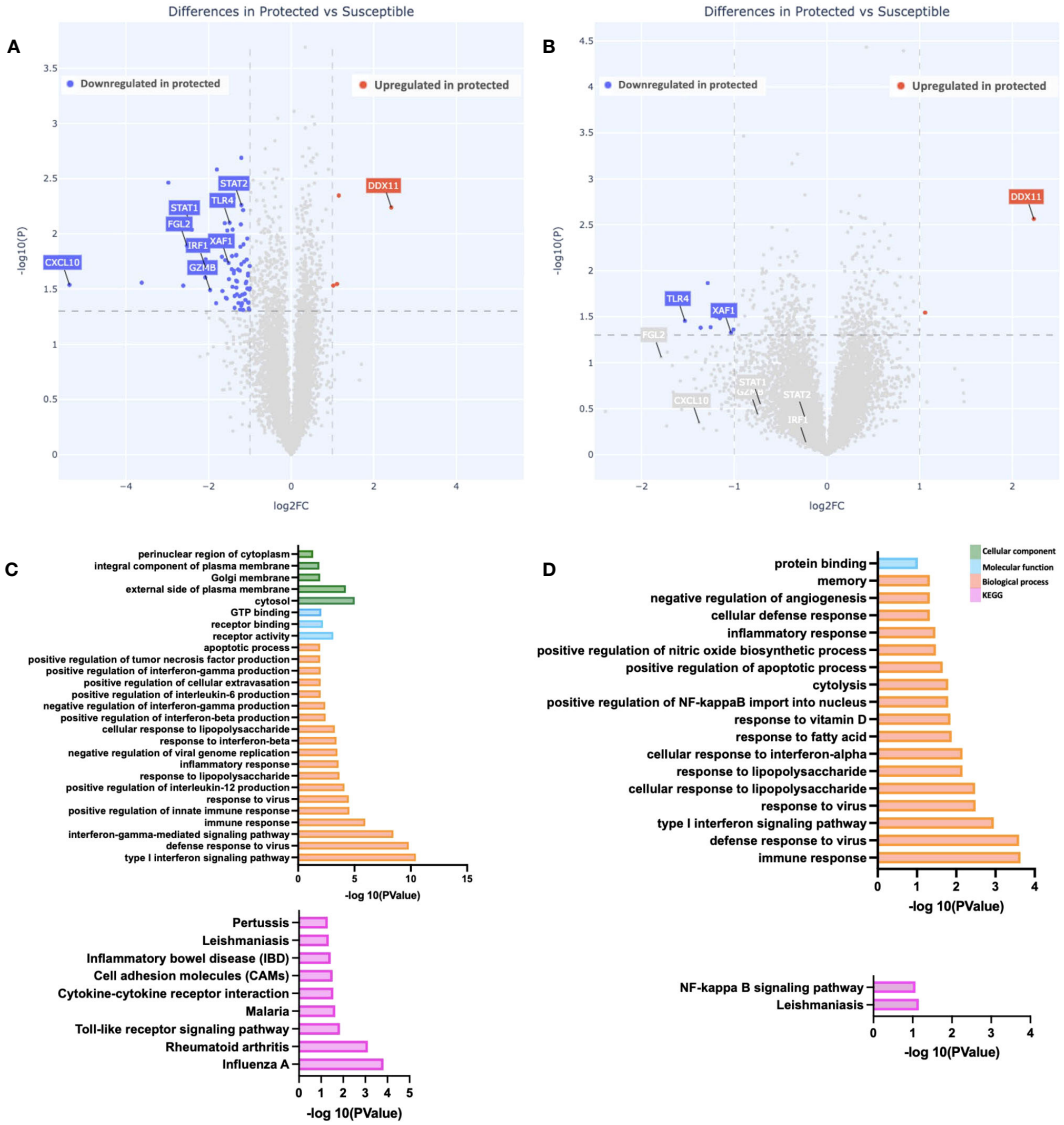

FIGURE 1
Differences in gene expression and immune pathways exist at baseline. **(A, B)** Depicted is a volcano plot of differential gene expression, with significant differences shown (blue, red), based on Welch's Test (log10(pval) is plotted against the log2 foldchange; significance: P value <0.05). **(A)** Unstimulated PBMCs. **(B)** PBMCs stimulated with malaria antigen (*P. falciparum* schizont, Pfsz). **(C, D)** Pathway enrichment analysis on differentially expressed genes (False discovery rate, FDR<0.05; gene expression log-fold change, LFC>1), using pathway enrichment software DAVID (26). **(C)** Pathways enriched in susceptible children before antigen stimulation. **(D)** Pathways enriched in susceptible children after Pfsz stimulation. Enrichment analyses were performed on differentially expressed genes that met the FDR and LFC thresholds; no genes overexpressed in protected children met this threshold.

important blood stage *P. falciparum* antigen, the responses to which decrease over time since a previous clinical malaria episode (42), for individuals in the same study. A comparative analysis of 25 samples for which data was available, twelve of which were from protected and 13 of which were from susceptible children, showed no significant differences in the baseline AMA1 antibodies present in the serum collected from the children in either cohort (Supplementary Figure 5). The lack of differences in antibody responses to PfEMP1 and AMA1, two major blood stage malaria antigens, suggest that the differences in gene and pathway expression between groups are not due to differences in malaria exposure between the two groups. Finally, we investigated the possibility of ongoing subclinical malaria infections in susceptible children at baseline. To this effect, we analyzed previously generated data on a screen to detect the presence of parasites based on PCR amplification of the AMA1 gene from the day 0 timepoint (15). Although 2/12 individuals from the protected group were asymptomatically positive at baseline compared to 0/13 individuals from the susceptible group, we observed no statistically significant differences (Fisher's exact test) in the percent of individuals testing positive for malaria for each study group (Supplementary Figures 6A, B), consistent with the

hypothesis that the observed patterns are not caused by differences in ongoing or recent malaria exposure.

Gene expression at peak malaria transmission

To evaluate how increased natural exposure to malaria impacts the differences observed at baseline, we evaluated gene expression differences between the two groups at day 90 (peak malaria transmission). At this time point, we identified 73 differentially expressed genes in the unstimulated PBMCs; 61 were downregulated while 12 were upregulated in PBMCs from protected children relative to susceptible children (Figures 2A, B). Pathway enrichment analyses revealed significantly enriched "inflammatory response" among biological processes, in susceptible children (Figures 2C, D). We also observed enrichment in other biological processes in this group, including "chemotaxis" and "response to IFNg," as well as enrichment in molecular functions including "chemokine activity" and "receptor activity" (Figures 2C, D). KEGG pathway analysis revealed multiple enriched pathways in susceptible children, including the "malaria" pathway (Figures 2C, D). Consistent with pre-stimulation observations, the biological process "inflammatory response" was significantly enriched, after Pfsz-stimulation, in susceptible children compared to protected children (Figure 2D).

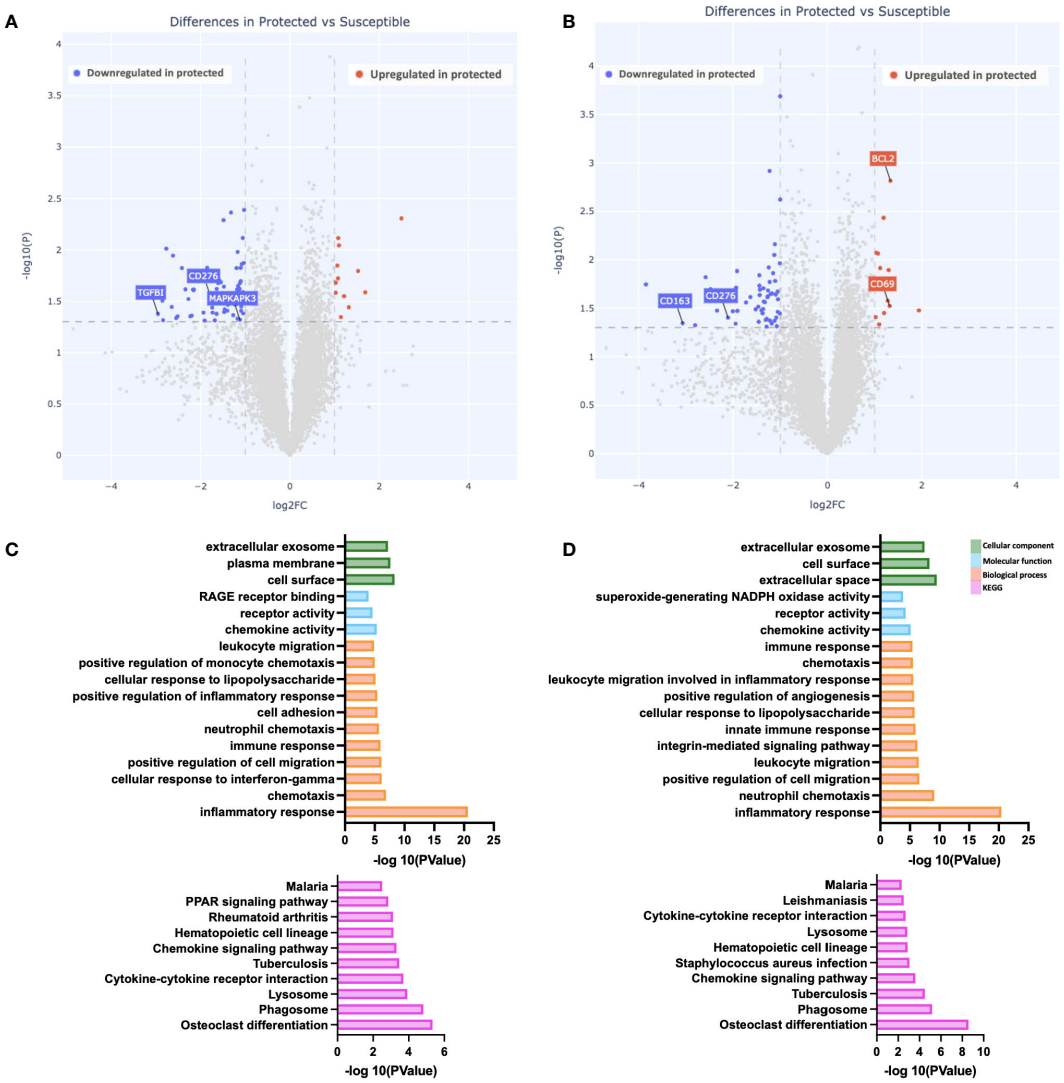

FIGURE 2
Gene expression differences during peak malaria transmission. **(A, B)** Depicted is a volcano plot of differential gene expression, with significant differences shown (blue, red), based on Welch's Test (log10(pval) is plotted against the log2 foldchange; significance: P value <0.05). **(A)** Unstimulated PBMCs. **(B)** PBMCs stimulated with malaria antigen (*P. falciparum* schizont, Pfsz). **(C, D)** Pathway enrichment analysis on differentially expressed genes (False discovery rate, FDR<0.05; gene expression log-fold change, LFC>1), using pathway enrichment software DAVID (26). Bar graphs depict Gene Ontology; Cellular component, molecular function, and biological processes that are enriched and KEGG pathways enriched at day 90. **(C)** Pathways enriched in susceptible children before antigen stimulation. **(D)** Pathways enriched in susceptible children after Pfsz stimulation. Enrichment analyses were performed on differentially expressed genes that met the FDR and LFC thresholds.

Reduced gene expression differences at the end of the malaria transmission season

We evaluated gene expression differences between the two groups at day 150 (end of the transmission season). We observed the fewest differences at this time point, with a total of 11 genes differentially expressed between the two groups. Six genes were downregulated compared to five genes upregulated in protected versus susceptible children (Figure 3A). Upregulated genes include the chemokine ligand CCL24 (Figures 3A, B), while downregulated genes included STAT1 and CD163 (Figures 3A). Pathway enrichment analysis revealed increased chemokine activity in susceptible children compared to protected children (Figures 3C, D). Chemokines play an important role during the host immune response to infection, as they recruit immune cells to the site of infection by binding chemokine receptors on the surface of immune cells (43). In malaria, high serum chemokine levels are associated with high parasite density and in some cases, severe malaria (44, 45).

Similar immune cell population clustering patterns between protected and susceptible children

To identify additional distinguishing properties between children with varying malaria susceptibility, we also investigated

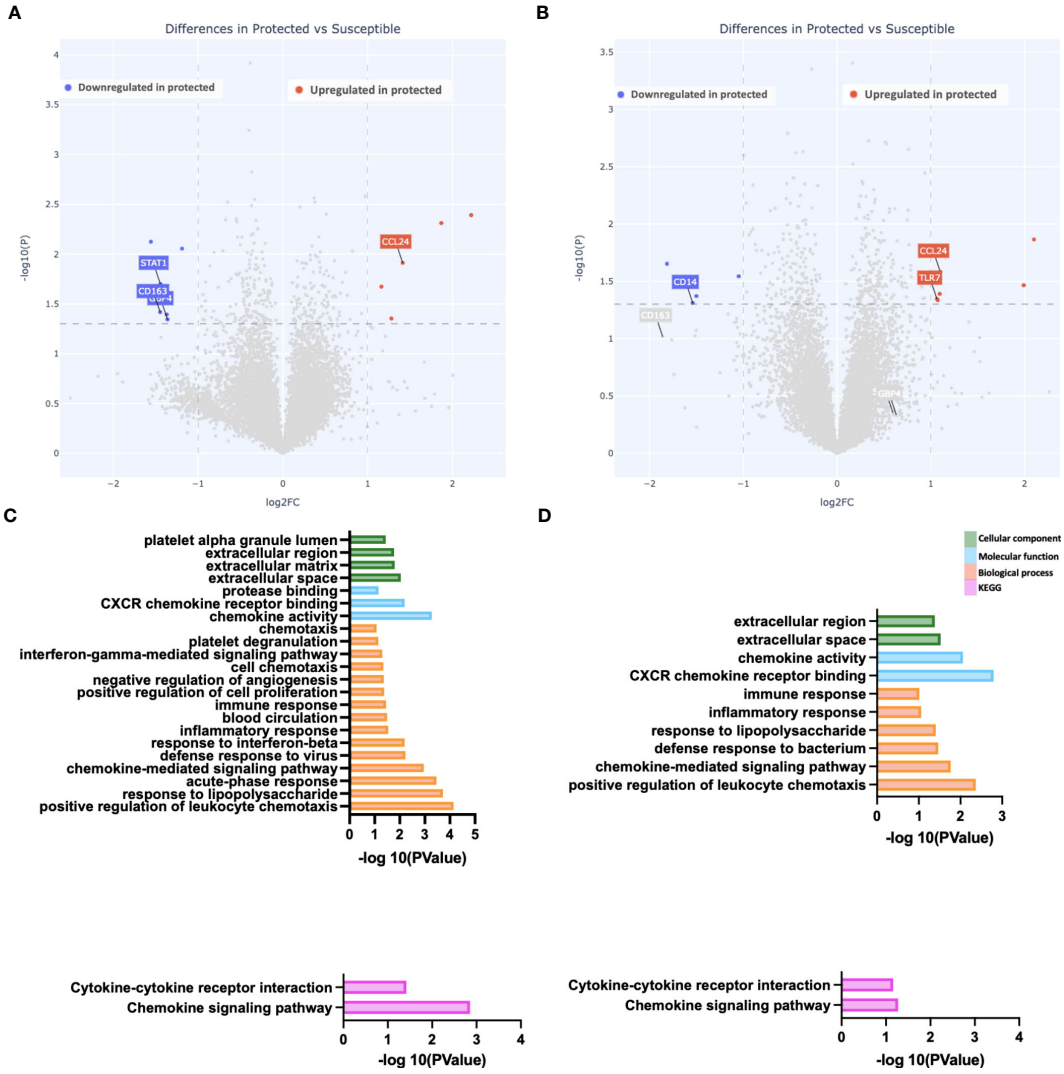

FIGURE 3
Reduced gene expression differences at the end of the malaria transmission season. **(A, B)** Depicted is a volcano plot of differential gene expression, with significant differences shown (blue, red), based on Welch's Test (log10(pval) is plotted against the log2 foldchange; significance: P value <0.05). **(A)** Unstimulated PBMCs. **(B)** PBMCs stimulated with malaria antigen (*P. falciparum* schizont, Pfsz). **(C, D)** Pathway enrichment analysis on differentially expressed genes (False discovery rate, FDR<0.05; gene expression log-fold change, LFC>1), using pathway enrichment software DAVID (26). Bar graphs depict Gene Ontology; Cellular component, molecular function, and biological processes that are enriched and KEGG pathways enriched at day 150. **(C)** Pathways enriched in susceptible children before antigen stimulation. **(D)** Pathways enriched in susceptible children after Pfsz stimulation. Enrichment analyses were performed on differentially expressed genes that met the FDR and LFC thresholds; no genes overexpressed in protected children met this threshold.

the phenotypes of immune cell populations. PBMCs were stimulated and analyzed *via* mass cytometry (see Methods). Using a panel specific for effector function $CD4^+$ T cell profiling (Supplementary Table 2), we performed high dimensional clustering on $CD3^+$ PBMCs collected at each timepoint and identified distinct cell populations (Figures 4A-C). Across all three timepoints, we were able to successfully identify $CD8^+$, gd and naïve and memory $CD4^+$ T cell populations, as well as a cluster annotated as "T cells" for cells that were not positive for either $CD4^+$, $CD8^+$ or gd TCR antibodies. Memory cell populations became more defined as the transmission season progressed. By day 150, we identified distinct memory $CD4^+$ T cell populations, including central memory (T_{CM}) ($CD4^+CD45RA^-CCR7^+$), effector memory (T_{EM}) ($CD4^+CD45RA^-CCR7^-$), and $CD45RA^+$ effector memory populations (T_{EMRA}) in both protected and susceptible individuals (Figures 4B, C). For each identified cluster, we performed both differential cell type abundance and differential state analyses using *diffcyt* package. We observed variable cell type abundances across all individuals regardless of protected or susceptible status (Figures 4D-F and Supplementary Figures 7A-F). Differential state analysis did not detect any significant differences in intracellular marker abundance between protected and susceptible children; however, we observed slightly elevated levels of Programmed Cell Death 1 (PD-1) at day 0 and day 90 (Figures 5A, B), elevated IL-4 across all three timepoints (Figures 5A-C) and elevated IL-6 at day 150 within all PBMCs in susceptible children compared to protected children (Figure 5C). Within this small subset, we did not observe significant differences in cytokine production within $CD4^+$ or $CD8^+$ T cells alone (Supplementary Figure 8).

The presence of slightly elevated levels of PD1 in the mass cytometry data along with the enrichment of cell death pathways in susceptible children prompted us to investigate the role of regulatory T cells at baseline and across the transmission season. Previous studies show that the presence of Tregs may promote increased *P. falciparum* parasitemia due to a reduction in host responses to infection, and that these effects are reversed under CD25 depleted conditions (18, 46). To probe how regulatory T cells from protected and susceptible children behave as exposure to *P. falciparum* increases, we stained stimulated PBMCs with a regulatory T cell panel (Supplementary Table 3). We assessed cell composition and cytokine secretion patterns of stimulated $CD3^+$ cells in the presence and absence of Tregs ($CD4^+CD25^+$). We were able to successfully identify a small subset of Tregs (200-1200 cells) at all three timepoints and, as expected, these cells were absent under the CD25 depleted conditions (Figures 6A-F). Additionally, we identified an HLA-DR^+ $CD4^+$ population across all three timepoints in both $CD25^+$ present and depleted conditions (Figures 6A-F). HLA-DR is a human MHC class II molecule that is expressed on a variety of lymphocytes, including activated T cells (47). Differential abundance and state analyses for PBMCs stained with the regulatory panel revealed differences in the frequency of HLA-DR^+ $CD4^+$ T cells at day 90, when protected children had a higher frequency of this population relative to susceptible children

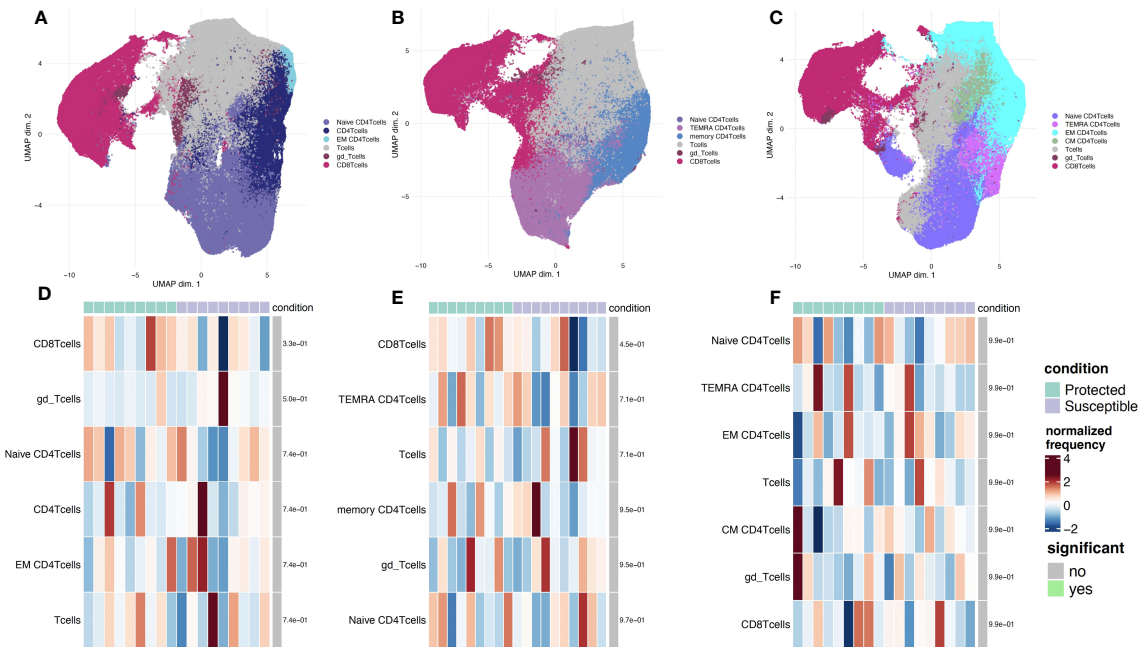

FIGURE 4
Phenotyping of $CD3^+$ immune cell populations to assess effector function and cell type abundance across a single malaria transmission season. **(A-C)** UMAP plots displaying immune cell populations identified though unsupervised clustering based on cell surface marker expression. **(A)** Clustering of cells from samples collected at the day 0 timepoint. **(B)** Cells from sampled collected at day 90. **(C)** Cells from samples collected at the day 150 timepoint. **(D-F)** Heatmap showing cell type frequencies of $CD3^+$ T cell populations present in protected (green) and susceptible (purple) children. High frequency populations are displayed in dark red and lowest frequencies are in dark blue. Population frequencies that are significantly different (FDR < 0.05) between protected and susceptible children are marked with a green bar. **(D)** heatmap of cell type frequencies at day 0. **(E)** Heatmap of cell type frequencies at day 90. **(F)** Heatmap of cell frequencies at day 150.

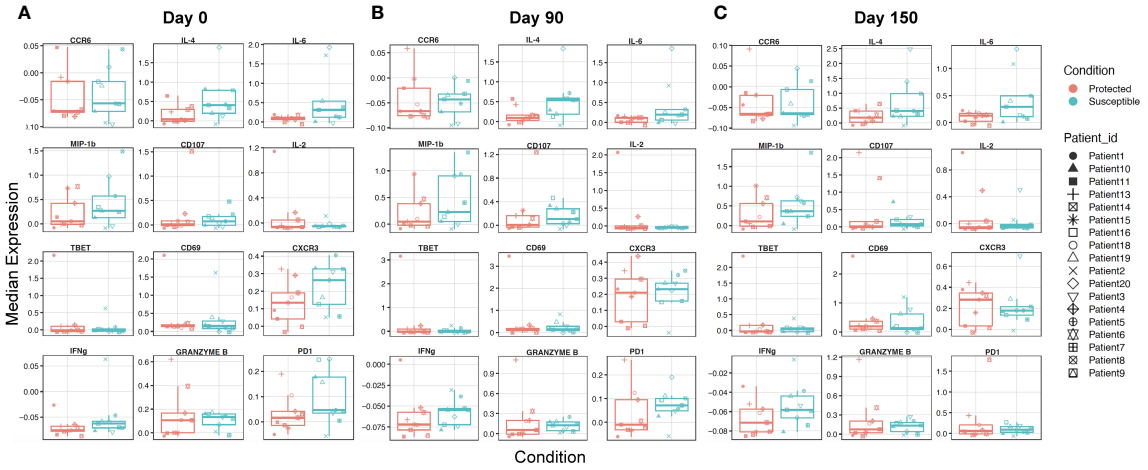

FIGURE 5
Characterizing overall expression of intracellular molecules and induced chemokine receptors in $CD3^+$ cells across a single transmission season. **(A-C)** Box plots displaying overall median expression of intracellular molecules and chemokine receptors from all T cells ($CD3^+$) in each Pfsz stimulated sample. Expression values were subjected to Z-score scaling, transforming the values to have a mean of 0 and a standard deviation of 1 across all cells. Negative expression values indicate that the average expression of a marker is lower relative to the other markers and positive expression values indicate that the average expression of a marker is higher relative to the other markers. Expression levels for protected children are indicated in red and expression levels for susceptible children are indicated in teal. Expression values from each child are indicated by a unique shape **(A)** Median expression for molecules at day 0. **(B)** Median expression for molecules at day 90. **(C)** Median expression for molecules at day 150.

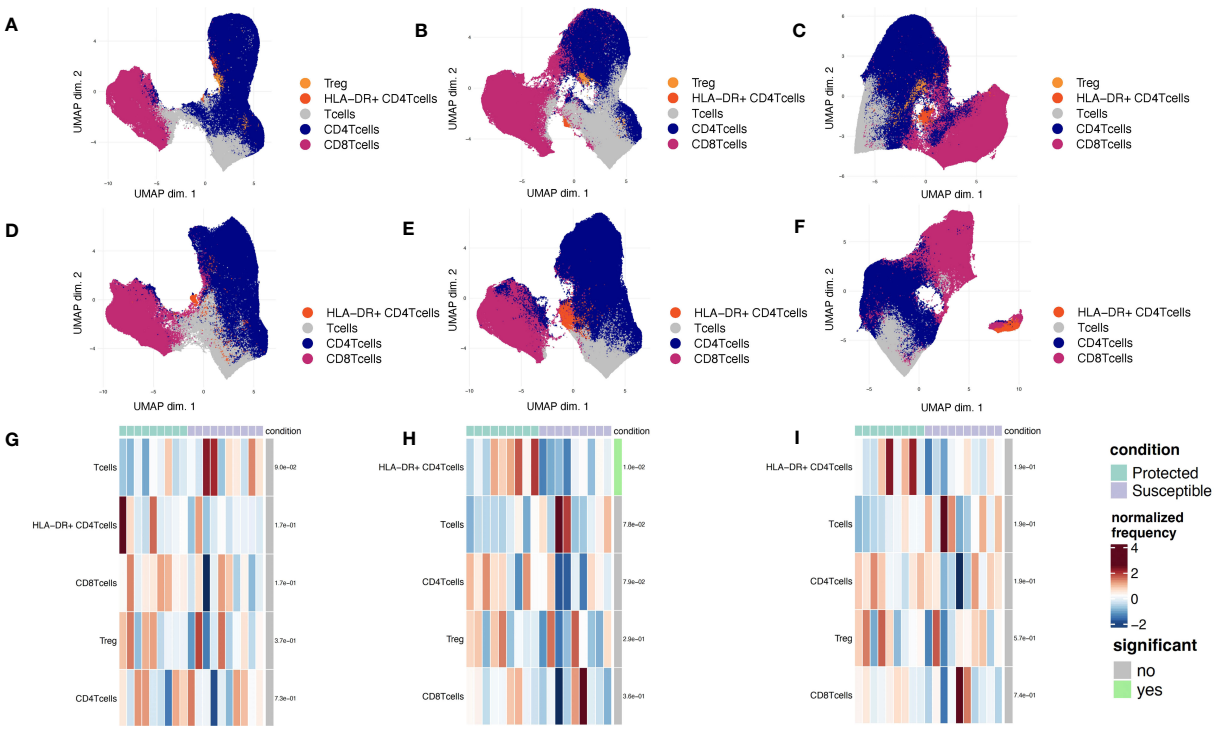

FIGURE 6
Phenotyping of $CD3^+$ immune cell populations to assess regulatory functions across a single malaria transmission season. **(A-C)** UMAP plots displaying immune cell populations identified though unsupervised clustering based of PBMCs stained with the regulatory panel. **(A)** Day 0, **(B)** Day 90, and **(C)** Day 150. **(D-F)** UMAP plots displaying immune cell populations identified though unsupervised clustering of CD25-depleted PBMC stained with the regulatory panel. **(D)** Day 0, **(E)** Day 90, and **(F)** Day 150. **(G-I)** Heatmap showing cell type frequencies of $CD3^+$ T cell populations present in children from each of two conditions (protected, teal; susceptible, purple). High frequency populations are displayed in dark red and lowest frequencies are in dark blue. Population frequencies that are significantly different (FDR<0.05) between protected and susceptible children are marked with a green bar (to the right of heat map). **(G)** Day 0, **(H)** Day 90, and **(I)** Day 150.

(Figures 6G-I). We did not observe significant differences in intracellular marker expression between the two groups (Supplementary Figure 9). Comparison of intracellular cytokine production in PBMCs before and after CD25 depletion revealed individual-specific changes, with no significant trend noted within the entire group (Supplementary Figures 10 A-F). Some individuals, patients 4, 6, 9, and 10 experienced slight increase in IFNg and IL-2 levels at day 0 while patients 2, 3, and 13 experienced decrease in these cytokines at the same time point (Supplementary Figures 10A, D). These data demonstrate inter-individual variation present in samples collected from individuals in an endemic setting.

Discussion

In this study, we used both bulk RNA sequencing and mass cytometry to identify host immune gene and protein expression patterns associated with varying susceptibility to clinical malaria disease. We used samples from a cohort of children who have high exposure to malaria, but who are early in the trajectory of acquiring immunity to malaria. We performed RNA sequencing on PBMCs to characterize gene expression patterns of children with different levels of malaria susceptibility. Through gene expression analyses, we identified higher baseline expression of CXCL10, STAT1, STAT2, GZMB, XAF1 and IRF1 in susceptible children relative to protected children. Our findings suggest that existing differences in gene expression, already in place before a malaria transmission season may impact susceptibility to subsequent infection. However, a new study with a larger cohort is needed to enable a study design with stronger statistical power and establish definitive conclusions. Furthermore, utilizing a regression approach can help determine the association between the number of malaria events and the enrichment of specific pathways.

Interferon gamma-induced protein 10 (CXCL10), a pro-inflammatory chemokine induced by multiple cytokines including IFNg, has been previously identified as a marker of malaria disease severity (48–50). A study of CXCL10 wildtype (WT) and Knockout (KO) mice showed efficient parasite control in KO mice while WT mice progressed to cerebral malaria (48). Additionally, a field study in Ghana found higher CXCL10 levels from postmortem cerebral spinal fluid (CSF) in cerebral malaria patients (51). Another gene downstream of IFNg signaling, STAT1, was also significantly overexpressed in the susceptible group relative to the protected group. STAT1 is a transcription factor activated by multiple interferons, and it regulates various cellular processes including cell proliferation and differentiation (52, 53). Although we did not see differential expression between groups with IFNg cytokine expression, we found evidence of gene expression differences for molecules downstream of IFN signaling, suggesting that gene expression studies may detect changes that are missed by cytokine studies.

Our pathway-level analyses revealed an enrichment of the apoptotic pathway in susceptible children. These observations are consistent with previous studies that have demonstrated increased apoptosis of immune cells (lymphopenia) in individuals with malaria infection (54, 55). Additional studies have found that malaria infection increases apoptotic processes, mediated through FAS, FASL and Tumor Necrosis Factor (TNF) (56–58). Although we did not observe increased expression of these specific genes, we observed higher expression of pro-apoptotic genes XAF1 and IRF1 in susceptible children at baseline. XAF1 is a transcriptional co-activator of IRF1, a protein that negatively regulates anti-apoptotic genes and promotes FASL expression in immune cells (59–62). The RNA-seq data were supported by mass cytometry results of slightly higher levels of PD-1 in susceptible children.

High dimension reduction and differential analysis of mass cytometry data identified higher frequencies of HLA-DR$^+$CD4$^+$ T cells in protected children when compared to susceptible children. HLA-DR is a late activation marker that is upregulated on the surface of either memory or naïve T cells after antigen encounter. Although the function of HLA-DR on the surface of T cells is poorly understood, studies on infectious pathogens including *Mycobacterium tuberculosis* (the causative agent of tuberculosis, or TB) and Human Immunodeficiency Virus (HIV), show that HLA-DR$^+$CD4$^+$ T cells have the ability to persist longer in the periphery and are more resistant to suppression mechanisms initiated by regulatory T cells (63–65).

Our data shows that inherent differences in inflammatory and apoptotic gene expression already exist at baseline between children who will go on to have two or more malaria episodes throughout a malaria season and those who will not experience clinical malaria. Recent studies report on the importance of baseline immune signatures on the subsequent response to disease progression, vaccine efficacy, and treatment failure or success (66). Tsang et al. showed a correlation between the extent of an immune response to influenza vaccination and the pre-vaccination status of an individual (67). Additionally, the importance of baseline immunity has been noted in cancer, where studies show that the presence of certain immune genes influences the activity of some immunotherapies as well as cancer metastasis (68). These studies also emphasize the importance of a systems approach to understanding overall immune signatures (66, 69).

Our current study corroborates and extends previous findings. We compared children with two or more episodes of clinical malaria (susceptible cohort) to age- and location-matched children without clinical malaria (protected cohort). Although the cohorts had similar risk of malaria exposure, we identified differences in gene expression patterns assessed before the onset of the malaria transmission season between the cohorts. This study emphasizes the importance of understanding the initial gene expression repertoire to accurately interpret clinical and immunological implications of field studies with human subjects. In conclusion, this study identifies potential genes and cell populations associated with, and which may play a causal role in, predicting malaria susceptibility.

Data availability statement

The datasets presented in this study can be found in online repositories. The names of the repository/repositories and accession

number(s) can be found below: PRJNA603324 (Bioproject- Genbank) and GEO Accession GSE234970.

Ethics statement

The studies involving human participants were reviewed and approved by Institutional Review Board for Human Subject Research at University of Maryland Baltimore. Written informed consent to participate in this study was provided by the participants' legal guardian/next of kin.

Author contributions

GM, JS, and KL were involved in study design and execution of current study. KL, ML, CP, and MAT were involved in the execution of the primary study. GM, KL, and RB contributed to protocol optimization. GM, AnD, and OOI contributed to bioinformatics analysis. TH and RA contributed to software optimization and training. MAT, OKD, AK, DC, and AB were responsible for study management in Mali. BS, AB, and MT contributed to microarray data generation and analysis. GM, JS, and KL contributed to interpretation and writing of the article. All authors participated in editing and approved the submitted version.

Funding

This project was funded in part by federal funds from the National Institute of Allergy and Infectious Diseases, National Institutes of Health, Department of Health and Human Services under grant number U19AI110820. Site development and the conduct of the original clinical trial were supported by contract N01AI85346 and cooperative agreement U19AI065683 from the National Institute of Allergy and Infectious Diseases, grant D43TW001589 from the Fogarty International Center, National Institutes of Health and contract W81XWH-06-1-0427 from the United States Department of Defense and the United States Agency for International Development for site development and the conduct of the trial.

Acknowledgments

We would like to acknowledge the community of Bandiagara, Mali, the volunteers, and their parents for their support and participation in the primary trial. The authors thank Danzele Coulibaly, Sekouba Mariko, and Moctar Traore for administrative support at the MRTC. We thank the team of the Bandiagara Malaria Project in Bandiagara for their dedication. In sorrow and gratitude, this work is dedicated to the memory of co-author Ogobara K. Doumbo, who passed away in June 2018. Professor Doumbo co-created the Malaria Research and Training Center at the University of Bamako and has been recognized during his prolific career as a global leader in malaria research. Additional thanks are extended to the Genome Resource Center at the Institute of Genome Sciences for assistance in generating the RNA sequencing data and the flow cytometry and mass cytometry core at the Center for Vaccine Development for assistance in processing the mass cytometry samples.

Conflict of interest

The authors declare that the research was conducted in the absence of any commercial or financial relationships that could be construed as a potential conflict of interest.

Publisher's note

Supplementary material

The Supplementary Material for this article can be found online at: https://www.frontiersin.org/articles/10.3389/fimmu.2023.1179314/full#supplementary-material

References

1. *World malaria report* (2022). Available at: https://www.who.int/publications-detail-redirect/9789240064898.

2. Doolan DL, Dobaño C, Baird JK. Acquired immunity to malaria. *Clin Microbiol Rev* (2009) 22(1):13–36. doi: 10.1128/CMR.00025-08

3. Lyke KE, Fernández-Viña MA, Cao K, Hollenbach J, Coulibaly D, Kone AK, et al. Association of HLA alleles with plasmodium falciparum severity in malian children. *Tissue Antigens* (2011) 77(6):562–71. doi: 10.1111/j.1399-0039.2011.01661.x

4. Lopera-Mesa TM, Doumbia S, Konaté D, Anderson JM, Doumbouya M, Keita AS, et al. Impact of red blood cell variants on childhood malaria in Mali: a prospective cohort study. *Lancet Haematol* (2015) 2(4):e140–9. doi: 10.1016/S2352-3026(15)00043-5

5. Hodgson SH, Muller J, Lockstone HE, Hill AVS, Marsh K, Draper SJ, et al. Use of gene expression studies to investigate the human immunological response to malaria infection. *Malar J* (2019) 18:418. doi: 10.1186/s12936-019-3035-0

6. Krupka M, Seydel K, Feintuch CM, Yee K, Kim R, Lin CY, et al. Mild plasmodium falciparum malaria following an episode of severe malaria is associated with induction of the interferon pathway in Malawian children. *Infect Immun* (2012) 80(3):1150–5. doi: 10.1128/IAI.06008-11

7. King T, Lamb T. Interferon-γ: the Jekyll and Hyde of malaria. *PloS Pathog* (2015) 11(10):e1005118. doi: 10.1371/journal.ppat.1005118

8. Kurup SP, Butler NS, Harty JT. T Cell-mediated immunity to malaria. *Nat Rev Immunol* (2019) 19(7):457–71. doi: 10.1038/s41577-019-0158-z

9. Frimpong A, Amponsah J, Adjokatseh AS, Agyemang D, Bentum-Ennin L, Ofori EA, et al. Asymptomatic malaria infection is maintained by a balanced pro- and anti-inflammatory response. *Front Microbiol* (2020) 11:2832. doi: 10.3389/fmicb.2020.559255

10. Perez-Mazliah D, Langhorne J. CD4 T-cell subsets in malaria: TH1/TH2 revisited. *Front Immunol* (2015) 5:671/full. doi: 10.3389/fimmu.2014.00671/full

11. Tran TM, Jones MB, Ongoiba A, Bijker EM, Schats R, Venepally P, et al. Transcriptomic evidence for modulation of host inflammatory responses during febrile plasmodium falciparum malaria. *Sci Rep* (2016) 6(1):31291. doi: 10.1038/srep31291

12. Illingworth J, Butler NS, Roetynck S, Mwacharo J, Pierce SK, Bejon P, et al. Chronic exposure to plasmodium falciparum is associated with phenotypic evidence of b and T cell exhaustion. *J Immunol Author Choice* (2013) 190(3):1038–47. doi: 10.4049/jimmunol.1202438

13. Ockenhouse CF, Hu WC, Kester KE, Cummings JF, Stewart A, Heppner DG, et al. Common and divergent immune response signaling pathways discovered in peripheral blood mononuclear cell gene expression patterns in presymptomatic and clinically apparent malaria. *Infect Immun* (2006) 74(10):5561–73. doi: 10.1128/IAI.00408-06

14. Tran TM, Guha R, Portugal S, Skinner J, Ongoiba A, Bhardwaj J, et al. A molecular signature in blood reveals a role for p53 in regulating malaria-induced inflammation. *Immunity* (2019) 51(4):750–765.e10. doi: 10.1016/j.immuni.2019.08.009

15. Thera MA, Doumbo OK, Coulibaly D, Laurens MB, Ouattara A, Kone AK, et al. A field trial to assess a blood-stage malaria vaccine. *N Engl J Med* (2011) 365(11):1004–13. doi: 10.1056/NEJMoa1008115

16. Coulibaly D, Rebaudet S, Travassos M, Tolo Y, Laurens M, Kone AK, et al. Spatio-temporal analysis of malaria within a transmission season in bandiagara, Mali. *Malar J* (2013) 12:82. doi: 10.1186/1475-2875-12-82

17. Lyke KE, Dabo A, Arama C, Diarra I, Plowe CV, Doumbo OK, et al. Long-term maintenance of CD4 T cell memory responses to malaria antigens in malian children coinfected with schistosoma haematobium. *Front Immunol* (2018) 8. doi: 10.3389/fimmu.2017.01995

18. Lyke KE, Dabo A, Arama C, Daou M, Diarra I, Wang A, et al. Reduced T regulatory cell response during acute plasmodium falciparum infection in malian children Co-infected with schistosoma haematobium. *PloS One* (2012) 7(2):e31647. doi: 10.1371/journal.pone.0031647

19. Fienberg H, Simonds EF, Fantl WJ, Nolan GP, Bodenmiller B. A platinum-based covalent viability reagent for single cell mass cytometry. *Cytom Part J Int Soc Anal Cytol* (2012) 81(6):10. doi: 10.1002/cyto.a.22067

20. Kim D, Langmead B, Salzberg SL. HISAT: a fast spliced aligner with low memory requirements. *Nat Methods* (2015) 12(4):357–60. doi: 10.1038/nmeth.3317

21. Anders S, Huber W. Differential expression analysis for sequence count data. *Genome Biol* (2010) 11(10):R106. doi: 10.1186/gb-2010-11-10-r106

22. Anders S, Pyl PT, Huber W. HTSeq–a Python framework to work with high-throughput sequencing data. *Bioinformatics* (2015) 31(2):166–9. doi: 10.1093/bioinformatics/btu638

23. Trapnell C, Hendrickson DG, Sauvageau M, Goff L, Rinn JL, Pachter L. Differential analysis of gene regulation at transcript resolution with RNA-seq. *Nat Biotechnol* (2013) 31(1):46–53. doi: 10.1038/nbt.2450

24. Orvis J, Gottfried B, Kancherla J, Adkins RS, Song Y, Dror AA, et al. gEAR: gene expression analysis resource portal for community-driven, multi-omic data exploration. *Nat Methods* (2021) 18(8):843–4. doi: 10.1038/s41592-021-01200-9

25. Huang DW, Sherman BT, Lempicki RA. Bioinformatics enrichment tools: paths toward the comprehensive functional analysis of large gene lists. *Nucleic Acids Res* (2009) 37(1):1–13. doi: 10.1093/nar/gkn923

26. Huang DW, Sherman BT, Lempicki RA. Systematic and integrative analysis of large gene lists using DAVID bioinformatics resources. *Nat Protoc* (2009) 4(1):44–57. doi: 10.1038/nprot.2008.211

27. Subramanian A, Tamayo P, Mootha VK, Mukherjee S, Ebert BL, Gillette MA, et al. Gene set enrichment analysis: a knowledge-based approach for interpreting genome-wide expression profiles. *Proc Natl Acad Sci* (2005) 102(43):15545–50. doi: 10.1073/pnas.0506580102

28. Hahne F, LeMeur N, Brinkman RR, Ellis B, Haaland P, Sarkar D, et al. flowCore: a bioconductor package for high throughput flow cytometry. *BMC Bioinf* (2009) 10:106. doi: 10.1186/1471-2105-10-106

29. Nowicka M, Krieg C, Crowell HL, Weber LM, Hartmann FJ, Guglietta S, et al. CyTOF workflow: differential discovery in high-throughput high-dimensional cytometry datasets. *F1000Research* (2019) 6:748. doi: 10.12688/f1000research.11622.3

30. Crowell HL, Chevrier S, Jacobs A, Sivapatham S, Consortium TP, Bodenmiller B, et al. An r-based reproducible and user-friendly preprocessing pipeline for CyTOF data. *F1000Research* (2020) 9:1263. doi: 10.12688/f1000research.26073.1

31. Van Gassen S, Callebaut B, Van Helden MJ, Lambrecht BN, Demeester P, Dhaene T, et al. FlowSOM: using self-organizing maps for visualization and interpretation of cytometry data. *Cytometry A* (2015) 87(7):636–45. doi: 10.1002/cyto.a.22625

32. Wilkerson MD, Hayes DN. ConsensusClusterPlus: a class discovery tool with confidence assessments and item tracking. *Bioinformatics* (2010) 26(12):1572–3. doi: 10.1093/bioinformatics/btq170

33. Weber LM, Nowicka M, Soneson C, Robinson MD. Diffcyt: differential discovery in high-dimensional cytometry *via* high-resolution clustering. *Commun Biol* (2019) 2(1):1–11. doi: 10.1038/s42003-019-0415-5

34. Thera MA, Doumbo OK, Coulibaly D, Diallo DA, Kone AK, Guindo AB, et al. Safety and immunogenicity of an AMA-1 malaria vaccine in malian adults: results of a phase 1 randomized controlled trial. *PloS One* (2008) 3(1):e1465. doi: 10.1371/journal.pone.0001465

35. Zhou AE, Jain A, Nakajima R, Shrestha B, Stucke EM, Joshi S, et al. Protein microarrays as a tool to analyze antibody responses to variant surface antigens expressed on the surface of plasmodium falciparum-infected erythrocytes. *Methods Mol Biol Clifton NJ* (2022) 2470:343–58. doi: 10.1007/978-1-0716-2189-9_25

36. Doolan DL, Mu Y, Unal B, Sundaresh S, Hirst S, Valdez C, et al. Profiling humoral immune responses to p. falciparum infection with protein microarrays. *Proteomics* (2008) 8(22):4680–94. doi: 10.1002/pmic.200800194

37. Davies DH, Liang X, Hernandez JE, Randall A, Hirst S, Mu Y, et al. Profiling the humoral immune response to infection by using proteome microarrays: high-throughput vaccine and diagnostic antigen discovery. *Proc Natl Acad Sci U S A* (2005) 102(3):547–52. doi: 10.1073/pnas.0408782102

38. van Schie JJM, Faramarz A, Balk JA, Stewart GS, Cantelli E, Oostra AB, et al. Warsaw Breakage syndrome associated DDX11 helicase resolves G-quadruplex structures to support sister chromatid cohesion. *Nat Commun* (2020) 11(1):4287. doi: 10.1038/s41467-020-18066-8

39. Crompton PD, Kayala MA, Traore B, Kayentao K, Ongoiba A, Weiss GE, et al. A prospective analysis of the ab response to plasmodium falciparum before and after a malaria season by protein microarray. *Proc Natl Acad Sci USA* (2010) 107(15):6958–63. doi: 10.1073/pnas.1001323107

40. Travassos MA, Niangaly A, Bailey JA, Ouattara A, Coulibaly D, Laurens MB, et al. Seroreactivity to plasmodium falciparum erythrocyte membrane protein 1 intracellular domain in malaria-exposed children and adults. *J Infect Dis* (2013) 208(9):1514–9. doi: 10.1093/infdis/jit339

41. Travassos MA, Niangaly A, Bailey JA, Ouattara A, Coulibaly D, Lyke KE, et al. Children with cerebral malaria or severe malarial anaemia lack immunity to distinct variant surface antigen subsets. *Sci Rep* (2018) 8(1):6281. doi: 10.1038/s41598-018-24462-4

42. Bailey JA, Berry AA, Travassos MA, Ouattara A, Boudova S, Dotsey EY, et al. Microarray analyses reveal strain-specific antibody responses to plasmodium falciparum apical membrane antigen 1 variants following natural infection and vaccination. *Sci Rep* (2020) 10:3952. doi: 10.1038/s41598-020-60551-z

43. Griffith JW, Sokol CL, Luster AD. Chemokines and chemokine receptors: positioning cells for host defense and immunity. *Annu Rev Immunol* (2014) 32(1):659–702. doi: 10.1146/annurev-immunol-032713-120145

44. Ioannidis LJ, Nie CQ, Hansen DS. The role of chemokines in severe malaria: more than meets the eye. *Parasitology* (2014) 141(5):602–13. doi: 10.1017/S0031182013001984

45. Dunst J, Kamena F, Matuschewski K. Cytokines and chemokines in cerebral malaria pathogenesis. *Front Cell Infect Microbiol* (2017) 7:324. doi: 10.3389/fcimb.2017.00324

46. Hisaeda H, Maekawa Y, Iwakawa D, Okada H, Himeno K, Kishihara K, et al. Escape of malaria parasites from host immunity requires CD4+CD25+ regulatory T cells. *Nat Med* (2004) 10(1):29–30. doi: 10.1038/nm975

47. Reddy M, Eirikis E, Davis C, Davis HM, Prabhakar U. Comparative analysis of lymphocyte activation marker expression and cytokine secretion profile in stimulated human peripheral blood mononuclear cell cultures: an *in vitro* model to monitor cellular immune function. *J Immunol Methods* (2004) 293(1):127–42. doi: 10.1016/j.jim.2004.07.006

48. Ioannidis LJ, Nie CQ, Ly A, Ryg-Cornejo V, Chiu CY, Hansen DS. Monocyte- and neutrophil-derived CXCL10 impairs efficient control of blood-stage malaria infection and promotes severe disease. *J Immunol* (2016) 196(3):1227–38. doi: 10.4049/jimmunol.1501562

49. Liu M, Guo S, Hibbert JM, Jain V, Singh N, Wilson NO, et al. CXCL10/IP-10 in infectious diseases pathogenesis and potential therapeutic implications. *Cytokine Growth Factor Rev* (2011) 22(3):121–30. doi: 10.1016/j.cytogfr.2011.06.001

50. Wilson NO, Jain V, Roberts CE, Lucchi N, Joel PK, Singh MP, et al. CXCL4 and CXCL10 predict risk of fatal cerebral malaria. *Dis Markers* (2011) 30(1):39. doi: 10.1155/2011/828256

51. Armah HB, Wilson NO, Sarfo BY, Powell MD, Bond VC, Anderson W, et al. Cerebrospinal fluid and serum biomarkers of cerebral malaria mortality in ghanaian children. *Malar J* (2007) 6:147. doi: 10.1186/1475-2875-6-147

52. Mogensen TH. IRF. And STAT transcription factors - from basic biology to roles in infection, protective immunity, and primary immunodeficiencies. *Front Immunol* (2019) 9:3047. doi: 10.3389/fimmu.2018.03047

53. Shi X, Qin L, Liu G, Zhao S, Peng N, Chen X. Dynamic balance of pSTAT1 and pSTAT3 in C57BL/6 mice infected with lethal or nonlethal plasmodium yoelii. *Cell Mol Immunol* (2008) 5(5):341–8. doi: 10.1038/cmi.2008.42

54. Kern P, Dietrich M, Hemmer C, Wellinghausen N. Increased levels of soluble fas ligand in serum in plasmodium falciparum malaria. *Infect Immun* (2000) 68(5):3061–3. doi: 10.1128/IAI.68.5.3061-3063.2000

55. Hviid L, Kemp K. What is the cause of lymphopenia in malaria? *Infect Immun* (2000) 68(10):6087–9. doi: 10.1128/IAI.68.10.6087-6089.2000

56. Kakani P, Suman S, Gupta L, Kumar S. Ambivalent outcomes of cell apoptosis: a barrier or blessing in malaria progression. *Front Microbiol* (2016) 7. doi: 10.3389/fmicb.2016.00302

57. Pinzon-Charry A, Woodberry T, Kienzle V, McPhun V, Minigo G, Lampah DA, et al. Apoptosis and dysfunction of blood dendritic cells in patients with falciparum and vivax malaria. *J Exp Med* (2013) 210(8):1635–46. doi: 10.1084/jem.20121972

58. Toure-Balde A, Sarthou JL, Aribot G, Michel P, Trape JF, Rogier C, et al. Plasmodium falciparum induces apoptosis in human mononuclear cells. *Infect Immun* (1996) 64(3):744–50. doi: 10.1128/iai.64.3.744-750.1996

59. Jeong SI, Kim JW, Ko KP, Ryu BK, Lee MG, Kim HJ, et al. XAF1 forms a positive feedback loop with IRF-1 to drive apoptotic stress response and suppress tumorigenesis. *Cell Death Dis* (2018) 9(8):806. doi: 10.1038/s41419-018-0867-4

60. Lee MG, Han J, Jeong SI, Her NG, Lee JH, Ha TK, et al. XAF1 directs apoptotic switch of p53 signaling through activation of HIPK2 and ZNF313. *Proc Natl Acad Sci* (2014) 111(43):15532–7. doi: 10.1073/pnas.1411746111

61. Xia Y, Novak R, Lewis J, Duckett CS, Phillips AC. Xaf1 can cooperate with TNFα in the induction of apoptosis, independently of interaction with XIAP. *Mol Cell Biochem* (2006) 286(1–2):67–76. doi: 10.1007/s11010-005-9094-2

62. Tanaka N, Ishihara M, Kitagawa M, Harada H, Kimura T, Matsuyama T, et al. Cellular commitment to oncogene-induced transformation or apoptosis is dependent on the transcription factor IRF-1. *Cell* (1994) 77(6):829–39. doi: 10.1016/0092-8674(94)90132-5

63. Tippalagama R, Singhania A, Dubelko P, Arlehamn CSL, Crinklaw A, Pomaznoy M, et al. HLA-DR marks recently divided antigen-specific effector CD4 T cells in active tuberculosis patients. *J Immunol* (2021) 207(2):523–33. doi: 10.4049/jimmunol.2100011

64. Ahmed A, Adiga V, Nayak S, Kumar JAJU, Dhar C, Sahoo PN, et al. Circulating HLA-DR+CD4+ effector memory T cells resistant to CCR5 and PD-L1 mediated suppression compromise regulatory T cell function in tuberculosis. *PloS Pathog* (2018) 14(9):e1007289. doi: 10.1371/journal.ppat.1007289

65. Lee E, Bacchetti P, Milush J, Shao W, Boritz E, Douek D, et al. Memory CD4 + T-cells expressing HLA-DR contribute to HIV persistence during prolonged antiretroviral therapy. *Front Microbiol* (2019) 10. doi: 10.3389/fmicb.2019.02214

66. Tsang JS, Dobaño C, VanDamme P, Moncunill G, Marchant A, Othman RB, et al. Improving vaccine-induced immunity: can baseline predict outcome? *Trends Immunol* (2020) 41(6):457–65. doi: 10.1016/j.it.2020.04.001

67. Tsang JS, Schwartzberg PL, Kotliarov Y, Biancotto A, Xie Z, Germain RN, et al. Global analyses of human immune variation reveal baseline predictors of post-vaccination responses. *Cell* (2014) 157(2):499–513. doi: 10.1016/j.cell.2014.03.031

68. Gnjatic S, Bronte V, Brunet LR, Butler MO, Disis ML, Galon J, et al. Identifying baseline immune-related biomarkers to predict clinical outcome of immunotherapy. *J Immunother Cancer* (2017) 5(1):44. doi: 10.1186/s40425-017-0243-4

69. Bucasas KL, Franco LM, Shaw CA, Bray MS, Wells JM, Niño D, et al. Early patterns of gene expression correlate with the humoral immune response to influenza vaccination in humans. *J Infect Dis* (2011) 203(7):921–9. doi: 10.1093/infdis/jiq156

frontiers | Frontiers in Immunology

TYPE Hypothesis and Theory
PUBLISHED 05 May 2023
DOI 10.3389/fimmu.2023.1028303

OPEN ACCESS

EDITED BY
Silvano Sozzani,
Sapienza University of Rome, Italy

REVIEWED BY
Paola Italiani,
National Research Council (CNR), Italy
Tiziana Musso,
University of Turin, Italy

*CORRESPONDENCE
Subulade A. Ademola
saademola@com.ui.edu.ng

RECEIVED 25 August 2022
ACCEPTED 25 April 2023
PUBLISHED 05 May 2023

CITATION
Ademola SA, Bamikole OJ and Amodu OK (2023) Is TNF alpha a mediator in the co-existence of malaria and type 2 diabetes in a malaria endemic population? *Front. Immunol.* 14:1028303. doi: 10.3389/fimmu.2023.1028303

Is TNF alpha a mediator in the co-existence of malaria and type 2 diabetes in a malaria endemic population?

Subulade A. Ademola*, Oluwayemi J. Bamikole and Olukemi K. Amodu

Molecular Genetics Unit, Institute of Child Health, College of Medicine, University of Ibadan, Ibadan, Nigeria

Malaria remains a disease of public health importance globally, especially in sub-Saharan Africa. Malaria deaths reduced globally steadily between 2000-2019, however there was a 10% increase in 2020 due to disruptions in medical service during the COVID-19 pandemic. Globally, about 96% of malaria deaths occurred in 29 countries; out of which, four countries (Nigeria, the Democratic Republic of the Congo, the Niger, and the United Republic of Tanzania) accounted for just over half of the malaria deaths. Nigeria leads the four countries with the highest malaria deaths (accounting for 31% globally). Parallelly, sub-Saharan Africa is faced with a rise in the incidence of Type 2 diabetes (T2D). Until recently, T2D was a disease of adulthood and old age. However, this is changing as T2D in children and adolescents is becoming an increasingly important public health problem. Nigeria has been reported to have the highest burden of diabetes in Africa with a prevalence of 5.77% in the country. Several studies conducted in the last decade investigating the interaction between malaria and T2D in developing countries have led to the emergence of the intra-uterine hypothesis. The hypothesis has arisen as a possible explanation for the rise of T2D in malaria endemic areas; malaria in pregnancy could lead to intra-uterine stress which could contribute to low birth weight and may be a potential cause of T2D later in life. Hence, previous, and continuous exposure to malaria infection leads to a higher risk of T2D. Current and emerging evidence suggests that an inflammation-mediated link exists between malaria and eventual T2D emergence. The inflammatory process thus, is an important link for the co-existence of malaria and T2D because these two diseases are inflammatory-related. A key feature of T2D is systemic inflammation, characterized by the upregulation of inflammatory cytokines such as tumor necrosis factor alpha (TNF-α) which leads to impaired insulin signaling. Malaria infection is an inflammatory disease in which TNF-α also plays a major role. TNF-α plays an important role in the pathogenesis and development of malaria and T2D. We therefore hypothesize that TNF-α is an important link in the increasing co-existence of T2D.

KEYWORDS

malaria, type 2 diabetes (T2D), TNF-α, malaria-endemic population, inflammation, cytokine, hypothesis, TCF7L2 gene

Introduction: the hypothesis

Type 2 diabetes is a non-communicable disease of serious public health importance globally. It is the most common type of diabetes mellitus, accounting for 90-95% of all diagnosed diabetes cases (1, 2). Worldwide, an estimated 537 million adults aged 20–79 years are currently living with diabetes (3, 4). The development of type 2 diabetes is mainly caused by two factors; impaired insulin secretion by pancreatic β-cells and the inability of insulin-sensitive tissues to respond to insulin (1, 5). Type 2 diabetes develops when the pancreas cannot produce enough insulin or when the insulin-sensitive tissues become resistant to insulin. Symptoms of T2D include excessive thirst and dry mouth, frequent urination, lack of energy, tiredness, slow healing wounds, recurrent infections in the skin, blurred vision, tingling or numbness in hands and feet (6). However, these symptoms can be mild or absent, making it possible for people with type 2 diabetes to live several years with the condition before being diagnosed.

Malaria is one of the most severe diseases of public health importance globally. With 247 million cases reported in 84 malaria endemic countries in 2021 (2), malaria remains a major cause of morbidity and mortality in many developing countries. The causative agent, the protozoan *Plasmodium*, malaria is transmitted to humans by infected female *Anopheles* mosquitoes. The human *Plasmodium* species include *Plasmodium vivax*, *Plasmodium ovale*, *Plasmodium malaria*, *Plasmodium falciparum* and *P. knowlesi* (2). The most dangerous of the plasmodia infecting humans is *P. falciparum* (7), and it is one of the most important causes of child mortality worldwide. The *P. falciparum* life cycle comprise a non-pathogenic symptomless extraerythrocytic stage, which is followed by the invasion of mature red blood cells by the infective forms (merozoites) and the initiation of pathogenic intraerythrocytic stages. Most of the clinical signs of malaria are caused by the parasite at stages in which it multiplies asexually in red blood cells. The most common clinical symptoms of severe malaria are high fever, progressing anemia, multi-organ dysfunction and unconsciousness or coma, which is one of the causes of death (7). The stages of the *P. falciparum* life cycle are complex, and this allows for the use of various evasion strategies by the malaria parasite. The immune response triggered against the malaria parasite is also complex and stage specific (8). Both the innate and adaptive immune responses are activated by the malaria parasite during malaria infection. The host immune responses play a key role in determining the efficiency of parasite clearance, resulting in immunological phenotype of individuals that are resistant or susceptible to malaria infection.

Several studies in recent times have reported the co-existence of malaria and type 2 diabetes in developing countries. However, most of the evidence reported in literature have been based on the effect of malaria on the risk of diabetes (9); the effect of diabetes on malaria outcome (10–12); and the effect of malaria on glycemic presentation (6). These findings have resulted in the emergence of hypotheses and pathways that have provided explanations for the co-existence of malaria and type 2 diabetes (13). The most popular of the hypotheses that has emerged to explain the co-existence of malaria and type 2 diabetes is the intra-uterine hypothesis. Summarily, the intra-uterine hypothesis is based on the effect of the malaria-induced inflammation which occurs during exposure to malaria *in utero* on the development of type 2 diabetes later in life.

The intra-uterine hypothesis arose as a plausible explanation for the increase in the burden of type 2 diabetes in malaria endemic populations. Low birth weight arising from of intra uterine stress has been linked with changes in skeletal muscle and pancreatic morphology function (14), leading to increased skeletal muscle insulin resistance and future risk of type 2 diabetes. Exposure to malaria *in utero* is associated with increased risk of preterm and low birthweight births (15) and may be a potential cause for later development of type 2 diabetes in life. A recent study reported subtle elevations of plasma glucose levels in young adult offspring of pregnancies affected by malaria which may be an early marker for the risk of later developing type 2 if these individuals are exposed to an obesogenic environment (16). Furthermore, malaria has been positively associated with insulin resistance (17) mediated by inflammation (18); which is an important risk factor for the development of type 2 diabetes (19). These findings give indirect evidence that inflammation is an important link for the co-existence of malaria and diabetes.

Cytokines are important mediators in the pathogenesis of malaria and T2D. Interestingly, the pro-inflammatory cytokines implicated in the pathogenesis of malaria such as IL-1β, IL-6, IL-8 and IL-12 (20, 21) have also been linked with the pathogenesis of T2D (22, 23). However, TNF- α is distinct among the main cytokines involved in the pathogenesis of malaria and T2D. TNF-α is a proinflammatory cytokine with pleiotropic properties (24). It is a multipotent cytokine produced by a wide range of immune cells such as B cells, T cells and macrophages. TNF- α is involved in various steps of immune responses and can initiate host defense, both innate and adaptive immune responses (25). TNF-α plays an important role in the pathogenesis of malaria (18, 26) and has also been implicated in the development of insulin resistance which contributes to the development of type 2 diabetes (27). In malaria infection, TNF- α is also involved in anti-Plasmodium responses that lead to intra-erythrocytic parasite killing and parasitemia reduction and it also plays a central role in the progression of malaria to cerebral malaria (21, 28). TNF-α upregulates the expression of adhesion receptors on endothelial cells, leading to an increase in the sequestration of parasite-infected RBCs on the endothelial cells in the brain. Furthermore, TNF-α is a major adipocyte cytokine; it interferes with insulin signaling after binding to its cognate receptor on muscle cells, thereby impairing insulin action (29–32). TNF-α has also been shown to increase leukocyte adhesion to endothelium, which results in endothelial dysfunction pathogenesis (33). *In vitro*, TNF-α has been shown to increase the transcriptional activity of TCF7L2 (a gene that has consistently been associated with type 2 diabetes) leading to reduced adipogenesis (34).

Functional studies

TNF-α is an important human cytokine that is implicated in malaria pathogenicity (35). Malaria infected individuals produce varying levels of TNF-α; the level of TNF-α production is directly

proportional to malaria severity (36). A high TNF production is associated with accelerated parasite clearance, while excessive TNF levels are associated with complications such as cerebral malaria or severe anemia (37). The pathway to TNF-α production in malaria infection begins at the pre-erythrocytic phase after the entry of *Plasmodium falciparum* parasite into the human host, sporozoite antigen stimulates the release of TNF-α before sporozoite invasion into the liver (38).

Following the release of merozoites from the liver, the merozoites infect red blood cells. In the red blood cells, molecular interactions occur between the merozoite and the red blood cell surface. Eventually, the merozoites develop into fully matured trophozoites which rupture to release merozoites, hemozoin and toxins such as *P. falciparum* glycosylphosphatidyl inositol into the bloodstream. This stimulates macrophages to produce TNF- α alongside other pro-inflammatory cytokines such as IFN-γ and IL-12 (39, 40), which coincides with the clinical manifestation of malaria. However, TNF- α is the main cytokine that has been associated with the severe forms of malaria, cerebral malaria (41–43).

Recent report shows that TNF-α plays dual role (which includes protective and pathogenic) in malaria physiopathology; as at higher levels, it promotes pathogenicity in cerebral malaria while it is protective against severe malaria at lower levels (44–46). This corroborates Clark et al. (47) findings, who reported that increased TNF- α production induces the cytoadherence of parasite-infected red blood cells to the endothelial cells lining blood vessels in the brain, a phenomenon known as sequestration which is characteristic of cerebral malaria.

Tumor necrosis factor (TNF)-α was the first proinflammatory cytokine to be implicated in the pathogenesis of insulin resistance and type 2 diabetes (48, 49). Several studies have demonstrated high levels of TNF- α in patients with type 2 diabetes. The major organs involved in the development of type 2 diabetes include the pancreas (β-cells and α-cells), liver, skeletal muscle, kidneys, brain, small intestine, and adipose tissue (50). TNF-α has been shown to reduce the expression of insulin-regulated glucose transporter type 4 (GLUT4), which is located mainly on adipocytes, and skeletal and cardiac muscles (48). The consequence of this is a reduction in insulin receptor substrate-1 (IRS-1) which results in impaired insulin sensitivity. Furthermore, TNF-α can act as an inhibitor of peripheral insulin action by inducing serine phosphorylation of insulin receptor substrate-1 which leads to insulin resistance (48).

Obesity is a major risk factor for type 2 diabetes (51). The level of mRNA of TNF-α and its protein has been shown to increase in the adipose tissues of diabetic individuals (52, 53). TNF-α impairs insulin sensitivity in adipose tissues is *via* the downregulation of protein level of insulin receptor substrate1 (IRS-1) and glucose transporter 4 (GLUT4) (53). The expression of TNF-α is increased in human adipose tissues with insulin resistance (27). In adipose tissues, TNF-alpha activates enhanced lipolysis leading to increased secretion of free fatty acids from adipose tissue into the circulation (49, 54). TNF-α mediates its biological effect in adipose tissues *via* the two receptors, TNFR1 and TNFR2. The TNFR1 is widely expressed on all cell types, while TNFR2 is expressed predominantly on leukocytes and endothelial cells. The two TNFRs have been shown to mediate distinct biological effects. The binding of TNF-α to TNFR1 mostly triggers pro-inflammatory pathways (55). The action of TNF-α on adipose tissues can also alter the production of many adipokines. This is relevant to the systemic effects of this TNF-α on insulin sensitivity and whole-body energy homeostasis (56). On the other hand, TNF-alpha upregulates the expression of genes like vascular cell adhesion molecule-1, plasminogen activator inhibitor-1, IL-6, IL-1b, angiotensinogen, resisting and leptin (57).

In obese individuals, TNF-α is over-expressed in adipose and muscle tissue (58). In obese type 2 diabetes patients, the TNF-α plasma level is related to the amount of visceral fat and is not instantly affected in poorly controlled diabetic patients by acute lowering of blood glucose level (59). Moreover, the levels of TNF-α expression strongly correlate with hyperinsulinemia and decreased insulin sensitivity (60). TNF-α also plays a vital role in the pathogenesis and development of obesity-induced insulin resistance as demonstrated by the augmented levels of TNF-α in systemic circulation, liver, and adipocytes (61–63). Impairment of normal functioning of the β-cells of pancreatic islets is one of the major causative factors for the suppression of insulin secretion. TNF-α can also induce the inflammation in pancreatic islets which lead to the induction of apoptosis in β-cells of pancreatic islets (64)

TNF-α in genetic studies

Genetic variations in the promoter region of the TNF-α gene may regulate TNF- α production, transcription and affect susceptibility to or protection from inflammatory-related diseases such as malaria and type 2 diabetes (26, 65, 66). Many studies have been carried out to determine whether the TNF- α polymorphisms are associated with levels of TNF- α production, disease susceptibility and or disease severity (67–69). The polymorphisms at positions -238 (rs361525), -308 (rs1800629), -857 (rs1799724), -863 (rs1800630) and -1031(rs1799964) have been associated with increased transcriptional activity and production of TNF-α in several studies (20, 70). The polymorphism at the -308G/A has been linked with various inflammatory and autoimmune diseases (71–74). The -238 G/A polymorphism has been associated with insulin resistance syndrome and obesity (75). The polymorphisms at positions -857, -863 and -1031 have been associated with both increased luciferase activity and increased concanavalin-A stimulated TNF-α production from peripheral blood mononuclear cells (76). In malaria, the aforementioned SNPs have been associated with control of parasitemia levels and increased anti-*P. falciparum* IgG levels (77, 78); suggesting that the TNF- α SNPs may play a role in the effectiveness of anti-parasite responses. However, the control of TNF- α gene expression by these polymorphisms seems to be context-dependent based on secreting cell types, cell activation status, and action of other inflammatory mediators such as IL-6 and CRP (79).

A previous study by McGuire et al. (80) associated the A allele of TNF-α -308 with cerebral malaria. Gimenez et al. (36) also reported that TNF-α and TNF-α receptors are involved in the

pathogenesis of cerebral malaria. Mohamedahmed and Abakar (81) implicated high TNF-α plasma levels with susceptibility to severe malaria, and this was corroborated with previous reports (26, 82, 83) that showed that TNF - 238G/A, a TNF-α SNP was associated with severe malaria and/or progression from uncomplicated malaria infection to severe malaria.

Single nucleotide variations in the TNF-α gene have also been implicated in increased insulin resistance typical of type 2 diabetes. The most widely studied of the TNF-α promoter variants are the *TNF-α* −308G/A and −238G/A polymorphisms. These TNF-α variants have been studied in association with the outcome of type 2 diabetes. Although several studies have focused on these associations, their conclusions have been controversial (84–86). An earlier meta-analysis on the association between *TNF-α* −308G/A and type 2 diabetes did not find any significant association (87). A more recent meta-analysis however, found the *TNF-α* −308G/A variant to be associated with susceptibility to type 2 diabetes (88). On other hand, the *TNF-α* −238G/A was not associated with type 2 diabetes in most of the previous meta-analyses carried out on the variant (87, 89). Generally, the association of 308G/A and 238G/A polymorphisms have been associated with insulin resistance, obesity and T2DM has been demonstrated in some ethnic groups (90–93).

Discussion: TNF-α, an important link in the co-existence of malaria and type 2 diabetes

Malaria has long been associated with inflammation (94). Tumor necrosis factor (TNF)-α is an important pro-inflammatory cytokine involved in immune responses to malaria infection. It plays an important role in both the innate and adaptive immune responses to malaria parasites during malaria infection. Although inflammation is a major host defense mechanism against pathogens such as the *Plasmodium* parasite, inflammation can be harmful to the host with resultant acute or chronic pathology if dysregulated (20). As discussed earlier, TNF-α promotes pathogenicity in cerebral malaria at higher levels, while it is protective against severe malaria at lower levels (44–46).This is evident in malaria infection as increased serum levels of TNF-α is characteristic of malaria episodes and elevated levels correlates with faster parasite clearance with the resolution of malaria episodes (95, 96). On the other hand, increased TNF serum levels were repeatedly found in children with severe malaria (94, 97), establishing the important role that TNF-α plays in malaria pathogenesis. Interestingly, the TNF-α-induced inflammation seen in malaria infection is similar to that observed in type 2 diabetes (98). Studies have demonstrated high levels of TNF-α in patients with type 2 diabetes. TNF-α reduces the expression of insulin-regulated glucose transporter type 4 (48), resulting in impaired insulin sensitivity. Also, increased levels of TNF-α expression is strongly correlated with hyperinsulinemia and decreased insulin sensitivity (60).

The inflammation link between malaria and type 2 diabetes is not direct due to the complex nature of the inflammatory process in the two diseases. Nevertheless, previous studies have associated malaria-induced inflammation with critical risk factors of T2DM. A good example is the malaria-induced inflammation in placental malaria that has been associated with low birth weight, which is an important risk factor for the development of type 2 diabetes later in life (19, 99). Similarly, malaria has been positively associated with insulin resistance mediated by inflammation (17, 18), which is a key risk factor for the development of type 2 diabetes (19). One of the most important inflammatory mediators that has been implicated in the development of insulin resistance (which is central to the development of type 2 diabetes) is TNF-α which is also involved in the pathogenesis of malaria (18, 100). These observations affirm inflammation *via* TNF-α as a mechanism which contributes to the co-existence of malaria and type 2 diabetes in malaria endemic regions.

The pertinent question then, is, how does TNF-α connect malaria and type 2 diabetes? The answer lies in the well-known type 2 diabetes marker, TCF4 also known as TCF7L2 (transcription factor 7-like 2). The transcription factor 7-like 2 (TCF7L2) is the most potent locus for type 2 diabetes; as the association of *TCF7L2* with type 2 diabetes has been consistently replicated in multiple populations with diverse genetic origins (101). TNF-α has been shown to enhance the transcriptional activity of TCF7L2 *in vitro*, leading to reduced adipogenesis (54). The transcriptional effects of TNF-a promote oxidative stress and mitochondrial dysfunction, lipolysis and altered adipokine expression, thereby compromising insulin signaling and adipocyte lipid metabolism (56). Cawthorn et al. (54), found that TNF- α enhanced TCF4-dependent transcriptional activity during early anti-adipogenesis suggesting that TNF-α and Wnt signaling pathways may converge to inhibit adipocyte development at the level of TCF4-dependent gene transcription. TCF7L2 is a transcription factor that forms a basic part of the Wnt signaling pathway (101). This evidence further strengthens the possibility of a link between TNF-α and TCF7L2 which may play an important role in the co-existence of malaria and type 2 diabetes.

In order to test this hypothesis, we genotyped a TCF7L2 gene variant (rs7903146) in Nigerian children with malaria in a pilot study and found the gene to be present in the population. The study was carried out among under-five children in Ibadan, southwest Nigeria, an area that is holoendemic for malaria. The children were categorized into, asymptomatic, uncomplicated and severe malaria groups as defined by World Health Organization. Genotyping was done using PCR-RFLP, we found the TCF7L2 gene variant, rs7903146 in the population with a minor allelic frequency of 0.139. We also found the TCF7L2 variant, rs7903146 to be associated with susceptibility to developing severe malaria in children from Ibadan southwest Nigeria. These results suggest an association between the type 2 diabetes gene (TCF7L2) and malaria in Ibadan, Nigeria, a population that is malaria endemic.

This evidence suggests a probable pathway that links TNF-α and TCF7L2 in the co-existence of malaria and type 2 diabetes. During malaria infection, infected erythrocytes lead to the activation of macrophages and natural killer cells which lead to

10.3389/fimmu.2023.1028303

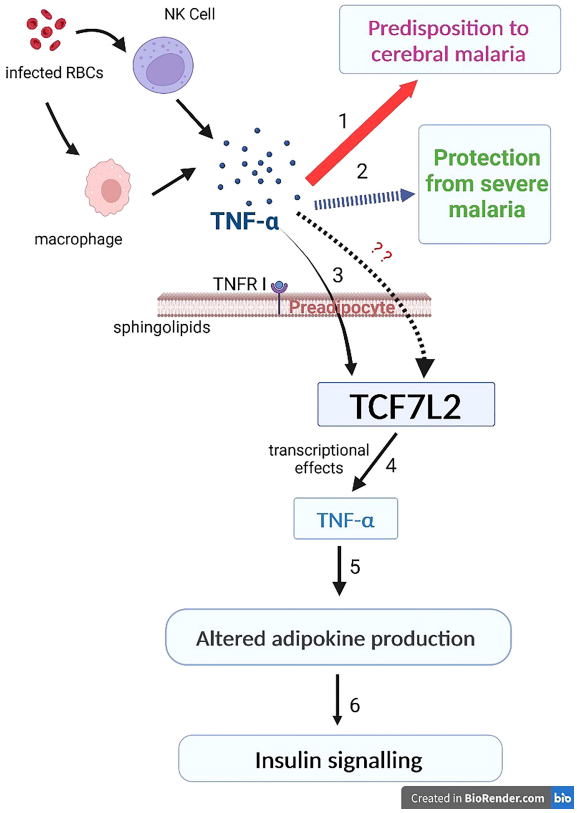

FIGURE 1
The inflammation link between malaria and type 2 diabetes. During malaria infection, infected erythrocytes lead to the activation of macrophages and natural killer cells which lead to the production of TNF-α. Varying levels of TNF-α determine the outcome of clinical malaria; the thick red arrow indicates high levels of TNF-α that promote cerebral malaria (1) while the dashed blue arrow indicates reduced levels of TNF-α that protects against severe malaria (2). 3-6: in type 2 diabetes, TNF-α mediates its biological effect in adipose tissues through its receptor, TNFR1. TNF-α binds to TNFR1, leading to the production of soluble forms of TNF-α. In preadipocytes, TNF-α can stimulate transcription via the type 2 diabetes gene, TCF7L2, leading to altered adipokine production, thereby compromising insulin signaling and adipocyte lipid metabolism (4-6; Figure 1). However, the effect (s) of varying levels of TNF-α on the transcriptional activity of TCF7L2 remains unknown (this is indicated by the red question marks).

the production of TNF-α. However, varying levels of TNF-α determine the outcome of clinical malaria; high levels of TNF-α promote cerebral malaria while reduced levels of TNF-α protects against severe malaria (1-3; Figure 1). In type 2 diabetes, TNF-α can mediate its biological effect in adipose tissues through its receptor, TNFR1. TNF-α binds to its receptor, TNFR1, leading to the production of soluble forms of TNF-α. In preadipocytes, TNF-α can stimulate transcription *via* the type 2 diabetes gene, TCF7L2, leading to altered adipokine production, thereby compromising insulin signaling and adipocyte lipid metabolism (4-6; Figure 1). However, the effect(s) of varying levels of TNF-α on the transcriptional activity of TCF7L2 remains unknown (7; Figure 1). Studies are needed to investigate the effect of varying levels of TNF-α on the transcription of TCF7L2.

There are critical knowledge gaps which requires further studies. One of these is the effect of the varying levels of TNF-α on the transcriptional activity of TCF7L2. This is important because TNFα is known to have differential effects depending on its level of production *in vivo*. However, the effect(s) of its elevated or reduced levels on the transcriptional activity of the type 2 diabetes gene, TCF7L2 remains unknown. Another knowledge gap is the dearth of studies on malaria and type 2 diabetes in children and adolescents. Most of the research that has been carried out on the co-existence of malaria with diabetes has been conducted using the adult population with little or no studies on children. This is important mainly because malaria is most severe in children and the incidence of type 2 diabetes is becoming more common in children and adolescents.

Data availability statement

The original contributions presented in the study are included in the article/Supplementary Material. Further inquiries can be directed to the corresponding author.

Ethics statement

The studies involving human participants were reviewed and approved by Oyo State Ministry of Health Ethics Review Board. Written informed consent to participate in this study was provided by the participants' legal guardian/next of kin.

Author contributions

SA and OA conceived and designed the idea behind the paper, OB analyzed the data and participated in the manuscript drafting and revision. All authors contributed to the article and approved the submitted version.

Acknowledgments

The authors sincerely appreciate the efforts of the doctoral students; Babajide Adedeji, Taiwo Olajide and Noah Bukoye for their assistance in proof reading the article.

Conflict of interest

The authors declare that the research was conducted in the absence of any commercial or financial relationships that could be construed as a potential conflict of interest.

Publisher's note

References

1. IDF. *International diabetes federation diabetes atlas* (2021). Available at: https://diabetesatlas.org/resources/.

2. WHO. *Diabetes. fact sheets*. World Health Organization (2022). Available at: https://www.who.int/news-room/fact-sheets/detail/diabetes.

3. Haamid B, Majid S, Khan M.S., K.S., Bhat MH, Hamid R, Ashraf R, et al. Impact of pro- and anti- inflammatory biomarkers on development and severity of type 2 diabetes mellitus – a case-control study. *Heliyon* (2022) 8(11):e11329. doi: 10.2139/ssrn.4071641

4. International Diabetes Federation. *International diabetes federation atlas(ninth edition)* (2019). Available at: www.diabetesatlas.org.

5. Roden M, Shulman GI. The integrative biology of type 2 diabetes. *Nature* (2019) 576:51–60. doi: 10.1038/s41586-019-1797-8

6. Metta E, Bailey A, Kessy F, Geubbels E, Hutter I, Haisma H. In a situation of rescuing life. In: *Meanings given to diabetes symptoms and care-seeking practices among adults in southeastern Tanzania: a qualitative inquiry*, vol. 15. BMC Public Health (2015). doi: 10.1186/s12889-015-1504-0

7. Trampuz A, Jereb M, Muzlovic I, Prabh MJ. Clinical review: severe malaria. *Crit Care* (2003) 7.4:315–23. doi: 10.1186/cc2183

8. Malaguarnera L, Musumeci S. The immune response to *Plasmodium falciparum* malaria. *Lancet Infect Dis* (2002) 2:472–8. doi: 10.1016/S1473-3099(02)00344-4

9. Kalra S, Khandelwal D, Singla R, Aggarwal S, Dutta D. Malaria and diabetes. *J Of Pakistan Med Assoc* (2017) 67(5):810–3.

10. Danquah I, Bedu-Addo G, Mockenhaupt FP. Type 2 diabetes mellitus and increased risk for malaria infection. *Emerg Infect Dis* (2010) 16(10):1601–4. doi: 10.3201/eid1610.100399

11. Ikekpeazu EJ, Ikekpeazu EJ, Neboh EE, Maduka IC, Nwagbara IJ, Nwobodo MW. Type-2 diabetes mellitus and malaria parasitaemia: effect on liver function tests. *Asian J Med Sci* (2010) 2(5):214–7.

12. Carrillo-Larco RM, Altez-Fernandez C, Ugarte-Gil C. Is diabetes associated with malaria and malaria severity? a systematic review of observational studies [version 3; peer review: 2 approved]. *Wellcome Open Res* (2019) 4. doi: 10.12688/wellcomeopenres.15467.1

13. Ch'Ng JH, Moll K, Wyss K, Hammar U, Rydén M, Kämpe O, et al. Enhanced virulence of plasmodium falciparum in blood of diabetic patients. *PloS One* (2021) 16(6 June). doi: 10.1371/journal.pone.0249666

14. Christensen DL, Kapur A, Bygbjerg IC. Physiological adaption to maternal malaria and other adverse exposure: low birth weight, functional capacity, and possible metabolic disease in adult life. *Int J Gynecol Obstet* (2011) 115(SUPPL. 1). doi: 10.1016/S0020-7292(11)60006-4

15. Thompson JM, Eick SM, Dailey C, Dale AP, Mehta M, Nair A, et al. Relationship between pregnancy-associated malaria and adverse pregnancy outcomes: a systematic review and meta-analysis. *J Trop Pediatr* (2020) 66(3):327–38. doi: 10.1093/TROPEJ/FMZ068

16. Grunnet LG, Bygbjerg IC, Mutabingwa TK, Lajeunesse-Trempe F, Nielsen J, Schmiegelow C, et al. Influence of placental and peripheral malaria exposure in fetal life on cardiometabolic traits in adult offspring. *BMJ Open Diabetes Res Care* (2022) 10(2). doi: 10.1136/bmjdrc-2021-002639

17. Acquah S, Boampong JN, Jnr BAE. Functional paradox of leptin and adiponectin in diabetes patients and controls in the cape coast metropolis of Ghana. *Med J Dr DY Patil Univ* (2017) 10(3):268. doi: 10.4103/MJDRDYPU.MJDRDYPU_271_16

18. Acquah S, Boampong JN, Jnr E, Ackon B. Increased oxidative stress and inflammation independent of body adiposity in diabetic and nondiabetic controls in falciparum malaria. *BioMed Res Int* (2016) 2016:5216913. doi: 10.1155/2016/5216913

19. Lontchi-Yimagou E, Sobngwi E, Matsha TE, Kengne AP. Diabetes mellitus and inflammation. *Curr Diabetes Rep* (2013) 13(3):435–44. doi: 10.1007/s11892-013-0375-y

20. Penha-Gonçalves C. Genetics of malaria inflammatory responses: a pathogenesis perspective. *Front Immunol* (2019) 10:1771. doi: 10.3389/fimmu.2019.01771

21. Popa GL, Popa MI. Recent advances in understanding the inflammatory response in malaria: a review of the dual role of cytokines. *J Immunol Res* (2021) 2021:1–9. doi: 10.1155/2021/7785180

22. Alexandraki K, Piperi C, Kalofoutis C, Singh J, Alaveras A, Kalofoutis A. Inflammatory process in type 2 diabetes: the role of cytokines. *Ann N Y Acad Sci* (2006) 1084:89–117. doi: 10.1196/annals.1372.039

23. Liu C, Feng X, Li Q, Wang Y, Li Q, Hua M. Adiponectin, TNF-α and inflammatory cytokines and risk of type 2 diabetes: a systematic review and meta-analysis. *Cytokine* (2016) 86:100–9. doi: 10.1016/j.cyto.2016.06.028

24. Horiuchi T, Mitoma H, Harashima SI, Tsukamoto H, Shimoda T. Transmembrane TNF-α: structure, function and interaction with anti-TNF agents. *Rheumatology* (Oxford) (2010) 49(7):1215–28. doi: 10.1093/rheumatology/keq031

25. Horiuchi T, Mitoma H, Harashima S, Tsukamoto H, Shimoda T. Review transmembrane TNF- a: structure, function and interaction with anti-TNF agents. (2010) :1215–28. doi: 10.1093/rheumatology/keq031

26. Olaniyan SA, Amodu OK, Bakare AA, Troye-Blomberg M, Omotade OO, Rockett KA. Tumour necrosis factor alpha promoter polymorphism, TNF-238 is associated with severe clinical outcome of falciparum malaria in ibadan southwest Nigeria. *Acta Tropica* (2016) 161(2015):62–7. doi: 10.1016/j.actatropica.2016.05.006

27. Peraldi P, Hotamisligil GS, Buurman WA, White MF, Spiegelman BM. Tumor necrosis factor (TNF)-β inhibits insulin signaling through stimulation of the p55 TNF receptor and activation of sphingomyelinase. *J Biol Chem* (1996) 271(22):13018–22. doi: 10.1074/jbc.271.22.13018

28. Clark IA, Virelizier JL, Carswell EA, Wood PR. Possible importance of macrophage-derived mediators in acute malaria. *Infect Immun* (1981) 32:1058–66. doi: 10.1128/iai.32.3.1058-1066.1981

29. Hotamisligil GS, Arner P, Caro JF, Atkinson RL, Spiegelman BM. Increased adipose tissue expression of tumor necrosis factor-alpha in human obesity and insulin resistance. *J Clin Invest* (1995) 95(5):2409–15. doi: 10.1172/JCI117936

30. Peraldi P, Spiegelman B. TNF-alpha and insulin resistance: summary and future prospects. *Mol Cell Biochem* (1998) 182(1-2):169–75. doi: 10.1023/A:1006865715292

31. Ruan H, Lodish HF. Insulin resistance in adipose tissue: direct and indirect effects of tumor necrosis factor alpha. *Cytokine Growth Factor Rev* (2003) 14:447–55. doi: 10.1016/S1359-6101(03)00052-2

32. Dandona P, Aljada A, Chaudhuri A, Mohanty P, Garg R. Metabolic syndrome: a comprehensive perspective based on interactions between obesity, diabetes, and inflammation. *Circulation* (2005) 111(11):1448–54. doi: 10.1161/01.CIR.0000158483.13093.9D

33. Zeng M, Zhang H, Lowell C, He P. Tumor necrosis factor-alpha-induced leukocyte adhesion and microvessel permeability. *Am J Physiol Heart Circ Physiol* (2002) 283(6):H2420–30. doi: 10.1152/ajpheart.00787.2001

34. Kabagambe EK, Glasser SP, Ordovas JM, Warodomwichit D, Tsai MY, Hopkins PN, et al. TCF7L2 polymorphisms and inflammatory markers before and after

treatment with fenofibrate. *Diabetol Metab Syndrome* (2009) 1(1). doi: 10.1186/1758-5996-1-16

35. Randall LM, Engwerda CR. Experimental parasitology TNF family members and malaria: old observations, new insights and future directions. *Exp Parasitol* (2010) 126(3):326–31. doi: 10.1016/j.exppara.2010.04.016

36. Gimenez F, Lagerie B, Fernandez C, Pino P, Mazier D. Tumor necrosis factor a in the pathogenesis of cerebral. *Cell Mol Life Sci* (2003) 60:1623–35. doi: 10.1007/s00018-003-2347

37. Grau GE, Taylor TE, Molyneux ME. Tumour necrosis factor and disease severity in children with falciparum malaria. *New Engl J Med* (1989) 320:1586–91.

38. Richards AL. Tumour necrosis factor and associated cytokines in the host's response to malaria. *Int J Parasitol* (1997) 27:1251–63. doi: 10.1016/S0020-7519(97)00122-7

39. Stevenson MM, Riley EM. Innate immunity to malaria. *Nat Rev Immunol* (2004) 4(3):169–80. doi: 10.1038/nri1311

40. Kwiatkowski D, Perlman P. Harwood Academic Publishers (1999).

41. Storm J, Craig AG. Pathogenesis of cerebral malaria–inflammation and cytoadherence. *Front Cell Infect Microbiol* (2014) 29;4:100. doi: 10.3389/fcimb.2014.00100

42. Mauduit M, Depinay N, Franetich JF, Gru AC, Chavatte M, Luty AJF, et al. Inhibitory effect of TNF- a on malaria pre-erythrocytic stage Development: influence of host Hepatocyte/Parasite combinations. *PLoS One* (2011) 6(3):e17464. doi: 10.1371/journal.pone.0017464

43. Perera MK, Herath NP, Pathirana SL, Alles HK, Mendis KN, Premawansa S, et al. Association of high plasma TNF-alpha levels and TNF-alpha/IL-10 ratios with TNF2 allele in severe p. falciparum malaria patients in Sri Lanka. *Pathog Glob Health* (2013) 107(1):21–9. doi: 10.1179/2047773212Y.0000000069

44. Pino P, Mazier D. Tumor necrosis factor a in the pathogenesis of cerebral. *Cell Mol Life Sci September* (2003). doi: 10.1007/s00018-003-2347-x

45. Awasthi G, Singh S, Dash AP, Das A. Genetic characterization and evolutionary inference of TNF- α through computational analysis. *Braz J Infect Dis* (2008) 12:374–9. doi: 10.1590/S1413-86702008000500006

46. Leão L, Puty B, Dolabela MF, Povoa MM, Gecy Y, Né DS, et al. Association of cerebral malaria and TNF- α levels: a systematic review. *BMC Infect Dis* (2020) 20(1):442. doi: 10.1186/s12879-020-05107-2

47. Clark IA, Alleva LM, Mills AC, Cowden WB. Pathogenesis of malaria and clinically similar conditions. *Clin Microbiol Rev* (2004) 17:509–39. doi: 10.1128/CMR.17.3.509-539.2004

48. Hotamisligil GS. Inflammation and endoplasmic reticulum stress in obesity and diabetes. *Int J Obes* (2009) 32(S7):S52–4. doi: 10.1038/ijo.2008.238

49. Sethi JK. The role of TNF in adipocyte metabolism. *Semin Cell Dev Biol* (1999) 10:19–29. doi: 10.1006/scdb.1998.0273

50. Defronzo RA. From the triumvirate to the ominous octet: a new paradigm for the treatment of type 2 diabetes mellitus. *Diabetes* (2009) 58:773–95. doi: 10.2337/db09-9028

51. Galicia-Garcia U, Benito-Vicente A, Jebari S, Larrea-Sebal A, Siddiqi H, Uribe KB, et al. Pathophysiology of type 2 diabetes mellitus. *Int J Mol Sci* (2020) 21(17):1–34. doi: 10.3390/ijms21176275

52. Akash MSH, Rehman K, Liaqat A. Tumor necrosis factor-alpha: role in development of insulin resistance and pathogenesis of type 2 diabetes mellitus. *J Cell Biochem* (2018) 119(1):105–10. doi: 10.1002/jcb.26174

53. el Hini SH, Ahmed ATZ, Hamed EMS, Mahmoud YZ, Eldin AMK, Abdelghany HM. Pivotal role of both tnf-α 238g/a and tcf7l2 c/t gene polymorphisms in type 2 diabetes. *Open Access Macedonian J Med Sci* (2020) 8(F):283–6. doi: 10.3889/oamjms.2020.5008

54. Cawthorn WP, Heyd F, Hegyi K, Sethi JK. Tumour necrosis factor-α inhibits adipogenesis *via* a β-catenin/TCF4(TCF7L2)-dependent pathway. *Cell Death Differentiation* (2007) 14(7):1361–73. doi: 10.1038/sj.cdd.4402127

55. Yang S, Wang J, Brand DD, Zheng SG. Role of TNF-TNF receptor 2 signal in regulatory T cells and its therapeutic implications. *Front Immunol* (2018) 19(9):784. doi: 10.3389/fimmu.2018.00784

56. Cawthorn WP, Sethi JK. TNF-α and adipocyte biology. *FEBS Lett* (2008) 582(1):117–31. doi: 10.1016/j.febslet.2007.11.051

57. Saghizadeh M, Ong JM, Garvey WT, Henry RR, Kern PA. The expression of TNF by human muscle relationship to insulin resistance. in. *J Clin Invest* (1996) 97(4). doi: 10.1172/JCI118504

58. Hoffmann C, Lorenz K, Braithwaite SS, Colca JR, Palazuk BJ, Hotamisligil GS, et al. Altered gene expression for tumor necrosis factor-alpha and its receptors during drug and dietary modulation of insulin resistance. *Endocrinology* (1994) 134:264–70. doi: 10.1210/endo.134.1.8275942

59. Alzamil H. Elevated serum TNF-α is related to obesity in type 2 diabetes mellitus and is associated with glycemic control and insulin resistance. *J Obese* (2020) 2020:5076858. doi: 10.1155/2020/5076858

60. Sethi JK, Hotamisligil GS. Metabolic messengers: tumour necrosis factor. *Nat Metab* (2021) 3(10):1302–12. doi: 10.1038/s42255-021-00470-z

61. Kabayama K, Sato T, Kitamura F, Uemura S, Kang BW, Igarashi Y, et al. TNFα-induced insulin resistance in adipocytes as a membrane microdomain disorder: involvement of ganglioside GM3. *Glycobiology* (2005) 15:21–9. doi: 10.1093/glycob/cwh135

62. Solomon S, Odunusi O, Carrigan D, Majumdar G, Kakoola D, Lenchik N, et al. TNF-α inhibits insulin action in liver and adipose tissue: a model of metabolic syndrome. *Hormone Metab Res* (2010) 42:115–21. doi: 10.1055/s-0029-1241834

63. da Rocha AF, Liboni TF, Kurauti MA, de Souza CO, Miksza DR, Moreira CCL, et al. Tumor necrosis factor alpha abolished the suppressive effect of insulin on hepatic glucose production and glycogenolysis stimulated by cAMP. *Pharmacol Rep* (2014) 66:380–5. doi: 10.1016/j.pharep.2013.12.005

64. Wang C, Guan Y, Yang J. Cytokines in the progression of pancreatic β-cell dysfunction. *Int J Endocrinol* (2010) 2010:515136. doi: 10.1155/2010/515136

65. Jamil K, Jayaraman A, Ahmad J, Joshi S, Kumar YS. TNF-alpha -308G/A and – 238G/A polymorphisms and its protein network associated with type 2 diabetes mellitus. *Saudi J Biol Sci* (2017) 24:1195–203. doi: 10.1016/j.sjbs.2016.05.012

66. Mahto H, Rina T, Meher BR, Prusty BK, Sharma M, Deogharia D, et al. TNF- α promoter polymorphisms (G-238A and G-308A) are associated with susceptibility to systemic lupus erythematosus (SLE) and p. falciparum malaria: a study in malaria endemic area. *Sci Rep* (2019) 9(1):11752. doi: 10.1038/s41598-019-48182-5

67. De Jong BA, Westendorp AM, Bakker AM, Huizinga M. Polymorphisms in or near tumour necrosis factor gene do not determine levels of endotoxin-induced TNF production. *Genes Immun* (2002) 3:25–9.

68. Feng R, Li Y, Zhao D, Wang C, Niu Y. Lack of association between TNF 238 G/A polymorphism and type 2 diabetes: a meta-analysis. *Acta Diabetol* (2009) 46:339–43. doi: 10.1007/s00592-009-0118-3

69. Sharma N, Joseph R, Arun R, Chandni R, Srinivas KL, Banerjee M. Cytokine gene polymorphism (interleukin-1β +3954, interleukin-6 [-597/-174] and tumor necrosis factor-a - 308) in chronic periodontitis with and without type 2 diabetes mellitus. *Indian J Dent Res* (2014) 25:375–80. doi: 10.4103/0970-9290.138343

70. Wilson AG, Symons JA, McDowell TL, McDevitt HO, Duff GW. Effects of a polymorphism in the human tumor necrosis factor alpha promoter on transcriptional activation. *Proc Natl Acad Sci USA* (1997) 94:3195–9. doi: 10.1073/pnas.94.7.3195

71. Verjans GM, Brinkman BNM, Van Doornik CEM. Polymorphism of tumour necrosis factor-alpha (TNF-α) at position -308 in relation to ankylosing spondylitis. *Clin Exp Immunol* (1994) 97:45–7.

72. Cabrera M, Shaw MA, Sharples C. Polymorphism in tumour necrosis factor genes associated with mucocutaneous leishmaniasis. *J Exp Med* (1995) 182:1259–64. doi: 10.1084/jem.182.5.1259

73. Wilson AG, Clay FE, Crane AM. Comparative genetic association of human leukocyte antigen class II and tumour necrosis factor alpha with dermatitis herpetiformis. *J Invest Dermatol* (1995) 104:856–8.

74. Nadel S, Newport MJ, Booy R. Variation in the tumour necrosis factor-alpha gene promoter region may be associated with death from meningococcal disease. *J Infect Dis* (1996) 174:878–80. doi: 10.1093/infdis/174.4.878

75. Rasmussen SK, Urhammer SA, Jensen JN. The -238 and -308 G/A polymorphisms of tumour necrosis factor alpha gene promoter are not associated with features of the insulin resistance syndrome or altered birth weight in Danish caucasians. *J Clin Endocrinol Metab* (2000) 85:1731–4.

76. Higuchi T, Seki N, Kamizono S, Yamada A, Kimura A, Kato H, et al. Polymorphism of the 5'-flanking region of the human tumor necrosis factor (TNF)-alpha gene in japanese. *Tissue antigens. 51* (1998), 605–12.

77. Wilson AG, Symons JA, McDowell TL, McDevitt HO, Duff GW. Effects of a polymorphism in the human tumor necrosis factor alpha promoter on transcriptional activation. *Proc Natl Acad Sci USA* (1997) 94:3195–9.

78. Basu M, Maji AK, Chakraborty A, Banerjee R, Mullick S, Saha P. Genetic association of toll-like-receptor 4 and tumor necrosis factor-a polymorphisms with plasmodium falciparum blood infection levels. *Infect Genet Evol* (2010) 10:686–96. doi: 10.1016/j.meegid.2010.03.008

79. El-Tahan RR, Ghoneim AM, El-Mashad N. TNF-a gene polymorphisms and expression. *Springerplus* (2016) 5:1508. doi: 10.1186/s40064-016-3197-y

80. McGuire W, Hill AV, Allsopp CE, Greenwood BM, Kwiatkowski D. Variation in the TNF-alpha promoter region associated with susceptibility to cerebral malaria. *Nature. 371* (1994), 508–10. doi: 10.1038/371508a0

81. Mohamedahmed KA, Abakar A. The role of TNF- α levels as predictive diagnostic biomarker among children with severe falciparum malaria in endemic area in Sudan. *International Journal of Academic Health and Medical Research (IJAHMR)* (2019) 3(7):1–6.

82. Flori L, Delahaye NF, Iraqi FA, Fumoux F, Rihet P. TNF as a malaria candidate gene: polymorphism-screening and family-based association analysis of mild malaria attack and parasitemia in Burkina Faso. *Genes Immun* (2005) 6(6):472–80. doi: 10.1038/sj.gene.6364231

83. Randall LM, Kenangalem E, Lampah DA, Tjitra E, Mwaikambo ED, Handojo T, et al. A study of the TNF/LTA/LTB locus and susceptibility to severe malaria in highland papuan children and adults. *Malar J* (2010) 9:302. doi: 10.1186/1475-2875-9-302

84. Kim EY, Priatel JJ, Teh SJ, The HS. TNF receptor type 2 (p75) functions as a costimulator for antigen-driven T cell responses *in vivo*. *J Immunol* (2006) 176(2):1026–35. doi: 10.4049/jimmunol.176.2.1026

85. Liu C, Batliwalla F, Li W. Genome-wide association scan identifies candidate polymorphisms associated with differential response to anti-TNF treatment in rheumatoid arthritis. *Mol Med* (2008) 14:575–81. doi: 10.2119/2008-00056

86. Golshani Y, Zarei M, Mohammadi S. Acute/Chronic pain relief: is althaea officinalis essential oil effective? *Avicenna J Neuro Psych Physiol* (2015) 2(4). doi: 10.17795/ajnpp-36586

87. Feng R-N, Zhao C, Sun C-H, Li Y. Meta-analysis of *TNF* 308 G/A polymorphism and type 2 diabetes mellitus. *PloS One* (2011) 6(4):e18480. doi: 10.1371/journal.pone.0018480

88. Guo Y, Ren M, Ge L, Sun C, Li R, Ma C, et al. Increased serum concentrations of TNF-like weak inducer of apoptosis predict higher 28-day mortality in patients with sepsis. *Emergency Med Int* (2019) 2019:1–7. doi: 10.1155/2019/7238705

89. Gao W, Zhu R, Yang L. Association of tumor necrosis factor-Alpha-308 G/A and -238 G/A polymorphism with diabetic retinopathy: a systematic review and updated meta-analysis. *Ophthalmic Res* (2021) 64(6):903–15. doi: 10.1159/000513586

90. Guzma´ n-Flores JM, Escalante M, Sa´nchez-Corona J, Garcıa-Zapie´n AG, Cruz Quevedo EG, Mun˜ oz-Valle JF, et al. Association analysis between -308G/A and -238G/A TNF-alpha gene promoter polymorphisms and insulin resistance in Mexican women with gestational diabetes mellitus. *J Invest Med* (2013) 61:265–9. doi: 10.2310/JIM.0b013e31827b98c9

91. Saxena M, Srivastava N, Banerjee M. Association of IL-6, TNF-a and IL 10 gene polymorphisms with type 2 diabetes mellitus. *Mol Biol Rep* (2013) 40:6271–9. doi: 10.1007/s11033-013-2739-4

92. Sikka R, Raina P, Matharoo K, Bandesh K, Bhatia R, Chakrabarti S, et al. TNF-a (g.-308 g> a) and ADIPOQ (g. +45 T >G) gene polymorphisms in type 2 diabetes and microvascular complications in the region of punjab (North-West India). *Curr Eye Res* (2014) 39:1042–51. doi: 10.3109/02713683.2014.892998

93. Wilson AG, di Giovine FS, Blakemore AIF, Duff GW. Single base polymorphism in the human tumor necrosis factor alpha (TNF-alpha) gene detectable by NcoI restriction of PCR product. *Hum Mol Genet* (1992) 1:353.

94. Kwiatkowski D, Hill AV, Sambou I, Twumasi P, Castracane J, Manogue KR, et al. TNF concentration in fatal cerebral, non-fatal cerebral, and uncomplicated plasmodium falciparum malaria. *Lancet* (1990) 336(8725):1201–4. doi: 10.1016/0140-6736(90)92827-5

95. Clark K, Nyambati VCS, Neitz AWH, Louw AI. In search of an amino acid falciparum. *Biochem Afr - 2nd FASBMB; 15th SASBMB* (1998).

96. McGuire W, D'Alessandro U, Stephens S, Olaleye BO, Langerock P, Greenwood BM, et al. Levels of tumour necrosis factor and soluble TNF receptors during malaria fever episodes in the community. *Trans R Soc Trop Med Hygiene* (1998) 92:50–3. doi: 10.1016/S0035-9203(98)90951-8

97. Tchinda VH, Tako EA, Tene G, Fogako J, Nyonglema P. Severe malaria in cameroonian children: correlation between plasma levels of three soluble inducible adhesion molecules and TNF-alpha. *Acta Trop* (2007) 102:20–8. doi: 10.1016/j.actatropica.2007.02.011

98. Acquah S. Linking malaria to type 2 diabetes mellitus: a review. *J Ghana Sci Assoc* (2019) 18(1):56–70.

99. Fitri LE, Sardjono TW, Rahmah Z, Siswanto B, Handono K, Dachlan YP. Low fetal weight is directly caused by sequestration of parasites and indirectly by IL-17 and IL-10 imbalance in the placenta of pregnant mice with malaria, (2015). *Korean J Parasitol* (2015) 53(2):189–96. doi: 10.3347/kjp.2015.53.2.189

100. Nasr A, Allam G, Hamid O. IFN-gamma and TNF associated with severe falciparum malaria infection in Saudi pregnant women. *Malar J* (2014) 13:314. doi: 10.1186/1475-2875-13-314

101. Del Bosque-Plata L, Martínez-Martínez E, Espinoza-Camacho MÁ, Gragnoli C. The role of *TCF7L2* in type 2 diabetes. *Diabetes* (2021) 70(6):1220–8. doi: 10.2337/db20-0573

frontiers | Frontiers in Immunology

TYPE Original Research
PUBLISHED 09 March 2023
DOI 10.3389/fimmu.2023.954054

OPEN ACCESS

EDITED BY
Diana Boraschi,
Shenzhen Institute of Advanced Technology (SIAT) (CAS), China

REVIEWED BY
Paola Italiani,
National Research Council (CNR), Italy
Benjamin Swartzwelter,
Colorado State University, United States
Giselle Penton-Rol,
Center for Genetic Engineering and Biotechnology (CIGB), Cuba

*CORRESPONDENCE
Liliane K. Siransy,
lsiransy@gmail.com
kouabla.siransy@ufhb.edu.ci

SPECIALTY SECTION
This article was submitted to Cytokines and Soluble Mediators in Immunity, a section of the journal Frontiers in Immunology

RECEIVED 26 May 2022
ACCEPTED 27 February 2023
PUBLISHED 09 March 2023

CITATION
Siransy LK, Dasse RS, Adou H, Kouacou P, Kouamenan S, Sekongo Y, Yeboah R, Memel C, Assi-Sahoin A, Moussa SY, Oura D and Seri J (2023) Are IL-1 family cytokines important in management of sickle cell disease in Sub-Saharan Africa patients? *Front. Immunol.* 14:954054. doi: 10.3389/fimmu.2023.954054

Are IL-1 family cytokines important in management of sickle cell disease in Sub-Saharan Africa patients?

Liliane K. Siransy[1,2*], Romuald S. Dasse[1], Honoré Adou[1], Patricia Kouacou[1], Sidonie Kouamenan[2], Yassongui Sekongo[2], Richard Yeboah[1], Charlene Memel[3], Aniella Assi-Sahoin[1], Salimata Y. Moussa[2], Doris Oura[2] and Jocelyne Seri[1]

[1]Immunology–Allergology Department, Medical Sciences, Felix Houphouet Boigny University, Abidjan, Côte d'Ivoire, [2]Transfusional therapeutic department, National Blood Transfusion Center, Abidjan, Côte d'Ivoire, [3]Immunology Department, CHU Bouake, Alassane Ouattara University, Bouake, Côte d'Ivoire

Introduction: Sickle cell disease (SCD) is the most common genetic disease found in Africa and throughout the world. It is responsible for a high rate of hemolysis, systemic inflammation, and modulation of the immune system with the involvement of immunological molecules, such as cytokines. IL-1β is a major inflammatory cytokine. IL-18 and IL-33, members of IL-1 family, also exhibit characteristics of inflammation-related cytokines. Thus, in order to contribute to the evaluation of the severity and prognosis of SCD in Africa, this study aimed to estimate the cytokine response, in particular the levels of cytokines of the IL-1 family, in sickle cell patients living in a Sub-Saharan country.

Methods: Ninety patients with a diagnosis of SCD were recruited with different hemoglobin types. Samples were assessed for cytokine levels using the Human Inflammation Panel assay from BioLegend. The assay allows the simultaneous quantification of 13 human inflammatory cytokines/chemokines, i.e., IL-1β, IFN-α2, IFN-γ, TNFα, MCP-1 (CCL2), IL-6, IL-8 (CXCL8), IL-10, IL-12p70, IL-17A, IL-18, IL-23, and IL-33.

Results and discussion: the assessment of plasma cytokines in SCD patients revealed significantly increased levels of IL-1 family cytokines in crisis compared to steady state, suggesting a substantial involvement of these cytokines in clinical exacerbation. This suggests the possibility of a causal effect in the SCD pathology and can open the way to define better care, pointing toward new therapeutic avenues for sickle disease in Sub-Saharan Africa.

KEYWORDS

sickle cell disease, cytokines, IL-1, IL-18, IL-33, Africa, chemokines

1 Introduction

Sickle cell disease (SCD) is the most common genetic disease in Africa, more than 23 countries in West and central Africa and throughout the world (1). Increasing global migration has introduced SCD into many areas where they were not originally endemic (1, 2), so that the disease has been designated by the World Health Organization (WHO) and United Nations as a global public health problem (1, 3). SCD is characterized by the formation of a particular hemoglobin called hemoglobin S (HbS), generated a single point mutation in the β globin chain of hemoglobin (Hb) that causes the substitution of the glutamate at position 6 with a valine (4). People who inherit the abnormal gene from both parents are homozygotes (SS or SSFA2) and develop SCD (5).

Other types of abnormal hemoglobin are frequently associated with HbS, e.g., hemoglobin C (HbC). Individuals with both HbS and HbC are heterozygotes HbSC (SC). Although the clinical complications of hemoglobin C disease are not severe, inheritance with other abnormal hemoglobin such as hemoglobin S may have significant consequences (6). Another frequent association described (SFA2*)* is the inheritance a thalassemia defect on one β gene that reduces the production of hemoglobin associated with the β S gene. Despite our understanding of the molecular basis and pathophysiology of these diseases, the burden is still heavy, particularly in countries that have medical settings with limited resources (4, 7).

The sickle cell gene is present in 10-45% of the population in many countries, resulting in an estimated prevalence of at least 2% (1). Clinical manifestations of SCD are of three main categories: chronic hemolytic anemia, vaso-occlusive phenomena and extreme susceptibility to infections that varies greatly from one individual to another. Deaths from SCD complications occur mostly in children under five, adolescents and pregnant women (1). Infant morbidity and mortality associated with SS homozygosity is very high among African children (50-90%) (8) and, under the age of five, it is related to acute, chronic and severe complications (9–11).

Inflammation is a fundamental component in SCD. HbS polymerization under deoxygenation conditions causes the red blood cells to adopt their characteristic sickle shape. This predisposes red cells to numerous intracellular and membrane alterations that make them more adhesive. Therefore, they interact with endothelial cells, activated neutrophils and platelets. Sickled red cells also release heme, which is highly inflammatory, and numerous other molecules with inflammatory potential, such as ATP, Cyclophilin A, and extracellular DNA (12). These molecules act as damage-associated molecular patterns (DAMPs) and participate in the activation of the innate immune system and the coagulation system. All these events participate in the chronic inflammatory processes in the SCD leading to numerous complications.

A very serious and dramatic complication is stroke, which causes severe motor and neurocognitive sequelae. The cerebrovascular accident exists in all forms of SCD (SS, SC, SFA2) ranging from 1.2 to 12% of prevalence according to the age of the patient and the country (13). By the age of 45, about 25% of patients have suffered an apparent stroke even with chronic transfusion therapy or a normal transcranial doppler (TCD) (13–15). In addition, after a first stroke, silent cerebral infarcts can occur despite regular blood transfusions (14). Although in SCD the incidence of first clinical stroke has fallen over the past decades in the USA and Europe, this is still a highly prevalent matter of concern in Africa, where the majority of people with this condition live. Prevention and care of stroke as well as other complications have been largely neglected in Africa. To improve quality of life, prevention and early recognition *via* cytokines may be a key to decrease morbidity and mortality in SCD. The involvement of immune reactions and their effector molecules, such as the cytokine response in SCD, are of increasing interest, due to cytokines' capacity to drive acute and chronic inflammatory states, thereby contributing to the pathology of SCD (16–18). Several cytokines and chemokines are involved in the chronic inflammatory state in SCD patients. Increased IL-1α and IL-1β are reported in SCD, which trigger inflammatory reactions leading to primary leukocyte recruitment, endothelial cell activation and production of other many inflammatory mediators, in particular IL-8. IL-8 is a very important chemokine, which facilitates the recruitment of leukocytes, such as neutrophils and eosinophils, to blood vessel walls (19, 20). The increased production of inflammatory cytokines could contribute to the pathophysiology of the disease and can be responsible for the damage to the different organs and the occurrence of common cyclic events in sickle cell patients (17, 21). Insightful understanding of the correlation between inflammatory mediators, such as cytokines, and stroke or other organ damage may provide new biomarkers or therapeutic approaches for SCD management.

Cytokines of the IL-1 family have multiple local and systemic effects, which regulate both innate and adaptive immune responses. Many IL-1 family cytokines have inflammatory activity (IL-1α, IL-1β, IL-18, IL-36α, IL-36β, IL-36γ), while others are mainly anti-inflammatory (IL-1Ra, IL-33, IL-36Ra, IL-37, IL-38) (22). IL-1β is a major inflammatory cytokine that has been associated with exacerbation of injury in stroke, but that was shown to exert both deleterious and protective functions in stroke (19).

Most studies involving cytokines have been conducted in high income countries. Unfortunately, in West Africa, access to such analysis is not possible due to lack of well-equipped infrastructures, absence of standardized management and too few skilled immunologists.

To our knowledge, very few studies have investigated the cytokines association with SCD in our area. This study is the first one done in sickle cells patients in Côte d'Ivoire and will help the evaluation of the significance of cytokines, in particularly those belonging to the IL-1 family, in the management, severity and prognosis of SCD in Sub-Saharan Africa.

2 Material and methods

2.1 Study population

This is a prospective case-control study of a population of 90 patients with SCD, aged 4 to 55 years, and followed at the

Therapeutic and Research Unit of the National Blood Transfusion Center in Abidjan, Côte d'Ivoire. It was conducted after approval by the national ethics committee (n°44_2018-SIHIOTS). Informed consents were obtained from the patients' parents or legal guardians before patients were enrolled in this study.

Patients were divided into two groups: patients admitted for crisis for and steady state patients.

Steady state was defined as a state without pain, illness, or infection during the last three months before the study; this group represents our control group compared with the crisis group.

The profile of homozygous or heterozygous sickle cell patients was determined by hemoglobin electrophoresis on cellulose acetate strips (pH 9.2).

Patients with crisis were admitted to the Unit, while those who were asymptomatic, i.e., at steady stat,e were present to the Unit of Therapeutic Transfusion for routine monitoring. Crisis was defined as an episode of acute diffuse pain with infection or anemia, requiring hospitalization and/or analgesic administration. Clinical investigations were evaluated by a specialist in hematology. Cytokine levels were compared in steady-state and crisis patients according to the type of hemoglobin and the complications. All subjects were from West African countries: Côte d'Ivoire, Ghana, Guinea, Mali, Nigeria and Togo.

2.2 Cytokine analysis

Blood samples were collected by venipuncture in EDTA tubes for basic determination of hematological indices and for cytokine dosage.

The blood count was obtained with an automated hematological cell count machine (Sysmex XN 550). Plasma was extracted by centrifugation at 1000xg at 4°C for 10 min and stored at -30°C for cytokine assays.

Before assay, samples were thawed, mixed and centrifuged, then assessed for cytokine levels using the BioLegend LEGENDplex™ Human Inflammation Panel assay (Cat. N°740118), an immunoassay based on immunofluorescent beads. The assay allows the simultaneous quantification of 13 human inflammatory cytokines/chemokines, i.e., IL-1β, IFN-α2, IFN-γ, TNFα, MCP-1 (CCL2), IL-6, IL-8 (CXCL8), IL-10, IL-12p70, IL-17A, IL-18, IL-23, and IL-33. The assay was performed in the BioLegend laboratory in San Diego, CA, USA.

All samples were processed and analyzed on the same day of thawing. A minimum of cytokine-specific 3000 beads were acquired with a BD FACSCalibur™ cytometer. Controls provided by the manufacturer were used. Data analysis was performed using LEGENDplex™ Data Analysis Software.

2.3 Statistical analysis

All results are expressed as mean ± SD. Data were analyzed using the SPSS version 22.0 program (SPSS Inc., Chicago, IL, USA). Statistical results with a p value ≤ 0.05 were significant.

For the comparison of cytokine means, we first used the Levene test to determine the equality of variances: if the Levene test was not significant ($p > 0.05$), we had an equality of variances and used the Student t-test for the 2-modality variables and the ANOVA test for the more than 2-modality variables. If the Levene test was significant (p ¾ 0.05), we had a variance inequality and in this case we use nonparametric tests such as the Mann-Whitney U test for the 2-modality variables and the Kruskal-Wallis for variables with more than 2 modalities.

3 Results

3.1 Biometric and epidemiological characteristics of sickle cell patients by clinical status

Ninety (90) patients with a diagnosis of SCD, comprising 48 women (53.3%) and 42 men (42.70%) were recruited.

Among the sickle cell patients, 34 (37.8%) were in steady state phase and represented our stable controls, while 56 (62.2%) were in crisis and represented the cases.

Our SCD patients show in general a low body mass index BMI (Table 1). We find an average BMI of 20.74 kg/m^2 ± 2.82 in SCD patients in crisis versus 20.24 kg/m^2 ± 5.63 in SCD patients in steady state phase. Few patients were overweight, and none was obese.

Cerebral stroke was found in 45.95% followed by leg ulcer (27.03%) and osteonecrosis (10.81%). Other complications such as heart disease, splenomegaly and hyperviscosity were found in patients in our study with prevalence of 5.41% (Figure 1). The minimum age for stroke patients was 7 years, with an average of 21 years and a maximum of 37 years.

3.2 Biological characteristics

3.2.1 Type and levels of hemoglobin and white blood cells

Regarding hemoglobin type, 46 were homozygous Hb SS (SSFA2) (51.1%), 28 were heterozygous SFA2 (31.1%) and 16 were Hb SC (17.8%) (Table 1).

SCD was associated with a decrease in the hemoglobin level in the 2 groups, steady state and crisis (8.7 ± 2 and 8.5 ± 2.1 g/l, respectively), compared to the normal blood level of hemoglobin but showing a non-significant difference ($p = 0.64$) (Table 1).

No significant difference was observed for white blood cells and leukocyte subpopulations for SCD in steady state phase or during crisis.

3.2.2 Cytokines in steady state and crisis

Thirteen cytokines were measured in our SCD patients. Three cytokines of the IL-1 family were assessed, i.e., IL-1β, IL-18 and IL-33. We have compared their levels to those of the most studied cytokines in SCD, i.e., TNFα, IL-6, IL-8 and IL-10. They were all increased in the crisis group except IL-10 and IL-33, with TNFα and

10.3389/fimmu.2023.954054

TABLE 1 Demographic and hematological characteristics of sickle cell patients.

Parameter	Steady state	Crisis	*p* value
Age (years) *			
All patients	20.9 ± 14.6 (4–50)	27.3 ± 13.1 (4–55)	0.09
4-9	6.3 ± 2.1	6.6 ± 1.7	
10-19	17.5 ± 0.7	15.1 ± 3.6	
20-29	23.6 ± 3.4	23.5 ± 3.2	
30-39	33.5 ± 4.4	34.5 ± 3.1	
40-55	44.3 ± 4.3	48.2 ± 4.4	
Sex ratio (M/F)	30.7	1.0	
BMI (kg/m^2) *	20.2 ± 5.6 (7.6-27.3)	20.7 ± 2.8 (13.7-26.2)	0.36
Hemoglobin (g/l) *	8.7 ± 2.0 (5.6-3.1)	8.5 ± 2.1 (4.8-14.3)	0.64
Hemoglobin type (%) **			
SSFA2(SS)	51	51.2	0.96
SFA2	29.4	32.8	0.68
SC	19.6	16	0.42
WBC (cells/µl) *	10431.3 ± 4631.4 (5100–18600)	10393.5 ± 4129.4 (3600-20600)	0.97
Lymphocytes (cells/µl) *	3691.2 ± 1305.7 (1769.7-5952)	4248.2 ± 1482.9 (1945.8-8049.6)	0.09
Neutrophils (cells/µl) *	5521.8 ± 3432.2 (623-11346)	5078.7 ± 1852.6 (1427.4-8793.4)	0.56
Monocytes (cells/µl) *	1225.1 ± 858 (316.2-4018)	1375.7 ± 2003.7 (285.2-10046.4)	0.69

*Mean ± SD (min-max).
**Mean percentage of hemoglobin types among all SCD patients (steady state and crisis) were: SSFA2, 51.1%; SFA2, 31.1%; SC, 17.8%.

IL-10 not reaching statistical significance (Table 2). By contrast, anti-inflammatory IL-33 and IL-10 were decreased in the crisis group, with significant difference for IL-33 (Table 2). Other cytokines (IFN-α2, IFN-γ, MCP-1, IL-12p70 and IL-17A, IL-23) were detected, which however did not differ between groups (Supplementary Table 1).

We also compared the mean levels of circulating cytokines in patients during crisis with those in steady state relative to the type of hemoglobin (Table 3).

In SSFA2 patients, a significantly a lower level was measured for IL-33 (p=0.000096) during crisis. In SFA2 patients, a higher level was observed for IL-1β (p=0.02) during crisis. In SC patients, higher

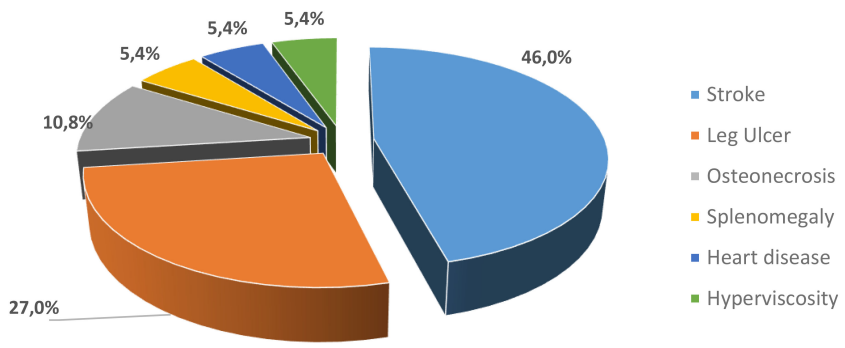

FIGURE 1
Frequency of complications in our SCD patients .

TABLE 2 General cytokines profile of the SCD patients.

Cytokines *(pg/ml)*	Steady state *mean ± SD (min-max)*	Crisis *mean ± SD (min-max)*	*p* value
IL-1β	3.50 ± 6.65 (0.00-27.26)	43.21 ± 181.42 (0.00-974.33)	0.03
IL-18	667.82 ± 1049.31 (48.76-2879.67)	1433.02 ± 1901.54 (96.18-9130.03)	0.01
IL-33	13.42 ± 29.18 (0.00-93.23)	6.13 ± 13.60 (0.00-28.45)	0.04
IL-6	53.26 ± 121.18 (0.00-473.4)	506.17 ± 2461.94 (0.00-13059.41)	0.01
IL-8	294.17 ± 671.05 (0.00-10693.45)	1133.98 ± 2602.06 (0.00-12000)	0.0024
IL-10	14.23 ± 25.73 (0.00-96.04)	8.78 ± 12.20 (0.00-57.85)	0.1
TNFα	2.03 ± 2.81 (0.00-15.08)	3.36 ± 9.80 (0.00-49.91)	0.2

level of IL-18 (p=0.01) and lower values for IL-33 (p=0.000029) were observed during crisis.

3.2.3 Cytokines in SCD complications

Complications have been observed in our SCD patients. Stroke was the most important (46%), followed by leg ulcer (27%) and osteonecrosis (10.8%) (Figure 1).

IL 1β and IL-18 were increased in stroke (p<0.001 stroke vs. steady state), while IL-33 was decreased (p<0.05 stroke vs. steady state) (Figure 2). In patients with osteonecrosis there was a tendency towards decreased levels of all three cytokines compared to steady state, which however did not reach statistical significance (Figure 2). In patients with leg ulcers the three cytokine levels did not significantly differ from those in steady state, although there was

TABLE 3 Comparison of circulating cytokines for HbSSFA2, HbSFA2 and HbSC steady state and crisis patients.

Cytokine *(pg/ml)*	Hb Type	Steady state *mean ± SD (min-max)*	Crisis *mean ± SD (min-max)*	*P value*
	SSFA2	9.3 ± 16.7 (0-27.3)	6.74 ± 13.1 (0-46.1)	0.28
IL-1β	SFA2	2.0 ± 1.4 (0-3.7)	60.4 ± 221.8 (0-974.3)	0.02
	SC	3.6 ± 4.2 (0-10.8)	1.9 ± 2.7 (0-6.6)	0.21
	SSFA2	868.6 ± 1388.8 (96.2-2879.7)	1394.7 ± 1337.5 (95.3-4091.3)	0.16
IL-18	SFA2	728.1 ± 749.7 (48.8-1759.2)	1388.3 ± 2069.8 (167.3-6806)	0.19
	SC	298.3 ± 256.8 (106.1-774.8)	1941.6 ± 4018.5 (120.1-9130)	0.01
	SSFA2	26.2 ± 38.2 (0-93.2)	3.0 ± 9.0 (0-29.4)	0.000096
IL-33	SFA2	4.6 ± 8.5 (0-18.4)	3.6 ± 9.3 (0-28.5)	0.33
	SC	34.7 ± 19.6 (0-46.2)	0.0 ± 0.0	0.000029
	SSFA2	2.0 ± 4.2 (0-15.8)	2.7 ± 3.3 (0-9.3)	0.28
TNFα	SFA2	0 ± 0	2.6 ± 11.5 (0-49.9)	0.23
	SC	4.8 ± 4.7 (0-10)	2.6 ± 2.3 (0-4.7)	0.11
	SSFA2	69.6 ± 158.1 (0-473.4)	41.8 ± 82.4 (0-309.1)	0.21
IL-6	SFA2	22.0 ± 46.5 (0-28.7)	2618.1 ± 55.0 (0-13059.4)	0.000035
	SC	14.1 ± 16.2 (0-28.1)	55.1 ± 84.8 (0-230.7)	0.12
	SSFA2	640.9 ± 1110.6 (3.5-3499.8)	1662.1 ± 3630.1 (0-12000)	0.0042
IL-8	SFA2	492.2± 1126.1 (0-10693)	2413.8 ± 5052.4 (0-344.5)	0.15
	SC	172.3 ± 198.9 (0-344.5)	345.2 ± 438.2 (3.3-1124.5)	0.12
	SSFA2	12.2 ± 17.7 (0-56.5)	8.8 ± 14.1 (1.8-57.9)	0.23
IL-10	SFA2	10.6 ± 14.5 (0-36.9)	9.3 ± 11.1 (0-29.8)	0.43
	SC	19.1 ± 36.1 (0-96.0)	5.1 ± 5.9 (0-11.9)	0.22

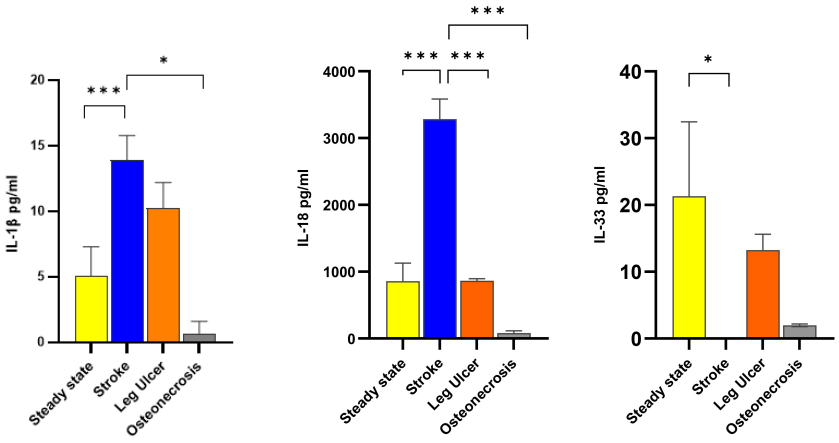

FIGURE 2
Comparison of IL-1 cytokine levels according to the 3 most common complications Cytokines levels were assessed in steady state SCD patients (34 patients; yellow columns), in crisis patients with stroke (17 patients; blue columns), in leg ulcers (10 patients; orange columns) and in osteonecrosis (4 patients; grey columns). Data are presented as mean pg/ml ± SD of IL-1β (left panel), IL-18 (center panel) and IL-33 (right panel). Statistical significances for complications vs. steady state were found for IL-1β (stroke vs. steady state, stroke vs. osteonecrosis), IL-18 (steady state vs. stroke, stroke vs. leg ulcer, stroke vs. osteonecrosis) and IL-33 (steady state vs stroke.). * p<0.05; *** p<0.001.

a tendency towards decrease (Figure 2). For the other cytokines, no significant difference was found (Supplementary Figure 1).

We also compared cytokines by type of crisis (hemolytic anemia, HA; vaso-occlusive crisis, VOC).

Among the crisis, HA accounted for 55%, followed by VOC (45%). A tendency (not statistically significant) towards higher levels of IL-1β, IL-6, IL-8, and TNFα and lower levels of IL-10 were observed in HA, compared to steady state, while IL-18 tended to be higher in VOC (Figure 3).

Discussion

In the present study, assessment of plasma cytokines in SCD patients revealed measurable circulating levels of the IL-1 family cytokines in both clinical presentations, crisis, and steady state (Table 2). We consider the cytokine levels in plasma of SCD patients in steady state as a benchmark, in order to assess the variations during crisis or with complications. How much these values compare to cytokine levels of healthy subjects is currently unknown (study ongoing), although from previously published data steady state SCD patients seem to have increased levels of IL-6, IL-8 and IL-18 (which in normal subjects are ≤ 10 pg/ml for IL-6 and IL-8, and around 200 pg/ml for IL-18), suggesting a partially upregulated inflammatory level in steady state SCD. Variability of conditions in different geographical settings and differences in detection assays makes impossible any quantitative comparison with data from other studies (23).

Patients in crisis showed higher levels of the inflammatory cytokines IL-1β, IL-6, IL-8 and IL-18 compared to those in steady state conditions and decreased levels of the anti-inflammatory factor IL-33 (Table 2). Differences were not statistically significant for IL-10 and TNFα.

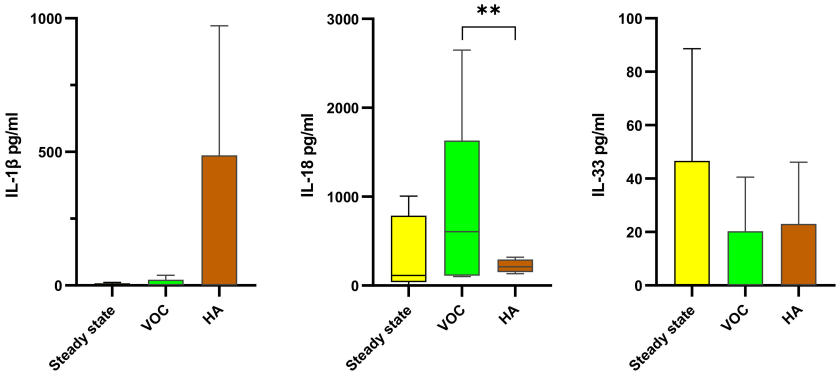

FIGURE 3
Comparison of IL-1 family cytokines according to the type of crisis in SCD patients The levels of IL-1β (left), IL-18 (center) and IL-33 (right) in SCD patients were compared between steady state (34 patients; yellow boxes), vaso-occlusive crisis (VOC; 24 patients; green boxes) and hemolytic anemia (HA; 32patients; brown boxes). Data are presented as median values and interquartile range in pg/ml. Statistical analysis was performed using Kruskal-Wallis. ** p<0.01 VOC, vaso-occlusive crisis; HA, hemolytic anemia.

IL-1β is a key mediator of the inflammatory response and shows a huge complexity. In addition to being essential for host response and resistance to pathogens, it also exacerbates the damage caused by chronic disease and acute tissue injury, as is the case in SCD (16, 24). Our study shows a significant increase of IL-1β levels in crisis subjects (p=0.03). The values found in sickle cell patients in crisis were 10 times greater compared with the steady state, suggesting an involvement of this cytokine in SCD crisis. Our values are similar to those observed by Pitanga et al., who found low IL-1β levels (below 10 pg/ml) both in normal children and in steady state SCD patients (18). The substantial increase in crisis patients that we have observed is in contrast to the data of Pathare et al., who found no change between steady state and crisis levels (24). It should be noted that the circulating IL-1β levels in healthy subjects reported in that study are exceedingly high and different from the low-undetectable levels commonly observed in healthy people (18, 25, 26), thus posing some questions on the reliability of the detection assay.

Although IL-1β has been well characterized, IL-18 and other members of the IL-1 family are less so (27, 28). In our study, IL-18 was detected at high levels both in steady state and, at even higher levels, during crisis. A study suggested a possible role for IL-18 in the physiopathology of crisis in SCD (29). High levels of IL-18 have been associated with high levels of LDH and uric acid, and patients with these indicators have poor prognosis (29). It should be noted that IL-18 is not an exclusively inflammatory cytokine (28). Its circulating levels are well detectable in healthy subjects and increase in essentially all inflammatory conditions (25, 28). IL-18 is an established biomarker of heart failure, so that it has been proposed that anti-IL-18 treatment may have therapeutic effects in patients with SCD at risk for cardiac arrhythmias and adverse outcomes (30).

Interleukin-33 (IL-33), another member of the IL-1 cytokine family, is widely expressed by various tissues, such as smooth muscle cells, epithelial cells, fibroblasts, and keratinocytes. IL-33 is mainly involved in type 2 inflammation, alternative to classical type 1 inflammation, and has anti-inflammatory protective effects in many diseases (31–33). In our study, IL-33 was significantly higher in steady state (Table 2). IL-33 has been proposed as a novel contributor to anemia in inflammatory disease through its effects on differentiation of erythroid cells and as a therapeutic target for this type of patients (34). This cytokine has been rarely investigated in SCD. A link between hemolysis and IL-33 has been proposed, although results might be biased by the fact that the evaluation was performed on stored red blood cells (35). In our study, IL-33 seems to behave as an anti-inflammatory cytokine. This may be due to the heterogeneity of patient genotypes, treatment, environmental impact, socio-economic status, nutrition, the presence of other associated inflammatory factors such as infections or other inflammatory stress and genetic polymorphism (36, 37).

SCD is characterized by common acute and chronic complications. In our study, five types of complications have been identified: stroke (46%), leg ulcer (27%), osteonecrosis (10.8%), hyperviscosity (5.4%), heart disease (5.4%), and splenomegaly (5.4%) and no patient has no more than one complication.

Stroke was the most important complication in our study and in other regions of the world (13) as it is a devastating complication and an important cause of death in SCD. Between 5 and 17% of SCD patients will suffer a first stroke during childhood or adolescence in the absence of screening and prophylactic treatment (10, 11, 13). The minimum age of stroke of our patients in our study was 7 years, a quite young age, and this could be explained by the precariousness of the management, lack of access to care, and inadequate plans for the management of sickle cell children (1). IL-1β has been associated with exacerbation of injury in stroke and has been implicated in the pathogenic processes associated with a number of central nervous system disorders (38–40), while IL-6 and IL-10 have been found to be neuroprotective (38). The mechanism by which IL-1β affects seizure is unknown. It is known that IL-1β administered with the excitatory neurotransmitter AMPA (α-amino-3-hydroxy-5-methyl- 4-isoxazole propionic acid) produces a widespread cortical cell death (38). Also, recent work in a murine model with SCD has shown that Interleukin-1 receptor inhibition reduced the size of stroke (41). Although there are indications of a detrimental role of IL-1β, a study showed that an increased IL-1β concentration was linked with protection from stroke development in HbSS children with abnormal transcranial doppler (TCD) (19). IL-1β has been therefore qualified as both beneficial and deleterious in cerebral ischemia depending on its plasma levels. Protective concentration ranges should be well identified to benefit from this predictive biomarker in the management of cerebrovascular events in SCD (19). This suggests that plasma IL-1β levels in combination with TCD measurements may be used to improve evaluation of stroke risk in HbSS patients, by early identification of those needing intensive prophylactic interventions, especially as these strokes can be asymptomatic or silent.

Sickle cell leg ulcers came in second position in our study (27.03%). It is the most important common cutaneous complication in SCD, severe, chronic, and disabling with intense and continuing pain (42). There is no official recommendations for treatment and a high rate of relapse (42). No significant differences was found for IL-1β or for any other cytokine, suggesting that these cytokines are not useful predictors for poor outcomes (Supplementary Figure 1) (43).

Osteonecrosis was the third most frequent complications in our study, with a prevalence of 10.81%. It is a form of ischemic bone injury that leads to degenerative joint disease, and SCD is an important cause of its occurrence (44). An estimated 50% of adults will develop an osteonecrosis by age 35 years old (45). The circulating IL-33 concentration is considered a biomarker of avascular necrosis of the femoral head in patients without SCD, since increased IL-33 levels correlate with osteonecrosis of the femoral head (46, 47). In our study, the IL-33 values in patients with osteonecrosis were very low, thus discounting this marker as an element of early diagnosis and progression of osteonecrosis. Our findings are consistent with those of Agrawal et al. in India (46), in which IL-33 plasma levels did not correlate with osteonecrosis of the femoral head in patients with SCD.

We also presented the results according to the hemoglobin type and the clinical status at the time of the blood sampling, to find a correlation between the hemoglobin type, the level of cytokines and the crisis (Table 3). Relative to the cytokines of the IL-1 family, significant differences between crisis and non-crisis states were found for phenotypes SFA2 (IL-1β), SSFA2 (IL-33) and SC (IL-18, IL-33). It is however difficult to determine an influence or a cause-effect correlation.

The clinical manifestations of SCD are multifaceted but we investigated the major features: vaso-occlusive (VOC) and hemolytic anemia (HA). In our study, HA was the most common with 55% followed by the VOC (45%). The lower frequency of VOC compared to other studies (48, 49) may be explained by the fact that VOC are mostly managed at home by patients and often not reported (50). We noted a tendency towards higher levels of IL-1β, IL-6, IL-8 and TNFα in HA compared to VOC, which however did not reach statistical significance, while IL-18 and IL-10 are significantly higher in VOC. None of them was however statistically different from the steady state levels. Since hemolysis triggers inflammation and participates in numerous multisystemic complications of SCD (51), and red blood cells could play a role in cytokine signaling (52), this could explain why inflammation-related cytokines are higher in HA. Conversely, the anti-inflammatory cytokine IL-10 was significantly increased in VOC compared to HA, in agreement with other studies (53, 54). The fact that IL-18 was also higher in VOC underlines the notion that this is not a classically inflammatory cytokine and supports previous indirect data hypothesizing the involvement of IL-18 in vascular occlusion in SCD (28). Furthermore, data in SCD mice showed that IL-18 is strongly involved in the entire process of leucocyte recruitment in VOC, while IL-1β is only involved in the late steps of the process (55).

Therapeutic options for SCD are limited to hematopoietic stem cell transplantation, which is a curative option but not available for our countries due to its high cost and the lack of resources. Therefore, anti-inflammatory drugs are important for us because they can neutralize key players in the SCD inflammatory scenario. Many are currently under investigation as potential therapeutics, and agents such as antibodies to anti-IL-1β, the IL-1 receptor antagonist or the IL-18 binding protein are expected to provide benefits for these patients (12).

In conclusion, few studies in Sub-Saharan countries describe the cytokine levels in SCD patients. Our data emphasize the role of inflammation in SCD in crisis, suggesting an important involvement of inflammation-related cytokines in the dynamics of SCD.

IL-1 family members are poorly studied in SCD, even though these cytokines are key mediators of the inflammatory response that enhances the damage caused by SCD. IL-1 family cytokines deserve further consideration with larger cohorts, as they can be useful predictors of poor or favourable outcome, depending on the circumstances. A better knowledge of these cytokines in the evolution of SCD in African countries, considering the specific aspects of patients' management due to extrinsic factors (such as the environment, access to care, socio-economic status), will improve survival and increase the quality of life of these patients in low-income countries.

Data availability statement

The original contributions presented in the study are included in the article/Supplementary Material. Further inquiries can be directed to the corresponding author.

Ethics statement

The studies involving human participants were reviewed and approved by Ethic Commitee of Faculty of Medecine-SIHIOTS 044_2018-sihiots. Written informed consent to participate in this study was provided by the participants' legal guardian/next of kin.

Author contributions

LS conceived and designed the experiments, conducted all the experiments, analyzed, and interpreted the data, assembled all the figures, supervised the study, and wrote the manuscript. RD co-supervised the study, contributed to the scientific discussion, and wrote the manuscript. HA contributed to the scientific concept, revised the manuscript, contributed to data interpretation, and performed the statistical analysis. YS, SK, AA-S, SM, DO and JS contributed to obtaining clinical data, and organized and implemented sample management. PK, RY and CM analyzed data and critically revised the manuscript. All authors contributed to the article and approved the submitted version.

Acknowledgments

We would like to thank all sickle cell patients who agreed to participate in this study. We acknowledge the help from the Immunology Department of Abidjan, Bouake, and the Therapeutic Unit of the National Blood Transfusion Center. We are particularly grateful to the staff of the BioLegend HQ facility in San Diego for help and assistance for immunocytometry evaluations, especially Drs Shaoquan Ji and Binggang Sun.

Conflict of interest

The authors declare that the research was conducted in the absence of any commercial or financial relationships that could be construed as a potential conflict of interest.

Publisher's note

Supplementary material

The Supplementary Material for this article can be found online at: https://www.frontiersin.org/articles/10.3389/fimmu.2023.954054/full#supplementary-material

References

1. Regional Committee for Africa 60. Sickle-cell disease: a strategy for the WHO African region, in: *Report no.: AFR/RC60/8. disponible sur* (2011). Available at: https://apps.who.int/iris/handle/10665/1682 (Accessed 19 déc 2022).

2. Conseil exécutif 118. Thalassémie et autres hémoglobinopathies : rapport du secrétariat, in: *Report no.: EB118/5. disponible sur* (2006). Organisation mondiale de la Santé. Available at: https://apps.who.int/iris/handle/10665/22195 (Accessed 19 déc 2022).

3. CDC. What is sickle cell disease?, in: (2022).CDC Centers for Disease Control and Prevention. Available at: https://www.cdc.gov/ncbddd/sicklecell/facts.html (Accessed 19 déc 2022).

4. Brandow AM, Liem RI. Advances in the diagnosis and treatment of sickle cell disease. *J Hematol OncolJ Hematol Oncol* (2022) 15(1):20. doi: 10.1186/s13045-022-01237-z

5. Hurley R. CHAPTER 46 - anemia and red blood cell disorders, in: *Immigrant medicine* (2007). Edinburgh: W.B. Saunders. Available at: https://www.sciencedirect.com/science/article/pii/B9780323034548500504 (Accessed 19 déc 2022).

6. Karna B, Jha SK, Al Zaabi E. Hemoglobin c disease, in: *StatPearls* (2022). Treasure Island (FLStatPearls Publishing. Available at: http://www.ncbi.nlm.nih.gov/books/NBK559043/ (Accessed 19 déc 2022).

7. McGann PT, Nero AC, Ware RE. Clinical features of β-thalassemia and sickle cell disease. *Adv Exp Med Biol* (2017) 1013:1–26. doi: 10.1007/978-1-4939-7299-9_1

8. Grosse SD, Odame I, Atrash HK, Amendah DD, Piel FB, Williams TN. Sickle cell disease in Africa: A neglected cause of early childhood mortality. *Am J Prev Med déc* (2011) 41(6 Suppl 4):S398–405. doi: 10.1016/j.amepre.2011.09.013

9. Guédéhoussou T, Gbadoé AD, Lawson-Evi K, Atakouma DY, Ayikoé AK, Vovor A, et al. .

10. Platt OS, Brambilla DJ, Rosse WF, Milner PF, Castro O, Steinberg MH, et al. Mortality in sickle cell disease. life expectancy and risk factors for early death. *N Engl J Med* (1994) 330(23):1639–44. doi: 10.1056/NEJM199406093302303

11. Platt OS. Preventing stroke in sickle cell anemia. *N Engl J Med* (2005) 353 (26):2743–5. doi: 10.1056/NEJMp058274

12. Conran N, Belcher JD. Inflammation in sickle cell disease. *Clin Hemorheol Microcirc* (2018) 68(2–3):263–99. doi: 10.3233/CH-189012

13. Kirkham FJ, Lagunju IA. Epidemiology of stroke in sickle cell disease. *J Clin Med* (2021) 10(18):4232. doi: 10.3390/jcm10184232

14. Hulbert ML, McKinstry RC, Lacey JL, Moran CJ, Panepinto JA, Thompson AA, et al. Silent cerebral infarcts occur despite regular blood transfusion therapy after first strokes in children with sickle cell disease. *Blood* (2011) 117(3):772–9. doi: 10.1182/blood-2010-01-261123

15. Ware RE, Davis BR, Schultz WH, Brown RC, Aygun B, Sarnaik S, et al. Hydroxycarbamide versus chronic transfusion for maintenance of transcranial doppler flow velocities in children with sickle cell anaemia-TCD with transfusions changing to hydroxyurea (TWiTCH): A multicentre, open-label, phase 3, non-inferiority trial. *Lancet Lond Engl* (2016) 387(10019):661–70. doi: 10.1016/S0140-6736(15)01041-7

16. Makis AC, Hatzimichael EC, Bourantas KL. The role of cytokines in sickle cell disease. *Ann Hematol* (2000) 79(8):407–13. doi: 10.1007/s002770000173

17. Olenscki Gilli SC, Pericole FV, Benites BD, Sippert EÂ, Castilho LM, Addas-Carvalho M, et al. Cytokine polymorphisms in sickle cell disease and the relationship with cytokine expression. *Exp Hematol* (2016) 44(7):583–9. doi: 10.1016/j.exphem.2016.03.008

18. Pitanga TN, Oliveira RR, Zanette DL, Guarda CC, Santiago RP, Santana SS, et al. Sickle red cells as danger signals on proinflammatory gene expression, leukotriene B4 and interleukin-1 beta production in peripheral blood mononuclear cell. *Cytokine* (2016) 83:75–84. doi: 10.1016/j.cyto.2016.03.016

19. Asare K, Gee BE, Stiles JK, Wilson NO, Driss A, Quarshie A, et al. Plasma interleukin-1beta concentration is associated with stroke in sickle cell disease. *Cytokine* (2010) 49(1):39–44. doi: 10.1016/j.cyto.2009.10.002

20. Qari MH, Dier U, Mousa SA. Biomarkers of inflammation, growth factor, and coagulation activation in patients with sickle cell disease. *Clin Appl Thromb Off J Int Acad Clin Appl Thromb* (2012) 18(2):195–200. doi: 10.1177/1076029611420992

21. Iughetti L, Bigi E, Venturelli D. Novel insights in the management of sickle cell disease in childhood. *World J Clin Pediatr* (2016) 5(1):25–34. doi: 10.5409/wjcp.v5.i1.25

22. Striz I. Cytokines of the IL-1 family: Recognized targets in chronic inflammation underrated in organ transplantations. *Clin Sci Lond Engl* (1979) 131(17):2241–56. doi: 10.1042/CS20170098

23. Silva-Junior AL, Garcia NP, Cardoso EC, Dias S, Tarragô AM, Fraiji NA, et al. Immunological hallmarks of inflammatory status in vaso-occlusive crisis of sickle cell anemia patients. *Front Immunol* (2021) 12. https://www.frontiersin.org/articles/10.3389/fimmu.2021.559925. doi: 10.3389/fimmu.2021.559925

24. Pathare A, Al Kindi S, Alnaqdy AA, Daar S, Knox-Macaulay H, Dennison D. Cytokine profile of sickle cell disease in Oman. *Am J Hematol* (2004) 77(4):323–8. doi: 10.1002/ajh.20196

25. Li Y, Yi JS, Russo MA, Rosa-Bray M, Weinhold KJ, Guptill JT. Normative dataset for plasma cytokines in healthy human adults. *Data Brief. avr* (2021) 35:106857. doi: 10.1016/j.dib.2021.106857

26. Kleiner G, Marcuzzi A, Zanin V, Monasta L, Zauli G. Cytokine levels in the serum of healthy subjects. *Mediators Inflamm* (2013) 2013:1–6. doi: 10.1155/2013/434010

27. Dinarello CA. Overview of the IL-1 family in innate inflammation and acquired immunity. *Immunol Rev* (2018) 281(1):8–27. doi: 10.1111/imr.12621

28. Dinarello CA, Novick D, Kim S, Kaplanski G. Interleukin-18 and IL-18 binding protein. *Front Immunol 8 oct* (2013) 4:289. doi: 10.3389/fimmu.2013.00289

29. Cerqueira BAV, Boas WV, Zanette AD, Reis MG, Goncalves MS. Increased concentrations of IL-18 and uric acid in sickle cell anemia: contribution of hemolysis, endothelial activation and the inflammasome. *Cytokine* (2011) 56(2):471–6. doi: 10.1016/j.cyto.2011.08.013

30. Gupta A, Fei YD, Kim TY, Xie A, Batai K, Greener I, et al. IL-18 mediates sickle cell cardiomyopathy and ventricular arrhythmias. *Blood* (2021) 137(9):1208–18. doi: 10.1182/blood.2020005944

31. Liew FY, Girard JP, Turnquist HR. Interleukin-33 in health and disease. *Nat Rev Immunol* (2016) 16(11):676–89. doi: 10.1038/nri.2016.95

32. Miller AM. Role of IL-33 in inflammation and disease. *J Inflammation Lond Engl* (2011) 8:22. doi: 10.1186/1476-9255-8-22

33. Guo H, Bossila EA, Ma X, Zhao C, Zhao Y. Dual immune regulatory roles of interleukin-33 in pathological conditions. *Cells 14* (2022) 11(20):3237. doi: 10.3390/cells11203237

34. Swann JW, Koneva LA, Regan-Komito D, Sansom SN, Powrie F, Griseri T. IL-33 promotes anemia during chronic inflammation by inhibiting differentiation of erythroid progenitors. *J Exp Med* (2020) 217(9):e20200164. doi: 10.1084/jem.20200164

35. Wei J, Zhao J, Schrott V, Zhang Y, Gladwin M, Bullock G, et al. Red blood cells store and release interleukin-33. *J Investig Med Off Publ Am Fed Clin Res* (2015) 63 (6):806–10. doi: 10.1097/JIM.0000000000000213

36. Gonçalves MS, Queiroz IL, Cardoso SA, Zanetti A, Strapazoni AC, Adorno E, et al. Interleukin 8 as a vaso-occlusive marker in Brazilian patients with sickle cell disease. *Braz J Med Biol Res* (2001) 34(10):1309–13. doi: 10.1590/s0100-879x2001001000011

37. Habara A, Steinberg MH. Minireview: Genetic basis of heterogeneity and severity in sickle cell disease. *Exp Biol Med Maywood NJ* (2016) 241(7):689–96. doi: 10.1177/1535370216636726

38. Allan SM, Rothwell NJ. Cytokines and acute neurodegeneration. *Nat Rev Neurosci* (2001) 2(10):734–44. doi: 10.1038/35094583

39. Shaftel SS, Griffin WST, O'Banion MK. The role of interleukin-1 in neuroinflammation and Alzheimer disease: an evolving perspective. *J Neuroinflammation.* (2008) 5:7. doi: 10.1186/1742-2094-5-7

40. Zoppo G, Ginis I, Hallenbeck JM, Iadecola C, Wang X, Feuerstein GZ. Inflammation and stroke: Putative role for cytokines, adhesion molecules and iNOS in brain response to ischemia. *Brain Pathol* (2006) 10(1):95–112. doi: 10.1111/j.1750-3639.2000.tb00247.x

41. Venugopal J, Wang J, Mawri J, Guo C, Eitzman D. Interleukin-1 receptor inhibition reduces stroke size in a murine model of sickle cell disease. *Haematologica.* (2021) 106(9):2469–77. doi: 10.3324/haematol.2020.252395

42. Granja PD, Quintão SBM, Perondi F, de Lima RBF, Martins CL de M, Marques MA, et al. Leg ulcers in sickle cell disease patients. *J Vasc Bras.* (2020) 19:e20200054. doi: 10.1590/1677-5449.200054

43. Domingos IF, Pereira-Martins DA, Sobreira MJVC, Oliveira RTD, Alagbe AE, Lanaro C, et al. High levels of proinflammatory cytokines IL-6 and IL-8 are associated with a poor clinical outcome in sickle cell anemia. *Ann Hematol* (2020) 99(5):947–53. doi: 10.1007/s00277-020-03978-8

44. Adesina OO, Neumayr LD. Osteonecrosis in sickle cell disease: An update on risk factors, diagnosis, and management. *Hematol Am Soc Hematol Educ Program* (2019) 2019(1):351–8. doi: 10.1182/hematology.2019000038

45. Milner PF, Kraus AP, Sebes JI, Sleeper LA, Dukes KA, Embury SH, et al. Sickle cell disease as a cause of osteonecrosis of the femoral head. *N Engl J Med* (1991) 325 (21):1476–81. doi: 10.1056/NEJM199111213252104

46. Agrawal AC, Mohapatra E, Nanda R, Bodhey NK, Sakale H, Garg AK. Plasma interleukin-33 cannot predict hip osteonecrosis in patients with sickle cell disease: A case-control study. *Cureus. mars* (2022) 14(3):e23556. doi: 10.7759/cureus.23556

47. Ma J, Guo W, Li Z, Wang B, Li S, Wang P. Hip osteonecrosis is associated with increased plasma IL-33 level. *Mediators Inflamm* (2017) 2017:1732638. doi: 10.1155/2017/1732638

48. Olabode JO, Shokunbi WA. Types of crises in sickle cell disease patients presenting at the haematology day care unit (HDCU), university college hospital (UCH), ibadan West Afr J med. *West Afr J Med* (2006) 25(4):284–8.

49. Shah N, Bhor M, Xie L, Paulose J, Yuce H. Sickle cell disease complications: Prevalence and resource utilization. *PloS One* (2019) 14(7):e0214355. doi: 10.1371/journal.pone.0214355

50. Smith WR, Penberthy LT, Bovbjerg VE, McClish DK, Roberts JD, Dahman B, et al. Daily Assessment of pain in adults with sickle cell disease. *Ann Intern Med* (2008) 148(2):94–101. doi: 10.7326/0003-4819-148-2-200801150-00004

51. Kato GJ, Piel FB, Reid CD, Gaston MH, Ohene-Frempong K, Krishnamurti L, et al. Sickle cell disease. *Nat Rev Dis Primer. 15 mars* (2018) 4:18010.

52. Karsten E, Breen E, Herbert BR. Red blood cells are dynamic reservoirs of cytokines. *Sci Rep 15 févr* (2018) 8(1):3101. doi: 10.1038/s41598-018-21387-w

53. Musa BOP, Onyemelukwe GC, Hambolu JO, Mamman AI, Isa AH. Pattern of serum cytokine expression and T-cell subsets in sickle cell disease patients in vaso-occlusive crisis. *Clin Vaccine Immunol CVI.* (2010) 17(4):602–8. doi: 10.1128/CVI.00145-09

54. Sarray S, Saleh LR, Lisa Saldanha F, Al-Habboubi HH, Mahdi N, Almawi WY. Serum IL-6, IL-10, and TNFα levels in pediatric sickle cell disease patients during vasoocclusive crisis and steady state condition. *Cytokine* (2015) 72(1):43–7. doi: 10.1016/j.cyto.2014.11.030

55. Torres LS, Gotardo EMF, Leonardo FC, Brito PL, Förster I, Kovarik J, et al. Neutralization of inflammasome-processed cytokines reduces inflammatory mechanisms and leukocyte recruitment in the vasculature of TNF-α-Stimulated sickle cell disease mice. *Blood.* (2021) 138(Supplement 1):856. doi: 10.1182/blood-2021-147436

frontiers | Frontiers in Immunology

TYPE Review
PUBLISHED 27 July 2023
DOI 10.3389/fimmu.2023.1134020

OPEN ACCESS

EDITED BY
Denis Sereno,
Institut de Recherche Pour le Développement (IRD), France

REVIEWED BY
Fernanda Nazaré Morgado,
Oswaldo Cruz Institute, Brazil
Sara M. Robledo,
University of Antioquia, Colombia

*CORRESPONDENCE
Sylviane Pied
sylviane.pied@pasteur-lille.fr

RECEIVED 29 December 2022
ACCEPTED 10 March 2023
PUBLISHED 27 July 2023

CITATION
Saidi N, Blaizot R, Prévot G, Aoun K, Demar M, Cazenave PA, Bouratbine A and Pied S (2023) Clinical and immunological spectra of human cutaneous leishmaniasis in North Africa and French Guiana.
Front. Immunol. 14:1134020.
doi: 10.3389/fimmu.2023.1134020

Clinical and immunological spectra of human cutaneous leishmaniasis in North Africa and French Guiana

Nasreddine Saidi[1,2], Romain Blaizot[1,3,4], Ghislaine Prévot[1], Karim Aoun[2,5], Magalie Demar[1,3,4], Pierre André Cazenave[1], Aida Bouratbine[2,5] and Sylviane Pied[1]*

[1]Univ. Lille, Univ. French Guiana, CNRS UMR 9017-INSERM U1019, Center for Infection and Immunity of Lille-CIIL, Institut Pasteur de Lille, Lille, France, [2]Laboratoire de Recherche, LR 16-IPT-06, Parasitoses Médicales, Biotechnologies et Biomolécules, Institut Pasteur de Tunis, Université Tunis El-Manar, Tunis, Tunisia, [3]Centre National de Référence des Leishmanioses, Laboratoire Associé, Hôpital Andrée Rosemon, Cayenne, French Guiana, France, [4]Service de Dermatologie, Hôpital de Cayenne, Cayenne, French Guiana, France, [5]Service de Parasitologie-Mycologie, Institut Pasteur de Tunis, Tunis, Tunisia

Cutaneous leishmaniasis (CL) caused by infection with the parasite *Leishmania* exhibits a large spectrum of clinical manifestations ranging from single healing to severe chronic lesions with the manifestation of resistance or not to treatment. Depending on the specie and multiple environmental parameters, the evolution of lesions is determined by a complex interaction between parasite factors and the early immune responses triggered, including innate and adaptive mechanisms. Moreover, lesion resolution requires parasite control as well as modulation of the pathologic local inflammation responses and the initiation of wound healing responses. Here, we have summarized recent advances in understanding the *in situ* immune response to cutaneous leishmaniasis: *i*) in North Africa caused by *Leishmania (L.) major*, *L. tropica*, and *L. infantum*, which caused in most cases localized autoresolutives forms, and *ii*) in French Guiana resulting from *L. guyanensis* and *L. braziliensis*, two of the most prevalent strains that may induce potentially mucosal forms of the disease. This review will allow a better understanding of local immune parameters, including cellular and cytokines release in the lesion, that controls infection and/or protect against the pathogenesis in new world compared to old world CL.

KEYWORDS

***L. major*, *L. infantum*, *L. tropica*, *L. guyanensis*, *L. braziliensis*, cutaneous leishmaniasis (CL), clinical manifestation, local immune response**

Introduction

Leishmaniasis is a parasitic disease caused by a vector-borne protozoan parasite belonging to the *Leishmania* genus. It is transmitted as a flagellated promastigote *via* the bite of an infected sandfly (1, 2). Following its inoculation, promastigotes are ingested by innate cells mainly macrophages, neutrophils, and dendritic cells, where they evolve into amastigotes. *Leishmania* parasite are distributed in more than 98 countries, with 350 million people exposed and 12 million infected (3, 4). The cutaneous form is the most frequent, with an estimation of 600 000 to 1 million new cutaneous leishmaniasis (CL) cases per year. This disease is also responsible for significant psychosocial impacts due to the scars that persist after recovery and the associated social stigma (5). In the Old World, specifically in North Africa (NA), CL is caused by three species: *L. major*, *L. tropica*, and *L. infantum*. Cutaneous leishmaniasis is highly prevalent in Morocco, Algeria, and Tunisia. In the New World (NW), CL is widely distributed in South and Central America. It is mainly caused by *L. amazonensis*, *L. guyanensis*, *L. panamensis*, *L. peruviana*, *L. mexicana*, and *L. braziliensis* (6). These species can cause cutaneous and sometimes mucosal leishmaniasis (ML), with only a small potential for self-healing. French Guiana (FG) is a good example of an endemic South American country, where numerous works have been published on CL. The disease is basically divided into four clinical phenotypes (1): Localized CL (LCL) (2), mucocutaneous leishmaniasis, and (3) diffuse and (4) disseminated CL (7–9). Skin lesions result from a deregulated immune response which is unable to eliminate the intracellular parasites. This could explain the high number of parasites in the inflammatory infected zone for some forms of CL (10). Unbalanced T helper (Th)1/Th2 responses has been associated with an increased tissue destruction and a worsening of skin lesions. Moreover, in a susceptible murine model of *L. major* infection, improved resistance to infection was linked to the production of cytokines in lymph nodes. In most mouse strains, Th1 cells bring resistance through the secretion of IFN-γ. In contrast, susceptible mice generate a Th2 cell response characterized by the production of IL-4 and IL-13, which hampers the ability of IFN-γ to trigger toxic metabolites (11). The evolution of lesions is determined by a complex interaction between many factors triggered by the early immune responses, including innate and acquired immune mechanisms (10). However, there is a significant lack of information on the cutaneous immune response within CL lesions determining the evolution of the disease both in NA and FG. A better knowledge of the pattern of immune mechanisms and related factors involved in lesion progression or healing might provide helpful information for identifying new immunotherapeutic targets and new drugs.

In this review, we will sum up the current knowledge on clinical manifestations, lesion evolution and local immune response associated with *L. infantum*, *L. major* and *L. tropica* in NA and *L. guyanensis* and *L. braziliensis* CL in FG. We will also discuss similarities and divergences in immune mechanisms induced in NA and FG.

Comparison of clinical manifestations and disease outcome between North Africa and French Guiana

The clinical presentation and the outcome of CL depend on multiple factors, including species involved, lesion location, sandfly infectivity, comorbidities, treatment modalities, skin microbiota and host immune responses against *Leishmania* (Figure 1) (23–25). The clinical appearance of CL is initially characterized by an erythematous, non-specific papule or patch following an incubation period after the bite of the *Leishmania* infected sandfly. This sub-clinical or early CL has the potential for self-healing; it then evolves into ulcerated (85%) or non-ulcerated (nodules, papules, plaques 15%) specific lesions. Some lesions have a very small potential for self-healing, especially those in the New World, and almost always require a treatment; the median incubation of CL in French Guiana is 25 days. Hypopigmented, hyperpigmented or atrophic scars can persist after treatment, depending on the skin phototype (26–31). In some cases, the lesions can persist for more than one year and become a chronic non-healing form (32, 33). Therefore, some infected patients leading to disfigured (34–36). However, the disease outcome also depends on the parasite species (Table 1).

Concerning *L. major*, this species is the most frequent in NA countries, where it remains a major public health problem, with more than 1000 to 8 000 cases yearly in Tunisia and 10,000 to 25,000 in Algeria (9, 40, 51, 52). Lesion can be single or multiple, usually with ulcerative nodules. These primary lesions can give birth to secondary peripheral lesions "satellite" (Figure 2) (9, 58). The most common type of ulcer is the ulcero-crusted form (59), also known as the "wet" or "rural" type. It is characterized by a painless ulcer with a clear raised border and a brownish scab covering it, commonly affecting the upper and lower limbs. CL caused by *L. major* has a wide range of clinical presentations, so it should be considered as a possibility in many skin diseases, including actinomycetoma, pyoderma gangrenosum, and various types of skin cancer. In Tunisia, about 11 uncommon clinical forms of CL due to *L. major* have been reported in zoonotic foci in Central and South regions of the country (60–62). This diversity may be due to the combination of the parasite's genetics and the host's immune response.

L. tropica, is responsible for chronic CL (CCL). Among the different countries of NA, Morocco presents the widest endemic areas and the highest incidence for this species (9). Compared with *L. major*, cutaneous lesions are distinguished by their chronicity; their appearance is dry and slightly inflamed. Therefore, this makes *L. tropica* CL more difficult to diagnose, which causes a delay in patient care (9, 63–66). Lesions in CCL are drier than in *L. major*, with papules, nodules, or crusty ulcers. Also, they are different in location and size compared to other species, as it mainly appears on the face and are typically smaller, with a diameter of less than 2 cm (41, 51, 67, 68).

The third CL causative species in NA is *L. infantum*, the primary responsible agent of visceral leishmaniasis (VL) (69).

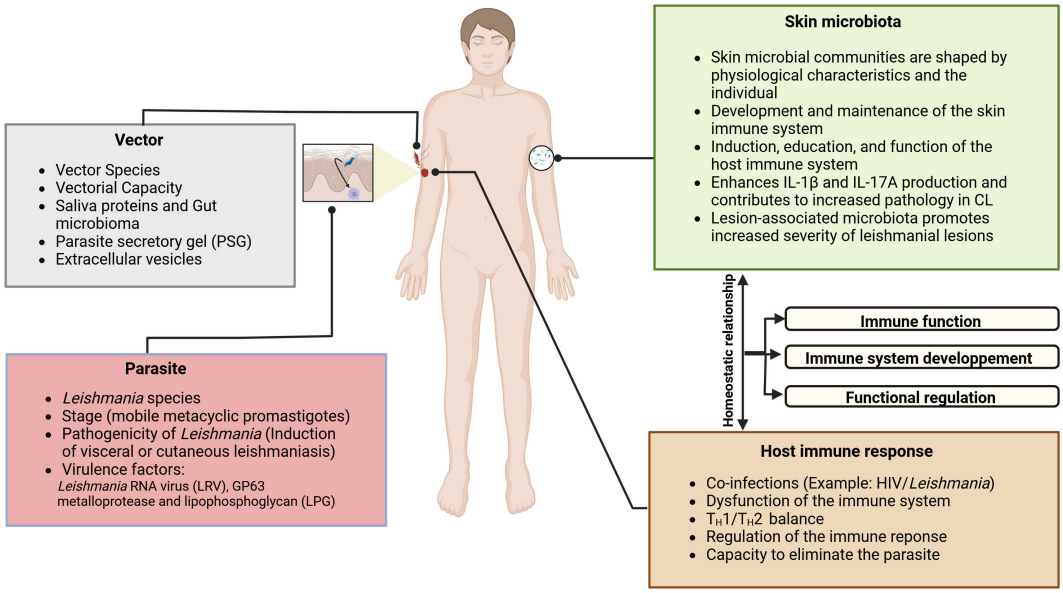

FIGURE 1
The pathogenesis of CL and the evolution of lesions are multifactorial; it depends on the complex interactions between the *Leishmania* parasite, the immune system, and the skin environment, including the vector-injected particles and the microbial skin communities. Sandfly saliva contains potent vasodilators, maxadilan, and adenosine, described respectively in *Lutzomyia longipalpis* and *P. papatasi*, that prevent clotting at the biting site (12), in addition of proteins that trigger a host immune response (13–15). As clearly demonstrated by several investigators, sandfly saliva contains immunomodulatory molecules that have been shown to enhance disease progression (16–18). Some of them, such as the parasite secretory gel (PSG), afford *Leishmania* protection from a hostile pro-inflammatory environment. They may directly regulate macrophages activation in dampening the early pro-inflammatory response and orchestrating wound repair and re-epithelialization (19). In fresh wounds, a robust pro-inflammatory response is required to sterilize the damaged tissue of potentially pathogenic bacteria. The skin microbiota plays a fundamental role in the host immune system's induction, education, and function. In turn, the host immune system has evolved multiple means to maintain its homeostatic relationship with the microbiota. It has been shown that *Staphylococcus* spp., *Streptococcus* spp., *Enterococcus spp*, *Pseudomonas spp*, and other opportunistic bacteria are present in CL lesions (20–22). It was proven using a *Leishmania*-infected mouse with dysbiotic skin microbiota that naturally acquired dysbiosis can cause a change in inflammatory responses and disease progression. It has been demonstrated that the skin microbiome could modulate the skin's immune response by enhancing IL17 production, which is essential in mediating inflammation in CL. While Th17 cells are a source of IL-17, it is possible that IL-17 produced by innate lymphoid cells present in the skin could contribute to disease progression. In effect, Scoot's team has suggested that following infection by *L. major*, RORγt+ILCs produced IL-17 in the skin may contribute to disease progression.

Between 50 and 150 cases are reported annually in Tunisia; few data are available for other countries (9). Compared to the previous two, the clinical appearance of wounds is more significant (58, 70). The duration between the bite of the infective sandfly and the onset of symptoms may vary between several weeks to 1 year (average 3-6 months) (51, 71). Another characteristic is that lesions may last longer than those with *L. major*, persisting for several months or years; such lesions are often slow to heal and may leave large, disfiguring, or disabling scars. Clinically, *L. infantum* lesions may present as papules or nodules, typically on the extremities and

TABLE 1 Summary of the different *Leishmania* species, clinical presentations, vector and transmission cycles in North African countries (Old World) and French Guiana (New World).

Leishmania species	Clinical presentation	Vectors	Transmission cycle	References
L. major	Localized	*P. papatasi*	Zoonotic	(9, 37–39)
L. infantum	Localized Visceral Leishmaniasis	*P. perfiliewi* *P. longicuspis* *P. ariasi*	Zoonotic	(9, 37, 38)
L. tropica	Localized	*P. sergenti*	Zoonotic	(9, 40, 41)
L. guyanensis	Single and multiple skin lesions Rare proportion of mucocutaneous cases Disseminated	*Lutzomyia (Ny.) umbratilis*	Zoonotic	(42–46)
L. braziliensis	Disseminated Important proportion of mucocutaneous cases	*Lutzomyia wellcomei* *Lu. (Ny.) neivai* *Lu. (Ny.) whitmani* *Lutzomyia ovallesi*	Zoonotic	(45, 47–50)

bordered by a large zone of infiltration (9, 37). Plaque is the most frequent clinical manifestation of cutaneous *L. infantum* involvement, followed by ulcers, nodules, and papules (72). The clinical presentation is a single small plaque on the face (9). Cases of mucosal involvement have recently been reported in travelers returning to Europe but are seldom described by North African teams (73).

In French Guiana, CL is caused by certain species belonging to the *Leishmania Viannia* subgenus, which is endemic to Central and South America (74). *L. guyanensis* represents more than 80% of cases in FG, while *L. braziliensis* has emerged in the 2000s and represents about 10-15% of cases (75). Other species, such as *L. lainsoni*, *L. naiffi*, and *L. amazonensis* can also be found but remain rare and are not part of this review (76). Though a complex clinical classification has not been proposed in FG, a very wide spectrum of clinical lesions can be observed, including impetigo-like, lupoid-like, sporotrichoid, crusted ulcers, patches, plaques, nodules, papules, or even extensive sores (Figure 2). These atypical forms

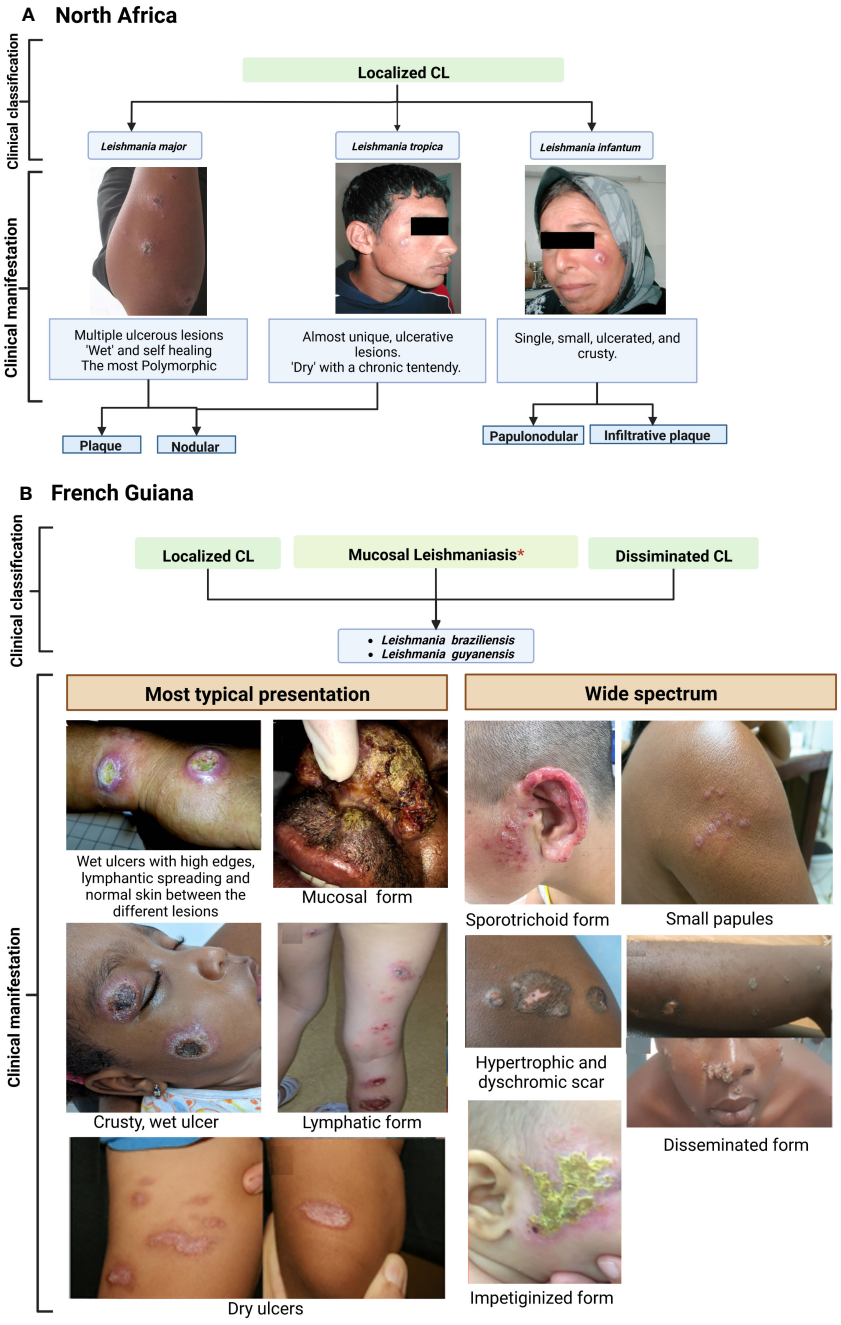

FIGURE 2
Clinical features of cutaneous leishmaniasis caused by *L. major*, *L. tropica* and *L. infantum* (Old world) **(A)** compared to *L. braziliensis* and *L. guyanensis* (New World) **(B)**. Case photos were provided by the laboratory of Medical Parasitology and Mycology. Institute Pasteur of Tunis. and Dermatology Department, Centre Hospitalier de Cayenne, French Guiana. *Risk for mucosal involvement is about 6% for *L. braziliensis* and 1% for *L. guyanensis*. Reference: North Africa; French Guiana (9, 53–57).

have also been described in other countries of South America, notably Brazil (77, 78). However, the typical form of CL in French Guiana and the rest of the Amazon basin consists of a wet, acute ulcer which is slightly painful and usually without secondary bacterial infection (44). Several lesions can be found, particularly when *L. guyanensis* is involved. The skin between the lesions is normal, without erythema. A lymphangitis with or without parasitic nodules can be observed. Compared to Old World (OW) leishmaniasis, New World (NW) forms are known for a greater tendency to disseminate systemically in the skin (6, 79).

In addition, a great number of lesions with lymphatic involvement are observed for *L. guyanensis* CL in FG (42, 43) (Figure 2). This species is known to occasionally cause mucosal issues, but it is less common than mucosal disease caused by *L. braziliensis* (44, 80–82). Indeed, less than 1% of *L. guyanensis* cases in FG display a mucosal involvement (81, 83). *L. braziliensis* CL can manifest in different ways, from a single ulcer on the skin, which is often associated with satellite adenomegaly, to the less frequently disseminated form (82, 84). Potentially severe mucosal involvement of the upper airways are typically described with this species (47, 82, 85–87). Single lesions are more frequent than with *L. guyanensis* (44, 83).

Cell-mediated immune responses associated with protection in the skin of CL patients

CL in NA and FG is characterized by various immunological features (Figure 3) (44, 47, 58, 74, 88–90). Once the *Leishmania* infected sandfly bites, the infection starts with an asymptomatic "silent phase" of variable duration, characterized by an inflammatory wave of poly morpho nuclear (PMN), dendritic cells (DC), and monocyte-derived macrophages which harbour a proliferation of amastigotes intracellular parasites (10, 91, 92). Then, a massive recruitment of $CD4^+$ and $CD8^+$ T lymphocytes, with enhanced pro-inflammatory responses participate in granuloma formation and parasite control. As a result, few parasites remain in the lesions and promote a delayed-type hypersensitivity (DTH) (Figure 4) (10, 93, 94). However, differences in intralesional immune profiles between the different CL forms are not well documented. Still, the infection outcome is clearly the consequence of a balance between pro and anti-inflammatory responses.

In *L. major* infection

During *L. major* infection, promastigotes deposition in the skin promotes neutrophils and dendritic cells (DCs) recruitment during the earliest stage of infection (95). In this stage, Chaves et al. demonstrated the anti-inflammatory functions of dermal tissue-resident macrophages, which was supported by the reduced parasite burdens observed in mice (96). The clearance and control of *L. major* multiplication involved mainly cytotoxic $CD8^+$ T cells and $CD4^+$ helper T cells and the production of IFN-γ (90, 97); in fact, non-healing lesions in mice are associated with a small number of $TCD4^+$ (98, 99). However, PWK mice strain develops prolonged but self-healing lesions, with an immune response characterized by a mixed Th1-plus-Th2 pattern acquiring resistance to a secondary challenge (100). Formaglio et al. recently showed the implication of the resident memory $CD4^+$ T cells in delayed-hypersensitivity response, without the involvement of circulating T cells but with the recruitment of activated inflammatory monocytes. These monocytes produce reactive oxygen species (ROS) and nitric oxide (NO) that play a role in the inhibition of *L. major* development in the mice (101). These findings underscore the central role of skin-resident $CD4^+$ T cells' in enhancing the protective immune response against *L. major* (102). Independently of the T resident memory cells, the acute availability of circulating $CD4^+$ T helper 1 effector cells (Th1EFF) at the time of secondary infection is critical for the Th1 immune response. Th1EFF cell-phagocyte interactions proved crucial in

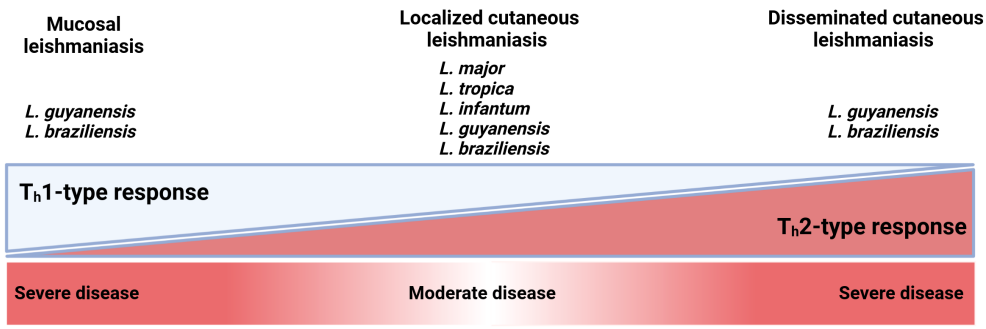

FIGURE 3
The T helper 1 (Th1)-type T helper 2 (Th2)-type balance across the cutaneous leishmaniasis severity. Mucosal and disseminated CL caused by *L. guyanensis* and *L. braziliensis* are the most severe form of the disease. They are on opposite sides of the Th1 and Th2 response, which enhances disease severity in an exaggerated response. An uncontrolled Th1 response in mucocutaneous leishmaniasis can cause an exaggerated cellular response, in which *Leishmania* amastigotes spread to the nasopharyngeal mucosa and cause tissue damage resulting in disfiguring lesions. For localized cutaneous leishmaniasis, mixed T_H1 and T_H2 responses have been observed during the active stage of infection; the Th1 profile is mainly associated with the healing of lesions.

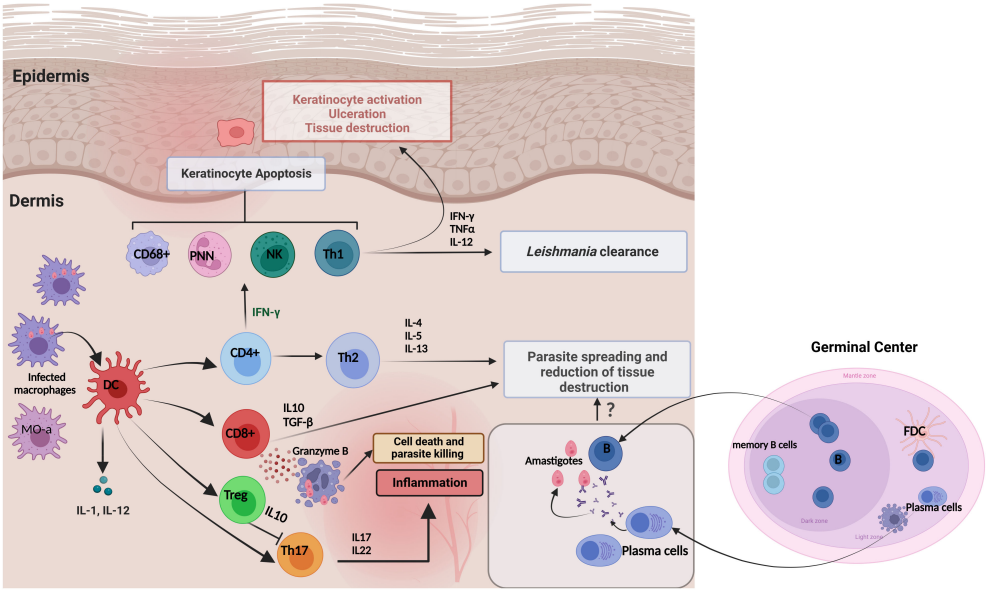

FIGURE 4
Immune responses and skin cytokine profile during cutaneous leishmaniasis infection. Pro-inflammatory cytokines are produced primarily to amplify the immune response to *Leishmania* infection. The major proinflammatory cytokines include TNF-α, IFN-γ, IL-1, IL-8, IL-12, IL-17 and Granzyme β. In contrast, anti-inflammatory cytokines are immunoregulatory molecules that counteract the effects of pro-inflammatory cytokines to limit the inflammation. These major anti-inflammatory cytokines include IL-5, IL-6, IL-4, IL-10, IL-13, and TGF-β. It has been proposed that the existence of Tregs in infected tissues could be an immune response from the host to maintain the balance to control Leishmania infection and reduce excessive inflammation that supports parasite survival. This is achieved by Tregs inhibiting Th17 cells through the production of IL-10. The role of the local humoral response to amastigote spreading and tissue destruction is still uncompletely understood.

preventing the establishment of a permissive *L. major* niche in lesions (103). However, if NK cells may play several roles in developing an effective T cell response against *Leishmania*, their contributions to the response to CL in humans are less clear. For instance, it has been shown that NK-cell-derived IFN-γ, in mice, is essential for activating the dendritic cells that mediate the T-cell-dependent protection against *L. major* infection (104). Another mechanism associated with Human skin lesions protection is granzyme B–dependent CD8 T-cell cytotoxicity, as it participates in controlling parasite multiplication through a cytotoxic process (88, 105). On the other hand, in mice, a negative regulatory role for IL-4 was identified in limiting the recruitment of Th1 cells to *L. major* infected tissues, which alters the *Leishmania* clearance (89, 106). Therefore, the study of the impact of IL-4 on lesion evolution could provide hints for a therapeutic trial (107–109). In addition, the cytokine balance IL-4/IFN-γ has also been demonstrated to participate in the commitment of local immune response. Indeed, IL-4 secretion at the site of *L. major* infection rather than low IFN-γ production may play a role in the prolongation of disease during acute and chronic CL lesions. A moderate increase of CD4 Tregs would be observed in chronic lesions. However, few studies have suggested the role of Tregs during human CL; Belkaid et al. demonstrated that Tregs are rapidly accumulated at sites of *L. major* infection, favoring the early parasite expansion, contributing to the maintenance of immunological self-tolerance, and coinciding with the expression of effective immune responses (98, 110). In a group of *L.major* infected patients, Hoseini et al. observed a significantly higher expression of Foxp3 in chronic lesions compared to acute lesions; The moderate increase of T reg in chronic lesions and their function in persistent infection is still not apparent (111).

In *L. infantum* infection

L. infantum is mostly responsible for visceral leishmaniasis (LV) but can also cause CL; little is known about the pathogenesis of this form. Recently, the level of INF-γ was evaluated for sporadic CL and zoonotic CL and was found to be significantly higher in *L. infantum* lesions than due to *L. major* (90). As mentioned above, for CL caused by *L. major*, $CD8^+$ T cells are an essential part of the defense mechanisms against the parasite; however, for *L. infantum* infection, IFN-γ has a long-range effect inducing skin tissue destruction and keratinocyte apoptosis (10, 112, 113). In addition, it has been shown that increased IL4 production in skin lesions of *L. infantum*- infected dogs is associated with severe clinical signs and a high parasite burden (114). Although the role of IL4 was little described for *L. major* infection, no data was found for *L. infantum* human cutaneous Leishmaniasis. Furthermore, there is still much to be learned regarding the role of T reg cells on skin lesions in human CL caused by *L. infantum*; authors have suggested that T reg cells and the regulatory cytokines, especially TGF-*β*, play an essential role in the immunopathogenesis of non-typical ulcerated leishmaniasis (NUCL), modulating the cellular immune response in the skin, avoiding tissue damage, and leading to low parasitic persistence in the skin (115, 116). These factors could play a role in

regulating the cellular immune response balance, resulting in the maintenance of a low tissue parasitism that avoids lesion growth.

In *L. tropica* infection

Although little is known about the *in situ* immune status of *L. tropica*-infected patients, cases develop a chronic CL with a strong delayed-type hypersensitivity (117). It has been recently, shown that *L. tropica* has an enhanced capacity to reduce NO production by macrophages *in vitro*, which could help to understand why *L. tropica* infection could induce chronic lesions (118). In a study by Ajdary et al., evaluating T-cell responses to *Leishmania* antigen *in vitro*, Th2 cell response was dominant in active CL cases, and Th1 characterized the group of healed patients (119). The level of specific cytokine was evaluated *in vitro* in the PBMC but not in the skin, and high levels of IFN-γ, IL-5, and IL-13 in non-healing patients were observed, suggesting a mixed Th1/Th2 response with chronic lesions. In contrast, patients with acute lesions respond to infection *via* a Th1-type response (119). However, such a result must be confirmed locally in skin lesions or animal models. It has been discovered that in the early stages of *L. tropica* infection, the amount of IL-4 is upregulated and linked to a higher parasite burden. This may play a role in the development of CL by inhibiting the protective immune response. These findings indicate that the parasites may rapidly multiply at the beginning of the infection, leading to a Th2-type immune response (120). Information on regulatory immune responses is lacking for *L. tropica* CL. However, *L. tropica*-infected lesions from Indian patients, the analysis of localized immune response reveals the presence of Th17 and T reg cells (121). Because of the difficulties in establishing infection *in vivo*, published data using animal models for leishmaniasis caused by *L. tropica* is limited (122). Nevertheless, it was suggested that the presence of Tregs in infected tissues may be a possible host immune response or homeostatic mechanism to control *L. tropica* infection and to reduce the excessive inflammation supporting parasite survival through IL-10. Still, additional investigations are needed to clarify this response.

In *L. braziliensis* infection

The severity of lesions that develop in patients infected by *L. braziliensis* is mainly associated with a highly inflammatory cutaneous environment. In fact, patients with *L. braziliensis* infection exhibit a strong T-helper 1 (Th1) immune response, which leads to excessive inflammation and tissue damage (123). High levels of both IFN-γ and TNF-α are observed in CL caused by this species. Still, while IFN-γ may have a protective function (124), there is strong evidence to support the role of TNF-α in the pathology of cutaneous and mucosal lesions (125–130). Thiago Cardoso and colleagues (2014) studied the protective and pathological functions of $CD8^+$ T Cells in *L. braziliensis* infection. The frequency of $CD8^+$ T cells expressing granzyme in the lesions of severe CL patients is more significant than that in patients during early stage of CL (131). However, cytotoxic CD8 T cells are harmful to both *L. braziliensis* and infected host cells because cytotoxicity is higher in mucocutaneous leishmaniasis than in the localized form (132, 133). Recently, it has been observed a high proportion of senescent T cells (Tsen) with high inflammatory profiles in *L. braziliensis* lesions with mucosal involvement (134, 135), which is linked to the severity and tissue damage (136). Therefore, *in vivo*, senescent CD8+ T cells appear to be the most important cell populations mediating skin pathology (137). Other cells, particularly Treg cells, accumulate in lesions caused by *L. braziliensis*, and *contribute* to the local control of effector T-cell functions (138). Campanelli et al. research suggests that Treg accumulated at the sites of *L. braziliensis infection* may contribute to the local control of effector T cell functions. Still, a direct correlation with the pathogenesis is yet to be detected (138).

In *L. guyanensis* infection

Little is known about the immune responses induced during human infection with *L. guyanensis*, which generally generates a mixed Th1/Th2/Th17 immune response. IL-13 is the main Th2 cytokine found in *L. guyanensis* LCL lesions, according to research by Bourreau and colleagues. As IL-13 has many similar effects with IL-4 (139), patients with *L. guyanensis* LCL are likely to have a Th2 response that includes the production of either IL-4 or IL-13. However, IL-13 plays a key role in maintaining the Th2 response in Human leishmaniasis by making certain cells resistant to IL-12 (140). In *L. guyanensis* infection, the levels of Foxp3 in the lesions were superior in chronic patients than in acute ones demonstrating the regulatory role of T reg. Furthermore, Tregs isolated from skin biopsy of *L. guyanensis* patients with acute CL had a suppressive effect on CD4+T effector (eff) cells. Also, Foxp3 expressions were higher in skin biopsies than in peripheral blood mononuclear cells (PBMC), confirming the recruitment of Tregs to the infection site (141, 142). *L. guyanensis* shows unique characteristics with a mixed immune response (Figures 5, 6), which warrants further investigation to uncover the mechanisms that regulate immune responses and control inflammation caused by this parasite. Recently, a proposed relationship between *Leishmania* RNA Virus (LRV) and the severity of leishmaniasis has been suggested, as various factors are linked to the pathogenicity of the disease (146). Zabala-Peñafiel and colleagues demonstrated that *L. guyanensis* metastatic strains had a higher rate of LRV1 positivity than non-metastatic strains (147). During macrophage infection, it caused over-expression of pro-inflammatory mediators such as TNF-α and IL-6. Ginouvès and colleagues found that 74% of the *Leishmania* (*Viannia*) subgenus clinical isolates in French Guiana contain LRV1, with the majority being *L. braziliensis* and *L. guyanensis*. Patients infected with LRV1-positive *L. guyanensis* have a high ratio of IL-17A and IFNγ in their skin lesions (146) (Figure 5). This is accompanied by higher levels of IL-17A in blood cell cultures after stimulation with live parasites, compared to those infected with LRV1-free *L. guyanensis* (148). This demonstrates that virus infection can exacerbate atypical tegumentary leishmaniasis caused by *L. guyanensis*. These findings suggest that the presence of LRV1 in the parasites not only increases the risk of developing

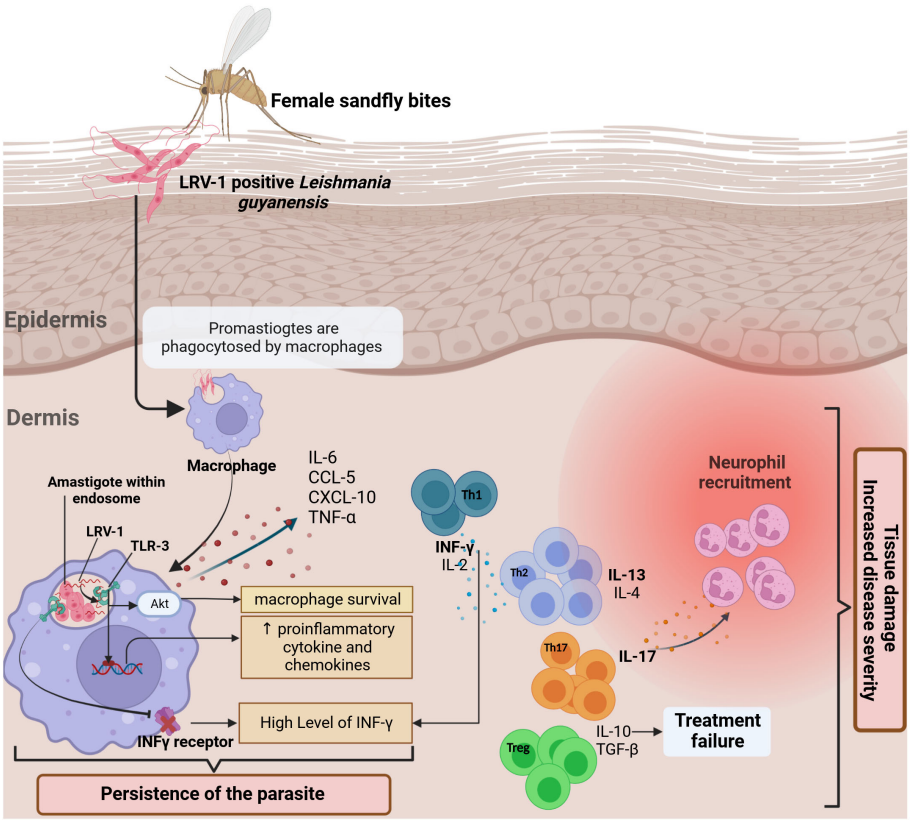

FIGURE 5
The *in situ* immune response against *L. guyanensis* contains a dsRNA virus called (LRV-1). The response to the virus is mediated by TLR 3 in the endosomal macrophage compartment, where the parasite lives and divides. A hypothesis is that after the infection, the viral RNA is released after parasite death and binds to TLR-3 (143), promoting pro-inflammatory cytokines and chemokines production such as IL-6, TNF-α, CXCL-10, and CCL-5 and controlling the severity of the disease (144). Generally, *L. guyanensis* infection induces a mixed Th1/Th2/Th17 immune response. Th-17 cells appear to predominate in lesions in the presence of *Leishmania* RNA with high production of IL17-A. TGF-β is essential for establishing infection and, together with IL-10, leads to therapeutic failures and increased disease severity. The stimulation of TLR3 results in the downregulating of IFN-γ receptor expression, reducing macrophage activation, which explains the high level of IFN-γ observed in lesions produced by Th-1. Indeed, *via* Akt (Protein kinase B) signaling, TLR3 activation by LRV1 promoted parasite persistence (145). Altogether, it enhances inflammation and thus exacerbates disease.

	***Leishmania* species in North Africa**			***Leishmania* species in French Guiana**	
	L. major	***L. infantum***	***L. tropica***	***L. guyanensis***	***L. braziliensis***
Pathogenesis and tissue destruction	• ↑ T_{h2} • ↑ T_{reg} (Chronic form) • ↑ IL-4 (Alter *Leishmania* clearance)	• ↑ LT CD8 • ↑ INF γ • ↑ IL-4 (↑Severity)	• ↑ T_{h1} • ↑ T_{h2} • ↑ IL-4 (*Leishmania* clearance)	• ↑ IL17-A ↑T_{h17} • ↑ INF γ • ↑ IL-4 • **↑ IL-13 (+++)**	• ↑ T_{h1} (Tissue damage • ↑ LT $CD8^+$(MCL and CL) • ↑ INF γ • ↑ TNF α • ↑Tsen
Protection and parasite clearance	• ↑ LT $CD4^+$ • ↑ LT $CD8^+$ • ↑ INFγ / Granzyme β	• ↑ T_{reg} (Ovoid tissue damage)	• ↑ T_{reg} • ↑ T_{h17}	• ↑ T_{reg} • ↑Th_1	• ↑ T_{reg} (control effectors T cells)

FIGURE 6
Comparison between the *in situ* immune profiles in lesions of patients infected with the five *Leishmania* species (*L. major, L. infantum, L. tropica, L. guyanensis, L. braziliensis*) and the implication for pathogenesis and the control of the diseases.

ML but also causes complications in CL. Contradictorily, in a study conducted by Ginouvès et al., no correlation was found between the presence of LRV1 or its genotypes in *L. guyanensis* parasites and treatment failure, either after the first or second course of treatment of pentamidine (149). Additional research is required to assess a possible link between LRV1-infected parasites and their clinical symptoms.

Conclusion

The outcome of *Leishmania* infection relies on the intricate equilibrium of pro- and anti-inflammatory immune responses generated by the host. Both innate and adaptive immunity are inextricably linked to each other as the cytokines produced by cells of the innate system determine the outcome and magnitude of the adaptive immune response. Therefore, the immune responses need to be tightly regulated to avoid immune-mediated pathology to host tissue. Here, we have highlighted recent progress made in understanding the immune response to cutaneous leishmaniasis caused by *Leishmania major*, *L. tropica*, and *L. infantum* in North Africa on the one hand, and by *L. guyanensis* and *L. braziliensis in* French Guiana on the other hand. If cellular and cytokines are released in the lesion during OW-CL, much remains to be known in NW-CL. Indeed, this review could significantly contribute to understanding local immune parameters that control and protect the pathogenesis during *Leishmania* infection. However, a better knowledge of the local immune response in Human CL may help to identify new mechanisms and targets to develop new and more adapted treatments. New local therapies for cutaneous leishmaniasis in NA, French Guiana, and all endemic countries are urgently needed. Drug development is considered a priority, as most current treatments are based on expensive drugs or potential side effects. The cost of anti-Leishmanial drugs is a crucial issue in low-income countries. Besides, therapeutic failures remain frequent, and cases of unresolved CL are often reported, possibly because all current drugs only target the parasite, not the host responses. This review demonstrates how these responses can shape the clinical lesions and lead to different forms. Research efforts should focus on testing immunotherapies that could reduce the severity of pathology seen in some cases of cutaneous leishmaniasis, which could consecutively lessen the duration of antiparasitic courses and their toxicity. In the last decade, several drugs have been developed for other skin inflammatory diseases or as immunotherapy for skin cancers. Some of these drugs inhibit IL-4 or cytotoxicity and might be helpful in combination with existing anti-parasitic drugs. Anti-IL 4 drugs could be useful for all species of *Leishmania*, while specific inhibitors of IL-13 and IL-17 could be used to dampen tissue damage in *L. guyanensis* infections (Figure 6). Dupilumab is currently used in atopic dermatitis both for its IL-4 and IL-13 effects and could be tested in association with antiparasitic drugs. Other candidates could include anti-IL17 used for inflammatory skin diseases, such as secukinumab, brodalimumab or ixekizumab. Furthermore, skin dysbiosis has been shown to drive the inflammatory response in *L. major* infected germ-free mice model (150). These observations emphasize the need to explore mechanisms by which skin microbiota is involved in the physiopathology of CL. In our opinion, it is essential that these advances in the role of microbiota should be included in the research for the development of new drugs and vaccines against CL.

Author contributions

SP designed, revised, and supervised the work. NS reviewed the literature, created the figures, and wrote the manuscript. RB, GP, KA, MD, PC, AB participated in the manuscript's analysis, drafting, and revising. All authors revised and approved the manuscript's final version.

Funding

This work was supported by LabEx PARAFRAP ANR-11-LABX-0024i and MALTOX FEDER CTG Guyane.

Acknowledgments

We wish to thank all the authors who have participated in this Research Topic and the reviewers for their insightful comments and suggestions. NS was funded by the Federation of African Immunological Societies (FAIS) Legacy Project (FLP), 2019, and the High-level scientific stays (SSHN) grant from the Minister of Europe and foreign affairs France, 2020.

Conflict of interest

The authors declare that the research was conducted in the absence of any commercial or financial relationships that could be construed as a potential conflict of interest.

Publisher's note

References

1. Sunter J, Gull K. Shape, form, function and leishmania pathogenicity: From textbook descriptions to biological understanding. *Open Biol* (2017) 7(9). doi: 10.1098/rsob.170165

2. Steverding D. The history of leishmaniasis. *Parasites Vectors* (2017) 10(1):82. doi: 10.1186/s13071-017-2028-5

3. Ruiz-Postigo JA, Jain S, Maia-Elkhoury AMAN, Valadas S, Warusavithana S, Osman M, et al. Global leishmaniasis surveillance: 2019-2020, a baseline for the 2030 Roadmap/Surveillance mondiale de la leishmaniose: 2019-2020, une periode de reference pour la feuille de route a l'horizon 2030. *Weekly Epidemiological Rec* (2021) 96:401–19.

4. Torres-Guerrero E, Quintanilla-Cedillo MR, Ruiz-Esmenjaud J, Arenas R. Leishmaniasis: A review. *F1000Research* (2017) 6:750. doi: 10.12688/f1000research.11120.1

5. Bennis I, Belaid L, De Brouwere V, Filali H, Sahibi H, Boelaert M. "The mosquitoes that destroy your face". social impact of cutaneous leishmaniasis in south-Eastern Morocco, a qualitative study. *PloS One* (2017) 12(12):e0189906. doi: 10.1371/journal.pone.0189906

6. Burza S, Croft SL, Boelaert M. Leishmaniasis. *Lancet (London England)* (2018) 392(10151):951–70. doi: 10.1016/s0140-6736(18)31204-2

7. Hashiguchi Y, Gomez EL, Kato H, Martini LR, Velez LN, Uezato H. Diffuse and disseminated cutaneous leishmaniasis: Clinical cases experienced in Ecuador and a brief review. *Trop Med Health* (2016) 44(1):2. doi: 10.1186/s41182-016-0002-0

8. Sinha S, Fernández G, Kapila R, Lambert WC, Schwartz RA. Diffuse cutaneous leishmaniasis associated with the immune reconstitution inflammatory syndrome. *Int J Dermatol* (2008) 47(12):1263–70. doi: 10.1111/j.1365-4632.2008.03804.x

9. Aoun K, Bouratbine A. Cutaneous leishmaniasis in north Africa: A review. *Parasite* (2014) 21:14. doi: 10.1051/parasite/2014014

10. Scott P, Novais FO. Cutaneous leishmaniasis: Immune responses in protection and pathogenesis. *Nat Rev Immunol* (2016) 16(9):581–92. doi: 10.1038/nri.2016.72

11. Reiner SL, Locksley RM. The regulation of immunity to leishmania major. *Annu Rev Immunol* (1995) 13(1):151–77. doi: 10.1146/annurev.iy.13.040195.001055

12. Maryam Ghafari S, Ebrahimi S, Nateghi Rostami M, Bordbar A, Parvizi P. Comparative evaluation of salivary glands proteomes from wild phlebotomus papatasi–proven vector of zoonotic cutaneous leishmaniasis in Iran. *Veterinary Med Sci* (2021) 7 (2):362–9. doi: 10.1002/vms3.368

13. Mahamdallie SS, Ready PD. No recent adaptive selection on the apyrase of Mediterranean phlebotomus: Implications for using salivary peptides to vaccinate against canine leishmaniasis. *Evolutionary Appl* (2012) 5(3):293–305. doi: 10.1111/j.1752-4571.2011.00226.x

14. Ready PD. Biology of phlebotomine sand flies as vectors of disease agents. *Annu Rev entomology* (2013) 58:227–50. doi: 10.1146/annurev-ento-120811-153557

15. Zahirnia AH, Bordbar A, Ebrahimi S, Spotin A, Mohammadi S, Ghafari SM, et al. Predominance of leishmania major and rare occurrence of leishmania tropica with haplotype variability at the center of Iran. *Braz J Infect Dis* (2018) 22(4):278–87. doi: 10.1016/j.bjid.2018.07.005

16. Titus RG, Ribeiro JMC. Salivary gland lysates from the sand fly lutzomyia longipalpis enhance leishmania infectivity. *Science* (1988) 239(4845):1306–8. doi: 10.1126/science.3344436

17. Rogers KA, Titus RG. Immunomodulatory effects of maxadilan and phlebotomus papatasi sand fly salivary gland lysates on human primary *in vitro* immune responses. *Parasite Immunol* (2003) 25(3):127–34. doi: 10.1046/j.1365-3024.2003.00623.x

18. Adly E, Shehata MG, El-Demerdash E, Alfarraj S, Ali Alharbi S, Soliman DE. Impact of anti-sandfly saliva antibodies on biological aspects of phlebotomus papatasi (Diptera: Psychodidae), vector of cutaneous leishmaniasis. *Saudi J Biol Sci* (2021) 28 (5):2695–700. doi: 10.1016/j.sjbs.2021.03.016

19. Leoni G, Neumann PA, Sumagin R, Denning TL, Nusrat A. Wound repair: Role of immune-epithelial interactions. *Mucosal Immunol* (2015) 8(5):959–68. doi: 10.1038/mi.2015.63

20. Shirazi MH, Ranjbar R, Asgari V, Mohebali M, Hamidian M. Study of bacterial infections among the patients with suspected cutaneous leishmaniasis. *Pakistan J Biol sciences: PJBS* (2007) 10(24):4555–8. doi: 10.3923/pjbs.2007.4555.4558

21. Vera LA, Macedo JL, Ciuffo IA, Santos CG, Santos JB. [Antimicrobial susceptibility of aerobic bacteria isolated from leishmaniotic ulcers in corte de pedra, ba]. *Rev da Sociedade Bras Medicina Trop* (2006) 39(1):47–50. doi: 10.1590/s0037-86822006000100009

22. Ziaei H, Sadeghian G, Hejazi SH. Distribution frequency of pathogenic bacteria isolated from cutaneus leishmaniasis lesions. *Korean J Parasitol* (2008) 46(3):191–3. doi: 10.3347/kjp.2008.46.3.191

23. Handler MZ, Patel PA, Kapila R, Al-Qubati Y, Schwartz RA. Cutaneous and mucocutaneous leishmaniasis: Clinical perspectives. *J Am Acad Dermatol* (2015) 73 (6):897–908. doi: 10.1016/j.jaad.2014.08.051

24. Rojas R, Valderrama L, Valderrama M, Varona MX, Ouellette M, Saravia NG. Resistance to antimony and treatment failure in human leishmania (Viannia) infection. *J Infect Dis* (2006) 193(10):1375–83. doi: 10.1086/503371

25. Hartley MA, Drexler S, Ronet C, Beverley SM, Fasel N. The immunological, environmental, and phylogenetic perpetrators of metastatic leishmaniasis. *Trends Parasitol* (2014) 30(8):412–22. doi: 10.1016/j.pt.2014.05.006

26. Laboudi M, Sahibi H, Elabandouni M, Nhammi H, Ait Hamou S, Sadak A. A review of cutaneous leishmaniasis in Morocco: A vertical analysisto determine appropriate interventions for control and prevention. *Acta tropica* (2018) 187:275–83. doi: 10.1016/j.actatropica.2018.07.019

27. Beniklef R, Aoun K, Boudrissa K, Ben Abid M, Cherif K, Aissi W, et al. Cutaneous leishmaniasis in algeria; highlight on the focus of m'sila. *Microorganisms* (2021) 9(5). doi: 10.3390/microorganisms9050962

28. Bachi F, Icheboudene K, Benzitouni A, Taharboucht Z, Zemmouri M. [Epidemiology of cutaneous leishmaniasis in algeria through molecular characterization]. *Bull la Societe pathologie exotique (1990)* (2019) 112(3):147–52. doi: 10.3166/bspe-2019-0087

29. Pearson RD, Sousa A. Clinical spectrum of leishmaniasis. *Clin Infect Dis* (1996) 22(1):1–13. doi: 10.1093/clinids/22.1.1

30. Davidson RN. 123 - leishmaniasis. In: Cohen J, Powderly WG, Opal SM, editors. *Infectious diseases (Fourth edition)*. Elsevier (2017). p. 1059–64.e1.

31. Yedidia Moser R, Ben-Shimol S, Sagi O, Horev A. Comparison between cutaneous leishmaniasis patients with facial and non-facial lesions. *Int J Dermatol* (2021) 60(9):1109–13. doi: 10.1111/ijd.15582

32. Akilov OE, Khachemoune A, Hasan T. Clinical manifestations and classification of old world cutaneous leishmaniasis. *Int J Dermatol* (2007) 46(2):132–42. doi: 10.1111/j.1365-4632.2007.03154.x

33. Mortazavi H, Sadeghipour P, Taslimi Y, Habibzadeh S, Zali F, Zahedifard F, et al. Comparing acute and chronic human cutaneous leishmaniasis caused by leishmania major and leishmania tropica focusing on arginase activity. *J Eur Acad Dermatol Venereol: JEADV* (2016) 30(12):2118–21. doi: 10.1111/jdv.13838

34. Bennis I, Thys S, Filali H, De Brouwere V, Sahibi H, Boelaert M. Psychosocial impact of scars due to cutaneous leishmaniasis on high school students in errachidia province, Morocco. *Infect Dis poverty* (2017) 6(1):46. doi: 10.1186/s40249-017-0267-5

35. Bennis I, De Brouwere V, Belrhiti Z, Sahibi H, Boelaert M. Psychosocial burden of localised cutaneous leishmaniasis: A scoping review. *BMC Public Health* (2018) 18 (1):358. doi: 10.1186/s12889-018-5260-9

36. Chraiet-Rezgani K, Bouafif-Ben Alaya N, Habboul Z, Hajjej Y, Aoun K. [Epidemiological and clinical features of cutaneous leishmaniasis in kairouan-Tunisia and characteristics in children]. *Bull la Societe pathologie exotique (1990)* (2016) 109(2):80–3. doi: 10.1007/s13149-016-0475-4

37. Aoun K, Bouratbine A, Harrat Z, Guizani I, Mokni M, Bel Hadj Ali S, et al. [Epidemiologic and parasitologic data concerning sporadic cutaneous leishmaniasis in northern Tunisia]. *Bull Soc Pathol Exot* (2000) 93(2):101–3.

38. Aoun K, Kalboussi Y, Ben Sghaier I, Souissi O, Hammami H, Bellali H, et al. Assessment of incubation period of cutaneous leishmaniasis due to leishmania major in Tunisia. *Am J Trop Med hygiene* (2020) 103(5):1934–7. doi: 10.4269/ajtmh.20-0439

39. Bellali H, Chemak F, Nouiri I, Ben Mansour D, Ghrab J, Chahed MK. Zoonotic cutaneous leishmaniasis prevalence among farmers in central Tunisia, 2014. *J agromedicine* (2017) 22(3):244–50. doi: 10.1080/1059924x.2017.1318725

40. Tabbabi A. Review of leishmaniasis in the middle East and north Africa. *Afr Health Sci* (2019) 19(1):1329–37. doi: 10.4314/ahs.v19i1.4

41. Bousslimi N, Ben-Ayed S, Ben-Abda I, Aoun K, Bouratbine A. Natural infection of north African gundi (Ctenodactylus gundi) by leishmania tropica in the focus of cutaneous leishmaniasis, southeast Tunisia. *Am J Trop Med hygiene* (2012) 86(6):962–5. doi: 10.4269/ajtmh.2012.11-0572

42. Dedet J, Pradinaud R, Gay F. Epidemiological aspects of human cutaneous leishmaniasis in French Guiana. *Trans R Soc Trop Med Hygiene* (1989) 83(5):616–20. doi: 10.1016/0035-9203(89)90375-1

43. Dedet J-P. Cutaneous leishmaniasis in French Guiana: A review. (1990). doi: 10.4269/ajtmh.1990.43.25

44. Loiseau R, Nabet C, Simon S, Ginouves M, Brousse P, Blanchet D, et al. American Cutaneous leishmaniasis in French Guiana: An epidemiological update and study of environmental risk factors. *Int J Dermatol* (2019) 58(11):1323–8. doi: 10.1111/ijd.14625

45. Gramiccia M, Gradoni L. The current status of zoonotic leishmaniases and approaches to disease control. *Int J Parasitol* (2005) 35(11):1169–80. doi: 10.1016/j.ijpara.2005.07.001

46. Couppié P, Clyti E, Sainte-Marie D, Dedet JP, Carme B, Pradinaud R. Disseminated cutaneous leishmaniasis due to leishmania guyanensis: Case of a patient with 425 lesions. *Am J Trop Med hygiene* (2004) 71(5):558–60. doi: 10.4269/ajtmh.2004.71.558

47. Marsden P. Clinical presentations of leishmania braziliensis braziliensis. *Parasitol Today* (1985) 1(5):129–33. doi: 10.1016/0169-4758(85)90057-2

48. Simon S, Veron V, Carme B, Leishmania S. Identification by polymerase chain reaction-restriction fragment length polymorphism analysis and its applications in

French Guiana. *Diagn Microbiol Infect Dis* (2010) 66(2):175–80. doi: 10.1016/j.diagmicrobio.2009.08.013

49. Rougeron V, Catzeflis F, Hide M, De Meeûs T, Bañuls AL. First clinical case of cutaneous leishmaniasis due to leishmania (Viannia) braziliensis in a domestic cat from French Guiana. *Veterinary Parasitol* (2011) 181(2-4):325–8. doi: 10.1016/j.vetpar.2011.04.028

50. Desjeux P, Dedet JP. Isoenzyme characterization of 112 leishmania isolates from French Guiana. *Trans R Soc Trop Med Hygiene* (1989) 83(5):610–2. doi: 10.1016/0035-9203(89)90373-8

51. Chaara D, Haouas N, Dedet JP, Babba H, Pratlong F. Leishmaniases in maghreb: An endemic neglected disease. *Acta tropica* (2014) 132:80–93. doi: 10.1016/j.actatropica.2013.12.018

52. Saïdi N, Galaï Y, Ben-Abid M, Boussoffara T, Ben-Sghaier I, Aoun K, et al. Imaging leishmania major antigens in experimentally infected macrophages and dermal scrapings from cutaneous leishmaniasis lesions in Tunisia. *Microorganisms* (2022) 10(6):1157.

53. Epelboin L, Abboud P, Abdelmoumen K, About F, Adenis A, Blaise T, et al. Panorama des pathologies infectieuses et non infectieuses de Guyane en 2022 [Overview of infectious and non-infectious diseases in French Guiana in 2022]. *Med Trop Sante Int* (2023) (1):mtsi.v3i1.2023.308. doi: 10.48327/mtsi.v3i1.2023.308

54. Malmontet T, Guarmit B, Gaillet M, Michaud C, Garceran N, Chanlin R, et al. Spectrum of skin diseases in Amerindian villages of the Upper Oyapock, French Guiana. *Int J Dermatol* (2020) 59(5):599–605. doi: 10.1111/ijd.14848

55. Henry K, Mayet A, Hernandez M, Frechard G, Blanc PA, Schmitt M, et al. Outbreak of Cutaneous Leishmaniasis among military personnel in French Guiana, 2020: Clinical, phylogenetic, individual and environmental aspects. *PLOS Negl Trop Dis* (2021) 15(11):e0009938. doi: 10.1371/journal.pntd.0009938

56. Valentin J, Niemetzky F, Gaillet M, Michaud C, Carbunar A, Demar M, et al. Spectrum of skin diseases in Maroon villages of the Maroni area, French Guiana. *Int J Dermatol* (2022) 61:1137–1144. doi: 10.1111/ijd.16324

57. Heleine M, Elenga N, Njuieyon F, Martin E, Piat C, Pansart C, et al. Using pentamidine to treat cutaneous leishmaniasis in children: a 10-year study in French Guiana. *Clin Exp Dermatol* (2023), llad146. doi: 10.1093/ced/llad146

58. Mokni M. [Cutaneous leishmaniasis]. *Annales dermatologie venereologie* (2019) 146(3):232–46. doi: 10.1016/j.annder.2019.02.002

59. Remadi L, Haouas N, Chaara D, Slama D, Chargui N, Dabghi R, et al. Clinical presentation of cutaneous leishmaniasis caused by leishmania major. *Dermatol (Basel Switzerland)* (2016) 232(6):752–9. doi: 10.1159/000456543

60. Masmoudi A, Hariz W, Marrekchi S, Amouri M, Turki H. Old world cutaneous leishmaniasis: Diagnosis and treatment. *J Dermatol Case Rep* (2013) 7(2):31. doi: 10.3315/jdcr.2013.1135

61. Masmoudi A, Ayadi N, Boudaya S, Meziou T, Mseddi M, Marrekchi S, et al. Clinical polymorphism of cutaneous leishmaniasis in centre and south of Tunisia. *Bull la Societe pathologie exotique (1990)* (2007) 100(1):36–40.

62. Masmoudi A, Kitar A, Rebai M, Bouassida S, Turki H, Zahaf A. [the cutaneous leishmaniasis of the face in gafsa area, Tunisia]. *Bull la Societe pathologie exotique (1990)* (2005) 98(5):374–9.

63. El Alem MMM, Hakkour M, Hmamouch A, Halhali M, Delouane B, Habbari K, et al. Risk factors and prediction analysis of cutaneous leishmaniasis due to leishmania tropica in southwestern Morocco. *Infection Genet Evol* (2018) 61:84–91. doi: 10.1016/j.meegid.2018.03.017

64. Baghad B, Razanapinaritra R, Maksouri H, El Bouri H, Outlioua A, Fellah H, et al. Possible introduction of leishmania tropica to urban areas determined by epidemiological and clinical profiles of patients with cutaneous leishmaniasis in Casablanca (Morocco). *Parasite Epidemiol control* (2020) 9:e00129. doi: 10.1016/j.parepi.2019.e00129

65. Chaara D, Ravel C, Bañuls A, Haouas N, Lami P, Talignani L, et al. Evolutionary history of leishmania killicki (Synonymous leishmania tropica) and taxonomic implications. *Parasites Vectors* (2015) 8:198. doi: 10.1186/s13071-015-0821-6

66. Dokhan MR, Jaouadi K, Salem S, Zenbil O, Gonzalez JP, Ben Salah A, et al. Natural infection of phlebotomus sergenti by leishmania tropica in Libya. *Am J Trop Med hygiene* (2018) 98(5):1339–42. doi: 10.4269/ajtmh.17-0814

67. Chiheb S, Guessous-Idrissi N, Hamdani A, Riyad M, Bichichi M, Hamdani S, et al. [Leishmania tropica cutaneous leishmaniasis in an emerging focus in north Morocco: New clinical forms]. *Annales dermatologie venereologie* (1999) 126(5):419–22.

68. Aoun K, Ben Abda I, Bousslimi N, Bettaieb J, Siala E, Ben Abdallah R, et al. Caractérisation comparative des trois formes de leishmaniose cutanée endémiques en tunisie. *Annales dermatologie venereologie* (2012) 139(6):452–8. doi: 10.1016/j.annder.2012.04.154

69. Hakkour M, El Alem MM, Hmamouch A, Rhalem A, Delouane B, Habbari K, et al. Leishmaniasis in northern Morocco: Predominance of leishmania infantum compared to leishmania tropica. *BioMed Res Int* (2019) 2019:5327287. doi: 10.1155/2019/5327287

70. del Giudice P, Marty P, Lacour JP, Perrin C, Pratlong F, Haas H, et al. Cutaneous leishmaniasis due to leishmania infantum. case reports and literature review. *Arch Dermatol* (1998) 134(2):193–8. doi: 10.1001/archderm.134.2.193

71. Meeting WECotCotL and Organization WH. *Control of the leishmaniases: Report of a meeting of the who expert committee on the control of leishmaniases, Geneva, 22-26 march 2010*. World Health Organization (2010).

72. Merino-Espinosa G, Corpas-López V, Díaz-Sáez V, Morillas-Márquez F, Tercedor-Sánchez J, Azaña-Defez JM, et al. Cutaneous leishmaniasis by leishmania infantum: Behind granulomatous lesions of unknown aetiology. *J Eur Acad Dermatol Venereol* (2018) 32(1):117–24. doi: 10.1111/jdv.14506

73. Guery R, Walker SL, Harms G, Neumayr A, Van Thiel P, Gangneux JP, et al. Clinical diversity and treatment results in tegumentary leishmaniasis: A European clinical report in 459 patients. *PloS Negl Trop Dis* (2021) 15(10):e0009863. doi: 10.1371/journal.pntd.0009863

74. Scorza BM, Carvalho EM, Wilson ME. Cutaneous manifestations of human and murine leishmaniasis. *Int J Mol Sci* (2017) 18(6):1296. doi: 10.3390/ijms18061296

75. Simon S, Nacher M, Carme B, Basurko C, Roger A, Adenis A, et al. Cutaneous leishmaniasis in French Guiana: Revising epidemiology with pcr-rflp. *Trop Med Health* (2017) 45:5. doi: 10.1186/s41182-017-0045-x

76. Ducharme O, Simon S, Ginouves M, Prévot G, Couppie P, Demar M, et al. Leishmania naiffi and lainsoni in French Guiana: Clinical features and phylogenetic variability. *PloS Negl Trop Dis* (2020) 14(8):e0008380. doi: 10.1371/journal.pntd.0008380

77. Meireles CB, Maia LC, Soares GC, Teodoro IPP, Gadelha M, da Silva CGL, et al. Atypical presentations of cutaneous leishmaniasis: A systematic review. *Acta Trop* (2017) 172:240–54. doi: 10.1016/j.actatropica.2017.05.022

78. Silveira FT, Lainson R, De Castro Gomes CM, Laurenti MD, Corbett CEP. Immunopathogenic competences of leishmania (V.) braziliensis and l. (L.) amazonensis in American cutaneous leishmaniasis. *Parasite Immunol* (2009) 31(8):423–31. doi: 10.1111/j.1365-3024.2009.01116.x

79. Rojas-Jaimes J, Rojas-Palomino N, Pence J, Lescano AG. Leishmania species in biopsies of patients with different clinical manifestations identified by high resolution melting and nested pcr in an endemic district in Peru. *Parasite Epidemiol control* (2019) 4:e00095–e. doi: 10.1016/j.parepi.2019.e00095

80. Santrich C, Segura I, Arias AL, Saravia NG. Mucosal disease caused by leishmania braziliensis guyanensis. *Am J Trop Med hygiene* (1990) 42(1):51–5. doi: 10.4269/ajtmh.1990.42.51

81. Naiff RD, Talhari S, Barrett TV. Isolation of leishmania guyanensis from lesions of the nasal mucosa. *Memorias do Instituto Oswaldo Cruz* (1988) 83(4):529–30. doi: 10.1590/s0074-02761988000400022

82. Marsden PD. Mucosal leishmaniasis ("Espundia" escomel, 1911). *Trans R Soc Trop Med Hygiene* (1986) 80(6):859–76. doi: 10.1016/0035-9203(86)90243-9

83. Borges AF, Gomes RS, Ribeiro-Dias F. Leishmania (Viannia) guyanensis in tegumentary leishmaniasis. *Pathog Dis* (2018) 76(4). doi: 10.1093/femspd/fty025

84. Costa J, Marsden P, Llanos-Cuentas E, Netto E, Carvalho E, Barral A, et al. Disseminated cutaneous leishmaniasis in a field clinic in bahia, Brazil: A report of eight cases. *J Trop Med hygiene* (1986) 89(6):319–23.

85. Llanos-Cuentas EA, Marsden PD, Lago EL, Barreto AC, Cuba CC, Johnson WD. Human mucocutaneous leishmaniasis in três braços, bahia-Brazil: An area of leishmania braziliensis braziliensis transmission. ii. cutaneous disease. presentation and evolution. *Rev da Sociedade Bras Medicina Trop* (1984) 17:169–77. doi: 10.1590/S0037-86821984000400003

86. Parise M, Pompeu M, Coehlo Filho J, Vasconcelos I, Lima J, Oliveira E, et al. Bubonic leishmaniasis: A common manifestation of leishmania (Viannia) braziliensis infection in ceara, Brazil. *Am J Trop Med hygiene* (1995) 53(4):380–5.

87. Romero GAS, de Farias Guerra MV, Paes MG, Macêdo V. Comparison of cutaneous leishmaniasis due to leishmania (Viannia) braziliensis and l. (V.) guyanensis in Brazil: Clinical findings and diagnostic approach. *Clin Infect Dis* (2001) 32(9):1304–12. doi: 10.1086/319990

88. Boussoffara T, Chelif S, Ben Ahmed M, Mokni M, Ben Salah A, Dellagi K, et al. Immunity against leishmania major infection: Parasite-specific granzyme b induction as a correlate of protection. *Front Cell infection Microbiol* (2018) 8:397. doi: 10.3389/fcimb.2018.00397

89. Louzir H, Melby PC, Ben Salah A, Marrakchi H, Aoun K, Ben Ismail R, et al. Immunologic determinants of disease evolution in localized cutaneous leishmaniasis due to leishmania major. *J Infect Dis* (1998) 177(6):1687–95. doi: 10.1086/515297

90. Boussoffara T, Boubaker MS, Ben Ahmed M, Mokni M, Guizani I, Ben Salah A, et al. Histological and immunological differences between zoonotic cutaneous leishmaniasis due to leishmania major and sporadic cutaneous leishmaniasis due to leishmania infantum. *Parasite (Paris France)* (2019) 26:9. doi: 10.1051/parasite/2019007

91. Misra P, Singh S. Site specific microbiome of leishmania parasite and its cross-talk with immune milieu. *Immunol Lett* (2019) 216:79–88. doi: 10.1016/j.imlet.2019.10.004

92. Dubie T, Mohammed Y. Review on the role of host immune response in protection and immunopathogenesis during cutaneous leishmaniasis infection. *J Immunol Res* (2020) 2020:2496713. doi: 10.1155/2020/2496713

93. Shamsi Meymandi S, Dabiri S, Eslammanesh T, Azadeh B, Nadji M, Shamsi Meymandi M, et al. Immunopathology of anthroponotic cutaneous leishmaniasis and incidental diagnostic tool of metastatic granuloma: A case-control study. *Microbial pathogenesis* (2021) 152:104654. doi: 10.1016/j.micpath.2020.104654

94. Wijesinghe H, Gunathilaka N, Semege S, Pathirana N, Manamperi N, de Silva C, et al. Histopathology of cutaneous leishmaniasis caused by leishmania donovani in Sri Lanka. *BioMed Res Int* (2020) 2020:4926819. doi: 10.1155/2020/4926819

95. Ribeiro-Gomes FL, Peters NC, Debrabant A, Sacks DL. Efficient capture of infected neutrophils by dendritic cells in the skin inhibits the early anti-leishmania response. *PloS Pathog* (2012) 8(2):e1002536. doi: 10.1371/journal.ppat.1002536

96. Chaves MM, Lee SH, Kamenyeva O, Ghosh K, Peters NC, Sacks D. The role of dermis resident macrophages and their interaction with neutrophils in the early establishment of leishmania major infection transmitted by sand fly bite. *PloS Pathog* (2020) 16(11):e1008674. doi: 10.1371/journal.ppat.1008674

97. Müller AJ, Filipe-Santos O, Eberl G, Aebischer T, Späth GF, Bousso P. Cd4+ T cells rely on a cytokine gradient to control intracellular pathogens beyond sites of antigen presentation. *Immunity* (2012) 37(1):147–57. doi: 10.1016/j.immuni.2012.05.015

98. Belkaid Y, Piccirillo CA, Mendez S, Shevach EM, Sacks DL. Cd4+Cd25+ regulatory T cells control leishmania major persistence and immunity. *Nature* (2002) 420(6915):502–7. doi: 10.1038/nature01152

99. Choi B-S, Kropf P. Evaluation of T cell responses in healing and nonhealing leishmaniasis reveals differences in T helper cell polarization *ex vivo* and *in vitro*. *Parasite Immunol* (2009) 31(4):199–209. doi: 10.1111/j.1365-3024.2009.01094.x

100. Babay BEC, Louzir H, Kebaïer C, Boubaker S, Dellagi K, Cazenave P-A. Inbred strains derived from feral mice reveal new pathogenic mechanisms of experimental leishmaniasis due to leishmania major. *Infection Immun* (2004) 72(8):4603–11. doi: 10.1128/IAI.72.8.4603-4611.2004

101. Formaglio P, Alabdullah M, Siokis A, Handschuh J, Sauerland I, Fu Y, et al. Nitric oxide controls proliferation of leishmania major by inhibiting the recruitment of permissive host cells. *Immunity* (2021) 54(12):2724–39.e10. doi: 10.1016/j.immuni.2021.09.021

102. Glennie ND, Volk SW, Scott P. Skin-resident Cd4+ T cells protect against leishmania major by recruiting and activating inflammatory monocytes. *PloS Pathog* (2017) 13(4):e1006349. doi: 10.1371/journal.ppat.1006349

103. Hohman LS, Mou Z, Carneiro MB, Ferland G, Kratofil RM, Kubes P, et al. Protective Cd4+ Th1 cell-mediated immunity is reliant upon execution of effector function prior to the establishment of the pathogen niche. *PloS Pathog* (2021) 17(9):e1009944. doi: 10.1371/journal.ppat.1009944

104. Remer KA, Roeger B, Hambrecht C, Moll H. Natural killer cells support the induction of protective immunity during dendritic cell-mediated vaccination against leishmania major. *Immunology* (2010) 131(4):570–82. doi: 10.1111/j.1365-2567.2010.03329.x

105. Trapani JA, Smyth MJ. Functional significance of the Perforin/Granzyme cell death pathway. *Nat Rev Immunol* (2002) 2(10):735–47. doi: 10.1038/nri911

106. Lazarski CA, Ford J, Katzman SD, Rosenberg AF, Fowell DJ. Il-4 attenuates Th1-associated chemokine expression and Th1 trafficking to inflamed tissues and limits pathogen clearance. *PloS One* (2013) 8(8):e71949. doi: 10.1371/journal.pone.0071949

107. McElrath MJ, Kaplan G, Nusrat A, Cohn ZA. Cutaneous leishmaniasis. the defect in T cell influx in Balb/C mice. *J Exp Med* (1987) 165(2):546–59. doi: 10.1084/jem.165.2.546

108. Nasseri M, Modabber FZ. Generalized infection and lack of delayed hypersensitivity in Balb/C mice infected with leishmania tropica major. *Infection Immun* (1979) 26(2):611–4. doi: 10.1128/iai.26.2.611-614.1979

109. Sadick MD, Heinzel FP, Holaday BJ, Pu RT, Dawkins RS, Locksley RM. Cure of murine leishmaniasis with anti-interleukin 4 monoclonal antibody. evidence for a T cell-dependent, interferon gamma-independent mechanism. *J Exp Med* (1990) 171(1):115–27. doi: 10.1084/jem.171.1.115

110. Suffia I, Reckling SK, Salay G, Belkaid Y. A role for Cd103 in the retention of $Cd4^+$ $Cd25^+$ TReg and control of leishmania major infection. *J Immunol* (2005) 174(9):5444–55. doi: 10.4049/jimmunol.174.9.5444

111. Hoseini SG, Javanmard SH, Zarkesh SH, Khamesipour A, Rafiei L, Karbalaie K, et al. Regulatory T-cell profile in early and late lesions of cutaneous leishmaniasis due to leishmania major. *J Res Med Sci* (2012) 17(6):513–8.

112. Antonelli LR, Dutra WO, Almeida RP, Bacellar O, Carvalho EM, Gollob KJ. Activated inflammatory T cells correlate with lesion size in human cutaneous leishmaniasis. *Immunol Lett* (2005) 101(2):226–30. doi: 10.1016/j.imlet.2005.06.004

113. Filipe-Santos O, Pescher P, Breart B, Lippuner C, Aebischer T, Glaichenhaus N, et al. A dynamic map of antigen recognition by Cd4 T cells at the site of leishmania major infection. *Cell Host Microbe* (2009) 6(1):23–33. doi: 10.1016/j.chom.2009.04.014

114. Brachelente C, Müller N, Doherr MG, Sattler U, Welle M. Cutaneous leishmaniasis in naturally infected dogs is associated with a T helper-2-Biased immune response. *Veterinary Pathol* (2005) 42(2):166–75. doi: 10.1354/vp.42-2-166

115. Araujo Flores GV, Sandoval Pacheco CM, Tomokane TY, Sosa Ochoa W, Zúniga Valeriano C, Castro Gomes CM, et al. Evaluation of regulatory immune response in skin lesions of patients affected by nonulcerated or atypical cutaneous leishmaniasis in Honduras, central America. *Mediators Inflammation* (2018) 2018:3487591. doi: 10.1155/2018/3487591

116. Abbehusen MMC, Cunha J, Suarez MS, Teixeira C, Almeida VDA, Pereira LDS, et al. Immunization of experimental dogs with salivary proteins from lutzomyia longipalpis, using DNA and recombinant canarypox virus induces immune responses consistent with protection against leishmania infantum. *Front Immunol* (2018) 9:2558. doi: 10.3389/fimmu.2018.02558

117. Sher A, Sacks DL, Scott PA. Host and parasite factors influencing the expression of cutaneous leishmaniasis. *Ciba Found Symp* (1983) 99:174–89. doi: 10.1002/9780470720806.ch10

118. Maksouri H, Dang PM-C, Rodrigues V, Estaquier J, Riyad M, Akarid K. Moroccan Strains of leishmania major and leishmania tropica differentially impact on nitric oxide production by macrophages. *Parasites Vectors* (2017) 10(1):506. doi: 10.1186/s13071-017-2401-4

119. Ajdary S, Riazi-Rad F, Alimohammadian MH, Pakzad SR. Immune response to leishmania antigen in anthroponotic cutaneous leishmaniasis. *J infection* (2009) 59(2):139–43. doi: 10.1016/j.jinf.2009.05.010

120. Kumar R, Bumb RA, Salotra P. Correlation of parasitic load with interleukin-4 response in patients with cutaneous leishmaniasis due to leishmania tropica. *FEMS Immunol Med Microbiol* (2009) 57(3):239–46. doi: 10.1111/j.1574-695X.2009.00607.x

121. Katara GK, Raj A, Kumar R, Avishek K, Kaushal H, Ansari NA, et al. Analysis of localized immune responses reveals presence of Th17 and treg cells in cutaneous leishmaniasis due to leishmania tropica. *BMC Immunol* (2013) 14:52. doi: 10.1186/1471-2172-14-52

122. Bastien P, Killick-Kendrick R. Leishmania tropica infection in hamsters and a review of the animal pathogenicity of this species. *Exp Parasitol* (1992) 75(4):433–41. doi: 10.1016/0014-4894(92)90256-a

123. Carvalho LP, Passos S, Schriefer A, Carvalho EM. Protective and pathologic immune responses in human tegumentary leishmaniasis. *Front Immunol* (2012) 3:301. doi: 10.3389/fimmu.2012.00301

124. Santos Cda S, Boaventura V, Ribeiro Cardoso C, Tavares N, Lordelo MJ, Noronha A, et al. Cd8(+) granzyme b(+)-mediated tissue injury vs. Cd4(+)Ifnγ(+)-mediated parasite killing in human cutaneous leishmaniasis. *J Invest Dermatol* (2013) 133(6):1533–40. doi: 10.1038/jid.2013.4

125. Faria DR, Gollob KJ, Barbosa JJr., Schriefer A, Machado PR, Lessa H, et al. Decreased in situ expression of interleukin-10 receptor is correlated with the exacerbated inflammatory and cytotoxic responses observed in mucosal leishmaniasis. *Infection Immun* (2005) 73(12):7853–9. doi: 10.1128/iai.73.12.7853-7859.2005

126. Carvalho LP, Passos S, Bacellar O, Lessa M, Almeida RP, Magalhães A, et al. Differential immune regulation of activated T cells between cutaneous and mucosal leishmaniasis as a model for pathogenesis. *Parasite Immunol* (2007) 29(5):251–8. doi: 10.1111/j.1365-3024.2007.00940.x

127. Gollob KJ, Antonelli LR, Faria DR, Keesen TS, Dutra WO. Immunoregulatory mechanisms and Cd4-Cd8- (Double negative) T cell subpopulations in human cutaneous leishmaniasis: A balancing act between protection and pathology. *Int Immunopharmacol* (2008) 8(10):1338–43. doi: 10.1016/j.intimp.2008.03.016

128. Da-Cruz AM, de Oliveira MP, De Luca PM, Mendonça SC, Coutinho SG. Tumor necrosis factor-alpha in human American tegumentary leishmaniasis. *Memorias do Instituto Oswaldo Cruz* (1996) 91(2):225–9. doi: 10.1590/s0074-02761996000200019

129. Miranda Lessa M, Andrade Lessa H, Castro TWN, Oliveira A, Scherifer A, Machado P, et al. Mucosal leishmaniasis: Epidemiological and clinical aspects. *Braz J otorhinolaryngol* (2007) 73(6):843–7. doi: 10.1016/s1808-8694(15)31181-2

130. Lessa HA, Machado P, Lima F, Cruz AA, Bacellar O, Guerreiro J, et al. Successful treatment of refractory mucosal leishmaniasis with pentoxifylline plus antimony. *Am J Trop Med hygiene* (2001) 65(2):87–9. doi: 10.4269/ajtmh.2001.65.87

131. Cardoso TM, Machado Á, Costa DL, Carvalho LP, Queiroz A, Machado P, et al. Protective and pathological functions of $Cd8^+$ T cells in leishmania braziliensis infection. *Infection Immun* (2015) 83(3):898–906. doi: 10.1128/IAI.02404-14

132. Melby PC, Andrade-Narvaez FJ, Darnell BJ, Valencia-Pacheco G, Tryon VV, Palomo-Cetina A. Increased expression of proinflammatory cytokines in chronic lesions of human cutaneous leishmaniasis. *Infection Immun* (1994) 62(3):837–42. doi: 10.1128/iai.62.3.837-842.1994

133. Bacellar O, Lessa H, Schriefer A, Machado P, Ribeiro de Jesus A, Dutra WO, et al. Up-regulation of Th1-type responses in mucosal leishmaniasis patients. *Infection Immun* (2002) 70(12):6734–40. doi: 10.1128/iai.70.12.6734-6740.2002

134. Covre LP, Martins RF, Devine OP, Chambers ES, Vukmanovic-Stejic M, Silva JA, et al. Circulating senescent T cells are linked to systemic inflammation and lesion size during human cutaneous leishmaniasis. *Front Immunol* (2019) 9:3001. doi: 10.3389/fimmu.2018.03001

135. Covre LP, Devine OP, Garcia de Moura R, Vukmanovic-Stejic M, Dietze R, Ribeiro-Rodrigues R, et al. Compartmentalized cytotoxic immune response leads to distinct pathogenic roles of natural killer and senescent Cd8(+) T cells in human cutaneous leishmaniasis. *Immunology* (2020) 159(4):429–40. doi: 10.1111/imm.13173

136. Fantecelle CH, Covre LP, Garcia de Moura R, Guedes HLM, Amorim CF, Scott P, et al. Transcriptomic landscape of skin lesions in cutaneous leishmaniasis reveals a strong Cd8(+) T cell immunosenescence signature linked to immunopathology. *Immunology* (2021) 164(4):754–65. doi: 10.1111/imm.13410

137. Milling S. Ageing dangerously; homing of senescent Cd8 T cells in cutaneous leishmaniasis. *Immunology* (2020) 159(4):355–6. doi: 10.1111/imm.13188

138. Campanelli AP, Roselino AM, Cavassani KA, Pereira MS, Mortara RA, Brodskyn CI, et al. Cd4+Cd25+ T cells in skin lesions of patients with cutaneous leishmaniasis exhibit phenotypic and functional characteristics of natural regulatory T cells. *J Infect Dis* (2006) 193(9):1313–22. doi: 10.1086/502980

139. Punnonen J, Aversa G, Cocks BG, McKenzie AN, Menon S, Zurawski G, et al. Interleukin 13 induces interleukin 4-independent Igg4 and ige synthesis and Cd23 expression by human b cells. *Proc Natl Acad Sci* (1993) 90(8):3730–4. doi: 10.1073/pnas.90.8.3730

140. Bourreau E, Prévot G, Pradinaud R, Launois P. Interleukin (Il)–13 is the predominant Th2 cytokine in localized cutaneous leishmaniasis lesions and renders specific Cd4+ T cells unresponsive to il-12. *J Infect Dis* (2001) 183(6):953–9. doi: 10.1086/319249

141. Bourreau E, Ronet C, Darcissac E, Lise MC, Marie DS, Clity E, et al. Intralesional regulatory T-cell suppressive function during human acute and chronic cutaneous leishmaniasis due to leishmania guyanensis. *Infection Immun* (2009) 77 (4):1465–74. doi: 10.1128/IAI.01398-08

142. Bourreau E, Ronet C, Darsissac E, Lise M-C, Sainte Marie D, Clity E, et al. In leishmaniasis due to leishmania guyanensis infection, distinct intralesional interleukin-10 and Foxp3 mrna expression are associated with unresponsiveness to treatment. *J Infect Dis* (2009) 199(4):576–9. doi: 10.1086/596508

143. Ives A, Ronet C, Prevel F, Ruzzante G, Fuertes-Marraco S, Schutz F, et al. Leishmania rna virus controls the severity of mucocutaneous leishmaniasis. *Science* (2011) 331(6018):775–8. doi: 10.1126/science.1199326

144. Hartley M-A, Ronet C, Zangger H, Beverley S, Fasel N. Leishmania rna virus: When the host pays the toll. *Front Cell Infection Microbiol* (2012) 2:99. doi: 10.3389/fcimb.2012.00099

145. Eren RO, Reverte M, Rossi M, Hartley MA, Castiglioni P, Prevel F, et al. Mammalian innate immune response to a leishmania-resident rna virus increases macrophage survival to promote parasite persistence. *Cell Host Microbe* (2016) 20 (3):318–28. doi: 10.1016/j.chom.2016.08.001

146. Ginouvès M, Simon S, Bourreau E, Lacoste V, Ronet C, Couppié P, et al. Prevalence and distribution of leishmania rna virus 1 in leishmania parasites from French Guiana. *Am J Trop Med hygiene* (2016) 94(1):102–6. doi: 10.4269/ajtmh.15-0419

147. Zabala-Peñafiel A, Fantinatti M, Dias-Lopes G, da Silva JL, Miranda LFC, Lyra MR, et al. First report of leishmania rna virus 1 in leishmania (Viannia) braziliensis clinical isolates from Rio de Janeiro state - Brazil. *Memorias do Instituto Oswaldo Cruz* (2022) 117:e210107. doi: 10.1590/0074-02760210107

148. Hartley MA, Bourreau E, Rossi M, Castiglioni P, Eren RO, Prevel F, et al. Leishmaniavirus-dependent metastatic leishmaniasis is prevented by blocking il-17a. *PloS Pathog* (2016) 12(9):e1005852. doi: 10.1371/journal.ppat.1005852

149. Ginouvès M, Couppié P, Simon S, Bourreau E, Rogier S, Brousse P, et al. Leishmaniavirus genetic diversity is not related to leishmaniasis treatment failure. *Clin Microbiol infection* (2021) 27(2):286.e1–.e5. doi: 10.1016/j.cmi.2020.04.037

150. Naik S, Bouladoux N, Wilhelm C, Molloy MJ, Salcedo R, Kastenmuller W, et al. Compartmentalized control of skin immunity by resident commensals. *Science* (2012) 337(6098):1115. doi: 10.1126/science.1225152

frontiers | Frontiers in Immunology

TYPE Original Research
PUBLISHED 16 May 2023
DOI 10.3389/fimmu.2023.1129398

OPEN ACCESS

EDITED BY
Erwan Mortier,
Centre National de la Recherche Scientifique (CNRS), France

REVIEWED BY
Henrique Borges da Silva,
Mayo Clinic Arizona, United States
Marisa Benagiano,
University of Florence, Italy

*CORRESPONDENCE
Zulma Vanessa Rueda
zulma.rueda@umanitoba.ca

RECEIVED 21 December 2022
ACCEPTED 26 April 2023
PUBLISHED 16 May 2023

CITATION
Herrera M, Keynan Y, Lopez L, Marín D, Vélez L, McLaren PJ and Rueda ZV (2023) Cytokine/chemokine profiles in people with recent infection by *Mycobacterium tuberculosis*. *Front. Immunol.* 14:1129398. doi: 10.3389/fimmu.2023.1129398

Cytokine/chemokine profiles in people with recent infection by *Mycobacterium tuberculosis*

Mariana Herrera[1,2], Yoav Keynan[2,3,4], Lucelly Lopez[4,5], Diana Marín[4,5], Lázaro Vélez[6], Paul J. McLaren[2,7] and Zulma Vanessa Rueda[2,4,5]*

[1]Epidemiology Doctorate, Facultad Nacional de Salud Pública, Universidad de Antioquia, Medellín, Colombia, [2]Department of Medical Microbiology & Infectious Diseases, University of Manitoba, Winnipeg, MB, Canada, [3]Departments of Internal Medicine and Community Health Sciences, University of Manitoba, Winnipeg, MB, Canada, [4]Facultad de Medicina, Universidad Pontificia Bolivariana, Medellín, Colombia, [5]Grupo de Investigación en Salud Pública, Universidad Pontificia Bolivariana, Medellín, Colombia, [6]Grupo Investigador de Problemas en Enfermedades Infecciosas (GRIPE), Facultad de Medicina, Universidad de Antioquia, Medellín, Colombia, [7]JC Wilt Infectious Diseases Research Centre, Public Health Agency of Canada, Winnipeg, MB, Canada

Introduction: The risk of progression to tuberculosis disease is highest within the first year after *M. tuberculosis* infection (TBI). We hypothesize that people with newly acquired TBI have a unique cytokine/chemokine profile that could be used as a potential biomarker.

Methods: We evaluated socio-demographic variables and 18 cytokines/chemokines in plasma samples from a cohort of people deprived of liberty (PDL) in two Colombian prisons: 47 people diagnosed with pulmonary TB, 24 with new TBI, and 47 non-infected individuals. We performed a multinomial regression to identify the immune parameters that differentiate the groups.

Results: The concentration of immune parameters changed over time and was affected by the time of incarceration. The concentration of sCD14, IL-18 and IP-10 differed between individuals with new TBI and short and long times of incarceration. Among people with short incarceration, high concentrations of MIP-3α were associated with a higher risk of a new TBI, and higher concentrations of Eotaxin were associated with a lower risk of a new TBI. Higher concentrations of sCD14 and TNF-α were associated with a higher risk of TB disease, and higher concentrations of IL-18 and MCP-1 were associated with a lower risk of TB disease.

Conclusions: There were cytokines/chemokines associated with new TBI and TB disease. However, the concentration of immune mediators varies by the time of incarceration among people with new TBI. Further studies should evaluate the changes of these and other cytokines/chemokines over time to understand the immune mechanisms across the spectrum of TB.

KEYWORDS

tuberculosis infection, TST conversion, *Mycobacterium tuberculosis*, cytokines, chemokines, tuberculosis

1 Introduction

To reduce the burden of Tuberculosis (TB) worldwide, two key components will be necessary: 1) prevention of new TB infection (TBI) and 2) prevention of the progression from TBI to TB disease (1). The global prevalence of TBI is 24.8% (95% CI: 19.7-30.0%) and 21.2% (95% CI: 17.9-24.4%) based on the results of the interferon-gamma release assays (IGRAs) and tuberculin skin test (TST), respectively (2). Prevalence among people who are at higher risk for TBI, including people deprived of liberty (PDL), is generally higher than the community at large in the same geographic location and can be as high as 88.8% (3).

Control of the progression to TB disease relies on accurate TBI diagnosis. However, this is one of the significant challenges in the path toward TB elimination. The main limitations of current tests (TST and IGRAs) are their inability to distinguish between TBI and TB disease or to predict TB progression to active disease (4–8). Despite numerous articles reporting immune markers associated with TBI and TB disease, there is high heterogeneity in the design, participant selection, sample processing (including the stimulation protocols), measured markers and analysis that limits comparing study results (9).

TB disease occurs most frequently among people newly infected with TB, mainly within the first year of acquiring mycobacterial infection (10). Identifying and prioritizing those with new TBI within the first year of mycobacterial infection to offer TBI treatment could be an effective measure to decrease TB transmission.

This study focused on incarcerated population because of the high risk of exposure to TB and progress to TB disease (11). We analyzed data and samples collected from two prisons where we have previously shown high rates of TB infection and disease (12, 13). This study aimed to determine the plasma concentration of 18 cytokines/chemokines associated with the presence of new *Mycobacterium tuberculosis* (MTB) infection and compare it with the concentration among people with pulmonary TB diagnosis and exposed but uninfected people.

2 Methods

2.1 Ethics statement

Approval for the study was obtained from the Ethics Committees of the Universidad Pontificia Bolivariana and the University of Manitoba. The Instituto Nacional Penitenciario y Carcelario (INPEC) and the director of each prison approved the project. In all cases, written consent forms were explained and signed in the presence of two witnesses (always people deprived of liberty -PDL).

2.2 Study design, settings, and population

This cohort study was conducted in Colombia between September 2016 and December 2018 in two medium and high-security men's prisons. According to the inclusion criteria, the cohort included 124 PDL with a negative two-step TST at enrolment (Supplementary Material 1). Complete information related to the protocol, procedures, eligibility, recruitment, follow-up and epidemiological data for this cohort study has been published elsewhere (13).

During the cohort study, the TBI incidence rates varied between 2,402.88 cases per 100,000 person-months (95% CI 1,364.62 - 4,231.10) in PDL with short time of incarceration to 419.66 issues per 100,000 person-months (95% CI 225.80 - 779.95) in individuals with a long time of incarceration (13). For this reason, the cohort was divided into two subgroups: 64 "PDL with short incarceration" for those who were enrolled in follow-up upon incarceration or within the first three months of incarceration, and 60 "PDL with long incarceration" for people who started their follow-up after one year or more of imprisonment.

The primary outcome in the cohort was a new TBI (documented TST conversion). In the end, there were 25 new TBIs among 124 people with a negative two-step TST at enrolment. Thirteen out of 25 were people with short incarceration, and 12/25 new TBIs were people with long incarceration. Ninety-nine individuals remained TST negative after the follow-up. Supplementary Material 1 has information about the new TBI diagnosis criteria.

In addition, we included 51 of 88 (57.95%) people with a new pulmonary TB diagnosis during the study period. The prison healthcare system performed the microbiological diagnoses, and we also collected sputum samples to confirm *Mycobacterium tuberculosis*. People were invited to participate in the study after the TB diagnosis. Supplementary Material 1 describes the eligibility criteria and the TB diagnosis.

2.3 Procedures

2.3.1 Data collection

The socio-demographic data were collected from all individuals at baseline: age; history and time of prior incarceration; use of drugs (inhaled, injected, or smoked), smoking, and alcohol consumption; comorbidities (chronic obstructive pulmonary disease, diabetes, chronic kidney disease, HIV, and any other immunosuppressive condition); contact with a person diagnosed with TB disease (outside and inside the prison); history of prior TB, including date of the last episode, and outcome; weight and height. To determine previous exposure to the BCG vaccine, the field team sought the presence of the BCG scar.

2.3.2 Blood sample collection

All PDL included in the study provided blood samples at baseline and every three months during their follow-up. The samples were collected in sodium heparin tubes, and plasma was separated and stored at -80°C until processing.

We processed 148 samples as follows: a) 58 samples of PDL with a new TBI (21 samples at baseline, 18 at pre-conversion [3 months before TST conversion], and 19 at the time of TST conversion); b) 43 samples of PDL of the last follow–up available among people that remain TST negative and had the longest follow-ups; c) and 47 samples at baseline of people diagnosed with TB disease (Figure 1).

We excluded 4/51 participants diagnosed with TB because 3 had HIV co-infection, and one did not have a plasma sample at baseline.

2.3.3 Cytokines and chemokine selection and detection

The cytokines/chemokines quantified in the study were selected based on: 1) a systematic review we conducted to identify the relevant cytokines/chemokines associated with TBI (14), 2) published reviews about the pathophysiology of *M. tuberculosis* infection (15–17), 3) results from animal models (guinea pig, macaques and mice) (15, 16, 18–20), 4) immune response to intracellular bacteria (21, 22), 5) *M. tuberculosis* pathway (23) (available at: http://www.genome.jp/kegg/pathway.html) and 6) our previous results among people diagnosed with TB disease (24).

Commercial multiplex and single bead-based fluorescent assay kits were used to quantify 18 cytokines/chemokines of interest from plasma samples as follows: Macrophage Inflammatory Protein 3α (MIP-3α/CCL20), Human Cytokine/Chemokine magnetic Panel III, Milliplex® Map kit); Interleukin 18 (IL-18), Human IL-18 Singleplex Magnetic Bead kit, Milliplex® Map kit; soluble CD14 (sCD14), Human Cardiovascular Disease (CVD) Panel 6 Magnetic Bead kit, Milliplex® Map kit; Eotaxin 1 (CCL11), Interferon gamma (INF-γ), Interleukin 5 (IL-5), Interleukin 6 (IL-6), Interleukin 10 (IL-10), Interleukin IL-12 p40 homodimer (IL-12[p40]), Interleukin 13 (IL-13), Interleukin 15 (IL-15), Interleukin (IL-17), Interleukin-1 receptor antagonist (IL-1RA), human interferon-inducible protein 10 (CXCL10/IP-10), monocyte chemoattractant protein-1 (CCL2/MCP-1), macrophage inflammatory protein 1α (CCL3/MIP-1α), macrophage inflammatory protein 1β (CCL4/MIP-1β), Tumor necrosis factor alpha (TNF-α), Human Cytokine/Chemokine magnetic Bead Panel, Milliplex® Map kit, Millipore Corporation, Billeria, MA, USA.

The assays were performed according to the manufacturer's instructions, using 25 µl of plasma per sample (5 µl to run the sCD14 assay) and overnight incubation. Standards were reconstituted and serially diluted to generate standard curves. Two controls with low and high concentrations, provided by the commercial kit, were included in each assay and considered positive controls for the experiment. Results were analyzed in the BioPlex-200 instrument (Bio-Rad, Mississauga, Canada), reported as mean fluorescence intensity, and converted to pg/ml or ng/ml using the BioPlex® Manager version 6.0 (Bio-Rad, Mississauga, ON).

To control for potential biases, all specimens were analyzed, blinded to the clinical status, and longitudinal samples were performed by the same person and analyzed on the same plate. Samples with values outside the standard curve range were assigned a value of one-half of the lower limit of detection (LOD divided by 2) in pg/mL.

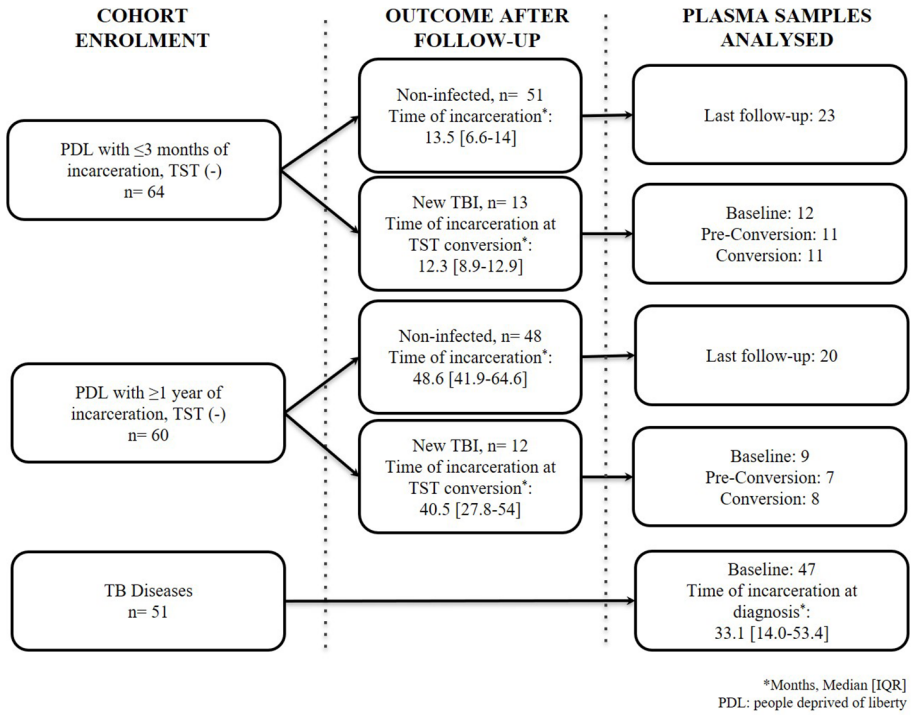

FIGURE 1
Flow chart of people included in the study. TB: tuberculosis; TST: tuberculin skin test. New TBI [people with negative two-step TST that became positive during follow-up were divided into TBI with short incarceration (they had ≤3 months of incarceration at enrolment) and TBI with long incarceration (they had ≥1 year of incarceration at enrolment)].

2.4 Analysis

We used descriptive statistics (median [IQR] and n [%]) to report cytokines/chemokines and socio-demographic variables, and chi-squared and Kruskal Wallis tests to evaluate differences between groups. The primary outcome of this study was a new TBI stratified by short and long incarceration.

In individuals with new TBI, we compared the concentration of the immune mediators at baseline, three months before the TST conversion (pre-conversion point) and TST conversion. Wilcoxon test was used to compare the changes in cytokines/chemokines over time. In addition, we used the Mann-Whitney test to compare each follow-up between individuals with a new TBI with short and long times of incarceration.

Then, we compared plasma concentration of cytokines/chemokines in people with new TBI with short and long incarceration to non-infected individuals and people diagnosed with pulmonary TB using the Kruskal-Wallis test. We used multinomial logistic regression to determine the association between each cytokine/chemokine and new TBI with short or long incarceration compared to TB disease and non-infected groups. All cytokines/chemokines were log-transformed to adjust for skewness before the multivariable analysis. Variables included in the final regression model were selected using the biological plausibility criteria, a manual backward elimination method. We adjusted the model by age, BCG scar, contact with a person diagnosed with TB and drug use. All models were adjusted by cluster effect (15 different courtyards in the two prisons).

All analyses were done using STATA® version 14. A two-tailed p-value <0.05 was considered significant. Considering the multiple comparisons were made when we evaluated the cytokine concentration between the groups, a *p*-value <0.01 was considered significant, applying the Bonferroni correction.

3 Results

3.1 Study participants

The median time of TST conversion (new TBI) among the short incarceration group was 12.3 months, and in the new TBI with long incarceration group was 40.5 months (Figure 1). The majority of new TBIs occurred in one prison (75%).

There was no significant difference between groups regarding the mean age (Table 1). Ten individuals in the study had a body mass index ≤18.5 kg/m^2, and 9 of them had a TB diagnosis. Individuals diagnosed with TB reported higher consumption of smoked drugs (61.7%) and inhaled drugs (34%) compared to the other groups (p ≤ 0.001). There was no difference in the frequency of alcohol consumption and tobacco use (p>0.051) (Table 1). Having contact with a person diagnosed with TB was reported in 8.3% of the new TBI group, 34% of people diagnosed with TB, and 19.2% in the non-infected group. Table 1 reports socio-demographic information at baseline.

IL-10, IL-12, IL-13, IL-15, IL-17A, IL-1RA, IL-5, IL-6 and MIP-1α had more than 40% of the results below the lower detection limit. We did not see consistent trends of these results within and between groups or by the follow-up time. Therefore, these cytokines/chemokines were excluded from the analysis and results.

3.2 The concentration of cytokines/chemokines among the new TBI group is affected by the time of incarceration

Supplementary Material S2 reports the median concentrations of all immune parameters at baseline, pre-conversion and TST conversion by short and long incarceration among the new TBI group.

Our results showed that there were no differences in the concentrations of MIP-3α (Figure 2A), Eotaxin (Figure 2B), INF-γ (Figure 2D) and MIP-1β (Figure 2F). We found higher concentrations of sCD14 at baseline compared to pre-conversion and TST conversion points; the change was more evident in PDL with long incarceration (Figure 2C). PDL with short incarceration showed increased plasma levels of IL-18 at baseline and pre-conversion, compared to the time of TST conversion (Figure 2E). MCP-1 showed an increased concentration over time, with a higher concentration at the time of TST conversion (Figure 2G). We also found that in PDL with short incarceration, IP-10 decreased three months before TST conversion (Figure 2H).

The concentrations of sCD14 (Figure 2C) and IL-18 (Figure 2E) were higher among people with new TBI and short incarceration compared to those with long incarceration ($p< 0.05$). The concentration of IP-10 (Figure 2H) was higher in people with long incarceration.

3.3 Cytokines/chemokines concentrations are different between groups

We found higher concentrations of sCD14 and TNF-α among people diagnosed with TB, MIP-3α among people with new TBI and short incarceration, and IL-18 and MCP-1 among people with new TBI and long incarceration (Table 2). We did not find differences in the concentration of Eotaxin, INF-γ, MIP-1β, and IP-10 among the groups (Figures 3B, 3D, 3F, 3H).

The concentration of sCD14 was higher in the TB disease group compared to non-infected individuals and new TBI with long incarceration group (Figure 3C). TNF-α was higher in the TB disease group compared to non-infected individuals (Figure 3I). MIP-3α was higher in the new TBI with short incarceration compared to the TB disease group (Figure 3A). MCP-1 was higher in the new TBI with long incarceration compared to the TB disease group (Figure 3G). IL-18 (Figure 3E) and MCP-1 (Figure 3G) concentrations were lower in the TB disease group compared to non-infected individuals.

3.4 There are cytokines/chemokines associated with a new TBI and TB disease

In the multivariable analysis, only having a BCG scar was associated with decreased risk of a new TBI in people with short

10.3389/fimmu.2023.1129398

TABLE 1 Baseline characteristics of study participants diagnosed with a new TBI (with short and long incarceration), TB disease, and non-infected people.

Variable	Not infected (n=47) n (%)	New TBI, short incarceration (n=11) n (%)	New TBI, long incarceration (n=13) n (%)	TB disease (n=47) n (%)	*p-value*
Age, years, median [IQR]	34 [30-44]	33 [30-39]	31 [25-56]	32 [26-37]	0.201
Time of current incarceration, months, median [IQR]	11.2 [1.6-39.4]	12.3 [8.9-12.9]	40.5 [27.8-54]	33.1 [14-53.4]	**0.001**
BMI ≤18.5	1 (2.2)	0	0	9 (19.1)	**0.013**
Prison					**<0.001**
Prison One	22 (46.8)	7 (63.6)	11 (84.6)	47 (100.0)	
Prison Two	25 (53.2)	4 (36.7)	2 (15.4)	0	
Comorbidities	9 (19.1)	0	4 (30.7)	9 (19.1)	0.284
COPD	3 (6.4)	0	1 (7.7)	3 (6.4)	0.849
Diabetes mellitus	1 (2.1)	0	2 (15.4)	2 (4.3)	0.173
Psychiatric illness	3 (6.4)	0	1 (7.7)	0	0.256
Others	3 (6.4)	1 (9.1)	0	4 (8.5)	0.736
Inhaled drug use					**0.001**
Never	32 (68.1)	6 (54.5)	9 (69.2)	14 (30.0)	
Past	11 (23.4)	5 (45.5)	3 (23.1)	16 (34.0)	
Current	4 (8.51)	0	1 (4.17)	17 (34.0)	
Smoked drug use					**<0.001**
Never	28 (59.6)	7 (63.6)	7 (53.8)	7 (14.9)	
Past	11 (23.4)	2 (18.2)	3 (23.1)	11 (23.4)	
Current	8 (17.0)	2 (18.2)	3 (23.1)	29 (61.7)	
Tobacco consumption					0.294
Never	18 (38.3)	6 (54.5)	3 (23.1)	11 (23.4)	
Past	12 (25.5)	1 (9.1)	4 (30.7)	10 (21.3)	
Current	17 (36.2)	4 (36.4)	6 (46.1)	26 (55.3)	
Alcohol use					0.051
Never	12 (25.5)	3 (27.4)	1 (7.7)	8 (17.0)	
Past	22 (46.8)	7 (63.6)	8 (61.5)	17 (36.1)	
Current	12 (25.5)	0	3 (23.1)	22 (46.8)	
Occasional	1 (2.13)	1 (9.1)	1 (7.7)	0	
History of contact with a TB case	9 (19.1)	1 (9.1)	1 (7.7)	16 (34.0)	0.087
Contact with prisoner	7 (14.9)	1 (9.1)	1 (7.7)	14 (29.8)	
Contact with relative	2 (4.3)	0	0	2 (4.1)	
BCG Scar	45 (95.7)	8 (72.2)	8 (61.5)	41 (87.2)	**0.007**

IQR, interquartile range; TB, tuberculosis; COPD, Chronic obstructive pulmonary disease; BCG, Bacillus Calmette-Guerin. New TBI [people with negative two-step TST that became positive during follow-up were divided into TBI with short incarceration (they had ≤3 months of incarceration at enrolment) and TBI with long incarceration (they had ≥1 year of incarceration at enrolment)]. *p-value using the Kruskal-Wallis test for quantitative variables and Chi-square test for qualitative variables. Variables with statistical significance are shown in bold.

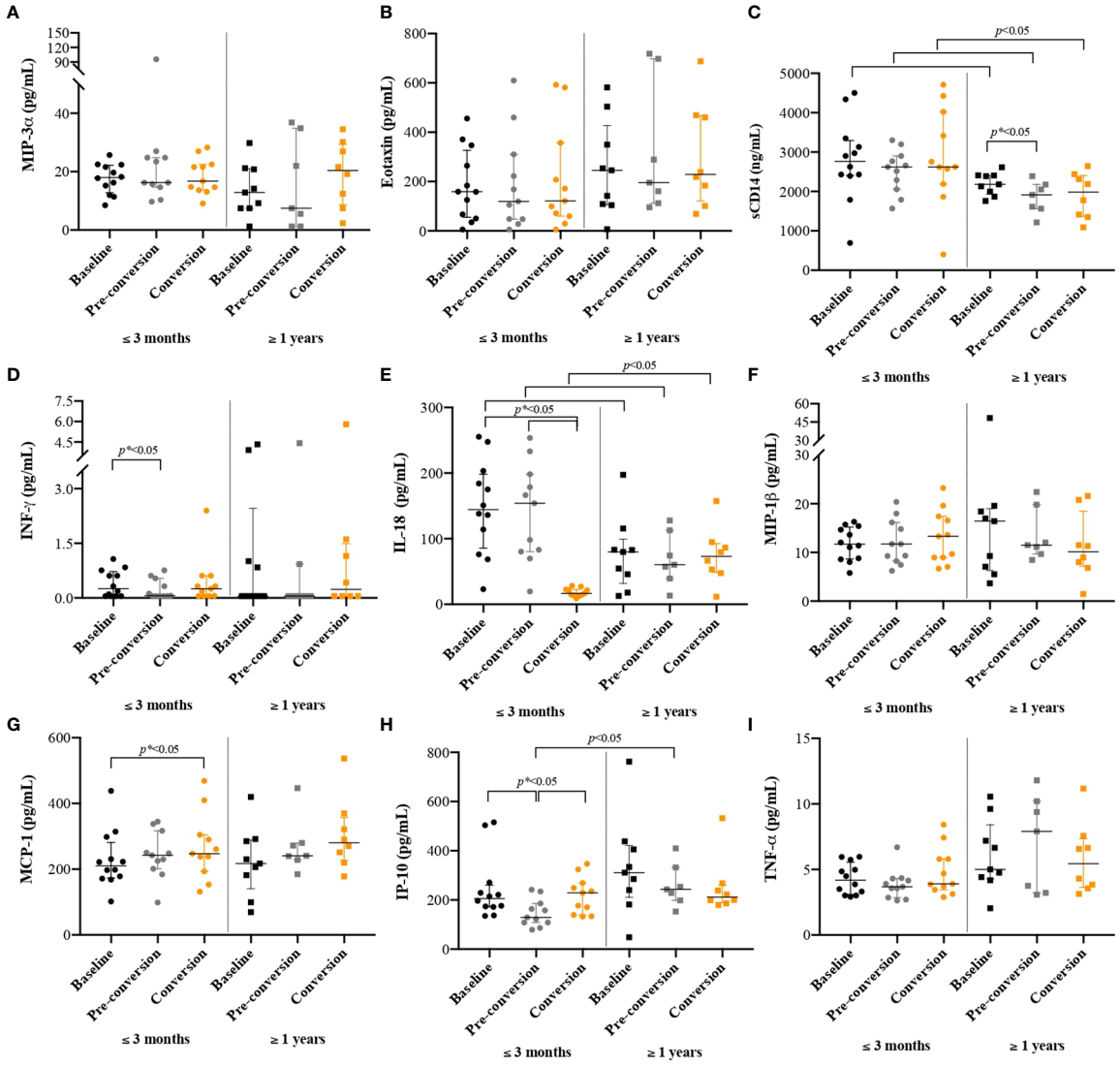

FIGURE 2
Cytokines/chemokines concentrations among people with new latent tuberculosis infection at baseline, pre-conversion, and TST conversion, by the time of incarceration. New TBI [people with negative two-step TST that became positive during follow-up were divided into new TBI with short incarceration (they had ≤3 months of incarceration at enrolment) and new TBI with long incarceration (they had ≥1 year of incarceration at enrolment)]. Values are reported in pg/ml for all cytokines/chemokines, except for sCD14 where results are reported in ng/ml. Boxplots are median and interquartile range. **(A)** MIP-3α; **(B)** Eotaxin; **(C)** sCD14; (ng/ml) **(D)** INF-γ; **(E)** IL-18; **(F)** MIP-1β; **(G)** MCP-1; **(H)** IP-10; **(I)** TNF-α.

incarceration. The other socio-demographic variables (age, history of having contact with a person diagnosed with TB, and drug use) were not associated with new TBI or TB disease. Although having a BMI of less than 18 kg/m^2 and alcohol consumption were significant factors, the multinomial model did not converge when we included those variables due to the low number of outcomes in the 'yes' category.

In the final multinomial model (Table 3), we identified that higher concentrations of MIP-3α were associated with a higher risk of a new TBI. The presence of a BCG scar and higher concentrations of Eotaxin were associated with a lower risk of a new TBI among people with short incarceration compared to non-infected individuals.

Higher plasma concentrations of sCD14 and TNF-α were associated with an increased risk of TB disease. Finally, we found that higher concentrations of IL-18 and MCP-1 were associated with a lower risk of TB disease compared to non-infected individuals (Table 3).

4 Discussion

The main results of our study were: 1) the concentration of immune mediators in persons with a new TBI varies according to the time of incarceration (short or long incarceration); and 2) Among people with short incarceration, high concentrations of MIP-3α were associated with a higher risk of a new TBI, and higher concentrations of Eotaxin was associated with a lower risk of a new TBI. Higher concentrations of sCD14 and TNF-α were associated with a higher risk of TB disease, and higher concentrations of IL-18 and MCP-1 were associated with a lower risk of TB disease.

TABLE 2 The concentration cytokine/chemokine and differences between the groups (new TBI [with short and long incarceration], TB disease, and non-infected).

Cytokines/ Chemokines	Non-infected pg/ml (IQR)	New TBI and short incarceration pg/ml (IQR)	New TBI and long incarceration pg/ml (IQR)	TB disease pg/ml (IQR)	*p-value**
sCD14 (ng/ml)	2213.8 (1851.9-2579.9)	2610.8 (1863.6-3413.0)	2314.9 (1596.8-2619.5)	3063.4 (2605.7-4233.1)	**0.0001**
MIP-3α	13.6 (10.9-18.2)	21.6 (14.8-26.9)	14.2 (9.9-24.9)	8.7 (4.1-13.4)	**0.0001**
IL-18	125.4 (84.5-220.8)	91.6 (86.3-198.9)	148.4 (59.9-191.1)	64.8 (38.1-100.5)	**0.0001**
Eotaxin	249.3 (141.3-375.9)	146.8 (59.8-218.8)	334.0 (100.4-587.2)	190.4 (118.3-333.4)	0.2421
INF-γ	0.19 (0.05-0.8)	0.4 (0.05-0.6)	0.12 (0.05-0.3)	1.44 (0.05-4.1)	0.1714
MIP-1β	11.1 (8.2-17.0)	12.4 (9,7-19.6)	8.5 (6.7-15.5)	15.0 (10.1-19.2)	0.1532
TNF-α	4.4 (3.7-6.3)	4.3 (3.5-5.8)	5.4 (3.8-7.0)	6.6 (5.2-8.5)	**0.0466**
IP-10	217.4 (133.2-303.6)	233.7 (177.1-267.5)	199.7 (174.8-280.2)	328.7 (179.7-518.6)	0.0842
MCP-1	246.9 (207.3-307.5)	253.9 (193.1-369.8)	256.0 (243.1-305.8)	174.2 (133.6-231.7)	**0.0006**

IQR: interquartile range; TB: tuberculosis; TBI: tuberculosis infection *p value using Kruskal-Wallis test. New TBI [people with negative two-step TST that became positive during follow-up were divided into TBI with short incarceration (they had ≤3 months of incarceration at enrolment) and TBI with long incarceration (they had ≥1 year of incarceration at enrolment)]. Variables with statistical significance are shown in bold.

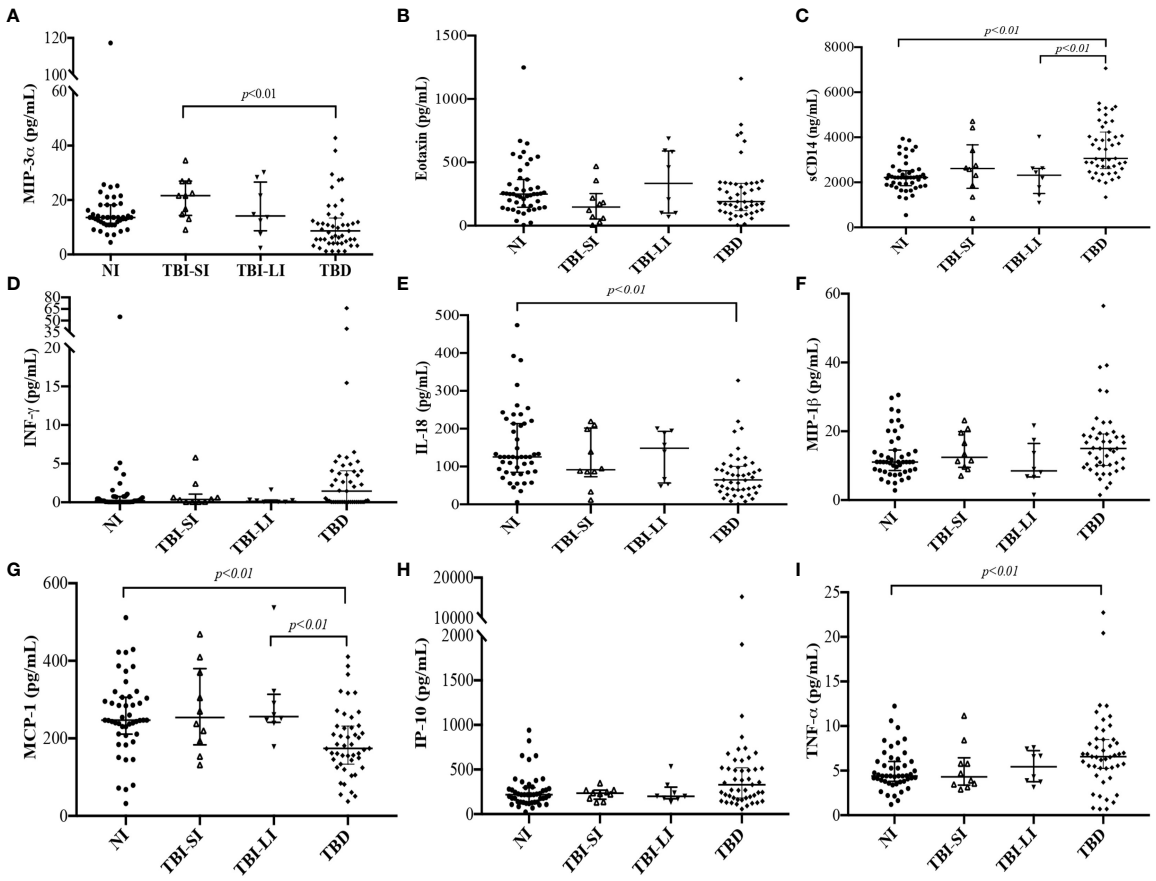

FIGURE 3
Immune parameters concentrations among people who converted the TST (new TBI with short incarceration [n= 11] and TBI with long incarceration [n= 13]), people diagnosed with TB disease (n=47), and non-infected people (n=47). New TBI [people with negative two-step TST that became positive during follow-up were divided into new TBI with short incarceration (they had ≤3 months of incarceration at enrolment) and new TBI with long incarceration (they had ≥1 year of incarceration at enrolment)]. **(A)** MIP-3α; **(B)** Eotaxin; **(C)** sCD14 (ng/ml); **(D)** INF-γ; **(E)** IL-18; **(F)** MIP-1β; **(G)** MCP-1; **(H)** IP-10; **(I)** TNF-α. Values reported in pg/ml for all cytokines, except for sCD14 reported in ng/ml. Boxplots are median and interquartile range. *p-value* using the Mann-Whitney U test and adjusted by multiple comparisons.

10.3389/fimmu.2023.1129398

TABLE 3 Cytokines/chemokines associated with new TBI with short or long incarceration, TB disease compared to non-infected people in a multinomial regression model.

Cytokines/ Chemokines (Log transformed)	New TBI with short incarceration		New TBI with long incarceration		TB disease	
	cRR^{+} [95% CI]	aRR*$^{+}$ [95% CI]	cRR^{+} [95% CI]	aRR*$^{+}$ [95% CI]	cRR^{+} [95% CI]	aRR*$^{+}$ [95% CI]
Non-infected	1 [Reference]	1 [Reference]	1 [Reference]	1 [Reference]	1 [Reference]	1 [Reference]
sCD14	1.17 [0.09-13.92]	2.62 [0.59-11.69]	0.87 [0.31-2.41]	0.76 [0.09-6.40]	24.17 [8.66-67.42]	**77.78 [7.60-796.16]**
MIP-3α	2.40 [1.47-3.93]	**7.46 [2.01-26.72]**	0.80 [0.29-2.18]	0.96 [0.32-2.93]	0.28 [0.11-0.66]	0.33 [0.09-1.19]
IL-18	0.55 [0.16-1.88]	0.31 [0.04-2.57]	0.86 [0.39-1.93]	1.00 [0.48-2.08]	0.30 [0.10-0.88]	**0.13 [0.02-0.91]**
Eotaxin	0.53 [0.35-0.83]	**0.35 [0.19-0.65]**	1.27 [0.56-2.90]	1.31 [0.60-2.84]	0.81 [0.53-1.25]	1.35 [0.61-2.98]
INF-γ	1.09 [0.76-1.56]	1.13 [0.60-2.13]	0.85 [0.52-1.39]	0.81 [0.35-1.87]	1.28 [1.05-1.56]	1.45 [0.91-2.30]
MIP-1β	1.56 [0.61-4.01]	6.87 [0.74-63.74]	0.49 [0.25-0.98]	0.50 [0.09-2.55]	1.78 [0.92-3.45]	2.91 [0.73-11.57]
TNF-α	1.10 [0.44-2.76]	0.27 [0.04-1.80]	1.34 [0.61-2.92]	2.53 [0.23-28.28]	2.00 [0.64-6.27]	**3.38 [1.01-11.24]**
IP-10	1.13 [0.72-1.77]	0.72 [0.17-2.95]	1.21 [0.65-2.27]	1.06 [0.16-6.80]	2.58 [1.51-4.42]	1.41 [0.29-6.97]
MCP-1	1.81 [0.35-9.40]	1.75 [0.10-29.26]	3.15 [1.74-5.69]	1.65 [0.30-8.91]	0.9 [0.15-0.55]	**0.03 [0.006-0.18]**
BCG scar	0.12 [0.01-1.04]	**0.04 [0.002-0.43]**	0.07 [0.01-0.57]	0.12 [0.003-5.67]	0.29 [0.05-1.52]	0.07 [0.003-1.32]
Age in years	0.98 [0.95-1.02]	0.95 [0.88-1.02]	1.02 [0.99-1.04]	1.01 [0.95-1.08]	0.98 [0.95-1.00]	0.98 [0.91-1.04]

cRR, crude relative risk *aRR: adjusted relative risk based on multinomial logistic regression analysis; TB, tuberculosis. New TBI [people with negative two-step TST that became positive during follow-up were divided into TBI with short incarceration (they had ≤3 months of incarceration at enrolment) and TBI with long incarceration (they had ≥1 year of incarceration at enrolment)]. All variables included in the multinomial regression model were selected through a manual backward elimination method. $^{+}$The bivariable and multivariate models are adjusted by cluster effect (15 courtyards). Variables with statistical significance are shown in bold.

In this study, immune mediators' concentration varied among people newly infected by the time of incarceration. Levels of sCD14 and IL-18 were increased in individuals with short incarceration and IP-10 in those with long incarceration. These variations between people could occur for several reasons: 1) early exposure to *M. tuberculosis* can induce increased macrophage activation, leading to elevated sCD14 concentration. 2) Continuously exposed individuals (≥1 year in prison) could eliminate the bacteria repeatedly, owing to an effective immune response. 3) Other factors associated with prison entry include stress, physical activity, or dietary patterns. Several studies have documented changes in the production of pro-inflammatory cytokines when people are under a chronic stressful situation (25), variable levels of physical activity/exercise (26), or when a stress-generating situation is compounded by an infectious process, such as influenza vaccination (27). People deprived of liberty are exposed to acute and chronic stressors, given the social and safety conditions that prevail in prisons in which they live or the changes associated with freedom deprivation (28). In other words- the inflammatory milieu induced by environmental factors related to imprisonment may alter the immune response, thereby increasing the risk of MTB infection (29).

We found that increased circulating levels of MIP-3α were associated with a higher risk of having new TBI after short incarceration. The MIP-3α/CCL20 is a dendritic cell, T cell, B cell and monocyte chemoattractant involved in lymphocyte homeostasis and trafficking, cell proliferation and activation (21, 30, 31). Rivero-Lezcano et al. reported that the expression of MIP-3α increased up to 39-fold when monocytes from healthy donors were infected with *M. tuberculosis* (32), and Lee et al. showed that MIP-3α was up-regulated in PBMC and bronchoalveolar lavage fluids from people diagnosed with TB compared to healthy controls after *in vitro* stimulation with the 30 kDa antigen (Ag) of *M. tuberculosis* (33). MIP-3α concentration in serum/plasma samples is an attractive target for further evaluation in newly acquired MTB infection studies among people with documented recent exposure. In our research, PDL with a new TBI and with short incarceration had lower circulating levels of Eotaxin. Eotaxin has been reported as inhibited after *in vitro* infection by *M. tuberculosis* (34), decreased in people diagnosed with TB disease, and with increasing levels after anti-TB treatment (35).

After adjusting for the other co-variables, individuals with elevated concentrations of MCP-1, a potent chemotactic factor for monocytes (36), had a lower risk of TB disease. In a model of macaques previously vaccinated with BCG, the production of β-chemokine MCP-1 increased in lung lesions of animals after five weeks of infection with MTB (37). These immune molecules are mainly associated with the recruitment of monocytes/macrophages, in keeping with the observation that animals had a higher frequency of macrophages (CD14+ CD68+) in peripheral blood three weeks post-infection with MTB (37). In this case, the increase in cells and β-chemokines may be a sign of the recruitment of these cells from peripheral blood to the site of infection in the lung. Our results show that the concentrations of MCP-1 were lower among the TB disease group compared to non-infected individuals; however, most reports about this chemokine have shown increased concentration among people diagnosed with TB (38, 39). Results may be different because of stimulation with mycobacterial antigens or the absence of stimulation in whole blood samples. Increased concentrations of MCP-1 have been reported in stimulated samples from individuals

diagnosed with active TB, but higher concentrations in unstimulated samples among non-infected individuals compared to individuals diagnosed with TB (40). Some additional explanations for those differences between the studies are the ancestry of the population, the specimen (serum, whole blood, or supernatants of cultured PBMC), and the presence of genetic polymorphisms regulating IL-18 or MCP-1 production (41) in the populations, which could alter the final structure, concentration, or function of the protein.

We also found that higher concentrations of sCD14 and TNF-α were associated with a higher risk of TB disease. These immune mediators are highly involved in monocyte/macrophage activation and trafficking pathways (42, 43). Macrophages are the main niche for the growth and survival of *M. tuberculosis* (44); likewise, macrophages are the most important cells for infection control in animal and human models and critical cells in the host response during active disease (44–46) trying to limit the systemic spread of mycobacteria (47). Soluble CD14, whose membrane-bound portion is highly expressed in these cells, is a mediator of macrophage activation and serves as a receptor for mycobacterial lipoarabinomannan (43). It has been reported among people diagnosed with TB disease (48, 49), with or without concurrent HIV infection (47, 50), and individuals with diabetes mellitus (51). A published article by Lawn SD et al. suggests that sCD14 might increase the concentration of TNF-α due to the high load of mycobacterial antigens among people living with HIV and co-infected with TB disease (47). In our study, people diagnosed with TB had higher plasma concentrations of TNF-α, presumably contributing to cell recruitment, the production of other pro-inflammatory cytokines, and apoptosis of MTB-infected cells (52). Similar to our study, TNF-α has been reported to be increased in adults (49, 53–56) and children (57) diagnosed with TB disease.

Our findings show lower concentrations of IL-18 and MCP-1 among the TB group compared to non-infected individuals. Other researchers have shown that *M. tuberculosis*-stimulated culture supernatants from people diagnosed with TB have lower concentrations of IL-18 compared to those from healthy TST converters (58). IL-18 has an important function in TB as a pro-inflammatory cytokine (59); it plays an important role in the T-cell-helper type 1 (Th1) response, primarily by its ability to induce IFN-γ production in T cells and natural killer (NK) cells (60) and in combination with IL-12 triggers the antimicrobial protein cathelicidin and autophagy, resulting in inhibition of intracellular mycobacteria in macrophages and lung epithelial cells (61). Still, studies in humans are not conclusive. For example, Yamada G et al. (62) showed that increased serum IL-18 concentrations were associated with TB disease compared to healthy individuals (including TST converters).

Future studies are needed to validate and complement our cytokine and chemokine findings.

We did not find associations between IP-10, IL-17, IL-10, and a new TBI (the first one was not different between groups, and the latter two had concentrations below the lower detection limit), contrary to other publications (63, 64). This discrepancy may be attributed to the measurement of immune mediators after mycobacterial antigen and mitogen stimulation in prior studies (53, 56, 65–75), in contrast to the unstimulated measurements in our study. In the case of IL-17, there are six members in the IL-17 family, including IL-17A. IL-17B, IL-17C, IL-17D, IL-17E, and IL-17F (76, 77). Our study only measured Il-17A. Therefore, it is possible that other not measured subunits, such as IL-17F, were increased in plasma samples. In the same way, IL-17 is described as essential in the lung during recent infection (60). Still, perhaps blood sampling in the context of recent infection may have contributed to the reduced systemic level of IL-17.

Another reason for discrepant results may be that individuals included in other longitudinal studies were evaluated with only one TST administration, and those with a negative TST may represent a false negative result (61). In our previous studies, a second administration of TST identified an additional 11.6% positive TST individuals (78).

Our study's most crucial distinguishing feature is the study design (cohort). In cross-sectional studies, the duration an individual has had TBI cannot be quantified. The main limitation of a cross-sectional approach is that human and primate studies have demonstrated there is a spectrum of TB stages (5, 6, 79, 80), on which there is little published work (4, 6), and that potentially could alter the concentration of the immune parameters according to the stage of the infection. The cohort design allowed us to quantify the concentration of cytokines at a temporal point close to the time of infection (new infection) and identify individuals in whom infection occurred recently. Borgstrom WE et al., using mathematical models and CD4+ T-cell flow-cytometry data, showed that the most specific prediction of recent TBI was a high proliferative CD4+ response to CFP-10 and PPD, and a low response to ESAT-6 at ≤1 month after exposure (81).

Our study has other strengths: rigorous selection criteria among people diagnosed with TB, including only those with microbiological confirmation and with less than 15 days of treatment, rule out of booster effect, and rigorous monitoring and follow-up every three months to all uninfected participants.

The main limitation of this study is that some bacterial factors may modify the response to cytokines, such as the virulence of some strains; however, in people with TBI, it is not feasible to isolate the mycobacterium, and therefore the role of MTB strain cannot be assessed yet.

5 Conclusion

Our study found that immune markers vary according to the time of incarceration. Among people with short incarceration, high concentrations of MIP-3α were associated with a higher risk of a new TBI, and higher concentrations of Eotaxin were associated with a lower risk of a new TBI. Higher concentrations of sCD14 and TNF-α were associated with a higher risk of TB disease, and higher concentrations of IL-18 and MCP-1 were associated with a lower risk of TB disease. It is necessary to have more cohort studies that evaluate the changes over time of these and other cytokines/chemokines to understand the immune mechanisms across the spectrum of TB.

Data availability statement

The raw data supporting the conclusions of this article will be made available by the authors, without undue reservation.

Ethics statement

The studies involving human participants were reviewed and approved by Ethics Committees of the Universidad Pontificia Bolivariana and the University of Manitoba. The patients/participants provided their written informed consent to participate in this study.

Author contributions

Substantial contributions to the conception or design of the work: MH, YK, ZR. Acquisition of data: MH. Analysis and interpretation of data: MH, YK, LL, DM, ZR. Drafting the article and revising it critically for important intellectual content: MH, YK, LV, PM, ZR. Final approval of the version to be published: MH, YK, LV, LL, DM, PM, ZR. Agreement to be accountable for all aspects of the work in ensuring that questions related to the accuracy or integrity of any part of the work are appropriately investigated and resolved: MH, YK, LL, DM, LV, PM, ZR. Principal investigator and funding acquisition: ZVR. All authors contributed to the article and approved the submitted version.

Funding

This article (the design of the study, the collection, analysis, and interpretation of data) was funded by The Administrative Department of Science, Technology and Innovation (Colciencias), as part of the research project entitled "Host gene expression profile used to identify latent TB infection and the transition to active disease - Perfil de la expresión génica del hospedero para identificar tuberculosis latente y la transición a enfermedad activa", grant number: 121071249878. And the project "Pro-inflammatory patterns of cytokine/chemokine associated with latent tuberculosis in people deprived of liberty (PDL)," grant number: 639B-06/16-55, funded by Universidad Pontificia Bolivariana. The Administrative Department of Science, Technology and Innovation (Colciencias), scholarship program #647 in Colombia, and Emerging Leaders of Americas Program, 2018, a scholarship from the Government of Canada support the Ph.D. student. This manuscript was also supported, in part, by the Canada Research Chairs Program for ZR. Award number: 950-232963.

Acknowledgments

The authors are grateful to all of the PDL who accepted to participate in the study, to INPEC (Instituto Nacional Penitenciario y Carcelario de Colombia), and to the director of each prison and all personnel working there for their support in performing the study.

Conflict of interest

The authors declare that the research was conducted in the absence of any commercial or financial relationships that could be construed as a potential conflict of interest.

Publisher's note

Supplementary material

The Supplementary Material for this article can be found online at: https://www.frontiersin.org/articles/10.3389/fimmu.2023.1129398/full#supplementary-material

References

1. Matteelli A, Sulis G, Capone S, D'Ambrosio L, Migliori GB, Getahun H. Tuberculosis elimination and the challenge of latent tuberculosis. *Presse Médicale* (2017) 46:e13–21. doi: 10.1016/j.lpm.2017.01.015

2. Cohen A, Mathiasen VD, Schön T, Wejse C. The global prevalence of latent tuberculosis: a systematic review and meta-analysis. *Eur Respir J* (2019) 54:13–21. doi: 10.1183/13993003.00655-2019

3. Al-Darraji HAA, Kamarulzaman A, Altice FL. Latent tuberculosis infection in a Malaysian prison: implications for a comprehensive integrated control program in prisons. *BMC Public Health* (2014) 14:22. doi: 10.1186/1471-2458-14-22

4. Behr MA, Edelstein PH, Ramakrishnan L. Is mycobacterium tuberculosis infection life long? *BMJ* (2019) 367:l5770. doi: 10.1136/bmj.l5770

5. 3rd CEB, Boshoff HI, Dartois V, Dick T, Ehrt S, Flynn J, et al. The spectrum of latent tuberculosis: rethinking the biology and intervention strategies. *Nat Rev Microbiol* (2009) 7:nrmicro2236. doi: 10.1038/nrmicro2236

6. Lin PL, Flynn JL. The end of the binary era: revisiting the spectrum of tuberculosis. *J Immunol Baltim Md 1950* (2018) 201:2541–8. doi: 10.4049/jimmunol.1800993

7. Schnappinger D, Ehrt S. A broader spectrum of tuberculosis. *Nat Med* (2016) 22:1076–7. doi: 10.1038/nm.4186

8. Kestler B, Tyler SK. Latent tuberculosis testing through the ages: the search for a sleeping killer. *Am J Physiol - Lung Cell Mol Physiol* (2022) 322:L412–9. doi: 10.1152/ajplung.00217.2021

9. Sudbury EL, Clifford V, Messina NL, Song R, Curtis N. Mycobacterium tuberculosis-specific cytokine biomarkers to differentiate active TB and LTBI: a systematic review. *J Infect* (2020) 81:873–81. doi: 10.1016/j.jinf.2020.09.032

10. Reichler MR, Khan A, Sterling TR, Zhao H, Moran J, McAuley J, et al. Risk and timing of tuberculosis among close contacts of persons with infectious tuberculosis. *J Infect Dis* (2018) 218:1000–8. doi: 10.1093/infdis/jiy265

11. Cords O, Martinez L, Warren JL, O'Marr JM, Walter KS, Cohen T, et al. Incidence and prevalence of tuberculosis in incarcerated populations: a systematic review and meta-analysis. *Lancet Public Health* (2021) 6:e300–8. doi: 10.1016/S2468-2667(21)00025-6

12. Arroyave L, Keynan Y, López L, Marin D, Arbeláez MP, Rueda ZV. Negative latent tuberculosis at time of incarceration: identifying a very high-risk group for infection. *Epidemiol Infect* (2017) 145:2491–9. doi: 10.1017/S0950268817001558

13. Herrera M, Keynan Y, López L, Marín D, Arroyave L, Arbeláez MP, et al. Incidence and risk factors associated with latent tuberculosis infection and pulmonary tuberculosis among people deprived of liberty in Colombian prisons. *Am J Trop Med Hyg* (2021) 106:66–74. doi: 10.4269/ajtmh.20-0307

14. Herrera M, Vera C, Keynan Y, Rueda ZV. Gaps in study design for immune parameter research for latent tuberculosis infection: a systematic review. *J Immunol Res* (2020) 2020:8074183. doi: 10.1155/2020/8074183

15. Etna MP, Giacomini E, Severa M, Coccia EM. Pro- and anti-inflammatory cytokines in tuberculosis: a two-edged sword in TB pathogenesis. *Semin Immunol* (2014) 26:543–51. doi: 10.1016/j.smim.2014.09.011

16. Ahmad S. Pathogenesis, immunology, and diagnosis of latent mycobacterium tuberculosis infection. *J Immunol Res* (2010) 2011:e814943. doi: 10.1155/2011/814943

17. Simmons JD, Stein CM, Seshadri C, Campo M, Alter G, Fortune S, et al. Immunological mechanisms of human resistance to persistent mycobacterium tuberculosis infection. *Nat Rev Immunol* (2018) 18:575–89. doi: 10.1038/s41577-018-0025-3

18. Zuñiga J, Torres-García D, Santos-Mendoza T, Rodriguez-Reyna TS, Granados J, Yunis EJ. Cellular and humoral mechanisms involved in the control of tuberculosis. *Clin Dev Immunol* (2012) 2012:193923. doi: 10.1155/2012/193923

19. Lyadova IV, Panteleev AV. Th1 and Th17 cells in tuberculosis: protection, pathology, and biomarkers. *Mediators Inflammation* (2015) 2015:1–13. doi: 10.1155/2015/854507

20. Lin PL, Flynn JL. Understanding latent tuberculosis: a moving target. *J Immunol Baltim Md 1950* (2010) 185:15–22. doi: 10.4049/jimmunol.0903856

21. *Cellular and molecular immunology* . Available at: https://www.elsevier.com/books/cellular-and-molecular-immunology/abbas/978-0-323-47978-3 (Accessed October 31, 2017).

22. Bennett JE, Dolin R, Bennett JE. *Enfermedades infecciosas. Principios y práctica. 9th Edition*. Chapter 6 Cell-Mediated Defense Against Infection. (2020) Pag 69–72.

23. Kanehisa M, Furumichi M, Tanabe M, Sato Y, Morishima K. KEGG: new perspectives on genomes, pathways, diseases and drugs. *Nucleic Acids Res* (2017) 45: D353–61. doi: 10.1093/nar/gkw1092

24. Keynan Y, Trajtman A, McLaren P, Aguilar Y, Velez L, Rueda ZV. Inflammatory cytokine and gene expression patterns correlate with etiologic agent causing pneumonia among patients with advanced HIV in medellin, Colombia. *J Clin Virol* (2016) 82:S93. doi: 10.1016/j.jcv.2016.08.186

25. Tian R, Hou G, Li D, Yuan T-F. A possible change process of inflammatory cytokines in the prolonged chronic stress and its ultimate implications for health. *Sci World J* (2014) 2014:780616. doi: 10.1155/2014/780616

26. Zhou X, Fragala MS, McElhaney JE, Kuchel GA. Conceptual and methodological issues relevant to cytokine and inflammatory marker measurements in clinical research. *Curr Opin Clin Nutr Metab Care* (2010) 13:541–7. doi: 10.1097/MCO.0b013e32833cf3bc

27. Sribanditmongkol V, Neal JL, Patrick TE, Szalacha LA, McCarthy DO. Effect of perceived stress on cytokine production in healthy college students. *West J Nurs Res* (2015) 37:481–93. doi: 10.1177/0193945914545658

28. Lauren C. Porter. being "on point": exploring the strees-related experiences of incarceration. *Soc Ment Health* (2018) 9:1–17. doi: 10.1177/2156869318771439

29. Tabung FK, Birmann BM, Epstein MM, Martínez-Maza O, Breen EC, Wu K, et al. Influence of dietary patterns on plasma soluble CD14, a surrogate marker of gut barrier dysfunction. *Curr Dev Nutr* (2017) 1:1–11. doi: 10.3945/cdn.117.001396

30. Baba T, Mukaida N. Role of macrophage inflammatory protein (MIP)-1α/CCL3 in leukemogenesis. *Mol Cell Oncol* (2014) 1:1–5. doi: 10.4161/mco.29899

31. Aziz N, Detels R, Chang LC, Butch AW. Macrophage inflammatory protein-3 alpha (MIP-3α)/CCL20 in HIV-1-Infected individuals. *J AIDS Clin Res* (2016) 7:1–14. doi: 10.4172/2155-6113.1000587

32. Rivero-Lezcano OM, González-Cortés C, Reyes-Ruvalcaba D, Diez-Tascón C. CCL20 is overexpressed in mycobacterium tuberculosis-infected monocytes and inhibits the production of reactive oxygen species (ROS). *Clin Exp Immunol* (2010) 162:289–97. doi: 10.1111/j.1365-2249.2010.04168.x

33. Lee J-S, Lee J-Y, Son JW, Oh J-H, Shin D-M, Yuk J-M, et al. Expression and regulation of the CC-chemokine ligand 20 during human tuberculosis. *Scand J Immunol* (2008) 67:77–85. doi: 10.1111/j.1365-3083.2007.02040.x

34. Riffo-Vasquez Y, Coates ARM, Page CP, Spina D. Mycobacterium tuberculosis chaperonin 60.1 inhibits leukocyte diapedesis in a murine model of allergic lung inflammation. *Am J Respir Cell Mol Biol* (2012) 47:245–52. doi: 10.1165/rcmb.2011-0412OC

35. Yang Q, Cai Y, Zhao W, Wu F, Zhang M, Luo K, et al. IP-10 and MIG are compartmentalized at the site of disease during pleural and meningeal tuberculosis and are decreased after antituberculosis treatment. *Clin Vaccine Immunol* (2014) 21:1635–44. doi: 10.1128/CVI.00499-14

36. Deshmane SL, Kremlev S, Amini S, Sawaya BE. Monocyte chemoattractant protein-1 (MCP-1): an overview. *J Interferon Cytokine Res* (2009) 29:313–26. doi: 10.1089/jir.2008.0027

37. Dutta NK, McLachlan J, Mehra S, Kaushal D. Humoral and lung immune responses to mycobacterium tuberculosis infection in a primate model of protection. *Trials Vaccinol* (2014) 3:47–51. doi: 10.1016/j.trivac.2014.02.001

38. Wang Y, Li H, Bao H, Jin Y, Liu X, Wu X, et al. Auxiliary diagnostic value of monocyte chemoattractant protein-1 of whole blood in active tuberculosis. *Int J Clin Exp Med* (2015) 8:9454–61.

39. Suzukawa M, Akashi S, Nagai H, Nagase H, Nakamura H, Matsui H, et al. Combined analysis of IFN-γ, IL-2, IL-5, IL-10, IL-1RA and MCP-1 in QFT supernatant is useful for distinguishing active tuberculosis from latent infection. *PloS One* (2016) 11: e0152483. doi: 10.1371/journal.pone.0152483

40. Ruhwald M, Bjerregaard-Andersen M, Rabna P, Eugen-Olsen J, Ravn P. IP-10, MCP-1, MCP-2, MCP-3, and IL-1RA hold promise as biomarkers for infection with m. tuberculosis in a whole blood based T-cell assay. *BMC Res Notes* (2009) 2:19. doi: 10.1186/1756-0500-2-19

41. Zhang Y, Zhang J, Zeng L, Huang H, Yang M, Fu X, et al. The -2518A/G polymorphism in the MCP-1 gene and tuberculosis risk: a meta-analysis. *PloS One* (2012) 7:e38918. doi: 10.1371/journal.pone.0038918

42. Menten P, Wuyts A, Van Damme J. Macrophage inflammatory protein-1. *Cytokine Growth Factor Rev* (2002) 13:455–81. doi: 10.1016/S1359-6101(02)00045-X

43. Yu W, Soprana E, Cosentino G, Volta M, Lichenstein HS, Viale G, et al. Soluble CD14(1-152) confers responsiveness to both lipoarabinomannan and lipopolysaccharide in a novel HL-60 cell bioassay. *J Immunol Baltim Md 1950* (1998) 161:4244–51. doi: 10.4049/jimmunol.161.8.4244

44. Guirado E, Schlesinger LS, Kaplan G. Macrophages in tuberculosis: friend or foe. *Semin Immunopathol* (2013) 35:563–83. doi: 10.1007/s00281-013-0388-2

45. Marino S, Cilfone NA, Mattila JT, Linderman JJ, Flynn JL, Kirschner DE. Macrophage polarization drives granuloma outcome during mycobacterium tuberculosis infection. *Infect Immun* (2015) 83:324–38. doi: 10.1128/IAI.02494-14

46. Flynn J, Chan J, Lin P. Macrophages and control of granulomatous inflammation in tuberculosis. *Mucosal Immunol* (2011) 4:271–8. doi: 10.1038/mi.2011.14

47. Lawn SD, Labeta MO, Arias M, Acheampong JW, Griffin GE. Elevated serum concentrations of soluble CD14 in HIV– and HIV+ patients with tuberculosis in Africa: prolonged elevation during anti-tuberculosis treatment. *Clin Exp Immunol* (2000) 120:483–7. doi: 10.1046/j.1365-2249.2000.01246.x

48. Ayaslioglu E, Kalpaklioglu F, Kavut AB, Erturk A, Capan N, Birben E. The role of CD14 gene promoter polymorphism in tuberculosis susceptibility. *J Microbiol Immunol Infect* (2013) 46:158–63. doi: 10.1016/j.jmii.2012.05.008

49. Zambuzi FA, Cardoso-Silva PM, Espindola MS, Soares LS, Galvão-Lima LJ, Brauer VS, et al. Identification of promising plasma immune biomarkers to differentiate active pulmonary tuberculosis. *Cytokine* (2016) 88:99–107. doi: 10.1016/j.cyto.2016.08.030

50. Wyndham-Thomas C, Corbière V, Selis E, Payen M-C, Goffard J-C, Van Vooren J-P, et al. Immune activation by mycobacterium tuberculosis in HIV-infected and -uninfected subjects. *J Acquir Immune Defic Syndr 1999* (2017) 74:103–11. doi: 10.1097/QAI.0000000000001157

51. Kumar NP, Moideen K, Bhootra Y, Nancy A, Viswanathan V, Shruthi BS, et al. Elevated circulating levels of monocyte activation markers among tuberculosis patients with diabetes co-morbidity. *Immunology* (2019) 156:249–58. doi: 10.1111/imm.13023

52. Lin PL, Plessner HL, Voitenok NN, Flynn JL. Tumor necrosis factor and tuberculosis. *J Investig Dermatol Symp Proc* (2007) 12(1):22–5. doi: 10.1038/sj.jidsymp.5650027

53. Won E-J, Choi J-H, Cho Y-N, Jin H-M, Kee HJ, Park Y-W, et al. Biomarkers for discrimination between latent tuberculosis infection and active tuberculosis disease. *J Infect* (2017) 74:281–93. doi: 10.1016/j.jinf.2016.11.010

54. Belay M, Legesse M, Mihret A, Bekele Y, Ottenhoff THM, Franken KLMC, et al. Pro- and anti-inflammatory cytokines against Rv2031 are elevated during latent tuberculosis: a study in cohorts of tuberculosis patients, household contacts and community controls in an endemic setting. *PloS One* (2015) 10:e0124134. doi: 10.1371/journal.pone.0124134

55. Wei M, Wu ZY, Lin JH, Li Y, Qian ZX, Xie YQ, et al. Regulation network of serum cytokines induced by tuberculosis-specific antigens reveals biomarkers for tuberculosis diagnosis. *Genet Mol Res GMR* (2015) 14:17182–92. doi: 10.4238/2015.December.16.18

56. Jeong YH, Hur Y-G, Lee H, Kim S, Cho J-E, Chang J, et al. Discrimination between active and latent tuberculosis based on ratio of antigen-specific to mitogen-induced IP-10 production. *J Clin Microbiol* (2015) 53:504–10. doi: 10.1128/JCM.02758-14

57. Tebruegge M, Dutta B, Donath S, Ritz N, Forbes B, Camacho-Badilla K, et al. Mycobacteria-specific cytokine responses detect tuberculosis infection and distinguish

latent from active tuberculosis. *Am J Respir Crit Care Med* (2015) 192:485–99. doi: 10.1164/rccm.201501-0059OC

58. Vankayalapati RR, Wizel B, Weis SE, Samten B, Girard WM, Barnes PF. Production of interleukin-18 in human tuberculosis. *J Infect Dis* (2000) 182:234–9. doi: 10.1086/315656

59. Schneider BE, Korbel D, Hagens K, Koch M, Raupach B, Enders J, et al. A role for IL-18 in protective immunity against mycobacterium tuberculosis. *Eur J Immunol* (2010) 40:396–405. doi: 10.1002/eji.200939583

60. Khader SA, Bell GK, Pearl JE, Fountain JJ, Rangel-Moreno J, Cilley GE, et al. IL-23 and IL-17 in the establishment of protective pulmonary CD4 + T cell responses after vaccination and during mycobacterium tuberculosis challenge. *Nat Immunol* (2007) 8:369–77. doi: 10.1038/ni1449

61. Menzies D. Interpretation of repeated tuberculin tests. boosting, conversion, and reversion. *Am J Respir Crit Care Med* (1999) 159:15–21. doi: 10.1164/ajrccm.159.1.9801120

62. Yamada G, Shijubo N, Shigehara K, Okamura H, Kurimoto M, Abe S. Increased levels of circulating interleukin-18 in patients with advanced tuberculosis. *Am J Respir Crit Care Med* (2000) 161:1786–9. doi: 10.1164/ajrccm.161.6.9911054

63. Buchwald UK, Adetifa IMO, Bottomley C, Owiafe PK, Donkor S, Bojang AL, et al. Broad adaptive immune responses to m. tuberculosis antigens precede TST conversion in tuberculosis exposed household contacts in a TB-endemic setting. *PloS One* (2014) 9:1–17. doi: 10.1371/journal.pone.0116268

64. Hussain R, Talat N, Shahid F, Dawood G. Biomarker changes associated with tuberculin skin test (TST) conversion: a two-year longitudinal follow-up study in exposed household contacts. *PloS One* (2009) 4:1–9. doi: 10.1371/journal.pone.0007444

65. Hur Y-G, Kang YA, Jang S-H, Hong JY, Kim A, Lee SA, et al. Adjunctive biomarkers for improving diagnosis of tuberculosis and monitoring therapeutic effects. *J Infect* (2015) 70:346–55. doi: 10.1016/j.jinf.2014.10.019

66. Kim K, Perera R, Tan DBA, Fernandez S, Seddiki N, Waring J, et al. Circulating mycobacterial-reactive CD4+ T cells with an immunosuppressive phenotype are higher in active tuberculosis than latent tuberculosis infection. *Tuberc Edinb Scotl* (2014) 94:494–501. doi: 10.1016/j.tube.2014.07.002

67. Hur Y-G, Gorak-Stolinska P, Ben-Smith A, Lalor MK, Chaguluka S, Dacombe R, et al. Combination of cytokine responses indicative of latent TB and active TB in Malawian adults. *PloS One* (2013) 8:1–10. doi: 10.1371/journal.pone.0079742

68. Hussain R, Kaleem A, Shahid F, Dojki M, Jamil B, Mehmood H, et al. Cytokine profiles using whole-blood assays can discriminate between tuberculosis patients and healthy endemic controls in a BCG-vaccinated population. *J Immunol Methods* (2002) 264:95–108. doi: 10.1016/S0022-1759(02)00092-3

69. Santin M, Morandeira-Rego F, Alcaide F, Rabuñal R, Anibarro L, Agüero-Balbín R, et al. Detection of interleukin-2 is not useful for distinguishing between latent and active tuberculosis in clinical practice: a prospective cohort study. *Clin Microbiol Infect Off Publ Eur Soc Clin Microbiol Infect Dis* (2016) 22:1007.e1–1007.e5. doi: 10.1016/j.cmi.2016.09.004

70. Wang S, Diao N, Lu C, Wu J, Gao Y, Chen J, et al. Evaluation of the diagnostic potential of IP-10 and IL-2 as biomarkers for the diagnosis of active and latent tuberculosis in a BCG-vaccinated population. *PloS One* (2012) 7:e51338. doi: 10.1371/journal.pone.0051338

71. Chegou NN, Black GF, Kidd M, van Helden PD, Walzl G. Host markers in quantiferon supernatants differentiate active TB from latent TB infection: preliminary report. *BMC Pulm Med* (2009) 9:21. doi: 10.1186/1471-2466-9-21

72. Sauzullo I, Mastroianni CM, Mengoni F, Ermocida A, Mascia C, Salotti A, et al. Long-term IFN-γ and IL-2 response for detection of latent tuberculosis infection in healthcare workers with discordant immunologic results. *J Immunol Methods* (2014) 414:51–7. doi: 10.1016/j.jim.2014.07.013

73. Anbarasu D, Raja CP, Raja A. Multiplex analysis of cytokines/chemokines as biomarkers that differentiate healthy contacts from tuberculosis patients in high endemic settings. *Cytokine* (2013) 61:747–54. doi: 10.1016/j.cyto.2012.12.031

74. Yao X, Liu Y, Liu Y, Liu W, Ye Z, Zheng C, et al. Multiplex analysis of plasma cytokines/chemokines showing different immune responses in active TB patients, latent TB infection and healthy participants. *Tuberculosis* (2017) 107:88–94. doi: 10.1016/j.tube.2017.07.013

75. Kamakia R, Kiazyk S, Waruk J, Meyers A, Ochanda J, Ball TB, et al. Potential biomarkers associated with discrimination between latent and active pulmonary tuberculosis. *Int J Tuberc Lung Dis Off J Int Union Tuberc Lung Dis* (2017) 21:278–85. doi: 10.5588/ijtld.16.0176

76. Jin W, Dong C. IL-17 cytokines in immunity and inflammation. *Emerg Microbes Infect* (2013) 2:e60. doi: 10.1038/emi.2013.58

77. Zenobia C, Hajishengallis G. Basic biology and role of interleukin-17 in immunity and inflammation. *Periodontol 2000* (2015) 69:142–59. doi: 10.1111/prd.12083

78. Rueda ZV, Arroyave L, Marin D, López L, Keynan Y, Giraldo MR, et al. High prevalence and risk factors associated with latent tuberculous infection in two Colombian prisons. *Int J Tuberc Lung Dis Off J Int Union Tuberc Lung Dis* (2014) 18:1166–71. doi: 10.5588/ijtld.14.0179

79. Mehra S, Golden NA, Dutta NK, Midkiff CC, Alvarez X, Doyle LA, et al. Reactivation of latent tuberculosis in rhesus macaques by co-infection with simian immunodeficiency virus. *J Med Primatol* (2011) 40:233–43. doi: 10.1111/j.1600-0684.2011.00485.x

80. Kaushal D, Mehra S, Didier PJ, Lackner AA. The non-human primate model of tuberculosis. *J Med Primatol* (2012) 41:191–201. doi: 10.1111/j.1600-0684.2012.00536.x

81. Borgström EW, Fröberg G, Correia-Neves M, Atterfelt FB, Bellbrant J, Szulkin R, et al. CD4+ T cell proliferative responses to PPD and CFP-10 associate with recent m. tuberculosis infection. *Tuberculosis* (2020) 123:101959. doi: 10.1016/j.tube.2020.101959

frontiers | Frontiers in Immunology

TYPE Original Research
PUBLISHED 15 September 2023
DOI 10.3389/fimmu.2023.1238391

OPEN ACCESS

EDITED BY
Jieh-Juen Yu,
University of Texas at San Antonio,
United States

REVIEWED BY
Sudeep Kumar,
Albany Medical College, United States
Althea Campuzano,
University of Texas at San Antonio,
United States

*CORRESPONDENCE
Anders Sjöstedt
anders.sjostedt@umu.se

RECEIVED 11 June 2023
ACCEPTED 24 August 2023
PUBLISHED 15 September 2023

CITATION
Lindgren H, Eneslätt K, Golovliov I, Gelhaus C and Sjöstedt A (2023) Analyses of human immune responses to *Francisella tularensis* identify correlates of protection. *Front. Immunol.* 14:1238391. doi: 10.3389/fimmu.2023.1238391

Analyses of human immune responses to *Francisella tularensis* identify correlates of protection

Helena Lindgren[1], Kjell Eneslätt[1], Igor Golovliov[1], Carl Gelhaus[2] and Anders Sjöstedt[1]*

[1]Department of Clinical Microbiology, Umeå University, Umeå, Sweden, [2]Appili Therapeutics, Halifax, NS, Canada

Francisella tularensis is the etiological agent of the potentially severe infection tularemia. An existing *F: tularensis* vaccine, the live vaccine strain (LVS), has been used to protect at-risk personnel, but it is not licensed in any country and it has limited efficacy. Therefore, there is a need of a new, efficacious vaccine. The aim of the study was to perform a detailed analysis of the characteristics of the human immune response to *F. tularensis*, since this will generate crucial knowledge required to develop new vaccine candidates. Nine individuals were administered the LVS vaccine and peripheral blood mononuclear cells (PBMC) were collected before and at four time points up to one year after vaccination. The properties of the PBMC were characterized by flow cytometry analysis of surface markers and intracellular cytokine staining. In addition, the cytokine content of supernatants from *F. tularensis*-infected PBMC cultures was determined and the protective properties of the supernatants investigated by adding them to cultures with infected monocyte-derived macrophages (MDM). Unlike before vaccination, PBMC collected at all four time points after vaccination demonstrated *F. tularensis*-specific cell proliferation, cytokine secretion and cytokine-expressing memory cells. A majority of 17 cytokines were secreted at higher levels by PBMC collected at all time points after vaccination than before vaccination. A discriminative analysis based on IFN-γ and IL-13 secretion correctly classified samples obtained before and after vaccination. Increased expression of IFN-γ, IL-2, and MIP-1β were observed at all time points after vaccination vs. before vaccination and the most significant changes occurred among the CD4 transient memory, CD8 effector memory, and CD8 transient memory T-cell populations. Growth restriction of the highly virulent *F. tularensis* strain SCHU S4 in MDM was conferred by supernatants and protection correlated to levels of IFN-γ, IL-2, TNF, and IL-17. The findings demonstrate that *F. tularensis* vaccination induces long-term T-cell reactivity, including T_{EM} and T_{TM} cell populations. Individual cytokine levels correlated with the degree of protection conferred by the supernatants. Identification of such memory T cells and effector mechanisms provide an improved understanding of the protective mechanisms against *F. tularensis*. mechanisms against *F. tularensis*.

KEYWORDS

***F. tularensis*, vaccination, immune response, memory cells, human correlates of protection**

Introduction

Tularemia is a disease caused by *Francisella tularensis* that affects many animal species as well as humans. The most severe form of tularemia in humans, with high mortality if untreated, is due to inhalation of *F. tularensis* subspecies *tularensis* (type A) (1). The vaccine against *F. tularensis*, a live vaccine of the less virulent subspecies *holarctica* (LVS), offers limited protection against this form of tularemia (2). Moreover, since the knowledge regarding the attenuation of LVS is incomplete, the vaccine is not licensed in any country. Tularemia is widespread over the Northern Hemisphere with local, unpredictable outbreaks, although rather uncommon in many countries (1). The highest total number of cases has been reported in Sweden, Finland, Turkey, Hungary, and Czech Republic. In these countries, as well as in other European countries, there are very marked annual and seasonal variations (3, 4). Although not a threat to the public health in most countries, there are endemic areas in, for example, Sweden and Finland with persistent high incidences, and in these areas, an efficacious vaccine would be of much value. In addition, there are at-risk groups that would benefit from vaccination, for example, clinical laboratory personnel and individuals regularly working outdoors, such as farmers.

F. tularensis is classified as a Category A Select Agent, due to its ease of spread by aerosol, extremely low infectious dose, and potential to cause severe morbidity and mortality, therefore considered to have the potential to pose a severe threat to public health and safety (1). The high virulence of *F. tularensis* relies on its ability to proliferate in many different cell types, including macrophages (5). As a consequence, a Th1-dependent cellular immune response is evoked to protect against the bacterium (6, 7). Detailed analysis of the characteristics of the immune response to *F. tularensis* has been performed by *in vivo* and *in vitro* studies, mostly using mice and rats, but also *ex vivo* studies using human cells (8–14). The efficacy of new vaccine candidates has been tested in mice, rats, and non-human primates, but human clinical trials are unlikely due to the low incidence and unpredictability of tularemia (7, 15). Thus, our knowledge regarding the human immune response to *F. tularensis* is based mostly on *ex vivo* studies of peripheral blood mononuclear cells (PBMCs) derived from immune individuals.

Studies of vaccine-mediated immune responses have demonstrated that there is an initial phase of rapid proliferation and expansion of antigen-specific T-cell clones and a majority of circulating T cells are antigen-specific. Subsequently, the responding cells contract and form a much smaller memory immune population (16). Experimental models have also demonstrated that the specificities of the T-cell responses are complex and composed of distinct epitope specificities with hierarchies of dominant, subdominant, and cryptic responses (17). The immunospecific T cells are characterized by their expression of surface receptors and markers, which are believed to identify the T-cell differentiation stage. However, the division of T-cell subpopulations into naïve, memory effector, and memory immunity T cells may not be unequivocal, since there is evidence that the expression of surface receptors and markers and their correlation to effector properties may vary between different infections and vaccinations (18, 19). This indicates that studies of specific infection models are necessary to identify the pathogen-specific T cells that constitute the long-term memory as well as those that effectuate the anti-microbial responses. By combining data on the specificities of responding T cells with characterization of their phenotypes, it will be possible to delineate the responsible subpopulations and to determine their reactivity.

In addition to vaccine-specific variations in the memory immune responses, there is always heterogeneity due to individual variation and some individuals may not mount an effective immune response to certain vaccines (18). Such differences can be utilized to understand what best protects against a given pathogen. The present study analyzed development of memory T cells and cytokine responses before and after *F. tularensis* vaccination. Furthermore, it was assessed how such variation affected the protective efficacy by analyzing the ability of supernatants collected from recall-stimulated PBMC to provide control of *F. tularensis* in monocyte cultures. Thereby, it was possible to identify cytokines and memory cells of importance for protection against highly virulent strains of *F. tularensis*.

Materials and methods

Vaccination

All individuals were vaccinated the same day with a variant of LVS designated NDBR 101, lot no. 11 (National Drug Company, Philadelphia, PA). The lyophilized material was dissolved in 2.0 ml of sterile H_2O to a concentration of 2.4×10^9 CFU/ml and 20 µl was inoculated by scarification in the skin of the upper arm. Ethical approvals for the study were received from the Swedish Ethical Review Authority, 2019-01567 and 2020-01860.

Preparation of PBMCs from blood

Venous blood was drawn from healthy individuals, five women and four men (22–53 years old at time of vaccination, mean age 36.3 ± 12.2 years) before vaccination and 2, 4, 12, 52, and 104 weeks after vaccination. The blood, approximately 100 ml, was collected in CPT-tubes (BD Biosciences NJ USA) and PBMCs were prepared according to the manufacturer's protocol. Purified PBMC was suspended in human serum (HS) (Innovative research, MI, USA) containing 10% DMSO (Sigma Aldrich, MO, USA) and aliquoted into cryovials, which was placed in a Cryo 1°C Freezing Container (NALGENE, NY, USA) at −80°C overnight before transferred into liquid nitrogen.

Recall stimulation PBMC

Cryovials with PBMC were thawed in a 37°C water bath and transferred to 20 ml of RPMI medium 1640 + GlutaMAX (RPMI), (Gibco, MA USA). The PBMC was collected by centrifugation at 200 × *g* for 10 min, washed with 40 ml of RPMI, and suspended in 1 ml

of RPMI + 10% HS + 10 μg/ml Gentamicin (complete RPMI). After resting at 37°C in 5% CO_2 for 2 h, the PBMCs were counted and diluted in complete RPMI. For FACS analysis, 8×10^5 cells were seeded per well in a round-bottom 96-well plate (Sarstedt, Nümbrecht, Germany). For the Lymphocyte proliferation assay (LPA), 2×10^5 cells were seeded per well. To some wells, *Ft* antigen (2.5 μg/ml), prepared from *F. tularensis* LVS as described previously (20) or Concavalin A (ConA) (2.5 μg/ml), was added (stimulated cells) whereas other wells contained complete RPMI only (resting cells). After 3 days of incubation, 300,000–500,000 cells per sample were collected and analyzed by FACS. From separate wells, supernatants were transferred to a 96-well plate and stored at −80°C until analyzed for cytokine content by multiplex cytokine analysis. For LPA, tritium-thymidine (0.003 mCi/ml) (Perkin Elmer MA USA) was added to the cells, and after 6 h, incorporated thymidine was measured using a 1450 microbeta liquid scintillation & luminescence counter (Trilux Chelmsford UK). All time points from two to three individuals were included in each experiment.

Flow cytometry analysis of surface markers and intracellular cytokine staining

Cells were collected after 72 h of recall stimulation and treated with 5 μg/ml of Brefeldin A and 5 μg/ml of Monensin for 4 h. Then, cells were centrifuged for 3 min at 500 × *g* and supernatants were removed. Cells were stained with Aqua Viability Dye (Molecular Probes/Invitrogen) for 20 min in RT and thereafter labeled with conjugated monoclonal antibodies (mAbs) against cell surface markers for 30 min at 4°C. After wash and treatment with perm/wash buffer (BD Biosciences) for 20 min at 4°C, the cells were stained for intracellular cytokines for 30 min at 4°C. The following mAb conjugates were used (BD Biosciences): CD3-APCH7 (clone SK7), CD4-FITC (clone RPA-T4), CD8-PerCPCy5.5 (clone SK1), CD45RO-APC (clone UCHL-1), CCR7-PECF594 (clone 2-L1-A), CD28-PE (clone CD28.2), CD95-BUV395 (clone DX2), IFNγ-PeCY7 (clone B27), MIP-1β-AF700 (clone D21-1351), IL2-BV711 (clone 5344.111), and TNF-BV421 (clone MAb11). CD14-V500 (clone M5E2) and CD19-V500 (clone H1B19) were included in the dump channel. PBMCs were acquired using a ZE5 flow cytometer (Bio-Rad) with Everest software (Bio-Rad). Results were analyzed using FlowJo software (BD Biosciences).

Multiplex cytokine analysis

Supernatants, 50 μl/well, were collected from cultures after 72 h of incubation. The supernatants were stored at −80°C until analyzed using a 17-plex kit (Bio-Rad Laboratories Inc., Hercules, CA, USA, M5000031YV) according to the manufacturer's instructions using a Bio-Plex 200 system (Bio-Rad Laboratories Inc., Hercules, CA, USA).

Isolation of monocytes and generation of monocyte-derived macrophages

PBMCs, 15×10^6 cells, prepared from buffy coat, were seeded in a 9-cm petri dish in 15 ml of complete RPMI. After 2 h, medium containing non-adherent cells was removed and the adherent cells were washed with 20 ml of 37°C RPMI. The adherent cells were detached by scraping and thereafter transferred to a 50-ml tube, which was centrifuged at 200 × *g* for 10 min. The cells were suspended in complete RPMI, viable cells were determined using trypan blue exclusion in a TC20 cell counter (Bio-Rad Laboratories Inc, Hercules, CA, USA), and 1×10^5 cells were seeded per well in a flat-bottom 96-well culture plate. After overnight incubation at 37°C in 5% of CO_2, cells were washed and thereafter complete RPMI with 40 ng/ml of GM-CSF was added. After 48 h incubation at 37°C in 5% CO_2, cells were washed and complete RPMI with 40 ng/ml of GM-CSF was added. Complete RPMI (100 μl) was added to each well after an additional 48 h of incubation.

Infection of MDMs

SCHU S4, grown overnight on Gc-agar plates, were resuspended in complete RPMI and added to the MDM monolayer at an MOI of 50. After 1 h, cells were washed and complete RPMI with 10 μg/ml of gentamicin was added for 30 min. To some wells, 20-fold diluted supernatant, collected from *Ft*-stimulated PBMCs from respective donor, was added to separate cultures. Complete RPMI was used as diluent. The number of intracellular bacteria was determined after 24 h lysis of the monolayers with 0.1% deoxycholate and spreading of 10-fold serial dilutions of the lysate in PBS on agar plates. Colonies were counted after 3 days of incubation of the plates at 37°C in 5% CO_2.

Data analysis and statistical methods

Two-tailed Student's *t*-test was used to identify significant differences ($p < 0.05$) between data sets. To analyze correlations between data sets, Spearman's rank correlation test was used. Cytokine data were used to derive a classifier that enables prediction of vaccination status, i.e., to predict if PBMCs were derived from individuals before vaccination with LVS or derived at 2, 4, 12, or 52 weeks after vaccination. Linear discriminant analysis (LDA), assuming homoscedasticity and no prior, was used to build the classifiers and cross-validation was used to predict the posterior probabilities (21). The LDA analyses were performed using the settings discriminant analysis and stepwise method (Wilks´ Lambda) with the criteria of F to enter 3.84 and F to remove 2.71 in the program SPSS version 28. SPSS was also used to perform two-tailed Student's *t*-test and Spearman's rank correlation test.

Results

Proliferative responses of PBMCs

PBMCs isolated from nine individuals before vaccination with LVS and 2, 4, 12, and 52 weeks after vaccination were stimulated with *Ft* antigen, ConA, or sham for 3 days. As expected, PBMCs responded to ConA with robust proliferation, whereas non-

stimulated PBMCs showed minor proliferation (Figure 1). The average *Ft*-specific proliferative responses of PBMCs isolated from the nine individuals after vaccination, regardless of time point, were significantly higher than that of PBMCs isolated prior to vaccination ($p < 0.05$–$p < 0.001$, Figure 1) The magnitude of the *Ft*-specific proliferative responses varied among individuals (Figure S1).

In summary, the PBMCs showed robust proliferation to ConA, whereas only PBMCs collected after vaccination proliferated in response to the *Ft* antigen.

Detection of intracellular cytokines

PBMCs stimulated with the *Ft* antigen for 3 days, or sham-stimulated PBMCs, were analyzed by FACS for intracellular expression of IFN-γ, IL-2, MIP-1β, or TNF. In previous studies, these cytokines have been identified to discriminate responses of immune vs. naïve individuals (12, 22). The cells were also stained for cell surface markers, which enabled identification of CD4 and CD8 lymphocytes and of various memory populations thereof (Figures 2, S2, S3 illustrate the gating strategies).

The number of CD4 T cells expressing IFN-γ was higher among PBMCs collected 2, 4, 12, and 52 weeks after vaccination, compared to PBMCs collected prior to vaccination ($p < 0.05$–$p < 0.01$, Figure 3A). For the other cytokines, there were no significant differences among the CD4 T cells at any of the time points (Figure 3A). The number of CD8 T cells expressing IFN-γ, IL-2, or MIP-1β was higher among PBMCs collected 2, 4, 12, and 52 weeks after vaccination, compared to PBMCs collected prior to vaccination ($p < 0.01$ or $p < 0.001$, Figure 3B). The number of CD4 or CD8 T cells expressing TNF was unchanged before and after vaccination (Figures 3A, B). When comparing various time points after vaccination, the sole difference identified was a lower number of IFN-γ-expressing CD8 T cells at the 52-week time point compared to the 4- and 12-week time points ($p < 0.01$, Figure 3B).

Cytokine expression by various T cell memory subpopulations was also analyzed. The most significantly increased expression of cytokines among CD4 T cells was identified in the transient memory (T_{TM}) population; IFN-γ-, IL-2-, and MIP-1β-expressing cells were increased at all time points after vaccination compared to prior to vaccination ($p < 0.05$–$p < 0.001$, Figure 4D). In the CD4 T-cell effector memory (T_{EM}) population, cells expressing MIP-1β were increased at all time points after vaccination and cells expressing IFN-γ were increased at the 52-week time point after vaccination ($p < 0.05$, Figure 4B). The number of CD4 central memory (T_{CM}) cells expressing IFN-γ or MIP-1β was higher in PBMCs collected 52 weeks after vaccination, but not at the other time points, compared to PBMCs collected prior to vaccination ($p < 0.05$, Figure 4A). The number of TNF-positive CD4 T cells was similar before and after vaccination, regardless of memory population (Figures 4A–E). Among the naïve and T_{SCM} CD4 T cells, the number of cytokine-expressing cells was similar before and after vaccination ($p > 0.05$, Figures 4A, E).

In the CD8 T-cell populations, the most significant expression of cytokines was identified in the T_{TM} and T_{EM} population; IFN-γ-, IL-2-, and MIP-1β-expressing cells were increased at all time points after vaccination compared to prior to vaccination ($p < 0.05$–$p < 0.001$, Figures 5B, D). In addition, the number of MIP-1β expressing cells was increased at all time points after vaccination in the T_{CM} and T_{EMRA} population, and IFN-γ- and IL-2-expressing cells were increased at various time points after vaccination in the T_{CM} population ($p < 0.05$–$p < 0.01$, Figures 5C, F). The number of TNF-positive CD8 T cells was similar before and after vaccination, regardless of memory population (Figures 5A–F). Among the naïve and T_{SCM} CD8 T cells, the number of cytokine-expressing cells was similar before and after vaccination ($p > 0.05$, Figures 5A, E).

To verify the longevity of the memory cell populations, PBMCs from six individuals were collected 2 years after vaccination and cytokine expression by the T-cell subpopulations was analyzed. As observed at the other four time points after vaccination, CD4 T_{TM}, CD8 T_{TM}, and CD8 T_{EM} cell populations showed increased expression of IFN-γ, IL-2, and MIP-1β ($p < 0.05$–$p < 0.001$, Figures S4, S5).

In summary, the CD4 T_{TM}, CD8 T_{TM}, and CD8 T_{EM} populations showed prominently increased expression of IFN-γ, IL-2, and MIP-1β in response to vaccination for a period of at least 2 years. Increased TNF expression was not detected in any of the memory populations.

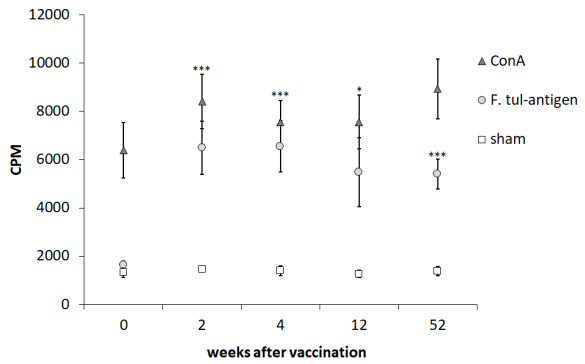

FIGURE 1
Proliferative responses of PBMCs after recall stimulation with *Ft* antigen. PBMCs collected from nine individuals before vaccination (0) and 2, 4, 12, and 52 weeks after vaccination were cultured in the presence or absence of *Ft* antigen for 3 days. Six hours after addition of tritium-thymidine, incorporation was measured. The proliferative responses of the sham, ConA-stimulated, or *Ft*-stimulated cells are expressed as CPM for each time point. The mean ± SEM of triplicate samples from nine individuals are shown for each time point. Asterisks indicate significant differences of the *Ft*-stimulated groups compared to *Ft*-stimulated cells obtained before vaccination, denoted week 0 (*$P < 0.05$; ***$P < 0.001$). There were no significant differences between the time points after vaccination for each of the stimuli.

Analysis of multifunctional cells

The FACS data were subjected to further analysis for the presence of multifunctional cells, i.e., cells simultaneously expressing more than one of the investigated cytokines IL-2, IFN-γ, MIP-1β, or TNF. Since their individual expression was significantly increased in the CD8 T_{TM} and CD8 T_{EM} populations, these were the focus of the analysis. Samples collected before vaccination and 2, 4, 12, and 52 weeks after

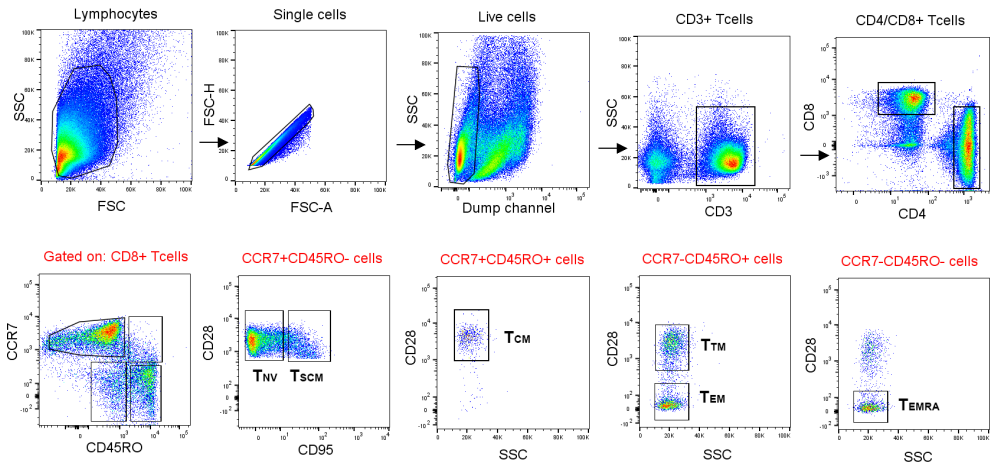

FIGURE 2
Gating strategy used for FACS analysis of memory populations. Lymphocytes were gated based on morphology detected with forward and side scatter, FSC and SSC. After gating for singlets, a gate for $CD14^-$ and $CD19^-$ live cells was created. $CD4^+$ and $CD8^+$ T cells were gated from $CD3^+$ T cells. The $CD45RO^-CCR7^+$ population were gated into naïve (T_{NV}) and stem cell-like memory T cells (T_{SCM}) by the expression of CD95. Memory populations [central memory (T_{CM}), transitional memory (T_{TM}), effector memory (T_{EM}), and effector memory RA^+ (T_{EMRA}) cells] were further gated according to the positive or negative expression of CD45RO, CCR7, and CD28. Finally, IFN-γ-, TNF-, MIP-1β-, and IL-2-expressing cells were gated from the naïve and memory populations, respectively.

vaccination were analyzed. There were significant differences for several of the groups with the highest significances ($p \leq 0.001$) among cells expressing IFN-γ and MIP-1β, or IFN-γ, MIP-1β, and IL-2 (Table S1). These groups were subjected to a *post-hoc* analysis using the Bonferroni *post-hoc* test to identify differences between each of the time points (Table S2). The numbers of CD8 T_{TM} and CD8 T_{EM} cells expressing IFN-γ and MIP-1β were increased at all time points after vaccination compared to before vaccination ($p < 0.05$–$p < 0.001$, Figures 6A, B). CD8 T_{EM} cells expressing IFN-γ, MIP-1β, and IL-2 were increased up to 12 weeks ($p < 0.05$–0.001, Figure 6A). CD8 T_{TM} cells expressing IFN-γ, MIP-1β, and IL-2 were increased at some of the time points after vaccination ($p < 0.05$–$p < 0.001$, Figure 6B). At the 2-year time point, CD8 T_{EM} cells expressing IFN-γ and MIP-1β, IL-2 and MIP-1β, or IL-2, IFN-γ, and IL-2 were present in higher numbers than in samples collected before vaccination ($p < 0.001$, Figure S6).

In summary, CD8 T_{TM} and CD8 T_{EM} cells co-expressing various combinations of cytokines were increased post vaccination. CD8 T_{TM} and CD8 T_{EM} cells expressing IFN-γ and MIP-1B showed the most consistent increases of cytokine expression. Multifunctional CD8 T_{EM} cells were detected up to 2 years after vaccination.

Detection of secreted cytokines and chemokines by LUMINEX

Supernatants from the *Ft* antigen-stimulated PBMCs collected prior to and after vaccination were analyzed for 17 cytokines, IL-1β, IL-2, IL-4, IL-5, IL-6, IL-7, IL-8, IL-10, IL-12p70, IL-13, IL-17, G-CSF, GM-CSF, IFN-γ, MCP-1, MIP-1β, and TNF. As aforementioned, the T_{EM} and T_{TM} cell populations demonstrated high intracellular expression of IFN-γ, IL-2, and MIP-1β, and levels of these cytokines were also high in supernatants from cultures with PBMCs collected at any of the four time points after vaccination ($p <$ 0.01 or < 0.001, Table 1). In addition, TNF was secreted at high levels in the same cultures ($p < 0.01$). All other cytokines measured, except for IL-10, were secreted at higher levels from PBMCs collected at 52 weeks after vaccination compared to PBMCs collected before vaccination ($p < 0.05$ or $p < 0.01$, Table 1). Most of these cytokines were also secreted at higher levels in cultures with PBMCs collected 2, 4, and 12 weeks after vaccination ($p < 0.05$ or $p < 0.01$, Table 1).

Determination of vaccination status based on cytokine patterns

Linear discriminant analysis was used to determine whether individual cytokines, or sets of cytokines, could differentiate between each of the five groups: PBMCs collected before vaccination, or collected 2, 4, 12, or 52 weeks after vaccination. Two canonical discriminant functions, based on IL-13 and IFN-γ, were used in the analysis (Wilks´ Lambda 0.222, $p < 0.001$) and 99.9% of the variance was explained by function 1 (F1). The standardized canonical discriminant function coefficients for IFN-γ and IL-13 were 0.804 and 0.787 in F1, respectively, indicating that the two variables contributed similarly to the model. To further illustrate the discriminative ability of the model, the data were plotted by discriminant loading using functions 1 and 2 (Figure 7). The results demonstrate that non-vaccinated individuals were correctly classified in 100% of the cases and therefore visualized as a distinct group in the plot. Importantly, none of the vaccinated individuals was classified as non-vaccinated (Table 2). However, the resolution among the post-vaccination groups was poor (Table 2 and Figure 7). As an example, the profiles of 64.3% of individuals sampled at 52 weeks overlapped with the profiles of individuals sampled at 2 weeks and there was no distinction between individuals sampled at 4 or 12 weeks (Table 2).

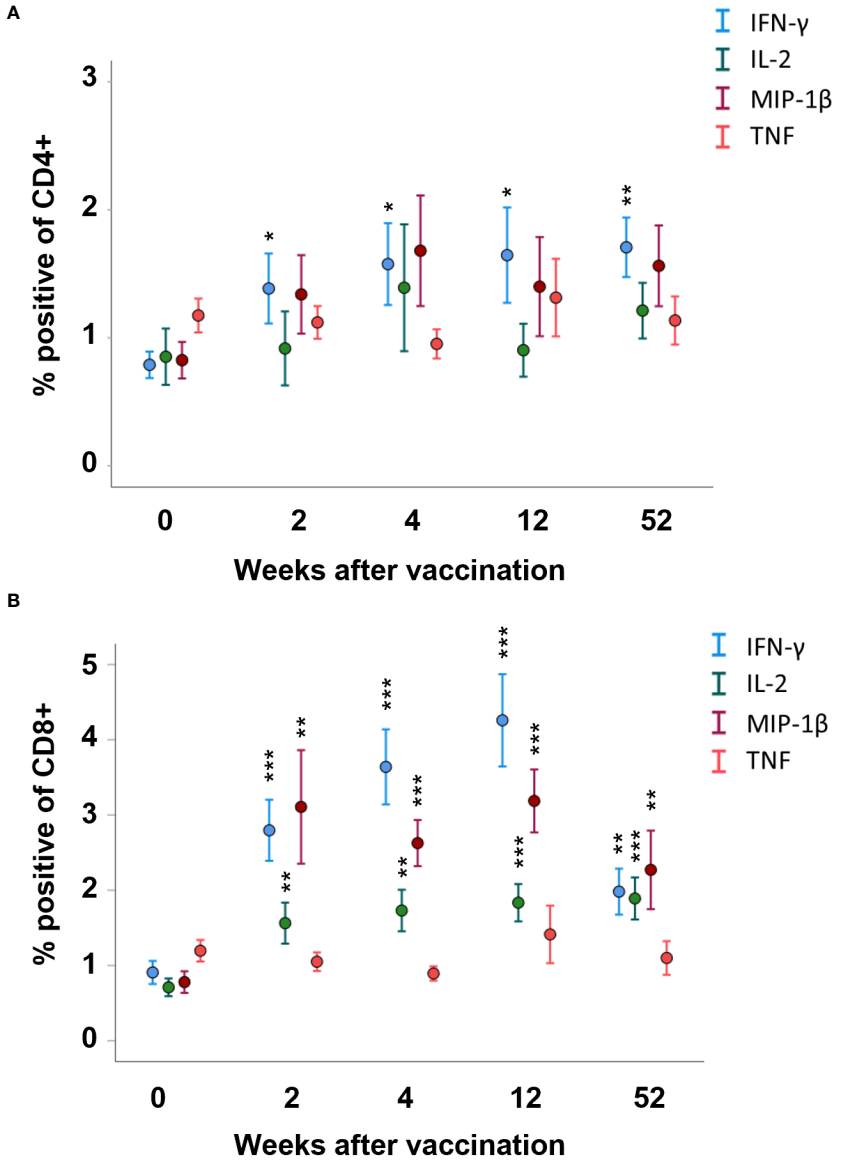

FIGURE 3
FACS analysis of intracellular cytokine expression of the CD4 and CD8 memory populations. PBMCs collected from nine individuals before vaccination (0) and 2, 4, 12, and 52 weeks after vaccination were recall-stimulated with *Ft* antigen for 3 days. The cells were analyzed to identify **(A)** CD4 and **(B)** CD8 memory populations for expression of IFN-γ, IL-2, MIP-1β, or TNF. The mean ± SEM of triplicate samples from nine individuals are shown for each time point and cytokine. Asterisks indicate significant differences of intracellular cytokine expression compared to time point 0. (*$P < 0.05$; **$P < 0.01$; ***$P < 0.001$).

In summary, using linear discriminant analysis, a model based on IL-13 and IFN-γ correctly predicted if an individual had been vaccinated or not, but failed to separate groups sampled at various time points after vaccination.

Capacity of supernatants collected from *Ft*-stimulated cells to confer protection

It was tested if the supernatants of stimulated cell cultures could activate monocyte-derived macrophages (MDMs) to control intracellular SCHU S4. Supernatants collected from *Ft*-stimulated cells from individual donors were added at a 20-fold dilution to cultures at the time of infection with SCHU S4. Concentration of the 17 cytokines in the 20-fold diluted supernatants varied among the individuals (Table S3). After 24 h, growth of SCHU S4 was reduced in all cultures supplemented with supernatants from *Ft* antigen-stimulated PBMCs compared to cultures with supernatants from sham-stimulated PBMCs (Figure 8A). The weakest growth inhibition of SCHU S4, 5-fold, was observed in cultures supplemented with supernatants from donor D129 ($p < 0.05$), and the strongest inhibition, 230-fold, was observed in cultures supplemented with supernatants from donor D135 ($p < 0.001$) (Figure 8A). Supernatants from all donors elicited a significantly better control of SCHU S4 in MDMs compared to recombinant IFN-γ ($p < 0.05$ for 136, $p < 0.01$ for 129, and $p < 0.001$ for all other donors, Figure 8A). The

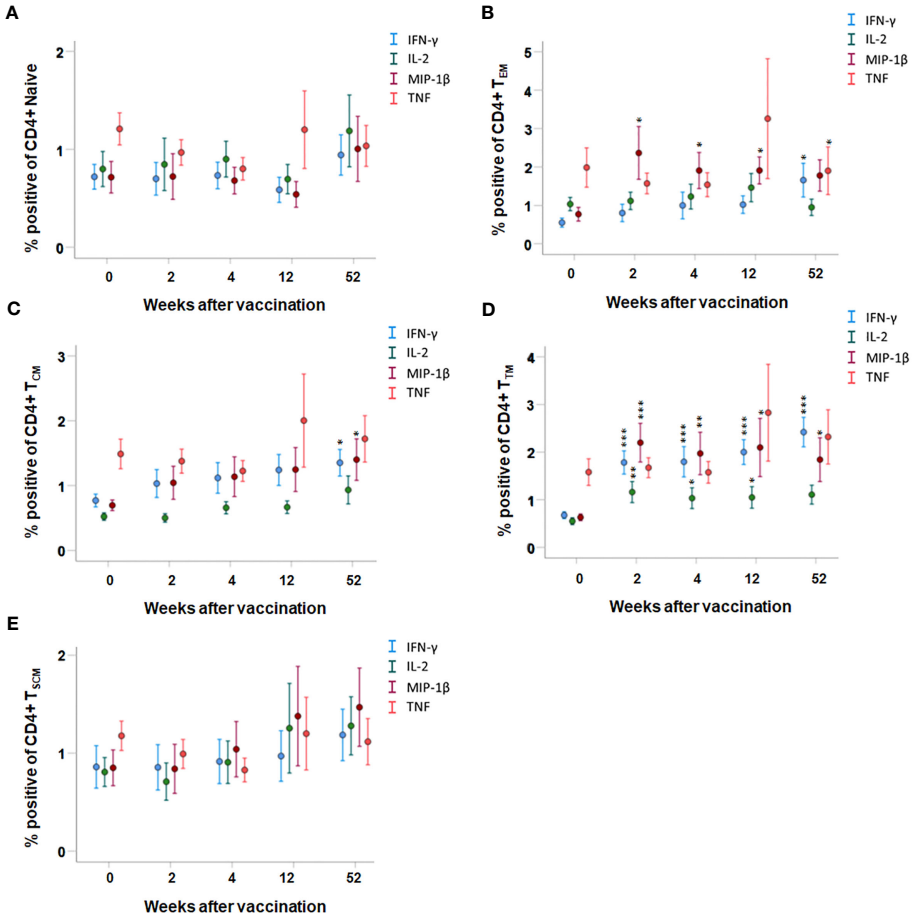

FIGURE 4
FACS analysis of intracellular cytokine expression of CD4 memory subpopulations. PBMCs collected from nine individuals before vaccination (0) and 2, 4, 12, and 52 weeks after vaccination were recall stimulated with *Ft* antigen for 3 days. The cells were stained to detect the following CD4 memory populations: **(A)** T_{Naive}, **(B)** T_{EM}, **(C)** T_{CM}, **(D)** T_{TM}, and **(E)** T_{SCM} and their expression of IFN-γ, IL-2, MIP-1β, or TNF. The mean ± SEM of triplicate samples from nine individuals are shown for each time point and cytokine. Asterisks indicate significant differences of intracellular cytokine expression compared to time point 0 (*$P < 0.05$; **$P < 0.01$; ***$P < 0.001$). The T_{EMRA} subpopulation was not detected in the $CD4^+$ population.

concentration of recombinant IFN-γ, 15 ng/ml, was at least 5-fold higher than the concentration of IFN-γ in any of the 20-fold diluted supernatants (Figure 8B). This suggested that the anti-*F. tularensis* effect elicited by IFN-γ was potentiated by other cytokines present in the supernatant. Potential candidates were IL-2, IL-7, MIP-1B, and TNF, the levels of which, as of IFN-γ, displayed a negative correlation to the number of bacteria in the cultures, i.e., higher concentrations correlated to lower bacterial numbers ($p < 0.05$, Table 3). Levels of IL-13 and G-CSF showed a positive correlation to the number of bacteria in the cultures ($p < 0.05$, Table 3).

Collectively, cells from vaccinated donors produced a mixture of cytokines in response to stimulation with *Ft* antigen that activated MDMs to control intracellular SCHU S4. The control elicited was significantly better than that conferred by recombinant IFN-γ.

Discussion

T-cell-mediated memory immunity is dependent on a pool of memory cells. The half-life of vaccine-induced immunity is one or several decades; however, most evidence indicates that individual memory cells may be comparatively short-lived, in the order of months, and therefore the only logical explanation for the persistence of cell-mediated immunity for decades is the sustainability of clonal populations of memory cells (23). This is achieved by balancing proliferation, death, and differentiation rates of the populations. Thus, the cells within the populations confer long-lived memory rather than being long-lived memory cells. The longevity of these clonal populations is generally ill-defined and possibly distinct for a given T-cell population. An improved understanding of how long-term memory immunity is sustained is critical to improve efficacy of vaccines that rely on cell-mediated immunity.

Previously, we demonstrated that T-cell-mediated immune responses to *F. tularensis* may persist many decades after natural infection or vaccination (24). Herein, we elaborate on this finding and describe the cell-mediated immune responses quantitatively and qualitatively during a 1-year period after vaccination with the live vaccine strain of *F. tularensis*. Importantly, the experimental system used is devoid of antibodies; thus, any influence of humoral

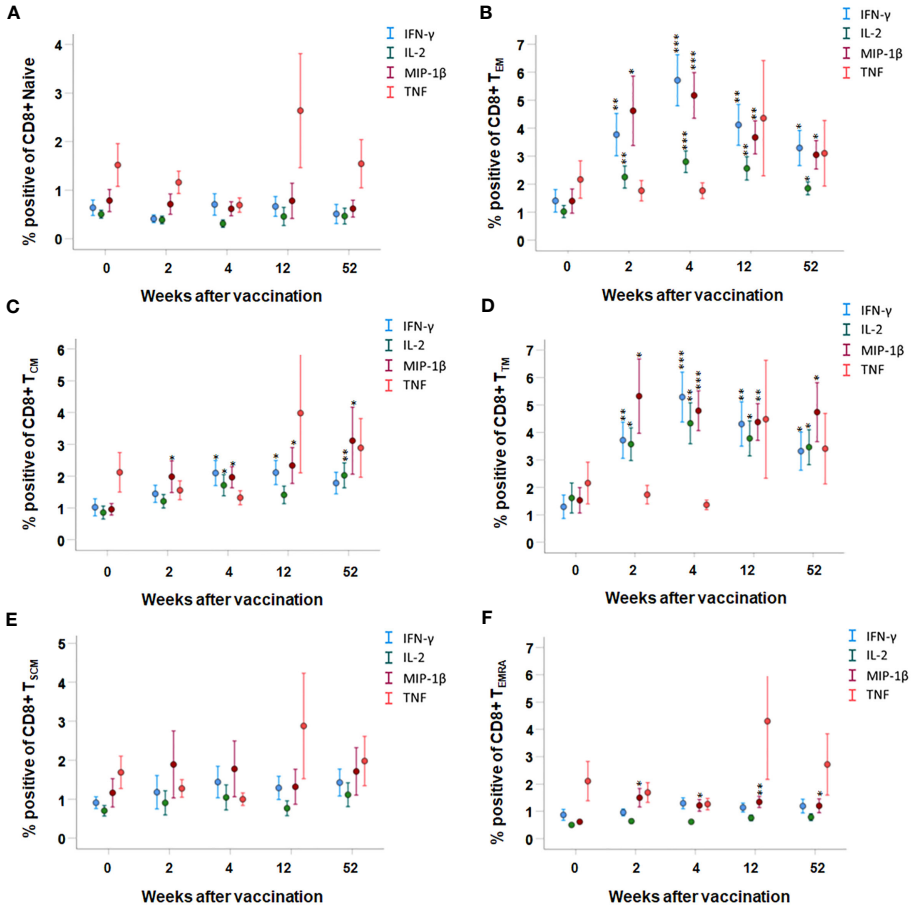

FIGURE 5
FACS analysis of the intracellular cytokine expression of CD8 memory subpopulations. PBMCs collected from nine individuals before vaccination (0) and 2, 4, 12, and 52 weeks after vaccination were recall-stimulated with *Ft* antigen for 3 days. The cells were stained to detect the following CD8 memory populations: **(A)** T_{Naive}, **(B)** T_{EM}, **(C)** T_{CM}, **(D)** T_{TM}, and **(E)** T_{SCM} and **(F)** T_{TEMRA} for their expression of IFN-γ, IL-2, MIP-1β, or TNF. The mean ± SEM of triplicate samples from nine individuals are shown for each time point and cytokine. Asterisks indicate significant differences of intracellular cytokine expression compared to time point 0. (*$P < 0.05$; **$P < 0.01$; ***$P < 0.001$).

immunity can be excluded. Proliferative responses, cytokine secretion, and the intracellular cytokine profiles of CD4 and CD8 cells and memory cell populations were mostly indistinguishable when PBMCs were analyzed at the three early time points after vaccination. However, absolute levels somewhat decreased thereafter, although still significantly increased compared to the responses of the PBMC obtained before vaccination. Antigenic cross-reactivity is unlikely to sustain the longevity since *F. tularensis* is not closely related to other human pathogens (25). Moreover, since tularemia is a rare disease in most regions of the world (26), reexposure is an unlikely reason for the extremely long-lived cell-mediated immunity and, therefore, the data support the notion that natural infection, or vaccination, may result in very long-lasting, persisting for many decades. The narrow immunoreactivity to *F. tularensis* is distinct from that to many other infections due to its antigenic uniqueness and rare occurrence of tularemia. In the case of *F. tularensis*, there is no direct evidence that the long-lasting cell-mediated immunity confers protection against subsequent challenge; however, indirect evidence strongly indicates that this may be the case, since tularemia has been very rarely recorded in vaccinated individuals and only a handful of cases of reinfection have been reported during the last century (27, 28).

Beyond the characterization of the longevity of the cell-mediated immune responses, we also identified the cytokine profiles indicative of the vaccine-induced immune responses by intracellular staining of the PBMC T-cell populations. A more detailed analysis of subpopulations revealed that CD4 cell expression of intracellular IFN-γ was increased after vaccination and sustained for the whole period of 1 year. CD8 cells expressed increased levels of IFN-γ, IL-2, and MIP-1β after vaccination. All three cytokines have been identified in our previous studies of human vaccine-mediated immune responses (12, 22). When memory T-cell subpopulations were analyzed, the most nuanced cytokine expression was detected in the CD4 T_{EM} subpopulation with regard to MIP-1β and in the CD4 T_{TM} subpopulation with regard to IFN-γ, IL-2, and MIP-1β, since the expression of each of the cytokines was increased at all time points after vaccination. Also, the CD8 T_{EM} and T_{TM} subpopulations showed increased expression of IFN-γ, IL-2, and MIP-1β at all time points. Thus, the

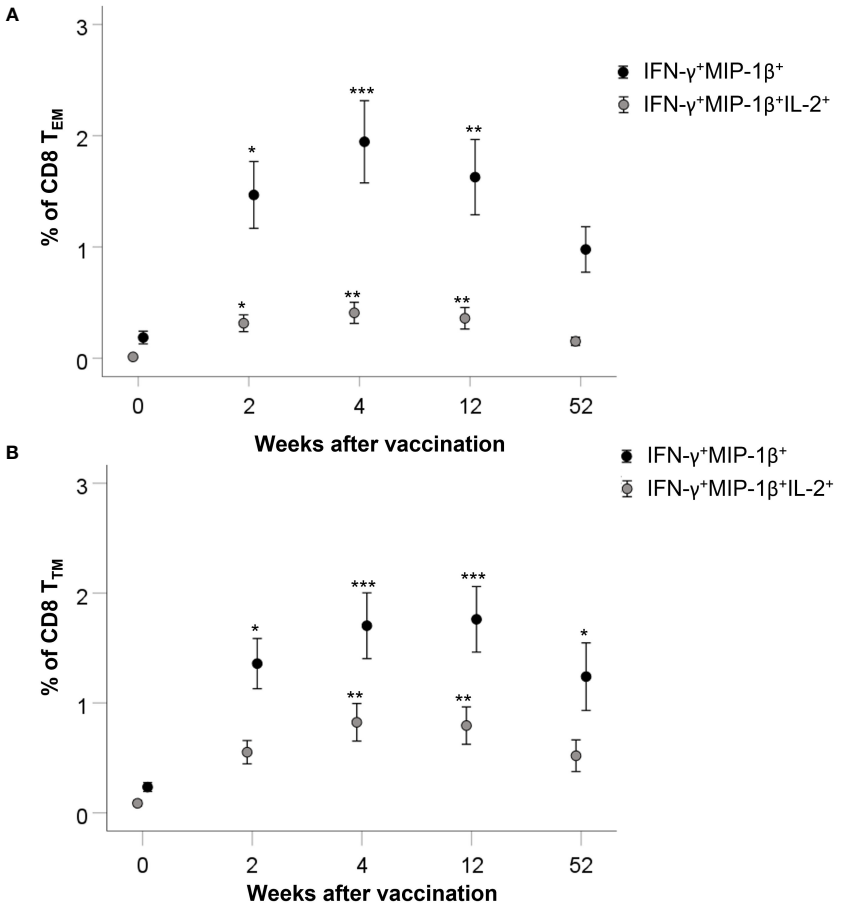

FIGURE 6
Multifunctional memory cell populations. Data were subjected to Boolean gating in order to detect multifunctional memory cell populations. The mean ± SEM of triplicate samples from nine individuals are shown for each time point and cytokine combination. Asterisks indicate significant differences of number of cells positive for intracellular cytokine expression compared to time point 0. (*$P < 0.05$; **$P < 0.01$; ***$P < 0.001$).

findings corroborate previously published data regarding the relevance of these cytokines in the memory immune response against *F. tularensis* after vaccination and demonstrate that the T_{EM} and T_{TM} populations exhibit the most diversified cytokine expression.

The identification of the CD4 T_{TM} and CD8 T_{EM} and T_{TM} subpopulations as the predominant reservoirs for cytokine secretion was not entirely surprising. The T_{EM} subpopulation is known to rapidly upregulate effector functions and to also express homing receptors for migration to nonlymphoid sites of inflammation and to possess high levels of gut-homing molecules and chemokine receptors (29). T_{TM} cells display an intermediate phenotype between T_{EM} and T_{CM} subpopulations, since some transcript expression levels closely align with those of T_{EM} cells, e.g., *CD62L* and *PIM2*, whereas others with those of T_{CM} cells, e.g., *FasL* and *IFN-γ* (30). Thus, the T_{EM} and T_{TM} subpopulations represent potential effector populations and the identification of their potent upregulation of multiple cytokines is therefore logical and identify them as important for the effective protective responses present after tularemia vaccination. In contrast, we did not detect the same broadly increased cytokine secretion by the T_{CM} and T_{EMRA} subpopulations. This reinforces the general concept that the T_{CM} subpopulation constitutes quiescent cells that require very strong stimulation and costimulation to respond to the cognate antigens (31). Their most important role with regard to protection against tularemia may be to serve as a reservoir that can be clonally expanded and differentiated into the T_{EM} and T_{TM} subpopulations. In fact, it cannot be ruled out that the *in vitro* antigen stimulation utilized in the present study led to differentiation of some T_{CM} cells to T_{EM} or T_{TM} cells. As for the T_{CM} subpopulation, the T_{SCM} subpopulation may also serve as a reservoir of cells for subsequent differentiation to effector memory cells. This would be in line with previous observations regarding the T_{SCM} subpopulation (32). The relevance of the T_{EMRA} subpopulation appears to be infection-dependent; e.g., HIV-specific T cells predominantly belong to the T_{EM} subpopulation, while CMV-specific T cells are mainly of the T_{EMRA} phenotype (33). Our findings indicate a rather modest role for the T_{EMRA} subpopulation after tularemia vaccination.

Linear discriminant analysis of patterns of secreted cytokines was utilized and a model was created based on the levels of IFN-γ and IL-13. This analysis revealed that discrimination between non-vaccination and vaccination was 100%, but that resolution between the groups after vaccination was low. This indicates that the

10.3389/fimmu.2023.1238391

TABLE 1 Cytokine levels in supernatants collected from recall-stimulated PBMCs.

Cytokine	Weeks after vaccination				
	Before	2	4	12	52
IL-1β	2.63 ± 0.11[1]	2.97 ± 0.12*[2]	3.03 ± 0.09**	3.23 ± 0.05***	3.12 ± 0.10**
IL-2	1.92 ± 0.06	2.21 ± 0.05**	2.17 ± 0.06**	2.27 ± 0.04***	2.22 ± 0.07**
IL-4	1.44 ± 0.06	1.71 ± 0.05**	1.74 ± 0.05**	1.82 ± 0.03***	1.79 ± 0.05***
IL-5	2.54 ± 0.05	2.71 ± 0.05*	2.73 ± 0.04**	2.80 ± 0.03***	2.82 ± 0.03***
IL-6	4.19 ± 0.06	4.39 ± 0.08	4.43 ± 0.08	4.49 ± 0.06**	4.61 ± 0.03***
IL-7	0.62 ± 0.18	1.60 ± 0.06***	1.62 ± 0.14***	1.46 ± 0.21**	1.56 ± 0.14***
IL-8	6.39 ± 0.29	7.19 ± 0.29	7.05 ± 0.29	6.55 ± 0.26	7.60 ± 0.26**
IL-10	1.42 ± 0.11	1.56 ± 0.06	1.63 ± 0.07	1.68 ± 0.04*	1.62 ± 0.04
Il-12p70	1.24 ± 0.19	1.77 ± 0.06*	1.80 ± 0.07*	1.93 ± 0.06**	1.79 ± 0.11*
IL-13	0.31 ± 0.10	1.25 ± 0.08***	1.24 ± 0.13***	1.36 ± 0.09***	1.23 ± 0.10***
IL-17	1.93 ± 0.08	2.21 ± 0.08*	2.24 ± 0.07**	2.37 ± 0.04***	2.31 ± 0.06**
G-CSF	2.78 ± 0.08	2.89 ± 0.06	2.99 ± 0.05*	2.95 ± 0.07	2.98 ± 0.06
GM-CSF	1.83 ± 0.12	1.95 ± 0.10	2.09 ± 0.08	2.12 ± 0.08*	2.22 ± 0.09*
IFN-γ	2.41 ± 0.09	3.75 ± 0.10***	3.80 ± 0.19***	3.98 ± 0.18***	3.82 ± 0.19***
MCP-1	4.10 ± 0.07	4.38 ± 0.03**	4.30 ± 0.06*	4.29 ± 0.05*	4.49 ± 0.06***
MIP-1β	3.80 ± 0.04	3.98 ± 0.05**	3.95 ± 0.06	3.99 ± 0.05**	4.09 ± 0.05***
TNF	3.73 ± 0.07	4.05 ± 0.06**	3.93 ± 0.07	4.03 ± 0.06**	4.05 ± 0.09**

[1]Cytokine content was determined in supernatants obtained from Ft-stimulated PBMC cultures. Average pg/ml (log_{10}) ± SEM were determined from duplicate samples of seven individuals.
[2]Two-sided t-test of differences compared to cytokine levels in cultures with Ft-stimulated PBMCs collected before vaccination. *p < 0.05, **p < 0.01, and ***p < 0.001.

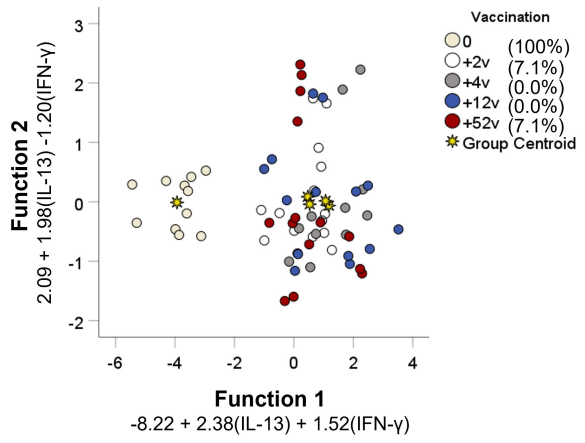

FIGURE 7
Discriminant analysis of individuals with regard to vaccination status. Seventeen cytokines measured in supernatants from recall-stimulated cell cultures were included in a stepwise discriminant function analysis to identify predictors of vaccination status. Functions 1 and 2 are depicted on the *x*- and *y*-axis, respectively. Each data point corresponds to each individual replicate of each group and the asterisks represent the group centroid. The percentage values of group classification correctness are presented in the brackets.

qualitative and quantitative responses observed after vaccination did not change during the observation period of 1 year. This finding agrees with our previous studies demonstrating that recall responses are sustained for three decades without evidence of decline (22). Various types of logistical modeling, similar to the linear discriminant analysis used herein, have been used in previous studies on tularemia secreted cytokines, cytokine gene expression, and lymphocyte stimulation indices, and these have been linked to protective capacity or immune status (12, 13, 22, 24, 34). Also in the mouse model, similar modeling has been utilized and combined results from *in vivo* gene expression and a co-culture method (35). Such results from animal and human models of tularemia are highly relevant with regard to the FDA Animal Rule (36). The rule stipulates that vaccine efficacy and approval can be assessed based on data from animal models only, provided that protective mechanisms are well characterized and the animal data therefore can be extrapolated to the human situation. Thus, the aforementioned data fulfill the criteria and will form an important basis for the approval of new tularemia vaccines. The identification of IL-13 in the context is intriguing since it was long ago demonstrated that the cytokine inhibits nitric oxide production by activated macrophages and thereby most likely will also mitigate the protective responses to *F. tularensis* (37).

Our

TABLE 2 Prediction of individuals according to vaccination using LDA[1].

Predicted	Time after vaccination				
	Before	2 weeks	4 weeks	12 weeks	52 weeks
Before	100	0	0	0	0
2 weeks	0	7.1	0	57.1	35.7
4 weeks	0	0	0	50	50
12 weeks	0	42.9	42.9	0	14.3
52 weeks	0	64.3	14.3	14.3	7.1

[1]Prediction was performed based on the following: function 1: −8,223 + 2.382 (IL-13) + 1.52 (IFN-γ); function 2: 2.093 + 1.198 (IL-13) − 1.197 (IFN-γ).

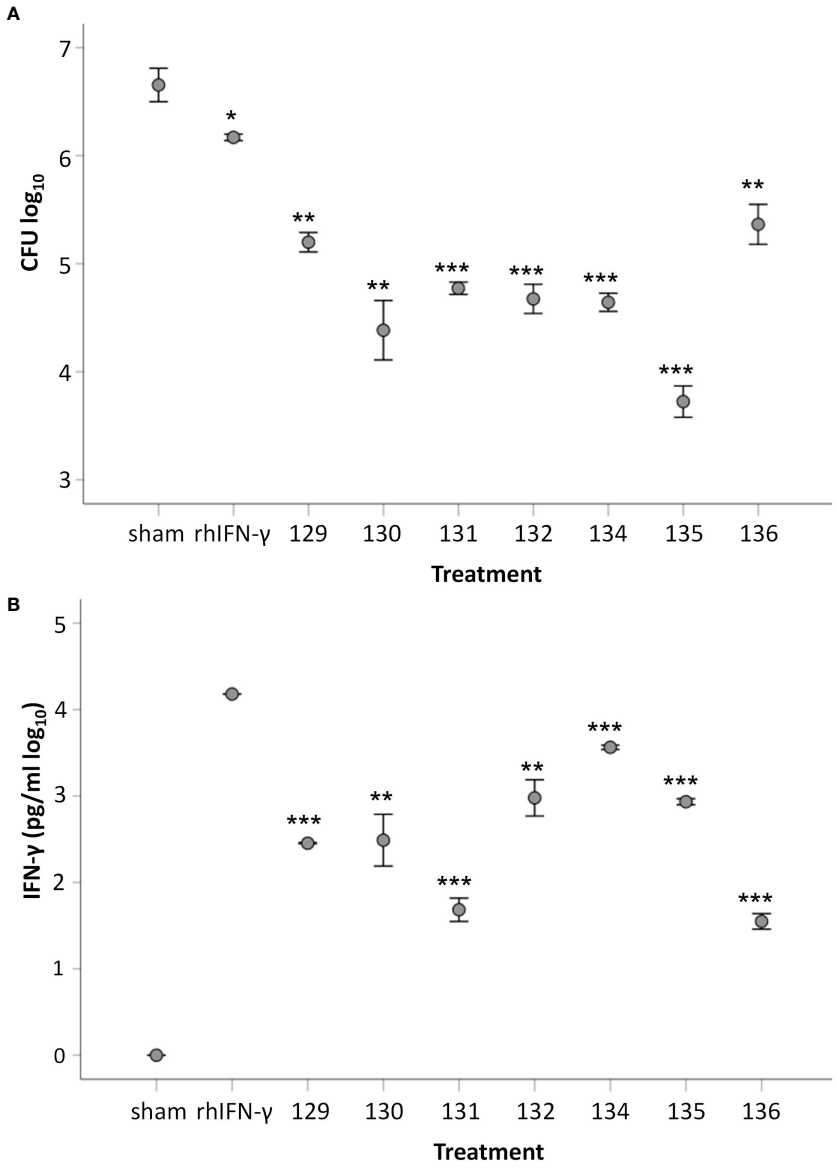

FIGURE 8
Capacity of supernatants from *Ft*-stimulated cells to induce protection against SCHU S4 in MDM. **(A)** Number of intracellular SCHU S4 after 24 h of infection. MDMs were infected with SCHU S4 and supernatants collected from *Ft*-stimulated cells from respective donor were added to separate cultures. Number of phagocytosed bacteria after 2 h of incubation with an MOI of 50 were 3.4 ± 0.02. **(B)** Concentration of IFN-γ in SCHU S4-infected cultures supplemented with supernatants collected from *Ft*-stimulated cells or with recombinant IFN-γ. The bars show the mean ± SEM of three observations. Statistical evaluation of differences between groups were analyzed using two-sided Student's *t*-test. In diagram A, asterisksindicate significant differences vs. sham. In diagram B, asterisks indicate significant differences vs. cultures with recombinant IFN-γ (*$p < 0.05$, **$p < 0.01$, ***$p < 0.001$).

TABLE 3 Correlation of intracellular bacteria to concentration of cytokines in supernatants.

	IL-2	IL-7	IL-13	G-CSF	IFN-γ	MIP-1β	TNF
CFU[1]	−0.635[2]*[3]	−0.576*	0.638*	0.599*	−0.643*	−0.853***	−0.782*

[1] Colony-forming units, numbers of intracellular bacteria at 24 h.
[2] Spearman´s Rho and Spearman's rank correlation test were used to correlate numbers of intracellular bacteria after 24 h to cytokine concentrations in the supernatant. Cytokines not displaying significant correlation are not included in the table.
[3] Asterisks indicate significant correlation between the indicated cytokine and numbers of intracellular bacteria. *p < 0.05, **p < 0.01, and ***p < 0.001.

findings identified IFN-γ as a key cytokine being expressed at high levels after vaccination by both CD4 and CD8 T cells. This finding was not unexpected, since the crucial role of the cytokine for protection against tularemia was first identified more than 30 years ago using various animal models (38–45). Moreover, we have previously used a human co-culture model and demonstrated the protective ability of IFN-γ (12). In animal models, mechanisms dependent on guanylate-binding proteins GBP2 and GBP5 are crucial to effectuate the IFN-γ-mediated control (46, 47). This was first demonstrated for the closely related bacterium *F. novicida* and subsequently also for the LVS strain using infection of mononuclear cells; however, control of the highly virulent SCHU S4 strain was not observed in the model (48). Later, it was demonstrated that control of infection with each of the three *F. tularensis* strains occurred in a mouse co-culture model, but, again, control was critically dependent on GBPs (49). Thus, the evidence from animal models indicate that the control of highly virulent strains is distinct from that of attenuated *F. tularensis* strains and demonstrates that the use of such strains in the models is necessary to identify relevant correlates of immunity and protection.

The strategy used in the present study, to directly assess the protective ability of supernatants elicited during *F. tularensis*-specific immune responses allowed identification of cytokines that correlated to protection in the model. The supernatants demonstrated protective capability even at a 20-fold dilution. However, there were distinct individual differences and the inhibitory effects varied from 5-fold to 230-fold, but this was still as efficacious, or superior to the effect mediated by high levels of recombinant IFN-γ, despite the fact that this concentration of IFN-γ was at least 5-fold higher than the concentrations in the supernatants. Thus, the supernatants provided additional, strongly protective effects besides that of IFN-γ. Of relevance, the levels of several other cytokines were found to correlate to the degree of protection observed. Specifically, IL-2, MIP-1β, TNF, and IL-7 all fulfilled the criterion and the former three of these cytokines have previously been observed to correlate the control of infection in a human co-culture model and also in an animal models of tularemia (12, 34, 50, 51). The strategy was found to be useful and can later be combined with direct assessment of the contribution of individual cytokines, e.g., by depletion of one or several together with the assessment of the protective ability or by supplementation of combinations of recombinant cytokines.

The findings herein serve to identify both correlates of immunity and protection. In fact, even correlates of immunity are very challenging to identify with regard to cell-mediated immune responses. In the case of the most common global infection, tuberculosis, the identification of potential immune correlates is challenging, e.g., the relevance of multifunctional cytokine-producing T cells as correlates has been questioned (52), although there are still considerable efforts trying to identify such correlates (53). With regard to tularemia, most work to identify correlates has been based on animal models, particularly the mouse model. A general finding has been the identification of Th1-related cytokines in these models; e.g., the demonstration of increased levels of IFN-γ, TNF, and MCP-1 has been consistent. Moreover, the levels of these cytokines correlated to protection after vaccination with attenuated *F. tularensis* mutants (34, 35). Studies on immunity after tularemia vaccination, or natural infection of humans, have identified multifunctional T cells similar to findings described for tuberculosis patients (22, 52, 54). When a human co-culture system was used, correlations between levels of IFN-γ, TNF, and MIP-1β and protection were observed (12). Thus, there is substantial indirect evidence that levels of Th1 cytokines, such as IFN-γ, TNF, and MIP-1β, are correlates of protection in various animal and human tularemia models, thereby in much agreement with the present findings (12, 22, 34, 35, 54). Of note, none of the studies on *F. tularensis* has included neutralization of cytokines as a direct demonstration of their contribution to protection.

The present study exclusively utilized PBMCs, and this may affect the results, since memory immunity expressed by this cell type is sometimes distinct compared to that of tissue-resident immune cells. For example, it has been demonstrated that mouse lung T cells require repeated antigen stimulation to sustain memory immunity for 1 year, whereas memory immunity among circulating T cells was preserved during the same time without restimulation (55). Also, with regard to tularemia, evidence indicates that systemic and organ-specific cell-mediated immunity is distinct, e.g., an attenuated mutant of *F. tularensis* conferred superior protection after intranasal vs. intradermal vaccination (35). It was hypothesized that there are organ-specific differences between immune cells and therefore certain routes of immunization confer optimal protection. If memory immunity to some extent will be cell-specific, this may be a caveat when characterizing human protective immunity since cell sources other than peripheral blood will be severely limited. It should be noted that although intranasal vaccination can confer immunological benefits, there may be an increased risk of adverse events with this route as shown for certain vaccines (56).

Collectively, the findings herein identify characteristics of long-term immunospecific T cells, including T_{EM} and T_{TM}

subpopulations secreting an array of cytokines, following vaccination against *F. tularensis*. Moreover, individual cytokines were identified, the levels of which correlated with the degree of protection. Thus, the data provide important information about memory T cells and effector mechanisms that form the basis for the protective mechanisms operative against *F. tularensis*.

Data availability statement

The original contributions presented in the study are included in the article/Supplementary Material. Further inquiries can be directed to the corresponding author.

Ethics statement

The studies involving humans were approved by Swedish Ethical Review Authority, permits 2019-01567 and 2020-01860. The studies were conducted in accordance with the local legislation and institutional requirements. The participants provided their written informed consent to participate in this study.

Author contributions

HL, KE, and IG performed the experiments. AS and HL designed the study. HL, KE, and AS analyzed the data and wrote the manuscript. HL, KE, IG, CG, and AS reviewed the manuscript. All authors contributed to the article and approved the submitted version.

Funding

We acknowledge research funding for this work by grants from Region Västerbotten, Centrala ALF-medel, RV-939171, and Basenhets-ALF, RV-941049 and from Insamlingsstiftelsen, no. 963943, from the Medical Faculty, Umeå University, Umeå, Sweden. Research funding from the Swedish Laboratory Network within Microbiology is also acknowledged.

Conflict of interest

The authors declare that the research was conducted in the absence of any commercial or financial relationships that could be construed as a potential conflict of interest.

Publisher's note

Supplementary material

The Supplementary Material for this article can be found online at: https://www.frontiersin.org/articles/10.3389/fimmu.2023.1238391/full#supplementary-material

References

1. Sjöstedt A. Tularemia: history, epidemiology, pathogen physiology, and clinical manifestations. *Ann N Y Acad Sci* (2007) 1105:1–29. doi: 10.1196/annals.1409.009

2. Conlan JW. Tularemia vaccines: recent developments and remaining hurdles. *Future Microbiol* (2011) 6(4):391–405. doi: 10.2217/fmb.11.22

3. Hestvik G, Warns-Petit E, Smith LA, Fox NJ, Uhlhorn H, Artois M, et al. The status of tularemia in europe in a one-health context: a review. *Epidemiol Infect* (2015) 143(10):2137–60. doi: 10.1017/S0950268814002398

4. European Center for Disease Control. *Tularaemia. In: ECDC. Annual epidemiological report for 2019*. Stockholm: ECDC (2021).

5. Celli J, Zahrt TC. Mechanisms of *Francisella tularensis* intracellular pathogenesis. *Cold Spring Harb Perspect Med* (2013) 3(4):a010314. doi: 10.1101/cshperspect.a010314

6. Elkins KL, Cowley SC, Bosio CM. Innate and adaptive immunity to *Francisella*. *Ann N Y Acad Sci* (2007) 1105:284–324. doi: 10.1196/annals.1409.014

7. Roberts LM, Powell DA, Frelinger JA. Adaptive immunity to *Francisella tularensis* and considerations for vaccine development. *Front Cell Infect Microbiol* (2018) 8:115. doi: 10.3389/fcimb.2018.00115

8. Glynn AR, Alves DA, Frick O, Erwin-Cohen R, Porter A, Norris S, et al. Comparison of experimental respiratory tularemia in three nonhuman primate species. *Comp Immunol Microbiol Infect Dis* (2015) 39:13–24. doi: 10.1016/j.cimid.2015.01.003

9. Lyons CR, Wu TH. Animal models of *Francisella tularensis* infection. *Ann N Y Acad Sci* (2007) 1105:238–65. doi: 10.1196/annals.1409.003

10. Twine S, Shen H, Harris G, Chen W, Sjostedt A, Ryden P, et al. BALB/C Mice, but not C57bl/6 mice immunized with a Delta*clpB* mutant of *Francisella tularensis* subspecies *tularensis* are protected against respiratory challenge with wild-type bacteria: association of protection with post-vaccination and post-challenge immune responses. *Vaccine* (2012) 30(24):3634–45. doi: 10.1016/j.vaccine.2012.03.036

11. Golovliov I, Lindgren H, Eneslätt K, Conlan W, Mosnier A, Henry T, et al. An *in vitro* co-culture mouse model demonstrates efficient vaccine-mediated control of *Francisella tularensis* SCHU S4 and identifies nitric oxide as a predictor of efficacy. *Front Cell Infect Microbiol* (2016) 6:152. doi: 10.3389/fcimb.2016.00152

12. Eneslätt K, Golovliov I, Ryden P, Sjöstedt A. Vaccine-mediated mechanisms controlling replication of *francisella tularensis* in human peripheral blood mononuclear cells using a co-culture system. *Front Cell Infect Microbiol* (2018) 8:27. doi: 10.3389/fcimb.2018.00027

13. De Pascalis R, Frey B, Rice HM, Bhargava V, Wu TH, Peterson RL, et al. Working correlates of protection predict SCHU S4-derived-vaccine candidates with improved efficacy against an intracellular bacterium. *Francisella tularensis. NPJ Vaccines* (2022) 7(1):95. doi: 10.1038/s41541-022-00506-9

14. Lindgren H, Eneslätt K, Golovliov I, Gelhaus C, Ryden P, Wu T, et al. Vaccine-mediated mechanisms controlling francisella tularensis SCHU S4 growth in a rat co-culture system. *Pathogens* (2020) 9(5):388. doi: 10.3390/pathogens9050338

15. Conlan JW, Oyston PC. Vaccines against *Francisella tularensis*. *Ann N Y Acad Sci* (2007) 1105:325–50. doi: 10.1196/annals.1409.012

16. Ratajczak W, Niedzwiedzka-Rystwej P, Tokarz-Deptula B, Deptula W. Immunological memory cells. *Cent Eur J Immunol* (2018) 43(2):194–203. doi: 10.5114/ceji.2018.77390

17. Farber DL, Yudanin NA, Restifo NP. Human memory T cells: generation, compartmentalization and homeostasis. *Nat Rev Immunol* (2014) 14(1):24–35. doi: 10.1038/nri3567

18. Pulendran B, Davis MM. The science and medicine of human immunology. *Science* (2020) 369(6511):1582. doi: 10.1126/science.aay4014

19. Pulendran B, Ahmed R. Immunological mechanisms of vaccination. *Nat Immunol* (2011) 12(6):509–17. doi: 10.1038/ni.2039

20. Sandström G, Tärnvik A, Wolf-Watz H, Löfgren S. Antigen from *Francisella tularensis*: nonidentity between determinants participating in cell-mediated and humoral reactions. *Infect Immun* (1984) 45(1):101–6. doi: 10.1128/iai.45.1.101-106.1984

21. Tharwat A, Tarekc G, Ibrahim A, Hassanien AE. Linear discriminant analysis: a detailed tutorial. *AI Commun* (2017) 30(2):169–90. doi: 10.3233/AIC-170729

22. Eneslätt K, Normark M, Björk R, Rietz C, Zingmark C, Wolfraim LA, et al. Signatures of T cells as correlates of immunity to *Francisella tularensis*. *PloS One* (2012) 7(3):e32367. doi: 10.1371/journal.pone.0032367

23. Baliu-Pique M, Verheij MW, Drylewicz J, Ravesloot L, de Boer RJ, Koets A, et al. Short lifespans of memory T-cells in bone marrow, blood, and lymph nodes suggest that T-cell memory is maintained by continuous self-renewal of recirculating cells. *Front Immunol* (2018) 9:2054. doi: 10.3389/fimmu.2018.02054

24. Eneslätt K, Rietz C, Ryden P, Stöven S, House RV, Wolfraim LA, et al. Persistence of cell-mediated immunity three decades after vaccination with the live vaccine strain of *Francisella tularensis*. *Eur J Immunol* (2011) 41(4):974–80. doi: 10.1002/eji.201040923

25. Sjöstedt A, Genus I. Francisella. In: Brenner DJ, editor. *Bergey's manual of systematic bacteriology*. New York, NY: Springer-Verlag (2005). Family Xvii. *Francisellaceae*.

26. Desvars-Larrive A, Liu X, Hjertqvist M, Sjöstedt A, Johansson A, Ryden P. High-risk regions and outbreak modelling of tularemia in humans. *Epidemiol Infect* (2017) 145(3):482–90. doi: 10.1017/S0950268816002478

27. Burke DS. Immunization against tularemia: analysis of the effectiveness of live *Francisella tularensis* vaccine in prevention of laboratory-acquired tularemia. *J Infect Dis* (1977) 135(1):55–60. doi: 10.1093/infdis/135.1.55

28. Tärnvik A, Berglund L. Tularaemia. *Eur Respir J* (2003) 21(2):361–73. doi: 10.1183/09031936.03.00088903

29. Martin MD, Badovinac VP. Defining memory CD8 T cells. *Front Immunol* (2018) 9:2692. doi: 10.3389/fimmu.2018.02692

30. Lugli E, Goldman CK, Perera LP, Smedley J, Pung R, Yovandich JL, et al. Transient and persistent effects of IL-15 on lymphocyte homeostasis in nonhuman primates. *Blood* (2010) 116(17):3238–48. doi: 10.1182/blood-2010-03-275438

31. Abdelsamed HA, Moustaki A, Fan Y, Dogra P, Ghoneim HE, Zebley CC, et al. Human memory cd8 T cell effector potential is epigenetically preserved during *in vivo* homeostasis. *J Exp Med* (2017) 214(6):1593–606. doi: 10.1084/jem.20161760

32. Costa Del Amo P, Lahoz-Beneytez J, Boelen L, Ahmed R, Miners KL, Zhang Y, et al. Human tscm cell dynamics *in vivo* are compatible with long-lived immunological memory and stemness. *PloS Biol* (2018) 16(6):e2005523. doi: 10.1371/journal.pbio.2005523

33. Appay V, Dunbar PR, Callan M, Klenerman P, Gillespie GM, Papagno L, et al. Memory CD8+ T cells vary in differentiation phenotype in different persistent virus infections. *Nat Med* (2002) 8(4):379–85. doi: 10.1038/nm0402-379

34. Ryden P, Twine S, Shen H, Harris G, Chen W, Sjöstedt A, et al. Correlates of protection following vaccination of mice with gene deletion mutants of *Francisella tularensis* subspecies *tularensis* strain, SCHU S4 that elicit varying degrees of immunity to systemic and respiratory challenge with wild-type bacteria. *Mol Immunol* (2012) 54 (1):58–67. doi: 10.1016/j.molimm.2012.10.043

35. De Pascalis R, Chou AY, Ryden P, Kennett NJ, Sjöstedt A, Elkins KL. Models derived from *in vitro* analyses of spleen, liver, and lung leukocyte functions predict vaccine efficacy against the *francisella tularensis* Live Vaccine Strain (LVS). *mBio* (2014) 5(2):e00936. doi: 10.1128/mBio.00936-13

36. Snoy PJ. Establishing efficacy of human products using animals: the US food and drug administration's "Animal rule". *Vet Pathol* (2010) 47(5):774–8. doi: 10.1177/0300985810372506

37. Doherty TM, Kastelein R, Menon S, Andrade S, Coffman RL. Modulation of murine macrophage function by IL-13. *J Immunol* (1993) 151(12):7151–60. doi: 10.4049/jimmunol.151.12.7151

38. Anthony LS, Ghadirian E, Nestel FP, Kongshavn PA. The requirement for gamma interferon in resistance of mice to experimental tularemia. *Microb Pathog* (1989) 7(6):421–8. doi: 10.1016/0882-4010(89)90022-3

39. Karttunen R, Surcel HM, Andersson G, Ekre HP, Herva E. *Francisella tularensis*-Induced *in vitro* gamma interferon, tumor necrosis factor alpha, and interleukin 2 responses appear within 2 weeks of tularemia vaccination in human beings. *J Clin Microbiol* (1991) 29(4):753–6. doi: 10.1128/jcm.29.4.753-756.1991

40. Surcel HM, Syrjala H, Karttunen R, Tapaninaho S, Herva E. Development of *Francisella tularensis* antigen responses measured as T-Lymphocyte proliferation and cytokine production (Tumor necrosis factor alpha, gamma interferon, and interleukin-2 and -4) during human tularemia. *Infect Immun* (1991) 59(6):1948–53. doi: 10.1128/iai.59.6.1948-1953.1991

41. Fortier AH, Polsinelli T, Green SJ, Nacy CA. Activation of macrophages for destruction of *francisella tularensis*: identification of cytokines, effector cells, and effector molecules. *Infect Immun* (1992) 60(3):817–25. doi: 10.1128/iai.60.3.817-825.1992

42. Conlan JW, Sjöstedt A, North RJ. CD4+ and CD8+ T-cell-dependent and -independent host defense mechanisms can operate to control and resolve primary and secondary *Francisella tularnsis* LVS infection in mice. *Infect Immun* (1994) 62 (12):5603–7. doi: 10.1128/iai.62.12.5603-5607.1994

43. Elkins KL, Rhinehart-Jones TR, Culkin SJ, Yee D, Winegar RK. Minimal requirements for murine resistance to infection with *Francisella tularensis* LVS. *Infect Immun* (1996) 64(8):3288–93. doi: 10.1128/iai.64.8.3288-3293.1996

44. Sjöstedt A, North RJ, Conlan JW. The requirement of tumour necrosis factor-alpha and interferon-gamma for the expression of protective immunity to secondary murine tularaemia depends on the size of the challenge inoculum. *Microbiology* (1996) 142:1369–74. doi: 10.1099/13500872-142-6-1369

45. Cowley SC, Meierovics AI, Frelinger JA, Iwakura Y, Elkins KL. Lung CD4- CD8-double-negative T cells are prominent producers of IL-17a and IFN-gamma during primary respiratory murine infection with *Francisella tularensis* live vaccine strain. *J Immunol* (2010) 184(10):5791–801. doi: 10.4049/jimmunol.1000362

46. Man SM, Karki R, Malireddi RK, Neale G, Vogel P, Yamamoto M, et al. The transcription factor IRF1 and guanylate-binding proteins target activation of the AIM2 inflammasome by *Francisella* infection. *Nat Immunol* (2015) 16(5):467–75. doi: 10.1038/ni.3118

47. Meunier E, Wallet P, Dreier RF, Costanzo S, Anton L, Ruhl S, et al. Guanylate-binding proteins promote activation of the AIM2 inflammasome during infection with. *Francisella novicida*. *Nat Immunol* (2015) 16(5):476–84. doi: 10.1038/ni.3119

48. Wallet P, Benaoudia S, Mosnier A, Lagrange B, Martin A, Lindgren H, et al. IFN-gamma extends the immune functions of guanylate binding proteins to inflammasome-independent antibacterial activities during *Francisella novicida* infection. *PloS Pathog* (2017) 13(10):e1006630. doi: 10.1371/journal.ppat.1006630

49. Mohammadi N, Lindgren H, Golovliov I, Eneslätt K, Yamamoto M, Martin A, et al. Guanylate-binding proteins are critical for effective control of *Francisella tularensis* strains in a mouse co-culture system of adaptive immunity. *Front Cell Infect Microbiol* (2020) 10:594063. doi: 10.3389/fcimb.2020.594063

50. Paranavitana C, Zelazowska E, DaSilva L, Pittman PR, Nikolich M. Th17 cytokines in recall responses against *Francisella tularensis* in humans. *J Interferon Cytokine Res* (2010) 30(7):471–6. doi: 10.1089/jir.2009.0108

51. Cowley S, Elkins K. Immunity to *Francisella*. *Front Microbiol* (2011) 2:26. doi: 10.3389/fmicb.2011.00026

52. Derrick SC, Yabe IM, Yang A, Morris SL. Vaccine-induced anti-tuberculosis protective immunity in mice correlates with the magnitude and quality of multifunctional CD4 T cells. *Vaccine* (2011) 29(16):2902–9. doi: 10.1016/j.vaccine.2011.02.010

53. Choi HG, Kwon KW, Choi S, Back YW, Park HS, Kang SM, et al. Antigen-specific IFN-gamma/IL-17-co-producing CD4(+) T-cells are the determinants for protective efficacy of tuberculosis subunit vaccine. *Vaccines (Basel)* (2020) 8(2):300. doi: 10.3390/vaccines8020300

54. Paranavitana C, Pittman P, Velauthapillai M, DaSilva L. Temporal cytokine profiling of *Francisella tularensis*-infected human peripheral blood mononuclear cells. *J Microbiol Immunol Infect* (2008) 41(3):192–9.

55. Uddback I, Cartwright EK, Scholler AS, Wein AN, Hayward SL, Lobby J, et al. Long-term maintenance of lung resident memory T cells is mediated by persistent antigen. *Mucosal Immunol* (2021) 14(1):92–9. doi: 10.1038/s41385-020-0309-3

56. Izurieta HS, Haber P, Wise RP, Iskander J, Pratt D, Mink C, et al. Adverse events reported following live, cold-adapted, intranasal influenza vaccine. *JAMA* (2005) 294 (21):2720–5. doi: 10.1001/jama.294.21.2720

frontiers | Frontiers in Immunology

TYPE Mini Review
PUBLISHED 22 November 2022
DOI 10.3389/fimmu.2022.1048505

OPEN ACCESS

EDITED BY
Marita Troye Blomberg,
Stockholm University, Sweden

REVIEWED BY
Fintan Thomas Moriarty,
AO Research Institute, Switzerland
Diana Boraschi,
Chinese Academy of Science (CAS), China

*CORRESPONDENCE
Cristina Sobacchi
cristina.sobacchi@humanitasresearch.it

SPECIALTY SECTION
This article was submitted to Cytokines and Soluble Mediators in Immunity, a section of the journal Frontiers in Immunology

RECEIVED 19 September 2022
ACCEPTED 03 November 2022
PUBLISHED 22 November 2022

CITATION
Granata V, Possetti V, Parente R, Bottazzi B, Inforzato A and Sobacchi C (2022) The osteoblast secretome in *Staphylococcus aureus* osteomyelitis. *Front. Immunol.* 13:1048505. doi: 10.3389/fimmu.2022.1048505

The osteoblast secretome in *Staphylococcus aureus* osteomyelitis

Valentina Granata[1,2], Valentina Possetti[1,3], Raffaella Parente[1], Barbara Bottazzi[1], Antonio Inforzato[1,3] and Cristina Sobacchi[1,2]*

[1]IRCCS Humanitas Research Hospital, Rozzano, Italy, [2]Milan Unit, National Research Council - Institute for Genetic and Biomedical Research (CNR-IRGB), Milan, Italy, [3]Department of Biomedical Sciences, Humanitas University, Pieve Emanuele, Italy

Osteomyelitis (OM) is an infectious disease of the bone predominantly caused by the opportunistic bacterium *Staphylococcus aureus* (*S. aureus*). Typically established upon hematogenous spread of the pathogen to the musculoskeletal system or contamination of the bone after fracture or surgery, osteomyelitis has a complex pathogenesis with a critical involvement of both osteal and immune components. Colonization of the bone by *S. aureus* is traditionally proposed to induce functional inhibition and/or apoptosis of osteoblasts, alteration of the RANKL/OPG ratio in the bone microenvironment and activation of osteoclasts; all together, these events locally subvert tissue homeostasis causing pathological bone loss. However, this paradigm has been challenged in recent years, in fact osteoblasts are emerging as active players in the induction and orientation of the immune reaction that mounts in the bone during an infection. The interaction with immune cells has been mostly ascribed to osteoblast-derived soluble mediators that add on and synergize with those contributed by professional immune cells. In this respect, several preclinical and clinical observations indicate that osteomyelitis is accompanied by alterations in the local and (sometimes) systemic levels of both pro-inflammatory (e.g., IL-6, IL-1α, TNF-α, IL-1β) and anti-inflammatory (e.g., TGF-β1) cytokines. Here we revisit the role of osteoblasts in bacterial OM, with a focus on their secretome and its crosstalk with cellular and molecular components of the bone microenvironment and immune system.

KEYWORDS

osteomyelitis, infection, bone, osteoblast, staphylococcus aureus, cytokines, chemokines

Introduction

Osteomyelitis is a severe bone infection arising from hematogenous spread of pathogens, mainly in pediatric patients (1), or direct contamination of the bone after fracture or surgery, more commonly in adults (2). Typically associated with comorbidities, osteomyelitis has a relatively high incidence amongst diabetics, where it develops secondary to vascular and neuropathic complications of hyperglycemia, and may require extreme clinical measures (i.e., limb amputation) (3). Osteomyelitis occurs also in in the absence of known risk factors for invasive infections, which underlines the complexity of its etiopathogenesis. Several pathogens, including bacteria, fungi, and viruses, can cause bone infections, but the most common etiologic agent of the disease is the Gram-positive bacterium *Staphylococcus aureus* (*S. aureus*), which is responsible for up to 60% of the cases (4). Different classification schemes have been proposed for osteomyelitis, based on a range of clinical and microbiological characteristics (5). Most commonly, the disease is classified as either acute or chronic, according to its duration, and either hematogenous or contiguous, according to the origin of infection. During a bone infection, the serum levels of several cytokines [e.g., IL-6, IL-8, IL-1β, IL-12(p70)], angiogenic factors (e.g., VEGF), and acute phase proteins (e.g., C reactive protein, CRP) increase, which is of diagnostic value in the clinical handling of the disease; nevertheless, specific infection markers with diagnostic value are still sought for (6, 7).

The first line of defense against invading pathogens, including *S. aureus*, is represented by cells of the innate immune system (neutrophils, monocytes, macrophages), which detect the pathogens through germline-encoded pattern-recognition receptors (PRRs), including Toll-like receptors (TLRs) and cytoplasmic receptors. PRRs recognize specific microbial components known as pathogen-associated molecular patterns (PAMPs), such as LPS, lipoteichoic acid, lipoproteins, and peptidoglycans, and convey the biochemical signals that are ultimately responsible for activation of the immune cells (8). PRRs are also made by non-immune cells, including cells of the osteoclast and osteoblast lineage in the bone. All TLRs but TLR2 and TLR4 are downregulated during osteoclast differentiation, and relative timing of TLR and RANKL/MCSF stimulation of osteoclast precursors elicit opposite effect on osteoclast formation (9). Very recently it has been reported that TLR2 and TLR9 signaling contributes marginally to the inflammatory bone loss and enhanced osteoclast formation that accompany *S. aureus*-dependent osteomyelitis (see *Osteoclasts and their progenitors*) (10). However, it is generally accepted that osteoblasts use TLRs and NODs to recognize and respond to *S. aureus*, which leads to secretion of the master osteoclastogenic cytokine RANKL as well as other factors (11), as discussed below.

In line with the general paradigm of immunological activation upon PRR engagement, in the context of a bone infection, polymorphonuclear leukocytes (PMNs) and macrophages migrate into the bone microenvironment and therein release several diverse inflammatory mediators, including cytokines, chemokines (e.g., IL-1β, IL-6, and TNF-α, CCL3 and CXCL2), and other factors. The immune reaction that mounts in the bone alters the local homeostasis profoundly, which adds on the direct effects of *S. aureus* on skeletal cells (8). Proinflammatory mediators promote formation and activation of osteoclasts, thus enhancing bone resorption; in parallel, new, poorly structured bone is deposited at the periosteum (periosteal bone reaction) by osteoblasts to confine the infection. These opposing processes collectively result into progressive disruption of the bone microarchitecture. The crosstalk between immune and skeletal cells in the context of bone infections sustained by *S. aureus* (a paradigmatic example of osteoimmunology) is schematically depicted in Figure 1.

Besides their function in bone homeostasis, both osteoclasts and osteoblasts exert immune regulatory functions by orchestrating synthesis and release of various inflammatory molecules (12). In the present review, we present and discuss the roles of osteoblasts in the pathogenesis of osteomyelitis, with a focus on osteoblast-derived soluble factors and their contribution to the long-term fate of bone infections (Figure 2).

Mainstays in bone biology and basic microbiology of *S. aureus* osteomyelitis

Bone is a dynamic tissue that undergoes constant remodeling throughout life (13). Osteoclasts and osteoblasts are the two cell types primarily involved in bone remodeling, responsible for bone resorption and bone formation, respectively. Osteoclasts are of hematopoietic origin, and unique in their ability to degrade the inorganic (hydroxyapatite) and organic (mostly collagen) matrix of the bone (14) through acidification of the resorption lacuna and release of hydrolytic enzymes (e.g., cathepsin K). Conversely, osteoblasts arise from cells of the mesenchymal lineage, and produce the whole set of components of the mineralized extracellular matrix of the bone, which comprises collagen, proteoglycans and several non-collagenous proteins, and an extremely dense hydroxyapatite-based mineral (15). As the matrix grows, some osteoblasts are enclosed in it and become osteocytes. These are terminally differentiated cells that communicate with each other and other cell types by means of cellular processes that penetrate the canaliculi in the bone extracellular matrix.

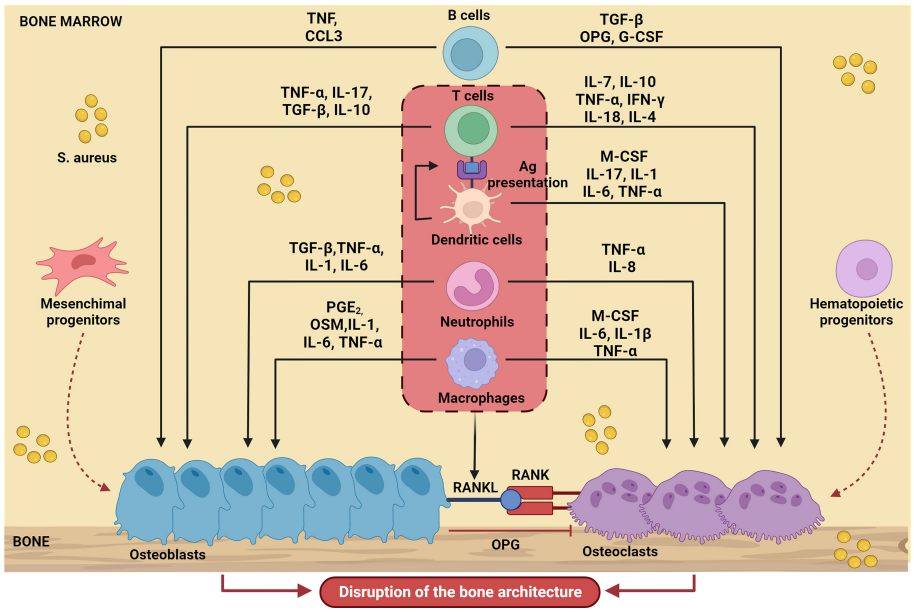

FIGURE 1
Schematic representation of bone cell regulation by the main soluble factors produced by immune cells during S. aureus-induced osteomyelitis. Upon infection, immune cells migrate into the bone microenvironment and release cytokines (IL-17, IL-10, IL-1, IL-1β, IL-6, IL-7, IL-18, IL-4, IL-8), chemokines (CCL3), growth factors (M-CSF, G-CSF) and other several inflammatory mediators (TNF-α, PGE_2, TGFβ, INF-γ, OSM) that influence osteoblast and osteoclast activity. The result is massive disruption of the normal bone architecture. The Figure was created with BioRender.com.

The crosstalk between osteoclasts and osteoblasts shapes the extracellular matrix. Their mutual interaction relies on a series of membrane-bound molecules and soluble factors (e.g., EFNB2-EPHB4, FASL-FAS and SEMA3A-NRP1). Among the latter, M-CSF and RANKL, produced by osteoblasts and acting on their specific receptors on the osteoclast surface (C-FMS and RANK, respectively), have a pivotal role in bone homeostasis (14). In addition, osteoblasts release OPG, the decoy receptor for RANKL that hinders RANK-RANKL interaction, reducing osteoclast formation and bone resorption. In fact, RANKL/OPG ratio is commonly used as an indicator of the balance between bone formation and resorption (16).

S. aureus can invade, colonize, and thrive in the bone. Microbial surface components recognizing adhesive matrix molecules (MSCRAMMs), such as fibronectin-binding protein A and B (FnBPA and B), collagen adhesin (Cna) and Staphylococcus protein A (SpA) (17), initiate adhesion to the bone extracellular matrix. Once bound to the matrix, *S. aureus* can activate diverse mechanisms to escape the host immune response, survive in the bone microenvironment, and establish chronic infection. A primary strategy of immune evasion is biofilm formation, a complex process that involves synthesis and release of extracellular polymeric substances (i.e., polysaccharides and extracellular DNA) and is controlled both by microbial (i.e., the Agr quorum-sensing system) (18) and host factors (i.e., mineral components of the bone matrix, such as Mg^{2+} and Ca^{2+}, oxygen and nutrient availability) (18). Biofilms reduce osteoblast viability and increase RANKL production, thus promoting bone resorption (19). Moreover, in an *in vitro* dynamic model of biofilm deposition, the supernatant of TNFα-treated osteoblasts was found to affect *S. aureus* adhesion and biofilm formation (20). Abscess formation is another survival strategy for *S. aureus*, whereby following upon the engagement of fibrinogen by the bacterial clamping factors A and B (ClfA and B) and its conversion to fibrin (by coagulase, CoA, and von Willebrand factor-binding protein, vWbp), a fibrous pseudocapsule is formed that encases a core of staphylococcal abscess communities (SACs) and is surrounded by a layer of necrotic leukocytes (mostly, neutrophils) (2). Furthermore, *S. aureus* is able to invade the osteocyte lacunocanalicular network through bacteria deformation (whereby a key role has been proposed for the transpeptidases penicillin-binding proteins 3 and 4), entry and migration into the canaliculi *via* asymmetric binary fission at the leading edge (21, 22); these mechanisms are particularly relevant to long term bacterial persistence and eradication. Finally, intracellular infection and survival is a bacterial strategy to evade immune surveillance; of note, all skeletal cells are potential targets, as discussed in the following section.

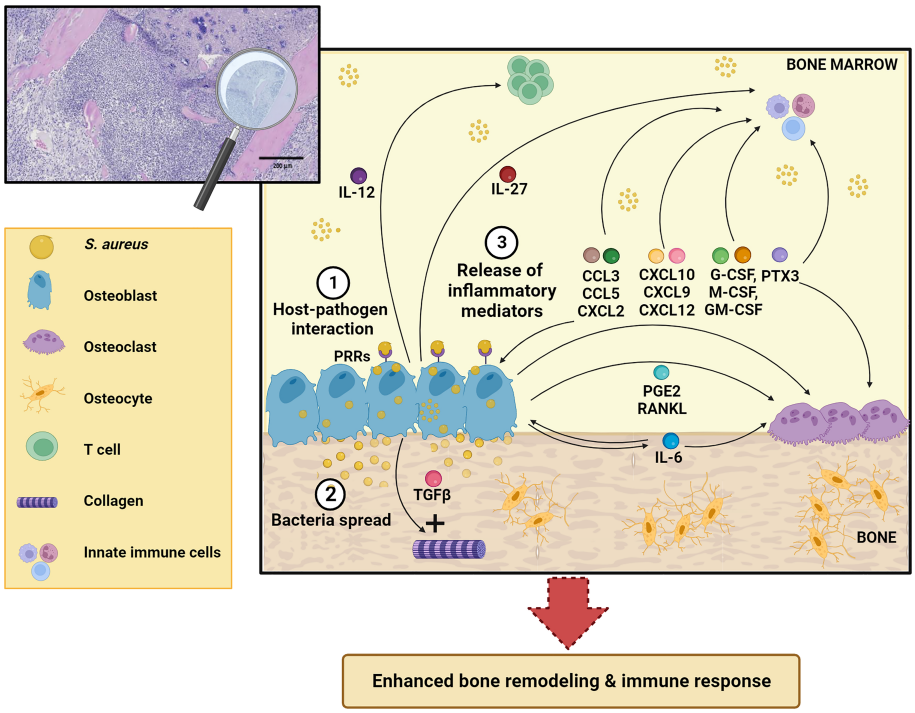

FIGURE 2
Schematic representation of osteoblast response to *S. aureus* infection. After osteoblast infection (1), *S. aureus* can grow and spread further in the bone (2) and induce synthesis and release of different inflammatory mediators (IL-12, IL-27, IL-6, CCL3, CCL5, CXCL2, CXCL10, CXCL9, CXCL12, TGFβ, G-CSF, M-CSF, GM-CSF, PTX3, RANKL, PGE_2) (3) that act both on skeletal and immune cells. This leads to enhanced bone remodeling and immune response. See the main text for more details. The Figure was created with BioRender.com.

Skeletal cell infection in the context of *S. aureus* osteomyelitis

Osteoclasts and their progenitors

A growing body of evidence supports the concept of osteoclasts working as the innate immune cells of the bone (23, 24); accordingly, it is expected that they play a role in the framework of osteomyelitis. Bacterial infection has the potential to influence osteoclast formation directly, through receptor ligation on progenitor cells (9), and indirectly, through enhanced cytokine release from neighboring cells (8). In particular, *in vitro S. aureus* infection of murine bone marrow-derived osteoclast precursors has been shown to induce their differentiation into activated macrophages that actively secrete proinflammatory cytokines, such as CCL5, MIP-1α, MIP-1β, G-CSF, IL-12p40, and MCP-1 (25). These cytokines enhance the bone resorption capacity of uninfected mature osteoclasts and differentiation of uninfected precursors. Moreover, infection of mature osteoclasts directly promotes cell fusion, which contributes to enhance their ability to resorb bone (25). A similar effect has been also demonstrated upon exposure of human monocyte-derived osteoclasts to Staphylococcal superantigen TSST-1, while the Panton-Valentine leukocidin, known as one of the most powerful pore-forming toxins, and hemolysin-α induced osteoclast death, indicating that the clinical presentation and outcome of bone and joint infection could be related, at least partly, to the toxin profile of the *S. aureus* isolate involved (26). The osteoclast intracellular infection, which has been demonstrated also *in vivo* (27), has been recently studied exploiting fluorescently labelled bacterial strains visualized by confocal and time-lapse microscopy (28). Intracellular penetration of bacteria occurred *in vitro* in a short timeframe; bacterial proliferation started two-four hours post-infection, but the bacterial load in the intracellular compartment of infected osteoclasts did not change over time (28). Osteoclast colonization was accompanied by reduced bactericidal potential compared to non-infected osteoclast precursors (29). Moreover, the proliferative capacity of *S. aureus* within osteoclasts was dependent on the signaling cascade activated by the osteoclastogenic master transcription factor NFATc1, and varied to some extent amongst individual osteoclasts (29).

Osteoblasts and their progeny

S. aureus has been shown to infect osteoblasts and downstream mature cells (osteocytes) both in *in vitro* and *in vivo* animal models and clinical biopsies (21, 30–33). The interaction of osteoblasts with *S. aureus* involves several pathogen-derived factors and components of the osteoblast plasma membrane. For example, a major virulence factor of *S. aureus*, SpA, interacts directly with osteoblasts *via* TNFR1, and activates intracellular signaling cascades that result into reduced proliferation, enhanced apoptosis, and impaired mineralizing potential of cultured osteoblasts (34). The binding of *S. aureus* FnBPA and FnBPB to the extracellular matrix protein fibronectin is recognized as another important process in osteoblast infection. Indeed, fibronectin is believed to act as a "molecular bridge" in linking osteoblasts to the pathogen through α5β1 integrin (35). In this respect, the supramolecular structure of fibronectin in the bone extracellular matrix has been recently shown to play an essential role in bacterial uptake by osteoblasts (36).

Whether bacteria internalization in osteoblasts is achieved passively or through an active process has been debated. It is likely that in fact both mechanisms are in place (37, 38). Intracellular infection has been proposed to occur very rapidly upon exposure to *S. aureus*. Indeed, bacteria have been detected by immunofluorescence microscopy inside murine calvaria osteoblast-like MC3T3-E1 cells as early as 15 minutes after infection, and the rate of bacteria internalization was found to increase over time (39). Invasion likely requires actin rearrangement at the cell surface; in fact, treatment with the actin depolymerization agent Cytochalasin D significantly reduced *S. aureus* invasion (40).

Mouton and colleagues recently demonstrated that *S. aureus* internalization (assessed *in vitro* through a gentamycin/lysostaphin protection assay that allows eliminating adherent and non-adherent bacteria, while sparing intracellular pathogen) induced an impairment in early osteoblast differentiation by interfering with β1 integrin signaling, leading to decreased expression of RUNX2 and COL1α1 and ALP activity. Accordingly, an internalization defective *S. aureus* strain lacking fnbpA expression did not elicit this effect (41). Consistent with this, *in vivo* infection with the *S. aureus* strain capable of cell internalization altered some bone histomorphometric parameters, supporting the hypothesis that osteoblast functions are impaired upon intracellular bacterial infection (41).

Osteoblast colonization by *S. aureus* stimulates the focal adhesion kinase (FAK)/epidermal growth factor receptor (EGFR) and c-Src signaling pathways by enhancing their phosphorylation in a time-dependent fashion; on the contrary, inhibition of the EGFR/FAK or c-Src signaling pathways significantly reduces the rate of pathogen internalization (39). Consequently, these pathways could be targeted in parallel to standard antibiotic therapy of chronic *S. aureus* osteomyelitis.

Osteoblast infection by *S. aureus* has been confirmed also in the presence of invasive MRSA infection of the human MG-63 osteosarcoma cell line, using imaging flow cytometry (IFC) which is more sensitive and reproducible than conventional cell culture methods (42). Pathogen uptake is known to vary depending on the strain irrespectively of antibiotic resistance (43). Statistical analysis of results obtained by IFC assays demonstrated that intracellular persistence capacity of several different MRSA strains over a 24 hour-timeframe was correlated with the total number of infected cells at 24 hour-post-infection and not with the number of bacteria that managed to enter/replicate in each single cell, defined by spot counting after cell transient permeabilization and pathogen staining with a membrane-impermeable green-fluorochrome vancomycin analogue (42). This would suggest that other factors besides the specific clone define the bacteria ability to internalize and persist inside osteoblasts. Future research is needed on this point that is relevant to chronicization of infection.

The encounter of the pathogen with osteoblasts results into release of cytokines and chemokines (as discussed later on) that recruit and activate immune cells; increased RANKL production that sustains osteoclast activity; impaired bone matrix production and mineralization; and ultimately osteoblast death through upregulation of the cell death signal transducer TRAIL and its cell surface death receptors, and concomitant decrease of the decoy receptor OPG (44, 45). All these events contribute to bone loss. Progression from acute to chronic bone and joint infections is accompanied by phenotypic adaptation of the pathogen to a less virulent form, called "small colony variant". This is characterized by increased intracellular persistence and antibiotics resistance, and reduced cytokine release induction and immune system stimulation (46, 47). In particular, osteocytes have been recently demonstrated to constitute a reservoir for silent or persistent infection owing to reduced antimicrobial capacity to eliminate intracellular bacteria, and higher pathogen survival in the form of small colony variants (11, 48). Moreover, infected osteocytes can also elicit an inflammatory response that contributes to communication with other skeletal cells, immune cell recruitment and bone disruption (11).

The mechanisms described above are specific for *S. aureus* and not shared by other opportunistic bacteria involved in orthopedic infections, which points to the evolution of bacterial species-specific ways of interaction with eukaryotic cells that need to be further elucidated.

Osteoblasts as inflammatory cells

The osteoblast secretome in a non-infected setting

The secretory function is highly relevant in the framework of osteoblast activities. It comprises the release of the diverse

components of the extracellular matrix, essentially calcium-deficient apatite and trace elements, for the inorganic part; type I collagen and other types of collagens, and non-collagenous proteins (γ-carboxyglutamate-containing proteins, proteoglycans, glycoproteins, and small integrin-binding ligands N-linked glycoproteins), for the organic part (49). Osteoblasts also release a variety of cytokines, chemokines, and growth factors (i.e., the osteoblast secretome) that regulate osteoclast formation and resorptive activity (e.g., M-CSF, RANKL, OPG, WNT5A, WNT16, IL-6, GM-CSF) (14), enhance the osteoblast anabolic function (e.g., IGFs and IGFBPs) (50), support hematopoiesis (e.g., G-CSF, osteopontin, thrombopoietin, angiopoietin 1, CXCL12, SCF and IL-7) (51) and act as immune modulators (e.g., IL-6, GM-CSF, CCL5) (52). In this respect, an intimate crosstalk takes place in the bone between skeletal cells and the immune system, which also involves the release of cytokines and chemokines in diverse pathophysiological contexts (53). Systemic and local factors such as inflammation and infection elicit marked changes in bone cell functions, as further described in the following sections.

The osteoblast secretome in S. aureus osteomyelitis: Cytokines and growth factors

At sites of infection, soluble factors deriving from activated immune and skeletal cells make up an inflammatory milieu that mediates reciprocal regulation of the osteal and immune components and provides host defense against pathogens. In this regard, osteoblasts play an active role, and cannot be regarded as inert niches for bacterial colonization. In fact, not only do they strive to kill intracellular bacteria by increasing the production of reactive oxygen species and oxidative stress, but they also take part in the immune response orchestrated by professional innate immune cells through production of antimicrobial peptides (beta-defensins), as shown in *in vitro* and *in vivo* models and *ex vivo* in human specimens (54, 55). In addition, the osteoblast secretome further boosts the inflammatory response and affect the behavior of skeletal cells (see Figure 2).

Cytokine synthesis and release involve several intracellular signaling pathways including the NF-kB pathway, which regulates the secretion of IL-6 and MCP1 (CCL2; see below) (56), and the JNK pathway, which is activated downstream of *S. aureus* SpA binding to TNFR1 on the osteoblast plasma membrane and leads to increased TLR2 and RANKL protein levels and TNF-α and IL-6 secretion (56).

The transcriptomic profile of infected osteoblasts has been recently comprehensively investigated by RNAseq analysis of FACS-sorted *S. aureus*-bearing MG-63 cells, and compared to that of non-infected cells and of a mixed cell population comprising both infected and not-infected MG-63 cells (57). Specifically, this work indicated enhanced immune and inflammatory responses in a model of long-term infection, taking advantage of engineered bacterial strains expressing a fluorescent reporter gene that allowed isolation of infected cells 6 days after infection. Top up-regulated genes included several cytokines such as IL-33, IL-32, IL-6, IL-1β, IL-1α, IL-24, G-CSF, TRAIL and TNFSF14, with higher protein levels in culture supernatants. Accordingly, in the Gene Set Enrichment Analysis, several pathways enriched in FACS-sorted infected MG-63 were related to the immune response, including functional categories such as antigen processing and presentation (of note, CD44 and HLA-DR expression has been reported in cultured human osteoblasts) (58) complement and coagulation cascade, platelet activation, Th17 cell differentiation, IL-17 pathway, NOD-like and TLR signal cascades (known to be involved in bacteria recognition), and cytokine signaling (57).

At the protein level, IL-6 has been found to be upregulated in infected murine osteoblasts (in various experimental settings) and human bone tissues (59, 60). Increased IL-6 induces COX-2 and thereby PGE2 and RANKL, which modulate osteoclast recruitment and differentiation, contributing to progressive inflammatory damage and bone loss (61). Enhanced RANKL production by osteoblasts, without concomitant significant change in OPG expression, occurs also downstream of TLR2 recognition of *S. aureus*; accordingly, RANKL increase is abrogated in osteoblasts from Tlr2 knockout mice. This mechanism would support pronounced bone resorption and periosteal osteoclast formation in *S. aureus*-infected bones (62).

IL-12 also is secreted by osteoblasts in *S. aureus*-induced osteomyelitis (59). It has been proposed to strengthen Th1 immune responses and favor elimination of intracellular bacteria (63), a mechanism that could be potentially used to develop novel strategies for infection prevention (64, 65). Since IL-12 in the bone microenvironment promotes myeloid-derived suppressor cell recruitment, it is plausible that osteoblasts contribute to this mechanism (66).

Expression of the highly conserved anti-inflammatory cytokine TGFβ1 has been reported to change in MG-63 cells infected with four different clinically isolated *S. aureus* strains (43), with 2 of them causing downregulation in the short and one upregulation in the long timeframe (3 and 24 hours post infection, respectively). Among other functions, TGFβ1 stimulates type I collagen production (67), therefore an increase of this factor might explain the abnormal matrix deposition that occurs in the periosteum during an infection.

IL-1β and TNF-α increased in the bone of animals with *S. aureus*-induced OM (43, 68, 69), and both cytokines stimulated osteoclast maturation and function. However, some findings regarding to IL-1β are contradictory: *in vitro* infection of murine primary osteoblasts with *S. aureus* resulted in increased transcription, but not in increased protein synthesis or secretion. Of note, the same was observed for IL-18 (70), a

potent inflammatory molecule, structurally and functionally closely related to IL-1β: in fact, it favors osteoclast differentiation by expanding the inflammatory response and inhibits the osteogenic function (71). Owing to the fine line between intense or exaggerated immune response, it is reasonable that IL-1β and IL-18 production is strictly controlled (70), however their regulation deserves further investigation. In parallel, the specific IL-18 inhibitor *IL-18BP* was upregulated *in vitro* in human primary osteoblasts 2 hours after *S. aureus* infection (https://www.ebi.ac.uk/arrayexpress/E-MTAB-6700), while no data are available regarding IL18-BP protein production by osteoblasts in this specific context, to the best of our knowledge. Therefore, at present, activated immune cells, not osteoblasts, are the most likely source of these ILs in the bone microenvironment during bone infections.

Also, while low levels of TNF-α were detected in *in vitro* differentiated human osteoblasts and in the MG-63 cell line in basal conditions (72), a marked increase was observed in MG-63 upon infection (43, 73). A recent study described a novel signaling cascade comprising TNF-α/miR-129-5p/endothelial nitric oxide synthase (eNOS) in the pathogenesis of osteomyelitis (74). Briefly, TNF-α and miR-129-5p were upregulated while eNOS was downregulated in *S. aureus*-infected MC3T3-E1 cells and in osteomyelitis patients' blood. Accordingly, a TNF-α blocker inhibited miR-129-5p and elevated eNOS expression, likely contributing to rescue the mineralization defect caused by *S. aureus* infection in MC3T3-E1 cells (74).

IL-27 expression has been recently demonstrated to be induced early (on day 1) in the infected bone in a transtibial model of *S. aureus*-induced osteomyelitis and upon *in vitro* infection of MC3T3-E1 cells and primary osteoblasts (75). This cytokine likely contributes to host innate immune response in the early phases of the infection by stimulating local neutrophil recruitment and activation.

Finally, there is preliminary evidence of IFN-β secretion by mature murine osteoblasts in response to *S. aureus* infection (76). This type I interferon has been reported to be a negative regulator of RANKL-mediated osteoclastogenesis by inhibiting the translation of the critical signaling component c-Fos (77). Based on these data, *S. aureus* would stimulate osteoblasts to release factors with opposing effects on osteoclastogenesis (78); it can be speculated that the production of IFN-β represents a compensatory response to restore bone homeostasis.

Cytokine production from infected osteoblasts has been shown also in the framework of three-dimensional (3D) models of *S. aureus*-induced osteomyelitis, which more closely reproduce composition and structure of the natural bone compared to conventional 2D culture systems. For example, in a 3D model of osteomyelitis based on the coculture of MC3T3-E1 cells and *S. aureus* on magnesium-doped hydroxyapatite/collagen I scaffolds, *Tnf-α* expression increased over time during infection. The same was observed for the long pentraxin *Ptx3*, a key pattern recognition molecule with emerging roles in bone pathophysiology, known to be induced by TNF-α. On the contrary, *Tgf-β*(a reported repressor of Ptx3 transcription) decreased over time. In the conditioned medium of the 3D cocultures, TNF-α was not detected, while PTX3 and OPG levels were stable over time (79). Importantly, the expression of selected osteogenic (Bmp2, Alp, Spp1), and antioxidant (Nrf-2, Ho-1) genes were substantially affected by the applied 3D setting, indicating matrix-dependent effects on osteoblasts during an *S. aureus* infection (79).

In *S. aureus* osteomyelitis, mRNA and serum protein levels of G-CSF significantly increase in infected patients, contributing to bone loss through suppression of osteoblast function in favor of osteoclast formation (80), and to enhanced phagocytic activity of immune cells. G-CSF is also released directly by osteoblasts upon *S. aureus* infection, as well as GM-CSF and M-CSF. In fact, GM-CSF and G-CSF mRNA expression and protein secretion were substantially upregulated in cultured mouse and human osteoblasts following interaction with *S. aureus* (81). Furthermore, these cytokines were induced in unexposed osteoblasts separated from infected osteoblasts by means of a transwell system, thus pointing to a paracrine-autocrine regulatory mechanism. On the contrary, M-CSF secretion increased only in cultures of infected human osteoblasts (81). These CSFs allow osteoblasts to modulate the cellular composition of the bone microenvironment, favoring differentiation of myeloid progenitors towards osteoclasts and various innate immune cell fates (66).

The osteoblast secretome: Chemokines

In response to *S. aureus* infection, osteoblasts also produce chemokines, members of the C-X-C-motif chemokine ligand (CXCL) and CC-motif (CCL) families, such as CCL2, CCL5, CCL7, CCL8, CCL10, CCL11, CCL13, CCL20, CCL26, and CXCL1, CXCL2, CXCL3, CXCL5, CXCL6 and CX3CL1 (57). Chemokines are traditionally known to act as immune cell chemoattractants, recruiting and activating components of the innate and adaptive immunity, however skeletal cells also are endowed with autocrine and paracrine chemokine signaling, which modulates bone turnover (82).

CCL3 and CXCL2 are known inflammatory mediators enhancing osteoclast formation and osteolysis (83). Their expression was documented in samples from osteolytic sites of patients with implant-associated infection (83). *In vitro* experiments showed that human primary osteoblasts released CCL3 and CXCL2 upon *S. aureus* infection (83). This indicates that, besides monocytes, also osteoblasts contribute to the sustained local production of these factors and the related enhanced RANKL-dependent bone resorption (82), in line with previous evidence in a mouse model (84) of *S. aureus*-

induced osteomyelitis. Overexpression of CXCL2 would also result into inhibition of osteoblast formation through downmodulation of the ERK1/2 signaling upstream of RUNX2 (85). In accordance with a role of the CCL2-CCR2 axis in *S. aureus*-induced osteomyelitis, Ccr2-deficient mice had a higher bacterial load than wild type mice in a model of implant-associated *S. aureus* infection in which a bioluminescent bacterial strain was inoculated directly into the knee joint after implantation of an orthopedic-grade titanium pin. The infection was monitored *in vivo* by means of bioluminescence and *ex vivo* by colony-forming unit counting in the infected joint tissue (86). While the specific contribution of osteoblast-derived CCR2 could not be established in this model, the higher bacterial burden in Ccr2-deficient mice was ascribed to lower T cell and myeloid cell infiltration and overall reduced host defense against the pathogen in the absence of a functional CCR2/CCL2 axis.

In vitro S. aureus infection of human primary osteoblasts also causes a strong upregulation and release of CCL5 (also known as RANTES) compared to other cell types, such as endothelial and epithelial cells (87). The levels of this chemokine influence osteoclast and osteoblast formation and function, as highlighted in the CCL5-deficient mouse (88), besides acting as chemoattractant for monocytes/macrophages and T lymphocytes (89).

Additionally, in a mouse model of implant-associated osteomyelitis, CXCL10 and CXCL9 were up-regulated in the infected femurs versus controls at 3- and 14-days post-infection (90), suggesting a possible role of these chemokines (produced also by osteoblasts through TLR4 activation (91, 92)) in the pathological bone turnover occurring during Osteomyelitis. Of note, in clinical samples from *S. aureus*-infected patients and from a mouse model of MRSA skin infection, CXCL10 and CXCL9 have also been found to enhance the spontaneous release of the virulence factor SpA, however the underlying mechanism and the biological significance of this process are yet to be defined (93). In this regard, there is evidence that extracellular SpA contributes to biofilm formation by *S. aureus* (39), therefore the ability of certain chemokines to induce its release could paradoxically help the pathogen skip immune recognition *via* encasing in a protective layer of biofilm (94). A similar process could occur in principle in bone infections, further increasing the complexity of molecular interactions that underpin osteomyelitis.

Moreover, in a mouse model of endodontic infection-induced inflammation that mimics osteomyelitis of the jaw, the chemokines *Cxcl5*, *Cxcl2*, and *Cxcl13* were among the top upregulated genes in bone lesions (95).

Furthermore, osteoblasts express both CXCL12 (also known as SDF-1) and its receptor CXCR4. This signaling axis has been extensively studied in relation to the bone marrow niche (96) and implicated in skeletal homeostasis (97). Its involvement in bone remodeling during Osteomyelitis is quite likely, though not specifically investigated thus far, to the best of our knowledge.

Finally, the neutrophil chemoattractants CCL5, CXCL1, and CXCL8 and the chemokines related to T cell activation CXCL9, CXCL10, and CXCL11, were strongly upregulated in human-osteocyte-like cells in response to *S. aureus* invasion, in *ex vivo* infected human bone and in bone specimens from the infected acetabulum site of patients suffering from periprosthetic joint infection (48). CCL5 and CXCL10 proteins, but not CXCL8 were also confirmed to be secreted by infected osteocyte-like cells.

Limitations of *in vitro* and *in vivo* models

Dissection of the mechanisms underlying bone infection is hindered by the involvement of a variety of cells within a complex, not easily accessible microenvironment. *In vivo* models have contributed significantly to our understanding of osteomyelitis and remain a valuable tool, even though they have inherent limitations (e.g., difficulties related to joint dimension and surgery procedures in small animals; different cortical bone composition and structure), as recently reviewed (98, 99).

Conventional *in vitro* 2D models and advanced microfluidics systems allow addressing specific hypotheses in a simplified environment (2, 100, 101), however, they also present some drawbacks: for instance, the effort to simplify the model may overlook molecules and/or cellular populations that are of pathogenetic relevance. Moreover, results achieved using cell lines may present inconsistencies with respect data obtained using primary cells. For example, *S. aureus* internalization has been shown to be 30-fold lower in human primary osteoblasts than in the human osteoblast cell line hFOB. On the other hand, human primary osteoblasts displayed significantly lower cell death and higher cytokine and chemokine production (87). These findings indicate that immortalized cell lines, though widely used, do not (always) faithfully reflect post-invasion and post-infection events occurring in primary cells and raise some doubts on the physiological relevance of cell line-based *in vitro* infection models. Conversely, the use of primary cells has drawbacks due to limited availability of material and inter-donor variability.

3D models that closely resemble the *in vivo* conditions have been implemented (79, 102, 103). In this regard, manufacturing of bioactive bone mimetic scaffolds that recapitulate texture and chemistry of the natural bone matrix provide unique experimental tools to study the interface between pathogens (including *S. aureus*) and both skeletal and immune cells in a tightly controlled setting. Yet, it is problematic to reproduce in 3D models the cellular and molecular complexity of the bone microenvironment.

Overall, consistency and translation of findings from both *in vivo* and *in vitro* settings is often problematic, and integration of different models and expertise is warranted.

Conclusions and perspectives

In conclusion, our concise overview shows that osteoblasts are actively involved in the response to infection in *S. aureus* osteomyelitis. In this framework, they are engaged in complex osteoimmunological interactions. This implies the release of a variety of factors collectively described as the osteoblasts secretome, which, on one hand, recruit and activate immune cells, on the other modulate skeletal cell function. The major source of most inflammatory mediators in the bone marrow are professional innate and adaptive immune cells enrolled from the periphery or differentiated locally in the infected bone (8) (see Figure 1), as cell subsets specifically endowed with this function. Nevertheless, osteoblasts have turned out to be partners in defense (and crime) in *S. aureus* osteomyelitis through an arsenal of diverse factors (see Figure 2). Based on the established osteoblast-osteoclast bidirectional communication occurring in pathophysiological conditions (14), we would expect bone resorbing cells in turn impact on osteoblast function during infection. This aspect would be worth investigating, also considering the increasing heterogeneity recognized within the osteoclast lineage and its possible translational implications (24, 104).

The osteoblast secretome appears to be specific to the infectious agent, but whether any of its components or combinations of them can be used as specific biomarkers of the bone infection in the clinic remains to be evaluated. The possibility to manipulate the arsenal represented by the OB secretome for therapeutic purposes in addition to standard antibiotics treatments should also be considered. The double-faced nature of several cytokines and chemokines, which foster professional immune cells but sustain bone metabolism overbalance, makes this putative strategy challenging, though worth investigating, as prompted by an unmet medical need.

Author contributions

GV and SC drafted the manuscript. GV and SC generated the figures. All authors contributed to the article and approved the submitted version.

Funding

This work was partially supported by Fondazione Beppe e Nuccy Angiolini Onlus.

Acknowledgments

GV and PV are supported by Fondazione Beppe e Nuccy Angiolini Onlus. We gratefully acknowledge their generous contribution to our research.

Conflict of interest

BB receives royalties for reagents related to innate immunity and is inventor of patents related to PTX3 and other innate immunity molecules.

The remaining authors declare that the research was conducted in the absence of any commercial or financial relationships that could be construed as a potential conflict of interest.

Publisher's note

References

1. McNeil JC. Acute hematogenous osteomyelitis in children: Clinical presentation and management. *Infection Drug Resistance* (2020) 13:4459–73. doi: 10.2147/IDR.S257517

2. Hofstee MI, Muthukrishnan G, Atkins GJ, Riool M, Thompson K, Morgenstern M, et al. Current concepts of osteomyelitis: From pathologic mechanisms to advanced research methods. *Am J Pathol* (2020) 190(6):1151–63. doi: 10.1016/j.ajpath.2020.02.007

3. Rubitschung K, Sherwood A, Crisologo AP, Bhavan K, Haley RW, Wukich DK, et al. Pathophysiology and molecular imaging of diabetic foot infections. *Int J Mol Sci* (2021) 22(21):11552. doi: 10.3390/ijms222111552

4. Masters EA, Ricciardi BF, Bentley KLM, Moriarty TF, Schwarz EM, Muthukrishnan G. Skeletal infections: Microbial pathogenesis, immunity and clinical management. *Nat Rev Microbiol* (2022) 20(7):385–400. doi: 10.1038/s41579-022-00686-0

5. Hotchen AJ, McNally MA, Sendi P. The classification of long bone osteomyelitis: A systemic review of the literature. *J Bone Joint Infection* (2017) 2 (4):167–74. doi: 10.7150/jbji.21050

6. Brinkmann J, Zeissler EC, Scharrenberg JS, Schenk J, Majjouti M, Oberste M, et al. The diagnostic value of cytokines for the discrimination of vertebral osteomyelitis and degenerative diseases of the spine. *Cytokine* (2022) 150:155782. doi: 10.1016/j.cyto.2021.155782

7. Evans CA, Jellis J, Hughes SP, Remick DG, Friedland JS. Tumor necrosis factor-alpha, interleukin-6, and interleukin-8 secretion and the acute-phase response in patients with bacterial and tuberculous osteomyelitis. *J Infect Dis* (1998) 177(6):1582–7. doi: 10.1086/515313

8. Brandt SL, Putnam NE, Cassat JE, Serezani CH. Innate immunity to staphylococcus aureus: Evolving paradigms in soft tissue and invasive infections. *J Immunol* (2018) 200(12):3871–80. doi: 10.4049/jimmunol.1701574

9. Souza PPC, Lerner UH. Finding a toll on the route: The fate of osteoclast progenitors after toll-like receptor activation. *Front Immunol* (2019) 10. doi: 10.3389/fimmu.2019.01663

10. Petronglo JR, Putnam NE, Ford CA, Cruz-Victorio V, Curry JM, Butrico CE, et al. Context-dependent roles for toll-like receptors 2 and 9 in the

pathogenesis of staphylococcus aureus osteomyelitis. *Infection Immun*, e0041722. doi: 10.1128/iai.00417-22

11. Garcia-Moreno M, Jordan PM, Gunther K, Dau T, Fritzsch C, Vermes M, et al. Osteocytes serve as a reservoir for intracellular persisting staphylococcus aureus due to the lack of defense mechanisms. *Front Microbiol* (2022) 13:937466. doi: 10.3389/fmicb.2022.937466

12. Dapunt U, Giese T, Stegmaier S, Moghaddam A, Hänsch GM. The osteoblast as an inflammatory cell: Production of cytokines in response to bacteria and components of bacterial biofilms. *BMC Musculoskeletal Disord* (2016) 17(1):243. doi: 10.1186/s12891-016-1091-y

13. Siddiqui JA, Partridge NC. Physiological bone remodeling: Systemic regulation and growth factor involvement. *Physiol (Bethesda)* (2016) 31(3):233–45. doi: 10.1152/physiol.00061.2014

14. Kim JM, Lin C, Stavre Z, Greenblatt MB, Shim JH. Osteoblast-osteoclast communication and bone homeostasis. *Cells* (2020) 9(9):2073. doi: 10.3390/cells9092073

15. Al-Bari AA, Al Mamun A. Current advances in regulation of bone homeostasis. *FASEB bioAdvances* (2020) 2(11):668–79. doi: 10.1096/fba.2020-00058

16. Martin TJ, Sims NA. RANKL/OPG; critical role in bone physiology. *Rev Endocrine Metab Disord* (2015) 16(2):131–9. doi: 10.1007/s11154-014-9308-6

17. Stracquadanio S, Musso N, Costantino A, Lazzaro LM, Stefani S, Bongiorno D. Staphylococcus aureus internalization in osteoblast cells: Mechanisms, interactions and biochemical processes. What did we learn from experimental models? *Pathogens* (2021) 10(2):239. doi: 10.3390/pathogens10020239

18. Le KY, Otto M. Quorum-sensing regulation in staphylococci–an overview. *Front Microbiol* (2015) 6. doi: 10.3389/fmicb.2015.01174

19. Sanchez CJJr., Ward CL, Romano DR, Hurtgen BJ, Hardy SK, Woodbury RL, et al. Staphylococcus aureus biofilms decrease osteoblast viability, inhibits osteogenic differentiation, and increases bone resorption *in vitro*. *BMC Musculoskelet Disord* (2013) 14:187. doi: 10.1186/1471-2474-14-187

20. Reffuveille F, Josse J, Velard F, Lamret F, Varin-Simon J, Dubus M, et al. Bone environment influences irreversible adhesion of a methicillin-susceptible staphylococcus aureus strain. *Front Microbiol* (2018) 9:2865. doi: 10.3389/fmicb.2018.02865

21. de Mesy Bentley KL, Trombetta R, Nishitani K, Bello-Irizarry SN, Ninomiya M, Zhang L, et al. Evidence of staphylococcus aureus deformation, proliferation, and migration in canaliculi of live cortical bone in murine models of osteomyelitis. *J Bone Mineral Res* (2017) 32(5):985–90. doi: 10.1002/jbmr.3055

22. de Mesy Bentley KL, MacDonald A, Schwarz EM, Oh I. Chronic osteomyelitis with staphylococcus aureus deformation in submicron canaliculi of osteocytes: A case report. *JBJS Case connector* (2018) 8(1):e8. doi: 10.2106/JBJS.CC.17.00154

23. Wu Y, Humphrey MB, Nakamura MC. Osteoclasts–the innate immune cells of the bone. *Autoimmunity* (2008) 41(3):183–94. doi: 10.1080/08916930701693180

24. Madel M-B, Ibáñez L, Wakkach A, de Vries TJ, Teti A, Apparailly F, et al. Immune function and diversity of osteoclasts in normal and pathological conditions. *Front Immunol* (2019) 10. doi: 10.3389/fimmu.2019.01408

25. Trouillet-Assant S, Gallet M, Nauroy P, Rasigade J-P, Flammier S, Parroche P, et al. Dual impact of live staphylococcus aureus on the osteoclast lineage, leading to increased bone resorption. *J Infect Dis* (2014) 211(4):571–81. doi:10.1093/infdis/jiu386

26. Flammier S, Rasigade J-P, Badiou C, Henry T, Vandenesch F, Laurent F, et al. Human monocyte-derived osteoclasts are targeted by staphylococcal pore-forming toxins and superantigens. *PLoS One* (2016) 11(3):e0150693. doi: 10.1371/journal.pone.0150693

27. Garzoni C, Kelley WL. Staphylococcus aureus: new evidence for intracellular persistence. *Trends Microbiol* (2009) 17(2):59–65. doi: 10.1016/j.tim.2008.11.005

28. Yu K, Song L, Kang HP, Kwon H-K, Back J, Lee FY. Recalcitrant methicillin-resistant staphylococcus aureus infection of bone cells: Intracellular penetration and control strategies. *Bone Joint Res* (2020) 9(2):49–59. doi: 10.1302/2046-3758.92.BJR-2019-0131.R1

29. Krauss JL, Roper PM, Ballard A, Shih CC, Fitzpatrick JAJ, Cassat JE, et al. Staphylococcus aureus infects osteoclasts and replicates intracellularly. *mBio* (2019) 10(5):1128. doi: 10.1128/mBio.02447-19

30. Reilly SS, Hudson MC, Kellam JF, Ramp WK. *In vivo* internalization of staphylococcus aureus by embryonic chick osteoblasts. *Bone* (2000) 26(1):63–70. doi: 10.1016/S8756-3282(99)00239-2

31. Bosse MJ, Gruber HE, Ramp WK. Internalization of bacteria by osteoblasts in a patient with recurrent, long-term osteomyelitis. *A Case Rep J Bone Joint Surg Am Volume* (2005) 87(6):1343–7. doi: 10.2106/jbjs.d.02649

32. Hamza T, Li B. Differential responses of osteoblasts and macrophages upon staphylococcus aureus infection. *BMC Microbiol* (2014) 14(1):207. doi: 10.1186/s12866-014-0207-5

33. Josse J, Guillaume C, Bour C, Lemaire F, Mongaret C, Draux F, et al. Impact of the maturation of human primary bone-forming cells on their behavior in acute or persistent staphylococcus aureus infection models. *Front Cell Infection Microbiol* (2016) 6:64. doi: 10.3389/fcimb.2016.00064

34. Claro T, Widaa A, O'Seaghdha M, Miajlovic H, Foster TJ, O'Brien FJ, et al. Staphylococcus aureus protein a binds to osteoblasts and triggers signals that weaken bone in osteomyelitis. *PLoS One* (2011) 6(4):e18748. doi: 10.1371/journal.pone.0018748

35. Sinha B, François PP, Nüsse O, Foti M, Hartford OM, Vaudaux P, et al. Fibronectin-binding protein acts as staphylococcus aureus invasin *via* fibronectin bridging to integrin alpha5beta1. *Cell Microbiol* (1999) 1 (2):101–17. doi: 10.1046/j.1462-5822.1999.00011.x

36. Niemann S, Nguyen MT, Eble JA, Chasan AI, Mrakovcic M, Bottcher RT, et al. More is not always better-the double-headed role of fibronectin in staphylococcus aureus host cell invasion. *mBio* (2021) 12(5):e0106221. doi: 10.1128/mBio.01062-21

37. Hudson MC, Ramp WK, Nicholson NC, Williams AS, Nousiainen MT. Internalization of staphylococcus aureus by cultured osteoblasts. *Microbial Pathogenesis* (1995) 19(6):409–19. doi: 10.1006/mpat.1995.0075

38. Jevon M, Guo C, Ma B, Mordan N, Nair SP, Harris M, et al. Mechanisms of internalization of staphylococcus aureus by cultured human osteoblasts. *Infection Immunity* (1999) 67(5):2677–81. doi: 10.1128/IAI.67.5.2677-2681.1999

39. Ji Z, Su J, Hou Y, Yao Z, Yu B, Zhang X. EGFR/FAK and c-src signalling pathways mediate the internalisation of staphylococcus aureus by osteoblasts. *Cell Microbiol* (2020) 22(10):e13240. doi: 10.1111/cmi.13240

40. Mohamed W, Sommer U, Sethi S, Domann E, Thormann U, Schütz I, et al. Intracellular proliferation of s. aureus in osteoblasts and effects of rifampicin and gentamicin on s. aureus intracellular proliferation and survival. *Eur Cells Materials* (2014) 28:258–68. doi: 10.22203/eCM.v028a18

41. Mouton W, Josse J, Jacqueline C, Abad L, Trouillet-Assant S, Caillon J, et al. Staphylococcus aureus internalization impairs osteoblastic activity and early differentiation process. *Sci Rep* (2021) 11(1):17685. doi: 10.1038/s41598-021-97246-y

42. Bongiorno D, Musso N, Lazzaro LM, Mongelli G, Stefani S, Campanile F. Detection of methicillin-resistant staphylococcus aureus persistence in osteoblasts using imaging flow cytometry. *MicrobiologyOpen* (2020) 9(5):e1017. doi: 10.1002/mbo3.1017

43. Musso N, Caruso G, Bongiorno D, Grasso M, Bivona DA, Campanile F, et al. Different modulatory effects of four methicillin-resistant staphylococcus aureus clones on MG-63 osteoblast-like cells. *Biomolecules* (2021) 11(1):72. doi: 10.3390/biom11010072

44. Reott MAJr., Ritchie-Miller SL, Anguita J, Hudson MC. TRAIL expression is induced in both osteoblasts containing intracellular staphylococcus aureus and uninfected osteoblasts in infected cultures. *FEMS Microbiol Letters* (2008) 278 (2):185–92. doi: 10.1111/j.1574-6968.2007.00988.x

45. Young AB, Cooley ID, Chauhan VS, Marriott I. Causative agents of osteomyelitis induce death domain-containing TNF-related apoptosis-inducing ligand receptor expression on osteoblasts. *Bone* (2011) 48(4):857–63. doi: 10.1016/j.bone.2010.11.015

46. Trouillet-Assant S, Lelièvre L, Martins-Simões P, Gonzaga L, Tasse J, Valour F, et al. Adaptive processes of staphylococcus aureus isolates during the progression from acute to chronic bone and joint infections in patients. *Cell Microbiol* (2016) 18 (10):1405–14. doi: 10.1111/cmi.12582

47. Tuchscherr L, Kreis CA, Hoerr V, Flint L, Hachmeister M, Geraci J, et al. Staphylococcus aureus develops increased resistance to antibiotics by forming dynamic small colony variants during chronic osteomyelitis. *J Antimicrobial Chemother* (2016) 71(2):438–48. doi: 10.1093/jac/dkv371

48. Yang D, Wijenayaka AR, Solomon LB, Pederson SM, Findlay DM, Kidd SP, et al. Novel insights into staphylococcus aureus deep bone infections: the involvement of osteocytes. *mBio* (2018) 9(2):e00415–18. doi: 10.1128/mBio.00415-18

49. Lin X, Patil S, Gao Y-G, Qian A. The bone extracellular matrix in bone formation and regeneration. *Front Pharmacol* (2020) 11. doi: 10.3389/fphar.2020.00757

50. Govoni KE. Insulin-like growth factor-I molecular pathways in osteoblasts: potential targets for pharmacological manipulation. *Curr Mol Pharmacol* (2012) 5 (2):143–52. doi: 10.2174/1874467211205020143

51. Galán-Díez M, Kousteni S. The osteoblastic niche in hematopoiesis and hematological myeloid malignancies. *Curr Mol Biol Rep* (2017) 3(2):53–62. doi: 10.1007/s40610-017-0055-9

52. Terashima A, Takayanagi H. The role of bone cells in immune regulation during the course of infection. *Semin Immunopathol* (2019) 41(5):619–26. doi: 10.1007/s00281-019-00755-2

53. Guder C, Gravius S, Burger C, Wirtz DC, Schildberg FA. Osteoimmunology: A current update of the interplay between bone and the immune system. *Front Immunol* (2020) 11. doi: 10.3389/fimmu.2020.00058

54. Varoga D, Tohidnezhad M, Paulsen F, Wruck CJ, Brandenburg L, Mentlein R, et al. The role of human beta-defensin-2 in bone. *J Anatomy* (2008) 213(6):749–57. doi: 10.1111/j.1469-7580.2008.00992.x

55. Varoga D, Wruck CJ, Tohidnezhad M, Brandenburg L, Paulsen F, Mentlein R, et al. Osteoblasts participate in the innate immunity of the bone by producing human beta defensin-3. *Histochem Cell Biol* (2009) 131(2):207–18. doi: 10.1007/s00418-008-0522-8

56. Ning R, Zhang X, Guo X, Li Q. Staphylococcus aureus regulates secretion of interleukin-6 and monocyte chemoattractant protein-1 through activation of nuclear factor kappaB signaling pathway in human osteoblasts. *Braz J Infect Diseases* (2011) 15(3):189–94. doi: 10.1016/s1413-8670(11)70173-8

57. Nicolas A, Deplanche M, Commere P-H, Diot A, Genthon C, Marques da Silva W, et al. Transcriptome architecture of osteoblastic cells infected with staphylococcus aureus reveals strong inflammatory responses and signatures of metabolic and epigenetic dysregulation. *Front Cell infection Microbiol* (2022) 12. doi: 10.3389/fcimb.2022.854242

58. Reyes-Botella C, Montes MJ, Vallecillo-Capilla MF, Olivares EG, Ruiz C. Expression of molecules involved in antigen presentation and T cell activation (HLA-DR, CD80, CD86, CD44 and CD54) by cultured human osteoblasts. *J Periodontol* (2000) 71(4):614–7. doi: 10.1902/jop.2000.71.4.614

59. Bost KL, Ramp WK, Nicholson NC, Bento JL, Marriott I, Hudson MC. Staphylococcus aureus infection of mouse or human osteoblasts induces high levels of interleukin-6 and interleukin-12 production. *J Infect Diseases* (1999) 180 (6):1912–20. doi: 10.1086/315138

60. Marriott I, Gray DL, Tranguch SL, Fowler VG, Stryjewski M, Scott Levin L, et al. Osteoblasts express the inflammatory cytokine interleukin-6 in a murine model of staphylococcus aureus osteomyelitis and infected human bone tissue. *Am J Pathol* (2004) 164(4):1399–406. doi: 10.1016/S0002-9440(10)63226-9

61. Somayaji SN, Ritchie S, Sahraei M, Marriott I, Hudson MC. Staphylococcus aureus induces expression of receptor activator of NF-kappaB ligand and prostaglandin E2 in infected murine osteoblasts. *Infection Immunity* (2008) 76 (11):5120–6. doi: 10.1128/IAI.00228-08

62. Kassem A, Lindholm C, Lerner UH. Toll-like receptor 2 stimulation of osteoblasts mediates staphylococcus aureus induced bone resorption and osteoclastogenesis through enhanced RANKL. *PloS One* (2016) 11(6):e0156708. doi: 10.1371/journal.pone.0156708

63. Hamza T, Barnett JB, Li B. Interleukin 12 a key immunoregulatory cytokine in infection applications. *Int J Mol Sci* (2010) 11(3):789–806. doi: 10.3390/ijms11030789

64. Li B, Jiang B, Boyce BM, Lindsey BA. Multilayer polypeptide nanoscale coatings incorporating IL-12 for the prevention of biomedical device-associated infections. *Biomaterials* (2009) 30(13):2552–8. doi: 10.1016/j.biomaterials.2009.01.042

65. Li B, Jiang B, Dietz MJ, Smith ES, Clovis NB, Rao KMK. Evaluation of local MCP-1 and IL-12 nanocoatings for infection prevention in open fractures. *J Orthopaedic Res Off Publ Orthopaedic Res Society* (2010) 28(1):48–54. doi: 10.1002/jor.20939

66. Heim CE, Vidlak D, Scherr TD, Hartman CW, Garvin KL, Kielian T. IL-12 promotes myeloid-derived suppressor cell recruitment and bacterial persistence during staphylococcus aureus orthopedic implant infection. *J Immunol* (2015) 194 (8):3861–72. doi: 10.4049/jimmunol.1402689

67. Kasagi S, Chen W. TGF-beta1 on osteoimmunology and the bone component cells. *Cell Biosci* (2013) 3(1):4. doi: 10.1186/2045-3701-3-4

68. Littlewood-Evans AJ, Hattenberger MR, Lüscher C, Pataki A, Zak O, O'Reilly T. Local expression of tumor necrosis factor alpha in an experimental model of acute osteomyelitis in rats. *Infection Immunity* (1997) 65(8):3438–43. doi: 10.1128/iai.65.8.3438-3443.1997

69. Garcia-Alvarez F, Navarro-Zorraquino M, Castro A, Grasa JM, Pastor C, Monzon M, et al. Effect of age on cytokine response in an experimental model of osteomyelitis. *Biogerontology* (2009) 10(5):649–58. doi: 10.1007/s10522-008-9211-1

70. Marriott I, Hughes FMJr., Bost KL. Bacterial infection of osteoblasts induces interleukin-1beta and interleukin-18 transcription but not protein synthesis. *J Interferon Cytokine Res* (2002) 22(10):1049–55. doi: 10.1089/107999002760624288

71. Jiang N, An J, Yang K, Liu J, Guan C, Ma C, et al. NLRP3 inflammasome: A new target for prevention and control of osteoporosis? *Front Endocrinol (Lausanne)* (2021) 12:752546–. doi: 10.3389/fendo.2021.752546

72. Bu R, Borysenko CW, Li Y, Cao L, Sabokbar A, Blair HC. Expression and function of TNF-family proteins and receptors in human osteoblasts. *Bone* (2003) 33(5):760–70. doi: 10.1016/j.bone.2003.07.006

73. Chen Q, Hou T, Wu X, Luo F, Xie Z, Xu J. Knockdown of TNFR1 suppresses expression of TLR2 in the cellular response to staphylococcus aureus infection. *Inflammation* (2016) 39(2):798–806. doi: 10.1007/s10753-016-0308-4

74. Ma X, Xia W, Zong Y, Jiang C, Shan H, Lin Y, et al. Tumor necrosis factor-α promotes staphylococcus aureus-induced osteomyelitis through downregulating endothelial nitric oxide synthase. *J Microbiol Immunol Infection = Wei mian yu gan ran za zhi* (2021) 54(6):1018–27. doi: 10.1016/j.jmii.2020.08.002

75. Morita Y, Saito M, Rangel-Moreno J, Franchini AM, Owen JR, Martinez JC, et al. Systemic IL-27 administration prevents abscess formation and osteolysis *via* local neutrophil recruitment and activation. *Bone Res* (2022) 10(1):56. doi: 10.1038/s41413-022-00228-7

76. Johnson MB, Suptela SR, Sipprell SE, Marriott I. Substance p exacerbates the inflammatory and pro-osteoclastogenic responses of murine osteoclasts and osteoblasts to staphylococcus aureus. *Inflammation* (2022) 10:1007. doi: 10.1007/s10753-022-01731-z

77. Hayashida C, Ito J, Nakayachi M, Okayasu M, Ohyama Y, Hakeda Y, et al. Osteocytes produce interferon-β as a negative regulator of osteoclastogenesis. *J Biol Chem* (2014) 289(16):11545–55. doi: 10.1074/jbc.M113.523811

78. Takayanagi H, Kim S, Taniguchi T. Signaling crosstalk between RANKL and interferons in osteoclast differentiation. *Arthritis Res Ther* (2002) 4(3):S227. doi: 10.1186/ar581

79. Parente R, Possetti V, Schiavone ML, Campodoni E, Menale C, Loppini M, et al. 3D cocultures of osteoblasts and staphylococcus aureus on biomimetic bone scaffolds as a tool to investigate the host-pathogen interface in osteomyelitis. *Pathog (Basel Switzerland)* (2021) 10(7):837. doi: 10.3390/pathogens10070837

80. Hou Y, Qin H, Jiang N, Liu G, Wu H, Bai L, et al. G-CSF partially mediates bone loss induced by staphylococcus aureus infection in mice. *Clin Science* (2019) 133(12):1297–308. doi: 10.1042/CS20181001

81. Bost KL, Bento JL, Ellington JK, Marriott I, Hudson MC. Induction of colony-stimulating factor expression following staphylococcus or salmonella interaction with mouse or human osteoblasts. *Infection Immunity* (2000) 68 (9):5075–83. doi: 10.1128/IAI.68.9.5075-5083.2000

82. Brylka LJ, Schinke T. Chemokines in physiological and pathological bone remodeling. *Front Immunol* (2019) 10:2182. doi: 10.3389/fimmu.2019.02182

83. Dapunt U, Maurer S, Giese T, Gaida MM, Hansch GM. The macrophage inflammatory proteins MIP1alpha (CCL3) and MIP2alpha (CXCL2) in implant-associated osteomyelitis: linking inflammation to bone degradation. *Mediators Inflammation* (2014) 2014:728619. doi: 10.1155/2014/728619

84. Marriott I, Gray DL, Rati DM, Fowler VGJr., Stryjewski ME, Levin LS, et al. Osteoblasts produce monocyte chemoattractant protein-1 in a murine model of staphylococcus aureus osteomyelitis and infected human bone tissue. *Bone* (2005) 37(4):504–12. doi: 10.1016/j.bone.2005.05.011

85. Yang N, Liu Y. The role of the immune microenvironment in bone regeneration. *Int J Med Sci* (2021) 18(16):3697–707. doi: 10.7150/ijms.61080

86. Wang Y, Dikeman D, Zhang J, Ackerman N, Kim S, Alphonse MP, et al. CCR2 contributes to host defense against staphylococcus aureus orthopedic implant-associated infections in mice. *J Orthopaedic Res* (2022) 40(2):409–19. doi: 10.1002/jor.25027

87. Strobel M, Pfortner H, Tuchscherr L, Volker U, Schmidt F, Kramko N, et al. Post-invasion events after infection with staphylococcus aureus are strongly dependent on both the host cell type and the infecting s. aureus strain. *Clin Microbiol Infection* (2016) 22(9):799–809. doi: 10.1016/j.cmi.2016.06.020

88. Wintges K, Beil FT, Albers J, Jeschke A, Schweizer M, Claass B, et al. Impaired bone formation and increased osteoclastogenesis in mice lacking chemokine (C-c motif) ligand 5 (Ccl5). *J Bone Mineral Res* (2013) 28(10):2070–80. doi: 10.1002/jbmr.1937

89. Josse J, Velard F, Gangloff SC. Staphylococcus aureus vs. osteoblast: Relationship and consequences in osteomyelitis. *Front Cell Infection Microbiol* (2015) 5:85. doi: 10.3389/fcimb.2015.00085

90. Lin Y, Su J, Wang Y, Xu D, Zhang X, Yu B. mRNA transcriptome analysis of bone in a mouse model of implant-associated staphylococcus aureus osteomyelitis. *Infection Immun* (2021) 89(5):e00814–20. doi: 10.1128/IAI.00814-20

91. Gasper NA, Petty CC, Schrum LW, Marriott I, Bost KL. Bacterium-induced CXCL10 secretion by osteoblasts can be mediated in part through toll-like receptor 4. *Infection Immun* (2002) 70(8):4075–82. doi: 10.1128/IAI.70.8.4075-4082.2002

92. Huang B, Wang W, Li Q, Wang Z, Yan B, Zhang Z, et al. Osteoblasts secrete Cxcl9 to regulate angiogenesis in bone. *Nat Commun* (2016) 7:13885. doi: 10.1038/ncomms13885

93. Yung SC, Parenti D, Murphy PM. Host chemokines bind to staphylococcus aureus and stimulate protein a release. *J Biol Chem* (2011) 286(7):5069–77. doi: 10.1074/jbc.M110.195180

94. Merino N, Toledo-Arana A, Vergara-Irigaray M, Valle J, Solano C, Calvo E, et al. Protein a-mediated multicellular behavior in staphylococcus aureus. *J Bacteriol* (2009) 191(3):832–43. doi: 10.1128/JB.01222-08

95. Sasaki H, Furusho H, Rider DB, Dobeck JM, Kuo WP, Fujimura A, et al. Endodontic infection-induced inflammation resembling osteomyelitis of the jaws in toll-like receptor 2/Interleukin 10 double-knockout mice. *J Endodontics* (2019) 45(2):181–8. doi: 10.1016/j.joen.2018.10.007

96. Aoki K, Kurashige M, Ichii M, Higaki K, Sugiyama T, Kaito T, et al. Identification of CXCL12-abundant reticular cells in human adult bone marrow. *Br J Haematol* (2021) 193(3):659–68. doi: 10.1111/bjh.17396

97. Shahnazari M, Chu V, Wronski TJ, Nissenson RA, Halloran BP. CXCL12/CXCR4 signaling in the osteoblast regulates the mesenchymal stem cell and osteoclast lineage populations. *FASEB J* (2013) 27(9):3505–13. doi: 10.1096/fj.12-225763

98. Meroni G, Tsikopoulos A, Tsikopoulos K, Allemanno F, Martino PA. Soares filipe JF. A journey into animal models of human osteomyelitis: A review. *Microorganisms* (2022) 10(6):1135. doi: 10.3390/microorganisms10061135

99. Roux KM, Cobb LH, Seitz MA, Priddy LB. Innovations in osteomyelitis research: A review of animal models. *Anim Models Exp Med* (2021) 4(1):59–70. doi: 10.1002/ame2.12149

100. Lee J-H, Wang H, Kaplan JB, Lee WY. Effects of staphylococcus epidermidis on osteoblast cell adhesion and viability on a Ti alloy surface in a microfluidic co-culture environment. *Acta Biomaterialia* (2010) 6(11):4422–9. doi: 10.1016/j.actbio.2010.05.021

101. Masters EA, Salminen AT, Begolo S, Luke EN, Barrett SC, Overby CT, et al. An *in vitro* platform for elucidating the molecular genetics of s. aureus invasion of the osteocyte lacuno-canalicular network during chronic osteomyelitis. *Nanomedicine: Nanotechn Biol Med* (2019) 21:102039. doi: 10.1016/j.nano.2019.102039

102. Lee J-H, Gu Y, Wang H, Lee WY. Microfluidic 3D bone tissue model for high-throughput evaluation of wound-healing and infection-preventing biomaterials. *Biomaterials* (2012) 33(4):999–1006. doi: 10.1016/j.biomaterials.2011.10.036

103. Lee J-H, Wang H, Kaplan JB, Lee WY. Microfluidic approach to create three-dimensional tissue models for biofilm-related infection of orthopaedic implants. *Tissue Eng Part C: Methods* (2010) 17(1):39–48. doi: 10.1089/ten.tec.2010.0285

104. Madel MB, Ibáñez L, Ciucci T, Halper J, Rouleau M, Boutin A, et al. Dissecting the phenotypic and functional heterogeneity of mouse inflammatory osteoclasts by the expression of Cx3cr1. *eLife* (2020) 9:e54493. doi: 10.7554/eLife.54493

10.3389/fimmu.2022.1048505

Glossary

IL-6	Interleukin 6
IL-8	Interleukin 8
IL-1β	Interleukin-1 beta
IL-12	Interleukin 12
VEGF	Vascular-Endothelial Growth Factor
CRP	C reactive protein
PRRs	Pattern-Recognition Receptors
TLRs	Toll-Like Receptors
PAMPs	Pathogen-Associated Molecular Patterns
LPS	Lipopolysaccharides
TLR2	Toll-like Receptor 2
TLR4	Toll-like Receptor 4
RANKL	Receptor Activator of Nuclear Factor κappa B Ligand
M-CSF	Macrophage Colony-Stimulating Factor
NOD	Nucleotide oligomerization domain
PMNs	Polymorphonuclear leukocytes
TNF-α	Tumor Necrosis Factor-alfa
CCL3	Chemokine (C-C motif) ligand 3
CXCL2	Chemokine (C-X-C motif) ligand 2
EFNB2	Membrane-bound ligand Ephrin B2
EPHB4	Ephrin receptor B4
FASL	Fas cell surface death receptor-ligand
FAS	Fas cell surface death receptor
SEMA3A	Semaphorin 3A
NRP1	Neuropilin-1
C-FMS	Colony-stimulating factor-1 receptor
RANK	Receptor Activator of Nuclear Factor κappa B
OPG	Osteoprotegerin
MSCRAMMs	Microbial Surface Components Recognizing Adhesive Matrix Molecules
FnBPA and B	Fibronectin-Binding Protein A and B
Cna	Collagen adhesin
SpA	Staphylococcus protein A
ClfA and B	clamping factor A and B
vWbp	von Willebrand factor-binding protein
SACs	Staphylococcal abscess communities
CCL5	Chemokine (C-C motif) ligand 5
MIP-1α	Macrophage Inflammatory Protein-1 alpha
MIP-1β	Macrophage Inflammatory Protein-1 beta
G-CSF	Granulocyte Colony-Stimulating Factor
MCP1	Monocyte Chemoattractant Protein-1
TSST-1	Toxic Shock Syndrome Toxin 1
NFATc1	Nuclear Factor Of Activated T Cells 1
TNFR1	Tumor Necrosis Factor Receptor 1
RUNX2	Runt-related transcription factor 2
COL1a1	Collagen type I alpha 1 chain
ALP	Alkaline phosphates

(Continued)

Continued

FAK	Focal Adhesion Kinase
EGFR	Epidermal Growth Factor Receptor
c-Src	Proto-oncogene
cellular Src	
MRSA	Methicillin-Resistant Staphylococcus aureus
IFC	imaging flow cytometry
TRAIL	Tumor Necrosis Factor-Related Apoptosis-Inducing Ligand
WNT5A	WNT family member 5A
WNT16	WNT family member 16
GM-CSF	Granulocyte-Macrophage Colony-Stimulating Factor
IGF	insulin growth factor
IGFBP	insulin growth factor-binding protein
CXCL12	Chemokine (C-X-C motif) ligand 12
SCF	Stem cell factor
IL-7	Interleukin 7
NF-kB	Nuclear factor kappa-light-chain-enhancer of activated B cells
JNK	c-Jun N-terminal kinase
IL-33	Interleukin 33
IL-32	Interleukin 32
IL-1α	Interleukin 1 alfa
IL-24	Interleukin 24
TNFSF14	Tumor Necrosis Factor Superfamily Member 14
Th17	T helper 17
IL-17	Interleukin 17
COX2	Cyclooxygenase 2
PGE2	Prostaglandin E2
Th1	T helper 1
TGFβ1	Transforming Growth Factor beta 1
IL-18	Interleukin 18
IL-18BP	Interleukin 18 Binding Protein
eNOS	Endothelial Nitric Oxide Synthase
IL-27	Interleukin 27
PTX3	Pentraxin 3
Bmp2	Bone morphogenetic protein 2
Spp1	Secreted Phosphoprotein 1
Nrf-2	Nuclear factor erythroid 2-related factor 2
Ho-1	heme oxygenase-1
CCL2	Chemokine (C-C motif) ligand 2
CCL7	Chemokine (C-C motif) ligand 7
CCL8	Chemokine (C-C motif) ligand 8
CCL10	Chemokine (C-C motif) ligand 10
CCL11	Chemokine (C-C motif) ligand 11
CCL13	Chemokine (C-C motif) ligand 13
CCL20	Chemokine (C-C motif) ligand 20
CCL26	Chemokine (C-C motif) ligand 26
CXCL1	Chemokine (C-X-C motif) ligand 1
CXCL2	Chemokine (C-X-C motif) ligand 2
CXCL3	Chemokine (C-X-C motif) ligand 3
CXCL5	Chemokine (C-X-C motif) ligand 5
CXCL6	Chemokine (C-X-C motif) ligand 6
CX3CL1	chemokine (C-X3-C Motif) ligand 1

(Continued)

10.3389/fimmu.2022.1048505

Continued

ERK1/2	Extracellular signal-regulated kinase 1/2
CCR2	C-C chemokine receptor type 2
CXCL10	Chemokine (C-X-C motif) ligand 10
CXCL9	Chemokine (C-X-C motif) ligand 9
CXCL13	Chemokine (C-X-C motif) ligand 13
CXCR4	C-X-C chemokine receptor type 4
CXCL11	Chemokine (C-X-C motif) ligand 11
hFOB	Human fetal osteoblast

frontiers | Frontiers in Immunology

TYPE Original Research
PUBLISHED 15 September 2022
DOI 10.3389/fimmu.2022.979232

OPEN ACCESS

EDITED BY
Daniela Novick,
Weizmann Institute of Science, Israel

REVIEWED BY
Diana Boraschi,
Shenzhen Institute of Advanced Technology (SIAT), (CAS), China
Francesca Innocenti,
Careggi University Hospital, Italy

*CORRESPONDENCE
Barbara Bottazzi
barbara.bottazzi@humanitasresearch.it
Alberto Mantovani
Alberto.mantovani@humanitasresearch.it

SPECIALTY SECTION
This article was submitted to Inflammation, a section of the journal Frontiers in Immunology

RECEIVED 27 June 2022
ACCEPTED 29 August 2022
PUBLISHED 15 September 2022

CITATION
Davoudian S, Piovani D, Desai A, Mapelli SN, Leone R, Sironi M, Valentino S, Silva-Gomes R, Stravalaci M, Asgari F, Madera A, Piccinini D, Fedeli C, Comina D, Bonovas S, Voza A, Mantovani A and Bottazzi B (2022) A cytokine/PTX3 prognostic index as a predictor of mortality in sepsis.
Front. Immunol. 13:979232.
doi: 10.3389/fimmu.2022.979232

A cytokine/PTX3 prognostic index as a predictor of mortality in sepsis

Sadaf Davoudian[1], Daniele Piovani[2], Antonio Desai[2,3], Sarah N. Mapelli[1], Roberto Leone[1], Marina Sironi[1], Sonia Valentino[1], Rita Silva-Gomes[1], Matteo Stravalaci[1], Fatemeh Asgari[1], Alessandra Madera[2], Daniele Piccinini[2], Carlo Fedeli[3], Denise Comina[3], Stefanos Bonovas[2], Antonio Voza[2,3], Alberto Mantovani[1,2,4]* and Barbara Bottazzi[1]*

[1]Department of Research in Inflammation and Immunology, IRCCS Humanitas Research Hospital, Milan, Italy, [2]Department of Biomedical Science, Humanitas University, Milan, Italy, [3]Department of Emergency, IRCCS Humanitas Research Hospital, Milan, Italy, [4]The William Harvey Research Institute, Queen Mary University of London, London, United Kingdom

Background: Early prognostic stratification of patients with sepsis is a difficult clinical challenge. Aim of this study was to evaluate novel molecules in association with clinical parameters as predictors of 90-days mortality in patients admitted with sepsis at Humanitas Research Hospital.

Methods: Plasma samples were collected from 178 patients, diagnosed based on Sepsis-3 criteria, at admission to the Emergency Department and after 5 days of hospitalization. Levels of pentraxin 3 (PTX3), soluble IL-1 type 2 receptor (sIL-1R2), and of a panel of pro- and anti-inflammatory cytokines were measured by ELISA. Cox proportional-hazard models were used to evaluate predictors of 90-days mortality.

Results: Circulating levels of PTX3, sIL-1R2, IL-1β, IL-6, IL-8, IL-10, IL-18, IL-1ra, TNF-α increased significantly in sepsis patients on admission, with the highest levels measured in shock patients, and correlated with SOFA score (PTX3: r=0.44, p<0.0001; sIL-1R2: r=0.35, p<0.0001), as well as with 90-days mortality. After 5 days of hospitalization, PTX3 and cytokines, but not sIL-1R2 levels, decreased significantly, in parallel with a general improvement of clinical parameters. The combination of age, blood urea nitrogen, PTX3, IL-6 and IL-18, defined a prognostic index predicting 90-days mortality in Sepsis-3 patients and showing better apparent discrimination capacity than the SOFA score (AUC=0.863, 95% CI: 0.780–0.945 *vs.* AUC=0.727, 95% CI: 0.613-0.840; p=0.021 respectively).

Conclusion: These data suggest that a prognostic index based on selected cytokines, PTX3 and clinical parameters, and hence easily adoptable in clinical

practice, performs in predicting 90-days mortality better than SOFA. An independent validation is required.

KEYWORDS

sepsis, biomarkers, cytokines, PTX3, disease severity

Introduction

Sepsis is a life-threatening condition due to a dysregulated response to infection which can lead to shock, multiple organ failure, and death. The estimated number of incident cases of sepsis increased to almost 50 million worldwide (1–4) and, despite massive efforts, the mortality rate has not improved over time. Early diagnosis of sepsis and prognostic assessment are crucial to prevent progression to severe disease and to make use of timely and appropriate treatments to reduce mortality (1–4).

Despite the recent revision of the definition of sepsis, diagnosis is still challenging for clinicians, in particular in the identification of patients at early stages (5). Alongside the diagnostic question, also important is the need to have early prognostic indications allowing clinicians to activate the most appropriate therapies based on the mortality risk of each individual patient (2, 6–10). A recent review collected 5367 studies identifying 258 different biomarkers of sepsis with potential diagnostic and/or prognostic functions (11). Among the different molecules, procalcitonin (PCT) and C-reactive protein (CRP) resulted as the most studied candidate biomarkers. However, the clinical implication and molecular involvement of these proteins still needs to be clarified and currently there is not a single molecule validated as the "gold standard" biomarker for sepsis (11). In particular the comprehensive analysis of the literature reported by Pierrakos et al. underlined the limited value of studies evaluating a single biomarker as a prognostic factor, given that mortality in septic patients is related to multiple pathophysiological processes. Therefore, investigation on multiple sepsis-related molecules is strongly suggested as a strategy to develop a validated prognostic model (12–18).

Here we focused on two proteins of the innate immune system, the long pentraxin 3 (PTX3) and the soluble form of the Interleukin-1 type 2 receptor (sIL-1R2). PTX3 is a distant relative of CRP (19, 20) and a key component of the innate immunity. The molecule is expressed by different cell types, at highest levels by phagocytes (monocytes/macrophages and myeloid dendritic cells), in response to primary pro-inflammatory signals, TLR engagement, microbial recognition and tissue damage (21–23). sIL-1R2 is generated by enzymatic cleavage of membrane-bound IL-1R2 and is released from neutrophils and macrophages in response to both pro- and anti-inflammatory signals, acting as a "decoy receptor" which negatively regulates the IL-1 signaling pathway (24–28).

Increased levels of PTX3 have been associated with infectious disorders, including sepsis and septic shock, tuberculosis, dengue and meningitis (29–33). In all these conditions, PTX3 plasma levels correlated with severity and had prognostic value. In sepsis, available data were mainly obtained in ICU patients and indicated that PTX3 is associated with disease severity, organ dysfunction and 28-days or 90-days mortality (29, 31, 34–39). Only few reports were obtained in patients enrolled in emergency rooms, such as the work by Uusitalo-Seppälä et al., underlining the role of PTX3 as a prognostic biomarker of 28-days mortality (40) in that setting.

Similarly, circulating levels of sIL-1R2 are documented to increase in many inflammatory disorders, correlating with disease severity (41–45). Early studies also reported increased levels of sIL-1R2 in small cohorts of sepsis patients or in experimental endotoxemia models (46–48). Elevated levels of sIL-1R2 were measured in patients with clinically defined sepsis (45, 49), and in a group of ICU patients with systemic infections categorized according with Sepsis-1 criteria (44). Despite the correlation with severity, contrasting results were reported in terms of prediction of mortality: Van Der Poll et al. showed higher levels of sIL-1R2 in non-survivors compared to survivors (45), while Muller et al. reported no difference of sIL-1R2 levels in relation to mortality (44).

Reflecting the co-occurrence of inflammation and immunosuppressive mechanisms, both pro- and anti-inflammatory cytokines increase concurrently in the plasma of septic patients. Tumor necrosis factor (TNF-α) and Interleukin 1 beta (IL-1β), the most important primary pro-inflammatory mediators, are the cytokines most extensively studied in sepsis patients (50–52). Other pro-inflammatory cytokines in sepsis response include IL-6, IL-8, IL-12, interferon (INF)-γ, granulocyte-colony stimulating factor (G-CSF), IL-12, IL-17 and IL-18 (50, 53, 54). Among the specific anti-inflammatory mediators enriched in sepsis, IL-1ra, IL-4 and IL-10 are the most studied (47, 53, 55, 56). So far, data showed a complex network of interactions between different cytokines in sepsis. While some

patients are characterized by rapid production of both pro and anti-inflammatory cytokines (57, 58), other septic individuals release predominantly anti-inflammatory mediators or show reduction of both types of molecules (59–62). Therefore, the available literature does not provide conclusive results. Of note, the circulating levels of cytokines differ massively from subject to subject and even within the same patient during the evolution of the disease. Hence it might be relevant to screen a set of different cytokines for monitoring sepsis patients (63, 64).

Due to the complexity of sepsis, the measurement of a set of markers related to different pathways may be more beneficial than relying on a single biomarker (11, 16–18). Thus, the aim of this study was to evaluate the prognostic value of a selection of promising innate immunity molecules, namely PTX3 and sIL-1R2, in combination with a set of pro- and anti-inflammatory cytokines. Circulating biomarkers will be integrated with clinical parameters, in order to improve the early prognostic assessment of sepsis patients in ED setting.

Materials and methods

Ethics approval

This study complied with the provisions of the Declaration of Helsinki and was approved by the Institutional Review Board of Humanitas Research Hospital (Approval n° 820/18). Patients were enrolled only after the signature of a written informed consent. In the case the patient was unable to provide consent, this was obtained from their relatives. Confidentiality of patient data was preserved and no patient identifiers were used in the dataset.

Study design

We conducted a single center prospective observational study enrolling patients with suspected sepsis admitted to the Emergency Department (ED) of Humanitas Research Hospital (from now on referred as Humanitas Hospital) between October 2017 and February 2020. Patients presenting at the Emergency Department were evaluated based on the Sepsis-3 criteria defined by the Third International Consensus Definitions for Sepsis and Septic Shock (65). Sepsis-3 criteria are based on the following recommendations: i) presence of an infection; ii) presence of organ dysfunction, represented by an increase in the Sequential [Sepsis-related] Organ Failure Assessment (SOFA) score of 2 points or more; iii) presence of at least two of the following clinical criteria, that together constitute a new bedside clinical score termed quick SOFA (qSOFA): altered mentation, a respiratory rate of 22/min or greater, and systolic blood pressure of 100 mm Hg or less. Septic shock is defined as a subset of sepsis patients clinically identified by a vasopressor requirement to maintain a mean arterial pressure of 65 mm Hg or greater, serum lactate levels greater than 2 mmol/L (>18 mg/dL) in the absence of hypovolemia or altered mentation (Glasgow coma scale score < 15). All non-sepsis patients had a proof of infectious disease.

A cohort of 178 patients aged 35-98 years old was enrolled in this study (Figure 1), representing approximately 25% of the individuals presenting at the ED of Humanitas Hospital with suspected sepsis during the recruitment period. Six patients were excluded due to missing data. The remaining population of 172 patients was stratified according to Sepsis-3 criteria as detailed above (65). Based on these criteria, the population was divided as follows: 37 patients with SOFA score < 2 were assigned to the "non-sepsis" group diagnosed with infections; 135 patients with SOFA≥2 were divided into two groups: sepsis, (n=99), and septic shock (n=36). The SOFA score was also used to determine the levels of organ dysfunction and mortality risk.

A group of healthy controls (HC) was enrolled among volunteers with age higher than 50 years (n=70). Median age and 25% and 75% quartiles (Q1–Q3) were 63 years (58–67); 56% were males and 43% were females.

Sample collection and preparation

Blood samples were collected in EDTA tubes on the day of arrival at ED or when, within 24-72 hours of observation in ED, the patient was diagnosed as sepsis or septic shock. The day of first blood withdrawal was considered as day1. For those patients admitted to Humanitas Hospital, a second collection was done on day 5 ± 1. Blood samples were centrifuged at 1800 rpm for 10 minutes, then plasma was aliquoted and stored at -20°C until analysis. To ensure the reproducible quality of samples, blood tubes were processed within 2 hours after collection.

Data collection

Demographic information (age, sex, prior medical history), ED stay, hospital stay, ICU admission and blood pressure were collected and documented. In addition, the progression of sepsis and survival outcome at 90 days were recorded. Routine laboratory tests were performed by methods applied in the Clinical Laboratory of Humanitas Hospital.

Biomarker measurement

PTX3 and sIL-1R2 levels were measured using sandwich enzyme-linked immunosorbent assay (ELISA). PTX3 was measured by an in-house assay based on original reagents developed at Humanitas Hospital (detection limit 100 pg/ml; inter-assay and intra-assay variability ranges from 8 to 10%), as

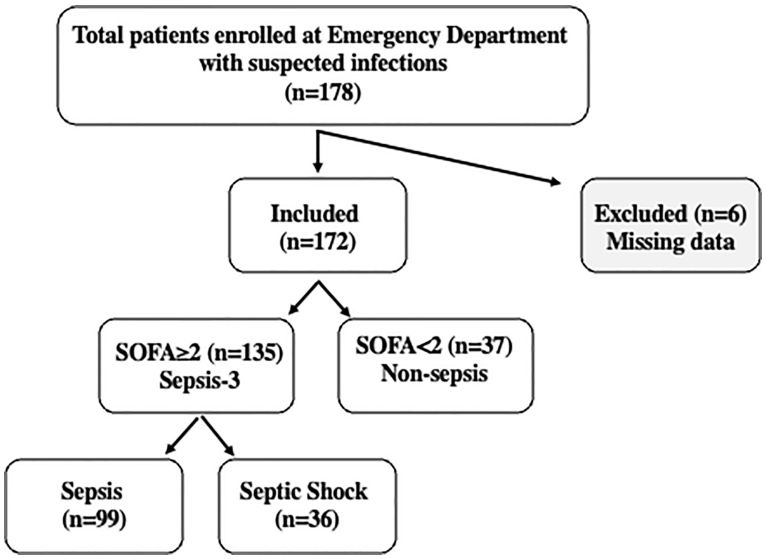

FIGURE 1
Flowchart of the study. A cohort of 178 patients was enrolled at the Emergency Department of Humanitas Research Hospital with suspected sepsis. 172 patients were included in the study and stratified based on Sepsis-3 criteria. Patients with SOFA<2 were classified as "non-sepsis" (n=37), while the 135 patients with SOFA_2, were classified as "sepsis" (n=99) or "septic shock" (n=36) according to clinical evaluation. Septic shock patients were characterized by vasopressor requirement to maintain a mean arterial blood pressure of 65 mmHg or greater and serum lactate levels >2mm/L in the absence of hypovolemia or altered mentation (Glasgow coma scale score < 15).

previously described (66). sIL-1R2 levels were measured using a commercial ELISA (Human sIL-1R2 Quantikine ELISA Kit, BioTechne; detection limit: less than 10 pg/ml) following the recommended protocol of the supplier. PCT and CRP concentrations were measured in the Clinical Laboratory of Humanitas Hospital.

A set of pro and anti-inflammatory cytokines, including IL-10, IL-6, IL-1β, TNF-α, IL-18, IL-8 and IL-1ra was measured using a customized assay in the ELLA Automated Immunoassay System (ProteinSimple, San Jose, CA, USA). The assay was performed following instructions provided by the manufacturer; concentrations of the different cytokines were directly provided by the software of the ELLA instrument. The lower limits of detection were: 0.46 pg/ml for IL-10; 0.41 pg/ml for IL-6; 0.16 pg/ml for IL-1β; 0.30 pg/ml for TNF-α; 0.96 pg/ml for IL-18; 0.19 pg/ml for IL-8; 3.39 pg/ml for IL-1ra.

Statistical analysis

All statistical tests were two-sided. Stata 16.1 (StataCorp LLC, College Station, TX, USA), R software and GraphPad Prism 7.0 (GraphPad Software Inc., CA) were used for statistical analyses and graphics. All significant *P* values are reported in figures and tables legends.

Quantitative data were presented as means ± standard deviations (SD) or medians and interquartile ranges (Q1-Q3) according to normality (analyzed by the D'Agostino-Pearson test). Qualitative data were summarized as frequency (percentage). Parametric (Student's *t*-test and one-way analysis of variance [ANOVA]) and non-parametric methods (two-sample Wilcoxon rank-sum [Mann-Whitney] test; Kruskal-Wallis (two-sample Wilcoxon rank-sum [Mann-Whitney] test; Kruskal-Wallis [equality-of-populations] rank test; Pearson's chi-squared; and Fisher's exact test) were used to detect differences between groups. Correlations were assessed by the Spearman's rank correlation coefficient and the respective *p*-value. For hypothesis testing, a probability level lower than 0.05 was considered as statistically significant.

Multivariable model and prognostic index development

The outcome considered for model development was 90-days mortality. We used time-to-event (survival) methods for censored observations. Time to event was defined as the time from the baseline visit (admission to emergency department) until the date of event or censoring. Kaplan–Meier estimates were used to draw cumulative incidence curves, compared by log-rank tests, as well as by univariable Cox proportional hazards (PH) analysis.

Candidate predictors for the multivariable model included the following variables at baseline: age, gender, SOFA and qSOFA scores, white blood cells, lymphocytes, neutrophils, platelets, C-reactive protein, capillary refill time, hemoglobin, hematocrit,

sodium, vitamin K, fasting blood sugars, prothrombin time, partial thromboplastin time, body temperature, heart rate, systolic and diastolic blood pressure, blood urea nitrogen, paO_2, spO_2, ratio of paO_2/fiO_2, biomarkers of inflammation (pentraxin-3, soluble IL-1R2, IL-1β, IL-1ra, IL-6, IL-8, IL-10, IL-18, TNFα), presence of cardiovascular disease, hypertension, malignancy, neurological disorders, diabetes type 2, chronic obstructive pulmonary disease, chronic kidney disease and other comorbidities. As the distribution of inflammatory biomarkers levels was severely positively skewed, we applied a log10-transformation prior to any analysis.

To avoid extreme collinearity, we first inspected pair-wise correlations among continuous predictors. In a few cases (e.g. hemoglobin and hematocrit) variables showed substantial collinearity (ρ-Spearman ≥0.80). In these cases, the variable most associated with mortality (highest likelihood ratio chi-squared test) was further considered for multivariable modelling. To assess associations between each candidate predictor and 90-days survival, we conducted explorative univariable Cox PH analysis. Except for the biomarkers of inflammation, candidate predictors showing a p-value <0.20 were considered for multivariable modelling. Given that the focus of the study was an in-depth screening of biomarkers of inflammation as potential predictors of mortality in septic patients, we explored systematically every potential interaction, also considering non-linearity through fractional polynomial terms (67). Potential interactions were screened across the other predictors at the final stage of model selection. The best fitting model was initially selected according to the lowest Akaike information criterion (68). Given the high number of candidate predictors relative to the limited sample size and number of events, we further simplified the resulting model through a backward selection procedure and eliminated variables not significant at a strict significance level of $p<0.005$. This process was deemed necessary to ensure a parsimonious multivariable model and avoid substantial overfitting of the data. The proportionality of hazard assumption was tested based on Shoenfeld residuals. Model fit was assessed through the Groennesby and Borgan test (69).

We assessed model discrimination using the Harrell's c-statistic, which quantifies the ability to identify correctly those patients who will die over the study period (68). Each variable entering the final multivariable model was also assessed in term of individual discrimination capacity (continuous), and sensitivity and specificity (dichotomous) in predicting mortality at 90 days of follow-up. The optimal cut-point for each predictor was determined through the maximally selected rank statistics, providing a threshold value corresponding to the most significant association with mortality (70). To estimate sensitivity and specificity at 90 days of follow-up, we used time-dependent receiver operating characteristic (ROC) curve analysis by means of inverse probability of censoring weighting (71). In time-dependent ROC-curve analysis, the status of an individual is observed and updated at each time point taking into account censored observations.

A preliminary prognostic index was built by multiplying the multivariable model beta coefficients (including interactions) by each patient's characteristics (age, blood urea nitrogen, and the log10-transformed PTX3, IL-6 and IL-18 levels) (68). Internal calibration was evaluated by plotting the observed proportion *vs.* predicted survival probability and reporting the calibration slope (which should equal one for a perfectly calibrated model) (68). We also performed a test for calibration intercept equals 0 and slope equals 1, as appropriate (68). The area under the curve of our preliminary prognostic index at 90-days were formally compared with those of SOFA and qSOFA scores, which represent the current gold standards for prediction of mortality in septic patients in different clinical settings.

A nomogram plot was produced to transform all possible total point scores into individual risks of death. We calculated the optimal cut-point of the continuous index by maximally selected rank statistics. This allowed estimating the sensitivity and specificity of this classification rule (i.e. patients scoring less points than the threshold are classified as "alive", those scoring more or equal to the threshold are classified as "dead") in predicting the 90-days risk of death.

Results

Patient demographics

Figure 1 reports the flowchart of the population analyzed in this study: 178 patients with suspected sepsis were enrolled during admission to the ED of Humanitas Hospital. Six patients were excluded due to missing data. Following evaluation by clinicians, the remaining population of 172 patients included 135 patients with SOFA≥ 2, 99 patients with sepsis and 36 with septic shock, while 37 patients with SOFA< 2 did not meet the Sepsis-3 criteria, despite the presence of infections. These patients were categorized as "non-sepsis".

Table 1 summarizes the clinical characteristics of the overall population. The mean age was significantly increased with the severity, while no differences between males and females in the three subgroups of patients were observed. Most frequent infections were at the urinary tract (24% in non-sepsis and 41% in septic shock groups) and the respiratory tract (44% in sepsis group). Almost all the patients with sepsis and septic shock had at least one comorbidity. The most frequent comorbidity in non-sepsis and sepsis groups is represented by hypertension (40% and 34% respectively), while cardiovascular disease was the most frequent comorbidity in septic shock patients (50%). Among the laboratory and clinical results, SOFA score and levels of lactate, PCT, creatinine, d-dimer, potassium and urea were higher in septic shock patients than in the other groups of patients. Also, vasopressor need and hypotension increased significantly in septic shock patients.

10.3389/fimmu.2022.979232

TABLE 1 Demographic, laboratory and clinical characteristics of the entire patients population on day 1.

Variables	Non-sepsis (n=37)	Sepsis (n=99)	Septic shock (n=36)	*p* value
Demographic Characteristics				
Age, median [Q1-Q3]	70 [57-81]	78 [70-84]	78 [71-85]	**0.02**
Male sex, n (%)	21 (56.8)	68 (68.7)	21 (58.3)	0.32
Female sex, n (%)	16 (43.2)	31 (31.3)	15 (41.7)	0.27
Comorbidities n (%)				
Cardiovascular disease	10 (27.0%)	33 (33.3%)	18 (50.0%)	0.06
Hypertension	15 (40.5%)	34 (34.3%)	12 (33.3%)	0.76
Malignancy	13 (35.1%)	31 (31.3%)	14 (38.8%)	0.69
Neurological disease	9 (24.3%)	22 (22.2%)	7 (19.4%)	0.88
Diabetes type 2	5 (13.5%)	19 (19.1%)	6 (16.6%)	0.73
COPD	6 (16.2%)	17 (17.1%)	10 (27.7%)	0.33
Chronic kidney disease	1 (2.7%)	19 (19.1%)	5 (13.8%)	**0.01**
Others	9 (24.3%)	27 (27.2%)	8 (22.2%)	0.97
Site of infection n (%)				
Respiratory system	7 (18.9%)	44 (44.4%)	9 (25.0%)	**0.008**
Urinary tract	9 (24.3%)	29 (29.2%)	15 (41.6%)	0.24
Liver	5 (13.5%)	4 (4.0%)	4 (11.1%)	0.11
Abdomen	2 (5.4%)	4 (4.0%)	0 (0%)	0.40
Blood	1 (2.7%)	4 (4.0%)	2 (5.5%)	0.82
Skin and soft tissue	3 (8.1%)	4 (4.0%)	1 (2.7%)	0.50
Unknown	4 (10.8%)	6 (6.0%)	3 (8.3%)	0.63
Others	6 (16.2%)	4 (4.0%)	2 (5.5%)	0.04
Vital signs, median [Q1-Q3]				
Body temperature (°C)	37.6 [36.7-38.4]	37.3 [36.3-38.4]	36.8 [36.0-38.5]	0.67
Body mass index (kg/m^2)	26.8 [24.2-32.3]	26.3 [22.3-31.3]	24.5 [21.1-25.6]	0.25
Respiratory rate (per min)	16 [15-18]	18 [16-21]	18 [16-20]	**0.03**
Heart rate (bpm)	97.5 [85.5-109.5]	97 [78-110]	99 [82.5-119.5]	0.70
SBP (mmHg)	116 [103-130]	110 [95-134]	83 [76-92]	**0.0001**
DBP (mmHg)	65 [60-79]	65 [50-80]	51 [40-60]	**0.0001**
MAP (mmHg)	85 [77-93]	77 [67-90]	60 [53-65]	**0.0001**
GCS	15 [15-15]	15 [15-15]	15 [13-15]	0.06
Laboratory values, median [Q1-Q3]				
WBC (10^3/mm^3)	11.9 [8.3-16.6]	11.6 [8.4-18.8]	16.1 [7.6-20.0]	0.46
Lymphocytes (10^3/mm^3)	0.8 [0.5-1.2]	0.7 [0.4-1.1]	0.7 [0.4-1.0]	0.30
Neutrophils (10^3/mm^3)	9.8 [6.7-13.9]	9.2 [6.8-16.4]	14.3 [6.6-17.5]	0.29
Platelets (10^3/mm^3)	204 [170-301]	172 [123-270]	166 [117-272]	0.10
Lactate (mmol/L)	1.6 [1.1-3.0]	2.6 [1.6-4.0]	4.8 [2.7-7.1]	**0.0002**
INR (sec)	1.2 [1.1-1.4]	1.3 [1.1-1.5]	1.3 [1.2-1.7]	0.09
Creatinine (mg/dL)	0.8 [0.6-1.0]	1.6 [1.0-2.5]	1.9 [1.2-3.2]	**0.0001**
D-dimer (ng/ml)	743 [416-2485]	685 [383-1896]	1728 [787-4735]	**0.01**
Fibrinogen (mg/dL)	633 [459-798]	512 [414-714]	504 [386-665]	0.39
Hemoglobin (g/dl)	12.0 [10.4-12.7]	11.6 [10.5-13.1]	10.5 [9.0-12.4]	0.12
Hematocrit (%)	36.6 [31.2-37.7]	35.6 [32.0-39.8]	34.3 [27.9-38.5]	0.30
Bilirubin (mg/dL)	0.7 [0.5-1.0]	0.8 [0.6-1.1]	0.9 [0.6-1.4]	0.15
Sodium (mmol/L)	137 [134-139]	137 [133-140]	138 [135-141]	0.56
Potassium (mmol/L)	3.8 [3.5-4.1]	4.0 [3.6-4.5]	4.3 [3.7-5.1]	**0.009**
Urea (mg/dL)	39.0 [31.0-59.7]	74.3 [49.9-115.3]	89.5 [52.8-148.4]	**0.0001**
Fasting blood sugar (mg/dL)	124 [106-165]	124 [105-169]	109 [85-184]	0.22

(Continued)

TABLE 1 Continued

Variables	Non-sepsis (n=37)	Sepsis (n=99)	Septic shock (n=36)	*p* value
PT (second)	1.2 [1.2-1.4]	1.3 [1.1-1.5]	1.3 [1.2-1.6]	0.28
PTT (second)	1.0 [0.9-1.0]	0.9 [0.9-1.1]	1.0 [0.8-1.1]	0.46
Bicarbonate (mmol/L)	24.4 [24.0-26.3]	22.6 [20.0-27.1]	19.1 [16.7-23.4]	**0.04**
PH value	7.5 [7.4-7.5]	7.5 [7.4-7.5]	7.4 [7.4-7.5]	0.18
PCT (ng/ml)	0.4 [0.1-1.3]	3.6 [0.6-17.5]	14.6 [2.3-75.5]	**0.0001**
CRP (mg/dL)	9.7 [3.6-19.6]	15.4 [6.7-24.1]	16.6 [12.2-22.4]	0.10
PTX3 (ng/ml)	34.6 [11.6-68.2]	52.5 [22.4-177.0]	210.9 [103.8-613.8]	**0.0001**
sIL-1R2 (ng/ml)	17.1 [14.6-20.0]	23.5 [16.1-34.6]	31.0 [22.0-50.1]	**0.0001**
Clinical factors, median [Q1-Q3] or n (%)				
SOFA score	1 [0-1]	4 [3-6]	8 [5-9]	**0.0001**
qSOFA score	0 [0-0]	1 [0-1]	1.5 [1-2]	**0.0001**
ICU admission	0 (0)	3 (3.0)	5 (17.2)	0.39
Vasopressor need	0 (0)	2 (2.0)	22 (61.1)	**0.0001**
Hypotension	1 (2.7)	26 (26.3)	32 (88.9)	**0.0001**
Hospital stays (days)	11 [7-17]	10 [7-18]	15 [4-24]	0.76

Data are reported as median [Q1-Q3] or n (%). Kruskal-Wallis equality-of-populations rank test was used for the comparisons of the different variables across the three groups of patients. Statistically significant values are in bold character. Abbreviations: COPD, Chronic obstructive pulmonary disease; DBP, diastolic blood pressure; GCS, Glasgow coma scale; ICU, intensive care unit; INR, international normalized ratio; MAP, mean arterial pressure; PCT, procalcitonin; PT, prothrombin time; PTT, partial thromboplastin time; SBP, systolic blood pressure; SOFA, Sequential Organ Failure Assessment; qSOFA, quick Sequential Organ Failure Assessment; WBC, white blood cells.

PTX3 and sIL-1R2 levels in sepsis and association with severity

The levels of PTX3 and sIL-1R2 in HC and in non-sepsis, sepsis and septic shock patients on day 1 of ED admission are reported in Figure 2 and Table 1. PTX3 levels were significantly increased in all the three groups of patients compared to HC (Figure 2A; PTX3 levels in HC: 2.52 [1.88-3.6], median ng/ml [Q1-Q3]). In the same cohort, sIL-1R2 levels were also increased in sepsis and septic shock patients compared to HC (median and Q1-Q3] 16.29 ng/ml [13.52-20.25]), while normal levels of sIL-1R2 were observed in non-sepsis patients (Figure 2B). The increased severity among the three groups of patients is supported by the upregulated levels of several clinical parameters, which are indicative of sepsis severity (Table 1). In parallel, both PTX3 and sIL-1R2 are increased with the increasing of severity from non-sepsis to sepsis and septic shock (Figure 2 and Table 1).

For the patients admitted to wards we collected a second blood sample after 5 days of hospitalization (non-sepsis n=23, sepsis n=62, septic shock n=17). In most of the patients with matched samples at day 1 and 5 we observed a significant decrease of PTX3 after 5 days of hospitalization, while sIL-1R2 levels did not change (Table 2). PCT and CRP, two molecules widely used as biomarkers indicative of sepsis severity (72, 73), were also elevated in our cohort of patients compared to levels in healthy population [CRP<0.5 mg/dl; PCT 0.05-0.5 ng/ml (74–76)], and were higher in Sepsis-3 patients compared to non-sepsis individuals (CRP: p=0.04; PCT: p<0.0001, Mann-Whitney test). In addition, a decrease was observed from day 1 to day 5 (not shown).

Univariable Spearman's rank correlation analysis of PTX3 and sIL-1R2 with SOFA score showed a positive correlation (PTX3: r=0.44, p<0.0001; sIL-1R2: r=0.35, p<0.0001, Table S1). In addition, PTX3 and sIL-1R2 correlated with different clinical parameters evaluated at enrollment in ED (e.g. creatinine and D-dimer, Table S1) as well as with PCT and CRP. Finally, a correlation was observed between PTX3 and sIL-1R2 evaluated on day 1.

Cytokine levels in Sepsis-3 population

In the same samples we measured a panel of pro-inflammatory (IL-6, IL-1β, TNF-α, IL-18 and IL-8) and anti-inflammatory cytokines (IL-10, IL-1ra). On day 1 all the cytokines were highly increased in patients compared to HC, with a gradual trend of progressively higher levels from non-sepsis to sepsis and septic shock patients (Table 3). In particular, there was approximately a 2-fold increase of all cytokines except IL-18 in septic shock patients compared to sepsis patients on day 1. When we limited the analysis to those patients admitted to wards, circulating levels of all cytokines decreased from day 1 to day 5, with the only exception of IL-1β in septic shock patients and IL-18 in sepsis patients (Table S2).

PTX3 and sIL-1R2 showed a positive correlation with all the pro- and anti-inflammatory cytokines considered in the present analysis, except IL-18 and IL-1β (Table 4). The strongest correlations were observed between the C-X-C chemokine IL-8, a main chemotactic

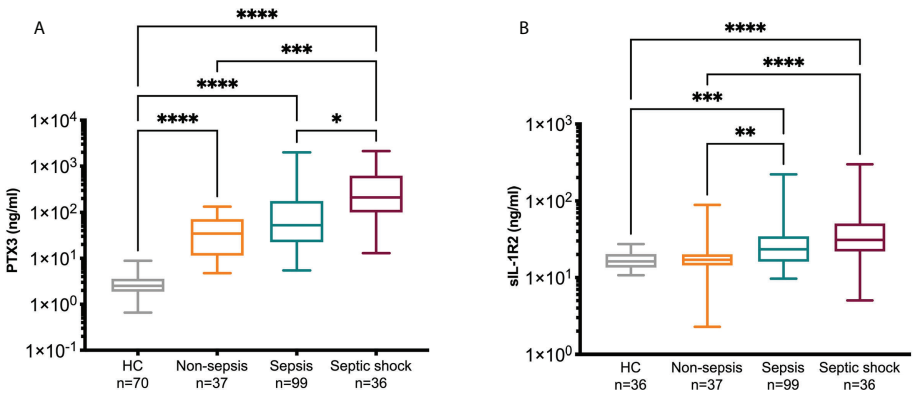

FIGURE 2
PTX3 and sIL-1R2 levels on day 1. PTX3 **(A)** and sIL-1R2 **(B)** plasma concentration were measured in non-sepsis, sepsis and septic shock patients admitted to ED. A group of healthy controls (HC) was also included. Kruskal-Wallis equality-of-populations rank test was used for the comparisons, * $p \leq 0.05$; ** $p \leq 0.01$; *** $p \leq 0.001$; **** $p \leq 0.0001$.

factor for neutrophils, and PTX3 (r=0.62, $p<0.0001$) or sIL-1R2 (r=0.50, $p<0.0001$) respectively. In addition, both pro and anti-inflammatory cytokines were positively correlated with SOFA score on day 1 of admission. Among them, TNF-α showed the strongest correlation (r=0.60, $p<0.0001$, Table 4).

Distribution of PTX3, sIL-1R2 and cytokines between survivors and non-survivors in Sepsis-3 patients

The 90-days survival analysis in the total Sepsis-3 population showed 99 survivors (73%) and 36 non-survivors (27%). Mortality rate was 20% among sepsis patients and 44% among septic shock patients. Of note, among the non-sepsis patients, four subjects (11%) did not survive following the 90-days follow up.

Clinical data, PTX3, sIL-1R2 and cytokines levels among survivors and non-survivors are summarized in Table 5. SOFA score, lactate, CRP, creatinine, d-dimer and urea on day 1 were remarkably higher in non-survivors compared to survivors. Similarly, PTX3 and sIL-1R2 levels at enrollment were significantly higher in patients who died within 90 days from ED admission compared to those who survived. In addition, both pro- and anti-inflammatory cytokines levels were upregulated in non-survivors. Additional data are reported in Table S3.

Multivariable model development

The association between candidate predictors measured at the arrival at the ED, and 90-days mortality was first explored by univariable Cox proportional analysis. Variables not associated with mortality in this cohort of patients are reported in Table S4, while predictors with a significant hazard ratio are listed in Table 6. According to the analysis, PTX3 and sIL-1R2 emerged as strong predictors of mortality, with a hazard ratio respectively of 3.09 [1.80-5.30] and 5.31 [2.05-13.74] and $p \leq 0.001$ (Table 6). Combinations including the different biomarkers and clinical variables were then investigated. The most parsimonious multivariable Cox proportional hazard model comprising independent predictors of 90-days mortality included five variables: age, blood urea nitrogen, PTX3, IL-6 and IL-18 as

TABLE 2 PTX3 and sIL-1R2 levels at day 1 and day 5 in non-sepsis, sepsis and septic shock patients.

	PTX3 Day 1	PTX3 Day 5	p value	sIL-1R2 Day 1	sIL-1R2 Day 5	p value
Non-sepsis (n=23)	48.9 [28.1-82.5]	16.6 [10.0-30.7]	**0.001**	17.0 [12.0-20.0]	18.1 [13.1-21.1]	0.66
Sepsis (n=62)	69.4 [34.1-220.6]	17.6 [10.2-28.9]	**<0.0001**	23.9 [17.9-35.1]	25.0 [17.28-35.6]	0.69
Septic shock (n=17)	219.8 [69.9-832.0]	30.31 [10.0-48.7]	**0.0001**	34.37 [21.3-72.2]	41.6 [15.9-82.4]	0.54

Data are reported as median ng/ml and [Q1-Q3], and refer only to those patients with available samples for both the time points. Number of patients is indicated for each group. The Wilcoxon signed-ranks test was used for the comparisons of PTX3 and sIL-1R2 levels on day 1 and day 5 in the different groups of patients. Statistically significant values are in bold character.

TABLE 3 Cytokine levels in healthy controls, non-sepsis, sepsis and septic shock patients on day 1 of admission to Emergency Department.

Cytokine	Healthy control (n=20)	Non-sepsis (n=37)	Sepsis (n=99)	Septic shock (n=36)	*p* value
IL-10	1.0 [0.7-1.4]	11.4 [5.8-29.0]	16.3 [8.3-41.0]	46.5 [15.2-333.5]	**0.0001**
IL-1β	0.1 [0.0-0.3]	0.8 [0.5-1.4]	0.8 [0.5-1.3]	1.3 [0.7-2.9]	**0.0001**
IL-6	1.6 [1.0-2.9]	82.0 [30.6-128.2]	112.9 [35.2-230.3]	342.7 [125.7-8450.4]	**0.0001**
TNF-α	4.9 [4.2-6.0]	14.9 [11.1-20.8]	23.1 [14.0-37.1]	45.5 [21.4-164.7]	**0.0001**
IL-18	138.9 [87.9-203.5]	262.6 [201.7-387.8]	328.8 [226.9-525.7]	376.3 [256.6-625.2]	**0.0001**
IL-1ra	183.5 [141.4-259.9]	2218.8 [1206.0-3258.2]	4005.4 [1418.5-9393.3]	15527.6 [4123.4-46700.6]	**0.0001**
IL-8	5.2 [4.1-8.5]	16.1 [10.9-27.5]	29.6 [15.1-73.0]	74.7 [42.2-352.3]	**0.0001**

Data are reported as median pg/ml and [Q1-Q3]; Kruskal-Wallis equality-of-population test was used for the comparison of cytokines levels among the non-sepsis, sepsis and septic shock groups of patients. Number of subjects with available data is indicated for each group. Statistically significant values are in bold character.

continuous predictors. The three biomarkers of inflammation were log10-transformed. The model included a strong positive interaction (synergistic effect) between IL-6 and IL-18 (i.e. due to this strong interaction term, despite their negative coefficients, IL-6 and IL-18 should be interpreted as positively associated with 90-days mortality, though in a non-linear fashion). All variables were significant at the conservative threshold of $p<0.005$. For each predictor we calculated a threshold from the maximally selected rank statistics. The biomarkers threshold included: age (87 years), blood urea nitrogen (117 mg/dL), PTX3 (240 ng/ml), IL-6 (175 pg/ml), IL-18 (526 pg/ml). According to these thresholds, patients were categorized in two groups (i.e. high *vs.* low). In Figure 3 are reported the Kaplan-Meier curves for each predictor included in the final multivariable model.

The c-statistics, sensitivity and specificity of each of these predictors are reported in Table 7. PTX3 showed the highest apparent c-statistic (0.716; 95% CI: 0.636–0.796) and sensitivity and specificity (threshold: 240 ng/ml; sensitivity: 48.4%, 95% CI: 31.9 –64.9; specificity: 89.9%, 95% CI: 82.7–97.0) in our cohort of patients.

Multivariable model specifications, including the baseline hazard at 90 days, are reported in Table 8. There was no evidence of violation of the proportionality of hazard assumption ($p=0.192$) and the Groennesby and Borgan test showed a reasonable model fit ($p=0.783$). The calibration plot showed good internal calibration (Figure S1), as indicated by a calibration slope equal to 1.146 (95% CI: 0.605–1.687) with an intercept not significantly different than zero ($p=0.876$). The Harrel c-statistic was 0.808 (95% CI: 0.734–0.882), indicating good discrimination performance.

We built a preliminary prognostic index by multiplying the multivariable model beta coefficients (including the interaction) by each patient's characteristics:

$$\begin{aligned} &\textit{Prognostic Index} \\ &= 0.066 \times Age + 1.343 \times log_{10}(\text{PTX3}) - 4.961 \\ &\quad \times log_{10}(\text{IL}-6) \; -3.437 \times log_{10}(\text{IL}-18) + 0.008 \times Urea \\ &\quad + 1.903 \times log_{10}(\text{IL}-18) \times log_{10}(\text{IL}-6) \end{aligned}$$

TABLE 4 Univariable correlations of PTX3, sIL-1R2 and SOFA score with cytokines in the Sepsis-3 population (n=135).

	PTX3		sIL-1R2		SOFA score	
Cytokine	**Spearman r**	***p***	**Spearman r**	***p***	**Spearman r**	***p***
IL-10	0.50	**<0.0001**	0.43	**<0.0001**	0.43	**<0.0001**
IL-1β	0.20	**0.01**	0.09	0.27	0.31	**0.0002**
IL-6	0.51	**<0.0001**	0.41	**<0.0001**	0.44	**<0.0001**
TNF-α	0.49	**<0.0001**	0.35	**<0.0001**	0.60	**<0.0001**
IL-18	0.12	0.13	0.31	**0.0002**	0.25	**0.0036**
IL-1ra	0.56	**<0.0001**	0.42	**<0.0001**	0.53	**<0.0001**
IL-8	0.62	**<0.0001**	0.50	**<0.0001**	0.58	**<0.0001**

Spearman's rank correlation test was used. Statistically significant values are in bold character.

TABLE 5 Distribution of selected clinical parameters and biomarkers among survivors and non survivors in the Sepsis-3 population.

Variables	Survivors (n=99)	n	Non-Survivors (n=36)	n	*p* value
SOFA score	4 [3-6]	99	6.5 [4-8.5]	36	**0.0005**
qSOFA score	1 [0-1]	99	1 [1-2]	36	**0.001**
Neutrophils (10^3/mm^3)	9.5 [6.1-15.8]	98	14.1 [7.9-18.8]	36	**0.05**
Lactate (mmol/L)	2.7 [1.6-4.4]	57	4.5 [3.1-6.9]	21	**0.007**
Creatinine (mg/dL)	1.5 [1.1-2.3]	99	2.3 [1.4-4.5]	36	**0.01**
D-dimer (ng/ml)	685 [398-1821]	51	2843 [1256-4057]	21	**0.003**
Urea (mg/dL)	69.4 [49.9-105.7]	98	122.8 [63.4-177.6]	36	**0.002**
Body temperature (°C)	37.7 [36.4-38.5]	97	36.5 [36.0-38.0]	35	**0.01**
MAP (mmHg)	73 [62-88]	99	66 [55-77]	35	**0.02**
DBP (mmHg)	60 [50-75]	99	52 [44-70]	36	**0.03**
GCS	15 [15-15]	99	15 [13-15]	36	**0.003**
FiO2 (%)	21 [21-28]	99	21 [21-36]	36	**0.01**
Haemoglobin (g/dl)	11.7 [10.5-13.1]	99	10.6 [9.4-12.4]	36	**0.03**
CRP (mg/dL)	15.4 [6.6-21.9]	98	17.4 [13.1-26.9]	36	**0.01**
PTX3 (ng/ml)	59.9 [19.9-177.0]	99	237.0 [61.1-557.0]	36	**0.0001**
sIL-1R2 (ng/ml)	22.8 [15.8-33.8]	99	34.6 [24.9-50.9]	36	**0.0002**
IL-10 (pg/ml)	15.5 [8.6-32.8]	99	48.0 [16.8-137.2]	36	**0.0004**
IL-1β (pg/ml)	0.8 [0.5-1.4]	99	1.2 [0.7-2.0]	36	**0.01**
IL-6 (pg/ml)	113.8 [41.1-297.7]	99	239.3 [92.8-730.5]	36	**0.03**
TNF-α (pg/ml)	25.2 [15.6-42.2]	99	36.1 [19.0-82.7]	36	**0.05**
IL-18 (pg/ml)	307 [222.4-472.8]	99	418.3 [284.6-684.4]	36	**0.05**
IL-1ra (pg/ml)	4099.7 [1595.1-10281.7]	99	9569.6 [3668.2-34912.4]	36	**0.01**
IL-8 (pg/ml)	29.6 [16.0-73.4]	99	73.8 [34.7-204.4]	36	**0.0003**

Data are reported as median and [Q1-Q3]; Mann-Whitney test was used for the comparisons. Only variables statistically significant are reported in the table. Abbreviations: DBP, diastolic blood pressure; FiO2, fraction of inspired oxygen; GCS, Glasgow coma scale; MAP, mean arterial pressure; SOFA, Sequential Organ Failure Assessment; qSOFA, quick Sequential Organ Failure Assessment. Statistically significant values are in bold character.

A nomogram plot associating each possible score with the individual 90-days risk of death is provided in Figure S2. The index was then dichotomized by applying the optimal threshold derived by maximally selected rank-statistics (threshold value = 0.112, corresponding to a predicted 90-days risk of death of 35.3%). This allowed patient stratification into high *vs.* low 90-

TABLE 6 Univariable Cox proportional hazard analysis of candidate predictors of 90-days mortality.

Variable (n)	Hazard ratio	95% CI	*p* value
SOFA score (n=135)	1.24	1.11–1.38	**<0.001**
qSOFA score (n=135)	2.03	1.37–3.02	**<0.001**
Sodium (n=135)	1.04	1.01–1.08	**0.011**
Blood urea nitrogen (n=134)	1.00	1.00–1.01	**0.001**
PaO_2/FiO_2 (n=135)	0.65	0.45–0.95	**0.026**
Biomarkers (n=135)			
PTX3 (n=135)	3.09	1.80–5.30	**<0.001**
sIL-1R2 (n=135)	5.30	2.05–13.74	**0.001**
CRP (n=134)	1.03	1.01–1.06	**0.003**
IL-10 (n=135)	1.63	1.17–2.26	**0.003**
IL-1ra (n=135)	1.72	1.12–2.63	**0.012**
IL-1β (n=135)	2.49	1.32–4.70	**0.005**
IL-6 (n=135)	1.33	0.99–1.80	**0.055**
IL-8 (n=135)	1.75	1.24–2.47	**0.001**

Levels of biomarkers were log10 transformed before statistical analysis. Number of patients with available data are indicated in parenthesis. Abbreviations: CI, confidence interval; FiO2, fraction of inspired oxygen; PaO2, partial pressure of oxygen in arterial blood; SOFA, Sequential Organ Failure Assessment; qSOFA, quick Sequential Organ Failure Assessment. Statistically significant values are in bold character.

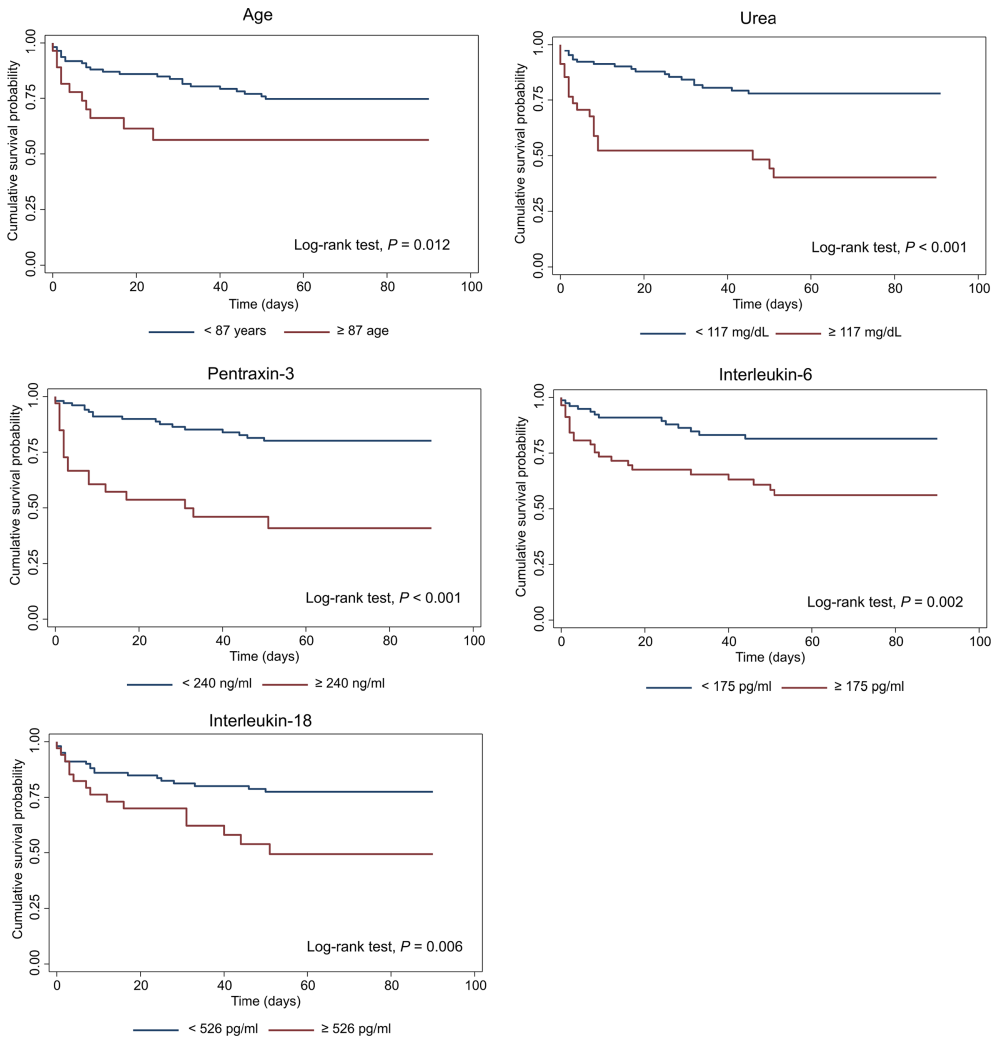

FIGURE 3
Kaplan-Meier survival curves of predictors included in the multivariable Cox model of 90-days mortality. Patients were categorized in two groups in accordance to continuous predictors dichotomized based on the maximally selected rank statistic. PTX3, IL-6 and IL-18 were log10-transformed before analysis. For each predictor, survival was analyzed by Log-rank test and correspondent *p* values are reported on the graphs.

days risk of death. The Kaplan Meier curves of patients belonging to the two groups are reported in Figure 4. Patients categorized by the index in the high mortality group had an observed cumulative 90-days risk of death of 73.3% (95% CI: 57.5–87.0), whereas patients in the low mortality group had a cumulative risk of 10.0% (95% CI: 5.12–19.1). The hazard ratio corresponding to the high mortality group was 12.0 (95% CI: 5.41–26.5). The sensitivity (76.9%; 95% CI: 62.8–91.0) and

TABLE 7 Harrel C-statistics, sensitivity and specificity of each predictor included in the multivariable Cox model of 90-days mortality.

	Threshold	*C-statistic [95% CI]*	*Sensitivity (%) [95% CI]*	*Specificity (%) [95% CI]*
Age	87 years	0.60 [0.50–0.70]	29.0 [14.3–43.7]	91.3 [84.6–98.0]
Blood urea nitrogen	117 mg/dL	0.66 [0.56–0.76]	50.9 [34.4–67.4]	86.8 [78.7–94.8]
PTX3	240 ng/ml	0.72 [0.64–0.80]	48.4 [31.9–64.9]	89.9 [82.7–97.]
IL-6	175 pg/ml	0.62 [0.53–0.71]	63.3 [47.4–79.2]	65.2 [53.9–76.5]
IL-18	526 pg/ml	0.58 [0.48–0.67]	42.2 [25.9–58.5]	84.1 [75.4–92.7]

Reported thresholds were calculated for each predictor once dichotomized based on the maximally selected rank statistic. Abbreviations: CI, confidence interval.

TABLE 8 Multivariable Cox model of 90-days mortality: full model specification[1].

	β coefficient	95% CI	*p*-value
Age	+0.066	+0.029 to +0.103	**0.001**
Blood urea nitrogen	+0.008	+0.003 to +0.012	**<0.001**
PTX3	+1.343	+0.630 to +2.056	**<0.001**
IL-6	-4.961	-7.583 to -2.339	**<0.001**
IL-18	-3.437	-5.355 to -1.518	**<0.001**
IL-6*IL-18 (interaction term)	+1.903	+0.926 to +2.880	**<0.001**

[1] H_0 = 0.3894 (90-days baseline hazard). Values of PTX3, IL-6 and IL-18 were log10 transformed before analysis. Abbreviations: CI, confidence interval. Statistically significant values are in bold character.

specificity (91.2%; 95% CI: 84.4–97.9) associated with this threshold showed a good performance of this classification rule in our sample of patients.

Comparison of the prognostic index with SOFA and qSOFA

SOFA and qSOFA scores were used to identify patients with sepsis according with the Sepsis-3 criteria, however it is well known that this scoring system is also useful in predicting the clinical outcomes of critically ill patients (77, 78). We thus compared formally the AUC of our preliminary prognostic index with that of SOFA and qSOFA scores. The 90-days AUC of our preliminary index was 0.863 (95% CI: 0.780 –0.945). The 90-days AUC of SOFA score was 0.727 (95% CI: 0.613–0.840), while the AUC for qSOFA at the same time-point was 0.660 (95% CI: 0.558–0.762). The AUC of our preliminary index was significantly greater than both SOFA (p=0.021) and qSOFA scores (p<0.001) in our cohort of patients, meaning that it was able to discriminate between patients dying from those surviving more accurately than the current gold standards.

Discussion

Aim of this study was to evaluate the prognostic value of molecules of the innate immune response, namely PTX3 and sIL-1R2, in association with a set of pro- and anti-inflammatory cytokines (IL-1β, IL-6, IL-8, IL-10, IL-18, TNF-α and IL-1ra) and clinical parameters, in patients presenting at the Emergency Department with a suspicious or diagnosis of sepsis defined according to the Sepsis-3 criteria (65). At ED arrival, a progressive increase in the circulating levels of PTX3, sIL-1R2 and both pro- and anti-inflammatory cytokines was observed from non-sepsis to sepsis and septic shock patients. In univariable Cox analysis, PTX3, sIL-1R2 and all the cytokines analyzed in this study, except IL-18, were significant predictors of 90-days mortality. The combination of circulating levels of PTX3, IL-6 and IL-18, with age and blood urea nitrogen, constituted a preliminary prognostic index of 90-days mortality with high sensitivity and specificity, and more efficient than the gold standards SOFA and qSOFA scores, providing a useful tool to stratify sepsis patients on arrival at the ED.

The emergency department plays a pivotal role in the prompt recognition of septic status and activation of optimal therapeutic approaches (79–81). Biomarkers predicting mortality risk would represent invaluable tools to quickly provide patients with the most appropriate hospital care (82, 83). The biomarkers described here are in principle amenable to evolution to rapid point-of-care tests better addressing emergency department needs. Different platforms are available or under development, potentially useful in this context, including the ELLA microfluidic immunoassay system used in our work or multiplexed label-free biosensors (84–86)

Several reports addressed the role of PTX3 as a biomarker of sepsis (29, 31, 33–40), while scanty and contrasting data are available on sIL-1R2 (44–49), and a general consensus on its role in sepsis has not yet been reached. The present work has the merit to analyze patients arriving at the ED and diagnosed according to the latest Sepsis-3 definition, without excluding any pre-existing comorbidity, including cancer. The model developed can be used for the early prediction of 90-days mortality risk, a timing no longer affected by the different therapies. PTX3 and sIL-1R2 circulating levels were increased, reflecting the augmented tissue damage and inflammation associated with the increased severity. In addition, both molecules strongly correlated with SOFA score in sepsis and septic shock patients (PTX3: r=0.44, p<0.0001; sIL-1R2: r=0.35, p<0.0001), confirming data obtained in earlier studies (31, 44), as well as with PCT, CRP and clinical parameters of severity. These data demonstrated that PTX3 and sIL-1R2 could be useful in monitoring the severity of disease in early hours of admission to ED.

The role of the immune system in sepsis is generally recognized and involves multiple processes, ranging from activation of pro-inflammatory mechanisms to immunosuppression, often occurring simultaneously (87–89). Early activation of the inflammatory response is involved in the pathogenesis of sepsis, and the altered levels of several cytokines observed in septic patients compared to healthy controls are likely involved in the organ injury observed in

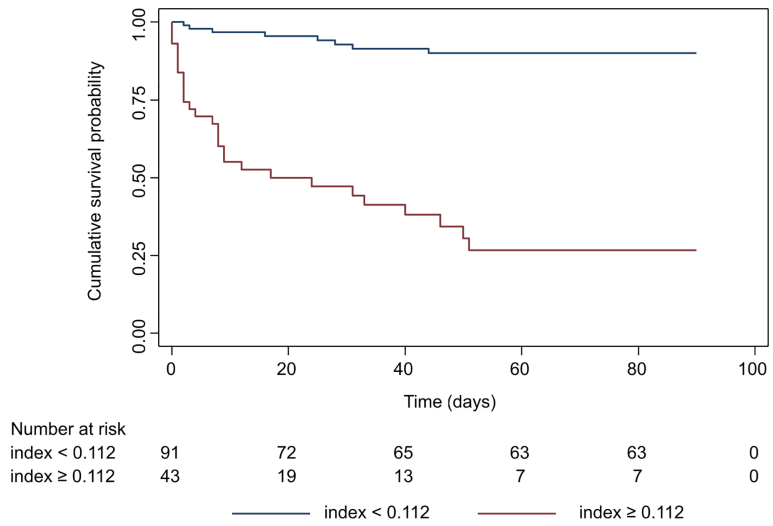

FIGURE 4
Kaplan-Meier survival curve of the prognostic index once dichotomized by maximally selected rank statistics. Patients were categorized in high and low mortality risk groups based on the threshold value of the prognostic index. Survival in the two groups was analyzed by Log-rank test (p<0.0001).

sepsis (9, 90). In our cohort of patients, we observed significant changes in the levels of the panel of pro-inflammatory (IL-1β, IL-6, IL-8, IL-18, TNF-α) and anti-inflammatory (IL-10, IL-1ra) cytokines. All the molecules were augmented in patients compared to HC and correlated with SOFA score, evidencing, as for PTX3 and sIL-1R2, the progressive increase of their circulating levels with the severity of disease. The concomitant upregulation of PTX3, CRP and pro-inflammatory cytokines (IL-6, IL-8, TNF-α) on one side, and of the anti-inflammatory molecules sIL-1R2, IL-10 and IL-1ra on the other side, further supports the coexistence of pro-inflammatory and immunosuppressive mechanisms throughout the host response to sepsis.

After 5 days of hospitalization, a general decrease of PTX3 circulating levels was observed, in parallel with an improvement of patients' conditions and a reduction of the inflammation and/or infection burden. In parallel, a reduction of CRP, PCT and cytokines levels was observed in the cohort of patients, together with the general improvement of clinical parameters. On the contrary, no significant changes were recorded in circulating levels of sIL-1R2 in this time frame. Considering that sIL-1R2 is a key negative regulator of the IL-1 system, the maintenance of high levels of the molecule could tightly regulate the responses to IL-1 family members, contributing to protect from an exaggerated inflammatory response (26).

PTX3, sIL-1R2 and all cytokines investigated in our study were significantly higher in non-survivors compared to 90-days survivors, and were strong predictors of mortality. These results are in agreement with several studies reporting the association of cytokines such as IL-6 or IL-18 with poor outcome in septic patients (91, 92). In another study of a small cohort of sepsis, severe sepsis and shock patient admitted to ICU, the levels of IL-6, IL-8 and IL-18 resulted higher in non-survivors compared to survivors, although following multivariable logistic regression analysis only IL-18 remained related to mortality (93). In addition, a positive synergistic effect has been observed between IL-18 and IL-6 that likely contributes to the association of these molecules with mortality, despite IL-18 not being a significant predictor of mortality by Cox proportional analysis. Our study was limited to a selected number of soluble mediators, and we are aware that other molecules could also play relevant roles. Growing interest has been observed for circulating antagonists of the IL-1 pathway, such as IL-18 binding protein (IL-18BP) and IL-1R4, also known as ST2 (94, 95), even for possible therapeutic implications (96). In a sub-group of patients, we measured both IL-18BP and IL-1R4: the two molecules were mildly increased in patients compared to healthy controls (data not shown). Although an increasing trend was seen from non-sepsis to sepsis and shock patients, IL-18BP and IL-1R4 were not significantly associated with mortality, in contrast to what reported by others (93, 96–98). A future comprehensive analysis of all the different molecules belonging to the IL-1 pathway would be helpful to fully define the strength of this essential family of inflammatory mediators in assessing sepsis patients.

Overall, the literature shows that none of the cytokines is a robust biomarker of mortality by itself (6, 11, 99). For this reason, the most recent investigations have mainly focused on the analysis of a combination of multiple biomarkers to predict outcome in sepsis patients (12–18). In a recent prospective observational analysis on septic patients arriving at the ED,

Song et al. showed that the combination of PTX3, IL-6, PCT and lactate was effective in predicting 28-days mortality with a good performance and better than SOFA score (100, 101). IL-6 alone, in combination with other molecules (102–104) or with neutrophil-to-lymphocyte ratio can be a marker of mortality in sepsis patients (74). Similarly, Matsumoto et al. suggested the involvement of a cytokine network including IL-6, IL-8, MCP-1 and IL-10 in the acute phase of sepsis and proposed the development of a combined score including IL-6 which is significantly correlated with prognosis (90). On the same line, our data argue in favor of the usefulness of testing a combination of multiple biomarkers to improve the prognostic capacity.

In multivariable Cox regression analysis, the combination of PTX3, urea, IL-6 and IL-18 levels with age showed the best prognostic value. Since this study includes a relatively low number of patients and death events, we ensured to select a parsimonious model with a very conservative threshold for significance ($p<0.005$). This model showed good internal calibration properties and could predict 90-days death significantly better than the SOFA score in our sample of patients, though these findings should be externally validated in an independent cohort in order to be generalizable.

Despite these limitations, these results could help to generate new hypotheses on the prognostic, but also etiological, role of IL-6 and IL-18 in sepsis. Similar to the study by Mierzchala-Pasierb et al. (105), we did not observe significant differences of IL-18 levels in survivors *vs.* non-survivors. However, both IL-18 and IL-6 were significant predictors of mortality in the full model. Additionally, when PTX3, urea levels and age were left unchanged, there was a highly significant interaction (positive synergistic effect) between IL-6 and IL-18, meaning there was a non-linear association between these two variables and 90-days mortality. This suggests that, although at low levels, IL-6 and IL-18 do not significantly affect the risk of mortality, thus, after a certain threshold, each increase becomes very importantly associated with the predicted mortality. This could perhaps be explained by the fact that IL-18 can induce the production of huge quantities of IL-6 from a variety of cell types through the activation of the NLRP3 inflammasome and caspase 1, effectively amplifying other pro-inflammatory signals (106). In our study, the variance of IL-18 values in sepsis patients was much lower (range from 6 pg/ml to about 2000 pg/ml) than what was observed for IL-6 (from 6 pg/ml to almost 1 million pg/ml). This may point toward a different magnitude of production of IL-6 in certain high-risk septic patients, in presence of relatively similar levels of IL-18. Further studies are necessary to characterize the physio-pathological role of these cytokines in sepsis patients.

Besides the aforementioned low number of participants, its monocentric nature, and the need for external validation, this study has other limitations. Patient demographics in our study cohort differed from other sepsis studies, including enrollment of patients at ED admission instead of later in the ICU setting. This adds novelty to our study, but also adds heterogeneity to our results. Some clinical data are missing for a fraction of patients, such as lactate and PCT levels, and we did not have other clinical scores, such as Simplified Acute Physiology Score (SAPS) II, SAPS III, and/or Acute Physiology and Chronic Health Evaluation II (APACHE II) scores. In our cohort, 31% of sepsis patients and 39% of septic shock patients had a malignancy as comorbidity, whereas many studies exclude malignancy-linked sepsis. However, we believe that considering all sepsis cases regardless of comorbidities could have added diagnostic value in the ED setting. Given the different comorbidities in our cohort of patients, the inflammatory markers such as CRP and PCT may be also influenced, potentially affecting the results; however, the reduction observed in patients after 5 days of hospitalization suggested that comorbidities had a limited impact on the overall inflammatory status of the patients. These preliminary results need to be confirmed with multicentric studies involving larger cohorts of patients. Overall, the increasing development of point-of-care testing systems for the rapid and accurate measurement of circulating molecules makes the evaluation of multiple soluble mediators feasible even in the emergency room (85, 86).

In conclusion, we concur with other reports that a combination of inflammatory mediators and clinical parameters can improve risk stratification of sepsis patients. Our data indicate that high levels of PTX3 in plasma of patients with suspected sepsis admitted to the emergency room can be used as a prognostic marker for risk stratification. In addition, measurement of PTX3 in combination with cytokine levels (IL-6 and IL-18), and other routine clinical parameters rapidly available in ED (e.g., age, urea), can provide a promising approach for 90-days mortality prediction for sepsis patients, better than the use of a single biomarker.

Data availability statement

The raw data supporting the conclusions of this article will be made available by the authors, without undue reservation.

Ethics statement

The studies involving human participants were reviewed and approved by the Institutional Review Board of Humanitas Hospital (Approval n° 820/18). The patients/participants provided their written informed consent to participate in this study.

Author contributions

SD, AV, AlbM, and BB made substantial contributions to the conception and design of the study; AD, AleM, DPv, CF, and DC collected patient samples and clinical data; SD, RL, MSi, SV and RS-G performed the experiments; SD, DP, SM, MSt and SB performed the data analyses; SD, DP, AD, SB, AV, AlbM, MSt and BB interpreted the results; SD, DP, AlbM, and BB wrote the paper. All authors were involved in the analysis and interpretation of data, drafting the manuscript and revising it critically, and approved the final version.

Funding

SD was supported by European Sepsis Academy/Innovative Training Networks (ESA/ITN) from the European Commission (H2020-MSCA-ITN-2015, Grant agreement Number: 676129). RS-G acknowledge financial support from Fundação para a Ciência e a Tecnologia (FCT) for Ph.D. grant PD/BD/114138/2016. This study has received funding from Associazione Italiana Ricerca sul Cancro (AIRC) [Special Program Metastatic disease: the key unmet need in oncology AIRC 5X1000 grant n° 21147 and "Regulatory pathways of myeloid cells, inflammation and cancer" grant IG-2019 N. 23465].

Acknowledgments

We thank all the physicians, nurses, and laboratory personnel of the Emergency Department and wards of Humanitas Research Hospital for their active collaboration. Also, a special thanks to all the patients who participated in this study.

Conflict of interest

AlbM and BB are inventors of a patent (EP20182181) on PTX3 and obtain royalties on related reagents.

The remaining authors declare that the research was conducted in the absence of any commercial or financial relationships that could be construed as a potential conflict of interest.

Publisher's note

Supplementary materials

The Supplementary Material for this article can be found online at: https://www.frontiersin.org/articles/10.3389/fimmu.2022.979232/full#supplementary-material.

References

1. Saeed K, Wilson DC, Bloos F, Schuetz P, van der Does Y, Melander O, et al. The early identification of disease progression in patients with suspected infection presenting to the emergency department: A multi-centre derivation and validation study. *Crit Care* (2019) 23(1):40. doi: 10.1186/s13054-019-2329-5

2. Kumar S, Tripathy S, Jyoti A, Singh SG. Recent advances in biosensors for diagnosis and detection of sepsis: A comprehensive review. *Biosens Bioelectron* (2019) 124-125:205–15. doi: 10.1016/j.bios.2018.10.034

3. Rudd KE, Johnson SC, Agesa KM, Shackelford KA, Tsoi D, Kievlan DR, et al. Global, regional, and national sepsis incidence and mortality, 1990-2017: Analysis for the global burden of disease study. *Lancet* (2020) 395(10219):200–11. doi: 10.1016/S0140-6736(19)32989-7

4. Cecconi M, Evans L, Levy M, Rhodes A. Sepsis and septic shock. *Lancet* (2018) 392(10141):75–87. doi: 10.1016/S0140-6736(18)30696-2

5. Ward NS, Levy MM. Sepsis: Definitions, pathophysiology and the challenge of bedside management. *Humana Press* (2019). doi: 10.1007/978-3-319-48470-9

6. Pierrakos C, Vincent JL. Sepsis biomarkers: A review. *Crit Care* (2010) 14(1): R15. doi: 10.1186/cc8872

7. Kyriazopoulou E, Giamarellos-Bourboulis EJ. Antimicrobial stewardship using biomarkers: Accumulating evidence for the critically ill. *Antibiot (Basel)* (2022) 11(3):367. doi: 10.3390/antibiotics11030367

8. van Engelen TSR, Wiersinga WJ, Scicluna BP, van der Poll T. Biomarkers in sepsis. *Crit Care Clin* (2018) 34(1):139–52. doi: 10.1016/j.ccc.2017.08.010

9. D'Onofrio V, Heylen D, Pusparum M, Grondman I, Vanwalleghem J, Meersman A, et al. A prospective observational cohort study to identify inflammatory biomarkers for the diagnosis and prognosis of patients with sepsis. *J Intensive Care* (2022) 10(1):13. doi: 10.1186/s40560-022-00602-x

10. Niederman MS, Baron RM, Bouadma L, Calandra T, Daneman N, DeWaele J, et al. Initial antimicrobial management of sepsis. *Crit Care* (2021) 25(1):307. doi: 10.1186/s13054-021-03736-w

11. Pierrakos C, Velissaris D, Bisdorff M, Marshall JC, Vincent JL. Biomarkers of sepsis: Time for a reappraisal. *Crit Care* (2020) 24(1):287. doi: 10.1186/s13054-020-02993-5

12. Mearelli F, Fiotti N, Giansante C, Casarsa C, Orso D, De Helmersen M, et al. Derivation and validation of a biomarker-based clinical algorithm to rule out sepsis from noninfectious systemic inflammatory response syndrome at emergency department admission: A multicenter prospective study. *Crit Care Med* (2018) 46(9):1421–9. doi: 10.1097/CCM.0000000000003206

13. Teggert A, Datta H, Ali Z. Biomarkers for point-of-Care diagnosis of sepsis. *Micromachines (Basel)* (2020) 11(3):286. doi: 10.3390/mi11030286

14. Kyriazopoulou E, Poulakou G, Giamarellos-Bourboulis EJ. Biomarkers in sepsis: Can they help improve patient outcome? *Curr Opin Infect Dis* (2021) 34 (2):126–34. doi: 10.1097/qco.0000000000000707

15. Gao L, Shi Q, Li H, Guo Q, Yan J, Zhou L. Prognostic value of the combined variability of mean platelet volume and neutrophil percentage for short-term

clinical outcomes of sepsis patients. *Postgrad Med* (2021) 133(6):604–12. doi: 10.1080/00325481.2020.1823137

16. Kim H, Hur M, Moon HW, Yun YM, Di Somma S, Network G. Multi-marker approach using procalcitonin, presepsin, galectin-3, and soluble suppression of tumorigenicity 2 for the prediction of mortality in sepsis. *Ann Intensive Care* (2017) 7(1):27. doi: 10.1186/s13613-017-0252-y

17. Shukeri W, Ralib AM, Abdulah NZ, Mat-Nor MB. Sepsis mortality score for the prediction of mortality in septic patients. *J Crit Care* (2018) 43:163–8. doi: 10.1016/j.jcrc.2017.09.009

18. Walborn A, Rondina M, Fareed J, Hoppensteadt D. Development of an algorithm to predict mortality in patients with sepsis and coagulopathy. *Clin Appl Thromb Hemost* (2020) 26:1076029620902849. doi: 10.1177/1076029620902849

19. Garlanda C, Bottazzi B, Bastone A, Mantovani A. Pentraxins at the crossroads between innate immunity, inflammation, matrix deposition, and female fertility. *Annu Rev Immunol* (2005) 23:337–66. doi: 10.1146/annurev.immunol.23.021704.115756

20. Garlanda C, Bottazzi B, Magrini E, Inforzato A, Mantovani A. Ptx3, a humoral pattern recognition molecule, in innate immunity, tissue repair, and cancer. *Physiol Rev* (2018) 98(2):623–39. doi: 10.1152/physrev.00016.2017

21. Bottazzi B, Doni A, Garlanda C, Mantovani A. An integrated view of humoral innate immunity: Pentraxins as a paradigm. *Annu Rev Immunol* (2010) 28:157–83. doi: 10.1146/annurev-immunol-030409-101305

22. Jeannin P, Bottazzi B, Sironi M, Doni A, Rusnati M, Presta M, et al. Complexity and complementarity of outer membrane protein a recognition by cellular and humoral innate immunity receptors. *Immunity* (2005) 22(5):551–60. doi: 10.1016/j.immuni.2005.03.008

23. Doni A, Musso T, Morone D, Bastone A, Zambelli V, Sironi M, et al. An acidic microenvironment sets the humoral pattern recognition molecule Ptx3 in a tissue repair mode. *J Exp Med* (2015) 212(6):905–25. doi: 10.1084/jem.20141268

24. Garlanda C, Riva F, Bonavita E, Gentile S, Mantovani A. Decoys and regulatory "Receptors" of the il-1/Toll-Like receptor superfamily. *Front Immunol* (2013) 4:180. doi: 10.3389/fimmu.2013.00180

25. Garlanda C, Riva F, Bonavita E, Mantovani A. Negative regulatory receptors of the il-1 family. *Semin Immunol* (2013) 25(6):408–15. doi: 10.1016/j.smim.2013.10.019

26. Molgora M, Supino D, Mantovani A, Garlanda C. Tuning inflammation and immunity by the negative regulators il-1r2 and il-1r8. *Immunol Rev* (2018) 281 (1):233–47. doi: 10.1111/imr.12609

27. Peters VA, Joesting JJ, Freund GG. Il-1 receptor 2 (Il-1r2) and its role in immune regulation. *Brain Behav Immun* (2013) 32:1–8. doi: 10.1016/j.bbi.2012.11.006

28. Slack JL, Schooley K, Bonnert TP, Mitcham JL, Qwarnstrom EE, Sims JE, et al. Identification of two major sites in the type I interleukin-1 receptor cytoplasmic region responsible for coupling to pro-inflammatory signaling pathways. *J Biol Chem* (2000) 275(7):4670–8. doi: 10.1074/jbc.275.7.4670

29. Muller B, Peri G, Doni A, Torri V, Landmann R, Bottazzi B, et al. Circulating levels of the long pentraxin Ptx3 correlate with severity of infection in critically ill patients. *Crit Care Med* (2001) 29(7):1404–7. doi: 10.1097/00003246-200107000-00017

30. Azzurri A, Sow OY, Amedei A, Bah B, Diallo S, Peri G, et al. Ifn-Gamma-Inducible protein 10 and pentraxin 3 plasma levels are tools for monitoring inflammation and disease activity in mycobacterium tuberculosis infection. *Microbes Infect* (2005) 7(1):1–8. doi: 10.1016/j.micinf.2004.09.004

31. Caironi P, Masson S, Mauri T, Bottazzi B, Leone R, Magnoli M, et al. Pentraxin 3 in patients with severe sepsis or shock: The albios trial. *Eur J Clin Invest* (2017) 47(1):73–83. doi: 10.1111/eci.12704

32. Mairuhu AT, Peri G, Setiati TE, Hack CE, Koraka P, Soemantri A, et al. Elevated plasma levels of the long pentraxin, pentraxin 3, in severe dengue virus infections. *J Med Virol* (2005) 76(4):547–52. doi: 10.1002/jmv.20397

33. Porte R, Davoudian S, Asgari F, Parente R, Mantovani A, Garlanda C, et al. The long pentraxin Ptx3 as a humoral innate immunity functional player and biomarker of infections and sepsis. *Front Immunol* (2019) 10:794. doi: 10.3389/fimmu.2019.00794

34. Hamed S, Behnes M, Pauly D, Lepiorz D, Barre M, Becher T, et al. Diagnostic value of pentraxin-3 in patients with sepsis and septic shock in accordance with latest sepsis-3 definitions. *BMC Infect Dis* (2017) 17(1):554. doi: 10.1186/s12879-017-2606-3

35. Jie H, Li Y, Pu X, Ye J. Pentraxin 3, a predicator for 28-day mortality in patients with septic shock. *Am J Med Sci* (2017) 353(3):242–6. doi: 10.1016/j.amjms.2017.01.003

36. Lee YT, Gong M, Chau A, Wong WT, Bazoukis G, Wong SH, et al. Pentraxin-3 as a marker of sepsis severity and predictor of mortality outcomes: A systematic review and meta-analysis. *J Infect* (2018) 76(1):1–10. doi: 10.1016/j.jinf.2017.10.016

37. Mauri T, Bellani G, Patroniti N, Coppadoro A, Peri G, Cuccovillo I, et al. Persisting high levels of plasma pentraxin 3 over the first days after severe sepsis and septic shock onset are associated with mortality. *Intensive Care Med* (2010) 36 (4):621–9. doi: 10.1007/s00134-010-1752-5

38. Chen H, Li T, Yan S, Liu M, Liu K, Zhang H, et al. Pentraxin-3 is a strong biomarker of sepsis severity identification and predictor of 90-day mortality in intensive care units *Via* sepsis 3.0 definitions. *Diagn (Basel)* (2021) 11(10):1906. doi: 10.3390/diagnostics11101906

39. Wang G, Jiang C, Fang J, Li Z, Cai H. Pentraxin-3 as a predictive marker of mortality in sepsis: An updated systematic review and meta-analysis. *Crit Care* (2022) 26(1):167. doi: 10.1186/s13054-022-04032-x

40. Uusitalo-Seppala R, Huttunen R, Aittoniemi J, Koskinen P, Leino A, Vahlberg T, et al. Pentraxin 3 (Ptx3) is associated with severe sepsis and fatal disease in emergency room patients with suspected infection: A prospective cohort study. *PloS One* (2013) 8(1):e53661. doi: 10.1371/journal.pone.0053661

41. Arend WP, Malyak M, Smith MFJr., Whisenand TD, Slack JL, Sims JE, et al. Binding of il-1 alpha, il-1 beta, and il-1 receptor antagonist by soluble il-1 receptors and levels of soluble il-1 receptors in synovial fluids. *J Immunol* (1994) 153 (10):4766–74.

42. Dinarello CA. Biologic basis for interleukin-1 in disease. *Blood* (1996) 87 (6):2095–147. doi: 10.1182/blood.V87.6.2095.bloodjournal8762095

43. Jouvenne P, Vannier E, Dinarello CA, Miossec P. Elevated levels of soluble interleukin-1 receptor type ii and interleukin-1 receptor antagonist in patients with chronic arthritis: Correlations with markers of inflammation and joint destruction. *Arthritis Rheum* (1998) 41(6):1083–9. doi: 10.1002/1529-0131(199806)41:6<1083::AID-ART15>3.0.CO;2-9

44. Muller B, Peri G, Doni A, Perruchoud AP, Landmann R, Pasqualini F, et al. High circulating levels of the il-1 type ii decoy receptor in critically ill patients with sepsis: Association of high decoy receptor levels with glucocorticoid administration. *J Leukoc Biol* (2002) 72(4):643–9. doi: 10.1189/jlb.72.4.643

45. van der Poll T, de Waal Malefyt R, Coyle SM, Lowry SF. Antiinflammatory cytokine responses during clinical sepsis and experimental endotoxemia: Sequential measurements of plasma soluble interleukin (Il)-1 receptor type ii, il-10, and il-13. *J Infect Dis* (1997) 175(1):118–22. doi: 10.1093/infdis/175.1.118

46. Giri JG, Wells J, Dower SK, McCall CE, Guzman RN, Slack J, et al. Elevated levels of shed type ii il-1 receptor in sepsis. potential role for type ii receptor in regulation of il-1 responses. *J Immunol* (1994) 153(12):5802–9.

47. Pruitt JH, Welborn MB, Edwards PD, Harward TR, Seeger JW, Martin TD, et al. Increased soluble interleukin-1 type ii receptor concentrations in postoperative patients and in patients with sepsis syndrome. *Blood* (1996) 87 (8):3282–8. doi: 10.1182/blood.V87.8.3282.bloodjournal8783282

48. van Deuren M, van der Ven-Jongekrijg J, Vannier E, van Dalen R, Pesman G, Bartelink AK, et al. The pattern of interleukin-1beta (Il-1beta) and its modulating agents il-1 receptor antagonist and il-1 soluble receptor type ii in acute meningococcal infections. *Blood* (1997) 90(3):1101–8. doi: 10.1182/blood.V90.3.1101

49. Pruitt JH, Copeland EM, Moldawer LL3rd. Interleukin-1 and interleukin-1 antagonism in sepsis, systemic inflammatory response syndrome, and septic shock. *Shock* (1995) 3(4):235–51. doi: 10.1097/00024382-199504000-00001

50. Hotchkiss RS, Karl IE. The pathophysiology and treatment of sepsis. *N Engl J Med* (2003) 348(2):138–50. doi: 10.1056/NEJMra021333

51. Seeley EJ, Bernard GR. Therapeutic targets in sepsis: Past, present, and future. *Clin Chest Med* (2016) 37(2):181–9. doi: 10.1016/j.ccm.2016.01.015

52. van der Poll T, Opal SM. Host-pathogen interactions in sepsis. *Lancet Infect Dis* (2008) 8(1):32–43. doi: 10.1016/S1473-3099(07)70265-7

53. Chousterman BG, Swirski FK, Weber GF. Cytokine storm and sepsis disease pathogenesis. *Semin Immunopathol* (2017) 39(5):517–28. doi: 10.1007/s00281-017-0639-8

54. Grobmyer SR, Lin E, Lowry SF, Rivadeneira DE, Potter S, Barie PS, et al. Elevation of il-18 in human sepsis. *J Clin Immunol* (2000) 20(3):212–5. doi: 10.1023/a:1006641630904

55. Friedman G, Jankowski S, Marchant A, Goldman M, Kahn RJ, Vincent JL. Blood interleukin 10 levels parallel the severity of septic shock. *J Crit Care* (1997) 12 (4):183–7. doi: 10.1016/s0883-9441(97)90030-7

56. Gardlund B, Sjolin J, Nilsson A, Roll M, Wickerts CJ, Wretlind B. Plasma levels of cytokines in primary septic shock in humans: Correlation with disease severity. *J Infect Dis* (1995) 172(1):296–301. doi: 10.1093/infdis/172.1.296

57. Gogos CA, Drosou E, Bassaris HP, Skoutelis A. Pro- versus anti-inflammatory cytokine profile in patients with severe sepsis: A marker for prognosis and future therapeutic options. *J Infect Dis* (2000) 181(1):176–80. doi: 10.1086/315214

58. van Dissel JT, van Langevelde P, Westendorp RG, Kwappenberg K, Frolich M. Anti-inflammatory cytokine profile and mortality in febrile patients. *Lancet* (1998) 351(9107):950–3. doi: 10.1016/S0140-6736(05)60606-X

59. Ertel W, Kremer JP, Kenney J, Steckholzer U, Jarrar D, Trentz O, et al. Downregulation of proinflammatory cytokine release in whole blood from septic patients. *Blood* (1995) 85(5):1341–7. doi: 10.3171/jns.1990.72.4.0572

60. Rigato O, Salomao R. Impaired production of interferon-gamma and tumor necrosis factor-alpha but not of interleukin 10 in whole blood of patients with sepsis. *Shock* (2003) 19(2):113–6. doi: 10.1097/00024382-200302000-00004

61. Sinistro A, Almerighi C, Ciaprini C, Natoli S, Sussarello E, Di Fino S, et al. Downregulation of Cd40 ligand response in monocytes from sepsis patients. *Clin Vaccine Immunol* (2008) 15(12):1851–8. doi: 10.1128/CVI.00184-08

62. Weighardt H, Heidecke CD, Emmanuilidis K, Maier S, Bartels H, Siewert JR, et al. Sepsis after major visceral surgery is associated with sustained and interferon-Gamma-Resistant defects of monocyte cytokine production. *Surgery* (2000) 127 (3):309–15. doi: 10.1067/msy.2000.104118

63. Oberholzer A, Souza SM, Tschoeke SK, Oberholzer C, Abouhamze A, Pribble JP, et al. Plasma cytokine measurements augment prognostic scores as indicators of outcome in patients with severe sepsis. *Shock* (2005) 23(6):488–93. doi: 10.1097/01.shk.0000163802.46355.59

64. Pinsky MR, Vincent JL, Deviere J, Alegre M, Kahn RJ, Dupont E. Serum cytokine levels in human septic shock. relation to multiple-system organ failure and mortality. *Chest* (1993) 103(2):565–75. doi: 10.1378/chest.103.2.565

65. Singer M, Deutschman CS, Seymour CW, Shankar-Hari M, Annane D, Bauer M, et al. The third international consensus definitions for sepsis and septic shock (Sepsis-3). *JAMA* (2016) 315(8):801–10. doi: 10.1001/jama.2016.0287

66. Knoflach M, Kiechl S, Mantovani A, Cuccovillo I, Bottazzi B, Xu Q, et al. Pentraxin-3 as a marker of advanced atherosclerosis results from the bruneck, army and arfy studies. *PloS One* (2012) 7(2):e31474. doi: 10.1371/journal.pone.0031474

67. Royston P, Sauerbrei W. *Multivariable model - building: A pragmatic approach to regression anaylsis based on fractional polynomials for modelling continuous variables*. Chichester, England: John Wiley & Sons (2008).

68. Moons KG, Altman DG, Reitsma JB, Collins GS. New guideline for the reporting of studies developing, validating, or updating a prediction model. *Clin Chem* (2015) 61(3):565–6. doi: 10.1373/clinchem.2014.237883

69. Gronnesby JK, Borgan O. A method for checking regression models in survival analysis based on the risk score. *Lifetime Data Anal* (1996) 2(4):315–28. doi: 10.1007/BF00127305

70. Hothorn T, Lausen B. On the exact distribution of maximally selected rank statistics. *Comput Stat Data Anal* (2003) 43(2):121–37. doi: 10.1016/S0167-9473 (02)00225-6

71. Kamarudin AN, Cox T, Kolamunnage-Dona R. Time-dependent roc curve analysis in medical research: Current methods and applications. *BMC Med Res Methodol* (2017) 17(1):53. doi: 10.1186/s12874-017-0332-6

72. Henriquez-Camacho C, Losa J. Biomarkers for sepsis. *BioMed Res Int* (2014) 2014:547818. doi: 10.1155/2014/547818

73. So-Ngern A, Leelasupasri S, Chulavatnatol S, Pummangura C, Bunupuradah P, Montakantikul P. Prognostic value of serum procalcitonin level for the diagnosis of bacterial infections in critically-ill patients. *Infect Chemother* (2019) 51(3):263–73. doi: 10.3947/ic.2019.51.3.263

74. Liu B, Chen YX, Yin Q, Zhao YZ, Li CS. Diagnostic value and prognostic evaluation of presepsin for sepsis in an emergency department. *Crit Care* (2013) 17 (5):R244. doi: 10.1186/cc13070

75. Niederman MS. Biological markers to determine eligibility in trials for community-acquired pneumonia: A focus on procalcitonin. *Clin Infect Dis* (2008) 47(Supplement_3):S127–S32. doi: 10.1086/591393

76. Petrovic J, Turnic TN, Zivkovic V, Andjic M, Draginic N, Stojanovic A, et al. Correlation of redox status with procalcitonin and c-reactive protein in septic patients. *Oxid Med Cell Longev* (2020) 2020:5147364. doi: 10.1155/2020/5147364

77. Gruyters I, De Ridder T, Bruckers L, Geebelen L, Gharmaoui S, Callebaut I, et al. Predictive value of serial evaluation of the sequential organ failure assessment (Sofa) score for intensive care unit mortality in critically ill patients with covid-19: A retrospective cohort study. *Anaesthesiol Intensive Ther* (2022) 54(1):3–11. doi: 10.5114/ait.2022.114048

78. Vincent JL, de Mendonça A, Cantraine F, Moreno R, Takala J, Suter PM, et al. Use of the sofa score to assess the incidence of organ Dysfunction/Failure in intensive care units: Results of a multicenter, prospective study. working group on "Sepsis-related problems" of the European society of intensive care medicine. *Crit Care Med* (1998) 26(11):1793–800. doi: 10.1097/00003246-199811000-00016

79. Dellinger RP, Levy MM, Rhodes A, Annane D, Gerlach H, Opal SM, et al. Surviving sepsis campaign: International guidelines for management of severe sepsis and septic shock, 2012. *Intensive Care Med* (2013) 39(2):165–228. doi: 10.1007/s00134-012-2769-8

80. Mouncey PR, Osborn TM, Power GS, Harrison DA, Sadique MZ, Grieve RD, et al. Trial of early, goal-directed resuscitation for septic shock. *N Engl J Med* (2015) 372(14):1301–11. doi: 10.1056/NEJMoa1500896

81. Levy MM, Evans LE, Rhodes A. The surviving sepsis campaign bundle: 2018 update. *Crit Care Med* (2018) 46(6):997–1000. doi: 10.1097/CCM.0000000000003119

82. Simpson SQ. Sepsis biomarkers and physician judgment in the emergency room. *Crit Care Med* (2019) 47(11):1656–7. doi: 10.1097/CCM.0000000000003983

83. Bloos F, Ruddel H, Thomas-Ruddel D, Schwarzkopf D, Pausch C, Harbarth S, et al. Effect of a multifaceted educational intervention for anti-infectious measures on sepsis mortality: A cluster randomized trial. *Intensive Care Med* (2017) 43(11):1602–12. doi: 10.1007/s00134-017-4782-4

84. Albert Vega C, Mommert M, Boccard M, Rimmele T, Venet F, Pachot A, et al. Source of circulating pentraxin 3 in septic shock patients. *Front Immunol* (2018) 9:3048. doi: 10.3389/fimmu.2018.03048

85. Bonavia AS, Samuelsen A, Chroneos ZC, Halstead ES. Comparison of rapid cytokine immunoassays for functional immune phenotyping. *Front Immunol* (2022) 13:940030. doi: 10.3389/fimmu.2022.940030

86. Bottazzi B, Fornasari L, Frangolho A, Giudicatti S, Mantovani A, Marabelli F, et al. Multiplexed label-free optical biosensor for medical diagnostics. *J BioMed Opt* (2014) 19(1):17006. doi: 10.1117/1.JBO.19.1.017006

87. Hotchkiss RS, Monneret G, Payen D. Sepsis-induced immunosuppression: From cellular dysfunctions to immunotherapy. *Nat Rev Immunol* (2013) 13 (12):862–74. doi: 10.1038/nri3552

88. Xiao H, Siddiqui J, Remick DG. Mechanisms of mortality in early and late sepsis. *Infect Immun* (2006) 74(9):5227–35. doi: 10.1128/IAI.01220-05

89. Rubio I, Osuchowski MF, Shankar-Hari M, Skirecki T, Winkler MS, Lachmann G, et al. Current gaps in sepsis immunology: New opportunities for translational research. *Lancet Infect Dis* (2019) 19(12):e422–e36. doi: 10.1016/s1473-3099(19)30567-5

90. Matsumoto H, Ogura H, Shimizu K, Ikeda M, Hirose T, Matsuura H, et al. The clinical importance of a cytokine network in the acute phase of sepsis. *Sci Rep* (2018) 8(1):13995. doi: 10.1038/s41598-018-32275-8

91. Emmanuilidis K, Weighardt H, Matevossian E, Heidecke CD, Ulm K, Bartels H, et al. Differential regulation of systemic il-18 and il-12 release during postoperative sepsis: High serum il-18 as an early predictive indicator of lethal outcome. *Shock* (2002) 18(4):301–5. doi: 10.1097/00024382-200210000-00002

92. Tschoeke SK, Oberholzer A, Moldawer LL. Interleukin-18: A novel prognostic cytokine in bacteria-induced sepsis. *Crit Care Med* (2006) 34 (4):1225–33. doi: 10.1097/01.CCM.0000208356.05575.16

93. Eidt MV, Nunes FB, Pedrazza L, Caeran G, Pellegrin G, Melo DA, et al. Biochemical and inflammatory aspects in patients with severe sepsis and septic shock: The predictive role of il-18 in mortality. *Clin Chim Acta* (2016) 453:100–6. doi: 10.1016/j.cca.2015.12.009

94. De la Fuente M, MacDonald TT, Hermoso MA. The il-33/St2 axis: Role in health and disease. *Cytokine Growth Factor Rev* (2015) 26(6):615–23. doi: 10.1016/j.cytogfr.2015.07.017

95. Dinarello CA, Novick D, Kim S, Kaplanski G. Interleukin-18 and il-18 binding protein. *Front Immunol* (2013) 4:289. doi: 10.3389/fimmu.2013.00289

96. Novick D, Schwartsburd B, Pinkus R, Suissa D, Belzer I, Sthoeger Z, et al. A novel il-18bp Elisa shows elevated serum il-18bp in sepsis and extensive decrease of free il-18. *Cytokine* (2001) 14(6):334–42. doi: 10.1006/cyto.2001.0914

97. Krychtiuk KA, Stojkovic S, Lenz M, Brekalo M, Huber K, Wojta J, et al. Predictive value of low interleukin-33 in critically ill patients. *Cytokine* (2018) 103:109–13. doi: 10.1016/j.cyto.2017.09.017

98. Kyriakoudi A, Rovina N, Koltsida O, Kostakou E, Konstantelou E, Kardara M, et al. Weaning failure in critically ill patients is related to the persistence of sepsis inflammation. *Diagnostics* (2022) 12:92. doi: 10.3390/diagnostics12010092

99. Faix JD. Biomarkers of sepsis. *Crit Rev Clin Lab Sci* (2013) 50(1):23–36. doi: 10.3109/10408363.2013.764490

100. Song J, Moon S, Park DW, Cho HJ, Kim JY, Park J, et al. Biomarker combination and sofa score for the prediction of mortality in sepsis and septic shock: A prospective observational study according to the sepsis-3 definitions. *Med (Baltimore)* (2020) 99(22):e20495. doi: 10.1097/MD.0000000000020495

101. Song J, Park DW, Moon S, Cho HJ, Park JH, Seok H, et al. Diagnostic and prognostic value of interleukin-6, pentraxin 3, and procalcitonin levels among sepsis and septic shock patients: A prospective controlled study according to the sepsis-3 definitions. *BMC Infect Dis* (2019) 19(1):968. doi: 10.1186/s12879-019-4618-7

102. Friedland JS, Porter JC, Daryanani S, Bland JM, Screaton NJ, Vesely MJ, et al. Plasma proinflammatory cytokine concentrations, acute physiology and chronic health evaluation (Apache) iii scores and survival in patients in an

intensive care unit. *Crit Care Med* (1996) 24(11):1775–81. doi: 10.1097/00003246-199611000-00003

103. Hack CE, De Groot ER, Felt-Bersma RJ, Nuijens JH, Strack Van Schijndel RJ, Eerenberg-Belmer AJ, et al. Increased plasma levels of interleukin-6 in sepsis. *Blood* (1989) 74(5):1704–10. doi: 10.1182/blood.V74.5.1704.1704

104. Jiang Y, Jiang FQ, Kong F, An MM, Jin BB, Cao D, et al. Inflammatory anemia-associated parameters are related to 28-day mortality in patients with sepsis admitted to the icu: A preliminary observational study. *Ann Intensive Care* (2019) 9(1):67. doi: 10.1186/s13613-019-0542-7

105. Mierzchala-Pasierb M, Krzystek-Korpacka M, Lesnik P, Adamik B, Placzkowska S, Serek P, et al. Interleukin-18 serum levels in sepsis: Correlation with disease severity and inflammatory markers. *Cytokine* (2019) 120:22–7. doi: 10.1016/j.cyto.2019.04.003

106. Ridker PM, MacFadyen JG, Thuren T, Libby P. Residual inflammatory risk associated with interleukin-18 and interleukin-6 after successful interleukin-1beta inhibition with canakinumab: Further rationale for the development of targeted anti-cytokine therapies for the treatment of atherothrombosis. *Eur Heart J* (2020) 41(23):2153–63. doi: 10.1093/eurheartj/ehz542

frontiers | Frontiers in Immunology

TYPE Original Research
PUBLISHED 06 September 2023
DOI 10.3389/fimmu.2023.1250488

OPEN ACCESS

EDITED BY
Gabor Laszlo Kovacs,
University of Pécs, Hungary

REVIEWED BY
Tamás Kőszegi,
Pécs University, Hungary
Raj Raghupathy,
Kuwait University, Kuwait

*CORRESPONDENCE
Izabela Nowak
izabela.nowak@hirszfeld.pl

RECEIVED 30 June 2023
ACCEPTED 23 August 2023
PUBLISHED 06 September 2023

CITATION
Piekarska K, Dratwa M, Radwan P, Radwan M, Bogunia-Kubik K and Nowak I (2023) Pro- and anti-inflammatory cytokines and growth factors in patients undergoing *in vitro* fertilization procedure treated with prednisone. *Front. Immunol.* 14:1250488. doi: 10.3389/fimmu.2023.1250488

Pro- and anti-inflammatory cytokines and growth factors in patients undergoing *in vitro* fertilization procedure treated with prednisone

Karolina Piekarska[1], Marta Dratwa[2], Paweł Radwan[3], Michał Radwan[3,4], Katarzyna Bogunia-Kubik[2] and Izabela Nowak[1]*

[1]Laboratory of Immunogenetics and Tissue Immunology, Department of Clinical Immunology, Hirszfeld Institute of Immunology and Experimental Therapy, Polish Academy of Sciences, Wrocław, Poland, [2]Laboratory of Clinical Immunogenetics and Pharmacogenetics, Department of Clinical Immunology, Hirszfeld Institute of Immunology and Experimental Therapy, Polish Academy of Sciences, Wrocław, Poland, [3]Department of Reproductive Medicine, Gameta Hospital, Rzgów, Poland, [4]Faculty of Health Sciences, The Mazovian Academy in Plock, Płock, Poland

Embryo implantation is a key moment in pregnancy. Abnormal production of pro- and anti-inflammatory cytokines, their receptors and other immune factors may result in embryo implantation failure and pregnancy loss. The aim of this study was to determine the profile of selected pro- and anti-inflammatory factors in the blood plasma of patients undergoing *in vitro* fertilization (IVF) and control women who achieved pregnancy after natural conception. The examined patients were administered steroid prednisone. We present results concern the plasma levels of IFN-ɣ, BDNF, LIF, VEGF-A, sTNFR1 and IL-10. We found that IVF patients receiving steroids differed significantly from patients who were not administered such treatment in terms of IFN-γ and IL-10 levels. Moreover, IVF patients differed in secretion of all tested factors with the fertile controls. Our results indicated that women who secrete at least 1409 pg/ml of sTNFR1 have a chance to become pregnant naturally and give birth to a child, while patients after IVF must achieve a concentration of 962.3 pg/ml sTNFR1 in blood plasma for successful pregnancy. In addition, IVF patients secreting VEGF-A above 43.28 pg/ml have a greater risk of miscarriage or a failed transfer in comparison to women secreting below this value. In conclusion, fertile women present a different profile of pro- and anti-inflammatory cytokines, and growth factors compared to patients with recurrent implantation failure (RIF).

KEYWORDS

***in vitro* fertilization embryo transfer, recurrent implantation failure, cytokines, proinflammatory, anti-inflammatory**

1 Introduction

Embryo implantation is a crucial process in the development and maintenance of a pregnancy. It begins with blastocyst adhesion to the surface of the uterus. Trophoblast cells, derived from the trophectoderm, form columns of anchoring villi and differentiate into syncytiotrophoblast and extravillous trophoblast (EVT). Furthermore, extravillous trophoblast migrate to the maternal uterus and develop into a placenta (1, 2). Implantation failure may occur during early stages of embryo development. Inability to naturally conceive is the primary reason behind couples using assisted reproductive techniques (ART). Despite significant advances in ART, such as *in vitro* fertilization (IVF), women undergoing these procedures experience recurrent implantation failure (RIF) (3, 4). The exact definition of RIF is difficult to determine, but most clinicians define RIF as a failure to achieve a pregnancy after three subsequent IVF cycles in which four good-quality embryos are transferred into women under the age 40 years (4–6). The pathogenesis of recurrent embryo implantation failure is ambiguous. There are many risk factors that may contribute to RIF, with the primary causes being maternal, male or embryo factors (4). During pregnancy the immune system has the dual purpose to protect the mother and the developing fetus against pathogens while also allowing tolerance for the semi-allogenic fetus, which expresses antigens from both the mother and the father. During trophoblast invasion and at birth, the decidua is dominated by pro-inflammatory factors, while anti-inflammatory factors are dominant in the second and third trimesters of pregnancy to facilitate fetal growth (7, 8).

Cytokines mediate signals between the endometrium during embryo implantation and throughout pregnancy. They may promote trophoblast invasion and placental formation. Maintaining the right balance between pro-inflammatory and anti-inflammatory cytokines is essential for pregnancy development and disorders or infections can alter cytokine expression (9). Cytokines can be secreted by endometrial cells and by immune system cells recruited into the uterus to the site of implantation. They are mostly uterine natural killer cells, macrophages, and dendritic cells (10–14). T cells also exhibit complex and variable cytokine production. Th1 cells are mainly involved in the elimination of cells infected with viruses and intracellular pathogens. Th1 cytokines (considered as pro-inflammatory) include interferon-ɣ (IFN-ɣ), tumor necrosis factor-α (TNF-α) and the interleukins: IL-1, IL-2, IL-12, IL-15, IL-18 (15, 16). Th1 cytokines predominate during the early stages of implantation and are thought to promote trophoblast invasion. Higher levels of TNF-α before embryo transfer have been shown to be associated with clinical pregnancy in RIF patients, emphasizing that pro-inflammatory factors are needed for embryo implantation (17, 18). However, studies concerning TNF-α are ambiguous because a meta-analysis performed by Zhang et al. showed an increased level of this cytokine in patients with recurrent spontaneous miscarriage in comparison to the controls (19). TNF-α works by binding to the TNF-α receptors (TNFR1 and TNFR2). Moreover, TNF receptors (TNFR1 and also TNFR2) expressed on trophoblasts may play a role in regulating development of fetus in pregnancy (20–22). After embryo implantation, in the second trimester of pregnancy, a noticeable shift occurs and the Th2 (anti-inflammatory) cytokines begin to predominate in the uterus, these include: IL-4, IL-5, IL-10, IL-13 and granulocyte-macrophage colony-stimulating factor (GM-CSF). Th2 cytokines are responsible for fetal growth and maintenance of the pregnancy. The prevalence of the Th1 response over Th2 may be associated with various complications of pregnancy, for example recurrent miscarriages, pre-eclampsia and embryo implantation failure after *in vitro* fertilization (9, 23–25). In the third trimester of pregnancy, the Th1 inflammatory response returns. Of great importance in this phase is the infiltration of immune cells into the myometrium, which supports uterine contractions, labor and placental separation (10, 26).

Cytokines may have an effect on endometrial decidualization. This is the process of endometrial stromal cell differentiation into specialized decidual cells that create the lining for the implanting embryo. Cytokines promote blood vessel formation and increase blood flow in the decidua. Uterine NK cells (uNK) are capable of secreting angiogenic factors such as vascular endothelial growth factor (VEGF) and placental growth factor (PlGF) (27). PlGF may have both a pro-angiogenic or anti-angiogenic effect, therefore effective decidualization requires the appropriate expression levels of this factor (28). VEGF can regulate the proliferation and survival of endothelial cells and increases the permeability of blood vessels. Therefore, VEGF supports the differentiation of trophoblast cells and is responsible for angiogenesis in the decidua (28, 29). It is reported that VEGF-A is the most important and potent factor in angiogenesis (30). Brain-derived neurotrophic factor (BDNF), which belongs to the neurotrophin family, is involved in the proliferation, differentiation and survival of neuronal cells. BDNF also plays a role in placental development, differentiation and proliferation of trophoblasts (31). Reduced circulating levels of BDNF in the sera of women undergoing IVF were probably associated with adverse peri- and/or post-implantation events and subsequent pregnancy failure (32).

A significant role in embryo implantation may also be played by leukemia inhibitory factor (LIF). It is expressed in the endometrium at the time of implantation by uNK cells and its receptor is located both in the endometrium and on the trophoblast (33, 34). By regulating prostaglandin synthesis, LIF may affect embryo implantation and decidualization. Studies have shown that LIF can enhance the expression of human leukocyte antigen (HLA-G) in choriocarcinoma cell line JEG3, used as a model for trophoblasts (35). This induction occurred in the presence of endoplasmic reticulum aminopeptidase-1 (ERAP1), which is involved in HLA class I antigenic peptide presentation through the trimming peptides to their optimal length.

Pro-inflammatory and anti-inflammatory cytokines and cytokine receptor profiles may change in the plasma of patients before and after the *in vitro* fertilization procedure. Abnormal production of cytokines and other immune factors may result in embryo implantation failure and pregnancy loss. Measurement of the level of these factors in the plasma of patients undergoing IVF before and after the procedure may potentially be useful and have

prognostic value in the diagnosis of RIF. Therefore, the aim of this study was to determine the immunological profile of pro- and anti-inflammatory cytokines in the blood plasma of patients undergoing *in vitro* fertilization before and after embryo transfer and control women who achieved pregnancy after natural conception. We investigated plasma levels of IFN-ɣ, GM-CSF, TNF-α, PlGF, BDNF, LIF, VEGF-A, VEGF-D, TNFR1 and interleukins: IL-10, IL-4, IL-6. The patients under examination were administered the steroid prednisone, which prompted our novel investigation into the influence of steroids on the secretion of specific cytokines.

2 Materials and methods

2. 1 Study design

One hundred eighty-seven patients were involved in this study (age range: 22-46), all underwent *in vitro* fertilization embryo transfer. Patients were enrolled into the study in years 2015 to 2020. They were qualified at the Gameta Assisted Reproduction Clinic in Rzgów, a centre certified by the European Society for Human Reproduction and Embryology (ESHRE ART Centre Certification for good clinical practice) and at the Department of Surgical, Endoscopic and Oncologic Gynecology, Department of Gynecology and Gynecologic Oncology, Polish Mothers' Memorial Hospital–Research Institute. Patients underwent an average 3 unsuccessful transfers and each had 3 good quality embryos transferred. In 67 patients (35.82%) IVF was indicated due to male only fertility factors, while female factors accounted for 45 patients (24.06%). Twenty-eight patients (14.97%) were infertile due to male and female factors, while idiopathic infertility was found in 47 patients (25.13%).

Eighty-seven percent of all patients (164 women) were administered prednisone. In the standard IVF procedure, patients were instructed to take 5 mg of prednisone on a routine basis (Encorton, Adamed, Poland) once a day in the morning orally, starting from the day of embryo transfer (ET/frozen ET). Patients with RIF received higher doses of prednisone (10–20 mg) for 2–3 weeks before ET and up to 8 weeks if pregnancy developed after transfer. Among those patients taking prednisone, 85 women achieved clinical pregnancy, 42 women experienced a miscarriage and in the case of 37 patients the embryo transfer resulted in a lack of pregnancy.

In order to supplement the luteal phase, all patients were intravaginally administered 2 × 200 mg micronized progesterone (Luteina, Adamed, Poland) and oral dydrogesterone 3 × 10 mg (Duphaston, Solvay Pharmaceuticals, Netherlands) until 12 weeks of gestation. Detailed information on the preparation of patients for IVF [ovarian stimulation, fertilization procedure, assessment of endometrial thickness for initiation progesterone supplementation and frozen ET (FET)] has been described in an earlier by Nowak et al. (36).

The fertile control group was recruited from the Institute of Immunology and Experimental Therapy of the Polish Academy of Sciences in the years 2018-2020. This group consisted of 67 healthy women (age range: 19–68) with at least 1 healthy-born child after natural conception and no history of miscarriage or endocrinological or immunological diseases, except five women, who had hypothyroidism. Among fertile control, we had samples from 27 pregnant women from natural conception. The gestational age of these women was from 6 to 37 weeks at the moment of blood donation. None of the fertile control patients were administered any steroid treatment.

All tested patients were of Polish origin. Experiments were carried out after obtaining the approval of the Ethics Committee of the Polish Mothers' Memorial Hospital–Research Institute in Łódź (No: 25/2019). The necessary consent was obtained from all individual participants. IVF patients differed significantly in mean

TABLE 1 Characteristics of patients and the fertile control groups.

Parameter		IVF	Fertile control	Fertile pregnant control
Number of women		N = 187	N = 40	N = 27
Age of women	Mean ± SD	32.99 ± 4.15	32.93 ± 6.03	31.69 ± 5.13
	Range	22-46	22-68	19-42
Indications for IVF-ET (%)	Male only factor	67 (35.82)	–	–
	Female only factor	45 (24.06)	–	–
	Both factors	28 (14.97)	–	–
	Unknown factor	47 (25.13)	–	–
Number of IVF-ET in all cycles	Mean ± SD	3.08 ± 0.15	–	–
	Range	1-11	–	–
Number of embryos in all cycles	Mean ± SD	3.39 ± 2.38	–	–
	Range	1-13	–	–

age from fertile women (p = 0.0414). The clinical characteristics of patients and fertile women are described in Table 1.

2.2 Measurement of pro- and anti-inflammatory cytokines and growth factors levels in plasma

Plasma samples from patients were taken before and after IVF-ET [at the moment of testing for beta-subunit of human chorionic gonadotropin (β-hCG)] between 11 and 15 days following the ET date) and also from fertile women. Samples were stored at -80 °C until the time of assay. Plasma levels of GM-CSF, IFN-ɣ, IL-10, IL-4, TNF-α (pg/ml) were detected by Human ProcartaPlex High Sensitivity assay (Thermo Fisher Scientific, USA) using the Luminex 200 system (Luminex Corp., USA). Concentrations of BDNF, IL-6, PlGF, LIF, TNF-R1, VEGF-A, VEGF-D (pg/ml) were measured by the commercial Human ProcartaPlex assay (Thermo Fisher Scientific, USA) also using the Luminex 200 system (Luminex Corp., USA). All measurements were performed following the protocol of the manufacturer. Luminex technology is based on colored magnetic microspheres coated with antibodies that capture specific analytes in a multiplex ELISA. The median fluorescence intensity was compared to the standard curve to calculate the analyte concentration in pg/mL with xPonent 4.2 software. Standard curves for each analyte were generated using the premixed lyophilized standards provided in the kits. Serial 4-fold dilutions of the standards were run to generate a 7-standard concentration set, and the diluent alone was used as a blank. The analyte concentrations in the samples were determined from the standard curve using a 5-parameter logistic fit curve to transform the mean fluorescence intensities into concentrations. There is a different detection range for each analyte. Standard curves measured the concentration were: for IFN-ɣ from 1.44 to 5900 pg/ml, for IL-10 from 0.19 to 765 pg/ml, for BDNF from 1.71 to 7000 pg/ml, for LIF from 11.06 to 45300 pg/ml, for TNFR1 from 158.96 to 651100 pg/ml, for VEGF-A from 5.49 to 22500 pg/ml.

2.3 Statistical analysis

To assess the differences in the concentration of the selected cytokines and growth factors in patient plasma before and after ET, the Mann–Whitney test was performed (GraphPad Prism 5 software). The normality of the data distributions was assessed by the D'Agostino-Pearson test. Statistical significance was considered as p value < 0.05. All parameters of statistical analyses (numbers, medians, means, standard deviation and errors, min, max and 25-75% percentiles) are part of Supplementary Tables 1-12. Results of the statistical analysis referring to cytokines and growth factors such as GM-CSF, IL-4, TNF-α, IL-6, PlGF and VEGF-D failed to yield any conclusions due to undetectable levels of cytokines. The median fluorescence intensities of tested analytes were not intensive enough to calculate their concentration. Therefore they were omitted from this manuscript.

3 Results

3.1 Secretion of IFN-ɣ in patients and the fertile control groups

We found that IVF patients who were prescribed steroids differed significantly from patients who were not. IVF patients without steroid treatment had higher levels of IFN-ɣ before and after ET in comparison to patients receiving steroid treatment (p = 0.0005, median 0.28 vs. 0.00 pg/ml and p < 0.0001, median 0.26 vs. 0.00 pg/ml, respectively; Figure 1A; Supplementary Table 1). Fertile women who had given birth in the past and women who were pregnant at the time of blood collection differed in terms of IFN-ɣ concentrations compared to IVF patients taking prednisone before and after ET (p < 0.0001 for comparisons with IVF steroid treatment patients, median 0.29 vs. 0.00 pg/ml before and after ET, median 0.28 vs. 0.00 pg/ml before and after ET). IVF women untreated with steroid secreted less IFN-ɣ after ET than fertile women and fertile pregnant women (p = 0.0041, median 0.26 vs. 0.29 pg/ml and p = 0.0148, median 0.26 vs. 0.28 pg/ml, respectively).

IVF patients taking prednisone, the overwhelming majority, did not secrete IFN-ɣ (all medians 0.000 pg/ml), therefore we only found statistically significant differences between those patients and women from control groups (median 0.29 and 0.28 pg/ml). The concentration of IFN-ɣ measured before and after ET differed in patients who became pregnant and fertile women who had given birth in the past and pregnant control (p < 0.0001 for both patient groups before and after ET; Figure 1B; Supplementary Table 2). We observed the same differences (p < 0.0001 or p = 0.0002) in the analysis of patients who experienced a lack of pregnancy or had miscarriages and women from the control groups.

3.2 IL-10 secretion in IVF patients and the fertile control groups

We observed that patients undergoing steroid treatment secreted significantly more IL-10 into plasma than patients without steroid treatment (p = 0.0063, median 0.31 vs. 0.05 pg/ml before ET; p = 0.0007, median 0.34 vs. 0.04 pg/ml after ET; Figure 2A; Supplementary Table 3). Most fertile women did not secrete IL-10 (median 0.00 pg/ml) and they differed to IVF patients receiving steroid treatment and those without in terms of IL-10 plasma levels (for patients with steroid treatment: p = 0.0027, median 0.00 vs. 0.05 pg/ml before ET, p = 0.009, median 0.00 vs. 0.04 pg/ml after ET; for patients without steroid treatment: p < 0.0001, median 0.00 vs. 0.31 pg/ml before ET; p < 0.0001, median 0.00 vs. 0.34 pg/ml after ET).

The concentration of IL-10 measured before and after ET did not differ in IVF women using steroid and achieved pregnancy (median 0.34 pg/ml before and 0.35 pg/ml after ET) and patients who experienced a lack of pregnancy (median 0.24 pg/ml before and 0.50 pg/ml after ET) or patients who experienced a miscarriage (median 0.30 pg/ml before and 0.24 pg/ml after ET) (Figure 2B;

10.3389/fimmu.2023.1250488

Supplementary Table 4). However, we noticed a decreased level of IL-10 in women who conceived naturally and gave birth to a child (median 0.00 pg/ml). The difference in concentrations between the fertile controls and all these patients was $p < 0.0001$, both before and after embryo transfer (Figure 2B; Supplementary Table 4).

3.3 Secretion of BDNF in IVF patients and the fertile control groups

We found no significant differences between patients who received steroid treatment and patients who did not in terms of

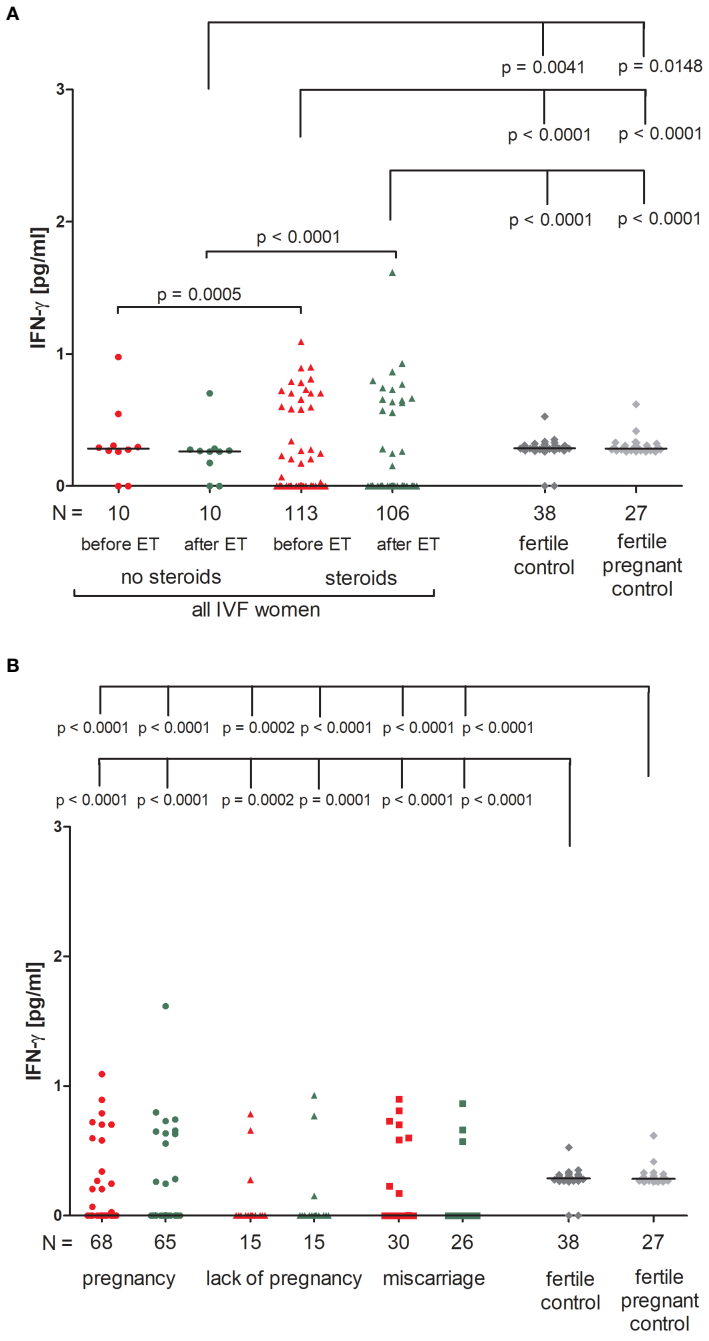

FIGURE 1
Concentration of plasma IFN-ɣ measured before and after embryo transfer in all patients and fertile controls. **(A)** Concentration of IFN-ɣ (pg/ml) measured before and after embryo transfer in patients receiving steroid or no steroid treatment and in fertile controls (without steroid treatment); **(B)** Concentration of IFN-ɣ (pg/ml) measured before and after embryo transfer in steroid treatment patients who achieved clinical pregnancy, experienced a lack of pregnancy or miscarriage and in fertile controls (without steroid treatment). Red points indicate measurement before embryo transfer; green, after embryo transfer; dark grey points, fertile control; light grey points, fertile pregnant control. *N* is the numer of women. Black horizontal lines represent medians. P values are calculated by Mann-Whitney test.

10.3389/fimmu.2023.1250488

BDNF secretion into plasma (Figure 3A; Supplementary Table 5). On the other hand, fertile women who were pregnant at the moment of blood collection had the lowest level of BDNF (median 0.00 pg/ml). Therefore, this group of women differed in secretion of BDNF with patients receiving steroid treatment (p = 0.0047, median 6.52 pg/ml before ET) and patients without steroid treatment (p = 0.0062, median 0.00 pg/ml before ET; p = 0.0006, median 5.38 pg/ml after ET). Women with a current natural

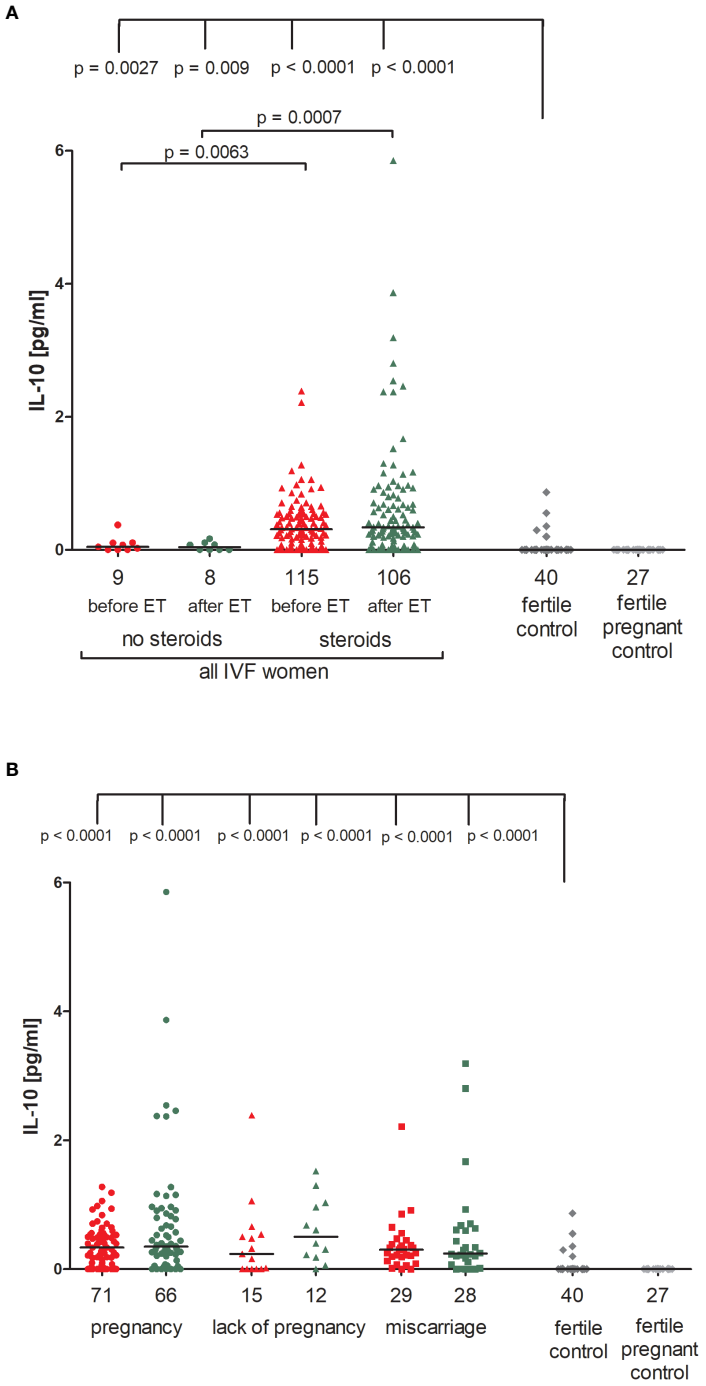

FIGURE 2
Concentration of plasma IL-10 measured before and after embryo transfer in all patients and fertile controls. **(A)** Concentration of IL-10 (pg/ml) measured before and after embryo transfer in patients receiving steroid or no steroid treatment and in fertile controls (without steroid treatment); **(B)** Concentration of IL-10 (pg/ml) measured before and after embryo transfer in steroid treatment patients who achieved clinical pregnancy, experienced a lack of pregnancy or miscarriage and in fertile controls (without steroid treatment). Red points indicate measurement before embryo transfer; green, after embryo transfer; dark grey points, fertile control; light grey points, fertile pregnant control. *N* is the numer of women. Black horizontal lines represent medians. P values are calculated by Mann-Whitney test.

10.3389/fimmu.2023.1250488

pregnancy also had a lower level of BDNF than women who had given birth in the past previously from natural conception (p = 0.0106, median 0.00 vs. 0.30 pg/ml).

When we divided patients receiving steroid treatment according to their pregnancy outcome after embryo transfer, we observed significant differences between all patients and the fertile pregnant controls (Figure 3B; Supplementary Table 6). The most striking difference in concentration of BDNF was observed in fertile pregnant women and patients for whom the embryo transfer did not result in a pregnancy (p = 0.0011, median 0.00 vs. 13.53 pg/ml after ET, respectively). Furthermore, the level of BDNF before ET in patients with a lack of pregnancy was higher than in the fertile pregnant controls (p = 0.0047, median 0.11 vs. 0.00 pg/ml, respectively). When embryo transfer resulted in pregnancy, we

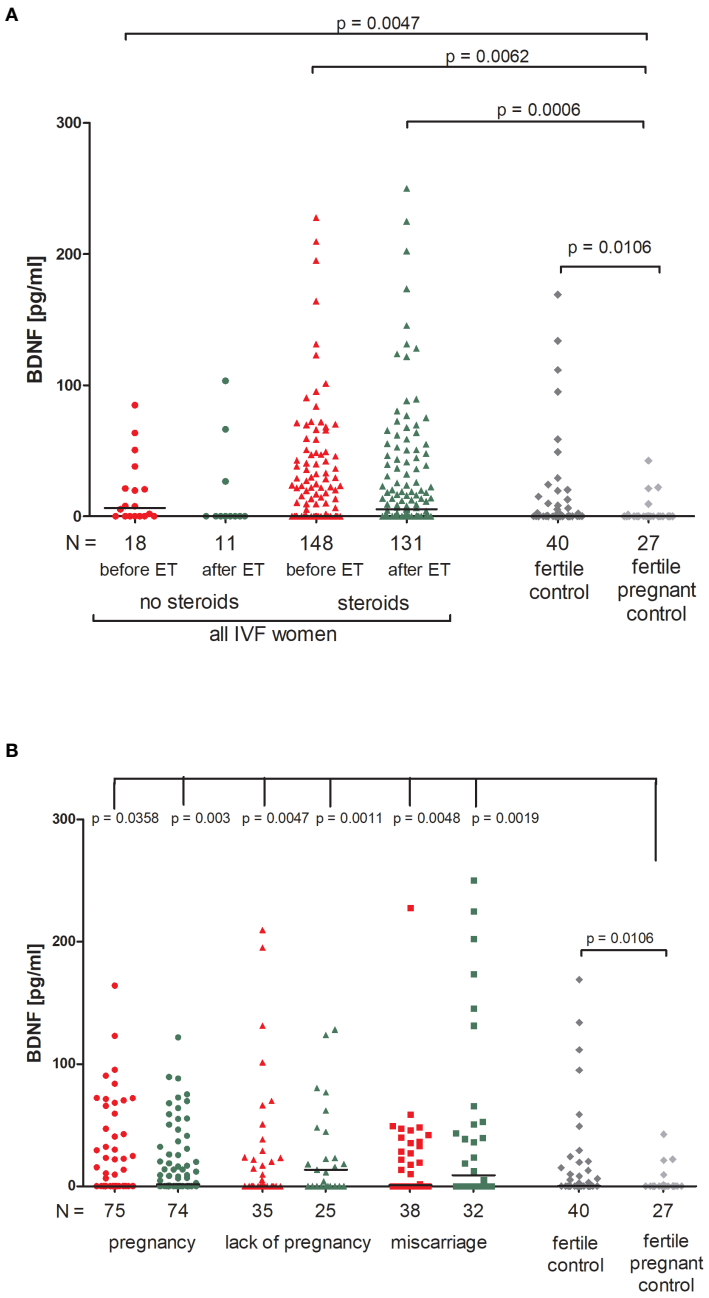

FIGURE 3
Concentration of plasma BDNF measured before and after embryo transfer in all patients and fertile controls. **(A)** Concentration of BDNF (pg/ml) measured before and after embryo transfer in patients receiving steroid or no steroid treatment and in fertile controls (without steroid treatment); **(B)** Concentration of BDNF (pg/ml) measured before and after embryo transfer in steroid treatment patients who achieved clinical pregnancy, experienced a lack of pregnancy or miscarriage and in fertile controls (without steroid treatment). Red points indicate measurement before embryo transfer; green, after embryo transfer; dark grey points, fertile control; light grey points, fertile pregnant control. *N* is the numer of women. Black horizontal lines represent medians. P values are calculated by Mann-Whitney test.

also observed statistically significant differences between patients and the fertile pregnant controls (p = 0.0358, median 0.00 before ET vs. 0.00 pg/ml, p = 0.003, median 1.63 vs. 0.00 pg/ml, respectively). Additionally, patients who experienced a miscarriage had a higher secretion of BDNF than in the fertile pregnant controls (p = 0.0048, median 0.94 before ET vs. 0.00 pg/ml; p = 0.0019, median 8.93 vs. 0.00 pg/ml).

3.4 LIF secretion in IVF patients and fertile groups

Patients who were not receiving steroid treatment had higher LIF values both before and after ET, but the differences compared to patients using prednisone were not significant (Figure 4A; Supplementary Table 7). All patients had a higher concentration

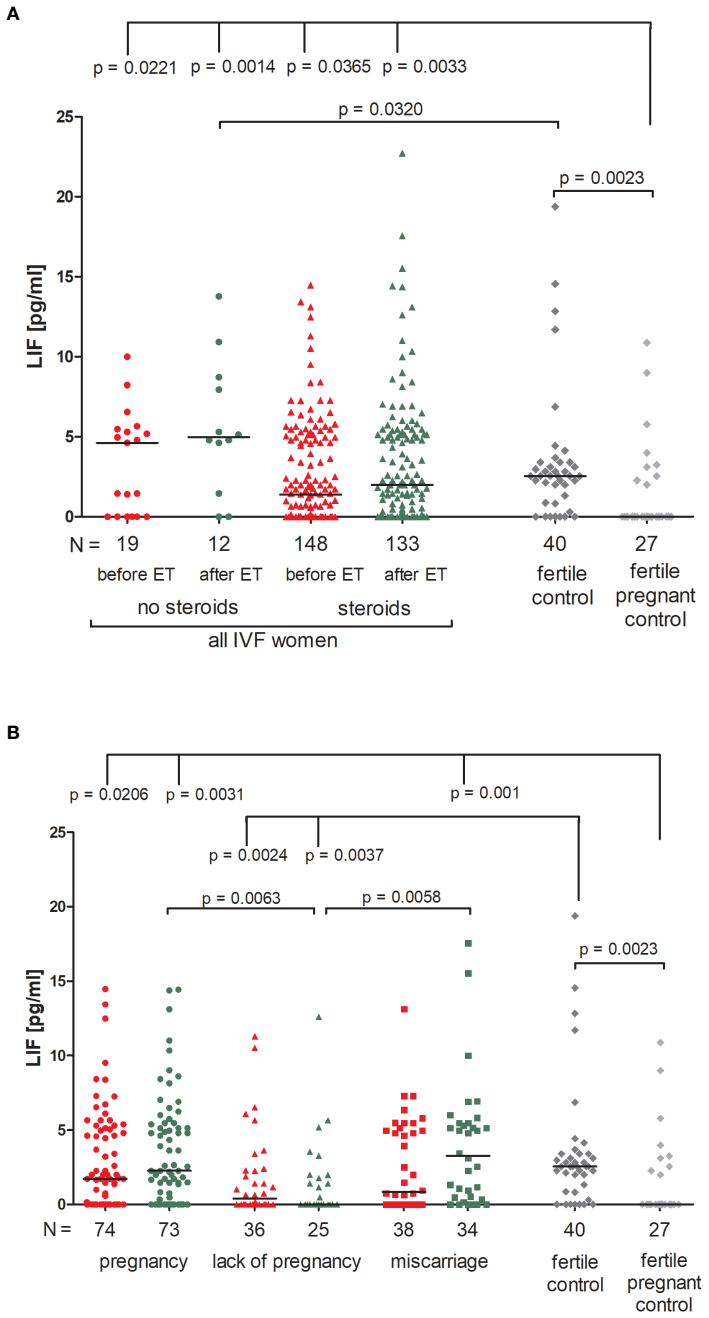

FIGURE 4
Concentration of plasma LIF measured before and after embryo transfer in all patients and fertile controls. **(A)** Concentration of LIF (pg/ml) measured before and after embryo transfer in patients receiving steroid or no steroid treatment and in fertile controls (without steroid treatment); **(B)** Concentration of LIF (pg/ml) measured before and after embryo transfer in steroid treatment patients who achieved clinical pregnancy, experienced a lack of pregnancy or miscarriage and in fertile controls (without steroids treatment). Red points mean measurement before embryo transfer; green, after embryo transfer; dark grey points, fertile control; light grey points, fertile pregnant control. *N* is the numer of women. Black horizontal lines represent medians. P values are calculated by Mann-Whitney test.

of LIF than in the fertile pregnant controls (p = 0.0221, median 4.62 before ET vs. 0.00 pg/ml and p = 0.0014, median 4.94 after ET vs. 0.00 pg/ml for patients not receiving steroid treatment; p = 0.0365, median 1.38 before ET vs. 0.00 pg/ml and p = 0.0033, median 2.00 after ET vs. 0.00 pg/ml for patients receiving steroid treatment). In addition, patients with no steroid treatment had a higher level of LIF after ET in comparison to the fertile controls (p = 0.0320, median 4.96 vs. 2.55 pg/ml, respectively). We also observed different secretion levels of LIF in fertile women and fertile pregnant women (p = 0.0023, median 2.55 vs. 0.00 pg/ml, respectively; Figure 4A; Supplementary Table 7).

When we compared patients according to various pregnancy outcomes, we observed that the lowest level of LIF in plasma was found in those patients who experienced a lack of pregnancy, in particular there was a concentration decrease after embryo transfer (Figure 4B; Supplementary Table 8). Comparison between patients who experienced a lack of pregnancy and patients who achieved pregnancy after ET (p = 0.0063, median 0.00 vs. 2.27 pg/ml after ET) and also between patients who had a miscarriage (p = 0.0058, median 0.00 vs. 3.27 pg/ml after ET) was significant. P values were also significant in comparison of the LIF secretion between patients with a lack of pregnancy and fertile women (p = 0.0024, median 0.40 before ET vs. 2.55 pg/ml; p = 0.0037, median 0.00 after ET vs. 2.55 pg/ml). Moreover, patients who achieved pregnancy after ET and also patients who experienced a miscarriage had higher levels of LIF than the fertile pregnant controls (p = 0.0206, median 1.73 before ET vs. 0.00 pg/ml; p = 0.0031, median 2.27 after ET vs. 0.00 pg/ml and p = 0.001, median 3.27 after ET vs. 0.00 pg/ml; respectively; Figure 4B; Supplementary Table 8).

3.5 Secretion of soluble TNFR1 in IVF patients and the fertile control groups

There were no significant differences between patients receiving steroid treatment and those that did not in terms of the secretion of soluble TNFR1 (sTNFR1) (Figure 5A; Supplementary Table 9). The highest amount of soluble TNFR1 was excreted by fertile women who gave birth in the past (median 1843 pg/ml). These women differed in their plasma concentration of sTNFR1 to IVF patients not receiving steroid treatment (p = 0.0069, median 1843 vs. 962.80 pg/ml before ET) and also with patients who did receive steroid treatment (p < 0.0001, median 1843 vs. 676.50 pg/ml before ET; p = 0.0007, median 1843 vs. 998.70 pg/ml after ET).

Among those patients receiving steroid treatment, the lowest levels of sTNFR1 were observed in patients experiencing a lack of pregnancy (median 0.00 and 143.30 pg/ml, before and after ET, respectively; Figure 5B; Supplementary Table 10). Patients who achieved pregnancy secreted higher levels of sTNFR1 than those with a lack of pregnancy (p <0.0001, median 1134 vs. 0.00 pg/ml before ET; p = 0.0015, median 1207.00 vs. 143.30 pg/ml after ET) the same was observed in the case of patients who experienced miscarriage in comparison to patients with a lack of pregnancy (p = 0.0420, median 414.70 vs. 0.00 pg/ml before ET). When embryo transfer resulted in pregnancy, patients had higher levels of sTNFR1 than those who had miscarried (p = 0.0066, median 1134.00 vs. 414.70 pg/ml before ET and p = 0.0504, median 1207.00 vs. 721.30 pg/ml after ET). All patients differed to the fertile controls in terms of the concentration of sTNFR1, but the most significant distinction was between patients with a lack pregnancy and the fertile controls (p < 0.0001, median 0.00 before ET vs. 1843 pg/ml and p < 0.0001, median 143.30 after ET vs. 1843 pg/ml). These patients also secreted less sTNFR1 than the fertile pregnant controls (p = 0.0005, median 0.00 pg/ml before ET vs. 523.80 pg/ml and p = 0.0162, median 143.30 pg/ml after ET vs. 523.80 pg/ml).

3.6 VEGF-A secretion in IVF patients and fertile control groups

Patients receiving steroid treatment and patients without steroid treatment had a similar concentration of VEGF-A in blood plasma (Figure 6A; Supplementary Table 11). The lowest quantities of VEGF-A were detected in the fertile pregnant controls (median 22.62 pg/ml). Significant differences between fertile pregnant control women and patients receiving steroid treatment (p < 0.0001, median 22.62 vs. 62.73 pg/ml before ET and p < 0.0001, median 22.62 vs. 66.30 pg/ml after ET) and patients with no steroid treatment were observed (p = 0.0023, median 22.62 vs. 58.44 pg/ml before ET and p = 0.0102, median 22.62 vs. 67.48 pg/ml after ET). Fertile women who gave birth in the past secreted more VEGF-A than fertile pregnant women (p = 0.0204, median 36.80 vs. 22.62 pg/ml) but less than patients receiving steroid treatment (p = 0.0003, median 36.80 vs. 62.73 pg/ml before ET and p = 0.0072, median 36.80 vs. 66.30 pg/ml after ET).

Patients divided according to their pregnancy outcome had higher levels of VEGF-A than fertile pregnant control women (Figure 6B; Supplementary Table 12). The most striking difference was found between fertile pregnant women and patients who did not achieve pregnancy (p < 0.0001, median 22.62 vs. 143.10 pg/ml before ET and p = 0.0005, median 22.62 vs. 78.41 pg/ml after ET). We also observed a higher level of VEGF-A in patients who experienced a lack of pregnancy in comparison to patients who became pregnant after IVF-ET (p = 0.003, median 143.10 vs. 57.19 pg/ml before ET) and those who miscarried (p = 0.003, median 143.10 vs. 52.72 pg/ml before ET).

3.7 ROC analyses for secretion of soluble TNFR1 and VEGF-A

We also performed a receiver–operator curve (ROC) analyses on the secretion of all the examined cytokines, but only in the case of sTNFR1 and VEGF-A did we find statistical significance. We determined the threshold value of sTNFR1 to be 962.3 pg/ml, which allowed us to distinguish IVF patients who achieved and maintained pregnancy from those who did not get pregnant or had a miscarriage (area under the curve (AUC) = 0.66, p = 0.00186,

10.3389/fimmu.2023.1250488

sensitivity 62.71%, specificity 62.16%, and likelihood ratio (LR) = 1.66; Figure 7A). When we compared fertile women who gave birth in the past to those who experienced a lack of pregnancy or had miscarriage, the threshold value was 1409 pg/ml (AUC = 0.76, p < 0.0001, sensitivity 77.97%, specificity 69.23%, LR = 2.53; Figure 7B).

ROC analysis for IVF patients indicated only the lack of significant differences in reproductive success. But the threshold value 48.04 pg/ml was the value differentiating fertile women who gave birth in the past with patients who did not achieve pregnancy or miscarried after IVF-ET (AUC = 0.69, p = 0.0016, sensitivity 65.52%, specificity 65.79%, LR = 1.92; Figure 8A). Patients who secreted VEGF-A above this value had a greater risk of miscarriage or failed transfer than women secreting below this value. Additionally, when we compared the fertile pregnant controls with patients who experienced a lack of pregnancy or miscarriage, we achieved a threshold value of 43.28 pg/ml, but the ROC analysis was stronger (AUC = 0.78, p < 0.0001, sensitivity 74.14%, specificity 81.48%, LR = 4.00; Figure 8B).

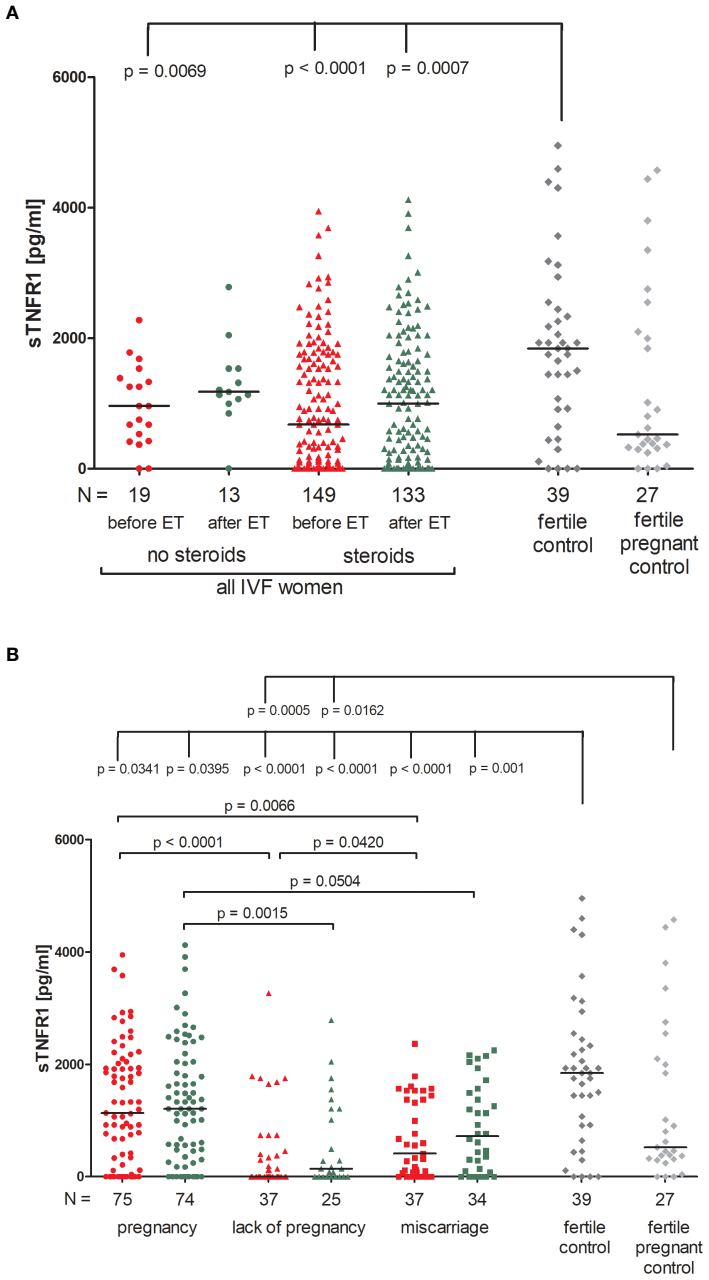

FIGURE 5
Concentration of soluble TNFR1 measured before and after embryo transfer in all patients and fertile controls. **(A)** Concentration of soluble TNFR1 (pg/ml) measured before and after embryo transfer in patients receiving steroid or no steroid treatment and in fertile controls (without steroid treatment); **(B)** Concentration of soluble TNFR1 (pg/ml) measured before and after embryo transfer in steroid treatment patients who achieved clinical pregnancy, experienced a lack of pregnancy or miscarriage and in fertile controls (without steroid treatment). sTNFR1 – soluble TNFR1. Red points indicate measurement before embryo transfer; green, after embryo transfer; dark grey points, fertile control; light grey points, fertile pregnant control. *N* is the numer of women. Black horizontal lines represent medians. P values are calculated by Mann-Whitney test.

4 Discussion

In successful embryo implantation and maintenance of pregnancy, the proper interaction between the embryo and endometrium is needed. Secretion of pro- and anti-inflammatory cytokines and their changing profile is one of the most crucial factors during embryo implantation and throughout the various stages of pregnancy (37, 38). In this study we investigated cytokine and growth factor levels measured in plasma before and after embryo transfer of patients undergoing IVF and also in the fertile controls. Patients being administered the steroid prednisone were compared in terms of the secretion of cytokines with patients who received no treatment with steroid, which may give a new insight into research on recurrent implantation failure and steroid

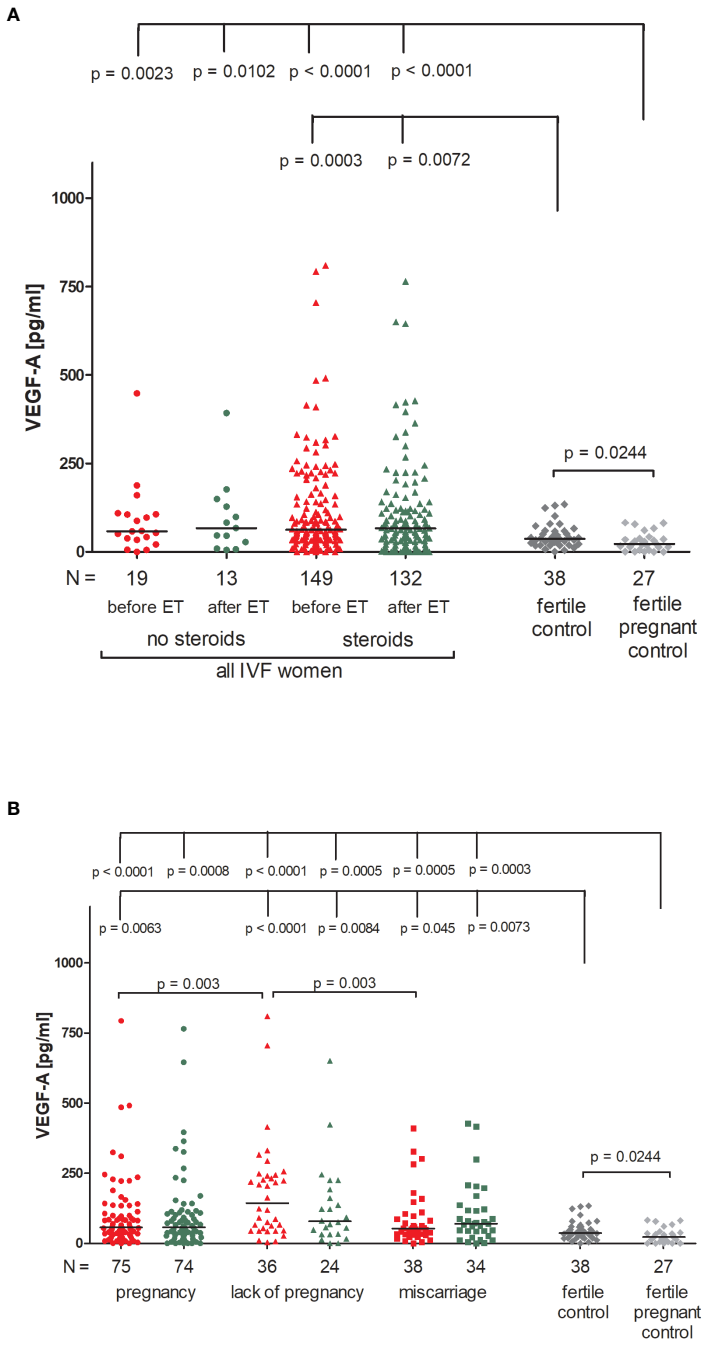

FIGURE 6
Concentration of plasma VEGF-A measured before and after embryo transfer in all patients and fertile controls. **(A)** Concentration of VEGF-A (pg/ml) measured before and after embryo transfer in patients receiving steroid or no steroid treatment and in fertile controls (without steroid treatment); **(B)** Concentration of VEGF-A (pg/ml) measured before and after embryo transfer in steroid treatment patients who achieved clinical pregnancy, experienced a lack of pregnancy or miscarriage and in fertile controls (without steroid treatment). Red points indicate measurement before embryo transfer; green, after embryo transfer; dark grey points, fertile control; light grey points, fertile pregnant control. *N* is the numer of women. Black horizontal lines represent medians. P values are calculated by Mann-Whitney test.

treatment during *in vitro* fertilization. We wanted also to examine whether an individual cytokine level could serve as an indicator of pregnancy outcome after embryo transfer. In addition, comparison with fertile controls identified those factors that may be associated with susceptibility to infertility.

Our study on the plasma level of IFN-ɣ indicates that taking prednisone reduces secretion of this cytokine in patients undergoing IVF-ET. Fertile controls, who did not use this steroid, had a similar level of IFN-ɣ as patients without steroid treatment. It indicates that approximately 0.28 pg/ml of IFN-ɣ must be detectable in women planning pregnancy. The role of IFN-ɣ in pregnancy has been confirmed in other studies (16, 39). IFN-ɣ, which is found in the human endometrium, plays a role in the maintenance of a pregnancy via up-regulating the expression of IL-6, monocyte chemotactic protein (MCP)-1, and macrophage colony stimulating factor (M-CSF) by endometrial stromal cells (40, 41). However, as previously mentioned, during implantation and early pregnancy, there are rapid changes in the immune response in decidua that affect the embryo implantation and pregnancy (42). It is believed that Th1 cytokines like IFN-ɣ and TNF-α are unfavorable to a pregnancy, while Th2 cytokines as IL-4 and IL-10 are significant in the successful development of a fetus. It follows that an increase in the Th1/Th2 ratio may lead to increased cytotoxicity against the embryo and subsequently to implantation failure (43). When a Th1 environment is dominant in the endometrium, uterine NK cells may become killer cells acting upon trophoblast cells and destroying them as a consequence. Thus, proper immune balance is required for embryo implantation (44). Liang et al. reported that both the concentration of IFN-ɣ in blood plasma and also the ratios of pro- and anti-inflammatory cytokines were higher in patients with RIF compared to the control group (45). Most studies have shown that IFN-γ expression is increased in spontaneous abortion or recurrent pregnancy loss patients (46–48). Higher levels of IFN-γ were found in serum samples of women in first trimester of pregnancy who have experienced preeclampsia and fetal growth restriction (49). Therefore, it is considered that inhibiting and regulation of the immune system by immunomodulators or

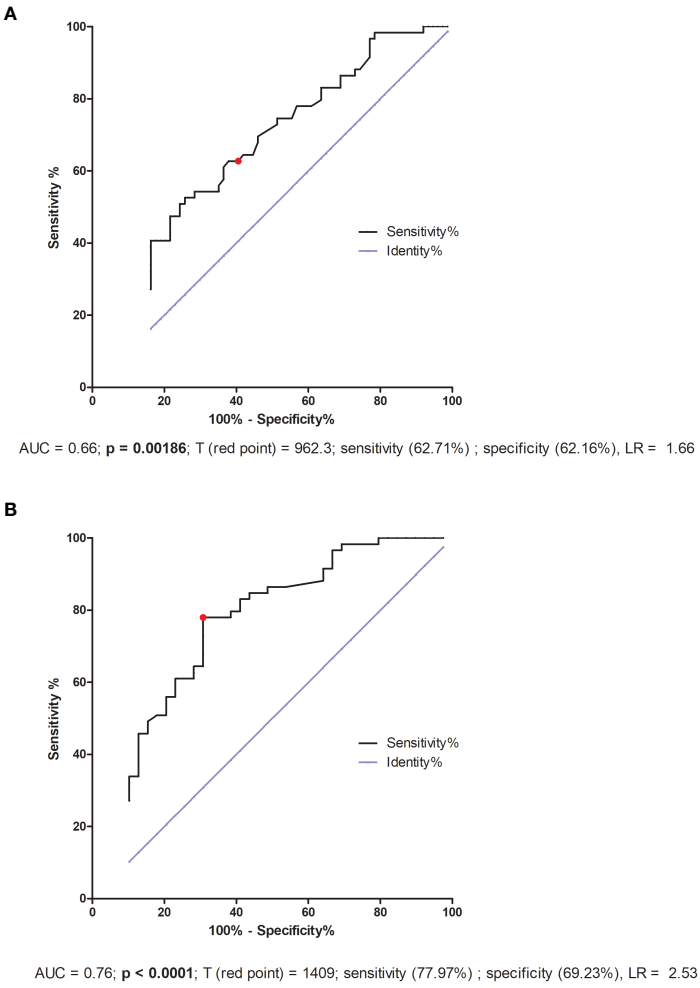

FIGURE 7
ROC analyses of sTNFR1 concentration in IVF patients and fertile controls. **(A)** Comparison of patients who became pregnant after IVF-ET and maintained it to patients who failed to conceive or had a miscarriage. AUC (Area under curve), T (red point) - limit value, LR – likelihood ratio. **(B)** Comparison of patients who did not become pregnant after IVF-ET to fertile women who gave birth in the past. AUC (Area under curve), T (red point) - limit value, LR – likelihood ratio.

immunosuppressive agents could be an effective treatment strategy to resolve RIF (50, 51). Corticosteroids are often used as immunotherapy for patients suffering from RIF or recurrent miscarriage because of their anti-inflammatory and immune-suppressive properties (52). However, the effect of prednisone on the IFN-γ level did not change in reproductive success of our patients. There were no differences in its secretion in patients achieving pregnancy after ET, patients without pregnancy after ET and also patients experiencing miscarriage.

In the case of IL-10, prednisone treatment increased its concentration in the blood plasma of the patients, while in both the non-treated non-pregnant fertile women and pregnant fertile women, its level was mostly undetectable. Other studies by Dibble et al. and Holmes et al. have reported higher levels of IL-10 in the plasma of pregnant women in comparison to non-pregnant women at different stages of pregnancy and postpartum (53, 54). However, the association between IL-10 concentration in peripheral blood during pregnancy and gestational period is inconclusive. Some studies showed no association (54, 55), while others, for example, by Dibble et al. and Allswede et al. found that plasma IL-10 levels increased with advanced gestational weeks throughout normal pregnancy (53, 56). On the other hand, our pregnant control women were mainly at 25 weeks of gestation and we were not able to detect this cytokine in their plasma. Furthermore, decreased IL-10 levels were associated with pregnancy losses, preeclampsia, and preterm delivery (48, 53, 57, 58). An elegant study was presented by Zhao et al., 2022, who determined the level of anti-inflammatory cytokines and chemokines in the period before and after embryo implantation in patients after IVF (59). During the peri-implantation period (ET+0 to ET+9 days), the serum cytokine profiles were similar between pregnancies which miscarried or did not miscarry. Yet, the profiles from day ET+16 indicated a significant difference concerning an increase of the pro-inflammatory cytokines IL-17, IFN-γ and TNF-α in the miscarriage group, but a sustained increase of anti-inflammatory cytokines IL-10 and TGF-β1 in the live birth group. Moreover, a change in the anti-inflammatory response at 3–6 days after ET occurred in all pregnancies whether they resulted in live birth or miscarriage. Therefore, the researchers concluded that the most exact day for measurement of pro- and anti-inflammatory cytokines

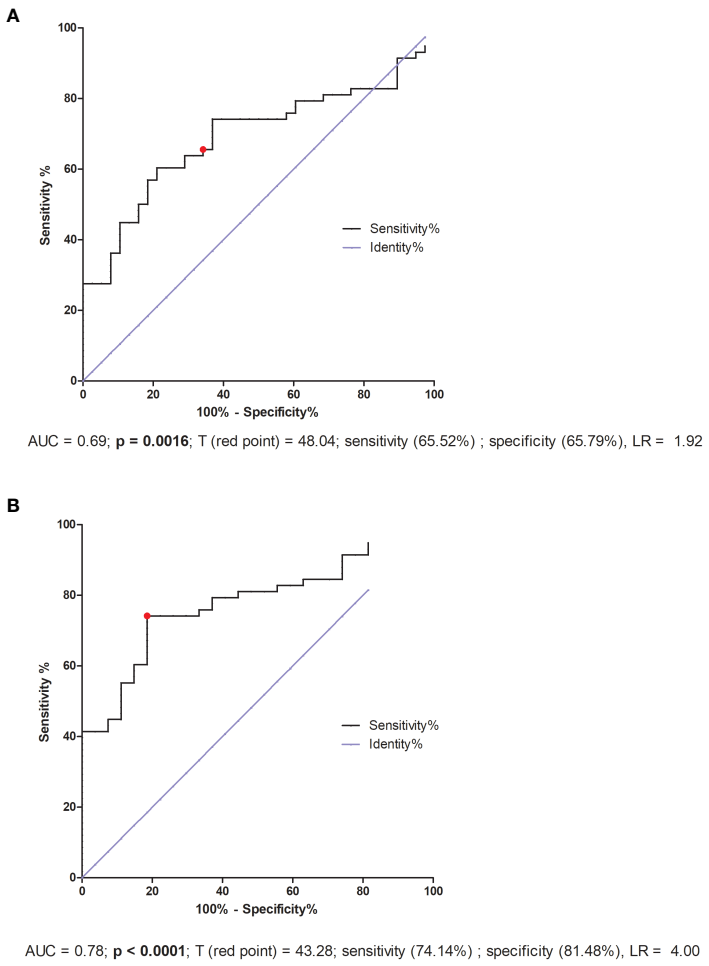

FIGURE 8
ROC analyses of VEGF-A concentration in IVF patients and fertile controls. **(A)** Comparison of patients who became pregnant after IVF and maintained it to patients who failed to conceive or had a miscarriage. AUC (Area under curve), T (red point) - limit value, LR – likelihood ratio. **(B)** Comparison of patients who did not become pregnant after *in vitro* fertilization to fertile women who gave birth in the past. AUC (Area under curve), T (red point) - limit value, LR – likelihood ratio.

monitoring the pregnancy outcome was ET+16. In our study, plasma was collected between 11 to 15 days after embryo transfer. Probably, the differences between our study and the one quoted resulted from the day of material collection for testing, as well as from prednisone treatment. In addition, we did not detect differences in the concentration of all tested cytokines and growth factors between plasma collected before and after embryo transfer. It should also be emphasized that some measurements could not be evaluated, e.g., TNF-α, GM-CSF, IL-4, IL-6, PlGF and VEGF-D. Glucocorticoids acting on antigen presenting cells (APCs) inhibit the production of IL-12, the main inducer of the Th1 response, resulting in a change in the Th1/Th2 balance. IL-12 stimulates IFN-γ production and inhibits IL-4 synthesis by T cells (60). Moreover, glucocorticoid-treated monocytes/macrophages produce significantly less IL-12, leading to a decreased capacity of these cells to induce IFN-γ production by antigen-primed CD4+ T cells (61). In addition, glucocorticoids downregulate the expression of IL-12 receptors on T and NK cells. It has been shown that lymphocyte-derived IL-10 production appears to be upregulated by glucocorticoids. In multiple sclerosis patients with an acute relapse, treatment with glucocorticoids was associated with increased plasma IL-10 secretion (62). A similar steroidal effect was observed in our patients.

Neutrophins like BDNF ensure the survival, differentiation or death of neurons at the embryonic and postnatal stages of development. They also maintain the viability of neurons at a later age (31, 63). Moreover, BDNF and its receptors are expressed in different regions of the human placenta, indicating the diverse functions of BDNF signaling in placental development (64, 65). Our findings point out that fertile pregnant women differ in BDNF secretion in peripheral blood from IVF patients. Moreover, they also differ from fertile women who gave birth in the past. Prednisone administration did not influence the level of BDNF in the plasma of IVF patients. Among our IVF patients, we did not find differences in pregnancy outcome, although the median concentration of BDNF was 8.93 pg/ml in patients experiencing miscarriage and 13.53 pg/ml in patients without a pregnancy. During pregnancy, this level decreased to 0.00 pg/ml for the control group and IVF patients (measured in plasma collected before embryo transfer; Supplementary Table 6). A similar observation was found in a study performed by Garces et al. (66). BDNF levels have been reported to be higher in non-pregnant women than in pregnant women. Moreover, they did not vary during menstrual cycle phases and were lowest in pregnant women during the 1st trimester and similar during the 2nd and 3rd trimesters (66). The question arises: Is BDNF taken up from peripheral blood and directed to the uterus when a woman becomes pregnant to fulfill its function in the development of fetus and thus is undetectable in blood of pregnant women? However, a study by Ramer does not support our results (32). Diminished circulating BDNF early in an IVF cycle was associated with implantation and subsequent pregnancy failure (32). The primary difference between our study and their study was the lack of prednisone administration and the time frame for serum collection.

LIF, an IL-6 cytokine family member, is expressed by the endometrium during the menstrual cycle in healthy women, with a remarkable increase during the mid-secretory to late-secretory phase (67–69). It initiates multiple factors and signaling pathways in the luminal epithelium for uterine receptivity and successful implantation (70–72). In our IVF patients, a lack of pregnancy was associated with a decreased level of LIF measured in plasma. Women achieving a pregnancy after IVF secreted LIF at a median concentration over 2 pg/ml. Surprisingly, the median LIF of our pregnant control group was 0.0 pg/ml, and that of women who gave birth in the past was over 2.5 pg/ml. However, we do not have information concerning in which phase of the menstrual cycle were women giving birth in the past. Perhaps LIF levels decline with gestational age. The pregnant women in our study were on average 25 weeks pregnant. Elevated levels of LIF have been observed in the development and progression of tumors (73). Undoubtedly, at the beginning of a pregnancy when trophoblast invasion occurs, elevated levels of LIF are required. Meanwhile, in a study by Basatvat et al., there was no reported difference in LIF gene expression level from the endometrial biopsies of healthy women and IVF-failure patients (74). In another study, a low concentration of LIF in uterine flushing fluid at day 26 was predictive of subsequent implantation and the LIF concentration was significantly lower in the pregnant group (75). Prednisolone treatment reduced the expression of human endometrial stromal fibroblasts (hESFs) cytokines (IL-6, IL-11, IL-18, LIF, and LIFR), however it had no effect on classic decidualization marker gene expression (prolactin or insulin like growth factor binding protein 1) or secretion by decidualized hESF (76).

TNFR1, also known as tumor necrosis factor receptor 1A superfamily member and CD120a, is a ubiquitous membrane receptor that binds tumor necrosis factor alpha (TNF-α). Membrane TNFα, as well as its receptors TNFR1 and TNFR2, after cleavage by the proteinase TACE (TNF-α converting enzyme), occur in a soluble form (sTNFR) in many body fluids. Elevated levels of sTNFR have been observed in serum, plasma and urine and are often found to be in connection with endotoxinemia, infections and malignancies, as well as chronic autoimmune diseases. The shedding of TNF receptors may lead to a transiently reduced cellular response to TNF-α. Depending on the sTNFR concentration, it has been suggested that sTNFRs block the binding of TNF-α to transmembrane TNFR and thus delay biological responses (77). However, it is also possible that shedding of TNFR in inflammation may initiate direct signaling effects through the binding of sTNFR to transmembrane TNF-α (mTNF-α) (78, 79). Therefore, the higher the concentration of circulating sTNFR, the lower the bioavailability of TNF-α, which may reduce the inflammatory response. Thus, it seems reasonable to ask whether it makes sense to administer steroids to patients who have a higher level of sTNFR1? sTNFR1 can fulfill its function by either blocking membrane TNF-α on cells or capturing TNF-α circulating in peripheral blood. The role of sTNFR1 has been described in pre-eclampsia and pregnancy-induced hypertension in several studies (80–85) alongside early miscarriage (86, 87). Our study shows the secretion of sTNFR1 into the plasma tested before embryo transfer and at a very early stage of pregnancy (2-3 weeks after embryo transfer to the uterus) in patients who have undergone an IVF procedure. The lowest sTNFR1 concentration was observed

in women who did not become pregnant after ET, and the highest in fertile controls who gave birth in the past. It should be noted that fertile pregnant women secreted sTNFR1 at an intermediate level (median 523.80 pg/ml). These women had an average of 25 weeks of gestation. There is a study showing that sTNFR1 expression decreases with gestational age. In the first trimester, secretion of sTNFR1 and sTNFR2 by placental macrophages were 46- and 260-fold higher than TNF-α concentration, respectively, whereas in the third trimester, a 15- and 1.7-fold excess was observed (88). Our results also indicate that women who secrete at least 1409 pg/ml sTNFR1 have a chance to become pregnant naturally and give birth to a child, while patients after IVF-ET with simultaneous support of the luteal phase and prednisone administration must achieve a concentration of 962.3 pg/ml sTNFR1 in the blood plasma.

VEGF-A (also called VEGF) is a multi-functional factor engaged in the regulation of proliferation, differentiation and survival of endothelial cells and it is also involved in blood vessel permeability. VEGF participates in embryonic vasculogenesis and angiogenesis during pregnancy (27). Progesterone and estrogen significantly promote VEGF production (89, 90). Therefore, in our study IVF patients, who were taking micronized progesterone, secreted more VEGF-A than in our control group. In general, we observed higher VEGF concentrations in IVF patients compared to fertile women, regardless of whether the patients were receiving steroid treatment or not. Moreover, the highest concentrations were observed in women who did not become pregnant after IVF-ET. Similar to our study, Bansal et al. showed that VEGF-A levels were significantly increased in women with RIF compared to healthy controls, however there was no correlation between VEGF-A or VEGF-R1 and the absolute levels of circulating NK cells, CD69 activated NK cells or NK cytotoxicity (91). In contrast to our research, Benkhalifa et al. reported decreased concentration of VEGF in RIF women compared to women with a successful of IVF-ET with an AUC of 0.742 in ROC curve analysis and a cut-off at 55.80 pg/ml (92). The threshold value 43.28 pg/ml of our ROC analysis differentiated fertile pregnant women from IVF patients who did not become pregnant or who miscarried. Our study differs from those previously mentioned not only in the fact that patients took prednisone and progesterone alongside differences in group size but also in that they did not compare the IVF patients with a healthy fertile control group. Thus, the analysis of VEGF levels should take into consideration the impact of estrogen, progesterone and other potential influential factors to understand the role of VEGF during embryo implantation.

One of the beneficial effects of prednisolone might be its suppressive impact on uterine NK cells. A study by Cooper et al. showed a relatively high prevalence of increased uNK cells in women with recurrent reproductive failure and confirmed the role of prednisolone in reducing uNK cell concentrations (93). Nevertheless, they did not find any evidence for a significant beneficial effect of prednisolone therapy on pregnancy outcomes. In turn, Giulini et al. suggest the advantage of prednisone and antibiotic treatment on the live birth rate in a subsequent IVF cycle (94). Indeed, the reported effectiveness of prednisolone/prednisone in prevention of miscarriage/recurrent implantation failure is highly variable between studies (93, 95–100). Therefore, the Practice Committee of the American Society for Reproductive Medicine since 2018 has not recommended the routine use of corticosteroids during ovarian stimulation to improve the outcome of live birth in ART cycles in the general population (101). ASRM has also not recommended the routine use of corticosteroids during the implantation window to improve the outcome of live births in ART cycles in the general population. In addition, the latest recommendations of the European Society of Human Reproduction and Embryology concerning recurrent implantation failure treatment do not contain guidelines for steroid treatment (102). According to the latest European recommendations (strong quality evidence), corticosteroids should be administered to women at a gestational age between 24 + 0 and 33 + 6 weeks, when preterm birth is expected in the next seven days. This treatment reduced neonatal mortality and morbidity by approximately 20% and neonatal respiratory distress syndrome by approximately 30% (103).

However, our research has limitations. Firstly, we tested only selected immunological factors that did not give a full picture of the immunological condition of the women studied. One of the weaknesses of our study was also the lack of information about the day of the menstrual cycle of the tested women who gave birth in the past, which may have influenced the results obtained. However, these were women of reproductive age (except for 1). Therefore, we added a control who was naturally pregnant at the time of blood sampling to compare the women in terms of conception method. Moreover, the group of women not treated with the steroid (N = 19 before ET) seems small compared to that treated. Despite the use of modern Luminex technology, we were unable to obtain unequivocal conclusions for all analytes tested. Panels of tested analytes need to be more refined.

Conclusions

i. Fertile women present a different profile of pro- and anti-inflammatory cytokines and growth factors from patients with RIF.
ii. Women who secrete at least 1409 pg/ml sTNFR1 have a chance to become pregnant naturally and give birth to a child, while patients after IVF-ET with simultaneous luteal phase support and receiving steroid treatment must achieve a concentration of 962.3 pg/ml sTNFR1 in the blood plasma.
iii. IVF patients secreting VEGF-A above 43.28 pg/ml have a greater risk of miscarriage or failed transfer than women secreting below this value.
iv. The use of steroid treatment by infertile patients should be carefully considered due to the changes they cause in the immune environment of the uterus and in the peripheral blood.

Data availability statement

The original contributions presented in the study are included in the article/Supplementary Materials, further inquiries can be directed to the corresponding author.

Ethics statement

The studies involving humans were approved by Ethics Committee of the Polish Mothers' Memorial Hospital–Research Institute in Łódź (No: 25/2019). The studies were conducted in accordance with the local legislation and institutional requirements. The participants provided their written informed consent to participate in this study.

Author contributions

KP, IN conceived and designed the experiments. KP, MD performed the experiments. KP, MD, IN, PR analyzed the data. PR, MR contributed to patient and control recruitment. KP and IN wrote the paper. KB-K contributed to the research methodology, provided equipment for the study and critically reviewed the manuscript. All authors contributed to the article and approved the submitted version.

Funding

This study was funded by the National Science Centre, grant number 2018/29/N/NZ5/00940. Open access was covered by Hirszfeld Institute of Immunology and Experimental Therapy, Polish Academy of Sciences, Wrocław and Gameta Hospital in Rzgów.

Acknowledgments

We would like to thank all patients and controls who participated in this study.

Conflict of interest

The authors declare that the research was conducted in the absence of any commercial or financial relationships that could be construed as a potential conflict of interest.

Publisher's note

Supplementary material

The Supplementary Material for this article can be found online at: https://www.frontiersin.org/articles/10.3389/fimmu.2023.1250488/full#supplementary-material

References

1. Gauster M, Moser G, Wernitznig S, Kupper N, Huppertz B. Early human trophoblast development: from morphology to function. *Cell Mol Life Sci* (2022) 79 (6):345. doi: 10.1007/s00018-022-04377-0

2. Huppertz B. Traditional and new routes of trophoblast invasion and their implications for pregnancy diseases. *Int J Mol Sci* (2019) 21(1):289. doi: 10.3390/ijms21010289

3. Ali SB, Jeelall Y, Pennell CE, Hart R, McLean-Tooke A, Lucas M. The role of immunological testing and intervention in reproductive medicine: A fertile collaboration? *Am J Reprod Immunol* (2018) 79(3):e12784. doi: 10.1111/aji.12784

4. Bashiri A, Halper KI, Orvieto R. Recurrent Implantation Failure-update overview on etiology, diagnosis, treatment and future directions. *Reprod Biol Endocrinol* (2018) 16(1):121. doi: 10.1186/s12958-018-0414-2

5. Coughlan C, Ledger W, Wang Q, Liu F, Demirol A, Gurgan T, et al. Recurrent implantation failure: Definition and management. *Reprod BioMed Online* (2014) 28 (1):14–38. doi: 10.1016/j.rbmo.2013.08.011

6. Sheikhansari G, Pourmoghadam Z, Danaii S, Mehdizadeh A, Yousefi M. Etiology and management of recurrent implantation failure: A focus on intra-uterine PBMC-therapy for RIF. *J Reprod Immunol* (2020) 139:103121. doi: 10.1016/j.jri.2020.103121

7. Cornish EF, Filipovic I, Åsenius F, Williams DJ, McDonnell T. Innate immune responses to acute viral infection during pregnancy. *Front Immunol* (2020) 11:572567. doi: 10.3389/fimmu.2020.572567

8. Abu-Raya B, Michalski C, Sadarangani M, Lavoie PM. Maternal immunological adaptation during normal pregnancy. *Front Immunol* (2020) 11:575197. doi: 10.3389/fimmu.2020.575197

9. Munro SK, Balakrishnan B, Lissaman AC, Gujral P, Ponnampalam AP. Cytokines and pregnancy: Potential regulation by histone deacetylases. *Mol Reprod Dev* (2021) 88 (5):321–37. doi: 10.1002/mrd.23430

10. Liu S, Diao L, Huang C, Li Y, Zeng Y, Kwak-Kim JYH. The role of decidual immune cells on human pregnancy. *J Reprod Immunol* (2017) 124:44–53. doi: 10.1016/j.jri.2017.10.045

11. Mor G, Cardenas I, Abrahams V, Guller S. Inflammation and pregnancy: the role of the immune system at the implantation site. *Ann N Y Acad Sci* (2011) 1221(1):80–7. doi: 10.1111/j.1749-6632.2010.05938.x

12. Nagamatsu T, Schust DJ. The contribution of macrophages to normal and pathological pregnancies. *Am J Reprod Immunol* (2010) 63(6):460–71. doi: 10.1111/j.1600-0897.2010.00813.x

13. Yang F, Zheng Q, Jin L. Dynamic function and composition changes of immune cells during normal and pathological pregnancy at the maternal-fetal interface. *Front Immunol* (2019) 10:2317. doi: 10.3389/fimmu.2019.02317

14. Olmos-Ortiz A, Flores-Espinosa P, Mancilla-Herrera I, Vega-Sánchez R, Díaz L, Zaga-Clavellina V. Innate immune cells and toll-like receptor-dependent responses at the maternal-fetal interface. *Int J Mol Sci* (2019) 20(15):3654. doi: 10.3390/ijms20153654

15. Kitazawa J, Kimura F, Nakamura A, Morimune A, Takahashi A, Takashima A, et al. Endometrial immunity for embryo implantation and pregnancy establishment. *Tohoku J Exp Med* (2020) 250(1):49–60. doi: 10.1620/tjem.250.49

16. Yang X, Tian Y, Zheng L, Luu T, Kwak-Kim J. The update immune-regulatory role of pro- and anti-inflammatory cytokines in recurrent pregnancy losses. *Int J Mol Sci* (2023) 24:132. doi: 10.3390/ijms24010132

17. Mekinian A, Cohen J, Alijotas-Reig J, Carbillon L, Nicaise-Roland P, Kayem G, et al. Unexplained recurrent miscarriage and recurrent implantation failure: is there a place for immunomodulation? *Am J Reprod Immunol* (2016) 76(1):8–28. doi: 10.1111/aji.12493

18. Boomsma CM, Kavelaars A, Eijkemans MJ, Lentjes EG, Fauser BC, Heijnen CJ, et al. Endometrial secretion analysis identifies a cytokine profile predictive of pregnancy in IVF. *Hum Reprod* (2009) 24(6):1427–35. doi: 10.1093/humrep/dep011

19. Zhang C, Deng X, Zhang X, Pan Z, Zhao W, Zhang Y, et al. Association between serum TNF-alpha levels and recurrent spontaneous miscarriage: a meta-analysis. *Am J Reprod Immunol* (2016) 75(2):86–93. doi: 10.1111/aji.12447

20. Haider S, Knöfler M. Human tumour necrosis factor: physiological and pathological roles in placenta and endometrium. *Placenta* (2009) 30(2):111–23. doi: 10.1016/j.placenta.2008.10.012

21. Okuda K. Sakumoto R Multiple roles of TNF super family members in corpus luteum function. *Reprod Biol Endocrinol* (2003) 1:95. doi: 10.1186/1477-7827-1-95

22. Huppertz B, Rote NS, Nelson DM, Reister F, Black S, Hunt JS. Apoptosis: molecular control of placental function – a workshop report. *Placenta* (2001) 22 (SupplA):S101e3. doi: 10.1053/plac.2001.0645

23. Guven MA, Coskun A, Ertas IE, Aral M, Zencirci B, Oksuz H. Association of maternal serum CRP, IL-6, TNF-alpha, homocysteine, folic acid and vitamin B12 levels with the severity of preeclampsia and fetal birth weight. *Hypertens Pregnancy* (2009) 28 (2):190–200. doi: 10.1080/10641950802601179

24. Wang W, Sung N, Gilman-Sachs A, Kwak-Kim J. T helper (Th) cell profiles in pregnancy and recurrent pregnancy losses: Th1/Th2/Th9/Th17/Th22/Tfh cells. *Front Immunol* (2020) 11:2025. doi: 10.3389/fimmu.2020.02025

25. Jin LP, Fan DX, Zhang T, Guo PF, Li DJ. The costimulatory signal upregulation is associated with Th1 bias at the maternal-fetal interface in human miscarriage. *Am J Reprod Immunol* (2011) 66(4):270–8. doi: 10.1111/j.1600-0897.2011.00997.x

26. Magatti M, Stefani FR, Papait A, Cargnoni A, Masserdotti A, Silini AR. Perinatal mesenchymal stromal cells and their possible contribution to fetal-maternal tolerance. *Cells* (2019) 8(11):1401. doi: 10.3390/cells8111401

27. Guo X, Yi H, Li TC, Wang Y, Wang H, Chen X. Role of vascular endothelial growth factor (VEGF) in human embryo implantation: clinical implications. *Biomolecules* (2021) 11(2):253. doi: 10.3390/biom11020253

28. Sang Y, Li Y, Xu L, Li D, Du M. Regulatory mechanisms of endometrial decidualization and pregnancy-related diseases. *Acta Biochim Biophys Sin (Shanghai)* (2020) 52(2):105–15. doi: 10.1093/abbs/gmz146

29. Sharma S, Godbole G, Modi D. Decidual control of trophoblast invasion. *Am J Reprod Immunol* (2016) 75(3):341–50. doi: 10.1111/aji.12466

30. Melincovici CS, Boşca AB, Şuşman S, Mărginean M, Mihu C, Istrate M, et al. Vascular endothelial growth factor (VEGF) - Key factor in normal and pathological angiogenesis. *Rom J Morphol Embryol* (2018) 59:455–67.

31. Kawamura K, Kawamura N, Sato W, Fukuda J, Kumagai J, Tanaka T. Brain-derived neurotrophic factor promotes implantation and subsequent placental development by stimulating trophoblast cell growth and survival. *Endocrinology* (2009) 150(8):3774–82. doi: 10.1210/en.2009-0213

32. Ramer I, Kruczek A, Doulaveris G, Orfanelli T, Shulman B, Witkin SS, et al. Reduced circulating concentration of brain-derived neurotrophic factor is associated with peri- and post-implantation failure following *in vitro* fertilization-embryo transfer. *Am J Reprod Immunol* (2016) 75(1):36–41. doi: 10.1111/aji.12430

33. Sharkey AM, King A, Clark DE, Burrows TD, Jokhi PP, Charnock-Jones DS, et al. Localization of leukemia inhibitory factor and its receptor in human placenta throughout pregnancy. *Biol Reprod* (1999) 60(2):355–64. doi: 10.1095/biolreprod60.2.355

34. Dimitriadis E, Menkhorst E, Salamonsen LA, Paiva P. Review: LIF and IL11 in trophoblast-endometrial interactions during the establishment of pregnancy. *Placenta* (2010) 31 Suppl:S99–104. doi: 10.1016/j.placenta.2009.12.027

35. Shido F, Ito T, Nomura S, Yamamoto E, Sumigama S, Ino K, et al. Endoplasmic reticulum aminopeptidase-1 mediates leukemia inhibitory factor-induced cell surface human leukocyte antigen-G expression in JEG-3 choriocarcinoma cells. *Endocrinology* (2006) 147(4):1780–8. doi: 10.1210/en.2005-1449

36. Nowak I, Wilczyńska K, Radwan P, Wiśniewski A, Krasiński R, Radwan M, et al. Association of soluble HLA-G plasma level and HLA-G genetic polymorphism with pregnancy outcome of patients undergoing *in vitro* fertilization embryo transfer. *Front Immunol* (2020) 10:2982. doi: 10.3389/fimmu.2019.02982

37. Seshagiri PB, Vani V, Madhulika P. Cytokines and blastocyst hatching. *Am J Reprod Immunol* (2016) 75(3):208–17. doi: 10.1111/aji.12464

38. Pantos K, Grigoriadis S, Maziotis E, Pistola K, Xystra P, Pantou A, et al. The role of interleukins in recurrent implantation failure: a comprehensive review of the literature. *Int J Mol Sci* (2022) 23(4):2198. doi: 10.3390/ijms23042198

39. Murphy SP, Tayade C, Ashkar AA, Hatta K, Zhang J, Croy BA. Interferon gamma in successful pregnancies. *Biol Reprod* (2009) 80:848–59. doi: 10.1095/biolreprod.108.073353

40. Nasu K, Matsui N, Narahara H, Tanaka Y, Miyakawa I. Effects of interferon-gamma on cytokine production by endometrial stromal cells. *Hum Reprod* (1998) 13:2598–601. doi: 10.1093/humrep/13.9.2598

41. Yeaman GR, Collins JE, Currie JK, Guyre PM, Wira CR, Fanger MW. IFN-gamma is produced by polymorphonuclear neutrophils in human uterine endometrium and by cultured peripheral blood polymorphonuclear neutrophils. *J Immunol* (1998) 160:5145–53. doi: 10.4049/jimmunol.160.10.5145

42. PrabhuDas M, Bonney E, Caron K, Dey S, Erlebacher A, Fazleabas A, et al. Immune mechanisms at the maternal-fetal interface: perspectives and challenges. *Nat Immunol* (2015) 16(4):328. doi: 10.1038/ni.3131

43. Kwak-Kim JYH, Chung-Bang HS, Ng SC, Ntrivalas EI, Mangubat CP, Beaman KD, et al. Increased T helper 1 cytokine responses by circulating T cells are present in women with recurrent pregnancy losses and in infertile women with multiple implantation failures after IVF. *Hum Reprod* (2003) 18(4):767–73. doi: 10.1093/humrep/deg156

44. Chaouat G. The Th1/Th2 paradigm: still important in pregnancy? *Semin Immunopathol* (2007) 29(2):95–113. doi: 10.1007/s00281-007-0069-0

45. Liang P-Y, Diao L-H, Huang C-Y, Lian R-C, Chen X, Li G-G, et al. The pro-inflammatory and anti-inflammatory cytokine profile in peripheral blood of women with recurrent implantation failure. *Reprod BioMed Online* (2015) 31(6):823–6. doi: 10.1016/j.rbmo.2015.08.009

46. Raghupathy R, Makhseed M, Azizieh F, Omu A, Gupta M, Farhat R. Cytokine production by maternal lymphocytes during normal human pregnancy and in unexplained recurrent spontaneous abortion. *Hum Reprod* (2000) 15:713–8. doi: 10.1093/humrep/15.3.713

47. Hossein H, Mahroo M, Abbas A, Firouzeh A, Nadia H. Cytokine production by peripheral blood mononuclear cells in recurrent miscarriage. *Cytokine* (2004) 28:83–6. doi: 10.1016/j.cyto.2004.07.002

48. Calleja-Agius J, Jauniaux E, Pizzey AR, Muttukrishna S. Investigation of systemic inflammatory response in first trimester pregnancy failure. *Hum Reprod* (2012) 27:349–57. doi: 10.1093/humrep/der402

49. Vafaei H, Faraji S, Ahmadi M, Tabei SMB, Fereidoni S, Shiravani Z, et al. Alteration in IFN-γ and CCL2 serum levels at first trimester of pregnancy contribute to development of preeclampsia and fetal growth restriction. *Taiwan J Obstet Gynecol* (2023) 62(1):71–6. doi: 10.1016/j.tjog.2022.09.005

50. Abdolmohammadi-Vahid S, Danaii S, Hamdi K, Jadidi-Niaragh F, Ahmadi M, Yousefi M. Novel immunotherapeutic approaches for treatment of infertility. *BioMed Pharmacother* (2016) 84:1449–59. doi: 10.1016/j.biopha.2016.10.062

51. Ghasemnejad-Berenji H, Ghaffari Novin M, Hajshafiha M, Nazarian H, Hashemi SM, Ilkhanizadeh B, et al. Immunomodulatory effects of hydroxychloroquine on Th1/Th2 balance in women with repeated implantation failure. *BioMed Pharmacother* (2018) 107:1277–85. doi: 10.1016/j.biopha.2018.08.027

52. Franchimont D. Overview of the actions of glucocorticoids on the immune response: a good model to characterize new pathways of immunosuppression for newtreatment strategies. *Ann N Y Acad Sci* (2004) 1024:124–37. doi: 10.1196/annals.1321.009

53. Dibble S, Andersen A, Lassen MR, Cunanan J, Hoppensteadt D, Fareed J. Inflammatory and procoagulant cytokine levels during pregnancy as predictors of adverse obstetrical complications. *Clin Appl Thromb Hemost* (2014) 20(2):152–8. doi: 10.1177/1076029613494467

54. Holmes VA, Wallace JMW, Gilmore WS, McFaul P, Alexander HD. Plasma levels of the immunomodulatory cytokine interleukin-10 during normal human pregnancy: a longitudinal study. *Cytokine* (2003) 21(6):265–9. doi: 10.1016/s1043-4666(03)00097-8

55. Reyes-Lagos JJ, Peña-Castillo MÁ, Echeverría JC, Pérez-Sánchez G, Álvarez-Herrera S, Becerril-Villanueva E, et al. Women serum concentrations of the IL-10 family of cytokines and IFN-γ Decrease from the third trimester of pregnancy to active labor. *Neuroimmunomodulation* (2017) 24:162–70. doi: 10.1159/000480734

56. Allswede DM, Yolken RH, Buka SL, Cannon TD. Cytokine concentrations throughout pregnancy and risk for psychosis in adult offspring: a longitudinal case-control study. *Lancet Psychiatry* (2020) 7(3):254–61. doi: 10.1016/S2215-0366(20)30006-7

57. Kaislasuo J, Simpson S, Petersen JF, Peng G, Aldo P, Lokkegaard E, et al. IL-10 to TNFα ratios throughout early first trimester can discriminate healthy pregnancies from pregnancy losses. *Am J Reprod Immunol* (2020) 83(1):e13195. doi: 10.1111/aji.13195

58. Nath MC, Cubro H, McCormick DJ, Milic NM, Garovic VD. Preeclamptic women have decreased circulating IL-10 (Interleukin-10) values at the time of preeclampsia diagnosis: systematic review and meta-analysis. *Hypertension* (2020) 76 (6):1817–27. doi: 10.1161/HYPERTENSIONAHA.120.15870

59. Zhao Y, Man G, Zhang R, Wong C-K, Chen X, Pui-Wah Chung J, et al. A prospective study comparing the inflammation-related cytokine and chemokine profile from the day of blastocyst transfer to 7 weeks of gestation between pregnancies that did or did not result in a miscarriage. *J Reprod Immunol* (2022) 154:103755. doi: 10.1016/j.jri.2022.103755

60. Elenkov IJ, Chrousos GP, Wilder RL. Neuroendocrine regulation of IL-12 and TNF-alpha/IL-10 balance. Clinical implications. *Ann N Y Acad Sci* (2000) 917:94–105. doi: 10.1111/j.1749-6632.2000.tb05374.x

61. Dekruyff RH, Fang Y, Umetsu DT. Corticosteroids enhance the capacity of macrophages to induce Th2 cytokine synthesis in CD4+ lymphocytes by inhibiting IL-12 production. *J Immunol* (1998) 160(5):2231–7. doi: 10.4049/jimmunol.160.5.2231

62. Gayo A, Mozo L, Suárez A, Tuñon A, Lahoz C, Gutiérrez C. Glucocorticoids increase IL-10 expression in multiple sclerosis patients with acute relapse. *J Neuroimmunol* (1998) 85(2):122–30. doi: 10.1016/s0165-5728(97)00262-2

63. Milyutina YP, Arutjunyan AV, Korenevsky AV, Selkov SA, Kogan IY. Neurotrophins: are they involved in immune tolerance in pregnancy? *Am J Reprod Immunol* (2023) 89(4):e13694. doi: 10.1111/aji.13694

64. Marchese MJ, Li S, Liu B, Zhang JJ, Feng L. Perfluoroalkyl substance exposure and the BDNF pathway in the placental trophoblast. *Front Endocrinol (Lausanne)* (2021) 12:694885. doi: 10.3389/fendo.2021.694885

65. Sahay AS, Jadhav AT, Sundrani DP, Wagh GN, Joshi SR. Differential expression of nerve growth factor (NGF) and brain derived neurotrophic factor (BDNF) in different regions of normal and preeclampsia placentae. *Clin Exp Hypertens* (2020) 42 (4):360–4. doi: 10.1080/10641963.2019.1665677

66. Garces MF, Sanchez E, Torres-Sierra AL, Ruiz-Parra AI, AngelMuller E, Alzate JP, et al. Brain-derived neurotrophic factor is expressed in rat and human placenta and its serum levels are similarly regulated throughout pregnancy in both species. *Clin Endocrinol* (2014) 81:141–51. doi: 10.1111/cen.12391

67. Charnock-Jones DS, Sharkey AM, Fenwick P, Smith SK. Leukaemia inhibitory factor mRNA concentration peaks in human endometrium at the time of implantation and the blastocyst contains mRNA for the receptor at this time. *J Reprod Fertil* (1994) 101(2):421–6. doi: 10.1530/jrf.0.1010421

68. Arici A, Engin O, Attar E, Olive DL. Modulation of leukemia inhibitory factor gene expression and protein biosynthesis in human endometrium. *J Clin Endocrinol Metab* (1995) 80(6):1908–15. doi: 10.1210/jcem.80.6.7775640

69. Vogiagis D, Marsh MM, Fry RC, Salamonsen LA. Leukaemia inhibitory factor in human endometrium throughout the menstrual cycle. *J Endocrinol* (1996) 148(1):95–102. doi: 10.1677/joe.0.1480095

70. Rosario GX, Stewart CL. The multifaceted actions of leukaemia inhibitory factor in mediating uterine receptivity and embryo implantation. *Am J Reprod Immunol* (2016) 75(3):246–55. doi: 10.1111/aji.12474

71. Salleh N, Giribabu N. Leukemia inhibitory factor: roles in embryo implantation and in nonhormonal contraception. *Sci World J* (2014) 2014:201514. doi: 10.1155/2014/201514

72. Mrozikiewicz AE, Ożarowski M, Jędrzejczak P. Biomolecular markers of recurrent implantation failure - A review. *Int J Mol Sci* (2021) 22(18):10082. doi: 10.3390/ijms221810082

73. Viswanadhapalli S, Dileep KV, Zhang KYJ, Nair HB, Vadlamudi RK. Targeting LIF/LIFR signaling in cancer. *Genes Dis* (2022) 9(4):973–80. doi: 10.1016/j.gendis.2021.04.003

74. Basatvat S, Russell JM, Saare M, Thurston LM, Salumets A, Fazeli A. Potential innate immunity-related markers of endometrial receptivity and recurrent implantation failure (RIF). *Reprod Biol* (2021) 21(4):100569. doi: 10.1016/j.repbio.2021.100569

75. Lédée-Bataille N, Laprée-Delage G, Taupin J-L, Dubanchet S, Frydman R, Chaouat G. Concentration of leukaemia inhibitory factor (LIF) in uterine flushing fluid is highly predictive of embryo implantation. *Hum Reprod* (2002) 17(1):213–8. doi: 10.1093/humrep/17.1.213

76. Grbac E, So T, Varshney S, Williamson N, Dimitriadis E, Menkhorst E. Prednisolone alters endometrial decidual cells and affects decidual-trophoblast interactions. *Front Cell Dev Biol* (2021) 9:647496. doi: 10.3389/fcell.2021.647496

77. Van Zee KJ, Kohno T, Fischer E, Rock CS, Moldawer LL, Lowry SF. Tumor necrosis factor soluble receptors circulate during experimental and clinical inflammation and can protect against excessive tumor necrosis factor alpha in vitro and in *vivo*. *Proc Natl Acad Sci U.S.A.* (1992) 89(11):4845–9. doi: 10.1073/pnas.89.11.4845

78. Idriss HT, Naismith JH. TNF alpha and the TNF receptor superfamily: structure-function relationship(s). *Microsc Res Tech* (2000) 50(3):184–95. doi: 10.1002/1097-0029(20000801)50:3<184::AID-JEMT2>3.0.CO;2-H

79. Waetzig GH, Rosenstiel P, Arlt A, Till A, Bräutigam K, Schäfer H, et al. Soluble tumor necrosis factor (TNF) receptor-1 induces apoptosis via reverse TNF signaling and autocrine transforming growth factor-beta1. *FASEB J* (2005) 19(1):91–3. doi: 10.1096/fj.04-2073fje

80. Nevalainen J, Korpimaki T, Kouru H, SaIranen M, Ryynanen M. Performance of first trimester biochemical markers and mean arterial pressure in prediction of early-onset pre-eclampsia. *Metabolism* (2017) 75:6–15. doi: 10.1016/j.metabol.2017.07.004

81. Leal AM, Poon LC, Frisova V, Veduta A, Nicolaides KH. First-trimester maternal serum tumor necrosis factor receptor-1 and pre-eclampsia. *Ultrasound Obstet Gynecol* (2009) 33:135–41. doi: 10.1002/uog.6275

82. Estensen ME, Grindheim G, Remme EW, Godang K, Henriksen T, Aukrust P, et al. Elevated inflammatory markers in preeclamptic pregnancies, but no relation to systemic arterial stiffness. *Pregnancy Hypertens* (2015) 5(4):325–9. doi: 10.1016/j.preghy.2015.09.003

83. Yliniemi A, Makikallio K, Korpimaki T, Kouru H, Marttala J, Ryynanen M. Combination of PAPPA, fhCGβ, AFP, PlGF, sTNFR1, and Maternal Characteristics in Prediction of Early-onset Preeclampsia. *Clin Med Insights Reprod Health* (2015) 9:13–20. doi: 10.4137/CMRH.S21865

84. Minuz P, Fava C, Hao S, Pedraza P, Amen G, Meneguzzi A, et al. Differential regulation of TNF receptors in maternal leukocytes is associated with severe preterm preeclampsia. *J Matern Fetal Neonatal Med* (2015) 28(8):869–75. doi: 10.3109/14767058.2014.937695

85. Laskowska M, Laskowska K, Leszczyńska-Gorzelak B, Oleszczuk J. Maternal and umbilical sTNF-R1 in preeclamptic pregnancies with intrauterine normal and growth retarded fetus. *Hypertens Pregnancy* (2007) 26(1):13–21. doi: 10.1080/10641950601146483

86. Yu XW, Li X, Ren YH, Li XC. Tumour necrosis factor-alpha receptor 1 polymorphisms and serum soluble TNFR1 in early spontaneous miscarriage. *Cell Biol Int* (2007) 31(11):1396–9. doi: 10.1016/j.cellbi.2007.06.005

87. Chernyshov VP, Vodyanik MA, Pisareva SP. Lack of soluble TNF-receptors in women with recurrent spontaneous abortion and possibility for its correction. *Am J Reprod Immunol* (2005) 54(5):284–91. doi: 10.1111/j.1600-0897.2005.00308.x

88. Pavlov OV, Niauri DA, Selutin AV, Selkov SA. Coordinated expression of TNFα- and VEGF-mediated signaling components by placental macrophages in early and late pregnancy. *Placenta* (2016) 42:28–36. doi: 10.1016/j.placenta.2016.04.008

89. Kim M, Park HJ, Seol JW, Jang JY, Cho YS, Kim KR, et al. VEGF-A regulated by progesterone governs uterine angiogenesis and vascular remodelling during pregnancy. *EMBO Mol Med* (2013) 5:1415–30. doi: 10.1002/emmm.201302618

90. Okada H, Tsutsumi A, Imai M, Nakajima T, Yasuda K, Kanzaki H. Estrogen and selective estrogen receptor modulators regulate vascular endothelial growth factor and soluble vascular endothelial growth factor receptor 1 in human endometrial stromal cells. *Fertil Steril* (2010) 93:2680–6. doi: 10.1016/j.fertnstert.2009.08.056

91. Bansal R, Ford B, Bhaskaran S, Thum M, Bansal A. Elevated levels of serum vascular endothelial growth factor-A are not related to NK cell parameters in recurrent IVF failure. *J Reprod Infertil* (2017) 18(3):280–7.

92. Benkhalifa M, Zidi W, Bahri H, Mahjoub S, Boudhraa K, Sanhaji H, et al. Circulating MMP-7 and VEGF as potential predictive biomarkers for recurrent implantation failures. *Zygote* (2021) 29(5):365–71. doi: 10.1017/S0967199421000113

93. Cooper S, Laird SM, Li MN, Metwally MTC. The effect of prednisolone on endometrial uterine NK cell concentrations and pregnancy outcome in women with reproductive failure. A retrospective cohort study. *J Reprod Immunol* (2019) 131:1–6. doi: 10.1016/j.jri.2018.10.001

94. Giulini S, Grisendi V, Sighinolfi G, Di Vinci P, Tagliasacchi D, Botticelli L, et al. Chronic endometritis in recurrent implantation failure: Use of prednisone and IVF outcome. *J Reprod Immunol* (2022) 153:103673. doi: 10.1016/j.jri.2022.103673

95. Tang AW, Alfirevic Z, Turner MA, Drury JA, Small R, Quenby S. A feasibility trial of screening women with idiopathic recurrent miscarriage for high uterine natural killer cell density and randomizing to prednisolone or placebo when pregnant. *Hum Reprod* (2013) 28(7):1743–52. doi: 10.1093/humrep/det117

96. Gomaa MF, Elkholy AG, El-Said MM, Abdel-Salam NE. Combined oral prednisolone and heparin versus heparin: the effect on peripheral NK cells and clinical outcome in patients with unexplained recurrent miscarriage. A double-blind placebo randomized controlled trial. *Arch Gynecol Obstet* (2014) 290(4):757–62. doi: 10.1007/s00404-014-3262-0

97. Dan S, Wei W, Yichao S, Hongbo C, Shenmin Y, Jiaxiong W, et al. Effect of prednisolone administration on patients with unexplained recurrent miscarriage and in routine intracytoplasmic sperm injection: a meta-analysis. *Am J Reprod Immunol* (2015) 74(1):89–97. doi: 10.1111/aji.12373

98. Woon EV, Day A, Bracewell-Milnes T, Male V, Johnson M. Immunotherapy to improve pregnancy outcome in women with abnormal natural killer cell levels/activity and recurrent miscarriage or implantation failure: A systematic review and meta-analysis. *J Reprod Immunol* (2020) 142:103189. doi: 10.1016/j.jri.2020.103189

99. Sung N, Khan SA, Yiu ME, Jubiz G, Salazar MD, Skariah A, et al. Reproductive outcomes of women with recurrent pregnancy losses and repeated implantation failures are significantly improved with immunomodulatory treatment. *J Reprod Immunol* (2021) 148:103369. doi: 10.1016/j.jri.2021.103369

100. Nyborg KM, Kolte AM, Larsen EC, Christiansen OB. Immunomodulatory treatment with intravenous immunoglobulin and prednisone in patients with recurrent miscarriage and implantation failure after in *vitro* fertilization/intracytoplasmic sperm injection. *Fertil Steril* (2014) 102(6):1650–5. doi: 10.1016/j.fertnstert.2014.08.029

101. Practice Committee of the American Society for Reproductive Medicine. The role of immunotherapy in *in vitro* fertilization: a guideline. *Fertil Steril* (2018) 110 (3):387–400. doi: 10.1016/j.fertnstert.2018.05.009

102. ESHRE Working Group on Recurrent Implantation Failure, Cimadomo D, de Los Santos MJ, Griesinger G, Lainas G, Le Clef N, et al. ESHRE good practice recommendations on recurrent implantation failure. *Hum Reprod Open* (2023) 2023 (3):hoad023. doi: 10.1093/hropen/hoad023

103. Daskalakis G, Pergialiotis V, Domellöf M, Ehrhardt H, Di Renzo GC, Koç E, et al. European guidelines on perinatal care: corticosteroids for women at risk of preterm birth. *J Matern Fetal Neonatal Med* (2023) 36(1):2160628. doi: 10.1080/14767058.2022.2160628

frontiers | Frontiers in Immunology

ORIGINAL RESEARCH
published: 01 July 2022
doi: 10.3389/fimmu.2022.930582

First-Trimester Serum Cytokine Profile in Pregnancies Conceived After Assisted Reproductive Technology (ART) With Subsequent Pregnancy-Induced Hypertension

Xiangxin Lan[1,2,3†], *Ling Guo*[1,2,3†], *Shiqin Zhu*[1,2,3†], *Yongzhi Cao*[1,2], *Yue Niu*[1,2,3], *Shuwen Han*[4], *Zeyan Li*[3], *Yan Li*[1,2,3,5*] *and Junhao Yan*[1,2*]

[1] Center for Reproductive Medicine, Shandong University, Jinan, China, [2] Key Laboratory of Reproductive Endocrinology of Ministry of Education, Shandong University, Jinan, China, [3] Medical Integration and Practice Center, Shandong University, Jinan, China, [4] School of Biomedical Sciences, Shandong University, Jinan, China, [5] Suzhou Research Institute, Shandong University, Suzhou, China

Pregnancy-induced hypertension (PIH) is one of the most common pregnancy complications that seriously affects the mother and fetus. The incidence of PIH is higher in pregnancies conceived after assisted reproductive technology (ART) than in spontaneous pregnancies; thus, exploring potential serum biomarkers before PIH onset is of great significance for effective early prediction and prevention of PIH in the ART population. Cytokines are involved in the inflammatory response and immune regulation, which play an essential role in the pathogenesis of PIH. A description of the cytokine profile in the first trimester of pregnancy could help identify new diagnostic tools and develop targeted therapies for PIH in the ART population. The concentrations of classical predictive markers for PIH and another 48 cytokines were measured in the first-trimester pregnancy serum samples from 33 PIH patients and 33 matched normotensive controls (NC), both of whom conceived after ART treatment. The measured values were compared and analyzed between NC and PIH, followed by comprehensive bioinformatic analysis and logistic regression analysis. There was no significant difference in classical predictive markers, including Activin A, PlGF, sFLT1 (VEGFR), and sFLT1/PlGF, between the PIH and NC groups ($P > 0.05$), while 29 cytokines were significantly lower in the PIH group than in the NC group ($P < 0.05$). Logistic regression analysis revealed that 17 cytokines (IL-2Rα, M-CSF, IL-6, IL-2, β-NGF, IL-7, IL-12 (p70), SCF, IL-10, IL-9, MIG, GM-CSF, LIF, IL-1α, MCP-3, IL-4, and HGF) in the first-trimester pregnancy serum were significantly negatively correlated with the subsequent onset of PIH. With the top 3 cytokines (IL-7, MIG, and SCF) of receiver operating characteristic (ROC) analysis, we constructed an efficient multifactor combined detection and prediction model for PIH in ART pregnancy. Classical early predictors for

OPEN ACCESS

Edited by:
Diana Boraschi, Shenzhen Institute of Advanced Technology (SIAT) (CAS), China

Reviewed by:
Paola Migliorini, University of Pisa, Italy
Benjamin Swartzwelter, Colorado State University, United States

***Correspondence:**
Junhao Yan
yyy306@126.com
Yan Li
yanli.sdu@gmail.com

[†]*These authors have contributed equally to this work*

Specialty section:
This article was submitted to Cytokines and Soluble Mediators in Immunity, a section of the journal Frontiers in Immunology

Received: *28 April 2022*
Accepted: *08 June 2022*
Published: *01 July 2022*

Citation:
Lan X, Guo L, Zhu S, Cao Y, Niu Y, Han S, Li Z, Li Y and Yan J (2022) First-Trimester Serum Cytokine Profile in Pregnancies Conceived After Assisted Reproductive Technology (ART) With Subsequent Pregnancy-Induced Hypertension. Front. Immunol. 13:930582. doi: 10.3389/fimmu.2022.930582

hypertensive disorder complicating pregnancy cannot distinguish PIH from their normal peers in ART pregnancy. In comparison, the description of the cytokine profile in the first trimester of pregnancy enables us to distinguish high-risk ART pregnancy for PIH, permitting enough time for PIH prevention therapy. The cytokine profile we described also provides immunological insight into the further mechanistic exploration of PIH.

Keywords: cytokine profile, first trimester of pregnancy, pregnancy-induced hypertension, assisted reproductive technology, biomarker

INTRODUCTION

Pregnancy-induced hypertension (PIH) is one of the most common pregnancy complications, affecting 6% to 10% of pregnancies (1, 2). It is defined as a new onset of hypertension (systolic pressure ≥ 140 mmHg and/or diastolic pressure ≥ 90 mmHg) with or without proteinuria after the 20th week of gestation, which includes preeclampsia (3). PIH is characterized by maternal hypertension and multiorgan involvement resulting from systemic endothelial dysfunction, and it is also a major cause of maternal and fetal morbidity and mortality (4, 5). However, the clinical intervention of PIH stagnates in passive treatment after symptoms appear, resulting in poor prognosis. Hence, early prediction markers for PIH are of great significance for presymptomatic prophylaxis.

To date, there are several well-studied molecular markers related to placental hypoperfusion, such as placental growth factor (PlGF), soluble Fms-like tyrosine kinase-1 (sFlt-1) or vascular endothelial growth factor receptor (VEGFR) and Activin A. Although a high sFlt-1:PlGF ratio (6–8), high Activin A serum level (9) and low PlGF serum level (8) have been proven to be able to separate PIH from normotensive pregnant women, they all share low predictive accuracy in the first trimester of pregnancy (10, 11). Unfortunately, it has recently been found that the incidence of PIH in the ART population is higher than that in spontaneous pregnancy (12). Guidelines suggest that oral aspirin should be started at $11\text{-}14^{+6}$ gestational weeks in high-risk populations to achieve effective prevention (13). Therefore, it is urgent to explore biomarkers for the first-trimester prediction of PIH in the ART population.

The pathophysiological mechanisms of the development of PIH remain unclear. One of the more deeply studied mechanisms is fetal-maternal immunity (14). There is increasing evidence that PIH may originate from poor maternal immune tolerance and abnormal interactions between immune cells, trophoblast cells, and decidual stromal cells after embryo implantation. Immune cells such as natural killer cells, dendritic cells, and T regulatory lymphocytes in the decidua have impaired immune tolerance to spiral artery remodeling and the emergence of fetal trophoblasts, leading to increased placental shedding, exaggerated systemic inflammation, and subsequent endothelial dysfunction (15).

Cytokines are a family of small soluble proteins expressed by various cell and tissue types that serve as immune mediators. Their expression profiles have been used to classify immune responses and functional states of the immune system. Evidence suggests that cytokines play a crucial role in ovulation, implantation, placentation, and parturition during pregnancy (16, 17). Recent research indicates that PIH is related to immune dysregulation and that components of the immune system may interact with angiogenic and antiangiogenic factors (12). In this study, the cytokine profiles were characterized in paired PIH and normotensive women following ART treatment to determine the specific cytokine signature involved, which would be of great value to explain the occurrence of PIH after ART and provide new avenues for early diagnosis, monitoring, and intervention.

MATERIALS AND METHODS

Participants

In this study, 33 women diagnosed with PIH and 33 controls were selected from patients who underwent *in vitro* fertilization (IVF)/ intracytoplasmic sperm injection (ICSI) cycles based on a large prospective cohort conducted at the Research Center of the Reproductive Hospital Affiliated to Shandong University from January 2018 to June 2019. All patients were < 40 years and achieved singleton pregnancy by assisted reproductive technology in this pregnancy. Patients diagnosed with chronic autoimmune disease (such as systemic lupus erythematosus, thyroid autoimmunity, or antiphospholipid syndrome), preexisting secondary/essential hypertension, gestational diabetes mellitus, and other diseases that may affect the inflammatory process were excluded. Pregnancies after embryo transfer were followed by periodic reviews of electronic medical records until delivery. PIH was defined as a new onset of hypertension (systolic pressure ≥ 140 mmHg and/or diastolic pressure ≥ 90 mmHg) with or without proteinuria after the 20th week of gestation. According to clinical and laboratory evaluations, 33 patients diagnosed with PIH were included in the PIH group. To achieve a balanced baseline characteristics, propensity score matching (PSM) was applied to control for potential confounders, including age, BMI, cause of infertility, fertilization method, and embryo transfer proposal, which were weighted equally. The NC group included 33 healthy women who were matched in a 1:1 ratio to PIH based on the propensity score with a standard caliper width of 0.1. This study protocol was approved by the Ethical Committee of Reproductive Medicine of Shandong University, and all participants signed informed consent forms.

Sample Collection

At 11-13 gestational weeks following IVF/ICSI, 6 ml fasting blood samples of the participants were collected by venipuncture.

After centrifugation at 1300 × g for 10 minutes, serum samples were separated and stored at −80°C until measurement.

ELISA Analysis

The serum levels of Activin A, PlGF and sFLT1 were measured using commercial ELISA kits (R&D, Cat # DAC00B, Human/Mouse/Rat Activin A Quantikine ELISA Kit; Cat # DPG00, Human PLGF Quantikine ELISA Kit; Cat # DVR100C, Human VEGFR1/Flt-1 Quantikine ELISA Kit).

Cytokine Profiling

Individual serum samples were subjected to cytokine profile measurement by the Bio-Plex Pro Human Cytokine Screening Panel, 48-plex (BioRad). The protocol of the kit was followed for the analysis of a total of 48 cytokines, chemokines or growth factors. These included interleukin-1β (IL-1β), IL-1α, IL-1ra, IL-2, IL-2Rα, IL-3, IL-4, IL-5, IL-6, IL-7, IL-8, IL-9, IL-10, IL-12 (p40), IL-12 (p70), IL-13, IL-15, IL-16, IL-17A, IL-18, interferon-α2 (IFN-α2), interferon-γ (IFN-γ), tumor necrosis factor-α (TNF-α), tumor necrosis factor-β (TNF-β), granulocyte colony-stimulating factor (G-CSF), macrophage colony-stimulating factor (M-CSF), granulocyte-macrophage colony-stimulating factor (GM-CSF), leukemia inhibitory factor (LIF), stem cell factor (SCF), vascular endothelial growth factor (VEGF), Eotaxin, macrophage inflammatory protein-1α (MIP-1α), macrophage inflammatory protein-1β (MIP-1β), basic fibroblast growth factor (FGF basic), monocyte chemotactic protein-1 (MCP-1) or monocyte chemoattractant activating factor (MCAF), monocyte chemotactic protein-3 (MCP-3), nerve growth factor-β (β-NGF), RANTES, stromal cell derived factor-1α (SDF-1α), platelet-derived growth factor-BB (PDGF-BB), growth related oncogene-α (GRO-α), hepatocyte growth factor (HGF), interferon inducible protein-10 (IP-10), cutaneous T-cell attracting chemokine (CTACK), mifepristone (MIF), gamma-interferon-induced monokine (MIG), stem cell growth factor-β (SCGF-β), and TNF-related apoptosis-inducing ligand (TRAIL).

Statistical Analysis

Statistical analysis and graphical representations were completed in IBM SPSS Statistics 21 and GraphPad Prism. Normality was assessed by Kolmogorov–Smirnov tests. Normally distributed data are presented as the mean ± SEM, and the t test was used to compare the significant differences between groups. For data with a nonnormal distribution, the median with interquartile range was applied, and the Mann–Whitney U test was used for data comparison. Values of $P < 0.05$ were considered statistically significant. Principal component analysis (PCA), heatmap and cluster analysis, forest map, and half-violin plots were conducted using the website www.bioinformatics.com.cn. Univariate logistic regression analysis was performed to assess the longitudinal association between first-trimester serum cytokine levels and the occurrence of PIH. OR > 1 indicates a risk factor, and OR < 1 indicates a protective factor. Cytokines with $P < 0.05$ were considered to be related to the occurrence of PIH and included in Receiver operating characteristic (ROC) analysis. ROC curves were drawn to analyze the independent predictive value of specific cytokines for PIH. Additionally, IL-7, MIG, and SCF were selected to build a combined prediction model, and the combined diagnostic value of the prediction model for PIH was analyzed.

RESULTS

Baseline Characteristics and Perinatal Outcomes of the Participants

Table 1 displays the baseline characteristics and perinatal outcomes of 33 women who developed PIH in later pregnancy and their 33 matched normotensive controls (NC). The systolic pressure (NC 115.48 ± 2.15 vs. PIH 127.07 ± 2.17, $P < 0.01$) and mean arterial pressure (NC 85.30 ± 1.86 vs. PIH 92.66 ± 1.83, $P = 0.01$) before pregnancy were higher in the PIH group than in the NC group. There were no significant differences between the two groups in other prepregnancy baseline characteristics. The incidence of cesarean section was significantly higher in the PIH group than in the NC group (NC 66.70% vs. PIH 96.97%, $P < 0.01$). The gestational age at delivery was lower in the PIH group than in the NC group (NC 275 days vs. PIH 269 days, $P = 0.02$). Lower gestational age and higher cesarean section rate are related to each other and exactly reflect the characteristics of PIH.

Classical Serum Biomarker Levels in Pregnancy After Assisted Reproductive Technology

First, we wanted to verify whether classical serum biomarkers can distinguish PIH from NC in ART pregnancy. Activin A, PlGF and sFLT1 levels tested by ELISA and accordingly calculated sFlt1/PlGF are shown in **Table 2**. In the first-trimester serum of ART pregnancy, classical biomarkers appeared to have no predictive validity with no significant difference between NC and the women who developed PIH later in pregnancy.

Cytokine Profile in First-Trimester Serum in ART Pregnancy

To explore serum markers with potential predictive/diagnostic value for PIH in the first trimester of ART pregnancy, 48 cytokine expression levels were detected in patients with PIH and NC. PCA showed that the NC and PIH groups could be well distinguished by the first principal component (PC1), and a variety of cytokines contributed to PC1 and served as the main reason for the variation (**Figure 1A**). Heatmap and cluster analysis showed that the expression level of first-trimester serum cytokines in the PIH group was lower than that in the NC group (**Figure 1B**). In total, we found 29 differentially expressed cytokines between the two groups: IL-1β, IL-1α, IL-2, IL-2Rα, IL-4, IL-5, IL-6, IL-7, IL-9, IL-12 (p40), IL-12 (p70), IL-16, IL-17A, TNF-α, M-CSF, GM-CSF, LIF, SCF, Eotaxin, MIP-1β, FGF basic, MCP-1 (MCAF), β-NGF, SDF-1α, PDGF-BB, GRO-α, HGF, MIG, and TRAIL (**Figure 1C** and **Table 3**). Notably, compared with the NC group, the expression levels of all these cytokines were significantly lower in the PIH group ($P < 0.05$). In addition, we generated ROC curves for every cytokine that showed a significant difference (**Supplementary Figure 1**).

TABLE 1 | Baseline characteristics and perinatal outcomes of the participants.

		NC (N = 33)	PIH (N = 33)	P Value
Prepregnancy baseline characteristics				
Age (yr)-Mean ± SD		30.21 ± 4.29	29.94 ± 3.75	0.78
BMI (kg/m²)-Mean ± SD		25.17 ± 3.92	25.21 ± 3.94	0.97
Blood pressure (mmHg)-Mean ± SD				
	Systolic pressure	115.48 ± 2.15	127.07 ± 2.17	< 0.01*
	Diastolic pressure	70.21 ± 1.90	75.45 ± 1.87	0.06
	Mean arterial pressure	85.30 ± 1.86	92.66 ± 1.83	0.01*
Primigravida-no. (%)		29 (87.88)	29 (87.88)	> 0.99
PCOS-no. (%)		6 (46.2)	7 (53.8)	0.80
Cause of infertility-no. (%)				0.96
	Pelvic factor	10 (30.30)	9 (27.27)	
	Male factor	2 (6.06)	2 (6.06)	
	Confounding factor	21 (63.64)	22 (66.67)	
Endometrial preparation protocol-no. (%)				0.80
	Natural cycle	14 (42.42)	13 (39.39)	
	Hormonally controlled	19 (57.58)	20 (60.61)	
Mode of fertilization-no. (%)				0.60
	IVF	21 (63.64)	23 (69.70)	
	ICSI	12 (36.36)	10 (30.30)	
Perinatal outcomes				
Delivery mode-no. (%)				< 0.01*
	Vaginal delivery	11 (33.33)	1 (3.03)	
	Cesarean delivery	22 (66.67)	32 (96.97)	
Gestational age at delivery (day)-Median (P25, P75)		275.00 (269.00,279.50)	269.00 (263.50, 273.00)	0.02*
Delivery at <37 wk-no. (%)		4 (12.12)	5 (15.15)	> 0.99
Neonatal birth weight (g)-Mean ± SD		3319.09 ± 107.72	3137.19 ± 93.48	0.21
Low birth weight infants (<2500 g)-no. (%)		3 (9.09)	2 (6.06)	0.64

*Values are the mean ± SD/median (P25, P75) or n. (%). BMI, body mass index; PCOS, polycystic ovarian syndrome; IVF, in vitro fertilization; ICSI, intracytoplasmic sperm injection. Significant difference (P < 0.05, marked by *).*

TABLE 2 | Classical serum biomarker levels in pregnancy after assisted reproductive technology.

Cytokine	NC (N = 33)	PIH (N = 33)	*P* Value
Activin A (pg/mL)	2168.54 (1247.21, 3105.89)	1917.64 (1340.23, 2754.65)	0.621
PlGF (pg/mL)	56.43 (43.23, 71.14)	44.48 (36.06, 71.30)	0.221
sFlt1 (VEGFR) (pg/mL)	14401.52 (9859.96, 19593.74)	11592.32 (7951.62, 14677.62)	0.052
sFlt1/PlGF	243.43 (178.763, 315.70)	229.72 (163.65, 314.83)	0.485

Values are median (P25, P75). PlGF, placental growth factor; sFLT1, soluble fms-like tyrosine kinase-1. Significant difference (P < 0.05).

Relationship Between the First-Trimester Serum Cytokine Profile and Subsequent PIH

We further analyzed the relationship between serum cytokine levels in the first trimester of pregnancy and the occurrence of PIH in later pregnancy by logistic regression analysis. Univariate logistic regression analysis showed that 35 cytokines were associated with subsequent PIH (**Figure 2A**). After adjusting for the influence of prepregnancy mean arterial pressure, 17 cytokines in early pregnancy serum were found to be negatively associated with an increased risk of PIH in later pregnancy, including IL-2Rα, M-CSF, IL-6, IL-2, β-NGF, IL-7, IL-12 (p70), SCF, IL-10, IL-9, MIG, GM-CSF, LIF, IL-1α, MCP-3, IL-4, and HGF (**Figure 2B**).

Predictive Value of Serum Cytokines in Early Pregnancy for PIH in ART Pregnancy

We selected the above 17 cytokines related to PIH and further explored their predictive value as potential target molecules for PIH. The ROC curve analysis results are shown in **Table 4**. Among the above 17 PIH-related cytokines, IL-7, MIG and SCF are the top three cytokines with pronounced predictive values for PIH. We then selected IL-7, MIG, and SCF to construct a combined prediction model, which was found to have good predictive value for PIH. (AUC 0.821, 95% CI: 0.718-0.924, $P < 0.001$) (**Figure 3**). The AUC of the combination of IL-7, MIG, and SCF was larger than that of every single cytokine, which proved that the combined prediction model had a better ability to predict PIH than other individual indicators. The sensitivity (true-positive rate) was 81.8%, and the specificity (true-negative rate) was 72.7%. Other analyses for variable selection and the suboptimal combined prediction model are graphically represented in **Supplementary Table 1** and **Supplementary Figure 2**. In addition, we evaluated the predictive value of decreased cytokine levels on pregnancy outcome, including delivery mode, delivery at <37wk, and low birth weight infants. We found IL-2Rα, M-CSF, SCF, and MIG are individual risk factors for cesarean delivery, and a combination of these four risk factors provide a good predictive value (AUC=0.722, $P = 0.004$) for cesarean delivery mode (**Supplementary Figure 3**).

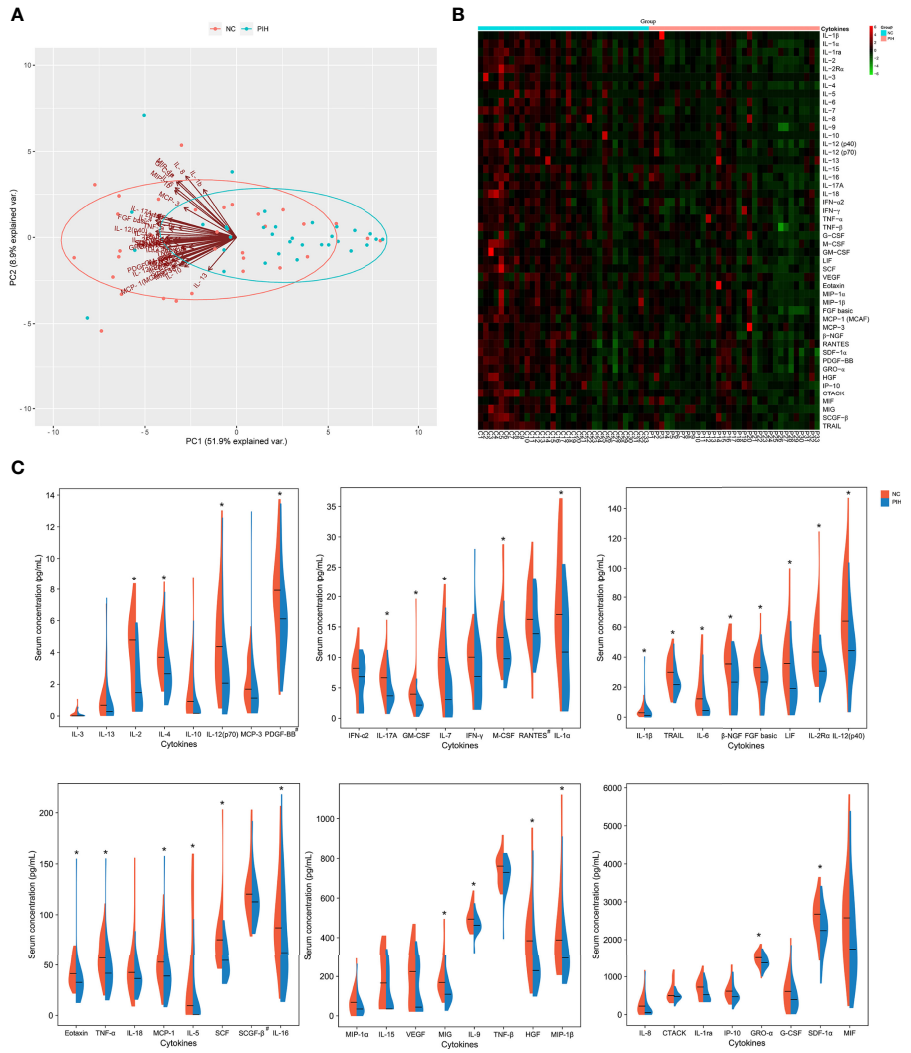

FIGURE 1 | Analysis of 48 cytokine profiles in the first-trimester pregnancy serum of the NC group vs. the PIH group. **(A)**, PCA of 48 cytokine profiles in the first-trimester pregnancy serum. The points in the diagram represent the samples, red for the NC group and blue for the PIH group. The arrows represent the contribution and correlation of the corresponding original variables to the principal component. **(B)**, Heatmap analysis of 48 cytokine profiles in the first-trimester pregnancy serum. The row displays the cytokines, and the column represents the sample number. The color key represents the deviation of global median concentrations for each cytokine. These median values (homogenized to 0 and displayed in dark) were calculated after homogenization treatment and used as a cut-off to separate high and low cytokine concentrations. Color gradation from red to green indicates high to low cytokine concentrations, respectively, with homogenized values ranging from 6 to -6. **(C)**, Half-violin plots showing the expression distributions of 48 cytokines in the first-trimester pregnancy serum between the NC group and the PIH group. Six boxes were plotted according to general cytokine concentrations. The ordinate indicates the serum concentration of cytokines, with pg/mL as the concentration unit, except for the concentration units of PDGF-BB, RANTES, and SCGF-β (marked by #) being ng/mL. Every different cytokine is shown as density (violin shap) and median value (horizontal lines) for NC vs. PIH. The left half (red) of each plot represents the NC group, and the right half (blue) represents the PIH group. Asterisk (*) represents a significant difference in cytokine expression in the first-trimester pregnancy serum between the two groups.

DISCUSSION

PIH is a common pregnancy-specific complication that threatens both maternal and fetal safety (18–20). As a result of the lack of definitive therapies except for early delivery of the feto-placental unit once PIH occurs, in recent years, guidelines have placed greater emphasis on early warning, early detection and early intervention (21–23). Low-dose aspirin (LDA) is suggested to be used beginning from 11 gestational weeks for better prevention efficacy in high-risk women (13, 23–25). In regard to ART pregnancy, the evaluation and prediction methods of PIH remain to be elucidated. In this study, we brought forward the serum cytokine testing time to as early as 11-13 gestational weeks for a potential timely prediction for PIH after ART. It is worth noting that even the routinely used predictive parameters, such as Activin A, PlGF, sFlt1 and sFlt1/PlGF, were not able to differ PIH from controls in ART women, which is in line with another recent study targeting the IVF population, reporting no

TABLE 3 | Cytokine profile in first-trimester serum in ART pregnancy.

Cytokine (pg/mL)	Controls (N = 33)	PIH (N = 33)	*P* Value	Cytokine (pg/mL)	Controls (N = 33)	PIH (N = 33)	*P* Value
*IL-1β	2.93 (1.48, 6.24)	1.21 (0.82,3.57)	0.011	G-CSF	615.19 (191.61, 866.13)	399.05 (180.65,654.47)	0.132
*IL-1α	19.14 (12.91, 27.63)	12.91 (5.90,18.10)	0.001	*M-CSF	13.26 (10.39, 17.04)	9.78 (8.06,12.48)	< 0.001
IL-1ra	754.61 (563.53, 931.41)	621.73 (490.48,806.13)	0.132	*GM-CSF	3.97 (2.97, 5.02)	2.18 (1.62,2.97)	< 0.001
*IL-2	4.79 (3.33, 6.23)	2.78 (1.13,4.34)	< 0.001	*LIF	35.99 (23.57, 48.17)	19.35 (10.74,35.99)	0.005
*IL-2Rα	43.69 (32.21, 62.07)	30.92 (24.50,38.92)	< 0.001	*SCF	75.37 (56.95, 87.72)	54.54 (41.27,68.84)	< 0.001
IL-3	0.21 (0.04, 0.42)	0.18 (0.06,0.44)	0.746	VEGF	241.12 (147.15, 342.22)	231.61 (84.03,272.58)	0.197
*IL-4	3.70 (2.89, 5.22)	2.66 (1.64,3.77)	0.002	*Eotaxin	41.31 (32.02, 54.46)	32.69 (22.51,39.91)	0.001
*IL-5	64.32 (26.94, 126.01)	14.91 (8.41,58.69)	0.007	MIP-1α	68.56 (10.83, 106.22)	34.84 (9.81,71.25)	0.099
*IL-6	12.51 (6.06, 29.49)	5.24 (2.44,14.71)	0.002	*MIP-1β	388.30 (262.23, 529.08)	294.13 (234.93,379.84)	0.029
*IL-7	9.96 (5.51, 12.08)	5.51 (3.07,7.78)	< 0.001	*FGF basic	33.27 (25.93, 41.14)	25.94 (18.56,33.76)	0.03
IL-8	230.33 (36.70, 408.97)	86.52 (21.61,207.12)	0.052	*MCP-1 (MCAF)	52.70 (38.31, 73.37)	38.95 (24.46,52.13)	0.014
*IL-9	494.05 (452.60, 537.36)	462.89 (438.57,499.35)	0.022	MCP-3	1.83 (1.35, 3.49)	1.42 (0.91,1.96)	0.116
IL-10	1.68 (0.92, 3.14)	0.73 (0.17,1.68)	0.188	*β-NGF	41.57 (29.74, 46.19)	25.47 (17.27,36.90)	0.004
*IL-12 (p40)	64.38 (52.06, 93.65)	44.61 (34.61,54.53)	< 0.001	RANTES	1624.35 (13493.87, 21797.75)	1388.68 (11416.12, 18478.29)	0.095
*IL-12 (p70)	4.37 (2.48, 6.53)	2.28 (1.67,3.95)	0.01	*SDF-1α	2652.52 (2290.04, 2996.44)	2215.57 (1867.89,2593.89)	0.007
IL-13	0.86 (0.63, 1.45)	0.68 (0.28,1.04)	0.176	*PDGF-BB	7927.44 (5971, 9627.23)	6115.82 (4231.42, 7319.49)	0.031
IL-15	290.99 (166.36, 350.68)	198.59 (157.51,265.26)	0.164	*GRO-α	1517.16 (1367.91, 1618.30)	1377.92 (1269.18,1521.83)	0.022
*IL-16	87.15 (70.04, 123.29)	62.67 (43.89,110.71)	0.041	*HGF	384.31 (271.83, 493.41)	229.67 (189.72,348.35)	0.002
*IL-17A	6.66 (4.43, 8.54)	3.69 (2.96,6.66)	0.003	IP-10	622.64 (439.78, 779.46)	473.83 (386.64,608.99)	0.054
IL-18	42.53 (29.65, 55.84)	36.53 (25.78,48.17)	0.14	CTACK	501.42 (405.36, 715.20)	476.80 (400.04,550.13)	0.197
IFN-α2	8.22 (6.66, 10.26)	7.53 (5.42,8.90)	0.176	MIF	2552.33 (1572.57, 3226.17)	1720.26 (1015.06,2776.20)	0.106
IFN-γ	10.16 (7.21, 12.61)	9.35 (4.77,11.33)	0.4	*MIG	169.31 (135.75, 237.82)	109.68 (72.98,160.12)	< 0.001
*TNF-α	56.98 (45.56, 76.22)	41.73 (29.39,54.70)	0.003	SCGF-β	1203.12 (106619.85, 136337.81)	1127.04 (99055.56, 129400.67)	0.108
TNF-β	761.20 (687.85, 796.32)	729.31 (662.35,768.62)	0.064	*TRAIL	29.92 (21.70, 39.14)	21.70 (18.06,27.57)	0.01

Values are median (P25, P75). P < 0.05 was considered statistically significant and indicated by an asterisk.

significant difference in first-trimester serum Activin A between normotensive controls and pregnancies with subsequent PE/PIH (26). This is possibly ascribed to the potentially undefined population specificity, emphasizing the importance of exploring novel biomarkers for PIH in the ART population. Our results show that the cytokine profile in the first trimester of ART pregnancy demonstrated a significantly downregulated trend in ART women destined to develop PIH. We found 17 cytokines in the serum of first-trimester pregnancy related to the increased risk of PIH, including 10 interleukins (IL): IL-1α, IL-2Rα, IL-2, IL-4, IL-6, LIF, IL-7, IL-9, IL-10, and IL-12 (p70); three colony stimulating factors (CSF): M-CSF, GM-CSF, and SCF; two chemokines: MIG and MCP-3; and two growth factors (GF): β-NGF and HGF. Moreover, we constructed a first-trimester prediction model using IL-7, MIG, and SCF for screening out the cases at high risk of developing PIH preceding clinical manifestations in ART pregnancy.

With increasing knowledge, the antecedents of poor placentation of PIH are considered to be immunological in origin (14, 27, 28). At the maternal-fetal interface during early pregnancy, the adaptive regulation of maternal immunity is mainly characterized by the transformation of T helper type 1 (Th1) cytokines to Th2 cytokines (29, 30). Studies have shown that the shift toward Th2 may be hindered in PIH, with the cytokine profile in peripheral blood being mainly Th1 (31, 32). Our results support this theory; that is, IL-4, IL-9 and IL-10, which are related to Th2 in the serum of PIH patients during early pregnancy, are significantly downregulated.

The cytokine profile of PIH in previous studies was usually demonstrated during middle and late pregnancy, which is generally characterized by a pro-inflammatory state, showing a higher level of proinflammatory cytokines, such as IL-1, IL-6, IL-8, IL-17, and TNF-α, and a lower level of anti-inflammatory interleukins, especially IL-10, IL-33, and IL-35 (15, 33–35). Compared to the pro-inflammatory state in middle and late pregnancy, our assay in the ART population showed that proinflammatory factors such as IL-6 and IL-12 were downregulated in the first-trimester serum of PIH patients. A study in rats indicated that IL-6-mediated arterial pressure elevation is due to a response to chronic reductions in uterine perfusion pressure during pregnancy (36). Therefore, we hypothesized that in ART pregnancy, the shift toward a

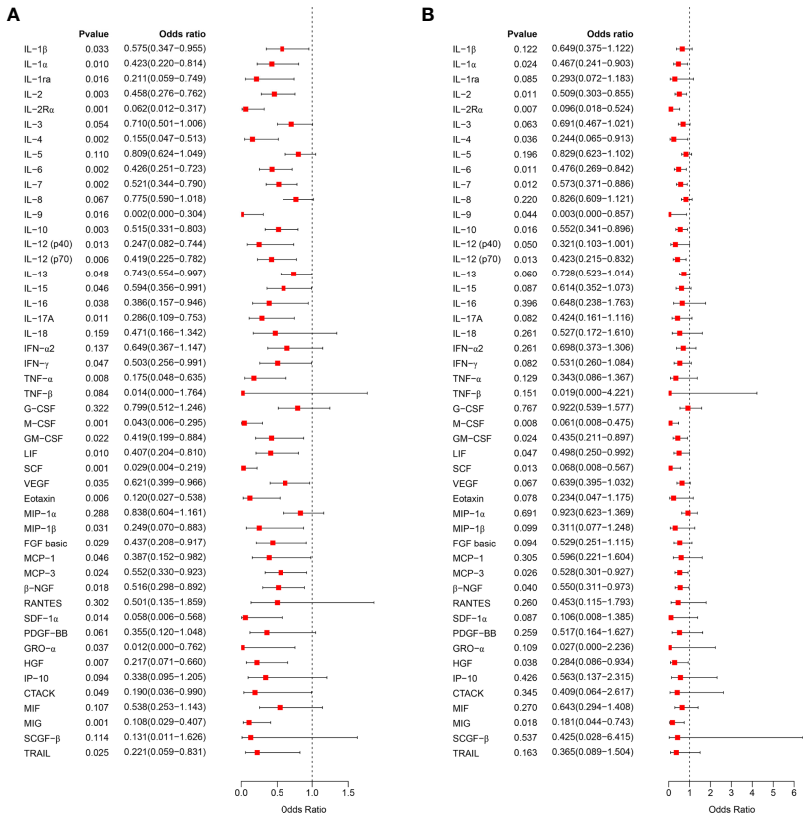

FIGURE 2 | Correlation analysis of early pregnancy serum cytokines and PIH. **(A)**, The relationship between the expression level of 48 cytokines in early pregnancy serum and the occurrence of PIH in later pregnancy was analyzed by univariate logistic regression analysis and visualized as a forest map. **(B)**, After correcting the mean arterial pressure before pregnancy, the relationship between the expression level of 48 serum cytokines in early pregnancy and the occurrence of PIH in later pregnancy was analyzed by logistic regression analysis. OR > 1 indicates a risk factor, and OR < 1 indicates a protective factor.

TABLE 4 | ROC analysis of serum cytokines in early pregnancy for PIH predictive/diagnostic value.

Cytokines	AUC (95% CI)	*P* value
IL-7	0.787 (0.676-0.899)	< 0.001
MIG	0.766 (0.651-0.882)	< 0.001
SCF	0.763 (0.649-0.876)	< 0.001
M-CSF	0.759 (0.644-0.875)	< 0.001
GM-CSF	0.759 (0.637-0.881)	< 0.001
IL-2	0.758 (0.641-0.876)	< 0.001
IL-2Rα	0.756 (0.64-0.873)	< 0.001
IL-6	0.737 (0.617-0.857)	0.001
IL-4	0.736 (0.616-0.857)	0.001
IL-12 (p70)	0.729 (0.607-0.852)	0.001
β-NGF	0.729 (0.607-0.850)	0.001
LIF	0.723 (0.599-0.847)	0.002
HGF	0.721 (0.594-0.849)	0.002
IL-1α	0.716 (0.593-0.839)	0.003
IL-10	0.697 (0.567-0.826)	0.006
MCP-3	0.675 (0.545-0.805)	0.015
IL-9	0.664 (0.533-0.796)	0.022

AUC: area under the curve; CI: confidence interval. Significant difference (P < 0.05).

proinflammatory phenotype in PIH probably does not occur in the very early stages of the disease. Similarly, the association of IL-12 serum levels with the development of PIH has been assessed in various studies, drawing no certain conclusions because of conflicting evidence (37–41). In fact, a proinflammatory phenotype is the result of compensation for insufficient immune activation and early placental establishment in the first trimester. Therefore, most studies devoted to finding biomarkers in middle and late pregnancy to predict PIH failed to achieve good clinical application effects (42). The difference in serum proinflammatory factors in PIH patients at different pregnancy stages and the dynamic changes need to be further explored.

In spontaneous pregnancy, semen exposure between coitus and conception primes innate and adaptive immune cells for prepared maternal immune tolerance in advance of potential implantation (43–45). In contrast, ART pregnancy tends to directly transfer embryos under the premise of prohibiting sexual intercourse in the transfer cycle. This may at least partially explain why ART is associated with an increased risk of PIH and at the same time support our results that the PIH

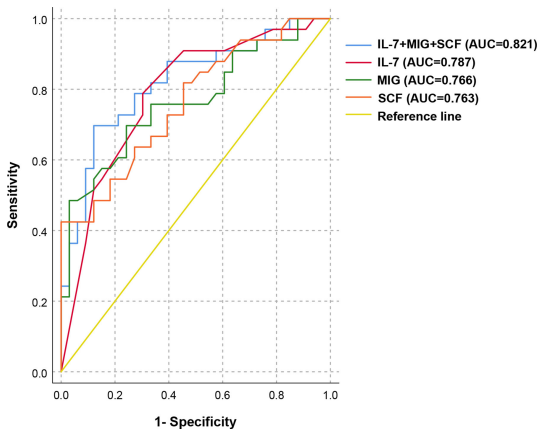

FIGURE 3 | ROC analysis of the combined prediction model for the prediction of PIH in ART pregnancy. ROC curves show the results of ROC analysis for differentiation between PIH and NC in ART pregnancy. ROC curve analysis revealed that IL-7, MIG, and SCF appeared to be potential biomarkers for the separation between PIH and NC in the first trimester of pregnancy (AUC = 0.821, 95% CI: 0.718-0.924, $P < 0.001$), with a sensitivity of 81.8% and a specificity of 72.7%.

group showed lower serum cytokine levels than the normotensive group at 11-13 weeks gestation. In other words, inadequate tolerance induction before embryo transfer results in a universally low level of serum cytokines in the first trimester of pregnancy, which may disrupt the inflammatory process of embryo implantation and is in turn involved in the shallow invasion of trophoblasts in early PIH (46).

The present study is based on the human biobank of our large-scale assisted reproductive cohort platform and is the first to delineate the first-trimester serum cytokine profile of PIH, especially for the ART population. We found that maternal serum concentrations of multiple immune-related cytokines were significantly decreased in the first trimester of ART pregnancy with subsequent PIH. With conjoint analysis of serum IL-7, MIG and SCF, we demonstrated a first-trimester prediction model before PIH onset and subsequent compensatory response. Admittedly, the number of participants included in the current study is still limited and further research with a large sample size is needed to support our findings.

The establishment and maintenance of pregnancy poses great challenges to the maternal immune system. Uncoordinated maternal immunization, especially in the first trimester of pregnancy, will be a potential cause of a series of pregnancy complications (47, 48). Currently, immunotherapy has been applied to the treatment of a variety of reproductive diseases, such as recurrent spontaneous abortion (RSA) and recurrent implantation failure (RIF) (49), while the immunotherapy against PIH still needs a long way to go. Our study described the first-trimester serum cytokine profile in pregnancies conceived after ART and provided a better understanding of the immunological etiology and pathophysiology of PIH in the specific population. Additionally, the first-trimester immune disturbance enables early prediction, which guarantees enough time for low-dose aspirin (LDA) prevention before the appearance of hypertension symptom and hopefully may also promote novel therapeutic strategies on immune regulation and shed light on the clinical management of PIH in the ART population.

DATA AVAILABILITY STATEMENT

The original contributions presented in the study are included in the article/**Supplementary Material**. Further inquiries can be directed to the corresponding authors.

ETHICS STATEMENT

The studies involving human participants were reviewed and approved by Ethical Committee of Reproductive Medicine of Shandong University. The patients/participants provided their written informed consent to participate in this study. Written informed consent was obtained from the individual(s) for the publication of any potentially identifiable images or data included in this article.

AUTHOR CONTRIBUTIONS

YL conceived and designed the project. XL, LG, and SZ performed the experiments and analyzed the data. XL, YC, and YN collected the clinical serum samples and information. XL, LG, SZ, SH, and ZL wrote the manuscript. YL and JY critically revised the manuscript. All authors have been involved in interpreting the data and approved the final version.

FUNDING

This study was supported by grants from the National Key Research and Development Program of China (2021YFC2700604), the National Natural Science Foundation of China (82101784, 82171648), the Key Research and Development Program of Shandong Province (2021LCZX02), the Natural Science Foundation of Shandong Province (ZR2020QH051), the Natural Science Foundation of Jiangsu Province (BK20200223), Taishan Scholars Program for Young Experts of Shandong Province (tsqn201812154) and the Young Scholars Program of Shandong University.

SUPPLEMENTARY MATERIAL

The Supplementary Material for this article can be found online at: https://www.frontiersin.org/articles/10.3389/fimmu.2022.930582/full#supplementary-material

REFERENCES

1. *WHO Recommendations for Prevention and Treatment of Pre-Eclampsia and Eclampsia*. Geneva: World Health Organization (2011).
2. Kintiraki E, Papakatsika S, Kotronis G, Goulis DG, Kotsis V. Pregnancy-Induced Hypertension. *Hormones (Athens)* (2015) 14(2):211–23. doi: 10.14310/horm.2002.1582
3. Berhe AK, Ilesanmi AO, Aimakhu CO, Bezabih AM. Awareness of Pregnancy Induced Hypertension Among Pregnant Women in Tigray Regional State, Ethiopia. *Pan Afr Med J* (2020) 35:71. doi: 10.11604/pamj.2020.35.71.19351
4. Redman CW, Sargent IL. Latest Advances in Understanding Preeclampsia. *Science* (2005) 308(5728):1592–4. doi: 10.1126/science.1111726
5. Reddy S, Jim B. Hypertension and Pregnancy: Management and Future Risks. *Adv Chronic Kidney Dis* (2019) 26(2):137–45. doi: 10.1053/j.ackd.2019.03.017
6. Zeisler H, Llurba E, Chantraine F, Vatish M, Staff AC, Sennström M, et al. Predictive Value of the Sflt-1:Plgf Ratio in Women With Suspected Preeclampsia. *N Engl J Med* (2016) 374(1):13–22. doi: 10.1056/NEJMoa1414838
7. Levine RJ, Lam C, Qian C, Yu KF, Maynard SE, Sachs BP, et al. Soluble Endoglin and Other Circulating Antiangiogenic Factors in Preeclampsia. *N Engl J Med* (2006) 355(10):992–1005. doi: 10.1056/NEJMoa055352
8. Verlohren S, Galindo A, Schlembach D, Zeisler H, Herraiz I, Moertl MG, et al. An Automated Method for the Determination of the Sflt-1/Pigf Ratio in the Assessment of Preeclampsia. *Am J Obstet Gynecol* (2010) 202(2):161.e1–.e11. doi: 10.1016/j.ajog.2009.09.016
9. Williamson RD, O'Keeffe GW, Kenny LC. Activin Signalling and Pre-Eclampsia: From Genetic Risk to Pre-Symptomatic Biomarker. *Cytokine* (2015) 71(2):360–5. doi: 10.1016/j.cyto.2014.11.017
10. Tarca AL, Romero R, Benshalom-Tirosh N, Than NG, Gudicha DW, Done B, et al. The Prediction of Early Preeclampsia: Results From a Longitudinal Proteomics Study. *PloS One* (2019) 14(6):e0217273. doi: 10.1371/journal.pone.0217273
11. Zhong Y, Zhu F, Ding Y. Serum Screening in First Trimester to Predict Pre-Eclampsia, Small for Gestational Age and Preterm Delivery: Systematic Review and Meta-Analysis. *BMC Pregnancy Childbirth* (2015) 15:191. doi: 10.1186/s12884-015-0608-y
12. Henriksson P. Cardiovascular Problems Associated With Ivf Therapy. *J Intern Med* (2021) 289(1):2–11. doi: 10.1111/joim.13136
13. Poon LC, Shennan A, Hyett JA, Kapur A, Hadar E, Divakar H, et al. The International Federation of Gynecology and Obstetrics (Figo) Initiative on Pre-Eclampsia: A Pragmatic Guide for First-Trimester Screening and Prevention. *Int J Gynaecol Obstet* (2019) 145 Suppl 1(Suppl 1):1–33. doi: 10.1002/ijgo.12802
14. Redman C. The Six Stages of Pre-Eclampsia. *Pregnancy Hypertens* (2014) 4 (3):246. doi: 10.1016/j.preghy.2014.04.020
15. Aggarwal R, Jain AK, Mittal P, Kohli M, Jawanjal P, Rath G. Association of Pro- and Anti-Inflammatory Cytokines in Preeclampsia. *J Clin Lab Anal* (2019) 33(4):e22834. doi: 10.1002/jcla.22834
16. Bowen JM, Chamley L, Mitchell MD, Keelan JA. Cytokines of the Placenta and Extra-Placental Membranes: Biosynthesis, Secretion and Roles in Establishment of Pregnancy in Women. *Placenta* (2002) 23(4):239–56. doi: 10.1053/plac.2001.0781
17. Osman I, Young A, Ledingham MA, Thomson AJ, Jordan F, Greer IA, et al. Leukocyte Density and Pro-Inflammatory Cytokine Expression in Human Fetal Membranes, Decidua, Cervix and Myometrium Before and During Labour at Term. *Mol Hum Reprod* (2003) 9(1):41–5. doi: 10.1093/molehr/gag001
18. Xiong T, Mu Y, Liang J, Zhu J, Li X, Li J, et al. Hypertensive Disorders in Pregnancy and Stillbirth Rates: A Facility-Based Study in China. *Bull World Health Organ* (2018) 96(8):531–9. doi: 10.2471/blt.18.208447
19. Ananth CV, Basso O. Impact of Pregnancy-Induced Hypertension on Stillbirth and Neonatal Mortality. *Epidemiology* (2010) 21(1):118–23. doi: 10.1097/EDE.0b013e3181c297af
20. Sutton ALM, Harper LM, Tita ATN. Hypertensive Disorders in Pregnancy. *Obstet Gynecol Clin North Am* (2018) 45(2):333–47. doi: 10.1016/j.ogc.2018.01.012
21. Askie LM, Duley L, Henderson-Smart DJ, Stewart LA. Antiplatelet Agents for Prevention of Pre-Eclampsia: A Meta-Analysis of Individual Patient Data. *Lancet* (2007) 369(9575):1791–8. doi: 10.1016/s0140-6736(07)60712-0
22. Chaemsaithong P, Sahota DS, Poon LC. First Trimester Preeclampsia Screening and Prediction. *Am J Obstet Gynecol* (2020) 226(2s):S1071-S97.e2. doi: 10.1016/j.ajog.2020.07.020
23. Sinkey RG, Battarbee AN, Bello NA, Ives CW, Oparil S, Tita ATN. Prevention, Diagnosis, and Management of Hypertensive Disorders of Pregnancy: A Comparison of International Guidelines. *Curr Hypertens Rep* (2020) 22 (9):66. doi: 10.1007/s11906-020-01082-w
24. National Guideline A. National Institute for Health and Care Excellence: Clinical Guidelines. In: *Hypertension in Pregnancy: Diagnosis and Management*. London: National Institute for Health and Care Excellence (UK) (2019).
25. Acog Committee Opinion No. 743: Low-Dose Aspirin Use During Pregnancy. *Obstet Gynecol* (2018) 132(1):e44–52. doi: 10.1097/aog.0000000000002708
26. Zhu S, Li Z, Cui L, Ban Y, Leung PCK, Li Y, et al. Activin a Increases Human Trophoblast Invasion by Upregulating Integrin β1 Through Alk4. *FASEB J* (2021) 35(2):e21220. doi: 10.1096/fj.202001604R
27. LaMarca B, Cornelius D, Wallace K. Elucidating Immune Mechanisms Causing Hypertension During Pregnancy. *Physiol (Bethesda)* (2013) 28 (4):225–33. doi: 10.1152/physiol.00006.2013
28. Laresgoiti-Servitje E, Gómez-López N, Olson DM. An Immunological Insight Into the Origins of Pre-Eclampsia. *Hum Reprod Update* (2010) 16(5):510–24. doi: 10.1093/humupd/dmq007
29. Lin H, Mosmann TR, Guilbert L, Tuntipopipat S, Wegmann TG. Synthesis of T Helper 2-Type Cytokines at the Maternal-Fetal Interface. *J Immunol* (1993) 151(9):4562–73.
30. Saito S, Sakai M, Sasaki Y, Tanebe K, Tsuda H, Michimata T. Quantitative Analysis of Peripheral Blood Th0, Th1, Th2 and the Th1:Th2 Cell Ratio During Normal Human Pregnancy and Preeclampsia. *Clin Exp Immunol* (1999) 117(3):550–5. doi: 10.1046/j.1365-2249.1999.00997.x
31. Arriaga-Pizano L, Jimenez-Zamudio L, Vadillo-Ortega F, Martinez-Flores A, Herrerias-Canedo T, Hernandez-Guerrero C. The Predominant Th1 Cytokine Profile in Maternal Plasma of Preeclamptic Women Is Not Reflected in the Choriodecidual and Fetal Compartments. *J Soc Gynecol Investig* (2005) 12 (5):335–42. doi: 10.1016/j.jsgi.2005.02.005
32. Hennessy A, Pilmore HL, Simmons LA, Painter DM. A Deficiency of Placental Il-10 in Preeclampsia. *J Immunol* (1999) 163(6):3491–5.
33. Stefańska K, Zieliński M, Jankowiak M, Zamkowska D, Sakowska J, Adamski P, et al. Cytokine Imprint in Preeclampsia. *Front Immunol* (2021) 12:667841. doi: 10.3389/fimmu.2021.667841
34. Ribeiro VR, Romao-Veiga M, Romagnoli GG, Matias ML, Nunes PR, Borges VTM, et al. Association Between Cytokine Profile and Transcription Factors Produced by T-Cell Subsets in Early- and Late-Onset Pre-Eclampsia. *Immunology* (2017) 152(1):163–73. doi: 10.1111/imm.12757
35. Bellos I, Karageorgiou V, Kapnias D, Karamanli KE, Siristatidis C. The Role of Interleukins in Preeclampsia: A Comprehensive Review. *Am J Reprod Immunol* (2018) 80(6):e13055. doi: 10.1111/aji.13055
36. Gadonski G, LaMarca BB, Sullivan E, Bennett W, Chandler D, Granger JP. Hypertension Produced by Reductions in Uterine Perfusion in the Pregnant Rat: Role of Interleukin 6. *Hypertension* (2006) 48(4):711–6. doi: 10.1161/01.Hyp.0000238442.33463.94
37. Celik H, Avcı B, Alper T. Comparison of Maternal Serum Levels of Interleukin-10, Interleukin-12, and Interleukin-2 in Normal and Preeclamptic Pregnancies. *Pregnancy Hypertens* (2012) 2(1):39–42. doi: 10.1016/j.preghy.2011.09.005
38. Omu AE, Makhseed M, al-Qattan F. Effect of Antihypertensive Therapy in Preeclampsia on Levels of Serum Interleukin-4. *Gynecol Obstet Invest* (1996) 42(4):230–6. doi: 10.1159/000291969
39. Daniel Y, Kupferminc MJ, Baram A, Jaffa AJ, Fait G, Wolman I, et al. Plasma Interleukin-12 Is Elevated in Patients With Preeclampsia. *Am J Reprod Immunol* (1998) 39(6):376–80. doi: 10.1111/j.1600-0897.1998.tb00372.x
40. Bachmayer N, Rafik Hamad R, Liszka L, Bremme K, Sverremark-Ekström E. Aberrant Uterine Natural Killer (Nk)-Cell Expression and Altered Placental and Serum Levels of the Nk-Cell Promoting Cytokine Interleukin-12 in Pre-Eclampsia. *Am J Reprod Immunol* (2006) 56(5-6):292–301. doi: 10.1111/j.1600-0897.2006.00429.x
41. Liang Z, Zhu J, Wang Y, Wang Y, Zhang Y, Lin J, et al. Three Transcription Factors and the Way Immune Cells Affected by Different Plasma Change in Opposite Ways in the Development of the Syndrome of Pre-Eclampsia. *Chin Med J (Engl)* (2014) 127(12):2252–8. doi: 10.3760/cma.j.issn.0366-6999.20140290

42. Hayes-Ryan D, Khashan AS, Hemming K, Easter C, Devane D, Murphy DJ, et al. Placental Growth Factor in Assessment of Women With Suspected Pre-Eclampsia to Reduce Maternal Morbidity: A Stepped Wedge Cluster Randomised Control Trial (Parrot Ireland). *Bmj* (2021) 374:n1857. doi: 10.1136/bmj.n1857
43. Robertson SA. Seminal Plasma and Male Factor Signalling in the Female Reproductive Tract. *Cell Tissue Res* (2005) 322(1):43–52. doi: 10.1007/s00441-005-1127-3
44. Robertson SA, Prins JR, Sharkey DJ, Moldenhauer LM. Seminal Fluid and the Generation of Regulatory T Cells for Embryo Implantation. *Am J Reprod Immunol* (2013) 69(4):315–30. doi: 10.1111/aji.12107
45. Robertson SA, Sharkey DJ. Seminal Fluid and Fertility in Women. *Fertil Steril* (2016) 106(3):511–9. doi: 10.1016/j.fertnstert.2016.07.1101
46. Harmon AC, Cornelius DC, Amaral LM, Faulkner JL, Cunningham MWJr., Wallace K, et al. The Role of Inflammation in the Pathology of Preeclampsia. *Clin Sci (Lond)* (2016) 130(6):409–19. doi: 10.1042/cs20150702
47. Mo HQ, Tian FJ, Ma XL, Zhang YC, Zhang CX, Zeng WH, et al. Pdia3 Regulates Trophoblast Apoptosis and Proliferation in Preeclampsia *Via* the Mdm2/P53 Pathway. *Reproduction* (2020) 160(2):293–305. doi: 10.1530/rep-20-0156
48. Qin S, Zhang Y, Zhang J, Tian F, Sun L, He X, et al. Spry4 Regulates Trophoblast Proliferation and Apoptosis *Via* Regulating Ifn-Γ-Induced Stat1 Expression and Activation in Recurrent Miscarriage. *Am J Reprod Immunol* (2020) 83(6):e13234. doi: 10.1111/aji.13234
49. Xu L, Li Y, Sang Y, Li DJ, Du M. Crosstalk Between Trophoblasts and Decidual Immune Cells: The Cornerstone of Maternal-Fetal Immunotolerance. *Front Immunol* (2021) 12:642392. doi: 10.3389/fimmu.2021.642392

Conflict of Interest: The authors declare that the research was conducted in the absence of any commercial or financial relationships that could be construed as a potential conflict of interest.

Publisher's Note: All claims expressed in this article are solely those of the authors and do not necessarily represent those of their affiliated organizations, or those of the publisher, the editors and the reviewers. Any product that may be evaluated in this article, or claim that may be made by its manufacturer, is not guaranteed or endorsed by the publisher.

frontiers | Frontiers in Immunology

TYPE Original Research
PUBLISHED 16 November 2023
DOI 10.3389/fimmu.2023.1297929

OPEN ACCESS

EDITED BY
Giselle Penton-Rol,
Center for Genetic Engineering and Biotechnology (CIGB), Cuba

REVIEWED BY
Estibalitz Laresgoiti-Servitje,
Tecnológico de Monterrey, Mexico
Maria Laura Manca,
University of Pisa, Italy

*CORRESPONDENCE
Rujin Zhuang
hmuzrj@163.com

RECEIVED 20 September 2023
ACCEPTED 06 November 2023
PUBLISHED 16 November 2023

CITATION
Guan S, Bai X, Ding J and Zhuang R (2023) Circulating inflammatory cytokines and hypertensive disorders of pregnancy: a two-sample Mendelian randomization study. *Front. Immunol.* 14:1297929. doi: 10.3389/fimmu.2023.1297929

Circulating inflammatory cytokines and hypertensive disorders of pregnancy: a two-sample Mendelian randomization study

Siqi Guan, Xiaoxu Bai, Jincheng Ding and Rujin Zhuang*

Department of Obstetrics and Gynecology, The Second Affiliated Hospital of Harbin Medical University, Harbin, China

Background: Hypertensive disorders of pregnancy (HDP) pose a significant risk to maternal and fetal well-being; however, the etiology and pathogenesis of HDP remain ambiguous. It is now widely acknowledged that inflammatory response and the immune system are closely related to HDP. Previous research has identified several inflammatory cytokines are associated with HDP. This study applied Mendelian randomization (MR) analysis to further assess causality.

Methods: Patients with HDP who participated in the MR analysis presented with four types of HDP: pre-eclampsia or eclampsia (PE); gestational hypertension (GH); pre-existing hypertension complicating pregnancy, childbirth and the puerperium (EH); and pre-eclampsia or poor fetal growth (PF). A two-sample MR analysis was used to analyze the data in the study. The causal relationship between exposure and outcome was analyzed with inverse variance weighting (IVW), MR Egger, weighted median, weighted mode, and simple mode methods, where IVW was the primary method employed.

Results: Our MR analysis demonstrated a reliable causative effect of Interleukin-9 (IL-9) and macrophage migration inhibitory factor (MIF) on reducing HDP risk, while macrophage inflammatory protein 1-beta (MIP1b), Interleukin-13 (IL-13), and Interleukin-16 (IL-16) were associated with promoting HDP risk.

Conclusions: This study demonstrated that IL-9, MIF, MIP1b, IL-13, and IL-16 may be cytokines associated with the etiology of HDP, and that a number of inflammatory cytokines are probably involved in the progression of HDP. Additionally, our study revealed that these inflammatory cytokines have causal associations with HDP and may likely be potential therapeutic targets for HDP.

KEYWORDS

hypertensive disorders of pregnancy, pre-eclampsia, inflammatory cytokine, Mendelian randomization, genome-wide association study

1 Introduction

Hypertensive disorders of pregnancy (HDP)—including pre-eclampsia/eclampsia, gestational hypertension, chronic hypertension, and pre-eclampsia superimposed on chronic hypertension (1)—is ranked as the second leading cause of maternal death globally, after maternal hemorrhage (2). Apart from causing harm to the mother, HDP is also associated with adverse fetal outcomes, such as preterm labor and fetal growth restriction (3). The exact pathogenesis of HDP is unclear, and current studies have found that endothelial dysfunction, insufficient trophoblastic invasion, abnormal angiogenesis, and aberrant uterine artery remodeling are considered to be key elements in its development (4–6). Among women in the gestational state, inappropriate immune activation and subsequent inflammation may result in maternal vasculopathy or placental dysfunction, thereby contributing to HDP (7).. Previous studies have revealed that certain inflammatory cytokines are strongly correlated with HDP, such as macrophage inflammatory protein 1-beta (MIP1b) and interleukin-18 (IL-18) (8, 9). However, the causal link of various cytokines and HDP is difficult to establish through observational studies because of interference from confounding variables and reverse causations (10).

Mendelian randomization (MR) is an instrumental variable (IV) analysis which utilizes genetic variation as the IV to assess the causality for exposure and outcome (11). The advantages of MR analysis are as follows: first, genetic variations are distributed at random during meiosis and, thus, the likelihood of correlation with environmental confounders is rare (12); second, genotype distribution precedes acquired exposure in time and the two are not impacted by reverse causality; third, exposure-related genetic variation generally accompanies individuals from birth to adulthood, thereby avoiding attenuation due to error in causal inference (regression dilution bias) (13). Additionally, Mendel's laws of inheritance are universal in the population, thereby avoiding the problem of representativeness in randomized controlled experiments. A two-sample MR analysis enables assessment of the relation between exposure and outcome in two independent populations, thereby expanding the scope of application and improving validity. MR analysis was performed on the basis of the following three hypotheses related to IVs. The first hypothesis is that the selected IVs are genetic variants highly correlated to the exposure. The second hypothesis is that IVs have no association with confounding factors between exposure and outcome. The third hypotheses is that IVs make no difference to outcome directly and merely affect outcome through exposure (14).

The aim of this study is to investigate the causal association between HDP and 41 inflammatory cytokines by using MR analysis and to identify inflammatory cytokines that can serve as potential biomarkers to facilitate early detection and treatment strategies for HDP.

2 Materials and methods

2.1 Study design

We used published summarized genome-wide association studies (GWAS) data for 41 circulating inflammatory cytokines and 4 types of HDP. In our study, a two-sample MR analysis was carried out in order to investigate bidirectional causality between inflammatory cytokines and HDP. This MR study was in accordance with the guidelines of Strengthening the Reporting of Observational Studies in Epidemiology using Mendelian Randomization (STROBE-MR) (15). The study design overview is presented in Figure 1.

2.2 Data sources

Data on inflammatory cytokines was taken from a GWAS meta-analysis that provided genomic variants in 8293 Finnish individuals (16). This study was conducted in three cohorts including The Cardiovascular Risk in Young Finns Study (YFS) and FINRISK surveys of the 1997 and 2002, which have already been completed. The average age of the participants in the YFS study was 37 years and that in the FINRISK survey was 60 years. The GWAS data of inflammatory cytokines used in this MR analysis were after adjusting for age, sex, and body-mass index (BMI). HDP-summarized GWAS data were retrieved from FinnGen database (https://www.finngen.fi/en) R9 version. According to the definition of HDP we included two cohorts of gestational hypertension; and pre-eclampsia/eclampsia. However, since the GWAS data for chronic hypertension were not available and the pre-eclampsia superimposed on chronic hypertension cohort had only 154 case samples, these two categories under the HDP definition were unable to be included in this MR study. In addition, we found two cohorts with larger sample sizes, pre-existing hypertension complicating pregnancy, childbirth and the puerperium and pre-eclampsia or poor fetal growth, which were thus included in the study. Finally, we selected four cohorts for inclusion in this MR analysis, including pre-eclampsia or eclampsia (PE); gestational hypertension (GH); pre-existing hypertension complicating pregnancy, childbirth and the puerperium (EH); and pre-eclampsia or poor fetal growth (PF). No overlap existed between the exposure and outcome groups in the population. Table S1 lists details of the four types of HDP.

2.3 Instrumental variable selection

First, we applied a genome-wide significance threshold of $p < 5 \times 10^{-8}$ so as to filter out single nucleotide polymorphisms (SNP) that were closely associated with HDP and inflammatory cytokines. A few inflammatory cytokines were found under this criterion that did not have a sufficient number of SNPs to perform MR analysis; thus, a higher cutoff value ($p < 5 \times 10^{-6}$) was selected. Second, when inflammatory cytokines were used as exposure, we clumped SNPs (kb = 10000, $r^2 = 0.01$), which implies that SNPs with $r^2 > 0.01$ in the 10000 kb range with the most significant SNPs were eliminated, thereby avoiding linkage disequilibrium (LD). Whereas for HDP as exposure, the number of SNPs was sufficient and, hence, a higher criterion for eliminating LD was set—kb = 10000, $r^2 = 0.001$. As we could not determine whether the palindromic SNPs were oriented in a consistent direction between exposure and outcome, these SNPs were not involved in MR analysis. Third, the R^2 value was calculated for each SNP, which indicates the extent of exposure

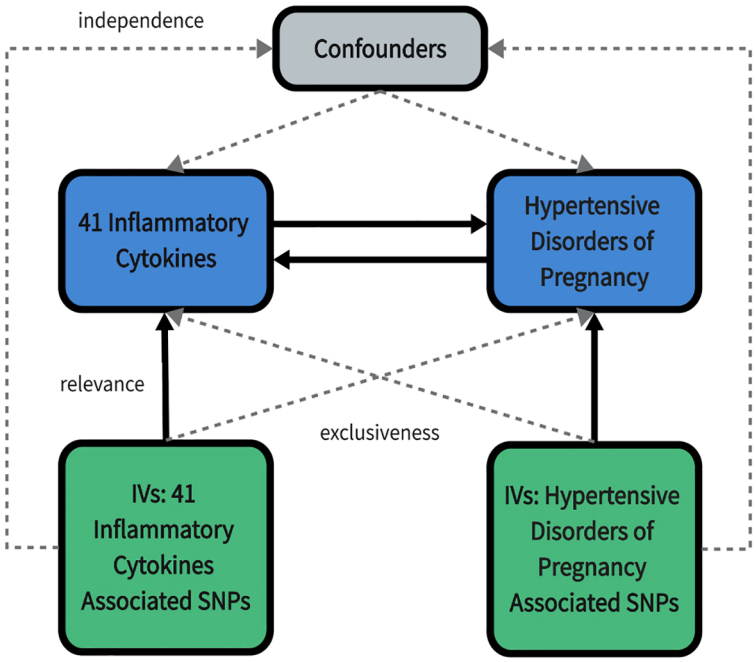

FIGURE 1
An overall design of the present study. IV, Instrumental variable; SNP, Single nucleotide polymorphism.

explained by IVs; moreover, to avoid weak instrumental bias, we evaluated the strength of the IV correlations by calculating the F-statistic and selected SNPs with F-statistic >10 for inclusion in this MR analysis. Finally, whenever unavailable SNPs are found, we use the LDlink Website (https://ldlink.nci.nih.gov/) to search for proxy SNPs ($r^2 > 0.8$) to replace them.

2.4 Statistical analysis

MR analysis is conducted utilizing the "TwoSampleMR" R package (Version 0.5.6) of the RStudio (version 4.2.3), which includes five MR analysis methods. Of these five methods, inverse variance weighting (IVW) was employed as the main method, with MR Egger regression, weighted median, simple mode, and weighted mode as complementary methods. The IVW method, which ignores the presence of the intercept term in the regression and takes the inverse of the result variance (quadratic of se) as the weight for the fit, assumes that all of the SNPs turned out to be valid instrumental variables and are completely independent of each other (17). MR Egger regression accounts for the existence of an intercept term. It assumes that the instrument-exposure and instrument-outcome associations are independent—that is, the instrument strength independent of the assumption of direct effect (18). The weighted median method requires a minimum of 50% of the IVs to be valid to obtain a robust estimate; this method tolerates more invalid IVs (19). Further, inflammatory cytokines that were ultimately identified as statistically significant were subject to the following conditions: The IVW results revealed that the 95% confidence intervals (CI) did not cross over with 1 (or 0), $p < 0.05$, and met the consistent trend of inflammatory cytokine effects derived from the five MR analyses.

We employed three sensitivity analysis methods to assess the sensitivity of MR results, including the heterogeneity test, pleiotropy test, and leave-one-out sensitivity test. Cochran's Q test and Rucker's Q test were used to detect the heterogeneity, and $p > 0.05$ was regarded as no heterogeneity. The intercept of the MR Eggar analysis results were used for testing the horizontal pleiotropy, with $p > 0.05$ considered as no pleiotropy (20). Additionally, the MR PRESSO method is capable of outlier identification and horizontal pleiotropy detection simultaneously (21). When applying MR PRESSO analysis, the NbDistribution parameter refers to the number of simulations calculated, and we set this parameter to 1000. Leave-one-out sensitivity was used to investigate whether the causal association was influenced by an SNP between exposure and outcome (22). Further, this study was not pre-registered on any platform.

3 Results

In this two-sample MR study, we investigated the correlation of each of the 4 types of HDP with 41 biomarkers—including interleukins, growth factors, and chemokines— thereby demonstrating that the inflammatory cytokines variably impact each disease type. Interleukin-9 (IL-9), macrophage migration inhibitory factor (MIF), MIP1b, interleukin-13 (IL-13), interleukin-16 (IL-16), and tumor necrosis factor-related apoptosis-inducing ligand (TRAIL) in PE; MIF and vascular

endothelial growth factor (VEGF) in GH; interleukin-18 (IL-18), TRAIL, and MIP1b in EH; and IL-9, MIP1b, IL-13 and IL-16 in PF may serve as potential upstream factors for disease when inflammatory cytokines are used as exposures and disease is used as an outcome. In addition, VEGF, interleukin-12p70 (IL-12p70), interleukin-1 beta (IL-1b), interleukin-1 receptor antagonist (IL-1ra), interleukin-4 (IL4), interleukin-7 (IL-7), interleukin-8 (IL-8), macrophage colony stimulating factor (MCSF) in PE and macrophage inflammatory protein 1-alpha (MIP1a), hepatocyte growth factor (HGF), IL-18, IL-8 in GH might cause alterations in the expression levels of these cytokines through the pathogenic pathway if the disease type is used as exposure. Further, there is no reciprocal causal association between individual biomarkers and diseases under each disease type. The results of bidirectional MR analysis among the four types of HDP and inflammatory cytokines are presented in Figures 2–5.

3.1 Bidirectional interactions between 41 inflammatory cytokines and PE

The results of bidirectional MR analysis of inflammatory cytokines correlated with PE are depicted in Figure 2. When 41 inflammatory cytokines were used as exposures, 6 inflammatory factors were causally associated with the pathogenesis of PE disease, including IL9 (odds ratio (OR) = 1.168, 95%CI = 1.027–1.327, p = 0.018) and MIF (OR = 1.120, 95% CI = 1.021–1.228, p = 0.016) as facilitators, MIP1b (OR = 0.957, 95% CI = 0.917–0.998, p = 0.042), IL13 (OR = 0.947, 95% CI = 0.898–

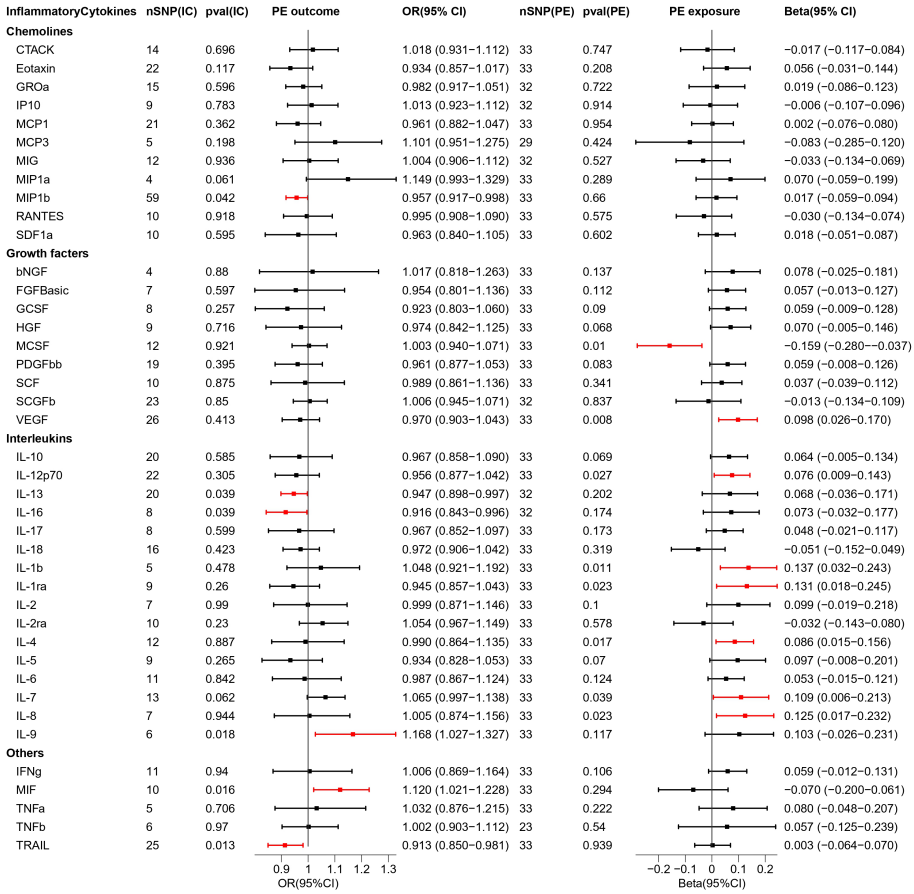

FIGURE 2
Causal estimations between 41 inflammatory cytokines and PE. The odds ratio (OR) was estimated using the random effect IVW method. The horizontal bars represent 95% confidence intervals (CI). SNP, Single nucleotide polymorphism; IC, Inflammatory Cytokine; pval, P-value; PE, Pre-eclampsia or eclampsia; OR, Odds ratio; CI, Confidence interval; CTACK, Cutaneous T cell-attracting chemokine; bNGF, Basic-nerve growth factor; FGFBasic, Basic fibroblast growth factor; GCSF, Granulocyte colony-stimulating factor; GROa, Gastroesophageal resuscitative occlusion of the aorta; HGF, Hepatocyte growth factor; IFNg, Interferon-gamma; IL-10, Interleukin-10; IL-12p70, Interleukin-12p70; IL-13, Interleukin-13; IL-16, Interleukin-16; IL-17, Interleukin-17; IL-18, Interleukin-18; IL-1b, Interleukin-1 beta; IL-1ra, Interleukin-1 receptor antagonist ; IL-2, Interleukin-2; IL-2ra, Interleukin-2 receptor antagonist; IL-4, Interleukin-4; IL-5, Interleukin-5; IL-6, Interleukin-6; IL-7, Interleukin-7; IL-8, Interleukin-8; IL-9, Interleukin-9; IP10, Interferon gamma-induced protein 10; MCP1, Monocyte chemotactic protein 1; MCP3, Monocyte chemotactic protein 3; MCSF, Macrophage colony stimulating factor; MIF, Macrophage migration inhibitory factor; MIG, Monokine induced by interferon (IFN)-gamma; MIP1a, Macrophage inflammatory protein 1-alpha; MIP1b, Macrophage inflammatory protein 1-beta; PDGFbb, Platelet derived growth factor bb; RANTES, Regulated upon activation normal T cell expressed and presumably secreted; SCF, Stem cell factor; SCGFb, Stem cell growth factor-beta; SDF1a, Stromal cell-derived factor-1alpha; TNFa, Tumor necrosis factor-alpha; TNFb, Tumor necrosis factor-beta; TRAIL, Tumor necrosis factor-related apoptosis-inducing ligand; VEGF, Vascular endothelial growth factor.

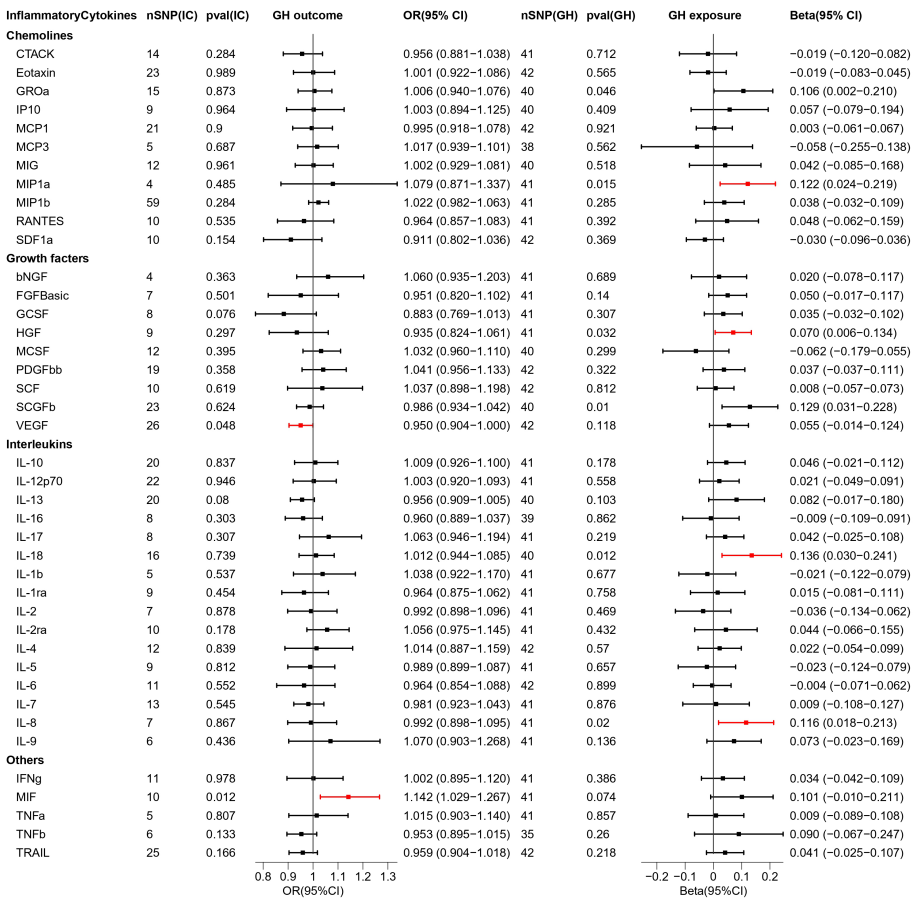

FIGURE 3
Causal estimations between 41 inflammatory cytokines and GH. The odds ratio (OR) was estimated using the random effect IVW method. The horizontal bars represent 95% confidence intervals (CI). SNP, Single nucleotide polymorphism; IC, Inflammatory Cytokine; pval, P-value; GH, Gestational hypertension; OR, Odds ratio; CI, Confidence interval; CTACK, Cutaneous T cell-attracting chemokine; bNGF, Basic-nerve growth factor; FGFBasic, Basic fibroblast growth factor; GCSF, Granulocyte colony-stimulating factor; GROa, Gastroesophageal resuscitative occlusion of the aorta; HGF, Hepatocyte growth factor; IFNg, Interferon-gamma; IL-10, Interleukin-10; IL-12p70, Interleukin-12p70; IL-13, Interleukin-13; IL-16, Interleukin-16; IL-17, Interleukin-17; IL-18, Interleukin-18; IL-1b, Interleukin-1 beta; IL-1ra, Interleukin-1 receptor antagonist ; IL-2, Interleukin-2; IL-2ra, Interleukin-2 receptor antagonist; IL-4, Interleukin-4; IL-5, Interleukin-5; IL-6, Interleukin-6; IL-7, Interleukin-7; IL-8, Interleukin-8; IL-9, Interleukin-9; IP10, Interferon gamma-induced protein 10; MCP1, Monocyte chemotactic protein 1; MCP3, Monocyte chemotactic protein 3; MCSF, Macrophage colony stimulating factor; MIF, Macrophage migration inhibitory factor; MIG, Monokine induced by interferon (IFN)-gamma; MIP1a, Macrophage inflammatory protein 1-alpha; MIP1b, Macrophage inflammatory protein 1-beta; PDGFbb, Platelet derived growth factor bb; RANTES, Regulated upon activation normal T cell expressed and presumably secreted; SCF, Stem cell factor; SCGFb, Stem cell growth factor-beta; SDF1a, Stromal cell-derived factor-1alpha; TNFa, Tumor necrosis factor-alpha; TNFb, Tumor necrosis factor-beta; TRAIL, Tumor necrosis factor-related apoptosis-inducing ligand; VEGF, Vascular endothelial growth factor.

0.997, p = 0.039), IL16 (OR = 0.916, 95% CI = 0.843–0.996, p = 0.039), and TRAIL (OR = 0.913, 95% CI = 0.850–0.981, p = 0.013) playing inhibitory roles. Scatter plots were used to demonstrate the trends of inflammatory cytokines under the five MR methods (Figure S1).

When PE was used as exposure, the remaining 33 SNPs were involved in the MR analysis. The results are depicted in Figure 2. Eight inflammatory cytokines were affected by PE, among which the growth factor MCSF (Beta = -0.159, 95% CI= -0.280–0.037, p = 0.01) was negatively regulated, while the others were positively regulated. The remaining seven inflammatory factors were VEGF (Beta = 0.098, 95% CI = 0.026–0.170, p = 0.008), IL12p70 (Beta = 0.076, 95% CI = 0.009–0.143, p = 0.027), IL1b (Beta = 0.137, 95% CI = 0.032–0.243, p = 0.011), IL1ra (Beta = 0.131, 95% CI = 0.018–0.245, p = 0.023), IL4 (Beta = 0.086, 95% CI = 0.015–0.156, p = 0.017), IL7 (Beta = 0.109, 95% CI = 0.006–0.213, p = 0.039), IL8 (Beta = 0.125, 95% CI = 0.017–0.232, p = 0.023). The scatter plot of the above inflammatory cytokines is presented in Figure S2.

3.2 Bidirectional interactions between 41 inflammatory cytokines and GH

As 41 inflammatory cytokines were used for MR analysis as exposure, MIF (OR = 1.142, 95% CI = 1.029–1.267, p = 0.012), which acted as a promoter, and VEGF (OR = 0.950, 95% CI = 0.904–0.9995, p = 0.048), which acted as an inhibitor, were identified. The scatter plot is depicted in Figure S3.

Next, we reversed the exposure and outcome. MR analysis revealed that four inflammatory cytokines were screened out and all of them had increased expression under the influence of GH. The four

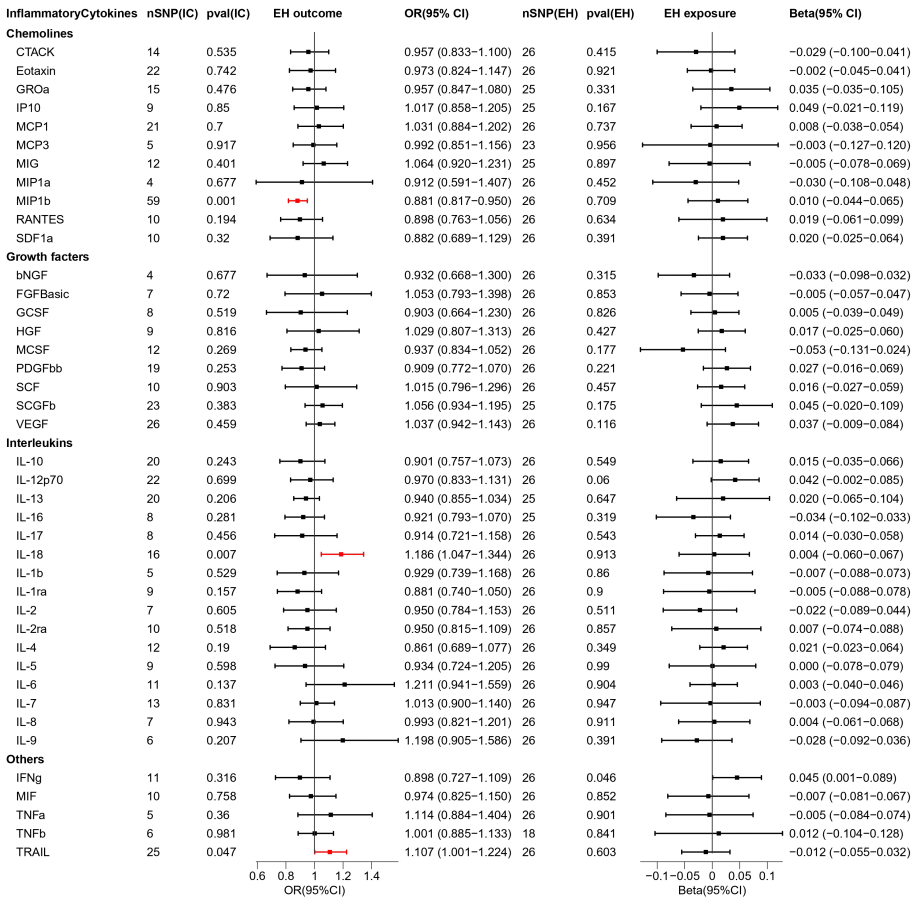

FIGURE 4
Causal estimations between 41 inflammatory cytokines and EH. The odds ratio (OR) was estimated using the random effect IVW method. The horizontal bars represent 95% confidence intervals (CI). SNP, Single nucleotide polymorphism; IC, Inflammatory Cytokine; pval, P-value; EH, Pre-existing hypertension complicating pregnancy, childbirth and the puerperium; OR, Odds ratio; CI, Confidence interval; CTACK, Cutaneous T cell-attracting chemokine; bNGF, Basic-nerve growth factor; FGFBasic, Basic fibroblast growth factor; GCSF, Granulocyte colony-stimulating factor; GROa, Gastroesophageal resuscitative occlusion of the aorta; HGF, Hepatocyte growth factor; IFNg, Interferon-gamma; IL-10, Interleukin-10; IL-12p70, Interleukin-12p70; IL-13, Interleukin-13; IL-16, Interleukin-16; IL-17, Interleukin-17; IL-18, Interleukin-18; IL-1b, Interleukin-1 beta; IL-1ra, Interleukin-1 receptor antagonist ; IL-2, Interleukin-2; IL-2ra, Interleukin-2 receptor antagonist; IL-4, Interleukin-4; IL-5, Interleukin-5; IL-6, Interleukin-6; IL-7, Interleukin-7; IL-8, Interleukin-8; IL-9, Interleukin-9; IP10, Interferon gamma-induced protein 10; MCP1, Monocyte chemotactic protein 1; MCP3, Monocyte chemotactic protein 3; MCSF, Macrophage colony stimulating factor; MIF, Macrophage migration inhibitory factor; MIG, Monokine induced by interferon (IFN)-gamma; MIP1a, Macrophage inflammatory protein 1-alpha; MIP1b, Macrophage inflammatory protein 1-beta; PDGFbb, Platelet derived growth factor bb; RANTES, Regulated upon activation normal T cell expressed and presumably secreted; SCF, Stem cell factor; SCGFb, Stem cell growth factor-beta; SDF1a, Stromal cell-derived factor-1alpha; TNFa, Tumor necrosis factor-alpha; TNFb, Tumor necrosis factor-beta; TRAIL, Tumor necrosis factor-related apoptosis-inducing ligand; VEGF, Vascular endothelial growth factor.

cytokines are MIP1a (Beta = 0.122,95% CI = 0.024–0.219, p = 0.015) HGF (Beta = 0.070, 95% CI = 0.006–0.134, p = 0.032), IL-18 (Beta = 0.136, 95% CI = 0.030–0.241, p = 0.012), and IL-8 (Beta = 0.116, 95% CI = 0.018–0.213, p = 0.02). The scatter plot is depicted in Figure S4. In addition, the 95% CIs for GROa and SCGFb did not pass through 0 (Figure 3). The beta values for MR Eggar were in the opposite direction as that of IVW; thus, GROa (IVW beta = 0.106, MR Eggar beta = -0.143) and SCGFb (IVW beta = 0.129, MR Eggar Beta = -0.263) were not considered as statistically significant cytokines.

3.3 Bidirectional interactions between 41 inflammatory cytokines and EH

We explored the causal association of 41 inflammatory cytokines with EH as outcome and obtained three inflammatory cytokines with causal potential—IL-18 (OR = 1.186, 95% CI = 1.047–1.344, p = 0.007) and TRAIL (OR = 1.107, 95% CI = 1.001–1.224, p = 0.047) factors produced positive regulatory effects, while MIP1b (OR = 0.881, 95% CI = 0.817–0.950, p = 0.001) factor exerted negative effects. The scatter plot is depicted in Figure S5.

When exploring the MR analysis of the role of EH as exposure, only the IFNg was revealed as a statistically significant responder by the IVW method. However, the MR Eggar method obtained results with the opposite trend to that of the former; thus, the IFNg (IVW beta = 0.045, MR Eggar beta = -0.004) was eliminated.

3.4 Bidirectional interactions between 41 inflammatory cytokines and PF

When MR analysis was performed with 41 inflammatory cytokines as exposure and PF as outcome, one facilitator, IL-9

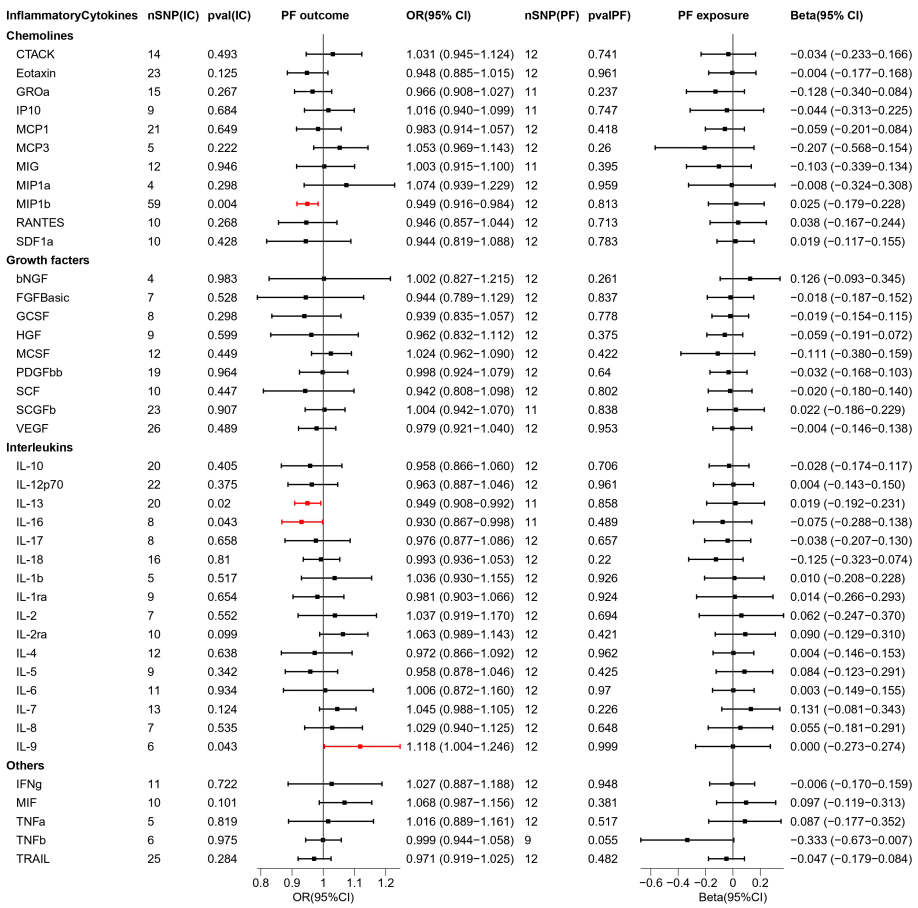

FIGURE 5
Causal estimations between 41 inflammatory cytokines and PF. The odds ratio (OR) was estimated using the random effect IVW method. The horizontal bars represent 95% confidence intervals (CI). SNP, Single nucleotide polymorphism; IC, Inflammatory Cytokine; pval, P-value; PF, Pre-eclampsia or poor fetal growth; OR, Odds ratio; CI, Confidence interval; CTACK, Cutaneous T cell-attracting chemokine; bNGF, Basic-nerve growth factor; FGFBasic, Basic fibroblast growth factor; GCSF, Granulocyte colony-stimulating factor; GROa, Gastroesophageal resuscitative occlusion of the aorta; HGF, Hepatocyte growth factor; IFNg, Interferon-gamma; IL-10, Interleukin-10; IL-12p70, Interleukin-12p70; IL-13, Interleukin-13; IL-16, Interleukin-16; IL-17, Interleukin-17; IL-18, Interleukin-18; IL-1b, Interleukin-1 beta; IL-1ra, Interleukin-1 receptor antagonist ; IL-2, Interleukin-2; IL-2ra, Interleukin-2 receptor antagonist; IL-4, Interleukin-4; IL-5, Interleukin-5; IL-6, Interleukin-6; IL-7, Interleukin-7; IL-8, Interleukin-8; IL-9, Interleukin-9; IP10, Interferon gamma-induced protein 10; MCP1, Monocyte chemotactic protein 1; MCP3, Monocyte chemotactic protein 3; MCSF, Macrophage colony stimulating factor; MIF, Macrophage migration inhibitory factor; MIG, Monokine induced by interferon (IFN)-gamma; MIP1a, Macrophage inflammatory protein 1-alpha; MIP1b, Macrophage inflammatory protein 1-beta; PDGFbb, Platelet derived growth factor bb; RANTES, Regulated upon activation normal T cell expressed and presumably secreted; SCF, Stem cell factor; SCGFb, Stem cell growth factor-beta; SDF1a, Stromal cell-derived factor-1alpha; TNFa, Tumor necrosis factor-alpha; TNFb, Tumor necrosis factor-beta; TRAIL, Tumor necrosis factor-related apoptosis-inducing ligand; VEGF, Vascular endothelial growth factor.

(OR = 1.118, 95% CI = 1.004–1.246, p = 0.043), and three inhibitory factors, MIP1b (OR = 0.949, 95% CI = 0.916–0.984, p = 0.004), IL-13 (OR = 0.949, 95% CI = 0.908–0.992, p = 0.02), and IL-16 (OR = 0.930, 95% CI = 0.867–0.998, p = 0.043) were found. The scatterplot is presented in Figure S6.

Reversing exposure and outcome, no significant inflammatory cytokines were found.

3.5 Sensitivity analysis

The results of the tests for heterogeneity and pleiotropy when inflammatory cytokines were used as exposures are presented in Table S2. The results of the tests for heterogeneity and pleiotropy when inflammatory cytokines were used as outcomes are presented in Table S4. In addition, the leave-one-out analysis results are presented in Figure S7-12. Details of SNPs when inflammatory cytokines were used as exposures are presented in Table S3. Details of SNPs when inflammatory cytokines were used as outcomes are presented in Table S5.

4 Discussion

Recently, numerous studies that explore the association of HDP with the immune system and the inflammatory cytokines produced by immune cells have been published. For example, TH17 cells and their secreted interleukin-17 (IL-17) levels are found to be increased in PE patients; TH17 cells induce pre-eclampsia by participating in placental ischemia, oxidative stress, and other pathways (23). It has

also been suggested that VEGF may be an important biomarker for pre-eclampsia and has significant value in predicting its severity (24, 25). Despite the rich results of previous observational studies, the causal association among numerous important inflammatory cytokines with HDP has not been established due to the limitations of traditional epidemiology (26). Observational studies often provide biased associations due to the presence of confounding factors or reverse causality, thereby making it difficult to obtain credible conclusions using this method (27). In terms of pregnancy disorders, it is difficult to identify the causes of changes in inflammatory cytokine levels in patients with HDP through general observational studies. The presence of the disease itself, side effects caused by therapeutic drugs, underlying pathological immune response, the state of hidden infection, and harmful lifestyle habits (such as alcohol abuse and smoking) can cause changes in the levels of inflammatory cytokines (28–30). Recently, it has been reported that cytokine storms are highlighted as a common feature in pre-eclampsia and severe forms of coronavirus disease 2019 disease (31).

Our study found that more inflammatory cytokines exhibited significant changes in the initiation and progression of PE compared to GH. Among the four types of HDP, the inflammatory cytokines that recurrently appear upstream of the disease are IL-9, MIF, MIP1b, IL-13, IL-16, and TRAIL. The IL-9/IL-9R pathway is involved in regulating trophectoderm function, and increased IL-9 levels were found to result in increased tissue proliferation and invasiveness (32). IL-9 and IL-9R increase fibroblast proliferation as well as induce pro-inflammatory cytokines and metalloproteinases, which are key pathological processes that promote the formation of vascular opacities (33). Prior studies have suggested that Th9 cells may be involved in immune-mediated diseases such as allergy and autoimmune inflammatory diseases (34). Th1 or Th17 cells can induce CD4+IL-9+ T cell differentiation by promoting factors such as IL-1b and IL-12 (35). Under condition of TGF-β presence, Th-17 cells can produce IL-9 to participate in pro-inflammatory response (36). At present, research on Th9 cells in human pregnancy is limited, and the possible role of Th9 cells in preeclampsia needs to be further investigated. In addition, MIF is involved in multiple biophysiological processes that contribute to cell proliferation and differentiation, innate immune responses, and angiogenic biological activities (37). Previous studies have confirmed that large amounts of pro-inflammatory mediators are produced by MIF stimulation, including cytokines tumor necrosis factor-alpha (TNFa), IL-1b, interleukin-6 (IL-6), interferon-gamma (IFNg), matrix metalloproteinases, and nitric oxide (38, 39). Circulating concentrations of MIF are elevated in infected patients, inflammatory conditions, and autoimmune diseases (40). Therefore, MIF is recognized as a biomarker or pharmacological target for different diseases (41, 42), and MIF inhibitors might have considerable therapeutic benefit for numerous inflammatory and autoimmune diseases (43–46). Similar conditions have been found in mothers with pathological pregnancies (preterm birth (47) and pre-eclampsia (48). MIP1b was revealed to have the potential to recruit macrophages and dendritic cells (49, 50), which have the ability to secrete a range of cytokines/chemokines and enzymes implicated in angiogenesis and tissue remodeling (51). Furthermore, it has been demonstrated that macrophages promote trophoblastic invasion in pregnant mice (52). IL-13 exerts its anti-inflammatory effects by binding to IL-4 receptor alpha (IL-4ra) (53). In addition, IL-13 can downregulate the expression of IL-1b, IL-8, TNFa, and MIP1a (54–56). The anti-inflammatory potential of IL-13 has been therapeutically investigated in a variety of pathologies, including psoriasis, arthritis, and Alzheimer's disease (57–59). Therefore, IL13 may be a key therapeutic target in pre-eclampsia. Currently, there are very few studies that investigate the correlation between IL-16 and HDP. It has been shown that IL-16 can initiate and amplify inflammatory responses through the release of cell signaling molecules that bind to CD4+ T cells (60). It is worth noting that Andrea L et al. found a noticeable decrease of IL-16 expression in hemolysis, elevated liver enzymes, and low platelet count (HELLP) syndrome (61). Due to the lack of clarity regarding how IL-16 is implicated in the etiopathogenesis of pre-eclampsia suggests, it is noteworthy that future research on IL-16 in such disorders is necessary. Tumor necrosis factor-related apoptosis-inducing ligand (TRAIL) is part of the TNF ligand family, and TRAIL and its receptor play essential roles in trophoblastic immunity and invasion during early pregnancy (62, 63). TRAIL induces apoptosis in vascular endothelial cells and vascular smooth muscle cells during the process of remodeling the uterine spiral arteries (64). It has recently been demonstrated that pregnant women who subsequently develop HDP have reduced plasma levels of TRAIL prior to 20 weeks gestation (65), thereby suggesting that TRAIL could serve as a new predictive, noninvasive biomarker for pregnant women with HDP.

Further, previous studies have revealed that IL-12p70, IL-1ra, IL-1b, IL-8, and IL-18 are considerably higher in PE group than in normal pregnant women (66, 67), which supports our findings. IL-1ra is elevated in PE, and elevated circulating IL-1ra reflect increased activity of the pro-inflammatory cytokines IL-1a and IL-1b, both of which are difficult to identify in serum levels because of their short circulating half-lives (68, 69). Moreover, it has been revealed that IL-1b and TNFa can significantly increase MCSF expression in early pregnancy decidual cells (70). IL-7 cytokine is necessary for the proliferation and survival of pathogenic Th17 cells, and has a promotional role in autoimmune diseases such as experimental autoimmune encephalomyelitis (71, 72).. In addition, previous evidence suggests that Th17 cells are observed to be increased in the decidual cells of patients with pre-eclampsia (73). IL-17 is a major effector molecule of Th17 cells, which plays an important role in inflammatory response, and IL-17 also induces the production of factors such as IL-6 and IL-8. However, IL-17 was not a statistically significant factor in the results of this MR analysis. In a meta-analysis published in 2020, the authors found no evidence that circulating IL-17 levels differed between pre-eclampsia and controls (74). Furthermore, Brewster et al. found that IL-17 levels were lower in patients with early-onset pre-eclampsia and higher in patients with late-onset compared to controls (75). Consequently, we consider that the role of IL-17 in pre-eclampsia needs to be approached with caution and further studies are still needed. Karol

Charkiewicz et al. demonstrated that HGF was expressed in the plasma of patients with PE at a higher level than that in healthy pregnant women (76).

Currently, the most effective way to deal with pre-eclampsia is the prompt delivery of the fetus and placenta (77). Symptoms of pre-eclampsia and eclampsia are usually greatly relieved when the fetus and placental tissue are delivered from the mother. In our study, circulating inflammatory cytokines were also no longer active in patients after delivery. Moreover, we found that IL-9, MIP1b, IL-13, and IL-16 might be associated with fetal dysplasia. Previous researches have suggested that IL-9 induces immune tolerance during pregnancy; if abnormalities occur, the fetus is no longer tolerated by the mother and has adverse outcomes for both the mother and fetus (78). MIP1b affects cytotoxicity and causes tissue damage in the developing fetal brain and is a potential mechanism for intrauterine fetal dysplasia (79). Fetal growth restriction (FGR) maternal IL-13 levels are lower than those in normal pregnancies (80). IL-13 is a Th2 cytokine with anti-inflammatory characteristics. IL-13 inhibits the production of IL-6, IL-8, TNFa, and IL-12 as well as suppresses cytotoxicity and blocks pathologic inflammation (81). Lower levels of IL13 in FGR may indicate a more pronounced Th1 bias or pro-inflammatory cytokine bias. Denihan et al. investigated that IL-16 participated in the process of fetal brain injury and that its level associated with the long-term prognosis of neonatal hypoxic-ischemic encephalopathy (82).

For the first time, we adopted bidirectional two-sample MR analysis to explore the causal association between circulating inflammatory cytokines and the four types of HDP. Additionally, attention has been focused on inflammatory cytokines in pre-eclampsia that may contribute to poor fetal growth and development. Prior literature reviewed upstream and downstream inflammatory cytokines in HDP, thereby providing strong evidence for our results. Our study obtained different inflammatory cytokine profiles for both the incidence and progression of the disease, which offers new directions in the prevention, surveillance, and treatment of HDP. The pathogenesis and pathophysiology of HDP, represented by pre-eclampsia, are very complex and multifactorial. This includes endothelial dysfunction, oxidative stress, angiogenesis, neutrophil activation, anti-angiogenic factors, and syncytiotrophoblast microparticles, which are all involved in the pathophysiologic process of pre-eclampsia. Inflammatory cytokines play an important role in disease progression, but not all. This study only included 41 inflammatory cytokines, which is obviously a limitation. With in-depth study of HDP, more cytokines will be explored by researchers in the future and bring new perspectives and insights for early detection and therapeutic strategies of HDP.

There are several strengths of this study. First, genetic variation is randomly distributed during gamete formation and conception; thus, MR analysis avoids the limitations of observational studies (confounding, regression dilution, and reverse causation bias) (11). Second, we used separate samples for the circulating inflammatory cytokines and HDP data, and two-sample data avoided bias from weak instrumental variables. Third, we included two large-scale cohorts were included for MR analysis, thereby applying a sufficiently large sample size to ensure generalizability of causality. Moreover, two sets of data were treated as exposure and outcome to perform bidirectional MR analysis, respectively. Finally, so as to test the validity of the IV hypotheses, we performed sensitivity analyses, which included heterogeneity, pleiotropy, and leave-one-out analyses.

Nevertheless, there are also a few limitations of this study that must be discussed. First, the number of IVs as exposure varied for each inflammatory cytokine. During our analysis, a few IVs were discarded after screening; thus, the final MR analysis results could be influenced by the limited number of IVs. Despite this, we calculated statistical efficacy for each IV and excluded IVs with low efficacies in order to ensure that the results presented in this study remain reliable. Second, HDP occurs only in the female population, whereas circulating inflammatory cytokine GWASs are found in both male and female populations; thus, the presence of gender differences could potentially impact MR results. Third, this research data pertains to European populations; therefore, it needs to be treated with caution when generalizing to other populations. Finally, the immune system in pregnancy is complex and variable, with multiple changes in inflammatory cytokines influenced by a variety of factors, whereas it is difficult to dynamically monitor such a complex process in our study. Early-onset preeclampsia (onset < 34 weeks of gestation) and late-onset preeclampsia (onset ≥ 34 weeks of gestation), have different pathophysiological and immunopathological origins. However, limited by the availability of GWAS data, this study did not conduct subgroup analyses. With regard to the causal association of circulating inflammatory cytokines with HDP, deeper and more extensive studies are required in the future.

Data availability statement

The datasets presented in this study can be found in online repositories. The names of the repository/repositories and accession number(s) can be found in the article/Supplementary Material.

Author contributions

SG: Data curation, Formal Analysis, Investigation, Methodology, Project administration, Resources, Visualization, Writing – original draft, Writing – review & editing. XB: Conceptualization, Investigation, Methodology, Project administration, Resources, Supervision, Visualization, Writing – original draft, Writing – review & editing. JD: Formal Analysis, Investigation, Validation, Visualization, Writing – original draft, Writing – review & editing. RZ: Conceptualization, Investigation, Project administration, Resources, Supervision, Writing – original draft, Writing – review & editing.

Funding

The author(s) declare financial support was received for the research, authorship, and/or publication of this article. This study

was funded by Wu Jieping Medical Foundation (Grant No. 320.6750.2020-06-83).

Acknowledgments

We sincerely thank the FinnGen database and Ari V. Aholai et al. and other related researchers for providing GWASs summary data.

Conflict of interest

The authors declare that the research was conducted in the absence of any commercial or financial relationships that could be construed as a potential conflict of interest.

Publisher's note

Supplementary material

The Supplementary Material for this article can be found online at: https://www.frontiersin.org/articles/10.3389/fimmu.2023.1297929/full#supplementary-material

References

1. Garovic VD, Dechend R, Easterling T, Karumanchi SA, McMurtry Baird S, Magee LA, et al. Hypertension in pregnancy: diagnosis, blood pressure goals, and pharmacotherapy: A scientific statement from the American heart association. *Hypertension (Dallas Tex: 1979)* (2022) 79(2):e21–41. doi: 10.1161/HYP.0000000000000208

2. GBD 2015 Maternal Mortality Collaborators. *Global, regional, and national levels of maternal mortality, 1990-2015: a systematic analysis for the Global Burden of Disease Study 2015* Vol. 388. London, England: Lancet (2016) p. 1775–812.

3. Bakker R, Steegers EA, Hofman A, Jaddoe VW. Blood pressure in different gestational trimesters, fetal growth, and the risk of adverse birth outcomes: the generation R study. *Am J Epidemiol* (2011) 174(7):797–806. doi: 10.1093/aje/kwr151

4. Staff AC, Benton SJ, von Dadelszen P, Roberts JM, Taylor RN, Powers RW, et al. Redefining preeclampsia using placenta-derived biomarkers. *Hypertension (Dallas Tex: 1979)* (2013) 61(5):932–42. doi: 10.1161/HYPERTENSIONAHA.111.00250

5. Garovic VD. The role of the podocyte in preeclampsia. *Clin J Am Soc Nephrol: CJASN* (2014) 9(8):1337–40. doi: 10.2215/CJN.05940614

6. Lyall F, Robson SC, Bulmer JN. Spiral artery remodeling and trophoblast invasion in preeclampsia and fetal growth restriction: relationship to clinical outcome. *Hypertension (Dallas Tex: 1979)* (2013) 62(6):1046–54. doi: 10.1161/HYPERTENSIONAHA.113.01892

7. Pierik E, Prins JR, van Goor H, Dekker GA, Daha MR, Seelen MAJ, et al. Dysregulation of complement activation and placental dysfunction: A potential target to treat preeclampsia? *Front Immunol* (2019) 10:3098. doi: 10.3389/fimmu.2019.03098

8. Hart PMB, Stephenson NL, Scime NV, Tough SC, Slater DM, Chaput KH. Second trimester cytokine profiles associated with gestational diabetes and hypertensive disorders of pregnancy. *PloS One* (2022) 17(12):e0279072. doi: 10.1371/journal.pone.0279072

9. Wang Y, Shi D, Chen L. Lipid profile and cytokines in hypertension of pregnancy: A comparison of preeclampsia therapies. *J Clin Hypertens (Greenwich Conn)* (2018) 20 (2):394–9. doi: 10.1111/jch.13161

10. Burgess S, Butterworth A, Thompson SG. Mendelian randomization analysis with multiple genetic variants using summarized data. *Genet Epidemiol* (2013) 37 (7):658–65. doi: 10.1002/gepi.21758

11. Verduijn M, Siegerink B, Jager KJ, Zoccali C, Dekker FW. Mendelian randomization: use of genetics to enable causal inference in observational studies. *Nephrol Dial Transplant* (2010) 25(5):1394–8. doi: 10.1093/ndt/gfq098

12. Smith GD, Lawlor DA, Harbord R, Timpson N, Day I, Ebrahim S. Clustered environments and randomized genes: a fundamental distinction between conventional and genetic epidemiology. *PloS Med* (2007) 4(12):e352. doi: 10.1371/journal.pmed.0040352

13. Smith GD, Ebrahim S. Mendelian randomization: prospects, potentials, and limitations. *Int J Epidemiol* (2004) 33(1):30–42. doi: 10.1093/ije/dyh132

14. Emdin CA, Khera AV, Kathiresan S. Mendelian randomization. *Jama* (2017) 318 (19):1925–6. doi: 10.1001/jama.2017.17219

15. Skrivankova VW, Richmond RC, Woolf BAR, Yarmolinsky J, Davies NM, Swanson SA, et al. Strengthening the reporting of observational studies in epidemiology using Mendelian randomization: the STROBE-MR statement. *Jama* (2021) 326(16):1614–21. doi: 10.1001/jama.2021.18236

16. Ahola-Olli AV, Würtz P, Havulinna AS, Aalto K, Pitkänen N, Lehtimäki T, et al. Genome-wide association study identifies 27 loci influencing concentrations of circulating cytokines and growth factors. *Am J Hum Genet* (2017) 100(1):40–50. doi: 10.1016/j.ajhg.2016.11.007

17. Lee YH. Causal association between smoking behavior and the decreased risk of osteoarthritis: a Mendelian randomization. *Z fur Rheumatol* (2019) 78(5):461–6. doi: 10.1007/s00393-018-0505-7

18. Bowden J. Misconceptions on the use of MR-Egger regression and the evaluation of the InSIDE assumption. *Int J Epidemiol* (2017) 46(6):2097–9. doi: 10.1093/ije/dyx192

19. Li C, Niu M, Guo Z, Liu P, Zheng Y, Liu D, et al. A mild causal relationship between tea consumption and obesity in general population: A two-sample Mendelian randomization study. *Front Genet* (2022) 13:795049. doi: 10.3389/fgene.2022.795049

20. Burgess S, Thompson SG. Interpreting findings from Mendelian randomization using the MR-Egger method. *Eur J Epidemiol* (2017) 32(5):377–89. doi: 10.1007/s10654-017-0255-x

21. Verbanck M, Chen CY, Neale B, Do R. Detection of widespread horizontal pleiotropy in causal relationships inferred from Mendelian randomization between complex traits and diseases. *Nat Genet* (2018) 50(5):693–8. doi: 10.1038/s41588-018-0099-7

22. Hemani G, Zheng J, Elsworth B, Wade KH, Haberland V, Baird D, et al. The MR-Base platform supports systematic causal inference across the human phenome. *eLife* (2018) 7. doi: 10.7554/eLife.34408

23. Cornelius DC, Hogg JP, Scott J, Wallace K, Herse F, Moseley J, et al. Administration of interleukin-17 soluble receptor C suppresses TH17 cells, oxidative stress, and hypertension in response to placental ischemia during pregnancy. *Hypertension (Dallas Tex: 1979)* (2013) 62 (6):1068–73. doi: 10.1161/HYPERTENSIONAHA.113.01514

24. Kurtoglu E, Avci B, Kokcu A, Celik H, Cengiz Dura M, Malatyalioglu E, et al. Serum VEGF and PGF may be significant markers in prediction of severity of preeclampsia. *J Maternal fetal Neonatal Med* (2016) 29(12):1987–92. doi: 10.3109/14767058.2015.1072157

25. Deshpande JS, Sundrani DP, Sahay AS, Gupte SA, Joshi SR. Unravelling the potential of angiogenic factors for the early prediction of preeclampsia. *Hypertens Res* (2021) 44(7):756–69. doi: 10.1038/s41440-021-00647-9

26. Davey Smith G, Hemani G. Mendelian randomization: genetic anchors for causal inference in epidemiological studies. *Hum Mol Genet* (2014) 23(R1):R89–98. doi: 10.1093/hmg/ddu328

27. Sekula P, Del Greco MF, Pattaro C, Köttgen A. Mendelian randomization as an approach to assess causality using observational data. *J Am Soc Nephrol: JASN.* (2016) 27(11):3253–65. doi: 10.1681/ASN.2016010098

28. Sayad B, Mohseni Afshar Z, Mansouri F, Salimi M, Miladi R, Rahimi S, et al. Pregnancy, preeclampsia, and COVID-19: susceptibility and mechanisms: A review study. *Int J Fertil Steril* (2022) 16(2):64–9. doi: 10.22074/IJFS.2022.539768.1194

29. Gaydos J, McNally A, Guo R, Vandivier RW, Simonian PL, Burnham EL. Alcohol abuse and smoking alter inflammatory mediator production by pulmonary and systemic immune cells. *Am J Physiol Lung Cell Mol Physiol* (2016) 310(6):L507–18. doi: 10.1152/ajplung.00242.2015

30. Deer E, Herrock O, Campbell N, Cornelius D, Fitzgerald S, Amaral LM, et al. The role of immune cells and mediators in preeclampsia. *Nat Rev Nephrol* (2023) 19 (4):257–70. doi: 10.1038/s41581-022-00670-0

31. Todros T, Masturzo B, De Francia S. COVID-19 infection: ACE2, pregnancy and preeclampsia. *Eur J Obstet Gynecol Reprod Biol* (2020) 253:330. doi: 10.1016/j.ejogrb.2020.08.007

32. Sun Y, Liu S, Hu R, Zhou Q, Li X. Decreased placental IL9 and IL9R in preeclampsia impair trophoblast cell proliferation, invasion, and angiogenesis. *Hypertens Pregnancy* (2020) 39(3):228–35. doi: 10.1080/10641955.2020.1754852

33. Raychaudhuri SK, Abria C, Maverakis EM, Raychaudhuri SP. IL-9 receptor: Regulatory role on FLS and pannus formation. *Cytokine* (2018) 111:58–62. doi: 10.1016/j.cyto.2018.08.001

34. Kaplan MH. Th9 cells: differentiation and disease. *Immunol Rev* (2013) 252 (1):104–15. doi: 10.1111/imr.12028

35. Wang W, Sung N, Gilman-Sachs A, Kwak-Kim J. T helper (Th) cell profiles in pregnancy and recurrent pregnancy losses: Th1/Th2/Th9/Th17/Th22/Tfh cells. *Front Immunol* (2020) 11:2025. doi: 10.3389/fimmu.2020.02025

36. Nowak EC, Weaver CT, Turner H, Begum-Haque S, Becher B, Schreiner B, et al. IL-9 as a mediator of Th17-driven inflammatory disease. *J Exp Med* (2009) 206 (8):1653–60. doi: 10.1084/jem.20090246

37. Harris J, VanPatten S, Deen NS, Al-Abed Y, Morand EF. Rediscovering MIF: new tricks for an old cytokine. *Trends Immunol* (2019) 40(5):447–62. doi: 10.1016/j.it.2019.03.002

38. Calandra T, Roger T. Macrophage migration inhibitory factor: a regulator of innate immunity. *Nat Rev Immunol* (2003) 3(10):791–800. doi: 10.1038/nri1200

39. Bucala R, Donnelly SC. Macrophage migration inhibitory factor: a probable link between inflammation and cancer. *Immunity* (2007) 26(3):281–5. doi: 10.1016/j.immuni.2007.03.005

40. Bilsborrow JB, Doherty E, Tilstam PV, Bucala R. Macrophage migration inhibitory factor (MIF) as a therapeutic target for rheumatoid arthritis and systemic lupus erythematosus. *Expert Opin Ther Targets* (2019) 23(9):733–44. doi: 10.1080/14728222.2019.1656718

41. Grieb G, Merk M, Bernhagen J, Bucala R. Macrophage migration inhibitory factor (MIF): a promising biomarker. *Drug News Perspect* (2010) 23(4):257–64. doi: 10.1358/dnp.2010.23.4.1453629

42. Hertelendy J, Reumuth G, Simons D, Stoppe C, Kim BS, Stromps JP, et al. Macrophage migration inhibitory factor - A favorable marker in inflammatory diseases? *Curr Medicinal Chem* (2018) 25(5):601–5. doi: 10.2174/0929867324666170714114200

43. Mikulowska A, Metz CN, Bucala R, Holmdahl R. Macrophage migration inhibitory factor is involved in the pathogenesis of collagen type II-induced arthritis in mice. *J Immunol (Baltimore Md: 1950)* (1997) 158(11):5514–7. doi: 10.4049/jimmunol.158.11.5514

44. Calandra T, Echtenacher B, Roy DL, Pugin J, Metz CN, Hültner L, et al. Protection from septic shock by neutralization of macrophage migration inhibitory factor. *Nat Med* (2000) 6(2):164–70. doi: 10.1038/72262

45. Amano T, Nishihira J, Miki I. Blockade of macrophage migration inhibitory factor (MIF) prevents the antigen-induced response in a murine model of allergic airway inflammation. *Inflammation Res* (2007) 56(1):24–31. doi: 10.1007/s00011-007-5184-9

46. Cavalli E, Ciurleo R, Petralia MC, Fagone P, Bella R, Mangano K, et al. Emerging role of the macrophage migration inhibitory factor family of cytokines in neuroblastoma. Pathogenic effectors and novel therapeutic targets? *Mol (Basel Switzerland)* (2020) 25(5). doi: 10.3390/molecules25051194

47. Pearce BD, Garvin SE, Grove J, Bonney EA, Dudley DJ, Schendel DE, et al. Serum macrophage migration inhibitory factor in the prediction of preterm delivery. *Am J Obstet Gynecol* (2008) 199(1):46.e1–6. doi: 10.1016/j.ajog.2007.11.066

48. Todros T, Bontempo S, Piccoli E, Ietta F, Romagnoli R, Biolcati M, et al. Increased levels of macrophage migration inhibitory factor (MIF) in preeclampsia. *Eur J Obstet Gynecol Reprod Biol* (2005) 123(2):162–6. doi: 10.1016/j.ejogrb.2005.03.014

49. Chiba K, Zhao W, Chen J, Wang J, Cui HY, Kawakami H, et al. Neutrophils secrete MIP-1 beta after adhesion to laminin contained in basement membrane of blood vessels. *Br J Haematol* (2004) 127(5):592–7. doi: 10.1111/j.1365-2141.2004.05242.x

50. Cheung R, Malik M, Ravyn V, Tomkowicz B, Ptasznik A, Collman RG. An arrestin-dependent multi-kinase signaling complex mediates MIP-1beta/CCL4 signaling and chemotaxis of primary human macrophages. *J Leuk Biol* (2009) 86 (4):833–45. doi: 10.1189/jlb.0908551

51. David Dong ZM, Aplin AC, Nicosia RF. Regulation of angiogenesis by macrophages, dendritic cells, and circulating myelomonocytic cells. *Curr Pharm Design* (2009) 15(4):365–79. doi: 10.2174/138161209787315783

52. Abrahams VM, Kim YM, Straszewski SL, Romero R, Mor G. Macrophages and apoptotic cell clearance during pregnancy. *Am J Reprod Immunol (New York NY: 1989)* (2004) 51(4):275–82. doi: 10.1111/j.1600-0897.2004.00156.x

53. Jiang H, Harris MB, Rothman P. IL-4/IL-13 signaling beyond JAK/STAT. *J Allergy Clin Immunol* (2000) 105(6 Pt 1):1063–70. doi: 10.1067/mai.2000.107604

54. Herbert JM, Savi P, Laplace MC, Lale A. IL-4 inhibits LPS-, IL-1 beta- and TNF alpha-induced expression of tissue factor in endothelial cells and monocytes. *FEBS Lett* (1992) 310(1):31–3. doi: 10.1016/0014-5793(92)81139-D

55. Berkman N, John M, Roesems G, Jose P, Barnes PJ, Chung KF. Interleukin 13 inhibits macrophage inflammatory protein-1 alpha production from human alveolar macrophages and monocytes. *Am J Respir Cell Mol Biol* (1996) 15(3):382–9. doi: 10.1165/ajrcmb.15.3.8810643

56. Standiford TJ, Kunkel SL, Liebler JM, Burdick MD, Gilbert AR, Strieter RM. Gene expression of macrophage inflammatory protein-1 alpha from human blood monocytes and alveolar macrophages is inhibited by interleukin-4. *Am J Respir Cell Mol Biol* (1993) 9(2):192–8. doi: 10.1165/ajrcmb/9.2.192

57. Kiyota T, Okuyama S, Swan RJ, Jacobsen MT, Gendelman HE, Ikezu T. CNS expression of anti-inflammatory cytokine interleukin-4 attenuates Alzheimer's disease-like pathogenesis in APP+PS1 bigenic mice. *FASEB J* (2010) 24(8):3093–102. doi: 10.1096/fj.10-155317

58. Horsfall AC, Butler DM, Marinova L, Warden PJ, Williams RO, Maini RN, et al. Suppression of collagen-induced arthritis by continuous administration of IL-4. *J Immunol (Baltimore Md: 1950)* (1997) 159(11):5687–96. doi: 10.4049/jimmunol.159.11.5687

59. Martin R. Interleukin 4 treatment of psoriasis: are pleiotropic cytokines suitable therapies for autoimmune diseases? *Trends Pharmacol Sci* (2003) 24(12):613–6. doi: 10.1016/j.tips.2003.10.006

60. Gu Y, Lewis DF, Deere K, Groome LJ, Wang Y. Elevated maternal IL-16 levels, enhanced IL-16 expressions in endothelium and leukocytes, and increased IL-16 production by placental trophoblasts in women with preeclampsia. *J Immunol (Baltimore Md: 1950)* (2008) 181(6):4418–22. doi: 10.4049/jimmunol.181.6.4418

61. Tranquilli AL, Landi B, Corradetti A, Giannubilo SR, Sartini D, Pozzi V, et al. Inflammatory cytokines patterns in the placenta of pregnancies complicated by HELLP (hemolysis, elevated liver enzyme, and low platelet) syndrome. *Cytokine* (2007) 40 (2):82–8. doi: 10.1016/j.cyto.2007.08.010

62. Whitley GS, Cartwright JE. Trophoblast-mediated spiral artery remodelling: a role for apoptosis. *J Anatomy* (2009) 215(1):21–6. doi: 10.1111/j.1469-7580.2008.01039.x

63. Chen L, Liu X, Zhu Y, Cao Y, Sun L, Jin B. Localization and variation of TRAIL and its receptors in human placenta during gestation. *Life Sci* (2004) 74(12):1479–86. doi: 10.1016/j.lfs.2003.07.044

64. Keogh RJ, Harris LK, Freeman A, Baker PN, Aplin JD, Whitley GS, et al. Fetal-derived trophoblast use the apoptotic cytokine tumor necrosis factor-alpha-related apoptosis-inducing ligand to induce smooth muscle cell death. *Circ Res* (2007) 100 (6):834–41. doi: 10.1161/01.RES.0000261352.81736.37

65. Zhou C, Long Y, Yang H, Zhu C, Ma Q, Zhang Y. TRAIL is decreased before 20 weeks gestation in women with hypertensive disorders of pregnancy. *PloS One* (2015) 10(6):e0128425. doi: 10.1371/journal.pone.0128425

66. Daniel Y, Kupferminc MJ, Baram A, Jaffa AJ, Fait G, Wolman I, et al. Plasma interleukin-12 is elevated in patients with preeclampsia. *Am J Reprod Immunol (New York NY: 1989)* (1998) 39(6):376–80. doi: 10.1111/j.1600-0897.1998.tb00372.x

67. Szarka A, Rigó J Jr., Lázár L, Beko G, Molvarec A. Circulating cytokines, chemokines and adhesion molecules in normal pregnancy and preeclampsia determined by multiplex suspension array. *BMC Immunol* (2010) 11:59. doi: 10.1186/1471-2172-11-59

68. Southcombe JH, Redman CW, Sargent IL, Granne I. Interleukin-1 family cytokines and their regulatory proteins in normal pregnancy and pre-eclampsia. *Clin Exp Immunol* (2015) 181(3):480–90. doi: 10.1111/cei.12608

69. Greer IA, Lyall F, Perera T, Boswell F, Macara LM. Increased concentrations of cytokines interleukin-6 and interleukin-1 receptor antagonist in plasma of women with preeclampsia: a mechanism for endothelial dysfunction? *Obstet Gynecol* (1994) 84 (6):937–40.

70. Wu ZM, Yang H, Li M, Yeh CC, Schatz F, Lockwood CJ, et al. Pro-inflammatory cytokine-stimulated first trimester decidual cells enhance macrophage-induced apoptosis of extravillous trophoblasts. *Placenta* (2012) 33(3):188–94. doi: 10.1016/j.placenta.2011.12.007

71. Bikker A, Hack CE, Lafeber FP, van Roon JA. Interleukin-7: a key mediator in T cell-driven autoimmunity, inflammation, and tissue destruction. *Curr Pharm Design* (2012) 18(16):2347–56. doi: 10.2174/138161212800165979

72. Arbelaez CA, Glatigny S, Duhen R, Eberl G, Oukka M, Bettelli E. IL-7/IL-7 receptor signaling differentially affects effector CD4+ T cell subsets involved in experimental autoimmune encephalomyelitis. *J Immunol (Baltimore Md: 1950)* (2015) 195(5):1974–83. doi: 10.4049/jimmunol.1403135

73. Toldi G, Rigó J Jr., Stenczer B, Vásárhelyi B, Molvarec A. Increased prevalence of IL-17-producing peripheral blood lymphocytes in pre-eclampsia. *Am J Reprod Immunol (New York NY: 1989)* (2011) 66(3):223–9. doi: 10.1111/j.1600-0897.2011.00987.x

74. Deng Z, Zhang L, Tang Q, Xu Y, Liu S, Li H. Circulating levels of IFN-γ, IL-1, IL-17 and IL-22 in pre-eclampsia: A systematic review and meta-analysis. *Eur J Obstet Gynecol Reprod Biol* (2020) 248:211–21. doi: 10.1016/j.ejogrb.2020.03.039

75. Brewster JA, Orsi NM, Gopichandran N, McShane P, Ekbote UV, Walker JJ. Gestational effects on host inflammatory response in normal and pre-eclamptic pregnancies. *Eur J Obstet Gynecol Reprod Biol* (2008) 140(1):21–6. doi: 10.1016/j.ejogrb.2007.12.020

76. Charkiewicz K, Jasinska E, Goscik J, Koc-Zorawska E, Zorawski M, Kuc P, et al. Angiogenic factor screening in women with mild preeclampsia - New and significant proteins in plasma. *Cytokine* (2018) 106:125–30. doi: 10.1016/j.cyto.2017.10.020

77. Hypertension in pregnancy. Report of the American College of Obstetricians and Gynecologists' Task Force on hypertension in pregnancy. *Obstet Gynecol* (2013) 122 (5):1122–31. doi: 10.1097/01.AOG.0000437382.03963.88

78. Sun Y, Wu S, Zhou Q, Li X. Trophoblast-derived interleukin 9 mediates immune cell conversion and contributes to maternal-fetal tolerance. *J Reprod Immunol* (2021) 148:103379. doi: 10.1016/j.jri.2021.103379

79. Akhtar F, Rouse CA, Catano G, Montalvo M, Ullevig SL, Asmis R, et al. Acute maternal oxidant exposure causes susceptibility of the fetal brain to inflammation and oxidative stress. *J Neuroinflamm* (2017) 14(1):195. doi: 10.1186/s12974-017-0965-8

80. Raghupathy R, Al-Azemi M, Azizieh F. Intrauterine growth restriction: cytokine profiles of trophoblast antigen-stimulated maternal lymphocytes. *Clin Dev Immunol* (2012) 2012:734865. doi: 10.1155/2012/734865

81. Yano S, Sone S, Nishioka Y, Mukaida N, Matsushima K, Ogura T. Differential effects of anti-inflammatory cytokines (IL-4, IL-10 and IL-13) on tumoricidal and chemotactic properties of human monocytes induced by monocyte chemotactic and activating factor. *J Leuk Biol* (1995) 57(2):303–9. doi: 10.1002/jlb.57.2.303

82. Denihan NM, Looney A, Boylan GB, Walsh BH, Murray DM. Normative levels of Interleukin 16 in umbilical cord blood. *Clin Biochem* (2013) 46(18):1857–9. doi: 10.1016/j.clinbiochem.2013.07.012

frontiers | Frontiers in Immunology

TYPE Original Research
PUBLISHED 16 August 2022
DOI 10.3389/fimmu.2022.960909

OPEN ACCESS

EDITED BY
Diana Boraschi,
Chinese Academy of Science (CAS), China

REVIEWED BY
Francesco Alviano,
University of Bologna, Italy
Paola Pontrelli,
University of Bari Aldo Moro, Italy

*CORRESPONDENCE
Ornella Parolini
ornella.parolini@unicatt.it

†These authors have equally contributed to this work

SPECIALTY SECTION
This article was submitted to Cytokines and Soluble Mediators in Immunity, a section of the journal Frontiers in Immunology

RECEIVED 03 June 2022
ACCEPTED 12 July 2022
PUBLISHED 16 August 2022

CITATION
Papait A, Ragni E, Cargnoni A, Vertua E, Romele P, Masserdotti A, Perucca Orfei C, Signoroni PB, Magatti M, Silini AR, De Girolamo L and Parolini O (2022) Comparison of EV-free fraction, EVs, and total secretome of amniotic mesenchymal stromal cells for their immunomodulatory potential: a translational perspective. *Front. Immunol.* 13:960909. doi: 10.3389/fimmu.2022.960909

Comparison of EV-free fraction, EVs, and total secretome of amniotic mesenchymal stromal cells for their immunomodulatory potential: a translational perspective

Andrea Papait[1,2†], Enrico Ragni[3†], Anna Cargnoni[4], Elsa Vertua[4], Pietro Romele[4], Alice Masserdotti[4], Carlotta Perucca Orfei[3], Patrizia Bonassi Signoroni[4], Marta Magatti[4], Antonietta R. Silini[4], Laura De Girolamo[3] and Ornella Parolini[1,2*]

[1]Department of Life Science and Public Health, Università Cattolica del Sacro Cuore, Rome, Italy, [2]Fondazione Policlinico Universitario "Agostino Gemelli" Istituto di Ricovero e Cura a Carattere Scientifico, IRCCS, Rome, Italy, [3]Istituto di Ricovero e Cura a Carattere Scientifico, IRCCS Istituto Ortopedico Galeazzi, Laboratorio di Biotecnologie Applicate all'Ortopedia, Milan, Italy, [4]Centro di Ricerca E. Menni, Fondazione Poliambulanza Istituto Ospedaliero, Brescia, Italy

Amniotic mesenchymal stromal cells (hAMSCs) have unique immunomodulatory properties demonstrated *in vitro* and *in vivo* in various diseases in which the dysregulated immune system plays a major role. The immunomodulatory and pro-regenerative effects of MSCs, among which hAMSCs lie in the bioactive factors they secrete and in their paracrine activity, is well known. The mix of these factors (i.e., secretome) can be either freely secreted or conveyed by extracellular vesicles (EV), thus identifying two components in the cell secretome: EV-free and EV fractions. This study aimed to discern the relative impact of the individual components on the immunomodulatory action of the hAMSC secretome in order to obtain useful information for implementing future therapeutic approaches using immunomodulatory therapies based on the MSC secretome. To this aim, we isolated EVs from the hAMSC secretome (hAMSC-CM) by ultracentrifugation and validated the vesicular product according to the International Society for Extracellular Vesicles (ISEV) criteria. EVs were re-diluted in serum-free medium to maintain the EV concentration initially present in the original CM. We compared the effects of the EV-free and EV fractions with those exerted by hAMSC-CM *in toto* on the activation and differentiation of immune cell subpopulations belonging to both the innate and adaptive immune systems.

We observed that the EV-free fraction, similar to hAMSC-CM *in toto*, a) decreases the proliferation of activated peripheral blood mononuclear cells (PBMC), b) reduces the polarization of T cells toward inflammatory Th subsets, and induces the induction of regulatory T cells; c) affects monocyte

polarization to antigen-presenting cells fostering the acquisition of anti-inflammatory macrophage (M2) markers; and d) reduces the activation of B lymphocytes and their maturation to plasma cells. We observed instead that all investigated EV fractions, when used in the original concentrations, failed to exert any immunomodulatory effect, even though we show that EVs are internalized by various immune cells within PBMC. These findings suggest that the active component able to induce immune regulation, tested at original concentrations, of the hAMSC secretome resides in factors not conveyed in EVs. However, EVs isolated from hAMSC could exert actions on other cell types, as reported by others.

KEYWORDS

amnion, secretome/conditioned medium, extracellular vesicles, mesenchymal stem/stromal cells, immune modulation

Introduction

Human amniotic mesenchymal stromal cells (hAMSCs) have attracted great attention thanks to their immunomodulatory properties (1, 2) that determine significant advantages for their application in the treatment of inflammatory or immune-mediated diseases (3). Indeed, hAMSCs exert strong antiproliferative and immunomodulatory actions on different immune cells. Several *in vitro* studies demonstrated that hAMSCs and their secretome inhibit the proliferation of T cells when activated through TCR stimulation. As a matter of fact, we previously reported that hAMSCs and their secretome prevent/reduce the development of cytotoxic T cells and the polarization toward inflammatory T helper subsets and enhance instead the polarization toward regulatory T cells (4, 5). Furthermore, they suppress the *in vitro* differentiation of monocytes toward inflammatory antigen-presenting cells, triggering instead the acquisition of phenotypical and functional features typical of M2 anti-inflammatory macrophages (5–8). We have also recently demonstrated that hAMSCs and their secretome are able to suppress the proliferation and differentiation of B lymphocytes to plasma cells (9).

The immunomodulatory properties of hAMSCs and their secretome have been shown to contribute to their ability to foster tissue regeneration and induce therapeutic effects in preclinical disease models. As a matter of fact, hAMSCs and their secretome have been successfully used to treat different inflammatory-related diseases including lung (10, 11) and liver fibrosis (12), wound healing (7, 13), collagen-induced arthritis (14), tendon-to-bone healing (15), bone defects (16), multiple sclerosis (14), inflammatory bowel disease (14), colitis (14, 17), sepsis (14), traumatic brain injury (18), and Huntington's disease (19). All these studies strongly indicate that hAMSCs provide immunoregulatory actions through paracrine signaling triggered by factors present in their secretome, which include both freely secreted factors and factors conveyed by extracellular vesicles (EVs).

EVs are a heterogeneous family of bilayer membrane vesicles that, according to their size and biogenesis, are classified into exosomes (40–200 nm; generated within the endosomal system) and microvesicles (50–1,000 nm; produced by outward budding of the plasma membrane). EVs carry molecules such as proteins, lipids, and coding and non-coding RNAs, which can contribute to the function of the cells of origin from which they are released (20, 21). Some studies suggest that EVs released from MSCs may have a therapeutic action comparable to that of parental cells and their derived secretomes, thus representing an enormous therapeutic potential for applications in regenerative medicine due to their easier management/storage and higher safety (i.e., lack of tumorigenicity) compared to cell-based therapy (22). Our previous studies evidence that the hAMSC secretome (hereinafter defined as hAMSC-conditioned medium: hAMSC-CM) contains free, soluble molecules and EV-conveyed miRNAs

Abbreviations: ANOVA, analysis of variance; AT, adipose tissue; BM, bone marrow; CFSE, carboxyfluorescein succinimidyl ester; CM, conditioned medium; DC, dendritic cell; Edu, 5-ethynyl-2′-deoxyuridine; EV, extracellular vesicles; GM-CSF, granulocyte-macrophage colony-stimulating factor; hAMSC, mesenchymal stromal cells derived from amniotic membrane; IFN-γ, interferon gamma; IL-4, interleukin-4; LPS, lipopolysaccharide; mAB, monoclonal antibody; mDC, mature dendritic cell; MFI, mean fluorescence intensity; Mo, monocyte; ns, not significant; NTA, nanoparticle tracking analysis; PBMC, peripheral blood mononuclear cells; PBS, phosphate buffered saline; P/S, penicillin/streptomycin; RPMI, Roswell Park Memorial Institute 1640 medium; RT, room temperature; Th, T helper cell; Treg, T regulatory cell; TEM, transmission electron microscopy; UC, umbilical cord.

with regulatory functions on different types of inflammatory cells (23). It is now crucial to define whether the EV fraction can exert biological activities comparable to those of the CM in toto. To this end, we compared the immunomodulatory potential of the different hAMSC secretome fractions. Indeed, no study has yet to specifically address the contribution that EVs and the freely secreted fraction have to the multifaceted immunomodulatory effects of hAMSC-CM. As a matter of fact, in this comparative study we aimed to discern the relative impact of the individual components of the hAMSC secretome, maintaining for each secretome fraction (EV-free and EV) the quantitative proportions in which they are represented in the secretome of origin.

Thus, herein for the first time we compared the immunomodulatory properties of the hAMSC secretome in toto with those of the different fractions (EV-free and EV fractions) to draw upon useful information for implementing future therapeutic approaches using immunomodulatory therapies (EV vs. secretome in toto) based on the MSC secretome.

Material and methods

Ethics statements

The collection of human peripheral blood mononuclear cells (PBMCs) for research purposes was approved by the Regional Departments of Transfusion Medicine (Rif. 523, July 7, 2016). PBMCs were obtained from healthy adult donors after informed consent and provided by the Center of Immune Transfusion of Spedali Civili of Brescia, Italy.

Human term placentae were collected from healthy women after vaginal delivery or caesarean section at term, after obtaining informed written consent, according to the guidelines set by the local ethical committee "Comitato Etico Provinciale di Brescia," Italy (number NP 2243, 19 January 2016).

Isolation of mesenchymal stromal cells from human amniotic membrane and CM preparation

Cells were isolated as previously described (24). The amniotic membrane was cut in fragments and digested at 37°C for 9 min with 2.5 U/ml dispase (VWR, Radnor, PA, USA). The digestion was then blocked by washing the amniotic fragments in RPMI complete medium composed of RPMI 1640 medium supplemented with 10% heat-inactivated fetal bovine serum (FBS), 1% penicillin/streptomycin (P/S), and 1% L-glutamine (all from Sigma-Aldrich, St. Louis, MO, USA). Enzymatic digestion continued with fragment incubation in the presence of 0.94 mg/ml collagenase and DNase I (both from Roche, Basel, Switzerland) for approximately 2.5–3 h at 37°C. The cell suspension obtained was centrifuged at low g, and the supernatant was filtered (100-µm cell strainer) (BD Falcon, Bedford, MA, USA), and the cells were collected by centrifugation. After isolation, hAMSCs (p0) were phenotypically characterized as previously reported (24). Cells with >80% expression of mesenchymal markers CD13 and CD90 and <10% expression of the hematopoietic marker CD45 and of the epithelial marker CD324 were used in this study.

Freshly isolated cells were expanded until passage 1 (p1) by plating at a density of 10^4 cells/cm^2 in Chang Medium C (Irvine Scientific, Santa Ana, CA, USA) supplemented with 2 mM L-glutamine at 37°C in the incubator at 5% CO2. To produce conditioned medium (CM), hAMSC p1 cells were seeded for 5 days in 24-well plates (Corning, NY, USA) at a density of 5×10^5 cells/well in 0.5 ml of DMEM-F12 medium (Sigma-Aldrich) without serum, supplemented with 2 mM L-glutamine (Sigma-Aldrich) and 1% P/S as described (25).

At the end of the 5-day culture, CM was collected, centrifuged at 300×g, and filtered through a 0.2-µm sterile filter (Sartorius Stedim, Florence, Italy). An aliquot of 5 ml was kept frozen at – 80°C until use (CM in toto for comparison with other fractions), while the remaining CM volume (15–20 ml) was used for EV isolation. After EV isolation, the EV-free fraction was maintained for comparison studies. Six placentas were used to obtain six different hAMSC-CM preparations. The number of CMs used for each experiment is indicated in the figure legends.

CM fractionation by ultracentrifugation

CM was centrifuged at 100,000 × g for 1, 3, 9, or 24 h at 4°C in a 70.1 Ti rotor (Beckman Coulter, Fullerton, CA, USA). To ensure optimal EV recovery, tubes were filled up to half nominal volume. After centrifugation, supernatants (EV-free fraction) were recovered and pellets (EV fraction) were suspended in a small volume of PBS or in a volume equivalent to the starting volume of CM used to isolate EVs (for example, EVs isolated from 12 ml of CM were resuspended in 12 ml of fresh medium without serum). Both EV-free and EV fractions were stored at 4° C and utilized within 24 h from isolation.

EV detection by nanoparticle tracking analysis

EVs in the CM in toto, EV-free fractions, or EV fractions were visualized by the NanoSight NS300 system (NanoSight

Ltd., Amesbury, UK). Dilutions with PBS were performed to ensure sample readings between 20 and 120 particles per frame. Pump flow was set to 30. Three to five recordings of 60 s were executed for each sample. Collected data were analyzed by the Nanoparticle Tracking Analysis (NTA) software, providing concentration measurements and high-resolution particle size distribution profiles.

EV characterization by flow cytometry

For analysis of EV integrity, an identical number of EVs in both CM in toto and EV fraction samples calculated from NTA data were supplemented with carboxyfluorescein succinimidyl ester (CFSE; Sigma-Aldrich, St Louis, MO, USA) (10 µM final) and incubated in the dark at 37°C for 30 min. CFSE-positive events were detected and counted using the FITC channel up to a maximum value of 10,000 events per second with a 10-µl/min flow rate using a CytoFLEX flow cytometer (Beckman Coulter). Unstained CM in toto and EV fraction samples were used as negative controls to set CFSE positivity. Integrity was calculated as the ratio of FITC+ events between the EV fraction and CM in toto. Before analysis, flow cytometer performance in the nanometer range was set with reference Megamix-Plus SSC beads (Biocytex, Marseille, France) composed of FITC fluorescent spheres (160, 200, 240, and 500 nm).

For EV marker detection, CM in toto and EV fraction samples were stained with CFSE as previously described. Afterward, one-seventh of the labeled samples were stored at 4°C, whereas the rest was divided into six aliquots and each stained for 30 min at 4°C in the dark with 1 µl of the following APC-conjugated Ab: anti-CD9 (312107, BioLegend, San Diego, CA, USA), CD63 (353007, BioLegend), CD81 (349509, BioLegend), CD44 (338805, BioLegend), CD73 (344005, BioLegend), and CD90 (328113, BioLegend). Antibodies were used singularly. A maximum value of 10,000 events per second were acquired with a 10-µl/min flow rate using a CytoFLEX flow cytometer, and APC-positive events were detected after FITC gating as previously described. Unstained samples were used as negative controls to set APC positivity.

EV characterization by transmission electron microscopy

EV fraction samples were suspended in PBS (100 µl per initial 5-ml volume). Five microliters was absorbed for 10 min at RT on formvar carbon-coated grids and drops blotted with filter paper. Two percent of uranyl acetate aqueous suspension was used to perform negative staining for 10 min, and excess was removed by filter paper. The grid was dried at RT. Samples were examined with a TALOS L120C transmission electron microscope (Thermo Fisher Scientific, Waltham, MA, USA) at 120 kV.

Protein quantification in purified EVs

After centrifugation, samples from EV fractions were analyzed with a NanoDrop ND-1000 spectrophotometer (Thermo Fisher Scientific, Waltham, MA, USA) with the Protein A280 protocol. The concentration was related with NTA data to obtain the number of EVs/µg protein value.

Analysis of T-cell proliferation

T-cell proliferation was induced by stimulating peripheral blood mononuclear cells (PBMCs) with an anti-CD3 monoclonal antibody. Human PBMCs were obtained from heparinized whole blood samples using density gradient centrifugation (Histopaque-1077, Sigma-Aldrich, St. Louis, MO, USA). PBMCs (1×10^5/well in a 96-well-plate) were activated with 125 ng/ml (final concentration) anti-CD3 (Orthoclone OKT3, Janssen-Cilag, Cologno Monzese, Italy). Activated PBMCs (PBMC + anti-CD3) were cultured in the presence of different volumes of CM or of its fractions (EV-free or EVs) (10, 25, 50, or 100 µl/well of CM 5%, 12.5%, 25%, or 50%, respectively, of the final volume), for 3 days. The final volume of each well was 200 µl. In all experiments, activated PBMCs cultured alone were used as controls. All conditions were performed in triplicate in RPMI 1640 medium (Cambrex, Verviers, Belgium) supplemented with 10% heat-inactivated FBS, 2 mM L-glutamine, and P/S.

T-cell proliferation was assessed by 5-ethynyl-2′-deoxyuridine (EdU) incorporation as previously described (26). Briefly, 10 µM EdU (Life Technologies, Carlsbad, CA, USA) was added to PBMCs at day 3 post-stimulation. After 16–18 h, cells were harvested and EdU incorporation was evaluated by adding 2.5 µM 3-azido-7-hydroxycoumarin (Jena Biosciences, Jena, Germany) in buffer solution (100 mM Tris–HCl pH 8.0, 10 mM L-ascorbic acid, 2 mM $CuSO_4$) at RT for 30 min. Cells were acquired using a FACSymphony A3 (BD Biosciences), and the percentage of proliferating EdU-positive cells was analyzed with FlowJo V10 (BD Biosciences). Cells were also stained with eFluor 780 (Thermo Fisher) for the exclusion of dead cells.

Analysis of $CD4^+$ T helper subsets and Treg subset polarization

Phenotypes were assessed by flow cytometry analysis of the expression of specific cell surface markers and transcription factors

to identify T helper subsets (Th1, Th2, and Th17) and Treg. After 5 days of coculture in the presence of CM, PBMCs stimulated with anti-CD3 were collected and centrifuged at 300g for 5 min. Cells were stained with eFluor 780 for the exclusion of dead cells. The staining was performed using antibodies for CD3 (clone UCHT1), CD4 (clone VIT-4), CD45RA (clone HI100), CD196 (clone 11A9), CD183 (clone 1C6/CXCR3), CD25 (clone M-A25), and FoxP3 (clone 259D/C7) which all came from BD Biosciences and CD194 (clone REA279) from Miltenyi. Intracellular staining for FoxP3 was performed after fixation and permeabilization using BD Cytofix/Cytoperm (BD Biosciences), followed by staining with anti-FoxP3 antibody. Samples were acquired using a FACSymphony A3 and analyzed with FlowJo V10. T-cell subsets were identified by a sequential gating strategy. T effector cells were first identified by gating CD4-positive and CD45RA-negative cell populations ($CD4^+CD45RA^-$ cells), and different T helper (Th) subsets were identified as follows: Th1 as $CD196^-CD183^+$, Th17/Th1 as CD196 +CD183+, and Th2 as $CD196^-CD183^-CD194^+$ (27). Furthermore, to investigate the ability of hAMSC-CM and its fraction to induce Treg polarization, we performed a mixed lymphocyte reaction (MLR-T) by coculturing T lymphocytes (1×10^5), previously isolated from PBMCs using the Pan T cell Isolation Kit (Miltenyi Biotech), with 1×10^5 gamma-irradiated allogeneic PBMCs. Activated T lymphocytes (MLR-T) were cultured in the presence of different volumes of CM or of its fractions (EV-free or EVs) (10, 25, 50, or 100 µl/well of CM (5%, 12.5%, 25%, or 50%, respectively, of the final volume), for 6 days. Tregs were evaluated as previously reported in the aforementioned gating strategy, and the % of Treg cells was evaluated as CD25 High and FoxP3-positive cells.

Analysis of monocyte differentiation toward antigen-presenting cells

Monocyte-derived M1 macrophages were differentiated starting from 5×10^5 PBMCs cultured or not (control condition) in the presence of CM or its fractions, in 24-well plates (Corning) for 4 days in the presence of 5 ng/ml GM-CSF (Miltenyi Biotec) in 0.5 ml RPMI 1640 complete medium. Cells were activated by adding 20 ng/ml interferon gamma (IFN-γ) (Miltenyi Biotec) for 1 h after which 0.1 µg/ml LPS (Sigma-Aldrich) was added and left for 2 days. For dendritic cell (DC) differentiation, 2.5×10^5 PBMCs were cultured in 48-well plates (Corning) for 4 days in the presence of 50 ng/ml recombinant human IL-4 (R&D Systems, Minneapolis, MN, USA) and 50 ng/ml GM-CSF in 0.5 ml RPMI 1640 complete medium. Complete maturation was reached by adding 0.1 µg/ml LPS for 2 days.

M1 macrophages, as well as DC, were collected after 6 days of differentiation in the absence or presence of 10, 25, 50, or 100 µl/well of CM or its fractions (EV-free or EVs) (2%, 5%, 10%, or 20%, respectively, of the final volume). Different CM products were added at day 0, concomitantly with the start of the differentiation protocol. Phenotype was investigated by flow cytometry. Prior to surface marker staining, cells were stained with eFluor 780 for the exclusion of dead cells. Cells stained with CD3 were excluded; CD11b (clone ICRF44)-positive cells were analyzed for the expression of CD163 (clone GHI/61), CD197 (clone 3D12), CD86 (clone 2331 (FUN-1)), and CD14 (clone MΦP9) to distinguish M1/M2 macrophage polarization. For mDC differentiation, the same protocol aforementioned for the macrophages was used and staining was performed for CD197 (clone 3D12), CD209 (clone DCN46), CD14 (clone MΦP9), CD83 (clone HB15e), and CD1a (clone HI149). All antibodies were purchased from BD Biosciences.

Analysis of B-cell proliferation and differentiation

To evaluate B lymphocyte proliferation, PBMCs were labeled with CFSE to monitor cell division (9). Stained PBMCs (1×10^5 cells) were seeded in 96-well tissue culture plates in 50% RPMI complete medium and 50% UltraCULTURE™ serum-free culture medium (Lonza, Basel, Switzerland). B-cell proliferation was induced by stimulating cells for 6 days with 2.5 µg/ml CpG-ODN 2006 (Aurogene s.r.l., Rome, Italy). Activated PBMCs were cultured in the presence of CM-hAMSC or its fractions, EV-free, or EVs (10, 25, 50, or 100 µl/well of CM 5%, 12.5%, 25%, or 50%, respectively, of the final volume).

Cells were stained with eFluor 780 for the exclusion of dead cells. The staining was performed using antibodies for CD3 (clone UCHT1), CD19 (clone SJ25C1), CD14 (clone MΦP9), CD27 (clone M-T271), CD24 (clone ML5), CD38 (clone HB7), and IgM (clone G20-127) which all came from BD Biosciences and CD138 (clone 44F9) from Miltenyi. Samples were acquired using a FACSymphony A3 and analyzed with FlowJo V10. B-cell subsets were identified by a sequential gating strategy. Plasmablasts were identified as $CD19^+CD27^{hi}CD38^{hi}CD138^-$ cells; plasma cells (PC) were identified by the co-expression of the CD138 marker ($CD19^+CD27^{hi}CD38^{hi}CD138^+$).

Quantification of hAMSC-EV uptake by PBMC

The spontaneous uptake of EVs by PBMC was analyzed by culturing unstimulated PBMC for 18 h with 5×10^9 vesicles stained with CFSE, as previously reported in the section entitled "EV characterization by flow cytometry". After incubation, the PBMCs were collected, extensively washed, and analyzed by flow cytometry for uptake. To evaluate the uptake ability of the different immune cell subsets, we stained the PBMCs with the following antibodies: CD3 (clone UCHT1), CD19 (clone

SJ25C1), and CD14 (clone MΦP9). The amount of immune cells positive for the expression of CFSE and indicative of the EV uptake was assessed with FACSymphony A3 and analyzed with FlowJo V10. The comparison was performed using untreated PBMC as baseline for basal autofluorescence.

Statistical analysis

The data are shown as violin-truncated plots with Tukey variations. The parameters were compared using one-way and two-way analyses of variance (ANOVA). Data are representative of at least three independent experiments. Statistical analysis was performed using Prism 8 (GraphPad Software, La Jolla, CA, USA). A p value lower than 0.05 was considered statistically significant.

Results

hAMSC-CM fractionation

In order to efficiently isolate EVs from the hAMSC-CM and obtain the EV-depleted counterpart, a tailored protocol was fine-tuned relying on a centrifugal force of 100,000 × g, as widely reported in the ISEV guidelines as an efficient method for EV isolation from CM (28). This was followed by several quality controls (Figure 1A). On a pilot hAMSC-CM lot ($15.3 \times 10^9 \pm 0.4$ EVs/ml), different centrifugation times were scored to identify via NTA technology the experimental condition coupling the highest EV removal and recovery with the most reduced operative time to avoid EV damage by long-lasting g-force (Figure 1B). The combination of 100,000 × g and 3-h centrifugation resulted in the best protocol with EV recovery up to 77.9% ± 4.2 (Figure 1C). Notably, increasing the centrifugation times did not allow for higher recovery (80.4% ± 0.8 and 72.6% ± 2.8, 9 and 24 h, respectively), whereas a shorter time (1 h) did not lead to efficient separation of particles from the supernatant that resulted to be contaminated (44.0% ± 4.0 of the initial EVs input with 46.6% ± 7.9 recovery). Moreover, the selected 3-h protocol led to the isolation of particles of comparable size with respect to EVs in the CM (133 nm ± 8 vs. 127 nm ± 7, CM vs. EVs, no significant ($p < 0.05$) difference) (Figure 1D), as scored by NTA data, while 1-h centrifugation resulted in particles of smaller size (96 nm ± 5), possibly due to the selection of a subpopulation as clearly evidenced in NTA plots where larger particles are mainly detected in the supernatant. NTA graphs also showed the absence of larger (>300 nm) events both before and after EV isolation, emphasizing that the procedure does not lead to particle aggregates or clumps, even after 24 h of centrifugation. Size was substantiated by transmission electron microscopy (TEM) analysis of isolated EVs, showing their typical cup-shaped morphology, with the majority of particles below 200 nm and few large ones (>250 nm) as reported by NTA (Figure 1E). The isolation of particles with dimensional parameters similar to those in the CM suggests the conservation of EV integrity after processing, a crucial step in order to subsequently attribute a biological effect. By flow cytometry analysis of CFSE-stained particles, compared to those in the unpurified CM, and by direct comparison with fluorescent nanobeads of predetermined size (160, 200, 240, and 500 nm), the dimensional range previously obtained with NTA technology was further confirmed to be around 150 nm (Figure 1F) both before and after purification of another parameter that confirmed the absence of major particle disruption or aggregation. Finally, we reported that EV integrity after centrifugation showed 76.4% ± 2.0 (Figure 1G). Flow cytometry also showed the low and high presence of CD9 and CD63/CD81 EV markers, respectively, as well as both the abundance of CD73/90 and the whole population shift of CD44 hAMSC markers (Supplementary Figure 1), as previously published by our group (23). Comparable data before and after centrifugation were a further support of absence of detrimental effects or isolation of subpopulation given by the isolation procedure. As a final quality control, the purity of isolated EVs was calculated and resulted to be $0.468 \times 10^9 \pm 0.095$ EVs/μg protein, a value falling within the range (10^8 to 10^{10}) reported for EV preparations from cell culture supernatants (29).

Characterization of EVs from hAMSC-CM

To try to discriminate the impact of the different components of the secretome, we compared the results obtained from the secretome in toto (hAMSC-CM) with those of the same secretome depleted from EVs (EV-free) and with the EV fraction resuspended in an equivalent volume of fresh medium. Specifically, in order to evaluate the effect due to EVs alone and discern it from that of soluble bioactive molecules contained in the EV-depleted secretome, we suspended EVs in the equivalent volume of fresh medium (DMEM-F12) (for example, EVs isolated from 12 ml of CM were resuspended in 12 ml of fresh medium). The products obtained were subsequently characterized as previously described (Table 1). The average EV concentration per ml resulted to be $12.0 \times 10^9 \pm 7.6$ in CM, $2.0 \times 10^9 \pm 2.9$ in EV-free, and $9.9 \times 10^9 \pm 5.5$ in EV fractions.

Overall, the recovery rate was similar to the values previously observed during protocol optimization resulting to be 85.8% ± 12.8. Mean EV size was calculated in 149 nm ± 21 and 147 nm ± 17 for CM and EV samples, respectively, with no significant ($p < 0.05$) difference between conditions. On three random EV samples, we monitored the presence of EV and hAMSC markers obtaining results almost identical to those previously observed with a very weak presence of CD9 (5% ± 1), abundant signal for CD63 (88% ± 1), CD81 (87% ± 2), CD73 (90% ± 2), and CD90 (81% ± 1), and weaker staining albeit with a whole

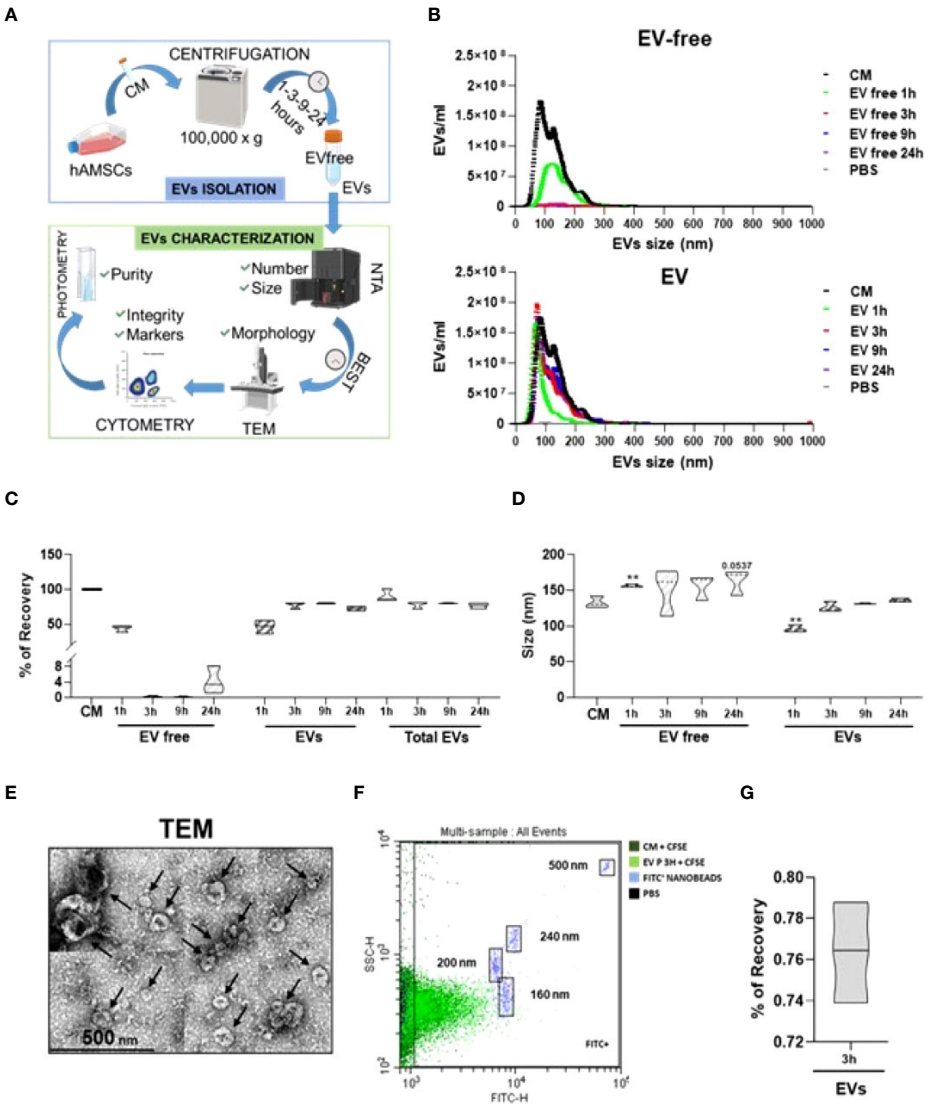

FIGURE 1
Definition of hAMSC-CM fractionation protocol and EV characterization. **(A)** Workflow of the protocol used to identify and validate the most efficient centrifugation procedure to obtain EV-depleted and EV-enriched fractions from hAMSC-CM. **(B)** Particle size and concentration profiles from NTA data for both fractions (EV free and EVs) after centrifugation for the indicated times (1, 3, 9, and 24 h). CM and PBS were used as starting condition and background, respectively (N = 3, values indicated as mean ± SD). **(C)** EV recovery or contamination in the EV-free fraction for the tested centrifugation times (1, 3, 9, and 24 h) calculated from the NTA data with respect to EVs in the CM set as 100% (N = 3, mean ± SD). **(D)** Size analysis from NTA data for the EVs identified in the CM, EVs, or EV-free fractions obtained after centrifugation for the indicated times (1, 3, 9, and 24 h) (N = 3, mean ± SD). **(E)** Transmission electron micrographs of EVs in the 3-h centrifugation pellets showing characteristic cup-shaped morphology and size compatible with NTA data. Black arrows indicate the EVs. **(F)** Visualization of EVs (in the unprocessed CM or in EV-fraction) after a 3-h centrifugation), after CFSE staining and comparison with nanometric FITC-fluorescent beads of indicated sizes. A representative cytogram is presented. **(G)** % of EVs recovery after 3 h of centrifugation.

population shift for CD44 (40% ± 9). Also, purity on four samples resulted to be 0.178 × 109 ± 0.060 EVs/μg protein. Analysis on a single sample showed 78% EV integrity. Given the reliability of the procedure, in all experimental conditions discussed in the following paragraphs, with exception when indicated, we compared the effect of a range of comparable doses of hAMSC-CM and EV-free and EV fractions (100, 50, 25, and 10 μl).

Ability of hAMSC-CM and EV-free and EV fractions to modulate T-cell proliferation

First, we evaluated and compared the effects of different doses of hAMSC-CM in toto and fractions obtained thereof (EV-free and EV fractions) on the proliferation of T lymphocytes stimulated with anti-CD3. The results obtained confirmed that CM in toto was able to inhibit the proliferation of T lymphocytes

10.3389/fimmu.2022.960909

TABLE 1 Summary table for concentration, recovery, size, and marker expression of EVs isolated from hAMSC-CM.

EV/ml ($\times 10^8$) (N = 6)		
	MEAN	**SD**
CM-hAMSC	12.0	7.6
EV-free	2.0	2.9
Evs	9.9	5.5
Recovery (%) (N = 6)		
	MEAN	**SD**
EV-free	12.9	10.9
Evs	85.8	12.8
Size (nm) (N = 6)		
	MEAN	**SD**
CM-hAMSC	149	21
EV-free	153	17
Evs	147	17
Markers (%) (N = 3)		
EV-CD9	5	1
EV-CD83	88	1
EV-CD81	87	2
EV-CD44	40	9
EV-CD73	90	2
EV-CD90	81	1
Purity (EV $\times 10^8$/µg) (N = 4)		
	MEAN	**SD**
EVs	0.178	0.06

in a dose-dependent manner (from 59.4 ± 6.6% to 15.2 ± 8.3% of proliferating T cells in control and in activated PBMCs treated with 100 µl of CM, respectively; $p < 0.001$) and that only at the lowest dose (10 µl) was this effect partially lost (Figure 2). A similar trend was appreciable for the EV-free fraction (15.9 ± 7.5% proliferating cells in activated PBMCs treated with 100 µl of EV-free fraction, $p < 0.001$) (Figure 1), whereas no appreciable effect was observed for EVs at any dose used (52.1 ± 13.1% proliferating cells in activated PBMCs treated with 100 µl of EVs, *p*=ns).

Ability of hAMSC-CM and EV-free and EV fractions to modulate Th subsets and Treg polarization

Given that EVs are carriers of miRNAs and given the importance that miRNAs have on modulating the cell differentiation process (30), we investigated the impact of hAMSC-CM and its fractions on the differentiation of effector T cells toward various Th subsets. This study was performed, as done

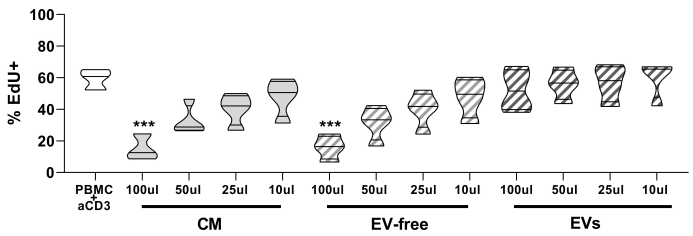

FIGURE 2
Effects of hAMSC-CM and its fractions (EV-free and EVs) on PBMC proliferation. Allogeneic PBMC (1×10^5) were stimulated with anti-CD3 antibody in the presence of 100, 50, 25, or 10 µl of hAMSC-CM *in toto* or with the same volume of the EV-free or EV fractions. Results are expressed as percentage of EdU+ cells representative of the proliferating cells. PBMCs stimulated with anti-CD3 mAb constitute the positive control. Results are displayed as violin plots showing median (thick line) and 25th and 75th quartiles (***$p < 0.001$ versus control (PBMC + anti-CD3), $N \geq 3$.

for T-cell proliferation analysis, by stimulating PBMCs with anti-CD3 monoclonal antibody in the presence of hAMSC-CM in toto or of its two fractions (EV-free or EVs). The commitment toward the different Th subsets was evaluated by flow cytometry, and the results were expressed as % of CD4-positive cells expressing specific markers identifying Th1, Th2, or Th1/Th17 subsets. As shown in Figure 3, hAMSC-CM decreased the median percentage of Th1 in PBMC stimulated with anti-CD3 with respect to control without CM treatment (40.0 ± 12.3% vs. 66.5 ± 5.7% in activated PBMC treated with 100 µl CM and in control activated PBMCs, respectively; $p < 0.05$). A similar trend was observed for the EV-free fraction (39.3 ± 6.3% in activated PBMCs treated with 100 µl of EV-free fraction, $p < 0.05$). When anti-CD3 stimulated PBMCs were cocultured in the presence of the EV fraction, we observed a slight reduction in Th1 median percentage (58.6 ± 6.6% in activated PBMCs treated with 100 µl EV fraction, p=ns), but this reduction was not statistically significant.

No significant differences were observed for Th2 polarization or the generation of Th1/Th17 subsets, for either hAMSC-CM in toto or the different fractions tested.

In addition, we investigated the effects of the hAMSC-CM in toto or its fractions (EV-free or EVs) on Treg subset polarization (Figure 3 lower panel). As previously reported, we confirmed that CM-hAMSC triggers the induction of Treg cells at the highest concentration (1.08 ± 0.46% vs. 3.34 ± 1.04%, respectively). Similar results were also obtained by the EV-free fraction at the intermediate and lowest concentrations (50 and 10 µl: 3.046 ± 1.03% and 3.094 ± 1.14%, respectively). Also in

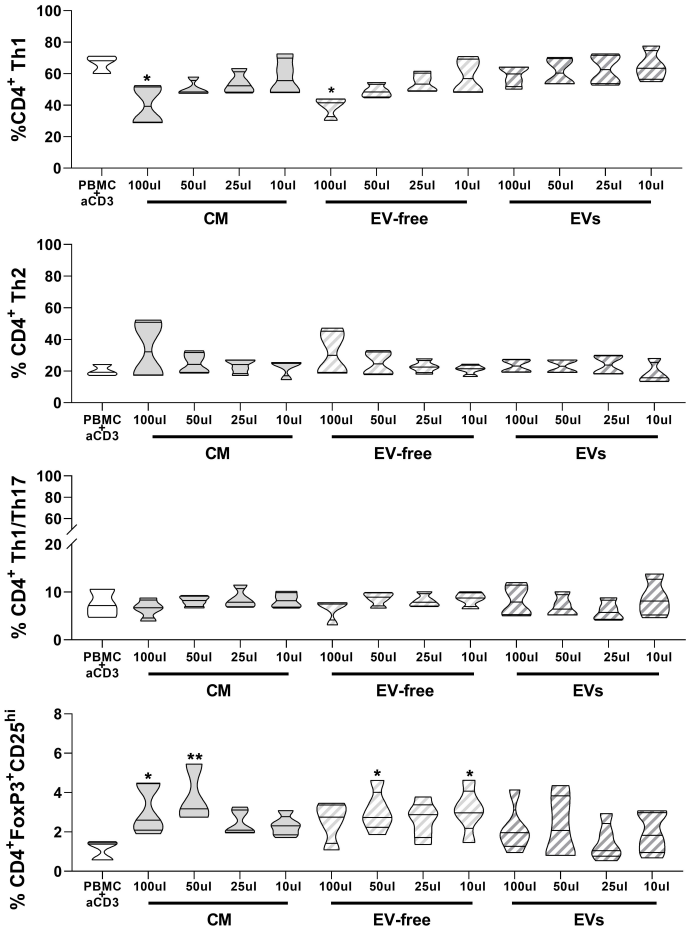

FIGURE 3
Effects of hAMSC-CM and its fractions (EV-free and EVs) on the differentiation of T lymphocytes toward Th1, Th2, Th1/Th17, and Treg subtypes. Allogeneic PBMCs were incubated with anti-CD3 mAb in the presence of 100, 50, 25, or 10 µl of hAMSC-CM in toto or with the same volumes of the EV-free or EV fractions. Samples were collected after 5 days of culture. Results are expressed as percentage of the different Th subsets investigated: Th1 ($CD183^+CD196^-$), Th2 ($CD183^-CD196^-CD194^+$), Th1/Th17 ($CD183^+CD196^+$), and Treg ($CD4^+CD25^{hi}FoxP3^+$). Results are displayed as violin plots showing median (thick line) and 25th and 75th quartiles (*$p < 0.05$, **$p < 0.01$, N ≥ 3 individual experiments).

10.3389/fimmu.2022.960909

this case, the EV fraction seems to be able to induce only a slight increase in the Treg subset polarization at the highest concentration used (2.14 ± 1.20%).

Ability of hAMSC-CM and EV-free and EV fractions to modulate monocyte differentiation to antigen-presenting cells

Our group previously demonstrated that hAMSC-CM hampers monocyte (Mo) differentiation toward M1-type macrophages and instead triggers the acquisition of anti-inflammatory M2 macrophage features (6). Here we wanted to clarify the impact that the EV-free fraction and EVs have on Mo-M1 differentiation comparing the results with those obtained with hAMSC-CM in toto.

Both hAMSC-CM as well as the EV-free fraction reduced monocyte differentiation toward M1 macrophages, both by maintaining the expression of the undifferentiated monocytic marker CD14 (11.2 ± 7.2% control Mo-M1 macrophages vs. 87.8 ± 8.85% hAMSC-CM 100 µl and 90.9 ± 3.34% EV-free fraction 100 µl) (Figure 4A) and by reducing the expression of markers associated with M1 differentiation, such as CD197 (chemokine receptor CCR7) (70.8 ± 18.2% control Mo-M1 macrophages vs. 43.7 ± 4.30% hAMSC-CM 100 µl and 41.6 ± 20.5% EV-free fraction 100 µl) and the co-stimulatory molecule CD86 (MFI 384.8 ± 122.8 control Mo-M1 macrophages vs. 133.7 ± 80.2 hAMSC-CM 100 µl and 171.4 ± 78.5% EV-free fraction 100 µl) (Figure 4A). In parallel, they promoted monocyte skewing toward alternatively activated (M2) macrophages, as indicated by the significant increase in the percentage of macrophages expressing the M2 marker CD163 (all the results refer to the 100-µl concentration: 2.29 ± 2.64% control Mo-M1 macrophages vs. 75.3 ± 15.4% hAMSC-CM and 73.8 ± 13.4% EV-free fraction). On the other hand, the EV fraction did not affect monocyte differentiation toward M1 macrophages. Indeed, no differences vs. control Mo-M1 macrophages were observed with the administration of EVs regardless of the concentration used (all the

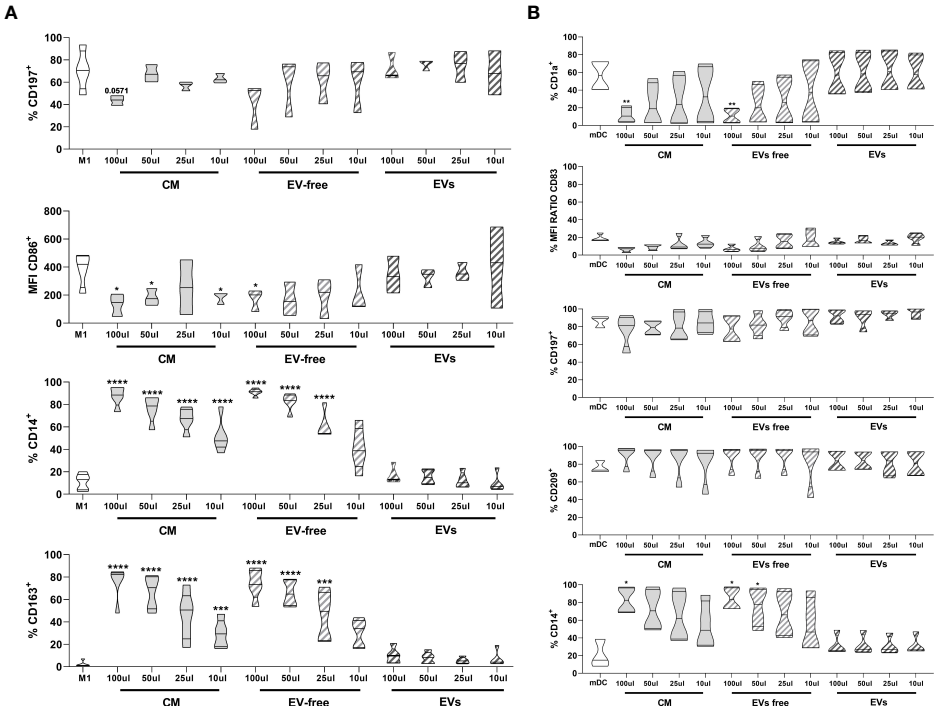

FIGURE 4
Effects of hAMSC-CM and its fractions (EV-free and EVs) on monocyte differentiation toward antigen-presenting cells **(A)** M1 macrophages were obtained by incubating PBMCs with GM-CSF for 4 days, followed by IFN-γ + LPS for other 2 days. At the end of the culture period, the expression of CD197 and of the co-stimulatory molecule CD86, together with the pro-monocytic marker CD14, was evaluated by flow cytometry for M1 macrophages. The M2 polarization was assessed by analyzing the expression of the CD163 marker. **(B)** mDC differentiation was carried out by incubating PBMCs with GM-CSF + IL-4 for 4 days followed by 2 days of LPS treatment. At the end of the culture period, expressions of CD1a, CD197, CD209, CD14, and the co-stimulatory molecule CD83 were evaluated by flow cytometry for mDC differentiation. Results are presented as a percentage of expression or mean fluorescence intensity (MFI) ratio (between MFI control and MFI treated samples) and are shown as violin plots with median (thick line) and 25th and 75th quartiles (*$P < 0.05$, **$P < 0.01$, ***$P < 0.001$, ****$P < 0.0001$ versus control M1 **(A)** or mDC **(B)**, N ≥ 3 individual experiments.

results refer to the 100-µl concentration: CD14 (16.76 ± 7.21%), CD197 (72.2 ± 12.65%), CD86 (MFI 341.97 ± 131.4), and CD163 (9.6 ± 7.14%) (Figure 4A).

In parallel, we investigated the ability of CM-hAMSC in toto and the two fractions to impact monocyte differentiation toward myeloid dendritic cells (mDC) (Figure 4B), while both the CM in toto and the EV-free fraction were able to impact monocyte-derived mDC (Mo-mDC) differentiation by lowering the expression of the maturation marker CD1a (56.5 ± 18.01% control Mo-mDC vs. 11.8 ± 8.45% hAMSC-CM 100 µl and 10.9 ± 8.3% EV-free fraction 100 µl) and of the costimulatory molecule CD83 (MFI 18.8 ± 4.14 control Mo-mDC vs. 6.5 ± 2.67 hAMSC-CM 100 µl and 7.2 ± 3.77 EV-free fraction 100 µl), with a slight effect on CD197 expression (86.4 ± 6.6% control Mo-mDC vs. 76.5 ± 18.3% hAMSC-CM 100 µl and 84.87 ± 12.14% EV-free fraction 100 µl). No differences were observed in the expression of the dendritic marker CD209 (76.6 ± 6.87% control Mo-mDC vs. 90.12 ± 12.5% hAMSC-CM 100 µl and 88.75 ± 14.25% EV-free fraction 100 µl). Furthermore, we confirmed the ability of CM-hAMSC to impair the monocyte differentiation fostering instead the maintenance of the promonocytic marker CD14 (20.5 ± 15.9% control Mo-mDC vs. 82.8 ± 14.76% hAMSC-CM 100 µl and 84.3 ± 13.02% EV-free fraction 100 µl). On the other hand, also for this subset no differences were attributable to the exogenous administration of the EVs regardless of the concentration used (all the results refer to the 100-µl concentration: CD1a (58.5 ± 25.7%), CD83 (MFI 15.03 ± 3.07), CD197 (91.6 ± 7.82%), CD209 (9.6 ± 7.14%), and CD14 (31.17 ± 11.76%) Figure 4B.

Ability of hAMSC-CM and EV-free and EV fractions to modulate B lymphocyte proliferation and differentiation toward antibody-secreting cells

In order to provide a comprehensive analysis of the immunomodulatory properties of hAMSC-CM and its fractions, we also evaluated their effects on B lymphocyte proliferation induced by PBMC stimulation with CpG.

B-cell proliferation and differentiation were evaluated by flow cytometry, and specifically by the percentage of CD19+-proliferating cells, and the expression of markers specific for B-cell differentiation toward antibody-secreting cells and specifically plasmablasts ($CD19^+CD27^{High}CD38^{High}CD138^-$ cells) and plasmacells ($CD19^+CD27^{High}CD38^{High}$ $CD138^+$ cells).

As shown in Figure 5, upper panel, the percentage of proliferating $CD19^+$ cells in the control condition represented by untreated PBMC activated with CpG (PBMC+CpG) was strongly reduced in the presence of hAMSC-CM (100 µl) (66.8 ± 10.74% to 38.6 ± 20.36%, respectively). When we analyzed the effect of the EV-free fraction, we observed results similar to those obtained with hAMSC-CM. The EV-free fraction (100 µl) indeed decreased the percentage of $CD19^+$-proliferating cells to 39.4 ± 19.9%. Finally, EVs induced a slight reduction of CD19+-proliferating cells in comparison to hAMSC-CM and the EV-free fraction (62.2 ± 8.9%).

Moreover, we observed a higher percentage of plasmablasts (Figure 5, middle panel) in the presence of hAMSC-CM (and consequently a lower percentage of plasma cells), with respect to that observed in the control PBMCs stimulated in the absence of hAMSC-CM (48.4 ± 1.27% vs. 75.75 ± 1.06%, respectively). We obtained comparable results when stimulated PBMCs were exposed to the EV-free fraction (75.45 ± 0.2%), while no differences were observed when we performed the test in the presence of EVs.

Conversely, we observed that the percentage of plasma cells was strongly increased in the control condition with respect to the PBMCs activated in the presence of hAMSC-CM and the EV-free fraction (51.9 ± 0.8% to 24.2 ± 1.06% and 24.5 ± 0.2%, respectively), while only small differences were appreciable in the presence of EVs (42.3 ± 4.94%) (Figure 5 lower panel).

Uptake of hAMSC-EVs by immune cells

In an effort to exclude the lack of uptake by PBMCs as a possible mechanism responsible for the negligible immunomodulatory effect of EVs, we performed an uptake experiment by labeling EVs with CFSE. The CFSE-labeled vesicles were added to the unstimulated PBMC. We chose to evaluate fluorescence-labeled exosome uptake under a condition that could be considered similar for all immune PBMC cell types, and thus we considered the quiescent condition since activation conditions can vary between different types of immune cells. After 18 h, whole PBMC and major immune populations were analyzed by flow-cytometry to evaluate CFSE-positive cells. We observed that PBMCs were 99.8% positive for CFSE staining (Figure 6), indicating that EVs were taken up by immune cells. Furthermore, we observed that among the different immune populations, $CD14^+$ cells, representative of the monocyte compartment, were highly positive for CFSE expression in comparison to the lymphocyte compartment, considering both T and the B lymphocytes (($CD3^-CD19^+$ cells), respectively).

Discussion

Our previous studies evidenced the strong immunomodulatory activities of mesenchymal stromal cells derived from amniotic membrane (hAMSC) and the essential role of the secreted bioactive factors in mediating these activities.

Given that these factors can be directly secreted as free molecules or conveyed in EVs, in this study we explored the contribution of all these components to the immunomodulatory activity of the hAMSC secretome. To this end, we compared the

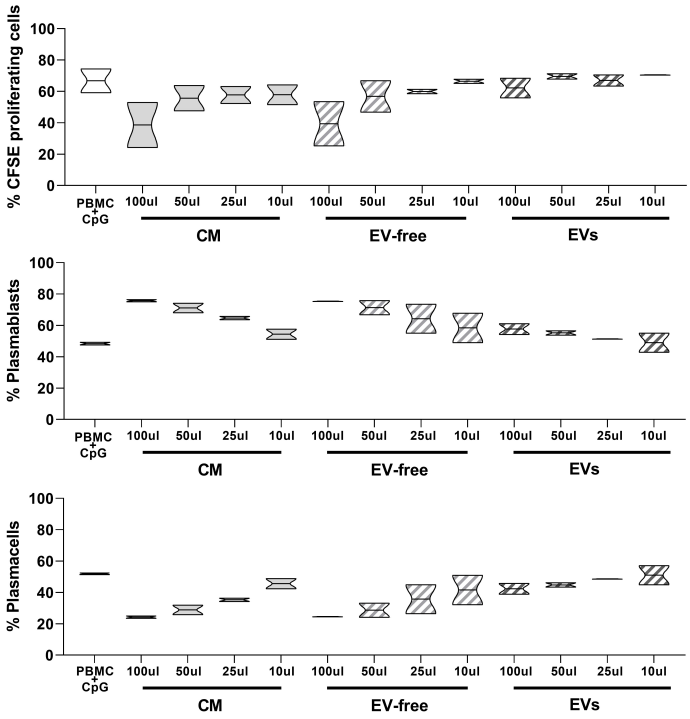

FIGURE 5
Effects of hAMSC-CM and its fractions (EV-free and EVs) on B lymphocyte proliferation and maturation. Allogeneic PBMCs (1 × 105) were stimulated with CpG in the presence of 100, 50, 25, or 10 µl of hAMSC-CM or with the same volume of the EV-free or EV fractions. B-cell proliferation was measured by the analysis of CFSE dilution and calculated as percentage of CD19+-proliferating cells. The impact that hAMSC-CM and its fractions have on B lymphocyte differentiation was evaluated analyzing the total amount of plasmablasts ($CD19^{+}CD27^{hi}CD38^{hi}CD138^{-}$) and plasma cells ($CD19^{+}CD27^{hi}CD38^{hi}CD138^{+}$) obtained from the different culture conditions and compared with the control condition. Results are presented as a percentage of expression and are shown as violin plots with median (thick line) and 25th and 75th quartiles versus control PBMC+CpG, N ≥ 2 individual experiments.

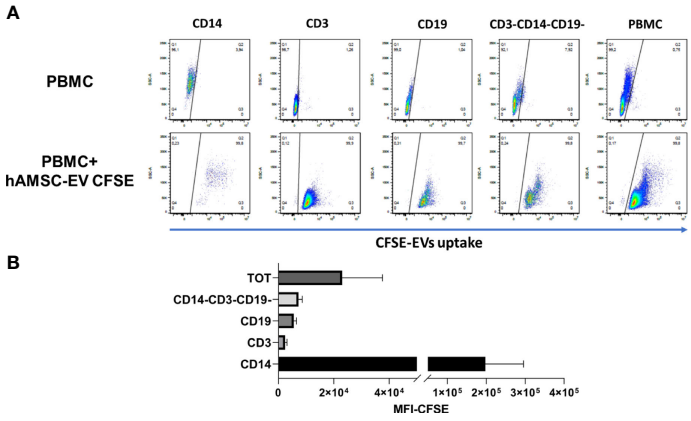

FIGURE 6
Flow cytometry analysis of hAMSC EV uptake by PBMC **(A)** PBMC were cultured without stimulation in presence or absence of 5 × 10^{9} EVs loaded with CFSE to evaluate uptake. A staining for the different immune subsets was performed to evaluate differences in the uptake capability. **(B)** Mean fluorescence analysis of the different immune subpopulations normalized on the negative fraction.

ability of the secretome in toto versus EV-free and EV fractions to affect immune cell subsets *in vitro*.

Our study deeply investigated the effects of the hAMSC secretome and its fractions on immune cells and was not limited to selected immune populations (31, 32) but included immune cells belonging to both innate and adaptive immune systems.

For the first time, EV and EV-free fractions were compared with the secretome in toto by maintaining the quantitative proportions as the secretome of origin. These study conditions allowed us to depict a reliable representation of the relative immunomodulatory potency of each secretome component.

Our data evidenced that the ability of the hAMSC secretome to modulate the immune cell response is mainly mediated by factors non-conveyed by EVs. In fact, the EV-free fraction, comparable to the secretome in toto, inhibited T-cell proliferation, reduced T-cell polarization toward the Th1 subset, and promoted the induction of Treg. In addition, the EV-free fraction, similar to the secretome in toto, maintained the ability to shift monocyte differentiation toward M2 instead of M1 macrophages, to reduce the maturation of dendritic cells and to reduce the CpG-induced B-cell proliferation and differentiation toward plasmablasts and plasmacells. The EV fraction instead did not affect any of these immune parameters despite that hAMSC EVs are taken up by all types of immune cells investigated.

Our results are in line with those published by Lange-Consiglio and colleagues (33) that showed that EVs derived from equine amniotic MSCs were not able to affect PBMC proliferation. However, no other study except ours has investigated the effects of EVs from hAMSC on a wide spectrum of immune cells.

EVs from other types of MSCs, including MSCs from the bone marrow (BM), umbilical cord (UC), and adipose tissue (AT), were investigated for their ability to control the proliferation of different immune cells among which are T cells, B cells, and NK cells, but with controversial results (31, 32, 34–37). For example, some studies have shown an immunosuppressive action of EVs on T cells (34, 38); other studies instead found lower effects of EVs in relation to parental MSC (31, 32, 36), while some demonstrated no effect at all of EVs (35, 39). Controversial results were also obtained by studies focusing on the effect of MSC-derived EVs on B cells (31, 37, 40).

These different findings can potentially derive from some methodological limitations that make the various studies incomparable. For example, different methods of EV quantification were applied, such as protein concentration or EV absolute counts by NanoSight, making it difficult to identify the possible effective dose. To this regard, we explored the effects of three increasing doses of EVs (10, 50, and 100 µl) corresponding to a wide range of EV absolute number (from 1.8×10^8 to 2.0×10^9 vesicles). This range covers and even exceeds the EV doses used in most of the reported studies: 5–100 $\times 10^6$ EVs (33), 3×10^6 EVs/10^4 immune cells (31), and 0.75 and 3×10^9 particles/ml (41) and 10^9 particles (34). Furthermore, to exclude the possibility that the lack of effect observed for hAMSC-EVs was due to a low concentration of EVs, we repeated the immunomodulatory tests using twice the concentration of EVs used in the tests (i.e., 200 µl instead of 100 µl); however, we still did not observe any effect on the different immune populations tested (data not shown). Although the EV-free fraction contained a residual amount of EVs, which represents an unavoidable compromise to obtain the highest EV removal avoiding EV damage, it is very unlikely that the residual EV amount can be responsible for the immunomodulatory activities observed for the EV-free fraction; otherwise, we would have observed some of these activities also for the EV fraction.

Another important factor that could heavily impact functions of MSC-derived EVs is the MSC culture conditions used to produce CM from which EVs are isolated. The extracellular microenvironment indeed affects the composition of EVs and the consequent biological activities (42). Likewise, different methodologies have been used to isolate EVs with different impact on EV biological functions (43, 44). For example, it has been recently reported (45) that contaminating soluble factors can increase the apparent bioactivity of EV even if the specific role on immunomodulatory properties has not been elucidated.

Moreover, it is to be considered that a given type of cell (i.e., MSC) may secrete heterogenous types of EVs characterized by differential exosome content and different subsets of exosomes with distinct proteomic profiles suggesting distinct biological functions (46–48). Thus, a specific function cannot be generalized to all MSCs and to all EVs/exosomes secreted from these cells.

Although we found that hAMSC EVs play a negligible role in determining the immunomodulatory properties of the hAMSC secretome, others have demonstrated that they exert *in vivo* beneficial effects on animal models of inflammation-driven diseases such as chronic endometritis (49), liver fibrosis, non-alcoholic steatohepatitis (50), and osteoarthritis (51). Furthermore, *in vitro* studies demonstrated that hAMSC EVs are able to reduce injury/activation in endometrial cells (52), in hepatic stellate cells (50), and in tenocytes (33). These findings, together with our recent unpublished results, that demonstrate the ability of hAMSC EVs to promote the expansion and the differentiation of dystrophic progenitor muscle cells suggest that hAMSC EVs might preferentially target injured organ/tissue specific cells by directly promoting their integrity and survival and differentiation.

Conclusion

Our study demonstrates that EVs are not responsible for the immunomodulatory activity of the hAMSC secretome. For the

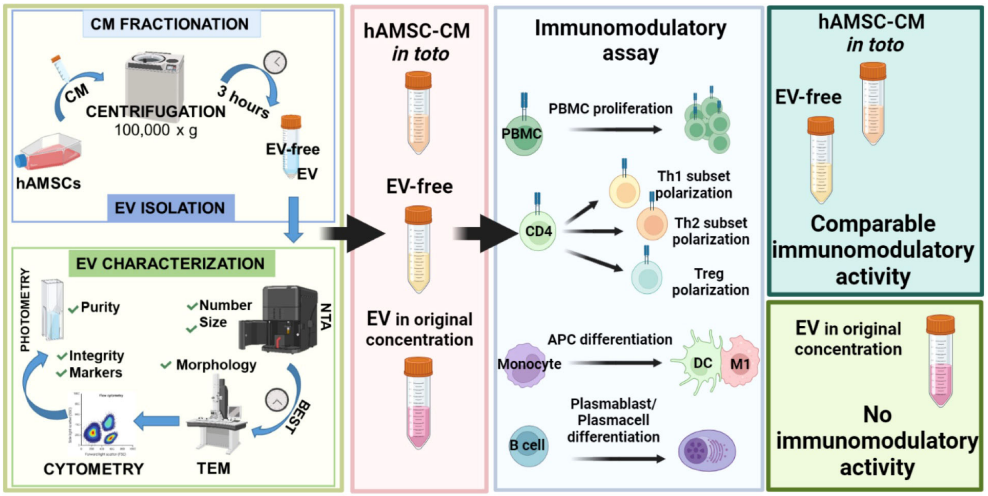

FIGURE 7
Summary figure hAMSC secrete factors able to modulate the immune system. This study demonstrates that the EV fraction of the hAMSC secretome has a negligible immunomodulatory effect while the EV-free fraction is the active component.

first time, we compare EV-enriched and EV-depleted fractions obtained from the hAMSC secretome and demonstrate that the immunomodulatory effect is exerted by secreted factors not conveyed by EVs (Figure 7). Many factors have been reported to contribute to the immunomodulatory properties of MSC, such as the TNF-α-induced gene/protein 6 (TSG-6) (53), IL-10 (54), indoleamine 2,3-dioxygenase (IDO) (55), and inducible nitric-oxide (NO)-synthase (iNOS) (56). Also, hepatocyte growth factor (HGF) (57, 58), transforming growth factor β (TGF-β) (59, 60), and prostaglandin E2 (PGE2) (25, 61) are some of the most studied. However, the secretome represents a repertoire of cytokines, chemokines, and growth factors that combined together can act synergistically to contribute to the immunomodulatory activity of MSC not only *in vitro* but also *in vivo*. Indeed, many studies report the ability of MSC to contribute to regenerative processes in inflammatory-mediated diseases by modulating the immune response (62). Furthermore, MSCs are now being used in numerous clinical trials to treat diseases where a dysregulated immune system plays a major role in pathogenesis (63).

Finally, our findings suggest the utilization of the hAMSC secretome in toto when a modulation of immune response is desired. In addition, these data open a new possible scenario for the clinical application of the hAMSC secretome in toto that indeed contains two fractions that target either inflammatory immune cells or also other cell types involved in tissue regeneration, a combination of potentially synergistic effects that are highly desirable for an effective regenerative medicine strategy. A further not secondary advantage of hAMSC secretome in toto is the use of a less manipulated product which could contain costs and variability

Data availability statement

The raw data supporting the conclusions of this article will be made available by the authors, without undue reservation. The datasets generated for this study can be found in the OSF Repository (https://osf.io/3ejxs/?view_only=40b9a42079ff43059d9236c56f61d465).

Author contributions

Designing research study: AP, ER, LDG, and OP. Conducting experiments and acquiring data: EV, PR, AM, CPO, PBS. Analyzing data: AP, ER, AC, MM. Result interpretation: AP, ER, AC, MM, ARS. Writing and reviewing the manuscript: AP, ER, AC, ARS, LDG, OP. Financial support: LDG, OP. Final approval of the manuscript: LDG, OP. All authors contributed to the article and approved the submitted version.

Funding

This work was supported by Ministero della Salute (Ricerca Corrente), Italian Ministry of Research and University (MIUR, 5x1000), PRIN 2017 program of the Italian Ministry of Research and University (MIUR, grant no. 2017RSAFK7), and Contributi per il funzionamento degli Enti privati che svolgono attività di ricerca - C.E.P.R. (2020-2021). Italian Ministry of Health, RCR-2021-23671217 project, under the The Italian Musculoskeletal Apparatus Network RAMS.

Acknowledgments

The authors thank the physicians and midwives of the Department of Obstetrics and Gynecology of Fondazione Poliambulanza, Brescia, Italy, and all of the mothers who donated placenta. This work contributes to the COST Action CA17116 International Network for Translating Research on Perinatal Derivatives into Therapeutic Approaches (SPRINT), supported by COST (European Cooperation in Science and Technology).

Conflict of interest

The authors declare that the research was conducted in the absence of any commercial or financial relationships that could be construed as a potential conflict of interest.

Publisher's note

Supplementary material

The Supplementary Material for this article can be found online at: https://www.frontiersin.org/articles/10.3389/fimmu.2022.960909/full#supplementary-material

References

1. Silini AR, Masserdotti A, Papait A, Parolini O. Shaping the future of perinatal cells: Lessons from the past and interpretations of the present. *Front Bioeng Biotechnol* (2019) 7:75. doi: 10.3389/fbioe.2019.00075

2. Magatti M, Vertua E, Cargnoni A, Silini A, Parolini O. The immunomodulatory properties of amniotic cells: The two sides of the coin. *Cell transplantation.* (2018) 27(1):31–44. doi: 10.1177/0963689717742819

3. Silini AR, Magatti M, Cargnoni A, Parolini O. Is immune modulation the mechanism underlying the beneficial effects of amniotic cells and their derivatives in regenerative medicine? *Cell Transplant* (2017) 26(4):531–9. doi: 10.3727/096368916X693699

4. Pianta S, Bonassi Signoroni P, Muradore I, Rodrigues MF, Rossi D, Silini A, et al. Amniotic membrane mesenchymal cells-derived factors skew T cell polarization toward treg and downregulate Th1 and Th17 cells subsets. *Stem Cell Rev* (2015) 11(3):394–407. doi: 10.1007/s12015-014-9558-4

5. Papait A, Vertua E, Magatti M. Mesenchymal stromal cells from fetal and maternal placenta possess key similarities and differences: Potential implications for their applications in regenerative medicine. (2020) 9(1):1–23. doi: 10.3390/cells9010127

6. Silini AR, Papait A, Cargnoni A, Vertua E, Romele P, Bonassi Signoroni P, et al. CM from intact hAM: an easily obtained product with relevant implications for translation in regenerative medicine. *Stem Cell Res Ther* (2021) 12(1):540. doi: 10.1186/s13287-021-02607-z

7. Magatti M, Vertua E, De Munari S, Caro M, Caruso M, Silini A, et al. Human amnion favours tissue repair by inducing the M1-to-M2 switch and enhancing M2 macrophage features. *J Tissue Eng regenerative Med* (2017) 11(10):2895–911. doi: 10.1002/term.2193

8. Magatti M, De Munari S, Vertua E, Nassauto C, Albertini A, Wengler GS, et al. Amniotic mesenchymal tissue cells inhibit dendritic cell differentiation of peripheral blood and amnion resident monocytes. *Cell transplantation.* (2009) 18 (8):899–914. doi: 10.3727/096368909X471314

9. Magatti M, Masserdotti A, Bonassi Signoroni P, Vertua E, Stefani FR, Silini AR, et al. B lymphocytes as targets of the immunomodulatory properties of human amniotic mesenchymal stromal cells. *Front Immunol* (2020) 11:1156. doi: 10.3389/fimmu.2020.01156

10. Cargnoni A, Piccinelli EC, Ressel L, Rossi D, Magatti M, Toschi I, et al. Conditioned medium from amniotic membrane-derived cells prevents lung fibrosis and preserves blood gas exchanges in bleomycin-injured mice-specificity of the effects and insights into possible mechanisms. *Cytotherapy* (2014) 16(1):17–32. doi: 10.1016/j.jcyt.2013.07.002

11. Cargnoni A, Romele P, Bonassi Signoroni P, Farigu S, Magatti M, Vertua E, et al. Amniotic MSCs reduce pulmonary fibrosis by hampering lung b-cell recruitment, retention, and maturation. *Stem Cells Trans Med* (2020) 9(9):1023–35. doi: 10.1002/sctm.20-0068

12. Lee PH, Tu CT, Hsiao CC, Tsai MS, Ho CM, Cheng NC, et al. Antifibrotic activity of human placental amnion membrane-derived CD34+ mesenchymal Stem/Progenitor cell transplantation in mice with thioacetamide-induced liver injury. *Stem Cells Trans Med* (2016) 5(11):1473–84. doi: 10.5966/sctm.2015-0343

13. Kim SW, Zhang HZ, Guo L, Kim JM, Kim MH. Amniotic mesenchymal stem cells enhance wound healing in diabetic NOD/SCID mice through high angiogenic and engraftment capabilities. *PLoS One* (2012) 7(7):e41105. doi: 10.1371/journal.pone.0041105

14. Parolini O, Souza-Moreira L, O'Valle F, Magatti M, Hernandez-Cortes P, Gonzalez-Rey E, et al. Therapeutic effect of human amniotic membrane-derived cells on experimental arthritis and other inflammatory disorders. *Arthritis Rheumatol* (2014) 66(2):327–39. doi: 10.1002/art.38206

15. Zhang J, Liu Z, Tang J, Li Y, You Q, Yang J, et al. Fibroblast growth factor 2-induced human amniotic mesenchymal stem cells combined with autologous platelet rich plasma augmented tendon-to-bone healing. *J orthopaedic translation.* (2020) 24:155–65. doi: 10.1016/j.jot.2020.01.003

16. Jiang F, Zhang W, Zhou M, Zhou Z, Shen M, Chen N, et al. Human amniotic mesenchymal stromal cells promote bone regeneration *via* activating endogenous regeneration. *Theranostics* (2020) 10(14):6216–30. doi: 10.7150/thno.45249

17. Onishi R, Ohnishi S, Higashi R, Watari M, Yamahara K, Okubo N, et al. Human amnion-derived mesenchymal stem cell transplantation ameliorates dextran sulfate sodium-induced severe colitis in rats. *Cell Transplantation* (2015) 24(12):2601–14. doi: 10.3727/096368915X687570

18. Pischiutta F, Brunelli L, Romele P, Silini A, Sammali E, Paracchini L, et al. Protection of brain injury by amniotic mesenchymal stromal cell-secreted metabolites. *Crit Care Med* (2016) 44(11):e1118–e31. doi: 10.1097/CCM.0000000000001864

19. Giampà C, Alvino A, Magatti M, Silini AR, Cardinale A, Paldino E, et al. Conditioned medium from amniotic cells protects striatal degeneration and ameliorates motor deficits in the R6/2 mouse model of huntington's disease. *J Cell Mol Med* (2019) 23(2):1581–92. doi: 10.1111/jcmm.14113

20. Yáñez-Mó M, Siljander PR, Andreu Z, Zavec AB, Borràs FE, Buzas EI, et al. Biological properties of extracellular vesicles and their physiological functions. *J Extracellular Vesicles* (2015) 4:27066. doi: 10.3402/jev.v4.27066

21. Seo Y, Kim HS. Stem cell-derived extracellular vesicles as immunomodulatory therapeutics. *Stem Cells Int* (2019) 2019:5126156. doi: 10.1155/2019/5126156

22. Keshtkar S, Azarpira N, Ghahremani MH. Mesenchymal stem cell-derived extracellular vesicles: novel frontiers in regenerative medicine. *Stem Cell Res Ther* (2018) 9(1):63. doi: 10.1186/s13287-018-0791-7

23. Ragni E, Papait A, Perucca Orfei C. Amniotic membrane-mesenchymal stromal cells secreted factors and extracellular vesicle-miRNAs: Anti-inflammatory and regenerative features for musculoskeletal tissues. *Stem Cells Transl Med* (2021) 10(7):1044–62. doi: 10.1002/sctm.20-0390

24. Magatti M, Pianta S, Silini A, Parolini O. Isolation, culture, and phenotypic characterization of mesenchymal stromal cells from the amniotic membrane of the human term placenta. *Methods Mol Biol (Clifton NJ)* (2016) 1416:233–44. doi: 10.1007/978-1-4939-3584-0_13

25. Rossi D, Pianta S, Magatti M, Sedlmayr P, Parolini O. Characterization of the conditioned medium from amniotic membrane cells: prostaglandins as key effectors of its immunomodulatory activity. *PLoS One* (2012) 7(10):e46956. doi: 10.1371/journal.pone.0046956

26. Pianta S, Magatti M, Vertua E, Bonassi Signoroni P, Muradore I, Nuzzo AM, et al. Amniotic mesenchymal cells from pre-eclamptic placentae maintain immunomodulatory features as healthy controls. *J Cell Mol Med* (2016) 20 (1):157–69. doi: 10.1111/jcmm.12715

27. Wingender G, Kronenberg M. OMIP-030: Characterization of human T cell subsets *via* surface markers. *Cytometry Part A: J Int Soc Analytical Cytology* (2015) 87(12):1067–9. doi: 10.1002/cyto.a.22788

28. Théry C, Witwer KW. Minimal information for studies of extracellular vesicles 2018 (MISEV2018): a position statement of the international society for extracellular vesicles and update of the MISEV2014 guidelines. *J Extracellular Vesicles* (2018) 7(1):1535750.

29. Webber J, Clayton A. How pure are your vesicles? *J Extracellular Vesicles* (2013) 2:1–6. doi: 10.3402/jev.v2i0.19861

30. Cargnoni A, Papait A, Masserdotti A, Pasotti A, Stefani FR, Silini AR, et al. Extracellular vesicles from perinatal cells for anti-inflammatory therapy. *Front Bioengineering Biotechnol* (2021) 9:637737. doi: 10.3389/fbioe.2021.637737

31. Di Trapani M, Bassi G, Midolo M, Gatti A, Kamga PT, Cassaro A, et al. Differential and transferable modulatory effects of mesenchymal stromal cell-derived extracellular vesicles on T, b and NK cell functions. *Sci Rep* (2016) 6:24120. doi: 10.1038/srep24120

32. Conforti A, Scarsella M, Starc N, Giorda E, Biagini S, Proia A, et al. Microvescicles derived from mesenchymal stromal cells are not as effective as their cellular counterpart in the ability to modulate immune responses in vitro. *Stem Cells Dev* (2014) 23(21):2591–9. doi: 10.1089/scd.2014.0091

33. Lange-Consiglio A, Perrini C, Tasquier R, Deregibus MC, Camussi G, Pascucci L, et al. Equine amniotic microvesicles and their anti-inflammatory potential in a tenocyte model in vitro. *Stem Cells Dev* (2016) 25(8):610–21. doi: 10.1089/scd.2015.0348

34. Franco da Cunha F, Andrade-Oliveira V, Candido de Almeida D, Borges da Silva T, Naffah de Souza Breda C, Costa Cruz M, et al. Extracellular vesicles isolated from mesenchymal stromal cells modulate CD4(+) T lymphocytes toward a regulatory profile. *Cells* (2020) 9(4):1–27. doi: 10.3390/cells9041059

35. Gouveia de Andrade AV, Bertolino G, Riewaldt J, Bieback K, Karbanová J, Odendahl M, et al. Extracellular vesicles secreted by bone marrow- and adipose tissue-derived mesenchymal stromal cells fail to suppress lymphocyte proliferation. *Stem Cells Dev* (2015) 24(11):1374–6. doi: 10.1089/scd.2014.0563

36. Del Fattore A, Luciano R, Pascucci L, Goffredo BM, Giorda E, Scapaticci M, et al. Immunoregulatory effects of mesenchymal stem cell-derived extracellular vesicles on T lymphocytes. *Cell Transplantation* (2015) 24(12):2615–27. doi: 10.3727/096368915X687543

37. Budoni M, Fierabracci A, Luciano R, Petrini S, Di Ciommo V, Muraca M. The immunosuppressive effect of mesenchymal stromal cells on b lymphocytes is mediated by membrane vesicles. *Cell Transplantation* (2013) 22(2):369–79. doi: 10.3727/096368911X582769b

38. Blazquez R, Sanchez-Margallo FM, de la Rosa O, Dalemans W, Alvarez V, Tarazona R, et al. Immunomodulatory potential of human adipose mesenchymal stem cells derived exosomes on *in vitro* stimulated T cells. *Front Immunol* (2014) 5:556. doi: 10.3389/fimmu.2014.00556

39. Lopatina T, Favaro E, Grange C, Cedrino M, Ranghino A, Occhipinti S, et al. PDGF enhances the protective effect of adipose stem cell-derived extracellular vesicles in a model of acute hindlimb ischemia. *Sci Rep* (2018) 8(1):17458. doi: 10.1038/s41598-018-36143-3

40. Carreras-Planella L, Monguió-Tortajada M, Borràs FE, Franquesa M. Immunomodulatory effect of MSC on b cells is independent of secreted extracellular vesicles. *Front Immunol* (2019) 10:1288. doi: 10.3389/fimmu.2019.01288

41. Kim H, Lee MJ, Bae EH, Ryu JS, Kaur G, Kim HJ, et al. Comprehensive molecular profiles of functionally effective MSC-derived extracellular vesicles in immunomodulation. *Mol therapy: J Am Soc Gene Ther* (2020) 28(7):1628–44. doi: 10.1016/j.ymthe.2020.04.020

42. Burrello J, Monticone S, Gai C, Gomez Y, Kholia S, Camussi G. Stem cell-derived extracellular vesicles and immune-modulation. *Front Cell Dev Biol* (2016) 4:83. doi: 10.3389/fcell.2016.00083

43. Witwer KW, Buzás EI, Bemis LT, Bora A, Lässer C, Lötvall J, et al. Standardization of sample collection, isolation and analysis methods in extracellular vesicle research. *J Extracellular Vesicles* (2013) 2:1–25. doi: 10.3402/jev.v2i0.20360

44. Gardiner C, Di Vizio D, Sahoo S, Théry C, Witwer KW, Wauben M, et al. Techniques used for the isolation and characterization of extracellular vesicles: results of a worldwide survey. *J Extracellular Vesicles* (2016) 5:32945. doi: 10.3402/jev.v5.32945

45. Whittaker TE, Nagelkerke A, Nele V, Kauscher U, Stevens MM. Experimental artefacts can lead to misattribution of bioactivity from soluble mesenchymal stem cell paracrine factors to extracellular vesicles. *J Extracell Vesicles* (2020) 9(1):1807674. doi: 10.1080/20013078.2020.1807674

46. Bobrie A, Théry C. Exosomes and communication between tumours and the immune system: are all exosomes equal? *Biochem Soc Trans* (2013) 41(1):263–7. doi: 10.1042/BST20120245

47. Kowal J, Arras G, Colombo M, Jouve M, Morath JP, Primdal-Bengtson B, et al. Proteomic comparison defines novel markers to characterize heterogeneous populations of extracellular vesicle subtypes. *Proc Natl Acad Sci USA* (2016) 113(8): E968–77. doi: 10.1073/pnas.1521230113

48. Zhang H, Freitas D, Kim HS, Fabijanic K, Li Z, Chen H, et al. Identification of distinct nanoparticles and subsets of extracellular vesicles by asymmetric flow field-flow fractionation. *Nat Cell Biol* (2018) 20(3):332–43. doi: 10.1038/s41556-018-0040-4

49. Lange-Consiglio A, Funghi F, Cantile C, Idda A, Cremonesi F, Riccaboni P. Case report: Use of amniotic microvesicles for regenerative medicine treatment of a mare with chronic endometritis. *Front Veterinary Science* (2020) 7:347. doi: 10.3389/fvets.2020.00347

50. Ohara M, Ohnishi S. Extracellular vesicles from amnion-derived mesenchymal stem cells ameliorate hepatic inflammation and fibrosis in rats. *Stem Cells Int* (2018) 2018:321264. doi: 10.1155/2018/3212643

51. Zavatti M, Beretti F, Casciaro F, Bertucci E, Maraldi T. Comparison of the therapeutic effect of amniotic fluid stem cells and their exosomes on monoiodoacetate-induced animal model of osteoarthritis. *BioFactors (Oxford England)* (2020) 46(1):106–17. doi: 10.1002/biof.1576

52. Perrini C, Strillacci MG, Bagnato A, Esposti P, Marini MG, Corradetti B, et al. Microvesicles secreted from equine amniotic-derived cells and their potential role in reducing inflammation in endometrial cells in an in-vitro model. *Stem Cell Res Ther* (2016) 7(1):169. doi: 10.1186/s13287-016-0429-6

53. Lo Sicco C, Reverberi D, Balbi C, Ulivi V, Principi E, Pascucci L, et al. Mesenchymal stem cell-derived extracellular vesicles as mediators of anti-inflammatory effects: Endorsement of macrophage polarization. *Stem Cells Trans Med* (2017) 6(3):1018–28. doi: 10.1002/sctm.16-0363

54. Abumaree MH, Al Jumah MA, Kalionis B, Jawdat D, Al Khaldi A, Abomaray FM, et al. Human placental mesenchymal stem cells (pMSCs) play a role as immune suppressive cells by shifting macrophage differentiation from inflammatory M1 to anti-inflammatory M2 macrophages. *Stem Cell Rev Rep* (2013) 9(5):620–41. doi: 10.1007/s12015-013-9455-2

55. Opitz CA, Litzenburger UM, Lutz C, Lanz TV, Tritschler I, Köppel A, et al. Toll-like receptor engagement enhances the immunosuppressive properties of human bone marrow-derived mesenchymal stem cells by inducing indoleamine-2,3-dioxygenase-1 *via* interferon-beta and protein kinase r. *Stem Cells (Dayton Ohio)* (2009) 27(4):909–19. doi: 10.1002/stem.7

56. Maria ATJ, Rozier P, Fonteneau G, Sutra T, Maumus M, Toupet K, et al. iNOS activity is required for the therapeutic effect of mesenchymal stem cells in experimental systemic sclerosis. *Front Immunol* (2018) 9:3056. doi: 10.3389/fimmu.2018.03056

57. Deng Y, Zhang Y, Ye L, Zhang T, Cheng J, Chen G, et al. Umbilical cord-derived mesenchymal stem cells instruct monocytes towards an IL10-producing phenotype by secreting IL6 and HGF. *Sci Rep* (2016) 6:37566. doi: 10.1038/srep37566

58. Melief SM, Geutskens SB, Fibbe WE, Roelofs H. Multipotent stromal cells skew monocytes towards an anti-inflammatory interleukin-10-producing phenotype by production of interleukin-6. *Haematologica* (2013) 98(6):888–95. doi: 10.3324/haematol.2012.078055

59. Melief SM, Schrama E, Brugman MH, Tiemessen MM, Hoogduijn MJ, Fibbe WE, et al. Multipotent stromal cells induce human regulatory T cells through a novel pathway involving skewing of monocytes toward anti-inflammatory macrophages. *Stem Cells (Dayton Ohio)* (2013) 31(9):1980–91. doi: 10.1002/stem.1432

60. Ko JH, Lee HJ, Jeong HJ, Kim MK, Wee WR, Yoon SO, et al. Mesenchymal stem/stromal cells precondition lung monocytes/

macrophages to produce tolerance against allo- and autoimmunity in the eye. *Proc Natl Acad Sci USA* (2016) 113(1):158–63. doi: 10.1073/pnas.1522905113

61. Wang J, Liu Y, Ding H, Shi X, Ren H. Mesenchymal stem cell-secreted prostaglandin E(2) ameliorates acute liver failure *via* attenuation of cell death and regulation of macrophage polarization. *Stem Cell Res Ther* (2021) 12(1):15. doi: 10.1186/s13287-020-02070-2

62. Klinker MW, Wei CH. Mesenchymal stem cells in the treatment of inflammatory and autoimmune diseases in experimental animal models. *World J Stem Cells* (2015) 7(3):556–67. doi: 10.4252/wjsc.v7.i3.556

63. Wang LT, Ting CH, Yen ML, Liu KJ, Sytwu HK, Wu KK, et al. Human mesenchymal stem cells (MSCs) for treatment towards immune- and inflammation-mediated diseases: review of current clinical trials. *J Biomed Science* (2016) 23(1):76. doi: 10.1186/s12929-016-0289-5

frontiers | Frontiers in Immunology

TYPE Original Research
PUBLISHED 24 July 2023
DOI 10.3389/fimmu.2023.1228647

OPEN ACCESS

EDITED BY
Diana Boraschi,
Chinese Academy of Science (CAS), China

REVIEWED BY
Maria Laura Manca,
University of Pisa, Italy
Estibalitz Laresgoiti-Servitje,
Tecnológico de Monterrey, Mexico

*CORRESPONDENCE
Keun-Young Lee
mfmlee@hallym.ac.kr

RECEIVED 25 May 2023
ACCEPTED 30 June 2023
PUBLISHED 24 July 2023

CITATION
Jeong S, Cho WK, Jo Y, Choi S-R, Lee N, Jeon K, Park M-J, Song W and Lee K-Y (2023) Immune-checkpoint proteins, cytokines, and microbiome impact on patients with cervical insufficiency and preterm birth. *Front. Immunol.* 14:1228647. doi: 10.3389/fimmu.2023.1228647

Immune-checkpoint proteins, cytokines, and microbiome impact on patients with cervical insufficiency and preterm birth

Seri Jeong[1], Won Kyong Cho[2], Yeonhwa Jo[2], Soo-Ran Choi[3], Nuri Lee[1], Kibum Jeon[4], Min-Jeong Park[1], Wonkeun Song[1] and Keun-Young Lee[5]*

[1]Department of Laboratory Medicine, Kangnam Sacred Heart Hospital, Hallym University College of Medicine, Seoul, Republic of Korea, [2]College of Biotechnology and Bioengineering, Sungkyunkwan University, Suwon, Republic of Korea, [3]Department of Obstetrics and Gynecology, Inha University College of Medicine, Inha University Hospital, Incheon, Republic of Korea, [4]Department of Laboratory Medicine, Hangang Sacred Heart Hospital, Hallym University College of Medicine, Seoul, Republic of Korea, [5]Division of Maternal-Fetal Medicine, Department of Obstetrics and Gynecology, Kangnam Sacred Heart Hospital, Hallym University College of Medicine, Seoul, Republic of Korea

Background: Microenvironmental factors, including microbe-induced inflammation and immune-checkpoint proteins that modulate immune cells have been associated with both cervical insufficiency and preterm delivery. These factors are incompletely understood. This study aimed to explore and compare interactions among microbiome and inflammatory factors, such as cytokines and immune-checkpoint proteins, in patients with cervical insufficiency and preterm birth. In particular, factors related to predicting preterm birth were identified and the performance of the combination of these factors was evaluated.

Methods: A total of 220 swab samples from 110 pregnant women, prospectively recruited at the High-Risk Maternal Neonatal Intensive Care Center, were collected between February 2020 and March 2021. This study included 63 patients with cervical insufficiency receiving cerclage and 47 control participants. Endo- and exocervical swabs and fluids were collected simultaneously. Shotgun metagenomic sequencing for the microbiome and the measurement of 34 immune-checkpoint proteins and inflammatory cytokines were performed.

Results: First, we demonstrated that immune-checkpoint proteins, the key immune-regulatory molecules, could be measured in endocervical and exocervical samples. Secondly, we identified significantly different microenvironments in cervical insufficiency and preterm birth, with precise cervical locations, to provide information about practically useful cervical locations in clinical settings. Finally, the presence of *Moraxella osloensis* (odds ratio = 14.785; P = 0.037) and chemokine CC motif ligand 2 levels higher than 73 pg/mL (odds ratio = 40.049; P = 0.005) in endocervical samples were associated with preterm birth. Combining *M. osloensis* and chemokine CC motif ligand 2 yielded excellent performance for predicting preterm birth (area under the receiver operating characteristic curve = 0.846, 95% confidence interval = 0.733-0.925).

Conclusion: Multiple relationships between microbiomes, immune-checkpoint proteins, and inflammatory cytokines in the cervical microenvironment were identified. We focus on these factors to aid in the comprehensive understanding and therapeutic modulation of local microbial and immunologic compositions for the management of cervical insufficiency and preterm birth.

KEYWORDS

cervix, cervical insufficiency, cytokines, immune-checkpoint proteins, inflammation, microbiome, preterm birth

1 Introduction

Preterm birth (before 37 completed weeks of gestation) occurs in approximately 15 million cases annually worldwide (1) and is the leading cause of neonatal death (2). Approximately 1.1 million babies die from complications of prematurity. Cervical insufficiency, defined as painless cervical dilation in the second trimester (3), has traditionally been associated with preterm birth (4). If cervical insufficiency is left untreated, most patients deliver within two to three weeks (5), resulting in miscarriage or extremely early preterm birth. Cervical cerclage has been used to treat cervical insufficiency to reduce perinatal mortality and recurrent preterm delivery (6). In particular, emergency cerclage is indicated when visible cervical dilatation or an unexpected finding of a shortened cervix on routine examination is present (7).

The cervix, located between the microbe-rich vaginal environment and the presumably sterile intrauterine space, provides a mechanical barrier for preventing ascending infection by remaining closed during pregnancy (8). The cervix has both innate and adaptive immune functions, mediated by diverse cell types and molecules (9, 10). Patients with cervical insufficiency are therefore vulnerable to ascending infection caused by the disruption of these barriers (8). Microenvironmental factors have been associated with disease pathogenesis and preterm delivery (11, 12). However, our understanding of the interactions among microbial composition, inflammatory factors, immune-checkpoint proteins, and the modulation of immunity in patients with cervical insufficiency and preterm birth is incomplete. Accordingly, we have studied these factors in patients with cervical insufficiency and preterm conditions, stratified by cervical location (endocervix and exocervix), to identify clinical diagnostic and therapeutic targets, particularly their predictive utility.

Abbreviations: sCD28, soluble cluster of differentiation 28; sTIM-3, soluble T-cell immunoglobulin and mucin-domain containing-3; sHVEM, soluble herpes virus entry mediator; sPD-L1, soluble programmed death-ligand 1; sCTLA-4, soluble cytotoxic T-lymphocyte-associated protein 4; sPD-1, soluble programmed cell death protein 1; sICOS, soluble B- and T-lymphocyte attenuator; CCL2, chemokine CC motif ligand 2; CXCL10, C-X-C motif chemokine ligand; GM-CSF, granulocyte-macrophage colony-stimulating factor; IFN, interferon; IL, interleukin; TNF, tumor necrosis factor; PCA, principal component analysis; ROC, receiver operating characteristic; AUC, area under the curve; PC, principal components; OR, odds ratio.

2 Materials and methods

2.1 Study design and sample collection

Subjects were pregnant women prospectively recruited at the High-Risk Maternal Neonatal Intensive Care Center in Kangnam Sacred Heart Hospital. Samples were collected between February 2020 and March 2021. All participants provided written informed consent and the study protocol was approved by the Institutional Review Board of Kangnam Sacred Heart Hospital (HKS 2019-11-024 and 2022-06-010). The inclusion criteria for patients with cervical insufficiency undergoing cerclage were as follows: length < 25 mm or internal os dilation of at least 1 cm, effacement of at least 50%, membranes visible at or beyond the external os, and gestational age between 16 and 24 weeks. The exclusion criteria were less than 18 years of age, multifetal gestations, major fetal malformations, ruptured membranes, vaginal bleeding, clinical chorioamnionitis, or persistent, regular contractions. Outpatients visiting our clinical center for the observation of normal pregnancy or for prophylactic cerclage due to history of previous preterm birth during the study period were included. For normal pregnant women as a control group, only gentle swab sampling without cerclage was performed during routine colposcopic examinations. Endo- and exocervical swabs and fluids were collected simultaneously and stored for analysis. The location of the endocervix is around the internal cervical os and the exocervix is near the vaginal fornix. A uniconcave balloon was used for cerclage (13, 14). After identification of the bulging fetal membranes, the cervix was retracted with two atraumatic forceps, and a sufficiently inflated balloon (Supplementary Figure S1) was used to push fetal membranes back into the uterus. Sutures were placed as high as possible using the McDonald technique with a 5-mm polyester tape. After deflating the balloon, a purse-string suture was placed and the instrument was withdrawn from the cervix. A physician working under the Maternal-Fetal Medicine division conducted all procedures using the same technique.

2.2 Shotgun metagenomic sequencing for microbiome

The OMNIgene OMR-130 kit (DNA Genotek Inc., Ottawa, Canada) was used to analyze swab samples. DNA extraction was performed using the Maxwell 16 LEV Blood DNA Purification Kit (Promega, Madison, WI, USA) within four weeks of sampling, based on the manufacturer's instructions. After assessing DNA quality using PCR and electrophoresis, libraries were prepared as per standard Illumina protocols. The TruSeq Nano DNA Library Prep kit was used for library preparation, and the quality of the sample pool was confirmed. Libraries were paired-end sequenced (2 × 150 bp) using the Illumina HiSeqXten platform (Illumina, San Diego, CA, USA). After trimming, reads aligned to the human reference genome (GRCh38) were removed using BBDuk software. Finally, clean reads mostly derived from microorganisms were used for metagenomic analyses using Kraken2 (15).

2.3 Immune-checkpoint proteins and inflammatory cytokines

Sterile Dacron swabs (Puritan Medical Products, Guilford, ME) were used to take samples from the endo- or exocervix. Soluble immune-checkpoint proteins were quantified using the MILLIPLEX Human Immuno-Oncology Checkpoint Protein Premixed 17-plex Panel (Merck, Darmstadt, Germany). The measured immune-checkpoint proteins were soluble cluster of differentiation 28 (sCD28), soluble T-cell immunoglobulin and mucin-domain containing-3 (sTIM-3), soluble herpes virus entry mediator (sHVEM), sCD40, lymphocyte activation gene 3 (sLAG-3), soluble Toll-like receptor 2 (sTLR-2), soluble programmed death-ligand 1 (sPD-L1), soluble cytotoxic T-lymphocyte-associated protein 4 (sCTLA-4), sCD80/B7-1, sCD86/B7-1, soluble programmed cell death protein 1 (sPD-1), sPD-L2, and soluble B- and T-lymphocyte attenuator (sICOS). Inflammatory cytokines were assayed using the Human XL Cytokine Luminex Performance Panel Premixed Kit (R&D Systems, Minneapolis, MN). The measured cytokines were chemokine CC motif ligand 2 (CCL2), CCL3, CCL4, C-X-C motif chemokine ligand (CXCL10), granulocyte-macrophage colony-stimulating factor (GM-CSF), interferon (IFN)-α, IFN-γ, interleukin (IL)-1α, IL-1β, IL-4, IL-6, IL-8, IL-10, IL-12, IL-13, IL-17A, and tumor necrosis factor-α (TNF-α). All assays were conducted using Luminex-based multiplex technology according to the manufacturer's protocols on a Bio-Plex 200 instrument (Bio-Rad, Hercules, CA).

2.4 Statistical analyses

Principal component analysis (PCA) was conducted to reduce the number of observed variables to a smaller number of principal components accounting for most of the variance in the observed variables. For pre-processing data, the pcaMethods R package was utilized for row scaling (16). The values were divided by standard deviations using the unit variance scaling method. The utilized default method for calculating principal components was singular value decomposition with imputation. The distribution of continuous variables, including mean, mean standard error, standard deviation, skewness, kurtosis, 1st quartile, median, 3rd quartile, and *P*-values for normality, are presented in Supplementary Table S1. The Anderson-Darling test was used for normality. For descriptive statistics for comparisons, the Chi-square test was applied to categorical variables and the Wilcoxon test was utilized for paired groups. The Mann-Whitney and Kruskal-Wallis tests were applied to two unpaired groups and three unmatched groups, respectively. For multiple comparisons, nonparametric multiple comparisons for relative effects were performed using the moonBook and nparcomp packages in R for the correction of *P*-values. Multivariate logistic regression analysis was performed, using the factors having a *P* value less than 0.05 in the univariate analysis as co-variables. A receiver operating characteristic (ROC) analysis was conducted to assess the performance of combined factors found to be significant in multivariate analyses to predict preterm birth. The area under the curve (AUC) of combined markers was classified as follows: acceptable (between 0.7 and 0.8), excellent (between 0.8 and 0.9), and outstanding (over 0.9) (17). Spearman's rank correlation analyses were performed to assess the associations of the microbiome with clinical significance, immune-checkpoint proteins, and inflammatory cytokines. Statistical analyses were performed using ClustVis (a web tool for visualizing clustering of multivariate data) (18); Analyse-it Method Evaluation Edition software, version 2.26 (Analyse-it Software Ltd., Leeds, UK); MedCalc software, version 19.8 (MedCalc Software Ltd., Ostend, Belgium); and the moonBook package in R (http://web-r.org/).

3 Results

3.1 Clinical and demographic information

A total of 220 samples (n = 110 for endocervix and n = 110 for exocervix) from pregnant women were analyzed (Supplementary Table S2). The study population consisted of 63 patients with cervical insufficiency receiving cerclage, 21 undergoing prophylactic cerclage, and 26 women with normal pregnancies. Membrane bulging was observed in 41 (37.3%) patients and the median gestational age at cerclage was 22.0 weeks (interquartile range = 5.0 weeks). Among participants with complete clinical information on their outcomes (n = 84; 76.4%), 13 (15.5%) of them exhibited preterm birth. Patients outcomes are presented in Supplementary Table S3.

3.2 Principal component analysis (PCA)

To investigate the overall profiles, including soluble immune-checkpoint proteins and inflammatory cytokines, according to clinical information such as sampling location, cervical insufficiency, and preterm birth, PCA was performed (Figure 1). The X and Y axes of the PCA plot for the endocervix samples show

principal components (PC) 1 and 2, respectively, which explain 37.9% and 14.6% of the total variance, respectively (Figure 1A). Meanwhile, PCA of the exocervix samples showed that PC1 accounted for 43.9% of the variance and PC2 accounted for 12.9% of the variance in the dataset (Figure 1B). Samples from patients exhibiting preterm birth varied more than those who did not and had a similar pattern to those for cervical insufficiency. These patterns were distinct in exocervical samples. PCA loading values for soluble immune-checkpoint proteins and inflammatory cytokines are presented in Supplementary Table S4 (endocervix) and Table S5 (exocervix).

3.3 Microbiomes, immune-checkpoint proteins, and cytokines according to sampling location

Comparisons between endocervix and exocervix samples were conducted (Supplementary Table S6). After taxonomic profiling of the microbiomes, clinically significant bacteria in the cervical environment, such as *Lactobacillus* spp., *Gardnerella vaginalis*, *Moraxella osloensis*, *Veillonella atypica*, *V. parvula*, *Streptococcus dysgalactiae*, *Ureaplasma urealyticum*, *U. parvum*, *Fusobacterium nucleatum*, *Mycoplasma hominis*, *Sneathia amnii*, *Prevotella enoeca*, *P. fusca*, *P. scopos*, *P. jejuni*, *Megasphaera elsdenii*, and *Megasphaera stantonii* were included in analyses. The median total microbiome reads (68577.5 versus 32169.0) and *Lactobacillus* spp. (41178.5 versus 21109.5) in exocervix samples were two-fold greater than in endocervix samples (Figure 2A). However, there were no significant differences at the species level. Among immune-checkpoint proteins, CD 28, TIM-3, LAG-3, PD-1, and PD-L2 showed significantly increased levels in the endocervix than the exocervix. Meanwhile, HVEM and CD40 were present at lower levels in the endocervix (Figures 2B–H). Regarding inflammatory cytokines, the endocervix had significantly increased median levels of CCL2, CCL3, CCL4, IL-6, and TNF-α but significantly decreased IL-1α levels (Supplementary Table S6). Taken together, the endo- and exocervical microenvironments showed significant differences in their microbiomes, soluble immune-checkpoint proteins, and inflammatory cytokines.

3.4 Immune-checkpoint proteins and cytokines in patients with cervical insufficiency

Significant differences were not observed among the endocervical microbiomes of patients undergoing cerclage and prophylactic, cerclage and normal individuals (Supplementary Table S7). The levels of five immune-checkpoint proteins, TIM-3, LAG-3, TLR2, PD-L2, and ICOS revealed significant differences. Among them, TIM-3 and LAG-3 with *P*-values less than 0.001 are illustrated in Figures 3A, B. For inflammatory cytokines in endocervix, the CCL2, CCL3, CCL4, GM-CSF, IFN-γ, IL-1β, IL-4, IL-6, and IL-13 were significantly different among included groups (Supplementary Table S7).

For exocervical samples, the highest total microbiome reads were observed in patients with cervical insufficiency undergoing cerclages (75822.0; $P = 0.002$). Four immune-checkpoint proteins, TIM-3, LAG-3, PD-1, and CD86/B7-2, showed differences. For the inflammatory cytokines, CCL2, CCL3, CCL4, GM-CSF, IFN-γ, IL-4, IL-6, IL-13, and TNF-α were significantly different (Supplementary Table S8).

3.5 Microbiomes, immune-checkpoint proteins, and cytokines in patients with preterm birth

Among clinical characteristics, membrane bulging was significantly different between patients with preterm birth and term participants ($P = 0.015$). Age, gestational age at sampling, and body mass index did not reveal differences. The outcomes for normal participants and patients receiving cerclages with uniconcave balloons were not different (Supplementary Table S9). In the microbiomes, *Moraxella osloensis*, *Veillonella atypica*, and *V.*

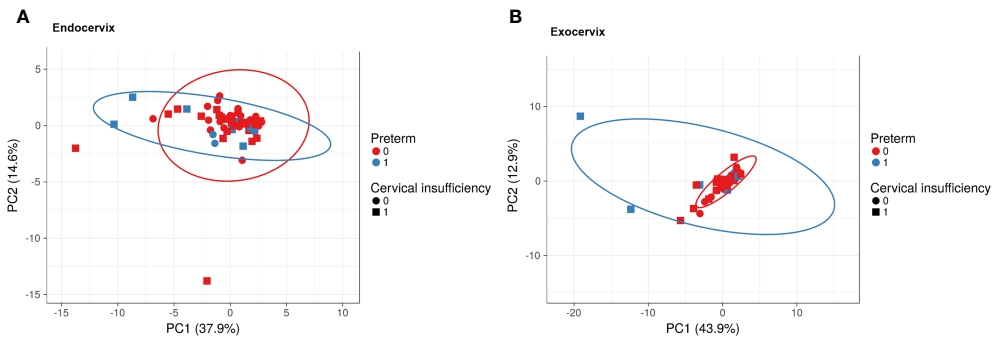

FIGURE 1
Principal component analysis plots for soluble immune-checkpoint proteins and inflammatory cytokines according to sampling location, cervical insufficiency, and preterm birth. **(A)** Endocervical samples; **(B)** Exocervical samples. Prediction ellipses illustrated as red and blue lines represent probabilities of 0.95.

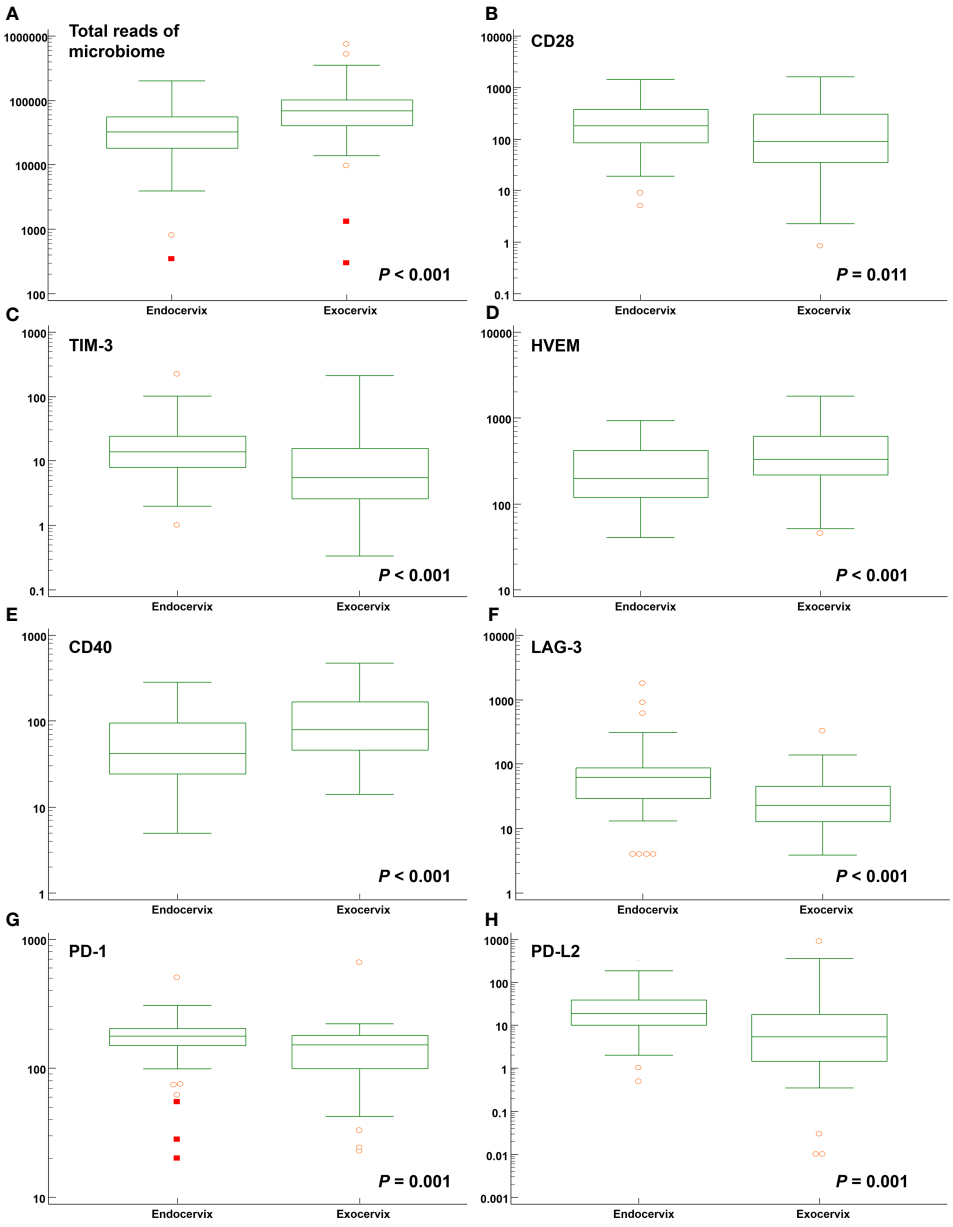

FIGURE 2
Distribution of total microbiome reads and levels of soluble immune-checkpoint proteins according to sampling locations such as the endocervix and exocervix. Plots for **(A)** total reads; **(B)** CD28; **(C)** TIM-3; **(D)** HVEM; **(E)** CD40; **(F)** LAG-3; **(G)** PD-1; and **(H)** PD-L2.

parvula were significantly increased in patients with preterm birth. The median levels of the TIM-3 immune-checkpoint protein as well as the cytokines CCL2, IL-6, and IL-17A were increased in the preterm group compared to the term group (Figures 4A–C and Supplementary Table S10). For exocervical samples, the median levels of CD80/B7-1, PD-L2, and IL-6 (Figures 4D–F and Supplementary Table S11) were significantly raised in women with preterm birth. In addition, analyses for patients undergoing cerclage were performed. For the endocervical samples, *V. atypica*, *V. parvula*, and *S. dysgalactiae* were significantly found in patients with preterm birth (Supplementary Table S12). Among them, only *S. dysgalactiae* showed significant association with preterm birth (odds ratio [OR] = 14.571; P = 0.029). In terms of exocervical samples, *V. atypica* and CD80/B7-1 revealed significant differences (Supplementary Table S13).

Both univariate and multivariate binary logistic regression analyses were applied to identify variables that correlated independently with the preterm state (Table 1). After univariate analyses, variables significantly associated with preterm birth were included in multivariate analyses. The presence of membrane bulging, *Moraxella osloensis*, TIM-3, CCL2, and IL-6 from endocervix were used as predictors. For exocervix, CD80/B7-1, PD-L2, and IL-6 were included as confounding variables for the multivariate analysis. The presence of *M. osloensis* (OR = 14.785; P = 0.037) and CCL2 levels higher than 73 pg/mL (OR = 40.049; P = 0.005) in the endocervical samples were associated with preterm birth. When factors

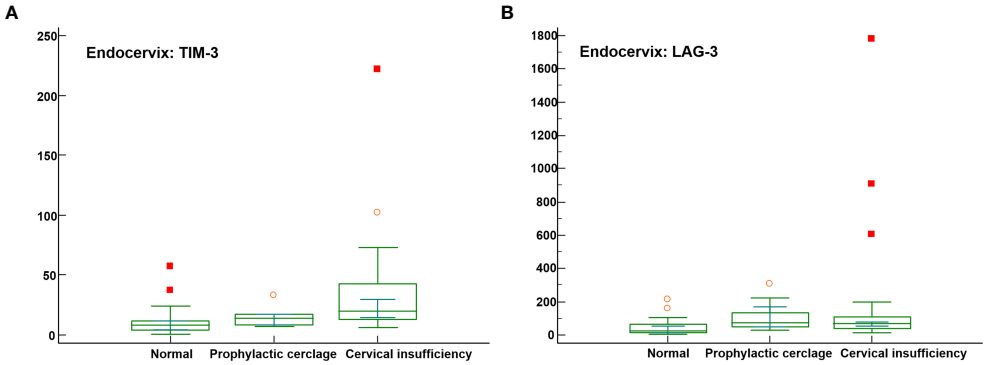

FIGURE 3
Distribution of soluble immune-checkpoint protein levels in the cervical insufficiency, prophylactic cerclage, and normal pregnant women groups. Plots for **(A)** Endocervical TIM-3; and **(B)** Endocervical LAG-3.

independently related to preterm birth after multivariate analyses were subjected to ROC analysis, the AUC was 0.846 (95% confidence interval [CI] = 0.733-0.925) (Figure 5).

3.6 Correlations of immune-checkpoint proteins with microbiomes and cytokines

Using Spearman's correlation coefficients, we focused on markers associated with preterm birth. For endocervix, *M. osloensis* was negatively correlated with TIM-3, CD80/B7-1, and PD-L2 (Figure 6A, Supplementary Table S14). Among the immune-checkpoint proteins, PD-L2 showed strong correlation with TIM-3 and CD80/B7-1. Among inflammatory cytokines, CCL2 and IL-6 showed no significant correlation with immune-checkpoint proteins (Figure 6B, Supplementary Table S15). In exocervical samples, CD80/B7-1 was positively correlated with CD28 and PD-1 (Figure 6C, Supplementary Table S16). PD-L2 also showed positive correlation with TIM-3. Similar to the endocervix, IL-6 in exocervical samples did not show significant correlation with any immune-checkpoint proteins (Figure 6D, Supplementary Table S17).

4 Discussion

We have shown that cervical immune-checkpoint proteins can be measured indicating the presence of their soluble forms in the cervical microenvironment. For cervical locations, total microbiome and

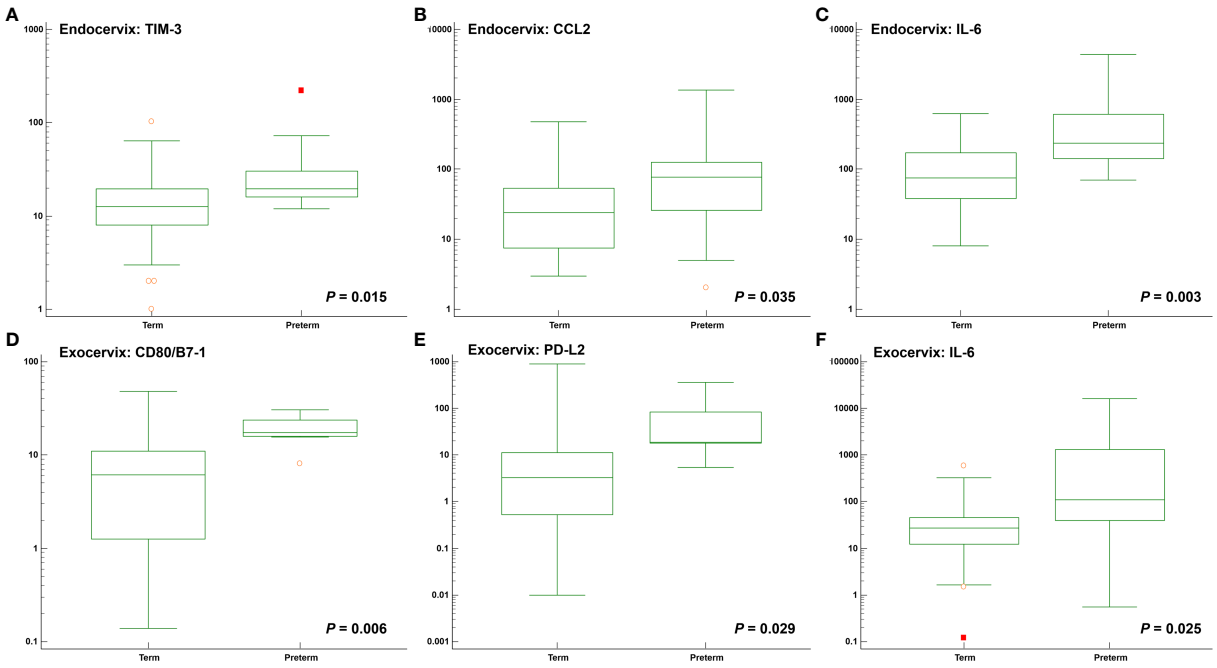

FIGURE 4
Distribution of soluble immune-checkpoint protein and inflammatory cytokine levels between participants with preterm and term birth. Plots for **(A)** Endocervical TIM-3; **(B)** Endocervical CCL2; **(C)** Endocervical IL-6; **(D)** Exocervical CD80/B7-1; **(E)** Exocervical PD-L2; and **(F)** Exocervical IL-6.

TABLE 1 Univariate and multivariate analyses for predicting preterm birth.

Variable	Univariate		Multivariate[a]	
	OR (95% CI)	*P*	OR (95% CI)	*P*
Clinical features				
Age	1.059 (0.909-1.233)	0.464		
Gestational age at sampling	0.997 (0.856-1.161)	0.968		
Body mass index	1.005 (0.879-1.149)	0.946		
Cervical insufficiency	3.429 (0.870-13.514)	0.078		
Membrane bulging	5.357 (1.485-19.333)	0.010	8.915 (0.950-83.667)	0.056
Endocervix				
Microbiota				
Moraxella osloensis	4.696 (1.308-16.862)	0.018	14.785 (1.173-186.389)	0.037
Immune-checkpoint protein[b]				
TIM-3	11.348 (1.339-96.188)	0.030	9.387 (0.157-561.688)	0.283
Inflammatory cytokine[b]				
CCL2	13.417 (3.011-59.789)	0.001	40.049 (3.040-527.575)	0.005
IL-6	9.000 (1.715-47.223)	0.009	1.204 (0.073-19.933)	0.897
Exocervix				
Immune-checkpoint protein[b]				
CD80/B7-1	31.500 (2.940-337.558)	0.004	20.314 (1.021-404.347)	0.049
PD-L2	18.000 (1.692-191.529)	0.017	13.680 (0.544-344.046)	0.112
Inflammatory cytokine[b]				
IL-6	7.636 (1.684-34.627)	0.008	1.139 (0.047-27.856)	0.936

[a] Variables with P-values less than 0.05 in univariate analyses were included in multivariate analyses.
[b] Cutoffs for continuous values for the immune-checkpoint proteins and inflammatory cytokines were estimated using the Youden index.
OR, odds ratio; CI, confidence interval.

Lactobacillus reads, seven immune-checkpoint proteins, and six inflammatory cytokines were different between endo- and exocervical samples. No significant differences were found in microbiome distributions among patients undergoing cerclage, patients undergoing prophylactic cerclage, and normal individuals for endocervical samples. Meanwhile, five immune-checkpoint proteins and nine inflammatory cytokines were different. For exocervical samples, total microbiome reads, four immune-checkpoint proteins, and nine inflammatory cytokines showed differences. For patients with preterm birth, two species, one immune-checkpoint protein, and three inflammatory cytokines from endocervical samples, as well as two immune-checkpoint proteins and one inflammatory cytokine from exocervical samples, were significantly different. The area under the ROC curve for the combined presence of *M. osloensis* and CCL2 was 0.846, suggesting excellent performance for predicting preterm birth.

Soluble immune-checkpoint proteins, which may function differently from their membrane-bound forms, have been measured in serum (19) and cervicovaginal lavages (20). However, their role in cervical insufficiency has not been examined. We found that they can be measured using minimally invasive procedures. Furthermore, our data showed differences between endocervix and exocervix in patients with cervical insufficiency. Other microbiome comparisons between vagina and cervical canal have been conducted in women with endometriosis (21) and pregnant women (22). However, there were no data for the comparison between endo- and exocervical samples in cervical insufficiency providing information about precise sampling locations. The locations evidently had an effect on microbiomes because only the exocervix, which is nearer to cervical canal and vagina, showed differences between cervical insufficiency and normal pregnancy.

Microbiome studies on patients with cervical insufficiency are rare. Our data showed non-significant differences in microbiomes, except for exocervical samples. A previous study reported no bacterial composition differences between vagina and cervical canal in patients with cervical insufficiency, suggesting that cervical incompetence enhances exchange between these communities (22). Another study has shown differences between these communities owing to cervical obstruction in normal pregnancies (23).

Inflammatory cytokines were measured in cervicovaginal fluid in a previous study on cervical insufficiency (24). The study

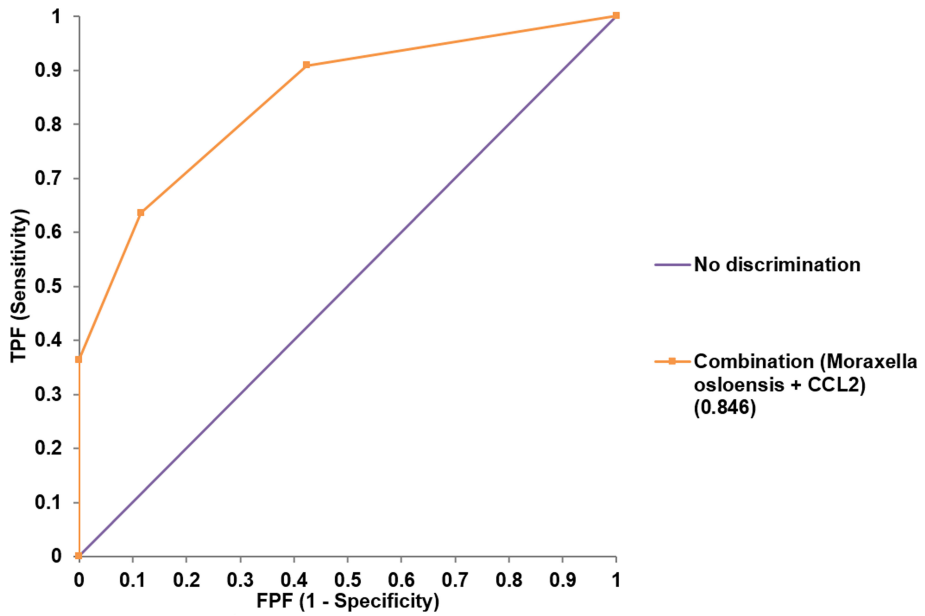

FIGURE 5
Receiver operating characteristic analysis for the performance of combined variables (*Moraxella osloensis* and CCL2 from endocervical samples) for predicting preterm delivery.

reported higher levels of IL-6, in agreement with our data from both the endo- and exocervical samples. Vaginal levels of IL-6 have been reported to be predictive (24, 25), consistent with our results. Data for immune-checkpoint proteins in cervical insufficiency have yet to be reported, to the best of our knowledge.

Preterm delivery is an important complication associated with cervical insufficiency (3, 24). Reduced abundance of *Lactobacillus* spp. has been correlated with premature cervical dilation, whereas *G. vaginalis* has been associated with unsuccessful rescue cerclage (3). The dominance of *L. iners* with *Lactobacillus* depletion was observed in women with cervical shortening, which often precedes preterm delivery (26). A network meta-analysis showed that women with low *Lactobacillus* spp. abundance were at increased risk (OR = 1.69) for preterm birth when compared to those with *L. crispatus* dominance (27). There are multiple reports of dysbiotic conditions in the vaginal microbiome, such as the emergence of *F. nucleatum*, *M. hominis, Ureaplasma* spp., *Sneathia* spp., *Prevotella* spp., and *Megasphaera* spp (20, 28, 29). With respect to the association of *M. osloensis* with preterm birth in our study, it has also been detected in the uterine microbiome in amniotic fluid (30, 31), which is close to the endocervix. In addition, septicemia in a preterm infant, neonatal early-onset sepsis, and ophthalmia caused by *M. osloensis* have been reported (32–34). Considering we used detection through sequencing and a relatively low study population, further studies to validate this species as a predictor of preterm birth are necessary because few studies on the uterine and cervical microbiome have been conducted (28).

Immune-checkpoint proteins are involved in the modulation of T cells (35). Regulatory T cells promote maternal-fetal tolerance, as well as fetal development, throughout gestation (36). Moreover, regulatory T cells express diverse immune-checkpoint molecules involved in immunosuppression, which is critical for effective immune intervention. Several immune-checkpoint proteins, including PD-1, TIM-3, and LAG-3, influence both decidual and peripheral regulatory T cells during pregnancy. According to our data, TIM-3 from endocervical samples was associated with preterm birth. The expression of TIM-3 downregulates signals inhibiting Th1 responses and apoptosis of antigen-specific cells (37). TIM-3 expression dysregulation has been associated with excessive or inhibited inflammatory responses, leading to autoimmune disease and pregnancy complications, including both preterm birth and recurrent spontaneous abortion (38). Thus, the TIM-3 pathway may serve as a potential target for immunotherapeutic approaches (39).

CD80, as a ligand of CTLA-4, is involved in regulating T-cell proliferation and differentiation (40). It was associated with preterm delivery in our exocervical samples. Consistent with our results, alterations in the maternal immune system, such as CD80, have been associated with preterm delivery (41). PD-L2, also associated with preterm delivery in exocervical samples, is another ligand for PD-1; innate immune activators and signaling downstream of cytokine receptors modulate its expression. PD-L2 mainly plays a role in the induction of Th2-driven T-cell immunity (42). Our understanding of PD-L2 is limited, necessitating more studies on this molecule. In addition, the strong correlation among microbiome and immune-checkpoint proteins found in our data has been consistently reported in other diseases (20, 43, 44).

Vaginal levels of the inflammatory cytokine IL-6 have been reported to be predictive in patients with cervical insufficiency (24, 25, 45), consistent with our results. CCL2 is a pro-inflammatory cytokine that is upregulated in the myometrium during labor (46). Abnormal levels of CCL2 have been associated with adverse outcomes such as spontaneous abortion, preeclampsia, and preterm labor (47). A previous study demonstrated that respondents with recurrent pregnancy loss expressed higher level

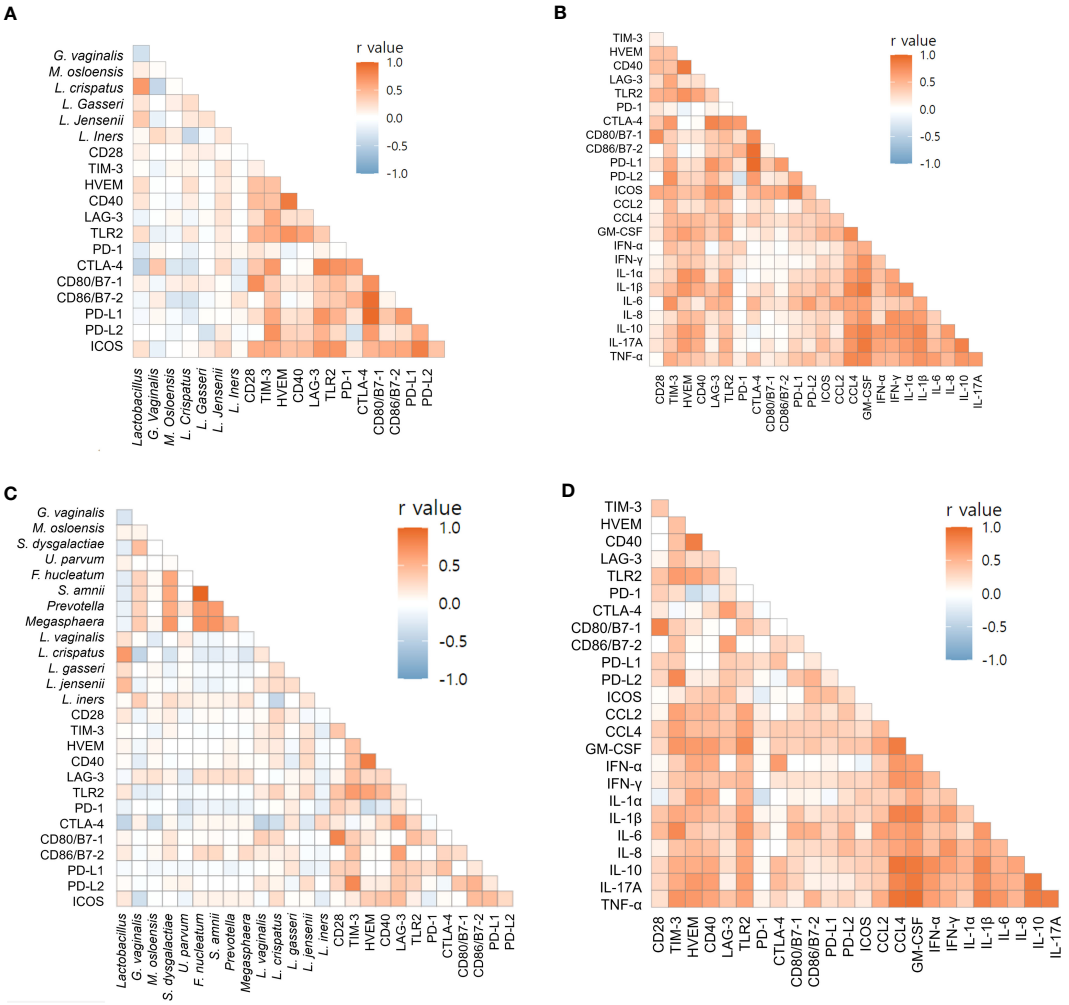

FIGURE 6
Correlations of soluble immune-checkpoint proteins with microbiomes and inflammatory cytokines based on Spearman's rank correlation analyses. **(A)** Soluble immune-checkpoint proteins with microbiomes in endocervical samples; **(B)** Soluble immune-checkpoint proteins with inflammatory cytokines in endocervical samples. **(C)** Soluble immune-checkpoint proteins with microbiome in exocervical samples; **(D)** Soluble immune-checkpoint proteins with inflammatory cytokines in exocervical samples.

of CCL2 than normal pregnant women (48). CCL2 levels were well above the normal range in plasma and placenta samples from patients with preeclampsia (49). CCL2 also integrates both mechanical and endocrine signals that influence preterm delivery, showing promise as a potential target for therapeutic prevention of preterm birth. Exploring and combining microbiomes, immune-checkpoint proteins, and inflammatory cytokines exhibited excellent performance for predicting preterm birth, supporting comprehensive approaches.

To the best of our knowledge, data for immune-checkpoint proteins in cervical insufficiency and preterm birth have yet to be reported. We found that immune-checkpoint proteins could be measured in both endo- and exocervical microenvironments and showed differences. Potential biomarkers for predicting preterm birth with precise sampling locations were identified for clinical settings. In addition, measuring soluble markers is beneficial because of easy accessibility and non-invasiveness. Limitations of our study include its relatively small sample size. Future studies with larger study populations are needed to validate and extend our findings. Furthermore, we were not able to measure the membrane-bound forms of studied markers, as tissues from normal participants and pregnant patients with cervical insufficiency were not available.

In conclusion, we showed that soluble immune-checkpoint proteins and inflammatory cytokines, as well as microbiomes, can be detected in the endo- and exocervical microenvironments, especially in patients with cervical insufficiency. Their distributions revealed differences between endo- and exocervical microenvironments. Significantly different levels of these markers were found in cervical insufficiency. These patterns were also observed in patients with preterm deliveries. For predicting preterm birth, combining *M. osloensis* and CCL2 from endocervical samples exhibited excellent performance, showing potential as a prognostic biomarker. Understanding the relationships among microbiomes, immune-checkpoint proteins, and inflammatory cytokines has potential in the development of

novel strategies for the management of cervical insufficiency and preterm states based on risk stratification.

Data availability statement

The data presented in the study are deposited in the NCBI Sequence Read Archive, accession number PRJNA836344 and HARVARD Dataverse, accession number https://doi.org/10.7910/DVN/4YF2FU.

Ethics statement

The studies involving human participants were reviewed and approved by Institutional Review Board of Kangnam Sacred Heart Hospital (HKS 2019-11-024 and 2022-06-010). The patients/participants provided their written informed consent to participate in this study.

Author contributions

SJ and K-YL conceived the study. WC and YJ analyzed the microbiome data. SC and K-YL led the sampling and clinical data generation. SJ, NL, and KJ generated immunologic data and performed the analyses. SJ wrote the manuscript. M-JP, WS, and K-YL reviewed and edited the manuscript. All authors contributed to the manuscript and approved the submitted version.

Funding

This research was funded by a National Research Foundation of Korea (NRF) grant (grant number NRF-2022R1A2C1003503). The funding source had no involvement in the study design, the collection, analysis, and interpretation of data, the writing of the report, and the decision to submit the article for publication.

Acknowledgments

The authors appreciate the staff at Macrogen, Inc. for performing experiments for DNA shotgun sequencing and Jin Hyun Ju for sample collection and coordinating metadata. We would like to thank Editage (www.editage.co.kr) for English language editing.

Conflict of interest

The authors declare that the research was conducted in the absence of any commercial or financial relationships that could be construed as a potential conflict of interest.

Publisher's note

Supplementary material

The Supplementary Material for this article can be found online at: https://www.frontiersin.org/articles/10.3389/fimmu.2023.1228647/full#supplementary-material

References

1. Fettweis JM, Serrano MG, Brooks JP, Edwards DJ, Girerd PH, Parikh HI, et al. The vaginal microbiome and preterm birth. *Nat Med* (2019) 25(6):1012–21. doi: 10.1038/s41591-019-0450-2

2. Delnord M, Hindori-Mohangoo AD, Smith LK, Szamotulska K, Richards JL, Deb-Rinker P, et al. Variations in very preterm birth rates in 30 high-income countries: are valid international comparisons possible using routine data? *BJOG* (2017) 124 (5):785–94. doi: 10.1111/1471-0528.14273

3. Brown RG, Chan D, Terzidou V, Lee YS, Smith A, Marchesi JR, et al. Prospective observational study of vaginal microbiota pre- and post-rescue cervical cerclage. *BJOG* (2019) 126(7):916–25. doi: 10.1111/1471-0528.15600

4. Iams JD, Goldenberg RL, Meis PJ, Mercer BM, Moawad A, Das A, et al. The length of the cervix and the risk of spontaneous premature delivery. national institute of child health and human development maternal fetal medicine unit network. *N Engl J Med* (1996) 334(9):567–72. doi: 10.1056/NEJM199602293340904

5. Pereira L, Cotter A, Gomez R, Berghella V, Prasertcharoensuk W, Rasanen J, et al. Expectant management compared with physical examination-indicated cerclage (EM-PEC) in selected women with a dilated cervix at 14(0/7)-25(6/7) weeks: results from the EM-PEC international cohort study. *Am J Obstet Gynecol* (2007) 197(5):483 e1.8. doi: 10.1016/j.ajog.2007.05.041

6. Owen J, Hankins G, Iams JD, Berghella V, Sheffield JS, Perez-Delboy A, et al. Multicenter randomized trial of cerclage for preterm birth prevention in high-risk women with shortened midtrimester cervical length. *Am J Obstet Gynecol* (2009) 201 (4):375 e1–8. doi: 10.1016/j.ajog.2009.08.015

7. Newnham JP, White SW, Meharry S, Lee HS, Pedretti MK, Arrese CA, et al. Reducing preterm birth by a statewide multifaceted program: an implementation study. *Am J Obstet Gynecol* (2017) 216(5):434–42. doi: 10.1016/j.ajog.2016.11.1037

8. Kim Y, Lee KY, Lee JJ, Tak H, Park ST, Song JE, et al. Expression of antimicrobial peptides in the amniotic fluid of women with cervical insufficiency. *Am J Reprod Immunol* (2022) 88(2):e13577. doi: 10.1111/aji.13577

9. Hein M, Helmig RB, Schonheyder HC, Ganz T, Uldbjerg N. An *in vitro* study of antibacterial properties of the cervical mucus plug in pregnancy. *Am J Obstet Gynecol* (2001) 185(3):586–92. doi: 10.1067/mob.2001.116685

10. Kawana K, Matsumoto J, Miura S, Shen L, Kawana Y, Nagamatsu T, et al. Expression of CD1d and ligand-induced cytokine production are tissue specific in mucosal epithelia of the human lower reproductive tract. *Infect Immun* (2008) 76 (7):3011–8. doi: 10.1128/IAI.01672-07

11. Goldenberg RL, Culhane JF, Iams JD, Romero R. Epidemiology and causes of preterm birth. *Lancet* (2008) 371(9606):75–84. doi: 10.1016/S0140-6736(08)60074-4

12. Elovitz MA, Gajer P, Riis V, Brown AG, Humphrys MS, Holm JB, et al. Cervicovaginal microbiota and local immune response modulate the risk of

spontaneous preterm delivery. *Nat Commun* (2019) 10(1):1305. doi: 10.1038/s41467-019-09285-9

13. Scheerer LJ, Lam F, Bartolucci L, Katz M. A new technique for reduction of prolapsed fetal membranes for emergency cervical cerclage. *Obstet Gynecol* (1989) 74(3 Pt 1):408–10.

14. Son GH, Chang KH, Song JE, Lee KY. Use of a uniconcave balloon in emergency cerclage. *Am J Obstet Gynecol* (2015) 212(1):114 e1–4. doi: 10.1016/j.ajog.2014.07.022

15. Cho WK, Jo Y, Jeong S. *De novo* assembly and annotation of the vaginal metatranscriptome associated with bacterial vaginosis. *Int J Mol Sci* (2022) 23(3):1621. doi: 10.3390/ijms23031621

16. Stacklies W, Redestig H, Scholz M, Walther D, Selbig J. pcaMethods–a bioconductor package providing PCA methods for incomplete data. *Bioinformatics* (2007) 23(9):1164–7. doi: 10.1093/bioinformatics/btm069

17. Kim J, Hwang IC. Drawing guidelines for receiver operating characteristic curve in preparation of manuscripts. *J Korean Med Sci* (2020) 35(24):e171. doi: 10.3346/jkms.2020.35.e17

18. Metsalu T, Vilo J. ClustVis: a web tool for visualizing clustering of multivariate data using principal component analysis and heatmap. *Nucleic Acids Res* (2015) 43 (W1):W566–70. doi: 10.1093/nar/gkv468

19. Wang Q, Zhang J, Tu H, Liang D, Chang DW, Ye Y, et al. Soluble immune checkpoint-related proteins as predictors of tumor recurrence, survival, and T cell phenotypes in clear cell renal cell carcinoma patients. *J Immunother Cancer* (2019) 7 (1):334. doi: 10.1186/s40425-019-0810-y

20. Laniewski P, Cui H, Roe DJ, Chase DM, Herbst-Kralovetz MM. Vaginal microbiota, genital inflammation, and neoplasia impact immune checkpoint protein profiles in the cervicovaginal microenvironment. *NPJ Precis Oncol* (2020) 4:22. doi: 10.1038/s41698-020-0126-x

21. Ata B, Yildiz S, Turkgeldi E, Brocal VP, Dinleyici EC, Moya A, et al. The endobiota study: comparison of vaginal, cervical and gut microbiota between women with stage 3/4 endometriosis and healthy controls. *Sci Rep* (2019) 9(1):2204. doi: 10.1038/s41598-019-39700-6

22. Sun M, Geng H, Bai J, Feng J, Xu N, Liu Y, et al. Characterization of cervical canal and vaginal bacteria in pregnant women with cervical incompetence. *Front Microbiol* (2022) 13:986326. doi: 10.3389/fmicb.2022.986326

23. Chen C, Song X, Wei W, Zhong H, Dai J, Lan Z, et al. The microbiota continuum along the female reproductive tract and its relation to uterine-related diseases. *Nat Commun* (2017) 8(1):875. doi: 10.1038/s41467-017-00901-0

24. Monsanto SP, Daher S, Ono E, Pendeloski KPT, Traina E, Mattar R, et al. Cervical cerclage placement decreases local levels of proinflammatory cytokines in patients with cervical insufficiency. *Am J Obstet Gynecol* (2017) 217(4):455 e1.e8. doi: 10.1016/j.ajog.2017.06.024

25. Diago Munoz DM, Martinez-Varea A, Roca Prats A, Alonso-Diaz R, Perales Marin A, Diago Almela VJ. Diagnosis of intraamniotic inflammation by measuring vaginal interleukin-6 in patients with cervical insufficiency: could amniocentesis be avoided? *J Matern Fetal Neonatal Med* (2022) 35(25):9303–7. doi: 10.1080/14767058.2022.2029838

26. Chan D, Bennett PR, Lee YS, Kundu S, Teoh TG, Adan M, et al. Microbial-driven preterm labour involves crosstalk between the innate and adaptive immune response. *Nat Commun* (2022) 13(1):975. doi: 10.1038/s41467-022-28620-1

27. Gudnadottir U, Debelius JW, Du J, Hugerth LW, Danielsson H, Schuppe-Koistinen I, et al. The vaginal microbiome and the risk of preterm birth: a systematic review and network meta-analysis. *Sci Rep* (2022) 12(1):7926. doi: 10.1038/s41598-022-12007-9

28. Parnell LA, Briggs CM, Mysorekar IU. Maternal microbiomes in preterm birth: recent progress and analytical pipelines. *Semin Perinatol* (2017) 41(7):392–400. doi: 10.1053/j.semperi.2017.07.010

29. Komesu YM, Dinwiddie DL, Richter HE, Lukacz ES, Sung VW, Siddiqui NY, et al. Defining the relationship between vaginal and urinary microbiomes. *Am J Obstet Gynecol* (2020) 222(2):154 e1– e10. doi: 10.1016/j.ajog.2019.08.011

30. Payne MS, Bayatibojakhi S. Exploring preterm birth as a polymicrobial disease: an overview of the uterine microbiome. *Front Immunol* (2014) 5:595. doi: 10.3389/fimmu.2014.00595

31. Romero R, Dey SK, Fisher SJ. Preterm labor: one syndrome, many causes. *Science* (2014) 345(6198):760–5. doi: 10.1126/science.1251816

32. Cortés AF, Feria PR, García EG, Sánchez AP. Moraxella osloensis septicemia in a preterm infant. *J Pediatr Infect Diseases* (2013) 8:149–51. doi: 10.3233/JPI-130395

33. Parodi E, Galletto C, Vinciguerra T, Stroppiana P, Casonato I, Frigerio M. Neonatal early onset sepsis due to moraxella osloensis: case-report and revision of the literature. *Signa Vitae* (2015) 10(2):202–7. doi: 10.22514/SV102.122015.14

34. Walls A, Wald E. Neonatal moraxella osloensis ophthalmia. *Emerg Infect Dis* (2005) 11(11):1803–4. doi: 10.3201/eid1111.050488

35. Cai H, Liu G, Zhong J, Zheng K, Xiao H, Li C, et al. Immune checkpoints in viral infections. *Viruses* (2020) 12(9):1051. doi: 10.3390/v12091051

36. Zhang YH, Sun HX. Immune checkpoint molecules in pregnancy: focus on regulatory T cells. *Eur J Immunol* (2020) 50(2):160–9. doi: 10.1002/eji.201948382

37. Rangachari M, Zhu C, Sakuishi K, Xiao S, Karman J, Chen A, et al. Bat3 promotes T cell responses and autoimmunity by repressing Tim-3-mediated cell death and exhaustion. *Nat Med* (2012) 18(9):1394–400. doi: 10.1038/nm.2871

38. Grossman T, Leizer J, Minis E, Bongiovanni AM, Witkin SS. 609: the contribution of the checkpoint inhibitor Tim-3 to immune tolerance during pregnancy is maximal in nulliparous women. *Am J Obstetrics Gynecol* (2018) 218(1): S363. doi: 10.1016/j.ajog.2017.10.458

39. Hu XH, Tang MX, Mor G, Liao AH. Tim-3: expression on immune cells and roles at the maternal-fetal interface. *J Reprod Immunol* (2016) 118:92–9. doi: 10.1016/j.jri.2016.10.113

40. Qureshi OS, Kaur S, Hou TZ, Jeffery LE, Poulter NS, Briggs Z, et al. Constitutive clathrin-mediated endocytosis of CTLA-4 persists during T cell activation. *J Biol Chem* (2012) 287(12):9429–40. doi: 10.1074/jbc.M111.304329

41. Evangelinakis NE, Polyzou EN, Salamalekis GE, Kotsaki AJ, Chrelias CG, Giamarellos-Bourboulis EJ, et al. Alterations in the cellular component of the maternal immune system in a murine preterm delivery model. *J Matern Fetal Neonatal Med* (2013) 26(10):1024–9. doi: 10.3109/14767058.2013.765848

42. Jeong S, Lee N, Park MJ, Jeon K, Song W. Currently used laboratory methodologies for assays detecting PD-1, PD-L1, PD-L2 and soluble PD-L1 in patients with metastatic breast cancer. *Cancers (Basel)* (2021) 13(20):5225. doi: 10.3390/cancers13205225

43. Kim E, Ahn H, Park H. A review on the role of gut microbiota in immune checkpoint blockade therapy for cancer. *Mamm Genome* (2021) 32(4):223–31. doi: 10.1007/s00335-021-09867-3

44. Laniewski P, Barnes D, Goulder A, Cui H, Roe DJ, Chase DM, et al. Linking cervicovaginal immune signatures, HPV and microbiota composition in cervical carcinogenesis in non-Hispanic and Hispanic women. *Sci Rep* (2018) 8(1):7593. doi: 10.1038/s41598-018-25879-7

45. Yoo HN, Park KH, Jung EY, Kim YM, Kook SY, Jeon SJ. Non-invasive prediction of preterm birth in women with cervical insufficiency or an asymptomatic short cervix (</=25 mm) by measurement of biomarkers in the cervicovaginal fluid. *PloS One* (2017) 12(7):e0180878. doi: 10.1371/journal.pone.0180878

46. Shynlova O, Tsui P, Dorogin A, Lye SJ. Monocyte chemoattractant protein-1 (CCL-2) integrates mechanical and endocrine signals that mediate term and preterm labor. *J Immunol* (2008) 181(2):1470–9. doi: 10.4049/jimmunol.181.2.1470

47. Lin Z, Shi JL, Chen M, Zheng ZM, Li MQ, Shao J. CCL2: an important cytokine in normal and pathological pregnancies: a review. *Front Immunol* (2022) 13:1053457. doi: 10.3389/fimmu.2022.1053457

48. Namli Kalem M, Akgun N, Kalem Z, Bakirarar B, Celik T. Chemokine (C-c motif) ligand-2 (CCL2) and oxidative stress markers in recurrent pregnancy loss and repeated implantation failure. *J Assist Reprod Genet* (2017) 34(11):1501–6. doi: 10.1007/s10815-017-0992-5

49. Ma Y, Ye Y, Zhang J, Ruan CC, Gao PJ. Immune imbalance is associated with the development of preeclampsia. *Med (Baltimore)* (2019) 98(14):e15080. doi: 10.1097/MD.0000000000015080

frontiers | Frontiers in Immunology

TYPE Original Research
PUBLISHED 05 April 2023
DOI 10.3389/fimmu.2023.1112608

OPEN ACCESS

EDITED BY
Diana Boraschi,
Shenzhen Institute of Advanced Technology (SIAT) (CAS), China

REVIEWED BY
Paola Italiani,
National Research Council (CNR), Italy
Cinzia Fionda,
Sapienza University of Rome, Italy

*CORRESPONDENCE
Anne Hilgendorff
A.Hilgendorff@med.uni-muenchen.de

†PRESENT ADDRESS
Hamid Hossain,
Institute of Microbiology, Infectious Diseases, Laboratory Medicine and Hospital Hygiene, City Hospital of Braunschweig, Braunschweig, Germany

‡These authors share first authorship

RECEIVED 30 November 2022
ACCEPTED 14 March 2023
PUBLISHED 05 April 2023

CITATION
Windhorst AC, Heydarian M, Schwarz M, Oak P, Förster K, Frankenberger M, Gonzalez Rodriguez E, Zhang X, Ehrhardt H, Hübener C, Flemmer AW, Hossain H, Stoeger T, Schulz C and Hilgendorff A (2023) Monocyte signature as a predictor of chronic lung disease in the preterm infant.
Front. Immunol. 14:1112608.
doi: 10.3389/fimmu.2023.1112608

Monocyte signature as a predictor of chronic lung disease in the preterm infant

Anita C. Windhorst[1‡], Motaharehsadat Heydarian[2‡], Maren Schwarz[2,3], Prajakta Oak[2], Kai Förster[3,4], Marion Frankenberger[2], Erika Gonzalez Rodriguez[2], Xin Zhang[2], Harald Ehrhardt[5,6], Christoph Hübener[7], Andreas W. Flemmer[3], Hamid Hossain[8†], Tobias Stoeger[2], Christian Schulz[9,10] and Anne Hilgendorff[2,4*]

[1]Institute of Medical Informatics, Justus-Liebig-University Giessen, Giessen, Germany, [2]Institute for Lung Health and Immunity and Comprehensive Pneumology Center, Helmholtz Zentrum München, German Center for Lung Research (DZL), Munich, Germany, [3]Department of Neonatology, Dr. von Hauner Childre's Hospital, University Hospital, Ludwig-Maximilian-University, Munich, Germany, [4]Center for Comprehensive Developmental Care (CDeCLMU) at the Social Pediatric Center, Dr. von Hauner Children`s Hospital, Ludwig Maximilian University (LMU) Hospital, Ludwig-Maximilian-University, Munich, Germany, [5]Division of Neonatology and Pediatric Intensive Care Medicine, University Medical Center Ulm, Ulm, Germany, [6]Department of General Pediatrics and Neonatology, Universities of Giessen and Marburg Lung Center (UGMLC), German Center for Lung Research (DZL), Justus-Liebig-University Giessen, Giessen, Germany, [7]Department of Gynecology and Obstetrics, Dr. von Hauner Children's Hospital, University Hospital, Ludwig-Maximilian-University, Munich, Germany, [8]Institute for Medical Microbiology, Justus-Liebig-University Giessen, Giessen, Germany, [9]German Center for Cardiovascular Research (DZHK), Partner Site Munich Heart Alliance, Munich, Germany, [10]Department of Medicine I, University Hospital, Ludwig Maximilian University, Munich, Germany

Introduction: Inflammation is a key driver of morbidity in the vulnerable preterm infant exposed to pre- and postnatal hazards and significantly contributes to chronic lung disease, *i.e.* bronchopulmonary dysplasia (BPD). However, the early changes in innate immunity associated with BPD development are incompletely understood.

Methods: In very immature preterm infants below 32 weeks gestational age (GA; n=30 infants), monocyte subtypes were identified by Flow Cytometry at birth and throughout the postnatal course including intracellular TNF expression upon LPS stimulation. Complementing these measurements, cytokine end growth factor expression profiles (Luminex® xMAP®; n=110 infants) as well as gene expression profiles (CodeLink™ Human I Bioarray; n=22) were characterized at birth.

Results: The abundance of monocyte subtypes differed between preterm and term neonates at birth. Specifically, $CD14^{++}CD16^{+}$ (intermediate) monocytes demonstrated a dependency on PMA and elevated levels of nonclassical ($CD14^{+}CD16^{++}$) monocytes characterized preterm infants with developing BPD. Postnatally, lung injury was associated with an increase in intermediate monocytes, while high levels of nonclassical monocytes persisted. Both subtypes were revealed as the main source of intracellular TNF-α expression in the preterm infant. We identified a cytokine and growth factor expression profile in cord blood specimen of preterm infants with developing BPD that corresponded to the disease-dependent regulation of monocyte abundances. Multivariate modeling of protein profiles revealed FGF2, sIL-2 Rα, MCP-1, MIP1a, and TNF-α as predictors of BPD when

considering GA. Transcriptome analysis demonstrated genes predicting BPD to be overrepresented in inflammatory pathways with increased disease severity characterized by the regulation of immune and defense response pathways and upstream regulator analysis confirmed TNF-α, interleukin (IL) -6, and interferon α as the highest activated cytokines in more severe disease. Whereas all BPD cases showed downstream activation of chemotaxis and activation of *inflammatory response pathways*, more severe cases were characterized by an additional activation of *reactive oxygen species (ROS) synthesis*.

Discussion: In the present study, we identified the early postnatal presence of nonclassical ($CD14^{+}CD16^{++}$) and intermediate ($CD14^{++}CD16^{+}$) monocytes as a critical characteristic of BPD development including a specific response pattern of monocyte subtypes to lung injury. Pathophysiological insight was provided by the protein and transcriptome signature identified at birth, centered around monocyte and corresponding granulocyte activation and highlighting TNFα as a critical regulator in infants with developing BPD. The disease severity-dependent expression patterns could inform future diagnostic and treatment strategies targeting the monocytic cell and its progeny.

KEYWORDS

bronchopulmonary dysplasia, monocytes, cytokines, preterm infants, prenatal injury, chronic lung disease

Introduction

Organ injury provoked by sustained inflammation is especially detrimental in the developing organism. Perinatal inflammation is linked to increased mortality and long-term morbidity in preterm infants (1). One of the most prevalent morbidities bearing significant long-term consequences is the development of neonatal chronic lung disease (CLD), known as bronchopulmonary dysplasia (BPD) with different severities ranging from mild to moderate and severe disease (2). BPD affects more than 30% of all very preterm infants (3, 4) and determines the lung`s capacity to undergo structural and functional maturation as well as its potential to cope with second and third hit injury (5, 6).

The dysregulation of developmentally relevant growth factor signaling underlies the incomplete formation of the gas exchange area that is subsequently dominated by apoptotic changes and fibrotic remodeling. These processes are substantially driven by a sustained inflammatory response observed in the BPD lung (7). Despite several attempts to characterize these immune phenomena in the context of different pre- and postnatal risk factors driving BPD, comprehensive knowledge that informs diagnostic and therapeutic strategies at an early disease stage is missing. In the injured neonatal lung, both clinical and experimental studies have confirmed the presence of lung macrophages (MΦ) and their respective signaling molecules (8, 9). These key players of innate immunity undergo a complex process of maturation and are in neonates characterized by shared and distinct functions when compared to adult MΦ including lipopolysaccharide-induced activation, Fc receptor-dependent phagocytosis, and differences in polarization with interferon-gamma (IFNγ) or interleukin (IL)-10 (10, 11).

To understand early changes in the neonatal immune response that likely drive sustained inflammation related to BPD development on a cellular level and beyond, we characterized monocyte subtypes at birth and in the first week of life when undergoing postnatal treatments, delineated the corresponding cytokine and growth factor expression profile, and analyzed the immune network by transcriptome analysis in preterm infants with and without BPD.

Material and methods

Patient characteristics

Preterm infants <32 weeks gestational age (GA) with and without BPD were prospectively included in the study cohorts, following identical in- and exclusion (congenital malformations, metabolic disorders) criteria (12). Patient monitoring comprised an extensive set of clinical and laboratory variables from birth to discharge, including the variables displayed in Table 1 (for definitions see table legend) (15). Specifically, BPD was diagnosed according to the NIH consensus statement (4) referring to oxygen requirement and/or ventilatory support at 36 weeks postmenstrual age (PMA) for disease severity. Incidences for BPD severity (no, mild, moderate and severe) are provided in each method section as well as in Table 1 and Supplemental Tables 1, 2.

TABLE 1 Description of cohorts used for transcriptome, protein, and monocyte analysis.

	Monocyte analysis		Protein analysis		Transcriptome analysis	
	no BPD	BPD	no BPD	BPD	no BPD	BPD
Number of patients	15	15	55	45	13	9
GA (weeks)	30.14 (25.43-31.57)	25.86 (23.57-29.57)	30.6 (24.1-31.9)	26.6 (23.6 - 31.6)	30.3 (28.4-31.1)	24. 7 (24.3 - 30.3)
Birth weight (g)	1160 (750-1760)	590 (510-1510)	1310 (510-2240)	760 (315-1550)	1400 (900-1760)	830 (590-1390)
Sex (female)	8 (53%)	7 (47%)	27 (49%)	15 (33%)	6 (46%)	7 (78%)
ANCS	12 (80%)	12 (80%)	36 (67%)	27 (60%)	9 (69%)	7 (78%)
AIS	5 (33%)	11 (73%)	32 (64%)	30 (67%)	1 (8%)	5 (56%)
RDS	11 (79%)	15 (100%)	42 (42%)	43 (96%)	12 (92%)	9 (100%)
EOI	1 (9.1%)	5 (33%)	4 (7%)	16 (36%)	6 (46%)	9 (100%)
Mechanical ventilation	7 (47%)	15 (100%)	20 (36%)	39 (87%)	6 (46%)	9 (100%)
Invasive ventilation (days)	0 (0-9)	19 (3-42)	2 (1-53)	16 (1-40)	7 (2-9)	6 (1-44)
CPAP/NIPPV (days)	6.5 (2-50)	40.5 (34-59)	9 (1-48)	50 (0-119)	2 (1-13)	11 (3-45)
Oxygen supplementation (days)	0 (0-1)	63 (30-176)	5 (0-97)	63 (0-138)	4 (1-18)	46 (28-138)
Surfactant therapy	5 (33%)	13 (87%)	18 (33%)	37 (67%)	6 (46%)	9 (100%)

Data are given as median and range or frequencies (percent of total in group).
BPD was defined according to the NICHD/NHLBI/ORD workshop (4) based on the need for oxygen supplementation (>FiO2 0.21) for at least 28 days, followed by a final assessment at 36 weeks postmenstrual age (PMA) or at discharge, whichever came first in preterm infants born <32 weeks GA.
AIS, amniotic infection syndrome; ANCS, antenatal corticosteroids; CPAP, continuous positive airway pressure; EOI, presence of early postnatal systemic infections/early-onset infection [diagnosis: one or more clinical and laboratory signs of infection according to Sherman et al. (13)]; GA, gestational age; NIPPV, non-invasive positive pressure ventilation; RDS, respiratory distress syndrome [diagnosis and severity: assessment of anterior-posterior chest radiographs according to Couchard et al. (14)].

The study was approved by the local ethic committees at LMU Munich (ethic vote #195-07) and JLU Giessen (ethic vote #file-79/01).

For monocyte subtype analysis by FACS samples of n=30 infants were available for analysis. Protein analysis included samples from n=110 preterm infants, and samples from n=22 preterm infants were available for transcriptome analysis.

Sample analysis

Flow cytometry (FACS)

In order to identify monocyte subtypes (16, 17) in volume limited (20-50µl) fresh, whole blood EDTA specimen of preterm infants with (n=15) and without (n=15) BPD, samples were incubated with CD45-APC (#IM2473), CD14(My4)-FITC (#6603511), CD16(3G8)-PE (#A07766) and HLA-DR-PC5 (#A07793) antibodies (Beckman Coulter, Germany) before adding blood volume equal amounts of counting beads (#7547053, Beckman Coulter, Germany). Data were analyzed on a four laser LSRII flow cytometer (Becton Dickinson, Germany). Monocyte subtypes were identified by gating on CD14/HLA-DR positive cells out of all CD45 positive leukocytes (Supplemental Figure 6). Further analysis for CD14 vs CD16 allowed us to define classical monocytes with high CD14 expression ($CD14^{++}CD16^{-}$), nonclassical monocytes with lower CD14 and high CD16 expression ($CD14^{+}CD16^{++}$), and intermediate monocytes with high CD14 and lower CD16 expression ($CD14^{++}CD16^{+}$) (18, 19). Data were analyzed by FlowJo® version 10.8.1. Intracellular TNF staining was performed in whole blood samples (PerFix -nc, Beckman Coulter # B10826) according to the manufactures' instructions. In brief, 50 µl of whole EDTA-blood and 10µg/ml Brefeldin A (Sigma #B-6542) were incubated with 100 ng/ml LPS (Lipopolysaccharide, Sigma #L6261) at 37°C for 4 hours or left without stimulus. Aliquots were stained after adding 2.5 µl Fixative Reagent 1 (15 min, RT) using 150 µl Permeabilizing Reagent 2 and monoclonal antibodies CD14-PC5 (Beckmann Coulter #A07765), CD16(3G8)-FITC (Becton Dickinson #555406) and TNF-PE (Beckman Coulter #IM3279) or TNF-PE + rTNF in a 10-fold molar excess as an isotype control (incubation for 20 min at RT). After adding 800 µl 1:10 diluted Final Reagent B, cells were analyzed using a LSR II flow cytometer. Monocyte subtypes were identified while gating on CD14-PE versus CD16-FITC. Corresponding iTNF expression was calculated while subtracting the mean fluorescence intensity of TNF-PE minus TNF-PE/rTNF for the respective monocyte subtypes and then calculating the delta mean fluorescence intensity after stimulation with LPS for the three analyzed monocyte subpopulations.

Protein analysis

For protein analysis, venous umbilical cord blood (CB) of 110 preterm infants (no BPD n=55, BPD (mild/moderate/severe) n=45) was centrifuged (1,000 rpm, 5 min) and stored (-20°C). All samples were analyzed using the 21-plex premixed human cytokine

milliplex panel (HPANLXM 2, Luminex® xMAP®, Luminex, TX, US) according to the manufacturer's instructions.

Transcriptome analysis

For transcriptome analysis, venous umbilical CB specimens of 22 preterm infants (no BPD n=13, BPD n=9), were stabilized using the PAXgene Blood RNA System (PreAnalytiX, Germany) before RNA extraction (PreAnalytiX) and quantification (NanoDrop Technologies, US). From a total of 61 array images for analysis, spot signals of CodeLink™ Human I Bioarrays (GE Healthcare/ Amersham Biosciences) were quantified according to the manufacturer's instructions (12) (CodeLink System Software (Batch Submission (V2.2.27), Expression Analysis (V2.2.25), GE Healthcare, Germany). Two to three technical replicates were prepared per sample. Microarrays were background corrected by subtracting and intra-slide normalized using Median normalization as recommended by the manufacturer. The 9945 transcripts were filtered for missingness (threshold >= 50% missing data per group), low expression (threshold >= 50% of values expressed below the detection threshold as defined by the manufacturer), and outliers per transcript probe and group over all microarrays (values deviating from the group median by more than 3). The remaining missing values were imputed by Bayesian Principal Component Analysis imputation in R ('pcaMethods' (20),). Subsequently, data were inter-slide normalized using Quantile normalization. The average expression of technical replicates was used for analysis. Transcriptome data were archived in Gene Expression Omnibus (GEO, Accession number: GSE225881).

Data analysis

Data analysis was conducted in R (Version 4.1.1) (21).

Monocyte subtypes were analyzed using a linear mixed-effects model (R-Package *nlme* (22) that was fitted by maximizing restricted log-likelihood in order to model log-transformed monocyte levels dependent on clinical conditions, i.e., BPD, preterm or term birth, PMA, status of invasive positive pressure ventilation (timepoints: birth, before IPPV, start of IPPV, during and 2 weeks after IPPV). To analyze the development of monocyte levels over time, random effects were added to the statistical model.

Protein expression was analyzed by the Wilcoxon test; orthogonal partial least squares discriminant analysis (OPLS-DA) (22) for multivariate data sets using the Bioconductor packages 'ropls' (version 1.24.0), gestational age was included in the analysis. Variable influences on projection (VIP) were calculated to explain intergroup variation, i.e., BPD and no BPD. Orthogonal VIPs were calculated to facilitate the interpretation and detection of latent variables in the protein assay explaining intragroup variation. VIPS greater than 1 are considered most relevant, VIPS smaller than 0.5 are considered irrelevant (23).

Transcriptome expression analysis included prediction [PAM; Bioconductor packages 'pamr' (version 1.56.1)] (24, 25) and differential expression analysis (linear modeling, limma open source software, Bioconductor release 3.14) (26). Predictive analysis for microarray data used a multivariate approach to differentiate between BPD and BPD severity grades (no BPD n=13, mild BPD n=6, moderate or severe BPD n=3), while differential analysis for microarray data focused on differences in single transcripts in a univariate approach. The significance level was adjusted for multiple testing using the False Discovery Rate (FDR) (27). Cut-off FDR for differential expression was set at FDR < 0.05 and a minimum absolute fold change of 2 between at least two groups.

Results

Characteristic monocyte signature in infants with BPD at birth

In order to identify early postnatal immune cell characteristics that indicate or drive morbidity development, we characterized monocyte subtypes in volume-limited CB and follow-up samples from n=30 preterm infants with and without BPD. Supporting a GA specific pattern of innate immune capacities, each monocyte subpopulation showed individual trajectories ($p<0.05$, two-way Analysis of Variance). Whereas levels of intermediates and nonclassical monocytes at birth decreased with increasing PMA towards stable expression levels exhibited by term newborns, classical ($CD14^{++}CD16^{-}$) monocytes showed PMA independent abundances at birth (Figure 1A). The abundance of $CD14^{++}CD16^{+}$ (intermediate) monocyte subtypes differed between preterm and term neonates at birth (p-value=0.067) and demonstrated a dependency on PMA (p-value=0.003) (Figure 1A). When considering disease, our analysis revealed elevated levels of nonclassical $CD14^{+}CD16^{++}$ monocytes in preterm infants with developing BPD at birth (p-value=0.004) (Figure 1B and Table 2). In the postnatal course, lung injury, *i.e.*, exposure to oxygen and invasive positive pressure ventilation (IPPV) was associated with an increase of $CD14^{+}$ $^{+}CD16^{+}$ (intermediate) monocytes (p-value < 0.001), while high levels of $CD14^{+}CD16^{++}$ monocytes persisted (Figure 1B and Table 2). A peak of all monocyte subtypes can be observed when preterm infants with developing BPD are exposed to oxygen and IPPV in contrast to infants without the disease (Figure 1B and Table 2). With regard to cellular function, intermediate $CD14^{+}$ $^{+}CD16^{+}$ and nonclassical $CD14^{+}CD16^{++}$ monocytes from preterm infants were revealed as the main source of intracellular TNF-α expression upon LPS stimulation (Figure 1C). The capacity of $CD14^{+}$ $^{+}CD16^{+}$ for TNF-α expression upon stimulation increased with PMA (Figure 1C).

Next, we identified a cytokine and growth factor expression profile by multiplexed protein analysis in CB EDTA plasma from n=110 infants that corresponded to the disease dependent regulation of monocyte abundances in preterm infants with developing BPD. Protein profiling demonstrated the upregulation of IL-6, IL-8, MCP-1, MIP1a, IL-1Rα, sIL-2 Rα, EGF, and FGF2 levels in preterm infants with BPD when compared to infants without the disease. Multivariate modeling revealed FGF2, sIL-2 Rα, MCP-1, MIP1a, and TNF-α as predictors of BPD when considering GA as a strong influencing factor (VIP). Further, TNF-α, IL1b, IL6, IL8, and IL-1Rα were identified as top mediators for protein abundance (Table 3, oVIPs). In line with these findings, transcriptome analysis in CB EDTA

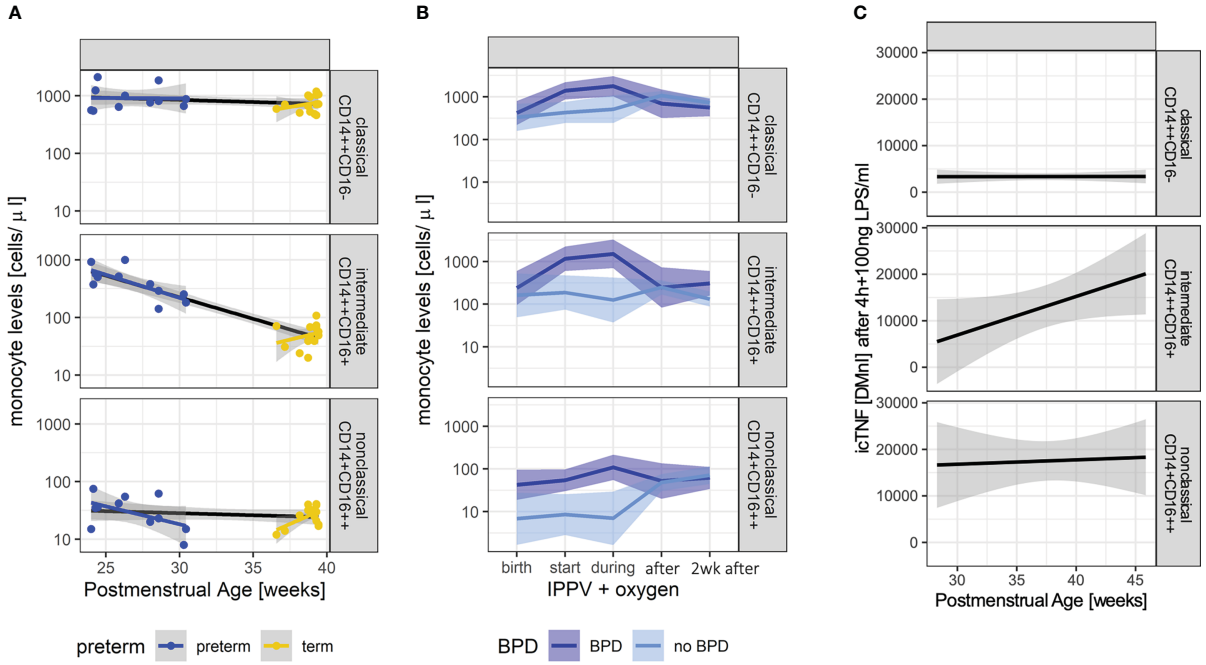

FIGURE 1
Characteristic monocyte subtypes at birth in infants developing BPD. **(A)**: Monocyte levels (upper panel: classical ($CD14^{++}CD16^{-}$), middle panel: intermediate ($CD14^{++}CD16^{+}$), lower panel: nonclassical $CD14^{+}CD16^{++}$) of preterm (n=11, blue) and term (n=14, yellow) infants at the day of birth (+72h if not done immediately). Overall trend dependent on PMA indicated by black lines. Group comparisons: abundancy preterm vs. term 0.695, p-value=0.067; development with PMA (slope): -0.017, p-value= 0.003. **(B)**: Monocyte levels (upper panel: classical ($CD14^{++}CD16^{-}$), middle panel: intermediate ($CD14^{++}CD16^{+}$), lower panel: nonclassical $CD14^{+}CD16^{++}$) in preterm infants with (n=15, dark blue) and without BPD (n=15, light blue) at birth up until 2 weeks after the start of invasive positive pressure ventilation (IPPV) and oxygen therapy. Linear mixed effect models take PMA into account. Levels of nonclassical monocytes are elevated at birth (pairwise comparison, p-value=0.004); nonclassical (BPD vs. no BPD p-value < 0.001), intermediate (BPD vs. no BPD p-value=0.011) and classical (BPD vs. no BPD p-value=0.004) differ during IPPV. **(C)**: Intracellular TNFα (icTNF) expression in response to LPS stimulation (4 hours after) in monocytes of preterm infants (n=9) (upper panel: classical ($CD14^{++}CD16^{-}$), middle panel: intermediate ($CD14^{++}CD16^{+}$), lower panel: nonclassical $CD14^{+}CD16^{++}$). Increases in icTNF are statistically significant in intermediate (p-value = 0.005) and nonclassical monocytes (p-value = 0.033). Levels of icTNF are displayed as delta mean intensities (DMnl).

samples of 22 very preterm infants identified a cluster of 28 transcripts differentiating between BPD and no BPD cases (Supplementary Figure 1 and Supplementary Table 1) with a cluster of 71 transcripts differentiating between disease severities (Supplementary Figure 2 and Supplementary Table 2). Genes predicting BPD are significantly overrepresented in *inflammatory* and *Galanin/GMAP prepropeptide* pathways (Supplementary Table 3) and increased disease severity is characterized by the regulation of immune and defense response pathways (Supplementary Table 4) including activated *chemotaxis of cells*, increased biological functions associated with *apoptosis*, *accumulation of leukocytes*, and decreased *phagocytosis by immune cells* (Supplementary Table 5). Differential gene expression analysis revealed 238 differentially expressed genes (DEG) out of 7,529 transcripts (FDR <0.05, and |FC|>2) when comparing cases with and without BPD (Supplementary Table 6). Upstream regulator

TABLE 2 Comparison of monocyte levels with before, during, and after start of invasive positive pressure ventilation (IPPV).

timepoint	classical CD14++CD16-	intermediates CD14++CD16+	nonclassical CD14+CD16++
BIRTH	-0.04 +/-0.21, p-value=0.8662	0.01 +/-0.32, p-value=0.9796	**1.05 +/-0.32, p-value=0.0036**
START IPPV	0 +/-0.2, p-value=0.9972	0.12 +/-0.31, p-value=0.7141	-0.04 +/-0.3, p-value=0.8914
DURING IPPV	**0.7 +/-0.21, p-value=0.0044**	**0.93 +/-0.32, p-value=0.011**	**1.47 +/-0.32, p-value=0.0003**
AFTER IPPV	-0.17 +/-0.13, p-value=0.2236	0.04 +/-0.19, p-value=0.8501	0.05 +/-0.19, p-value=0.7896
2 WKS AFTER IPPV	-0.11 +/-0.11, p-value=0.3388	*0.28 +/-0.15, p-value=0.086*	0.02 +/-0.14, p-value=0.8863

Repeated measurement analysis of variance for each monocyte subpopulation (classical, intermediate, nonclassical) with postmenstrual age as covariate. P-values and estimates for differences in log(cells) as well as standard deviation of comparison of BPD (n=15) vs no BPD (n=15) are displayed for each timepoint. Bold values show significance at a 95%-significance level; p-values < 0.05.

TABLE 3 Comparison of protein abundance at birth.

Protein	n	BPD (n=45)	no BPD (n=55)	p-value Wilcoxon-Test	oVIP	VIP
GA	100	26.6 (25.1-27.9)	30.6 (29.2-31.0)	<0.001	0.03	3.53
EGF	100	107.5 (86.9-372.3)	87.8 (66.7-118.9)	0.008	1.00	0.50
FGF2	98	135.1 (70.4-231.2)	96.6 (54.0-141.4)	0.032	0.88	1.23
GCSF	99	96.5 (57.5-392.8)	113.4 (62.3-209.6)	0.673	1.12	0.26
GMCSF	100	3.2 (3.2-6.2)	3.2 (3.2-5.6)	0.827	1.07	0.40
IFNg	100	3.2 (3.2-3.2)	3.2 (3.2-3.2)	0.904	1.04	0.02
IL-10	99	7.0 (3.2-13.7)	6.4 (3.2-11.7)	0.547	1.09	0.35
IL-12p40	100	14.8 (3.2-41.4)	13.4 (3.2-46.3)	0.603	1.01	0.56
IL-1a	100	18.1 (4.9-36.1)	12.2 (3.4-30.5)	0.191	0.98	0.49
IL-1b	100	3.2 (3.2-3.2)	3.2 (3.2-3.2)	0.193	1.29	0.20
IL1ra	100	55.6 (25.1-215.3)	22.4 (5.1-86.2)	0.023	1.24	0.25
IL–4	100	3.2 (3.2-3.2)	3.2 (3.2-3.2)	0.515	0.02	0.45
IL-6	100	9.6 (3.8-30.4)	3.3 (3.2-25.5)	0.031	1.26	0.65
IL-8	100	53.4 (31.8-107.0)	24.6 (11.7-53.1)	<0.001	1.26	0.69
IP10	100	200.1 (151.6-435.6)	190.1 (121.8-321.2)	0.369	0.93	0.47
MCP1	100	951.3 (545.5-1798.4)	596.3 (384.8-983.2)	0.005	1.12	1.15
MCP3	100	3.2 (3.2-3.2)	3.2 (3.2-3.8)	0.096	0.10	0.24
MIP1a	98	18.8 (3.2-28.4)	14.5 (3.2-22.7)	0.051	0.91	1.13
MIP1b	100	53.9 (38.1-94.2)	53.0 (37.4-66.4)	0.509	1.07	0.35
sIL2Rα	100	206.6 (100.4-402.7)	115.7 (47.9-274.9)	0.022	0.63	1.21
TNF-α	100	15.7 (10.8-19.7)	12.1 (9.8-17.2)	0.117	1.32	1.09
VEGF	96	119.4 (84.2-246.9)	136.2 (93.8-186.8)	0.887	0.98	0.10

Univariate analysis for protein values obtained by Wilcoxon tests and multivariate analysis using orthogonal partial least squares discriminant analysis (OPLSDA). Multivariate analysis considered also gestational age (GA). Median and upper and lower quartile are presented for continuous variables, n is the number of non-missing values. VIP, Variable influence on projection; oVIP, orthogonal Variable influence on projection from the orthogonal partial least squares discriminant analysis modeling BPD. GA, gestational age; protein names according to 21-plex premixed human cytokine milliplex panel.

analysis indicated TNF-α, interleukin (IL)-2, -6, -10, and interferons as the highest activated cytokines in moderate/severe BPD patients (Supplementary Table 7).

Mechanistic insight into BPD immune signature by transcriptome analysis at birth

Regulator effect networks consisting of upstream cytokines and downstream biological function demonstrated the activation of IL-6, TNF-α, and TNFRSF1A (tumor necrosis factor receptor superfamily, member 1a) together with the regulation of *CXCL9, LGALS3, MMP7, TLR3, IL-10*, as well as *TCR* and *LAT* in infants with BPD, indicating immune cell activation, cell-matrix interaction and remodeling at the same time. Prediction analysis revealed the activation of TNF-α as a possible regulator for the differentially regulated genes *CXCL9, IL10, LGALS3, MMP7, TLR3, TNFRSF1A* (Figure 2A), and also *BID, CAT, CDH13, TF, ZFP36* (Supplementary Figure 3), with functional analysis confirming the activation of *leukocyte chemotaxis*, increased neutrophil number, increased *apoptosis and necrosis* and the deactivation of the *accumulation of eosinophils* together with the regulation of *TNF-α homeostasis* (*ZFP36, TNFRSF1A*). Increased disease severity was characterized by *reactive oxygen species (ROS) synthesis*, whereas all BPD cases independent of disease severity showed downstream activation of chemotaxis and activation of inflammatory response pathways (Figure 2B and Supplemental Figure 4). The transcriptome signature that was dominated by immune system activation in upstream analysis, indicated the upregulation of IL-2, TNF-α IL-6, IL-10, Interferon (IF) alpha/beta, and IFNG in mild BPD, next to the involvement of interferons from the alpha group, IL27, EBI3 in moderate/severe BPD. When comparing mild and moderate/severe BPD, differences included the activation of IL-5 (upregulation in moderate/severe BPD), and WNT1 (Supplementary Table 8).

Discussion

There is a paucity of data providing insight into the immune cell characteristics that indicate or drive pulmonary morbidity in preterm infants early after birth.

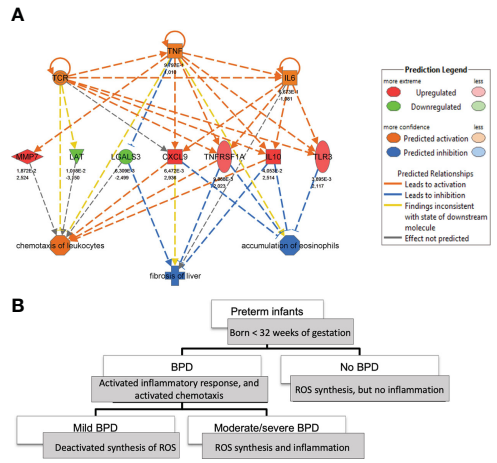

FIGURE 2
Tracking of monocyte-related cytokine expression in BPD at birth. **(A)**: Regulator-effects-network highlighting the role of TNFα in mild BPD (n=6) in comparison to no BPD (n=13) at birth. The network is derived from Ingenuity Pathway analysis of the transcripts differentiating between BPD severity grades (up- and downstream). **(B)**: The comparison of downstream effects of transcripts, able to predict BPD severity grades at birth, demonstrates involvement of inflammatory response, chemotaxis, and synthesis of Reactive Oxygen species (ROS) depending on BPD severity.

Significantly extending clinical and experimental studies that associated interleukin and cytokine expression levels with pre-and postnatal injury and adverse long-term development in preterm infants (28, 29), we were able to identify the early postnatal presence of nonclassical and intermediate monocytes as a critical component in BPD development including their response pattern to lung injury. This picture was supported and pathophysiologically deepened by the protein and transcriptome signature identified, centered around monocyte and corresponding granulocyte activation.

In our study, BPD infants were characterized by elevated levels of $CD14^{+}CD16^{++}$ (nonclassical) monocytes and demonstrated a peak of all monocyte subtypes studied upon lung injury, especially revealing an increase in intermediate monocytes. Identified as the main source of stimulated intracellular TNF-α expression in preterm neonates, the early postnatal predominance of nonclassical and intermediate monocytes in infants with lung injury that develop BPD was closely reflected by the immune response identified in protein and transcriptome profiling.

Results from multiplexed proteomics demonstrated the regulation of IL-6, IL-8, MCP-1, MIP1a, IL-1Rα, sIL-2 Rα, EGF, and FGF2 in BPD infants at birth. The signature is related to *monocyte activation*, *proliferation*, *chemotaxis*, and *recruitment* (30), and statistical modeling revealed the potential of these cytokines and growth factors to both predict BPD as well as mediate protein abundance in these infants under strong consideration of TNF-α. These results aligned with transcriptome analysis, where upstream regulator analysis identified TNF-α, interleukin (IL)-2, -6, -10, and interferons as the highest activated cytokines in BPD patients with moderate or severe disease.

The identification of TNF-α as an upstream regulator of gene expression and protein abundance in BPD in concert with the overall cytokine and growth factor signature described, links back to the predominance of nonclassical and intermediate monocytes observed in BPD infants, as they represent a main source of TNF-α production as shown by us and others (31, 32) Regarding functional relevance for BPD development, TNF-α, and interferon-gamma signaling are not only known to drive monocyte to macrophage polarization enhancing extravasation of these cells and accumulation of monocyte-derived alveolar macrophages, but they as well exhibit significant profibrotic potential in lung disease (33).

The image of monocyte and granulocyte activation portrayed by the protein and transcriptome analysis is further illustrated by the network that we identified to characterize preterm infants with BPD as early as birth. Here, regulator effect networks demonstrated the activation of IL-6, TNF-α, and TNFRSF1A side by side with the regulation of genes involved in immune cell activation, cell-matrix interaction, and remodeling (CXCL9, LGALS3, MMP7, TLR3, IL-10, TCR, LAT) in infants with BPD. Differential regulation of genes involved in leukocyte chemotaxis and accumulation of eosinophils (CAT, CDH13, IL-10, LGALS3, TNFRSF1A, BID, TF, ZFP36) were again predicted to be regulated by TNF-α. The underlying network of immune signals identified by functional transcriptome analysis further enabled us to associate increased disease severity with the activation of genes involved in leukocyte chemotaxis and apoptosis side-by-side with a decrease in phagocytosis, thereby closely reflecting findings of studies on neonatal MΦ function in BPD (10). Whereas all BPD cases, independent of disease severity, showed reactive oxygen species (ROS) synthesis, the main differences between mild and more severe BPD cases included the engagement of adaptive immune responses (IL-5) and developmental pathways (WNT1), in line with previous studies (34, 35).

Our results are supported by studies in preterm infants that demonstrated a predictive signature for inflammatory lung disease in preterm infants by transcriptional profiling of lung macrophages, highlighting IL-6, TNF, and CCL3 to be regulated in BPD, as well as studies that engaged protein profiling and revealed a comparable immune signature (36). Supported by a characteristic transcriptome and protein signature, the predominance of the nonclassical and intermediate monocyte subtypes identified in our study likely reflects critical processes for BPD development, including their impact on proliferative state, telomere length, cellular ROS levels, and mitochondrial membrane potential as critical functions in aging and cellular senescence (32, 37). The revelation of distinct developmental pathways from circulating monocytes to lung macrophages highlights the potential of specific monocyte subtypes to differentially contribute to populations of alveolar, interstitial, and pulmonary intravascular macrophages (38). While nonclassical blood monocytes give rise to intravascular macrophages in the lung, classical monocytes have been associated with interstitial and alveolar macrophages (38, 39). Intermediary CD14+ monocytes expressing macrophage markers exist reflecting stages of monocyte-macrophage transition (40). The role of monocyte-derived macrophages in tissue development (38), including their impact on growth factor signaling as well as their relation to a pro-fibrotic phenotype (33) further underlines their potential as critical regulators of BPD development (41, 42).

The disease-characteristic immune response aligns with the maturational effects observed in the monocyte subtypes studied, as intermediate and nonclassical monocyte levels both demonstrated an association with PMA and specifically intermediate ($CD14^{++}CD16^{+}$) monocytes were increased in premature infants at birth. The capacity of these cells to express TNF-α upon stimulation, however, increased with maturation.

Closing the knowledge gap or early drivers in chronic lung disease development, we successfully identified distinct signatures of monocyte subtypes in volume-limited CB specimen and follow-up samples in preterm infants with BPD, complemented by comprehensive protein and transcriptome profiling.

The identified immune response in preterm infants with developing BPD at birth holds potential for the design of diagnostic and therapeutic strategies but warrants future studies engaging large patient collectives to delineate the differential impact of prenatal complications as well as genetic background on these disease characteristic profiles.

Data availability statement

The data presented in the study are deposited in the GEO repository (https://www.ncbi.nlm.nih.gov/geo), accession number GSE225881.

Ethics statement

This study was confirmed by the local ethic committees at LMU Munich (ethic vote #195-07) and JLU Giessen (ethic vote #file-79/01), following the same in- and exclusion (congenital malformations, metabolic disorders) criteria. The patients/participants provided their written informed consent to participate in this study.

Author contributions

AH, HH, TS, and CS designed the study. PO, CH, KF, MF, AF, EG, and XZ acquired the data. AH, AW, MH, PO, HE, MS, MF, and HH analyzed and interpreted the data. AH, AW, MH, TS, and CS drafted the manuscript for important intellectual content. All authors contributed to the article and approved the submitted version.

Funding

The present study was supported by the National Genome Research Network (NGFN; IE-S08T03), the Pneumonia Research Network on Genetic Resistance and Susceptibility for the Evolution of Severe Sepsis (PROGRESS; 01KI07110), the Young Investigator Grant (Helmholtz Association; VH-NG-829), the German Center for Lung Research (DZL; BMBF) and Stiftung AtemWeg (Lung Science Foundation, Project LSS AIRR). Work was supported by the Deutsche Forschungsgemeinschaft (DFG, German Research Foundation) - TRR 359 - Project number 491676693.

Acknowledgments

We sincerely thank the patients and their families for their significant contribution to this study by providing biospecimen and clinical data.

Conflict of interest

The authors declare that the research was conducted in the absence of any commercial or financial relationships that could be construed as a potential conflict of interest.

Publisher's note

Supplementary material

The Supplementary Material for this article can be found online at: https://www.frontiersin.org/articles/10.3389/fimmu.2023.1112608/full#supplementary-material

References

1. Humberg A, Fortmann I, Siller B, Kopp MV, Herting E, Göpel W, et al. Preterm birth and sustained inflammation: Consequences for the neonate. *Semin Immunopathology* (2020) 42:451–68. doi: 10.1007/s00281-020-00803-2

2. Ali Z, Schmidt P, Dodd J, Jeppesen DL. Bronchopulmonary dysplasia: A review. *Arch Gynecol Obstet* (2013) 288:325–33. doi: 10.1007/s00404-013-2753-8

3. Walsh MC, Szefler S, Davis J, Allen M, Van Marter L, Abman S, et al. Summary proceedings from the bronchopulmonary dysplasia group. *Pediatrics* (2006) 117(3 Pt2): S52–6. doi: 10.1542/peds.2005-0620I

4. Jobe AH, Bancalari E. Bronchopulmonary dysplasia. *Am J Respir Crit Care Med* (2001) 163:1723–9. doi: 10.1164/ajrccm.163.7.2011060

5. Perrone S, Laschi E, Buonocore G. Biomarkers of oxidative stress in the fetus and in the newborn. *Free Radical Biol Med* (2019) 142:23–31. doi: 10.1016/j.freeradbiomed.2019.03.034

6. Heydarian M, Oak P, Zhang X, Kamgari N, Kindt A, Koschlig M, et al. Relationship between impaired BMP signalling and clinical risk factors at early-stage vascular injury in the preterm infant. *Thorax* (2022) 77(12):1176–86. doi: 10.1136/thoraxjnl-2021-218083

7. Goedicke-Fritz S, Härtel C, Krasteva-Christ G, Kopp MV, Meyer S, Zemlin M. Preterm birth affects the risk of developing immune-mediated diseases. *Front Immunol* (2017) 8:1266. doi: 10.3389/fimmu.2017.01266

8. Heydarian M, Schulz C, Stoeger T, Hilgendorff A. Association of immune cell recruitment and BPD development. *Mol Cell Pediatr* (2022) 9:16. doi: 10.1186/s40348-022-00148-w

9. Twisselmann N, Pagel J, Künstner A, Weckmann M, Hartz A, Glaser K, et al. Hyperoxia/Hypoxia exposure primes a sustained pro-inflammatory profile of preterm infant macrophages upon LPS stimulation. *Front Immunol* (2021) 12:762789. doi: 10.3389/fimmu.2021.762789

10. Dreschers S, Ohl K, Lehrke M, Möllmann J, Denecke B, Costa I, et al. Impaired cellular energy metabolism in cord blood macrophages contributes to abortive response toward inflammatory threats. *Nat Commun* (2019) 10:1685. doi: 10.1038/s41467-019-09359-8

11. Dreschers S, Ohl K, Schulte N, Tenbrock K, Orlikowsky TW. Impaired functional capacity of polarised neonatal macrophages. *Sci Rep* (2020) 10:1–12. doi: 10.1038/s41598-019-56928-4

12. Hilgendorff A, Windhorst A, Klein M, Tchatalbachev S, Windemuth-Kieselbach C, Kreuder J, et al. Gene expression profiling at birth characterizing the preterm infant with early onset infection. *J Mol Med* (2017) 95:169–80. doi: 10.1007/s00109-016-1466-4

13. Sherman MP, Goetzman BW, Ahlfors CE, Wennberg RP. Tracheal asiration and its clinical correlates in the diagnosis of congenital pneumonia. *Pediatrics* (1980) 65:258–63.

14. Couchard M, Polge J, Bomsel F. [Hyaline membrane disease: Diagnosis, radiologic surveillance, treatment and complications]. *Ann Radiol (Paris)* (1974) 17:669–83.

15. Förster K, Ertl-Wagner B, Ehrhardt H, Busen H, Sass S, Pomschar A, et al. Altered relaxation times in MRI indicate bronchopulmonary dysplasia. *Thorax* (2020) 75:184–7. doi: 10.1136/thoraxjnl-2018-212384

16. Ziegler-Heitbrock L, Ancuta P, Crowe S, Dalod M, Grau V, Hart DN, et al. Nomenclature of monocytes and dendritic cells in blood. *Blood* (2010) 116:e74–80. doi: 10.1182/blood-2010-02-258558

17. Passlick B, Flieger D, Ziegler-Heitbrock H. Identification and characterization of a novel monocyte subpopulation in human peripheral blood. *Blood* (1989) 74:2527–34. doi: 10.1182/blood.V74.7.2527.2527

18. Cros J, Cagnard N, Woollard K, Patey N, Zhang S-Y, Senechal B, et al. Human CD14dim monocytes patrol and sense nucleic acids and viruses *via* TLR7 and TLR8 receptors. *Immunity* (2010) 33:375–86. doi: 10.1016/j.immuni.2010.08.012

19. Ziegler-Heitbrock L. The CD14+ CD16+ blood monocytes: Their role in infection and inflammation. *J Leukocyte Biol* (2007) 81:584–92. doi: 10.1189/jlb.0806510

20. Stacklies W, Redestig H, Scholz M, Walther D, Selbig J. pcaMethods a bioconductor package providing PCA methods for incomplete data. *Bioinformatics* (2007) 23:1164–7. doi: 10.1093/bioinformatics/btm069

21. R Core Team. *R: A language and environment for statistical computing*. Vienna, Austria: R Foundation for Statistical Computing (2021). Available at: https://www.R-project.org/.

22. Bylesjö M, Rantalainen M, Cloarec O, Nicholson JK, Holmes E, Trygg J. OPLS discriminant analysis: Combining the strengths of PLS-DA and SIMCA classification. *J Chemometrics* (2006) 20:341–51. doi: 10.1002/cem.1006

23. Thévenot EA, Roux A, Xu Y, Ezan E, Junot C. Analysis of the human adult urinary metabolome variations with age, body mass index, and gender by implementing a comprehensive workflow for univariate and OPLS statistical analyses. *J Proteome Res* (2015) 14:3322–35. doi: 10.1021/acs.jproteome.5b00354

24. Huber W, Carey VJ, Gentleman R, Anders S, Carlson M, Carvalho BS, et al. Orchestrating high-throughput genomic analysis with bioconductor. *Nat Methods* (2015) 12:115–21. doi: 10.1038/nmeth.3252

25. Hastie AT, Tibshirani R, Narasimhan B, Chu G. Package 'pamr'. (2019). Available at: https://CRAN.R-project.org/package=pamr.

26. Ritchie ME, Phipson B, Wu D, Hu Y, Law CW, Shi W, et al. Limma powers differential expression analyses for RNA-sequencing and microarray studies. *Nucleic Acids Res* (2015) 43:e47–7. doi: 10.1093/nar/gkv007

27. Benjamini Y, Hochberg Y. *Controlling the false discovery rate: A practical and powerful approach to multiple testing*. *J R Stat Soc: Series B Stat (Methodol)* (1995) 57:289–300. doi: 10.1111/j.2517-6161.1995.tb02031.

28. de Jong E, Hancock DG, Wells C, Richmond P, Simmer K, Burgner D, et al. Exposure to chorioamnionitis alters the monocyte transcriptional response to the neonatal pathogen staphylococcus epidermidis. *Immunol Cell Biol* (2018) 96:792–804. doi: 10.1111/imcb.12037

29. Yoon BH, Romero R, Kim KS, Park JS, Ki SH, Il KB, et al. A systemic fetal inflammatory response and the development of bronchopulmonary dysplasia. *Am J Obstetrics Gynecology* (1999) 181:773–9. doi: 10.1016/S0002-9378(99)70299-1

30. Tang P, Jerebtsova M, Przygodzki R, Ray PE. Fibroblast growth factor-2 increases the renal recruitment and attachment of HIV-infected mononuclear cells to renal tubular epithelial cells. *Pediatr Nephrol* (2005) 20:1708–16. doi: 10.1007/s00467-005-2018-2

31. Belge K-U, Dayyani F, Horelt A, Siedlar M, Frankenberger M, Frankenberger B, et al. The proinflammatory CD14+CD16+DR++ monocytes are a major source of TNF. *J Immunol* (2002) 168:3536–42. doi: 10.4049/jimmunol.168.7.3536

32. Ong S-M, Hadadi E, Dang T-M, Yeap W-H, Tan CT-Y, Ng T-P, et al. The pro-inflammatory phenotype of the human non-classical monocyte subset is attributed to senescence. *Cell Death Dis* (2018) 9:266. doi: 10.1038/s41419-018-0327-1

33. Misharin AV, Morales-Nebreda L, Reyfman PA, Cuda CM, Walter JM, McQuattie-Pimentel AC, et al. Monocyte-derived alveolar macrophages drive lung fibrosis and persist in the lung over the life span. *J Exp Med* (2017) 214:2387–404. doi: 10.1084/jem.20162152

34. Lingappan K, Savani RC. The wnt signaling pathway and the development of bronchopulmonary dysplasia. *Am J Respir Crit Care Med* (2020) 201:1174–6. doi: 10.1164/rccm.202002-0277ED

35. D'Angio CT, Ambalavanan N, Carlo WA, McDonald SA, Skogstrand K, Hougaard DM, et al. Blood cytokine profiles associated with distinct patterns of bronchopulmonary dysplasia among extremely low birth weight infants. *J Pediatr* (2016) 174:45–51.e5. doi: 10.1016/j.jpeds.2016.03.058

36. Sahoo D, Zaramela LS, Hernandez GE, Mai U, Taheri S, Dang D, et al. Transcriptional profiling of lung macrophages identifies a predictive signature for inflammatory lung disease in preterm infants. *Commun Biol* (2020) 3:259. doi: 10.1038/s42003-020-0985-2

37. Yao H, Wallace J, Peterson AL, Scaffa A, Rizal S, Hegarty K, et al. Timing and cell specificity of senescence drives postnatal lung development and injury. *Nat Commun* (2023) 14:273. doi: 10.1038/s41467-023-35985-4

38. Evren E, Ringqvist E, Tripathi KP, Sleiers N, Rives IC, Alisjahbana A, et al. Distinct developmental pathways from blood monocytes generate human lung macrophage diversity. *Immunity* (2021) 54:259–275.e7. doi: 10.1016/j.immuni.2020.12.003

39. Travaglini KJ, Nabhan AN, Penland L, Sinha R, Gillich A, Sit RV, et al. A molecular cell atlas of the human lung from single-cell RNA sequencing. *Nature* (2020) 587:619–25. doi: 10.1038/s41586-020-2922-4

40. Madissoon E, Oliver AJ, Kleshchevnikov V, Wilbrey-Clark A, Polanski K, Richoz N, et al. A spatially resolved atlas of the human lung characterizes a gland-associated immune niche. *Nat Genet* (2023) 55:66–77. doi: 10.1038/s41588-022-01243-4

41. Eldredge LC, Creasy RS, Presnell S, Debley JS, Juul SE, Mayock DE, et al. Infants with evolving bronchopulmonary dysplasia demonstrate monocyte-specific expression of IL-1 in tracheal aspirates. *Am J Physiology-Lung Cell Mol Physiol* (2019) 317:L49–56. doi: 10.1152/ajplung.00060.2019

42. Ballabh P, Simm M, Kumari J, Krauss AN, Jain A, Califano C, et al. Neutrophil and monocyte adhesion molecules in bronchopulmonary dysplasia, and effects of corticosteroids. *Arch Dis Childhood: Fetal Neonatal Edition* (2004) 89:76–83. doi: 10.1136/fn.89.1.f76

frontiers | Frontiers in Immunology

TYPE Original Research
PUBLISHED 13 February 2023
DOI 10.3389/fimmu.2023.1067714

OPEN ACCESS

EDITED BY
Rowan S. Hardy,
University of Birmingham, United Kingdom

REVIEWED BY
Nicholas Veldhuis,
Monash University, Australia
Parisa Gazerani,
Oslo Metropolitan University, Norway

*CORRESPONDENCE
Patricia García-Fernández
garcia_P@ukw.de

SPECIALTY SECTION
This article was submitted to Cytokines and Soluble Mediators in Immunity, a section of the journal Frontiers in Immunology

RECEIVED 12 October 2022
ACCEPTED 31 January 2023
PUBLISHED 13 February 2023

CITATION
García-Fernández P, Höfflin K, Rausch A, Strommer K, Neumann A, Cebulla N, Reinhold A-K, Rittner H, Üçeyler N and Sommer C (2023) Systemic inflammatory markers in patients with polyneuropathies. *Front. Immunol.* 14:1067714. doi: 10.3389/fimmu.2023.1067714

Systemic inflammatory markers in patients with polyneuropathies

Patricia García-Fernández[1]*, Klemens Höfflin[1], Antonia Rausch[1], Katharina Strommer[2], Astrid Neumann[2], Nadine Cebulla[1], Ann-Kristin Reinhold[3], Heike Rittner[3], Nurcan Üçeyler[1] and Claudia Sommer[1]

[1]Department of Neurology, University Hospital of Würzburg, Würzburg, Germany, [2]Department of Bioanalytics, Bionorica research GmbH, Innsbruck, Austria, [3]Department of Anesthesiology, University Hospital of Würzburg, Würzburg, Germany

Introduction: In patients with peripheral neuropathies (PNP), neuropathic pain is present in 50% of the cases, independent of the etiology. The pathophysiology of pain is poorly understood, and inflammatory processes have been found to be involved in neuro-degeneration, -regeneration and pain. While previous studies have found a local upregulation of inflammatory mediators in patients with PNP, there is a high variability described in the cytokines present systemically in sera and cerebrospinal fluid (CSF). We hypothesized that the development of PNP and neuropathic pain is associated with enhanced systemic inflammation.

Methods: To test our hypothesis, we performed a comprehensive analysis of the protein, lipid and gene expression of different pro- and anti-inflammatory markers in blood and CSF from patients with PNP and controls.

Results: While we found differences between PNP and controls in specific cytokines or lipids, such as CCL2 or oleoylcarnitine, PNP patients and controls did not present major differences in systemic inflammatory markers in general. IL-10 and CCL2 levels were related to measures of axonal damage and neuropathic pain. Lastly, we describe a strong interaction between inflammation and neurodegeneration at the nerve roots in a specific subgroup of PNP patients with blood-CSF barrier dysfunction.

Conclusion: In patients with PNP systemic inflammatory, markers in blood or CSF do not differ from controls in general, but specific cytokines or lipids do. Our findings further highlight the importance of CSF analysis in patients with peripheral neuropathies.

KEYWORDS

cytokines, polyneuropathy, cerebrospinal fluid, neurofilament light chain, blood CSF barrier

Introduction

Polyneuropathy (PNP) is a term to describe a group of diseases with peripheral nerve dysfunction of various etiologies. Symptoms may affect the motor, sensory and/or autonomic system, and in 50% of the cases, patients experience neuropathic pain. Why some patients with PNP have pain and others not, is unknown, and even PNPs with the same etiology may be painful or painless (1). The available treatments have modest efficacy in reducing pain and present considerable side effects (2, 3). One approach toward better symptom control and potentially causative treatment might be to find common pathophysiologic pathways in PNP of different etiologies.

Although merely 14%-20% of PNP have a definite immune-related cause (4), inflammatory processes have been found to be involved in neuro-degeneration, -regeneration and pain in neuropathies of different origin (5–7). One of the main pro-inflammatory pathways that are activated upon damage is toll-like receptor (TLR) 4 mediated. Stimulation of TLR4 results in the activation of the nuclear factor k B (NFkB) pathway and the release of inflammatory cytokines, including tumor necrosis factor-alpha (TNF-α), interleukin (IL)-1β, IL-6, IL-8, IL-10, or chemokines such as the CC-chemokine ligand (CCL) 2 (8). This pathway can in turn be regulated by other mediators. For instance, the NAD-dependent deacetylase sirtuin 1 (SIRT1) has been suggested to be able to inhibit the pro-inflammatory cascade by deacetylating the p65 subunit of NFkB (9). Fractalkine (Cx3CL1) is an algesic chemokine which is cleaved from neurons and activates glial cells (10). Furthermore, small fragments of RNA, or microRNAs (miR), can regulate the expression of genes coding for pro- and anti-inflammatory proteins and have been found altered in different neuropathies of the central or peripheral nervous system, nociception and pain (11). While many miRs might be involved in the development of neuropathic pain, miR-146a-5p, miR-132-3p and miR-155-5p participate in the regulation of the NFkB pathway and have been described altered in patients with painful PNP (12–14). In addition, alterations in ion channels such as voltage gated sodium channels or those of the transient receptor potential cation channel subfamily like TRPV1 might lead to enhanced excitatory responses in nociceptors and promote axonal degeneration and the release of pro-inflammatory mediators, exacerbating the immune response (15). Furthermore, TRPV1 is expressed in blood mononuclear cells, and a direct role in cytokine production and immune responses has been proposed (16, 17).

Several lipid compounds, such as prostaglandins (PGs) or thromboxanes, are known to be involved in inflammation and pain, and can in turn be upregulated upon inflammation or tissue injury. Moreover, high levels of PGs have been described in serum from patients with peripheral neuropathies, as well as in the spinal cord of animal models with peripheral injury (18, 19). In fact, non-steroidal anti-inflammatory drugs (NSAIDs), a very common treatment against pain, have anti-inflammatory and analgesic properties mediated by blocking the synthesis of PGs and thromboxanes (18, 20, 21). Short-chain and long-chain acylcarnitines can be found upstream their synthesis pathway and have been reported upregulated in sera, nerve and spinal cord in animal models of neurodegeneration, in particular, palmitoylcarnitine (C16:0) and oleoylcarnitine (C18:1) (20, 22–24).

In PNP, signs and symptoms are typically length-dependent and thus more severe in the distal extremities of the body, such as feet and hands, than in the proximal regions or in the torso. Previous studies found a local upregulation of inflammatory mediators such as IL-2, IL-6, IL-8 or IL-10 in skin or nerve from patients with PNP (5, 25). The study of local inflammation, especially in the nerve, is difficult in humans, since it implies an invasive nerve biopsy, while systemic samples, such as blood and cerebrospinal fluid (CSF), are drawn and analyzed routinely. Since several inflammatory cytokines have been seen upregulated locally in patients with PNP, we studied whether some of these markers might be found systemically in sera or CSF. Different studies have shown a high variability in the cytokines present in serum from patients with PNP or nerve root compression, associated with the severity and symptoms of the neuropathy (26–31). Furthermore, extensive studies have shown that the CSF is directly altered by diseases of the central nervous system, while in diseases of the peripheral nervous system (PNS), differences in the levels of cytokines in CSF have yet to be explained. A factor that can influence these levels is the integrity of the barrier between blood and CSF, also called blood-CSF-barrier (B-CSF barrier) (32–34) or blood brain barrier (BBB) (35).

We hypothesized that PNP is associated with enhanced systemic inflammation that may correlate with the severity of the disease and the development of neuropathic pain. To test our hypothesis, we performed a comprehensive analysis of the protein, lipid, and gene expression of selected pro- and anti-inflammatory markers in blood and CSF from patients with PNP and controls. Furthermore, we measured the levels of neurofilament light-chain (NFL), as a cytoskeletal protein expressed by neurons and released upon cell damage, to assess the level of neurodegeneration present in patients with PNP (36), and to correlate NFL levels with the degree of inflammation. We also aimed to identify new systemic markers that might be important in the pursuit of a more accurate diagnosis and the prediction of neuropathic pain.

Materials and methods

Patient recruitment and diagnostic assessment

Between 2019 and 2021, 28 patients with PNP were prospectively recruited at the Department of Neurology, University of Würzburg, Germany, where they were seen for diagnostic work-up. In addition, 10 patients with acute headaches of unclear etiology were used as disease controls for the CSF analysis, and serum data from twelve healthy volunteers were included in the analysis to determine the inflammatory state of the headache group. Our study was approved by the Würzburg Medical Faculty Ethics Committee (# 15/19 and # 242/17) and all participants gave written informed consent prior to inclusion.

Diagnoses were based on history taking and neurological examination, laboratory studies, and nerve conduction examinations. All patients underwent laboratory tests including full

blood count, electrolytes, kidney and liver function tests, C-reactive protein, thyroid stimulating hormone, vitamin B12, HbA1c, oral glucose tolerance test (OGTT), screening for autoimmune antibodies (i.e., ANA, ENA, ANCA, anti-ganglioside antibodies), and lumbar puncture. Electrophysiological assessment with nerve conduction studies of the affected nerves including tibial motor nerve and sural sensory nerve was performed in all PNP patients.

To rate the severity of the neuropathy, we used standardized scales, including the modified Toronto clinical neuropathy score (mTCNS), the overall disability sum score (ODSS) and the Medical Research Council-sumscore (MRC-sumscore). Depression was assessed with the "Allgemeine Depressionsskala" (ADS) (37). Pain was evaluated by a numerical rating scale (NRS) from 0 (no pain) to 10 (worst pain), the neuropathic pain symptom inventory (NPSI) and the graded chronic pain scale (GCPS). After the diagnostic work-up, the examining neurologists categorized the neuropathies into a mild (1), moderate (2) or severe (3) clinical phenotype.

Sample collection

From each patient, venous blood was drawn in the morning between 8 a.m. and 9 a.m. into S-Monovette® Serum-Gel Tubes (Sarstedt, Nümbrecht, Germany) and Tempus™ Blood RNA Tubes (Thermo Fisher Scientific, Waltham, MA, USA). For the collection of sera, whole blood was left to clot for 30 min at room temperature and later centrifuged for 10 min at 1200 g. Supernatant was aliquoted and stored at -20°C until further analysis. Tempus™ Blood RNA Tubes were immediately shaken for 30 s to lyse the cells and stabilize the RNA and stored at -80°C until extraction.

CSF samples were obtained after a lumbar puncture at the L4/5 level. The amount of CSF taken varied between 10-15 ml. Samples of 2 ml were aliquoted and subsequently stored at -20 °C.

Gene expression analysis

RNA was extracted from Tempus™ Blood RNA Tubes following the manufacturer's protocol (38, 39) from the MagMAX™ for Stabilized Blood Tubes RNA Isolation Kit (Thermo Fisher Scientific, Waltham, MA, USA). RNA quality and quantity were assessed with a NanoDrop™ One (Thermo Fisher Scientific, Waltham, MA, USA), and RNA was stored at -80°C.

For cDNA synthesis from mRNA, TaqMan Reverse Transcription reagents (Thermo Fisher Scientific, Waltham, MA, USA) were used. 250 ng mRNA of each sample were pre-incubated with 5 µl random hexamer at 85°C for 3 min. Next, 10 µL 10× PCR buffer, 22 µL $MgCl_2$, 20 µL deoxyribonucleoside triphosphate, 6.25 µL multiscribe reverse transcriptase and 2 µL RNase inhibitor were added per sample. Lastly, reaction was performed under these conditions: annealing (25°C, 10 min), reverse transcription (48°C, 60 min), and enzyme inactivation (95°C, 5 min).

For miRNA, reverse transcription was carried out with the miRCURY LNA RT Kit (Qiagen, Hilden, Germany). 10 ng of RNA were mixed with 2 µL of 5x reaction buffer, 5 µL of nuclease free water and 1 µL of enzyme mix, per sample. Reaction was performed using the following program: reverse transcription (42°C, 60 min) and enzyme deactivation (95°C, 5 min).

Reactions were carried out on a PRISM 7700 Cycler (Applied Biosystems, Waltham, MA, USA) and transcribed cDNA was stored at -20°C until further analysis.

Real time qPCR of mRNA and miRNA targets was performed to analyze gene expression using the StepOnePlus Real-Time PCR System (Thermo Fisher Scientific, Waltham, MA, USA). For mRNA, RT-qPCR was carried out with TaqMan qRT-PCR reagents (all Thermo Fisher Scientific, Waltham, MA, USA) and pre-designed assays. For target normalization, different endogenous controls were used: ribosomal protein L13a (RPL13A), actin beta (ACTb), Hydroxymethylbilane Synthase (HMBS) and TATA-Box binding protein (TBP) were tested. TBP was the most stable across groups, and thus selected as suitable endogenous control. For each reaction, 3.5 µl cDNA (8.75 ng cDNA) was mixed with 0.5 µl nuclease free water, 5 µl Fast Advanced Mastermix and 0.5 µl TBP primer and 0.5 µl target primer (see list of primers in Table 1).

For miRNA, the miRCURY LNA SYBR Green PCR Kit (Qiagen, Hilden, Germany) and pre-designed miRCURY LNA miR PCR assays (Qiagen, Hilden, Germany) were used. Based on previous experience from our group (12, 13) and on the recommendations by TaqMan Advanced miRNA Assays (https://assets.thermofisher.com/TFS-Assets/GSD/Reference-Materials/identifying-mirna-normalizers-white-paper.pdf), the ribosomal RNA 5s and hsa-miR-16 were tested as endogenous controls. Due to differences found in the expression of 5s between groups, hsa-miR-16 was selected as suitable endogenous control, based on its comparability and standard deviation across groups and samples. Each miRNA was run adding 5 µl 2× miRCURY SYBR Green Master Mix with 1 µl ROX per 50 µl and 1 µl primer (see list of primers in Table 1) to 4 µl of 1:80 diluted cDNA.

Each mRNA and miRNA was amplified in triplicates and relative quantitation (RQ) values were obtained by the StepOnePlus™ Software v2.3 (Thermo Fisher Scientific, Waltham, MA, USA) using interplate calibrators through the 2-ΔΔCt method.

Protein analysis

Cytokine levels were measured in serum and CSF using the Ella™ technology (ProteinSimple, San Jose, Cal, USA). Ella™ is a fully automated cartridge-based system that allows you to perform multiple sample, multi-analyte immunoassays with the specificity of a traditional single-plex ELISA (enzyme-linked immunosorbent assay). Samples were thawed on ice and more than two freeze-thaw cycles were avoided. Samples were diluted 1:1 in the appropriate sample diluent from each kit and 50 µl were added to each sample well of the Simple Plex™ cartridge, after 1 ml of washing buffer was added to their corresponding wells. Each sample was measured in triplicates, and the levels of each cytokine were displayed in pg/ml.

Lipid analysis

Serum and CSF samples were quantitatively analyzed for their levels of the endogenous metabolites carnitine (CAR), palmitoylcarnitine (PC) and oleoylcarnitine (OC) by LC-MS/MS (liquid chromatography coupled with tandem mass spectrometry).

All samples were thawed on ice for the first time for this analysis, in order to avoid freeze-thaw cycles, and processed within two years upon collection. Serum samples were analyzed at a neat dilution and after applying a 1:10 dilution step in 70% (v/v) ethanol. For sample

TABLE 1 List of primer assays.

Taqman Primer*	Assay Number
TRPV1	Hs00218912_m1
TLR4	Hs00152939_m1
SIRT1	Hs01009006_m1
TNFα	Hs00174128_m1
IL-1β	Hs00174097_m1
IL-6	Hs00174131_m1
IL-8	Hs00174103_m1
CCL2	Hs00234140_m1
IL-10	Hs00174086_m1
TBP	Hs00427620_m1
SYBR Green Primer#	**Assay Number**
hsa-miR-132-3p	YP00206035
hsa-miR-146a-5p	YP00204688
hsa-miR-155-5p	YP00204308
hsa-miR-16-5p	YP00205702
5s rRNA	YP00203906

*Taqman Primers were purchased from Thermo Fisher Scientific, Waltham, MA, USA.
#SYBR Green Primers were purchased from Qiagen, Hilden, Germany.
TRPV1, transient receptor potential cation channel subfamily V member 1; TLR4, toll-like receptor 4; SIRT1, sirtuin 1; TNFα, tumor necrosis factor α; IL, interleukin; CCL2, CC-chemokine ligand 2; TBP, TATA-Box binding protein; miR, microRNA, rRNA, ribosomalRNA.

preparation, 50 µl of serum or CSF samples were mixed with 150 µl internal standard solution (100 ng/ml acetylcarnitine-d3 in acetonitrile). Samples were centrifuged (13000 rpm, 1.5 min) and the supernatant was used for analysis.

Chromatographic separation was performed with a UHPLC System (1290 Infinity series, Agilent) using a Waters Acquity UHPL CSH™ Fluoro-Phenyl (75 × 2.1 mm, 1.7 µm) column. The injection volume was 2 µl and the flow rate was set to 0.3 mL/min. For the chromatographic separation a gradient was run using 0.1% formic acid in water (solvent A) and 0.1% formic acid in acetonitrile (solvent B). Detection was performed by means of a triple quadrupole mass spectrometer (API 4000®, Sciex) in multiple reaction monitoring (MRM) mode. Measurements were carried out in the positive electrospray ionization (ESI) mode. The LC-MS/MS system was operated with the Software Analyst®, Version 1.7.1 (Sciex).

Calibration samples were prepared in 30% acetonitrile and covered calibration ranges of 5 - 500 ng/ml for PC and OC and 5 - 1500 ng/ml for CAR. To verify method performance at medium analyte concentrations, QC samples with a concentration of 50.00 ng/ml CAR, OC and PC were prepared in 30% acetonitrile or in a surrogate matrix comparable to the analyzed biological samples (2% bovine serum albumin (BSA) or PBS buffer pH 7.4 diluted 1:10 in 30% acetonitrile were used to mimic serum or CSF, respectively).

Correlation coefficients of 0.9996 (CAR, OC) and 0.9992 (PC) were obtained. Accuracies of the calibration samples were found within +/-15% or within +/-20% for the lowest calibration level, respectively. Mean accuracies for all QC samples were found between 87.07% and 109.77% with CVs < 15%, indicating an acceptable method performance for all matrices investigated.

Further analytical information can be found in the Supplementary Material.

Statistical analysis and visualization

Statistical analysis was performed in SPSS 27 (IBM, Armonk, NY, USA), where the Shapiro-Wilk test was used to determine the normal distribution of the data. For parametric data, a T-test was used for comparison between two groups and a Pearson test was performed for correlations. In non-parametric data, the Mann–Whitney U Test was applied for comparison of two groups, and the Spearman test was used for correlations. Data results were plotted in GraphPad Prism 9 (GraphPad Software, Inc., La Jolla, CA, USA) for visualization. Graphical images were incorporated from Smart Servier Medical Art, https://smart.servier.com/, under the Creative common Attribution 3.0 Unported Licence.

Results

Clinical characteristics of patient cohort

Baseline characteristics of the study group and the diagnostic subgroups are summarized in Table 2. Patients were included if they presented for diagnostic work-up for their PNP, including lumbar puncture. To be included, they further needed to have either no pain (NRS = 0) or pain ≥ 4 at the time of admission. Patients with an NRS between one and three were excluded from the cohort. After applying the exclusion criteria, twenty-eight patients with PNP of different etiologies were included [median body max index (BMI) 28.3, range 19.2-35.1; median age 54.5 years, range 20–80]. The median disease duration was 2.5 years (range 0.02–29 years). Nine patients were diagnosed with an inflammatory neuropathy including non-systemic vasculitis (six patients), chronic inflammatory demyelinating polyneuropathy (CIDP) (two patients) and multifocal motor neuropathy (MMN) (one patient). Nineteen patients were classified as non-inflammatory, including idiopathic neuropathy (nine patients), hereditary neuropathy (five patients), a neuropathy caused by vitamin B deficiency (three patients) or diabetic neuropathy (two patients).

Patients were classified as painless when they presented an NRS = 0 (fourteen patients; 50%), and as painful with an NRS ≥ 4 (fourteen patients; 50%). From the full cohort of PNP patients, at the time of inclusion fifteen patients had been treated for their neuropathy with either an immunosuppressive/immunomodulatory drug (six patients) and/or pain treatment (twelve patients), while thirteen received no treatment.

Further laboratory and electrophysiological data are given in Table 3. The median CRP value in serum was 0.24 mg/dl (range 0-2.37 mg/dl). In CSF, patients presented a median of 2 leukocytes/µl (range 0-6 cells/µl) and a median total protein of 46.3 mg/dl (range 19.3-194.6 mg/dl). Nerve conduction studies showed a median sural nerve sensory nerve action potential (SNAP) of 4.9 µV (range 2.5-12.6 µV) with a median nerve conduction velocity (NCV) of 45.9 m/s

TABLE 2 Description and diagnostic subgroups of patient cohort.

Item	Number (% of entire group)
M, F (*N*)	22, 6
Median BMI (range)	28.3 (19.2-35.1)
Median age (range)	54.5 years (20-80)
Median disease duration (range in years)	2.5 years (0.02-29)
Diagnostic subgroups (*N* and % of entire group):	
Idiopathic neuropathy	9 (32.1%)
Vasculitic neuropathy	6 (21.4%)
Hereditary neuropathy	5 (17.9%)
Vit B1/B6/B9/B12 deficiency	3 (10.7%)
Diabetic neuropathy	2 (7.1%)
CIDP	2 (7.1%)
Multifocal motor neuropathy (MMN)	1 (3.6%)
Analysis subgroups (*N*):	
Painless, painful	14, 14
Inflammatory, non-inflammatory neuropathy	9, 19
Patients with treatment, without treatment (*N*)*:	15, 13
Immunosupressory/immunomodulatory treatment (Corticoids, immunoglobulins, NSAIDs)	6
Pain treatment[#]	12
Anti-neuropathic analgesics	11
Opioids	4

Numbers add up to >28 (*) and >12 (#) because some patients had more than one treatment.

(range 32.4-57.3 m/s), and in the tibial nerve a median compound motor action potential (CMAP) upon stimulation at the ankle of 5.4 mV (range 0.1-23.4 mV) and a median nerve conduction velocity (NCV) of 38.3 m/s (range 26.8-52.2 m/s).

Control group

Patients that presented with acute headaches of unclear etiology (AH) and had a lumbar puncture to exclude meningitis or a subarachnoid bleed were used as controls for the CSF data. Only patients that had less than four leukocytes/µl in their CSF and normal protein values were included. After full clinical work-up, five of these patients had some signs of inflammation (elevated CRP, n = 3; sinusitis, n = 1; or elevated ANA and ANCA titers, n = 1). Thus, the AH group was divided into two groups (unclear headache, UH, and inflammatory headache, IH), and only patients with UH were further used as controls for inflammatory markers (Table 4, Figure 1A). Twelve healthy volunteers (HC) were included as controls for NFL and inflammatory markers in serum. HC and AH did not differ in age or NFL levels in pg/ml in serum (Figures 1B, C), and in both groups a positive correlation between age and NFL was present (HC, $p < 0.05$; AH, $p < 0.01$) (Figure 1D). When separating AH into UH and IH, NFL levels did not differ between groups, but IL-6 was higher in IH in comparison to HC ($p < 0.001$) (Figure 1E). These results supported our decision to continue the study on inflammatory markers with the UH exclusively, while the whole cohort (AH) was used for the NFL analysis.

NFL levels in serum and CSF from PNP patients

NFL was measured in serum and CSF in twenty-eight patients with PNP in comparison to ten age-matched AH (Figures 2A, B). PNP patients had higher serum levels of NFL than AH ($p < 0.01$) (Figure 2C). There was a positive correlation between age and NFL levels in AH ($p < 0.01$) but not in PNP patients (Figure 2D). NFL levels correlated negatively to sural nerve SNAP in PNP patients (Figure 2E), which translated into higher levels of NFL in patients with abnormal SNAP values (< 5 µV) in comparison to those with normal SNAP (≥ 5 µV) ($p < 0.01$) (Figure 2F).

The same analysis was performed with CSF samples (Figure 3A) and we observed higher levels of NFL in PNP patients in comparison to AH ($p < 0.001$) (Figure 3B). Again, a correlation between age and NFL was present in AH ($p < 0.001$) but not in PNP patients (Figure 3C). Furthermore, our results showed a negative correlation between the levels of NFL in CSF and the MRC sumscore (Figure 3D), therefore suggesting an involvement of NFL release in the severity of the neuropathy.

TABLE 3 Clinical findings in PNP patients versus controls.

Item	Normal range	PNP	AH	UH
N	NA	28	10	5
Serum findings				
Median CRP (mg/dl) (range)	≤0.5	0.24 (0-2.37)	0.23 (0-11.39)	0 (0-0.34)
Median NFL (pg/ml) (range)	NA	27.35 (8.3-2856)**/##	10.80 (3.04-48.90)	4.92 (3.04-26.90)
Lumbar puncture				
Median cells/µl (range)	≤4	2 (0-6)	0.5 (0-3)	0 (0-3)
Median CSF protein (mg/dl) (range)	≤50	46.3 (19.3-194.6)	27.6 (16.9-44)	30.1 (21.2-38.8)
Median NFL (pg/ml) (range)	NA	627.0 (155.0-8535)***/##	291.0 (134.0-489.0)	199.0 (123.0-413.0)
Median NFL Ratio (CSF/Serum)	NA	26.14 (1.9-75.9)	28.53 (8.4-66.1)	56.53 (15.35-66.06)
Electrophysiology				
Sural nerve				
Median SNAP (µV) (range)	≥5/10 (Age ≥65y/<65y)	4.9 (2.5-12.6)	NA	NA
Median NCV(m/s) (range)	≥40	45.9 (32.4-57.3)	NA	NA
Tibial nerve				
Median Distal CMAP (mV) (range)	≥10	5.4 (0.1-23.4)	NA	NA
Median NCV (m/s) (range)	≥40	38.3 (26.8-52.2)	NA	NA

Patients with polyneuropathies (PNP) were compared to the control group acute headaches (AH) (10), and to the subgroup unclear headaches (UH) (5/10). CRP, C-reactive protein; NFL, neurofilament light chain, CSF, cerebrospinal fluid; SNAP, sensory nerve action potential; NCV, nerve conduction velocity; CMAP, compound motor action potential. Kruskal-Wallis or T-test was performed between PNP and AH (*) or UH (#). **/##, $p < 0.01$; ***, $p < 0.001$.

TABLE 4 Description of the control groups.

Item	Number (% of entire group)		
	Acute headaches (AH)		Healthy controls (HC)
M, F (N)	6, 4		6,6
Median age (range)	52 years (22-78)		54 years (21-65)
Diagnostic subgroups (*N* and % of entire group):			
Unclear headaches (UH)	5 (50%)		NA
Infectious/inflammatory headaches (IH)	5 (50%)		NA
Median NFL pg/ml in serum (range)	10.80 (3.04-48.90)		13.85 (8.93-27.80)
	UH	IH	HC
Median NFL pg/ml in serum (range)	4.92 (3.04-26.90)	14.80 (10.00-38.90)	13.85 (8.93-27.80)
Median of cytokine levels in serum (range):			
TNFα pg/ml	6.78 (6.04-23.20)	9.89 (8.22-12.90)	8.94 (6.51-13.55)
IL-1β pg/ml	0.19 (0.05-0.54)	0.06 (0.05-0.4)	0.35 (0.03-2.11)
IL-6 pg/ml	1.36 (0.51-3.48)	7.04 (3.52-11.50)***	1.22 (0.33-2.80)
IL-8 pg/ml	9.38 (6.72-13.70)	14.40 (9.19-20.60)	11.65 (7.35-19.90)
CCL2 pg/ml	198 (190-454)	340 (179-531)	357 (201-470)
IL-10 pg/ml	3.06 (2.63-12.50)	3.55 (2.89-3.62)	3.95 (3.07-7.69)
NGF-β pg/ml	3.34 (2.66-5.00)	4.77 (3.52-5.99)	5.04 (3.76-13.50)

NFL, neurofilament light-chain; TNFα, tumor necrosis factor α; IL, interleukin; CCL2, CC-chemokine ligand2, NGF-β, nerve growth factor β. (*) Kruskal-Wallis test was performed between HC and UH or IH.***, $p < 0.001$.

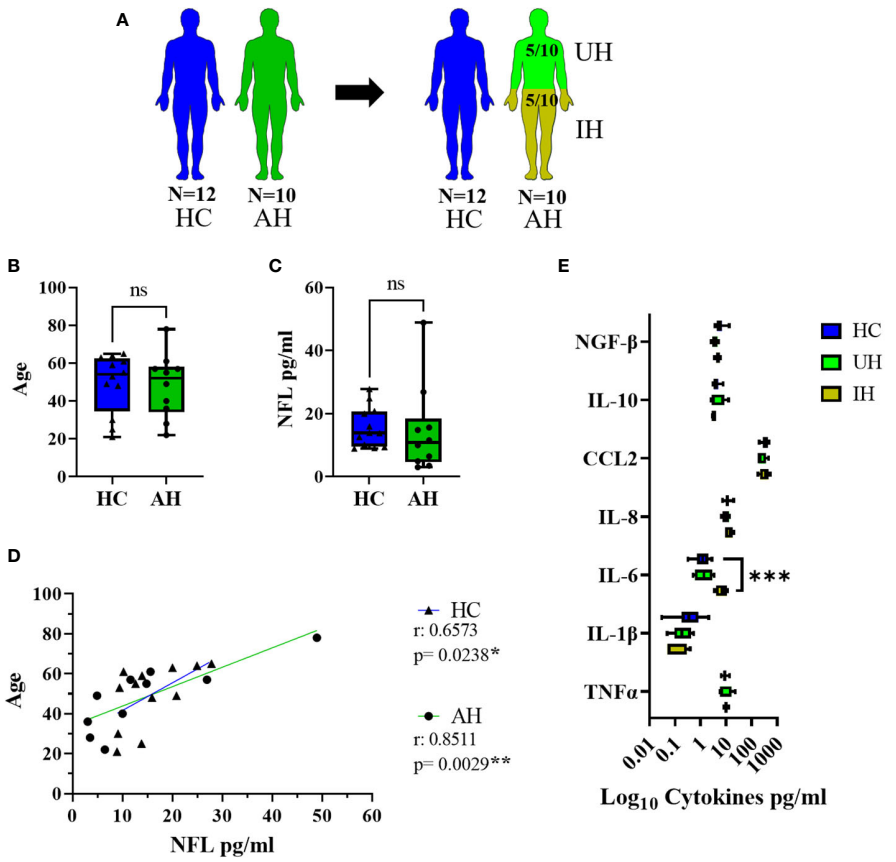

FIGURE 1
Description of the control groups. **(A)** Visual representation of the healthy controls (HC) (blue) and acute headaches group (AH) (green), further divided into unclear headaches (UH, light green) and inflammatory headaches (IH, olive green). **(B)** Age values in HC and AH. **(C)** NFL levels in serum in pg/ml between HC and AH. **(D)** Correlation between age and NFL levels in serum in pg/ml in HC and AH. **(E)** Log10 representation of cytokine values in serum from HC, UH and IH. ns, not significant; *, $p < 0.05$; **, $p < 0.01$; ***, $p < 0.001$. All graphical images were incorporated from Smart Servier Medical Art, https://smart.servier.com/, under the Creative common Attribution 3.0 Unported Licence.

Gene expression of pro- and anti-inflammatory markers in whole blood

In twenty-seven out of twenty-eight PNP patients and five UH, we analyzed the gene expression of the receptors TRPV1 and TLR4; the deacetylase SIRT1; the pro-inflammatory cytokines TNFα, IL-1β, IL-6 and IL-8, and chemokine CCL2; the anti-inflammatory cytokine IL-10; and the microRNAs miR-146a-5p, miR-132-3p and miR-155-5p in whole blood (Figure 4A). The expression results of PNP patients, with painful and painless PNP, and inflammatory and non-inflammatory PNP are displayed as fold change in comparison to UH in Table 5. Comparisons between PNP patients and controls, as well as between painful and painless PNP subgroups, and inflammatory and non-inflammatory did not show any differences in the expression of these components.

Interestingly, PNP patients were next grouped into patients with and without systemic inflammation based on increased CRP levels in the serum (cut-off 0.5 mg/dl). Patients with systemic inflammation had a higher expression of IL-10 in comparison to those with normal CRP levels (≤0.5 mg/dl) ($p < 0.001$) (Figure 4B) and a positive correlation was found between CRP levels and IL-10 expression ($p < 0.01$) (Figure 4E). Furthermore, PNP patients with high CSF total protein (> 50 mg/dl) also presented lower expression of TNFα (Figure 4C) and higher expression of miR-155 (Figure 4D) than those with normal levels (≤ 50 mg/dl). Moreover, a multivariate correlation analysis (Figure 4E) showed that CCL2 correlated positively with the duration of the disease ($p < 0.001$) while negatively with several neuropathy scores such as sural nerve SNAP amplitudes ($p < 0.01$) or GCPS, indicating a relation between inflammation and axonal degeneration.

Cytokine protein levels in sera

As indicators of systemic inflammation, we analyzed the levels of the pro-inflammatory cytokines TNFα, IL-1β, IL-6 and IL-8, the chemokine CCL2, and the anti-inflammatory cytokine IL-10 in sera from twenty-eight patients with PNP and five UH (Figure 5A). Furthermore, we measured the levels of nerve growth factor beta (NGF-β) in sera, since it is involved in nociceptive processing and a target of novel analgesics (40). The CSF from the same cohort was available and we measured the levels of the pro-inflammatory cytokines IL-6 and IL-8, and the chemokines CCL2 and fractalkine (Cx3CL1). TNFα, IL-1β and IL-10 were not detected in these samples (data not shown). All results are detailed in Table 6.

CCL2 was present in higher levels in serum in PNP in comparison to UH, while no differences were discovered for the other analyzed

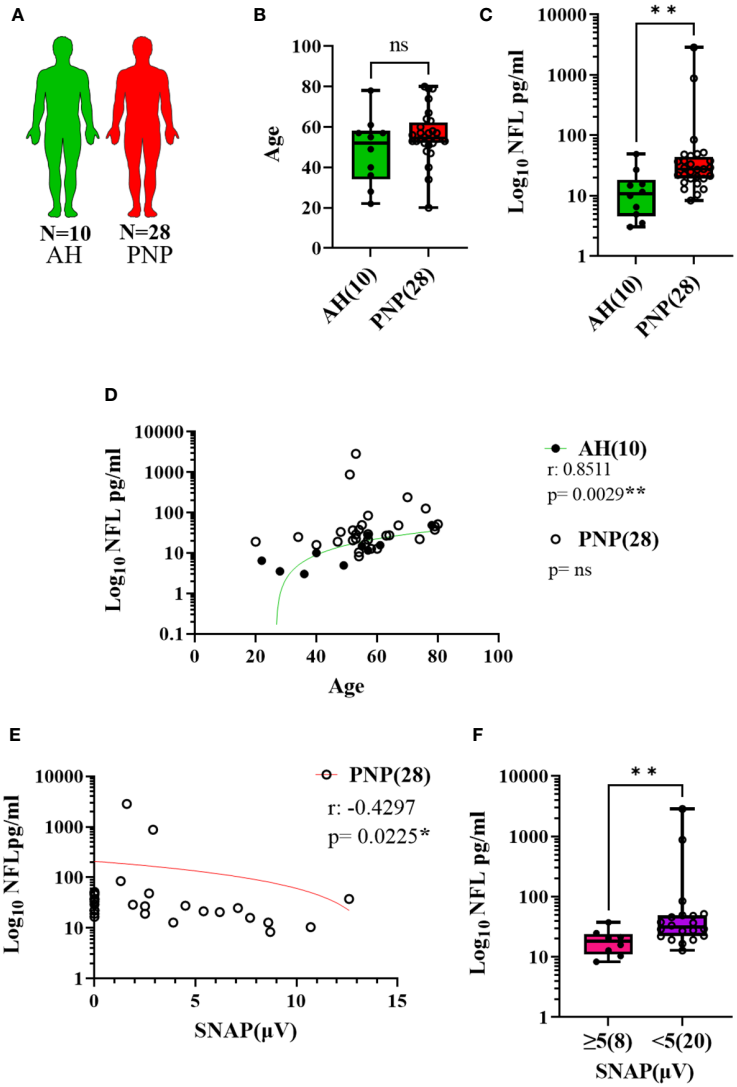

FIGURE 2
NFL levels in serum from patients with PNP. **(A)** Visual representation of the analyzed 10 AH (green) and 28 PNP patients (red). **(B)** Age values in AH and PNP. **(C)** Log 10 of NFL levels in pg/ml between AH and PNP. **(D)** Correlation between age and log 10 of NFL levels in pg/ml in AH and PNP. **(E)** Correlation between log10 of NFL levels in pg/ml and SNAP. **(F)** Log10 of NFL levels in pg/ml between PNP patients with normal (≥ 5µV) (pink) and abnormal (< 5µV) (purple) sural nerve SNAP. ns, not significant; *, $p < 0.05$; **, $p < 0.01$. All graphical images were incorporated from Smart Servier Medical Art, https://smart.servier.com/, under the Creative common Attribution 3.0 Unported Licence.

markers. CCL2 was specifically upregulated in PNP patients under analgesic treatment ($p < 0.05$, Figure 5B). No differences were discovered between the PNP subgroups inflammatory and non-inflammatory. On the other hand, patients with a painful PNP had higher levels of IL-10 in sera than those with no pain ($p < 0.01$, Figure 5C). A multivariate analysis showed that the levels of IL-10 positively correlated with the pain scores in NRS ($p < 0.01$), NPSI ($p < 0.05$) and GCPS ($p < 0.05$) (Figure 5D).

Analysis of the relation of proteins between sera and CSF in PNP patients

The proteins present in CSF, such as NFL or inflammatory components, may be intrathecally produced or have infiltrated from the blood vessels due to a permeabilization of the B-CSF barrier. In order to study the origin of NFL and cytokines in CSF, we compared the levels of albumin between CSF and serum (albumin ratio in CSF/in serum: Q_{Alb}) and divided the patients in subgroups according to the B-CSF barrier integrity: Normal B-CSF barrier integrity ($Q_{Alb} < 0.007$) and mild ($0.007 < Q_{Alb} < 0.01$), moderate ($0.01 < Q_{Alb} < 0.02$) and severe ($Q_{Alb} > 0.02$) B-CSF barrier dysfunction (Figure S1A) (41). Due to a low number of patients with severe B-CSF barrier dysfunction (2), moderate and severe groups were analyzed together. A moderate/severe B-CSF barrier dysfunction was present more often in inflammatory neuropathies than normal or mild dysfunction (Figure S1B). Furthermore, the albumin ratio (Q_{Alb}) correlated with the severity of the clinical phenotype (Figure S1C). As expected, the levels of total protein in CSF increased as the B-CSF barrier dysfunction became more severe (Figure S1D), thus indicating a higher permeabilization or a relation between an intrathecal production and a B-CSF barrier dysfunction.

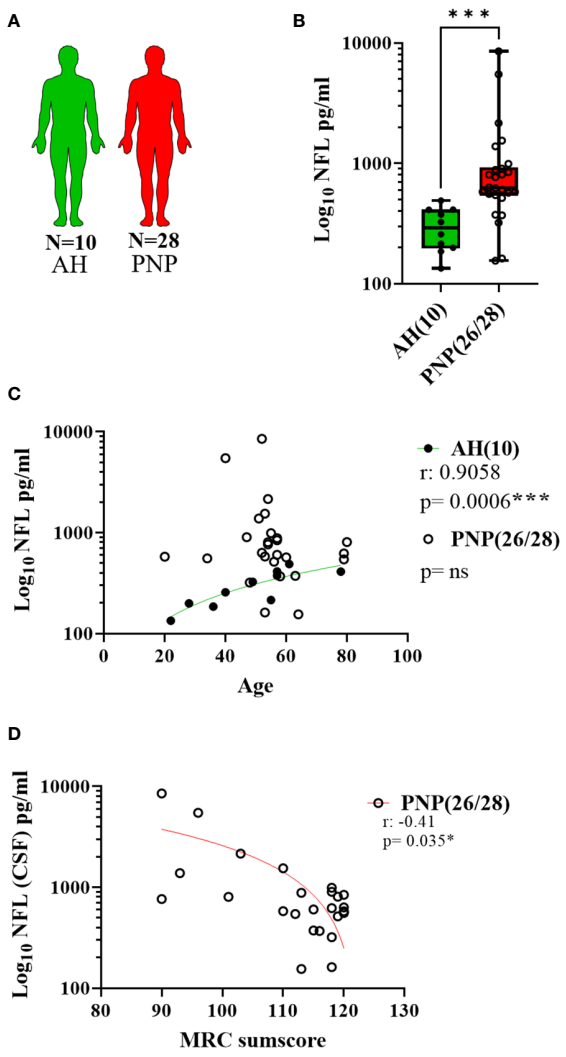

FIGURE 3
NFL levels in CSF from patients with PNP. **(A)** Visual representation of the analyzed 10 AH (green) and 28 PNP patients (red). **(B)** Log 10 of NFL levels in pg/ml between AH and PNP. **(C)** Correlation between age and log 10 of NFL levels in pg/ml in AH and PNP. **(D)** Correlation between the levels of NFL levels in pg/ml (Log10) and the MRC sumscore in PNP patients. ns, not significant; *, $p < 0.05$; ***, $p < 0.001$. All graphical images were incorporated from Smart Servier Medical Art, https://smart.servier.com/, under the Creative common Attribution 3.0 Unported Licence.

NFL measurements in serum and CSF in the different subgroups of twenty-eight PNP patients and ten AH (Figure 6A) showed higher levels in those patients with moderate/severe B-CSF barrier dysfunction in comparison to those with a normal B-CSF barrier integrity and to AH (Figures 6B, C). This resulted in a constant Q_{NFL} (NFL ratio in CSF/serum) among subgroups and between PNP and AH (Figure 6D). Furthermore, NFL in serum and CSF correlated positively with the severity of the clinical phenotype (Figure 6E), suggesting that the release of NFL might be a consequence of the severe neurodegeneration.

Interestingly, we found a correlation between the levels of NFL and IL-8 in CSF (Figure 6F), thus indicating a relation between neurodegeneration and inflammation. With this discovery, we decided to study the levels of cytokines between CSF and serum, in order to determine their origin, in the different subgroups of twenty-eight PNP patients and five UH (Figure 7A). This analysis showed that PNP patients with a moderate/severe B-CSF barrier dysfunction present higher levels of IL-6 and IL-8 in CSF and a higher $Q_{IL\text{-}6}$ and Q_{CCL2} (cytokine ratio in CSF/in serum), than those with a normal B-CSF barrier integrity (Figure 7B). A multivariate analysis showed that the levels of IL-6 in CSF correlated with the overall severity, thus indicating a relation between the production or release of IL-6 and severe PNP (Figure 7C). Interestingly, a second multivariate analysis showed that the levels of most cytokines analyzed in CSF correlated with each other (Figure 7D), therefore suggesting a common stimulus triggering their production, or their involvement in a common pathway

Acyl-carnitine levels in serum and CSF from PNP patients

In order to complete our study with the analysis of lipid compounds involved in pro-inflammatory pathways, we performed LC-MS to measure the levels of carnitine, palmitoylcarnitine and oleoylcarnitine in serum and CSF from twenty-three PNP patients and five UH (Figure 8A). While carnitine and palmitoylcarnitine in

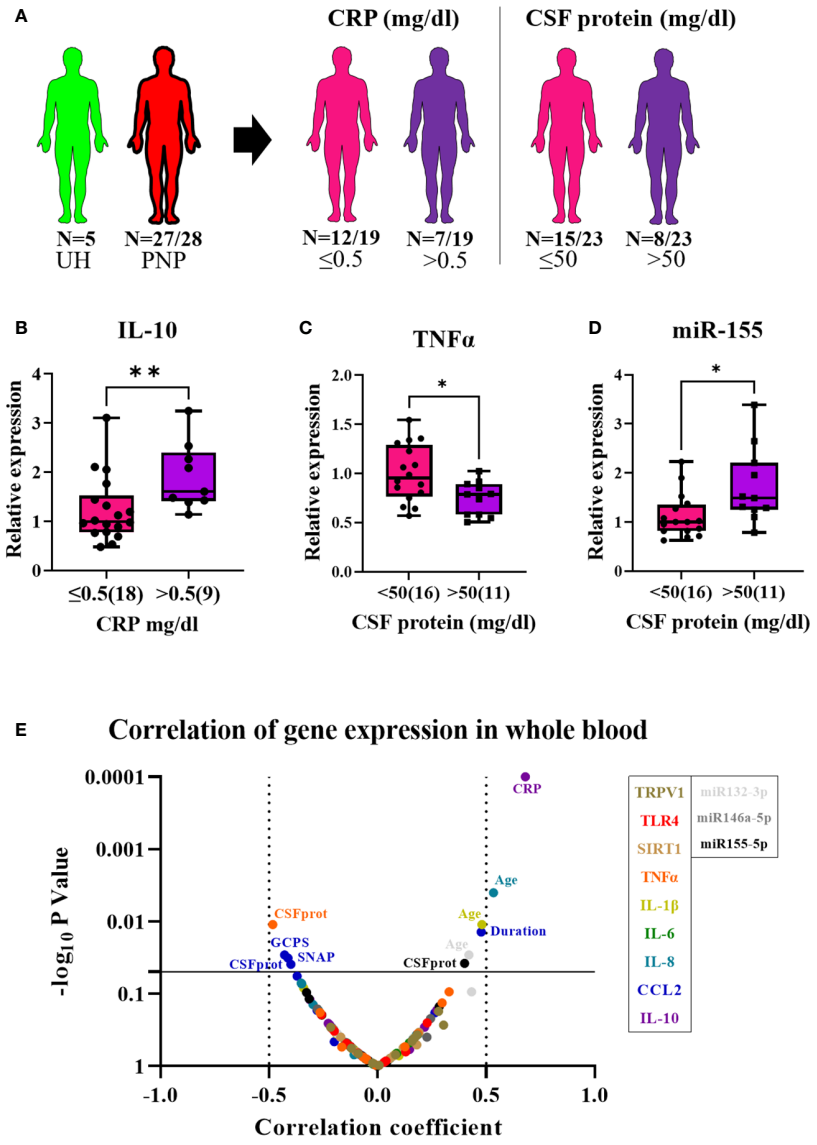

FIGURE 4
Relative gene expression of pro- and anti-inflammatory markers in whole blood from patients with PNP. **(A)** Visual representation of the analyzed 5 UH (light green) and 27 out of 28 PNP patients (red), further divided into 18 PNP patients with normal (≤0.5mg/dl, pink) and seven with increased (> 0.5 mg/dl, purple) CRP levels in serum, and into 16 PNP patients with normal (≤ 50 mg/dl, pink) and seven with abnormal (> 50 mg/dl, purple) protein levels in CSF. **(B)** Relative expression of IL-10 in PNP patients with increased CRP in comparison to those with normal values. Relative expression of TNFα **(C)** and miR-155 **(D)** in PNP patients with normal and abnormal protein levels in CSF. **(E)** Volcano plot of the Spearman multivariate correlations between each studied target and the neuropathy scores. *, $p < 0.05$; **, $p < 0.01$. All graphical images were incorporated from Smart Servier Medical Art, https://smart.servier.com/, under the Creative common Attribution 3.0 Unported Licence.

serum did not differ between PNP and UH, oleoylcarnitine was found in higher levels in patients with PNP in comparison to UH (Figure 8B). Carnitine was also not different in CSF between PNP patients and UH (Figure 8C). Palmitoylcarnitine and oleoylcarnitine were not detected in CSF samples (data not shown).

Our results also showed that PNP patients with high CSF protein (>50mg/dl) had higher levels of carnitine in CSF and a lower serum/CSF ratio than those with normal protein levels ($p < 0.001$) (Figure 8D).

Furthermore, we observed that the levels of palmitoylcarnitine and oleoylcarnitine in serum positively correlated in patients with PNP ($p < 0.0001$) and in UH ($p < 0.001$) (Figure 8E). Interestingly, a multivariate analysis found a positive correlation between the levels of carnitine in serum and the mTCNS ($p < 0.001$) as well as between the levels of carnitine in serum and the overall severity (Figure 8F).

Discussion

In this study, we investigated the gene expression, protein and lipid levels of different pro-inflammatory markers in blood and CSF from patients with PNP, in comparison to a control group of patients with acute headaches of unclear etiology.

Our results showed that, contrary to our initial hypothesis of PNP being associated with enhanced systemic inflammation, PNP patients and disease controls did not present major differences in systemic

10.3389/fimmu.2023.1067714

TABLE 5 Fold change of the gene expression of pro- and anti-inflammatory markers in whole blood from patients with PNP, in comparison to UH.

Item	PNP (Entire cohort)	Painful PNP	Painless PNP	Inflammatory PNP	Non-inflammatory PNP	UH
N	27	13	14	9	18	5
Mean (± SD)						
TRPV1	1.04 (± 0.24)	1.08 (± 0.11)	1.09 (± 0.14)	1.08 (± 0.10)	1.085 (± 0.13)	1.00 (± 0.17)
TLR4	1.02 (± 0.34)	1.06 (± 0.41)	0.97 (± 0.26)	1.05 (± 0.56)	1.00 (± 0.24)	1.00 (± 0.58)
SIRT1	0.91 (± 0.13)	0.92 (± 0.13)	0.90 (± 0.16)	0.86 (± 0.10)	0.93 (± 0.15)	1.00 (± 0.09)
TNFα	1.14 (± 0.35)	1.28 (± 0.25)	1.20 (± 0.43)	1.06 (± 0.23)	1.30 (± 0.37)	1.00 (± 0.36)
IL-1β	1.08 (± 0.28)	0.98 (± 0.32)	1.15 (± 0.29)	0.83 (± 0.14)	1.20 (± 0.30)	1.00 (± 0.45)
IL-6	0.79 (± 0.37)	0.62 (± 0.30)	0.78 (± 0.34)	0.68 (± 0.48)	0.72 (± 0.28)	1.00 (± 0.50)
IL-8	1.35 (± 0.99)	1.03 (0.50)	1.76 (± 0.43)	0.88 (± 0.45)	1.67 (± 1.29)	1.00 (± 0.49)
CCL2	0.80 (± 0.64)	0.69 (± 0.29)	1.24 (± 0.89)	0.60 (± 0.29)	1.17 (± 0.80)	1.00 (± 0.36)
IL-10	0.88 (± 0.48)	0.94 (± 0.49)	0.92 (± 0.56)	0.84 (± 0.53)	0.97 (± 0.52)	1.00 (± 0.33)
miR146	1.02 (± 0.31)	0.94 (± 0.29)	1.02 (± 0.30)	1.07 (± 0.37)	0.96 (± 0.27)	1.00 (± 0.27)
miR132	1.00 (± 0.33)	0.84 (± 0.21)	0.93 (± 0.38)	0.87 (± 0.27)	0.89 (± 0.33)	1.00 (± 0.29)
miR155	1.19 (± 0.57)	0.82 (± 0.21)	1.08 (± 0.42)	0.88 (± 0.22)	0.98 (± 0.40)	1.00 (0.27)

TRPV1, transient receptor potential cation channel subfamily V member 1; TLR4, toll-like receptor 4; SIRT1, sirtuin 1; TNFα, tumour necrosis factor α; IL, interleukin; CCL2, CC-chemokine ligand 2; TBP, TATA-Box binding protein; miR, microRNA, rRNA, ribosomalRNA.

inflammatory markers. Receptors of great interest in the fields of inflammation and pain, TLR4 and TRPV1, were not informative in our cohort. While only CCL2 and oleoylcarnitine were present in higher levels in sera from PNP patients than in controls, the levels of CCL2 were associated to pain treatment.

Oleoylcarnitine, as one of the long-chain acylcarnitines found upstream of the synthesis of prostaglandins and thromboxanes, has been described upregulated in patients with systemic inflammation, as well as in different neuronal tissues in models of neurodegeneration (20, 22, 24). This suggests that the levels of oleoylcarnitine indicate an inflammatory process or neurodegeneration taking place in patients with PNP. Since it did not correlate with any neuropathy scores, we postulate that oleoylcarnitine is upregulated in all patients with PNP, and it might be of interest to explore as a potential early diagnostic marker in larger groups of different types of PNP versus controls.

Secondly, we hypothesized that a systemic inflammation may correlate with the severity of the disease and the development of neuropathic pain. Our study showed that IL-10 was the only inflammatory mediator consistently upregulated at the gene and protein level in patients with severe pain, in comparison to those without pain. IL-10 is understood as an anti-inflammatory cytokine, mainly produced by anti-inflammatory macrophages, and secreted to suppress pro-inflammatory responses and maintain tissue homeostasis (42). In patients with different neuropathies, levels of IL-10 have been described downregulated in serum and CSF and negatively correlating with pain scores, therefore suggesting an increased systemic inflammation (26–30). Our study, on the other hand, showed a positive correlation between IL-10 and CRP, confirming the involvement of IL-10 in inflammatory responses, potentially in a counter-regulatory function. Our results are in accordance with previous studies where higher levels of IL-10 were reported in serum from patients with neuropathies (27, 43, 44). This suggests that the higher expression of IL-10 might act as a compensatory mechanism against the inflammation triggered by neuropathy-specific processes. However, high levels of IL-10 as well as of IL-10 expressing blood mononuclear cells have been found related to large nerve fiber sensory and motor axonal damage, as well as motor nerve demyelination (28, 45). Therefore, we cannot exclude the option that the overexpression of IL-10 might also play a direct role in the pathogenesis of nerve fiber damage

Severe neuropathy indicated by a low SNAP correlated with high gene expression of CCL2. CCL2 and its receptor CCR2 can cause hyperalgesia through the upregulation of cation channels (46–48). In addition, CCL2, also named monocyte chemoattractant protein-1 (MCP-1), is directly involved in the migration and infiltration of monocytes, memory T lymphocytes, and natural killer (NK) cells, therefore also promoting local inflammatory processes (49). High systemic levels of CCL2 might thus correlate with the development of neuropathic symptoms and could serve as a severity marker of the neuropathy. Furthermore, the high levels of CCL2 might also be due to the treatment of pain as previously mentioned. More specifically, PNP patients with the highest levels of CCL2 were those that had been treated with opioids. This could either be indicate of a molecular interaction or simply support that severe neuropathy is more likely to be painful and therefore being properly treated. Kaminski et al. provided evidence for a molecular interaction because inhibition of opioid receptors led to a downregulation of CCL2 (50). On the other hand, high levels of CCL2 can inhibit the activation of opioid receptors, thus attenuating analgesia (51, 52). This suggests that the high CCL2 levels might be a compensatory effect from the opioid treatment. Further studies need to elucidate the role of CCL2 in the development of PNP and its symptoms.

Interestingly, we found that patients with a severe B-CSF barrier dysfunction, determined by the CSF/serum albumin ratio (41), also presented higher levels of NFL in serum and CSF, as well as higher levels of IL-6 and IL-8 in CSF. NFL constitutes one of the subunits of

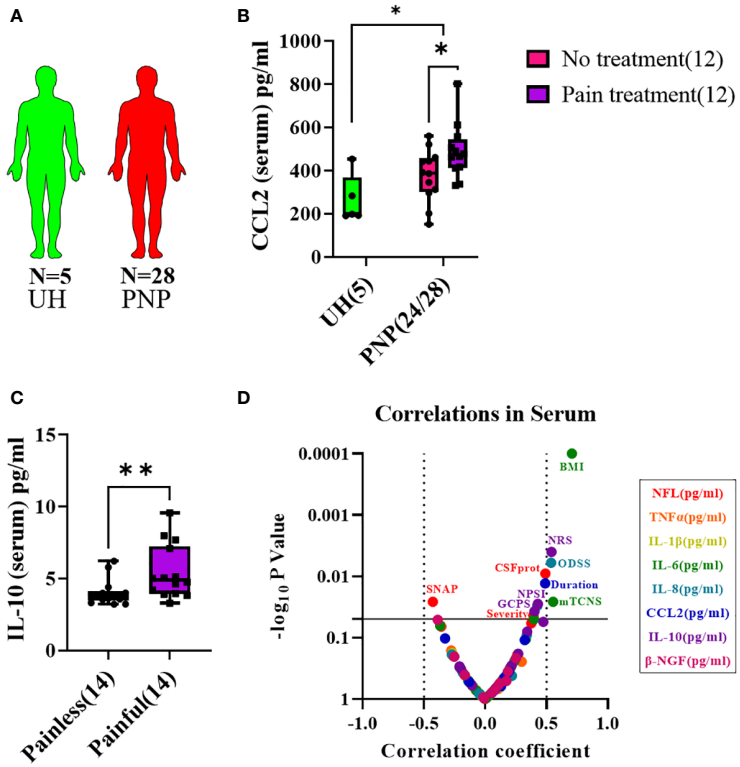

FIGURE 5
Cytokine levels in serum from patients with PNP. **(A)** Visual representation of the analyzed 5 UH (light green) and 28 PNP patients (red). **(B)** CCL2 levels in pg/ml in serum from UH and PNP patients, further divided between those without (pink) and with pain treatment (purple). **(C)** IL-10 levels in pg/ml in serum from PNP patients with painless (pink) and painful (purple) neuropathies. **(D)** Volcano plot of the Spearman multivariate correlations between each studied target and the neuropathy scores. *, $p < 0.05$; **, $p < 0.01$. All graphical images were incorporated from Smart Servier Medical Art, https://smart.servier.com/, under the Creative common Attribution 3.0 Unported Licence.

TABLE 6 Cytokine levels in serum and CSF from patients with PNP and UH.

Item	PNP (Entire cohort)	Painful PNP	Painless PNP	Inflammatory PNP	Non-inflammatory PNP	UH
N	28	14	14	9	19	5
Median findings in serum (range)						
TNFα pg/ml	9.71 (6.33-86.30)	9.87 (8.58-13.60)	9.39 (6.33-86.30)	9.77 (8.64-86.30)	9.64 (6.33-20.70)	6.78 (6.04-23.20)
IL-1β pg/ml	0.27 (0.04-0.61)	0.29 (0.04-0.50)	0.23 (0.12-0.61)	0.31 (0.09-0.58)	0.27 (0.04-0.61)	0.19 (0.05-0.54)
IL-6 pg/ml	2.94 (1.10-10.09)	3.05 (1.10-10.09	2.90 (1.27-5.87)	2.37 (1.10-10.09)	2.94 (1.12-9.36)	1.36 (0.51-3.48)
IL-8 pg/ml	12.60 (5.48-62.40)	14.80 (8.12-41.20)	12.50 (5.48-62.40)	12.60 (8.12-22.0)	13.00 (5.48-62.40)	9.380 (6.72-13.70)
CCL2 pg/ml	442.0* (151.0-802.0)	464.5 (201.0-802.0)	411.0 (151.0-560.0)	417.0 (201.0-611.0)	443.0 (151.0-802.0)	198.0 (190.0-454.0)
IL-10 pg/ml	4.00 (3.22-9.57)	4.89## (3.29-9.57)	3.79 (3.22-6.22)	4.40 (3.22-7.69)	3.99 (3.23-9.57)	3.06 (2.63-12.50)
NGF-β pg/ml	4.28 (2.17-9.49)	4.58 (2.92-8.32)	3.89 (2.17-9.49)	3.53 (2.39-5.03)	4.50 (2.17-9.49)	3.34 (2.66-5.00)
Median findings in CSF (range)						
IL-6 pg/ml	3.32 (1.23-27.60)	3.79 (1.66-11.80)	2.81 (1.23-27.60)	5.19 (1.82-27.60)	3.21 (1.23-11.90)	5.37 (1.40-23.00)

(Continued)

TABLE 6 Continued

Item	PNP (Entire cohort)	Painful PNP	Painless PNP	Inflammatory PNP	Non-inflammatory PNP	UH
N	28	14	14	9	19	5
IL-8 pg/ml	42.25 (14.70-180.0)	40.35 (19.40-180.0)	45.45 (14.70-124.0)	44.60 (19.40-180.0)	39.40 (14.70-124.0)	32.20 (21.80-117.0)
CCL2 pg/ml	415.5 (169.0-937.0)	359.0 (260.0-937.0)	422.5 (169.0-829.0)	411.0 (260.0-937.0)	414.0 (169.0-767.0)	271.0 (222.0-672.0)
CX3CL1 pg/ml	261.5 (89.70-500.0)	218.0 (104.0-500.0)	282.0 (89.7-444.0)	253.0 (104.0-397.0)	272.0 (89.70-500.0)	223.0 (138.0-247.0)

TNFα, Tumor necrosis factor alpha; IL, Interleukin; CCL2, CC-chemokine ligand 2, NGF-β, nerve growth factor beta; Cx3CL1, fractalkine or C-X3-C motif chemokine 1. Kruskal-Wallis or T-test was performed between PNP and UH (*), painful and painless PNP (#) and inflammatory and non-inflammatory PNP.
*, $p < 0.05$; ##, $p < 0.01$.

the neurofilament that forms the cytoskeleton in neurons. Neurofilaments are especially abundant in large myelinated axons, while relatively scarce in dendrites, and their release has been described as a marker of neurodegeneration or upon neuroaxonal damage (36, 53–59). As expected, NFL levels in CSF and serum of our PNP group were increased in comparison to the controls, indicating neurodegeneration. This increase seemed to be present especially in those PNP patients with B-CSF barrier dysfunction, both in serum and CSF, while no difference was found in PNP patients with a normal B-CSF barrier and controls. The correlation we found between the albumin ratio (Q_{Alb}) and the severity of the neuropathy may indicate that patients with a moderate to severe B-CSF barrier dysfunction also present more severe neuropathy and thus, more neurodegeneration, explaining the higher levels of NFL in these patients. Furthermore, while a break of the B-CSF barrier would allow the exchange of proteins between serum and CSF, the levels of NFL were consistently higher in CSF than in sera, thus indicating an intrathecal production. Since we found higher NFL levels in serum

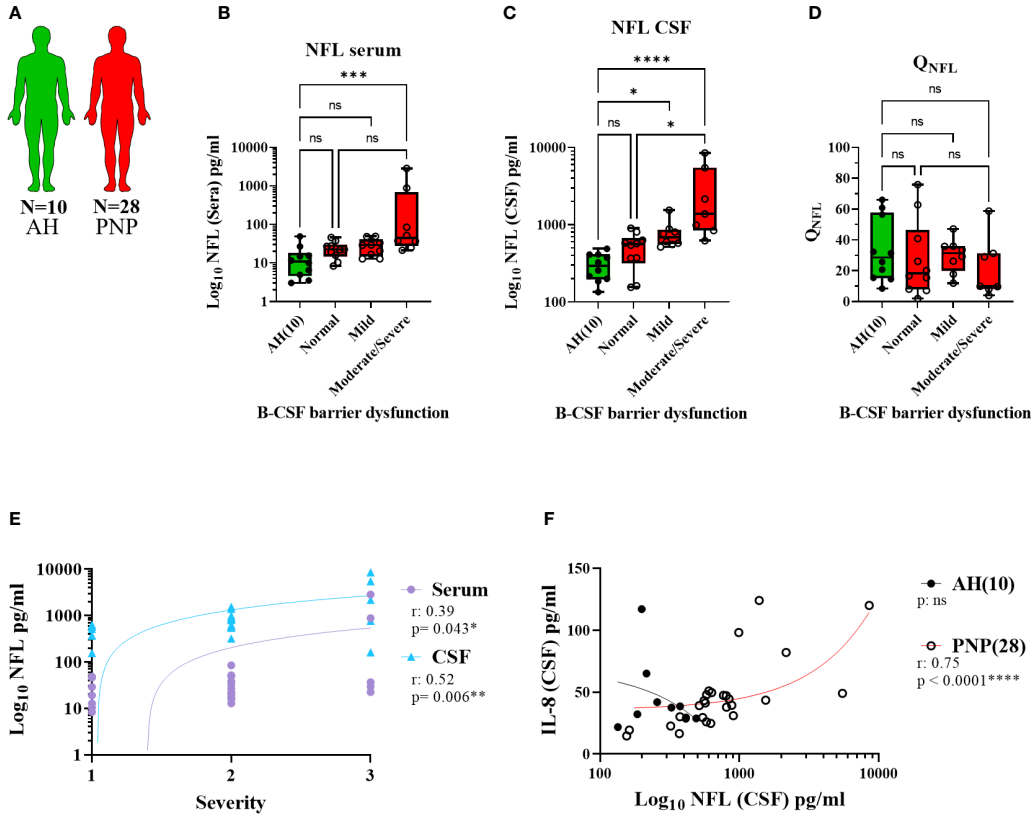

FIGURE 6
Levels of NFL between CSF and serum from patients with PNP. **(A)** Visual representation of the analyzed 5 AH (green) and 28 PNP patients (red). Levels of NFL in serum **(B)** and CSF **(C)** in patients with normal B-CSF barrier function, or mild, moderate and severe B-CSF barrier dysfunction. **(D)**. NFL ratio between CSF and serum (Q_{NFL}) in AH and the subgroups of PNP patients according to their B-CSF barrier dysfunction. **(E)** Correlation between the levels of NFL in serum (●) and CSF (▲) and the subjective severity. **(F)** Correlations between the levels of IL-8 and NFL in CSF in pg/ml. ns, not significant; *, $p < 0.05$; **, $p < 0.01$; ***, $p < 0.001$; ****, $p < 0.0001$. All graphical images were incorporated from Smart Servier Medical Art, https://smart.servier.com/, under the Creative common Attribution 3.0 Unported Licence.

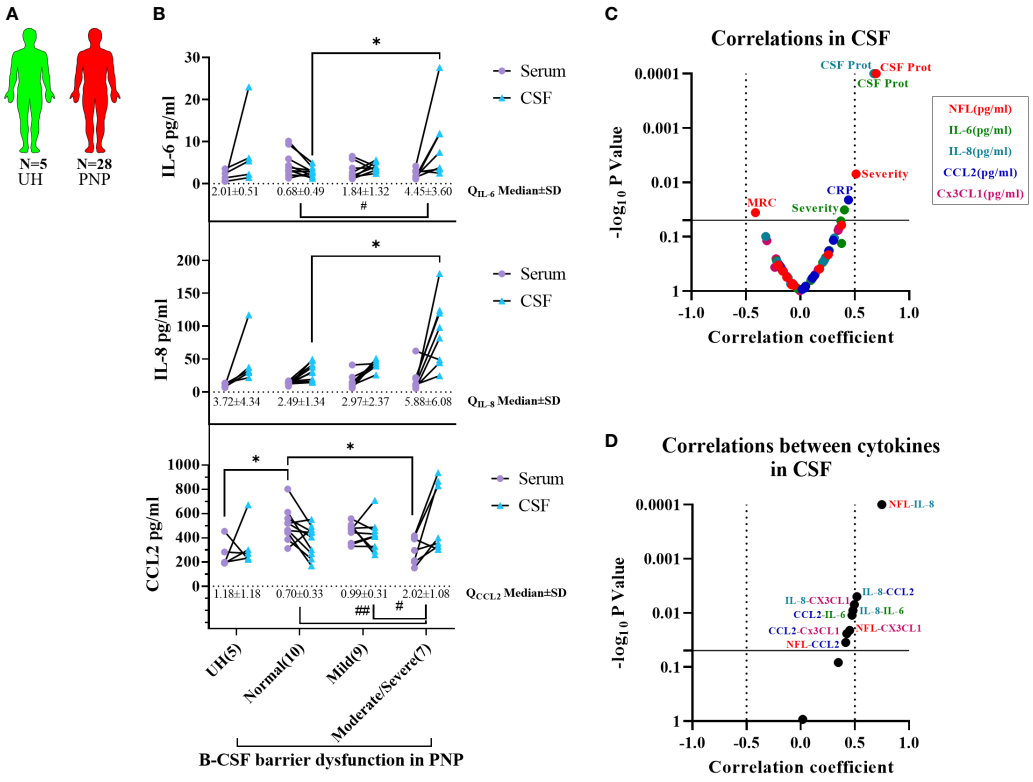

FIGURE 7
Comparison of cytokine levels between CSF and serum from patients with PNP. **(A)** Visual representation of the analyzed 5 UH (light green) and 28 PNP patients (red). **(B)** Levels of IL-6, IL-8 and CCL2 in serum (●) and CSF (▲) in patients with normal B-CSF barrier function, or mild, moderate and severe B-CSF barrier dysfunction. **(C)** Volcano plot of the Spearman multivariate correlations between each cytokine in CSF and the neuropathy scores **(C)**, and among each cytokine in CSF **(D)** */# $p < 0.05$; ##, $p < 0.01$. All graphical images were incorporated from Smart Servier Medical Art, https://smart.servier.com/, under the Creative common Attribution 3.0 Unported Licence.

related with a decreased SNAP, and in accordance with previous studies (59–62), we believe that in diseases of the PNS, NFL in serum could come from the degeneration of peripheral axons. Since the prognosis of a neuropathy is often uncertain in an individual patient, NFL in serum could be used prospectively to monitor progress and eventually to detect unexpected accelerations of the progression. In CSF, on the other hand, differences in the levels of NFL in peripheral neuropathies have yet to be explained. In 2018, Axelsson et al. described for the first time higher NFL levels in CSF in patients with Guillain-Barré syndrome (GBS), a neuropathy of the PNS, than in controls. This increase was postulated to be due to axonal damage of nerve roots, which are surrounded by CSF in the subarachnoid space of the spinal cord (63). This idea has been restated in a more recent study in acute and chronic inflammatory polyneuropathies (57). Later in 2018, similar levels of NFL were found in CSF by Mariotto et al. in a cohort of acquired peripheral neuropathies. This study, however, discusses a possible ongoing axonal damage in both the CNS and PNS, and that the levels of NFL might be affected by a disrupted blood nerve barrier (64). Following the idea raised by Axelsson et al., we postulate that neurodegeneration takes place at the nerve roots, which constitute the very beginning of the PNS, leading to the intrathecal release of NFL. Recent studies have also found a lowered NFL CSF/Serum ratio in patients with peripheral neuropathies, therefore proposing peripheral axonal damage contributing to higher levels of NFL in serum (64, 65). Our results showed a constant CSF/serum ratio among PNP subgroups and controls, suggesting a constant increment of NFL in both tissues and therefore neurodegeneration taking place at the nerve roots as well as in peripheral nerves.

Interestingly, patients with a severe B-CSF barrier dysfunction also presented higher levels of IL-6 and IL-8 in CSF, while the levels in sera remained constant, therefore causing an increment of their CSF/serum ratio. Since 1993, high levels of IL-6 and IL-8 have been reported in CSF of patients with GBS and CIDP. This study as well as more recent ones suggest a prominent intrathecal activation of cells of the monocyte/macrophage lineage, leading to the intrathecal production of the cytokines (66–68). Following a similar line of thought, we postulate that inflammation is present at the level of the nerve roots and leads to the release of pro-inflammatory cytokines directly to the CSF. Furthermore, this inflammation may cause neuronal damage and disruption of the axonal cell membrane, inducing the releases of NFL into the CSF compartment (69). The finding of a strong correlation between the levels of IL-8 and NFL in CSF supports this assumption and leads to the question whether they are simultaneously released from the same cell type, or whether they consecutively induce each other's release. Moreover, the levels of IL-6 in CSF correlated with the severity of neuropathy, thus indicating that the inflammation at the nerve roots might be the cause or consequence of the

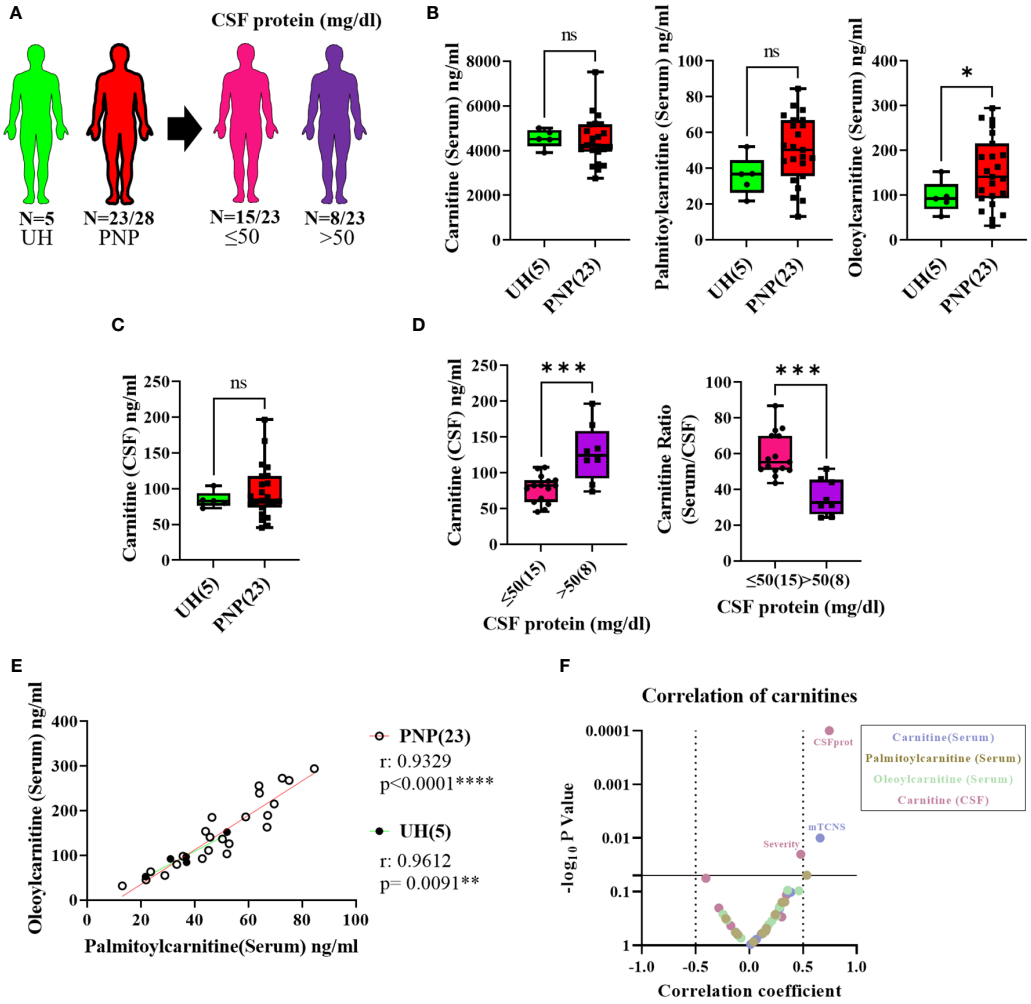

FIGURE 8
Levels of pro-inflammatory lipids in serum and CSF from patients with PNP. **(A)** Visual representation of the analyzed 5 UH (light green) and 23 out of 28 PNP patients (red), further divided into 15 PNP patients with normal (≤ 50 mg/dl) (pink) and 8 with an abnormal (> 50 mg/dl) (purple) CSF total protein. **(B)** Levels of carnitine, palmitoylcarnitine and oleoylcarnitine in ng/ml in serum from UH and PNP patients. **(C)** Levels of carnitine in ng/ml in CSF from UH and PNP patients. **(D)** Levels of carnitine in ng/ml in CSF (left) and its ratio (serum/CSF) (right) in PNP patients with normal and abnormal CSF total protein. Correlations can be found between oleoylcarnitine and palmitoylcarnitine (ng/ml) in serum from UH and PNP patients **(E)**. **(F)** Volcano plot of the Spearman multivariate correlations between each carnitine and the neuropathy scores. * $p < 0.05$; **, $p < 0.01$; ***, $p < 0.001$; ****, $p < 0.0001$. All graphical images were incorporated from Smart Servier Medical Art, https://smart.servier.com/, under the Creative common Attribution 3.0 Unported Licence.

neurodegeneration. This would indicate that patients with more severe neuropathic symptoms would present an affection of the nerve roots and a break of the B-CSF barrier, supporting the importance of CSF analysis as a diagnostic tool for patients with PNP (70). Being an invasive procedure, lumbar puncture to obtain CSF is not without risks, and patients need to sign informed consent, however, the risk of headache, the most frequent adverse effect of lumbar puncture, can be markedly reduced by that use of an atraumatic needle (71). Other adverse effects are extremely rare when the lumbar puncture is properly performed.

Although our study includes the analysis of a large number of pro- and anti-inflammatory markers, non-biased omics-based analysis might be necessary to identify all involved markers and elucidate the specific pathways taking place in PNP. Furthermore, our results are limited by the very well characterized but low number of recruited patients and the variance in etiologies. A larger cohort might help separating the patients into males and females and into diagnostic subgroups that could lead to clearer results.

We conclude that in patients with PNP systemic inflammatory markers in blood or CSF do not differ from controls in general, but specific cytokines or lipids do. Nevertheless, we found several indications of a correlation between inflammation and the neuropathy severity and symptoms. In particular, we described a strong interaction between inflammation and neurodegeneration at the nerve roots in a specific subgroup of PNP patients with B-CSF barrier dysfunction, which highlights the importance of CSF analysis in patients with peripheral neuropathies. We believe that the diagnostic marker panel provided in our study may help improving patient stratification not only to increase diagnostic validity, but also to guide treatment decisions.

Data availability statement

The original contributions presented in the study are included in the article/Supplementary Material. Further inquiries can be directed to the corresponding author.

Ethics statement

The studies involving human participants were reviewed and approved by Würzburg Medical Faculty Ethics Committee (# 15/19 and # 242/17). The patients/participants provided their written informed consent to participate in this study.

Author contributions

PG-F, NÜ and CS contributed to conception and design of the study. AR performed the gene expression analysis. KH and NC performed the protein analysis. KS and AN performed the lipid analysis. KH, NC, A-KR, HR, NÜ and CS contributed to recruitment of patients and collection of clinical data. A-KR and HR provided samples from healthy controls. PG-F organized the database and performed the statistical analysis. PG-F wrote the first draft of the manuscript. KS and AN wrote a section of the manuscript. All authors contributed to the article and approved the submitted version.

Funding

This project has received funding from the European Union's Horizon 2020 research and innovation programme under the Marie Skłodowska-Curie Grant Agreement No. 764860. This publication was supported by the Open Access Publication Fund of the University of Würzburg

Acknowledgments

The authors thank Sonja Gommersbach for her skillful technical assistance and Christoph Erbacher, MSc for his advice on data analysis and figures.

Conflict of interest

Author CS has been a consultant for Merz, Omega, Ipsen and Bayer on the subject of neuropathic pain. She has given educational talks for GSK and Pfizer. Authors KS and AN are employed by Bionorica research GmbH.

The remaining authors declare that the research was conducted in the absence of any commercial or financial relationships that could be construed as a potential conflict of interest.

Publisher's note

All claims expressed in this article are solely those of the authors and do not necessarily represent those of their affiliated organizations, or those of the publisher, the editors and the reviewers. Any product that may be evaluated in this article, or claim that may be made by its manufacturer, is not guaranteed or endorsed by the publisher.

Supplementary material

The Supplementary Material for this article can be found online at: https://www.frontiersin.org/articles/10.3389/fimmu.2023.1067714/full#supplementary-material

References

1. JA R. General approach to peripheral nerve disorders. *Am Acad Neurology. Continuum (Minneap Minn)* (2017) 23:1241–62. doi: 10.1212/CON.0000000000000519

2. Finnerup NB, Attal N, Haroutounian S, McNicol E, Baron R, Dworkin RH, et al. Pharmacotherapy for neuropathic pain in adults: a systematic review and meta-analysis. *Lancet Neurol* (2015) 14(2):162–73. doi: 10.1016/S1474-4422(14)70251-0

3. Cavalli E, Mammana S, Nicoletti F, Bramanti P, Mazzon E. The neuropathic pain: An overview of the current treatment and future therapeutic approaches. *Int J Immunopathol Pharmacol* (2019) 33:2058738419838383. doi: 10.1177/2058738419838383

4. Tavee JO. Immune axonal polyneuropathy. *Am Acad Neurology. Continuum (Minneap Minn)* (2017) 23:1394–410. doi: 10.1212/CON.0000000000000523

5. Sommer C, Leinders M, Üçeyler N. Inflammation in the pathophysiology of neuropathic pain. *Pain* (2018) 159(3):595–602. doi: 10.1097/j.pain.0000000000001122

6. Fakhoury M. Immune-mediated processes in neurodegeneration: where do we stand? *J Neurol* (2016) 263(9):1683–701. doi: 10.1007/s00415-016-8052-0

7. Grace PM, Hutchinson MR, Maier SF, Watkins LR. Pathological pain and the neuroimmune interface. *Nat Rev Immunol* (2014) 14(4):217–31. doi: 10.1038/nri3621

8. Liu T, Zhang L, Joo D, Sun SC. NF-kappaB signaling in inflammation. *Signal Transduct Target Ther* (2017) 2. doi: 10.1038/sigtrans.2017.23

9. Kauppinen A, Suuronen T, Ojala J, Kaarniranta K, Salminen A. Antagonistic crosstalk between NF-kappaB and SIRT1 in the regulation of inflammation and metabolic disorders. *Cell Signal* (2013) 25(10):1939–48. doi: 10.1016/j.cellsig.2013.06.007

10. Liu W, Jiang L, Bian C, Liang Y, Xing R, Yishakea M, et al. Role of CX3CL1 in diseases. *Arch Immunol Ther Exp (Warsz)* (2016) 64(5):371–83. doi: 10.1007/s00005-016-0395-9

11. Bali KK, Gandla J, Rangel DR, Castaldi L, Mouritzen P, Agarwal N, et al. A genome-wide screen reveals microRNAs in peripheral sensory neurons driving painful diabetic neuropathy. *Pain* (2021) 162(5):1334–51. doi: 10.1097/j.pain.0000000000002159

12. Leinders M, Üçeyler N, Pritchard RA, Sommer C, Sorkin LS. Increased miR-132-3p expression is associated with chronic neuropathic pain. *Exp Neurol* (2016) 283(Pt A):276–86. doi: 10.1016/j.expneurol.2016.06.025

13. Leinders M, Üçeyler N, Thomann A, Sommer C. Aberrant microRNA expression in patients with painful peripheral neuropathies. *J Neurol Sci* (2017) 380:242–9. doi: 10.1016/j.jns.2017.07.041

14. Juzwik CA, S SD, Zhang Y, Paradis-Isler N, Sylvester A, Amar-Zifkin A, et al. microRNA dysregulation in neurodegenerative diseases: A systematic review. *Prog Neurobiol* (2019) 182:101664. doi: 10.1016/j.pneurobio.2019.101664

15. Hoeijmakers JG, Faber CG, Merkies IS, Waxman SG. Painful peripheral neuropathy and sodium channel mutations. *Neurosci Lett* (2015) 596:51–9. doi: 10.1016/j.neulet.2014.12.056

16. Parenti A, De Logu F, Geppetti P, Benemei S. What is the evidence for the role of TRP channels in inflammatory and immune cells? *Br J Pharmacol* (2016) 173(6):953–69. doi: 10.1111/bph.13392

17. Cakir M, Sacmaci H, Sabah-Ozcan S. Selected transient receptor potential channel genes' expression in peripheral blood mononuclear cells of multiple sclerosis. *Hum Exp Toxicol* (2021) 40(12_suppl):S406–13. doi: 10.1177/09603271211043476

18. Ito S, Okuda-Ashitaka E, Minami T. Central and peripheral roles of prostaglandins in pain and their interactions with novel neuropeptides nociceptin and nocistatin. *Neurosci Res* (2001) 41(4):299–332. doi: 10.1016/S0168-0102(01)00289-9

19. Hu W, Mathey E, Hartung HP, Kieseier BC. Cyclo-oxygenases and prostaglandins in acute inflammatory demyelination of the peripheral nerve. *Neurology* (2003) 61 (12):1774–9. doi: 10.1212/01.WNL.0000098884.75756.4D

20. To KK, Lee KC, Wong SS, Lo KC, Lui YM, Jahan AS, et al. Lipid mediators of inflammation as novel plasma biomarkers to identify patients with bacteremia. *J Infect* (2015) 70(5):433–44. doi: 10.1016/j.jinf.2015.02.011

21. Maroon JC, Bost JW, Borden MK, Lorenz KM, Ross NA. Natural antiinflammatory agents for pain relief in athletes. *Neurosurg Focus* (2006) 21(4):E11. doi: 10.3171/foc.2006.21.4.12

22. McGill MR, Li F, Sharpe MR, Williams CD, Curry SC, Ma X, et al. Circulating acylcarnitines as biomarkers of mitochondrial dysfunction after acetaminophen overdose in mice and humans. *Arch Toxicol* (2014) 88(2):391–401. doi: 10.1007/s00204-013-1118-1

23. Viader A, Sasaki Y, Kim S, Strickland A, Workman CS, Yang K, et al. Aberrant schwann cell lipid metabolism linked to mitochondrial deficits leads to axon degeneration and neuropathy. *Neuron* (2013) 77(5):886–98. doi: 10.1016/j.neuron.2013.01.012

24. Quanico J, Hauberg-Lotte L, Devaux S, Laouby Z, Meriaux C, Raffo-Romero A, et al. 3D MALDI mass spectrometry imaging reveals specific localization of long-chain acylcarnitines within a 10-day time window of spinal cord injury. *Sci Rep* (2018) 8 (1):16083. doi: 10.1038/s41598-018-34518-0

25. Üçeyler N, Riediger N, Kafke W, Sommer C. Differential gene expression of cytokines and neurotrophic factors in nerve and skin of patients with peripheral neuropathies. *J Neurol* (2015) 262(1):203–12. doi: 10.1007/s00415-014-7556-8

26. Andrade P, Cornips EMJ, Sommer C, Daemen MA, Visser-Vandewalle V, Hoogland G. Elevated inflammatory cytokine expression in CSF from patients with symptomatic thoracic disc herniation correlates with increased pain scores. *Spine J* (2018) 18(12):2316–22. doi: 10.1016/j.spinee.2018.07.023

27. Stork ACJ, Rijkers GT, Vlam L, Cats EA, de Jong BAW, Fritsch-Stork RDE, et al. Serum cytokine patterns in immunoglobulin m monoclonal gammopathy-associated polyneuropathy. *Muscle Nerve* (2019) 59(6):694–8. doi: 10.1002/mus.26462

28. Magrinelli F, Briani C, Romano M, Ruggero S, Toffanin E, Triolo G, et al. The association between serum cytokines and damage to Large and small nerve fibers in diabetic peripheral neuropathy. *J Diabetes Res 2015* (2015) p:547834. doi: 10.1155/2015/547834

29. Beppu M, Sawai S, Misawa S, Sogawa K, Mori M, Ishige T, et al. Serum cytokine and chemokine profiles in patients with chronic inflammatory demyelinating polyneuropathy. *J Neuroimmunol* (2015) 279:7–10. doi: 10.1016/j.jneuroim.2014.12.017

30. Baka P, Escolano-Lozano F, Birklein F. Systemic inflammatory biomarkers in painful diabetic neuropathy. *J Diabetes Complications* (2021) 35(10):108017. doi: 10.1016/j.jdiacomp.2021.108017

31. Purohit S, Tran PMH, Tran LKH, Satter KB, He M, Zhi Wb , et al. Serum levels of inflammatory proteins are associated with peripheral neuropathy in a cross-sectional type-1 diabetes cohort. *Front Immunol* (2021) 12:654233. doi: 10.3389/fimmu.2021.654233

32. Redzic Z. Molecular biology of the blood-brain and the blood-cerebrospinal fluid barriers: similarities and differences. *Fluids Barriers CNS* (2011) 8(1):3. doi: 10.1186/2045-8118-8-3

33. Puthenparampil M, Tomas-Ojer P, Hornemann T, Lutterotti A, Jelcic I, Ziegler M, et al. Altered CSF albumin quotient links peripheral inflammation and brain damage in MS. *Neurol Neuroimmunol Neuroinflamm* (2021) 8(2). doi: 10.1212/NXI.0000000000000951

34. Solar P, Zamani A, Kubickova L, Dubovy P, Joukal M. Choroid plexus and the blood-cerebrospinal fluid barrier in disease. *Fluids Barriers CNS* (2020) 17(1):35. doi: 10.1186/s12987-020-00196-2

35. Meixensberger S, Bechter K, Dersch R, Feige B, Maier S, Schiele MA, et al. Sex difference in cerebrospinal fluid/blood albumin quotients in patients with schizophreniform and affective psychosis. *Fluids Barriers CNS* (2020) 17(1):67. doi: 10.1186/s12987-020-00223-2

36. van Ballegoij WJC, van de Stadt SIW, Huffnagel IC, Kemp S, Willemse EAJ, Teunissen CE, et al. Plasma NfL and GFAP as biomarkers of spinal cord degeneration in adrenoleukodystrophy. *Ann Clin Transl Neurol* (2020) 7(11):2127–36. doi: 10.1002/acn3.51188

37. L.S. R. The CES-d scale: a self-report depression scale for research in the general population. *Appl Psychol Meas.* (1977) 1(3):385–401. doi: 10.1177/014662167700100306

38. Duale N, Lipkin WI, Briese T, Aarem J, Ronningen KS, Aas KK, et al. Long-term storage of blood RNA collected in RNA stabilizing tempus tubes in a large biobank–evaluation of RNA quality and stability. *BMC Res Notes* (2014) 7:633. doi: 10.1186/1756-0500-7-633

39. Aarem J, Brunborg G, Aas KK, Harbak K, Taipale MM, Magnus P, et al. Comparison of blood RNA isolation methods from samples stabilized in tempus tubes and stored at a large human biobank. *BMC Res Notes* (2016) 9(1):430. doi: 10.1186/s13104-016-2224-y

40. Barker PA, Mantyh P, Arendt-Nielsen L, Viktrup L, Tive L. Nerve growth factor signaling and its contribution to pain. *J Pain Res* (2020) 13:1223–41. doi: 10.2147/JPR.S247472

41. Csuka E, Morganti-Kossmann MC, Lenzlinger PM, Joller H, Trentz O, Kossmann T. IL-10 levels in cerebrospinal fluid and serum of patients with severe traumatic brain injury: relationship to IL-6, TNF-alpha, TGF-beta1 and blood-brain barrier function. *J Neuroimmunol* (1999) 101(2):211–21. doi: 10.1016/S0165-5728(99)00148-4

42. Ouyang W, Rutz S, Crellin NK, Valdez PA, Hymowitz SG. Regulation and functions of the IL-10 family of cytokines in inflammation and disease. *Annu Rev Immunol* (2011) 29:71–109. doi: 10.1146/annurev-immunol-031210-101312

43. Üçeyler N, Kafke W, Riediger N, He L, Necula G, Toyka KV, et al. Elevated proinflammatory cytokine expression in affected skin in small fiber neuropathy. *Neurology* (2010) 74(22):1806–13. doi: 10.1212/WNL.0b013e3181e0f7b3

44. Azevedo EP, Guimaraes-Costa AB, Bandeira-Melo C, Chimelli L, Waddington-Cruz M, Saraiva EM, et al. Inflammatory profiling of patients with familial amyloid polyneuropathy. *BMC Neurol* (2019) 19(1):146. doi: 10.1186/s12883-019-1369-4

45. Press R, Deretzi G, Zou LP, Zhu J, Fredman P, Lycke J, et al. IL-10 and IFN-gamma in Guillain-barre syndrome. network members of the Swedish epidemiological study group. *J Neuroimmunol* (2001) 112(1-2):129–38. doi: 10.1016/s0165-5728(00)00388-x

46. White FA, Wilson NM. Chemokines as pain mediators and modulators. *Curr Opin Anaesthesiol* (2008) 21(5):580–5. doi: 10.1097/ACO.0b013e32830eb69d

47. Dansereau MA, Midavaine E, Begin-Lavallee V, Belkouch M, Beaudet N, Longpre JM, et al. Mechanistic insights into the role of the chemokine CCL2/CCR2 axis in dorsal root ganglia to peripheral inflammation and pain hypersensitivity. *J Neuroinflamm* (2021) 18(1):79. doi: 10.1186/s12974-021-02125-y

48. Kao DJ, Li AH, Chen JC, Luo RS, Chen YL, Lu JC, et al. CC chemokine ligand 2 upregulates the current density and expression of TRPV1 channels and Nav1.8 sodium channels in dorsal root ganglion neurons. *J Neuroinflamm* (2012) 9:189. doi: 10.1186/1742-2094-9-189

49. Deshmane SL, Kremlev S, Amini S, Sawaya BE. Monocyte chemoattractant protein-1 (MCP-1): an overview. *J Interferon Cytokine Res* (2009) 29(6):313–26. doi: 10.1089/jir.2008.0027

50. Kaminsky DE, Rogers TJ. Suppression of CCL2/MCP-1 and CCL5/RANTES expression by nociceptin in human monocytes. *J Neuroimmune Pharmacol* (2008) 3 (2):75–82. doi: 10.1007/s11481-007-9086-y

51. Kwiatkowski K, Popiolek-Barczyk K, Piotrowska A, Rojewska E, Ciapala K, Makuch W, et al. Chemokines CCL2 and CCL7, but not CCL12, play a significant role in the development of pain-related behavior and opioid-induced analgesia. *Cytokine* (2019) 119:202–13. doi: 10.1016/j.cyto.2019.03.007

52. Heles M, Mrozkova P, Sulcova D, Adamek P, Spicarova D, Palecek J. Chemokine CCL2 prevents opioid-induced inhibition of nociceptive synaptic transmission in spinal cord dorsal horn. *J Neuroinflamm* (2021) 18(1):279. doi: 10.1186/s12974-021-02335-4

53. Mattsson N, Cullen NC, Andreasson U, Zetterberg H, Blennow K. Association between longitudinal plasma neurofilament light and neurodegeneration in patients with Alzheimer disease. *JAMA Neurol* (2019) 76(7):791–9. doi: 10.1001/jamaneurol.2019.0765

54. Preische O, Schultz SA, Apel A, Kuhle J, Kaeser SA, Barro C, et al. Serum neurofilament dynamics predicts neurodegeneration and clinical progression in presymptomatic alzheimer's disease. *Nat Med* (2019) 25(2):277–83. doi: 10.1038/s41591-018-0304-3

55. Backstrom D, Linder J, Jakobson Mo S, Riklund K, Zetterberg H, Blennow K, et al. NfL as a biomarker for neurodegeneration and survival in Parkinson disease. *Neurology* (2020) 95(7):e827–38. doi: 10.1212/WNL.0000000000010084

56. Graham NSN, Zimmerman KA, Moro F, Heslegrave A, Maillard SA, Bernini A, et al. Axonal marker neurofilament light predicts long-term outcomes and progressive neurodegeneration after traumatic brain injury. *Sci Transl Med* (2021) 13(613):eabg9922. doi: 10.1126/scitranslmed.abg9922

57. Kmezic I, Samuelsson K, Finn A, Upate Z, Blennow K, Zetterberg H, et al. Neurofilament light chain and total tau in the differential diagnosis and prognostic evaluation of acute and chronic inflammatory polyneuropathies. *Eur J Neurol* (2022) 29 (9):2810–22. doi: 10.1111/ene.15428

58. Yuan A, Rao MV, Veeranna Nixon RA. Neurofilaments and neurofilament proteins in health and disease. *Cold Spring Harb Perspect Biol* (2017) 9(4). doi: 10.1101/cshperspect.a018309

59. Huehnchen P, Schinke C, Bangemann N, Dordevic AD, Kern J, Maierhof SK, et al. Neurofilament proteins as a potential biomarker in chemotherapy-induced polyneuropathy. *JCI Insight* (2022) 7(6). doi: 10.1172/jci.insight.154395

60. Ticau S, Sridharan GV, Tsour S, Cantley WL, Chan A, Gilbert JA, et al. Neurofilament light chain as a biomarker of hereditary transthyretin-mediated amyloidosis. *Neurology* (2021) 96(3):e412–22. doi: 10.1212/WNL.0000000000011090

61. Hayashi T, Nukui T, Piao JL, Sugimoto T, Anada R, Matsuda N, et al. Serum neurofilament light chain in chronic inflammatory demyelinating polyneuropathy. *Brain Behav* (2021) 11(5):e02084. doi: 10.1002/brb3.2084

62. Millere E, Rots D, Simren J, Ashton NJ, Kupats E, Micule I, et al. Plasma neurofilament light chain as a potential biomarker in charcot-Marie-Tooth disease. *Eur J Neurol* (2021) 28(3):974–81. doi: 10.1111/ene.14689

63. Axelsson M, Sjogren M, Andersen O, Blennow K, Zetterberg H, Lycke J. Neurofilament light protein levels in cerebrospinal fluid predict long-term disability of Guillain-barre syndrome: A pilot study. *Acta Neurol Scand* (2018) 138(2):143–50. doi: 10.1111/ane.12927

64. Mariotto S, Farinazzo A, Magliozzi R, Alberti D, Monaco S, Ferrari S. Serum and cerebrospinal neurofilament light chain levels in patients with acquired peripheral neuropathies. *J Peripher Nerv Syst* (2018) 23(3):174–7. doi: 10.1111/jns.12279

65. Kortvelyessy P, Kuhle J, Duzel E, Vielhaber S, Schmidt C, Heinius A, et al. Ratio and index of neurofilament light chain indicate its origin in Guillain-barre syndrome. *Ann Clin Transl Neurol* (2020) 7(11):2213–20. doi: 10.1002/acn3.51207

66. Maimone D, Annunziata P, Simone IL, Livrea P, Guazzi GC. Interleukin-6 levels in the cerebrospinal fluid and serum of patients with Guillain-barre syndrome and chronic inflammatory demyelinating polyradiculoneuropathy. *J Neuroimmunol* (1993) 47(1):55–61. doi: 10.1016/0165-5728(93)90284-6

67. Sivieri S, Ferrarini AM, Lolli F, Mata S, Pinto F, Tavolato B, et al. Cytokine pattern in the cerebrospinal fluid from patients with GBS and CIDP. *J Neurol Sci* (1997) 147 (1):93–5. doi: 10.1016/S0022-510X(96)00319-X

68. Sainaghi PP, Collimedaglia L, Alciato F, Leone MA, Naldi P, Molinari R, et al. The expression pattern of inflammatory mediators in cerebrospinal fluid differentiates Guillain-barre syndrome from chronic inflammatory demyelinating polyneuropathy. *Cytokine* (2010) 51(2):138–43. doi: 10.1016/j.cyto.2010.05.005

69. Kuhle J, Gaiottino J, Leppert D, Petzold A, Bestwick JP, Malaspina A, et al. Serum neurofilament light chain is a biomarker of human spinal cord injury severity and outcome. *J Neurol Neurosurg Psychiatry* (2015) 86(3):273–9. doi: 10.1136/jnnp-2013-307454

70. Ludwig J, Binder A, Steinmann J, Wasner G, Baron R. Cytokine expression in serum and cerebrospinal fluid in non-inflammatory polyneuropathies. *J Neurol Neurosurg Psychiatry* (2008) 79(11):1268–73. doi: 10.1136/jnnp.2007.134528

71. Sjulstad AS, Odeh F, Baloch FK, Berg DH, Arntzen K, Alstadhaug KB. Occurrence of postdural puncture headache-a randomized controlled trial comparing 22G sprotte and quincke. *Brain Behav* (2020) 10(12):e01886. doi: 10.1002/brb3.1886

frontiers | Frontiers in Immunology

TYPE Systematic Review
PUBLISHED 04 October 2022
DOI 10.3389/fimmu.2022.950275

OPEN ACCESS

EDITED BY
Marita Troye Blomberg,
Stockholm University, Sweden

REVIEWED BY
Benjamin Swartzwelter,
Colorado State University,
United States
Paola Italiani,
National Research Council (CNR), Italy
Harumi Jyonouchi,
Rutgers, The State University of New Jersey, United States

*CORRESPONDENCE
Abeer R. Al-Shammari
aalshammari@hbku.edu.qa

SPECIALTY SECTION
This article was submitted to Cytokines and Soluble Mediators in Immunity, a section of the journal Frontiers in Immunology

RECEIVED 22 May 2022
ACCEPTED 21 September 2022
PUBLISHED 04 October 2022

CITATION
Nour-Eldine W, Ltaief SM, Abdul Manaph NP and Al-Shammari AR (2022) In search of immune cellular sources of abnormal cytokines in the blood in autism spectrum disorder: A systematic review of case-control studies.
Front. Immunol. 13:950275.
doi: 10.3389/fimmu.2022.950275

In search of immune cellular sources of abnormal cytokines in the blood in autism spectrum disorder: A systematic review of case-control studies

Wared Nour-Eldine, Samia M. Ltaief, Nimshitha P. Abdul Manaph and Abeer R. Al-Shammari*

Neurological Disorders Research Center, Qatar Biomedical Research Institute, Hamad Bin Khalifa University, Qatar Foundation, Doha, Qatar

Abnormal cytokine levels in circulating blood have been repeatedly reported in autism; however, the underlying cause remains unclear. This systematic review aimed to investigate cytokine levels in peripheral blood compartments and identify their potential immune cellular sources in subjects with autism through comparison with controls. We conducted an electronic database search (PubMed, Scopus, ProQuest Central, Ovid, SAGE Journals, and Wiley Online Library) from inception (no time limits) to July 9, 2020, and identified 75 relevant articles. Our qualitative data synthesis focused on results consistently described in at least three independent studies, and we reported the results according to the PRISMA protocol. We found that compared with controls, in subjects with autism, cytokines IL-6, IL-17, TNF-α, and IL-1β increased in the plasma and serum. We also identified monocytes, neutrophils, and CD4+ T cells as potential sources of these elevated cytokines in autism. Cytokines IFN-γ, TGF-β, RANTES, and IL-8 were increased in the plasma/serum of subjects with autism, and IFN-γ was likely produced by CD4+ T cells and natural killer (NK) cells, although conflicting evidence is present for IFN-γ and TGF-β. Other cytokines—IL-13, IL-10, IL-5, and IL-4—were found to be unaltered in the plasma/serum and post-stimulated blood immune cells in autistic individuals as compared with controls. The frequencies of T cells, monocytes, B cells, and NK cells were unchanged in subjects with autism as opposed to controls, suggesting that abnormal cytokines were unlikely due to altered cell numbers but might be due to altered functioning of these cells in autism. Our results support existing studies of abnormal cytokines in autism and provide comprehensive evidence of potential cellular sources of these altered cytokines in the context of autism.

Systematic Review Registration: https://www.crd.york.ac.uk/prospero/display_record.php?ID=CRD42020205224, identifier [CRD42020205224].

KEYWORDS

immune cells, cytokines, blood, autism, systematic review, case-control

Introduction

Autism spectrum disorder (ASD) is a heterogeneous neurodevelopmental disorder characterized by stereotyped behaviors and interests, impaired communication skills, and difficulties in social interactions. Autism is present in early childhood and affects approximately 1 in 100 children (1), according to World Health Organization epidemiological data (2022). Despite the high prevalence of autism, the etiologies and pathogenesis are still not clearly defined but are known to involve genetic and environmental factors and complex interactions between them.

Emerging evidence supports the link between immune disruption and autism. Epidemiological studies indicate that maternal infection during pregnancy is associated with an increased risk of autism development in the offspring (2–4). These correlation studies are also supported by animal models of maternal immune activation; these models give rise to offspring that exhibit behavioral and neuropathological deficits relevant to autism (3). In addition, a family history of autoimmunity and autoantibodies is also associated with an increased risk of autism (5, 6). An increased number of autoantibodies are produced by mothers with a family history of autoimmunity; these autoantibodies may target specific proteins in the fetal brain that affect neurodevelopment, which might lead to autism-related behaviors in the offspring (5, 6). In contrast, neonatal studies have shown that immune dysregulation has been detected at birth in children who later develop autism. For example, several studies have identified a correlation between abnormal levels of several cytokines in neonatal bloodspots, such as IL-1β, IL-6, IL-8, and RANTES, and increased risk of developing autism (7–11). Together, these studies indicate that abnormal immune factors are present during early development, before the onset of autism symptoms, and accordingly suggest that immune dysfunction is more likely to be a contributing cause of autism rather than an outcome (12).

Remarkably, immune dysregulation persists postnatally, and ongoing inflammation has been observed in individuals with autism. Several studies have revealed abnormal cytokine levels in the peripheral blood of subjects with autism, which were also associated with increased severity of autism symptoms (13, 14). Similarly, there is evidence of increased inflammatory cytokines in brain tissues and cerebrospinal fluid, as well as active neuroinflammation in the brains of individuals with autism (13–15). Cytokines play a substantial role in the brain by signaling other cells to remove dead and damaged neurons and conducting physiological and neuroprotective functions. Increased levels of inflammatory cytokines in the peripheral immune system are also correlated with increased expression of these cytokines in brain neurogenic niches, which could lead to disrupted synaptic plasticity and impaired behavioral outcomes in autism (6, 16, 17). Therefore, persistent abnormalities in peripheral cytokine levels in subjects with autism might reflect changes in cytokine levels in the brain, which are correlated with behavioral deficits in autism.

In this review, we focus on studies that investigated immune profiles in the peripheral blood of subjects with autism compared with controls. Various studies have addressed the implications of peripheral cytokines in the pathophysiology of autism, as reported in previous systematic reviews and meta-analyses (18, 19). However, these reviews focused on the peripheral levels of cytokines in autism without considering their potential cells of origin. This is important for targeted therapies for autism. The objective of this systematic review is to provide an update on the dysregulation of cytokine levels in autism and associate these altered cytokines with their cellular immune sources. To our knowledge, this is the first review to integrate altered cytokines and their specific cellular sources in autism.

Methods

This study was designed, reported, and executed based on the Preferred Requirements for Systematic Reviews and Meta-Analyses (PRISMA) (20). The review protocol was registered in the International Prospective Register of Systematic Reviews (registration number CRD42020205224) (21). The registered protocol was amended twice to correct a minor typing error and update the current status of the review by adding more details to the protocol sections without changing the original protocol. The PRISMA checklist used in this study is presented in Table S1.

Inclusion and exclusion criteria

This review focused on studies of immune cells and cytokines in the blood of subjects with autism compared with their matching controls. The inclusion criteria were the following: (1) original articles; (2) case-control studies; (3) sample type: peripheral blood, plasma, or serum; (4) analysis of immune cell percentages; (5) analysis of cytokine levels in plasma, serum, or bloodspot; (6) analysis of cytokine levels in immune cells at baseline or after *in vitro* stimulation; and (7) analysis of protein or gene expression. The exclusion criteria were as follows: (1) animal work; (2) sample type: cerebrospinal fluid, tissues, brain, or cell lines; (3) cases without controls; (4) subjects under medication; (5) analysis of treatment or intervention; (6) analysis of immune cell receptors, transcription factors, or activation markers; and (7) genetic (DNA) analysis.

Search strategy

We performed electronic searches of six different databases (PubMed, Scopus, ProQuest Central, Ovid, SAGE Journals, and

Wiley Online Library) using consistent terms. We applied a search filter to the English language results and original journal articles. No other limits were applied. The search was conducted from inception to July 9, 2020, which means no time limits were applied at the time of our database search on July 9, 2020. The search terms used in the PubMed database are as follows: (autism OR autistic OR ASD) AND (human OR subject OR child OR participant OR patient OR volunteer) AND (blood OR plasma OR serum OR immune OR peripheral OR circulating) AND ((cytokine OR chemokine OR "growth factor" OR interferon OR "tumor necrosis factor" OR "colony stimulating factor" OR interleukin) OR (lymphocyte OR monocyte OR "B cell" OR "T cell" OR "natural killer" OR "dendritic cell" OR neutrophil OR basophil OR eosinophil OR myeloid)). The search terms for the remaining databases are listed in Table S2.

After removing duplicates, we screened the records for relevance based on title and abstract. The full texts of potentially relevant records were retrieved and assessed for eligibility according to our pre-defined inclusion and exclusion criteria, as detailed above. We then assessed the quality and risk of bias of each eligible study using the NIH Quality Assessment Tool of Case-Control Studies (available at: https://www.nhlbi.nih.gov/health-topics/study-quality-assessment-tools), which includes 12 evaluation criteria, and a final rating for each study was given based on the following criteria: 7–12 (good), 4–6 (fair), or 0–3 (poor). Studies with good or fair quality ratings were included in the qualitative synthesis of this review. All steps in the identification, screening, eligibility, and selection of records were performed by two authors independently, followed by discussion and consensus between the two authors, and any disagreement was resolved through discussion with a third author. A PRISMA flow diagram is shown in Figure 1.

Data extraction

We extracted data from the included studies and separated them into two tables in Word documents. These tables list the main outcome (increase, decrease, or no change) in autism compared with controls for either immune cell percentage or cytokine release from immune cells (Table S3) and cytokine levels in plasma, serum, or bloodspot (Table S4). Other data, such as sample size, age range, sample type, and analysis technique, are also included in Tables S3 and S4. From these two tables, we identified results that were consistently reported in at least three studies and placed these data into three sub-tables (Tables 1, 2, and 3), which formed the basis of this review. Data were extracted by two authors, and all data were re-checked by at least two independent authors to verify accuracy.

Results

Study characteristics

We identified a total of 3316 records in our search of six electronic databases: PubMed (N = 893), Scopus (N = 633), ProQuest Central (N = 1205), Ovid (N = 119), SAGE Journals (N = 52), and Wiley Online Library (N = 414), as illustrated in the PRISMA flow diagram in Figure 1. We screened the titles and abstracts of 2627 records after duplicate removal and identified 277 potentially relevant records. We retrieved the full-text articles of 277 records to assess eligibility according to our pre-defined inclusion and exclusion criteria. A total of 131 studies were excluded for the following reasons: non-original article (N = 11); non-autism subjects (N = 5); full-text articles not found (N = 2); non-English articles (N = 1); studies not pertaining to immune cells or cytokines or only on genetic DNA (N = 74); sample type not blood, plasma, or serum (N = 6); autism cases without controls (N = 16); studies on immune-related receptors, transcription factors, or activation markers (N = 5); and studies involving treatment or intervention (N = 11). The results of the quality assessments of the 146 eligible studies are listed in Table S5. Seventy-five studies had an overall rating of at least fair quality and were thus included in the qualitative data synthesis of this review.

Data synthesis

We generated two comprehensive tables that summarize the reported findings from all 75 studies included in this review (Table S3 and S4). Data related to immune cell percentages and cytokine production in immune cells are listed in Table S3, whereas data related to cytokine levels in the plasma, serum, or neonatal bloodspot are included in Table S4.

Of note, we did not include results from studies that were unrelated to cell quantification, such as activation markers, transcription factors, and immune cell receptors (e.g., IL-1Ra, CXCR3, CCR6, and IL-6sR). We also excluded results that were not related to cytokines, such as adhesion molecules (e.g., sPECAM-1, sVCAM-1, sP-selectin, and ICAM-1), and enzymes or enzyme inhibitors (e.g., thioredoxin, TIMP-1, and TIMP-2). Growth factors that are not cytokines, such as BDNF, GDNF, EGF, FGF2, NT-3, VEGF, PDGF-BB, and hepatocyte growth factor (HGH), were excluded from this review. Although we included "growth factor" in the search terms, this, in fact, refers to "transforming growth factor" (e.g., TGF-β) and "hematopoietic growth factors" (e.g., GM-CSF, G-CSF, IL-3), which are also cytokines. One study investigated immune responses in autism compared with controls and included

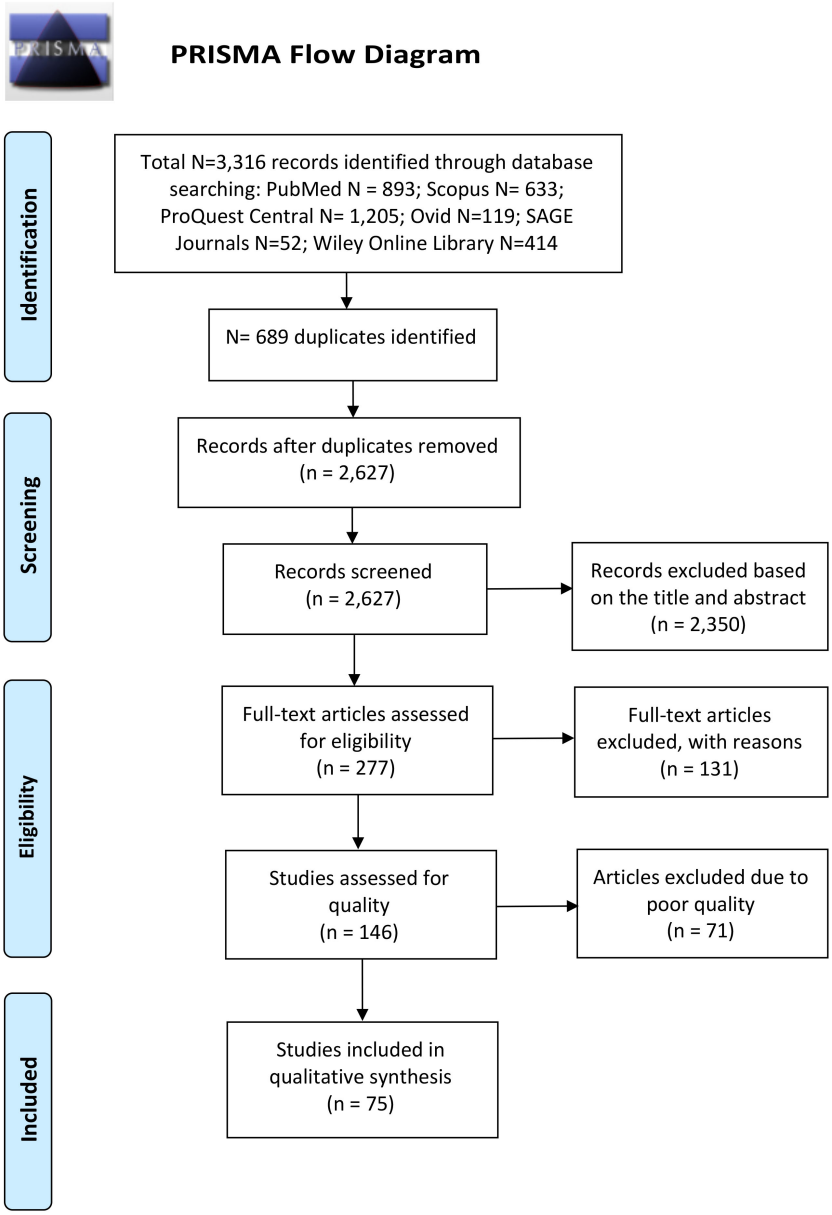

FIGURE 1
PRISMA flow diagram displaying the different stages of this systematic review and the number of records identified in each stage.

other subgroups with and without gastrointestinal complications (66). As we were interested in results on autism as compared with controls in this review, we excluded results from the subgroups that included gastrointestinal complications (66).

Based on the results from Tables S3 and S4, we identified findings that were consistently reported in at least three references. We generated three tables that focused on basal cytokine levels (Table 1), levels of cytokines produced by immune cells (Table 2), and the percentage of the immune cell population (Table 3) in autism relative to controls. A final list of the 62 studies, which formed the basis of this review, is included in Tables 1–3 and described in the data summary section.

Study population and sample analysis methods

We have included a detailed description of the study population and analysis methods in Tables 1–3, based on the data extracted from individual studies in Supplementary Tables S3 and S4. Data

TABLE 1 Baseline levels of cytokines in the blood of individuals with autism compared with controls.

Cytokine affected	Sample type	No. of studies	Age range (in years) (mean ± SD)		Total sample size		% Males	Reported findings in autism compared with controls (in at least N = 3 references)		
			Autism	Controls	Autism	Controls	Autism; Controls	↑	↓	≈
IL-6	Plasma and serum	12	2 to 21 (6.85 ± 2.21)	2 to 21 (7.04 ± 2.08)	540	470	86;75	(22–28)		(29–33)
	Plasma	4	3 to 8 (6.78 ± 2.73)	3 to 8 (6.36 ± 2.43)	134	122	85;73			(29–32)
	Serum	5	2 to 21 (5.91 ± 1.82)	2 to 21 (6.60 ± 1.97)	244	202	86;74	(22–26)		
IL-17	Plasma	5	2.1 to 11.8 (7.11 ± 2.35)	2.6 to 12 (6.83 ± 2.41)	200	168	82;71			(29–31, 34, 35)
	Serum	3	3 to 14.5 (6.70 ± 1.86)	3 to 11 (7.06 ± 1.56)	127	98	89;83	(22, 33, 36)		
TNF-α	Plasma and serum	13	2 to 21 (6.18 ± 2.29)	2 to 21 (7.03 ± 2.17)	615	446	84;70	(24, 29, 33, 37–40		(25, 27, 30–32, 41)
	Plasma	3	3 to 8 (6.67 ± 2.34)	3 to 8 (6.23 ± 1.92)	94	87	89;77			(30–32)
	Serum	5	2 to 21 (5.23 ± 2.11)	2 to 21 (7.33 ± 2.51)	156	142	84;64	(24, 33, 37, 38, 40)		
IL-1β	Plasma and serum	15	2 to 21 (6.43 ± 2.63)	2 to 21 (7.08 ± 2.31)	659	496	85;73	(23–25, 27, 33, 37, 42, 43)		(22, 29, 30, 32, 40, 41, 44)
	Plasma	4	NR (8.08 ± 3.80)	NR (7.43 ± 2.93)	119	102	83;80			(29, 30, 32, 44)
	Serum	6	2 to 21 (5.25 ± 1.95)	2 to 21 (5.76 ± 1.81)	243	202	84;70	(24, 25, 33, 37, 42, 43)		
IFN-γ	Plasma and serum	11	1.58 to 14.5 (6.02 ± 2.21)	2.3 to 12 (7.00 ± 2.08)	564	374	88;73			(22, 25, 27, 29–31, 33, 39–41, 45)
	Plasma	10	2.2 to 16 (6.98 ± 2.51)	2.3 to 16 (6.61 ± 2.30)	474	344	85;77	(32, 46, 47)		(27, 29–31, 39, 41, 45)
	Serum	4	2 to 14.5 (5.17 ± 1.87)	3 to 16 (7.55 ± 1.63)	154	92	93;71			(22, 25, 33, 40)

(Continued)

10.3389/fimmu.2022.950275

TABLE 1 Continued

Cytokine affected	Sample type	No. of studies	Age range (in years) (mean ± SD)		Total sample size		% Males	Reported findings in autism compared with controls (in at least N = 3 references)		
			Autism	Controls	Autism	Controls	Autism; Controls	↑	↓	≈
TGF-β	Plasma and serum	8	2 to 28 (11.46 ± 1.73)	2 to 26 (14.16 ± 2.15)	349	243	89;77	(39, 40, 46, 48)	(35, 49–51)	
	Plasma	6	1.6 to 13 (8.70 ± 1.20)	2 to 14 (9.10 ± 1.70)	300	208	83;73	(39, 46, 48)	(35, 50, 51)	
RANTES	Plasma	3	3 to 8 (4.40 ± 0.83)	2.8 to 8 (4.21 ± 0.98)	167	131	88;59	(31, 52, 53)		
IL-13	Plasma and serum	4	2 to 21 (6.31 ± 2.17)	2 to 21 (5.75 ± 1.99)	196	179	93;79			(24, 27, 30, 31)
IL-12p70	Plasma	4	2.2 to 10 (6.79 ± 2.00)	2.3 to 10 (6.36 ± 1.91)	186	119	87;77			(30, 31, 41, 45)
IL-12p40	Plasma	3	3 to 10 (6.79 ± 2.00)	3 to 10 (6.36 ± 1.91)	169	103	89;75			(30, 31, 41)
IL-10	Plasma and serum	7	2.2 to 10 (6.44 ± 2.32)	2.3 to 12 (6.48 ± 2.11)	225	186	86;74			(25, 29–33, 45)
	Plasma	5	2.2 to 8 (6.78 ± 2.73)	2.3 to 8 (6.36 ± 2.43)	151	138	85;75			(29–32, 45)
IL-8	Plasma and serum	10	1.58 to 10 (5.68 ± 2.03)	2 to 16 (6.97 ± 2.01)	710	397	88;73	(27, 31, 37, 54)		(7, 25, 30, 39–41)
IL-5	Plasma	4	2.2 to 8 (7.10 ± 1.84)	2.3 to 8 (6.86 ± 1.89)	160	133	84;73			(27, 30, 31, 45)
IL-4	Plasma and serum	8	2.2 to 14.5 (6.47 ± 2.46)	2.3 to 11 (6.38 ± 2.11)	330	283	87;78			(22, 27, 29–33, 45)
	Plasma	6	2.2 to 8 (6.78 ± 2.73)	2.3 to 8 (6.36 ± 2.43)	248	225	85;76			(27, 29–32, 45)
IL-2	Plasma and serum	5	2.9 to 10 (7.19 ± 2.32)	2.8 to 10 (7.08 ± 1.93)	277	204	85;81			(27, 30, 32, 33, 41)
	Plasma	4	2.9 to 10 (7.76 ± 2.67)	2.8 to 10 (7.41 ± 2.23)	245	176	84;82			(27, 30, 32, 41)

(Continued)

10.3389/fimmu.2022.950275

TABLE 1 Continued

Cytokine affected	Sample type	No. of studies	Age range (in years) (mean ± SD)		Total sample size		% Males	Reported findings in autism compared with controls (in at least N = 3 references)		
			Autism	Controls	Autism	Controls	Autism; Controls	↑	↓	≈
MCP-1	Plasma	4	1.6 to 6 (5.63 ± 1.77)	3 to 6.6 (5.29 ± 1.69)	1141	1295	88;76			(30, 31, 39, 53)
	Bloodspot	3	Neonates	Neonates	942	1181	84;81			(7, 8, 11)
MIP-1α	Plasma	3	1.58 to 6.17 (8.11 ± 3.65)	2.8 to 6.58 (7.44 ± 3.12)	192	124	89;79			(30, 39, 52)
	Bloodspot	3	Neonates	Neonates	656	962	85;68			(7, 10, 11)
GM-CSF	Plasma	4	2.9 to 10 (6.79 ± 2.00)	2.8 to 10 (6.36 ± 1.91)	266	190	88;77			(27, 30, 31, 41)
Eotaxin	Plasma	4	3 to 10 (6.17 ± 1.74)	3 to 10 (5.86 ± 1.71)	211	138	89;67			(30, 31, 41, 53)

Symbols: ↑, increased; ↓, decreased; ≈, unchanged; in autism compared with controls
GM-CSF, granulocyte monocyte colony-stimulating factor; IFN-γ, interferon-γ; IL, interleukin; MCP-1, monocyte chemoattractant protein-1; MIP-1α, macrophage inflammatory protein; NR, not reported; RANTES, regulated upon activation, normal T cell expressed and presumably secreted; TGF-β, transforming growth factor-β; TNF-α, tumor necrosis factor-α.

TABLE 2 Level of cytokines produced by blood immune cells of individuals with autism, compared with controls, at either baseline or after *in vitro* stimulation conditions.

Cytokine affected	Cell type(s)	Condition (Stimuli[cell type])	No. of studies	Age range (in years) (mean ± SD)		Total sample size		% Males	Reported findings in autism compared with controls (in at least N = 3 references)		
				Autism	Controls	Autism	Controls	Autism; Controls	↑	↓	≈
IL-6	PBMCs, CD16+ Neutrophils, CD14+ Monocytes	Baseline	6	3 to 15 (6.96 ± 2.56)	4 to 12 (7.76 ± 2.45)	366	335	78;76	(55–60)		
	PBMCs[a], CD16+ Neutrophils[b], CD14+ Monocytes[c]	Post-stimulation (PMA/Ionomycin[a], LPS+ ATP[a], IL-17A[b], LTA[c])	4	2.2 to 12 (7.05 ± 2.12)	2.3 to 12 (6.32 ± 2.21)	132	111	86;84	(42, 45, 56, 61)		
IL-17	CD4+ T cells, CD16+ Neutrophils	Baseline	3	NR (6.70 ± 1.80)	NR (6.70 ± 1.76)	120	116	80;32	(56, 58, 62)		
	PBMCs[a], CD4+ T cells[d]	Post-stimulation (PHA[a], PMA/Ionomycin[d], anti-CD3/CD28[d])	3	2 to 6 (6.65 ± 1.20)	2 to 6 (6.70 ± 1.30)	120	129	86;86	(62–64)		

(Continued)

10.3389/fimmu.2022.950275

TABLE 2 Continued

Cytokine affected	Cell type(s)	Condition (Stimuli[cell type])	No. of studies	Age range (in years) (mean ± SD)		Total sample size		% Males	Reported findings in autism compared with controls (in at least N = 3 references)		
				Autism	Controls	Autism	Controls	Autism; Controls	↑	↓	≈
TNF-α	PBMCs, CD3+, CD8+ or CD4+ T cells	Baseline	3	2.5 to 4.8 (6.90 ± 3.80)	2.2 to 6.1 (8.40 ± 4.00)	252	209	83;76			(57, 59, 65)
	PBMCs[a], CD14+ Monocytes[c]	Post-stimulation (LPS[a], PHA[a], LTA[c])	3	2.2 to 11.2 (NR)	2.3 to 8.3 (NR)	109	124	82;73	(45, 66, 67)		
IL-1β	PBMCs	Baseline	4	2 to 10 (6.60 ± 2.60)	2 to 17 (7.60 ± 2.70)	277	244	79;76			(57–59, 68)
	PBMCs[a], CD14+ Monocytes[c], CD4+ T cells[d]	Post-stimulation (PMA/Ionomycin[a], LPS+ ATP[a], LPS+BDE-47[a], LPS[a,c], LTA[c], anti-CD3/ CD28[d])	6	2.2 to 11.2 (7.28 ± 2.40)	2.3 to 11 (7.56 ± 2.47)	167	182	77;75	(42, 45, 66, 69–71)		
IFN-γ	PBMCs, CD56+ NK cells	Baseline	3	2.2 to 56 (16.87 ± NR)	2 to 56 (16.70 ± NR)	118	83	84;81	(68, 72, 73)		
	PBMCs[a], CD4+ T cells[d], CD56+ NK cells[e]	Post-stimulation (PMA/Ionomycin[a], tetanus toxoid[a], PGN[a], anti-CD3/ CD28[a,d], IL-12+IL-18[e], K562 cells[e])	7	2.2 to 56 (10.66 ± 2.04)	2.3 to 56 (10.71 ± 2.15)	294	275	82;78	(61, 69, 70)	(66, 67, 72, 73)	
IL-13	PBMCs	Post-stimulation (PGN, PHA, LPS, tetanus toxoid)	3	2.2 to 11.2 (6.90 ± 2.00)	2 to 10.1 (6.80 ± 2.00)	91	124	80;80			(64, 66, 74)
IL-10	PBMCs	Post-stimulation (PGN, PHA, LPS, tetanus toxoid)	3	3.2 to 11.2 (6.90 ± 2.00)	2.7 to 10.1 (6.80 ± 2.00)	112	128	82;74			(66, 67, 74)
IL-5	PBMCs	Post-stimulation (PGN, PHA, LPS, tetanus toxoid)	3	3.2 to 11.2 (6.90 ± 2.00)	2.7 to 10.1 (6.80 ± 2.00)	112	128	82;74			(66, 67, 74)
IL-4	PBMCs	Post-stimulation (PGN, PHA, LPS, tetanus toxoid)	3	2.2 to 11.2 (6.90 ± 2.00)	2 to 10.1 (6.80 ± 2.00)	91	124	80;80			(64, 66, 74)

Symbols: ↑, increased; ↓, decreased; ≈, unchanged; in autism compared with controls.

ATP, adenosine triphosphate; BDE-47, 2,2',4,4'-tetrabromodiphenyl ether; CD, cluster of differentiation; IFN-γ, interferon-γ; IL, interleukin; LPS, lipopolysaccharide; LTA, lipoteichoic acid; NK, natural killer; NR, not reported; PBMCs, peripheral blood mononuclear cells; PGN, polymeric peptidoglycan; PHA, phytohemagglutinin; PMA, phorbol myristate acetate; TNF-α, tumor necrosis factor-α.

10.3389/fimmu.2022.950275

TABLE 3 Percentages of blood immune cells in autism under baseline conditions compared with controls.

Cell type	Markers	No. of studies	Age range (in years) (mean ± SD)		Total sample size		% Males	Reported findings in autism compared with controls (in at least N = 3 references)		
			Autism	Controls	Autism	Controls	Autism; Controls	↑	↓	≈
T cells	CD3+	4	2.5 to 9 (4.25 ± 1.70)	2.2 to 9 (4.25 ± 2.20)	168	155	90;82			(65, 67, 75, 76)
T helper cells	CD4+	5	2.5 to 14.5 (5.21 ± 2.14)	2.2 to 11 (5.50 ± 2.06)	246	189	90;85			(22, 65, 67, 76, 77)
T suppressor cells	CD8+	5	2.5 to 14.5 (5.21 ± 2.14)	2.2 to 11 (5.50 ± 2.06)	210	180	91;84			(22, 65, 67, 76, 77)
Monocytes	CD14+, CD16+	5	2.5 to 14.5 (6.17 ± 2.58)	2.2 to 11 (6.75 ± 1.92)	213	138	87;82			(22, 45, 75, 77, 78)
B cells	CD19+	3	3 to 14.5 (6.17 ± 2.58)	3 to 11 (6.75 ± 1.92)	126	87	90;83			(22, 75, 78)
NK cells	CD3-CD56+, CD56+CD16+	3	3 to 56 (14.29 ± 3.09)	1 to 56 (13.9 ± 2.66)	189	96	83;76			(22, 72, 79)

Symbols: ↑, increased; ↓, decreased; ≈, unchanged; in autism compared with controls.
CD, cluster of differentiation; NK, natural killer.

related to the study population include age, total sample size, and sex, whereas data related to the analysis methods include sample type, *in vitro* stimulus, and analysis technique.

Overall, the mean age and age range of the study population in this review were comparable between the autism and control groups. The mean age ± standard deviation (SD) was 7.06 ± 0.70 and 7.17 ± 0.46 years for the autism and control groups, respectively. In Table 1, the age of subjects ranged from 2 to 12 years, apart from seven studies in which subjects reached 13, 14, 16, 21, and 28 years (22–24, 40, 46, 48, 49). Studies on MCP-1 and MIP-1α bloodspots were performed using neonatal samples (7, 8, 10, 11). In Tables 2 and 3, the age of subjects ranged from 2 to 12 years, except in a few studies in which the subjects' ages reached 15, 17, and 56 years (Table 2) (55, 68, 72) and 14.5 and 56 years (Table 3) (22, 72). Regarding gender distribution, most of the studies in Tables 1–3 involved the recruitment of male subjects (at least 70% of total subjects), which was similar between the autism and control groups. However, in a few studies, the overall percentage of male subjects only reached 67%, 64%, 59%, and 32% in the control group (Tables 1 and 2).

Meanwhile, the sample type was either plasma or serum for all cytokines included in Table 1, except the bloodspot samples used in the MCP-1 and MIP-1α analyses. The sample types were blood immune cells, including peripheral blood mononuclear cells (PBMCs), neutrophils, monocytes, T cells, and natural killer (NK) cells in Table 2 and T cells, monocytes, B cells, and NK cells in Table 3. The techniques used in the analysis of the samples in Table 1 were either ELISA or cytokine multiplex, as listed in Supplementary Table S4. The analysis techniques for samples in Tables 2–3 include flow cytometry, ELISA, cytokine multiplex, qPCR, and western blot, as illustrated in Supplementary Table S3.

The stimuli used in the *in vitro* poststimulation studies are shown in Table 2. Different types of stimuli were used to assess cytokine production from various immune cells in autism, as compared with the control group. Studies on PBMCs and CD4+ T cells consistently showed differential responses from these cells in autism when stimulated with PMA/ionomycin and anti-CD3/CD28, respectively, as compared with the control group (61, 63, 69, 70). However, studies that used LPS, PHA, PGN or tetanus toxoid to stimulate PBMCs showed conflicting results, which might be due to differences in the type of cytokines analyzed in these studies (42, 64, 66, 67, 70, 71, 74). Therefore, the use of PMA/Ionomycin and anti-CD3/CD28 to stimulate PBMCs and CD4+ T cells, respectively, may represent a good model for studying cytokine production in autism. However, it should be noted that PMA/Ionomycin is a potent stimulant that bypasses receptor-mediated signal transduction mechanisms and directly activates intracellular signaling pathways that result in the production of various cytokines. Meanwhile, monocytes stimulated with LTA, neutrophils stimulated with IL-17A, and NK cells stimulated with IL-12/IL-18 or K562 cells showed differential responses in each of these cell types in autism, as compared with the controls (45, 56, 72, 73). However, the number of studies on these cell types is still limited, which makes it difficult to predict whether these stimuli can be effectively used for studying cytokine production in these cell types in autism.

Data summary

In this review, we found that IL-6, IL-17, TNF-α, and IL-1β were increased in the in the serum but unchanged in the plasma in subjects with autism (Table 1). Interestingly, the increase in IL-6, IL-17, TNF-α, and IL-1β in the serum was in accordance with the elevated levels of these cytokines in *in vitro* stimulated neutrophils, monocytes, and CD4+ T cells in individuals with autism, as compared with controls (Table 2). Additionally, the levels of IL-6 and IL-17, but not TNF-α and IL-1β, were consistently higher in the unstimulated neutrophils, monocytes, and CD4+ T cells in autism subjects, as opposed to the controls (Table 2).

Meanwhile, studies have shown conflicting results for IFN-γ, as it is not only reported to be both increased and unchanged in plasma but also unchanged in the serum of subjects with autism (Table 1). This discrepancy in IFN-γ levels is also found in the response of blood immune cells after *in vitro* challenge, in which studies have delineated both increased and decreased IFN-γ levels in post-stimulated NK cells and CD4+ T cells, in addition to consistently increased levels in NK cells under baseline conditions (Table 2).

Likewise, reports on TGF-β are also conflicting, whereby it was found to be both increased and decreased in the plasma of autism subjects (Table 1), and little or no data pertaining to its cell of origin for autism are available. The two isoforms of TGF-β (β1 and β2) as well as the functional forms of TGF-β were treated equally during our data synthesis, which might have accounted for the variability observed in the TGF-β results (Table 1).

Studies have indicated an increase in the cytokine levels of RANTES and IL-8 relative to controls in subjects with autism (Table 1). In addition, reports consistently delineate unchanged IL-13, IL-10, IL-5, and IL-4 levels in the plasma/serum and post-stimulated blood immune cells in individuals with autism as compared with controls (Tables 1 and 2). Other cytokines, IL-12, IL-2, MCP-1, MIP-1α, GM-CSF, and eotaxin, were unchanged in the plasma of subjects with autism (Table 1).

Interestingly, the overall reported outcomes described above are unlikely to be caused by changes in the percentage of immune cells in subjects with autism compared with controls. As shown in Table 3, the frequency of CD3+ T cells and their subsets, CD4+ and CD8+ cells, as well as the frequency of monocytes, B cells, and NK cells were comparable between subjects with autism and controls. This might indicate that increased cytokine levels are not due to differences in immune cell numbers but rather due to the abnormal functional responses of these immune cells in individuals with autism as compared with controls. Based on the results in Tables 1 and 2, we present a schematic diagram illustrating our proposed model for the immune cells of origin of the altered cytokines in autism (Figure 2).

Discussion

This systematic review was undertaken to investigate alterations in peripheral blood cytokines in autism and identify the immune cells contributing to abnormal cytokine profiles in individuals with this disorder. We focused on findings that showed a difference between autism and control subjects. Remarkably, we identified a list of specific cytokines that were altered in both plasma and serum, as well as in *in vitro* stimulated blood immune cells in autism. Collectively, we found increased levels of IL-6, IL-17, TNF-α, IL-1β, IFN-γ, RANTES, and IL-8 in the plasma/serum in autism, which is overall consistent with the findings from previous systematic reviews (18, 19). We reviewed autism studies that investigated cytokine production by *in vitro* stimulated blood immune cells and identified monocytes, neutrophils, CD4+ T cells, and NK cells as the major cellular sources of these altered cytokines. Conversely, we found TGF-β to be both increased and decreased in the plasma of patients with autism relative to controls, and there is as yet no conclusive evidence concerning its cellular sources. Interestingly, the immune cells identified in our review that produce certain cytokines in autism are also known to produce these cytokines. In this review, we also found that the percentage of the immune cell population is consistently unaltered in autism, suggesting that abnormal cytokine levels might be due to changes in the functionality or activation status of these cells rather than their numbers in autism.

In this review, we found elevated levels of IL-6, TNF-α, and IL-1β in the plasma/serum of individuals with autism. IL-6, TNF-α, and IL-1β are early proinflammatory cytokines released from immune cells in response to inflammatory stimuli. Importantly, these cytokines can cross from the peripheral blood into the brain, where they directly affect brain function and behavior (6, 16, 17). Previous studies have shown that high levels of IL-6, TNF-α, and IL-1β are correlated with the severity of autism symptoms, which include stereotypical behaviors and impaired communication skills (27, 33, 43, 45, 52). Interestingly, we found some evidence in our review for the potential cellular sources of these cytokines in autism. Elevated IL-6 levels have been described in monocytes and neutrophils at both baseline (56, 60) and after *in vitro* stimulation (45, 56) in autism, whereas augmented TNF-α levels have been described only in the post-stimulated monocytes of individuals with autism (45). In addition, IL-1β levels are markedly increased in post-stimulated monocytes and CD4+ T cells in autism (45, 70). Altogether, we suggest that monocytes are the predominant cells contributing to the elevated cytokine levels of IL-6, TNF-α, and IL-1β in autism, along with CD4+ T cells, which act as another source of IL-1β, whereas neutrophils are another source of IL-6. Previous studies have shown that TNF-α enhances T cell proliferation, augments IL-2R (interleukin-2 receptor) on T cells, and sustains T cell survival during the initiation of T cell responses (81). Similarly, IL-1β acts synergistically with IL-2 to promote the expansion of CD4 and CD8 T cells (82) and induces a robust and durable primary and secondary CD4 response (83). Therefore, we suggest that elevated TNF-α and IL-1β levels would promote naïve

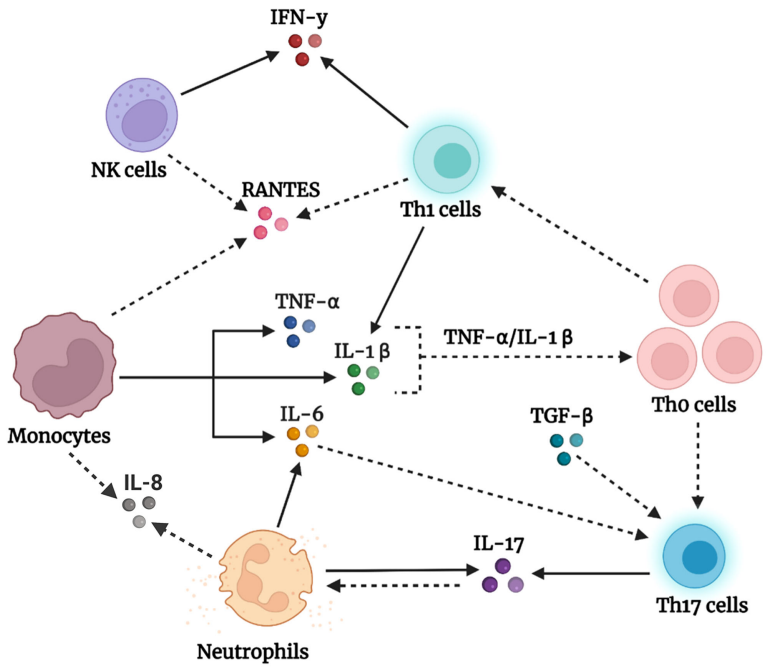

FIGURE 2
Schematic representation of our proposed model of peripheral immune dysregulation in autism.Activated monocytes produce high amounts of the triad of proinflammatory cytokines, TNF-α, IL-1β, and IL-6. Accordingly, TNF-α and IL-1β promote the activation, priming, and proliferation of naïve and effector T cells, whereas IL-6, in the presence of dysregulated levels of TGF-β, drives the polarization of naïve T helper (Th0) cells into effector Th17 subsets. The latter produces its signature cytokine IL-17, which initiates several events that result in neutrophil recruitment and activation (80). Neutrophils in individuals with autism produce IL-17 and IL-6, which add to the observed large pool of IL-17 and IL-6. In addition, naïve T helper (Th0) cells under the influence of cytokines in the milieu differentiate into Th1 cells, which impart high IFN-γ levels and enrich the IL-1β pool. Natural killer (NK) cells, on the other hand, tend to be dysfunctional in autism and chronically produce IFN-γ, which augments the IFN-γ pool. Furthermore, the high levels of the chemotactic factor RANTES might be derived from activated monocytes, T cells, or NK cells, whereas IL-8 might be produced by monocytes and neutrophils, and function to recruit cells to the scene. The solid arrows represent confirmed findings in the tables we formulated, whereas the dashed arrows are based on well-known facts in the literature that we suggest occur in the context of autism. Created using BioRender.com

T helper (Th0) cell proliferation and expansion in the context of autism, as illustrated in our proposed model in Figure 2.

However, results for TGF-β are conflicting, whereby it is reported to be both increased (39, 46, 48) and decreased (35, 50, 51) in the plasma of individuals with autism, and there is scarce evidence concerning its cell of origin in autism. This discrepancy in TGF-β results might be due to differences between the studies in the isoforms or functional forms being assessed. TGF-β exists in three isoforms (β1, β2, and β3), which are structurally similar and share approximately 71%–79% sequence identity (84, 85). Although the three isoforms show similar functions *in vitro*, isoform-specific knockout mice show phenotypic differences, suggesting distinctive functions for these isoforms *in vivo* (84, 85). Unlike other cytokines that are produced in their active forms, TGF-β is secreted in an inactive form and stored in the extracellular matrix as a latent complex with its prodomain, which can then be converted into the active form through multiple mechanisms (86). In this review, studies showing decreased TGF-β levels specifically involved the TGF-β1 isoform (35, 50, 51), whereas increased levels of TGF-β were found for either the TGF-β2 or TGF-β1 isoform (39, 46, 48). Among these studies, only the functional form of TGF-β was reported in some studies, in which the activated form of TGF-β was specifically analyzed (35, 46, 50). Based on this evidence, we speculate that the activated TGF-β1 isoform is decreased, whereas the activated TGF-β2 isoform is increased in autism, which needs to be further investigated in future studies.

Given the dysregulated levels of TGF-β in autism, we speculate that this dysregulation may disrupt several immune processes in autism. TGF-β is an immunosuppressive cytokine produced by the immune system guardian-regulatory T (Treg) cells, which maintain immune homeostasis (49, 50) and are involved in diverse cellular functions, including the promotion of cell growth, proliferation, and differentiation (18). Alternatively, TGF-β can empower naïve T cell differentiation into effector T helper 17 (Th17) cells (87, 88), which are important for host defense and associated with inflammation and autoimmune conditions (89). This highly dynamic function of TGF-β is contextual; when it is produced in the presence of IL-6, TGF-β directs Th17 cell development and differentiation (90, 91) whereas when it is produced in the presence of IL-2, TGF-β promotes the

development of induced regulatory T cells (92). Therefore, we suggest that dysregulated TGF-β levels, together with elevated IL-6 levels, may disrupt immune homeostasis in autism and affect Th17 cells, as shown in our proposed model in Figure 2.

In this review, we found evidence of increased IL-17 levels in the serum of subjects with autism (22, 33, 36). Interestingly, previous studies have shown that IL-17 signaling is responsible for autism-like symptoms in the offspring of maternal immune-activated mice (93, 94). From the studies we included, we identified neutrophils (56) and CD4+ T cells (62) as potential sources of IL-17 in the steady state of autism, in addition to IL-17 production by stimulated CD4+ T cells (62–64). IL-17 exerts important functions on T cells and neutrophils, including priming T cells and acting on neutrophils to promote the production of the proinflammatory cytokines IL-1, IL-6, and TNF-α (95). Although neutrophils are recruited to inflammatory sites under the influence of chemokines induced by IL-17 (80), they can become the main producers of IL-17 under certain circumstances, as in the case of kidney ischemia-reperfusion injury (96). The biological activity of IL-17 relies on the formation of multimeric receptors composed of IL-17RA and IL-17RC subunits (80). Interestingly, neutrophils of individuals with autism were found to express the IL-17RC subunit, which was absent in the neutrophils of control subjects. This enabled neutrophils to potently respond to IL-17A/IL-17R signaling and release IL-6 (56), leading to increased IL-17 production in autism. Taken together, these results suggest that Th17 cells and neutrophils are potential sources of upregulated IL-17 levels in autism (Figure 2).

Furthermore, we found increased levels of RANTES, IL-8, and IFN-γ in the plasma/serum of subjects with autism. However, there is still no clear evidence concerning the cellular sources of RANTES and IL-8 in our review. Given that RANTES is mainly produced by T cells, monocytes, and NK cells (97), we suggest that these cells also produce RANTES in autism (Figure 2), which does not exclude the possibility of the presence of other sources. Meanwhile, IL-8 is produced by monocytes and neutrophils, and we propose that these cell types in the circulating blood might also be potential sources of IL-8 in autism (Figure 2). In contrast, our review identified elevated production of IFN-γ in *in vitro* stimulated CD4+ T cells (70) and NK cells in the basal state in autism (72, 73). However, reduced levels of IFN-γ were observed in NK cells in autism after introducing an external stimulus, such as IL-12/IL-18 or K562 target cells (72, 73). These observations suggest that NK cells in autism are persistently activated and produce abnormal amounts of IFN-γ under baseline conditions; however, they tend to be hypofunctional (exhausted) after an *in vitro* immune challenge. Interestingly, the same NK cell phenotype has also been reported in other psychiatric disorders, including obsessive-compulsive disorder, chronic stress, and depression (98, 99). Future studies are needed to further investigate the exhausted NK cell phenotype in autism, where this phenotype might be representative of a subpopulation of subjects with autism.

It is worth mentioning that the studies presented in this review suggest the prevalence of T helper 1 (Th1) and Th17 phenotypes rather than the Th2 phenotype in autism. CD4+ T helper (Th) cells are subdivided into different subsets distinguished by their unique transcription factors and cytokine production. These subsets include IFN-γ-producing Th1 cells, IL-4-producing Th2 cells, IL-17-producing Th17 cells, and Foxp3-expressing Treg cells. Importantly, T helper cell differentiation toward a specific subset actively inhibits the transcriptional program of the other subset and its ability to produce characteristic cytokines (100). Therefore, our findings indicate that increased production of Th1 cytokines (IFN-γ) and Th17 cytokines (IL-17), along with no change in Th2 cytokines (IL-4, IL-5, and IL-13), might suggest a skewing toward the Th1/Th17 phenotype and dampening of the Th2 phenotype in the context of autism (Figure 2). Interestingly, Th1 cytokines were shown to be associated with autism severity and impaired behavior, whereas Th2 cytokines were correlated with better behavioral and developmental scores (67).

In addition, there are some limitations that should be considered in our systematic review. We restricted our search to articles written in English only and, thus, may have neglected results from articles in other languages. Other limitations include differences in the age range of subjects among the different studies, in addition to technical variations, such as the use of different analysis methods, sample types, and *in vitro* stimuli, which together might have contributed to the variability in the observed results across studies. The overall age range of subjects from the studies included in this review was between 2 and 12 years; however, it is important to emphasize that the immune system undergoes dynamic changes during this developmental period from early childhood to adolescence (101), which might introduce some variability when combining results from different studies. Therefore, future studies should consider restricting the age range of subjects for a more comprehensive understanding of immune changes in autism.

In our review, we also observed differences in some cytokines when measured in serum versus plasma samples, which is also supported by previous studies (102–104). This inconsistency in the results between plasma and serum might be attributed to differences in the preparation methods for these sample types. Serum samples are obtained after blood coagulation, whereas the preparation of plasma samples involves the use of various anticoagulants that affect cytokine measurement (102–104). Although the studies included in this review have used standard methods for cytokine detection, such as ELISA, cytokine multiplex, or flow cytometry, significant differences might still exist regarding sample handling and processing methods, the analysis platforms used, and the sensitivity and specificity of the antibodies used across different studies. In addition, there are variations in the type of *in vitro* stimuli, such as LPS, PHA, or PGN, used in PBMCs culture models, which could lead to variations in cell responses.

Currently, there are a limited number of studies investigating cytokine production at the level of a specific immune cell type in autism, and much of the present evidence pertains to total PBMCs.

Although we found consistent results regarding the type of altered cytokines produced by blood immune cells in autism, these results were not representative of a specific immune cell type and may include results from PBMCs. In addition, the results presented in this review and the proposed model are based on currently available evidence from the autism literature; therefore, it does not exclude the fact that other cellular sources, such as innate lymphoid cells and NK T cells, although present in very small numbers in the circulating blood, might also contribute to the production of IL-17, IFN-γ, and other T cell cytokines, which have yet to be investigated. Furthermore, endothelial cells and tissue-resident cells are other potential sources for cytokine production, however we focused in our review on peripheral immune cells in the circulating blood in autism, which are less invasive and have current evidence in the literature. Finally, most of the studies included in this review were cross-sectional in nature and lacked details of the clinical features and comorbid conditions of autism subjects, which can be considered other limitations of the current studies in the field. These highlight the need for more longitudinal analyses in future studies in a well-characterized study population for more accurate detection of time-dependent changes in immune phenotypes in autism and their correlation with clinical and behavioral changes in autism.

Conclusions

This systematic review supports the existing evidence of abnormal cytokine levels in the peripheral blood of individuals with autism. Given that cytokines are ubiquitous molecules circulating in the bloodstream, determining their cellular sources is crucial for targeted therapeutics. To our knowledge, this is the first review to identify the potential immune cells of origin of the altered cytokines in autism, and we propose a network model that integrates these altered cytokines and their specific cellular sources in autism. Although certain areas presented in this review still lack solid evidence, this review summarizes the current knowledge in the field and highlights the gaps that need to be considered in future studies. Most current studies on autism have focused on cytokine levels in the blood or analyzed cytokine production from a population of PBMCs. We emphasize the importance of future studies on autism to further elucidate immune sources of altered cytokines at the single-cell level and combine multi-omics approaches, such as proteomics, cell phenotyping, and single-cell transcriptomic analyses, which may reveal cell-specific immune pathways underlying autism. Since autism is a heterogeneous condition, immune phenotypes may vary widely within a group of subjects with autism. Future studies should consider the utilization of advanced bioinformatics and machine learning techniques to segregate autism groups into different subgroups based on their exhibited immune and clinical phenotypes, which might also lead to the identification of novel characteristics of subclusters of subjects with autism for a better understanding of the pathophysiology of autism.

Data availability statement

The original contributions presented in the study are included in the article/Supplementary Material. Further inquiries can be directed to the corresponding author.

Author contributions

AA-S conceived the review. WN-E, SL, NM, and AA-S collected and summarized the review data. WN-E and AA-S wrote the manuscript. All authors contributed to the article and approved the submitted version.

Funding

This publication was made possible by ECRA Award number ECRA01-001-3-001 from the Qatar National Research Fund (a member of Qatar Foundation), and start-up fund from Qatar Biomedical Research Institute (Grant code VR03).

Acknowledgments

We would like to thank Editage (www.editage.com) for English language editing.

Conflict of interest

The authors declare that the research was conducted in the absence of any commercial or financial relationships that could be construed as a potential conflict of interest.

Publisher's note

Author disclaimer

The findings achieved herein are solely the responsibility of the authors.

Supplementary material

The Supplementary Material for this article can be found online at: https://www.frontiersin.org/articles/10.3389/fimmu.2022.950275/full#supplementary-material

References

1. World Health Organization. *Autism* (2022). Available at: https://www.who.int/news-room/fact-sheets/detail/autism-spectrum-disorders.

2. Atladottir HO, Thorsen P, Ostergaard L, Schendel DE, Lemcke S, Abdallah M, et al. Maternal infection requiring hospitalization during pregnancy and autism spectrum disorders. *J Autism Dev Disord* (2010) 40(12):1423–30. doi: 10.1007/s10803-010-1006-y

3. Estes ML, McAllister AK. Maternal immune activation: Implications for neuropsychiatric disorders. *Science* (2016) 353(6301):772–7. doi: 10.1126/science.aag3194

4. Zerbo O, Iosif AM, Delwiche L, Walker C, Hertz-Picciotto I. Month of conception and risk of autism. *Epidemiology* (2011) 22(4):469–75. doi: 10.1097/EDE.0b013e31821d0b53

5. Edmiston E, Ashwood P, Van de Water J. Autoimmunity, autoantibodies, and autism spectrum disorder. *Biol Psychiatry* (2017) 81(5):383–90. doi: 10.1016/j.biopsych.2016.08.031

6. Estes ML, McAllister AK. Immune mediators in the brain and peripheral tissues in autism spectrum disorder. *Nat Rev Neurosci* (2015) 16(8):469–86. doi: 10.1038/nrn3978

7. Krakowiak P, Goines PE, Tancredi DJ, Ashwood P, Hansen RL, Hertz-Picciotto I, et al. Neonatal cytokine profiles associated with autism spectrum disorder. *Biol Psychiatry* (2017) 81(5):442–51. doi: 10.1016/j.biopsych.2015.08.007

8. Heuer LS, Croen LA, Jones KL, Yoshida CK, Hansen RL, Yolken R, et al. An exploratory examination of neonatal cytokines and chemokines as predictors of autism risk: The early markers for autism study. *Biol Psychiatry* (2019) 86(4):255–64. doi: 10.1016/j.biopsych.2019.04.037

9. Abdallah MW, Larsen N, Mortensen EL, Atladottir HO, Norgaard-Pedersen B, Bonefeld-Jorgensen EC, et al. Neonatal levels of cytokines and risk of autism spectrum disorders: an exploratory register-based historic birth cohort study utilizing the Danish newborn screening biobank. *J neuroimmunol* (2012) 252(1-2):75–82. doi: 10.1016/j.jneuroim.2012.07.013

10. Zerbo O, Yoshida C, Grether JK, Van de Water J, Ashwood P, Delorenze GN, et al. Neonatal cytokines and chemokines and risk of autism spectrum disorder: the early markers for autism (EMA) study: a case-control study. *J Neuroinflamm* (2014) 11:113. doi: 10.1186/1742-2094-11-113

11. Abdallah MW, Larsen N, Grove J, Bonefeld-Jorgensen EC, Norgaard-Pedersen B, Hougaard DM, et al. Neonatal chemokine levels and risk of autism spectrum disorders: findings from a Danish historic birth cohort follow-up study. *Cytokine* (2013) 61(2):370–6. doi: 10.1016/j.cyto.2012.11.015

12. McAllister AK. Immune contributions to cause and effect in autism spectrum disorder. *Biol Psychiatry* (2017) 81(5):380–2. doi: 10.1016/j.biopsych.2016.12.024

13. Gladysz D, Krzywdzinska A, Hozyasz KK. Immune abnormalities in autism spectrum disorder-could they hold promise for causative treatment? *Mol Neurobiol* (2018) 55(8):6387–435. doi: 10.1007/s12035-017-0822-x

14. Onore C, Careaga M, Ashwood P. The role of immune dysfunction in the pathophysiology of autism. *Brain Behav Immun* (2012) 26(3):383–92. doi: 10.1016/j.bbi.2011.08.007

15. Vargas DL, Nascimbene C, Krishnan C, Zimmerman AW, Pardo CA. Neuroglial activation and neuroinflammation in the brain of patients with autism. *Ann Neurol* (2005) 57(1):67–81. doi: 10.1002/ana.20315

16. Gottfried C, Bambini-Junior V, Francis F, Riesgo R, Savino W. The impact of neuroimmune alterations in autism spectrum disorder. *Front Psychiatry* (2015) 6:121. doi: 10.3389/fpsyt.2015.00121

17. Siniscalco D, Schultz S, Brigida AL, Antonucci N. Inflammation and neuro-immune dysregulations in autism spectrum disorders. *Pharm (Basel)* (2018) 11(2):56. doi: 10.3390/ph11020056

18. Masi A, Quintana DS, Glozier N, Lloyd AR, Hickie IB, Guastella AJ. Cytokine aberrations in autism spectrum disorder: a systematic review and meta-analysis. *Mol Psychiatry* (2015) 20(4):440–6. doi: 10.1038/mp.2014.59

19. Zhao H, Zhang H, Liu S, Luo W, Jiang Y, Gao J. Association of peripheral blood levels of cytokines with autism spectrum disorder: A meta-analysis. *Front Psychiatry* (2021) 12:670200. doi: 10.3389/fpsyt.2021.670200

20. Moher D, Liberati A, Tetzlaff J, Altman DG. Preferred reporting items for systematic reviews and meta-analyses: The PRISMA statement. *Ann Internal Med* (2009) 151(4):264–9. doi: 10.7326/0003-4819-151-4-200908180-00135

21. *Immune cellular sources of abnormal cytokines in the blood in autism spectrum disorder: a systematic review of case-control studies* (2020). Available at: https://www.crd.york.ac.uk/prospero/display_record.php?ID=CRD42020205224.

22. Basheer S, Venkataswamy MM, Christopher R, Van Amelsvoort T, Srinath S, Girimaji SC, et al. Immune aberrations in children with autism spectrum disorder: a case-control study from a tertiary care neuropsychiatric hospital in India. *Psychoneuroendocrinology* (2018) 94:162–7. doi: 10.1016/j.psyneuen.2018.05.002

23. El Wakkad ASED, Saleh MT. The proinflammatory cytokines in children with autism. *Pakistan J Biol Sci* (2006) 9(14):2593–9. doi: 10.3923/pjbs.2006.2593.2599

24. Ricci S, Businaro R, Ippoliti F, Lo Vasco VR, Massoni F, Onofri E, et al. Altered cytokine and BDNF levels in autism spectrum disorder. *Neurotoxicity Res* (2013) 24(4):491–501. doi: 10.1007/s12640-013-9393-4

25. Kordulewska NK, Kostyra E, Piskorz-Ogórek K, Moszyńska M, Cieślińska A, Fiedorowicz E, et al. Serum cytokine levels in children with spectrum autism disorder: Differences in pro- and anti-inflammatory balance. *J Neuroimmunol* (2019) 337:577066. doi: 10.1016/j.jneuroim.2019.577066

26. Ning J, Xu L, Shen CQ, Zhang YY, Zhao Q. Increased serum levels of macrophage migration inhibitory factor in autism spectrum disorders. *NeuroToxicology* (2019) 71:1–5. doi: 10.1016/j.neuro.2018.11.015

27. Ashwood P, Krakowiak P, Hertz-Picciotto I, Hansen R, Pessah I, Van de Water J. Elevated plasma cytokines in autism spectrum disorders provide evidence of immune dysfunction and are associated with impaired behavioral outcome. *Brain behavior Immun* (2011) 25(1):40–5. doi: 10.1016/j.bbi.2010.08.003

28. Yang CJ, Liu CL, Sang B, Zhu XM, Du YJ. The combined role of serotonin and interleukin-6 as biomarker for autism. *Neuroscience* (2015) 284:290–6. doi: 10.1016/j.neuroscience.2014.10.011

29. Guloksuz SA, Abali O, Aktas Cetin E, Bilgic Gazioglu S, Deniz G, Yildirim A, et al. Elevated plasma concentrations of S100 calcium-binding protein b and tumor necrosis factor alpha in children with autism spectrum disorders. *Braz J Psychiatry* (2017) 39(3):195–200. doi: 10.1590/1516-4446-2015-1843

30. Napolioni V, Ober-Reynolds B, Szelinger S, Corneveaux JJ, Pawlowski T, Ober-Reynolds S, et al. Plasma cytokine profiling in sibling pairs discordant for autism spectrum disorder. *J Neuroinflamm* (2013) 10:38. doi: 10.1186/1742-2094-10-38

31. Shen Y, Li Y, Shi L, Liu M, Wu R, Xia K, et al. Autism spectrum disorder and severe social impairment associated with elevated plasma interleukin-8. *Pediatr Res* (2020) 89:591–7. doi: 10.1038/s41390-020-0910-x

32. Tostes MHFS, Teixeira HC, Gattaz WF, Brandão MAF, Raposo NRB. Altered neurotrophin, neuropeptide, cytokines and nitric oxide levels in autism. *Pharmacopsychiatry* (2012) 45(6):241–3. doi: 10.1055/s-0032-1301914

33. Xie J, Huang L, Li X, Li H, Zhou Y, Zhu H, et al. Immunological cytokine profiling identifies TNF-α as a key molecule dysregulated in autistic children. *Oncotarget* (2017) 8(47):82390–8. doi: 10.18632/oncotarget.19326

34. Enstrom A, Onore C, Hertz-Picciotto I, Hansen R, Croen L, Van De Water J, et al. Detection of IL-17 and IL-23 in plasma samples of children with autism. *Am J Biochem Biotechnol* (2008) 4(2):114–20. doi: 10.3844/ajbbsp.2008.114.120

35. Hashim H, Abdelrahman H, Mohammed D, Karam R. Association between plasma levels of transforming growth factor-β1, IL-23 and IL-17 and the severity of autism in Egyptian children. *Res Autism Spectr Disord* (2013) 7(1):199–204. doi: 10.1016/j.rasd.2012.08.007

36. Al-Ayadhi LY, Mostafa GA. Elevated serum levels of interleukin-17A in children with autism. *J Neuroinflamm* (2012) 9:158. doi: 10.1186/1742-2094-9-158

37. Abd-Allah NA, Ibrahim OM, Elmalt HA, Shehata MA, Hamed RA, Elsaadouni NM, et al. Thioredoxin level and inflammatory markers in children with autism spectrum disorders. *Middle East Curr Psychiatry* (2020) 27(1):11. doi: 10.1186/s43045-020-00021-4

38. Ghaffari MA, Mousavinejad E, Riahi F, Mousavinejad M, Afsharmanesh MR. Increased serum levels of tumor necrosis factor-alpha, resistin, and visfatin in the children with autism spectrum disorders: A case-control study. *Neurol Res Int* (2016) 2016:7. doi: 10.1155/2016/9060751

39. Hu CC, Xu X, Xiong GL, Xu Q, Zhou BR, Li CY, et al. Alterations in plasma cytokine levels in chinese children with autism spectrum disorder. *Autism Res* (2018) 11(7):989–99. doi: 10.1002/aur.1940

40. Carissimi C, Laudadio I, Palone F, Fulci V, Cesi V, Cardona F, et al. Functional analysis of gut microbiota and immunoinflammation in children with autism spectrum disorders. *Digestive Liver Dis* (2019) 51(10):1366–74. doi: 10.1016/j.dld.2019.06.006

41. Manzardo AM, Henkhaus R, Dhillon S, Butler MG. Plasma cytokine levels in children with autistic disorder and unrelated siblings. *Int J Dev Neurosci* (2012) 30(2):121–7. doi: 10.1016/j.ijdevneu.2011.12.003

42. Saresella M, Piancone F, Marventano I, Zoppis M, Hernis A, Zanette M, et al. Multiple inflammasome complexes are activated in autistic spectrum disorders. *Brain Behavior Immun* (2016) 57:125–33. doi: 10.1016/j.bbi.2016.03.009

43. Saad K, Abdallah AM, Abdel-Rahman AA, Al-Atram AA, Abdel-Raheem YF, Gad EF, et al. Polymorphism of interleukin-1β and interleukin-1 receptor antagonist genes in

children with autism spectrum disorders. *Prog Neuropsychopharmacol Biol Psychiatry* (2020) 103:109999. doi: 10.1016/j.pnpbp.2020.109999

44. Barbosa IG, Rodrigues DH, Rocha NP, Sousa LFDC, Vieira ELM, Simões-e-Silva AC, et al. Plasma levels of alarmin IL-33 are unchanged in autism spectrum disorder: A preliminary study. *J Neuroimmunol* (2015) 278:69–72. doi: 10.1016/j.jneuroim.2014.11.021

45. Enstrom AM, Onore CE, Van de Water JA, Ashwood P. Differential monocyte responses to TLR ligands in children with autism spectrum disorders. *Brain Behavior Immun* (2010) 24(1):64–71. doi: 10.1016/j.bbi.2009.08.001

46. El-Ansary A, Al-Ayadhi L. Neuroinflammation in autism spectrum disorders. *J Neuroinflamm* (2012) 9:265. doi: 10.1186/1742-2094-9-265

47. El-Ansary A, Al-Ayadhi L. GABAergic/glutamatergic imbalance relative to excessive neuroinflammation in autism spectrum disorders. *J Neuroinflamm* (2014) 11:189. doi: 10.1186/s12974-014-0189-0

48. Hamed NO, Laila Al A, Osman MA, Elkhawad AO, Bjørklund G, Qasem H, et al. Determination of neuroinflammatory biomarkers in autistic and neurotypical Saudi children. *Metab Brain Dis* (2019) 34(4):1049–60. doi: 10.1007/s11011-019-00420-5

49. Okada K, Hashimoto K, Iwata Y, Nakamura K, Tsujii M, Tsuchiya KJ, et al. Decreased serum levels of transforming growth factor-β1 in patients with autism. *Prog Neuropsychopharmacol Biol Psychiatry* (2007) 31(1):187–90. doi: 10.1016/j.pnpbp.2006.08.020

50. Ashwood P, Enstrom A, Krakowiak P, Hertz-Picciotto I, Hansen RL, Croen LA, et al. Decreased transforming growth factor beta1 in autism: A potential link between immune dysregulation and impairment in clinical behavioral outcomes. *J Neuroimmunol* (2008) 204(1-2):149–53. doi: 10.1016/j.jneuroim.2008.07.006

51. El Gohary TM, El Aziz NA, Darweesh M, Sadaa ES. Plasma level of transforming growth factor β 1 in children with autism spectrum disorder. *Egyptian J Ear Nose Throat Allied Sci* (2015) 16(1):69–73. doi: 10.1016/j.ejenta.2014.12.002

52. Ashwood P, Krakowiak P, Hertz-Picciotto I, Hansen R, Pessah IN, Van de Water J. Associations of impaired behaviors with elevated plasma chemokines in autism spectrum disorders. *J Neuroimmunol* (2011) 232(1-2):196–9. doi: 10.1016/j.jneuroim.2010.10.025

53. Shen Y, Oua J, Liu M, Shi L, Li Y, Xiao L, et al. Altered plasma levels of chemokines in autism and their association with social behaviors. *Psychiatry Res* (2016) 244:300–5. doi: 10.1016/j.psychres.2016.07.057

54. Singh S, Yazdani U, Gadad B, Zaman S, Hynan LS, Roatch N, et al. Serum thyroid-stimulating hormone and interleukin-8 levels in boys with autism spectrum disorder. *J Neuroinflamm* (2017) 14:113. doi: 10.1186/s12974-017-0888-4

55. Atwan H, Assarehzadegan MA, Shekarabi M, Jazayeri SM, Barfi S, Shoormasti RS, et al. Assessment of miR-181b-5p, miR-23a-3p, BCL-2, and IL-6 in peripheral blood mononuclear cells of autistic patients; likelihood of reliable biomarkers. *Iranian J Allergy Asthma Immunol* (2020) 19(1):74–83. doi: 10.18502/ijaai.v19i1.2420

56. Nadeem A, Ahmad SF, Attia SM, Al-Ayadhi LY, Bakheet SA, Al-Harbi NO. Oxidative and inflammatory mediators are upregulated in neutrophils of autistic children: Role of IL-17A receptor signaling. *Prog Neuropsychopharmacol Biol Psychiatry* (2019) 90:204–11. doi: 10.1016/j.pnpbp.2018.12.002

57. Abruzzo PM, Matté A, Bolotta A, Federti E, Ghezzo A, Guarnieri T, et al. Plasma peroxiredoxin changes and inflammatory cytokines support the involvement of neuro-inflammation and oxidative stress in autism spectrum disorder. *J Trans Med* (2019) 17:322. doi: 10.1186/s12967-019-2076-z

58. Eftekharian MM, Ghafouri-Fard S, Noroozi R, Omrani MD, Arsang-jang S, Ganji M, et al. Cytokine profile in autistic patients. *Cytokine* (2018) 108:120–6. doi: 10.1016/j.cyto.2018.03.034

59. Kutuk MO, Tufan E, Gokcen C, Kilicaslan F, Karadag M, Mutluer T, et al. Cytokine expression profiles in autism spectrum disorder: A multi-center study from Turkey. *Cytokine* (2020) 133:155152. doi: 10.1016/j.cyto.2020.155152

60. Nadeem A, Ahmad SF, Al-Ayadhi LY, Attia SM, Al-Harbi NO, Alzahrani KS, et al. Differential regulation of Nrf2 is linked to elevated inflammation and nitrative stress in monocytes of children with autism. *Psychoneuroendocrinology* (2020) 113:104554. doi: 10.1016/j.psyneuen.2019.104554

61. Ahmad SF, Ansari MA, Nadeem A, Bakheet SA, Al-Ayadhi LY, Alasmari AF, et al. Involvement of CD45 cells in the development of autism spectrum disorder through dysregulation of granulocyte-macrophage colony-stimulating factor, key inflammatory cytokines, and transcription factors. *Int Immunopharmacol* (2020) 83:106466. doi: 10.1016/j.intimp.2020.106466

62. Nadeem A, Ahmad SF, Attia SM, Al-Ayadhi LY, Al-Harbi NO, Bakheet SA. Dysregulation in IL-6 receptors is associated with upregulated IL-17A related signaling in CD4+ T cells of children with autism. *Prog Neuropsychopharmacol Biol Psychiatry* (2020) 97:109783. doi: 10.1016/j.pnpbp.2019.109783

63. Nadeem A, Ahmad SF, Al-Harbi NO, Alasmari AF, Al-Ayadhi LY, Alasmari F, et al. Upregulation of enzymatic antioxidants in CD4+ T cells of autistic children. *Biochimie* (2020) 171-172:205–12. doi: 10.1016/j.biochi.2020.03.009

64. Akintunde ME, Rose M, Krakowiak P, Heuer L, Ashwood P, Hansen R, et al. Increased production of IL-17 in children with autism spectrum disorders and co-morbid asthma. *J Neuroimmunol* (2015) 286:33–41. doi: 10.1016/j.jneuroim.2015.07.003

65. Ashwood P. Differential T cell levels of tumor necrosis factor receptor-II in children with autism. *Front Psychiatry* (2018) 9. doi: 10.3389/fpsyt.2018.00543

66. Rose DR, Yang H, Serena G, Sturgeon C, Ma B, Careaga M, et al. Differential immune responses and microbiota profiles in children with autism spectrum disorders and co-morbid gastrointestinal symptoms. *Brain Behavior Immun* (2018) 70:354–68. doi: 10.1016/j.bbi.2018.03.025

67. Ashwood P, Krakowiak P, Hertz-Picciotto I, Hansen R, Pessah IN, Van de Water J. Altered T cell responses in children with autism. *Brain Behav Immun* (2011) 25(5):840–9. doi: 10.1016/j.bbi.2010.09.002

68. Balestrieri E, Cipriani C, Matteucci C, Benvenuto A, Coniglio A, Argaw-Denboba A, et al. Children with autism spectrum disorder and their mothers share abnormal expression of selected endogenous retroviruses families and cytokines. *Front Immunol* (2019) 10(SEP). doi: 10.3389/fimmu.2019.02244

69. Ahmad SF, Ansari MA, Nadeem A, Bakheet SA, Al-Ayadhi LY, Alotaibi MR, et al. Dysregulation of T cell immunoglobulin and mucin domain 3 (TIM-3) signaling in peripheral immune cells is associated with immune dysfunction in autistic children. *Mol Immunol* (2019) 106:77–86. doi: 10.1016/j.molimm.2018.12.020

70. Ahmad SF, Nadeem A, Ansari MA, Bakheet SA, Al-Ayadhi LY, Attia SM. Upregulation of IL-9 and JAK-STAT signaling pathway in children with autism. *Prog Neuropsychopharmacol Biol Psychiatry* (2017) 79:472–80. doi: 10.1016/j.pnpbp.2017.08.002

71. Ashwood P, Schauer J, Pessah IN, Van de Water J. Preliminary evidence of the in vitro effects of BDE-47 on innate immune responses in children with autism spectrum disorders. *J Neuroimmunol* (2009) 208(1-2):130–5. doi: 10.1016/j.jneuroim.2008.12.012

72. Bennabi M, Tarantino N, Gaman A, Scheid I, Krishnamoorthy R, Debré P, et al. Persistence of dysfunctional natural killer cells in adults with high-functioning autism spectrum disorders: stigma/consequence of unresolved early infectious events? *Mol Autism* (2019) 10:22. doi: 10.1186/s13229-019-0269-1

73. Enstrom AM, Lit L, Onore CE, Gregg JP, Hansen RL, Pessah IN, et al. Altered gene expression and function of peripheral blood natural killer cells in children with autism. *Brain Behavior Immun* (2009) 23(1):124–33. doi: 10.1016/j.bbi.2008.08.001

74. Molloy CA, Morrow AL, Meinzen-Derr J, Schleifer K, Dienger K, Manning-Courtney P, et al. Elevated cytokine levels in children with autism spectrum disorder. *J Neuroimmunol* (2006) 172(1-2):198–205. doi: 10.1016/j.jneuroim.2005.11.007

75. Heuer LS, Rose M, Ashwood P, Van de Water J. Decreased levels of total immunoglobulin in children with autism are not a result of b cell dysfunction. *J Neuroimmunol* (2012) 251(1-2):94–102. doi: 10.1016/j.jneuroim.2012.07.001

76. Wasilewska J, Kaczmarski M, Stasiak-Barmuta A, Tobolczyk J, Kowalewska E. Low serum IgA and increased expression of CD23 on b lymphocytes in peripheral blood in children with regressive autism aged 3-6 years old. *Arch Med Sci* (2012) 8(2):324–31. doi: 10.5114/aoms.2012.28561

77. Ashwood P, Corbett BA, Kantor A, Schulman H, van de Water J, Amaral DG. In search of cellular immunophenotypes in the blood of children with autism. *PloS One* (2011) 6(5):e19299. doi: 10.1371/journal.pone.0019299

78. Onore C, Enstrom A, Krakowiak P, Hertz-Picciotto I, Hansen R, Van de Water J, et al. Decreased cellular IL-23 but not IL-17 production in children with autism spectrum disorders. *J Neuroimmunol* (2009) 216(1-2):126–9. doi: 10.1016/j.jneuroim.2009.09.005

79. Siniscalco D, Mijatovic T, Bosmans E, Cirillo A, Kruzliak P, Lombardi VC, et al. Decreased numbers of CD57+CD3-cells identify potential innate immune differences in patients with autism spectrum disorder. *In Vivo* (2016) 30(2):83–90.

80. Pelletier M, Maggi L, Micheletti A, Lazzeri E, Tamassia N, Costantini C, et al. Evidence for a cross-talk between human neutrophils and Th17 cells. *Blood* (2010) 115(2):335–43. doi: 10.1182/blood-2009-04-216085

81. Mehta AK, Gracias DT, Croft M. TNF activity and T cells. *Cytokine* (2018) 101:14–8. doi: 10.1016/j.cyto.2016.08.003

82. Ben Aribia MH, Leroy E, Lantz O, Métivier D, Autran B, Charpentier B, et al. rIL 2-induced proliferation of human circulating NK cells and T lymphocytes: synergistic effects of IL 1 and IL 2. *J Immunol* (1987) 139(2):443–51.

83. Ben-Sasson SZ, Hu-Li J, Quiel J, Cauchetaux S, Ratner M, Shapira I, et al. IL-1 acts directly on CD4 T cells to enhance their antigen-driven expansion and differentiation. *Proc Natl Acad Sci U.S.A.* (2009) 106(17):7119–24. doi: 10.1073/pnas.0902745106

84. Huang T, Schor SL, Hinck AP. Biological activity differences between TGF-beta1 and TGF-beta3 correlate with differences in the rigidity and arrangement of their component monomers. *Biochemistry* (2014) 53(36):5737–49. doi: 10.1021/bi500647d

85. Travis MA, Sheppard D. TGF-beta activation and function in immunity. *Annu Rev Immunol* (2014) 32:51–82. doi: 10.1146/annurev-immunol-032713-120257

86. Kubiczkova L, Sedlarikova L, Hajek R, Sevcikova S. TGF-β - an excellent servant but a bad master. *J Transl Med* (2012) 10:183. doi: 10.1186/1479-5876-10-183

87. Lohr J, Knoechel B, Wang JJ, Villarino AV, Abbas AK. Role of IL-17 and regulatory T lymphocytes in a systemic autoimmune disease. *J Exp Med* (2006) 203 (13):2785–91. doi: 10.1084/jem.20061341

88. Tran DQ. TGF-β: the sword, the wand, and the shield of FOXP3(+) regulatory T cells. *J Mol Cell Biol* (2012) 4(1):29–37. doi: 10.1093/jmcb/mjr033

89. Korn T, Bettelli E, Oukka M, Kuchroo VK. IL-17 and Th17 cells. *Annu Rev Immunol* (2009) 27:485–517. doi: 10.1146/annurev.immunol.021908.132710

90. Volpe E, Servant N, Zollinger R, Bogiatzi SI, Hupé P, Barillot E, et al. A critical function for transforming growth factor-beta, interleukin 23 and proinflammatory cytokines in driving and modulating human T(H)-17 responses. *Nat Immunol* (2008) 9(6):650–7. doi: 10.1038/ni.1613

91. Yoshimura A, Wakabayashi Y, Mori T. Cellular and molecular basis for the regulation of inflammation by TGF-beta. *J Biochem* (2010) 147(6):781–92. doi: 10.1093/jb/mvq043

92. Andersson J, Tran DQ, Pesu M, Davidson TS, Ramsey H, O'Shea JJ, et al. CD4+ FoxP3+ regulatory T cells confer infectious tolerance in a TGF-beta-dependent manner. *J Exp Med* (2008) 205(9):1975–81. doi: 10.1084/jem.20080308

93. Choi H, Song J, Park G, Kim J. Modeling of autism using organoid technology. *Mol Neurobiol* (2017) 54(10):7789–95. doi: 10.1007/s12035-016-0274-8

94. Hsiao EY, McBride SW, Chow J, Mazmanian SK, Patterson PH. Modeling an autism risk factor in mice leads to permanent immune dysregulation. *Proc Natl Acad Sci U.S.A.* (2012) 109(31):12776–81. doi: 10.1073/pnas.1202556109

95. O'Connor W, Zenewicz LA, Flavell RA. The dual nature of TH17 cells: shifting the focus to function. *Nat Immunol* (2010) 11(6):471–6. doi: 10.1038/ni.1882

96. Li L, Huang L, Vergis AL, Ye H, Bajwa A, Narayan V, et al. IL-17 produced by neutrophils regulates IFN-gamma-mediated neutrophil migration in mouse kidney ischemia-reperfusion injury. *J Clin Invest* (2010) 120(1):331–42. doi: 10.1172/JCI38702

97. Seo W, Shimizu K, Kojo S, Okeke A, Kohwi-Shigematsu T, S-i F, et al. Runx-mediated regulation of CCL5 *via* antagonizing two enhancers influences immune cell function and anti-tumor immunity. *Nat Commun* (2020) 11(1):1562. doi: 10.1038/s41467-020-15375-w

98. Denys D, Fluitman S, Kavelaars A, Heijnen C, Westenberg H. Decreased TNF-alpha and NK activity in obsessive-compulsive disorder. *Psychoneuroendocrinology* (2004) 29(7):945–52. doi: 10.1016/j.psyneuen.2003.08.008

99. Evans DL, Folds JD, Petitto JM, Golden RN, Pedersen CA, Corrigan M, et al. Circulating natural killer cell phenotypes in men and women with major depression. relation to cytotoxic activity and severity of depression. *Arch Gen Psychiatry* (1992) 49(5):388–95. doi: 10.1001/archpsyc.1992.01820050052009

100. Mosmann TR, Cherwinski H, Bond MW, Giedlin MA, Coffman RL. Two types of murine helper T cell clone. i. definition according to profiles of lymphokine activities and secreted proteins. *J Immunol* (1986) 136(7):2348–57.

101. Simon AK, Hollander GA , McMichael A. Evolution of the immune system in humans from infancy to old age. *Proc Biol Sci* (2015) 282 (1821):20143085. doi: 10.1098/rspb.2014.3085

102. Biancotto A, Feng X, Langweiler M, Young NS, McCoy JP. Effect of anticoagulants on multiplexed measurement of cytokine/chemokines in healthy subjects. *Cytokine* (2012) 60(2):438–46. doi: 10.1016/j.cyto.2012.05.019

103. Liu C, Chu D, Kalantar-Zadeh K, George J, Young HA, Liu G. Cytokines: From clinical significance to quantification. *Adv Sci (Weinh)* (2021) 8(15): e2004433. doi: 10.1002/advs.202004433

104. Parkitny L, McAuley JH, Kelly PJ, Di Pietro F, Cameron B, Moseley GL. Multiplex cytokine concentration measurement: how much do the medium and handling matter? *Mediators Inflammation* (2013) 2013:890706. doi: 10.1155/2013/890706

frontiers | Frontiers in Immunology

TYPE Brief Research Report
PUBLISHED 21 June 2023
DOI 10.3389/fimmu.2023.1157265

OPEN ACCESS

EDITED BY
Arnaud Zaldumbide,
Leiden University Medical Center (LUMC), Netherlands

REVIEWED BY
Sally C. Kent,
University of Massachusetts Medical School, United States
Xiaofan Jia,
University of Colorado Anschutz Medical Campus, United States

*CORRESPONDENCE
Tuure Kinnunen
tuure.kinnunen@uef.fi

RECEIVED 02 February 2023
ACCEPTED 05 June 2023
PUBLISHED 21 June 2023

CITATION
Schroderus AM, Poorbaugh J, McElyea S, Beasley S, Zhang L, Näntö-Salonen K, Rintamäki R, Pihlajamäki J, Knip M, Veijola R, Toppari J, Ilonen J, Benschop RJ and Kinnunen T (2023) Evaluation of plasma IL-21 as a potential biomarker for type 1 diabetes progression. *Front. Immunol.* 14:1157265. doi: 10.3389/fimmu.2023.1157265

Evaluation of plasma IL-21 as a potential biomarker for type 1 diabetes progression

Anna-Mari Schroderus[1], Josh Poorbaugh[2], Samantha McElyea[2], Stephanie Beasley[2], Lin Zhang[2], Kirsti Näntö-Salonen[3], Reeta Rintamäki[4], Jussi Pihlajamäki[4,5], Mikael Knip[6,7,8], Riitta Veijola[9], Jorma Toppari[3,10], Jorma Ilonen[11], Robert J. Benschop[2] and Tuure Kinnunen[1,12]*

[1]Department of Clinical Microbiology, Institute of Clinical Medicine, University of Eastern Finland, Kuopio, Finland, [2]Eli Lilly and Company, Indianapolis, IN, United States, [3]Department of Pediatrics, Turku University Hospital, Turku, Finland, [4]Department of Medicine, Endocrinology and Clinical Nutrition, Kuopio University Hospital, Kuopio, Finland, [5]Institute of Public Health and Clinical Nutrition, University of Eastern Finland, Kuopio, Finland, [6]Tampere Center for Child Health Research, Tampere University Hospital, Tampere, Finland, [7]Pediatric Research Center, New Children's Hospital, Helsinki University Hospital, Helsinki, Finland, [8]Research Program for Clinical and Molecular Metabolism, Faculty of Medicine, University of Helsinki, Helsinki, Finland, [9]PEDEGO Research Unit, Department of Pediatrics, Medical Research Center, Oulu University Hospital and University of Oulu, Oulu, Finland, [10]Institute of Biomedicine, Research Centre for Integrative Physiology and Pharmacology, Centre for Population Health Research, University of Turku, Turku, Finland, [11]Immunogenetics Laboratory, Institute of Biomedicine, University of Turku, Turku, Finland, [12]ISLAB Laboratory Centre, Kuopio, Finland

IL-21 is a multifunctional cytokine linked with the pathophysiology of several autoimmune diseases, including type 1 diabetes. In this study, our aim was to examine plasma IL-21 levels in individuals at different stages of type 1 diabetes progression. We measured plasma IL-21 levels, as well as levels of other key pro-inflammatory cytokines (IL-17A, TNF-α and IL-6), from 37 adults with established type 1 diabetes and 46 healthy age-matched adult controls, as well as from 53 children with newly diagnosed type 1 diabetes, 48 at-risk children positive for type 1 diabetes-associated autoantibodies and 123 healthy age-matched pediatric controls using the ultrasensitive Quanterix SiMoA technology. Adults with established type 1 diabetes had higher plasma IL-21 levels compared to healthy controls. However, the plasma IL-21 levels showed no statistically significant correlation with clinical variables, such as BMI, C-peptide, HbA1c, or hsCRP levels, evaluated in parallel. In children, plasma IL-21 levels were almost ten times higher than in adults. However, no significant differences in plasma IL-21 levels were detected between healthy children, autoantibody-positive at-risk children, and children with newly diagnosed type 1 diabetes. In conclusion, plasma IL-21 levels in adults with established type 1 diabetes were increased, which may be associated with autoimmunity. The physiologically high plasma IL-21 levels in children may, however, reduce the potential of IL-21 as a biomarker for autoimmunity in pediatric subjects.

KEYWORDS

autoimmunity, autoimmune diseases, interleukin-21, IL-21, human, type 1 diabetes

1 Introduction

Type 1 diabetes (T1D) is a chronic autoimmune disease, in which autoreactive T cells mediate the progressive destruction of insulin-producing beta cells in the pancreas. T1D is preceded by a preclinical phase of variable length, during which circulating autoantibodies (AAb) to islet autoantigens are almost invariably detected (1). It is well-established that T cells play a central role in the T1D disease process (2). However, the exact T-cell phenotypes or immune pathways involved remain largely elusive. Recently, the interleukin-21 (IL-21) pathway has gained attention, as it has been associated with the development of T1D both in murine models (3) as well as in human studies (4–6).

IL-21 is a pleiotropic cytokine with multiple functions. It is a hallmark cytokine of $CD4^+CXCR5^+$ T follicular helper (Tfh) cells (7, 8). In addition, it is produced by Th17 cells (7) and a recently identified population, coined T peripheral helper (Tph) cells (9, 10). IL-21 has a fundamental role in B-cell helper functions. In order to activate, expand and produce antibodies, B cells are largely dependent on the help provided by IL-21-producing Tfh cells in lymph nodes (7, 8), and possibly also by Tph cells within inflamed tissues (10). Importantly, IL-21 is also known to support the effector functions and cytotoxicity of $CD8^+$ T cells (7). IL-21 produced by $CD4^+$ T cells may therefore contribute to the T1D disease process also by activating autoreactive $CD8^+$ T cells in the pancreas (11–13).

Interestingly, an expansion of circulating Tfh and Tph cells and increased IL-21 production by T cells has been observed both in children with newly diagnosed T1D (6, 14), as well as in adults with established T1D (4, 5). Moreover, Th17 cells, another potential source of IL-21, appear to be increased both in the blood and pancreatic lymph nodes of patients with T1D (15, 16). These findings implicate the IL-21 pathway to be an appealing candidate for immunotherapy of T1D. Promisingly, in a recently completed phase 2 trial, an anti-IL-21 antibody combined with liraglutide was shown to preserve beta-cell function in patients with recent-onset T1D (17).

Given the importance of IL-21 for autoimmunity, blood IL-21 levels could serve as a potential biomarker of disease activity in autoimmune disorders. Indeed, in some autoimmune diseases, such as Sjögren's syndrome (18) and systemic lupus erythematosus (SLE) (19), plasma and/or serum IL-21 levels are elevated in patients. Recently, limitations in the specificity and sensitivity of commercially available human IL-21 ELISA kits have been identified, and as a result, a new ultrasensitive assay for detecting IL-21 based on the Quanterix SiMoA (Single Molecule Array) technology was developed (20). With this assay, it was demonstrated that IL-21 concentrations in plasma and serum are considerably lower than previously published data using less sensitive and less specific assays suggested. Importantly, higher plasma IL-21 levels in patients with Sjögren's syndrome and SLE compared to healthy individuals were also validated with this ultrasensitive assay (20).

To our knowledge, plasma IL-21 levels have previously been investigated in a limited number of studies related to T1D, all of which have suggested that patients with T1D (21, 22) and AAb^+ at-risk children (23) have higher IL-21 levels in blood than controls. In this study, we analyzed plasma IL-21, as well as levels of other key pro-inflammatory cytokines (IL-17A, TNF-α and IL-6) with the ultrasensitive Quanterix SiMoA technology at different stages of T1D development, utilizing samples from cross-sectional cohorts of adults with established T1D, children with newly diagnosed T1D, and AAb^+ at-risk children together with age-matched controls.

2 Materials and methods

2.1 Study subjects

The adult cohort comprised 37 patients with established T1D and 46 healthy age-matched controls (Table 1). The pediatric cohort consisted of 53 children with newly diagnosed T1D (0 to 7 days after clinical diagnosis), 48 autoantibody-positive (AAb^+) at-risk children, and 123 healthy control children who were autoantibody-negative and age-matched with the T1D and AAb^+ cases (Table 2). The AAb^+ and healthy control children participated in the Finnish Type 1 Diabetes Prediction and Prevention (DIPP) follow-up study and carried HLA genotypes associated with increased risk for T1D. Autoantibody-positivity was analyzed, as previously described (24). Autoantibody-positivity was defined based on the presence of one or more biochemical autoantibodies (insulin autoantibodies [IAA], insulinoma-associated-2 antibodies [IA-2A] and glutamic acid decarboxylase antibodies [GADA]).

Plasma samples were collected between May 2013 and January 2016 for the pediatric cohort at the DIPP study center in Turku, Finland, and between February 2012 and March 2020 for the adult cohort at the University of Eastern Finland, Kuopio, Finland. Plasma was collected from heparinized peripheral blood samples after centrifugation at 700 x g for 10 min and stored at -80°C until analysis.

All participants and/or their legal guardians provided written informed consent, as mandated by the Declaration of Helsinki. The study was approved by local ethics committees of the University Hospitals of Turku and Kuopio, and for the DIPP study by the ethics committee of the Hospital District of Northern Ostrobothnia.

2.2 Quanterix SiMoA assays

The heparin plasma samples were randomized for plating, then thawed and aliquoted in batches to reduce freeze-thaw cycles. For all samples, assessment of IL-21 levels was performed using the Quanterix SiMoA assay as previously reported (20). Assessment of IL-17A, IL-6 and TNF-α levels was performed using the Cytokine 3 Plex B Quanterix SiMoA assay, according to manufacturer's instructions.

The spike recoveries were determined by comparing the spike samples of the observed back-calculated concentration from calibration curve against known spiked concentration. Limits of detection (LODs) were determined by the selection criteria of 75%–125% of the calibration recovery (i.e., comparing the calibration samples of the calculated concentration to expected concentration). Limits of Quantitation (LOQs) were determined by the selection criteria of 75%–125% of the spike recovery (i.e., comparing the spike samples of the calculated concentration to expected

concentration). The analyses for the adult cohort were performed in two batches, with slightly different LOD and Lower Limit of Quantitation (LLOQ) values, and batch correction was calculated using linear model in R (25).

2.3 C-peptide and hsCRP measurements

C-peptide was measured from heparinized plasma with electrochemiluminescence immunoassay (detection limit 0.007 nmol/L, Cobas, Roche Diagnostics) and high-sensitivity C-reactive protein (hsCRP) from heparinized plasma with particle enhanced immunoturbidimetric assay (detection limit 0.15 mg/L, Cobas, Roche Diagnostics).

2.4 Statistical analyses

Graphpad Prism version 9.1.0 (GraphPad Software, San Diego, California USA) was used for statistical analyses. Kruskal-Wallis test followed by Dunn's multiple comparison test was applied when comparing more than two groups. Mann-Whitney test or Wilcoxon matched-pairs signed-rank test was used when comparing two groups. No power calculations were made as the study was exploratory in nature with very limited previous data to support the calculations, and sample sizes were determined in part by feasibility. Spearman's correlation was calculated when relationships between plasma cytokine concentrations and different variables were assessed. Simple linear regression was used to calculate regression lines for each group. Slopes and intercepts of the regression lines were compared, and two-tailed P-values were calculated for them in Prism. P-values <0.05 were considered to indicate statistical significance.

3 Results

3.1 Plasma IL-21 levels are higher in adults with established type 1 diabetes than in healthy controls

Plasma IL-21, as well as IL-17A, TNF-α, and IL-6 levels were analyzed in 37 adults with established T1D and in 47 age-matched healthy controls. Plasma IL-21 levels were 2.5-fold higher in T1D patients (median 0.05 pg/mL) compared to healthy controls (median 0.02 pg/mL, $P < 0.001$, Figure 1A). Plasma IL-6 levels were also elevated in T1D patients compared to controls (median 1.03 pg/mL vs. 0.61 pg/mL, $P < 0.05$), but plasma IL-17A and TNF-α levels were similar between the study groups (Supplementary Figure 1).

Next, we examined whether selected clinical variables were associated with plasma IL-21 levels. No correlations were observed between age, hsCRP, C-peptide levels, HbA1c values, body-mass index (BMI), or disease duration with plasma IL-21 levels in the T1D patients (Figure 1B, Supplementary Figure 1). However, plasma IL-21 levels correlated positively with both TNF-α ($P < 0.001$, r=0.40) and IL-6 ($P < 0.05$, r=0.27) levels. Moreover, IL-17A levels correlated with TNF-α ($P < 0.001$, r=0.57) and IL-6 ($P < 0.001$, r=0.60) levels, while TNF-α levels correlated with hsCRP ($P < 0.05$, r=0.26) (Supplementary Figure 1).

3.2 Plasma IL-21 levels are similar in children with newly diagnosed type 1 diabetes, children at-risk for type 1 diabetes and healthy controls

Next, we analyzed the plasma cytokine levels in samples from 53 children with newly diagnosed T1D and 48 AAb^+ at-risk children, as well as from 123 healthy age-matched controls. In the pediatric

TABLE 1 Characteristics of the adult cohort.

Study group	Healthy controls	T1D patients
n	46	37
Age (years), mean ± SD	26.1 ± 4.3	26.6 ± 6.4
Age range (years)	20–38	18–39
Disease duration (years), mean ± SD	N/A*	11.7 ± 8.1
Disease duration range (years)	N/A	0–36
Male	40% (20/46)	57% (21/37)
Female	60% (26/46)	43% (16/37)
Clinical variables:		
HbA1c (mmol/mol), mean ± SD	ND†	64.6 ± 13.7 (n=32)
C-peptide (nmol/L), mean ± SD	ND	0.11± 0.17
BMI (kg/m^2), mean ± SD	ND	26.6 ± 5.1 (n=29)
hsCRP (mg/L), mean ± SD	1.31± 1.96	3.15 ± 5.14

*not applicable, †not determined.

cohort, plasma IL-21 levels (Figure 2A), as well as IL-17A, TNF-α, and IL-6 levels Supplementary Figure 2) were similar between children with T1D, AAb$^+$ at-risk children, and healthy controls. Of note, plasma IL-21 levels in children (median 0.26 pg/mL for the whole pediatric cohort) were around ten-fold higher compared to those observed in the adult cohort (Figures 1A, 2A). Accordingly, a strong negative correlation between age and IL-21 levels ($P < 0.001$, r=-0.35), as well as to a lesser extent between age and IL-17A ($P < 0.01$, r=-0.20) and TNF-α ($P < 0.001$, r=-0.24) levels, was observed in the pediatric cohort (Figure 2B, Supplementary Figure 2). However, even after stratification with age, no differences in plasma IL-21 levels between the pediatric study groups were detected (Figure 2B, Supplementary Figure 2). Finally, these results were further corroborated by a stringent pairwise analysis of a subset of samples from T1D and AAb$^+$ children that were drawn and processed in parallel with a sample from an age-matched healthy control child on the same day (Supplementary Figure 3). In addition, we analyzed correlation between selected clinical variables and plasma cytokine levels in children with newly diagnosed T1D. We did not observe correlations between cytokine levels and clinical variables at diagnosis (plasma glucose, HbA1c, blood pH, or beta-hydroxybutyrate levels) (Supplementary Figure 2). Of note, similar to the adult cohort, IL-17A levels correlated with TNF-α ($P < 0.001$, r=0.66) and IL-6 ($P < 0.001$, r=0.48) levels also in the pediatric cohort (Supplementary Figure 2).

We have previously observed that the frequency of both circulating Tfh (6) and Tph (14) cells was increased in children with newly diagnosed T1D positive for at least two AAbs but not in those positive for one AAb or none. Hence, we next stratified both AAb$^+$ children and children with T1D into two subgroups based on the number of autoantibodies detected (≤1 or ≥2) in these children. However, plasma IL-21, as well as IL-17A, TNF-α, and IL-6 levels were again similar in AAb$^+$ children and children with T1D positive for either ≤1 or ≥2 autoantibodies (Figures 2C, D, Supplementary Figure 4). In addition, we analyzed whether plasma cytokine levels differed between those AAb$^+$ at-risk children who had progressed to T1D (mean time to T1D after sampling 2.6 ± 1.4 years) and those who had not. However, again, no differences were detected between the groups (Figure 2E, Supplementary Figure 5).

Finally, flow cytometry data were available on selected T-cell subset frequencies for the pediatric samples (6, 26). Hence, we examined the correlation between plasma IL-21 levels and selected T-cell subset frequencies. The frequencies of activated Tfh cells (PD-1$^+$ICOS$^+$ of CXCR5$^+$ memory CD4$^+$ T cells) (6) positively correlated with plasma IL-21 levels ($P < 0.001$, r=0.29, Figure 2F). A weaker positive correlation was also observed with the frequency of

TABLE 2 Characteristics of the pediatric cohort.

Study group	Healthy children	AAb$^+$ at-risk children	Newly diagnosed T1D patients
n	123	48	53
Age (years), mean ± SD	8.9 ± 4.0	8.6 ± 4.7	8.5 ± 3.8
Age range (years)	2.0–15.7	2.0–17.2	2.4–17.5
Male	63% (77/123)	54% (26/48)	51% (27/53)
Female	37% (46/123)	46% (22/48)	49% (26/53)
Progressors*	N/A†	52% (25/48)	N/A
Time (years) from sampling to clinical T1D, mean ± SD	N/A	2.6 ± 1.4	N/A
Time (years) from birth to clinical T1D, mean ± SD	N/A	10.0 ± 4.1	N/A
Autoantibodies:			
GADA	N/A	63% (30/48)	68% (36/53)
IA-2A	N/A	67% (32/48)	75% (40/53)
IAA	N/A	48% (23/48)	25% (13/53)
Number of autoantibodies:			
≤1 AAb	N/A	31% (15/48)	30% (16/53)
≥2 AAb	N/A	69% (33/48)	70% (37/53)
Clinical variables at diagnosis:			
Plasma glucose (mmol/L), mean ± SD	N/A	N/A	24.3 ± 10.7 (n=43)
HbA1c (mmol/mol), mean ± SD	N/A	N/A	79.0 ± 30.1 (n=31)
Blood pH, mean ± SD	N/A	N/A	7.34 ± 0.11 (n=42)
Beta-hydroxybutyrate (mmol/L), mean ± SD	N/A	N/A	2.83 ± 2.79 (n=44)

*individuals, who have progressed from AAb$^+$ stage to clinical T1D during follow-up, †not applicable.

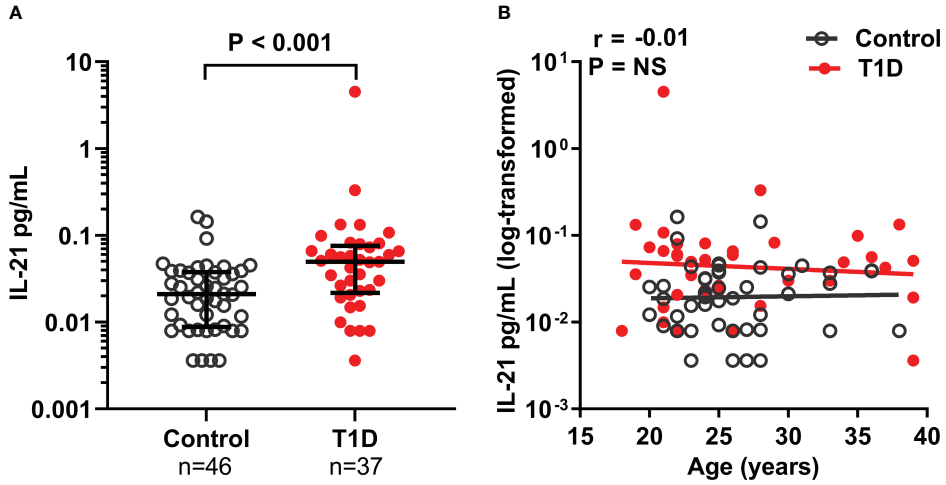

FIGURE 1
Plasma IL-21 levels are elevated in adults with T1D. **(A)** Plasma IL-21 levels in adults with established T1D and healthy controls. Mann-Whitney U-test was used for statistical analysis. **(B)** Correlation between age and $\log_{10}$-transformed plasma IL-21 levels was examined using Spearman's correlation by pooling the data from both study groups and is expressed together with the P value on the plot. The elevations of the linear regression lines were significantly different between the study groups (P = 0.001). Medians and IQRs are shown in the **(A)**.

regulatory T cells (Treg; $CD25^{+}CD127^{low}$ of $CD4^{+}$ T cells) (26) and plasma IL-21 levels ($P < 0.05$, r=0.17, Supplementary Figure 6). However, no correlation was observed between the frequency of Th17 cells ($CCR6^{+}CXCR3^{-}$ of memory $CD4^{+}$ T cells) (26) and plasma IL-21 levels (Supplementary Figure 6).

4 Discussion

In this study, we demonstrated that adults with established T1D had significantly elevated plasma IL-21 and IL-6 levels compared to age-matched controls. IL-21 levels did not correlate with the time from diagnosis or C-peptide levels, a marker of residual beta-cell function. Moreover, no correlation between plasma IL-21 levels and HbA1c levels, a marker related to glycemic control, or hsCRP, a marker related to inflammation, was observed. Therefore, the elevated plasma IL-21 levels do not appear to be associated with the extent of beta-cell destruction, hyperglycemia itself, or with underlying inflammation in T1D patients in the cohort studied.

In the pediatric cohort, we did not observe differences in plasma IL-21 levels between patients with newly diagnosed T1D, AAb^{+} at-risk children, and healthy age-matched children. Similar to adults, no correlation between plasma IL-21 levels and clinical variables, such as level of hyperglycemia (blood glucose and HbA1c levels at diagnosis) or markers of ketoacidosis (blood pH and beta-hydroxybutyrate levels) were found in children with T1D. Moreover, no associations between plasma IL-21 levels and autoantibody status or the risk of progression to clinical T1D in AAb^{+} at-risk children were observed.

An important observation in our study was that plasma IL-21 levels appear to be physiologically around ten-fold higher in children than in adults. Importantly, for the other cytokines, IL-17A, TNF-α, and IL-6, assessed in this study, no such phenomenon was observed. This observation could potentially explain the discrepancy that higher plasma IL-21 levels were observed only in adult T1D patients but not in children with T1D. As the plasma IL-21 levels were only modestly elevated in adult T1D patients compared to controls, a corresponding small change would be masked by the considerably higher physiological background levels in children. Another interesting finding in the pediatric cohort was that plasma IL-21 levels correlated with the frequency of activated Tfh cells in blood, potentially implicating Tfh cells as a major source of plasma IL-21.

Three previous studies have reported slightly elevated plasma IL-21 levels in both adult and pediatric patients with T1D (21, 22), as well as in AAb^{+} at-risk children (23). However, in these studies either ELISA or Luminex xMAP technologies were used, and the IL-21 levels reported were >100-fold higher than in our study using the ultrasensitive Quanterix SiMoA technology. Previous validation results strongly suggest that these conspicuously higher IL-21 levels reported in the previous studies may not accurately reflect physiological cytokine levels, as these older methods lack both the sensitivity and specificity required to detect endogenous IL-21 levels reliably (20).

In addition to using an ultrasensitive analysis method, the major strengths of our study are the large cohort sizes and the stringent matching with HLA background, age, and sampling date in the pediatric cohort, which all considerably strengthen the validity of our results. One caveat of our study is that we were only able to analyze cross-sectional cohorts. In the future, longitudinal analyses could potentially better detect subtle intraindividual alterations in cytokine levels occurring during T1D progression. Moreover, the analysis of patients with type 2 diabetes could help confirm whether the increased plasma IL-21 levels in adults with T1D are truly associated with autoimmunity and are not secondary to hyperglycemia and/or exogenous insulin use.

In conclusion, for the first time, IL-21 was quantified using an ultrasensitive and specific method and found to be elevated in adults with established T1D, supporting a potential role of IL-21 in the T1D disease process. In contrast, in the pediatric cohort, comprising children with newly diagnosed T1D, AAb^{+} children at-risk for T1D,

10.3389/fimmu.2023.1157265

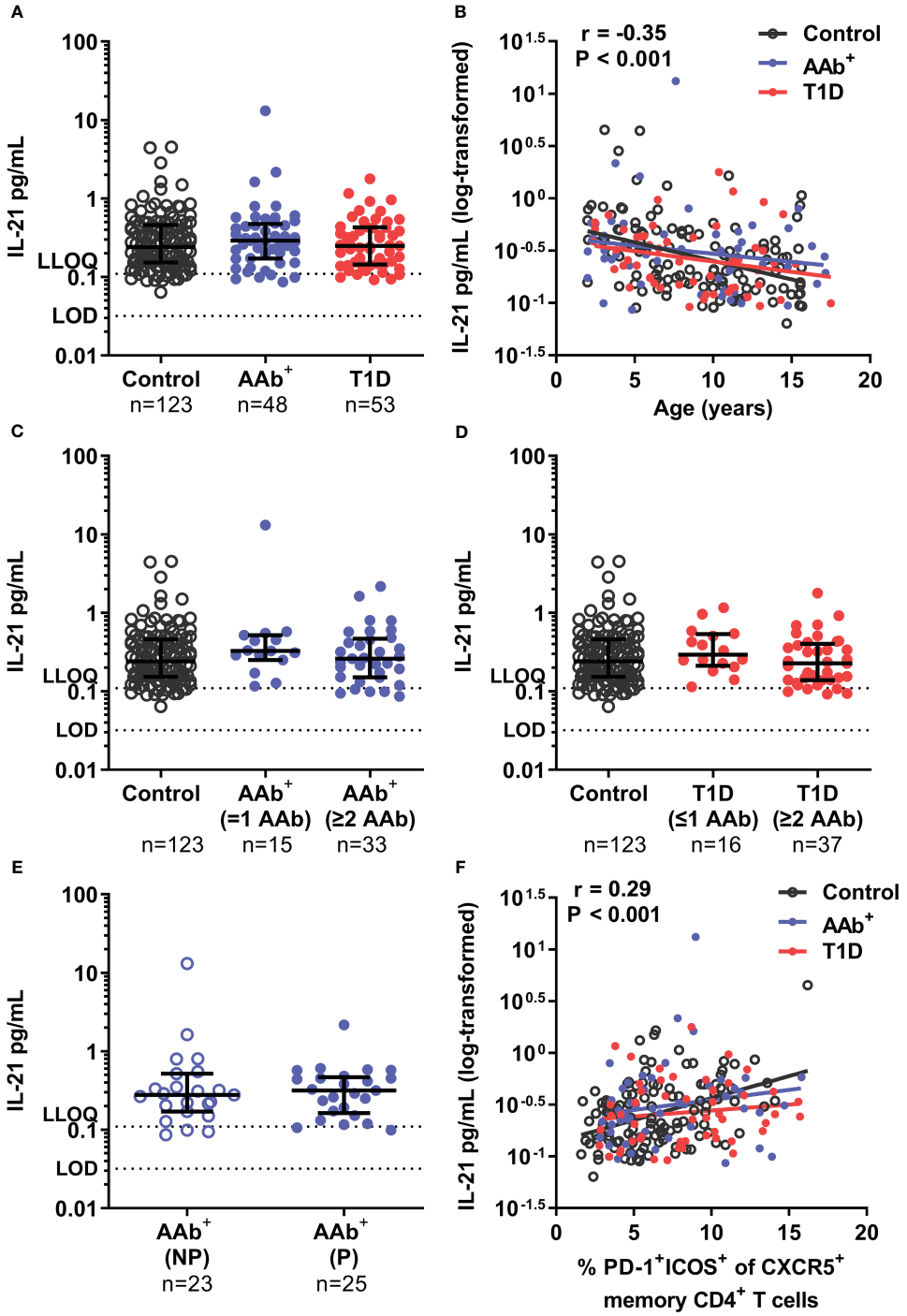

FIGURE 2
Similar plasma IL-21 levels in children with newly diagnosed T1D, AAb+ at-risk children and healthy children. **(A)** Plasma IL-21 levels in children with newly diagnosed T1D, AAb^+ at-risk children and control children. **(B)** Correlation between age and log_{10}-transformed plasma IL-21 levels was examined using Spearman's correlation by pooling the data from all study groups and is presented together with the P value on the plot. The elevations of the linear regression lines were comparable between the study groups. AAb^+ at-risk children **(C)** and children with newly diagnosed T1D **(D)** were stratified into two subgroups based on the number of persistent autoantibodies detected at sampling (positive for ≤1 autoantibodies and ≥2 autoantibodies). **(E)** AAb^+ at-risk children were divided into non-progressors (NP) and progressors (P) depending on whether they had later progressed to T1D during follow-up. Kruskal-Wallis with Dunn's multiple comparisons test or Mann-Whitney U-test was used for statistical analyses. Medians with IQRs are shown, and limit of detection (LOD) and lower limit of quantification (LLOQ) are represented with dotted lines in A, C–E. **(F)** Correlation between the frequency of circulating activated Tfh ($PD\text{-}1^+ICOS^+$ of $CXCR5^+$ memory $CD4^+$ T cells) and log_{10}-transformed plasma IL-21 levels was examined using Spearman's correlation by pooling the data from all study groups, and is expressed together with the P value on the plot. The elevations of the linear regression lines were comparable between the study groups.

and age-matched healthy controls, we did not observe differences in plasma IL-21 levels between the study groups. The physiologically higher plasma IL-21 levels in children may, however, mask potential changes caused by T1D autoimmunity. Taken together, the direct detection of plasma IL-21 levels, even by the ultrasensitive method capable of detecting fg/mL concentrations of cytokines employed here, may have limited potential as a biomarker of T1D progression, particularly in children.

Data availability statement

The raw data supporting the conclusions of this article will be made available by the authors, without undue reservation.

Ethics statement

The studies involving human participants were reviewed and approved by local ethics committees of the University Hospitals of Turku and Kuopio and the ethics committee of the Hospital District of Northern Ostrobothnia. Written informed consent to participate in this study was provided by the participants or participants' legal guardian/next of kin.

Author contributions

JPo, SM and SB measured the cytokines. RR, JPi, KN-S and JT provided the clinical research samples. MK and RV were responsible for the islet autoantibody analyses of the pediatric cohort. JI was responsible for the HLA screening of the pediatric study subjects. A-MS, JPo, SM, SB, LZ, RJB and TK analyzed the data and drafted the manuscript. TK is the guarantor of this work and, as such, had full access to all the data in the study and takes responsibility for the integrity of the data and the accuracy of the data analysis. All authors contributed to the article and approved the submitted version.

Funding

This work was supported by the Academy of Finland (decision no. 331282) and the Sigrid Jusélius Foundation.

Acknowledgments

We thank the skillful technical assistance of Hanna Eskelinen (University of Eastern Finland), Anne Suominen (University of Turku), Matti Laitinen (Kuopio University Hospital) and Satu Miettinen (Eastern Finland Laboratory Centre).

Conflict of interest

JPo, SM, SB, LZ, and RB are employees of Eli Lilly & Company and may own stock.

The remaining authors declare that the research was conducted in the absence of any commercial or financial relationships that could be constructed as a potential conflict of interest.

Publisher's note

Supplementary material

The Supplementary Material for this article can be found online at: https://www.frontiersin.org/articles/10.3389/fimmu.2023.1157265/full#supplementary-material

References

1. Ziegler AG, Rewers M, Simell O, Simell T, Lempainen J, Steck A, et al. Seroconversion to multiple islet autoantibodies and risk of progression to diabetes in children. *JAMA - J Am Med Assoc* (2013) 309:2473–9. doi: 10.1001/jama.2013.6285

2. Atkinson MA, Eisenbarth GS, Michels AW. Type 1 diabetes. *Lancet* (2014) 383:69–82. doi: 10.1016/S0140-6736(13)60591-7

3. Sutherland APR, Van Belle T, Wurster AL, Suto A, Michaud M, Zhang D, et al. Interleukin-21 is required for the development of type 1 diabetes in nod mice. *Diabetes* (2009) 58:1144–55. doi: 10.2337/db08-0882

4. Kenefeck R, Wang CJ, Kapadi T, Wardzinski L, Attridge K, Clough LE, et al. Follicular helper T cell signature in type 1 diabetes. *J Clin Invest* (2015) 125:292–303. doi: 10.1172/JCI76238

5. Ferreira RC, Simons HZ, Thompson WS, Cutler AJ, Dopico XC, Smyth DJ, et al. IL-21 production by CD4+ effector T cells and frequency of circulating follicular helper T cells are increased in type 1 diabetes patients. *Diabetologia* (2015) 58:781–90. doi: 10.1007/s00125-015-3509-8

6. Viisanen T, Ihantola E-L, Näntö-Salonen K, Hyöty H, Nurminen N, Selvenius J, et al. Circulating CXCR5 + PD-1 + ICOS + follicular T helper cells are increased close to the diagnosis of type 1 diabetes in children with multiple autoantibodies. *Diabetes* (2017) 66:437–47. doi: 10.2337/db16-0714

7. Spolski R, Leonard WJ. Interleukin-21: basic biology and implications for cancer and autoimmunity. *Annu Rev Immunol* (2008) 26:57–79. doi: 10.1146/annurev.immunol.26.021607.090316

8. Crotty S. T Follicular helper cell biology: a decade of discovery and diseases. *Immunity* (2019) 50:1132–48. doi: 10.1016/j.immuni.2019.04.011

9. Rao DA, Gurish MF, Marshall JL, Slowikowski K, Fonseka CY, Liu Y, et al. Pathologically expanded peripheral T helper cell subset drives b cells in rheumatoid arthritis. *Nature* (2017) 542:110–4. doi: 10.1038/nature20810

10. Rao DA. T Cells that help b cells in chronically inflamed tissues. *Front Immunol* (2018) 9:1924. doi: 10.3389/fimmu.2018.01924

11. McGuire HM, Walters S, Vogelzang A, Lee CMY, Webster KE, Sprent J, et al. Interleukin-21 is critically required in autoimmune and allogeneic responses to islet tissue in murine models. *Diabetes* (2011) 60:867–75. doi: 10.2337/db10-1157

12. McGuire HM, Vogelzang A, Ma CS, Hughes WE, Silveira PA, Tangye SG, et al. A subset of interleukin-21+ chemokine receptor CCR9+ T helper cells target accessory

organs of the digestive system in autoimmunity. *Immunity* (2011) 34:602–15. doi: 10.1016/j.immuni.2011.01.021

13. Sutherland APR, Joller N, Michaud M, Liu SM, Kuchroo VK, Grusby MJ. IL-21 promotes CD8+ CTL activity *via* the transcription factor T-bet. *J Immunol* (2013) 190:3977–84. doi: 10.4049/jimmunol.1201730

14. Ekman I, Ihantola EL, Viisanen T, Rao DA, Näntö-Salonen K, Knip M, et al. Circulating CXCR5^{-}PD-1^{hi} peripheral T helper cells are associated with progression to type 1 diabetes. *Diabetologia* (2019) 62:1681–8. doi: 10.1007/s00125-019-4936-8

15. Honkanen J, Nieminen JK, Gao R, Luopajarvi K, Salo HM, Ilonen J, et al. IL-17 immunity in human type 1 diabetes. *J Immunol* (2010) 185:1959–67. doi: 10.4049/jimmunol.1000788

16. Ferraro A, Socci C, Stabilini A, Valle A, Monti P, Piemonti L, et al. Expansion of Th17 cells and functional defects in T regulatory cells are key features of the pancreatic lymph nodes in patients with type 1 diabetes. *Diabetes* (2011) 60:2903–13. doi: 10.2337/db11-0090

17. von Herrath M, Bain SC, Bode B, Clausen JO, Coppieters K, Gaysina L, et al. Anti-interleukin-21 antibody and liraglutide for the preservation of β-cell function in adults with recent-onset type 1 diabetes: a randomised, double-blind, placebo-controlled, phase 2 trial. *Lancet Diabetes Endocrinol* (2021) 9:212–24. doi: 10.1016/S2213-8587(21)00019-X

18. Kang KY, Kim HO, Kwok SK, Ju JH, Park KS, Sun D, et al. Impact of interleukin-21 in the pathogenesis of primary sjögren's syndrome: increased serum levels of interleukin-21 and its expression in the labial salivary glands. *Arthritis Res Ther* (2011) 13. doi: 10.1186/ar3504

19. Wang L, Zhao P, Ma L, Shan Y, Jiang Z, Wang J, et al. Increased interleukin 21 and follicular helper T-like cells and reduced interleukin 10+ b cells in patients with new-onset systemic lupus erythematosus. *J Rheumatol* (2014) 41:1781–92. doi: 10.3899/jrheum.131025

20. Poorbaugh J, Samanta T, Bright SW, Sissons SE, Chang CY, Oberoi P, et al. Measurement of IL-21 in human serum and plasma using ultrasensitive MSD s-PLEX® and quanterix SiMoA methodologies. *J Immunol Methods* (2019) 466:9–16. doi: 10.1016/j.jim.2018.12.005

21. Alnek K, Kisand K, Heilman K, Peet A, Varik K, Uibo R. Increased blood levels of growth factors, proinflammatory cytokines, and Th17 cytokines in patients with newly diagnosed type 1 diabetes. *PloS One* (2015) 10:1–16. doi: 10.1371/journal.pone.0142976

22. Xu X, Shi Y, Cai Y, Zhang Q, Yang F, Chen H, et al. Inhibition of increased circulating tfh cell by anti-CD20 monoclonal antibody in patients with type 1 diabetes. *PloS One* (2013) 8. doi: 10.1371/journal.pone.0079858

23. Yeung WCG, Al-Shabeeb A, Pang CNI, Wilkins MR, Catteau J, Howard NJ, et al. Children with islet autoimmunity and enterovirus infection demonstrate a distinct cytokine profile. *Diabetes* (2012) 61:1500–8. doi: 10.2337/db11-0264

24. Siljander HTA, Simell S, Hekkala A, Lähde J, Simell T, Vähäsalo P, et al. Predictive characteristics of diabetes-associated autoantibodies among children with HLA-conferred disease susceptibility in the general population. *Diabetes* (2009) 58:2835–42. doi: 10.2337/db08-1305

25. R Core Team. *R: a language and environment for statistical computing* (2021). Vienna, Austria: R Foundation for Statistical Computing. Available at: https://www.R-project.org/ (Accessed February 28, 2022).

26. Viisanen T, Gazali AM, Ihantola EL, Ekman I, Näntö-Salonen K, Veijola R, et al. FOXP3+ regulatory T cell compartment is altered in children with newly diagnosed type 1 diabetes but not in autoantibody-positive at-risk children. *Front Immunol* (2019) 10:19. doi: 10.3389/fimmu.2019.00019

frontiers | Frontiers in Immunology

TYPE Review
PUBLISHED 30 September 2022
DOI 10.3389/fimmu.2022.950049

OPEN ACCESS

EDITED BY
Diana Boraschi,
Chinese Academy of Science (CAS), China

REVIEWED BY
Paola Italiani,
National Research Council (CNR), Italy
Paola de Candia,
University of Naples Federico II, Italy

*CORRESPONDENCE
Olga Sierawska
olga.sierawska@phd.usz.edu.pl

SPECIALTY SECTION
This article was submitted to Cytokines and Soluble Mediators in Immunity, a section of the journal Frontiers in Immunology

RECEIVED 22 May 2022
ACCEPTED 01 September 2022
PUBLISHED 30 September 2022

CITATION
Sierawska O and Niedźwiedzka-Rystwej P (2022) Adipokines as potential biomarkers for type 2 diabetes mellitus in cats. *Front. Immunol.* 13:950049. doi: 10.3389/fimmu.2022.950049

Adipokines as potential biomarkers for type 2 diabetes mellitus in cats

Olga Sierawska[1,2]* and Paulina Niedźwiedzka-Rystwej[2]

[1]Doctoral School, University of Szczecin, Szczecin, Poland, [2]Institute of Biology, University of Szczecin, Szczecin, Poland

Type 2 diabetes mellitus (T2DM) is no longer only a disease of humans, but also of domestic animals, and it particularly affects cats. It is increasingly thought that because of its unique characteristics, T2DM may belong not only to the group of metabolic diseases but also to the group of autoimmune diseases. This is due to the involvement of the immune system in the inflammation that occurs with T2DM. Various pro- and anti-inflammatory substances are secreted, especially cytokines in patients with T2DM. Cytokines secreted by adipose tissue are called adipokines, and leptin, adiponectin, resistin, omentin, TNF-α, and IL-6 have been implicated in T2DM. In cats, approximately 90% of diabetic cases are T2DM. Risk factors include older age, male sex, Burmese breed, presence of obesity, and insulin resistance. Diagnosis of a cat requires repeated testing and is complicated compared to human diagnosis. Based on similarities in the pathogenesis of T2DM between humans and cats, adipokines previously proposed as biomarkers for human T2DM may also serve in the diagnosis of this disease in cats.

KEYWORDS

feline, diabetes mellitus, adipokines, leptin, adiponektin

1 Introduction

Chronic low-grade inflammation is common in pathologies such as obesity, cancer, type 2 diabetes (T2DM), and cardiovascular diseases (1). The immune system is usually described in terms of its protective function against infections and its role in the development of autoimmunity. In contrast, interactions between the immune system and metabolic processes have been reported for more than a decade, resulting in a field of research termed immunometabolism. So far, it has been shown (2) that the development of metabolic diseases can be linked to inflammation, which in some cases reflects the activation of immune responses. There are many evolutionarily conservative interactions between the immune response and metabolism. Proper maintenance of this delicate balance is critical for health and has important implications for many pathological conditions such as obesity, diabetes mellitus, and other chronic non-communicable

diseases (3). Metabolic dysregulation results in immune cell involvement. If the organism is obese, pro-inflammatory M1 macrophages make up the majority of the macrophage population in adipose tissue, with more anti-inflammatory M2 in lean individuals. They secrete pro-inflammatory cytokines (TNF-α, IL-6, IL-1β, IL-12, and MCP-1), which not only have a role in promoting insulin resistance but also recruit other immune cells to the site of inflammation (4). Among the cells recruited are neutrophils, lymphocytes, and innate lymphoid cells (ILC), including natural killer (NK) cells, mast cells, and eosinophils (4, 5). Elevated levels of neutrophil, have been observed in both obese humans and mouse models fed a high-fat diet (HFD), and are therefore thought to be involved in modulating adipose tissue inflammation in the early stages of obesity (6). Lymphocytes are recruited to the site of inflammation by specific cytokines. In obesity, reduced levels of CD4 + CD25 + Foxp3+ lymphocytes are observed, indicating their depletion, which contributes to the development of insulin resistance. In contrast, CD8 T-lymphocyte levels increase in adipose tissue as early as 2 weeks of HFD feeding, and levels are high in obesity. The important role of CD8 T lymphocytes in the development of inflammation lies in their ability to induce the differentiation of macrophages from monocytes. B lymphocytes influence adipose tissue inflammation by modulating T lymphocyte activity (7). Mast cells have also been shown to be involved in the regulation of adipose tissue in obesity. Eosinophils, on the other hand, induce a faster rate of macrophage differentiation into the M2 phenotype by secreting the cytokines IL-4 and IL-13, which have an anti-inflammatory effect on adipose tissue inflammation (5).

The site of many inflammatory processes is in adipose tissue. Adipose tissue is classified as connective tissue, as a specialized tissue composed mainly of adipocytes (fat cells). Adipocytes are composed of a single, large lipid droplet with a thin envelope of cytoplasm between it and the plasma membrane (3). Currently, it is widely agreed that adipose tissue is a strongly active and complex hormonal and metabolic gland consisting of adipocytes, connective tissue matrix, neural tissue, stromal cells, and immune cells (8). The link between adipose tissue metabolism and the immune system is indicated by the fact that immune responses often lead to loss of body weight, and in obese individuals, the immune system malfunctions, causing them to suffer an increased incidence and severity of infectious diseases (9, 10). In obese individuals, only half the number of the monocytes mature into macrophages, compared to patients without obesity (10). In addition, macrophages contribute to the adipose organ in the generation of inflammation (11). Animal studies also yield similar data. Decreased immunocompetence, decreased activity of cellular immune components, decreased resistance to infection, and decreased macrophage killing capacity are observed in obese individuals (10).

Studies suggest (2) that T2DM, like type 1 diabetes (T1DM), may belong to the autoimmune diseases, and the two types of diabetes may have more in common than previously thought (3). In T2DM with obesity, adipocyte size is increased. This alters the levels of circulating pro-inflammatory cytokines contributing to the recruitment of immune cells to the site of inflammation, which is adipose tissue (12). Additionally, the insulin resistance in T2DM may be the result of attacks by immune system cells that are designed to produce antibodies that fight pathogens on body tissues (3). Although T2DM has been classified as a metabolic disease for more than 30 years, autoimmunity in T2DM is a growing topic (13). Chronic inflammation induced by obesity, a major causative factor in T2DM, affects the activation of innate and adaptive immunity, including the secretion of pro-inflammatory cytokines that activate T lymphocytes, B lymphocytes and macrophages. As a result of the strong impact of inflammatory and autoimmune reactions, β-cells undergo apoptosis, and impaired insulin secretion in β-cells affects the development of hyperglycemia (13, 14). Another important feature of autoimmunity in T2DM is impaired B lymphocyte function. People with T2DM do not secrete the anti-inflammatory cytokine, interleukin-10, and they secrete a much higher amount of pro-inflammatory cytokines (13, 14). Patients with T2DM have reduced resistance to infection, which may be due to the reduced ability of B lymphocytes to produce de novo antibodies (14). Additionally, T lymphocytes are an important aspect in autoimmunity in T2DM. Self-reactive T lymphocytes are in decline in patients with T2DM (13). T-cell receptors (TCRs), which are designed to recognize antigen and are differentially expressed in healthy individuals, are limited in T2DM patients (15). T-lymphocytes, together with macrophages, by releasing pro-inflammatory cytokines, contribute to increased pancreatic islet inflammation (13). A role for dysbiosis of the gut microbiota in toll-like receptor (TLR) activation in adipocytes and production of pro-inflammatory adipokines is also indicated (15). Current immunomodulatory therapies in T2DM target IL-1β, block the NF-kB pathway and increase circulating adiponectin with positive results (13).

Because of differences in the structure of adipose tissue in rodents, the most popular model organism for humans, research on it is not fully developed. Murine adipocytes differ in structure from those of humans: mouse adipocytes contain many fat droplets, while human adipocytes contain one (3). There are differences in adipogenesis too. Additionally, molecular differences adversely affect the use of mouse models: in mice, TNF-α is a major factor in haptoglobin expression, and in humans, it induces downregulation of haptoglobin mRNA (16). Cats, unlike rodents, develop all the symptoms of T2DM: insulin resistance, impaired β-cell function and reduced numbers of them, and pancreatic amyloid deposition (17).

2 T2DM in cats

In cats, T2DM is the most common among the various types of diabetes, with about 90% of diabetes cases being T2DM (18). By comparison, in dogs, most cases of diabetes are type 1 diabetes (19). T2DM is characterized by insulin resistance and decreased insulin secretion due to pancreatic β-cell failure (18, 20). Insulin resistance is differentiated by impaired tissue response to insulin and can lead to hyperglycemia and excessive pancreatic insulin secretion leading to balance (20). Although T2DM in cats is the most common type of DM and is very similar to human T2DM, unlike in humans, treatment may include insulin therapy (21). This is because DM in cats has been proposed to be divisible into insulin-dependent DM (IDDM) and non-insulin-dependent diabetes mellitus (NIDDM), and T2DM in cats qualifies as IDDM (22). In this paper, however, we will use the term T2DM and note that it is a type of IDDM in cats.

2.1 Risk factors

Risk factors for developing T2DM in cats include both genetic and environmental conditions, like advancing age, male sex (including being neutered), genetic aspects (breed), diet-dependent obesity and physical inactivity (18, 21, 23, 24).

2.1.1 Age

The probability of cats developing DM has been shown to increase beyond the age of 6 years, and it is highest at 11-13 years (25–28). This may be because insulin sensitivity and β-cell functionality decrease with age, and amyloid deposition in the pancreas may be high (26).

2.1.2 Sex

An increased risk of developing T2DM has been observed in male cats. The more their body weight increased, the higher the risk was. Interestingly, this pattern did not occur in female cats — despite increasing body weight, there was no significant increase in the risk of developing T2DM (25). This may be because male cats may be naturally more insulin resistant than female cats. Additionally, the mere fact of being a female purebred cat rather than a mixed-breed cat was protective against developing T2DM (25). Males, regardless of breed, were at the same risk of developing the disease (25). In males, neutering also appears to have an impact on the development of T2DM disease, as they are 2-9 time more likely to develop the disease then uncastrated males (21, 29). After neutering there are changes in hormone levels: an increase in prolactin, leptin, and insulin-like growth factor 1 (IGF-1), and a decrease in testosterone and estrogen. Among estrogens, estradiol has been shown to regulate normal food intake. In neutered males, estradiol levels are significantly reduced, by up to half in plasma (30). Therefore, especially in males, ad libitum access to food is a large risk factor for the development of obesity and resulting T2DM. The exceptions are Burmese cats, in which the gender factor does not affect the chances of developing T2DM — both male and female cats are equally susceptible to the disease (29).

2.1.3 Breed and other genetic factors

Remarkably, there is one breed that is particularly prone to developing diabetes: the Burmese cat (22, 23, 31). Type 2 diabetes is up to 4 times more common in Australian-bred Burmese cats (32), and the New Zealand population is also at increased risk (33). This is probably due to the presence of an inborn metabolic deficiency in certain of these cats. This results in postprandial hypertriglyceridemia after high-fat meals. In Burmese cats with postprandial hypertriglyceridemia, lipoprotein lipase (LPL) deficiency and elevated very-low-density lipoprotein (VLDL) concentrations have been observed (31). This may be because the breed was developed from a small number of individuals and the propensity for the disease is passed down generationally. A genetic factor is also indicated by the fact that USA-bred Burmese cats, a population quite isolated from others because Burmese breeders in Australia, New Zealand, and the United Kingdom have not approved Burmese cats from the USA for more than 20 years, do not suffer from an increased risk of developing T2DM (34). With further genetic studies of Burmese cats, it would be possible to locate the alleles responsible for the increased risk of developing type 2 diabetes in cats.

In addition to the Burmese breed, high incidence rates of DM risk were also found in the Russian blue, Norwegian forest cat, European shorthair, and Abyssinian breeds (27).

Additionally, in cats mutations in the sequence of the gene encoding the melanocortin 4 receptor (MC4-R), decreased expression levels of the insulin receptor substrate 1 (IRS-1), insulin receptor substrate 2 (IRS-2) and phosphoinositide 3-kinase (PI3-K) genes, or decreased expression levels of the gene encoding the glucose transporter type 4 (GLUT4) in muscle and adipose tissues have also been observed (21). As in cats, in humans genetic factors are also important in the pathogenesis of T2DM (33). A mutation in the gene encoding the melanocortin 4 receptor (MC4-R) causing it to be defective in humans is one of the most common causes of obesity, glucose intolerance and T2DM (35, 36). MC4-R inhibition leads to increased fat cell accumulation (37). Polymorphisms in the IRS-1 gene in humans are associated with an increased risk of developing gestational diabetes, and the gene itself is involved in the development of insulin resistance in T2DM (38). Notable among the polymorphisms in IRS-1 affecting the development of T2DM and insulin resistance are IRS-1 substitutions by Gly to Arg 972 (39). IRS-2 also plays an important role in the initiation and progression of T2DM. It has been shown that increasing its

expression in patients with insulin resistance can positively delay the development of diabetes (40), and its reduced expression can induce β-cell apoptosis (41). PI3-K is involved in the IRS substrate pathway, which is impaired by insulin inefficiency and hyperglycemia (42). GLUT4 is involved in glucose uptake in muscle and adipose tissues, and changes in its expression affect glycemic control in the human body (43). Similarities in the expression changes of genes involved in the pathogenesis of T2DM between humans and cats deserve special attention and suggest similarities in the pathogenesis of the disease.

2.1.4 Nutrition

In their natural environment, cats feed on small mammals and birds: food that is rich in protein, moderately rich in fat, and with minimal carbohydrates (19). Proteins in cats' diet are needed to maintain blood glucose levels, as cats do not have many adaptations to regulate carbohydrate digestion. Cats do not secrete salivary amylase and have low intestinal and pancreatic amylase and intestinal disaccharidase activity (19). In addition, hepatic glucokinase activity is low and is not adaptive to increased carbohydrate consumption and the feline liver does not secrete fructokinase. Consequently, the cat's body's ability to minimize hyperglycemia is severely compromised when there is a large amount of glucose in the diet (19, 25). Additionally, large amounts of carbohydrates in a cat's diet reduce the digestibility of proteins (19).

A high-protein/low-carbohydrate (HP) diet is recommended for feeding obese cats because its use affects the maintenance of normal insulin sensitivity of fat metabolism (44). The HP diet has the effect of increasing heat production and consequently facilitating fat loss (44). Cats fed an HP diet are less likely to develop obesity and show less insulin resistance compared to cats fed the same amount of calories but on a high-carbohydrate/low-protein (HC) diet (44). HC diets during obesity therapy have been shown to reduce lean body mass loss and promote fat loss (45–47). Additionally, compared to HP diets, HC diets decrease insulin sensitivity and cause hyperinsulinemia (24). As in obese cats, in cats with T2DM, the use of the HP diet is beneficial and leads to an improvement in insulin requirements (44).

The cat has a similar narrative in the "Carnivore Connection" theory as humans. This theory states that the cause of the current epidemic of obesity and diabetes in humans is potentially because, over the last two million years of evolution humans have consumed a predominantly low-carbohydrate, high-protein diet. As a result, they developed insulin resistance, which was beneficial with such a diet because it allowed them to control the balance of glucose levels and had a positive effect on fetal development. With the development of agriculture and the industrialization of the population, the diet changed, and man began to consume more cereals and starches. Populations that have recently adopted agriculture and have been on a high-carbohydrate diet for a shorter time, such as the Pima Indians, are more likely to develop T2DM, while Europeans, who have used agriculture for 12,000 years, have a lower incidence of diabetes (48). Domestic cats may have experienced a similar situation with a change from a natural, protein-rich diet to a diet consisting primarily of high-carbohydrate commercial food. Although high-carbohydrate diets lead to elevated postprandial glucose and insulin levels, and low-carbohydrate diets have been shown to improve glycemic control in cats with DM, it cannot currently be concluded with certainty that a high-carbohydrate diet is a risk factor for the development of T2DM (49).

2.1.5 Obesity

The next risk factor, obesity is the condition of increased body fat mass due to too many nutrients being provided to the body than needed and may be a consequence of incorrect nutrition (20, 50). In cats, there is a strong link between obesity and diseases such as cancer, lower urinary tract diseases, especially feline idiopathic cystitis, constipation, lameness and orthopedic diseases, altered hemostasis, liver lipidosis, dermatological diseases, musculoskeletal diseases, hypertrophic cardiomyopathy, respiratory diseases, oral conditions, diabetes mellitus, atopic dermatitis, hypertension, asthma, diarrhea, ocular conditions, and allergic conditions (11, 30, 51).

Hoeing et al. (44) reported that 1 kilogram of weight gain in cats resulted in a loss of insulin sensitivity and glucose effectiveness by approximately 30% (44). Adipose tissue regulates the storage, release, degradation, and hydrolysis of fatty acids (FA). During the normal process of lipolysis, fatty acids esterify, resulting a decrease in their serum levels decrease. In obesity, there is impaired inhibition of lipolysis by insulin, resulting in increased levels of fatty acids and glycerol, and adipose tissue secretes cytokines and other pro-inflammatory molecules that antagonize the action of insulin and contribute to inflammation (52).

Additionally, the distribution of body fat in an animal is associated with insulin resistance. In cats, unlike humans, there is no gender difference in body fat distribution. Abdominal fat, which is the major site of fat accumulation in cats, is evenly distributed subcutaneously and in the abdominal cavity (44). In contrast, obese cats may deposit fatty acids into the muscle and have increased lipid levels there, which may be associated with insulin resistance (53).

It is important to note that not all obese cats develop T2DM because other genetic, environmental, and metabolic factors are involved in the pathogenesis of the disease. Obesity increases the diabetes risk by 3 to 5 times (24). However, obesity is considered to be one of the main factors in the development of T2DM and it is thought that this may be due to an increase in endogenous glucose production caused by hepatic insulin resistance, resulting in β-cell impairment and/or decreased insulin

secretion due to amyloid deposition in the pancreatic islets, and as a result of β-cell failure, hypoinsulinemia and increased EGP production by the liver (54, 55).

2.1.6 Insulin resistance development

In humans, obesity is thought to lead to the development of insulin resistance through a number of mechanisms. The first is the accumulation of FA in the liver and muscle as a result of abnormal FA transport and incomplete fatty acid oxidation. Additionally, oxidative stress and inflammatory response caused by adipocyte hypertrophy, including the release of pro-inflammatory cytokines resulting in elevated phosphorylation of insulin receptor substrates (iRSs). Subsequently, the secretion of adipokines by adipocytes, e.g., adiponectin increases insulin sensitivity. As the mechanism of insulin resistance in obese cats has not been studied in detail, it is presumed that its mechanisms are similar to those in obese humans. This may be indicated by reduced expression of GLUT-4 in muscle and adipose tissue, increased triglyceride content in muscle and liver, and high levels of muscle-fat ratio lipoprotein lipase expression. Unlike humans, cats (excluding the Burmese breed) do not have most of their fat stored in the abdominal cavity. In addition, insulin resistance in cats does not cause systemic inflammation as it does in humans (56).

As weight increases in the cat, insulin sensitivity and the effectiveness of insulin in lowering plasma glucose levels decrease (57, 58). As a result of the persistent state of producing excess insulin, the β-cells eventually become depleted and stop producing insulin (57). In a study by Appleton et al. (57), more than half of the cats also developed impaired glucose tolerance after gaining weight. A 30% decrease in insulin sensitivity was observed for each kilogram of excess body weight in cats (56). As mentioned, the development of insulin resistance is closely related to the development of obesity (59). This is a reversible mechanism and if the animal loses weight, the insulin resistance disappears (17, 59). Interestingly, not all obese cats develop diabetes, and the mechanisms of the obesity–insulin resistance–diabetes interaction are not yet fully understood (59). In cats with T2DM, insulin sensitivity is lower by about 6 times (17).

2.2 Complications of untreated type 2 diabetes in cats

The consequences of unrecognized and untreated type 2 diabetes in cats are severe. The main complications of diabetes that have been studied in cats are diabetic neuropathy and diabetic retinopathy. Diabetic neuropathy is one of the most common post-diabetic complications in cats. Although it affects 90% of individuals, only 10% of them show neurological signs. Neuropathy in cats mainly affects the pelvic limbs and motor nerve conduction, and clinical signs include hindlimb paresis, muscle atrophy most prominent in the distal parts of the pelvic limbs, plantigrade posture, difficulty or inability to jump, abnormal postural responses, ataxia, poor patellar reflex, and increased flatulence and irritability in response to touch (60, 61). Damage in nerves includes changes in Schwann cells with cleavage and ballooning of the myelin sheath, followed by demyelination, and axons of myelinated fibers involving dystrophic accumulation of axoplasmic membrane debris and glycogen, and degenerative fiber loss (61, 62). The changes observed in Schwann cells seen in cats are similar to those seen in humans with diabetes (60). Diabetic retinopathy damages blood vessels in the retina. A model of oxygen-induced retinopathy in cats was proposed as early as the 1950s, but the long development time of diabetic retinopathy and limitations in research reagents means that it is not the most popular model (63). In feline diabetics, however, diabetic cataracts often develop along with linear opacification of the posterior cortex and cortical cataracts or posterior subcapsular plaques. Complete blindness due to diabetic cataracts is very rare in adult cats, but kittens can develop more severe cataracts resulting in blindness (64, 65). Diabetic nephropathy is a serious complication of diabetes in humans, but diabetes-induced nephropathy is rare in cats (66). However, since kidney disease in older cats can be as common as diabetes, it is difficult to determine whether it is due to damage from diabetes or whether it is a comorbid condition. The incidence of chronic kidney disease in -cats ranges from 17 to 63%, and in cats newly diagnosed, 13% developed the disease during a follow-up 6-month study (67–69). In addition to the described complications, about one-third of cats with diabetes develop hypersomatotropism, resulting in the development of acromegaly. Diabetes may also be implicated in the increased development of heart disease and echocardiographic changes, but there are still few studies evaluating the impact of diabetes on heart disease in cats (70).

2.3 Diagnosis of type 2 diabetes in cats

Clinical signs of type 2 diabetes mellitus in cats include persistent hyperglycemia, polyuria, polyphagia, polydipsia, and decreased muscle mass with, as a consequent, weight loss, and liver enlargement (18, 22, 71).

The diagnosis of insulin sensitivity and type 2 diabetes mellitus in cats is not the same as in humans. In humans, the homeostatic model assessment (HOMA) and the quantitative insulin sensitivity method are used to assess insulin sensitivity (54). However, in cats the HOMA method is considered insufficient to reflect changes in insulin sensitivity (54). Additionally, stress-induced hyperglycemia has been observed in cats (71). A study by Ray et al. (72) showed that more than half of healthy cats without T2DM admitted to the hospital exhibited hyperglycemia (72). As cats are particularly susceptible to stress, it

can be triggered by several factors, e.g., travel, being in the waiting room of a veterinary clinic, or having blood drawn for a test (71). The increase in blood glucose levels due to stress is rapid - it is observed after about 5 minutes and can last for up to 3 hours (18). Because of this unique characteristic of cats, type 2 diabetes can be diagnosed using methods that are not as influenced by stress. To diagnose a cat, it is advisable to perform a general urine test with glucose detection and relative density and a serum fructosamine determination (71). Urinary glucose occurs when serum glucose levels in cats exceed 200-288 mg/dl (11-16 mmol/l). As for the relative density of urine, it is typically 1.026-1.035 (71). Fructosamine is defined as the total of plasma proteins that have undergone the process of protein glycation. Its concentration in the blood can determine the blood glucose concentration up to 2-3 weeks before its determination. Decreased fructosamine levels are also observed when plasma protein levels are decreased and in hyperthyroidism (71). Unfortunately, the use of fructosamine is not always effective because healthy cats with naturally elevated fructosamine levels and T2DM cats with normal fructosamine levels have been reported (18). Cats with suspected T2DM may also have glycosylated hemoglobin, which indicates glucose levels approximately 70 days before the test. Additionally, this method has disadvantages, the results may be reduced in the case of anemia, and the too-long time required to reflect blood glucose concentration makes it an innefective diagnostic tool (71).

3 Adipokines

All substances secreted by adipose tissue are called adipokines, although the types differ. Adipokines can be hormones, such as leptin, adiponectin, plasminogen activator inhibitor-1 (PAI-1), or cytokines, such as interleukin 8 (IL-8) or tumor necrosis factor-alpha (TNFα) and chemokines (73). Among adipokines, leptin, adiponectin, resistin, and omentin, as well as cytokines and chemokines (TNF-α, IL-6), result in chronic inflammation, which may play a key role in the development of insulin resistance and T2DM and increase the risk of obesity-related cardiovascular disease, collectively referred to as the metabolic syndrome (1, 2, 74, 75).

The view of adipose tissue changed significantly after 1994, when the Ob gene and its product, leptin, were identified and characterized, and now adipose tissue is known to be an organ involved in endocrine function, the central nervous system, the immune system, and energy metabolism (8).

The observed increase in adipokines in obese patients includes cytokines, e.g., interleukin 6 (IL-6), interleukin 8 (IL-8), interleukin 18 (IL-18), TNF-α; acute phase proteins, e.g., C-reactive protein (CRP), plasminogen activator inhibitor-1 (PAI-1), haptoglobin; and chemokines, e.g., monocyte chemoattractant protein-1 (MCP-1) (16, 76). The increase in adiponectin concentration is inversely proportional to body weight gain. It has been observed that there is diurnal variation in adiponectin levels, with an increase in the morning and a decrease at night (20). Adipokines play important roles in the pathophysiology of obesity and diabetes in humans (77). There is a need to determine what role they play in T2DM in cats and whether they could be used as biomarkers of disease progression in the future (Table 1).

3.1 Leptin

Leptin is known as the central satiety signal because it regulates body composition and energy expenditure (20). It also influences sympathetic nervous system activity, hematopoiesis, and reproductive function and modulates the immune responses by having a pro-inflammatory effect and activating T cells (9, 16, 20). Additionally, is known to regulate nutritional intake, which may impact thermogenesis because it increases energy expenditure, stimulates lipolysis, and inhibits lipogenesis (24, 98). Leptin is produced by adipocytes and in minor amounts by the central nervous system (CNS), skeletal muscles, stomach, and placenta (20, 99). Although leptin has an inhibitory effect on adipose tissue cell differentiation, its secretion increases during adipocyte maturation from preadipocytes. Leptin release is initiated by TNFα and

TABLE 1 Changes in levels of selected adipokines in cats and humans with T2DM and obesity compared to healthy individuals.

Adipokine	T2DM cat	T2DM human	Obese cat	Obese human
Leptin	↑	↑	↑	↑
Adiponectin	↓	↓	↓	↓
Resistin	ND	↑	↑	↑
Omentin	ND	↓	–	↓
TNF-α	ND	↑	↑	↑
IL-6	ND	↑	↑	↑

↑, increased levels; ↓, decreased levels; –, no change; ND, no data. Based on (17, 44, 58, 77–97). The similarities in the course of T2DM in humans and cats may allow us to predict how selected adipokines will change levels in T2DM in cats on the basis of data obtained in humans, but more studies are needed. Omentin, in particular, appears to be an interesting case, as it did not change the range of levels in obese cats, unlike its levels in obese humans. In the case given, one study was conducted. To obtain more data, additional studies should be conducted.

chemokines (9). High leptin levels are closely associated with high body fat mass and may lead to further weight gain and therefore the development of insulin resistance (100). Thus, along with IL-6, resistin, and TNF-α, leptin acts as an indicator of obesity initiation and insulin resistance (22).

In humans, leptin is a marker for the development of obesity, and as body fat increases, leptin levels increase (90). Additionally, it has been proposed as a biomarker for type 2 diabetes. In addition, although leptin levels increase in obese and T2DM patients, interestingly, it has been noted that diabetics with high BMI have lower leptin levels than non-diabetics with high BMI (85, 86). It has been indicated that low leptin levels have a significant effect on increasing the risk of developing insulin resistance and type 2 diabetes (86). Leptin affects the body's insulin sensitivity by decreasing the storage capacity of triglycerides in muscle tissues and increasing fatty acid oxidation (90). Because of these unique abilities, leptin has been proposed as a potential therapeutic agent in obesity and type 2 diabetes (101).

Correlations between increased leptin levels and increased BCS and body fat mass have been demonstrated in cats (44, 58, 78–80, 87–89). Leptin levels are not dependent on the sex of the animal (88). In a study by Zapata et al. (58), diabetic cats had leptin levels 221% higher than those in normal-weight cats. Healthy cats that were obese had levels 172% higher compared to those of normal weight (58). In a study by Appleton et al. (89), lower insulin sensitivity, with higher insulin concentrations and indices, was observed in healthy, lean cats aged 1-5 years driven to overweight/obesity. Following an increased in body weight, the cats that had the highest fasting plasma leptin concentrations also had the highest fasting insulin concentrations, along with decreased insulin sensitivity (89). Increased leptin levels are also correlated with increased cat insulin resistance not only in obese but also in lean individuals (24, 89). Additionally, increased insulin levels in obese cats stimulate leptin production as in other animal species (89). As the animal's weight decreased, serum leptin concentrations gradually decreased (81). Leptin levels in lean cats have been shown to increase with increasing age (102). It has been shown that the HC/HB diet has no effect on blood leptin levels in cats (44).

3.2 Adiponectin

Adiponectin is secreted by adipocytes in white adipose tissue (103). Adiponectin has anti-inflammatory effects (16). Adiponectin has several important functions, such as improving glucose and lipid metabolism, modulating insulin action, preventing inflammation, and preventing atherosclerosis (20, 104). Adiponectin receptors are located in the liver and skeletal muscle, and it has been suggested that the greatest increase in insulin sensitivity occurs in the liver. Adiponectin, together with AMP-activated protein kinase, increases glucose uptake in skeletal muscle, oxidizes fatty acids in muscle and liver, initiates the insulin signal transduction cascade in these two tissues, and increases insulin sensitivity (20, 24). Hosogai et al. (104) showed that the presence of ER stress concurrently with obesity affects the downregulation of adiponectin mRNA (104).

In humans, adiponectin levels are lower in patients with obesity, insulin resistance, and T2DM and its reduced levels can be used to predict the development of these diseases (77). Adiponectin in humans has been proposed as a biomarker for diabetes-related cardiac complications and for assessing vascular changes in peripheral type 2 diabetes. Adiponectin levels have also been proposed as a risk factor for cardiovascular disease and coronary artery disease (91). Interestingly, adiponectin has also been indicated as a target for the treatment of type 2 diabetes (77, 91, 101).

Most studies have shown that, in cats, with increasing BCS, adiponectin levels decrease (44, 78–84). However, contrary studies have also been published (82, 105, 106). Adiponectin levels in cats are not dependent on the sex of the animal (88). According to the study by Öhlund et al. (107), adiponectin levels do not differ between healthy individuals of Burmese breed, prone to developing T2DM, and Birman breed with low risk of developing DM (107). In a study by Takashima et al. (81) on healthy cats with normal BCS suffering from obesity that then lost 8% of their weight during a 9-week weight-loss period, it was shown that adipokine levels did not significantly increase in association with weight loss (81). Therefore, the hypothesis was proposed that it is not the degree of obesity that affects adiponectin levels, but other factors, such as, for example, low muscle mass (81). In the same study, a correlation between adiponectin and insulin levels was not found (81). Zapata et al. (58) showed, that compared to healthy cats of normal weight, cats with diabetes had 61% lower adiponectin levels, and cats with diabetes had 45% lower levels compared to healthy obese cats. High molecular-weight (HMW) adiponectin multimers, which are associated with insulin sensitivity, account for approximately 80% of adiponectin in cats, whereas they only account for 30% in humans (17). It has been shown that the HC/HB diet had no effect on blood adiponectin levels in cats (44).

3.3 Resistin

Because resistin's mRNA has been detected in humans in circulating mononuclear cells, not adipocytes, and is released from non-fat adipose tissue cells, Fain (3) proposed that resistin is a cytokine secreted by cells of the immune system (3). Resistin is insulin-resistant and impairs glucose homeostasis. Its function is to downregulate inflammation in macrophages, peripheral blood mononuclear cell (PBMC) and vascular cells (108).

Resistin levels are elevated in obese humans, and also in humans with T2DM, but there are no data for cats with T2DM (91). Resistin is involved in the development of insulin resistance

and T2DM, and for this reason, it too has been proposed as a biomarker for these diseases. In addition, in humans, it has also been proposed as a biomarker for diabetes complications related to chronic periodontitis and cardiovascular disease (91, 109).

It has been reported that resistin levels increase with increasing BCS and body fat mass in cats (78, 79). Cats with obesity have higher resistin mRNA expression in adipose tissue compared to lean cats (78). In addition to adipose tissue, in cats resistin expression may also occur in the lung and spleen (81). However, in the previously described study by Takashima et al. (81), resistin levels also did not change significantly. Resistin was negatively correlated with insulin in the blood of the cats studied (81), which is confusing, since an important role in the pathogenesis of insulin resistance and T2DM has also been indicated (79).

3.4 Omentin

Omentin, although not yet studied in cats with T2DM, deserves consideration because of its unique properties. It has regulatory functions, modulates insulin secretion and insulin sensitivity, and can increase insulin action, affecting fat accumulation, adverse fat breakdown, and inflammation (55, 110). In humans, omentin-1 levels are lower in individuals with T2DM compared to healthy controls (110).

In people with obesity and T2DM, omentin levels are lower than in healthy people, but not in patients with type 1 diabetes (91, 92). Omentin has anti-inflammatory, anti-obesity and anti-diabetic properties, and these are indicated when omentin is proposed as a therapeutic target (90, 91). Omentin has also been proposed as a marker for predicting obesity and T2DM risk (90).

In cats, Williams et al. showed that blood concentrations of omentin are not dependent on BCS, but are 56% higher in males (88). In cats, omentin levels were also not correlated with insulin or glucose levels, as has been reported in humans (88).

3.5 TNF-α

TNF-α has various important functions related to adipose tissue regulation, it responds to inflammation, induces apoptosis, stimulates lipolysis, modulates insulin sensitivity, induces insulin resistance, inhibits adipocyte differentiation, disrupts leptin homeostasis, and induces chemokine secretion (9, 16). TNF-α stimulates IL-6 and MCP-1 expression and inhibits adiponectin mRNA expression. Wang et al. (16) described the lack of effect of TNF-α on leptin expression in humans (16). Among the roles of TNF-α are also the promotion of lipid mobilization, inhibition of adipocyte differentiation, and reduction of lipid storage capacity (79).

In humans, TNF-α levels are elevated in people with T2DM and obesity, and TNF-α itself plays roles in the development of insulin resistance (93). TNF-α and its receptors have been indicated to be biomarkers for the progression of diabetic kidney disease (111, 112) and for assessing the degree of diabetic retinopathy (93).

In cats, TNF-α levels increase with increasing BCS and body weight, and increased levels of TNF-α expression have been shown in adipose tissue and skeletal muscle in obese cats (94, 95). However, in a study by Hoenig et al. in cats that were driven to obesity, TNF-α levels did not show significant changes (80).

3.6 IL-6

IL-6 is a pro-inflammatory cytokine secreted from leukocytes, endothelial cells, and adipocytes. Its plasma levels in obese patients are directly proportional to weight loss and fat loss. It regulates the development of chronic diseases such as cardiovascular disease (CVD), where it induces the secretion of a risk marker, hepatic C-reactive protein, and type 2 diabetes mellitus (113). By decreasing lipoprotein lipase (LPL) activity, it increases blood lipid levels (113). By inhibiting the expression of the insulin receptor, insulin receptor substrate-1, and glucose transporter type 4 in 3T3-L1 adipocytes, IL-6 suppresses insulin activity (113) A correlation has been shown between increased IL-6 levels and the occurrence of insulin resistance (3). Additionally, attenuating adiponectin mRNA synthesis and secretion, and inhibition of insulin signaling in hepatocytes contribute to insulin resistance (113).

In humans, IL-6 levels increase in patients with T2DM and obesity (96, 97). IL-6 has been shown to be correleted with the development of complications in diabetes, including diabetic neuropathy, in which high levels of IL-6 are associated with increased nerve degeneration (90, 114).

Plasma IL-6 levels are elevated in obese cats (17). Here again, Hoeing et al. showed no significant changes in IL-6 levels in cats that had gained weight (80).

4 Conclusion

T2DM is a serious disease that an increasing number of domestic cats are suffering from. The multitude of factors that can cause this disease indicate its severity. Some of the risk factors, such as nutrition and the development of obesity, can be influenced by the pet's caregiver. Therefore, it is worthwhile for veterinary professionals to educate cat guardians on the proper management of the animal to limit the development of the disease.

The domestic cat is still a very poorly studied species in terms of the pathogenesis of diabetes mellitus. Most of the information on the subject is still based on data obtained from humans. This is enabled by the high similarity of feline diabetes to human T2DM. In order to better understand the exact mechanisms of the disease, especially regarding adipokines,

studies focusing not only on obesity, which is indeed also an important factor in the development of T2DM, but also on cats already suffering from diabetes themselves, are needed.

The data collected in the above review indicate a promising role for the presented adipokines as biomarkers of type 2 diabetes in cats. Adipokines may be a promising means to control disease progression and recovery in the animal. Notably, adipokines have been proposed as biomarkers of disease in humans, e.g., resistin as a biomarker for diabetes complications related to chronic periodontitis and cardiovascular disease. Biomarkers are useful in the course of disease progress, as they can be used not only for risk assessment and screening, but also to determine the severity of the disease and to select and monitor therapy (109). It is particularly important to discover rapid, sensitive and effective methods for risk assessment in feline type 2 diabetes.

Author contributions

Conceptualization, OS and PN-R. Methodology, OS and PN-R. Software, OS. Validation, OS. Formal analysis, OS. Investigation, OS and PN-R. Resources, PN-R. Data curation, OS. Writing—original draft preparation, OS. Writing—review and editing, OS and PN-R. Visualization, OS. Supervision, PN-R. Project administration, PN-R. Funding acquisition, PN-R. All authors have read and agreed to the published version of the manuscript.

Conflict of interest

The authors declare that the research was conducted in the absence of any commercial or financial relationships that could be construed as a potential conflict of interest.

Publisher's note

All claims expressed in this article are solely those of the authors and do not necessarily represent those of their affiliated organizations, or those of the publisher, the editors and the reviewers. Any product that may be evaluated in this article, or claim that may be made by its manufacturer, is not guaranteed or endorsed by the publisher.

References

1. Niedźwiedzka-Rystwej P, Deptuła W. Adipose tissue and immunity system. *Alergia Astma Immunol* (2009) 14:101–5.

2. Majid S, Farooq R, Bhat SA. Adipocytokines: unravelling the missing link in diabetes and metabolic syndrome. *MOJ Biol Med* (2017) 2:271–2. doi: 10.15406/mojbm.2017.02.00054

3. Fain JN. Release of interleukins and other inflammatory cytokines by human adipose tissue is enhanced in obesity and primarily due to the nonfat cells. *Vitam Horm* (2006) 74:443–77. doi: 10.1016/S0083-6729(06)74018-3

4. Saitoh S, Van Wijk K, Nakajima O. Crosstalk between metabolic disorders and immune cells. *Int J Mol Sci* (2021) 22:10017. doi: 10.3390/ijms221810017

5. Huh JY, Park YJ, Ham M, Kim JB. Crosstalk between adipocytes and immune cells in adipose tissue inflammation and metabolic dysregulation in obesity. *Mol Cells* (2014) 37:365–71. doi: 10.14348/molcells.2014.0074

6. Keeter WC, Moriarty AK, Galkina EV. Role of neutrophils in type 2 diabetes and associated atherosclerosis. *Int J Biochem Cell Biol* (2021) 141:106098. doi: 10.1016/j.biocel.2021.106098

7. Lu J, Zhao J, Meng H, Zhang X. Adipose tissue-resident immune cells in obesity and type 2 diabetes(2019) (Accessed August 13, 2022).

8. Kershaw EE, Flier JS. Adipose tissue as an endocrine organ. *J Clin Endocrinol Metab* (2004) 89:2548–56. doi: 10.1210/jc.2004-0395

9. Gerhardt CC, Romero IA, Cancello R, Camoin L, Strosberg AD. Chemokines control fat accumulation and leptin secretion by cultured human adipocytes. *Mol Cell Endocrinol* (2001) 175:81–92. doi: 10.1016/s0303-7207(01)00394-x

10. Cousin B, Munoz O, Andre M, Fontanilles AM, Dani C, Cousin JL, et al. A role for preadipocytes as macrophage-like cells. *FASEB J* (1999) 13:305–12. doi: 10.1096/fasebj.13.2.305

11. Corrêa LH, Heyn GS, Magalhaes KG. The impact of the adipose organ plasticity on inflammation and cancer progression. *Cells* (2019) 8:662. doi: 10.3390/cells8070662

12. Tataranni PA, Ortega E. A burning question: Does an adipokine-induced activation of the immune system mediate the effect of overnutrition on type 2 diabetes? *Diabetes* (2005) 54:917–27. doi: 10.2337/diabetes.54.4.917

13. Itariu BK, Stulnig TM. Autoimmune aspects of type 2 diabetes mellitus - a mini-review. *GER* (2014) 60:189–96. doi: 10.1159/000356747

14. de Candia P, Prattichizzo F, Garavelli S, De Rosa V, Galgani M, Di Rella F, et al. Type 2 diabetes: How much of an autoimmune disease?(2019) (Accessed July 14, 2022).

15. Prasad M, Chen EW, Toh S-A, Gascoigne NRJ. Autoimmune responses and inflammation in type 2 diabetes. *J Leukocyte Biol* (2020) 107:739–48. doi: 10.1002/jlb.3mr0220-243r

16. Wang B, Jenkins JR, Trayhurn P. Expression and secretion of inflammation-related adipokines by human adipocytes differentiated in culture: integrated response to TNF-α. *Am J Physiology-Endocrinol Metab* (2005) 288:e731–40. doi: 10.1152/ajpendo.00475.2004

17. Osto M, Zini E, Reusch CE, Lutz TA. Diabetes from humans to cats. *Gen Comp Endocrinol* (2013) 182:48–53. doi: 10.1016/j.ygcen.2012.11.019

18. Gottlieb S, Rand J. Managing feline diabetes: Current perspectives. *Vet Med (Auckl)* (2018) 9:33–42. doi: 10.2147/vmrr.s125619

19. Zoran DL. The carnivore connection to nutrition in cats. *J Am Vet Med Assoc* (2002) 221:1559–67. doi: 10.2460/javma.2002.221.1559

20. Gil-Campos M, Cañete RR, Gil A. Adiponectin, the missing link in insulin resistance and obesity. *Clin Nutr* (2004) 23:963–74. doi: 10.1016/j.clnu.2004.04.010

21. Gadomska J, Gójska-Zygner O, Wieczorek M, Jaros S. Cukrzyca u kotów. część i. etiologia i patogeneza. *Życie Weterynaryjne* (2013) 88:458–62.

22. Niaz K, Maqbool F, Khan F, Hassan FI, Momtaz S, Abdollahi M. Comparative occurrence of diabetes in canine, feline, and few wild animals and their association with pancreatic diseases and ketoacidosis with therapeutic approach. *Vet World* (2018) 11:410–22. doi: 10.14202/vetworld.2018.410-422

23. Lewitt MS, Strage E, Church D. An individual approach to feline diabetes care: a case report and literature review. *Acta Vet Scand* (2016) 58:63. doi: 10.1186/s13028-016-0245-0

24. Rotlewicz NB, Gallelli F, Blatter MFC, Miceli D, Castillo V. Pathophysiology of diabetes mellitus and its relationship with obesity in cats. *Slovenian Veterinary Res* (2010) 47:29–34.

25. Prahl A, Guptill L, Glickman NW, Tetrick M, Glickman LT. Time trends and risk factors for diabetes mellitus in cats presented to veterinary teaching hospitals. *J Feline Med Surg* (2007) 9:351–8. doi: 10.1016/j.jfms.2007.02.004

26. O'Neill DG, Gostelow R, Orme C, Church DB, Niessen SJM, Verheyen K, et al. Epidemiology of diabetes mellitus among 193,435 cats attending primary-care veterinary practices in England. *J Vet Intern Med* (2016) 30:964–72. doi: 10.1111/jvim.14365

27. Öhlund M, Fall T, Ström Holst B, Hansson-Hamlin H, Bonnett B, Egenvall A. Incidence of diabetes mellitus in insured Swedish cats in relation to age, breed and sex. *J Veterinary Internal Med* (2015) 29:1342–7. doi: 10.1111/jvim.13584

28. Jotha-Mattos L, Vieira AB, Castelo M da SM, Queiroz AS de M, de Souza HJM, de Alencar NX, et al. Amyloidogenesis of feline amylin and plasma levels in cats with diabetes mellitus or pancreatitis. *Domest Anim Endocrinol* (2021) 74:106532. doi: 10.1016/j.domaniend.2020.106532

29. McCann TM, Simpson KE, Shaw DJ, Butt JA, Gunn-Moore DA. Feline diabetes mellitus in the UK: The prevalence within an insured cat population and a questionnaire-based putative risk factor analysis. *J Feline Med Surg* (2007) 9:289–99. doi: 10.1016/j.jfms.2007.02.001

30. Larsen JA. Risk of obesity in the neutered cat. *J Feline Med Surg* (2017) 19:779–83. doi: 10.1177/1098612X16660605

31. Kluger EK, Hardman C, Govendir M, Baral RM, Sullivan DR, Snow D, et al. Triglyceride response following an oral fat tolerance test in Burmese cats, other pedigree cats and domestic crossbred cats. *J Feline Med Surg* (2009) 11:82–90. doi: 10.1016/j.jfms.2008.05.005

32. Lederer R, Rand J, Jonsson N, Hughes I, Morton J. Frequency of feline diabetes mellitus and breed predisposition in domestic cats in Australia. *Veterinary J* (2009) 179(2):254–8. doi: 10.1016/j.tvjl.2007.09.019

33. O'Leary C, Duffy D, Gething M, McGuckin C, Rand J. Investigation of diabetes mellitus in Burmese cats as an inherited trait: A preliminary study. *New Z Veterinary J* (2013) 61:354–8. doi: 10.1080/00480169.2013.817295

34. Panciera DL, Thomas CB, Eicker SW, Atkins CE. Epizootiologic patterns of diabetes mellitus in cats: 333 cases (1980-1986). *J Am Vet Med Assoc* (1990) 197:1504–8.

35. Mergen M, Mergen H, Ozata M, Oner R, Oner C. RAPID COMMUNICATION: A novel melanocortin 4 receptor (MC4R) gene mutation associated with morbid obesity. *J Clin Endocrinol Metab* (2001) 86:3448. doi: 10.1210/jcem.86.7.7809

36. Piotrowicz Z, Chalimoniuk M, Czuba M, Langfort J. Rola neurotroficznego czynnika pochodzenia mózgowego w kontroli łaknienia. *Postępy Biochemii* (2020) 66:205â 212–205â 212. doi: 10.18388/pb.2020_340

37. Hajam YA, Rani R, Ganie SY, Sheikh TA, Javaid D, Qadri SS, et al. Oxidative stress in human pathology and aging: Molecular mechanisms and perspectives. *Cells* (2022) 11:552. doi: 10.3390/cells11030552

38. Wu L, Cui L, Tam WH, Ma RCW, Wang CC. Genetic variants associated with gestational diabetes mellitus: A meta-analysis and subgroup analysis. *Sci Rep* (2016) 6:30539. doi: 10.1038/srep30539

39. Yousef AA, Behiry EG, Allah WMA, Hussien AM, Abdelmoneam AA, Imam MH, et al. IRS-1 genetic polymorphism (r.2963G>A) in type 2 diabetes mellitus patients associated with insulin resistance. *Appl Clin Genet* (2018) 11:99–106. doi: 10.2147/TACG.S171096

40. Brady MJ. IRS2 takes center stage in the development of type 2 diabetes. *J Clin Invest* (2004) 114:886–8. doi: 10.1172/JCI23108

41. Lin Y, Sun Z. Current views on type 2 diabetes. *J Endocrinol* (2010) 204:1. doi: 10.1677/JOE-09-0260

42. Kobayashi T, Matsumoto T, Kamata K. The PI3-K/Akt pathway: Roles related to alterations in vasomotor responses in diabetic models. *J Smooth Muscle Res* (2005) 41:283–302. doi: 10.1540/jsmr.41.283

43. Passarelli M, Machado UFF. AGEs-induced and endoplasmic reticulum Stress/Inflammation-mediated regulation of GLUT4 expression and atherogenesis in diabetes mellitus. *Cells* (2022) 11:104. doi: 10.3390/cells11010104

44. Hoenig M, Thomaseth K, Waldron M, Ferguson DC. Insulin sensitivity, fat distribution, and adipocytokine response to different diets in lean and obese cats before and after weight loss. *Am J Physiol Regul Integr Comp Physiol* (2007) 292: R227–234. doi: 10.1152/ajpregu.00313.2006

45. Szabo J, Ibrahim WH, Sunvold GD, Dickey KM, Rodgers JB, Toth IE, et al. Influence of dietary protein and lipid on weight loss in obese ovariohysterectomized cats. *Am J Vet Res* (2000) 61:559–65. doi: 10.2460/ajvr.2000.61.559

46. Laflamme D, Hannah S. Increased dietary protein promotes fat loss and reduces loss of lean body mass during weight loss in cats. *Int J Appl Res Veterinary Med* (2005) 3:62–8.

47. Blanchard G, Nguyen P, Gayet C, Leriche I, Siliart B, Paragon B-M. Rapid weight loss with a high-protein low-energy diet allows the recovery of ideal body composition and insulin sensitivity in obese dogs. *J Nutr* (2004) 134:2148S–50S. doi: 10.1093/jn/134.8.2148S

48. Brand-Miller JC, Griffin HJ, Colagiuri S. The carnivore connection hypothesis: Revisited. *J Obes* (2012) 2012:258624. doi: 10.1155/2012/258624

49. Samaha G, Beatty J, Wade CM, Haase B. The Burmese cat as a genetic model of type 2 diabetes in humans. *Anim Genet* (2019) 50:319–25. doi: 10.1111/age.12799

50. Pluta W, Dudzińska W, Lubkowska A. Metabolic obesity in people with normal body weight (MONW)–review of diagnostic criteria. *Int J Environ Res Public Health* (2022) 19:624. doi: 10.3390/ijerph19020624

51. Teng KT, McGreevy PD, Toribio J a. LML, Raubenheimer D, Kendall K, Dhand NK. Associations of body condition score with health conditions related to overweight and obesity in cats. *J Small Anim Pract* (2018) 59(10):603–15. doi: 10.1111/jsap.12905

52. Smith U, Kahn BB. Adipose tissue regulates insulin sensitivity: Role of adipogenesis, *de novo* lipogenesis and novel lipids. *J Intern Med* (2016) 280:465–75. doi: 10.1111/joim.12540

53. Wilkins C, Long RC, Waldron M, Ferguson DC, Hoenig M. Assessment of the influence of fatty acids on indices of insulin sensitivity and myocellular lipid content by use of magnetic resonance spectroscopy in cats. *Am J Vet Res* (2004) 65:1090–9. doi: 10.2460/ajvr.2004.65.1090

54. Hoenig M. The cat as a model for human obesity and diabetes. *J Diabetes Sci Technol* (2012) 6:525–33. doi: 10.1177/193229681200600306

55. Zähringer D, Svoboda M. Endocrine changes related to obesity and diabetes mellitus in cats – a review. *Veterinářství* (2018) 68:250–3.

56. Clark M, Hoenig M. Feline comorbidities: Pathophysiology and management of the obese diabetic cat. *J Feline Med Surg* (2021) 23:639–48. doi: 10.1177/1098612X211021540

57. Appleton D, Rand J, Sunvold G. Insulin sensitivity decreases with obesity, and lean cats with low insulin sensitivity are at greatest risk of glucose intolerance with weight gain. *J Feline Med Surg* (2001) 3:211–28. doi: 10.1053/jfms.2001.0138

58. Zapata RC, Meachem MD, Cardoso NC, Mehain SO, McMillan CJ, Snead ER, et al. Differential circulating concentrations of adipokines, glucagon and adropin in a clinical population of lean, overweight and diabetic cats. *BMC Vet Res* (2017) 13:85. doi: 10.1186/s12917-017-1011-x

59. Nelson RW, Reusch CE. Classification and etiology of diabetes in dogs and cats. *J Endocrinol* (2014) 222:T1–9. doi: 10.1530/joe-14-0202

60. Henson MS, O'Brien TD. Feline models of type 2 diabetes mellitus. *ILAR J* (2006) 47:234–42. doi: 10.1093/ilar.47.3.234

61. Mizisin AP, Shelton GD, Burgers ML, Powell HC, Cuddon PA. Neurological complications associated with spontaneously occurring feline diabetes mellitus. *J Neuropathol Exp Neurol* (2002) 61:872–84. doi: 10.1093/jnen/61.10.872

62. Mizisin AP, Nelson RW, Sturges BK, Vernau KM, LeCouteur RA, Williams DC, et al. Comparable myelinated nerve pathology in feline and human diabetes mellitus. *Acta Neuropathol* (2007) 113:431. doi: 10.1007/s00401-006-0163-8

63. Quiroz J, Yazdanyar A. Animal models of diabetic retinopathy. *Ann Transl Med* (2021) 9:1272. doi: 10.21037/atm-20-6737

64. Thoresen S, Bjerkås E, Aleksandersen M, Peiffer R. Diabetes mellitus and bilateral cataracts in a kitten. *J Feline Med Surg* (2002) 4:115–22. doi: 10.1053/jfms.2001.0161

65. Williams DL, Fred Heath M. Prevalence of feline cataract: results of a cross-sectional study of 2000 normal animals, 50 cats with diabetes and one hundred cats following dehydrational crises. *Veterinary Ophthalmol* (2006) 9:341–9. doi: 10.1111/j.1463-5224.2006.00497.x

66. Zini E, Benali S, Coppola L, Guscetti F, Ackermann M, Lutz TA, et al. Renal morphology in cats with diabetes mellitus. *Vet Pathol* (2014) 51:1143–50. doi: 10.1177/0300985813516645

67. Roomp K, Rand J. Intensive blood glucose control is safe and effective in diabetic cats using home monitoring and treatment with glargine. *J Feline Med Surg* (2009) 11:668–82. doi: 10.1016/j.jfms.2009.04.010

68. Callegari C, Mercuriali E, Hafner M, Coppola LM, Guazzetti S, Lutz TA, et al. Survival time and prognostic factors in cats with newly diagnosed diabetes mellitus: 114 cases (2000–2009). *J Am Veterinary Med Assoc* (2013) 243:91–5. doi: 10.2460/javma.243.1.91

69. Hafner M, Lutz TA, Reusch CE, Zini E. Evaluation of sensor sites for continuous glucose monitoring in cats with diabetes mellitus. *J Feline Med Surg* (2013) 15:117–23. doi: 10.1177/1098612X12463925

70. Borgeat K, Niessen SJM, Wilkie L, Harrington N, Church DB, Fuentes VL, et al. Time spent with cats is never wasted: Lessons learned from feline acromegalic cardiomyopathy, a naturally occurring animal model of the human disease. *PloS One* (2018) 13:e0194342. doi: 10.1371/journal.pone.0194342

71. Gójska-Zygner O, Gadomska J, Wieczorek M, Jaros S. Cukrzyca u kotów. część II. diagnostyka i leczenie. *Życie Weterynaryjne* (2013) 88:543–8.

72. Ray CC, Callahan-Clark J, Beckel NF, Walters PC. The prevalence and significance of hyperglycemia in hospitalized cats. *J Vet Emerg Crit Care (San Antonio)* (2009) 19:347–51. doi: 10.1111/j.1476-4431.2009.00435.x

73. Fain JN, Madan AK, Hiler ML, Cheema P, Bahouth SW. Comparison of the release of adipokines by adipose tissue, adipose tissue matrix, and adipocytes from visceral and subcutaneous abdominal adipose tissues of obese humans. *Endocrinology* (2004) 145:2273–82. doi: 10.1210/en.2003-1336

74. Niedźwiedzka-Rystwej P, Trzeciak-Ryczek A, Deptuła W. Adipose tissue and its role in immunity - new. *Alergia Astma Immunol* (2012) 17:16–21.

75. Depta J, Małkowska P, Wysokińska M, Todorska K, Sierawska O, Hrynkiewicz R, et al. Therapeutic role of antimicrobial peptides in diabetes mellitus. *Biologics* (2022) 2:92–106. doi: 10.3390/biologics2010008

76. Skurk T, Herder C, Kräft I, Müller-Scholze S, Hauner H, Kolb H. Production and release of macrophage migration inhibitory factor from human adipocytes. *Endocrinology* (2005) 146:1006–11. doi: 10.1210/en.2004-0924

77. Kim WK, Bae K-H, Lee SC, Oh K-J. The latest insights into adipokines in diabetes. *J Clin Med* (2019) 8:1874. doi: 10.3390/jcm8111874

78. Takashima S, Nishii N, Kato A, Matsubara T, Shibata S, Kitagawa H. Molecular cloning of feline resistin and the expression of resistin, leptin and adiponectin in the adipose tissue of normal and obese cats. *J Vet Med Sci* (2016) 78:23–8. doi: 10.1292/jvms.15-0233

79. Radin MJ, Sharkey LC, Holycross BJ. Adipokines: A review of biological and analytical principles and an update in dogs, cats, and horses. *Veterinary Clin Pathol* (2009) 38:136–56. doi: 10.1111/j.1939-165x.2009.00133.x

80. Hoenig M, Pach N, Thomaseth K, Le A, Schaeffer D, Ferguson DC. Cats differ from other species in their cytokine and antioxidant enzyme response when developing obesity. *Obesity* (2013) 21:e407–14. doi: 10.1002/oby.20306

81. Takashima S, Nishii N, Kobatake Y, Kiyosue M, Kimura S, Kitagawa H. Concentrations of leptin, adiponectin, and resistin in the serum of obese cats during weight loss. *J Vet Med Sci* (2019) 81:1294–300. doi: 10.1292/jvms.19-0091

82. Ishioka K, Omachi A, Sasaki N, Kimura K, Saito M. Feline adiponectin: molecular structures and plasma concentrations in obese cats. *J Vet Med Sci* (2009) 71:189–94. doi: 10.1292/jvms.71.189

83. Muranaka S, Mori N, Hatano Y, Saito TR, Lee P, Kojima M, et al. Obesity induced changes to plasma adiponectin concentration and cholesterol lipoprotein composition profile in cats. *Res Vet Sci* (2011) 91:358–61. doi: 10.1016/j.rvsc.2010.09.012

84. Hatano Y, Mori N, Asada M, Mori A, Yamamoto I, Muranaka S, et al. Hypertriglyceridemia with increased plasma insulin concentrations in cats. *Res Vet Sci* (2010) 88:458–60. doi: 10.1016/j.rvsc.2009.12.012

85. Sun Q, van Dam RM, Meigs JB, Franco OH, Mantzoros CS, Hu FB. Leptin and soluble leptin receptor levels in plasma and risk of type 2 diabetes in U.S. women: A prospective study. *Diabetes* (2009) 59:611–8. doi: 10.2337/db09-1343

86. Al-Harithy RN, Alomari AS. Expression of leptin mRNA as non-invasive biomarker in type 2 diabetes mellitus. *Int J Clin Pract* (2021) 75:e14844. doi: 10.1111/ijcp.14844

87. Sieber-Ruckstuhl NS, Zini E, Osto M, Franchini M, Boretti FS, Meli ML, et al. Effect of hyperlipidemia on 11β-hydroxysteroid-dehydrogenase, glucocorticoid receptor, and leptin expression in insulin-sensitive tissues of cats. *Domest Anim Endocrinol* (2010) 39:222–30. doi: 10.1016/j.domaniend.2010.06.003

88. Williams MC, McMillan CJ, Snead ER, Takada K, Chelikani PK. Association of circulating adipokine concentrations with indices of adiposity and sex in healthy, adult client owned cats. *BMC Vet Res* (2019) 15:332. doi: 10.1186/s12917-019-2080-9

89. Appleton DJ, Rand JS, Sunvold GD. Plasma leptin concentrations are independently associated with insulin sensitivity in lean and overweight cats. *J Feline Med Surg* (2002) 4:83–93. doi: 10.1053/jfms.2002.0166

90. Lee M-W, Lee M, Oh K-J. Adipose tissue-derived signatures for obesity and type 2 diabetes: Adipokines, batokines and MicroRNAs. *J Clin Med* (2019) 8:854. doi: 10.3390/jcm8060854

91. Liang W, dong Y. The potential of adipokines as biomarkers and therapeutic agents for vascular complications in type 2 diabetes mellitus. *Cytokine Growth Factor Rev* (2019) 48:32–9. doi: 10.1016/j.cytogfr.2019.06.002

92. As´habi A, Sadeghi M, Arab A, Hajianfar H. The association between omentin and diabetes: A systematic review and meta-analysis of observational studies. *Diabetes Metab Syndr Obes* (2019) 12:1277–86. doi: 10.2147/DMSO.S206981

93. Costagliola C, Romano V, De Tollis M, Aceto F, dell'Omo R, Romano MR, et al. TNF-alpha levels in tears: A novel biomarker to assess the degree of diabetic retinopathy. *Mediators Inflammation* (2013) 2013:e629529. doi: 10.1155/2013/629529

94. Hoenig M, McGoldrick JB, deBeer M, Demacker PNM, Ferguson DC. Activity and tissue-specific expression of lipases and tumor-necrosis factor α in lean and obese cats. *Domest Anim Endocrinol* (2006) 30:333–44. doi: 10.1016/j.domaniend.2005.09.001

95. Miller C, Bartges J, Cornelius L, Norton N, Barton M. Tumor necrosis factor-α levels in adipose tissue of lean and obese cats. *J Nutr* (1998) 128:2751S–2S. doi: 10.1093/jn/128.12.2751S

96. Fedullo AL, Schiattarella A, Morlando M, Raguzzini A, Toti E, De Franciscis P, et al. Mediterranean Diet for the prevention of gestational diabetes in the covid-19 era: Implications of il-6 in diabesity. *Int J Mol Sci* (2021) 22:1213. doi: 10.3390/ijms22031213

97. Rodrigues KF, Pietrani NT, Bosco AA, Campos FMF, Sandrim VC, Gomes KB. IL-6, TNF-α, and IL-10 levels/polymorphisms and their association with type 2 diabetes mellitus and obesity in Brazilian individuals. *Arch Endocrinol Metab* (2017) 61:438–46. doi: 10.1590/2359-3997000000254

98. Whittle AJ, López M, Vidal-Puig A. Using brown adipose tissue to treat obesity – the central issue. *Trends Mol Med* (2011) 17:405–11. doi: 10.1016/j.molmed.2011.04.001

99. Pluta W, Radecka A, Dudzińska W, Lubkowska A. Adipose tissue and its proinflammatory properties. *J Education Health Sport* (2020) 10:138–49. doi: 10.12775/JEHS.2020.10.08.016

100. Scuderi MA, Ribeiro Petito M, Unniappan S, Waldner C, Mehain S, McMillian CJ, et al. Safety and efficacy assessment of a GLP-1 mimetic: Insulin glargine combination for treatment of feline diabetes mellitus. *Domest Anim Endocrinol* (2018) 65:80–9. doi: 10.1016/j.domaniend.2018.04.003

101. Blüher M. Clinical relevance of adipokines. *Diabetes Metab J* (2012) 36:317–27. doi: 10.4093/dmj.2012.36.5.317

102. Ferguson DC, Caffall Z, Hoenig M. Obesity increases free thyroxine proportionally to nonesterified fatty acid concentrations in adult neutered female cats. *J Endocrinol* (2007) 194:267–73. doi: 10.1677/JOE-07-0064

103. Choi HM, Doss HM, Kim KS. Multifaceted physiological roles of adiponectin in inflammation and diseases. *Int J Mol Sci* (2020) 21:1219. doi: 10.3390/ijms21041219

104. Hosogai N, Fukuhara A, Oshima K, Miyata Y, Tanaka S, Segawa K, et al. Adipose tissue hypoxia in obesity and its impact on adipocytokine dysregulation. *Diabetes* (2007) 56:901–11. doi: 10.2337/db06-0911

105. Bjornvad CR, Rand JS, Tan HY, Jensen KS, Rose FJ, Armstrong PJ, et al. Obesity and sex influence insulin resistance and total and multimer adiponectin levels in adult neutered domestic shorthair client-owned cats. *Domest Anim Endocrinol* (2014) 47:55–64. doi: 10.1016/j.domaniend.2013.11.006

106. Tvarijonaviciute A, German AJ, Martínez-Subiela S, Tecles F, Ceron JJ. Analytical performance of commercially-available assays for feline insulin-like growth factor 1 (IGF-1), adiponectin and ghrelin measurements. *J Feline Med Surg* (2012) 14:138–46. doi: 10.1177/1098612X11432236

107. Öhlund M, Müllner E, Moazzami A, Hermansson U, Pettersson A, Anderson F, et al. Differences in metabolic profiles between the Burmese, the Maine coon and the Birman cat–three breeds with varying risk for diabetes mellitus. *PloS One* (2021) 16:e0249322. doi: 10.1371/journal.pone.0249322

108. Tripathi D, Kant S, Pandey S, Ehtesham NZ. Resistin in metabolism, inflammation, and disease. *FEBS J* (2020) 287:3141–9. doi: 10.1111/febs.15322

109. Devanoorkar A, Kathariya R, Guttiganur N, Gopalakrishnan D, Bagchi P. Resistin: A potential biomarker for periodontitis influenced diabetes mellitus and diabetes induced periodontitis. *Dis Markers* (2014) 2014:e930206. doi: 10.1155/2014/930206

110. Pan X, Kaminga AC, Wen SW, Acheampong K, Liu A. Omentin-1 in diabetes mellitus: A systematic review and meta-analysis. *PloS One* (2019) 14:e0226292. doi: 10.1371/journal.pone.0226292

111. Murakoshi M, Gohda T, Suzuki Y. Circulating tumor necrosis factor receptors: A potential biomarker for the progression of diabetic kidney disease. *Int J Mol Sci* (2020) 21:1957. doi: 10.3390/ijms21061957

112. Barutta F, Bruno G, Grimaldi S, Gruden G. Inflammation in diabetic nephropathy: Moving toward clinical biomarkers and targets for treatment. *Endocrine* (2015) 48:730–42. doi: 10.1007/s12020-014-0437-1

113. Harkins JM, Moustaid-Moussa N, Chung Y-J, Penner KM, Pestka JJ, North CM, et al. Expression of interleukin-6 is greater in preadipocytes than in adipocytes of 3T3-L1 cells and C57BL/6J and ob/ob mice. *J Nutr* (2004) 134:2673–7. doi: 10.1093/jn/134.10.2673

114. Jin HY, Park TS. Role of inflammatory biomarkers in diabetic peripheral neuropathy. *J Diabetes Investig* (2018) 9:1016–8. doi: 10.1111/jdi.12794

frontiers | Frontiers in Immunology

TYPE Original Research
PUBLISHED 13 October 2022
DOI 10.3389/fimmu.2022.987937

OPEN ACCESS

EDITED BY
Diana Boraschi,
Shenzhen Institute of Advanced Technology (SIAT), Chinese Academy of Science (CAS), China

REVIEWED BY
Barbara Cassani,
University of Milan, Italy
Alberto Cintado,
Cigb, Cuba

*CORRESPONDENCE
Baoxin Zhang
z197218275@yeah.net
Zhenqun Zhao
doctorqun@126.com

†These authors have contributed equally to this work and share first authorship

‡These authors have contributed equally to this work

SPECIALTY SECTION
This article was submitted to Cytokines and Soluble Mediators in Immunity, a section of the journal Frontiers in Immunology

RECEIVED 06 July 2022
ACCEPTED 27 September 2022
PUBLISHED 13 October 2022

CITATION
Wang X, Pei Z, Hao T, Ariben J, Li S, He W, Kong X, Chang J, Zhao Z and Zhang B (2022) Prognostic analysis and validation of diagnostic marker genes in patients with osteoporosis. *Front. Immunol.* 13:987937. doi: 10.3389/fimmu.2022.987937

Prognostic analysis and validation of diagnostic marker genes in patients with osteoporosis

Xing Wang[1†], Zhiwei Pei[2†], Ting Hao[3], Jirigala Ariben[1], Siqin Li[1], Wanxiong He[2], Xiangyu Kong[2], Jiale Chang[2], Zhenqun Zhao[3*‡] and Baoxin Zhang[3*‡]

[1]Bayannur Hospital, Bayannur City, China, [2]Inner Mongolia Medical University, Hohhot, China, [3]The Second Affiliated Hospital of Inner Mongolia Medical University, Hohhot, China

Backgrounds: As a systemic skeletal dysfunction, osteoporosis (OP) is characterized by low bone mass and bone microarchitectural damage. The global incidences of OP are high.

Methods: Data were retrieved from databases like Gene Expression Omnibus (GEO), GeneCards, Search Tool for the Retrieval of Interacting Genes/Proteins (STRING), Gene Expression Profiling Interactive Analysis (GEPIA2), and other databases. R software (version 4.1.1) was used to identify differentially expressed genes (DEGs) and perform functional analysis. The Least Absolute Shrinkage and Selection Operator (LASSO) logistic regression and random forest algorithm were combined and used for screening diagnostic markers for OP. The diagnostic value was assessed by the receiver operating characteristic (ROC) curve. Molecular signature subtypes were identified using a consensus clustering approach, and prognostic analysis was performed. The level of immune cell infiltration was assessed by the Cell-type Identification by Estimating Relative Subsets of RNA Transcripts (CIBERSORT) algorithm. The hub gene was identified using the CytoHubba algorithm. Real-time fluorescence quantitative PCR (RT-qPCR) was performed on the plasma of osteoporosis patients and control samples. The interaction network was constructed between the hub genes and miRNAs, transcription factors, RNA binding proteins, and drugs.

Results: A total of 40 DEGs, eight OP-related differential genes, six OP diagnostic marker genes, four OP key diagnostic marker genes, and ten hub genes (TNF, RARRES2, FLNA, STXBP2, EGR2, MAP4K2, NFKBIA, JUNB, SPI1, CTSD) were identified. RT-qPCR results revealed a total of eight genes had significant differential expression between osteoporosis patients and control samples. Enrichment analysis showed these genes were mainly related to MAPK signaling pathways, TNF signaling pathway, apoptosis, and Salmonella infection. RT-qPCR also revealed that the MAPK signaling pathway (p38, TRAF6) and NF-kappa B signaling pathway (c-FLIP, MIP1β) were significantly different

between osteoporosis patients and control samples. The analysis of immune cell infiltration revealed that monocytes, activated CD4 memory T cells, and memory and naïve B cells may be related to the occurrence and development of OP.

Conclusions: We identified six novel OP diagnostic marker genes and ten OP-hub genes. These genes can be used to improve the prognostic of OP and to identify potential relationships between the immune microenvironment and OP. Our research will provide insights into the potential therapeutic targets and pathogenesis of osteoporosis.

KEYWORDS

osteoporosis, GEO, WGCNA, immune cells, bioinformatics analysis

Introduction

Osteoporosis (OP) is a systemic bone disease characterized by low bone mass and destruction of bone microarchitecture (1), which increases the fragility of the bone and fracture risk (2, 3). OP is the fourth leading chronic disease after heart disease, dementia, and lung cancer (4). Bone homeostasis depends on osteoclast resorption and osteoblast formation, and an imbalance in this tightly coupled process can lead to the development of osteoporosis (5). Hip and vertebral fractures are two common osteoporotic fractures (6). Elderly patients with osteoporotic fractures often require hospitalization, resulting in poor quality of life, long-term medical care, disability, and even death (7). This creates a substantial economic and social burden worldwide and is a global public health challenge (8, 9). Due to its asymptomatic nature, patients with OP are often not diagnosed until the first osteoporotic fracture occurs. Therefore, it is very important to find biomarkers that enable early diagnosis.

In recent years, it has been established that bone and immune cells share the same progenitor cells and are affected by the same cytokines (3). They are functionally linked, and the infiltration of immune cells plays a vital role in the occurrence and development of OP (10). Factors such as the balance between Th1/Th2/Treg cells (3), inflammatory T cells (Th17) (4, 10), regulatory B cells (Bregs) (4), and macrophages (11) play an important role in regulating osteoblasts and osteoclast homeostasis, which in turn affects osteoporosis (12). Regarding the immune system, assessing the varying degrees of immune cell infiltration and identifying the compositional differences in the infiltrating immune cells can help elucidate the molecular pathological mechanism of OP and develop new immunotherapeutic targets.

In this study, to explore the potential diagnostic marker genes for OP, six OP diagnostic marker genes were screened for prognosis of OP, which can predict the prevalence of OP. First, the two OP immune signature subgroups were divided using a consensus clustering method, and differential expression analysis was performed to obtain 40 differentially expressed genes (DEGs). Secondly, eight OP-related differential genes were screened using Weighted gene co-expression network analysis (WGCNA), Gene Ontology (GO) functional annotation, Kyoto Encyclopedia of Genes and Genomes (KEGG) pathway enrichment, and Gene Set Enrichment (GSEA) analysis disease ontology (DO) disease annotation, and Gene Set Variation Analysis (GSVA) were performed on eight DEG. To conduct network analysis, we identified 10 hub genes using the cytoHubba function of Cytoscape software. RT-qPCR was performed on the plasma of osteoporosis patients and control samples. The results revealed a total of eight genes that had significantly different expression levels, and the following signaling pathways such asMAPK signaling pathway (p38, TRAF6) and NF-kappa B signaling pathway (c-FLIP, MIP1β), had significant different expressions. Out of the eight OP-related DEGs, six diagnostic marker genes were tested using Least Absolute Shrinkage and Selection Operator (lasso) regression and random forest using the new dataset. The Cell-type Identification by Estimating Relative Subsets of RNA Transcripts (CIBERSORT) algorithm was used to evaluate the level of immune cell infiltration in the two clusters, and the results showed that there were significant differences in proportions of monocytes, CD4 memory activated T cells, memory, and naïve B cells. Based on six OP-related diagnostic marker genes, two distinct molecular subtypes were identified using a consensus clustering approach. Prognostic analysis was carried out, and four key diagnostic marker genes were identified. Finally, the interaction network with miRNA, transcription factors (TF), RNA binding protein (RBP), and the drugs were constructed for key genes. Our study suggests that targeting these six diagnostic marker genes and ten hub genes may enhance the diagnosis and treatment of OP.

Materials and methods

Data downloaded

Download GSE56815 (13), GSE7158 (14) and GSE56116 (15) datasets from GEO database, In which GSE56815 contains 40 osteoporosis samples (OP) and 40 control samples from GPL96 sequencing platform, GSE7158 contains 12 osteoporosis samples Osteoporosis samples (OP) and 14 control samples were obtained from the GPL570 sequencing platform, and GSE56116 included 10 osteoporosis samples (OP) and 3 control samples from the GPL1433 sequencing platform, all of which were human peripheral blood sample. The above data were integrated for downstream analysis, the R package sva (16) was used to correct for batch effects between different datasets and log2 normalization was performed, and then the batch-corrected expression distribution was visualized using boxplots, where 62 osteoporosis samples and 57 control samples were included.

In order to analyze the expression of osteoporosis-related genes in all samples, we first obtained osteoporosis-related genes from the GeneCards database (17) through the keyword "Osteoporosis", a total of 4657 genes, and intersected with the existing expression profiles. All 4657 genes were retained.

Unsupervised clustering of samples

The R package factoextra (18) was used to determine the optimal number of clusters. The k-means clustering method was used for unsupervised clustering of all patients based on the optimal number of clusters, and the samples were divided into two categories. Finally, the R package was used to see the final clustering effect. Heatmap was used to visualize the gene expression profile of the two groups. The R package ggpubr (19) was used to construct the grouping histogram based on the sample clustering label. The Wilcoxon rank-sum test method was used to study the statistically significant differences between the groups. $P<0.05$ was considered to be statistically significant.

Immune infiltration analysis

CIBERSORT is a deconvolution algorithm based on the principle of linear support vector regression to study the expression matrix of immune cell subtypes. It uses RNA-Seq data to estimate the abundance of immune cells in a sample (20). CIBERSORT: R package was used to estimate the quantity of 22 immune cells between disease and control samples in the datasets. The immune cell composition was visualized using boxplots. Differences in immune cell proportions were calculated using the Wilcoxon test, and $P< 0.05$ was considered statistically significant.

Pearson correlation was used to investigate the correlation between the immune cell expression in all patients. The two genes were correlated if the absolute value of the correlation coefficient > 0.3 and the $P< 0.05$. Correlations between matching gene pairs were plotted using the R package ggplot2 (21).

Osteoporosis-related DEGs

In order to analyze the effect of different gene expression levels on patients with different subtypes of osteoporosis, the R package limma (22) was used to perform differential gene analysis between the two groups of patient samples in the integrated dataset. The significant differential genes (DEGs) were screened. Log2 (fold change) (log2FC) > 1.5 and Padj < 0.05 was set as the thresholds of DEGs. Genes with log2FC> 1.5 and Padj < 0.05 were up-regulated DEG, and genes with log 2FC <-1.5 and Padj < 0.05 were down-regulated DEG. The volcano plot shows the up-regulated DEG, and the R package pheatmap (23) shows the expression heat map of these DEG in all the samples. The R package ggpubr (19) was used to analyze the expression of osteoporosis-related genes in the two groups and construct grouped box plots based on the two subtype samples. Wilcoxon rank sum test method was used to test the statistically significant difference between the groups. $P< 0.05$ was considered statistically significant.

Weighted gene co-expression network analysis

Weighted gene co-expression network analysis (WGCNA) is a systems biology method used to describe gene association patterns between different samples, and can be used to identify gene sets with highly coordinated changes. And identify candidate biomarker genes or therapeutic targets based on the interconnectivity of gene sets and the association between gene sets and phenotypes. We used the R package WGCNA (24) to calculate the key gene sets associated with the disease and normal two groups of samples and used them for subsequent analysis.

Functional enrichment analysis

To investigate the biological differences between sample groups, gene set enrichment analysis (GSEA) was performed on DEG. Gene Ontology (GO) enrichment analysis is commonly used for large-scale functional enrichment analysis of genes at different dimensions and levels, mainly:

biological process (BP), molecular function (MF), and cellular component (CC) (25). Kyoto Encyclopedia of Genes and Genomes (KEGG) pathway enrichment analysis is widely used for storing information about genomes, biological pathways, diseases, and drugs (26). Disease Ontology (DO) is the annotation of genes in the context of the disease. All the significantly DEG were subjected to GO, KEGG pathway enrichment, and disease annotation using the R package clusterProfiler (27) and the DOSE: R Package (28) to identify significantly enriched biological processes. The enrichment results were represented as bubble graphs for visualization. The significance threshold for the enrichment analysis was set at a corrected p-value < 0.05.

Gene Set Enrichment Analysis (GSEA) is a computational method used to determine whether a predefined gene set shows statistical differences between the two biological states. It is typically used to estimate expression in a dataset sample, changes in biological process, pathways, and activity (29). To investigate the differences in biological processes between the two groups of samples, based on the gene expression profiling dataset, the reference gene sets "c5.go.v7.5.1.entrez.gmt" and "c2.cp. kegg.v7.5.1.entrez.gmt" were downloaded from the Molecular Signatures Database MSigDB (30), for enrichment analysis and visualization of the dataset using the GSEA method included in the R package "clusterProfiler." Adjusted p-values < 0.05 were considered statistically significant.

Gene Set Variation Analysis (GSVA) (31), is a non-parametric unsupervised analysis method. It mainly converts the gene expression matrix between different samples into the gene expression sets between samples. Quantity matrices were used to evaluate gene set enrichment results from microarray transcriptome data. To evaluate whether different pathways are enriched in different samples, the "c5.go.v7.5.1.entrez.gmt" and "c2.cp.kegg.v7.5.1.entrez.gmt" gene sets were retrieved from the MSigDB. Further, GSVA was performed at the gene expression level to calculate the differences in functional enrichment between groups (disease and control groups).

Validation of osteoporosis marker genes

The identified diagnostic marker genes were validated using the osteoporosis dataset GSE7429 (32) retrieved from the GEO. The sequencing platform used for this dataset was GPL96 for humans. Data was first log-normalized and then divided into disease and control groups based on gene expression data of each marker. Lasso regression analysis was performed for univariate and multivariate analysis. The receiver operating characteristic (ROC) curve was used to evaluate the performance of marker genes in predicting the groups. ROC curves were drawn using the R package pROC (33).

Network analysis

The Search Tool for the Retrieval of Interacting Genes/Proteins (STRING) (34) database searches for interactions between known and predicted proteins. The STRING database was used to select genes with a combined score greater than 400 to construct a protein-protein interaction (PPI) network related to DEG. Cytoscape (v3.7.2) (35) is used to visualize the PPI network model. PPI network analysis was performed using the CytoHubba (36) function in Cytoscape.

Estimation of key genes

Ridge regression was first used to screen for osteoporosis-related genes. The analysis was performed using the R package glmnet (37) and was used to select the best lambda value. Only genes with coefficients other than zero were retained after regression analysis. The genes were further screened using logistic regression. The genes used to construct the model, and their corresponding coefficients were displayed in the form of forest plots using the R package forestplot (38).

To examine the multivariate influence of eigengenes in the diagnostic model, a new logistic multivariate regression model was constructed using the R package rms (39) on the genes with significant absolute weights in the previous model. To verify the predictive grouping efficacy of key genes, the ROC package pROC (33) was used to draw the ROC curve of the model and calculate the area under the curve (AUC).

Panorama of key genes

The R package RCircos (40) was used to map the location of genes on the chromosomes. The chromosome data were provided by the R package, and the information regarding the location of genes on chromosomes was downloaded from the ENSEMBL (41) database. Boxplot was constructed using R package ggplot2 to analyze the differences in the expression of key genes in all the patients. The Gene Expression Profiling Interactive Analysis (GEPIA2, 42) explores the RNA-seq expression data from tumor and normal tissues retrieved from TCGA and GTEx databases. GEPIA2 was used to obtain the expression of key genes in tumor and normal samples from various human tissues.

Multidimensional network analysis of key genes

TF controls gene expression by interacting with target genes at the transcriptional stage. miRNet database (43) was used to

construct the regulatory network of key genes, TFs, and miRNAs. RBP is an important protein of the cells, which interacts with RNA by recognizing certain RNA binding domains. It is widely involved in RNA splicing, transport, sequence editing, intracellular localization, translation control, and post-transcriptional regulation. The regulatory network of key genes-RBP was constructed using the RBP2GO database (44). RNAactDrug database (45) was used to build a key gene-drug regulatory network.

Real-time fluorescence quantitative PCR

Peripheral blood of four clinical osteoporosis patients and three healthy adults were obtained from the Second Affiliated Hospital of Inner Mongolia Medical University. (This study was performed in line with the principles of the Declaration of Helsinki. Approval was granted by the Ethics Committee of Second Affiliated Hospital of Inner Mongolia Medical University. The ethical review number: YKD202002055). 5ml peripheral venous blood was collected with EDTA-K2 anticoagulant blood collection tube. After centrifugation at 1500 r/min for 15 minutes, the uppermost plasma was obtained. Total RNA was extracted from plasma samples. The genomic DNA was removed from the RNA sample, and RNA was reverse transcribed using the PrimeScript™ RT reagent Kit with gDNA Eraser (RR047A, Takara, Japan). Real-Time quantitative PCR was performed using the SYBR® Premix Ex Taq (Takara, Japan, RR820A) kit using a real-time PCR machine (ABI-7500, Applied Biosystems, USA). The PCR amplification was carried out for a total of 42 cycles. The mean + standard error of three independent experiments were calculated, with each experiment repeated three times. Relative mRNA expression levels were calculated using *GAPDH* as an internal reference.

Statistical analysis

All data processing and analysis were conducted using R software (version 4.1.1). The student's t-test was used to compare the two continuous variables groups and evaluate the statistical significance of normally distributed variables. The independent and the differences among non-normally distributed variables were analyzed using the Mann-Whitney U test (i.e., the Wilcoxon rank sum test). Chi-squared test or Fisher's exact test was used to compare and analyze statistical significance between two groups of categorical variables. Correlation coefficients between different genes were calculated using Pearson correlation analysis. The t-test was used to compare the mean values of two groups of samples, and the analysis of variance (ANOVA) test was used to compare the mean values of multiple groups of samples. All statistical P values were two-sided. $P < 0.05$ considered statistically significant.

Results

Gene Expression Omnibus data preprocessing

In order to clearly show the specific process of this study, the bioinformatics analysis process is specially summarized as shown in the figure (Figure 1). To construct a panorama of osteoporosis-related genes in all samples, the expression profiles of all three datasets were integrated. Datasets from different sources generally have severe batch effects. Hence the raw data was first analyzed and then corrected for batch effects and log normalization. Boxplots were drawn using the data OP and Normal groups retrieved from datasets GSE56815, GSE7158, and GSE56116 (Figures 2A, B). The results show that after batch correction and log normalization, the distribution of expression profiles of all the samples tends to be overall consistent., which

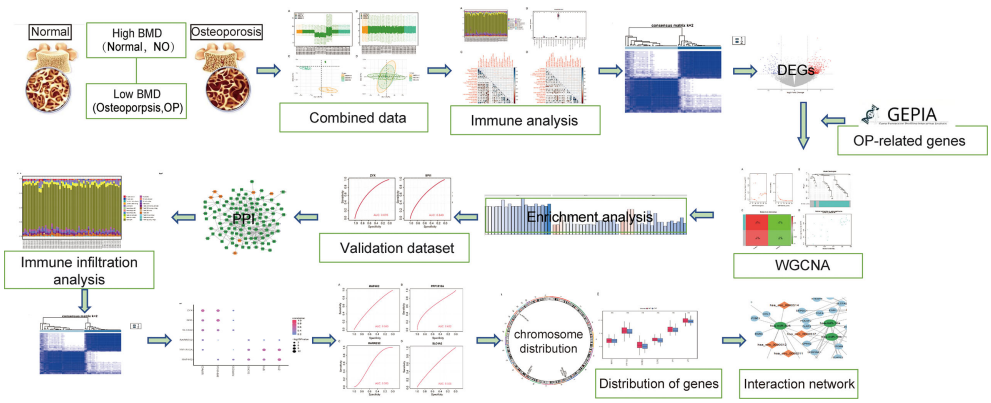

FIGURE 1
Flowchart.

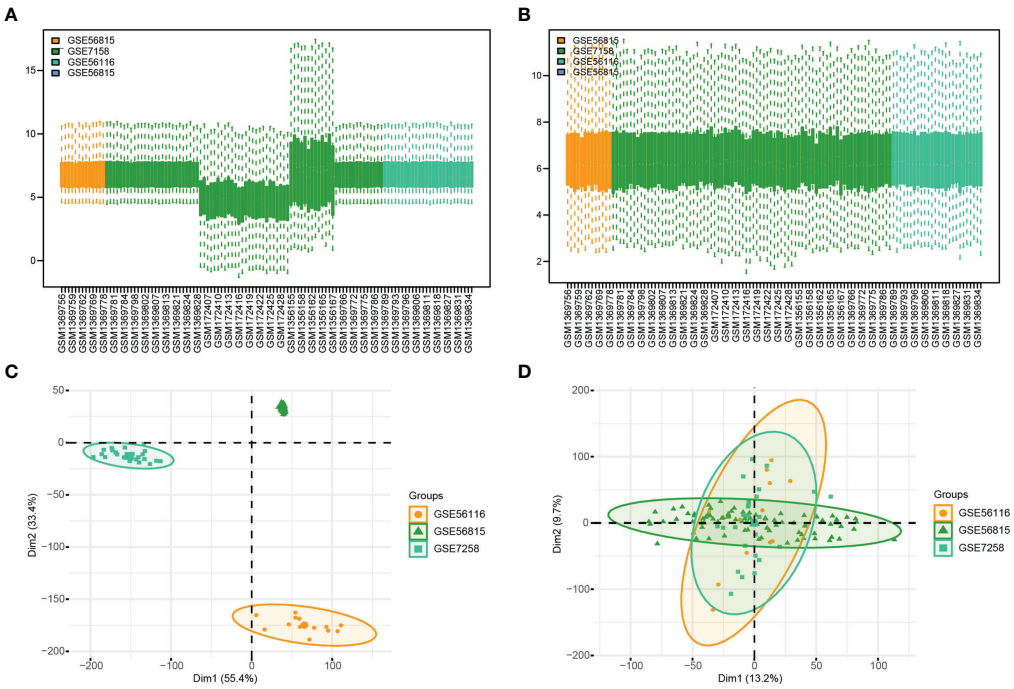

FIGURE 2
Gene Expression Omnibus (GEO) data preprocessing. **(A, B)** are the differences in data distribution before and after data set processing. **(C, D)** results from PCA dimensionality reduction before and after data set processing.

was more conducive to improving the accuracy and robustness of the downstream analysis (Figure 2). The batch effect was removed to obtain an integrated dataset, which included 62 osteoporosis and 57 control samples.

Overall immune level analysis and differential analysis of immune signature subtypes in osteoporosis

The immune microenvironment is a complex integrated system composed mainly of immune cells, inflammatory cells, fibroblasts, interstitial cells, various cytokines, and chemokines. The analysis of infiltrated immune cells in samples plays an important role in understanding the pathology, prognosis, and treatment of the disease. To analyze the differences in immune levels between normal and disease states, we analyzed the overall immune profile of normal (NO) and osteoporotic (OP) patient samples (Figures 3A–D). CIBESORT analysis of immune infiltration analysis (Figure 3A) reveals that the content of monocytes was high in OP and normal samples. Compared to normal samples, the OP patient samples only showed significant differences in the expression levels of M0, M1 Macrophages, and activated dendritic cells (Figure 3B). Further, the correlation of immune cell content in normal and OP patient samples was analyzed. The results revealed a significant correlation between the memory B cells and monocyte content in normal samples and various immune cells (Figure 3C). In OP patient samples, a significant correlation between the content of the activated mast cells and M0 macrophages, and various other immune cells (Figure 3D).

Here, a consensus clustering method commonly used in tumor typing is used. We wanted to use this method to divide the 62 OP patient samples from the 3 datasets into an appropriate number of subgroups. Furthermore, differential expression analysis was performed on its different subgroups. The obtained differential expression results can not only represent the difference between OP and normal samples, but also reflect the differential genes between different types (or grades) of OP. Different expression patterns were identified in 62 osteoporosis patient samples using a consensus clustering method (ConsensusClusterPlus package in the R software). Figures 3E, F show the matrix heatmaps for k=2 and k=6, and the clustering results are better separated when k=2. Secondly, considering the consistent Cumulative Distribution Function (CDF) plot and the Delta Area Plot, the CDF at k=2 had a lower slope of decline and a lower change in the AUC (Figures 3G, H). Two osteoporosis subtypes (cluster1 and cluster2) were finally identified (Figures 3E–H), with cluster 1 containing 34 samples and cluster 2 containing 28 samples. (Figure 3E).

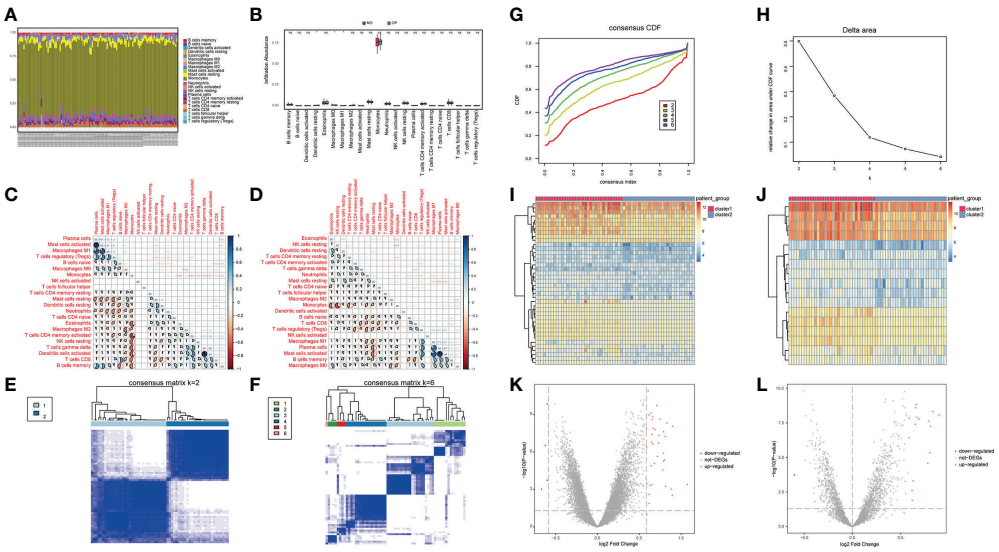

FIGURE 3
Overall immune level analysis and differential analysis of immune signature subtypes in osteoporosis. **(A)** The content of immune cells between the osteoporosis (OP) and the control group. Different colors represent different immune cells, and the horizontal axis represents the patient id. **(B)** Histogram of immune cell content, the horizontal axis represents immune cells, the vertical axis represents cell content, red represents the control group samples, and blue represents the disease group samples. 3C-D: Correlation of immune cell content in the normal group **(C)** and disease group samples **(D)**; red indicates a negative correlation, and blue indicates a positive correlation. **(E, F)** Consistent clustering result graph, different colors represented different groups. **(G)** Cumulative Distribution Function (CDF) plot of consensus clustering, showing the curve of the CDF as the number of clusters changes. **(H)** Delta Area plot, calculating the relative change in the area under the curve (AUC) of the CDF as the number of clusters increases. **(I, J)** Heatmaps of differentially expressed genes (DEG), where red is for cluster 1 and blue is for cluster 2. **(K, L)** the volcano plot for DEG, the abscissa is log2FoldChange, the ordinate is -log10 (adjust P-value), red nodes indicate up-regulated DEG, gray nodes indicate genes that are not significantly differentially expressed, and blue nodes indicate down-regulated genes DEG.

To understand the biological differences between the two patient subgroups, the DEG analysis was first performed on the two patients' subgroups. The threshold was set as padj<0.05 and foldchange>1.5 or foldchange<-1.5. and a total of 40 DEGs were identified during the analysis. There were 36 up-regulated genes and four down-regulated genes (Figures 3I, K). The OP-related genes retrieved from GeneCards were intersected, and a total of 17 genes that were significantly different between the two groups of patients and related to OP were retained (Figures 3J, L).

Functional enrichment analysis between samples

To explore the relationship between the differentially expressed OP-related genes, WGCNA analysis was performed on the DEG between the two groups of patients (Figure S1A). A co-expression module was identified (Figure S1B), and the gene set with the highest correlation was identified and subjected to subsequent analysis (Figures S1C, D) 1198 key genes were obtained. After intersecting with differentially expressed OP-related genes, eight genes were obtained for subsequent analysis (Table S1).

To explore the influence of the differential genes on the biological functions of different patient subtypes, GO enrichment analysis was performed on the differential genes. The biological processes enriched by these differential genes were myeloid cell differentiation, regulation of stress-activated MAPK cascade (Figure 4A), and cell groups such as vesicle lumen and tertiary granule (Figure 4B). The molecular functions enriched by these differential genes were ubiquitin protein ligase binding and ubiquitin-like protein ligase binding (Figure 4C). KEGG pathway enrichment analysis revealed these differential genes significantly enriched pathways such as Salmonella infection and MAPK signaling pathway (Figure 4D). In addition, Disease ontology analysis (DOSE) was performed on the differential genes. The results revealed that the DEG between different patient subtypes was significantly enriched in heart valve disease (Figures 4E, F).

GSEA analysis was performed on the differential genes, and the results revealed significant differences in the following biological processes between the two groups of patient samples. In cluster 1 patient samples, the regulation of response to stimulus, negative regulation of the cellular process, and negative regulation of biological and other biological processes were activated (Figures 4G, H).

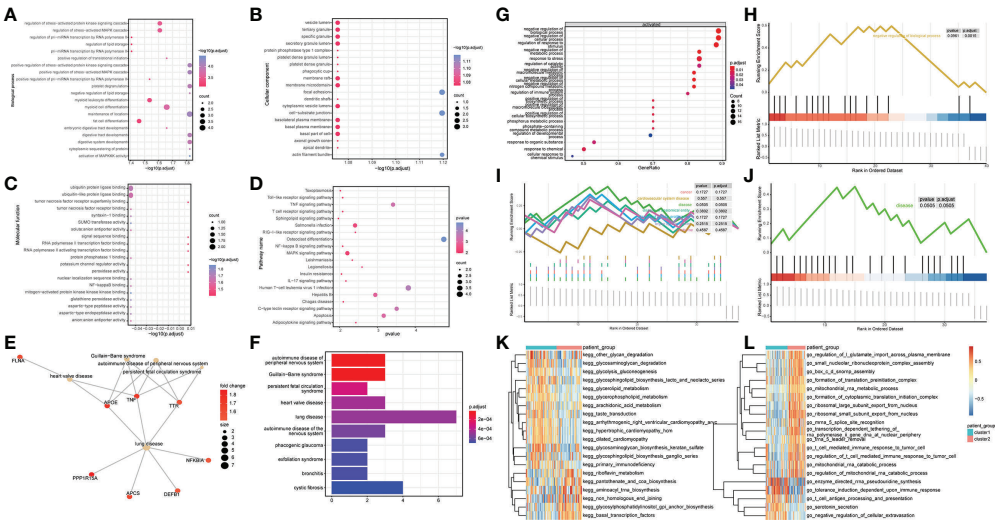

FIGURE 4
DEGs identification and functional enrichment analysis between samples. **(A-C)** GO enrichment analysis was performed on up-regulated, and down-regulated genes, and biological process (BP), molecular function (MF), and cellular component (CC) were displayed. Node size indicates the number of genes enriched in the pathway, and node color indicates -log10 (p-value). **(D)** Results of KEGG pathway analysis, the node size represents the number of genes enriched in the pathway, and the node color represents the p-value. **(E, F)** DOSE enrichment results. **(G)** Overall Gene Ontology enrichment analysis results. **(H)** gsea-go enrichment pathway analysis results. **(I, J)** The overall and partial gsea_dose enrichment results are displayed. **(K, L)** GSVA enrichment results.

Simultaneously, among the seven related pathways annotated by DOSE, the disease pathway was significantly annotated (Figures 4I, J).

The results of GSVA analysis showed that go_chloride_transprt was activated in the cluster 2 patient samples, and in the cluster 1 patient samples, kegg_ubiquitin_mediated_proteolysis was inhibited (Figures 4K, L).

Validation of diagnostic marker genes in a new dataset

To evaluate if the key identified genes could serve as diagnostic marker genes for osteoporosis and to test the robustness of the predicted diagnostic marker genes, new datasets (GSE7429, GPL96) were retrieved from GEO. The data were preprocessed consistently, and the association of genes with OP was first tested using lasso regression and random forest. Univariate analysis (Figures 5A–C) revealed that none of the eight key genes were significant associated (EGR2, RARRES2, ZYX, SLC4A2, MAP4K2, MAT1A, PPP1R15A, SPI1). Hence, the performance of key genes in predicting disease samples was evaluated by plotting the ROC curves of the key genes. There were eight key genes related to OP differences. ROC curves of each of the eight key genes associated with OP in normal and OP tissue samples were constructed. The results revealed six key genes with predicted AUC > 0.6, namely RARRES2, ZYX, SLC4A2, EGR2, MAT1A, and SPI1 (Figure 5D). The results show that these six genes could successfully distinguish between OP and normal samples.

Verification of Hub genes and signaling pathway molecules in clinical samples

To understand the relationship between the DEG-related to OP in the biological network, eight OP-related differential genes were analyzed using WGCNA, and 11 PPI regulatory networks were downloaded from the STRING database (Figure S2A). The regulatory relationship was imported into Cytoscape for network analysis, and the top ten hub genes were identified (Figure S2B). Hub genes were TNF, RARRES2, FLNA, STXBP2, EGR2, MAP4K2, NFKBIA, JUNB, SPI1, CTSD. Figure S2C shows the diagnostic genes that distinguish OP samples from control samples scattered in the PPI network, further reiterating that the research focus was still on validating the diagnostic genes.

The peripheral blood from clinical samples was collected to explore the expression of hub genes. The mRNA expression of TNF, RARRES2, FLNA, STXBP2, EGR2, MAP4K2, NFKBIA, JUNB, SPI1, and CTSD in the plasma of the control group and the OP group was detected (Figures 6A–J). The RT-qPCR results showed that compared to the control group, the mRNA

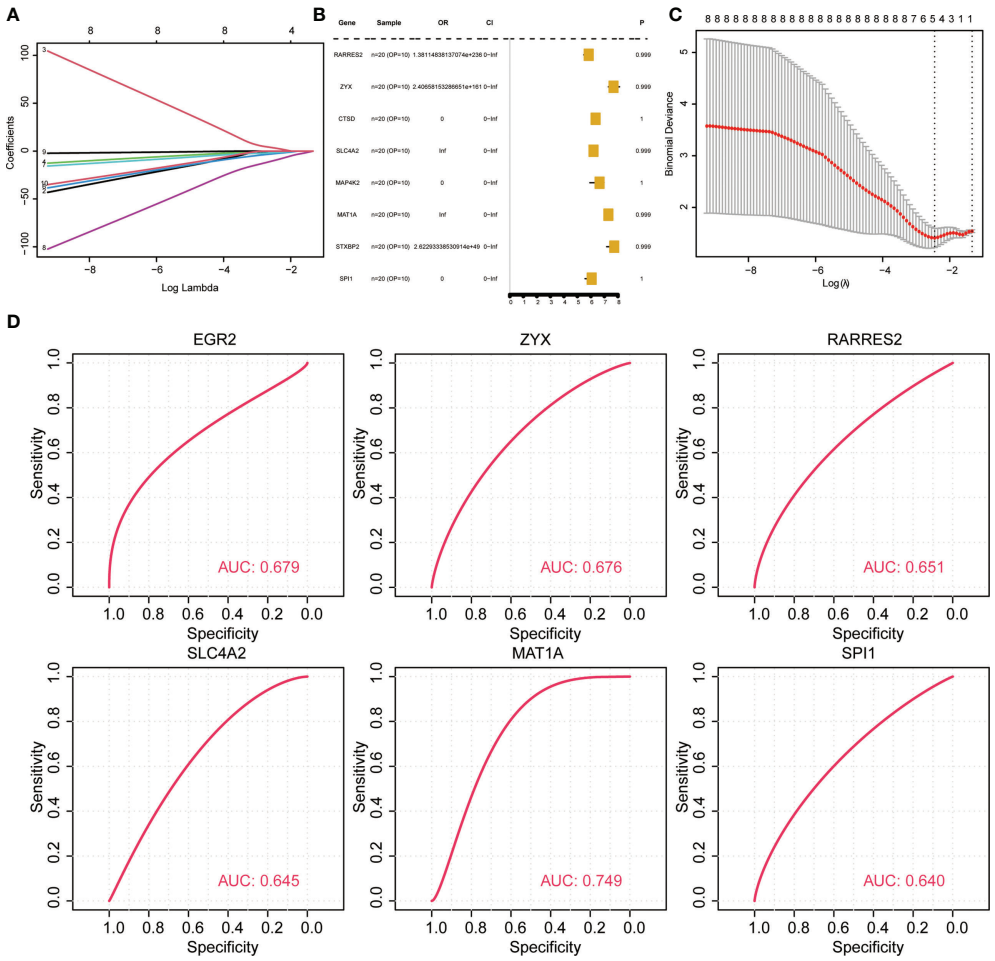

FIGURE 5
Validation of diagnostic marker genes in a new dataset. **(A, C)** lasso regression analysis results. **(B)** Univariate analysis results. **(D)** ROC curve, indicating the diagnostic performance of the genes.

expression levels of TNF, RARRES2, FLNA, MAP4K2, and SPI1 in the plasma of the OP group were significantly increased, the mRNA expression levels of EGR2, JUNB, and CTSD were significantly decreased in the OP group. There was no significant difference in the mRNA expression levels of STXBP2 and NFKBIA between the two groups.

To further explore the expression of MAPK and NF-kappa B signaling pathway-related genes, the peripheral blood from clinical samples was collected, and total RNA was extracted to study the expression levels of c-FLIP, MIP1β, p38, and TRAF6 in the plasma of the control group (Control) and the osteoporosis group (OP) (Figures 6K–N). The results of RT-qPCR showed that compared to the control group, a significant decrease in the mRNA expression level of c-FLIP in the plasma of the OP group was observed, and a significant increase in the mRNA expression levels of MIP1β, p38, and TRAF6 was observed.

Immune infiltration analysis and molecular subtype construction based on key OP-related diagnostic marker genes

The CIBERSORT results showed (Figure 7A) that the monocyte content was significantly high in the two groups of OP patients. Compared to cluster 1, OP patients in cluster 2 had lower levels of CD8 in Monocytes and T cells (Figure 7B). OP patients in cluster 1 had a low content of activated dendritic cells, resting mast cells, neutrophils, and activated CD4 memory T cells compared to cluster 2 (Figure 7B). The correlation between differentially expressed characteristic genes related to OP, the diagnostic marker genes, and immune cell content was analyzed. The results showed a significant positive correlation between the expression levels of monocytes and various differentially expressed

10.3389/fimmu.2022.987937

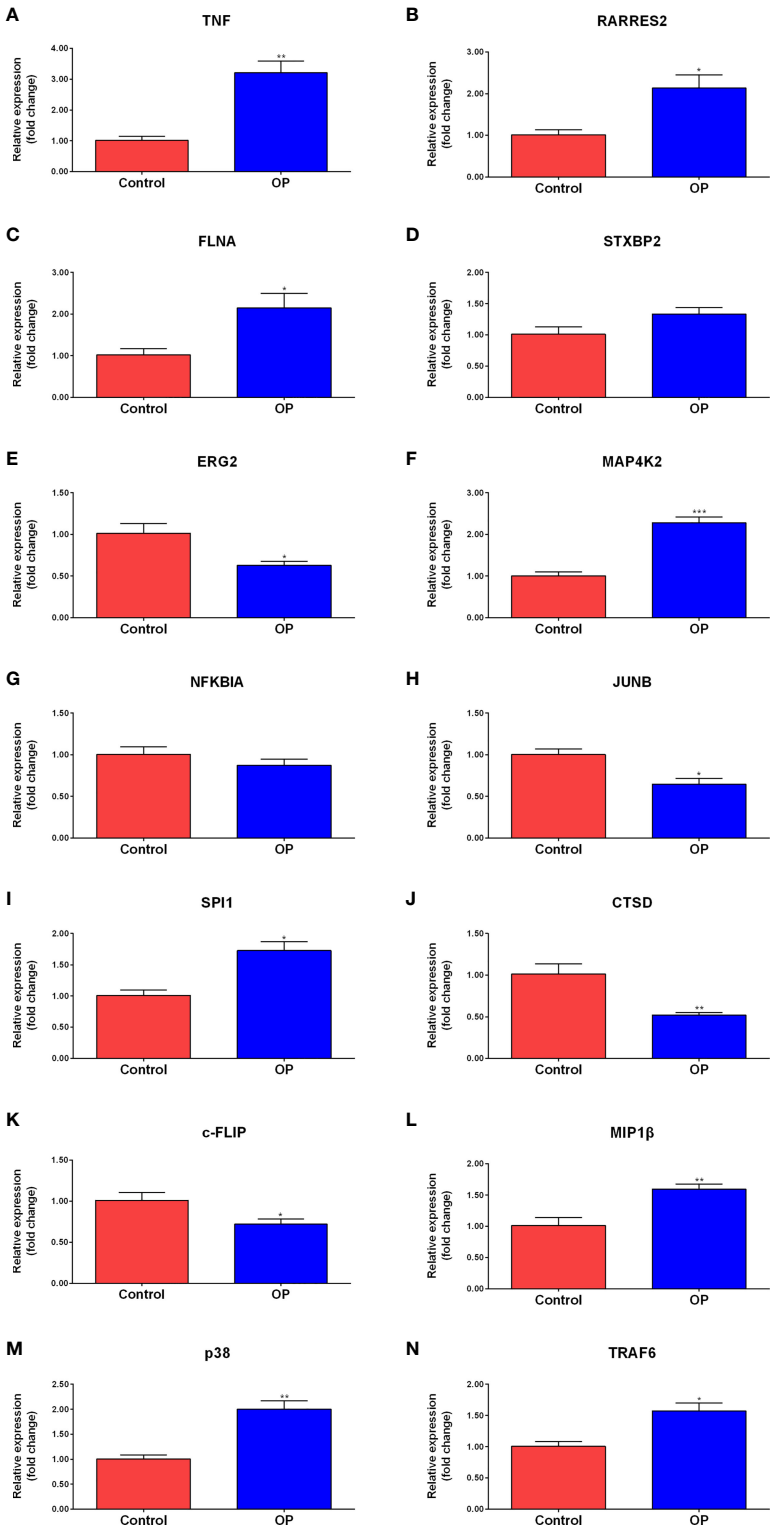

FIGURE 6
RT-qPCR results of the expression level of Hub genes and signaling pathway molecules. Comparison of mRNA expression levels of 10 Hub genes and 4 signaling pathway molecules in plasma of control group (n=3) and OP group (n=4). Among them, the mRNA expression levels of TNF **(A)**, RARRES2 **(B)**, FLNA **(C)**, MAP4K2 **(F)**, SPI1 **(I)**,MIP1b **(L)**, p38 **(M)**, and TRAF6 **(N)** in the plasma of the OP group were significantly increased. the mRNA expression levels of EGR2 **(E)**, JUNB **(H)**, CTSD **(J)** and c-FLIP **(K)** were significantly decreased in the OP group. There was no significant difference in the mRNA expression levels of STXBP2 **(D)** and NFKBIA **(G)** between the two groups. P-values were calculated using a two-sided unpaired Student's t-test. (*P < 0.05, **P < 0.01,***P < 0.001 vs. Control).

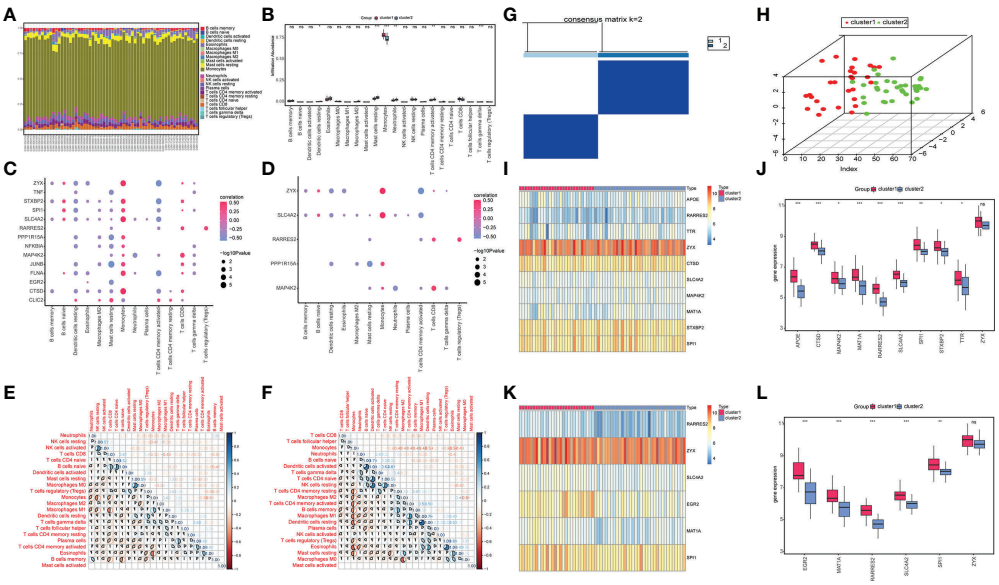

FIGURE 7
Immune infiltration analysis and molecular subtype construction based on key OP-related diagnostic marker genes. **(A)** The accumulation of immune cells between cluster 1 and cluster 2, different colors represent different immune cells, and the horizontal axis represents the patient id. **(B)** Histogram of immune cell content, the horizontal axis represents immune cells, the vertical axis represents cell content, red represents cluster 1 samples, and blue represents cluster 2 samples. **(C)** Correlation diagram between OP differentially expressed genes and immune cells, the horizontal axis represents immune cells, the vertical axis represents genes, the color of nodes represents the size of the correlation, and the size of the nodes represents the level of significance. **(D)** Correlation diagram between key genes and immune cells, the horizontal axis represents immune cells, the vertical axis represents key genes, the color of the nodes represents the size of the correlation, and the size of the nodes represents the level of significance. **(E, F)** Correlation of immune cell content in cluster 1 **(E)** and cluster 2 samples **(F)**; red indicates a negative correlation, and blue shows a positive correlation. **(G)** Graph of Consistent clustering results. **(H)** PCA analysis of cluster1 and cluster2. **(I, J)** Heat map **(I)** and box plot **(J)** shows the expression of OP-related differentially expressed genes between the two groups. **(K, L)** Heatmap **(K)** and boxplot **(L)** show the expression levels of key genes between the two groups. Red represents cluster1, and blue represents cluster2. (*P < 0.05, **P < 0.01, ***P < 0.001, ns P > 0.05 no significance vs. Control).

characteristic genes related to OP (Figure 7C). Monocytes positively correlated with multiple diagnostic marker genes, and a negative correlation was observed between activated CD4 memory T cells and multiple diagnostic marker genes (Figure 7D). Simultaneously, the correlation between the immune cell content of samples from patients in cluster 1 and samples from patients in cluster 2 was calculated. The results showed a significant correlation between the content of the memory B cells and various immune cells in samples from cluster 1 (Figure 7E). The content of monocytes in the samples significantly correlated with the content of various other immune cells (Figure 7F).

Based on the six OP-related diagnostic key genes, two different molecular subtypes and two patient subgroups (cluster1 and cluster2) were identified (Figure 7G) using a consensus clustering method ("ConsensusClusterPlus" package in the R software). Cluster 1 contained 28 samples, and cluster 2 had 34 samples. The PCA clustering results showed significant differences between the two clusters (Figure 7H).

The heatmaps and box plots were constructed based on the expression to observe changes in isoforms and gene expression. WGCNA analysis revealed a significant increase in the OP-related DEG in cluster1 (Figures 7I, J). Simultaneously, the expression of diagnostic marker genes in cluster1 was significantly higher compared to cluster2 (Figures 7K, L).

Key gene correlation analysis based on osteoporosis subtypes

To analyze the influence of key diagnostic genes on patients with different subtypes of OP, logistic univariate regression analysis was used to identify six genes with poor influence on OP (Figure 8C). Coefficients for six genes were calculated based on LASSO analysis (Figures 8A, B). The correlation between the expression of key genes was calculated, and the RARRES2 gene showed a significant positive correlation with multiple other genes (Figure 8D).

To analyze whether the key genes could better distinguish the two molecular subtypes, the gene expression was multiplied by the corresponding coefficient and added to establish the OP prediction score. The final prediction score of each sample was calculated. The results revealed that these four genes (RARRES2, SLC4A2, SPI1, ZYX) could better predict different subtypes of OP patients (Figures 8E–H).

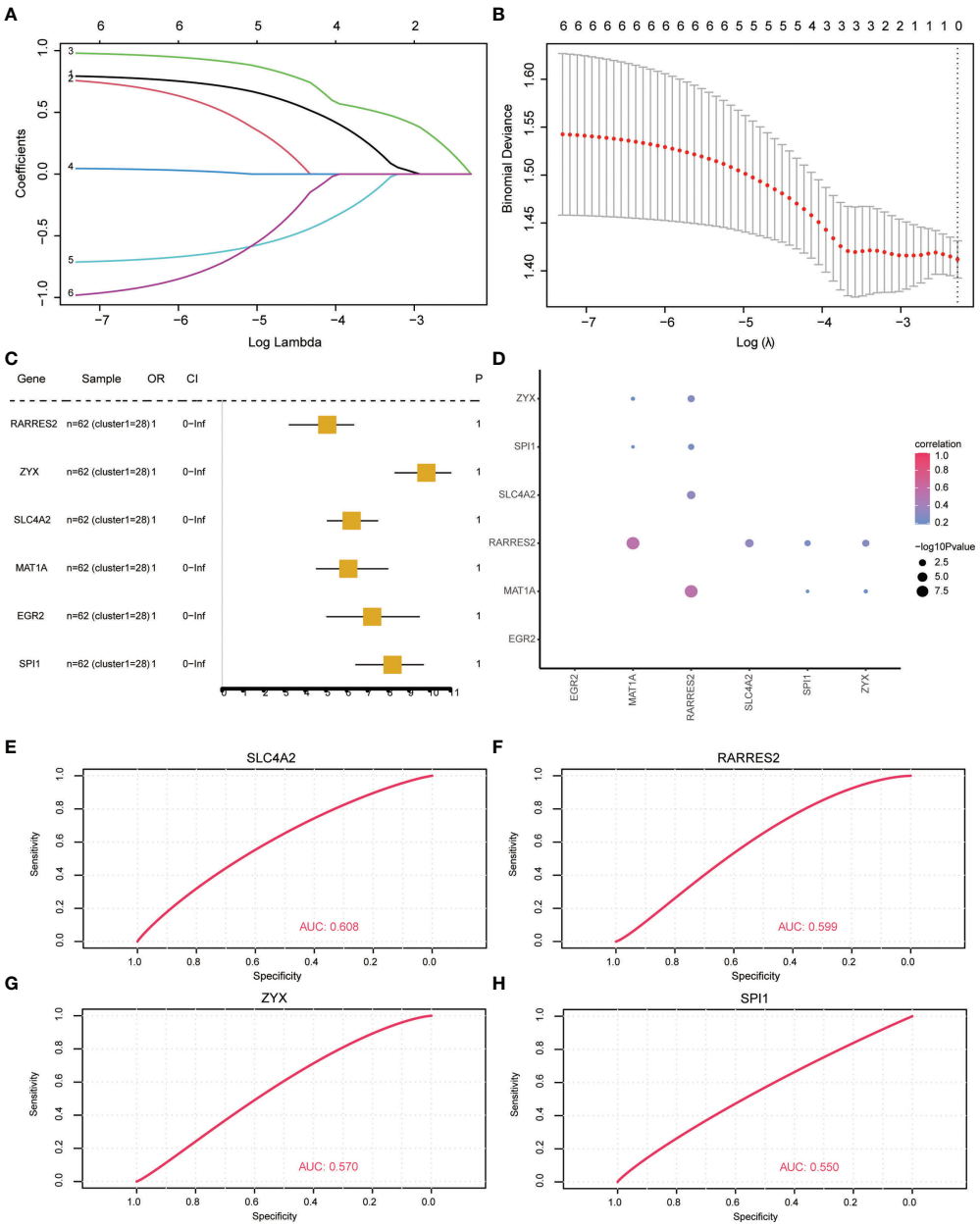

FIGURE 8
Key gene correlation analysis based on osteoporosis subtypes. **(A, B)** Lasso regression analysis results. **(C)** Univariate analysis results. **(D)** Similarity between key genes, the size of the point represents significance; the larger the point, the more significant the color indicates the correlation, and the redder the color, the more relevant. **(E–H)**: ROC curve, indicating the diagnostic performance of the genes.

Discussion

In recent years, due to the lack of reliable early diagnostic tools and methods, most OP patients have suffered pathological fractures, which would require internal fixation and surgical interventions. This causes causing severe physical, mental, and economic burdens to the patients. Previous studies have shown that the immune microenvironment may play an important role in the occurrence and development of OP (4, 11, 46). However, the specific targets and therapeutic mechanisms of OP remain unclear and require further investigation. Our study screened 40 DEGs, eight OP-related differential genes, ten hub genes, six OP diagnostic marker genes, and four OP diagnostic marker key genes. Furthermore, the correlation between OP prognostic models and immune signatures and immune cell infiltration profile revealed that the immune microenvironment might be involved in the pathogenesis of OP.

WGCNA analysis screened eight OP-related differential genes. GO, KEGG, GSEA, DOSE, and GSVA enrichment analysis was also performed. The results showed that OP-related genes mainly enriched the MAPK signaling pathway, TNF signaling pathway, apoptosis, and Salmonella infection. RT-qPCR results showed significant differences in the MAPK signaling pathway (p38, TRAF6) and NF-kappaB signaling pathway (c-FLIP, MIP1β). Previous studies have shown that OPG/RANK/RANKL (9), IL-1β (47),TRAF6 (48), NFATc1, OSCAR and NF-κB (49), and other genes related to apoptosis, inflammation, and osteogenic differentiation (6). These genes regulate bone metabolism *via* the MAPK signaling pathway and TNF signaling pathway, which affects OP. Salmonella infection can lead to mild intestinal inflammation, which releases cytokines and other factors like interleukin-6 (IL-6), IL-8, IL-12, LPS-induced tumor necrosis factor alpha (LITAF) and interferon gamma (IFN-γ). The increases in expression of these pro-inflammatory cytokines affect bone metabolism, leading to bone loss (50). The above findings further corroborate the reliability of our analysis and prediction.

Further, the network analysis using the CytoHubba function in Cytoscape software identified ten hub genes. RT-qPCR results showed a significant increase in the mRNA expression levels of TNF, RARRES2, FLNA, MAP4K2, and SPI1 in the plasma of the OP patients group compared to the control group. Further, the mRNA expression levels of EGR2, JUNB, and CTSD were significantly decreased compared to the control sample group. Lastly, the mRNA expression levels of STXBP2 and NFKBIA were no significant difference. Previous studies have shown that TNF-α can act as an osteoclast factor, and TNF-β acts as an anti-osteoclast factor (4), which affects bone metabolism by regulating RANKL expression (3). Han L et al. (51) showed that RARRES2 protein secreted by adipocytes (52) has an inhibitory effect on osteoblast differentiation and proliferation by inhibiting Wnt/β-catenin signaling and activating RANK signaling. Osteocyte differentiation and proliferation are stimulatory. Therefore, maintaining low RARRES2 levels could be a strategic approach for OP prevention and treatment. Yang C et al. (53) showed that FLNA accumulates in the osteoblasts, and the osteoclasts were observed in the human OP samples. A report suggests that negative regulation of FLNA in mice is age-related and postmenopausal osteoporosis *in vitro* osteogenic differentiation in OP promotes RANKL-induced osteoclast differentiation (54). Zhang X et al. (55) showed an increase in MAP4K2 expression upstream of JNK in aged osteoblasts. Yang C et al. (56) showed the involvement ofSPI1 in OP development by regulating autophagy. Previous studies have shown that EGR2 is a zinc finger transcription factor, and EGFR signaling activates the MAPK/ERK pathway to stimulate EGR2 expression (57). Further, mounting evidence indicates that IL-27 inhibits RANKL-mediated osteoclast differentiation (8) in an EGR2-dependent manner (10). A previous report suggests that BMP-2-induced Smad1 protein activation leads to JUNB synthesis, which is involved in the trans-differentiation of myoblasts to osteoblasts and contributes to bone repair after OP (58). CTSD deficiency can lead to lysosomal autophagy, which plays a protective role in OP development (59). Previous studies show that STXBP2regulates vascular homeostasis in endothelial cells (60), along with various factors NFKBIA which significantly affect osteoclastogenesis (7, 61). However, in our study, there was no significant difference in the expression of STXBP2 and NFKBIA, as shown by RT-qPCR. Therefore, in the future, increasing the sample size would be a need for in-depth analysis. Taken together, it is suggested that the above molecules may play an important role in the diagnosis and treatment of OP.

In addition, for these eight OP-related differential genes, six diagnostic marker genes were tested by lasso regression and random forest using the new dataset. In recent years, osteoporosis treatment has focused on modulating the local immunity of the bone tissues. This provides a suitable microenvironment for positive regulation of bone metabolism, promotion of osteogenic differentiation, and inhibition of osteoclast differentiation (12). A report suggests that bone cells and the immune system share common progenitor cells, cytokines, and growth factors that interact during normal conditions and pathological states (3). However, the specific role of the immune system in OP is not fully understood. In this study, the CIBERSORT evaluated the immune cell infiltration in the two clusters. The results showed significant differences in monocytes, activated CD4 memory T cells, and memory and naïve B cells. Liu P et al (62) showed that monocytes express high levels of glucocorticoid receptors, which accumulate in the bone marrow during GC-induced osteoporosis, and have osteoclast differentiation potential. Gazzola L et al (63) revealed that higher levels of activated CD4+/CD8+ T cells are an independent predictor of osteopenia and osteoporosis. Titanji K et al (64) showed that individuals with HIV infection had significantly higher bone resorption and osteopenia, which were associated with B cell dysfunction. It is likely that a significant increase in RANKL-expressing B cells and a significant decrease in OPG-expressing B cells could be related to the induction of B cells naïve (46). Taken together, the immune microenvironment is under the tight regulation of cell-associated factors, which may play an important role in OP.

Moreover, two distinct molecular subtypes were identified using a consensus clustering approach based on six OP-related diagnostic marker genes. Prognostic analysis identified four key diagnostic marker genes (RARRES2, SLC4A2, MAP4K2, PPP1R15A). Among them, RARRES2, MAP4K2, and SPI1 could be used as hub genes, and significant difference in expression in OP have been established. ZYX can repair the

vascular endothelial injury by regulating endothelial cell exocytosis to reorganize the local actin network (65). Previous studies have shown that SLC4A2-mediated osteoclast anion exchange affects bone resorption by regulating pHi (66, 67). PPP1R15A promotes apoptosis, alleviating stress-induced osteoblast damage (68, 69). Finally, interaction networks with miRNAs, TFs, RBPs, and drugs for key genes were constructed. The study's results suggest that ten hub genes and six diagnostic marker genes could be used as diagnostic markers for OP.

However, this study has some obvious limitations. First, this study used bioinformatics analysis and proposed a theoretical diagnostic model. We have conducted a preliminary investigation to study the expression levels of Hub genes and pathway-related genes. A specific regulatory relationship needs to be further verified, for which a large sample size would be required to validate and enhance the clinical translational value of our diagnostic and prognostic model. Secondly, the immune characterization and cellular infiltration analysis were based on limited genetic data; thus, heterotypic cellular interactions and disturbances caused by different diseases may lead to bias in the immune analysis. Finally, further experimental validation using RT-qPCR, western blotting, and immunohistochemical analysis is required to fully understand the role of Hub genes and their underlying regulatory mechanisms associated with OP.

Conclusion

In conclusion, we identified genes that may be differentially expressed in the OP and performed functional enrichment analysis on eight OP-related differential genes. CytoHubba function of Cytoscape software was used to conduct network analysis, and as a result, ten hub genes were identified. Further, RT-qPCR results confirmed that eight genes were significantly differential expressed, of which MAPK signaling pathway (p38, TRAF6), NF-kappa B signaling pathway (c-FLIP, MIP1β) were significantly differentially expressed between OP and control samples. The molecular features of OP prognosis based on six diagnostic marker genes were constructed. The immune infiltration analysis showed significant differences in monocytes, activated CD4 memory T cells, memory, and naïve B cells. Two different molecular subtypes of OP were identified using the consensus clustering method. Four key diagnostic marker genes were obtained from the prognostic analysis. Further, an interaction network with miRNA, TF, RBP, and drug was constructed for this purpose. We have identified a more accurate and reliable prognosis strategy for patients with early OP, which has enhanced our understanding of OP pathogenesis.

Data availability statement

The datasets involved in the present study are available in the NCBI repository, accession numbers GSE56815, GSE7158, GSE56116 and GSE7429.

Ethics statement

The studies involving human participants were reviewed and approved by the Second Affiliated Hospital of Inner Mongolia Medical University (ethical review number: YKD202002055). The patients/participants provided their written informed consent to participate in this study.

Author contributions

XW, ZP, BZ and ZZ are responsible for the research concept and design. ZP and BZ wrote the manuscript. XW, ZP, TH, JA, SL, WH, XK, JC, ZZ, BZ participated in data collection and interpretation. All authors approved the final version of the manuscript. All authors contributed to the article and approved the submitted version.

Funding

Science and Technology Planning Project of Inner Mongolia Science and Technology Department (2021GG0174; Inner Mongolia Education Department Project (NJZZ22665); Inner Mongolia Autonomous Region "14th Five-Year" social welfare field key research and development and achievement transformation plan project (2022YFSH0022); Science and Technology Planning Project of Inner Mongolia Science and Technology Department (2020GG0195); Inner Mongolia Autonomous Region "14th Five-Year" social welfare field key research and development and achievement transformation plan project (2022YFSH0021).

Acknowledgments

Thanks to the Inner Mongolia Nature Foundation, Bayannaoer City Hospital, the Second Affiliated Hospital of Inner Mongolia Medical University.

Conflict of interest

The authors declare that the research was conducted in the absence of any commercial or financial relationships that could be construed as a potential conflict of interest.

Publisher's note

All claims expressed in this article are solely those of the authors and do not necessarily represent those of their affiliated organizations, or those of the publisher, the editors and the reviewers. Any product that may be evaluated in this article, or claim that may be made by its manufacturer, is not guaranteed or endorsed by the publisher.

Supplementary material

The Supplementary Material for this article can be found online at: https://www.frontiersin.org/articles/10.3389/fimmu.2022.987937/full#supplementary-material

References

1. Zhang YL, Chen Q, Zheng L, Zhang ZW, Chen YJ, Dai YC, et al. Jianpi qingchang bushen decoction improves inflammatory response and metabolic bone disorder in inflammatory bowel disease-induced bone loss. *World J Gastroenterol* (2022) 28(13):1315–28. doi: 10.3748/wjg.v28.i13.1315

2. Lin S, Wu J, Chen B, Li S, Huang H. Identification of a potential MiRNA-mRNA regulatory network for osteoporosis by using bioinformatics methods: A retrospective study based on the gene expression omnibus database. *Front Endocrinol (Lausanne)* (2022) 13:844218. doi: 10.3389/fendo.2022.844218

3. Zhang W, Zhao W, Li W, Geng Q, Zhao R, Yang Y, et al. The imbalance of cytokines and lower levels of tregs in elderly Male primary osteoporosis. *Front Endocrinol (Lausanne)* (2022) 13:779264. doi: 10.3389/fendo.2022.779264

4. Sapra L, Shokeen N, Porwal K, Saini C, Bhardwaj A, Mathew M, et al. Bifidobacterium longum ameliorates ovariectomy-induced bone loss *via* enhancing anti-osteoclastogenic and immunomodulatory potential of regulatory b cells (Bregs). *Front Immunol* (2022) 13:875788. doi: 10.3389/fimmu.2022.875788

5. Zhang H, Feng J, Lin Z, Wang S, Wang Y, Dai S, et al. Identification and analysis of genes underlying bone mineral density by integrating microarray data of osteoporosis. *Front Cell Dev Biol* (2020) 8:798. doi: 10.3389/fcell.2020.00798

6. Marycz K, Kowalczuk A, Turlej E, Zachanowicz E, Tomaszewska A, Kulpa-Greszta M, et al. Impact of polyrhodanine manganese ferrite binary nanohybrids (PRHD@MnFe(2)O(4)) on osteoblasts and osteoclasts activities-a key factor in osteoporosis treatment. *Mater (Basel)* (2022) 15(11):3990. doi: 10.3390/ma15113990

7. Yu T, Xiong Y, Luu S, You X, Li B, Xia J, et al. The shared KEGG pathways between icariin-targeted genes and osteoporosis. *Aging (Albany NY)* (2020) 12 (9):8191–201. doi: 10.18632/aging.103133

8. Changani H, Parikh P. Molecular insights for an anti-osteoporotic properties of litsea glutinosa on saos-2 cells: An *in-vitro* approach. *J Ayurveda Integr Med* (2021) 13(2):100501. doi: 10.1016/j.jaim.2021.07.017

9. He Q, Yang J, Chen D, Li Y, Gong D, Ge H, et al. 12-Deoxyphorbol-13-Hexadecanoate abrogates OVX-induced bone loss in mice and osteoclastogenesis *via* inhibiting ROS level and regulating RANKL-mediated NFATc1 activation. *Front Pharmacol* (2022) 13:899776. doi: 10.3389/fphar.2022.899776

10. Shukla P, Mansoori MN, Kakaji M, Shukla M, Gupta SK, Singh D. Interleukin 27 (IL-27) alleviates bone loss in estrogen-deficient conditions by induction of early growth response-2 gene. *J Biol Chem* (2017) 292(11):4686–99. doi: 10.1074/jbc.M116.764779

11. Wang X, Liu X, He P, Guan K, Yang Y, Lei Y, et al. The imbalance of mitochondrial homeostasis of peripheral blood-derived macrophages mediated by MAFLD may impair the walking ability of elderly patients with osteopenia. *Oxid Med Cell Longev* (2022) 2022:5210870. doi: 10.1155/2022/5210870

12. Zheng L, Zhuang Z, Li Y, Shi T, Fu K, Yan W, et al. Bone targeting antioxidative nano-iron oxide for treating postmenopausal osteoporosis. *Bioact Mater* (2022) 14:250–61. doi: 10.1016/j.bioactmat.2021.11.012

13. Zhou Y, Gao Y, Xu C, Shen H, Tian Q, Deng HW. A novel approach for correction of crosstalk effects in pathway analysis and its application in osteoporosis research. *Sci Rep* (2018) 8(1):668. doi: 10.1038/s41598-018-19196-2

14. Chen J, Wang L, Shen Y, Yu J, Ye T, Zhuang C, et al. Key genes associated with osteoporosis revealed by genome wide gene expression analysis. *Mol Biol Rep* (2014) 41(9):5971–7. doi: 10.1007/s11033-014-3474-1

15. Xu F, Gao F. Liuwei dihuang pill cures postmenopausal osteoporosis with kidney-yin deficiency: Potential therapeutic targets identified based on gene expression profiling. *Med (Baltimore)* (2018) 97(31):e11659. doi: 10.1097/MD.0000000000011659

16. Kazezian Z, Gawri R, Haglund L, Ouellet J, Mwale F, Tarrant F, et al. Gene expression profiling identifies interferon signalling molecules and IGFBP3 in human degenerative annulus fibrosus. *Sci Rep* (2015) 5:15662. doi: 10.1038/srep15662

17. Safran M, Dalah I, Alexander J, Rosen N, Iny Stein T, Shmoish M, et al. GeneCards version 3: the human gene integrator. (2010) 2010:baq020 doi: 10.1093/database/baq020

18. Wu S, Liu S, Chen N, Zhang C, Zhang H, Guo X, et al. Genome-wide identification of immune-related alternative splicing and splicing regulators involved in abdominal aortic aneurysm. *Front Genet* (2022) 13:816035. doi: 10.3389/fgene.2022.816035

19. Whitehead MJ, McCanney GA, Willison HJ, Barnett SC . MyelinJ: an ImageJ macro for high throughput analysis of myelinating cultures. *Bioinformatics* 35(21):4528–30. doi: 10.1093/bioinformatics/btz403.

20. Newman AM, Steen CB, Liu CL, Gentles AJ, Chaudhuri AA, Scherer F, et al. Determining cell type abundance and expression from bulk tissues with digital cytometry. *Nat Biotechnol* (2019) 37(7):773–82. doi: 10.1038/s41587-019-0114-2

21. Wu X, Sui Z, Zhang H, Wang Y, Yu Z. Integrated analysis of lncrna-mediated ceRNA network in lung adenocarcinoma. *Front Oncol* (2020) 10:554759. doi: 10.3389/fonc.2020.554759

22. Wang J, Cong S, Wu H, He Y, Liu X, Sun L, et al. Identification and analysis of potential autophagy-related biomarkers in endometriosis by WGCNA. *Front Mol Biosci* (2005) 8:743012. doi: 10.3389/fmolb.2021.743012

23. Tian X, Liu B, Chen L, Xie Y, Liang J, Yang Y, et al. RNA-seq identifies marked th17 cell activation and altered cftr expression in different atopic dermatitis subtypes in chinese han populations. *Front Immunol* (2015) 12:628512. doi: 10.3389/fimmu.2021.628512

24. Langfelder P, Horvath S. WGCNA: an r package for weighted correlation network analysis. *BMC Bioinformatics* (2008) 9(1):1–13. doi: 10.1186/1471-2105-9-559

25. Harris MA, Clark J, Ireland A, Lomax J, Ashburner M, Foulger R, et alGene Ontology Consortium. The gene ontology (GO) database and informatics resource. *Nucleic Acids Res* (2004) 32(suppl_1):D258–D61. doi: 10.1093/nar/gkh036

26. Kanehisa M, Goto SJNar. KEGG. Kyoto encyclopedia of genes and genomes. *Nucleic Acids Res* (2000) 28(1):27–30. doi: 10.1093/nar/28.1.27

27. Wu T, Hu E, Xu S, Chen M, Guo P, Dai Z, et al. clusterProfiler 4. *: A Universal Enrichment Tool Interpreting Omics Data* (2021) 2(3):100141. doi: 10.1016/j.xinn.2021.100141

28. Yu G, Wang LG, Yan GR, He QY. DOSE: an R/Bioconductor package for disease ontology semantic and enrichment analysis. *Bioinformatics* (2015) 31 (4):608–9. doi: 10.1093/bioinformatics/btu684

29. Subramanian A, Tamayo P, Mootha VK, Mukherjee S, Ebert BL, Gillette MA, et al. Gene set enrichment analysis: a knowledge-based approach for interpreting genome-wide expression profiles. *Proc Natl Acad Sci U S A* (2005) 102(43):15545–50. doi: 10.1073/pnas.0506580102

30. Liberzon A, Birger C, Thorvaldsdottir H, Ghandi M, Mesirov JP, Tamayo P. The molecular signatures database (MSigDB) hallmark gene set collection. *Cell Syst* (2015) 1(6):417–25. doi: 10.1016/j.cels.2015.12.004

31. Hänzelmann S, Castelo R, Guinney JJBb. GSVA. Gene set variation analysis for microarray and RNA-seq data. *BMC Bioinformatics* (2013) 14(1):1–15. doi: 10.1186/1471-2105-14-7

32. Yang C, Ren J, Li B, Jin C, Ma C, Cheng C, et al. Identification of gene biomarkers in patients with postmenopausal osteoporosis. *Mol Med Rep* (2019) 19 (2):1065–73. doi: 10.3892/mmr.2018.9752

33. Robin X, Turck N, Hainard A, Tiberti N, Lisacek F, Sanchez J-C, et al. pROC: an open-source package for r and s+ to analyze and compare ROC curves. *BMC Bioinformatics* (2011) 12(1):1–8. doi: 10.1186/1471-2105-12-77

34. Von Mering C, Jensen LJ, Snel B, Hooper SD, Krupp M, Foglierini M, et al. STRING: known and predicted protein–protein associations, integrated and transferred across organisms. *Nucleic Acids Res.* (2005) 33(suppl_1):D433–D7. doi: 10.1093/nar/gki005

35. Shannon P, Markiel A, Ozier O, Baliga NS, Wang JT, Ramage D, et al. Cytoscape: a software environment for integrated models of biomolecular interaction networks. *Genome Res* (2003) 13(11):2498–504. doi: 10.1101/gr.1239303

36. Chin C-H, Chen S-H, Wu H-H, Ho C-W, Ko M-T, Lin C-Y. cytoHubba: identifying hub objects and sub-networks from complex interactome. *BMC Syst Biol* (2014) 8(4):1–7. doi: 10.1186/1752-0509-8-S4-S11

37. Engebretsen S, Bohlin J. Statistical predictions with glmnet. *Clin Epigenetics* (2019) 11(1):123. doi: 10.1186/s13148-019-0730-1

38. Fang Y, Huang S, Han L, Wang S, Xiong B. Package 'forestplot'. *Cancer Manag Res* (2021) 13:5599–611. doi: 10.2147/CMAR.S318704

39. Liu TT, Li R, Huo C, Li JP, Yao J, Ji XL, et al. Comprehensive analysis of peritoneal metastasis sequencing data to identify linc00924 as a prognostic biomarker in gastric cancer. *Front Cell Dev Biol* (2021) 9:682002. doi: 10.3389/fcell.2021.682002

40. Zhang H, Meltzer P, Davis S. RCircos: an r package for circos 2D track plots. *BMC Bioinf* (2013) 14:244. doi: 10.1186/1471-2105-14-244

41. Cunningham F, Achuthan P, Akanni W, Allen J, Amode MR, Armean IM, et al. Ensembl 2019. *Nucleic Acids Res* (2019) 47(D1):D745–d51. doi: 10.1093/nar/gky1113

42. Tang Z, Kang B, Li C, Chen T, Zhang Z. GEPIA2: an enhanced web server for large-scale expression profiling and interactive analysis. *Nucleic Acids Res* (2019) 47(W1):W556–W60. doi: 10.1093/nar/gkz430

43. Chang L, Zhou G, Soufan O, Xia JJNAR. miRNet 2.0: network-based visual analytics for miRNA functional analysis and systems biology. *Nucleic Acids Res* (2020) 48(W1):W244–W51. doi: 10.1093/nar/gkaa467

44. Caudron-Herger M, Jansen RE, Wassmer E, Diederichs S. RBP2GO: a comprehensive pan-species database on RNA-binding proteins, their interactions and functions. *Nucleic Acids Res* (2021) 49(D1):D425–D36. doi: 10.1093/nar/gkaa1040

45. Dong Q, Li F, Xu Y, Xiao J, Xu Y, Shang D, et al. RNAactDrug: a comprehensive database of RNAs associated with drug sensitivity from multi-omics data. *Brief Bioinform* (2020) 21(6):2167–74. doi: 10.1093/bib/bbz142

46. Titanji K, Ofotokun I, Weitzmann MN. Immature/transitional b-cell expansion is associated with bone loss in HIV-infected individuals with severe CD4+ T-cell lymphopenia. *Aids* (2020) 34(10):1475–83. doi: 10.1097/QAD.0000000000002563

47. Tao H, Tao Y, Yang C, Li W, Zhang W, Li X, et al. Gut metabolite urolithin a inhibits osteoclastogenesis and senile osteoporosis by enhancing the autophagy capacity of bone marrow macrophages. *Front Pharmacol* (2022) 13:875611. doi: 10.3389/fphar.2022.875611

48. Liu T, Jiang L, Xiang Z, Li J, Zhang Y, Xiang T, et al. Tereticornate a suppresses RANKL-induced osteoclastogenesis *via* the downregulation of c-src and TRAF6 and the inhibition of RANK signaling pathways. *BioMed Pharmacother* (2022) 151:113140. doi: 10.1016/j.biopha.2022.113140

49. Kim H, Lee K, Kim JM, Kim MY, Kim JR, Lee HW, et al. Selenoprotein W ensures physiological bone remodeling by preventing hyperactivity of osteoclasts. *Nat Commun* (2021) 12(1):2258. doi: 10.1038/s41467-021-22565-7

50. Raehtz S, Hargis BM, Kuttappan VA, Pamukcu R, Bielke LR, McCabe LR. High molecular weight polymer promotes bone health and prevents bone loss under salmonella challenge in broiler chickens. *Front Physiol* (2018) 9:384. doi: 10.3389/fphys.2018.00384

51. Han L, Zhang Y, Wan S, Wei Q, Shang W, Huang G, et al. Loss of chemerin triggers bone remodeling *in vivo* and *in vitro*. *Mol Metab* (2021) 53:101322. doi: 10.1016/j.molmet.2021.101322

52. Guo Y, Huo J, Wu D, Hao H, Ji X, Zhao E, et al. Simvastatin inhibits the adipogenesis of bone marrow–derived mesenchymal stem cells through the downregulation of chemerin/CMKLR1 signaling. *Int J Mol Med* (2020) 46 (2):751–61. doi: 10.3892/ijmm.2020.4606

53. Yang C, Yang P, Liu P, Wang H, Ke E, Li K, et al. Targeting filamin a alleviates ovariectomy-induced bone loss in mice *via* the WNT/β-catenin signaling pathway. *Cell Signal* (2022) 90:110191. doi: 10.1016/j.cellsig.2021.110191

54. Goldberg S, Glogauer J, Grynpas MD, Glogauer M. Deletion of filamin a in monocytes protects cortical and trabecular bone from post-menopausal changes in bone microarchitecture. *Calcif Tissue Int* (2015) 97(2):113–24. doi: 10.1007/s00223-015-9994-4

55. Zhang X, Zhao G, Zhang Y, Wang J, Wang Y, Cheng L, et al. Activation of JNK signaling in osteoblasts is inversely correlated with collagen synthesis in age-related osteoporosis. *Biochem Biophys Res Commun* (2018) 504(4):771–6. doi: 10.1016/j.bbrc.2018.08.094

56. Yang C, Tao H, Zhang H, Xia Y, Bai J, Ge G, et al. TET2 regulates osteoclastogenesis by modulating autophagy in OVX-induced bone loss. *Autophagy* (2022) 24:1–13. doi: 10.1080/15548627.2022.2048432

57. Chandra A, Lan S, Zhu J, Siclari VA, Qin L. Epidermal growth factor receptor (EGFR) signaling promotes proliferation and survival in osteoprogenitors by increasing early growth response 2 (EGR2) expression. *J Biol Chem* (2013) 288 (28):20488–98. doi: 10.1074/jbc.M112.447250

58. Lin DPL, Carnagarin R, Dharmarajan A, Dass CR. Transdifferentiation of myoblasts into osteoblasts - possible use for bone therapy. *J Pharm Pharmacol* (2017) 69(12):1661–71. doi: 10.1111/jphp.12790

59. Deng YX, He WG, Cai HJ, Jiang JH, Yang YY, Dan YR, et al. Analysis and validation of hub genes in blood monocytes of postmenopausal osteoporosis patients. *Front Endocrinol (Lausanne)* (2021) 12:815245. doi: 10.3389/fendo.2021.815245

60. Schillemans M, Karampini E, Hoogendijk AJ, Wahedi M, van Alphen FPJ, van den Biggelaar M, et al. Interaction networks of weibel-palade body regulators syntaxin-3 and syntaxin binding protein 5 in endothelial cells. *J Proteom* (2019) 205:103417. doi: 10.1016/j.jprot.2019.103417

61. Yang L, Zhang B, Liu J, Dong Y, Li Y, Li N, et al. Protective effect of acteoside on ovariectomy-induced bone loss in mice. *Int J Mol Sci* (2019) 20(12):2974. doi: 10.3390/ijms20122974

62. Liu P, Gao Y, Luo P, Yu H, Guo S, Liu F, et al. Glucocorticoid-induced expansion of classical monocytes contributes to bone loss. *Exp Mol Med* (2022) 54 (6):765–76. doi: 10.1038/s12276-022-00764-6

63. Gazzola L, Bellistri GM, Tincati C, Ierardi V, Savoldi A, Del Sole A, et al. Association between peripheral T-lymphocyte activation and impaired bone mineral density in HIV-infected patients. *J Transl Med* (2013) 11:51. doi: 10.1186/1479-5876-11-51

64. Titanji K, Vunnava A, Sheth AN, Delille C, Lennox JL, Sanford SE, et al. Dysregulated b cell expression of RANKL and OPG correlates with loss of bone mineral density in HIV infection. *PloS Pathog* (2014) 10(10):e1004497. doi: 10.1371/journal.ppat.1004497

65. Han X, Li P, Yang Z, Huang X, Wei G, Sun Y, et al. Zyxin regulates endothelial von willebrand factor secretion by reorganizing actin filaments around exocytic granules. *Nat Commun* (2017) 8:14639. doi: 10.1038/ncomms14639

66. Xue JY, Grigelioniene G, Wang Z, Nishimura G, Iida A, Matsumoto N, et al. SLC4A2 deficiency causes a new type of osteopetrosis. *J Bone Miner Res* (2022) 37 (2):226–35. doi: 10.1002/jbmr.4462

67. Wu C, Liu X, Sun R, Qin Y, Liu Z, Yang S, et al. Targeting anion exchange of osteoclast, a new strategy for preventing Wear particles induced- osteolysis. *Front Pharmacol* (2018) 9:1291. doi: 10.3389/fphar.2018.01291

68. Chang IC, Chiang TI, Lo C, Lai YH, Yue CH, Liu JY, et al. Anemone altaica induces apoptosis in human osteosarcoma cells. *Am J Chin Med* (2015) 43 (5):1031–42. doi: 10.1142/S0192415X15500597

69. Lin CC, Chao PY, Shen CY, Shu JJ, Yen SK, Huang CY, et al. Novel target genes responsive to apoptotic activity by ocimum gratissimum in human osteosarcoma cells. *Am J Chin Med* (2014) 42(3):743–67. doi: 10.1142/S0192415X14500487

frontiers | Frontiers in Immunology

TYPE Original Research
PUBLISHED 11 September 2023
DOI 10.3389/fimmu.2023.1246777

OPEN ACCESS

EDITED BY
Diana Boraschi,
Chinese Academy of Science (CAS), China

REVIEWED BY
Giselle Penton-Rol,
Center for Genetic Engineering and Biotechnology (CIGB), Cuba
Giacomo De Luca,
Vita-Salute San Raffaele University, Italy

*CORRESPONDENCE
Carlo Selmi
carlo.selmi@hunimed.eu

†These authors have contributed equally to this work and share first authorship

RECEIVED 24 June 2023
ACCEPTED 28 August 2023
PUBLISHED 11 September 2023

CITATION
Motta F, Tonutti A, Isailovic N, Ceribelli A, Costanzo G, Rodolfi S, Selmi C and De Santis M (2023) Proteomic aptamer analysis reveals serum biomarkers associated with disease mechanisms and phenotypes of systemic sclerosis. *Front. Immunol.* 14:1246777. doi: 10.3389/fimmu.2023.1246777

Proteomic aptamer analysis reveals serum biomarkers associated with disease mechanisms and phenotypes of systemic sclerosis

Francesca Motta[1,2†], Antonio Tonutti[1,2†], Natasa Isailovic[2], Angela Ceribelli[1,2], Giovanni Costanzo[1,2], Stefano Rodolfi[1,2], Carlo Selmi[1,2*] and Maria De Santis[1,2]

[1]Department of Biomedical Sciences, Humanitas University, Pieve Emanuele, Italy, [2]Rheumatology and Clinical Immunology, Istituti di Ricovero e Cura a Carattere Scientifico (IRCCS) Humanitas Research Hospital, Rozzano, Italy

Background: Systemic sclerosis (SSc) is an autoimmune connective tissue disease that affects multiple organs, leading to elevated morbidity and mortality with limited treatment options. The early detection of organ involvement is challenging as there is currently no serum marker available to predict the progression of SSc. The aptamer technology proteomic analysis holds the potential to correlate SSc manifestations with serum proteins up to femtomolar concentrations.

Methods: This is a two-tier study of serum samples from women with SSc (including patients with interstitial lung disease - ILD - at high-resolution CT scan) and age-matched healthy controls (HC) that were first analyzed with aptamer-based proteomic analysis for over 1300 proteins. Proposed associated proteins were validated by ELISA first in an independent cohort of patients with SSc and HC, and selected proteins subject to further validation in two additional cohorts.

Results: The preliminary aptamer-based proteomic analysis identified 33 proteins with significantly different concentrations in SSc compared to HC sera and 9 associated with SSc-ILD, including proteins involved in extracellular matrix formation and cell-cell adhesion, angiogenesis, leukocyte recruitment, activation, and signaling. Further validations in independent cohorts ultimately confirmed the association of specific proteins with early SSc onset, specific organ involvement, and serum autoantibodies.

Conclusions: Our multi-tier proteomic analysis identified serum proteins discriminating patients with SSc and HC or associated with different SSc subsets, disease duration, and manifestations, including ILD, skin involvement, esophageal disease, and autoantibodies.

KEYWORDS

connective tissue disease, interstitial lung disease, proteomics, aptamer technology, immunology

Introduction

Systemic sclerosis (SSc) is a connective tissue disease characterized by a pathogenetic triad composed of microangiopathy, immune system activation, and fibrosis. SSc is associated with significant morbidity and mortality largely dependent on the early detection of organ involvement including skin, lung, gastrointestinal tract, and heart (1–3).

Serum autoantibodies are the only available biomarkers for precision medicine in SSc as anti-centromere antibodies (ACA) are commonly observed in the limited form (lcSSc) and associated with an increased risk of pulmonary arterial hypertension (PAH) while anti-RNA polymerase III antibodies are linked to scleroderma renal crisis and anti-topoisomerase I (anti-Scl-70) antibodies are observed in the diffuse form (dcSSc) with a higher incidence of interstitial lung disease (ILD) (4, 5). However, autoantibodies are of limited use to predict the onset of specific complications (6–8); other biomarkers, such as uric acid and NT-ProBNP are instrumental to assess the risk of having PAH (9), KL-6 may predict the progression of SSc-ILD (10), while the combination of serum NT-ProBNP and troponins may be evocative of myocardial involvement (11, 12).

In recent years, proteomic analysis has been broadly used to identify biomarkers as it illustrated by the transcriptional profile changes associated with specific disease manifestations (13–19). Aptamers are short single-stranded oligonucleotides capable of folding into various structures, and have the ability to bind to proteins, peptides, and small molecules at concentrations ranging from femtomolar to micromolar, with high reproducibility and low variability rates (20) and holds promising in SSc to elucidate the molecular mechanisms of disease pathogenesis and internal organ involvement (21). We took advantage of proteomic aptamer analysis and different validation cohorts of SSc patients with and without ILD to identify biomarkers for SSc phenotypes.

Methods

Patients

Six patients who met the 2013 European League Against Rheumatism/American College of Rheumatology classification criteria for SSc (22) were enrolled from the Scleroderma Unit, Rheumatology and Clinical Immunology, IRCCS Humanitas Research Hospital in Rozzano, Italy. Clinical data were recorded, including organ involvement based on clinical features, laboratory results, and findings from diagnostic imaging (radiological imaging, echocardiography, lung function tests, and other relevant examinations). SSc-ILD was diagnosed based on high resolution computed tomography (HRCT) scans, following the guidelines set by the Fleischner Society (23). PAH was defined using right-heart catheterization in the presence of suspected/suggestive signs, symptoms, echocardiographic abnormalities, or pulmonary function abnormalities (24). Myocardial involvement was diagnosed based on compatible findings at cardiac magnetic resonance (25) in patients with suspected/suggestive signs or symptoms, electrocardiographic and 24-hour Holter ECG alterations, or elevated serum myocardial enzymes (11, 12). Serum autoantibodies were assessed using commercially available kits in routine laboratory analysis. Early SSc was defined as a disease duration less than 3 years from the onset of the first non-Raynaud manifestation (26). Patients were naïve to any immunosuppressive or vasoactive treatment. Seven healthy controls (HC) were enrolled (2 females, 5 males, median age 54 years, interquartile 46-67 years).

We also used two separate and independent cohorts of SSc patients and HC to validate our findings, as described below.

In all cases and controls, serum samples were collected using serum separator tubes, allowed to clot, aliquoted, and stored at -80° C.

This study was conducted in accordance with the Declaration of Helsinki, and the research protocol was approved by the local ethics committee (study number 831); all subjects provided their informed consent.

Aptamer proteomic analysis

Serum aliquots of 150 µL were prepared from all collected samples and subjected to proteome profiling using a high throughput multiplexing aptamer-based SOMAscan® assay, targeting 1310 serum proteins (Somalogic Inc., Boulder, CO), as previously described (27). The technique utilizes a panel of protein-specific Slow Off-rate Modified DNA aptamers (SOMAmers), which are constructed from chemically modified nucleotides capable of specifically recognizing and binding proteins with high specificity and affinity. The SOMAmer reagents are labeled with a 5'fluorophore and a biotin, immobilized on streptavidin coated beads, and incubated with serum samples. Complexes consisting of SOMAmer reagents and target proteins are formed on the beads. The SOMAmer reagents are then quantified through fluorescence using microarrays containing specific sequences. The relative intensity of fluorescence correlates to the amount of protein in the original sample.

Validation with ELISA tests

Proteins that showed significantly different concentrations at the proteomic aptamer analysis (SomaSuite, *vide infra*) were selected for further validation and clinical correlations based on their pathogenic significance (as supported by previous literature) or if their relative fluorescence intensity was notably elevated. For validation, solid-phase enzyme immunoassays, ELISA tests, were employed to quantitatively determine the levels of the most relevant proteins in separate cohorts of SSc patients and HC. The following kits were used for ELISA testing: Human CD177, Eotaxin1, Leptin, Angiopoietin 2 (Ang2), Kininogen HMW, TPSB2, MMP12, IL-22BP (Raybiotech, USA), and Human Calpain 1, Aldolase A, BAFFR, Fractalkine, and Calgranulin B (S100 A9) (Mybiosuorce, Vancouver Canada), following the manufacturer's instructions. All

10.3389/fimmu.2023.1246777

candidate proteins were first validated in an independent cohort of 30 patients with SSc and 10 HC (8 women, median age 71 years, interquartile range 62-74 years). Three proteins (Ang2, IL-22BP, and TPSB2) that exhibited statistical significance for multiple variables and displayed critical and innovative correlations with disease pathogenesis were further validated in an expanded cohort consisting of 89 patients with SSc and 43 HC (35 females, 8 males, median age 65 years, interquartile range 50-70 years).

Statistical analysis

Data analysis of the SomaLogic results was conducted using SomaSuite software (Somalogic, Boulder, CO, USA). Statistical analysis of the ELISA data was performed using Stata16 software (StataCorp. 2019. Stata Statistical Software: Release 16. College Station, TX: StataCorp LLC). Non-parametric data were analyzed using the Wilcoxon rank-sum (Mann-Whitney) test for individual comparisons. To account for multiple comparisons, the Kruskal-Wallis correction was applied. A significance level of $p < 0.05$ was considered statistically significant. Variables that reached statistical significance in the univariate analysis were entered into a logistic regression analysis with both forward and backward stepwise selection procedure to identify independent risk factors for selected variables.

Pathway analysis was performed by Reactome peer-reviewed pathway database (https://reactome.org) through the over-representation analysis: a statistical test (hypergeometric distribution) that determines whether certain Reactome pathways are over-represented (enriched) in the submitted data. The probability score was corrected for false discovery rate using the Benjamani-Hochberg method.

Results

Patients

The characteristics of the three cohorts of patients, namely the SOMAscan, first ELISA validation, and extended ELISA validation groups, are illustrated in Table 1, with slight differences in terms of rarer organ involvements. Among the six patients studied with the SOMAscan proteomic aptamer analysis, all were female, with a median age of 64.5 years (interquartile range – IQR 41-73). One (17%) had dcSSc, 3 (50%) were ACA-positive, and 2 (33%) were anti-Scl-70 positive. Three patients (50%) had ILD and 5 (83%) had gastrointestinal involvement, while no patient had PAH.

In the first validation cohort there were 30 patients, with a median age of 63.5 years (IQR 48-75). Seven (23%) had dcSSc, 14 (47%) were ACA-positive, and 13 (43%) were anti-Scl-70 positive. Additionally, 3 (10%) had anti-RNA polymerase III antibodies. Out of the 30 patients, 14 (47%) were in the early stage of SSc, 12 (40%) had ILD, 6 (20%) had cardiomyopathy, 14 (47%) had gastrointestinal involvement, and 2 (7%) had PAH.

The extended validation cohort consisted of 89 patients, with a median age of 64 years (IQR 52-73.5). Seventeen (19%) had dcSSc, 47 (53%) were ACA-positive, and 30 (34%) were anti-Scl-70 positive. Moreover, 6 (7%) had anti-RNA polymerase III antibodies. Among the 89 patients, 38 (43%) were in the early stage of SSc, 30 (34%) had ILD,

TABLE 1 Demographic features of SSc patients analyzed by SomaLogic, the initial and extended validation cohorts.

	Aptamer cohort (n = 6)	First validation cohort (n = 30)	Extended validation cohort (n = 89)
Female, n (%)	6 (100)	26 (87)	82 (92)
Age, median (IQR)	64.5 (41-73)	63.5 (48-75)	64 (52-73.5)
dcSSc, n (%)	1 (17)	7 (23)	17 (19)
Sine scleroderma, n (%)	0 (0)	4 (13)	20 (22)
ACA, n (%)	3 (50)	14 (47)	47 (53)
Anti-Scl-70, n (%)	2 (33)	13 (43)	30 (34)
Anti-RNA polymerase III, n (%)	0 (0)	3 (10)	6 (7)
Early SSc, n (%)	3 (50)	14 (47)	38 (43)
ILD, n (%) dcSSc with ILD, n (%)	3 (50) 1 (17)	12 (40) 2 (7)	30 (34) 10 (11)
Cardiomyopathy, n (%)	1 (17)	6 (20)	17 (19)
PAH, n (%)	0 (0)	2 (7)	14 (16)
Gastrointestinal involvement, n (%)	5 (83)	14 (47)	43 (48)
Cancer, n (%)	1 (17)	5 (17)	14 (16)

ACA, anticentromere antibodies; dcSSc, diffuse cutaneous subset of SSc; ILD, interstitial lung disease; IQR, interquartile range; PAH, pulmonary arterial hypertension.

17 (19%) had cardiomyopathy, 43 (48%) had gastrointestinal involvement, and 14 (16%) had PAH.

Proteomics of SSc and SSc-ILD using aptamers

Our first-tier proteomic analysis using SOMAscan technology revealed significant differences in serum levels of 33 proteins between patients with SSc and HC (Table 2). Patients with SSc exhibited altered expression of proteins involved in various biological processes, including extracellular matrix formation and cell-to-cell adhesion (elevated Calpain, EphA5, IDS, MATN2, MMP-12, TNR4, and reduced levels of desmoglein-1, SNP25), angiogenesis (increased levels of anti-angiogenic factors such as Ang2 and high molecular weight kininogen), lymphocyte recruitment, activation, and signaling (elevated levels of CXCL-1, LAG3 and decreased levels of SH21A), and overall inhibition of neutrophil function (decreased levels of G-CSF-R, CD177, calgranulin B; Figure 1). Nine proteins differentiated patients with SSc-ILD and without ILD or HC (Table 3). SSc-ILD patients showed elevated serum levels of proteins involved in intracellular signaling and cell cycle regulation (FCRL3, PDE11, Stratifin), as well as increased levels of MCP-3, a monocyte chemoattractant, and sICAM-5, the ligand for leukocyte adhesion protein LFA-1, compared to patients without ILD. Patients with SSc-ILD exhibited higher levels of IL-22BP, the decoy receptor for IL-22, and lower levels of BAFF.

TABLE 2 Significantly different ($p < 0.05$) protein serum levels in SSc patients compared with HC as assessed using the aptamer (SomaLogic) proteomics platform.

Increased in SSc	Reduced in SSc
Aldolase A	Adrenomedullin
Angiopoietin-2*	ASGR1
C1QR1	C1s
Calpain	C5
COLEC12	Calgranulin B
Eotaxin	CD177
EphA5	Desmoglein-1
Fractalkine/CXCL-1	Flt-3 ligand
Granulins	G-CFS-R
IDS	IL-1Ra
Kininogen HMW	Leptin
LAG-3	Lypd3
Lamin-B1	SH21A
LRP1b	SNAP25
MATN2	TPSB2
MMP-12	
STAT1	
TNR4	

ASGR1, asialoglycoprotein receptor 1; C1QR1, complement component C1q receptor 1; C1s, complement fraction 1s; C5, complement fraction 5; COLEC12, collectin-12; EphA5, ephrin type-A receptor 5; G-CSF-R, receptor for granulocyte colony stimulating factor; HMW, high molecular weight; IDS, iduronate 2-sulfatase; IL-1Ra, interleukin-1 receptor antagonist; LAG-3, lymphocyte-activation gene 3; LRP1b, low-density lipoprotein receptor-related protein 1B; Lypd3, LY6/PLAUR domain containing 3; MATN2, matrilin 2; MMP-12, matrix metalloproteinase 12.
SH21A, SH2 domain-containing protein 1A; SNAP25, synaptosome associated protein 25; STAT1, signal transducer and activator of transcription 1; TNR4, TNF receptor superfamily member 4; TPSB2, tryptase beta-2.
* Significantly increased also at ELISA validation ($p < 0.0001$).

Validation of protein biomarkers and association with disease manifestations

In the second-tier analysis, we selected 13 proteins from the first analysis to be validated in the independent cohort (Tables 4–7).

We observed significantly higher levels of serum Ang2 in SSc, especially in SSc-ILD compared to HC [median (IQR): 1.15 ng/mL (0.60-2.41) in SSc, 1.45 ng/mL (0.79-3.09) in SSc-ILD, 0.58 ng/mL (0.34-0.82) in HC; $p = 0.0001$ for both comparisons]. IL-22BP was also present at higher concentrations in sera from patients with SSc-ILD [36.3 ng/mL (18.7-57.8)], with a progressive decrease in SSc without ILD [24.7 ng/mL (13.7-50.8)] and HC [20.4 ng/mL (13.9-37.6); $p = 0.02$ SSc-ILD vs. HC].

Concentrations of MMP-12 were significantly lower in SSc, particularly in SSc-ILD, compared to HC [0.10 ng/mL (0.06-0.16) in SSc, 0.09 ng/mL (0.05-0.13) in SSc-ILD, 0.20 ng/mL (0.16-0.33) in HC; $p = 0.003$ for SSc vs. HC and $p = 0.01$ for SSc-ILD vs. HC].

In terms of skin involvement, patients with SSc were stratified into three subsets (28), namely dcSSc, lcSSc, and SSc *sine scleroderma* (Table 5). Higher levels of calgranulin B were observed in dcSSc compared to other SSc forms [65.7 ng/mL (62.2-81.8) in dcSSc vs. 25.6 ng/mL (16.6-40.8) in the other subsets; $p = 0.02$]. In comparison to patients with skin involvement (i.e., dcSSc and lcSSc), patients with SSc *sine scleroderma* exhibited lower serum levels of leptin [0.18 ng/mL (0-1.21) in sine vs. 2.58 ng/mL (0.79-4.70) in the other subsets; $p = 0.03$], and higher levels of aldolase A [123 ng/mL (116-148) in sine vs. 84.7 ng/mL (74.7-96) in the other subsets; $p = 0.003$].

Results comparing disease duration (early SSc vs. long-standing disease) are illustrated in Table 6. Serum levels of MMP-12 were significantly lower in the early SSc group [0.07 ng/mL (0.03-0.10) in early SSc vs. 0.15 ng/mL (0.09-0.20) in long-standing disease; $p = 0.003$] and CD177 [9.13 ng/mL (6.24-11.3) in early SSc vs. 12.3 ng/mL (9.34-20.0) in long-standing disease; $p = 0.03$]. Multivariate analysis confirmed that MMP-12 is independently associated to early SSc [OR 5.7×10^{-10}; 95% CI (7.2×10^{-19}-0.45); $p = 0.04$].

Lower concentrations of fractalkine [1.62 ng/mL (10.8-3.22) vs. 2.95 ng/mL (2.77-4.61); $p = 0.02$] and higher concentrations of eotaxin [1.16 ng/mL (0.88-3.12) vs. 0.74 ng/mL (0.43-1.08); $p = 0.03$] were associated with gastrointestinal involvement, along with a non-significant increase in MMP-12 [0.13 ng/mL (0.09-0.20) vs. 0.09 ng/mL (0.03-0.14); $p = 0.08$] (Table 6). No significant differences were found when stratifying patients with SSc based on the presence of PAH or cardiomyopathy (Table 6).

We also compared patients based on autoantibody profiling, specifically ACA, anti-Scl-70, and anti-RNA polymerase III (Table 7). Patients with ACA had significantly higher levels of MMP-12 [0.14 ng/mL (0.10-0.20) for ACA vs. 0.07 ng/mL (0.04-0.11) for anti-Scl-70 vs. 0.03 ng/mL (0.03-0.09) for anti-RNA polymerase III; $p = 0.01$]. Calgranulin B showed the lowest values in ACA-positive subjects [24.2 ng/mL (15.2-33.1) for ACA vs. 59.7 ng/mL (28.2-75.7) for other antibodies; $p = 0.01$] and the highest

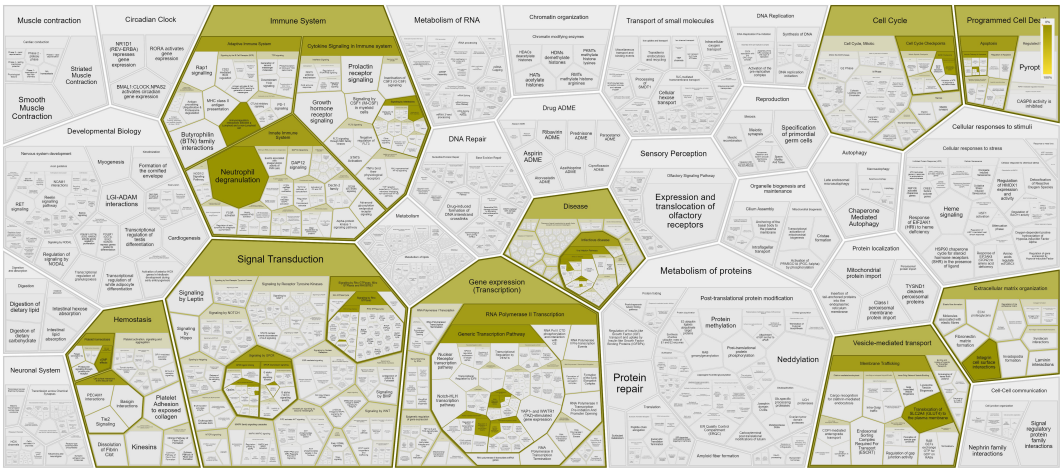

FIGURE 1
Pathways and interactions (https://reactome.org) of proteins showing significantly different ($p < 0.05$) serum levels in SSc patients compared with HC, as assessed using the aptamer (SomaLogic) proteomics platform.

levels with anti-Scl-70 [62.2 ng/mL (28.3-79.4) for anti-Scl-70 vs. 25.3 ng/mL (16.6-40.8) for other autoantibodies; $p = 0.03$].

Discussion

The complex pathogenesis of SSc encompasses aberrant inflammation, dysregulated fibrosis, and microvascular disease (2). Comprehensive proteomic analysis is an ideal approach for identifying relevant molecules involved in various disease mechanisms, including potential prognostic factors, predictive molecules, and therapeutic targets. Proteomic analyses have already been performed and associated to clinical phenotype in SSc (29–32), as shown by the report that the higher expression of CXCL4 from peripheral blood and skin plasmacytoid dendritic cells in association with the incidence and progression of ILD and PAH in SSc (33). In addition, altered serum levels of collagen IV, endostatin, IGFBP-2, IGFBP-7, MMP-2, neuropilin-1, NT-proBNP, and RAGE have been described in SSc-PAH patients (34). Further, patients with a prominent signature based on CD40 ligand, CXCL4, and anti-PM/Scl-100 antibodies have shown a preferential positive response to treatment with the tyrosine kinase inhibitor imatinib (35).

TABLE 3 Significantly different ($p < 0.05$) protein serum levels in SSc with ILD compared with SSc without ILD and HC as assessed using SomaLogic proteomics.

Increased in SSc-ILD	Reduced in SSc-ILD
FCRL3	BAFF
IL-22BP**	DERM
MCP-3	
PDE11	
PGP9.5	
sICAM-5	
Stratifin	

BAFF, B cell activating factor; DERM, dermatopontin; FCRL3, Fc receptor-like protein 3; IL-22BP, interleukin-22 binding protein; MCP-3, human monocyte chemotactic protein-3; PDE11, phosphodiesterase 11; PGP9.5, protein gene product 9.5; sICAM-5, soluble intercellular adhesion molecule 1.
**Significantly increased also at ELISA validation comparing patients with SSc-ILD and HC ($p < 0.0001$).

Only a few studies have been conducted using the aptamer tools for proteomics in SSc (36–39). Within the studies investigating the preclinical phase of SSc (36, 39) one identified three proteins involved in the dysregulated angiogenesis and fibrosis being differentially expressed in patients with preclinical SSc at risk of evolving into overt disease, thus confirming the importance of microvascular disease in the earliest phases of SSc pathogenesis (36). Piera-Velazquez and Colleagues elegantly demonstrated that proteomic analysis of serum exosomes differs between patients with primary Raynaud's phenomenon and patients with Raynaud's phenomenon at risk of evolving into SSc (39). In the other two studies available (37, 38), the aptamer analysis was applied to describe longitudinal changes in patients with established SSc and organ damage. It was indeed demonstrated that serum levels of ST2 and spondin-1 predicted the changes in mRSS, also providing evidence of a peculiar cytokine signature (i.e., TNF, IFN-γ, TGF-β, and IL-13) (37). Additionally, chemerin was identified as a potential biomarker with pathogenic significance for increased pulmonary vascular resistances in patients with SSc-PAH (38). In another study, 82 proteins were found to be differentially expressed in sera from SSc-PAH patients compared to SSc patients without lung vascular involvement, including an IFN-γ signature and two other proteins of interest, Midkine (implicated in the pathogenesis of arterial hypertension, renal disease, and lung fibrosis) and Follistatin-like 3 (FSTL3, regulated by TGF-β) in association with SSc-PAH (40). A composite three-biomarker index (including Ca15-3, surfactant protein D, and ICAM-1) has been recently described to predict ILD in patients with SSc, and is associated to disease severity (41). Several reasons could explain the differences found in the proteomic profile between previous studies and our results. First, the types of samples, such as whole blood, serum, and exosomes, is expected to provide different analytical outcomes. Second, the correlation between the duration of the disease

TABLE 4 Serum concentration -median (IQR)- of validated proteins in HC, and SSc according to the presence or absence of SSc-ILD.

	HC	SSc	SSc-ILD	SSc without ILD
Aldolase A	71.9 (67.0-97.4)	91.9 (78.3-102)	92.6 (76.7-95.8)	88.4 (78.3-110)
Ang2	0.58 (0.34-0.82)*°	1.15 (0.60-2.41)*	1.45 (0.79-3.09)°	1.08 (0.58-2.12)
BAFFR	1.04 (0.38-1.28)	1.05 (0.64-2.38)	0.85 (0.58-1.54)	1.39 (0.80-2.62)
Calgranulin B	24.0 (11.6-45.4)	29.0 (16.6-65.0)	31.4 (21.7-60.1)	26.9 (16.6-65.0)
Calpain	12.7 (11.6-13.2)	13.4 (12.6-14.0)	13.0 (12.1-13.7)	13.6 (12.7-14.2)
CD177	12.3 (10.5-16.1)	10.9 (7.28-15.5)	10.4 (6.34-20.0)	10.9 (7.36-14.7)
Eotaxin	1.09 (0.74-1.65)	0.94 (0.62-1.35)	1.03 (0.56-1.36)	0.93 (0.62-1.35)
Fractalkine	2.37 (1.38-3.29)	2.82 (1.39-3.49)	2.37 (1.38-4.35)	2.87 (1.39-3.49)
IL-22BP	20.4 (13.9-37.6)°	26.2 (16.1-51.0)	36.3 (18.7-57.8)°	24.7 (13.7-50.8)
Kininogen	596 (506-765)	522 (352-707)	604 (299-807)	515 (433-689)
Leptin	2.11 (0.83-3.66)	1.92 (0.60-4.10)	2.09 (1.02-3.85)	1.92 (0.33-4.10)
MMP-12	0.20 (0.16-0.33)*°	0.10 (0.06-0.16)*	0.09 (0.05-0.13)°	0.12 (0.06-0.18)
TPSB2	42.6 (17.9-84.3)	59.6 (23.4-123)	67.5 (16.6-190)	56.9 (27.2-98.3)

HC, healthy controls; SSc-ILD, SSc-associated interstitial lung disease.
*$p < 0.05$ comparing SSc vs. HC.
°$p < 0.05$ comparing SSc-ILD vs. HC.
$p > 0.05$ comparing SSc without ILD vs HC.

history and the timing of sample collection might have played a role, not only in the case of early vs. longstanding SSc but also in patients with isolated Raynaud's phenomenon at risk of evolving towards established disease. Third, such results ultimately reflect the heterogeneity of SSc, indicating various internal organ involvements, as well as multiple nuances of disease severity and rates of disease progression.

Our multi-tier study including an aptamer-based analysis and a validation on independent cohorts supports the alterations in different biomarkers to reflect abnormal extracellular matrix formation, angiogenesis, vascular remodeling, and immune cell recruitment and function, which recapitulate the fundamental pathogenic aspects of SSc and some of the proposed biomarkers (Ang2, IL-22BP, and TPSB2) require a detailed discussion.

TABLE 5 Serum concentration -median (IQR)- of validated proteins in SSc patients, according to the cutaneous subset.

	dcSSc	lcSSc	sine SSc	lcSSc + sine SSc
Aldolase A	85.5 (80.5-104)°	83.7 (74.0-95.5)°	123 (116-148)^°	92.5 (74.7-102.4)
Ang2	1.58 (0.80-2.72)	1.17 (0.66-2.39)	0.58 (0.37-1.65)	1.08 (0.58-2.12)
BAFFR	1.67 (0.80-3.20)	1.01 (0.60-1.84)	0.60 (0.34-1.62)	1.01 (0.56-1.84)
Calgranulin B	65.7 (62.2-81.8)*°	25.3 (16.5-33.1)°	49.0 (34.5-64.7)°	25.6 (16.6-40.8)*
Calpain	13.6 (12.7-14.7)	13.4 (12.4-14.0)	12.8 (12.5-14.4)	13.4 (12.4-14.0)
CD177	7.28 (4.97-14.7)	12.2 (8.79-19.9)	8.97 (3.68-10.9)	11.3 (8.17-19.9)
Eotaxin	1.35 (0.83-1.75)	0.95 (0.65-1.21)	0.55 (0.40-0.80)	0.94 (0.49-1.18)
Fractalkine	2.90 (1.07-3.32)	2.00 (1.35-4.01)	3.24 (2.89-4.72)	2.78 (1.39-4.08)
IL-22BP	24.9 (16.8-86.4)	27.8 (15.3-52.7)	23.6 (15.7-36.9)	26.6 (15.8-50.9)
Kininogen	505 (286-707)	591 (390-717)	384 (352-416)	564 (371-699)
Leptin	1.74 (0.79-3.00)	2.87 (0.77-4.92)	0.18 (0-1.21)^	2.09 (0.48-4.70)
MMP-12	0.07 (0.03-0.20)	0.13 (0.09-0.18)	0.05 (0.03-0.09)	0.11 (0.08-0.16)
TPSB2	23.5 (0-72.3)	71.7 (30.7-162)	64.6 (33.5-103)	71.7 (31.3-151)

dcSSc, diffuse cutaneous subset of SSc; lcSSc, limited cutaneous subset of SSc; sine SSc, SSc sine scleroderma.
*$p < 0.05$ comparing dcSSc vs. lcSSc and SSc sine scleroderma.
^$p < 0.05$ comparing SSc sine scleroderma vs. dcSSc and lcSSc.
°$p < 0.05$ comparing dcSSc vs. lcSSc vs. SSc sine scleroderma (three-group Kruskal-Wallis).

TABLE 6 Serum concentration -median (IQR)- of validated proteins in SSc patients, according to disease duration and organ involvement.

	Early SSc	Long SSc	Cardiomyopathy	PAH	GI
Aldolase A	97.6 (80.5-122)	83.8 (76.5-93.3)	87.8 (74.7-92.7)	132.8 (93.8-172)	91.9 (78.4-96.0)
Ang2	1.06 (0.56-1.65)°^	1.16 (0.65-3.46)^	1.28 (0.62-2.74)	1.38 (0.57-2.72)	1.25 (0.63-2.25)
BAFFR	1.08 (0.56-2.43)	1.05 (0.66-1.78)	1.25 (0.68-1.72)	0.94 (0.86-1.01)	1.36 (0.68-2.43)
Calgranulin B	36.9 (28.1-65.7)	25.3 (16.6-49.1)	33.1 (23.1-62.2)	57.3 (28.1-86.5)	30.7 (16.6-79.4)
Calpain	13.4 (12.7-14.0)	13.4 (12.1-14.1)	13.2 (12.7-13.9)	12.1 (11.8-12.4)	13.0 (12.4-13.9)
CD177	9.13 (6.24-11.3)*	12.3 (9.34-20.0)*	14.3 (6.15-19.9)	5.65 (0-11.3)	10.8 (6.15-12.4)
Eotaxin	0.91 (0.41-1.18)	1.01 (0.71-2.64)	0.80 (0.45-1.35)	0.85 (0.49-1.21)	1.16 (0.88-3.12)#
Fractalkine	2.90 (1.35-3.32)	2.66 (1.62-4.66)	3.27 (2.85-3.46)	3.90 (1.85-5.96)	1.62 (10.8-3.22)#
IL-22BP	26.2 (14.7-60.7)	26.4 (16.3-50.9)	28.2 (25.8-54.6)	28.3 (24.4-56.0)	27.5 (20.7-50.8)
Kininogen	501 (325-682)	579 (416-717)	638 (505-682)	310	591 (508-717)
Leptin	1.63 (0.48-2.93)	2.76 (0.69-4.81)	2.12 (1.02-2.65)	1.43 (0.77-2.09)	1.63 (0.60-5.45)
MMP-12	0.07 (0.03-0.10)*°^	0.15 (0.09-0.20)*^	0.14 (0.09-0.20)	0.03	0.13 (0.09-0.20)
TPSB2	48.0 (0-151)	66.2 (31.3-123)	65.7 (23.0-315)	71.7 (47.9-151)	67.9 (38.6-105)

GI, gastrointestinal involvement; HC, healthy controls; PAH, pulmonary arterial hypertension.
*p < 0.05 comparing early SSc vs. long standing disease.
°p < 0.05 comparing early SSc vs. HC.
^p < 0.05 comparing HC vs. early SSc vs. long standing disease (three-group Kruskal-Wallis).
#p < 0.05 comparing patients with and without gastrointestinal involvement (GI).

Angiopoietin-2 (Ang2) is a vascular growth factor secreted by endothelial cells that induces their own activation and promotes leukocyte chemotaxis. In the presence of a pro-inflammatory cytokine environment, this signaling pathway leads to vascular instability and endothelial inflammation (42). By stimulating the release of IL-6 and IL-8 from monocytes, Ang2 enhances the inflammatory-driven fibrogenic process, a hallmark of SSc (43). Our analysis revealed significantly increased serum levels of Ang2 in SSc patients compared to HC, which is consistent with previous literature findings (44). Furthermore, we observed significantly higher levels of serum Ang2 in early SSc and SSc-ILD patients compared to HC. Previous studies have shown that serum Ang2

TABLE 7 Serum concentration -median (IQR)- of validated proteins in SSc patients, according to autoantibody profile.

	ACA	Scl-70	RNApol III
Aldolase A	83.8 (78.3-96.0)	95.5 (73.5-104)	92.7 (85.5-110)
Ang2	1.07 (0.63-1.59)	1.58 (0.58-3.03)	1.79 (0-7.89)
BAFFR	1.36 (0.68-1.84)	1.01 (0.64-2.43)	0.80 (0.34-1.08)
Calgranulin B	24.2 (15.2-33.1)*$^	62.2 (28.3-79.4)*$#	57.2 (20.3-65.0)*
Calpain	13.6 (12.8-14.0)	12.9 (12.4-13.6)	14.7 (10.7-15.8)
CD177	11.0 (8.79-14.0)	11.3 (6.24-15.8)	7.36 (7.28-22.1)
Eotaxin	1.03 (0.77-2.17)	0.88 (0.41-1.21)	0.62 (0.34-1.75)
Fractalkine	1.98 (1.31-3.46)	2.99 (1.85-3.98)	2.90 (2.78-7.50)
IL-22BP	25.9 (13.7-52.7)	31.8 (20.7-49.2)	22.4 (18.3-23.8)
Kininogen	604 (522-682)	390 (299-807)	416 (111-496)
Leptin	2.76 (0.48-4.92)	1.74 (1.28-2.93)	0.79 (0.33-11.1)
MMP-12	0.14 (0.10-0.20)*^	0.07 (0.04-0.11)	0.03 (0.03-0.09)
TPSB2	67.9 (29.2-92.8)	34.8 (14.1-153)	70.5 (0-305)

ACA, anticentromere antibodies; RNApol III, anti-RNA polymerase III antibodies.
*p < 0.05 comparing ACA vs. anti-Scl-70 vs. anti-RNA polymerase III (three-group Kruskal-Wallis).
$p < 0.05 comparing anti-Scl-70 vs. ACA.
^p < 0.05 comparing ACA vs. other autoantibodies.
#p < 0.05 comparing anti-Scl-70 vs. other autoantibodies.

levels decrease after treatment with intravenous cyclophosphamide in SSc-ILD patients, and this reduction correlates with concentrations of KL-6, an established biomarker of lung involvement (45). Overall, these results support the crucial role of aberrant angiogenesis across the pathogenic processes underlying SSc since the earliest phases, throughout the development of established disease, along with providing further support for the correlation between serum Ang2 concentrations and SSc-ILD.

IL-22 is an inflammatory cytokine produced by CD4+ T cells and innate T cells, including NKT, γδ T cells, and innate lymphoid cells (ILC) (46); IL-22BP is a soluble decoy receptor that acts as an IL-22 inhibitor (46). Ambivalent proinflammatory and modulating functions have been attributed to both IL-22 and IL-22BP in a tissue- and disease-dependent manner (47–49). A protective anti-inflammatory effect of IL-22 has been demonstrated in the case of pulmonary inflammation, with lower levels being detectable in the bronchoalveolar lavage fluid (BALF) of patients with acute respiratory distress syndrome and sarcoidosis (50). Moreover, IL-22 is essential to allow alveolar repair following Influenza pneumonia (51), while elevated IL-22BP expression increases the risk of severe pulmonary infections (52). On the other hand, a prominent IL-22-based inflammatory signature has been described in patients with SSc (53), with increased circulating Th22 cells (54) and serum IL-22 levels being associated with SSc-ILD (55). Expression of IL-22 in scleroderma skin is linked to both the inflammatory (56) and fibrotic responses that are responsible for disease progression (57). In our study, serum levels of IL-22BP were significantly increased in patients with SSc-ILD compared with HC. This points towards a role for reduced IL-22 function in the pathogenesis of SSc-ILD. A mouse model study reported that bleomycin-induced lung fibrosis leads to a decrease in IL-22, and administering exogenous IL-22 can inhibit the inflammatory and fibrotic process (58). We speculate that the protective role of IL-22 may be compromised in patients with SSc-ILD and modulating the IL-22/IL-22BP system could be a promising therapeutic target. Further studies are needed to clarify the role of cells producing IL-22 in the pathogenesis of scleroderma lung disease, with a particular focus on innate-like lymphocytes (59), which represent an intriguing crossroad between the environment, innate, and adaptive immunity.

Conflicting evidence has been reported regarding matrix metalloproteinase (MMP)-12, an enzyme with critical functions in extracellular matrix remodeling in animal models of lung fibrosis (60, 61). *In vitro* studies have shown that dermal fibroblasts from SSc patients overexpress MMP-12, thus affecting angiogenic homeostasis (62). Increased levels of MMP-12 in serum and tissue have been reported in SSc patients, and these levels are associated with longer disease duration and more severe skin and lung involvement (63). Furthermore, the rs2276109 polymorphism of the MMP-12 gene has been linked to SSc susceptibility in a large Italian cohort (64). Our results partially contrast with previous evidence. While we initially observed higher MMP-12 levels in SSc patients during SOMAscan analysis, we found significantly lower values during ELISA validation, especially in SSc-ILD, early SSc, and anti-Scl-70 or anti-RNA polymerase III positivity, suggesting a potential correlation between serum MMP-12 levels and milder forms of the disease. Such observations could suggest the presence of an ineffective extracellular matrix turnover, as reflected by lower levels of MMP-12, in those patients with a higher burden of fibro-inflammatory lesions. This is notably the case of individuals with SSc-ILD, as well as rapidly progressive cutaneous fibrosis associated with anti-RNA polymerase III antibodies. However, due to the discrepancy of previous evidence, further research is warranted also in this case to clarify these associations.

Dysfunction of the myeloid cell compartment has been implicated in both the inflammatory and fibrotic phases of SSc pathogenesis (65). To support this view, we found significant differences in serum concentrations of myeloid-derived proteins in SSc patients compared to HC, including calgranulin B, and CD177. Calgranulin B is a calcium-binding protein expressed in neutrophils, monocytes, and macrophages, and it is overexpressed in the lungs of patients with idiopathic pulmonary fibrosis and nonspecific interstitial pneumonia (66). Our analysis showed that SSc-ILD patients and dcSSc patients have higher circulating levels of calgranulin B. CD177 is a neutrophil membrane molecule involved in the regulation of diapedesis (67), and CD177+ neutrophils produce large amounts of IL-22 (68). As mentioned earlier, the ambivalent role of IL-22 may help explain the mild reduction in soluble CD177 that we observed in patients with early SSc. Further research is required to elucidate the role of the myeloid compartment in the pathogenesis of different subsets of SSc.

Two proteins associated with gastrointestinal involvement in patients with SSc are eotaxin and fractalkine. Eotaxin's role in recruiting eosinophils and mast cells has been extensively studied in asthma (69), and its pro-fibrotic effects have been demonstrated in both animal models (70) and human conditions (71, 72). Recently, Piera-Velazquez and colleagues demonstrated that patients with early SSc have higher levels of eotaxin in circulating exosomes compared to subjects with primary Raynaud's phenomenon (39). We are the first to report that increased serum levels of eotaxin and lower serum concentrations of fractalkine are significantly associated with esophageal involvement in patients with SSc.

Leptin warrants also a discussion as this is a metabolic hormone produced by adipose tissue cells and has potential, albeit conflicting, roles in autoimmune inflammation (73) and fibrosis (74). Its effects on the fibrotic process appear to be tissue- or organ-dependent (74). Contradictory data have been reported on serum leptin concentrations in patients with SSc (75–78), and it has been suggested that these variations may reflect heterogeneity in disease duration, activity, and different phenotypes and endotypes. We are the first to report low levels of leptin in patients with SSc *sine scleroderma* compared to subjects with cutaneous involvement (both lcSSc and dcSSc).

To our knowledge, this is the first study to investigate serum proteins using proteomic aptamer analysis in a deeply phenotyped and endotyped cohort of SSc patients to assess the potential pathogenetic roles, spanning from extracellular matrix formation, angiogenesis, and immune cell homing and function. The strength

of our study is that patient sera were obtained at the time of diagnosis, prior to any immunosuppressive or vasoactive treatment initiation, therefore our findings are expected to accurately represent the serum proteome of treatment-naïve individuals with SSc. Functionality assays, including gene expression and epigenetic studies, could serve as powerful tools to test and enhance the pathogenic validity of our observations. For instance, by studying the modulation of angiogenic pathways (mainly represented by Ang2 in our dataset), extracellular matrix remodeling (such as MMP-12), or myeloid cell function, we could gain a deeper understanding of whether these processes play a "disease-modifying" role at various stages of the disease or in different organs. Silencing IL-22 in mice-models of SSc lung disease may prove helpful to understand if IL-22 has a different role in the lung compared to the skin. Functionality analysis could reveal critical and potentially practice-changing information while the checkpoint driving dysregulated fibrosis could be intercepted, or it might be revealed that targeting certain pathways (e.g., aberrant angiogenesis, lymphocyte activation) is crucial but only in certain disease phases. Among the limitations of our study, the small sample size used for the aptamer analysis and the validation performed on a larger cohort should be noted, as well as the arbitrary choice of the candidate proteins, based on their presumed pathogenic significance and available data from previous literature. Furthermore, while the composition of the validation cohorts adequately reflects the distribution of different disease subsets and organ manifestations, this is not the case for the SOMAscan cohort due to the low prevalence of dcSSc, absence of subjects with SSc *sine scleroderma*, anti-RNA polymerase III antibodies, and PAH.

Conclusions

Serum and tissue proteomics offer valuable tools for characterizing various aspects of the disease, aligning with the principles of precision medicine, while prospective validation of these biomarkers is warranted. The potential biomarkers that distinguish patients with SSc from HC identified in this work play functional roles in extracellular matrix metabolism, angiogenesis, and immune cell function, which are critical checkpoints in the pathogenesis of the disease. Biomarkers related to altered angiogenesis can differentiate patients with early SSc from HC, while other molecules exhibit differential expression in patients with SSc depending on factors such as disease subset, autoantibody profile, extent of skin fibrosis, and internal organ involvement, including ILD.

Data availability statement

The raw data supporting the conclusions of this article will be made available by the authors, without undue reservation.

Ethics statement

The studies involving humans were approved by IRCCS Humanitas Research Hospital ethics committee. The studies were conducted in accordance with the local legislation and institutional requirements. The participants provided their written informed consent to participate in this study.

Author contributions

Conceptualization and coordination: MS and CS. Laboratory investigations: NI, AC. Data collection and statistical analysis: FM, AT, MS, AC, and NI. Literature review: FM, AT, and GC. Manuscript preparation—original draft: FM and AT; supervision: MS and CS. All authors contributed to the article and approved the submitted version.

Funding

This work was partially supported by "Ricerca Corrente" funding from Italian Ministry of Health to IRCCS Humanitas Research Hospital.

Conflict of interest

The authors declare that the research was conducted in the absence of any commercial or financial relationships that could be construed as a potential conflict of interest.

Publisher's note

References

1. Gabrielli A, Avvedimento EV, Krieg T. Scleroderma. *N Engl J Med* (2009) 360 (19):1989–2003. doi: 10.1056/NEJMra0806188

2. Denton CP, Khanna D. Systemic sclerosis. *Lancet* (2017) 390(10103):1685–99. doi: 10.1016/S0140-6736(17)30933-9

3. Volkmann ER, Andréasson K, Smith V. Systemic sclerosis. *Lancet* (2023) 401 (10373):304–18. doi: 10.1016/S0140-6736(22)01692-0

4. Kowal-Bielecka O, Fransen J, Avouac J, Becker M, Kulak A, Allanore Y, et al. Update of EULAR recommendations for the treatment of systemic sclerosis. *Ann Rheum Dis* (2017) 76(8):1327–39. doi: 10.1136/annrheumdis-2016-209909

5. Roofeh D, Jaafar S, Vummidi D, Khanna D. Management of systemic sclerosis-associated interstitial lung disease. *Curr Opin Rheumatol* (2019) 31(3):241–9. doi: 10.1097/BOR.0000000000000592

6. Skaug B, Assassi S. Biomarkers in systemic sclerosis. *Curr Opin Rheumatol* (2019) 31(6):595–602. doi: 10.1097/BOR.0000000000000656

7. Cavazzana I, Vojinovic T, Airo' P, Fredi M, Ceribelli A, Pedretti E, et al. Systemic sclerosis-specific antibodies: novel and classical biomarkers. *Clin Rev Allergy Immunol* (2023) 64(3):412–30. doi: 10.1007/s12016-022-08946-w

8. Domsic RT. Scleroderma: the role of serum autoantibodies in defining specific clinical phenotypes and organ system involvement. *Curr Opin Rheumatol* (2014) 26 (6):646–52. doi: 10.1097/BOR.0000000000000113

9. Coghlan JG, Denton CP, Grünig E, Bonderman D, Distler O, Khanna D, et al. Evidence-based detection of pulmonary arterial hypertension in systemic sclerosis: the DETECT study. *Ann Rheum Dis* (2014) 73(7):1340–9. doi: 10.1136/annrheumdis-2013-203301

10. Watanabe S, Kase K, Saeki K, Ohkura N, Murata A, Waseda Y, et al. Kinetic changes in serum KL-6 levels predict disease progression in patients with systemic sclerosis-associated interstitial lung disease. *Respir Med* (2022) 191:106689. doi: 10.1016/j.rmed.2021.106689

11. Bosello S, De Luca G, Berardi G, Canestrari G, de Waure C, Gabrielli FA, et al. Cardiac troponin T and NT-proBNP as diagnostic and prognostic biomarkers of primary cardiac involvement and disease severity in systemic sclerosis: A prospective study. *Eur J Intern Med* (2019) 60:46–53. doi: 10.1016/j.ejim.2018.10.013

12. Bosello S, De Luca G, Ferraccioli G. Troponin in stable ischemic heart disease and diabetes. *N Engl J Med* (2015) 373(20):1977–8. doi: 10.1056/NEJMc1511645

13. Lourido L, Blanco FJ, Ruiz-Romero C. Defining the proteomic landscape of rheumatoid arthritis: progress and prospective clinical applications. *Expert Rev Proteomics* (2017) 14(5):431–44. doi: 10.1080/14789450.2017.1321481

14. Butt S, Jeppesen JL, Iversen LV, Fenger M, Eugen-Olsen J, Andersson C, et al. Association of soluble urokinase plasminogen activator receptor levels with fibrotic and vascular manifestations in systemic sclerosis. *PloS One* (2021) 16(2):e0247256. doi: 10.1371/journal.pone.0247256

15. Chularojanamontri L, Charoenpipatsin N, Silpa-Archa N, Wongpraparut C, Thongboonkerd V. Proteomics in psoriasis. *Int J Mol Sci* (2019) 20(5):1141. doi: 10.3390/ijms20051141

16. Ling HZ, Xu SZ, Leng RX, Wu J, Pan HF, Fan YG, et al. Discovery of new serum biomarker panels for systemic lupus erythematosus diagnosis. *Rheumatol (Oxford)* (2020) 59(6):1416–25. doi: 10.1093/rheumatology/kez634

17. Cecchettini A, Finamore F, Puxeddu I, Ferro F, Baldini C. Salivary extracellular vesicles versus whole saliva: new perspectives for the identification of proteomic biomarkers in Sjögren's syndrome. *Clin Exp Rheumatol* (2019) 37 Suppl 118(3):240–8.

18. Landi C, Bargagli E, Bianchi L, Gagliardi A, Carleo A, Bennett D, et al. Towards a functional proteomics approach to the comprehension of idiopathic pulmonary fibrosis, sarcoidosis, systemic sclerosis and pulmonary Langerhans cell histiocytosis. *J Proteomics* (2013) 83:60–75. doi: 10.1016/j.jprot.2013.03.006

19. Szél E, Bozó R, Hunyadi-Gulyás É, Manczinger M, Szabó K, Kemény L, et al. Comprehensive proteomic analysis reveals intermediate stage of non-lesional psoriatic skin and points out the importance of proteins outside this trend. *Sci Rep* (2019) 9 (1):11382. doi: 10.1038/s41598-019-47774-5

20. Gramolini A, Lau E, Liu PP. Identifying low-abundance biomarkers: aptamer-based proteomics potentially enables more sensitive detection in cardiovascular diseases. *Circulation* (2016) 134(4):286–9. doi: 10.1161/CIRCULATIONAHA.116.022940

21. Wermuth PJ, Piera-Velazquez S, Jimenez SA. Identification of novel systemic sclerosis biomarkers employing aptamer proteomic analysis. *Rheumatol (Oxford)* (2018) 57(10):1698–706. doi: 10.1093/rheumatology/kex404

22. van den Hoogen F, Khanna D, Fransen J, Johnson SR, Baron M, Tyndall A, et al. 2013 classification criteria for systemic sclerosis: an American college of rheumatology/ European league against rheumatism collaborative initiative. *Ann Rheum Dis* (2013) 72 (11):1747–55. doi: 10.1136/annrheumdis-2013-204424

23. Hansell DM, Bankier AA, MacMahon H, McLoud TC, Müller NL, Remy J. Fleischner Society: glossary of terms for thoracic imaging. *Radiology* (2008) 246 (3):697–722. doi: 10.1148/radiol.2462070712

24. Hassoun PM. Pulmonary arterial hypertension. *N Engl J Med* (2021) 385 (25):2361–76. doi: 10.1056/NEJMra2000348

25. Mavrogeni S, Pepe A, Gargani L, Bruni C, Quaia E, Kitas GD, et al. Cardiac inflammation and fibrosis patterns in systemic sclerosis, evaluated by magnetic resonance imaging: An update. *Semin Arthritis Rheumatol* (2022) 58:152126. doi: 10.1016/j.semarthrit.2022.152126

26. Allanore Y, Simms R, Distler O, Trojanowska M, Pope J, Denton CP, et al. Systemic sclerosis. *Nat Rev Dis Primers* (2015) 1:15002. doi: 10.1038/nrdp.2015.2

27. Lollo B, Steele F, Gold L. Beyond antibodies: new affinity reagents to unlock the proteome. *Proteomics* (2014) 14(6):638–44. doi: 10.1002/pmic.201300187

28. LeRoy EC, Black C, Fleischmajer R, Jablonska S, Krieg T, Medsger TA, et al. Scleroderma (systemic sclerosis): classification, subsets and pathogenesis. *J Rheumatol* (1988) 15(2):202–5.

29. Dumit VI, Küttner V, Käppler J, Piera-Velazquez S, Jimenez SA, Bruckner-Tuderman L, et al. Altered MCM protein levels and autophagic flux in aged and systemic sclerosis dermal fibroblasts. *J Invest Dermatol* (2014) 134(9):2321–30. doi: 10.1038/jid.2014.69

30. Aden N, Shiwen X, Aden D, Black C, Nuttall A, Denton CP, et al. Proteomic analysis of scleroderma lesional skin reveals activated wound healing phenotype of epidermal cell layer. *Rheumatol (Oxford)* (2008) 47(12):1754–60. doi: 10.1093/rheumatology/ken370

31. Zian Z, Bakkach J, Barakat A, Ghailani Nourouti N, Bennani Mechita M. Salivary biomarkers in systemic sclerosis disease. *BioMed Res Int* (2018) 2018:3921247. doi: 10.1155/2018/3921247

32. Landi C, Bargagli E, Carleo A, Refini RM, Bennett D, Bianchi L, et al. Bronchoalveolar lavage proteomic analysis in pulmonary fibrosis associated with systemic sclerosis: S100A6 and 14-3-3ϵ as potential biomarkers. *Rheumatol (Oxford)* (2019) 58(1):165–78. doi: 10.1093/rheumatology/key223

33. van Bon L, Affandi AJ, Broen J, Christmann RB, Marijnissen RJ, Stawski L, et al. Proteome-wide analysis and CXCL4 as a biomarker in systemic sclerosis. *N Engl J Med* (2014) 370(5):433–43. doi: 10.1056/NEJMoa1114576

34. Bauer Y, de Bernard S, Hickey P, Ballard K, Cruz J, Cornelisse P, et al. Identifying early pulmonary arterial hypertension biomarkers in systemic sclerosis: machine learning on proteomics from the DETECT cohort. *Eur Respir J* (2021) 57 (6):2002591. doi: 10.1183/13993003.02591-2020

35. Haddon DJ, Wand HE, Jarrell JA, Spiera RF, Utz PJ, Gordon JK, et al. Proteomic analysis of sera from individuals with diffuse cutaneous systemic sclerosis reveals a multianalyte signature associated with clinical improvement during imatinib mesylate treatment. *J Rheumatol* (2017) 44(5):631–8. doi: 10.3899/jrheum.160833

36. Bellocchi C, Assassi S, Lyons M, Marchini M, Mohan C, Santaniello A, et al. Proteomic aptamer analysis reveals serum markers that characterize preclinical systemic sclerosis (SSc) patients at risk for progression toward definite SSc. *Arthritis Res Ther* (2023) 25(1):15. doi: 10.1186/s13075-023-02989-w

37. Rice LM, Mantero JC, Stifano G, Ziemek J, Simms RW, Gordon J, et al. A proteome-derived longitudinal pharmacodynamic biomarker for diffuse systemic sclerosis skin. *J Invest Dermatol* (2017) 137(1):62–70. doi: 10.1016/j.jid.2016.08.027

38. Sanges S, Rice L, Tu L, Valenzi E, Cracowski JL, Montani D, et al. Biomarkers of haemodynamic severity of systemic sclerosis-associated pulmonary arterial hypertension by serum proteome analysis. *Ann Rheum Dis* (2023) 82(3):365–73. doi: 10.1136/ard-2022-223237

39. Piera-Velazquez S, Dillon ST, Gu X, Libermann TA, Jimenez SA. Aptamer proteomics of serum exosomes from patients with Primary Raynaud's and patients with Raynaud's at risk of evolving into Systemic Sclerosis. *PloS One* (2022) 17(12): e0279461. doi: 10.1371/journal.pone.0279461

40. Rice LM, Mantero JC, Stratton EA, Warburton R, Roberts K, Hill N, et al. Serum biomarker for diagnostic evaluation of pulmonary arterial hypertension in systemic sclerosis. *Arthritis Res Ther* (2018) 20(1):185. doi: 10.1186/s13075-018-1679-8

41. Jee AS, Stewart I, Youssef P, Adelstein S, Lai D, Hua S, et al. A composite serum biomarker index for the diagnosis of systemic sclerosis-associated interstitial lung disease: A multicenter, observational cohort study. *Arthritis Rheumatol* (2023) 75 (8):1424–33. doi: 10.1002/art.42491

42. Wu Q, Xu WD, Huang AF. Role of angiopoietin-2 in inflammatory autoimmune diseases: A comprehensive review. *Int Immunopharmacol* (2020) 80:106223. doi: 10.1016/j.intimp.2020.106223

43. Carvalheiro T, Lopes AP, van der Kroef M, Malvar-Fernandez B, Rafael-Vidal C, Hinrichs AC, et al. Angiopoietin-2 promotes inflammatory activation in monocytes of systemic sclerosis patients. *Int J Mol Sci* (2020) 21(24):9544. doi: 10.3390/ijms21249544

44. Michalska-Jakubus M, Kowal-Bielecka O, Chodorowska G, Bielecki M, Krasowska D. Angiopoietins-1 and -2 are differentially expressed in the sera of patients with systemic sclerosis: high angiopoietin-2 levels are associated with greater severity and higher activity of the disease. *Rheumatol (Oxford)* (2011) 50(4):746–55. doi: 10.1093/rheumatology/keq392

45. Takahashi T, Asano Y, Akamata K, Aozasa N, Taniguchi T, Noda S, et al. Dynamics of serum angiopoietin-2 levels correlate with efficacy of intravenous pulse cyclophosphamide therapy for interstitial lung disease associated with systemic sclerosis. *Mod Rheumatol* (2013) 23(5):884–90. doi: 10.3109/s10165-012-0755-1

46. Dudakov JA, Hanash AM, van den Brink MRM. Interleukin-22: immunobiology and pathology. *Annu Rev Immunol* (2015) 33:747–85. doi: 10.1146/annurev-immunol-032414-112123

47. Zenewicz LA. IL-22 binding protein (IL-22BP) in the regulation of IL-22 biology. *Front Immunol* (2021) 12:766586. doi: 10.3389/fimmu.2021.766586

48. Voglis S, Moos S, Kloos L, Wanke F, Zayoud M, Pelczar P, et al. Regulation of IL-22BP in psoriasis. *Sci Rep* (2018) 8(1):5085. doi: 10.1038/s41598-018-23510-3

49. Pelczar P, Witkowski M, Perez LG, Kempski J, Hammel AG, Brockmann L, et al. A pathogenic role for T cell-derived IL-22BP in inflammatory bowel disease. *Science* (2016) 354(6310):358–62. doi: 10.1126/science.aah5903

50. Whittington HA, Armstrong L, Uppington KM, Millar AB. Interleukin-22: a potential immunomodulatory molecule in the lung. *Am J Respir Cell Mol Biol* (2004) 31 (2):220–6. doi: 10.1165/rcmb.2003-0285OC

51. Pociask DA, Scheller EV, Mandalapu S, McHugh KJ, Enelow RI, Fattman CL, et al. IL-22 is essential for lung epithelial repair following influenza infection. *Am J Pathol* (2013) 182(4):1286–96. doi: 10.1016/j.ajpath.2012.12.007

52. Hebert KD, Mclaughlin N, Galeas-Pena M, Zhang Z, Eddens T, Govero A, et al. Targeting the IL-22/IL-22BP axis enhances tight junctions and reduces inflammation during influenza infection. *Mucosal Immunol* (2020) 13(1):64–74. doi: 10.1038/s41385-019-0206-9

53. Mathian A, Parizot C, Dorgham K, Trad S, Arnaud L, Larsen M, et al. Activated and resting regulatory T cell exhaustion concurs with high levels of interleukin-22 expression in systemic sclerosis lesions. *Ann Rheum Dis* (2012) 71(7):1227–34. doi: 10.1136/annrheumdis-2011-200709

54. Truchetet ME, Brembilla NC, Montanari E, Allanore Y, Chizzolini C. Increased frequency of circulating Th22 in addition to Th17 and Th2 lymphocytes in systemic sclerosis: association with interstitial lung disease. *Arthritis Res Ther* (2011) 13(5):R166. doi: 10.1186/ar3486

55. Kardum Ž, Milas-Ahić J, Šahinović I, Masle AM, Uršić D, Kos M. Serum levels of interleukin 17 and 22 in patients with systemic sclerosis: a single-center cross-sectional study. *Rheumatol Int* (2023) 43(2):345–54. doi: 10.1007/s00296-022-05250-w

56. Brembilla NC, Dufour AM, Alvarez M, Hugues S, Montanari E, Truchetet ME, et al. IL-22 capacitates dermal fibroblast responses to TNF in scleroderma. *Ann Rheum Dis* (2016) 75(9):1697–705. doi: 10.1136/annrheumdis-2015-207477

57. Sawamura S, Jinnin M, Inoue K, Yamane K, Honda N, Kajihara I, et al. Regulatory mechanisms of collagen expression by interleukin-22 signaling in scleroderma fibroblasts. *J Dermatol Sci* (2018) 90(1):52–9. doi: 10.1016/j.jdermsci.2017.12.017

58. Qu Z, Dou W, Zhang K, Duan L, Zhou D, Yin S. IL-22 inhibits bleomycin-induced pulmonary fibrosis in association with inhibition of IL-17A in mice. *Arthritis Res Ther* (2022) 24:280. doi: 10.1186/s13075-022-02977-6

59. Van Kaer L, Postoak JL, Song W, Wu L. Innate and innate-like effector lymphocytes in health and disease. *J Immunol* (2022) 209(2):199–207. doi: 10.4049/jimmunol.2200074

60. Matute-Bello G, Wurfel MM, Lee JS, Park DR, Frevert CW, Madtes DK, et al. Essential role of MMP-12 in Fas-induced lung fibrosis. *Am J Respir Cell Mol Biol* (2007) 37(2):210–21. doi: 10.1165/rcmb.2006-0471OC

61. Manoury B, Nenan S, Guenon I, Boichot E, Planquois JM, Bertrand CP, et al. Macrophage metalloelastase (MMP-12) deficiency does not alter bleomycin-induced pulmonary fibrosis in mice. *J Inflammation (Lond)* (2006) 3:2. doi: 10.1186/1476-9255-3-2

62. Serratì S, Cinelli M, Margheri F, Guiducci S, Del Rosso A, Pucci M, et al. Systemic sclerosis fibroblasts inhibit in *vitro* angiogenesis by MMP-12-dependent cleavage of the endothelial cell urokinase receptor. *J Pathol* (2006) 210(2):240–8. doi: 10.1002/path.2048

63. Manetti M, Guiducci S, ROmano E, Bellando-Randone S, Conforti ML, Ibba-Manneschi L, et al. Increased serum levels and tissue expression of matrix metalloproteinase-12 in patients with systemic sclerosis: correlation with severity of skin and pulmonary fibrosis and vascular damage. *Ann Rheum Dis* (2012) 71(6):1064–72. doi: 10.1136/annrheumdis-2011-200837

64. Manetti M, Ibba-Manneschi L, Fatini C, Guiducci S, Cuomo G, Bonino C, et al. Association of a functional polymorphism in the matrix metalloproteinase-12 promoter region with systemic sclerosis in an Italian population. *J Rheumatol* (2010) 37(9):1852–7. doi: 10.3899/jrheum.100237

65. Kania G, Rudnik M, Distler O. Involvement of the myeloid cell compartment in fibrogenesis and systemic sclerosis. *Nat Rev Rheumatol* (2019) 15(5):288–302. doi: 10.1038/s41584-019-0212-z

66. Bennett D, Salvini M, Fui A, Cillis G, Cameli P, Mazzei MA, et al. Calgranulin B and KL-6 in bronchoalveolar lavage of patients with IPF and NSIP. *Inflammation* (2019) 42(2):463–70. doi: 10.1007/s10753-018-00955-2

67. Bai M, Grieshaber-Bouyer R, Wang J, Schmider AB, Wilson ZS, Zeng L, et al. CD177 modulates human neutrophil migration through activation-mediated integrin and chemoreceptor regulation. *Blood* (2017) 130(19):2092–100. doi: 10.1182/blood-2017-03-768507

68. Zhou G, Yu L, Fang L, Yang W, Yu T, Miao Y, et al. CD177+ neutrophils as functionally activated neutrophils negatively regulate IBD. *Gut* (2018) 67(6):1052–63. doi: 10.1136/gutjnl-2016-313535

69. Pease JE, Williams TJ. Eotaxin and asthma. *Curr Opin Pharmacol* (2001) 1 (3):248–53. doi: 10.1016/S1471-4892(01)00044-3

70. Zweifel M, Matozan K, Dahinden C, Schaffner T, Mohacsi P. Eotaxin/CCL11 levels correlate with myocardial fibrosis and mast cell density in native and transplanted rat hearts. *Transplant Proc* (2010) 42(7):2763–6. doi: 10.1016/j.transproceed.2010.05.152

71. Mari A, Kadah A, Mahamid M, Sbeit W, Khoury T. IgG4 related autoimmune pancreatitis: an overview and the emerging role of serum eotaxin as a potential treatment target. *Isr Med Assoc J* (2019) 21(9):620–3.

72. Cheng E, Zhang X, Wilson KS, Wang DH, Park JY, Huo X, et al. JAK-STAT6 pathway inhibitors block eotaxin-3 secretion by epithelial cells and fibroblasts from esophageal eosinophilia patients: promising agents to improve inflammation and prevent fibrosis in eoe. *PloS One* (2016) 11(6):e0157376. doi: 10.1371/journal.pone.0157376

73. La Cava A. Leptin in inflammation and autoimmunity. *Cytokine* (2017) 98:51–8. doi: 10.1016/j.cyto.2016.10.011

74. Liu Y, Li Y, Liang J, Sun Z, Wu Q, Liu Y, et al. Leptin: an entry point for the treatment of peripheral tissue fibrosis and related diseases. *Int Immunopharmacol* (2022) 106:108608. doi: 10.1016/j.intimp.2022.108608

75. Michalska-Jakubus M, Sawicka K, Potembska E, Kowal M, Krasowska D. Clinical associations of serum leptin and leptin/adiponectin ratio in systemic sclerosis. *Postepy Dermatol Alergol* (2019) 36(3):325–38. doi: 10.5114/ada.2018.75809

76. Lee YH, Song GG. Meta-analysis of circulating adiponectin, leptin, and resistin levels in systemic sclerosis. *Z Rheumatol* (2017) 76(9):789–97. doi: 10.1007/s00393-016-0172-5

77. Budulgan M, Dilek B, Dağ ŞB, Batmaz I, Yıldız İ, Sarıyıldız MA, et al. Relationship between serum leptin level and disease activity in patients with systemic sclerosis. *Clin Rheumatol* (2014) 33(3):335–9. doi: 10.1007/s10067-013-2459-0

78. Pehlivan Y, Onat AM, Ceylan N, Turkbeyler IH, Buyukhatipoglu H, Comez G, et al. Serum leptin, resistin and TNF-α levels in patients with systemic sclerosis: the role of adipokines in scleroderma. *Int J Rheum Dis* (2012) 15(4):374–9. doi: 10.1111/j.1756-185X.2012.01755.x

frontiers | Frontiers in Immunology

TYPE Brief Research Report
PUBLISHED 13 October 2022
DOI 10.3389/fimmu.2022.1034570

OPEN ACCESS

EDITED BY
Jeremy P. McAleer,
Marshall University, United States

REVIEWED BY
Ahmet Eken,
Erciyes University, Turkey
Jay K. Kolls,
Tulane Medical Center, United States

*CORRESPONDENCE
Jérôme C. Martin
jerome.martin@univ-nantes.fr
Régis Josien
regis.josien@univ-nantes.fr

†These authors have contributed equally to this work and share second authorship

SPECIALTY SECTION
This article was submitted to Inflammation, a section of the journal Frontiers in Immunology

RECEIVED 01 September 2022
ACCEPTED 03 October 2022
PUBLISHED 13 October 2022

CITATION
Fantou A, Lagrue E, Laurent T, Delbos L, Blandin S, Jarry A, Beriou G, Braudeau C, Salabert N, Marin E, Moreau A, Podevin J, Bourreille A, Josien R and Martin JC (2022) IL-22BP production is heterogeneously distributed in Crohn's disease. *Front. Immunol.* 13:1034570. doi: 10.3389/fimmu.2022.1034570

IL-22BP production is heterogeneously distributed in Crohn's disease

Aurélie Fantou[1,2], Eric Lagrue[3†], Thomas Laurent[1†], Laurence Delbos[1], Stéphanie Blandin[4], Anne Jarry[5], Gaëlle Beriou[1], Cécile Braudeau[1,2], Nina Salabert[1,2], Eros Marin[1], Aurélie Moreau[1], Juliette Podevin[6], Arnaud Bourreille[6], Régis Josien[1,2*] and Jérôme C. Martin[1,2*]

[1]Nantes Université, CHU Nantes, Inserm, Centre de Recherche Translationnelle en Transplantation et Immunologie, UMR 1064, Nantes, France, [2]CHU Nantes, Nantes Université, Laboratoire d'Immunologie, CIMNA, Nantes, France, [3]CHU Nantes, Nantes Université, Service d'Anatomie et Cytologie Pathologiques, Nantes, France, [4]Nantes Université, CHU Nantes, CNRS, Inserm, BioCore, US16, SFR Bonamy, Nantes, France, [5]Nantes Université, Univ Angers, INSERM, CNRS, Immunology and New Concepts in ImmunoTherapy, INCIT, UMR 1302/EMR6001, Nantes, France, [6]CHU Nantes, Institut des Maladies de l'Appareil Digestif, Nantes, France

Crohn's disease (CD), a form of inflammatory bowel disease (IBD), is characterized by impaired epithelial barrier functions and dysregulated mucosal immune responses. IL-22 binding protein (IL-22BP) is a soluble inhibitor regulating IL-22 bioactivity, a cytokine proposed to play protective roles during CD. We and others have shown that IL-22BP is produced in IBD inflamed tissues, hence suggesting a role in CD. In this work, we extended the characterization of IL-22BP production and distribution in CD tissues by applying enzyme-linked immunosorbent assays to supernatants obtained from the culture of endoscopic biopsies of patients, and reverse transcription-quantitative polymerase chain reaction on sorted immune cell subsets. We reveal that IL-22BP levels are higher in inflamed ileums than colons. We observe that in a cell-intrinsic fashion, populations of mononuclear phagocytes and eosinophils express IL-22BP at the highest levels in comparison to other sources of T cells. We suggest the enrichment of intestinal eosinophils could explain higher IL-22BP levels in the ileum. In inflamed colon, we reveal the presence of increased IL-22/IL22BP ratios compared to controls, and a strong correlation between IL-22BP and CCL24. We identify monocyte-derived dendritic cells (moDC) as a cellular subtype co-expressing both cytokines and validate our finding using *in vitro* culture systems. We also show that retinoic acid induces the secretion of both IL-22BP and CCL24 by moDC. Finally, we report on higher IL-22BP levels in active smokers. In conclusion, our work provides new information relevant to therapeutic strategies modulating IL-22 bioactivity in CD, especially in the context of disease location.

KEYWORDS

IL-22BP, IL-22, Crohn's disease, mononuclear phagocytes, eosinophils, disease location

Introduction

Inflammatory bowel disease (IBD) is a group a chronic inflammatory conditions of the gastrointestinal tract, the main clinical entities of which are Crohn's disease (CD) and ulcerative colitis (UC) (1). IBD results from dysregulated mucosal immune responses against the microbiota, triggered by environmental factors in genetically susceptible individuals (2). Inflammatory responses in IBD alter the intestinal epithelial barrier, further amplifying immune pathogenicity. The cytokine interleukin-(IL) 22 is proposed to play central roles during IBD inflammation (3, 4). IL-22 is induced during IBD flares, as a result of increased production by $CD4^+$ T cells and group 3 innate lymphoid cells (ILC3) (5). IL-22 receptor (IL-22R) expression is mostly limited to epithelial cells and protective functions for IL-22 on the gut epithelium have been suggested in several rodent models of intestinal inflammation (6, 7). IL-22 supports gut epithelial barrier properties by inducing the secretion of antimicrobial peptides (6) and mucins (7), as well as intestinal epithelial cell (IEC) survival and proliferation (8). When dysregulated, however, IL-22 actions on IEC can promote tumor cell proliferation (9, 10). IL-22 binding protein (IL-22BP; encoded by the gene *IL22RA2*) is a soluble inhibitor specific for IL-22 (11), which regulates the level of IL-22 bioactivity *in vivo* (12, 13). Concordantly, we have observed increased IL-22-dependent protection against DSS-induced colitis in IL-22BP-deficient rats (14). In mice, IL-22BP worsens T cell-dependent colitis (15) but prevents tumorigenic long-lasting pro-proliferative actions of IL-22 (12). We and others have shown that the expression of *IL22RA2* is down-regulated during infectious colitis but not in IBD inflamed tissues, hence suggesting possible pathophysiological relevance for the IL-22BP-dependent modulation of IL-22 bioactivity (14, 15). IL-22BP is produced by various cell types, which include subsets of intestinal dendritic cells (DCs) and macrophages in the gut lamina propria (LP) and secondary lymphoid structures (12, 15–18). In human, we have revealed that IL-22BP is also produced by gut eosinophils in the LP of both healthy and inflamed IBD tissues (14). Finally, $CD4^+$ T cells have also been proposed to contribute to IL-22BP levels detected in IBD (15, 19).

Several layers of disease heterogeneity exist in CD. It has so far remained unclear whether the general findings about IL-22BP regulation in IBD discussed above can be extrapolated homogenously to patients with CD, especially when considering intestinal segments of disease location. In the light of therapeutic strategies modulating IL-22 bioactivity in IBD that are currently under evaluation, we thus sought to extend further the characterization of IL-22BP production and distribution in intestinal tissues from a cohort of CD patients.

Material and methods

Patients

Patients were recruited, from January 2016 to October 2019, from the Institut des Maladies de l'Appareil Digestif (IMAD), the gastroenterology department and the digestive endoscopy unit at CHU Nantes Hospital. The protocol was approved, and informed consent was obtained from all participants in accordance with the institutional review board (DC-2008-402). A cohort 1 of CD patients was constituted to explore cytokine secretions in supernatants from *ex vivo* biopsy cultures. Cohort 1 included a total of 43 CD patients for whom endoscopic biopsies in involved areas were collected during colonoscopies planned for routine care (Supplementary Table 1). Control biopsies were also analyzed and collected from surgical specimens of colon cancers, on unaffected areas of the colon or the ileum, at least 10 cm distant from the tumor. A cohort 2 that included mesenteric lymph nodes and intestinal mucosa obtained from ileocecal resections of 6 patients with active CD was constituted for gene expression analyses in sorted immune cell subsets (Supplementary Table 2).

Ex vivo cultures of gut biopsies

During the colonoscopy procedure, biopsies were collected with forceps directly in ice cold RPMI and processed within 2h. Biopsies (controlled for weight) were put into 4-well Petri dishes filled with in 500µL serum-free medium (RPMI 1640, Gibco™) supplemented with BSA (0.01%), 200µg/mL Penicillin/Streptomycin (Gibco ™; ref 15140-122) and 0.25µg/mL Fungizone (Gibco™; ref 15290-026), and cultured *ex vivo* during 6 h at +37°C in a 95% O_2/5% CO_2 atmosphere on a low-speed rocking platform. Supernatants were collected and stored at -80°C until use.

ELISA assay for 22BP

IL-22BP quantification was performed with the Human IL-22BP ELISA DuoSet kit (R&D System, ref DY-1087-05) according to manufacturer's instruction. Briefly, a 96-well microplate was coated with a rabbit monoclonal anti-IL-22BP [4µg/mL] and incubated at room temperature (RT) overnight. The next day, after blocking with Reagent Diluent (R&D System, ref DY006), 100-µL standard dilutions and samples were added to each well and incubated 2 hours at RT. Then, 100µL/well of goat anti-IL-22BP [70ng/mL] were added and 2 h incubation at RT was performed. Finally, ELISA was revealed and plates were read at 450 nm with TECAN Spark® instrument. Of note, the combination of antibodies used in this assay has the potential to detect all three isoforms of IL-22BP existing in humans (20).

Multiplex assay

Levels of soluble cytokines (CCL4, CXCL10, CXCL2, CCL24, CCL11, IFNγ, IL-10, IL-17A, IL-22, IL-27, IL-6, IL-8, CCL2, OSM, CXCL1, CXCL11, CXCL5, CCL26, IL-1β, IL-18, IL-23, IL-33, IL-7, CXCL9, TNF) were quantified in supernatants obtained after *ex vivo* biopsy cultures with a multiplex assay from Biotechne (Rennes, France) and a Luminex MAGPIX® instrument (Supplementary Table 3).

Eosinophil counts

Eosinophil counts were scored in a blinded fashion by a trained pathologist. Hematoxylin and eosin-stained slides from intestinal tissues of 36 CD patients were analyzed with an Olympus BH2 microscope. A high-power field (HPF) included an area of 0.196mm^2. For each slide, eosinophil counts were defined by averaging the results obtained in 5 different HPFs selected randomly. Results of eosinophil counts were reported as the number of eosinophils/mm^2.

Isolation of intestinal lamina propria cells

Tissues from surgical resections were collected in ice cold RPMI 1640 (Gibco™) and processed within one hour after the end of the surgery. The mucosa was stripped and cut into small pieces before transfer into complete RPMI media. Epithelial cells were dissociated in an EDTA-enriched dissociation medium (HBSS w/o Ca^{2+} Mg^{2+} (Gibco™) - HEPES 10mM (Gibco™) - EDTA 5mM at +37°C through two 15 min cycles of agitation at 100 rpm. After each cycle, intestinal fragments were hand-shaken for 30 s and vortexed vigorously for another 30 s. Epithelium-free fragments were washed in PBS, and transferred in the digestion medium (HBSS with Ca^{2+} Mg^{2+} - Fetal Calf serum (FCS) 2% - DNase I 0.1mg/mL (Sigma-Aldrich, ref 11284932001) – Collagenase IV 0.5mg/mL (Sigma-Aldrich, ref C5138) for 40 min at +37°C under 100 rpm agitation; and vortexing every 20 min. Cell suspensions were filtered through 70µm pore size cell strainers (BD Biosciences) and washed with FACS-buffer (with EDTA 1mM) twice before being processed for cell sorting.

Intestinal mesenteric lymph nodes isolation

Tissues were collected in ice cold RPMI 1640 (Gibco™) from the resected specimens and processed within one hour after the end of the surgery. After removing the adipose tissue, mesenteric lymph nodes were cut in small pieces and transferred into the digestion medium (10mL of complete RPMI with Collagenase D (2mg/mL- Sigma-Aldrich, ref 1108882001) and DNase I (0,1 mg/mL)). After 30 min of incubation at +37°C 100 rpm, EDTA (1mM) was added to block the reaction. Cell suspensions were filtered through 70µm pore size cell strainers (BD Biosciences) and processed for cell sorting.

Cells sorting

Single cell suspensions were incubated in PBS containing the flow cytometry antibody cocktail (Supplementary Table 4) for 20 min at 4°C in the dark. Dead cells were excluded by gating on 4',6-diamidino-2-phenylindole (DAPI)-negative cells. Cell sorting was performed on a BD FACS Aria Cell sorter (BD Biosciences) using the gating strategies shown in Figure 2.

Real-time quantitative PCR

Sorted cells were suspended in TRIzol reagent (Thermo Fisher Scientific) and frozen at -80°C. Total RNA was extracted using an RNeasy mini kit (Qiagen,Valencia, CA) according to manufacturer's instructions. Reverse transcription was performed using Murine Moloney Leukemia Virus Reverse Transcriptase (Thermo Fisher Scientific) following manufacturer's instructions. Gene expressions were assessed with the TaqMan Fast Advanced Master Mix reagent (Applied Biosystems, Foster City, Calif). Primers and probes were from Applied Biosystems (Supplementary Table 5). With regard to *IL22RA2* mRNA detection, all three isoforms can be detected with the probe used in this study. Real-time PCR was performed using the StepOne Plus System (Applied Biosystems). Relative expression was normalized to hypoxanthine-guanine phosphoribosyltransferase and calculated using $2^{\wedge -ddct}$ method. Results were expressed in arbitrary units (a.u.).

Monocyte-derived dendritic cells

Monocytes from healthy volunteers were isolated either by elutriation of PBMCs (Clinical Development and Transfer Platform, Nantes, France) or by magnetic labelling (untouched cells, Human monocyte Isolation kit II). To obtain monocyte-derived DC (moDC), 2.5x10^6 monocytes were incubated in a 6-well plate in 5 mL of complete medium (RPMI 1640 medium containing 10% FCS, 1% L-glutamine, 1% antibiotics, 1mM Sodium Pyruvate, 1mM HEPES, 1% non-essential amino

acids) supplemented with recombinant human IL-4 (200U/mL) and recombinant human GM-CSF (100U/mL) for 6 days at 37°C with 5% CO_2. When indicated, cells were treated with retinoic acid (RA) (100nM, Sigma Aldrich), LPS (1 µg/mL, Sigma Aldrich) and TNF (50 ng/mL, Miltenyi). After 6 days, moDC and supernatants were collected and frozen at −80°C until use.

Immunofluorescence staining from mesenteric lymph nodes

Lymph nodes isolated from 3 CD patients were frozen in tissue-Tek. Sections were fixed for 15 min in paraformaldehyde. After rehydration, a 10 min step saturation was performed with H2O2 (3%). For double staining, mouse IgG anti-hIL-22BP (MAB 1087 from R&D System, [1/800]) or isotype control (mouse IgG1, DDXCMO1P from Dendritic products [1/800] were incubated at room temperature (RT) for 1 hour. After washing, several steps are carried out in order to amplify the IL-22BP signal: polymer enhancer (M023 from ImPath) then HRP-2 (M024 from ImPath) and finally Opal 650 (FP1496A from Akoya) following manufacturer's instruction. Then, after washing and a second step of saturation with goat serum 1.5%, a second purified antibody: rabbit anti-hCD3 (A0452 from Dako, [1/800]) or isotype control rabbit IgG (I-1000 from Vector) was added and incubated at RT during 1 hour. Purified antibody was revealed with adapted secondary antibody labelled withAlexa488 (goat anti-rabbit, A11008) from Life Technologies. After washing, DAPI (Molecular Probes, D1306) was incubated 30 min. Slides were mounted with Vectashield® Vibrance™ Antifade Mounting Medium (H-1700 Vector Laboratories). Images were obtained with A1 R Si Confocal microscope (MicroPICell).

Cytokine correlation plots

Pairwise correlations between cytokines were calculated and visualized as a correlogram using R function corrplot. Spearman's rank correlation coefficient (ρ) was indicated by heat scale; significance was indicated by *P < 0.05, **P < 0.01, and ***P < 0.001.

Statistical analysis

Statistical analysis was performed with GraphPad Prism Software (GraphPad Software, San Diego, CA). Means comparisons of unpaired samples were performed using the Mann–Whitney U-test or the Kruskal–Wallis test with Dunn's post-test. The Wilcoxon signed-rank test was used for paired samples. P-values <0.05 were considered statistically significant.

Multiple linear regression analysis: Since, the distribution of IL-22BP values was not Gaussian, we transformed it by ranking the values and converting them to a normal distribution using the R function qnorm. Multiple linear regression was then performed using the lm() function. Adjusted P-values were calculated after multiple-comparison using *post hoc* Bonferroni correction.

Results

IL22BP levels are higher in the ileum than in the colon of Crohn's disease patients

Both IL-22 and IL-22BP mediate their biological functions as secreted soluble proteins (11, 21). To explore IL-22BP production in a biologically relevant manner in CD, we thus quantified secreted levels released after short *ex vivo* culture of intestinal biopsies. Soluble IL-22BP was consistently detected in supernatants from both controls and CD biopsies (see Supplementary Table 1 for patient characteristics), and though means were not statistically significant, the highest levels were detected in a subset of CD patients (Figure 1A). To begin explore what factors would preferentially associate with IL-22BP heterogenous distributions in CD, we ran a multiple linear regression analysis that included several disease-relevant clinical parameters such as age, sex, disease location, disease phenotype and medication (Table 1). This analysis revealed disease location as the strongest factor (Bonferroni adjusted P-value <0.0001). Accordingly, higher levels of IL-22BP were detected in the supernatants of ileal vs. colonic CD biopsies (Figure 1B). IL-22 levels in turn, were similar between biopsy supernatants from both locations, which translated into IL-22/IL-22BP ratios, a surrogate to infer IL-22 bioactivity, higher in the colon as compared to the ileum of CD patients (Figures 1C, D). In fact, the analysis of IL-22BP and IL-22 in control patients indicated that both proteins were produced at higher levels in ileal vs. colonic biopsies (Figures 1E, F), an observation confirming previous reports about the physiological distribution of IL-22 across intestinal segments (22). Remarkably, however, IL-22 induction was largely limited to CD colons (Figures 1G, H). IL-22BP mean levels in turn, remained similar between controls and CD patients when controlling for gut segments (Figures 1I, J). Concordantly, in comparison to controls, IL-22/IL-22BP ratios were unchanged in the ileum but increased significantly in CD colons (Figures 1K, L).

Altogether, these results suggest that regional specialization in the intestine are characterized by higher levels of IL-22BP production in the ileum as compared to the colon in both controls and CD patients.

10.3389/fimmu.2022.1034570

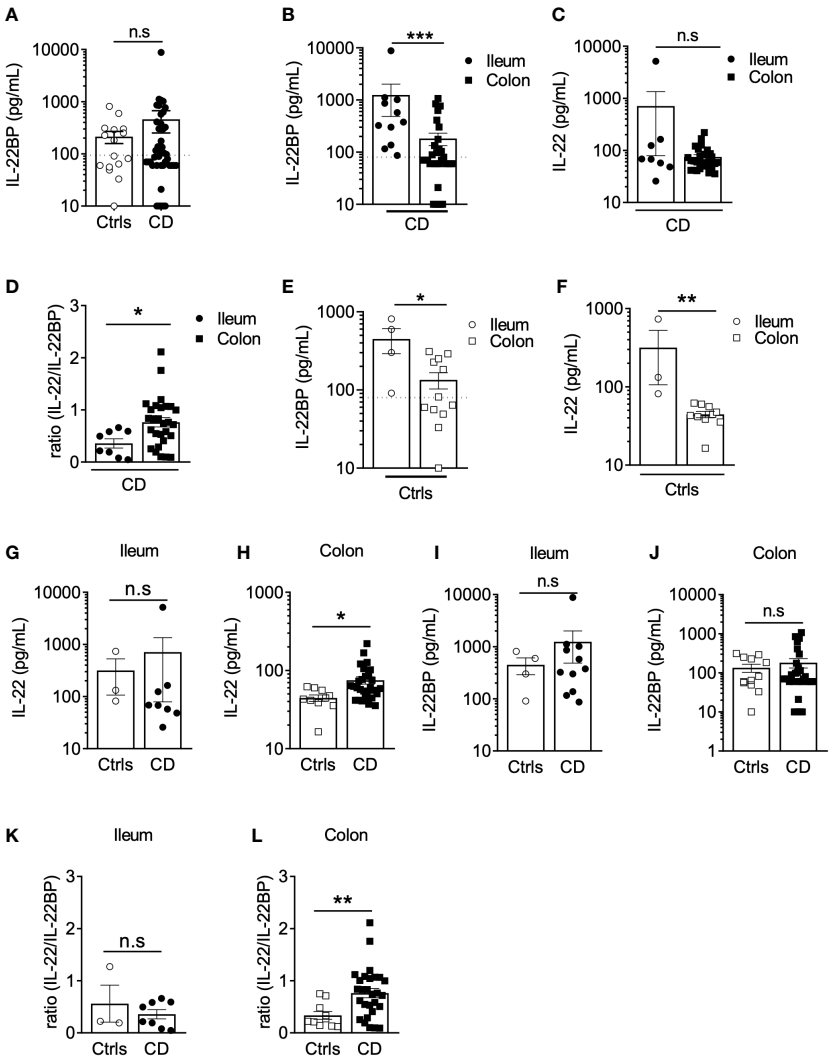

FIGURE 1
IL22BP levels are higher in the ileum than in the colon of Crohn's disease patients. **(A)** Levels of soluble IL-22BP were quantified by ELISA in the supernatant of gut (both ileum and colon locations) endoscopic biopsies from controls (Ctrls) (n=16) and Crohn's disease (CD) (n=43) patients after 6 hours of ex vivo culture. **(B, C)** Quantification of soluble IL-22BP **(B)** and IL-22 **(C)** in culture supernatants of biopsies from CD patients with inflamed lesions in the ileum (n=11) or in the colon (n=32). **(D)** Comparison of IL-22/IL-22BP ratios in the supernatants of CD patients with inflamed ileum and colon. **(E, F)** Quantification of soluble IL-22BP **(E)** and IL-22 **(F)** levels in the supernatant of gut biopsies from Ctrls ileum (n=4) and colon (n=12). **(G, H)** Comparison of IL-22 levels in the ileum **(G)** and the colon **(H)** of Ctrls and CD patients. **(I, J)** Comparison of IL-22BP levels in the ileum **(I)** and the colon **(J)** of Ctrls and CD patients. **(K, L)** Comparison of IL-22/IL-22BP ratios in the ileum **(K)** and the colon **(L)** of Ctrls and CD patients. Statistical significance for mean comparisons was assessed by the Mann-Whitney U-test in a two-sided manner, using a nominal significance threshold of $P < 0.05$. *$P < 0.05$, **$P < 0.01$, ***$P < 0.001$ ns, not significant.

The highest levels of IL22BP expression are detected in CD MNP and eosinophils

Various cell types can produce IL-22BP in IBD intestinal tissues, including populations of mononuclear phagocytes (MNP), which encompass dendritic cells (DCs) and macrophages, $CD4^+$ T cells and eosinophils (14, 15, 19). So far, however, no systematic direct comparison of *IL22RA2* levels of expression by these different immune cell subsets has been performed specifically in intestinal tissues of CD patients. We thus analyzed *IL22RA2* expression in FACS-sorted populations of MNP ($CD45^+$ $HLA\text{-}DR^+$ $CD11c^+$), eosinophils ($CD45^+$ $SIGLEC\text{-}8^+$), $CD4^+$ T cells ($CD45^+$ $CD3^+$ $CD4^+$), $CD4^-$ T cells ($CD45^+$ $CD3^+$ $CD4^-$), and B cells ($CD45^+$ $CD3^-$ $CD19^+$) isolated

10.3389/fimmu.2022.1034570

TABLE 1 Multiple linear regression to assess associations between clinical parameters of CD and IL-22BP levels.

Variable	Adj. P-value
Sex	0.01439
Age	0.30812
Localization	<0.0001
Tobacco	0.27988
Disease evolution	1.00000
Phenotype	1.00000
Perianal involvement	1.00000
Treatment: anti-TNF	1.00000
Treatment: IS	1.00000
Surgical resection	1.00000
Clinical score	0.01013

from surgically resected intestinal tissues of CD patients (Figures 2A, B; Supplementary Figure 1A). Compared to the three lymphocytes fractions, MNP and eosinophils expressed higher levels of IL-22BP mRNA (Figure 2B). We observed similar trends between MNP and T cells isolated from CD mesenteric lymph nodes (MLN) (Figures 2C, D; Supplementary Figure 1B). Of note, similar mRNA levels were detected between populations of naïve and non-naïve T cells. Using indirect immunofluorescence (IIF) approaches, we previously verified IL-22BP protein expression in major basic protein $(MBP)^+$ eosinophils and HLA-DR^+ MNP in the gut LP but not in $CD3^+$ T cells (14). We could not detect IL-22BP in $CD3^+$ MLN cells either (Supplementary Figure 1C), hence possibly reflecting a lack of method sensitivity to capture lower expression levels in T cells. Finally, while we could observe increased expression levels of activation-induced *IL2RA* (encoding for CD25) in sorted gut and MLN T cells upon simulation with PMA and ionomycin, no difference existed for *IL22RA2* (Supplementary Figures 1D-G).

Taken together, these data suggest that in a cell-intrinsic fashion, MNP and eosinophils express IL-22BP at the highest levels in intestinal tissues of CD patients.

High levels of IL22BP in the ileum associate with higher proportions of eosinophils

In inflamed CD tissues, the strongest factor linked to IL-22BP variability was disease location (Table 1), and as for controls, IL-22BP secretion in biopsy supernatants was higher in the ileum than in the colon (Figure 1). Interestingly, the levels of CCL11 (aka. eotaxin-1), the main driver of eosinophil homeostatic recruitment in the intestine (23), were also higher in biopsy supernatants from the ileum than from the colon of controls (Figure 2E), concordant with the reported increased abundance of gut resident eosinophils in the small intestine (24–26). This suggested that the higher levels of IL-22BP we detected in inflamed CD ileums as compared to CD colons could in part be explained by the heterogenous distribution of resident-eosinophils across intestinal segments. Accordingly, we confirmed the existence of higher eosinophil numbers in CD ileums than in CD colons (Figures 2F, G). Blood-derived eosinophil infiltration has been reported during colonic inflammation, including in CD (27–29), and CCL11 levels were indeed moderately increased in CD colons as compared to controls (Figure 2E). Median-based stratification of colonic CD patients into $eosinophil^{high}$ and $eosinophil^{low}$, however, did not reveal differences in IL-22BP production between the two subgroups (Figure 2H). Importantly, we previously reported that *IL22RA2* expression was undetectable in human peripheral blood eosinophils (14). This suggested that the contribution of eosinophil-derived IL-22BP detected in CD lesions could in fact reflect a pre-established production by tissue-imprinted gut-resident eosinophils but not by recently recruited eosinophils in inflamed tissues.

In consequence, our interpretation of these data is that homeostatic enrichment of tissue-resident eosinophil contributes to create an IL-22BP-rich environment that is maintained upon inflammation induction in CD ileums and participate to limit the extent of IL-22 bioavailability.

IL22BP levels correlate with CCL24 produced by monocyte-derived dendric cells in the colon of CD patients

In the colon of CD patients, IL-22BP detected in biopsy supernatants spanned a wide range of concentrations, and while means did not differ from controls, a subset of patients nevertheless exhibited levels reaching those observed in the ileum (Figures 1B). As described above, this variability could not be explained by colonic eosinophil abundance (Figure 2H), which suggested a role for other IL-22BP sources (i.e. MNP and/or T cells). We were unable to examine IL-22BP production by flow cytometry because in our hands none of the anti-IL-22BP antibodies commercially available could be confidently validated. To infer possible sources, we hypothesized that IL-22BP secretion should be correlated with other cytokines in biopsy supernatants, in part as a consequence of shared cellular origins. We characterized the cytokine milieu associated with IL-22BP secretion in the CD colon through a multiplex analysis on the same biopsy supernatants as used for IL-22BP quantification. We then realized a correlation matrix to identify possible

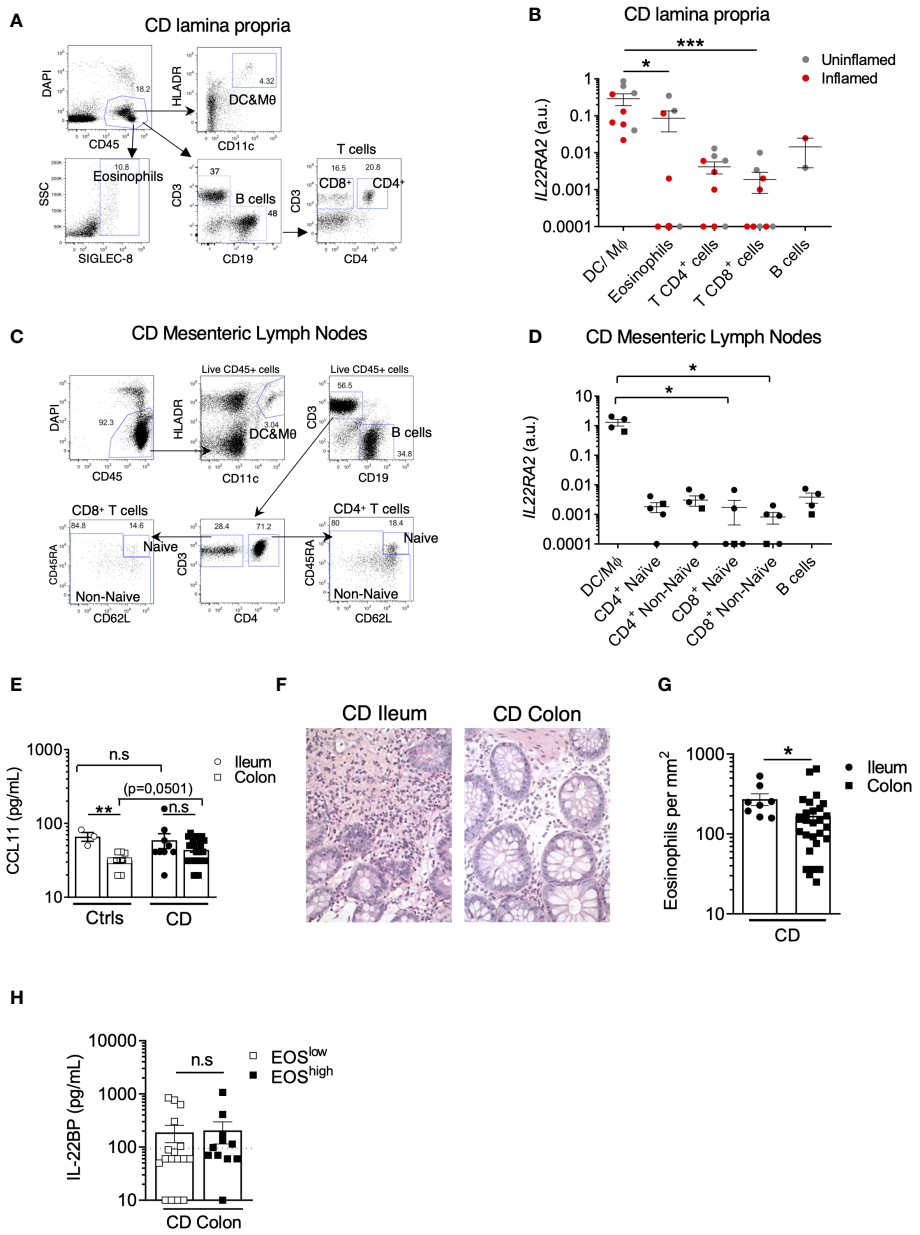

FIGURE 2
The highest levels of IL22BP expression are detected in CD MNP and eosinophils. **(A)** Representative dot plots of the gating strategy used to sort indicated cell subsets from the lamina propria (LP) of intestinal surgical resections from Crohn's disease (CD) patients. **(B)** *IL22RA2* expression was analyzed by RT-qPCR in indicated FACS-sorted cell subsets from CD patient gut LP samples (n=6). Grey and red dots refer to cells sorted from surgical resections respectively defined as non-inflamed and inflamed after pathology examination. **(C)** Representative dot plots of the gating strategy used to sort indicated cell subsets from mesenteric lymph nodes (MLN) of CD patients. **(D)** *IL22RA2* expression was analyzed by RT-qPCR in indicated FACS-sorted cell subsets from CD patient MLNs (n=5) with inflamed ileum (circles) or colon (square). **(E)** Levels of soluble CCL11 were quantified in gut endoscopic biopsy supernatants from controls (Ctrls) (n=12) and CD (n=37) patients after 6 hours of ex vivo culture. Dots and squares refer to ileum and colon tissues respectively. **(F)** Representative pictures of slides from formalin-fixed, paraffin-embedded (FFPE) sections of CD tissues stained with standard hematoxylin and eosin (HES) coloration. Original magnification x 200. **(G)** Eosinophil counts were scored in a blinded manner by a trained pathologist on HES slides from CD patients (n=36). Each count was obtained by averaging the results obtained from the analysis of 5 different fields and was expressed as eosinophils per mm^2. **(H)** Comparison of soluble IL-22BP levels in the supernatant of endoscopic colonic biopsies of CD patients stratified into eosinophils $(EOS)^{high}$ and EOS^{low} based on the median value. Mean comparisons of unpaired samples were performed using the Kruskal Wallis (for > 2 conditions) or the Mann-Whitney U-test. P-value < 0.05 were considered statistically significant. *P < 0.05, **P < 0.01, ***P < 0.001 ns, not significant.

cytokines sharing similar regulation of expression as IL-22BP (Figure 3A). The strongest correlate of IL-22BP secreted levels was CCL24 (aka. eotaxin-2; spearman r=0,7; P<0,0001). Accordingly, the median-based stratification of CD patients based on their CCL24 levels in the colon showed that almost all $CCL24^{low}$ patients had IL-22BP levels below the lower limit of quantification, while it was the opposite for $CCL24^{high}$ patients (Figure 3B). We thus compared *CCL24* expression between T cells and MNP isolated from the CD lamina propria. The highest levels were detected in MNP (Figure 3C), which suggested they could be the privileged source responsible for heterogenous IL-22BP secreted levels across colonic CD patients.

In an attempt to further refine the nature of a possible MNP subset producing both IL-22BP and CCL24, we reanalyzed a CD single-cell RNA-sequencing (scRNA-seq) dataset we published recently (30). While the contribution of eosinophils could not be evaluated in these data because of known technical limitations to capture intestinal granulocytes with the scRNAseq 10x Genomics Chromium Single Cell 3' v2 Chemistry [see (30, 31)], our analysis confirmed the highest expression levels of *IL22RA2* were present in MNP populations of DCs followed by lymphocyte populations including Type 3 cytokine-producing T cells, while *CCL24* was preferentially detected in macrophages (Figure 3D) (see (30) for detailed description about cluster annotations). Interestingly, only monocyte-derived dendritic cells (moDC) displayed shared detectable expression of both genes (Figure 3D), and we validated that moDC differentiated *ex vivo* co-secreted IL-22BP and CCL24 (Figures 3E–G). Importantly, we previously showed that retinoic acid (RA) was a potent inducer of *IL22RA2* expression in moDC (16), which we could further confirm at the protein level in moDC supernatants (Figures 3E, F). Rather interestingly, the same held true for CCL24 (Figure 3G), suggesting IL-22BP and CCL24 inductions could share similar regulatory pathways, such as RA activity in moDC. In turn, the activation of moDC with LPS for 24h had no effect on CCL24 secreted levels but decreased the production of IL-22BP (Figures 3E, F), hence supporting ours and others previous observations (16, 32).

Other myeloid-derived cytokines showed significant positive correlations with IL-22BP, though weaker than for CCL24 (Spearman; P <0,05) (Figure 3A). These included IL-6, IL-27 and IL-23, the most potent inducer of IL-22 in $CD4^+$ T cells and ILC3 (33, 34). Concordantly, IL-22 correlated with IL-22BP and was also increased in $CCL24^{high}$ patients, hence leading to similar IL-22/IL-22BP ratios between the two subgroups of $CCL24^{high}$ and $CCL24^{low}$ patients (Figures 3H, I). The co-regulation of IL-22/IL-22BP secretion in the colon of CD patients was in agreement with previous results we and others reported in IBD (14, 15). Because $CD4^+$ T cells also produce IL-22BP in IBD tissues (15), it is thus possible that Type 3 cytokine-producing T cells contribute to increase both IL-22 and IL-22BP levels in the colon of CD patients.

Higher levels of IL-22BP are detected in the colon of actively smoking CD patients

Finally, we analyzed IL-22BP secretion in the colon of CD patients based on their smoking status. The production of IL-22BP was significantly higher in actively smoking patients (Figure 3J). A role for tobacco smoking has been suggested for the reprogramming of macrophages into the production of more immunoregulatory molecules, including CCL24 among others (corresponding to *in vitro* so-called "M2" macrophages) (35–37). Because a strong association existed between IL-22BP and CCL24 secretions in CD colons, we compared the proportions of smokers and non-smokers between $CCL24^{high}$ and $CCL24^{low}$ CD patients and verified an enrichment of smokers in the $CCL24^{high}$ subgroup, though not reaching statistical significance (Figure 3K). While this would deserve further investigations, it is thus possible that tobacco-derived metabolites be part of the signals shaping moDC toward higher production of IL-22BP and CCL24 in the CD colon.

Discussion

Our understanding of the pathophysiological functions assumed by the IL-22/IL-22BP axis in IBD is currently described in a rather homogenous way, frequently intermixing conclusions obtained from mouse and human studies, and including results generated in both CD and UC. By providing new insights focused on a more detailed characterization of IL-22BP biology in tissues from CD patients specifically, our study unravels a more complex picture arguing against a such generalization. Our work reveals that the distribution of IL-22BP production is not homogenous between CD patients and we suggest this could be the product of multiple factors related to IL-22BP complex biology in the human gut. First, we show that IL-22BP levels are higher in both control and inflamed ileums when comparing to control and inflamed colons of CD patients respectively, and we suggest this could be explained by distinct homeostatic distributions of gut resident-eosinophils between the two segments. This is of particular relevance as the injection of recombinant IL-22 is currently under evaluation in IBD clinical trials (NCT03650413), and it is thus unclear whether the IL-22BP-rich environment created in the ileum could lead to more interference with the biological actions of the drug in involved ileum vs. colon of CD patients. In addition, our data suggest that a raise of IL-22 bioactivity is more likely to be achieved in inflammatory responses developing in the colon, hence indicating that greater clinical benefits of IL-22 injections may nevertheless be expected in involved ileums of CD patients. More human studies will be needed to address this important question, as we previously showed that lL-22BP expression in

10.3389/fimmu.2022.1034570

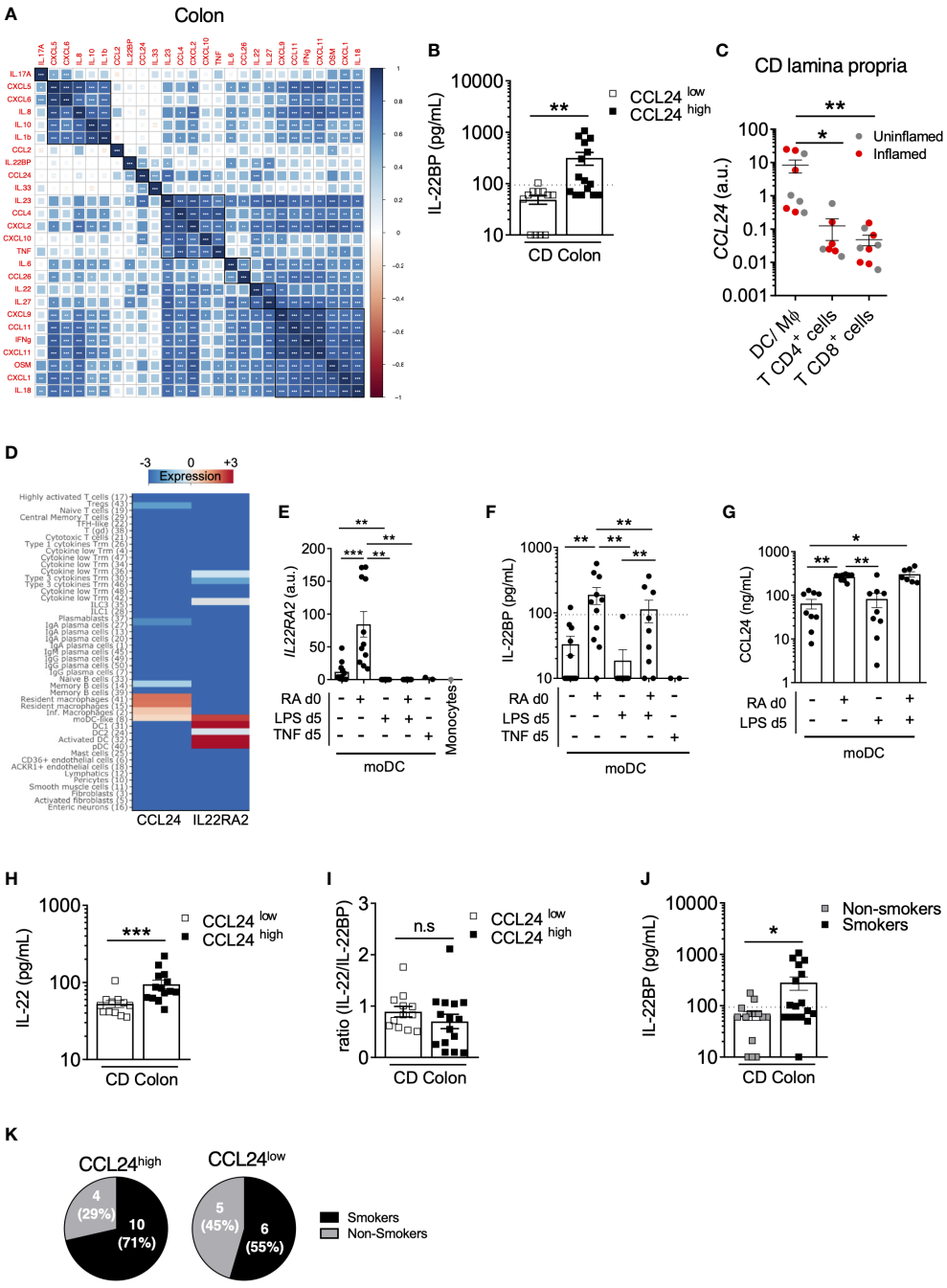

FIGURE 3
IL22BP levels correlate with CCL24 produced by monocyte-derived dendric cells in the CD colon. **(A)** Spearman correlation and hierarchical clustering of indicated cytokines quantified in culture supernatants of endoscopic colonic biopsies from 28 CD patients. **(B)** Comparison of soluble IL-22BP levels in CD patients stratified into CCL24^{low} and CCL24^{high} patients based on the median level. **(C)** *CCL24* expression was analyzed by RT-qPCR on FACS-sorted cells from CD lamina propria, as in Figure 2A. **(D)** Heatmap representing the expression of *IL22RA2* and *CCL24* in indicated cell types using the clustering analysis of a previously published single-cell RNA-sequencing (scRNA-seq) dataset (Martin JC, Cell, 2019). **(E–G)** Human blood classical monocytes from healthy donors were differentiated into monocyte-derived DC (moDC) with GM-CSF and IL-4 for 6 days in the presence of indicated ligands. At day 6 of culture *IL22RA2* mRNA expression was analyzed by RT–qPCR in moDC **(E)**, and levels of IL-22BP **(F)** and CCL24 **(G)** were quantified in culture supernatants. **(H, I)** Comparison of soluble IL-22 **(H)** and IL-22/IL-22BP ratios **(I)** in culture supernatants of colonic CD biopsies from CCL24^{high} or CCL24^{low} patients. **(J)** Comparison of soluble IL-22BP levels in culture supernatants of colonic CD biopsies (n=32) from patients stratified according to their smoking status. **(K)** Pie charts representing the proportion of active smokers vs. non-smokers in the colon of CCL24^{high} or CCL24^{low} CD patients. *P < 0.05, **P < 0.01, ***P < 0.001 ns, not significant.

gut resident-eosinophils is a feature not conserved in rodents (14). The reason why IL-22 is not induced in inflamed ileums despite higher homeostatic production in control tissues would also deserve more investigations. Beyond the difference of IL-22BP production created by regional specializations across gut segments, we also uncover additional heterogeneity in inflamed colons of CD patients. In particular, we observe a strong correlation between IL-22BP and CCL24 secretion and suggest this could be the consequence of a shared production by moDC with variable intensity across subsets of patients. Importantly, while, CCL24 was initially described as an eosinophil chemoattractant trough the receptor CCR3, experiments in rodents suggested it was not involved in eosinophil infiltration during colitis (29, 38). Our data further suggest that IL-22BP variability among inflamed CD colons was likely not explained by the level of infiltration of blood-derived eosinophils but relied more on other IL-22BP cellular sources such as moDC. CCR3 is also expressed by subsets of T cells (39) and it is possible that CCL24-mediated T cell infiltration participates to the total production of IL-22BP in the colon of CD patients (15).

Importantly, three isoforms of IL-22BP exist in humans (11). Experimental evidences suggest that contrary to isoforms 2 and 3, IL-22BP isoform 1 is not spontaneously secreted owing to the presence of an additional 32-amino acids exon responsible for endoplasmic reticulum retention (20, 32, 40). Intracellular isoform 1 is in fact proposed to participate in the regulation of the unfolded protein response (20). Both isoforms 2 and 3, however, can antagonize IL-22, isoform 2 being the most potent, hence indicating secreted IL-22BP is necessarily bioactive (32). We showed in our previous studies that gut DC/Macs and eosinophils, as well as monocyte-derived dendritic cells dominantly express IL-22BP bioactive isoform 2, and to a lower extent isoform 1, but not isoform 3 (14, 16). Overall, this indicates that all three subsets produce bioactive IL-22BP, dominantly through their expression of IL-22BP isoform 2.

Supporting the existence of similar regulatory pathways for both IL-22BP and CCL24 in inflamed CD colons, we report that retinoic acid increases the secretion of both proteins by moDC. As suggested by the higher IL-22BP levels we noticed in tobacco smokers, it is likely that additional factors contribute to differential regulations of IL-22BP production across patients. In that regard, it is interesting to note that IL-22BP levels also correlated with those of IL-22 and IL-23, the main driver of IL-22 expression in lymphocytes. Recent evidence suggests that lymphotoxin (LT)α1β2 upregulates IL-22BP *via* the noncanonical NF-κB pathway in moDC (19). Because NF-κB is involved in the generation of IL-22-producing T cells, in part indirectly through the induction of IL-23 secretion in MNP (41), one may speculate that privileged cellular circuits exist in inflamed colons of a subset of CD patients, in which LTα1β2 from CD4 T cells drives both IL-22BP and IL-23 expression in moDC (42, 43). The latter in turn can promote IL-22 production in CD4 T cells. While this would deserve further investigations, specific cellular niches in subsets of CD patients could thus participate to increase both IL-22 and IL-22BP global levels associated with a more localized impact on epithelial cell biology (44). Clarifying the existence, tissue distribution and pathophysiological actions of such cellular circuits would be especially relevant in light of the upcoming IL-23 blockers in the CD therapeutic armamentarium (45, 46).

In conclusion, our work provides new important information about the biology of IL-22BP in CD, which can open the way to therapeutically relevant future studies with regard to the modulation of the IL-22/IL-22BP axis in patients.

Data availability statement

The original contributions presented in the study are included in the article/Supplementary Material. Further inquiries can be directed to the corresponding authors.

Ethics statement

The studies involving human participants were reviewed and approved by Centre de Protection des Personnes Ouest IV - CHU de Nantes. The patients/participants provided their written informed consent to participate in this study.

Author contributions

JCM, RJ, and AF designed experiments and interpreted the data; JCM wrote the manuscript; AF, RJ, and JCM edited the manuscript; AF, EL, TL, LD, SB, and GB performed experiments and analyses; CB and NS performed cytokine multiplex assays; EM and AM performed *in vitro* moDC experiments; JP and AB managed the biobank and selected the patients included in the study. All authors contributed to the article and approved the submitted version.

Acknowledgments

The authors warmly thank Dr Mathieu Uzzan (Hopital Henri Mondor, Assistance Publique-Hôpitaux de Paris) for his critical reading of the manuscript and meaningful comments. The authors also warmly thank Dr Ephraim Kenigsberg (Icahn School of Medicine at Mount Sinai, New York, NY) for his critical help with statistical analyses. This work was supported

by grants Association Francois Aupetit (AFA), the European Crohn and Colitis Organization (ECCO), and Région Pays de la Loire (INSET) to RJ. JCM is supported by NExT "Junior Talent" and ANR JCJC (ANR-20-CE17-0009). AF was supported by a fellowship from CHU de Nantes ("Année supplémentaire d'Internat").

Conflict of interest

The authors declare that the research was conducted in the absence of any commercial or financial relationships that could be construed as a potential conflict of interest.

Publisher's note

Supplementary Material

The Supplementary Material for this article can be found online at: https://www.frontiersin.org/articles/10.3389/fimmu.2022.1034570/full#supplementary-material

SUPPLEMENTARY TABLE 1
Clinical characteristic of controls and Crohn's disease patients cohort 1.

SUPPLEMENTARY TABLE 2
Clinical characteristic of Crohn's disease patients cohort 2.

SUPPLEMENTARY FIGURE 1
(A, B) Representative dot plots showing the post-sort purity of indicated cell subsets sorted from the lamina propria of intestinal surgical resections **(A)** and mesenteric lymph nodes (MLN) **(B)** of CD patients. **(C)** Representative IFI pictures of slides from formalin-fixed, paraffin-embedded (FFPE) sections of CD MLN stained with mAbs against IL-22BP (red) and CD3 (green), as well as with DAPI (blue) (n=3 CD patients). Original magnification x 630. **(D–G)** Indicated T cell subsets were sorted from CD lamina propria intestinal surgical resections (n=5) **(D, F)** and MLN (n=3) **(E, G)** and cultured with or without PMA (50ng/mL) and Ionomycin (250ng/mL) (PMA/Iono). After 20 hours, expressions of *IL2RA* **(D–E)** and *IL22RA2* **(F–G)** were analyzed by RT-qPCR. IL22RA2 expression levels of freshly isolated DC/Macrophages and eosinophils are indicated for reference. Means comparisons were performed with the Kruskal–Wallis test for unpaired samples and with the Wilcoxon test for paired samples. P-value < 0.05 were considered statistically significant. CD: Crohn's disease; DC: dendritic cells, EOS: eosinophils; Mθ: macrophages.

References

1. Baumgart DC, Sandborn WJ. Inflammatory bowel disease: clinical aspects and established and evolving therapies. *Lancet* (2007) 369:1641–57. doi: 10.1016/S0140-6736(07)60751-X

2. Graham DB, Xavier RJ. Pathway paradigms revealed from the genetics of inflammatory bowel disease. *Nature* (2020) 578:527–39. doi: 10.1038/s41586-020-2025-2

3. Keir ME, Yi T, Lu TT, Ghilardi N. The role of IL-22 in intestinal health and disease. *J Exp Med* (2020) 217:1-9. doi: 10.1084/jem.20192195

4. Mizoguchi A, Yano A, Himuro H, Ezaki Y, Sadanaga T, Mizoguchi E. Clinical importance of IL-22 cascade in IBD. *J Gastroenterol* (2018) 53:465–74. doi: 10.1007/s00535-017-1401-7

5. Geremia A, Arancibia-Cárcamo CV, Fleming MPP, Rust N, Singh B, Mortensen NJ, et al. IL-23-responsive innate lymphoid cells are increased in inflammatory bowel disease. *J Exp Med* (2011) 208:1127–33. doi: 10.1084/jem.20101712

6. Zheng Y, Valdez PA, Danilenko DM, Hu Y, Sa SM, Gong Q, et al. Interleukin-22 mediates early host defense against attaching and effacing bacterial pathogens. *Nat Med* (2008) 14:282–9. doi: 10.1038/nm1720

7. Sugimoto K, Ogawa A, Mizoguchi E, Shimomura Y, Andoh A, Bhan AK, et al. IL-22 ameliorates intestinal inflammation in a mouse model of ulcerative colitis. *J Clin Invest* (2008) 118:534–44. doi: 10.1172/JCI33194

8. Lindemans CA, Calafiore M, Mertelsmann AM, O'Connor MH, Dudakov JA, Jenq RR, et al. Interleukin-22 promotes intestinal-stem-cell-mediated epithelial regeneration. *Nature* (2015) 528:560–4. doi: 10.1038/nature16460

9. Hernandez P, Gronke K, Diefenbach A. A catch-22: Interleukin-22 and cancer. *Eur J Immunol* (2018) 48:15–31. doi: 10.1002/eji.201747183

10. Kirchberger S, Royston DJ, Boulard O, Thornton E, Franchini F, Szabady RL, et al. Innate lymphoid cells sustain colon cancer through production of interleukin-22 in a mouse model. *J Exp Med* (2013) 210:917–31. doi: 10.1084/jem.20122308

11. Dumoutier L, Lejeune D, Colau D, Renauld JC. Cloning and characterization of IL-22 binding protein, a natural antagonist of IL-10-related T cell-derived inducible factor/IL-22. *J Immunol* (2001) 166:7090–5. doi: 10.4049/jimmunol.166.12.7090

12. Huber S, Gagliani N, Zenewicz LA, Huber FJ, Bosurgi L, Hu B, et al. IL-22BP is regulated by the inflammasome and modulates tumorigenesis in the intestine. *Nature* (2012) 491:259–63. doi: 10.1038/nature11535

13. Martin JC, Wolk K, Bériou G, Abidi A, Witte-Händel E, Louvet C, et al. Limited presence of IL-22 binding protein, a natural IL-22 inhibitor, strengthens psoriatic skin inflammation. *J Immunol* (2017) 198:3671–8. doi: 10.4049/jimmunol.1700021

14. Martin JC, Bériou G, Heslan M, Bossard C, Jarry A, Abidi A, et al. IL-22BP is produced by eosinophils in human gut and blocks IL-22 protective actions during colitis. *Mucosal Immunol* (2016) 9:539–49. doi: 10.1038/mi.2015.83

15. Pelczar P, Witkowski M, Perez LG, Kempski J, Hammel AG, Brockmann L, et al. A pathogenic role for T cell-derived IL-22BP in inflammatory bowel disease. *Science* (2016) 354:358–62. doi: 10.1126/science.aah5903

16. Martin JCJ, Bériou G, Heslan M, Chauvin C, Utriainen L, Aumeunier A, et al. Interleukin-22 binding protein (IL-22BP) is constitutively expressed by a subset of conventional dendritic cells and is strongly induced by retinoic acid. *Mucosal Immunol* (2014) 7:101–13. doi: 10.1038/mi.2013.28

17. Jinnohara T, Kanaya T, Hase K, Sakakibara S, Kato T, Tachibana N, et al. IL-22BP dictates characteristics of peyer's patch follicle-associated epithelium for antigen uptake. *J Exp Med* (2017) 214:1607–18. doi: 10.1084/jem.20160770

18. Savage AK, Liang H-E, Locksley RM. The development of steady-state activation hubs between adult LTi ILC3s and primed macrophages in small intestine. *J Immunol* (2017) 199:1912–22. doi: 10.4049/jimmunol.1700155

19. Kempski J, Giannou AD, Riecken K, Zhao L, Steglich B, Lücke J, et al. IL22BP mediates the antitumor effects of lymphotoxin against colorectal tumors in mice and humans. *Gastroenterology* (2020) 159:1417–1430.e3. doi: 10.1053/j.gastro.2020.06.033

20. Gómez-Fernández P, Urtasun A, Paton AW, Paton JC, Borrego F, Dersh D, et al. Long interleukin-22 binding protein isoform-1 is an intracellular activator of the unfolded protein response. *Front Immunol* (2018) 9:2934. doi: 10.3389/fimmu.2018.02934

21. Dudakov JA, Hanash AM, van den Brink MRM. Interleukin-22: immunobiology and pathology. *Annu Rev Immunol* (2015) 33:747–85. doi: 10.1146/annurev-immunol-032414-112123

22. Krämer B, Goeser F, Lutz P, Glässner A, Boesecke C, Schwarze-Zander C, et al. Compartment-specific distribution of human intestinal innate lymphoid cells is altered in HIV patients under effective therapy. *PloS Pathog* (2017) 13:e1006373. doi: 10.1371/journal.ppat.1006373

23. Adar T, Shteingart S, Ben Ya'acov A, Bar-Gil Shitrit A, Goldin E. From airway inflammation to inflammatory bowel disease: eotaxin-1, a key regulator of intestinal inflammation. *Clin Immunol* (2014) 153:199–208. doi: 10.1016/j.clim.2014.04.012

24. Matsushita T, Maruyama R, Ishikawa N, Harada Y, Araki A, Chen D, et al. The number and distribution of eosinophils in the adult human gastrointestinal tract: a study and comparison of racial and environmental factors. *Am J Surg Pathol* (2015) 39:521–7. doi: 10.1097/PAS.0000000000000370

25. DeBrosse CW, Case JW, Putnam PE, Collins MH, Rothenberg ME. Quantity and distribution of eosinophils in the gastrointestinal tract of children. *Pediatr Dev Pathol* (2006) 9:210–8. doi: 10.2350/11-05-0130.1

26. Loktionov A. Eosinophils in the gastrointestinal tract and their role in the pathogenesis of major colorectal disorders. *World J Gastroenterol* (2019) 25:3503–26. doi: 10.3748/wjg.v25.i27.3503

27. Lampinen M, Waddell A, Ahrens R, Carlson M, Hogan SP. CD14+CD33+ myeloid cell-CCL11-eosinophil signature in ulcerative colitis. *J Leukoc Biol* (2013) 94:1061–70. doi: 10.1189/jlb.1212640

28. Adar T, Shteingart S, Ben-Ya'acov A, Shitrit AB-G, Livovsky DM, Shmorak S, et al. The importance of intestinal eotaxin-1 in inflammatory bowel disease: New insights and possible therapeutic implications. *Dig Dis Sci* (2016) 61:1915–24. doi: 10.1007/s10620-016-4047-z

29. Ahrens R, Waddell A, Seidu L, Blanchard C, Carey R, Forbes E, et al. Intestinal Macrophage/Epithelial cell-derived CCL11/Eotaxin-1 mediates eosinophil recruitment and function in pediatric ulcerative colitis. *J Immunol* (2008) 181:7390–9. doi: 10.4049/jimmunol.181.10.7390

30. Martin JC, Chang C, Boschetti G, Ungaro R, Giri M, Grout JA, et al. Single-cell analysis of crohn's disease lesions identifies a pathogenic cellular module associated with resistance to anti-TNF therapy. *Cell* (2019) 178:1493–1508.e20. doi: 10.1016/j.cell.2019.08.008

31. Smillie CS, Biton M, Ordovas-Montanes J, Sullivan KM, Burgin G, Graham DB, et al. Intra- and inter-cellular rewiring of the human colon during ulcerative colitis. *Cell* (2019) 178:714–730.e22. doi: 10.1016/j.cell.2019.06.029

32. Lim C, Hong M, Savan R. Human IL-22 binding protein isoforms act as a rheostat for IL-22 signaling. *Sci Signal* (2016) 9:ra95. doi: 10.1126/scisignal.aad9887

33. Rutz S, Eidenschenk C, Ouyang W. IL-22, not simply a Th17 cytokine. *Immunol Rev* (2013) 252:116–32. doi: 10.1111/imr.12027

34. Wolk K, Kunz S, Asadullah K, Sabat R. Cutting edge: immune cells as sources and targets of the IL-10 family members? *J Immunol* (2002) 168:5397–402. doi: 10.4049/jimmunol.168.11.5397

35. Yang DC, Chen C-H. Cigarette smoking-mediated macrophage reprogramming: Mechanistic insights and therapeutic implications. *J Nat Sci* (2018) 4:e539.

36. Lee SH, Chaves MM, Kamenyeva O, Gazzinelli-Guimaraes PH, Kang B, Pessenda G, et al. M2-like, dermal macrophages are maintained *via* IL-4/CCL24-mediated cooperative interaction with eosinophils in cutaneous leishmaniasis. *Sci Immunol* (2020) 5:eaaz4415. doi: 10.1126/sciimmunol.aaz4415

37. Murray PJ, Allen JE, Biswas SK, Fisher EA, Gilroy DW, Goerdt S, et al. Macrophage activation and polarization: nomenclature and experimental guidelines. *Immunity* (2014) 41:14–20. doi: 10.1016/j.immuni.2014.06.008

38. Forssmann U, Uguccioni M, Loetscher P, Dahinden CA, Langen H, Thelen M, et al. Eotaxin-2, a novel CC chemokine that is selective for the chemokine receptor CCR3, and acts like eotaxin on human eosinophil and basophil leukocytes. *J Exp Med* (1997) 185:2171–6. doi: 10.1084/jem.185.12.2171

39. Sallusto F, Mackay CR, Lanzavecchia A. Selective expression of the eotaxin receptor CCR3 by human T helper 2 cells. *Science* (1997) 277:2005–7. doi: 10.1126/science.277.5334.2005

40. Gómez-Fernández P, Urtasun A, Astobiza I, Mena J, Alloza I, Vandenbroeck K. Pharmacological targeting of the ER-resident chaperones GRP94 or cyclophilin b induces secretion of IL-22 binding protein isoform-1 (IL-22BPi1). *Int J Mol Sci* (2019) 20:1-13. doi: 10.3390/ijms20102440

41. Liu T, Zhang L, Joo D, Sun S-C. NF-κB signaling in inflammation. *Sig Trans Target Ther* (2017) 2:1–9. doi: 10.1038/sigtrans.2017.23

42. Upadhyay V, Poroyko V, Kim T, Devkota S, Fu S, Liu D, et al. Lymphotoxin regulates commensal responses to enable diet-induced obesity. *Nat Immunol* (2012) 13:947–53. doi: 10.1038/ni.2403

43. Upadhyay V, Fu Y-X. Lymphotoxin organizes contributions to host defense and metabolic illness from innate lymphoid cells. *Cytokine Growth Factor Rev* (2014) 25:227–33. doi: 10.1016/j.cytogfr.2013.12.007

44. Macho-Fernandez E, Koroleva EP, Spencer CM, Tighe M, Torrado E, Cooper AM, et al. Lymphotoxin beta receptor signaling limits mucosal damage through driving IL-23 production by epithelial cells. *Mucosal Immunol* (2015) 8:403–13. doi: 10.1038/mi.2014.78

45. Sands BE, Peyrin-Biroulet L, Kierkus J, Higgins PDR, Fischer M, Jairath V, et al. Efficacy and safety of mirikizumab in a randomized phase 2 study of patients with crohn's disease. *Gastroenterology* (2022) 162:495–508. doi: 10.1053/j.gastro.2021.10.050

46. Bossuyt P, Ferrante M, Baert F, Danese S, Feagan BG, Loftus EVJr., et al. OP36 risankizumab therapy induces improvements in endoscopic endpoints in patients with moderate-to-Severe crohn's disease: Results from the phase 3 ADVANCE and MOTIVATE studies. *J Crohn's Colitis* (2021) 15:S033–4. doi: 10.1093/ecco-jcc/jjab075.035

frontiers | Frontiers in Immunology

TYPE Original Research
PUBLISHED 19 April 2023
DOI 10.3389/fimmu.2023.1040493

OPEN ACCESS

EDITED BY
Marita Troye Blomberg,
Stockholm University, Sweden

REVIEWED BY
Mikael Adner,
Karolinska Institutet (KI), Sweden
Vadim Pivniouk,
The University of Arizona, United States

*CORRESPONDENCE
Olga Krysko
olga.krysko@uzgent.be

†PRESENT ADDRESS
Olga Krysko,
Department of Laboratory Medicine, Ghent University Hospital, Ghent, Belgium and Cell Death Investigation and Therapy (CDIT) Laboratory, Department of Human Structure and Repair, Ghent University, Ghent, Belgium

SPECIALTY SECTION
This article was submitted to Cytokines and Soluble Mediators in Immunity, a section of the journal Frontiers in Immunology

RECEIVED 09 September 2022
ACCEPTED 27 March 2023
PUBLISHED 19 April 2023

CITATION
Krysko O, Korsakova D, Teufelberger A, De Meyer A, Steels J, De Ruyck N, van Ovost J, Van Nevel S, Holtappels G, Coppieters F, Ivanchenko M, Braun H, Vedunova M, Krysko DV and Bachert C (2023) Differential protease content of mast cells and the processing of IL-33 in *Alternaria alternata* induced allergic airway inflammation in mice.
Front. Immunol. 14:1040493.
doi: 10.3389/fimmu.2023.1040493

Differential protease content of mast cells and the processing of IL-33 in *Alternaria alternata* induced allergic airway inflammation in mice

Olga Krysko[1*†], Darya Korsakova[2], Andrea Teufelberger[1,3], Amse De Meyer[1], Jill Steels[1], Natalie De Ruyck[1], Judith van Ovost[1], Sharon Van Nevel[1], Gabriele Holtappels[1], Frauke Coppieters[4], Mikhail Ivanchenko[5], Harald Braun[6,7], Maria Vedunova[2], Dmitri V. Krysko[8,9] and Claus Bachert[1,10,11]

[1]Upper Airways Research Laboratory, Department of Head and Skin, Ghent University, Ghent, Belgium, [2]Institute of Biology and Biomedicine, National Research Lobachevsky State University of Nizhny Novgorod, Nizhny Novgorod, Russia, [3]Department of Dermatology and Venereology, Medical University of Graz, Graz, Austria, [4]Center for Medical Genetics Ghent (CMGG), Department of Biomolecular Medicine, Ghent University, Ghent, Belgium, [5]Institute of Information Technology, Mathematics and Mechanics, National Research Lobachevsky State University of Nizhny Novgorod, Nizhny Novgorod, Russia, [6]Unit for Structural Biology, VIB-UGent Center for Inflammation Research, Ghent University, Ghent, Belgium, [7]Unit for Structural Biology, Department of Biochemistry and Microbiology, Ghent University, Ghent, Belgium, [8]Cell Death Investigation and Therapy Laboratory, Department of Human Structure and Repair, Ghent University, Ghent, Belgium, [9]Department of Pathophysiology, Sechenov First Moscow State Medical University (Sechenov University), Moscow, Russia, [10]Department of Otorhinolaryngology - Head and Neck Surgery, University Hospital of Münster, Münster, Germany, [11]First Affiliated Hospital, Sun Yat-Sen University, International Airway Research Center, Guangzhou, China

Background: Recent *in vitro* studies strongly implicated mast cell-derived proteases as regulators of IL-33 activity by enzymatic cleavage in its central domain. A better understanding of the role of mast cell proteases on IL-33 activity *in vivo* is needed. We aimed to compare the expression of mast cell proteases in C57BL/6 and BALB/c mice, their role in the cleavage of IL-33 cytokine, and their contribution to allergic airway inflammation.

Results: *In vitro*, full-length IL-33 protein was efficiently degraded by mast cell supernatants of BALB/c mice in contrast to the mast cell supernatants from C57BL/6 mice. RNAseq analysis indicated major differences in the gene expression profiles of bone marrow-derived mast cells from C57BL/6 and BALB/c mice. In *Alternaria alternata (Alt)* - treated C57BL/6 mice the full-length form of IL-33 was mainly present, while in BALB/c mice, the processed shorter form of IL-33 was more prominent. The observed cleavage pattern of IL-33 was associated with a nearly complete lack of mast cells and their proteases in the lungs of C57BL/6 mice. While most inflammatory cells were similarly increased in *Alt*-treated C57BL/6 and BALB/c mice, C57BL/6 mice had significantly more eosinophils in the bronchoalveolar lavage fluid and IL-5 protein levels in their lungs than BALB/c mice.

10.3389/fimmu.2023.1040493

Conclusion: Our study demonstrates that lung mast cells differ in number and protease content between the two tested mouse strains and could affect the processing of IL-33 and inflammatory outcome of *Alt* -induced airway inflammation. We suggest that mast cells and their proteases play a regulatory role in IL-33-induced lung inflammation by limiting its proinflammatory effect *via* the IL-33/ST2 signaling pathway.

KEYWORDS

IL-33, mast cells, allergy, type 2 inflammation, protease

Introduction

Asthma is a heterogeneous inflammatory airway disease with different underlying pathophysiologic mechanisms and disease endotypes, which often manifest by similar clinical complaints (1, 2). In mild asthma, mostly the type 2 phenotype, an eosinophilic immune response is observed, while only a minor percentage of patients show a non-type 2 phenotype (3). In severe asthma, a mixed inflammatory phenotype is also characterized by increased IL-33 levels. Of interest, in children, severe asthma is more common in the case of sensitization to the fungus *Alternaria alternata (Alt)* and is strongly associated with increased IL-33 sputum levels (4). In this regard, a clinical trial has shown that IL-33 targeting could efficiently reduce exacerbations in patients with severe asthma (5). In contrast, patients with mild or moderate asthma have less clinical benefit from an IL-33 targeting therapy. IL-33 is an alarmin, which in allergic airway inflammation is mainly secreted by epithelial cells in response to aeroallergens and signals through a cell surface receptor complex of ST2 (IL-1 receptor-like 1, IL1RL1) and IL-1 receptor accessory protein (IL1RAcP) to stimulate cytokine production in type 2 ILCs and T helper 2 cell, inducing the production of IL-4, IL-5, and IL-13 (6–8). Endogenous serine proteases and cysteine proteases, such as calpains, were suggested to regulate the activity of IL-33 *via* enzymatic cleavage (9–11). Recently, we have demonstrated the contribution of neutrophilic proteases in IL-33 processing in an allergic asthma mouse model using *Alt* (12). IL-33 is produced as a full-length protein lacking a signal sequence by a not entirely clear release mechanism. The cleavage of full-length IL-33 (IL-33_{FL}) by human mast cell tryptase, chymase, and cathepsin G *in vitro* results in cleaved IL-33 (IL-33_{C}), which is up to 30-fold more potent towards innate lymphoid cells type 2 (ILC2s) (9). It is known that the functional, inflammatory parameters in severe asthma are linked to the presence of activated mast cells (13–15) which, *via* their release of cytokines, proteases, and alarmins, could potentially contribute to the persistence and the exacerbation of the airway inflammation (13, 16, 17); and possibly to the loss of corticosteroid sensitivity in severe asthma (18). In asthmatic patients, bronchoalveolar lavage fluid (BALF) contains increased levels of tryptase (19, 20). The presence of an active form of IL-33 acting on ST2-expressing immune cells could contribute to the sustained type 2 immune response in the airway epithelium (8, 21). Remarkably, in humans, the phenotype of mast cells seems to be different in the same disease with different inflammatory profiles: In mild asthma, tryptase-positive mast cells localize in the submucosa while in severe asthma, mast cells are mostly localized in the airway submucosa and epithelium and express chymase (13, 20). We showed earlier that different inbred mouse strains respond differently to an IL-33 mediated asthma model, using the bacterial allergen, *S. aureus* protease-like protein D (22).

In the current study, we analysed the link between the type of inflammatory response towards *Alt* and the characteristics of mast cells in the two inbred mouse strains C57BL/6 and BALB/c. The strain-dependent mast cell heterogeneity in the regulation of IL-33 processing *in vivo* was addressed.

Results

Differential inflammatory response of BALB/c and C57BL/6 mice towards Alt

The IL-33-dependent model of *Alt*-induced airway inflammation was chosen to evaluate an impact on the processing of IL-33 and inflammatory parameters in two commonly used mouse strains (6, 14, 23). C57BL/6 and BALB/c mice received six intratracheal (i.t.) applications of 20 µg *Alt* extract every 48 hours (Figure 1A), in a slightly modified application schedule from our previous work (14). The *Alt*-treated BALB/c and C57BL/6 mice showed higher numbers of total BALF cells compared to PBS-treated mice (Figure 1B). The BALF of *Alt*-treated C57BL/6 mice contained more eosinophils in BALF as compared to *Alt*-treated BALB/c mice (Figures 1C, D). In turn, BALB/c mice had higher neutrophil numbers in the BALF (Figures 1E, F). The percentage of $CD4^+$ (Figure 1G) cells was stronger increased in BALF of BALB/c mice compared to C57BL/6 mice. $CD8^+$ cells were higher in BALF of BALB/c mice (Figure 1H). Furthermore, in the lungs of both mouse strains, marked eosinophilia was observed (Figure 1I), while the percentage of neutrophils remained comparable between *Alt*-treated mice and controls of both mouse strains (Figure 1J). Of note, no major difference in the percentages of lung $CD4^+$ and $CD8^+$ cells was seen (Figures 1K, L). Serum IgE levels were higher in *Alt*-treated mice as compared to PBS -treated controls (Figure 1M).

10.3389/fimmu.2023.1040493

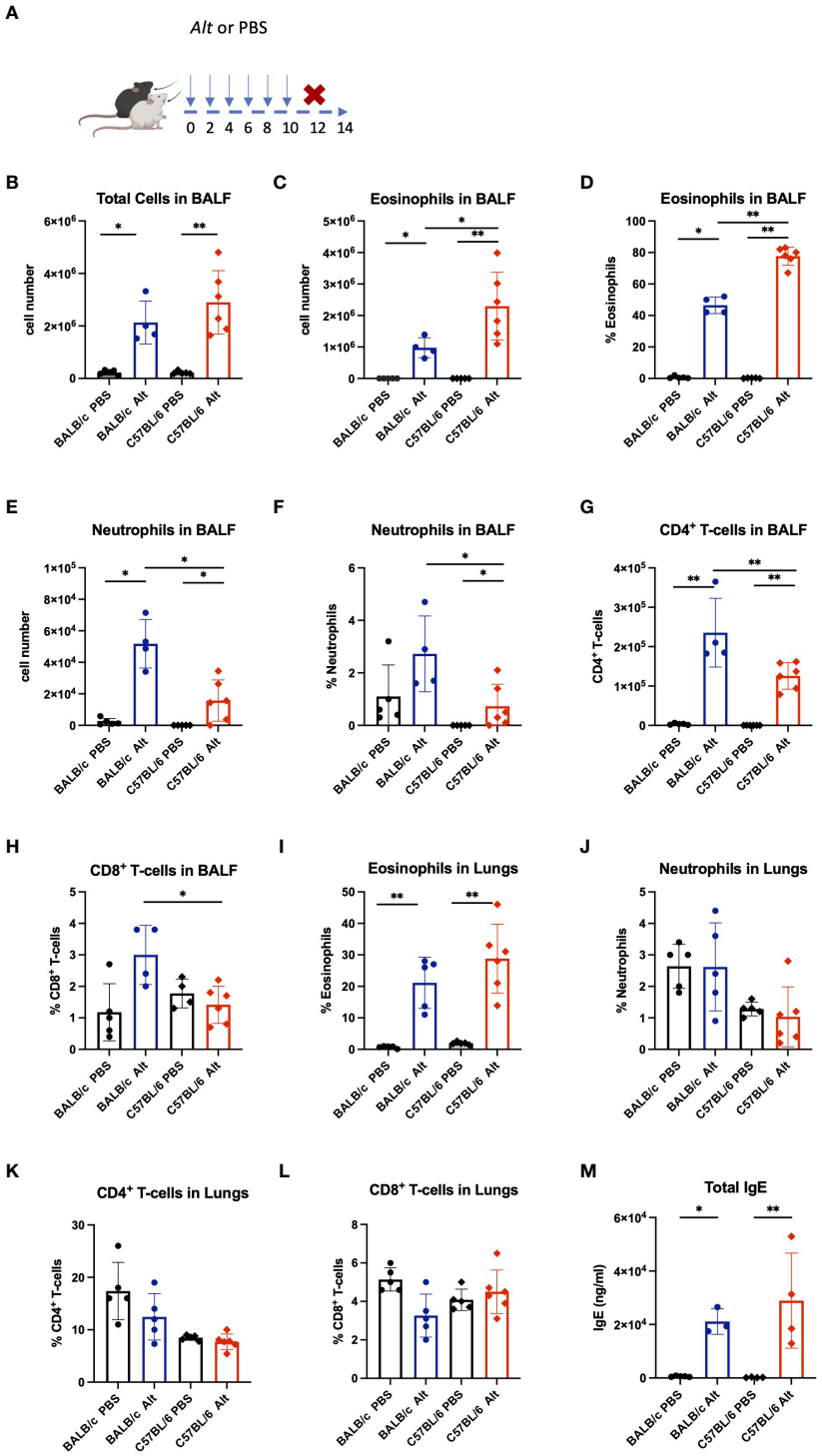

FIGURE 1
BALB/c and C57BL/6 mice were given six intratracheal applications of 20 μg *Alternaria alternata* (*Alt*) extract in PBS, controls received PBS alone. Forty-eight hours after the last application mice were sacrificed, and experimental samples were collected **(A)**. The absolute cell numbers in the bronchial lavage fluid (BALF) are presented for total cell counts **(B)**, eosinophils **(C)** and neutrophils **(E)** in BALF. The percentage of eosinophils **(D)** and neutrophils **(F)** in BALF are presented. The BALF and lungs were analysed by flow cytometry and the infiltration of eosinophils **(I)**, neutrophils **(J)**, $CD4^+$ T cells **(G, K)** and $CD8^+$ T cells **(H, L)** in the BALF and lungs are presented as percentage. Mouse serum was collected 48h following the final *Alt* application and the levels of total IgE in serum were determined using enzyme-linked immunosorbent assay **(M)**. The data are presented as scatter plots ± standard deviation (S.D.). Statistical significance between the groups was determined by one-way ANOVA with Dunn's test for multiple comparisons. N=4-6 per group. *p < 0.05, **p < 0.01.

10.3389/fimmu.2023.1040493

Processing of IL-33 in *Alt*-induced allergic airway inflammation in C57BL/6 and BALB/c mice

Notably, despite the comparable degree of inflammatory response in the lungs of C57BL/6 and BALB/c mice, IL-33 levels were significantly higher in BALB/c than in C57BL/6 (Figure 2A). The expression of a cleaved/mature form of IL-33 (IL-33_C; ~ 18 kDa) was higher in the lungs of BALB/c mice, while in C57BL/6 mice, the non-processed full-length form of IL-33 (IL-33_{FL} ~ 30 kDa) was more abundant (Figures 2B, C). IL-33 positive cells were abundantly present in the lungs of mice after *Alt* treatment (Figure 2D). RT-PCR didn't show differences between both strains in the respective treatment groups in the expression of IL-33 receptor *IL1Rl1* (Figure 2E). Interestingly, IL-5 and IL-13 levels tend to increase in both mouse strains treated with *Alt* (Figures 2F, G), while IL-4 and G-CSF were slightly but not significantly increased in both mouse strains, and IL-25 levels in the lungs were comparable in all experimental groups tested (Figure S1).

Increased mast cell numbers and mast cell protease expression in the lungs of *Alt*-treated BALB/c mice

The lungs of *Alt*-treated BALB/c mice showed increased numbers of mast cells, positive for toluidine blue and chymase compared to PBS controls (Figures 3A-D). In agreement with the immunohistochemical staining, the lungs of BALB/c mice treated with *Alt* extract showed increased expression levels of genes encoding mast cell proteases such as *Mcpt1*, *Mcpt2*, *Mcpt4*, *Tpsab1*, *Tpsb2*, *Cma1*, *Cpa3* (Figures 3E–L). As expected, PBS-treated mice lacking significant numbers of mast cells did not express the proteases mentioned above. Only very few mast cells

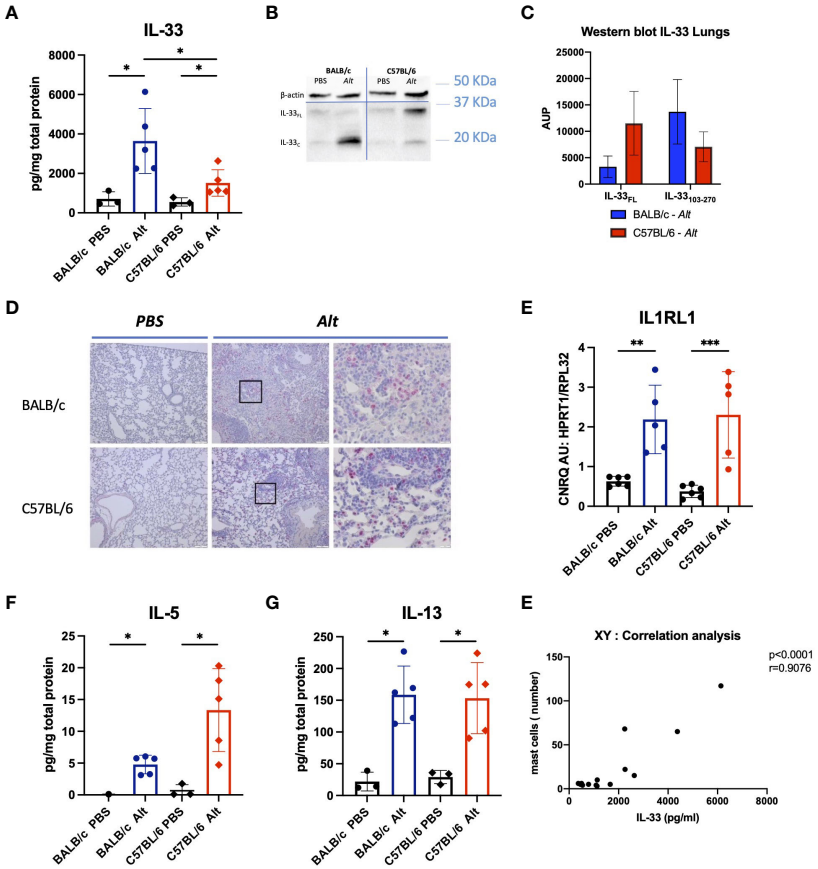

FIGURE 2
The analysis of cytokine response in the lungs of mice with intratracheal applications of 20 μg of *Alt* extract and PBS-treated controls. The levels of IL-33 **(A)** in the lung homogenates were measured by Luminex. Full-length IL-33 (IL-33_{FL}) and cleaved forms (IL-33_C) were analysed by western blotting and one representative blot is shown **(B)** and area under the peak (AUP) was quantified using ImageJ software **(C)**. Representative images of IL-33 immunostaining in the lungs of C57BL/6 and BALB/c treated with PBS or the *Alt* extract for six times every 48 hours **(D)**. *IL1rl1* gene expression levels analysed in lungs by RT-qPCR **(E)**. The levels of IL-5 **(F)**, IL-13 **(G)** in the lung homogenates were measured by Luminex. The data are presented as scatter plot with a bar ± standard deviation (S.D). Statistical significance between the groups was determined by one-way ANOVA with Dunn's test for multiple comparisons. N=4-6 per group. *p < 0.05, **p < 0.01, ***p < 0.001.

10.3389/fimmu.2023.1040493

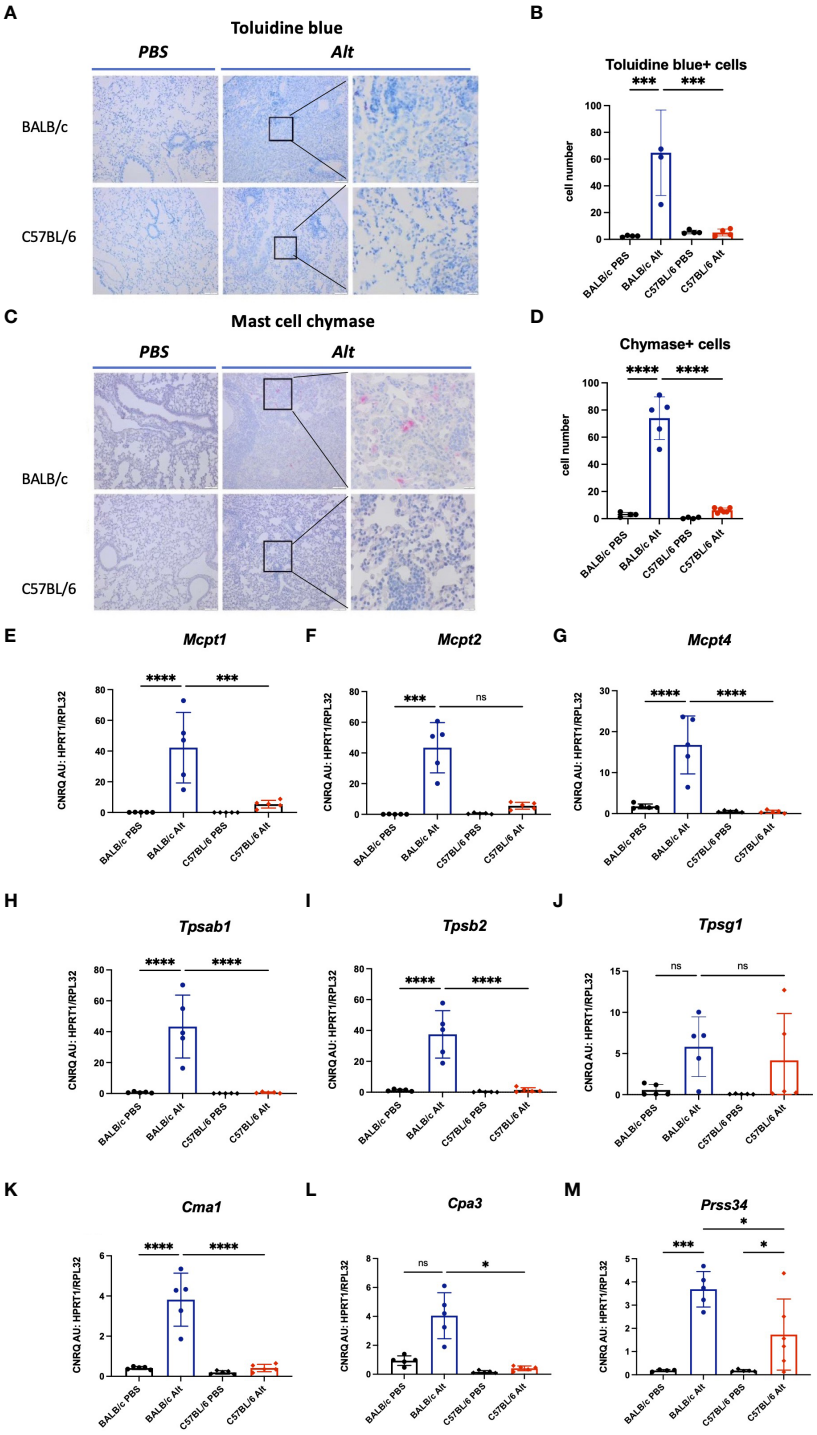

FIGURE 3
To visualize mast cells, formalin-fixed paraffin-embedded lung sections were stained with toluidine blue **(A)** and the number of mast cells was quantified in four different fields per mouse under magnification of forty times **(B)**. Chymase - positive mast cells in the lungs of mice were visualized by immunohistochemistry **(C)** and quantified **(D)**. Expression of mast cell proteases in the lungs of BALB/c and C57BL/6 mice treated with six intratracheal applications of 20 µg *Alt* extract or PBS. Values of gene expression of *Mcpt1* **(E)**, *Mcpt2* **(F)**, *Mcpt4* **(G)**, *Tpsab1* **(H)**, *Tpsab2* **(I)**, *Tpsg1* **(J)**, *Cma1* **(K)**, *Cpa3* **(L)** and *Prss34* **(M)** were normalised using reference genes *Hprt1* and *Rpl32*. The data are presented as scatter plot with a bar ± standard deviation (S.D.). Statistical significance between the groups was determined by one-way ANOVA with Sidak's test for multiple comparisons. n=4-6 per group. *p < 0.05, ***p < 0.001, ****p < 0.0001. ns, not significant.

could be found in the lung sections of PBS or *Alt*-treated C57BL/6 mice demonstrating nearly complete lack of mast cell response in C57BL/6 mice treated with *Alt* extract. The gene expression levels of mast cell proteases in the lungs of *Alt*-treated C57BL/6 mice were almost undetectable. The gene expression levels of *Prss34* (*Mcpt11*) were upregulated in both mouse strains with slightly higher levels in *Alt*-treated BALB/c mice than in *Alt*-treated C57BL/6 mice (Figure 3M).

10.3389/fimmu.2023.1040493

Differential protease expression profiles in bone marrow-derived mast cells of BALB/c versus C57BL/6 mice

To test if the enzymatic content of mast cells from C57BL/6 mice might be different from BALB/c mast cells, we have used BMMCs differentiated *in vitro* in the presence of IL-3 as earlier described (24). The purity of BMMCs reached about 97% on day 20 and was consistent from day 20 to day 40 as analysed by expression of c-kit and FcεRI by flow cytometry (Figure 4A). The total RNA was isolated from BMMCs on days 20, 30, and 40 of *in vitro* culture, and the expression levels of several mast cell proteases were tested. RT-qPCR showed a gradual increase from day 20 to day 40 in *Mcpt1*, *Mcpt2*, and *Mcpt4* gene expression in differentiating BMMCs of both mouse strains (Figures 4B–D). Remarkably, while BMMCs from BALB/c mice showed very high expression levels of *Tpsab1* at all differentiation stages tested (Figure 4E), the BMMCs from C57BL/6 mice had higher levels of *Tpsb2*, *Tpsg1*, and *Prss34* (Figures 4F–H). The gene expression of *Ctsg* and *Cma1* were significantly lower in BMMCs from C57BL/6 compared to BALB/c mice on days 30 and 40 (Figures 4I, J). Thus, despite identical culture conditions, mast cells differentiated *in vitro* from the bone

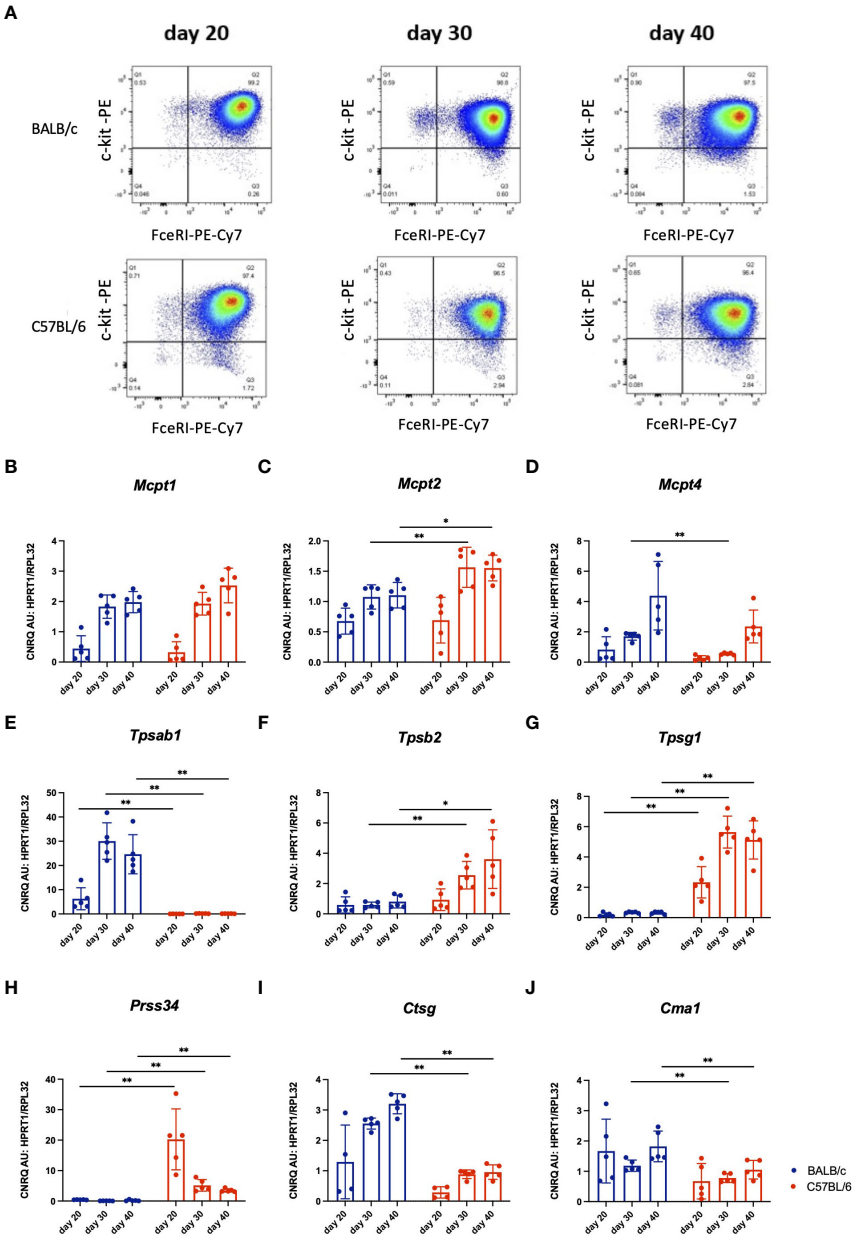

FIGURE 4
Representative dot plots of *in vitro* differentiated BMMCs from BALB/c and C57BL/6 mice cultured *in vitro* for 20, 30 or 40 days, respectively. Viable mast cells were analyzed for their expression of FceRI and c-kit using flow cytometry **(A)**. Next, gene expression analysis by RT-qPCR of mast cell proteases in these cultured BMMCs from I BALB/c and C57BL/6 mice was performed. Values of gene expression of *Mcpt1* **(B)**, *Mcpt2* **(C)**, *Mcpt4* **(D)**, *Tpl1* **(E)**, *Tpsb2* **(F)**, *Tpsg1* **(G)**, *Prss34* **(H)**, *Ctsg* **(I)** and *Cma1* **(J)** were normalised to reference genes *Hprt1* and *Rpl32*. The data represent individual values, bars ± standard deviation (S.D.). Statistical significance between the groups was determined by Mann-Whitney test comparing BALB/c and C57BL/6 mice at each individual time point. The BMMCs were collected from two separate experiments, n=5 per group. *p < 0.05, **p < 0.01.

marrow of C57BL/6 and BALB/c mice show a differential protease expression profile.

The difference observed on RT-qPCR between mast cells derived from C57BL/6 versus BALB/c prompted us to perform RNA sequencing (RNAseq) analysis to deeper characterize the phenotype of mast cells derived from different mouse strains. RNAseq analysis was performed in BMMCs of BALB/c and C57BL/6 mice on day 20. In total, 460 genes were upregulated and 263 downregulated in BMMCs of BALB/c mice compared to C57BL/6 mice. A full list of genes is provided in Supplementary Data and online repository, accession number GSE216642. 17 genes encoding proteases and 4 protease inhibitors that were differentially expressed between the BMMCs of BALB/c and C57BL/6 are summarized in (Table 1). Importantly, the expression of proteases involved in the cleavage of IL-33 is different between the two mouse strains at the baseline, showing that *Cma1* and *Cma2* were upregulated, while *Mcpt4* and *Ctsg* were downregulated in the BMMCs of C57BL/6 mice compared to BALB/c mice.

BMMCs from BALB/c mice rapidly degraded IL-33

Next, we tested whether the full-length IL-33 protein could be processed *in vitro* by mast cell supernatants of BMMCs of both mouse strains. GFP-murine IL-33-mCherry fusion protein (Figure 5A) was used for a cleavage assay with BMMCs supernatants. DNP-IgE/DNP activated BMMCs of C57BL/6 mice did not degrade IL-33, while supernatants of similarly activated BALB/c BMMCs effectively degraded IL-33 after 10 min of co-incubation (Figures 5B, C). Importantly, the efficiency of IL-33 cleavage was linked to the degree of mast cell degranulation after IgE crosslinking. C57BL/6 BMMCs showed a much weaker release of β-hexosaminidase in response to IgE-DNP complex formation than BALB/c BMMCs (Figure 5D).

Discussion

It is well-known that mast cells play a central role in mediating allergic diseases. Mast cells contribute to the activation of immune cells through their broad range of mediators. Next to proteases and histamine, they can also release cytokines. It is known that TNF-α, IL-4, and IL-13 release is triggered by IL-33 and drives the type 2 inflammatory pattern seen in asthma (25–29). We have previously shown that the inflammatory response to *S. aureus* protease like protein D (SplD) and *Alt* extract, which are IL-33 dependent asthma models, can vary among different genetic backgrounds in mice. In these models, a stronger eosinophilic response was found in C57BL/6 than BALB/c mice (12, 30, 31). Similar observations were made in other type 2 response inducing asthma models of ovalbumin-alum and house dust mite (32–35). We, therefore, hypothesized in this work that mast cells might differ between C57BL/6 and BALB/c mice, leading to a different inflammatory response.

In this study, we provide a comprehensive comparative analysis of BMMCs from BALB/c and C57BL/6 mice showing significant differences in expression of major mast cell proteases and protease inhibitors. RNA sequencing analysis of BMMCs *in vitro* from both strains has shown that tryptase genes were differentially expressed, namely C57BL/6 mice lacked *Tpsab1* expression but had higher levels of *Tpsb2* and *Tpsg1* instead, while *Ctsg* and *Cma1* were higher in BMMCs from BALB/c mice. It is known that mast cell chymase and cathepsin G can also generate more potent forms of IL-33 through its enzymatic processing (9). Some genetic differences were reported earlier, such as mutations in mMCP-7 of C57BL/6 mice that leads to its loss of expression (36). A frameshift mutation in the protease inhibitor *Serpina3i* that leads to a truncated and probably unfunctional protein in BALB/c mice (31). Their role in the differential regulation of IL-33 has been suggested (30).

Moreover, we here demonstrate *in vitro* that activated BMMCs from C57BL/6 and BALB/c mice show different enzymatic activity towards IL-33. Mast cells are known to regulate the processing of IL-33 in a dichotomic way: their proteases degrade IL-33 (37, 38) or generate active processed forms of IL-33 *in vitro* (9), generating a more functionally potent form of IL-33. The observed functional differences between mast cells of C57BL/6 and BALB/c mice could be explained by their different protease content and their IgE-dependent activation potential. A lower degranulation activity by IgE cross linkage of C57BL/6 bone marrow mast cells than BALB/c mast cells has also recently been demonstrated elsewhere (39). However, the exact mechanisms leading to this immune phenotypic difference need to be addressed in future studies. Mast cells of rodents are classically distinguished into two different phenotypes, mucosal and connective tissue mast cells. Connective tissue mast cells express high levels of chymases (Mcpt-4, Mcpt-5) and tryptases (Mcpt-6, Mcpt-7), while mucosal tissue mast cells mostly show an upregulation of Mcpt-1 and Mcpt-2 (40). The transcription program of mast cells varies depending on their differentiation stage (41, 42) and organ-specific localization (43). The studies were mostly performed in C57BL/6 mice, while the information on BALB/c mast cell expression profile is scarce (41, 42). In our experiments, we have seen an upregulation of markers characteristic for both types of mast cells in the lungs of BALB/c mice receiving *Alt* extract with a strong increase of *Mcpt-1, Mcpt-2, Mcpt-4, Mcpt-6* and *Mcpt-7* next to an upregulation of *Cma1* and *Cpa3*. In C57BL/6 mice, a nearly complete absence of mast cells and their proteases was seen in the lungs after the treatment with *Alt*. Even though *Prss34* expression was increased in *Alt*-treated C57BL/6 mice, BALB/c mice treated with the *Alt* extract had even higher levels of *Prss34*.

In our model, we repeatedly exposed mice to *Alt* extract as an *in vivo* mouse model of allergic IL-33-dependent airway inflammation, because *Alt* triggers the airway epithelium resulting in the release of alarmins, including ATP, IL-33, and TSLP, which induce ILC2 proliferation and a type 2-driven immune response (4, 44). In our study, BALB/c mice respond to *Alt* with features of allergic airway inflammation, including strong eosinophilic inflammation and neutrophilia in the BALF and lungs, in agreement with previous studies (4, 12, 44). Further, as seen previously, C57BL/6 mice presented an even higher eosinophilic

10.3389/fimmu.2023.1040493

TABLE 1 List of selected genes differentially expressed by RNAseq analysis in three biological replicates of *in vitro* differentiated mast cells from C57BL/6 as compared to BALB/c.

Genes	Number of reads in C57BL/6 mice	Fold change C57BL/6 compared to BALB/c mice	p - value	p - adj	Protein name	Molecular function
Proteases						
Cma2	1610,69	3,58	1,0E-125	1,5E-123	Chymase-2	serine protease
Fgl2	18084,38	2,24	2,4E-83	1,9E-81	Fibroleukin	protease
Gzma	71,83	7,73	1,1E-18	1,5E-17	Granzyme A	serine protease
Gzmd	233,68	8,38	6,2E-69	4,0E-67	Granzyme D	serine protease
Gzme	69,27	16,48	7,3E-26	1,4E-24	Granzyme E	serine protease
Hgfac	6281,16	2,41	9,9E-114	1,2E-111	Hepatocyte growth factor	serine protease
Htra1	1184,94	4,61	1,8E-28	3,7E-27	High-temperature requirement A serine peptidase 1	serine protease
Cma1/ Mcpt8	4273,77	2,16	2,4E-112	3,0E-110	Chymase-1/Mast cell protease 8	serine protease
Mcpt9	1220,34	8,56	2,0E-256	8,9E-254	Mast cell protease 9	serine protease
Plau	3686,77	2,00	5,7E-86	4,8E-84	Urokinase-type plasminogen activator	serine protease
Prcp	338,50	4,62	2,5E-60	1,4E-58	Lysosomal Pro-X carboxypeptidase	carboxypeptidase
Prss34	100,62	48,60	9,2E-33	2,3E-31	Mast cell protease 11	serine protease
Tpsb2	99140,01	4,88	3,3E-49	1,4E-47	Tryptase beta-2	serine protease
Tpsg1	24719,65	35,37	0,0E+00	0,0E +00	Tryptase gamma	serine protease
Mcpt1	5886,78	2,58	4,67E-196	1,38E-193	Mast cell protease 1	serine protease
Mcpt4	4770,70	-2,16	2,9E-07	1,7E-06	Mast cell protease 4 chymotrypsin-like activity serine protease	serine protease
Ctsg	8137,29	-2,37	1,99E-10	1,60E-09	Cathepsin G	serine protease
protease inhibitors						
Serpine1	332,62	9,8	8,33E-86	6,99E-84	Plasminogen activator inhibitor 1	Serine protease inhibitor
Spink2	1241,65	-2,3	7,58E-44	2,67E-42	Serine protease inhibitor Kazal-type 2	Serine protease inhibitor
Serpina3f	1054,53	-6,39	3,44E-183	8,89E-181	SERPIN domain-containing protein	Serine protease inhibitor
Serpina3i	898,69	-3,70	1,15E-89	1,01E-87	Serine (or cysteine) peptidase inhibitor, clade A, member 3I	Serine protease inhibitor

Number of reads, fold difference between the groups, p-value and adjusted p-value (p adj) are presented. The full list of differentially regulated genes is provided in online repository, accession number GSE216642.

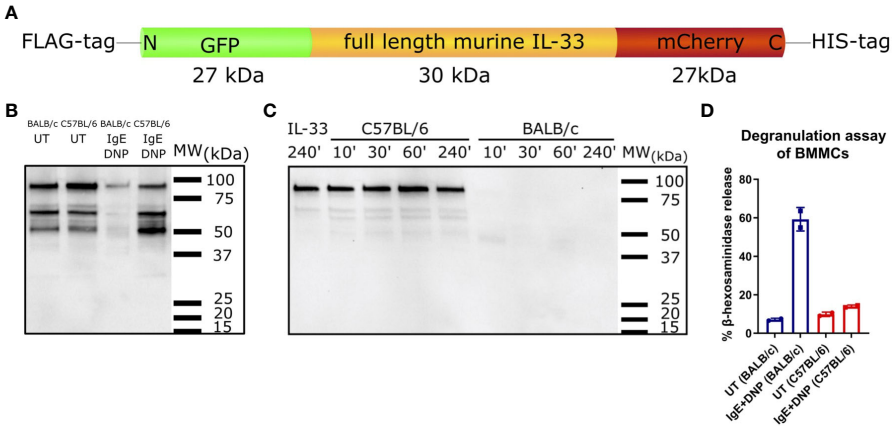

FIGURE 5
IL-33 degrading abilities of supernatants from C57BL/6 and BALB/c BMMCs. Schematic representation of the GFP-murine IL-33-mCherry fusion protein used for IL-33 cleavage assay with BMMCs supernatants **(A)**. Supernatants from C57BL/6 or BALB/c BMMCs, which were either stimulated with IgE+DNP or left untreated were incubated with GFP-murine IL-33-mCherry for 1 h **(B)**. IL-33 degradation was analysed by western blotting. Supernatants from IgE +DNP stimulated C57BL/6 or BALB/c BMMCs were incubated with GFP-murine IL-33-mCherry for 10, 30, 60, or 240 min at 37°C. IL-33 incubated only in buffer for 240 min at 37°C served as negative control. IL-33 degradation was analysed by western blotting **(C)**. Beta-hexosaminidase degranulation assay of untreated or IgE+DNP stimulated BMMCs from C57BL/6J or BALB/c mice **(D)**. Data are presented as mean ± SEM.

response in the BALF as well as higher lung IL-5 levels than BALB/c mice. Based on the low numbers of mast cells and the low mast cell protease expression levels in the lungs of C57BL/6 mice compared to BALB/c mice, we suggest a protective effect of mast cells, that dampen IL-5 and the eosinophilic response in BALB/c mice.

Interestingly, IL-33 protein levels were remarkably higher in the lungs of BALB/c mice treated with *Alt*. We have noted before that IL-33 protein levels by Luminex, however, do not reflect the levels of cleaved IL-33 (IL-33$_C$) found by western blotting (12). We demonstrated different processing patterns of IL-33 seen by western blotting between BALB/c mice with the prevailing IL-33$_C$ and C57BL/6 mice, where also full-length IL-33 was detected. Therefore, we hypothesize that this different cleavage pattern is a consequence of different proteolytic regulation of IL-33 by endogenous proteases upon intratracheal treatment with the *Alt* extract. Based on our previous results, we expect that Mcpt-4 present in the lungs of BALB/c mice degrades IL-33 (31). Next to mast cell proteases, also neutrophilic proteases, such as proteinase 3, and caspases can degrade IL-33 and inactivate it (10, 45). We recently demonstrated the importance of neutrophil proteases in the regulation of IL-33 in a comparable *Alt*-induced asthma model (12). Consistent with our previous results, we here showed that BALB/c mice respond with a stronger neutrophilic inflammation than C57BL/6 mice, which, in addition to the mast cell proteases, influences the IL-33 signaling pathway. In our previous study, depletion of neutrophils *in vivo* by *i.p.* injections of anti-Ly6G antibodies in *Alt*-treated BALB/c mice resulted in a significant decrease of elastase and reduced processing of IL-33$_C$ supporting the additional effect of neutrophilic proteases in the regulation of IL-33 processing (12). However, in our previously used SplD-induced asthma model, where C57BL/6 mice also presented a stronger eosinophilic response than BALB/c mice, the neutrophilic response was negligibly weak, and still IL-33 was processed in a comparable way to the here shown *Alt*-induced allergic airway inflammation model, which underlines the importance of mast cell proteases in the regulation of IL-33 (22). Remarkably, the expression levels of ST2 receptor were comparable between the lungs of *Alt* -treated C57BL/6 and BALB/c mice, excluding the role of possible deficient IL-33/ST2 signaling axis in this regulation.

To conclude, our study demonstrates that mast cells differ in number and protease content between the two mouse strains most often used in asthma and allergy research. These differences might influence the phenotypic outcome in IL-33-dependent models of type 2 inflammation which are unlikely to be related to different efficiency of the IL-33/ST2 signalling axis. The mast cells and their proteases play a regulatory role in IL-33-induced inflammation by limiting its proinflammatory effect *via* the IL-33 signalling pathway because the models of allergic inflammation tested including BALB/c mice show a weaker eosinophilic response compared to C57BL/6 mice.

Materials and methods

Mice: experimental procedures

All experimental procedures were approved by the local Ethical Committee of Ghent University. Seven-week-old female BALB/c or C57BL/6J wild-type mice (Janvier, Saint-Berthevin, France) received six intratracheal applications of 50 µl PBS alone or 20 µg of *Alt* extract (Stallergenes Greer, London, UK) in 50 µl PBS. Animals were kept in individually ventilated cages in a 12-hour/12-hour light/dark cycle. The experiments were performed under light gaseous anaesthesia with isoflurane/air (Ecuphar, Breda, The Netherlands). Mice were euthanized with an intraperitoneal (i.p.) injection of 150 µl Dolethal (Vétoquinol, Lure, France). Lungs were perfused with 0.9% NaCl. For the cytokine analysis, a piece of the lung was snap-frozen in liquid nitrogen and stored at -80°C for further analysis. To perform immunohistochemical staining a piece

of the lung was immersed in 10% formalin and paraffin-embedded. The 5µm sections were cut and used for the subsequent staining.

Flow cytometry

BALFs were collected with PBS containing protease inhibitor cocktail (Roche, Mannheim, Germany), 0.5% bovine serum albumin and ethylenediaminetetraacetic acid (EDTA) (Sigma-Aldrich, Bornem, Belgium). The lungs were enzymatically dissociated by incubation in 1 mg/ml collagenase type II (Worthington Biochemical, New Jersey, USA) at 37°C for one hour shaking to obtain single cell suspension. Red blood cells were lysed by cell lysis solution (VersaLyse Lysing solution, Beckman Coulter, Marseille, France). 1 x 10^6 cells were stained with the following antibodies: purified CD16/CD32 (clone 93), CD4-FITC (clone RM4-4), CD8a-PerCp-Cy5.5 (clone 53-6.7), CD11c-PE-Cy7 (clone HL3), CD11b-PerCP-Cy5.5 (clone M1/70) and Gr1-FITC (clone RB6-8C5) purchased from Thermo Fisher Scientific and Siglec F-PE (clone ES22-10D8) from Miltenyi Biotec (Bergisch Gladbach, Germany). To exclude the dead cells the LIVE/DEAD Fixable Near-IR Dead Cell Stain Kit (Merck Millipore, Massachusetts, USA) was used. The following gating strategy was applied for flow cytometry to analyze eosinophils and neutrophils in BALF and lungs. First, the subset of viable cells was gated through the selection of singlets viable cells. Next from $CD11c^-$ population eosinophils were defined as $CD11b^+$, $SiglecF^+$, and neutrophils as SSC^{low}, $CD11b^+$, $Gr1^+$ as earlier described in (12). $CD4^+$ and $CD8^+$ T cells were gated as subsets of singlet/viable SSC^{low} cells. Murine lungs and BALF were analysed by flow cytometry using the FACS Canto II (BD Biosciences, Erembodegem, Belgium).

Luminex assays

A Luminex analysis was performed to measure the protein concentration of IL-4, IL-5, IL-13, IL-25, IL-33, and G-CSF in mouse lung homogenates. The mouse magnetic Luminex kit (R&D Systems, Minnesota, USA) was used and all steps were performed according to the manufacturer's protocol. The lung homogenates (1 mg/ml) were diluted 1/2 by adding 25 µl of each sample to 25 µl Calibrator Diluent RD6-52. A standard curve for each cytokine analysed was generated using a series of dilution (diluted 1/3) of the Standard Cocktails in Calibrator Diluent RD6-52. A diluted biotin-antibody cocktail and streptavidin- phycoerythrin (PE) solution were made according to the manufacturer's protocol in a 1/10 dilution. The plate was read using the Bio-Rad analyzer, Bioplex 200 system with Luminex xMAP technology (Bio-Rad, California, USA).

Total IgE analysis

The levels of total IgE in serum of mice were analyzed with an ELISA kit from ThermoFisher Scientific according to manufacturer instructions. The reaction was read using automated spectrophotometric plate reader and the SkanIt Software (Multiscan FC, Thermo Fisher Scientific).

In vitro differentiation of murine bone marrow-derived mast cells

The mast cells were differentiated *in vitro* from BMMCs of naive wild type BALB/c and C57BL/6 mice. The BMMCs were differentiated for 40 days in Dulbecco's modified Eagle's medium with 10% fetal bovine serum, L-glutamine, penicillin/streptomycin and 1 mM sodium pyruvate (all from Thermo Fisher Scientific) supplemented with 5 ng/ml IL-3, 5 ng/ml IL-9, 1 ng/ml TGF-β1 and 30 ng/ml stem cell factor (all from PeproTech, London, UK). On days 20, 30 and 40 of the culture, the purity of obtained mast cells was tested by flow cytometry using anti-c-Kit-PE and anti-FcεRI-PE-Cy7 antibodies (Thermo Fisher Scientific). The representative dot plots are provided in Figure 4A. The experiment was repeated with four separate cultures. RNA from murine bone marrow-derived mast cells was isolated on days 20, 30 and 40.

BMMCs stimulation

BMMCs were stimulated by DNP-IgE complex formation. 2x10^7cells/mL of BMMCs were preincubated with 0.15 µg/mL anti-DNP IgE (Sigma-Aldrich) overnight and stimulated for 1 h with 200 ng/mL DNP-HSA (Sigma-Aldrich) in Tyrodes buffer (10 mM HEPES, 130 mM NaCl, 6.2 mM D-glucose, 3.0 mM KCl, 1.4 mM $CaCl_2$, 1.0 mM $MgCl_2$ and 0.1% BSA, pH 7.15, sterile filtered) at 37°C. Supernatants were frozen and stored at -20°C until usage.

IL-33 cleavage assay

Supernatants were incubated with 1µg of a full-length murine IL-33 GFP and mCherry fusion protein in a total volume of 20µL for 10, 30, 60 or 240 min. IL-33 degradation was detected by Western blot using mouse IL-33 antigen affinity-purified polyclonal goat IgG (dilution 1:300; R&D Systems) with polyclonal peroxidase labelled anti-goat IgG (H+L) (1:1000; Vector Laboratories Inc., Burlingame, CA, USA).

Beta-hexosaminidase degranulation assay

Degranulation of BMMCs from C57BL/6 and BALB/c mice was tested as previously described (22).

Immunohistochemistry

Formalin-fixed paraffin-embedded lung sections were deparaffinized and dehydrated. The slides were exposed to citrate buffer for antigen retrieval and endogenous peroxidase was blocked by incubation in 3% H_2O_2. Lung sections were stained with anti-

mast cell chymase (Abcam) and anti- IL-33 (R&D systems). The ImmPRESS®-AP Horse Anti-Goat IgG Polymer Detection Kit, Alkaline Phosphatase (Vectorlabs, Burlington, California, USA) and Dako REALTM Detection System, Alkaline Phosphatase/ RED, Rabbit/Mouse (Agilent Technologies, Santa-Clara, California, USA) was used to visualize the binding. The slides were counterstained with haematoxylin and mounted with Aquatex (Sigma-Aldrich). The cells positive for IL-33 or chymase were counted in five power fields per mouse lung at magnification of forty times.

Toluidine blue staining

Formalin-fixed paraffin-embedded murine lung sections were deparaffinized and dehydrated and stained for 15 minutes with toluidine blue (Sigma-Aldrich) working solution at pH 2.3. The slides were air-dried and mounted with a non-aqueous medium (Pertex, 00811, Histolab). The images were taken using Nikon Eclipse Ni-U upright microscope with NIS BR imaging software.

Reverse transcription quantitative polymerase chain reaction

Snap frozen mouse tissue samples (± 20-25 mg) were disrupt using a mortar and pestle containing liquid nitrogen and thawed directly into lysis solution (QIAGEN, Antwerp, Belgium), while murine bone marrow-derived mast cells were directly vortexed for 5 min in lysis solution. The lysate was then homogenized using a QIAshredder homogenizer (QIAGEN). The RNA isolation was further performed using the RNeasy Mini Kit (QIAGEN) following the manufacturer's instructions. The RNA concentration was measured with Nanodrop (Thermo Fisher Scientific, Waltham, Massachusetts, United States) and the quality of the RNA was assessed with the Fragment Analyzer™ Automated CE System (Agilent technologies, California, USA). 500 ng of the isolated RNA was transcribed into cDNA with the iScript Advanced cDNA Synthesis Kit (Bio-Rad) and subsequently diluted with nuclease-free water to 2.5 ng/µl cDNA (total RNA equivalent). Real-time PCR amplifications were performed in a 384-well plate LightCycler LC480 System (Roche Diagnostics, Mannheim, Germany). qPCR reactions (5 µl) contain 5 ng cDNA, 2x SsoAdvanced Universal SYBR Green Supermix (Bio-Rad) and 250 nM forward and reverse primer (Table 2). The PCR protocol consisted of 2 minutes polymerase activation at 95°C and 44 cycles of 5 seconds at 95°C, 30 seconds at 60°C and 1 second at 72°C followed by a dissociation curve analysis from 60°C to 95°C. For murine BMMCs, RT-qPCR was performed for mouse mast cell proteases (*Mcpt*1, Mcpt2, Mcpt4), tryptase α/β1 (*Tpsab1*), tryptase β2 (*Tpsb2*), tryptase γ1 (*Tpsg1*), serine protease 34 (*Prss34*), cathepsin G (*Ctsg*) and mast cell chymase 1 (*Cma1*). For mouse lung tissue, RT-qPCR was performed for mouse mast cell proteases (*Mcpt*1, Mcpt2, Mcpt4), tryptase α/β1 (*Tpsab1*), tryptase β2 (*Tpsb2*), tryptase γ1 (*Tpsg1*), mast cell chymase 1 (*Cma1*), carboxypeptidase A3 (*Cpa3*) and serine protease 34 (*Prss34*). The primer sequences of all target genes were shown in Table 2. *IL1rl1* (encoding ST2) Taqman (QuantiTect Probe PCR kit; Mm00516117_ml) was purchased from Applied Biosystems. The expression of 2 reference genes, hypoxanthine phosphoribosyltransferase 1 (*Hprt1*) and ribosomal protein L32 (*Rpl32*) was used to normalize for transcription and amplification variations among samples after a validation with geNorm (Biogazelle, Zwijnaarde, Belgium). The normalized relative quantities (NRQs) were calculated with the qBase+ software (Biogazelle, Belgium) and the final gene expression levels are expressed as NRQs per 5 ng cDNA.

Western blotting

Tissue homogenates of 20 - 25 mg of mouse lung tissue were made by a mechanical dissociation in a mixture of tissue lysis buffer

TABLE 2 List of primers used in the study.

Gene name	Primer sequence FW (5′-3′)	Primer sequence RW (5′-3′)
Hprt1	CCTAAGATGAGCGCAAGTTGAA	CCACAGGACTAGAACACCTGCTAA
Rpl32	GGCACCAGTCAGACCGATATG	CCTTCTCCGCACCCTGTTG
Mcpt1	AAAAACAGCATACATGGGAG	CATATGCAGAGATTCTGGTG
Mcpt2	CAATAGGACAAGGAGATTCTG	TAATAGGAGATTCGGGTGAAG
Mcpt4	CACTGTAGTGGAAGAGAAATC	GAGGAATTACATTCACAGAGG
Tpsab1	AAACCCTGTGAACATTTCTG	TACACCATTGTCGATGTTAC
Tpsb2	GACATTGATAATGACGAGCC	GACAATGGGAAAATCATCTCC
Tpsg1	TTCTCTGGGTCTGTGAAC	GTTTTACAGTGGAGAAGTGG
Prss34	AGTCTATGGTGTCCCTTAAC	ATGGTAAGGAGGGAATATGG
Ctsg	TGACCTTTATTCTACTCCAAGG	GTAACATTTATGGAGCTTCCC
Cma1	GTATACAAGGGAGACTCTGG	CAGAGTTAATTCTCCCTCAAG
Cpa3	ATGGCTACACATTCAAACTG	TATTGGGCCGTAGATGTAAC

(Thermo Fisher Scientific) and protease inhibitor cocktail (Roche, Sigma-Aldrich, Merck KGaA, Darmstadt, Germany) with a TissueLyser LT (QIAGEN). The supernatant was collected and centrifuged for 10 min at 3000 rpm at 4°C. The tissue homogenate was stored in -20°C. For spectrophotometric determination of the concentration of total proteins in the tissue homogenate, a standard series of dilution with bovine serum albumin (Sigma- Aldrich, Merck KGaA, Darmstadt, Germany) was used. Homogenate samples were diluted 1:20 with NaCl (0,9%) (Versylene Fresenius). The dye solution was prepared by diluting 1 part protein assay dye reagent concentrate (Bio-Rad) with 4 parts distilled water. Subsequently, the optical density was measured at a wavelength of 570 nm using the SkanIt Software (Multiscan FC, Thermo Fisher Scientific). Samples of mouse lung homogenates were prepared for gel electrophoresis with 25 µg protein. For gel electrophoresis, Mini-protean TGX stain-free precast gels (Bio-Rad) were used and 10 µl of the Precision Plus Protein Dual Color Standards (Bio-Rad) was added. The proteins were blotted on a nitrocellulose membrane (Bio-Rad). After blotting, the membrane was washed with a washing buffer and adding a blocking buffer (5% skim milk powder in 1x TBST), the membrane was incubated with the primary antibody (goat anti-IL-33, 0,6 µg/ml)) overnight at 4°C while shaking. After washing, the membrane was incubated with the appropriate secondary antibody (anti-goat IgG horseradish peroxidase (HRP) (1 µg/ml)). Visualization was done with the Chemidoc imaging system (Bio-Rad) after incubation with SuperSignal West Dura (Thermo Fisher Scientific).

RNAseq analysis, RNAseq pipeline and data quantification

RNA was isolated from $1*10^6$ murine mast cells per condition as described above. The integrity of RNA was tested using Fragment Analyzer and 100 ng of total RNA was used for RNA sequencing analysis. The TruSeq Stranded mRNA kit (Illumina) was used to prepare a RNAseq library according to the manufacturer's protocol, followed by PE100 cycles sequencing on one lane of a NovaSeq 6000 S1 run (Illumina).

Bioinformatics

All fastq files passed quality control with FastQC v0.11.5 (46). Salmon v0.8.2 (47) was used to align raw RNAseq reads against Ensembl *Mus musculus* GRCm39 and get quantification estimates at the transcript level. All subsequent analyses were conducted in R software v 4.0.3 (48). Differential analysis was computed using tximport v1.10.0 (49) and the negative binomial generalized linear modeling implemented in DESeq2 package version 1.30.1 (50) Genes were regarded to be differentially expressed when the q value cutoff (FDR adjusted p-value using Benjamini–Hochberg mode l (51) was lower than 0.05. In order to obtain significantly different genes, we set the selection criteria as: the multiple of difference| Fold Change| > 2. To visualize the differentially - expressed (DE) genes identified using the methods described above, the Bioconductor Enhanced Volcano (52) and g plots (53) packages were used. Enhanced Volcano was used to display each gene's shrunken log2 fold change (LFC) against its adjusted p-value. A gene classification and functional annotation analysis were performed using the 'Gene Functional Classification' and 'Functional Annotation Charts' tools of the Database for Annotation, Visualization and Integrated Discovery (DAVID Bioinformatics Resources 6.8, NIAID/NIH) (54). As annotation category, KEGG_PATHWAYS was selected for pathways analysis.

Statistical analysis

The data were analysed using D'Agostino & Pearson test for normal (Gaussian) distribution (alpha = 0.05). When three or more experimental groups were compared, the normally distributed data were analysed by parametric one-way ANOVA with Dunnett's multiple comparisons test. The data, which were not normally distributed, were analysed by non-parametric Kruskal-Wallis test with Dunn's test for multiple comparisons. Significance was determined as followed: * $p<0.05$, ** $p<0.01$, *** $p<0.001$, **** $p<0.0001$.

Data availability statement

The data presented in the study are deposited in the GEO repository, accession number GSE216642.

Ethics statement

The animal study was reviewed and approved by Ethical Committee of Ghent University, Faculty of Medicine and Health Sciences.

Author contributions

OK designed and performed experiments, analyzed data and wrote the original draft. DK and MI performed the bioinformatics analysis of the RNA sequencing dataset. AT performed experiments and revised the manuscript. JV, JS and AD collected experimental material, did immunohistochemistry and western blotting, analyzed data, revised the manuscript. SV contributed to the collection of the murine samples and revised the manuscript. GH performed and analyzed Luminex data. ND performed and analyzed RT-qPCR data. FC performed RNA seq analysis. HB provided a genetic construct encoding full length IL-33. MV, and DVK supervised the study, provided analysis tools, revised the manuscript. CB supervised the study, provided analysis tools, revised the manuscript. All authors discussed the results and approved the manuscript. All authors contributed to the article and approved the submitted version.

Funding

The research was supported by FWO-Flanders 3G065319N to OK and CB. DVK lab is supported by Ghent University BOF (Special Research Fund 01/O3618; BOF/IOP/2022/033; BOF23/GOA/029). MV and MI acknowledge the Ministry of Science and Higher Education of the RF, agreement No. 075-15-2020-808.

Conflict of interest

The authors declare that the research was conducted in the absence of any commercial or financial relationships that could be construed as a potential conflict of interest.

Publisher's note

All claims expressed in this article are solely those of the authors and do not necessarily represent those of their affiliated organizations, or those of the publisher, the editors and the reviewers. Any product that may be evaluated in this article, or claim that may be made by its manufacturer, is not guaranteed or endorsed by the publisher.

Supplementary material

The Supplementary Material for this article can be found online at: https://www.frontiersin.org/articles/10.3389/fimmu.2023.1040493/full#supplementary-material

SUPPLEMENTARY FIGURE 1
The levels of IL-4 **(A)**, G-CSF **(B)**, and IL-25 **(C)** in the lung homogenates were measured by Luminex. The data are presented as a scatter plot with a bar ± standard deviation (S.D). Statistical analysis was performed by one-way ANOVA with Dunn's test for multiple comparisons. N=4-6 per group.

SUPPLEMENTARY TABLE 1
List of genes differentially expressed in RNA-Seq analysis of *in vitro* differentiated mast cells (BMMCs) from naïve BALB/c and C57BL/6 mice obtained from three biological replicates.

References

1. Wenzel SE. Severe adult asthmas: Integrating clinical features, biology, and therapeutics to improve outcomes. *Am J Respir Crit Care Med* (2021) 203(7):809–21. doi: 10.1164/rccm.202009-3631CI

2. Traister RS, Uvalle CE, Hawkins GA, Meyers DA, Bleecker ER, Wenzel SE. Phenotypic and genotypic association of epithelial IL1RL1 to human T(H)2-like asthma. *J Allergy Clin Immunol* (2015) 135(1):92–9. doi: 10.1016/j.jaci.2014.06.023

3. Hinks TSC, Levine SJ, Brusselle GG. Treatment options in type-2 low asthma. *Eur Respir J* (2021) 57(1):2000528. doi: 10.1183/13993003.00528-2020

4. Castanhinha S, Sherburn R, Walker S, Gupta A, Bossley CJ, Buckley J, et al. Pediatric severe asthma with fungal sensitization is mediated by steroid-resistant IL-33. *J Allergy Clin Immunol* (2015) 136(2):312–22. doi: 10.1016/j.jaci.2015.01.016

5. Kelsen SG, Agache IO, Soong W, Israel E, Chupp GL, Cheung DS, et al. Astegolimab (anti-ST2) efficacy and safety in adults with severe asthma: A randomized clinical trial. *J Allergy Clin Immunol* (2021) 148(3):790–8. doi: 10.1016/j.jaci.2021.03.044

6. Lambrecht BN, Hammad H. Allergens and the airway epithelium response: gateway to allergic sensitization. *J Allergy Clin Immunol* (2014) 134(3):499–507. doi: 10.1016/j.jaci.2014.06.036

7. Cayrol C, Duval A, Schmitt P, Roga S, Camus M, Stella A, et al. Environmental allergens induce allergic inflammation through proteolytic maturation of IL-33. *Nat Immunol* (2018) 19(4):375–85. doi: 10.1038/s41590-018-0067-5

8. Cayrol C, Girard JP. Interleukin-33 (IL-33): A nuclear cytokine from the IL-1 family. *Immunol Rev* (2018) 281(1):154–68. doi: 10.1111/imr.12619

9. Lefrancais E, Duval A, Mirey E, Roga S, Espinosa E, Cayrol C, et al. Central domain of IL-33 is cleaved by mast cell proteases for potent activation of group-2 innate lymphoid cells. *Proc Natl Acad Sci U States A* (2014) 111(43):15502–7. doi: 10.1073/pnas.1410700111

10. Clancy DM, Sullivan GP, Moran HBT, Henry CM, Reeves EP, McElvaney NG, et al. Extracellular neutrophil proteases are efficient regulators of IL-1, IL-33, and IL-36 cytokine activity but poor effectors of microbial killing. *Cell Rep* (2018) 22(11):2937–50. doi: 10.1016/j.celrep.2018.02.062

11. Scott IC, Majithiya JB, Sanden C, Thornton P, Sanders PN, Moore T, et al. Interleukin-33 is activated by allergen- and necrosis-associated proteolytic activities to regulate its alarmin activity during epithelial damage. *Sci Rep* (2018) 8(1):3363. doi: 10.1038/s41598-018-21589-2

12. Van Nevel S, van Ovost J, Holtappels G, De Ruyck N, Zhang N, Braun H, et al. Neutrophils affect IL-33 processing in response to the respiratory allergen alternaria alternata. *Front Immunol* (2021) 12:677848. doi: 10.3389/fimmu.2021.677848

13. Balzar S, Fajt ML, Comhair SAA, Erzurum SC, Bleecker E, Busse WW, et al. Mast cell phenotype, location, and activation in severe asthma data from the severe asthma research program. *Am J Respir Crit Care Med* (2011) 183(3):299–309. doi: 10.1164/rccm.201002-0295OC

14. Balzar S, Chu HW, Strand M, Wenzel S. Relationship of small airway chymase-positive mast cells and lung function in severe asthma. *Am J Respir Crit Care Med* (2005) 171(5):431–9. doi: 10.1164/rccm.200407-949OC

15. Winter NA, Qin L, Gibson PG, McDonald VM, Baines KJ, Faulkner J, et al. Sputum mast cell/basophil gene expression relates to inflammatory and clinical features of severe asthma. *J Allergy Clin Immunol* (2021) 148(2):428–38. doi: 10.1016/j.jaci.2021.01.033

16. Lezmi G, Galmiche-Rolland L, Rioux S, Jaubert F, Tillie-Leblond I, Scheinmann P, et al. Mast cells are associated with exacerbations and eosinophilia in children with severe asthma. *Eur Respir J* (2016) 48(5):1320–8. doi: 10.1183/13993003.00947-2016

17. Brightling CE, Bradding P, Symon FA, Holgate ST, Wardlaw AJ, Pavord ID. Mast-cell infiltration of airway smooth muscle in asthma. *New Engl J Med* (2002) 346 (22):1699–705. doi: 10.1056/NEJMoa012705

18. Alzahrani A, Hussain A, Alhadian F, Hakeem J, Douaoui S, Tliba O, et al. Potential role of mast cells in regulating corticosteroid insensitivity in severe asthma. *Lung Inflammation Health Dis Vol I* (2021) 1303:1–12. doi: 10.1007/978-3-030-63046-1_1

19. Rao R, Frederick JM, Enander I, Gregson RK, Warner JA, Warner JO. Airway function correlates with circulating eosinophil, but not mast cell, markers of inflammation in childhood asthma. *Clin Exp Allergy* (1996) 26(7):789–93. doi: 10.1111/j.1365-2222.1996.tb00609.x

20. Dougherty RH, Sidhu SS, Raman K, Solon M, Solberg OD, Caughey GH, et al. Accumulation of intraepithelial mast cells with a unique protease phenotype in T(H)2-high asthma. *J Allergy Clin Immunol* (2010) 125(5):1046–53. doi: 10.1016/j.jaci.2010.03.003

21. Gabryelska A, Kuna P, Antczak A, Bialasiewicz P, Panek M. IL-33 mediated inflammation in chronic respiratory diseases-understanding the role of the member of IL-1 superfamily. *Front Immunol* (2019) 10. doi: 10.3389/fimmu.2019.00692

22. Teufelberger AR, Nordengrun M, Braun H, Maes T, De Grove K, Holtappels G, et al. The IL-33/ST2 axis is crucial in type 2 airway responses induced by staphylococcus aureus-derived serine protease-like protein d. *J Allergy Clin Immunol* (2018) 141(2):549–59 e7. doi: 10.1016/j.jaci.2017.05.004

23. Holgado A, Braun H, Van Nuffel E, Detry S, Schuijs MJ, Deswarte K, et al. IL-33trap is a novel IL-33-neutralizing biologic that inhibits allergic airway inflammation. *J Allergy Clin Immunol* (2019) 144(1):204–15. doi: 10.1016/j.jaci.2019.02.028

24. Ito T, Smrz D, Jung MY, Bandara G, Desai A, Smrzova S, et al. Stem cell factor programs the mast cell activation phenotype. *J Immunol (Baltimore Md: 1950)* (2012) 188(11):5428–37. doi: 10.4049/jimmunol.1103366

25. Bradding P, Walls AF, Holgate ST. The role of the mast cell in the pathophysiology of asthma. *J Allergy Clin Immunol* (2006) 117(6):1277–84. doi: 10.1016/j.jaci.2006.02.039

26. Wernersson S, Pejler G. Mast cell secretory granules: armed for battle. *Nat Rev Immunol* (2014) 14(7):478–94. doi: 10.1038/nri3690

27. Mendez-Enriquez E, Hallgren J. Mast cells and their progenitors in allergic asthma. *Front Immunol* (2019) 10:821. doi: 10.3389/fimmu.2019.00821

28. Sjoberg LC, Nilsson AZ, Lei Y, Gregory JA, Adner M, Nilsson GP. Interleukin 33 exacerbates antigen driven airway hyperresponsiveness, inflammation and remodeling in a mouse model of asthma. *Sci Rep* (2017) 7(1):4219. doi: 10.1038/s41598-017-03674-0

29. Saluja R, Zoltowska A, Ketelaar ME, Nilsson G. IL-33 and thymic stromal lymphopoietin in mast cell functions. *Eur J Pharmacol* (2016) 778:68–76. doi: 10.1016/j.ejphar.2015.04.047

30. Krysko O, Teufelberger A, Van Nevel S, Krysko DV, Bachert C. Protease/antiprotease network in allergy: The role of staphylococcus aureus protease-like proteins. *Allergy* (2019) 74(11):2077–86. doi: 10.1111/all.13783

31. Teufelberger AR, Van Nevel S, Hulpiau P, Nordengrun M, Savvides SN, De Graeve S, et al. Mouse strain-dependent difference toward the staphylococcus aureus allergen serine protease-like protein d reveals a novel regulator of IL-33. *Front Immunol* (2020) 11:582044. doi: 10.3389/fimmu.2020.582044

32. Gueders MM, Paulissen G, Crahay C, Quesada-Calvo F, Hacha J, Van Hove C, et al. Mouse models of asthma: a comparison between C57BL/6 and BALB/c strains regarding bronchial responsiveness, inflammation, and cytokine production. *Inflammation Res* (2009) 58(12):845–54. doi: 10.1007/s00011-009-0054-2

33. Van Hove CL, Maes T, Cataldo DD, Gueders MM, Palmans E, Joos GF, et al. Comparison of acute inflammatory and chronic structural asthma-like responses between C57BL/6 and BALB/c mice. *Int Arch Allergy Immunol* (2009) 149(3):195–207. doi: 10.1159/000199715

34. Kelada SN, Wilson MS, Tavarez U, Kubalanza K, Borate B, Whitehead GS, et al. Strain-dependent genomic factors affect allergen-induced airway hyperresponsiveness in mice. *Am J Respir Cell Mol Biol* (2011) 45(4):817–24. doi: 10.1165/rcmb.2010-0315OC

35. Serra-Pages M, Torres R, Plaza J, Herrerias A, Costa-Farre C, Marco A, et al. Activation of the prostaglandin E2 receptor EP2 prevents house dust mite-induced airway hyperresponsiveness and inflammation by restraining mast cells' activity. *Clin Exp Allergy* (2015) 45(10):1590–600. doi: 10.1111/cea.12542

36. Hunt JE, Stevens RL, Austen KF, Zhang J, Xia Z, Ghildyal N. Natural disruption of the mouse mast cell protease 7 gene in the C57BL/6 mouse. *J Biol Chem* (1996) 271(5):2851–5. doi: 10.1074/jbc.271.5.2851

37. Waern I, Jonasson S, Hjoberg J, Bucht A, Abrink M, Pejler G, et al. Mouse mast cell protease 4 is the major chymase in murine airways and has a protective role in allergic airway inflammation. *J Immunol (Baltimore Md: 1950)* (2009) 183(10):6369–76. doi: 10.4049/jimmunol.0900180

38. Waern I, Lundequist A, Pejler G, Wernersson S. Mast cell chymase modulates IL-33 levels and controls allergic sensitization in dust-mite induced airway inflammation. *Mucosal Immunol* (2013) 6(5):911–20. doi: 10.1038/mi.2012.129

39. Nagashima M, Koyanagi M, Arimura Y. Comparative analysis of bone marrow-derived mast cell differentiation in C57BL/6 and BALB/c mice. *Immunol Invest* (2019) 48(3):303–20. doi: 10.1080/08820139.2018.1523924

40. Reynolds DS, Stevens RL, Lane WS, Carr MH, Austen KF, Serafin WE. Different mouse mast-cell populations express various combinations of at least 6 distinct mast-cell serine proteases. *Proc Natl Acad Sci U States A* (1990) 87(8):3230–4. doi: 10.1073/pnas.87.8.3230

41. Hamey FK, Lau WWY, Kucinski I, Wang X, Diamanti E, Wilson NK, et al. Single-cell molecular profiling provides a high-resolution map of basophil and mast cell development. *Allergy* (2021) 76(6):1731–42. doi: 10.1111/all.14633

42. Dahlin JS, Hamey FK, Pijuan-Sala B, Shepherd M, Lau WWY, Nestorowa S, et al. A single-cell hematopoietic landscape resolves 8 lineage trajectories and defects in kit mutant mice. *Blood* (2018) 131(21):e1–e11. doi: 10.1182/blood-2017-12-821413

43. Akula S, Paivandy A, Fu Z, Thorpe M, Pejler G, Hellman L. Quantitative in-depth analysis of the mouse mast cell transcriptome reveals organ-specific mast cell heterogeneity. *Cells* (2020) 9(1):2118. doi: 10.3390/cells9010211

44. Holgado A, Braun H, Verstraete K, Vanneste D, Callewaert N, Savvides SN, et al. Single-chain soluble receptor fusion proteins as versatile cytokine inhibitors. *Front Immunol* (2020) 11:1422. doi: 10.3389/fimmu.2020.01422

45. Afonina IS, Muller C, Martin SJ, Beyaert R. Proteolytic processing of interleukin-1 family cytokines: Variations on a common theme. *Immunity* (2015) 42(6):991–1004. doi: 10.1016/j.immuni.2015.06.003

46. Andrews S. *FastQC: a quality control tool for high throughput sequence data*. (2010).

47. Patro R, Duggal G, Love MI, Irizarry RA, Kingsford C. Salmon provides fast and bias-aware quantification of transcript expression. *Nat Methods* (2017) 14(4):417–9. doi: 10.1038/nmeth.4197

48. Team RC. *R: A language and environment for statistical computing*. Vienna, Austria: R Foundation for Statistical Computing (2018).

49. Soneson C, Love MI, Robinson MD. Differential analyses for RNA-seq: Transcript-level estimates improve gene-level inferences. *F1000Res* (2015) 4(1521). doi: 10.12688/f1000research.7563.1

50. Love MI, Huber W, Anders S. Moderated estimation of fold change and dispersion for RNA-seq data with DESeq2. *Genome Biol* (2014) 15(12):1070. doi: 10.1186/s13059-014-0550-8

51. Benjamini Y, Hochberg Y. Controlling the false discovery rate - a practical and powerful approach to multiple testing. *J R Stat Soc Ser B Statistical Methodol* (1995) 57(1):289–300. doi: 10.1111/j.2517-6161.1995.tb02031.x

52. Blighe K. *Enhanced volcano: publication-ready volcano plots with enhanced colouring and labelin*. New Jersey, NJ (2019). https://github.com/kevinblighe/EnhancedVolcano.

53. Warnes GR, Bolker B, Bonebakker L, Gentleman R, Liaw WHA, Lumley T, et al. *Gplots: various r programming tools for plotting data*. New Jersey, NJ (2019). https://github.com/talgalili/gplots.

54. Dennis G, Sherman BT, Hosack DA, Yang J, Gao W, Lane HC, et al. DAVID: Database for annotation, visualization, and integrated discovery. *Genome Biol* (2003) 4(9):R70. doi: 10.1186/gb-2003-4-9-r60

CYTOKINES/SOLUBLE FACTORS IN PATHOGENIC MECHANISMS

frontiers | Frontiers in Immunology

TYPE Perspective
PUBLISHED 08 May 2023
DOI 10.3389/fimmu.2023.1128190

OPEN ACCESS

EDITED BY
Bodduluri Haribabu,
University of Louisville, United States

REVIEWED BY
Robert Friedland,
University of Louisville, United States
Jin Bao,
The Brain Cognition and Brain Disease Institute, Chinese Academy of Sciences (CAS), China

*CORRESPONDENCE
Diana Boraschi
diana.boraschi@itb.cnr.it
Paola Bossù
p.bossu@hsantalucia.it

RECEIVED 20 December 2022
ACCEPTED 11 April 2023
PUBLISHED 08 May 2023

CITATION
Boraschi D, Italiani P, Migliorini P and Bossù P (2023) Cause or consequence? The role of IL-1 family cytokines and receptors in neuroinflammatory and neurodegenerative diseases.
Front. Immunol. 14:1128190.
doi: 10.3389/fimmu.2023.1128190

Cause or consequence? The role of IL-1 family cytokines and receptors in neuroinflammatory and neurodegenerative diseases

Diana Boraschi[1,2,3,4]*, Paola Italiani[2,3,4], Paola Migliorini[5] and Paola Bossù[6]*

[1]Shenzhen Institute of Advanced Technology (SIAT), Chinese Academy of Sciences (CAS), Shenzhen, China, [2]Institute of Biochemistry and Cell Biology (IBBC), National Research Council (CNR), Naples, Italy, [3]Stazione Zoologica Anton Dohrn (SZN), Napoli, Italy, [4]China-Italy Joint Laboratory of Pharmacobiotechnology for Medical Immunomodulation, Shenzhen, China, [5]Clinical Immunology and Allergy Unit, Department of Clinical and Experimental Medicine, University of Pisa, Pisa, Italy, [6]Laboratory of Experimental Neuro-psychobiology, Department of Clinical and Behavioral Neurology, Santa Lucia Foundation, Rome, Italy

Cytokines and receptors of the IL-1 family are key mediators in innate immune and inflammatory reactions in physiological defensive conditions, but are also significantly involved in immune-mediated inflammatory diseases. Here, we will address the role of cytokines of the IL-1 superfamily and their receptors in neuroinflammatory and neurodegenerative diseases, in particular Multiple Sclerosis and Alzheimer's disease. Notably, several members of the IL-1 family are present in the brain as tissue-specific splice variants. Attention will be devoted to understanding whether these molecules are involved in the disease onset or are effectors of the downstream degenerative events. We will focus on the balance between the inflammatory cytokines IL-1β and IL-18 and inhibitory cytokines and receptors, in view of future therapeutic approaches.

KEYWORDS

IL-1 family cytokines, IL-1 family receptors, neuroinflammation, neurodegeneration, Alzheimer's disease, multiple sclerosis

1 Introduction

The interleukin-1 (IL-1) superfamily encompasses eleven structurally and evolutionarily related cytokines that mainly act by binding to specific receptors (1). The IL-1 receptor (IL-1R) complexes are formed by a ligand-binding chain and an accessory chain necessary for signal transduction. The IL-1R family comprises ten related transmembrane molecules with extracellular Ig-like domains and intracellular TIR (Toll-Like Receptor/IL-1 Receptor) domains (2). Most IL-1 and IL-1R molecules are involved in inflammation/immunostimulation and its regulation. It is notable that, while IL-1R are derived from invertebrate TIR-containing receptors involved in innate immunity, IL-1 cytokines only appeared in vertebrates (likely linked to the development of adaptive immunity) and the majority of them is only present in mammals (3, 4).

In mammals, eleven cytokines of the IL-1 family have been identified, the inflammatory IL-1α, IL-1β, IL-18, IL-36α, IL-36β, IL-36γ, and the regulatory/anti-inflammatory IL-1Ra, IL-33, IL-36Ra, IL-37 and IL-38 (overview in 1). IL-1 family cytokines mainly act by binding to receptor complexes, composed by a ligand binding chain and an accessory signal transducing chain. Signalling is initiate by the pairing of the intracellular TIR domains of the two receptor chains. Receptors of the IL-1R family are ten structurally related transmembrane proteins, which may also give rise to soluble receptors upon gene splicing or proteolysis of the membrane chains (overview in 2). IL-1R1 binds the agonist ligands IL-1α and IL-1β, and its signalling depends on the engagement of the accessory chain IL-1R3. IL-1R1 also binds IL-1Ra but in this case fails to recruit the IL-1R3, and no activation occurs. Binding of IL-38 has also been reported. IL-1R2 is similar to IL-1R1 in its ligand binding capacity and IL-1R3 engagement, but it lacks the intracellular TIR domain and its therefore an inhibitory receptor. IL-1R4 is the receptor for IL-33, an uses the same IL-1R3 as accessory chain for signalling. IL-1R5 is the receptor for IL-18, and uses its specific accessory chain IL-1R7. It was reported that IL-37 also binds to IL-1R5 but is unable to recruit IL-1R7. IL-1R6 is the ligand binding chain for all the IL-36 isoforms (IL-36α, IL-36β, IL-36γ) and uses the promiscuous IL-1R3 as accessory chain. IL-1R6 also binds the receptor antagonist IL-36Ra and fails to engage the accessory chain. Binding of IL-38 has also been reported. IL-1R8 is an inhibitory receptor, which can interact with several IL-1R complexes and interfere with their signalling and may also act as inhibitory accessory chain for IL-37 bound to IL-1R5 and IL-38 bound to IL-1R6. IL-1R9 is an orphan receptor, although binding to IL-38 has been reported, predominantly expressed in neurons and likely involve in IL-1-independent neuronal functions. Likewise, IL-1R10 is abundantly expressed in the brain and has no IL-1-dependent functions (for complete references, please see the reference lists of 1, 2).

IL-1 and IL-1R molecules expressed in brain have as their main role the modulation of neuronal plasticity and function, in addition to mediating immune protective functions, in both physiologic and pathologic condition (5–8). IL-1, originally described as endogenous pyrogen or leukocytic pyrogen, is mainly produced in the hypothalamus in response to inflammatory agents and can induce fever by upregulating cyclooxygenase-2, the enzyme responsible for the synthesis of the vasoactive and inflammatory prostaglandin E_2 (9, 10). A central nervous system (CNS)-restricted expression of splice variants of different IL-1 and IL-1R family members, as truncated forms with regulatory functions, have been identified for both IL-1 (11) and IL-18 (12–14). In the case of IL-37, only one of its five splice variants (IL-37a) is present in the brain (15). Some IL-1R members are only present in the brain, including a particular variant of the accessory receptor chain IL-1R3 (IL-1R3b), expressed in neurons and involved in IL-1-mediated neuroprotection. Notably, the receptor complex for IL-1α and β in the brain can be the canonical one (IL-1R1 plus IL-1R3, present everywhere in the body) that mediates inflammatory effects, or the alternative one (IL-1R1 plus IL-1R3b, specific for the brain) that mediates neuroprotective effects (2, 16–18). Other brain-specific receptors are the two orphan receptors IL-1R9 and IL-1R10, which are mostly expressed in neurons. IL-1R9 is likely involved in memory and learning capacity, as its mutations are linked to X-linked mental retardation and autism (2, 19, 20). The functions of IL-18 in the brain are also peculiar, since the cytokine is active (inflammation and homeostasis) even in the absence of its receptor IL-1R5, while IL-1R5 seems to be involved in the pathogenesis of experimental allergic encephalomyelitis (EAE, the mouse model of multiple sclerosis) in the absence of its IL-18 ligand (21, 22). This suggests that a CNS-specific network of IL-1 family cytokines and receptors is crucial in maintaining brain homeostasis, thus highlighting the limitation of a simplistic inflammatory paradigm to explain the function of these cytokines in neuroinflammatory diseases.

In this perspective, we examine the available experimental and clinical evidence of the involvement of these molecules in two major neurodegenerative diseases, Alzheimer's disease (AD) and multiple sclerosis (MS), and propose a more global picture of the pathogenic and pathological role of the IL-1/IL-1R system.

2 Alzheimer's disease

2.1 Disease pathogenesis and inflammation

Alzheimer's disease (AD) in its sporadic form is the most common dementia diagnosis, characterized by a long progressive process of neuronal damage that affects memory and thinking and ultimately leads to death, in general preceded by a preclinical condition named mild cognitive impairment (MCI) (23).

The main pathological hallmarks of AD are the extracellular accumulation of amyloid β (Aβ) peptides and the intraneuronal neurofibrillary tangles (NFT) formed by aggregation of hyperphosphorylated tau proteins. Neuroinflammation is the third core feature of the disease (24, 25). Many inflammation-related genes have been identified as important AD risk factors (26), and increased inflammatory responses in the brain and periphery have been widely reported in AD (27, 28). Innate immune cells, primarily brain-resident microglia, have a dual role in AD neuroinflammation (29–33). Microglia have a protective function by releasing neurotrophic factors and clearing misfolded proteins, and can degrade Aβ thereby reducing its accumulation. Indeed, a transition of microglia from homeostatic to disease-associated populations endowed with protective potential has been described as a function of the disease progression (34). However, during the course of AD, microglia can be hyperactivated by accumulating danger-associated molecular patterns (DAMPs), mainly Aβ and tau, and secrete neurotoxic and inflammatory cytokines that cause persistent neuroinflammation and initiate/exacerbate neurodegeneration (35–38). The focus on neuroinflammation and inflammasome activation as cause of neuronal damage in AD (39–43) leads to assessing the role of the inflammatory cytokines generated by inflammasome activation, in particular the IL-1 family cytokines IL-1β and IL-18 (44).

2.1.1 IL-1

In the brain, IL-1β is required for learning and memory processes, but, when expressed at aberrant levels, it is involved in infection- and sterile inflammation-induced cognitive dysfunction (45, 46). It has also been suggested that low levels of IL-1 act in the CNS to perform non-immunological functions, while higher

concentrations could engage brain non-neuronal cells to produce neuroinflammation (47). Notably, brain IL-1β is produced by and target different cells, ranging from microglia, infiltrating leukocytes, astrocytes, to neurons. By activating different specific cell types, including endothelial cells, neurons and choroid plexus cells, IL-1 may exert different functions of both immunological and non-immunological nature, and neuroinflammation itself may be the result of multiple responses to IL-1 by different brain cell types (8).

In AD, IL-1β is an important mediator of neuroinflammation (48, 49), but also a protective factor (50), able to influence the balance between beneficial and detrimental outcomes (51). In mice lacking the gene encoding the IL-1 inhibitor IL-1Ra the AD-like pathology is exacerbated (52), while the IL-1R1 blockade results in decreased neuroinflammation, attenuated tau pathology and reversal of cognitive deficits (53). Modulation of levels of IL-1Ra or different IL-1R has been observed in brain and blood of AD patients (54–58). Overall, the available experimental and clinical data do not support an exclusively detrimental role of IL-1-driven inflammation in AD.

2.1.2 IL-18

IL-18, its receptors IL-1R5 and IL-1R7 and its inhibitory protein (IL-18BP) are normally expressed in the brain and modulated in both experimental and clinical AD conditions (21). Similar to IL-1, IL-18 could exert both detrimental and protective functions in AD. Thus, while IL-18 dysregulation has been observed in AD patients in association with severity of symptoms and correlated to increased Aβ production *in vitro* (59–62), a protective function has been also reported in IL-18-deficient mice in both physiological (63) and AD-like conditions (64).

2.1.3 IL-33

A third IL-1 family cytokine, IL-33, is being explored in CNS diseases (65). IL-33 is constitutively expressed in astrocytes and to a minor extent in oligodendrocytes, microglia and neurons; its receptor IL-1R4 is expressed on astrocytes, endothelial cells, glial cells and neurons (6). IL-33 can induce microglia cell proliferation and production of inflammatory IL-1β and TNFα, and anti-inflammatory IL-10 (66). In animal models, IL-33 decreases inflammatory responses and improves AD-like pathology (67). In patients, IL-33 expression in the brain is variably modulated relative to healthy subjects (68, 69). Patients with measurable circulating IL-33 levels have preserved cognitive functions, compared with those that do not express the cytokine (70). Eventually, in MCI patients treated with the neuroprotective compound homotaurine, the improvement of cognitive functions correlates with increased IL-33 plasma levels (71), confirming the potential protective role of this cytokine in AD development.

2.2 Mechanisms of IL-1/IL-1R family in AD pathology

IL-1β, IL-18 and IL-33 are dysregulated in AD and likely exerting a dual role: driving the inflammatory pathogenic processes associated with the disease and providing protection to the damaged CNS. The functions of these mediators in brain homeostasis and pathology can be pleiotropic, redundant, synergic and cross-regulating, aiming to switch off or amplify the inflammatory response in a context-dependent manner. In this scenario, the IL-1R signaling could lead to the production of inflammatory cytokines and participate in Aβ-induced inflammasome activation in microglia, while it might even increase the Amyloid Precursor Protein non-amyloidogenic processing in neurons, thereby preventing neurotoxic Aβ generation (72). Overall, whether and when the different molecules belonging to the IL-1/IL-1R family are either beneficial or detrimental to neuronal function in the course of AD, and how their negative feedback mechanisms influence this, is still a matter of intense research (39). However, the general deregulation of IL-1 family members observed in patients consistently reflect the AD-linked activation of the innate immune system, strongly suggesting that an inflammatory condition, although not exclusively detrimental or beneficial, is indisputably present in AD.

It is likely that neuroinflammation is both a response to Aβ and tau NFT that exacerbates their deleterious effects, and a cause of the disease, that increases brain deposit of Aβ and tau phosphorylation starting before onset of symptoms (73, 74). Convincing new data in patients show that microglia activation and consequent neuroinflammation are associated with disease development and progression (75). The infectious hypothesis (76, 77) offers a fascinating explanation of the etiological meaning of inflammation in the disease and the underlying role of IL-1 family cytokines. According to the observation that Aβ has antimicrobial functions (78), several microbial infections (herpesviruses, periodontal bacteria, gut microbiota dysbiosis) have been associated to AD. By inducing inflammasome activation, infectious agents can induce the release of IL-1 family cytokines, which can contribute to blood brain barrier alterations, amplify pre-existing inflammation in the brain, influence Aβ pathology (note that infections upregulate Aβ production) and tau-related neurodegeneration. Indeed, it has been proposed that the AD pathology can be modulated by innate immune mechanisms associated with infectious burden, including long-term innate memory, which affect epigenetic reprogramming of microglia and the release of IL-1 family cytokines (79, 80).

3 Multiple sclerosis

3.1 Pathology and inflammation

Multiple sclerosis (MS) is a chronic inflammatory neurological disorder driven by myelin-targeting $CD4^+$ T cells. The two main disease phenotypes are the relapsing-remitting form (RRMS) and the primary progressive MS, with a steady loss of function (PPMS) (81, 82). RRMS patients may evolve to a progressive disease course, diagnosed as secondary progressive MS (SPMS). The characteristic demyelinating lesions are localized in both white and grey matter, and contain an abundant inflammatory infiltrate with activated macrophages, microglia, $CD8^+$ and $CD4^+$ T cells, B and plasma cells (83). Inflammatory mediators released by innate and adaptive

immune cells lead to damage of oligodendrocytes, the cells responsible for myelin deposition, and axonal injury. A wealth of information, in particular in experimental models, suggests a role for the gut microbiota in bidirectionally modulating brain inflammation in MS, with changes in bacterial composition inducing upregulation *vs*. downregulation of the production of IL-1β and other inflammation-related factors (84–87).

3.1.1 IL-1β

Acting on astrocytes and endothelial cells, IL-1β increases the permeability of the blood-brain barrier and allows leukocyte recruitment (88); acting on T cells, it induces the encephalitogenic phenotype of Th17 (89). *IL1B* transcript and IL-1β protein are detected in CNS lesions of MS patients (88), and microglia display an intense IL-1β staining (90). Changes in IL-1 levels in sera and cerebro-spinal fluid (CSF) are non-univocal, possibly due to patients' heterogeneity and the interference of therapies. Elevated serum levels of IL-1β were reported (91), and the difference with normal subjects was higher for untreated RRMS patients with active disease (92). Other authors report normal levels of IL-1α and IL-1β in active patients, who however had received immunosuppressive therapy (93). Conflicting data have been obtained also in the analysis of CSF. Markedly increased levels of IL-1β in CSF were reported by some authors (91, 94) but not confirmed by others (95, 96). The possible relationship between IL-1β levels and disease activity is also challenged by the observation that in a group of active patients neither serum nor CSF levels were affected by high dose steroid treatment (91).

Soluble inhibitors and decoy receptors are also modulated in MS. IL-1Ra, undetectable in normal CNS, is expressed in lesional foamy macrophages, which also express the anti-inflammatory factors IL-10 and Transforming Growth Factor β, and markers typical of anti-inflammatory M2 macrophages (97). IL-1Ra levels are significantly higher in CSF but not in serum, and even if not correlated with disease activity, they are further increased by steroid treatment (91). IL-1Ra levels are strongly related with disability index, suggesting the potential role of IL-1Ra as serum biomarker of disease progression (98). On the contrary, the soluble decoy receptor IL-1R2 is not elevated in serum compared to normal controls, but steroid treatment induces an increase of its levels (91). In CSF, sIL-1R2 is undetectable irrespective of the disease stage. Finally, soluble IL-1R3 levels are significantly elevated in sera and CSF of MS patients, but not related to disease activity and not modulated by therapy.

3.1.2 IL-18

IL-18 levels were elevated in sera (99–101) and also in CSF, especially in patients with active lesions (99). The findings in CSF, however, were not confirmed in other studies (102). An increase in serum IL-18 levels is detected in untreated RRMS (93) but also in SPMS (102). As observed in most inflammatory disorders, the increase in IL-18 serum levels is accompanied by a parallel increase in its soluble inhibitor IL-18BP, aimed at counteracting the IL-18 inflammatory effects. Although free IL-18 was not evaluated, the IL-18BP/IL-18 ratio was higher in RRMS patients than in controls (93).

3.1.3 Other IL-1 family members

IL-33 has been extensively investigated in MS and EAE. The expression levels of both the cytokine and its receptor IL-1R4 are increased in lesions of MS patients and EAE mice (65, 103). Serum levels of IL-33 are elevated in patients and decreased by treatment with IFNβ (103). Longitudinal assessment of peripheral expression of IL-33 in RRMS revealed peak expression after relapses, but a clear correlation with clinical recovery was not demonstrated (104). In EAE mice, administration of IL-33 attenuates the disease, while antibody-mediated or genetic blockade exacerbates it (105–107). Similarly, IL-1R4 deficient mice develop a severe form of EAE. In this model, IL-33 induces M2 macrophage polarization indirectly, by stimulating mast cells to produce IL-13, and M2 cells then limit the expansion of pathogenic Th17 cells (108). The contribution of IL-1R4$^+$ Treg, activated by IL-33, should also be taken into account. Controversial results have been obtained on the direct effect of IL-33 on myelination (109, 110), but on the whole the data are consistent with the notion that IL-33 is involved in neuroprotection and repair.

Interesting data underline the role of IL-37, an anti-inflammatory member of the IL-1 family. Intracellularly, IL-37 acts as an anti-inflammatory transcriptional regulator. Extracellularly, IL-37 signaling is allegedly mediated by a receptor complex formed by IL-1R5 and IL-1R8. IL-37 is barely detectable in PBMC from normal or MS patients; in the brain, its low expression levels are further downregulated in active MS lesions (111). Notably, the level of IL-37 gene expression in PBMC of MS patients is associated with a lower number of relapses (112). IL-1R5 and IL-1R8 are expressed at similar levels in PBMC and brain from normal or MS patients, and the levels of IL-1R5 (which is also the receptor for IL-18) tend to increase in active lesions. In sera, IL-37 is detectable in 8% of RRMS patients in a stable disease phase and 42% in the active stage; its levels are increased by treatment with a disease-modifying agent, fingolimod (112). Data from patients suggest that the anti-inflammatory activity of IL-37 may be defective in MS, as also confirmed by animal experiments. EAE is milder in transgenic mice expressing human IL-37, with reduced inflammatory infiltrate and decreased numbers of Th1 cells and inflammatory macrophages in lesions (111). This beneficial effect of IL-37 on EAE is lost in mice lacking IL-1R8, indicating that the cytokine confers protection acting through the inhibitory receptor IL-1R8. Moreover, administration of recombinant IL-37 reduces neurological deficits and demyelination in EAE mice. Thus, IL-37 is protective in neuroinflammation and may represent a novel treatment in MS.

4 The NLRP3 inflammasome

The NOD-like receptor 3 (NLRP3) inflammasome, a multiprotein complex that regulates production and release of inflammatory cytokines, in the brain is mainly expressed in microglia but also in astrocytes and neurons. Besides being involved in protection from bacterial, fungal and viral agents, NLRP3 plays a role in neurodevelopment and neuroprotection, but its aberrant activation is crucial in neuroinflammation (113).

Different pathways, including impaired autophagy and dysregulated cell death mechanisms, upregulate NLRP3 activity in AD (114). Aβ and tau can directly activate NLRP3 in microglia (115–117), and several compounds that ameliorate AD-associated pathology reduce NLRP3 activity.

Strong evidence points to a critical role of inflammasome activation in MS. Caspase-1 is more expressed in peripheral blood mononuclear cells (PBMC) of MS patients than in controls (118). Its serum levels can be considered a biomarker of MS, even if they do not identify more active or more severe patients (101). In untreated patients, upregulation of NLRP3 gene expression and higher caspase 1 activity were detected in circulating monocytes (119). NLRP3 upregulation characterized patients with PPMS and was associated with hyperexpression of several inflammatory chemokines and cytokines. IL-1β was one of the most expressed genes, correlated with faster disease progression in PPMS (119). There is a marked increase in the number of IL-1β, caspase-1, and gasdermin D (GSDMD)-positive cells in white matter of MS versus non-MS patients. GSDMD, activated by inflammatory caspases, forms membrane pores responsible for pyroptosis an inflammasome-driven programmed cell death (120). In MS lesions, inflammasome activation and pyroptosis are detected in microglia and oligodendrocytes, suggesting a role in demyelination. Inhibition of inflammasome activation and caspase-1-dependent IL-1β production have already been exploited in MS therapy: IFNβ treatment reduces NLRP3 activity and induces IL-10, thus decreasing the production of pro-IL-1α, pro-IL-1β and mature cytokines (121).

In experimental autoimmune encephalomyelitis (EAE), the mouse MS model, blockade of caspase-1 expression or activity attenuates neuroinflammation (122). Caspase-1 inhibition also reduces GSDMD activation and pyroptosis, limiting oligodendrocyte death and demyelination (120). Similarly, NLRP3 KO or IL-18 KO mice have a less severe disease course, with a marked reduction of CNS inflammatory infiltrate (123, 124). Microglia-specific deletion of the gene encoding the NFκB regulatory protein A20 leads to microglial cell proliferation, susceptibility to LPS-induced inflammation and increased EAE severity, reversed by NLRP3 or caspase-1 genetic deletion (125), indicating a critical role of microglia in MS, mediated by inflammasome activation. The inflammasome involvement in neuroinflammation is also suggested by data in a cohort of MS patients, in which low penetrance mutations of the NLRP3 gene were detected in 16% of the cases (126). These mutations are associated with mild symptoms (suggestive of autoinflammatory disease) and increased production of IL-1β and IL-18 (127).

5 IL-1 family molecules in other main neurodegenerative diseases

Inflammation is involved in other neurological diseases, both neurodegenerative (see below) and of traumatic or other origin (trauma, stroke, autism, schizophrenia, epilepsy). Focusing on neurodegenerative disorders, these are classified in four main groups: amyloidoses, tauopathies, alpha-synucleinopathies, and TDP (transactivation response DNA binding protein)-43 proteinopathies, all characterised by abnormal protein conformations and the formation of protein aggregates in neuronal cells in different brain areas (128, 129). AD is the most common and prevalent of both amyloidoses and tauopathies, along with frontotemporal dementia with parkinsonism and some forms of prion diseases. Main α-synuclein-related diseases include Parkinson's disease (PD), Dementia with Lewy Bodies, and Multiple System Atrophy, while Amyotrophic Lateral Sclerosis (ALS) is mainly associated with TDP-43 pathology. The Huntington disease (HD) is associated with mutations in the huntingtin protein, which clumps within neurons provoking cell damage and death (130).

Although it is well known and documented that all neurodegenerative diseases share the chronic aberrant inflammation (131), less is known on the role of IL-1 family cytokines and receptors in specific neurodegenerative diseases (132). In addition to AD and MS, reviewed in the previous sections, here we will briefly examine the involvement of IL-1 family molecules in PD, HD, and ALS.

PD is characterised by the death of dopaminergic neurons in the *substantia nigra* and by the cytoplasmatic aggregation of fibrillar α-synuclein in Lewy bodies (133). Increase of α-synuclein released outside the cells drives the activation of microglia, and the microglia-dependent production of TNF-α, NO, and IL-1β sustains the neuroinflammatory process in PD (134). Recent results in the 6-OHDA mouse model showed that the increased levels of IL-1β and TNF-α have a different kinetics, with TNF-α appearing in the advanced disease stage, while increased level of IL-1β in serum were already evident with a moderate degree of lesion in *substantia nigra*, suggesting a prognostic value for this inflammatory cytokine (135). Although the results on the level and role of IL-1β in PD patients are conflicting (136), the activation of the NLRP3 inflammasome seems to be determinant for the development of PD at least *in vitro*. Indeed, when activated, the inflammasome can cause the aggregation of α-synuclein in a neuronal cell model of PD, as caspase-1 directly cleaves α-synuclein generating a truncated protein highly prone to aggregation and able to provoke cell death (137). The involvement of the NLRP3 inflammasome activation in PD also includes two additional mechanisms, the interaction with the parkin protein, whose mutations are responsible of autosomal recessive familial and sporadic early-onset PD (138, 139); and the association with mitochondrial dysfunction that affects neuron performance and favours neuronal degeneration (140). Although IL-1β is a major product of the NLRP3 inflammasome activation, its role in causing/sustaining inflammation in PD patients is still debated (141).

Increasing evidence suggest that inflammation contributes to the development of HD, but the involvement of IL-1 family is still poorly known. The role of IL-1β has been investigated in mice expressing a mutant and pathogenic huntingtin crossed with animals knocked out for IL-1R1 (142). These mice showed more severe neurological symptoms compared to control mice expressing IL-1R1, suggesting a protective role for IL-1R1 signalling in preventing the HD neuropathology. Whether IL-1β is the

molecule that activates IL-1R1 signalling is not known. Although IL-1β has been identified as one of the inflammation-related markers of the disease in the porcine HD model (143), its level does not increase in plasma of HD patients, at variance with IL-6 or other inflammatory factors (144, 145). An involvement of the NLRP3 inflammasome has been also suggested for HD, although evidence is still poor and mostly from pre-clinical studies (146).

ALS is a neuromuscular disorder characterized by the progressive loss of anterior-lateral horn spinal cord motoneurons (147). Sporadic ALS affects the 90-95% of patients, while the familiar form affects the remaining 5-10% of patients. The two most relevant genetic mutations associated with ALS are a defect in the hexanucleotide repeat expansion (HRE) in intron 1 of the *C9orf72* gene (which makes a protein that regulates actin dynamics and endosomal recycling of GluR1 at the synapse) (148), and in the free radical scavenging enzyme Cu,Zn-superoxide dismutase (SOD1) gene (149). The involvement of inflammation in the etiopathogenesis of ALS is starting to be investigated, but studies are still limited (150, 151). In a recent study, the authors suggest hyperinflammation and immunodeficiency as primary triggers of motoneuron death in ALS, and underline the complex link between the development ALS and T cell and monocyte profiles of patients, as well as polymorphisms in cytokine and chemokine receptors, suggesting a need for personalised therapies based on immunophenotyping (152). In this regard, recently new polymorphisms in the gene encoding IL-1β and in genes involved in oxidative stress (*e.g.*, SOD2) have been identified as modifiers of ALS progression (153). IL-1β is one of the main biomarkers of inflammation in ALS (151, 152). Even if it is not the best marker of ALS severity (154), its plasma levels negatively correlate with survival in ALS patients with genetic variant *C9orf72HRE* (155). Among the IL-1 family cytokines and receptors, it has been observed that only IL-18 is associated with sporadic ALS, whereas the serum levels of the cytokines IL-33 and IL-36 and the soluble receptors sIL-1R2 and sIL-1R4 were comparable between ALS patients and healthy controls, and IL-1β, IL-1Ra and IL-37 were below detection (156). The possible pathogenic role of IL-18 in ASL has been also recently underlined by a Whole Genome Sequencing study, which identified a genetic variant in a noncoding region of the gene encoding the IL-18 receptor accessory protein (*IL18RAP*) able to reduce mRNA stability and motor neuron neurotoxicity, thereby decreasing 5x the risk of developing ALS (157). A protective role has been suggested for another member of IL-1 family, IL-33 (158). In the ALS mouse model transgenic for G93A-superoxide dismutase 1 (*SOD1-G93A*), long-term IL-33 administration delays disease onset in females but not males, probably through peripheral Th2 response (159).

6 Conclusions and perspectives

The role of IL-1 family cytokines and receptors in the etiology and pathogenesis of neurodegenerative diseases is still poorly understood. However, there is strong evidence of their involvement in the initiation

TABLE 1 IL-1 family cytokines and receptors in brain physiology and pathology.

Cytokine/ receptor	Physiological role	Role in pathogenesis	Role in pathology	References
IL-1β	• Learning and memory processes •Thermoregulation	• Induction of inflammation •Induction of fever	• Persistence of inflammation •Neurodegeneration	(7–10, 45–51, 88–92)
IL-1Ra	• Unknown (regulation of IL-1 activity)	• Unknown	•Increased with disease (feedback mechanism)?	(52, 91, 97, 98)
IL-18	•Neuroprotective	•Induction of inflammation	•Persistence of inflammation	(21, 59–64)
IL-18BP	• Unknown (regulation of IL-18 activity)	• Unknown	• Increases with disease (feedback mechanism)?	(93)
IL-33	• Regulates microglia proliferation • Regulates the microglial inflammatory/anti-inflammatory balance	• Anti-inflammatory protective effects	• Upregulated in pathology • Negative correlation with disease severity	(6, 65–71, 103, 108)
IL-37	• Unknown	• Anti-inflammatory protective effects	• Downregulated in active disease • Negative correlation with disease severity	(111, 112)
IL-1R3b	• Accessory receptor mediating the neuroprotective effects of IL-1	• Unknown	• Unknown	(16, 18)
IL-1R4	• Mediates the homeostatic activities of IL-33	• Unknown	• Soluble form upregulated during disease (feedback mechanism)?	(6, 108)
IL-1R5	• Mediates the homeostatic activities of IL-18	• Associated with disease pathogenesis in EAE	• Unknown	(21, 111)
IL-1R8	• Anti-inflammatory orphan receptor; physiological role unknown	• Unknown	• Necessary for the neuroprotective role of IL-37	(111)
IL-1R9	• Orphan receptor, involved in learning and memory processes	• Unknown (mutations are associated with X-linked mental retardation, schizophrenia and autism)	• Unknown	(19, 20)

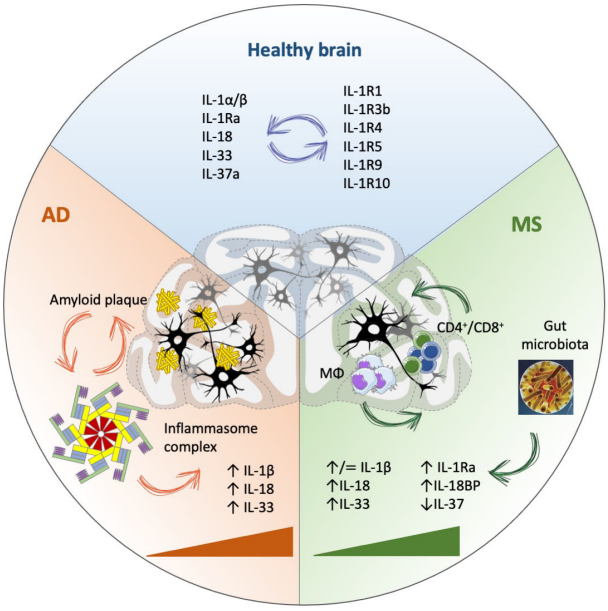

FIGURE 1
IL-1 family involvement in Alzheimer's disease (AD) and Multiple Sclerosis (MS). IL-1 family cytokines and receptors are crucial in maintaining brain homeostasis, with an important role in the modulation of neuronal plasticity and function, in addition to mediating immune protective functions. In physiological conditions, many activities of IL-1 family cytokines depend on binding to specific receptors, but independent functions have been observed for both cytokines (*e.g.*, IL-18) and receptors (*e.g.*, IL-1R9). In disease conditions (AD, MS), IL-1 family members are substantially modulated during disease progression (triangles), associated with increased inflammation (partly dependent on inflammasome activation) and likely involved in all disease phases, from initiation and establishment to progression, without a clear association with either disease initiation or progression. MΦ, macrophages.

and regulation of inflammation associated to most CNS diseases, and their participation to neuroinflammation has been widely described in AD an MS. This is evident despite the limitations due to the current lack of reliable animal models that realistically recapitulate the pathological features of the human diseases, such as in the case of sporadic AD (160). In humans, longitudinal molecular monitoring of inflammation is also hampered by the reduced accessibility of human brain and the limited availability of clinical studies with extensive follow-ups (161, 162).

From the combined *in vivo* and *in vitro* functional and molecular evidence, it is clear that these factors play a homeostatic and neuroprotective role in healthy conditions. It is notable that the IL-1 family system in the CNS includes several molecules and functions that are CNS-restricted, implying tissue-specific needs and consequent functional adaptation. Disease conditions imply an imbalance of the IL-1 system network (Table 1).

From the available experimental and clinical evidence, we can draw the following conclusions and suggestions.

- IL-1 family cytokines and receptors are altered in AD and MS and related to the neuroinflammatory conditions.
- Alterations in the amount of produced inflammatory cytokines (IL-1, IL-18) likely switch their role from neuroprotection/homeostasis to pathological inflammation.
- The excess of inflammatory cytokines causes an excessive induction of feedback mechanisms, *e.g.*, the production of downregulating factors (IL-1Ra, IL-18BP, IL-33, IL-37), which however do not succeed in rebalancing the excessive inflammation.
- Unbalanced IL-1 family molecules contribute to alterations in adaptive immune responses, thereby amplifying the autoimmune aspects of neurodegenerative diseases.
- Whether anomalies in the IL-1 family cytokine and receptor network are cause or effect of neuroinflammation and neurodegeneration in AD and MS is not an appropriate question, as it seems that these factors are involved in all steps of disease, from its induction to its establishment and downstream symptoms (Figure 1).
- The CNS-restricted peculiarities of the network of IL-1 family cytokines and receptors suggest a tissue-specific physiological balance and pathological dysregulation. A more thorough understanding of the CNS specificities in the IL-1 family system will open the way to a precision rebalancing approach for therapeutic purposes.

Author contributions

DB, PM, PI and PB wrote the manuscript and critically revised it. DB and PI contributed to figures and tables. All authors contributed to the article and approved the submitted version.

Funding

This work was supported by the EU Commission H2020 projects PANDORA (GA671881) and ENDONANO (GA 812661) (PI, DB), the project MIUR/PRIN-20173ZECCM of the Italian Ministry of Research (PI) and the projects RC 2018-2021, ADIMB, CoEN 2019-Pathfinder IV and RF-2021-12374301 by the Italian Ministry of Health (PB).

Conflict of interest

The reviewer JB declared a shared affiliation, with no collaboration, with one of the authors, DB, to the handling editor at the time of the review.

The remaining authors declare that the research was conducted in the absence of any commercial or financial relationships that could be construed as a potential conflict of interest.

Publisher's note

References

1. Dinarello CA. Overview of the IL-1 family in innate inflammation and acquired immunity. *Immunol Rev* (2018) 281:8–27. doi: 10.1111/imr.12621

2. Boraschi D, Italiani P, Weil S, Martin MU. The family of the interleukin-1 receptors. *Immunol Rev* (2018) 281:197–232. doi: 10.1111/imr.12606

3. Rivers-Auty J, Daniels MJD, Colliver I, Robertson DL, Brough D. Redefining the ancestral origins of the interleukin-1 superfamily. *Nat Commun* (2018) 9:1156. doi: 10.1038/s1467-018-03362-1

4. Boraschi D. What is IL-1 for? the functions of IL-1 across evolution. *Front Immunol* (2021) 13:872155. doi: 10.3389/fimmu.2022.872155

5. Alboni S, Cervia D, Sugama S, Conti B. Interleukin 18 in the CNS. *J Neuroinflamm* (2010) 7:9. doi: 10.1186/1742-2094-7-9

6. Fairlie-Clarke K, Barbour M, Wilson C, Hridi SU, Allan D, Jiang H-R. Expression and function of IL-33/ST2 axis in the central nervous system under normal and diseased conditions. *Front Immunol* (2018) 9:2596. doi: 10.3389/fimmu.2018.02596

7. Liu X, Quan N. Microglia and CNS interleukin-1: beyond immunological concepts. *Front Neurol* (2018) 9:8. doi: 10.3389/fneur.2018.00008

8. Liu X, Nemeth DP, McKim DB, Zhu L, DiSabato DJ, Berdysz O, et al. Cell-type-specific interleukin 1 receptor 1 signaling in the brain regulates distinct neuroimmune activities. *Immunity* (2019) 50:317. doi: 10.1016/j.immuni.2018.12.012

9. Dinarello CA. Cytokines as endogenous pyrogens. *J Infect Dis* (1999) 179:S294–304. doi: 10.1086/513856

10. El-Rahi AS. Pathogenesis of fever. In: *Clinical manual of fever in children, nature public health emergency collection* (2019). Springer, Cham. p. 53–68. doi: 10.1007/978-3-319-92336-9_3

11. Smith DE, Lipsky BP, Russell C, Ketchem RR, Kirchner J, Hensley K, et al. A novel CNS-restricted isoform of the IL-1R accessory protein modulates neuronal responses to IL-1. *Immunity* (2009) 30:817. doi: 10.1016/j.immuni.2009.03.020

12. Andre R, Wheeler RD, Collins PD, Luheshi GN, Pickering-Brown S, Kimber I, et al. Identification of a truncated IL-18Rβ mRNA: a putative regulator of IL-18 expressed in rat brain. *J Neuroimmunol* (2003) 145:40–5. doi: 10.1016/j.jneuroim.2003.09.005

13. Alboni S, Cervia D, Ross B, Montanari C, Gonzalez AS, Sanchez-Alavez M, et al. Mapping of the full length and the truncated interleukin-18 receptor alpha in the mouse brain. *J Neuroimmunol* (2009) 214:43–54. doi: 10.1016/j.jneuroim.2009.06.016

14. Alboni S, Montanari C, Benatti C, Blom JMC, Simone ML, Brunello N, et al. Constitutive and LPS-regulated expression of interleukin-18 receptor beta variants in the mouse brain. *Brain Behav Immun* (2011) 25:483–93. doi: 10.1016/j.bbi.2010.11.011

15. Boraschi D, Lucchesi D, Hainzl S, Leitner M, Maier E, Mangelberger D, et al. IL-37: an anti-inflammatory cytokine of the IL-1 family. *Eur Cytokine Netw* (2011) 22:127–47. doi: 10.1684/ecn.2011.0288

16. Smith DE, Lipsky BP, Russell C, Ketchem RR, Kirchner J, Hensley K, et al. A central nervous system-restricted isoform of the interleukin-1 receptor accessory protein modulates neuronal responses to interleukin-1. *Immunity* (2009) 30:817–31. doi: 10.1016/j.immuni.2009.03.020

17. Nguyen L, Rothwell NJ, Pinteaux E, Boutin H. Contribution of interleukin-1 receptor accessory protein b to interleukin-1 actions in neuronal cells. *Neurosignals* (2011) 19:222–30. doi: 10.1159/000330803

18. Huang Y, Smith DE, Ibáñez-Sandoval O, Sims JE, Fridman WJ. Neuron-specific effects of interleukin-1β are mediated by a novel isoform of the IL-1 receptor accessory protein. *J Neurosci* (2011) 31:18048–59. doi: 10.1523/JNEUROSCI.4067-11.201

19. Carrié A, Jun L, Bienvenu T, Vinet MC, McDonell N, Couvert P, et al. A new member of the IL-1 receptor family highly expressed in hippocampus and involved in X-linked mental retardation. *Nat Genet* (1999) 23:25–31. doi: 10.1038/12623

20. Piton A, Michaud JL, Peng H, Aradhya S, Gauthier J, Mottron L, et al. Mutations in the calcium-related gene IL1RAPL1 are associated with autism. *Hum Mol Genet* (2008) 17:3965–74. doi: 10.1093/hmg/ddn300

21. Bossù P, Ciaramella A, Salani F, Vanni D, Palladino I, Caltagirone C, et al. Interleukin-18, from neuroinflammation to alzheimer's disease. *Curr Pharm Des* (2010) 16:4213–24. doi: 10.2174/138161210794519147

22. Gutcher I, Urich E, Wolter K, Prinz M, Becher B. Interleukin 18-independent engagement of interleukin 18 receptor-α is required for autoimmune inflammation. *Nat Immunol* (2006) 7:946–53. doi: 10.1038/ni1377

23. 2022 alzheimer's disease facts and figures. *Alzheimer's Dementia* (2022) 18:700–89. doi: 10.1002/alz.12638

24. McGeer PL, McGeer EG. The amyloid cascade-inflammatory hypothesis of Alzheimer disease: implications for therapy. *Acta Neuropathol* (2013) 126:479–97. doi: 10.1007/s00401-013-1177-7

25. Kinney JW, Bemiller SM, Murtishaw AS, Leisgang AM, Salazar AM, Lamb BT. Inflammation as a central mechanism in alzheimer's disease. *Alzheimers Dement* (2018) 4:575–90. doi: 10.1016/j.trci.2018.06.014

26. Bellenguez C, Küçükali F, Jansen IE, Kleineidam L, Moreno-Grau S, Amin N, et al. New insights into the genetic etiology of alzheimer's disease and related dementias. *Nat Genet* (2022) 54:412–36. doi: 10.1038/s41588-022-01024-z

27. Heneka MT, Carson MJ, El Khoury J, Landreth GE, Brosseron F, Feinstein DL, et al. Neuroinflammation in alzheimer's disease. *Lancet Neurol* (2015) 14:388–405. doi: 10.1016/S1474-4422(15)70016-5

28. Ennerfelt HE, Lukens JR. The role of innate immunity in alzheimer's disease. *Immunol Rev* (2020) 297:225–46. doi: 10.1111/imr.12896

29. Rezai-Zadeh K, Gate D, Town T. CNS infiltration of peripheral immune cells: d-day for neurodegenerative disease? *J Neuroimmune Pharmacol* (2009) 4:462–75. doi: 10.1007/s11481-009-9166-2

30. Mildner A, Schlevogt B, Kierdorf K, Bottcher C, Erny D, Kummer MP, et al. Distinct and non-redundant roles of microglia and myeloid subsets in mouse models of alzheimer's disease. *J Neurosci* (2011) 31:11159–71. doi: 10.1523/JNEUROSCI.6209-10.2011

31. Le Page A, Dupuis G, Frost EH, Larbi A, Pawelec G, Witkowski JM, et al. Role of the peripheral innate immune system in the development of alzheimer's disease. *Exp Gerontol* (2018) 107:59–66. doi: 10.1016/j.exger.2017.12.019

32. Fani Maleki A, Rivest S. Innate immune cells: monocytes, monocyte-derived macrophages and microglia as therapeutic targets for alzheimer's disease and multiple sclerosis. *Front Cell Neurosci* (2019) 13:355. doi: 10.3389/fncel.2019.00355

33. Leng F, Edison P. Neuroinflammation and microglial activation in Alzheimer disease: where do we go from here? *Nat Rev Neurol* (2020) 17:157–72. doi: 10.1038/s41582-020-00435-y

34. Keren-Shaul H, Spinrad A, Weiner A, Matcovitch-Natan O, Dvir-Szternfeld R, Ulland TK, et al. A unique microglia type associated with restricting development of alzheimer's disease. *Cell* (2017) 169:1276–90.e17. doi: 10.1016/j.cell.2017.05.018

35. Cuello AC. Early and late CNS inflammation in alzheimer's disease: two extremes of a continuum? *Trends Pharmacol Sci* (2017) 38:956–66. doi: 10.1016/j.tips.2017.07.005

36. Hickman S, Izzy S, Sen P, Morsett L, El Khoury J. Microglia in neurodegeneration. *Nat Neurosci* (2018) 21:1359–69. doi: 10.1038/s41593-018-0242-x

37. Hansen DV, Hanson JE, Sheng M. Microglia in alzheimer's disease. *J Cell Biol* (2018) 217:459–72. doi: 10.1083/jcb.201709069

38. Cai Y, Liu J, Wang B, Sun M, Yang H. Microglia in the neuroinflammatory pathogenesis of alzheimer's disease and related therapeutic targets. *Front Immunol* (2022) 13:856376. doi: 10.3389/fimmu.2022.856376

39. Lau S-F, Fu AKY, Ip NY. Cytokine signaling convergence regulates the microglial state transition in alzheimer's disease. *Cell Mol Life Sci* (2021) 78:4703–12. doi: 10.1007/s00018-021-03810-0

40. Passaro AP, Lebos AL, Yao Y, Stice SL. Immune response in neurological pathology: emerging role of central and peripheral immune crosstalk. *Front Immunol* (2021) 12:676621. doi: 10.3389/fimmu.2021.676621

41. Bai H, Zhang Q. Activation of NLRP3 inflammasome and onset of alzheimer's disease. *Front Immunol* (2021) 12:701282. doi: 10.3389/fimmu.2021.701282

42. Milner MT, Maddugoda M, Götz J, Burgener SS, Schroder K. The NLRP3 inflammasome triggers sterile neuroinflammation and alzheimer's disease. *Curr Opin Immunol* (2021) 68:116–24. doi: 10.1016/j.coi.2020.10.011

43. Liang T, Zhang Y, Wu S, Chen Q, Wang L. The role of NLRP3 inflammasome in alzheimer's disease and potential therapeutic targets. *Front Pharmacol* (2022) 13:845185. doi: 10.3389/fphar.2022.845185

44. Chan AH, Schroder K. Inflammasome signaling and regulation of interleukin-1 family cytokines. *J Exp Med* (2019) 217:e20190314. doi: 10.1084/jem.20190314

45. Yirmiya R, Goshen I. Immune modulation of learning, memory, neural plasticity and neurogenesis. *Brain Behav Immun* (2011) 25:181–213. doi: 10.1016/j.bbi.2010.10.015

46. Skelly DT, Griffin ÉW, Murray CL, Harney S, O'Boyle C, Hennessy E, et al. Acute transient cognitive dysfunction and acute brain injury induced by systemic inflammation occur by dissociable IL-1-dependent mechanisms. *Mol Psychiatry* (2019) 24:1533–48. doi: 10.1038/s41380-018-0075-8

47. An Y, Chen Q, Quan N. Interleukin-1 exerts distinct actions on different cell types of the brain in vitro. *J Inflammation Res* (2011) 2011:11. doi: 10.2147/JIR.S15357

48. Mrak RE, Griffin WST. Interleukin-1 and the immunogenetics of Alzheimer disease. *J Neuropathol Exp Neurol* (2000) 59:471. doi: 10.1093/jnen/59.6.471

49. Allan SM, Tyrrell PJ, Rothwell NJ. Interleukin-1 and neuronal injury. *Nat Rev Immunol* (2005) 5:629–40. doi: 10.1038/nri1664

50. Shaftel SS, Kyrkanides S, Olschowka JA, Miller JH, Johnson RE, O'Banion MK. Sustained hippocampal IL-1β overexpression mediates chronic neuroinflammation and ameliorates Alzheimer plaque pathology. *J Clin Invest* (2007) 117:1595. doi: 10.1172/JCI31450

51. Shaftel SS, Griffin WST, O'Banion MK. The role of interleukin-1 in neuroinflammation and Alzheimer disease: an evolving perspective. *J Neuroinflamm* (2008) 5:1–12. doi: 10.1186/1742-2094-5-7

52. Craft JM, Watterson DM, Hirsch E, Van Eldik LJ. Interleukin 1 receptor antagonist knockout mice show enhanced microglial activation and neuronal damage induced by intracerebroventricular infusion of human beta-amyloid. *J Neuroinflamm* (2005) 2:15. doi: 10.1186/1742-2094-2-15

53. Kitazawa M, Cheng D, Tsukamoto MR, Koike MA, Wes PD, Vasilevko V, et al. Blocking IL-1 signaling rescues cognition, attenuates tau pathology, and restores neuronal β-catenin pathway function in an alzheimer's disease model. *J Immunol* (2011) 187:6539–49. doi: 10.4049/jimmunol.1100620

54. Yasuhara O, Matsuo A, Terai K, Walker DG, Berger AE, Akiguchi I, et al. Expression of interleukin-1 receptor antagonist protein in post-mortem human brain tissues of alzheimer's disease and control cases. *Acta Neuropathol* (1997) 93:414–20. doi: 10.1007/s004010050633

55. Taipa R, das Neves SP, Sousa AL, Fernandes J, Pinto C, Correia AP, et al. Proinflammatory and anti-inflammatory cytokines in the CSF of patients with alzheimer's disease and their correlation with cognitive decline. *Neurobiol Aging* (2019) 76:125–32. doi: 10.1016/j.neurobiolaging.2018.12.019

56. Garlind A, Brauner A, Höjeberg B, Basun H, Schultzberg M. Soluble interleukin-1 receptor type II levels are elevated in cerebrospinal fluid in alzheimer's disease patients. *Brain Res* (1999) 826:112–6. doi: 10.1016/S0006-8993(99)01092-6

57. Italiani P, Puxeddu I, Napoletano S, Scala E, Melillo D, Manocchio S, et al. Circulating levels of IL-1 family cytokines and receptors in alzheimer's disease: new markers of disease progression? *J Neuroinflamm* (2018) 15:342. doi: 10.1186/s12974-018-1376-1

58. Zettergren A, Höglund K, Kern S, Thorvaldsson V, Johan Skoog M, Hansson O, et al. Association of IL1RAP-related genetic variation with cerebrospinal fluid concentration of Alzheimer-associated tau protein. *Sci Rep* (2019) 9:2460. doi: 10.1038/s41598-018-36650-3

59. Motta M, Imbesi R, Di Rosa M, Stivala F, Malaguarnera L. Altered plasma cytokine levels in alzheimer's disease: correlation with the disease progression. *Immunol Lett* (2007) 114:46–51. doi: 10.1016/j.imlet.2007.09.002

60. Bossù P, Ciaramella A, Salani F, Bizzoni F, Varsi E, Di Iulio F, et al. Interleukin-18 produced by peripheral blood cells is increased in alzheimer's disease and correlates with cognitive impairment. *Brain Behav Immun* (2008) 22:487–92. doi: 10.1016/j.bbi.2007.10.001

61. Ojala J, Alafuzoff I, Herukka S-K, van Groen T, Tanila H, Pirttilä T. Expression of interleukin-18 is increased in the brains of alzheimer's disease patients. *Neurobiol Aging* (2009) 30:198–209. doi: 10.1016/j.neurobiolaging.2007.06.006

62. Sutinen EM, Pirttilä T, Anderson G, Salminen A, Ojala JO. Pro-inflammatory interleukin-18 increases alzheimer's disease-associated amyloid-β production in human neuron-like cells. *J Neuroinflamm* (2012) 9:199. doi: 10.1186/1742-2094-9-199

63. Yamanishi K, Doe N, Mukai K, Ikubo K, Hashimoto T, Uwa N, et al. Interleukin-18-deficient mice develop hippocampal abnormalities related to possible depressive-like behaviors. *Neuroscience* (2019) 408:147–60. doi: 10.1016/j.neuroscience.2019.04.003

64. Tzeng T-C, Hasegawa Y, Iguchi R, Cheung A, Caffrey DR, Thatcher EJ, et al. Inflammasome-derived cytokine IL18 suppresses amyloid-induced seizures in Alzheimer-prone mice. *Proc Natl Acad Sci USA* (2018) 115:9002–7. doi: 10.1073/pnas.1801802115

65. Sun Y, Wen Y, Wang L, Wen L, You W, Wei S, et al. Therapeutic opportunities of interleukin-33 in the central nervous system. *Front Immunol* (2021) 12:654626. doi: 10.3389/fimmu.2021.654626

66. Yasuoka S, Kawanokuchi J, Parajuli B, Jin S, Doi Y, Noda M, et al. Production and functions of IL-33 in the central nervous system. *Brain Res* (2011) 1385:8–17. doi: 10.1016/j.brainres.2011.02.045

67. Fu AKY, Hung K-W, Yuen MYF, Zhou X, Mak DSY, Chan ICW, et al. IL-33 ameliorates alzheimer's disease-like pathology and cognitive decline. *Proc Natl Acad Sci USA* (2016) 113:E2705–13. doi: 10.1073/pnas.1604032113

68. Chapuis J, Hot D, Hansmannel F, Kerdraon O, Ferreira S, Hubans C, et al. Transcriptomic and genetic studies identify IL-33 as a candidate gene for alzheimer's disease. *Mol Psychiatry* (2009) 14:1004–16. doi: 10.1038/mp.2009.10

69. Xiong Z, Thangavel R, Kempuraj D, Yang E, Zaheer S, Zaheer A. Alzheimer's disease: evidence for the expression of interleukin-33 and its receptor ST2 in the brain. *J Alzheimers Dis* (2014) 40:297–308. doi: 10.3233/JAD-132081

70. Liang C-S, Su K-P, Tsai C-L, Lee J-T, Chu C-S, Yeh T-C, et al. The role of interleukin-33 in patients with mild cognitive impairment and alzheimer's disease. *Alzheimers Res Ther* (2020) 12:86. doi: 10.1186/s13195-020-00652-z

71. Toppi E, Sireno L, Lembo M, Banaj N, Messina B, Golesorkhtafti S, et al. IL-33 and IL-10 serum levels increase in MCI patients following homotaurine treatment. *Front Immunol* (2022) 13:813951. doi: 10.3389/fimmu.2022.813951

72. Wang H, Wang X. Interleukin 1 receptor and alzheimer's disease-related neuroinflammation. in mechanisms of neuroinflammation. *InTech* (2017) 2017. doi: 10.5772/intechopen.69067

73. Zhang B, Gaiteri C, Bodea L-G, Wang Z, McElwee J, Podtelezhnikov AA, et al. Integrated systems approach identifies genetic nodes and networks in late-onset alzheimer's disease. *Cell* (2013) 153:707. doi: 10.1016/j.cell.2013.03.030

74. Zhao J, Zhao D, Wang J, Luo X, Guo R. Inflammation–cause or consequence of late onset alzheimer's disease or both? a review of the evidence. *Eur J Inflammation* (2022) 20. doi: 10.1177/1721727X221095383

75. Pascoal TA, Benedet AL, Ashton NJ, Kang MS, Therriault J, Chamoun M, et al. Microglial activation and tau propagate jointly across braak stages. *Nat Med* (2021) 27:1592–9. doi: 10.1038/s41591-021-01456-w

76. Fulop T, Witkowski JM, Bourgade K, Khalil A, Zerif E, Larbi A, et al. Can an infection hypothesis explain the beta amyloid hypothesis of alzheimer's disease? *Front Aging Neurosci* (2018) 10:224. doi: 10.3389/fnagi.2018.00224

77. Itzhaki RF, Golde TE, Heneka MT, Readhead B. Do infections have a role in the pathogenesis of Alzheimer disease? *Nat Rev Neurol* (2020) 16:193–7. doi: 10.1038/s41582-020-0323-9

78. Soscia SJ, Kirby JE, Washicosky KJ, Tucker SM, Ingelsson M, Hyman B, et al. The alzheimer's disease-associated amyloid β-protein is an antimicrobial peptide. *PLoS One* (2010) 5:e9505. doi: 10.1371/journal.pone.0009505

79. Wendeln A-C, Degenhardt K, Kaurani L, Gertig M, Ulas T, Jain G, et al. Innate immune memory in the brain shapes neurological disease hallmarks. *Nature* (2018) 556:332–8. doi: 10.1038/s41586-018-0023-4

80. Salani F, Sterbini V, Sacchinelli E, Garramone M, Bossù P. Is innate memory a double-edge sword in alzheimer's disease? a reappraisal of new concepts and old data. *Front Immunol* (2019) 10:1768. doi: 10.3389/fimmu.2019.01768

81. Dobson R, Giovannoni G. Multiple sclerosis: a review. *Eur J Neurol* (2019) 26:27–40. doi: 10.1111/ene.13819

82. Cree BAC, Arnold DL, Chataway J, Chitnis T, Fox RJ, Pozo Ramajo A, et al. Secondary progressive multiple sclerosis. *New Insights Neurol* (2021) 97:378–88. doi: 10.1212/WNL.0000000000012323

83. Attfield KE, Torp Jensen L, Kaufmann M, Friese MA, Fugger L. The immunology of multiple sclerosis. *Nat Rev Immunol* (2022) 22:734–50. doi: 10.1038/s41577-022-00718-z

84. Chen J, Chia N, Kalari KR, Yao JZ, Novitna M, Soldan MMP, et al. Multiple sclerosis patients have a distinct gut microbiota compare to healthy controls. *Sci Rep* (2016) 6:1–10. doi: 10.1038/srep28484

85. Cekanaviciute E, Yoo BB, Runia TF, Debelius JW, Singh S, Nelson CA, et al. Gut bacteria from multiple sclerosis patients modulate human T cells and exacerbate

symptoms in mouse models. *Proc Natl Acad Sci USA* (2017) 114:10713–8. doi: 10.1073/pnas.1711235114

86. Rutsch A, Kantsjö JB, Ronchi F. The gut-brain axis: how microbiota and hist inflammasome influence brain physiology and pathology. *Front Immunol* (2020) 11:604179. doi: 10.3389/fimmu.2020.604179

87. Mestre L, Carrillo-Salinas FJ, Feliú A, Mecha M, Alonso G, Espejo C, et al. How oral probiotics affect the severity of an experimental model of progressive multiple sclerosis? bringing commensal bacteria into the neurodegenerative process. *Gut Microbes* (2020) 12:1813532. doi: 10.1080/19490976.2020.1813532

88. Lin CC, Edelson BT. New insights into the role of IL-1β in experimental autoimmune encephalomyelitis and multiple sclerosis. *J Immunol* (2017) 198:4553–60. doi: 10.4049/jimmunol.1700263

89. Lukens JR, Barr MJ, Chaplin DD, Chi H, Kanneganti TD. Inflammasome-derived IL-1β regulates the production of GM-CSF by CD4(+) T cells and γδ T cells. *J Immunol* (2012) 188:3107–15. doi: 10.4049/jimmunol.1103308

90. Burm SM, Peferoen LA, Zuiderwijk-Sick EA, Haanstra KG, 't Hart BA, van der Valk P, et al. Expression of IL-1β in rhesus EAE and MS lesions is mainly induced in the CNS itself. *J Neuroinflamm* (2016) 13:138. doi: 10.1186/s12974-016-0605-8

91. Dujmovic I, Mangano K, Pekmezovic T, Quattrocchi C, Mesaros S, Stojsavljevic N, et al. The analysis of IL-1β and its naturally occurring inhibitors in multiple sclerosis: the elevation of IL-1 receptor antagonist and IL-1 receptor type II after steroid therapy. *J Neuroimmunol* (2009) 207:101–6. doi: 10.1016/j.neuroim.2008.11.004

92. D'Angelo C, Reale M, Costantini E, Di Nicola M, Porfilio I, de Andrés C, et al. Profiling of canonical and non-traditional cytokine levels in interferon-β-treated relapsing-remitting-multiple sclerosis patients. *Front Immunol* (2018) 9:1240. doi: 10.3389/fimmu.2018.01240

93. Thöne J, Kleiter I, Stahl A, Ellrichmann G, Gold R, Hellwig K. Relevance of endoglin, IL-1α, IL-1β and anti-ovarian antibodies in females with multiple sclerosis. *J Neurol Sci* (2016) 362:240–3. doi: 10.1016/j.jns.2016.01.057

94. Hauser SL, Doolittle TH, Lincoln R, Brown RH, Dinarello CA. Cytokine accumulations in CSF of multiple sclerosis patients: frequent detection of interleukin-1 and tumor necrosis factor but not interleukin-6. *Neurology* (1990) 40:1735–9. doi: 10.1212/wnl.40.11.1735

95. Maimone D, Gregory S, Arnason BG, Reder AT. Cytokine levels in the cerebrospinal fluid and serum of patients with multiple sclerosis. *J Neuroimmunol* (1991) 32:67–74. doi: 10.1016/0165-5728(91)90073-g

96. Tsukada N, Miyagi K, Matsuda M, Yanagisawa N, Yone K. Tumor necrosis factor and interleukin-1 in the CSF and sera of patients with multiple sclerosis. *J Neurol Sci* (1991) 104:230–4. doi: 10.1016/0022-510x(91)90315-x

97. Boven LA, Van Meurs M, Van Zwam M, Wierenga-Wolf A, Hintzen RQ, Boot RG, et al. Myelin-laden macrophages are anti-inflammatory, consistent with foam cells in multiple sclerosis. *Brain* (2006) 129:517–26. doi: 10.1093/brain/awh707

98. Blandford SN, Galloway DA, Williams JB, Arsenault S, Brown J, MacLean G, et al. Interleukin-1 receptor antagonist: an exploratory plasma biomarker that correlates with disability and provides pathophysiological insights in relapsing-remitting multiple sclerosis. *Mult Scler Relat Disord* (2021) 52:103006. doi: 10.1016/j.msard.2021.103006

99. Chen YC, Chen SD, Miao L, Liu ZG, Li W, Zhao ZX, et al. Serum levels of interleukin (IL)-18, IL-23 and IL-17 in Chinese patients with multiple sclerosis. *J Neuroimmunol* (2012) 243:56–60. doi: 10.1016/j.jneuroim.2011.12.008

100. Losy J, Niezgoda A. IL-18 in patients with multiple sclerosis. *Acta Neurol Scand* (2001) 104:171–3. doi: 10.1034/j.1600-0404.2001.00356.x

101. Keane RW, Dietrich WD, de Rivero Vaccari JP. Inflammasome proteins as biomarkers of multiple sclerosis. *Front Neurol* (2018) 9:135. doi: 10.3389/fneur.2018.00135

102. Nicoletti F, Di Marco R, Mangano K, Patti F, Reggio E, Nicoletti A, et al. Increased serum levels of interleukin-18 in patients with multiple sclerosis. *Neurology* (2001) 57:342–4. doi: 10.1212/wnl.57.2.342

103. Christophi GP, Gruber RC, Panos M, Christophi RL, Jubelt B, Massa PT. Interleukin-33 upregulation in peripheral leukocytes and CNS of multiple sclerosis patients. *Clin Immunol* (2012) 142:308–19. doi: 10.1016/j.clim.2011.11.007

104. Sriram S, Shaginurova G, Tossberg JT, Natarajan C, Spurlock CF3rd, Aune TM. Longitudinal changes in the expression of IL-33 and IL-33 regulated genes in relapsing remitting MS. *PloS One* (2018) 13:e0208755. doi: 10.1371/journal.pone.0208755

105. Chen H, Sun Y, Lai L, Wu H, Xiao Y, Ming B, et al. Interleukin-33 is released in spinal cord and suppresses experimental autoimmune encephalomyelitis in mice. *Neuroscience* (2015) 308:157–68. doi: 10.1016/j.neuroscience.2015.09.019

106. Jiang HR, Milovanović M, Allan D, Niedbala W, Besnard AG, Fukada SY, et al. IL-33 attenuates EAE by suppressing IL-17 and IFN-γ production and inducing alternatively activated macrophages. *Eur J Immunol* (2012) 42:1804–14. doi: 10.1002/eji.201141947

107. Xiao Y, Lai L, Chen H, Shi J, Zeng F, Li J, et al. Interleukin-33 deficiency exacerbated experimental autoimmune encephalomyelitis with an influence on immune cells and glia cells. *Mol Immunol* (2018) 101:550–63. doi: 10.1016/j.molimm.2018.08.026

108. Finlay CM, Cunningham KT, Doyle B, Mills KHG. IL-33-stimulated murine mast cells polarize alternatively activated macrophages, which suppress T cells that mediate experimental autoimmune encephalomyelitis. *J Immunol* (2020) 205:1909–19. doi: 10.4049/jimmunol.1901321

109. Allan D, Fairlie-Clarke KJ, Elliott C, Schuh C, Barnett SC, Lassmann H, et al. Role of IL-33 and ST2 signalling pathway in multiple sclerosis: expression by oligodendrocytes and inhibition of myelination in central nervous system. *Acta Neuropathol Commun* (2016) 4:75. doi: 10.1186/s40478-016-0344-1

110. Natarajan C, Yao SY, Sriram S. TLR3 agonist poly-IC induces IL-33 and promotes myelin repair. *PloS One* (2016) 11:e0152163. doi: 10.1371/journal.pone.0152163

111. Sánchez-Fernández A, Zandee S, Amo-Aparicio J, Charabati M, Prat A, Garlanda C, et al. IL-37 exerts therapeutic effects in experimental autoimmune encephalomyelitis through the receptor complex IL-1R5/IL-1R8. *Theranostics* (2021) 11:1–13. doi: 10.7150/thno.47435

112. Cavalli E, Mazzon E, Basile MS, Mammana S, Pennisi M, Fagone P, et al. In silico and *in vivo* analysis of IL-37 in multiple sclerosis reveals its probable homeostatic role on the clinical activity, disability, and treatment with fingolimod. *Molecules* (2019) 25:20. doi: 10.3390/molecules25010020

113. Jha D, Bakker ENTP, Kumar R. Mechanistic and therapeutic role of NLRP3 inflammasome in the pathogenesis of alzheimer's disease. *J Neurochem* (2023) 00:1–25. doi: 10.1111/jnc.15788

114. Kumar S, Budhathoki S, Oliveira CB, Kahle AD, Calhan OY, Lukens JR, et al. Role of the caspase-8/RIPK3 axis in alzheimer's disease pathogenesis and aβ-induced NLRP3 inflammasome activation. *JCI Insight* (2023) 8:e157433. doi: 10.1172/jci.insight.157433

115. Heneka MT, Kummer MP, Stutz A, Delekate A, Schwartz S, Vieira-Saecker A, et al. NLRP3 is activated in alzheimer's disease and contributes to pathology in APP/PS1 mice. *Nature* (2013) 493:674–8. doi: 10.1038/nature11729

116. Ising C, Venegas C, Zhang S, Scheiblich H, Schmidt SV, Vieira-Saecker A, et al. NLRP3 inflammasome activation drives tau pathology. *Nature* (2019) 575:669–73. doi: 10.1038/s41586-019-1769-z

117. Tejera D, Mercan D, Sanchez-Caro JM, Hanan M, Greenberg D, Soreq H, et al. Systemic inflammation impairs microglial aβ clearance through NLRP3 inflammasome. *EMBO J* (2019) 38:e101064. doi: 10.15252/embj.2018101064

118. Huang WX, Huang P, Hillert J. Increased expression of caspase-1 and interleukin-18 in peripheral blood mononuclear cells in patients with multiple sclerosis. *Mult Scler* (2004) 10:482–7. doi: 10.1191/1352458504ms1071oa

119. Malhotra S, Cost C, Eixarch H, Keller CW, Amman L, Martinez-Banaclocha H, et al. NLRP3 inflammasome as prognostic factor and therapeutic target in primary progressive multiple sclerosis patients. *Brain* (2020) 143:1414–30. doi: 10.1093/brain/awaa084

120. McKenzie BA, Mamik MK, Saito LB, Boghozian R, Monaco MC, Major EO, et al. Caspase-1 inhibition prevents glial inflammasome activation and pyroptosis in models of multiple sclerosis. *Proc Natl Acad Sci USA* (2018) 115:E6065–74. doi: 10.1073/pnas.1722041115

121. Guarda G, Braun M, Staehli F, Tardivel A, Mattmann C, Förster I, et al. Type I interferon inhibits interleukin-1 production and inflammasome activation. *Immunity* (2011) 34:213–23. doi: 10.1016/j.immuni.2011.02.006

122. Furlan R, Martino G, Galbiati F, Poliani PL, Smiroldo S, Bergami A, et al. Caspase-1 regulates the inflammatory process leading to autoimmune demyelination. *J Immunol* (1999) 163:2403–9. doi: 10.4049/jimmunol.163.5.2403

123. Gris D, Ye Z, Iocca HA, Wen H, Craven RR, Gris P, et al. NLRP3 plays a critical role in the development of experimental autoimmune encephalomyelitis by mediating Th1 and Th17 responses. *J Immunol* (2010) 185:974–81. doi: 10.4049/jimmunol.0904145

124. Inoue M, Williams KL, Gunn MD, Shinohara ML. NLRP3 inflammasome induces chemotactic immune cell migration to the CNS in experimental autoimmune encephalomyelitis. *Proc Natl Acad Sci USA* (2012) 109:10480–5. doi: 10.1073/pnas.1201836109

125. Voet S, Mc Guire C, Hagemeyer N, Martens A, Schroeder A, Wieghofer P, et al. A20 critically controls microglia activation and inhibits inflammasome-dependent neuroinflammation. *Nat Commun* (2018) 9:2036. doi: 10.1038/s41467-018-04376-5

126. Schuh E, Lohse P, Ertl-Wagner B, Witt M, Krumbholz M, Frankenberger M, et al. Expanding spectrum of neurologic manifestations in patients with NLRP3 low-penetrance mutations. *Neurol Neuroimmunol Neuroinflamm* (2015) 2:e109. doi: 10.1212/NXI.0000000000000109

127. Verma D, Särndahl E, Andersson H, Eriksson P, Fredrikson M, Jönsson JI, et al. The Q705K polymorphism in NLRP3 is a gain-of-function alteration leading to excessive interleukin-1β and IL-18 production. *PLoS One* (2012) 7:e34977. doi: 10.1371/journal.pone.0034977

128. Kovacs GG. Molecular pathological classification of neurodegenerative diseases: turning towards precision medicine. *Int J Mol Sci* (2016) 17:189. doi: 10.3390/ijms17020189

129. Dugger BN, Dickson DW. Pathology of neurodegenerative diseases. *Cold Spring Harb Perspect Biol* (2017) 9:a028035. doi: 10.1101/cshperspect.a028035

130. Nopoulos PC. Huntington disease: a single-gene degenerative disorder of the striatum. *Dialogues Clin Neurosci* (2016) 18:91–8. doi: 10.31887/DCNS.2016.18.1/pnopoulos

131. Guzman-Martinez L, Maccioni RB, Andrade V, Navarrete LP, Pastor MG, Ramos-Escobar N. Neuroinflammation as a common feature of neurodegenerative disorders. *Front Pharmacol* (2019) 10:1008. doi: 10.3389/fphar.2019.01008

132. Luís JP, Simões CJV, Brito RMM. The therapeutic prospects of targeting IL-1R1 for the modulation of neuroinflammation in central nervous system disorders. *Int J Mol Sci* (2022) 23:1731. doi: 10.3390/ijms23031731

133. Petrucci S, Consoli F, Valente EM. Parkinson Disease genetics: a "continuum" from mendelian to multifactorial inheritance. *Curr Mol Med* (2014) 14:1079–88. doi: 10.2174/1566524014666141010155509

134. Hirsch EC, Hunot S. Neuroinflammation in parkinson's disease: a target for neuroprotection? *Lancet Neurol* (2009) 8:382–97. doi: 10.1016/S1474-4422(09)70062-6

135. Sophiabadi M, Rastgoo N, Haghdoost-Yazdi H. Dopaminergic neuronal death in substantia nigra associates with serum levels of total bilirubin, selenium, and zinc: evidences from 6-hydroxydopamine animal model of parkinson's disease. *Biol Trace Elem Res* (2022) 200:4058–67. doi: 10.1007/s12011-021-03012-6

136. Saghazadeh A, Ferrari CC, Rezaei N. Deciphering variability in the role of interleukin-1β in parkinson's disease. *Rev Neurosci* (2016) 27:635–50. doi: 10.1515/revneuro-2015-0059

137. Wang W, Nguyen LT, Burlak C, Chegini F, Guo F, Chataway T, et al. Caspase-1 causes truncation and aggregation of the parkinson's disease-associated protein α-synuclein. *Proc Natl Acad Sci U S A* (2016) 113:9587–92. doi: 10.1073/pnas.1610099113

138. Yan YQ, Fang Y, Zheng R, Pu JL, Zhang BR. NLRP3 inflammasomes in parkinson's disease and their regulation by parkin. *Neuroscience* (2020) 446:323–34. doi: 10.1016/j.neuroscience.2020.08.004

139. Ahmed S, Kwatra M, Ranjan Panda S, Murty USN, Naidu VGM. Andrographolide suppresses NLRP3 inflammasome activation in microglia through induction of parkin-mediated mitophagy in *in vitro* and *in vivo* models of Parkinson disease. *Brain Behav Immun* (2021) 91:142–58. doi: 10.1016/j.bbi.2020.09.017

140. Khot M, Sood A, Tryphena KP, Khan S, Srivastava S, Singh SB, et al. NLRP3 inflammasomes: a potential target to improve mitochondrial biogenesis in parkinson's disease. *Eur J Pharmacol* (2022) 934:175300. doi: 10.1016/j.ejphar.2022.175300

141. Piancone F, La Rosa F, Marventano I, Saresella M, Clerici M. The role of the inflammasome in neurodegenerative ddiseases. *Molecules* (2021) 26:953. doi: 10.3390/molecules26040953

142. Wang CE, Li S, Li XJ. Lack of interleukin-1 type 1 receptor enhances the accumulation of mutant huntingtin in the striatum and exacerbates the neurological phenotypes of huntington's disease mice. *Mol Brain* (2010) 3:33. doi: 10.1186/1756-6606-3-33

143. Valekova I, Jarkovska K, Kotrcova E, Bucci J, Ellederova Z, Juhas S, et al. Revelation of the IFNα, IL-10, IL-8 and IL-1β as promising biomarkers reflecting immuno-pathological mechanisms in porcine huntington's disease model. *J Neuroimmunol* (2016) 293:71–81. doi: 10.1016/j.jneuroim.2016.02.012

144. Corey-Bloom J, Fischer RS, Kim A, Snell C, Parkin GM, Granger DA, et al. Levels of interleukin-6 in saliva, but not plasma, correlate with clinical metrics in huntington's disease patients and healthy control subjects. *Int J Mol Sci* (2020) 21:6363. doi: 10.3390/ijms21176363

145. Bjorkqvist M, Wild EJ, Thiele J, Silvestroni A, Andre R, Lahiri N, et al. A novel pathogenic pathway of immune activation detectable before clinical onset in huntington's disease. *J Exp Med* (2008) 205:1869–77. doi: 10.1084/jem.20080178

146. de Oliveira Furlam T, Roque IG, Machado da Silva EW, Vianna PP, Costa Valadão PA, Guatimosim C, et al. Inflammasome activation and assembly in huntington's disease. *Mol Immunol* (2022) 151:134–42. doi: 10.1016/j.molimm.2022.09.002

147. Hardiman O, Al-Chalabi A, Chio A, Corr EM, Logroscino G, Robberecht W, et al. Amyotrophic lateral sclerosis. *Nat Rev Dis Primers* (2017) 5:17071. doi: 10.1038/nrdp.2017.71

148. Smeyers J, Banchi E-G and Latouche M. C9ORF72: what it is, what it does, and why it matters. *Front Cell Neurosci* (2021) 15:661447. doi: 10.3389/fncel.2021.661447

149. Zou ZY, Zhou ZR, Che CH, Liu CY, He RL, Huang HP. Genetic epidemiology of amyotrophic lateral sclerosis: a systematic review and meta-analysis. *J Neurol Neurosurg Psychiatry* (2017) 88:540–9. doi: 10.1136/jnnp-2016-315018

150. Lyon MS, Wosiski-Kuhn M, Gillespie R, Caress J, Milligan C. Inflammation, immunity, and amyotrophic lateral sclerosis: i. etiology and pathology. *Muscle Nerve* (2019) 59:10–22. doi: 10.1002/mus.26289

151. Staats KA, Borchelt DR, Tansey MG, Wymer J. Blood-based biomarkers of inflammation in amyotrophic lateral sclerosis. *Mol Neurodegeneration* (2022) 17:11. doi: 10.1186/s13024-022-00515-1

152. Béland LC, Markovinovic A, Jakovac H, De Marchi F, Bilic E, Mazzini L, et al. Immunity in amyotrophic lateral sclerosis: blurred lines between excessive inflammation and inefficient immune responses. *Brain Commun* (2020) 2:fcaa124. doi: 10.1093/braincomms/fcaa124

153. Ravnik-Glavač M, Goričar K, Vogrinc D, Koritnik B, Lavrenčič JG, Glavač D, et al. Genetic variability of inflammation and oxidative stress genes affects onset, progression of the disease and survival of patients with amyotrophic lateral sclerosis. *Genes* (2022) 13:757. doi: 10.3390/genes13050757

154. Brodovitch A, Boucraut J, Delmont E, Parlanti A, Grapperon AM, Attarian S, et al. Combination of serum and CSF neurofilament-light and neuroinflammatory biomarkers to evaluate ALS. *Sci Rep* (2021) 11:703. doi: 10.1038/s41598-020-80370-6

155. Olesen MN, Wuolikainen A, Nilsson AC, Wirenfeldt M, Forsberg K, Madsen JS, et al. Inflammatory profiles relate to survival in subtypes of amyotrophic lateral sclerosis. *Neurol Neuroimmunol Neuroinflamm* (2020) 7:e697. doi: 10.1212/NXI.0000000000000697

156. Italiani P, Carlesi C, Giungato P, Puxeddu I, Borroni B, Bossù P, et al. Evaluating the levels of interleukin-1 family cytokines in sporadic amyotrophic lateral sclerosis. *J Neuroinflamm* (2014) 11:94. doi: 10.1186/1742-2094-11-94

157. Eitan C, Siany A, Barkan E, Olender T, van Eijk KR, Moisse M, et al. Whole-genome sequencing reveals that variants in the interleukin 18 receptor accessory protein 3'UTR protect against ALS. *Nat Neurosci* (2022) 25:433–45. doi: 10.1038/s41593-022-01040-6

158. Lin CY, Pfluger CM, Henderson RD, McCombe PA. Reduced levels of interleukin 33 and increased levels of soluble ST2 in subjects with amyotrophic lateral sclerosis. *J Neuroimmunol* (2012) 249:93–5. doi: 10.1016/j.jneuroim.2012.05.001

159. Korhonen P, Pollari E, Kanninen KM, Savchenko E, Lehtonen S, Wojciechowski S, et al. Long-term interleukin-33 treatment delays disease onset and alleviates astrocytic activation in a transgenic mouse model of amyotrophic lateral sclerosis. *IBRO Rep* (2019) 6:74–86. doi: 10.1016/j.ibror.2019.01.005

160. Dawson TM, Golde TE, Tourenne CL. Animal models of neurodegenerative diseases. *Nat Neurosci* (2018) 21:1370. doi: 10.1038/s41593-018-0236-8

161. Zhou R, Ji B, Kong Y, Qin L, Ren W, Guan Y, et al. PET imaging of neuroinflammation in alzheimer's disease. *Front Immunol* (2021) 12:739130. doi: 10.3389/fimmu.2021.739130

162. Haage V, De Jager PL. Neuroimmune contributions to alzheimer's disease: a focus on human data. *Mol Psychiatry* (2022) 27:3164–81. doi: 10.1038/s41380-022-01637-0s

frontiers | Frontiers in Immunology

TYPE Original Research
PUBLISHED 28 June 2023
DOI 10.3389/fimmu.2023.1211730

OPEN ACCESS

EDITED BY
Giselle Penton-Rol,
Center for Genetic Engineering and Biotechnology (CIGB), Cuba

REVIEWED BY
Paola Allavena,
University of Milan, Italy
Chiara Colarusso,
University of Salerno, Italy

*CORRESPONDENCE
Lina H. K. Lim
linalim@nus.edu.sg

†These authors have contributed equally to this work

RECEIVED 25 April 2023
ACCEPTED 08 June 2023
PUBLISHED 28 June 2023

CITATION
Chew ZH, Cui J, Sachaphibulkij K, Tan I, Kar S, Koh KK, Singh K, Lim HM, Lee SC, Kumar AP, Gasser S and Lim LHK (2023) Macrophage IL-1β contributes to tumorigenesis through paracrine AIM2 inflammasome activation in the tumor microenvironment. *Front. Immunol.* 14:1211730. doi: 10.3389/fimmu.2023.1211730

Macrophage IL-1β contributes to tumorigenesis through paracrine AIM2 inflammasome activation in the tumor microenvironment

Zhi Huan Chew[1,2,3,4†], Jianzhou Cui[1,2,3†], Karishma Sachaphibulkij[1,2,3], Isabelle Tan[1,2,3], Shreya Kar[5,6], Kai Kiat Koh[1,2,3], Kritika Singh[5], Hong Meng Lim[1,2,3], Soo Chin Lee[5,7,8], Alan Prem Kumar[5,6,8], Stephan Gasser[3,9,10] and Lina H. K. Lim[1,2,3,4*]

[1]Department of Physiology, Yong Loo Lin School of Medicine, National University of Singapore, Singapore, Singapore, [2]Immunology Translational Research Program, Yong Loo Lin School of Medicine, National University of Singapore, Singapore, Singapore, [3]Immunology Program, Life Sciences Institute, National University of Singapore, Singapore, Singapore, [4]Graduate School for Integrative Sciences and Engineering, National University of Singapore, Singapore, Singapore, [5]Cancer Science Institute of Singapore, National University of Singapore, Singapore, Singapore, [6]Department of Pharmacology, Yong Loo Lin School of Medicine, National University of Singapore, Singapore, Singapore, [7]Centre for Cancer Research, Yong Loo Lin School of Medicine, National University of Singapore, Singapore, Singapore, [8]Department of Haematology-Oncology, National University Hospital, Singapore, Singapore, [9]Department of Microbiology and Immunology, Yong Loo Lin School of Medicine, National University of Singapore, Singapore, Singapore, [10]Roche Pharma Research and Early Development, Roche Innovation Center, Roche Glycart AG, Schlieren, Switzerland

Intracellular recognition of self and non-self -nucleic acids can result in the initiation of effective pro-inflammatory and anti-tumorigenic responses. We hypothesized that macrophages can be activated by tumor-derived nucleic acids to induce inflammasome activation in the tumor microenvironment. We show that tumor conditioned media (CM) can induce IL-1β production, indicative of inflammasome activation in primed macrophages. This could be partially dependent on caspase 1/11, AIM2 and NLRP3. IL-1β enhances tumor cell proliferation, migration and invasion while coculture of tumor cells with macrophages enhances the proliferation of tumor cells, which is AIM2 and caspase 1/11 dependent. Furthermore, we have identified that DNA-RNA hybrids could be the nucleic acid form which activates AIM2 inflammasome at a higher sensitivity as compared to dsDNA. Taken together, the tumor-secretome stimulates an innate immune pathway in macrophages which promotes paracrine cancer growth and may be a key tumorigenic pathway in cancer. Broader understanding on the mechanisms of nucleic acid recognition and interaction with innate immune signaling pathway will help us to better appreciate its potential application in diagnostic and therapeutic benefit in cancer.

KEYWORDS

innate immunity, inflammasome, cytosolic DNA, tumor microenvironment, AIM2 inflammasome

Introduction

The innate immune system serves as the first-line defense against bacteria, viruses, and other pathogens(1). DNA is typically found in the nucleus of eukaryotic cells, and the presence of DNA in aberrant locations, such as the cytoplasm and endosomes triggers immune activation, sensed by a group of proteins collectively known as DNA sensors(2). We and others have reported that cytosolic DNA is found in cancer cells and tissues and not in healthy tissues, suggesting that it is a unique cancer phenotype (3). Whether the tumor cells or innate immune cells in the tumor microenvironment recognizes cancer derived cytosolic nucleic acids has been recently questioned, and the involvement of DNA sensors has appeared to be important both intrinsically and for tumor surveillance (4). Another class of DNA sensors are the inflammasomes and namely, the AIM2 inflammasome senses dsDNA(5) and has been implicated in the development (6) as well as regulation (7) of various cancers.

The inflammasomes are a family of oligomeric protein complex made up of the sensor component which, upon sensing of PAMPs and DAMPs, binds adaptor protein ASC, which activates caspase-1, and triggers the release of pro-inflammatory cytokines such as IL-1β, making the inflammasomes one of the critical drivers of inflammation(8). Inflammasomes are defined by their sensor, which include AIM2, Pyrin, and NLRP1 and NLRP3. The diversity and specificity of sensors allow responsiveness to a broad range of stimuli, either extrinsic (microbial molecules) or intrinsic (danger signals). Activation of inflammasomes requires two different signals, encompassing a priming step which usually involves microbial molecules which would induce nuclear factor kappa B (NF-κB)-dependent expression of the sensor protein and pro-IL-1β and a second signal provided by various structurally unrelated microbial molecules such as toxins or danger signals (e.g., DNA, ATP or uric acid), which, together with the first signal, will trigger inflammasome multimerization and activation(9). The AIM2 inflammasome consists of AIM2, an adaptor molecule ASC (apoptosis-associated speck-like protein containing a CARD), and pro-caspase-1. Upon inflammasome activation, caspase-1 is cleaved, which in turn, cleaves IL-1β and gasdermin-D which frees the N-terminal effector domain from the C-terminal inhibitory domain. Oligomerization of the gasdermin-D N terminal subsequently forms a pore in the membrane and leads to membrane rupture and pyroptosis.

As mentioned, AIM2 is a cytosolic DNA sensor protein which can have inflammasome dependent and independent functions. AIM2 has been implicated in the development of various cancers including prostate cancer, squamous cell carcinoma (10, 11), as well as non-small cell lung cancer through the regulation of mitochondrial dynamics (12) and renal cell carcinoma through FOXO3a-ACSL4 inhibition of ferroptosis(13). However, other studies have reported that AIM2 acts as a tumor suppressor gene in many cancers including colon cancer and endometrial cancer (6, 14),inhibiting cancer proliferation, invasion and migration through various mechanisms, including suppressing glioma-associated oncogene-1 (GLi1) (15), inactivating PI3K/AKT/mTOR signaling (16), Moreover, the trigger mechanisms of the AIM2 inflammasome remain unknown. Cytosolic DNA, including ssDNA, dsDNA, and DNA/RNA hybrids, are present in all tested cancer cell lines and cancer samples (3, 17). Strikingly, cytosolic DNA is not found in healthy tissues, suggesting that it is a unique cancer phenotype and hence giving us a clue to study the link between cancer cells and AIM2 inflammasome activation.

Based on previous reports that cancer cells contain cytosolic nucleic acids (3) and cancer cells can activate macrophages, we hypothesized that macrophages can be activated by tumor-derived nucleic acids to induce inflammasome activation in the tumor microenvironment, which in turn, can affect cancer progression.

Materials and methods

Mice

All animal work was approved by the National University of Singapore Institutional Animal Care and Use Committee (IACUC), an AALAAC accredited institution and was in accordance with the National Advisory Committee for laboratory Animal Research (NACLAR) Guidelines. TRAMP-C2 cells were injected subcutaneously into C57BL6 mice or AIM2-/- mice on the same background. Tumors were homogenized or treated with collagenase before isolating CD11b+ cells through a column and incubating overnight, after which supernatants were collected for ELISA analysis.

Cell lines, drugs and treatments

Human THP-1, U937, HeLa cells, A549, HCT-116, and mouse TRAMP-C2 cells were purchased from ATCC (USA). A549, HeLa and TRAMP-C2 cells were grown in DMEM medium (Invitrogen, USA), while HCT116 cells were cultured in McCoy's 5A medium (Invitrogen, USA), and both mediums are supplemented with 10% heat-inactivated FCS (Hyclone, USA) and 1% pen/strep (Invitrogen). THP-1 and U937 cells were cultured in RPMI medium (Hyclone, USA) supplemented with 10% heat-inactivated FCS (Hyclone, USA). All cells were grown at 37°C in a humidified 5% CO2 incubator (Thermo Scientific, USA). THP1 cells were differerentiated in PMA (#tlrl-pma, InvivoGen, USA) and stimulated with 1 μg/ml LPS (#tlrl-peklps, InvivoGen, USA) overnight before fresh cell medium was replaced and the cells were either treated with 50% cancer CM or transfected with 1 μg/ml poly (dA:dT) (#tlrl-patc, InvivoGen, USA) with lyovec transfection reagent. *Inhibitors* THP1 Cells were primed with 100 ng/ml PMA, followed by LPS (1 μg/ml) for 3 hours prior to treatment 1 hour with 1 μg/ml Poly(dA:dT) complexes (AIM2 inflammasome inducer) or A549 tumor CM in the presence of ODN TTAGGG (A151; AIM2 inhibitor, 0.5 μM) or MCC950 (NLRP3 inhibitor, 0.5 μM). Cell supernatants were detected using ELISA.

Bone marrow derived macrophage isolation and differentiation

Bone marrow derived macrophages (BMDMs) from mice were obtained by flushing the femurs and tibias of mice with DMEM media. Briefly, red blood cells were removed through osmotic lysis and the bone marrow cell suspension was washed twice with PBS and cultured with BMDM media (DMEM medium containing 10% FBS (v/v), 100 U/mL penicillin, 100 µg/mL streptomycin, 2 mM L-glutamine and 20% L-929-conditioned DMEM (v/v) as a source of M-CSF). After 3 days of culture, the cells were supplemented with fresh BMDM media. At day 7, culture media and non-adherent cells were removed, and the remaining adherent cells were replenished with fresh BMDM media before experiments.

Tumor conditioned media preparation

A549, Hela, MCF7 cells are cultured in T-75 flasks until 80% confluency before the existing media was replaced by new DMEM medium. The cells were grown for another 24 h in the new DMEM media before the conditioned media was collected and filtered using 0.45 µm filter (Millipore, USA) prior to use.

Flow cytometry

Cells were stained with Fixable Viability Dye eFluor 506 (1:1000) in 1x PBS for 30 min at 4°C (Thermo Fisher Scientific, USA) before incubated with Fc block (BioLegend, USA) for 15 min at 4°C. Cells were stained with fluorescence-conjugated antibodies (BioLegend, USA) diluted in FACS buffer and incubated on ice for 30 min in the dark. Macrophages were identified as CD45+ Ly6G-Gr1- F4/80+ CD11b+ cells. Cells were analyzed on a BD LSRFortessa (BD Biosciences, USA) or Attune NxT Flow Cytometer (Thermo Fisher Scientific, USA). Data analysis was performed using FlowJo software (FlowJo, USA).

Immunohistochemistry

Immunohistochemistry (IHC) was performed using the Leica Bond max autostainer (Leica Biosystems, Nussloch GmbH) and bond polymer refine detection kit (DS9800, Leica Biosystems) following the manufacturer's instructions. Briefly, tissues were fixed in formalin, dehydrated and cleared before adding paraffin (pre-heated to 60oC) and left overnight. Sectioning was performed with a microtome. Formalin-fixed tissue sections were de-waxed, rehydrated and antigen retrieval was achieved using citrate buffer at pH 6 for 20 minutes. Endogenous peroxidase activity was quenched in 0.3% hydrogen peroxide for 10 minutes and non-specific sites were blocked with 3% bovine serum albumin for 20 minutes. Further, single immunostaining with primary antibodies for CD68 (1:50, Bio-Rad), inducible nitric oxide synthase (iNOS, 1:50, Abcam), mannose receptor CD206 (1:200, Abcam) followed by incubation with respective HRP-linked secondary antibodies (for CD68: goat anti-rat antibody Bio-Rad; for iNOS and CD206: goat anti-rabbit antibody, DAKO) was performed. 3,3'-diaminobenzidine (DAB) was used as the chromogen to obtain the brown colour. Counterstaining was with hematoxylin for 10 min. The mean score of five high-power fields (HPF) (×400) was counted for each slide under a light microscope (Olympus BX43) and digital images were acquired using Olympus cellSens Entry imaging software. In the IHC stained sections, macrophages observed with their cytoplasm stained tan or brown were considered positive.

Immunofluorescence

Cytosolic dsDNA and DNA-RNA staining were performed as described previously (16). Briefly, 50% formamide (VWR International, USA) diluted in PBS was added for 10 mins at room temperature, followed by incubation for 15 mins at 75°C to denature dsDNA. Cells were washed with PBS and incubated with blocking buffer (1% BSA (Sigma Aldrich), 2% goat serum (Hyclone) in PBS) for 1 h to prevent non-specific binding of antibodies. Cells were then stained with dsDNA (1:200, Sigma-Aldrich, USA) or S9.6 DNA-RNA hybrids (1:100, Kerafast, Boston, USA) antibodies overnight in 4°C. Cells were subsequently washed with PBST (0.1% Tween) thrice followed by anti-mouse IgG coupled with Cy3 (Millipore, Singapore) or anti-rabbit IgG coupled to Alexa Fluor 488 (Invitrogen, Singapore). Finally, DNA fluorophore DAPI (0.5 µg/ml in PBS, KPL Inc., USA) was added for 10 min. Slides were washed once in PBS before mounted with Da-/- fluorescent mounting medium (Da-/-, UK). Confocal images of staining were captured using a Zeiss Axio Imager Z1 fluorescent microscope equipped with AxioVision 4.8 software (Carl Zeiss MicroImaging, USA) or confocal TCS SP5 (Leica, Singapore). Images were analyzed using Photoshop CS4 (Adobe, USA) or ImageJ. Colocalisation of AIM2 with DNA or other proteins were quantified using Metamorph (Metamorph NX, version 8.12, Molecular Devices, USA).

Western blot

Cells were lysed with RIPA (Radio-Immunoprecipitation Assay) buffer containing protease inhibitors (Calbiochem, USA). 30 µg of total protein was loaded onto a SDSPAGE gel and electroblotted onto Hybond ECL membrane (GE Healthcare, UK). The blots were stained with primary antibodies (AIM2 (1:1000, Cell Signaling Technology, USA), NLRP1 (1:200, Santa Cruz Biotechnology, USA), NLRP2 (1:1000, Proteintech, USA), NLRP3 (1:1000, Adipogen, USA), NAIP (1:1000, Adipogen, USA), ASC (1:1000, Cell Signaling Technology, USA), Caspase 1 (1:200, Santa Cruz Biotechnology, USA), IL1β (1:1000, R & D, USA), Tubulin (!;1000, Cell Signaling Technology, USA), Actin (1:1000, Cell Signaling Technology, USA) overnight at 4° C after blocked with 5% low fat milk (Bio-Rad, USA). The blots were washed with TBST and incubated with a secondary HRP-linked antibody (1:5000, Santa Cruz Biotechnology, USA). Blots were

washed TBST before visualization using ECL reagents according to manufacturer's instructions (Perkin Elmer, USA). Each protein bands' intensities were normalized against its loading control band intensity for quantification using ImageJ. Briefly, an area of interest rectangle was created around each band and the integrated density was measured, background subtracted, and divided by its specific loading control band.

ELISA assay

Cytokines in culture supernatant and tissue lysates were measured by ELISA using commercially available kits. Mouse IL-1β (88-7013, eBioscience, USA) and human IL-1β (88-7261-86, eBioscience, USA) were used in accordance with the manufacturer's protocol. Absorbance was read with a Tecan Spark 10M microplate reader (Tecan, USA) at absorbance values as indicated in the manufacturer's protocol.

Isolation of CD11b+ tumor-associated macrophages

Tumors were mechanically dissociated and strained through a 40 μm nylon mesh before digestion into single cells with collagenase type II (0.5 mg mL−1), collagenase type IV (0.5 mg mL−1), hyaluronidase (10 U/mL) and DNase I (0.01 mg mL−1) for 2 h at 37 °C. The dissociated cells were collected, lysed by RBC lysis buffer before CD11b+ tumor associated macrophages were isolated out of these suspensions by the MACS technology according to the manufacturer's instructions using 10 μl CD11b microbeads (130049601; Miltenyi, USA) per $1x10^7$ cells. The isolated CD11b+ cells were grown overnight in complete RPMI media overnight before the cells and cell supernatants were collected for analysis.

siRNA transfection

AIM2-specific siRNA and scrambled siRNA (Thermo Fisher) were used according to manufacturer's instructions. THP-1 cells were seeded at a concentration of 5x105/well in a 12 well plate (Greiner Bio-science) before silencing with a final concentration 10 nM of siRNA and grown overnight before treatment with or without 100ng/ml PMA, 1 μg/ml LPS, and 50% A549 tumor conditioned media for another 24 h.

MTT cell proliferation assay

A549 cells were seeded in 24 well plates and treated with IL-1β (#29-8018-65, Thermo Scientific, USA) at the indicated concentrations for 72 h, after which cell viability was measured using an MTT Cell Proliferation and Cytotoxicity Assay Kit (Boster Bio), according to the manufacturer's instructions. Absorbance was measured using a TECAN spectrophotometer (Tecan Trading AG, Switzerland) at 490 nm.

Migration and invasion assay

A549 cells were seeded into cell migration chambers (SPL, Korea) of PET membrane with 8.0 μm pore size. IL-1β was added to the cells and the chambers were incubated for 24 h in a humidified chamber at 37°C, 5% CO2. For the invasion assay, inserts were coated with 10% Matrigel prior to cell seeding. For co-culture, the bottom chamber was seeded with mouse BMDM cells stimulated with LPS (1 μg/ml) one day prior to TRAMPC2 cell seeding before the chambers were incubated for 24 h. At the end of the incubation period, the inserts were washed using 1xPBS. Inserts were fixed with 100% methanol for 15 minutes before washing and air drying, followed by cell staining using 0.5% crystal violet (filtered) for 30 minutes. The upper membrane of the inserts was rinsed and cleaned to remove excess stain and non-migrated cells. Five microscopic fields of each insert were captured using Nikon Stereoscopic Microscope SMZ1500 and Digital Camera DXM1200F (Nikon, Melvile, NY, USA).

Statistics

Unpaired Student's T-Test or One-way/Two-way analysis of variance (ANOVA) with Tukey's post-test was performed when appropriate. Results are presented as mean values ± standard error (SE).

A p-value of < 0.05 or less was deemed significant.

Results

Higher dsDNA and infiltration of CD68+ and CD206+ cells in the mouse mammary tumor microenvironment

The presence of nucleic acids have been reported in cancer tissues and cell lines (3) which could activate DAMPs in tumor associated macrophages (TAMs). We first confirmed the expression of dsDNA and in a spontaneous breast cancer mouse model which develops tumors at ~6-9 months of age- MMTV-Wnt+ mice, compared to non-tumor fat pads. Indeed, tumors expressed more dsDNA compared to normal mammary tissue (Figure S1A). We next investigated the tumor microenvironment in MMTV-Wnt+ fatpads and tumor (which developed at 9 months) and MMTV-Wnt- fat pads. Many more CD11b+F480+ cells were present in tumor tissue (Figure S1B). Interestingly macrophage infiltration occurs early before tumor development, confirmed by immunohistochemistry of MMTV-Wnt+ and MMTV-Wnt- fat pads stained with CD68 and counterstained with Haemotoxylin (at 2,4,6 and 9 months of age). Figure 1A shows mouse mammary tissue composed of fat pads (black arrow), ducts (red arrow) and acinar structures (yellow arrow). MMTV-Wnt+ pads exhibit ductal and acinar proliferation with branching and budding, progressing from 2 months to 6 months in comparison to their respective age matched control littermates. Formation of malignant tumor is observed at 9 months which

10.3389/fimmu.2023.1211730

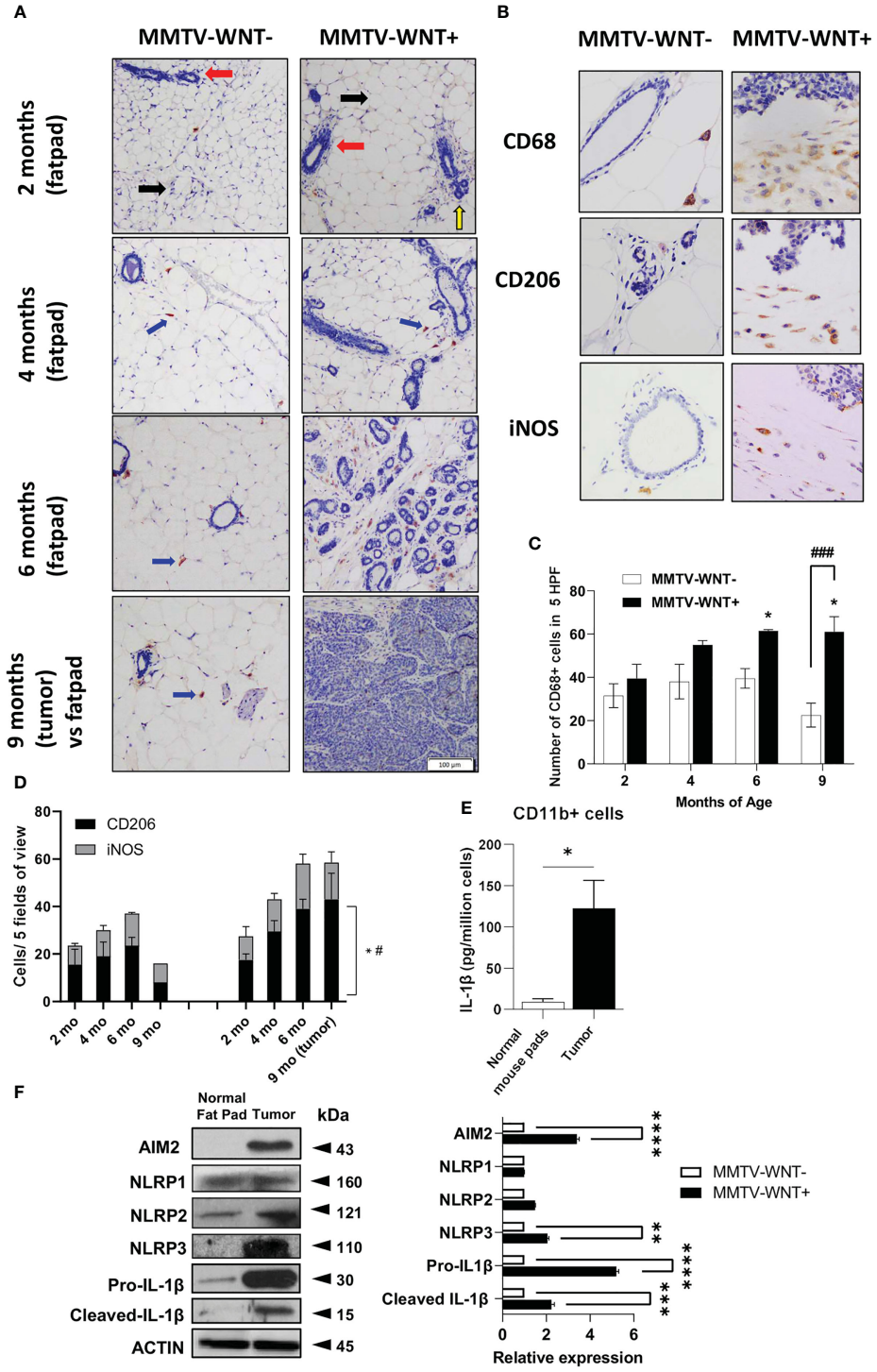

FIGURE 1
Higher dsDNA and infiltration of CD11b+ cells in the mouse mammary tumor microenvironment. **(A)** Immunohistochemical expression of CD68 and Haemotoxylin and Eosin staining of MMTV-WNT- and MMTV-WNT+ mammary fat pads at 2,4,6 and 9 months and upon tumor resection at 9 months. (Magnification, 100x). **(B)** Immunohistochemical expression of CD68 in 9-month MMTV-WNT- mammary fat pads and MMTV-WNT+ tumors. Blue corresponds to nuclear staining and brown corresponds to positive staining (magnification, 400x). **(C)** CD68+ cells were counted in 5 high power fields. **(D)** iNOS+ and CD206+ cells were counted in 5 high power fields. * P<0.05 vs 2 months; # P<0.05, ### P<0.001 vs MMTV-WNT- at same time point. 2 replicates per age were performed **(E)** CD11b+ macrophages were isolated from normal mouse pads and MMTV tumors and grown overnight. IL1β production was analyzed using ELISA. **(F)** Inflammasome components (IL1β, AIM2, NLRP1,2,3) and activation (cleaved) were analyzed using western blotting. Graph shows the quantification of immunoblots using Image J (fold change vs Actin) * P<0.05 from n=3-4 mice. **p<0.01; ***p<0.001 **** p<0.0001.

shows atypical epithelial cells forming enlarged irregular glands with intraluminal papillary projections. At places, there is also formation of cysts filled with secretory material and many solid areas of tumor cells can be seen. Macrophages were stained with CD68 (400x) and a significant increase in CD68+ cells was seen in fat pads from MMTV-WNT+ mice progressing from 2-6 months and tumors at 9 months (Figures 1B, C). In addition, staining of sections with an inflammatory macrophage marker, iNOS or an alternatively activated macrophage marker CD206 demonstrated a time-dependent and significant increase in the number of CD206 expressing cells at 9 months of age, when the tumor had formed (Figure 1D). Next to assess if tumor-derived nucleic acids can activate the inflammasome in leukocytes in the tumor microenvironment, CD11b+ cells isolated and cultured overnight from MMTV-Wnt+ tumors secreted more IL-1β and expressed higher levels of inflammasome components AIM2 and NLRP3 as compared to CD11b+ cells derived from normal fat pads (Figures 1E, F).

Tumor secretome increases IL-1β production from macrophages

To determine if tumors secrete mediators which can enhance the IL-1β and inflammasome activation in macrophages, we collected conditioned media (CM) from TRAMPC2 mouse prostate cancer cells overnight. TRAMPC2 CM induced a high level of IL-1β production in LPS-primed bone marrow derived macrophages (BMDM) (Figure 2A). This was confirmed with human monocytic THP-1 cells either resting (monocytic) or differentiated with PMA (macrophage-like) and stimulated with CM from several human cancer cells (Figure 2B). Monocytic THP1 cells did not secrete IL-1β in response to LPS or LPS + CM, while macrophage-like THP1 cells secreted more IL-1β basally, when stimulated with LPS and significantly more when stimulated with both LPS+CM (Figure S2A). In addition, A549 tumor CM significantly enhanced the cleavage and maturation of inflammasome components caspase-1 and IL-1β and upregulated AIM2 (Figures 2C, D). Surprisingly, despite the presence of cytosolic DNA or exogenous DNA transfection, epithelial cancer cells do not produce appreciable amounts of IL-1β compared to myeloid THP-1 cells, implying that the IL-1β in the tumor microenvironment does not originate from the tumor cells themselves (Figure S2B).

Silencing or inhibiting AIM2 or NLRP3 in macrophages reverses IL1β production induced by tumor CM

Next, AIM2 was either silenced with siRNA ((Figure 3A) or treated with A151, an inhibitor of AIM2 and TLR9 (Figure 3B) which resulted in the inhibition of IL-1β and inflammatory components after A549 CM in human THP1 cells, with quantified densitometry (Figure 3C). AIM2-/- and caspase 1-/- BMDM, treated with LPS and either dsDNA or tumor CM, similarly produced significantly less IL-1β compared to WT BMDM (Figures 3D, E). This shows that macrophage AIM2 is important for IL-1β secretion in response to tumor CM. However, as Caspase-1 plays a role here, we examined if other inflammasomes could also be involved. Inhibition of NLRP3 with MCC950 partially inhibited the release and cleavage of IL-1β and induced by LPS+ATP as well as A549 CM, indicating that the NLRP3 inflammasome activation is partially responsible (Figure S3).

AIM2-dependent IL1β production stimulates tumor cell proliferation

Exogenous IL-1β stimulated proliferation of TRAMPC2 cancer cells, and addition of exogenous IL-1β stimulated proliferation of TRAMPC2 cancer cells similarly in the presence of WT and AIM2-/- or Caspase1/11-/- macrophages (Figure 4A). However, coculture of TRAMPC2 cancer cells with BMDM increased their proliferation which was AIM2 and Caspase 1/11 dependent as this was not observed with AIM2-/- or Caspase1/11-/- BMDM (Figures 4B, C). In addition, IL-1β enhanced the migration and invasion of TRAMPC2 cancer cells (Figure 4D) which implies a pro-tumorigenic role for IL-1β.

Cytosolic DNA and DNA/RNA hybrids are increased in tumors and colocalize with AIM2

The presence of dsDNA and DNA-RNA hybrids has been reported in cancer tissues and cell lines (3, 17–19). We hypothesized that these cytosolic nucleic acids may act as intracellular ligands to stimulate AIM2 inflammasome activation. Therefore, we next determined if cytosolic DNA or DNA-RNA hybrids were present in the spontaneous mammary tumors in MMTV-Wnt+mice by staining MMTV-Wnt+ tumors and non-tumor fat pads from MMTV-Wnt- for both DNA-RNA hybrids and dsDNA using immunofluorescence staining. Both cytosolic dsDNA and DNA-RNA hybrids are constitutively present in tumor tissues and are not found in non-tumor mammary fat pads (Figure 5A). In addition, AIM2 colocalized with cytosolic DNA and DNA-RNA hybrids in A549 cells (Figures 5B, C) as well as other tested cell lines (U937, THP-1, Hela, and HCT-116, Figure S4).

To determine which nucleic acid species in the tumor CM could be responsible for inflammasome activation, DNAase, RNAase H, and RNAase A which degrade dsDNA, DNA-RNA hybrids, and dsRNA, respectively, was added to A549 CM prior to addition to THP-1 cells. Tumor CM stimulated the production of IL-1β which was significantly inhibited with RNAase H, and not RNAase A. Interestingly, only a slight reduction was observed with DNAase treatment (Figure 5D). Furthermore, treatment with RNAase H significantly reduced the maturation of IL-1β, and inhibited gasdermin D-N expression (Figure 5E). Treatment with DNAase, to a smaller extent, reduced the maturation of IL-1β, but did not inhibit the IL1β release, suggesting that DNA-RNA hybrids present in tumor CM, could be responsible for the IL-1β secretion and inflammasome activation in THP1 macrophages, rather than dsDNA.

10.3389/fimmu.2023.1211730

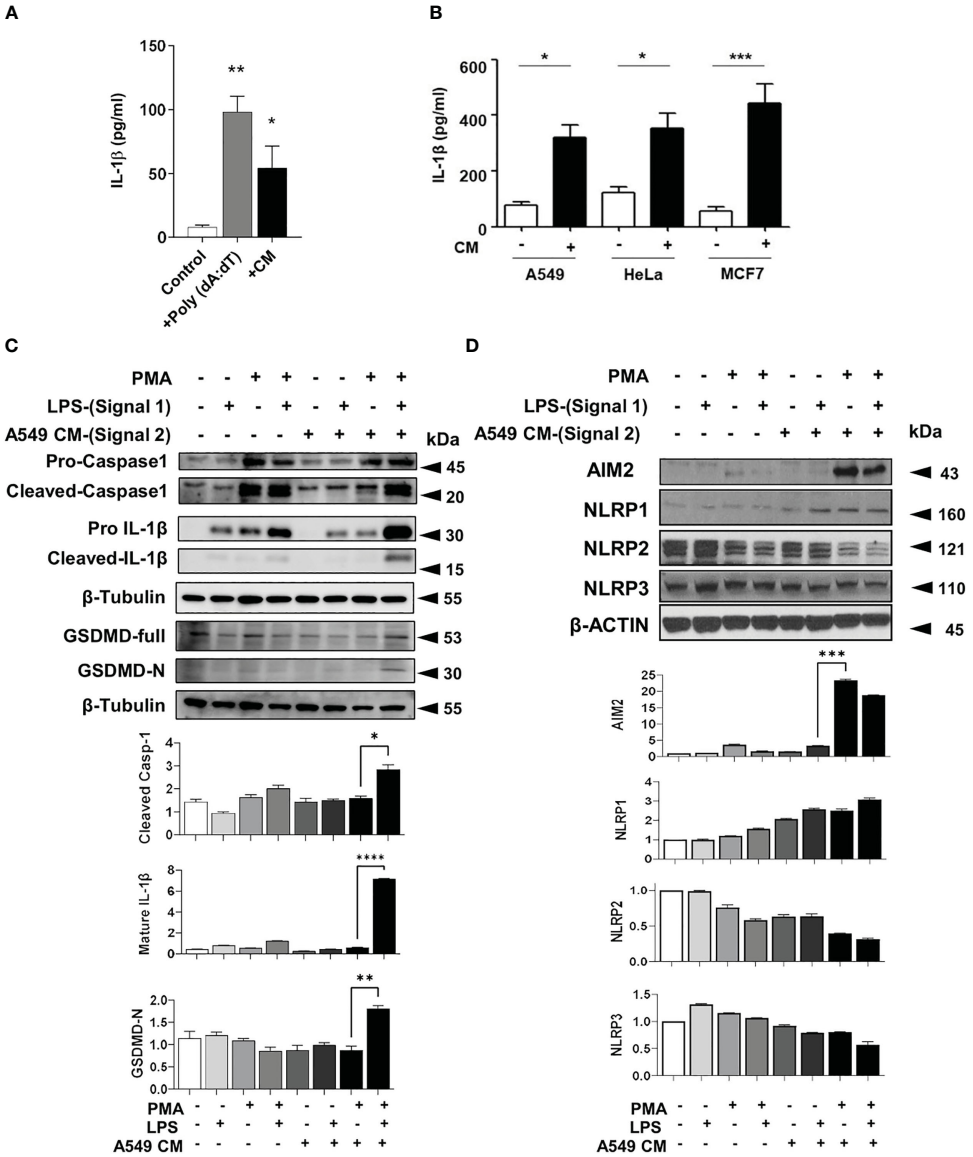

FIGURE 2
Tumor conditioned media stimulates inflammasomes in macrophages **(A)** IL-1β production in bone marrow derived macrophages primed with LPS and treated with either poly (dA: dT) or TRAMPC2 prostate cancer conditioned media (CM). **(B)** IL-1β production from PMA and LPS treated THP-1 treated with CM from A549, Hela or MCF7 cells (+) or DMEM only for 24 h (-). **(C, D)** Inflammasome components from PMA and LPS treated THP-1 treated with CM from A549 cells. Graph shows the quantification of immunoblots using Image J (fold change vs Actin) *p<0.05; **p<0.01; ***p<0.001; ****p<0.0001. Data represents the mean ± SEM of at 3-5 independent experiments.

Finally, to validate that the AIM2 inflammasome can sense dsDNA and DNA-RNA hybrids, BMDM from WT and AIM2-/- mice were generated and transfected with different concentrations of DNA-RNA hybrids or dsDNA poly (dA: dT). The lowest concentration of DNA-RNA hybrid transfection (0.1μg/ml) increased IL-1β secretion which was AIM2 dependent. Interestingly, transfection of DNA-RNA hybrids at higher concentrations (1μg/ml and 5 μg/ml) did not increase IL-1β secretion compared to the transfected control. (Figure 5F). However, only higher concentrations of poly (dA: dT) stimulated IL-1β production. This data suggests that AIM2 can respond to both DNA-RNA hybrids and dsDNA, but is more sensitive to DNA-RNA hybrids as compared to dsDNA

In summary, this study shows that macrophage AIM2 is activated by nucleic acids secreted from the cancer cells, which leads to inflammasome activation, IL-1β cleavage and release from macrophages. IL-1β and coculture of tumor cells with macrophages enhances the proliferation of tumor cells which is AIM2 and caspase 1/11 dependent (Gigure 6). AIM2 is more sensitive to stimulation with DNA-RNA hybrids compared to dsDNA,

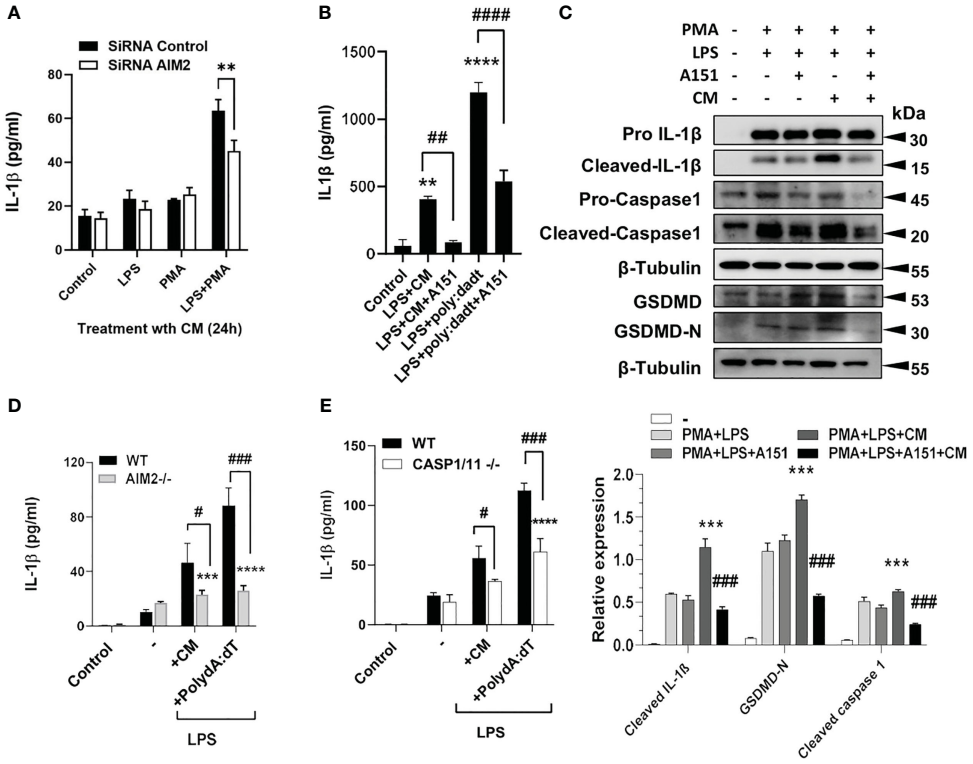

FIGURE 3
Silencing or inhibiting AIM2 in macrophages reverses IL1β production induced by tumor CM. **(A)** IL-1β levels from control, LPS or PMA Primed THP-1 cells transfected with AIM2 siRNAs or scrambled siRNAs (siRNA Control) and treated with A549 CM. **(B, C)** IL-1β levels and inflammasome activation in LPS and PMA primed THP-1 cells pre-treated with A151 for 1h prior to treatment with A549 CM. Graph shows the quantification of immunoblots using Image J (fold change vs Actin) **(D,E)** IL-1β levels in LPS-primed WT and AIM2-/- or Caspase1/11-/- BMDM treated with mouse TRAMP-C2 CM or Poly(dA:dT). Data represents mean ± SEM of at least 3 independent experiments. **p<0.01; ***p<0.001, **** p<0.0001. # p<0.05; ##p<0.01; ###p<0.001; ####p<0.0001.

suggesting that both dsDNA and DNA-RNA hybrids can activate AIM2 inflammasome in tumor associated macrophages in the tumor microenvironment.

Discussion

Understanding the tumor microenvironment and the intrinsic relationship between tumor cells and immune cells is essential for developing potential therapy options. The critical role of inflammation in the tumor microenvironment is beginning to be appreciated, with many tumor types showing an inflammatory signature (20). Although cancer inflammation is described as a double-edged sword (21), it is without question a key mediator of cancer development with both tumor-promoting and inhibiting properties. Inflammasomes are multimeric protein complexes that are key drivers of inflammation and can recognize DNA to trigger innate immune responses. The AIM2 inflammasome is a DNA sensor that has been reported to be activated by dsDNA (22). In particular, the AIM2 inflammasome has been reported to be an important tumor regulator with inflammasome-dependent and independent roles in cancer but its exact role remains unclear (6, 23–25). The complex role of AIM2 in the tumor microenvironment may be more complicated through its inhibition of several signaling pathways including AKT (16) as well as STING-type 1 interferon signaling (7b) Most importantly, how AIM2 gets activated in cancer remains unknown.

A strength of the paper is the use of the MMTV-WNT mouse model as we wished primarily to look at spontaneous cancer growth. The MMTV-WNT mouse develops tumors at ~6-9 months of age so it was possible to determine if the numbers of infiltrating macrophages increases with time pre-tumor. *In vitro*, other tumor cell lines were used, such as human Hela (cervical cancer), human HCT116 (colon cancer) and human A549 (lung cancer) as well as mouse TRAMPC2 (prostate cancer). This demonstrates that all cancer cell lines could stimulate AIM2 inflammasome activation in macrophages exposed to the conditioned media from these cell lines. Thus our observations are not tumor type specific, but we believe a reflection of cancer cells in general.

The role of IL-1β in cancer has both positive and negative functions and may be dependent on the cancer type and stage. Our study has shown that IL-1β enhances proliferation of prostate cancer cells at physiological concentrations. This is in line with studies showing that host IL-1β is required for *in vivo* angiogenesis and invasiveness of melanoma, prostate and breast tumor cells through the production of VEGF and cytokines by macrophages (26). Similarly, IL1 was shown to be produced by tumor infiltrating

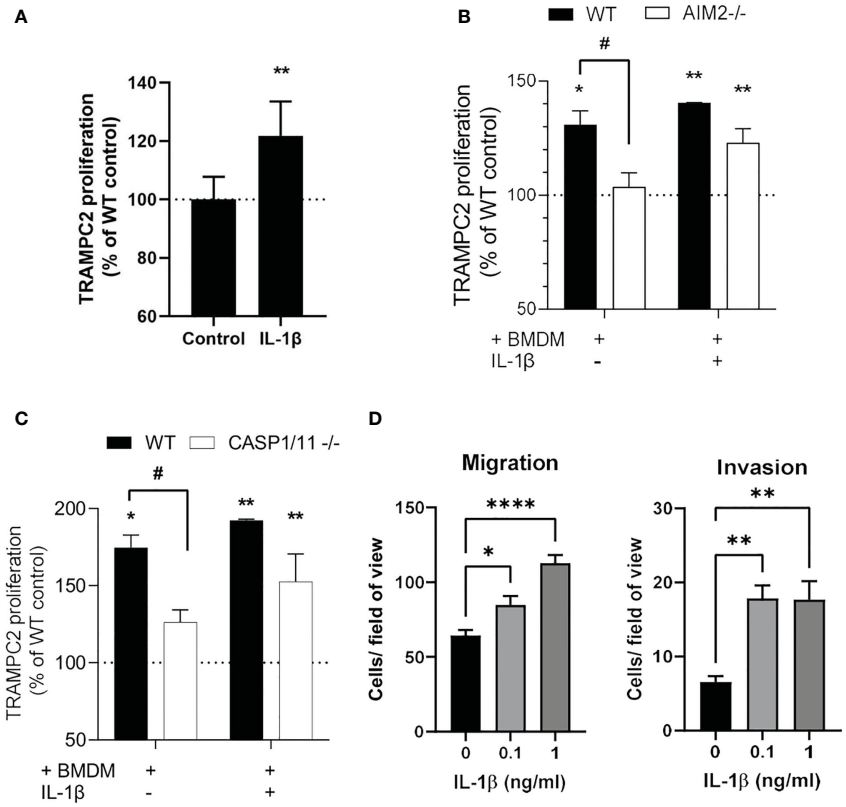

FIGURE 4
IL1β production from macrophages induces TRAMPC2 proliferation and migration/invasion **(A-C)** Proliferation rates of TRAMPC2 cells co-cultured with C57BL6, AIM2 -/- or Caspase 1/11 -/- bone marrow derived macrophages for 24h, with and without 0.25 ng/ml mouse IL-1β. *p<0.05, ** p<0.01 vs WT control; # p<0.05 vs WT+BMDM **(D)** Migration and invasion of TRAMPC2 cells cultured with IL-1β. Data are from n=3 mice *p<0.05; **p<0.01; ****p<0.0001.

myeloid cells in the tumor microenvironment and neutralizing IL1 receptor inhibits breast cancer progression *in vivo* in a humanized mouse model(27), indicating the importance of paracrine IL-1β in tumor growth and progression. In other studies, monocyte-derived IL-1β inhibited prostate cancer proliferation and induced apoptosis (28). However, interestingly, IL-1β inhibits differentiation and metastasis of metastasis initiating cells and among patients with lymph node-positive breast cancer, high primary tumor IL-1β expression is associated with better overall survival and distant metastasis-free survival (29).

The other players in the inflammasome pathway such as Gasdermin-D are is also involved in the macrophage inflammasome-dependent proliferation of cancer where lung metastasis in Gasdermin D -/- mice was reduced (30). Similar to our study, macrophage gasdermin-D plays a role in the tumor microenvironment. In addition, Caspase-1 and Gasdermin-D deficient macrophages enhance the activation of cGAS-STING dependent type-1 interferon pathway. However, this was reported to be pytoptosis, IL1 and IL-18 independent and through K+ depletion and suppression of cGAS activation (31). NLRP3 also has been reported in a multitude of studies to be involved in tumor growth and development both as an oncogene and as a tumor suppressor gene. (32). The spatial and temporal activation and expression of AIM2 and NLRP3 in varying tumor types may explain the conflicting reports but more studies are needed to fully understand the importance of the inflammasomes and its components in cancer.

Although implicated in different types of cancer, the trigger for AIM2 in these cancers remains unknown. Our results show that DNA-RNA hybrids may be the trigger for AIM2 inflammasome in cancers. Firstly, macrophages exhibited a significant decrease in IL-1β release when treated with DNA-RNA hybrid-depleted tumor conditioned media. This effect is not seen using dsDNA-depleted tumor conditioned media. Secondly, AIM2 -/- macrophages have impaired levels of IL-1β following transfection with DNA-RNA hybrids. Thirdly, immunostaining revealed that AIM2 colocalizes with cytosolic DNA-RNA hybrids to a larger extent than dsDNA in various cells tested. Taken together, our results indicate AIM2 indeed interacts with DNA-RNA hybrids. To the best of our knowledge, DNA-RNA hybrids have not been previously linked to AIM2 inflammasome in cancer. However, AIM2 was reported to be activated by RNA viruses such as influenza viruses (33, 34), Chikungunya virus and West Nile virus (35). Given that DNA-RNA hybrids are generated as intermediates during replication of the various viruses within infected cells (36, 37), RNA viruses may activate AIM2 via direct sensing of the DNA-RNA hybrids produced when the viral RNA is reverse transcribed into DNA. However, one report finds that bacterial DNA-RNA hybrids from Enterohemorrhagic Escherichia coli are sensed by NLRP3

10.3389/fimmu.2023.1211730

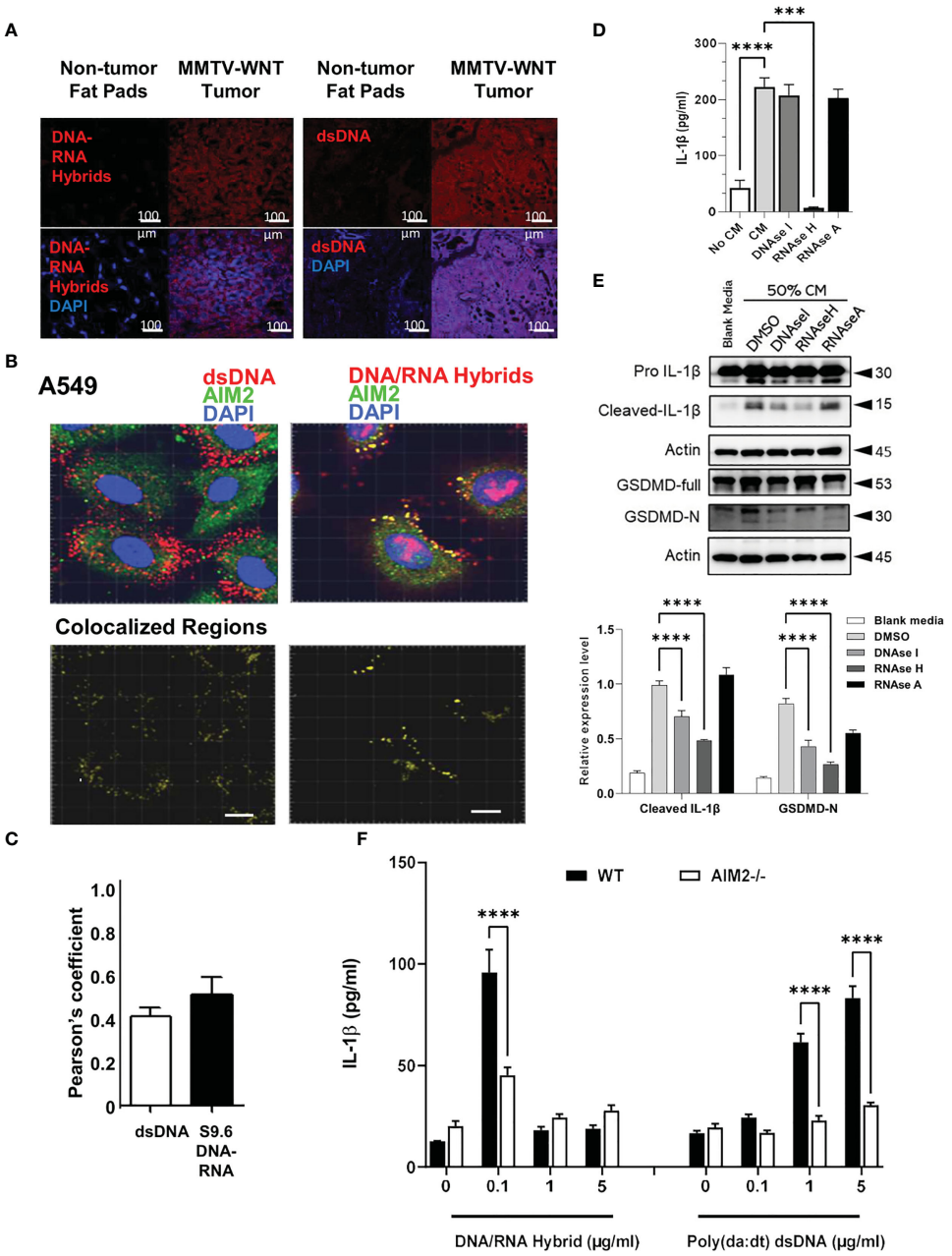

FIGURE 5
Tumor derived DNA-RNA hybrids activate AIM2 inflammasome. **(A)** MMTV Tissues and non-cancerous fat pads from mice were co-labelled for dsDNA or DNA/RNA hybrids (red) in the presence of DAPI (blue). **(B, C)** A549 cancer cells were co-labelled for AIM2 (green) and dsDNA (red) or -DNA-RNA hybrids (red) in presence of DAPI (blue). Co-localized regions are shown in yellow. Bar=20µm. Pearson's correlation of colocalization between AIM2 and either dsDNA or S9.6 DNA-RNA hybrids is shown. **(D)** A549 CM was treated with DMSO, sDNAase I (10 µg/ml), RNAase H (10U/ml) or RNAase A (10 µg/ml) for 2h and added to primed and differentiated THP-1 cells for 24h. Cell supernatants were collected and IL-1β levels analyzed using ELISA. **(E)** Cells were treated as above and inflammasome components (IL-1β and Gasdermin-D) and activation (cleaved, GasderminD-N) were analyzed using western blotting. Graph shows the quantification of immunoblots using Image J (fold change vs Actin) **(F)** AIM2-/- and WT BMDMs were treated with LPS (1 µg/ml) for 6h and increasing concentrations of DNA-RNA hybrids or Poly (dA: dT). Oligonucleotides were transfected with lyovec transfection reagent for the indicated time according to the manufacturer's recommendations. Cell supernatants were collected 24 h post- LPS priming, and IL-1β levels were quantified using ELISA. Data represents the mean ± SEM of at least 3 independent experiments. ***p<0.001; ****p<0.0001.

inflammasome (38). Our preliminary data indicates that while tumors express high levels of AIM2 and NLRP3, tumor CM increases the expression of AIM2, but not NLRP1, NLRP2 or NLRP3 inflammasomes, suggesting that AIM2 and NLRP3 inflammasomes may play complementary roles in inflammasome activation in response to tumor-derived mediators. It is important to note that our model here reports AIM2 sensing of endogenous self-DNA-RNA hybrids and not foreign bacterial hybrids.

Given the understanding that AIM2 recognizes dsDNA (10, 39), our study is one of the first to describe AIM2 recognition of DNA-RNA hybrids and at a higher sensitivity than dsDNA. It may be possible that AIM2 is only capable of sensing dsDNA more than

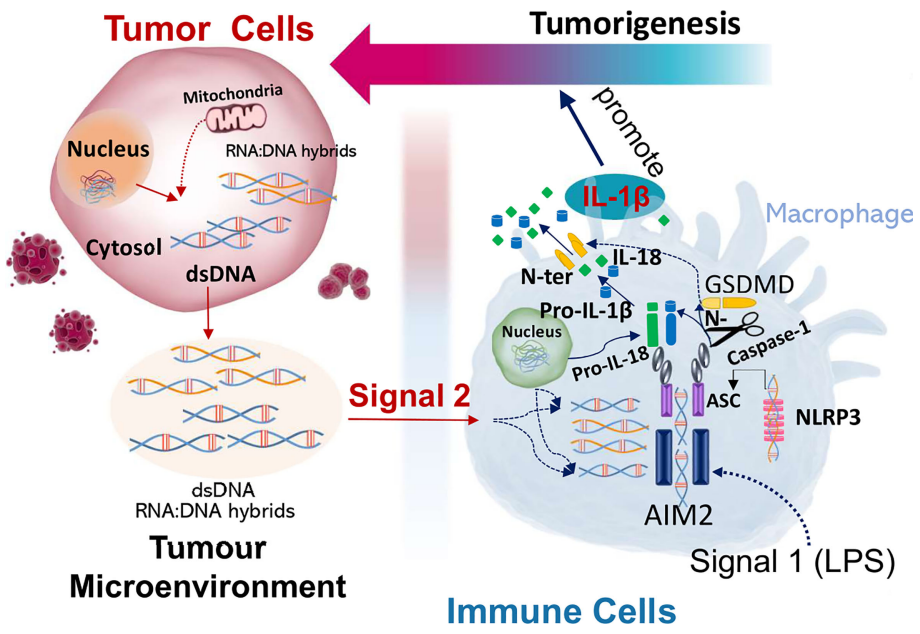

FIGURE 6
DNA-RNA hybrids and dsDNA in the tumor microenvironment activate and trigger AIM2 induced inflammation in macrophages to produce a pro-tumor response. Cancer cells secrete cytosolic DNA into the tumor microenvironment which is taken up by the macrophages. DNA-RNA hybrids and dsDNA bind and activate AIM2 inflammasome in macrophages, which produce pro-tumorigenic responses.

80bp in length (40). While the length of dsDNA in the tumor cells we used (A549, Hela, MCF-7) remains elucidated, it is certainly possible that the dsDNA present in these tumor cells is too short to trigger AIM2 activation in this model.

In summary, we show that tumors express cytosolic DNA and have higher numbers of infiltrating macrophages. Macrophages release IL-1β indicative of inflammasome activation after stimulation with LPS and tumor-CM, which is AIM2 dependent. IL-1β and coculture of tumor cells with macrophages enhances the proliferation of tumor cells which is AIM2 and Casp1/11 dependent. We propose that cancer cells release nucleic acids into the tumor microenvironment, which activates macrophages to produce an acute pro-tumor response (Figure 6). Accordingly, understanding paracrine tumor cytosolic DNA and immune cell interactions in cancer pathogenesis is a critical step for therapeutic development. Broader understanding of the mechanisms of nucleic acid interaction with innate immune signaling pathways would provide novel targets for anticancer research and future molecular therapy.

Data availability statement

The original contributions presented in the study are included in the article/Supplementary Material. Further inquiries can be directed to the corresponding author.

Ethics statement

The animal study was reviewed and approved by National University of Singapore IACUC, (AAALAC-accredited institution).

Author contributions

ZC, LL: Conception and design. ZC, JC, KaS, KrS, and KK: Investigation. ZC, JC, and LL: Analysis and interpretation of data. ZC: Roles/Writing original draft. JC, SG, and LL: Writing, review & editing. HL, AK, SL: Administrative, technical, or material support. LL, and SG: Study supervision and funding acquisition. All authors contributed to the article and approved the submitted version.

Funding

This research was funded by grants from the Ministry of Education (MOE2014T2-1-133) and (MOE2013-T2-2-032) awarded to LL. ZC was supported by a scholarship from the NUS Graduate School of Science and Technology.

Acknowledgments

We would like to thank Prof Jenny Ting (University of North Carolina at Chapel Hill, USA) for providing the AIM2-/- C57BL/6 mice and Prof David Virshup (Duke NUS, Singapore) for providing MMTV-Wnt (Mouse Mammary Tumor Virus-Wingless-related integration site) mice, and Dr Chen Kaiwen for providing the Caspase 1/11-/- mice.

Conflict of interest

Author SG was employed by company Roche.

The remaining authors declare that the research was conducted in the absence of any commercial or financial relationships that could be construed as a potential conflict of interest.

Publisher's note

Supplementary material

The Supplementary Material for this article can be found online at: https://www.frontiersin.org/articles/10.3389/fimmu.2023.1211730/full#supplementary-material

References

1. Isaacs A, Cox R, Rotem Z. Foreign nucleic acids as the stimulus to make interferon. *Lancet* (1963) 113–6. doi: 10.1016/S0140-6736(63)92585-6

2. Paludan SR, Bowie AG. Immune sensing of DNA. *Immunity* (2013) 38:870–80. doi: 10.1016/j.immuni.2013.05.004

3. Shen YJ, Le Bert N, Chitre AA, Koo CXE, Nga XH, Ho SS, et al. Genome-derived cytosolic DNA mediates type I interferon-dependent rejection of b cell lymphoma cells. *Cell Rep* (2015) 11:460–73. doi: 10.1016/j.celrep.2015.03.041

4. Woo S-R, Fuertes MB, Corrales L, Spranger S, Furdyna MJ, Leung MY, et al. STING-dependent cytosolic DNA sensing mediates innate immune recognition of immunogenic tumors. *Immunity* (2014) 41:830–42. doi: 10.1016/j.immuni.2014.10.017

5. Xiao TS. The nucleic acid-sensing inflammasomes. *Immunol Rev* (2015) 265:103–11. doi: 10.1111/imr.12281

6. Wilson JE, Petrucelli AS, Chen L, Koblansky AA, Truax AD, Oyama Y, et al. Inflammasome-independent role of AIM2 in suppressing colon tumorigenesis via DNA-PK and akt. *Nat Med* (2015) 21:906. doi: 10.1038/nm.3908

7. Fukuda K, Okamura K, Riding RL, Fan X, Afshari K, Haddadi N-S, et al. AIM2 regulates anti-tumor immunity and is a viable therapeutic target for melanoma. *J Exp Med* (2021) 218:e20200962. doi: 10.1084/jem.20200962

8. Broz P, Dixit VM. Inflammasomes: mechanism of assembly, regulation and signalling. *Nat Rev Immunol* (2016) 16:407. doi: 10.1038/nri.2016.58

9. Chan AH, Schroder K. Inflammasome signaling and regulation of interleukin-1 family cytokines. *J Exp Med* (2019) 217:e20190314. doi: 10.1084/jem.20190314

10. Ponomareva L, Liu H, Duan X, Dickerson E, Shen H, Panchanathan R, et al. AIM2, an IFN-inducible cytosolic DNA sensor, in the development of benign prostate hyperplasia and prostate cancer. *Mol Cancer Res* (2013) 11:1193–202. doi: 10.1158/1541-7786.MCR-13-0145

11. Farshchian M, Nissinen L, Siljamaki E, Riihila P, Piipponen M, Kivisaari A, et al. Tumor cell-specific AIM2 regulates growth and invasion of cutaneous squamous cell carcinoma. *Oncotarget* (2017) 8:45825–36. doi: 10.18632/oncotarget.17573

12. Qi M, Dai D, Liu J, Li Z, Liang P, Wang Y, et al. AIM2 promotes the development of non-small cell lung cancer by modulating mitochondrial dynamics. *Oncogene* (2020) 39:2707–23. doi: 10.1038/s41388-020-1176-9

13. Wang Q, Gao S, Shou Y, Jia Y, Wei Z, Liu Y, et al. AIM2 promotes renal cell carcinoma progression and sunitinib resistance through FOXO3a-ACSL4 axis-regulated ferroptosis. *Int J Biol Sci* (2023) 19:1266–83. doi: 10.7150/ijbs.79853

14. Woerner SM, Kloor M, Schwitalle Y, Youmans H, Doeberitz M, Gebert J, et al. The putative tumor suppressor AIM2 is frequently affected by different genetic alterations in microsatellite unstable colon cancers. *Genes Chromosomes Cancer* (2007) 46:1080–9. doi: 10.1002/gcc.20493

15. Xu M, Wang J, Li H, Zhang Z, Cheng Z. AIM2 inhibits colorectal cancer cell proliferation and migration through suppression of Gli1. *Aging (Albany NY)* (2020) 13:1017–31. doi: 10.18632/aging.202226

16. Zheng J, Liu C, Shi J, Wen K, Wang X. AIM2 inhibits the proliferation, invasion and migration, and promotes the apoptosis of osteosarcoma cells by inactivating the PI3K/AKT/mTOR signaling pathway. *Mol Med Rep* (2022) 25:1–11. doi: 10.3892/mmr.2021.12569

17. Lam AR, Le Bert N, Ho SS, Shen YJ, Tang ML, Xiong GM, et al. RAE1 ligands for the NKG2D receptor are regulated by STING-dependent DNA sensor pathways in lymphoma. *Cancer Res* (2014) 74:2193–203. doi: 10.1158/0008-5472.CAN-13-1703

18. Ho SS, Zhang WY, Tan NYJ, Khatoo M, Suter MA, Tripathi S, et al. The DNA structure-specific endonuclease MUS81 mediates DNA sensor STING-dependent host rejection of prostate cancer cells. *Immunity* (2016) 44:1177–89. doi: 10.1016/j.immuni.2016.04.010

19. Poh L, Fann DY, Wong P, Lim HM, Foo SL, Kang S-W, et al. AIM2 inflammasome mediates hallmark neuropathological alterations and cognitive impairment in a mouse model of vascular dementia. *Mol Psychiatry* (2021) 26 (8):4544–60. doi: 10.1038/s41380-020-00971-5

20. Wang M, Zhao J, Zhang L, Wei F, Lian Y, Wu Y, et al. Role of tumor microenvironment in tumorigenesis. *J Cancer* (2017) 8:761. doi: 10.7150/jca.17648

21. Hagemann T, Balkwill F, Lawrence T. Inflammation and cancer: a double-edged sword. *Cancer Cell* (2007) 12:300–1. doi: 10.1016/j.ccr.2007.10.005

22. Fernandes-Alnemri T, Yu J-W, Datta P, Wu J, Alnemri ES. AIM2 activates the inflammasome and cell death in response to cytoplasmic DNA. *Nature* (2009) 458:509–13. doi: 10.1038/nature07710

23. Patsos G, Germann A, Gebert J, Dihlmann S. Restoration of absent in melanoma 2 (AIM2) induces G2/M cell cycle arrest and promotes invasion of colorectal cancer cells. *Int J Cancer* (2010) 126:1838–49. doi: 10.1002/ijc.24905

24. Ma X, Guo P, Qiu Y, Mu K, Zhu L, Zhao W, et al. Loss of AIM2 expression promotes hepatocarcinoma progression through activation of mTOR-S6K1 pathway. *Oncotarget* (2016) 7:36185. doi: 10.18632/oncotarget.9154

25. Fukuda K. Immune regulation by cytosolic DNA sensors in the tumor microenvironment. *Cancers (Basel)* (2023) 15. doi: 10.3390/cancers15072114

26. Voronov E, Shouval DS, Krelin Y, Cagnano E, Benharroch D, Iwakura Y, et al. IL-1 is required for tumor invasiveness and angiogenesis. *Proc Natl Acad Sci* (2003) 100:2645–50. doi: 10.1073/pnas.0437939100

27. Wu T-C, Xu K, Martinek J, Young RR, Banchereau R, George J, et al. IL1 receptor antagonist controls transcriptional signature of inflammation in patients with metastatic breast cancer. *Cancer Res* (2018) 78:5243–58. doi: 10.1158/0008-5472.CAN-18-0413

28. Culig Z, Hobisch A, Herold M, Hittmair A, Thurnher M, Eder I, et al. Interleukin 1β mediates the modulatory effects of monocytes on LNCaP human prostate cancer cells. *Br J Cancer* (1998) 78:1004–11. doi: 10.1038/bjc.1998.619

29. Castaño Z, San Juan BP, Spiegel A, Pant A, Decristo MJ, Laszewski T, et al. IL-1β inflammatory response driven by primary breast cancer prevents metastasis-initiating cell colonization. *Nat Cell Biol* (2018) 20:1084–97. doi: 10.1038/s41556-018-0173-5

30. Traughber CA, Deshpande GM, Neupane K, Bhandari N, Khan MR, Mcmullen MR, et al. Myeloid-cell-specific role of gasdermin d in promoting lung cancer progression in mice. *iScience* (2023) 26:106076. doi: 10.1016/j.isci.2023.106076

31. Banerjee I, Behl B, Mendonca M, Shrivastava G, Russo AJ, Menoret A, et al. Gasdermin d restrains type I interferon response to cytosolic DNA by disrupting ionic homeostasis. *Immunity* (2018) 49:413–426.e415. doi: 10.1016/j.immuni.2018.07.006

32. Hamarsheh S, Zeiser R. NLRP3 inflammasome activation in cancer: a double-edged sword. *Front Immunol* (2020) 11:1444. doi: 10.3389/fimmu.2020.01444

33. Schattgen SA, Gao G, Kurt-Jones EA, Fitzgerald KA. Cutting edge: DNA in the lung microenvironment during influenza virus infection tempers inflammation by engaging the DNA sensor AIM2. *J Immunol* (2016) 196:29–33. doi: 10.4049/jimmunol.1501048

34. Zhang H, Luo J, Alcorn JF, Chen K, Fan S, Pilewski J, et al. AIM2 inflammasome is critical for influenza-induced lung injury and mortality. *J Immunol* (2017) 198:4383–93. doi: 10.4049/jimmunol.1600714

35. Ekchariyawat P, Hamel R, Bernard E, Wichit S, Surasombatpattana P, Talignani L, et al. Inflammasome signaling pathways exert antiviral effect against chikungunya virus in human dermal fibroblasts. *Infection Genet Evol* (2015) 32:401–8. doi: 10.1016/j.meegid.2015.03.025

36. Summers J, Mason WS. Replication of the genome of a hepatitis b-like virus by reverse transcription of an RNA intermediate. *Cell* (1982) 29:403–15. doi: 10.1016/0092-8674(82)90157-X

37. Prichard MN, Jairath S, Penfold ME, Jeor SS, Bohlman MC, Pari GS. Identification of persistent RNA-DNA hybrid structures within the origin of replication of human cytomegalovirus. *J Virol* (1998) 72:6997–7004. doi: 10.1128/JVI.72.9.6997-7004.1998

38. Vanaja SK, Rathinam VA, Atianand MK, Kalantari P, Skehan B, Fitzgerald KA, et al. Bacterial RNA: DNA hybrids are activators of the NLRP3 inflammasome. *Proc Natl Acad Sci* (2014) 111:7765–70. doi: 10.1073/pnas.1400075111

39. Hornung V, Ablasser A, Charrel-Dennis M, Bauernfeind F, Horvath G, Caffrey DR, et al. AIM2 recognizes cytosolic dsDNA and forms a caspase-1-activating inflammasome with ASC. *Nature* (2009) 458:514–8. doi: 10.1038/nature07725

40. Jin T, Perry A, Jiang J, Smith P, Curry JA, Unterholzner L, et al. Structures of the HIN domain: DNA complexes reveal ligand binding and activation mechanisms of the AIM2 inflammasome and IFI16 receptor. *Immunity* (2012) 36:561–71. doi: 10.1016/j.immuni.2012.02.014

frontiers | Frontiers in Immunology

TYPE Original Research
PUBLISHED 28 August 2023
DOI 10.3389/fimmu.2023.1252384

OPEN ACCESS

EDITED BY
Timur O. Yarovinsky,
Yale University, United States

REVIEWED BY
Amelie Vromman,
Harvard Medical School, United States
Melanie Rae Gubbels Bupp,
Randolph–Macon College, United States

*CORRESPONDENCE
Christina Maeder
christina.maeder@medizin.uni-leipzig.de

†These authors have contributed equally to this work

RECEIVED 04 July 2023
ACCEPTED 10 August 2023
PUBLISHED 28 August 2023

CITATION
Maeder C, Speer T, Wirth A, Boeckel J-N, Fatima S, Shahzad K, Freichel M, Laufs U and Gaul S (2023) Membrane-bound Interleukin-1α mediates leukocyte adhesion during atherogenesis. *Front. Immunol.* 14:1252384. doi: 10.3389/fimmu.2023.1252384

Membrane-bound Interleukin-1α mediates leukocyte adhesion during atherogenesis

Christina Maeder[1*], Thimoteus Speer[2,3], Angela Wirth[4,5], Jes-Niels Boeckel[1], Sameen Fatima[6], Khurrum Shahzad[6], Marc Freichel[4,5], Ulrich Laufs[1†] and Susanne Gaul[1†]

[1]Klinik und Poliklinik für Kardiologie, Universitätsklinikum Leipzig, Leipzig University, Leipzig, Germany, [2]Medizinische Klinik 4, Nephrologie, Goethe-Universität Frankfurt, Frankfurt am Main, Germany, [3]Else Kroener Fresenius Zentrum für Nephrologische Forschung, Goethe-Universität Frankfurt, Frankfurt am Main, Germany, [4]Institute of Pharmacology, Heidelberg University, Heidelberg, Germany, [5]DZHK (German Centre for Cardiovascular Research), Partner Site Heidelberg/Mannheim, Heidelberg, Germany, [6]Department of Diagnostics, Laboratory Medicine, Clinical Chemistry and Molecular Diagnostic, Universitätsklinikum Leipzig, Leipzig University, Leipzig, Germany

Introduction: The interleukin-1 (IL-1) family and the NLR family pyrin domain-containing 3 (NLRP3) inflammasome contribute to atherogenesis but the underlying mechanisms are incompletely understood. Unlike IL-1β, IL-1α is not dependent on the NLRP3 inflammasome to exert its pro-inflammatory effects. Here, a non-genetic model was applied to characterize the role of IL-1α, IL-1β, and NLRP3 for the pathogenesis of atherosclerosis.

Methods: Atherogenesis was induced by gain-of-function PCSK9-AAV8 mutant viruses and feeding of a high-fat western diet (WTD) for 12 weeks in C57Bl6/J wildtype mice (WT) and in Il1a$^{-/-}$, Nlrp3$^{-/-}$, and Il1b$^{-/-}$ mice.

Results: PCSK9-Il1a$^{-/-}$ mice showed reduced atherosclerotic plaque area in the aortic root with lower lipid accumulation, while no difference was observed between PCSK9-WT, PCSK9-Nlrp3$^{-/-}$ and PCSK9-Il1b$^{-/-}$ mice. Serum proteomic analysis showed a reduction of pro-inflammatory cytokines (e.g., IL-1β, IL-6) in PCSK9-Il1a$^{-/-}$ as well as in PCSK9-Nlrp3$^{-/-}$ and PCSK9-Il1b$^{-/-}$ mice. Bone marrow dendritic cells (BMDC) of PCSK9-WT, PCSK9-Nlrp3$^{-/-}$, and PCSK9-Il1b$^{-/-}$ mice and primary human monocytes showed translocation of IL-1α to the plasma membrane (csIL-1α) upon stimulation with LPS. The translocation of IL-1α to the cell surface was regulated by myristoylation and increased in mice with hypercholesterolemia. CsIL-1α and IL1R1 protein-protein interaction on endothelial cells induced VCAM1 expression and monocyte adhesion, which was abrogated by the administration of neutralizing antibodies against IL-1α and IL1R1.

Conclusion: The results highlight the importance of IL-1α on the cell surface of circulating leucocytes for the development of atherosclerosis. PCSK9-Il1a$^{-/-}$ mice, but not PCSK9-Nlrp3$^{-/-}$ or PCSK9-Il1b$^{-/-}$ mice, are protected from atherosclerosis after induction of hypercholesterolemia independent of circulating cytokines. Myristoylation and translocation of IL-1α to the cell surface in myeloid cells facilitates leukocyte adhesion and contributes to the development of atherosclerosis.

KEYWORDS

atherosclerosis, inflammation, hyperlipidemia, interleukin - 1, mouse model

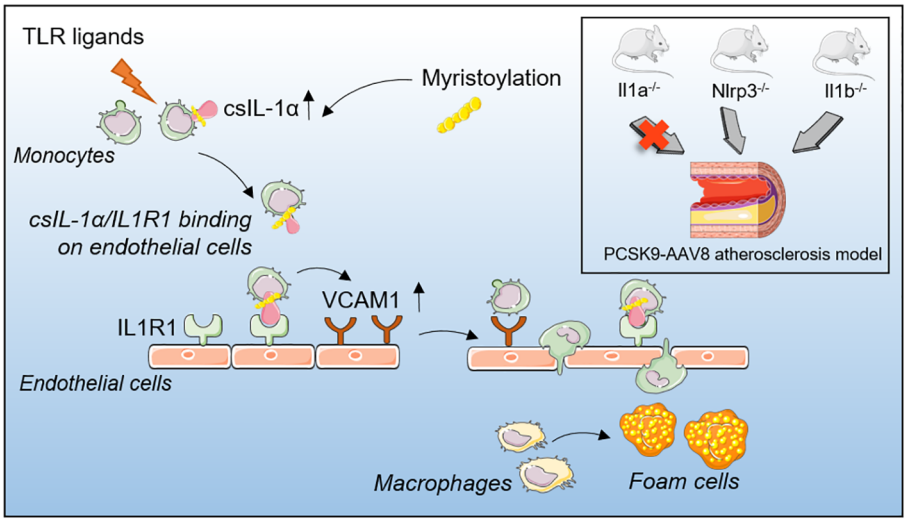

GRAPHICAL ABSTRACT
The role of cell-surface (cs) IL-1α in the initiation of atherosclerosis.

Introduction

Atherosclerosis is a chronic inflammatory disease driven by intimal lipid accumulation (1, 2). Reactive oxygen species modify plasma lipoproteins in the subendothelial space, where they are engulfed and digested by macrophages (3). Processing of oxidized lipoproteins inside the cell leads to cholesterol crystal formation and activation of the NOD-, LRR- and pyrin domain-containing protein 3 (NLRP3) inflammasome, initiating the release of pro-inflammatory cytokines such as IL-1β (4, 5). During plaque progression, different subsets of leukocytes adhere to endothelial cells and infiltrate the atherosclerotic plaque contributing to the inflammatory environment (6, 7).

IL-1 cytokines are considered inflammatory mediators of atherosclerosis (8). Two related but distinct IL-1 genes, *IL1A*, and *IL1B*, encode IL-1α and IL-1β, respectively. Both share the same receptor, and upon binding of either cytokine, interleukin 1 receptor type I (IL1R1) associates with interleukin 1 receptor accessory protein (IL1RAP/IL1R3) to form a trimeric structure that mediates NfκB-dependent pro-inflammatory signaling (9). The inactive IL-1β precursor protein is cleaved by caspase 1 to the mature form of IL-1β (10).

In contrast to IL-1β, both the precursor and the cleaved form of IL-1α are biologically active. Pro-IL-1α can also be presented on the cell surface (csIL-1α) upon activation of the TLR, e.g., in the presence of lipopolysaccharides (LPS) (11). The precise mechanism of binding IL-1α to the outer cell membrane is incompletely understood (12). It was observed that csIL-1α plays a role in acute myocardial infarction (AMI) and chronic kidney disease (CKD) and is associated with an increased risk of cardiovascular events (13). However, its functional role in atherogenesis is not fully elucidated.Previous studies of atherogenesis in mice depended on cross-breeding with either Ldlr- or ApoE-deficient animals. Both models exhibit high plasma cholesterol levels and the development of atherosclerotic lesions in susceptible areas (14). Studies on genes involved in atherosclerosis require inbreeding in either $Ldlr^{-/-}$ or $ApoE^{-/-}$ animals with the associated potential confounders. However, studies of gene candidates without the genetic bias of the atherosclerosis model itself were not available. We therefore applied a nongenetic gain-of-function PCSK9-AAV8 atherosclerosis model to address the question whether atherosclerosis development depends on IL-1α or the NLRP3 inflammasome and whether IL-1α expressed at the cell surface is involved in the development of atherosclerosis (15).

Materials and methods

Mice

$Il1a^{-/-}$ (n=6) and $Il1b^{-/-}$ (n=5) mice were a kind gift from Prof. Timotheus Speer (Goethe-Universität Frankfurt, Frankfurt am Main, Germany) (13). WT C57Bl6/J (n=10) and $Nlrp3^{-/-}$ (B6.129S6-Nlrp3tm1Bhk/J backcrossed to a C57BL/6J background, n=5) were purchased from Charles River (Sulzfeld, Germany). To induce atherosclerosis, the mice were injected with a mutated AAV8 virus, as described previously (15). Briefly, age-matched littermates were injected with rAAV8-$PCSK9^{D377Y}$ (1.0×10^{11} viral genomes/mouse) or saline as control at 10 weeks (Figure 1A). Mice received a western high-fat diet (Ssniff, 21% fat, 0.21% cholesterol) one-week post-virus injection for 12 weeks (referred as PCSK9-WT). Saline-treated control mice were fed a normal chow diet. Body weights were measured weekly. Mice were sacrificed after the given time point, and organs were harvested. In brief, the mice were anesthetized with 4-5% isoflurane. The absence of the pedal reflex confirmed successful anesthesia. Afterward, blood was collected, and mice were perfused for organ harvest. All protocols were approved by the Institutional Animal Care

10.3389/fimmu.2023.1252384

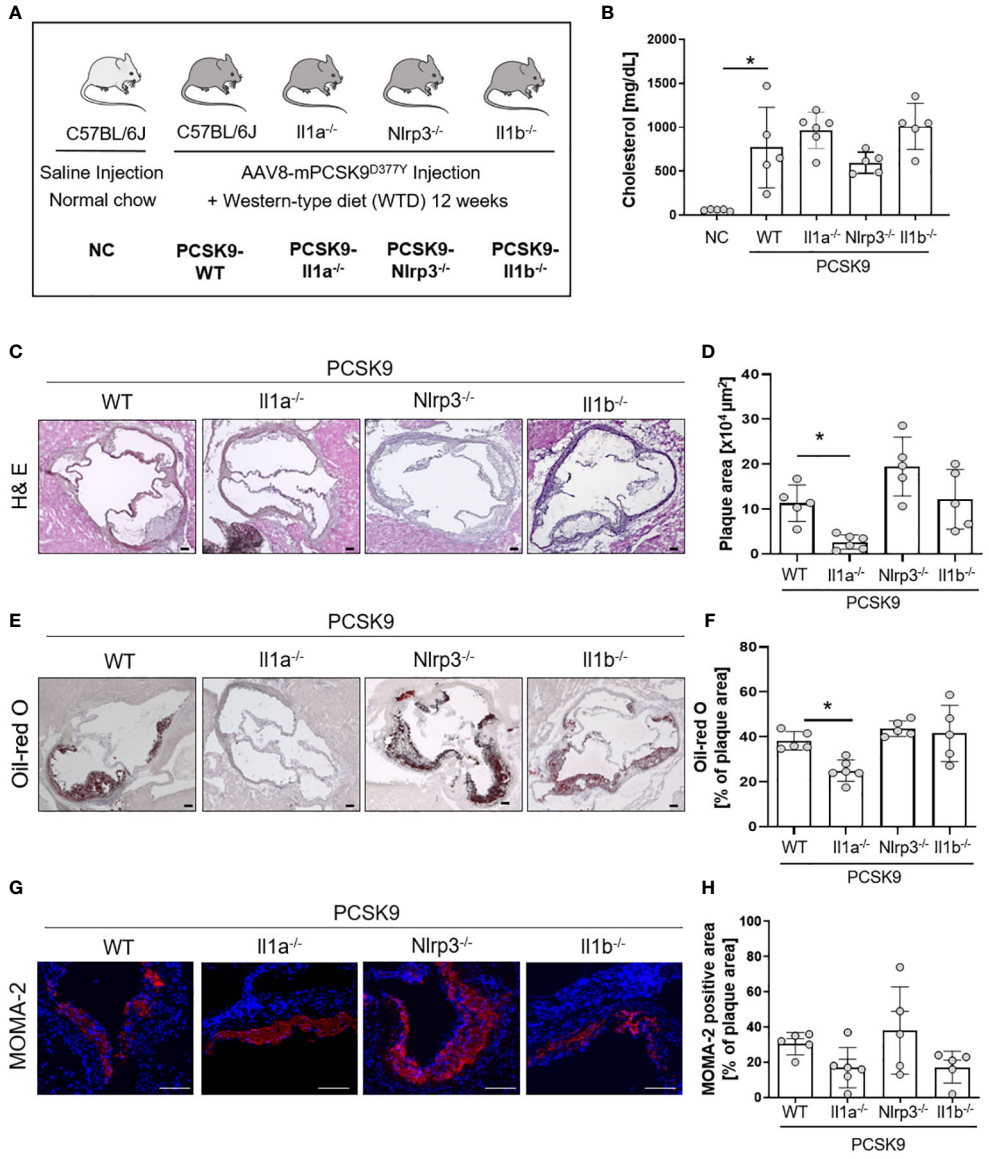

FIGURE 1
Il1a knockout mice are protected from hyperlipidemic-induced atherosclerosis independent of the NLRP3-inflammasome. **(A)** Schematic overview of the experimental groups. Mice were injected with either rAAV8-PCSK9^{D377Y} or Saline. One-week post-injection, mice were fed a western-type diet (21% fat, 0.21% cholesterol) for 12 weeks. Saline-injected mice received a normal chow (NC) diet. **(B)** Bar graph of plasma cholesterol [mg/dL] after 12 weeks of diet intervention. **(C–H)**: Representative histological images of the aortic root stained with Hematoxylin/Eosin (H& E, **(C)**, Oil-red O (ORO, **E)**, and monocyte and macrophage (MOMA-2) staining **(G)** with their corresponding bar graphs **(D, F, H)**. One-way ANOVA was performed with Sidak's multiple comparisons posthoc test (*p < 0.05). H& E and ORO stainings were imaged with 4 × magnification, scale bar 100 µm **(C, E)**, MOMA-2 staining with 10 × magnification, scale bar 100 µm **(G)**. Data are presented as mean ± SD of PCSK9-WT (n=5), PCSK9-Il1a$^{-/-}$ (n=6), PCSK9-Nlrp3$^{-/-}$ (n=5), and PCSK9-Il1b$^{-/-}$ (n=5) animals.

(42/2019, Veterinary Office of the Saarland) and were consistent with the guidelines from Directive 2010/63/EU of the European Parliament.

Histology

Characterization of atherosclerotic lesions was performed in the aortic root. Cryopreserved sections (10 µm) were used for Hematoxylin and Eosin (H& E), MOMA-2, and Oil-red O (ORO) staining. MOMA-2 and ORO staining were performed as described previously (15). H& E staining was performed by fixation of cryoslides with Xylene 3x 5 min, followed by a descending series with alcohol. Slides were washed with H2O before the hematoxylin staining for 4 min. Then, sections were washed with H2O and incubated with Scott's bluing water for 20 seconds, followed by 1 min in 95% EtOH. Staining with Eosin was performed for 1 min, and sections were incubated in an ascending series of alcohol followed by 3x 5 min in xylene. Stained sections were then covered with xylene-based mounting solution and coverslips. ImageJ software (Version 1.53k) was used for image analysis. MOMA-2 staining was imaged with a ZEISS Elyra microscope.

The percentage of MOMA-2 positive area per lesion was calculated by measuring the MOMA-2 positive area and dividing it by the plaque area.

Isolation and culture of murine bone marrow-derived dendritic cells

Bone marrow cells were isolated from wildtype mice (16). 2×10^6 bone marrow cells were plated on a 10-cm dish in RPMI-1640 medium (Sigma Aldrich, USA) containing 10% fetal calf serum (Gibco, Thermo Fisher Scientific, USA), 1% Penicillin-Streptomycin, and 50 mM β-Mercaptoethanol (Gibco, Thermo Fisher Scientific, USA). To induce dendritic cell differentiation, the medium was supplemented with 20 ng/ml GM-CSF (Preprotech, Thermo Fisher Scientific, USA) and 10 ng/ml IL-4 (Preprotech, Thermo Fisher Scientific, USA) (17). Cells were harvested on day 7 by collecting the suspension cells in the supernatant. Differentiation was confirmed using flow cytometry by detecting the MHC-II and Cd11c double-positive cells (min. 70% double-positive cells) (Figure S2A). Harvested cells were replated for further experiments in a fresh culture dish.

Isolation and stimulation of human primary monocytes

Human primary monocytes were isolated from buffy coats of healthy volunteers via Ficoll (Cytiva, USA) gradient centrifugation. The study was conducted in accordance with the Declaration of Helsinki on Ethical Principles and was approved by the Ethical Committee of the Medical Faculty, University of Leipzig (ethics license: 272-12-13082012). Isolated PBMCs were incubated with CD14 beads (Milteny Biotech, Germany) for 15 min at 4°C and isolated with MACS magnetic separator. Isolated monocytes were cultured in RPMI-1640 (Sigma Aldrich, USA) with 10% Fetal calf serum and 10 mM Sodium Pyruvate (Merck, Germany). Cells were stimulated with 100 ng/ml ultrapure LPS (upLPS, Invivogen, USA) overnight.

Culture of human umbilical vein endothelial cells

Human Umbilical Vein Cells (HUVECs) were cultured in EBM Endothelial Cell Growth Basal Medium (Lonza, Swiss) supplemented with EGMTM Endothelial Cell Growth Medium SingleQuots (Lonza, Swiss). Passages 4 to 8 were used for experiments.

Serum analysis

Serum was collected for the measurement of plasma lipids and plasma proteins. 500-700 µl of blood were collected from each mouse and centrifuged at 3.500× g for 10 min at room temperature. Blood serum was transferred to a fresh 1.5 ml tube and snap-frozen in liquid nitrogen. Cholesterol was measured using LabAssay Cholesterol (Fuji Film, Japan) following the manufacturer's instructions.

The Olink Mouse Exploratory Panel was used to measure circulating proteins. Serum was prepared according to the manufacturer's instructions (Olink, Sweden) and measured with the Mouse Exploratory 96 panel. Protein concentration was determined using the proximity extension assay (PEA) technology described elsewhere (18). Briefly, oligonucleotide-labeled antibodies bind to their target proteins where they come into proximity with other labeled antibodies that bind to the same target. The oligonucleotides hybridize in proximity and form a basis for qPCR and quantification. The number of qPCR cycles stands in relation to the protein concentration and gives the arbitrary unit normalized protein expression ("NPX") as the readout. To examine changes in the secretome in the hyperlipidemic mouse model vs. mice fed a normal chow (NC) diet, two-sideded t-test was performed, followed by enrichment analysis of the significant regulated proteins (FDR cutoff= 0.1).

Subcellular fractionation

Mouse BMDC were incubated overnight with culture medium or 100 ng/ml upLPS. Human monocytes were stimulated overnight with 100 ng/ml upLPS. Subcellular fractionation was performed using the Cell Signaling Kit (Cell signaling, USA) according to the manufacturer's instructions. NaK- ATPase was used as a marker for the membrane fraction and GAPDH for the cytoplasmic fraction in immunoblotting.

Immunoblotting

Cytoplasm and membrane fractions were mixed with 4x Laemmli and β-mercaptoethanol. Equal volumes of fractions were directly loaded in a 4-12% pre-cast gradient gel (BioRad, USA) and separated by SDS-Page. Proteins were transferred to a nitrocellulose membrane (BioRad, USA), blocked with 5% non-fat dietary milk (NFDM, Carl Roth, Germany), and washed and incubated with the primary antibodies were either diluted in 5% NFDM or 5% bovine serum albumin (BSA, Serva, USA) overnight at 4°C: hIL-1α (1:500, sc-271618, clone G10, Santa Cruz, USA), mIL-1α (1:1,000, AF-400-SP, R&D, USA), GAPDH (1:5,000, sc-47724, clone 0411, Santa Cruz, USA), NaK ATPase (1:10,000, ab76020, Abcam, United Kingdom). The membrane was incubated with the secondary antibody coupled with horse radish peroxidase diluted in 5% NFDM for 1h on the following day. Classico Western HRP Substrate (Millipore) or SuperSigna West Femto (Thermo Fisher Scientific, USA) were used for development on iBright 1500 (Thermo Fisher Scientific, USA).

Proximity ligation assay

Duolink *In Situ* Red Starter Kit Mouse/Rabbit (Sigma Aldrich, USA) was used and performed following the manufacturer's

instructions. Briefly, HUVEC cells were seeded on a µ-slide Angiogenesis (ibidi, Germany) and were pre-stimulated with neutralizing IL1R1 antibody (10 µg/ml, #AB-269-NA, R&D Systems, USA) as indicated for 1h. Unstimulated or upLPS-stimulated monocytes were then added for 4h per well. Monocytes were washed 4 times to eliminate residual upLPS before seeding on HUVEC cells. After 4h, the supernatant was aspirated carefully, and cells were fixed with ROTI Histofix 4% (Carl Roth, Germany) for 20 min at room temperature. The primary antibodies hIL-1α (1:50, sc-271618, clone G10, Santa Cruz, USA) and IL1R1 Polyclonal Antibody (1:100, PA5-117479, Invitrogen, USA) were diluted in Duolink antibody dilution and stained overnight. 1 µg/ml rabbit IgG (Dianova, RIgG, Germany) was included as an isotype control.

Monocyte adhesion assay

To determine monocyte-to-endothelial adhesion, HUVEC cells 3were seeded on 96-well Flat Clear Bottom Black Polystyrene Microplates (Corning, USA). Isolated primary monocytes were stimulated with upLPS overnight or kept in culture medium. The next day, stimulated monocytes were pre-incubated with a neutralizing IL-1α antibody (1 µg/ml, mabg-hil1a-3, Invivogen, USA) as indicated for 1h. Afterward, monocytes were labeled with CellTrace™ Calcein Red-Orange, AM (Invitrogen, USA) for 30 min at 37° C. Monocytes were washed 4 times to eliminate residual upLPS and were co-incubated with HUVECs. After 4 h, fluorescence intensity was measured, as well as the remaining intensity after up to 4 washing steps. %adhesion of monocytes was calculated as stated: $((F_{remaining\ fluorescence} - F_{blanc})/(F_{total} - F_{blanc}))x100$.

Flow cytometry analysis of csIL-1α and VCAM1

For the staining of cell-surface IL-1α (12), cells were harvested and washed once with PBS. The cell number was adjusted to $1x10^6$/ml, and cells were resuspended in FACS buffer (1% BSA, 0.05% sodium azide in PBS). Trustain mouse or human Fc block (1µg/ml, Biolegend, USA) was added and incubated for 10 min on ice. Anti-biotin IL-1α antibody (human: 10µg/ml, #531304, Biolegend, USA; mouse: 10µg/ml, #512503, Biolegend, USA) or appropriate IgG isotype control (human: Goat IgG Biotinylated control, 10 µg/ml, BAF108, Bio Techne, USA; mouse: Biotin Rat IgG1, 10 µg/ml, #400403, Biolegend, USA) was added and incubated for 30 min on ice. Anti-Streptavidin PE was added (2,5 µg/ml, eBioscience, USA) and incubated for 30 min on ice in the dark. Cells were incubated with 5 µl of 7AAD (BD Bioscience, USA) for 10 min at room temperature; cells were immediately measured. For the assessment of total IL-1α, cells were fixed after harvest with 250 µl of Cytofix (Biolegend, USA) for 20 min at 4°C. Staining of IL-1α was performed as described, but FACS buffer was exchanged with Permeabilisation buffer (Biolegend, USA). To detect VCAM1 on HUVECs, cells were pre-stimulated with neutralizing IL1R1 antibody (10 µg/ml, #AB-269-NA, R&D Systems, USA) as indicated for 1h. Unstimulated and upLPS-stimulated monocytes were added for 4h. Tnfα served as a positive control. Monocytes were washed 4 times to eliminate residual upLPS before seeding on HUVEC cells. Up-LPS stimulated HEK293 and handled as stimulated monocytes and were included as a control to verify the successful elimination of LPS (Figure S3A). After 4h, the supernatant was discarded, and cells were fixed with 0.5% Roti-Histofix (Carl Roth, Germany) and harvested. Staining was performed using 5 µg/ml anti-human CD106 APC Antibody (#305810, Biolegend, USA) or mouse IgG2a kappa Isotype control (eBM2a) APC (5 µg/ml, #17-4724-81, Thermo Fisher Scientific, USA) as the isotype control, for 45 min on a rotator at 4°C. Cells were measured at the BD FACS Lyrica. FlowJo® Software (Version 10.8.1) was used for further analysis.

Myristoylation assay

Myristoylation was detected using a myristoylated protein assay kit (abcam, USA) following the manufacturer's instructions. Cells without myristic acid labeling served as background controls. To test the myristoylation inhibitor, cells were pre-incubated with 1 µM n-myristoyltransferase inhibitor IMP-1088 (Cayman Chemical, USA) for 1h before stimulation with 100 ng/ml upLPS overnight.

ELISA

Human (R&D Systems, USA) and mouse IL-1α (R&D Systems, USA) DuoSet ELISA kits, as well as human (R&D Systems, USA) and mouse IL-1β (R&D Systems, USA) DuoSet ELISA kits, were used in combination with DuoSet ELISA Ancillary Reagent kit (R&D Systems, USA). The assays were performed following the manufacturer's instructions.

Illustrations

Graphical abstract and schematic overviews were generated by using icons from Servier Medical Art, provided by Servier, licensed under a Creative Commons Attribution 3.0 unported license.

Statistical analysis

Statistical analyses were performed with GraphPad Prism (version 8; GraphPad Software Inc., La Jolla, CA, USA). Data were tested for a gaussian distribution using the Kolmogorov–Smirnov or D'Agostino-Pearson normality test. Two-tailed unpaired t-test was performed to compare groups if not otherwise stated. One-way ANOVA with Sidak's multiple comparisons test was performed to compare more than two groups. The significance level was set to $p < 0.05$.

Results

PCSK9-Il1a$^{-/-}$ mice are protected from hyperlipidemia-induced atherosclerosis, whereas PCSK9-Nlrp3$^{-/-}$ and PCSK9-Il1b$^{-/-}$ mice are not

To investigate the role of IL-1α and the NLRP3 inflammasome in a nongenetic mouse model of atherosclerosis, we induced hypercholesterolemia in WT, Il1a$^{-/-}$, Nlrp3$^{-/-}$, and Il1b$^{-/-}$ mice by a single injection of a hyperactive pro-protein convertase subtilisin/kexin type 9 (PCSK9)-adeno-associated virus (rAAV) followed by a Western-type diet (PCSK9) for 12 weeks (Figure 1A). PCSK9 control mice (PCSK9-WT) develop hypercholesterolemia and spontaneous atherosclerosis (Figures 1B–H), as recently described by our group (15). Cholesterol levels were similar in PCSK9-WT and PCSK9-Il1a$^{-/-}$, PCSK9-Nlrp3$^{-/-}$, and PCSK9-Il1b$^{-/-}$ animals (Figure 1B). PCSK9-Il1a$^{-/-}$ mice showed reduced atherosclerotic lesions (-76%) (Figures 1C, D) and lower lipid accumulation (Oil-red O, Figures 1E, F) than PCSK9 control mice. The development of atherosclerosis in PCSK9-Nlrp3$^{-/-}$ and PCSK9-Il1b$^{-/-}$ mice did not differ from the control wildtype animals (Figures 1C–F). No significant difference in macrophage infiltration in plaques (MOMA-2 positive cells) was observed in PCSK9-Il1a$^{-/-}$, PCSK9-Il1b$^{-/-}$, and PCSK9-Nlrp3$^{-/-}$ mice compared to PCSK9-WT animals (Figures 1G, H).

PCSK9-Il1a$^{-/-}$, PCSK9-Nlrp3$^{-/-}$ and PCSK9-Il1b$^{-/-}$ mice show reduced levels of circulating cytokines

To determine whether the atheroprotective effect in PCSK9-Il1a$^{-/-}$ mice are associated with changes in the serum protein profile, we used the Olink Target 96 Mouse Exploratory Panel. The 92 proteins measured encompass various biological processes and thus provide an overview of regulated signaling pathways. The serum of PCSK9-WT control mice showed increased proteins annotated to cell-activating signaling pathways and vasculature-regulating mechanisms (Figures 2A, B). PCSK9-Il1a$^{-/-}$ led to a significant downregulation of pro-inflammatory proteins, such as IL-6, IL-1β, and CCL-2, compared to PCSK9-WT (Figure 2C). IL-6 was also downregulated in PCSK9-Nlrp3$^{-/-}$ and PCSK9-Il1b$^{-/-}$ but both groups show similar plaque development to PCSK9-WT (Figure 1C). Normal chow control group (NC) and PCSK9-Il1a$^{-/-}$ animals did not share similar regulated proteins (Figure 2D). Even though IL-1β was significantly upregulated in PCSK9-WT group, serum IL-1α levels did not show a significant difference between NC and PCSK9-WT (Figure 2E).

Cell surface translocation of IL-1α is not influenced by NLRP3 and IL-1β in murine BMDC

Since serum levels of IL-1α were not increased in atherosclerotic PCSK9-WT mice (Figure 2E), we investigated the membrane-bound form of IL-1α. The shuttle from the cytoplasm to the plasma membrane requires *de-novo* synthesis of IL-1α, mediated by the TLR/NFκB signaling pathway. BMDCs, as an important representative of circulating immune cells, were used to study the translocation of IL-1α from the cytoplasm to the plasma membrane after a single stimulus of 100 ng/ml ultrapure LPS (upLPS) and cell fractionation (Figure 3A). Stimulation of the TLR leads to the accumulation of pro-IL-1α in the plasma membrane fraction (Figures 3B, C). The purity of the cell fractions was confirmed with markers for cytoplasm (glyceraldehyde-3-phosphate dehydrogenase (GAPDH)) and for plasma membrane (sodium-potassium ATPase (NaK- ATPase)). GAPDH was not detected in the membrane fraction, confirming no contamination of cytoplasmic IL-1α. The translocation to the plasma membrane was validated by flow cytometry on stimulated, unfixed cells (Figure 3D). 7-AAD was used to discriminate between dead and live cells and analyze the cell-surface IL-1α only in unfixed 7-AAD negative cells (Figure 3D). LPS increased *de-novo* synthesis of total IL-1α from 4.9 ± 6.6% to 42.9 ± 7.6% (fixed cells, Figure 3E) and induced the translocation of IL-1α to the plasma membrane (unfixed 7-AAD- cells, Figure 3F). LPS did not increase the permeability of the cells (Figure 3G). FACS analysis demonstrated that 5.3 ± 1.9% of the cells showed IL-1α plasma membrane localisation after LPS stimulation (Figure 3F). Stimulated BMDCs of PCSK9-WT, PCSK9-Nlrp3$^{-/-}$, and PCSK9-Il1b$^{-/-}$ expressed IL-1α in their cytoplasm, which was translocated to the plasma membrane upon LPS stimulation (Figures 3H, I). Even though LPS alone was sufficient for the translocation of IL-1α to the plasma membrane, BMDCs did not secrete IL-1α or IL-1β to the extent of the positive control (LPS+ ATP, Figures S2B, C), which is in line with our *in vivo* findings.

IL-1α surface expression on human monocytes induces IL1R1-mediated VCAM1 expression and monocyte adhesion on endothelial cells

To confirm the interaction of monocytic csIL-1α with endothelial IL1R1, a close proximity ligation assay (PLA) was performed. Incubation of LPS-stimulated monocytes with primary human endothelial cells (HUVEC) resulted in a positive PLA fluorescence signal which was not observed under control conditions (Figure 4A). To validate the pro-atherogenic effect of csIL-1α, VCAM1 expression on HUVECs was measured after treatment with upLPS-stimulated monocytes. Stimulated monocytes increased VCAM1 expression compared to treatment with unstimulated monocytes (25.9 ± 7.1% vs. 2.5 ± 1.4% VCAM pos. cells) on HUVECs, which was significantly reduced by the administration of neutralizing IL1R1 antibody (18.6 ± 6.3% VCAM1 pos. cells) (Figures 4B, C) indicating that csIL-1α/IL1R1 binding and signaling plays a major role in VCAM1 expression and can be abrogated by blocking of IL1R1. In addition, the induced VCAM1 expression through csIL-1α/IL1R1 binding promoted the adhesion of monocytes to HUVECs. Therefore, calcein-labeled monocytes were incubated with HUVECs, and the remaining

10.3389/fimmu.2023.1252384

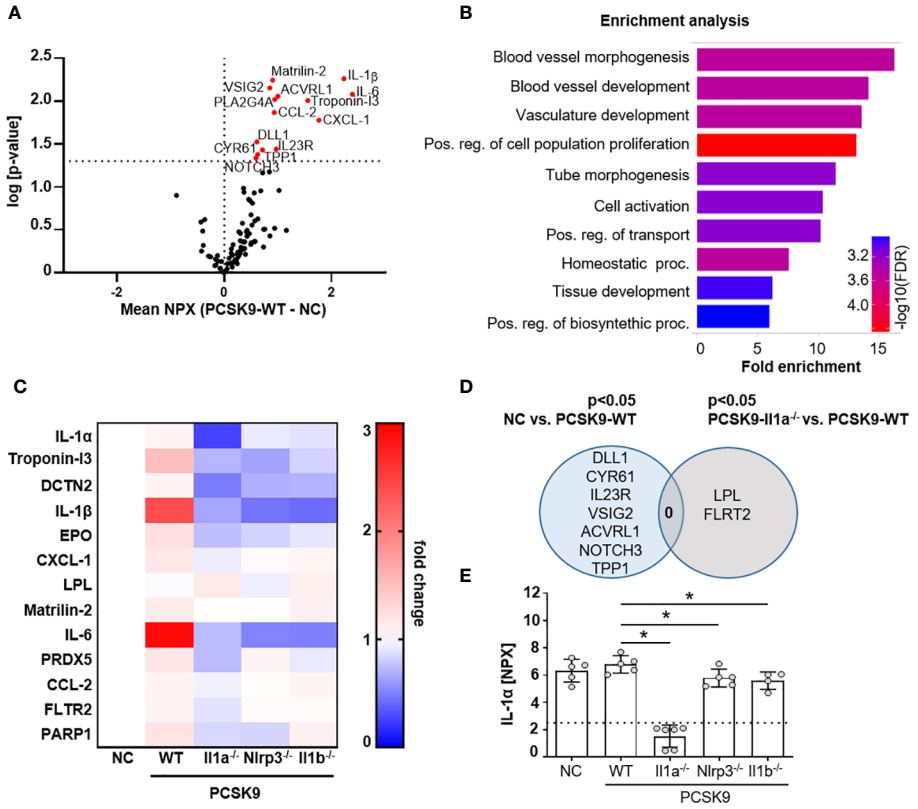

FIGURE 2
PCSK9-Il1a$^{-/-}$, PCSK9-Nlrp3$^{-/-}$, and PCSK9-Il1b$^{-/-}$ mice show reduced levels of circulating cytokines. **(A)** Volcano plot of proteins regulated in Olink mouse exploratory panel comparing serum protein levels of mice fed a NC vs. PCSK9-WT mice. Red data points indicate the difference of the NPX mean between PCSK9-WT and NC for each protein. The dashed line intersecting the y-axis indicates the significance of p<0.05. **(B)** Shiny GO (19) (Version 0.77) enrichment analysis annotating the significantly regulated proteins to the Gene Ontology (GO) Biological Process (false detection rate (FDR) cutoff: 0.1). The top 10 regulated pathways are presented as a barplot with the colors indicating the -log10 FDR, with red as the highest and blue as the lowest. **(C)** Heatmap depicting the dynamics of proteins significantly regulated in Il1a$^{-/-}$ compared to PCSK9-WT. Data is presented as fold change of PCSK9-WT, PCSK9-Il1a$^{-/-}$, PCSK9-Nlrp3$^{-/-}$, and PCSK9-Il1b$^{-/-}$ to NC. **(D)** Venn Diagram representing serum proteins specifically regulated in only NC or PCSK9-Il1a$^{-/-}$ animals compared to PCSK9-WT. Shared regulated proteins are displayed at the intersection of both areas. **(E)** Bargraphs of serum IL-1α levels measured in the Olink 96 mouse exploratory panel. The dashed line indicates the limit of detection of the assay. Data is presented with the Olink NPX value as mean ± SD, *p<0.05. PCSK9-WT (n=5), PCSK9-Il1a$^{-/-}$ (n=6), PCSK9-Nlrp3$^{-/-}$ (n=5), and PCSK9-Il1b$^{-/-}$ (n=4).

fluorescence after washing was measured (Figure 4D). Monocytes pre-stimulated with LPS showed more endothelial adhesion than non-stimulated monocytes (6.7 ± 3.6% vs. 3.5 ± 2.5%). To study whether monocyte adhesion is dependent on csIL-1α expression and binding on endothelial IL1R1, the cells were co-stimulated with neutralizing IL-1α antibody, which reduced the monocyte adhesion to baseline level (Figure 4E).

Myristoylation regulates csIL-1α translocation in murine bone marrow cells and in human monocytes

The N- terminus of the 31-kDa IL-1α precursor is myristoylated on lysine residues Lys82 and Lys83 (20). Bone-marrow cells from the hyperlipidemic atherosclerotic mice (PCSK9-WT) showed significantly more protein myristoylation than cells from control mice on normal chow (10.0 ± 4.0% in control vs. 76.0 ± 35.7% in PCSK9-WT mice) (Figure 5A). Blocking of N-myristoyltransferases 1 and 2 (NMT1/2) with IMP-1088 [1μM] reduced protein myristoylation by 62 ± 12.9% (p< 0.05) (Figure 5B) in human monocytes under control conditions. Pre-incubation of human monocyte cells with IMP-1088 [1μM] for 1h before LPS treatment reduced the cell surface expression of IL-1α by 35 ± 8.7%, p<0.05 (Figure 5C).

Discussion

The present study provides evidence for a significant contribution of IL-1α during the development of atherosclerosis. Our results revealed that circulating pro-inflammatory cytokines are not the only driving factor in atherogenesis. At the observed time points in early atherogenesis, IL-1α at the cell surface mediates leukocyte adhesion to endothelial cells independently of the NLRP3 inflammasome.

Cytokines are an important factor in immune cell activation and mediators of sterile inflammation. The study demonstrates that pro-inflammatory proteins such as IL-1β, IL-6, and CCL-2 are upregulated in the serum of PCSK9-WT animals (Figures 2D–F). However, PCSK9-Nlrp3$^{-/-}$ and PCSK9-Il1b$^{-/-}$ animals showed

10.3389/fimmu.2023.1252384

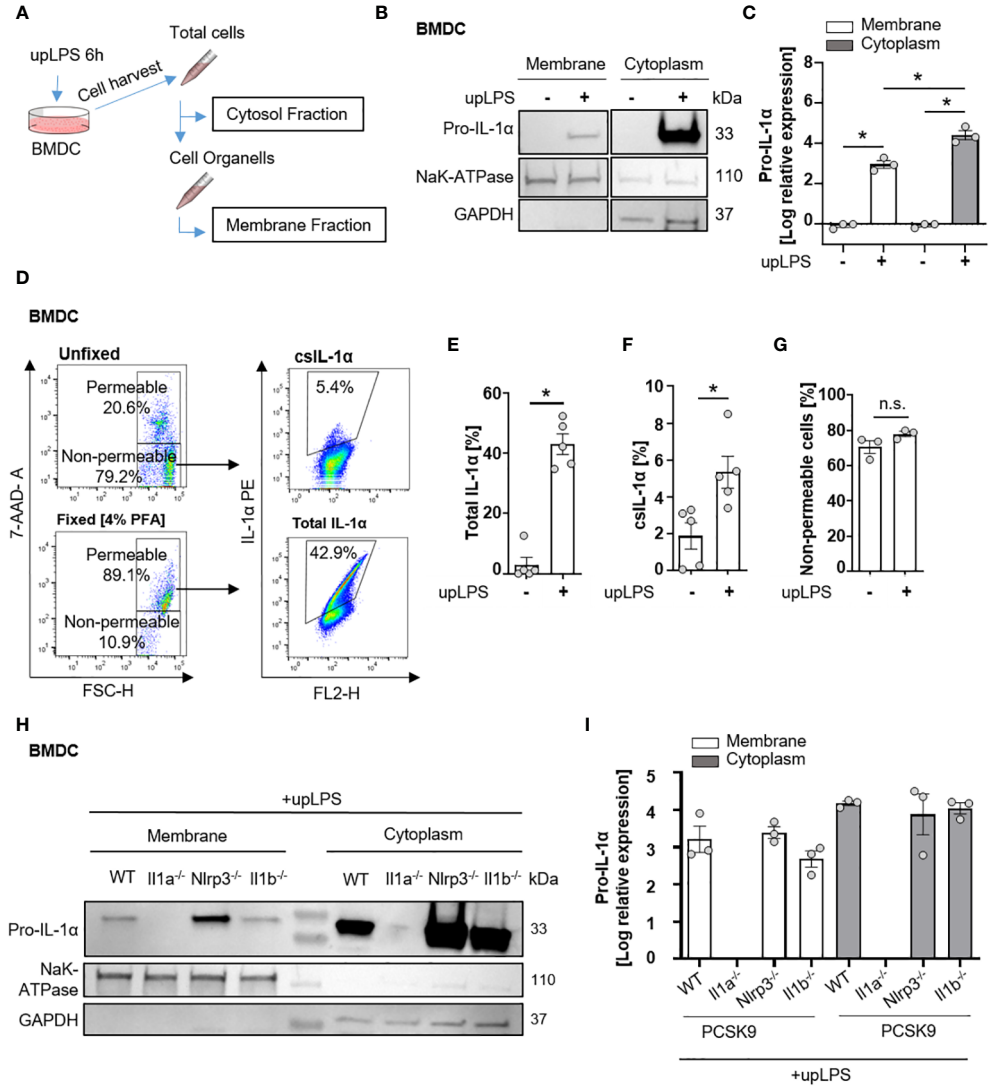

FIGURE 3
Cell surface translocation of IL-1α is not influenced by NLRP3 and IL-1β in murine BMDC. **(A)** Schematic overview of the experimental setup. Bone marrow-derived dendritic cells (BMDCs) were replated after 7 days of differentiation and stimulated with 100 ng/ml ultrapure Lipopolysaccharide (upLPS) overnight. Afterward, cells were harvested, and fractions were isolated using a detergent-based method. **(B)** Representative immunoblot of the membrane and cytoplasmic fraction of BMDCs with or without upLPS stimulation. Protein levels of IL-1α, GAPDH (glycerinaldehyde-3-phosphate-dehydrogenase, cytoplasmatic marker), and NaK ATPase (sodium–potassium ATPase, membrane marker) are presented. **(C)** Densiometric quantification of IL-1α in cytoplasmic fraction normalized to GAPDH and IL-1α in membrane fraction normalized to NaK ATPase. **(D)** Representative flow cytometry scatter plot of staining for IL-1α on stimulated BMDCs after gating for viable, non-fixated (7AAD-) cells. Total IL-1α was measured on fixed cells. **(E)** Barplot depicting the percentage of total IL-1α positive monocytes (7AAD+) with or without upLPS stimulation. **(F)** Barplot depicting the percentage of csIL-1α positive monocytes (7AAD-) with or without upLPS stimulation. **(G)** Barplot representing the percentage of non-permeable monocytes with or without upLPS stimulation. **(H)** Representative immunoblot of membrane and cytosolic fraction from upLPS-stimulated BMDCs of PCSK9-WT, PCSK9-Il1a$^{-/-}$, PCSK9-Nlrp3$^{-/-}$, and PCSK9-Il1b$^{-/-}$ animals. Protein levels of IL-1α, GAPDH (cytoplasmatic marker), and NaK ATPase (membrane marker) are presented with corresponding densiometric quantification **(I)** of log-transformed IL-1α expression. All data are presented as mean ± SEM, *p<0.05.

significantly reduced serum protein levels of IL-1β and IL-6 compared to PCSK9-WT mice despite similar plaque areas. The novel observation is that plaque development after 12 weeks of a high-fat diet appears to be largely independent of circulating pro-inflammatory cytokines.

Interestingly, circulating IL-1α was not significantly increased in PCSK9-WT animals (Figure 2C). However, the lack of Il1a resulted in a reduction in atherosclerotic lesions, suggesting a significant role of membrane-bound IL-1α protein in atherogenesis. Il1a knockout mice also had significantly lower serum levels of CCL-2 and CXCL-1 (Figures 2C, D). We also demonstrated that csIL-1α/IL1R1 binding and signaling plays an important role in VCAM1 expression on endothelial cells and that this expression can be abrogated by blocking IL1R1. This finding highlights the important role of IL-1α in monocyte adhesion and initiation of atherosclerosis.

PCSK9-Il1a$^{-/-}$ animals also show a reduction in circulating IL-1β (Figure 2C, dashed line), which are consistent with results

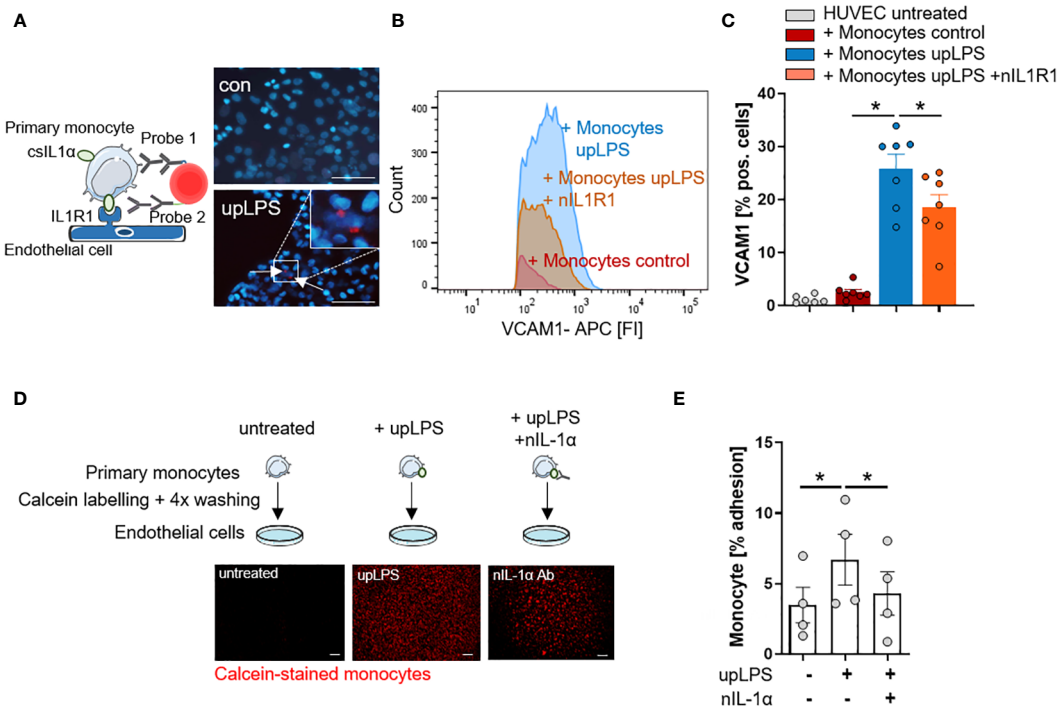

FIGURE 4
IL-1α surface expression on human monocytes induces VCAM1 expression and leads to increased adhesion on endothelial cells. **(A)** Schematic principle of proximity ligation assay (PLA) and representative picture of PLA. Direct binding of csIL-1α to the Interleukin-1 receptor 1 (IL1R1) leads to a fluorescence signal detectable at 594 nm. Human umbilical vein endothelial cells (HUVECs) were treated with monocytes for 6h, stimulated with and without upLPS (100 ng/ml). Cells were imaged at a 40× magnification (scale bar 50µm). HUVECs and monocytes are presented in blue, IL-1α/IL1R1 PLA signal is visible as red dots. **(B)** Representative flow cytometry histogram of vascular cell adhesion molecule–1 (VCAM1) stained HUVECs after 4h treatment with upLPS-stimulated monocytes. 10 µg/ml neutralizing IL1R1 (nIL1R1) antibody was added 1h before HUVEC-monocyte co-incubation. **(C)** Bar graph depicting the percentage of VCAM1- positive HUVECs after treatment with unstimulated and upLPS-stimulated monocytes. HUVECs were incubated with and without nIL1R1 antibody (10 µg/ml) for 1h before co-incubation. Data are presented as mean ± SEM of seven independent experiments; *p< 0.05. **(D)**: Schematic experimental setup of monocyte adhesion assay. Primary monocytes were treated as indicated, labeled with Calcein and 4x washings. HUVECs were treated with and without 1 µg/ml neutralizing IL-1α antibody (nIL-1α) 1h before co-incubation. Then, HUVECs were treated with labeled monocytes for 4h. The initial fluorescence of adhering monocytes was measured as well as after two washes. Cells were imaged (4× magnification), scalebar 100 µM. **(E)** Quantification of adhering monocytes to HUVECs presented as mean ± SEM of four independent experiments. Repeated measure ANOVA was performed, followed by Sidak's multiple comparison test (*p< 0.05).

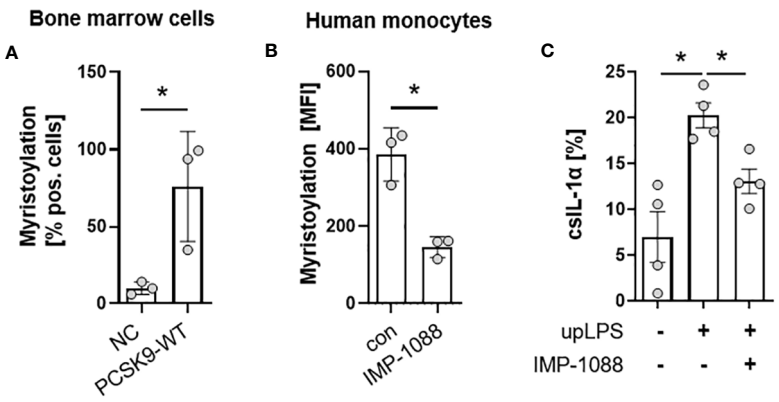

FIGURE 5
Myristoylation regulates csIL-1α in murine bone marrow cells and human monocytes. **(A)** Barplot depicting the percentage of murine bone marrow cells with myristoylated proteins. Bone marrow cells were cultured and myristoylated proteins were labeled overnight. Data are presented as mean ± SEM of NC (n=3) and PCSK9-WT (n=3), *p<0.05. **(B)** Mean fluorescence intensity of human primary monocytes under culture conditions (con) or with overnight incubation of N-myristoyltransferase inhibitor IMP-1088 [1 µM]. Data are presented as mean ± SEM of three independent experiments. One-sided paired t-test was performed, *p<0.05. **(C)** Percentage of csIL-1α presenting monocytes stimulated with 100 ng/ml upLPS and 1 µM IMP-1088 as indicated. Data are presented as mean ± SEM of four independent experiments, *p<0.05.

from previous publications (21, 22). However, although PCSK9-Il1a$^{-/-}$ animals show reduced IL-1β secretion, this does not appear to be the driving factor for atherosclerosis, because PCSK9-Il1b$^{-/-}$ animals do not show a reduction in plaque size.

Although Il1a knock out animals show greatly reduced atherosclerosis development compared with PCSK9-WT animals, macrophage infiltration per plaque is unchanged. We found no significant differences in MOMA-2 expression per plaque in the Il1a-deficient mice. Thus, Il1a is thought to play a critical role in monocyte adhesion to the endothelium but has no protective effect on macrophage infiltration in existing plaques. However, there are other risk factors, such as elevated cholesterol levels, which are also elevated in Il1a knockout mice, and may lead to endothelial damage and thus macrophage infiltration in plaques.

Chen et al. provided a mechanism for IL-1α surface presentation via IL1R2 and GPI anchors (12). They showed that Il1r2 deficiency in mice reduced levels of csIL-1α, but the mechanism remained unclear. Our data show that csIL-1α is reduced in primary monocytes by adding the myristoylation inhibitor IMP-1088 before stimulation (Figure 5C). Protein N-myristoylation is an essential fatty acylation catalyzed by N-myristoyltransferases (NMTs), which is vital for proteins participating in various biological functions, including signal transduction, cellular localization, and oncogenesis (23). Lately, myristoylated IL-1α was linked to the mitochondrial membrane by binding to cardiolipin. The myristoylation at the lysine residues 82 and 83 increased the association between proteins and lipids and, thus, the integration of IL-1α in the membrane lipid bilayer in the presence of Ca^{2+} (24). CsIL-1α levels do not return to baseline, indicating that the different mechanisms of tethering IL-1α to the membrane are essential for the presentation, even though the exact mechanism of transport from IL-1α to the membrane remains elusive. Metabolic stimuli and TLR ligands can induce csIL-1α expression on myeloid cells, making this cytokine a considerable candidate in atherosclerosis initiation, driven by high levels of circulating free fatty acids or other metabolic stimuli, such as cholesterol or high glucose (25).

Nlrp3 deficiency did not reduce atherosclerotic lesion size compared to PCSK9-WT animals in the presented data. Previous PCSK9-Nlrp3$^{-/-}$ studies are controversial and differ in their genetic background and diet composition. Using ApoE$^{-/-}$ mice crossed with either Nlrp3$^{-/-}$, Casp1$^{-/-}$ or Asc$^{-/-}$, mice did not show a reduction in plaque size, macrophage infiltration, or plaque stability after 11 weeks of high-fat diet compared to ApoE$^{-/-}$ mice (4). However, chimeric Ldlr$^{-/-}$ mice transplanted with bone marrow from Nlrp3$^{-/-}$, Asc$^{-/-}$, and Il1a$^{-/-}$ mice revealed reduced plaque area after 4 weeks of a high-fat diet (26). The PCSK9-AAV8 atherosclerosis model used in this study has the advantage of being independent of genetic alterations to induce atherosclerosis. Knockout of Nlrp3 results in a reduction in circulating cytokines but not in plaque size, lipid accumulation, or macrophage infiltration. Thus, the study contributes to the observation that a constitutive Nlrp3 knockout does not protect against the development of atherosclerotic plaques.

Previous studies have shown that csIL-1α has an implication in different pathologies and is tested as a therapeutic target in different diseases. Monocytes from patients with acute myocardial infarction (AMI) and chronic kidney disease (CKD) exhibit increased levels of csIL-1α. The expression of csIL-1α was associated with an increased risk for atherosclerotic cardiovascular disease events (13). Bermekimab (MABp1) is a human antibody targeting IL-1α and was used in patients with refractory cancer. It was well tolerated and led to a decrease in plasma IL-6 (27). The antibody was also assessed in phase II clinical study with patients suffering from type II diabetes mellitus. MABp1 improved glycemia and reduced C-reactive protein, an important prognostic marker of systemic inflammation (28). Anakinra, an IL1R antagonist, has already been approved by the FDA and is beneficial for patients with rheumatoid arthritis and autoimmune diseases (29). Treatment of ApoE$^{-/-}$ mice with anakinra reduced plaque size of the aortic arch and serum triglycerides (30). However, anakinra blocks both IL-1α/IL1R and IL-1β/IL1R signaling, which may exert differential or opposite functions in certain diseases. Due to the diverse nature of IL-1α and its associated functions, it is critical to know precisely which IL-1α isoform to target in immunotherapy. Therefore, it appears highly relevant to uncover the detailed role of IL-1α isoforms and their regulation (e.g., by myristoylation) in various diseases.

Knockout of Il1b did not affect lesion size in the PCSK9-AAV8 model of hypercholesterolemia (Figure 1D). However, other studies show a plaque size reduction in ApoE$^{-/-}$/Il1b$^{-/-}$ animals (31, 32). These controversies could be related to the animal model. Ldlr-deficient animals exhibit significantly smaller lesion sizes and necrotic cores than ApoE$^{-/-}$ mice at similar time points (33). In addition, Kamari et al. pointed out that Il1b$^{-/-}$ leads to only 32% plaque reduction, whereas Il1a$^{-/-}$ reduces plaque size by 52% in ApoE double knockout animals (32). Vromman et al. investigated the effects of monoclonal antibodies against IL-1α and IL-1β in atherosclerosis *in vivo* which demonstrated that IL-1β has a profound effect on late-stage atherosclerosis by increasing IL-10 in the plasma. In contrast, IL-1α appeard to be more critical in early atherosclerosis due to its influence on arterial outward remodelling (34). Therefore, the effect of Il1b-knockout might not be as pronounced in the PCSK9-AAV8 model compared to ApoE$^{-/-}$ animals but might be detectable at a later time point exhibiting progressed atherosclerotic lesions.

A limitation is that our study describes only a single time point in early atherogenesis (12 weeks). Our previous study observed that the inflammatory cytokines such as TNF-α increase significantly when comparing the PCSK9-AAV8 model at 12 weeks vs. 20 weeks (15). IL-1β may have a greater impact on atherosclerosis in established plaques. Therefore, it would be interesting to examine the changes in secretome as well as plaque characteristics in the applied knockout animals in combination with the PCSK9-AAV8 model at later time points in the future.

In conclusion, IL-1α deficiency reduces atherosclerotic plaque development. Low levels of pro-inflammatory cytokines in the knockout animals indicated independence of plaque development from circulating cytokines at this time point of the disease since csIL-1α mediates initial leucocyte-to-endothelial adhesion and activation of endothelial cells. Importantly, these data highlight the importance of IL-1α in atherosclerosis and the need for detailed understanding of the mechanisms of the translocation and

presentation of IL-1α to the plasma membrane as a target for novel therapies, such as myristoylation inhibitors.

Data availability statement

The original contributions presented in the study are included in the article/Supplementary Material. Further inquiries can be directed to the corresponding author.

Ethics statement

The studies involving humans were approved by Ethik-Kommission der Medizinischen Fakultät der Universität Leipzig. The studies were conducted in accordance with the local legislation and institutional requirements. The participants provided their written informed consent to participate in this study. The animal studies were approved by Veterinary Office of the Saarland. The studies were conducted in accordance with the local legislation and institutional requirements. Written informed consent was obtained from the owners for the participation of their animals in this study.

Author contributions

CM and SG interpreted the experimental work and prepared the manuscript. AW and CM performed and conducted the *in vivo* experiments. CM and SG performed histological analyses and figure preparation. J-NB assisted with Olink Serum Analysis. SA and KS assisted in histology. MF and UL interpreted the data and assisted in manuscript preparation. UL, TS, and SG designed the study and assisted in manuscript preparation. UL and SG supervised the study. All authors contributed to the article and approved the submitted version.

Funding

This work was supported by the German Research Foundation DFG (GA 3049/3-1 to SG).

Acknowledgments

We thank Anja Barnikol-Oettler, Andreas Hauck, Ellen Becker, and Ihsan Gadi for their excellent technical support.

Conflict of interest

The authors declare that the research was conducted in the absence of any commercial or financial relationships that could be construed as a potential conflict of interest.

Publisher's note

Supplementary material

The Supplementary Material for this article can be found online at: https://www.frontiersin.org/articles/10.3389/fimmu.2023.1252384/full#supplementary-material

SUPPLEMENTARY FIGURE 1
A: Representative immunoblot of the LDL-receptor (LDLR) expression and β-actin expressed in liver tissue **B**: Densiometric quantification of LDLR normalized to β-actin.

SUPPLEMENTARY FIGURE 2
A: Representative flow cytometry scatter plot of staining for double positive BMDCs for CD11c and MHC II on BMDCs at the first day of differentiation (D0) and 7 days of differentiation (D7). **B**: Secreted IL-1α after overnight upLPS stimulation in the supernatant of PCSK9-WT, PCSK9-Nlrp3$^{-/-}$, and PCSK9-Il1b$^{-/-}$. UpLPS (100ng/ml) stimulation with 5mM ATP stimulation for the last 30 min served as the positive control (pos). **C**: Secreted IL-1β after overnight upLPS stimulation in the supernatant of PCSK9-WT, PCSK9-Nlrp3$^{-/-}$, and PCSK9-Il1b$^{-/-}$. UpLPS (100ng/ml) stimulation with 5mM ATP stimulation for the last 30 min served as the positive control (pos).

SUPPLEMENTARY FIGURE 3
A: Bar graph depicting the percentage of VCAM1- positive HUVECs after treatment with unstimulated and upLPS-stimulated monocytes. Supernatant after the 4th wash, as well as upLPS, stimulated HEK293 cells and served as the negative control. Data are presented as mean± SEM of three independent experiments; *p< 0.05.

References

1. Libby P. Inflammation in atherosclerosis. *Nature* (2002) 420:868–74. doi: 10.1038/nature01323

2. Lusis AJ. Atherosclerosis. *Nature* (2000) 407:233–41. doi: 10.1038/35025203

3. Moore KJ, Sheedy FJ, Fisher EA. Macrophages in atherosclerosis: a dynamic balance. *Nat Rev Immunol* (2013) 13:709–21. doi: 10.1038/nri3520

4. Duewell P, Kono H, Rayner KJ, Sirois CM, Vladimer G, Bauernfeind FG, et al. NLRP3 inflammasomes are required for atherogenesis and activated by cholesterol crystals. *Nature* (2010) 464:1357–61. doi: 10.1038/nature08938

5. Rajamäki K, Lappalainen J, Oörni K, Välimäki E, Matikainen S, Kovanen PT, et al. Cholesterol crystals activate the NLRP3 inflammasome in human macrophages: a novel link between cholesterol metabolism and inflammation. *PloS One* (2010) 5:e11765. doi: 10.1371/journal.pone.0011765

6. Gerhardt T, Ley K. Monocyte trafficking across the vessel wall. *Cardiovasc Res* (2015) 107:321–30. doi: 10.1093/cvr/cvv147

7. Winkels H, Ehinger E, Vassallo M, Buscher K, Dinh HQ, Kobiyama K, et al. Atlas of the immune cell repertoire in mouse atherosclerosis defined by single-cell RNA-sequencing and mass cytometry. *Circ Res* (2018) 122:1675–88. doi: 10.1161/CIRCRESAHA.117.312513

8. Abbate A, Toldo S, Marchetti C, Kron J, van Tassell BW, Dinarello CA. Interleukin-1 and the inflammasome as therapeutic targets in cardiovascular disease. *Circ Res* (2020) 126:1260–80. doi: 10.1161/CIRCRESAHA.120.315937

9. Dinarello CA. Overview of the IL-1 family in innate inflammation and acquired immunity. *Immunol Rev* (2018) 281:8–27. doi: 10.1111/imr.12621

10. Afonina IS, Müller C, Martin SJ, Beyaert R. Proteolytic processing of interleukin-1 family cytokines: variations on a common theme. *Immunity* (2015) 42:991–1004. doi: 10.1016/j.immuni.2015.06.003

11. Fettelschoss A, Kistowska M, LeibundGut-Landmann S, Beer H-D, Johansen P, Senti G, et al. Inflammasome activation and IL-1β target IL-1α for secretion as opposed to surface expression. *Proc Natl Acad Sci U.S.A.* (2011) 108:18055–60. doi: 10.1073/pnas.1109176108

12. Chan JN, Humphry M, Kitt L, Krzyzanska D, Filbey KJ, Bennett MR, et al. Cell surface IL-1α trafficking is specifically inhibited by interferon-γ, and associates with the membrane via IL-1R2 and GPI anchors. *Eur J Immunol* (2020) 50:1663–75. doi: 10.1002/eji.201948521

13. Schunk SJ, Triem S, Schmit D, Zewinger S, Sarakpi T, Becker E, et al. Interleukin-1α Is a central regulator of leukocyte-endothelial adhesion in myocardial infarction and in chronic kidney disease. *Circulation* (2021) 144:893–908. doi: 10.1161/CIRCULATIONAHA.121.053547

14. Oppi S, Lüscher TF, Stein S. Mouse models for atherosclerosis research-which is my line? *Front Cardiovasc Med* (2019) 6:46. doi: 10.3389/fcvm.2019.00046

15. Gaul S, Shahzad K, Medert R, Gadi I, Mäder C, Schumacher D, et al. Novel nongenetic murine model of hyperglycemia and hyperlipidemia-associated aggravated atherosclerosis. *Front Cardiovasc Med* (2022) 9:813215. doi: 10.3389/fcvm.2022.813215

16. Amend SR, Valkenburg KC, Pienta KJ. Murine hind limb long bone dissection and bone marrow isolation. *J Vis Exp*. 2016 (110):53936. doi:10.3791/53936

17. Matheu MP, Sen D, Cahalan MD, Parker I. Generation of bone marrow derived murine dendritic cells for use in 2-photon imaging. *J Vis Exp* (2008). doi: 10.3791/773

18. Fredriksson S, Gullberg M, Jarvius J, Olsson C, Pietras K, Gústafsdóttir SM, et al. Protein detection using proximity-dependent DNA ligation assays. *Nat Biotechnol* (2002) 20:473–7. doi: 10.1038/nbt0502-473

19. Ge SX, Jung D, Yao R. ShinyGO: a graphical gene-set enrichment tool for animals and plants. *Bioinformatics* (2020) 36:2628–9. doi: 10.1093/bioinformatics/btz931

20. Stevenson FT, Bursten SL, Fanton C, Locksley RM, Lovett DH. The 31-kDa precursor of interleukin 1 alpha is myristoylated on specific lysines within the 16-kDa N-terminal propiece. *Proc Natl Acad Sci U.S.A.* (1993) 90:7245–9. doi: 10.1073/pnas.90.15.7245

21. Freigang S, Ampenberger F, Spohn G, Heer S, Shamshiev AT, Kisielow J, et al. Nrf2 is essential for cholesterol crystal-induced inflammasome activation and exacerbation of atherosclerosis. *Eur J Immunol* (2011) 41:2040–51. doi: 10.1002/eji.201041316

22. Horai R, Asano M, Sudo K, Kanuka H, Suzuki M, Nishihara M, et al. Production of mice deficient in genes for interleukin (IL)-1alpha, IL-1beta, IL-1alpha/beta, and IL-1 receptor antagonist shows that IL-1beta is crucial in turpentine-induced fever development and glucocorticoid secretion. *J Exp Med* (1998) 187:1463–75. doi: 10.1084/jem.187.9.1463

23. Udenwobele DI, Su R-C, Good SV, Ball TB, Varma Shrivastav S, Shrivastav A. Myristoylation: an important protein modification in the immune response. *Front Immunol* (2017) 8:751. doi: 10.3389/fimmu.2017.00751

24. Dagvadorj J, Mikulska-Ruminska K, Tumurkhuu G, Ratsimandresey RA, Carriere J, Andres AM, et al Recruitment of pro-IL-1α to mitochondrial cardiolipin, via shared LC3 binding domain, inhibits mitophagy and drives maximal NLRP3 activation. *Proc Natl Acad Sci U S A* (2020) 118(1):e2015632118. doi:10.1073/pnas.2015632118

25. Freigang S, Ampenberger F, Weiss A, Kanneganti T-D, Iwakura Y, Hersberger M, et al. Fatty acid-induced mitochondrial uncoupling elicits inflammasome-independent IL-1α and sterile vascular inflammation in atherosclerosis. *Nat Immunol* (2013) 14:1045–53. doi: 10.1038/ni.2704

26. Menu P, Pellegrin M, Aubert J-F, Bouzourene K, Tardivel A, Mazzolai L, et al. Atherosclerosis in ApoE-deficient mice progresses independently of the NLRP3 inflammasome. *Cell Death Dis* (2011) 2:e137. doi: 10.1038/cddis.2011.18

27. Hong DS, Hui D, Bruera E, Janku F, Naing A, Falchook GS, et al. MABp1, a first-in-class true human antibody targeting interleukin-1α in refractory cancers: an open-label, phase 1 dose-escalation and expansion study. *Lancet Oncol* (2014) 15:656–66. doi: 10.1016/S1470-2045(14)70155-X

28. Timper K, Seelig E, Tsakiris DA, Donath MY. Safety, pharmacokinetics, and preliminary efficacy of a specific anti-IL-1alpha therapeutic antibody (MABp1) in patients with type 2 diabetes mellitus. *J Diabetes Complications* (2015) 29:955–60. doi: 10.1016/j.jdiacomp.2015.05.019

29. Cohen SB. The use of anakinra, an interleukin-1 receptor antagonist, in the treatment of rheumatoid arthritis. *Rheum Dis Clin North Am* (2004) 30:365–80. doi: 10.1016/j.rdc.2004.01.005

30. Ku EJ, Kim B-R, Lee J-I, Lee YK, Oh TJ, Jang HC, et al. The anti-atherosclerosis effect of anakinra, a recombinant human interleukin-1 receptor antagonist, in apolipoprotein e knockout mice. *Int J Mol Sci* (2022) 23(9):4906. doi:10.3390/ijms23094906

31. Kirii H, Niwa T, Yamada Y, Wada H, Saito K, Iwakura Y, et al. Lack of interleukin-1beta decreases the severity of atherosclerosis in ApoE-deficient mice. *Arterioscler Thromb Vasc Biol* (2003) 23:656–60. doi: 10.1161/01.ATV.0000064374.15232.C3

32. Kamari Y, Shaish A, Shemesh S, Vax E, Grosskopf I, Dotan S, et al. Reduced atherosclerosis and inflammatory cytokines in apolipoprotein-E-deficient mice lacking bone marrow-derived interleukin-1α. *Biochem Biophys Res Commun* (2011) 405:197–203. doi: 10.1016/j.bbrc.2011.01.008

33. Roselaar SE, Kakkanathu PX, Daugherty A. Lymphocyte populations in atherosclerotic lesions of apoE -/- and LDL receptor -/- mice. Decreasing density with disease progression. *Arterioscler Thromb Vasc Biol* (1996) 16:1013–8. doi: 10.1161/01.atv.16.8.1013

34. Vromman A, Ruvkun V, Shvartz E, Wojtkiewicz G, Santos Masson G, Tesmenitsky Y, et al. Stage-dependent differential effects of interleukin-1 isoforms on experimental atherosclerosis. *Eur Heart J* (2019) 40:2482–91. doi: 10.1093/eurheartj/ehz008

frontiers | Frontiers in Immunology

TYPE Original Research
PUBLISHED 01 September 2023
DOI 10.3389/fimmu.2023.1194733

OPEN ACCESS

EDITED BY
Philip Bufler,
Charité University Medicine Berlin,
Germany

REVIEWED BY
Javier Mora,
University of Costa Rica, Costa Rica
Cornelius Engelmann,
Charité University Medicine Berlin,
Germany

*CORRESPONDENCE
Zoe Waibler
zoe.waibler@pei.de

RECEIVED 27 March 2023
ACCEPTED 16 August 2023
PUBLISHED 01 September 2023

CITATION
Anzaghe M, Niles MA, Korotkova E, Dominguez M, Kronhart S, Ortega Iannazzo S, Bechmann I, Bachmann M, Mühl H, Kochs G and Waibler Z (2023) Interleukin-36γ is causative for liver damage upon infection with Rift Valley fever virus in type I interferon receptor-deficient mice. *Front. Immunol.* 14:1194733. doi: 10.3389/fimmu.2023.1194733

Interleukin-36γ is causative for liver damage upon infection with Rift Valley fever virus in type I interferon receptor-deficient mice

Martina Anzaghe[1], Marc A. Niles[1], Eugenia Korotkova[1], Monica Dominguez[1], Stefanie Kronhart[1], Samira Ortega Iannazzo[1], Ingo Bechmann[2], Malte Bachmann[3], Heiko Mühl[3], Georg Kochs[4] and Zoe Waibler[1]*

[1]Division of Immunology, Paul-Ehrlich-Institut, Langen, Germany, [2]Medical Faculty, Institute for Anatomy, University Leipzig, Leipzig, Germany, [3]Pharmazentrum Frankfurt/ZAFES, University Hospital Frankfurt, Goethe-University Frankfurt am Main, Frankfurt am Main, Germany, [4]Institute of Virology, Medical Center, Faculty of Medicine, University of Freiburg, Freiburg, Germany

Type I interferons (IFN) are pro-inflammatory cytokines which can also exert anti-inflammatory effects via the regulation of interleukin (IL)-1 family members. Several studies showed that interferon receptor (IFNAR)-deficient mice develop severe liver damage upon treatment with artificial agonists such as acetaminophen or polyinosinic:polycytidylic acid. In order to investigate if these mechanisms also play a role in an acute viral infection, experiments with the *Bunyaviridae* family member Rift Valley fever virus (RVFV) were performed. Upon RVFV clone (cl)13 infection, IFNAR-deficient mice develop a severe liver injury as indicated by high activity of serum alanine aminotransferase (ALT) and histological analyses. Infected IFNAR$^{-/-}$ mice expressed high amounts of IL-36γ within the liver, which was not observed in infected wildtype (WT) animals. In line with this, treatment of WT mice with recombinant IL-36γ induced ALT activity. Furthermore, administration of an IL-36 receptor antagonist prior to infection prevented the formation of liver injury in IFNAR$^{-/-}$ mice, indicating that IL-36γ is causative for the observed liver damage. Mice deficient for adaptor molecules of certain pattern recognition receptors indicated that IL-36γ induction was dependent on mitochondrial antiviral-signaling protein and the retinoic acid-inducible gene-I-like receptor. Consequently, cell type-specific IFNAR knockouts revealed that type I IFN signaling in myeloid cells is critical in order to prevent IL-36γ expression and liver injury upon viral infection. Our data demonstrate an anti-inflammatory role of type I IFN in a model for virus-induced hepatitis by preventing the expression of the novel IL-1 family member IL-36γ.

KEYWORDS

rift valley fever virus, type I interferon, interleukin-36γ, anti-inflammatory, immune pathology, dysregulation, liver injury

1 Introduction

Type I interferons (IFN) are a family of cytokines which are expressed early upon infection in order to guarantee the survival of the host until the adaptive immunity is activated. In order to elicit their pro-inflammatory function, type I IFN are induced e.g. upon sensing of pathogen-associated molecular patterns (PAMPs). PAMPs are recognized by pattern recognition receptors (PRRs) such as toll-like receptors (TLR) and the retinoic acid-inducible gene (RIG)-I-like receptors (RLR). Whereas most TLR signal via the adaptor protein myeloid differentiation primary response 88 (MyD88), signaling of RLR is dependent on the adaptor protein mitochondrial antiviral signaling protein (MAVS) (1). Type I IFN can be subdivided into 13 isoforms of IFN-α, one IFN-β, as well as IFN-ϵ, IFN-τ, IFN-κ, IFN-ω, IFN-δ, IFN-ζ, and IFN-v (2). All type I IFN bind to a common type I IFN receptor (IFNAR) in order to regulate the expression of hundreds of IFN-stimulated genes (ISG) (2, 3). It has been shown by several studies in the past that a positive feedback loop via the IFNAR is necessary for the formation of robust type I IFN responses. Small amounts of early type I IFN, mainly IFN-α_4 and IFN-β, bind to the IFNAR in order to induce the production of high amounts of type I IFN (4–6). Nevertheless, depending on dose and route of infection, the IFNAR feedback loop is not strictly necessary for robust type I IFN expression upon infection with a variety of RNA-encoded viruses (7).

Even though type I IFN are generally considered as pro-inflammatory cytokines, they can also exert anti-inflammatory functions. Impaired induction of type I IFN in a model of TLR9 ligand-induced liver injury resulted in increased inflammation and liver damage. Here, the protective role of type I IFN was mediated via the attenuation of IL-1β expression and induction of the IL-1 receptor antagonist (RA) (8). Moreover, IL-1 family member-mediated immune pathology was shown for alcohol-induced hepatitis, fatty liver disease, as well as in a mouse model investigating lipopolysaccharide (LPS)/d-galactosamine (D-GalN)-induced liver injury (9, 10). In addition, in a previous study we showed that the artificial double-stranded RNA polyinosinic: polycytidylic acid (poly(I:C)) induced severe liver injury in IFNAR-deficient mice ($IFNAR^{-/-}$). Deficient type I IFN signaling was associated with increased levels of IL-1β, which in turn was causative for the induction of severe liver damage as shown e.g. by high activity of serum alanine aminotransferase (ALT) (11, 12). As many viruses produce double-stranded RNA during their life cycle, poly(I:C) resembles a good model for a viral infection. To further explore the anti-inflammatory role of type I IFN upon a 'real' acute viral infection, we aimed to investigate the regulation of IL-1 family members in virus-induced hepatitis.

Rift Valley fever is an emerging zoonotic disease endemic in sub-Saharan African countries and the Arabian Peninsula. The disease is caused by the Rift Valley fever virus (RVFV), which is an enveloped virus with a segmented negative-sensed single-stranded RNA genome. It belongs to the *Bunyaviridae* family, genus *Phlebovirus*, and is primarily transmitted via *Aedes mcintoshi* mosquitos (13–18). RVFV outbreaks in the human population vary in extent, intensity, and location. Thus far, the largest outbreak was documented in Egypt 1977 with 10,000-20,000 cases and a mortality rate of up to 20% (16). RVFV predominantly infects domestic ruminant animals including sheep, cattle, goats, and camels (16). In humans, infection with RVFV usually causes a self-limiting mild disease with influenza-like symptoms. Nevertheless, a small percentage of patients develop complications with clinical symptoms ranging from hemorrhagic fever to acute hepatitis, severe encephalitis, or thrombosis (13, 17, 19). The liver is considered the major target organ for RVFV and viral replication was shown to induce apoptosis in hepatocytes accompanied by necrosis (13, 15, 18). In line with that, RVFV pathogenesis in mice is associated with a loss of liver function due to liver necrosis and hepatitis (15, 16, 20).

RVFV was described to mainly infect epithelial cells (such as hepatocytes), mesenchymal cells, neural cells, hematopoietic cells such as mononuclear phagocytes, and cells morphologically consistent with dendritic cells (DC) (15). Other studies identified macrophages to be the primarily virus shedding cells while DC and granulocytes are additional target cells for RVFV replication (17).

The genome of RVFV consists of three segments: large (L), medium (M), and small (S) (16, 18). RVFV clone (cl)13 is an avirulent virus variant, which harbors a large deletion in the S segment. It is naturally attenuated and was obtained by plaque purification from a field isolate obtained from a nonfatal human case during an outbreak in 1974 (19). RVFV cl13 has no pathogenicity for mice or hamsters and the animals survive infections with up to 10^6 plaque-forming units (pfu) without developing any signs of disease. Nevertheless, type I IFN are critical for the survival of mice upon RVFV cl13 infection as $IFNAR^{-/-}$ mice show up to 100-fold higher titers when compared to their wildtype (WT) counterparts and finally succumb to infection (19).

In order to investigate if type I IFN also exert anti-inflammatory effects upon an acute viral infection, we used RVFV cl13 and analyzed the induction of IL-1 family members. Interestingly, data revealed a critical role for the novel IL-1 family member IL-36γ which was known thus far to play a pro-inflammatory role in some human disorders such as psoriasis, inflammatory bowel disease, pulmonary disease, or rheumatoid arthritis (21–24). IL-36 cytokines are new members of the IL-1 family which comprise IL-36α, IL-36β, and IL-36γ (25–27). All bind to a heterodimeric receptor composed of the IL-36 receptor (IL-36R) and IL-1 receptor accessory protein (IL-1RAcP). IL-36 receptor antagonist (IL-36RA) and IL-38 have been shown to negatively regulate the IL-36 signaling pathway via competitive binding to IL-36R, suppressing agonist recognition and IL-1RAcP recruitment (21, 28–30). IL-36R is expressed in skin (especially on keratinocytes), epithelial cells within the lung, the gastrointestinal tract, and other tissues. Furthermore, several types of immune cells were shown to express IL-36R and respond to stimulation. In addition, human and mouse DC express IL-36R and binding of IL-36 promotes DC maturation and improves antigen presentation via upregulation of HLA-DR, CD83, and CD86 (21, 29, 31–33). IL-36 stimulates the production of various cytokines, chemokines, adhesion molecules, and pro-inflammatory mediators. IL-36 cytokines can be induced upon stimulation with different agents including cytokines, TLR ligands, bacterial or viral infections, or other pathological conditions (30, 34, 35).

In this study, we provide for the first time a mechanism for the type I IFN-mediated regulation of IL-36γ induction in the context of an acute viral infection.

2 Materials and methods

2.1 Mice

C57BL/6 WT mice were purchased from Harlan Winkelmann (Borchen, Germany). IFNAR$^{-/-}$ mice (6) were backcrossed at least 20 times on the C57BL/6 background. ISRE-eGFP mice express eGFP under the control of an interferon-stimulated response element (ISRE) (36). CD4Cre IFNAR$^{flox/flox}$ and CD19Cre IFNAR$^{flox/flox}$ mice (37), LysMCre IFNARflox/flox mice (38), and CD11cCre IFNARflox/flox (6) have been described before. To obtain MyD88$^{-/-}$IFNAR$^{-/-}$ double-deficient mice and MAVS$^{-/-}$ IFNAR$^{-/-}$ double-deficient mice, MyD88$^{-/-}$ mice or MAVS$^{-/-}$ mice were intercrossed with IFNAR$^{-/-}$ mice as described before (7). All mice were bred under specific pathogen free conditions at the Zentrale Tierhaltung of the Paul-Ehrlich-Institut. Correct gene knock outs were verified by PCR analyses for all genotypes used. Health monitoring results of sentinel mice for all knock out mice showed no differences when compared to WT mice in our breeding. Fur structure, bearing, nutrition, and mating behavior of all knock out mice were inconspicuous. Mouse experimental work was carried out using 8 to 12 week old mice in compliance with regulations of German animal welfare.

2.2 Viruses and stimuli

For infection experiments RVFV cl13 (19) was used (under BSL2 conditions). Virus was propagated and titrated on Vero cells. Virus supernatants were harvested without further purification. Plaque assay analyses were performed as described earlier (39). *In vivo* infections were performed with 2x10^4 pfu RVFV cl13 in 200 µl via the intraperitoneal (i.p.) route. Recombinant human IL-1RA (Anakinra, kindly provided by Swedish Orphan Biovitrum) was diluted in PBS and i.p. injected 6 hours before, simultaneously with, and 10 hours after infection with 100 µg/g bodyweight in a maximal volume of 200 µl. Recombinant mouse IL-36γ/IL-1F9 (aa 13-164; R&D) was diluted in PBS and intravenously (i.v.) injected (1 µg in a volume of 200 µl). Recombinant mouse IL-36RA (R&D) was diluted in PBS and i.v. injected 12 hours and 24 hours hours after infection (6 µg in a volume of 200 µl).

2.3 Quantification of cytokine production and ALT activity

To determine serum cytokine levels and ALT activity, peripheral blood was taken retro-orbitally upon anesthetization using Isofluran (CP-Pharma) and serum was prepared. IL-36γ was determined by enzyme-linked immunosorbent assay (ELISA) according to manufacturer's instructions (Cloud-Clone Corp). Levels of eight different cytokines were measured via ProcartaPlex multiplex immunoassay kit (Thermo Fisher Scientific) according to manufacturer's instructions. ALT activity was determined using a commercially available kit (Hiss Diagnostics GmbH).

2.4 Histology

For histological analysis, livers were fixed in 10% buffered formalin and embedded in paraffin. Sections were stained with hematoxylin and eosin (H&E) as described before (11) and examined by light microscopy.

2.5 Quantitative real-time PCR

Total RNA was prepared from liver, spleen, and peritoneal exudate cells (PEC) using Trizol (Invitrogen)/chloroform extraction. Isolation of liver and spleen was described earlier (11). Samples were treated with DNaseI (Roche) for 15 min at 37°C. Absence of genomic DNA contamination was confirmed by standard PCR using a glyceraldehyde 3-phosphate dehydrogenase (GAPDH)-specific primer pair. Target- and reference-mRNA levels were examined by qRT-PCR using QuantiFast SYBR Green PCR kit (Qiagen). Primer pairs used were the following: GAPDH forward 5'-ACCACAGTCCATGCCATCAC-3', GAPDH reverse 5'-TCCACCACCCTGTTGCTGTA-3', pro-IL-1β forward 5'-TCTTTGAAGTTGACGGACCC-3', pro-IL-1β reverse 5'-TGAGT GATACTGCCTGCCTG-3', IL-1RA forward 5'-TCAGATCT GCACTCAATGCC-3', IL-1RA reverse 5'-CTGGTGTTT GACCTGGGAGT-3', IL-36γ forward 5'-CAGGCCCTT GTGACAGTTCCA-3', IL-36γ reverse 5'- TTAGCAGCAAA GTAGGGTGTCCATTA-3', IL-36α forward 5'- CCGATGAGC TGCCTGTTCTGC -3', IL-36α reverse 5'- GTGGGCAGC TCCCTTTAGAGC -3', IL-36β forward 5'- AATGTCAAGC CTGTCATTCTTAGC -3', IL-36β reverse 5'- GTGGGCAGCT CCCTTTAGAGC -3', IL-36RA forward 5'- CGCAGAGAAGG TCATTAAAGG -3', IL-36RA reverse 5'- AGCTCTTTGA TTCCTTGGC -3'. The expression levels of all target genes were normalized against GAPDH (ΔCt). Gene expression values were calculated based on the ΔΔCt method using the mean of the untreated control group as calibrator to which all other samples were compared. Relative quantities (RQ) were determined using the equation $RQ=2^{-\Delta\Delta Ct}$.

2.6 Flow cytometry

Isolation of PEC was described elsewhere (7, 11). For FACS analyses, cells were stained for 20 min at 4°C with the following fluorochrome-labeled monoclonal antibodies: anti-CD11c-allophycocyanin (APC), anti-B220-PE (both from BD PharMingen), anti-CD11b-Pacific Blue (from Caltag/Invitrogen), and anti-F4/80-APC (AbD Serotec). Cells were washed and analyzed with a LSRII flow cytometer (Becton Dickinson). Analyses were performed using BD FACSDiva™ 8.0.1 and FlowJo® 7.6.5 and 10.7.1.

2.7 Statistics

For all animal experiments, the statistical evaluation was exploratory. All observed effects were described by specifying key statistical metrics (mean value, standard deviation, etc.). For normally distributed data, 95% confidence intervals are given for the mean estimates (also for mean differences). Statistical tests were decided at the two-sided significance level α=5%. For paired comparisons between several treatment groups, the associated p-values were adjusted. Data that are not normally distributed were transformed accordingly. If a transformation is not possible, non-parametric methods were used. All animal experiments were approved by the Regierungspräsidium Darmstadt with the license number F107_1027.

Either Welch's t-test or Mann Whitney test were performed using GraphPad Prism 9.2.0.Values with $p \leq 0.05$ are statistically significant which is illustrated by the number of stars: (*) for $p \leq 0.05$, (**) for $p \leq 0.01$, (***) and for $p \leq 0.001$; ns = not significant.

3 Results

3.1 IFNAR$^{-/-}$ mice develop severe liver damage upon infection with RVFV

As shown before (7), IFNAR$^{-/-}$ mice succumb to infection with RVFV cl13, which is accompanied by body weight loss and a drop in body temperature, while their WT counterparts survive the infection and do not show such symptoms (Figures 1A-C). In line with this, WT mice mount IFN-α responses 12 hpi while IFNAR$^{-/-}$ mice produced high amounts of IFN-α (up to ~4500 pg/ml) at 30 hpi indicating uncontrolled IFN-α production in the course of infection (Supplementary Figure 1). As given in Figure 1D, infection with RVFV induces viremia with high viral loads in all organs tested in IFNAR$^{-/-}$ but not WT mice resulting in the death of IFNAR$^{-/-}$ mice 30 hours post infection (7). In addition, IFNAR$^{-/-}$ but not WT mice show high ALT activity in the peripheral blood 30 h post infection indicating a severe liver injury in these animals (Figure 1E). In conclusion, IFNAR$^{-/-}$ but not WT mice develop a severe liver damage upon infection with RVFV cl13.

3.2 Liver damage in RVFV-infected IFNAR$^{-/-}$ mice is caused by IL-1 family member IL-36γ

Next, we aimed to investigate if liver damage upon RVFV cl13 infection is mediated by a dysregulation of the IL-1 family members IL-1β and/or IL-1RA as it has been shown before for poly(I:C) treatment (11, 12). Thus, we isolated livers of IFNAR$^{-/-}$ and WT mice 30 hours post RVFV cl13 infection and analyzed IL-1β (Figure 2A) and IL-1RA (Figure 2B) induction by ELISA. Unlike poly(I:C)-treated animals (11, 12), RVFV cl13-infected IFNAR$^{-/-}$ mice showed high IL-1β as well as IL-1RA expression while WT mice did not show any IL-1β or IL-1RA induction upon infection. To confirm that an IL-1β/IL-1RA imbalance is indeed not involved in RVFV cl13-mediated liver injury, RVFV cl13-infected IFNAR$^{-/-}$ mice were treated with recombinant IL-1RA (Anakinra) and analyzed for the development of liver damage by analyzing ALT activity within the serum (Figure 2C). Here, the administration of recombinant IL-1RA could not prevent the development of severe liver injury in RVFV cl13-infected IFNAR$^{-/-}$ mice indicating that IL-1β/IL-1RA are not involved in RVFV cl13-induced liver injury.

In a model of paracetamol (acetaminophen, APAP)-induced liver damage, the IL-1 family member IL-36γ and its antagonist IL-36RA were shown to play a role in the onset and regeneration of liver damage (40). Hence, we presumed that these IL-1 family members might be type I IFN regulated and thus involved in the RVFV cl13-induced liver damage in absence of IFNAR-signaling. To obtain a first insight, we analyzed the expression of IL-36γ upon RVFV cl13 infection by an ELISA method. As given in Figure 3A, IFNAR$^{-/-}$ but not WT mice show high levels of IL-36γ 30 hours post infection. To investigate if IL-36γ is sufficient to cause liver injury, we i.p. injected WT animals with 1 µg recombinant IL-36γ and analyzed ALT activity (Figure 3B). Indeed, WT mice developed a severe liver injury within 3 hours post IL-36γ injection as indicated by high ALT activity within the serum.

To further verify that IL-36γ was causative for the liver damage upon RVFV cl13 infection, RVFV cl13-infected IFNAR$^{-/-}$ mice were treated with recombinant IL-36RA 12 and 24 hours post infection (Figure 3C). Analyses of IFNAR$^{-/-}$ mice revealed that the administration of recombinant IL-36RA significantly reduced ALT activity (Figure 3C) and overall liver damage as indicated by histological analyses (Figure 3D). Of note, viral titers within all organs analyzed were not affected by IL-36RA treatment (Figure 3E). These data strongly indicate that the dysregulated IL-36γ expression in absence of type I IFN-signaling is causative for the liver injury observed upon RVFV cl13 infection.

3.3 Macrophage-like cells within the peritoneum are the main source of IL-36 γ in the absence of type I IFN signaling

To gain insight in which cells or organs are the source of IL-36γ upon RVFV cl13 infection, we analyzed spleens (as an organ harboring many immune cells), livers (as the site where the damage occurs), and PEC (because of the intraperitoneal route of infection) of WT and IFNAR$^{-/-}$ mice. To ensure that both genotypes show a comparable basal expression of IL-36γ, we analyzed uninfected mice by qRT-PCR analysis. As given in Figure 4A, spleen, liver, and PEC of WT and IFNAR$^{-/-}$ mice showed comparable basal levels of IL-36γ mRNA. Next, we infected WT and IFNAR$^{-/-}$ mice with RVFV for 24 hours and isolated spleen, liver, and PEC RNA for qRT-PCR analyses. As shown in Figure 4B, IFNAR$^{-/-}$ mice express high levels of IL-36γ mRNA in all organs/cells tested with the highest expression in PEC (up to 4000-fold induction) while WT mice did not show upregulation in spleen and liver and only minor upregulation (up to 80-fold) in PEC. These results strongly indicate that PEC are the main source of IL-36γ in

IFNAR$^{-/-}$ mice upon RVFV cl13 infection and that type I IFN signaling in these cells prevents IL-36γ induction.

In order to clarify which cells within the peritoneum directly sense type I IFN upon infection, we used reporter mice expressing eGFP under the control of the ISRE for further experiments. Flow cytometric analyses of PEC derived from RVFV-infected mice demonstrated that eGFP-positive cells are mainly CD11b^{+}F4/80^{+} and therefore show a myeloid/macrophage-like phenotype (Figure 4C).

To investigate if sensing of type I IFN in myeloid/macrophage-like cells is critical for IL-36γ expression, we used conditional knockout mice, deficient for the IFNAR in certain types of immune cells (DC-IFNAR$^{-/-}$ with specific IFNAR deletion in DC, Mye-IFNAR$^{-/-}$ with specific IFNAR deletion in myeloid cells, T-IFNAR$^{-/-}$ with specific IFNAR deletion in T cells, whereas all other cell types remain IFNAR-competent as described in (11)) and infected these mice with RVFV cl13. IFNAR$^{-/-}$ mice served as control. As given in Figure 5A, mice deficient for the IFNAR in myeloid cells (Mye-IFNAR$^{-/-}$) and DC (DC-IFNAR$^{-/-}$) develop a severe liver injury upon infection which was even more pronounced when compared to IFNAR$^{-/-}$ mice. In contrast, T-IFNAR$^{-/-}$ control-mice did not show enhanced ALT activity upon infection. In line with this, qRT-PCR analyses of PEC derived from those animals show IL-36γ induction in Mye-IFNAR$^{-/-}$ (350-fold) and DC-IFNAR$^{-/-}$ (500-fold) which was not observed in T-IFNAR$^{-/-}$ mice. As shown before, IFNAR$^{-/-}$ mice strongly upregulate IL-36γ mRNA upon infection (1000-fold) (Figure 5B). Of note, IL-36γ induction in Mye-IFNAR$^{-/-}$ mice was comparable to IFNAR$^{-/-}$ mice. These results indicate that upon RVFV cl13 infection the absence of IFNAR-signaling in myeloid cells/DC results in IL-36γ expression, which in turn mediates a severe liver damage.

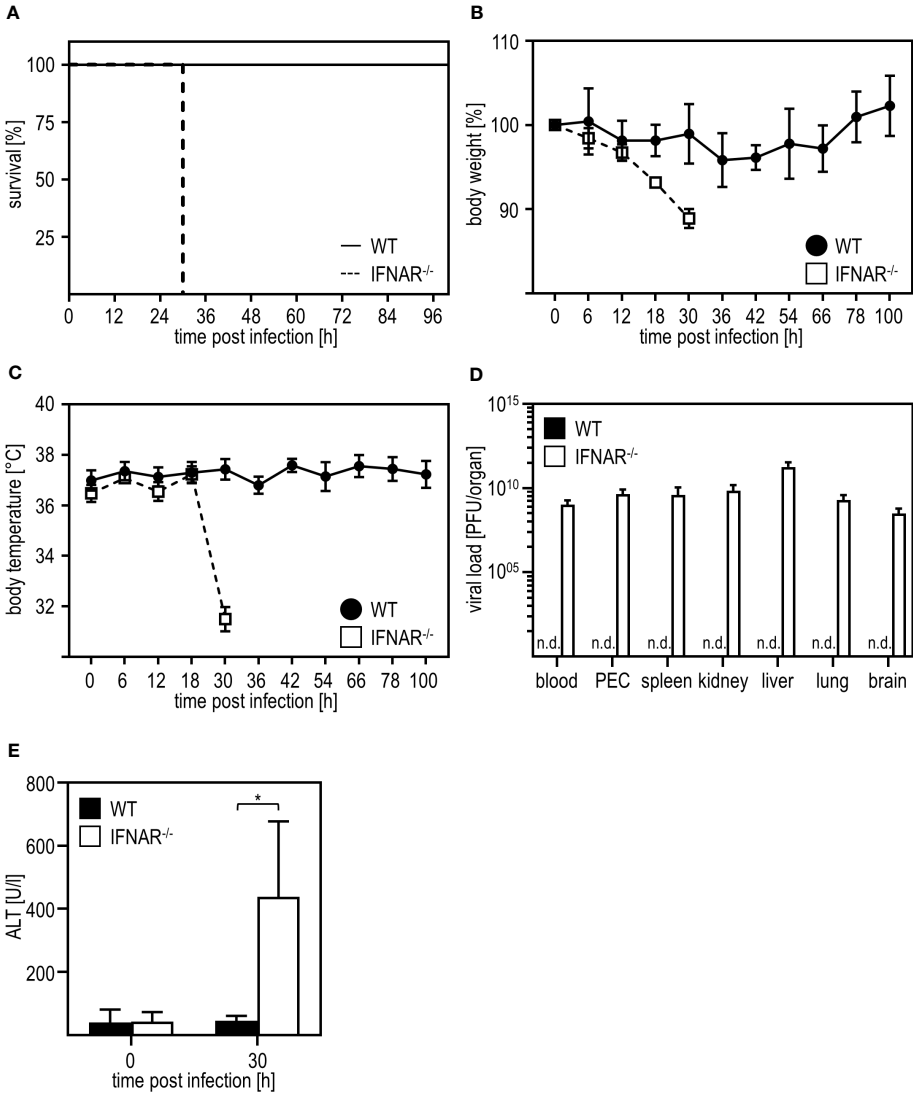

FIGURE 1
Infection with RVFV cl13 induces liver damage in type I IFN-deficient mice. C57BL/6 (WT) and IFNAR$^{-/-}$ mice were i.p. infected with 2x10^{4} pfu/200 µl RVFV cl13 (n=4-7) and **(A)** survival, **(B)** body weight, and **(C)** body temperature was monitored at the indicated time points post infection. **(D)** Viral loads were analyzed 30 hours post infection (hpi) in the indicated organs by plaque assay (n=4). **(E)** ALT activity was measured 30 hpi within the serum of WT and IFNAR$^{-/-}$ mice (n=6). Error bars indicate standard deviations. * < 0.05 (Welch's t-test); n.d., not detectable.

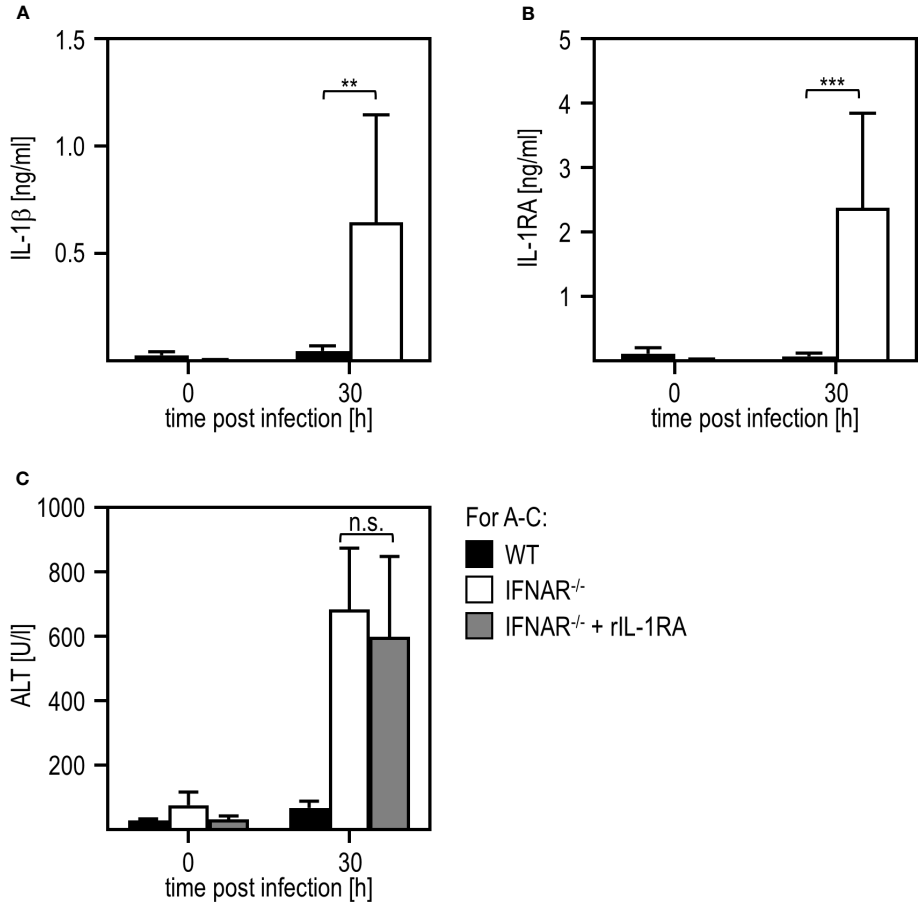

FIGURE 2
Liver injury in RVFV cl13-infected IFNAR$^{-/-}$ mice is not mediated by a dysregulation of IL-1β/IL-1RA. C57BL/6 (WT) and IFNAR$^{-/-}$ mice were i.p. infected with 2x10^4 pfu/200 µl RVFV cl13. Levels of IL-1β **(A)** and IL-1RA **(B)** were measured 30 hpi within the serum by an ELISA method (n=4-13). **(C)** WT and IFNAR$^{-/-}$ mice were infected with 2x10^4 pfu/200 µl RVFV cl13. Then, a subset of infected IFNAR$^{-/-}$ animals was treated with 100 µg recombinant IL-1RA (Anakinra) per g body weight as described in material methods. ALT activity was measured 30 hpi within the serum (n=4-13) Error bars indicate standard deviations. ** < 0.01; *** < 0.001 (Welch's t-test); n.s., not significant.

3.4 MAVS is critically involved in the production of IL-36γ upon RVFV infection of IFNAR$^{-/-}$ mice

Viral infections can be sensed via different pathways such as those involving TLR or RLR (41, 42). To uncover which signaling pathway is involved in IL-36γ induction and liver damage upon RVFV infection, we used IFNAR$^{-/-}$ mice additionally deficient for MyD88 (MyD88$^{-/-}$IFNAR$^{-/-}$ affecting most TLR pathways) and IFNAR$^{-/-}$ mice additionally deficient for MAVS (MAVS$^{-/-}$ IFNAR$^{-/-}$ not capable of using the RLR pathway). qRT-PCR analysis of PEC derived from those mice revealed that MAVS$^{-/-}$ IFNAR$^{-/-}$ did not induce any IL-36γ mRNA upon RVFV cl13 infection while IFNAR$^{-/-}$ and MyD88$^{-/-}$IFNAR$^{-/-}$ showed high levels of IL-36γ mRNA. Interestingly, IL-36γ mRNA-levels were even significantly higher in MyD88$^{-/-}$IFNAR$^{-/-}$ mice when compared to IFNAR$^{-/-}$ mice (Figure 6A). These data show that for IL-36γ mRNA expression by IFNAR$^{-/-}$ PEC, the MAVS-adapted RLR pathway is used while the MyD88-adapted TLR are of no relevance. Finally, we analyzed the ALT activity in the serum of these different knockout mice. While MyD88$^{-/-}$IFNAR$^{-/-}$ showed levels comparable to those in IFNAR$^{-/-}$ mice, no ALT activity was detected in MAVS$^{-/-}$IFNAR$^{-/-}$ mice indicating that these mice were indeed protected from the RVFV cl13-induced IL-36γ-mediated liver injury. Of note, plaque assay analyses revealed high viral loads in all organs tested, irrespective of the genotype of mice investigated (Figure 6C). Of note, higher levels of IL-36γ expression in MyD88$^{-/-}$ IFNAR$^{-/-}$ could not be correlated with increased viral loads in these mice.

In conclusion, our study demonstrated a critical role for the IL-1 family member IL-36γ for the induction of liver damage in the course of viral infection. In line with results obtained using the artificial double-stranded RNA poly(I:C), the dysregulation of IL-1 family members in the absence of type I IFN results in severe liver injury independent of viral titers.

4 Discussion

It was shown before that members of the IL-1 family, especially IL-1β, play an important role in liver injury (11, 43). The current study demonstrates a pathological role for IL-36γ upon an acute

viral infection. The pro-inflammatory cytokine IL-36γ was known before to be critically involved in several inflammatory disorders such as psoriasis (29, 44, 45), inflammatory bowel disease (23, 32, 44), rheumatoid arthritis (21), or systemic lupus erythematosus (SLE) (24). Accumulating evidences suggest that IL-36γ also plays a role during infectious diseases (24). Nevertheless, it is not fully understood yet if it promotes infection, drives immune-pathology, or rather plays a protective role.

A study by Wang et al. using a mouse model for influenza A virus (IAV) infection revealed that IL-36 contributes to lung damage and mortality by promoting inflammation. Mice deficient for the IL-36R were protected from IAV-induced lung injury and mortality. Furthermore, IL-36R$^{-/-}$ mice showed reduced lymphocyte activation, accumulation of myeloid cells, reduced permeability of the alveolar epithelial barrier, and less production of pro-inflammatory cytokines and chemokines (24, 46). In line with that, patients with IAV-induced acute respiratory syndrome (ARDS) show higher concentrations of IL-36γ in the plasma when compared to healthy individuals (47). In addition, IL-36γ and IL-36α are significantly upregulated in patients with pulmonary tuberculosis, bacterial pneumonia, or chronic hepatitis B virus (HBV) infection (47, 48).

Others reported a protective role for IL-36. Upon infection of mice, pretreatment with IL-36γ increased the resistance against Herpes simplex virus (HSV)-2 infection and disease (21). Mice lacking IL-36γ showed increased morbidity and mortality upon IAV

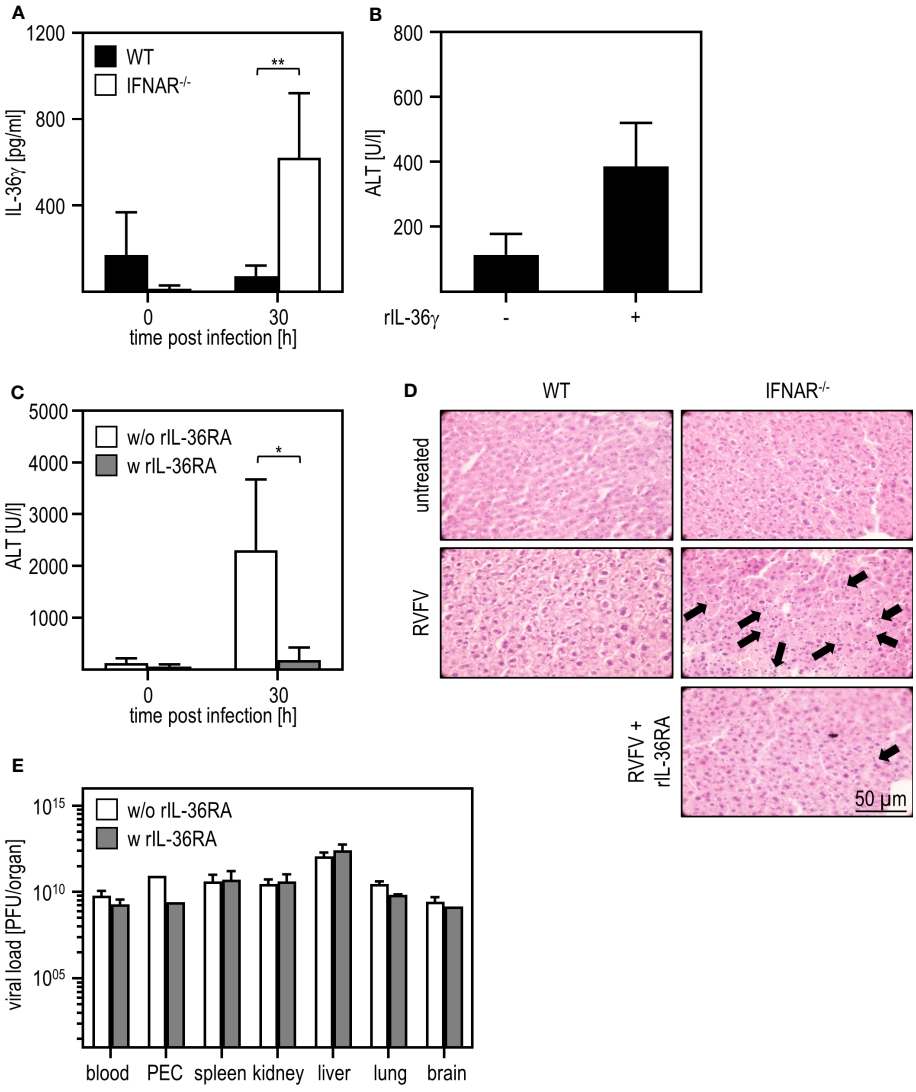

FIGURE 3
IL-36γ is causative for the liver injury in RVFV cl13-infected IFNAR$^{-/-}$ mice. C57BL/6 (WT) and IFNAR$^{-/-}$ mice were i.p. infected with 2x10^4 pfu/200 µl RVFV cl13. **(A)** IL-36γ was measured 30 hpi within the serum using an ELISA method (n=4-6). **(B)** C57BL/6 (WT) mice were i.v. injected with 1 µg recombinant IL-36γ. ALT activity within the serum was measured 3 hours post treatment (n=3). **(C)** RVFV cl13-infected IFNAR$^{-/-}$ mice were i.v injected with 6 µg rIL-36RA in 200 µl 12 and 24 hpi. RVFV cl13-infected IFNAR$^{-/-}$ mice served as control. ALT activity was measured 30 hpi (n=5). **(D)** Histological analyses were performed using H&E staining. Liver sections of RVFV cl13-infected WT and IFNAR$^{-/-}$ mice were prepared 30 hpi as described earlier (11). Additionally, RVFV cl13-infected IFNAR$^{-/-}$ mice were rIL-36RA-treated (all n=2). Untreated animals served as controls. Arrows exemplarily indicate apoptotic bodies within the tissue. **(E)** Organs of WT and IFNAR$^{-/-}$ mice were harvested 30 hours post RVFV infection and analyzed for the viral load by plaque assay (n=2-6). Error bars indicate standard deviations. * < 0.05; ** < 0.01 (Welch's t-test).

infection which was associated with increased virus titers and higher levels of inflammatory cytokines (46). Furthermore, IL-36γ$^{-/-}$ mice showed higher bacterial load in the lung, systemic dissemination, and higher mortality upon infection with *Staphylococcus pneumoniae* when compared to WT mice (45). Blocking IL-36γ receptor binding and using recombinant IL-36γ (see Figure 3), we found IL-36γ to be causative for the liver damage induced upon infection with RVFV cl13 in absence of intact type I IFN signaling. Interestingly, neither IL-36α, IL-36β, nor IL-36RA were elevated in organs of RVFV cl13-infected IFNAR$^{-/-}$ mice when compared to untreated IFNAR$^{-/-}$ or WT mice (see Supplementary Figure 2).

IL-36γ was shown before to play a role in drug-induced liver injury. In a model of acetaminophen (APAP)-induced hepatitis, Scheiermann et al. showed elevated levels of IL-36γ within the liver of IFNAR$^{-/-}$ mice. However, application of IL-36RA increased the late phase of liver injury indicating a potential role for IL-36γ as a cytokine contributing to the decision between tissue damage and liver regeneration (40). Moreover, treatment with IL-36RA significantly reduced the production of pro-inflammatory

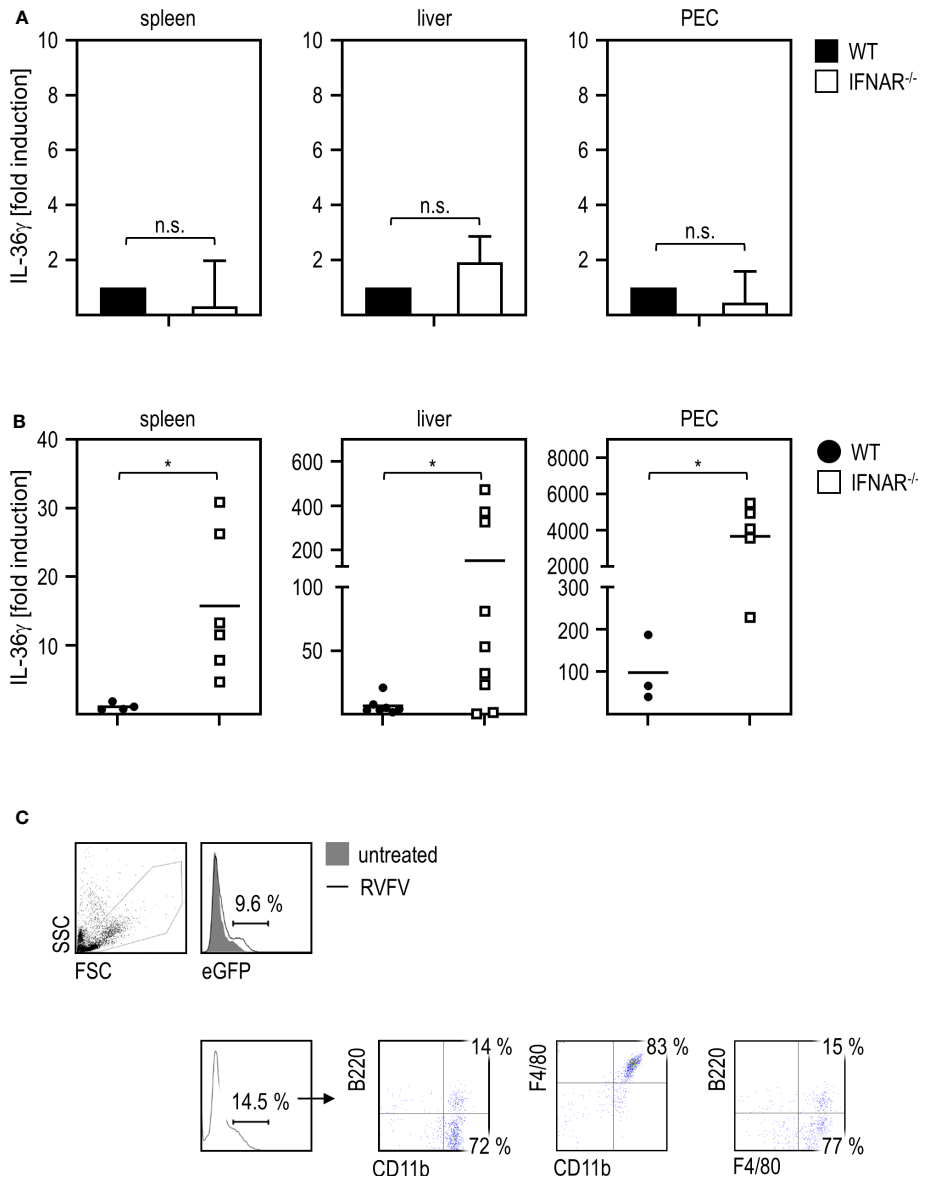

FIGURE 4
PEC are the main source of IL-36γ upon RVFV cl13 infection of IFNAR$^{-/-}$ mice. **(A)** To exclude genotype-specific differences in basal expression levels, spleen, liver, and peritoneal exudate cells (PEC) of C57BL/6 (WT) and IFNAR$^{-/-}$ mice (each n=4) were isolated and RNA was prepared as described elsewhere (11). Expression of IL-36γ was determined by qRT-PCR analyses. All values were normalized to WT animals; n.s.=not significant (Mann Whitney test). **(B)** C57BL/6 (WT) and IFNAR$^{-/-}$ mice (n=4-9) were i.p. infected with 2x10^4 pfu RVFV cl13 in 200 µl. Spleen, liver, and PEC were isolated 24 hpi infection and RNA was prepared as described earlier (11). Expression of IL-36γ was determined by qRT-PCR analyses. **(C)** ISRE-eGFP mice were either left untreated or infected with RVFV cl13 for 30 hours. PEC were isolated and analyzed for eGFP expression by flow cytometry. eGFP-positive cells were further characterized as CD11b$^+$F4/80$^+$ (one representative staining out of three is shown). Error bars indicate standard deviations; * < 0.05 (Welch's t-test); n.s., not significant.

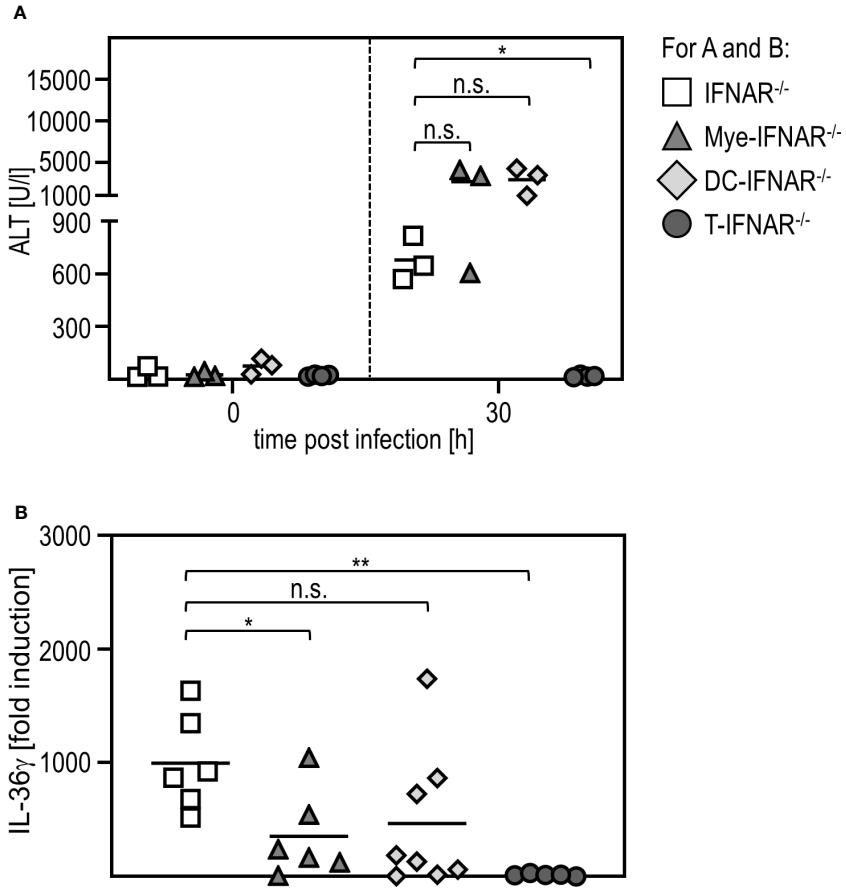

FIGURE 5
Myeloid cells need to sense type I IFN in order to protect from IL-36γ-mediated liver injury. IFNAR$^{-/-}$, Mye-IFNAR$^{-/-}$, DC-IFNAR$^{-/-}$, and T-IFNAR$^{-/-}$ mice were i.p. infected with 2x10^4 pfu RVFV cl13 in 200 µl. **(A)** ALT activity was measured 0 and 30 hpi infection (n=3-4). **(B)** Induction of IL-36γ within the PEC was determined by qRT-PCR analyses (n=5-8); * < 0.05; ** < 0.01 (Welch's t-test); n.s., not significant.

cytokines in BALB/c mice in a model of Concanavalin (Con)A-induced liver injury (49). ConA-treated IL-36R$^{-/-}$ animals exhibited exaggerated T cell responses as shown by increased infiltration of effector T cells into the liver accompanied by the production of pro-inflammatory cytokines (29).

Interestingly, in our study, IL-36γ-mediated liver injury upon RVFV infection was completely independent from viral loads in various organs tested. In particular, while viral titers in MAVS$^{-/-}$ IFNAR$^{-/-}$ animals are comparable to those in IFNAR$^{-/-}$ mice (Figures 1, 6), ALT activity in these double-deficient mice is comparable to WT animals (Figure 6). This suggests an immunopathology caused by IL-36γ expression in an IFNAR-deficient situation, whereas the hepatocellular tropism of RVFV and thus a virus-induced hepatitis seem to play a minor role.

Upon drug-induced liver injury, hepatocytes were shown to be the major source of IL-36 promoting the inflammatory response (50). In line with this, IL-6, TNF-α, and IFN-γ were slightly elevated in RVFV cl13-infected IFNAR$^{-/-}$ mice when compared to RVFV cl13-infected WT mice (for all p-value = 0.0571, Mann-Whitney-Test). In addition, a minor expression of IL-12p70 and IL-18 was observed in RVFV cl13-infected IFNAR$^{-/-}$ mice while other cytokines such as IL2, IL-4 or IL-5 did not differ between RVFV cl13-infected IFNAR$^{-/-}$ and WT mice (Supplementary Figure 3). Our study revealed that type I IFN sensing by macrophages as well as DC is critical for the prevention of IL-36γ production and thus the IL-36γ-induced liver injury upon RVFV cl13 infection (see Figure 5). The protective role of myeloid cells was also shown before for poly(I:C)-induced liver damage. Here, myeloid-derived suppressor cells infiltrated the liver in a type I IFN-dependent manner in order to produce IL-1RA and therefore prevent IL-1β-mediated liver injury (11). Interestingly, in the current study, no enhanced IL-36RA expression was detected in qRT-PCR analyses of organs of WT mice (see Supplementary Figure 2) indicating that other factors are involved in order to regulate the expression of IL-36γ. Within the poly(I:C)-induced model of liver damage as well as in our current study, myeloid cells within the peritoneum are of particular importance. Along this line, deficient type I IFN signaling was associated with decreased liver recruitment of DC in a model of TLR9 ligand-induced liver damage (8). In addition, a study by Pinto et al. demonstrated that deletion of the IFNAR on subsets of myeloid cells such as macrophages and DC, resulted in uncontrolled replication of West Nile virus (WNV), production of pro-inflammatory cytokines, organ damage, and death (51). Interestingly, particularly cells of the macrophage lineage show

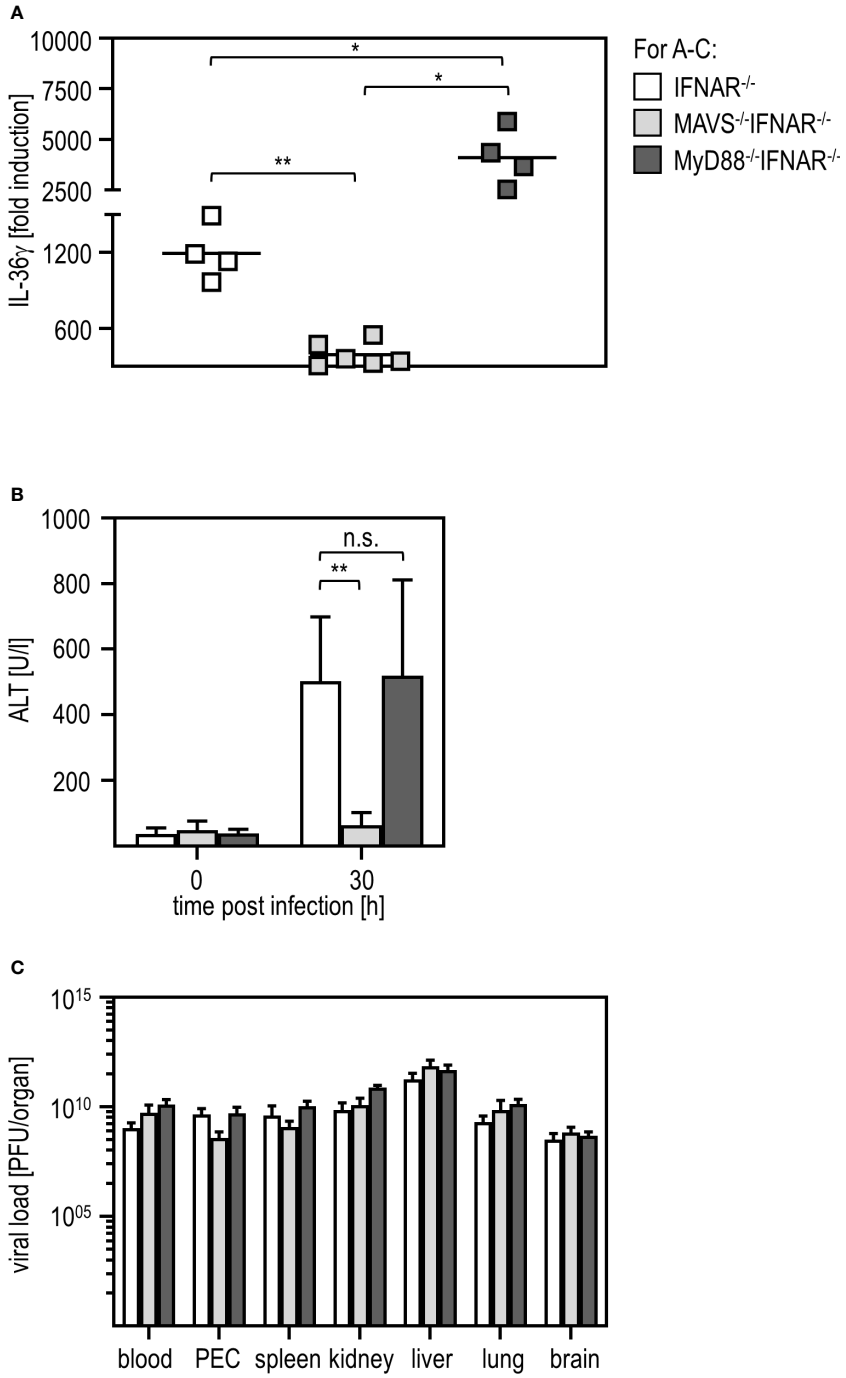

FIGURE 6
MAVS is critically involved in IL-36γ induction and IL-36γ-mediated liver injury upon RVFV cl13 infection of IFNAR$^{-/-}$ mice. IFNAR$^{-/-}$, MAVS$^{-/-}$IFNAR$^{-/-}$, and MyD88$^{-/-}$IFNAR$^{-/-}$ mice were i.p. infected with 2x10^4 pfu RVFV cl13 in 200 µl for 30 hours. **(A)** IL-36γ induction was investigated by qRT-PCR analyses of the PEC (n=4-6). **(B)** ALT activity was measured in serum samples at 30 hours post infection (n=4-8). **(C)** Viral load in different organs was analyzed by plaque assay (n=4-7). Error bars indicate standard deviations; * < 0.05; ** < 0.01; n.s., not significant.

increased susceptibility to RVFV cl13 infection in the absence of type I IFN. During initial stages of infection of IFNAR$^{-/-}$ mice, RVFV cl13 replicates within macrophages and DC (17). Ermler et al. demonstrated that murine conventional DC and macrophages express type I IFN in response to RVFV cl13 (14, 18).

In addition, RVFV cl13-infected human monocyte-derived macrophages were shown to secrete TNF-α and type I IFN (18). This together with our data implies that production as well as sensing of type I IFN by myeloid cells such as macrophages and DC, is critical in order to prevent IL-36γ production and thus the IL-36γ-induced liver damage upon RVFV cl13 infection. Besides immune cells, human lung fibroblasts and human bronchial epithelial cells were shown to produce IL-6 and CXCL8 upon treatment with IL-36 (30). Thus, other cells than immune cells such as hepatocytes might

contribute to a production of pro-inflammatory cytokines and dysregulated immune reaction upon RVFV cl13 infection.

It was shown in several studies that myeloid cells sense PAMPs rather via RLRs than TLRs. For example, Dutta et al. revealed that MAVS signaling in myeloid cells was critical for the resistance to Ebola virus infection in mice (52). In line with this, a variety of RNA-encoded viruses were shown to induce IFNAR-independent type I IFN responses in a MAVS-dependent manner (7). Here, we show that IL-36γ production and accordingly liver damage were dependent on MAVS in RVFV cl13-infected IFNAR$^{-/-}$ mice while MyD88-adapted TLR are of no importance for IL-36γ production (see Figure 6). Along this line, others showed that upon infection with WNV no cytokine production was observed in MAVS$^{-/-}$ IFNAR$^{-/-}$ mice (51). Of note, production of pro-inflammatory cytokines by DC or fibroblasts upon IL-36γ stimulation was shown to be dependent on MyD88 indicating that induction and sensing of IL-36γ can be mediated by different pathways (23, 45).

The interaction between type I IFN and IL-36 was previously observed also in psoriasis patients. Here, the expression of IL-36 strongly correlated with type I IFN overexpression (53). In addition, IL-36 serum levels in patients correlate with SLE disease activity, a disorder characterized by an enhanced type I IFN signature (53). In epithelial cells, IL-36 was shown to increase antiviral immunity by enhancing the expression of type I IFN stimulated genes (ISG) via the IFNAR (54). This mechanism may have evolved in order to control viruses that developed immune evasion strategies by blocking the production of type I IFN.

In conclusion, our study demonstrated that pro-inflammatory IL-36γ is causative for the observed liver injury in IFNAR$^{-/-}$ mice upon an acute viral infection. The expression of IL-36γ is regulated by type I IFN, which need to be sensed by myeloid cells in order to prevent liver damage.

Data availability statement

The raw data supporting the conclusions of this article will be made available by the authors, without undue reservation.

Ethics statement

The animal study was approved by Regierungspräsidium Darmstadt, license number F107-1027. The study was conducted in accordance with the local legislation and institutional requirements.

Author contributions

All authors contributed either to research design (MA, ZW, and GK) and/or the acquisition (MA, MN, EK, MD, SK, IB, SO-I), data analysis (MA, ZW, MN, EK, MD, SK, IB, SO-I), or interpretation of data (all authors). MA and ZW drafted the manuscript, which was critically revised by all other authors. All authors contributed to the article and approved the submitted version.

Acknowledgments

We thank Dorothea Kreuz, Björn Becker, and Yvonne Krebs for expert technical assistance.

Conflict of interest

The authors declare that the research was conducted in the absence of any commercial or financial relationships that could be construed as a potential conflict of interest.

Publisher's note

Supplementary material

The Supplementary Material for this article can be found online at: https://www.frontiersin.org/articles/10.3389/fimmu.2023.1194733/full#supplementary-material

SUPPLEMENTARY FIGURE 1
RVFV cl13-infected IFNAR$^{-/-}$ mice express high levels of IFN-α in the serum 30 hpi while WT mice show low amounts 12 hpi. C57BL/6 (WT) and IFNAR$^{-/-}$ mice (n= 2-14) were i.p. infected with 2x10^4 pfu RVFV cl13 in 200 µl. Serum was collected prior to infection as well as 30 hpi and tested using a multiplex kit for the presence of IL-6, TNF-α, and IFN-γ as described in the material and methods section. Error bars indicate standard deviations; *< 0.05; ** < 0.01; **** < 0.0001 (Welch's t-test); n.s., not significant.

SUPPLEMENTARY FIGURE 2
Spleen, liver, and PEC of RVFV cl13-infected IFNAR$^{-/-}$ mice do not upregulate IL-36α, Il-36β, or IL-36RA when compared to WT mice. C57BL/6 (WT) and IFNAR$^{-/-}$ mice (for IL-36α and IL-36β n=3-5; for IL-36RA n= 2-11) were i.p. infected with 2x10^4 pfu RVFV cl13 in 200 µl. Spleen, liver, and PEC were isolated 24 hpi infection and RNA was prepared as described earlier (11). Expression of IL-36α, IL-36β, and IL-36RA was determined by qRT-PCR analyses. n.s., not significant (Welch's t-test).

SUPPLEMENTARY FIGURE 3
RVFV cl13-infected IFNAR$^{-/-}$ mice show slightly enhanced levels of IL-6, TNF-α, and IFN-γ within the serum when compared to WT mice. C57BL/6 (WT) and IFNAR$^{-/-}$ mice (n= 3-4) were i.p. infected with 2x10^4 pfu RVFV cl13 in 200 µl. Serum was collected prior to infection as well as 30 hpi and tested using a multiplex kit for the presence of a panel of eight different cytokines as described in the material and methods section. n.s., not significant (Mann-Whitney-Test).

References

1. Chen H, Jiang Z. The essential adaptors of innate immune signaling. *Protein Cell* (2013) 4:27–39. doi: 10.1007/s13238-012-2063-0

2. Schneider WM, Chevillotte MD, Rice CM. Interferon-stimulated genes: a complex web of host defenses. *Annu Rev Immunol* (2014) 32:513–45. doi: 10.1146/annurev-immunol-032713-120231

3. Trinchieri G. Type I interferon: friend or foe? *J Exp Med* (2010) 207:2053–63. doi: 10.1084/jem.20101664

4. Honda K, Yanai H, Takaoka A, Taniguchi T. Regulation of the type I IFN induction: a current view. *Int Immunol* (2005) 17:1367–78. doi: 10.1093/intimm/dxh318

5. Ma F, Li B, Yu Y, Iyer SS, Sun M, Cheng G. Positive feedback regulation of type I interferon by the interferon-stimulated gene STING. *EMBO Rep* (2015) 16:202–12. doi: 10.15252/embr.201439366

6. Müller U, Steinhoff U, Reis LF, Hemmi S, Pavlovic J, Zinkernagel RM, et al. Functional role of type I and type II interferons in antiviral defense. *Science* (1994) 264:1918–21. doi: 10.1126/science.8009221

7. Anzaghe M, Kronhart S, Niles MA, Höcker L, Dominguez M, Kochs G, et al. Type I interferon receptor-independent interferon-α induction upon infection with a variety of negative-strand RNA viruses. *J Gen Virol* (2021) 102. doi: 10.1099/jgv.0.001616

8. Petrasek J, Dolganiuc A, Csak T, Kurt-Jones EA, Szabo G. Type I interferons protect from Toll-like receptor 9-associated liver injury and regulate IL-1 receptor antagonist in mice. *Gastroenterology* (2011) 140:697–708.e4. doi: 10.1053/j.gastro.2010.08.020

9. Gehrke N, Hövelmeyer N, Waisman A, Straub BK, Weinmann-Menke J, Wörns MA, et al. Hepatocyte-specific deletion of IL1-RI attenuates liver injury by blocking IL-1 driven autoinflammation. *J Hepatol* (2018) 68:986–95. doi: 10.1016/j.jhep.2018.01.008

10. Tilg H, Moschen AR, Szabo G. Interleukin-1 and inflammasomes in alcoholic liver disease/acute alcoholic hepatitis and nonalcoholic fatty liver disease/nonalcoholic steatohepatitis. *Hepatology* (2016) 64:955–65. doi: 10.1002/hep.28456

11. Conrad E, Resch TK, Gogesch P, Kalinke U, Bechmann I, Bogdan C, et al. Protection against RNA-induced liver damage by myeloid cells requires type I interferon and IL-1 receptor antagonist in mice. *Hepatology* (2014) 59:1555–63. doi: 10.1002/hep.26915

12. Anzaghe M, Resch T, Schaser E, Kronhart S, Diez C, Niles MA, et al. Organ-specific expression of IL-1 receptor results in severe liver injury in type I interferon receptor deficient mice. *Front Immunol* (2019) 10:1009. doi: 10.3389/fimmu.2019.01009

13. Ikegami T, Makino S. The pathogenesis of Rift Valley fever. *Viruses* (2011) 3:493–519. doi: 10.3390/v3050493

14. Ermler ME, Traylor Z, Patel K, Schattgen SA, Vanaja SK, Fitzgerald KA, et al. Rift Valley fever virus infection induces activation of the NLRP3 inflammasome. *Virology* (2014) 449:174–80. doi: 10.1016/j.virol.2013.11.015

15. Smith DR, Steele KE, Shamblin J, Honko A, Johnson J, Reed C, et al. The pathogenesis of Rift Valley fever virus in the mouse model. *Virology* (2010) 407:256–67. doi: 10.1016/j.virol.2010.08.016

16. Gray KK, Worthy MN, Juelich TL, Agar SL, Poussard A, Ragland D, et al. Chemotactic and inflammatory responses in the liver and brain are associated with pathogenesis of Rift Valley fever virus infection in the mouse. *PloS Negl Trop Dis* (2012) 6:e1529. doi: 10.1371/journal.pntd.0001529

17. Gommet C, Billecocq A, Jouvion G, Hasan M, Zaverucha do Valle T, Guillemot L, et al. Tissue tropism and target cells of NSs-deleted rift valley fever virus in live immunodeficient mice. *PloS Negl Trop Dis* (2011) 5:e1421. doi: 10.1371/journal.pntd.0001421

18. Terasaki K, Makino S. Interplay between the virus and host in rift valley fever pathogenesis. *J Innate Immun* (2015) 7:450–8. doi: 10.1159/000373924

19. Bouloy M, Janzen C, Vialat P, Khun H, Pavlovic J, Huerre M, et al. Genetic evidence for an interferon-antagonistic function of rift valley fever virus nonstructural protein NSs. *J Virol* (2001) 75:1371–7. doi: 10.1128/JVI.75.3.1371-1377.2001

20. McGavran MH, Easterday BC. Rift valley fever virus hepatitis: light and electron microscopic studies in the mouse. *Fort Belvoir VA: Defense Tech Inf Center* (1963). doi: 10.21236/AD0410394

21. Byrne J, Baker K, Houston A, Brint E. IL-36 cytokines in inflammatory and Malignant diseases: not the new kid on the block anymore. *Cell Mol Life Sci* (2021) 78:6215–27. doi: 10.1007/s00018-021-03909-4

22. Elias M, Zhao S, Le HT, Wang J, Neurath MF, Neufert C, et al. IL-36 in chronic inflammation and fibrosis - bridging the gap? *J Clin Invest* (2021) 131. doi: 10.1172/JCI144336

23. Kanda T, Nishida A, Takahashi K, Hidaka K, Imaeda H, Inatomi O, et al. Interleukin(IL)-36α and IL-36γ Induce proinflammatory mediators from human colonic subepithelial myofibroblasts. *Front Med (Lausanne)* (2015) 2:69. doi: 10.3389/fmed.2015.00069

24. Wang X, Yi P, Liang Y. The role of IL-36 in infectious diseases: potential target for COVID-19? *Front Immunol* (2021) 12:662266. doi: 10.3389/fimmu.2021.662266

25. Palomo J, Mastelic-Gavillet B, Woldt E, Troccaz S, Rodriguez E, Palmer G, et al. IL-36-induced toxicity in neonatal mice involves TNF-α Production by liver myeloid cells. *J Immunol* (2016) 197:2239–49. doi: 10.4049/jimmunol.1600700

26. Winkle SM, Throop AL, Herbst-Kralovetz MM. IL-36γ Augments host defense and immune responses in human female reproductive tract epithelial cells. *Front Microbiol* (2016) 7:955. doi: 10.3389/fmicb.2016.00955

27. Tsutsui H, Cai X, Hayashi S. Interleukin-1 family cytokines in liver diseases. *Mediators Inflammation* (2015) 2015:630265. doi: 10.1155/2015/630265

28. Towne JE, Renshaw BR, Douangpanya J, Lipsky BP, Shen M, Gabel CA, et al. Interleukin-36 (IL-36) ligands require processing for full agonist (IL-36α, IL-36β, and IL-36γ) or antagonist (IL-36Ra) activity. *J Biol Chem* (2011) 286:42594–602. doi: 10.1074/jbc.M111.267922

29. Wang X, Liang Y, Wang H, Zhang B, Soong L, Cai J, et al. The protective role of IL-36/IL-36R signal in con A-induced acute hepatitis. *J Immunol* (2022) 208:861–9. doi: 10.4049/jimmunol.2100481

30. Zhang J, Yin Y, Lin X, Yan X, Xia Y, Zhang L, et al. IL-36 induces cytokine IL-6 and chemokine CXCL8 expression in human lung tissue cells: Implications for pulmonary inflammatory responses. *Cytokine* (2017) 99:114–23. doi: 10.1016/j.cyto.2017.08.022

31. Foster AM, Baliwag J, Chen CS, Guzman AM, Stoll SW, Gudjonsson JE, et al. IL-36 promotes myeloid cell infiltration, activation, and inflammatory activity in skin. *J Immunol* (2014) 192:6053–61. doi: 10.4049/jimmunol.1301481

32. Queen D, Ediriweera C, Liu L. Function and regulation of IL-36 signaling in inflammatory diseases and cancer development. *Front Cell Dev Biol* (2019) 7:317. doi: 10.3389/fcell.2019.00317

33. Vigne S, Palmer G, Lamacchia C, Martin P, Talabot-Ayer D, Rodriguez E, et al. IL-36R ligands are potent regulators of dendritic and T cells. *Blood* (2011) 118:5813–23. doi: 10.1182/blood-2011-05-356873

34. Gabay C, Towne JE. Regulation and function of interleukin-36 cytokines in homeostasis and pathological conditions. *J Leukoc Biol* (2015) 97:645–52. doi: 10.1189/jlb.3RI1014-495R

35. Lian L-H, Milora KA, Manupipatpong KK, Jensen LE. The double-stranded RNA analogue polyinosinic-polycytidylic acid induces keratinocyte pyroptosis and release of IL-36γ. *J Invest Dermatol* (2012) 132:1346–53. doi: 10.1038/jid.2011.482

36. Mitani Y, Takaoka A, Kim SH, Kato Y, Yokochi T, Tanaka N, et al. Cross talk of the interferon-alpha/beta signalling complex with gp130 for effective interleukin-6 signalling. *Genes Cells* (2001) 6:631–40. doi: 10.1046/j.1365-2443.2001.00448.x

37. Waibler Z, Anzaghe M, Ludwig H, Akira S, Weiss S, Sutter G, et al. Modified vaccinia virus Ankara induces Toll-like receptor-independent type I interferon responses. *J Virol* (2007) 81:12102–10. doi: 10.1128/JVI.01190-07

38. Malmgaard L. Induction and regulation of IFNs during viral infections. *J Interferon Cytokine Res* (2004) 24:439–54. doi: 10.1089/1079990041689665

39. Kochs G, Bauer S, Vogt C, Frenz T, Tschopp J, Kalinke U, et al. Thogoto virus infection induces sustained type I interferon responses that depend on RIG-I-like helicase signaling of conventional dendritic cells. *J Virol* (2010) 84:12344–50. doi: 10.1128/JVI.00931-10

40. Scheiermann P, Bachmann M, Härdle L, Pleli T, Piiper A, Zwissler B, et al. Application of IL-36 receptor antagonist weakens CCL20 expression and impairs recovery in the late phase of murine acetaminophen-induced liver injury. *Sci Rep* (2015) 5:8521. doi: 10.1038/srep08521

41. Akira S, Uematsu S, Takeuchi O. Pathogen recognition and innate immunity. *Cell* (2006) 124:783–801. doi: 10.1016/j.cell.2006.02.015

42. Takeuchi O, Akira S. Pattern recognition receptors and inflammation. *Cell* (2010) 140:805–20. doi: 10.1016/j.cell.2010.01.022

43. Petrasek J, Bala S, Csak T, Lippai D, Kodys K, Menashy V, et al. IL-1 receptor antagonist ameliorates inflammasome-dependent alcoholic steatohepatitis in mice. *J Clin Invest* (2012) 122:3476–89. doi: 10.1172/JCI60777

44. Walsh PT, Fallon PG. The emergence of the IL-36 cytokine family as novel targets for inflammatory diseases. *Ann N Y Acad Sci* (2018) 1417:23–34. doi: 10.1111/nyas.13280

45. Kovach MA, Singer BH, Newstead MW, Zeng X, Moore TA, White ES, et al. IL-36γ is secreted in microparticles and exosomes by lung macrophages in response to bacteria and bacterial components. *J Leukoc Biol* (2016) 100:413–21. doi: 10.1189/jlb.4A0315-087R

46. Wein AN, Dunbar PR, McMaster SR, Li Z-RT, Denning TL, Kohlmeier JE. IL-36γ Protects against severe influenza infection by promoting lung alveolar macrophage survival and limiting viral replication. *J Immunol* (2018) 201:573–82. doi: 10.4049/jimmunol.1701796

47. Liu S, Li H, Wang Y, Li H, Du S, Zou X, et al. High expression of IL-36γ in influenza patients regulates interferon signaling pathway and causes programmed cell death during influenza virus infection. *Front Immunol* (2020) 11:552606. doi: 10.3389/fimmu.2020.552606

48. Gong Y, Tingxi Z, Qing L, Guozhen Z, Bing T, Xiaoliang Y, et al. Elevated production of IL-36α in chronic hepatitis B virus-infected patients correlates with viral load. *Microb Pathog* (2017) 113:412–5. doi: 10.1016/j.micpath.2017.11.023

49. Peng X, Pan X, Tan J, Li Y, Li M. Protective effect of interleukin-36 receptor antagonist on liver injury induced by concanavalin A in mice. *Iran J Basic Med Sci* (2020) 23:623–8. doi: 10.22038/ijbms.2020.35614.8492

50. Shang Y, Yang H-X, Li X, Zhang Y, Chen N, Jiang X-L, et al. Modulation of interleukin-36 based inflammatory feedback loop through the hepatocyte-derived IL-36R-P2X7R axis improves steatosis in alcoholic steatohepatitis. *Br J Pharmacol* (2022) 179:4378–99. doi: 10.1111/bph.15858

51. Pinto AK, Ramos HJ, Wu X, Aggarwal S, Shrestha B, Gorman M, et al. Deficient IFN signaling by myeloid cells leads to MAVS-dependent virus-induced sepsis. *PloS Pathog* (2014) 10:e1004086. doi: 10.1371/journal.ppat.1004086

52. Dutta M, Robertson SJ, Okumura A, Scott DP, Chang J, Weiss JM, et al. A systems approach reveals MAVS signaling in myeloid cells as critical for resistance to ebola virus in murine models of infection. *Cell Rep* (2017) 18:816–29. doi: 10.1016/j.celrep.2016.12.069

53. Catapano M, Vergnano M, ROmano M, Mahil SK, Choon S-E, Burden AD, et al. IL-36 promotes systemic IFN-I responses in severe forms of psoriasis. *J Invest Dermatol* (2020) 140:816–826.e3. doi: 10.1016/j.jid.2019.08.444

54. Wang P, Gamero AM, Jensen LE. IL-36 promotes anti-viral immunity by boosting sensitivity to IFN-α/β in IRF1 dependent and independent manners. *Nat Commun* (2019) 10:4700. doi: 10.1038/s41467-019-12318-y

10.3389/fimmu.2023.1194733

Glossary

ALT	alanine aminotransferase
APAP	acetaminophen
CD	cluster of differentiation
cl	clone
ConA	concanavalin A
DC	dendritic cell(s)
D-GalN	d-galactosamine
ELISA	enzyme-linked immunosorbent assay
Figure	figure(s)
GFP	green fluorescent protein
HBV	hepatits B virus
hpi	hours post infection
HSV	herpes simplex virus
IAV	influenza A virus
IFN	type I interferon(s)
IFNAR	type I interferon receptor
IL	interleukin
IL-1RA	interleukin-1 receptor antagonist
IL-1RAcP	interleukin-1 receptor accessory protein
IL-36RA	interleukin-36 receptor antagonist
i.p.	intraperitoneal
ISG	IFN-stimulated gene(s)
i.v.	intravenously
LPS	lipopolysaccharide
MAVS	mitochondrial antiviral-signaling protein
MyD88	myeloid differentiation primary response 88
RVFV	Rift Valey fever virus
PAMP	pathogen associated molecular pattern
PBMC	peripheral mononuclear cells
PEC	peritoneal exudate cells
poly(I:C)	polyinosinic-polycytidylic acid
PRR	pattern recognition receptor(s)
RIG	retinoic acid-inducible gene
RLR	retinoic acid-inducible gene RIG-I-like receptors
SLE	systemic lupus erythematosus
TLR	toll like receptor(s)
WT	wildtype

frontiers | Frontiers in Immunology

TYPE Original Research
PUBLISHED 17 May 2023
DOI 10.3389/fimmu.2023.1128239

OPEN ACCESS

EDITED BY
Diana Boraschi,
Shenzhen Institute of Advanced Technology (SIAT) (CAS), China

REVIEWED BY
Bernhard Ryffel,
Centre National de la Recherche Scientifique (CNRS), France
Piersante Sestini,
University of Siena, Italy

*CORRESPONDENCE
Carola Voss
carola.voss@helmholtz-muenchen.de
Anne Hilgendorff
anne.hilgendorff@med.uni-muenchen.de

RECEIVED 20 December 2022
ACCEPTED 23 March 2023
PUBLISHED 17 May 2023

CITATION
Kastlmeier MT, Gonzalez-Rodriguez E, Cabanis P, Guenther EM, König A-C, Han L, Hauck SM, See F, Asgharpour S, Bukas C, Burgstaller G, Piraud M, Lehmann M, Hatz RA, Behr J, Stoeger T, Hilgendorff A and Voss C (2023) Cytokine signaling converging on *IL11* in ILD fibroblasts provokes aberrant epithelial differentiation signatures. *Front. Immunol.* 14:1128239. doi: 10.3389/fimmu.2023.1128239

Cytokine signaling converging on *IL11* in ILD fibroblasts provokes aberrant epithelial differentiation signatures

Miriam T. Kastlmeier[1], Erika Gonzalez-Rodriguez[1], Phoebe Cabanis[1], Eva M. Guenther[1], Ann-Christine König[2], Lianyong Han[1], Stefanie M. Hauck[2], Fenja See[1], Sara Asgharpour[1], Christina Bukas[3], Gerald Burgstaller[1], Marie Piraud[3], Mareike Lehmann[1,4], Rudolf A. Hatz[5], Jürgen Behr[6], Tobias Stoeger[1], Anne Hilgendorff[1,7]* and Carola Voss[1]*

[1]Institute of Lung Health and Immunity, Helmholtz Center Munich, German Research Center for Environmental Health (GmbH), Comprehensive Pneumology Center Munich with the CPC-M bioArchive, Member of the German Center of Lung Research (DZL), Munich, Germany, [2]Metabolomics and Proteomics Core (MPC), Helmholtz Center Munich, German Research Center for Environmental Health (GmbH), Munich, Germany, [3]Helmholtz AI, Helmholtz Center Munich, German Research Center for Environmental Health (GmbH), Munich, Germany, [4]Institute for Lung Research, Philipps-University Marburg, Universities of Giessen and Marburg Lung Center, Member of the German Center for Lung Research (DZL), Marburg, Germany, [5]Klinik für Thoraxchirurgie, Asklepios Fachkliniken München-Gauting, Thoraxchirurgie, Munich, Germany, [6]Department of Medicine V, University Hospital, Ludwig-Maximilians University Munich, Comprehensive Pneumology Center, Member of the German Center for Lung Research (DZL), Munich, Germany, [7]Dr. von Haunersche Children's Hospital, Hospital of the Ludwig-Maximilians University, Member of the German Lung Research Center (DZL), Munich, Germany

Introduction: Interstitial lung disease (ILD) is a heterogenous group of lung disorders where destruction and incomplete regeneration of the lung parenchyma often results in persistent architectural distortion of the pulmonary scaffold. Continuous mesenchyme-centered, disease-relevant signaling likely initiates and perpetuates the fibrotic remodeling process, specifically targeting the epithelial cell compartment, thereby destroying the gas exchange area.

Methods: With the aim of identifying functional mediators of the lung mesenchymal-epithelial crosstalk with potential as new targets for therapeutic strategies, we developed a 3D organoid co-culture model based on human induced pluripotent stem cell-derived alveolar epithelial type 2 cells that form alveolar organoids in presence of lung fibroblasts from fibrotic-ILD patients, in our study referring to cases of pulmonary fibrosis, as well as control cell line (IMR-90).

Results: While organoid formation capacity and size was comparable in the presence of fibrotic-ILD or control lung fibroblasts, metabolic activity was significantly increased in fibrotic-ILD co-cultures. Alveolar organoids cultured with fibrotic-ILD fibroblasts further demonstrated reduced stem cell function as reflected by reduced Surfactant Protein C gene expression together with an aberrant basaloid-prone differentiation program indicated by elevated Cadherin

2, Bone Morphogenic Protein 4 and Vimentin transcription. To screen for key mediators of the misguided mesenchymal-to-epithelial crosstalk with a focus on disease-relevant inflammatory processes, we used mass spectrometry and characterized the secretome of end stage fibrotic-ILD lung fibroblasts in comparison to non-chronic lung disease (CLD) patient fibroblasts. Out of the over 2000 proteins detected by this experimental approach, 47 proteins were differentially abundant comparing fibrotic-ILD and non-CLD fibroblast secretome. The fibrotic-ILD secretome profile was dominated by chemokines, including CXCL1, CXCL3, and CXCL8, interfering with growth factor signaling orchestrated by Interleukin 11 (IL11), steering fibrogenic cell-cell communication, and proteins regulating extracellular matrix remodeling including epithelial-to-mesenchymal transition. When in turn treating alveolar organoids with IL11, we recapitulated the co-culture results obtained with primary fibrotic-ILD fibroblasts including changes in metabolic activity.

Conclusion: We identified mediators likely contributing to the disease-perpetuating mesenchymal-to-epithelial crosstalk in ILD. In our alveolar organoid co-cultures, we were able to highlight the importance of fibroblast-initiated aberrant epithelial differentiation and confirmed IL11 as a key player in fibrotic-ILD pathogenesis by unbiased fibroblast secretome analysis.

KEYWORDS

cytokine, *IL11*, secretome, interstitial lung disease, organoids, human pluripotent stem cells, disease modeling, co-culture model

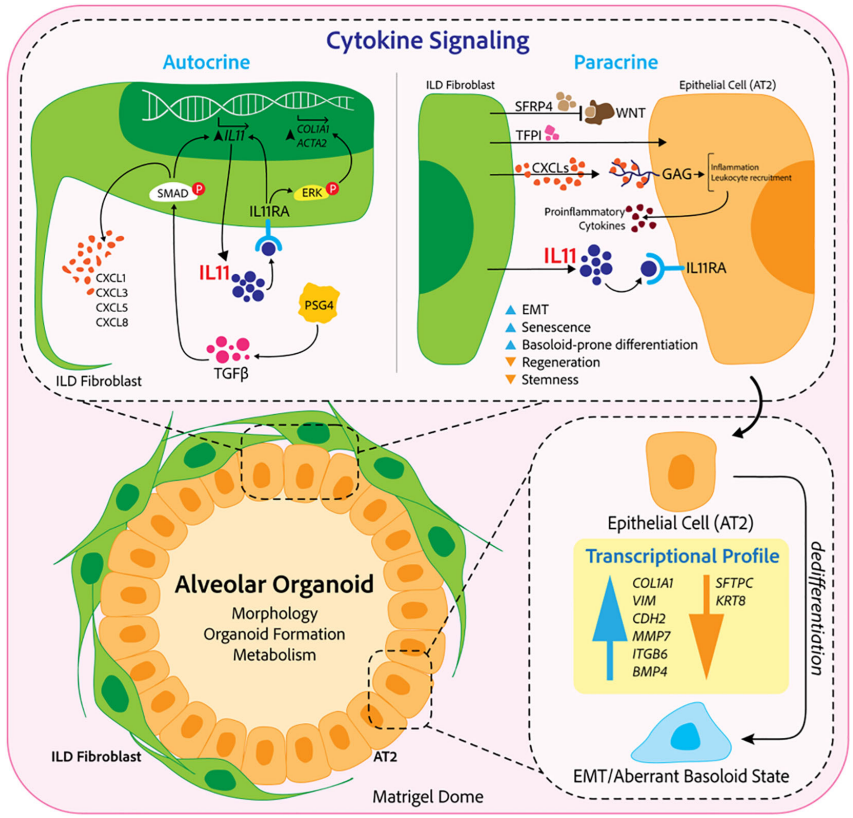

GRAPHICAL ABSTRACT

1 Introduction

Interstitial lung diseases (ILDs) comprise a variety of chronic pulmonary conditions that are characterized by structural remodeling of the gas exchange area (1). ILD pathophysiology is centered on sustained inflammation and progressive scarring, ultimately resulting in irreversible tissue destruction and organ failure. Despite the exact pathogenesis of ILD still being unclear, genetic predisposition, age, sex and environmental exposure are known drivers of the disease (2, 3).

In ILD pathogenesis, fibroblast activation occurs through the impact of exogenous stimuli side-by-side with their activation through innate immune cells, especially monocytes and neutrophils, communicating *via* growth factor signaling and cytokine secretion. Subsequently, lactic acid release from fibroblasts as well as epithelial cells, induced by matrix metalloproteinases (MMPs), fibroblast growth factors and metabolic changes in turn further enhances fibroblast activation and accumulation (4). As a result, fibroblasts become the main loci of extracellular matrix (ECM) production and deposition. Induced by repeated inflammatory epithelial injury that leads to further leucocyte attraction and infiltration of the airspace and further perpetuating the pro-fibrotic circle of events, activated fibroblasts are discussed to induce epithelial-to-mesenchymal transition (EMT) in alveolar epithelial cells *via* SMAD and MAPK signaling (5), (6).

Driving and upholding the outlined pathophysiologic processes in ILD that ultimately result in severe tissue destruction and loss of the alveolar epithelium in end-stage ILD, a tightly knit crosstalk between the activated fibroblast and the damaged epithelium has been proposed (7–9). Here, the role of pathologic growth factor signaling and secreted cytokines such as *transforming growth factor ß (TGF-β)* and *Interleukin 17 (IL17)* were highlighted.

Adding to their detrimental role, activated fibroblasts – next to their capacity for pro-fibrotic signaling and EMT induction – have been shown to alter repair and regeneration of the injured gas-exchange area by affecting alveolar epithelial type 2 stem cell potential (10).

To address apparent knowledge gaps in the cytokine-driven, disease-relevant mesenchymal-to-epithelial crosstalk, we used lung organoids derived from human induced pluripotent stem cells (hiPSCs) through chemical directed differentiation into a sophisticated co-culture model. hiPSC-derived alveolar type 2 cells (iAT2s) are recognized as a useful tool to study lung diseases and regeneration capacities, and are recently emerging as a novel tool in environmental and occupational hazard assessment (11, 12). iAT2-derived alveolar organoids recapitulate the characteristic three-dimensional (3D) structure of alveoli and are thereby ideal to mimic important functions of the gas exchange area *in vitro*. Their potential to study pulmonary disease *in vitro* (13, 14) is particularly versatile when targeting underlying molecular mechanisms (3).

By the integration of this sophisticated methodology in a novel co-culture model, we were able to investigate the impact of primary lung fibroblasts from ILD patients, in our study referring to cases of pulmonary fibrosis, on critical functions of hiPSC-derived alveolar organoids. The combination of this approach with unbiased secretome analysis allowed us to delineate functionally relevant signals of the pathologic crosstalk from the lung mesenchyme towards the alveolar epithelium with the aim to identify potential therapeutic targets.

2 Material and methods

2.1 Human induced pluripotent stem cells (hiPSCs) and directed differentiation into lung progenitors

The hiPSC line BU3NGST was kindly provided by Prof. Darrell Kotton, Boston University, Center for Regenerative Medicine. This cell line is a dual-reporter construct composed of fluorochrome-encoding cassettes targeted to the endogenous NKX2.1 and SFTPC loci (BU3 NKX2.1^{GFP}; SFTPC^{tdTomato}) (15). hiPSCs were maintained in mTeSR1 (StemCell Technologies), on Matrigel (Corning) coated cell culture plates at 37°C/5% CO_2 in a cell culture CO_2 incubator. Cells were subcultured by using ReLeSR (StemCell Technologies) or Gentle Cell Dissociation Reagent (StemCell Technologies) (16, 17).

BU3NGSTs were differentiated into NKX2.1$^+$ lung progenitor cells and iAT2s as described previously by Jacob et al. (16, 17). In short, hiPSCs were checked for their pluripotency *via* Alkaline Phosphatase staining (ES Cell Characterization Kit, CHEMICON International) or immunofluorescence staining of TRA 181 and SSEA 4 (ES cell characterization Kit, CHEMICON International). Induction of definitive endoderm was conducted *via* STEMdiff Definitive Endoderm Kit, (StemCell Technologies). On day 14 of differentiation, lung progenitor specification was evaluated by immunofluorescence staining of NKX2.1 (Invitrogen) and Albumin (ALB, R&D Systems). NKX2.1^{GFP+} lung progenitor cells were enriched by GFP signal for NKX2.1 based on a previously described protocol. The sorting was performed by FACS cell sorting at MACSQuant Tyto Cell Sorter (Miltenyi Biotec). For data evaluation FlowJo Version 7.2.1 and v10 was used. Purified lung progenitors were seeded in Matrigel (Corning) domes at a cell density of 50 cells/µL and passaged every second week. To increase SFTPC$^{tdTomato+}$ cells CHIR withdrawal and addback was performed. At day 45 of differentiation, iAT2s were enriched by flow cytometry (MACSQuant Tyto Cell Sorter, Miltenyi Biotec) using tdTomato signal for SFTPC expression and subsequently cultured as 3D alveolar organoids. Differentiated SFTPC$^{tdTomato+}$ iAT2s in 3D Matrigel were grown in CK+DCI medium, with media changes every 48 – 72 h. Alveolar organoids were passaged every 14 days.

2.2 Primary human fibroblast culture

Primary human lung fibroblasts from ILD patients, in our study referring to cases of pulmonary fibrosis,and non-CLD (P4) for co-culture experiments (ILD fibroblasts) and MS based secretome

analysis (ILD and non-CLD fibroblasts) were isolated according to a published protocol (18) and obtained through the CPC-M bioArchive at the Comprehensive Pneumology Center in Munich, Germany.

All patients underwent surgery at the LMU Hospital and the Asklepios Pulmonary Hospital Munich-Gauting. Tissue from ILD patients (n = 3, Table 1) was provided through lung transplantation. Control fibroblasts were derived from lung tissue resections of age-matched non-CLD patients (female n = 1, = 3, male n = 2).

The study was approved by the local ethics committee of the Ludwig-Maximilians University of Munich, Germany (Ethic vote #333-10) and written informed consent form was obtained for all study participants.

Human fetal lung fibroblasts (IMR-90, P8) for control co-cultures were obtained from ATCC (Catalog # CCL-186^{TM}) and grown in Dulbecco's Modified Eagle Medium: Nutrient F-12 (DMEM/F12; Gibco) with 20% fetal bovine serum (FBS SUPERIOR, Sigma) and 1% penicillin-streptomycin (Pen Strep, Gibco).

Cells were seeded in 6-well plates. at a density of 1x10^5 cells in 2 mL media (DMEM/F12, 20% FBS, 1% penicillin/streptomycin) per well until reaching 80% confluency. Once confluent, each well was washed three times with a 15-minute incubation per wash with 1 mL of FBS-free culturing medium (DMEM/F12, 1% penicillin/streptomycin) to eliminate remaining FBS. Fibroblasts were cultured for 48 h in FBS-free medium, supernatants were collected and stored at -80°C for further analysis.

2.3 Secretome analysis by mass spectrometry

2.3.1 Sample preparation for proteomics

Each 500 µL supernatant was subjected to tryptic digest applying a modified filter aided sample preparation procedure (19, 20). After protein reduction and alkylation using DTT and iodoacetamide, samples were denatured in UA buffer (8 M urea in 0.1 M Tris/HCl pH 8.5) and centrifuged on a 30 kDa cut-off filter device (PALL or Sartorius) and washed thrice with UA buffer and twice with 50 mM ammoniumbicarbonate (ABC). Proteins were proteolysed for 2 h at room temperature using 0.5 µg Lys-C (Wako) and subsequently for 16 h at 37°C using 1 µg trypsin (Promega). Peptides were collected by centrifugation and acidified with 0.5% trifluoroacetic acid.

2.3.2 Mass spectrometric measurements

LC-MSMS analysis was performed on a Q-Exactive HF mass spectrometer (Thermo Scientific) each online coupled to a nano-RSLC (Ultimate 3000 RSLC; Dionex). For subsequent analysis on the Q-Exactive HF, tryptic peptides were accumulated on a nano trap column (300 µm inner diameter × 5 mm, packed with Acclaim PepMap100 C18, 5 µm, 100 Å; LC Packings) and then separated by reversed phase chromatography (nanoEase MZ HSS T3 Column, 100 Å, 1.8 µm, 75 µm X 250 mm; Waters) in a 80 minutes non-linear gradient from 3 to 40% acetonitrile in 0.1% formic acid at a flow rate of 250 nL/min. Eluted peptides were analyzed by the Q-Exactive HF mass spectrometer equipped with a PepSep PSS1 source. Full scan MS spectra (from m/z 300 to 1500) and MSMS fragment spectra were acquired in the Orbitrap with a resolution of 60.000 or 15.000 respectively, with maximum injection times of 50 ms each. The up to ten most intense ions were selected for HCD fragmentation depending on signal intensity (TOP10 method). Target peptides already selected for MS/MS were dynamically excluded for 30 seconds. Data are available *via* ProteomeXchange with identifier PXD039554 (21, 22).

2.3.3 Protein identification and label-free quantification

Proteome Discoverer 2.5 software (Thermo Fisher Scientific; version 2.5.0.400) was used for peptide and protein identification *via* a database search (Sequest HT search engine, SequestHT score:1) against Swissprot human database (Release 2020_02, 20432 sequences), considering full tryptic specificity, allowing for up to two missed tryptic cleavage sites, precursor mass tolerance 10 ppm, fragment mass tolerance 0.02 Da. Carbamidomethylation of Cys was set as a static modification. Dynamic modifications included deamidation of Asn, Gln and Arg, oxidation of Pro and Met; and a combination of Met loss with acetylation on protein N-terminus. Percolator was used for validating peptide spectrum matches and peptides, accepting only the top-scoring hit for each spectrum, and satisfying the cutoff values for false discovery rate (FDR) < 5%, and posterior error probability < 0.01.

The quantification of proteins was based on abundance values for unique peptides. Abundance values were normalized on total peptide amount and protein abundances were calculated summing up the abundance values for admissible peptides. The final protein ratio was calculated using median abundance values. The statistical significance of the ratio change was ascertained employing the T-test approach

TABLE 1 Patient characteristics.

Patient	Diagnosis	Age at sample collection (years)	Sex	Surgery	Smoking history
1	Connective Tissue Disease related ILD	48	F	Lung transplantation (single)	no
2	Idiopathic pulmonary fibrosis	62	M	Lung transplantation (single)	no
3	Hypersensitivity Pneumonitis, Rheumatoid arthritis	57	F	Lung transplantation	no

described in 23 (23), which is based on the presumption that we look for expression changes for proteins that are just a few in comparison to the number of total proteins being quantified. The quantification variability of the non-changing "background" proteins can be used to infer which proteins change their expression in a statistically significant manner. Proteins with increased or decreased abundance were filtered with the following criteria: proteins were considered to be decreased in abundance below an abundance of ratio of 0.5 fold and increased abundance above 2 fold, proteins identified with a single peptide were excluded and just significant proteins were considered (P value < 0.05, P values were adjusted for multiple testing by Benjamini-Hochberg correction). Additionally, at least two MSMS identifications had to be identified to include the protein ratio.

2.3.4 Enrichment analysis

Pathway enrichment analyses were performed in Cytoscape (3.9.0) with the ClueGo plugin (v2.5.8) for significantly increased or decreased proteins. The following ontologies were used: KEGG (8093), GO_MolecularFunction-EBI-UniProt (18336), GO_BiologicalProcess-EBI-UniProt (18058). Accession IDs were used as identifiers and the analysis was performed with the standard software settings provided in the ClueGo app (24).

2.4 Mesenchymal-epithelial co-culture

Primary lung ILD fibroblasts and IMR-90 (control fibroblast cell line) were grown in cell culture flasks until 70% confluency. A single cell suspension was prepared using 0.25% EDTA-Trypsin (Gibco). iAT2s were grown into alveolar organoids for up to two weeks in Matrigel domes. Single cell suspension was obtained with Dispase (Corning) and 0.25% EDTA-Trypsin as described by Jacob et al. (17). Human ILD and IMR-90 fibroblasts as well as iAT2s were counted and directly seeded either in equal 1:1 (F_{low}) or 1:5 (F_{high}) iAT2s to fibroblasts seeding densities in undiluted Matrigel domes in 8-chamber wells (20 µL Drops, Falcon), 96-well plates (50 µL Drops, Greiner) or 12-well plates (50 µL Drops, Greiner). Co-cultures used CK+DCI media that was changed every 48 h to 72 h for up to 12 days of cultivation.

2.5 Immunofluorescence microscopy

3D alveolar organoids mono- and co-cultures as described in section 2.1 (mono-culture) and 2.4 (co-culture) were cultured in 8-chamber wells for immunofluorescence analysis (Nunc Lab-Tek Chamber Slide System, 8-well, Permanox slide, 0.8 cm^2/well). After alveolar organoids were formed, fixation was achieved with ice cold methanol and acetone (1:1v/v) for 5 minutes at -20°C. Cells were washed with PBS and stained with the respective primary antibody in buffer containing 0.1% BSA and 0.1% Triton X-100 overnight at 4°C. The next day, cells were washed 3 times with PBS and incubated in buffer with the respective fluorescent conjugated secondary antibody at a dilution of 1:500 and DAPI diluted 1:1.000 overnight at 4°C. The following day, cells were washed gently, growth camber removed and remaining microscope slide mounted with fluorescent mounting media (Dako) and covered with a coverslip. Slides were stored at 4°C until imaging. Imaging was performed using a confocal laser scanning microscope (CLSM) Zeiss LSM 880 with Airyscan and edited afterwards using ZEN 2.5 software (Zeiss). Detailed information on the primary and secondary antibodies are given in Supplementary Table 1.

2.6 Operetta high content imaging and Napari organoid counter

Live imaging of all alveolar organoid mono- and co-cultures was performed using the Operetta CLS high-content analysis system (Operetta CLS, PerkinElmer) at time points 5, 8 and 12 days during the co-culture experimental set-up. Pictures were analyzed by the Harmony 3.5.2 high-content imaging and analysis software with PhenoLOGIC.

Multi-plane confocal 3D images were visualized in Napari image viewer (Python) as maximum intensity projections and the automatic measurements obtained from the "Napari organoid counter" (25) were visually checked and manually curated, resulting in output of size and numbers of formed alveolar organoids between iAT2s and human fibroblasts (ILD and control IMR-90). The Canny Edge Detection (26) algorithm is used for identifying the organoids, while pre- and post-processing steps have been included, to ensure the image matches the detector's expected input and the number of detected organoids along with their size is returned. More specifically, the organoids are approximated to ellipses and the algorithm fits orthogonal bounding boxes around each, with the height and width of each box corresponding to the two diameters of the organoid which are then in turn used to approximate the object's area.Quantitative real-time PCR

Co-cultures were lysed in RLT Plus Lysis Buffer (Qiagen) and RNA isolation was performed with the RNeasy Mini Kit (Qiagen) according to the manufacturer's instructions. Cell lysis from organoids and co-culture assays was performed with peqGOLD TriFast (VWR Life Science) as recommended by the manufactures followed by RNA isolation with the RNeasy Mini Kit (Qiagen). RNA was transcribed into cDNA by reverse transcriptase using the High-Capacity cDNA Reverse Transcription Kit (Thermo Fisher Scientific) according to the manufacturer's instructions. 5 ng of cDNA was added to a final concentration volume of 10 µL, Random Nonamers (Metabion) and master mix (Invitrogen, Thermo Fisher Scientific) was added to each RNA sample. cDNA was diluted with ultrapure H_2O. qPCR was performed in 96-well format using the quantitative real-time PCR System (Roche 480 LightCycler). 2 µL cDNA were added to a final reaction volume of 10 µL containing H_2O, 480 SYBR Green (LightCycler, Roche Diagnostics) and the primer mix (100 µM). Gene expression was normalized to *ß-Actin* control for genes *Vimentin* (*VIM*), *Integrin Subunit Beta 6* (*ITGB6*) and *Cadherin 2* (*CDH2*), and normalized to an average of *ß-Actin* and *HRPT* control for genes *Surfactant Protein C* (*SFTPC*), *Keratin 8* (*KRT8*), *Collagen 1A1* (*Col1A1*), *Matrix Metallopeptidase* (*MMP7*) and *Bone*

Morphogenic Protein 4 (*BMP4*), the fold change was calculated using the 2^ (-ddC) method. Sequence information of used primers are given in Supplementary Table 2. Data obtained from qPCR are presented relative to respective control co-cultures, to demonstrate influence of disease background.

2.7 Metabolic activity estimated by WST-1 assay

WST-1 assays were performed at day 2, 3, 5 and 7 of alveolar organoid co-cultures (human ILD or IMR-90 control fibroblasts). WST-1 reagent (Roche Diagnostics) was added to the culture medium in a 1:10 dilution. The culture medium was used as background control. After 2 h of incubation at 37°C and 5% CO_2, 100 µL of media from every sample was transferred to a microplate (Thermo Scientific; Fisher Scientific) and the absorbance of the sample against the background was measured with a TECAN reader (TECAN; infinite M200 PRO).

3 Results

3.1 Fibroblast induced changes in organoid formation and metabolic activity in co-cultured alveolar organoids

An overview of the experimental workflow is provided in Supplementary Figures 1A–C. iAT2s (Figure 1A) were successfully co-cultured with both ILD, in our study referring to cases of pulmonary fibrosis, or IMR-90 control fibroblasts, resulting in the formation of proliferative alveolar organoids (Figure 1B). Cell-cell contact of iAT2s and fibroblasts in (ILD) co-culture was demonstrated by partial encapsulation of alveolar organoids by α-SMA expressing fibroblasts (Figure 1C, white arrows).

Image analysis of the 3D co-cultures revealed a reduction in organoid formation capacity in the presence of human fibroblasts (Figure 1D). Although alveolar organoid size was not significantly affected by fibroblast co-culture (Figures 1B, E), quantitative assessment of organoid size (area, μm^2) and number of images obtained from alveolar organoids and co-cultures with either ILD or IMR-90 control fibroblasts in 1:1 ($F_{ILD/Control\ low}$) or 1:5 ($F_{ILD/Control\ high}$) seeding density (Figures 1B, D) demonstrated a negative correlation of fibroblast seeding density (ILD or IMR-90) with the alveolar organoid formation capacity.

In contrast, co-culture with ILD fibroblasts significantly increased metabolic activity of alveolar organoid in comparison to IMR-90 control co-cultures (Figure 1F).

3.2 Presence of ILD fibroblasts leads to aberrant epithelial gene expression changes

In order to relate the observed changes in organoid formation capacity and metabolic activity (Figure 1) to changes in gene expression, we measured critical markers of stem cell function and epithelial differentiation in co-cultured organoids.

Indicating changes in (stem) cell function and epithelial injury, we showed decreased expression of the alveolar stem cell marker *SFTPC* in the presence of ILD fibroblasts in both seeding ratios (F_{low} and F_{high}; Figure 2A). In line with this, *Keratin 8* (*KRT8*) expression levels were reduced under the impact of ILD primary fibroblasts (Figure 2A). Further, the distal epithelial marker *Integrin Subunit Beta 6* (*ITGB6*) as well as *Bone Morphogenetic Protein 4* (*BMP4*) showed increased transcription in ILD co-cultures when high seeding densities were applied (Figure 2A). Genes associated with regulation of extracellular matrix formation and remodeling including *Collagen 1A1* (*Col1A1*), *N-Cadherin 2* (*CDH2*) and *Vimentin* (*VIM*) showed increased expression in alveolar organoids co-cultured with ILD fibroblasts in high seeding ratios (Figure 2B). Likewise, expression levels of *Matrix Metallopeptidase 7* (*MMP7*) were increased in ILD co-cultures compared to control co-cultures. (Figure 2B).

3.3 ILD fibroblast secretome reveals proinflammatory signaling converging on *IL11* stimulating epithelial remodeling

To characterize fibroblast driven communication resulting in gene expression and phenotypical changes in the alveolar epithelium in ILD, supernatants of ILD and non-CLD fibroblasts were subjected to mass spectrometry (MSMS).

MS analysis detected an overall of 2625 expressed proteins, of which 47 were significantly more and 55 significantly less abundant when comparing ILD-derived fibroblast to non-CLD controls (Supplementary Table 3, 4, Figure 3A). The top 15 differentially expressed proteins (increased and decreased abundance) are listed in Supplementary Tables 1, 2.

Proteins with increased abundance predominantly belonged to the C-X-C motif chemokine family (*CXCL1, CXCL3*, and *CXCL8*), as well as to the interleukin family (*IL13RA, IL11*) and included gap junction proteins (*connexin 43*, *GJA1*). Further, *Pregnancy Specific Beta-1-Glycoprotein 4 (PSG4)* as well as WNT signaling modulator *SFRP4* were found amongst the top 15 proteins.

Accordingly, pathway enrichment analysis of proteins with increased abundance classified the responses as cytokine activity, chemokine-mediated signaling pathway and TNF-signaling pathway. Furthermore, cellular/response to chemokines, *IL17* signaling pathways and neutrophil chemotaxis were identified, indicative of a strong inflammatory response.

ClueGo, a Cytoscape plug-in for network analysis, highlighted proteins associated with rheumatoid arthritis, a disease often complicated by the development of lung fibrosis and characterized by the presence of inflammatory chemokines (Figure 3B).

Proteins with decreased abundance in the in ILD secretome were dominated by candidates involved in ECM production, ECM assembly or ECM reorganization as well as coordination of myofibroblast differentiation (*PDGFRL*) together with a downregulation of proteins involved in complement and coagulation cascade pathways (Figure 3C).

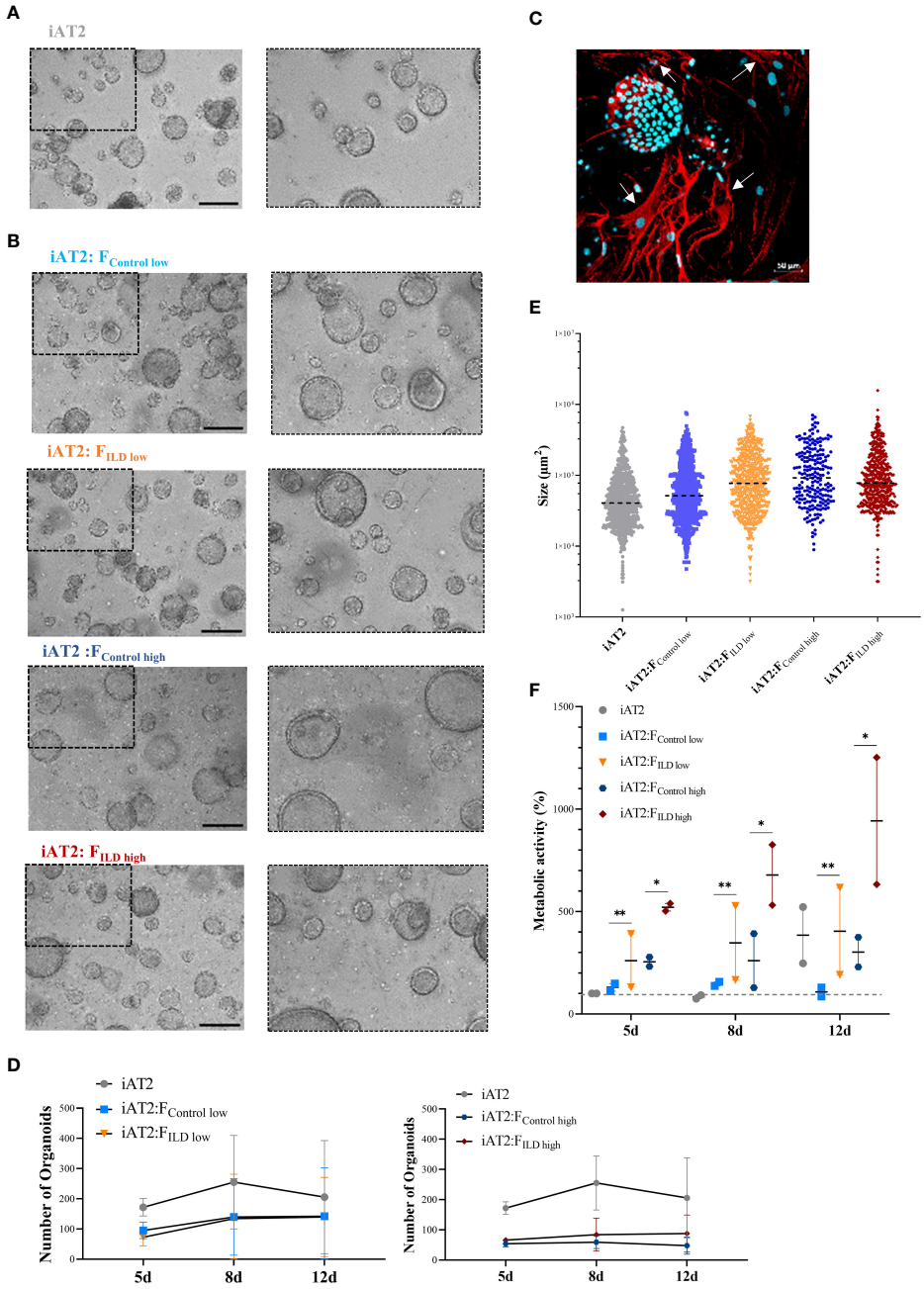

FIGURE 1
(A) Representative maximum intensity projections from high-content images of iAT2s growing as alveolar organoids at day 12. Scale bar 500µm. **(B)** Immunofluorescence of 3D co-culture of iAT2s with ILD fibroblasts at day 12 (α-SMA: red, DAPI: cyan). Scale bar 50 µm. **(C)** Representative maximum intensity projections from high-content images of different co-culture conditions showing iAT2s growing with human fibroblasts for 12 days. Scale bar 500 µm. Zoom-ins show a 3x optical magnification. **(D)** Scatter plots (dashed black lines: median) indicate size (µm2) of organoids in co-cultures at day 12 across three independent biological replicates. **(E)** Number of formed organoids in co-cultures at day 12, N = 3. **(F)** Metabolic activity of co-cultured organoids at 5, 8 and 12 days of co-culture. Results show the increase in percentage across two biological replicates in comparison to d5 iAT2 organoids alone, representing the baseline of 100% metabolic activity (dashed grey line across dataset). Statistics: unpaired t-Test, *p<0.05, **p<0.01.

3.4 *IL11* acts as a driver for aberrant signatures in hiPSC-derived alveolospheres

Based on the MSMS secretome analysis, *IL11* emerged as a top player in the mesenchymal-to-epithelial disease crosstalk. In consequence, we exposed alveolar organoids (Figure 4A) to *IL11* in order to investigate its functional relevance. Experiments ($Dose_{low}$ = 0.5 ng/mL, $Dose_{high}$ = 5 ng/mL) (Figures 4B–D) recapitulated the results observed in epithelial-fibroblasts co-cultures (section 3.1), *i.e.*, we demonstrated reduced organoid formation capacity (Figures 4Biii, C) and increased metabolic activity (WST-1) in *IL11* treated alveolar organoids (treatment

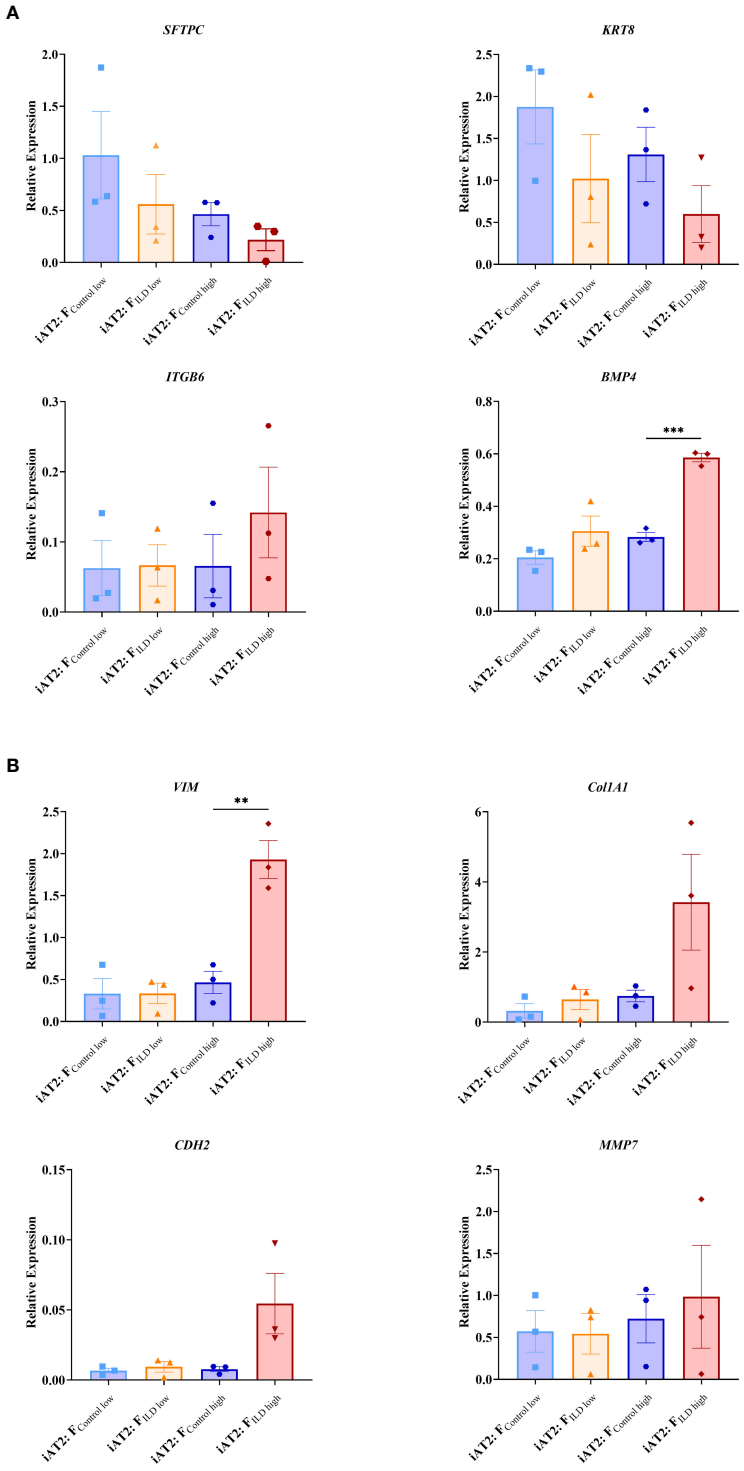

FIGURE 2
Relative gene expression at day 12 measured in AT2s co-cultures with ILD or IMR90 control fibroblasts in two seeding densities (high or low) compared to reference gene expression (HK; average of ß-Actin *(ACTB)* and hypoxanthine guanine phosphoribosyl transferase (*HRPT)*). **(A)** Epithelial and stem cell markers and **(B)** Genes associated with aberrant differentiation of epithelium. N = 3, unpaired t-Test, **p<0.005, ***p<0.0005.

from day 7 - 14 of culture) (Figure 4D). In addition, treatment of growing alveolar organoid monocultures with *IL11* (20 ng/mL) led to an increase in alveolar organoid size followed by apoptosis within 5 days of culture.

4 Discussion

In ILD, sustained inflammation and scarring of the gas exchange area ultimately result in destruction of the pulmonary

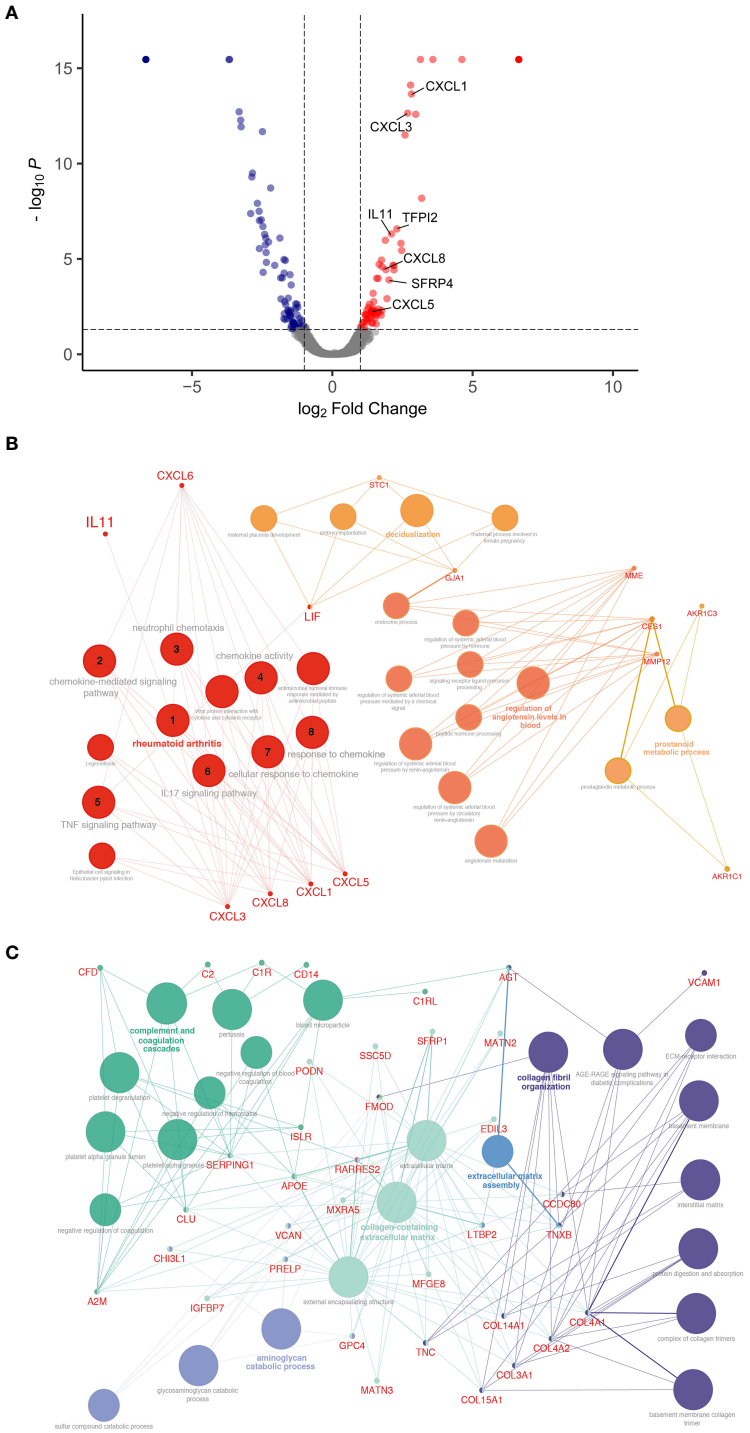

FIGURE 3
Differential protein expression comparing ILD fibroblasts (F_{ILD}) vs. non-chronic lung disease fibroblasts ($F_{control}$). **(A)** Volcano plot visualizing significantly regulated proteins (47 up, 55 down) detected by MS secretome analysis of ILD or non-CLD control fibroblasts. Data showing log_2 fold change against the adjusted P value [log10]. Significantly upregulated proteins are depicted in red and significantly downregulated proteins in blue. (Total: 102 significantly regulated proteins with 5% FDR < 0.05, adj. p_value < 0.05). Pathway enrichment and protein interaction network of proteins with **(B)** increased and **(C)** decreased abundance using the Cytoscape plugin ClueGo. The following ontologies were used: KEGG, molecular functions and biological processes. The connectivity of the pathways is described by functional nodes and edges that are shared between proteins with a kappa score of 0.4. Only enriched pathways are visualized and the node size indicates the p-value (p-value ≤ 0.05). Proteins from the same pathway share the same node color and the bold fonts indicate the most important functional pathways that define the names of each group. Enriched Pathways: 1. rheumatoid arthritis, 2. chemokine-mediated signaling pathway, 3. neutrophil chemotaxis, 4. chemokine activity, 5. *TNF* signaling pathway, 6. *IL17* signaling pathway, 7. cellular response to chemokine, 8. response to chemokine.

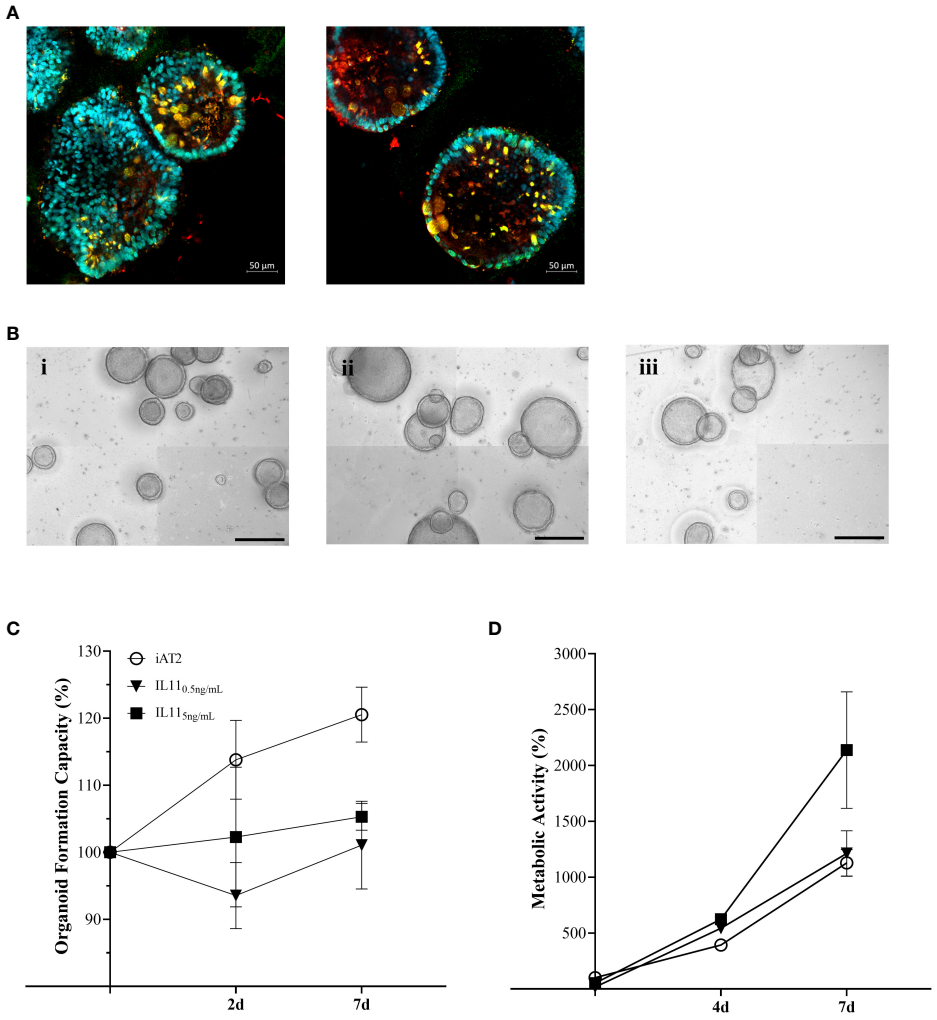

FIGURE 4
(A) Immunofluorescence of untreated alveolar organoids at day 14 of culture (*SFTPC*: red, *NKX2.1*: green, DAPI: cyan). **(B)** Representative maximum intensity projections from high-content images of (i) untreated alveolar organoids, (ii) 0.5 ng/mL or (iii) 5 ng/mL *IL11* treatment. Treatment started at day 7 of culture every 48h. Scale bar, 500 µm. **(C)** Organoid formation capacity of alveolar organoids treated with 0.5 or 5ng/mL *IL11*. **(D)** Metabolic activity of alveolar organoids treated with 0.5 or 5ng/mL *IL11*. **(C, D)** Each value is graphed as percentage of the respective starting culture at day 7 set to 100%.

scaffold and organ failure. Excessive deposition of ECM as well as epithelial damage and dedifferentiation is widely transmitted by the misguided interaction of fibroblasts and epithelial cells (27). Therefore, improved understanding of the mesenchymal-to-epithelial crosstalk remains a centerpiece in finding new avenues to monitor and treat ILD. However, signaling factors with functional relevance and their distinct role in ILD pathogenesis remain understudied.

This study aimed at deciphering disease-relevant candidates of mesenchymal-to-epithelial crosstalk that could serve as potential targets for future therapeutic strategies. By advancing a sensitive human iPSC-derived alveolar organoid culture into a human fibroblast co-culture model, we successfully demonstrated the importance of fibroblast-driven, cytokine-centered signaling in inducing the impairment of key epithelial cell functions, including differentiation and metabolism. In combination with an unbiased proteomic approach, we were able to identify important mediators that translate these effects such as *IL11*, one of the top 15 proteins with increased abundance in ILD, in our study referring to cases of pulmonary fibrosis. The previously identified role of *IL11* in chronic inflammatory lung diseases in line with its potential to drive pro-fibrotic mesenchymal-epithelial crosstalk, supported the relevance of our approach on the one hand, while we were able to contribute the important functional consequences of its signaling in our human alveolar organoid model on the other (7, 8, 28).

In our *in vitro* co-culture approach, primary human pulmonary fibroblasts and iAT2s formed alveolar organoids that successfully recapitulated tissue characteristics of the distal lung in three dimensions, in contrast to 2D, plastic culture conditions (Figure 1). Primary human fibroblasts, both ILD-derived and IMR-90 control cells, demonstrated effects that correlated with seeding density leading to reduced organoid number and increased organoid size after 12 days of co-culture. The findings indicate that the co-culture with fibroblasts per se is able to change

the microenvironment of iAT2s, thereby impacting organoid formation. As studies indicated, that the activation of primary lung fibroblasts in a disease-comparable fashion is easily achieved (29), our findings likely explain the disease-independent fibroblast effects in alveolar organoids.

In contrast, the significant increase in metabolic activity was provoked by diseased human fibroblasts in high-seeding ratios, indicating their potential to impact on the metabolic program of the epithelial cell, potentially indicating epithelial dedifferentiation or EMT (30–32). These considerations are supported by the expression signature characterizing the co-cultures: The decrease in *SFTPC* expression (33–36) we observed in the ILD co-cultures points towards the loss of epithelial stem cell characteristics, as *SFTPC* expression is sensitive to epithelial inflammation and injury, lately supported by studies in Sars-CoV-2 infected alveolar organoids (10). Differentiation of AT2s is key for regeneration in injured alveoli marked by their expression of transient basaloid features such as *Keratin 5* (*KRT5*) and the amount of alveolar *KRT5*$^{+}$ basaloid cells directly correlates with disease progression in pulmonary fibrosis (29, 37, 38), mirrored by the decreased expression observed in our study. Closely related, downregulation of *KRT8*, an important marker of AT2 to (pre)AT1 transdifferentiation during epithelial regeneration (38, 39) was associated with the increased expression of EMT markers in a murine bleomycin lung injury model including pro-fibrogenic proteins such as *ITGB6* (39). In line with these findings, we demonstrated increased *ITGB6* expression in ILD co-cultures. Its release from the plasma membrane potentially reflects the activation of EMT-like processes in lung organoids, accompanied by the decrease of expressed *KRT8*. Further supporting these findings, we showed the elevated expression of *BMP4* and *MMP7*, critical regulators of EMT in pulmonary fibrosis (40), in lung organoids co-cultured with ILD fibroblasts. *MMP7* has furthermore been highlighted for its function as a plasma biomarker in idiopathic pulmonary fibrosis (33, 41), in line with its detection in our study.

Co-culture of alveolar organoids with ILD fibroblasts also specifically changed the expression of genes involved in ECM biosynthesis including the increased transcription of *Col1A1*, *VIM* and *CDH2*, well-known players in fibrotic lung disease (33, 34) (38), as compared to organoid monocultures. Linking back to the indications of aberrant basal transdifferentiation in fibroblast co-culture discussed above (29), the basaloid cells show increased ECM protein expression, next to their increase in *BMP4* and *ITGB6* expression, again successfully detected in our model.

We next were able to provide deeper insight into the relevant mediators of mesenchymal-to-epithelial crosstalk related to the observed changes in organoid phenotype by screening the supernatant of ILD or control fibroblasts using mass spectrometry (42). Cytokines that belong to the C-X-C motif family dominated the protein signature in the secretome, demonstrating their increased abundance in ILD. These signaling molecules act on the *CXCR1* and *CXCR2* receptor, as well as regulate the expression of cytokines from the interleukin family, central to the pathogenesis of fibrotic and inflammatory lung diseases such as IPF and acute respiratory distress syndrome (3, 8, 36, 43). The majority of the differentially abundant proteins are proinflammatory cytokines that primarily act on neutrophil, monocyte or lymphocyte recruitment (*CXCL1, CXCL3, CXCL5, CXCL8*). The proinflammatory response is complemented by the regulation of proteins that play a role in cellular senescence and activation of *TGF-ß* such as the Pregnancy-Specific Glycoprotein (PSG) family, *PSG 4, 5, 6* or in the induction of a hypercoagulable tissue state (*TFPI2*). Other important proteins such as *SFRP4* directly inhibit WNT signaling, thereby modulating cell growth and differentiation, particularly of AT2s to AT1s (44). *WNT* serum levels are discussed as biomarkers for lung fibrosis and EMT. *WNT* modulation and *TGF-ß* solubilization in particular could account for the change in organoid number and size and support our observations in gene expression levels that indicate epithelial transdifferentiation into aberrant basaloid cells or EMT in the presence of ILD fibroblasts.

IL11, centrally orchestrating the ILD protein profile as observed by pathway enrichment, was identified among the top 15 candidates in the ILD fibroblast secretome. *IL11* is known to be expressed in pro-inflammatory fibroblasts extracted from IPF lungs. The cytokine belongs to the *IL6* family and is induced by *TGF-ß* and other proinflammatory mediators [*IL1β, IL17, IL22*, reactive oxygen species (ROS)]. It can either activate fibroblasts to differentiate into myofibroblasts in an autocrine fashion through ERK/SMAD canonical signaling, which results in pro-fibrotic protein expression (*COL1A1, ACTA2*), or it stimulates epithelial cells (paracrine loop) through activating *ERK* signaling cascades, thereby inducing cellular senescence, EMT, cellular dysfunction and impaired regeneration (8). Results from our co-culture model indicate both autocrine and paracrine signaling of *IL11* as we demonstrated indication of EMT, stem cell dysfunction as well as ECM production, i.e., upregulation of collagen expression in line with 8 (8). Similar to the results obtained from ILD fibroblast co-culture in different seeding densities, *IL11* treatment of alveolar organoid monocultures resulted in a dose dependent increase in metabolic activity, elevated expression of mesenchymal markers and decreased AT2 stemness and identity. Dose-dependent, *IL11* even induced apoptotic cell death, in line with its role in senescence and stem cell function observed in alveolar organoids (36). Similarly, *IL11* alone induced fibrotic changes in healthy alveolar organoids whereas knock-out of *IL11* expression in diseased organoids reversed organoid fibrosis in a model of the Hermansky-Pudlak syndrome-associated interstitial pneumonia, a disease with high similarity to IPF (3). Supporting our co-culture findings in this regard, *IL11* exposure impacts on AT2 progenitor function, thereby likely suppressing the formation of mature AT2s as described by Kortekaas and colleagues (35, 36).

Taken together, our results strongly support the central role of *IL11* signaling as the cytokine holds the potential to strongly influence the intricate crosstalk between the (then activated (myo)) fibroblasts and the injured epithelium, central in the progression of fibrosis in ILD. We successfully demonstrated the potential of our lung organoid co-culture model derived from hiPSCs and primary fibroblasts to display critical consequences of the malfunctional crosstalk such as aberrant dedifferentiation and basaloid-prone signatures (33, 45). In this context, *IL11* likely holds an important role in misguided alveolar function, differentiation

and thereby regeneration, important functions as a potential therapeutic target to regain alveolar crosstalk homeostasis (46).

Data availability statement

The datasets presented in this study can be found in online repositories. The names of the repository/repositories and accession number(s) can be found in the article. The mass spectrometry proteomics data presented in the study have been deposited to the ProteomeXchange Consortium via the PRIDE partner repository with the dataset identifier PXD039554..

Ethics statement

The studies involving human participants were reviewed and approved by Ludwig-Maximilians University of Munich, Germany. (Ethic vote #333-10). The patients/participants provided their written informed consent to participate in this study.

Author contributions

MK, AH and CV conceived and planned the experiments. MK, EG-R, PC and EMG carried out the main experiments. FS and SA contributed to sample preparation. A-CK and SH performed the mass spectrometry analysis. LH performed additional data analysis and figure composition. CB, GB, MP and ML conceived, discussed and developed the AI based organoid counter. RAH headed patient sample retrieval and documentation and contributed clinical background to the study. MK, CV, TS, A-CK, SH, JB and AH contributed substantially to the interpretation of the results. MK and CV took the lead in writing the manuscript. All authors provided critical feedback and helped shape the research, analysis and drafting of the manuscript.

Funding

This project was supported by the Research Training Group GRK2338 of the DFG, LMU Munich. Further funding was received by the German Center of Lung Research (DZL) and Helmholtz Munich.

Acknowledgments

We gratefully acknowledge the provision of human biomaterial (primary human fibroblasts) and clinical data from the CPC-M bioArchive and its partners at the Asklepios Biobank Gauting, the LMU Hospital and the Ludwig-Maximilians-Universität München. We thank the patients and their families for their support. We wish to thank the Kotton Lab especially Prof. Darrell Kotton by providing the hiPSC cell line. We are grateful to David Kutschke (LHI, Helmholtz Center Munich) for technical assistance. We thank Dr. Kenji Schorpp and Dr. Kamyar Hadian (Research Unit Signaling and Translation, Molecular Targets and Therapeutics Center, Helmholtz Zentrum München, Germany) for their excellent support with the Operetta System. We thank the Research Unit Analytical Pathology (AAP, Helmholtz Center Munich) with Dr. Ulrike Buchholz and Dr. Annette Feuchtinger for their assistance during confocal imaging. We thank Benoite Champon and Dr. Minodora Brimpari for their help with the cell sorting at the MACSQuant Tyto Cell Sorter. We thank Zeynep Ertüz for creating the graphical abstract. Graphics were created with BioRender.com. The manuscript has been published as a preprint on Biorxiv under (47).

Conflict of interest

The authors declare that the research was conducted in the absence of any commercial or financial relationships that could be construed as a potential conflict of interest.

Publisher's note

Supplementary material

The Supplementary Material for this article can be found online at: https://www.frontiersin.org/articles/10.3389/fimmu.2023.1128239/full#supplementary-material

References

1. Glasser SW, Hardie WD, Hagood JS. Pathogenesis of interstitial lung disease in children and adults. *Pediatr Allergy Immunol Pulmonol* (2010) 23(1):9–14. doi: 10.1089/ped.2010.0004

2. Lederer DJ, Martinez FJ. Idiopathic pulmonary fibrosis. *N Engl J Med* (2018) 378 (19):1811–23. doi: 10.1056/NEJMra1705751

3. Strikoudis A, Cieślak A, Loffredo L, Chen YW, Patel N, Saqi A, et al. Modeling of fibrotic lung disease using 3D organoids derived from human pluripotent stem cells. *Cell Rep* (2019) 27(12):3709–3723.e3705. doi: 10.1016/j.celrep.2019.05.077

4. Dwyer AR, Ellies LG, Holme AL, Pixley FJ. A three-dimensional co-culture system to investigate macrophage-dependent tumor cell invasion. *J Biol Methods* (2016) 3(3):e49. doi: 10.14440/jbm.2016.132

5. Kim KK, Sheppard D, Chapman HA. TGF-β1 signaling and tissue fibrosis. *Cold Spring Harb Perspect Biol* (2018) 10(4):a022293. doi: 10.1101/cshperspect.a022293

6. O'Dwyer DN, Ashley SL, Moore BB. Influences of innate immunity, autophagy, and fibroblast activation in the pathogenesis of lung fibrosis. *Am J Physiology-Lung Cell Mol Physiol* (2016) 311(3):L590–601. doi: 10.1152/ajplung.00221.2016

7. Ng B, Dong J, D'Agostino G, Viswanathan S, Widjaja AA, Lim WW, et al. Interleukin-11 is a therapeutic target in idiopathic pulmonary fibrosis. *Sci Transl Med* (2019) 11(511):eaaw1237. doi: 10.1126/scitranslmed.aaw1237

8. Ng B, Cook SA, Schafer S. Interleukin-11 signaling underlies fibrosis, parenchymal dysfunction, and chronic inflammation of the airway. *Exp Mol Med* (2020) 52(12):1871–8. doi: 10.1038/s12276-020-00531-5

9. Yao L, Zhou Y, Li J, Wickens L, Conforti F, Rattu A, et al. Bidirectional epithelial-mesenchymal crosstalk provides self-sustaining profibrotic signals in pulmonary fibrosis. *J Biol Chem* (2021) 297(3):101096. doi: 10.1016/j.jbc.2021.101096

10. Mou H. Induced pluripotent stem cell-derived alveolar type II heterogeneity: Revealed by SFTPC expression. *Am J Respir Cell Mol Biol* (2021) 65(4):345–6. doi: 10.1165/rcmb.2021-0242ED

11. Kong J, Wen S, Cao W, Yue P, Xu X, Zhang Y, et al. Lung organoids, useful tools for investigating epithelial repair after lung injury. *Stem Cell Res Ther* (2021) 12(1):95. doi: 10.1186/s13287-021-02172-5

12. Kastlmeier MT, Guenther EM, Stoeger T, Voss C. Lung organoids for hazard assessment of nanomaterials. *Int J Mol Sci* (2022) 23(24):15666. doi: 10.3390/ijms232415666

13. Nikolić MZ, Sun D, Rawlins EL. Human lung development: recent progress and new challenges. *Development* (2018) 145(16):dev163485. doi: 10.1242/dev.163485

14. Nikolić MZ, Hogan MZN. Lung stem cells in development, health and disease. In: *ERS monograph* (2021). doi: 10.1183/2312508X.erm9121

15. Hawkins F, Kramer P, Jacob A, Driver I, Thomas DC, McCauley KB, et al. Prospective isolation of NKX2-1-expressing human lung progenitors derived from pluripotent stem cells. *J Clin Invest* (2017) 127(6):2277–94. doi: 10.1172/jci89950

16. Jacob A, Morley M, Hawkins F, McCauley KB, Jean JC, Heins H, et al. Differentiation of human pluripotent stem cells into functional lung alveolar epithelial cells. *Cell Stem Cell* (2017) 21(4):472–488.e410. doi: 10.1016/j.stem.2017.08.014

17. Jacob A, Vedaie M, Roberts DA, Thomas DC, Villacorta-Martin C, Alysandratos K-D, et al. Derivation of self-renewing lung alveolar epithelial type II cells from human pluripotent stem cells. *Nat Protoc* (2019) 14(12):3303–32. doi: 10.1038/s41596-019-0220-0

18. Heinzelmann K, Lehmann M, Gerckens M, Noskovičová N, Frankenberger M, Lindner M, et al. Cell-surface phenotyping identifies CD36 and CD97 as novel markers of fibroblast quiescence in lung fibrosis. *Am J Physiol Lung Cell Mol Physiol* (2018) 315 (5):L682–l696. doi: 10.1152/ajplung.00439.2017

19. Wiśniewski JR, Zougman A, Nagaraj N, Mann M. Universal sample preparation method for proteome analysis. *Nat Methods* (2009) 6(5):359–62. doi: 10.1038/nmeth.1322

20. Grosche A, Hauser A, Lepper MF, Mayo R, von Toerne C, Merl-Pham J, et al. The proteome of native adult müller glial cells from murine retina. *Mol Cell Proteomics* (2016) 15(2):462–80. doi: 10.1074/mcp.M115.052183

21. Deutsch EW, Bandeira N, Sharma V, Perez-Riverol Y, Carver JJ, Kundu DJ, et al. The ProteomeXchange consortium in 2020: enabling 'big data' approaches in proteomics. *Nucleic Acids Res* (2019) 48(D1):D1145–52. doi: 10.1093/nar/gkz984

22. Perez-Riverol Y, Bai J, Bandla C, García-Seisdedos D, Hewapathirana S, Kamatchinathan S, et al. The PRIDE database resources in 2022: a hub for mass spectrometry-based proteomics evidences. *Nucleic Acids Res* (2021) 50(D1):D543–52. doi: 10.1093/nar/gkab1038

23. Navarro P, Trevisan-Herraz M, Bonzon-Kulichenko E, Núñez E, Martínez-Acedo P, Pérez-Hernández D, et al. General statistical framework for quantitative proteomics by stable isotope labeling. *J Proteome Res* (2014) 13(3):1234–47. doi: 10.1021/pr4006958

24. Bindea G, Mlecnik B, Hackl H, Charoentong P, Tosolini M, Kirilovsky A, et al. ClueGO: a cytoscape plug-in to decipher functionally grouped gene ontology and pathway annotation networks. *Bioinformatics* (2009) 25(8):1091–3. doi: 10.1093/bioinformatics/btp101

25. Bukas C. *HelmholtzAI-Consultants-Munich/napari-organoid-counter: Latest versions of dependencies (v0.1.1)*. Zenodo (2022). doi: 10.5281/zenodo.7065206

26. Canny J. (1986). "A computational approach to edge detection," in: *IEEE Transactions on Pattern Analysis and Machine Intelligence*, Vol. PAMI-8. pp. 679–98. doi: 10.1109/TPAMI.1986.4767851

27. Lewis KJR, Hall JK, Kiyotake EA, Christensen T, Balasubramaniam V, Anseth KS. Epithelial-mesenchymal crosstalk influences cellular behavior in a 3D alveolus-fibroblast model system. *Biomaterials*. (2018) 115:124–34. doi: 10.1016/j.biomaterials.2017.11.008

28. Cook SA, Schafer S. Hiding in plain sight: Interleukin-11 emerges as a master regulator of fibrosis, tissue integrity, and stromal inflammation. *Annu Rev Med* (2020) 71:263–76. doi: 10.1146/annurev-med-041818-011649

29. Kathiriya JJ, Wang C, Zhou M, Brumwell A, Cassandras M, Le Saux CJ, et al. Human alveolar type 2 epithelium transdifferentiates into metaplastic KRT5+ basal cells. *Nat Cell Biol* (2022) 24(1):10–23. doi: 10.1038/s41556-021-00809-4

30. Kalluri R. EMT: When epithelial cells decide to become mesenchymal-like cells. *J Clin Invest* (2009) 119(6):1417–9. doi: 10.1172/JCI39675

31. Kalluri R, Weinberg RA. The basics of epithelial-mesenchymal transition. *J Clin Invest* (2009) 119(6):1420–8. doi: 10.1172/JCI39104

32. Wang Y, Dong C, Zhou BP. Metabolic reprogram associated with epithelial-mesenchymal transition in tumor progression and metastasis. *Genes Dis* (2020) 7 (2):172–84. doi: 10.1016/j.gendis.2019.09.012

33. Adams TS, Schupp JC, Poli S, Ayaub EA, Neumark N, Ahangari F, et al. Single-cell RNA-seq reveals ectopic and aberrant lung-resident cell populations in idiopathic pulmonary fibrosis. *Sci Adv* (2020) 6(28):eaba1983. doi: 10.1126/sciadv.aba1983

34. Katzen J, Beers MF. Contributions of alveolar epithelial cell quality control to pulmonary fibrosis. *J Clin Invest* (2020) 130(10):5088–99. doi: 10.1172/JCI139519

35. Kortekaas RK, Burgess JK, Webster M, Gosens R. IL11 negatively impacts adult lung alveolar organoid formation. *ERJ Open Res* (2021) 7(suppl 6):81. doi: 10.1183/23120541.Lsc-2021.81

36. Kortekaas R, Geillinger-Kästle K, Borghuis T, Belharch K, Webster M, Timens W, et al. IL-11 disrupts alveolar epithelial progenitor function. *bioRxiv* (2022). doi: 10.1101/2022.11.11.516088

37. Khan P, Roux J, Blumer S, Knudsen L, Jonigk D, Kuehnel MP, et al. Alveolar basal cells differentiate towards secretory epithelial- and aberrant basaloid-like cells *In vitro*. *Cells* (2022) 11(11):1820. doi: 10.3390/cells11111820

38. Ng B, Huang KY, Pua CJ, Lim W-W, Kuthubudeen F, Hii AA, et al. Interleukin-11 causes alveolar type 2 cell dysfunction and prevents alveolar regeneration. *bioRxiv* (2022). doi: 10.1101/2022.11.11.516109

39. Strunz M, Simon LM, Ansari M, Kathiriya JJ, Angelidis I, Mayr CH, et al. Alveolar regeneration through a Krt8+ transitional stem cell state that persists in human lung fibrosis. *Nat Commun* (2020) 11(1):3559. doi: 10.1038/s41467-020-17358-3

40. Molloy EL, Adams A, Moore JB, Masterson JC, Madrigal-Estebas L, Mahon BP, et al. BMP4 induces an epithelial-mesenchymal transition-like response in adult airway epithelial cells. *Growth Factors* (2008) 26(1):12–22. doi: 10.1080/08977190801987166

41. Bauer Y, White ES, de Bernard S, Cornelisse P, Leconte I, Morganti A, et al. MMP-7 is a predictive biomarker of disease progression in patients with idiopathic pulmonary fibrosis. *ERJ Open Res* (2017) 3(1):00074-2016. doi: 10.1183/23120541.00074-2016

42. Strieter RM, Gomperts BN, Keane MP. The role of CXC chemokines in pulmonary fibrosis. *J Clin Invest* (2007) 117(3):549–56. doi: 10.1172/jci30562

43. Mukaida N. Pathophysiological roles of interleukin-8/CXCL8 in pulmonary diseases. *Am J Physiology-Lung Cell Mol Physiol* (2003) 284(4):L566–77. doi: 10.1152/ajplung.00233.2002

44. Abdelwahab EMM, Rapp J, Feller D, Csongei V, Pal S, Bartis D, et al. Wnt signaling regulates trans-differentiation of stem cell like type 2 alveolar epithelial cells to type 1 epithelial cells. *Respir Res* (2019) 20(1):204. doi: 10.1186/s12931-019-1176-x

45. Habermann AC, Gutierrez AJ, Bui LT, Yahn SL, Winters NI, Calvi CL, et al. Single-cell RNA sequencing reveals profibrotic roles of distinct epithelial and mesenchymal lineages in pulmonary fibrosis. *Sci Adv* (2020) 6(28):eaba1972. doi: 10.1126/sciadv.aba1972

46. Lin CR, Bahmed K, Kosmider B. Impaired alveolar re-epithelialization in pulmonary emphysema. *Cells* (2022) 11(13):2055. doi: 10.3390/cells11132055

47. Kastlmeier MT, Rodriguez EG, Cabanis P, Guenther EM, König A-C, Han L, et al. Cytokine signaling converging on IL11 in ILD fibroblasts provokes aberrant epithelial differentiation signatures. *bioRxiv* (2022). doi: 10.1101/2022.12.20.521114

frontiers | Frontiers in Immunology

TYPE Original Research
PUBLISHED 23 March 2023
DOI 10.3389/fimmu.2023.1089098

OPEN ACCESS

EDITED BY
Jawed A Siddiqui,
University of Nebraska Medical Center, United States

REVIEWED BY
Surendra Sharma,
Women & Infants Hospital of Rhode Island, United States
Vishal Chandra,
University of Oklahoma Health Sciences Center, United States

*CORRESPONDENCE
Chandrakant Tayade
tayadec@queensu.ca

SPECIALTY SECTION
This article was submitted to Cytokines and Soluble Mediators in Immunity, a section of the journal Frontiers in Immunology

RECEIVED 03 November 2022
ACCEPTED 08 March 2023
PUBLISHED 23 March 2023

CITATION
Zutautas KB, Sisnett DJ, Miller JE, Lingegowda H, Childs T, Bougie O, Lessey BA and Tayade C (2023) The dysregulation of leukemia inhibitory factor and its implications for endometriosis pathophysiology.
Front. Immunol. 14:1089098.
doi: 10.3389/fimmu.2023.1089098

The dysregulation of leukemia inhibitory factor and its implications for endometriosis pathophysiology

Katherine B. Zutautas[1], Danielle J. Sisnett[1], Jessica E. Miller[1], Harshavardhan Lingegowda[1], Timothy Childs[1,2], Olga Bougie[1,3], Bruce A. Lessey[4] and Chandrakant Tayade[1*]

[1]Department of Biomedical and Molecular Sciences, Queen's University, Kingston, ON, Canada, [2]Department of Pathology and Molecular Medicine, Kingston Health Sciences Centre, Kingston, ON, Canada, [3]Department of Obstetrics and Gynaecology, Kingston Health Sciences Centre, Kingston, ON, Canada, [4]School of Medicine, Wake Forest University, Winston-Salem, NC, United States

Endometriosis is an estrogen dominant, chronic inflammatory disease characterized by the growth of endometrial-like tissue outside of the uterus. The most common symptoms experienced by patients include manifestations of chronic pelvic pain- such as pain with urination, menstruation, or defecation, and infertility. Alterations to Leukemia Inhibitory Factor (LIF), a cytokine produced by the luminal and glandular epithelium of the endometrium that is imperative for successful pregnancy, have been postulated to contribute to infertility. Conditions such as recurrent implantation failure, unexplained infertility, and infertility associated diseases such as adenomyosis and endometriosis, have demonstrated reduced LIF production in the endometrium of infertile patients compared to fertile counterparts. While this highlights the potential involvement of LIF in infertility, LIF is a multifaceted cytokine which plays additional roles in the maintenance of cell stemness and immunomodulation. Thus, we sought to explore the implications of LIF production within ectopic lesions on endometriosis pathophysiology. Through immunohistochemistry of an endometrioma tissue microarray and ELISA of tissue protein extract and peritoneal fluid samples, we identify LIF protein expression in the ectopic lesion microenvironment. Targeted RT qPCR for LIF and associated signaling transcripts, identify *LIF* to be significantly downregulated in the ectopic tissue compared to eutopic and control while its receptor, *LIFR*, is upregulated, highlighting a discordance in ectopic protein and mRNA LIF expression. *In vitro* treatment of endometriosis representative cell lines (12Z and hESC) with LIF increased production of immune-recruiting cytokines (MCP-1, MCP-3) and the angiogenic factor, VEGF, as well as stimulated tube formation in human umbilical vein endothelial cells (HUVECs). Finally, LIF treatment in a syngeneic mouse model of endometriosis induced both local and peripheral alterations to immune cell phenotypes, ultimately reducing immunoregulatory $CD206^{+}$ small peritoneal macrophages and T regulatory cells. These findings suggest that LIF is present in the ectopic lesions of endometriosis patients and could be contributing to lesion vascularization and immunomodulation.

KEYWORDS

leukemia inhibitory factor (LIF), endometriosis, vascularization, cytokine, immunomodulation, infertility

1 Introduction

Endometriosis, a chronic inflammatory gynaecological disease, is defined by the growth of endometrial like tissue outside of the uterus (1). Lesions, referred to as ectopic tissue, can manifest throughout the abdominal cavity constituting the subtypes of endometriosis based on lesion placement and depth: superficial peritoneal, deep infiltrating, and ovarian (2). While lesion presentation provides a means for categorizing disease stage, there is currently no relationship between endometriosis subtype and patient symptomatology. Symptoms such as chronic pelvic pain, pain with urination, and infertility, vary across patients and disease stages (3, 4). Of note, infertility is experienced by approximately 30-50% of endometriosis patients (5). The cause and effect are still unclear surrounding the association between infertility and endometriosis, however there are numerous mechanisms that have been proposed. In this context, Leukemia Inhibitory Factor (LIF) has been implicated as a contributor to endometriosis associated infertility (6, 7).

LIF is a pleiotropic cytokine of the interleukin (IL)-6 family, with involvements in reproductive processes such as embryo implantation and decidualization, as well as regulation of the immune response. LIF is produced by the endometrial luminal and glandular epithelium during the mid to late secretory phase and is imperative for successful pregnancy through the orchestration of stromal cell decidualization (8, 9). Pivotal findings determined that LIF knock out mice were unable to support blastocyst implantation, implicating a critical role for LIF in fertility (10). As such, LIF mRNA and protein, both content and localization within the endometrium, have been studied in a variety of infertility cohorts including unexplained infertility (11, 12), recurrent implantation failure (13, 14), as well as in diseases associated with infertility such as adenomyosis (15, 16) and endometriosis (6, 7). Consistently it has been shown through immunohistochemistry (IHC) of the endometrium that the infertile cohorts- regardless of cause, have reduced endometrial LIF protein expression compared to fertile controls. This is in concert with cervical lavage samples from infertile adenomyosis patients obtained during the mid to late secretory phase, which had significantly lower LIF protein compared to fertile controls (15). In patients with mild to moderate endometriosis who are experiencing infertility, LIF expression was reduced in endometrial samples obtained during the mid-secretory phase, combined with elevated IL-6 and IL-1α in the peritoneal fluid (PF) (7). These inflammatory mediators were hypothesized to be a contributor to patient infertility yet the broader implications of LIF dysregulation within endometriosis pathophysiology have not been speculated upon and remain to be explored.

The role of LIF throughout the body is dynamic. In development, LIF is a regulator of embryonic stem cells, facilitating their pluripotency (17). In adults, LIF is produced in the uterus (18), lung (19), and central nervous system (20, 21), situated as a mediator between neuro-immune crosstalk and a regulator of anti-inflammatory pathways. The LIF receptor (LIFR) can be found on various cell types such as stromal, endothelial, epithelial, and immune cells- most notably T cells and macrophages (9, 22). However, the specific function of LIF is dependent on the local microenvironment, leading to both an inflammatory and anti-inflammatory response. LIF signaling activates three primary pathways known as- janus kinase (JAK)- signal transducer and activator of transcription (STAT3), mitogen activated protein kinase (MAPK), phosphatidylinositol-3 kinase (PI3k), which are associated with cellular proliferation and self-renewal (17). LIFs activation of these pathways has been demonstrated not only within reproductive processes and homeostatic immune regulation but additionally, within the pathological context of cancer. Specifically, breast (23–25), ovarian (26), pancreatic (27), and nasopharyngeal cancers (28), have demonstrated that LIF overexpression by tumours contributes to tumor growth and metastasis as mediated by the STAT3 pathway. Within these contexts, LIFs' capacity to modulate immune phenotypes serves to promote immune evasion and treatment resistance. LIF has been shown to induce regulatory phenotypes in both myeloid and lymphoid cells, primarily working through alternatively activated macrophages (M2) to increase T regulatory (Treg) cell function (29–31). These mechanisms of tissue maintenance, growth, and immune evasion can be paralleled with endometriosis pathophysiology. Thus, LIFs production by ectopic tissue and potential contribution to lesion sustainment and immunomodulation warrants investigation.

To date, LIF has only been studied within the context of endometriosis-associated infertility however its potential contributions to disease pathophysiology remains to be understood. Through human patient data, endometriosis representative human cell lines, and a syngeneic mouse model of endometriosis, we demonstrate that LIF is present in the lesion microenvironment of endometriosis patients and could be contributing to endometriosis-associated lesion vascularization and immune dysregulation. These findings provide novel insight to the role of LIF within endometriosis.

2 Methods

2.1 Ethics statement

Ethics was approved for this study by the Health Sciences Research Ethics Board at Kingston Health Sciences Centre (KHSC), Queen's University (Kingston, Ontario, Canada), Greenville Health System (Greenville, South Carolina, USA), the University of North Carolina at Chapel Hill (Chapel Hill, North Carolina, USA), and Wake Forest Baptist Health (Winston-Salem, NC, USA). Human ectopic and eutopic samples from endometriosis patients and control samples, from healthy fertile women, were collected as per institutional approved protocols and guidelines. Written, informed consent was acquired from all patients before acquisition and storage of samples.

2.2 Detection of LIF in endometriosis patient peritoneal fluid and tissue samples using ELISA

Endometriosis patient PF (n=5) and tissue protein extract (matched ectopic (n=13) and eutopic (n=12)) were analyzed to determine the concentration of LIF using an ELISA kit (BMS242, ThermoFisher). Protein extract and PF samples were obtained from separate endometriosis patient cohorts, resulting in n=17 samples. Briefly, 37mg of tissue was weighed and manually homogenized using ceramic power bead tubes (13113-50, QIAGEN) with the addition of tissue protein extraction reagent (78510, ThermoFisher) and protease inhibitor cocktail (535140, Sigma-Aldrich). Protein content was determined using a microplate bicinchoninic acid (BCA) protein assay kit (23532, ThermoFisher) and normalized to the lowest concentration (1202ug). For the ELISA, standards and samples were added to the plate and incubated at room temperature for 2hrs on a plate shaker. After incubation, the plate was washed with wash buffer before the addition of streptavidin and then incubated for 1hr in the same conditions. After washing, horseradish-peroxidase (HRP) was added, and the plate incubated for 30mins. Finally, a substrate solution of tetramethyl-benzidine was added and incubated for 10mins in the dark, after which stop solution was added. The plate was analyzed in a SpectraMax iD5 microplate reader (Molecular devices, California, USA) at an absorbance of 450nm with a reference wavelength of 620nm.

2.3 Immunohistochemistry for LIF on an endometrioma tissue microarray

A tissue microarray (TMA) was created with human patient samples from Kingston General Hospital as previously outlined (32). From a separate patient cohort, matched ectopic (endometrioma samples) and eutopic tissues collected from endometriosis patients (n=19) were compared to endometrium from healthy controls (n=22). Patients were identified as one of three menstrual states by pathologist review: proliferative, secretory, or inactive. The breakdown of patients by menstrual stage are as follows: Endometriosis (proliferative = 7, secretory = 8, inactive= 4), controls (proliferative= 18, secretory= 7, inactive= 1). For IHC, a 5µm section of the TMA was taken, subjected to xylene, and rehydrated with various concentrations of ethanol and citrisolv solutions. Antigen retrieval was performed with a citrate buffer for 20mins and subsequently stained with a polyclonal LIF antibody (26757-1-AP, ThermoFisher, 1:500) using a Leica Bond RX autostainer (Leica Biosystems- Microsystems Inc., IL, USA). The slide was scanned using an Olympus VS120 Virtual Slide Microscope (Olympus, USA) and analyzed using HALO image analysis software (Indica Labs, USA). Quantification of percent area positive for anti-LIF stain was performed on the total core area and the luminal and glandular epithelium respectively. As LIF is produced within the luminal and glandular epithelium, this delineation in area quantification provided a more accurate representation of LIF staining as cores differed in their stromal and epithelial composition.

2.4 Targeted RT qPCR array for LIF associated genes in endometriosis and control tissues

Total RNA was extracted from patient samples (n=8 matched endometriosis eutopic/ectopic tissues, n=9 healthy controls) using a total RNA isolation kit (17200, Norgen Biotek Corp., ON, Canada). Briefly, 20mg of tissue was added to a ceramic power bead tube (13113-50, QIAGEN, Hilden, Germany) with 600µL lysate buffer solution and digested using the Omni Bead Ruptor (PerkinElmer Comp., GA, USA). Samples were subsequently centrifuged at 10000g for 5min to pellet tissue debris. The resultant supernatant was aspirated and passed through a pre-assembled column to remove genomic DNA and collect total RNA. RNA was purified and reverse transcribed into complimentary DNA (cDNA) using a RT^2 First Strand Kit (330401, QIAGEN). Quality of RNA and cDNA samples were tested using a Nanodrop 2000 Spectrophotometer (ThermoScientific, MA, USA). cDNA was used with targeted RT^2 qPCR custom array plates (CLAH41769-(330171)), QIAGEN) to detect 19 key gene transcripts for downstream LIF family proteins and transcription factors, selected after extensive literature review. RT qPCR was conducted using the LightCycler 480 Real-Time PCR system (Roche Molecular Systems, Inc. Basel, Switzerland) with QuantiTect SYBR Green PCR mastermix (330501, QIAGEN). Relative gene expression values were calculated by delta delta CT method after normalization to housekeeping genes (*ACTB* and *GAPDH*). Primers for the following proteins and transcription factors were used: *LIF, LIFR, OSM, IL-6, IL6ST, CNTF, PRL, IGFBP-1, SOX2, SOCS3, JAK1, MAPK1, AKT, mTOR, POU5F1, PTPN11, PI3KR1, NANOG, STAT3.*

2.5 Human cell lines

Immortalized human endometriotic epithelial- 12Z cells (provided by Dr. Anna StarzinskiPowitz), human umbilical vein endothelial cells (HUVEC; CRL-1730, ATCC, VA, USA), and human endometrial stromal cells (hESCs; T0533 ABM, BC, Canada). Immortalized 12Z cells were maintained in DMEM/F-12 (11320033, ThermoFisher) supplemented with 10% fetal bovine serum (FBS; 97068-085, VWR), 1% penicillin/streptomycin (15140122, ThermoFisher) and 1% (100mM) sodium pyruvate (11360070, ThermoFisher). HUVEC cells were maintained with complete endothelial cell growth medium (211-500, Cell Application). hESCs were maintained in PriGrow (TM004, ABM) with 10% charcoal stripped FBS (12676029, ThermoFisher), 1% L-glutamine (A2916801, ThermoFisher) and 1% penicillin/streptomycin. All cell lines were cultured in T75 flasks and maintained until 70-80% confluence, with media changes every 2-3 days. Cells were kept in a humidified cell culture incubator at 37°C and with 5% CO_2.

2.6 Multiplex cytokine analysis of endometriosis representative cell lines following rhLIF treatment

12Z, HUVEC, and hESCs were cultured in 24-well plates at $2.5x10^4$ cells/well. Cells were rested for 24hrs prior to treatment with PBS or rhLIF in the following concentrations: 1, 20, and 100ng/mL. Following a 24hr incubation period, cell supernatant was collected and stored at -80°C prior to multiplex cytokine analysis (HD-48 plex, EveTechnologies, AL, Canada). Exhaustive cytokine list as follows: sCD40L, EGF, Eotaxin, FGF-2, Flt-3 ligand, Fractalkine, G-CSF, GM-CSF, GROα, IFNα2, IFNγ, IL-1α, IL-1β, IL-1ra, IL-2, IL-3, IL-4, IL-5, IL-6, IL-7, IL-8, IL-9, IL-10, IL-12p40, IL-12p70, IL-13, IL-15, IL-17A, IL-17E/IL-25, IL-17F, IL-18, IL-22, IL-27, IP-10, MCP-1, MCP-3, M-CSF, MDC (CCL22), MIG, MIP-1α, MIP-1β, PDGF-AA, PDGF-AB/BB, RANTES, TGFα, TNFα, TNFβ, VEGF-A.

2.7 Proliferation and apoptosis assays in endometriosis representative cell lines treated with rhLIF

Cell proliferation and apoptosis were measured in 12Zs, HUVECs, and hESCs following treatment with PBS or varying concentrations of recombinant human LIF (rhLIF; 7734-LF, R&D Systems, MN, USA). Briefly, cells were seeded at $5x10^3$ cells/well in 96 well plates (hESCs and 12Zs used phenol red free DMEM F-12 (21041025, ThermoFisher) and rested for 24hrs. Media was then changed with media containing either PBS or rhLIF at 1,20, or 100ng/mL, and incubated for an additional 24hrs. Proliferation was determined using a WST-1 assay (0501594400, Sigma-Aldrich, MO, USA) and apoptosis determined using Caspase Glo 3/7 reagent (G8091, Promega, WI, USA). Briefly, 10μL of WST-1 reagent was added per well to achieve a 1:10 dilution before a 2hr incubation at 37°C. To determine apoptosis, 100μL of Caspase Glo 3/7 reagent was added per well to achieve a 1:1 dilution before incubation at room temperature for 2hrs. A SpectraMax iD5 microplate reader (Molecular Devices) was used to obtain the absorbance and luminescence for the proliferation and apoptosis assays respectively. The absorbance of formazan dye produced during the WST-1 reaction was recorded at 450nm with a reference wavelength of 650nm. Each proliferation and apoptosis experiment was repeated at least 3 times per individual cell line, thus data shown is representative.

2.8 Endothelial tube formation assay

HUVEC cells were utilized for a tube formation assay as per the protocol of the manufacturer in a μ-slide assay format. Briefly, IBIDI microplates (81506 Ibidi, Germany) were loaded with 10μL of Matrigel™ (354230, Corning, USA) and incubated for 1hr to allow for Matrigel™ polymerization. HUVEC cells were plated in triplicates at $1x10^4$ cells/well above the polymerized Matrigel™ in 50μL of media with one of the following treatments: VEGF, PBS, LIF (1, 20, 100ng/mL). Cells were incubated at 37°C and with 5% CO_2 for 4hrs. Images were taken on a Nikon TE200 inverted epifluorescence microscope using a 10× objective and a cooled CCD camera and analyzed by WimTube: Tube Formation Assay Image Analysis Solution (33).

2.9 Murine model of endometriosis

Seven-to-eight-week-old female C57BL/6 mice (n=17; Charles River Laboraties, MA, USA) were housed in conventional housing with an automated watering system and 12-hr light-dark cycle at 3-4 animals per cage. To induce endometriosis, uterine horns were harvested from donor mice (n=3) and dermal biopsy punches ($3mm^3$) were used to obtain uterine fragments to be explanted into recipient mice. For surgery, mice were anesthetized with 2.5% isofluorane. Briefly, an incision was made into the abdomen to allow access to the peritoneum, upon which two $3mm^3$ uterine fragments were attached with Vetbond adhesive (1469SB, 3M, MN, USA) to the peritoneal wall. A suture and two staples were used to close the peritoneum and skin respectively. To understand the influence of LIF on endometrial lesion growth and immune cell populations, mice received daily intraperitoneal (i.p) injections of either PBS (control; n=6) or recombinant mouse LIF (rmLIF; n=6; 8878-LF-100/CF, R&D Systems) for 14 days. This experiment was duplicated with varying rmLIF doses (300ng and 1μg). On day 14, animals were sacrificed and peritoneal lavage was performed with ice-cold PBS before the spleen, uterine horns, and endometriosis-like lesions were excised. Lesions were placed in 4% paraformaldehyde and kept in 4°C for 24hrs. Fixed lesions were then transferred to 70% ethanol before processing for paraffin embedding. PF and splenocytes were used for flow cytometry. Spleens were excised and immediately placed in RPMI 1640 supplemented with 5% FBS. To isolate splenocytes, spleens were mechanically digested through a 70μm strainer and centrifuged at 300g for 5min at 4°C. Both PF and splenocytes were pelleted and resuspended in FBS with 10% dimethyl sulfoxide (DMSO; Sigma-Aldrich) for cryopreservation.

2.10 Flow cytometry

Mouse PF and splenocytes were thawed in a water bath at 37°C and reconstituted in 15mL of FACs buffer (PBS with 10% FBS). Cells were centrifuged at 300g for 5min 4°C and supernatant decanted. Following the addition of DNAse 1 (10104159001, Millipore Sigma; 100μg/μL) samples were incubated for 10min at 4°C as per manufacturers guidelines. Cells were neutralized with 10mL of FACS, centrifuged at 300g for 5min 4°C, then resuspended for cell counting by an automated cell counter (Countess 3, ThermoFisher). Samples of $5x10^5$ cells were used for staining for flow cytometry. To limit non-specific antigen binding, samples were stained with anti-mouse TruStainFcX (101320, BioLegend; 1:50) and incubated for 10min at 4°C. Subsequently, extracellular staining for myeloid and lymphoid markers was performed with a 30min incubation period. All products were obtained from BioLegend unless otherwise stated: fixable viability dye, eFluor780 (65-0865-14, ThermoFisher; 1:500), Brilliant Violet (BV)510-anti-CD3 (100234; 1:40), BV785-anti-CD4

(100552; 1:80), BV605-anti-CD8 (100744; 1:40), FITC-anti-CD25 (102005; 1:50), PB- anti-CD11b (1012224; 1:50), PE-Cy7-anti-F4/80 (123114; 1:80), AF700-anti-MHCII (107621; 1:200). Cells were fixed and permeabilized using a FOXP3 Fixation and Permeabilization Kit (00-5523-00, eBioscience) following the manufacturers recommendation. After permeabilization, cells were stained intracellularly with PE-anti-FOXP3 (126404; 1:20) and APC-anti-CD206 (141708; 1:40). Following a 30min staining incubation, cells were washed with FACS.

All data was acquired on the CytoFLEX S flow cytometer (Beckman Coulter, CA, USA) and analyzed using FlowJo software (version 10). Half-heat killed cells were used to detect viability and fluorescence minus one (FMO) controls used to set positive population gates.

2.11 Immunohistochemistry of mouse lesions

Paraffin embedded blocks were sectioned to 5μm thickness and subjected to deparaffinization with xylene before rehydration with various concentrations of ethanol and citrisolv solutions. Antigen retrieval was performed with citrate buffer for 20mins and subsequent staining with polyclonal antibodies for mouse Ki67 (ab15580, Abcam, 1:1000), CD31 (77699S, New England Biolab, 1:100), LIF (PA5-115510, Invitrogen, 1:50), and LIFR (101228, Abcam ab, 1:2000) were completed using a Leica Bond RX autostainer. Lesions were analyzed using a singular computer-generated algorithm created for each stain (Ki67, CD31, LIF, LIFR). Percent area quantification for positive stain was used for CD31, LIF, and LIFR. A cytonuclear algorithm was used to detect individual cell expression of Ki67 after which the percent of proliferating cells ($Ki67^+$) could be expressed as a percent of the total cells. Slides were scanned using an Olympus VS120 Virtual Slide Microscope (Olympus) and image analysis performed using HALO image analysis software (Indica Labs).

2.12 Statistics

All statistical analyses were performed on GraphPad Prism9 (CA, USA). Unpaired students T-test used for analysis between two groups, and one way-ANOVA with Tukey *post-hoc* used for multiple group comparisons. A p value equal or less than 0.05 was considered statistically significant.

3 Results

3.1 LIF is present in the ectopic lesions of endometriosis patients and is dysregulated across the ectopic and eutopic tissues

Previous reports have analyzed LIF within the endometrial tissue of endometriosis patients as it pertains to fertility status, however it has yet to be identified within the ectopic lesion. To gain insight into the presence of LIF within the lesion microenvironment, endometriosis patient tissues and PF samples were analyzed for LIF by ELISA. LIF was detected in all tissue extracts (Figure 1A) and PF samples (Figure 1B) at varying levels; ectopic= 45.08 ± 28.34, eutopic=43.52 ± 20.87, PF=50.49 ± 46.48. No significant differences in protein expression were found between the eutopic and ectopic tissues of endometriosis patients. PF samples from healthy, fertile controls could not be obtained due to logistical difficulties; however, demonstrating the presence of LIF in the PF of women with endometriosis represents a novel finding in and of itself as it demonstrates that LIF is present in the endometriotic microenvironment.

Our next step was to gain spatial understanding of LIF within the lesion microenvironment, thus, IHC was performed on a TMA of endometrioma and control endometrium samples (endometriosis matched; n=19, controls; n=21) (Figures 1C–K). When specified to the epithelium, eutopic tissues demonstrated significantly less percent area positive for LIF stain than the control ($p=0.0096$), as previously noted in literature (Figure 1I). Percentage positive for LIF stain was elevated in ectopic lesions compared to eutopic but was not statistically significant. However, when patients were stratified by menstrual phase, there was a significant difference between ectopic and eutopic LIF staining ($p<0.001$) (Figure 1K) illustrating a dysregulation in the production of LIF within endometriosis patients during the secretory phase.

Finally, we performed targeted RT qPCR using a custom array with select genes involved in the LIF signaling pathway and including members of the IL-6 family of cytokines, to identify differentially expressed transcripts (Figure 2). Of the 19 genes studied, *LIFR, IL-6, NANOG* were upregulated and *LIF, IGFBP-1* were downregulated in the ectopic tissue, compared to the eutopic endometrium from endometriosis patients and healthy controls (Figures 2A, B).

3.2 LIF treatment promotes the production of immune recruiting cytokines and induces tube formation in human umbilical vein endothelial cells

LIF is a known immunomodulator, working as both an inflammatory and anti-inflammatory cytokine depending on the microenvironment. Additionally, as LIF can promote vascularization and proliferation, we sought to determine the effects of LIF on endometriosis lesion representative cell lines. We used 12Zs- an endometriotic epithelial cell line, and hESCs- a human endometrial stromal cell line, to represent the two primary cellular components of the endometrium and ectopic tissue being epithelial and stromal cells. Additionally, we utilized HUVECs- human umbilical vein endothelial cells, as they are a well-established model for angiogenesis. All cell lines were treated with varying rhLIF concentrations (1, 20, 100ng). Proliferation and apoptosis were measured using a WST-1 and caspase 3/7 glo assay respectively. LIF treatment did not result in detectable proliferation in any of the cell lines, but rather at the lowest dose decreased proliferation compared to the PBS control (Figures 3A–C). This

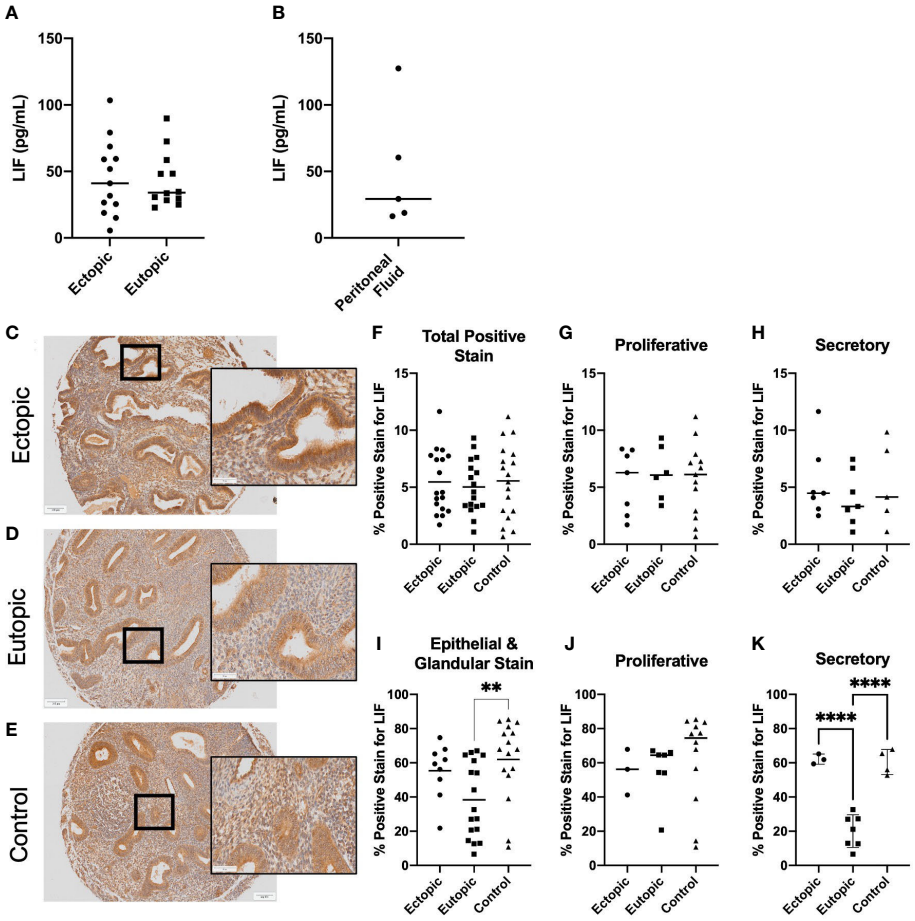

FIGURE 1
LIF is present in the ectopic lesion microenvironment of endometriosis patients. Ectopic and eutopic tissues **(A)** and PF **(B)** from endometriosis patients contain LIF as detected through ELISA. No significant differences in LIF values were seen across tissue type. Analysis performed as unpaired Student's T-test. **(C–E)**, Endometrioma TMA of matched endometriosis (eutopic and ectopic; n=19) and control endometrium (n=22) was stained with an anti-LIF antibody. Area quantification of percent positive stain was calculated for the total core area **(F–H)** and luminal and glandular epithelium **(I–K)** respectively. Patients were stratified by menstrual phase- proliferative **(G, J)** and secretory **(H, K)**, for both area quantifications. Patient samples used in **(A–C, E)** reflect 3 separate patient cohorts. Magnification provided at 4x and 20x; scale bar 100μm. Analysis performed as one-way ANOVA with Tukey post-hoc, **P<0.01, ****P<0.0001.

reduced proliferation was not attributed to apoptosis, however, as the caspase assay showed no alterations to apoptosis regardless of the dose of LIF treatment (Figures 3D–F).

Cell supernatant, collected in response to rhLIF treatment (1, 20, 100ng/mL), was analyzed using a multiplex cytokine array for predominant pro-inflammatory/immunoregulatory cytokines, chemokines, and growth factors (Figures 3G–M). Significant production of immune recruiting cytokines such as monocyte chemoattractant protein (MCP)-1 and MCP-3 were produced in 12Zs and HUVECs upon LIF treatment (Figures 3J–L), but not in hESCs. Further, 12Zs secreted significantly higher concentrations of vascular endothelial growth factor (VEGF) with all treatment doses compared to PBS, indicating LIF as a potential promoter of angiogenesis *in vitro* (Figure 3G). Additional cytokines detected in the cell supernatants can be found in Supplemental Figure 1.

To determine LIFs influence on angiogenesis, a tubulogenesis assay was performed with HUVECs (Figure 4). Significantly elevated tube length ($p<0.05$) and number of total branching points ($p<0.05$) were seen with the 100ng rhLIF treatment compared to the PBS control (Figures 4F, G).

3.3 LIF treatment in a syngeneic mouse model of endometriosis alters the local and peripheral immune response

To understand the influence of LIF on immune cell recruitment and polarization, we surgically induced endometriosis in C57BL/6 mice and performed daily i.p. injections of recombinant mouse LIF [rmLIF; 300ng and 1μg, based on available literature (28, 30)] or PBS for 14 days. To capture alterations to the local and peripheral immune response, PF (Figure 5) and splenocytes (Figure 6) were harvested for flow cytometric analysis of myeloid and lymphoid immune cell subsets. With LIF treatment, regardless of dose, there

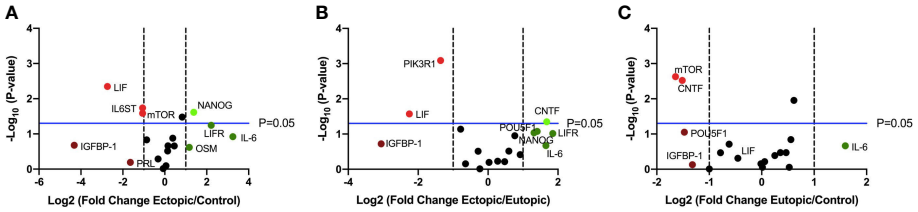

FIGURE 2
LIF gene expression is significantly downregulated in ectopic tissue compared to eutopic and control. Volcano plots showing differentially expressed genes in the LIF signaling pathway between **(A)** ectopic (n=9) and control (n=10), **(B)** ectopic and eutopic (n=9), **(C)** eutopic and control tissue samples. Vertical dashed lines indicate a fold change of +/-1 and horizontal blue line denotes a significance value of P=0.05.

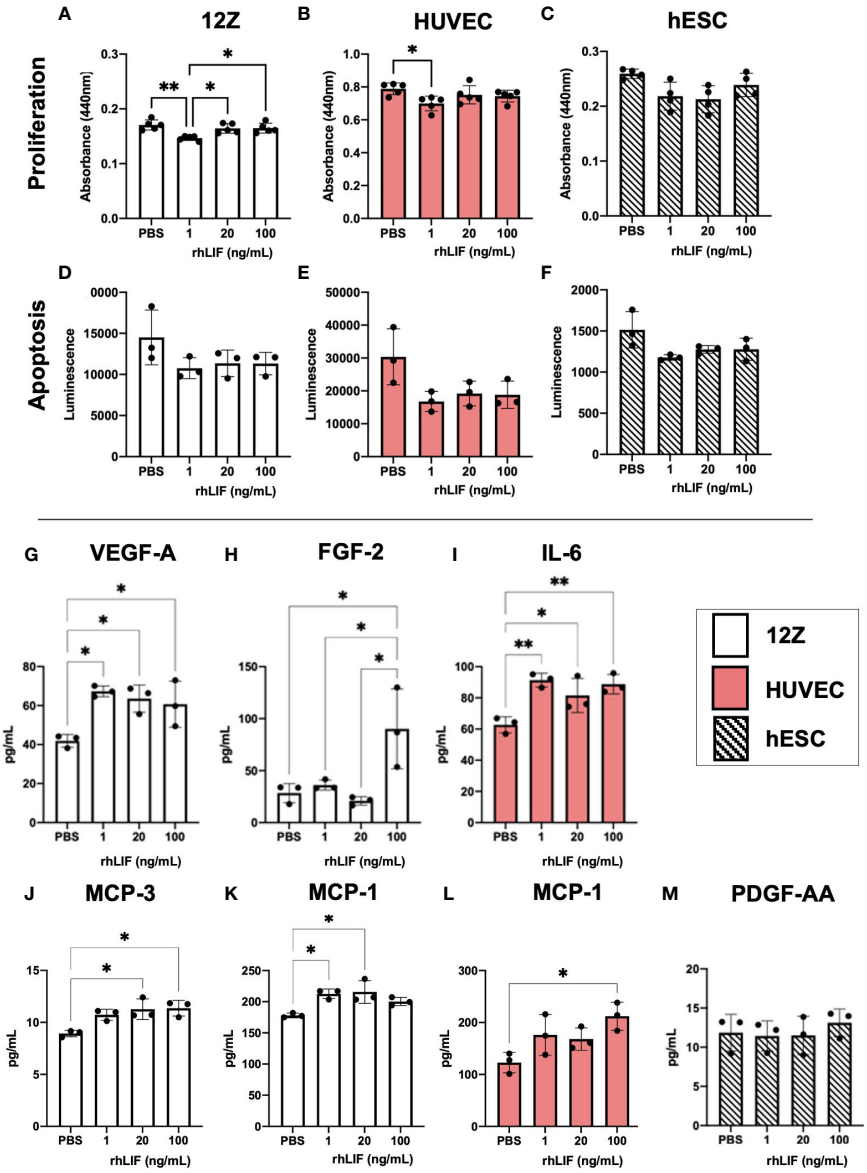

FIGURE 3
LIF treatment *in vitro* did not alter proliferation or apoptosis in endometriosis representative cell lines but stimulated the release of growth factors and immune recruiting cytokines. WST-1 **(A–C)** and Caspase **(D–F)** assays were conducted in endometriosis representative cell lines- 12Zs (white bars), HUVECs (red bars), and hESCs (dashed bars), to detect LIF influence on proliferation and apoptosis respectively. **(G–M)**, Cell lines were treated for 24hrs with PBS or varying rhLIF concentrations (1, 20, 100ng/mL) and supernatant analyzed for 48 cytokines pertaining to angiogenesis, inflammation, and cell growth (HD48-Multi-plex Analysis, EveTech). Analysis performed as one-way ANOVA with Tukey *post-hoc*, *P<0.05, **P<0.01.

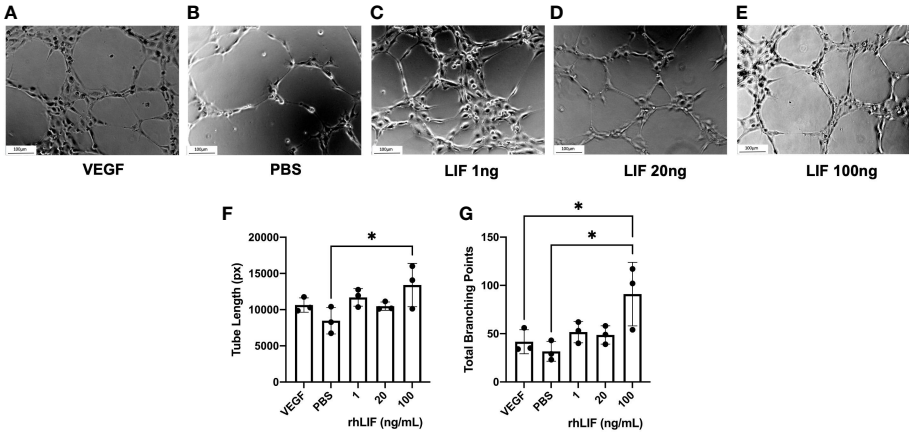

FIGURE 4
LIF treatment promotes tubulogenesis in HUVEC cell line. HUVEC were treated with VEGF, PBS, or rhLIF (1, 20, 100ng/mL) and incubated for 4hrs before image acquisition- representative images provided for each treatment condition **(A–E)**. Images were analyzed by WIMASIS Software to determine metrics of tube formation including **(F)** tube length and **(G)** total branching points. Analysis performed as one-way ANOVA with Tukey post-hoc, *P<0.05. Scale bar 100μm.

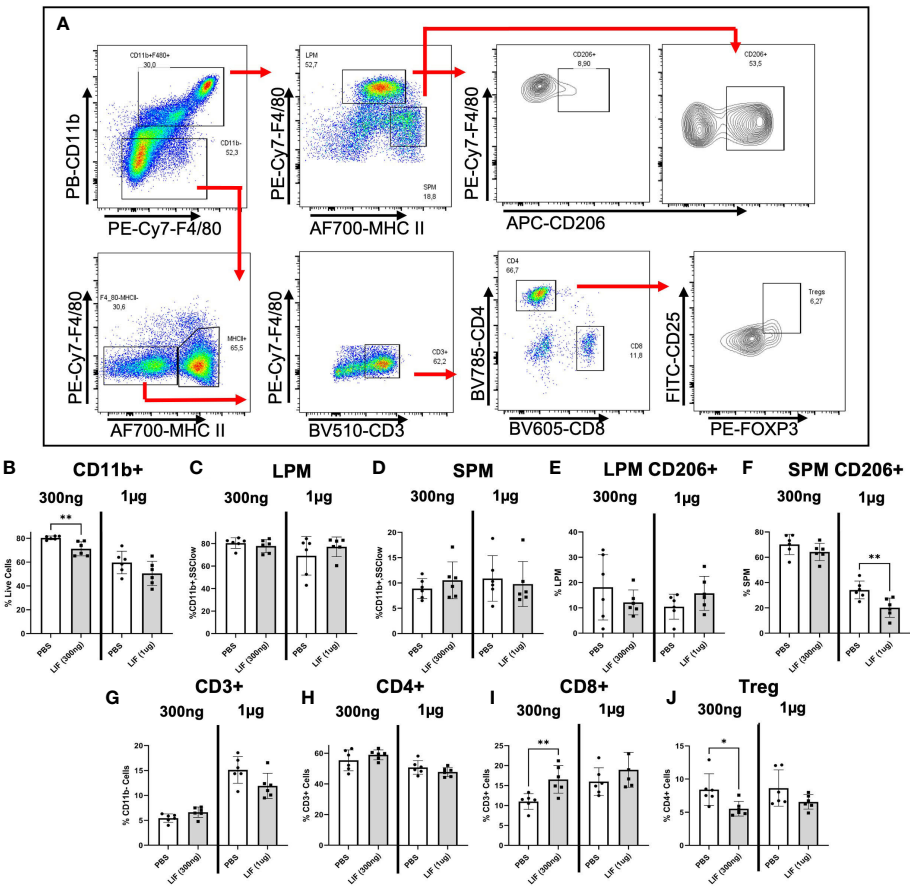

FIGURE 5
LIF treatment in a mouse model of endometriosis alters the local peritoneal immune response. **(A)** Gating strategy for flow cytometric analysis of myeloid **(B–F)** and lymphoid **(G–J)** markers on immune cells from the PF of mice injected i.p with PBS (white bars) or rmLIF (grey bars; 300ng, 1μg) for 14 days. LPM gated as: single cells, live, SSC^{low}, $CD11b^{+}$, $F4/80^{hi}$, $MHCII^{low}$. SPM gated as: single cells, live, SSC^{low}, $CD11b^{+}$, $F4/80^{mid}$, $MHCII^{hi}$. Tregs gated as: single cells, live, SSC^{low}, $CD11b^{-}$, $F4/80^{-}$, $MHCII^{-}$, $CD3^{+}$, $CD4^{+}$, $CD25^{+}$, $FOXP3^{+}$. Results reflect duplicate experiments- one per rmLIF dosage. Analysis performed as unpaired Student's T-test, *P<0.05, **P<0.01. LPM, large peritoneal macrophages, SPM, small peritoneal macrophages.

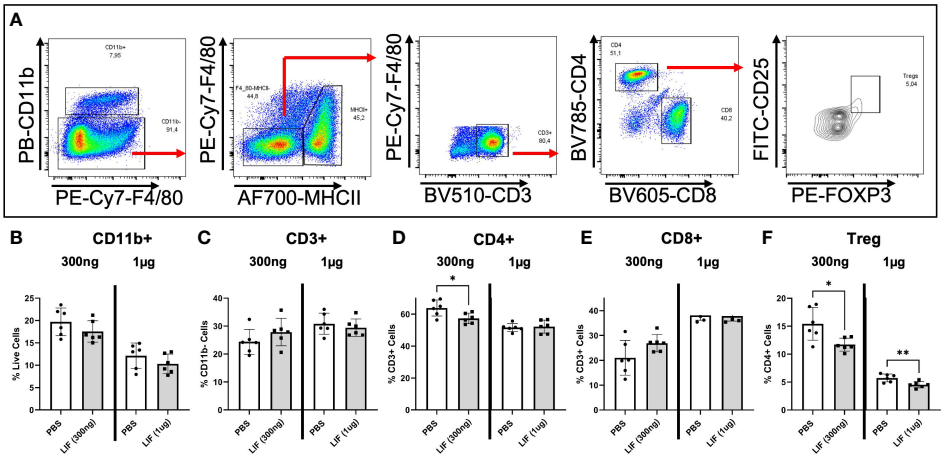

FIGURE 6
LIF treatment in a mouse model of endometriosis alters the peripheral immune response. **(A)** Gating strategy for flow cytometric analysis of myeloid **(B)** and lymphoid markers **(C–F)** on immune cells from the spleen of mice injected i.p with PBS (white bars) or rmLIF (grey bars; 300ng, 1µg) for 14 days. Tregs gated as: single cells, live, SSC^{low}, $CD11b^{-}$, $F4/80^{-}$, $MHCII^{-}$, $CD3^{+}$, $CD4^{+}$, $CD25^{+}$, $FOXP3^{+}$. Results reflect duplicate experiments- one per rmLIF dosage. Analysis performed as unpaired Student's T-test, *P<0.05, **P<0.01.

was a reduction in immunoregulatory phenotypes in the PF and spleen. In the PF, $CD206^{+}$ small peritoneal macrophages (SPMs; gated as: singlet, live, side scatter $(SSC)^{low}$, $CD11b^{+}$, $F4/80^{mid}$, $MHCII^{hi}$, $CD206^{+}$) and Treg (gated as: singlet, live, SSC^{low}, $CD11b^{-}$, $F4/80^{-}$, $MHCII^{-}$, $CD3^{+}$, $CD4^{+}$, $CD25^{+}$, $FOXP3^{+}$) cells were significantly decreased compared to PBS control (Figures 5E, J). Similarly in the spleen, Treg cells were significantly reduced with LIF treatment, as were $CD4^{+}$ cells (Figures 6D, F). Of note, the PF of mice receiving the low LIF dose had significantly more $CD8^{+}$ T cells compared to PBS ($p<0.01$) (Figure 5I).

3.4 LIF treatment did not alter lesion associated proliferation or angiogenesis in a syngeneic mouse model of endometriosis

LIF has been shown to promote tumor growth and vascularization in cancer, thus we sought to determine if those effects were withstanding in our syngeneic mouse model of endometriosis. Lesions harvested from LIF (300ng and 1µg) and PBS treated mice were fixed in paraformaldehyde and embedded in paraffin for IHC. Lesions were stained for markers of angiogenesis- CD31 and proliferation- Ki67, as well as LIF and LIFR (Figure 7). No differences were detected in any of the markers regardless of LIF dosage.

4 Discussion

Foundational knowledge of LIF is centered on its role in maintaining embryonic stem cell pluripotency (17), facilitating successful pregnancy through stromal cell decidualization and trophoblast implantation (8, 34), and participation in neuroimmune modulation (21). These situate LIF as a primary regulator of various homeostatic and pathologic signaling pathways within the body. Recent cancer literature has revealed that LIF is a contributor to immune evasion and facilitation of tumor growth and metastasis (28, 35). In endometriosis, LIF has only been investigated for its contributions to infertility (6, 7) however its presence within the lesion microenvironment and impact on lesion maintenance and the immune contexture remained unexplored.

Our findings identify LIF in the lesion microenvironment, with detection of LIF in the PF and protein extracts of both ectopic and eutopic endometriosis tissues. Spatial localization of LIF in endometriosis patients and control tissues, as provided by our IHC data, further corroborates that LIF is present in ectopic lesions with LIF staining localized to the luminal and glandular epithelium. Across both the proliferative and secretory phases, LIF expression by the ectopic luminal and glandular epithelium is similar to that of the control endometrium. Interestingly, within the secretory phase, ectopic LIF expression is significantly greater than eutopic. This reduced eutopic LIF expression is in accordance with infertility research (7), demonstrating that the endometrium of endometriosis patients has aberrant LIF expression during the secretory phase. Together, these results indicate that ectopic LIF production is rescued in endometriosis patients, highlighting a dysregulation of LIF between endometriosis tissues. The mechanism behind this recued phenotype requires further investigation as does the source of LIF production within the lesion microenvironment. LIF is produced by a variety of cell types including but not limited to endometrial luminal and glandular epithelium, endothelial cells (36), macrophages, and T cells (21). As patient PF and tissue protein extract consist of contributions from heterogenous cell types, continued investigation into the primary contributors of LIF to the lesion microenvironment is needed.

Targeted RT qPCR data provides further insight into LIF production within ectopic lesions. Our findings revealed that *LIF* gene expression is significantly downregulated while its primary

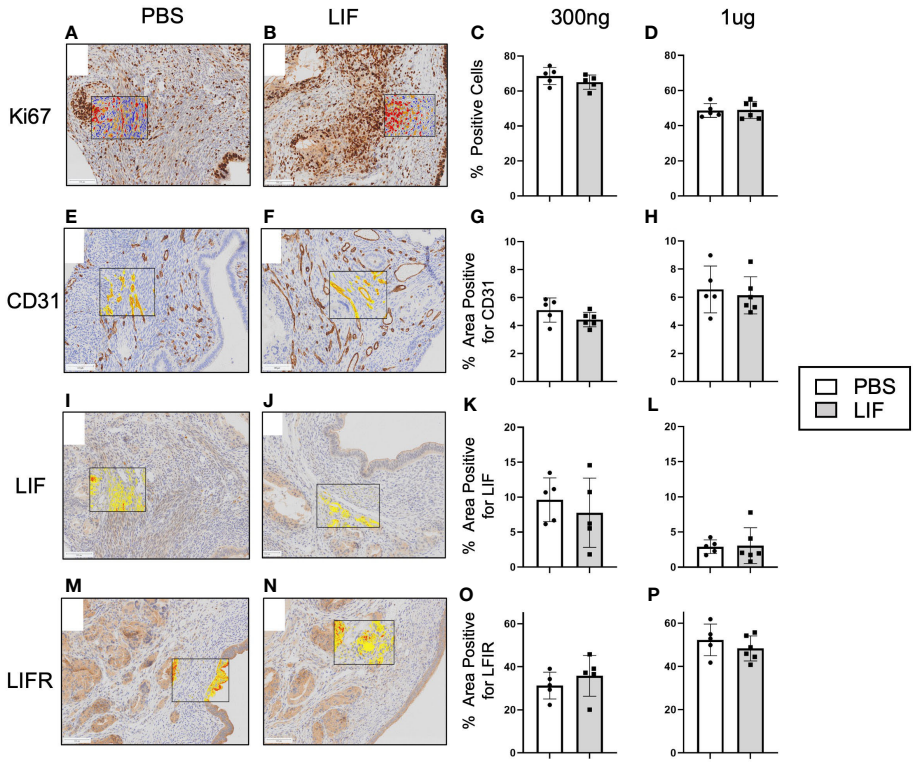

FIGURE 7
LIF treatment did not alter lesion growth or proliferation in a mouse model of endometriosis. I.p injections of PBS (white bars) or rmLIF (grey bars; 300ng, 1µg) were administered to C57BL/6 mice (n=6 for all groups) for 14 days, one week after endometriosis inducing surgery. Endometriosis-like lesions were collected upon sacrifice and subjected to IHC for markers of proliferation-Ki67 **(A, B)** and angiogenesis-CD31 **(E, F)**, as well as LIF **(I, J)** and LIFR **(M, N)**. Representative stain analysis provided for each marker from both the PBS and LIF treatment groups. Ki67 was analyzed as percent of cells expressing Ki67 over the total cell number as detected by a cytonuclear algorithm **(C, D)**, while all other stains (CD31, LIF, LIFR) were analyzed by percent area quantification of stain **(G, H, K, L, O, P)**. No statistical differences were detected across the four stains. Analysis performed as unpaired Student's T-test. Scale bar 100µm.

receptor *LIFR* is upregulated in the ectopic tissue compared to eutopic and healthy control samples. This suggests that ectopic tissue is likely receptive to LIF but not producing it, potentially due to the high levels of LIF detected within the lesion microenvironment. In support of LIF signaling, *NANOG*, a downstream transcription factor of LIF associated with the maintenance of cell stemness, was significantly upregulated in the ectopic tissues compared to control and upregulated, though not significantly, compared to eutopic tissue. NANOG production is present in embryonic stem cells to maintain cell pluripotency and if present in adult tissues, serves as an oncogene, contributing to tumorigenesis (37). Our findings are in accordance with other endometriosis literature identifying downstream LIF targets NANOG, OCT-3/4, and SOX2 to be elevated in ectopic lesions compared to control endometrium (38, 39). These studies however do not mention LIF as a mediator of these pathways, thus our findings offer a novel perspective to view the activation of these stemness transcription factors within endometriosis. It is notable however, that NANOG can be regulated in the absence of LIF. E-cadherin can signal through STAT3 to increase NANOG transcription, while p53 can inhibit NANOG transcription through binding of its promoter region (37, 40). Thus, further investigation is required to confirm whether the upregulation of *NANOG* is due specifically to LIF signaling or other mediators in endometriosis.

Additionally, it is worth noting that other IL-6 family proteins (such as ciliary neurotrophic factor (CNTF) and oncostatin-M (OSM)) use the LIF receptor for signaling and have been implicated in various aspects of endometriosis. CNTF has been investigated for its potential association with sensitization and pain (41, 42), while OSM has been shown to inhibit endometrial stromal cell growth, with endometriotic stromal cells being resistant to this inhibitory effect (43). Our customized RT qPCR array included both CNTF and OSM to determine whether IL-6 family proteins or LIF specifically were dysregulated within endometriosis. Our findings demonstrate a significant upregulation of CNTF within the ectopic tissue compared to eutopic and significant downregulation in the eutopic tissue compared to the control. While OSM is upregulated, though not significantly, within the ectopic tissue compared to control. These findings suggest that the IL-6 family proteins are dysregulated within the ectopic tissue, with further research needed to determine the impact on lesion sensitization and growth.

LIF has been shown to promote tumor growth and metastasis through carcinoma cell proliferation, however in our *in vitro* models there were limited alterations to proliferation across

various cell types- 12Z, hESC, and HUVEC. Yet treatment of these endometriosis representative cell lines with rhLIF yielded the production of immune recruiting and inflammatory cytokines MCP-1, MCP-3, and IL-6, as well as the angiogenic factor VEGF. The role of LIF as an angiogenic factor is contentious throughout the literature, reflecting the nuances through which microenvironments modulate LIF signaling. LIF has been demonstrated to regulate vascularization in concert with oxygen availability, meaning that it can prevent or promote the formation of blood vessels as seen in mouse models of ocular vascularization (44). Our findings, suggest that LIF is a promoter of angiogenesis both indirectly through the promotion of the angiogenic factor VEGF from 12Zs and directly by increasing endothelial tube formation in HUVECs. We sought to visualize these effects of LIF treatment within our mouse model through examination of indirect alterations to lesion architecture including proliferation and angiogenesis, however no significant changes were found. This discordance in angiogenesis can in part be attributed to temporal variations in experimental end points, where the tubulogenesis assay demonstrated short term response and our mouse model captures a more chronic response. Additionally, these are varying endothelial cell types, thus further investigation of LIF specifically on endometriotic endothelial cells is needed to elucidate its role within endometriosis.

LIFs role as an immunomodulator is co-opted in pathologies like cancer, as the immunoregulatory environment perpetuates tumor immune evasion and promotes resistance to treatment (23, 28). As our human data highlights the presence of LIF in the lesion microenvironment and our *in vitro* evidence suggests a role in angiogenesis and immune recruitment, we wanted to understand the impact of elevated LIF on lesion development and the immune contexture in our syngeneic immunocompetent mouse model of endometriosis. LIF treated mice did not demonstrate an increased number of infiltrating immune cells, but the composition of immune cell phenotypes was altered both locally and systemically. At both a low (300ng) and high (1μg) dose of rmLIF, there were significant reductions in immunoregulatory myeloid and lymphoid phenotypes, mainly CD206$^+$ SPMs and Tregs. Further, CD8$^+$ T cells were upregulated in the PF of the low dose rmLIF treated group. LIF has been demonstrated to assist in polarizing macrophages to an M2 phenotype and works through these cells to increase Treg functioning (29–31). Further, LIF provides barriers to CD8$^+$ T cell infiltration due to its influence on M2 macrophages. In a mouse model of breast cancer, LIF was shown to operate through M2 like- tumor associated macrophages to silence CD8$^+$ T cells *via* epigenetic modification (30). Our results appose these findings, potentially providing insight into a novel endometriosis associated LIF pathway whereby LIF intervention is reducing immunoregulatory phenotypes and promoting a potential cytotoxic response. Further phenotypic characterizations are needed to clarify the activation status of the CD8$^+$ T cells present. Notably IL-6 has been identified as a key factor in assisting LIF polarization of macrophages to an M2 phenotype (26). Multiplex cytokine analysis of the PF demonstrated undetectable or negligible levels (<4pg/mL) of IL-6 (data not shown) suggesting that IL-6 was not produced in sufficient quantities in our mouse model with this treatment and time course for macrophage polarization to occur. Finally, direct comparison between rmLIF doses was not possible due to batch effect variations. Despite this limitation, the trend of reduced immunoregulatory phenotypes was consistent between LIF treatments supporting its role as an immunomodulator within endometriosis.

While we provide previously unexplored dimensions of LIF in endometriosis pathophysiology beyond infertility, we acknowledge some of the limitations of the work that are inherent to endometriosis research. Access to representative patient samples from each disease subtype and severity is limited. Additionally, as most patients have irregular menstrual cycles, there are limitations to identifying specific occurrences within defined menstrual phases. Due to limited access to PF samples from healthy controls only endometriosis LIF expression in the PF was shown. While we present this data to document LIF presence in endometriosis PF samples, future studies are needed to provide a comparison between endometriosis and control samples. Further, infertility is not a symptom that all patients experience yet it is one that is common, being present in around 30-50% of cases (5). Within our patient samples fertility status was not known preventing us from including this as a factor within our analysis. Thus, continued investigation is needed to determine whether LIF dysregulation is specific to endometriosis patients with infertility or whether it can be found in fertile patients as well. Finally, as the endometrioma TMA data was more conclusive for LIF presence within the ectopic tissue than the ELISA data (which contained mixed endometriosis subtypes), perhaps the type of endometriosis is a factor in the degree of LIF dysregulation, thus further investigation within endometriosis subtypes is needed.

In conclusion, this study demonstrates that LIF is present in ectopic endometriosis lesions and provides insight to the potential contributions it has to endometriosis pathophysiology. While it is known that some endometriosis patients experience alterations to eutopic LIF production, it is still not known whether this is a consequence of endometriosis associated infertility or whether this contributes to endometriosis pathophysiology. Ultimately, further investigation into the role of LIF across endometriosis subtypes and stages is required to better address its role within both endometriosis-associated infertility and pathophysiology.

Data availability statement

The original contributions presented in the study are included in the article/Supplementary Material. Further inquiries can be directed to the corresponding author.

Ethics statement

The studies involving human participants were reviewed and approved by Health Sciences Research Ethics Board at Kingston Health Sciences Centre, Queen's University Health Sciences Research Ethics Board, Greenville Health System, and Wake Forest Baptist Health. The patients/participants provided their

written informed consent to participate in this study. The animal study was reviewed and approved by Queen's University Animal Care Committee.

Author contributions

KZ conceived and conducted experiments, analyzed data, and wrote the manuscript. DS, JM, and HL conducted experiments. TC, OB, and BL contributed human patient samples. CT contributed reagents, conceived experiments, provided financial support. All authors read and edited the manuscript.

Funding

This research was supported with funds from the Canadian Institutes of Health Research (CIHR 394570, CT).

Acknowledgments

We thank Lee Boudreau in the Department of Pathology and Molecular Medicine (Queen's University) for his technical contributions to all IHC processing. We also thank Dr. Bruce Banfield (Queen's University) for the use of his Nikon TE200 inverted epifluorescence microscope and Safara Holder for assistance in image acquisition.

Conflict of interest

The authors declare that the research was conducted in the absence of any commercial or financial relationships that could be construed as a potential conflict of interest.

Publisher's note

Supplementary material

The Supplementary Material for this article can be found online at: https://www.frontiersin.org/articles/10.3389/fimmu.2023.1089098/full#supplementary-material

References

1. Giudice LC, Kao LC. Endometriosis. *Lancet* (2004) 364(9447):1789–99. doi: 10.1016/S0140-6736(04)17403-5

2. Zondervan KT, Becker CM, Koga K, Missmer SA, Taylor RN, Vigano P. Endometriosis. *Nat Rev Dis Primers* (2018) 4(1):9. doi: 10.1038/s41572-018-0008-5

3. Agarwal SK, Chapron C, Giudice LC, Laufer MR, Leyland N, Missmer SA, et al. Clinical diagnosis of endometriosis: a call to action. *Am J Obstet Gynecol* (2019) 220 (4):354.e1– e12. doi: 10.1016/j.ajog.2018.12.039

4. Giudice LC. Endometriosis. *New Engl J Med* (2010) 362:2389–98. doi: 10.1056/NEJMcp1000274

5. Holoch K, Lessey BA. Endometriosis and infertility. *Clin Obstetrics Gynecol* (2010) 53(2):429–38. doi: 10.1097/GRF.0b013e3181db7d71

6. Dimitriadis E, Stoikos C, Stafford-Bell M, Clark I, Paiva P, Kovacs G, et al. Interleukin-11, IL-11 receptor alpha and leukemia inhibitory factor are dysregulated in endometrium of infertile women with endometriosis during the implantation window. *J Reprod Immunol* (2006) 69(1):53–64. doi: 10.1016/j.jri.2005.07.004

7. Moberg C, Bourlev V, Ilyasova N, Olovsson M. Endometrial expression of LIF and its receptor and peritoneal fluid levels of IL-1alpha and IL-6 in women with endometriosis are associated with the probability of pregnancy. *Arch Gynecol Obstet* (2015) 292(2):429–37. doi: 10.1007/s00404-015-3626-0

8. Shuya LL, Menkhorst EM, Yap J, Li P, Lane N, Dimitriadis E. Leukemia inhibitory factor enhances endometrial stromal cell decidualization in humans and mice. *PloS One* (2011) 6(9):e25288. doi: 10.1371/journal.pone.0025288

9. Nicola NA, Babon JJ. Leukemia inhibitory factor (LIF). *Cytokine Growth Factor Rev* (2015) 26(5):533–44. doi: 10.1016/j.cytogfr.2015.07.001

10. Stewart C, Kaspart P, Brunet JL, BhaU H, Gadi I, Kontgen F, et al. Blastocyst implantation depends on maternal expression of leukaemia inhibitory factor. *Nature* (1992) 359:76–9. doi: 10.1038/359076a0

11. Franasiak JM, Holoch KJ, Yuan L, Schammel DP, Young SL, Lessey BA. Prospective assessment of midsecretory endometrial leukemia inhibitor factor expression versus alphanubeta3 testing in women with unexplained infertility. *Fertil Steril* (2014) 101(6):1724–31. doi: 10.1016/j.fertnstert.2014.02.027

12. Aghajanova L, Altmae S, Bjuresten K, Hovatta O, Landgren BM, Stavreus-Evers A. Disturbances in the LIF pathway in the endometrium among women with unexplained infertility. *Fertil Steril* (2009) 91(6):2602–10. doi: 10.1016/j.fertnstert.2008.04.010

13. Mariee N, Li TC, Laird SM. Expression of leukaemia inhibitory factor and interleukin 15 in endometrium of women with recurrent implantation failure after IVF; correlation with the number of endometrial natural killer cells. *Hum Reprod* (2012) 27 (7):1946–54. doi: 10.1093/humrep/des134

14. Comba C, Bastu E, Dural O, Yasa C, Keskin G, Ozsurmeli M, et al. Role of inflammatory mediators in patients with recurrent pregnancy loss. *Fertil Steril* (2015) 104(6):1467–74 e1. doi: 10.1016/j.fertnstert.2015.08.011

15. Xiao Y, Sun X, Yang X, Zhang J, Xue Q, Cai B, et al. Leukemia inhibitory factor is dysregulated in the endometrium and uterine flushing fluid of patients with adenomyosis during implantation window. *Fertil Steril* (2010) 94(1):85–9. doi: 10.1016/j.fertnstert.2009.03.012

16. Yen CF, Liao SK, Huang SJ, Tabak S, Arcuri F, Lee CL, et al. Decreased endometrial expression of leukemia inhibitory factor receptor disrupts the STAT3 signaling in adenomyosis during the implantation window. *Reprod Sci* (2017) 24 (8):1176–86. doi: 10.1177/1933719116681515

17. Niwa H, Ogawa K, Shimosato D, Adachi K. A parallel circuit of LIF signalling pathways maintains pluripotency of mouse ES cells. *Nature* (2009) 460(7251):118–22. doi: 10.1038/nature08113

18. Cullinan EB, Abbondanzo SJ, Anderson PS, Pollard JW, Lessey BA, Stewart CL. Leukemia inhibitory factor (LIF) and LIF receptor expression in human endometrium suggests a potential autocrine/paracrine functioninregulating embryoimplantation. *Proc Natl Acad Sci* (1996) 93:3115–20. doi: 10.1073/pnas.93.7.3115

19. Traber KE, Symer EM, Allen E, Kim Y, Hilliard KL, Wasserman GA, et al. Myeloid-epithelial cross talk coordinates synthesis of the tissue-protective cytokine leukemia inhibitory factor during pneumonia. *Am J Physiol Lung Cell Mol Physiol* (2017) 313(3):L548–L58. doi: 10.1152/ajplung.00482.2016

20. Davis SM, Collier LA, Winford ED, Leonardo CC, Ajmo CTJr., Foran EA, et al. Leukemia inhibitory factor modulates the peripheral immune response in a rat model of emergent large vessel occlusion. *J Neuroinflamm* (2018) 15(1):288. doi: 10.1186/s12974-018-1326-y

21. Hendriks JJ, Slaets H, Carmans S, de Vries HE, Dijkstra CD, Stinissen P, et al. Leukemia inhibitory factor modulates production of inflammatory mediators and myelin phagocytosis by macrophages. *J Neuroimmunol* (2008) 204(1-2):52–7. doi: 10.1016/j.jneuroim.2008.07.015

22. Metcalfe SM. LIF in the regulation of T-cell fate and as a potential therapeutic. *Genes Immun* (2011) 12(3):157–68. doi: 10.1038/gene.2011.9

23. Li M, Viswanadhapalli S, Santhamma B, Pratap UP, Luo Y, Liu J, et al. LIFR inhibition enhances the therapeutic efficacy of HDAC inhibitors in triple negative breast cancer. *Commun Biol* (2021) 4(1):1235. doi: 10.1038/s42003-021-02741-7

24. Li X, Yang Q, Yu H, Wu L, Zhao Y, Zhang C, et al. LIF promotes tumorigenesis and metastasis of breast cancer through the AKT-mTOR pathway. *Oncotarget* (2014) 5:788–801. doi: 10.18632/oncotarget.1772

25. Viswanadhapalli S, Luo Y, Sareddy GR, Santhamma B, Zhou M, Li M, et al. EC359: A first-in-Class small-molecule inhibitor for targeting oncogenic LIFR signaling in triple-negative breast cancer. *Mol Cancer Ther* (2019) 18(8):1341–54. doi: 10.1158/1535-7163.MCT-18-1258

26. McLean K, Tan L, Bolland DE, Coffman LG, Peterson LF, Talpaz M, et al. Leukemia inhibitory factor functions in parallel with interleukin-6 to promote ovarian cancer growth. *Oncogene* (2019) 38(9):1576–84. doi: 10.1038/s41388-018-0523-6

27. Wang MT, Fer N, Galeas J, Collisson EA, Kim SE, Sharib J, et al. Blockade of leukemia inhibitory factor as a therapeutic approach to KRAS driven pancreatic cancer. *Nat Commun* (2019) 10(1):3055. doi: 10.1038/s41467-019-11044-9

28. Liu SC, Tsang NM, Chiang WC, Chang KP, Hsueh C, Liang Y, et al. Leukemia inhibitory factor promotes nasopharyngeal carcinoma progression and radioresistance. *J Clin Invest* (2013) 123(12):5269–83. doi: 10.1172/JCI63428

29. Duluc D, Delneste Y, Tan F, Moles MP, Grimaud L, Lenoir J, et al. Tumor-associated leukemia inhibitory factor and IL-6 skew monocyte differentiation into tumor-associated macrophage-like cells. *Blood* (2007) 110(13):4319–30. doi: 10.1182/blood-2007-02-072587

30. Pascual-Garcia M, Bonfill-Teixidor E, Planas-Rigol E, Rubio-Perez C, Iurlaro R, Arias A, et al. LIF regulates CXCL9 in tumor-associated macrophages and prevents CD8(+) T cell tumor-infiltration impairing anti-PD1 therapy. *Nat Commun* (2019) 10 (1):2416. doi: 10.1038/s41467-019-10369-9

31. Gao W, Thompson L, Zhou Q, Putheti P, Fahmy TM, Strom TB, et al. Treg versus T17 lymphocyte lineages are cross-regulated by LIF versus IL-6. *Cell Cycle* (2009) 8(9):1444–50. doi: 10.4161/cc.8.9.8348

32. Symons LK, Miller JE, Tyryshkin K, Monsanto SP, Marks RM, Lingegowda H, et al. Neutrophil recruitment and function in endometriosis patients and a syngeneic murine model. *FASEB J* (2020) 34(1):1558–75. doi: 10.1096/fj.201902272R

33. *Wimasis* (2016). Available at: https://www.wimasis.com/en/products/13/WimTube.

34. Rosario GX, Hondo E, Jeong JW, Mutalif R, Ye X, Yee LX, et al. The LIF-mediated molecular signature regulating murine embryo implantation. *Biol Reprod* (2014) 91(3):66. doi: 10.1095/biolreprod.114.118513

35. Liu B, Lu Y, Li J, Liu Y, Liu J, Wang W. Leukemia inhibitory factor promotes tumor growth and metastasis in human osteosarcoma *via* activating STAT3. *APMIS* (2015) 123(10):837–46. doi: 10.1111/apm.12427

36. Mi H, Haeberle H, Barres BA. Induction of astrocyte differentiation by endothelial cells. *J Neurosci* (2001) 21(5):1538–47. doi: 10.1523/JNEUROSCI.21-05-01538.2001

37. Gawlik-Rzemieniewska N, Bednarek I. The role of NANOG transcriptional factor in the development of malignant phenotype of cancer cells. *Cancer Biol Ther* (2016) 17(1):1–10. doi: 10.1080/15384047.2015.1121348

38. Shariati F, Favaedi R, Ramazanali F, Ghoraeian P, Afsharian P, Aflatoonian B, et al. Increased expression of stemness genes REX-1, OCT-4, NANOG, and SOX-2 in women with ovarian endometriosis versus normal endometrium: A case-control study. *Int J Reprod BioMed* (2018) 16(12):783–90. doi: 10.18502/ijrm.v16i12.3684

39. Song Y, Xiao L, Fu J, Huang W, Wang Q, Zhang X, et al. Increased expression of the pluripotency markers sex-determining region y-box 2 and nanog homeobox in ovarian endometriosis. *Reprod Biol Endocrinol* (2014) 12(42):1–7. doi: 10.1186/1477-7827-12-42

40. Gong S, Li Q, Jeter CR, Fan Q, Tang DG, Liu B. Regulation of NANOG in cancer cells. *Mol Carcinog* (2015) 54(9):679–87. doi: 10.1002/mc.22340

41. Browne AS, Yu J, Huang R, Francisco AM, Sidell N, Taylor RN. Proteomic identification of neurotrophins in the eutopic endometrium of women with endometriosis. *Fertil Steril* (2012) 98(3):713–9. doi: 10.1016/j.fertnstert.2012.05.027

42. Suzumori NS K. Peritoneal fluid concentrations of ciliary neutrophic growth factor, a gp130 cytokine, in women with endometriosis. *Gynecol Obstet Invest* (2003) 56:51–4. doi: 10.1159/000072694

43. Ohata Y, Harada T, Fujii A, Yoshida S, Iawbe T, Terakaw N. Menstrual cycle-specific inhibition of endometrial stromal cell proliferation by oncostatin m. *Mol Hum Reprod* (2001) 7(7):665–70. doi: 10.1093/molehr/7.7.665

44. Kubota Y, Hirashima M, Kishi K, Stewart CL, Suda T. Leukemia inhibitory factor regulates microvessel density by modulating oxygen-dependent VEGF expression in mice. *J Clin Invest* (2008) 118(7):2393–403. doi: 10.1172/JCI34882

frontiers | Frontiers in Immunology

TYPE Original Research
PUBLISHED 28 July 2022
DOI 10.3389/fimmu.2022.942640

OPEN ACCESS

EDITED BY
Diana Boraschi,
Shenzhen Institute of Advanced Technology (SIAT) (CAS), China

REVIEWED BY
Simona Sivori,
University of Genoa, Italy
Kyoung-Ho Pyo,
Yonsei University, South Korea

*CORRESPONDENCE
Cinzia Fionda
cinzia.fionda@uniroma1.it
Helena Stabile
helena.stabile@uniroma1.it

†These authors have contributed equally to this work and share senior authorship

SPECIALTY SECTION
This article was submitted to Cytokines and Soluble Mediators in Immunity, a section of the journal Frontiers in Immunology

RECEIVED 12 May 2022
ACCEPTED 04 July 2022
PUBLISHED 28 July 2022

CITATION
Kosta A, Mekhloufi A, Lucantonio L, Zingoni A, Soriani A, Cippitelli M, Gismondi A, Fazio F, Petrucci MT, Santoni A, Stabile H and Fionda C (2022) GAS6/TAM signaling pathway controls MICA expression in multiple myeloma cells.
Front. Immunol. 13:942640.
doi: 10.3389/fimmu.2022.942640

GAS6/TAM signaling pathway controls MICA expression in multiple myeloma cells

Andrea Kosta[1], Abdelilah Mekhloufi[2], Lorenzo Lucantonio[1], Alessandra Zingoni[1], Alessandra Soriani[1], Marco Cippitelli[1], Angela Gismondi[1], Francesca Fazio[3], Maria Teresa Petrucci[3], Angela Santoni[1,4,5], Helena Stabile[1*†] and Cinzia Fionda[1*†]

[1]Department of Molecular Medicine, Sapienza University of Rome, Rome, Italy, [2]Department of Biomedical Engineering, Emory University, Atlanta, GA, United States, [3]Division of Hematology, Department of Translational Medicine and Precision, Sapienza University of Rome, Rome, Italy, [4]Istituto di Ricovero e Cura a Carattere Scientifico (IRCCS) Neuromed, Pozzilli, Italy, [5]Istituto Pasteur-Fondazione Cenci Bolognetti, Sapienza University of Rome, Rome, Italy

NKG2D ligands play a relevant role in Natural Killer (NK) cell -mediated immune surveillance of multiple myeloma (MM). Different levels of regulation control the expression of these molecules at cell surface. A number of oncogenic proteins and miRNAs act as negative regulators of NKG2D ligand transcription and translation, but the molecular mechanisms sustaining their basal expression in MM cells remain poorly understood. Here, we evaluated the role of the growth arrest specific 6 (GAS6)/TAM signaling pathway in the regulation of NKG2D ligand expression and MM recognition by NK cells. Our data showed that GAS6 as well as MERTK and AXL depletion in MM cells results in MICA downregulation and inhibition of NKG2D-mediated NK cell degranulation. Noteworthy, GAS6 derived from bone marrow stromal cells (BMSCs) also increases MICA expression at both protein and mRNA level in human MM cell lines and in primary malignant plasma cells. NF-kB activation is required for these regulatory mechanisms since deletion of a site responsive for this transcription factor compromises the induction of *mica* promoter by BMSCs. Accordingly, knockdown of GAS6 reduces the capability of BMSCs to activate NF-kB pathway as well as to enhance MICA expression in MM cells. Taken together, these results shed light on molecular mechanism underlying NKG2D ligand regulation and identify GAS6 protein as a novel autocrine and paracrine regulator of basal expression of MICA in human MM cells.

KEYWORDS

GAS6, AXL, MERTK, MICA, NKG2D ligand, multiple myeloma, natural killer cells, bone marrow stromal cells

Introduction

Natural Killer (NK) cells are innate lymphocytes playing a prominent role in antitumor-immune response (1, 2). A complex repertoire of activating and inhibitory receptors controls their ability to recognize and kill target cells (3). Because high tumor-associated expression of ligands MICA, MICB and ULBPs, the stimulatory receptor NKG2D strongly contributes to NK cell response against solid and hematologic cancers (4, 5), including multiple myeloma (MM) (6), a neoplasia caused by accumulation of malignant plasma cells (PCs) in the bone marrow (BM). Advanced-stage MM is associated with defective recognition of cancerous PCs and suppression of NK cell function (7). Indeed, promising strategies to treat this incurable cancer include NK cell therapeutic approaches (8, 9). To this aim, several studies have focused on the comprehension of mechanisms underlying the expression of NKG2D ligands on MM cells. Of note, a number of oncoproteins, such as Hsp90, STAT3, IRF4, C-MYC and IKAROS/AIOLOS, emerged as negative regulators of *MICA* gene transcription (10–13). However, pathways driving basal expression of these ligands on MM cells remain largely unexplored. It is also completely unknown whether BM microenvironment plays a role in these mechanisms. The survival, proliferation and drug resistance of malignant PCs depend on autocrine and paracrine loops involving many cellular and non-cellular components of BM (14, 15). In particular, adhesive interaction as well as soluble factors released by BM stromal cells (BMSCs) strongly promote MM pathogenesis and progression (16). Our recent findings identified BMSCs as regulators of NK cell anti-MM response. We reported a role for IL-8-bearing microvesicles released by BMSCs in the regulation of the expression of Poliovirus receptor (PVR/CD155) (17), a ligand of the receptors DNAM-1, TIGIT and TACTILE/CD96 expressed by NK cells (18, 19).

Accumulating evidence demonstrated the contribution of GAS6/TAM pathway as an oncogenic signaling in MM pathogenesis (20–23). The TAM subfamily of tyrosine kinase receptors (RTK) includes TYRO3, AXL and MERTK (TAM) which are able to bind two vitamin-K dependent proteins, Growth arrest-specific gene 6 (GAS6) and Protein S (PROS1). Ligand binding induces dimerization and autophosphorylation of TAM receptors, followed by activation of many downstream pathways like MEK/ERK, PI3K/AKT and JAK/STAT signaling (24, 25).

MM cells express TAM receptors, mainly MERTK, and produce high amount of GAS6, which is also largely secreted by BMSCs (20, 22). In MM cells, TAM receptor activation triggers MAPK/ERK, PI3K/Akt and NF-kB signaling and promotes the survival and proliferation. Blockade of MERTK on MM cells or pharmacologic targeting of GAS6 reduces myeloma burden and increases survival of mice bearing an orthotopic myeloma model (22). Such effects support a role for GAS6/TAM receptors as novel therapeutic targets for this malignancy.

Importantly, TAM pathway can exert a direct regulatory activity on diverse immune cells, including NK cells. It is required for NK cell development and functional maturation in human and mice (26, 27). NK cells isolated from TAM-deficient mice have poor cytotoxic activity because of impaired expression of inhibitory and activating receptors. On the other hand, TAM-mediated signaling was shown to attenuate NK cell response in mouse metastasis models in a Cbl-b-dependent manner (28, 29). More recently, it was reported that activated human NK cells rapidly acquired TYRO3 from tumor cells *via* trogocytosis and become more cytotoxic (30).

However, the role of GAS6 and its receptors TYRO3, AXL and MERTK in the regulation of activating ligands and immunosurveillance of MM is unknown.

In this study, we investigated the impact of GAS6/TAM pathway on NKG2D-dependent recognition of MM cells. We demonstrated that defective TAM signaling causes a selective reduction of surface MICA expression on MM cells, compromising their ability to induce NKG2D-dependent NK cell degranulation. We also found that BMSC-derived GAS6 can promote the expression of this NKG2D ligand on MM cell lines and primary PCs *via* activation of NF-kB pathway.

Our findings provide evidence of a role for GAS6 protein as a novel autocrine and paracrine regulator of basal expression of MICA in human MM cells.

Materials and methods

Cell lines and clinical samples

Human MM cell lines SKO-007(J3) and ARP-1 were kindly provided by Prof. P. Trivedi (Sapienza, University of Rome, Italy). The human MM cell line U266 was kindly provided by Prof. Nicola Giuliani (University of Parma, Italy). These cell lines were maintained at 37°C and 5% CO_2 in RPMI 1640 (Life Technologies, Gaithersburg, MD) supplemented with 10% FCS, and were authenticated by IRCCS Azienda Ospedaliera Universitaria San Martino-IST, S.S. Banca Biologica e Cell factory (Genova, IT). The human 293T embryonic kidney cells were purchased from ATCC (Manassas, VA) and were maintained in Dulbecco's modified Eagle's supplemented with 10% FCS. All cell lines were mycoplasma-free (EZ-PCR Mycoplasma Test Kit, Biological Industries).

Bone marrow (BM) samples from MM patients were managed at the Division of Haematology, Department of Translational Medicine and Precision, Sapienza University of Rome. Informed consent in accordance with the Declaration of Helsinki was obtained from all patients, and approval was obtained from the

Ethics Committee of the Sapienza University of Rome (RIF.CE: 5191). BM aspirates were processed as described in (31). MM cells were selected using anti-CD138 magnetic beads (Miltenyi Biotec, Auburn, CA, USA). More than 95% of the purified cells expressed CD138 and CD38. Bone Marrow Stromal Cells (BMSCs) were obtained from $CD138^-$ fraction, phenotypically characterized and assessed for their capacity of osteogenic and adipogenic differentiation as previously described (17).

Reagents and antibodies

Monoclonal antibodies (mAbs) anti-CD138/FITC, anti-CD38/APC, anti-CD107a/APC, anti-CD45/Pecy7, anti-CD3/APC-H7, CD14/APC-H7, CD19/APC-H7 anti-CD56/BV421, anti-MERTK/BB700 (125518) and anti-Axl/BV711 (108724) were purchased from BD Biosciences (San Jose, California, USA). Unconjugated mAbs anti-MICA (MAB159227), anti-MICB (MAB236511), anti-ULBP1 (MAB170818), anti-ULBP2/5/6 (MAB165903), anti-ULBP3 (MAB166510), anti-NKG2D (MAB149810), anti-B7/H6 (MAB71444), anti-ICAM-1 (BBA3), anti-MICA/AF488 (MAB159227) and anti-Tyro3/AF488 (FAB859G) conjugated mAbs were all purchased from R&D System (Minneapolis, USA). Anti-PVR (SKII.4) was kindly provided by Prof. M. Colonna (Washington University, St Louis, MO). Anti-MHC class I (W6/32) mAb was purchased from ATCC (Manassas, Virginia, USA). Allophycocyanin conjugated with goat anti mouse (GAM-APC) (Poly4053) mAb was purchased from Jackson Immuno-Research Laboratories (Cambridgeshire, UK). Anti-GAS6 (D3A3G) mAb, anti-phosphorylated p65, anti-phosphorylated AXL and anti-AXL were purchased from Cell Signaling Technology (Danvers, MA, USA). Anti-p65 was purchased from Santa Cruz Biotechnologies (Dallas, TX, USA). Anti-β-Actin (AC-15) mAb was purchased from Sigma-Aldrich (St. Louis, MO, USA). Donkey anti-rabbit (NA934V) or sheep anti-mouse (NA931V) secondary Hrp-linked mAbs were purchased from GE Healthcare (Wisconsin, MA, USA). The inhibitor UNC2250 was purchased from Selleck (Houston, TX, USA).

Flow cytometry and degranulation assay

MM cell lines (1,5 x 10^5 cells/mL) were cultured for 72h in complete medium or in BMSC-conditioned medium (BMSCs-CM). Cells were stained with anti-MICA mAb followed by secondary goat anti-mouse APC Ab. In all experiments, cells were stained with Propidium Iodide (PI) (1 μg/mL) in order to assess cell viability (always higher than 90% after the different treatments). Nonspecific fluorescence was assessed by using an isotype-matched irrelevant mAb (R&D System, Minneapolis, USA) followed by the same secondary Ab. Patient-derived plasma cells (2x10^6 cells/mL) were cultured for 48h in BMSC-CM or complete medium supplemented with IL-3 (20 ng/mL) and IL-6 (2 ng/mL). The membrane expression of MICA was analyzed by immunofluorescence staining with anti-MICA/AF488 or matched isotype control. All samples were also stained with Fixable Viability Stain 450 (FVS450) (BD Biosciences, San Jose, California, USA) to discriminate cell viability.

NK cell-mediated degranulation was evaluated using the lysosomal marker CD107a as previously described (32, 33). As source of effector cells, we used PBMCs purified from healthy donor blood by Ficoll–Hypaque centrifugation or freshly cultured NK cells. SKO-007(J3) cells were incubated with PBMCs or with NK cells at effector:target (E:T) ratio of 1:1 and 2.5:1 respectively, in a U-bottom 96-well tissue culture plate in complete medium at 37°C and 5% CO2 for 2h. When PBMCs were used, cells were stained with Fixable Viability Stain APC-H7, anti-CD3/APC-H7, anti-CD19/APC-H7, anti-CD14/APC-H7, anti-CD45/Pecy7, anti-CD56/BV421 and anti-CD107a/APC. When cultured NK cells were used, cells were stained with Fixable Viability Stain APC-H7, anti-CD3/APC-H7, anti-CD56/BV421 and anti-CD107a/APC. In some experiments, cells were pre-treated for 20 min at room temperature with anti-NKG2D neutralizing mAb. Fluorescence was analyzed using a FACSCanto or FACS LRSFORTESSA flow cytometer (BD Biosciences, San Jose, California, USA) and data were analyzed by FlowJo V10 Cytometric Analysis Software (BD Biosciences, San Jose, California, USA).

Western-blot analysis

For Western-Blot analysis, whole cell extracts were obtained from SKO-007(J3) cells as previously described (34). Protein concentration was determined by the BCA method (Thermo Fisher Scientific, Waltham, MA USA). Thirty to 50 μg was resolved by SDSPAGE and transferred to nitrocellulose membranes (Whatman GmbH, Dassel, Germany). After blocking in bovine serum albumin, membranes were probed with specific Abs. An HRP-conjugated secondary Ab and an ECL detection system (Amersham, GE Healthcare, Wisconsin, MA, USA) were used to reveal immunoreactivity.

Plasmids

The pGL3 Basic -270bp MICA and −270bp MICA/Luc DEL 1 promoter constructs have been already described in (10). The lentiviral vector pHAGE-3xNF-kB-LUC-GFP expressing the green fluorescence gene insert and containing the luciferase gene driven by NF-kB-responsive consensus sequences and the plasmids pVSG-5, pPAX2, pGAg-Pol-Env, and pTK-Green Renilla (TK Renyl) were purchased from Addgene (Cambridge, Massachusetts, USA). The lentiviral vectors pLKO.1sh-GAS6, pLKO.1sh-AXL and pLKO.1sh-PROS1

expressing a short hairpin RNA for GAS6, AXL and PROS1 respectively, and the puromycin gene resistance, were generated by inserting shRNA sequences in pLKO.1 lentiviral vector purchased from Addgene (Cambridge, Massachusetts, USA). The following forward and reverse shRNA sequences were used: human GAS6 shRNA forward, 5'CCGGGCAGACA ATCTCTGTTGAGGACTCGAGTCCTCAACAGAGATTGT CTGCTTTTTG-3'; human GAS6 shRNA reverse: 5'-AATTCAAAAAGCAGACAACTCTGTTGAGGACTCGAGTC CTCAACAGAGATTGTCTGC-3'; human AXL shRNA forward: 5'-CCGGCGAAATCCTCTATGTCAACATCTCGAG ATGTTGACATAGAGGATTTCGTTTTTG-3'; human AXL shRNA reverse: 5'-AATTCAAAAACGAAATCCTCTATG TCAACATCTCGAGATGTTGACATAGAGGATT TCG-3'; human PROS1 shRNA forward, 5' CCGG CCTACAAAT GACAGTTTCAAT CTCGAG ATTGAAACTGTCATTTGTA GGTTTTTG -3'; human PROS1 shRNA reverse: 5'- AATT CAAAAA CCTACAAATGACAGTTTCAAT CTCGAGATT GAAACTGTCATTTGTAGG-3'. All constructs were verified by DNA sequence analysis. For knocking down MERTK, we used pLKO.1-shMERTK (TRCN0000442967) lentiviral vector and the control vector pLKO.1 non-targeting shRNA (MISSION^{TM} Sigma-Aldrich, St. Louis, MO, USA).

DNA transfections, virus production and *in vitro* transduction

For virus production, HEK293T was transfected with viral DNA together with packaging vectors, using Lipofectamine 2000 (Life Technologies, Gaithersburg, MD) as previously described (35). SKO-007(J3) and BMSCs cells were infected as previously described (17). SKO-007(J3) cell stable clones expressing pHAGE-3xNF-kB-LUC-GFP were previously described (17). For GAS6, PROS1, AXL and MERTK silencing, MM cell lines were allowed to expand for 24 h and were then selected for 3 days for puromycin resistance (1 µg/mL). SKO-007(J3) cells were transfected using Amaxa nucleofection procedure (Lonza Bioscience, Morrisville, USA) as already described (17) and treated with BMSC-conditioned medium. After 48h, cells were collected, and protein extracts were prepared for the luciferase assay. A TK-renilla expression vector was co-transfected each time to normalize DNA uptake. Luciferase and renilla activity were read using Dual-Luciferase Reporter Assay and the Glomax Multi Detection System (Promega, Madison, USA) following the manufacturer's instructions.

RNA isolation and quantitative real-time polymerase chain reaction (qRT-PCR)

Total RNA was extracted using the total RNA mini-Kit following instructions provided by the manufacturer (Geneaid Biotech Ltd, Taiwan) and 2 µg were used for cDNA first-strand synthesis in a 25 µl reaction volume according to the manufacturer's protocol for M-MLV reverse transcriptase (Promega, Madison, USA). MICA, GAS6 and GAPDH mRNA expression were analyzed by real-time PCR using the following specific TaqMan Gene Expression Assays (Applied Biosystems, Foster City, CA): MICA (Hs00792195_m1), GAS6 (Hs1090305_m1), PROS1 (Hs00165590_m1) and GAPDH (Hs03929097_g1) conjugated with fluorochrome FAM.

The level of expression was measured using Ct (threshold cycle). Relative expression of each gene versus the housekeeping gene was calculated according to the $2^{-\Delta\Delta Ct}$ method. The analysis was performed using the SDS version 2.4 software (Applied Biosystems, Foster City, CA).

Annexin V

Apoptotic cell death was evaluated using APC Annexin-V Apoptosis Detection Kit with PI (Thermo Fisher Scientific, Waltham, MA USA). Briefly, 1.5×10^4/mL SKO-007(J3) cells infected with lentivirus pLKO.1-shRNA-GAS6 or non-target shRNA were culture in 24-well plates for 72h. Cells were then stained using Annexin-V/APC and PI according to the manufacturer's instruction. Cell populations were acquired using FACS Canto II flow cytometer (BD Biosciences, San Jose, California, USA). Flow cytometric analysis was performed using Flow Jo Flow Cytometric Analysis Software.

Enzyme-linked immunosorbent assay (ELISA)

BMSC-conditioned medium and bone marrow plasma were analyzed for GAS6 by ELISA following instructions provided by the manufacturer (R&D System, Minneapolis, USA). BMSC-CM was collected from 72h culture of $20x10^3$ BMSCs in 1 mL of serum free-medium in a 24-well plate. Absorbance was measured at 450/540nm with Victor2 Microplate Reader (Perkin Elmer – GMI Waltham, Massachusetts, USA), and GAS6 concentration was calculated in correlation to a standard curve of control samples.

Preparation of BMSC-CM

Medium collected from 72h-culture of confluent BMSCs ($2x10^4$ cells) (BMSCs-CM) was used to stimulate MM cell lines for 72h. In some experiments, BMSCs-CM was treated with Proteinase K (250µg/mL) (Sigma-Aldrich, St. Louis, MO, USA) for 1h at 65°C. BMSCs-CM and complete RPMI1640 medium were separated in different fractions by Amicon Ultra-15 centrifugal filter devices (Merck Millipore,

Darmstadt, Germany) according to the manufacturer's instructions.

Statistical analysis

Statistical significance between two groups was determined by performing two-tailed, Student's t-test, Anova. Prism 6 (GraphPad) software was used. Graphs show mean values, and error bars represent the SD or SEM.We used non-parametric t-test (Mann Whitney test). P-value of < 0.05 (*), < 0.01 (**), < 0.001 (***), and < 0.0001 (****) was considered statistically significant, when not indicated, data were not statistically significant. Multiple comparisons were performed using univariate analysis of variance (Two-way Anova with Bonferroni's post-test).

Results

GAS6/TAM signaling pathway regulates MICA expression in human MM cells

GAS6 and its receptors TYRO3, AXL and MERTK contribute to MM pathobiology (21, 22), however the role of these molecules in the regulation of immune attack of malignant PCs remains to be elucidated.

Here, we investigated the effect of GAS6/TAM signaling pathway on the regulation of NKG2D ligands in three MM cell lines [SKO-007(J3), U266 and ARP1]. Among TAM receptors, these MM cell lines lack TYRO3 but express MERTK, while AXL is present only on SKO-007(J3) cells (Supplementary Figures 1A, 2A–E). Thus, we performed a flow cytometric analysis on MM cells silenced for the ligands GAS6 and PROS1 or the receptors AXL and/or MERTK by lentiviral-transduced small-hairpin RNAs (shRNAs). Since stable depletion of these proteins is cytotoxic for MM cells (20, 22), these experiments were performed using transient infection without any significant effect on cell viability (as assessed by Annexin V staining) (Supplementary Figure 1C). We found that knockdown of GAS6, PROS1, AXL or MERTK was able to significantly reduce MICA surface levels in MM cell lines (Figures 1C, E, G, I and Supplementary Figures 2B, C, F, G). Differently, depletion of GAS6 did not affect the expression of other NKG2D ligands (MICB and ULBPs), NKp30 ligand B7/H6, DNAM-1 ligand PVR, MHC class I and of the adhesion molecule ICAM-1 (Supplementary Figure 1B).

These results indicate a role for TAM pathway in sustaining the basal expression of MICA in MM cells.

We then examined whether MICA downregulation could be the consequence of a decreased mRNA expression. To this aim, total RNA was isolated from SKO-007(J3) cells infected with lentivirus pLKO.1-shRNA GAS6, PROS1, AXL or MERTK or non-target shRNA, and analyzed by real-time quantitative RT-PCR. Consistent with FACS analysis, silencing of these proteins decreased basal *MICA* mRNA levels (Figure 1J).

To evaluate the functional consequences of changes in MICA expression, we analyzed the degranulation of healthy donor NK cells against SKO-007(J3) cells or U266 infected with lentivirus pLKO.1-shRNA GAS6 or non-target shRNA (pLKO.1-control). As shown in Figures 2B–E, expression of CD107a on NK cells was decreased when co-cultured with GAS6 depleted-SKO-007(J3) or U266 target cells. Moreover, a blocking anti-NKG2D mAb impaired NK cell degranulation against SKO-007(J3) or U266 pLKO.1-control, and U266 pLKO.1-GAS6 shRNA; however, it failed to reduce the activation of NK cells contacting SKO-007(J3) pLKO.1-GAS6 shRNA.

In lines with previous studies (6, 10, 11, 36), these findings demonstrate that constitutive NK cell degranulation against MM cells involves NKG2D. More importantly, they indicate that MICA downregulation on GAS6 depleted- SKO-007(J3) and U266 cells compromises their NKG2D-dependent recognition by NK cells.

BMSC-derived GAS6 increases MICA surface expression in MM cells

Myeloma BM microenvironment is highly enriched in GAS6 (22), which is also largely produced by BMSCs and tumor cells (Figure 3A and Supplementary Table 1). We thus analyzed the possible effects of MM patient derived-BMSCs on MICA expression in MM cells. We observed that conditioned medium (BMSCs-CM) collected after 72h culture of MM-BMSCs could induce AXL phosphorylation in SKO-007(J3) (Figure 3B) and up-regulated the basal membrane expression of MICA on SKO-007(J3), ARP-1 and U266 cell lines (Figures 3C, D). Moreover, we found that MM patient-derived PCs cultured in autologous or heterologous BMSC-CM for 48h expressed higher levels of MICA than primary myeloma cells cultured in RPMI1640 medium alone (Figure 3E and Supplementary Table 2). However, BMSC-CM did not affect the expression of MICB on these cells (data not shown). Consistently, BMSC-CM-treated SKO-007(J3) were more capable to activate NK cell degranulation. This effect was significantly inhibited by a blocking anti-NKG2D mAb, indicating that stimulation of NK cell degranulation was dependent on NKG2D activation (Figures 3F, G).

To gain insight into the nature of the BMSCs-derived factor (s) capable of enhancing MICA expression on MM cells, BMSC-CM was pre-treated with the serine protease Proteinase K for 1h before to be used to stimulate SKO-007(J3) cells for 72h. As shown in Figure 4A, we found that pre-treatment with this enzyme able to degrade proteins abolished the capability of BMSC-CM to increase the expression of MICA on MM cells. These findings indicate that soluble factor(s) produced by

BMSCs involved in these mechanisms are protein(s). Then, using centrifugal filtration with a semi permeable membrane of different molecular weight cutoff, we separated BMSC-CM and complete RPMI1640 medium, used as a control, into fractions ranging from 100 to 10 KDa. Fractioned BMSC-CM or complete RPMI1640 medium were used to stimulate SKO-007(J3) cells for 72h. In line with our data implying GAS6 (75 KDa) in MICA up-regulation, we observed that this NKG2D ligand augmented in SKO-007(J3) cells exposed to the fraction >50KDa (Figure 4B). Consistently, CM derived from BMSCs lacking GAS6 (Figures 4C, D) was not able to augment MICA expression on SKO-007(J3) cells (Figure 4E).

Taken together, these results demonstrate that autocrine and paracrine production of GAS6 is implicated in the regulation of MICA on MM cells.

Role of NF-kB in MICA up-regulation by BMSCs

To examine the molecular mechanisms underlying MICA up-regulation, we performed real-time quantitative RT-PCR on total RNA isolated from SKO-007(J3) cells and PCs isolated from different MM patients cultured in BMSC-CM for 48h. We found a significant increase of *MICA* mRNA levels in treated MM cells (Figures 5A, B). Thus, we investigated the direct effect of BMSC-CM on the activity of the *MICA* promoter. As shown in Figure 5C, by transient transfection assays, we observed that BMSC-CM enhanced the luciferase reporter activity driven by a 270bp 5′-flank of *MICA* promoter.

Collectively, these data indicate that *MICA* mRNA expression and promoter activity are enhanced by BMSC-CM in MM cells.

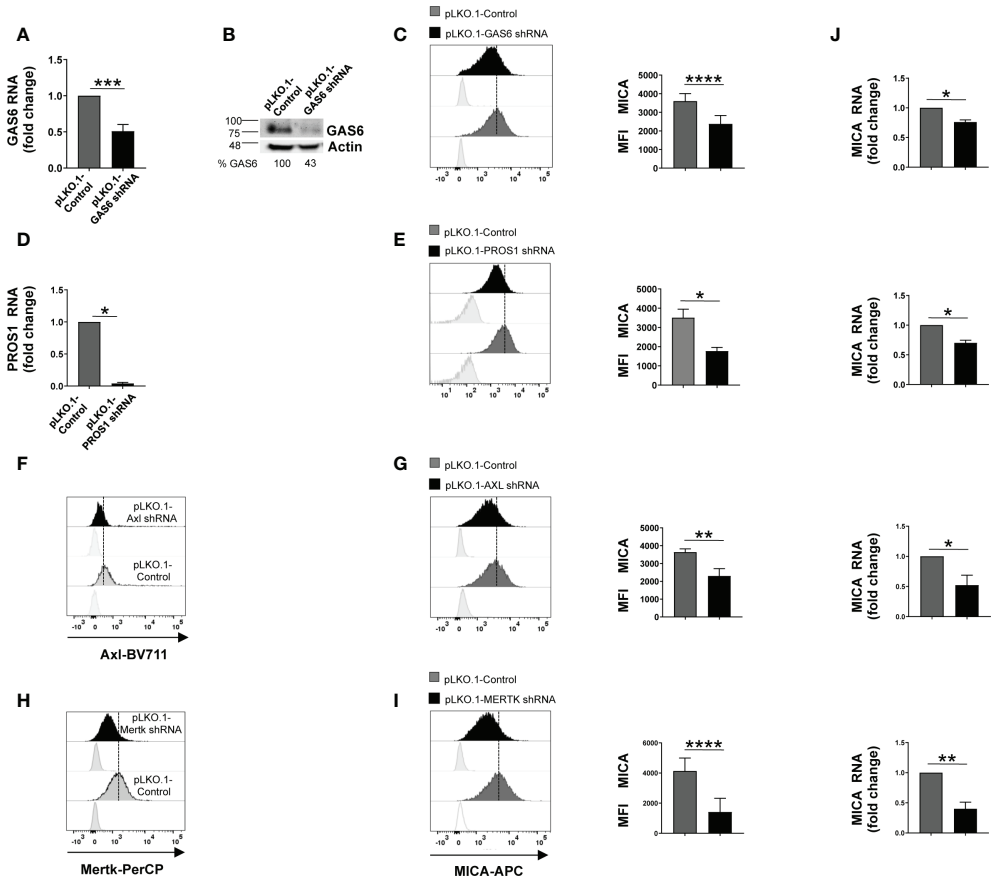

FIGURE 1
Silencing of GAS6, PROS1 or TAM receptors reduces MICA expression in SKO-007(J3) cells. Total mRNA and protein extracts obtained from SKO-007(J3) pLKO.1-GAS6 shRNA or pLKO.1-PROS1 shRNA and pLKO.1-Control were analyzed for GAS6 or PROS1 expression by real-time PCR **(A–D)** and Western Blot **(B)**. AXL and MERTK receptor expression was analyzed by FACS on SKO-007(J3) pLKO.1-Control, pLKO.1-AXL shRNA **(F)** or pLKO.1-MERTK shRNA **(H)**. MICA expression was analyzed by flow cytometry and real-time PCR in SKO-007(J3) pLKO.1-GAS6 shRNA (n=6) **(C)**, pLKO.1-PROS1 shRNA (n=3) **(E)**, pLKO.1-AXL shRNA (n=6) **(G)**, pLKO.1-MERTK shRNA (n=6) **(I)** or pLKO.1-Control. Histograms represent the MFI of specific mAb subtracted of MFI of isotype control. Data are shown as mean ± SD (****p < 0.001; ***p < 0.005; **p < 0.01; *p < 0.05 Mann-Whitney Test). For real-Time PCR analysis **(J)**, data, expressed as fold change units, were normalized with GAPDH and referred to pLKO.1-Control, considered as calibrator. Data are shown as mean ± SD (**p < 0.01; *p < 0.05; Mann-Whitney Test).

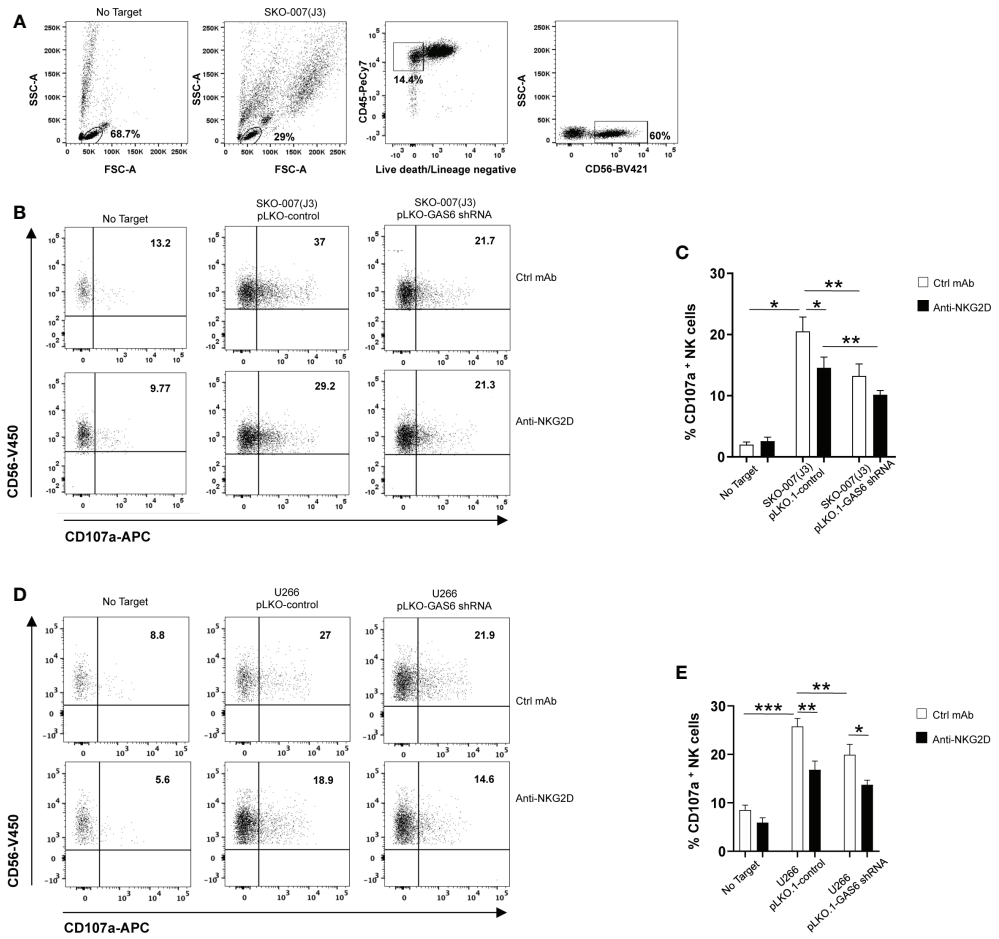

FIGURE 2
Impaired NKG2D-dependent recognition of GAS6-depleted MM cells. Healthy donor-derived PBMCs were incubated with SKO-007(J3) **(A–C)** or U266 **(D, E)** pLKO.1-GAS6 shRNA or pLKO.1-Control at E/T ratio of 1:1. CD107a expression was analyzed on $CD3^{-}CD19^{-}CD14^{-}CD45^{+}CD56^{+}$ NK cells as shown in **(A, B)**. To evaluate the role of NKG2D, the assay was performed in parallel treating NK cells with blocking anti-NKG2D or anti-IgG mAb used as control (Ctrl). Results are expressed as the percentage of $CD107a^{+}$ NK cells. A representative experiment for each MM cell line is shown in **(B, D)**. Histogram represents the mean ± SD from three independent experiments **(C, E)** (*$p < 0.05$; **$p < 0.001$; ***$p < 0.005$ ANOVA).

Previous reports demonstrated a role for NF-kB in the regulation of MICA expression in different types of cells (e.g. T lymphocytes, endothelial cells and MM cells) (37, 38) NF-kB proteins are constitutively active in MM cells but BMSCs produce many soluble factors, including GAS6, which further trigger this signaling pathway in these tumor cells (16, 20, 39, 40). For this reason, we investigated the role for NF-kB in MICA regulation by BMSCs.

First, we observed that GAS6 depleted-BMSC-CM has a reduced capability to induce phosphorylation of p65 and to enhance NF-kB transcriptional activity in SKO-007(J3) cells; moreover, the TAM receptor inhibitor UNC2250 partially blocks phosphorylation of p65 by BMSC-CM in these cells (Figures 5D, E). Accordingly, we found reduced levels of phosphorylated p65 in GAS6 silenced SKO-007(J3) cells (Figure 5F). These findings indicate a direct contribute of autocrine and paracrine GAS6 as a regulator of NF-kB pathway in MM cells.

Second, we revealed that the stimulatory effect of BMSC-CM was significantly diminished on a mutated version of *MICA* promoter (indicated as DEL1), in which a putative NF-kB site (41) was removed by site-directed mutagenesis (Figure 5G), thus indicating that binding of this transcription factor to this region is required for promoter activation.

Taken together, these findings demonstrate that NF-kB can act as an activator of MICA expression in MM cells in response to GAS6 secreted by BMSCs.

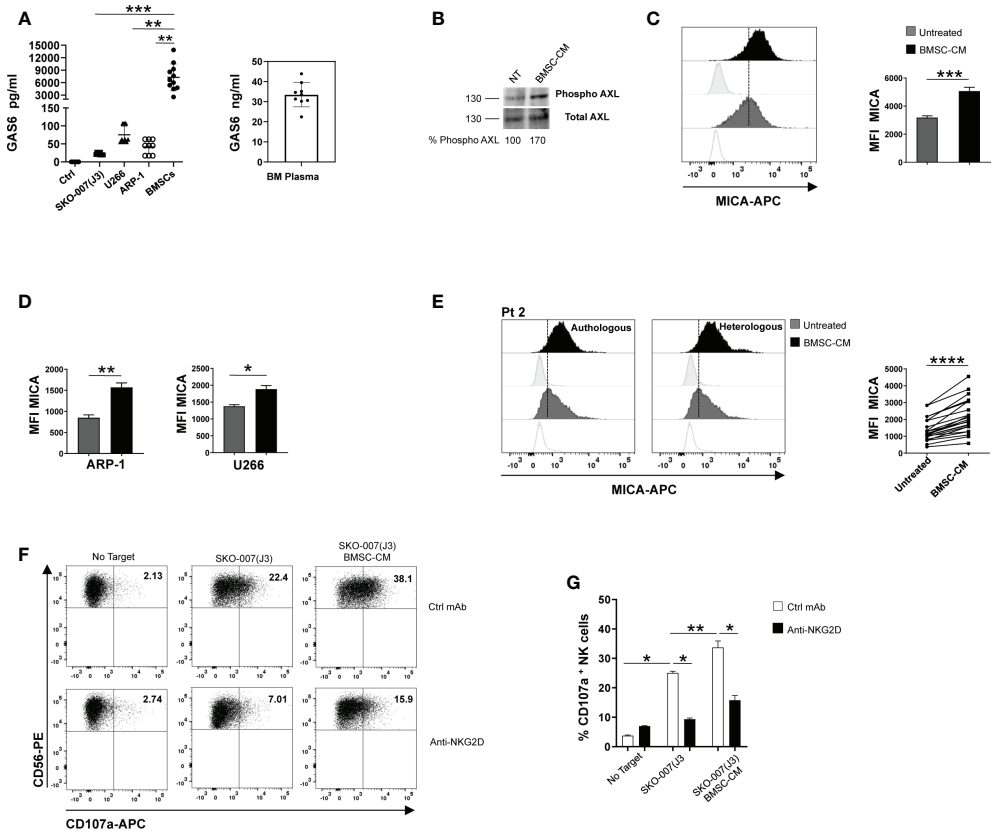

FIGURE 3
BMSC-CM up-regulates MICA surface expression in MM cells. GAS6 protein was quantified by ELISA in conditioned medium (CM) derived from the indicated MM cell lines, BMSCs and plasma from BM aspirates of MM patients. Serum free medium was used as control (Ctrl) **(A)**. Total protein extracts obtained from SKO-007(J3) untreated or treated for 1h with BMSC-CM were analyzed for phosphorylated and total AXL expression by Western Blot **(B)**. Numbers represent densitometric analysis of phosphorylated AXL normalized relative to untreated cells. MICA surface expression was analyzed by flow cytometry in SKO-007(J3) (n=8) **(C)**, ARP-1 (n=6) or U266 (n=5) MM cell line **(D)** or in primary malignant PCs (n=12) **(E)** untreated or treated with BMSC-CM for 72h or 48h, respectively. A representative experiment is shown. Histograms represent the MFI of specific mAb subtracted of MFI of isotype control. Data show mean ± SD (*****p* < 0.001; ****p* < 0.005; ***p* < 0.05; Mann -Whitney Test). NK cells derived from healthy donor PBMCs were incubated with SKO-007(J3) cells, untreated or cultured for 72h with BMSC-CM and used as target cells in a degranulation assay as described above. Results are expressed as the percentage of $CD107a^+$ NK cells **(F)**. A representative experiment is shown in **(E)**. Histogram represents the mean ± SD from three independent experiments **(G)** (**p* < 0.05; ***p* < 0.001 ANOVA).

Discussion

Natural Killer cells are important effectors of anti-MM immune response. Yet, malignant PCs acquire the ability to elude NK cell recognition and suppress their function (7, 42). To overcome NK cell dysfunctions associated to disease progression, innovative treatments include the adoptive NK cell therapy and monoclonal antibodies to enhance NK cell-versus-MM effect (8, 9); in parallel, tumor modulating agents able to render MM cells more susceptible to NK cell attack also represent promising therapeutic tools. NKG2D is a key activating receptor involved in these mechanisms (6, 43), thus understanding how expression of its ligands is regulated on malignant PCs could be helpful to address these approaches.

Regulation of NKG2D ligand expression in MM cells mainly relays on transcriptional and post-translational mechanisms (44). A number of transcription factors, highly expressed and active in these tumor cells, where they control aberrant and malignancy-specific gene expression program, are also involved in the regulation of NKG2D ligand expression. Our group identified Hsp90, STAT3, IRF4, C-MYC and IKAROS/AIOLOS as repressors of *MICA* and/or *MICB* gene transcription (10–13). These findings indicate that MM cells have developed the capability to exploit the same pathways to promote their growth as well as to reduce immune recognition. Further, a relevant immune escape mechanism is represented by the down-regulation of NKG2D ligands on the surface of MM cells by proteolytic shedding (45). In particular, soluble MICA is

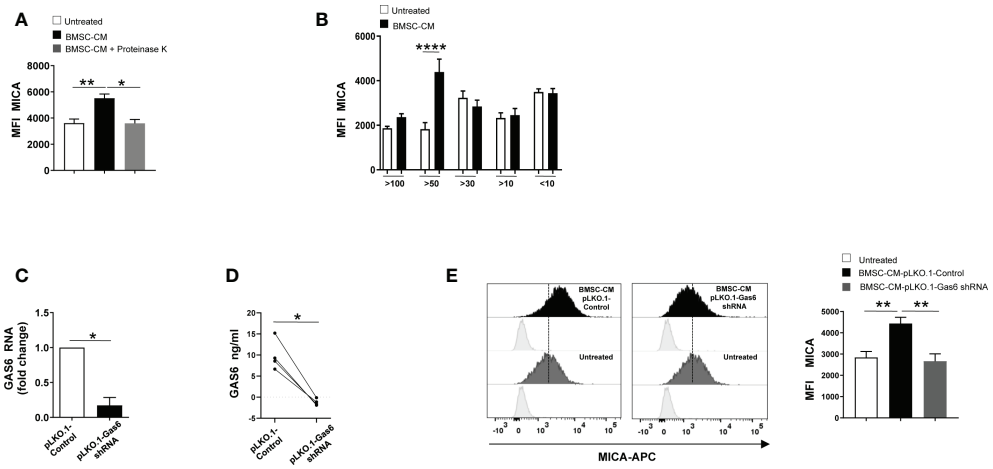

FIGURE 4
GAS6 controls MICA up-regulation in BMSC-CM-treated MM cells. Flow cytometry analysis of MICA surface expression on SKO-007(J3) cells cultured for 72h in BMSC-CM, pre-treated or not with proteinase K **(A)**, or in fractions of different molecular weight obtained from BMSC-CM (n=8) **(B)**. Histograms represent the MFI of specific mAb subtracted of MFI of isotype control. Data show mean ± SD (*$p < 0.05$; **$p < 0.005$; ****$p < 0.001$; ANOVA). Analysis of *GAS6* mRNA **(C)** and protein **(D)** in BMSCs infected with lentiviral vector expressing GAS6 shRNA (pLKO.1-GAS6 shRNA) or scramble control (pLKO.1-Control) (n=4). Data show mean ± SD (*$p < 0.05$; Mann-Whitney Test). MICA surface expression was analyzed by FACS on SKO-007(J3) treated for 72h with CM derived from BMSCs pLKO.1-GAS6 shRNA or pLKO.1-Control (n=3) **(E)**. Histograms represent the MFI of specific mAb subtracted of MFI of isotype control. Data show mean ± SEM (**$p < 0.001$; ANOVA).

overexpressed in the serum of MM patients, and its levels correlate with tumor progression (46).

However, little is currently known about signaling events and molecular mechanisms responsible for basal expression of NKG2D ligands in MM cells.

Here, we provide first evidence that surface MICA expression is regulated by GAS6/TAM pathway in MM cells. We demonstrate that: (1) GAS6/AXL and MERTK signaling, in a cell-autonomous way, sustains MICA expression in MM cells; (2) GAS6 secreted by BMSCs augments membrane MICA expression on MM cells at transcriptional level; (3) NF-kB pathway mediates MICA up-regulation by GAS6.

GAS6/TAM signaling components are overexpressed in MM cells and support their survival and proliferation (20, 22). We found that MM cells silenced for the ligand GAS6 or PROS1, or the receptors AXL and MERTK by lentiviral-transduced shRNAs express reduced levels of MICA, both at protein and mRNA level, and are less susceptible to NKG2D mediated-recognition by NK cells.

The contribution of soluble factors in the regulation of this ligand has been previously described. A number of cytokines and growth factors, such as TGF-β, IL-10, IFN-γ and EGF function as regulators of MICA expression in different types of cancer cells (47–50).

Here, we demonstrate that a peculiar regulatory circuitry, involving both autocrine and paracrine GAS6, assures MICA expression on MM cells. Indeed, MM BM microenvironment is highly enriched in GAS6 (22), which is largely produced by BMSCs. We found a significant up-regulation of membrane MICA expression on MM cell lines as well as on patient-derived PCs by BMSC-CM. However, knockdown of GAS6 in BMSCs abolished these effects. Interestingly, we have already described that BMSCs enhance PVR surface expression on MM cells and promote their NK cell-mediated recognition (17). Our novel findings confirm that expression of NK cell activating ligands on malignant PCs is highly dependent on BM microenvironment.

Our data also indicate that the transcription factor NF-kB is critically involved in MICA regulation by GAS6/BMSCs.

NF-kB was found to be a positive regulator of *MICA* gene in different cellular contexts. In activated T lymphocytes and epithelial cancer cell lines, NF-kB acts by binding to a specific sequence in the long intron 1 of the *MICA* gene (37, 38). Furthermore, in human endothelial cells TNF-α-induced NF-kB binds a regulatory control site at -130 bp upstream of the *MICA* transcription start site (41).

Here, we first observed reduced NF-kB activation in MM cells lacking GAS6 and after treatment with GAS6 depleted-BMSC-CM, thus revealing that TAM receptor signaling controls NF-kB activity in these tumor cells. Second, by a site-directed mutagenesis approach, we proved that deletion of an NF-kB responsive element (41) compromises the induction of *MICA* promoter by BMSC-CM. Based on these observations, we propose a role for NF-kB as a direct positive regulator of *MICA* promoter in MM cells.

Previous studies have described a negative impact of TAM pathway on immunological visibility of tumor cells *via*

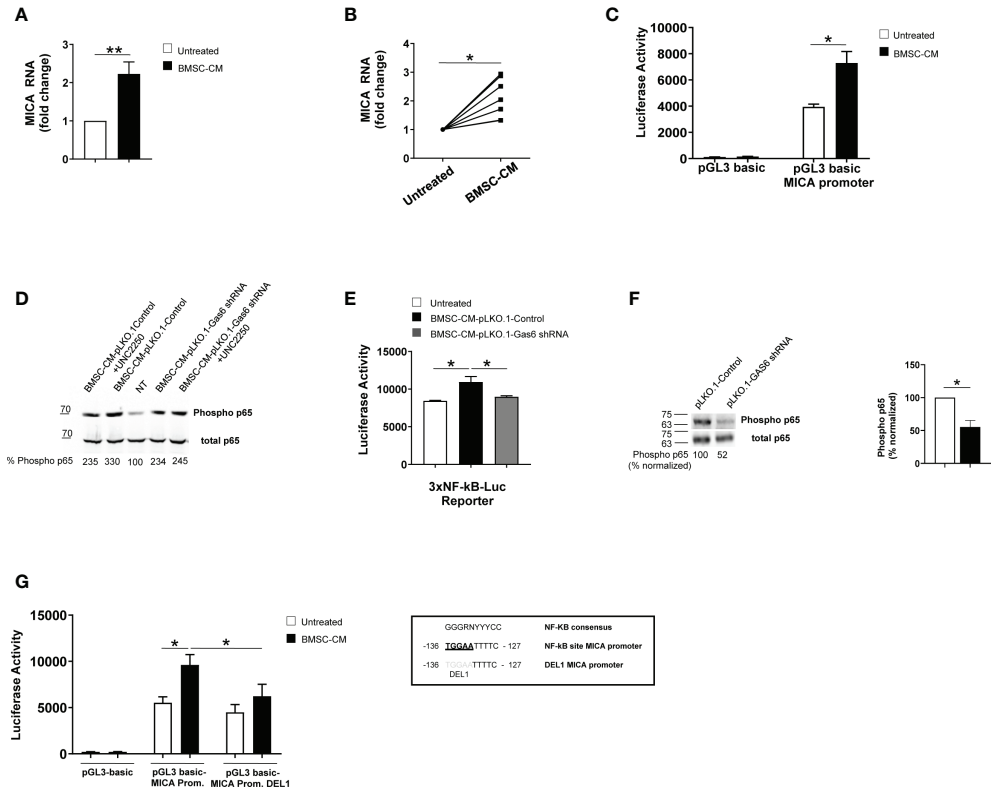

FIGURE 5
BMSC-CM increases *MICA* mRNA expression and promoter activity *via* NF-kB activation. Real time PCR analysis of total mRNA obtained from SKO-007(J3) cells **(A)** or patient-derived PCs **(B)** after 48h stimulation with BMSC-CM or complete medium. Data, expressed as fold change units, were normalized with GAPDH and referred to the untreated cells, considered as calibrator. For SKO-007(J3) cells, histograms represent the mean ± SD from six independent experiments. For primary PCs, data from 7 MM patients are shown where each dot represents a single patient. (*P< 0.05; **P<0.005; Mann-Whitney Test). SKO-007(J3) cells were transiently transfected with pGL3 basic empty vector/MICA 270bp promoter plasmid **(C)** and/or a DEL1-270bp MICA promoter plasmid (in which a putative NF-kB site indicated in the figure was removed by site-directed mutagenesis) **(G)** or infected with lentivirus pHAGE-3xNF-kB-LUC-GFP **(E)** as described in materials and methods. After 48h of treatment with BMSC-CM, SKO-007(J3) cells were harvested, and protein extracts were prepared for the luciferase assay. Data, expressed as relative luciferase activity, were normalized to protein concentration and renilla activity and represent the mean±± SEM from three independent experiments (*p < 0.05; ANOVA). Total protein extracts obtained from SKO-007(J3) treated with CM derived from BMSCs pLKO.1-GAS6 shRNA or pLKO.1-Control in the absence or in the presence of UCN2250 (1 μM) **(D)** or SKO-007(J3) infected with lentivirus pLKO.1-GAS6 shRNA or pLKO.1-Control **(F)** were analyzed for phosphorylated and total p65 expression by Western Blot. Numbers represent densitometric analysis of phosphorylated p65 normalized relative to untreated cells.

upregulation of NK cell inhibitory ligands. As an immune evasion mechanism, AXL signaling was shown to increase surface expression of MHC-class I molecules and PDL-1 in lung, renal and breast cancer cell lines (51–53). In our experimental setting, either silencing of GAS6 or culture with BMSC-CM did not affect MHC-class I expression in MM cells, while the possible effects on other NK cell inhibitory ligands were not investigated. However, the absence of GAS6 in MM cells reduces their capability to activate NK cells, whereas BMSC-CM renders MM more susceptible to recognition by both NK cells from healthy donors and MM patients (17). Such functional consequences do not suggest any relevant change of inhibitory pathways by GAS6/TAM signaling in MM cells, but further studies are needed to address this possibility.

Although unexcepted, our data are not the first demonstration on the positive regulation of MICA by an oncogenic pathway. Another major cell-autonomous component of tumor progression, EGFR, was shown to drive basal expression of NKG2D ligands in epithelial cancer cells (50). Together these and our observations indicate that oncogenic signaling pathways may be relevant at the early stages of cancer when they become dysregulated, and expression of activating ligands is key for immune surveillance.

Remarkably, GAS6/TAM pathway is also a key regulator of immune homeostasis (25). Innate and adaptive immune cells, in

humans and mice, express TAM receptor/ligands and blocking TAM signaling causes severe defects in the clearance of apoptotic cells, widespread inflammation and over-activation of the immune system, and development of systemic autoimmunity (54).

This axis signaling is also known to regulate NK cell differentiation and function. Binding of GAS6 to TAM receptors inhibits murine NK cell function by phosphorylating Cbl-b, which promotes the degradation of LAT1. Consistently, administration of GAS6 or TAM receptor inhibitors leads to rejection of metastatic tumors (28, 29). However, to our knowledge, there is no evidence of these inhibitory effects on human NK cells. In contrast, a recent study proposed TYRO3 as an NK cell activating receptor showing that activated human NK cells can acquire the receptor upon contact with tumor cells *via* trogocytosis and that TYRO3$^+$ NK cells are more cytotoxic and produce more IFN-γ (30). Activating effects were also reported for MERTK in human CD8$^+$ T cells, where the receptor functions as a co-stimulatory signal promoting proliferation and generation of memory T cells (55).

The role of TAM receptors in the regulation of NK cells in MM has never been investigated. In the context of a study on NK cells from newly diagnosed and refractory relapsed MM, an RNA seq analysis showed a reduction of *AXL* and *GAS6* gene expression (56), thus suggesting that inhibitory signals generated by GAS6/TAM components may not be related to NK cell dysregulation in this malignancy. However, these mechanisms remain to be studied.

Due to their pro-oncogenic and putative immune-inhibitory effects, TAM receptors have emerged as promising targets for cancer therapy. Indeed, many clinical trials are currently investigating TAM targeting therapies in solid and hematologic cancers. However, further investigations are required to elucidate the contribute of different TAM receptors on distinct immune cell types during anti-tumor immune response. Indeed, the impact on immune system and immune surveillance are relevant aspects to evaluate in design drugs targeting cancer cells. In this context, our data suggest that the modulation of MICA on tumor cells may be a potential limiting effect of GAS6/TAM inhibitors on immune surveillance. To this regard, a recent report demonstrated the feasibility of using autologous NK cells bearing NKG2D-CAR to treat MM. These cells have robust cytotoxic activity against MM cells *in vitro* and exhibit high efficiency *in vivo* in a mouse model of MM (57). In this therapeutic perspective, it would be important to preserve and/or enhance NKG2D ligand expression on tumor cells, and our finding could be helpful in setting the right combined therapy.

Overall, these data reveal a novel immunoregulatory role for the GAS6/TAM pathway and shed light on molecular mechanisms underlying basal MICA expression in MM cells.

Data availability statement

The original contributions presented in the study are included in the article/**Supplementary Material**. Further inquiries can be directed to the corresponding authors.

Ethics statement

The studies involving human participants were reviewed and approved by RIF.CE: 5191. The patients/participants provided their written informed consent to participate in this study.

Author contributions

CF, AK, AM, LL, and HS performed the experiments and analyzed the results; HS, ASo, AZ, and MC contributed with analytic tools and analyzed the results; MP and FF provided and managed bone marrow samples from patients; AG and ASa critically reviewed the manuscript. CF and HS contributed to design research and write the manuscript. All authors contributed to the article and approved the submitted version.

Funding

This work was supported by grants from andMinistero dell'Istruzione, dell'Università e della Ricerca (PRIN cod. 20174T7NXL and 2017NTK4HY), Ricerca Universitaria (RP120172A7CD4ACB).

Acknowledgments

The authors thank all patients who contributed to this study.

Conflict of interest

The authors declare that the research was conducted in the absence of any commercial or financial relationships that could be construed as a potential conflict of interest.

Publisher's note

Supplementary material

The Supplementary Material for this article can be found online at: https://www.frontiersin.org/articles/10.3389/fimmu.2022.942640/full#supplementary-material

SUPPLEMENTARY FIGURE 1
Defective TAM signaling causes a selective reduction of MICA expression in SKO-007(J3). TAM (TYRO3, AXL, MERTK) receptor expression was analyzed by FACS on SKO-007(J3) cells **(A).** A representative experiment is shown. Flow cytometry analysis of the indicated surface molecules on SKO-007(J3) pLKO.1-GAS6 shRNA or pLKO.1-Control (n=3). A representative experiment is shown (**B**, left panel). Histograms represent the MFI of specific mAb subtracted of MFI of isotype control. Data are shown as mean ± SD (*P< 0.05; Mann-Whitney) (**B**, right panel). SKO-007(J3) pLKO.1-GAS6 shRNA or pLKO.1-Control were stained using Annexin-V/APC and Propidium Iodide. A representative experiment is shown (**C,** left panel). Histograms indicate the percentage of Annexin V or propidium positive cells and were calculated based on at least three independent experiments (**C**, right panel).

SUPPLEMENTARY FIGURE 2
Depletion of GAS6 or TAM receptors reduces MICA expression in U266 and ARP-1 cells. TAM (TYRO3, AXL, MERTK) receptor expression was analyzed by FACS on U266 **(A)** and ARP-1 cells **(E)**. A representative experiment is shown. MERTK and MICA surface expression was analyzed by FACS on U266 **(B)** or ARP-1 **(F)** pLKO.1-Control and pLKO.1-MERTK shRNA or pLKO.1-GAS6 shRNA **(C, F)** (n=3). In pLKO.1-GAS6 shRNA transduced U266 **(D)** or ARP-1 **(H)** ULBPs, B7/H6, PVR and ICAM1 expression was also analyzed. Histograms represent the MFI of specific mAb subtracted of MFI of isotype control. Data are shown as mean ± SD (*P< 0.05; Mann-Whitney). Total mRNA obtained from U266 **(C)** or ARP-1 **(G)** pLKO.1-GAS6 shRNA or pLKO.1-Control were analyzed for *GAS6* expression by real-time PCR (n=3). Data, expressed as fold change units, were normalized with GAPDH and referred to pLKO.1-Control, considered as calibrator. Data are shown as mean ± SD (*p < 0.05; Mann-Whitney Test).

SUPPLEMENTARY TABLE 1
Clinical parameters of MM patients used for the analysis of GAS6 in condition medium derived from BMSCs and BM plasma. Patients were classified according to Durie and Salmon's Staging System.

SUPPLEMENTARY TABLE 2
Clinical parameters of MM patients used for the analysis of MICA surface expression and mRNA. Patients were classified according to Durie and Salmon's Staging System.

References

1. Morvan MG, Lanier LL. NK cells and cancer: You can teach innate cells new tricks. *Nat Rev Cancer* (2016) 16:7–19. doi: 10.1038/nrc.2015.5

2. Liu S, Galat V, Galat Y, Lee YKA, Wainwright D, Wu J. NK cell-based cancer immunotherapy: From basic biology to clinical development. *J Hematol Oncol* (2021) 14. doi: 10.1186/s13045-020-01014-w

3. Crinier A, Narni-Mancinelli E, Ugolini S, Vivier E. SnapShot: Natural killer cells. *Cell* (2020) 180. doi: 10.1016/j.cell.2020.02.029

4. Dhar P, Wu JD. NKG2D and its ligands in cancer. *Curr Opin Immunol* (2018) 51. doi: 10.1016/j.coi.2018.02.004

5. Sheppard S, Ferry A, Guedes J, Guerra N. The paradoxical role of NKG2D in cancer immunity. *Front Immunol* (2018) 9:1808. doi: 10.3389/fimmu.2018.01808

6. El-Sherbiny YM, Meade JL, Holmes TD, McGonagle D, Mackie SL, Morgan AW, et al. The requirement for DNAM-1, NKG2D, and NKp46 in the natural killer cell-mediated killing of myeloma cells. *Cancer Res* (2007) 67. doi: 10.1158/0008-5472.CAN-06-4230

7. Fionda C, Stabile H, Molfetta R, Soriani A, Bernardini G, Zingoni A, et al. Translating the anti-myeloma activity of natural killer cells into clinical application. *Cancer Treat Rev* (2018) 70. doi: 10.1016/j.ctrv.2018.10.005

8. Alfarra H, Weir J, Grieve S, Reiman T. Targeting NK cell inhibitory receptors for precision multiple myeloma immunotherapy. *Front Immunol* (2020) 11:575609. doi: 10.3389/fimmu.2020.575609

9. Sperling AS, Anderson KC. Facts and hopes in multiple myeloma immunotherapy. *Clin Cancer Res* (2021) 27. doi: 10.1158/1078-0432.CCR-20-3600

10. Fionda C, Abruzzese MP, Zingoni A, Cecere F, Vulpis E, Peruzzi G, et al. The IMiDs targets IKZF-1/3 and IRF4 as novel negative regulators of NK cell-activating ligands expression in multiple myeloma. *Oncotarget* (2015) 6. doi: 10.18632/oncotarget.4603

11. Fionda C, Malgarini G, Soriani A, Zingoni A, Cecere F, Iannitto ML, et al. Inhibition of glycogen synthase kinase-3 increases NKG2D ligand MICA expression and sensitivity to NK cell-mediated cytotoxicity in multiple myeloma cells: Role of STAT3. *J Immunol* (2013) 190. doi: 10.4049/jimmunol.1201426

12. Fionda C, Soriani A, Malgarini G, Iannitto ML, Santoni A, Cippitelli M. Heat shock protein-90 inhibitors increase MHC class I-related chain a and b ligand expression on multiple myeloma cells and their ability to trigger NK cell degranulation. *J Immunol* (2009) 183. doi: 10.4049/jimmunol.0901797

13. Abruzzese MP, Bilotta MT, Fionda C, Zingoni A, Soriani A, Vulpis E, et al. Inhibition of bromodomain and extra-terminal (BET) proteins increases NKG2D ligand MICA expression and sensitivity to NK cell-mediated cytotoxicity in multiple myeloma cells: Role of cMYC-IRF4-miR-125b interplay. *J Hematol Oncol* (2016) 9. doi: 10.1186/s13045-016-0362-2

14. Hideshima T, Anderson KC. Signaling pathway mediating myeloma cell growth and survival. *Cancers (Basel)* (2021) 13. doi: 10.3390/cancers13020216

15. Giannakoulas N, Ntanasis-Stathopoulos I, Terpos E. The role of marrow microenvironment in the growth and development of malignant plasma cells in multiple myeloma. *Int J Mol Sci* (2021) 22. doi: 10.3390/ijms22094462

16. Maiso P, Mogollón P, Ocio EM, Garayoa M. Bone marrow mesenchymal stromal cells in multiple myeloma: Their role as active contributors to myeloma progression. *Cancers (Basel)* (2021) 13. doi: 10.3390/cancers13112542

17. Mekhloufi A, Kosta A, Stabile H, Molfetta R, Zingoni A, Soriani A, et al. Bone marrow stromal cell-derived IL-8 upregulates pvr expression on multiple myeloma cells *via* NF-KB transcription factor. *Cancers (Basel)* (2020) 12. doi: 10.3390/cancers12020440

18. Bottino C, Castriconi R, Pende D, Rivera P, Nanni M, Carnemolla B, et al. Identification of PVR (CD155) and nectin-2 (CD112) as cell surface ligands for the human DNAM-1 (CD226) activating molecule. *J Exp Med* (2003) 198. doi: 10.1084/jem.20030788

19. Stanietsky N, Simic H, Arapovic J, Toporik A, Levy O, Novik A, et al. The interaction of TIGIT with PVR and PVRL2 inhibits human NK cell cytotoxicity. *Proc Natl Acad Sci USA* (2009) 106. doi: 10.1073/pnas.0903474106

20. Furukawa M, Ohkawara H, Ogawa K, Ikeda K, Ueda K, Shichishima-Nakamura A, et al. Autocrine and paracrine interactions between multiple myeloma cells and bone marrow stromal cells by growth arrest-specific gene 6 cross-talk with interleukin-6. *J Biol Chem* (2017) 292. doi: 10.1074/jbc.M116.733030

21. Yan S, Vandewalle N, de Beule N, Faict S, Maes K, de Bruyne E, et al. AXL receptor tyrosine kinase as a therapeutic target in hematological malignancies: Focus on multiple myeloma. *Cancers (Basel)* (2019) 11. doi: 10.3390/cancers11111727

22. Waizenegger JS, Ben-Batalla I, Weinhold N, Meissner T, Wroblewski M, Janning M, et al. Role of growth arrest-specific gene 6-mer axis in multiple myeloma. *Leukemia* (2015) 29. doi: 10.1038/leu.2014.236

23. Khoo WH, Ledergor G, Weiner A, Roden DL, Terry RL, McDonald MM, et al. A niche-dependent myeloid transcriptome signature defines dormant myeloma cells. *Blood* (2019) 134. doi: 10.1182/blood.2018880930

24. Aehnlich P, Powell RM, Peeters MJW, Rahbech A, Straten PT. Tam Receptor inhibition–implications for cancer and the immune system. *Cancers (Basel)* (2021) 13. doi: 10.3390/cancers13061195

25. Paolino M, Penninger JM. The role of TAM family receptors in immune cell function: Implications for cancer therapy. *Cancers (Basel)* (2016) 8. doi: 10.3390/cancers8100097

26. Walzer T, Vivier E. NK cell development: Gas matters. *Nat Immunol* (2006) 7. doi: 10.1038/ni0706-702

27. Caraux A, Lu Q, Fernandez N, Riou S, di Santo JP, Raulet DH, et al. Natural killer cell differentiation driven by Tyro3 receptor tyrosine kinases. *Nat Immunol* (2006) 7. doi: 10.1038/ni1353

28. Paolino M, Choidas A, Wallner S, Pranjic B, Uribesalgo I, Loeser S, et al. The E3 ligase cbl-b and TAM receptors regulate cancer metastasis *via* natural killer cells. *Nature* (2014) 507. doi: 10.1038/nature12998

29. Chirino LM, Kumar S, Okumura M, Sterner DE, Mattern M, Butt TR, et al. TAM receptors attenuate murine NK-cell responses *via* E3 ubiquitin ligase cbl-b. *Eur J Immunol* (2020) 50. doi: 10.1002/eji.201948204

30. Lu T, Ma R, Li Z, Mansour AG, Teng KY, Chen L, et al. Hijacking TYRO3 from tumor cells *via* trogocytosis enhances NK-cell effector functions and proliferation. *Cancer Immunol Res* (2021) 9. doi: 10.1158/2326-6066.CIR-20-1014

31. Soriani A, Borrelli C, Ricci B, Molfetta R, Zingoni A, Fionda C, et al. p38 MAPK differentially controls NK activating ligands at transcriptional and post-transcriptional level on multiple myeloma cells. *OncoImmunology* (2017) 6. doi: 10.1080/2162402X.2016.1264564

32. Stabile H, Nisti P, Peruzzi G, Fionda C, Pagliara D, Brescia PL, et al. Reconstitution of multifunctional CD56lowCD16low natural killer cell subset in children with acute leukemia given α/β T cell-depleted HLA-haploidentical haematopoietic stem cell transplantation. *OncoImmunology* (2017) 6(9): e1342024. doi: 10.1080/2162402X.2017.1342024

33. Stabile H, Nisti P, Fionda C, Pagliara D, Gaspari S, Locatelli F, et al. NK cell reconstitution in paediatric leukemic patients after T-cell-depleted HLA-haploidentical haematopoietic stem cell transplantation followed by the reinfusion of iCasp9-modified donor T cells. *J Clin Med* (2019) 8. doi: 10.3390/jcm8111904

34. Fionda C, Nappi F, Piccoli M, Frati L, Santoni A, Cippitelli M. Inhibition of trail gene expression by cyclopentenonic prostaglandin 15-deoxy-Δ12,14-prostaglandin J2 in T lymphocytes. *Mol Pharmacol* (2007) 72. doi: 10.1124/mol.107.038042

35. Zitti B, Molfetta R, Fionda C, Quatrini L, Stabile H, Lecce M, et al. Innate immune activating ligand SUMOylation affects tumor cell recognition by NK cells. *Sci Rep* (2017) 7. doi: 10.1038/s41598-017-10403-0

36. Soriani A, Zingoni A, Cerboni C, Lannitto ML, Ricciardi MR, Gialleonardo VD, et al. ATM-ATR-dependent up-regulation of DNAM-1 and NKG2D ligands on multiple myeloma cells by therapeutic agents results in enhanced NK-cell susceptibility and is associated with a senescent phenotype. *Blood* (2009) 113. doi: 10.1182/blood-2008-08-173914

37. Molinero LL, Fuertes MB, Girart MV, Fainboim L, Rabinovich GA, Costas MA, et al. NF-κB regulates expression of the MHC class I-related chain a gene in activated T lymphocytes. *J Immunol* (2004) 173. doi: 10.4049/jimmunol.173.9.5583

38. Cerboni C, Zingoni A, Cippitelli M, Piccoli M, Frati L, Santoni A. Antigen-activated human T lymphocytes express cell-surface NKG2D ligands *via* an ATM/ATR-dependent mechanism and become susceptible to autologous NK-cell lysis. *Blood* (2007) 110. doi: 10.1182/blood-2006-10-052720

39. Markovina S, Callander NS, O'Connor SL, Kim J, Werndli JE, Raschko M, et al. Bortezomib-resistant nuclear factor-κB activity in multiple myeloma cells. *Mol Cancer Res* (2008) 6. doi: 10.1158/1541-7786.MCR-08-0108

40. Markovina S, Callander NS, O'Connor SL, Xu G, Shi Y, Leith CP, et al. Bone marrow stromal cells from multiple myeloma patients uniquely induce bortezomib resistant NF-κB activity in myeloma cells. *Mol Cancer* (2010) 9. doi: 10.1186/1476-4598-9-176

41. Lin D, Lavender H, Soilleux EJ, O'Callaghan CA. NF-κB regulates MICA gene transcription in endothelial cell through a genetically inhibitable control site. *J Biol Chem* (2012) 287. doi: 10.1074/jbc.M111.282152

42. Vulpis E, Stabile H, Soriani A, Fionda C, Petrucci MT, Mariggio' E, et al. Key role of the CD56lowCD16low natural killer cell subset in the recognition and killing of multiple myeloma cells. *Cancers (Basel)* (2018) 10. doi: 10.3390/cancers10120473

43. Fionda C, Soriani A, Zingoni A, Santoni A, Cippitelli M. NKG2D and DNAM-1 ligands: Molecular targets for NK cell-mediated immunotherapeutic intervention in multiple myeloma. *BioMed Res Int* (2015) 2015. doi: 10.1155/2015/178698

44. Zingoni A, Fionda C, Borrelli C, Cippitelli M, Santoni A, Soriani A. Natural killer cell response to chemotherapy-stressed cancer cells: Role in tumor immunosurveillance. *Front Immunol* (2017) 8:1194. doi: 10.3389/fimmu.2017.01194

45. Zingoni A, Vulpis E, Nardone I, Soriani A, Fionda C, Cippitelli M, et al. Targeting NKG2D and NKp30 ligands shedding to improve NK cell–based immunotherapy. *Crit Rev Immunol* (2016) 36. doi: 10.1615/CritRevImmunol.2017020166

46. Zingoni A, Vulpis E, Cecere F, Amendola MG, Fuerst D, Saribekyan T, et al. MICA-129 dimorphism and soluble MICA are associated with the progression of multiple myeloma. *Front Immunol* (2018) 9:926. doi: 10.3389/fimmu.2018.00926

47. Serrano AE, Menares-Castillo E, Garrido-Tapia M, Ribeiro CH, Hernández CJ, Mendoza-Naranjo A, et al. Interleukin 10 decreases MICA expression on melanoma cell surface. *Immunol Cell Biol* (2011) 89. doi: 10.1038/icb.2010.100

48. Wu D, Zhang J, Qian T, Dai Y, Mashaghi A, Xu J, et al. IFN-γ regulates the expression of MICA in human corneal epithelium through miRNA4448 and NFκB. *Front Immunol* (2018) 9:1530. doi: 10.3389/fimmu.2018.01530

49. Trinh T, Kandell WM, Donatelli SS, Tu N, Tejera MM, Gilvary DL, et al. Immune evasion by TGFβ-induced miR-183 repression of MICA/B expression in human lung tumor cells. *OncoImmunology* (2019) 8. doi: 10.1080/2162402X.2018.1557372

50. Vantourout P, Willcox C, Turner A, Swanson CM, Haque Y, Sobolev O, et al. Immunological visibility: Posttranscriptional regulation of human NKG2D ligands by the EGF receptor pathway. *Sci Trans Med* (2014) 6. doi: 10.1126/scitranslmed.3007579

51. Skinner HD, Giri U, Yang LP, Kumar M, Liu Y, Story MD, et al. Integrative analysis identifies a novel AXL-PI3 kinase-PD-L1 signaling axis associated with radiation resistance in head and neck cancer. *Clin Cancer Res* (2017) 23. doi: 10.1158/1078-0432.CCR-16-2586

52. Tsukita Y, Fujino N, Miyauchi E, Saito R, Fujishima F, Itakura K, et al. Axl kinase drives immune checkpoint and chemokine signalling pathways in lung adenocarcinomas. *Mol Cancer* (2019) 18. doi: 10.1186/s12943-019-0953-y

53. Terry S, Abdou A, Engelsen AST, Buart S, Dessen P, Corgnac S, et al. AXL targeting overcomes human lung cancer cell resistance to NK- and CTL-mediated cytotoxicity. *Cancer Immunol Res* (2019) 7. doi: 10.1158/2326-6066.CIR-18-0903

54. Lu Q, Lemke G. Homeostatic regulation of the immune system by receptor tyrosine kinases of the tyro 3 family. *Science* (2001) 293. doi: 10.1126/science.1061663

55. Peeters MJW, Dulkeviciute D, Draghi A, Ritter C, Rahbech A, Skadborg SK, et al. MERTK acts as a costimulatory receptor on human cd8 t cells. *Cancer Immunol Res* (2019) 7. doi: 10.1158/2326-6066.CIR-18-0841

56. D'Souza C, Keam SP, Yeang HXA, Neeson M, Richardson K, Hsu AK, et al. Myeloma natural killer cells are exhausted and have impaired regulation of activation. *Haematologica* (2021) 106. doi: 10.3324/haematol.2020.277525

57. Leivas A, Valeri A, Córdoba L, García-Ortiz A, Ortiz A, Sánchez-Vega L, et al. NKG2D-CAR-transduced natural killer cells efficiently target multiple myeloma. *Blood Cancer J* (2021) 11. doi: 10.1038/s41408-021-00537-w

frontiers | Frontiers in Immunology

TYPE Original Research
PUBLISHED 08 June 2023
DOI 10.3389/fimmu.2023.1200725

OPEN ACCESS

EDITED BY
Michael V. Volin,
Midwestern University, United States

REVIEWED BY
Blanca Molins,
August Pi i Sunyer Biomedical Research Institute (IDIBAPS), Spain
Talat Malik,
Imperial College London, United Kingdom
Svetlana Hakobyan,
Cardiff University, United Kingdom

*CORRESPONDENCE
Olaf Strauß
olaf.strauss@charite.de

RECEIVED 05 April 2023
ACCEPTED 23 May 2023
PUBLISHED 08 June 2023

CITATION
Busch C, Rau S, Sekulic A, Perie L, Huber C, Gehrke M, Joussen AM, Zipfel PF, Wildner G, Skerka C and Strauß O (2023) Increased plasma level of terminal complement complex in AMD patients: potential functional consequences for RPE cells.
Front. Immunol. 14:1200725.
doi: 10.3389/fimmu.2023.1200725

Increased plasma level of terminal complement complex in AMD patients: potential functional consequences for RPE cells

Catharina Busch[1], Saskia Rau[2], Andjela Sekulic[2], Luce Perie[3], Christian Huber[2], Miranda Gehrke[4], Antonia M. Joussen[2], Peter F. Zipfel[3,5], Gerhild Wildner[4], Christine Skerka[3] and Olaf Strauß[2]*

[1]Department of Ophthalmology, University Hospital Leipzig, Leipzig, Germany, [2]Experimental Ophthalmology, Department of Ophthalmology, Charité - Universitätsmedizin Berlin, Corporate Member of Freie Universität, Berlin Institute of Health, Humboldt-University, Berlin, Germany, [3]Department of Infection Biology, Leibniz Institute for Natural Product Research and Infection Biology, Hans-Knoell-Institute, Jena, Germany, [4]Section of Immunobiology, Department of Ophthalmology, University Hospital, Ludwig-Maximilians-Universität (LMU) Munich, Munich, Germany, [5]Institute of Microbiology, Friedrich-Schiller-University, Jena, Germany

Purpose: Polymorphisms in complement genes are risk-associated for age-related macular degeneration (AMD). Functional analysis revealed a common deficiency to control the alternative complement pathway by risk-associated gene polymorphisms. Thus, we investigated the levels of terminal complement complex (TCC) in the plasma of wet AMD patients with defined genotypes and the impact of the complement activation of their plasma on second-messenger signaling, gene expression, and cytokine/chemokine secretion in retinal pigment epithelium (RPE) cells.

Design: Collection of plasma from patients with wet AMD (n = 87: 62% female and 38% male; median age 77 years) and controls (n = 86: 39% female and 61% male; median age 58 years), grouped for risk factor smoking and genetic risk alleles *CFH* 402HH and *ARMS2* rs3750846, determination of TCC levels in the plasma, *in vitro* analysis on RPE function during exposure to patients' or control plasma as a complement source.

Methods: Genotyping, measurement of TCC concentrations, ARPE-19 cell culture, Ca^{2+} imaging, gene expression by qPCR, secretion by multiplex bead analysis of cell culture supernatants.

Main outcome measures: TCC concentration in plasma, intracellular free Ca^{2+}, relative mRNA levels, cytokine secretion.

Results: TCC levels in the plasma of AMD patients were five times higher than in non-AMD controls but did not differ in plasma from carriers of the two risk alleles. Complement-evoked Ca^{2+} elevations in RPE cells differed between patients and controls with a significant correlation between TCC levels and peak amplitudes.

Comparing the Ca^{2+} signals, only between the plasma of smokers and non-smokers, as well as heterozygous (*CFH 402YH*) and *CFH 402HH* patients, revealed differences in the late phase. Pre-stimulation with complement patients' plasma led to sensitization for complement reactions by RPE cells. Gene expression for surface molecules protective against TCC and pro-inflammatory cytokines increased after exposure to patients' plasma. Patients' plasma stimulated the secretion of pro-inflammatory cytokines in the RPE.

Conclusion: TCC levels were higher in AMD patients but did not depend on genetic risk factors. The Ca^{2+} responses to patients' plasma as second-messenger represent a shift of RPE cells to a pro-inflammatory phenotype and protection against TCC. We conclude a substantial role of high TCC plasma levels in AMD pathology.

KEYWORDS

retinal pigment epithelium, terminal complement complex, age-related macular degeneration, AMD serum, genetic risk factors

1 Introduction

Age-related macular degeneration (AMD) is one of the major causes of vision loss in industrialized countries (1). The disease shows two clinically defined end stages. One is the loss of cells of the retinal pigment epithelium (RPE) and photoreceptors, which progresses slowly. This form, the so-called "dry AMD" or geographic atrophy, accounts for approximately 80% of the cases but due to its low progression for approximately 20% of blindness. The other end stage is characterized by the proliferation of endothelial cells, resulting in pathologic neo-angiogenesis that leads to bleeding due to low grade of blood vessel differentiation and thus too fast loss of vision (2). This end stage, the so-called choroidal neovascularization or "wet AMD", represents the majority of cases of blindness. AMD is a multifactorial disease for which environmental risk factors like smoking and genetic risk factors like polymorphisms in genes such as *ARMS2* (age-related macular susceptibility-2) or genes of the complement components are known (3–5).

The identification of complement deposits in drusen as well as polymorphisms in complement genes as risk factors suggested that the complement system is associated with the development of AMD. Recent reports confirmed that an over-activated complement system due to reduced regulation represents a risk for AMD (3, 4, 6–10). However, recent clinical trials failed to establish a complement inhibition-based therapy for the dry form of AMD (11–13). Therefore, the role of activated complement proteins is more complex, and the chronic AMD-associated complement activity is still not fully understood (12).

Another reason why complement-targeting clinical trials failed might be the fact that the systemic over-activity of the complement cascade has a life-long impact on the retina. This would explain why acute intervention into complement activity might not immediately reverse chronic events that have affected the outer retina for decades (12). Complement activation may have a lifelong systemic impact on the outer retina with strong local pathologic changes. The impact of the end product of the complement cascade, the terminal complement complex (TCC; also termed C5b-9), is not clear so far. The TCC is a complex of five different proteins (C5b, C6, C7, C8, and C9). When this complex is formed on a cell surface, several C9 components are aggregated and form a ring, inserting a pore into the cell membrane, which leads to cell lysis and is also called membrane attack complex (MAC). Indeed, depending on age, AMD status, and risk allele, TCC accumulates in the outer retina. TCC is increasingly found in the tissue complex of the choroid, Bruch's membrane, and RPE during its lifetime (14–17). AMD patients with C9 risk alleles show increased plasma levels of C9 or TCC compared to healthy non-carriers (18–20), although no differences were reported among AMD with or without C9 risk alleles. This might be explained by the fact that AMD patients with the absence of C9 risk alleles generally display increased systemic complement activities (21–23). In the plasma of patients carrying various C9 risk alleles, higher levels of C9 but no differences in TCC plasma levels were found (19). When comparing different C9 risk alleles, it appeared that some are associated with higher C9 or TCC plasma levels (20). This suggests an important role of TCC in AMD pathology.

Acting as MAC, the consequence of TCC accumulation in the outer retina would destabilize RPE cells, which results in the loss of RPE cells (24–26). The RPE itself is a close interaction partner of the light-sensitive photoreceptors, supporting their function and even contributing to visual function (27). Thus, the loss of RPE cells in AMD ultimately causes loss of photoreceptors and blindness. Several observations about the general nature of TCC effects and the concept of the specific complement impact on the RPE are still unclear. In the RPE, the human plasma-derived complement ignites a well-orchestrated Ca^{2+} signal that depends on the activation of endogenously expressed Ca^{2+} and K^+ channels. The induction of an

unspecific pore could not be detected in measurements of the membrane conductance by means of the patch-clamp technique (28). The different complement activation products' consequence is that the RPE cells change their gene expression pattern toward a more pro-inflammatory profile in response to anaphylatoxins via the Akt–kinase pathway and the transcription factor FoxP3 (29–33).

TCC's influence on gene expression emerged as the concept of sub-lytic MAC in studies that investigated the effects of different TCC concentrations and combinations at various cell types (25, 34–39). The concept bases on the ability of cells to remove MAC from the plasma membrane. As long as the cell's ability to remove MAC from the plasma membrane can cope with the rate of extracellular TCC formation and membrane insertion, the cell will not undergo lysis (35). Soluble TCC is generally accepted as a marker of *in vivo* complement activation (40). These studies defined TCC concentrations that do not lyse cells but lead to functional changes as sub-lytic (34, 35, 37, 38). The functional changes require intracellular signaling such as an increase in intracellular Ca^{2+}, activation of different types of kinases, and even the activation of G proteins (25, 34, 35, 37–39, 41). The activation of these intracellular signaling pathways then lead to secondary effects such as changes in the gene expression profile and represent the basic sub-lytic MAC effects onto cellular functions. Several studies demonstrated functional changes of the RPE by sub-lytic MAC, mainly in the secretory activity of, e.g., VEGF-A or MCP-1, or reduced stress response (5, 30, 33, 42, 43). This might be explained by CD59, which inactivates MAC formation (7, 44) and represents a target for further therapeutic approaches (26). However, Cipriani et al. found no risk association of TCC regulators CD46, CD55, and CD59 with AMD, especially not for CD59 (45).

As a consequence, the enhanced generation of TCC in AMD patients might not directly lead to RPE cell death but promote a change of the RPE's immunogenic phenotype toward low-grade chronic inflammation. To test this concept, we have used human plasma from AMD patients with defined genetic risk factors as a complement source to test RPE cell reactions to dysregulated complement. Depending on the patients' genotype, these plasma contained different levels of TCC and caused different Ca^{2+} signals as well as different regulatory effects on gene expression. Our hypothesis is that TCC complexes in AMD patients generate Ca^{2+} signals with profound physiological changes in the RPE.

2 Materials and methods

2.1 Blood samples and determination of TCC concentration

A total of 87 AMD patients with wet AMD (62% female and 38% male) with a mean age of 77.9 years (median = 77 years) and 86 age-matched controls (39% female and 61% male) with a mean age of 55.1 years (median = 58) were included; further information is presented in the tables of Supplementary Material Suppl. 1, 2. The samples were anonymized. Blood samples were collected with EDTA and centrifuged, and plasma was stored at −80°C. The concentration of TCC was determined by ELISA as previously described (46). In brief, plasma samples were pre-incubated (37°C; 15 min) and incubated on lipopolysaccharide (LPS)-coated plates. Plates were analyzed at 450-nm wavelength using TCC mAB from TECOmedical (Sissach, Switzerland). The polymorphisms in this patient cohort were determined as described earlier for *ARMS* (47) and *CFH* (9, 48).

2.2 RPE cell culture

For our study, the ARPE-19 cell line was used, which shows limitations for conclusions about native RPE cells. Here, these cells were used to monitor the biological activity of activated complement proteins in human plasma rather than to investigate specific RPE cell functions. The cells were grown on glass coverslips to confluence prior to the Ca^{2+} imaging experiments. The culture conditions were using Dulbecco's modified Eagle medium (DMEM)/F12 (Thermo Fisher, Darmstadt, Germany) with GlutaMAX (stable glutamine) supplemented with 10% fetal calf serum (FCS) and 50 U penicillin/50 mg streptomycin at 37°C and 5% CO_2. The medium was changed twice a week.

2.3 Ca^{2+} imaging experiments

As a readout of biological responses to the activated complement, intracellular free Ca^{2+} as a second messenger was measured by means of Ca^{2+} imaging techniques based on fluorescence microscopy using the Ca^{2+}-sensitive fluorescence dye fura-2. Confluent ARPE-19 cells grown on glass coverslips were incubated in the membrane-diffusible fura-2 ester fura-2-AM (2 µM) for 40 min at room temperature. Fura-2 loaded cells were mounted onto the stage of a Zeiss Axiovert 40 CFL inverted microscope (Carl Zeiss, Oberkochen, Germany) with an attached Visitron Polychromator (Visitron Systems, Puchheim, Germany) and a high-sensitivity color event camera (CED) camera (CoolSNAP EZ, Photometrics, Tucson, AZ, USA). Experiments were conducted using the MetaFlour software (Visitron Systems, Puchheim, Germany). The cells were bathed in an extracellular solution containing (mM): 138 NaCl, 5.8 KCl, 0.41 $MgSO_4$, 0.48 $MgCl_2$, 0.95 $CaCl_2$, 4.17 $NaHCO_3$, 1.1 NaH_2PO_4, and 25 HEPES; pH = 7.2 adjusted with Tris base. Fura-2 fluorescence was measured at 505-nm wavelength and excited by the wavelengths 340 and 380 nm through a semiconducting mirror. The changes in intracellular free Ca^{2+} were given as fluorescence ratio (dF/F) from baseline (ddF/F) between the excitation wavelengths 340 and 380 nm. Human plasma samples were directly applied to the cells on the stage of the microscope at a concentration of 20%. C6-depleted plasma was purchased from CompTech (Complement Technology, Tyler, TX, USA).

2.4 qPCR

In order to assess the functional consequences of complement-activated intracellular Ca^{2+} signaling, gene expression activity was

measured by quantification of mRNA in ARPE-19 cells. Confluent ARPE-19 cells were exposed to different human plasma and in some conditions in combination with L-type channel blocker nifedipine (10 μM). After cell harvest, RNA isolation and cDNA synthesis were performed using RNeasy Mini and QuantiTect Reverse Transcription Kit (Qiagen, Hilden, Germany). mRNA levels were measured in triplicates for the target genes and GAPDH as a housekeeping gene for standardization in a Rotor-Gene Q (Qiagen, Hilden, Germany) by using the Rotor-Gene SYBR Green PCR Kit (Qiagen, Hilden, Germany); primer sequences are shown in Table 1. The mRNA levels of the target genes were calculated and presented as a comparative CT (threshold cycle, ΔΔCT) method using Rotor-Gene Q software 2.2.3 (Qiagen) (49). Of note, the primers for *CFH*, IL-1β, and CD46 showed reduced efficacy in the presence of dimethyl sulfoxide (DMSO) needed for the solubilization of nifedipine; thus, respective results from nifedipine-treated cultures could not be obtained.

2.5 Cytokine secretion of ARPE-19 cells in response to human plasma

ARPE-19 cells were grown in 96-well plates to confluency. Three days later, cultures were switched to serum-free DMEM/Ham's F12 medium for 24 h before triplicate cultures were set up with 10% human plasma from smokers or non-smokers who were either homozygous (*CFH 402HH*) or heterozygous (*CFH 402YH*) or low-risk allele carriers (*CFH 402YY*), respectively, and incubated for another 3 days. Identical cultures were set up with 50 μM PI3 K-inhibitor LY294002 (Cayman Chemical, Ann Arbor, MI, USA). Plasma from age-matched, non-AMD donors without *CFH* mutations was used as the control.

Supernatants were collected after 24, 48, and 72 h; immediately shock frozen at −80°C; pooled in equal volumes before being tested for cytokines by human Bio-Plex bead analysis (Bio-Rad Laboratories, Inc., Hercules, CA, USA); and measured with a Bio-Plex 200 reader (Bio-Rad Laboratories, Inc.) according to the manufacturer's instruction. Tested analytes were IL-1β, IL-1RA, IL-6, IL-8/CXCL8, IL-10, IL-12(p70), IFN-gamma, MCP-1/CCL2, and VEGF. Only results from those cytokines and chemokines that were secreted by the ARPE-19 cells are shown. Experiments were performed twice with ARPE-19 cells from different sources in different passages (as indicated, p6, p15, and p25) with comparable results. Data are shown as means + SE from triplicate cultures of one representative experiment with two different cell lines; experiments were performed twice.

2.6 Data analysis and statistical testing

All data are presented as mean values ± SEM or ± SD. Statistical significance was calculated using Mann–Whitney *U* test for Ca^{2+} imaging data and qPCR data (*$p < 0.05$, **$p < 0.01$, and ***$p < 0.005$). All calculations were performed in SPSS 26 and Excel 2010.

3 Results

To re-test the hypothesis of systemic complement activation in AMD, the TCC plasma levels in probes from AMD patients (the details of the patient cohort and controls in Supplementary Material Tables S1, S2) were compared with probes from age-matched controls (Figure 1) and found significantly, approximately five times, higher levels of TCC in AMD patients (0.44 ± 0.06 versus 2.15 ± 0.08 μg/ml; $p < 0.001$) (Figure 1A). The levels of TCC in healthy donors were in accordance with those that we published earlier (46). However, when comparing TCC concentrations in plasma from AMD patients carrying risk alleles, a different picture evolved. Comparing carriers of the low-risk allele of *ARMS2* versus high-risk allele carriers (*ARMS2* rs3750846) revealed no differences between low-risk and heterozygous or homozygous carriers (Figure 1B). Similar results were obtained among *CFH* polymorphism carriers with no differences between low-risk (*CFH 402YY*), heterozygous high-risk (*CFH 402YH*), or homozygous high-risk (*CFH 402HH*) allele carriers in AMD patients. Furthermore, no differences between the *ARMS2* and the *CFH* risk carriers were identified. The same applies to the environmental risk factor that we have analyzed in more detail, the smoking status (Figure 1D). In AMD patients without these genetic risk factors, no differences in the TCC concentrations were observed depending on their smoking status.

To test the biological relevance of increased TCC levels in the plasma of AMD patients, we used Ca^{2+} imaging techniques to explore the acute reaction of ARPE-19 cells on the patients' plasma. Earlier studies showed that an increase in intracellular free Ca^{2+} that was evoked by exposure to human plasma as the source of complement reflects the concerted activity of all activated complement factors (28). Thus, changes were expected in

TABLE 1 Primer sequences.

Gene	Forward sequence	Reverse sequence
C3	TTCCGATTGAGGATGGCTCG	ATGTCACTGCCTGAGTGCAA
C3aR	GGCTGTCTTTCTTGTCTGCTG	GACTGCCTTGCTTTCTTCCTAA
C5	ACACTGGTACGGCACGTATG	GGCATTGATTGTGTCCTGGG
C5aR	ThermoFisher TaqMan Primer Hs00704891_s1	
GAPDH	TCAACGACCACTTTGTCAAGCTCA	GCTGGTGGTCCAGGGGTCTTACT

10.3389/fimmu.2023.1200725

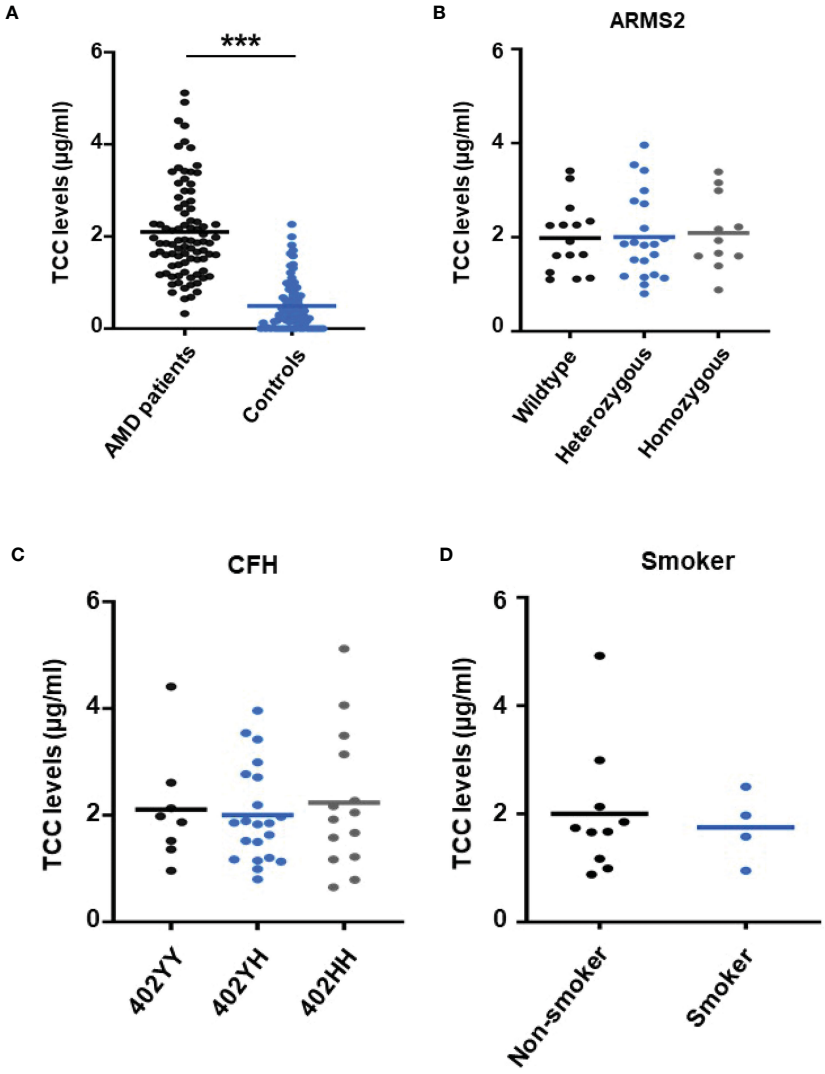

FIGURE 1
Plasma levels of terminal complement complex (TCC) in plasma from healthy donors and age-related macular degeneration (AMD) patients with AMD risk alleles. **(A)** Plasma levels of TCC (µg/ml) in AMD patients (n = 87) *vs.* healthy controls (n = 86) showing significantly higher TCC levels in AMD patients ($p < 0.001$). **(B)** TCC levels stratified for *Age-related maculopathy-susceptibility 2* (*ARMS2*) risk alleles, with all patients carrying one *Complement factor H* (*CFH 402YH*) risk allele. No significant difference in TCC levels among patients with no (wild type (WT), n = 15), one (heterozygous, n = 21), and two (homozygous, n = 11) *ARMS2* risk alleles existed. **(C)** TCC levels stratified for *CFH* risk alleles, with all patients carrying one *ARMS2* risk allele. No significant difference in TCC levels among patients with no (*CFH 402YY*, n = 8), one (*CFH 402YH*, n = 21), and two (*CFH 402HH*, n = 14) *CFH* risk alleles. The horizontal lines represent the means of the TCC levels. ***$p < 0.001$ (Mann–Whitney *U* test). **(D)** TCC levels stratified for the risk factor smoking and non-smoking among patients who do not carry one of the investigated genetic risk alleles. As the "heterozygous patients" are heterozygous for *CFH* (*CFH 402YH*) and *ARMS2*, the same set of plasma samples from these patients was used for the comparison with homozygous deficient *CFH* **(B)** and *ARMS2* **(C)** as well as with respective WT plasma.

intracellular Ca^{2+} transients by human plasma from AMD patients. As a first step, we investigated whether the Ca^{2+} response to human plasma was dependent on TCC in normal human plasma (NHP). We compared Ca^{2+} transients induced by C6-depleted plasma with those induced with NHP (Figure 2). Indeed, without C6, the plasma induced a Ca^{2+} response half in amplitude compared to that of the control plasma (Figures 2A, B). As the peak in C6-depleted plasma is much smaller, the peak in C6-depleted plasma is reached in a shorter time (Figure 2C). Furthermore, C6-depleted plasma failed to develop a sustained phase of an intracellular Ca^{2+} increase (Figure 2D).

Since C6-depleted human plasma indicated a substantial contribution of TCC in a complement-induced Ca^{2+} increase, the plasma from AMD patients versus control plasma was then tested in a similar experiment (Figure 3). The waveform of Ca^{2+} transients evoked by AMD patients' plasma was different from that of control plasma (Figure 3A). Although the peak was slightly reduced (Figure 3B) and the same level was reached in the sustained phase (Figure 3C), the latency was shorter, and the slope of the Ca^{2+} was steeper with a faster time-to-peak (Figure 3D) in response to AMD patients' plasma. To find out whether the patients' plasma evoked Ca^{2+} increases that resulted exclusively from activated

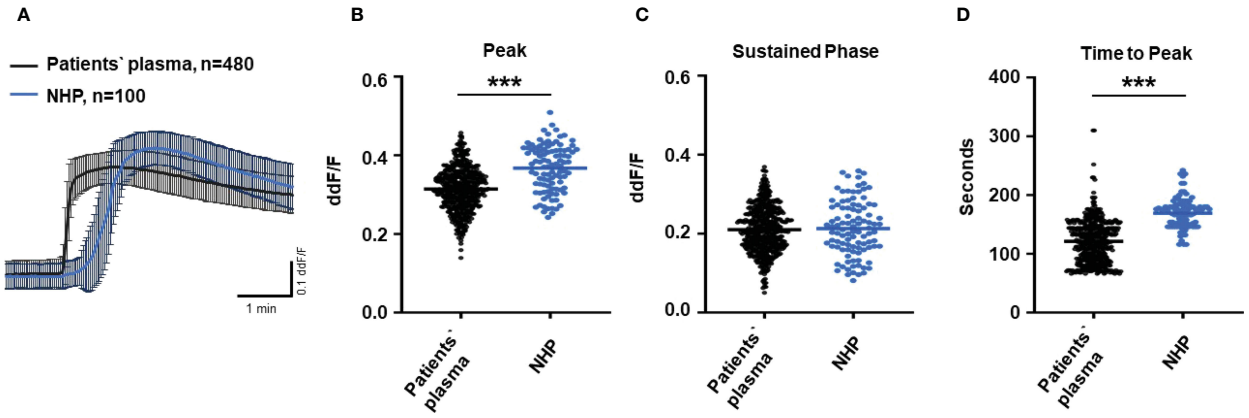

FIGURE 2
Changes in Ca^{2+} transients activated by C6-depleted plasma and normal human plasma (NHP) in ARPE-19 cells. **(A)** Ca^{2+} transients are given as differences to the baseline in fluorescence ratio between the two excitation wavelengths 340 and 380 nm; plasma concentrations were 10%. Data are mean ± SEM. **(B–D)** Ca^{2+} transient changes at the initial peak phase and the late sustained phase. C6-depleted plasma induced a significantly lower change in intracellular free Ca^{2+} compared to NHP. The horizontal line represents the mean change in Ca^{2+} transients from baseline. ***$p < 0.001$ (Mann–Whitney *U* test).

complement proteins, heat-inactivated plasma was used as a control in a similar experiment. Complement as a heat-labile component of the plasma in AMD patients was denatured by incubation at 57°C for 45 min. The heat-inactivated patients' plasma showed a strongly reduced Ca^{2+} reaction when compared to the untreated plasma from the same AMD patients. The resulting levels did not significantly differ from the baseline before the application of heat-inactivated plasma (Supplementary Material Figure S2). These results suggest that the observed differences in the Ca^{2+} signals mainly depended on activated complement components, where some minor effects of other heat-labile plasma compounds cannot be fully excluded. Therefore, a correlation analysis between measured plasma TCC levels and the peak of the single plasma-induced Ca^{2+} signal (Figure 4) was performed. For that purpose, TCC levels were compared with the Ca^{2+} amplitude in a scatter plot, and the data were analyzed using a generalized estimating equation (GEE) model. The analysis revealed a significant negative correlation between TCC levels and the Ca^{2+} peak amplitude: the higher the TCC level, the lower the Ca^{2+} peak, which correlates with the significantly lower Ca^{2+} peaks induced by patients' plasma compared to the controls (Figures 2, 3).

To further evaluate the role of TCC, we investigated the Ca^{2+} responses from AMD patients' plasma with defined risk alleles (Figures 5, 6). According to the lack of differences among plasma levels of TCC, we also expected no differences in the Ca^{2+} signals evoked by the patients' plasma. Indeed, we observed no differences between plasma from heterozygous and homozygous carriers of *ARMS2* risk alleles (Figures 5A–C), as well as with plasma from heterozygous or homozygous carriers of *CFH* risk alleles (Figures 6A–C). However, we observed subtle differences between the plasma samples of patients with the two investigated risk haplotypes *ARMS2* and *CFH*. We found a higher Ca^{2+} level at the sustained phase of the Ca^{2+} signal in response to plasma of homozygous *CFH 402YY* compared to heterozygous (*CFH 402YH*) individuals, in contrast to plasma derived from patients with the ARMS2 risk allele.

As smoking is a relevant risk factor for AMD, we compared smokers and non-smokers within the AMD patients' cohort (Figure 7). Plasma from smokers and non-smokers induced Ca^{2+} signals in ARPE cells with the same latency and slope of Ca^{2+} increase reaching the same peak. However, plasma from smokers revealed significantly higher sustained phases of the Ca^{2+} signal when compared to that of non-smokers. We observed a comparable effect on the plasma-evoked Ca^{2+} increase with plasma from patients who were homozygous carriers of *CFH 402HH*.

So far, our experimental results suggest a potential impact of TCC on the RPE. To mimic the effects of chronic complement stimulation, we pre-incubated ARPE-19 monolayers for 24 h with patients' plasma before we measured Ca^{2+} increases (Figure 8). Pre-stimulation with patients' plasma led to a marked increase in evoked Ca^{2+} transients (Figure 8A) with significantly higher peaks and sustained phases (Figure 8B). As the patients' plasma contents caused ARPE-19 cells to be more sensitive to complement, this "pathological" effect was further analyzed by varying the pre-incubation conditions and using control plasma (NHP) for pre-incubation of the cells. In addition, pre-incubation with NHP changed the Ca^{2+} transients evoked by patients' plasma but in a different way (Figure 8C). Again, the peak was significantly increased, but the sustained phase was markedly reduced (Figure 8D). Normal human plasma seemed to lack those components, which were required for complement sensitization. This was also seen in the comparison of the subsequently evoked Ca^{2+} transients with patients' plasma after pre-incubating the cells with either standard control plasma or patients' plasma (Figure 9A). The peaks from both pre-incubation conditions looked very similar, but the sustained phase of cells pre-incubated with patients' plasma was substantially higher than that of cells pre-incubated with normal humans (Figure 9B).A central paradigm in Ca^{2+} signaling is that Ca^{2+} signals specify the cell

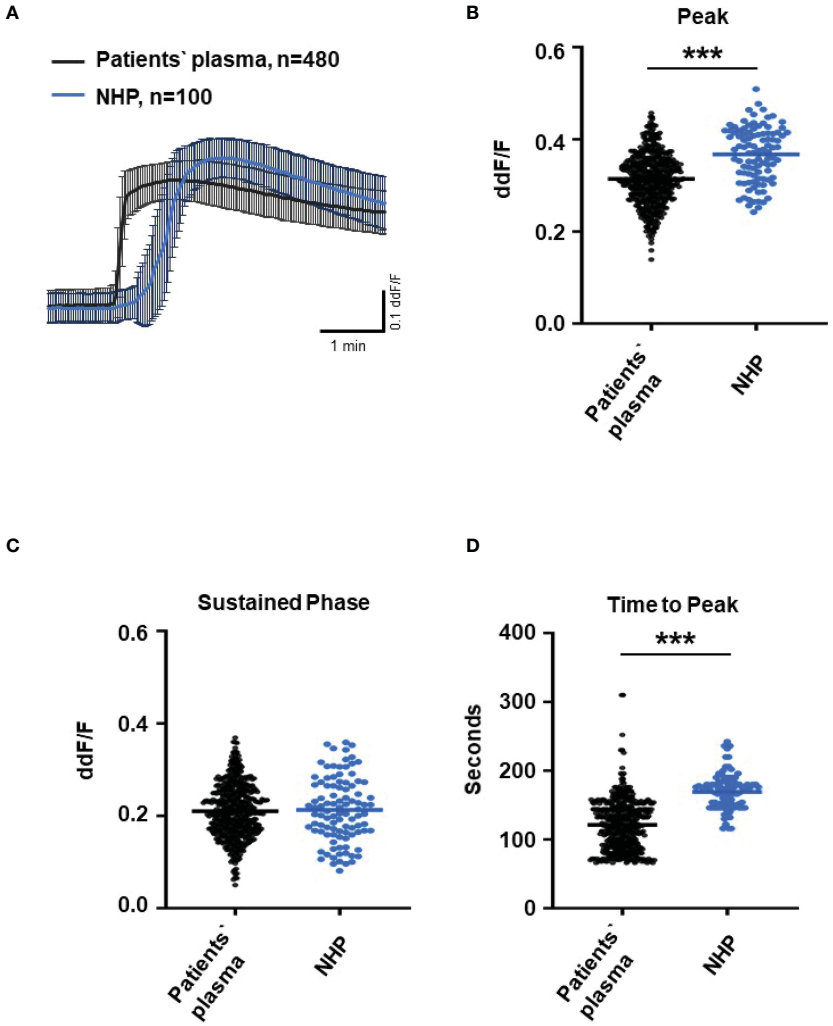

FIGURE 3
Changes in Ca^{2+} transients activated by plasma from age-related macular degeneration patients. **(A)** Ca^{2+} transients are given as differences to the baseline in fluorescence ratio between the two excitation wavelengths 340 and 380 nm. Experiments were conducted with plasma (10%) from 16 different patients (30 cells per patient) and normal human plasma (NHP) in ARPE-19 cells. Data are mean ± SD. **(B)** Ca^{2+} transient changes at the initial peak phase and the late sustained phase. NHP induced a significantly higher change in intracellular free Ca^{2+} in the initial phase compared to patients' plasma. **(C, D)** Mean time until maximum Ca^{2+} transient change. Patients' plasma induced significantly faster maximum Ca^{2+} transients to change compared to NHP. The horizontal line represents the mean change in Ca^{2+} transients from baseline **(B)** and mean time until peak **(C)**. ***$p < 0.001$ (Mann–Whitney *U* test).

function changes by its waveform and spatial distribution as a code (50–52). Thus, differences in the waveforms have different effects on the cell's function. These waveform differences might change intracellular signaling and gene expression profiles. Therefore, gene expression activities in ARPE-19 cells stimulated by patients' plasma and control plasma were quantified, as well as cells that were kept overnight under plasma-free conditions (Figure 10), thereby concentrating our analysis on genes of the complement system, the pro-inflammatory cytokine IL-1β, and the surface receptors CD46 (cleavage of C3b and C4b), CD55 (accelerated decay of complement proteins), and CD59 (TCC formation inhibition).

To identify the contribution by L-type channels, nifedipine (10 μM), an L-type Ca^{2+} channel blocker, was used. Incubation of cells with patients' plasma resulted in an upregulation of C5, C5aR, CD55, CD59, and CFH (Figure 10A). In parallel, C3 and IL1-β were downregulated (Figure 10A). The differential regulation by patients' plasma of C3, C5, C5aR, and CD59 was nifedipine sensitive, indicating that these expression changes depend on complement action, with a great likelihood of the presence of TCC. Comparing standard control plasma with plasma/plasma-free conditions, we found that the ARPE-19 cell reacted with a selective downregulation in the C5aR 1 (there are two C5a receptors) and CFH expression but an increase in the expression of C3aR and IL-1β (Figure 10B) in response to control plasma.

To substantiate the hypothesis that the patients' plasma promotes an immune stimulatory phenotype of RPE cells, we analyzed the secretory profile of ARPE-19 cells under 3 days of stimulation with AMD patients' plasma (Figure 11). Here, we used plasma from patients heterozygous (*CFH 402YH*) or homozygous (*CFH 402HH*) for the *CFH* risk allele who were additionally differentiated by their smoking status. In a third, independent assay, we tested plasma pools

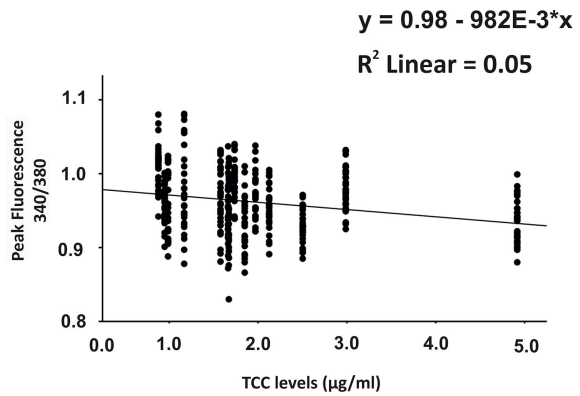

FIGURE 4
Correlation analysis between plasma terminal complement complex (TCC) levels and the height of the plasma-induced Ca^{2+} peaks. Scatter plot of Ca^{2+} peak induced by patients' plasma (given in 340/380 fluorescence ratio) over the individual TCC concentrations in the patients' plasma. Correlation analysis was performed using the generalized estimated equation (GEE) model for longitudinal versus repeated measures (* = multiplies).

from elderly patients of different age groups but without AMD for the induction of cytokine secretion by ARPE-19 cells (see Supplementary Material).

Using the multiplex technology, we analyzed a broad profile of immune and angiogenesis-relevant factors. We plotted only those factors that were induced by patients' plasma in ARPE-19 cell lines from two different laboratories: one in passage 25 (Figures 11A, C) and the other in passage 15 (Figures 11B, D). In general, we found induction of IL-6, IL-8/CXCL8, MCP-1/CCL2, and VEGF-A, with the predominant secretion of VEGF-A and MCP-1, while the other tested cytokines, IL-1β, IL-1RA, IL-10, IL-12(p70), and IFN-γ, were not detected.

Among the risk types with homozygous *CFH* deficiency (*CFH 402HH*) or smoker status, we found comparably strong induction of cytokine secretion. However, an exception appeared to be the group of non-smokers with *CFH* polymorphisms. In this group, we found increased MCP-1 levels compared to the smoker group, especially when the donors were homozygous for *CFH 402HH*. The MCP-1 secretion was twice as high as in the heterozygous *CFH 402YH* non-smoker group and increased three- to fourfold compared to the group of smokers with *CFH 402HH* risk polymorphism. Concerning VEGF secretion, homozygous *CFH 402HH* donors, irrespective of their smoking status, displayed a slightly decreased secretion when compared to the heterozygous groups. The addition of the PI3K inhibitor resulted in a significantly reduced secretion to less than 50%, while the pattern of secretion remained the same.

In our experiments, ARPE-19 cells of the higher passages 15 and 25 secreted higher levels of cytokines than those of passage 6 (Supplementary Material Figure S3), potentially reflecting the situation of aged RPE.

4 Discussion

As polymorphisms in complement genes are associated with the risk of AMD, it is questioned whether this leads to systemic or only local effects. Chirco et al. (17) did not find a difference in TCC levels in the plasma of AMD patients with low-risk and high-risk *CFH* alleles, whereas in the retinas of patients with high-risk *CFH* alleles, higher local TCC concentrations were detected. The current literature indicates an important role of TCC in the etiology of AMD in two ways. On the one hand, systemic changes by increased complement activity and higher TCC levels in AMD patients are discussed, as well as higher risks for AMD associated with polymorphisms in C9. On the other hand, the exploration of complement affecting RPE cells at a cellular level followed the concept of "sub-lytic" MAC influencing cell function. Our study provides a direct link between the mechanistic levels: the patients' observations and the cellular effects of isolated TCC on RPE cells. The most relevant observation of our study is that AMD patients showed higher plasma levels of TCC when compared to age-matched controls, but there were no differences among carriers with different risk alleles of complement genes. These systemic changes affect the Ca^{2+} signaling that regulates the expression activity of complement genes in the RPE and thus the control of the local activity of the complement system.

In our study, we investigated the TCC levels from the plasma of AMD patients and compared them with those from the plasma of AMD patients and age-matched controls as well as carriers of risk alleles *CFH* and *ARMS2*. Whereas AMD patients' plasma showed higher TCC levels, there were no differences between plasma from AMD patients with either *CFH* or *ARMS2* risk alleles. The same applies to the comparison between smokers and non-smokers in the patients' cohort. This observation matches well with that from other publications. First, our data confirmed the conclusions by Chirco et al. (17), who found no differences in TCC levels in the plasma between carriers of polymorphism *CFH 402HH* and *CFH 402YY* controls. Thus, the increased TCC levels in the plasma correlate with the diagnosis of AMD and, thus, clinically relevant degenerative changes in the retina. This assumption would also explain why there are no differences between AMD patients in the comparison of genetic and smoking-associated risk profiles. In the measurement of complement activity markers in the plasma, such as C3d/C3 ratio, C3a-desarg, or TCC, the different risk allele *CFH*, *ARMS*, or *CFI* carriers display comparable levels of those markers, while healthy donor's plasma displayed increased levels of complement activity (18, 19, 21, 23, 53–58). Increased markers for complement activity were found when compared to those in control plasma in both patients with dry and wet AMD. Our study included patients with wet AMD showing that not only dry AMD patients are affected by increased complement activity in the plasma. In contrast to these data, the C9 risk alleles have differential effects on TCC or C9 plasma levels (19, 20, 58). C9 risk allele carriers show higher levels of TCC when comparing AMD versus non-AMD patients, and also among AMD patients, the carriers of the C9 risk allele have higher TCC levels than non-carriers, which also varies within the group of C9 risk allele carriers depending on specific polymorphisms. Thus, considering our data and data from existing literature, we conclude that increased TCC or C9 levels in the plasma are associated with the disease AMD. However, the increased plasma levels originate at different steps of the complement cascade: either at the insufficient control of the

10.3389/fimmu.2023.1200725

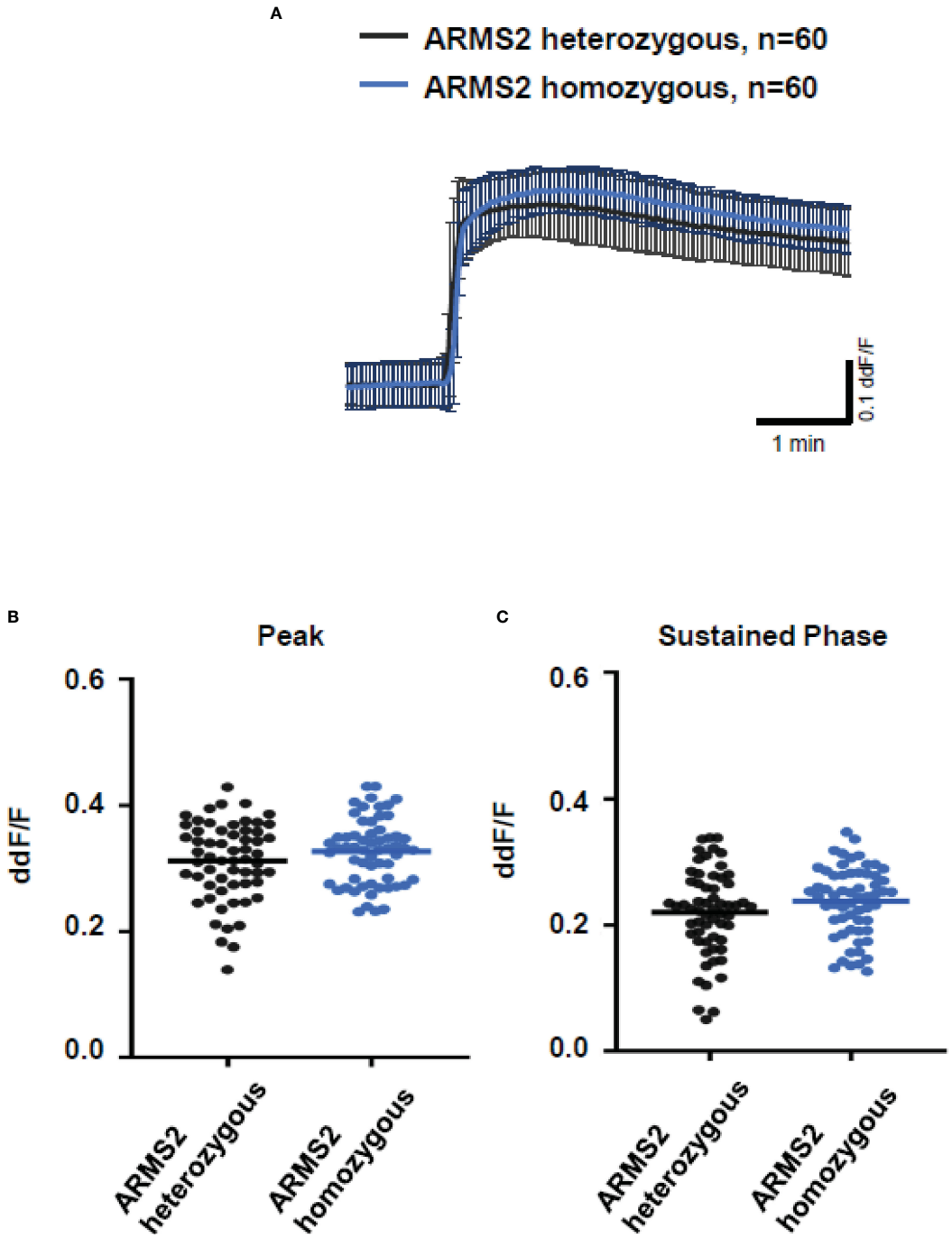

FIGURE 5
Changes in Ca^{2+} transients activated by plasma from age-related macular degeneration patients, stratified for *age-related maculopathy susceptibility 2 (ARMS2)* risk allele status. Plasma from patients carrying one (heterozygous) *vs.* two (homozygous) *ARMS2* risk alleles (2 different patients per risk allele status, 30 cells per patient). All patients were age-matched and had no additional *Complement factor H* risk alleles. **(A)** Ca^{2+} transients are given as differences to the baseline in fluorescence ratio between the two excitation wavelengths 340 and 380 nm; plasma was used in concentrations of 10%. Data are mean ± SD. **(B, C)** Ca^{2+} transient changes at the initial peak phase and the late sustained phase induced by plasma from patients with one *vs.* two *ARMS2* risk alleles, showing no significant differences in induced Ca^{2+} transients. The horizontal line represents the mean change in Ca^{2+} transients from baseline.

alternative activation pathway or directly by determining the gain-of-function effects by altered C9 proteins. In summary, our data further support the prominent role of the TCC in the etiology of AMD.

To determine whether these differences in plasma TCC levels are of biological relevance, we incubated these plasma probes with ARPE-19 cells. Although this RPE cell line is under debate for being representative of the native RPE and might thus limit our

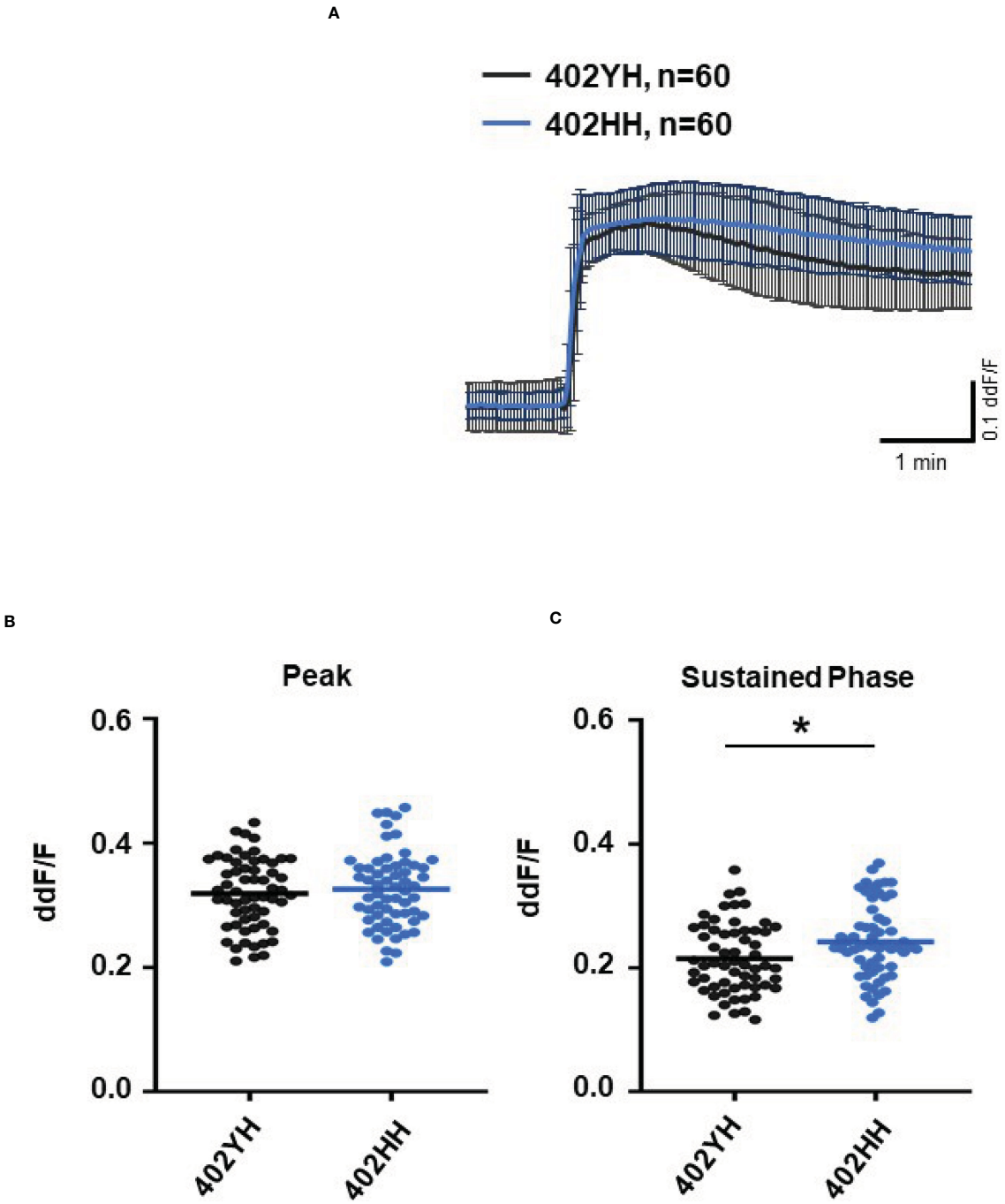

FIGURE 6
Changes in Ca^{2+} transients activated by plasma from age-related macular degeneration patients, stratified for *Complement factor H (CFH)* risk allele status. Plasma from patients *CFH 402YH* carriers vs. *CFH 402HH* carriers (2 different patients per risk allele status, 30 cells per patient). All patients were age-matched and had no additional *Age-related maculopathy susceptibility 2 (ARMS2)* risk allele. Data are mean ± SD. **(A)** Ca^{2+} transients are given as differences to the baseline in fluorescence ratio between the two excitation wavelengths 340 and 380 nm; plasma was used in concentrations of 10%. **(B, C)** Ca^{2+} transient changes at the initial peak phase and the late sustained phase. Plasma from *CFH 402HH* carriers induced a significantly higher change in intracellular free Ca^{2+} in the sustained phase compared to plasma from carriers of *CFH 402YH*. The horizontal line represents the mean change in Ca^{2+} transients from baseline. *$p < 0.05$ (Mann–Whitney *U* test).

conclusions for the pathogenic mechanisms possibly taking place *in vivo*, these cells will reflect the differences in the biological activity of patients' plasma. As in many other and also in our own recent studies, we used the Ca^{2+} imaging technique to monitor the cell reactions to plasma as a complement resource (28, 35, 59). We know from our own studies that activated complement compounds produced by the complement cascade induced by human plasma evoke orchestrated Ca^{2+} signals by activation of endogenously expressed ion channels (28). The central paradigm for coding the desired specific change of cell function activated by an increase in

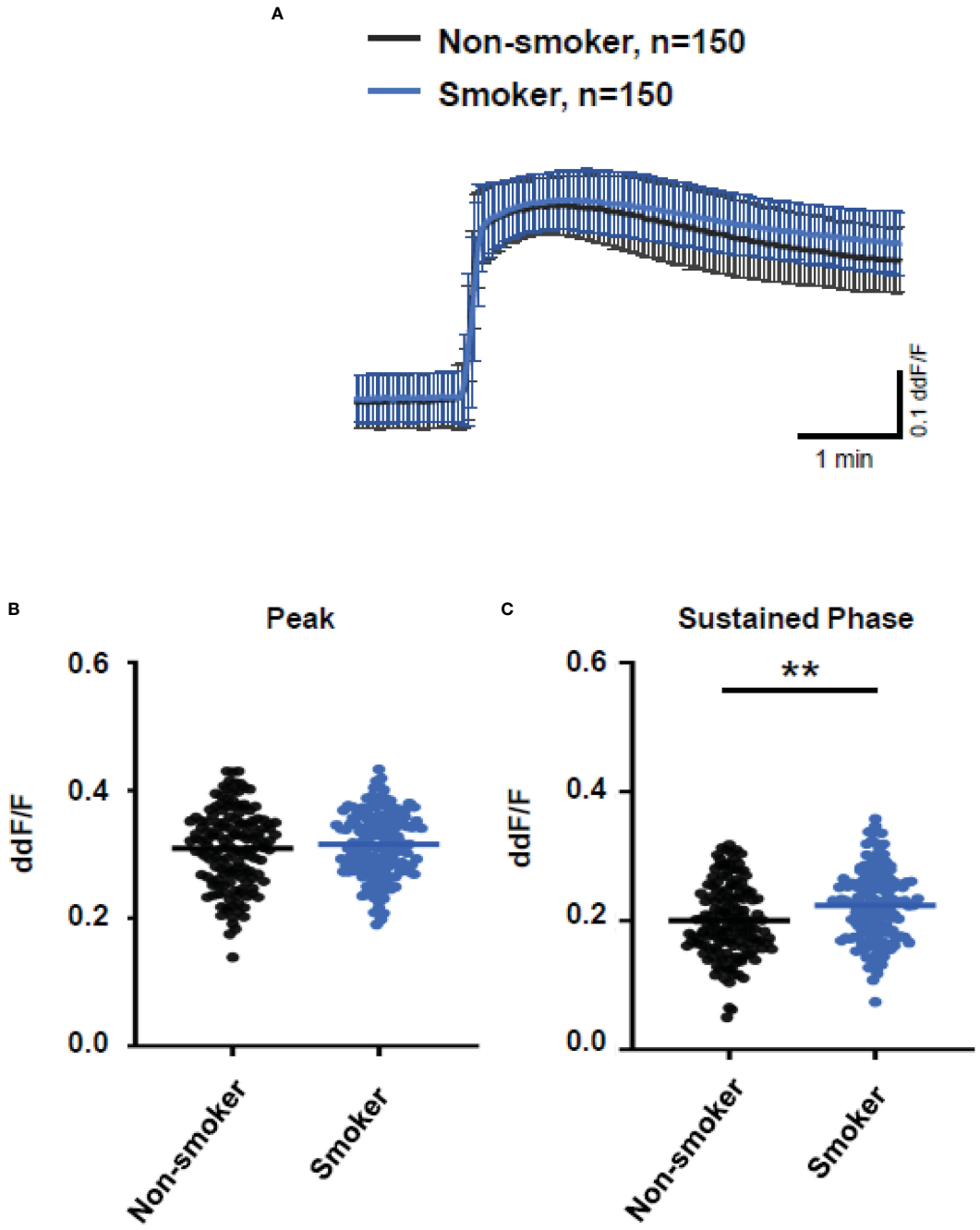

FIGURE 7
Changes in Ca^{2+} transients activated by plasma from age-related macular degeneration patients, stratified for smoking status (non-smoker *vs.* smoker). Plasma from five different patients per group was compared, with 30 cells per patient. All patients were matched for age, *age-related maculopathy susceptibility 2*, and *complement-factor H* risk alleles. Data are mean ± SD. **(A)** Ca^{2+} transients are given as differences to the baseline in fluorescence ratio between the two excitation wavelengths 340 and 380 nm; plasma was used in concentrations of 10%. **(B, C)** Ca^{2+} transient changes at the initial peak phase and the late sustained phase. Plasma from smoking patients induced a significantly higher change in intracellular free Ca^{2+} in the sustained phase compared to plasma from non-smoking patients. The horizontal line represents the mean change in Ca^{2+} transients from baseline. $^{**}p < 0.01$ (Mann–Whitney *U* test).

intracellular free Ca^{2+} states its origins in the time-dependent shape and the spatial distribution of the signal (50–52). Thus, differences in shape and distribution represent different changes in cellular functions.

Considering the importance of the shape of Ca^{2+} transients to represent specific cellular functions (50–52) and taking into account the reproducibility of complement-evoked Ca^{2+} increases (28, 33), we tested the effects of patients' plasma on intracellular free Ca^{2+} as a second messenger. Before we used patients' plasma, we tested C6-depleted plasma to identify the parts of the Ca^{2+} signal under the influence of TCC. The Ca^{2+} signal evoked by C6-depleted plasma was strongly reduced in peak amplitude and showed an absence of a

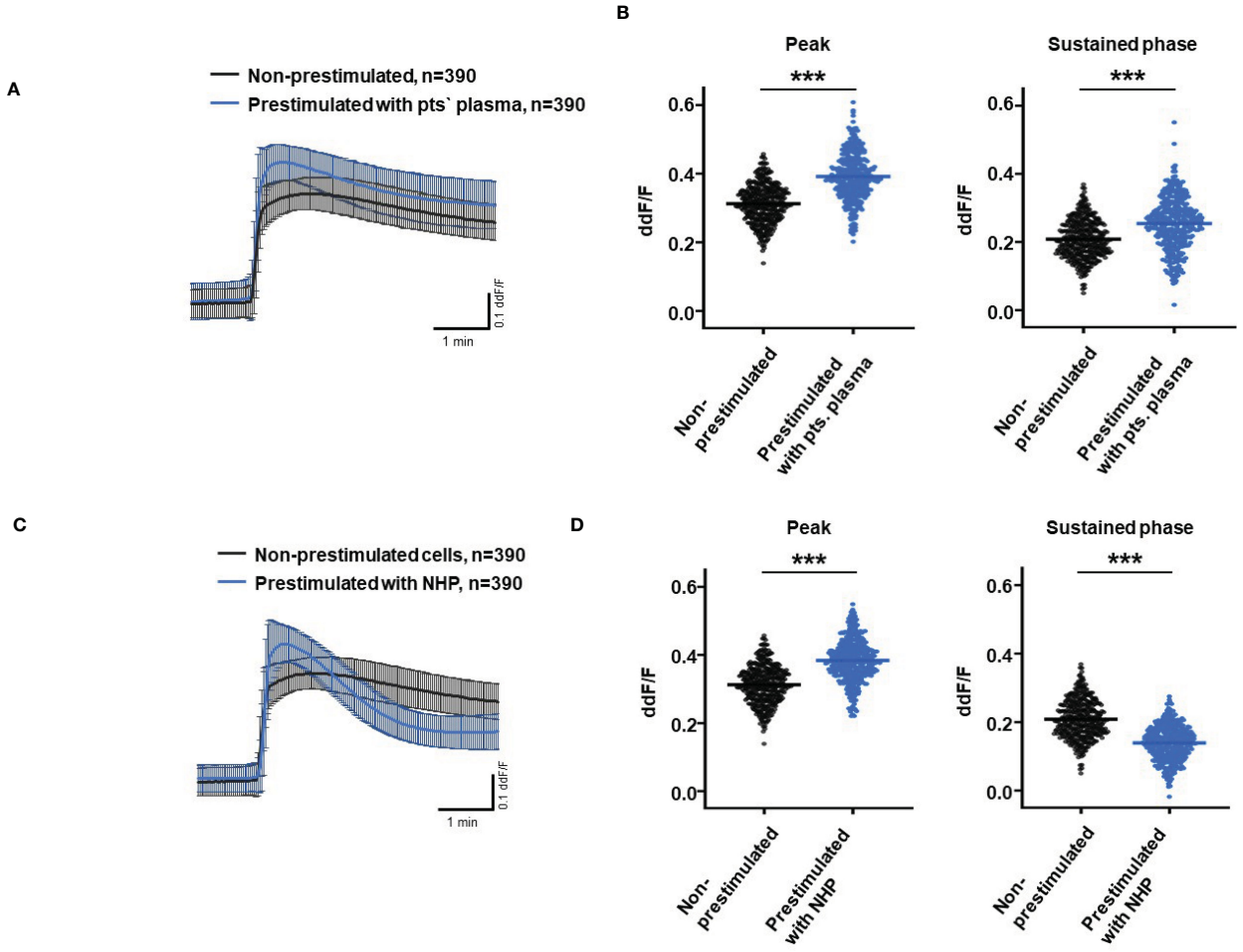

FIGURE 8
Effects of pre-stimulation with either plasma from age-related macular degeneration patients or controls on Ca^{2+} transients in ARPE-19 cells. The experimental conditions were pre-incubation with serum-free media **(A–D)**, media with 10% patients' (pts.) plasma (A, B, E, F), or media with 10% normal human plasma (NHP; C–F) for 24 h. Data are mean ± SD. **(A, C)** Ca^{2+} transients are given as differences to the baseline in the fluorescence ratio between the two excitation wavelengths 340 and 380 nm. **(B, D)** Ca^{2+} transient changes at the initial peak phase and the late sustained phase. Cells, pre-stimulated with patients' plasma, showed a significantly higher change in intracellular free Ca^{2+} compared to non-pre-stimulated cells **(B)**. Cells pre-stimulated with NHP showed a significantly higher change in intracellular free Ca^{2+} at the initial peak phase but a significantly lower amplitude in the sustained late phase compared to non-pre-stimulated cells **(D)**. The horizontal line represents the mean change in Ca^{2+} transients from baseline. ***$p < 0.001$ (Mann–Whitney *U* test). The dataset for "non-prestimulated" for "peak" and "sustained" were statistically tested two times: Once against "pre-stimulation patients' plasma" and a second time against "pre-stimulated NHP"; thus, the data for "non-stimulated" "peak" and "sustained" in the **(B, D)** are identical.

sustained phase. Thus, TCC that is formed in human plasma during the first seconds of exposure to the cells already determines the first phase of the Ca^{2+} increase and additionally paves the full development signal. As the later parts of the plasma-induced Ca^{2+} are activated by anaphylatoxins (28, 33), the early increase by TCC is of importance for anaphylatoxin signaling. In a recent study, we showed that isolated anaphylatoxins exhibit monophasic Ca^{2+} transients with amplitudes (33) that are far smaller than those of complete plasma, which shows biphasic Ca^{2+} transients consisting of an initial peak and a sustained phase (28). Thus, the C6-depleted plasma indicates that especially the early increase of intracellular Ca^{2+} stems from the presence of TCC.

Indeed, comparing Ca^{2+} transients evoked from control plasma to those evoked from patients' plasma, we found that the Ca^{2+} transients from AMD plasma increased faster with shorter latency and a steeper increase to a slightly reduced peak, whereas the sustained phases remained unchanged. For the peak level of the Ca^{2+} signals, we found a negative correlation with the TCC levels in the plasma of individual patients. Thus, the plasma with higher levels of TCC especially showed changes in the first phase of the signal as hypothesized from the data with C6-depleted plasma. Heat inactivation of patients' plasma to inhibit complement activity revealed no increased intracellular free Ca^{2+}, which suggests that the Ca^{2+} signal from patients' plasma depends on the activity of complement, although the minor contribution of other heat-labile factors cannot be fully excluded. Indeed, we found a correlation between the plasma TCC levels in the patients and the peak amplitude of the Ca^{2+} increase, evidencing that the major

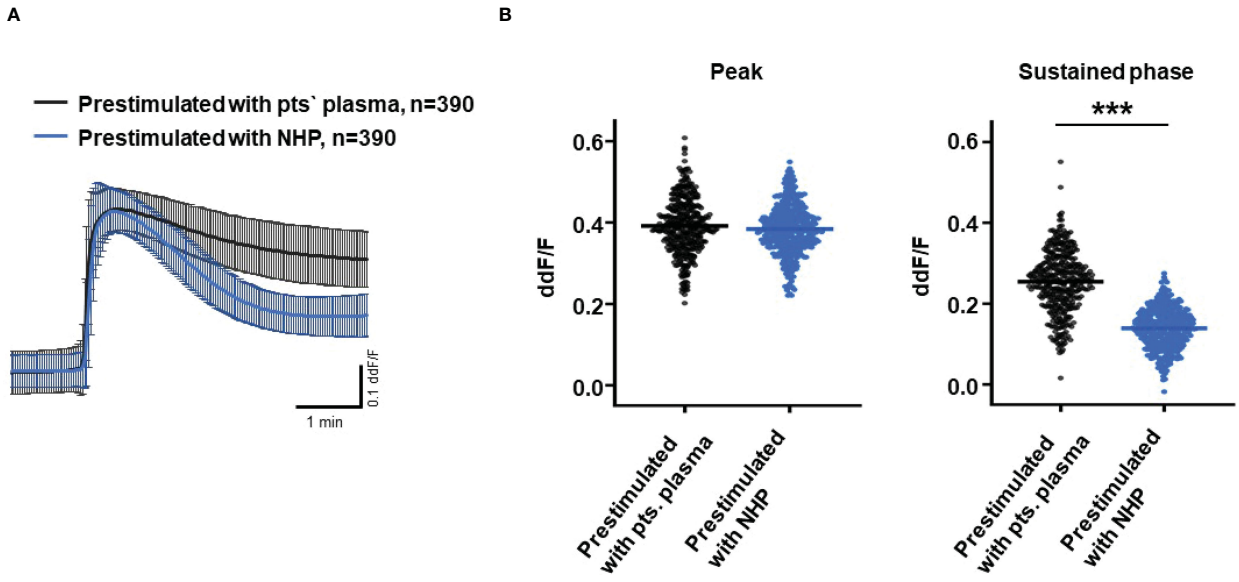

FIGURE 9
Direct comparison of pre-stimulation effects between patients' plasma and control plasma on Ca^{2+} transients in ARPE-19 cells. **(A)** Ca^{2+} transients are given as differences to the baseline in the fluorescence ratio between the two excitation wavelengths 340 and 380 nm; plasma was used in concentrations of 10%. Data are mean ± SD. **(B)** Compared to pre-stimulation with normal human plasma (NHP), cells showed a significantly higher change in intracellular free Ca^{2+} in the sustained phase after pre-stimulation with patients' plasma. The horizontal line represents the mean change in Ca^{2+} transients from baseline. ***$p < 0.001$ (Mann–Whitney *U* test).

differences in the Ca^{2+} signals between control plasma and patients' plasma result from the differences in the plasma TCC levels. Thus, any changes resulting in Ca^{2+} signals and also changes in gene expression should be attributed to the higher TCC levels in the patients' plasma.

In general, we found no differences in the plasma TCC levels between the carriers of risk alleles *ARMS2* and *CFH*. However, when comparing the plasma-evoked Ca^{2+} signals from carriers of different risk alleles, we observed subtle differences. With *ARMS2* genotypes, the Ca^{2+} signals were indistinguishable between heterozygous and homozygous carriers, while the *CFH 402HH* carrier's plasma showed higher amplitudes in the late phase than plasma from *CFH 402YH* individuals. We observed the same when comparing plasma from smokers with non-smokers. In addition, only the late phase was increased. A decreased CFH efficiency to control the alternative complement pathway by either polymorphic CFH or by cigarette smoke (3, 6, 7, 44, 60–62) leads to increased complement activity markers in the patients' sera (57, 60, 63). Because of this, we assume that sera of smokers or patients carrying *CFH* risk alleles contain higher levels of anaphylatoxins, which in turn increase the late Ca^{2+} signals. The study by Smailhodzic et al. supports this conclusion (21). The study reports that sera from *CFH* risk allele carriers show higher systemic complement activity determined as C3d/C3 ratio compared to *ARMS2* risk allele carriers. However, we found no differences in the TCC levels in the plasma of mutated *CFH* and *ARMS2* allele carriers. We explain this difference by the fact that C3d/C3 measurements reflect a more dynamic parameter based on complement factors that are more unstable than TCC.

Given the above conclusions, the Ca^{2+} transients evoked in ARPE-19 cells by plasma as a complement source represent integrals of the biological activity of activated complement. To shift these observations toward more translational conclusions, we performed pre-stimulation experiments with plasma to mimic a sustained exposure to complement as it likely occurs in the patients' eye. After pre-incubation with patients' plasma, both the peak and sustained phases are higher than those without pre-stimulation. Thus, the pro-inflammatory complement composition in the patients' sera sensitizes ARPE-19 cells for complement reactions. In contrast, after pre-stimulation with control plasma, the patients' sera show a differentially regulated response. Although the peak increases in the same manner, the sustained phase is much smaller in amplitude. Thus, control plasma also sensitizes the cells for the initial reaction but leads to a faster termination of the Ca^{2+} signal. The composition of activated complement in control sera maintains the immune inhibitory activity of RPE cells against the pro-inflammatory complement activity of patients' sera.

To support this conclusion, we investigated gene expression profiles of ARPE-19 cells in response to stimulation by control and patients' sera. The RPE cell reaction to complement under healthy conditions includes the secretion of CFH to prevent local complement reactions at the moment they would occur (44, 62–66). Thus, we investigated the effects of the patients' sera on complement gene expression in ARPE-19 cells. In previous publications, we have shown that the complete Ca^{2+} signal evoked by complement is blocked by the inhibition of L-type channels (28). Furthermore, the steepness of the Ca^{2+} increase was profoundly reduced. This matches well with the kinetic

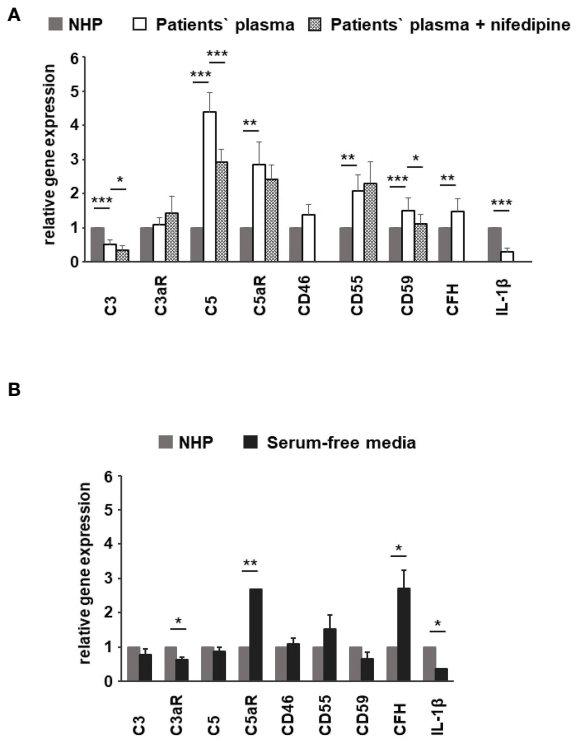

FIGURE 10
Effects of patients' plasma on differential gene expression of complement genes in ARPE-19 cells. Effect of patients' plasma ± nifedipine **(A)** and serum-free media **(B)** and plasma compared to normal human plasma (NHP; 10%) on gene expression of C3, C3aR, C5, C5aR, CD46, CD55, CD59, complement factor H (*CFH*), and interleukin-1beta (IL-1β) in ARPE-19 cells. NHP and patients' plasma were applied at a total concentration of 10% with nifedipine at 10 μM for 24 h. Data are expressed as mean values + SD. For serum-free media, n = 2–3. For patients' plasma, n = 16, except for C5aR, n = 6. Patients' plasma + nifedipine, n = 9, except for C5aR, n = 5. For NHP, n = 3. *$p < 0.05$, **$p < 0.01$, ***$p < 0.001$ (Student's t-test).

alterations associated with patients' plasma that contains higher levels of TCC. However, when investigating the Ca^{2+} signals evoked by isolated anaphylatoxins, we found that these Ca^{2+} signals were insensitive to L-type channel blockers (33). Thus, the blocking effects of the L-type channel blocker nifedipine indicate the contribution of TCC to gene expression. We compared gene expression using control plasma versus plasma-free conditions and observed a decrease in the C3aR expression, in parallel to an increase in C5aR and CFH expression. Furthermore, the IL-1β expression decreased. This effect on IL-1β expression might result from anaphylatoxin C5a as shown by Brandstetter et al. (67), who also reported that the expression profile induced by C5a increased further inflammasome priming by IL-1β. When studying the effects of the isolated anaphylatoxins, we found no effects on the C3, C5, or anaphylatoxin receptor expression (33). Thus, the additional presence of TCC is required to produce the differential gene expression changes as shown by Brandstetter et al. (67), and in our study, such an interactive effect between activated complement components that we have previously described (33) demonstrates interactive signaling of C3a and C5a. In combination with our new data, the picture is widening to an effect in which control plasma causes the cell reactions to have a higher sensibility for the C3 convertase level: more signaling with C3aR and increased C3 convertase activity by CFH downregulation and likely less C5aR1 and C5aR2 signaling. In contrast, with patients' plasma incubation, the expression of C3 decreased, but C5 is now more strongly expressed. This goes along with increases in C5aR1 expression and increased expression of TCC surface inhibitors CD55 and CD59. Thus, in contrast to control plasma, AMD plasma shifts the cell activity toward the C5 convertase level with higher C5a signaling and preparation for higher levels of TCC. Compared to control plasma, IL-1β expression is further decreased. These observations and the observations of Brandstetter et al. (67) led us to the conclusion that the patients' plasma turns the expression profile into a more pro-inflammatory phenotype in ARPE-19 cells. The reduction in C3 expression along with increases in C5 and CD59 expression is sensitive to the L-type channel blocker nifedipine and thus induced under contribution by TCC. With an increased production of C5, the RPE would at the same time lead to more formation of TCC and thus increase its protection against TCC impact. Our observations of the secretory activity under the influence of patients' plasma support this conclusion. Also, under treatment with AMD plasma, ARPE-19 cells showed increased secretion of pro-inflammatory cytokines IL-1, IL-6, IL-8, MCP-1, and the angiogenic factor VEGF-A; among them, the secretion of MCP-1 and VEGF-A was the highest. Interestingly, we found differences between smokers and non-smokers for MCP-1 secretion. The non-smoker group showed generally higher MCP-1 secretion rates with differences between the *CFH* risk haplotypes when compared to the smoker group, in which we also found no differences between the *CFH* haplotypes. This corresponds to the differences in the Ca^{2+} signal patterns. The comparison between smokers and non-smokers showed no differences in the peak, only in the sustained phase, whereas the peak was dependent on the TCC concentration. This indicates that there is no general pattern of secretion activity associated with the different risk factors, but, in general, the risk factors lead to increased secretion of pro-inflammatory cytokines. Thus, under the influence of TCC, the RPE's phenotype is changing into a pro-inflammatory one including a self-protection of the RPE against TCC.

Here, we have investigated the reaction of ARPE-19 cells to AMD patients' plasma, which indicated a biological impact on the cells, rendering the immune reactions toward a more pro-inflammatory type. Although the ARPE-19 cell line might not reliably represent properties of RPE cells *in vivo*, we can principally draw conclusions on the capabilities of the patients' plasma themselves. Here, the main conclusion is that in AMD, a systemic impact like the complement system acts on vulnerable cells of the outer blood–retina barrier. AMD risk alleles exacerbate local immune reactions, and the systemic pre-activated complement system might affect the outer retina even without local complement activity. The TCC might play an important role among the systemic factors, leading to a local effect on the tissue,

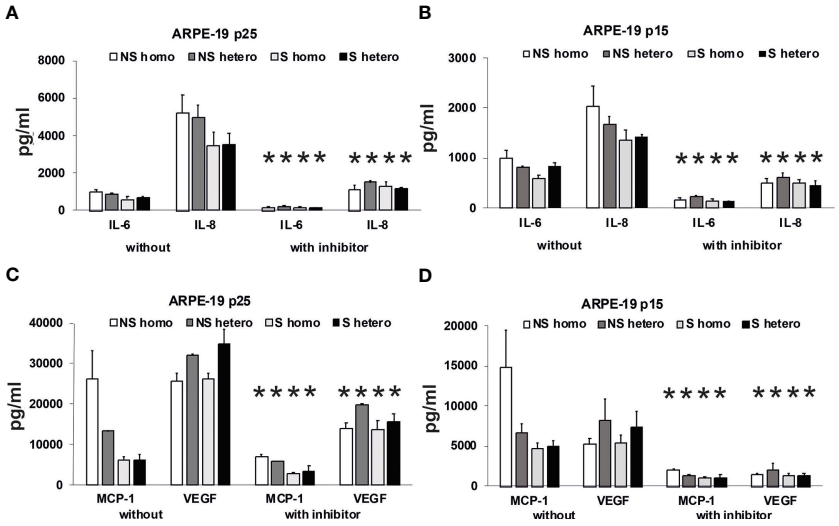

FIGURE 11
Effects of plasma on differential secretion activities of ARPE-19 cells. Cytokine and chemokine secretion of ARPE-19 cell lines. **(A, C)** ARPE-19 in passage 25. **(B, D)** ARPE-19 in passage 15. **(A–D)** Plasma (all 10%) from non-smoking (NS) or smoking (S) age-related macular degeneration (AMD) patients, carriers *CFH 402HH* versus carriers *CFH 402YH*. Plasma samples with or without PI3K-inhibitor LY294002 (50 μM) were incubated with ARPE-19 cells and cyto-/chemokine concentrations determined from culture supernatants. n = 2–4 for CHF mutant plasma (* = p< 0.05 for all respective values of supernatants from cultures with inhibitor vs. without).

which might not be primarily fatal for RPE cells. We assume that this effect drives the chronic low-grade inflammation known to occur in AMD patients and is reflected by observations such as a life-long accumulation of TCC in the outer retina (15–17) by increased levels of terminal complement complex in the blood (20, 21, 68).

Data availability statement

The original contributions presented in the study are publicly available. This data can be found here: https://doi.org/10.5281/zenodo.7797381 or DOI 10.5281/zenodo.7797381 (Zenodo repository).

Ethics statement

The studies involving human participants were reviewed and approved by Charité ethics committee, registration number EA2/004/14. The patients/participants provided their written informed consent to participate in this study.

Author contributions

Conceptualization: CB, PZ, AJ, CS and OS. Methodology: CB, SR, AS, LP, CH and MG. Formal analysis: CB, SR, LP, CS, GW and OS. Investigation: CB, SR, AS, LP, CH and MG. Writing—original draft preparation: OS, CB, CS and GW. Writing—review and editing: OS, SC, GW and JP. All authors contributed to the article and approved the submitted version.

Funding

This is supported by the Deutsche Forschungsgemeinschaft (DFG) grant STR480/26-1 and the Jackstaedt Foundation. Furthermore, this work was supported by a grant from the Friedrich-Baur-Foundation. We acknowledge support from the German Research Foundation (DFG) and the Open Access Publication Fonds of the Charite—Universitätsmedizin Berlin.

Acknowledgments

The authors thank Ina Löschmann and Monika von der Heide for excellent technical support and Roman Hennel for his help and access to the multiplex reader. Further, we gratefully thank Julian Pottier for the expert English and scientific language editing.

Conflict of interest

The authors declare that the research was conducted in the absence of any commercial or financial relationships that could be construed as a potential conflict of interest.

Publisher's note

All claims expressed in this article are solely those of the authors and do not necessarily represent those of their affiliated organizations, or those of the publisher, the editors and the reviewers. Any product that may be evaluated in this article, or claim that may be made by its manufacturer, is not guaranteed or endorsed by the publisher.

Supplementary material

The Supplementary Material for this article can be found online at: https://www.frontiersin.org/articles/10.3389/fimmu.2023.1200725/full#supplementary-material

SUPPLEMENTARY FIGURE 1
Tables of patients' and risk factors. Upper table shows the age and gender distribution in the patients cohort and the group of healthy donors. The lower table shows the distribution of risk factors among the AMD patient cohort.

SUPPLEMENTARY FIGURE 2
Properties of patients whose plasma was used for Ca^{2+} imaging, qPCR and secretion assay. Table shows detailed properties of the patient donors whose plasma was used for biological analyses. Note: the numbers are not suitable to identify certain patients.

SUPPLEMENTARY FIGURE 3
Heat-inactivation control for patient's plasma. Changes in Ca^{2+} transients activated by plasma from age-related macular degeneration patients (16 different patients, 30 cells per patients) and heat-inactivated patients' plasma (16 different patients, 10 cells per patients). Ca^{2+} transients are given as differences to the baseline in fluorescence ratio between the two excitation wavelengths 340 nm and 380 nm. Data are mean ± SD.

SUPPLEMENTARY FIGURE 4
Complement-dependent activation of basal secretion by ARPE-19 cells. ARPE-19 cells in passage 6 were stimulated with normal human plasma (NHP, 10%) from age-matched, non-smoking donors without AMD, *CFH* mutations unknown. Secretion of different cytokines was measured in supernatants with a multiplex bead assay; cytokine concentrations are given as mean + SEM; n = 17. In a second, independent experiment, pooled plasma samples of age-matched donors without AMD were tested for their ability to induce cytokine secretion by ARPE-19 cells in their sixth passage. In this experiment, the plasma pools displayed slight differences in their ability to induce cytokine secretion in ARPE-19 cells, the "oldest" pool (mean donor age: 82.7 years) induced more IL-6 and IL-8 and less MCP-1 compared to the pools of younger donors (means of 77.4 and 73 years, respectively). Data not shown. Interestingly, the used plasma pools already contained a high concentration of MCP-1, which decreased fivefold during the incubation with ARPE-19 cells, suggesting that MCP-1 was obviously used by the ARPE-19 cells, while IL-8 was produced by the RPE cells themselves and not provided by the plasma. VEGF concentrations remained unaltered, not allowing any conclusion on use or production by the ARPE-19 cells.

References

1. van Leeuwen R, Klaver CC, Vingerling JR, Hofman A, De Jong PT. Epidemiology of age-related maculopathy: a review. *Eur J Epidemiol* (2003) 18:845–54. doi: 10.1023/A:1025643303914

2. Campochiaro PA. Ocular neovascularization. *J Mol Med (Berl)* (2013) 91:311–21. doi: 10.1007/s00109-013-0993-5

3. Zipfel PF, Lauer N, Skerka C. The role of complement in AMD. *Adv Exp Med Biol* (2010) 703:9–24. doi: 10.1007/978-1-4419-5635-4_2

4. Armstrong RA, Mousavi M. Overview of risk factors for age-related macular degeneration (AMD). *J Stem Cells* (2015) 10:171–91.

5. Tan PL, Bowes Rickman C, Katsanis N. AMD And the alternative complement pathway: genetics and functional implications. *Hum Genomics* (2016) 10:23. doi: 10.1186/s40246-016-0079-x

6. Skerka C, Lauer N, Weinberger AA, Keilhauer CN, Suhnel J, Smith R, et al. Defective complement control of factor h (Y402H) and FHL-1 in age-related macular degeneration. *Mol Immunol* (2007) 44:3398–406. doi: 10.1016/j.molimm.2007.02.012

7. Zipfel PF, Skerka C. Complement regulators and inhibitory proteins. *Nat Rev Immunol* (2009) 9:729–40. doi: 10.1038/nri2620

8. Anderson DH, Radeke MJ, Gallo NB, Chapin EA, Johnson PT, Curletti CR, et al. The pivotal role of the complement system in aging and age-related macular degeneration: hypothesis re-visited. *Prog Retin Eye Res* (2010) 29:95–112. doi: 10.1016/j.preteyeres.2009.11.003

9. Fritsche LG, Lauer N, Hartmann A, Stippa S, Keilhauer CN, Oppermann M, et al. An imbalance of human complement regulatory proteins CFHR1, CFHR3 and factor h influences risk for age-related macular degeneration (AMD). *Hum Mol Genet* (2010) 19:4694–704. doi: 10.1093/hmg/ddq399

10. McHarg S, Clark SJ, Day AJ, Bishop PN. Age-related macular degeneration and the role of the complement system. *Mol Immunol* (2015) 67:43–50. doi: 10.1016/j.molimm.2015.02.032

11. Troutbeck R, Al-Qureshi S, Guymer RH. Therapeutic targeting of the complement system in age-related macular degeneration: a review. *Clin Experiment Ophthalmol* (2012) 40:18–26. doi: 10.1111/j.1442-9071.2011.02581.x

12. Kassa E, Ciulla TA, Hussain RM, Dugel PU. Complement inhibition as a therapeutic strategy in retinal disorders. *Expert Opin Biol Ther* (2019) 19:335–42. doi: 10.1080/14712598.2019.1575358

13. Jaffe GJ, Westby K, Csaky KG, Mones J, Pearlman JA, Patel SS, et al. C5 inhibitor avacincaptad pegol for geographic atrophy due to age-related macular degeneration: a randomized pivotal phase 2/3 trial. *Ophthalmology* (2021) 128:576–586. doi: 10.1016/j.ophtha.2020.08.027

14. Lommatzsch A, Hermans P, Weber B, Pauleikhoff D. Complement factor h variant Y402H and basal laminar deposits in exudative age-related macular degeneration. *Graefes Arch Clin Exp Ophthalmol* (2007) 245:1713–6. doi: 10.1007/s00417-007-0649-7

15. Mullins RF, Schoo DP, Sohn EH, Flamme-Wiese MJ, Workamelahu G, Johnston RM, et al. The membrane attack complex in aging human choriocapillaris: relationship to macular degeneration and choroidal thinning. *Am J Pathol* (2014) 184:3142–53. doi: 10.1016/j.ajpath.2014.07.017

16. Chirco KR, Tucker BA, Stone EM, Mullins RF. Selective accumulation of the complement membrane attack complex in aging choriocapillaris. *Exp Eye Res* (2016) 146:393–397. doi: 10.1016/j.exer.2015.09.003

17. Chirco KR, Flamme-Wiese MJ, Wiley JS, Potempa LA, Stone EM, Tucker BA, et al. Evaluation of serum and ocular levels of membrane attack complex and c-reactive protein in CFH-genotyped human donors. *Eye (Lond)* (2018) 32:1740–2. doi: 10.1038/s41433-018-0170-8

18. Geerlings MJ, Kremlitzka M, Bakker B, Nilsson SC, Saksens NT, Lechanteur YT, et al. The functional effect of rare variants in complement genes on C3b degradation in patients with age-related macular degeneration. *JAMA Ophthalmol* (2017) 135:39–46. doi: 10.1001/jamaophthalmol.2016.4604

19. Kremlitzka M, Geerlings MJ, De Jong S, Bakker B, Nilsson SC, Fauser S, et al. Functional analyses of rare genetic variants in complement component C9 identified in patients with age-related macular degeneration. *Hum Mol Genet* (2018) 27:2678–88. doi: 10.1093/hmg/ddy178

20. McMahon O, Hallam TM, Patel S, Harris CL, Menny A, Zelek WM, et al. The rare C9 P167S risk variant for age-related macular degeneration increases polymerization of the terminal component of the complement cascade. *Hum Mol Genet* (2021) 30:1188–99. doi: 10.1093/hmg/ddab086

21. Smailhodzic D, Klaver CC, Klevering BJ, Boon CJ, Groenewoud JM, Kirchhof B, et al. Risk alleles in CFH and ARMS2 are independently associated with systemic complement activation in age-related macular degeneration. *Ophthalmology* (2012) 119:339–46. doi: 10.1016/j.ophtha.2011.07.056

22. Paun CC, Ersoy L, Schick T, Groenewoud JM, Lechanteur YT, Fauser S, et al. Genetic variants and systemic complement activation levels are associated with serum lipoprotein levels in age-related macular degeneration. *Invest Ophthalmol Vis Sci* (2015) 56:7766–73. doi: 10.1167/iovs.15-17035

23. Lores-Motta L, Paun CC, Corominas J, Pauper M, Geerlings MJ, Altay L, et al. Genome-wide association study reveals variants in CFH and CFHR4 associated with systemic complement activation: implications in age-related macular degeneration. *Ophthalmology* (2018) 125:1064–74. doi: 10.1016/j.ophtha.2017.12.023

24. Khandhadia S, Cipriani V, Yates JR, Lotery AJ. Age-related macular degeneration and the complement system. *Immunobiology* (2012) 217:127–46. doi: 10.1016/j.imbio.2011.07.019

25. Triantafilou K, Hughes TR, Triantafilou M, Morgan BP. The complement membrane attack complex triggers intracellular Ca2+ fluxes leading to NLRP3 inflammasome activation. *J Cell Sci* (2013) 126:2903–13. doi: 10.1242/jcs.124388

26. Kumar-Singh R. The role of complement membrane attack complex in dry and wet AMD - from hypothesis to clinical trials. *Exp Eye Res* (2019) 184:266–77. doi: 10.1016/j.exer.2019.05.006

27. Strauss O. The retinal pigment epithelium in visual function. *Physiol Rev* (2005) 85:845–81. doi: 10.1152/physrev.00021.2004

28. Genewsky A, Jost I, Busch C, Huber C, Stindl J, Skerka C, et al. Activation of endogenously expressed ion channels by active complement in the retinal pigment epithelium. *Pflugers Arch* (2015) 467:2179–91. doi: 10.1007/s00424-014-1656-2

29. Thurman JM, Renner B, Kunchithapautham K, Ferreira VP, Pangburn MK, Ablonczy Z, et al. Oxidative stress renders retinal pigment epithelial cells susceptible to

complement-mediated injury. *J Biol Chem* (2009) 284:16939–47. doi: 10.1074/jbc.M808166200

30. Kunchithapautham K, Bandyopadhyay M, Dahrouj M, Thurman JM, Rohrer B. Sublytic membrane-attack-complex activation and VEGF secretion in retinal pigment epithelial cells. *Adv Exp Med Biol* (2012) 723:23–30. doi: 10.1007/978-1-4614-0631-0_4

31. Joseph K, Kulik L, Coughlin B, Kunchithapautham K, Bandyopadhyay M, Thiel S, et al. Oxidative stress sensitizes retinal pigmented epithelial (RPE) cells to complement-mediated injury in a natural antibody-, lectin pathway-, and phospholipid epitope-dependent manner. *J Biol Chem* (2013) 288:12753–65. doi: 10.1074/jbc.M112.421891

32. Kunchithapautham K, Atkinson C, Rohrer B. Smoke exposure causes endoplasmic reticulum stress and lipid accumulation in retinal pigment epithelium through oxidative stress and complement activation. *J Biol Chem* (2014) 289:14534–46. doi: 10.1074/jbc.M114.564674

33. Busch C, Annamalai B, Abdusalamova K, Reichhart N, Huber C, Lin Y, et al. Anaphylatoxins activate Ca(2+), Akt/PI3-kinase, and FOXO1/FoxP3 in the retinal pigment epithelium. *Front Immunol* (2017) 8:703. doi: 10.3389/fimmu.2017.00703

34. Morgan BP, Campbell AK. The recovery of human polymorphonuclear leucocytes from sublytic complement attack is mediated by changes in intracellular free calcium. *Biochem J* (1985) 231:205–8. doi: 10.1042/bj2310205

35. Carney DF, Hammer CH, Shin ML. Elimination of terminal complement complexes in the plasma membrane of nucleated cells: influence of extracellular Ca2 + and association with cellular Ca2+. *J Immunol* (1986) 137:263–70. doi: 10.4049/jimmunol.137.1.263

36. Reiter Y, Ciobotariu A, Jones J, Morgan BP, Fishelson Z. Complement membrane attack complex, perforin, and bacterial exotoxins induce in K562 cells calcium-dependent cross-protection from lysis. *J Immunol* (1995) 155:2203–10. doi: 10.4049/jimmunol.155.4.2203

37. Kilgore KS, Flory CM, Miller BF, Evans VM, Warren JS. The membrane attack complex of complement induces interleukin-8 and monocyte chemoattractant protein-1 secretion from human umbilical vein endothelial cells. *Am J Pathol* (1996) 149:953–61.

38. Kilgore KS, Schmid E, Shanley TP, Flory CM, Maheswari V, Tramontini NL, et al. Sublytic concentrations of the membrane attack complex of complement induce endothelial interleukin-8 and monocyte chemoattractant protein-1 through nuclear factor-kappa b activation. *Am J Pathol* (1997) 150:2019–31.

39. Niculescu F, Rus H, Van Biesen T, Shin ML. Activation of ras and mitogen-activated protein kinase pathway by terminal complement complexes is G protein dependent. *J Immunol* (1997) 158:4405–12. doi: 10.4049/jimmunol.158.9.4405

40. Mollnes TE, Lea T, Froland SS, Harboe M. Quantification of the terminal complement complex in human plasma by an enzyme-linked immunosorbent assay based on monoclonal antibodies against a neoantigen of the complex. *Scand J Immunol* (1985) 22:197–202. doi: 10.1111/j.1365-3083.1985.tb01871.x

41. Reiter Y, Ciobotariu A, Fishelson Z. Sublytic complement attack protects tumor cells from lytic doses of antibody and complement. *Eur J Immunol* (1992) 22:1207–13. doi: 10.1002/eji.1830220515

42. Kunchithapautham K, Rohrer B. Sublytic membrane-attack-complex (MAC) activation alters regulated rather than constitutive vascular endothelial growth factor (VEGF) secretion in retinal pigment epithelium monolayers. *J Biol Chem* (2011) 286:23717–24. doi: 10.1074/jbc.M110.214593

43. Lueck K, Wasmuth S, Williams J, Hughes TR, Morgan BP, Lommatzsch A, et al. Sub-Lytic C5b-9 induces functional changes in retinal pigment epithelial cells consistent with age-related macular degeneration. *Eye (Lond)* (2011) 25:1074–82. doi: 10.1038/eye.2011.109

44. Weismann D, Hartvigsen K, Lauer N, Bennett KL, Scholl HP, Charbel Issa P, et al. Complement factor h binds malondialdehyde epitopes and protects from oxidative stress. *Nature* (2011) 478:76–81. doi: 10.1038/nature10449

45. Cipriani V, Matharu BK, Khan JC, Shahid H, Stanton CM, Hayward C, et al. Genetic variation in complement regulators and susceptibility to age-related macular degeneration. *Immunobiology* (2012) 217:158–61. doi: 10.1016/j.imbio.2011.09.002

46. Chen Q, Wiesener M, Eberhardt HU, Hartmann A, Uzonyi B, Kirschfink M, et al. Complement factor h-related hybrid protein deregulates complement in dense deposit disease. *J Clin Invest* (2014) 124:145–55. doi: 10.1172/JCI71866

47. Micklisch S, Lin Y, Jacob S, Karlstetter M, Dannhausen K, Dasari P, et al. Age-related macular degeneration associated polymorphism rs10490924 in ARMS2 results in deficiency of a complement activator. *J Neuroinflamm* (2017) 14:4. doi: 10.1186/s12974-016-0776-3

48. Lauer N, Mihlan M, Hartmann A, Schlotzer-Schrehardt U, Keilhauer C, Scholl HP, et al. Complement regulation at necrotic cell lesions is impaired by the age-related macular degeneration-associated factor-h His402 risk variant. *J Immunol* (2011) 187:4374–83. doi: 10.4049/jimmunol.1002488

49. Morrison TB, Weis JJ, Wittwer CT. Quantification of low-copy transcripts by continuous SYBR green I monitoring during amplification. *Biotechniques* (1998) 24:954–8, 960, 962.

50. Berridge MJ, Lipp P, Bootman MD. The versatility and universality of calcium signalling. *Nat Rev Mol Cell Biol* (2000) 1:11–21. doi: 10.1038/35036035

51. Berridge MJ. Unlocking the secrets of cell signaling. *Annu Rev Physiol* (2005) 67:1–21. doi: 10.1146/annurev.physiol.67.040103.152647

52. Berridge MJ. The inositol Trisphosphate/Calcium signaling pathway in health and disease. *Physiol Rev* (2016) 96:1261–96. doi: 10.1152/physrev.00006.2016

53. Sivaprasad S, Adewoyin T, Bailey TA, Dandekar SS, Jenkins S, Webster AR, et al. Estimation of systemic complement C3 activity in age-related macular degeneration. *Arch Ophthalmol* (2007) 125:515–9. doi: 10.1001/archopht.125.4.515

54. Scholl HP, Charbel Issa P, Walier M, Janzer S, Pollok-Kopp B, Borncke F, et al. Systemic complement activation in age-related macular degeneration. *PloS One* (2008) 3:e2593. doi: 10.1371/journal.pone.0002593

55. Reynolds R, Hartnett ME, Atkinson JP, Giclas PC, Rosner B, Seddon JM. Plasma complement components and activation fragments: associations with age-related macular degeneration genotypes and phenotypes. *Invest Ophthalmol Vis Sci* (2009) 50:5818–27. doi: 10.1167/iovs.09-3928

56. Ristau T, Paun C, Ersoy L, Hahn M, Lechanteur Y, Hoyng C, et al. Impact of the common genetic associations of age-related macular degeneration upon systemic complement component C3d levels. *PloS One* (2014) 9:e93459. doi: 10.1371/journal.pone.0093459

57. Rohrer B, Frazer-Abel A, Leonard A, Ratnapriya R, Ward T, Pietraszkiewicz A, et al. Association of age-related macular degeneration with complement activation products, smoking, and single nucleotide polymorphisms in south carolinians of European and African descent. *Mol Vis* (2019) 25:79–92.

58. Schultz H, Song Y, Baumann BH, Kapphahn RJ, Montezuma SR, Ferrington DA, et al. Increased serum proteins in non-exudative AMD retinas. *Exp Eye Res* (2019) 186:107686. doi: 10.1016/j.exer.2019.05.026

59. Tan LX, Toops KA, Lakkaraju A. Protective responses to sublytic complement in the retinal pigment epithelium. *Proc Natl Acad Sci U.S.A.* (2016) 113:8789–94. doi: 10.1073/pnas.1523061113

60. Kew RR, Ghebrehiwet B, Janoff A. Cigarette smoke can activate the alternative pathway of complement *in vitro* by modifying the third component of complement. *J Clin Invest* (1985) 75:1000–7. doi: 10.1172/JCI111760

61. Woodell A, Coughlin B, Kunchithapautham K, Casey S, Williamson T, Ferrell WD, et al. Alternative complement pathway deficiency ameliorates chronic smoke-induced functional and morphological ocular injury. *PloS One* (2013) 8:e67894. doi: 10.1371/journal.pone.0067894

62. Toomey CB, Johnson LV, Bowes Rickman C. Complement factor h in AMD: bridging genetic associations and pathobiology. *Prog Retin Eye Res* (2018) 62:38–57. doi: 10.1016/j.preteyeres.2017.09.001

63. Marazita MC, Dugour A, Marquioni-Ramella MD, Figueroa JM, Suburo AM. Oxidative stress-induced premature senescence dysregulates VEGF and CFH expression in retinal pigment epithelial cells: implications for age-related macular degeneration. *Redox Biol* (2016) 7:78–87. doi: 10.1016/j.redox.2015.11.011

64. Fett AL, Hermann MM, Muether PS, Kirchhof B, Fauser S. Immunohistochemical localization of complement regulatory proteins in the human retina. *Histol Histopathol* (2012) 27:357–64. doi: 10.14670/HH-27.357

65. Wyatt MK, Tsai JY, Mishra S, Campos M, Jaworski C, Fariss RN, et al. Interaction of complement factor h and fibulin3 in age-related macular degeneration. *PloS One* (2013) 8:e68088. doi: 10.1371/journal.pone.0068088

66. Zhang Y, Huang Q, Tang M, Zhang J, Fan W. Complement factor h expressed by retinal pigment epithelium cells can suppress neovascularization of human umbilical vein endothelial cells: an *in vitro* study. *PloS One* (2015) 10:e0129945. doi: 10.1371/journal.pone.0129945

67. Brandstetter C, Holz FG, Krohne TU. Complement component C5a primes retinal pigment epithelial cells for inflammasome activation by lipofuscin-mediated photooxidative damage. *J Biol Chem* (2015) 290:31189–98. doi: 10.1074/jbc.M115.671180

68. Mullins RF, Russell SR, Anderson DH, Hageman GS. Drusen associated with aging and age-related macular degeneration contain proteins common to extracellular deposits associated with atherosclerosis, elastosis, amyloidosis, and dense deposit disease. *FASEB J* (2000) 14:835–46. doi: 10.1096/fasebj.14.7.835

frontiers | Frontiers in Immunology

TYPE Review
PUBLISHED 28 April 2023
DOI 10.3389/fimmu.2023.1163316

OPEN ACCESS

EDITED BY
Martin Perez-Andres,
University of Salamanca, Spain

REVIEWED BY
Sharat Chandra,
Cincinnati Children's Hospital Medical Center, United States
Vijaya Knight,
University of Colorado Anschutz Medical Campus, United States
Catarina Gregório Martins,
New University of Lisbon, Portugal

*CORRESPONDENCE
Jana Pachlopnik Schmid
jana.pachlopnik@kispi.uzh.ch

†PRESENT ADDRESS
Matthias Felber,
Department of Pediatrics, Division of Stem Cell Transplantation and Regenerative Medicine, Stanford University, Stanford, CA, United States
Stefano Vavassori,
Immunology, Cellerys AG, Schlieren, Switzerland

RECEIVED 10 February 2023
ACCEPTED 11 April 2023
PUBLISHED 28 April 2023

CITATION
Planas R, Felber M, Vavassori S and Pachlopnik Schmid J (2023) The hyperinflammatory spectrum: from defects in cytotoxicity to cytokine control.
Front. Immunol. 14:1163316.
doi: 10.3389/fimmu.2023.1163316

The hyperinflammatory spectrum: from defects in cytotoxicity to cytokine control

Raquel Planas[1,2], Matthias Felber[1†], Stefano Vavassori[1†] and Jana Pachlopnik Schmid[1,3*]

[1]Division of Immunology, University Children's Hospital Zurich, Zurich, Switzerland, [2]Department of Cell Biology, Physiology and Immunology, University of Barcelona, Barcelona, Spain, [3]Pediatric Immunology, University of Zurich, Zurich, Switzerland

Cytotoxic lymphocytes kill target cells through polarized release of the content of cytotoxic granules towards the target cell. The importance of this cytotoxic pathway in immune regulation is evidenced by the severe and often fatal condition, known as hemophagocytic lymphohistiocytosis (HLH) that occurs in mice and humans with inborn errors of lymphocyte cytotoxic function. The clinical and preclinical data indicate that the damage seen in severe, virally triggered HLH is due to an overwhelming immune system reaction and not the direct effects of the virus *per se*. The main HLH-disease mechanism, which links impaired cytotoxicity to excessive release of pro-inflammatory cytokines is a prolongation of the synapse time between the cytotoxic effector cell and the target cell, which prompts the former to secrete larger amounts of cytokines (including interferon gamma) that activate macrophages. We and others have identified novel genetic HLH spectrum disorders. In the present update, we position these newly reported molecular causes, including CD48-haploinsufficiency and ZNFX1-deficiency, within the pathogenic pathways that lead to HLH. These genetic defects have consequences on the cellular level on a gradient model ranging from impaired lymphocyte cytotoxicity to intrinsic activation of macrophages and virally infected cells. Altogether, it is clear that target cells and macrophages may play an independent role and are not passive bystanders in the pathogenesis of HLH. Understanding these processes which lead to immune dysregulation may pave the way to novel ideas for medical intervention in HLH and virally triggered hypercytokinemia.

KEYWORDS

hemophagocytic lymphohistiocytosis, inflammation, hyperinflammatory syndromes, cytotoxic lymphocytes, cytokines, immune dysregulation, inborn errors of immunity

1 Introduction

Over the last few years, the use of whole-exome and whole-genome sequencing has broadened the spectrum of HLH disorders. In-depth characterization of genetic causes and related molecular dysfunctions in hemophagocytic lymphohistiocytosis (HLH) provides us with a better understanding of immune regulation processes. HLH is a unique clinical entity. Primary forms of HLH (pHLH) are caused by genetic defects that impair lymphocytes' cytotoxic machinery. For instance, individuals with deleterious mutations in the gene coding for perforin (*PRF1*) develop HLH (1, 2). pHLH disorders include autosomal recessive mutations in genes involved in the perforin-dependent cytotoxic lymphocyte granule release, causing familial HLH (FHL) and other genetic defects such as *RAB27A*, *LYST* and *SH2D1A* mutations. Moreover, HLH-like manifestations can occur in association with other genetic defects, i.e. inborn errors of immunity (IEI). In these cases, HLH is often considered as an acquired event secondary to the concomitant disease, even though patients may fulfil the HLH diagnostic criteria (3).

Primary forms of HLH are distinct from autoinflammatory diseases. Despite clinical manifestations can be similar, posing a challenge to the clinicians during initial assessments, the genetics and underlying causes of pHLH and autoinflammatory diseases are different. Autoinflammatory diseases are caused by dysregulation that mainly affect the innate immune system and the activation of pro-inflammatory pathways; they include inflammasomopathies, interferonopathies, and a group of non-inflammasome-related diseases associated with the nucleotide-binding oligomerization domain-containing protein 2 (NOD2) pathway and the interleukin (IL)-1β pathway leading to sustained cytokine release by innate cells. In genetic terms, both polygenic and monogenic autoinflammatory diseases have been described (4). A viral infection leading to hyperinflammation is not an autoinflammation, because auto-inflammation, by definition, requires a lack of infectious trigger. This is in contrast to pHLH, which is known to be triggered by viruses.

The release of granules containing cytolytic effector molecules by cytotoxic lymphocytes is not only essential in the host's defense against viruses and other pathogens but also serves to terminate immune responses (5). The latter is evidenced by the development of systemic hyperinflammation in patients who lack perforin, the pore-forming molecule delivered to target cells during granule-mediated cytotoxicity (1, 2). This sepsis-like disease is characterized by a number of clinical and laboratory criteria that include fever, splenomegaly, bicytopenia, hemophagocytosis, and hyperferritinemia, among others. According to the current diagnostic criteria (HLH-2004), HLH is diagnosed in a patient when fulfilling the following criteria: either 1) a molecular diagnosis consistent with a mutation previously associated with HLH or 2) 5 of 8 of the following clinical parameters: fever; splenomegaly: bicytopenia, affecting at least two of three lineages in peripheral blood (hemoglobin<90g/L (in infants <4 weeks: hemoglobin <100 g/L), platelets < $100x10^9$/L, neutrophils <$1.0x10^9$/L); hypertriglyceridemia (fast triglycerides >265mg/dl) and/or hypofibrinogenemia (fibrinogen ≤1.5g/L); hemophagocytosis in the bone marrow or spleen or lymph nodes; low or absent natural killer (NK) cell activity; high ferritin levels (≥500μg/L); high levels of soluble CD25 (≥2,400U/mL) (6).

HLH can also occur in individuals with germline mutations in genes not related to any defect in the cytotoxic machinery. Furthermore, the so called "acquired" forms of HLH develop concomitantly to other infectious, malignant, autoimmune and rheumatological diseases such as systemic juvenile idiopatic arthritis (sJIA) (7, 8). By contrast to pHLH, these forms have been also named secondary HLH (sHLH). In particular, sHLH associated with rheumatologic/autoimmune conditions is often named macrophage activation syndrome (MAS). pHLH and MAS share clinical symptoms but MAS lacks the familial link and/or genetic causative mutation.

HLH is a cytokine storm syndrome. pHLH and MAS cause similar clinical manifestations and share some (but not all) impairments in immune pathways. Episodes of pHLH and episodes of MAS can both be triggered by infections (9). The immune responses to the trigger become persistent and go out of control, which leads to multiorgan damage and a sustained hyperinflammatory response - the main dangers, rather than impaired clearance of the viral trigger. However, in some disorders with HLH (e.g. XLP-1), the initial viral infection is poorly controlled. The immune dysregulation in HLH leads to an exaggerated, prolonged immune activation. This prompts the cytotoxic cell to secrete larger amounts of cytokines (including IFNγ), which directly activate macrophages. The defects in granule-mediated cytotoxicity in HLH compromise the ability of NK cells and CD8+ T cells to kill their target cells. Perforin-deficient CD8+ T cells interact with APCs for longer than usual (10, 11). Defective disengagement between the cytotoxic cell and its target leads to repetitive calcium release in the cytotoxic lymphocyte and increased production of proinflammatory cytokines. IFNγ and TNFα (a) stimulate hemophagocytic activity in macrophages, (b) continuously activate T cells during antigen presentation, and (c) induce the production of other proinflammatory cytokines, leading to a cytokine storm. Macrophage-secreted cytokines (such as IL-1α, IL-1β, IL–6, IL1β and IL-18, in MAS) maintain the $CD8^+$ T cells in an activated state and thus create a cytokine storm feedback loop.

Reduced fratricide killing furthermore contributes to the pathogenesis of HLH: during viral infections, NK cells have an immunoregulatory role by controlling overactivated $CD4^+$ and $CD8^+$ T cells (12, 13), a function which is disabled in the context of defective granule-dependent cytotoxicity.

The characterization of novel monogenic HLH disorders has revealed additional disease mechanisms. On one hand, APC resistance to killing may inhibit timely resolution of inflammation. Target cells themselves have an active role in determining susceptibility to granule-mediated cytotoxicity, through the cell-surface expression of cytotoxicity receptor ligands (14). On the other hand, cell-intrinsic overproduction of cytokines or dysregulated cytokine control may contribute to HLH. Systemic hyperinflammation can be triggered by inflammasome activation or by the dysregulation of cytokine mRNA transcription (15–18).

Thus, HLH can occur in a whole array of clinical settings and so is considered as a group of inflammatory disorders. Whole-exome and whole-genome sequencing methods have immensely amplified the ability to identify novel, pathogenic gene variants causing IEI (19). We and others have used these technologies to discover novel genetic inflammatory syndromes with HLH (14, 15, 20–22). Here, we propose a model that positions a number of conventional and novel monogenic inflammatory disorders on the HLH spectrum that ranges from inborn errors of cytotoxicity to inborn errors of cytokine control – all of which converge clinically to HLH (Figure 1A).

2 Cytotoxic lymphocyte subsets and granule-mediated cytotoxicity

Cytotoxic lymphocytes correspond to various subsets of innate and adaptive cells that recognize and attack malignant, stressed or virally infected cells. These include innate NK cells, adaptive cytotoxic T lymphocytes (CTLs), and other less abundant unconventional T lymphocytes. NK cells and CTLs are both capable of death receptor activation and the release of granules containing cytolytic effector molecules. These cytotoxic cells also produce proinflammatory cytokines, such as interferon gamma (IFNγ). CTLs have a CD8 complexed T cell-receptor (TCR) that recognizes peptides derived from (for example) intracellular pathogens or malignant cells. The peptides are presented by major histocompatibility complex (MHC) class I molecules on APCs (23). Specific peptide recognition triggers $CD8^+$ T cell activation, the acquisition of cytotoxic effector functions, and the development of the CTL memory program (24).

As an evasion strategy, some pathogens and malignant cells can downregulate MHC I expression. However, NK cells (the main innate lymphoid cell subset) complement CTLs by detecting and killing target cells that have downregulated their cell-surface expression of MHC class I. Furthermore, the cytotoxic activities of CTLs and NK cells have complementary time scales; whereas NK are innate cells that rapidly induce cell cytotoxicity, adaptive CTL responses require an antigen encounter and the development of effector status (25). As innate immune cells, NK cells lack specific, rearranged lymphocyte receptors and mount rapid, first-line effector responses against infected, malignant or stressed cells. They integrate signals of an array of germline-encoded HLA-specific and non-HLA-specific activating and inhibitory receptors. An NK cell combines and integrates the inputs of its various receptors, which fine-tunes its effector outcome (25, 26). For example, the lack of MHC class I ligands (detected by inhibiting receptors such as killer immunoglobulin (Ig)-like receptors and NKG2A) triggers cytotoxicity. The detection of ligands present in altered cells by activating receptors (e.g. NKG2D and natural cytotoxicity receptors) also promotes cytotoxicity. CD16 is another activating receptor present in the $CD56^{dim}$ cytotoxic

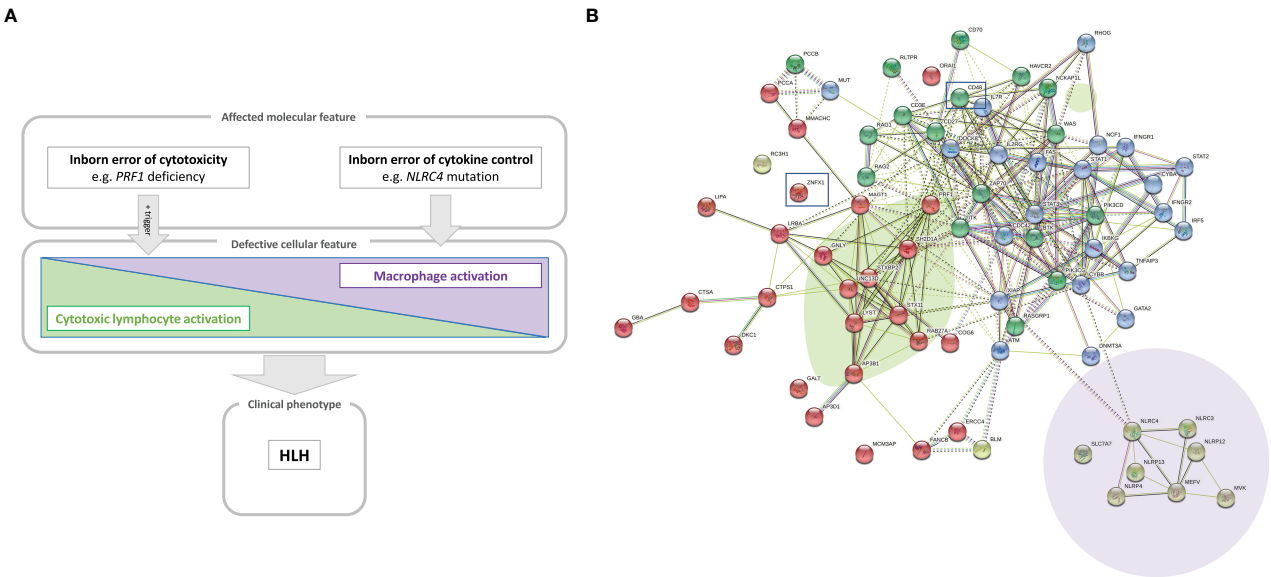

FIGURE 1
(A) A model of the hyperinflammatory spectrum, ranging from errors of cytotoxicity to lack of cytokine control with macrophage activation. From the molecular point of view, HLH-associated gene mutations can be divided into inborn errors of cytotoxicity and inborn errors of cytokine control (upper panel). These genetic defects have consequences on the cellular level on a spectrum ranging from impaired lymphocyte cytotoxicity to macrophage activation. A trigger (e.g. a viral infection) for HLH is commonly found in the case of impaired lymphocyte cytotoxicity (middle panel). Both entities, inborn errors of cytotoxicity and inborn errors of cytokine control, may converge clinically to HLH (lower panel). **(B)** Genetic determinants of HLH and hyperinflammatory diseases. HLH-associated genes identified by searching the literature for reported cases are shown with their known and predicted protein-protein interaction network linked graphically using the STRING database and algorithm (182). The green oval highlights genes whose products are involved in granule-mediated cytotoxicity. Genes whose products interact with *NLRC4* are highlighted by the mauve oval. HLH has also been described to occur in chronic granulomatous disease (genes marked in dark blue in the upper right corner) and (severe) combined immunodeficiency (genes in the upper left corner, such as IL2RG, ZAP70 and IL7RA). Two newly reported molecular causes, CD48 and ZNFX1, are highlighted (by squares), which we position here within the pathogenic pathways that lead to HLH.

subset of NK cells; it binds the Fc portion of IgG antibodies in antibody-coated target cells and triggers antibody-dependent cell cytotoxicity (ADCC). Other activating and inhibitory receptors (including 2B4, CD2, DNAX accessory molecule-1 (DNAM-1) and T cell immunoglobulin and mucin domain-containing protein 3 (TIM-3)) help to fine-tune NK cell cytotoxicity and are discussed below because of their roles in immune regulation and hyperinflammation. Despite the NK cells' clear role in innate immunity, it has recently been discovered that these cells also develop "memory-like" responses. Hence, NK cell subsets can expand, contract and later vigorously respond to previously encountered haptens, viral antigens and vaccines (27). This exciting new discovery has changed the paradigm for the link between immune memory and adaptive responses. However, the mechanisms that contribute to the NK cells' immune memory have not yet been identified and characterized in detail (28).

Other less abundant cytotoxic cell subsets are important for immune regulation in hyperinflammatory diseases. Unconventional T cells (such as NKT cells, γδ T cells, invariant NKT (iNKT) cells, and mucosa-associated invariant T cells) share features of both NK and T cells. They recognize antigens other than classic peptides (such as microbial metabolites or lipid antigens) presented by non-polymorphic molecules other than MHC (such as CD1d and butyrophillins) and semi-invariant or γδ TCRs (29, 30). Peripherally induced regulatory T cells can also exert cytotoxicity towards myeloid APCs in a perforin-, granzyme B- and HLA class I-dependent manner, assisted by lymphocyte function-associated antigen 1, CD2-CD58, and CD226-CD155 (31, 32).

Granule-mediated cytotoxicity is the cytotoxic lymphocyte's main killing mechanism. Upon activation, cytotoxic lymphocytes polarize secretory lysosomes that are anchored to microtubules and contain cytotoxicity effector molecules. The secretory lysosomes and the microtubule-organizing center move progressively towards the immune synapse formed between the killer cell and the target cell. Cytotoxic granules dock at the inner leaflet of the effector cell plasma membrane, near a cluster of TCRs (the central supramolecular activation cluster) and release their contents into the synaptic cleft *via* exocytosis (5). Perforin is a pore-forming protein present in the lymphocytes' cytotoxic granules. It is released as a monomer but can form oligomeric pre-pores that can dock with (but do not insert into) the target membrane (33). Insertion into the target membrane occurs only upon a conformational change of the perforin, enabling polymerization and formation of 22-mer pores in the target cell membrane, which then facilitate the entry of soluble cytotoxic effectors into the target cell (34). Although both target and killer cell are exposed to perforin in the immune synapse, only the target cell membrane is disrupted. Indeed, two protective mechanisms prevent the CTL from being killed during the cytotoxicity response: (i) the formation of highly ordered lipid rafts, and (ii) the exposure of negatively charged phosphatidylserines, which inactivate residual perforin (35).

Granzymes are the main cytotoxic effectors in secretory granules. Of the various types of granzymes, granzymes A and B the most abundant and best characterized. Granzyme B engages caspase-dependent apoptosis of the target cell and cleave initiator pro-caspases, such as pro-caspase-3 and the pro-apoptotic molecule Bid. Granzyme A triggers caspase-independent cell death *via* the disruption of mitochondrial metabolism and the generation of reactive oxygen species, which enable the formation of the SET complex of nucleases. Upon translocation to the nucleus, Granzyme A cleaves and releases SET complex nucleases, which eventually leads to DNA damage (36). The less studied granzyme K is present in the immunoregulatory $CD56^{bright}$ NK cell subset (37). The latter are also able to kill autologous activated T cells in a granzyme K dependent manner (38). Interestingly, $CD56^{bright}$ NK cells expand during disorders of hyperinflammation and cytotoxic cell disturbance (14, 39). Perforin and granzymes have a synergistic effect on granule-mediated cell cytotoxicity. Granzymes A, K and M are differentially expressed on cytotoxic T and NK cell subsets (37). Data from experiments in granzyme-deficient mouse models indicate that the granzymes have redundant functions, in order to overcome viral evasion strategies (37, 40). Redundant, compensatory granzyme functions can mediate tumor rejection in granzyme-deficient mice (41). It is noteworthy that only mice lacking both granzymes A and B are susceptible to lymphocytic choriomeningitis virus (LCMV) and the poxvirus ectromelia but are still resistant to other viruses. In contrast, perforin has an essential, non-redundant role in cytotoxicity (41, 42). This might also be why granzyme deficiency has not (yet) been linked to HLH per se, given that most gene-hunting workflows in the field of IEI are based on a monogenic disease hypothesis.

Granulysin is another membrane-disrupting effector molecule present in cytotoxic granules of CTLs and NK cells. It primarily attacks cardiolipin-rich microbial cell membranes rather than cholesterol-rich mammalian cell membranes (43) but does appear to be somehow involved in human cell cytotoxicity (44). However, granulysin and has not been studied in the context of HLH.

In addition to granule-mediated cytotoxicity, cytotoxic cells can also induce target cell killing through death receptors. The main death receptors are Fas (CD95) and TNF-related apoptosis-inducing ligand (TRAIL) receptors. After ligand binding, Fas ligand and TRAIL transmembrane death receptors recruit Fas-associated protein with death domain (FADD) adapter proteins to their death receptor domain and activate caspase-dependent apoptosis (45). A small proportion of NK cells can kill several target cells consecutively. This process is known as "serial killing" and is important for the elimination of infected and malignant cells (46). During serial killing, cytotoxicity mechanisms are tightly regulated by NK cells. The first kills result from granule-mediated fast cytolysis, whereas later events switch to slower death receptor killing following upon a decrease in the granule count and the upregulation of FAS ligand (47). Both mechanisms are enhanced by cytokines like IL-2, IFNγ and tumor necrosis factor alpha (TNF-α), which also promote inflammation. The importance of FAS and FAS ligand for immune regulation is obvious in patients with autoimmune lymphoproliferative syndrome (ALPS) due to mutations in the *FAS* and *FASLG* genes (48). Although perforin deficiency is a fatal disorder, patients with ALPS easily reach adulthood.

Cell death caused by limited availability of growth factors, such as following the resolving of an immune response, is more dependent on the proapoptotic factor BCL-2 interacting mediator

of cell death (BIM) (49, 50).This is independent of other death receptors, such as FAS. Therefore, BIM-dependent cell death has been implicated in controlling lymphocyte contraction following resolution of an immune response, where conditions of lower pro-inflammatory cytokines and growth factors are created. On the other side, during chronic infections, where antigen persists and lymphocyte expansion is promoted, lymphocyte expansion is mainly controlled by FAS-dependent cell death (51). BIM could also be implicated in the resolution of lymphoproliferation in ALPS (52). In humans, a common deletion polymorphism in BIM that enables the synthesis of an alternatively spliced isoform has been associated to low efficacy of tyrosine kinase inhibitors in cancer (53). In addition, mice experiments have shown a role of this protein in controlling autoimmunity, but also in controlling APCs expansion (54), therefore raising a possibility of a predisposition for HLH.

An additional indirect mechanism that cytotoxic lymphocytes use to promote killing is the production of proinflammatory cytokines, such as IFNγ and TNFα. IFNγ directly enhances the cytolytic activity of NK cells and CTLs (55). TNFα binds to TNF receptors 1 and 2 and can thus trigger cell death upon FADD adaptor recruitment or trigger pro-inflammation through nuclear factor kappa B activation (56). Lastly, another indirect mechanism is the competitive advantage given to activated CD8+ T cells by homeostatic cytokines such as IL-2, to the detriment of regulatory T cells (Tregs) in the context of HLH (57, 58).

3 HLH and HLH-like hyperinflammatory syndromes

HLH corresponds to a clinical phenotype with diverse triggers and disease mechanisms. A comprehensive overview of the functional networks of proteins encoded by genes reportedly linked to HLH is given in Figure 1B.

3.1 Primary HLH

Primary HLH (pHLH) corresponds to a group of disorders caused by IEI affecting genes, whose products are involved in granule-mediated cytotoxicity. The signs and symptoms of pHLH usually appear at an early age, although the disorder may also develop later in life. The clinical manifestations of pHLH include fever, hepatosplenomegaly, and multiorgan infiltration and damage (e.g. bone marrow failure and damage to the central nervous system) (59–61). The presence of tissue macrophages with hemophagocytic activity (referred to as histiocytes) is a hallmark of pHLH. Other observed clinical abnormalities include bicytopenia, hypercytokinemia, overactivated T lymphocytes, elevated ferritin levels, and elevated levels of soluble interleukin 2 (IL-2) receptor α (also referred to as soluble CD25 (sCD25)). Primary HLH is diagnosed when the patient meets at least five of the eight established clinical criteria (6) or has compatible molecular findings. The estimated incidence of pHLH is 1 per 3000 inpatients in tertiary care pediatric hospitals and 1 per 50000 newborns (59, 62). Primary HLH is a potentially fatal sepsis-like disease; for survival, immunosuppressive treatment and then hematopoietic stem cell transplantation (HSCT) are generally required (63). Episodes of hyperinflammation are caused by uncontrolled, excessive immune responses, mostly upon exposure to viral or bacterial triggers (9). However, a triggering event or infection cannot be found in all individuals with HLH, e.g. some patients with intrauterine HLH. Rather than being a direct effect of an infectious trigger, pHLH develops because of impaired regulation of inflammation and lacking termination of immune responses by the granule-mediated cytotoxicity pathway (64).

Primary HLH is caused by inherited pathogenic variants in genes involved in different stages of the perforin-dependent granule-mediated cytotoxic pathway. Familial HLH type 2 (FHL2) is caused by biallelic deleterious mutations in the gene coding for perforin (*PRF1*). To date, more than 120 different *PRF1* mutations have been described (65) and account for 20-50% of cases of pHLH. However, some mutations are found also in healthy older adults – sometimes even in their homozygous form (66). The perforin knock-out mouse infected with LCMV is the "gold standard" model of pHLH and has provided valuable information on the pathogenesis of this disorder (58, 64, 67, 68).

Other HLH-associated mutations affect genes whose products are involved in the docking, priming and membrane fusion of cytotoxic granules (64, 69, 70). Familial HLH (FHL) type 3 (FHL3), type 4 (FHL4) and type 5 (FHL5) patients show degranulation defects. FHL3 is caused by pathogenic variants in the *UNC13D* gene encoding the Munc13-4 protein involved in priming the secretory granules. *UNC13D* mutations account for 30-35% of pHLH cases, although the prevalence varies as a function of the ethnicity and the geographic area; for example, the prevalence of *UNC13D* mutations is higher in northern Europe (71). FHL4 patients present mutations in the syntaxin 11 gene (*STX11*) involved in the membrane fusion between the cytotoxic granule and the target cell (72). Mutations in the *STXBP2* gene (coding for syntaxin-binding protein 2, which assists membrane fusion in exocytosis) cause FHL5 (73). There is also a related group of disorders characterized by concomitant HLH and hypopigmentation. For instance, Griscelli syndrome type 2 is caused by pathogenic variants of the *RAB27A* gene; the encoded GTPase signaling protein is expressed in many (but not in the central nervous system (74)) and is involved in late granule exocytosis stages. Hence, *RAB27A* pathogenic gene variants affect not only cytotoxic granules but also melanosome degranulation. Some patients also present neuropathy associated with the sequelae of HLH (75). Chediak-Higashi syndrome is another rare disease associated with hypopigmentation, HLH, impaired cytotoxicity, and the presence of enlarged lysosomal structures in cells and hair shafts. In this syndrome, pathogenic gene variants of *LYST* (coding for a lysosomal traffic regulator) impair the release of cytotoxic granules into the immune synapse. Lysosomal trafficking is an important process in neurons. Some *LYST* mutations are associated with neuronal affectations. Moreover, a mouse model bearing a mutation in the LYST protein's conserved WD40 domain shows a neurodegenerative phenotype with Purkinje cell loss, rather than alterations in the immune system (76). Furthermore, patients with Chediak-Higashi syndrome may

develop a neurodegenerative disease marked by cerebellar ataxia and peripheral neuropathy – even after successful HSCT (77). Hermansky-Pudlak syndrome 2 is another rare, multisystem disorder associated with HLH. It is caused by *AP3B1* pathogenic gene variants that affect lysosomal protein sorting and lead to cytotoxic lymphocyte defects in patients. A summary of the genetic, epidemiological, clinical and immunological characteristics of pHLH, together with secondary and novel forms of HLH are compiled in Table 1.

3.2 X-linked lymphoproliferative disease

X-linked lymphoproliferative disease (XLP-1) is a life-threatening lymphoproliferative disorder that arises in male patients with mutations in the X-linked *SH2D1A* gene (78, 79). The incidence of XLP-1 is 1 to 3 per million males, and 45-70% of patients with XLP-1 develop HLH (78, 79). Patients with XLP-1 have an impaired ability to clear EBV infections. The seroprevalence of EBV in adults is 90%. Diseases caused by EBV are mild in children, moderate-to-severe in teenagers and immunocompetent adults but life-threatening in patients with *SH2D1A* mutations; the survival rate in the latter is 20%, and the disease features lymphoproliferation, multiple organ infiltration and multiple organ failure (80). 25-30% of patients with XLP-1 develop B-cell lymphoma associated with EBV infection (80). In addition, 35% of patients have not been exposed to EBV but are diagnosed because of their family medical history (81). At the time of writing, 100 patients with XLP-1 have been described in the literature (82). It is not completely understood how viral infections trigger HLH episodes in susceptible individuals. Putative mechanisms include the direct interference of antiviral responses with cytokine balances, the direct infection of cytotoxic cells or other key cells in HLH, disturbance of immune homeostasis, the capacity of viruses to

TABLE 1 Conventional and novel HLH, HLH-like and HLH-associated disorders: genetics, epidemiology, clinical manifestations, and immune dysregulations.

Disease	Gene symbol	Protein name (s)	Cellular expression	Impaired function	Clinical manifestations and concomitant diseases	Trigger	Mouse model
Primary HLH (FHL1)	Unknown	Unknown	Unknown	Cytotoxicity	HLH	Intracellular infections (viruses, bacteria, parasites	Not described
Primary HLH (FHL2)	*PRF1*	Perforin-1 (PERF)	Cytotoxic lymphocytes	Cytotoxicity	HLH	Viruses (EBV, CMV, other herpesviruses, parvovirus B19, adenoviruses)	Perforin-deficient mice infected with LCMV
Primary HLH (FHL3)	*UNC13D*	Protein unc-13 homolog D (Munc13-4)	Leukocytes, lung, placenta	Degranulation, cytotoxicity	HLH	Viruses (EBV, CMV, other herpesviruses, parvovirus B19, adenoviruses)	*Unc13d* mutated "jinx" mice infected with LCMV
Primary HLH (FHL4)	*STX11*	Synthaxin-11 (STX11)	Cytotoxic lymphocytes	Degranulation, cytotoxicity	HLH	Viruses (EBV, CMV, other herpesviruses, parvovirus B19, adenoviruses)	*Stx11*-deficient mice infected with LCMV
Primary HLH (FHL5)	*STXBP2*	Syntaxin-binding protein 2 (STXBP2, Munc18-2)	Cytotoxic lymphocytes, intestinal and renal epithelium	Degranulation, cytotoxicity	HLH	Viruses (EBV, CMV, other herpesviruses, parvovirus B19, adenoviruses)	Not described
Griscelli syndrome type 2	*RAB27A*	Ras-related protein Rab-27-A (RAB27A	Leukocytes and melanocytes	Degranulation, cytotoxicity	HLH. Concomitant hypopigmentation.	Viruses (EBV, CMV, other herpesviruses, parvovirus B19, adenoviruses)	*Rab27a*-deficient *ashen* mice infected with LCMV
Chediak-Higashi syndrome	*LYST*	Lysosomal-trafficking regulator (LYST)	Leukocytes, melanocytes and neurons	Lysosome trafficking, cytotoxicity	HLH. Concomitant hypopigmentation.	Viruses (EBV, CMV, other herpesviruses, parvovirus B19, adenoviruses)	Lyst mutated mice (*souris* strain) infected with LCMV
Hermansky-Pudlak syndrome type 2 (HPS2)	*AP3B1*	Adaptor protein complex 3	Multiple cell types, including	Lysosome storage and trafficking, cytotoxicity	Multisystem disease. Concomitant	Viruses (EBV, CMV, other herpesviruses,	*Ap3b1*-deficient *pearl* mice infected with LCMV

(Continued)

10.3389/fimmu.2023.1163316

TABLE 1 Continued

Disease	Gene symbol	Protein name (s)	Cellular expression	Impaired function	Clinical manifestations and concomitant diseases	Trigger	Mouse model
		(AP-3) complex subunit beta 1 (AP3B1)	melanocytes, fibroblasts, platelets, and monocytes.		hypopigmentation, bleeding.	parvovirus B19, adenoviruses)	
Secondary HLH (MAS)	-	–	–	Regulation of hyperinflammation/ diverse	HLH. Concomitant rheumatic, inflammatory, malignant or infectious diseases.	Underlying autoimmune or autoinflammatory disease, lymphoma, viral infection (herpes viruses, HIV, influenza), bacterial (mycobacteria), fungal and parasitic infections	Toll-like receptor 9 stimulation in wild-type and IL-6 transgenic mice or in combination with IL-10 receptor-blocking antibody. Infection with *Salmonella* or *Trypanosoma* in wild-type mice. Humanized mouse models with transfer of the patient's immune cells to immunodeficient mice.
Secondary HLH (MAS)	*NLRC4*	NLR Family CARD Domain Containing 4	Leukocytes, higher expression in macrophages	Inflammasome activation	HLH	Inflammasome	*Nlrc4* mutant mice, with or without cold exposure
XLP-1	*SH2D1A*	SH2 domain-containing protein 1A (SAP)	Cytotoxic lymphocytes	Signaling triggering cytotoxicity	HLH. Concomitant hypogammaglobulinemia, lymphoma.	EBV, occasionally other viruses	*Sh2d1a*-deficient mice infected with LCMV or MHV-68
HLH	*HAVCR2*	Hepatitis A virus cellular receptor 2 (TIM-3)	T lymphocytes and other immune cells	Checkpoint inhibitor regulation	HLH. Concomitant subcutaneous panniculitis-like T cell lymphoma.	Not described	Not described
HLH and autoinflammation	*NCKAP1L*	NCK associated protein 1 like	Hematopoietic cells	Cytoskeleton regulation, T cell homeostasis	HLH, autoinflammation, neonatal pancytopenia	Not described	Not described
HLH and hyperinflammation	*RC3H1*	Roquin-1	Leukocytes	mRNA post-transcriptional regulation on immune genes	Hyperinflammation	Not described	Toll-like receptor 9 stimulation in sanroque mice
NOCARH	*CDC42*	Cell division cycle 42, isoform 1	Ubiquitously expressed	Cytoskeleton rearrangement, migration and cell proliferation	Neonatal onset of pancytopenia, autoinflammation, rash and HLH	Not described	Not described
Recurrent hyperinflammation	*CD48*	CD48	Immune cells	Signaling triggering cytotoxicity	HLH-like	Not described	*Cd48*-deficient mice infected with LCMV
XLP-2	*BIRC4*	XIAP	Ubiquitously expressed	Apoptosis, inflammation signaling, inflammatory cell death,	HLH. Concomitant hypogammaglobulinemia, colitis.	EBV, occasionally other viruses	*Birc4*-deficient mice infected with MHV-68
Multisystem inflammation,	*ZNFX1*	NFX1-*type zinc finger*-	Ubiquitously expressed, greater	IFN-dependent transcript regulation	HLH and HLH-like	Viral and mycobacterial infections	Not described

(Continued)

TABLE 1 Continued

Disease	Gene symbol	Protein name (s)	Cellular expression	Impaired function	Clinical manifestations and concomitant diseases	Trigger	Mouse model
vulnerability to infections		*containing* protein *1*.	expression in hematopoietic tissue				
HLH (occasionally)	*STAT1*	STAT1	Ubiquitously expressed, greater expression on leukocytes	IFN-dependent signaling	HLH	*Mycobacterium bovis* (1 case)	Multiorgan immune infiltration and hypercytokinemia in *Stat1*-deficient mice infected with LCMV (although not described as an HLH model)

CMV, cytomegalovirus; EBV, Epstein-Barr virus; FHL, familial hemophagocytic lymphohistiocytosis; HLH, hemophagocytic lymphohistiocytosis; LCMV, lymphocytic choriomeningitis virus; MAS, macrophage activation síndrome; MHV-68, murine gammaherpesvirus 68; NFX, nuclear transcription factor X-box binding; NOCARH, neonatal onset of pancytopenia, autoinflammation, rash, and episodes of hemophagocytic lymphohistiocytosis; STAT, signal transducer and activator of transcription; XIAP, X-linked inhibitor of apoptosis; XLP, X-linked lymphoproliferative syndrome.

encode anti-apoptotic proteins delaying the apoptosis of infected immune cells or the chronic stimulation of pattern recognition receptors. Other viral evasion strategies that might promote HLH are the downregulation of MHC class I on NK cells or the suppression of the cytotoxic function of NK cells by downregulating the expression of perforin and SAP or encoding Fc receptors that block viral-specific antibodies diminishing antibody-dependent cell cytotoxicity (9).

SH2D1A encodes SAP, a small intracellular molecule belonging to a family of adaptors containing a Src homology 2 domain and a short C-terminal tail, that includes Ewing's sarcoma-activated transcript-2 (EAT-2) and EAT-2-related transduced. SAP binds to phosphorylated immunoreceptor tyrosine-based "switch" motifs (ITSM) of the SLAM family (SLAMF) of receptors within the CD2 family of leukocyte surface receptors, triggering lymphocyte cytotoxicity upon recruitment of the tyrosine kinase FynT and also preventing the binding of other inhibitory phosphatases (83, 84). The impediment to bind SAP to 2B4 SLAMF receptor enables the binding of other inhibitory proteases to intracellular 2B4 ITSMs, triggering the receptor's inhibitory function rather than the SAP-mediated activating signal (85). Various *SH2D1A* mutations have been described as affecting the binding to interactants (such as SLAMF receptors and FynT) or decreasing the half-life of the SAP protein (86, 87). Along with the molecular identification of SAP mutations, other methods for the rapid diagnosis of XLP-1 have been suggested. However, the measurement of intracellular SAP expression might not be relevant for mutations affecting SAP's function or half-life.

SAP pathogenic gene variants lead to a reduction in NK cell cytotoxic activity (79, 88–91). Patients with XLP-1 have abnormally low levels of NK and CD8+ T cell cytolytic activity towards EBV-infected B cells. A rapid screen that combines intracellular SAP expression and a 2B4-directed reverse ADCC (R-ADCC) assay of murine Fc receptor-expressing target cells has shown promising results (92). In this study, SAP^- and SAP^+ NK clones from healthy female heterozygous carriers of SAP mutations provided information on the molecular defects in SAP deficiency. SAP^- clones showed low cytotoxic activity towards $CD48^+$ target cells in an R-ADCC assay triggered by 2B4 crosslinking. In contrast, SAP^+ NK clones exerted cytotoxicity upon 2B4 crosslinking, giving an overall neutral response at a polyclonal level in bulk populations (92). Patients with XLP-1 have defective NK cell cytotoxicity towards SLAMF-expressing hematopoietic cells. Moreover, SAP-deficient mice and patients with XLP-1 display enhanced NK responses to non-hematopoietic cells (93). This difference has been attributed to a defect in NK cell education (a mechanism for fine-tuning the NK cells' sensitivity to activating and inhibitory signals) in XLP-1 (94). Signaling during NK cell education is mediated by SLAMF6 and depends on SAP, which blocks the binding of the inhibitor phosphatase SHP1 to the SLAMF receptor. As mentioned before, SAP not only mediates SLAMF-activated signaling but also prevents inhibitory SH2-containing proteases from binding to SLAMF receptors (84, 95). Natural cytotoxicity receptors (such as NKp46 and CD16) have compensatory activity in patients with XLP-1 (93). SAP is crucial for the development of NKT cells because the latter are absent in patients with XLP-1 and in SAP-deficient mice (78, 96). Mice with a SAP mutation that abolishes the recruitment of Fyn have a defect in NKT cell development in the thymus and a lack of invariant NKT (iNKT) cells (97). NKT developmental defects have been found in mice with mutations in all SLAMF receptors (98–100). NKT cells are also absent/very reduced in patients. For instance, NKT cells showed undetectable levels with α-galactosylceramide-loaded CD1d tetramers and/or antibodies targeting the invariant Vα24 Vβ11 TCR, when compared with controls or patients with other IEI (101). Thus, it has been suggested that low/absent NKT cell frequencies could be a diagnostic parameter for XLP1. However, data from other studies indicate that the frequency of NKT cells in adult and pediatric XLP1 patients is variable and point against the use of NKT cell levels to exclude a diagnosis of XLP1 (102). In SAP-deficient patients, high levels of T cell proliferation have been observed upon viral infection, despite the inability to eliminate virus-infected cells or to produce IFNγ. In mice, T cells proliferate and survive the acute infection (88). SAP-deficient mice have problems controlling chronic LCMV infections, due to defects in humoral response (89). These defects can be rescued by

reconstitution with wild-type $CD4^+$ T cells (103). Patients with XLP-1 also have profound defects in the humoral response. 50% of patients with XLP-1 have hypogammaglobulinemia (82). Defective T follicular helper (TFH) and T helper 2 (Th2) cell development and defective Th2 cytokine production are also observed (88, 89, 91, 104). SAP-deficient mice have a defect in TFH cell development in the germinal centers. The TFH cell type is crucial for the generation of high-affinity antibody responses (78). In the absence of SAP, SLAM family receptor signaling to TFH is inhibitory, since mice with mutations in all the SLAM family receptors do not have a defect in TFH development (98). XLP1 patients also display a deficiency in the formation of germinal centers in the spleen (105). In tune with this defect, patients show a reduction of germinal center-dependent isotype-switched CD27+ memory B cells in peripheral blood. However, despite this reduction, the few patient's IgM+ CD27+ B lymphocytes present in circulation have the capacity to undergo somatic hypermutation (105).

The XLP-1-related disorder XLP-2 has been linked to a deficiency of X-linked inhibitor of apoptosis (XIAP) protein, caused by pathogenic gene variants in the *XIAP*/*BIRC4* gene. More than 90 such mutations have been described since 2006 (106, 107). XIAP deficiency has similarities with SAP deficiency, such as EBV-triggered HLH, splenomegaly, cytopenia and hypogammaglobulinemia. However, patients with XLP-2 do not suffer from lymphoma; Other inflammatory symptoms (such as colitis, hepatitis, uveitis and arthritis) are considered a hallmark of XLP-2 (81). The anti-apoptotic protein XIAP is involved in innate immune signaling of pattern recognition receptors like dectin-1 and nucleotide oligomerization domain (NOD)-like receptors and also the regulation of the NOD-, LRR- and pyrin domain-containing protein 3 (NLRP3) inflammasome (106). Indeed, a functional assay demonstrating the XIAP-deficient monocytes' inability to produce TNFα upon NOD2 stimulation had been established as a diagnostic tool (107, 108). XIAP also regulates adaptive immune functions such as activation-induced cell death (AICD), an important homeostatic mechanism for controlling and limiting activated T cells in conventional and unconventional T cells. In XLP-2 patients, AICD is also impaired in T cells (106). In contrast to XLP-1, patients with XLP-2 have a normal iNKT cell compartment (106). Regarding the humoral compartment, one third of XLP-2 patients experience mild hypogammaglobulinemia but the switched B cell compartment is not affected (106).

3.3 Secondary HLH or MAS

The term sHLH (or sometimes "sporadic" or "acquired" HLH) has generally been used to describe patients with (i) a disease meeting the clinical criteria for a diagnosis of HLH, (ii) none of the genetic defects mentioned in the above section on pHLH, and (iii) no XLP-1/2 syndrome. In addition and as later discussed, sHLH can also occur in patients with other IEI not related to cytotoxicity defects. Most patients with sHLH suffer from an inherited or acquired underlying disease or are receiving treatment that predisposes them to immune dysregulation. Secondary HLH can occur in autoinflammatory syndromes and is most frequently reported in systemic juvenile idiopathic arthritis (sJIA). Many rheumatologists prefer to use the term macrophage activation syndrome (MAS), rather than sHLH (8, 109–111) MAS appears later in life than pHLH but may also be life-threatening. pHLH and MAS have similar clinical manifestations. Although patients with pHLH have a permanent impairment in the granule-mediated cytotoxic activity of T lymphocytes and NK cells, there might be no impairment of granule-mediated cytotoxicity in patients with MAS or the impairment is only partial or transient. Animal models of MAS have been established by stimulating toll-like receptors in wildtype and IL-6 transgenic mice; these experiments highlighted the importance of IFNγ in MAS, while lymphocytes were not required for the induction of the disease, although critical to induce maximal disease (112–114).

In contrast to pHLH, inflammasome activation and IL-18 hypercytokinemia are the hallmarks of MAS pathogenesis in patients with *NLRC4* pathogenic gene variants. While impaired lymphocyte cytotoxicity is essential for a diagnosis of pHLH, intrinsically activated macrophages are essential for MAS in NLRC4-mutated patients. Furthermore, new mutations in the inflammasome-associated gene *NLRC4* reportedly cause some of the features of MAS (16, 17). We suggest a model in which NLRC4- and perforin pathogenic gene variants represent the two prototypes in this hyperinflammatory spectrum (Figure 1A). NLRC4 triggers the formations of inflammasomes, i.e. multimeric complexes assembled after stimulation by pathogens and that lead to the production of IL-1β and IL-18 and pyroptosis cell death after caspase-1 activation. Indeed, IL-18 hypercytokinemia has been linked to MAS in patients with sJIA and in animal models (115, 116). CD163, a scavenger receptor associated with phagocytosis in macrophages, is also a biomarker associated with MAS and EBV-triggered HLH (117). Strikingly, the A91V *PRF1* variant and mutations in *UNC13D* are more prevalent in patients with sJIA who developed MAS (118, 119). MAS is the most severe complication of sJIA and adult-onset Still's disease and is also observed in patients with systemic lupus erythematosus. sJIA is a chronic, autoinflammatory disease of childhood characterized by the clinical features arthritis, fever, rash, swollen lymph nodes, hepatomegaly, and serositis. MAS-associated symptoms are observable clinically in 10% of sJIA cases and subclinically in 30-40% of cases. Nonsteroidal anti-inflammatory drugs constitute the first-line treatment, and corticosteroids and methotrexate are used as a second-line treatments. In treatment-resistant cases and in patients with sHLH, HSCT and monoclonal antibodies against the pathogenic proinflammatory cytokines are used. However, the treatment of sJIA has not been standardized.

In addition to MAS, patients infected with intracellular pathogens and patients being treated with immunomodulatory monoclonal antibodies or chimeric antigen receptor T cells may develop a cytokine release syndrome that resembles HLH. Secondary HLH can also develop in patients with inborn errors of metabolism, such as lysinuric protein intolerance, multiple sulfatase deficiency, galactosemia, Gaucher disease, Pearson disease, galactosialidosis, propionic acidemia, Niemann-Pick disease, and congenital disorders of glycosylation (120, 121).

3.4 Novel genetic inflammatory syndromes with HLH

The area of cell-cell contact between the cytotoxic lymphocyte and its target cell, the so called immunological synapse, is a highly organized area involving cytoskeletal rearrangement. Efficient killing by T cells and NK cells requires function of the actin cytoskeleton. Several mutations in genes with a role in active cytoskeleton remodeling have been associated with HLH. Indeed, pathogenic gene variants in *WAS*, *DOCK8* and *NCKAP1L* genes coding for cytoskeleton regulators in immune cells cause hyperinflammatory disorders with HLH hyperinflammation (20). Another novel HLH disorder associated with hematological impairments and features of autoinflammation was recently identified in five patients with a unique *de novo* missense mutation in the cell division cycle 42 (*CDC42*) gene (22, 122). This one specific mutation was associated with neonatal onset of cytopenia, autoinflammation, rash, and episodes of HLH (NOCARH). *CDC42* is a Ras-homologous (Rho) signaling GTPase protein involved in cytoskeleton rearrangement and cell migration. The p.R186C missense mutation identified affected the subcellular localization of the protein -aberrantly concentrated in the Golgi apparatus-, cell polarity, migration, proliferation and signaling. It profoundly affected hematopoiesis and compromised the normal composition and migration of bone marrow cells. This is a multisystem inflammatory disease with a strong autoinflammatory component, with characteristics similar to NLRC4 inflammosopathies. The autoinflammatory symptoms were attributed to the high spontaneous release of IL-18 by mononuclear cells from the bone marrow and the high IL-1β levels. In addition, the 4 identified patients developed HLH, lethal in all the patients but one, that survived upon anti-IFNγ treatment with emapalumab and HSCT. Indeed, IL-18 is a co-stimulatory factor for IFNγ production. An additional mechanism contributing to HLH in this novel hyperinflammatory syndrome was the defect in the NK cell capacity to form conjugates and to migrate, that diminished its cytotoxic potential (111, 116, 123). Differently than the NOCARH and HLH responsive to anti-IFNγ caused by the p.R186C mutation in the *CDC42* gene, novel additional mutations in *CDC42* C-terminus region have been recently associated to a clinical autoinflammatory syndrome responsive to IL-1 inhibitors (124).

Over the last few years, the establishment of novel associations between inborn errors of immunity (IEI) and HLH has broadened to beyond genes involved in cytotoxicity, cytoskeleton reorganization, and inflammasome activation, but also to the ones involved in checkpoint control, receptor signaling, and mRNA regulation. For instance, a novel association between HLH and loss-of-function mutations in the *HAVCR2* gene (coding for T cell immunoglobulin and mucin domain-containing protein 3 (TIM-3)) was identified in patients with subcutaneous panniculitis-like T cell lymphoma with associated HLH. TIM-3 is an inhibitory molecule expressed by T lymphocytes and other immune cells (21, 125). The TIM-3 negative checkpoint is a critical regulator of innate immunity and inflammatory responses and suppresses effector T cells by decreasing IFNγ-driven inflammation. The predisposition to HLH in individuals with defective TIM-3 function might therefore be explained by a defect in downregulating the T-cell response to IFNγ. Importantly, TIM-3 also regulates monocyte/macrophage activation. Thus, it is possible that TIM-3 deficiency leads in multiple ways to an increased inflammatory response and thereby to HLH.

Lymphocyte cytotoxicity is triggered upon contact with a target cell if sufficient activating signals are received. This implies that target cells are not passive bystanders during granule-dependent cytotoxicity. Indeed, we could gain insight in the role of resistance to cytotoxicity in the pathogenesis of HLH by studying a patient with a novel IEI affecting the 2B4-CD48 interaction. 2B4 (CD244) is a SLAMF receptor that signals through SAP and is crucial for controlling CTL responses to EBV (126). 2B4 is the SLAMF receptor with greatest number of ITSM SAP-binding motifs and is also the only heterotypic SLAMF receptor. Thus, 2B4 is not a self-ligand, but it interacts with CD48. In mice, signaling through 2B4 can be either costimulatory or coinhibitory, whereas there is evidence of a predominantly activating role in human subjects (127, 128). We recently identified a novel hyperinflammatory disorder with HLH caused by a *de novo* heterozygous mutation in the *CD48* gene ($CD48^{S220Yhet}$) (14). This disorder is characterized by recurrent episodes of hyperinflammation, rash and IL-6 hypercytokinemia, while only moderately elevated sCD25 levels. A similar inflammatory pattern was triggered by LCMV infection in CD48+/- and CD48-/- mice (14). CD48 is expressed by almost all leukocytes (except for some long-term hematopoietic stem cell precursors) and functions mainly as a co-stimulatory and adhesion molecule (129). The $CD48^{S220}$ residue is essential for the protein's subcellular localization and serves as the attachment site for a glycosylphosphatidylinositol cell surface anchor. The S220Y pathogenic gene variant is associated with lower cell-surface CD48 expression and a lower cytotoxic ability for NK cells. The diminished expression of CD48 appears to be involved in a novel mechanism that contributes to hyperinflammation; target cells are less susceptible to killing and CD48-haploinsufficient immune cells are more resistant to elimination by granule-mediated cytotoxicity. Along with these functional alterations, maturation defects were also observed in cytotoxic lymphocytes. Thus, target cells' resistance mechanisms to cytotoxicity can significantly contribute to immune dysregulation.

A novel homozygous mutation in the *RC3H1* gene (coding for roquin-1, a post-transcriptional regulator of mRNAs involved in immune responses) led to HLH and hyperinflammation in a patient and in a mouse model (18).

Signal transducer and activator of transcription 1 (STAT1) mediates both type I and type II IFN responses. Patients with a gain-of-function (GOF) mutation in *STAT1* can occasionally present HLH, despite the absence of IFNγ hypercytokinemia (130, 131). Conversely, *Stat1* knock-out mice develop multiorgan immune infiltration and hypercytokinemia upon LCMV infection (132). This data seem to be paradoxical. In the experimental *Stat1* knock-out mice model challenged with LCMV, the lethal multi-organic infiltration is dependent on highly expanded antigen-specific CD4+ T cells. In the clinical setting, *STAT1* GOF mutations have been linked to a permanent phosphorylated status of the transcription factor due

to an impaired dephosphorylation and are associated to a broad clinical spectrum, from infection susceptibility to autoimmune manifestations, this later probably due to a strong type I IFN signaling mediated by the hyperphosphorylated STAT1 (131). In the clinical case with *STAT1* GOF linked to HLH, the hyperphosphorylated status of STAT1 was associated with a persistent overactivity of APCs, previously activated by innate immune receptors in the context of an infection (130). Interestingly, deficiencies in STAT2 and IRF9, the other two components that together with STAT1 form the heterotrimeric complex named Interferon Stimulated Gene Factor 3 (ISGF3), induce a prolonged type I IFN response due to lack of negative feedback of the IFN receptor (133). STAT2 and IRF9 mutations have been also recently linked to HLH episodes (134, 135).

ZNFX1 (NFX1-type zinc-finger-containing 1) is a highly conserved IFN-stimulated dsRNA sensor that restricts the replication of RNA viruses in mice and contributes to transgenerational inheritance in *C. elegans*, by binding to mRNA complexed to short non-coding RNAs (15, 136, 137). In humans, homozygous ZNFX1 destabilizing pathogenic gene variants were associated with multisystem inflammation, including HLH, monocytosis, and a predisposition to viral infections and mycobacterial disease (15, 138). Recent studies on patients suffering from COVID19 propose an anti-SARS-COV-2 role for ZNFX1 and other ZNF proteins, where ZNF protein activity positively correlated with the abundance of multiple immune cells implying an effective antiviral response (139). While the underlying mechanisms still need further investigation, the role of ZNFX1 in immune regulation highlights the importance of time and context in tuning innate response, to allow for proper elimination of viral material while preventing hyper-inflammatory responses. With regards to the spatial context, ZNFX1 has been shown to localize to liquid-like perinuclear condensates in *C.elegans* germ cells (136, 137), to stress granules of virally or chemically stressed cells (138), and to the proximity of the outer mitochondrial membrane in steady-state (137). We have shown that in the absence of ZNFX1, the half-life of the mRNA of interferon sensitive genes is prolonged (15). We therefore propose a mechanism whereby the helicase function of ZNFX1 is needed to remove mRNAs which has been formed in consequence of a viral infection. In the absence of ZNFX1, the mRNA of interferon sensitive genes remains more stable, allowing it to be translated again instead of being degraded. This prevents a return to homeostasis leading to the described hyperinflammatory syndrome. Overall, ZNFX1 plays a central role at both the very early and late stages of nucleic acids driven interferon responses, by regulating sensing and the return to homeostasis. As a consequence, patients with homozygous ZNFX1 destabilizing mutations suffered from multisystem inflammation, including HLH, and a predisposition to viral infections (118).

The molecular changes caused by inborn errors of granule-mediated cytotoxicity or cytokine control contribute variably to cellular impairments (such as impaired lymphocyte cytotoxicity or macrophage activation) that lead to uncontrolled hyperinflammation. Thus, the pathophysiological spectrum of HLH-associated disorders ranges from impaired lymphocyte cytotoxicity to macrophage activation (Figure 1A).

4 HLH-like manifestations in other immune-mediated diseases

4.1 Inborn errors of immunity

As described above, biallelic *PRF1* pathogenic gene variants cause pHLH. However, *PRF1* mutations concomitant to other IEI have been also described. ALPS is an immune dysregulation disorder that causes splenomegaly, lymphadenopathy, autoimmunity, susceptibility to lymphoma, and blood accumulation of double-negative $CD4^-$ $CD8^-$ T cells. Dianzani autoimmune lymphoproliferative disease (DALD) is a variant of ALPS that lacks the expansion of double-negative $CD4^-$ $CD8^-$ T lymphocytes (140). In most cases, ALPS is caused by a genetic mutation related to the FAS-mediated pathway of apoptosis. More than 70% of the mutations affect the *FAS* gene directly but mutations in *FASLG*, *CASP10*, *CASP8* and other genes have also been observed (48). A combination of a heterozygous *PRF1* mutation and a *FAS* mutation was identified in an ALPS patient with aggressive lymphoma (141). A larger study found that 2 of 14 ALPS patients and 6 of 28 DALD patients had an FHL-associated *PRF1* mutation, leading to diminished NK cell activity (121). Perforin-dependent activation-induced cell death operates as a compensatory mechanism in FAS-deficient T cells from ALPS patients (142). Mutations in the FHL3-associated *UNC13D* gene have been detected in six ALPS/DALD patients; although the patients' NK cells showed normal levels of activity, granule exocytosis release was impaired in transfected cell lines (143). Furthermore, a SAP polymorphism affecting a key methylation site for the protein's expression was significantly more frequent in ALPS/DALD patients than in controls (144).

A multicenter analysis identified 63 patients with other IEI meeting the diagnostic criteria for HLH (6). In a systematic evaluation of the patients' clinical and immunological features, 30 had combined immunodeficiencies (including 12 with severe combined immunodeficiencies (SCIDs)) and 22 had chronic granulomatous disease (CGD) (145). 80% of patients with other IEI and who met the diagnostic criteria for HLH had either SCID or CGD. Although this study did not cover all known IEI, it is noteworthy that SCID and CGD were markedly over-represented because they account for only 15% of IEI overall. The remaining 20% (i.e. those not meeting the diagnostic criteria for HLH) included two patients with ALPS due to *FAS* mutations. In 79% of the affected cases, the HLH episode was associated with an infectious trigger. When comparing the subgroups with regard to their immunological and clinical variables, the serum level of sCD25 was lower in patients with T cell-dependent IEI than in patients with FHL. Thus, the study of other IEI associated with HLH provides data on the respective contributions of leukocyte subsets

to hyperinflammatory diseases. In addition to rare complications of CGD and SCID (146, 147), rare cases of HLH have been also reported among patients with DiGeorge syndrome and Wiskott-Aldrich syndrome (148, 149).

4.2 The role of perforin in immune system cancers and bone marrow diseases

Inherited *PRF1* pathogenic gene variants cause FHL in early childhood. However, compound heterozygous missense *PRF1* mutations that do not fully abrogate perforin activity may have effects later in life (150). Granule-mediated cell cytotoxicity is a crucial mechanism for killing tumor cells. One study identified biallelic *PRF1* mutations in 4 out of 29 patients with primary lymphoma (151). Another study showed that 50% of cases of late-onset of FHL presented with lymphoma or leukemia. Interestingly, the mutations were not fully deleterious but caused protein misfolding that could be restored by a permissive protein folding temperature in *in vitro* assays (150). Missense mutations are also linked to a predisposition to cancer (152). *PRF1* mutations and decreased NK cell cytotoxic activity have been observed in patients with acquired aplastic anemia (a form of bone marrow failure) (153).

5 Novel insights into pathogenesis

Different dysregulated pathways contribute to HLH development. Deficient perforin-granule-dependent cytotoxicity leads to (i) reduced clearance of triggering intracellular pathogens within APCs, which leads to an increase in the CTL-APC synapse time and repetitive Ca^{2+} release within (and thus activation of) the CTL (11) and (ii) defective fratricidal killing (12); both resulting in excessive cytokine production by CTLs. Tregs are crucial regulators of immune responses and express high levels of CD25, the α subunit of the high affinity receptor for IL-2. The growth factor IL-2 is essential for T lymphocytes. A Treg dysfunction has been postulated in both patients with pHLH and in experimental models of pHLH, due to the preferential consumption of IL-2 by abundant, highly activated $CD25^{high}$ $CD8^{+}$ T cells (58). The precise role of Tregs in HLH needs further characterization. An important feedback loop which is critical for immune homeostasis and which fails in perforin-deficiency is the elimination of antigen-presenting dendritic cells. In a murine model of HLH has been shown that the persistence of potent, immunostimulatory dendritic cells, contributes to the pathogenesis (154), thus demonstrating a reciprocal relationship between perforin in CTLs and APCs' function. This is consistent with our own observations made in a patient with heterozygous pathogenic gene variant in CD48 suffering from recurrent hyperinflammation (25). We have shown that reduced CD48 expression leads to an increased resistance of human APCs to killing. This provides evidence that immunostimulatory APCs contribute to the pathogenesis of HLH, also in humans. A hallmark of HLH is macrophage activation. On one hand excessive cytokine production by CTLs leads to macrophage activation in HLH. On the other hand, a defect in cytokine control, as in NLRC mutations and ZNFX1 deficiency can, independently of CTLs, lead to macrophage activation in an HLH context. Disease mechanisms linking deficient cytotoxicity and deficient cytokine control to HLH spectrum diseases are summarized in Figure 2.

5.1 Dysregulation of CD48-triggered SLAMF-dependent cytotoxicity in HLH

As in the case for other IEI, monogenic HLH diseases are excellent models for improving our knowledge of how the immune system works. In-depth studies of immune dysregulation in patients with HLH and animals models of conventional HLH have provided invaluable information on the important role of granule-mediated cytotoxicity in eliminating virus-infected cells and in terminating immune responses. The newly identified CD48 haploinsufficiency and XLP-1 are clinically distinct but immunologically related disorders. Both CD48 and SAP mutations affect the 2B4-triggered cytotoxicity pathway, by either diminishing cell-surface expression of the 2B4 ligand or affecting the stability or binding capacity of a signaling adapter molecule (14, 79). SAP and CD48 pathogenic gene variants cause partially overlapping features, such as cytotoxicity defects and hyperinflammation. However, the disorders differ with regard to clinical signs, the extent of cytotoxicity impairment, and the immune compensatory mechanisms (Figure 3 and Table 1). While in XLP-1 all SAP-dependent pathways are impaired, in CD48 haploinsufficiency only CD48-triggered 2B4-dependent SAP signaling is affected. This is probably the underlying mechanism setting the differences between these two disorders.

The viral triggers associated with HLH and hyperinflammatory syndromes are mainly DNA herpesviruses (such as EBV and human cytomegalovirus (CMV)) and more rarely herpes simplex virus, human herpesvirus 6 and 8, and varicella zoster virus (9). Hyperinflammatory episodes in CD48 haploinsufficiency are not currently known to be associated with greater vulnerability to a specific pathogen (14). CD48 haploinsufficiency appears to be less aggressive clinically and immunologically than XLP-1. This novel disorder is characterized by normal perforin-dependent T cell cytotoxicity and an NK cell degranulation towards K562 cells within reference values but lower cytotoxicity towards autologous EBV-immortalized lymphoblastoid cells. Phenotypic and functional analyses of the NK cells of patient with CD48 haploinsufficiency have nevertheless evidenced an impact of CD48 on NK cell maturation, since the patient presented a high number of immunoregulatory-immature $CD56^{bright}$ $CD94^{high}$ NK cells, high levels of IFNγ production by NK cells upon IL-12 stimulation, and a low number of the more differentiated, highly cytotoxic $CD56^{dim}$ $CD94^{low}$ cells. Interestingly, a similarly immature NK profile has been observed in patients with an IEI affecting the IL-2/CD25 pathway (39). It is noteworthy that HLH-episodes in CD48 haploinsufficiency were not associated with high serum sCD25 levels as opposed to the high levels observed in FHL (14).

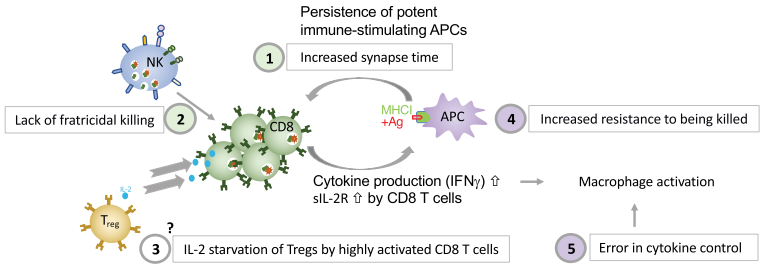

FIGURE 2
Five major disease mechanisms linking defective cytotoxicity and error in cytokine control with HLH (1). reduced clearance of triggering intracellular pathogens within APCs, which leads to an increase in the CTL-APC synapse time and repetitive Ca2+ release within (and thus activation of) the CTL (11); **(2)** defective NK-cell- and CTL-mediated immune regulation by fratricidal killing (12, 155), **(3)** excessive consumption of IL-2 by CTLs, which deprives Tregs, postulated by Humblet-Baron et al. (58), **(4)** persistence of immunostimulatory APCs (either due to increased resistance of APCs to killing as shown in a patient with CD48 deficiency (14) or due to persistence of immunostimulatory APCs due to CTL defect as demonstrated by Terrell & Jordan (154) in a murine model, and **(5)** error in cytokine control leading to macrophage activation.

A remarkable novelty that CD48 haploinsufficiency provided to HLH knowledge is the importance of the target cell in perforin-dependent cytotoxicity. Of note, CD48 is expressed on both the cytotoxic cell and the target cell. In CD48 haploinsufficiency, the target cells themselves might have an active role in the pathogenesis of HLH because CD48 expression might be a "kill me" signal as a ligand for 2B4 receptors on the killer cell promoting cytotoxicity. A similar mechanism has been described for controlling activated CD155-expressing T cells upon DNAM-1 interaction on NK cells, in the context of immune regulation in autoimmunity (156). Indeed, cell-surface CD48 expression in target cells determines the degree of susceptibility to NK cell killing in hyperinflammation, as shown by experiments on cell lines transfected with a plasmid encoding wildtype and mutated CD48 or experiments in which the target cell is pre-coated with blocking antibodies (14). The interactive feedback loop between target cells and cytotoxic lymphocytes is crucial for the elimination of APCs and a return to immune homeostasis (154).

CD48 signaling defects affect also T lymphocytes. In a CD48 knock-out model, low $CD4^+$ and $CD8^+$ T cell proliferation has been observed (157). However, it must be born in mind that CD48 has an additional low affinity receptor (CD2) which, in humans, has a high affinity ligand (CD58); this is not the case in mice. In patients, it has not yet been established whether CD48-associated alterations are mediated by low-affinity CD2 receptor signaling. AICD is impaired in CD48 haploinsufficiency, as in SAP mutations (158, 159). CD48 protects against restimulation-induced cell death by maintaining basal autophagy and inhibiting p53 signaling in a SAP-independent manner (160). Finally and concerning the humoral branch of the adaptive immune system, CD48 haploinsufficiency causes slight alterations in IgG subtypes (such as low IgG2 levels) but not profound hypogammaglobulinemia (14).

5.2 Dysregulated cytokine control in novel HLH spectrum disorders

HLH is characterized by hypercytokinemia and systemic inflammation. IFNγ is a key pathogenic cytokine in both pHLH and MAS (161) and is produced by overactivated CTLs (67, 68). In pHLH, a mouse model with genetically depleted IFNγ demonstrates that this cytokine is responsible for the hematologic features of the disease, such as anemia (162). Indeed, the monoclonal anti-IFNγ antibody emapalumab is the first cytokine-targeted therapy approved for pHLH patients that have a refractory or relapsing disease or do not tolerate first-line therapies (63, 163). This contrasts with low IFNγ responses to EBV-infected B cells in patients with XLP-1 (164). Patients with XLP-2 present elevated levels of cytokines such as IFNγ, IL-6, TNFα and IL-18 (106).

The cytokine IL-33 is released by stressed and necrotic cells. Thus, it is considered an "alarmin" that activates immune responses upon injury. IL-33 binds its receptor ST2 resulting in a MyD88-dependent signaling. In the context of HLH, experimental models blocking ST2 have demonstrated that IL-33 enhances the IFNγ-driven pathology in HLH (165).

IL-6 is another proinflammatory cytokine associated with HLH hyperinflammation. In CD48 haploinsufficiency, PBMCs upregulate the linker for activation of T cells-regulated cytokine and phospholipase Cγ transcript upon activation (14). This disorder is associated with IL-6 hypercytokinemia, both in the patient with CD48 deficiency and in the CD48 knock-out mouse model upon LCMV infection. In HLH, defective killer cell-target cell disengagement promotes persistent activation of the killer cells and the production of proinflammatory cytokines that induce IL-6 secretion by macrophages. Interestingly, IL-6 hypercytokinemia and cytotoxicity defects were observed during the cytokine storms in severe COVID-19 (166) and MAS (167) – two hyperinflammatory disorders with overlapping features. Monoclonal antibodies against the IL-6 receptor, IFNγ and Janus kinases 1 and 2 (which act downstream of the cytokines) are being tested as an immunomodulatory treatment for HLH (81, 163, 168, 169). In MAS, lack of cytotoxicity-induced apoptosis in target cells favors the lytic death of the latter; this releases alarmins that activate inflammasomes and leads to a hyperinflammatory situation (170).

Mutations in genes involved in the regulation of cytokine transcription have been recently linked to HLH (Figure 4). NLRC4 is an intracellular pattern recognition receptor that activates inflammasomes. NLRC4-triggered inflammasomes

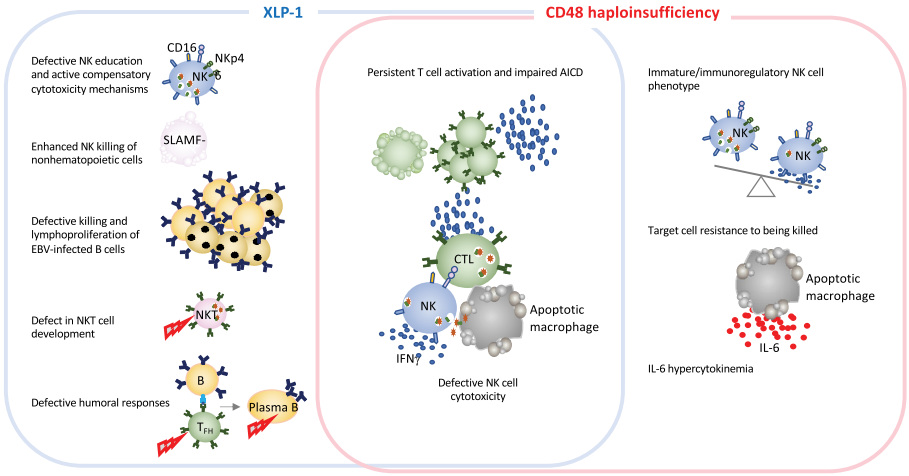

FIGURE 3
Schematic representation of immune defects in two related inborn errors of cytotoxicity: XLP-1 (SAP deficiency) and CD48 haploinsufficiency. In humans and animal models, XLP-1 and CD48 haploinsufficiency are related because SAP is an adapter molecule for the high-affinity CD48 receptor. However, the two diseases also present differences. XLP-1 disorder in humans and/or SAP deficiency in mice (in the blue box) cause NK cell abnormalities, such as the defective killing of EBV-infected target cells, subsequent EBV-infected B cell lymphoproliferation and NK education defects. These affects are partially countered by compensatory NK killing mechanism. Profound NKT cell developmental defects and defective humoral responses are also hallmarks of XLP-1. SAP deficiency and CD48 haploinsufficiency (in the red box) trigger some of the same generic dysregulations, such as defective NK cell cytotoxicity and impaired activation-induced cell death. Furthermore, CD48 haploinsufficiency impairs the maturation of NK cells. Given that CD48 is a ligand of the cytotoxicity triggering receptor 2B4, CD48 haploinsufficiency enables the target cell to better resist granule-mediated cytotoxicity. Moreover, the hypercytokinemia in this disease is characterized by a high serum IL-6 level, as observed in a CD48 haploinsufficient patient and the $CD48^{-/-}$ mouse model (11).

induce the activation of caspase 1 and the production of proinflammatory cytokines IL-1β and IL-18 (171). *NLRC4* pathogenic gene variants have been linked to spontaneous inflammasome activation and IL-1β and IL-18 hypercytokinemia (16). An imbalance between IL-18 and its natural antagonist (IL-18 binding protein) might be related to the development of MAS (172). In contrast, IL-10 appears to have a protective role (112). CXCL9 is an inflammatory chemokine induced by IFNγ recently linked to MAS as disease biomarker (173, 174). In addition to the cytokine effect per se, novel hyperinflammatory disorders with HLH disorders highlight the importance of post-transcriptional RNA regulators of cytokine transcripts to control hyperinflammation. For instance, genetic mutations responsible for a deficiency in roquin-1 (a regulator of RNA transcripts involved in immune responses) can also cause a dysregulation in cytokine synthesis and lead to hyperinflammation as described above for ZNFX1 (18).

6 Concluding remarks and open questions

A better understanding of the genetic disease mechanisms underlying HLH is essential for more accurate, more personalized diagnoses. Pathway-related pathogenic gene variants associated with HLH (such as inborn errors of cytotoxicity or cytokine control) can manifest themselves to different extents with regard to aggressiveness, clinical signs, and immune cell defects.

CTLs and NK cells are crucial cytotoxic lymphocytes for controlling overactivated immune responses, as has been demonstrated for HLH. NK cells have been extensively studied in HLH and are widely used to screen for cytotoxicity and degranulation defects in HLH (175). In the future, research should also focus on the roles of $CD8^+$ CTLs and unconventional cytotoxic T cells (such as polyclonal cytotoxic $CD4^+$ T terminally differentiated cells, which are enriched in pHLH) (176, 177).

Two novel HLH disease mechanisms have been revealed by the identification and characterization of additional monogenic immune disorders with HLH. The target cell's active role in susceptibility to killing (by regulating the expression of cytotoxicity receptor ligands) is a novel HLH-associated dysregulation seen in CD48 haploinsufficiency. CD48 is also a candidate molecular target for controlling not only HLH but also autoimmunity (156), and cancer (178). The cell-intrinsic production of cytokines caused by inborn errors of cytokine control might also improve our understanding of systemic hyperinflammation in other fields, such as autoinflammatory diseases or severe COVID-19.

The enormous power of whole-exome and whole-genome sequencing will certainly help to identify links between novel genetic mutations and HLH in the future. However, in order to confirm novel genetic associations and characterize their phenotypical consequences,

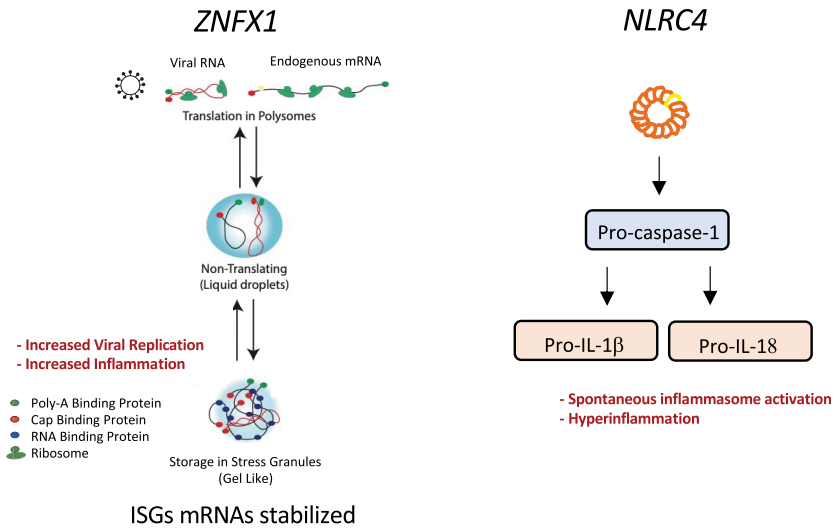

FIGURE 4
Graphical representation of the molecular pathways affected by two inborn errors of cytokine control leading to HLH: *ZNFX1* and *NLCR4* pathogenic gene variants. ZNFX1 deficiency (left panel) causes susceptibility to viral infections. At later stages of infection, increased expression of interferon-stimulated genes is driven by greater mRNA stability; this prevents a return to homeostasis and leads to hyperinflammation and multiple organ failure. ZNFX1 localizes to stress granules. We hypothesize that ZNFX1's helicase function is needed to remove mRNAs stored in stress granules formed upon viral infection. In the absence of ZNFX1, the more stable mRNA is translated and not degraded, preventing a return to homeostasis and leading to a hyperinflammatory syndrome. *NLRC4* mutations can cause intrinsic macrophage activation (right panel). A mutation in the nucleotide-binding domain of the NLRC4 sensor activates inflammasomes and leads to pro-caspase-1 cleavage. Subsequent caspase-1 dependent activation of pro-IL-1b and pro-IL-18 results in macrophage activation and hyperinflammation.

it will still be necessary to continue the development of functional immunological assays and animal models. For instance, novel autoinflammatory syndromes with HLH due to IEI evidence the need to better understand what to what extend HLH and autoinflammation overlap, in order to provide disease-specific treatments. Hypercytokinemia contributes to link this two disorders, with a predominant role for IL-18 and IL-1 in autoinflammation that enhance the production of IFNγ, key effector molecule in HLH immunopathology. Translational studies from patients with autoinflammation and/or HLH responsive to cytokine oriented therapies will help dissecting the role for IL-18, IL-1, IFNγ and others (IL-6) in different hyperinflammatory disorders. In addition to IFNγ hypercytokinemia, viral triggers, poor viral control -sometimes associated with IEI- and defects in cytotoxic lymphocytes are other key factors more specifically contributing to HLH development. Larger, collaborative studies of patients with the novel genetic disorders with HLH will also be essential for defining typical and atypical disease manifestations and developing personalized therapies.

Author contributions

RP wrote the manuscript and prepared figures. MF collected and visualized clinical data and figures. SV contributed to manuscript writing and prepared figures. JPS wrote the manuscript and prepared figures. All the authors reviewed and edited the manuscript. All authors contributed to the article and approved the submitted version.

Funding

This work was funded by the Swiss National Science Foundation (Project number: 320030_205097) and the University of Zurich (the University Research Priority Program ITINERARE – Innovative Therapies in Rare Diseases (to JS) and the Clinical Research Priority Program CYTIMM-Z (to RP and JS).

Conflict of interest

JPS received honorary from Pharming for participation in a data monitoring committee DMC for Leniolisib. MF received a grant by Jazz Pharmaceuticals.

The remaining authors declare that the research was conducted in the absence of any commercial or financial relationships that could be construed as a potential conflict of interest.

Publisher's note

References

1. Schmid JP, Côte M, Ménager MM, Burgess A, Nehme N, Ménasché G, et al. Inherited defects in lymphocyte cytotoxic activity. *Immunol Rev* (2010) 235:10–23. doi: 10.1111/j.0105-2896.2010.00890.x

2. Stepp SE, Dufourcq-Lagelouse R, le Deist F, Bhawan S, Certain S, Mathew PA, et al. Perforin gene defects in familial hemophagocytic lymphohistiocytosis. *Sci (1979)* (1999) 286(5446):1957–9. doi: 10.1126/science.286.5446.1957

3. Sepulveda FE, de Saint Basile G. Hemophagocytic syndrome: primary forms and predisposing conditions. *Curr Opin Immunol* (2017) 49:20–6. doi: 10.1016/j.coi.2017.08.004

4. Doria A, Zen M, Bettio S, Gatto M, Bassi N, Nalotto L, et al. Autoinflammation and autoimmunity: bridging the divide. *Autoimmun Rev* (2012) 12:22–30. doi: 10.1016/j.autrev.2012.07.013

5. de Saint Basile G, Ménasché G, Fischer A. Molecular mechanisms of biogenesis and exocytosis of cytotoxic granules. *Nat Rev Immunol* (2010) 10:568–79. doi: 10.1038/nri2803

6. Henter JI, Horne AC, Aricó M, Egeler RM, Filipovich AH, Imashuku S, et al. HLH-2004: diagnostic and therapeutic guidelines for hemophagocytic lymphohistiocytosis. *Pediatr Blood Cancer* (2007) 48:124–31. doi: 10.1002/pbc.21039

7. Hayden A, Park S, Giustini D, Lee AYY, Chen LYC. Hemophagocytic syndromes (HPSs) including hemophagocytic lymphohistiocytosis (HLH) in adults: a systematic scoping review. *Blood Rev* (2016) 30:411–20. doi: 10.1016/j.blre.2016.05.001

8. Grom AA, Mellins ED. Macrophage activation syndrome: advances towards understanding pathogenesis. *Curr Opin Rheumatol* (2010) 22:561–6. doi: 10.1097/01.bor.0000381996.69261.71

9. Brisse E, Wouters CH, Andrei G, Matthys P. How viruses contribute to the pathogenesis of hemophagocytic lymphohistiocytosis. *Front Immunol* (2017) 8:1102. doi: 10.3389/fimmu.2017.01102

10. Jenkins MR, Griffiths GM. The synapse and cytolytic machinery of cytotoxic T cells. *Curr Opin Immunol* (2010) 22(3):308–13. doi: 10.1016/j.coi.2010.02.008

11. Jenkins MR, Rudd-Schmidt JA, Lopez JA, Ramsbottom KM, Mannering SI, Andrews DM, et al. Failed CTL/NK cell killing and cytokine hypersecretion are directly linked through prolonged synapse time. *J Exp Med* (2015) 212(3):307–17. doi: 10.1084/jem.20140964

12. Waggoner SN, Cornberg M, Selin LK, Welsh RM. Natural killer cells act as rheostats modulating antiviral T cells. *Nature* (2012) 481(7381):394–8. doi: 10.1038/nature10624

13. Lang PA, Crome SQ, Xu HC, Lang KS, Chapatte L, Deenick EK, et al. NK cells regulate CD8+ T cell mediated autoimmunity. *Front Cell Infect Microbiol* (2020) 10:36. doi: 10.3389/fcimb.2020.00036

14. Volkmer B, Planas R, Gossweiler E, Lünemann A, Opitz L, Mauracher A, et al. Recurrent inflammatory disease caused by a heterozygous mutation in CD48. *J Allergy Clin Immunol* (2019) 144(5):1441–1445.e17. doi: 10.1016/j.jaci.2019.07.038

15. Vavassori S, Chou J, Faletti LE, Haunerdinger V, Opitz L, Joset P, et al. Multisystem inflammation and susceptibility to viral infections in human ZNFX1 deficiency. *J Allergy Clin Immunol* (2021) 148(2):381–93. doi: 10.1016/j.jaci.2021.03.045

16. Canna SW, de Jesus AA, Gouni S, Brooks SR, Marrero B, Liu Y, et al. An activating NLRC4 inflammasome mutation causes autoinflammation with recurrent macrophage activation syndrome. *Nat Genet* (2014) 46(10):1140–6. doi: 10.1038/ng.3089

17. Romberg N, al Moussawi K, Nelson-Williams C, Stiegler AL, Loring E, Choi M, et al. Mutation of NLRC4 causes a syndrome of enterocolitis and autoinflammation. *Nat Genet* (2014) 46(10):1135–9. doi: 10.1038/ng.3066

18. Tavernier SJ, Athanasopoulos V, Verloo P, Behrens G, Staal J, Bogaert DJ, et al. A human immune dysregulation syndrome characterized by severe hyperinflammation with a homozygous nonsense roquin-1 mutation. *Nat Commun* (2019) 10(1):4779. doi: 10.1038/s41467-019-12704-6

19. Meyts I, Bosch B, Itan Y. Whole-exome sequencing for detecting inborn errors of immunity: overview and perspectives. *F1000Res* (2017) 6:2056. doi: 10.12688/f1000research.12365.1

20. Castro CN, Rosenzwajg M, Carapito R, Shahrooei M, Konantz M, Khan A, et al. NCKAP1L defects lead to a novel syndrome combining immunodeficiency, lymphoproliferation, and hyperinflammation. *J Exp Med* (2020) 217(12):e20192275. doi: 10.1084/jem.20192275

21. Gayden T, Sepulveda FE, Khuong-Quang DA, Pratt J, Valera ET, Garrigue A, et al. Germline HAVCR2 mutations altering TIM-3 characterize subcutaneous panniculitis-like T cell lymphomas with hemophagocytic lymphohistiocytic syndrome. *Nat Genet* (2018) 50:1650–7. doi: 10.1038/s41588-018-0251-4

22. Lam MT, Coppola S, Krumbach OHF, Prencipe G, Insalaco A, Cifaldi C, et al. A novel disorder involving dyshematopoiesis, inflammation, and HLH due to aberrant CDC42 function. *J Exp Med* (2019) 216(12):2778–99. doi: 10.1084/jem.20190147

23. Zinkernagel RF, Doherty PC. Immunological surveillance against altered self components by sensitised T lymphocytes in lymphocytes choriomeningitis. *Nature* (1974) 251(5475):547–8. doi: 10.1038/251547a0

24. Zhang N, Bevan MJ. CD8+ T cells: foot soldiers of the immune system. *Immunity* (2011) 35:161–8. doi: 10.1016/j.immuni.2011.07.010

25. Lanier LL. NK cell recognition. *Annu Rev Immunol* (2005) 23:225–74. doi: 10.1146/annurev.immunol.23.021704.115526

26. Quatrini L, della Chiesa M, Sivori S, Mingari MC, Pende D, Moretta L. Human NK cells, their receptors and function. *Eur J Immunol* (2021) 51:1566–79. doi: 10.1002/eji.202049028

27. Nikzad R, Angelo LS, Aviles-Padilla K, Le DT, Singh VK, Bimler L, et al. Human natural killer cells mediate adaptive immunity to viral antigens. *Sci Immunol* (2019) 4(35):eaat8116. doi: 10.1126/sciimmunol.aat8116

28. von Andrian UH. NK cell memory: discovery of a mystery. *Nat Immunol* (2021) 22:669–71. doi: 10.1038/s41590-021-00890-9

29. de Libero G, Mori L. Recognition of lipid antigens by T cells. *Nat Rev Immunol* (2005) 5:485–96. doi: 10.1038/nri1631

30. Vavassori S, Kumar A, Wan GS, Ramanjaneyulu GS, Cavallari M, Daker S, et al. Butyrophilin 3A1 binds phosphorylated antigens and stimulates human γδ T cells. *Nat Immunol* (2013) 14(9):908–16. doi: 10.1038/ni.2665

31. Sayitoglu EC, Freeborn RA, Roncarolo MG. The yin and yang of type 1 regulatory T cells: from discovery to clinical application. *Front Immunol* (2021) 12. doi: 10.3389/fimmu.2021.693105

32. Magnani CF, Alberigo G, Bacchetta R, Serafini G, Andreani M, Roncarolo MG, et al. Killing of myeloid APCs *via* HLA class I, CD2 and CD226 defines a novel mechanism of suppression by human Tr1 cells. *Eur J Immunol* (2011) 41(6):1652–62. doi: 10.1002/eji.201041120

33. Leung C, Hodel AW, Brennan AJ, Lukoyanova N, Tran S, House CM, et al. Real-time visualization of perforin nanopore assembly. *Nat Nanotechnol* (2017) 12(5):467–73. doi: 10.1038/nnano.2016.303

34. Voskoboinik I, Dunstone MA, Baran K, Whisstock JC, Trapani JA. Perforin: structure, function, and role in human immunopathology. *Immunol Rev* (2010) 235:35–54. doi: 10.1111/j.0105-2896.2010.00896.x

35. Rudd-Schmidt JA, Hodel AW, Noori T, Lopez JA, Cho HJ, Verschoor S, et al. Lipid order and charge protect killer T cells from accidental death. *Nat Commun* (2019) 10(1):5396. doi: 10.1038/s41467-019-13385-x

36. Chowdhury D, Lieberman J. Death by a thousand cuts: granzyme pathways of programmed cell death. *Annu Rev Immunol* (2008) 26:389–420. doi: 10.1146/annurev.immunol.26.021607.090404

37. Bade B, Boettcher HE, Lohrmann J, Hink-Schauer C, Bratke K, Jenne DE, et al. Differential expression of the granzymes a, K and m and perforin in human peripheral blood lymphocytes. *Int Immunol* (2005) 17(11):1419–28. doi: 10.1093/intimm/dxh320

38. Jiang W, Chai NR, Maric D, Bielekova B. Unexpected role for granzyme K in CD56 bright NK cell-mediated immunoregulation of multiple sclerosis. *J Immunol* (2011) 187(2):781–90. doi: 10.4049/jimmunol.1100789

39. Caldirola MS, Broggi MGR, Gaillard MI, Bezrodnik L, Zwirner NW. Primary immunodeficiencies unravel the role of IL-2/CD25/STAT5b in human natural killer cell maturation. *Front Immunol* (2018) 9(JUN). doi: 10.3389/fimmu.2018.01429

40. Ebnet K, Hausmann M, Lehmann-Grube F, Müllbacher A, Kopf M, Lamers M, et al. Granzyme a-deficient mice retain potent cell-mediated cytotoxicity. *EMBO J* (1995) 14(17):4230–9. doi: 10.1002/j.1460-2075.1995.tb00097.x

41. Davis J, Smyth M, Trapani J. Granzyme a and b-deficient killer lymphocytes are defective in eliciting DNA fragmentation but retain potent *in vivo* anti-tumor capacity. *Eur J Immunol* (2001) 31(1):39–47. doi: 10.1002/1521-4141(200101)31:1<39::AID-IMMU39>3.0.CO;2-1

42. Müllbacher A, Hla RT, Museteanu C, Simon MM. Perforin is essential for control of ectromelia virus but not related poxviruses in mice. *J Virol* (1999) 73(2):1665–7. doi: 10.1128/JVI.73.2.1665-1667.1999

43. Dotiwala F, Lieberman J. Granulysin: killer lymphocyte safeguard against microbes. *Curr Opin Immunol* (2019) 60:19–29. doi: 10.1016/j.coi.2019.04.013

44. Chung WH, Hung SI, Yang JY, Su SC, Huang SP, Wei CY, et al. Granulysin is a key mediator for disseminated keratinocyte death in stevens-Johnson syndrome and toxic epidermal necrolysis. *Nat Med* (2008) 14(12):1343–50. doi: 10.1038/nm.1884

45. Golstein P, Griffiths GM. An early history of T cell-mediated cytotoxicity. *Nat Rev Immunol* (2018) 18(8):527–35. doi: 10.1038/s41577-018-0009-3

46. Vanherberghen B, Olofsson PE, Forslund E, Sternberg-Simon M, Khorshidi MA, Pacouret S, et al. Classification of human natural killer cells based on migration behavior and cytotoxic response. *Blood* (2013) 121(8):1326–34. doi: 10.1182/blood-2012-06-439851

47. Prager I, Liesche C, van Ooijen H, Urlaub D, Verron Q, Sandström N, et al. NK cells switch from granzyme b to death receptor-mediated cytotoxicity during serial killing. *J Exp Med* (2019) 216(9):2113–27. doi: 10.1084/jem.20181454

48. Li P, Huang P, Yang Y, Hao M, Peng H, Li F. Updated understanding of autoimmune lymphoproliferative syndrome (ALPS). *Clin Rev Allergy Immunol* (2016) 50:55–63. doi: 10.1007/s12016-015-8466-y

49. Hughes PD, Belz GT, Fortner KA, Budd RC, Strasser A, Bouillet P. Apoptosis regulators fas and bim cooperate in shutdown of chronic immune responses and prevention of autoimmunity. *Immunity* (2008) 28(2):197–205. doi: 10.1016/j.immuni.2007.12.017

50. Hutcheson J, Scatizzi JC, Siddiqui AM, Haines GK, Wu T, Li QZ, et al. Combined deficiency of proapoptotic regulators bim and fas results in the early onset of systemic autoimmunity. *Immunity* (2008) 28(2):206–17. doi: 10.1016/j.immuni.2007.12.015

51. Green DR. Fas bim boom! *Immunity* (2008) 28:141–3. doi: 10.1016/j.immuni.2008.01.004

52. Niss O, Sholl A, Bleesing JJ, Hildeman DA. IL-10/Janus kinase/signal transducer and activator of transcription 3 signaling dysregulates bim expression in autoimmune lymphoproliferative syndrome. *J Allergy Clin Immunol* (2015) 135(3):762–70. doi: 10.1016/j.jaci.2014.07.020

53. Ng KP, Hillmer AM, Chuah CTH, Juan WC, Ko TK, Teo ASM, et al. A common BIM deletion polymorphism mediates intrinsic resistance and inferior responses to tyrosine kinase inhibitors in cancer. *Nat Med* (2012) 18(4):521–8. doi: 10.1038/nm.2713

54. Chen M, Huang L, Wang J. Deficiency of bim in dendritic cells contributes to overactivation of lymphocytes and autoimmunity. *Blood* (2007) 109(10):4360–7. doi: 10.1182/blood-2006-11-056424

55. Bhat P, Leggatt G, Waterhouse N, Frazer IH. Interferon-γ derived from cytotoxic lymphocytes directly enhances their motility and cytotoxicity. *Cell Death Dis* (2017) 8(6):e2836. doi: 10.1038/cddis.2017.67

56. Wajant H, Beilhack A. Targeting regulatory T cells by addressing tumor necrosis factor and its receptors in allogeneic hematopoietic cell transplantation and cancer. *Front Immunol* (2019) 10. doi: 10.3389/fimmu.2019.02040

57. Whyte CE, Singh K, Burton OT, Aloulou M, Moudra A, Roca CP, et al. Context-dependent effects of IL-2 rewire immunity into distinct cellular circuits. *bioRxiv* (2020) 219(7):e20212391. doi: 10.1101/2020.12.18.423431

58. Humblet-Baron S, Franckaert D, Dooley J, Bornschein S, Cauwe B, Schönefeldt S, et al. IL-2 consumption by highly activated CD8 T cells induces regulatory T-cell dysfunction in patients with hemophagocytic lymphohistiocytosis. *J Allergy Clin Immunol* (2016) 138(1):200–209.e8 . doi: 10.1016/j.jaci.2015.12.1314

59. George MR. Journal of blood medicine dovepress hemophagocytic lymphohistiocytosis: review of etiologies and management. *J Blood Med* (2014) 5:69–86. doi: 10.2147/JBM.S46255

60. Usmani GN, Woda BA, Newburger PE. Advances in understanding the pathogenesis of HLH. *Br J Haematol* (2013) 161:609–22. doi: 10.1111/bjh.12293

61. Janka GE. Familial hemophagocytic lymphohistiocytosis. *Eur J Pediatr* (1983) 140:221–30. doi: 10.1007/BF00443367

62. Allen CE, Yu X, Kozinetz CA, McClain KL. Highly elevated ferritin levels and the diagnosis of hemophagocytic lymphohistiocytosis. *Pediatr Blood Cancer* (2008) 50(6):1227–35. doi: 10.1002/pbc.21423

63. Vallurupalli M, Berliner N. Emapalumab for the treatment of relapsed/refractory hemophagocytic lymphohistiocytosis. *Blood* (2019) 134(21):1783–6. doi: 10.1182/blood.2019002289

64. Pachlopnik Schmid J, de Saint Basile G. Inherited hemophagocytic lymphohistiocytosis (HLH). *Klin Padiatr* (2010) 222(6):345–50. doi: 10.1055/s-0029-1246165

65. Sieni E, Cetica V, Hackmann Y, Coniglio ML, da Ros M, Ciambotti B, et al. Familial hemophagocytic lymphohistiocytosis: when rare diseases shed light on immune system functioning. *Front Immunol* (2014) 5(APR). doi: 10.3389/fimmu.2014.00167

66. Voskoboinik I, Lacaze P, Jang HSI, Flinsenberg T, Fernando SL, Kerridge I, et al. Prevalence and disease predisposition of p.A91V perforin in an aged population of European ancestry. *Blood* (2020) 135:582–4. doi: 10.1182/blood.2019003487

67. Schmid JP, Ho CH, Chrétien F, Lefebure JM, Pivert G, Kosco-Vilbois M, et al. Neutralization of IFNγ defeats haemophagocytosis in LCMV-infected perforin - and Rab27a-deficient mice. *EMBO Mol Med* (2009) 1(2):112–24. doi: 10.1002/emmm.200900009

68. Jordan MB, Hildeman D, Kappler J, Marrack P. An animal model of hemophagocytic lymphohistiocytosis (HLH): CD8 + T cells and interferon gamma are essential for the disorder. *Blood* (2004) 104(3):735–43. doi: 10.1182/blood-2003-10-3413

69. Sepulveda FE, Debeurme F, Ménasché G, Kurowska M, Côte M, Schmid JP, et al. Distinct severity of HLH in both human and murine mutants with complete loss of cytotoxic effector PRF1, RAB27A, and STX11. *Blood* (2013) 121(4):595–603. doi: 10.1182/blood-2012-07-440339

70. Zhang K, Jordan MB, Marsh RA, Johnson JA, Kissell D, Meller J, et al. Hypomorphic mutations in PRF1, MUNC13-4, and STXBP2 are associated with adult-onset familial HLH. *Blood* (2011) 118(22):5794–8. doi: 10.1182/blood-2011-07-370148

71. Meeths M, Chiang SCC, Wood SM, Entesarian M, Schlums H, Bang B, et al. Familial hemophagocytic lymphohistiocytosis type 3 (FHL3) caused by deep intronic mutation and inversion in UNC13D. *Blood* (2011) 118(22):5783–93. doi: 10.1182/blood-2011-07-369090

72. Rudd E, Göransdotter Ericson K, Zheng C, Uysal Z, Ozkan A, Gürgey A, et al. Spectrum and clinical implications of syntaxin 11 gene mutations in familial haemophagocytic lymphohistiocytosis: association with disease-free remissions and haematopoietic malignancies. *J Med Genet* (2006) 43(4):e14. doi: 10.1136/jmg.2005.035253

73. Pagel J, Beutel K, Lehmberg K, Koch F, Maul-Pavicic A, Rohlfs AK, et al. Distinct mutations in STXBP2 are associated with variable clinical presentations in patients with familial hemophagocytic lymphohistiocytosis type 5 (FHL5). *Blood* (2012) 119(25):6016–24. doi: 10.1182/blood-2011-12-398958

74. Chen D, Guo J, Miki T, Tachibana M, Gahl WA. Molecular cloning and characterization of rab27a and rab27b, novel human rab proteins shared by melanocytes and platelets. *Biochem Mol Med* (1997) 60(1):27–37. doi: 10.1006/bmme.1996.2559

75. Schmid JP, Moshous D, Boddaert N, Neven B, Dal Cortivo L, Tardieu M, et al. Hematopoietic stem cell transplantation in griscelli syndrome type 2: a single-center report on 10 patients. *Blood* (2009) 114(1):211–8. doi: 10.1182/blood-2009-02-207845

76. Rudelius M, Osanger A, Kohlmann S, Augustin M, Piontek G, Heinzmann U, et al. A missense mutation in the WD40 domain of murine lyst is linked to severe progressive purkinje cell degeneration. *Acta Neuropathol* (2006) 112(3):267–76. doi: 10.1007/s00401-006-0092-6

77. Tardieu M, Lacroix C, Neven B, Bordigoni P, de Saint Basile G, Blanche S, et al. Progressive neurologic dysfunctions 20 years after allogeneic bone marrow transplantation for chediak-higashi syndrome. *Blood* (2005) 106:40–2. doi: 10.1182/blood-2005-01-0319

78. Cannons JL, Tangye SG, Schwartzberg PL. SLAM family receptors and SAP adaptors in immunity. *Annu Rev Immunol* (2011) 29:665–705. doi: 10.1146/annurev-immunol-030409-101302

79. Morra M, Howie D, Grande MS, Sayos J, Wang N, Wu C, et al. X-Linked lymphoproliferative disease: a progressive immunodeficiency. *Annu Rev Immunol* (2001) 19:657–82. doi: 10.1146/annurev.immunol.19.1.657

80. Booth C, Gilmour KC, Veys P, Gennery AR, Slatter MA, Chapel H, et al. X-Linked lymphoproliferative disease due to SAP/SH2D1A deficiency: a multicenter study on the manifestations, management and outcome of the disease. *Blood* (2011) 117(1):5060. doi: 10.1182/blood-2010-06-284935

81. Panchal N, Booth C, Cannons JL, Schwartzberg PL. X-Linked lymphoproliferative disease type 1: a clinical and molecular perspective. *Front Immunol* (2018) 9. doi: 10.3389/fimmu.2018.00666

82. Latour S, Winter S. Inherited immunodeficiencies with high predisposition to Epstein-Barr virus-driven lymphoproliferative diseases. *Front Immunol* (2018) 9. doi: 10.3389/fimmu.2018.01103

83. Latour S, Roncagalli R, Chen R, Bakinowski M, Shi X, Schwartzberg PL, et al. Binding of SAP SH2 domain to FynT SH3 domain reveals a novel mechanism of receptor signalling in immune regulation. *Nat Cell Biol* (2003) 5(2):149–54. doi: 10.1038/ncb919

84. Sayos J, Wu C, Morra M, Wang N, Zhang X, Allen D, et al. The X-linked lymphoproliferative-disease gene product SAP regulates signals induced through the co-receptor SLAM. *Nature* (1998) 395(6701):462–9. doi: 10.1038/26683

85. Chen S, Dong Z. NK cell recognition of hematopoietic cells by SLAM-SAP families. *Cell Mol Immunol* (2019) 16:452–9. doi: 10.1038/s41423-019-0222-4

86. Morra M, Simarro-Grande M, Martin M, Chen ASI, Lanyi A, Silander O, et al. Characterization of SH2D1A missense mutations identified in X-linked lymphoproliferative disease patients. *J Biol Chem* (2001) 276(39):36809–16. doi: 10.1074/jbc.M101305200

87. Torralba-Raga L, Tesi B, Chiang SCC, Schlums H, Nordenskjöld M, Horne AC, et al. Diagnostic challenges for a novel SH2D1A mutation associated with X-linked lymphoproliferative disease. *Pediatr Blood Cancer* (2020) 67(4):e28184. doi: 10.1002/pbc.28184

88. Czar MJ, Kersh EN, Mijares LA, Lanier G, Lewis J, Yap G, et al. Altered lymphocyte responses and cytokine production in mice deficient in the X-linked lymphoproliferative disease gene SH2D1A/DSHP/SAP. *Proc Natl Acad Sci USA* (2001) 98(13):7449–54. doi: 10.1073/pnas.131193098

89. Crotty S, Kersh EN, Cannons J, Schwartzberg PL, Ahmed R. SAP is required for generating long term humoral immunity. *Nature* (2003) 421(6920):282–7. doi: 10.1038/nature01318

90. Yin L, Al-Alem U, Liang J, Tong WM, Li C, Badiali M, et al. Mice deficient in the X-linked lymphoproliferative disease gene sap exhibit increased susceptibility to murine gammaherpesvirus-68 and hypo-gammaglobulinemia. *J Med Virol* (2003) 71(3):446–55. doi: 10.1002/jmv.10504

91. Davidson D, Shi X, Zhang S, Wang H, Nemer M, Ono N, et al. Genetic evidence linking SAP, the X-linked lymphoproliferative gene product, to src-related kinase FynT in TH2 cytokine regulation. *Immunity* (2004) 21(5):707–17. doi: 10.1016/j.immuni.2004.10.005

92. Meazza R, Tuberosa C, Cetica V, Falco M, Parolini S, Grieve S, et al. Diagnosing XLP1 in patients with hemophagocytic lymphohistiocytosis. *J Allergy Clin Immunol* (2014) 134(6):1381–1387.e7. doi: 10.1016/j.jaci.2014.04.043

93. Wu N, Zhong MC, Roncagalli R, Pérez-Quintero LA, Guo H, Zhang Z, et al. A hematopoietic cell-driven mechanism involving SLAMF6 receptor, SAP adaptors and SHP-1 phosphatase regulates NK cell education. *Nat Immunol* (2016) 17(4):387–96. doi: 10.1038/ni.3369

94. Orr MT, Lanier LL. Natural killer cell education and tolerance. *Cell* (2010) 142:847–56. doi: 10.1016/j.cell.2010.08.031

95. Wu N, Veillette A. SLAM family receptors in normal immunity and immune pathologies. *Curr Opin Immunol* (2016) 38:45–51. doi: 10.1016/j.coi.2015.11.003

96. Schmid JP, Canioni D, Moshous D, Touzot F, Mahlaoui N, Hauck F, et al. Clinical similarities and differences of patients with X-linked lymphoproliferative syndrome type 1 (XLP-1/SAP deficiency) versus type 2 (XLP-2/XIAP deficiency). *Blood* (2011) 117(5):1522–9. doi: 10.1182/blood-2010-07-298372

97. Nichols KE, Hom J, Gong SY, Ganguly A, Ma CS, Cannons JL, et al. Regulation of NKT cell development by SAP, the protein defective in XLP. *Nat Med* (2005) 11 (3):340–5. doi: 10.1038/nm1189

98. Chen S, Cai C, Li Z, Liu G, Wang Y, Blonska M, et al. Dissection of SAP-dependent and SAP-independent SLAM family signaling in NKT cell development and humoral immunity. *J Exp Med* (2017) 214(2):475–89. doi: 10.1084/jem.20161312

99. Huang B, Gomez-Rodriguez J, Preite S, Garrett LJ, Harper UL, Schwartzberg PL. CRISPR-mediated triple knockout of SLAMF1, SLAMF5 and SLAMF6 supports positive signaling roles in NKT cell development. *PloS One* (2016) 11(6):e0156072. doi: 10.1371/journal.pone.0156072

100. Hu JK, Crampton JC, Locci M, Crotty S. CRISPR-mediated Slamf1Δ/Δ Slamf5Δ/Δ Slamf6Δ/Δ triple gene disruption reveals NKT cell defects but not T follicular helper cell defects. *PloS One* (2016) 11(5):e0156074. doi: 10.1371/journal.pone.0156074

101. Pasquier B, Yin L, Fondanèche MC, Relouzat F, Bloch-Queyrat C, Lambert N, et al. Defective NKT cell development in mice and humans lacking the adapter SAP, the X-linked lymphoproliferative syndrome gene product. *J Exp Med* (2005) 201(5):695–701. doi: 10.1084/jem.20042432

102. Ralph E, Evans J, Booth C, Gilmour K. Patients with XLP type 1 have variable numbers of NKT cells. *Br J Haematol* (2022) 198(1):151–4. doi: 10.1111/bjh.18159

103. Cannons JL, Yu LJ, Jankovic D, Crotty S, Horai R, Kirby M, et al. SAP regulates T cell-mediated help for humoral immunity by a mechanism distinct from cytokine regulation. *J Exp Med* (2006) 203(6):1551–65. doi: 10.1084/jem.20052097

104. Ma CS, Hare NJ, Nichols KE, Dupré L, Andolfi G, Roncarolo MG, et al. Impaired humoral immunity in X-linked lymphoproliferative disease is associated with defective IL-10 production by CD4+ T cells. *J Clin Invest* (2005) 115(4):1049–59. doi: 10.1172/JCI200523139

105. Ma CS. Selective generation of functional somatically mutated IgM+CD27+, but not ig isotype-switched, memory b cells in X-linked lymphoproliferative disease. *J Clin Invest* (2006) 116(2):322–33. doi: 10.1172/JCI25720

106. Mudde ACA, Booth C, Marsh RA. Evolution of our understanding of XIAP deficiency. *Front Pediatr* (2021) 9. doi: 10.3389/fped.2021.660520

107. Jost PJ, Vucic D. Regulation of cell death and immunity by xiap. *Cold Spring Harb Perspect Biol* (2020) 12(8):a036426. doi: 10.1101/cshperspect.a036426

108. Ammann S, Elling R, Gyrd-Hansen M, Dückers G, Bredius R, Burns SO, et al. A new functional assay for the diagnosis of X-linked inhibitor of apoptosis (XIAP) deficiency. *Clin Exp Immunol* (2014) 176(3):394–400. doi: 10.1111/cei.12306

109. Crayne CB, Albeituni S, Nichols KE, Cron RQ. The immunology of macrophage activation syndrome. *Front Immunol* (2019) 10. doi: 10.3389/fimmu.2019.00119

110. Grom AA, Horne A, de Benedetti F. Macrophage activation syndrome in the era of biologic therapy. *Nat Rev Rheumatol* (2016) 12:259–68. doi: 10.1038/nrrheum.2015.179

111. Billiau AD, Roskams T, van Damme-Lombaerts R, Matthys P, Wouters C. Macrophage activation syndrome: characteristic findings on liver biopsy illustrating the key role of activated, IFN-γ-producing lymphocytes and IL-6- and TNF-α-producing macrophages. *Blood* (2005) 105(4):1648–51. doi: 10.1182/blood-2004-08-2997

112. Behrens EM, Canna SW, Slade K, Rao S, Kreiger PA, Paessler M, et al. Repeated TLR9 stimulation results in macrophage activation syndrome: like disease in mice. *J Clin Invest* (2011) 121(6):2264–77. doi: 10.1172/JCI43157

113. Schulert GS, Canna SW. Convergent pathways of the hyperferritinemic syndromes. *Int Immunol* (2018) 30:195–203. doi: 10.1093/intimm/dxy012

114. Strippoli R, Carvello F, Scianaro R, de Pasquale L, Vivarelli M, Petrini S, et al. Amplification of the response to toll-like receptor ligands by prolonged exposure to interleukin-6 in mice: implication for the pathogenesis of macrophage activation syndrome. *Arthritis Rheum* (2012) 64(5):1680–8. doi: 10.1002/art.33496

115. Girard-Guyonvarc'h C, Palomo J, Martin P, Rodriguez E, Troccaz S, Palmer G, et al. Unopposed IL-18 signaling leads to severe TLR9-induced macrophage activation syndrome in mice. *Blood* (2018) 131(13):1430–41. doi: 10.1182/blood-2017-06-789552

116. Weiss ES, Girard-Guyonvarc'h C, Holzinger D, de Jesus AA, Tariq Z, Picarsic J, et al. Interleukin-18 diagnostically distinguishes and pathogenically promotes human and murine macrophage activation syndrome. *Blood* (2018) 131(13):1442–55. doi: 10.1182/blood-2017-12-820852

117. Sakumura N, Shimizu M, Mizuta M, Inoue N, Nakagishi Y, Yachie A. Soluble CD163, a unique biomarker to evaluate the disease activity, exhibits macrophage activation in systemic juvenile idiopathic arthritis. *Cytokine* (2018) 110:459–65. doi: 10.1016/j.cyto.2018.05.017

118. Vastert SJ, van Wijk R, D'Urbano LE, de Vooght KMK, de Jager W, Ravelli A, et al. Mutations in the perforin gene can be linked to macrophage activation syndrome in patients with systemic onset juvenile idiopathic arthritis. *Rheumatology* (2009) 49 (3):441–9. doi: 10.1093/rheumatology/kep418

119. Zhang K, Biroschak J, Glass DN, Thompson SD, Finkel T, Passo MH, et al. Macrophage activation syndrome in patients with systemic juvenile idiopathic arthritis is associated with MUNC13-4 polymorphisms. *Arthritis Rheum* (2008) 58(9):2892–6. doi: 10.1002/art.23734

120. Althonaian N, Alsultan A, Morava E, Alfadhel M. Secondary hemophagocytic syndrome associated with cog6 gene defect: report and review. *JIMD Rep (Wiley-Blackwell)* (2018) 42:105–11. doi: 10.1007/8904_2018_88

121. Gokce M, Unal O, Hismi B, Gumruk F, Coskun T, Balta G, et al. Secondary hemophagocytosis in 3 patients with organic acidemia involving propionate metabolism. *Pediatr Hematol Oncol* (2012) 29(1):92–8. doi: 10.3109/08880018.2011.601402

122. He T, Huang Y, Ling J, Yang J. A new patient with NOCARH syndrome due to CDC42 defect. *J Clin Immunol* (2020) 40:571–5. doi: 10.1007/s10875-020-00786-7

123. Toplak N, Blazina Š, Avčin T. The role of IL-1 inhibition in systemic juvenile idiopathic arthritis: current status and future perspectives. *Drug Design Dev Ther* (2018) 12:1633–43. doi: 10.2147/DDDT.S114532

124. Coppola S, Insalaco A, Zara E, di Rocco M, Marafon DP, Spadaro F, et al. Mutations at the c-terminus of CDC42 cause distinct hematopoietic and autoinflammatory disorders. *J Allergy Clin Immunol* (2022) 150(1):223–8. doi: 10.1016/j.jaci.2022.01.024

125. Wegehaupt O, Groß M, Wehr C, Marks R, Schmitt-Graeff A, Uhl M, et al. TIM-3 deficiency presenting with two clonally unrelated episodes of mesenteric and subcutaneous panniculitis-like T-cell lymphoma and hemophagocytic lymphohistiocytosis. *Pediatr Blood Cancer* (2020) 67(6):e28302. doi: 10.1002/pbc.28302

126. Chijioke O, Marcenaro E, Moretta A, Capaul R, Münz C. Role of the 2B4 receptor in CD8+ T-cell-dependent immune control of Epstein-Barr virus infection in mice with reconstituted human immune system components. *J Infect Dis* (2015) 212 (5):803–7. doi: 10.1093/infdis/jiv114

127. Tangye SG, Phillips JH, Lanier LL, Nichols KE. Cutting edge: functional requirement for SAP in 2B4-mediated activation of human natural killer cells as revealed by the X-linked lymphoproliferative syndrome. *J Immunol* (2000) 165 (6):2932–6. doi: 10.4049/jimmunol.165.6.2932

128. Bloch-Queyrat C, Fondanèche MC, Chen R, Yin L, Relouzat F, Veillette A, et al. Regulation of natural cytotoxicity by the adaptor SAP and the src-related kinase fyn. *J Exp Med* (2005) 202(1):181–92. doi: 10.1084/jem.20050449

129. McArdel SL, Terhorst C, Sharpe AH. Roles of CD48 in regulating immunity and tolerance. *Clin Immunol* (2016) 164:10–20. doi: 10.1016/j.clim.2016.01.008

130. Liu N, Zhao FY, Xu XJ. Hemophagocytic lymphohistiocytosis caused by STAT1 gain-offunction mutation is not driven by interferon-γ: a case report. *World J Clin Cases* (2020) 8(23):6130–5. doi: 10.12998/wjcc.v8.i23.6123

131. Toubiana J, Okada S, Hiller J, Oleastro M, Gomez ML, Becerra JCA, et al. Heterozygous STAT1 gain-of-function mutations underlie an unexpectedly broad clinical phenotype. *Blood* (2016) 127(25):3154–64. doi: 10.1182/blood-2015-11-679902

132. Hofer MJ, Li W, Manders P, Terry R, Lim SL, King NJC, et al. Mice deficient in STAT1 but not STAT2 or IRF9 develop a lethal CD4 + T-Cell-Mediated disease following infection with lymphocytic choriomeningitis virus. *J Virol* (2012) 86 (12):6932–46. doi: 10.1128/JVI.07147-11

133. Gothe F, Stremenova Spegarova J, Hatton CF, Griffin H, Sargent T, Cowley SA, et al. Aberrant inflammatory responses to type I interferon in STAT2 or IRF9 deficiency. *J Allergy Clin Immunol* (2022) 150(4):955–64.e16. doi: 10.1016/j.jaci.2022.01.026

134. Alosaimi MF, Maciag MC, Platt CD, Geha RS, Chou J, Bartnikas LM. A novel variant in STAT2 presenting with hemophagocytic lymphohistiocytosis. *J Allergy Clin Immunol* (2019) 144(2):611–3.e3. doi: 10.1016/j.jaci.2019.05.008

135. Bravo García-Morato M, Calvo Apalategi A, Bravo-Gallego LY, Blázquez Moreno A, Simón-Fuentes M, Garmendia Jv, et al. Impaired control of multiple viral infections in a family with complete IRF9 deficiency. *J Allergy Clin Immunol* (2019) 144 (1):309–12.e10. doi: 10.1016/j.jaci.2019.02.019

136. Ishidate T, Ozturk AR, Durning DJ, Sharma R, Shen Ez, Chen H, et al. ZNFX-1 functions within perinuclear nuage to balance epigenetic signals. *Mol Cell* (2018) 70 (4):639–49.e6. doi: 10.1016/j.molcel.2018.04.009

137. Wang Y, Yuan S, Jia X, Ge Y, Ling T, Nie M, et al. Mitochondria-localised ZNFX1 functions as a dsRNA sensor to initiate antiviral responses through MAVS. *Nat Cell Biol* (2019) 21(11):1346–56. doi: 10.1038/s41556-019-0416-0

138. le Voyer T, Neehus AL, Yang R, Ogishi M, Rosain J, Alroqi F, et al. Inherited deficiency of stress granule ZNFX1 in patients with monocytosis and mycobacterial disease. *Proc Natl Acad Sci USA* (2021) 118(15):e2102804118. doi: 10.1073/pnas.2102804118

139. Qin S, Xu W, Wang C, Jiang S, Dai W, Yang Y, et al. Analyzing master regulators and scRNA-seq of COVID-19 patients reveals an underlying anti-SARS-CoV-2 mechanism of ZNF proteins. *Brief Bioinform* (2021) 22(5):bbab118. doi: 10.1093/bib/bbab118

140. Clementi R, Chiocchetti A, Cappellano G, Cerutti E, Ferretti M, Orilieri E, et al. Variations of the perforin gene in patients with autoimmunity/lymphoproliferation and defective fas function. *Blood* (2006) 108(9):3079–84. doi: 10.1182/blood-2006-02-001412

141. Clementi R, Dagna L, Dianzani U, Dupré L, Dianzani I, Ponzoni M, et al. Inherited perforin and fas mutations in a patient with autoimmune lymphoproliferative syndrome and lymphoma. *New Engl J Med* (2004) 351(14):1419–24. doi: 10.1056/NEJMoa041432

142. Mateo V, Ménager M, de Saint-Basile G, Stolzenberg MC, Roquelaure B, André N, et al. Perforin-dependent apoptosis functionally compensates fas deficiency in activation-induced cell death of human T lymphocytes. *Blood* (2007) 110(13):4285–92. doi: 10.1182/blood-2007-05-088286

143. Aricò M, Boggio E, Cetica V, Melensi M, Orilieri E, Clemente N, et al. Variations of the UNC13D gene in patients with autoimmune lymphoproliferative syndrome. *PloS One* (2013) 8(7):e68045. doi: 10.1371/journal.pone.0068045

144. Boggio E, Melensi M, Bocca S, Chiocchetti A, Comi C, Clemente N, et al. The -346T polymorphism of the SH2D1A gene is a risk factor for development of autoimmunity/lymphoproliferation in males with defective fas function. *Hum Immunol* (2012) 73(5):585–92. doi: 10.1016/j.humimm.2012.02.025

145. Bode SFN, Ammann S, Al-Herz W, Bataneant M, Dvorak CC, Gehring S, et al. The syndrome of hemophagocytic lymphohistiocytosis in primary immunodeficiencies: implications for differential diagnosis and pathogenesis. *Haematologica* (2015) 100(7):978–88. doi: 10.3324/haematol.2014.121608

146. Marzollo A, Conti F, Rossini L, Rivalta B, Leonardi L, Tretti C, et al. Neonatal manifestations of chronic granulomatous disease: MAS/HLH and necrotizing pneumonia as unusual phenotypes and review of the literature. *J Clin Immunol* (2022) 42(2):299–311. doi: 10.1007/s10875-021-01159-4

147. Shi B, Chen M, Xia Z, Xiao S, Tang W, Qin C, et al. Hemophagocytic syndrome associated with mycobacterium bovis in a patient with X-SCID: a case report. *BMC Infect Dis* (2020) 20(1):711. doi: 10.1186/s12879-020-05421-9

148. Pasic S, Micic D, Kuzmanovic M. Epstein-Barr Virus-associated haemophagocytic lymphohistiocytosis in wiskott-Aldrich syndrome. *Acta Paediatr* (2007) 92(7):859–61. doi: 10.1111/j.1651-2227.2003.tb02548.x

149. Arico M, Bettinelli A, Maccario R, Clementi R, Bossi G, Danesino C. Hemophagocytic lymphohistiocytosis in a patient with deletion of 22q11.2. *Am J Med Genet* (1999) 87(4):329–30. doi: 10.1002/(SICI)1096-8628(19991203)87:4<329::AID-AJMG9>3.0.CO;2-M

150. Brennan AJ, Chia J, Trapani JA, Voskoboinik I. Perforin deficiency and susceptibility to cancer. *Cell Death Differ* (2010) 17:607–15. doi: 10.1038/cdd.2009.212

151. Clementi R, Locatelli F, Dupré L, Garaventa A, Emmi L, Bregni M, et al. A proportion of patients with lymphoma may harbor mutations of the perform gene. *Blood* (2005) 105(11):4424–8. doi: 10.1182/blood-2004-04-1477

152. Chaudhry MS, Gilmour KC, House IG, Layton M, Panoskaltsis N, Sohal M, et al. Missense mutations in the perforin (PRF1) gene as a cause of hereditary cancer predisposition. *Oncoimmunology* (2016) 5(7):e1179415. doi: 10.1080/2162402X.2016.1179415

153. Solomou EE, Gibellini F, Stewart B, Malide D, Berg M, Visconte V, et al. Perforin gene mutations in patients with acquired aplastic anemia. *Blood* (2007) 109(12):5234–7. doi: 10.1182/blood-2006-12-063495

154. Terrell CE, Jordan MB. Perforin deficiency impairs a critical immunoregulatory loop involving murine CD81 T cells and dendritic cells. *Blood* (2013) 121(6):5184–91. doi: 10.1182/blood-2013-04-495309

155. Lang PA, Lang KS, Xu HC, Grusdat M, Parish IA, Recher M, et al. Natural killer cell activation enhances immune pathology and promotes chronic infection by limiting CD8 + T-cell immunity. *Proc Natl Acad Sci USA* (2012) 109(4):1210–5. doi: 10.1073/pnas.1118834109

156. Gross CC, Schulte-Mecklenbeck A, Rünzi A, Kuhlmann T, Posevitz-Fejfár A, Schwab N, et al. Impaired NK-mediated regulation of T-cell activity in multiple sclerosis is reconstituted by IL-2 receptor modulation. *Proc Natl Acad Sci USA* (2016) 113(21):E2973–82. doi: 10.1073/pnas.1524924113

157. González-Cabrero J, Wise CJ, Latchman Y, Freeman GJ, Sharpe AH, Reiser H. CD48-deficient mice have a pronounced defect in CD4+ T cell activation. *Proc Natl Acad Sci USA* (1999) 96(3):1019–23. doi: 10.1073/pnas.96.3.1019

158. Chen G, Tai AK, Lin M, Chang F, Terhorst C, Huber BT. Increased proliferation of CD8+ T cells in SAP-deficient mice is associated with impaired activation-induced cell death. *Eur J Immunol* (2007) 37(3):663–74. doi: 10.1002/eji.200636417

159. Snow AL, Marsh RA, Krummey SM, Roehrs P, Young LR, Zhang K, et al. Restimulation-induced apoptosis of T cells is impaired in patients with X-linked lymphoproliferative disease caused by SAP deficiency. *J Clin Invest* (2009) 119 (10):2976–89. doi: 10.1172/JCI39518

160. Voss K, Lake C, Luthers CR, Lott NM, Dorjbal B, Arjunaraja S, et al. FOXP3 protects conventional human T cells from premature restimulation-induced cell death. *Cell Mol Immunol* (2021) 18(1):194–205. doi: 10.1038/s41423-019-0316-z

161. de Benedetti F, Prencipe G, Bracaglia C, Marasco E, Grom AA. Targeting interferon-γ in hyperinflammation: opportunities and challenges. *Nat Rev Rheumatol* (2021) 17:678–91. doi: 10.1038/s41584-021-00694-z

162. Humblet-Baron S, Franckaert D, Dooley J, Ailal F, Bousfiha A, Deswarte C, et al. IFN-γ and CD25 drive distinct pathologic features during hemophagocytic lymphohistiocytosis. *J Allergy Clin Immunol* (2019) 143(6):2215–26.e7. doi: 10.1016/j.jaci.2018.10.068

163. Locatelli F, Jordan MB, Allen C, Cesaro S, Rizzari C, Rao A, et al. Emapalumab in children with primary hemophagocytic lymphohistiocytosis. *New Engl J Med* (2020) 382(19):1811–22. doi: 10.1056/NEJMoa1911326

164. Hislop AD, Palendira U, Leese AM, Arkwright PD, Rohrlich PS, Tangye SG, et al. Impaired Epstein-Barr virus-specific CD8 + T-cell function in X-linked lymphoproliferative disease is restricted to SLAM family-positive b-cell targets. *Blood* (2010) 116(17):3249–57. doi: 10.1182/blood-2009-09-238832

165. Rood JE, Rao S, Paessler M, Kreiger PA, Chu N, Stelekati E, et al. ST2 contributes to T-cell hyperactivation and fatal hemophagocytic lymphohistiocytosis in mice. *Blood* (2016) 127(4):426–35. doi: 10.1182/blood-2015-07-659813

166. Mazzoni A, Salvati L, Maggi L, Capone M, Vanni A, Spinicci M, et al. Impaired immune cell cytotoxicity in severe COVID-19 is IL-6 dependent. *J Clin Invest* (2020) 130(9):4694–703. doi: 10.1172/JCI138554

167. Cifaldi L, Prencipe G, Caiello I, Bracaglia C, Locatelli F, de Benedetti F, et al. Inhibition of natural killer cell cytotoxicity by interleukin-6: implications for the pathogenesis of macrophage activation syndrome. *Arthritis Rheumatol* (2015) 67 (11):3037–46. doi: 10.1002/art.39295

168. Dufranc E, del Bello A, Belliere J, Kamar N, Faguer S, Dufranc E, et al. IL6-r blocking with tocilizumab in critically ill patients with hemophagocytic syndrome. *Crit Care* (2020) 24(1):166. doi: 10.1186/s13054-020-02878-7

169. Keenan C, Nichols KE, Albeituni S. Use of the JAK inhibitor ruxolitinib in the treatment of hemophagocytic lymphohistiocytosis. *Front Immunol* (2021) 12. doi: 10.3389/fimmu.2021.614704

170. Andersson U. Hyperinflammation: on the pathogenesis and treatment of macrophage activation syndrome. *Acta Paediatrica Int J Paediatrics* (2021) 110:2717–22. doi: 10.1111/apa.15900

171. Duncan JA, Canna SW. The NLRC4 inflammasome. *Immunol Rev* (2018) 281:115–23. doi: 10.1111/imr.12607

172. Mazodier K, Marin V, Novick D, Farnarier C, Robitail S, Schleinitz N, et al. Severe imbalance of IL-18/IL-18BP in patients with secondary hemophagocytic syndrome. *Blood* (2005) 106(10):3483–9. doi: 10.1182/blood-2005-05-1980

173. Bracaglia C, Marafon DP, Caiello I, de Graaf K, Guilhot F, Ferlin W, et al. High levels of interferon-gamma (IFNγ) in macrophage activation syndrome (MAS) and CXCL9 levels as a biomarker for IFNγ production in MAS. *Pediatr Rheumatol* (2015) 13(1):O84. doi: 10.1186/1546-0096-13-S1-O84

174. Mizuta M, Shimizu M, Inoue N, Nakagishi Y, Yachie A. Clinical significance of serum CXCL9 levels as a biomarker for systemic juvenile idiopathic arthritis associated macrophage activation syndrome. *Cytokine* (2019) 119:182–7. doi: 10.1016/j.cyto.2019.03.018

175. Hines MR, Nichols KE. Go with the flow: perforin and CD107a in HLH. *Blood* (2017) 129:2954–5. doi: 10.1182/blood-2017-04-773192

176. Ammann S, Lehmberg K, Stadt U, Janka G, Rensing-Ehl A, Klemann C, et al. Primary and secondary hemophagocytic lymphohistiocytosis have different patterns of T-cell activation, differentiation and repertoire. *Eur J Immunol* (2017) 47(2):364–73. doi: 10.1002/eji.201646686

177. Cheroutre H, Husain MM. CD4 CTL: living up to the challenge. *Semin Immunol* (2013) 25:273–81. doi: 10.1016/j.smim.2013.10.022

178. Hosen N, Ichihara H, Mugitani A, Aoyama Y, Fukuda Y, Kishida S, et al. CD48 as a novel molecular target for antibody therapy in multiple myeloma. *Br J Haematol* (2012) 156(2):213–24. doi: 10.1111/j.1365-2141.2011.08941.x

frontiers | Frontiers in Immunology

TYPE Review
PUBLISHED 29 September 2023
DOI 10.3389/fimmu.2023.1239732

OPEN ACCESS

EDITED BY
Hui-Rong Jiang,
University of Strathclyde, United Kingdom

REVIEWED BY
Weiwei Xue,
Chongqing University, China
Vassilis Valatas,
University Hospital of Heraklion, Greece
Qingqing du,
Second Affiliated Hospital of Chongqing Medical University, China

*CORRESPONDENCE
Cheryl L. Jorcyk
cjorcyk@boisestate.edu

†These authors have contributed equally to this work

RECEIVED 13 June 2023
ACCEPTED 30 August 2023
PUBLISHED 29 September 2023

CITATION
Wolf CL, Pruett C, Lighter D and Jorcyk CL (2023) The clinical relevance of OSM in inflammatory diseases: a comprehensive review. *Front. Immunol.* 14:1239732. doi: 10.3389/fimmu.2023.1239732

The clinical relevance of OSM in inflammatory diseases: a comprehensive review

Cody L. Wolf[1†], Clyde Pruett[2†], Darren Lighter[2] and Cheryl L. Jorcyk[1,2*]

[1]Department of Biomolecular Sciences, Boise State University, Boise, ID, United States, [2]Department of Biological Sciences, Boise State University, Boise, ID, United States

Oncostatin M (OSM) is a pleiotropic cytokine involved in a variety of inflammatory responses such as wound healing, liver regeneration, and bone remodeling. As a member of the interleukin-6 (IL-6) family of cytokines, OSM binds the shared receptor gp130, recruits either OSMRβ or LIFRβ, and activates a variety of signaling pathways including the JAK/STAT, MAPK, JNK, and PI3K/AKT pathways. Since its discovery in 1986, OSM has been identified as a significant contributor to a multitude of inflammatory diseases, including arthritis, inflammatory bowel disease, lung and skin disease, cardiovascular disease, and most recently, COVID-19. Additionally, OSM has also been extensively studied in the context of several cancer types including breast, cervical, ovarian, testicular, colon and gastrointestinal, brain,lung, skin, as well as other cancers. While OSM has been recognized as a significant contributor for each of these diseases, and studies have shown OSM inhibition is effective at treating or reducing symptoms, very few therapeutics have succeeded into clinical trials, and none have yet been approved by the FDA for treatment. In this review, we outline the role OSM plays in a variety of inflammatory diseases, including cancer, and outline the previous and current strategies for developing an inhibitor for OSM signaling.

KEYWORDS

oncostatin M (OSM), oncostatin M receptor beta (OSMRβ), inflammatory diseases, cytokine, cancer, metastasis, drug development, therapeutics

1 Introduction

Oncostatin-M (OSM) is an interleukin-6 (IL-6) family cytokine first isolated in 1986 from human histiocytic lymphoma U937 cells (1). It was initially identified as a cytostatic protein for melanoma cells, thus deriving its name ('onco' for cancer and 'statin' for inhibitor) (1). Other than OSM, the IL-6 family members consist of the parent protein IL-6, leukemia inhibitory factor (LIF), IL-11, IL-27, cardiotrophin-1 (CT-1), ciliary neurotrophic factor (CNTF), and cardiotrophin-like cytokine factor 1 (CLCF1). The human *OSM* gene encodes for a 2 kb mRNA transcript that is translated and cleaved into a soluble 227 amino acid pro-OSM polypeptide with a 28 kDa molecular weight (2). Mature OSM is synthesized

after a C-terminal cleavage of 31 amino acids, yielding a 196 amino acid, ~22kDa protein (3, 4). OSM, like all other IL-6 family members, has a crystal structure consisting of a four alpha-helical up-up-down-down configuration (5). LIF and OSM are structurally and genetically the most similar members of the IL-6 family, resulting from an ancestral gene duplication event (6). Similar to other IL-6 family cytokine members, OSM utilizes the shared receptor protein membrane glycoprotein 130 (gp130; also known as IL-6Rβ) and a unique receptor protein to create a complete signaling receptor complex (7–10). In the case of OSM, it possesses the capability to interact and transduce signaling through two separate complexes (7–10). OSM first binds to the extracellular cytokine-binding homology region (CHR) domain of gp130 with a high affinity (~10^{-8} M) and subsequently recruits either the leukemia inhibitory factor receptor beta (LIFRβ) or oncostatin M receptor beta (OSMRβ); to form either a type I or type II receptor complex (LIFRβ/gp130 and OSMRβ/gp130, respectively) (Figures 1A, B) (11–16). While the OSMR (type II) complex has been studied extensively in various human cell lines, it remains unclear how OSM interacting with the LIFR (type I) complex affects signaling or disease progression; however, recent research has indicated that OSM binds to LIFR with significantly lower affinity than its specific receptor (17, 18). After binding to the OSMR complex, several signaling pathways are activated, including the Janus-activated kinase/signal transducer and activator of transcription 3 (JAK/STAT3), the mitogen-activated protein kinase/extracellular regulator kinase (MAPK/ERK), the c-Jun N-terminal Kinase (JNK), and the phosphatidylinositol-3-kinase/protein kinase B (PI3K/AKT) pathways (Figure 1C) (19–21). To a lesser extent OSM signaling may also activate additional STAT proteins, including STAT1 and STAT5, depending on the cell type (22, 23). OSM is synthesized and secreted by a variety of cells; primarily activated macrophages, monocytes, T cells, dendritic cells, and neutrophils (1, 2, 24). OSM acts in a pleiotropic fashion, contributing towards a variety of physiological functions such as hematopoiesis, stem cell differentiation, liver regeneration, and inflammation. While some of these effects are similar to other IL-6 family members, many are unique (5, 11, 15). Over the course of

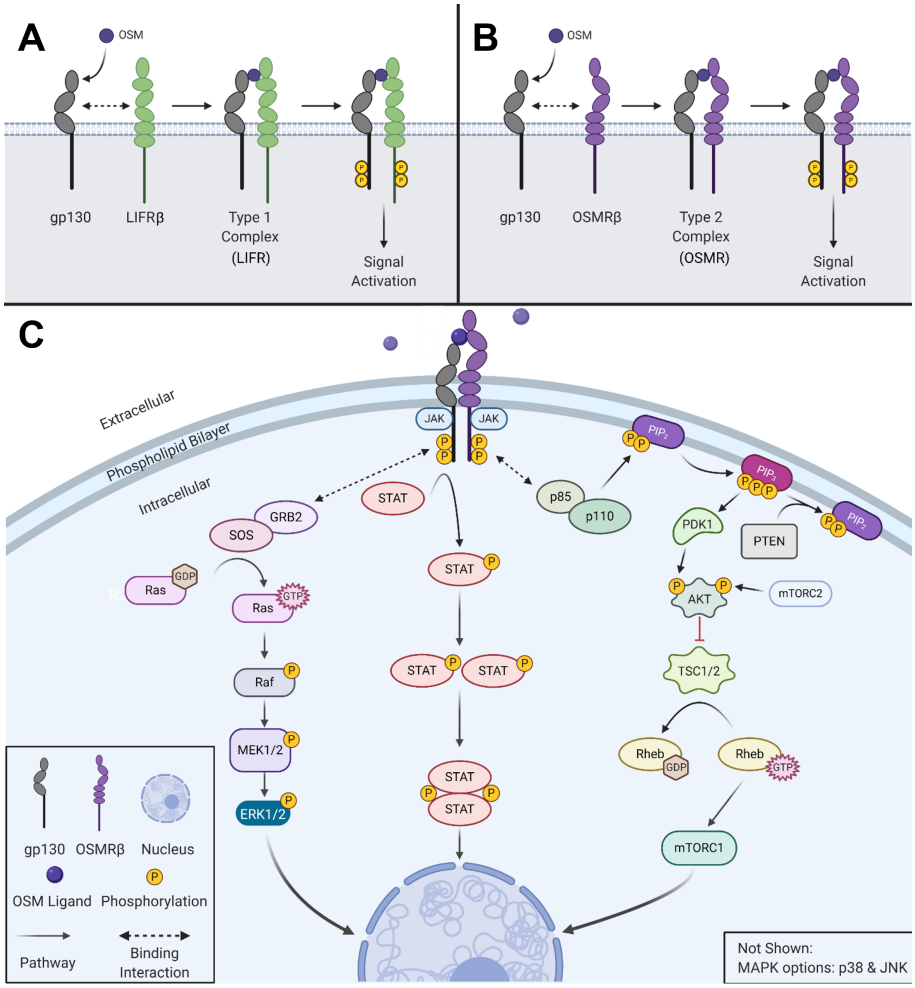

FIGURE 1
OSM activates multiple signaling cascades. **(A)** OSM binds to gp130 and then recruits LIFRβ to form a type I complex (LIFR). **(B)** OSM binds to gp130 and then recruits its major receptor complex subunit OSMRβ to form a type II complex. **(C)** Visual representation of the signaling pathways used by OSM type II complex. Created with BioRender.com.

the last 30 years OSM has been demonstrated to play a significant role in a variety of processes and diseases, yet successful development of an anti-OSM clinical therapeutic has not yet reached FDA approval despite mounting evidence that such a therapeutic is necessary for a multitude of diseases. In this review, we will describe: i) the different roles that OSM plays within the human body regarding its function in inflammatory diseases; ii) the role of OSM in multiple cancer types; and iii) a detailed analysis of current targeted therapies designed to disrupt OSM signaling.

2 OSM in diseases

A significant difficulty with developing treatment strategies to block OSM stems from the pleiotropic nature of the cytokine. As indicated in Table 1, OSM has a variety of positive and negative effects on several diseases in the body. Systemic inhibition of OSM signaling in the body for extended periods of time may be beneficial with respect to some diseases, but detrimental in cases that rely on the proinflammatory response for healing. This section will describe the role OSM plays in a variety of diseases.

2.1 Arthritis

Arthritis is a disease referring to chronic inflammation in one or more joints of the body, with the two most common and studied types being: rheumatoid arthritis and osteoarthritis. Rheumatoid arthritis (RA) is a chronic autoimmune disease involving inflammation of the lining of joints. It has been shown that the presence of OSM and another proinflammatory cytokine, interleukin-1β (IL-1β), play an important role in development of the rheumatoid joint (25, 26). In multi-cell culture systems, OSM-mediated signaling has been identified as an initiator of extracellular matrix (ECM) turnover as well as human cartilage degradation; potentially though the secretion of matrix metalloproteinase (MMP) -1 and -13 (23). Through regulation of various proinflammatory mediators, OSM in rheumatoid arthritis synovial fibroblasts (RAFLS), increases the detrimental effects of tumor necrosis factor alpha (TNFα) via activation of STAT3 signaling (27). Inhibition of JAK/STAT signaling with tofacitinib (a JAK inhibitor) resolved inflammation through metabolic reprograming of biopsied RALFS (28). *In vivo* studies demonstrated that both collagen-induced and pristane-induced

TABLE 1 OSM in Diseases.

Disease	Type	Impact of OSM	References
Diseases associated with OSM signaling			
Arthritis	Rheumatoid and Osteoarthritis	ECM turnover, cartilage degradation, osteoblast proliferation/ differentiation	(23, 25–32)
Bone	Neurogenic Heterotopic Ossification	Osteoclast/osteoblast imbalance	(33–37)
Inflammatory Bowel Disease	Chron's Disease, Ulcerative Colitis	Presence in intestinal mucosal cells signify anti-TNF therapy resistance	(38–45)
Lung Diseases	Pulmonary Fibrosis, Asthma	ECM and Pro-fibrotic macrophage accumulation, airway remodeling	(46–50)
Cutaneous Inflammatory Diseases	Psoriasis, Atopic Dermatitis	Increase in keratinocyte proliferation and differentiation	(51–57)
Oral Disease	Gingivitis, Periodontal Disease	Increase presence and activation of Th1 cells	(58–62)
Liver Diseases	Fibrosis, Cirrhosis	Increased TIMP-1 expression, reduction in fibrinolysis, increase in myofibroblasts	(63–72)
Central Nervous System Disorders	HIV-1 Associated Neurocognitive Disorders, Alzheimer's	Inhibits glutamate uptake, BBB impairment	(73–77)
Heart	Atherosclerosis	Proinflammatory response in smooth muscle cells	(78–86)
COVID-19	Cytokine Storm	Present in Cytokine Storm associated with severe COVID-19 infection.	(87–91)
Cancer	Many	Tumor cell detachment, invasion, metastasis	See Table 2
Normal conditions associated with OSM signaling			
Liver	Regeneration, development, acute injury	Hepatocyte differentiation, proliferation, tissue remodeling	(63–72)
Bone	Bone homeostasis, fracture repair	Osteoblast differentiation/proliferation	(33–37)
Central Nervous System	Multiple Sclerosis, Spinal Cord Injury	Increase TIMP-1 and MCL-1 expression, remyelination, neuroprotective effects	(73–77)
Heart	Post myocardial infarction	Increase in angiogenesis, dedifferentiation	(78–86)
Wound Healing	Early Wound Healing, Scar Formation	Neutrophil recruitment, excessive scar prevention	(92–95)
Pregnancy	Placental development, Trophoblast invasion	Increase MMP2/9, regulation of HCG	(96–98)

arthritis mouse models, showed significant improvement in severity ($p<0.01$) and number of affected paws ($p<0.01$) when administered an anti-OSM antibody (29). In response to the strong association of OSM with RA, two clinical therapeutics have entered clinical trials (GSK315234 and GSK2330811) discussed in further detail below (see Anti-OSM Therapeutics).

The effects of OSM are not limited to rheumatoid arthritis, as studies have shown its effects in the development of the much more prevalent osteoarthritis (OA). OA is characterized by articular cartilage destruction and an inflammatory response due to mechanical wear on joints (30). *In vitro* analysis in primary OA osteoblasts has demonstrated that degradation and inflammation could be due to endothelin-1 (ET-1) trans-activating OSM via Ets-1 (31). Increased levels of OSM in synovial tissues induce bone formation through osteoblast proliferation and differentiation following cartilage degradation by inhibition of Notch signaling (32). Currently no clinical trials have evaluated the efficacy of anti-OSM therapeutics for OA.

2.2 Bone

OSM signaling regarding bone tissue is complicated, as there is evidence to suggest benefit and harm from its activation. It is well known that OSM induces differentiation of mesenchymal stem cells (MSCs) into osteoblasts though the STAT3 signaling pathway (17, 33, 34). This can be beneficial in respect to new bone formation in osteoporosis and arthritis as well as remodeling of bone during fracture repair (33). However, there is significant research suggesting that OSM has an overall negative effect in respect to bone. While osteogenesis is being stimulated, the anabolic signal suppresses the reabsorption signal-controlled receptor activator of nuclear factor-kappa beta ligands (RANKL) signaling, repressing osteoblast-mediated osteoclast differentiation in bones (34). OSM-mediated STAT3 signaling has also been associated with the development of neurogenic heterotopic ossifications, which is the formation of bone tissue in periarticular muscles, an incapacitating complication of traumatic brain and spinal cord injuries (35). Other studies have indicated that STAT3 signaling through OSM is necessary for osteoclast formation and subsequent bone resorption (36, 37). It is clear that OSM plays a role in bone remodeling, however there is evidence suggesting it promotes the differentiation of both osteoblasts and osteoclasts, leading to some potential questions about the true effects of OSM signaling among bones.

2.3 Inflammatory bowel disease

Inflammatory bowel disease (IBD) is a collective term describing disorders that involve chronic inflammation of the small intestine. The two main forms of IBD are ulcerative colitis (UC) and Chron's disease (CD) (38). It has been demonstrated that OSM and OSMR are overexpressed in many IBD lesions (39). While anti-tumor necrosis factor alpha (TNFα) antibodies such as infliximab, adalimumab, certolizumab, and golimumab have long been available as treatment strategies for CD and UC, they are far from perfect. Approximately one third of patients do not respond to infliximab initially, and between 23% and 46% develop resistance to anti-TNFα therapies within 12 months of treatment (40, 41). A recent retrospective cohort study demonstrates that patients with increased levels of OSM had a lower chance of remaining in remission 1 year after starting anti-TNFα therapies (42). There are other IBD treatment options available, some of the more viable options include JAK/STAT inhibitors, indicating OSM inhibition upstream may be beneficial (43). In a study analyzing over 200 patients with IBD, those with high OSM and OSMR expression before treatment with infliximab demonstrated reduced efficacy of the therapy from 69-85% to just 10-15% (39). *In vivo* IBD mouse studies comparing wildtype and *Osm-/-* showed that lack of OSM signaling led to a decrease in overall pathology ($p<0.0001$), leukocyte infiltration ($p<0.0001$), epithelial and goblet cell disruption ($p<0.0001$), area affected ($p<0.0001$), and severity of disease features ($p<0.0005$) (39). Additionally, OSM has been shown to mediate STAT3-dependent upregulation of serin protease inhibitors (SERPINS), which have anti-apoptotic effects in intestinal epithelial cells that lead to inflammation and a disrupted intestinal epithelial barrier (44). Recent studies have also shown that the use of berberine, an isoquinoline alkaloid used to treat chronic UC, interferes with the production of OSM from T cells, neutrophils, dendritic cells, and macrophages, as well as inhibiting OSM activation of stromal cells and recruitment of immune cells (45). As seen in other diseases with inflammation as a hallmark, OSM signaling is a key component in disease pathogenesis, and in this case, it also appears to interfere with pharmacological treatments.

2.4 Lung diseases

OSM plays an important role in the development and progression of pulmonary fibrosis and chronic lung inflammatory diseases such as asthma. OSM levels are upregulated in patients with pulmonary fibrosis, due to increased lung inflammation as well as accumulation of ECM proteins (46). Evidence suggests that an increase in OSM and IL-6 leads to the accumulation of profibrotic macrophages, in turn increasing bleomycin-induced lung fibrosis (47). Chronic inflammatory diseases of the lung such as asthma also showed a significant increase in OSM expression (48). In severe asthma, poor disease prognosis is characterized by an increase in number of epithelial mucus producing cells, peribronchial fibrosis, and smooth muscle contractility through follistatin-like 1 induction of OSM expression (49). Recent studies have also demonstrated that overexpression of OSM leads to an increase in resistin-like molecule alpha in airway epithelial cells, leading to rearrangement of the ECM in mouse lungs (50). The increase in OSM signaling in the lungs with respect to these chronic inflammatory diseases demonstrates its potential to be used as a therapeutic target.

2.5 Cutaneous inflammatory diseases

Being the human body's largest organ, and our first line of defense, the skin plays an important role in inflammatory processes

and responses. Diseases such as psoriasis and atopic dermatitis are chronic inflammatory skin diseases that affect over 7.5 million individuals within the United States and are characterized by keratinocyte hyperplasia, proliferation, and altered differentiation (51, 52). These diseases demonstrate an increase in skin infiltrating T lymphocytes that lead to secretion of OSM and an increase in OSMRβ on keratinocytes, increasing keratinocyte activation through STAT3 signaling (52). When OSM is overexpressed in the skin, its proinflammatory effects have been demonstrated both *in vitro* and *in vivo* (53). Studies conducted in mice show that intradermal injection of OSM, but not IL-6, regulates the expression of genes responsible for skin inflammation and epidermal differentiation, including S100A8/9, cytokeratin-10, filaggrin, and a number of other cytokines (52). Additionally, OSM has recently been identified as a significant contributor to chronic pruritus (itching). *Tsen and Hoon et al.* discovered that OSMRβ is preferentially expressed by itch-selective sensory neurons and that OSM can directly modulate itch-selective neurons during chronic skin inflammation (54). Functional studies showed that OSM acts in a unique fashion compared to other pruritogens, being that OSM causes potentiation of neural response to pruritogens and that OSM increases sensitization of sensory neurons, resulting in tonic action potential firing of itch-selective neurons. Another study showed that OSM and IL-31 stimulate dermal cells expressing IL-31RA and OSMRβ, which may further promote itch and inflammation in patients with prurigo nodularis, a chronic skin dermatosis (55).

Scleroderma is an inflammatory autoimmune disease that is characterized by increased activation of fibroblasts leading to accumulation of connective tissue that results in chronic inflammation on the surface on the skin and internal organs (56). Elevated OSMRβ levels have been found in fibroblasts as well as dermal endothelial cell of scleroderma patients. *In vitro* of human dermal microvascular endothelial cells treated with OSM and IL-6 displayed induced cell migration and proliferation, as well as stimulation of proinflammatory genes, and genes associated with endothelial to mesenchymal transition including STAT3, ET-1, zinc finger protein SNAI1 (SNAIL1), transforming growth factor-β 3 (TGFβ3), and its receptor TGFβ3R (57). There is currently a clinical trial for a monoclonal antibody against OSM, in patients with systemic scleroderma, which will be discussed in greater detail in Anti-OSM therapeutics.

2.6 Oral diseases

OSM and other cytokines play an important role in the progression of periodontal disease, a gum infection typically caused by poor brushing and flossing habits. In studies investigating levels of OSM in patients' gingival crevicular fluid, OSM concentrations increase as disease severity progresses from early-stage disease to chronic periodontitis (58–60). Another study focused on T-helper type 1 (Th1) cells, which have detrimental effects in regard to periodontal disease through the stimulation of alveolar bone loss (61). OSM and IL-1β together increased the expression of chemokine (C-X-C motif) ligand 10 (CXCL10), a chemokine related to Th1 cell migration, as well as intracellular adhesion molecule 1 (ICAM-1) that is important in retention and activation of Th1 cells in inflamed tissue (62). CXCL10 and ICAM-1 expression were both suppressed when inhibitors of NF-κB and STAT3 were introduced, indicating that OSM-mediates STAT3 signaling and IL-1β-mediated NF-κB signaling may promote infiltration and retention of Th1 cells, leading to periodontal disease (62). Overall OSM signaling continues to demonstrate negative downstream effects through activation of several different signaling molecules.

2.7 Liver

Inflammation is a key driver in liver disease, and it has been demonstrated that OSM plays a profibrogenic role in the progression of chronic liver disease (63–65). Administration of OSM to human hepatocellular HepG2 cells in culture increased expression of GP73 (a glycoprotein biomarker for cirrhosis and hepatic cell carcinoma), indicative of the effects OSM has on promoting chronic liver disease progression (63). OSM's role in fibrosis is characterized by promoting the expression of tissue inhibitor of metalloproteinase 1 (TIMP-1), which both suppresses fibrinolysis in hepatic stellate cells (HSCs) as well as promotes fibrogenesis through induction of Type 1 collagen expression (64). Recent research also suggests that OSM promotes fibrosis in non-alcoholic fatty acid liver disease (NAFLD) through stimulating migration of hepatic myofibroblasts (MFs) that originate from HSCs (65). A recent study analyzed serum levels of 83 patients with NAFLD and non-alcoholic steatohepatitis (NASH) who also have hepatocellular carcinoma (HCC) and found that the presence of HCC further increased OSM concentrations (66). It has also been found in chronic hepatitis C that antigen presenting cells release OSM following interaction with CD40L present on active CD4+ T cells (67). This OSM does not result in a large notable effect, as OSMRβ and LIFR expression is also downregulated both *in vitro* and in patients with chronic hepatitis C; however, the increase in ligand is thought to be noteworthy (67).

In addition to affecting liver fibrosis and progression of chronic liver disease, OSM also plays an important role in liver regeneration (64, 68–71). Following acute liver injury, it is primarily oval cells that are responsible for liver regeneration (72). More research has shown that OSM is able to induce the differentiation of these oval cells into hepatocytes *in vitro* (69). *In vivo* studies demonstrated that OSMRβ knockout mice had impaired hepatocyte proliferation and tissue remodeling following induced liver injury, indicating its importance in regeneration (71). Furthermore, administration of OSM in wild type mice mitigated liver injury through prevention of apoptosis and tissue destruction (71). It was also demonstrated that OSM gene therapy in rats effectively increases proliferation and the anti-apoptotic effects of on hepatocytes, leading to liver regeneration (70). Through the upregulation of hypoxia-inducible factory 1 α (HIF1α) and HIF1 transcription, OSM demonstrates its importance as an upstream mediator of vascular endothelial growth factor (VEGF) and plasminogen activator inhibitor 1 (PAI1), both of which are important for angiogenesis and tissue remodeling respectively (68). While OSM does appear to play an important role

in regeneration following acute liver injuries, continuous activation of OSM has a very different effect with respect to fibrosis and chronic liver disease suggesting its prolonged presence may be harmful.

2.8 Central nervous system

In diseases related to the central nervous system, research has indicated that OSM plays various roles with both detrimental and beneficial outcomes. Studies have been conducted displaying various negative effects that OSM has on the central nervous system. Diseases such as HIV-1-associated neurocognitive disorders and Alzheimer's disease have displayed elevated levels of OSM (73). Specifically, through JAK/STAT3 signaling, OSM inhibits glutamate uptake in astrocytes resulting in neuronal excitotoxicity (73). OSM also induces blood brain barrier impairment in mice, through prolonged STAT3 signaling in pericytes (74). As discussed previously, STAT3 activation initiated through OSM signaling *in vivo* has also been shown to increase neurogenic heterotrophic ossifications in damaged muscles following spinal cord injuries (35).

In diseases characterized by the loss of myelination such as multiple sclerosis, overexpression of OSM has been shown to mediate the expression of tissue inhibitor of TIMP-1, promoting a beneficial remyelination (75). Following mild and severe spinal cord injuries, elevated OSM signaling results in improved recovery and neuroprotective effects by promoting neurite outgrowth, increasing serotonergic fiber plasticity, and protecting primary neurons from cell death (76). OSM also stimulates the expression of myeloid cell lukemia-1 (MCL-1), in turn enhancing mitochondrial bioenergetics and increasing neuroprotective effects against 3-nitropropionic acid in cortical neurons (77). The pleotropic nature of OSM is clearly demonstrated with respect to the central nervous system, especially concerning the inflammatory response following spinal cord injuries.

2.9 Heart

When it comes to function of the heart, research has indicated that OSM plays various roles with both detrimental and beneficial outcomes. Regarding atherosclerosis development and progression, the vast majority of research suggests that prolonged STAT3 activation through OSM signaling has a negative impact on arterial vessels, which leads to atherogenesis (78–81). However, one recent study showed that chronic OSM administration in mice reduced atherosclerosis development, and patients with higher levels of serum OSM had improved coronary heart disease survival probability (82). This differing research continues to cloud the role OSM plays in the heart.

Cardiomyocytes are the workhorse of the heart, and OSM plays a key role in the dedifferentiation of cardiomyocytes (83, 84). This dedifferentiation leads to protective effects during and following acute myocardial infarction (MI) (83–85). Knockout of OSM signaling following MI in mouse models suppressed cardiomyocyte dedifferentiation, resulting in decreased heart function, while OSM treatment induced remodeling, stem cell marker expression, and improved cardiac function (84). Inhibition of OSM treatment reduced cardiomyocyte function following MI, however, improved performance in dilated cardiomyopathy (DCM) indicates negative effects of OSM long-term (84). Other studies done in mice have shown that OSM increases cardiac function following MI through the inhibition of apoptosis and fibrosis, while stimulating angiogenesis. OSM treated mice had significantly increased capillary density as well as increased expression of pAKT and the angiogenic factors, VEGF and basic fibroblast growth factor (bFGF) (85). More *in vivo* studies have indicated that OSM alleviates post MI dysfunction by enhancing cardiomyocyte autophagy through the inhibition of mammalian Ste20-like kinase 1 (Mst1) (86). Activation of Mst1 has been shown to cause (DCM) as well as inhibit cardiomyocyte autophagy (86). OSM signaling is a crucial component to the heart's response to acute stressors, but when its presence is prolonged, it can have other effects.

2.10 Wound healing

It is well known that following almost any cut or abrasion an inflammatory response is triggered. OSM has been shown to be an important player in the early stages of the wound healing process under normal and diabetic-impaired healing conditions *in vivo* (92). This increase in OSM at the site of inflammation has been tied to the early influx of polymorphonuclear neutrophils into the wound site, but if OSM is around for too long it can actually impair the healing process in chronic diabetic wound conditions (92). Other studies have demonstrated the role OSM has in the scarring process (93, 94). Hypertrophic and keloid scars are both abnormal wound responses to trauma, inflammation, surgery, or burns. Keloid scars are typically considered worse than hypertrophic scars as keloid scars often increase in size, can develop months after surgery, and fail to improve appearance over time even with surgical intervention (93). Increased levels of OSM have been found in hypertrophic scars but not keloid scars, and it has been demonstrated that the increase in OSM served as protection against excessive scarring through suppression of TGFβ1-induced ECM protein expression (94). Other studies have shown similar benefits that OSM has in respect to late and early wound healing, differentially demonstrating an anti-inflammatory effect (95). It again seems that in the case of wound healing and scarring, more research is needed to clarify the contributions of OSM.

2.11 Pregnancy

A lot of changes take place in a person's body during pregnancy. Studies done in humans have shown OSM is present in high concentrations in pregnant women when compared to non-pregnant women, as well as in placental tissue in all three trimesters (96). OSM is especially relevant in the early stages of

pregnancy through the upregulation of human chorionic gonadotropin, demonstrating importance in placental endocrine function (96). Through STAT3 and ERK1/2 signaling, OSM and LIF are responsible for trophoblast invasion and placental development, both important steps in the early stages of pregnancy (97). *In vitro* studies show trophoblast invasion is induced through the upregulation of matrix metalloprotease 2 (MMP2) and MMP9 by both OSM and LIF, either synergistically or separately, in some but not all cell types used (97). Other studies also suggest that OSM increases protein expression and enzymatic activity of MMP2 and MMP9, leading to the invasion of primary trophoblasts through STAT3 signaling under hypoxic conditions typically found during trophoblast invasion in early pregnancy (98). While OSM presence is increased during pregnancy and is a known STAT3 activator, there is more research suggesting LIF signaling is primarily responsible during early pregnancy.

2.12 Cytokine storm and COVID-19

The coronavirus disease 19 (COVID-19) is caused by the novel severe acute respiratory syndrome coronavirus 2 (SARS-CoV-2) and has sparked a global pandemic since its introduction in humans in late 2019. It is well known that cytokines play an important role in developing an innate immune response during viral infection. There has been evidence suggesting that cytokine storms, characterized by an excessive and dysregulated immune response, play a significant role in pathogenesis of SARS-Cov-2 infection (87–89). Retrospective research studies conducted around the world have shown that a hyperinflammatory state, indicated by the presence of IL-6, IL-10, and TNF-α, is a significant predictor of mortality (89). A different study found increased OSM along with a number of other inflammatory proteins present in lung and spleen tissue in 13 postpartum subjects with fatal COVID-19 infections (90). Other retrospective studies done in Hong Kong and Atlanta Georgia have demonstrated an increase in cytokines and proinflammatory mediators such as IL-6, TNSF14, EN-RAGE, and OSM are correlated with disease severity (91). While there is a lot to be said about the role of cytokines in COVID-19, OSM's role has yet to be fully elucidated.

3 OSM in cancer

As previously stated, the pleiotropic nature of OSM causes it to exert differing effects on various cell types. While OSM has been investigated in a multitude of diseases, a particular area of interest is cancer biology. In the tumor environment, OSM often acts in a deleterious fashion through multiple different mechanisms, though it is noted that OSM can have a positive effect on specific cancer types, making it a particularly interesting cytokine to study (99–101). In this section, we will provide a thorough analysis of the role OSM plays in a multitude of cancers. Table 2 provides a list of the cancers that will be discussed in the following section.

3.1 Breast

Breast cancer is the most common cancer among women, and the second leading cause of cancer-related deaths in the United States. While OSM has historically been identified as an inhibitor of breast cancer proliferation (15, 102, 103), overexpression of OSM and OSMRβ has been linked to decreased overall survival, decreased reoccurrence-free survival and decreased metastasis free survival in breast cancer patients (104–107). Immunohistochemical analysis in benign human breast lesions have shown low expression of OSMRβ (11.7%) and gp130 (23.5%) proteins. However, in infiltrating carcinomas; high expression of OSMRβ (77.5%) and gp130 (74.1%) proteins have been seen, with OSM localized in 100% of tumor samples studied (107). At the molecular level, OSM via STAT3 signaling has been shown to inhibit c-Myc expression in human mammary epithelial (HMEC) cells, but constitutively overexpressing c-Myc HMEC cells gain the capacity for anchorage-independent growth in the presence of OSM-mediated PI3K-AKT signaling, suggesting c-Myc acts as a molecular switch to alter response of mammary epithelial cells (108). OSM has also been shown to promote a cancer stem cell (CSC)-like phenotype and pro-survival phenotype for breast cancer cells (36, 109). It can also create a pre-metastatic environment in bone by inducing osteoclast differentiation, increasing the possibility of bone metastases for breast cancer cells expressing a high level of OSM suggesting that the role of OSM in breast cancer is not tumor proliferation, but rather migration and invasion (36, 110, 111).

Examining patient tissue using microarray analysis, OSM expression was revealed to be the highest in patients with ductal carcinoma *in situ* (DCIS) (109). This highlights the possible role that OSM could have in progressing early grade tumors. Paracrine and autocrine signaling of OSM has been shown *in vivo* to increase the amount of circulating tumor cells (CTC), epithelial to mesenchymal transition (EMT), as well as increased metastasis to lungs and decreased survival (109). OSM can also induce $CD44^{high}/CD24^{low}$ phenotype allowing OSM to promote a CSC- like property, as well as increase detachment and migration of ER+ cells, while EMT remains independent of CD44 induction (112).

Recently, there has been increasing evidence that OSM operates differently in the varying subtypes of breast cancer (104, 106). At diagnosis, breast cancer patients are categorized into different subtypes based on expression of three receptors: estrogen receptor-alpha (ERα), progesterone receptor (PR), and human epidermal growth factor receptor 2 (HER2) (113–120). ERα status is important for clinical management of breast cancer since tumor cells that are ERα+ are usually less aggressive and can be treated with endocrine therapies (121). OSM has shown the ability to downregulate the expression of ERα, which in turn increases the OSM signaling cascade and migratory effects that its pathways have *in vitro* (105). *In vivo*, high OSM expression was correlated with decreased ERα ($p < 0.01$) and PR ($p < 0.05$) expression, and a shorter reoccurrence-free survival ($p < 0.0001$) (105). OSM has also been shown to promote secretion of IL-6 in ERα- cells and not in ERα+ cells, further suggesting that OSM plays unique roles in ERα+ versus ERα- breast cancer (104, 106). This illustrates that OSM can

TABLE 2 OSM in Cancer.

Location	Cancer Type	Impact of OSM	Reference
Pro-tumorigenic Effects of OSM			
Breast	Ductal Carcinoma	Overexpression linked with poor prognosis and creates a more CSC phenotype; Increases EMT, motility, invasion, and metastasis; Recruits neutrophils and surrounding tissue to express OSM	(20, 102–135)
Cervical	Squamous Cell Carcinoma	OSMRβ overexpression leading to EMT and increased skeletal metastasis	(135–143)
Ovarian	Epithelial Carcinoma	Auto/paracrine signaling loop in malignant OC; Increased proliferation, and metastasis dependent on STAT3 Increase in keratinocyte proliferation and differentiation	(144–148)
Prostate	Ductal Adenocarcinoma	Increased VEGF and u-PA expression and induced EMT in prostate epithelial cells	(149–155)
Testicular	Leydig Cell Carcinoma	Upregulation of OSM in functioning neoplasms	(156, 157)
Colon	Adenocarcinoma	More advanced and aggressive CRC have higher OSM serum level and lower survival; OSMRβ polymorphisms	(158–163)
Gastrointestinal	Adenocarcinoma	Differential expression of OSM in the grades of GI cancers could be used as biomarker.	(164–169)
Pancreatic	Ductal Adenocarcinoma	Overexpressed OSM in the serum, causes EMT, and greater metastasis to the lung *in vivo* dependent on STAT3	(170–175)
Bladder	Urothelial	Genetic mutations can cause an overexpression of the OSMRβ, leading to increased signaling	(176–178)
Lung	Adenocarcinoma	Induce EMT, increase fibroblast activation, OSMRβ overexpression is correlated to poor prognosis	(179–187)
Brain	Astroglioma, astrocytoma, adenoma, glioblastoma, glioma, medulloblastoma, meningioma	Three-fold increase in VEGF, seven-fold when in conjunction with IL-1β	(52, 182–184, 188–198)
Squamous Cell Carcinoma	Cutaneous & Oral Squamous Cell Carcinoma	Promotes proliferation, migration, and inflammation *in vitro* and *in vivo*	(199–210)
Kaposi's Sarcoma	Sarcoma	Mitogen and autocrine growth factor, promoter of bFGF	(4, 136, 211–217)
Misc. Sarcomas	Osteosarcoma, Chondrosarcoma, Ewing Sarcoma	Increased MMP2, VEGF, and proliferation	(218–227)
Melanoma	Melanoma	Antigen-silencing, resistance to inhibitory OSM singling in > Stage 3 patients	(225, 228–240)
Anti-tumorigenic Effects of OSM			
Multiple	Chondrosarcoma	Cell cycle arrest through JAK3/STAT1 signaling, decreased proliferation and enhanced apoptosis	(225)
Skin	Melanoma	Activates STAT5B and MAPK inhibiting proliferation; Increased SOCS3 with decreased OSMRβ expression	(225, 228–240)

increase the metastatic potential of breast cancer cells as well as make them more difficult to treat in a clinical setting.

Triple negative breast cancers (TNBCs) are highly aggressive, metastatic, and therapeutically difficult to treat due to their lack of, or low expression of receptors commonly targeted for therapeutics (122, 123). It has been shown that patients with TNBC and high OSM expression have a greater abundance of cells with a cancer stem cell (CSC) phenotype due to OSM/STAT3/SMAD3 signaling, which promotes growth of the tumor and leads to poor clinical outcomes for patients (111, 124). Similar research also evaluated OSM-mediated MEK/ERK signaling and found that blocking ERK abolished the growth inhibition characterized by OSM, but only in triple-negative MDA-MB-231 cells (21). Interestingly, interferon-β (IFN-β) can repress this OSM-mediated tumor initiation and CSC phenotype, but mRNA of endogenous IFN-β is repressed directly by OSM. IFN-β is suggested as a possible therapeutic to OSM in TNBCs, following a more comprehensive investigation of the relationship between these two cytokines (125). OSM can also perpetuate a chronic inflammatory environment that is detrimental to the prognosis of breast cancer patients due to the recruitment and/or induction of other inflammatory cytokines that are known to promote a metastatic phenotype in breast cancer. Induction of IL-6 is directly caused by the synergistic effects of both OSM and IL-1β (106). Analysis of The Cancer Genome Atlas (TCGA) breast cancer dataset shows that these three cytokines in high concentrations lower patient's survival rate ($p < 2.2x10^{-23}$) (106).

The tumor microenvironment (TME) plays a large role in the progression of breast cancer, through the complex interactions of tumor cell-to-cell communications, secretions of infiltrating

immune cells, and communications of surrounding tissues (126–129). OSM has been shown to directly bind to extracellular matrix proteins, which can protect it from proteases and preserve bioactive accumulation of OSM near within the TME for long periods of time (130). Stromal OSM production has also been recently shown to play a significant role in breast cancer progression by reprogramming fibroblasts within the TME towards a more tumorigenic phenotype and increase proinflammatory myeloid cell recruitment (131). OSM signaling also leads to TME remodeling in breast cancer as OSM induces the expression of lysyl-oxidase like 2 (LOXL2), which leads to crosslinking and alignment of collagen I fibers present in the stromal ECM (132). Presence of OSM within the breast tumor microenvironment has been shown to be provided by tumor associated neutrophils (TAN's), tumor associated macrophages (TAM's), and monocytes. Stromal OSM/OSMRβ has recently been shown to play a distinct role in breast cancer progression (131). TAN's co-cultured with human breast cancer cell lines have also been shown to increase TAN-mediated secretion of OSM throughout the tumor microenvironment, which in turn leads to increased secretion of the pro-angiogenic factor VEGF from human breast cancer cells (133). Neutrophils co-cultured with human breast cancer cells, MDA-MB-231 and T47D, also increased the number of viable cells that underwent detachment and increased invasive capacity *in vitro*, as measured by cell-cell/cell-substratum detachment and Matrigel invasion assays (133). This suggests that TANs can increase the expression of OSM at the site of the tumor and promote angiogenesis and metastasis of breast cancer cells.

Adipose tissue has also been shown to play a role in the progression of breast cancer, with obese post-menopausal women having twice as high of a mortality rate as compared to low body-mass-index post-menopausal women (134). Breast cancer-associated adipose tissue from patient tumors display high secretion of OSM, alluding to the paracrine signaling that could initiate a metastatic phenotype in breast cancer cells (20). When co-cultured with breast cancer cells, the adipose tissue induced EMT and increased the invasiveness of the breast cancer cells in a STAT3 dependent manner (20). Another direct target for OSM/STAT3 signaling is fascin, an actin-bundling protein that localizes to filopodia and functions in cell-to-cell interactions and cellular motility. STAT3 can directly bind to the promoter region of the fascin gene to upregulate its expression to increase cellular migration (241).

All of this evidence collectively highlights the role OSM has in breast cancer progression and metastasis. As metastatic breast cancer has the poorest survival rate at 29% (135), developing a therapeutic to inhibit OSM may dramatically prolong the life of patients and lead to better survival outcomes.

3.2 Cervical cancer

Cervical carcinoma ranks as the second most common cause of cancer deaths among women, with approximately 270,000 deaths per year globally (135). A vast majority of cervical carcinomas are squamous cell carcinomas (SCC) that arise from precursor squamous intraepithelial lesions (199). In 2007, *Ng et al* evaluated potential genes showing high-frequency copy number-driven changes in expression in cervical SCC and discovered that the OSMR gene was significantly higher in cervical SCC cases when compared to patients with precursor cervical squamous intraepithelial legions and gain of OSMR was significantly associated with adverse overall patient survival, (p=0.046) and may increase radio-resistance in cervical SCC (242). Additional work by this group directly examined the consequences of *OSMR* overexpression in vitro and discovered that OSM signaling dramatically increases cell migration, invasion, and induction of tumorigenic factors such as IL-6, HIF2-α, VEGF, and transglutamase 2 (TGM2) a calcium-dependent crosslinking enzyme that catalyzes post-translational protein modifications, yet no evidence of OSMR overexpression improving radio-resistance was found (243–245). A separate group investigated the sensitivity of cisplatin therapy of cervical SCC cells and found that while STAT3 phosphorylation dramatically increased in pre-cancerous cervical cancer legions, it declined when comparing to cervical SCC, and cervical SCC cells pre-treated with OSM were more responsive toward cisplatin-based chemoradiotherapy, via upregulation of STAT3-mediated interferon-regulatory factor 1 (IRF1) expression (246, 247). More recent work has also evaluated *OSMR* overexpression utilizing clinical data from the TCGA CESC (cervical cancer) database and found that patients with high OSMR expression display increased expression of mesenchymal makers such as SNAI1, SNAI2 and zinc finger E-box-binding homeobox (ZEB1) (248). Additionally, using 3D culture models and mouse *in vivo* models and found that OSMRβ-overexpressing cervical SCC cells exhibit increased EMT, stem cell-like properties as well as increased lung colonization and skeletal metastases *in vivo* (248). These studies together suggest that cervical cancer cells with increased OSM signaling and OSMRβ overexpression are more aggressive, and lead to worse overall survival in cervical SCC patients. While few studies have implicated a possible radioresistant role for high OSMRβ patients, it has not been fully evaluated. Nonetheless, OSMRβ overexpression may be a potential clinical marker for cervical cancer patients, HER2 in breast cancer, and an anti-OSMRβ monoclonal antibody could improve outcome for patients with cervical cancer.

3.3 Ovarian

Ovarian cancer is the fifth most common cancer in woman and the leading cause of death among gynecological cancers (135). While IL-6 family cytokine members have been evaluated in the progression of ovarian cancer, OSM has not been extensively studied (136). A small study consisting of 29 malignant ovarian carcinoma patients revealed OSM was expressed in all 29 primary malignant ovarian carcinomas (MOC). Additionally, the same group analyzed 25 primary ovarian carcinomas samples (OC) for LIFRβ and OSMRβ expression and found all 25 primary OC samples expressed LIFRβ and 14 out of 25 expressed OSMRβ (137). Overexpression of both LIFRβ and OSMRβ in turn has been shown to constitutively activate STAT3 nuclear signaling in

74% of MOC's tested, suggesting OSM signaling is frequently present in malignant ovarian carcinoma (137). *Li et al.* further supported this work, showing that OSM treatment enhanced proliferation of OC cells *in vitro* in a STAT3 dependent manner (138). Interestingly, in contrast to these studies, a group evaluating 239 epithelial ovarian cancer patients (19 with low stage and 220 with high stage) and 169 controls identified that OSM was significantly downregulated (-2.62-fold change in early stage and -2.65 in late stage) in the leukocytes fraction of ovarian cancer patients compared to healthy patients (139). More recent research however has further evaluated the role of OSM in ovarian cancer and found that *OSMR* is highly expressed in ovarian cancer cells, cancer associated fibroblasts, and endothelial cells of patient samples, and is highly expressed when compared to normal adjacent tissues. Additionally, this study showed human ovarian cancer cell lines overexpressing OSMRβ were found to promote colony formation, migration, invasion, and spheroid-forming capabilities, and that an anti-OSMRβ monoclonal antibody reduced the growth and peritoneal spread of ovarian cancer cells using a mouse *in vivo* ovarian cancer model (140). From this evidence, while the presence of OSM in ovarian cancer patients is not confounded, OSM-mediated STAT3 signaling does impact ovarian cancer progression. It could be hypothesized that similarly to cervical cancer, OSMRβ rather than OSM is the more favorable target against ovarian cancer metastasis and could be used as a clinical marker for disease progression and patient outcomes.

3.4 Prostate

Prostate cancer (PC) is both the second most common cancer and second leading cause of cancer related deaths in men. PC is one of the four most common cancer types, and with reduction rates within the population plateauing, there is a need to better understand the mechanisms that PC utilizes to persistently remain present within the population (141).

OSM treatment on prostate carcinoma cells (DU145) *in vitro* has been shown to increase the amount of urokinase-type plasminogen activator (u-PA), a serine protease that degrades ECM proteins leading to increased invasion and metastasis *in vitro*, as well as VEGF measured by means of ELISA (142). This correlation was also seen clinically evaluating 47 male patients: 20 with benign prostatic hyperplasia (BPH), 20 with non-metastatic PC, and 7 with metastatic PC. Patients with metastatic PC displayed a significant increase in plasma levels of IL-6 ($p<0.0001$), OSM ($p<0.009$), VEGF ($p<0.016$), and u-PA ($p<0.0001$) compared to the other disorders (142). Interestingly, OSM was also shown to induce tumorigenic properties, including EMT progression and migration of non-transformed human prostate epithelial cells via STAT3 signaling (143). A separate study also highlighted miR-181b-5p as a potential inhibitor of OSM-mediated prostate cancer progression using *in vitro* mouse prostate cancer cell lines. In the presence of OSM, miR-181b-5p was shown to inhibit proliferation, invasion and metastasis of mouse cell lines, while also repressing the levels of osteoclastogenic factors such as IL-6, AREG, and OPG that could prevent prostate cancer metastasis to bone (144).

PC commonly starts as an androgen-dependent tumor, making androgen-depriving therapeutics a useful first-round treatment strategy; however, 20-30% of patients exhibit recurrence of PC with a more aggressive androgen-negative phenotype that is difficult to treat (142, 145). Recent research has examined how exercise affects patients with advanced prostate cancer or patients receiving androgen deprivation therapy and have noticed elevated levels of OSM (146, 147). The implications of this, however, are not very well understood. All of this evidence combined shows that the OSM plays a pivotal role in the development and progression of prostate cancer and could be a valuable therapeutic target to improve stage outcomes in PC patients.

3.5 Testicular carcinoma

Testicular cancer is relatively rare, affecting only 1 in 250 males, however it develops in patients at a younger age, with an average diagnosis age at 33 years old (135). The role of OSM in testicular cancer has not been extensively studied, however *De Miguel et al.* in 1999 evaluated the presence of OSM in Leydig cells (cells in the testes responsible for testosterone production) as well as in various testicular carcinomas, including carcinoma-*in-situ* (CIS), germ cell tumors, and benign functioning Leydig cell tumors (148). OSM has been shown to cause a two-fold increase in the amount of Leydig cell progenitors, through stem Leydig cell differentiation in normal tissue samples. It was also found to be present in normal functioning and differentiated Leydig cells, therefore suggesting a role in normal Leydig cell differentiation and maintenance as shown by immunohistochemical staining (148, 149). OSM was also found within Leydig cells of patients with carcinoma-*in-situ* and in the parenchyma of neoplastic cells, however immunoreaction between cancerous and non-cancerous controls were similar, indicating OSM did not affect immune cell recruitment (148). Interestingly, functioning Leydig cell neoplasms showed a very strong immunoreaction to OSM, suggesting an upregulation of OSM in Leydig cell carcinoma may impact recruitment of immune cells (148). These preliminary studies evaluating OSM in testicular cancer suggest a possible role for OSM in Leydig cell differentiation and function of mature Leydig cells and recognize the presence of OSM in Leydig cell carcinoma and carcinoma in situ. However, no studies have yet to evaluate the tumorigenic properties of OSM in testicular cancer.

3.6 Colon

Colon cancer is the third most common type of malignancy and third leading cause of cancer-related deaths among men and women world-wide (135). The first connection of OSM in colorectal cancer was through discovering that the *OSMR* gene is highly methylated in non-invasive colorectal cancer patients, but not in normal controls, and has been suggested as a highly specific prognostic marker for colon cancer detection and severity of disease (150–152). In addition, a direct correlation between colorectal carcinoma (CRC) tumor grade and OSM expression level has

been identified after examining the blood serum levels of OSM in colorectal cancer patients. High T staged CRCs (stages 3 and 4) have significantly higher levels ($p < 0.001$) of OSM present in the serum compared to low stage CRC as well as in healthy patient controls (153). Additionally, *Rajamaki et al.* identified hypomethylation and subsequent overexpression of *OSMR* in inflammatory bowel disease-associated CRC (IBD-CRC) patients, which may result in EMT of CRC cells and promote resistance to anti-TNFα therapies (mentioned in the Inflammatory Bowel Disease section) (154).

Camptothecin (CPT) is a chemotherapeutic agent frequently used in CRC and is aimed at the inhibition of topoisomerases (153). CPT has been shown to increase the expression of programmed death-ligand 1 (PD-L1) as well as other cytokines, including OSM (155). Examination of the TCGA colorectal cancer (COAD) and pan-cancer (PANCAN) database of ~4500 patients where high and low OSM expression was analyzed showing that high OSM expression was correlated with decreased patient survival ($p < 0.001$) further correlating the role of OSM in progression and metastasis in CRC (155).

3.7 Gastrointestinal

Every year, almost 1 million patients are diagnosed with gastric cancer worldwide, and almost 750,000 die, making it the second most common cause of cancer death worldwide (156–158). The role of OSM in gastric cancer has yet to be studied, but OSM has been shown to be overexpressed in pre-cancerous lesions and in gastric cancer (GC) when compared to normal gastric tissue, as well as in cancer-derived mesenchymal stem cells isolated from patients (159, 160). OSM expression in gastric high-grade intraepithelial neoplasia (HGIN) and early gastric cancer (EGC) tissues was significantly higher than that of low-grade intraepithelial neoplasia (LGIN) tissues based on expression profiling ($p < 0.001$) (159). RT-qPCR analysis of the OSM gene in EGC patients had a higher expression of OSM mRNA than that in HGIN ($p < 0.05$) and LGIN ($p < 0.01$), while immunohistochemical staining of OSM in LGIN was significantly lower than that in HGIN ($p= 0.008$) and EGC ($p = 0.044$) (159). These studies show that OSM could be a useful independent biomarker for possible staging of gastric cancer, and that the difference in OSM staining between HGIN and LGIN could be used as an early marker for gastric cancer.

OSMRβ has also been shown to be overexpressed in GC, highlighting the possibility of increased OSM-OSMR signaling in GC patients (161). Treatment with OSM increased proliferation and EMT *in vitro*. GC cells transfected with shRNA to knockdown OSMRβ expression had a reduction in the rate of proliferation (37.5%) as well as a reversal of EMT (161). These effects have been shown to be dependent on the activation of STAT3, FAK, and SRC through OSM OSM-OSMR signaling (161). Treatment with OSM increased GC tumor size and incidence of peritoneal dissemination *in vivo* with attenuation being reached through OSMRβ inhibition (161). These findings underline the effects of OSM within GC, resulting in increased proliferation, cell migration, invasion, and EMT dependent on OSM-OSMR signaling, as well as its potential as a T staging biomarker.

3.8 Pancreas

While pancreatic cancer has a low incidence rate due to lack of symptoms and early detection screening methods, pancreatic cancer has one of the worst prognosis rates, with 5-year survival at 12% for late-stage pancreatic cancer (135). OSM has been shown to play an important role in the progression of pancreatic ductal adenocarcinoma (PDAC), the most common form of pancreatic cancer originating from ductal cells within the pancreas by promoting EMT and by creating a more CSC phenotype in the pancreatic tumor microenvironment (162). Treatment of multiple human pancreatic cancer cell lines with recombinant human OSM (rhOSM) induced EMT via reduction of E-cadherin and induction of ZEB1 as well as upregulation of OSMRβ, leading to a positive feedback loop of increased OSM-mediated STAT3 signaling that maintains the malignant phenotype of these cells (162). *In vivo* analysis using xenografts of OSM producing PDAC cells showed that increased amounts of OSM in the TME caused greater primary tumor burden, increased metastatic spread, and led to a greater capacity to colonize the lungs (162). Co-culture models of human pancreatic cancer cells (HPAC) and human fibroblast overexpressing OSM also induced a CSC phenotype when compared to HPAC cells co-cultured with control fibroblasts (162). *Lee et al.* also found that OSM-OSMR signaling induces inflammatory fibroblasts within the TME in an *in vivo* PDAC model and promotes tumor growth and metastasis (163). A separate study also identified that similarly in breast cancer, OSM induces LOXL2 expression, subsequent collagen fiber alignment, and metastasis *in vivo* (164). Due to the low survival rate of PDAC patients, and lack of screening methods for early diagnosis, OSM, along with an array of other cytokines, have been shown to be overexpressed in the serum of pancreatic cancer patients and recent bioinformatics data has implicated OSM to promote radio resistance and poor prognosis in patients (163, 165, 166). This suggests OSM may be a useful clinical marker for diagnosis, and a therapeutic may increase survivability for pancreatic cancer patients. In contrast to these studies, *Nistal-Villan et al.* developed two oncolytic virus models encoding human OSM and, when administered to an aggressive orthotopic pancreatic cancer model in Syrian hamsters, was found to stimulate immune responses against cancer cells and had a significant anti-tumor effect (167). This work has not been examined further but may suggest a possible mechanism for recruitment of anti-tumorigenic immune cells to prevent cancer progression in pancreatic cancer.

3.9 Bladder

According to the American Cancer Society, in 2022 there are expected to be over 80,000 patients diagnosed with bladder cancer and nearly 17,000 deaths (135). While the role of OSM in bladder cancer has not been extensively studied, in 2019 *Deng et al.* published a study of 306 bladder cancer patients of Han residents within the Sichuan province of China and identified two novel single nucleotide polymorphisms (SNPs) within the promoter region of the *OSMR* gene (168). The two SNPs identified,

rs2278329 and rs2292016 were identified in bladder cancer patients as well as healthy control patients. While rs2278329 allele variants showed no risk factors for bladder cancer progression, and patients with rs2292016 allele variants were associated with higher tumor grade and higher recurrence rate when compared to healthy control patients (168). Furthermore, a recent study performing whole exome sequencing of patients with bladder squamous cell carcinoma, also displayed significantly higher expression of OSM, OSMRβ, and IL-31, suggesting both OSM-OSMR and IL-31-OSMR signaling may impact bladder cancer progression (169). Recent evidence also suggests upregulation of OSM in metastatic bladder cancer patients (170). These studies illustrate that while the role of OSM and OSMRβ in bladder cancer has yet to be fully elucidated, OSMRβ allele variants may serve as a biomarker prognosis test for patients with bladder cancer, and therapeutics targeting OSMRβ may be a beneficial target for bladder cancer patients.

3.10 Lung

Lung cancer is the leading cause of cancer related deaths in both men and women, and the second most commonly diagnosed cancer (135). The current body of literature is conflicted on the role OSM plays in lung cancer progression. Some studies suggest OSM may repress lung cancer growth (171), but can promote lung cancer metastasis via activation of STAT3 and STAT5, thus increasing expression of tumorigenic factors such as tissue type plasminogen activator (tPA) (172, 173). Early work examining OSM in lung adenocarcinoma suggested it as a tumor promoter, including *in vitro* work showing OSM, and IL-6 to a lesser degree, as a potent inducer of human lung cancer differentiation. OSM combined TGF-β1 was also shown to regulate hyaluronan and may modulate lung cancer metastasis (174, 175). More recent work has also identified OSM as a tumor promoter *in vivo*. Adenovirus vector expressing mouse OSM induced a 13-fold increase in lung tumor burden and an increase in tumor size when compared to control cell lines. This effect was mitigated in OSMRβ KO mice, suggesting OSM-OSMRβ signaling is necessary (176). Other studies confirmed the pro-metastatic nature of OSM, demonstrating that it induces EMT in non-small cell lung cancer. Additionally, when lung cancer cells were co-cultured with cancer associated fibroblasts, there was an upregulation of phosphorylated-STAT3, OSMRβ, and LIFRβ, coupled with the downregulation of E-cadherin, suggesting an important role for fibroblasts in the activation of OSM signaling and the progression of lung tumors while protecting the cells from targeted therapies in an OSMRβ/JAK1/STAT3 dependent manner (177). This theory is also supported by *Wysoczynski et al.* who showed that lung cancer cells secrete an increased number of microvesicles when in the presence of stress factors like hypoxia and irradiation. Increased microvesicles lead to the activation of cancer associated fibroblasts and subsequent overexpression of pro-angiogenic factors such as OSM, IL-8, IL-11, VEGF, LIF, MMP-9, and tissue-type plasminogen activator (tPA) (172, 178). *Shien et al.* also analyzed patient data using the TCGA and PROSPECT lung adenocarcinoma databases and found a positive correlation of OSM, IL-6 and LIF in lung cancer patients, while also showing high OSMRβ expression had a significantly poorer prognosis compared to patients with a low OSMRβ expression ($p = 0.0096$ for recurrent-free survival), indicating that OSM and OSMRβ play a significant role in lung cancer (177). However, there is research that suggests OSM can suppress lung metastasis by inhibiting the EMT promoter SLUG, modulating mesenchymal-epithelial transition of lung cells by reducing EMT markers via STAT1 (179, 180). This combined research has not yet fully parsed out the mechanism of OSM in lung cancer, however patient data suggests a pro-tumorigenic and pro-metastatic role for OSM. Additionally, a study published by *Chen et al.* evaluated the expression of a short non-functioning form of OSMRβ, dubbed OSMRs, that is highly expressed in lung cancer patients, and acts a decoy receptor for OSM and thus resulting in mitigating OSMs oncogenic capabilities (181). This confounding factor may explain the contradictory results in lung cancer.

3.11 Brain

Brain cancer is a blanket term related to a variety of tumors based upon the cell type that becomes cancerous and includes both benign and malignant tumors. OSM has been shown to play a factor in a variety of brain tumor types including astrogliomas, astrocytomas, pituitary adenomas, glioblastomas, gliomas, medulloblastomas, and meningiomas (182–186, 189, 249). *In vitro*, OSM mediates tumorigenesis by activating STAT3 or STAT1 thus promoting expression of genes responsible for cell migration, ECM remodeling, and angiogenesis including, PLAU (plasminogen activator of urokinase), CHI3L3 (chitinase-like protein 1) and VEGF in several different human brain tumor cell types (183, 187, 249). In astroglioma cells, OSM induces an approximately three-fold increase in VEGF, while OSM and IL-1β together induce an approximately seven-fold increase of VEGF after 48 hours in astroglioma cells, in a STAT3 dependent manner (183). Additionally, OSM stimulation has been shown initiate the activation of the RelB/p50 proteins of the NF-κB pathway both *in vitro* and *in vivo*, perpetuating a tumor inflammatory environment in brain cancer cells (183). OSM-OSMR signaling mediated through STAT3, promoted MMP-9 upregulation over two-fold and increased the invasive potential of glioblastoma cells. OSM itself, however, did not influence tumor cell viability or proliferation (183). Two studies in fact suggest OSM may inhibit proliferation of glioma, astroglioma, and glioblastoma, although these studies have not been further evaluated (190, 191). Interestingly, *Jahani-Asl et al.* identified that OSMRβ is an essential co-receptor for EGFRvIII, and knockdown of OSMRβ strongly suppressed cell proliferation and tumor growth in mouse glioblastoma cells and human brain tumor stem cells in a xenograft mouse model (184). *Waters M. R., et al.* analyzed the correlation of OSM in brain cancer using brain tumor TCGA database and found OSM expression was most strongly correlated with poor glioblastoma multiforme (GBM; a heterogeneous mixture of cells containing brain tumor stem cells that are both tumorigenic and self-renewing) patient survival (182). They also discovered that OSM is produced in the brain solely by macrophages and microglia, and that chronic elevation of OSM

leads to the progression of GBM (182). Macrophage-derived OSM has been shown to increase the mesenchymal like phenotype of OSM, mediated via STAT3 signaling both *in vitro* and *in vivo* (183, 186). Most recently, *Chen et al.* found that high OSM level is correlated with poor prognosis in several cancers, particularly with GBM, and found that OSM promotes migration and invasion of U251 glioblastoma cells while also exhibiting a more mesenchymal phenotype indicative of aggressive disease (192). OSMRβ has also been shown to be overexpressed in aggressive GBMs via STAT3 signaling and is correlated to a decrease in survival among patients (183, 184). Studies targeting OSMRβ and STAT3 suggest that a clinical therapeutic that disrupts OSM/OSMRβ/STAT3 signaling can repress brain tumor growth and increase chemoresistance in aggressive brain tumors (183, 249).

3.12 Squamous cell carcinoma

Cutaneous squamous cell carcinoma (cSCC) is the second most common keratinocyte malignancy, being responsible for 20% of skin-cancer deaths due to the lack of therapies (193). While OSM has not been extensively analyzed in all varieties of skin cancer, OSM has been shown to promote normal keratinocyte proliferation, migration, skin inflammation, and epidermal hyperplasia both *in vitro* and *in vivo* (52). OSM has also been shown to be overexpressed in cSCC patients, and overexpression of OSM *in vitro* and shown to induce STAT3 and ERK phosphorylation and activation, as well as increased proliferation and migratory capacity *in vitro* (194–196). Interestingly, during *in vivo* studies OSM was not found in the keratinocyte cells, but rather, it was found in large quantities at the periphery of the tumor due to infiltration of neutrophils, macrophages, and other inflammatory cells that secrete OSM in a paracrine fashion (194). OSM has also been shown to be highly expressed in keratoacanthoma; originally believed to be a benign form of skin cancer, but rare cases act in a similar form to skin SCC have been reported (195). In OSM-knockout mice, cSCC tumor volume was reduced by approximately 30% when compared to wild-type mice after one month, however there were still significant amounts of IL-6, IL-1β, IL-23α, CXCL1, IL-4, and IFNγ present in the tumor tissue compared to normal skin (194). The most understood environmental cause of cSCC is ultraviolet (UV) radiation (197). OSM signaling has been shown to suppress UV induce apoptosis of human keratinocytes and may be crucial towards early cancer progression *in vitro via* an increase in cell motility through ECM remodeling (197). This indicates that OSM may not only be crucial for cSCC progression, but also may lead to a higher incidence of squamous cell carcinoma, via repression of apoptosis in keratinocytes.

In addition to cSCC, OSM has also been implicated in oral squamous cell carcinoma (OSCC). In OSCC cells, treated with the known oral carcinogen arecoline, induced the expression of IL-6, STAT3, and c-Myc (198). The upregulation of c-Myc has been shown to suppress the expression of micro-RNA-22 (MiR-22) subsequently leading to an upregulation of OSM (198). This is reinforced by the observation that the expression of OSM and MiR-22 are inversely related (198). MiR-22 overexpression was able to suppress cell proliferation and migration by directly inhibiting OSM, suggesting the role of OSM in OSCC may be dependent on miRNA regulation (198).

Esophageal squamous cell carcinoma (ESCC) is the seventh most common malignancy in the world and is common among Asian populations (199). Due to difficulties of early screening, nearly half of patients are diagnosed as having locally advanced disease (200). The effect of OSM in ESCC has not been extensively studied, and preliminary reports suggest OSM plays a minor role. A recent study evaluating inflammation biomarkers in ESCC patients in Japan identified OSM as negatively correlated to the disease, while another study evaluating 173 cases in the ESCC TCGA dataset correlated OSM with a worse prognosis (201, 202). However, *Kausar et al.* identified a soluble form of OSMRβ (sOSMRβ) to be present in 9 out of 11 cell ESCC cell lines, and the presence of sOSMRβ protein was detected in the sera of patients. Furthermore, while high expression of OSM (94% of patients) was confirmed via IHC, full length OSMRβ was only detected in 23% of patients, suggesting that sOSMRβ may be acting as a neutralizing receptor for OSM in ESCC (203).

3.13 Kaposi's sarcoma

OSM was first identified as a major growth factor in Kaposi's sarcoma (KS) in 1992 when evaluating media from patients with AIDS-associated KS (4). Kaposi's sarcoma is a relatively rare form of cancer but is endemic in several regions of the world and is estimated to be the leading cause of cancer incidence and mortality in several countries in Southern and Eastern Africa (199). When evaluating AIDS-KS cell lines, OSM was found to be a potent mitogen and autocrine growth factor (204, 205). Other studies showed OSM as a promoter of basic fibroblast growth factor (bFGF) which in turns promotes growth of Kaposi's sarcoma and endothelial cells through activation of AP-1 response elements in the bFGF promoter (206, 207). It has also been proposed that KS-encoded cyclin K inhibits the anti-proliferative effects of OSM by directly inhibiting STAT3, although previous work suggests OSM signaling promotes growth via MAPK/ERK and JNK signaling (208, 209). Further studies also suggest that in KS, OSM and bFGF induce RAFTK, a focal adhesion kinase downstream of JNK, which acts as a convergence site for intracytoplasmic kinases and adapter molecules and increase cytokine signaling cascades and promoting cell growth (210). Additionally, AIDS-associated KS cells have been shown to express OSMRβ but not LIFRβ or IL-6 receptor, and inhibition of gp130 blocks the growth stimulating effects of OSM in AIDS-KS cells suggesting inhibition of OSM signaling may be beneficial strategy for patients with KS (211).

3.14 Miscellaneous sarcomas

Osteosarcoma (OSA) is the most common malignant bone disease in humans (135). *Fossey et al.* discovered that several OSA cell lines express OSM, OSMRβ, and gp130 receptor complex proteins, but interestingly not IL-6 or IL-6R. Activation of these receptor complexes occur with the binding of OSM leading to a

time dependent increase in the levels of pSTAT3, pJAK2, and pSrc. While OSM does not increase proliferation of OSA cells (212–214), it does increase invasion via expression of glial fibrillary acidic protein (GFAP); a protein responsible for cytoskeletal reorganization in osteoblasts, MMP-2, cathepsin secretion and activity, as well as VEGF in a STAT3 dependent manner (212, 215–217). These features of OSM in OSA can increase the metastatic potential of OSA cells *in vivo*.

Chondrosarcomas (CSA) are difficult to treat, with chemotherapy and radiotherapy resistance, surgery remains the singular treatment option (218). Treatment with OSM induced cell cycle arrest in the S phase of murine SRC cell line *in vitro* and in G0/G1 of three other cells *in vitro* and is dependent on the JAK3/STAT1 pathway (218). Overexpression of OSM in the tumor cells, by adenovirus gene transfer, led to decreased tumor proliferation and enhanced apoptosis *in vivo* (218). These findings show that OSM treatment locally to the tumor environment of CSA could be a possible therapy to improve the prognosis of CSA patients.

Very little evidence exists for OSM and Ewing sarcoma (ES); however, the OSM gene has been shown to be differentially methylated in an ES microarray dataset (65% compared to healthy patients), although this did not significantly correlate with survival rate (219). Unlike OSA or CSA, OSM has been shown to increase the proliferation of ES cells in an OSMRβ/STAT3 dependent manner via upregulation of c-Myc (220). Based on the information given above, OSM inhibition would benefit CSA patients but burden OSA and ES patients.

3.15 Melanoma

Invasive melanoma accounts for only 1% of all skin cancer cases but is responsible for the vast majority of skin cancer deaths (135). Historically, OSM has been identified as a strong inhibitor of melanoma (221–223). Exogenous OSM has been shown to activate STAT3, STAT5b and the MAPK pathways via OSMRβ to strongly inhibit the proliferation of melanoma cells (221, 222, 224–226). OSM is also able to bind to collagens in a bioactive form and inhibit proliferation of A375 melanoma cells *in vitro* (227). Interestingly, OSM has also been shown to promote LIF expression, which could prolong the inflammatory effects of OSM (228). OSM also increases expression of membrane bound ICAM-1 *in vitro*, which also may suggest higher immune surveillance in human myeloma (229).

As melanoma reaches an advanced stage, cells appear to become resistant to the inhibitory effects of OSM (225). This has been shown *in vitro* and *in vivo* to be partly caused by the constitutive expression of suppressor of cytokine signaling-3 (SOCS-3) mRNA and subsequent high level of SOCS-3 protein (230). Accompanying the increase in SOCS-3 mRNA/protein is a downregulation of the OSMRβ subunit, due to a decrease in the amount of histone acetylation in the promoter region of the OSMRβ gene (231). Paracrine signaling of OSM in antigen-negative melanoma cells to antigen-positive will lead to antigen-silencing, possibly affecting the outcome of antitumor vaccine immunotherapies (232). OSM sensitivity in human melanoma cells also has importance for tumor-infiltrating lymphocyte (TIL) treatment of stage 3 melanoma (233). Patients that were unresponsive to OSM expressing TILs due to phosphorylation defects of STAT3 on Ser-727, as well as activation of AKT on Ser-473, were shown to have an increased resistance to OSM anti-proliferative activity (233). The development of OSM resistance in melanoma cells has a significant role in creating a more aggressive phenotype, which appears to be specific to melanoma. This could be treated by increasing the amount of OSM ligand in the system through the use of an OSM therapeutic.

4 Therapeutic intervention of OSM

As mentioned in the previous sections, developing an effective targeted therapeutic against OSM signaling could be crucial for the treatment of numerous diseases, including a variety of cancers. While several therapies have been developed and approved that target IL-6 and other IL-6 family members, currently no FDA approved treatments exist for OSM. This section will outline previous and current strategies for developing effective therapeutics against OSM and OSM receptor, including unique strategies that are in early stages of testing. The specific drugs and patents for drugs against OSM and OSMRβ are described in Table 3.

4.1 Anti-OSM therapeutics

In 2000, *Deller et al.* published the first molecular structure for OSM, paving the way for the development of potential anti-OSM therapeutics (5). OSM's tertiary structure consists of four α-helical bundles (helices A-D; Figure 2A) and has two distinct sites responsible for receptor complex binding (Figure 2B) (5). The Site II motif, consisting of regions of helices A and C, is responsible for OSM's binding to gp130. Site-directed mutagenesis has revealed four amino acid residues: Gln-16, Gln-20, Gly-120, and Asn-124, shown to be the primary residues responsible for this interaction (5, 16). The Site III epitope, located within a loop between helices A-B (Figure 2A), and near the N-terminal end of helix D, is the primary site by which OSM binds to OSMRβ and LIFRβ. This region is highly conserved for both OSM and LIF, thus making it difficult to generate a specific therapeutic against OSM. However, recent research efforts have shown that OSM possesses a unique amino acid composition that is necessary for specific interactions with OSMRβ. Alanine-scanning experiments and substitution experiments comparing OSM and LIF revealed that Tyr-34, Gln-38, Gly-39, and Leu-45 (in AB loop) and Pro-153 (in helix D) are responsible for OSMRβ binding, while Phe-160 and Lys-163 of D-helix are necessary for interaction with both OSMRβ and LIFRβ (16, 234, 235).

The pharmaceutical giant GlaxoSmithKline (GSK) has supported the production of two separate anti-OSM neutralizing antibodies, both of which target the Site II region of OSM, and to date, these are the only anti-OSM therapeutics to advance into clinical trials. GSK315234 is a humanized anti-OSM IgG

TABLE 3 Anti-OSM and Anti- OSMRβ Therapeutics.

Drug Name/Patent Number	Company /University	Type	Disease	Progress	References
Anti-OSM therapeutics					
GSK315234	GlaxoSmithKline	mAb	Rheumatoid Arthritis	Stage II clinical trial (*failed*)	(236)
GSK233081	GlaxoSmithKline	mAb	Systemic Scleroderma	Stage II clinical trial (*failed*)	(237–240, 250)
US7858753B2	GlaxoSmithKline	mAb	Non-specific	Pre-clinical	(240)
US6706266B1 WO2020127884A1	GlaxoSmithKline Universite de Poiters	Aptamer mAb	Rheumatoid Arthritis Inflammatory Skin Disease/ Cancer	Pre-clinical Pre-clinical	(240) (251)
US20170327573A1	University of Padua	Broad Therapeutic	Diabetes/Cardiovascular diseases	Pre-clinical	(252)
US9550828B2	Boise State University	SMI	Cancer	Pre-clinical	(253)
Anti-OSMR therapeutics					
US9663571B2	Kiniksa Pharmaceutical	mAb	Atopic Dermatitis	Pre-clinical	(254)
US10493149B2	Kiniksa Pharmaceutical	mAb	Non-specific	Pre-clinical	(255)
WO2013168829A1	Wakayama Medical University	mAb	Atopic Dermatits/Puritis	Pre-clinical	(256)
US20090300776A1	Universitie D'angers	siRNA	Inflammatory Skin Diseases	Pre-clinical	(257)
US7572896B2	Raven Biotechnologies	mAb	Cancer	Pre-clinical	(258)
WO 2010139742A1	Max Plank Society	Broad Therapeutics	Heart Failure	Pre-clinical	(259)

monoclonal antibody developed for the treatment of patients with active rheumatoid arthritis (RA), designed to bind to the Site II region of OSM and prevent dimerization with gp130 (236). A phase two clinical trial was initiated with the goal of investigating the safety, pharmacokinetics (PK), and pharmacodynamics (PD) of GSK315234 in patients with RA. The study contained a total of 135 patients with RA, was divided into four groups (double-blind, placebo-controlled, and randomized, and evaluated the following: i) an intravenous (IV) method of delivery, ii) a subcutaneous (SC) method of delivery, iii) a single dose delivery (single versus multiple

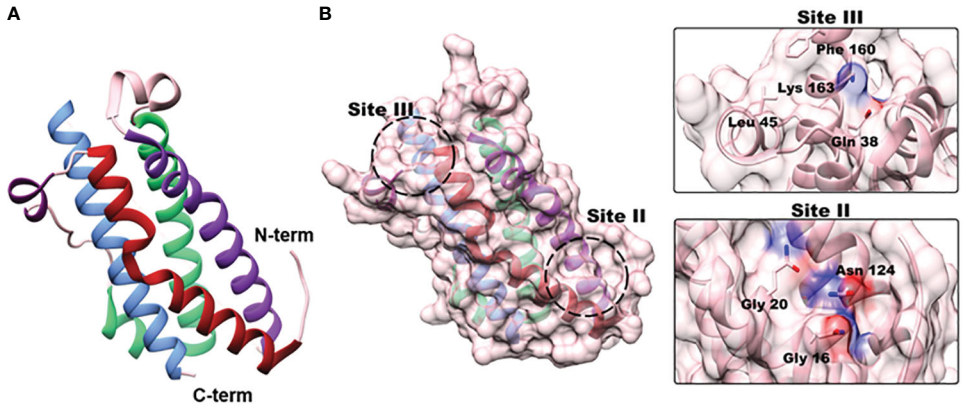

FIGURE 2
OSM structure and receptor binding sites. **(A)** OSM is a four α-helical bundle protein consisting of helices A (red; aa 10 −37), B (green; aa 66-90), C (purple; aa 106-131), and D (blue; aa 159-185) (truncated X-ray crystallography PDB:1EVS). **(B)** Site-directed mutagenesis experiments have identified two separate binding sites responsible for receptor-ligand interactions. Site II is located near the N-terminal region in helices A and C, and three amino acids (Gly-16, Gly-20, Asn-124) have been identified as crucial for OSM interaction with gp130. Site III is located in the A- B loop with a small portion of the D helix (dark purple) that is responsible for binding of OSM to LIFRβ and OSMRβ. Substitution experiments with OSM and LIF revealed that Lys-163, and Phe-160 are required to bind to both receptor complexes, but Tyr-34, Gln-38, Gly-39 and Leu-45 are specifically needed for interactions with OSMRβ.

delivery) and iv) a multiple dose delivery, all over a period of 154 days. Patients selected to participate in the study were required to have active RA with a Disease Activity Score 28 (DAS28) of > 4.2 at screening. DAS28 is a composite score analyzing the number of swollen/tender joints (that includes 28 joints), as well as examining concentration of erythrocyte sedimentation rate (ESR) and C-reactive protein (CRP) in the blood stream. Patients selected to participate in the study were also required to have had previously received at least three months of treatment with methotrexate.

Overall, evidence from this study suggests that repeated dosing with GSK315234 did not demonstrate statistically significant efficacy. While there appears to be minimal toxicity in patients who received GSK315234, the monoclonal antibody exhibited poor binding affinity (2.5 nM) and a rapid off-rate (1.73 x 10^3) when compared to the higher affinity of OSMRβ (approximately 150 pM). Interestingly, patients in the group which received a single 3 mg/kg dose of GSK315234 by IV displayed a statistically significant reduction in DAS28 score compared to the placebo group (p-value <0.05 at days 56, 84, and 91), as did the patients that received a 10 mg/kg dose by IV (at day 84). However, groups receiving larger single doses (20 and 30 mg/kg IV), repeated dosing (6 mg/kg IV), or SC injection (500 mg) exhibited no significant difference in clinical score. Due to the high off-rate and binding affinity, as well as the poor significance and inconclusive results in the study, GSK315234 clinical trials were halted.

Another GSK anti-OSM monoclonal antibody, GSK2330811, has entered clinical trials for treatment of systemic scleroderma (237, 238). A phase one, randomized, double-blind, placebo-controlled SC administered clinical trial with 30 healthy subjects showed a favorable safety profile in participants. Patients were divided into 6 groups, with patients given either placebo or varying concentration of a single SC dose of GSK2330811 (0.1, 0.3, 1, 3 or 6 mg/kg respectively). No clinically relevant change from baseline laboratory values were observed in any of the groups, and GSK2330811 exhibited pharmacokinetics over all five of the dose ranges with a binding affinity estimated at approximately 0.58 nM (95% CI 0.455, 0.710). This drug has recently finished evaluation in phase two clinical trials for patients with diffuse cutaneous systemic scleroderma involving 35 patients randomized to placebo receiving 100 mg or 300 mg treatment subcutaneously every other week for 12 weeks. There were no clinical differences between GSK2330811 and placebo groups. Additionally, all patients in the 300 mg treatment group reported at least one adverse effect; including decreased hemoglobin, anemia of varying severity, decreased platelet counts, decreased neutrophil counts, and thrombocytopenia (239). A separate clinical trial (NCT04151225) was also initiated with GSK2330811 for patients with Crohn's disease; however, the study was halted by an internal sponsor before patient enrollment began due to a potentially narrow therapeutic window (238, 240, 250).

In addition to the previously mentioned monoclonal antibodies that have advanced to clinical trials, GlaxoSmithKline possesses a patent (US7858753B2) (240) for another anti-OSM antibody. While the previous ones were designed to specifically interact with Site II of OSM (Figure 2), this is designed to inhibit OSM/gp130 interaction without directly binding to any amino acids within Site II. Instead, it is designed to interact with amino acids; Pro82, Ser83, Glu84, Leu90, Gly94, Pro112, Gln115, Asp122, Leu123, and Cys152 of OSM. It is unclear how this antibody interferes with OSM/gp130 dimerization, but further studies may reveal its mechanism. Within a separate patent (US6706266B1) (240), GlaxoSmithKline also has RNA aptamer designs that are highly specific towards OSM with a K_D at approximately 7 nM; however, both of these patents have yet to be tested *in vitro, in vivo*, or through clinical trials.

Researchers at the Universite de Poiters have also developed a patent (WO2020127884A1) relating to specific binding proteins, such as an antibody, that binds specifically to OSM to inhibit interaction with OSM and gp130, and/or LIFR, to be used with any disease associated with elevated levels of OSM, with a particular interest in inflammatory skin diseases and cancer (251).

A different patent, submitted by the University of Padua (US20170327573A1) (252), is designed to develop an anti-OSM therapeutic that will increase mobilization of bone marrow stem cells in patients with diabetes. This patent allows for the design of a variety of inhibitors that would inhibit OSM production or OSMRβ signaling at the cellular level such as enzyme inducers, an enzyme or receptor inhibitor, a ligand for a receptor, a compound that is toxic for cells, or an antisense RNA.

Utilizing a separate approach, Boise State University has submitted a patent (US9550828B2) (253) developing small molecule inhibitors against the Site III region of OSM, preventing OSM binding to OSMRβ. The compounds proposed in this patent are designed to reduce tumor cell detachment, invasion, and metastasis. Recently, a specific small molecule inhibitor named SMI-10B was characterized and shown to bind to specific amino acids within Site III of OSM via HSQC-NMR (260), and was subsequently confirmed by an independent group using molecular dynamics simulation (261). To date, this is the only patent designed for small molecule inhibition of OSM.

4.2 Anti-OSMRβ therapeutics

As outlined in Figure 1, OSM interacts with gp130, which then results in the dimerization of both LIFRβ and OSMRβ, however it is thought that human OSM binds with a much stronger affinity to OSMRβ than to LIFRβ. Another cytokine, IL-31, also uses OSMRβ as part of its receptor complex (along with its receptor IL-31RA), making OSMRβ, specifically, a beneficial target to inhibit OSM as well as IL-31 signaling (262, 263). Challenges exist for this strategy due to the unknown structure of OSMRβ. Recent work utilizing computational *in silico* analysis and homology modeling of the structurally similar LIFRβ has provided framework for structural modeling of the OSM-OSMR complex, providing more detailed information for those designing therapeutics against OSMRβ (257). Furthermore, with the recent advancement in molecular modelling, particularly with *AlphaFold*, a predicted structure for OSMRβ has been created, which may help pave the way for specific targets against the receptor protein (264, 265). Currently, no therapeutics targeted against OSMRβ are clinically available, and to date, none have advanced into clinical trial stages. However, several patents have

been submitted for a variety of compounds designed as inhibitors of OSMRβ and will be outlined below (see Table 3).

As highlighted previously, OSM has been shown to play a role in various inflammatory skin diseases. To combat this, Kiniksa Pharmaceutical currently has two patents, all describing monoclonal antibodies, that are designed to inhibit OSMRβ in inflammatory skin conditions. The first (US9663571B2) (254) is designed for the treatment of atopic dermatitis and chronic puritis in patients who have yet to receive treatment with a corticosteroid, or for patients with serum IgE levels lower than 300 IU/mL. Both OSM and IL-31 have been linked to atopic dermatitis. OSMRβ, which is part of the receptor complex for both proteins, makes it a desirable target to inhibit both OSM and IL-31 signaling. This patent outlines three separate antibodies that describe an IC_{50} range between 157 pM and 1.35 nM and an average K_D of 0.2 nM. Kiniksa Pharmaceutical's second patent, (US10493149B2) (255) is also a monoclonal antibody is for unspecified diseases. Furthermore, two other patents have been developed for inflammatory skin disorders. Wakayama Medical University has submitted a patent (WO2013168829A1) (256) for a monoclonal antibody against OSMRβ designed to inhibit both OSM and IL-31 induced inflammation in patients with atopic dermatitis. Universitie D'angers has also written a patent (US20090300776A1) (257) for a small interfering RNA (siRNA) that is designed to inhibit OSMRβ mRNA expression in keratinocytes that would subsequently result in repressed inflammation in a variety of inflammatory skin diseases. This patent also encompasses molecules designed to inhibit a variety of cytokines linked with keratinocyte-mediated inflammation, including OSM, IL-17, TNFα, IL-31, and IFN-γ.

Additionally, two pharmaceutical companies have patents targeting OSMRβ in both cancer and heart disease. Raven Biotechnologies has developed an anti-OSMRβ antibody (US7572896B2) (258) designed for diagnosis of human cancers with high OSMRβ expression, as well as treatment for a variety of human cancers. Mouse model experiments using human ovarian and lung cancer cells indicate this antibody is effective at reducing proliferation both *in vitro* and *in vivo*. Furthermore, the Max Plank Society has written a patent (WO 2010139742A1) to develop an anti-OSMRβ therapeutic for the treatment and/or prevention of heart failure (259). The patent is broad in nature, and is written to encompass an aptamer, siRNA, shRNA miRNA, and/or ribozyme. While current efforts for an anti-OSM or anti-OSMRβ drug have not yet succeeded in making it through clinical trials, it is clear that a therapeutic is needed for a variety of diseases. Developing novel therapies that target OSM or OSMRβ with high specificity and low toxicity will hopefully provide the necessary therapeutics for patients with abnormal OSM or OSMRβ expression.

5 Discussion

Throughout the course of this review, we have shown the important role OSM plays in a variety of diseases including many types of cancer. OSM activates several signaling pathways, frequently leading to inflammation, migration, or regeneration and differentiation (19–23). OSM can be produced and secreted by many different cell types, mostly activated immune cells such as macrophages and neutrophils, to intensify some inflammatory diseases, as shown in Table 1 (1, 2, 24). Several studies have linked OSM overexpression with an overall worse prognosis for a variety of diseases, including arthritis, IBD, and most recently COVID-19 (25, 26, 39, 42, 90). However, OSM expression has the possibility to be beneficial to healing injuries, particularly regarding the CNS, bone, liver, heart, and general external skin wounds (33, 37, 64, 68–72, 75–77, 83–85, 92). Negative effects due to chronic expression of OSM may outweigh its positives, yet inhibiting the signaling systemically may cause issues within other physiological processes.

The role of OSM in cancer has also been mysterious (see Table 2). While OSM was initially discovered as an inhibitor of cancer cell growth in melanoma cells (221–223), OSM has been shown to play an important role in cancer progression. In fact, while OSM expression has been shown to repress tumor growth in some cancer types it also may promote tumor growth in other types (15, 102, 103, 161, 162, 171). The specific mechanisms by which OSM operates under different cancer subtypes has yet to be fully explored. However, increased OSM signaling has been shown to increase the proliferation, motility, and metastatic potential of multiple cancers (36, 109, 140, 143, 162, 177, 183, 186, 248). It is also interesting to consider OSM or OSMRβ as a possible biomarker for certain types of cancers such as cervical, colon, GI, and pancreatic cancer (153, 159, 165, 242). Overexpression of OSM and/or OSMRβ is seen more commonly in a multitude of advanced tumors and is linked to decreased patient survival in several cancer types, including breast, cervical, colon, pancreatic, lung, and brain cancer (109, 153, 165, 177, 192, 242). Patients in a clinical setting could benefit greatly from an anti-OSM therapeutic, but the market remains empty for oncologists and their patients.

There are several therapeutics currently in development designed to inhibit the OSM signaling cascade, some by binding to OSM and others by binding its receptor, OSMRβ (see Table 3). The current strategies being implemented represent diverse and novel approaches to develop the most effective inhibitor. Significant inhibition of cytokines has proven to be a challenge clinically. To date, IL-6 remains the only member of its family to have FDA approved clinical therapeutics (266, 267). Targeting OSM, however, has proven to be more challenging. While two monoclonal antibodies against OSM have been the only potential therapies to reach clinical trial stages, both struggled with poor binding affinity and lack of clinical significance (236, 237). It is possible an alternative strategy is needed for an effective anti-OSM therapeutic. Monoclonal antibodies tend to have lengthy half-lives (on the order of days or weeks) that may affect normal inflammatory response mechanisms in cases of infection or injury, and serious wound healing might require pausing therapy (268). In the case of GSK2330811, the half-life was reported to be approximately 24 days (237). Furthermore, both clinical trials of GSK315234 and GSK233081 reported long-term accumulation of OSM-mAb complexes, directly resulting from their long half-life, which in combination with rapid off rate and poor binding affinity, may result in lengthening active OSM in the bloodstream of subjects (236, 237). The wide variety of techniques being implemented, including small molecule inhibitors, aptamers, and other biologics, may eliminate long-term issues with accumulation, provide a highly

specific and minimally toxic therapeutic for patients, and allow for therapy to be paused when necessary.

In addition to targeting OSM, several drugs are currently in development to inhibit OSMRβ rather than OSM. While targeting OSMRβ is a valid strategy, and several attempts have been initiated, none of them have entered into clinical trials. As a target, OSMRβ possesses its own unique challenges, lacking a completed crystalized structure; forcing medical chemists to rely on computational modeling for targeting amino acids necessary for OSM/OSMRβ (269). Furthermore, targeting the other OSMR subunit gp130 itself is a risky venture due to its diverse role in all IL-6 family cytokine receptor complexes, although one group is investigating inhibition of gp130 for specific cytokines in the context of inflammatory diseases and multiple cancers (270–272).

6 Conclusion

Throughout this review, we have outlined the evidence for identifying OSM as a therapeutic target for numerous diseases, as well as a variety of cancers. While efforts have been initiated to develop clinical therapeutic for patients, to date, none exist. Creating an anti-OSM or an anti-OSMRβ therapeutic is a much-needed venture for patients and clinicians alike, and work must be continued to synthesize and generate an FDA approved therapeutic.

Author contributions

CW contributed to conceptualization, original draft reparation, creation of figures and tables, and final review & editing. CP contributed to conceptualization and original draft preparation, and creation of figures and tables, and final review & editing. DL contributed to conceptualization and original draft preparation, and creation of figures and tables. CJ contributed to conceptualization, original draft reparation, creation of figures and tables, and review & editing, supervision of the project, and funding acquisition. All authors contributed to the article and approved the submitted version.

Funding

Funding was provided by NIH grants R15CA242471, P20GM103408, P20GM109095, and R25GM123927, the Murdock (M.J.) Charitable Trust 2000000722, *BSF* 2017237, the METAvivor Quinn Davis Northwest Arkansas METSquerade Fund, and the Smylie Family Cancer Fund.

Conflict of interest

The authors declare that the research was conducted in the absence of any commercial or financial relationships that could be construed as a potential conflict of interest.

Publisher's note

References

1. Zarling JM, Shoyab M, Marquardt H, Hanson MB, Lioubin MN, Todaro GJ. Oncostatin M: a growth regulator produced by differentiated histiocytic lymphoma cells. *Proc Natl Acad Sci* (1986) 83(24):9739–43. doi: 10.1073/pnas.83.24.9739

2. Malik N, Kallestad JC, Gunderson NL, Austin SD, Neubauer MG, Ochs V, et al. Molecular cloning, sequence analysis, and functional expression of a novel growth regulator, oncostatin M. *Mol Cell Biol* (1989) 9(7):2847–53. doi: 10.1128/mcb.9.7.2847-2853.1989

3. Linsley PS, Kallestad J, Ochs V, Neubauer M. Cleavage of a hydrophilic C-terminal domain increases growth-inhibitory activity of oncostatin M. *Mol AND Cell Biol* (1990) 10(5):1882–90. doi: 10.1128/MCB.10.5.1882

4. Nair B, Chandran, Devico AL. Identification of a major growth factor for AIDS-kaposi's sarcoma cells as oncostatin M. *Science* (1992) 255(5050). doi: 10.1126/science.1542792

5. Deller MC, Hudson KR, Ikemizu S, Bravo J, Yvonne Jones E, Heath JK. Crystal structure and functional dissection of the cytostatic cytokine oncostatin M. *Structure* (2000) 8(8):863–74. doi: 10.1016/S0969-2126(00)00176-3

6. Rose TM, Bruce AG. Oncostatin M is a member of a cytokine family that includes leukemia-inhibitory factor, granulocyte colony-stimulating factor, and interleukin 6. *Proc Natl Acad Sci U S A.* (1991) 88(19):8641–5. doi: 10.1073/pnas.88.19.8641

7. Hibi M, Murakami M, Saito M, HIrano T, Taga T, Kishimoto T. Molecular cloning and expression of an IL-6 signal transducer, gp130. *Cell* (1990) 63:1149–57. doi: 10.1016/0092-8674(90)90411-7

8. Murakami M, Hibi M, Nakagawa N, Nakagawa T, Yasukawa K, Yamanishi K, et al. IL-6-induced homodimerization of gp130 and associated activation of a tyrosine kinase. *Sci (1979).* (1993) 260(5115):1808–10. doi: 10.1126/science.8511589

9. Heinrich PC, Behrmann I, MüLler-Newen G, Schaper F, Graeve L. Interleukin-6-type cytokine signalling through the gp130/Jak/STAT pathway. *Biochem J* (1998) 334:297–314. doi: 10.1042/bj3340297

10. Heinrich PC, Behrmann I, Haan S, Hermanns HM, Schaper F. Principles of interleukin (IL)-6-type cytokine signalling and its regulation. *Biochem J* (2003) 374:1–20. doi: 10.1042/bj20030407

11. Gearing DP, Comeau MR, Friend DJ, Gimpel SD, Thut CJ, McGourty J, et al. The IL-6 signal transducer, gp130: an oncostatin M receptor and affinity converter for the LIF receptor. *Sci (1979)* (1992) 255(505):1434–7. doi: 10.1126/science.1542794

12. Mosley B, de Imus C, Friend D, Boiani N, Thoma B, Park LS, et al. Dual oncostatin M (OSM) receptors. Cloning and characterization of an alternative signaling subunit conferring OSM-specific receptor activation. *J Biol Chem* (1996) 271 (51):32635–43. doi: 10.1074/jbc.271.51.32635

13. Auguste P, Guillet C, Fourcin M, Olivier C, Lle Veziers J, Pouplard-Barthelaix A, et al. Signaling of type II oncostatin M receptor. *J Biol Chem* (1997) 272(25):15760–4. doi: 10.1074/jbc.272.25.15760

14. Hudson KR, Vernallis AB, Heath JK. Characterization of the receptor binding sites of human leukemia inhibitory factor and creation of antagonists. *THE J OF Biol Chem* (1996) 271:11971–8. doi: 10.1074/jbc.271.20.11971

15. Tanaka M, Miyajima A. Oncostatin M, a multifunctional cytokine. *Rev physiology Biochem Pharmacol* (2003) 149:39–52. doi: 10.1007/s10254-003-0013-1

16. Chollangi S, Mather T, Rodgers KK, Ash JD. A unique loop structure in oncostatin M determines binding affinity toward oncostatin M receptor and leukemia inhibitory factor receptor. *J Biol Chem* (2012) 287(39):32848–59. doi: 10.1074/jbc.M112.387324

17. Walker EC, McGregor NE, Poulton IJ, Solano M, Pompolo S, Fernandes TJ, et al. Oncostatin M promotes bone formation independently of resorption when signaling through leukemia inhibitory factor receptor in mice mice. *J Clin Invest* (2010) 120 (2):582–92. doi: 10.1172/JCI40568

18. Walker EC, Johnson RW, Hu Y, Brennan HJ, Poulton IJ, Zhang JG, et al. Murine oncostatin m acts via leukemia inhibitory factor receptor to phosphorylate signal transducer and activator of transcription 3 (STAT3) but not STAT1, an effect that protects bone mass. *J Biol Chem* (2016) 291(41):21703–16. doi: 10.1074/jbc.M116.748483

19. Smith DA, Kiba A, Zong Y, Witte ON. Interleukin-6 and oncostatin-M synergize with the PI3K/AKT pathway to promote aggressive prostate Malignancy in mouse and human tissues. *Mol Cancer Res* (2013) 11(10):1159–65. doi: 10.1158/1541-7786.MCR-13-0238

20. Lapeire L, Hendrix A, Lambein K, Van Bockstal M, Braems G, Den Van Broecke R, et al. Cancer-associated adipose tissue promotes breast cancer progression by paracrine oncostatin M and Jak/STAT3 signaling. *Cancer Res* (2014) 74(23):6806–19. doi: 10.1158/0008-5472.CAN-14-0160

21. Li C, Ahlborn TE, Kraemer FB, Liu J. Oncostatin M-induced growth inhibition and morphological changes of MDA-MB231 breast cancer cells are abolished by blocking the MEK/ERK signaling pathway. *Breast Cancer Res Treat* (2001) 66:111–21. doi: 10.1023/A:1010614724664

22. Pereira de Sousa FL, Chaiwangyen W, Morales-Prieto DM, Ospina-Prieto S, Weber M, Photini SM, et al. Involvement of STAT1 in proliferation and invasiveness of trophoblastic cells. *Reprod Biol* (2017) 17(3):218–24. doi: 10.1016/j.repbio.2017.05.005

23. Fearon U, Mullan R, Markham T, Connolly M, Sullivan S, Poole AR, et al. Oncostatin M induces angiogenesis and cartilage degradation in rheumatoid arthritis synovial tissue and human cartilage cocultures. *Arthritis Rheumatol* (2006) 54 (10):3152–62. doi: 10.1002/art.22161

24. Suda T, Chida K, Todate A, Ide K, Asada K, Nakamura Y, et al. Oncostatin M production by human dendritic cells in response to bacterial products. *Cytokine* (2002) 17(6):335–40. doi: 10.1006/cyto.2002.1023

25. Cawston TE, Curry VA, Summers CA, Clark IM, Riley GP, Life PF, et al. The role of oncostatin M in animal and human connective tissue collagen turnover and its localization within the rheumatoid joint. *Arthritis Rheum* (1998) 41(10):1760–71. doi: 10.1002/1529-0131(199810)41:10<1760::AID-ART8>3.0.CO;2-M

26. McInnes IB, Schett G. Cytokines in the pathogenesis of rheumatoid arthritis. *Nat Rev Immunol* (2007) 7(6):429–42. doi: 10.1038/nri2094

27. Hanlon MM, Rakovich T, Cunningham CC, Ansboro S, Veale DJ, Fearon U, et al. STAT3 mediates the differential effects of oncostatin M and TNFα on RA synovial fibroblast and endothelial cell function. *Front Immunol* (2019) 10(AUG). doi: 10.3389/fimmu.2019.02056

28. McGarry T, Orr C, Wade S, Biniecka M, Wade S, Gallagher L, et al. JAK/STAT blockade alters synovial bioenergetics, mitochondrial function, and proinflammatory mediators in rheumatoid arthritis. *Arthritis Rheumatol* (2018) 70(12):1959–70. doi: 10.1002/art.40569

29. Plater-Zyberk C, Buckton J, Thompson S, Spaull J, Zanders E, Papworth J, et al. Amelioration of arthritis in two murine models using antibodies to oncostatin M. *Arthritis Rheumatol* (2001) 44(11):2697–702. doi: 10.1002/1529-0131(200111)44:11<2697::AID-ART450>3.0.CO;2-#

30. Xia B, Chen DI, Zhang J, Hu S, Jin H, Tong P. Osteoarthritis pathogenesis: A review of molecular mechanisms. *Calcified Tissue Int* (2014) 95:495–505. doi: 10.1007/s00223-014-9917-9

31. Wu R, Wang W, Huang G, Mao X, Chen Y, Tang Q, et al. Endothelin-1 induces oncostatin M expression in osteoarthritis osteoblasts by trans-activating the oncostatin M gene promoter via Ets-1. *Mol Med Rep* (2016) 13(4):3559–66. doi: 10.3892/mmr.2016.4960

32. Ni J, Yuan XM, Yao Q, Peng LB. OSM is overexpressed in knee osteoarthritis and Notch signaling is involved in the effects of OSM on MC3T3-E1 cell proliferation and differentiation. *Int J Mol Med* (2015) 35(6):1755–60. doi: 10.3892/ijmm.2015.2168

33. Nicolaidou V, Wong MM, Redpath AN, Ersek A, Baban DF, Williams LM, et al. Monocytes induce STAT3 activation in human mesenchymal stem cells to promote osteoblast formation. *PloS One* (2012) 7(7):e39871. doi: 10.1371/journal.pone.0039871

34. Guihard P, Danger Y, Brounais B, David E, Brion R, Delecrin J, et al. Induction of osteogenesis in mesenchymal stem cells by activated monocytes/macrophages depends on oncostatin M signaling. *Stem Cells* (2012) 30(4):762–72. doi: 10.1002/stem.1040

35. Alexander KA, Tseng HW, Fleming W, Jose B, Salga M, Kulina I, et al. Inhibition of JAK1/2 tyrosine kinases reduces neurogenic heterotopic ossification after spinal cord injury. *Front Immunol* (2019) 10(MAR). doi: 10.3389/fimmu.2019.00377

36. Bolin C, Tawara K, Sutherland C, Redshaw J, Aranda P, Moselhy J, et al. Oncostatin M promotes mammary tumor metastasis to bone and osteolytic bone degradation. *Genes Cancer* (2012) 3(2):117–30. doi: 10.1177/1947601912458284

37. Persson E, Souza PPC, Floriano-Marcelino T, Conaway HH, Henning P, Lerner UH. Activation of Shc1 allows oncostatin M to induce RANKL and osteoclast formation more effectively than leukemia inhibitory factor. *Front Immunol* (2019) 10 (MAY). doi: 10.3389/fimmu.2019.01164

38. Zhang YZ, Li YY. Inflammatory bowel disease: Pathogenesis. *World J Gastroenterol* (2014) 20(1):91–9. doi: 10.3748/wjg.v20.i1.91

39. West NR, Hegazy AN, Owens BMJ, Bullers SJ, Linggi B, Buonocore S, et al. Oncostatin M drives intestinal inflammation and predicts response to tumor necrosis factor–neutralizing therapy in patients with inflammatory bowel disease. *Nat Med* (2017) 23:579–89. doi: 10.1038/nm.4307

40. Ben-Horin S, Chowers Y. Tailoring anti-TNF therapy in IBD: Drug levels and disease activity. *Nat Rev Gastroenterol Hepatology*. (2014) 11:243–55. doi: 10.1038/nrgastro.2013.253

41. Bermejo F, Guerra I. Management of inflammatory bowel disease in poor responders to infliximab. *Clin Exp Gastroenterol* (2014) :359. doi: 10.2147/CEG.S45297

42. Guo A, Ross C, Chande N, Gregor J, Ponich T, Khanna R, et al. High oncostatin M predicts lack of clinical remission for patients with inflammatory bowel disease on tumor necrosis factor α antagonists. *Sci Rep* (2022) 12(1):1185. doi: 10.1038/s41598-022-05208-9

43. Chudy-Onwugaje KO, Christian KE, Farraye FA, Cross RK. A state-of-the-art review of new and emerging therapies for the treatment of IBD. *Inflammation Bowel Dis* (2019) 25(5):820–30. doi: 10.1093/ibd/izy327

44. Beigel F, Friedrich M, Probst C, Sotlar K, Göke B, Diegelmann J, et al. Oncostatin M mediates STAT3-dependent intestinal epithelial restitution via increased cell proliferation, decreased apoptosis and upregulation of SERPIN family members. *PloS One* (2014) 9(4):e93498. doi: 10.1371/journal.pone.0093498

45. Li H, Feng C, Fan C, Yang Y, Yang X, Lu H, et al. Intervention of oncostatin M-driven mucosal inflammation by berberine exerts therapeutic property in chronic ulcerative colitis. *Cell Death Dis* (2020) 11(4):271. doi: 10.1038/s41419-020-2470-8

46. Mozaffarian A, Brewer AW, Trueblood ES, Luzina IG, Todd NW, Atamas SP, et al. Mechanisms of oncostatin M-induced pulmonary inflammation and fibrosis. *J Immunol* (2008) 181(10):7243–53. doi: 10.4049/jimmunol.181.10.7243

47. Ayaub EA, Dubey A, Imani J, Botelho F, Kolb MRJ, Richards CD, et al. Overexpression of OSM and IL-6 impacts the polarization of pro-fibrotic macrophages and the development of bleomycin-induced lung fibrosis. *Sci Rep* (2017) 7(1):13281. doi: 10.1038/s41598-017-13511-z

48. Simpson JL, Baines KJ, Boyle MJ, Scott RJ, Gibson PG. Oncostatin m (osm) is increased in asthma with incompletely reversible airflow obstruction. *Exp Lung Res* (2009) 35(9):781–94. doi: 10.3109/01902140902906412

49. Miller M, Beppu A, Rosenthal P, Pham A, Das S, Karta M, et al. Fstl1 promotes asthmatic airway remodeling by inducing oncostatin M. *J Immunol* (2015) 195 (8):3546–56. doi: 10.4049/jimmunol.1501105

50. Ho L, Yip A, Lao F, Botelho F, Richards CD. RELMα is induced in airway epithelial cells by oncostatin M without requirement of STAT6 or IL-6 in mouse lungs *in vivo*. *Cells* (2020) 9(6):1338. doi: 10.3390/cells9061338

51. Rabeony H, Petit-Paris I, Garnier J, Barrault C, Pedretti N, Guilloteau K, et al. Inhibition of keratinocyte differentiation by the synergistic effect of IL-17A, IL-22, IL-1α, TNFα and oncostatin M. *PloS One* (2014) 9(7):e101937. doi: 10.1371/journal.pone.0101937

52. Boniface K, Diveu C, Morel F, Pedretti N, Froger J, Ravon E, et al. Oncostatin M secreted by skin infiltrating T lymphocytes is a potent keratinocyte activator involved in skin inflammation. *J Immunol* (2007) 178(7):4615–22. doi: 10.4049/jimmunol.178.7.4615

53. Pohin M, Guesdon W, Mekouo AAT, Rabeony H, Paris I, Atanassov H, et al. Oncostatin M overexpression induces skin inflammation but is not required in the mouse model of imiquimod-induced psoriasis-like inflammation. *Eur J Immunol* (2016) 46(7):1737–51. doi: 10.1002/eji.201546216

54. Tseng PY, Hoon MA. P A I N Oncostatin M can sensitize sensory neurons in inflammatory pruritus. *Sci Transl Med* (2021) 13(619). doi: 10.1126/scitranslmed.abe3037

55. Hashimoto T, Nattkemper LA, Kim HS, Kursewicz CD, Fowler E, Shah SM, et al. Itch intensity in prurigo nodularis is closely related to dermal interleukin-31, oncostatin M, IL-31 receptor alpha and oncostatin M receptor beta. *Exp Dermatol* (2021) 30 (6):804–10. doi: 10.1111/exd.14279

56. Gyftaki-Venieri DA, Abraham DJ, Ponticos M. Insights into myofibroblasts and their activation in scleroderma: Opportunities for therapy? *Curr Opin Rheumatol* (2018) 30(6):581–7. doi: 10.1097/BOR.0000000000000543

57. Marden G, Wan Q, Wilks J, Nevin K, Feeney M, Wisniacki N, et al. The role of the oncostatin M/OSM receptor β axis in activating dermal microvascular endothelial cells in systemic sclerosis. *Arthritis Res Ther* (2020) 22(1):179. doi: 10.1186/s13075-020-02266-0

58. Thorat Manojkumar S, Pradeep AR, Garg G, Raju A. Gingival crevicular fluid levels of oncostatin M in periodontal conditions. *Cytokine* (2010) 50(3):248–52. doi: 10.1016/j.cyto.2010.02.002

59. Thorat MK, Pradeep AR, Garg G. Correlation of levels of oncostatin M cytokine in crevicular fluid and serum in periodontal disease. *Int J Oral Sci* (2010) 2(4):198–207. doi: 10.4248/IJOS10077

60. Pradeep AR, Thorat Manojkumar S, Garima G, Raju A. Serum levels of oncostatin M (a gp 130 cytokine): An inflammatory biomarker in periodontal disease. *Biomarkers* (2010) 15(3):277–82. doi: 10.3109/13547500903573209

61. Stashenko P, Gonçalves RB, Lipkin B, Ficarelli A, Sasaki H, Campos-Neto A. Th1 immune response promotes severe bone resorption caused by Porphyromonas gingivalis. *Am J Pathology*. (2007) 170(1):203–13. doi: 10.2353/ajpath.2007.060597

62. Hosokawa Y, Hosokawa I, Ozaki K, Nakae H, Matsuo T. Oncostatin M synergistically induces CXCL10 and ICAM-1 expression in IL-1β-stimulated-human gingival fibroblasts. *J Cell Biochem* (2010) 111(1):40–8. doi: 10.1002/jcb.22648

63. Liang H, Block TM, Wang M, Nefsky B, Long R, Hafner J, et al. Interleukin-6 and oncostatin M are elevated in liver disease in conjunction with candidate hepatocellular carcinoma biomarker GP73. *Cancer Biomarkers.* (2012) 11(4):161–71. doi: 10.3233/CBM-2012-00276

64. Matsuda M, Tsurusaki S, Miyata N, Saijou E, Okochi H, Miyajima A, et al. Oncostatin M causes liver fibrosis by regulating cooperation between hepatic stellate cells and macrophages in mice. *Hepatology* (2017) 67(1):296–312. doi: 10.1002/hep.29421

65. Foglia B, Sutti S, Pedicini D, Cannito S, Bocca C, Maggiora M, et al. A profibrogenic mediator overexpressed in non-alcoholic fatty liver disease, stimulates migration of hepatic myofibroblasts. *Cells* (2019) 9(1):28. doi: 10.3390/cells9010028

66. di Maira G, Foglia B, Napione L, Turato C, Maggiora M, Sutti S, et al. Oncostatin M is overexpressed in NASH-related hepatocellular carcinoma and promotes cancer cell invasiveness and angiogenesis. *J Pathology.* (2022) 257(1):82–95. doi: 10.1002/path.5871

67. Larrea E, Echeverria I, Riezu-Boj JI, Aldabe R, Guembe L, Sola I, et al. Characterization of the CD40L/Oncostatin M/Oncostatin M receptor axis as an antiviral and immunostimulatory system disrupted in chronic HCV infection. *J Hepatol* (2014) 60(3):482–9. doi: 10.1016/j.jhep.2013.10.016

68. Vollmer S, Kappler V, Kaczor J, Flügel D, Rolvering C, Kato N, et al. Hypoxia-inducible factor 1α is up-regulated by oncostatin M and participates in oncostatin M signaling. *Hepatology* (2009) 50(1):253–60. doi: 10.1002/hep.22928

69. Okaya A, Kitanaka J, Kitanaka N, Satake M, Kim Y, Terada K, et al. Oncostatin M inhibits proliferation of rat oval cells, OC15-5, inducing differentiation into hepatocytes. *Pathol Am J Pathol* (2005) 166:709–19. doi: 10.1016/S0002-9440(10)62292-4

70. Hamada T, Sato A, HIrano T, Yamamoto T, Son G, Onodera M, et al. Oncostatin M gene therapy attenuates liver damage induced by dimethylnitrosamine in rats. *Am J Pathology.* (2007) 171(3):872–81. doi: 10.2353/ajpath.2007.060972

71. Nakamura K, Nonaka H, Saito H, Tanaka M, Miyajima A. Hepatocyte proliferation and tissue remodeling is impaired after liver injury in oncostatin M receptor knockout mice. *Hepatology* (2004) 39(3):635–44. doi: 10.1002/hep.20086

72. Fausto N, Campbell JS. The role of hepatocytes and oval cells in liver regeneration and repopulation. *Mech Dev* (2003) 120(1):117–30. doi: 10.1016/s0925-4773(02)00338-6

73. Moidunny S, Matos M, Wesseling E, Banerjee S, Volsky DJ, Cunha RA, et al. Oncostatin M promotes excitotoxicity by inhibiting glutamate uptake in astrocytes: Implications in HIV-associated neurotoxicity. *J Neuroinflamm* (2016) 13(1), 144. doi: 10.1186/s12974-016-0613-8

74. Takata F, Dohgu S, Sakaguchi S, Sakai K, Yamanaka G, Iwao T, et al. Oncostatin-M-reactive pericytes aggravate blood–brain barrier dysfunction by activating JAK/STAT3 signaling in vitro. *Neuroscience* (2019) 422:12–20. doi: 10.1016/j.neuroscience.2019.10.014

75. Houben E, Janssens K, Hermans D, Vandooren J, Van Den Haute C, Schepers M, et al. Oncostatin M-induced astrocytic tissue inhibitor of metalloproteinases-1 drives remyelination. *Proc Natl Acad Sci U S A* (2020) 117(9):5028–38. doi: 10.1073/pnas.1912910117

76. Slaets H, Nelissen S, Janssens K, Vidal PM, Lemmens E, Stinissen P, et al. Oncostatin M reduces lesion size and promotes functional recovery and neurite outgrowth after spinal cord injury. *Mol Neurobiol* (2014) 50(3):1142–51. doi: 10.1007/s12035-014-8795-5

77. Chang SH, Hwang CS, Yin JH, Der Chen S, Yang DI. Oncostatin M-dependent Mcl-1 induction mediated by JAK1/2-STAT1/3 and CREB contributes to bioenergetic improvements and protective effects against mitochondrial dysfunction in cortical neurons. *Biochim Biophys Acta Mol Cell Res* (2015) 1853(10):2306–25. doi: 10.1016/j.bbamcr.2015.05.014

78. Schnittker D, Kwofie K, Ashkar A, Trigatti B, Richards CD. Oncostatin M and TLR-4 ligand synergize to induce MCP-1, IL-6, and VEGF in human aortic adventitial fibroblasts and smooth muscle cells. *Mediators Inflamm* (2013) 2013:317503. doi: 10.1155/2013/317503

79. Zhang X, Li J, Qin JJ, Cheng WL, Zhu X, Gong FH, et al. Oncostatin M receptor β deficiency attenuates atherogenesis by inhibiting JAK2/STAT3 signaling in macrophages. *J Lipid Res* (2017) 58(5):895–906. doi: 10.1194/jlr.M074112

80. Albasanz-Puig A, Murray J, Preusch M, Coan D, Namekata M, Patel Y, et al. Oncostatin M is expressed in atherosclerotic lesions: A role for Oncostatin M in the pathogenesis of atherosclerosis. *Atherosclerosis* (2011) 216(2):292–8. doi: 10.1016/j.atherosclerosis.2011.02.003

81. van Keulen D, Pouwer MG, Pasterkamp G, van Gool AJ, Gelpke MDS, Princen HMG, et al. Inflammatory cytokine oncostatinMinduces endothelial activation in macro- and microvascular endothelial cells and in APOE &z.txt 3Leiden.CETP mice. *PloS One* (2018) 13(10):e0204911. doi: 10.1371/journal.pone.0204911

82. van Keulen D, Pouwer MG, Emilsson V, Matic LP, Pieterman EJ, Hedin U, et al. Oncostatin M reduces atherosclerosis development in APOE3Leiden.CETP mice and is associated with increased survival probability in humans. *PloS One* (2019) 14:e0221477. doi: 10.1371/journal.pone.0221477

83. Szibor M, Pöling J, Warnecke H, Kubin T, Braun T. Remodeling and dedifferentiation of adult cardiomyocytes during disease and regeneration. *Cell Mol Life Sci* (2014) 71:1907–16. doi: 10.1007/s00018-013-1535-6

84. Kubin T, Pöling J, Kostin S, Gajawada P, Hein S, Rees W, et al. Oncostatin M is a major mediator of cardiomyocyte dedifferentiation and remodeling. *Cell Stem Cell* (2011) 9(5):420–32. doi: 10.1016/j.stem.2011.08.013

85. Zhang X, Zhu D, Wei L, Zhao Z, Qi X, Li Z, et al. OSM enhances angiogenesis and improves cardiac function after myocardial infarction. *BioMed Res Int* (2015) 2015:317905. doi: 10.1155/2015/317905

86. Hu J, Zhang L, Zhao Z, Zhang M, Lin J, Wang J, et al. OSM mitigates post-infarction cardiac remodeling and dysfunction by up-regulating autophagy through Mst1 suppression. *Biochim Biophys Acta Mol Basis Dis* (2017) 1863(8):1951–61. doi: 10.1016/j.bbadis.2016.11.004

87. Ruan Q, Yang K, Wang W, Jiang L, Song J. Clinical predictors of mortality due to COVID-19 based on an analysis of data of 150 patients from Wuhan, China. *Intensive Care Med Springer;* (2020) 46:846–8. doi: 10.1007/s00134-020-05991-x

88. Zhou F, Yu T, Du R, Fan G, Liu Y, Liu Z, et al. Clinical course and risk factors for mortality of adult inpatients with COVID-19 in Wuhan, China: a retrospective cohort study. *Lancet* (2020) 395(10229):1054–62. doi: 10.1016/S0140-6736(20)30566-3

89. Copaescu A, Smibert O, Gibson A, Phillips EJ, Trubiano JA. The role of IL-6 and other mediators in the cytokine storm associated with SARS-CoV-2 infection. *J Allergy Clin Immunol* (2020) 146(3):518–534.e1. doi: 10.1016/j.jaci.2020.07.001

90. Russell CD, Valanciute A, Gachanja NN, Stephen J, Penrice-Randal R, Armstrong SD, et al. Tissue proteomic analysis identifies mechanisms and stages of immunopathology in fatal COVID-19. *Am J Respir Cell Mol Biol* (2022) 66(2):196–205. doi: 10.1165/rcmb.2021-0358OC

91. Arunachalam PS, Wimmers F, Mok CKP, Perera RAPM, Scott M, Hagan T, et al. Systems biological assessment of immunity to mild versus severe COVID-19 infection in humans. *Science* (1979) . 2020:eabc6261. doi: 10.1126/science.abc6261

92. Goren I, Kämpfer H, Müller E, Schiefelbein D, Pfeilschifter J, Frank S. Oncostatin M expression is functionally connected to neutrophils in the early inflammatory phase of skin repair: Implications for normal and diabetes-impaired wounds. *J Invest Dermatol* (2006) 126(3):628–37. doi: 10.1038/sj.jid.5700136

93. Wolfram D, Tzankov A, Pülzl P, Piza-Katzer H. Hypertrophic scars and keloids - A review of their pathophysiology, risk factors, and therapeutic management. *Dermatologic Surgery.* (2009) 35:171–81. doi: 10.1111/j.1524-4725.2008.34406.x

94. Huguier V, Giot JP, Simonneau M, Levillain P, Charreau S, Garcia M, et al. Oncostatin M exerts a protective effect against excessive scarring by counteracting the inductive effect of TGFβ1 on fibrosis markers. *Sci Rep* (2019) 9(1):2113. doi: 10.1038/s41598-019-38572-0

95. Ganesh K, Das A, Dickerson R, Khanna S, Parinandi NL, Gordillo GM, et al. Prostaglandin E 2 induces oncostatin M expression in human chronic wound macrophages through axl receptor tyrosine kinase pathway. *J Immunol* (2012) 189(5):2563–73. doi: 10.4049/jimmunol.1102762

96. Ogata I, Shimoya K, Moriyama A, Shiki Y, Matsumura Y, Yamanaka K, et al. Oncostatin M is produced during pregnancy by decidual cells and stimulates the release of HCG. *Mol Hum Reprod* (2000) 6:1188. doi: 10.1093/molehr/6.8.750

97. Chaiwangyen W, Ospina-Prieto S, Morales-Prieto DM, Pereira De Sousa FL, Pastuschek J, Fitzgerald JS, et al. Oncostatin M and leukaemia inhibitory factor trigger signal transducer and activator of transcription 3 and extracellular signal-regulated kinase 1/2 pathways but result in heterogeneous cellular responses in trophoblast cells. *Reprod Fertil Dev* (2016) 28(5):608–17. doi: 10.1071/RD14121

98. Wie JH, Ko HS, Choi SK, Park IY, Kim A, Kim HS, et al. Effects of oncostatin M on invasion of primary trophoblasts under normoxia and hypoxia conditions. *Yonsei Med J* (2018) 59(7):879–86. doi: 10.3349/ymj.2018.59.7.879

99. Masjedi A, Hajizadeh F, Beigi Dargani F, Beyzai B, Aksoun M, Hojjat-Farsangi M, et al. Oncostatin M: A mysterious cytokine in cancers. *Int Immunopharmacol* (2021) 90:107158. doi: 10.1016/j.intimp.2020.107158

100. Horn D, Fitzpatrick WC, Gompper PT, Ochs V, Bolton-Hansen M, Zarling J, et al. Regulation of cell growth by recombinant oncostatin M. *Growth Factors* (1990) 2(2–3):157–65. doi: 10.3109/08977199009071502

101. Zhang XG, Gu JJ, Lu Z-Y, Yasukawa K, Yancopoulos GD, Turner K, et al. Ciliary neurotropic factor, interleukln 11, leukemia inhibitory factor, and oncostatin M are growth factors for human myeloma cell lines using the interleukin 6 signal transducer GP130. *J Exp Med* (1994) 179(4):1337–42. doi: 10.1084/jem.179.4.1337

102. Underhill-Day N, Heath JK, Oncostatin M. (OSM) cytostasis of breast tumor cells: Characterization of an OSM receptor β-specific kernel. *Cancer Res* (2006) 66(22):10891–901. doi: 10.1158/0008-5472.CAN-06-1766

103. Liu J, Spence MJ, Wallace PM, Forcier K, Hellström I, Vestal RE. Oncostatin M-specific receptor mediates inhibition of breast cancer cell growth and down-regulation of the c-myc proto-oncogene. *Cell Growth Differ* (1997) 8(6):667–76.

104. Omokehinde T, Johnson RW. Gp130 cytokines in breast cancer and bone. *Cancers* (2020) 12:326. doi: 10.3390/cancers12020326

105. West NR, Murphy LC, Watson PH. Oncostatin M suppresses oestrogen receptor-α expression and is associated with poor outcome in human breast cancer. *Endocr Relat Cancer.* (2012) 19(2):181–95. doi: 10.1530/ERC-11-0326

106. Tawara K, Scott H, Emathinger J, Wolf C, Lajoie D, Hedeen D, et al. HIGH expression of OSM and IL-6 are associated with decreased breast cancer survival:

synergistic induction of IL-6 secretion by OSM and IL-1β. *Oncotarget* (2019) 10:2068–85. doi: 10.18632/oncotarget.26699

107. García-Tuñón I, Ricote M, Ruiz A, Fraile B, Paniagua R, Royuela M. OSM, LIF, its receptors, and its relationship with the Malignance in human breast carcinoma (*in situ* and in infiltrative). *Cancer Invest* (2009) 26(3):222–9. doi: 10.1080/07357900701638491

108. Kan CE, Cipriano R, Jackson MW. c-MYC functions as a molecular switch to alter the response of human mammary epithelial cells to oncostatin M. *Cancer Res* (2011) 71(22):6930–9. doi: 10.1158/0008-5472.CAN-10-3860

109. Tawara K, Bolin C, Koncinsky J, Kadaba S, Covert H, Sutherland C, et al. OSM potentiates preintravasation events, increases CTC counts, and promotes breast cancer metastasis to the lung. *Breast Cancer Res* (2018) 20(1):53. doi: 10.1186/s13058-018-0971-5

110. Hicks MJ, Hu Q, Macrae E, DeWille J. Mitogen-activated protein kinase signaling controls basal and oncostatin M-mediated JUNB gene expression. *Mol Cell Biochem* (2015) 403(1–2):115–24. doi: 10.1007/s11010-015-2342-1

111. Bryson BL, Junk DJ, Cipriano R, Jackson MW. STAT3-mediated SMAD3 activation underlies Oncostatin M-induced Senescence. *Cell Cycle* (2017) 16(4):319–34. doi: 10.1080/15384101.2016.1259037

112. Covert H, Mellor LF, Wolf CL, Ankenbrandt N, Emathinger JM, Tawara K, et al. OSM-induced CD44 contributes to breast cancer metastatic potential through cell detachment but not epithelial-mesenchymal transition. *Cancer Manag Res* (2019) 11:7721–37. doi: 10.2147/CMAR.S208721

113. Goldhirsch A, Glick JH, Gelber RD, Senn HJ. Meeting highlights–International Consensus Panel on the treatment of primary breast cancer. *J Natl Cancer Inst* (2002) 90(21):347–63. doi: 10.1093/jnci/90.21.1601

114. Eifel P, Axelson JA, Costa J, Crowley J, Curran WJ, Deshler A, et al. National Institutes of Health Consensus Development Conference Statement: adjuvant therapy for breast cancer, November 1-3, 2000. *J Natl Cancer Inst* (2001) 93(13):979–89. doi: 10.1093/jnci/93.13.979

115. Perou CM, Jeffrey SS, de van Rijn M, Rees CA, Eisen MB, Ross DT, et al. Distinctive gene expression patterns in human mammary epithelial cells and breast cancers. *Genetics* (1999) 96:9212–7. doi: 10.1073/pnas.96.16.9212

116. Sørlie T, Perou CM, TibshIrani R, Aas T, Geisler S, Johnsen H, et al. *Gene Expression Patterns Of Breast Carcinomas Distinguish Tumor Subclasses With Clinical Implications*. *Proc Natl Acad Sci U S A* (2001) 98(19):10869–74. doi: 10.1073/pnas.191367098

117. van't Veer LJ, Dai H, van de Vijver MJ, He YD, Hart AAM, Mao M, et al. Gene expression profiling predicts clinical outcome of breast cancer. *Nature* (2002) 415 (6871):530–6. doi: 10.1038/415530a

118. Slamon DJ, Clark GM, Wong SG, Levin WJ, Ullrich A, McGuire WL. Human breast cancer: correlation of relapse and survival with amplification of the HER-2/neu oncogene. *Science* (1987) 235(4785):177–82. doi: 10.1126/science.3798106

119. Goldhirsch A, Winer EP, Coates AS, Gelber RD, Piccart-Gebhart M, Thürlimann B, et al. Personalizing the treatment of women with early breast cancer: Highlights of the st gallen international expert consensus on the primary therapy of early breast Cancer 2013. *Ann Oncol* (2013) 24(9):2206–23. doi: 10.1093/annonc/mdt303

120. Wolff AC, Hammond MEH, Hicks DG, Dowsett M, McShane LM, Allison KH, et al. Recommendations for human epidermal growth factor receptor 2 testing in breast. *J Clin Oncol* (2013) 31(31):3997–4013. doi: 10.1200/JCO.2013.50.9984

121. Abe O, Abe R, Enomoto K, Kikuchi K, Koyama H, Masuda H, et al. Effects of chemotherapy and hormonal therapy for early breast cancer on recurrence and 15-year survival: An overview of the randomised trials. *Lancet* (2005) 365(9472):1687–717. doi: 10.1016/S0140-6736(05)66544-0

122. Dent R, Trudeau M, Pritchard KI, Hanna WM, Kahn HK, Sawka CA, et al. Triple-negative breast cancer: Clinical features and patterns of recurrence. *Clin Cancer Res* (2007) 13(15):4429–34. doi: 10.1158/1078-0432.CCR-06-3045

123. Perou CM, Sørlie T, Eisen MB, van de Rijn M, Jeffrey SS, Rees CA, et al. Molecular portraits of human breast tumours. *Nature* (2000) 406(6797):747–52. doi: 10.1038/35021093

124. Junk DJ, Bryson BL, Smigiel JM, Parameswaran N, Bartel CA, Jackson MW. Oncostatin M promotes cancer cell plasticity through cooperative STAT3-SMAD3 signaling. *Oncogene* (2017) 36(28):4001–13. doi: 10.1038/onc.2017.33

125. Doherty MR, Parvani JG, Tamagno I, Junk DJ, Bryson BL, Cheon HJ, et al. The opposing effects of interferon-beta and oncostatin-M as regulators of cancer stem cell plasticity in triple-negative breast cancer. *Breast Cancer Res* (2019) 21(1):54. doi: 10.1186/s13058-019-1136-x

126. Soysal SD, Tzankov A, Muenst SE. Role of the tumor microenvironment in breast cancer. *Pathobiology. S.* (2015) 82:142–52. doi: 10.1159/000430499

127. Hu M, Yao J, Cai L, Bachman KE, van den Brûle F, Velculescu V, et al. Distinct epigenetic changes in the stromal cells of breast cancers. *Nat Genet* (2005) 37(8):899–905. doi: 10.1038/ng1596

128. Coleman RE, Gregory W, Marshall H, Wilson C, Holen I. The metastatic microenvironment of breast cancer: Clinical implications. *Breast* (2013) 22(S2):50–6. doi: 10.1016/j.breast.2013.07.010

129. Finak G, Bertos N, Pepin F, Sadekova S, Souleimanova M, Zhao H, et al. Stromal gene expression predicts clinical outcome in breast cancer. *Nat Med* (2008) 14 (5):518–27. doi: 10.1038/nm1764

130. Ryan RE, Martin B, Mellor L, Jacob RB, Tawara K, McDougal OM, et al. Oncostatin M binds to extracellular matrix in a bioactive conformation: Implications for inflammation and metastasis. *Cytokine* (2015) 72(1):71–85. doi: 10.1016/j.cyto.2014.11.007

131. Araujo AM, Abaurrea A, Azcoaga P, López-Velazco JI, Manzano S, Rodriguez J, et al. Stromal oncostatin M cytokine promotes breast cancer progression by reprogramming the tumor microenvironment. *J Clin Invest* (2022) 132(7):e148667. doi: 10.1172/JCI148667

132. Dinca SC, Greiner D, Weidenfeld K, Bond L, Barkan D, Jorcyk CL. Novel mechanism for OSM-promoted extracellular matrix remodeling in breast cancer: LOXL2 upregulation and subsequent ECM alignment. *Breast Cancer Res* (2021) 23 (1):56. doi: 10.1186/s13058-021-01430-x

133. Queen MM, Ryan RE, Holzer RG, Keller-Peck CR, Jorcyk CL. Breast cancer cells stimulate neutrophils to produce oncostatin M: Potential implications for tumor progression. *Cancer Res* (2005) 65(19):8896–904. doi: 10.1158/0008-5472.CAN-05-1734

134. Lorincz AM, Sukumar S. Molecular links between obesity and breast cancer. *Endocrine-Related Cancer.* (2006) 13:279–92. doi: 10.1677/erc.1.00729

135. Siegel RL, Miller KD, Wagle NS, Jemal A. Cancer statistics, 2023. *CA Cancer J Clin* (2023) 73(1):17–48. doi: 10.3322/caac.21763

136. Browning L, Patel MR, Horvath EB, Tawara K, Jorcyk CL. IL-6 and ovarian cancer: Inflammatory cytokines in promotion of metastasis. *Cancer Manag Res* (2018) 10:6685–93. doi: 10.2147/CMAR.S179189

137. Savarese TM, Campbell CL, McQuain C, Mitchell K, Guardiani R, Quesenberry PJ, et al. Coexpression of oncostatin M and its receptors and evidence for STAT3 activation in human ovarian carcinomas. *Cytokine* (2002) 17(6):324–34. doi: 10.1006/cyto.2002.1022

138. Li Q, Zhu J, Sun F, Liu L, Liu X, Yue Y. Oncostatin M promotes proliferation of ovarian cancer cells through signal transducer and activator of transcription 3. *Int J Mol Med* (2011) 28(1):101–8. doi: 10.3892/ijmm.2011.647

139. Pils D, Tong D, Hager G, Obermayr E, Aust S, Heinze G, et al. *A Combined Blood Based Gene Expression and Plasma Protein Abundance Signature for Diagnosis of Epithelial Ovarian Cancer-a Study of the OVCAD Consortium*. *BMC Cancer* (2013) 13:178. doi: 10.1186/1471-2407-13-178

140. Geethadevi A, Nair A, Parashar D, Ku Z, Xiong W, Deng H, et al. Oncostatin M Receptor-targeted antibodies suppress STAT3 signaling and inhibit ovarian cancer growth. *Cancer Res* (2021) 81(20):5336–52. doi: 10.1158/0008-5472.CAN-21-0483

141. Siegel RL, Miller KD, Jemal A. Cancer statistics, 2016. *CA Cancer J Clin* (2016) 66(1):7–30. doi: 10.3322/caac.21332

142. Sidenius N, Blasi F. The urokinase plasminogen activator system in cancer: Recent advances and implication for prognosis and therapy. *Cancer Metastasis Rev* (2003) 22(2–3):205–22. doi: 10.1023/A:1023099415940

143. Sterbova S, Karlsson T, Persson E. Oncostatin M induces tumorigenic properties in non-transformed human prostate epithelial cells, in part through activation of signal transducer and activator of transcription 3 (STAT3). *Biochem Biophys Res Commun* (2018) 498(4):769–74. doi: 10.1016/j.bbrc.2018.03.056

144. Han Z, Zhan R, Chen S, Deng J, Shi J, Wang W. miR-181b/Oncostatin m axis inhibits prostate cancer bone metastasis via modulating osteoclast differentiation. *J Cell Biochem* (2020) 121(2):1664–74. doi: 10.1002/jcb.29401

145. Brawley OW. Trends in prostate cancer in the United States. *JNCI Monographs.* (2012) 2012(45):152–6. doi: 10.1093/jncimonographs/lgs035

146. Kim JS, Wilson RL, Taaffe DR, Galvão DA, Gray E, Newton RU. Myokine Expression and Tumor-Suppressive Effect of Serum after 12 wk of Exercise in Prostate Cancer Patients on ADT. *Med Sci Sports Exerc.* (2022) 54(2):197–205. doi: 10.1249/MSS.0000000000002783

147. Kim JS, Taaffe DR, Galvão DA, Hart NH, Gray E, Ryan CJ, et al. Exercise in advanced prostate cancer elevates myokine levels and suppresses *in-vitro* cell growth. *Prostate Cancer Prostatic Dis* (2022) 25(1):86–92. doi: 10.1038/s41391-022-00504-x

148. de Miguel MP, Regadera J, Martinez-Garcia F, Nistal M, Paniagua R. Oncostatin M in the normal human testis and several testicular disorders. *J Clin Endocrinol Metab* (1999) 84(2):768–74. doi: 10.1210/jcem.84.2.5480

149. Teerds KJ, van Dissel-Emiliani FMF, de Miguel MP, de Boer-Brouwer M, Körting LM, Rijntjes E. Oncostatin-M inhibits luteinizing hormone stimulated Leydig cell progenitor formation in *vitro*. *Reprod Biol Endocrinol* (2007) 5:43. doi: 10.1186/1477-7827-5-43

150. Kim MS, Louwagie J, Carvalho B, Terhaar sive Droste JS, Park HL, Chae YK, et al. Promoter DNA methylation of Oncostatin M receptor-β as a novel diagnostic and therapeutic marker in colon cancer. *PloS One* (2009) 4(8):e6555. doi: 10.1371/journal.pone.0006555

151. Hibi K, Goto T, Sakaraba K, Shirahata A, Saito M, Ishibashi K, et al. Methylation of OSMR gene is frequently observed in non-invasive colorectal cancer. *Anticancer Res* (2011) 31(4):1293–6.

152. Deng G, Kakar S, Okudiara K, Choi E, Sleisenger MH, Kim YS. Unique methylation pattern of oncostatin M receptor gene in cancers of colorectum and other digestive organs. *Clin Cancer Res* (2009) 15(5):1519–26. doi: 10.1158/1078-0432.CCR-08-1778

153. Gurluler E, Tumay LV, Guner OS, Kucukmetin NT, Hizli B, Zorluoglu A. Oncostatin-M as a novel biomarker in colon cancer patients and its association with clinicopathologic variables. *Eur Rev Med Pharmacol Sci* (2014) 18(14):2042–7.

154. Rajamäki K, Taira A, Katainen R, Välimäki N, Kuosmanen A, Plaketti RM, et al. Genetic and epigenetic characteristics of inflammatory bowel disease–associated colorectal cancer. *Gastroenterology* (2021) 161(2):592–607. doi: 10.1053/j.gastro.2021.04.042

155. Bedi D, Henderson H, Manne U, Samuel T. Camptothecin induces PD-L1 and immunomodulatory cytokines in colon cancer cells. *Medicines* (2019) 6(2):51. doi: 10.3390/medicines6020051

156. Jemal A, Bray F, Ferlay J. Global cancer statistics: 2011. *CA Cancer J Clin* (1999) 49(2):1,33–64. doi: 10.3322/caac.20107

157. Ferlay J, Shin HR, Bray F, Forman D, Mathers C, Parkin DM. Estimates of worldwide burden of cancer in 2008: GLOBOCAN 2008. *Int J Cancer.* (2010) 127 (12):2893–917. doi: 10.1002/ijc.25516

158. Karimi P, Islami F, Anandasabapathy S, Freedman ND, Kamangar F. Gastric cancer: Descriptive epidemiology, risk factors, screening, and prevention. *Cancer Epidemiol Biomarkers Prev* (2014) 23:700–13. doi: 10.1158/1055-9965.EPI-13-1057

159. Shi J, Xu X, Du J, Cui H, Luo Q. Expression of oncostatin M in early gastric cancer and precancerous lesions. *Gastroenterol Res Pract* (2019) 2019:3616140. doi: 10.1155/2019/3616140

160. Zhu Q, Zhang X, Zhang L, Li W, Wu H, Yuan X, et al. The IL-6-STAT3 axis mediates a reciprocal crosstalk between cancer-derived mesenchymal stem cells and neutrophils to synergistically prompt gastric cancer progression. *Cell Death Dis* (2014) 5(6):e1295. doi: 10.1038/cddis.2014.263

161. Yu Z, Li Z, Wang C, Pan T, Chang X, Wang X, et al. Oncostatin M receptor, positively regulated by SP1, promotes gastric cancer growth and metastasis upon treatment with Oncostatin M. *Gastric Cancer.* (2019) 22(5):955–66. doi: 10.1007/s10120-019-00934-y

162. Smigiel JM, Parameswaran N, Jackson MW. Potent EMT and CSC phenotypes are induced by oncostatin-M in pancreatic cancer. *Mol Cancer Res* (2017) 15(4):478–88. doi: 10.1158/1541-7786.MCR-16-0337

163. Lee BY, Hogg EKJ, Below CR, Kononov A, Blanco-Gomez A, Heider F, et al. Heterocellular OSM-OSMR signalling reprograms fibroblasts to promote pancreatic cancer growth and metastasis. *Nat Commun* (2021) 12(1):7336. doi: 10.1038/s41467-021-27607-8

164. Alonso-Nocelo M, Ruiz-Canãs L, Sancho P, Görgülü K, Alcalá S, Pedrero C, et al. Macrophages direct cancer cells through a LOXL2-mediated metastatic cascade in pancreatic ductal adenocarcinoma. *Gut* (2022) 72(2):345–59. doi: 10.1136/gutjnl-2021-325564

165. Torres C, Perales S, Alejandre MJ, Iglesias J, Palomino RJ, Martin M, et al. Serum cytokine profile in patients with pancreatic cancer. *Pancreas* (2014) 43(7):1042–9. doi: 10.1097/MPA.0000000000000155

166. Nguyen AM, Zhou J, Sicairos B, Sonney S, Du Y. Upregulation of CD73 confers acquired radioresistance and is required for maintaining irradiation-selected pancreatic cancer cells in a mesenchymal state. *Mol Cell Proteomics.* (2020) 19(2):375–89. doi: 10.1074/mcp.RA119.001779

167. Nistal-Villan E, Bunuales M, Poutou J, Gonzalez-Aparicio M, Bravo-Perez C, Quetglas JI, et al. Enhanced therapeutic effect using sequential administration of antigenically distinct oncolytic viruses expressing oncostatin M in a Syrian hamster orthotopic pancreatic cancer model. *Mol Cancer* (2015) 14(1):210. doi: 10.1186/s12943-015-0479-x

168. Deng S, He SY, Zhao P, Zhang P. The role of oncostatin M receptor gene polymorphisms in bladder cancer. *World J Surg Oncol* (2019) 17(1):30. doi: 10.1186/s12957-018-1555-7

169. Hurst CD, Cheng G, Platt FM, Alder O, Black EVI, Burns JE, et al. Molecular profile of pure squamous cell carcinoma of the bladder identifies major roles for OSMR and YAP signalling. *J Pathology: Clin Res* (2022) 8(3):279–93. doi: 10.1002/cjp2.261

170. Olkhov-Mitsel E, Hodgson A, Liu SK, Vesprini D, Bayani J, Bartlett J, et al. Immune gene expression profiles in high-grade urothelial carcinoma of the bladder: a NanoString study. *J Clin Pathol* (2021) 74(1):53–7. doi: 10.1136/jclinpath-2020-206631

171. Ouyang L, Shen LY, Liu J. Inhibition effect of Oncostatin M on metastatic human lung cancer cells 95-D in vitro and on murine melanoma cells B16BL6 in vivo. *Biomed Res* (2006) 27:197–202. doi: 10.2220/biomedres.27.197

172. Spence MJ, Streiff R, Day D, Ma Y. Oncostatin M induces tissue-type plasminogen activator and plasminogen activator inhibitor-1 in Calu-1 lung carcinoma cells. *Cytokine* (2002) 18(1):26–34. doi: 10.1006/cyto.2001.1018

173. Chattopadhyay S, Tracy E, Liang P, Robledo O, Rose-John S, Baumann H. Interleukin-31 and oncostatin-M mediate distinct signaling reactions and response patterns in lung epithelial cells. *J Biol Chem* (2007) 282(5):3014–26. doi: 10.1074/jbc.M609655200

174. McCormick C, Freshney RI. Activity of growth factors in the IL-6 group in the differentiation of human lung adenocarcinoma. *Br J Cancer.* (2000) 82(4):881–90. doi: 10.1054/bjoc.1999.1015

175. Cichy J, Puré E. Oncostatin M and transforming growth factor-β1 induce post-translational modification and hyaluronan binding to CD44 in lung-derived epithelial tumor cells. *J Biol Chem* (2000) 275(24):18061–9. doi: 10.1074/jbc.M907962199

176. Lauber S, Wong S, Cutz JC, Tanaka M, Barra N, Lhoták Š, et al. Novel function of Oncostatin M as a potent tumour-promoting agent in lung. *Int J Cancer.* (2015) 136 (4):831–43. doi: 10.1002/ijc.29055

177. Shien K, Papadimitrakopoulou VA, Ruder D, Behrens C, Shen L, Kalhor N, et al. JAK1/STAT3 activation through a proinflammatory cytokine pathway leads to resistance to molecularly targeted therapy in non–small cell lung cancer. *Mol Cancer Ther* (2017) 16(10):2234–45. doi: 10.1158/1535-7163.MCT-17-0148

178. Wysoczynski M, Ratajczak MZ. Lung cancer secreted microvesicles: Underappreciated modulators of microenvironment in expanding tumors. *Int J Cancer.* (2009) 125(7):1595–603. doi: 10.1002/ijc.24479

179. Pan CM, Wang ML, Chiou SH, Chen HY, Wu CW. Oncostatin M Suppresses Metastasis of Lung Adenocarcinoma by Inhibiting SLUG Expression Through Coordination of STATs and PIASs Signalings. *Oncotarget* (2016) 7(37):60395–406. doi: 10.18632/oncotarget.10939

180. Wang ML, Pan CM, Chiou SH, Chen WH, Chang HY, Lee OKS, et al. Oncostatin M modulates the mesenchymal-epithelial transition of lung adenocarcinoma cells by a mesenchymal stem cell-mediated paracrine effect. *Cancer Res* (2012) 72(22):6051–64. doi: 10.1158/0008-5472.CAN-12-1568

181. Chen DR, Chu CY, Chen CY, Yang HC, Chiang YY, Lin TY, et al. Expression of short-form oncostatin M receptor as a decoy receptor in lung adenocarcinomas. *J Pathology.* (2008) 215(3):290–9. doi: 10.1002/path.2361

182. Waters MR, Gupta AS, Mockenhaupt K, Brown LSN, Biswas DD, Kordula T. RelB acts as a molecular switch driving chronic inflammation in glioblastoma multiforme. *Oncogenesis* (2019) 8(6). doi: 10.1038/s41389-019-0146-y

183. Natesh K, Bhosale D, Desai A, Chandrika G, Pujari R, Jagtap J, et al. Oncostatin-M differentially regulates mesenchymal and proneural signature genes in gliomas via STAT3 signaling. *Neoplasia* (2015) 17(2):225–37. doi: 10.1016/j.neo.2015.01.001

184. Jahani-As A, Yin H, Soleimani VD, Haque T, Luchman HA, Chang NC, et al. Control of glioblastoma tumorigenesis by feed-forward cytokine signaling. *Nat Neurosci* (2016) 19(6):798–806. doi: 10.1038/nn.4295

185. Repovic P, Fears CY, Gladson CL, Benveniste EN. Oncostatin-M induction of vascular endothelial growth factor expression in astroglioma cells. *Oncogene* (2003) 22 (50):8117–24. doi: 10.1038/sj.onc.1206922

186. Hara T, Chanoch-Myers R, Mathewson ND, Myskiw C, Atta L, Bussema L, et al. Interactions between cancer cells and immune cells drive transitions to mesenchymal-like states in glioblastoma. *Cancer Cell* (2021) 39(6):779–92. doi: 10.1016/j.ccell.2021.05.002

187. Schaefer LK, Menter DG, Schaefer TS. Activation of Stat3 and Stat1 DNA binding and transcriptional activity in human brain tumour cell lines by gp130 cytokines. *Cell Signalling* (2000) 12:143–51. doi: 10.1016/S0898-6568(99)00077-7

188. Krona A, Aman P, Orndal C, Josefsson A. Oncostatin M-induced genes in human astrocytomas. *Int J Oncol* (2007) 31(6):1457–63. doi: 10.3892/ijo.31.6.1457

189. Hanisch A, Dieterich KD, Dietzmann K, Lüdecke K, Buchfelder M, Fahlbusch R, et al. Expression of members of the interleukin-6 family of cytokines and their receptors in human pituitary and pituitary adenomas. *J Clin Endocrinol Metab* (2000) 85(11):4411–1. doi: 10.1210/jcem.85.11.7122

190. Chen SH, Gillespie GY, Benveniste EN. Divergent effects of oncostatin M on astroglioma cells: Influence on cell proliferation, invasion, and expression of matrix metalloproteinases. *Glia* (2006) 53(2):191–200. doi: 10.1002/glia.20264

191. Halfter H, Lotfi R, Westermann R, Young P, Ringelstein EB, Stögbauer FT. Inhibition of growth and induction of differentiation of glioma cell lines by oncostatin M (OSM). *Growth Factors.* (1998) 15(2):135–47. doi: 10.3109/08977199809117189

192. Chen M, Ren R, Lin W, Xiang L, Zhao Z, Shao B, et al. (OSM) feed-forward signaling of glioblastoma via STAT3 in pan-cancer analysis. *Cancer Cell Int* (2021) 21 (1):565. doi: 10.1186/s12935-021-02260-9

193. Stratigos AJ, Garbe C, Dessinioti C, Lebbe C, Bataille V, Bastholt L, et al. European interdisciplinary guideline on invasive squamous cell carcinoma of the skin: Part 1. epidemiology, diagnostics and prevention. *Eur J Cancer.* (2020) 128:60–82. doi: 10.1016/j.ejca.2020.01.007

194. Simonneau M, Frouin E, Huguier V, Jermidi C, François Jégou J, Godet J, et al. Oncostatin M is overexpressed in skin squamous-cell carcinoma and promotes tumor progression. *Oncotarget* (2018) 9(92):36457–73. doi: 10.18632/oncotarget.26355

195. Tran TA, Ross JS, Sheehan CE, Carlson JA. Comparison of oncostatin M expression in keratoacanthoma and squamous cell carcinoma. *Mod Pathol* (2000) 13 (4):427–32. doi: 10.1038/modpathol.3880073

196. Smigiel J, Parvani JG, Tamagno I, Polak K, Jackson MW. Breaking the oncostatin M feed-forward loop to suppress metastasis and therapy failure. *J Pathol* (2018) 245:6–8. doi: 10.1002/path.5063

197. Nguyen TN, Rajapakshe K, Nicholas C, Tordesillas L, Ehli EA, Davis CM, et al. Integrative transcriptomic analysis for linking acute stress responses to squamous cell carcinoma development. *Sci Rep* (2020) 10(1):17209. doi: 10.1038/s41598-020-74051-7

198. Chuerduangphui J, Ekalaksananan T, Chaiyarit P, Patarapadungkit N, Chotiyano A, Kongyingyoes B, et al. Effects of arecoline on proliferation of oral squamous cell carcinoma cells by dysregulating c-Myc and miR-22, directly targeting oncostatin M. *PloS One* (2018) 13(1):e0192009. doi: 10.1371/journal.pone.0192009

199. Bray F, Ferlay J, Soerjomataram I, Siegel RL, Torre LA, Jemal A. 394 CA: A cancer journal for clinicians global cancer statistics 2018: GLOBOCAN estimates of incidence and mortality worldwide for 36 cancers in 185 countries. *CA Cancer J Clin* (2018) 68:394–424. doi: 10.3322/caac.21492

200. Abnet CC, Arnold M, Wei WQ. Epidemiology of esophageal squamous cell carcinoma. *Gastroenterology* (2018) 154(2):360–73. doi: 10.1053/j.gastro.2017.08.023

201. Aversa J, Song M, Shimazu T, Inoue M, Charvat H, Yamaji T, et al. Prediagnostic circulating inflammation biomarkers and esophageal squamous cell carcinoma: A case–cohort study in Japan. *Int J Cancer.* (2020) 147(3):686–91. doi: 10.1002/ijc.32763

202. Lian L, Teng SB, Xia YY, Shen XM, Zheng Y, Han SG, et al. Development and verification of a hypoxia- and immune-associated prognosis signature for esophageal squamous cell carcinoma. *J Gastrointest Oncol* (2022) 13(2):462–77. doi: 10.21037/jgo-22-69

203. Kausar T, Sharma R, Hasan MR, Saraya A, Chattopadhyay TK, Gupta SD, et al. Overexpression of a splice variant of oncostatin M receptor beta in human esophageal squamous carcinoma. *Cell Oncol* (2011) 34(3):177–87. doi: 10.1007/s13402-011-0011-2

204. Miles SA, Martinez-Maza O, Rezai A, Magpantay L, Kishimoto T, Nakamura S, et al. Oncostatin M as a potent mitogen for AIDS-Kaposi's sarcoma-derived cells. *Science* (1979) 1992:1432–44. doi: 10.1126/science.1542793

205. Cai J, Gill PS, Masood R, Chandrasoma P, Jung B, Law RE, et al. Oncostatin-M is an autocrine growth factor in Kaposi's sarcoma. *Am J Pathology.* (1994) 145(1):74–9.

206. Faris M, Ensoli B, Kokot N, Nel AE. Inflammatory cytokines induce the expression of basic fibroblast growth factor (bFGF) isoforms required for the growth of Kaposi's sarcoma and endothelial cells through the activation of AP-1 response elements in the bFGF promoter. *AIDS* (1998) 198AD:19–27. doi: 10.1097/00002030-199801000-00003

207. Faris M, Ensoli B, Stahl N, Yancopoulos G, Nguyen A, Wang S, et al. Differential activation of the extracellular signal-regulated kinase, Jun Kinase and Janus Kinase-Stat pathways by oncostatin M and basic fibroblast growth factor in AIDS-derived Kaposi's sarcoma cells. *AIDS* (1996) 10(4):369–78. doi: 10.1097/00002030-199604000-00004

208. Lundquist A, Barré B, Bienvenu F, Hermann J, Avril S, Coqueret O. Kaposi sarcoma-associated viral cyclin K overrides cell growth inhibition mediated by oncostatin M through STAT3 inhibition. *Blood* (2003) 101(10):4070–7. doi: 10.1182/blood-2002-07-1994

209. Amaral MC, Miles S, Kumar G, Nel AE. Oncostatin-M stimulates tyrosine protein phosphorylation in parallel with the activation of p42MAPK/ERK-2 in Kaposi's cells: Evidence that this pathway is important in Kaposi cell growth. *J Clin Invest* (1993) 92(2):848–57. doi: 10.1172/JCI116659

210. Liu ZY, Ganju RK, Wang JF, Ona MA, Hatch WC, Zheng T, et al. Cytokine signaling through the novel tyrosine kinase RAFTK in kaposi's sarcoma cells. *J Clin Invest* (1997) 99:1798–804. doi: 10.1172/JCI119344

211. Murakami-Mori K, Taga T, Kishimoto T, Nakamura S. AIDS-associated Kaposi's Sarcoma (KS) Cells Express Oncostatin M (OM)-specific Receptor but Not Leukemia Inhibitory Factor/OM Receptor or Interleukin-6 Receptor Complete Block of OM-induced KS Cell Growth and OM Binding by Anti-gp130 Antibodies Key words: cytokine receptor * growth fac-tor * biological signaling * binding sites * growth inhibition. *J Clin Invest* (1995) 96(3):1319–27. doi: 10.1172/JCI118167

212. Fossey SL, Bear MD, Kisseberth WC, Pennell M, London CA. Oncostatin M promotes STAT3 activation, VEGF production, and invasion in osteosarcoma cell lines. *BMC Cancer* (2011) 11:125. doi: 10.1186/1471-2407-11-125

213. Brounais B, Chipoy C, Mori K, Charrier C, Battaglia S, Pilet P, et al. Oncostatin M induces bone loss and sensitizes rat osteosarcoma to the antitumor effect of midostaurin in *vivo*. *Clin Cancer Res* (2008) 14(17):5400–9. doi: 10.1158/1078-0432.CCR-07-4781

214. Brounais B, David E, Chipoy C, Trichet V, Ferré V, Charrier C, et al. Long term oncostatin M treatment induces an osteocyte-like differentiation on osteosarcoma and calvaria cells. *Bone* (2009) 44(5):830–9. doi: 10.1016/j.bone.2008.12.021

215. Chipoy C, Berreur M, Couillaud S, Pradal G, Vallette F, Colombeix C, et al. Downregulation of osteoblast markers and induction of the glial fibrillary acidic protein by oncostatin M in osteosarcoma cells require PKCδ and STAT3. *J Bone Mineral Res* (2004) 19(11):1850–61. doi: 10.1359/JBMR.040817

216. Damiens C, Grimaud E, Rousselle AV, Charrier C, Fortun Y, Heymann D, et al. Cysteine protease production by human osteosarcoma cells (MG63, SaOS2) and its modulation by soluble factors. *Cytokine* (2000) 12(5):539–42. doi: 10.1006/cyto.1999.0593

217. Damiens C, Fortun Y, Charrier C, Heymann D, Padrines M. Modulation by soluble factors of gelatinase activities released by osteoblastic cells. *Cytokine* (2000) 12 (11):1727–31. doi: 10.1006/cyto.2000.0765

218. David E, Guihard P, Brounais B, Riet A, Charrier C, Battaglia S, et al. Direct anti-cancer effect of oncostatin M on chondrosarcoma. *Int J Cancer.* (2011) 128 (8):1822–35. doi: 10.1002/ijc.25776

219. Park HR, Jung WW, Kim HS, Park YK. Microarray-based DNA methylation study of Ewing's sarcoma of the bone. *Oncol Lett* (2014) 8(4):1613–7. doi: 10.3892/ol.2014.2322

220. David E, Tirode F, Baud'Huin M, Guihard P, Laud K, Delattre O, et al. Oncostatin M is a growth factor for Ewing sarcoma. *Am J Pathology.* (2012) 181 (5):1782–95. doi: 10.1016/j.ajpath.2012.07.023

221. Brown TJ, Lioubin MN, Marquardt H. Purification and characterization of cytostatic lymphokines produced by activated human T lymphocytes. Synergistic antiproliferative activity of transforming growth factor beta 1, interferon-gamma, and oncostatin M for human melanoma cells. *J Immunol* (1987) 139(9):2977–83.

222. Lu C, Rak JW, Kobayashi H, Kerbel RS. Increased resistance to oncostatin M-induced growth inhibition of human melanoma cell lines derived from advanced-stage lesions. *Cancer Res* (1993) 53(12):2708–11.

223. McDonald VL, Dick KO, Malik N, Shoyab M. Selection and characterization of a variant of human melanoma cell line, A375 resistant to growth inhibitory effects of oncostatin M (OM): coresistant to interleukin 6 (IL-6). *Growth Factors.* (1993) 9 (3):167–75.

224. Kortylewski M, Heinrich PC, Mackiewicz A, Schniertshauer U, Klingmuè Ller U, Nakajima K, et al. Interleukin-6 and Oncostatin M-induced Growth Inhibition of human A375 Melanoma Cells is STAT-dependent and Involves Upregulation of the Cyclin-dependent Kinase Inhibitor p27/Kip1. *Oncogene* (1999) 18(25):3742–53. doi: 10.1038/sj.onc.1202708

225. Lázár-Molnár E, Hegyesi H, Tóth S, Falus A. Autocrine and paracrine regulation by cytokines and growth factors in melanoma. *Cytokine* (2000) 12:547–54. doi: 10.1006/cyto.1999.0614

226. Gibbs P, Chen Q, Robinson WA. Effects of oncostatin M and tamoxifen on human melanoma cells. *Melanoma Res* (1998) 8(3):221–6. doi: 10.1097/00008390-199806000-00004

227. Somasundaram R, Ruehl M, Schaefer B, Schmid M, Ackermann R, Riecken EO, et al. Interstitial collagens I, III, and VI sequester and modulate the multifunctional cytokine oncostatin M. *J Biol Chem* (2002) 277(5):3242–6. doi: 10.1074/jbc.M110011200

228. Heymann D, Blanchard F, Raher S, de Groote D, Godard A. Modulation of LIF expression in human melanoma cells by Oncostatin M. *Immunol Lett* (1995) 46:245–51. doi: 10.1016/0165-2478(95)00049-B

229. Heymann D, Godard A, Raher S, Ringeard S, Lassort D, Blanchard F, et al. Human interleukin for DA cells/leukemia inhibitory factor and oncostatin M enhance membrane expression of intercellular adhesion molecule-1 on melanoma cells but not the shedding of its soluble form. *Cytokine* (1995) 7(2):111–7. doi: 10.1006/cyto.1995.1015

230. Komyod W, Böhm M, Metze D, Heinrich PC, Behrmann I. Constitutive suppressor of cytokine signaling 3 expression confers a growth advantage to a human melanoma cell line. *Mol Cancer Res* (2007) 5(3):271–81. doi: 10.1158/1541-7786.MCR-06-0274

231. Lacreusette A, Nguyen JM, Pandolfino MC, Khammari A, Dreno B, Jacques Y, et al. Loss of oncostatin M receptor β in metastatic melanoma cells. *Oncogene* (2007) 26 (6):881–92. doi: 10.1038/sj.onc.1209844

232. Durda PJ, Dunn IS, Rose LB, Butera D, Benson EM, Pandolfi F, et al. Induction of 'Antigen silencing'. In: Melanomas by Oncostatin M: Down-Modulation of Melanocyte Antigen Expression. *Mol Cancer Res* (2003) 1(6):411–9.

233. Lacreusette A, Lartigue A, Nguyen JM, Barbieux I, Pandolfino MC, Paris F, et al. Relationship between responsiveness of cancer cells to Oncostatin M and/or IL-6 and survival of stage III melanoma patients treated with tumour-infiltrating lymphocytes. *J Pathology.* (2008) 216(4):451–9. doi: 10.1002/path.2416

234. Adrian-Segarra JM, Schindler N, Gajawada P, Lörchner H, Braun T, Pöling J. The AB loop and D-helix in binding site III of human Oncostatin M (OSM) are required for OSM receptor activation. *J Biol Chem* (2018) 293(18):7017–29. doi: 10.1074/jbc.RA118.001920

235. Du Q, Qian Y, Xue W. Cross-reactivity of two human IL-6 family cytokines OSM and LIF explored by protein-protein docking and molecular dynamics simulation. *Biochim Biophys Acta Gen Subj* (2021) 1865(7):129907. doi: 10.1016/j.bbagen.2021.129907

236. Choy EH, Bendit M, McAleer D, Liu F, Feeney M, Brett S, et al. Safety, tolerability, pharmacokinetics and pharmacodynamics of an anti- oncostatin M monoclonal antibody in rheumatoid arthritis: Results from phase II randomized, placebo-controlled trials. *Arthritis Res Ther* (2013) 15(5):R132. doi: 10.1186/ar4312

237. Reid J, Zamuner S, Edwards K, Rumley SA, Nevin K, Feeney M, et al. *In vivo* affinity and target engagement in skin and blood in a first-time-in-human study of an anti-oncostatin M monoclonal antibody. *Br J Clin Pharmacol* (2018) 84(10):2280–91. doi: 10.1111/bcp.13669

238. Shire SJ. *American Association of Pharmaceutical Scientists. Dosage Regimen: WO 2018/041823 A3*. Springer (2018).

239. Denton CP, del Galdo F, Khanna D, Vonk MC, Chung L, Johnson SR, et al. *Biological and clinical insights from a randomised phase II study of an anti-oncostatin M monoclonal antibody in systemic sclerosis* . Available at: https://academic.oup.com/rheumatology/advance-article/doi/10.1093/rheumatology/keac300/6588063.

240. Life PF. *Oncostatin M Antagonists: US6706266B1*. (2004).

241. Snyder M, Huang XY, Zhang JJ. Signal Transducers and Activators of Transcription 3 (STAT3) directly regulates cytokine-induced fascin expression and is required for breast cancer cell migration. *J Biol Chem* (2011) 286(45):38886–93. doi: 10.1074/jbc.M111.286245

242. Ng G, Winder D, Muralidhar B, Gooding E, Roberts I, Pett M, et al. Gain and overexpression of the oncostatin M receptor occur frequently in cervical squamous cell carcinoma and are associated with adverse clinical outcome. *J Pathology.* (2007) 212 (3):325–34. doi: 10.1002/path.2184

243. Winder DM, Chattopadhyay A, Muralidhar B, Bauer J, English WR, Zhang X, et al. Overexpression of the oncostatin M receptor in cervical squamous cell carcinoma cells is associated with a pro-angiogenic phenotype and increased cell motility and

invasiveness. *Journal of Pathology*. (2011) 225(3):448–62. doi: 10.3389/fmolb.2020.00029

244. Caffarel MM, Chattopadhyay A, Araujo AM, Bauer J, Scarpini CG, Coleman N. Tissue transglutaminase mediates the pro-malignant effects of oncostatin M receptor over-expression in cervical squamous cell carcinoma. *Journal of Pathology*. (2013) 231 (2):168–79.

245. Caffarel MM, Coleman N. Oncostatin M receptor is a novel therapeutic target in cervical squamous cell carcinoma. *Journal of Pathology*. (2014) 232:386–90.

246. Walch-Rückheim B, Pahne-Zeppenfeld J, Fischbach J, Wickenhauser C, Horn LC, Tharun L, et al. STAT3/IRF1 pathway activation sensitizes cervical cancer cells to chemotherapeutic drugs. *Cancer Res.* (2016) 76(13):3872–83.

247. Stroeder R, Walch-Rückheim B, Fischbach J, Juhasz-Böss I, Rübe C, Solomayer EF, et al. Oncostatin M treatment increases the responsiveness toward cisplatin-based chemoradiotherapy in cervical cancer cells in a STAT3-dependent mannerrussalina stroeder1. *Oncol Lett.* (2018) 16(3):3351–8.

248. Kucia-Tran JA, Tulkki V, Smith S, Scarpini CG, Hughes K, Araujo AM, et al. Overexpression of the oncostatin-M receptor in cervical squamous cell carcinoma is associated with epithelial-mesenchymal transition and poor overall survival. *Br J Cancer*. (2016) 115(2):212–22. doi: 10.1038/bjc.2016.199

249. Sreenivasan L, Li LV, Leclair P, Lim CJ. Targeting the gp130/STAT3 axis attenuates tumor microenvironment mediated chemoresistance in group 3 medulloblastoma cells. *Cells* (2022) 11(3):381. doi: 10.3390/cells11030381

250. Bembridge GP, Chung CW, Feeney M, Ford SK, Kirby I, McAdam R. *Antigen Binding Proteins to Oncostatin M (OSM): US8916695B2*. (2014).

251. Bernard FX, Danger Y, Froger J, Gascan H, Jegou JF, Lecron JC, et al. *Specific Binding Protein Capable of Binding Specifically to Human Oncostatin M (hOSM) Uses Therof: WO 2020/127884 A1*. (2021).

252. Fadini GP, Albiero M, Ciciliot S. *Composition To Induce Bone Marrow Stem Cell Mobilization: US 2017/0327573 A1*. (2017).

253. Jorcyk C, Xu D, Oncostatin M. *(OSM) Antagonists for Preventing Cancer Metastasis and IL-6 Related Disorders: US9550828B2*. (2017).

254. Arnett HA, Escobar SS, King CT, Lim AC, Narayanan S, Weinreb PH, et al. *Oncostatin M Receptor Antigen Binding Proteins: US9663571B2*. (2017).

255. Manning MC, Shahrokh Z, Nichols D, Levesque P, Holcomb RE. *Stable Anti-OSMR Antibody Formulation :US 10493149B2*. (2019).

256. Morikawa Y, Komori T, Esashi E, Kotaki A. Anti Oncostatin M receptor beta antibody. (2013).

257. Lecron JC, Gascan H, Morel F, Chevalier S, Bernarn FX, Boniface K, et al. *Compositions for Preventing, Reducing or Treating Keratinocyte-Mediated Inflammation: US2009/0300776AI*. (2009).

258. Mather JP, Roberts PE. *Antibodies to Oncostatin M Receptor: US7572896B2*. (2009).

259. Braun T, Kubin T. *Henning, Wolfgang, Jochen. Treatment of Oncostatin Receptor β Mediated Heart Failure: WO 2010/139742 A1*. (2010).

260. Mass OA, Tuccinardi J, Woodbury L, Wolf CL, Grantham B, Holdaway K, et al. Bioactive recombinant human oncostatin M for NMR-based screening in drug discovery. *Sci Rep* (2021) 11(1):16174. doi: 10.1038/s41598-021-95424-6

261. Du Q, Tu G, Qian Y, Yang J, Yao X, Xue W. Unbiased molecular dynamics simulation of a first-in-class small molecule inhibitor binds to oncostatin M. *Comput Biol Med* (2023) 155:106709. doi: 10.1016/j.compbiomed.2023.106709

262. Diveu C, Lelièvre E, Perret D, Lak-Hal AHL, Froger J, Guillet C, et al. GPL, a novel cytokine receptor related to GP130 and leukemia inhibitory factor receptor. *J Biol Chem* (2003) 278(50):49850–9. doi: 10.1074/jbc.M307286200

263. Diveu C, Lagrue Lak-Hal AH, Froger J, Ravon E, Grimaud L, Barbier F, et al. Predominant expression of the long isoform of GP130-like (GPL) receptor is required for interleukin-31 signaling. *Eur Cytokine Netw* (2004) 15(4):291–302.

264. Jumper J, Evans R, Pritzel A, Green T, Figurnov M, Ronneberger O, et al. Highly accurate protein structure prediction with AlphaFold. *Nature* (2021) 596 (7873):583–9. doi: 10.1038/s41586-021-03819-2

265. Varadi M, Anyango S, Deshpande M, Nair S, Natassia C, Yordanova G, et al. AlphaFold Protein Structure Database: Massively expanding the structural coverage of protein-sequence space with high-accuracy models. *Nucleic Acids Res* (2022) 50(D1): D439–44. doi: 10.1093/nar/gkab1061

266. Nishimoto N, Sasai M, Shima Y, Makagawa M, Matsumoto T, Shirai T, et al. Improvement in Castleman's disease by humanized anti-interleukin-6 receptor antibody therapy. *Clin Observations Interventions Ther Trials* (1999) 95:56–61.

267. Deisseroth A, Ko CW, Nie L, Zirkelbach JF, Zhao L, Bullock J, et al. FDA approval: Siltuximab for the treatment of patients with multicentric castleman disease. *Clin Cancer Res* (2015) 21(5):950–4. doi: 10.1158/1078-0432.CCR-14-1678

268. Keizer RJ, Huitema ADR, Schellens JHM, Beijnen JH. Clinical pharmacokinetics of therapeutic monoclonal antibodies. *Clin Pharmacokinet* (2010) 49(8):493–507. doi: 10.2165/11531280-000000000-00000

269. Du Q, Qian Y, Xue W. Molecular simulation of oncostatin M and receptor (OSM–OSMR) interaction as a potential therapeutic target for inflammatory bowel disease. *Front Mol Biosci* (2020) 7. doi: 10.3389/fmolb.2020.00029

270. Wei J, Ma L, Lai YH, Zhang R, Li H, Li C, et al. Bazedoxifene as a novel GP130 inhibitor for Colon Cancer therapy. *J Exp Clin Cancer Res* (2019) 38(1):63. doi: 10.1186/s13046-019-1072-8

271. Wu X, Cao Y, Xiao H, Li C, Lin J. Bazedoxifene as a novel GP130 inhibitor for pancreatic cancer therapy. *Mol Cancer Ther* (2016) 15(11):2609–19. doi: 10.1158/1535-7163.MCT-15-0921

272. Tian J, Chen X, Fu S, Zhang R, Pan L, Cao Y, et al. Bazedoxifene is a novel IL-6/GP130 inhibitor for treating triple-negative breast cancer. *Breast Cancer Res Treat* (2019) 175(3):553–66. doi: 10.1007/s10549-019-05183-2

frontiers | Frontiers in Immunology

TYPE Review
PUBLISHED 05 September 2022
DOI 10.3389/fimmu.2022.1000927

OPEN ACCESS

EDITED BY
Diana Boraschi,
Shenzhen Institute of Advanced Technology (SIAT), Chinese Academy of Science (CAS), China

REVIEWED BY
Yan Wang,
Chinese Academy of Medical Sciences & Peking Union Medical College, China
Yeqaing Liu,
Shanghai Dermatology Hospital, China
XueFeng Wan,
The First Affiliated Hospital of Xinjiang Medical University, China

*CORRESPONDENCE
Jianglin Zhang
zhangjl@csu.edu.com
Shanze Chen
chenshanze@mail.sustech.edu.cn

SPECIALTY SECTION
This article was submitted to Cytokines and Soluble Mediators in Immunity, a section of the journal Frontiers in Immunology

RECEIVED 22 July 2022
ACCEPTED 15 August 2022
PUBLISHED 05 September 2022

CITATION
Xiong K, Qi M, Stoeger T, Zhang J and Chen S (2022) The role of tumor-associated macrophages and soluble mediators in pulmonary metastatic melanoma.
Front. Immunol. 13:1000927.
doi: 10.3389/fimmu.2022.1000927

The role of tumor-associated macrophages and soluble mediators in pulmonary metastatic melanoma

Kaifen Xiong[1,2,3], Min Qi[4], Tobias Stoeger[5], Jianglin Zhang[2,6,7]* and Shanze Chen[1,2]*

[1]The Department of Respiratory Diseases and Critic Care Unit, Shenzhen Institute of Respiratory Disease, Shenzhen Key Laboratory of Respiratory Disease, Shenzhen People's Hospital (The Second Clinical Medical College), Jinan University, Guangdong, China, [2]The First Affiliated Hospital, Southern University of Science and Technology, Shenzhen, China, [3]Department of Dermatology, Xiangya Hospital of Central South University, Changsha, China, [4]Department of Plastic Surgery, Xiangya Hospital, Central South University, Changsha, China, [5]Institute of Lung Health and Immunity (LHI), Comprehensive Pneumology Center (CPC), Helmholtz Munich, Member of the German Center for Lung Research (DZL), Munich, Germany, [6]Department of Dermatology, Shenzhen People's Hospital, The Second Clinical Medical College, Jinan University, Guangdong, China, [7]Candidate Branch of National Clinical Research Center for Skin Diseases, Shenzhen, China

Skin malignant melanoma is a highly aggressive skin tumor, which is also a major cause of skin cancer-related mortality. It can spread from a relatively small primary tumor and metastasize to multiple locations, including lymph nodes, lungs, liver, bone, and brain. What's more metastatic melanoma is the main cause of its high mortality. Among all organs, the lung is one of the most common distant metastatic sites of melanoma, and the mortality rate of melanoma lung metastasis is also very high. Elucidating the mechanisms involved in the pulmonary metastasis of cutaneous melanoma will not only help to provide possible explanations for its etiology and progression but may also help to provide potential new therapeutic targets for its treatment. Increasing evidence suggests that tumor-associated macrophages (TAMs) play an important regulatory role in the migration and metastasis of various malignant tumors. Tumor-targeted therapy, targeting tumor-associated macrophages is thus attracting attention, particularly for advanced tumors and metastatic tumors. However, the relevant role of tumor-associated macrophages in cutaneous melanoma lung metastasis is still unclear. This review will present an overview of the origin, classification, polarization, recruitment, regulation and targeting treatment of tumor-associated macrophages, as well as the soluble mediators involved in these processes and a summary of their possible role in lung metastasis from cutaneous malignant melanoma. This review particularly aims to provide insight into mechanisms and potential therapeutic targets to readers, interested in pulmonary metastasis melanoma.

KEYWORDS

tumor-associated macrophages (TAMs), pulmonary metastatic melanoma, targeted therapy, soluble mediators, melanoma

Introduction

Cutaneous melanoma is a fatal skin malignant tumor derived from skin melanocytes. It is highly aggressive and is a major cause of skin cancer-related mortality; most patients have metastases the first time coming into the hospital (1, 2). The typical characteristics of cutaneous melanoma are early dissemination and subsequent metastatic colonization of multiple organs, for instance, lymph nodes, lung, liver, bone, and brain are common metastatic sites of skin melanoma (3). It's worth noting that metastatic melanoma is the main cause of its high mortality and among multiple organs that may be colonized by cutaneous melanoma, the lung is one of the most common distant metastatic sites of melanoma (3–6). The incidence of pulmonary metastasis of melanoma accounts for 5% of all malignant metastases, and the mortality rate of pulmonary metastasis of melanoma is also very high (7). Primary melanoma is another condition of pulmonary melanoma, but the incidence of primary melanoma is only 0.01%, and its pathophysiology and therapeutic intervention are still unclear (7, 8). This review focuses on pulmonary metastatic melanoma, which accounts for the majority of cases of pulmonary melanoma. Hoping this review could provide some possible explanations for the relationship between melanoma lung metastases and TAMs, which may not only help provide possible explanations for cutaneous melanoma lung metastases but also provide potential new therapeutic targets for the treatment of melanoma lung metastases.

Tumor metastasis is not only driven by the intrinsic changes of tumor cells, the implicated cross-talk between tumor cells and their altered microenvironmental components all also play an important role in tumor metastasis. In addition, tumor cell metastasis is usually a stepwise cascading process, which mainly includes (1) tumor cell invasion in the primary site, (2) tumor cells intravasated into the vasculature, (3) tumor cell survival in the circulations, (4) tumor cells extravasated out of the vasculature, (5) tumor cells adapt, colonize and grow at the metastatic site (9, 10). The tumor microenvironment (TME) is considered to have a strong influence on tumorigenesis and the occurrence of tumor metastasis. The macrophages that accumulate around the TME are usually called tumor-associated macrophages(TAMs) (11). A large number of studies have shown that the TEM significantly promotes tumor metastasis usually caused by the increasing infiltration of TAMs, and TAMs are almost involved in the five cascade steps of tumor metastasis (12, 13). Recent studies have found that TAMs play an important role in tumor metastasis. For example, Prune-1 enhances the M2 polarization of TAMs in triple-negative breast cancer (TNBC) and promotes TNBC lung metastasis (14). In the development, metastasis, and invasion of ovarian cancer, programmed death-ligand 1 (PD-L1), an immunomodulation point factor of tumor-associated macrophages, plays an important role (15). Moreover, a study suggests that genetic variants in TAMs can predict clinical outcomes of bevacizumab therapy in patients with metastatic colorectal cancer (16). The elevated number of TAM in the melanoma TEM is often correlated with its poor prognosis, and TAMs targeted drugs have several clinical trials in the targeted therapy of melanoma, breast cancer, pancreatic cancer, prostate cancer, and other tumors (17–19). However, there is no definite hypothesis on the role of TAMs in the mechanism and targeted therapy of melanoma pulmonary metastasis at present.

This article will review the origin, classification, polarization, recruitment, regulation and targeting of TAMs, as well as the soluble mediators involved in these processes, and summarize their possible role in pulmonary metastases from cutaneous malignant melanoma. This review shall provide some possible mechanistic explanations and potential targeted therapy options for TAMs in pulmonary metastasis melanoma for readers.

TAMs definition, origin, classification, and recruitment

TAMs definition

Macrophages are a highly heterogeneous class of immune cells that are found in almost all tissues. Macrophages clustered around the TEM are called tumor-associated macrophages (TAMs) and are the most common immune cells in the TEM (20, 21). A large number of studies have shown that the increased accumulation of TAMs in tumor tissue is related to the poor prognosis of tumor patients (15, 22). With increasing the infiltration of TAMs, the tumor cell proliferation, and invasion could be promoted and angiogenesis could be stimulated. Moreover, TAMs can exert anti-tumor immune responses by mediating the production of growth factors, chemokines, and other immune components by T cells, thus regulating tumor metastasis (15, 22–25).

TAMs origin

Blood monocytes derived from bone marrow hematopoietic stem cells were previously considered the generic origin of macrophages (20, 26). However, recent studies revealed that tissue macrophages of various organs such as the lung, brain, and liver embryonically originate from yolk sac progenitor cells (27). Consistent with this, there are two possible explanations for the origin of TAMs (1) tissue-resident TAMs: yolk sac progenitor-derived macrophages in various tissues may alter their phenotype or activation during tumorigenesis status; (2) tumor-induced TAMs (Monocyte-derived TAMs): Monocytes themselves undergo a distinct differentiation stage during tumor

growth and eventually become macrophages (26, 28). In different stages of tumorigenesis and development, the source of dominant macrophages may be different. Tissue-resident TAMs may predominate in the early stages of tumor growth, while tumor-induced TAMs may predominate in the later stages of tumor growth. About 30% of tumor cells in melanoma are TAMs mainly derived from circulating monocytes, which are considered to be the most abundant leukocytes in melanoma lesions (29).

TAMs classification

Macrophages are generally classified according to their function and their response to polarizing agents. Naive/unpolarized macrophages are called M0, and polarized macrophages are generally divided into M1 (classically activated macrophages) and M2 (alternatively activated macrophages), M2 macrophages can be further divided into Ma, Mb, Mc, Md subtypes (30, 31). Although, with the deepening of the understanding of macrophage polarization conditions, numerous new macrophage phenotypes, for example, Christian A. Gleissner, et al. identified M4 macrophages by comparing the transcriptome of M-CSF (macrophage colony-stimulation factor) and CXCL (4CXC Chemokine Ligand 4) induced macrophages *in vitro*, providing a novel starting point for atherosclerosis and other disease-related research; macrophages defined as M17 for secreting IL17 are also new macrophage phenotypes that have been recently identified (32, 33). The continued discovery of new macrophage phenotypes amply demonstrates the heterogeneity and plasticity of macrophages; however, the commonly used classification remains M1-M2, which differ in metabolic characteristics, markers, and gene expression profiles (31). M1 macrophages are involved in the anti-infective response together with helper T1 cells (Th1). It exerts its pro-inflammatory and anti-tumor effects by secreting pro-inflammatory cytokines such as interferon (IFN)-γ, IL-6, IL-12, tumor necrosis factor (TNF)-α, lipopolysaccharide (LPS) or molecules that regulate inflammation, and by producing substances such as nitric oxide synthase (NOS, a synthase involved in arginine metabolism) and reactive oxygen species (ROS) (15, 34). While the characteristics of M2 macrophages tend to favor tissue repair and tumor progression. M2 macrophages exert anti-inflammatory effects by secreting anti-inflammatory cytokines, such as IL-4, IL-10, IL-13, and TGF-β, and producing scavenger receptors and other substances; promoting proliferation, invasion and metastasis of tumor cells by inhibiting T-cell activity (15, 35, 36). The biological process of conversion between M1 (anti-tumor) and M2 (pro-tumor) in response to microenvironmental signals is termed "macrophage polarization" (35). Studies have shown that TAMs exist either two phenotypes on the tumor, for example, a study revealed that malignant melanoma TAMs as a heterogeneous phenotype with both M1 and M2 markers (37); However, the term "TAMs" now mainly refers to M2 macrophages because the functional characteristics of TAMs are more similar to M2 macrophages rather than to M1 macrophages (38).

TAMs recruitment

Expansion of tissue-resident TAMs and/or increased recruitment of monocyte-derived TAMs are important features of cancer. Cytokines, chemokines, growth factors, and other signals from tumor cells and stromal cells can induce the recruitment of TAMs to tumor sites (22, 39, 40). Several studies have found high levels of accumulation of tissue-resident macrophages and monocyte-derived macrophages in tumors such as glioblastoma, hepatocellular carcinoma and lung cancers (41–43). We therefore pondered whether the recruitment of TAMs also plays an important role in melanoma lung metastasis?

Colony-stimulating factor 1 (CSF-1), also known as macrophage colony-stimulating factor (M-CSF), is a secreted cytokine that differentiates hematopoietic stem cells into monocytes, macrophages, or other related cell types (44). CSF-1 acts as a major lineage regulator of macrophages and is also a recognized recruiter of macrophages. CSF-1 affects macrophages and monocytes through increased phagocytic, chemotactic activity and tumor cytotoxicity or other ways to affect macrophages and monocytes (44). Extensive overexpression of CSF-1 can be observed at the invasive edge of the various tumor, and it is involved in the polarization of M2 macrophages by interacting with its ligand CSF-1R; Its overexpression is also associated with a significant increase in metastasis (22, 45). Depletion of CSF-1/CSF-1R was shown to significantly inhibit tumour progression and metastasis in various tumour models (22, 44, 46). On the contrary, restoration of CSF-1 expression can accelerate tumor progression and metastasis in a CSF-1 mutant mouse xenograft model (46).

CCL2 is another well-established macrophage recruiter and M2 stimulator in addition to CSF-1. It is reported that CCL2 could induce the differentiation of macrophage into protumor phenotypes through CC chemokine receptor 2 (CCR2); In mouse tumor models such as colorectal cancer, prostate cancer, and melanoma, CCL2 recruit TAMs to tumor sites through ligand-receptor interactions with CCR2 or other forms of action (47–50). When the CCL2/CCR2 interaction was blocked, the metastatic dissemination of tumors in the mouse was significantly inhibited, the survival of the mouse was prolonged and the expression levels of tumor-promoting cytokines were reduced (47, 51). In a study by Xiaojing Chen, Yuanrun Deng et al. CCL8 act as another ligand for CCR2 was found to be highly overexpressed in human cervical cancer, which involved in the recruitment of TAMs in hypoxic regions (52). Moreover, the high expression of CCL2 in tumors such as esophageal carcinogenesis and clear cell renal cell carcinoma is associated with increased TAMs infiltration and metastatic events (53, 54).

It is well known that hypoxia promotes malignant tumor behavior through multiple mechanisms, including promoting glycolysis, antagonizing apoptosis, inducing immune escape, and inducing drug resistance, and is a common feature of most solid tumors (55–57). Studies have shown that hypoxia has an important impact on the recruitment of TAMs and that hypoxia captures disseminated macrophages by downregulating chemokine receptors expressed on macrophages (38). In addition, TAMs are recruited to the hypoxic TME through CCL2, VEGF-A, endothelin-2, semaphorin 3A (SEMA3A), stromal cell-derived factor 1α (SDF1α), and oncostatin M, etc. (38, 58, 59). TAMs are involved in angiogenesis and tumor spread through upregulation of hypoxia-inducible factor (HIF)-1a and HIF-2a when they are recruited to the hypoxic environment (38). The recruitment of TAMs by hypoxia facilitates the conversion of the TME into more hospitable sites for a tumor cell.

Besides, ligand-receptor interactions such as CCL3/CCR1, CCL3/CCR5, CCL5/CCR5, CX3CL1/CX3CR1, and VEGF-A/VEGFR1 and chemokines such as CCL7, CCL8, CCL9, CCL18, CCL20, IL-13…all can contribute to the survival, progression, and metastasis of various tumor including melanoma by recruiting TAMs to TEM (40). For example, the chemokine CCL20 is recognized by the CCR6 ligand expressed in melanoma and promotes melanoma growth and metastasis *in vivo* (60). It is reasonable to speculate that the recruitment of TAMs has a potential role in pulmonary metastatic melanoma. We still further describe the source, function, classification, and recruitment of TAMs in detail, as shown in Figure 1, hoping to better help readers understand the relevant definitions of TAMs.

The roles of TAMs in pulmonary metastatic melanoma

Pulmonary metastatic melanoma

Invasion and metastasis are the main causes of tumor death, and it is reported that the mortality caused by malignant tumor metastasis accounts for more than 90% of cancer mortality (61). Metastasis generally refers to the migration and spread of cancer cells from the primary sites to surrounding and distant organs; most malignant solid tumors could metastasize from the primary organ to other organs, such as the lung, liver, brain, and bone. Such a metastatic process is a gradual process termed the “metastatic cascade” (62). Like most solid tumors, melanoma also metastasizes to other organs. Early lymph node metastasis is one of the typical features of melanoma, the lung is one of the most common distant metastases of melanoma, and it is reported that about 18% of melanoma patients developed lung metastases during follow-up (63, 64). Moreover, the clinical prognosis of melanoma lung metastases is poor, and the 1-year survival rate of patients with melanoma lung metastases has been reported to be only about 30%-60% (65).

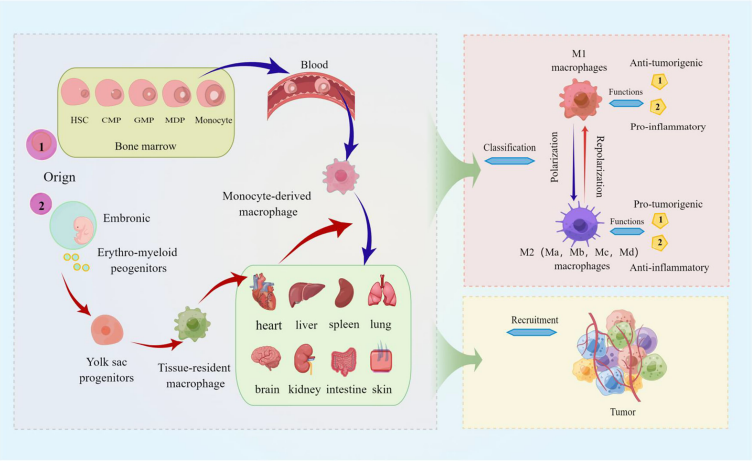

FIGURE 1
The source, function, classification, and recruitment of TAMs. The picture displayed that TAMs are derived from blood mononuclear cells from bone marrow hematopoietic stem cells, called monocyte-derived TAMs (or tumor-induced TAMs) and yolk sac progenitors, and reside in organs such as the lung, brain, liver, and skin. Macrophages polarized in tumors are divided into M1 (classically activated macrophages) and M2 (alternatively activated macrophages), and M2 macrophages can be further divided into Ma, Mb, Mc, and Md subtypes. M1 macrophages are characterized by the secretion of pro-inflammatory cytokines involved in anti-infective responses, and the immunosuppressive phenotype of M2 macrophages tends toward tissue repair and tumor progression; TAMs are activated by cytokines, growth factors, etc. can be recruited to tumor sites.

Epithelial-mesenchymal transition (EMT) is the process by which epithelial cells acquire mesenchymal properties and is associated with multiple functions such as tumour progression, metastasis and drug resistance (66). Recently, a series of studies have shown that TAMs are involved not only almost in each step of the metastatic cascade, such as the formation of pre-metastatic ecological niches, infiltration of tumour cells, survival of circulating tumour cells, extravasation and colonization of tumour cells, but also in the regulation of the EMT process (12, 15, 67–69). TAMs exhibit many important biological functions from different aspects during tumor progression. Here, we mainly focus on the role of TAMs in the process of pulmonary metastasis of melanoma. TAMs are involved in almost every step of metastasis as described below, also shown in Figure 2.

Pulmonary metastatic melanoma and TAMs

TAMs promote invasion of melanoma tumor cells

Invasion is generally considered to be the initiation of tumor metastasis. EMT and TAMs plays an important role in tumor invasion. On the one hand, EMT is a major event in the morphological transformation of tumor cells that acquire the invasive ability to escape from the border of the basement membrane to the surrounding mesenchyme, which contributes to tumor cells invasion and metastasis (70). On the other hand, compatibility factors secreted by TAMs, such as IL-8, TNF-α, and transforming growth factor-β (TGF-β), are involved in the regulation of the EMT process and promote metastasis (67, 71).

Abundant shreds of evidence indicate that the proportion of TAMs infiltrating melanoma is increased, and the high expression level of macrophage markers in melanoma tissue is closely related to poor prognosis (72, 73). A study suggests that high levels of reactive oxygen species (ROS) in primary melanoma may increase cytokine-tumor necrosis factor-α (TNF-α) secretion through MAPK/ERK kinase 1-mediated peroxisome proliferator-activated receptor γ (PPARγ) translocation to the nucleus, and it thus enhanced the invasion of TAMs in melanoma (37). These studies all provide favorable evidence to support the idea that TAMs promote invasion and cause melanoma lung metastasis.

TAMs promote vascularization of melanoma tumor cells

The process of forming new blood vessels from existing blood vessels is called angiogenesis. Angiogenesis is a vital condition for tumor cell proliferation and generation (74). Many tumors, including melanoma, metastasize through the vascular system and/or the lymphatic system. Existing evidence strongly supports that TAMs drive tumor angiogenesis through vascular endothelial growth factor (VEGF) matrix metalloproteinase (MMP9); TAMs stimulate the remodeling of established vasculature into a more tortuous and leaky form, which is beneficial to tumors dissemination of cells (15, 75, 76). When TAMs are absent, vessel density can be reduced by approximately 40% (76). In addition,

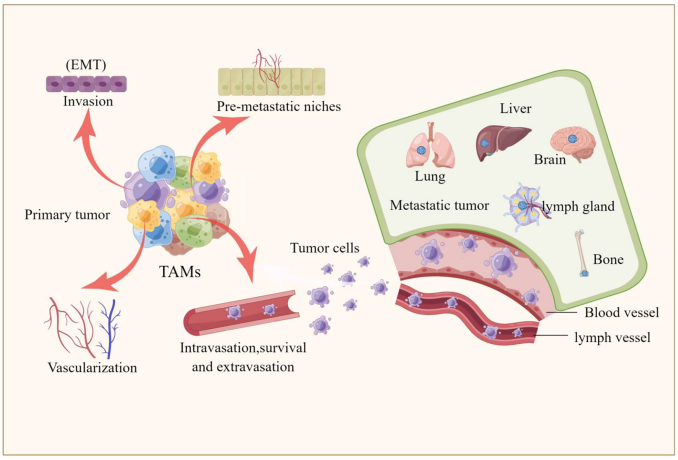

FIGURE 2
TAMs are involved tumor metastasis. The picture illustrated that TAMs are involved in every step of the metastatic cascade, including the formation of pre-metastatic ecological sites, invasion of tumor cells, survival of circulating tumor cells, extravasation and colonization of tumor cells, and the involvement of TAMs in regulating the epithelial-mesenchymal transition (EMT) process that promotes the formation of liver, brain, lung, bone and lymph node metastases.

studies have shown that pro-angiogenic molecules such as nitric oxide (iNOS), MMP7, CXCL8, IL1, and fibroblast growth factor (FGF)-2 can regulate tumor angiogenesis through TAMs (75, 77).

Studies show that the process of VEGF-C (tumor overexpressed ligand)/VEGFR-3 (receptor for VEGF-C expressed on TAMs) promotes lymphangiogenesis by directly affecting the activity of lymphatic endothelial cells (lymphatic endothelial cells) or indirectly increasing the secretion of ductal proteins to promote lymphangiogenesis, which supports the hypothesis that lymphangiogenesis is closely related to TAMs and also further suggests that TAMs play an important role in tumor invasion and metastasis (78, 79). The research carried out by Peiwen Chen et al.shows that TAMs promote angiogenesis and melanoma growth through paracrine and autocrine adrenomedullin. When adrenomedullin levels are reduced or secretion is inhibited, angiogenesis and melanoma growth *in vivo* are correspondingly inhibited (80). Monocyte chemoattractant protein-1 (MCP-1) is a member of the CC-motif chemokine family (as CCL2); MCP-1, a chemokine, is also one of the key agonists in the recruitment of macrophages to tumor sites (81). Both *in vivo* and *in vitro* studies have demonstrated that MCP-1 triggers a rich vascular network through M2 macrophages, and targeting TAMs to inhibit MCP-1 reduces angiogenesis and tumor growth in human melanoma xenografts (47).

Taken together, TAMs play an important role in regulating tumor angiogenesis and promote the vascularization of tumor cells (including melanoma cells)through different pathways, which may provide some explanation for melanoma lung metastasis.

TAMs promote the intravasation, survival in the circulation, and extravasation of melanoma tumor cells

Intravasation is defined as the process by which tumor cells leave the primary tumor and enter the circulation (generally into the blood circulation); tumor cells that enter the circulation survive and participate in the circulation and then leave the circulatory system, and the process of entering the secondary site from the primary tumor is called extravasation (82). Intravasation, survival, and extravasation of tumor cells in the circulatory system are all important steps in the cascade of events leading to tumor metastasis. Multiphoton *in vivo* imaging experiments showed that macrophages were mainly concentrated in the periphery of the tumor, and the density of macrophages in the center of the tumor decreased; the macrophages in the tumor were localized to the blood vessels and assisted the intravasation of tumor cells (83). Another study found that the intravasation of tumor cells was always accompanied by macrophages within one cell diameter (84). These studies provide strong evidence that TAMs enhance the ability of cancer cells to invade adjacent normal tissue.

Clinical observations suggest that the tumor metastasis microenvironment (TMEM) is composed of tumor cells, TAMs, and endothelial cells (15). In TMEM, TAMs can produce EGF (epidermal growth factor) and secrete chemokine CCL18, and tumor cells can also secrete chemokine CCL18 and produce cytokine CSF-1, all of which play important roles in the process of tumor cell invasion. For example, a study by Jingqi Chen et al. found that CCL18 secreted by TAMs in breast cancer induces integrin accumulation in cancer cells, which further promotes the adhesion of integrin-aggregated cancer cells to the extracellular matrix and then intravasation (85). The chemokine CCL18 produced by melanocytes itself can be increased and released under the induction of long non-coding RNA (LncRNA) CRNDE, and promote the proliferation, invasion, and metastasis of melanoma (86).

Tumor cells, which intravasated the circulation, also need to survive and circulate in the circulatory system. On the one hand, tumor cells evade recognition and killing by cytotoxic immune cells by clustering with platelets in the circulatory system; On the other hand, the survival of many tumor cells is protected by chemokines or cytokines secreted by macrophages (87, 88). Regarding the involvement of TAMs in tumor cell extravasation and tumor cell colonization, existing evidence supports that when tumor cells interact, macrophages have a higher extravasation rate. Therefore, the number of tumor cells that occurs extravasation was significantly reduced when macrophages are depleted (89).

Are TAMs also involved in promoting the endocytosis, circulating survival and extravasation of melanoma cells during pulmonary metastasis of melanoma? Based on the results of the above-mentioned studies, we believe that the answer is more than likely also in the affirmative.

TAMs prepare sites for melanoma tumor cells: pre-metastatic niches

The favorable microenvironment created by the primary tumour for secondary organs and/or tissues to which it subsequently metastasizes (metastatic target organs or tissues) is known as the pre-metastatic niche (PMN). the PMN is initiated and established through a complex interaction between growth factors, inflammatory factors, chemokines, bone marrow-derived cells and local stromal components in the primary tumour (90). Studies have shown that macrophages are one of the key determinants of PMN formation. Tissue-resident TAMs, such as osteoclasts and alveolar macrophages, are involved in PMN formation (91, 92). What're more, soluble mediators such as CSF-1, VEGF, TGF-α, and exosomes and tissue inhibitors of metallopeptidase (TIMP) that are involved in the recruitment of TAMs can also mobilize TAMs to aggregate in PMNs (92).

TAMs interact with dendritic cells(DC) and T helper cells (Th1 cells), impairing the antigen presentation and antitumor behavior of these immune cells; TAMs regulate tumor angiogenesis and extravasation through matrix-derived factors

(SDFs) and matrix metalloproteinases, etc., which in turn promote the formation of PMNs from tumor cells (CTCs) (15, 92, 93). Considering the preferential metastasis of lung-homing melanoma cells in melanoma metastasis and the important regulatory role of PNM in tumor metastasis, it is reasonable to speculate that TAMs and soluble mediators play an important role in melanoma lung metastasis by promoting PMN formation.

TAMs regulation and pulmonary metastasis melanoma

It has been reported that affecting TAM regulation at the transcriptional, epigenetic and metabolic levels could be an effective cancer treatment modality. The regulation of TAMs can influence its production, phenotype, and function, which in turn affect tumor development and metastasis, and drug resistance. The clinical application of corresponding activators or inhibitors for different regulatory modalities and related pathways is expected to target TAMs to improve the efficacy of tumor immunotherapy. We present the modalities of TAMs regulation in Figure 3.

We speculate whether regulating the production, phenotype and function of TAMs influence pulmonary metastasis from melanoma. Accordingly, does the application of activators or inhibitors that modulate key factors also improve the efficacy of therapy for lung metastases from melanoma?

Epigenetic regulation of TAMs and pulmonary metastasis melanoma

Epigenetics refers to developmental or environment-induced modifications that control the expression of information encoded in DNA in a tissue- and environment-specific manner without altering the genetic code (94). Various cellular functions, such as cell differentiation, cell activation, and transformation, are regulated by epigenetic changes in gene expression. Epigenetic dynamics of DNA methylation and histone modifications (such as methylation, acetylation, and phosphorylation) are associated with altered gene expression (95). The development, polarization, and activation of macrophages are also controlled by DNA and histone modifications. For example, DNA methylation and myeloid differentiation, Histone modifications in M1 macrophage activation, and M2 macrophage polarization by Jmjd3(an H3K27-specific demethylase) are currently clear mechanisms for the epigenetic regulation of macrophage phenotype and function (96). In addition to the epigenetic effects of DNA methylation and histone modification on the phenotype and function of TAMs, emerging data suggest that epigenetic changes in noncoding RNAs also have regulatory effects on TAMs. For example, many miRNAs involved in the production of IL-10 and the expression of PD-L1 in TAMs exert immunosuppressive effects in an epigenetic manner, helping to identify new therapeutic targets and providing a research reference for improving tumor sensitivity to immune responses (97).

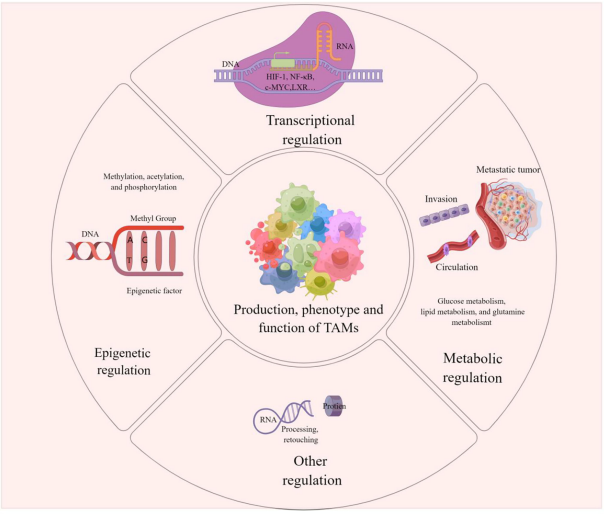

FIGURE 3
TAMs regulation This picture demonstrates that the production, phenotype and function of TAMs are regulated in epigenetic, transcriptional, metabolic or other different ways. These modulations influence tumorigenesis, metastasis and drug resistance on Pulmonary metastases in melanoma can also be influenced by the regulation of TAMs.

It is noteworthy that changing epigenetic regulation in macrophages selectively targets M2 macrophages and removes tumor-promoting TAMs while retaining only tumor-suppressed M1 macrophages (98, 99). Pharmacological modulators of many epigenetic enzymes are currently in clinical use and can be used to treat tumors with high TAM infiltration (99). Much research has been done on the epigenetic enzymes of M1s and their regulators, but much less is known about the epigenetic regulation of M2s, especially about cancer (99).

Taken together, epigenetic regulation affects tumorigenesis, progression, and metastasis by affecting the phenotype and function of TAMs. Given that melanoma is also one of the tumors subject to epigenetic regulation, it is reasonable to speculate that epigenetic regulation in TAMs may be an important reference direction for studying the mechanism and treatment of pulmonary metastatic melanoma.

Transcriptional regulation of TAMs and pulmonary metastasis melanoma

It is well known that malignant tumors usually have hypoxia, and the activation of two transcription factors, hypoxia-inducible factor-1 (HIF-1) and nuclear factor kappa b (NF-κB) is closely related to the occurrence of hypoxia. Circulating hypoxia affects the expression of angiogenesis-inducing cytokines such as VEGF-A, CCL2/MCP-1, etc., and recruits various cells into the tumor niche, where they are transformed into tumor-associated macrophages (TAM) involved in tumorigenesis, etc. Through the regulation of transcription factors HIF-1 and NF-κB and their related pathways, regulating the generation of TAMs may be one of the potential tumor-targeted therapeutic options (100). STAT-3 is also one of the key factors to initiate the transcriptional program of TAMs (101). In addition, research shows that transcription factor EB (TFEB) expression is significantly reduced in breast cancer. TFEB controls the phenotype and function of TAMs through multiple autophagy/lysosome-dependent and independent pathways, thereby promoting breast tumor development; Conversely, activation of TFEB is expected to be a target for TAMs for tumor immunotherapy strategies including breast cancer (102). The Liver X receptor (LXR) is one of the transcription factors in the nuclear receptor family that is activated by oxysterols and synthetic high-affinity agonists; A study shows that in a mouse model of lung cancer, pharmacological LXR activation can regulate TAM gene expression, thereby exerting an anti-tumor effect (103). In addition, studies show that the transcription factor c-Maf is a key controller of immunosuppressive macrophage polarization and function in cancer; Numerous M2 macrophage-related genes are controlled by c-Maf, which in turn promotes M2 macrophage-mediated T cell suppression and tumor progression. In a subcutaneous LLC tumor model, inhibition of c-Maf partially overcomes resistance to anti-PD-1 therapy; Likewise, c-Maf is expressed in human M2 and tumor-infiltrating macrophages/monocytes as well as circulating monocytes in human non-small cell lung cancer (NSCLC) patients and plays an important role in regulating its immunosuppressive activity (104).

Overall, various transcription factors including c-MYC, LXR, TFEB, etc., regulate the phenotype and function of TAMs in solid tumors such as lung cancer and breast cancer, thereby affecting tumor progression and metastasis. The clinical application of corresponding transcriptional activators or transcriptional inhibitors is expected to provide a new strategy for targeting TAMs in the treatment of tumors. Lung metastatic melanoma derived from melanoma has a close relationship with TAMs. The role of TAMs in pulmonary metastatic melanoma through transcriptional regulation needs more research, which not only contributes to providing a certain explanation for the development of pulmonary metastatic melanoma but may also provide possible strategies for targeting TAMs in the treatment of pulmonary metastatic melanoma.

Metabolic regulation of TAMs and pulmonary metastasis melanoma

As an important immune cell in TME, TAMs are closely related to poor tumor prognosis, drug resistance, enhanced angiogenesis, and tumor metastasis; A complete interpretation of the pro-tumor and anti-tumor metabolic switches in TAMS is critical for understanding immune escape mechanisms in cancer (105). Currently, a few of researches have been done on the intertwined relationship between metabolism and macrophages in the context of cancer, and the interaction between the two is not fully defined. Considering that pulmonary metastatic melanoma is closely related to TAMs like many solid tumors, the study of the regulation of TAMs may provide some explanation for the mechanism of pulmonary metastatic melanoma and its therapeutic direction.

A tumor hypoxic environment induces transcription of genes related to glucose and nitrogen metabolism. Hypoxia of the TME increases the levels of arginase-1 and man-ose receptor (CD206) on TAMs, and TAMs present in hypoxic regions induce the expression of HIF-1α, which induces a switch to glycolytic fermentation (106). Furthermore, a study shows that hypoxic TAMS strongly upregulated the expression of Redd1 (a TOR complex 1-MTORC1 inhibitor), a negative regulator of the mechanistic target of rapamycin (mTOR, a key nutrient, and energy sensor); Metabolic changes promote tumor angiogenesis and metastasis by inhibiting the glycolysis of hypoxic TAMs, inhibiting their angiogenesis and immunosuppressive effects (107). Moreover, exosomes derived from tumor cells can affect the differentiation of macrophages by altering the miRNA profiles of TAMs. For example, in the study of ovarian cancer,

it was found that hypoxia induced the expression of miR-940 in tumor exosomes and stimulated macrophages polarized toward the M2 phenotype; This also suggests that the metabolic program in TAMs is a combination of hypoxia and cytokines in the microenvironment (108, 109). Glucose metabolism, lipid metabolism, and glutamine metabolism all play an important role in the regulation of TAMs metabolism, and therapeutics targeting metabolic pathways in TAMs is also one of the alternative strategies for cancer treatment (105).

In general, some studies have shown that metabolic alterations of TAMs in a variety of solid tumors promote or inhibit their progression and metastasis. The metabolic effects on substances such as sugar and liposomes in melanoma TEM may also cause alterations in TAMs, which may affect melanoma lung metastasis. How alterations in the metabolism of TAMs affect their phenotype and function, and their impact on tumor growth and metastasis, including melanoma, remains to be revealed by more studies. The role of metabolic regulation of TAMs in pulmonary metastatic melanoma is also worthy of further investigation, as this may provide possible mechanistic explanations and even potential therapeutic targets for pulmonary metastatic melanoma.

TAMs targeted treatment strategies in pulmonary metastatic melanoma

As a key component of TEM and/or TMEM, TAMs infiltration is closely related to the survival rate and poor prognosis of tumor patients, and targeting TAMs is becoming an attractive tumor therapeutic intervention strategy (19, 60, 110). Multiple studies have demonstrated that inhibiting the recruitment or proliferation of TAMs, TAMs depletion, TAMs reprogramming, and targeting TAMs-related immune checkpoints are all effective strategies to target TAMs for tumor therapy, the specific treatment methods are shown in Figure 4.

Inhibiting the recruitment or proliferation of TAMs

The recruitment or proliferation of TAMs, which cause the number of TAMs to increase, is a key link in promoting the occurrence, development, and metastasis of tumors. Inhibiting the recruitment or proliferation of monocyte-derived TAMs is considered to be an effective anti-tumor therapeutic strategy targeting TAMs.

Targeting the soluble mediators CSF-1/CSF-1R and CCL2/CCR2, which induce recruitment of TAMs as described above, are currently the main potential targets to inhibit recruitment of TAMs for antitumor effects (111). CSF-1 (CSF-1) interacts with its ligand CSF-1R to promote tumour progression and metastasis by participating in the phenotypic differentiation of M2-type macrophages. Anti-CSF-1R antibodies and CSF-1R inhibitors retard tumour progression by regulating the polarization of TAMs (112, 113). Currently, CSF-1R inhibitors such as PLX3397 and ARRY-382 and anti-CSF-1R antibodies

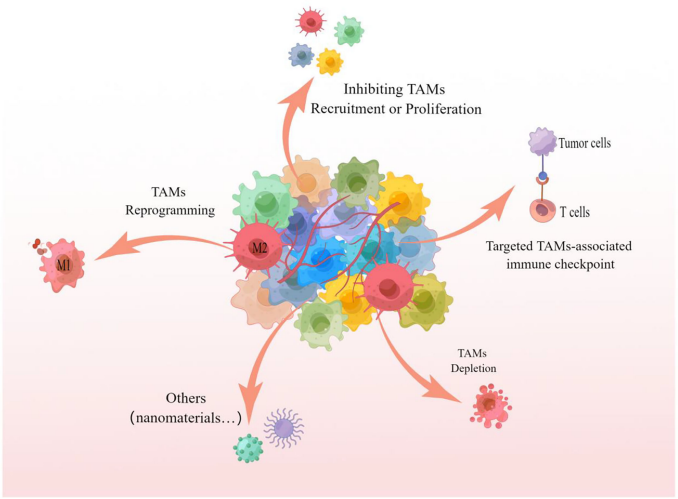

FIGURE 4
TAMs targeted treatment strategies The picture showed that inhibition of recruitment or proliferation of TAMs, depletion of TAMs, reprogramming of TAMs and targeting of TAMs-associated immune checkpoints are all capable of targeting TAMs for effective anti-tumor therapy. These strategies can likewise be referred to for targeting TAMs for the treatment of pulmonary metastatic melanoma.

FPA008 and RG7155 are under clinical development or evaluation (114–116). In the mouse xenograft model, the combination of CSF-R inhibitor and anti-PD-1 antibody showed a good therapeutic effect on melanoma (117).

Targeting the CCL2/CCR2 axis exhibits antitumor therapeutic effects by inhibiting the recruitment and polarization of TAMs. The anti-CCL2 antibody Carlumab (CNTO888) can cause a temporary decrease in the level of CCL2 in patients with prostate cancer so that the patient's disease state can be stabilized (118); CCR2 inhibitor PF-04136309) Combined with FOLFIRINOX (Oxaliplatin + Irinotecan + Leucovorin + Fluorouracil), the clinical outcome of patients with pancreatic adenocarcinoma was significantly improved (18). However, there may also be side effects, when CCR2 inhibitors are combined with chemotherapy or another therapeutic method (119). In a mouse melanoma model, combined treatment of CCR2 inhibitor RS504393 and anti-PD-1 improved the efficacy of melanoma lung metastases in mice (120).

In addition, targeting the CD40 receptor, targeting CX3CL1/CX3CR1, etc. have also been revealed to exert anti-tumor effects by effectively inhibiting the recruitment or proliferation of TAMs (111, 121, 122).CD40, which is expressed on antigen-presenting cells such as dendritic cells, is a member of the TNF receptor superfamily. CD40 plays an anti-tumor effect by promoting the activation of anti-tumor T cells and the polarization of M1 phenotype cells (123). Usually CD40 agonists are used in combination with anti-CSF-1R antibodies to enhance anti-tumour responses by inducing an increase in pro-inflammatory macrophages and eliminating the effects of populations that cause suppressive immune responses (124). For example, a phase I trial of the CD40 agonist APX005M (sotigalimab) and cabiralizumab in combination or not with the PD-1/PD-L1 inhibitor nivolumab for the treatment of anti-PD-1/PD-L1 resistant melanoma, kidney cancer and non-small cell lung cancer (125). There are also multiple clinical trials underway with anti-CD40 antibodies and recombinant CD40 ligands, alone or in combination with other treatments. Such as SGN-40, SEA-CD40, ADC-1013, etc (126).

Overall, Antibodies or small molecules targeting TAMs, alone or in combination with other therapeutic modalities, to inhibit the recruitment or proliferation of TAMs have proven to be a promising therapeutic technique for the treatment of solid tumors including melanoma lung metastases. However, inhibiting the recruitment or proliferation of TAMs also has side effects, so other strategies to target TAMs are also in full swing.

Depletion of TAMs

Since TAMs are involved in different stages of cancer development and progression, reducing or depleting TAMs is an attractive cancer treatment strategy. Elevated TAM numbers in TEM are often associated with poor prognosis in melanoma patients, therefore, reducing or depleting TAMs can be an effective targeted therapy for melanoma (127, 128).

Numerous of antitumor drugs have cytotoxic effects on TAMs while killing tumor cells (31, 129). Non-cytotoxic doses of commonly used chemotherapeutic drug paclitaxel have been reported to have inhibitory effects on immunosuppressive macrophages in mouse melanoma models, reducing bone marrow-derived suppressor cells (MDSCs), and even blocking the immunosuppressive potential of MDSCs (130). Due to the short biological half-life and renal toxicity of the drug itself, the direct use of TAMs cytotoxic drugs is limited. Combining TAMs cytotoxic drugs with nanomaterials can effectively improve the above problems (131–134). For example, novel clodronate-containing liposomes significantly reduced the number of lung nodules in a B16/F10 lung metastatic melanoma model; This study demonstrated that deletion of TAMs exhibited antitumor effects in metastatic melanoma by inhibiting angiogenesis and regulating inflammation-related cytokines (127). In addition, inhibition of M-CSF receptors can also deplete TAMs and enhance antitumor therapeutic effects (135).

In general terms, TAMs depletion therapy holds great potential as novel cancer (including pulmonary metastatic melanoma) treatment. However, the therapy has also caused a reduction in the number of systemic macrophages, which are the first line of defense for the innate immune response, which can cause adverse effects on the organism (131, 132, 136). Nanomaterials that reduce or deplete TAMs could largely limit the adverse effects of this therapeutic approach on the organism, and as such, much research is underway to target TAMs depleting nanomaterials, which also promises to provide better options for treating lung metastases from melanoma.

TAMs reprogramming

Due to the plasticity of macrophages themselves and the functional characteristics of TAMs more similar to M2 (pro-tumorigenic) macrophages rather than to M1 (anti-tumorigenic) macrophages, reprogramming M2-like macrophages into M1-like macrophages (also known as "repolarization") is one of the most attractive antitumor therapeutic modalities for targeting TAMs.

Activation of CD206 (mannose receptor) and toll-like receptors (TLRs) plays an important role in the repolarization of M2 macrophages to M1 macrophages. Studies have shown that activation of CD206 promotes the conversion of M2 to M1 through endocytosis, phagosome-lysosome formation, and autophagy, and enhances the phagocytosis of tumor cells (137). Moreover, studies have shown that the U.S. Food and Drug Administration (FDA)-approved clinical TLR agonist TLR

agonist Imiquimod has shown significant antitumor activity in preclinical models of melanoma (138, 139). Another study revealed that the FAD-approved cancer-common chemotherapy drugs sorafenib and paclitaxel can cause repolarization of TAMs (140, 141). Furthermore, if NF-kB inhibition, TAMs differentiate into M2 macrophages, and upon NF-kB activation, TAMs can be redirected to an M1-like phenotype with tumoricidal activity. Studies suggest that immunomodulators such as type I IFN (IFN-α, IFN-β) and type II IFN (IFN-γ) are effective in repolarizing TAMs in skin tumors such as melanoma (142, 143). It has been reported that the M2-specific clearance receptor MARCO is associated with poor prognosis in malignant tumors such as non-cellular lung cancer and metastatic melanoma, suggesting that targeting MARCO may promote the repolarization of M2 macrophages to M1 macrophages (144).

Overall, reprogramming of TAMs is showing promise as a novel anti-tumor targeted therapeutic strategy for advanced or metastatic tumors including melanoma lung metastases. However, clinical data on the therapeutic effect of repolarizers are limited, and more strong evidence is needed to support the efficacy and safety of repolarizers.

Targeting TAMs–associated immune checkpoints

Immune checkpoint inhibitors (ICIs) are a promising tumor immunotherapy approach for a variety of advanced/metastatic solid tumors, including melanoma, and are now widely accepted by clinicians (145, 146). Numbers of literature show that TAMs involvement in the failure of anti-tumor immune surveillance, as well as the failure of ICIs immunotherapy (146), suggests that targeting TAMs-related immune checkpoints can provide more options for tumor immunotherapy.

Immune checkpoint molecules such as programmed cell death 1 (PD-1), programmed cell death protein ligand 1 (PD-L1) and cytotoxic T lymphocyte-associated protein 4 (CTLA-4) are the most common immune checkpoints in clinical practice's target. Anti-PD-1/PDL-1 or anti-CTLA-4 therapy mainly maintains an effective immune system against cancer cells by activating tumor-specific cytotoxic T cells (147, 148). One study found that TAMs expressed PD-1 in both mouse and human tumor models; the phagocytic ability of TAMs in a mouse tumor model was negatively correlated with PD-1 expression. When PD-1/PD-L1 expression was inhibited, the phagocytic ability of TAMs *in vivo* was increased, tumor growth was delayed, and mouse survival was prolonged (149). In addition, studies have shown that a specific metabolic enzyme, indoleamine 2,3-dioxygenase (IDO), is involved in T cell exhaustion, which can serve as a target to avoid TAMs-mediated immune escape and improve anti-ICIs efficacy. The combination of IDO and pembrolizumab has good efficacy in the treatment of advanced and metastatic melanoma, and it is worthy of further evaluation (150). A completed Phase 1/2 clinical trial (NCT02073123) of the IDO inhibitor indoximod in combination with ICIs (ipilimumab, pembrolizumab, and nivolumab) in adult patients with metastatic stage III/IV melanoma, the results of the study showed that although the combined treatment method had side effects of fatigue, nausea, and itching, the patients showed good tolerability and efficacy.

Taken together, targeting TAMs-related immune checkpoints has attracted much attention as one of the options for tumor immunotherapy or adjuvant therapy. Regarding the targeting of immune checkpoints related to TAMs, there are not only many mechanism studies but also several clinical trials underway. Immunotherapy is still the common clinical treatment modality for melanoma, especially for advanced and metastatic melanoma. Can targeted TMAs therapy improve the efficacy of conventional immunotherapy? This is undoubtedly worthy of investigation and anticipation.

Other TAMs targeted therapy strategies and pulmonary metastatic melanoma

Targeted anti-tumor therapy for TAMs in addition to the above-mentioned methods, for example, because TAMs play a key role in angiogenesis and phagocytosis in the process of tumor development and metastasis, there are also corresponding targeted therapy methods (122).

Studies suggested that milk fat globule epidermal growth factor 8 (MFG-E8) promotes melanoma growth by stimulating mesenchymal stromal cell-induced angiogenesis and the differentiation of TAMs to the M2 phenotype, so targeting MFG-E8 to inhibit melanoma angiogenesis may be one of the effective targets for anti-melanoma therapy (151). Monocyte chemoattractant protein (MCP)-1, a chemokine, is one of the key agonists for attracting macrophages to tumors, and a study shows that in melanoma xenografts, inhibition of MCP-1 can inhibit TAMs recruitment and anti-angiogenesis, which is a highly anticipated melanoma therapeutic target (47). In addition, studies revealed a new mechanism by which TAMs promote angiogenesis and melanoma growth through derived adrenomedullin (ADM), which is expected to provide a potential target for melanoma therapy (80).

TAMs have a good phagocytic function for nanomaterials. Studies show that some nanomaterials can induce the intrinsic activity of macrophage phenotype differentiation so that TAMs can repolarize to the M1 phenotype to achieve the purpose of anti-tumor therapy (152, 153). For example, a hyaluronic acid-coated, mannan-conjugated MnO2 nanoparticle (Man-HA-

MnO2 NPs) repolarized TAMs to the M1 phenotype, alleviated tumor hypoxia by significantly enhancing tumor oxygenation, and thus Anti-tumor therapeutic effect; and this nanomaterial combined with doxorubicin can synergistically inhibit the growth and proliferation of tumor cells (154). Nanomaterials can also resist the progression of melanoma by anti-tumor angiogenesis and other means (94, 154, 155).

The above studies suggest that targeting TAMs therapy is an attractive and potential cancer treatment strategy. However, the specific choice of a treatment strategy for melanoma lung metastases or other different types of tumors should be based on the actual situation of the tumor and the role of targeted TAMs.

Conclusion and perspective

It is generally believed that macrophages play an important role in the development and metastasis of various solid tumors, including melanoma. Early dissemination and late multi-organ metastasis colonization are typical features of melanoma. Among the multiple organs that skin melanoma may colonize, the lung is one of the most common distant metastatic sites of melanoma. Lung metastases from melanoma account for 5% of all malignant metastases and have a high lethality rate. The macrophages involved in the lung metastasis of melanoma can refer to the macrophages in the occurrence and development of other tumors, and their sources may be monocyte-macrophages or tissue sources. Generally divided into two types: M1 macrophages and M2 macrophages. M1 has pro-inflammatory and anti-tumor properties, while M2 has anti-inflammatory and pro-tumor properties. TAMs are considered to belong to the M2 phenotype because their functions in promoting tumorigenesis, tumor angiogenesis, and metastasis are more similar to M2 macrophages.

Several studies have revealed the effect of TME on tumorigenesis and development and the effect of TMEM on tumor metastasis. TAMs, as the main component of the TME and TMEM, is a complex heterogeneous population of cells that contribute to the malignant features of solid tumors. This paper summarizes the role of TAMs in promoting tumor cell invasion and in participating in various steps of the tumor metastasis cascade, and the ways in which regulation such as epigenetics affects the function of TAMs and thus tumor progression and metastasis, which may provide some explanation for the role of TAMs in melanoma lung metastasis. In addition, the heterogeneity and specificity of TAMs lay the foundation for the development of therapeutic approaches targeting TAMs. In this paper, we also summarized anti-tumor therapeutic approaches targeting TAMs such as, inhibiting the recruitment and proliferation of TAMs, depleting TAMs, repro- gramming TAMs and targeting angiogenesis. It is also worth noting that in solid tumors including melanoma, both basic and clinical trials on TAMs are in full swing, suggesting that targeting TAMs strategies are expected to form a precise treatment and will be a valuable anti-tumor treatment strategy in the future.

In conclusion, TAMs have diverse functions in TME and TMEM and play complex roles in various solid tumors. Studying the role of TAMs in the process of melanoma pulmonary metastasis and the therapeutic strategies targeting TAMs is expected to provide more possible mechanism explanations and treatment options for melanoma pulmonary metastasis.

Author contributions

KX and SC drafted an outline of the manuscript. KX drafted the abstract, generated the figure, and edited the manuscript. MQ drafted the discussion and edited the manuscript. TS edited the manuscript. JZ added to and edited the manuscript. All authors contributed to the article and approved the submitted version.

Funding

This work was supported by the National Natural Science Foundation of China (under Grants 82073018, and 82073019) and also funded by the Shenzhen Science and Technology Innovation Committee (JCYJ20210324114212035).

Conflict of interest

The authors declare that the research was conducted in the absence of any commercial or financial relationships that could be construed as a potential conflict of interest.

Publisher's note

References

1. Siegel RL, Miller KD, Fuchs HE, Jemal A. Cancer statistics, 2021. *CA Cancer J Clin* (2021) 71(1):7–33. doi: 10.3322/caac.21654

2. Skudalski L, Waldman R, Kerr PE, Grant-Kels JM. Melanoma: An update on systemic therapies. *J Am Acad Dermatol* (2022) 86(3):515–24. doi: 10.1016/j.jaad.2021.09.075

3. Braeuer RR, Watson IR, Wu CJ, Mobley AK, Kamiya T, Shoshan M, Bar-EliE. Why is melanoma so metastatic? *Pigment Cell Melanoma Res* (2014) 27(1):19–36. doi: 10.1111/pcmr.12172

4. Papp O, Doma V, Gil J, Markó-Varga G, Kárpáti S, Tímár J, et al. Organ specific copy number variations in visceral metastases of human melanoma. *Cancers (Basel)* (2021) 13(23):5984. doi: 10.3390/cancers13235984

5. Borghesi A, Tironi A, Michelini S, Scrimieri A, Benetti D, Maroldi R. Two synchronous lung metastases from malignant melanoma: The same patient but different morphological patterns. *Eur J Radiol Open* (2019) 6:287–90. doi: 10.1016/j.ejro.2019.08.001

6. Murakami T, Cardones AR, Hwang ST. Chemokine receptors and melanoma metastasis. *J Dermatol Sci* (2004) 36(2):71–8. doi: 10.1016/j.jdermsci.2004.03.002

7. Zhang KS, Pelleg T, Campbell S, Rubio C, Loschner AL, Ie S. Pulmonary metastatic melanoma: current state of diagnostic imaging and treatments. *Melanoma Manag* (2021) 8(3):Mmt58. doi: 10.2217/mmt-2021-0001

8. Wilson RW, Moran CA. Primary melanoma of the lung: A clinicopathologic and immunohistochemical study of eight cases. *Am J Surg Pathol* (1997) 21 (10):1196–202. doi: 10.1097/00000478-199710000-00010

9. Fidler IJ, Kripke ML. The challenge of targeting metastasis. *Cancer Metastasis Rev* (2015) 34(4):635–41. doi: 10.1007/s10555-015-9586-9

10. Scully OJ, Bay BH, Yip G, Yu Y. Breast cancer metastasis. *Cancer Genomics Proteomics* (2012) 9(5):311–20.

11. Ruffell B, Affara NI, Coussens LM. Differential macrophage programming in the tumor microenvironment. *Trends Immunol* (2012) 33(3):119–26. doi: 10.1016/j.it.2011.12.001

12. Komohara Y, Jinushi M, Takeya M. Clinical significance of macrophage heterogeneity in human malignant tumors. *Cancer Sci* (2014) 105(1):1–8. doi: 10.1111/cas.12314

13. Ruffell B, Coussens LM. Macrophages and therapeutic resistance in cancer. *Cancer Cell* (2015) 27(4):462–72. doi: 10.1016/j.ccell.2015.02.015

14. Ferrucci V, Asadzadeh F, Collina F, Siciliano R, Boccia A, Marrone L, et al. Prune-1 drives polarization of tumor-associated macrophages (TAMs) within the lung metastatic niche in triple-negative breast cancer. *iScience* (2021) 24(1):101938. doi: 10.1016/j.isci.2020.101938

15. Lin Y, Xu J, Lan H. Tumor-associated macrophages in tumor metastasis: Biological roles and clinical therapeutic applications. *J Hematol Oncol* (2019) 12 (1):76. doi: 10.1186/s13045-019-0760-3

16. Sunakawa Y, Stintzing S, Cao S, Heinemann V, Cremolini C, Falcone A, et al. Variations in genes regulating tumor-associated macrophages (TAMs) to predict outcomes of bevacizumab-based treatment in patients with metastatic colorectal cancer: Results from TRIBE and FIRE3 trials. *Ann Oncol* (2015) 26 (12):2450–6. doi: 10.1093/annonc/mdv474

17. Gnant M, Mlineritsch B, Stoeger H, Luschin-Ebengreuth G, Heck D, Menzel C, et al. Adjuvant endocrine therapy plus zoledronic acid in premenopausal women with early-stage breast cancer: 62-month follow-up from the ABCSG-12 randomised trial. *Lancet Oncol* (2011) 12(7):631–41. doi: 10.1016/S1470-2045(11)70122-X

18. Nywening TM, Wang-Gillam A, Sanford DE, Belt BA, Panni BM, Cusworth RZ, et al. Targeting tumour-associated macrophages with CCR2 inhibition in combination with FOLFIRINOX in patients with borderline resectable and locally advanced pancreatic cancer: A single-centre, open-label, dose-finding, non-randomised, phase 1b trial. *Lancet Oncol* (2016) 17(5):651–62. doi: 10.1016/S1470-2045(16)00078-4

19. Yang L, Zhang Y. Tumor-associated macrophages: From basic research to clinical application. *J Hematol Oncol* (2017) 10(1):58. doi: 10.1186/s13045-017-0430-2

20. Liu Y, Cao X. The origin and function of tumor-associated macrophages. *Cell Mol Immunol* (2015) 12(1):1–4. doi: 10.1038/cmi.2014.83

21. Wynn TA, Chawla A, Pollard JW. Macrophage biology in development, homeostasis and disease. *Nature* (2013) 496(7446):445–55. doi: 10.1038/nature12034

22. Qian BZ, Pollard JW. Macrophage diversity enhances tumor progression and metastasis. *Cell* (2010) 141(1):39–51. doi: 10.1016/j.cell.2010.03.014

23. Williams CB, Yeh ES, Soloff AC. Tumor-associated macrophages: Unwitting accomplices in breast cancer malignancy. *NPJ Breast Cancer* (2016) 2:15025–. doi: 10.1038/npjbcancer.2015.25

24. Mantovani A, Marchesi F, Malesci A, Laghi L, Allavena P. Tumour-associated macrophages as treatment targets in oncology. *Nat Rev Clin Oncol* (2017) 14(7):399–416. doi: 10.1038/nrclinonc.2016.217

25. Fu LQ, Du WL, Cai MH, Yao JY, Zhao YY, Mou XZ. The roles of tumor-associated macrophages in tumor angiogenesis and metastasis. *Cell Immunol* (2020) 353:104119. doi: 10.1016/j.cellimm.2020.104119

26. Franklin RA, Liao W, Sarkar A, Kim M.V, Bivona MR, Liu K, et al. The cellular and molecular origin of tumor-associated macrophages. *Science* (2014) 344 (6186):921–5. doi: 10.1126/science.1252510

27. Hashimoto D, Chow A, Noizat C, Teo P, Beasley M.B, Leboeuf M, et al. Tissue-resident macrophages self-maintain locally throughout adult life with minimal contribution from circulating monocytes. *Immunity* (2013) 38(4):792–804. doi: 10.1016/j.immuni.2013.04.004

28. Franklin RA, Li MO. Ontogeny of tumor-associated macrophages and its implication in cancer regulation. *Trends Cancer* (2016) 2(1):20–34. doi: 10.1016/j.trecan.2015.11.004

29. Hussein MR. Tumour-associated macrophages and melanoma tumourigenesis: integrating the complexity. *Int J Exp Pathol* (2006) 87(3):163–76. doi: 10.1111/j.1365-2613.2006.00478.x

30. Pan Y, Yu Y, Wang X, Zhang T. Tumor-associated macrophages in tumor immunity. *Front Immunol* (2020) 11:583084. doi: 10.3389/fimmu.2020.583084

31. Hourani T, Holden JA, Li W, Lenzo JC, Hadjigol S, O'Brien-Simpson N.M. Tumor associated macrophages: Origin, recruitment, phenotypic diversity, and targeting. *Front Oncol* (2021) 11:788365. doi: 10.3389/fonc.2021.788365

32. Gleissner CA, Shaked I, Little KM, Ley K. CXC chemokine ligand 4 induces a unique transcriptome in monocyte-derived macrophages. *J Immunol* (2010) 184 (9):4810–8. doi: 10.4049/jimmunol.0901368

33. Zizzo G, Cohen PL. IL-17 stimulates differentiation of human anti-inflammatory macrophages and phagocytosis of apoptotic neutrophils in response to IL-10 and glucocorticoids. *J Immunol* (2013) 190(10):5237–46. doi: 10.4049/jimmunol.1203017

34. Ostuni R, Kratochvill F, Murray PJ, Natoli G. Macrophages and cancer: From mechanisms to therapeutic implications. *Trends Immunol* (2015) 36(4):229–39. doi: 10.1016/j.it.2015.02.004

35. Mantovani A, Sozzani S, Locati M, Allavena P, Sica A. Macrophage polarization: Tumor-associated macrophages as a paradigm for polarized M2 mononuclear phagocytes. *Trends Immunol* (2002) 23(11):549–55. doi: 10.1016/S1471-4906(02)02302-5

36. Hao Z, Li R, Meng L, Han Z, Hong Z. Macrophage, the potential key mediator in CAR-T related CRS. *Exp Hematol Oncol* (2020) 9:15. doi: 10.1186/s40164-020-00171-5

37. Lin X, Zheng W, Liu J, Zhang Y, Qin H, et al. Oxidative stress in malignant melanoma enhances tumor necrosis factor-α secretion of tumor-associated macrophages that promote cancer cell invasion. *Antioxid Redox Signal* (2013) 19 (12):1337–55. doi: 10.1089/ars.2012.4617

38. Henze AT, Mazzone M. The impact of hypoxia on tumor-associated macrophages. *J Clin Invest* (2016) 126(10):3672–9. doi: 10.1172/JCI84427

39. DeNardo DG, Ruffell B. Macrophages as regulators of tumour immunity and immunotherapy. *Nat Rev Immunol* (2019) 19(6):369–82. doi: 10.1038/s41577-019-0127-6

40. Lee HW, Choi HJ, Ha SJ, Lee KT, Kwon YG. Recruitment of monocytes/macrophages in different tumor microenvironments. *Biochim Biophys Acta* (2013) 1835(2):170–9. doi: 10.1016/j.bbcan.2012.12.007

41. Chen Z, Feng X, Herting CJ, Garcia VA, Nie K, Pong WW, et al. Cellular and molecular identity of tumor-associated macrophages in glioblastoma. *Cancer Res* (2017) 77(9):2266–78. doi: 10.1158/0008-5472.CAN-16-2310

42. Tian Z, Hou X, Liu W, Han Z, Wei L. Macrophages and hepatocellular carcinoma. *Cell Biosci* (2019) 9:79. doi: 10.1186/s13578-019-0342-7

43. Loyher PL, Hamon P, Laviron M, Meghraoui-Kheddar A, Goncalves E, Deng Z, et al. Macrophages of distinct origins contribute to tumor development in the lung. *J Exp Med* (2018) 215(10):2536–53. doi: 10.1084/jem.20180534

44. Hume DA, MacDonald KP. Therapeutic applications of macrophage colony-stimulating factor-1 (CSF-1) and antagonists of CSF-1 receptor (CSF-1R) signaling. *Blood* (2012) 119(8):1810–20. doi: 10.1182/blood-2011-09-379214

45. Lin EY, Nguyen AV, Russell RG, Pollard JW. Colony-stimulating factor 1 promotes progression of mammary tumors to malignancy. *J Exp Med* (2001) 193 (6):727–40. doi: 10.1084/jem.193.6.727

46. Abraham D, Zins K, Sioud M, Lucas T, Schäfer R, Stanley ER, et al. Stromal cell-derived CSF-1 blockade prolongs xenograft survival of CSF-1-negative neuroblastoma. *Int J Cancer* (2010) 126(6):1339–52. doi: 10.1002/ijc.24859

47. Gazzaniga S, Bravo AI, Guglielmotti A, Rooijen van N, Maschi F, Vecchi A, et al. Targeting tumor-associated macrophages and inhibition of MCP-1 reduce angiogenesis and tumor growth in a human melanoma xenograft. *J Invest Dermatol* (2007) 127(8):2031–41. doi: 10.1038/sj.jid.5700827

48. Grossman JG, Nywening TM, Belt BA, Panni RZ, Krasnick BA, DeNardo DG, et al. Recruitment of CCR2(+) tumor associated macrophage to sites of liver metastasis confers a poor prognosis in human colorectal cancer. *Oncoimmunology* (2018) 7(9):e1470729. doi: 10.1080/2162402X.2018.1470729

49. Gwak J, Jeong H, Lee K, Shin JY, Sim T, Na J, et al. SFMBT2-mediated infiltration of preadipocytes and TAMs in prostate cancer. *Cancers (Basel)* (2020) 12(9):2718. doi: 10.3390/cancers12092718

50. Idorn M, Skadborg SK, Kellermann L, Halldórsdóttir HR, Olofsson Holmen G, Met Ö, et al. Chemokine receptor engineering of T cells with CXCR2 improves homing towards subcutaneous human melanomas in xenograft mouse model. *Oncoimmunology* (2018) 7(8):e1450715. doi: 10.1080/2162402X.2018.1450715

51. Sierra-Filardi E, Nieto C, Domínguez-Soto A, Barroso R, Sánchez-Mateos P, Puig- Kroger A, et al. CCL2 shapes macrophage polarization by GM-CSF and m-CSF: identification of CCL2/CCR2-dependent gene expression profile. *J Immunol* (2014) 192(8):3858–67. doi: 10.4049/jimmunol.1302821

52. Chen XJ, Deng YR, Wang ZC, Wei WF, Zhou CF, Zhang YM, et al. Hypoxia-induced ZEB1 promotes cervical cancer progression *via* CCL8-dependent tumour-associated macrophage recruitment. *Cell Death Dis* (2019) 10(7):508. doi: 10.1038/s41419-019-1748-1

53. Yang H, Zhang Q, Xu M, Wang L, Chen X, Feng Y, et al. CCL2-CCR2 axis recruits tumor associated macrophages to induce immune evasion through PD-1 signaling in esophageal carcinogenesis. *Mol Cancer* (2020) 19(1):41. doi: 10.1186/s12943-020-01165-x

54. Arakaki R, Yamasaki T, Kanno T, Shibasaki N, Sakamoto H, Utsunomiya N, et al. CCL2 as a potential therapeutic target for clear cell renal cell carcinoma. *Cancer Med* (2016) 5(10):2920–33. doi: 10.1002/cam4.886

55. Chae YC, Vaira V, Caino MC, Tang HY, Seo JH, Kossenkov AV, et al. Mitochondrial akt regulation of hypoxic tumor reprogramming. *Cancer Cell* (2016) 30(2):257–72. doi: 10.1016/j.ccell.2016.07.004

56. Barsoum IB, Hamilton TK, Li X, Cotechini T, Miles EA, Siemens DR, et al. Hypoxia induces escape from innate immunity in cancer cells *via* increased expression of ADAM10: Role of nitric oxide. *Cancer Res* (2011) 71(24):7433–41. doi: 10.1158/0008-5472.CAN-11-2104

57. Vaupel P, Harrison L. Tumor hypoxia: causative factors, compensatory mechanisms, and cellular response. *Oncologist* (2004) 9 Suppl 5:4–9. doi: 10.1634/theoncologist.9-90005-4

58. Chen B, Yang Y, Yang C, Duan J, Chen L, Lu K, et al. M2 macrophage accumulation contributes to pulmonary fibrosis, vascular dilatation, and hypoxemia in rat hepatopulmonary syndrome. *J Cell Physiol* (2021) 236 (11):7682–97. doi: 10.1002/jcp.30420

59. Meng Q, Guo P, Jiang Z, Bo L, Bian J, et al. Dexmedetomidine inhibits LPS-induced proinflammatory responses *via* suppressing HIF1α-dependent glycolysis in macrophages. *Aging (Albany NY)* (2020) 12(10):9534–48. doi: 10.18632/aging.103226

60. Samaniego R, Gutiérrez-González A, Gutiérrez-Seijo A, Sánchez-Gregorio S, García- Giménez J, Mercader E, et al. CCL20 expression by tumor-associated macrophages predicts progression of human primary cutaneous melanoma. *Cancer Immunol Res* (2018) 6(3):267–75. doi: 10.1158/2326-6066.CIR-17-0198

61. Seyfried TN, Huysentruyt LC. On the origin of cancer metastasis. *Crit Rev Oncog* (2013) 18(1-2):43–73. doi: 10.1615/CritRevOncog.v18.i1-2.40

62. Banerjee R, Smith J, Eccles MR, Weeks RJ, Chatterjee A. Epigenetic basis and targeting of cancer metastasis. *Trends Cancer* (2022) 8(3):226–41. doi: 10.1016/j.trecan.2021.11.008

63. Younes R, Abrao FC, Gross J. Pulmonary metastasectomy for malignant melanoma: Prognostic factors for long-term survival. *Melanoma Res* (2013) 23 (4):307–11. doi: 10.1097/CMR.0b013e3283632cbe

64. Soliman M, Petrella T, Tyrrell P, Wright F, Hong Look NJ, Lu H, et al. The clinical significance of indeterminate pulmonary nodules in melanoma patients at baseline and during follow-up chest CT. *Eur J Radiol Open* (2019) 6:85–90. doi: 10.1016/j.ejro.2019.02.003

65. Balch CM, Gershenwald JE, Soong SJ, Thompson JF, Atkins MB, Byrd DR, et al. Final version of 2009 AJCC melanoma staging and classification. *J Clin Oncol* (2009) 27(36):6199–206. doi: 10.1200/JCO.2009.23.4799

66. Pastushenko I, Blanpain C. EMT transition states during tumor progression and metastasis. *Trends Cell Biol* (2019) 29(3):212–26. doi: 10.1016/j.tcb.2018.12.001

67. Fu XT, Dai Z, Song K, Zhang ZJ, Zhou ZJ, Zhou SL, et al. Macrophage-secreted IL-8 induces epithelial-mesenchymal transition in hepatocellular carcinoma cells by activating the JAK2/STAT3/Snail pathway. *Int J Oncol* (2015) 46(2):587–96. doi: 10.3892/ijo.2014.2761

68. Ravi J, Elbaz M, Wani NA, Nasser MW, Ganju RK. Cannabinoid receptor-2 agonist inhibits macrophage induced EMT in non-small cell lung cancer by downregulation of EGFR pathway. *Mol Carcinog* (2016) 55(12):2063–76. doi: 10.1002/mc.22451

69. Su S, Liu Q, Chen J, Chen J, Chen F, He C, et al. A positive feedback loop between mesenchymal-like cancer cells and macrophages is essential to breast cancer metastasis. *Cancer Cell* (2014) 25(5):605–20. doi: 10.1016/j.ccr.2014.03.021

70. Savagner P. The epithelial-mesenchymal transition (EMT) phenomenon. *Ann Oncol* (2010) 21 Suppl 7:vii89–92. doi: 10.1093/annonc/mdq292

71. Kawata M, Koinuma D, Ogami T, Umezawa K, Iwata C, Watabe T, et al. TGF-β-induced epithelial-mesenchymal transition of A549 lung adenocarcinoma cells is enhanced by pro-inflammatory cytokines derived from RAW 264.7 macrophage cells. *J Biochem* (2012) 151(2):205–16. doi: 10.1093/jb/mvr136

72. Jensen TO, Schmidt H, Møller HJ, Høyer M, Maniecki MB, Sjoegren P, et al. Macrophage markers in serum and tumor have prognostic impact in American joint committee on cancer stage I/II melanoma. *J Clin Oncol* (2009) 27(20):3330–7. doi: 10.1200/JCO.2008.19.9919

73. Varney ML, Johansson SL, Singh RK. Tumour-associated macrophage infiltration, neovascularization and aggressiveness in malignant melanoma: Role of monocyte chemotactic protein-1 and vascular endothelial growth factor-a. *Melanoma Res* (2005) 15(5):417–25. doi: 10.1097/00008390-200510000-00010

74. Ramjiawan RR, Griffioen AW, Duda DG. Anti-angiogenesis for cancer revisited: Is there a role for combinations with immunotherapy? *Angiogenesis* (2017) 20(2):185–204. doi: 10.1007/s10456-017-9552-y

75. Lin EY, Li JF, Gnatovskiy L, Deng Y, Zhu L, Grzesik DA, et al. Macrophages regulate the angiogenic switch in a mouse model of breast cancer. *Cancer Res* (2006) 66(23):11238–46. doi: 10.1158/0008-5472.CAN-06-1278

76. Lin EY, Pollard JW. Tumor-associated macrophages press the angiogenic switch in breast cancer. *Cancer Res* (2007) 67(11):5064–6. doi: 10.1158/0008-5472.CAN-07-0912

77. Giraudo E, Inoue M, Hanahan D. An amino-bisphosphonate targets MMP-9-expressing macrophages and angiogenesis to impair cervical carcinogenesis. *J Clin Invest* (2004) 114(5):623–33. doi: 10.1172/JCI200422087

78. Alishekevitz D, Gingis-Velitski S, Kaidar-Person O, Gutter-Kapon L, Scherer Z, Raviv SD, et al. Macrophage-induced lymphangiogenesis and metastasis following paclitaxel chemotherapy is regulated by VEGFR3. *Cell Rep* (2016) 17(5):1344–56. doi: 10.1016/j.celrep.2016.09.083

79. Riabov V, Gudima A, Wang N, Mickley A, Orekhov A, Kzhyshkowska J. Role of tumor associated macrophages in tumor angiogenesis and lymphangiogenesis. *Front Physiol* (2014) 5:75. doi: 10.3389/fphys.2014.00075

80. Chen P, Huang Y, Bong R, Ding Y, Song N, Wang X, et al. Tumor-associated macrophages promote angiogenesis and melanoma growth *via* adrenomedullin in a paracrine and autocrine manner. *Clin Cancer Res* (2011) 17(23):7230–9. doi: 10.1158/1078-0432.CCR-11-1354

81. Mulholland BS, Forwood MR, Morrison NA. Monocyte chemoattractant protein-1 (MCP-1/CCL2) drives activation of bone remodelling and skeletal metastasis. *Curr Osteoporos Rep* (2019) 17(6):538–47. doi: 10.1007/s11914-019-00545-7

82. Gómez-Cuadrado L, Tracey N, Ma R, Qian B, Brunton VG. Mouse models of metastasis: Progress and prospects. *Dis Model Mech* (2017) 10(9):1061–74. doi: 10.1242/dmm.030403

83. Sidani M, Wyckoff J, Xue C, Segall JE, Condeelis J. Probing the microenvironment of mammary tumors using multiphoton microscopy. *J Mammary Gland Biol Neoplasia* (2006) 11(2):151–63. doi: 10.1007/s10911-006-9021-5

84. Wang J, Cao Z, Zhang XM, Nakamura M, Sun M, Hartman J, et al. Novel mechanism of macrophage-mediated metastasis revealed in a zebrafish model of tumor development. *Cancer Res* (2015) 75(2):306–15. doi: 10.1158/0008-5472.CAN-14-2819

85. Chen J, Yao Y, Gong C, Yu F, Su S, Chen J, et al. CCL18 from tumor-associated macrophages promotes breast cancer metastasis *via* PITPNM3. *Cancer Cell* (2011) 19(4):541–55. doi: 10.1016/j.ccr.2011.02.006

86. Xu L, Zhang Y, Zhao Z, Chen Z, Wang Z, Xu S, et al. The long non-coding RNA CRNDE competed endogenously with miR-205 to promote proliferation and metastasis of melanoma cells by targeting CCL18. *Cell Cycle* (2018) 17(18):2296–308. doi: 10.1080/15384101.2018.1526602

87. Schumacher D, Strilic B, Sivaraj KK, Wettschureck N, Offermanns S. Platelet-derived nucleotides promote tumor-cell transendothelial migration and metastasis *via* P2Y2 receptor. *Cancer Cell* (2013) 24(1):130–7. doi: 10.1016/j.ccr.2013.05.008

88. Gil-Bernabé AM, Ferjancic S, Tlalka M, Zhao L, Allen PD, Im JH, et al. Recruitment of monocytes/macrophages by tissue factor-mediated coagulation is essential for metastatic cell survival and premetastatic niche establishment in mice. *Blood* (2012) 119(13):3164–75. doi: 10.1182/blood-2011-08-376426

89. Qian B, Deng Y, Im JH, Muschel RJ, Zou Y, Li J, et al. A distinct macrophage population mediates metastatic breast cancer cell extravasation, establishment and growth. *PloS One* (2009) 4(8):e6562. doi: 10.1371/journal.pone.0006562

90. Liu Y, Cao X. Characteristics and significance of the pre-metastatic niche. *Cancer Cell* (2016) 30(5):668–81. doi: 10.1016/j.ccell.2016.09.011

91. Sanmartin MC, Borzone FR, Giorello MB, Pacienza N, Yannarelli G, Chasseing NA. Bone marrow/bone pre-metastatic niche for breast cancer cells colonization: The role of mesenchymal stromal cells. *Crit Rev Oncol Hematol* (2021) 164:103416. doi: 10.1016/j.critrevonc.2021.103416

92. Jiang K, Chen H, Fang Y, Chen L, Zhong C, Bu T, et al. Exosomal ANGPTL1 attenuates colorectal cancer liver metastasis by regulating kupffer cell secretion pattern and impeding MMP9 induced vascular leakiness. *J Exp Clin Cancer Res* (2021) 40(1):21. doi: 10.1186/s13046-020-01816-3

93. Sceneay J, Smyth MJ, Möller A. The pre-metastatic niche: Finding common ground. *Cancer Metastasis Rev* (2013) 32(3-4):449–64. doi: 10.1007/s10555-013-9420-1

94. Cao M, Yan H, Han X, Weng L, Wei Q, Sun X, et al. Ginseng-derived nanoparticles alter macrophage polarization to inhibit melanoma growth. *J Immunother Cancer* (2019) 7(1):326. doi: 10.1186/s40425-019-0817-4

95. Andrisani O. Epigenetic mechanisms in hepatitis b virus-associated hepatocellular carcinoma. *Hepatoma Res* (2021) 7:12. doi: 10.20517/2394-5079.2020.83

96. Takeuch O, Akira S. Epigenetic control of macrophage polarization. *Eur J Immunol* (2011) 41(9):2490–3. doi: 10.1002/eji.201141792

97. Ahmad A. Epigenetic regulation of immunosuppressive tumor-associated macrophages through dysregulated microRNAs. *Semin Cell Dev Biol* (2022) 124:26–33. doi: 10.1016/j.semcdb.2021.09.001

98. Van den Bossche J, Neele AE, Hoeksema MA, Winther MP. Macrophage polarization: The epigenetic point of view. *Curr Opin Lipidol* (2014) 25(5):367–73. doi: 10.1097/MOL.0000000000000109

99. de Groot AE, Pienta KJ. Epigenetic control of macrophage polarization: Implications for targeting tumor-associated macrophages. *Oncotarget* (2018) 9 (29):20908–27. doi: 10.18632/oncotarget.24556

100. Korbecki J, Simińska D, Gassowska-Dobrowolska M, Listos J, Gutowska I, Chlubek D, et al. Chronic and cycling hypoxia: Drivers of cancer chronic inflammation through HIF-1 and NF-κB activation: A review of the molecular mechanisms. *Int J Mol Sci* (2021) 22(19):10701. doi: 10.3390/ijms221910701

101. Quatromoni JG, Eruslanov E. Tumor-associated macrophages: Function, phenotype, and link to prognosis in human lung cancer. *Am J Transl Res* (2012) 4 (4):376–89.

102. Li Y, Hodge J, Liu Q, Wang J, Wang Y, Evans TD, et al. TFEB is a master regulator of tumor-associated macrophages in breast cancer. *J Immunother Cancer* (2020) 8(1):e000543. doi: 10.1136/jitc-2020-000543

103. Carbó JM, León TE, Font-Díaz J, Rosa De JV, Castrillo A, Picard FR, et al. Pharmacologic activation of LXR alters the expression profile of tumor-associated macrophages and the abundance of regulatory T cells in the tumor microenvironment. *Cancer Res* (2021) 81(4):968–85. doi: 10.1158/0008-5472.CAN-19-3360

104. Liu M, Tong Z, Ding C, Luo F, Wu S, Wu C, et al. Transcription factor c-maf is a checkpoint that programs macrophages in lung cancer. *J Clin Invest* (2020) 130(4):2081–96. doi: 10.1172/JCI131335

105. Puthenveetil A, Dubey S. Metabolic reprograming of tumor-associated macrophages. *Ann Transl Med* (2020) 8(16):1030. doi: 10.21037/atm-20-2037

106. Laoui D, Van Overmeire E, Di Conza G, Aldeni C, Keirsse J, Morias Y, et al. Tumor hypoxia does not drive differentiation of tumor-associated macrophages but rather fine-tunes the M2-like macrophage population. *Cancer Res* (2014) 74(1):24–30. doi: 10.1158/0008-5472.CAN-13-1196

107. Wenes M, Shang M, Di Matteo M, Goveia J, Martín-Pérez R, Serneels J, et al. Macrophage metabolism controls tumor blood vessel morphogenesis and metastasis. *Cell Metab* (2016) 24(5):701–15. doi: 10.1016/j.cmet.2016.09.008

108. Meng W, Hao Y, He C, Li L, Zhu G. Exosome-orchestrated hypoxic tumor microenvironment. *Mol Cancer* (2019) 18(1):57. doi: 10.1186/s12943-019-0982-6

109. Chen X, Zhou J, Li X, Wang X, Lin Y, Wang X. Exosomes derived from hypoxic epithelial ovarian cancer cells deliver microRNAs to macrophages and elicit a tumor-promoted phenotype. *Cancer Lett* (2018) 435:80–91. doi: 10.1016/j.canlet.2018.08.001

110. Aras S, Zaidi MR. TAMeless traitors: macrophages in cancer progression and metastasis. *Br J Cancer* (2017) 117(11):1583–91. doi: 10.1038/bjc.2017.356

111. Peyraud F, Cousin S, Italiano A. CSF-1R inhibitor development: Current clinical status. *Curr Oncol Rep* (2017) 19(11):70. doi: 10.1007/s11912-017-0634-1

112. Ao JY, Zhu XD, Chai ZT, Cai H, Zhang YY, Zhang KZ, et al. Colony-stimulating factor 1 receptor blockade inhibits tumor growth by altering the polarization of tumor-associated macrophages in hepatocellular carcinoma. *Mol Cancer Ther* (2017) 16(8):1544–54. doi: 10.1158/1535-7163.MCT-16-0866

113. Aharinejad S, Paulus P, Sioud M, Hofmann M, Zins K, Schäfer R, et al. Colony-stimulating factor-1 blockade by antisense oligonucleotides and small interfering RNAs suppresses growth of human mammary tumor xenografts in mice. *Cancer Res* (2004) 64(15):5378–84. doi: 10.1158/0008-5472.CAN-04-0961

114. Tap WD, Wainberg ZA, Anthony SP, Ibrahim PN, Zhang C, Healey JH, et al. Structure-guided blockade of CSF1R kinase in tenosynovial giant-cell tumor. *N Engl J Med* (2015) 373(5):428–37. doi: 10.1056/NEJMoa1411366

115. Edwards VD, Sweeney DT, Ho H, Eide CA, Rofelty A, Agarwal A, et al. Targeting of colony-stimulating factor 1 receptor (CSF1R) in the CLL microenvironment yields antineoplastic activity in primary patient samples. *Oncotarget* (2018) 9(37):24576–89. doi: 10.18632/oncotarget.25191

116. Ries CH, Cannarile MA, Hoves S, Benz J, Wartha K, Runza V, et al. Targeting tumor-associated macrophages with anti-CSF-1R antibody reveals a strategy for cancer therapy. *Cancer Cell* (2014) 25(6):846–59. doi: 10.1016/j.ccr.2014.05.016

117. Neubert NJ, Schmittnaegel M, Bordry N, Nassiri S, Wald N, Martignier C, et al. T Cell-induced CSF1 promotes melanoma resistance to PD1 blockade. *Sci Transl Med* (2018) 10(436):eaan3311. doi: 10.1126/scitranslmed.aan3311

118. Pienta KJ, Machiels JP, Schrijvers D, Alekseev B, Shkolnik M, Crabb SJ, et al. Phase 2 study of carlumab (CNTO 888), a human monoclonal antibody against CC-chemokine ligand 2 (CCL2), in metastatic castration-resistant prostate cancer. *Invest New Drugs* (2013) 31(3):760–8. doi: 10.1007/s10637-012-9869-8

119. Noel M, O'Reilly EM, Wolpin BM, Ryan DP, Bullock AJ, Britten CD, et al. Phase 1b study of a small molecule antagonist of human chemokine (C-c motif) receptor 2 (PF-04136309) in combination with nab-paclitaxel/gemcitabine in first-line treatment of metastatic pancreatic ductal adenocarcinoma. *Invest New Drugs* (2020) 38(3):800–11. doi: 10.1007/s10637-019-00830-3

120. Tu MM, Abdel-Hafiz HA, Jones RT, Jean A, Hoff KJ, Duex JE, et al. Inhibition of the CCL2 receptor, CCR2, enhances tumor response to immune checkpoint therapy. *Commun Biol* (2020) 3(1):720. doi: 10.1038/s42003-020-01441-y

121. Zhu S, Yi M, Wu Y, Dong B, Wu K. Correction to: Roles of tumor-associated macrophages in tumor progression: Implications on therapeutic strategies. *Exp Hematol Oncol* (2022) 11(1):4. doi: 10.1186/s40164-022-00258-1

122. Zhu S, Yi M, Wu Y, Dong B, Wu K. Roles of tumor-associated macrophages in tumor progression: Implications on therapeutic strategies. *Exp Hematol Oncol* (2021) 10(1):60. doi: 10.1186/s40164-021-00252-z

123. Vonderheide RH. CD40 agonist antibodies in cancer immunotherapy. *Annu Rev Med* (2020) 71:47–58. doi: 10.1146/annurev-med-062518-045435

124. Wiehagen KR, Girgis NM, Yamada DH, Smith AA, Chan SR, Grewal IS, et al. Combination of CD40 agonism and CSF-1R blockade reconditions tumor-associated macrophages and drives potent antitumor immunity. *Cancer Immunol Res* (2017) 5(12):1109–21. doi: 10.1158/2326-6066.CIR-17-0258

125. Weiss SA, Djureinovic D, Jessel S, Krykbaeva I, Zhang L, Jilaveanu L, et al. A phase I study of APX005M and cabiralizumab with or without nivolumab in patients with melanoma, kidney cancer, or non-small cell lung cancer resistant to anti-PD-1/PD-L1. *Clin Cancer Res* (2021) 27(17):4757–67. doi: 10.1158/1078-0432.CCR-21-0903

126. Pathria P, Louis TL, Varner JA. Targeting tumor-associated macrophages in cancer. *Trends Immunol* (2019) 40(4):310–27. doi: 10.1016/j.it.2019.02.003

127. Piaggio F, Kondylis V, Pastorino F, Paolo Di D, Perri P, Cossu I, et al. A novel liposomal clodronate depletes tumor-associated macrophages in primary and metastatic melanoma: Anti-angiogenic and anti-tumor effects. *J Control Release* (2016) 223:165–77. doi: 10.1016/j.jconrel.2015.12.037

128. Pieniazek M, Matkowski R, Donizy P. Macrophages in skin melanoma-the key element in melanomagenesis. *Oncol Lett* (2018) 15(4):5399–404. doi: 10.3892/ol.2018.8021

129. von Moos R, Costa L, Gonzalez-Suarez E, Terpos E, Niepel D, Body JJ. Management of bone health in solid tumours: From bisphosphonates to a monoclonal antibody. *Cancer Treat Rev* (2019) 76:57–67. doi: 10.1016/j.ctrv.2019.05.003

130. Sevko A, Michels T, Vrohlings M, Umansky L, Beckhove P, Kato M, et al. Antitumor effect of paclitaxel is mediated by inhibition of myeloid-derived suppressor cells and chronic inflammation in the spontaneous melanoma model. *J Immunol* (2013) 190(5):2464–71. doi: 10.4049/jimmunol.1202781

131. Kimmel DB. Mechanism of action, pharmacokinetic and pharmacodynamic profile, and clinical applications of nitrogen-containing bisphosphonates. *J Dent Res* (2007) 86(11):1022–33. doi: 10.1177/154405910708601102

132. Abrahamsen B. Bisphosphonate adverse effects, lessons from large databases. *Curr Opin Rheumatol* (2010) 22(4):404–9. doi: 10.1097/BOR.0b013e32833ad677

133. Zang X, Zhang X, Hu H, Qiao M, Zhao X, Deng Y, et al. Targeted delivery of zoledronate to tumor-associated macrophages for cancer immunotherapy. *Mol Pharm* (2019) 16(5):2249–58. doi: 10.1021/acs.molpharmaceut.9b00261

134. Li X, Valdes SA, Alzhrani RF, Hufnagel S, Hursting SD, Cui Z. Zoledronic acid-containing nanoparticles with minimum premature release show enhanced activity against extraskeletal tumor. *ACS Appl Mater Interfaces* (2019) 11(7):7311–9. doi: 10.1021/acsami.8b16588

135. Mitchem JB, Brennan DJ, Knolhoff BL, Belt BA, Zhu Y, Sanford DE, et al. Targeting tumor-infiltrating macrophages decreases tumor-initiating cells, relieves immunosuppression, and improves chemotherapeutic responses. *Cancer Res* (2013) 73(3):1128–41. doi: 10.1158/0008-5472.CAN-12-2731

136. Demetri GD, Mehren von M, Jones RL, Hensley ML, Schuetze SM, Staddon A, et al. Efficacy and safety of trabectedin or dacarbazine for metastatic liposarcoma or leiomyosarcoma after failure of conventional chemotherapy: Results of a phase III randomized multicenter clinical trial. *J Clin Oncol* (2016) 34(8):786–93. doi: 10.1200/JCO.2015.62.4734

137. Jaynes JM, Sable R, Ronzetti M, Bautista W, Knotts Z, Abisoye- Ogunniyan A, et al. Mannose receptor (CD206) activation in tumor-associated macrophages enhances adaptive and innate antitumor immune responses. *Sci Transl Med* (2020) 12(530):eaax6337. doi: 10.1126/scitranslmed.aax6337

138. Narayan R, Nguyen H, Bentow JJ, Moy L, Lee DK, Greger S, et al. Immunomodulation by imiquimod in patients with high-risk primary melanoma. *J Invest Dermatol* (2012) 132(1):163–9. doi: 10.1038/jid.2011.247

139. Wang Y, Zhang S, Li H, Wang H, Zhang T, Hutchinson MR, et al. Small-molecule modulators of toll-like receptors. *Acc Chem Res* (2020) 53(5):1046–55. doi: 10.1021/acs.accounts.9b00631

140. Sprinzl MF, Puschnik A, Schlitter AM, Schad A, Ackermann K, Esposito I, et al. Sorafenib inhibits macrophage-induced growth of hepatoma cells by interference with insulin-like growth factor-1 secretion. *J Hepatol* (2015) 62 (4):863–70. doi: 10.1016/j.jhep.2014.11.011

141. Wanderley CW, Colón DF, Luiz JPM, Oliveira FF, Viacava PR, Leite CA, et al. Paclitaxel reduces tumor growth by reprogramming tumor-associated macrophages to an M1 profile in a TLR4-dependent manner. *Cancer Res* (2018) 78(20):5891–900. doi: 10.1158/0008-5472.CAN-17-3480

142. Kakizaki A, Fujimura T, Furudate S, Kambayashi Y, Yamauchi T, Yagita H., et al. Immunomodulatory effect of peritumorally administered interferon-beta on melanoma through tumor-associated macrophages. *Oncoimmunology* (2015) 4 (11):e1047584. doi: 10.1080/2162402X.2015.1047584

143. Fujimura T, Yamasaki K, Hidaka T, Ito Y, Aiba S. A synthetic NOD2 agonist, muramyl dipeptide (MDP)-lys (L18) and IFN-β synergistically induce dendritic cell maturation with augmented IL-12 production and suppress melanoma growth. *J Dermatol Sci* (2011) 62(2):107–15. doi: 10.1016/j.jdermsci.2011.02.002

144. La Fleur L, Boura VF, Alexeyenko A, Berglund A, Pontén V, Mattsson JSM, et al. Expression of scavenger receptor MARCO defines a targetable tumor-associated macrophage subset in non-small cell lung cancer. *Int J Cancer* (2018) 143(7):1741–52. doi: 10.1002/ijc.31545

145. Sharma P, Allison JP. The future of immune checkpoint therapy. *Science* (2015) 348(6230):56–61. doi: 10.1126/science.aaa8172

146. Ceci C, Atzori MG, Lacal PM, Graziani G. Targeting tumor-associated macrophages to increase the efficacy of immune checkpoint inhibitors: A glimpse into novel therapeutic approaches for metastatic melanoma. *Cancers (Basel)* (2020) 12(11):3401. doi: 10.3390/cancers12113401

147. Ribas A, Wolchok JD. Cancer immunotherapy using checkpoint blockade. *Science* (2018) 359(6382):1350–5. doi: 10.1126/science.aar4060

148. Wu K, Yi M, Qin S, Chu Q, Zheng X, Wu K. The efficacy and safety of combination of PD-1 and CTLA-4 inhibitors: A meta-analysis. *Exp Hematol Oncol* (2019) 8:26. doi: 10.1186/s40164-019-0150-0

149. Gordon SR, Maute RL, Dulken BW, Hutter G, George BM, McCracken MN, et al. PD-1 expression by tumour-associated macrophages inhibits phagocytosis and tumour immunity. *Nature* (2017) 545(7655):495–9. doi: 10.1038/nature22396

150. Zakharia Y, McWilliams RR, Rixe O, Drabick J, Shaheen MF, Grossmann KF, et al. Phase II trial of the IDO pathway inhibitor indoximod plus pembrolizumab for the treatment of patients with advanced melanoma. *J Immunother Cancer* (2021) 9(6):e002057. doi: 10.1136/jitc-2020-002057

151. Yamada K, Uchiyama A, Uehara A, Perera B, Ogino S, Yokoyama Y, et al. MFG-E8 drives melanoma growth by stimulating mesenchymal stromal cell-induced angiogenesis and M2 polarization of tumor-associated macrophages. *Cancer Res* (2016) 76(14):4283–92. doi: 10.1158/0008-5472.CAN-15-2812

152. Fuchs AK, Syrovets T, Haas KA, Loos C, Musyanovych A, Mailänder V, et al. Carboxyl- and amino-functionalized polystyrene nanoparticles differentially affect the polarization profile of M1 and M2 macrophage subsets. *Biomaterials* (2016) 85:78–87. doi: 10.1016/j.biomaterials.2016.01.064

153. Fu X, Yu J, Yuan A, Liu L, Zhao H, Huang Y, et al. Polymer nanoparticles regulate macrophage repolarization for antitumor treatment. *Chem Commun (Camb)* (2021) 57(56):6919–22. doi: 10.1039/D1CC02678J

154. Song M, Liu T, Shi C, Zhang X, Chen X. Bioconjugated manganese dioxide nanoparticles enhance chemotherapy response by priming tumor-associated macrophages toward M1-like phenotype and attenuating tumor hypoxia. *ACS Nano* (2016) 10(1):633–47. doi: 10.1021/acsnano.5b06779

155. Qian Y, Qiao S, Dai Y, Xu G, Dai B, Lu L, et al. Molecular-targeted immunotherapeutic strategy for melanoma *via* dual-targeting nanoparticles delivering small interfering RNA to tumor-associated macrophages. *ACS Nano* (2017) 11(9):9536–49. doi: 10.1021/acsnano.7b05465

frontiers | Frontiers in Immunology

TYPE Mini Review
PUBLISHED 28 September 2022
DOI 10.3389/fimmu.2022.1000996

OPEN ACCESS

EDITED BY
Giselle Penton-Rol,
Center for Genetic Engineering and Biotechnology (CIGB), Cuba

REVIEWED BY
Andrea Biondi,
University of Milano-Bicocca, Italy
Federica Benvenuti,
International Centre for Genetic Engineering and Biotechnology, Italy

*CORRESPONDENCE
Jutta Horejs-Hoeck
jutta.horejs_hoeck@plus.ac.at

SPECIALTY SECTION
This article was submitted to Cytokines and Soluble Mediators in Immunity, a section of the journal Frontiers in Immunology

RECEIVED 22 July 2022
ACCEPTED 14 September 2022
PUBLISHED 28 September 2022

CITATION
Luciano M, Krenn PW and Horejs-Hoeck J (2022) The cytokine network in acute myeloid leukemia. *Front. Immunol.* 13:1000996. doi: 10.3389/fimmu.2022.1000996

The cytokine network in acute myeloid leukemia

Michela Luciano[1,2], Peter W. Krenn[1,2] and Jutta Horejs-Hoeck[1,2]*

[1]Department of Biosciences and Medical Biology, Paris Lodron University of Salzburg, Salzburg, Austria, [2]Cancer Cluster Salzburg, Salzburg, Austria

Acute myeloid leukemia (AML) is a highly heterogeneous malignancy of the blood and bone marrow, characterized by clonal expansion of myeloid stem and progenitor cells and rapid disease progression. Chemotherapy has been the first-line treatment for AML for more than 30 years. Application of recent high-throughput next-generation sequencing technologies has revealed significant molecular heterogeneity to AML, which in turn has motivated efforts to develop new, targeted therapies. However, due to the high complexity of this disease, including multiple driver mutations and the coexistence of multiple competing tumorigenic clones, the successful incorporation of these new agents into clinical practice remains challenging. These continuing difficulties call for the identification of innovative therapeutic approaches that are effective for a larger cohort of AML patients. Recent studies suggest that chronic immune stimulation and aberrant cytokine signaling act as triggers for AML initiation and progression, facets of the disease which might be exploited as promising targets in AML treatment. However, despite the greater appreciation of cytokine profiles in AML, the exact functions of cytokines in AML pathogenesis are not fully understood. Therefore, unravelling the molecular basis of the complex cytokine networks in AML is a prerequisite to develop new therapeutic alternatives based on targeting cytokines and their receptors.

KEYWORDS

acute myeloid leukemia, cytokine signaling, inflammation, tumor microenvironment, cytokine inhibitors

Introduction

Acute Myeloid Leukemia (AML) is a highly aggressive and heterogenous hematological cancer characterized by the accumulation of molecular and cytogenetic mutations within hematopoietic stem and/or progenitor cells (HSPCs), leading to the establishment of leukemic stem cells (LSCs). LSCs are the source of immature myeloid progenitor cells, so-called myeloblasts or leukemic blasts, which accumulate in the bone marrow (BM), displace normal HSPCs, impair normal hematopoiesis, and eventually

spread into the peripheral blood (PB), lymph nodes, liver, spleen, testes, and central nervous system (1–4). Whereas many AML patients follow an aggressive clinical course with an overall 5-year survival rate of only 28%, individual patient survival strongly depends on the underlying tumor-driving genetic alterations and individual risk factors, including age, gender, prior chemotherapy, radiation exposure and genetic predisposition (1, 2, 5–8). However, irrespective of the molecular driver mutations initiating the disease, AML onset and development always go hand in hand with significant remodeling of the BM into a tumor-promoting microenvironment that supports and protects LSCs at the expense of normal HSPCs (9–15). In this review we discuss how cytokine signaling networks contribute to these maladaptations, fuel AML tumorigenesis and progression, and enable chemoresistance and immune evasion. We further shed some light on promising therapeutic approaches targeting cytokine signaling to irradicate the LSC population and prevent relapse after chemotherapy.

Role of cytokines in AML

Within the healthy BM microenvironment, hematopoietic stem cells (HSCs) are normally maintained in a delicate balance between quiescence, self-renewal, and differentiation to ensure life-long steady-state hematopoiesis and replenishment of the blood effector cell population under stress conditions such as infection, acute and chronic inflammation, aging or bleeding (16). During infection and inflammation, an array of cytokines, including Interleukin (IL)-1β (17, 18), IL-3 (19, 20), IL-6 (21–23), Tumor necrosis factor-α (TNF-α) (24–27) and Interferon (IFN) (28, 29) together with hematopoietic growth factors (HGFs) such as M-CSF, G-CSF and GM-CSF (17, 30), orchestrates the switch from steady-state to emergency hematopoiesis (31–33). In patients with preleukemic and leukemic conditions, including AML, the tight regulation of these cytokines is impaired, leading to aberrant cytokine secretion (32–38). Studies evaluating pro- and anti-inflammatory cytokine and growth factor levels in serum revealed that GM-CSF, IL-1β, IL-3, IL-4, IL-5, IL-6, IL-8, IL-10, IL-12p70, IL-27, IL-35, osteopontin and stem cell factor (SCF) are upregulated in all or in distinct AML patient groups compared to age-matched controls (39–43). In contrast to most cytokines, TRAIL and TGF-β levels are decreased in the serum of AML patients (39, 43, 44). To gain insights into the specific functions of individual cytokines and growth factors in AML, numerous studies have characterized the effects of recombinant cytokines and HGFs on proliferation and colony formation of primary AML cells and cell lines *in vitro*, thereby establishing *ex vivo* AML cell culture conditions (see Table 1).

Suggestive of a supportive feedback loop, some patient-derived LSCs and blasts can produce a variety of cytokines (e.g., IL-1β, IL-1α, IL-6, GM-CSF, and TNF-α) and proliferate *in vitro* without the addition of exogenous cytokines and HGFs (99–101). In particular, IL-1β was shown to act as an autocrine growth factor for AML blasts by inducing the production of HGFs and cytokines, including GM-CSF and IL-6 (50, 59, 99, 102–105). Moreover, IL-1-stimulated AML blast cells secreted increased levels of TNF-α, which synergized with IL-3- or GM-CSF-induced AML cell proliferation and colony formation (106). Of note, increased autonomous and/or HGF- and cytokine-induced *in vitro* proliferation of patient-derived leukemic cells correlated with negative clinical outcomes, including lower complete remission rates, higher risk for relapse, and shorter AML patient survival (107–109). *In vivo*, however, LSC and blast growth, survival, and protection from therapeutic agents do not exclusively rely on endogenous cytokine signaling, but strongly depend on AML cell interactions with the leukemic BM microenvironment and the latter's provisioning of supporting ligands and soluble factors, including cytokines (Figure 1), some of which are discussed in the following sections (110).

AML supporting cytokines

Osteopontin

Osteopontin, a secreted matrix glycoprotein produced by many cell types (e.g., stomal, endothelial, epithelial and immune cells), is crucial for the regulation and/or induction of inflammation, angiogenesis, proliferation, migration, and apoptosis throughout the body. During normal hematopoiesis, osteopontin is predominantly produced by osteoblasts within in the endosteal BM region, to guide and maintain healthy HSCs within supportive niches (111). Interestingly, PB and BM osteopontin levels were significantly increased in AML patients compared to healthy controls, and high osteopontin BM levels were associated with reduced overall and event-free survival (82, 83). Osteopontin was not, however, exclusively expressed by cells of the osteolineage within the leukemic BM, although it was strongly expressed by AML blasts (82). Additionally, it was shown that AML patient-derived mesenchymal stromal cells (MSCs) or healthy MSCs co-cultured with AML cells undergo osteogenic differentiation and produce increased amounts of osteopontin (112). Functionally, osteopontin was shown to upregulate AKT, mTOR, PTEN, and β-catenin mRNA expression in AML cells *in vitro* (113) and increase AML LSC self-renewal, proliferation, and expression of anti-apoptotic and cell-cycle-associated genes, thereby leading to accelerated disease progression in an MLL-AF9 driven AML mouse model (84). Direct targeting of osteopontin is difficult due to its ubiquitous expression and, so far, has been limited to approaches utilizing RNAi or blocking antibodies and aptamers in breast cancer models. Although delivered without specificity to cell type, these

10.3389/fimmu.2022.1000996

TABLE 1 Cytokines and growth factors supporting or inhibiting AML cells.

Cytokine	Expression in AML patients compared to healthy individuals	Physiologic function	Function *ex vivo* in AML cell culture
G-CSF	Not determined	Hematopoietic growth factor	Supports AML cell proliferation and clonogenicity (45–48)
GM-CSF	Elevated PB plasma levels and unchanged BM levels (42, 49)	Hematopoietic growth factor	Supports AML cell growth and self-renewal (44, 45, 50)
IFN-α	Not determined	Anti-/Pro-inflammatory cytokine	Reduces AML cell proliferation and IL-1, IL-6, GM-CSF expression (51, 52)
IFN-γ	Unchanged PB levels and reduced BM levels (39, 53)	Pro-inflammatory cytokine	Reduces AML cell proliferation and survival; increases spontaneous clonogenicity of AML cells (54, 55)
IL-1Ra	Elevated PB and reduced BM serum levels (42, 56)	Anti-inflammatory cytokine	Reduces AML cell proliferation (57, 58)
IL-1β	Unchanged or elevated PB and unchanged BM levels (39, 41, 42)	Pro-inflammatory cytokine	Supports AML cell proliferation and survival; increases GM-CSF, IL-6 and TNF expression (41, 45, 50, 51, 59, 60)
IL-3	Elevated PB levels (43)	Pro-inflammatory cytokine	Supports AML cell proliferation and self-renewal (45, 47, 61–63)
IL-4	Elevated PB levels in patients > 65 years (39, 53)	Anti-inflammatory cytokine	Inhibits IL-1- and HGF-induced AML cell proliferation (60, 64, 65)
IL-6	Elevated plasma levels (39, 53, 66)	Pro-inflammatory cytokine	Partially supports AML cell proliferation (45, 48, 67–71).
IL-8	Elevated PB and BM levels (39, 44, 66, 72)	Chemoattractant cytokine (chemokine)	Not determined
IL-10	Elevated PB levels (39, 53, 56, 73)	Anti-inflammatory cytokine	Inhibits AML cell proliferation; reduces IL-1α, IL-1β, IL-6, GM-CSF and TNF-α expression (74–76)
IL-12p70	Elevated PB levels in patients > 65 years (39)	Pro-inflammatory cytokine	Inhibits AML cell-induced angiogenesis; supports T cell-mediated cytotoxicity and possibly AML tumor growth (77–79)
IL-27	Elevated PB and BM levels (40)	Anti-inflammatory cytokine	Not determined
IL-35	Elevated PB and BM levels (40, 80, 81)	Anti-inflammatory cytokine	Supports AML cell proliferation and survival; promotes Treg function (80)
Osteopontin	Elevated PB and BM levels (44, 82, 83)	Matrix glycoprotein with pro-inflammatory cytokine properties	Supports AML cell self-renewal, proliferation and survival (84)
SCF	Elevated PB and BM levels (42)	Hematopoietic growth factor	Supports AML cell proliferation and survival (85–87)
TGF-β	Reduced PB and BM levels (39, 53)	Anti-inflammatory cytokine	Inhibits AML cell proliferation and survival (88–90)
TNF-α	Elevated PB levels (39, 44, 56, 66)	Pro-inflammatory cytokine	Supports AML cell chemoresistance and maintains proliferating LSCs (91)
TRAIL	Reduced PB levels (44)	Pro-inflammatory cytokine	Not determined
CXCL12	Reduced expression in AML blasts (92–94)	Chemoattractant cytokine (chemokine)	Promotes AML cell growth, survival, chemoresistance and adhesion (95–98)

Importantly, not all patient-derived AML cells or cell lines respond to HGF and cytokine treatment equally well. These observations reflect AML heterogeneity and suggest the presence of leukemic cell subpopulations. PB: peripheral blood; BM: bone marrow.

initial treatment studies confirm the antitumoral effect of osteopontin inhibition (114) and call for testing in AML disease models.

Interleukin-1

Due to its pleiotropic effects, IL-1-mediated signaling is recognized as a central hub between inflammation and cancer, including leukemia development and progression (32, 115–119). In AML patients, multiple studies have reported increased levels of IL-1β and IL-1 receptors as well as decreased levels of interleukin-1 receptor antagonist (IL-1RA) in PB and BM (41, 42, 56, 120). In an MLL-AF9-driven leukemic mouse model, chronic exposure to IL-1β accelerated leukemia progression and impaired normal hematopoiesis by modulating stromal niche support. Using both *in vitro* and *in vivo* AML models it was shown that depletion or deletion of IL-1RA resulted in reduced expansion of AML progenitor cells and partially restored normal hematopoiesis (121). This was confirmed by targeting IL-1 receptor signaling *via* inhibition of p38 MAPK, which enabled normal HSPCs to expand in the presence of IL-1β (41). Of note, *in vivo* AML development was curbed by knockout of IL-1 receptor in the MLL-AF9 mouse model but was increased in FLT3-ITD-driven leukemic mice (122), suggesting different dependencies on IL-1 signaling. Additionally, it was shown that AML HSPCs express high levels of IL-1 receptor accessory protein (IL-1RAP), which contributed to increased IL-1β production, AML cell proliferation and survival, but reduced normal hematopoiesis. This phenotype was further promoted when co-culturing AML $CD34^+$ HSPCs on MSCs (123, 124).

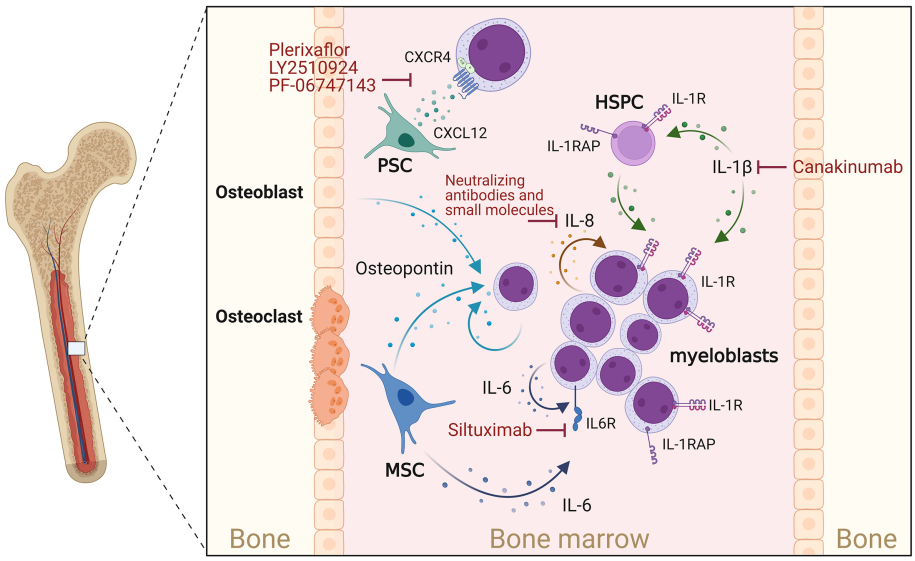

FIGURE 1
Cytokines supporting AML progression. Osteoblasts, myeloblasts and mesenchymal stromal cells (MSCs) secrete osteopontin. This in turn promotes AML cell proliferation and disease progression. CXCL12 is mainly secreted by perivascular stromal cells (PSCs), and osteoblasts and promotes growth and survival of AML blasts cell *via* the chemokine receptor CXCR4. IL-1β acts on myeloblasts and HSPCs, which express the IL-1 receptor (IL-1R) as well as the IL-1 receptor accessor protein (IL-1RAP), thereby enhancing IL-1β production, AML cell proliferation and survival. IL-1 signaling can be blocked by Canakinumab, a human monoclonal antibody targeting IL-1β. IL-8 is constitutively produced by AML myeloblasts and acts in an autocrine way. MSCs and myeloblasts are potent sources of IL-6, which can be blocked by IL-6-blocking antibodies such as Siltuximab. Created with Biorender.com.

Inhibition of IL-1RAP signaling antagonized this effect and enabled HSC proliferation in the presence of AML cell-conditioned media (124). In line with these AML cell-supporting functions, gene expression analysis revealed reduced overall survival (OS) of AML patients who expressed high levels of IL-1RAP (123). These observations suggest an important role for the IL-1β signaling pathway in the pathogenesis of AML and encourage studies to evaluate the therapeutic effects of targeting IL-1 signaling (117, 120). Multiple US Food and Drug Administration (FDA)-approved IL-1 blockers [Anakinra (Kineret); Rilonacept (Arcalyst); Canakinumab (Ilaris)] are already available. In particular, the effect of Canakinumab is being intensely evaluated in the CANTOS trail (NCT01327846), a randomized, double-blind, placebo-controlled phase 3 study involving 10,061 patients with solid tumors as well as hematological malignancies like chronic myelomonocytic leukemia (CMML) and myelodysplastic syndrome (MDS) (125, 126). However, additional studies will be required to fully understand the therapeutic value of targeting IL-1 and in particular IL-1β in hematological malignancies, including AML.

Interleukin-6

IL-6 is a potent pro-inflammatory cytokine which is crucial for a rapid and coordinated immune response during infections and tissue injuries, but also helps to maintain the hematopoietic system (127–129). Deregulated expression of IL-6 is associated with inflammatory and autoimmune diseases as well as skewed hematopoiesis and leukemia (104, 127, 130). In AML patients with reduced OS, blood and BM serum levels of IL-6 are increased (39, 53, 131). Further studies confirm these findings and suggest that IL-6 levels correlate with poor prognosis, rapid disease progression, and resistance to chemotherapy (39, 132–134). The combined assessment of PB IL-6 and FLT3-ligand levels during AML induction therapy revealed that patients with persistent high IL-6 levels display lower survival rates compared to patients with decreasing IL-6 and increasing FLT3-ligand levels (134). Similarly, low IL-6 levels accompanied by high IL-10 levels have been linked to better prognosis (39). Although AML blasts are clearly exposed to microenvironment-derived (135–137) and self-produced IL-6 (104), it is disputed how IL-6 contributes to AML progression. Curiously, all AML samples express the IL-6 receptor but only a subset responds to IL-6 treatment *in vitro* (48, 67, 69, 70, 131, 138). However, multiple studies suggest that IL-6-induced STAT3 signaling promotes AML by inducing chemoresistance (132, 135, 139). Hou and colleagues showed that BM MSCs promote chemoresistance against daunorubicin and cytosine arabinoside (Ara-c) by increasing IL-6 secretion and

activation of STAT3 signaling and the oxidative phosphorylation metabolic pathway in AML cells (135). Zhang et al. showed that IL-6-induced STAT3 signaling promotes CD36 expression, CD36-mediated uptake of fatty acids, and chemoresistance against Ara-c (139). Several IL-6 or IL-6 receptor-blocking antibodies have demonstrated promising results in (pre-) clinical studies for the treatment of cancers, chronic inflammation, and autoimmune diseases (130). While Siltuximab (CNTO 328; IL-6-blocking antibody) has been proposed as a treatment option for myelodysplastic syndrome (MDS) and multiple myeloma and is FDA-approved for the treatment of idiopathic multicentric Castleman's disease (140), Siltuximab in the AML setting has so far only been investigated in an AML xenograft mouse model that mimics end-stage BM failure. In that study, Siltuximab treatment antagonized AML-induced anemia and BM failure and prolonged mouse OS (141).

Interleukin-8

IL-8 (CXCL8) belongs to the CXC family of chemokines and is best known for its role as a chemoattractant for neutrophils (142). While production of IL-8 can be induced by various stimuli, including lipopolysaccharide, IL-1, and TNF in healthy cells, many tumor cells express IL-8 constitutively (142) or in a hypoxia-, acidosis-, or chemotherapy-induced manner, leading to anti-apoptotic and growth-supporting MAPK, PI3K, FAK and SRC18 signaling (143). In AML, constitutive production of IL-8 has been observed in both AML cell lines and primary AML samples, together with expression of functional IL-8 receptors [IL-8RA (CXCR1) and IL-8RB (CXCR2)] (144–146). Interestingly, AML cell-derived IL-8 also signals in a paracrine manner and affects neighboring non-leukemic cells in the BM microenvironment. Hypoxia-induced IL-8 secretion by AML cells resulted in increased migration of MSCs into the leukemic BM niche (147). MSCs, in turn, prevent apoptosis and confer drug resistance on leukemic cells by up-regulation of anti-apoptotic proteins and secretion of growth factors, cytokines, and extracellular vesicles (148, 149). Importantly, it has been shown that IL-8 production and secretion by MSCs, fibroblasts, and endothelial cells is induced or increased upon their co-culture with AML cells, thereby contributing to reduced apoptosis and increased proliferation and chemoresistance of the AML cells (150–152). In patients, this bidirectional signaling seems to result in elevated IL-8 levels in PB and BM levels (72), which additionally might contribute to impaired neutrophil migration and hematopoiesis (153). However, further confirmation, especially in the context of AML, is required. Inhibition of the IL-8–IL-8R axis has been proposed as a novel therapeutic intervention targeting the aberrant leukemic BM microenvironment. Blocking the IL-8 pathway with neutralizing antibodies has been shown to restore the sensitivity of malignant cells to chemotherapeutics and reduce AML cell proliferation (150, 151). Using knockdown or pharmacological inhibition approaches, Schinke and colleagues showed that inhibition of IL-8RB-mediated signaling leads to a significant reduction in proliferation and G0/G1 cell cycle arrest in several leukemic cell lines and primary MDS/AML samples (119).

CXC motif chemokine 12

The chemotactic cytokine (chemokine) CXCL12, also referred to as SDF-1, is secreted by a variety of cells including stromal cells, fibroblasts, and epithelial cells (154). CXCL12 initiates signaling by binding to its receptors CXCR4 and CXCR7 and plays a crucial role in regulating hematopoiesis (proliferation, differentiation, survival) and hematopoietic cell trafficking to and within the BM (95, 155), but also contributes to tumor growth, survival, metastasis, vascularization, and chemoresistance of several types of cancer (95, 156–160). In AML, low expression of CXCL12, high expression of CXCR4 and low to intermediate expression of CXCR7 have been measured on AML blasts in comparison to normal HSPCs (92–94). Interestingly, decreased CXCL12 and increased CXCR4 expression by AML blasts was associated with reduced patient relapse-free and overall survival OS (161–164). Within the healthy BM, CXCL12 is mainly secreted by perivascular stromal cells [mesenchymal stem and CXCL12-abundant reticular (CAR) cells], endothelial cells, and osteoblasts, thereby guiding, retaining, and regulating HSPCs to and within supportive BM niches (16). Within the AML BM microenvironment, it has not yet been determined which and to what extent cell populations produce and secrete CXCL12. *In vitro*, CXCL12 was shown to promote AML cell growth, survival, and chemoresistance (95–98) by activating or inducing the pro-survival proteins PI3K/AKT, MAP3K/ERK1/2, MYC, Bcl-2, and Bcl-XL (93, 96, 165). *In vivo*, however, while the deletion of CXCR4 in AML MLL-AF9^{+} HSPCs prolonged leukemic mouse survival, deletion of CXCL12 within the AML microenvironment did not alter the development and progression of the disease (166). This surprising finding suggests that CXCR4 signaling can support AML cells in a CXCL12-independent manner. Nevertheless, blocking the CXCL12/CXCR4 axis represents an attractive therapeutic strategy and several CXCR4 and CXCL12 inhibitors have been developed and used in preclinical and clinical models to induce the mobilization of the AML cells from the BM into the circulation with the aim of increasing their exposure to chemotherapeutic agents (95, 167). Plerixaflor (NCT01319864,

NCT01352650, NCT01027923), LY2510924 (NCT02652871), and PF-06747143 (NCT02954653) are among the antagonists that have been under Phase 1 clinical trials to test for safety, tolerability and clinical activity, either alone or in combination with standard chemotherapy in AML patients.

AML inhibiting cytokines

Interferon-γ

Interferon-γ (IFN-γ) is one of the lead cytokines of cellular immunity. It is mainly secreted by activated lymphocytes (168) and orchestrates tumor defense by regulating AML blast survival and apoptosis (118). While T cells obtained from AML patients at primary diagnosis exhibit increased IFN-γ production, strongly reduced levels of IFN-γ were observed in $CD8^+$ T cells from patients who developed relapsed AML after allogeneic HCT (allo-HCT), whereas patients without relapse did not show reduced IFN-γ production (169). This suggests that lower IFN-γ levels may elevate the risk of relapse. An early phase 1 trial was recently started to evaluate the potential of IFN-γ treatment in AML patients with reoccurring disease after allo-HCT (NCT04628338). However, manipulation of IFN-γ levels in AML patients should be carefully assessed, because systemic administration of IFN-γ is limited by rapid IFN-γ clearance and insufficient distribution to tumor sites. Moreover, while IFN-γ can restore T cell-mediated anti-cancer immunity and the surface expression of HLA class II molecules, the loss of which has been shown to impair AML recognition by donor T cells (170), IFN-γ is also capable of promoting PD-L1 and PD-L2 expression in AML (171, 172). Indeed, high expression of PD-L1 and PD-L2 is associated with poor OS in AML patients (173, 174). Binding of PD-L1/PD-L2 to the receptor PD-1 increases T cell exhaustion, promotes effector T cell apoptosis, induces the resistance to effector T cell-mediated killing (175) and increases the conversion and development of Tregs which have strong immune-suppressive abilities (176). Thus, the potential induction of PD-L1 and PD-L2 by IFN-γ may have unfavorable consequences, because the PD-1/PD-L1/PD-L2 axis helps the tumor to maintain an immunosuppressive microenvironment, thereby promoting immune evasion and survival of cancer cells (177). In addition to T cells, innate lymphoid cells type I (ILC1s) are another potent source of IFN-γ in healthy individuals. ILCs are important players of innate immune responses by reacting promptly to signals, or inducer cytokines, expressed by tissue-resident cells. ILC1s function as a first line of defense against intracellular pathogens, such as viruses, and tumors (178). By secreting IFN-γ, healthy ILC1s induce apoptosis and block differentiation by modulating JAK-STAT or PI3K/AKT signaling. However, in AML, ILC1s exhibit reduced IFN-γ secretion and lose their ability to suppress the development of LSCs and antagonize AML progression (179). ILC1s thus seem pivotal as an anti-cancer immune cell, and administration of *ex vivo*-expanded ILC1s could provide a new immunotherapeutic approach to ensure that IFN-γ levels are locally increased within leukemic niches. Importantly, this approach would significantly decrease toxicity for AML patients in comparison to systemic delivery of IFN-γ (179).

Interleukin-4

IL-4 is a signature cytokine of type II inflammation and regulates many aspects of Th2-mediated immunity (180). In epithelial cancers, IL-4 is generally considered to have pro-tumorigenic and pro-metastatic functions, suggesting that inhibition of the IL-4/IL-4R axis may be beneficial to limiting diseases (181, 182). Yet, in hematological cancers, a tumor-promoting role of IL-4 is controversial. Already in the early 1990s there were studies reporting that IL-4 might also have tumor-limiting functions, by suppressing IL-1-induced proliferation of AML cells (60, 64, 65). More recent findings substantiate those earlier observations and show that IL-4 has the potential to inhibit survival of AML cell lines as well as patient-derived AML cells, irrespective of their cytogenetic status and French-American-British (FAB) subtype, without affecting normal HSPCs. Anti-leukemic effects of IL-4 are at least partially dependent on STAT6 and Caspase-3, which agrees with the crucial role of STAT6 in mediating IL-4's effects downstream of the IL-4 receptor (183). In addition, IL-4-induced STAT6, in cooperation with the nuclear receptor protein proliferator-activated receptor gamma (PPARγ), upregulates the expression of prostaglandins. In particular, COX (cyclooxygenase)-dependent prostaglandins, so-called CyPGs, play an important role in apoptosis (184). After stimulation by IL-4, these lipid mediators are increasingly produced *via* the COX/prostaglandin axis, which leads to activation of p53 and caspase-3 and subsequently stimulates apoptosis of leukemic cells (185). The fact that IL-4 treatment specifically acts on AML blasts, but does not affect HSCs, even upon long-term treatment, makes IL-4 an interesting candidate for therapeutic intervention in AML. Yet, despite its promising role as an anti-leukemic cytokine, IL-4 additionally promotes the differentiation of immune cells, including M2 macrophages, which are regarded as having a leukemia-supporting

phenotype. M2 macrophages release various cytokines and growth factors that promote blast survival and proliferation, induce proangiogenic effects and can directly inhibit $CD8^+$ T cell-mediated killing of blast cells (186, 187). Therefore, more detailed studies are required to assess the value of IL-4 as an antileukemic molecule.

Interleukin-10

IL-10, an anti-inflammatory cytokine produced by several immune cells, is crucial for limiting immune responses and damage caused by long-lasting inflammation (188). In AML patients, significantly higher levels of plasma IL-10 are observed (53, 56, 73) which directly correlate with prolonged overall patient survival, event-free survival and higher complete remission rates (39, 189, 190). *In vitro*, IL-10 treatment of AML blasts inhibited spontaneous AML blast proliferation and colony formation by negatively affecting the production and secretion of pro-leukemic cytokines (IL-1α, IL-1β, TNF-α, GM-CSF, GM-CSF, and IL-6) (74–76, 191). However, contrary to these findings, there is also evidence that IL-10 together with IL-35 — the latter a $CD4^+$ and $CD8^+$ T cell-suppressing and T regulatory cell (Treg)-supporting cytokine upregulated in AML (118) — promotes AML cell proliferation, survival and chemoresistance. So far, $ICOS1^+$ and $PD1^+$ Treg cells as well as BM-MSCs have been suggested as a source for IL-10 in the AML microenvironment (176, 192), contributing to the establishment of an IL-10-induced immunosuppressive and anti-inflammatory niche which ensures LSC survival and stemness (193, 194). Therefore, despite the direct correlation between IL-10 serum level and prolonged patient survival and treatment response (39, 189), antagonizing IL-10 signaling could support current chemotherapeutic approaches to irradicate LSCs and decrease the patient relapse rate (195). However, so far, no combinatory studies have been performed. Interestingly, Chen et al. recently highlighted the IL-10 receptor as a potential candidate for AML immunotherapy as it is significantly upregulated on AML cells in patients and is required for LSC stemness. CAR-T cells harboring an IL-10 peptide structure within their antigen-binding domain were shown to recognize and bind to the IL-10 receptor of multiple AML cell lines (MV4-11, Kasumi-1, U937, THP-1 and MOLM-13) and primary AML cells, thereby inducing the CAR T-cell mediated killing of these cells *in vitro* and *in vivo* (196). Although the function of IL-10 may be patient-dependent, immunomodulatory agents that block IL-10 could offer an interesting approach for treatment of AML.

Interleukin-12p70: a new trick for an old cytokine

More than a decade ago, IL-12p70 was shown to inhibit the angiogenic potential but not the survival or proliferation of AML cells (77) and to increase T-cell proliferation and cytotoxicity against leukemic cells *in vitro* (78, 79). Multiple *in vitro* co-culture studies overexpressing IL-12p70 in dendritic cells have confirmed these findings (197, 198) and paved the way for initial immunotherapies using genetically modified dendritic cells (phase 1 clinical trial NCT01734304) (199), thereby trying to avoid the toxicity of systemic administration of IL-12. Recently, another elegant therapeutic approach based on transplantation of genetically modified AML blasts constitutively expressing IL-12 in a vaccine-like manner was successfully established in murine and human cells (197) and is currently under investigation in a phase 1 clinical trial (NCT02483312).

Conclusion and future perspectives

Despite intensive research leading to new and targeted therapeutic strategies for AML in recent years, the prognosis for a large proportion of patients remains poor. Due to the highly heterogeneous nature of AML, current therapies often only eliminate specific subclones but cannot permanently halt disease progression. As in many other cancers, chronic inflammation, characterized by the release of pro-inflammatory cytokines and growth factors, which significantly influence the interaction of tumor and immune cells in the tumor microenvironment, can also be observed in AML. On the one hand these cytokines may ensure survival of cancer cells by promoting tumor cell proliferation while inhibiting the antitumor immune responses; on the other hand, some cytokines contribute to cancer cell elimination by supporting the body's own immunological defense mechanisms. Therapeutic application of cytokines, or therapies that specifically target cytokines and/or their receptors, may provide new avenues for the treatment of AML patients in the coming years. In particular, IL-1β, IL-6 and CXCL12 might be promising new druggable targets. However, due to the pleiotropic effects of most cytokines, which control both tumor growth and anti-tumor immune responses, we are faced with the challenge of establishing new therapies, which on the one hand inhibit tumor growth and at the same time specifically enhance the anti-tumor response. The use of combination therapies, in which potential inhibitors of inflammatory cytokines are combined with other therapeutic molecules and agents, may prove promising for this purpose.

Author contributions

Conceptualization, JH-H, ML, PWK, writing—original draft preparation, ML and PWK, writing—review and editing, JH-H, visualization, ML and funding acquisition, JH-H. All authors contributed to the article and approved the submitted version.

Funding

This work was supported by the County of Salzburg, Cancer Cluster Salzburg [grant number 20102-P1601064-FPR01-2017], the Austrian Science Fund (FWF) [grant numbers W1213 and P33969], the Biomed Center Salzburg (project 20102-F1901165-KZP), the European Interreg project EPIC (grant number ITAT1054), and by the Priority program ACBN, University of Salzburg.

Conflict of interest

The authors declare that the research was conducted in the absence of any commercial or financial relationships that could be construed as a potential conflict of interest.

Publisher's note

References

1. Dohner H, Weisdorf DJ, Bloomfield CD. Acute myeloid leukemia. *N Engl J Med* (2015) 373(12):1136–52. doi: 10.1056/NEJMra1406184

2. Estey E, Döhner H. Acute myeloid leukaemia. *Lancet (London England)* (2006) 368(9550):1894–907. doi: 10.1016/S0140-6736(06)69780-8

3. Pelcovits A, Niroula R. Acute myeloid leukemia: A review. *Rhode Island Med J* (2013) (2020) 103(3):38–40.

4. Papayannidis C, Sartor C, Marconi G, Fontana MC, Nanni J, Cristiano G, et al. Acute myeloid leukemia mutations: Therapeutic implications. *Int J Mol Sci* (2019) 20(11):2721. doi: 10.3390/ijms20112721

5. Noone AM HN, Krapcho M, Miller D, Brest A, Yu M, Ruhl J, Tatalovich Z, Mariotto A, Lewis DR, Chen HS, Feuer EJ, Cronin KA eds. *SEER cancer statistics review, 1975-2015*. Bethesda, MD: National Cancer Institute (2018). Available at: https://seer.cancer.gov/csr/1975_2015/.

6. Prada-Arismendy J, Arroyave JC, Rothlisberger S. Molecular biomarkers in acute myeloid leukemia. *Blood Rev* (2017) 31(1):63–76. doi: 10.1016/j.blre.2016.08.005

7. De Kouchkovsky I, Abdul-Hay M. Acute myeloid leukemia: a comprehensive review and 2016 update *Blood Cancer J* (2016) 6(7):e441. doi: 10.1038/bcj.2016.50

8. Narayanan D, Weinberg OK. How I investigate acute myeloid leukemia. *Int J Lab Hematol* (2020) 42(1):3–15. doi: 10.1111/ijlh.13135

9. Krause DS, Scadden DT. A hostel for the hostile: the bone marrow niche in hematologic neoplasms *Haematologica*. (2015) 100(11):1376–87. doi: 10.3324/haematol.2014.113852

10. Lane SW, Scadden DT, Gilliland DG. The leukemic stem cell niche: current concepts and therapeutic opportunities. *Blood* (2009) 114(6):1150–7. doi: 10.1182/blood-2009-01-202606

11. Schepers K, Campbell TB, Passegué E. Normal and leukemic stem cell niches: insights and therapeutic opportunities. *Cell Stem Cell* (2015) 16(3):254–67. doi: 10.1016/j.stem.2015.02.014

12. Bhatia R, McGlave PB, Dewald GW, Blazar BR, Verfaillie CM. Abnormal function of the bone marrow microenvironment in chronic myelogenous leukemia: role of malignant stromal macrophages. *Blood* (1995) 85(12):3636–45. doi: 10.1182/blood.V85.12.3636.bloodjournal85123636

13. Somervaille TC, Cleary ML. Identification and characterization of leukemia stem cells in murine MLL-AF9 acute myeloid leukemia. *Cancer Cell* (2006) 10(4):257–68. doi: 10.1016/j.ccr.2006.08.020

14. Reynaud D, Pietras E, Barry-Holson K, Mir A, Binnewies M, Jeanne M, et al. IL-6 controls leukemic multipotent progenitor cell fate and contributes to chronic myelogenous leukemia development. *Cancer Cell* (2011) 20(5):661–73. doi: 10.1016/j.ccr.2011.10.012

15. Schemionek M, Spieker T, Kerstiens L, Elling C, Essers M, Trumpp A, et al. Leukemic spleen cells are more potent than bone marrow-derived cells in a transgenic mouse model of CML. *Leukemia* (2012) 26(5):1030–7. doi: 10.1038/leu.2011.366

16. Krenn PW, Montanez E, Costell M, Fässler R. Integrins, anchors and signal transducers of hematopoietic stem cells during development and in adulthood. *Curr Top Dev Biol* (2022) 149:203–61. doi: 10.1016/bs.ctdb.2022.02.009

17. Boettcher S, Manz MG. Regulation of inflammation- and infection-driven hematopoiesis. *Trends Immunol* (2017) 38(5):345–57. doi: 10.1016/j.it.2017.01.004

18. Pietras EM, Mirantes-Barbeito C, Fong S, Loeffler D, Kovtonyuk LV, Zhang S, et al. Chronic interleukin-1 exposure drives haematopoietic stem cells towards precocious myeloid differentiation at the expense of self-renewal. *Nat Cell Biol* (2016) 18(6):607–18. doi: 10.1038/ncb3346

19. Weber GF, Chousterman BG, He S, Fenn AM, Nairz M, Anzai A, et al. Interleukin-3 amplifies acute inflammation and is a potential therapeutic target in sepsis. *Science* (2015) 347(6227):1260–5. doi: 10.1126/science.aaa4268

20. Ihle JN. Interleukin-3 and hematopoiesis. *Chem Immunol* (1992) 51:65–106. doi: 10.1159/000420755

21. Ishihara K, Hirano T. IL-6 in autoimmune disease and chronic inflammatory proliferative disease. *Cytokine Growth Factor Rev* (2002) 13(4-5):357–68. doi: 10.1016/S1359-6101(02)00027-8

22. Reynaud D, Pietras E, Barry-Holson K, Mir A, Binnewies M, Jeanne M, et al. IL-6 controls leukemic multipotent progenitor cell fate and contributes to chronic myelogenous leukemia development. *Cancer Cell* (2011) 20(5):661–73. doi: 10.1016/j.ccr.2011.10.012

23. Maeda K, Baba Y, Nagai Y, Miyazaki K, Malykhin A, Nakamura K, et al. IL-6 blocks a discrete early step in lymphopoiesis. *Blood* (2005) 106(3):879–85. doi: 10.1182/blood-2005-02-0456

24. Tian T, Wang M, Ma D. TNF-alpha, a good or bad factor in hematological diseases? *Stem Cell Investig* (2014) 1:12. doi: 10.3978/j.issn.2306-9759.2014.04.02.

25. Selleri C, Maciejewski JP, Sato T, Young NS. Interferon-gamma constitutively expressed in the stromal microenvironment of human marrow cultures mediates potent hematopoietic inhibition. *Blood.* (1996) 87(10):4149–57. doi: 10.1182/blood.V87.10.4149.bloodjournal87104149

26. Jacobsen SE, Ruscetti FW, Dubois CM, Keller JR. Tumor necrosis factor alpha directly and indirectly regulates hematopoietic progenitor cell proliferation: role of colony-stimulating factor receptor modulation. *J Exp Med* (1992) 175(6):1759–72. doi: 10.1084/jem.175.6.1759

27. Rezzoug F, Huang Y, Tanner MK, Wysoczynski M, Schanie CL, Chilton PM, et al. TNF-alpha is critical to facilitate hemopoietic stem cell engraftment and function. *J Immunol* (2008) 180(1):49–57. doi: 10.4049/jimmunol.180.1.49

28. Baldridge MT, King KY, Boles NC, Weksberg DC, Goodell MA. Quiescent haematopoietic stem cells are activated by IFN-gamma in response to chronic infection. *Nature* (2010) 465(7299):793–7. doi: 10.1038/nature09135

29. Essers MA, Offner S, Blanco-Bose WE, Waibler Z, Kalinke U, Duchosal MA, et al. IFNalpha activates dormant haematopoietic stem cells *in vivo*. *Nature* (2009) 458(7240):904–8. doi: 10.1038/nature07815

30. Ushach I, Zlotnik A. Biological role of granulocyte macrophage colony-stimulating factor (GM-CSF) and macrophage colony-stimulating factor (M-CSF) on cells of the myeloid lineage. *J Leukoc Biol* (2016) 100(3):481–9. doi: 10.1189/jlb.3RU0316-144R

31. Mirantes C, Passegue E, Pietras EM. Pro-inflammatory cytokines: emerging players regulating HSC function in normal and diseased hematopoiesis. *Exp Cell Res* (2014) 329(2):248–54. doi: 10.1016/j.yexcr.2014.08.017

32. Hemmati S, Haque T, Gritsman K. Inflammatory signaling pathways in preleukemic and leukemic stem cells. *Front Oncol* (2017) 7:265. doi: 10.3389/fonc.2017.00265

33. King KY, Goodell MA. Inflammatory modulation of HSCs: viewing the HSC as a foundation for the immune response. *Nat Rev Immunol* (2011) 11(10):685–92. doi: 10.1038/nri3062

34. Camacho V, McClearn V, Patel S, Welner RS. Regulation of normal and leukemic stem cells through cytokine signaling and the microenvironment. *Int J Hematol* (2017) 105(5):566–77. doi: 10.1007/s12185-017-2184-6

35. Vilchis-Ordoñez A, Contreras-Quiroz A, Vadillo E, Dorantes-Acosta E, Reyes-López A, Quintela-Nuñez del Prado HM, et al. Bone marrow cells in acute lymphoblastic leukemia create a proinflammatory microenvironment influencing normal hematopoietic differentiation fates. *BioMed Res Int* (2015) 2015:386165. doi: 10.1155/2015/386165

36. Hoermann G, Greiner G, Valent P. Cytokine regulation of microenvironmental cells in myeloproliferative neoplasms. *Mediators Inflamm* (2015) 2015:869242. doi: 10.1155/2015/869242

37. Kiss C, Benko I, Kovács P. Leukemic cells and the cytokine patchwork. *Pediatr Blood Cancer* (2004) 42(2):113–21. doi: 10.1002/pbc.10436

38. Pietras EM. Inflammation: a key regulator of hematopoietic stem cell fate in health and disease. *Blood* (2017) 130(15):1693–8. doi: 10.1182/blood-2017-06-780882

39. Sanchez-Correa B, Bergua JM, Campos C, Gayoso I, Arcos MJ, Banas H, et al. Cytokine profiles in acute myeloid leukemia patients at diagnosis: survival is inversely correlated with IL-6 and directly correlated with IL-10 levels. *Cytokine* (2013) 61(3):885–91. doi: 10.1016/j.cyto.2012.12.023

40. Ahmed HA, Maklad AM, Khaled SA, Elyamany A. Interleukin-27 and interleukin-35 in *de novo* acute myeloid leukemia: expression and significance as biological markers. *J Blood Med* (2019) 10:341–9. doi: 10.2147/JBM.S221301

41. Carey A, DKt E, CA E, Newell L, Traer E, BC M, et al. Identification of interleukin-1 by functional screening as a key mediator of cellular expansion and disease progression in acute myeloid leukemia. *Cell Rep* (2017) 18(13):3204–18. doi: 10.1016/j.celrep.2017.03.018

42. Tao M, Li B, Nayini J, Andrews CB, Huang RW, Devemy E, et al. SCF, IL-1beta, IL-1ra and GM-CSF in the bone marrow and serum of normal individuals and of AML and CML patients. *Cytokine* (2000) 12(6):699–707. doi: 10.1006/cyto.2000.0666

43. Elbaz O, Shaltout A. Implication of granulocyte-macrophage colony stimulating factor (GM-CSF) and interleukin-3 (IL-3) in children with acute myeloid leukaemia (AML); malignancy. *Hematology* (2001) 5(5):383–8.

44. Islam M, Mohamed EH, Esa E, Kamaluddin NR, Zain SM, Yusoff YM, et al. Circulating cytokines and small molecules follow distinct expression patterns in acute myeloid leukaemia. *Br J Cancer* (2017) 117(10):1551–6. doi: 10.1038/bjc.2017.316

45. Carlo-Stella C, Mangoni L, Almici C, Frassoni F, Fiers W, Rizzoli V. Growth of CD34+ acute myeloblastic leukemia colony-forming cells in response to recombinant hematopoietic growth factors. *Leukemia* (1990) 4(8):561–6.

46. Delwel R, Salem M, Pellens C, Dorssers L, Wagemaker G, Clark S, et al. Growth regulation of human acute myeloid leukemia: effects of five recombinant hematopoietic factors in a serum-free culture system. *Blood* (1988) 72(6):1944–9. doi: 10.1182/blood.V72.6.1944.1944

47. Pebusque MJ, Fay C, Lafage M, Sempere C, Saeland S, Caux C, et al. Recombinant human IL-3 and G-CSF act synergistically in stimulating the growth of acute myeloid leukemia cells. *Leukemia* (1989) 3(3):200–5.

48. Suzuki T, Morio T, Tohda S, Nagata K, Yamashita Y, Imai Y, et al. Effects of interleukin-6 and granulocyte colony-stimulating factor on the proliferation of leukemic blast progenitors from acute myeloblastic leukemia patients. *Jpn J Cancer Res* (1990) 81(10):979–86. doi: 10.1111/j.1349-7006.1990.tb03335.x

49. Kassem NM, Ayad AM, El Husseiny NM, El-Demerdash DM, Kassem HA, Mattar MM. Role of granulocyte-macrophage colony-stimulating factor in acute myeloid Leukemia/Myelodysplastic syndromes. *J Glob Oncol* (2018) 4:1–6. doi: 10.1200/JGO.2017.009332

50. Hoang T, Haman A, Goncalves O, Letendre F, Mathieu M, Wong GG, et al. Interleukin 1 enhances growth factor-dependent proliferation of the clonogenic cells in acute myeloblastic leukemia and of normal human primitive hemopoietic precursors. *J Exp Med* (1988) 168(2):463–74. doi: 10.1084/jem.168.2.463

51. Carter A, Silvian-Draxler I, Tatarsky I. Effect of interleukin-1, tumor necrosis factor-alpha, and interferon-alpha on the blast cells of acute myeloblastic leukemia. *Am J Hematol* (1992) 40(4):245–51. doi: 10.1002/ajh.2830400402

52. Sissolak G, Hoffbrand AV, Mehta AB, Ganeshaguru K. Effects of interferon-alpha (IFN) on the expression of interleukin 1-beta (IL-1), interleukin 6 (IL-6), granulocyte-macrophage colony-stimulating factor (GM-CSF) and tumor necrosis factor-alpha (TNF) in acute myeloid leukemia (AML) blasts. *Leukemia.* (1992) 6 (11):1155–60.

53. Sun YX, Kong HL, Liu CF, Yu S, Tian T, Ma DX, et al. The imbalanced profile and clinical significance of T helper associated cytokines in bone marrow microenvironment of the patients with acute myeloid leukemia. *Hum Immunol* (2014) 75(2):113–8. doi: 10.1016/j.humimm.2013.11.014

54. Corradi G, Bassani B, Simonetti G, Sangaletti S, Vadakekolathu J, Fontana MC, et al. Release of IFN-γ by acute myeloid leukemia cells remodels bone marrow immune microenvironment by inducing regulatory T cells. *Clin Cancer Res* (2022) 28(14):3141–55. doi: 10.1158/1078-0432.CCR-21-3594

55. Ersvaer E, Skavland J, Ulvestad E, Gjertsen BT, Bruserud Ø. Effects of interferon gamma on native human acute myelogenous leukaemia cells. *Cancer Immunol Immunother.* (2007) 56(1):13–24. doi: 10.1007/s00262-006-0159-1

56. Tsimberidou AM, Estey E, Wen S, Pierce S, Kantarjian H, Albitar M, et al. The prognostic significance of cytokine levels in newly diagnosed acute myeloid leukemia and high-risk myelodysplastic syndromes. *Cancer.* (2008) 113(7):1605–13. doi: 10.1002/cncr.23785

57. Yin M, Gopal V, Banavali S, Gartside P, Preisler H. Effects of an IL-1 receptor antagonist on acute myeloid leukemia cells. *Leukemia* (1992) 6(9):898–901.

58. Estrov Z, Kurzrock R, Estey E, Wetzler M, Ferrajoli A, Harris D, et al. Inhibition of acute myelogenous leukemia blast proliferation by interleukin-1 (IL-1) receptor antagonist and soluble IL-1 receptors. *Blood* (1992) 79(8):1938–45. doi: 10.1182/blood.V79.8.1938.1938

59. Cozzolino F, Rubartelli A, Aldinucci D, Sitia R, Torcia M, Shaw A, et al. Interleukin 1 as an autocrine growth factor for acute myeloid leukemia cells. *Proc Natl Acad Sci USA.* (1989) 86(7):2369–73. doi: 10.1073/pnas.86.7.2369

60. Wagteveld AJ, Esselink MT, Limburg P, Halie MR, Vellenga E. The effects of IL-1 beta and IL-4 on the proliferation and endogenous secretion of growth factors by acute myeloblastic leukemic cells. *Leukemia* (1992) 6(10):1020–4.

61. Delwel R, Dorssers L, Touw I, Wagemaker G, Lowenberg B. Human recombinant multilineage colony stimulating factor (interleukin-3): stimulator of acute myelocytic leukemia progenitor cells *in vitro*. *Blood* (1987) 70(1):333–6. doi: 10.1182/blood.V70.1.333.333

62. Lemoli RM, Gulati SC, Strife A, Lambek C, Perez A, Clarkson BD. Proliferative response of human acute myeloid leukemia cells and normal marrow enriched progenitor cells to human recombinant growth factors IL-3, GM-CSF and G-CSF alone and in combination. *Leukemia* (1991) 5(5):386–91.

63. Santoli D, Yang YC, Clark SC, Kreider BL, Caracciolo D, Rovera G. Synergistic and antagonistic effects of recombinant human interleukin (IL) 3, IL-1 alpha, granulocyte and macrophage colony-stimulating factors (G-CSF and m-CSF) on the growth of GM-CSF-dependent leukemic cell lines. *J Immunol* (1987) 139(10):3348–54.

64. Tuyt LM, Dokter WH, Esselink MT, Vellenga E. Divergent effects of IL-10 and IL-4 on the proliferation and growth factor secretion by acute myeloblastic leukemic cells. *Eur Cytokine Netw* (1995) 6(4):231–5.

65. Akashi K. The role of interleukin-4 in the negative regulation of leukemia cell growth. *Leuk Lymphoma* (1993) 9(3):205–9. doi: 10.3109/10428199309147371

66. Negaard HF, Iversen N, Bowitz-Lothe IM, Sandset PM, Steinsvik B, Ostenstad B, et al. Increased bone marrow microvascular density in haematological malignancies is associated with differential regulation of angiogenic factors. *Leukemia* (2009) 23(1):162–9. doi: 10.1038/leu.2008.255

67. Sugiyama H, Inoue K, Ogawa H, Yamagami T, Soma T, Miyake S, et al. The expression of IL-6 and its related genes in acute leukemia. *Leuk Lymphoma* (1996) 21(1-2):49–52. doi: 10.3109/10428199609067579

68. Hoang T, Haman A, Goncalves O, Wong GG, Clark SC. Interleukin-6 enhances growth factor-dependent proliferation of the blast cells of acute myeloblastic leukemia. *Blood* (1988) 72(2):823–6. doi: 10.1182/blood.V72.2.823.823

69. Säily M, Koistinen P, Zheng A, Savolainen ER. Signaling through interleukin-6 receptor supports blast cell proliferation in acute myeloblastic leukemia *Eur J Haematol* (1998) 61(3):190–6. doi: 10.1111/j.1600-0609.1998.tb01083.x.

70. Lopez M, Maroc N, Kerangueven F, Bardin F, Courcoul M, Lavezzi C, et al. Coexpression of the genes for interleukin 6 and its receptor without apparent

involvement in the proliferation of acute myeloid leukemia cells. *Exp Hematol* (1991) 19(8):797–803.

71. Suzuki T, Bessho M, Hirashma K, Tohda S, Nagata K, Imai Y, et al. Interleukin-6 reduces the optimal growth *in vitro* of leukemic blast progenitors from acute myeloblastic leukemia patients. *Acta Haematol* (1992) 87(1-2):63–8. doi: 10.1159/000204718

72. Çelik H, Lindblad KE, Popescu B, Gui G, Goswami M, Valdez J, et al. Highly multiplexed proteomic assessment of human bone marrow in acute myeloid leukemia. *Blood Adv* (2020) 4(2):367–79. doi: 10.1182/bloodadvances.2019001124

73. Wu H, Li P, Shao N, Ma J, Ji M, Sun X, et al. Aberrant expression of treg-associated cytokine IL-35 along with IL-10 and TGF-β in acute myeloid leukemia. *Oncol Lett* (2012) 3(5):1119–23. doi: 10.3892/ol.2012.614

74. Westermann F, Kube D, Haier B, Bohlen H, Engert A, Zuehlsdorf M, et al. Interleukin 10 inhibits cytokine production of human AML cells. *Ann Oncol* (1996) 7(4):397–404. doi: 10.1093/oxfordjournals.annonc.a010607

75. Bruserud O, Tore Gjertsen B, Brustugun OT, Bassøe CF, Nesthus I, Espen Akselsen P, et al. Effects of interleukin 10 on blast cells derived from patients with acute myelogenous leukemia. *Leukemia* (1995) 9(11):1910–20.

76. Asano Y, Shibata S, Kobayashi S, Okamura S, Niho Y. Interleukin-10 inhibits the autocrine growth of leukemic blast cells from patients with acute myeloblastic leukemia. *Int J Hematol* (1997) 66(4):445–50. doi: 10.1016/S0925-5710(97)00070-4

77. Ferretti E, Di Carlo E, Cocco C, Ribatti D, Sorrentino C, Ognio E, et al. Direct inhibition of human acute myeloid leukemia cell growth by IL-12. *Immunol Lett* (2010) 133(2):99–105. doi: 10.1016/j.imlet.2010.08.002

78. Orleans-Lindsay JK, Deru A, Craig JI, Prentice HG, Lowdell MW. *In vitro* co-stimulation with anti-CD28 synergizes with IL-12 in the generation of T cell immune responses to leukaemic cells; a strategy for ex-vivo generation of CTL for immunotherapy. *Clin Exp Immunol* (2003) 133(3):467–75. doi: 10.1046/j.1365-2249.2003.02235.x

79. Pan L, Ohnishi K, Zhang WJ, Yoshida H, Maksumova L, Muratkhodjaev F, et al. *In vitro* IL-12 treatment of peripheral blood mononuclear cells from patients with leukemia or myelodysplastic syndromes: increase in cytotoxicity and reduction in WT1 gene expression. *Leukemia* (2000) 14(9):1634–41. doi: 10.1038/sj.leu.2401872

80. Tao Q, Pan Y, Wang Y, Wang H, Xiong S, Li Q, et al. Regulatory T cells-derived IL-35 promotes the growth of adult acute myeloid leukemia blasts. *Int J Cancer* (2015) 137(10):2384–93. doi: 10.1002/ijc.29563

81. Wang J, Tao Q, Wang H, Wang Z, Wu F, Pan Y, et al. Elevated IL-35 in bone marrow of the patients with acute myeloid leukemia. *Hum Immunol* (2015) 76 (9):681–6. doi: 10.1016/j.humimm.2015.09.020

82. Liersch R, Gerss J, Schliemann C, Bayer M, Schwöppe C, Biermann C, et al. Osteopontin is a prognostic factor for survival of acute myeloid leukemia patients. *Blood* (2012) 119(22):5215–20. doi: 10.1182/blood-2011-11-389692

83. Lee CY, Tien HF, Hou HA, Chou WC, Lin LI. Marrow osteopontin level as a prognostic factor in acute myeloid leukaemia. *Br J Haematol* (2008) 141(5):736–9. doi: 10.1111/j.1365-2141.2008.07082.x

84. Zhou J, Chen X, Zhou P, Sun X, Chen Y, Li M, et al. Osteopontin is required for the maintenance of leukemia stem cells in acute myeloid leukemia. *Biochem Biophys Res Commun* (2022) 600:29–34. doi: 10.1016/j.bbrc.2022.02.022

85. Carlesso N, Pregno P, Bresso P, Gallo E, Pileri A, Zsebo KM, et al. Human recombinant stem cell factor stimulates *in vitro* proliferation of acute myeloid leukemia cells and expands the clonogenic cell pool. *Leukemia* (1992) 6(7):642–8.

86. Hassan HT, Zander A. Stem cell factor as a survival and growth factor in human normal and malignant hematopoiesis. *Acta Haematol* (1996) 95(3-4):257–62. doi: 10.1159/000203893

87. Bendall LJ, Makrynikola V, Hutchinson A, Bianchi AC, Bradstock KF, Gottlieb DJ. Stem cell factor enhances the adhesion of AML cells to fibronectin and augments fibronectin-mediated anti-apoptotic and proliferative signals. *Leukemia* (1998) 12(9):1375–82. doi: 10.1038/sj.leu.2401136

88. Wu Y, Chen P, Huang HF, Huang MJ, Chen YZ. Reduction of transforming growth factor-β1 expression in leukemia and its possible role in leukemia development. *Leuk Lymphoma* (2012) 53(1):145–51. doi: 10.3109/10428194.2011.603446

89. Nara N, Tohda S, Nagata K, Suzuki T, Yamashita Y. Inhibition of the *in vitro* growth of blast progenitors from acute myeloblastic leukemia patients by transforming growth factor-beta (TGF-beta). *Leukemia* (1989) 3(8):572–7.

90. Tessier N, Hoang T. Transforming growth factor beta inhibits the proliferation of the blast cells of acute myeloblastic leukemia. *Blood* (1988) 72 (1):159–64. doi: 10.1182/blood.V72.1.159.159

91. Zhou X, Zhou S, Li B, Li Q, Gao L, Li D, et al. Transmembrane TNF-α preferentially expressed by leukemia stem cells and blasts is a potent target for antibody therapy. *Blood* (2015) 126(12):1433–42. doi: 10.1182/blood-2015-01-624833

92. Sison EA, Magoon D, Li L, Annesley CE, Rau RE, Small D, et al. Plerixafor as a chemosensitizing agent in pediatric acute lymphoblastic leukemia: efficacy and potential mechanisms of resistance to CXCR4 inhibition. *Oncotarget* (2014) 5 (19):8947–58. doi: 10.18632/oncotarget.2407

93. Yu X, Munoz-Sagredo L, Streule K, Muschong P, Bayer E, Walter RJ, et al. CD44 loss of function sensitizes AML cells to the BCL-2 inhibitor venetoclax by decreasing CXCL12-driven survival cues. *Blood* (2021) 138(12):1067–80. doi: 10.1182/blood.2020006343

94. Wang SS, Xu ZJ, Jin Y, Ma JC, Xia PH, Wen X, et al. Clinical and prognostic relevance of CXCL12 expression in acute myeloid leukemia. *PeerJ* (2021) 9:e11820. doi: 10.7717/peerj.11820

95. Mehrpouri M. The contributory roles of the CXCL12/CXCR4/CXCR7 axis in normal and malignant hematopoiesis: A possible therapeutic target in hematologic malignancies. *Eur J Pharmacol* (2022) 920:174831. doi: 10.1016/j.ejphar.2022.174831

96. Cho BS, Kim HJ, Konopleva M. Targeting the CXCL12/CXCR4 axis in acute myeloid leukemia: from bench to bedside. *Korean J Intern Med* (2017) 32(2):248–57. doi: 10.3904/kjim.2016.244

97. Peled A, Klein S, Beider K, Burger JA, Abraham M. Role of CXCL12 and CXCR4 in the pathogenesis of hematological malignancies. *Cytokine* (2018) 109:11–6. doi: 10.1016/j.cyto.2018.02.020

98. Ladikou EE, Chevassut T, Pepper CJ, Pepper AG. Dissecting the role of the CXCL12/CXCR4 axis in acute myeloid leukaemia. *Br J Haematol* (2020) 189 (5):815–25. doi: 10.1111/bjh.16456

99. Rodriguez-Cimadevilla JC, Beauchemin V, Villeneuve L, Letendre F, Shaw A, Hoang T. Coordinate secretion of interleukin-1 beta and granulocyte-macrophage colony-stimulating factor by the blast cells of acute myeloblastic leukemia: role of interleukin-1 as an endogenous inducer. *Blood* (1990) 76(8):1481–9. doi: 10.1182/blood.V76.8.1481.1481

100. Russell NH. Autocrine growth factors and leukaemic haemopoiesis. *Blood Rev* (1992) 6(3):149–56. doi: 10.1016/0268-960X(92)90026-M

101. Murohashi I, Tohda S, Suzuki T, Nagata K, Yamashita Y, Nara N. Autocrine growth mechanisms of the progenitors of blast cells in acute myeloblastic leukemia *Blood* (1989) 74(1):35–41. doi: 10.1182/blood.V74.1.35.35

102. Delwel R, Schipper P, van Buitenen C, van Agthoven T, Touw I, Löwenberg B. Comparative analysis of IL-1 regulated and spontaneous growth of acute myeloid leukemia *in vitro*. *Bone marrow Transplant* (1990) 6 Suppl 1:22–6.

103. Bradbury D, Rogers S, Reilly IA, Kozlowski R, Russell NH. Role of autocrine and paracrine production of granulocyte-macrophage colony-stimulating factor and interleukin-1 beta in the autonomous growth of acute myeloblastic leukaemia cells–studies using purified CD34-positive cells. *Leukemia* (1992) 6(6):562–6.

104. Oster W, Cicco NA, Klein H, Hirano T, Kishimoto T, Lindemann A, et al. Participation of the cytokines interleukin 6, tumor necrosis factor-alpha, and interleukin 1-beta secreted by acute myelogenous leukemia blasts in autocrine and paracrine leukemia growth control. *J Clin Invest* (1989) 84(2):451–7. doi: 10.1172/JCI114186

105. Beauchemin V, Villeneuve L, Rodriguez-Cimadevilla JC, Rajotte D, Kenney JS, Clark SC, et al. Interleukin-6 production by the blast cells of acute myeloblastic leukemia: regulation by endogenous interleukin-1 and biological implications. *J Cell Physiol* (1991) 148(3):353–61. doi: 10.1002/jcp.1041480305

106. Delwel R, van Buitenen C, Salem M, Oosterom R, Touw I, Löwenberg B. Hemopoietin-1 activity of interleukin-1 (IL-1) on acute myeloid leukemia colony-forming cells (AML-CFU) *in vitro*: IL-1 induces production of tumor necrosis factor-alpha which synergizes with IL-3 or granulocyte-macrophage colony-stimulating factor. *Leukemia* (1990) 4(8):557–60.

107. Tsuzuki M, Ezaki K, Maruyama F, Ino T, Kojima H, Okamoto M, et al. Proliferative effects of several hematopoietic growth factors on acute myelogenous leukemia cells and correlation with treatment outcome. *Leukemia* (1997) 11 (12):2125–30. doi: 10.1038/sj.leu.2400870

108. Russell NH, Hunter AE, Bradbury D, Zhu YM, Keith F. Biological features of leukaemic cells associated with autonomous growth and reduced survival in acute myeloblastic leukaemia. *Leuk Lymphoma* (1995) 16(3-4):223–9. doi: 10.3109/10428199509049761

109. Lowenberg B, van Putten WL, Touw IP, Delwel R, Santini V. Autonomous proliferation of leukemic cells *in vitro* as a determinant of prognosis in adult acute myeloid leukemia *N Engl J Med* (1993) 328(9):614–9. doi: 10.1056/NEJM199303043280904

110. Pimenta DB, Varela VA, Datoguia TS, Caraciolo VB, Lopes GH, Pereira WO. The bone marrow microenvironment mechanisms in acute myeloid leukemia. *Front Cell Dev Biol* (2021) 9:764698. doi: 10.3389/fcell.2021.764698

111. Nilsson SK, Johnston HM, Whitty GA, Williams B, Webb RJ, Denhardt DT, et al. Osteopontin, a key component of the hematopoietic stem cell niche and

regulator of primitive hematopoietic progenitor cells. *Blood* (2005) 106(4):1232–9. doi: 10.1182/blood-2004-11-4422

112. Battula VL, Le PM, Sun JC, Nguyen K, Yuan B, Zhou X, et al. AML-induced osteogenic differentiation in mesenchymal stromal cells supports leukemia growth. *JCI Insight* (2017) 2(13):e90036. doi: 10.1172/jci.insight.90036

113. Zahed Panah M, Nikbakht M, Sajjadi SM, Rostami S, Norooznezhad AH, Kamranzadeh Fumani H, et al. Anti-apoptotic effects of osteopontin *via* the up-regulation of AKT/mTOR/β-catenin loop in acute myeloid leukemia cells. *Int J Hematol Oncol Stem Cell Res* (2017) 11(2):148–57.

114. Bandopadhyay M, Bulbule A, Butti R, Chakraborty G, Ghorpade P, Ghosh P, et al. Osteopontin as a therapeutic target for cancer. *Expert Opin Ther Targets* (2014) 18(8):883–95. doi: 10.1517/14728222.2014.925447

115. Mantovani A, Dinarello CA, Molgora M, Garlanda C. Interleukin-1 and related cytokines in the regulation of inflammation and immunity. *Immunity* (2019) 50(4):778–95. doi: 10.1016/j.immuni.2019.03.012

116. Mantovani A, Ponzetta A, Inforzato A, Jaillon S. Innate immunity, inflammation and tumour progression: double-edged swords. *J Intern Med* (2019) 285(5):524–32. doi: 10.1111/joim.12886

117. Arranz L, Arriero MDM, Villatoro A. Interleukin-1beta as emerging therapeutic target in hematological malignancies and potentially in their complications. *Blood Rev* (2017) 31(5):306–17. doi: 10.1016/j.blre.2017.05.001

118. Binder S, Luciano M, Horejs-Hoeck J. The cytokine network in acute myeloid leukemia (AML): A focus on pro- and anti-inflammatory mediators. *Cytokine Growth Factor Rev* (2018) 43:8–15. doi: 10.1016/j.cytogfr.2018.08.004

119. Zhang W, Borcherding N, Kolb R. IL-1 signaling in tumor microenvironment. *Adv Exp Med Biol* (2020) 1240:1–23. doi: 10.1007/978-3-030-38315-2_1

120. de Mooij CEM, Netea MG, van der Velden W, Blijlevens NMA. Targeting the interleukin-1 pathway in patients with hematological disorders. *Blood* (2017) 129(24):3155–64. doi: 10.1182/blood-2016-12-754994

121. Wang Y, Sun X, Yuan S, Hou S, Guo T, Chu Y, et al. Interleukin-1β inhibits normal hematopoietic expansion and promotes acute myeloid leukemia progression *via* the bone marrow niche. *Cytotherapy* (2020) 22(3):127–34. doi: 10.1016/j.jcyt.2020.01.001

122. Höckendorf U, Yabal M, Herold T, Munkhbaatar E, Rott S, Jilg S, et al. RIPK3 restricts myeloid leukemogenesis by promoting cell death and differentiation of leukemia initiating cells. *Cancer Cell* (2016) 30(1):75–91. doi: 10.1016/j.ccell.2016.06.002

123. Barreyro L, Will B, Bartholdy B, Zhou L, Todorova TI, Stanley RF, et al. Overexpression of IL-1 receptor accessory protein in stem and progenitor cells and outcome correlation in AML and MDS. *Blood* (2012) 120(6):1290–8. doi: 10.1182/blood-2012-01-404699

124. De Boer B, Sheveleva S, Apelt K, Vellenga E, Mulder AB, Huls G, et al. The IL1-IL1RAP axis plays an important role in the inflammatory leukemic niche that favors acute myeloid leukemia proliferation over normal hematopoiesis. *Haematologica* (2020) 106(12):3067–78. doi: 10.3324/haematol.2020.254987

125. Svensson EC, Madar A, Campbell CD, He Y, Sultan M, Healey ML, et al. TET2-driven clonal hematopoiesis and response to canakinumab: An exploratory analysis of the CANTOS randomized clinical trial. *JAMA Cardiol* (2022) 7(5):521–8. doi: 10.1001/jamacardio.2022.0386

126. Wong CC, Baum J, Silvestro A, Beste MT, Bharani-Dharan B, Xu S, et al. Inhibition of IL1β by canakinumab may be effective against diverse molecular subtypes of lung cancer: An exploratory analysis of the CANTOS trial. *Cancer Res* (2020) 80(24):5597–605. doi: 10.1158/0008-5472.CAN-19-3176

127. Tanaka T, Narazaki M, Kishimoto T. IL-6 in inflammation, immunity, and disease. *Cold Spring Harbor Perspect Biol* (2014) 6(10):a016295. doi: 10.1101/cshperspect.a016295

128. Leary AG, Ikebuchi K, Hirai Y, Wong GG, Yang YC, Clark SC, et al. Synergism between interleukin-6 and interleukin-3 in supporting proliferation of human hematopoietic stem cells: comparison with interleukin-1 alpha. *Blood* (1988) 71(6):1759–63. doi: 10.1182/blood.V71.6.1759.1759

129. Ikebuchi K, Wong GG, Clark SC, Ihle JN, Hirai Y, Ogawa M. Interleukin 6 enhancement of interleukin 3-dependent proliferation of multipotential hemopoietic progenitors. *Proc Natl Acad Sci USA* (1987) 84(24):9035–9. doi: 10.1073/pnas.84.24.9035

130. Yao X, Huang J, Zhong H, Shen N, Faggioni R, Fung M, et al. Targeting interleukin-6 in inflammatory autoimmune diseases and cancers. *Pharmacol Ther* (2014) 141(2):125–39. doi: 10.1016/j.pharmthera.2013.09.004

131. Inoue K, Sugiyama H, Ogawa H, Yamagami T, Azuma T, Oka Y, et al. Expression of the interleukin-6 (IL-6), IL-6 receptor, and gp130 genes in acute leukemia. *Blood* (1994) 84(8):2672–80. doi: 10.1182/blood.V84.8.2672.2672

132. Stevens AM, Miller JM, Munoz JO, Gaikwad AS, Redell MS. Interleukin-6 levels predict event-free survival in pediatric AML and suggest a mechanism of chemotherapy resistance. *Blood Adv* (2017) 1(18):1387–97. doi: 10.1182/bloodadvances.2017007856

133. Saadi MI, Ramzi M, Hosseinzadeh M, Ebrahimi N, Owjfard M, Abdolyousefi EN, et al. Expression levels of il-6 and il-18 in acute myeloid leukemia and its relation with response to therapy and acute GvHD after bone marrow transplantation. *Indian J Surg Oncol* (2021) 12(3):465–71. doi: 10.1007/s13193-021-01358-w

134. Peterlin P, Gaschet J, Guillaume T, Garnier A, Eveillard M, Le Bourgeois A, et al. A new cytokine-based dynamic stratification during induction is highly predictive of survivals in acute myeloid leukemia. *Cancer Med* (2021) 10(2):642–8. doi: 10.1002/cam4.3648

135. Hou D, Wang B, You R, Wang X, Liu J, Zhan W, et al. Stromal cells promote chemoresistance of acute myeloid leukemia cells *via* activation of the IL-6/STAT3/OXPHOS axis. *Ann Transl Med* (2020) 8(21):1346. doi: 10.21037/atm-20-3191

136. Reikvam H, Brenner AK, Hagen KM, Liseth K, Skrede S, Hatfield KJ, et al. The cytokine-mediated crosstalk between primary human acute myeloid cells and mesenchymal stem cells alters the local cytokine network and the global gene expression profile of the mesenchymal cells. *Stem Cell Res* (2015) 15(3):530–41. doi: 10.1016/j.scr.2015.09.008

137. O'Hagan-Wong K, Nadeau S, Carrier-Leclerc A, Apablaza F, Hamdy R, Shum-Tim D, et al. Increased IL-6 secretion by aged human mesenchymal stromal cells disrupts hematopoietic stem and progenitor cells' homeostasis. *Oncotarget* (2016) 7(12):13285–96. doi: 10.18632/oncotarget.7690

138. Säily M, Koistinen P, Savolainen M, Rantala M, Savolainen ER. Expression of interleukin-6 (IL-6) receptor gene in acute myeloblastic leukemia and response of leukemic cells to exogenous IL-6. *A Comp study between Cell line Cells corresponding native Cells Growth Factors* (1998) 15(4):243–57. doi: 10.3109/08977199809017481

139. Zhang Y, Guo H, Zhang Z, Lu W, Zhu J, Shi J. IL-6 promotes chemoresistance *via* upregulating CD36 mediated fatty acids uptake in acute myeloid leukemia. *Exp Cell Res* (2022) 415(1):113112. doi: 10.1016/j.yexcr.2022.113112

140. Chen R, Chen B. Siltuximab (CNTO 328): a promising option for human malignancies. *Drug Des Devel Ther* (2015) 9:3455–8. doi: 10.2147/DDDT.S86438

141. Zhang TY, Dutta R, Benard B, Zhao F, Yin R, Majeti R. IL-6 blockade reverses bone marrow failure induced by human acute myeloid leukemia. *Sci Transl Med* (2020) 12(538):eaax5104. doi: 10.1126/scitranslmed.aax5104

142. Xie K. Interleukin-8 and human cancer biology. *Cytokine Growth Factor Rev* (2001) 12(4):375–91. doi: 10.1016/S1359-6101(01)00016-8

143. Campbell LM, Maxwell PJ, Waugh DJ. Rationale and means to target pro-inflammatory interleukin-8 (CXCL8) signaling in cancer. *Pharm (Basel.* (2013) 6 (8):929–59. doi: 10.3390/ph6080929

144. Vinante F, Rigo A, Vincenzi C, Ricetti MM, Marrocchella R, Chilosi M, et al. IL-8 mRNA expression and IL-8 production by acute myeloid leukemia cells. *Leukemia* (1993) 7(10):1552–6.

145. Tobler A, Moser B, Dewald B, Geiser T, Studer H, Baggiolini M, et al. Constitutive expression of interleukin-8 and its receptor in human myeloid and lymphoid leukemia. *Blood* (1993) 82(8):2517–25. doi: 10.1182/blood.V82.8.2517.2517

146. Schinke C, Giricz O, Li W, Shastri A, Gordon S, Barreyro L, et al. IL8-CXCR2 pathway inhibition as a therapeutic strategy against MDS and AML stem cells. *Blood* (2015) 125(20):3144–52. doi: 10.1182/blood-2015-01-621631

147. Kuett A, Rieger C, Perathoner D, Herold T, Wagner M, Sironi S, et al. IL-8 as mediator in the microenvironment-leukaemia network in acute myeloid leukaemia *Sci Rep* (2015) 5:18411. doi: 10.1038/srep18411

148. Konopleva M, Konoplev S, Hu W, Zaritskey AY, Afanasiev BV, Andreeff M. Stromal cells prevent apoptosis of AML cells by up-regulation of anti-apoptotic proteins. *Leukemia* (2002) 16(9):1713–24. doi: 10.1038/sj.leu.2402608

149. Nefedova Y, Landowski TH, Dalton WS. Bone marrow stromal-derived soluble factors and direct cell contact contribute to *de novo* drug resistance of myeloma cells by distinct mechanisms. *Leukemia* (2003) 17(6):1175–82. doi: 10.1038/sj.leu.2402924

150. Ryningen A, Wergeland L, Glenjen N, Gjertsen BT, Bruserud O. *In vitro* crosstalk between fibroblasts and native human acute myelogenous leukemia (AML) blasts *via* local cytokine networks results in increased proliferation and decreased apoptosis of AML cells as well as increased levels of proangiogenic interleukin 8. *Leukemia Res* (2005) 29(2):185–96. doi: 10.1016/j.leukres.2004.06.008

151. Vijay V, Miller R, Vue GS, Pezeshkian MB, Maywood M, Ast AM, et al. Interleukin-8 blockade prevents activated endothelial cell mediated proliferation and chemoresistance of acute myeloid leukemia*Leukemia Res* (2019) 84:106180. doi: 10.1016/j.leukres.2019.106180

152. Abdul-Aziz AM, Shafat MS, Mehta TK, Di Palma F, Lawes MJ, Rushworth SA, et al. MIF-induced stromal PKCβ/IL8 is essential in human acute myeloid leukemia. *Cancer Res* (2017) 77(2):303–11. doi: 10.1158/0008-5472.CAN-16-1095

153. Simonet WS, Hughes TM, Nguyen HQ, Trebasky LD, Danilenko DM, Medlock ES. Long-term impaired neutrophil migration in mice overexpressing human interleukin-8. *J Clin Invest* (1994) 94(3):1310–9. doi: 10.1172/JCI117450

154. Shi Y, Riese DJ. 2nd. *Role CXCL12/CXCR4/CXCR7 Chemokine Axis Cancer. Front Pharmacol* (2020) 11:574667. doi: 10.3389/fphar.2020.574667

155. Teicher BA, Fricker SP. CXCL12 (SDF-1)/CXCR4 pathway in cancer. *Clin Cancer Res* (2010) 16(11):2927–31. doi: 10.1158/1078-0432.CCR-09-2329

156. Khare T, Bissonnette M, Khare S. CXCL12-CXCR4/CXCR7 axis in colorectal cancer: Therapeutic target in preclinical and clinical studies. *Int J Mol Sci* (2021) 22(14):7371. doi: 10.3390/ijms22147371

157. Liao YX, Zhou CH, Zeng H, Zuo DQ, Wang ZY, Yin F, et al. The role of the CXCL12-CXCR4/CXCR7 axis in the progression and metastasis of bone sarcomas (Review). *Int J Mol Med* (2013) 32(6):1239–46. doi: 10.3892/ijmm.2013.1521

158. Daniel SK, Seo YD, Pillarisetty VG. The CXCL12-CXCR4/CXCR7 axis as a mechanism of immune resistance in gastrointestinal malignancies. *Semin Cancer Biol* (2020) 65:176–88. doi: 10.1016/j.semcancer.2019.12.007

159. Nazari A, Khorramdelazad H, Hassanshahi G. Biological/pathological functions of the CXCL12/CXCR4/CXCR7 axes in the pathogenesis of bladder cancer. *Int J Clin Oncol* (2017) 22(6):991–1000. doi: 10.1007/s10147-017-1187-x

160. Chen N, Jiang X, Wang J, Wu T, Cheng B, Xia J. CXCL12-CXCR4/CXCR7 axis contributes to cell motilities of oral squamous cell carcinoma. *Tumour Biol* (2016) 37(1):567–75. doi: 10.1007/s13277-015-3803-6

161. Spoo AC, Lübbert M, Wierda WG, Burger JA. CXCR4 is a prognostic marker in acute myelogenous leukemia. *Blood* (2007) 109(2):786–91. doi: 10.1182/blood-2006-05-024844

162. Du W, Lu C, Zhu X, Hu D, Chen X, Li J, et al. Prognostic significance of CXCR4 expression in acute myeloid leukemia. *Cancer Med* (2019) 8(15):6595–603. doi: 10.1002/cam4.2535

163. Zhao H, Guo L, Zhao H, Zhao J, Weng H, Zhao B. CXCR4 over-expression and survival in cancer: a system review and meta-analysis. *Oncotarget* (2015) 6 (7):5022–40. doi: 10.18632/oncotarget.3217

164. Ahn JY, Seo K, Weinberg OK, Arber DA. The prognostic value of CXCR4 in acute myeloid leukemia. *Appl Immunohistochem Mol Morphol* (2013) 21(1):79–84. doi: 10.1097/PAI.0b013e3182606f4d

165. Chen Y, Jacamo R, Konopleva M, Garzon R, Croce C, Andreeff M. CXCR4 downregulation of let-7a drives chemoresistance in acute myeloid leukemia. *J Clin Invest* (2013) 123(6):2395–407. doi: 10.1172/JCI66553

166. Ramakrishnan R, Peña-Martínez P, Agarwal P, Rodriguez-Zabala M, Chapellier M, Högberg C, et al. CXCR4 signaling has a CXCL12-independent essential role in murine MLL-AF9-Driven acute myeloid leukemia. *Cell Rep* (2020) 31(8):107684. doi: 10.1016/j.celrep.2020.107684

167. Cancilla D, Rettig MP, DiPersio JF. Targeting CXCR4 in AML and ALL. *Front Oncol* (2020) 10:1672. doi: 10.3389/fonc.2020.01672

168. Castro F, Cardoso AP, Gonçalves RM, Serre K, Oliveira MJ. Interferon-gamma at the crossroads of tumor immune surveillance or evasion. *Front Immunol* (2018) 9:847. doi: 10.3389/fimmu.2018.00847

169. Uhl FM, Chen S, O'Sullivan D, Edwards-Hicks J, Richter G, Haring E, et al. Metabolic reprogramming of donor T cells enhances graft-versus-leukemia effects in mice and humans. *Sci Transl Med* (2020) 12(567):eabb8969. doi: 10.1126/scitranslmed.abb8969

170. Toffalori C, Zito L, Gambacorta V, Riba M, Oliveira G, Bucci G, et al. Immune signature drives leukemia escape and relapse after hematopoietic cell transplantation. *Nat Med* (2019) 25(4):603–11. doi: 10.1038/s41591-019-0400-z

171. Garcia-Diaz A, Shin DS, Moreno BH, Saco J, Escuin-Ordinas H, Rodriguez GA, et al. Interferon receptor signaling pathways regulating PD-L1 and PD-L2 expression. *Cell Rep* (2017) 19(6):1189–201. doi: 10.1016/j.celrep.2017.04.031

172. Berthon C, Driss V, Liu J, Kuranda K, Leleu X, Jouy N, et al. In acute myeloid leukemia, B7-H1 (PD-L1) protection of blasts from cytotoxic T cells is induced by TLR ligands and interferon-gamma and can be reversed using MEK inhibitors. *Cancer Immunol Immunother* (2010) 59(12):1839–49. doi: 10.1007/s00262-010-0909-y

173. Chen C, Liang C, Wang S, Chio CL, Zhang Y, Zeng C, et al. Expression patterns of immune checkpoints in acute myeloid leukemia. *J Hematol Oncol* (2020) 13(1):28. doi: 10.1186/s13045-020-00853-x

174. Haroun F, Solola SA, Nassereddine S, Tabbara I. PD-1 signaling and inhibition in AML and MDS. *Ann Hematol* (2017) 96(9):1441–8. doi: 10.1007/s00277-017-3051-5

175. Xu L, Liu L, Yao D, Zeng X, Zhang Y, Lai J, et al. PD-1 and TIGIT are highly Co-expressed on CD8(+) T cells in AML patient bone marrow. *Front Oncol* (2021) 11:686156. doi: 10.3389/fonc.2021.686156

176. Dong Y, Han Y, Huang Y, Jiang S, Huang Z, Chen R, et al. PD-L1 is expressed and promotes the expansion of regulatory T cells in acute myeloid leukemia. *Front Immunol* (2020) 11:1710. doi: 10.3389/fimmu.2020.01710

177. Yang X, Ma L, Zhang X, Huang L, Wei J. Targeting PD-1/PD-L1 pathway in myelodysplastic syndromes and acute myeloid leukemia. *Exp Hematol Oncol* (2022) 11(1):11. doi: 10.1186/s40164-022-00263-4

178. Vivier E, Artis D, Colonna M, Diefenbach A, Di Santo JP, Eberl G, et al. Innate lymphoid cells: 10 years on. *Cell* (2018) 174(5):1054–66. doi: 10.1016/j.cell.2018.07.017

179. Li Z, Ma R, Ma S, Tian L, Lu T, Zhang J, et al. ILC1s control leukemia stem cell fate and limit development of AML. *Nat Immunol* (2022) 23(5):718–30. doi: 10.1038/s41590-022-01198-y

180. Junttila IS. Tuning the cytokine responses: An update on interleukin (IL)-4 and IL-13 receptor complexes. *Front Immunol* (2018) 9:888. doi: 10.3389/fimmu.2018.00888

181. Bankaitis KV, Fingleton B. Targeting IL4/IL4R for the treatment of epithelial cancer metastasis. *Clin Exp Metastasis* (2015) 32(8):847–56. doi: 10.1007/s10585-015-9747-9

182. Li Z, Jiang J, Wang Z, Zhang J, Xiao M, Wang C, et al. Endogenous interleukin-4 promotes tumor development by increasing tumor cell resistance to apoptosis. *Cancer Res* (2008) 68(21):8687–94. doi: 10.1158/0008-5472.CAN-08-0449

183. Peña-Martínez P, Eriksson M, Ramakrishnan R, Chapellier M, Högberg C, Orsmark-Pietras C, et al. Interleukin 4 induces apoptosis of acute myeloid leukemia cells in a Stat6-dependent manner. *Leukemia* (2018) 32(3):588–96. doi: 10.1038/leu.2017.261

184. Finch ER, Tukaramrao DB, Goodfield LL, Quickel MD, Paulson RF, Prabhu KS. Activation of PPARγ by endogenous prostaglandin J(2) mediates the antileukemic effect of selenium in murine leukemia. *Blood* (2017) 129(13):1802–10. doi: 10.1182/blood-2016-08-736405

185. Qian F, Arner BE, Kelly KM, Annageldiyev C, Sharma A, Claxton DF, et al. Interleukin-4 treatment reduces leukemia burden in acute myeloid leukemia *FASEB J* (2022) 36(5):e22328. doi: 10.1096/fj.202200251R

186. Miari KE, Guzman ML, Wheadon H, Williams MTS. Macrophages in acute myeloid leukaemia: Significant players in therapy resistance and patient outcomes. *Front Cell Dev Biol* (2021) 9:692800. doi: 10.3389/fcell.2021.692800

187. Pan Y, Yu Y, Wang X, Zhang T. Tumor-associated macrophages in tumor immunity. *Front Immunol* (2020) 11:583084. doi: 10.3389/fimmu.2020.583084

188. Saraiva M, O'Garra A. The regulation of IL-10 production by immune cells. *Nat Rev Immunol* (2010) 10(3):170–81. doi: 10.1038/nri2711

189. Kornblau SM, McCue D, Singh N, Chen W, Estrov Z, Coombes KR. Recurrent expression signatures of cytokines and chemokines are present and are independently prognostic in acute myelogenous leukemia and myelodysplasia. *Blood* (2010) 116(20):4251–61. doi: 10.1182/blood-2010-01-262071

190. Dong Q, Li G, Fozza C, Wang S, Yang S, Sang Y, et al. Levels and clinical significance of regulatory b cells and T cells in acute myeloid leukemia. *BioMed Res Int* (2020) 2020:7023168. doi: 10.1155/2020/7023168

191. Bruserud O. IL-4, IL-10 and IL-13 in acute myelogenous leukemia. *Cytokines Cell Mol Ther* (1998) 4(3):187–98.

192. Han Y, Dong Y, Yang Q, Xu W, Jiang S, Yu Z, et al. Acute myeloid leukemia cells express ICOS ligand to promote the expansion of regulatory T cells. *Front Immunol* (2018) 9:2227. doi: 10.3389/fimmu.2018.02227

193. Musuraca G, De Matteis S, Napolitano R, Papayannidis C, Guadagnuolo V, Fabbri F, et al. IL-17/IL-10 double-producing T cells: new link between infections, immunosuppression and acute myeloid leukemia. *J Transl Med* (2015) 13:229. doi: 10.1186/s12967-015-0590-1

194. Xu Y, Mou J, Wang Y, Zhou W, Rao Q, Xing H, et al. Regulatory T cells promote the stemness of leukemia stem cells through IL10 cytokine-related signaling pathway. *Leukemia* (2022) 36(2):403–15. doi: 10.1038/s41375-021-01375-2

195. Jimbu L, Mesaros O, Neaga A, Nanut AM, Tomuleasa C, Dima D, et al. The potential advantage of targeting both PD-L1/PD-L2/PD-1 and IL-10-IL-10R pathways in acute myeloid leukemia. *Pharm (Basel)* (2021) 14(11):1105. doi: 10.3390/ph14111105

196. Chen N, Xu Y, Mou J, Rao Q, Xing H, Tian Z, et al. Targeting of IL-10R on acute myeloid leukemia blasts with chimeric antigen receptor-expressing T cells. *Blood Cancer J* (2021) 11(8):144. doi: 10.1038/s41408-021-00536-x

197. Huang J, Liu Y, Au BC, Barber DL, Arruda A, Schambach A, et al. Preclinical validation: LV/IL-12 transduction of patient leukemia cells for immunotherapy of AML. *Mol Ther Methods Clin Dev* (2016) 3:16074. doi: 10.1038/mtm.2016.74

198. Curti A, Pandolfi S, Aluigi M, Isidori A, Alessandrini I, Chiodoni C, et al. Interleukin-12 production by leukemia-derived dendritic cells counteracts the inhibitory effect of leukemic microenvironment on T cells. *Exp Hematol* (2005) 33(12):1521–30. doi: 10.1016/j.exphem.2005.08.005

199. Schnorfeil F, Lichtenegger F, Geiger C, Köhnke T, Bücklein V, Altmann T, et al. Next-generation dendritic cells for immunotherapy of acute myeloid leukemia. *J Immunother Cancer* (2014) 2:P84. doi: 10.1186/2051-1426-2-S3-P84

CYTOKINES AND CYTOKINE MODULATION IN THERAPY

frontiers | Frontiers in Immunology

TYPE Mini Review
PUBLISHED 16 February 2023
DOI 10.3389/fimmu.2023.1151620

OPEN ACCESS

EDITED BY
Giselle Penton-Rol,
Center for Genetic Engineering and Biotechnology (CIGB), Cuba

REVIEWED BY
Diana Boraschi,
Shenzhen Institute of Advanced Technology (SIAT), Chinese Academy of Science (CAS), China

*CORRESPONDENCE
Daniela Novick
daniela.novick@weizmann.ac.il

SPECIALTY SECTION
This article was submitted to Cytokines and Soluble Mediators in Immunity, a section of the journal Frontiers in Immunology

RECEIVED 26 January 2023
ACCEPTED 03 February 2023
PUBLISHED 16 February 2023

CITATION
Novick D (2023) A natural goldmine of binding proteins and soluble receptors simplified their translation to blockbuster drugs, all in one decade.
Front. Immunol. 14:1151620.
doi: 10.3389/fimmu.2023.1151620

A natural goldmine of binding proteins and soluble receptors simplified their translation to blockbuster drugs, all in one decade

Daniela Novick*

Molecular Genetics, The Weizmann Institute of Science, Rehovot, Israel

Human urinary proteins are a goldmine of natural proteins a feature that simplifies their translation to biologics. Combining this goldmine together with the ligand-affinity-chromatography (LAC) purification method, proved a winning formula in their isolation. LAC specificity, efficiency, simplicity and inherent indispensability in the search for predictable and unpredictable proteins, is superior to other separation techniques. Unlimited amounts of recombinant cytokines and monoclonal antibodies (mAb) accelerated the "triumph". My approach concluded 35 years of worldwide pursuit for Type I IFN receptor (IFNAR2) and advanced the understanding of the signal transduction of this Type of IFN. TNF, IFNγ and IL-6 as baits enabled the isolation of their corresponding soluble receptors and N-terminal amino acid sequence of the isolated proteins facilitated the cloning of their cell surface counterparts. IL-18, IL-32, and heparanase as the baits yielded the corresponding unpredictable proteins: the antidote IL-18 Binding Protein (IL-18BP), the enzyme Proteinase 3 (PR3) and the hormone Resistin. IFNβ proved beneficial in Multiple Sclerosis and is a blockbuster drug, Rebif®. TNF mAbs translated into Remicade® to treat Crohn's disease. Enbrel® based on TBPII is for Rheumatoid Arthritis. Both are blockbusters. Tadekinig alfa™, a recombinant IL-18BP, is in phase III clinical study for inflammatory and autoimmune diseases. Seven years of continuous compassionate use of Tadekinig alfa™ in children born with mutations (NLRC4, XIAP) proved life-saving and is an example of tailored made medicine. IL-18 is a checkpoint biomarker in cancer and IL-18BP is planned recently to target cytokine storms resulting from CAR-T treatment and in COVID 19.

KEYWORDS

ligand affinity chromatography, TBPII, IFNAR2, IL-18BP, Enbrel®, Rebif®, Tadekinig alfa ™, COVID 19

1 Introduction

Soluble cytokine receptors and binding proteins are present in normal body fluids is the concept I established in 1989 once I isolated four such receptors in one month: TNF Binding Proteins I and II (TBPI and TBPII), interferon gamma receptor (IFNγR) and IL-6 receptor (IL-6R) (1, 2). The others, interferon alpha/beta receptor (later named IFNAR2) (3), a soluble fragment of LDL receptor (LDLR) (4), IL-18 Binding Protein (IL-18BP) (5), IL-32 Binding Protein, the enzyme Proteinase 3 (PR3) (6) and Heparanse Binding Protein, the hormone Resistin (7), quickly followed. My approach involved the use of a body fluid, the urine, reflecting naturally occurring proteins, and a highly specific and efficient separation method, ligand affinity chromatography (8). Urine and plasma contain similar repertoire of proteins yet urine has an advantage over plasma since it hardly contains albumin and immunoglobulins, that are too big to be filtered by the kidney, thus stands a concentration of 1000-fold, which is crucial when targeting proteins present in traces amount. Moreover, employing ligand affinity chromatography as the separation method rather than methods based on the chemistry of the target proteins, promises not only the isolation of all binding proteins to a given ligand but also points to its biological activity since it binds the ligand through its active site and also preserves its bioactivity. Yet strategy does not suffice to guarantee success. High amounts of the relevant cytokines and the corresponding monoclonal antibodies are required for purification, monitoring and characterization of the products and we worked out these tools prior to the endeavor of isolation of binding proteins (9). We developed concomitantly the corresponding ELISAs thus we could establish worldwide collaborations to measure the levels of the cytokines and their binding proteins in real life, namely, in health and disease. Moreover, we introduced the concept of free cytokine levels in pathology and calculated it. Free cytokine results from an imbalance of the players and is most probably responsible for the pathology (10, 11). Drug companies recognized the therapeutic potential of the various soluble receptors and binding proteins and translated some into drugs.

2 The discovery of cytokine receptors and binding proteins

In 1987, encouraged by the isolation of the EGF receptor *via* affinity chromatography (12), I purified the IFNγR. The protein source was a detergent-extract of huge batches of primary cells (10^{11} foreskin fibroblasts/batch) and the separation method was ligand affinity chromatography, namely, a column of an in-house recombinant IFNγ covalently coupled to a resin (13). Based on this experience I was confident that ligand affinity chromatography would work for other target proteins too provided ligands in milligram amounts are available and so is a rich source of naturally occurring proteins. From now on the source was 500 to 1000-fold concentrated normal human urine.

Soluble receptors are by definition homologous to the extracellular domains of their cell surface counterparts and are thus encoded by the same genes and are generated by a mechanism of alternative splicing or protease cleavage. Binding Proteins deviate from this definition, are not the corresponding receptors and are encoded by separate genes. The advantage of my approach is that it isolates both types of these molecules provided a given ligand has a sufficient affinity to the putative soluble receptor or binding protein.

2.1 Soluble TNF receptors (1989) and anti TNF therapy

The ultimate proof that my strategy works beyond expectations was the isolation of TBPI and TBPII. 20,000-fold purification in one step and over 80% recovery of bioactivity were achieved (1). It should be noted that purification *via* the canonical multistep laborious and inefficient chromatographic procedures yielded TBPI only (14). Of particular note is the fact that my approach, namely ligand affinity chromatography of urine on covalently coupled TNF to a resin, yielded not only the TBPI but also the novel at that time TBPII and it was the TBPII that proved beneficial in patients with Rheumatoid Arthritis. TBPI and TBPII were hypothesized to be soluble receptors and indeed based on their amino acid sequence their cell surface counterparts were easily cloned. Discovered in 1975, the TNF cytokine (15) proved with years to be a master cytokine involved in opposing biological activities. Together with its receptors and transcription factors TNF was shown to play a role in cell death and cell survival, to regulate immune functions and to be involved in many pathologies (16). TNF blockers were spotted by drug companies and translated to biologics that soon became blockbuster drugs. The TBPII was translated into Etanercept/Enbrel®, a fusion protein with the Fc portion of immunoglobulin, for the treatment of mainly Rheumatoid Arthritis but also other autoimmune and inflammatory pathologies such as Psoriatic arthritis, Juvenile idiopathic arthritis and Ankylosing spondylitis. TNF mAbs were translated into e.g. Remicade® and Humira® for the treatment of Crohn's disease and Ulcerative Colitis in addition to the pathologies treated by Enbrel®. The difference in the mechanism of action between these TNF blockers is addressed by Levin AD et al. (17). In a way, I had been involved in the monoclonal antibody anti TNF therapy too. In 1985 Hahn et al. generated anti TNF mAbs (18). I contributed a unique screening procedure for the selection of these mAbs, a screening developed by our laboratory for the selection of mAbs to various interferons (9). As stated later on, this screening assay was a crucial step in the selection of the TNF mAbs.

The discovery of the TNF receptors lead to a flood of world-wide research on the mechanism of action, signal transduction, immune response, cross talk with other cytokines and involvement in health and disease and this is what placed TNF high in the hierarchy of master cytokines. Biologics that neutralize TNF are amongst the most successful drugs for the treatment of chronic inflammatory and autoimmune pathologies (19, 20). In 1998 a modification of our TBPII and our anti TNF mAbs were the first TNF blockers to be approved by the FDA. I had the privilege to have a major part in their discovery and development.

2.2 Soluble receptors to IL-6 and IFNγ (1989)

I had no doubt that in addition to the TBPs urine contains other soluble receptors. Indeed, using different baits, my approach pulled

out two additional proteins, the soluble IL-6 receptor (IL-6R) and the soluble Type II interferon receptor (IFNγR). To our surprise, unlike the antagonistic soluble receptors to TNF and to IFNγ, the soluble IL-6R behaved as an agonist (21). In a mechanism named trans-signaling it was shown that it binds its corresponding ligand, the circulating IL-6, and presents it directly to the transducing IL-6R chain, gp130, present on cells that lack the binding IL-6R chain (22). The discovery of this player, the soluble IL-6R, uncovered this additional mode of signaling of IL-6 on top of the IL-6 classical signaling. It also added an important dimension in the development of inhibitors to IL-6 and IL-6R yet additional treatment for Rheumatoid Arthritis and a variety of inflammatory and autoimmune diseases (23, 24).

The type II IFN, IFNγ, named also and immune IFN, is also a master cytokine and is involved in pro-inflammatory and autoimmune pathologies. Obviously, we and others generated monoclonal antibodies to these cytokines and their receptors (9). Anti IFNγ mAbs developed by others translated to Emapalumab®, a drug approved in 2018 for primary hemophagocytic lymphohistiocytosis (HLH) (25). In the current pandemic these blocking agents are being considered for the treatment of severe cases of COVID 19.

2.3 Soluble IFNα/β Receptor (1992)

Type I interferons were discovered by Isaacs and Lindenmann in 1957 (26) but it took 35 years to uncover their receptor though laboratories all over the world were engaged in seeking it. Once again, my unique approach of isolation came to rescue and my "goldmine" yielded both the desired receptor and an eureka moment for me that I will never forget. Passing an equivalent of 500 Liter of normal human urine on a resin to which IFNα or IFNβ were covalently coupled yielded a few micrograms of a soluble Type I IFN receptor. By definition a soluble receptor is homologous to the extracellular domain of the cell bound receptor, thus the N-terminal amino acid sequence of our soluble receptor served to clone its self-surface counterpart. Two cell bound ligand binding receptors were discovered, ours, named IFNα/β receptor, a decoy receptor with a short intracellular domain (3) and the transducing receptor with the full intracellular length, later named IFNAR2 (27).

The discovery of the Type I IFN receptor was followed by a burst of publications on the mechanism of action of this yet another master cytokine. We showed the stepwise ligand induced formation of the trimeric complex (28) that include the IFN that first binds the ligand binding chain (IFNAR2) and then the chain, discovered earlier by Uze et al., that transduces the signal joins (29). We were the first to demonstrate the physical interaction of the ligand binding receptor with the transcription factor JAK1 (3), and our neutralizing mAbs raised against this receptor pointed to the fact that the JAK-STAT pathway does not explain all tested biological activities of Type I IFN (30).

JAKs have a pivotal role in a variety of immune mediated inflammatory and autoimmune diseases thus their targeted inhibition results in effective disease control (31). The use of JAK blocking drugs is extended in the present pandemic and there are ongoing clinical studies with these agents aiming at attenuation of the over-production of proinflammatory cytokines in severe Covid 19 (32).

Type I IFN was discovered 65 years ago as an antiviral agent. Being a bridge between innate and adaptive immunity, being essential in host defense and involved in cancer and autoimmunity, placed interferon in the limited list of master cytokines. As such it is being continuously revisited and is a source for drug discovery (33).

Forty years after the discovery, one of the Type I IFNs, IFNβ, had been approved for the treatment of multiple sclerosis (34). My persistence and daring paid, and in 1982 I generated monoclonal antibodies to this IFN (9, 35). These tools accelerated the CHO-expressed recombinant IFNβ characterization, monitoring of its scaled-up production, and submission of its file to the FDA. I am proud to have a part in its translation to a blockbuster drug, the REBIF®.

Interferons are extensively studied in the present pandemic, the SARS-2 Covid 19. Big data analyses revealed interferon deficiency, inborn errors in IFN signaling and autoantibodies to Type I IFN in severely ill patients. The latter accounts for more than 10% of these patients (36–42).

2.4 IL-18 Binding Protein (1997)

Having isolated 5 soluble receptors, gave me confidence that my approach would yield any unknown receptor provided it is present in the goldmine, the urine. But here I experienced a twist to my story. Based on my expertise I had been asked by Prof. Charles Dinarello, known in the field of IL-1, to isolate the receptor for an additional member of the IL-1 family, the pro-inflammatory cytokine, IL-18, first named IFNγ inducing factor (IGIF). To my surprise, all my attempts to isolate the soluble IL-18 receptor from the concentrated urine failed not because it does not exist but because in retrospect it turned out that its concentration in the urine and its affinity to the IL-18 are too low. Characterization of the protein that I did pull out instead, revealed a novel family of proteins, the Binding Proteins, osteoprotegerin being then its only member. These proteins bind the same ligand as the corresponding receptor does, but are encoded by a separate gene and have no cell surface counterpart. The protein I isolated was a unique binding protein, that we named IL-18BP (5). It has an exceptionally high affinity to its ligand (0.4 nM or 0.05 nM) (43, 44) and as such was proposed to serve as an antidote in a fatal inherited IL-18BP deficiency in human fulminant viral hepatitis A caused by toxic levels of IL-18 (45). Serono (Merck) translated recombinant IL-18BP to a drug and named it Tadekinig alfa™. There is an ongoing phase III clinical trial by AB2 bio (https://www.ab2bio.com) in children born with a mutation in the inflammasome e.g. *NLRC4* and in *XIAP/BIRC4* (ClinicalTrials.gov Identifier: NCT03113760). These mutations lead to an over expression of IL-18 that results in organ damage due to Macrophage Activation Syndrome (MAS) or hemophagocytic lymphohistiocytosis (HLH). On a compassionate basis Tadekinig alfa™ saved several children lives and let them lead almost normal life by being treated continuously for 7 years now. A successful phase II clinical study in the autoimmune Still's disease is completed and awaiting phase III. Tadekinig alfa™ treatment protocol was also submitted to the FDA to be tested in patients succumbing to a devastating MAS, resulting from cancer and viral diseases that otherwise has no cure and has up to 50% mortality. Tadekinig

alfa™ is considered in the treatment of a cytokine storm in patients undergoing CAR T therapy (46) and in severe cases of COVID 19 (47). The complete story referring to IL-18BP discovery can be found in my recent review (9).

2.5 Soluble LDL receptor, IL-32 and heparanase binding proteins

My approach proved indispensable in the isolation of binding proteins not only to cytokines but also to other key molecules such as LDL and heparanase. We found that a soluble LDL receptor, present in urine, has an unanticipated antiviral activity and that its cell surface counterpart, present in all types of cells, is the entry receptor of VSV (4, 48). These findings explain the pantropism of this virus used successfully in gene therapy.

An attempt to isolate the receptor to the IL-18 induced proinflammatory cytokine, the IL-32, failed and I isolated Proteinase 3 (PR3) instead (6). PR3 is the auto-antigen of an autoimmune blood vessel disease, Wegener's disease renamed Granulomatosis with polyangiitis (GPA). Blood levels of IL-32 were reported to be upregulated in these patients.

The receptor to heparanase was not isolated either but instead we have shown that the human resistin, present in urine, binds heparanse specifically and with a high affinity (7). Resistin is an adipogen in mice and a pro-inflammatory cytokine in humans (49, 50). The heparanase receptor is unknown till today.

3 Concluding remarks

The notion coined back in 1968 by Cuatrecasas et al. (8) that almost any given biomolecule has an inherent recognition site through which it recognizes a partner molecule served as the basis to my approach. My findings upgraded the status of normal human urine to a goldmine position, and the convenience in its handling placed it high in the list of sources of natural proteins such as soluble receptors and binding proteins. No doubt being self-proteins facilitated their translation into drugs.

It is clear now that the balance between the cytokines and their antagonists, agonists, or carrier proteins, namely, the soluble receptors and binding protein, dictate the outcome of a pathology. This is where I introduced the concept of a free cytokine (10, 51).

A spectacular comeback at the present pandemic, SARS-2 Covid 19, of these master cytokines and their receptors reminded all how crucial they are. TNF, IL-6, both types of IFNs and IL-18 were reported to be involved in the cytokine storm of severely ill Covid 19 patients. Blockers of these cytokines are being tested as possible therapeutic agents.

Though the journey taken to generate the tools and to discover the various receptors and binding proteins seems simple and straightforward it was not. The details of the "struggle" that lead to my success where others failed, my discoveries, the rationale behind and the "tricks" engaged, are described in my historical review titled "Nine receptors and binding proteins, four drugs, and one woman: Historical and personal perspectives" (9). I should stress that at those days all our research was basic-science oriented with a desire to solve Nature's enigmas yet also with a remote dream that part of it will prove beneficial to humanity. Mine did in a form of Rebif®, Enbrel®, Remicade® and Tadekinig alfa™.

Author contributions

DN is the sole author. She conceived and wrote the manuscript.

Acknowledgments

The author is grateful to all members of the lab and collaborators whose names can be found in the text of my historical review (9) and under other references.

Conflict of interest

The author declares that the research was conducted in the absence of any commercial or financial relationships that could be construed as a potential conflict of interest.

Publisher's note

References

1. Engelmann H, Novick D, Wallach D. Two tumor necrosis factor-binding proteins purified from human urine. evidence for immunological cross- reactivity with cell surface tumor necrosis factor receptors. *J Biol Chem* (1990) 265(3):1531–6.

2. Novick D, Engelmann H, Wallach D, Rubinstein M. Soluble cytokine receptors are present in normal human urine. *J Exp Med* (1989) 170(4):1409–14. doi: 10.1084/jem.170.4.1409

3. Novick D, Cohen B, Rubinstein M. The human interferon a/b receptor: Characterization and molecular cloning. *Cell* (1994) 77(3):391–400. doi: 10.1016/0092-8674(94)90154-6

4. Finkelshtein D, Werman A, Novick D, Barak S, Rubinstein M. LDL receptor and its family members serve as the cellular receptors for vesicular stomatitis virus. *Proc Natl Acad Sci* (2013) 110(18):7306–11. doi: 10.1073/pnas.1214441110

5. Novick D, Kim SH, Fantuzzi G, Reznikov LL, Dinarello CA, Rubinstein M. Interleukin-18 binding protein: A novel modulator of the Th1 cytokine response. *Immunity* (1999) 10(1):127–36. doi: 10.1016/S1074-7613(00)80013-8

6. Novick D, Rubinstein M, Azam T, Rabinkov A, Dinarello CA, Kim SH. Proteinase 3 is an IL-32 binding protein. *Proc Natl Acad Sci USA* (2006) 103:3316–21. doi: 10.1073/pnas.0511206103

7. Novick D, Barak S, Ilan N, Vlodavsky I. Heparanase interacts with resistin and augments its activity. *PloS One* (2014) 9(1):e85944. doi: 10.1371/journal.pone.0085944

8. Cuatrecasas P, Wilchek M, Anfinsen CB. Selective enzyme purification by affinity chromatography. affinity chromatography. *Proc Natl Acad Sci U S A* (1968) 61:636–43. doi: 10.1073/pnas.61.2.636

9. Novick D. Nine receptors and binding proteins, four drugs, and one woman: Historical and personal perspectives. *Front Drug Discovery* (2022) 9. doi: 10.3389/fddsv.2022.1001487

10. Novick D, Schwartsburd B, Pinkus R, Suissa D, Belzer I, Sthoeger Z, et al. A novel IL-18BP ELISA shows elevated serum IL-18BP in sepsis and extensive decrease of free IL-18. *Cytokine* (2001) 14(6):334–42. doi: 10.1006/cyto.2001.0914

11. Mazodier K, Marin V, Novick D, Farnarier C, Robitail S, Schleinitz N, et al. Severe imbalance of IL-18/IL-18BP in patients with secondary hemophagocytic syndrome. *Blood* (2005) 106(10):3483–9. doi: 10.1182/blood-2005-05-1980

12. Yarden Y, Schlessinger J. Epidermal growth factor induces rapid, reversible aggregation of the purified epidermal growth factor receptor. *Biochem* (1987) 26:1443–51. doi: 10.1021/bi00379a035

13. Novick D, Orchansky P, Revel M, Rubinstein M. The human interferon-gamma receptor. purification, characterization, and preparation of antibodies. *J Biol Chem* (1987) 262:8483–7. doi: 10.1016/S0021-9258(18)47439-X

14. Engelmann H, Aderka D, Rubinstein M, Rotman D, Wallach D. Tumor necrosis factor-binding protein purified to homogeneity from human urine protects cells from tumor necrosis factor toxicity. *J Biol Chem* (1989) 264:11974–80. doi: 10.1016/S0021-9258(18)80162-4

15. Carswell E, Old LJ, Kassel RL, Green S, Fiore N, Williamson B. An endotoxin-induced serum factor that causes necrosis of tumours. *Proc Natl Acad Sci* (1975) 72(9):3666–70. doi: 10.1073/pnas.72.9.3666

16. van Loo G, Bertrand MJM. Death by TNF: A road to inflammation. *Nat Rev Immunol* (2022):1–15. doi: 10.1038/s41577-022-00792-3

17. Levin AD, Wildenberg ME, van den Brink GR. Mechanism of action of anti-TNF therapy in inflammatory bowel disease. *J Crohns Colitis* (2016) 10:989–97. doi: 10.1093/ecco-jcc/jjw053

18. Hahn T, Toker L, Budilovsky S, Aderka D, Eshhar Z, Wallach D. Use of monoclonal antibodies to a human cytotoxin for its isolation and for examining the self-induction of resistance to this protein. *Proc Nati Acad Sci USA* (1985) 82(11):3814–8. doi: 10.1073/pnas.82.11.3814

19. Balkwill F. Tumour necrosis factor and cancer. *Nat Rev Cancer* (2009) 9(5):361–71. doi: 10.1038/nrc2628

20. Feldmann M, Maini RN. Lasker clinical medical research award. TNF defined as a therapeutic target for rheumatoid arthritis and other autoimmune diseases. *Nat Med* (2003) 9:1245–50. doi: 10.1038/nm939

21. Novick D, Shulman LM, Chen L, Revel M. Enhancement of interleukin 6 cytostatic effect on human breast carcinoma cells by soluble IL-6 receptor from urine and reversion by monoclonal antibody. *Cytokine* (1992) 4(1):6–11. doi: 10.1016/1043-4666(92)90029-Q

22. Reeh H, Rudolph N, Billing U, Christen H, Streif S. Bullinger, e. et al., Response to IL-6 trans- and IL-6 classic signalling is determined by the ratio of the IL-6 receptor α to gp130 expression: Fusing experimental insights and dynamic modelling. *Cell Commun Signal* (2019) 17. doi: 10.1186/s12964-019-0356-0

23. Hunter CA, Jones SA. IL-6 as a keystone cytokine in health and disease. *Nat Immunol* (2015) 16:448–57. doi: 10.1038/ni.3153

24. Choy. EH., De Benedetti F, Takeuchi. T, Hashizume M, John MR, Kishimoto T. Translating IL-6 biology into effective treatments. *Nat Rev Rheumatol* (2020) 16:335–45. doi: 10.1038/s41584-020-0419-z

25. Cheloff A, Al-Samkari H. Emapalumab for the treatment of hemophagocytic lymphohistiocytosis. *Drugs Today (Barc)* (2020) 56(7):439–46. doi: 10.1358/dot.2020.56.7.3145359

26. Isaacs A, Lindenmann J. Virus interference. i. the interferon. *Proc R Soc Lond B Biol Sci* (1957) 147:258–67. doi: 10.1098/rspb.1957.0048

27. Domanski P, Witte M, Kellum M, Rubinstein M, Hackett R, Pitha P, et al. Cloning and expression of a long form of the beta subunit of the interferon alpha beta receptor that is required for signaling. *J Biol Chem* (1995) 270:21606–11. doi: 10.1074/jbc.270.37.21606

28. Cohen B, Novick D, Barak S, Rubinstein M. Ligand-induced association of the type I interferon receptor components. *Mol Cell Biol* (1995) 15(8):4208–14. doi: 10.1128/MCB.15.8.4208

29. Uzé G, Lutfalla G, Gresser I. Genetic transfer of a functional human interferon a receptor into mouse cells: Cloning and expression. *Cell* (1990) 60(2):225–34. doi: 10.1016/0092-8674(90)90738-Z

30. Novick D, Nabioullin RR, Ragsdale W, McKenna S, Weiser W, Garone L, et al. The neutralization of type I IFN biologic actions by anti-IFNAR-2 monoclonal antibodies is not entirely due to inhibition of jak-stat tyrosine phosphorylation. *J Interferon Cytokine Res* (2000) 20(11):971–82. doi: 10.1089/10799900050198417

31. Tanaka Y, Luo Y, O'Shea JJ, Nakayamada S. Janus kinase-targeting therapies in rheumatology: A mechanisms-based approach. *Nat Rev Rheumatol* (2022) 18:133–45. doi: 10.1038/s41584-021-00726-8

32. Nissen C, Sciascia S, de Andrade D, Atsumi T, Bruce IN, Cron RQ, et al. The role of antirheumatics in patients with COVID-19. *Lancet Rheumatol* (2021) 3:e447–59. doi: 10.1016/S2665-9913(21)00062-X

33. Castro L, Lobo GS, Pereira P, Freire MG, Neves MC, Pedro AQ. Interferon-based biopharmaceuticals: Overview on the production, purification, and formulation. *Vaccines (Basel)* (2021) 9. doi: 10.3390/vaccines9040328

34. Jaber A, Driebergen R, Giovannoni G, Schellekens H, Simsarian J, Antonelli M. The rebif® new formulation story. *Drugs R&D* (2007) 8(6):335–48. doi: 10.2165/00126839-200708060-00002

35. Chernajovsky Y, Mory Y, Chen L, Marks Z, Novick D, Rubinstein M, et al. Efficient constitutive production of human fibroblast interferon by hamster cells transformed with the IFN-beta 1 gene fused to an SV40 early promoter. *DNA* (1984) 3:297–308. doi: 10.1089/dna.1.1984.3.297

36. Pathak G, Singh K, Miller-Fleming TW, Wendt FR, Ehsan N, Hou K, et al. Integrative genomic analyses identify susceptibility genes underlying COVID-19 hospitalization. *Nat Commun* (2021) 12(1):4569. doi: 10.1038/s41467-021-24824-z

37. Zhang Q, Bastard P, Liu Z, Le Pen J, Moncada-Velez M, Chen J. Ogishi, M et al. Inborn errors of type I IFN immunity in patients with life-threatening COVID-19. *Science* (2020) 370(6515):eabd4570. doi: 10.1126/science.abd4570

38. Zhang Q MD, Le Pen J, Lee D, Moens L, Asano T, Bohlen J, et al. Recessive inborn errors of type I IFN immunity in children with COVID-19 pneumonia. *J Exp Med* (2022) 219(8):e20220131. doi: 10.1084/jem.20220131

39. Bastard P, Rosen LB, Zhang Q, Michailidis E, Hoffmann HH, Zhang Y, et al. Autoantibodies against type I IFNs in patients with life-threatening COVID-19. *Science* (2020) 370(6515):eabd4585. doi: 10.1126/science.abd4585

40. Solanich X, Rigo-Bonnin R, Gumucio VD, Bastard P, Rosain J, Philippot Q, et al. Pre-existing autoantibodies neutralizing high concentrations of type I interferons in almost 10% of COVID-19 patients admitted to intensive care in Barcelona. *J Clin Immunol* (2021) 41(8):1733–44. doi: 10.1007/s10875-021-01136-x

41. Casanova JL, Abel L. From rare disorders of immunity to common determinants of infection: Following the mechanistic thread. *Cell* (2022) 185:3086–103. doi: 10.1016/j.cell.2022.07.004

42. Arrestier R, Bastard P, Belmondo T, Voiriot G, Urbina T. Luyt, CE. et al. Auto-antibodies against type I IFNs in > 10% of critically ill COVID-19 patients: a prospective multicentre study. *Ann Intensive Care* (2022) 12. doi: 10.1186/s13613-022-01095-5

43. Kim S, Eisenstein M, Reznikov L, Fantuzzi G, Novick D, Rubinstein M, et al. Structural requirements of six naturally occurring isoforms of the IL-18 binding protein to inhibit IL-18. *Proc Natl Acad Sci USA* (2000) 97(3):1190–5. doi: 10.1073/pnas.97.3.1190

44. Girard C, Rech J, Brown M, Allali A, Roux-Lombard P, Spertini F, et al. Elevated serum levels of free interleukin-18 in adult-onset still's disease. *Rheumatol (Oxford)* (2016) 55(12):2237–47. doi: 10.1093/rheumatology/kew300

45. Belkaya S, Michailidis E, Korol CB, Kabbani M, Cobat A, Bastard P, et al. Inherited IL-18BP deficiency in human fulminant viral hepatitis. *J Exp Med* (2019) 216(8):1777–90. doi: 10.1084/jem.20190669

46. Lichtenstein D, Schischlik F, Shao L, Steinberg SM, Yates B, Wang HW, et al. Characterization of HLH-like manifestations as a CRS variant in patients receiving CD22 CAR T cells. *Blood* (2021) 138(24):2469–84. doi: 10.1182/blood.2021011898

47. Sefik E, Qu R, Junqueira C, Kaffe E, Mirza H, Zhao J, et al. Inflammasome activation in infected macrophages drives COVID-19 pathology. *Nature* (2022) 606(7914):585–93. doi: 10.1038/s41586-022-04802-1

48. Fischer D, Tal N, Novick D, Barak S, Rubinstein M. An antiviral soluble form of the LDL receptor induced by interferon. *Sci* (1993) 262(5131):250–3. doi: 10.1126/science.8211145

49. Steppan C, Bailey ST, Bhat S, Brown EJ, Banerjee RR, Wright CM. The hormone resistin links obesity to diabetes. *Nature* (2001) 409(6818):307–12. doi: 10.1038/35053000

50. Tripathi D, Kant S, Pandey S, Ehtesham NZ. Resistin in metabolism, inflammation, and disease. *FEBS J* (2020) 287(15):3141–9. doi: 10.1111/febs.15322

51. Novick D, Kim S, Kaplanski G, Dinarello CA. Interleukin-18, more than a Th1 cytokine. *Semin Immunol* (2013) 25(6):439–48. doi: 10.1016/j.smim.2013.10.014

frontiers | Frontiers in Immunology

TYPE Original Research
PUBLISHED 13 July 2023
DOI 10.3389/fimmu.2023.1202157

OPEN ACCESS

EDITED BY
Catherine Sautes-Fridman,
INSERM U1138 Centre de Recherche des Cordeliers (CRC), France

REVIEWED BY
María Moreno,
Universidad de la República, Uruguay
Leticia Moreno-Fierros,
National Autonomous University of Mexico, Mexico

*CORRESPONDENCE
Renate Pichler
Renate.Pichler@i-med.ac.at

†These authors have contributed equally to this work and share first authorship

‡These authors have contributed equally to this work and share senior authorship

RECEIVED 07 April 2023
ACCEPTED 26 June 2023
PUBLISHED 13 July 2023

CITATION
Pichler R, Diem G, Hackl H, Koutník J, Mertens LS, D'Andrea D, Pradere B, Soria F, Mari A, Laukhtina E, Krajewski W, Teoh JY-C, Del Guidice F, Moschini M, Thurnher M and Posch W (2023) Intravesical BCG in bladder cancer induces innate immune responses against SARS-CoV-2. *Front. Immunol.* 14:1202157. doi: 10.3389/fimmu.2023.1202157

Intravesical BCG in bladder cancer induces innate immune responses against SARS-CoV-2

Renate Pichler[1*†], Gabriel Diem[2†], Hubert Hackl[3], Jiří Koutník[4], Laura S. Mertens[5], David D'Andrea[6], Benjamin Pradere[6,7], Francesco Soria[8], Andrea Mari[9], Ekaterina Laukhtina[6,10], Wojciech Krajewski[11], Jeremy Yuen-Chun Teoh[12], Francesco Del Guidice[13], Marco Moschini[14], Martin Thurnher[15‡] and Wilfried Posch[2‡] for the European Association of Urology-Young Academic Urologists (EAU-YAU): Urothelial carcinoma working group

[1]Department of Urology, Comprehensive Cancer Center Innsbruck, Medical University of Innsbruck, Innsbruck, Austria, [2]Institute of Hygiene and Medical Microbiology, Medical University of Innsbruck, Innsbruck, Austria, [3]Institute of Bioinformatics, Biocenter, Medical University of Innsbruck, Innsbruck, Austria, [4]Institute of Cell Genetics, Medical University of Innsbruck, Innsbruck, Austria, [5]Department of Urology, The Netherlands Cancer Institute - Antoni van Leeuwenhoek Hospital, Amsterdam, Netherlands, [6]Department of Urology, Medical University of Vienna, Vienna, Austria, [7]Department of Urology, Croix Du Sud Hospital, Quint-Fonsegrives, France, [8]Department of Urology, Molinette Hospital, University of Turin, Turin, Italy, [9]Department of Experimental and Clinical Medicine, University of Florence - Unit of Oncologic Minimally-Invasive Urology and Andrology, Careggi Hospital, Florence, Italy, [10]Institute for Urology and Reproductive Health, Sechenov University, Moscow, Russia, [11]Department of Minimally Invasive and Robotic Urology, Wrocław Medical University, Wroclaw, Poland, [12]Department of Surgery, S.H. Ho Urology Centre, The Chinese University of Hong Kong, Hong Kong, Hong Kong SAR, China, [13]Department of Maternal Infant and Urologic Sciences, 'Sapienza' University of Rome, Policlinico Umberto I Hospital, Rome, Italy, [14]Department of Urology, IRCCS Ospedale San Raffaele and Vita-Salute San Raffaele University, Milan, Italy, [15]Immunotherapy Unit, Department of Urology, Medical University of Innsbruck, Innsbruck, Austria

BCG is the most efficient adjuvant therapy for high-risk, non-muscle-invasive bladder cancer (NMIBC). Both innate and adaptive immune responses have been implicated in BCG-mediated effects. BCG vaccination can boost innate immune responses via trained immunity (TI), resulting in an increased resistance to respiratory viral infections. Here we evaluated for the first time whether intravesical application of BCG triggers increased immunity against SARS-CoV-2 in patients with high-risk NMIBC. Serum and peripheral blood mononuclear cells (PBMCs) from heparinized whole blood samples of 11 unvaccinated SARS-CoV-2-naïve high-risk NMIBC patients were collected at baseline and during BCG treatment in a pre-COVID-19 era. To examine B-cell or T cell-dependent adaptive immunity against SARS-CoV-2, sera were tested for the presence of SARS-CoV-2 neutralizing antibodies. Using a SARS-CoV-2 peptide pool, virus-specific T cells were quantified via IFNγ ELISpot assays. To analyze innate immune responses, mRNA and protein expression levels of pro- and anti-inflammatory cytokines were measured after a 24-hour stimulation of PBMCs with either BCG or SARS-CoV-2 wildtype. ATAC- sequencing was performed to identify a potential epigenetic reprogramming in immune cells. We neither identified SARS-CoV-2 neutralizing antibodies nor SARS-CoV-2- reactive T cells, indicating that intravesical BCG did not induce adaptive immunity against

SARS-CoV-2. However, a significant increase in mRNA as well as protein expression of IL-1β, IL-6 and TNFα, which are key cytokines of trained immunity, could be observed after at least four intravesical BCG instillations. Genomic regions in the proximity of TI genes (*TLR2, IGF1R, AKT1, MTOR, MAPK14, HSP90AA1*) were more accessible during BCG compared to baseline. Although intravesical BCG did not induce adaptive immune responses, repetitive intravesical instillations of BCG induced circulating innate immune cells that produce TI cytokines also in response to SARS-CoV-2.

KEYWORDS

BCG, bladder cancer, COVID-19, SARS-CoV-2, trained immunity, viral infections

Introduction

Intravesical Bacillus Calmette-Guérin (BCG) immunotherapy has been considered the most successful adjuvant treatment in preventing recurrence and progression of high-risk non- muscle-invasive bladder cancer (NMIBC) for more than 40 years (1, 2). Urology practices have also been affected by the global COVID-19 pandemic (3, 4). Clinical adjustments in the use of BCG schedule in high-risk NMIBC were the consequence of the COVID-19 pandemic. In detail, BCG maintenance ongoing for longer than 1 year could be safely terminated for high-risk NMIBC patients, according to the EAU´s COVID-19 recommendations to protect both patients and healthcare workers (3, 4).

The protective effect of BCG against several viral respiratory infections is mediated via a process termed trained immunity (TI). TI comprises epigenetic as well as metabolic reprogramming of innate immune cells, facilitating the enhanced production of the pro- inflammatory TI cytokines IL-1β, IL-6 and TNFα, when challenged with a secondary irrelevant bacterial or viral stimulus (5, 6). Through TI, BCG vaccination can boost innate immune responses, resulting in reduced viremia, increased TI cytokine production and faster viral elimination (5, 7). Consequently, the development of TI is desirable to generate protection against COVID-19. First data already indicate that BCG might also provide protection against COVID-19 infection (7–9). However, these observational reports cannot confirm a causal association between BCG vaccination and decreased COVID-19 infection as well as mortality rate. Thus, various randomized controlled clinical trials are still ongoing (NCT04384549, NCT04659941, NCT04461379) to determine whether BCG vaccine can prevent COVID-19 infection and severity, especially in healthcare workers or elderly people (10).

When focusing on bladder cancer, the repetitive intravesical BCG application induces a local immune response that ultimately translates into TI. Consequently, intravesical BCG has not only a local but also systemic effects. Recently, BCG-induced TI has been shown to significantly decrease the risk for respiratory viral infections in NMIBC patients (11, 12). However, a possible protective effect also against SARS-CoV-2 through intravesical BCG-induced TI in NMIBC has not been shown to date. We hypothesized that boosting innate immune cells by intravesical BCG instillations with induction of TI could also induce innate immunity against SARS-CoV-2 in NMIBC patients. Therefore, the objective of this study was to analyze, for the first time, the innate and adaptive immune responses against SARS-CoV-2 wildtype in blood samples of patients with (very) high-risk NMIBC who underwent intravesical BCG treatment in the pre-COVID-19 era.

Materials and methods

Patients

To rule out preexisting immunity to SARS-CoV-2 either by vaccination or infection, we used blood samples from our biobank of consecutive patients with the diagnosis of a primary or recurrent (very) high-risk papillary NMIBC (Ta high-grade or T1) with or without concomitant carcinoma *in situ* (CIS) of the bladder during a pre-COVID-19 era (2014-2015). The SARS-CoV- 2-naïve status was confirmed in all patients by testing cellular and humoral adaptive immunity (neutralization assay and IFNγ ELISpot). All patients were free of visible papillary tumor at the start of BCG induction as determined via second TURB (except primary, isolated CIS) or negative cystoscopy and/or cytology at most 4 weeks before start of BCG therapy. The study was approved by the local ethical committee of the Medical University of Innsbruck (study number AN2014-0121; 336/4.3).

Interventions, follow-up and blood sample collection

The BCG treatment schedule at the Department of Urology of the Medical University of Innsbruck was based on a standard regimen of a 6-week induction course followed by 3- weekly maintenance courses at 3, 6, 12, 18, 24, 30, and 36 months according to the current EAU guidelines (1). Each instillation contained 2×10^8 - 3×10^9 viable units from live attenuated BCG

bacteria strain seed RIVM derived from seed 1173-P2 (BCG Medac, Wedel, Germany). Follow-up examinations were performed according to institutional practice including cystoscopy and cytology (voided urine as well as bladder washing) 3-monthly for 2 years and every 6 months thereafter until 5 years, and then yearly. Upper urinary tract imaging (CT urography) was performed once a year or in case of recurrence (1). Blood sample collection was performed in the pre-COVID-19 era (2014-2015) as described previously (13). In brief, serum and heparinized whole blood (40-50 mL in EDTA tubes) was collected before each BCG bladder instillation. Peripheral blood mononuclear cells (PBMCs) were prepared from heparinized whole blood by Ficoll density centrifugation and aliquots (5×10^6 cells) were cryopreserved in liquid nitrogen. Serum samples were obtained under standard conditions, clotted at 4–8°C and then centrifuged at 3200 rpm for 6 min. Aliquots of 1.8 ml were stored at −80°C (13). For this follow-up study, we selected 4 samples at 4 different time points for each patient: baseline (before

the first BCG induction) and during BCG (1-2 weeks/early, 3-4 weeks/mid and 6-12 weeks time interval/late) treatment. The study flow chart is presented in Figure 1.

Determination of SARS-CoV-2 RBD-specific antibody titers

Sera from BCG treated patients as well as untreated but SARS-CoV-2 recovered individuals were analyzed for SARS-CoV-2 RBD-specific antibodies using SARS-CoV-2 IgG II Quant Assay (Abbott, USA). Results from this chemiluminescent microparticle immunoassay (CMIA) were calculated to BAU/ml and the cut-off value for positive results was defined at 7.1 BAU/ml according to manufacturer instructions.

Virus neutralization assay

Serum was serially diluted (1:8 – 1:2048) and incubated with replication competent SARS-CoV-2 wildtype virus (SARS-CoV-2 USA/WA1/2020, $2.5\text{x}10^2$ PFU/ml) for 1h at 37°C as described previously by our group (14). The dilutions were used as inoculum on Vero- TMPRSS2-ACE2 cells for 1h at 37°C, 5% CO2. After medium exchange, cells were further cultivated for 16h. Subsequently, plaque forming units (PFU) were measured after fixation and permeabilization using immunofluorescently labelled antibodies targeting SARS-CoV-2 nucleocapsid. Imaging and counting were performed using an ImmunoSpot analyser (Cellular Technology Limited, OH, USA).

SARS-CoV-2 or BCG-specific T cell response (IFNγ ELISpot)

PBMCs ($0.5\text{x}10^5$) were treated with CEF/CEFTA (1µg/ml each) as positive control, SARS-CoV-2 peptide pool (spike, matrix and nucleocapsid proteins, Mabtech, Sweden) or a mixture of

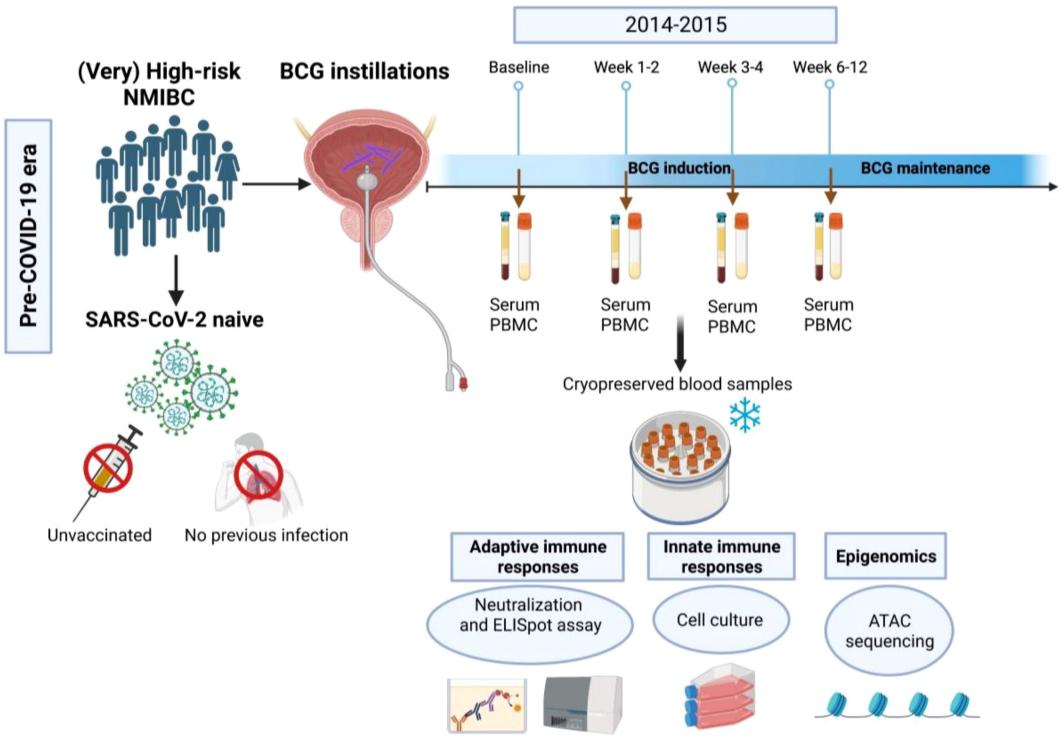

FIGURE 1
Flow chart of the study. In this study we used blood samples that have been collected from (very) high-risk NMIBC patients undergoing intravesical BCG therapy in the pre- COVID-19 era (2014-2015) using four time points (baseline, 1-2 weeks, 3-4 weeks and 6-12 weeks during BCG).

Mycobacterium tuberculosis peptides for 24h as previously described (15, 16). The CEF peptide pool consists of 23 MHC class I-restricted viral peptides from human CMV, EBV, and influenza virus induces secretion cytokine secretion from antigen-specific human CD8 T cells. The CEFTA peptide pool consists of 35 MHC class II-restricted peptides from human CMV, EBV, influenza virus, tetanus toxin, and adenovirus 5 to induce cytokine secretion of specific CD4 T cells. The SARS-CoV-2 peptide pools is a mixture of 100 peptides from the viral spike, membrane and nucleocapsid respectively and used at a concentration of 1 µg/ml each. The *Mycobacterium tuberculosis* peptide pool consists of a mixture of peptides pools from the antigenic targets ESAT-6, CFP-10 and EspC (1µg/ml each). After IFNγ detection, spots were imaged and counted using an ImmunoSpot analyser (Cellular Technology Limited, OH, USA).

In vitro induction of trained immunity

PBMCs (3 x 106) from three healthy donors were isolated using Ficoll isolation and primed for 24h with LPS (100 ng/ml), BCG (MOI 0.1) or left untreated (unprimed). Cells were then incubated at 37°C and 5% CO2 for 5 days before a 24h re-stimulation with LPS (100 ng/ml), BCG (MOI 0.1), SARS-CoV-2 (MOI 0.1) or mock treatment. Trained immunity was assessed by measuring the IL-1β mRNA expression levels in each condition and calculation of the delta delta CT as previously described by Livak et al. (17), relative to the unprimed and untreated cells.

Cell culture and cytokine analysis

Frozen PBMC stocks of each donor and each time point were thawed and cultured in RPMI- 1640 medium supplemented with 10% FCS and 1% L-glutamine for 2-3h before treatment (all reagents were obtained from Sigma Aldrich, MO, USA). Cells were then either left untreated, stimulated with LPS (*E. coli* O26: B6, 100 ng/ml, Sigma Aldrich, St. Louis, MO, USA) a live attenuated BCG strain RIVM (BCG Medac, Wedel, Germany; MOI: 1) or replication competent SARS-CoV-2 wildtype virus (SARS-CoV-2 USA/WA1/2020; MOI: 0.1) for 24h. For quantification of cytokine mRNA expression PBMCs were harvested and lysed 24h after treatment and RNA was extracted using a commercially available kit (Dr. P Kit, BioChain, CA, USA) following cDNA synthesis (LunaScript RT Supermix, New England Biolabs, MA, USA). Expression of IL-1β, IL-6, TNFα, IL-12A, IL-18, IFNγ and IL-10 mRNA was analyzed by PrimePCR Assays via multiplex qPCR using iQ Multiplex Powermix (Bio-Rad laboratories, CA; USA). Relative quantification of target genes was performed using the delta-delta CT method as previously described and normalized to the respective untreated controls (18). Cytokine protein concentrations of IL-1β, IL-6, IL-10, IL-18, TNFα and IFNγ in cell culture supernatants 24h post stimulation were measured using Bio-Plex systems (Bio-Rad Laboratories, CA, USA) according to the manufacturers' instructions.

Next generation sequencing

Assay for transposase accessible chromatin (ATAC), including tagmentation, library preparation and sequencing were performed by Genewiz (Azenta Life Sciences, MA, USA) on PBMCs from two BCG-treated NMIBC patients (responder) at baseline and during BCG (mid) as well as from two healthy donors. Raw data were preprocessed including mapping to the hg38 reference genome using bowtie2 and peak calling by MACS2. Differentially accessible regions in proximity to annotated genes including TI genes (TIDB) between the two time points (during BCG versus baseline) were identified using the R packages csaw and edgeR. We only focused on consensus regions with sufficient normalized counts (logCPM>1), which were more than three-fold enriched and annotated in the promoter or intron of coding genes excluding X, Y chromosomes and blacklisted regions. Overrepresentation analysis of biological processes (GO) and pathways (Reactome) were performed using DAVID, ConsensusPathDB, and ClueGO (Supplementary dataset S1).

Statistical analysis

All statistical analyses were performed on GraphPad Prism 9 (GraphPad Software Inc., San Diego, CA, USA). Paired t-test was used for neutralization assays comparing patients' sera before and after BCG treatment or Mann-Whitney test for SARS-CoV-2 vaccinated/unvaccinated individuals. ELISpot data were analyzed via 2-way ANOVA with Šidák's correction for multiple comparisons. For cytokine analysis, non-parametric Kruskal Wallis test with Dunn's correction for multiple comparisons was applied. A p-value of < 0.05 was considered significant. Graphics were produced with BioRender (www.biorender.com).

Results

Dynamic blood samples of eleven high-risk NMIBC patients during intravesical BCG treatment were available for further analysis. Descriptive patient and tumor characteristics are shown in Table 1. All patients were classified as BCG responders during a mean (range) follow-up of 41 (18-50) months, respectively.

To examine adaptive immune responses, we analyzed plasma antibodies against SARS-CoV-2 RBD and found no positive titers in all tested patients regardless of BCG instillation time interval, Figure 2. Next, we performed virus neutralization and IFNγ ELISpot assays. We found no cross-reactive antibodies against SARS-CoV-2 wildtype in BCG-treated NMIBC patients at baseline and during BCG therapy (mean, 228.8 *vs.* 215.6 PFU/mL; p=0.266), Figure 3A. As a control, we performed neutralization assays also in healthy, non-NMIBC blood donors who were either COVID-19 unvaccinated (n=8) or 3x COVID-19 vaccinated (n=8). Neutralizing antibodies could only be detected in vaccinated individuals (mean, unvaccinated *vs.* 3x vaccinated: 242.9 *vs.* 0.9 PFU/mL; p<0.0001), Figure 3B. Furthermore, to evaluate a potential cross-reactive T cell induction,

10.3389/fimmu.2023.1202157

TABLE 1 Clinicopathologic features of (very) high-risk NMIBC patients treated with intravesical BCG therapy (n=11).

Age, mean (SD), *years*	65.3 (6.7)
Sex, n (%)	
female	2 (18.2%)
male	9 (81.8%)
Smoking status, n (%)	
never smoker	1 (9.1%)
former smoker	3 (27.3%)
current smoker	7 (63.6%)
History of BCa, n (%)	
primary NMIBC	9 (81.8%)
recurrent NMIBC	2 (18.2%)
Tumor diameter, n (%)	
< 3 cm	8 (72.7%)
≥ 3 cm	3 (27.3%)
Number of tumors, n (%)	
1	7 (63.6%)
2-7	4 (36.4%)
> 7	–
pT stage, n (%)	
Ta	3 (27.3%)
T1	8 (72.7%)
Tumor grade (WHO 2004/2016), n (%)	
LG	4 (36.4%)
HG	7 (63.6%)
Tumor grade (WHO 1973), n (%)	
G1	2 (18.2%)
G2	2 (18.2%)
G3	7 (63.6%)
Concomitant CIS, n (%)	6 (54.5%)

CIS, carcinoma in situ; LG, low grade; HG, high grade; BCa, bladder cancer; NMIBC, non-muscleinvasive bladder cancer.

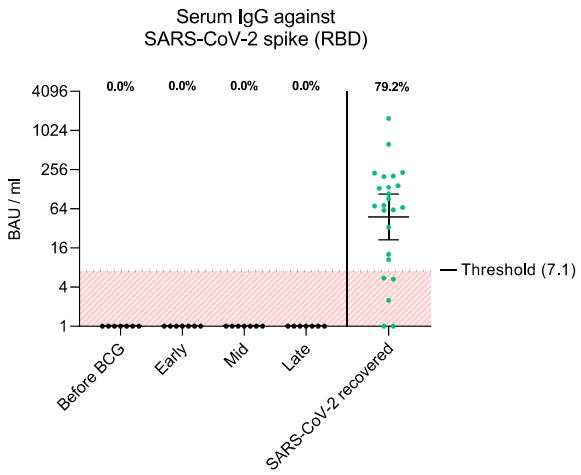

FIGURE 2
The graph shows antibody titers against wildtype SARS-CoV-2 spike RBD in BAU/ml (binding antibody units per ml) from each patient and time interval (black dots). As comparison, antibody titers from SARS-CoV-2 recovered individuals 1 month post infection are shown (green dots, n=24). Fraction of positive titers are indicated as percentages above each group. Titers >7.1 BAU/ml were defined as positive according to the manufacturer's instructions. Time points: 1-2 weeks/early, 3-4 weeks/mid and 6-12 week-interval/late during BCG. Data is presented as geometric mean (horizontal line) with 95% confidence interval (whiskers).

we challenged T cells with either SARS-CoV-2 wildtype-specific or BCG-specific peptide pools as well as CEF/CEFTA as positive control for 24h and measured the presence of pathogen-specific T cells via IFNγ ELISpot assays. We could not detect SARS-CoV-2 reactive T cells in our patients, Figure 3C.

Next, we investigated whether BCG instillations result in altered innate immune responses in patients with NMIBC. After a 24h stimulation of PBMCs with either BCG or SARS-CoV-2 wildtype, cytokine mRNA and protein expression levels were measured via multiplex qPCR. We found a significant increase in mRNA expression of the pro-inflammatory cytokines IL-1β, IL-6 and TNFα in response to BCG stimulation relative to the respective untreated controls, Figure 4A, lower panel, blue bars. The highest peak of these cytokines was detected after at least four BCG instillations (late time interval), while no response was detected during the early or mid-time intervals, Figure 4A. A very similar cytokine profile was observed after 24h exposure with SARS-CoV-2 wildtype, Figure 4A, upper panel, orange bars. No change in IL-12A, IL-18, IFNγ and IL-10 mRNA expression was identified in response to stimulation with BCG or SARS-CoV-2 wildtype relative to untreated, Figures 4B, C.

In accordance with the increase of mRNA expression, we also found significantly elevated secretion of IL-1β but also of IL-6 and TNFα protein after at least four BCG instillations (late time interval), Figure 5A. Importantly, these cytokines are considered the key markers of trained immunity. However, expression of the Th1 cytokines IL-18 and IFNγ as well as the anti-inflammatory cytokine IL-10 did not change, Figures 5B, 5C. To test if these changes are specific to the BCG or SARS-CoV-2 stimulus, we included a bacterial LPS treatment as potent activator of innate immune cells and observed a strong induction of the pro-inflammatory cytokines IL-1β, IL-6 and TNFα after 24h, independent of patient or instillation time interval, Figure 6.

To establish our experimental protocol for assessing trained immunity, we initially investigated the *in vitro* induction of trained immunity as described by Arts et al. (19) with LPS and BCG using PBMCs from fresh, healthy human blood donations. Cells were primed for 24h with LPS (100 ng/ml) or BCG (MOI: 0.1) or left untreated (i.e. unprimed). After 5 days, cells were re-stimulated with the same conditions and additionally with SARS-CoV-2 (MOI 0.1). We measured the IL-1β mRNA expression in these cells and calculated the fold-change compared to the unprimed and

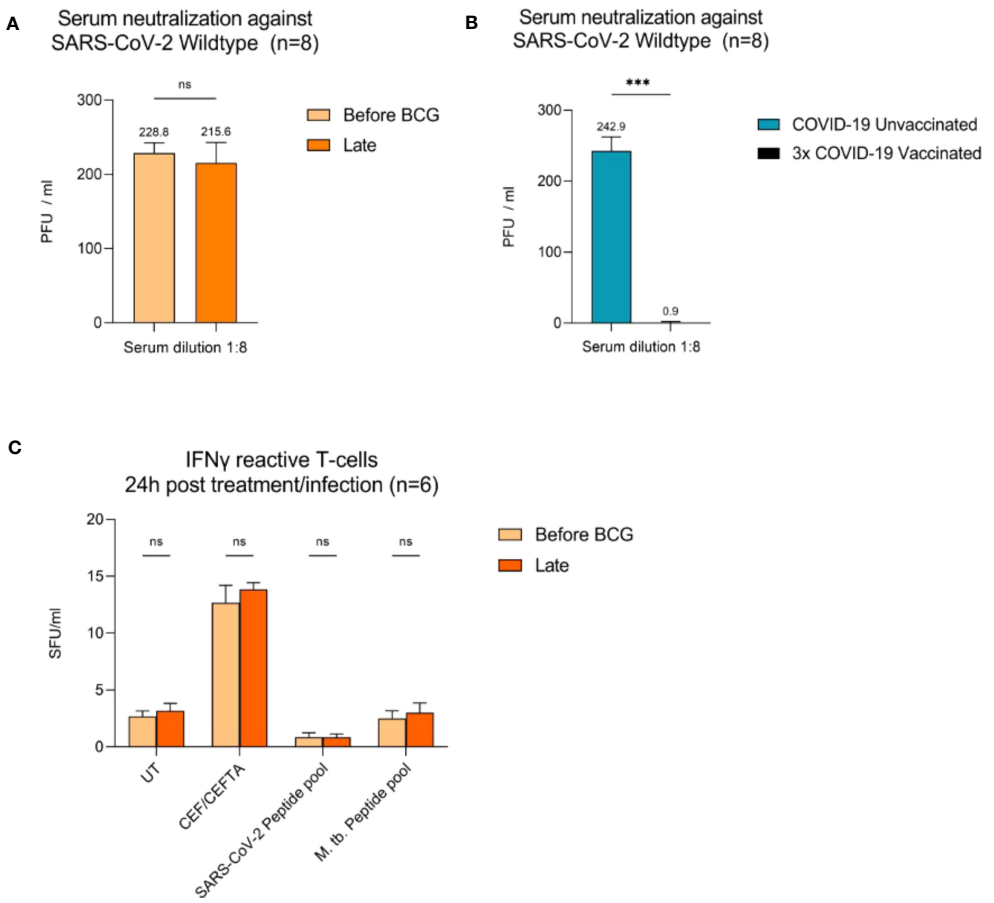

FIGURE 3
Virus neutralization assays and SARS-CoV-2/BCG specific IFNγ T cell responses. **(A)** Serum neutralization against SARS-CoV-2 wildtype in eight BCG-treated high-risk NMIBC patients (baseline and during BCG). **(B)** Serum neutralization in the internal control group (COVID-19 unvaccinated and 3x vaccinated patients, n=8). **(C)** IFNγ reactive T cells 24h post BCG/SARS-CoV-2 peptide pool (n=6). PBMCs ($0.5x10^5$) were treated with CEF/CEFTA as positive control. Data represent mean with SD; *p <.05, **p <.01; ***p <.001.

untreated condition, Figure S1, black bars. We observed a strong induction of IL-1β expression in the unprimed but LPS-treated conditions (Figure S1, LPS treated, black bars) which was greatly enhanced (>3 times more) when cells previously primed with LPS, Figure S1, LPS treated, pink bars. Similar results were obtained for cells treated with BCG, Figure S1, turquoise bars. Here, IL-1β mRNA expression was higher (>5 times more) in cells that were previously primed and stimulated with BCG compared to unprimed cells, Figure S1, BCG, turquoise bars. At the same time, in BCG-primed cells we could also observe a stronger cytokine induction in presence of SARS-CoV-2, which is in line with the results using our patient samples. One basis of trained immunity are epigenetic changes to facilitate a rapid and increased innate immune response. To address this aspect, we performed ATAC-seq analysis. Comparing two time points (during BCG vs. baseline), we identified differentially accessible genomic regions in proximity to 1697 genes. Among 64 TI candidate genes, 6 genes were overlapping (*TLR2, IGF1R, AKT1, MTOR, MAPK14, HSP90AA1)*, Figure 7A. We also performed an analysis of the overrepresented immune-related pathways and biological processes of the more accessible genes during BCG compared with baseline. Especially, myeloid differentiation was affected (Figure 7B). We particularly assessed an H3K4me3 signal in the identified regions near the TI genes, confirming H3K4me3 modifications at a more accessible region near transcription start site of all 6 genes. Next, as an example we show TLR2, which is one of the two BCG-specific toll-like receptors (TLR), Figure 7C.

Discussion

Despite 40 years of clinical research (2), the exact immune mechanism of BCG-mediated antitumor activity is still not fully established (17). However, activation of a predominant Th1- type immune response by infiltrating effector cells into the bladder wall is essential for a subsequent clinical BCG response (13, 20–22). Accordingly, BCG responders showed a significant increase of Th1-type urinary cytokines during BCG therapy (13, 20, 21). In contrast, BCG was totally ineffective in IFNγ or IL-12 knockout mice in a syngeneic orthotopic model of bladder cancer (23). The Th1-type immune response is elicited by dendritic cells, which are the most potent antigen presenting cells. BCG induces the activation/maturation of dendritic cells (24), and thus initiates the Th1-type immune cascade (20, 21). In summary, intravesical BCG elicits a

10.3389/fimmu.2023.1202157

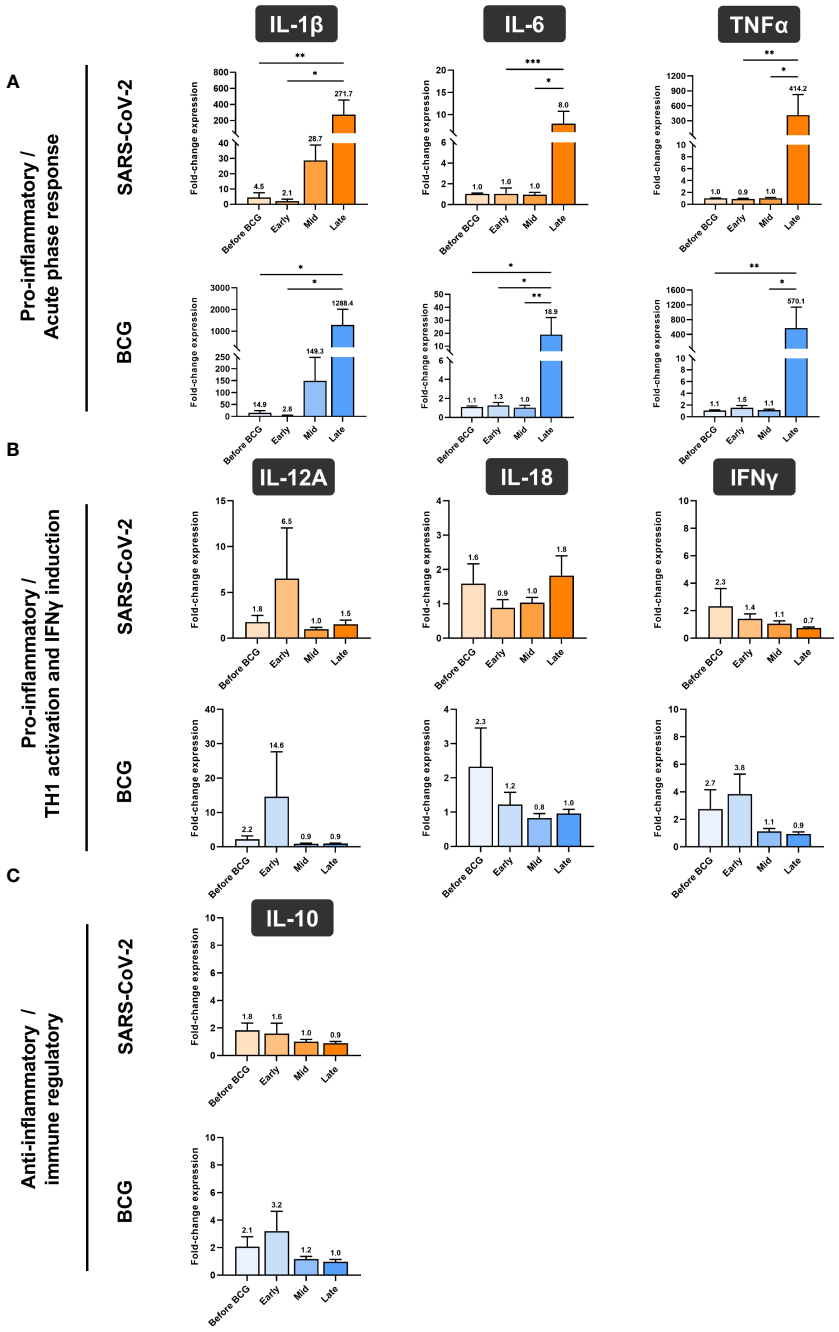

FIGURE 4
Relative quantification of cytokine mRNA expression by multiplex qPCR. **(A)** Pro- inflammatory cytokines IL-1β, IL-6 and TNFα, **(B)** cytokines associated with Th1 response IL- 12A, IL-18 and IFNγ and **(C)** anti-inflammatory cytokine IL-10 after a 24h stimulation of PBMCs with either BCG or SARS-CoV-2 wildtype are shown. PBMCs were taken before the start of BCG induction (baseline) and at early, mid and late time intervals during BCG treatment. Data is presented as fold-change expression relative to untreated control group (mean with SEM and mean values annotated above each individual bar; *p <.05, **p <.01; ***p <.001). Time points: baseline (before BCG induction), 1-2 weeks/early, 3-4 weeks/mid and 6-12 week-interval/late during BCG.

potent local immune response and recruits effector T cells into the NMIBC tumor microenvironment, suggesting that T lymphocytes are critical to BCG-mediated clinical efficacy resulting in BCG response (25). Our ClueGO analysis, including BCG responders, supports these findings, highlighting a strong alteration in lymphocyte differentiation and T cell response as well.

Activated myeloid cells such as dendritic cells and macrophages can further increase Th1 immune responses by producing cytokines such as IL-1β, IL-6, TNFα, as well as IL-12 and IL-18 after stimulation of toll-like and NOD-like receptors by BCG (26, 27). Myeloid cells can also develop TI following BCG vaccination. TI is characterized by an epigenetic and functional reprogramming, which facilitates the production of the pro-inflammatory cytokines IL-1β, IL- 6 and TNFα, in response to a secondary irrelevant bacterial or viral stimulus (28, 29). Althoughmonocytes, macrophages and NK cells have dominant roles in innate immune

10.3389/fimmu.2023.1202157

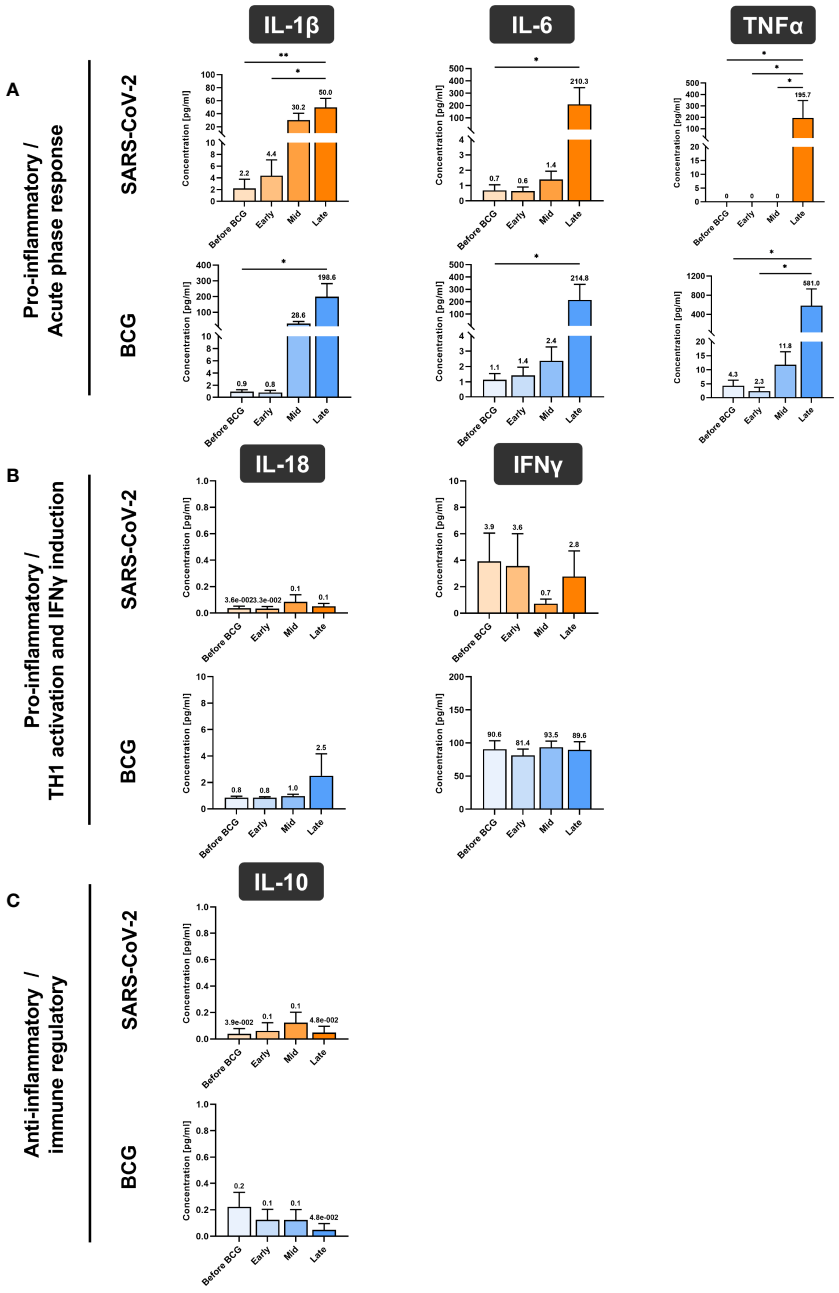

FIGURE 5
Cytokine quantification using Luminex xMAP technology. **(A)** Pro-inflammatory cytokines IL-1β, IL-6 and TNFα, **(B)** cytokines associated with Th1 response IL-18 and IFNγ and **(C)** anti-inflammatory cytokine IL-10 were measured in cell culture supernatant of PMBCs after 24h stimulation with either BCG or SARS-CoV-2 wildtype are presented. PBMCs were prepared before the start of BCG induction (baseline) and at early, mid and late time intervals during BCG treatment. Data represent means with SEM and mean values annotated above each individual bar (*p <.05, **p <.01; ***p <.001). Time points: baseline (before BCG induction), 1-2 weeks/early, 3-4 weeks/mid and 6-12 week-interval/late during BCG. IL-12A data are not shown as their levels were not detectable and samples for repetition were no more available.

memory, other mature innate immune cells, but also hematopoietic stem cells as well as progenitor cells have been implicated in TI (30). BCG is the most potent agent that induces TI through TLR2 and TLR4 activation and downstream signaling via Akt/mTOR and NOD2. Both pathways are required for epigenetic modifications of H3K4me3, thus facilitating an increased pro-inflammatory cytokine production (Figure 8) (31). Enhanced neutrophil function through BCG vaccination is associated with genome-wide epigenetic modification of H3K4me3 (32). Moreover, macrophages are trained to increase the expression of various pattern recognition receptors, chemokine receptors and costimulatory and/or signaling molecules that also correlated with modification of H3K4me3 (33). Accordingly, we also demonstrated H3K4me3 modifications at a more accessible region near transcription start site of TI genes such

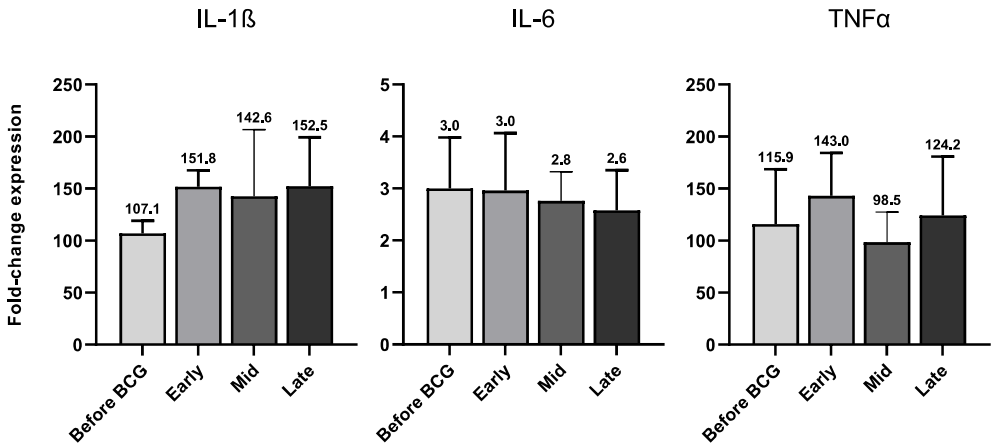

FIGURE 6
IL-1β, IL-6 and TNFα mRNA expression after 24h of LPS (100 ng/ml) treated PBMCs from patients before and during various time-points of BCG treatment. Data is presented as foldchange expression relative to untreated control group (mean with SEM). Time points: 1-2 weeks/early, 3-4 weeks/mid and 6-12 week-interval/late during BCG.

as the BCG receptor *TLR2* induced by BCG instillations. Arts et al. showed that BCG-induced TI was accompanied by a metabolic shift towards glycolysis through activation of the Akt/mTOR pathway (34). Thus, BCG-induced epigenetic and metabolic reprogramming influence each other. This fact means that inhibition of metabolism can reverse epigenetic changes in an *in vitro* TI model, resulting in reduced cytokine responses upon re-stimulation (35).

The repetitive activation of innate immune cells with BCG is the most important driver of enhanced innate immune responsiveness. Along this line, repetitive BCG administration has been shown to decrease the susceptibility to respiratory viral infections with respiratory syncytial virus, influenza A virus and herpes simplex virus type 2 (36, 37). This prompted us to test whether intravesical BCG might also induce TI-like innate immunity against SARS-CoV-2 in NMIBC. Several observational studies have already attempted to show a possible link between intravesical BCG instillations and COVID-19 infections (5, 38–40). No differences in the incidence of COVID-19 infections in BCG-treated NMIBC patients could be

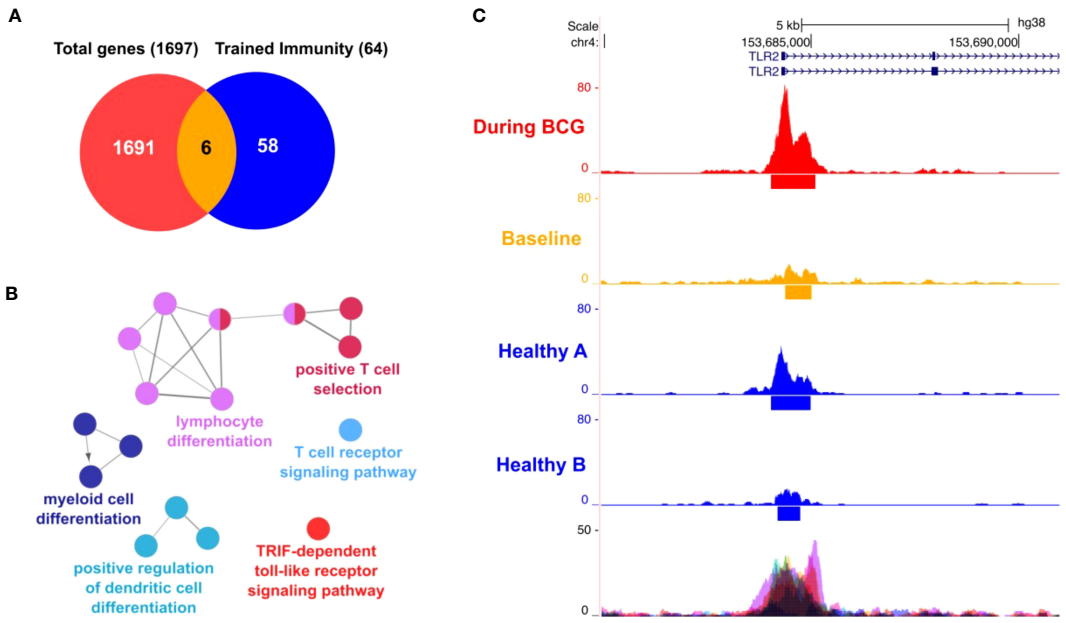

FIGURE 7
ATAC-seq analysis. **(A)** Venn diagram showing 6 genes (*AKT1, HSP90AA1, IGF1R, MAPK14, MTOR, TLR2*) overlapping between 64 trained immunity genes and 1697 genes with differentially accessible regions in their promoter or introns. **(B)** Differential affected immune system related processes (during BCG versus baseline) using ClueGO **(C)** Representative sequencing tracks for the TLR2 locus showing significantly higher ATAC-seq peaks at the promoter during BCG compared with baseline. Modifications of H3K4me3 were shown at the same region near the transcription start site of *TLR2*.

10.3389/fimmu.2023.1202157

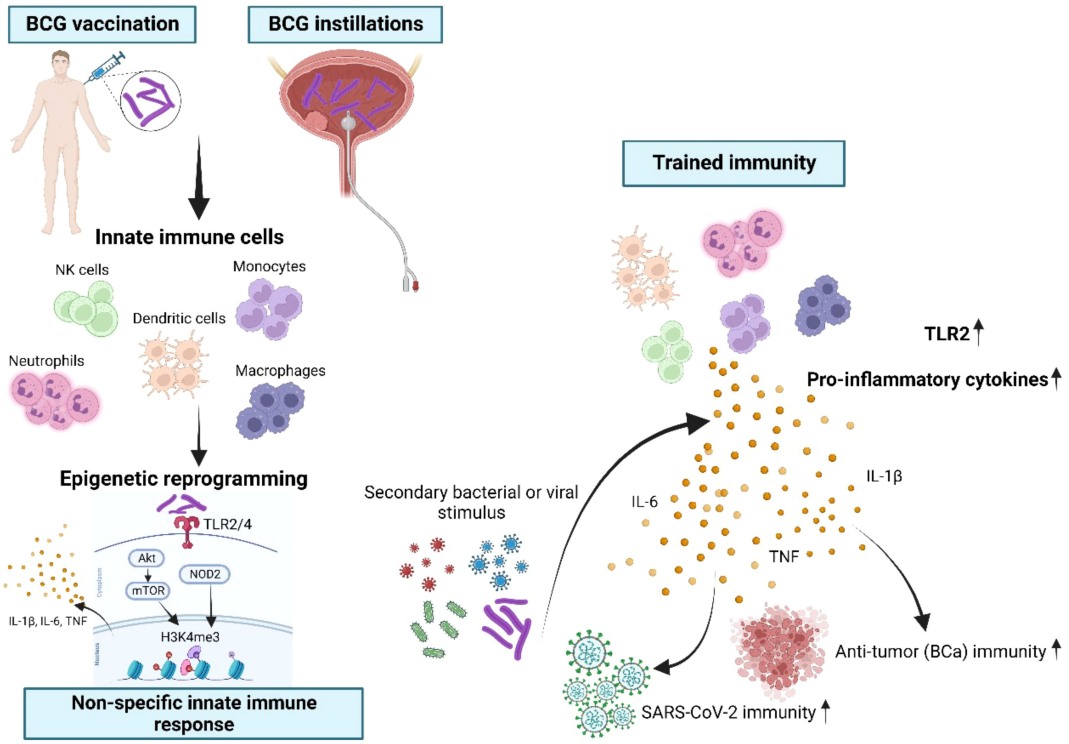

FIGURE 8
Schematic overview of BCG-induced trained immunity (TI). Innate immune cells such as monocytes, NK cells, dendritic cells, neutrophils, macrophages and their progenitor cells can be trained through repetitive BCG administration, which induces epigenetic and metabolic reprogramming of these cells. BCG is binding to the toll-like receptors (TLR)2 and TLR4 and thus leads to downstream epigenetic modifications at H3K4me3 through both the Akt/mTOR and NOD2 pathways. As a consequence, this specific modification of H3K4me3 facilitates the enhanced production of IL-1β, IL-6 and TNFα, known as the key cytokines of trained immunity (26–28). During a secondary bacterial or viral stimulation trained innate immune cells display an increased capacity to produce pro-inflammatory cytokines, resulting in improved protection also against unrelated pathogens. Importantly, in our study intravesical instillations as a route of BCG administration were suitable to induce TI, reflected by increased production of TI cytokines after at least four BCG instillations at mRNA and protein levels. BCG administration also resulted in epigenetic modifications of TI-related metabolic genes and of the gene encoding TLR2, which is a specific receptor for BCG. Most importantly, we demonstrated for the first time that high-risk NMIBC patients undergoing intravesical BCG showed an increased SARS-CoV-2 innate immune responsiveness indicative of TI.

shown. However, these findings must be interpreted with caution because they did not examine causal and mechanistic associations between intravesical BCG application and immunity against SARS-CoV-2 (5, 38–40). With regard to severity of the disease, we believe that BCG-induced TI may indeed help prevent detrimental hyperinflammation associated with viremia. Severe cases of Covid-19 tend to have lower lymphocyte counts (lymphopenia) (41). Intriguingly, a recent study also assessed short-term effects of BCG on innate immune responses during the BCG induction regimen and found that one week after the first BCG instillation the total number of white blood cells in the circulation was significantly increased compared to pre-BCG-1. Obviously, BCG treatment also appears appropriate to counteract lymphopenia and may thus improve the clinical course of Covid-19. In addition, the early local innate response to SARS-CoV-2 infection, which is facilitated by TI, may support rapid virus control, keeping systemic inflammation low and enabling recovery. In contrast, absence of TI may increase the risk of hyperinflammation and severe complications associated with viremia (7).

In the present study we show for the first time that intravesical BCG also induces innate immune responses against SARS-CoV-2. The major new findings of the present study are: (i) BCG did not induce B cell or T cell-dependent adaptive immunity against SARS-CoV-2; (ii) BCG-treated NMIBC patients expressed key cytokines of trained immunity at the mRNA and protein levels after stimulation with SARS-CoV-2; (iii) ATAC sequencing revealed that repeated BCG instillations cause an increased accessibility of important TI genes (*TLR2*, *IGF1R*, *AKT1*, *MTOR*, *MAPK14*, *HSP90AA1*). Collectively, intravesical BCG indeed causes TI, which is the basis of innate immunity against SARS-CoV-2 (Figure 6). An important aspect of our findings is that the local administration of BCG into the bladder also promotes systemic immunity after at least six BCG instillations, reflected by the increased responsiveness of circulating immune cells. In general, epigenetic and metabolic reprogramming leading to TI needs some time. With regard to BCG instillations in

NMIBC patients, repetitive administrations are required to observe an increase in innate immunity. In our study, TI cytokines appeared after 6 weeks. This is in accordance with recent work proposing TI as a molecular mechanism for BCG immunotherapy in bladder cancer (11). Although van Puffelen and coworkers assessed numbers of circulating leukocytes in whole blood early, i.e. one week after BCG1, changes in cytokine production were also not reported before BCG6 (11). The authors argue that late time points of cytokine measurements are most informative for TI (42).

In accordance with our current findings, a recent study has also shown that intravesical instillations of BCG induce TI at a systemic level (11). While these authors observed BCG-induced immunity against pneumonia and common cold in bladder cancer patients (11), we report for the first time on BCG-driven innate immunity against SARS-CoV-2. Of note, all blood samples analyzed in our study have been collected from NMIBC patients in the pre-Covid-19 era (2014-2015), most likely excluding the possibility of previous contact with SARS-CoV-2, which is also supported by the complete absence of RBD specific antibodies in these individuals. Accordingly, SARS-CoV-2-induced pro-inflammatory cytokine production could not be detected in control samples collected before BCG initiation. On the contrary, repetitive BCG administration was required to observe SARS-CoV-2-induced production of TI cytokines. Moreover, we could not detect adaptive immune responses (neutralizing antibodies, T cells) against SARS-CoV-2 excluding the existence of virus-specific memory lymphocytes.

One limitation of the study is the small number of patients, which is due to the fact that we used samples from a pre-COVID-19 era. Moreover, our data cannot be generalized as different BCG strains with immune-reactive differences in elicited immune responses are used in clinical practice (43). However, the BCG strain RIVM which was used in this study is mainly adopted across all EU countries.

Finally, our data reinforce the fact that adjustments to BCG induction and maintenance schedules, as recommended at the early onset of the COVID-19 pandemic (3, 4), are not necessary in clinical practice. Although our data support the development of BCG-induced TI, we did not have the opportunity to study TI-mediated protection against SARS-CoV-2 infection. However, it should be emphasized that research leading to the discovery of TI has been prompted by epidemiological studies showing that BCG vaccination at birth results in reduced child mortality and by subsequent randomized controlled trials demonstrating, that the beneficial effects of BCG were mainly due to protection against neonatal sepsis and respiratory infections (19). The BCG-induced TI observed in our study that includes responsiveness against SARS-CoV-2 in NMIBC patients is thus likely to mediate protection against Covid-19. Thus, every effort should be made to administer full BCG maintenance in high-risk NMIBC patients as recommended even during the pandemic period. Moreover, BCG-induced trained immunity could be one of the most important mechanisms mediating efficacy to BCG in bladder cancer (11, 44). Thus, further trials are urgently needed to evaluate how trained immunity influences the antitumor immune responses in BCG-treated NMIBC patients, improving personalized medicine in NMIBC (11, 44).

Conclusions

Here we present the first study showing that repetitive intravesical BCG instillations in high- risk NMIBC also induces innate immune responsiveness against SARS-CoV-2 via mechanisms of TI. The increased fitness of the innate immune system that is induced by repetitive BCG administrations may be important in the context of various therapeutic and preventive strategies.

Data availability statement

The datasets presented in this study can be found in online repositories. The names of the repository/repositories and accession number(s) can be found below: https://zenodo.org/record/7825968.

Ethics statement

The studies involving human participants were reviewed and approved by AN2014-0121; 336/4.3. The patients/participants provided their written informed consent to participate in this study.

Author contributions

RP, GD, JK, MT and WP processed and analyzed data and wrote the manuscript. RP, LM, DD, EL, AM, BP, FS, WK, MM, FG and JT were involved in patient recruiting, collection processing and analysis of samples and clinical data. GD, JK and WP performed and analyzed cell culture, neutralization and ELISpot assays. HH performed and analyzed ATAC sequencing. GD and JK performed experiments and analyzed data. MT, WP, MM, LM, DD, AM and FS helped with manuscript preparation, provided expertise and discussed the data. MT and WP were responsible for supervision. All authors contributed to the article and approved the submitted version.

Funding

This work was supported by the Austrian Science Fund (FWF; P34070-B13 to WP). JK receives DOC Fellowship from the Austrian Academy of Sciences.

Acknowledgments

We thank our technicians Sophie Ann Erckert, Viktoria Kozubowski, Christina Witting, Andrea Windisch (Institute of

Hygiene and Medical Microbiology, Medical University of Innsbruck, Innsbruck, Austria), as well as Hubert Gander and Andrea Rahm (Immunotherapy Unit, Department of Urology, Medical University of Innsbruck, Innsbruck, Austria) for their valuable help and support regarding this study. SARS-Related Coronavirus 2, Isolate USA-WA1/2020 NR-5228 was deposited by the Centers for Disease Control and Prevention and obtained through BEI Resources, NIAID, NIH.

Conflict of interest

The authors declare that the research was conducted in the absence of any commercial or financial relationships that could be construed as a potential conflict of interest.

Publisher's note

Supplementary material

The Supplementary Material for this article can be found online at: https://www.frontiersin.org/articles/10.3389/fimmu.2023.1202157/full#supplementary-material

References

1. Babjuk M, Burger M, Capoun O, Cohen D, Compérat EM, Dominguez Escrig JL, et al. European Association of urology guidelines on non-muscle- invasive bladder cancer (Ta, T1, and carcinoma in situ). *Eur Urol* (2022) 81(1):75–94. doi: 10.1016/j.eururo.2021.08.010

2. Morales A, Eidinger D, Bruce AW. Intracavitary bacillus calmette-guerin in the treatment of superficial bladder tumors. *J Urol* (1976) 116(2):180–3. doi: 10.1016/S0022-5347(17)58737-6

3. Lenfant L, Seisen T, Loriot Y, Rouprêt M. Adjustments in the use of intravesical instillations of bacillus calmette-guérin for high-risk non-muscle-invasive bladder cancer during the COVID-19 pandemic. *Eur Urol* (2020) 78(1):1–3.

4. Ribal MJ, Cornford P, Briganti A, Knoll T, Gravas S, Babjuk M, et al. European Association of urology guidelines office rapid reaction group: an organisation-wide collaborative effort to adapt the European association of urology guidelines recommendations to the coronavirus disease 2019 era. *Eur Urol* (2020) 78(1):21–8. doi: 10.1016/j.eururo.2020.04.056

5. O'Neill LAJ, Netea MG. BCG-Induced trained immunity: can it offer protection against COVID-19? *Nat Rev Immunol* (2020) 20(6):335–7. doi: 10.1038/s41577-020-0337-y

6. Mathurin KS, Martens GW, Kornfeld H, Welsh RM. CD4 T-cell-mediated heterologous immunity between mycobacteria and poxviruses. *J Virol* (2009) 83 (8):3528–39. doi: 10.1128/JVI.02393-08

7. Netea MG, Giamarellos-Bourboulis EJ, Domınguez-Andres J, Curtis N, van Crevel R, van de Veerdonk FL, et al. Trained immunity: a tool for reducing susceptibility to and the severity of SARS-CoV-2 infection. *Cell.* (2020) 181(5):969–77. doi: 10.1016/j.cell.2020.04.042

8. Noval Rivas M, Ebinger JE, Wu M, Sun N, Braun J, Sobhani K, et al. BCG Vaccination history associates with decreased SARS-CoV-2 seroprevalence across a diverse cohort of healthcare workers. *J Clin Invest* (2021) 131(2):e145157.

9. Escobar LE, Molina-Cruz A, Barillas-Mury C. BCG Vaccine protection from severe coronavirus disease 2019 (COVID-19). *Proc Natl Acad Sci U S A* (2020) 117 (30):17720–6. doi: 10.1073/pnas.2008410117

10. Curtis N, Sparrow A, Ghebreyesus TA, Netea MG. Considering BCG vaccination to reduce the impact of COVID-19. *Lancet.* (2020) 395(10236):1545–6. doi: 10.1016/S0140-6736(20)31025-4

11. van Puffelen JH, Novakovic B, van Emst L, Kooper D, Zuiverloon TCM, Oldenhof UTH, et al. Intravesical BCG in patients with non-muscle invasive bladder cancer induces trained immunity and decreases respiratory infections. *J Immunother Canc* (2023) 11(1):e005518. doi: 10.1136/jitc-2022-005518

12. Buffen K, Oosting M, Quintin J, Ng A, Kleinnijenhuis J, Kumar V, et al. Autophagy controls BCG- induced trained immunity and the response to intravesical BCG therapy for bladder cancer. *PloS Pathog* (2014) 10(10):e1004485. doi: 10.1371/journal.ppat.1004485

13. Pichler R, Gruenbacher G, Culig Z, Brunner A, Fuchs D, Fritz J, et al. Intratumoral Th2 predisposition combines with an increased Th1 functional phenotype in clinical response to intravesical BCG in bladder cancer. *Cancer Immunol Immunother* (2017) 66(4):427–40. doi: 10.1007/s00262-016-1945-z

14. Diem G, Lafon E, Bauer A, Lass-Flörl C, Reindl M, Wilflingseder D, et al. Salivary IgAs and their role in mucosal neutralization of SARS-CoV-2 variants of concern. *J Clin Microbiol* (2022) 60(9):e0106522. doi: 10.1128/jcm.01065-22

15. Jäger M, Diem G, Sahanic S, Fux V, Griesmacher A, Lass-Flörl C, et al. Immunity of heterologous and homologous boosted or convalescent individuals against omicron BA.1, BA.2 and BA.4/5 variants. *J Infect Dis* (2023) 4:jiad057. doi: 10.1093/infdis/jiad057

16. Jäger M, Dichtl S, Bellmann-Weiler R, Reindl M, Lass-Flörl C, Wilflingseder D, et al. Serum neutralization against SARS-CoV-2 variants is heterogenic and depends on vaccination regimen. *J Infect Dis* (2023) 227(4):528–32. doi: 10.1093/infdis/jiac432

17. Livak KJ, Schmittgen TD. Analysis of relative gene expression data using real-time quantitative PCR and the 2(-delta delta C(T)) method. *Methods.* (2001) 25 (4):402–8. doi: 10.1006/meth.2001.1262

18. Jäger M, Sonnleitner ST, Dichtl S, Lafon E, Diem G, Walder G, et al. Immune responses against SARS-CoV-2 WT and delta variant in elderly BNT162b2 vaccinees. *Front Immunol* (2022) 13:868361. doi: 10.3389/fimmu.2022.868361

19. Arts RJW, Moorlag SJCFM, Novakovic B, Li Y, Wang SY, Oosting M, et al. BCG Vaccination protects against experimental viral infection in humans through the induction of cytokines associated with trained immunity. *Cell Host Microbe* (2018) 23(1):89–100.e5. doi: 10.1016/j.chom.2017.12.010

20. Li R, Gilbert SM, Kamat AM. Unraveling the mechanism of the antitumor activity of bacillus calmette-guérin. *Eur Urol* (2021) 80(1):1–3.

21. Watanabe E, Matsuyama H, Matsuda K, Ohmi C, Tei Y, Yoshihiro S, et al. Urinary interleukin-2 may predict clinical outcome of intravesical bacillus calmette-guérin immunotherapy for carcinoma *in situ* of the bladder. *Cancer Immunol Immunother* (2003) 52(8):481–6. doi: 10.1007/s00262-003-0384-9

22. Saint F, Patard JJ, Groux Muscatelli B, Lefrere Belda MA, Gil D, de Medina S, et al. Evaluation of cellular tumour rejection mechanisms in the peritumoral bladder wall after bacillus calmette-guérin treatment. *BJU Int* (2001) 88(6):602–10. doi: 10.1046/j.1464-410X.2001.02394.x

23. Ratliff TL, Ritchey JK, Yuan JJ, Andriole GL, Catalona WJ. T-Cell subsets required for intravesical BCG immunotherapy for bladder cancer. *J Urol* (1993) 150 (3):1018–23. doi: 10.1016/S0022-5347(17)35678-1

24. Riemensberger J, Böhle A, Brandau S. IFN-gamma and IL-12 but not IL-10 are required for local tumour surveillance in a syngeneic model of orthotopic bladder cancer. *Clin Exp Immunol* (2002) 127(1):20–6. doi: 10.1046/j.1365-2249.2002.01734.x

25. Kates M, Nirschl T, Sopko NA, Matsui H, Kochel CM, Reis LO, et al. Intravesical BCG induces $CD4^+$T-cell expansion in an immune competent model of bladder cancer. *Cancer Immunol Res* (2017) 5(7):594–603. doi: 10.1158/2326-6066.CIR-16-0267

26. Thurnher M, Ramoner R, Gastl G, Radmayr C, Böck G, Herold M, et al. Bacillus calmette-guérin mycobacteria stimulate human blood dendritic cells. *Int J Canc* (1997) 70 (1):128–34. doi: 10.1002/(SICI)1097-0215(19970106)70:1<128::AID-IJC19>3.0.CO;2-H

27. Croft M. The role of TNF superfamily members in T-cell function and diseases. *Nat Rev Immunol* (2009) 9(4):271–85. doi: 10.1038/nri2526

28. Kumar P, Tyagi R, Das G, Bhaskar S. Mycobacterium indicus pranii and mycobacterium bovis BCG lead to differential macrophage activation in toll-like receptor-dependent manner. *Immunology.* (2014) 143(2):258–68. doi: 10.1111/imm.12306

29. Netea MG, Domínguez-Andrés J, Barreiro LB, Chavakis T, Divangahi M, Fuchs E, et al. Defining trained immunity and its role in health and disease. *Nat Rev Immunol* (2020) 20(6):375–88. doi: 10.1038/s41577-020-0285-6

30. Kleinnijenhuis J, Quintin J, Preijers F, Joosten LA, Ifrim DC, Saeed S, et al. Bacille calmette-guerin induces NOD2-dependent nonspecific protection from reinfection via epigenetic reprogramming of monocytes. *Proc Natl Acad Sci U S A* (2012) 109(43):17537–42. doi: 10.1073/pnas.1202870109

31. van Leent MMT, Priem B, Schrijver DP, de Dreu A, Hofstraat SRJ, Zwolsman R, et al. Regulating trained immunity with nanomedicine. *Nat Rev Mater* (2022) 7:465–81. doi: 10.1038/s41578-021-00413-w

32. Moorlag SJCFM, Rodriguez-Rosales YA, Gillard J, Fanucchi S, Theunissen K, Novakovic B, et al. BCG Vaccination induces long-term functional reprogramming of human neutrophils. *Cell Rep* (2020) 33(7):108387. doi: 10.1016/j.celrep.2020.108387

33. Jeljeli M, Riccio LGC, Doridot L, Chêne C, Nicco C, Chouzenoux S, et al. Trained immunity modulates inflammation-induced fibrosis. *Nat Commun* (2019) 10 (1):5670. doi: 10.1038/s41467-019-13636-x

34. Arts RJW, Carvalho A, La Rocca C, Palma C, Rodrigues F, Silvestre R, et al. Immunometabolic pathways in BCG-induced trained immunity. *Cell Rep* (2016) 17 (10):2562–71. doi: 10.1016/j.celrep.2016.11.011

35. Bekkering S, Blok BA, Joosten LA, Riksen NP, van Crevel R, Netea MG. *In vitro* experimental model of trained innate immunity in human primary monocytes. *Clin Vaccine Immunol* (2016) 23(12):926–33. doi: 10.1128/CVI.00349-16

36. Brueggeman JM, Zhao J, Schank M, Yao ZQ, Moorman JP. Trained immunity: an overview and the impact on COVID-19. *Front Immunol* (2022) 13:837524. doi: 10.3389/fimmu.2022.837524

37. Moorlag SJCFM, Arts RJW, van Crevel R, Netea MG. Non-specific effects of BCG vaccine on viral infections. *Clin Microbiol Infect* (2019) 25(12):1473–8. doi: 10.1016/j.cmi.2019.04.020

38. Fedeli U, Porreca A, Colicchia M, Schievano E, Artibani W, Biasio LR, et al. Intravescical instillation of calmette-guérin bacillus and COVID-19 risk. *Hum Vaccin Immunother* (2021) 17(2):416–7. doi: 10.1080/21645515.2020.1805994

39. Karabay O, Köse O, Tocoglu A, Uysal B, Dheir H, Yaylaci S, et al. 5Investigation of the frequency of COVID-19 in patients treated with intravesical BCG. *Rev Assoc Med Bras (1992)* (2020) 66Suppl 2(Suppl 2):91–5. doi: 10.1590/1806-9282.66.S2.91

40. Hurle R, Soria F, Contieri R, Avolio PP, Mancon S, Lazzeri M, et al. Evaluating the protective effect of intravesical bacillus calmette-guerin against SARS-CoV-2 in non-muscle invasive bladder cancer patients: a multicenter observational trial. *Cancers (Basel)* (2023) 15(5):1618. doi: 10.3390/cancers15051618

41. Qin C, Zhou L, Hu Z, Zhang S, Yang S, Tao Y, et al. Dysregulation of immune response in patients with coronavirus 2019 (COVID-19) in wuhan, China. *Clin Infect Dis* (2020) 71(15):762–8. doi: 10.1093/cid/ciaa248

42. Divangahi M, Aaby P, Khader SA, Barreiro LB, Bekkering S, Chavakis T, et al. Trained immunity, tolerance, priming and differentiation: distinct immunological processes. *Nat Immunol* (2021) 22(1):2–6. doi: 10.1038/s41590-020-00845-6

43. Del Giudice F, Flammia RS, Chung BI, Moschini M, Pradere B, Mari A, et al. Compared efficacy of adjuvant intravesical BCG-TICE vs. BCG-RIVM for high-risk non-muscle invasive bladder cancer (NMIBC): a propensity score matched analysis. *Cancers (Basel)* (2022) 14(4):88.

44. van Puffelen JH, Keating ST, Oosterwijk E, van der Heijden AG, Netea MG, Joosten LAB, et al. Trained immunity as a molecular mechanism for BCG immunotherapy in bladder cancer. *Nat Rev Urol* (2020) 17(9):513–25. doi: 10.1038/s41585-020-0346-4

frontiers | Frontiers in Immunology

TYPE Original Research
PUBLISHED 13 October 2023
DOI 10.3389/fimmu.2023.1258691

OPEN ACCESS

EDITED BY
Diana Boraschi,
Chinese Academy of Sciences (CAS), China

REVIEWED BY
Seyed Ali Reza Mousavi,
Adamas Pharmaceuticals, United States
Khalil Karimi,
University of Guelph, Canada

*CORRESPONDENCE
Alireza Haghparast
alireza.haghparast@gmail.com;
haghparast@um.ac.ir

RECEIVED 14 July 2023
ACCEPTED 06 September 2023
PUBLISHED 13 October 2023

CITATION
Hajiabadi S, Alidadi S, Montakhab Farahi Z, Ghahramani Seno MM, Farzin H and Haghparast A (2023) Immunotherapy with STING and TLR9 agonists promotes synergistic therapeutic efficacy with suppressed cancer-associated fibroblasts in colon carcinoma.
Front. Immunol. 14:1258691.
doi: 10.3389/fimmu.2023.1258691

Immunotherapy with STING and TLR9 agonists promotes synergistic therapeutic efficacy with suppressed cancer-associated fibroblasts in colon carcinoma

Sare Hajiabadi[1], Soodeh Alidadi[1], Zohreh Montakhab Farahi[1], Mohammad M. Ghahramani Seno[2], Hamidreza Farzin[3] and Alireza Haghparast[1*]

[1]Department of Pathobiology, Faculty of Veterinary Medicine, Ferdowsi University of Mashhad, Mashhad, Iran, [2]Program for Genetics and Genome Biology, The Hospital for Sick Children, Toronto, ON, Canada, [3]Razi Vaccine and Serum Research Institute, Agriculture Research, Education and Extension Organization (AREEO), Mashhad, Iran

The innate immune sensing of nucleic acids using effective immunoadjuvants is critical for increasing protective immune responses against cancer. Stimulators of interferon genes (STING) and toll-like receptor 9 (TLR9) agonists are considered promising candidates in several preclinical tumor models with the potential to be used in clinical settings. However, the effects of such treatment on tumor stroma are currently unknown. In this study, we investigated the immunotherapeutic effects of ADU-S100 as a STING agonist and CpG ODN1826 as a TLR9 agonist in a preclinical model of colon carcinoma. Tumor-bearing mice were treated intratumorally on days 10 and 16 post-tumor inoculation with ADU-S100 and CpG ODN1826. Cytokine profiles in the tumor and spleen, tumor cell apoptosis, the infiltration of immune cells, and cancer-associated fibroblasts (CAFs) in the tumor microenvironment (TME) were evaluated to identify the immunological mechanisms after treatment. The powerful antitumor activity of single and combination treatments, the upregulation of the expression of pro-inflammatory cytokines in the tumor and spleen, and the recruitment and infiltration of the TME by immune cells revealed the synergism of immunoadjuvants in the eradication of the colon carcinoma model. Remarkably, the significant downregulation of CAFs in the TME indicated that suppression of tumorigenesis occurred after immunoadjuvant therapy. The results illustrate the potential of targeting the STING and TLR9 pathways as powerful immunoadjuvants in the treatment of preclinical colon carcinoma and the possibility of harnessing these pathways in future therapeutic approaches.

KEYWORDS

STING, TLR9, immunoadjuvants, CAFs, colon carcinoma

1 Introduction

Despite extensive research and recent improvements in prognosis, prevention, and treatment, cancer is a leading cause of death worldwide. Colon carcinoma is the third most prevalent cancer and the second most lethal cancer in the world (1–3).

It is well known that immunotherapy, as a promising strategy, modulates the immune system for the treatment of cancer by stimulating the body's immune response against tumor growth and metastasis (4). However, there is still a need for the development and improvement of more effective therapies.

In immunotherapy, multiple approaches and different compounds have been studied so far, several of which work by inducing innate immune responses (5, 6). Nucleic acid-based immunoadjuvants are regarded as safe and powerful immunostimulatory compounds in therapeutic and vaccine settings. CpG oligodeoxynucleotides (CpG ODNs) are synthetic ligands of toll-like receptor 9 (TLR9), which is located in the endosomal compartment of cells (7). CpG ODNs, as an adjuvant approved by the U.S. Food and Drug Administration (FDA), demonstrate remarkable efficacy in phase I clinical trials of infectious diseases and cancer (8–10). As a result of CpG ODN binding to the TLR9 receptor, the myeloid differentiation primary response 88–interferon regulatory factor 7 (MyD88–IRF7) pathway is activated and stimulates the production of type I interferons (IFNs), thereby promoting the pro-inflammatory status of cells in a nuclear factor kappa B (NF-κB)-dependent manner (11). Moreover, CpG ODNs can trigger Th1-type immune responses through the polarization of plasmacytoid dendritic cells (pDCs) to produce type I IFNs, thereby enhancing the recruitment of T cells, induction of B cells, and pDC activation, which consequently promotes effector antitumor immunity (8, 12). A class B CpG ODN that is distinct for mouse TLR9 is CpG ODN1826, containing a full phosphorothioate backbone that is nuclease-resistant and has been well studied in several preclinical studies so far (8, 13).

Another well-known immunostimulatory compound is the stimulator of interferon genes (STING), which is present in the endoplasmic reticulum and activated by double-stranded DNA (dsDNA) (14–16). The production of type I interferon and pro-inflammatory cytokines by a variety of cells in the TANK-binding kinase 1–interferon regulatory factor 3 (TBK1–IRF3)- and TBK1–NFκB-dependent pathways is a consequent cascade of STING activation (17, 18), leading to the polarization of antigen-presenting cells (APCs) and the recruitment of cytotoxic T cells (19, 20).

Studies have revealed that DNA sensing by STING has a significant function in the immune recognition of tumors, which is crucial to effective cancer immunotherapy (21).

The application of the STING agonist cyclic GMP-AMP (cGAMP) as an immunoadjuvant in cancer is partially limited because it does not penetrate the cell membrane (22). To overcome the limitations of natural cGAMP, rational modifications of cyclic dinucleotides (CDNs) led to the introduction of a newly synthesized CDN called ML RRS2 CDA (MIW815 or ADU-S100), which had improved features such as high stability and lipophilicity and demonstrated stronger antitumor effects in various cancer models (23, 24). It induced effective tumor regression via intratumoral injection in the B16 melanoma, CT-26 colon cancer, and 4T1 breast cancer models (20, 25–30). In addition to mouse STING, this compound is able to activate all known human STING allelic variants. This agonist shows significant potential as a therapeutic agent to promote tumor microenvironment (TME) activation in many tumor types by activating efficient and lasting antitumor $CD8^+$ T cell responses (20).

The TME includes an extracellular matrix and a variety of cells consisting of infiltrating inflammatory cells, endothelial cells, and cancer-associated fibroblasts (CAFs) (31). CAFs form the dominant component of many tumors and promote tumorigenesis and cancer metastasis in several ways, including the production of growth factors, cytokines, and chemokines; the degradation of extracellular matrix (ECM) proteins; the promotion of angiogenesis; and the immunosuppression and prevention of drug penetration (31–35). Recent studies have demonstrated the presence of a heterogeneous population of CAFs in the TME, including tumor-promoting CAFs and tumor-restraining CAFs (34, 35). Different biomarkers such as vimentin (VIM), alpha-smooth muscle actin (α-SMA), fibroblast activation protein (FAP), fibroblast-specific protein 1 (FSP1), and platelet-derived growth factor receptor (PDGFR), have been used to identify CAFs (33, 35).

Myofibroblasts' contractile abilities, led by the expression of α-SMA, which is an isoform of actin, induce a positive feedback loop that amplifies the fibrotic cycle, which in turn results in tumor growth (36). There are different methods for detecting CAFs and their heterogenicity in tissues, which corresponds to their biological functions and subtypes. The CAFs are clustered into three subpopulations, namely antigen-presenting CAFs (apCAFs), myofibroblastic CAFs (myCAFs), and inflammatory CAFs (iCAFs) (37–39). Single-cell RNA-sequencing, multiplex immunostaining, and genetic mouse models have been used for the identification and biological functions of different subtypes of CAFs in pancreatic ductal adenocarcinoma (PDAC), colorectal cancer (CRC), breast cancer, and liver fibrosis progression (40–44).

Although several recent studies have highlighted the importance of combination therapy using STING and TLR agonists in preclinical cancer models (45–48), the relationship between such immunoadjuvants and CAFs as key players in stromal tumorigenesis has not yet been determined. Therefore, in this study, the synergistic effects of STING and TLR9 agonists and the immunological mechanisms underlying tumor regression and CAFs' infiltration of the TME were studied in a preclinical colorectal tumor model. In addition, several important cellular markers of immunity, pro-inflammatory cytokine expression, apoptosis, and pro-tumorigenesis were studied.

Our results suggest that the combination of ADU-S100 and CpG ODN1826 shows synergistic therapeutic effects with enhanced antitumor immune responses and suppressed tumorigenesis markers and, therefore, can be considered a promising target for further cancer immunotherapy investigation.

2 Materials and methods

2.1 Cell line

The CT-26 cell line was purchased from The Research Institute of Biotechnology (Mashhad, Iran) and cultured in Roswell Park Memorial Institute (RPMI) 1640 medium (Gibco®, Grand Island, NE, USA), supplemented with 10% heat-inactivated fetal bovine serum (Gibco), 2 mM L-glutamine (Invitrogen, San Diego, USA), 25 mM β-mercaptoethanol (Merck, Munich, Germany), and 100 IU/mL penicillin/streptomycin (Gibco) at 37°C and in a 5% CO_2 atmosphere.

2.2 Animals

Female BALB/c mice (6–8 weeks old) were obtained from the Royan Institute (Tehran, Iran). All the animals were kept at the animal housing of the Faculty of Veterinary Medicine, Ferdowsi University of Mashhad, Mashhad, Iran. The ***in vivo*** experiments were reviewed, approved, and conducted in accordance with the ethics guidelines of the Animal Care and Use Committee of Ferdowsi University of Mashhad (license number 46013-M).

2.3 *In vivo* tumor model

The CT-26 adenocarcinoma cells (3×10^5) were injected subcutaneously (SC) into the right flank of the mouse in 100 µL of phosphate-buffered saline (PBS). Every other day, the tumor size was measured with a digital caliper for a total of 30 days, and the tumor volume was calculated using the equation 1:

$V = (L \times W^2)/2$ (1)

where the letter "L" represents the large diameter and "W" represents the small diameter of the tumor (49, 50). The mice were divided into five groups ($n = 7$), as depicted in Table 1, and treatment with ADU-S100 (MedChemExpress, South Brunswick Township, NJ, USA) and CpG ODN1826 (InvivoGen, San Diego, CA, USA) was administered intratumorally on days 10 and 16 post tumor inoculation. The mice were euthanized on day 30 post-tumor induction and their body weights were recorded. Subsequently, the tumors were extracted and weighed. After conducting a necropsy of the mice, samples of their tumor, spleen, and liver tissues were taken. The tumor inhibition rate was calculated using the equation 2 (6):

Tumor inhibition rate (%) = [(mean tumor weight of control group − mean tumor weight in treated group)/mean tumor weight of control group] × 100% (2).

The spleen index was calculated using the equation 3 (51):

Spleen index = weight of spleen (mg)/body weight (g). (3)

TABLE 1 Treatment groups used in this study.

Treatment	Dose per mouse
PBS	–
ADU-S100	20 µg
ADU-S100	40 µg
CpG ODN1826	40 µg
ADU-S100 + CpG ODN1826	20 µg + 20 µg

PBS, phosphate-buffered saline.

2.4 RNA extraction and quantitative real-time polymerase chain reaction analysis

Total RNA was extracted from the spleen and tumor tissues using a total RNA isolation kit (DENAzist Asia, Mashhad, Iran). The extracted total RNA was subjected to 1U of DNase I (RNase free) (Thermo Scientific Fisher, Waltham, MA, USA) at 37°C for 15 **min**. The inactivation of the DNase was conducted by adding 1 µL of 50 mM ethylenediaminetetraacetic acid (EDTA) (Merck). Moloney murine leukemia virus (M-MLV) reverse transcriptase (Thermo Fisher Scientific) was used to convert RNA samples to cDNA. The quantitative real-time polymerase chain reactions (qRT-PCR) were carried out using RealQ Plus 2x Master Mix Green (Ampliqon A/S, Odense, Denmark) in a Rotor-Gene® Q real-time PCR cycler (QIAGEN, Hilden, Germany). The amplification steps were as follows: 15 **min** at 95°C (1 cycle), followed by 30 s at 95°C, 30 s at 58°C–62°C, and 25 s at 72°C (35–40 cycles). Three replicates were considered for qRT-PCR readout. The β-actin gene served as the internal control. Table 2 gene-specific primers and their accession numbers used in this study.

2.5 Hematoxylin and eosin staining

The samples obtained from the tumor, liver, and spleen tissues were fixed in 10% neutral buffered formalin (Merck) for 24 **h**. The 4-µm-thick sections of the tissue samples were stained with hematoxylin and eosin (H&E) (Merck), mounted on the slide, and finally, examined under a light microscope (Labomed Inc., Los Angeles, CA, USA). The mitotic cells were counted in 10 fields of the tumor slides, and, subsequently, the mean number of mitotic cells was calculated.

2.6 Immunohistochemical staining of tumor tissues

Sections of formalin-fixed paraffin-embedded tumor tissues were prepared. The sections were deparaffinized and rehydrated, and the retrieval of antigens was carried out using Tris-ethylenediaminetetraacetic acid (EDTA) buffer (10 mM Tris base, 1 mM EDTA solution, 0.05% Tween 20, pH 9.0) (Merck) for 20 min at 98°C. Subsequently, the slides were quenched using 0.3% [volume to volume (v/v)] methanol-diluted hydrogen peroxide (Merck). The sections were incubated for 30 min with different concentrations of primary antibodies, e.g., anti-CD8-α (1 out of 200) (cat. number sc-

TABLE 2 Gene-specific primer sequences used in the qRT-PCR analysis.

Gene	Primer sequence	Product (bp)	Annealing temperature (°C)	Accession number
β-actin	5′–TTCGCCATGGATGACGATATC–3′ 3′–GGCCTCGTCACCCACATAG–5′	180	58 60	NM_007393.5
IFN-β	5′–GATGAACTCCACCAGCAGACA–3′ 3′–CACCATCCAGGCGTAGCTG–5′	168	60 60	NM_010510.1
IFN-γ	5′–CTGCGGCCTAGCTCTGAGAC–3′ 3′–CTGGCTCTGCAGGATTTTCATG–5′	228	62 60	NM_008337.4
TNF-α	5′–GCCACCACGCTCTTCTGTCTA–3′ 3′–GAGGGTCTGGGCCATAGAAC–5′	105	62 60	NM_001278601.1
IL-12	5′–GTTGGAAGCACGGCAGCAG–3′ 3′–AGGGAGAAGTAGGAATGGGGAG–5′	177	62 60	NM_001303244.1
IL-6	5′–GGATACCACTCCCAACAGACC–3′ 3′–GTTTTCTGCAAGTGCATCATCG–5′	148	60 59	NM_001314054.1

IFN-β, interferon beta; IFN-γ, interferon-gamma; TNF-α, tumor necrosis factor alpha; IL-12, interleukin 12; IL-6, interleukin 6; qRT-PCR, quantitative real-time polymerase chain reaction.

7970; RRID: AB_627208; Santa Cruz Biotechnology, Dallas, TX, USA), anti-cleaved caspase 3 (1 out of 300) (cat. number 9661; RRID: AB_2341188; Cell Signaling Technology, Danvers, MA, USA), anti-vimentin (1 out of 400) (cat. number 5741; RRID: AB_10695459; Cell Signaling Technology), anti-CD45 (1 out of 3,200) (cat. number sc-53665, RRID: AB_629093; Santa Cruz Biotechnology), and anti-α-SMA (1 out of 500) (cat. number 65001, RRID: AB_2920672; Progen, Heidelberg, Germany). After washing with Tris-buffered saline (TBS) (0.5M Tris base, 9% NaCl, pH 8.4) (Merck), the slides were incubated with secondary antibodies in accordance with the protocol. Images of the stained slides were obtained using a light microscope from 10 different fields of high-power fields (×400 overall magnification) and then analyzed using QuPath software (RRID: SCR_018257). The caspase-3 labeling index was calculated using the following equation (52):

Caspase-3 labeling index = (number of activated caspase-3-positive cells × 100)/total number of nuclei. (4)

2.7 Measurements of hematological parameters

Before the animals were euthanized on day 30, whole blood was immediately collected from the hearts of the mice in a tube containing an anticoagulant. A complete blood count (CBC) analysis was performed using a cell counter (Nihon Kohden, Nima Pouyesh Teb, Iran).

2.8 MTT test

The CT26 cells were seeded in 96-well culture plates at 7×10^3 cells per well. The cells were incubated with different concentrations of ADU-S100, CpG ODN (10 μg/mL, 20 μg/mL, 40 μg/mL, and 60 μg/mL), or ADU-S100 (20 μg/mL) + CpG ODN (20 μg/mL) at 37°C for 24 h. The cells were further incubated with 10 μL per well of 3-(4,5-dimethylthiazol-2-yl)-2,5-diphenyl-2H-tetrazolium bromide (MTT) (5 mg/mL; Sigma, USA) for 3 h. Subsequently, the medium was removed and 100 μL per well of dimethyl sulfoxide (DMSO) was added. The absorbance was measured at 490 nm. The experiment was conducted in triplicate ($n = 3$).

2.9 Statistical analysis

Statistical analysis was conducted using GraphPad Prism software version 9.0 (RRID: SCR_002798; GraphPad Software Inc., San Diego, CA, USA). One-way analysis of variance and Mann–Whitney U–tests were used to analyze the data. The results are shown as mean ± SD and a p-value ≤ 0.05 is considered to be statistically significant. The relative expression software tool version 2.0.13 (REST 2009; RRID: SCR_023755) was used to analyze the qRT-PCR results by way of a pairwise fixed reallocation randomization test. Significant differences among the groups were indicated as $^{****}p \leq 0.0001$, $^{***}p \leq 0.001$, $^{**}p \leq 0.01$, and $^{*}p \leq 0.05$.

3 Results

3.1 Inhibition of tumor growth and increased survival rate of colon adenocarcinoma-bearing mice by single or combination therapy with CpG ODN1826 and ADU-S100

ADU-S100 is a STING agonist with a potent antitumor effect that has been validated in several preclinical tumor models. We hypothesized that the combination of ADU-S100 and CpG ODN 1826 at a reduced (i.e., 50% lower) concentration, compared with a single form of the agonist, would have an additive and robust anticancer effect in suppressing the tumor growth in a CT-26 colon cancer model. The cytotoxic effects of a single, or a combination of, agonist(s) were evaluated using an MTT assay. ADU-S100 and CpG ODN1826, alone or in combination, did not show any adverse

effects on the viability of CT-26 cells *in vitro* (Figure S1). The injection of a CT-26 cell suspension was administered subcutaneously into the right flanks of the mice. When palpable tumors appeared, mice were treated with intratumoral injections of PBS, ADU-S100 (20 μg and 40 μg), CpG ODN1826 (40 μg), or a combination of ADU-S100 (20 μg) and CpG ODN1826 (20 μg). Every other day, tumor volumes and mouse weights were recorded. To evaluate the immunological mechanisms underlying tumor regression, in a second experiment, all mice were euthanized on day 30 post tumor inoculation (Figure 1A). The standard survival curve (Kaplan–Meier), which describes the direct effects of treatment on tumor growth, showed that both single and combination therapy were able to prolong the survival rate of tumor-bearing mice. Notably, the combination treatment eradicated all CT-26 tumors. Specifically, the combination treatment group exhibited a higher survival rate (100%) than the single treatment groups treated with ADU-S100 (40 μg) (86%), CpG ODN (40 μg) (71%), and ADU-S100 (20 μg) (43%) (Figure 1B). Figures 1C, D illustrate how the tumor volume in all treatment groups was significantly reduced in comparison to the control group. The combination group [ADU-S100 (20 μg) + CpG ODN (20 μg)] showed the highest growth inhibition, from 1,952 mm^3 to 32 mm^3, and was therefore more effective than a single injection of each compound. In addition, in the ADU-S100 (40 μg) group, the tumor regression size reached 44.8 mm^3 and 144 mm^3 in the CpG ODN (40 μg) treatment group. These results indicate that the antitumor effects of ADU-S100 when combined with CpG ODN are approximately equal to those of monotherapy with ADU-S100 when administered at higher doses (i.e., at twice the concentration). The average tumor weight was significantly reduced from 2.09 g in the control group to 0.08 g and 0.1 g in the combination and the ADU-S100 (40 μg) groups, respectively (Figure 1E). The curve of

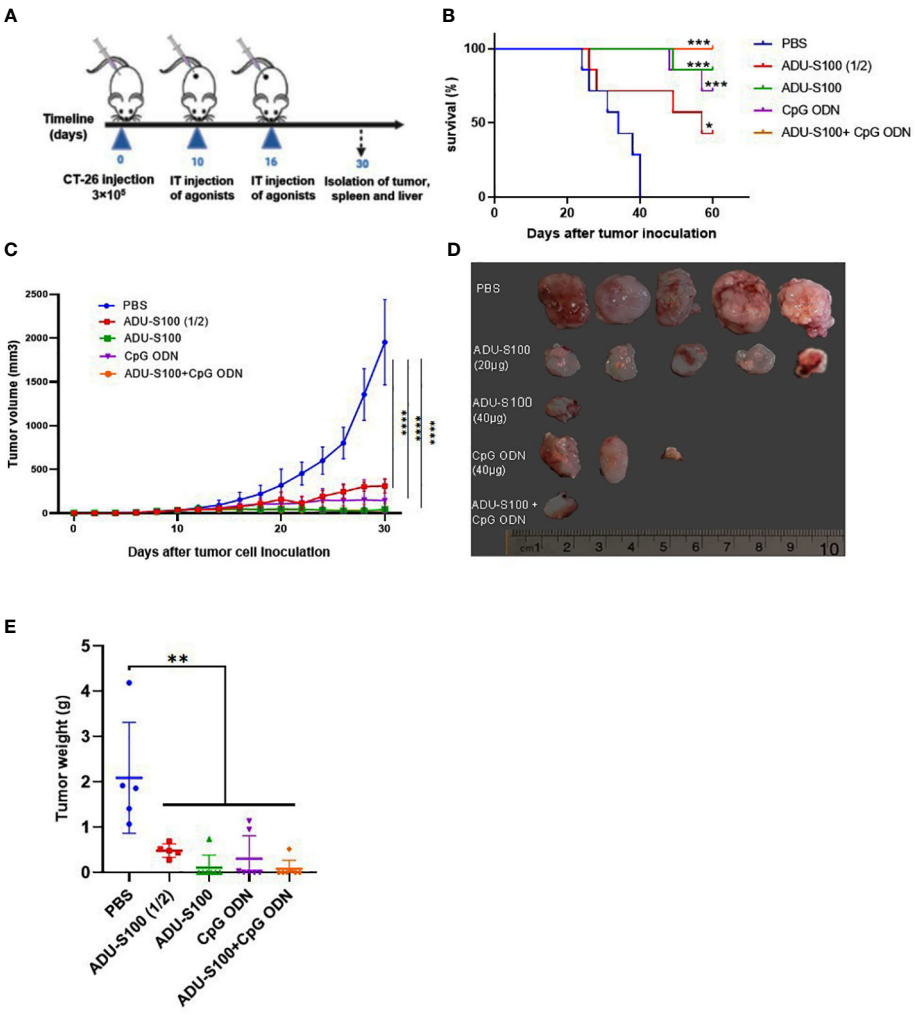

FIGURE 1
Intratumoral (IT) administration of ADU-S100 and CpG ODN1826 reduces tumor volume in the CT-26 adenocarcinoma model. **(A)** Mice were injected subcutaneously with 3 × 10^5 CT-26 cells (in 100 μL of PBS) on day 0. On days 10 and 16, mice were given IT injections of PBS, ADU-S100 (20 μg or 40 μg), CpG ODN (40 μg), ADU-S100 (20 μg) + CpG ODN (20 μg) (n = 7). **(B)** Kaplan–Meier survival curve of the animals. **(C)** Tumor volumes were monitored every other day for 30 days. **(D)** Photographs of dissected tumor tissues from treated mice on day 30 of treatment. **(E)** Average tumor weight in different treatment groups at the end of the experiment. Data are presented as mean ± SD. Significant differences in the survival plot were measured using a weighted log-rank test. Other data were analyzed using one-way ANOVA and Mann–Whitney tests. Statistically significant differences are indicated as ****$p \leq 0.0001$, ***$p \leq 0.001$, **$p \leq 0.01$, and *$p \leq 0.05$. PBS, phosphate-buffered saline.

the tumor inhibition rate is displayed in Figure S2A. The results show that ADU-S100 exhibited powerful antitumor activity that is dose-dependent, meaning that ADU-S100 at 20 μg suppressed CT-26 tumor growth by 77% on day 30, whereas for the 40-μg dose, the tumor inhibition rate was 95%. Furthermore, the combination of ADU-S100 and CpG ODN1826 showed the highest tumor inhibition rate (96%), whereas in the CpG ODN (40-μg) group, the tumor inhibitory rate was decreased to 85%. In the second *in vivo* experiment, on day 30 post-tumor inoculation, mice were sacrificed, and their spleens and tumors were removed and weighed for further immunological analysis. Owing to the importance of the spleen as an extramedullary hematopoietic tissue that produces immunosuppressive myeloid cells in tumor-bearing mice (53), we measured the spleen index (mg/g) in this study. The curve of the spleen index is presented in Figure S2B and shows that the spleen index was positively correlated with tumor weight. Furthermore, during the immunotherapy period, the body weight of the mice was recorded, and no considerable weight change was observed compared with the control group (Figure S2C). Overall, these data suggest that either the ADU-S100 treatment or the combination treatment had a profound inhibitory effect on the tumor growth progression, but that the combination of ADU-S100 (20 μg) + CpG ODN (20 μg) at a reduced concentration (i.e., 50% lower) was able to effectively control tumor growth and significantly prolong the survival of CT-26 tumor-bearing mice.

3.2 Upregulation of pro-inflammatory cytokine expression in tumor tissues

The induction of pro-inflammatory cytokine expression by CpG ODNs and CDNs has already been reported (46, 54). To determine whether ADU-S100 and CpG ODN1826 could induce effective immune responses and generate antitumor immunity, we evaluated the expression of several key pro-inflammatory cytokines (e.g., IFN-β, IFN-γ, TNF-α, IL-12, and IL-6) using qRT-PCR analysis. We observed that in tumor tissues, the combination treatment [ADU-S100 (20 μg) + CpG ODN (20 μg)] upregulated the expression level of IFN-β, IL-12, and TNF-α in a synergistic manner compared with the other treatments (Figures 2A–E). All treatment groups displayed a significant upregulation of IFN-β expression compared with the control group ($p \leq 0.05$) (Figure 2A). The expression level of IFN-γ, as one of the most potent cytokine hallmarks of antitumor immunity, was significantly upregulated in the combination [ADU-S100 (20 μg) + CpG ODN (20 μg)] and CpG ODN groups compared with the control group ($p \leq 0.05$)

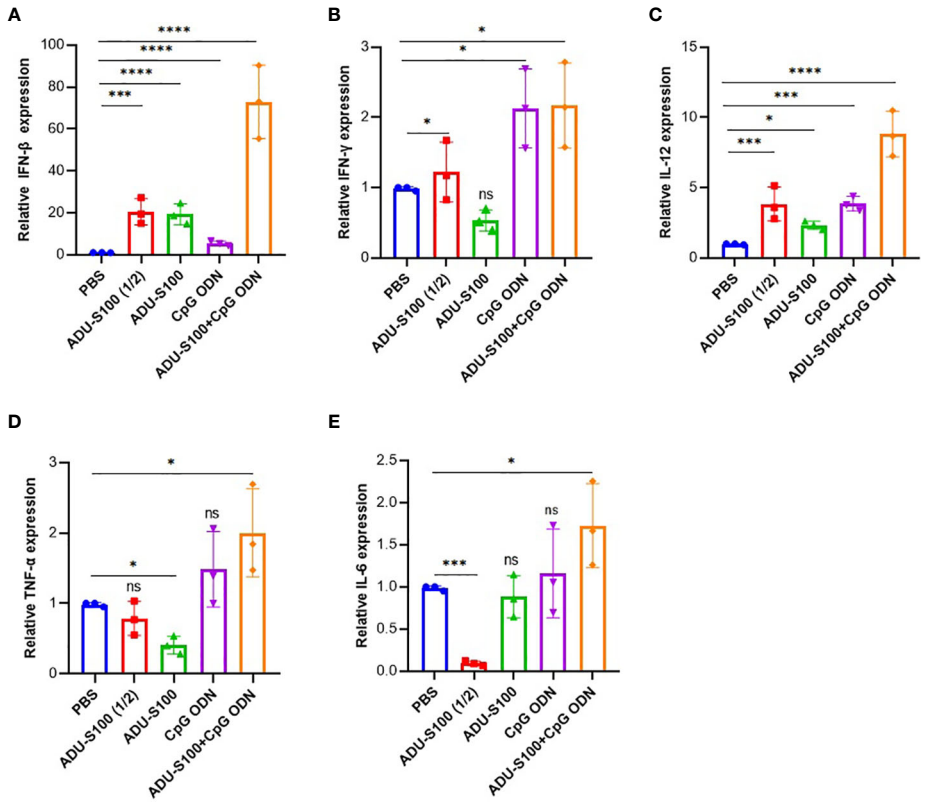

FIGURE 2
Expression profile of pro-inflammatory cytokines in the tumor. Quantitative real-time polymerase chain reaction (qRT-PCR) analysis of **(A)** IFN-β, **(B)** IFN-γ, **(C)** TNF-α, **(D)** IL-12, and **(E)** IL-6 in tumor tissues of treated mice on day 30 post tumor inoculation (n = 3 independent experiments). The transcripts for each gene were quantified relative to β-actin expression levels in each group. Data are presented as mean ± SD. Data were analyzed using REST software and statistically significant differences are indicated as ****$p \leq 0.0001$, ***$p \leq 0.001$, and *$p \leq 0.05$. IFN-β, interferon beta; IFN-γ, interferon-gamma; IL-12, interleukin 12; IL-6, interleukin 6; qRT-PCR, quantitative real-time polymerase chain reaction; TNF-α, tumor necrosis factor-alpha.

(Figure 2B). In our experiment, IL-12 expression was significantly upregulated in all treatment groups compared with the control group ($p \leq 0.05$) (Figure 2C). In addition to the combination group, which showed the highest level of expression of TNF-α and IL-6 compared with the control group, the CpG ODN group also showed increased expression of these cytokines compared with the control group, although the difference was not significant (Figures 2D, E). These results demonstrated that immunoadjuvant therapy with ADU-S100 and CpG ODN promotes the robust and synergistic expression of several important pro-inflammatory and immune-effector cytokines in CT-26 tumor tissues.

3.3 Upregulation of pro-inflammatory cytokine expression in the spleen

The spleen is the largest lymphoid organ in the body and contains many immune cells with a crucial role in immune response. In addition to the tumor, we measured the expression profile of pro-inflammatory cytokines (IFN-γ, IFN-β, TNF-α, IL-12, and IL-6) in the spleen tissue as the main secondary host lymphoid compartment (Figure 3). In the spleen, the highest level of expression of IFN-β and IL-6 was observed in the combination group [ADU-S100 (20 μg) + CpG ODN (20 μg)], which was increased compared with the control group (Figures 3A, E). The group treated with CpG ODN displayed the highest level of expression of IFN-γ and IL-12 compared with the control group ($p \leq 0.05$) (Figures 3B, C). The highest level of TNF-α expression was observed in the ADU-S100 (20 μg) group, which displayed a larger tumor size than the other treatment groups (Figure 3D).

3.4 Immunohistochemical and histological analysis of tumor tissues showed typical features of apoptosis and inflammation after immunotherapy

To explore the primary effects of immunoadjuvants in tumor tissue, H&E staining was performed. The tumor cells were characterized by scarce eosinophilic cytoplasm with a round, polygonal, spindle-like polymorphic nucleus of variable size. They contained one or more nuclei, within a scarce stroma (Figure 4). The tumor tissues of all mice treated with ADU-S100 (20 μg and 40 μg), CpG ODN (40 μg), and combination groups [ADU-S100 (20

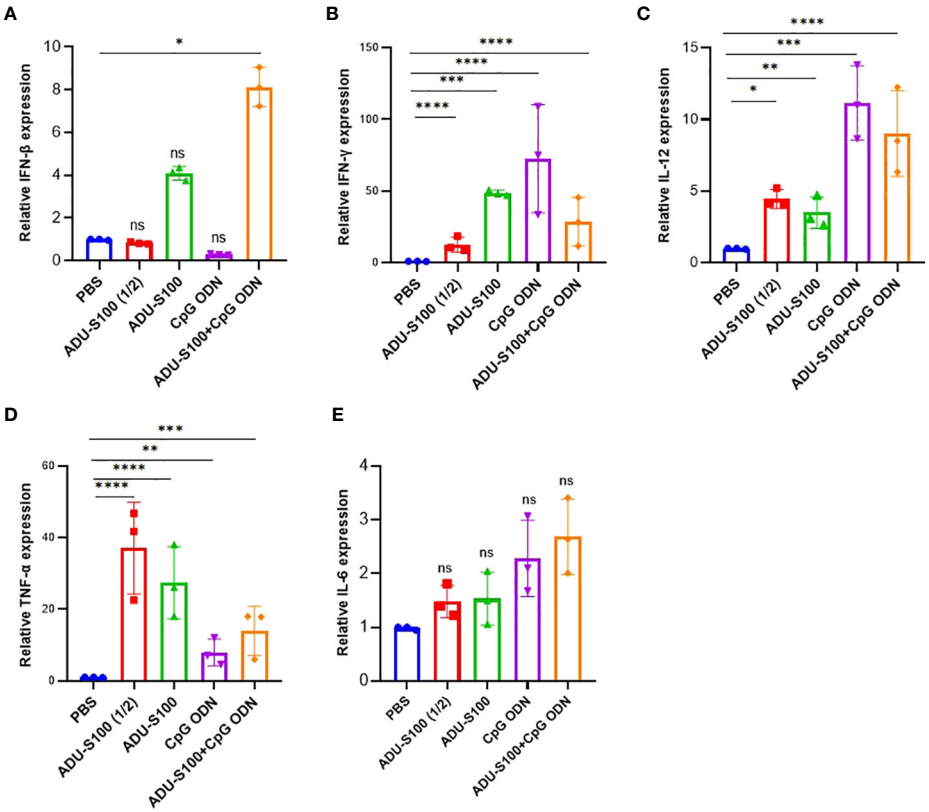

FIGURE 3
Expression profile of pro-inflammatory cytokines in the spleen. We conducted qRT-PCR analysis of **(A)** IFN-β, **(B)** IFN-γ, **(C)** TNF-α, **(D)** IL-12, and **(E)** IL-6 in the spleen tissues of treated mice on day 30 post-tumor inoculation (n = 3 independent experiments). The expression levels were quantified relative to β-actin as a reference gene. Data are presented as mean ± SD. Data were analyzed by REST software and statistically significant differences are indicated as $^{****}p \leq 0.0001$, $^{***}p \leq 0.001$, $^{**}p \leq 0.01$, and $^{*}p \leq 0.05$. IFN-β, interferon beta; IFN-γ, interferon-gamma; IL-12, interleukin 12; IL-6, interleukin 6; qRT-PCR, quantitative real-time polymerase chain reaction; REST, relative software expression tool; TNF-α, tumor necrosis factor-alpha.

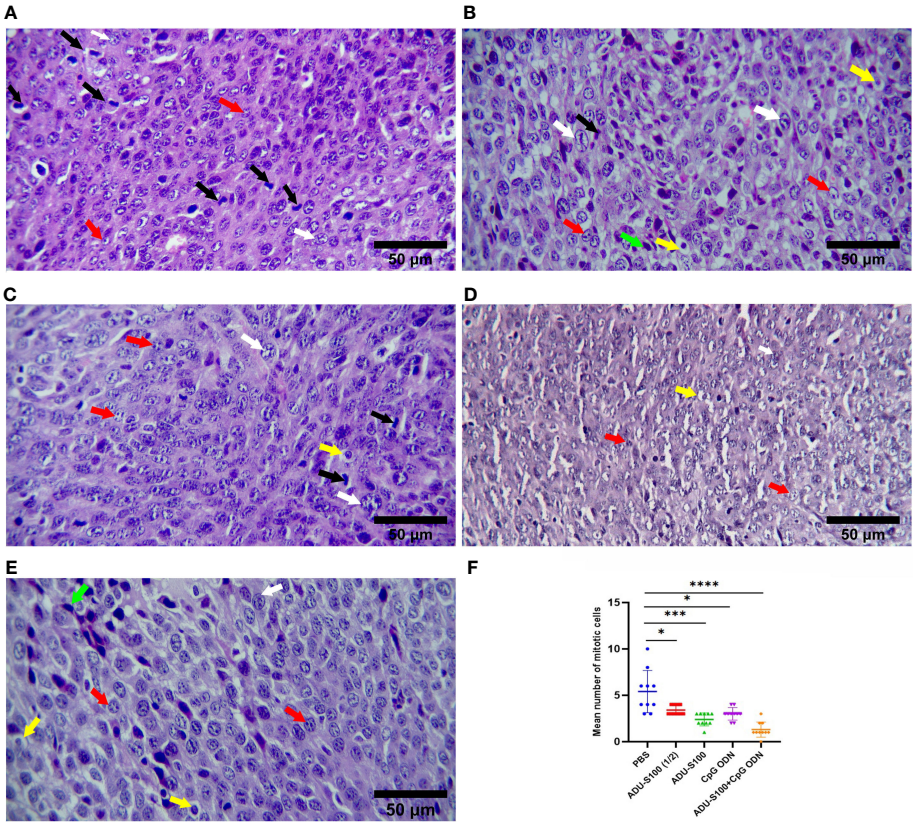

FIGURE 4
Microphotographs of tumor tissues in the **(A)** control, **(B)** ADU-S100 (20 µg), **(C)** ADU-S100 (40 µg), **(D)** CpG ODN (40 µg), and **(E)** ADU-S100 (20 µg) + CpG ODN (20 µg) groups. Scale bars = 50 µm. (**A–E**, H&E staining, ×400 magnification). Tumor cells undergoing mitosis (black arrows), apoptotic tumor cells (yellow arrows), pleomorphism of the tumor cells (white arrows), tumor cells with one or more nucleoli (red arrows), and mononuclear inflammatory cells infiltrating into the tumor tissue (lymphocytes, green arrows) are shown. **(F)** The mean number of mitotic cells in the tumor tissues (n = 3). Statistically significant differences were analyzed using Mann–Whitney tests and indicated as ****$p \leq 0.0001$, ***$p \leq 0.001$, and *$p \leq 0.05$. H&E, hematoxylin, and eosin.

µg) + CpG ODN (20 µg)], showed typical features of apoptosis and inflammation, indicating the effectiveness of the treatment in tumor clearance (Figures 4B–E). The number of mitotic cells in the control group was significantly increased compared with those in the treatment groups (Figure 4F). In addition, features of malignancy, such as hemorrhage and necrosis, were observed in the control group (Figure S3A). However, no tumor malignancies were observed in the treatment groups (Figures S3B–E).

Histopathological analysis of the liver and spleen was performed using H&E staining to assess the probability of tumor metastasis and toxicity linked to the treatment. The microstructure of the spleen in the control and all treatment groups was normal with no histological changes. The liver tissue displayed metastasis in control mice (Figures 5A, B), but treatment groups were normal (Figures 5C–F). To confirm that the necrotic cells observed in H&E-stained sections were apoptotic, cleaved caspase-3 expression was detected in the tumor tissues using immunohistochemistry (IHC). The results showed a remarkable and highly significant increase of cleaved caspase-3 as the main apoptotic marker in the combination group [ADU-S100 (20 µg) + CpG ODN (20 µg)]. Furthermore, we observed a significant caspase-3 increase in the single-agonist treatment groups compared with the control group (Figure 6).

3.5 Immunohistochemical analysis showed the abundant infiltration of tumor tissues by CD45$^+$ and CD8$^+$ cells after immunotherapy

To assess how ADU-S100 and CpG ODN1826 eradicated tumor growth and increased mice survival rate, immune cell infiltration of the tumor tissues was performed using IHC. CD45, as the most important marker of all nucleated hematopoietic cells (except platelets and erythrocytes), was used to sort the immune cells by IHC. The results showed that in all treatment groups, the level of CD45 expression was significantly increased compared with that of the control group ($p \leq 0.05$). However, the most abundant expression of this biomarker was observed in the combination group represented (Figure 7). Furthermore, due to the crucial role of CD8$^+$ T cells in antitumor activity, the expression of this cellular marker was determined using IHC, which exhibited a significant upregulation in the recruitment of CD8$^+$ cells in tumor tissues in all treatment groups. The greatest increase in recruitment was observed in the combination group [ADU-S100 (20 µg) + CpG ODN (20 µg], compared with the control group ($p \leq 0.05$), followed by the CpG ODN (40 µg), ADU-S100 (20 µg), and ADU-S100 (40 µg) groups, respectively (Figure 8). These results were

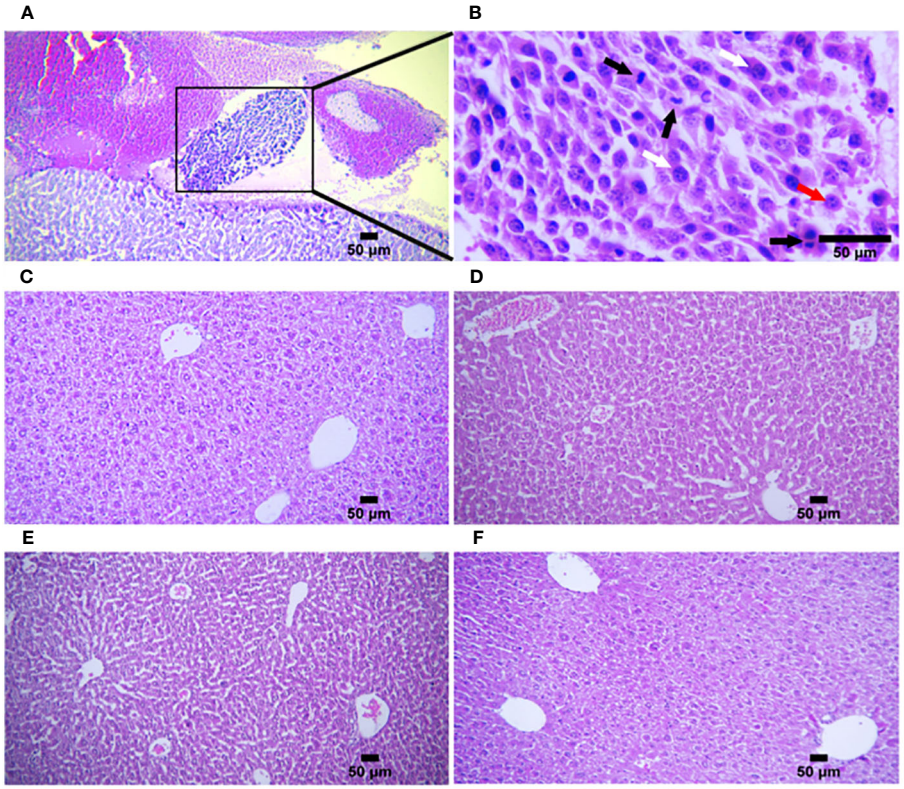

FIGURE 5
Histologic structures of liver tissues in the control and treatment groups. **(A)** Liver metastasis was observed in only one mouse in the control group (n = 5) (H&E staining, ×100 magnification). **(B)** Higher magnification of **(A)** In the metastatic tumor tissue, pleomorphic tumor cells (white arrows) have a vesicular nucleus containing one or more nucleoli (red arrow) with several mitotic figures (black arrows) (H&E staining, ×400 magnification). Liver tissues from **(C)** ADU-S100 (20 µg), **(D)** ADU-S100 (40 µg), **(E)** CpG ODN (40 µg), and **(F)** ADU-S100 (20 µg) + CpG ODN (20 µg) groups show normal structure without metastasis (n = 5 for ADU-S100 (20 µg) and n = 7 for other treatment groups). Scale bars = 50 µm. (C–F, H&E staining, ×100 magnification). H&E, hematoxylin, and eosin.

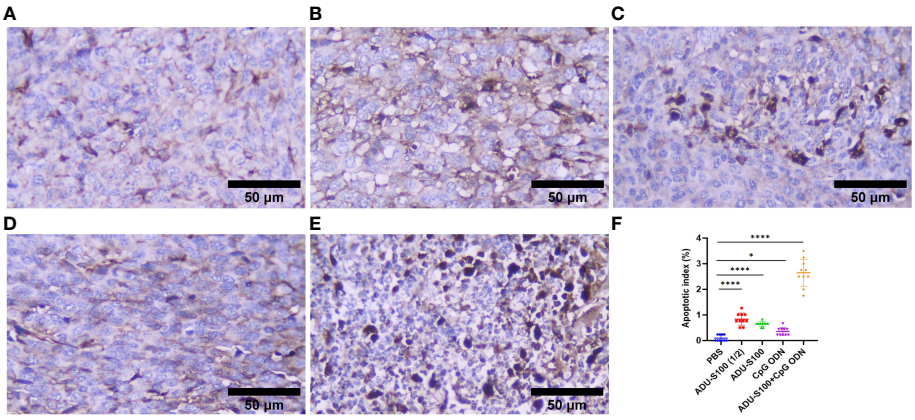

FIGURE 6
Cleaved caspase-3 expression obtained using IHC in tumor tissues. **(A)** PBS, **(B)** ADU-S100 (20 µg), **(C)** ADU-S100 (40 µg), **(D)** CpG ODN (40 µg), **(E)** ADU-S100 (20 µg) + CpG ODN (20 µg), and **(F)** quantitative analysis of the apoptotic index (n = 3). Data are presented as mean ± SD. Statistically significant differences were analyzed using Mann–Whitney tests and indicated as ****$p \leq 0.0001$ and *$p \leq 0.05$. Scale bars = 50 µm. IHC, immunohistochemistry; PBS, phosphate-buffered saline.

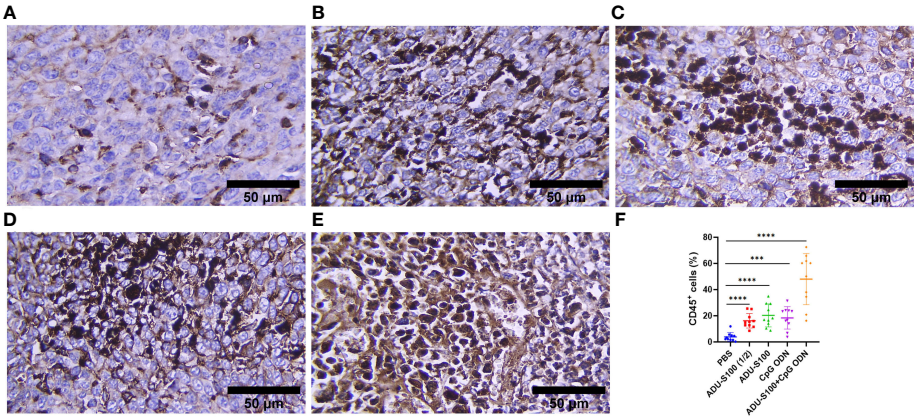

FIGURE 7
CD45 expression analyzed using IHC in tumor tissues. **(A)** PBS, **(B)** ADU-S100 (20 µg), **(C)** ADU-S100 (40 µg), **(D)** CpG ODN (40 µg), **(E)** ADU-S100 (20 µg) + CpG ODN (20 µg), and **(F)** quantitative analysis of $CD45^+$ cells (n = 3). Data are presented as mean ± SD. Statistically significant differences were analyzed using Mann–Whitney tests and indicated as ****$p \leq 0.0001$ and ***$p \leq 0.001$. Scale bars = 50 µm. IHC, immunohistochemistry; PBS, phosphate-buffered saline.

consistent with a CBC analysis that showed that the number of lymphocytes in the combination group was significantly increased compared with the control group ($p \leq 0.05$). In addition, in the CpG ODN (40 µg) and ADU-S100 (20 µg) groups, the level of total blood lymphocytes exhibited a greater than twofold increase compared with the control group (Figure S4).

3.6 Synergistic effect of ADU-S100 and CpG ODN in the suppression of CAFs' infiltration of tumor tissues

CAFs, as the most important stromal cells in the TME, contribute to tumor growth and metastasis through the production of growth factors and cytokines (31). To address the effects of ADU-S100 and CpG ODN on CAF abundance, the expression of α-SMA and VIM were assessed in the formalin-fixed paraffin-embedded tumor tissues using IHC (Figures 9, 10). The results indicated that the expression of these CAF biomarkers was significantly reduced in all treatment groups in comparison to the control group. This reduced expression of α-SMA and VIM was highly significant in the combination group [ADU-S100 (20 µg) + CpG ODN (20 µg)] compared with the other treatment groups. Therefore, the combined effect of the two agonists was remarkably effective in increasing tumor eradication and inhibiting the infiltration of the TME by tumor-supporting cells.

4 Discussion

Despite the recent advances and progress made in our understanding of cancer immunotherapy, the field still faces

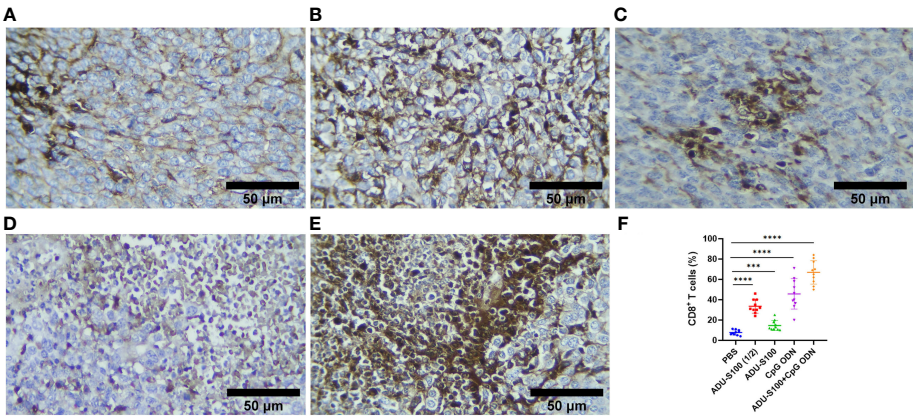

FIGURE 8
CD8 expression analyzed using IHC in tumor tissues. **(A)** PBS, **(B)** ADU-S100 (20 µg), **(C)** ADU-S100 (40 µg), **(D)** CpG ODN (40 µg), **(E)** ADU-S100 (20 µg) + CpG ODN (20 µg), and **(F)** quantitative analysis of $CD8^+$ T cells (n = 3). Data are presented as mean ± SD. Statistically significant differences were analyzed using Mann–Whitney tests and indicated as ****$p \leq 0.0001$ and ***$p \leq 0.001$. Scale bars = 50 µm. IHC, immunohistochemistry; PBS, phosphate-buffered saline.

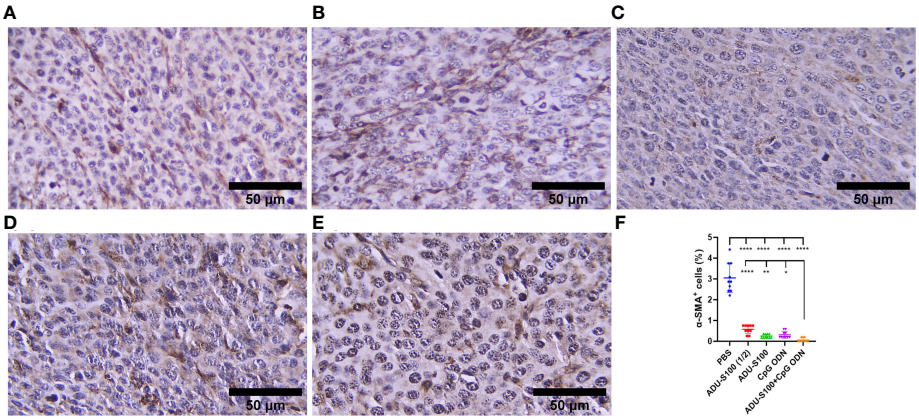

FIGURE 9
α-SMA expression analyzed by IHC in tumor tissues. **(A)** PBS, **(B)** ADU-S100 (20 µg), **(C)** ADU-S100 (40 µg), **(D)** CpG ODN (40 µg), **(E)** ADU-S100 (20 µg) + CpG ODN (20 µg), and **(F)** quantitative analysis of α-SMA$^+$ cells (n = 3). Data are presented as mean ± SD. Statistically significant differences were analyzed using Mann–Whitney tests and indicated as ****$p \leq 0.0001$, **$p \leq 0.01$ and *$p \leq 0.05$. Scale bars = 50 µm. IHC, immunohistochemistry; PBS, phosphate-buffered saline.

many challenges. Preclinical tumor models, the TME, and their expressed and secreted molecules are considered essential components to better understanding anticancer targeted therapy. This study revealed the immunotherapeutic effects of powerful innate immunity agonists in a mouse model of colon cancer. Tumor-bearing mice were treated intratumorally on days 10 and 16 post-tumor inoculation with ADU-S100, as a STING agonist, and CpG ODN1826, as a TLR9 agonist; both of these are powerful, safe, and effective immunoadjuvants with clinically translational potential. Several mechanistic studies, including on cytokine profiles, immune cells, and CAFs' infiltration of the TME, were performed to investigate the immunological mechanisms of tumor eradication and the extended survival rate after treatment. The results revealed the powerful antitumor activity of combination treatment even with a reduced (i.e., 50% lower) dose of each agonist and the upregulation of pro-inflammatory cytokine expression and recruitment and infiltration of the TME by immune cells. A remarkable finding of this study was that the level of CAFs in the TME was significantly reduced after immunotherapy with STING and TLR9 agonists.

CT-26 is a non-inflamed and cold tumor of the gastrointestinal tract exhibiting low levels of cytokine expression and a lack of immune cell infiltration (55). The underlying mechanism, according to our data, is that ADU-S100 combined with CpG ODN initiates local inflammation in the CT-26 tumor, which subsequently establishes systemic immune responses, for example, cellular immunity as observed in the TME and spleen. This result is consistent with previous findings that STING and TLR9 agonists promote robust antitumor inflammatory responses (8, 45–47). This revealed the promising outcomes of combination therapy in extending survival rate, inhibiting tumor growth, and suppressing tumorigenesis, accompanied by a stronger inflammatory state within the tumor

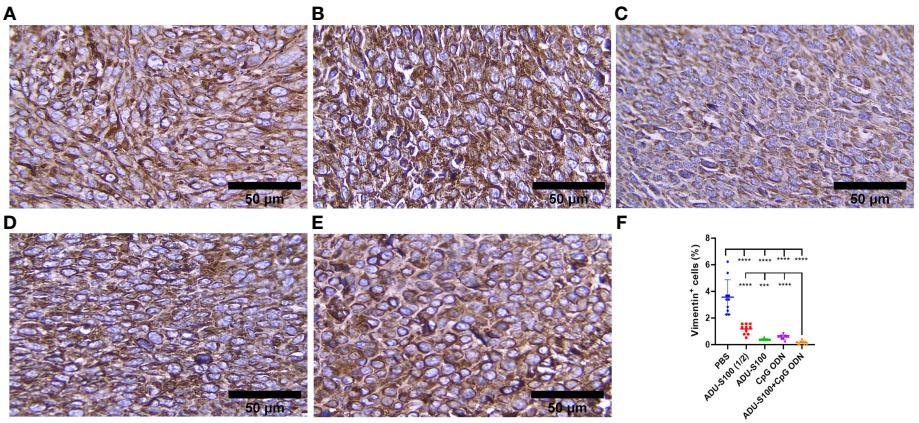

FIGURE 10
Vimentin expression analyzed by IHC in tumor tissues. **(A)** PBS, **(B)** ADU-S100 (20 µg), **(C)** ADU-S100 (40 µg), **(D)** CpG ODN (40 µg), **(E)** ADU-S100 (20 µg) + CpG ODN (20 µg), and **(F)** quantitative analysis of vimentin$^+$ cells (n = 3). Data are presented as mean ± SD. Statistically significant differences were analyzed using Mann–Whitney tests and indicated as ****$p \leq 0.0001$ and ***$p \leq 0.001$. Scale bars = 50 µm. IHC, immunohistochemistry; PBS, phosphate-buffered saline.

and spleen due to the increased expression of pro-inflammatory cytokines, which play a key role during the initial inflammation and the transition to T cell-mediated immune responses.

In this study, for the first time, we present evidence of biomarkers of tumor progression inhibition in CT-26 colon carcinoma following immunoadjuvant therapy. To our knowledge, although several preclinical studies have investigated the efficiency and immunological mechanisms of innate immunoadjuvant therapy in preclinical colon carcinoma models (56–58), the effect of such treatment on CAFs' infiltration of the TME has not been reported.

CAFs, as the key component of tumor stroma, play a significant role in many features of tumor biology, such as collagen deposition, tumor development, and immunosuppression (39).

CAFs are abundant in colorectal cancer and, within CT-26 tumors, constitute 25% of all live cells (55). CAFs, as important components of the TME, are associated with poor prognosis and therapeutic resistance (59).

Considering the upregulation of immune cell infiltration, cytokine production, and robust antitumor responses obtained by the combination of ADU-S100 and CpG ODN1826, we observed the downregulation of α-SMA and VIM as the main biomarkers of CAFs and predictive markers of cancer progression (Figures 9, 10), suggesting that immunoadjuvant therapy employing STING and TLR9 agonists in single or combination forms suppresses the tumorigenesis potential of CAFs in the colon carcinoma model. Although there are alternative methods for detecting CAFs, α-SMA, as the most studied marker, is used for determining the heterogenicity and phenotype of CAFs in tumor types (35, 60). In this study, we observed that tumor growth inhibition is directly related to α-SMA and VIM expression. The combination of ADU-S100 and CpG ODN1826 exhibited the greatest downregulation of these markers, which was accompanied by the highest tumor inhibition rate (96%) in comparison to a single form of agonist (Figure S2A and Figures 9 , 10).

The significant decrease in the levels of CAFs in all treatment groups is probably due to the activation of the STING signaling pathway, as Kabashima et al. demonstrated that in pancreatic ductal adenocarcinoma tissues, the activation of the cyclic GMP-AMP synthase (cGAS)–STING pathway led to an increase in the markers of tumor-suppressing CAFs and the infiltration of tumor tissues by immune cells (34). The intravenous injection of a chemically modified STING agonist (diABZI) in an established CT-26 tumor model abolished 98% of the CD140b$^+$ CAFs in the tumor stroma (55). Consistent with these data and our findings, the assumption relies on the interplay between the activation of the STING and TLR9 pathways and direct killing effects on CAFs in the TME. However, the underlying mechanisms of these findings have yet to be identified.

IL-6, as a cytokine produced by CAFs (39), demonstrated contrasting effects in our study. While monotherapy with ADU-S100 (20 μg) led to the downregulation of IL-6 compared with the control group, in the combination group the expression of IL-6 was significantly upregulated compared with the control group. This may be due to the direct effect of STING pathway activation on the inhibition of CAFs in the TME in monotherapy treatment, as in combination with CpG ODN1826, we found that IL-6 simultaneously diminished the abundance of CAFs and participated in the activation and proliferation of lymphocytes, as suggested in previous studies (6, 39, 61).

Type I and type II IFNs play a critical role in both innate and adaptive immunity and are essential for antitumor immune responses (62). The STING and TLR9 signaling pathways led to the production of type I IFNs in the TME (63, 64). Type I IFNs stimulate the apoptosis of tumor cells and prevent tumor cell proliferation and metastasis. The robust upregulation of IFN-β expression in the tumor and spleen tissue, along with the increased infiltration of CD8$^+$ cells and reduced tumor cell mitosis observed in our study, was mainly due to the synergetic effect of STING and TLR9 agonists when administered in combination forms (Figures 2A, 3A, 4F, 8). Type I IFNs enhance the accumulation of DCs in the TME and promote their maturation and migration into lymph nodes for activation of CD8$^+$ T cells (65). In contrast to the spleen, in tumor tissues, the combined effects of STING and TLR9 agonists resulted in an approximately 70-fold increase in IFN-β expression compared with the control group, which is a remarkable finding and indicates the pro-inflammatory status in the TME (Figures 2A, 3A).

The basal expression of type-I IFN by DCs resulted in the secretion of IFN-γ (6). Alternatively, activated T lymphocytes, as a result of the type I interferon signaling pathway, produce IFN-γ, which plays a crucial role in antitumor immunity (62). In our study, the tumoral expression of IFN-**γ** in the combination group was upregulated approximately twofold compared with the control group (Figure 2B). We also identified IL-12 as an important pro-inflammatory cytokine that regulates innate and adaptive immune responses and showed that IL-12 was upregulated in the tumor and spleen tissues of mice in all treatment groups (Figures 3C, 4C) and that it may be effective in the induction of Th1 responses along with type I IFN production, in turn leading to the observed antitumor effects.

As a result of STING and TLR9 signaling pathways and the production of type I and II IFNs, the cross-priming of tumor antigens by CD8$^+$ T cells facilitates antitumor immune responses (66–68). Our results suggest that the synergistic effects of immunoadjuvants toward polarization of T-cell-mediated immunity within the TME are evident by the IHC analysis of CD8$^+$ cell infiltration and TNF-α expression (Figures 8, 2D). As a hallmark cytokine in CD8$^+$ T-cell activation and tumor infiltration (69), the synergistic effects of the combination treatment with both immunoadjuvants increased the tumoral expression of TNF-α twofold, whereas reduced expression of this cytokine was detected when single forms of immunoadjuvants were administered (Figure 2D). Consistent with this finding, the expression of CD8$^+$ cells in the combination group was 59% higher than in the control group, which was remarkable compared with a single form of agonist (Figure 8). On the other hand, an increase in CDN concentration led to a decrease in T-cell infiltration of the tumor (70, 71). In support of these findings, our IHC results indicated that there was decreased infiltration by CD8$^+$ cells in the ADU-S100 (40-μg) group. However, when a lower dose of ADU-S100 (20 μg) was used as a monotherapy or in the combination group, a greater than twofold increase in CD8$^+$ cell

infiltration of the TME was observed. These results are consistent with the expression of IFN-γ in the tumor. In addition, the expression of CD45, which has an essential function in regulating immune responses, showed similar level of upregulation in all groups treated with a single agonist. However, the synergy of the agonists led to a higher (twofold) increase in CD45 expression, which was probably due to the greater recruitment of T cells to the TME in this group (Figure 7). H&E staining, along with the expression of cleaved caspase-3 as a positive marker for the efficiency of cancer treatment (72), revealed that there was a remarkable increase in the apoptotic index of caspase-3 in the combination group, suggesting *in situ* cell apoptosis compared with treatment with single agonists (Figure 6).

Studies showed that STING and TLR9 agonists promote the activation of DCs in the spleen (6, 45). We showed that, despite the intratumoral injection of agonists, the upregulation of cytokines occurred in the spleen, indicating a systemic immune response to agonists. In the combination group, the splenic expression of all cytokines was significantly upregulated compared with the control (Figure 3). It probably indicates the additive effects of both agonists on the activation of immune cells within the secondary lymphoid tissues. However, the splenic expression of IFN-γ, IL-12, and TNF-α in the combination group showed different results. The expression of IFN-γ in the combination group was lower than in the ADU-S100 (40 μg) and CpG ODN (40-μg) groups. The CpG ODN (40 μg) group showed the highest level of splenic expression of IL-12, followed by the combination group. The splenic expression of TNF-α in the combination group was lower than in the ADU-S100 (20 μg) and ADU-S100 (40 μg) groups. These results might be due to the different inflammatory properties of immunoadjuvants in single or combination forms in secondary lymphoid tissues when they are administered locally in the tumor. Studies have shown that the intratumoral injection of the STING agonist developed systemic immune responses in the spleen and tumor-draining lymph nodes, which were indicated by increased levels of IFN-γ-producing $CD8^+$T cells in these organs (73). In addition, in mice immunized with ovalbumin/STING/TLR7/8 agonists, the activation of antigen-specific $CD8^+$ T cells in the spleen and lymph nodes was induced, which was significant compared with that observed in the control group, whereas a significant increase was not observed in the mice treated with a single form of agonist (74). Furthermore, this combination induces enhanced infiltration of T cells into distant tumors, indicating that systemic immune responses occurred (75). Contrary to these findings, we observed a lower level of splenic expression of IFN-γ, IL-12, and TNF-α in the combination group after local immunotherapy, and, therefore, this suggests that further studies are required to explore the detailed mechanisms behind the splenic expression of these cytokines after intratumoral immunotherapy with ADU-S100 and CpG ODN1826. In conclusion, our results demonstrated that monotherapy with either CpG ODN or ADU-S100 and a combination of both agonists induced tumor regression, extended survival, and reduced infiltration of the TME by CAFs, underscoring the potential of immunoadjuvant therapy in inhibiting CAF-induced tumorigenesis. Mechanistic studies can reveal how the STING and TLR9 signaling pathways modulate and inhibit CAFs' tumorigenicity and immunosuppressive state. Therefore, CAF-mediated immune modulation may be considered a potential cellular target in immunotherapy strategies for colorectal cancer. Considering the heterogeneity and plasticity of CAFs and their crosstalk with immune and cancer cells, are key challenges that must be addressed for effective clinical translation of these findings.

Data availability statement

The original contributions presented in the study are included in the article/Supplementary Material. Further inquiries can be directed to the corresponding author.

Ethics statement

The animal study was approved under the ethical guidelines of the Animal Care and Use Committee of Ferdowsi University of Mashhad (license number 46013-M). The study was conducted in accordance with the local legislation and institutional requirements.

Author contributions

SH: Data curation, Formal Analysis, Investigation, Methodology, Project administration, Software, Validation, Visualization, Writing – original draft, Writing – review & editing. SA: Data curation, Formal Analysis, Visualization, editing. ZM: Methodology. MG: Methodology. HF: Resources. AH: Conceptualization, Data curation, Formal Analysis, Funding acquisition, Investigation, Methodology, Project administration, Resources, Supervision, Validation, Writing – original draft, Writing – review & editing, Visualization, Software.

Funding

The author(s) declare financial support was received for the research described in this article. This study was partially supported by grant number 46013 from the Ferdowsi University of Mashhad to AH. Financial support was also received from the Iranian Biotechnology Initiative Council.

Acknowledgments

Dr. Lukas J. A. C. Hawinkels (Department of Gastroenterology and Hepatology, Leiden University Medical Center, Leiden, the Netherlands) is acknowledged for providing several antibodies for IHC and for critical reading of the manuscript. Zahra Hosseininia and Zahra Fekri Rad are appreciated for their technical assistance.

Conflict of interest

The authors declare that the research was conducted in the absence of any commercial or financial relationships that could be construed as a potential conflict of interest.

Publisher's note

Supplementary material

The Supplementary Material for this article can be found online at: https://www.frontiersin.org/articles/10.3389/fimmu.2023.1258691/full#supplementary-material

SUPPLEMENTARY FIGURE 1
The cell viability of CT-26 cells after 24 hours culture with different concentrations of agonists was determined by the MTT test (n=3). **(A)** ADU-S100, **(B)** CpG ODN, and **(C)** ADU-S100 (20μg/ml) + CpG ODN (20μg/ml).

SUPPLEMENTARY FIGURE 2
(A) Tumor inhibition rate in treated versus control groups, **(B)** comparison of spleen index (mg/g) among control and treatment groups, **(C)** Body weight changes in different treatment groups during the course of the experiment, (n=7). Data are represented as mean ±SD. Statistical significance differences were analyzed by Mann-Whitney tests and indicated as **p ≤ 0.01 and *p ≤ 0.05).

SUPPLEMENTARY FIGURE 3
(A) Hemorrhage (thin arrows) and necrosis (star) in the control group. Necrotic cells have pyknotic (green arrows) and karyorrhectic (yellow arrows) nuclei or have lost their nucleus with highly eosinophilic cytoplasm. **(B–E)** Tumor tissues in the treatment groups without prominent hemorrhage and necrosis representing tumor malignancy. **(B)** ADU-S100 (20μg), **(C)** ADU-S100 (40μg), **(D)** CpG ODN (40μg), and **(D)** ADU-S100 (20μg) + CpG ODN (20μg). Scale bars = 50μm. (Hematoxylin-eosin staining, ×400 magnification).

SUPPLEMENTARY FIGURE 4
Increased number of lymphocytes (%) in blood samples obtained in control and treatment groups on day 30th (n=7). Data are represented as mean ±SD. Statistical significance differences were analyzed by Mann-Whitney tests and indicated as **p ≤ 0.01.

References

1. Temizoz B, Kuroda E, Kobiyama K, Aoshi T, Ishii KJ. Novel adjuvants. In: Yamaguchi Y, editor. *Immunotherapy of cancer: an innovative treatment comes of age*. Tokyo: Springer Japan (2016). p. 247–60. doi: 10.1007/978-4-431-55031-0_17

2. Xi Y, Xu P. Global colorectal cancer burden in 2020 and projections to 2040. *Transl Oncol* (2021) 14(10):101174. doi: 10.1016/j.tranon.2021.101174

3. Siegel RL, Miller KD, Wagle NS, Jemal A. Cancer statistics, 2023. *CA Cancer J Clin* (2023) 73(1):17–48. doi: 10.3322/caac.21763

4. Liu S, Sun Q, Ren X. Novel strategies for cancer immunotherapy: counter-immunoediting therapy. *J Hematol Oncol* (2023) 16(1):38. doi: 10.1186/s13045-023-01430-8

5. Dorostkar F, Arashkia A, Roohvand F, Shoja Z, Navari M, Mashhadi Abolghasem Shirazi M, et al. Co-administration of 2'3'-cGAMP STING activator and CpG-C adjuvants with a mutated form of HPV 16 E7 protein leads to tumor growth inhibition in the mouse model. *Infect Agent Cancer*. (2021) 16(1):7. doi: 10.1186/s13027-021-00346-7

6. Li T, Cheng H, Yuan H, Xu Q, Shu C, Zhang Y, et al. Antitumor Activity of cGAMP via Stimulation of cGAS-cGAMP-STING-IRF3 Mediated Innate Immune Response. *Sci Rep* (2016) 6:19049. doi: 10.1038/srep19049

7. Desmet CJ, Ishii KJ. Nucleic acid sensing at the interface between innate and adaptive immunity in vaccination. *Nat Rev Immunol* (2012) 12(7):479–91. doi: 10.1038/nri3247

8. Levy ES, Chang R, Zamecnik CR, Dhariwala MO, Fong L, Desai TA. Multi-immune agonist nanoparticle therapy stimulates type I interferons to activate antigen-presenting cells and induce antigen-specific antitumor immunity. *Mol Pharm* (2021) 18 (3):1014–25. doi: 10.1021/acs.molpharmaceut.0c00984

9. Sato-Kaneko F, Yao S, Ahmadi A, Zhang SS, Hosoya T, Kaneda MM, et al. Combination immunotherapy with TLR agonists and checkpoint inhibitors suppresses head and neck cancer. *JCI Insight* (2017) 2(18). doi: 10.1172/jci.insight.93397

10. Medrano RFV, Hunger A, Mendonça SA, Barbuto JAM, Strauss BE. Immunomodulatory and antitumor effects of type I interferons and their application in cancer therapy. *Oncotarget*. (2017) 8(41):71249–84. doi: 10.18632/oncotarget.19531

11. Krieg AM. Therapeutic potential of Toll-like receptor 9 activation. *Nat Rev Drug Discovery* (2006) 5(6):471–84. doi: 10.1038/nrd2059

12. Temizoz B, Kuroda E, Ishii KJ. Vaccine adjuvants as potential cancer immunotherapeutics. *Int Immunol* (2016) 28(7):329–38. doi: 10.1093/intimm/dxw015

13. Jie J, Zhang Y, Zhou H, Zhai X, Zhang N, Yuan H, et al. CpG ODN1826 as a promising mucin1-maltose-binding protein vaccine adjuvant induced DC maturation and enhanced antitumor immunity. *Int J Mol Sci* (2018) 19(3):920. doi: 10.3390/ijms19030920

14. Burdette DL, Monroe KM, Sotelo-Troha K, Iwig JS, Eckert B, Hyodo M, et al. STING is a direct innate immune sensor of cyclic di-GMP. *Nature*. (2011) 478 (7370):515–8. doi: 10.1038/nature10429

15. Burdette DL, Vance RE. STING and the innate immune response to nucleic acids in the cytosol. *Nat Immunol* (2013) 14(1):19–26. doi: 10.1038/ni.2491

16. Barber GN. STING: infection, inflammation and cancer. *Nat Rev Immunol* (2015) 15(12):760–70. doi: 10.1038/nri3921

17. Zhang X, Shi H, Wu J, Zhang X, Sun L, Chen C, et al. Cyclic GMP-AMP containing mixed phosphodiester linkages is an endogenous high-affinity ligand for STING. *Mol Cell* (2013) 51(2):226–35. doi: 10.1016/j.molcel.2013.05.022

18. Sun L, Wu J, Du F, Chen X, Chen ZJ. Cyclic GMP-AMP synthase is a cytosolic DNA sensor that activates the type I interferon pathway. *Science*. (2013) 339 (6121):786–91. doi: 10.1126/science.1232458

19. Sokolowska O, Nowis D. STING signaling in cancer cells: important or not? *Arch Immunol Ther Exp (Warsz)* (2018) 66(2):125–32. doi: 10.1007/s00005-017-0481-7

20. Corrales L, Glickman LH, McWhirter SM, Kanne DB, Sivick KE, Katibah GE, et al. Direct activation of STING in the tumor microenvironment leads to potent and systemic tumor regression and immunity. *Cell Rep* (2015) 11(7):1018–30. doi: 10.1016/j.celrep.2015.04.031

21. Woo SR, Fuertes MB, Corrales L, Spranger S, Furdyna MJ, Leung MY, et al. STING-dependent cytosolic DNA sensing mediates innate immune recognition of immunogenic tumors. *Immunity*. (2014) 41(5):830–42. doi: 10.1016/j.immuni.2014.10.017

22. Pépin G, Gantier MP. cGAS-STING activation in the tumor microenvironment and its role in cancer immunity. *Adv Exp Med Biol* (2017) 1024:175–94. doi: 10.1007/978-981-10-5987-2_8

23. Corrales L, Gajewski TF. Endogenous and pharmacologic targeting of the STING pathway in cancer immunotherapy. *Cytokine*. (2016) 77:245–7. doi: 10.1016/j.cyto.2015.08.258

24. Ji N, Wang M, Tan C. Liposomal delivery of MIW815 (ADU-S100) for potentiated STING activation. *Pharmaceutics*. (2023) 15(2). doi: 10.3390/pharmaceutics15020638

25. Chelvanambi M, Fecek RJ, Taylor JL, Storkus WJ. STING agonist-based treatment promotes vascular normalization and tertiary lymphoid structure formation in the therapeutic melanoma microenvironment. *J Immunother Cancer*. (2021) 9(2). doi: 10.1136/jitc-2020-001906

26. Sugimura N, Kubota E, Mori Y, Aoyama M, Tanaka M, Shimura T, et al. Reovirus combined with a STING agonist enhances anti-tumor immunity in a mouse model of colorectal cancer. *Cancer Immunol Immunother*. (2023). doi: 10.21203/rs.3.rs-2251036/v1

27. Wang Z, Celis E. STING activator c-di-GMP enhances the anti-tumor effects of peptide vaccines in melanoma-bearing mice. *Cancer Immunol Immunother.* (2015) 64 (8):1057–66. doi: 10.1007/s00262-015-1713-5

28. Wilson DR, Sen R, Sunshine JC, Pardoll DM, Green JJ, Kim YJ. Biodegradable STING agonist nanoparticles for enhanced cancer immunotherapy. *Nanomedicine.* (2018) 14(2):237–46. doi: 10.1016/j.nano.2017.10.013

29. Leach DG, Dharmaraj N, Piotrowski SL, Lopez-Silva TL, Lei YL, Sikora AG, et al. STINGel: Controlled release of a cyclic dinucleotide for enhanced cancer immunotherapy. *Biomaterials.* (2018) 163:67–75. doi: 10.1016/j.biomaterials.2018.01.035

30. Foote JB, Kok M, Leatherman JM, Armstrong TD, Marcinkowski BC, Ojalvo LS, et al. A STING agonist given with OX40 receptor and PD-L1 modulators primes immunity and reduces tumor growth in tolerized mice. *Cancer Immunol Res* (2017) 5 (6):468–79. doi: 10.1158/2326-6066.Cir-16-0284

31. Zhu HF, Zhang XH, Gu CS, Zhong Y, Long T, Ma YD, et al. Cancer-associated fibroblasts promote colorectal cancer progression by secreting CLEC3B. *Cancer Biol Ther* (2019) 20(7):967–78. doi: 10.1080/15384047.2019.1591122

32. Anggorowati N, Ratna Kurniasari C, Damayanti K, Cahyanti T, Widodo I, Ghozali A, et al. Histochemical and immunohistochemical study of α-SMA, collagen, and PCNA in epithelial ovarian neoplasm. *Asian Pac J Cancer Prev* (2017) 18(3):667–71. doi: 10.22034/apjcp.2017.18.3.667

33. Muchlińska A, Nagel A, Popęda M, Szade J, Niemira M, Zieliński J, et al. Alpha-smooth muscle actin-positive cancer-associated fibroblasts secreting osteopontin promote growth of luminal breast cancer. *Cell Mol Biol Lett* (2022) 27(1):45. doi: 10.1186/s11658-022-00351-7

34. Kabashima A, Matsuo Y, Ito S, Akiyama Y, Ishii T, Shimada S, et al. cGAS-STING signaling encourages immune cell overcoming of fibroblast barricades in pancreatic cancer. *Sci Rep* (2022) 12(1):10466. doi: 10.1038/s41598-022-14297-5

35. Mao X, Xu J, Wang W, Liang C, Hua J, Liu J, et al. Crosstalk between cancer-associated fibroblasts and immune cells in the tumor microenvironment: new findings and future perspectives. *Mol Cancer.* (2021) 20(1):131. doi: 10.1186/s12943-021-01428-1

36. Zeltz C, Primac I, Erusappan P, Alam J, Noel A, Gullberg D. Cancer-associated fibroblasts in desmoplastic tumors: emerging role of integrins. *Semin Cancer Biol* (2020) 62:166–81. doi: 10.1016/j.semcancer.2019.08.004

37. Elyada E, Bolisetty M, Laise P, Flynn WF, Courtois ET, Burkhart RA, et al. Cross-species single-cell analysis of pancreatic ductal adenocarcinoma reveals antigen-presenting cancer-associated fibroblasts. *Cancer Discovery* (2019) 9(8):1102–23. doi: 10.1158/2159-8290.CD-19-0094

38. Öhlund D, Handly-Santana A, Biffi G, Elyada E, Almeida AS, Ponz-Sarvise M, et al. Distinct populations of inflammatory fibroblasts and myofibroblasts in pancreatic cancer. *J Exp Med* (2017) 214(3):579–96. doi: 10.1084/jem.20162024

39. Caligiuri G, Tuveson DA. Activated fibroblasts in cancer: Perspectives and challenges. *Cancer Cell* (2023) 41(3):434–49. doi: 10.1016/j.ccell.2023.02.015

40. McAndrews KM, Chen Y, Darpolor JK, Zheng X, Yang S, Carstens JL, et al. Identification of functional heterogeneity of carcinoma-associated fibroblasts with distinct IL6-mediated therapy resistance in pancreatic cancer. *Cancer Discovery* (2022) 12(6):1580–97. doi: 10.1158/2159-8290.CD-20-1484

41. Zhao J, Chen Y. Systematic identification of cancer-associated-fibroblast-derived genes in patients with colorectal cancer based on single-cell sequencing and transcriptomics. *Front Immunol* (2022) 13:988246. doi: 10.3389/fimmu.2022.988246

42. Bartoschek M, Oskolkov N, Bocci M, Lövrot J, Larsson C, Sommarin M, et al. Spatially and functionally distinct subclasses of breast cancer-associated fibroblasts revealed by single cell RNA sequencing. *Nat Commun* (2018) 9(1):5150. doi: 10.1038/s41467-018-07582-3

43. Cords L, Tietscher S, Anzeneder T, Langwieder C, Rees M, de Souza N, et al. Cancer-associated fibroblast classification in single-cell and spatial proteomics data. *Nat Commun* (2023) 14(1):4294. doi: 10.1038/s41467-023-39762-1

44. Krenkel O, Hundertmark J, Ritz TP, Weiskirchen R, Tacke F. Single cell RNA sequencing identifies subsets of hepatic stellate cells and myofibroblasts in liver fibrosis. *Cells.* (2019) 8(5). doi: 10.3390/cells8050503

45. Temizoz B, Kuroda E, Ohata K, Jounai N, Ozasa K, Kobiyama K, et al. TLR9 and STING agonists synergistically induce innate and adaptive type-II IFN. *Eur J Immunol* (2015) 45(4):1159–69. doi: 10.1002/eji.201445132

46. Temizoz B, Hioki K, Kobari S, Jounai N, Kusakabe T, Lee MSJ, et al. Anti-tumor immunity by transcriptional synergy between TLR9 and STING activation. *Int Immunol* (2022) 34(7):353–64. doi: 10.1093/intimm/dxac012

47. Kocabas BB, Almacioglu K, Bulut EA, Gucluler G, Tincer G, Bayik D, et al. Dual-adjuvant effect of pH-sensitive liposomes loaded with STING and TLR9 agonists regress tumor development by enhancing Th1 immune response. *J Controlled Release.* (2020) 328:587–95. doi: 10.1016/j.jconrel.2020.09.040

48. Cai L, Du X, Zhang C, Yu S, Liu L, Zhao J, et al. Robust immune response stimulated by in *situ* injection of CpG/αOX40/cGAMP in αPD-1-resistant Malignancy. *Cancer Immunol Immunother.* (2022) 71(7):1597–609. doi: 10.1007/s00262-021-03095-z

49. Seth A, Lee H, Cho MY, Park C, Korm S, Lee JY, et al. Combining vasculature disrupting agent and Toll-like receptor 7/8 agonist for cancer therapy. *Oncotarget.* (2017) 8(3):5371–81. doi: 10.18632/oncotarget.14260

50. Luo M, Liu Z, Zhang X, Han C, Samandi LZ, Dong C, et al. Synergistic STING activation by PC7A nanovaccine and ionizing radiation improves cancer immunotherapy. *J Control Release.* (2019) 300:154–60. doi: 10.1016/j.jconrel.2019.02.036

51. Li B, Zhang S, Huang N, Chen H, Wang P, Li J, et al. Dynamics of the spleen and its significance in a murine H22 orthotopic hepatoma model. *Exp Biol Med (Maywood).* (2016) 241(8):863–72. doi: 10.1177/1535370216638772

52. Duan WR, Garner DS, Williams SD, Funckes-Shippy CL, Spath IS, Blomme EA. Comparison of immunohistochemistry for activated caspase-3 and cleaved cytokeratin 18 with the TUNEL method for quantification of apoptosis in histological sections of PC-3 subcutaneous xenografts. *J Pathol* (2003) 199(2):221–8. doi: 10.1002/path.1289

53. Jiang W, Li Y, Zhang S, Kong G, Li Z. Association between cellular immune response and spleen weight in mice with hepatocellular carcinoma. *Oncol Lett* (2021) 22(2):625. doi: 10.3892/ol.2021.12886

54. Adamus T, Kortylewski M. The revival of CpG oligonucleotide-based cancer immunotherapies. *Contemp Oncol (Pozn)* (2018) 22(1a):56–60. doi: 10.5114/wo.2018.73887

55. Moshnikova A, DuPont M, Visca H, Engelman DM, Andreev OA, Reshetnyak YK. Eradication of tumors and development of anti-cancer immunity using STINGa targeted by pHLIP. *Front Oncol* (2022) 12:1023959. doi: 10.3389/fonc.2022.1023959

56. Chattopadhyay S, Liu Y-H, Fang Z-S, Lin C-L, Lin J-C, Yao B-Y, et al. Synthetic immunogenic cell death mediated by intracellular delivery of STING agonist nanoshells enhances anticancer chemo-immunotherapy. *Nano Letters.* (2020) 20(4):2246–56. doi: 10.1021/acs.nanolett.9b04094

57. Nicolai CJ, Wolf N, Chang IC, Kirn G, Marcus A, Ndubaku CO, et al. NK cells mediate clearance of CD8(+) T cell-resistant tumors in response to STING agonists. *Sci Immunol* (2020) 5(45). doi: 10.1126/sciimmunol.aaz2738

58. Ohkuri T, Kosaka A, Ishibashi K, Kumai T, Hirata Y, Ohara K, et al. Intratumoral administration of cGAMP transiently accumulates potent macrophages for anti-tumor immunity at a mouse tumor site. *Cancer Immunol Immunother.* (2017) 66(6):705–16. doi: 10.1007/s00262-017-1975-1

59. Deng L, Jiang N, Zeng J, Wang Y, Cui H. The versatile roles of cancer-associated fibroblasts in colorectal cancer and therapeutic implications. *Front Cell Dev Biol* (2021) 9:733270. doi: 10.3389/fcell.2021.733270

60. Zhang J, Gu C, Song Q, Zhu M, Xu Y, Xiao M, et al. Identifying cancer-associated fibroblasts as emerging targets for hepatocellular carcinoma. *Cell Bioscience.* (2020) 10 (1):127. doi: 10.1186/s13578-020-00488-y

61. Fisher DT, Appenheimer MM, Evans SS. The two faces of IL-6 in the tumor microenvironment. *Semin Immunol* (2014) 26(1):38–47. doi: 10.1016/j.smim.2014.01.008

62. Karapetyan L, Luke JJ, Davar D. Toll-like receptor 9 agonists in cancer. *Onco Targets Ther* (2020) 13:10039–60. doi: 10.2147/OTT.S247050

63. Dongye Z, Li J, Wu Y. Toll-like receptor 9 agonists and combination therapies: strategies to modulate the tumour immune microenvironment for systemic anti-tumour immunity. *Br J Cancer.* (2022) 127(9):1584–94. doi: 10.1038/s41416-022-01876-6

64. Zheng J, Mo J, Zhu T, Zhuo W, Yi Y, Hu S, et al. Comprehensive elaboration of the cGAS-STING signaling axis in cancer development and immunotherapy. *Mol Cancer.* (2020) 19(1):133. doi: 10.1186/s12943-020-01250-1

65. Yu R, Zhu B, Chen D. Type I interferon-mediated tumor immunity and its role in immunotherapy. *Cell Mol Life Sci* (2022) 79(3):191. doi: 10.1007/s00018-022-04219-z

66. Yang H, Lee WS, Kong SJ, Kim CG, Kim JH, Chang SK, et al. STING activation reprograms tumor vasculatures and synergizes with VEGFR2 blockade. *J Clin Invest.* (2019) 129(10):4350–64. doi: 10.1172/JCI125413

67. Cheng N, Watkins-Schulz R, Junkins RD, David CN, Johnson BM, Montgomery SA, et al. A nanoparticle-incorporated STING activator enhances antitumor immunity in PD-L1-insensitive models of triple-negative breast cancer. *JCI Insight* (2018) 3(22). doi: 10.1172/jci.insight.120638

68. Krieg AM. Toll-like receptor 9 (TLR9) agonists in the treatment of cancer. *Oncogene.* (2008) 27(2):161–7. doi: 10.1038/sj.onc.1210911

69. Bertrand F, Rochotte J, Colacios C, Montfort A, Tilkin-Mariamé AF, Touriol C, et al. Blocking tumor necrosis factor α Enhances CD8 T-cell-dependent immunity in experimental melanoma. *Cancer Res* (2015) 75(13):2619–28. doi: 10.1158/0008-5472.CAN-14-2524

70. Jang SC, Economides KD, Moniz RJ, Sia CL, Lewis N, McCoy C, et al. ExoSTING, an extracellular vesicle loaded with STING agonists, promotes tumor immune surveillance. *Commun Biol* (2021) 4(1):497. doi: 10.1038/s42003-021-02004-5

71. Sivick KE, Desbien AL, Glickman LH, Reiner GL, Corrales L, Surh NH, et al. Magnitude of therapeutic STING activation determines CD8(+) T cell-mediated anti-tumor immunity. *Cell Rep* (2018) 25(11):3074–85.e5. doi: 10.1016/j.celrep.2018.11.047

72. Zhou M, Liu X, Li Z, Huang Q, Li F, Li CY. Caspase-3 regulates the migration, invasion and metastasis of colon cancer cells. *Int J Cancer.* (2018) 143(4):921–30. doi: 10.1002/ijc.31374

73. Vonderhaar EP, Barnekow NS, McAllister D, McOlash L, Eid MA, Riese MJ, et al. STING activated tumor-intrinsic type I interferon signaling promotes CXCR3 dependent antitumor immunity in pancreatic cancer. *Cell Mol Gastroenterol Hepatol* (2021) 12(1):41–58. doi: 10.1016/j.jcmgh.2021.01.018

frontiers | Frontiers in Immunology

TYPE Review
PUBLISHED 12 May 2023
DOI 10.3389/fimmu.2023.1197908

OPEN ACCESS

EDITED BY
Bruno Rivas-Santiago,
Unidad de Investigación Biomédica de Zacatecas (IMSS), Mexico

REVIEWED BY
Gill Diamond,
University of Louisville, United States
Cesar Rivas-Santiago,
National Council of Science and Technology (CONACYT), Mexico

*CORRESPONDENCE
Gudmundur Hrafn Gudmundsson
ghrafn@hi.is
Iwona T. Myszor
itm@hi.is

RECEIVED 31 March 2023
ACCEPTED 24 April 2023
PUBLISHED 12 May 2023

CITATION
Myszor IT and Gudmundsson GH (2023) Modulation of innate immunity in airway epithelium for host-directed therapy. *Front. Immunol.* 14:1197908. doi: 10.3389/fimmu.2023.1197908

Modulation of innate immunity in airway epithelium for host-directed therapy

Iwona T. Myszor[1]* and Gudmundur Hrafn Gudmundsson[1,2]*

[1]Faculty of Life and Environmental Sciences, Biomedical Center, University of Iceland, Reykjavik, Iceland, [2]Department of Laboratory Medicine, Karolinska Institutet, Stockholm, Sweden

Innate immunity of the mucosal surfaces provides the first-line defense from invading pathogens and pollutants conferring protection from the external environment. Innate immune system of the airway epithelium consists of several components including the mucus layer, mucociliary clearance of beating cilia, production of host defense peptides, epithelial barrier integrity provided by tight and adherens junctions, pathogen recognition receptors, receptors for chemokines and cytokines, production of reactive oxygen species, and autophagy. Therefore, multiple components interplay with each other for efficient protection from pathogens that still can subvert host innate immune defenses. Hence, the modulation of innate immune responses with different inducers to boost host endogenous front-line defenses in the lung epithelium to fend off pathogens and to enhance epithelial innate immune responses in the immunocompromised individuals is of interest for host-directed therapy. Herein, we reviewed possibilities of modulation innate immune responses in the airway epithelium for host-directed therapy presenting an alternative approach to standard antibiotics.

KEYWORDS

innate immunity, airway epithelium, microbiota metabolites, epigenetics, innate immune memory

Introduction

The airway epithelium of the respiratory tract is constantly exposed to particles and microbes inhaled with each breath that could possibly endanger the host. Hence, the highly specialized system of the host innate immune defenses is indispensable, as it keeps pathogens at bay and can limit the damaging effect of environmental pollutants. The airway epithelial cells together with stromal cells and tissue-residing immune cells shape immune responses in the local environment. Those immune responses protect the host from invading pathogens and maintain the local tissue homeostasis by producing signals for cell renewal and regeneration upon damage (1–4). In the first part of this review article, we provided an overview on innate immune functions of the airway epithelial cells covering recent developments like the identification of new cell types by single-cell transcriptomics.

In the second part, we described pathogens strategies to subvert host front-line defenses followed by the third part, where we reviewed research on how pathogens subversion mechanisms can be circumvented through modulation of host epithelial innate immune responses by different inducers for host-directed therapy.

Innate immunity components of the human respiratory epithelium

The airway epithelial cells are central players in the communication between the host and the external environment and together with stromal and immune cells present in local tissues, shape immune responses during homeostasis and disease. This is possible because of a highly complex innate immune system consisting of several components that we review in this section. All those components work together to provide protection of the host mucosal surfaces from the external environment and tissue regeneration upon damage (1–4).

Human airway and alveolar epithelium

The airway epithelium lining the upper and lower respiratory tract is composed of different types of epithelial cells forming a single-cell layer of pseudostratified epithelium with tight physical links to the basal lamina and communicating with underlaying stromal cells, such as fibroblasts, airway smooth muscle cells, peri-endothelial (pericytes), and endothelial cells embedded in the connective tissue matrix (2, 4, 5). The four major types of cells in the airway epithelial layer are secretory club cells, goblet cells, ciliated cells, and basal cells (Figure 1) (3). Secretory club cells are columnar non-ciliated cells producing factors responsible for the neutralization of inhaled toxic substances and displaying immunomodulatory functions (6). In a mouse model, club cells were shown to act as self-renewing stem cells and as progenitors for ciliated cells that constitute the majority in the airway epithelium (7, 8). Club cells can also differentiate to mucus-producing goblet cells in response to allergens (9). Basal cells are small cuboidal cells that replenish different types of mature cells maintaining epithelial cell turnover during homeostasis and regenerating damaged epithelial barrier (10, 11). In respect to the important role in self-renewal and tissue regeneration, the basal cells seem to be protected from directed exposition to the lumen of the airways by other epithelial cells (Figure 1). Additional protection is provided by advanced innate host defense mechanisms. The proportion of each cell type occurring in human airways varies depending on the diameter of the airways, which results in diverse innate immune responses at different levels of the anatomical and histological organization of the respiratory system. For instance, mucus-secreting goblet cells occurring in submucosal glands of the human trachea and large bronchus are replaced by secretory club cells in terminal bronchioles (8, 12). The submucosal glands are composed of four major types of the airway epithelial cells and myoepithelial cells that together form a sophisticated machinery releasing fluids, mucus, and antimicrobial effectors into the luminal space of the airways (1).

Additional types of the airway epithelial cells have been recently described (Figure 1) based on the increasing accessibility of the single-cell RNA sequencing, changing our view on the cellular landscape of the airway epithelium that is more heterogeneous than previously thought (3–5, 13). Rare types of airway epithelial cells were distinguished including brush cells (also called tuft cells) and solitary chemosensory cells identified in the human trachea and nasal cavity, respectively (14). The function of brush cells in humans remains largely uncharacterized and, based on the mouse studies, indicates regulation of type II immune responses, such as release of IL-25 in the nasal epithelium and protective reflexes, such

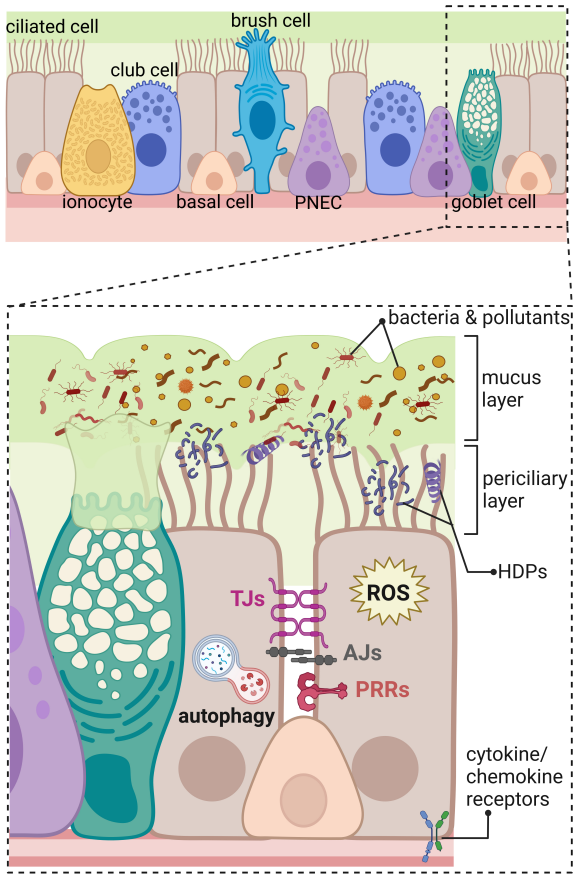

FIGURE 1
Innate immunity components of the human respiratory epithelium in the distal part of the respiratory tract. The upper panel shows an overview on the different types of cells composing respiratory epithelium of the distal part of the airways including ciliated cells, ionocytes, club cells, basal cells, brush (tuft) cells, pulmonary neuroendocrine cells (PNEC), and goblet cells. The lower panel represents magnified area showing a part of the respiratory epithelium with innate immunity components marked; beginning from the top: mucus layer with host defense peptides (HDPs) entrapping bacteria, and pollutants removed by beating cilia in the periciliary layer. The constant renewal of the mucus layer is provided by goblet cells. Transport of molecules through the paracellular space between neighboring cells is regulated by tight junctions (TJs) and adherens junctions (AJs). Danger signals are recognized by pathogen recognition receptors (PRRs) and cytokine/chemokine receptors. Intracellular components of the innate immunity in the respiratory epithelium include production of reactive oxygen species (ROS) and autophagy eliminating intracellular intruders and particles. Created with BioRender.com.

as sneezing (14, 15). Interestingly, brush cells do not occur in the healthy human alveolar epithelium. Expansion of brush cells in the upper airways and their *de novo* formation in the lower airways were observed after viral infections with severe acute respiratory syndrome coronavirus 2 (SARS-CoV-2) and influenza A subtype H1N1, respectively (15). Chemosensory cells in the human nasal epithelium detect and mediate reflex reactions in response to irritants and pathogens to prevent their passage down to the lower airways (16). Another rare cell type in the human airway epithelium are pulmonary neuroendocrine cells (PNECs) clustered into neuroendocrine bodies (NEB) (2, 17). Apart from olfactory epithelium in the nasal cavity (18), PNECs are the only cells in the airways supplied with nerves; therefore, they participate in the neurotransmission, act as sensory cells for the oxygen level, and detect and respond to inhaled allergens (2, 17). Another recently identified rare cell types are the ionocytes, showing high expression level of cystic fibrosis transmembrane receptor (CFTR), regulating the ionic microenvironment of the mucus (19, 20). In addition, novel subtypes of progenitor cells were identified, such as precursors of ciliated cells—deuterosomal cells containing numerous centrioles and mucous-ciliated differentiation intermediate cells (3). Moreover, the population of basal cells is more heterogeneous than what was thought. The new intermediate cells were distinguished between basal and 1) club cells—suprabasal cells, 2) PNEC, ionocytes, and brush cells—parabasal cells, and 3) luminal secretory cells—Hillock cells (3, 5, 11).

The distal part of human airways ends with terminal bronchioles mainly composed of club and ciliated cells with very few rare types of cells and almost no basal cells present (8). One can argue that only few basal cells are present in the distal part of human airways because, in principle, the portion of air reaching alveoli should be warmed, moistened, and cleared from pollutants, as the vital function of the alveolar epithelium is the gas exchange provided by epithelial alveolar type 1 cells (also known as AT1, ATI, and type I pneumocytes) (2). Frequently, these defense mechanisms of the proximal part of the respiratory system are not sufficient. Therefore, alveolar innate immune defense mechanisms are activated to protect the host, such as surfactant proteins produced by alveolar type 2 cells (also known as AT2, ATII, and type II pneumocytes), that also function as progenitor cells for AT1 cells in the adult lung (1, 2, 21). Overall, the recent advances in transcriptomic and proteomic analyses opened a new avenue for further characterization of innate immune functions of new epithelial cells subtypes and the signaling pathways guarding their differentiation.

Host defense peptides

Numerous antimicrobial effectors are produced by the airway epithelial cells for effective host innate defenses. Among them are host defense peptides (HDPs) (Figure 1), previously commonly called antimicrobial peptides (AMPs), divided into two main families of cathelicidins and defensins (22–24). HDPs can be produced constitutively and induced upon stimuli. Their constitutive expression can be enhanced upon stress conditions, like infection or injury. Most of HDPs are stored in the cellular granules as a pro-form, which is further released and processed upon a danger signal (22, 25). Human cathelicidins have one dominant mature peptide LL-37 encoded by *CAMP* gene (cathelicidin antimicrobial peptide). Human cathelicidin is produced as a pro-form (hCAP18; pro-LL-37) containing N-terminal cathelin domain that is cleaved off by serine proteases, such as kallikreins in the skin and proteinase 3 from neutrophiles to release the mature LL-37 peptide (25–28). LL-37 has an α-helical structure and a cationic, amphipathic character and can be processed in the skin to shorter peptides (26, 29). Human cathelicidin is constitutively expressed at rather low protein levels in airway epithelial cells showing only the pro-form to be secreted when the cells are cultured *in vitro*. The expression of cathelicidin is enhanced upon stimuli, indicating a highly responsive inducible system for host defense (30–32). During inflammation, the migration of neutrophiles to the site of infection contributes to the processing of the pro-form hCAP18 to the active LL-37 peptide in the lung, as neutrophiles are loaded with proteinase 3 and other enzymes. However, whether the processing of constitutively expressed pro-form hCAP18 to the active LL-37 peptide takes place on the airway epithelial surfaces in physiological conditions during homeostasis remains to be further elucidated, as the *in vitro* studies with the airway epithelial cells do not closely recapitulate the *in vivo* environment. On the other hand, the analysis of the airway surface liquid (ASL) indicated the presence of mature LL-37 (33). However, one may argue about fact that the source of mature LL-37 peptide in ASL might come from immune cells present in lungs. Therefore, the dynamics of the cathelicidin processing to the mature LL-37 peptide in the homeostatic conditions of the lung epithelium remains to be further investigated, similar to the identification of potential lung tissue specific enzymes responsible for the cleavage and confirmation if LL-37 is processed to shorter peptides with characterization of their potential role in shaping local lung innate immune responses. In contrast to cathelicidins, human defensins have several members and are divided in α-, β-, and θ-defensins (34). Alpha- and beta-defensins are produced in the airway epithelium constitutively and inducible as inactive precursors that undergo further processing to the active form (21, 22, 35, 36). In human genome, there are genes encoding the third group of θ-defensins; however, proteins are not produced because of premature codon stop (37). The expression of antimicrobial effectors in each cell type present in the airway epithelium has been explored and is available in Human Protein Atlas (HPA). According to HPA, the main sources of cathelicidin in bronchus are basal respiratory cells (https://www.proteinatlas.org/ENSG00000164047-CAMP/single+cell+type/bronchus).

The primary function of the HDPs is their bactericidal effect at the range of micromolar concentrations on both Gram-positive and Gram-negative bacteria, but they are also effective against viruses and fungi (26, 35, 38). The common antimicrobial activity of HDPs is associated with their cationic and amphipathic properties. Positively charged HDPs can strongly interact through electrostatic and hydrophobic interactions with negatively charged phospholipids of the bacterial cell membrane and pathogen-associated molecular patterns (PAMPs), such as LPS of Gram-

negative bacteria (39, 40). The interaction of HDPs with the bacterial membrane causes disruption, leakage of the intracellular components, and bacterial cell death (24). Another, less known antimicrobial mechanism of HDPs is the translocation of peptides through the membrane and binding to bacterial intracellular targets, for example, cardiolipin resulting in bacterial cell death (41). Furthermore, human β-defensin 3 has been shown to disrupt bacterial cell wall biosynthesis by binding to lipid II, which makes bacteria more vulnerable to damage (42). Hence, peptides have different activities against bacteria, but the membrane disruption seems of a major general importance. In case of the viral infections, HDPs bind and destabilize viral structures like viral envelope of influenza viruses, respiratory syncytial virus (RSV), Zika virus (38, 43, 44), and viral capsid of rhinoviruses (45). Similar mechanism takes place during fungal infections, like with *Candida albicans*, where HDPs permeabilize yeast cell membrane (46). Of note, at physiological concentrations, the HDPs do not damage human cell membranes due to its lack of negative charge in the outer leaflet of the membrane and presence of cholesterol (47). However, HDPs at higher concentrations might be able to damage host's cells, for instance when granulocytes are recruited to the site of infection in the lung (48, 49). Interestingly, recently, it has been described that the fragments of LL-37 peptide (17–29 aa residues) can cluster together to form highly organized oligomers resembling fibril-like tubules of unknown function (50). Some pathogens, such as *Staphylococcus aureus*, produce similar tubules what is recently discussed as an example of the bacterial mimicry, perhaps to evade host antimicrobial responses potentially exerted by such HDPs fibril-like oligomers (51). However, the existence and physiological relevance of such LL-37 fibrils in the lung epithelial surfaces have not been described so far.

Apart from antimicrobial activity, HDPs display immunomodulatory functions (24). HDPs are chemoattractant for immune cells, e.g., human β-defensin 2 (hBD2) is a chemoattractant for mast cells (52) and LL-37 for neutrophils, monocytes, and T cells (53, 54). HDPs also indirectly recruits leukocytes to the local site of infection or injury by inducing release of chemokines and cytokines (24). For instance, defensins can induce expression of proinflammatory IL-8, a chemoattractant for neutrophils, in human A549 lung epithelial cell line and therefore display proinflammatory function *in vitro* (55). HDPs interfere with the cell signaling cascades while displaying at the same time a dual pro- and anti-inflammatory role, depending on the local environment and the phase of infection. During infection when nuclear factor kappa B (NF-κB) pathway is activated by bacterial LPS binding Toll-like receptor 4 (TLR4) receptor, LL-37 peptide can selectively inhibit production of proinflammatory tumor necrosis factor (TNF) and reactive oxygen species (ROS) while at the same time stimulate IL-8 production in epithelial cells to attract immune cells (56). HDPs have pro- and anti-inflammatory effects that seem to be exerted depending on the stage of infection. In the early stage of bacterial infection with *Pseudomonas aeruginosa*, LL-37 enhances proinflammatory response in airway epithelial cells (57). Cathelicidins are also able to prevent activation of TLR2 and TLR4 signaling in macrophages by non-viable bacteria and their products at later stage of infection, resulting in reduced production of proinflammatory response that might protect local tissue from the injury (58). Therefore, HDPs can play a dual role in shaping both pro- and anti-inflammatory response and maintaining tissue homeostasis. HDPs also display additional functions by enhancing phagocytosis, ROS production, and participation in neutrophil extracellular trap (NET) formation, contributing to enhancement of the bacterial clearance (24). HDPs also initiate T-cell response by promoting Th17 differentiation (59) and could, therefore, play a role in the intersection of innate and adaptive immunity. Furthermore, local environment also affects immunomodulatory function of HDPs by their post-translational modifications (PTMs). The citrullinated LL-37 peptide was detected in human bronchoalveolar lavage; however, citrullination affected the net charge of the peptide that lost the ability for bacterial killing (60). Another evidence is citrullination of LL-37 by peptidyl arginine deaminase, where the peptide loses its ability to enhance proinflammatory response in macrophages (61). These studies indicate that PTMs regulate the mode of action of HDPs for the maintenance of the local tissue homeostasis, and future exploration of how additional PTMs affect function of HDPs in lungs is of interest.

Apart from HDPs, there are also several antimicrobial proteins like lysozyme, degrading bacterial peptidoglycans, and bacteriostatic lipocalin 2 and lactotransferrin (21). The bacteriostatic effect of lipocalin 2 and lactoferrin are linked to the inhibition of iron uptake by bacteria from the local environment, as they bind bacterial iron-chelating molecules. Lipocalin 2 has been shown to be effective against *Escherichia coli* causing pneumonia (62), and mutant mice lacking lipocalin 2 were more susceptible to *Klebsiella pneumoniae* infections (63). Similarly, S100A7 (psoriasin) protein from S100 protein family containing several antimicrobial effectors (e.g., S100A8/9 protein known as calprotectin) has been shown to kill *E. coli* by Zn^{2+} chelation (64). Airway epithelial cells and alveolar macrophages constitutively express S100A7 that is enhanced upon *S. aureus* challenge (65). Interestingly, the mechanical strain generated during breathing enhances expression of S100A7 protein in alveolus-on-chip model through activation of mechanosensitive ion channel TRPV4 (transient receptor potential vanilloid-type 4). Moreover, when TRPV4 and the S100A7 target receptor—receptor for advanced glycation end products (RAGE)—were blocked by inhibitors, the viral load of H3N2 influenza was increased, demonstrating the importance of S100A7 for lung defenses (66). Furthermore, antiproteases like secretory leukocyte protease inhibitor (SLPI) and elafin exhibit antimicrobial properties against pathogens *P. aeruginosa* and *S. aureus* in lung epithelial cells (67–69) and have anti-inflammatory potential, e.g., by inhibition of NF-κB pathway through reducing degradation of IκBα in macrophages and endothelial cells (70). Ribonuclease 7 (RNase7) discovered in the skin where it displays antimicrobial effects against several pathogens has also been shown to be expressed in human respiratory tract (71). Interestingly, the primary source of RNase7 in human airways are basal cells that express RNase7 upon stimulation with inactivated *H. influenzae* and cigarette smoke, therefore indicated as a second line of front-line defenses in case of injury of mature differentiated epithelial cells (72). Similarly, RNase7 has been induced in airway epithelial cells

upon infection with Mtb, where it marked intracellular bacteria to a limited extent. However, the direct effect of RNase7 on elimination of Mtb was not shown and requires further investigation (73). Additional components of the innate immunity in the lung epithelium are collectins, surfactant protein A and D (SP-A and SP-D), produced by alveolar type 2 cells (21). They tag bacteria for opsonization to increase phagocytosis by the alveolar macrophages (74). The immunomodulatory function of collectins can be exemplified by the inhibitory effect of the SP-A on the production of IL-8 by eosinophils present during allergic response (75). The antimicrobial and immunomodulatory functions are also displayed by plate-lung-nasal-clone (PLUNC) proteins shown to have antibacterial effect against *Mycoplasma pneumoniae* and reduce production of proinflammatory cytokine IL-8 (76). Of note, several chemokines like CXCL9 and CXCL11, present in the lung epithelium as a result of interferon gamma (IFNγ) stimulation, have antibacterial functions against *E. coli* and *L. monocytogenes* (77). Host defense effectors produced by club cells such as club cell protein 10 (CC-10) inhibit NF-κB signaling pathway and production of proinflammatory cytokines and chemokines in bronchial epithelial cells (78). Similar to CC-10, club cell secretory protein (CCSP) was shown to reduce inflammation and viral load during RSV infection (79). Next, the levels of secretoglobin A1A (SCGB1A1) also produced by club cells were reduced in the airways of patients with asthma in comparison to healthy individuals (80). Allergen-specific immunotherapy increased expression of SCGB1A1 considered as anti-inflammatory mediator in the lower airways (81). Secretoglobin A1A was also shown to affect alveolar macrophages by attenuation of the surge of inflammatory cytokines during activation of TLR receptors. Deficiency of secretoglobin A1A facilitated development of proinflammatory M1 phenotype of pulmonary macrophages, indicating the importance of physiological levels of SCGBA1A for innate immune defense and maintenance of local tissue homeostasis (82). Another important indirect link to HDP activity is the expression and function of CFTR and the non-gastric H^+/K^+ adenosine triphosphatase (ATP12A) in lung epithelial cells, including recently identified ionocytes. Both CFTR and ATP12A regulate pH of the airway surface liquid (ASL) by secretion of HCO_3^- and H^+, respectively, that is detrimental for antimicrobial activity of HDPs (83, 84).

A further important element of the innate immunity in the airway epithelial cells is the production of reactive oxygen species (ROS) (Figure 1). For many years, ROS were attributed to the lung tissue damage and tissue aging as a result of the oxidative stress (85, 86) but in fact ROS play an important function in the elimination of invading pathogens (21). Dual oxidases (DUOX) are key enzymes responsible for the generation of ROS in the lung epithelium, including superoxide and hydrogen peroxide, for effective pathogen elimination (87, 88). In addition, the protective role of NOX1 activity have been shown to limit inflammatory response and lung tissue damage exerted by influenza A at early stage of infection in mice (89) even though the NOX1 activity in different circumstances, such as hyperoxia, can cause tissue damage (85). The view on ROS generation and redox signaling in epithelial cells is developing to better understand their role in pathological situations and demonstrate that the physiological levels of ROS are important for cellular signaling during homeostasis (86, 90).

Mucus and mucociliary clearance

A physical component of the innate immune system is the airway surface liquid (ASL) composed of the mucus and periciliary layer on the airway epithelium (Figure 1) (91). The ASL provides a physical and chemical barrier for the invading pathogens and inhaled particles protecting the airway tissue from the damage (92). The chemical barrier of ASL is provided by the low salt content (93), pH maintained by HCO_3^- and H^+ (94, 95), and hydration maintained by Na^+ and Cl^- ion gradient (96). This environment facilitates the formation of MUC5B bundles (12) and keeps HDPs active for killing of entrapped pathogens in the mucus layer (83, 84) for their removal by mucociliary clearance of beating cilia (21, 93). The periciliary layer of ASL composed of transmembrane mucins and periciliary liquid reduces the friction of the constantly moving mucus that clears airways from bacteria and pollutants during homeostasis (12). The dynamic process of mucociliary clearance keeps the airways almost devoid of bacteria in healthy individuals (12, 93) causing the characterization of any existing lung microbiome very difficult and so far confirmed only by detection of bacterial nucleic acids (97, 98). In addition, the anaerobic bacterial fermentation products were detected in the lungs of patients with HIV (99, 100); however, those ground-breaking evidence shall be carefully interpreted and further confirmed by the characterization of additional microbiota metabolites and their original source of production. Impairment of the mucociliary clearance by primary ciliary dyskinesia (101) or defects in the function of ion channels in cystic fibrosis (CF) (92) cause clogging of the airways with mucus, creating a favorable environment for bacterial growth (12). Therefore, pre-existing bacteria during chronic respiratory diseases are sometimes referred in the literature as "lung microbiota" (102), although it should be emphasized that this terminology is used in the context of pathological conditions. In general, the studies on the mucus composition and physiology together with the interaction of innate immunity components with mucus are of interest and one of the future directions in the field investigating host defenses.

Pathogen recognition receptors

One of the initial functions of innate immunity in the airway epithelium is pathogen detection by pathogen recognition receptors (PRRs) (Figure 1), recognizing PAMPs. Upon stimulation, PRRs activate signaling cascade leading to the inflammation and clearance of the pathogens. Among different types of the PRRs, present in the airway epithelium are TLRs, NOD-like receptors (NLRs), RIG-I-like receptors (RLRs), C-type lectin receptors (CLRs), and formyl-peptide receptors (FPRs) (21, 103–105).

In the airway epithelium, all types of the TLRs (TLR2/1, TLR2/6, TLR3, TLR4, TLR5, TLR7, TLR8, TLR9, and TLR11) are present, anchored in the cell membrane and endosomes (21). However,

the mapping of TLRs with their exact spatial distribution within airway epithelial cell membranes at different regions of the respiratory tract, similar to the study done for the intestinal epithelium (106), is still missing. TLRs recognize bacterial lipopeptides, lipopolysaccharide (LPS), flagellin, DNA, and RNA by the leucine-rich repeat (LRR) motif that is linked through a single transmembrane domain to Toll/IL-1 receptor (TIR) intracellular motif. The activation of the receptor requires binding of the adaptor protein MyD88 or TIR-domain-containing adapter-inducing interferon-β (TRIF) to the TIR domain. MyD88 is an adaptor protein for all TLRs, except TLR3 and TRIF for TLR3 and TLR4. Other adaptor proteins like TIR domain containing adaptor protein (TIRAP), translocation associated membrane protein 1 (TRAM), sterile alpha and TIR motif containing (SARM) have been shown to be involved in the TLR signaling. The stimulation of TLRs initiates NF-κB and mitogen-activated protein kinase (MAPK) downstream signaling, leading to induction of proinflammatory cytokines and type I interferons (21, 107).

Unlike TLRs, apart from cell and endosomal membranes, NLRs occur as soluble receptors in the cytoplasm. In the airway epithelium, NLRs with caspase recruitment domain (CARD) are represented by NOD1 and NOD2 receptors, recognizing bacterial peptidoglycans and working in synergy with TLRs towards activation of NF-κB and MAPK pathways (108). The other types of NLRs, containing PYD (pyrin) and NLRB (baculoinhibitor of apoptosis protein) domains form inflammasome controlling cleavage of IL-1β and IL-18 pro-forms by caspase-1 (21, 103). For instance, in human lung epithelial cells NRLP3 receptor harboring pyrin domain forms NRLP3 inflammasome responsible for cleavage of IL-1β upon *C. albicans* or influenza A virus infection (109, 110).

Human airway epithelial cells have also cytoplasmic receptors for the detection of pathogen's nucleic acids (21). Among them are RIG-I-like receptors (RLRs), recognizing viral ss/dsRNA of influenza and paramyxoviruses causing respiratory diseases, e.g., RSV (111, 112). The group of RLR receptors include retinoic acid inducible gene-I (RIG-I), melanoma differentiation-associated gene 5 (MDA5) and RIG-I-like receptor dsRNA helicase (LGP2) (103). With the involvement of the adaptor proteins, e.g., mitochondrial antiviral-signaling protein (MAVS), RIG-I and MDA5 receptors transduce signals activating NF-κB, interferon regulatory factor 3 and 7 (IRF3 and IRF7) pathways leading to the production of proinflammatory cytokines and interferons (108). Other cytoplasmic receptors recognize bacterial DNA and bacterial signaling molecules such as cyclic dinucleotides (CDNs) (21). A prominent member of this family is the stimulator of IFN genes (STING) located on the ER membrane. STING recognizes CDNs and is an adaptor protein for other cytoplasmic receptors like interferon gamma inducible protein 16 (IFI16) recognizing *Streptococcus pneumoniae* dsDNA (113). Moreover, STING can by activated by cyclic GMP-AMP (cGAMP) synthetized by cGAMP synthase (cGAS) in human airway epithelial cells upon detection of not only microbial/viral DNA in the cytoplasm but also by self-DNA coming from the nucleus or damaged mitochondria (114).

Additional PRRs are C-type lectin receptors (CLRs) on the airway epithelial cells recognizing carbohydrates present on the pathogens and activating proinflammatory response (21, 103). The CLRs occur as membrane-anchored receptors like Dectin-1 recognizing *Haemophilus influenzae* and *Aspergillus fumigatus* infections (115, 116). The second form of CLRs are soluble collectins containing C-type lectin domain like SP-A and SP-D exhibiting antimicrobial activity through opsonization of bacterial, viral, and fungal pathogens (21). Formyl-peptide receptors (FPRs) are also expressed on the epithelial cells of the respiratory tract, where they recognize not only bacterial formylated peptides but also host-derived stimulants, such as mitochondrial proteins from damaged cells that chemoattract leukocytes promoting inflammation. Host LL-37 has also been shown to activate FPR2 (aka FPRL1) and is considered as a proinflammatory stimulus in chronic obstructive pulmonary disease (COPD). Depending on the local tissue environment, activation of FPRs can have a dual pro- or anti-inflammatory role, and it has been associated with the tissue regeneration and wound healing (105, 117).

Interestingly, it has recently been shown that PTMs of PRRs can be considered as contributing to a fine-tuning mechanism limiting inflammation; for instance, palmitoylation of NLR family pyrin domain containing 3 (NLRP3) prevents activation of inflammasome (118). Studies on how different PTMs affect PRRs downstream signaling in response to pathogens and during inflammation is one of the future directions for research in the host–pathogen interactions field.

Cell junctional complexes

The structural elements of the airway epithelial barrier integrity are tight (TJs) and adherens junctions (AJs) that determine the polarization of the epithelial cells into the apical and basolateral site providing physical barrier regulating paracellular flux through epithelial layers (119). Hence, the epithelial barrier integrity provided by TJs and AJs can be considered as part of the epithelial defense system (Figure 1). TJs and AJs are composed of transmembrane proteins, such as occludin, tricellulin, claudins, and junctional adhesion molecules (JAMs) and many others present in TJs together with E-cadherin and nectins in AJs. Transmembrane proteins of TJs interact with the proteins of the intracellular junctional plaque containing multiple interaction domains, such as zonula occludens-1 (ZO-1)—a well-defined protein from the junctional plaque complex—and its deletion is lethal in the mouse embryos. The examples of AJs intracellular junctional plaque proteins are α- and β- and p120 catenins and afadin (AF6) displaying similar functions. The intracellular junctional plaque proteins are coupled to cytoskeleton proteins, for example to actin through C-terminal domain of ZO-1 (119). The importance of the functional epithelial barrier sealing the deeper tissues from the external environment for the maintenance of the local tissue homeostasis seems to be explained by the epithelial barrier hypothesis (120). It highlights that the leaky epithelial layer caused by disruption of TJs and AJs by detergents, pollutants, allergens, and pathogens (121–125) contributes to increased incidence of allergies, asthma, and autoimmune diseases (120). The exposure to such environmental insults creates a positive feedback loop of further epithelial layer destruction. This process

includes a subsequent translocation of the microbiota and opportunistic pathogens through a disrupted epithelial layer to the lamina propria that activates macrophages and T cells, ultimately leading to inflammation (120). During inflammatory response, cytokines cause further disintegration of tight junctions in the airway epithelium (126, 127), exacerbating the inflammatory response that may become a chronic state. Therefore, the disruption of the net of TJs and AJs can be considered as one of the early onsets of the disease. Hence, the maintenance of the epithelial barrier integrity is crucial for balanced innate and adaptive immune responses in the airway epithelium.

Autophagy

Autophagy is a complex process involving interaction of several different proteins, leading to engulfment of the cytoplasmic cargo during autophagosome formation and its subsequent degradation upon fusion with lysosomes. Autophagy is one of the key cellular processes maintaining balance in cells exposed to a constantly changing environment. It plays a major "housekeeping" function on the cellular level where it is responsible for the degradation of damaged organelles and unfolded/misfolded proteins (128). An important function of the autophagy process in respect to innate immunity is the degradation of invading pathogens, when the initial innate immunity barrier—mucus, HDPs, and TJs—was not sufficient to halt the pathogen entering the cells (129). Pathogenic *P. aeruginosa* (130), conidia of *Aspergillus fumigatus* (131), and influenza A virus (132) can be effectively eliminated or restricted by autophagy in airway epithelial cells. Therefore, autophagy can be considered as part of cell autonomous innate immunity and an intracellular defense mechanism of the "last chance" for the prevention of pathogen dissemination and progression of infectious disease (133). The commonly used cell model to study the role of autophagy in innate immunity are phagocytic professional cells, such as macrophages. However, the importance of autophagy in epithelial cells should be highlighted due to the vital role of epithelial cells in the first line of the host defense and epithelial homeostasis (Figure 1). During homeostasis, autophagy can control ciliogenesis and ciliary function by regulating the length of motile cilia in airway cells (134). The biogenesis of primary cilia is regulated by autophagic degradation of centriole and centriolar satellite protein OFD1 (135) and the function of motile cilia by degradation of kinesin family member 19 (Kif19)—an essential protein controlling ciliary length that should be inhibited to maintain the correct length of cilia (136).

Moreover, the importance of autophagy in human lung is demonstrated in CF patients whose autophagy is impaired due to aggregating Beclin-1. In the cell and animal models of CF, this phenotype can be rescued upon Beclin-1 restoration, suggesting a key role of autophagy in the lung homeostasis (137). Autophagy was shown as a central contributor to IL-13-mediated mucus hypersecretion by airway epithelial cells in COPD and asthma (138). Moreover, autophagy regulates apical localization of DUOX1 in airway epithelial cells and ROS production in response to chronic IL-13 exposure (139). Furthermore, autophagy maintains the airway progenitor cells pool and regulates cell differentiation for epithelial regeneration (140). In addition, one of the clinical symptoms of the Hermansky–Pudlak syndrome type 1, a rare genetic disorder impairing vesicle trafficking, is lung fibrosis and impaired innate immune antimicrobial responses due to amplified mechanistic target of rapamycin kinase (mTOR) signaling resulting in reduced bacterial clearance, indicating autophagy as a key cellular process in physiological and pathological conditions (141, 142). Autophagy in the airway epithelium can be considered as a double-edge sword because in particulate-matter-induced airway inflammation, autophagy contributes to the epithelial injury (143). The basic research on the autophagy process and its regulation in different conditions remain future perspectives for the development of novel strategies for treating respiratory tract diseases.

Epigenetics and innate immunity

Innate immune responses in the airway epithelium are also regulated by epigenetic modifiers of DNA methylation and post-translational modifications of histones. The epigenetic regulation of gene expression by modulation leading to chromatin opening allows for a rapid response to environmental changes. These processes are tightly regulated by the equilibrium of epigenetic enzymes and their counterparts, for example by histone acetyltransferases (HATs)—histone deacetyltransferases (HDACs) and DNA methyltransferases (DMTs). The importance of the DNA methylation status seems to be highlighted by the studies showing that DNA methylation pattern is changed in respiratory tract diseases, such as increased DNA methylation in *NLRP3* gene of COPD patients (144). On the other hand, decreased methylation in the promoter region of *TLR2* contributed to enhanced inflammatory responses in the airway epithelium of CF patients in response to bacterial peptidoglycan (145). Different PTMs of histones can modulate the front-line innate immune defenses in response to pathogen invasion (Figure 2). For example, acetylation of histones allows for more permissive chromatin structure facilitating gene expression. Upon stimulation with LPS, the activation of MAPK pathway leads to phosphorylation of H3S10 and additional acetylation of H3S10K14 at the promoter of *IL12*, leading to chromatin opening for NF-κB and induction of IL-12 expression (146). Furthermore, an increased acetylation of H3K18 was observed in *STAT6* locus in the airway epithelial cells of asthmatic patients (147). Although that study did not show increased STAT6 expression, it is known that STAT6 signaling is affected in asthma and, together with elevated levels of IL-4 and IL-13 driven by Th2 immune responses, leads to mucus hypersecretion in mice, which is a characteristic for asthma, COPD, and CF (148). Moreover, the treatment of asthmatic airway epithelial cells with IL-4 and IL-13 caused the impairment of the airway epithelial barrier integrity concomitant with enhanced expression of HDACs (1 and 9) and sirtuins (SIRT6 and 7). Interestingly, inhibition of HDACs in asthmatic airway epithelial cells by quisinostat (class I and II HDAC inhibitor) improved the epithelial barrier integrity by increasing the expression of TJ proteins (149). On the other hand, inhibition of

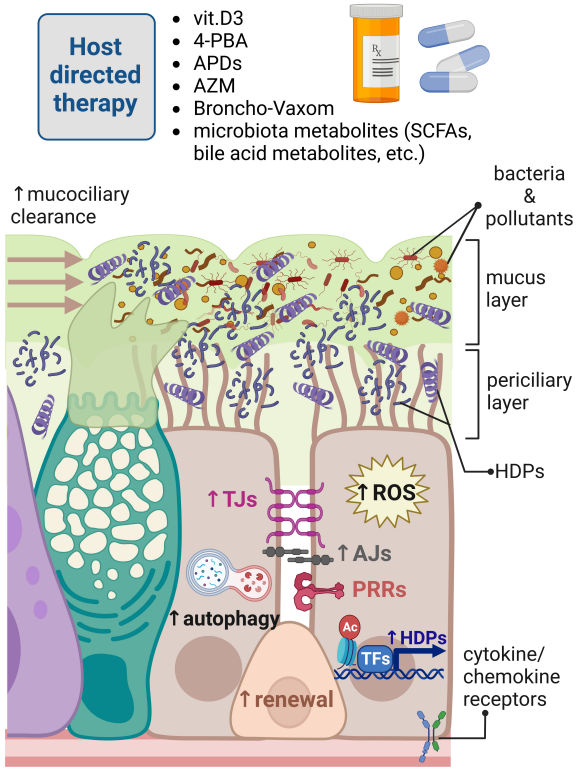

FIGURE 2
Modulation of innate immune responses in human respiratory epithelium for host-directed therapy. Different innate immunity inducers vitamin D3, 4-phenylbutyrate (4-PBA), aroylated phenylenediamines (APDs), Broncho-Vaxom (bacterial lysates), and microbiota metabolites can boost innate immune responses in the respiratory epithelium fending off pathogens invading mucosal surfaces of the respiratory tract. These responses are exerted by enhancement of the mucociliary clearance, removing dead bacteria and inhaled pollutants neutralized by increased expression of host defense peptides (HDPs) through the epigenetic modulation of histone epigenetic marks and transcriptional regulation. Innate immunity inducers and azithromycin (AZM) can also strengthen epithelial barrier integrity providing physical barrier for invading pathogens. Innate immunity modulators can increase autophagy and production of reactive oxygen species (ROS) for effective elimination of foreign molecules and microbes. Bacterial lysates, such as Broncho-Vaxom, can stimulate pathogen recognition receptors (PRRs), perhaps to train epithelial innate immunity through imprinting innate immune memory in renewing epithelial cells. Created with BioRender.com.

HDACs for example, by deletion of *Hdac1* in mice exposed to the allergen caused more stable Th2 immune responses resulting in mucus hypersecretion by goblet cells, demonstrating an important role of HDAC1 in allergic diseases (150). The enzyme HDAC2 can suppress NF-κB and AP-1 signaling leading to the inhibition of proinflammatory response caused by stimulation of TLR4. Interestingly, the downregulation of HDAC2 in lungs of COPD patients and rats exposed to cigarette smoke suggest that HDAC2 expression is modulated in response to environmental factors and protects from inflammation and mucus hypersecretion during homeostasis (148, 151, 152). Unlike HDAC2, exposition to cigarette smoke increased expression of HDAC6 enhancing autophagy. Rapid protein turnover due to increased autophagy led to shortening of the ciliary length that contributes to impaired mucociliary clearance observed in COPD. These effects were diminished in *Hdac6*$^{-/Y}$ mice exposed to cigarette smoke, suggesting the inhibition of HDAC6 as a potential therapeutic target for COPD treatment (153, 154). Apart from HDAC6, many epigenetic modifiers are suggested to regulate autophagy processes (155), such as EZH2 methyltransferase responsible for the trimethylation of H3K27 shown to inhibit autophagy (156). The importance of EZH2 was demonstrated to regulate differentiation of airway epithelial stem cells that is aberrant in *Ezh2*-deficient mice resembling an altered airway epithelial cell differentiation typical for COPD (157). Overall, the epigenetic regulation of innate immune responses is intensively investigated, and the studies showing epigenetic regulation of HDPs in the lung epithelium are ongoing (158).

How pathogens subvert host innate immune defenses in lungs

Efficient innate immune responses in airway mucosa are essential for maintaining respiratory functions. The mucosal surface of the airways is also an initial site for pathogens interaction with the host. Many pathogens can subvert airway mucosal defense mechanisms and cause disease, especially in immunocompromised individuals. In this section, we will discuss those strategies based on the selected examples of respiratory pathogens that mainly concentrate on bacteria, as those were extensively studied throughout the years in comparison to viruses and fungi. Viral subversions mechanisms of host innate immune responses in lungs has recently gained more attention due to SARS-CoV-2 pandemic, while little is known about fungal strategies that seems to be relevant, especially in the development of severe fungal infections in immunocompromised individuals.

Bacteria

Pseudomonas aeruginosa (Pa) is an opportunistic pathogen usually harmless for healthy people; however, it can cause pneumonia in vulnerable immunocompromised individuals like patients with chronic respiratory diseases, such as CF, COPD, and hospitalized patients with supportive mechanical ventilation. Pa is known to use different strategies and virulence factors for the effective colonization of the host mucosal surfaces (159). The bacteria utilize flagellin for movement and pili for adhesion to the host cells. Once the host–pathogen adhesion is established, Pa injects bacterial toxins, such as ExoS to the host cells by type 3 secretion system (T3SS) causing acute infection (160). Furthermore, lung tissue damage in pneumonia is caused by disruption of the airway TJs and AJs integrity by Pa elastase that also degrades collectins (SP-A and SP-D), collagen, complement components, and LL-37 (159, 161). Pa rhamnolipids also disrupt TJs integrity in the airway epithelium facilitating Pa invasion (162). As an additional virulence factor, pyocyanin impairs ciliary function and inhibits host catalase, which contributes to the oxidative lung damage (163, 164). Furthermore, Pa competes for the iron source

with host antimicrobial effectors, necessary for the activity of antimicrobial effector, lactoferrin, in the airway epithelium (165). Depending on the local environment of the host airway epithelium, especially during mucus clogging in CF and COPD, Pa can switch strategy of host colonization, from the invasive to a more adaptative one by formation of the biofilm. Quorum-sensing mechanisms allow for the communication of bacteria thriving in the biofilm and involve bacterial molecules, such as acyl homoserine lactones (AHL). At the same time, bacterial molecules involved in quorum sensing affect host cells; for example, AHL facilitates apoptosis of neutrophiles but not the host's airway epithelial cells (166). In addition, 2-aminoacetophenone enhances the host's HDAC1 activity suppressing proinflammatory response that facilitates bacterial survival (167). Moreover, Pa in biofilm produces alginate, a mucopolysaccharide used for bacterial encapsulation increasing bacterial fitness to persist on the mucosal surfaces of CF patients (168). These bacterial biofilm subversion and evasion mechanisms of the host's innate immune defenses facilitate chronic Pa infection that can be very difficult to eliminate by antibiotics and contributes to development of antibiotic resistance. Many opportunistic pathogens have gained resistance to antibiotics routinely used for the treatment of infections. Therefore, Pa has been included in a group of ESKAPE pathogens (ESKAPE stands for the group of pathogens: *Enterococcus faecium*, *Staphylococcus aureus*, *Klebsiella pneumoniae*, *Acinetobacter baumanii*, *Pseudomonas aeruginosa*, and *Enterobacter* spp.) that cause nosocomial infections (169).

Klebsiella pneumoniae (Kp) is another pathogen from the ESKAPE group causing pneumonia. Kp is well-known to contain several antibiotic resistance genes, including extended-spectrum beta-lactamase (ESBL), and carbapenemase encoding genes, which is referred to as a multidrug-resistant (MDR) Kp. Apart from gaining antibiotic resistance genes, Kp utilizes a variety of well-described strategies to evade host innate immune responses, especially affecting host innate immune cells (170), for instance, by interference with TLR signaling in macrophages exerted by targeting sterile alpha and TIR motif containing 1 (SARM1) protein to reduce inflammation and enhance IL-10 production (171). The interaction of Kp with the airway epithelial cells remains the first step of infection that is not well-characterized, and it is likely that Kp utilizes several strategies to compromise host epithelial front-line defenses. Kp secretes ytfL virulence factor that alters cytoskeleton organization in human and mouse airway epithelial cells by disassembling microtubules network (172). Kp translocation through airway epithelium mediated by induction of IFN-λ reduces the host airway epithelial barrier integrity that can facilitate bacterial invasion (173). Furthermore, the encapsulation of Kp with a polysaccharide coat has been considered as a determinant of bacterial virulence. Kp encapsulation limits bacterial binding by the complement component present on the airway mucosal surfaces and reduces bacterial clearance by the host epithelial cells (174). Recent studies showed that encapsulation helps Kp to overcome mouse innate immune defenses in the upper airways primed by microbiota through stimulation of IL-17A expression (175). Interestingly, a recent study indicates that asymptomatic colonization of the gut with MDR-Kp exacerbates pneumonia caused by Pa infection. Altered signaling on the gut–lung axis is caused by MDR-Kp-mediated dysbiosis resulting in reduced production of short-chain fatty acids (SCFAs) and reduced numbers of macrophages and DCs in the lung (176).

Streptococcus pneumoniae (Sp) is a respiratory pathogen frequently causing pneumonia (177). The virulence of Sp is associated with secretion of toxin, pneumolysin, exhibiting cytotoxic effect on the host cells accompanied with disintegration of TJs between host epithelial cells for Sp translocation (178). In addition, the cytotoxic effect of pneumolysin is caused by DNA damage associated with the cell cycle arrest (179). Another bacterial virulence factor is pyruvate oxidase SpxB responsible for H_2O_2 production and release of pneumolysin (180). Both virulence factors, pneumolysin with contribution of SpxB, were shown to reduce the host innate immune signaling through epigenetic mechanisms. Infection of mice and human airway epithelial cells with Sp led to the activation of the host phosphatase PP1 by its dephosphorylation, which further dephosphorylated histone 3 on serine 10 in the host cells promoting Sp intracellular expansion (181). Sp modifies a component of the cell wall, lipoteichoic acid, to increase its charge to resist host HDPs. Moreover, Sp serine protease PrtA is suggested to cleave HDPs (182, 183). The use of PrtA virulence factor as an antigen has been suggested to develop new vaccines in combination with other antigens to resolve problems of pneumococcal serotype specificity based on the fact that PrtA can also induce protective immunity in certain animal infection models (184). Another study by Biswas et al. showed that group A *Streptococcus*, mainly responsible for necrotizing fasciitis and rarely pneumonia, cleaves the host defense peptide LL-37 with ScpN protease into two shorter peptides that retained bactericidal properties. However, LL-37 cleavage products lost their immunomodulatory properties connected to the activation of P2X7 and EGFR signaling involved in neutrophil bacterial clearance and tissue regeneration, respectively (185, 186).

The respiratory pathogen *Mycobacterium tuberculosis* (Mtb) can bypass host immune defenses by hijacking host cell signaling in macrophages, neutrophiles, and DCs. This way, Mtb creates a favorable intracellular niche where bacteria can replicate and infect other cells or persist for decades in a latent state (187). In the initial step of bacterial colonization, Mtb infects respiratory epithelial cells and macrophages, while 7 days post-infection, the bacteria are present only in macrophages, indicating that bacteria do not replicate in epithelial cells (188). Interestingly, in the zebrafish model, a lipid component of *Mycobacterium marinum* outer membrane phthiocerol dimycocerosate (PDIM) spreads into the epithelial cell membrane and inhibits TLR/MyD88 signaling limiting recruitment of monocytes (189). In humans, Mtb selectively targets uptake by pulmonary macrophages that translocate to the lung interstitium and infect other types of cells. This process is mediated by Mtb virulence factor Esx-1 and the host IL-1β signaling (188). Despite activation of additional host innate immune components connected to the redox signaling, Mtb produces KatG and NuoG virulence proteins that neutralize and inhibit further production of ROS by macrophages and neutrophiles (190, 191). Moreover, CpsA allows Mtb to escape autophagic clearance in macrophages by blocking NADPH oxidase

recruitment to the Mtb-containing phagosomes and activation of LC3-associated phagocytosis (192). Mtb creates its own intracellular niche for survival by altering host lipid metabolism, creating the formation of foamy macrophages with characteristic lipid droplets (193). Mechanisms of Mtb evasion and subversion of host immune responses in macrophages and other immune cells are thoroughly described in a recent review (187) that explains why only approximately three Mtb bacterial cells are sufficient for effective colonization of the host (194), indicating a highly advanced Mtb virulence system.

A better understanding of how bacteria breach the host innate defenses on the airway mucosal surfaces to further hijack the host cellular machinery for intracellular survival could result in the development of more efficient therapies. Studies on the molecular mechanism of bacterial virulence factors for host colonization are especially important in the context of immunocompromised individuals suffering from severe infections.

Viruses

Viruses use a variety of different strategies to compromise the host innate immune defenses and effectively replicate within the host cells or remain in the latent state. Due to the recent pandemic, the majority of research has concentrated on the strategies used by SARS-CoV-2 coronavirus to evade host innate immune responses (195). Yin et al. showed that the host IFN response mediated through intracellular PRRs—MDA5, LGP2, and NOD2—is delayed by several hours in comparison to the kinetics of the viral replication, indicating the viral-strategy-limiting effects of IFNs (196). Moreover, SARS-CoV-2 produces viral endonuclease EndoU that cleaves viral RNA and blocks phosphorylation of STAT1 and STAT2 and their nuclear translocation to inhibit host innate immune responses (197, 198). Subsequently, the virus produces ORF8 protein that disrupts PTMs of host histones promoting closed chromatin state and suppression of host innate anti-viral responses, allowing for viral replication (199). Another virus commonly causing respiratory tract infections, especially harmful for newborns and infants, is RSV, and there is no vaccine available (200). An effective RSV replication within host cells is achieved by initial induction of autophagy and then by blocking autophagosome–lysosome fusion in human airway epithelial cells. This strategy most likely allows to form a replication-favorable niche for the virus inside the autophagosome vesicle (201). The "mimicry" of host chemokines is used to promote infection by RSV, more precisely by the interaction of viral G protein binding receptor with CX3CL1 that facilitates RSV infection (202). The group of Rhinoviruses are the common group of pathogens attacking the host respiratory system causing cold (203). Human rhinoviruses C group (HRV-C) were shown to disrupt epithelial barrier integrity and to alter host metabolism towards glycolysis and fatty acid biosynthesis, facilitating viral replication (204). Rhinoviruses also target another RNA RLRs, such as STING trafficking into viral replication organelles through interaction with PI4P (205). Interestingly, recently, it has been shown that disruption of the circadian clock and expression of immune response genes encoding chemokine receptors (Ccr2, Ccr3, Ccr5, Ccr6, etc.) due to sleep deprivation make mice more susceptible to viral infections, highlighting the importance of environmental factors determining host immune responses against viral infections (206).

Fungi

Fungal pathogens have developed specific strategies to evade the host immune responses (207). Among them are *C. albicans* triggering oropharyngeal candidiasis, *Aspergillus* ssp. causing pulmonary aspergillosis, and *Pneumocystis* and *Cryptococcus* causing pneumonia (208). *Candida albicans* avoids host responses by neutralization of the host complement components by proteolytic cleavage with aspartyl proteases (209). Moreover, *Aspergillus*, *Mucorales*, and *Candida* spp. cause coronavirus disease (COVID)-associated fungal infections, and aspergillosis was the most prevalent in the group of patients treated with corticosteroids and tocilizumab (210). *Cryptococcus neoformans* evades host innate immune responses, for example, by encapsulation with polysaccharides glucuronoxylomannan (GXM) that inhibits NETs formation (211). Furthermore, *C. neoformans* also produces giant fungal cells, the so-called titan cells, to avoid phagocytosis and killing by ROS, hence considered as a fungal strategy used to establish pulmonary infections (212). Fungal infections are often a complication of the antibiotic treatment because of microbiota dysbiosis, where opportunistic fungal species, such as mentioned *C. albicans*, expand on the host mucosal surfaces forming a biofilm. Those biofilms composed of fungal and bacterial components are hard to eradicate, especially in CF and immunocompromised patients (24); therefore, development of new therapies against such biofilms is needed.

Modulation of lung innate immunity to overcome pathogen subversion mechanisms

Pathogens quickly adapt to the changing environment, and this includes the presence of antibiotics. The excessive use of antibiotics in the healthcare and animal husbandry has led to the selection for antimicrobial resistance (AMR), which resulted in a global problem that caused 4.95 million of AMR-associated deaths in 2019 (213). Antibiotic resistance occurs in most countries, and many opportunistic pathogens have gained resistance to antibiotics routinely used for the treatment of infections. It is estimated that 63.5% of all infections caused by multidrug-resistant strains were connected to the healthcare (214). Despite of the increasing social awareness on the proper antibiotic use, general reduction in prescribed antibiotics, and a better control of nosocomial infections, the spreading of AMR genes in some pathogens remained unchanged (215, 216). In addition, the development of new antibiotics is a long and costly process, taking several years until the new drug is introduced to the market resulting, in only few developed drugs in the last decades (217). Therefore, alternative

strategies for the treatment of infectious diseases have gained more attention. By deciphering molecular pathways of host innate immunity and pathogen's infection strategies, an opportunity of modulating these mechanisms might result in the development of novel alternative treatment approaches, limiting and/or reducing the use of antibiotics and thereby reducing the selection of AMR strains. Therefore, in our research, we postulate the concept of host-directed therapy (Figure 2) executed through the modulation of epithelial and macrophages innate immune responses by enhancing expression of HDPs, improvement of the epithelial barrier integrity, and stimulation of autophagy. Our concept of host-directed therapy can be extended to the restoration of mucociliary clearance and ion balance, training innate immune system *via* controlled TLR stimulation and epigenetic modulation of host innate immune responses. The approach of host-directed therapy does not anticipate replacement of the antibiotics—it is rather a supplementary treatment that can reduce time of antibiotic use in case of persistent infections requiring a long antibiotic treatment, such as tuberculosis and infections requiring prolonged treatment due to poor bioavailability of the drug in the tissue (218). In this section, we will discuss different angles of host-directed therapy for modulation of lung epithelial innate immune responses.

One of the directions in the field is the direct use of HDPs and their analogues, mainly for topical administration (219). Synthetic analogues of HDPs have also been tested in a mouse model of severe lung infection caused by highly virulent *P. aeruginosa*. Nasal instillation of IDR-1002 peptide followed by bacterial infection reduced bacterial count in bronchoalveolar fluid and inflammatory response, indicating therapeutic potential of preventive administration of HDP analogues (220). Although promising, this approach usually uses only one peptide monotherapy, which carries a risk of development bacterial resistance to HDPs, which has been claimed to be limited, however a possible scenario (221). Therefore, the use of HDPs mixture would be a better strategy than a single peptide monotherapy to avoid AMR development, which seems to be highlighted by the fact that in physiological conditions, pathogens usually encounter a mixture of different antimicrobial effectors present on mucosal surfaces. Another aspect is the cost of the production of synthetic peptides and their purification on a bigger scale. Therefore, we suggest an alternative approach by inducing expression of natural HDPs in the epithelial cells and tissue-residing immune cells, which has several advantages in comparison to using synthetic HDPs and their derivatives. First, several antimicrobial effectors are induced, at the same time limiting the risk for the selection of antibiotic resistance. Second, using different innate immune modulators allows for the precise regulation of the HDPs induction and its cessation if needed. Third, the use of different non-peptide inducers for host-directed therapy is expected to reduce the cost of production, making it more accessible for pharmacological use. Those innate immune inducers/modulators were explored by our research group and collaborators and initially included nutrients and bacterial metabolites (like vitamin D3 and butyrate) and further expanded to synthetic chemical compounds (such as aroylated phenylenediamines (APDs)) (Figure 2) (218). Among the nutrients, vitamin D3 was shown to induce cathelicidin expression *via* activating vitamin D receptor (VDR) from the group of nuclear receptors binding to the vitamin D responsive elements (VDRE) present in human cathelicidin gene promoter (222, 223). Lung epithelial cells were shown to express the enzyme CYP27B1 involved in conversion of a precursor 25-hydroxyvitamin D3 to an active 1α,25-dihydroxyvitamin D3 that induced cathelicidin expression, indicating the importance of the vitamin D3 levels for mucosal antimicrobial defenses (30). Interestingly, VDREs are absent in mouse *CRAMP* promoter, making the translation of research on vitamin D3 inducer to mouse models difficult. For that reason, the novel transgenic model of humanized mice was established recently and contains human VDRE in the promoter of mouse *CRAMP* gene, opening a new avenue for the studies on vitamin D3 (224). Another inducer of cathelicidin expression in lung epithelium and macrophages is butyrate, a short-chain fatty acid produced by microbiota commensal bacteria from Firmicutes phylum (225). Butyrate constitutes the primary energy source for colonocytes, exerting local immunomodulatory effects on the colonic epithelia, tissue residing immune cells, and gastrointestinal (GI)-distant organs because butyrate is distributed with blood similar to other microbiota metabolites (218, 226). Butyrate is known from its strong odor; therefore, 4-phenylbuturate (hereafter phenylbutyrate or 4-PBA) was used in the studies as an odorless butyrate derivative, which is an FDA-approved drug for treatment of the urea cycle disorders used as ammonia scavenger (227). Phenylbutyrate was shown to induce cathelicidin expression in the airway epithelium (Figure 2) and induced autophagy in Mtb-infected macrophages through induction of LL-37 acting *via* P2X7 receptor (228, 229). Phenylbutyrate also counteracted the downregulation of cathelicidin expression in lungs of *Shigella*-infected rabbits, mitigating pathogens strategy of effective host colonization (230, 231). Phenylbutyrate is an inhibitor of histone deacetylases (HDACs)—histone-modifying enzymes facilitating chromatin opening state by acetylation of histones. Although *CAMP* gene expression was induced by phenylbutyrate, the increased acetylation of histone 3 and histone 4 was not observed in the promoter of *CAMP* gene (228). Therefore, the detailed mechanism of *CAMP* induction by phenylbutyrate remains unknown, perhaps requiring analysis of more specific histone modifications in *CAMP* promoter. The combination of 1,25-dihydroxyvitamin D3 and 4-PBA is so far the most potent inducer of cathelicidin expression in the human model of the lung epithelium, most likely by combing transcriptional regulation of vitamin D3 and epigenetic modulation by 4-PBA. Importantly, the combination of vitamin D3 and 4-PBA has clinical translational potential and was shown to be effective in the clinical trial of the Mtb treatment combined with standard antibiotics. Patients with tuberculosis receiving phenylbutyrate and vitamin D3 showed faster clearance of Mtb in sputum samples than the group receiving placebo, indicating beneficial effects of host-directed therapy combined with antibiotics (232, 233).

Moreover, in respect to the lung epithelium, other inducers of HDPs were tested from a novel class of compounds called aroylated phenylenediamines (APDs) (Figure 2). Two synthetic APD-compounds, derivatives of Entinostat, which is another HDAC

inhibitor known to induce *CAMP* gene expression, were shown to induce expression of antimicrobial effectors cathelicidin, calprotectin, lipocalin, and defensins. Of note, APDs were less toxic than Entinostat and did not induce proinflammatory responses (32, 234). Furthermore, innate immune inducers 4-PBA, vitamin D3, and APD compound were able to sensitize MDR *K. pneumoniae* to conventional antibiotics. The intracellular bacterial killing mechanism in infected macrophages was cathelicidin dependent for 4-PBA and vitamin D3 and ROS dependent for APD compound (235). This approach presents another angle on host-directed therapy, utilizing modulation of host innate immune responses and sensitization of multidrug-resistant pathogens to conventional antibiotics. Moreover, APD-compound induced autophagy in the differentiated lung epithelial cells through the epigenetic modulation of the H3K27 acetylation and AMP-activated protein kinase (AMPK) signaling (236). The preventive treatment of differentiated lung epithelial layers with APD compound enhanced the epithelial barrier integrity provided by tight junction's proteins occludin and ZO-1 when differentiated monolayer cells were challenged with *P. aeruginosa*-conditioned medium (32). Interestingly, one of the most often prescribed antibiotics, azithromycin, was shown independently of its microbicidal properties to modulate host's epithelial cell responses by strengthening epithelial integrity in the lung (Figure 2). This can be paradoxically considered as a positive side effect of azithromycin treatment that benefits cystic fibrosis patients by improving their condition (237). Azithromycin was shown to enhance epithelial barrier integrity by increasing trans-epithelial electrical resistance (TEER) and counteract the disruptive effect of *P. aeruginosa*-conditioned medium (238). Furthermore, azithromycin was shown to have a barrier protective effect and counteract proinflammatory response inflicted on the bronchial epithelia by cyclical mechanical stress during mechanical ventilation generated by a cyclical pressure air–liquid interface device (CPAD) (239). The supporting evidence suggest that the protective effect of azithromycin on lung epithelia is exerted by increased lamellar body formation and stimulation of epidermal differentiation (240). However, azithromycin is an antibiotic; therefore, prolonged use of azithromycin to strengthen the epithelial barrier is restricted because of the risk for antibiotic resistance development. Importantly, the mechanism behind strengthening of the lung epithelial barrier integrity by azithromycin and APDs remain unknown, and it is a subject of the ongoing research (32, 235, 236, 239, 240). On the contrary, vitamin D3 did not have this functional effect on the epithelial barrier strengthening while administered over the course of lung epithelial differentiation. Instead, it led to thickening of the lung epithelial layer *in vitro* displaying features of squamous metaplasia, indicating that this effect in the lung is tissue specific and is contrary to what has been observed in the gut (241). The group of Jun Sun showed that vitamin D3 regulates expression of a tight junction protein claudin-2, demonstrating the potential of VDR to regulate gut epithelial barrier integrity (242, 243). Different effects of innate immune inducers have been described depending on the tissue type, which may suggest possible epigenetic regulation of the epithelial barrier function. This concept seems to be additionally supported by the fact that many different respiratory tract diseases are associated with changes in the expression of histone-modifying enzymes, such as increased expression of histone deacetylases, HDACs (1 and 9) and sirtuins (SIRT6 and 7), in asthmatic bronchial epithelial cells. Inhibition of the HDACs with quisinostat (JNJ-26481585) in bronchial epithelial cells from asthmatic patients and allergic rhinitis improved epithelial barrier integrity by affecting expression and reorganization of TJs (149, 244). Recently, azithromycin was shown to attenuate wheezing in patients recovering from pulmonary inflammation. Azithromycin treatment helped to reduce time of wheezing for those patients, and these changes were associated with reduced expression of EZH2 (histone methyltransferase responsible for methylation of H3K27me3), reduced methylation of H3K27me3, and reduced expression of p65, suggesting that azithromycin exerts anti-inflammatory properties through epigenetic regulation (245). Overall, epigenetic modulation is part of the natural physiological regulation of innate immune responses in epithelial tissues and immune cells exerted by microbiota-produced metabolites of dietary products, highlighting the future directions for modulation of host innate immune responses through epigenetic therapies utilizing natural and synthetic epigenetic modulators. It is important to keep in mind that epigenetic therapies may exert off-target effects on other tissues, making the precise regulation difficult to control. However, transient epigenetic modulation over a short period of time with relatively rapidly degraded synthetic compounds and natural products, such as microbiota-produced butyrate, seems to be a reasonable approach.

In line with host-directed therapy is the concept of trained immunity responses for the treatment and prevention of respiratory tract infections. A type of immunotherapy with Broncho-Vaxom, a lyophilizate of the dead bacterial strains causing respiratory tract infections, such as *K. pneumoniae*, *S. aureus*, *Streptococcus pyogenes*, and *Neisseria catarrhalis*, is used to train immune responses in patients suffering from recurrent infections of upper and lower respiratory tract (Figure 2). Broncho-Vaxom showed efficiency in reducing recovery time and course of disease in pediatric patients with recurrent respiratory tract infections (246, 247). Beneficial effects of Broncho-Vaxom® (OM-85 BV) on human sinonasal epithelial cells were mediated through stimulation of the taste-receptor T2R signaling, leading to the production of nitric oxide (NO) responsible for direct bacterial killing and increased ciliary beating (248). Treatment of bronchial epithelial cells with bacterial lysates of Broncho-Vaxom protects epithelia from SARS-CoV-2 entry by reducing expression of host receptors used by the virus such as angiotensin-converting enzyme 2 (ACE2) (249, 250), suggesting that this form of host-directed therapy can be used as a preventive strategy to limit acute respiratory disease, for example in constantly exposed health workers (ClinicalTrials.gov Identifier: NCT04496245).

The concept of trained immunity refers to innate immunological memory previously attributed only to the adaptive immune responses. Trained immunity boosts secondary responses to infections or sterile inflammation after initial contact with the stimuli for the next faster and more efficient host responses. Although trained immunity responses are T- and B-cell

independent, they complement the adaptive immune responses to maximize chances for the host survival. The innate immunological memory can be achieved by stimulation of innate immune cells, such as macrophages, NK cells, DCs, fibroblasts, and tissue-specific stem cells (251, 252). The primary example of trained immunity is *Bacillus* Calmette–Guérin (BCG) vaccination used routinely in vaccination against tuberculosis and shown to reprogram hematopoietic stem cells to differentiate towards monocytes/macrophages with enhanced capabilities of Mtb clearance. Unlike subcutaneous BCG vaccination, intravenous BCG administration enhanced myelopoiesis and rewired epigenetic program in bone-marrow-derived macrophages connected to the changes in the H3K27ac and H3K4me3 marks for more efficient Mtb clearance that was IFNγ dependent (253). Microbiota metabolites have also been identified as elicitors of trained immunity. One of them is butyrate that affects the trajectory of antimicrobial responses in macrophages by imprinting antimicrobial program in differentiating macrophages through HDAC3 inhibition, resulting in the induction of calprotectin and enhanced bacterial clearance through autophagy (254). Another microbiota metabolite, deoxycholic acid (DCA), a secondary bile acid detected in the bloodstream, is shown to enhance differentiation of granulocyte-monocyte precursors in the bone marrow through epigenetic alterations, providing innate protection against parasite *E. histolytica*. Interestingly, DCA in sera of children from Bangladesh who previously have documented history of amebiasis had lower levels of DCA than those who never suffered from infection (255). Trained immunity was also described in the lung in the context of the allergic inflammatory memory inflicted on basal lung stem cells by IL-4 and IL-13 exposure. The chronic exposure of respiratory epithelial progenitor cells to the inflammatory type 2 immune responses shifts their differentiation program causing epithelial barrier dysfunction observed in chronic allergic diseases, resulting in rhinosinusitis and taking more extreme form of nasal polyps (256). Overall, trained immunity can be achieved by exposition of tissue-specific stem cells and their progenitors to different stimuli imprinting innate immune responses through metabolic and epigenetic reprogramming (257).

Future perspectives

Innate immunity of the lung epithelial surfaces is a complex system working together with the adaptive immune responses for host defense and survival. Many aspects of the innate immune regulation and the link between innate and adaptive immune responses remain to be further elucidated. These include characterization of the role of new types of cells in the respiratory epithelium identified by single-cell RNA sequencing in shaping local innate immune responses and epigenetic modulation of such responses. An exciting avenue is the exploration of how different microbiota metabolites shape host immune responses in lung epithelial cells for better protection against pathogens with defining molecular mechanism that can be further extended to the development of the synthetic compounds for host-directed therapy. Defining pathogen's effectors subverting host innate immune responses, especially in the context of compromised host innate immunity, include future steps of interest for the development of new treatment strategies. Furthermore, the concept of trained immunity mainly characterized in respect to immune cells remains to be further investigated in lung epithelial cells answering the questions on programming our epithelial cells, how innate immune memory confers to better host protection mechanisms, and whether there are any links to the development of chronic inflammatory diseases with defining environmental stimuli that shape such responses.

Author contributions

The conceptualization of the manuscript was based on ITM's PhD dissertation thesis from year 2021. ITM wrote and edited the manuscript including figures created with BioRender.com under license agreement. GHG commented and edited the manuscript. All authors contributed to the article and approved the submitted version.

Funding

GHG was supported by grants from Icelandic Research Fund (RANNÍS) and University of Iceland Research Fund.

Conflict of interest

GHG is a founder and stockholder in Akthelia Pharmaceuticals that holds a patent on APD compounds Patent No. US 9,957,226 B2.

The remaining author declare that the research was conducted in the absence of any commercial or financial relationships that could be construed as a potential conflict of interest.

Publisher's note

References

1. Whitsett JA, Alenghat T. Respiratory epithelial cells orchestrate pulmonary innate immunity. *Nat Immunol* (2015) 16:27–35. doi: 10.1038/ni.3045

2. Zepp JA, Morrisey EE. Cellular crosstalk in the development and regeneration of the respiratory system. *Nat Rev Mol Cell Biol* (2019) 20:551–66. doi: 10.1038/s41580-019-0141-3

3. Hewitt RJ, Lloyd CM. Regulation of immune responses by the airway epithelial cell landscape. *Nat Rev Immunol* (2021) 21:347–62. doi: 10.1038/s41577-020-00477-9

4. Davis JD, Wypych TP. Cellular and functional heterogeneity of the airway epithelium. *Mucosal Immunol* (2021) 14:978–90. doi: 10.1038/s41385-020-00370-7

5. Deprez M, Zaragosi LE, Truchi M, Becavin C, García SR, Arguel MJ, et al. A single-cell atlas of the human healthy airways. *Am J Respir Crit Care Med* (2020) 202:1636–45. doi: 10.1164/rccm.201911-2199OC

6. Reynolds SD, Malkinson AM. Clara Cell: progenitor for the bronchiolar epithelium. *Int J Biochem Cell Biol* (2010) 42:1–4. doi: 10.1016/j.biocel.2009.09.002

7. Rawlins EL, Okubo T, Xue Y, Brass DM, Auten RL, Hasegawa H, et al. The role of Scgb1a1+ Clara cells in the long-term maintenance and repair of lung airway, but not alveolar, epithelium. *Cell Stem Cell* (2009) 4:525–34. doi: 10.1016/j.stem.2009.04.002

8. Iwasaki A, Foxman EF, Molony RD. Early local immune defences in the respiratory tract. *Nat Rev Immunol* (2017) 17:7–20. doi: 10.1038/nri.2016.117

9. Chen G, Korfhagen TR, Xu Y, Kitzmiller J, Wert SE, Maeda Y, et al. SPDEF is required for mouse pulmonary goblet cell differentiation and regulates a network of genes associated with mucus production. *J Clin Invest* (2009) 119:2914–24. doi: 10.1172/JCI39731

10. Rock JR, Onaitis MW, Rawlins EL, Lu Y, Clark CP, Xue Y, et al. Basal cells as stem cells of the mouse trachea and human airway epithelium. *Proc Natl Acad Sci U.S.A.* (2009) 106:12771–5. doi: 10.1073/pnas.0906850106

11. Ruysseveldt E, Martens K, Steelant B. Airway basal cells, protectors of epithelial walls in health and respiratory diseases. *Front Allergy* (2021) 2:787128. doi: 10.3389/falgy.2021.787128

12. Hansson GC. Mucins and the microbiome. *Annu Rev Biochem* (2020) 89:769–93. doi: 10.1146/annurev-biochem-011520-105053

13. Garciá SR, Deprez M, Lebrigand K, Cavard A, Paquet A, Arguel MJ, et al. Novel dynamics of human mucociliary differentiation revealed by single-cell RNA sequencing of nasal epithelial cultures. *Development* (2019) 146:dev177428. doi: 10.1242/dev.177428

14. Ualiyeva S, Hallen N, Kanaoka Y, Ledderose C, Matsumoto I, Junger WG, et al. Airway brush cells generate cysteinyl leukotrienes through the ATP sensor P2Y2. *Sci Immunol* (2020) 43):eaax7224. doi: 10.1126/sciimmunol.aax7224

15. Strine MS, Wilen CB. Tuft cells are key mediators of interkingdom interactions at mucosal barrier surfaces. *PloS Pathog* (2022) 18:e1010318. doi: 10.1371/journal.ppat.1010318

16. Tizzano M, Gulbransen BD, Vandenbeuch A, Clapp TR, Herman JP, Sibhatu HM, et al. Nasal chemosensory cells use bitter taste signaling to detect irritants and bacterial signals. *Proc Natl Acad Sci U.S.A.* (2010) 107:3210–5. doi: 10.1073/pnas.0911934107

17. Branchfield K, Nantie L, Verheyden JM, Sui P, Wienhold MD, Sun X. Pulmonary neuroendocrine cells function as airway sensors to control lung immune response. *Science* (2016) 351:707–10. doi: 10.1126/science.aad7969

18. Harkema JR, Carey SA, Wagner JG. The nose revisited: a brief review of the comparative structure, function, and toxicologic pathology of the nasal epithelium. *Toxicol Pathol* (2006) 34:252–69. doi: 10.1080/01926230600713475

19. Montoro DT, Haber AL, Biton M, Vinarsky V, Lin B, Birket SE, et al. A revised airway epithelial hierarchy includes CFTR-expressing ionocytes. *Nature* (2018) 560:319–24. doi: 10.1038/s41586-018-0393-7

20. Plasschaert LW, Žilionis R, Choo-Wing R, Savova V, Knehr J, Roma G, et al. A single-cell atlas of the airway epithelium reveals the CFTR-rich pulmonary ionocyte. *Nature* (2018) 560:377–81. doi: 10.1038/s41586-018-0394-6

21. Leiva-Juárez MM, Kolls JK, Evans SE. Lung epithelial cells: therapeutically inducible effectors of antimicrobial defense. *Mucosal Immunol* (2018) 11:21–34. doi: 10.1038/mi.2017.71

22. Lai Y, Gallo RL. AMPed up immunity: how antimicrobial peptides have multiple roles in immune defense. *Trends Immunol* (2009) 30:131–41. doi: 10.1016/J.IT.2008.12.003

23. Mansour SC, Pena OM, Hancock REW. Host defense peptides: front-line immunomodulators. *Trends Immunol* (2014) 35:443–50. doi: 10.1016/J.IT.2014.07.004

24. Mookherjee N, Anderson MA, Haagsman HP, Davidson DJ. Antimicrobial host defence peptides: functions and clinical potential. *Nat Rev Drug Discovery* (2020) 19:311–32. doi: 10.1038/s41573-019-0058-8

25. Gudmundsson GH, Agerberth B, Odeberg J, Bergman T, Olsson B, Salcedo R. The human gene FALL39 and processing of the cathelin precursor to the antibacterial peptide LL-37 in granulocytes. *Eur J Biochem* (1996) 238:325–32. doi: 10.1111/j.1432-1033.1996.0325z.x

26. Agerberth B, Gunne H, Odeberg J, Kogner P, Boman HG, Gudmundsson GH. FALL-39, a putative human peptide antibiotic, is cysteine-free and expressed in bone marrow and testis. *Proc Natl Acad Sci U.S.A.* (1995) 92:195–9. doi: 10.1073/PNAS.92.1.195

27. Yamasaki K, Schauber J, Coda A, Lin H, Dorschner RA, Schechter NM, et al. Kallikrein-mediated proteolysis regulates the antimicrobial effects of cathelicidins in skin. *FASEB J* (2006) 20:2068–80. doi: 10.1096/fj.06-6075com

28. Sørensen OE, Follin P, Johnsen AH, Calafat J, Sandra Tjabringa G, Hiemstra PS, et al. Human cathelicidin, hCAP-18, is processed to the antimicrobial peptide LL-37 by extracellular cleavage with proteinase 3. *Blood* (2001) 97:3951–9. doi: 10.1182/blood.V97.12.3951

29. Murakami M, Lopez-Garcia B, Braff M, Dorschner RA, Gallo RL. Postsecretory processing generates multiple cathelicidins for enhanced topical antimicrobial defense. *J Immunol* (2004) 172:3070–7. doi: 10.4049/jimmunol.172.5.3070

30. Hansdottir S, Monick MM, Hinde SL, Lovan N, Look DC, Hunninghake GW. Respiratory epithelial cells convert inactive vitamin d to its active form: potential effects on host defense. *J Immunol* (2008) 181:7090–9. doi: 10.4049/jimmunol.181.10.7090

31. Kulkarni NN, Yi Z, Huehnken C, Agerberth B, Gudmundsson GH. Phenylbutyrate induces cathelicidin expression *via* the vitamin d receptor: linkage to inflammatory and growth factor cytokines pathways. *Mol Immunol* (2015) 63:530–9. doi: 10.1016/J.MOLIMM.2014.10.007

32. Myszor IT, Parveen Z, Ottosson H, Bergman P, Agerberth B, Strömberg R, et al. Novel aroylated phenylenediamine compounds enhance antimicrobial defense and maintain airway epithelial barrier integrity. *Sci Rep* (2019) 9:7114. doi: 10.1038/s41598-019-43350-z

33. Bals R, Wang X, Zasloff M, Wilson JM. The peptide antibiotic LL-37/hCAP-18 is expressed in epithelia of the human lung where it has broad antimicrobial activity at the airway surface. *Proc Natl Acad Sci U.S.A.* (1998) 95:9541. doi: 10.1073/PNAS.95.16.9541

34. Lehrer RI. Primate defensins. *Nat Rev Microbiol* (2004) 2:727–38. doi: 10.1038/nrmicro976

35. Diamond G, Zasloff M, Eck H, Brasseur M, Lee Maloy W, Bevins CL. Tracheal antimicrobial peptide, a cysteine-rich peptide from mammalian tracheal mucosa: peptide isolation and cloning of a cDNA. *Proc Natl Acad Sci U.S.A.* (1991) 88:3952–6. doi: 10.1073/pnas.88.9.3952

36. Wilson CL, Ouellette AJ, Satchell DP, Ayabe T, López-Boado YS, Stratman JL, et al. Regulation of intestinal α-defensin activation by the metalloproteinase matrilysin in innate host defense. *Science* (1999) 286:113–7. doi: 10.1126/science.286.5437.113

37. Selsted M. θ-defensins: cyclic antimicrobial peptides produced by binary ligation of truncated α-defensins. *Curr Protein Pept Sci* (2005) 5:365–71. doi: 10.2174/1389203043379459

38. Currie SM, Findlay EG, McHugh BJ, Mackellar A, Man T, Macmillan D, et al. The human cathelicidin LL-37 has antiviral activity against respiratory syncytial virus. *PloS One* (2013) 8(8):e73659. doi: 10.1371/journal.pone.0073659

39. Sochacki KA, Barns KJ, Bucki R, Weisshaar JC. Real-time attack on single *Escherichia coli* cells by the human antimicrobial peptide LL-37. *Proc Natl Acad Sci U.S.A.* (2011) 108:E77–81. doi: 10.1073/pnas.1101130108

40. Rosenfeld Y, Papo N, Shai Y. Endotoxin (lipopolysaccharide) neutralization by innate immunity host-defense peptides: peptide properties and plausible modes of action. *J Biol Chem* (2006) 281:1636–43. doi: 10.1074/jbc.M504327200

41. Schneider VAF, Coorens M, Tjeerdsma-van Bokhoven JLM, Posthuma G, van Dijk A, Veldhuizen EJA, et al. Imaging the antistaphylococcal activity of CATH-2: mechanism of attack and regulation of inflammatory response. *mSphere* (2017) 2(6): e00370–17. doi: 10.1128/msphere.00370-17

42. Sass V, Schneider T, Wilmes M, Körner C, Tossi A, Novikova N, et al. Human β-defensin 3 inhibits cell wall biosynthesis in staphylococci. *Infect Immun* (2010) 78:2793–800. doi: 10.1128/IAI.00688-09

43. Tripathi S, Verma A, Kim E-J, White MR, Hartshorn KL. LL-37 modulates human neutrophil responses to influenza a virus. *J Leukoc Biol* (2014) 96:931–8. doi: 10.1189/jlb.4a1113-604rr

44. He M, Zhang H, Li Y, Wang G, Tang B, Zhao J, et al. Cathelicidin-derived antimicrobial peptides inhibit zika virus through direct inactivation and interferon pathway. *Front Immunol* (2018) 9:722. doi: 10.3389/fimmu.2018.00722

45. Sousa FH, Casanova V, Findlay F, Stevens C, Svoboda P, Pohl J, et al. Cathelicidins display conserved direct antiviral activity towards rhinovirus. *Peptides* (2017) 95:76–83. doi: 10.1016/j.peptides.2017.07.013

46. Ordonez SR, Amarullah IH, Wubbolts RW, Veldhuizen EJA, Haagsman HP. Fungicidal mechanisms of cathelicidins LL-37 and CATH-2 revealed by live-cell imaging. *Antimicrob Agents Chemother* (2014) 58:2240–8. doi: 10.1128/AAC.01670-13

47. Zasloff M. Antimicrobial peptides of multicellular organisms. *Nature* (2002) 415:389–95. doi: 10.1038/415389a

48. Ganz T. Defensins: antimicrobial peptides of innate immunity. *Nat Rev Immunol* (2003) 3:710–20. doi: 10.1038/nri1180

49. Zhang H, Porro G, Orzech N, Müllen B, Liu M, Slutsky AS. Neutrophil defensins mediate acute inflammatory response and lung dysfunction in dose-related fashion. *Am J Physiol Lung Cell Mol Physiol* (2001) 280(5):L947–54. doi: 10.1152/ajplung.2001.280.5.l947

50. Engelberg Y, Landau M. The human LL-37(17-29) antimicrobial peptide reveals a functional supramolecular structure. *Nat Commun* (2020) 11:1–10. doi: 10.1038/s41467-020-17736-x

51. Tayeb-Fligelman E, Tabachnikov O, Moshe A, Goldshmidt-Tran O, Sawaya MR, Coquelle N, et al. The cytotoxic *Staphylococcus aureus* PSMα3 reveals a cross-α amyloid-like fibril. *Science* (2017) 355:831–3. doi: 10.1126/science.aaf4901

52. Niyonsaba F, Iwabuchi K, Matsuda H, Ogawa H, Nagaoka I. Epithelial cell-derived human b-defensin-2 acts as a chemotaxin for mast cells through a pertussis toxin-sensitive and phospholipase c-dependent pathway. *Int Immunl* (2002) 14:421–6. doi: 10.1093/intimm/14.4.421

53. De Yang B, Chen Q, Schmidt AP, Anderson GM, Wang JM, Wooters J, et al. LL-37, the neutrophil granule- and epithelial cell-derived cathelicidin, utilizes formyl peptide receptor-like 1 (FPRL1) as a receptor to chemoattract human peripheral blood neutrophils, monocytes, and T cells. *J Exp Med* (2000) 192:1069–74. doi: 10.1084/jem.192.7.1069

54. Agerberth B, Charo J, Werr J, Olsson B, Idali F, Lindbom L, et al. The human antimicrobial and chemotactic peptides LL-37 and α-defensins are expressed by specific lymphocyte and monocyte populations. *Blood* (2000) 96:3086–93. doi: 10.1182/BLOOD.V96.9.3086

55. Van Wetering S, Mannesse-Lazeroms SPG, Van Sterkenburg MAJA, Daha MR, Dijkman JH, Hiemstra PS. Effect of defensins on interleukin-8 synthesis in airway epithelial cells. *Am J Physiol Lung Cell Mol Physiol* (1997) 272(5 Pt 1):L888–96. doi: 10.1152/ajplung.1997.272.5.l888

56. Mookherjee N, Brown KL, Bowdish DME, Doria S, Falsafi R, Hokamp K, et al. Modulation of the TLR-mediated inflammatory response by the endogenous human host defense peptide LL-37. *J Immunol* (2006) 176:2455–64. doi: 10.4049/jimmunol.176.4.2455

57. McHugh BJ, Wang R, Li H-N, Beaumont PE, Kells R, Stevens H, et al. Cathelicidin is a "fire alarm", generating protective NLRP3-dependent airway epithelial cell inflammatory responses during infection with *Pseudomonas aeruginosa*. *PloS Pathog* (2019) 15:e1007694. doi: 10.1371/journal.ppat.1007694

58. Coorens M, Schneider VAF, de Groot AM, van Dijk A, Meijerink M, Wells JM, et al. Cathelicidins inhibit *Escherichia coli* –induced TLR2 and TLR4 activation in a viability-dependent manner. *J Immunol* (2017) 199:1418–28. doi: 10.4049/jimmunol.1602164

59. Minns D, Smith KJ, Alessandrini V, Hardisty G, Melrose L, Jackson-Jones L, et al. The neutrophil antimicrobial peptide cathelicidin promotes Th17 differentiation. *Nat Commun* (2021) 12:1–16. doi: 10.1038/s41467-021-21533-5

60. Al-Adwani S, Wallin C, Balhuizen MD, Veldhuizen EJA, Coorens M, Landreh M, et al. Studies on citrullinated LL-37: detection in human airways, antibacterial effects and biophysical properties. *Sci Rep* (2020) 10:1–14. doi: 10.1038/s41598-020-59071-7

61. Wong A, Bryzek D, Dobosz E, Scavenius C, Svoboda P, Rapala-Kozik M, et al. A novel biological role for peptidyl-arginine deiminases: citrullination of cathelicidin LL-37 controls the immunostimulatory potential of cell-free DNA. *J Immunol* (2018) 200:2327–40. doi: 10.4049/jimmunol.1701391

62. Wu H, Santoni-Rugiu E, Ralfkiaer E, Porse BT, Moser C, Høiby N, et al. Lipocalin 2 is protective against *E. coli* pneumonia. *Respir Res* (2010) 11:96. doi: 10.1186/1465-9921-11-96

63. Cramer EP, Dahl SL, Rozell B, Knudsen KJ, Thomsen K, Moser C, et al. Lipocalin-2 from both myeloid cells and the epithelium combats *Klebsiella pneumoniae* lung infection in mice. *Blood* (2017) 129:2813–7. doi: 10.1182/blood-2016-11-753434

64. Gläser R, Harder J, Lange H, Bartels J, Christophers E, Schröder JM. Antimicrobial psoriasin (S100A7) protects human skin from *Escherichia coli* infection. *Nat Immunol* (2004) 6:57–64. doi: 10.1038/ni1142

65. Andresen E, Lange C, Strodthoff D, Goldmann T, Fischer N, Sahly H, et al. S100A7/psoriasin expression in the human lung: unchanged in patients with COPD, but upregulated upon positive *S. aureus* detection. *BMC Pulm Med* (2011) 11:1–10. doi: 10.1186/1471-2466-11-10/FIGURES/7

66. Bai H, Si L, Jiang A, Belgur C, Zhai Y, Plebani R, et al. Mechanical control of innate immune responses against viral infection revealed in a human lung alveolus chip. *Nat Commun* (2022) 13:1–17. doi: 10.1038/s41467-022-29562-4

67. Williams SE, Brown TI, Roghanian A, Sallenave JM. SLPI and elafin: one glove, many fingers. *Clin Sci* (2006) 110:21–35. doi: 10.1042/CS20050115

68. Hiemstra PS, Maassen RJ, Stolk J, Heinzel-Wieland R, Steffens GJ, Dijkman JH. Antibacterial activity of antileukoprotease. *Infect Immun* (1996) 64:4520–4. doi: 10.1128/iai.64.11.4520-4524.1996

69. Simpson AJ, Maxwell AI, Govan JRW, Haslett C, Sallenave JM. Elafin (elastase-specific inhibitor) has anti-microbial activity against gram-positive and gram-negative respiratory pathogens. *FEBS Lett* (1999) 452:309–13. doi: 10.1016/S0014-5793(99)00670-5

70. Henriksen PA, Hitt M, Xing Z, Wang J, Haslett C, Riemersma RA, et al. Adenoviral gene delivery of elafin and secretory leukocyte protease inhibitor attenuates NF-κB-Dependent inflammatory responses of human endothelial cells and macrophages to atherogenic stimuli. *J Immunol* (2004) 172:4535–44. doi: 10.4049/jimmunol.172.7.4535

71. Harder J, Schröder JM. RNase 7, a novel innate immune defense antimicrobial protein of healthy human skin. *J Biol Chem* (2002) 277:46779–84. doi: 10.1074/JBC.M207587200

72. Amatngalim GD, van Wijck Y, de Mooij-Eijk Y, Verhoosel RM, Harder J, Lekkerkerker AN, et al. Basal cells contribute to innate immunity of the airway epithelium through production of the antimicrobial protein RNase 7. *J Immunol* (2015) 194:3340–50. doi: 10.4049/JIMMUNOL.1402169

73. Torres-Juarez F, Touqui L, Leon-Contreras J, Rivas-Santiago C, Enciso-Moreno JA, Hernández-Pando R, et al. RNase 7 but not psoriasin nor sPLA2-IIA associates with *Mycobacterium tuberculosis* during airway epithelial cell infection. *Pathog Dis* (2018) 76(2):1–8. doi: 10.1093/FEMSPD/FTY005

74. Han SH, Mallampalli RK. The role of surfactant in lung disease and host defense against pulmonary infections. *Ann Am Thorac Soc* (2015) 12:765–74. doi: 10.1513/AnnalsATS.201411-507FR

75. Cheng G, Ueda T, Nakajima H, Nakajima A, Kinjyo S, Motojima S, et al. Suppressive effects of SP-a on ionomycin-induced IL-8 production and release by eosinophils. *Int Arch Allergy Immunol* (1998) 117:59–62. doi: 10.1159/000053574

76. Chu HW, Thaikoottathil J, Rino JG, Zhang G, Wu Q, Moss T, et al. Function and regulation of SPLUNC1 protein in mycoplasma infection and allergic inflammation. *J Immunol* (2007) 179:3995–4002. doi: 10.4049/jimmunol.179.6.3995

77. Cole AM, Ganz T, Liese AM, Burdick MD, Liu L, Strieter RM. Cutting edge: IFN-inducible ELR – CXC chemokines display defensin-like antimicrobial activity. *J Immunol* (2001) 167:623–7. doi: 10.4049/jimmunol.167.2.623

78. Long X-B, Hu S, Wang N, Zhen H-T, Cui Y-H, Liu Z. Clara Cell 10-kDa protein gene transfection inhibits NF-κB activity in airway epithelial cells. *PloS One* (2012) 7:e35960. doi: 10.1371/journal.pone.0035960

79. Wang S-Z, Rosenberger CL, Bao Y-X, Stark JM, Harrod KS. Clara Cell secretory protein modulates lung inflammatory and immune responses to respiratory syncytial virus infection. *J Immunol* (2003) 171:1051–60. doi: 10.4049/jimmunol.171.2.1051

80. Zhu L, An L, Ran D, Lizarraga R, Bondy C, Zhou X, et al. The club cell marker SCGB1A1 downstream of FOXA2 is reduced in asthma. *Am J Respir Cell Mol Biol* (2019) 60(6):695–704. doi: 10.1165/rcmb.2018-0199OC

81. Zissler UM, Jakwerth CA, Guerth F, Lewitan L, Rothkirch S, Davidovic M, et al. Allergen-specific immunotherapy induces the suppressive secretoglobin 1A1 in cells of the lower airways. *Allergy: Eur J Allergy Clin Immunol* (2021) 76:2461–74. doi: 10.1111/all.14756

82. Xu M, Yang W, Wang X, Nayak DK. Lung secretoglobin Scgb1a1 influences alveolar macrophage-mediated inflammation and immunity. *Front Immunol* (2020) 11:584310. doi: 10.3389/fimmu.2020.584310

83. Pezzulo AA, Tang XX, Hoegger MJ, Abou Alaiwa MH, Ramachandran S, Moninger TO, et al. Reduced airway surface pH impairs bacterial killing in the porcine cystic fibrosis lung. *Nature* (2012) 487:109–13. doi: 10.1038/nature11130

84. Shah VS, Meyerholz DK, Tang XX, Reznikov L, Alaiwa MA, Ernst SE, et al. Airway acidification initiates host defense abnormalities in cystic fibrosis mice. *Science* (2016) 351:503–7. doi: 10.1126/science.aad5589

85. Carnesecchi S, Deffert C, Pagano A, Garrido-Urbani S, Métrailler-Ruchonnet I, Schäppi M, et al. NADPH oxidase-1 plays a crucial role in hyperoxia-induced acute lung injury in mice. *Am J Respir Crit Care Med* (2009) 180:972–81. doi: 10.1164/rccm.200902-0296OC

86. Schneider JL, Rowe JH, Garcia-de-Alba C, Kim CF, Sharpe AH, Haigis MC. The aging lung: physiology, disease, and immunity. *Cell* (2021) 184:1990–2019. doi: 10.1016/j.cell.2021.03.005

87. Forteza R, Salathe M, Miot F, Forteza R, Conner GE. Regulated hydrogen peroxide production by duox in human airway epithelial cells. *Am J Respir Cell Mol Biol* (2005) 32:462–9. doi: 10.1165/rcmb.2004-0302OC

88. Fischer H. Mechanisms and function of DUOX in epithelia of the lung. *Antioxid Redox Signal* (2009) 11:2453–65. doi: 10.1089/ars.2009.2558

89. Selemidis S, Seow HJ, Broughton BRS, Vinh A, Bozinovski S, Sobey CG, et al. Nox1 oxidase suppresses influenza a virus-induced lung inflammation and oxidative stress. *PloS One* (2013) 8:e60792. doi: 10.1371/journal.pone.0060792

90. Holmström KM, Finkel T. Cellular mechanisms and physiological consequences of redox-dependent signalling. *Nat Rev Mol Cell Biol* (2014) 15:411–21. doi: 10.1038/nrm3801

91. Haq IJ, Gray MA, Garnett JP, Ward C, Brodlie M. Airway surface liquid homeostasis in cystic fibrosis: pathophysiology and therapeutic targets. *Thorax* (2016) 71:284–7. doi: 10.1136/thoraxjnl-2015-207588

92. Fahy JV, Dickey BF. Airway mucus function and dysfunction. *N Engl J Med* (2010) 363:2233–47. doi: 10.1056/NEJMra0910061

93. Knowles MR, Boucher RC. Mucus clearance as a primary innate defense mechanism for mammalian airways. *J Clin Invest* (2002) 109:571–7. doi: 10.1172/JCI15217

94. Chen EYT, Yang N, Quinton PM, Chin WC. A new role for bicarbonate in mucus formation. *Am J Physiol Lung Cell Mol Physiol* (2010) 299:L542. doi: 10.1152/ajplung.00180.2010

95. Zajac M, Dreano E, Edwards A, Planelles G, Sermet-gaudelus I. Airway surface liquid pH regulation in airway epithelium current understandings and gaps in knowledge. *Int J Mol Sci* (2021) 22(7):3384. doi: 10.3390/ijms22073384

96. Tarran R, Button B, Boucher RC. Regulation of normal and cystic fibrosis airway surface liquid volume by phasic shear stress. *Annu Rev Physiol* (2006) 68:543–61. doi: 10.1146/ANNUREV.PHYSIOL.68.072304.112754

97. Charlson ES, Bittinger K, Haas AR, Fitzgerald AS, Frank I, Yadav A, et al. Topographical continuity of bacterial populations in the healthy human respiratory tract. *Am J Respir Crit Care Med* (2011) 184:957–63. doi: 10.1164/rccm.201104-0655OC

98. Dickson RP, Erb-Downward JR, Freeman CM, McCloskey L, Falkowski NR, Huffnagle GB, et al. Bacterial topography of the healthy human lower respiratory tract. *mBio* (2017) 8(1):e02287–16. doi: 10.1128/mBio.02287-16

99. Segal LN, Clemente JC, Li Y, Ruan C, Cao J, Danckers M, et al. Anaerobic bacterial fermentation products increase tuberculosis risk in antiretroviral-Drug-Treated HIV patients. *Cell Host Microbe* (2017) 21:530–537.e4. doi: 10.1016/j.chom.2017.03.003

100. Sulaiman I, Wu BG, Li Y, Tsay JC, Sauthoff M, Scott AS, et al. Functional lower airways genomic profiling of the microbiome to capture active microbial metabolism. *Eur Respir J* (2021) 58(1):2003434. doi: 10.1183/13993003.03434-2020

101. Kuek LE, Lee RJ. First contact: the role of respiratory cilia in host-pathogen interactions in the airways. *Am J Physiol Lung Cell Mol Physiol* (2020) 319:L603–19. doi: 10.1152/AJPLUNG.00283.2020

102. Chotirmall SH, Bogaert D, Chalmers JD, Cox MJ, Hansbro PM, Huang YJ, et al. Therapeutic targeting of the respiratory microbiome. *Am J Respir Crit Care Med* (2022) 206:535–44. doi: 10.1164/RCCM.202112-2704PP/SUPPL_FILE/DISCLOSURES.PDF

103. Takeuchi O, Akira S. Pattern recognition receptors and inflammation. *Cell* (2010) 140:805–20. doi: 10.1016/j.cell.2010.01.022

104. Hiemstra PS, McCray PB, Bals R. The innate immune function of airway epithelial cells in inflammatory lung disease. *Eur Respir J* (2015) 45:1150–62. doi: 10.1183/09031936.00141514

105. Jeong YS, Bae YS. Formyl peptide receptors in the mucosal immune system. *Exp Mol Med* (2020) 52:1694–704. doi: 10.1038/s12276-020-00518-2

106. Price AE, Shamardani K, Lugo KA, Deguine J, Roberts AW, Lee BL. Barton GM. a map of toll-like receptor expression in the intestinal epithelium reveals distinct spatial, cell type-specific, and temporal patterns. *Immunity* (2018) 49:560–575.e6. doi: 10.1016/j.immuni.2018.07.016

107. De Nardo D. Toll-like receptors: activation, signalling and transcriptional modulation. *Cytokine* (2015) 74:181–9. doi: 10.1016/j.cyto.2015.02.025

108. Brubaker SW, Bonham KS, Zanoni I, Kagan JC. Innate immune pattern recognition: a cell biological perspective. *Annu Rev Immunol* (2015) 33:257–90. doi: 10.1146/annurev-immunol-032414-112240

109. Thomas PG, Dash P, Aldridge JR, Ellebedy AH, Reynolds C, Funk AJ, et al. The intracellular sensor NLRP3 mediates key innate and healing responses to influenza a virus *via* the regulation of caspase-1. *Immunity* (2009) 30:566–75. doi: 10.1016/j.immuni.2009.02.006

110. Hise AG, Tomalka J, Ganesan S, Patel K, Hall BA, Brown GD, et al. An essential role for the NLRP3 inflammasome in host defense against the human fungal pathogen *Candida albicans*. *Cell Host Microbe* (2009) 5:487–97. doi: 10.1016/j.chom.2009.05.002

111. Kato H, Takeuchi O, Sato S, Yoneyama M, Yamamoto M, Matsui K, et al. Differential roles of MDA5 and RIG-I helicases in the recognition of RNA viruses. *Nature* (2006) 441:101–5. doi: 10.1038/nature04734

112. Bhoj VG, Sun Q, Bhoj EJ, Somers C, Chen X, Torres JP, et al. MAVS and MyD88 are essential for innate immunity but not cytotoxic T lymphocyte response against respiratory syncytial virus. *Proc Natl Acad Sci U.S.A.* (2008) 105:14046–51. doi: 10.1073/pnas.0804717105

113. Parker D, Prince A. Type I interferon response to extracellular bacteria in the airway epithelium. *Trends Immunol* (2011) 32:582–8. doi: 10.1016/j.it.2011.09.003

114. Chen Q, Sun L, Chen ZJ. Regulation and function of the cGAS-STING pathway of cytosolic DNA sensing. *Nat Immunol* (2016) 17:1142–9. doi: 10.1038/ni.3558

115. Heyl KA, Klassert TE, Heinrich A, Müller MM, Klaile E, Dienemann H, et al. Dectin-1 is expressed in human lung and mediates the proinflammatory immune response to nontypeable *Haemophilus influenzae*. *mBio* (2014) 5:e01492–14. doi: 10.1128/mBio.01492-14

116. Werner JL, Metz AE, Horn D, Schoeb TR, Hewitt MM, Schwiebert LM, et al. Requisite role for the dectin-1 β-glucan receptor in pulmonary defense against *Aspergillus fumigatus*. *J Immunol* (2009) 182:4938–46. doi: 10.4049/jimmunol.0804250

117. Le Y, Murphy PM, Wang JM. Formyl-peptide receptors revisited. *Trends Immunol* (2002) 23:541–8. doi: 10.1016/S1471-4906(02)02316-5

118. Wang L, Cai J, Zhao X, Ma L, Zeng P, Zhou L, et al. Palmitoylation prevents sustained inflammation by limiting NLRP3 inflammasome activation through chaperone-mediated autophagy. *Mol Cell* (2023) 83:281–297.e10. doi: 10.1016/J.MOLCEL.2022.12.002

119. Zihni C, Mills C, Matter K, Balda MS. Tight junctions: from simple barriers to multifunctional molecular gates. *Nat Rev Mol Cell Biol* (2016) 17:564–80. doi: 10.1038/nrm.2016.80

120. Akdis CA. Does the epithelial barrier hypothesis explain the increase in allergy, autoimmunity and other chronic conditions? *Nat Rev Immunol* (2021) 21:739–51. doi: 10.1038/s41577-021-00538-7

121. Wang M, Tan G, Eljaszewicz A, Meng Y, Wawrzyniak P, Acharya S, et al. Laundry detergents and detergent residue after rinsing directly disrupt tight junction barrier integrity in human bronchial epithelial cells. *J Allergy Clin Immunol* (2019) 143:1892–903. doi: 10.1016/j.jaci.2018.11.016

122. Shaykhiev R, Otaki F, Bonsu P, Dang DT, Teater M, Strulovici-Barel Y, et al. Cigarette smoking reprograms apical junctional complex molecular architecture in the human airway epithelium *in vivo*. *Cell Mol Life Sci* (2011) 68:877–92. doi: 10.1007/s00018-010-0500-x

123. Xian M, Ma S, Wang K, Lou H, Wang Y, Zhang L, et al. Akdis CA. particulate matter 2.5 causes deficiency in barrier integrity in human nasal epithelial cells. *Allergy Asthma Immunol Res* (2020) 12:56. doi: 10.4168/aair.2020.12.1.56

124. Heijink IH, Van Oosterhout A, Kapus A. Epidermal growth factor receptor signalling contributes to house dust mite-induced epithelial barrier dysfunction. *Eur Respir J* (2010) 36:1016–26. doi: 10.1183/09031936.00125809

125. Sintobin I, Siroux V, Holtappels G, Pison C, Nadif R, Bousquet J, et al. Sensitisation to staphylococcal enterotoxins and asthma severity: a longitudinal study in the EGEA cohort. *Eur Respir J* (2019) 54(3):1900198. doi: 10.1183/13993003.00198-2019

126. Petecchia L, Sabatini F, Usai C, Caci E, Varesio L, Rossi GA. Cytokines induce tight junction disassembly in airway cells *via* an EGFR-dependent MAPK/ERK1/2-pathway. *Lab Invest* (2012) 92:1140–8. doi: 10.1038/labinvest.2012.67

127. Schmidt H, Braubach P, Schilpp C, Lochbaum R, Neuland K, Thompson K, et al. IL-13 impairs tight junctions in airway epithelia. *Int J Mol Sci* (2019) 20:3222. doi: 10.3390/ijms20133222

128. Mizushima N, Komatsu M. Autophagy: renovation of cells and tissues. *Cell* (2011) 147:728–41. doi: 10.1016/j.cell.2011.10.026

129. Kimmey JM, Stallings CL. Bacterial pathogens versus autophagy: implications for therapeutic interventions. *Trends Mol Med* (2016) 22:1060–76. doi: 10.1016/j.molmed.2016.10.008

130. Junkins RD, Shen A, Rosen K, McCormick C, Lin TJ. Autophagy enhances bacterial clearance during *P. aeruginosa* lung infection. *PloS One* (2013) 8:e72263. doi: 10.1371/journal.pone.0072263

131. Croft CA, Culibrk L, Moore MM, Tebbutt SJ. Interactions of *Aspergillus fumigatus* conidia with airway epithelial cells: a critical review. *Front Microbiol* (2016) 7:472. doi: 10.3389/fmicb.2016.00472

132. Wang Y, Sharma P, Jefferson M, Zhang W, Bone B, Kipar A, et al. Non-canonical autophagy functions of ATG16L1 in epithelial cells limit lethal infection by influenza a virus. *EMBO J* (2021) 40:e105543. doi: 10.15252/embj.2020105543

133. Kinsella RL, Nehls EM, Stallings CL. Roles for autophagy proteins in immunity and host defense. *Vet Pathol* (2018) 55:366–73. doi: 10.1177/0300985818754967

134. Morleo M, Vieira HLA, Pennekamp P, Palma A, Bento-Lopes L, Omran H, et al. Crosstalk between cilia and autophagy: implication for human diseases. *Autophagy* (2022) 19(1):24–43. doi: 10.1080/15548627.2022.2067383

135. Tang Z, Lin MG, Stowe TR, Chen S, Zhu M, Stearns T, et al. Autophagy promotes primary ciliogenesis by removing OFD1 from centriolar satellites. *Nature* (2013) 502:254–7. doi: 10.1038/nature12606

136. Arora K, Lund JR, Naren NA, Zingarelli B, Naren AP. AC6 regulates the microtubule-depolymerizing kinesin KIF19A to control ciliary length in mammals. *J Biol Chem* (2020) 295:14250–9. doi: 10.1074/jbc.RA120.013703

137. Luciani A, Villella VR, Esposito S, Brunetti-Pierri N, Medina D, Settembre C, et al. Defective CFTR induces aggresome formation and lung inflammation in cystic fibrosis through ROS-mediated autophagy inhibition. *Nat Cell Biol* (2010) 12:863–75. doi: 10.1038/ncb2090

138. Dickinson JD, Alevy Y, Malvin NP, Patel KK, Gunsten SP, Holtzman MJ, et al. IL13 activates autophagy to regulate secretion in airway epithelial cells. *Autophagy* (2016) 12:397–409. doi: 10.1080/15548627.2015.1056967

139. Dickinson JD, Sweeter JM, Warren KJ, Ahmad IM, De Deken X, Zimmerman MC, et al. Autophagy regulates DUOX1 localization and superoxide production in airway epithelial cells during chronic IL-13 stimulation. *Redox Biol* (2018) 14:272–84. doi: 10.1016/j.redox.2017.09.013

140. Li K, Li M, Li W, Yu H, Sun X, Zhang Q, et al. Airway epithelial regeneration requires autophagy and glucose metabolism. *Cell Death Dis* (2019) 10:1–14. doi: 10.1038/s41419-019-2111-2

141. Huizing M, Helip-Wooley A, Westbroek W, Gunay-Aygun M, Gahl WA. Disorders of lysosome-related organelle biogenesis: clinical and molecular genetics. *Annu Rev Genomics Hum Genet* (2008) 9:359–86. doi: 10.1146/annurev.genom.9.081307.164303

142. Cavounidis A, Pandey S, Capitani M, Friedrich M, Cross A, Gartner L, et al. Hermansky-pudlak syndrome type 1 causes impaired anti-microbial immunity and inflammation due to dysregulated immunometabolism. *Mucosal Immunol* (2022) 15:1431–46. doi: 10.1038/s41385-022-00572-1

143. Wu YF, Li ZY, Dong LL, Li WJ, Wu YP, Wang J, et al. Inactivation of MTOR promotes autophagy-mediated epithelial injury in particulate matter-induced airway inflammation. *Autophagy* (2020) 16:435–50. doi: 10.1080/15548627.2019.1628536

144. Strom JE, Merid SK, Pourazar J, Blomberg A, Lindberg A, Ringh MV, et al. Chronic obstructive pulmonary disease is associated with epigenome-wide differential methylation in BAL lung cells. *Am J Respir Cell Mol Biol* (2022) 66:638–47. doi: 10.1165/rcmb.2021-0403OC

145. Shuto T, Furuta T, Oba M, Xu H, Li J, Cheung J, et al. Promoter hypomethylation of toll-like receptor-2 gene is associated with increased proinflammatory response toward bacterial peptidoglycan in cystic fibrosis bronchial epithelial cells. *FASEB J* (2006) 20:782–4. doi: 10.1096/fj.05-4934fje

146. Saccani S, Pantano S, Natoli G. p38-dependent marking of inflammatory genes for increased NF-κB recruitment. *Nat Immunol* (2002) 3:69–75. doi: 10.1038/ni748

147. Stefanowicz D, Lee JY, Lee K, Shaheen F, Koo HK, Booth S, et al. Elevated H3K18 acetylation in airway epithelial cells of asthmatic subjects. *Respir Res* (2015) 16 (1):95. doi: 10.1186/s12931-015-0254-y

148. Saco TV, Breitzig MT, Lockey RF, Kolliputi N. Epigenetics of mucus hypersecretion in chronic respiratory diseases. *Am J Respir Cell Mol Biol* (2018) 58:299–309. doi: 10.1165/rcmb.2017-0072TR

149. Wawrzyniak P, Wawrzyniak M, Wanke K, Sokolowska M, Bendelja K, Rückert B, et al. Regulation of bronchial epithelial barrier integrity by type 2 cytokines and histone deacetylases in asthmatic patients. *J Allergy Clin Immunol* (2017) 139:93–103. doi: 10.1016/j.jaci.2016.03.050

150. Grausenburger R, Bilic I, Boucheron N, Zupkovitz G, El-Housseiny L, Tschismarov R, et al. Conditional deletion of histone deacetylase 1 in T cells leads to enhanced airway inflammation and increased Th2 cytokine production. *J Immunol* (2010) 185:3489–97. doi: 10.4049/jimmunol.0903610

151. Marwick JA, Kirkham PA, Stevenson CS, Danahay H, Giddings J, Butler K, et al. Cigarette smoke alters chromatin remodeling and induces proinflammatory genes in rat lungs. *Am J Respir Cell Mol Biol* (2004) 31:633–42. doi: 10.1165/rcmb.2004-0006OC

152. Ito K, Ito M, Elliott WM, Cosio B, Caramori G, Kon OM, et al. Decreased histone deacetylase activity in chronic obstructive pulmonary disease. *New Engl J Med* (2005) 352:1967–76. doi: 10.1056/NEJMoa041892

153. Lam HC, Cloonan SM, Bhashyam AR, Haspel JA, Singh A, Sathirapongsasuti JF, et al. Histone deacetylase 6-mediated selective autophagy regulates COPD-associated cilia dysfunction. *J Clin Invest* (2013) 123:5212–30. doi: 10.1172/JCI69636

154. Lam HC, Cloonan SM, Bhashyam AR, Haspel JA, Singh A, Fah Sathirapongsasuti J, et al. Erratum: histone deacetylase 6–mediated selective autophagy regulates COPD-associated cilia dysfunction (Journal of clinical investigation (2013) 123:12 (5212-5230) DOI: 10.1172/JCI69636). *J Clin Invest* (2020) 130:6189. doi: 10.1172/JCI143863

155. Baek SH, Kim K. Epigenetic control of autophagy: nuclear events gain more attention. *Mol Cell* (2017) 65:781–5. doi: 10.1016/j.molcel.2016.12.027

156. Wei FZ, Cao Z, Wang X, Wang H, Cai MY, Li T, et al. Epigenetic regulation of autophagy by the methyltransferase EZH2 through an MTOR-dependent pathway. *Autophagy* (2015) 11:2309–22. doi: 10.1080/15548627.2015.1117734

157. Byrd AL, Qu X, Lukyanchuk A, Liu J, Chen F, Naughton KJ, et al. Dysregulated polycomb repressive complex 2 contributes to chronic obstructive pulmonary disease by rewiring stem cell fate. *Stem Cell Rep* (2023) 18:289–304. doi: 10.1016/J.STEMCR.2022.11.009

158. Barrier ML, Myszor IT, Sahariah P, Sigurdsson S, Carmena-Bargueño M, Pérez-Sánchez H, et al. Aroylated phenylenediamine HO53 modulates innate immunity, histone acetylation and metabolism. *Mol Immunol* (2023) 155:153–64. doi: 10.1016/J.MOLIMM.2023.02.003

159. Sadikot RT, Blackwell TS, Christman JW, Prince AS. Pathogen–host interactions in *Pseudomonas aeruginosa* pneumonia. *Am J Respir Crit Care Med* (2005) 171:1209–23. doi: 10.1164/rccm.200408-1044SO

160. Bucior I, Pielage JF, Engel JN. *Pseudomonas aeruginosa* pili and flagella mediate distinct binding and signaling events at the apical and basolateral surface of airway epithelium. *PloS Pathog* (2012) 8:e1002616. doi: 10.1371/journal.ppat.1002616

161. Schmidtchen A, Frick I-M, Andersson E, Tapper H, Björck L. Proteinases of common pathogenic bacteria degrade and inactivate the antibacterial peptide LL-37. *Mol Microbiol* (2002) 46:157–68. doi: 10.1046/j.1365-2958.2002.03146.x

162. Zulianello L, Canard C, Köhler T, Caille D, Lacroix J-S, Meda P. Rhamnolipids are virulence factors that promote early infiltration of primary human airway epithelia by *Pseudomonas aeruginosa*. *Infect Immun* (2006) 74:3134–47. doi: 10.1128/IAI.01772-05

163. Kanthakumar K, Taylor G T, Tsang KW, DR C, Rutman A, Smith S, et al. Mechanisms of action of *Pseudomonas aeruginosa* pyocyanin on human ciliary beat. *In Vitro.* (1993) 61(7):2848–53. doi: 10.1128/iai.61.7.2848-2853.1993

164. O'Malley YQ, Reszka KJ, Rasmussen GT, Abdalla MY, Denning GM, Britigan BE. The *Pseudomonas* secretory product pyocyanin inhibits catalase activity in human lung epithelial cells. *Am J Physiol Lung Cell Mol Physiol* (2003) 285(5):L1077–86. doi: 10.1152/ajplung.00198.2003

165. Cornelis P, Dingemans J. *Pseudomonas aeruginosa* adapts its iron uptake strategies in function of the type of infections. *Front Cell Infect Microbiol* (2013) 3:75. doi: 10.3389/fcimb.2013.00075

166. Tateda K, Ishii Y, Horikawa M, Matsumoto T, Miyairi S, Pechere JC, et al. The *Pseudomonas aeruginosa* autoinducer n-3-oxododecanoyl homoserine lactone accelerates apoptosis in macrophages and neutrophils. *Infect Immun* (2003) 71:5785–93. doi: 10.1128/IAI.71.10.5785-5793.2003

167. Bandyopadhaya A, Tsurumi A, Maura D, Jeffrey KL, Rahme LG. A quorum-sensing signal promotes host tolerance training through HDAC1-mediated epigenetic reprogramming. *Nat Microbiol* (2016) 1:1–9. doi: 10.1038/nmicrobiol.2016.174

168. Rossi E, La Rosa R, Bartell JA, Marvig RL, Haagensen JAJ, Sommer LM, et al. *Pseudomonas aeruginosa* adaptation and evolution in patients with cystic fibrosis. *Nat Rev Microbiol* (2021) 19:331–42. doi: 10.1038/s41579-020-00477-5

169. Rice LB. Federal funding for the study of antimicrobial resistance in nosocomial pathogens: no ESKAPE. *J Infect Dis* (2008) 197:1079–81. doi: 10.1086/533452

170. Gonzalez-Ferrer S, Peñaloza HF, Budnick JA, Bain WG, Nordstrom HR, Lee JS, et al. Finding order in the chaos: outstanding questions in *Klebsiella pneumoniae* pathogenesis. *Infect Immun* (2021) 89(4):e00693–20. doi: 10.1128/IAI.00693-20

171. Feriotti C, Sá-Pessoa J, Calderón-González R, Gu L, Morris B, Sugisawa R, et al. *Klebsiella pneumoniae* hijacks the toll-IL-1R protein SARM1 in a type I IFN-dependent manner to antagonize host immunity. *Cell Rep* (2022) 40:111167. doi: 10.1016/j.celrep.2022.111167

172. Chua MD, Liou C-H, Bogdan AC, Law HT, Yeh K-M, Lin J-C, et al. *Klebsiella pneumoniae* disassembles host microtubules in lung epithelial cells. *Cell Microbiol* (2019) 21(3):e12977. doi: 10.1111/cmi.12977

173. Ahn D, Wickersham M, Riquelme S, Prince A. The effects of IFN-l on epithelial barrier function contribute to *Klebsiella pneumoniae* ST258 pneumonia. *Am J Respir Cell Mol Biol* (2019) 60:158–66. doi: 10.1165/rcmb.2018-0021OC

174. Cortés G, Álvarez D, Saus C, Albertí S. Role of lung epithelial cells in defense against *Klebsiella pneumoniae* pneumonia. *Infect Immun* (2002) 70:1075–80. doi: 10.1128/IAI.70.3.1075-1080.2002

175. Sequeira RP, McDonald JAK, Marchesi JR, Clarke TB. Commensal Bacteroidetes protect against *Klebsiella pneumoniae* colonization and transmission through IL-36 signalling. *Nat Microbiol* (2020) 5:304–13. doi: 10.1038/s41564-019-0640-1

176. Le Guern R, Grandjean T, Stabler S, Bauduin M, Gosset P, Kipnis É, et al. Gut colonisation with multidrug-resistant *Klebsiella pneumoniae* worsens *Pseudomonas aeruginosa* lung infection. *Nat Commun* (2023) 14(1):78. doi: 10.1038/s41467-022-35767-4

177. Lucas R, Czikora I, Sridhar S, Zemskov E, Gorshkov B, Siddaramappa U, et al. Mini-review: novel therapeutic strategies to blunt actions of pneumolysin in the lungs. *Toxins* (2013) 5:1244–60. doi: 10.3390/toxins5071244

178. Jacques LC, Panagiotou S, Baltazar M, Senghore M, Khandaker S, Xu R, et al. Increased pathogenicity of pneumococcal serotype 1 is driven by rapid autolysis and release of pneumolysin. *Nat Commun* (2020) 11:1–13. doi: 10.1038/s41467-020-15751-6

179. Rai P, He F, Kwang J, Engelward BP, Chow VTK. Pneumococcal pneumolysin induces DNA damage and cell cycle arrest. *Sci Rep* (2016) 6:1–12. doi: 10.1038/srep22972

180. Bryant JC, Dabbs RC, Oswalt KL, Brown LR, Rosch JW, Seo KS, et al. Pyruvate oxidase of *Streptococcus pneumoniae* contributes to pneumolysin release. *BMC Microbiol* (2016) 16:1–12. doi: 10.1186/s12866-016-0881-6

181. Dong W, Rasid O, Chevalier C, Connor M, Eldridge MJG, Hamon MA. *Streptococcus pneumoniae* infection promotes histone H3 dephosphorylation by modulating host PP1 phosphatase. *Cell Rep* (2020) 30:4016–4026.e4. doi: 10.1016/J.CELREP.2020.02.116

182. Kovács M, Halfmann A, Fedtke I, Heintz M, Peschel A, Vollmer W, et al. A functional dlt operon, encoding proteins required for incorporation of d-alanine in teichoic acids in gram-positive bacteria, confers resistance to cationic antimicrobial peptides in *Streptococcus pneumoniae*. *J Bacteriol* (2006) 188:5797–805. doi: 10.1128/JB.00336-06

183. LaRock CN, Nizet V. Cationic antimicrobial peptide resistance mechanisms of streptococcal pathogens. *Biochim Biophys Acta Biomembr* (2015) 1848:3047–54. doi: 10.1016/j.bbamem.2015.02.010

184. McKenna S, Huse KK, Giblin S, Pearson M, Shibar MSMAl, Sriskandan S, et al. The role of streptococcal cell-envelope proteases in bacterial evasion of the innate immune system. *J Innate Immun* (2022) 14:69–88. doi: 10.1159/000516956

185. Biswas D, Ambalavanan P, Ravins M, Anand A, Sharma A, Lim KXZ, et al. LL-37-mediated activation of host receptors is critical for defense against group a streptococcal infection. *Cell Rep* (2021) 34:108766. doi: 10.1016/J.CELREP.2021.108766

186. Crum NF, Russell KL, Kaplan EL, Wallace MR, Wu J, Ashtari P, et al. Pneumonia outbreak associated with group a *Streptococcus* species at a military training facility. *Clin Infect Dis* (2005) 40:511–8. doi: 10.1086/427502

187. Chandra P, Grigsby SJ, Philips JA. Immune evasion and provocation by *Mycobacterium tuberculosis*. *Nat Rev Microbiol* (2022) 20(12):750–66. doi: 10.1038/s41579-022-00763-4

188. Cohen SB, Gern BH, Delahaye JL, Adams KN, Plumlee CR, Winkler JK, et al. Alveolar macrophages provide an early *Mycobacterium tuberculosis* niche and initiate dissemination. *Cell Host Microbe* (2018) 24:439–446.e4. doi: 10.1016/j.chom.2018.08.001

189. Cambier CJ, Banik SM, Buonomo JA, Bertozzi CR. Spreading of a mycobacterial cell surface lipid into host epithelial membranes promotes infectivity. *Elife* (2020) 9:1–68. doi: 10.7554/eLife.60648

190. Ng VH, Cox JS, Sousa AO, MacMicking JD, McKinney JD. Role of KatG catalase-peroxidase in mycobacterial pathogenesis: countering the phagocyte oxidative burst. *Mol Microbiol* (2004) 52:1291–302. doi: 10.1111/j.1365-2958.2004.04078.x

191. Miller JL, Velmurugan K, Cowan MJ, Briken V. The type I NADH dehydrogenase of *Mycobacterium tuberculosis* counters phagosomal NOX2 activity to inhibit TNF-α-Mediated host cell apoptosis. *PloS Pathog* (2010) 6:e1000864. doi: 10.1371/journal.ppat.1000864

192. Köster S, Upadhyay S, Chandra P, Papavinasasundaram K, Yang G, Hassan A, et al. *Mycobacterium tuberculosis* is protected from NADPH oxidase and LC3-associated phagocytosis by the LCP protein CpsA. *Proc Natl Acad Sci U.S.A.* (2017) 114:E8711–20. doi: 10.1073/pnas.1707792114

193. Peyron P, Vaubourgeix J, Poquet Y, Levillain F, Botanch C, Bardou F, et al. Foamy macrophages from tuberculous patients' granulomas constitute a nutrient-rich reservoir for *Mycobacterium tuberculosis* persistence. *PloS Pathog* (2008) 4:e1000204. doi: 10.1371/journal.ppat.1000204

194. Donald PR, Diacon AH, Lange C, Demers AM, Von Groote-Biddlingmeier F, Nardell E. Droplets, dust and Guinea pigs: an historical review of tuberculosis transmission research, 1878-1940. *Int J Tuberculosis Lung Dis* (2018) 22:972–82. doi: 10.5588/ijtld.18.0173

195. Paludan SR, Mogensen TH. Innate immunological pathways in COVID-19 pathogenesis. *Sci Immunol* (2022) 7:5505. doi: 10.1126/sciimmunol.abm5505

196. Yin X, Riva L, Pu Y, Martin-Sancho L, Kanamune J, Yamamoto Y, et al. MDA5 governs the innate immune response to SARS-CoV-2 in lung epithelial cells. *Cell Rep* (2021) 34:108628. doi: 10.1016/j.celrep.2020.108628

197. Hackbart M, Deng X, Baker SC. Coronavirus endoribonuclease targets viral polyuridine sequences to evade activating host sensors. *Proc Natl Acad Sci U.S.A.* (2020) 117:8094–103. doi: 10.1073/pnas.1921485117

198. Xia H, Cao Z, Xie X, Zhang X, Chen JYC, Wang H, et al. Evasion of type I interferon by SARS-CoV-2. *Cell Rep* (2020) 33:108234. doi: 10.1016/j.celrep.2020.108234

199. Kee J, Thudium S, Renner DM, Glastad K, Palozola K, Zhang Z, et al. SARS-CoV-2 disrupts host epigenetic regulation *via* histone mimicry. *Nature* (2022) 610:381–8. doi: 10.1038/s41586-022-05282-z

200. Battles MB, McLellan JS. Respiratory syncytial virus entry and how to block it. *Nat Rev Microbiol* (2019) 17:233–45. doi: 10.1038/s41579-019-0149-x

201. Das S, St. Croix C, Good M, Chen J, Zhao J, Hu S, et al. Interleukin-22 inhibits respiratory syncytial virus production by blocking virus-mediated subversion of cellular autophagy. *iScience* (2020) 23:101256. doi: 10.1016/j.isci.2020.101256

202. Tripp RA, Jones LP, Haynes LM, Zheng HQ, Murphy PM, Anderson LJ. CX3C chemokine mimicry by respiratory syncytial virus G glycoprotein. *Nat Immunol* (2001) 2:732–8. doi: 10.1038/90675

203. Blacklow SC. Catching the common cold. *Nat Struct Mol Biol* (2004) 11:388–90. doi: 10.1038/nsmb0504-388

204. Michi AN, Yipp BG, Dufour A, Lopes F, Proud D. PGC-1α mediates a metabolic host defense response in human airway epithelium during rhinovirus infections. *Nat Commun* (2021) 12:1–19. doi: 10.1038/s41467-021-23925-z

205. Triantafilou M, Ramanjulu J, Booty LM, Jimenez-Duran G, Keles H, Saunders K, et al. Human rhinovirus promotes STING trafficking to replication organelles to promote viral replication. *Nat Commun* (2022) 13:1–16. doi: 10.1038/s41467-022-28745-3

206. Taylor L, Von Lendenfeld F, Ashton A, Sanghani H, Di Pretoro S, Usselmann L, et al. Sleep and circadian rhythm disruption alters the lung transcriptome to predispose to viral infection. *iScience* (2022) 26(2):105877. doi: 10.1016/j.isci.2022.105877

207. Hernández-Chávez MJ, Pérez-García LA, Niño-Vega GA, Mora-Montes HM. Fungal strategies to evade the host immune recognition. *J Fungi* (2017) 3(4):51. doi: 10.3390/jof3040051

208. Lionakis MS, Drummond RA, Hohl TM. Immune responses to human fungal pathogens and therapeutic prospects. *Nat Rev Immunol* (2023), 1–20. Online ahead of print. doi: 10.1038/s41577-022-00826-w

209. Naglik JR, Challacombe SJ, Hube B. *Candida albicans* secreted aspartyl proteinases in virulence and pathogenesis. *Microbiol Mol Biol Rev* (2003) 67:400–28. doi: 10.1128/mmbr.67.3.400-428.2003

210. Hoenigl M, Seidel D, Sprute R, Cunha C, Oliverio M, Goldman GH, et al. COVID-19-associated fungal infections. *Nat Microbiol* (2022) 7:1127–40. doi: 10.1038/s41564-022-01172-2

211. Rocha JDB, Nascimento MTC, Decote-Ricardo D, Côrte-Real S, Morrot A, Heise N, et al. Capsular polysaccharides from *Cryptococcus neoformans* modulate production of neutrophil extracellular traps (NETs) by human neutrophils. *Sci Rep* (2015) 5:8008. doi: 10.1038/srep08008

212. Crabtree JN, Okagaki LH, Wiesner DL, Strain AK, Nielsen JN, Nielsen K. Titan cell production enhances the virulence of *Cryptococcus neoformans*. *Infect Immun* (2012) 80:3776–85. doi: 10.1128/IAI.00507-12

213. Murray CJ, Ikuta KS, Sharara F, Swetschinski L, Robles Aguilar G, Gray A, et al. Global burden of bacterial antimicrobial resistance in 2019: a systematic analysis. *Lancet* (2022) 399:629–55. doi: 10.1016/S0140-6736(21)02724-0

214. Cassini A, Högberg LD, Plachouras D, Quattrocchi A, Hoxha A, Simonsen GS, et al. Attributable deaths and disability-adjusted life-years caused by infections with antibiotic-resistant bacteria in the EU and the European economic area in 2015: a population-level modelling analysis. *Lancet Infect Dis* (2019) 19:56–66. doi: 10.1016/S1473-3099(18)30605-4

215. Laxminarayan R, Van Boeckel T, Frost I, Kariuki S, Khan EA, Limmathurotsakul D, et al. The lancet infectious diseases commission on antimicrobial resistance: 6 years later. *Lancet Infect Dis* (2020) 20:e51–60. doi: 10.1016/s1473-3099(20)30003-7

216. Laxminarayan R, Van Boeckel T, Frost I, Kariuki S, Khan EA, Limmathurotsakul D, et al. Correction to lancet infect dis 2020. *Lancet Infect Dis* (2020) 20:e50. doi: 10.1016/S1473-3099(20)30146-8

217. Lewis K. The science of antibiotic discovery. *Cell* (2020) 181:29–45. doi: 10.1016/j.cell.2020.02.056

218. Bergman P, Raqib R, Rekha RS, Agerberth B, Gudmundsson GH. Host directed therapy against infection by boosting innate immunity. *Front Immunol* (2020) 11:1209. doi: 10.3389/fimmu.2020.01209

219. De Breij A, Riool M, Cordfunke RA, Malanovic N, De Boer L, Koning RI, et al. The antimicrobial peptide SAAP-148 combats drug-resistant bacteria and biofilms. *Sci Transl Med* (2018) 10(423):eaan4044. doi: 10.1126/scitranslmed.aan4044

220. Wuerth K, Lee AHY, Falsafi R, Gill EE, Hancock REW. Characterization of host responses during *Pseudomonas aeruginosa* acute infection in the lungs and blood and after treatment with the synthetic immunomodulatory peptide IDR-1002. *Infect Immun* (2019) 87(1):e00661-18. doi: 10.1128/IAI.00661-18/SUPPL_FILE/IAI.00661-18-S0001.PDF

221. Lazzaro BP, Zasloff M, Rolff J. Antimicrobial peptides: application informed by evolution. *Science* (2020) 368:eaau5480. doi: 10.1126/science.aau5480

222. Wang T-T, Nestel FP, Bourdeau V, Nagai Y, Wang Q, Liao J, et al. Cutting edge: 1,25-dihydroxyvitamin D3 is a direct inducer of antimicrobial peptide gene expression. *J Immunol* (2004) 173:2909–12. doi: 10.4049/JIMMUNOL.173.5.2909

223. Gombart AF, Borregaard N, Koeffler HP. Human cathelicidin antimicrobial peptide (CAMP) gene is a direct target of the vitamin d receptor and is strongly up-regulated in myeloid cells by 1,25-dihydroxyvitamin D3. *FASEB J* (2005) 19:1067–77. doi: 10.1096/fj.04-3284com

224. Lowry MB, Guo C, Zhang Y, Fantacone ML, Logan IE, Campbell Y, et al. A mouse model for vitamin d-induced human cathelicidin antimicrobial peptide gene expression. *J Steroid Biochem Mol Biol* (2020) 198:105552. doi: 10.1016/j.jsbmb.2019.105552

225. Louis P, Flint HJ. Formation of propionate and butyrate by the human colonic microbiota. *Environ Microbiol* (2017) 19:29–41. doi: 10.1111/1462-2920.13589

226. Bilotta AJ, Cong Y. Gut microbiota metabolite regulation of host defenses at mucosal surfaces: implication in precision medicine. *Precis Clin Med* (2019) 2:110–9. doi: 10.1093/pcmedi/pbz008

227. Iannitti T, Palmieri B. Clinical and experimental applications of sodium phenylbutyrate. *Drugs R D* (2011) 11:227–49. doi: 10.2165/11591280-000000000-00000

228. Steinmann J, Halldórsson S, Agerberth B, Gudmundsson GH. Phenylbutyrate induces antimicrobial peptide expression. *Antimicrob Agents Chemother* (2009) 53:5127–33. doi: 10.1128/AAC.00818-09

229. Rekha RS, Rao Muvva SSVJ, Wan M, Raqib R, Bergman P, Brighenti S, et al. Phenylbutyrate induces LL-37-dependent autophagy and intracellular killing of *Mycobacterium tuberculosis* in human macrophages. *Autophagy* (2015) 11:1688–99. doi: 10.1080/15548627.2015.1075110

230. Islam D, Bandholtz L, Nilsson J, Wigzell H, Christensson B, Agerberth B, et al. Downregulation of bactericidal peptides in enteric infections: a novel immune escape mechanism with bacterial DNA as a potential regulator. *Nat Med* (2001) 7:180–5. doi: 10.1038/84627

231. Sarker P, Ahmed S, Tiash S, Rekha RS, Stromberg R, Andersson J, et al. Phenylbutyrate counteracts *Shigella* mediated downregulation of cathelicidin in rabbit lung and intestinal epithelia: a potential therapeutic strategy. *PloS One* (2011) 6:e20637. doi: 10.1371/journal.pone.0020637

232. Mily A, Rekha RS, Kamal SMM, Arifuzzaman ASM, Rahim Z, Khan L, et al. Significant effects of oral phenylbutyrate and vitamin D3 adjunctive therapy in pulmonary tuberculosis: a randomized controlled trial. *PloS One* (2015) 10:e0138340. doi: 10.1371/journal.pone.0138340

233. Bekele A, Gebreselassie N, Ashenafi S, Kassa E, Aseffa G, Amogne W, et al. Daily adjunctive therapy with vitamin d 3 and phenylbutyrate supports clinical recovery from pulmonary tuberculosis: a randomized controlled trial in Ethiopia. *J Intern Med* (2018) 284:292–306. doi: 10.1111/joim.12767

234. Miraglia E, Nylén F, Johansson K, Arnér E, Cebula M, Farmand S, et al. Entinostat up-regulates the CAMP gene encoding LL-37 *via* activation of STAT3 and HIF-1α transcription factors. *Sci Rep* (2016) 6:33274. doi: 10.1038/srep33274

235. Sultana Rekha R, Karadottir H, Ahmed S, Gudmundsson GH, Agerberth B, Bergman P. Innate effector systems in primary human macrophages sensitize multidrug-resistant *Klebsiella pneumoniae* to antibiotics. *Infect Immun* (2020) 88(8):e00186–20. doi: 10.1128/IAI.00186-20

236. Myszor IT, Sigurdsson S, Viktorsdottir AR, Agerberth B, Eskelinen EL, Ogmundsdottir MH, et al. The novel inducer of innate immunity HO53 stimulates autophagy in human airway epithelial cells. *J Innate Immun* (2022) 14(5):477–92. doi: 10.1159/000521602

237. Principi N, Blasi F, Esposito S. Azithromycin use in patients with cystic fibrosis. *Eur J Clin Microbiol Infect Dis* (2015) 34:1071–9. doi: 10.1007/s10096-015-2347-4

238. Halldorsson S, Gudjonsson T, Gottfredsson M, Singh PK, Gudmundsson GH, Baldursson O. Azithromycin maintains airway epithelial integrity during *Pseudomonas*

aeruginosa infection. *Am J Respir Cell Mol Biol* (2010) 42:62–8. doi: 10.1165/rcmb.2008-0357OC

239. Joelsson JP, Myszor IT, Sigurdsson S, Lehmann F, Page CP, Gudmundsson GH, et al. Azithromycin has lung barrier protective effects in a cell model mimicking ventilator-induced lung injury. *ALTEX* (2020) 37:545–60. doi: 10.14573/altex.2001271

240. Arason AJ, Joelsson JP, Valdimarsdottir B, Sigurdsson S, Gudjonsson A, Halldorsson S, et al. Azithromycin induces epidermal differentiation and multivesicular bodies in airway epithelia. *Respir Res* (2019) 20:129. doi: 10.1186/s12931-019-1101-3

241. Brockman-Schneider RA, Pickles RJ, Gern JE. Effects of vitamin d on airway epithelial cell morphology and rhinovirus replication. *PloS One* (2014) 9:e86755. doi: 10.1371/journal.pone.0086755

242. Zhang YG, Wu S, Lu R, Zhou D, Zhou J, Carmeliet G, et al. Tight junction CLDN2 gene is a direct target of the vitamin d receptor. *Sci Rep* (2015) 5:10642. doi: 10.1038/srep10642

243. Zhang Y, Garrett S, Carroll RE, Xia Y, Sun J. Vitamin d receptor upregulates tight junction protein claudin-5 against colitis-associated tumorigenesis. *Mucosal Immunol* (2022) 15(4):683–97. doi: 10.1038/s41385-022-00502-1

244. Steelant B, Wawrzyniak P, Martens K, Jonckheere AC, Pugin B, Schrijvers R, et al. Blocking histone deacetylase activity as a novel target for epithelial barrier defects in patients with allergic rhinitis. *J Allergy Clin Immunol* (2019) 144:1242–1253.e7. doi: 10.1016/j.jaci.2019.04.027

245. Wu S, Tian X, Mao Q, Peng C. Azithromycin attenuates wheezing after pulmonary inflammation through inhibiting histone H3K27me3 hypermethylation mediated by EZH2. *Clin Epigenet* (2023) 15:12. doi: 10.1186/s13148-023-01430-y

246. Berber AC, Del-Rio-Navarro BE. Use of broncho-vaxom® in private practice: phase IV trial in 587 children. *Clin Ther* (1996) 18:1068–79. doi: 10.1016/S0149-2918(96)80062-2

247. Yin J, Xu B, Zeng X, Shen K. Broncho-vaxom in pediatric recurrent respiratory tract infections: a systematic review and meta-analysis. *Int Immunopharmacol* (2018) 54:198–209. doi: 10.1016/j.intimp.2017.10.032

248. Triantafillou V, Workman AD, Patel NN, Maina IW, Tong CCL, Kuan EC, et al. Broncho-vaxom ®R (OM-85 BV) soluble components stimulate sinonasal innate immunity. *Int Forum Allergy Rhinol* (2019) 9:370–7. doi: 10.1002/alr.22276

249. Fang L, Zhou L, Tamm M, Roth M. OM-85 broncho-vaxom®, a bacterial lysate, reduces SARS-CoV-2 binding proteins on human bronchial epithelial cells. *Biomedicines* (2021) 9:1544. doi: 10.3390/biomedicines9111544

250. Pivniouk V, Pivniouk O, DeVries A, Uhrlaub JL, Michael A, Pivniouk D, et al. The OM-85 bacterial lysate inhibits SARS-CoV-2 infection of epithelial cells by downregulating SARS-CoV-2 receptor expression. *J Allergy Clin Immunol* (2022) 149:923–933.e6. doi: 10.1016/j.jaci.2021.11.019

251. Netea MG, Domínguez-Andrés J, Barreiro LB, Chavakis T, Divangahi M, Fuchs E, et al. Defining trained immunity and its role in health and disease. *Nat Rev Immunol* (2020) 20:375–88. doi: 10.1038/s41577-020-0285-6

252. Hamada A, Torre C, Drancourt M, Ghigo E. Trained immunity carried by non-immune cells. *Front Microbiol* (2019) 9:3225. doi: 10.3389/fmicb.2018.03225

253. Kaufmann E, Sanz J, Dunn JL, Khan N, Mendonça LE, Pacis A, et al. BCG Educates hematopoietic stem cells to generate protective innate immunity against tuberculosis. *Cell* (2018) 172:176–190.e19. doi: 10.1016/j.cell.2017.12.031

254. Schulthess J, Pandey S, Capitani M, Rue-Albrecht KC, Arnold I, Franchini F, et al. The short chain fatty acid butyrate imprints an antimicrobial program in macrophages. *Immunity* (2019) 50:432–445.e7. doi: 10.1016/j.immuni.2018.12.018

255. Burgess SL, Leslie JL, Uddin J, Oakland DN, Gilchrist C, Moreau GB, et al. Gut microbiome communication with bone marrow regulates susceptibility to amebiasis. *J Clin Invest* (2020) 140:4019–24. doi: 10.1172/JCI133605

256. Ordovas-Montanes J, Dwyer DF, Nyquist SK, Buchheit KM, Vukovic M, Deb C, et al. Allergic inflammatory memory in human respiratory epithelial progenitor cells. *Nature* (2018) 560:649–54. doi: 10.1038/s41586-018-0449-8

257. Fanucchi S, Domínguez-Andrés J, Joosten LAB, Netea MG, Mhlanga MM. The intersection of epigenetics and metabolism in trained immunity. *Immunity* (2021) 54:32–43. doi: 10.1016/j.immuni.2020.10.011

frontiers | Frontiers in Immunology

TYPE Original Research
PUBLISHED 01 August 2023
DOI 10.3389/fimmu.2023.1178909

OPEN ACCESS

EDITED BY
Giamila Fantuzzi,
University of Illinois Chicago, United States

REVIEWED BY
Hirofumi Hirao,
Kyoto University, Japan
Maria Pini,
Alira Health, United States

*CORRESPONDENCE
Carmen Peralta
cperalta@recerca.clinic.cat

RECEIVED 05 April 2023
ACCEPTED 11 July 2023
PUBLISHED 01 August 2023

CITATION
Casillas-Ramírez A, Micó-Carnero M, Sánchez-González A, Maroto-Serrat C, Trostchansky A and Peralta C (2023) NO–IL-6/10–IL-1β axis: a new pathway in steatotic and non-steatotic liver grafts from brain-dead donor rats. *Front. Immunol.* 14:1178909. doi: 10.3389/fimmu.2023.1178909

NO–IL-6/10–IL-1β axis: a new pathway in steatotic and non-steatotic liver grafts from brain-dead donor rats

Araní Casillas-Ramírez[1,2], Marc Micó-Carnero[3], Alfredo Sánchez-González[1], Cristina Maroto-Serrat[3], Andrés Trostchansky[4] and Carmen Peralta[3]*

[1]Department of Teaching and Research Sub-Direction, Hospital Regional de Alta Especialidad de Ciudad Victoria "Bicentenario 2010", Ciudad Victoria, Mexico, [2]Facultad de Medicina e Ingeniería en Sistemas Computacionales de Matamoros, Universidad Autónoma de Tamaulipas, Matamoros, Mexico, [3]Department of Liver, Digestive System and Metabolism, Institut d'Investigacions Biomèdiques August Pi i Sunyer, Barcelona, Spain, [4]Departamento de Bioquímica and Centro de Investigaciones Biomédicas (CEINBIO), Facultad de Medicina, Universidad de la República, Montevideo, Uruguay

Introduction: Brain death (BD) and steatosis are both risk factors for organ dysfunction or failure in liver transplantation (LT)

Material and methods: Here, we examine the role of interleukin 6 (IL- 6) and IL-10 in LT of both non-steatotic and steatotic liver recovered from donors after brain death (DBDs), as well as the molecular signaling pathways underlying the effects of such cytokines.

Results: BD reduced IL-6 levels only in nonsteatotic grafts, and diminished IL-10 levels only in steatotic ones. In both graft types, BD increased IL-1β, which was associated with hepatic inflammation and damage. IL-6 administration reduced IL-1β only in non-steatotic grafts and protected them against damage and inflammation. Concordantly, IL-1β inhibition via treatment with an IL-1 receptor antagonist caused the same benefits in non-steatotic grafts. Treatment with IL-10 decreased IL-1β only in steatotic grafts and reduced injury and inflammation specifically in this graft type. Blockading the IL-1β effects also reduced damage and inflammation in steatotic grafts. Also, blockade of IL-1β action diminished hepatic cAMP in both types of livers, and this was associated with a reduction in liver injury and inflammation, then pointing to IL-1β regulating cAMP generation under LT and BD conditions. Additionally, the involvement of nitric oxide (NO) in the effects of interleukins was evaluated. Pharmacological inhibition of NO in LT from DBDs prompted even more evident reductions of IL-6 or IL-10 in non-steatotic and steatotic grafts, respectively. This exacerbated the already high levels of IL-1β seen in LT from DBDs, causing worse damage and inflammation in both graft types. The administration of NO donors to non-steatotic grafts potentiated the beneficial effects of endogenous NO, since it increased IL-6 levels, and reduced IL-1β, inflammation, and damage. However, treatment with NO donors in steatotic grafts did not modify IL-10 or IL-1β levels, but induced more injurious effects tan the induction of BD alone, characterized by increased nitrotyrosine, lipid peroxidation, inflammation, and hepatic damage.

Conclusion: Our study thus highlights the specificity of new signaling pathways in LT from DBDs: NO–IL-6–IL-1β in non-steatotic livers and NO–IL-10–IL-1β in steatotic ones. This opens up new therapeutic targets that could be useful in clinical LT.

KEYWORDS

brain death, liver transplantation, nitric oxide, steatotic liver grafts, IL-10, IL-6, IL-1, ischemia-reperfusion

1 Introduction

At present, some 80% of hepatic grafts used in liver transplantation (LT) are recovered from donors after brain death (DBDs) (1, 2). It is well known that brain death (BD) of the donor is a factor that drastically increases the chance of a liver graft experiencing preservation/reperfusion injury and decreases graft survival rate (3). In clinical situations, there is a shortage of donors of hepatic grafts for LT (4). In order to reduce the time patients spend waiting for LT, many clinical centers are exploring ways in which to broaden the criteria used to decide if an organ from a so-called marginal donor can be accepted for LT (5, 6). Data from different countries such as USA, France, Australia, or Chile have indicated that as many as 30%–50% of livers recovered from deceased donors are in a state of steatosis, which is one of the key variables that predict negative outcomes after LT (6–10). This is because the risk of hepatic dysfunction and indeed of primary non-function of transplanted liver grafts that are steatotic is greater than that for liver grafts that are not steatotic (11). It is also the case that steatosis is becoming even more prevalent, which means that more steatotic livers are discarded, particularly if the infiltration of fat is severe. Clearly, this exacerbates the current shortage of donors, which has already been described as critical (12). Thus, in order to reduce the LT waiting lists, we need therapeutic strategies that will reduce the post-LT risks of organ dysfunction or failure that are inherent to steatotic livers from DBDs.

The multifunctional cytokine interleukin-6 (IL-6) has been recognized as playing an important role in providing hepatoprotection against warm I/R injury, particularly in reduced-size LT (13, 14). In addition, interleukin-10 (IL-10) has shown protective effects in non-steatotic and steatotic livers that undergo warm ischemia (15, 16). To the best of our knowledge, no study to date has assessed the role of both IL-6 and IL-10 in LT from DBDs. Of interest, a regulation mechanism could exist between IL-6 or IL-10 and interleukin-1 (IL-1), the latter being an interleukin that promotes processes of inflammation and damage (15), including when both steatotic and non-steatotic livers are subjected to warm ischemia-reperfusion (I/R) (15–17). A potential relationship setting up a signaling mechanism between IL-6, IL-10, and IL-1 should not be ruled out, as an interaction between IL-6 and IL-1 has been previously reported in several pathologies (18, 19), and the administration of IL-10 reduced IL-1β levels in both steatotic and non-steatotic livers under warm ischemic conditions (15, 16).

On the other hand, several studies show that nitric oxide (NO) is a crucial mediator of I/R injury in many organs, such as the heart, liver, lung, and kidney (20). NO action decreasing the expression of cytokines has been demonstrated (21–23); for instance, endogenous NO decreased IL-1 hepatic expression in the setting of ischemic preconditioning, thus reducing the deleterious effects of I/R injury (15, 23). In the same way, a relation between IL-10 and IL-6, on the one hand, and NO, on the other, has been reported in several I/R experimental models (15, 24, 25). Thus, in myocardial ischemia, inhibition of NO production resulted in an increase in IL-6 and a reduction in IL-10 (24). In the case of hepatic warm I/R, the therapeutic strategy of ischemic preconditioned triggered NO production, which, in turn, induced IL-10 in non-steatotic and steatotic livers alike (15). In partial LT with steatotic livers, application of venous-systemic oxygen persufflation with NO gas entering the grafts during cold storage caused a reduction in plasma IL-6 levels in the reperfusion period, which was associated with an improvement of graft viability and protection against hepatocellular damage (25).

Taking all this information into account, the current study aimed to evaluate (a) the role of IL-10 and IL-6 in LT of both non-steatotic and steatotic liver recovered from DBDs; (b) the involvement of IL-1 as part of signaling pathways underlying IL-10 and IL-6 effects in this pathology; and (c) if NO might affect the levels of such ILs in LT from DBDs. The results of this study could therefore lead to a description of the molecular signaling mechanisms for both non-steatotic and steatotic livers in LT from DBDs. This, in turn, could result in identifying therapeutic targets that would potentially improve post-LT outcomes in the case of marginal liver grafts recovered from DBDs. Clearly, findings such as these would potentially be of great importance in clinical settings where, as we have said, some 80% of LT grafts are obtained from BD donors, and moreover, it is estimated that hepatic steatosis is present to an important degree in some 30%–50% of deceased donors.

2 Materials and methods

2.1 Experimental animals

We carried out the study using homozygous (obese: Ob) and heterozygous (lean: Ln) Zucker rats (Iffa Credo, L'Arbresele, France) when they were aged 12 to 14 weeks. In such Zucker rats,

steatosis has not been associated with inflammation (26). However, the Ob rats do show severe macrovesicular and microvesicular infiltration of fat into the hepatocytes (>60% steatosis) (27–31), whereas the Ln rats do not show any signs of steatosis (32). We performed all the procedures in accordance with the European Union regulations pertaining to animal experiments (Directive 86/609 EEC).

2.2 Experimental design

1) **Sham** (n = 12, 6 Ln and 6 Ob). Ob and Ln Zucker rats were anesthetized, ventilated, and maintained normotensive for 6 h (26, 32).
2) **LT** (n = 24, 12 transplantations: 6 with non-steatotic grafts and 6 with steatotic grafts). In subgroup 2.1, Ln Zucker rats were anesthetized, ventilated, and maintained normotensive for 6 h. Then, the non-steatotic livers were flushed with University of Wisconsin (UW) solution, isolated, preserved in ice-cold UW solution for 4 h, and implanted into Ln Zucker rats. In subgroup 2.2, the same surgical procedure was repeated, but with Ob Zucker rats as donors and Ln Zucker rats as recipients (26).
3) **BD+LT** (n = 24, 12 transplantations: 6 with non-steatotic grafts and 6 with steatotic grafts). In subgroup 3.1, Ln Zucker rats were anesthetized and ventilated. To induce BD, a frontolateral trepanation was performed in the rats and a balloon catheter was introduced in the extradural space (26, 32). The intracranial pressure was increased by inflating the balloon for 1 min, which induced rapid brain injury, leading to immediate BD. Then, the rats were maintained normotensive for 6 h (32–34). Next, the non-steatotic livers were flushed with UW solution, isolated, preserved in ice-cold UW solution for 4 h, and implanted into Ln Zucker rats (26, 32–34). In subgroup 3.2, the same surgical procedure of BD and LT was repeated, but with Ob Zucker rats as donors and Ln Zucker rats as recipients.
4) **BD+IL-1ra+LT** (n = 24). Same as group 3, but donors were treated with Anakinra, an IL-1 receptor antagonist (Amgen, Thousand Oaks, CA) at doses of 40 mg/kg (i.v.) just after BD was induced (15, 23, 35).
5) **BD+anti-IL-6+LT** (n = 24). Same as group 3, but the donors were treated with an anti-IL-6 antibody (R&D Systems, Minneapolis, MN) at doses of 16.6 μg/kg (i.p.), just after BD was induced (36–38).
6) **BD+anti-IL-10+LT** (n = 24). Same as in group 3, but the donors were treated with an anti-IL-10 antibody (Biosource International, Camarillo, CA), at doses of 0.5 mg/kg (i.v.) just after BD was induced (15).
7) **BD+anti-IL-6+IL-1ra+LT** (n = 12). Same as group 3.1, but the donors were treated with an anti-IL-6 antibody (R&D Systems) at doses of 16.6 μg/kg (i.p.), and with Anakinra, (Amgen) at doses of 40 mg/kg (i.v.) just after BD was induced (15, 23, 35–38).
8) **BD+anti-IL-10+IL-1ra+LT** (n = 12). Same as group 3.2, but the donors were with an anti-IL-10 antibody (Biosource International), at doses of 0.5 mg/kg (i.v.) and with Anakinra (Amgen) at doses of 40 mg/kg (i.v.) just after BD was induced (15, 23, 35).
9) **BD+IL-6+LT** (n = 24). Same as group 3, but the donors were treated with recombinant rat IL-6 (R&D Systems, Minneapolis, MN) at doses of 500 μg/kg (i.p.), 24 and 12 h before BD was induced (14, 39).
10) **BD+IL-10+LT** (n = 24). Same as group 3, but the donors were treated with recombinant rat IL-10 (Peprotech EC Ltd., Rocky Hill, NJ) at doses of 10 μg/kg (i.v.), just after BD was induced (15, 40, 41).
11) **BD+IL-6+IL-1+LT** (n = 12). Same as group 3.1, but the donors were treated with recombinant rat IL-6 (R&D Systems) at doses of 500 μg/kg (i.p.), 24 and 12 h before BD was induced and with recombinant rat IL-1β (Peprotech EC Ltd.) at doses of 10 μg/kg (i.v.), just after BD was induced (14, 15, 19, 39).
12) **BD+IL-10+IL-1+LT** (n = 12). Same as group 3.2, but the donors were treated with recombinant rat IL-10 (Peprotech EC Ltd.) at doses of 10 μg/kg (i.v.) and with recombinant rat IL-1β (Peprotech EC Ltd.) at doses of 10 μg/kg (i.v.), just after BD was induced (15, 19, 39).
13) **BD+NAME+LT** (n = 24). Same as group 3, but the donors were treated with N-nitro-L-arginine methyl ester hydrochloride (NAME), an inhibitor of NO synthesis (Sigma Chemical Co., St. Louis, MO) at doses of 10 mg/kg (i.v.) immediately after BD was induced (15).
14) **BD+NO+LT** (n = 24). Same as group 3, but the donors were treated with a NO donor, spermine NONOate (Cayman Chemical, Ann Arbor, MI), at doses of 10 mg/kg (i.v.), just after BD was induced (23).

Blood and liver samples were collected at the end of protocols; this was 4 h post-LT. Blood was extracted via the infrahepatic vein in the afternoon and collected in tubes with heparin. Then, blood samples were centrifugated and plasma was immediately frozen in dry ice. Rats were fasted before the extraction. We chose the conditions under which the study was performed, such as doses and the administration times of the pretreatments for the drugs that were used, in accordance with previous studies cited above and also with the results of some preliminary studies we performed. In clinical practice, it is typical for a hepatic donor to be kept in an ICU for a period of 6 h once BD has been diagnosed. During this time, inflammatory alterations tend to occur, which have a negative effect on the quality of the liver, in terms of LT outcomes. A cold ischemia period of 4 h is long enough to induce damage after transplantation in non-steatotic and steatotic liver grafts and to allow high survival at 4 h after reperfusion. For these reasons, we believe that the conditions we used in the experiments that form part of our study were the best based on the available evidence and in order to assess the effects of the different ILs we studied on hepatic damage and also on the molecular signaling pathways of those ILs in both non-steatotic and steatotic livers from DBDs.

Considering that IL-6 and IL-10 might be generated in intestine and adipose tissue in the context of different liver diseases (42–44), we evaluated whether in addition to the liver, such tissues were contributing to the generation of both IL-6 or IL-10 observed in non-steatotic and steatotic liver grafts, respectively, at 4 h post-LT. For this, the levels of IL-1 and IL-6 were measured in adipose tissue and intestine from experimental groups 1, 2, and 3.

To explore at what point in the surgical process cytokines were originated in each type of liver, experiments on the following groups were performed:

15) **CI** (n = 12 rats, 6 Ob and 6 Ln Zucker rats): Animals were anesthetized, and livers were subsequently flushed with UW solution, isolated, and maintained in cold ischemia in UW solution for 4 h.

16) **BD** (n = 12 rats, 6 Ob and 6 Ln Zucker rats): Animals were anesthetized and ventilated. After BD induction, rats were maintained normotensive with colloid infusion for 6 h.

17) **BD+CI** (n = 12 rats, 6 Ob and 6 Ln Zucker rats): Animals were anesthetized and ventilated. After BD induction, rats were maintained normotensive with colloid infusion for 6 h, and then livers were flushed with UW solution, isolated, and maintained in cold ischemia in UW solution for 4 h.

To investigate whether differences in the levels of IL-1β are observed at earlier reperfusion times than 4 h, experiments on the following groups were carried out:

18) **LT 1h** (n = 24). Same as group 2, but reperfusion was allowed for 1 h.

19) **BD+LT 1h** (n = 24). Same as group 3, but reperfusion was allowed for 1 h.

20) **BD+anti-IL-6+LT 1h** (n = 12). Same as group 3.1, but the donors were treated with an anti-IL-6 antibody (R&D Systems, Minneapolis, MN) at doses of 16.6 μg/kg (i.p.), just after BD was induced (27–29), and reperfusion was allowed for 1 h.

21) **BD+anti-IL-10+LT 1h** (n = 12). Same as in group 3.2, but the donors were treated with an anti-IL-10 antibody (Biosource International, Camarillo, CA), at doses of 0.5 mg/kg (i.v.) just after BD was induced (9), and reperfusion was allowed for 1 h.

22) **LT 2h** (n = 24). Same as group 2, but reperfusion was allowed for 2 h.

23) **BD+LT 2h** (n = 24). Same as group 3, but reperfusion was allowed for 2 h.

24) **BD+anti-IL-6+LT 2h** (n = 12). Same as group 3.1, but the donors were treated with an anti-IL-6 antibody (R&D Systems, Minneapolis, MN) at doses of 16.6 μg/kg (i.p.), just after BD was induced (31–33), and reperfusion was allowed for 2 h.

25) **BD+anti-IL-10+LT 2h** (n = 12). Same as in group 3.2, but the donors were treated with an anti-IL-10 antibody (Biosource International, Camarillo, CA), at doses of 0.5 mg/kg (i.v.) just after BD was induced (13), and reperfusion was allowed for 2 h.

Liver and blood samples were collected from groups 15 to 25 at the end of the protocol.

2.3 Biochemical determinations

We followed standard experimental procedures to determine plasma levels of transaminases [alanine aminotransferase (ALT) and aspartate aminotransferase (AST)]. We established plasma levels of alkaline phosphatase (ALP), the total level of bilirubin, the Von Willebrand factor (vWF), and hyaluronic acid (HA) levels using the appropriate assay kits: colorimetric (ALP: Abcam, Cambridge, United Kingdom) or immunosorbent (Total Bilirubin: MyBioSource Inc., San Diego, CA; vWF: Cusabio, Wuhan, China; HA: R&D Systems, Minneapolis, MN). To determine hepatic edema, we weighed liver samples and then placed them in a drying oven at 55°C until they reached a constant weight. The increase in the wet-to-dry weight ratio represents hepatic edema (45, 46).

Hepatic levels of lipid peroxidation were determined via measurements of malondialdehyde (MDA) formation by using the thiobarbiturate reaction (45, 47). For this, frozen tissue samples were homogenized in 2 ml of Tris buffer at pH 7. For protein precipitation, 0.25 ml of 40% trichloroacetic acid was added to 0.25 ml of homogenate. After mixing and centrifuging at 3,000 g for 15 min at 4°C, 0.25 ml of 0.67% thiobarbiturate solution was added to the supernatant, and this mixture was boiled for 15 min. After cooling, optical density was read at 530 nm (48).

To function as an index of the level of accumulation of neutrophils, we determined hepatic levels of myeloperoxidase (MPO) photometrically using a substrate of 3,3′,5,5′-tetramethylbenzidine (45, 47). For this, liver samples were homogenized in phosphate buffer (0.05 M KH_2PO_4, pH 6) with 0.5% hexadecyltrimethylammonium bromide (HTBA), then sonicated for 30 s at 20% power. After spending three freeze/thaw cycles in dry ice, the samples were incubated for 2 h at 60°C to eliminate the activity of non-specific peroxidases and MPO inhibitors that could affect the determination. After incubation, the samples were centrifuged for 12 min at 4,000 g at 4°C, and the supernatant was recovered. Then, 10 μl of tetramethylbenzidine reagent dissolved in dimethyl sulfoxide at a concentration of 5 mg/ml was added to 5 μl of the supernatant. At time zero (t:0), 70 μl of phosphate buffer (8 mM KH_2PO_4, pH 5.4) with 0.05% H_2O_2 was added, and the MPO enzymatic kinetics were determined, reading the absorbance for 3 min every 15 s at a wavelength of 630 nm. One enzyme unit was defined as the amount of enzyme that produces an increase of one absorbance unit per minute (47).

We measured hepatic nitrotyrosine to function as a peroxynitrite formation index, using commercial kits (MyBioSource Inc.) (32). For the determination of nitrotyrosine levels in liver tissue, samples were homogenized in 1 ml of 50 mM Na_2HPO_4 buffer, pH 7.4, at 4°C, then centrifuged at 20,000 g for 30 min at 4°C, and the supernatant was recovered for determination of

nitrotirosines (48). cAMP was extracted and quantified with the cAMP enzyme-linked immunosorbent assay (Abcam, Cambridge, United Kingdom) according to the manufacturer's protocol (49). To obtain liver lysates, frozen tissue was homogenized in 0.5 ml of 0.1 M HCl. After that, lysates were centrifuged at top speed for 5 min and the supernatant was stored at −80°C for subsequent determination of cAMP.

Finally, we measured levels of ILs (IL-1α, IL-1β, IL-6, and IL-10) using enzyme-linked immunosorbent assays, as reported elsewhere, with commercial kits (R&D Systems) (15, 23). To determine IL-1α, IL-1β, and IL-10, frozen liver samples were homogenized in 50 mM phosphate buffer at pH 6, containing 2 mM PMSF, 1 mg/ml antipain, 1 mg/ml leupeptin, and 1 mg/ml pepstatin A. The homogenates were centrifuged at 100,000 *g* for 1 h at 15°C, and the supernatants were stored at −80°C for subsequent determination of interleukins (15). To determine IL-6, liver samples were homogenized in a buffer made up of 50 mM Tris-HCl, 150 mM NaCl, Triton X-100, and a cocktail of protease inhibitors (Complete mini, Merck, Darmstadt, Germany). The homogenate was centrifuged at 3,000 *g* for 15 min at 4°C. Finally, the supernatant was recovered to perform the IL-6 measurement (50).

2.4 Histology

Before performing experiments in experimental groups, we determined steatosis level in biopsy specimens of liver tissue from lean and obese Zucker rats (n = 12, 6 Ln and 6 Ob). Since an association between liver fibrosis and adverse LT outcome has been reported (L4), assessment of fibrosis was also performed in Zucker rats. The removed livers were immediately fixed in a 10% phosphate buffered formalin solution and then embedded in paraffin. Samples were cut and stained with hematoxylin–eosin (HE) stain reagent for light microscopic observation. Histopathological findings were evaluated by scoring methods according to the report of Kleiner et al. (51) through a microscope (Nikon, Tokyo, Japan) at ×100 and ×200 magnification. Steatosis was graded 0–3 according to the percentage of cells with fatty droplets (0, <5%; 1, 5%–33%; 2, >33%–66%; 3, >66%). Lobular inflammation was graded 0–3 according to overall assessment of all inflammatory foci (0, no foci; 1, <2 foci per ×200 field; 2, 2–4 foci per ×200 field; 3, >4 foci per ×200 field). Liver cell injury was graded 0–2 according to ballooning degeneration (0, none; 1, few balloon cells; 2, many cells/prominent ballooning). Fibrosis was graded 0–4 according to the extent of fibrosis (0, no fibrosis; 1, zone 3 fibrosis; 2, zone 3 and portal fibrosis; 3, zone 3 and portal fibrosis with bridging fibrosis; and 4, cirrhosis). These scores were added, and the sum was used as a histopathological score (52–55). This assessment was carried out by three independent researchers who were unaware of the experimental conditions. Average values of the three mean scores assessed by these researchers were then used as a histopathological score for each animal. The pathological findings of obese Zucker rats used in the study were classified into severe simple steatosis with neither inflammation nor fibrosis, and histological findings of lean Zucker rats were classified as normal. This difference of steatosis in the Ob versus Ln Zucker rats was confirmed by using specific lipid staining such as red oil staining. Liver tissue was frozen and red oil O staining was used according to standard procedures. The hepatic steatosis was determined by quantifying cells with stained lipid droplets in 30 randomly chosen high-power fields per section. Data were expressed as the percentage of stained cells with respect to the total number of hepatocytes. Ob Zucker rats showed severe and macrovesicular and microvesicular fatty infiltration in hepatocytes. In contrast, Ln Zucker rats show no evidence of steatosis (15, 45, 56). In addition, we also evaluated fibrosis presence or absence with Sirius Red staining in paraffin-embedded liver samples, as this staining is one of the best understood techniques able to selectively highlight collagen networks (57). The percent area of collagen deposition was calculated as collagen area/total area − vascular lumen area × 100 (26). Ln and Ob Zucker rats showed no evidence of fibrosis, which is in agreement with reports describing that Ob Zucker rats show resistance to developing fibrosis (58, 59).

In liver samples obtained from all experimental group studies, we assessed the degree of liver injury also by staining paraffin-embedded liver sections with H&E and then using a method of counting points to determine a histological score (47). An experienced pathologist blinded to the allocation of animals into different experimental groups reviewed biopsy specimens and scored the histologic findings according to the following scale: grade 0, zero or minimal evidence of injury; grade 1, the injury is mild, showing cytoplasmic vacuolation and focal nuclear pyknosis; grade 2, the injury is moderate ranging to severe with extensive nuclear pyknosis, cytoplasmic hypereosinophilia, and the loss of intercellular borders; grade 3, severe necrosis showing disintegration of the hepatic cords, hemorrhage, and neutrophil infiltration; and finally grade 4, very severe necrosis exhibiting disintegration of the hepatic cords, hemorrhaging, and neutrophil infiltration (41, 45).

2.5 Statistics

In all determinations represented in figures, biological replicates were used. That is, in each experimental group that was represented in the graphs, samples from six different transplants with the same treatment were included. Data are expressed as mean ± standard error of mean. We applied non-parametric Kruskal–Wallis tests to determine statistical significance when treating differing variables. In contrast, we used Mann–Whitney U tests for groups that showed significant differences, and we calculated adjusted p-values by the false discovery rate (FDR) method ($p < 0.05$ was considered significant).

3 Results

3.1 The role played by IL-6 and IL-10 in LT of non-steatotic and steatotic grafts recovered from DBDs

First, we determined the levels of endogenous IL-6 and IL-10 in steatotic and non-steatotic LT from DBDs.

Concerning alterations in anti-inflammatory interleukins (ILs), we observed increased levels of IL-6 and IL-10 in LT of both non-

10.3389/fimmu.2023.1178909

steatotic and steatotic livers, compared to the results of the Sham group (Figure 1A). The induction of BD (BD+LT) resulted in IL-6 levels in non-steatotic grafts lower than those observed in the LT group. However, such an effect was not observed in steatotic grafts, since in this type of liver, the IL-6 levels were similar in BD+LT and LT groups. With regard to IL-10, inducing BD (BD+LT) resulted in no changes for this interleukin in non-steatotic livers when compared to the LT group. However, when steatosis was present, we observed reduced levels of IL-10 in the BD+LT group, compared to the LT group (Figure 1A). Thus, depending on the presence or absence of steatosis, induction of BD downregulated different anti-inflammatory interleukins: IL-6 for non-steatotic and IL-10 for steatotic grafts.

Then, we assessed the role played by endogenous IL-6 and IL-10. To this end, we inhibited the action of either IL-6 or IL-10, always in liver grafts from DBDs, and evaluated the effects on inflammation and damage. The administration of antibodies against IL-6 (BD+anti-IL-6+LT) raised parameters of damage

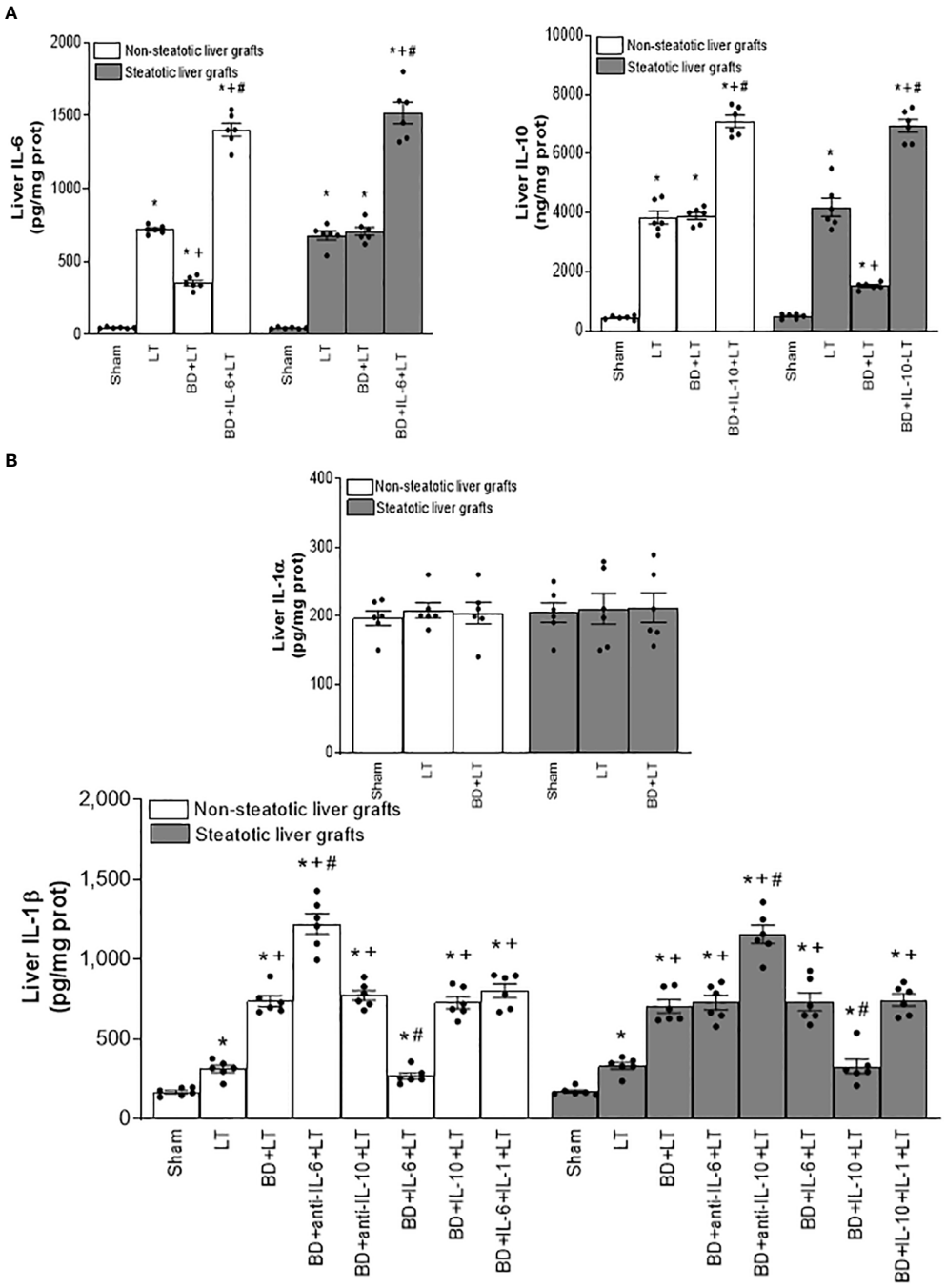

FIGURE 1
Interleukin levels in steatotic and non-steatotic LT from DBDs. **(A)** Levels of IL-6 and IL-10, and **(B)** levels of IL-1α and IL-1β, all in liver tissue. For A and B, six transplants per group in each measurement. *$p < 0.05$ versus Sham; $^{+}p < 0.05$ versus LT; $^{\#}p < 0.05$ versus BD+LT.

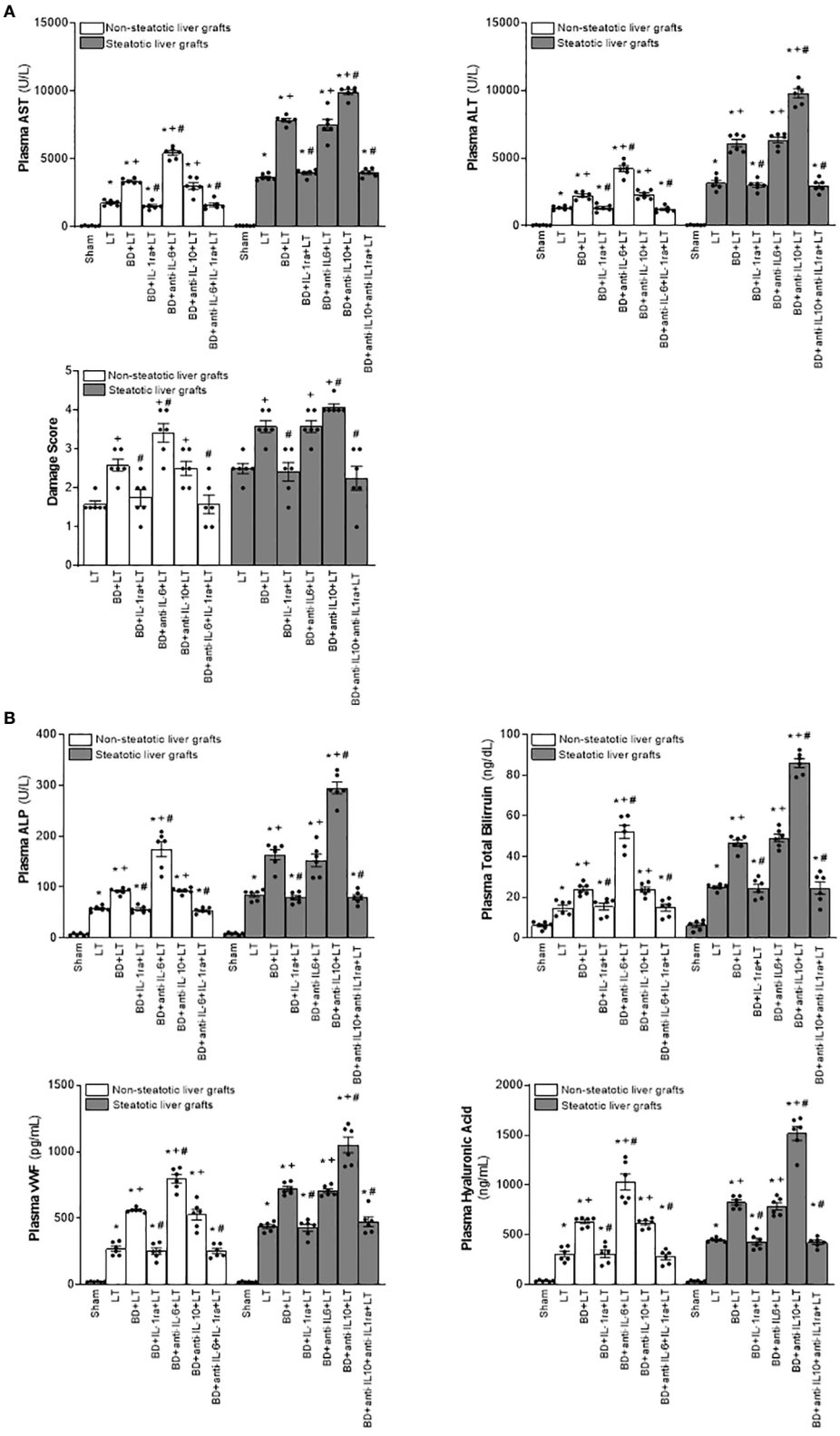

FIGURE 2
Relevance of endogenous interleukins for damage in steatotic and non-steatotic LT from DBDs. **(A)** ALT and AST levels in plasma and liver damage score. **(B)** ALP, total bilirubin, vWF, and HA levels in plasma. For A and B, six transplants per group in each measurement. *$p < 0.05$ versus Sham; +$p < 0.05$ versus LT; #$p < 0.05$ versus BD+LT.

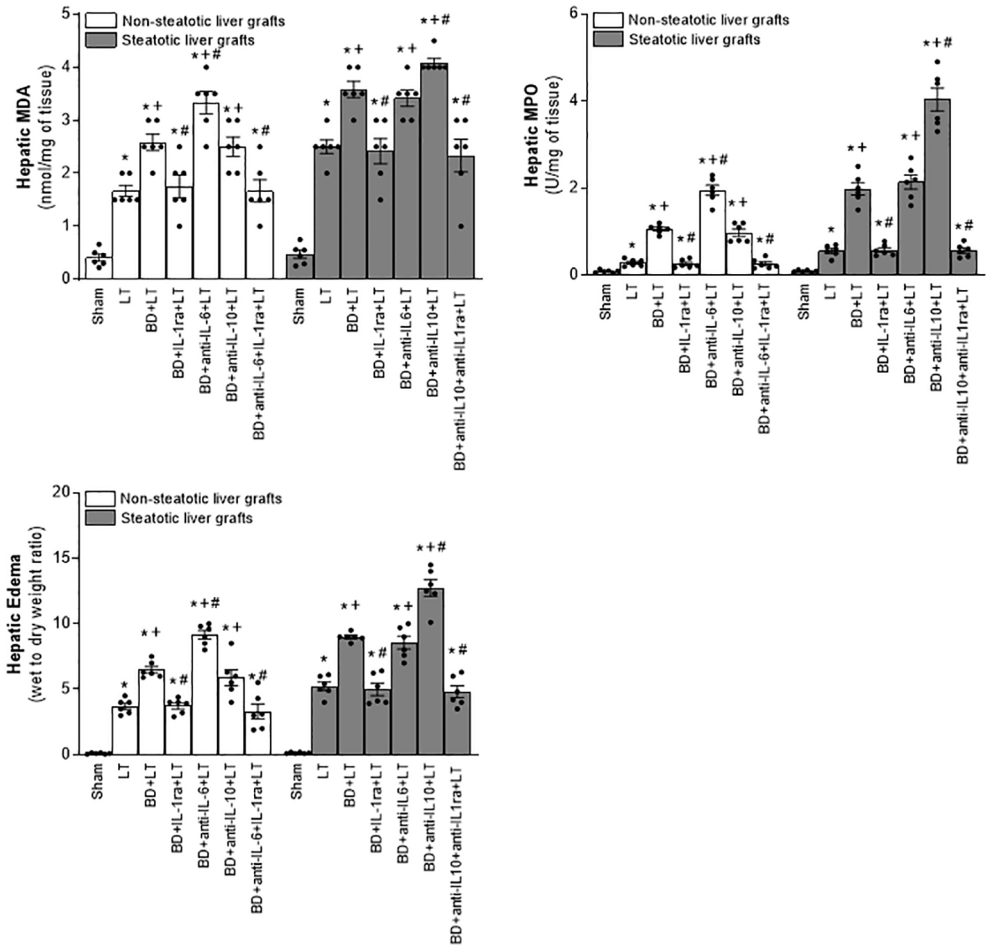

FIGURE 3
Effect of endogenous interleukins on inflammation in steatotic and non-steatotic LT from DBDs. Hepatic levels of MDA, MPO, and hepatic edema. For A and B, six transplants per group in each measurement. *$p < 0.05$ versus Sham; $^{+}p < 0.05$ versus LT; $^{\#}p < 0.05$ versus BD+LT.

(levels of transaminases, damage scores, ALP, total bilirubin, and also endothelial cell damage determined by vWF and HA levels) and inflammation (degree of neutrophil accumulation as measured by MPO, edema formation, and oxidative stress assessed using MDA) in non-steatotic grafts from DBDs, with respect to the results of the BD+LT group (Figures 2, 3). On the other hand, in steatotic liver grafts, no changes were observed in parameters of inflammation and damage (Figures 2, 3) when comparing the results of the BD+anti-IL-6+LT group to those of the BD+LT group. When we addressed the effects of endogenous IL-10, we observed that this cytokine was protective only in steatotic grafts since the administration of antibodies against IL-10 exacerbated hepatic damage and inflammation in steatotic liver grafts from DBDs, in comparison with LT from DBDs without treatment (that is, BD+anti-IL-10+LT vs. BD+LT) (Figures 2, 3). On the other hand, in the absence of steatosis, we observed that levels of these same parameters reflecting damage and inflammation were similar in the BD+anti-IL-10+LT group and in the BD+LT group. Thus, these results indicate that the protection offered by endogenous IL-6 and IL-10 is specific, according to the liver type: IL-6 provides protection in non-steatotic grafts and IL-10 in steatotic ones, within the context of LT from DBDs.

In consideration of the protection provided by endogenous IL-6 and IL-10 in LT from DBDs, we decided to evaluate whether treatments based on the administration of exogenous IL-6 and IL-10 might potentiate the benefits induced by the former regarding hepatic damage and inflammation in non-steatotic and steatotic livers, respectively. The administration of exogenous IL-6 (BD+IL-6+LT) increased IL-6 levels in both types of livers (Figure 1A) but livers obtained from DBDs were only protected against damage and inflammation in the absence of steatosis. In fact, for the BD+IL-6+LT group with non-steatotic livers, the liver injury parameters (levels of transaminases, damage scores, ALP, levels of total bilirubin, vWF, and HA; Figure 4) and inflammation indicators (MPO, edema, and MDA; Figure 5) were lower than those of the BD+LT group, while no changes were observed in those same experimental groups (BD+IL-6+LT and BD+LT) when steatotic grafts were used, when they were compared. The exogenous IL-10 supplementation (BD+IL-10+LT) increased IL-10 in non-steatotic and steatotic liver grafts (Figure 4); however, it did not abrogate the rise in parameters, indicating hepatic

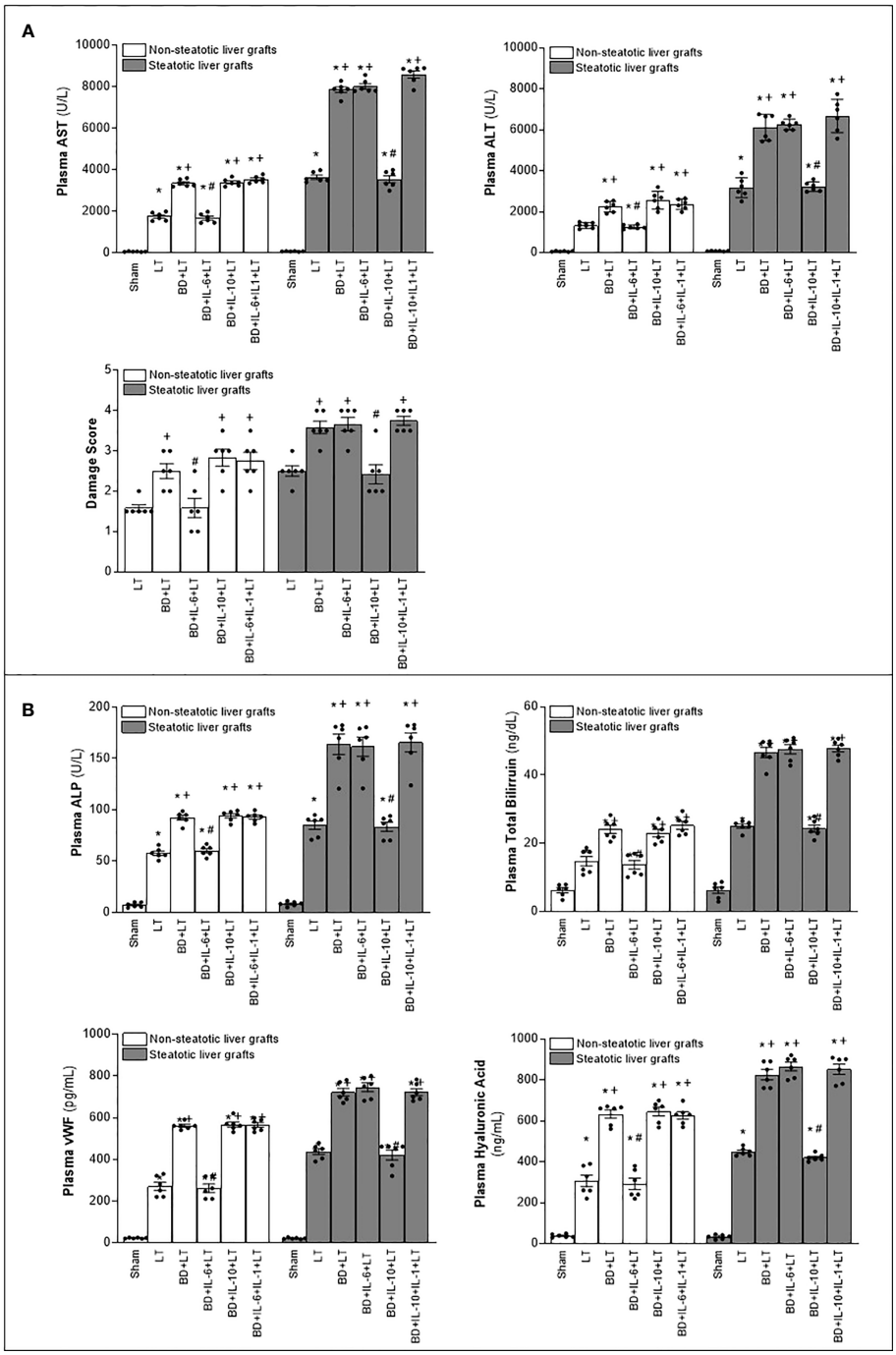

FIGURE 4
Relevance of exogenous IL-6 and IL-10 for damage in steatotic and non-steatotic LT from DBDs. **(A)** ALT and AST levels in plasma and liver damage score. **(B)** ALP, total bilirubin levels, vWF, and HA levels in plasma. For A and B, six transplants per group in each measurement. $^{*}p < 0.05$ versus Sham; $^{+}p < 0.05$ versus LT; $^{\#}p < 0.05$ versus BD+LT.

damage and inflammation in grafts obtained from DBDs in the absence of steatosis compared with the results of the BD+LT group (Figures 4, 5). In contrast, this intervention was effective as a therapeutic strategy in the presence of steatosis, since, in the BD +IL-10+LT treatment group, we observed reduced transaminase levels, damage scores, ALP, total levels of bilirubin, vWF, HA, MPO, edema, and MDA in grafts in the presence of steatosis with respect to the results of the BD+LT group (Figures 4, 5). Therefore, the benefits from exogenous IL-6 and IL-10 seem to be dependent on the type of liver: IL-6 was useful in non-steatotic livers and IL-10 was useful in steatotic ones. The dose of IL-6 and IL-10 used in the current study was the most effective because our preliminary results indicated that if these doses were increased threefold, this was not associated with more protection against damage (data not shown).

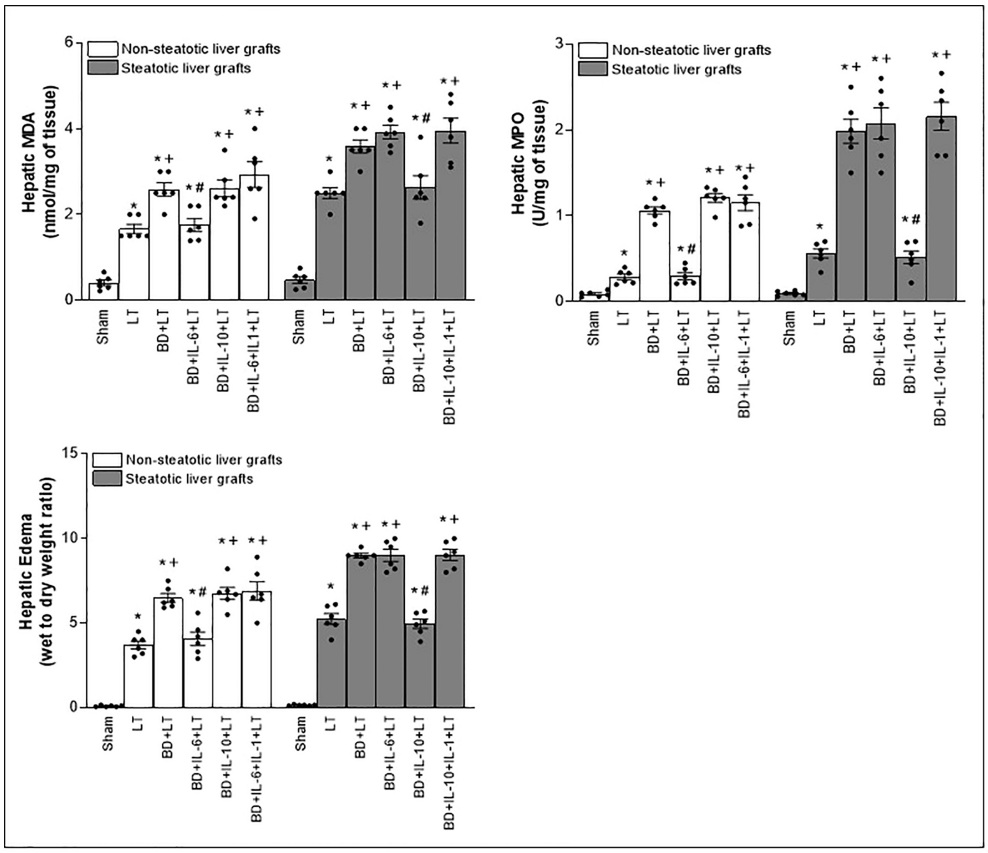

FIGURE 5
Effect of exogenous IL-6 and IL-10 on inflammation in steatotic and non-steatotic LT from DBDs. Hepatic levels of MDA, MPO, and hepatic edema (six transplants per group in each measurement). *$p < 0.05$ versus Sham; $^{+}p < 0.05$ versus LT; $^{\#}p < 0.05$ versus BD+LT.

3.2 Protective mechanisms of IL-6 and IL-10 in LT of non-steatotic and steatotic grafts recovered from DBDs

Considering previous publications that reported a regulatory role of IL-6 and IL-10 on IL-1 (11, 12, 14, 15), IL-1 was investigated as a possible mediator involved in signaling mechanism underpinning IL-6 and IL-10 beneficial effects. For this, hepatic levels of IL-1α and IL-1β in LT and BD surgical settings were first determined. Our results indicated that IL-1α does not mediate I/R injury in liver. This is because we observed levels of IL-1α in both non-steatotic and steatotic grafts obtained from DBDs (BD+LT), as well as in those grafts used in LT that had been obtained from donors that had not undergone BD (LT), similar to those of IL-1α in the Sham group (Figure 1B). Notwithstanding this, we did observe significant increases in levels of hepatic IL-1β in both grafts that were steatotic and those that were non-steatotic in the BD+LT group, compared to either the Sham group or the LT group (again, see Figure 1B). Then, the involvement of IL-1β in the damaging effects induced by BD in both types of liver grafts was evaluated. When we administered an IL-1 receptor antagonist (BD +IL-1ra+LT), we observed that damage in both types of liver was attenuated since, when compared to the BD+LT group, and all the following parameters were reduced: levels of transaminases, damage scores, ALP, total bilirubin, and endothelial cell damage (as determined by vWF and HA levels) (Figure 2). In conjunction with these effects, we also observed a reduced inflammatory response in both steatotic and non-steatotic grafts in the BD+IL-1ra+LT group compared to those of the BD+LT group, which was indicated by lower degrees of neutrophil accumulation (as measured by MPO), edema formation, and oxidative stress (as measured using MDA) (Figure 3). Thus, we observed that both in the presence and in the absence of steatosis, inhibition of IL-1 action was an effective strategy to reduce injury.

After demonstrating that IL-1β was involved in liver damage in LT with DBDs, we next evaluated whether IL-1β would be acting as a downstream mediator of IL-6 or IL-10. For this, we inhibited the action of either IL-6 or IL-10 in liver grafts from DBDs, to evaluate the effect of these endogenous cytokines on IL-1β. The administration of antibodies against IL-6 (BD+anti-IL-6+LT) increased IL-1β in non-steatotic grafts from DBDs, compared to those from the BD+LT group (this is shown in Figure 1B). In contrast to these findings, in grafts from steatotic livers, we found no changes in the levels of IL-1β when we compared the BD+anti-IL-6+LT group to the BD+LT group. Regarding endogenous IL-10, the administration of antibodies against IL-10 increased IL-1β in steatotic liver grafts from DBDs, in comparison with LT from DBDs without treatment (that is, BD+anti-IL-10+LT vs. BD+LT), whereas

the levels of IL-1β in liver grafts where there was an absence of steatosis were found to be similar in the BD+anti-IL-10+LT group and in the BD+LT group (Figure 1B). In addition, we investigated whether the benefits of exogenous IL-6 in non-steatotic livers and IL-10 in steatotic ones might be explained by their effects on IL-1β. In this sense, administration of IL-6 (BD+IL-6+LT) resulted in reduced IL-1β levels only in non-steatotic livers, whereas treatment with IL-10 (BD+IL-10+LT) led to reduced IL-1β levels only in steatotic livers (Figure 1B).

The above results showed that there is a relationship between IL-6 and IL-1β in non-steatotic grafts and between IL-10 and IL-1β in steatotic grafts, always from DBDs. Then, the relevance of such signaling pathways in liver inflammation and damage was investigated. For this, we evaluated whether the increased IL-1β levels were responsible for the exacerbated damage induced by the inhibition of either IL-6 or IL-10 action in liver grafts from DBDs, in the absence and presence of steatosis, respectively. We also found that, whereas blockade of IL-6 (BD+anti-IL-6+LT) increased IL-1β and damage in non-steatotic livers from DBDs more than in the BD +LT group, the inhibition of the action of both IL-6 and IL-1β (BD +anti-IL-6+IL-1ra+LT) gave rise to parameters that reflected liver damage and inflammation (Figures 2, 3), which were lower than those of the BD+LT group. In steatotic grafts from DBDs, suppression of IL-10 (BD+anti-IL-10+LT) increased IL-1β and the parameters of hepatic damage and inflammation when compared to the results in the BD+LT group, but no such effect was observed when both IL-10 and IL-1β effects were suppressed (BD+anti-IL-10+IL-1ra+LT). Indeed, the parameters of hepatic damage and inflammation in steatotic grafts from DBDs were decreased in the BD+anti-IL-10+IL-1ra+LT group, when we compared them with those of the experimental group BD+LT (Figures 2, 3). All of this confirms that in LT and BD, IL-6 in non-steatotic or IL-10 in steatotic livers reduces IL-1β levels, which is necessary to limit liver injury in each type of liver. If IL-6 in non-steatotic livers or IL-10 in steatotic ones is inhibited, IL-1β is increased and liver damage is more exacerbated than is seen with BD+LT. If IL-6 in non-steatotic grafts or IL-10 in steatotic grafts is inhibited but the action of IL-1β is also inhibited, there is no aggravated liver damage.

Next, we investigated whether the benefits of exogenous IL-6 in non-steatotic livers and IL-10 in steatotic ones might be explained by their effects on IL-1β. As previously described, administration of IL-6 (BD+IL-6+LT) resulted in reduced IL-1β levels and liver injury only in non-steatotic livers, whereas treatment with IL-10 (BD+IL-10+LT) led to reduced IL-1β levels and hepatic damage only in steatotic livers. In non-steatotic grafts from DBDs, IL-1β administration to the BD+IL-6+LT group (BD+IL-6+IL-1β+LT) increased IL-1β levels (Figure 1B) and this totally reversed the benefits seen from administration of IL-6 on hepatic damage and inflammation (Figures 4, 5). Similarly, in steatotic grafts from DBDs, IL-1β supplementation in the BD+IL-10+LT group (BD +IL-10+IL-1β+LT) raised IL-1β levels and abolished the benefits induced by IL-10, concerning liver injury and inflammatory response (Figures 1B, 4, 5). This demonstrates that IL-1β is a downstream mediator of IL-6 and IL-10 and its regulation is crucial as part of the signaling mechanisms to achieve the beneficial effects of IL-6 in non-steatotic grafts and IL-10 in steatotic ones when both are subjected to BD+LT.

To delve into the IL-6/IL-1β and IL-10/IL-1β signaling mechanism, we also investigated the IL-1β downstream mediator. Cyclic adenosine 3′,5′-monophosphate (cAMP) is produced by adenylate cyclase and acts as an intracellular second messenger for IL-1β (60, 61). In fact, it has been reported that IL-1β increased cAMP (61). When we measured hepatic cAMP levels, our results indicated that cAMP was higher in steatotic and non-steatotic livers of the BD+LT group when compared with the LT group. Of interest, the levels of cAMP were higher in experimental groups with steatotic livers than in those with non-steatotic ones. The inhibition of IL-1β effects through administration of IL-1β receptor antagonist (BD+IL-1ra+LT) reduced cAMP levels in both types of livers (Figure 6A). Then, blockade of IL-1β action and diminished hepatic cAMP were associated with a reduction in all parameters of hepatic damage and inflammation evaluated in the current study. Noticeably, the hepatic levels of cAMP induced by IL-1β were in parallel with the levels of liver damage observed in each type of graft; that is, steatotic livers subjected to LT or BD+LT have higher cAMP levels, compared to the levels recorded in non-steatotic livers. Hence, IL-1β regulates cAMP generation, and suppression of these both mediators downstream IL-6 or IL-10 was responsible for the protective effects of IL-6 in non-steatotic and IL-10 in steatotic livers in conditions of LT and BD.

3.3 Origin of IL-6, IL-10, and IL-1β in non-steatotic and steatotic LT from DBDs

Since IL-6 and IL-10 might be generated in intestine and adipose tissue in the context of different liver diseases (42–44), we evaluated whether, in addition to the liver, such tissues were contributing to the increased levels of both IL-6 or IL-10 observed in non-steatotic and steatotic liver grafts, respectively. In view of that, IL-6 and IL-10 were measured in adipose tissue and intestine. Our results showed that levels of IL-6 and IL-10 in intestine and adipose tissue in recipients with either non-steatotic or steatotic grafts, respectively, were similar in all experimental groups analyzed (Figure 6B). Therefore, neither adipose tissue nor intestine were responsible for changes in both ILs observed in liver grafts at 4 h post-LT.

We then considered that under experimental conditions of LT and BD, IL-6 and IL-10 are generated in liver tissue. Next, we explored whether these cytokines were originated in each type of liver at graft procurement, or just after BD procedure, and if the expression of IL-1β in liver tissue (which is induced by IL-6 or IL-10 in the experimental conditions evaluated in the present study) was already altered at those points in the surgical process. Results demonstrated that the levels of IL-6, IL-10, and IL-1β were similar in Sham (without any surgical intervention), CI (livers with cold ischemia, but without BD), BD (livers with BD but without cold ischemia), and in the BD+CI group (liver grafts experiencing BD and cold ischemia) (Figure 7A). Thus, hepatic levels for these three cytokines increase during the reperfusion in the recipient, and this means that IL-6, IL-10, or IL-1β did not

10.3389/fimmu.2023.1178909

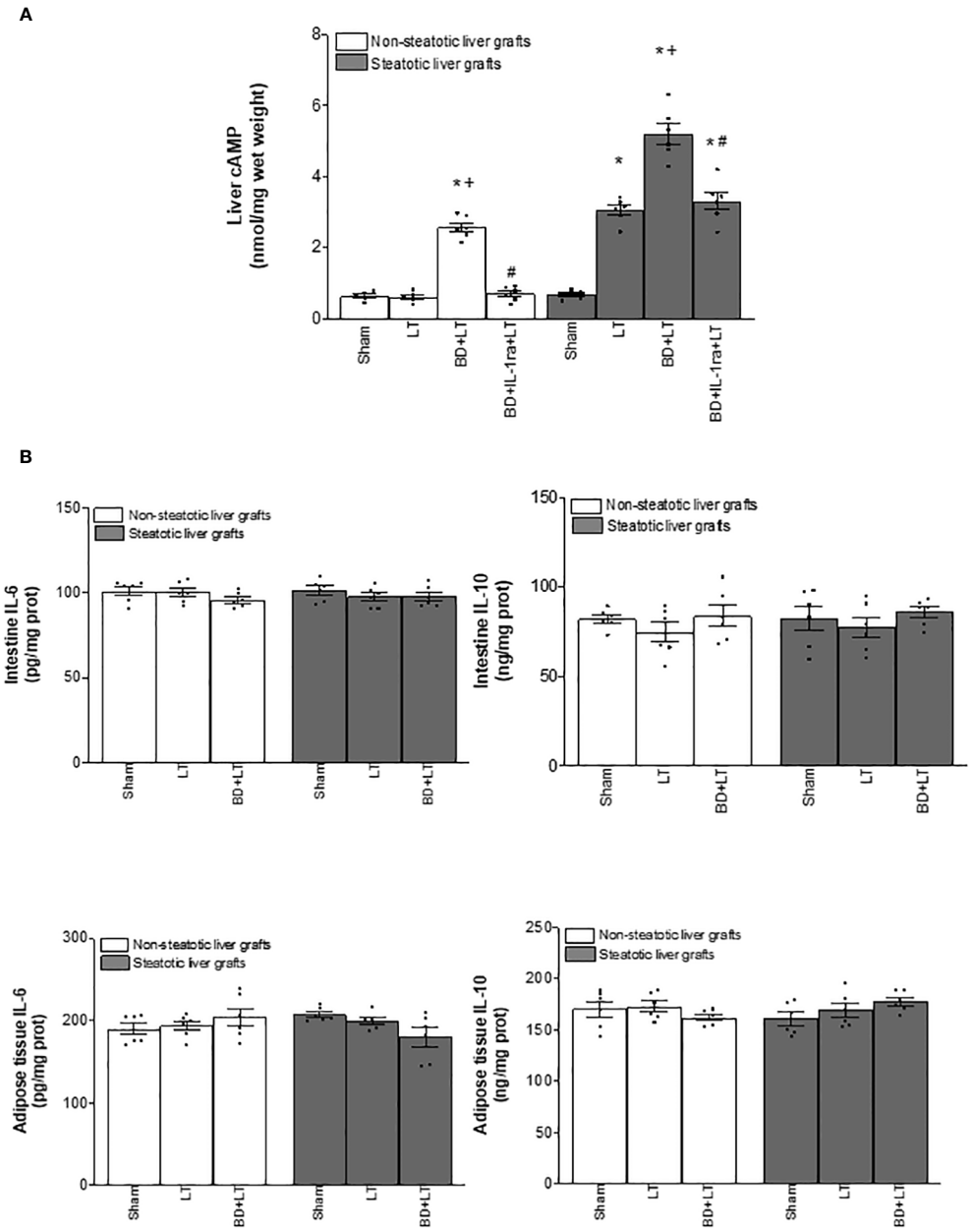

FIGURE 6
Effects of IL-1β on cAMP **(A)** and source of IL-6, IL-10, and IL-β **(B)** in steatotic and non-steatotic LT from DBDs. **(A)** Hepatic levels of cAMP. **(B)** IL-6, IL-10, and IL-1β in intestine and adipose tissue. For A and B, six transplants per group in each measurement. $^{*}p < 0.05$ versus Sham; $^{+}p < 0.05$ versus LT; $^{\#}p < 0.05$ versus BD+LT.

originate before the implantation of liver grafts in recipients, regardless of whether the graft comes from a BD or non-BD donor.

Finally, we evaluated whether differences in the levels of IL-1β altered by IL-6 or IL-10 were observed at earlier reperfusion times than 4 h in steatotic and non-steatotic livers. Then, liver samples were collected at 1 h and 2 h post-LT. Levels of IL-6 and IL-10 in non-steatotic and steatotic livers, respectively, gradually diminished as reperfusion occurs (Figure 7B). As it happened at 4 h of reperfusion, at 1 and 2 h of reperfusion, induction of BD (BD+LT) led to lower IL-6 levels in non-steatotic grafts than those observed in the LT group. In non-steatotic BD+LT groups, the higher levels of IL-6 were recorded at 1 h, whereas the lower levels were recorded at 4 h of reperfusion. On the other hand, in steatotic grafts, IL-6 levels were similar in BD+LT and LT groups at 1, 2, and 4 h of reperfusion (Figure 7B). In the case of IL-10, induction of BD (BD+LT) resulted in no changes for this interleukin in non-steatotic livers when compared to the LT group, at neither 1, 2, nor 4 h after reperfusion. However, when steatosis was present, a progressive reduction in the levels of IL-10 was observed as the reperfusion time proceeds. We observed reduced hepatic IL-10 in the BD+LT group, in comparison with the LT group, at 1, 2, and 4 h of reperfusion. Of interest, in BD+LT groups with steatotic livers, IL-10 was more elevated at 1 h and fewer at 4 h of reperfusion (Figure 7B).

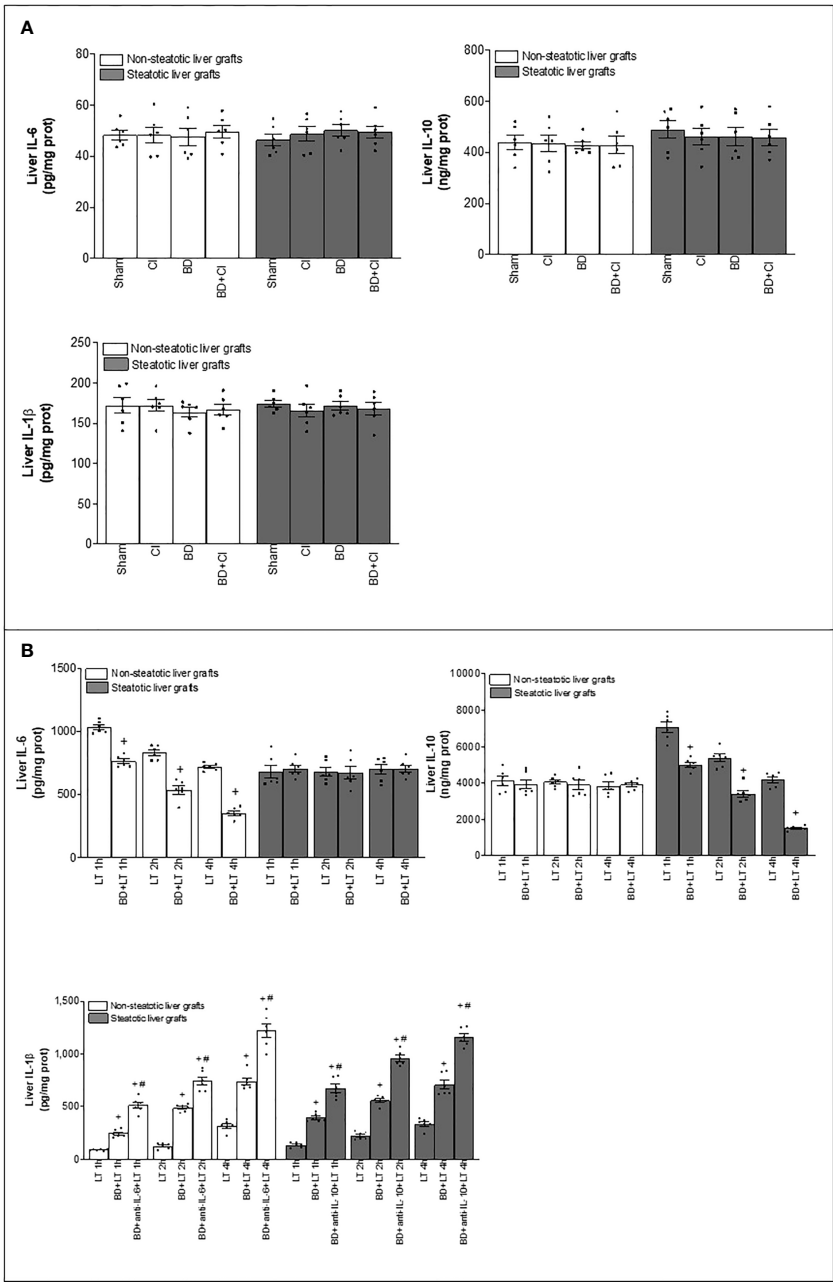

FIGURE 7
Generation of IL-6, IL-10, and IL-1β in the different stages of steatotic and non-steatotic LT from DBDs. **(A)** Hepatic levels of IL-6, IL-10, and IL-1β before implantation of liver grafts. **(B)** IL-6, IL-10, and IL-1β in liver grafts after transplantation. For A, six Ln or six Ob animals per group in each measurement; and for B, six transplants per group in each measurement. *$p < 0.05$ versus Sham; $^{+}p < 0.05$ versus LT; $^{\#}p < 0.05$ versus BD+LT.

Concerning IL-1β, hepatic levels were increased as reperfusion went on, and interestingly, at reperfusion times shorter than 4 h, hepatic IL-1β was higher in steatotic livers than in non-steatotic ones. In both types of liver from DBDs, IL-1β increased in the recipient at 4 h after LT (LT+BD groups), with such IL-1β levels being similar to steatotic and non-steatotic livers (Figure 7B). Treatment with antibodies against IL-6 (BD+anti-IL-6+LT) in non-steatotic livers, and against IL-10 (BD+anti-IL-10+LT) in steatotic grafts, augmented IL-1β even more compared to those levels from its respective BD+LT group, and levels were similar in the absence or presence of steatosis, at that reperfusion time (4 h post-LT) (Figure 7B). At 2 h after LT, levels of IL-1β were also higher in the BD+LT than in the LT group for non-steatotic and steatotic livers, but hepatic IL-1β in experimental groups with steatotic livers was more elevated than that recorded in respective analogous groups with non-steatotic livers (Figure 7B). In line with the above, when IL-6 in non-steatotic livers and IL-10 in steatotic livers were inhibited at 2 h post-LT, IL-1β levels increased in the BD +anti-IL-6+LT in grafts without steatosis and in the BD+anti-IL-10 +LT group in grafts with steatosis, compared with their respective BD+LT groups. Similar to what occurred in groups without cytokine modulation, the levels of IL-1β recorded were higher in

the group with steatotic livers than in non-steatotic ones (Figure 7B). Finally, when evaluating the hepatic levels of IL-1β in experimental groups at 1 h of reperfusion, the same pattern as observed at 2 and 4 h was registered between BD+LT and LT in both types of graft, as well as in BD+anti-IL-6+LT vs. BD+LT in non-steatotic livers and in the case of BD+anti-IL-10+LT vs. BD +LT in steatotic livers. Once again, in all the experimental groups analyzed at 1 h of reperfusion, the levels were higher in the presence of hepatic steatosis (Figure 7B). Contrary to what was observed during the reperfusion period for IL-6 and IL-10, the lowest levels of IL-1β in both types of grafts were recorded at 1 h of reperfusion, while the highest levels were observed at 4 h post-LT. These results demonstrated that IL-1β in non-steatotic and steatotic liver grafts is already being regulated by IL-6 and IL-10, respectively, at 1 h post-reperfusion. Remarkably, unlike what occurred in non-steatotic livers, the damaging effects of IL-1β are more intense as early as 1 h in steatotic livers, since IL-1β levels are higher in this type of liver at the start of reperfusion. This could be related to the exacerbated damage shown by steatotic livers in the conditions evaluated in the present study.

In different experimental groups, IL-1 receptor antagonist is administered to the donor since the liver graft obtained is the one that must be prepared to abolish high levels of IL-1β that will be generated later at reperfusion time. If the antagonist is administered to the recipient prior to transplantation, taking out the recipient's liver would remove a significant amount of the IL-1 receptor antagonist. Then, after implanting the donor-derived graft, the effects of the IL-1β inhibitor would no longer be present in the recipient at concentrations adequate to eliminate the effects of IL-β that will be generated rapidly at the beginning of reperfusion in the liver graft obtained from the donor. On the other hand, our preliminary control experiments demonstrated that when IL-1 receptor antagonist administration was performed in the recipient just after reperfusion, no effect was observed (data not shown). Then, it seems that this antagonist needs more than 4 h to exert its activity, and in consequence, when we administered IL-1 receptor antagonist immediately after reperfusion, no effect was demonstrated at the time of 4 h when the sacrifice is performed. Moreover, we tried to take advantage of the time frame between the declaration of BD and organ retrieval to prevent the side effects of the drug in other organs of the recipient. Because of this, in LT from DBD, a pharmacological treatment that could be administered in the donor that will be beneficial to the recipient would be most appropriate, as we performed in the case of IL-1 receptor antagonist.

Similarly, recombinant IL-1β was administered just after BD was induced since our experience and preliminary control assays indicated that it was the optimal pretreatment time to eliminate the protective effects of IL-6 or IL-10, which occur during reperfusion time in liver grafts. From our preliminary control experiments, we observed that administration of IL-1β just after induction of BD in the donor induced an increase of such cytokine in liver tissue after 6 h of BD, and this was maintained after 4 h of cold ischemia. In this sense, levels of IL-1β in steatotic and non-steatotic liver of the BD group (6 h after BD induction) were similar to those of the Sham group. However, an increase in IL-1β was observed in steatotic and non-steatotic livers of the BD+IL-6+IL-1, BD+IL-10+IL-1, BD+IL-6+IL-1+CI, and BD+Il-10+IL-1b+CI groups when compared with the results of either the Sham or BD group (data not shown). In this way, steatotic and non-steatotic grafts from DBDs had high levels of IL-1β to eliminate the protective effects of IL-6 or IL-10 that will be exercised precisely in those same grafts obtained from donors at the reperfusion stage. Moreover, supplementation of IL-1β just after BD induction in donors did not affect plasma levels at 6 h since BD, as IL-1β in plasma samples from experimental groups where it was technically possible to obtain them (Sham, BD, BD+IL-6+IL-1, and BD+IL-10-IL-1) was unchanged in all groups (at Sham levels, data not shown). Since liver grafts are isolated from circulation in BD +IL-6+IL-1+CI and BD+IL-10+IL-1+CI groups, it is not possible to collect plasma samples from them. These findings would mean that when recombinant IL-1β is administered in donors just after BD, it is not present in the circulation but in liver tissue, and then it would not have deleterious effects on other organs, which would be beneficial in the clinical context of LT. As it was the rationale for IL-1β receptor antagonist, if we deliver IL-1β to the recipient prior to LT, recipient liver extraction would remove a significant part of the recombinant IL-1β, so that after implanting the donor-derived graft, the IL-1β would no longer be present in the recipient at concentrations adequate to eliminate the effects of IL-6 or IL-10 during reperfusion time. From our previous control experiments, we observed that when administering IL-1β in the recipient post-LT, an increase in IL-1β levels in the plasma from recipients of groups BD+IL-6+IL-1+LT and BD+IL-10+IL-1+LT was registered at 4 h of reperfusion (data not shown). Therefore, we tried to avoid these high plasma IL-1β levels, in order to avoid a potential negative effect of this recombinant interleukin in other tissues from the recipient, which is crucial in the clinical scenario of LT.

3.4 Role of NO on IL levels in LT of steatotic and non-steatotic grafts recovered from DBDs

In consideration of the previous data that suggest that the effects resulting from NO could involve signaling mechanisms requiring interleukins (12, 16, 17, 19–21), we evaluated whether endogenous NO affects IL-6, IL-10, and IL-1β in non-steatotic and steatotic grafts from DBDs.

In non-steatotic grafts from DBDs, NO inhibition (BD+NAME +LT) resulted in reduced IL-6 and high IL-1β (Figure 8), and exacerbated liver injury and inflammatory response in comparison to the experimental group BD+LT (Figures 9, 10). In steatotic grafts, suppression of NO (BD+NAME+LT) reduced hepatic IL-10 and worsened hepatic damage and inflammation in comparison to the BD+LT group; all of this was associated with more elevated IL-1β levels than those in the BD+LT group (Figures 8–10).

In light of the beneficial effects of endogenous NO for hepatic grafts obtained from DBDs, we decided to assess if administration of exogenous NO would increase the benefits observed for endogenous NO. In grafts in the absence of steatosis obtained from DBDs, we observed that the administration of exogenous NO (BD+NO+LT) increased IL-6 and that this was associated with reduced IL-1β levels and protection against hepatic damage and inflammation, compared to the BD+LT group (Figures 8–10). In

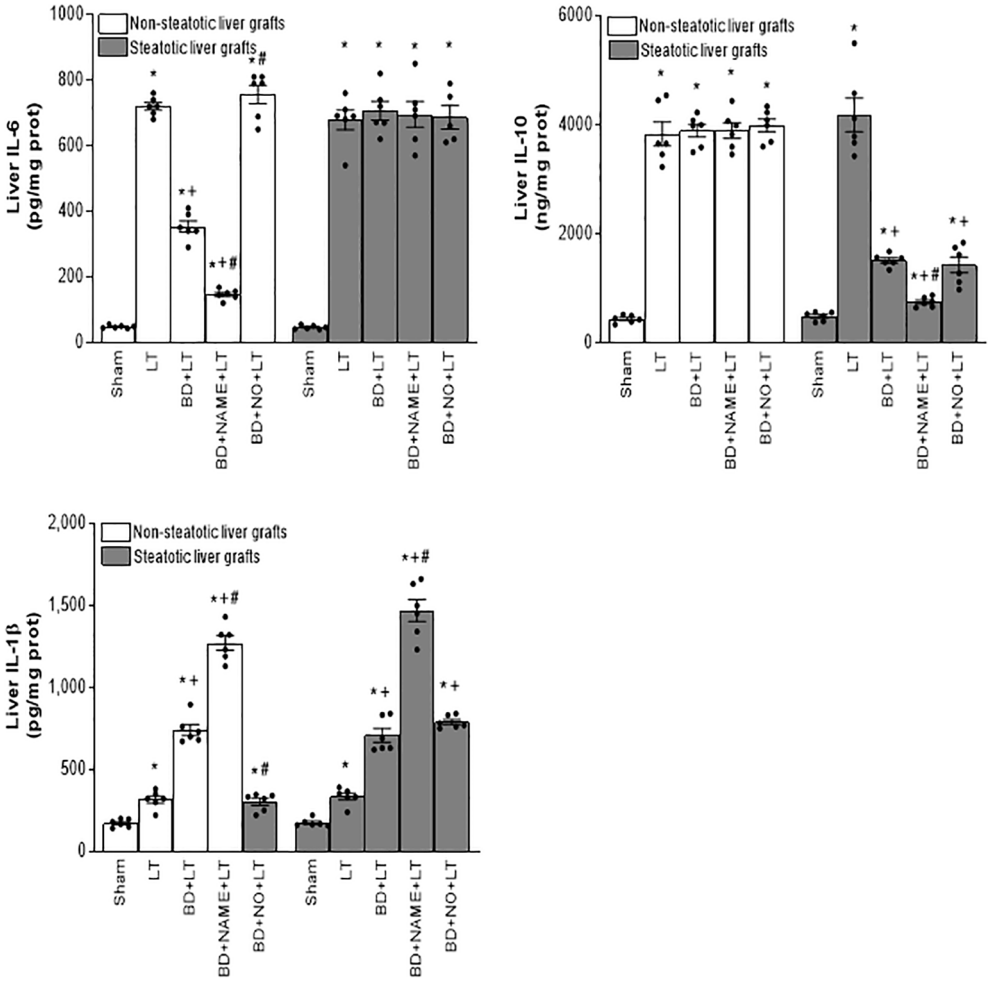

FIGURE 8
Effect of endogenous and exogenous NO on interleukin levels in steatotic and non-steatotic LT from DBDs. IL-6, IL-10, and IL-1β in liver. For A and B, six transplants per group in each measurement. *$p < 0.05$ versus Sham; $^{+}p < 0.05$ versus LT; $^{\#}p < 0.05$ versus BD+LT.

hepatic grafts from DBDs in which steatosis was present, the same level of administration of NO (BD+NO+LT) did not have an effect and was unable to induce changes in either IL-10 or IL-1β with respect to the experimental group BD+LT, without any treatment (Figure 8). In addition, NO supplementation severely aggravated all the parameters of hepatic damage and inflammation more than in the BD+LT group (Figures 9; 10). The effect induced by NO supplementation in steatotic grafts was related to an excess in nitrotyrosine generation, indicative of an increase of oxidative stress involving peroxynitrite ($ONOO^{-}$) formation, a highly oxidizing and cytotoxic reactive species. Thus, nitrotyrosine levels were notably increased in the experimental group BD+NO+LT, in comparison with the BD+LT group, for liver grafts in which steatosis was present; however, this did not occur with the same treatment in non-steatotic grafts from DBDs (Figure 10).

In Figure 11, we show representative histological images from the different interventions performed in the study aimed at protecting steatotic and non-steatotic liver grafts from DBDs. Our histological assessment of non-steatotic livers in the BD+LT group revealed a moderate presence of multifocal areas of coagulative necrosis and neutrophil infiltration, whose distribution across the parenchyma appeared to be random. In contrast to this, the necrotic areas in non-steatotic grafts from the experimental groups BD+IL-1ra+LT, BD+IL-6+LT, and BD+NO+LT were observed to be reduced in extent and number. In steatotic liver grafts from the BD+LT and BD+NO+LT groups, we observed areas with coagulative necrosis that were confluent, extensive, and severe. In contrast, there were fewer necrotic areas whose extent was reduced in grafts in which steatosis was present from the BD+IL-1ra+LT and BD+IL-10+LT groups.

4 Discussion

Herein, we show new endogenous signaling pathways in LT from DBDs, namely, IL-6/IL-1β in non-steatotic liver grafts and IL-10/L-1β in steatotic ones; these different mechanisms that depend on the presence of steatosis had not been reported to date. Our results indicated that when endogenous IL-6 in non-steatotic livers and IL-10 in steatotic livers, always from DBDs, are pharmacologically inhibited, then IL-1β is increased and the damage and inflammation are exacerbated. Thus, endogenous

10.3389/fimmu.2023.1178909

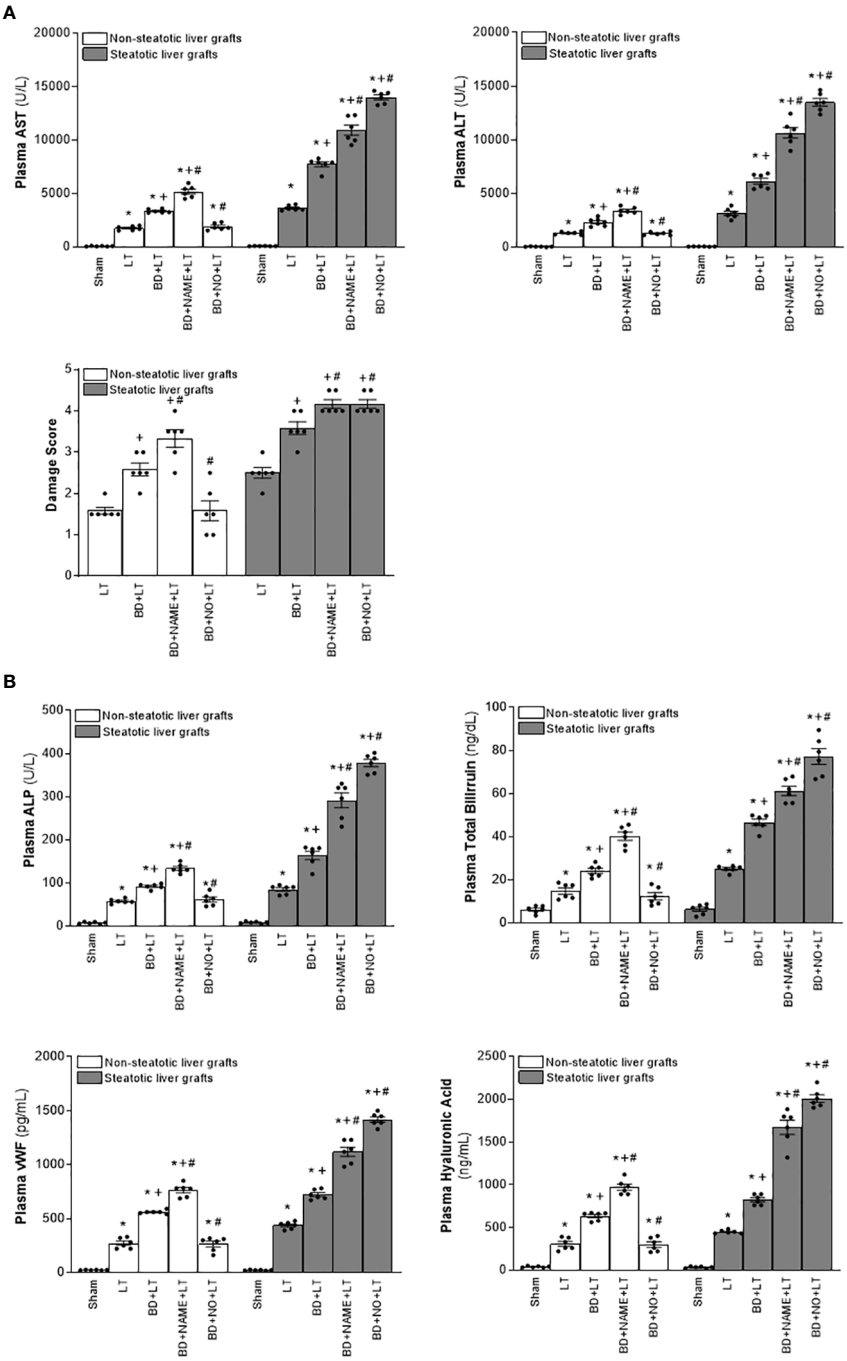

FIGURE 9
Involvement of interleukins in the effects of NO on damage in steatotic and non-steatotic LT from DBDs. **(A)** ALT and AST levels in plasma and liver damage score. **(B)** ALP, total bilirubin levels, vWF, and HA levels in plasma. For A and B, six transplants per group in each measurement. *$p < 0.05$ versus Sham; $^{+}p < 0.05$ versus LT; # $p < 0.05$ versus BD+LT.

IL-6 (for non-steatotic livers) and endogenous IL-10 (for steatotic ones) exert benefits through IL-1β inhibition, which, in turn, lessen cAMP generation. The suppression of both mediators (IL-1β and cAMP) downstream IL-6 or IL-10 is responsible for the protective effects of these cytokines. In addition, present research evidenced that NO is upstream of the endogenous IL-6 or IL-10 in the setting of LT from DBDs, thus defining the following endogenous signaling pathways: NO/IL-6/IL-1β in non-steatotic grafts from DBDs, and NO/IL-10/IL-1β for steatotic grafts from DBDs. Inhibition of NO synthesis abrogated the benefits of endogenous IL-6 and IL-10 in non-steatotic and steatotic grafts, respectively, consequently increasing hepatic IL-1β and cAMP, and exacerbating inflammation and damage, more than BD did by itself in LT.

In contrast to studies in the literature that report that there is a possible benefit of both exogenous IL-10 (15) and IL-6 (19) in both liver types under warm ischemia conditions, the results of the

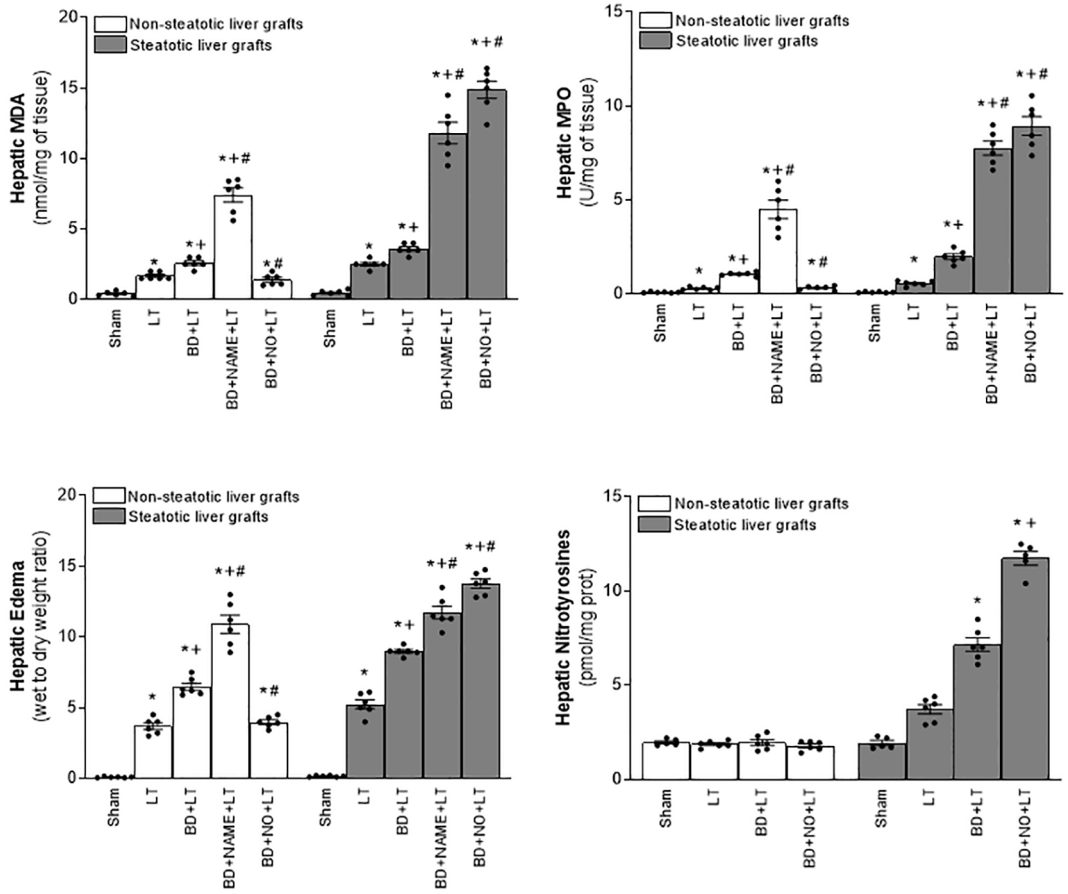

FIGURE 10
Involvement of interleukins in the effects of NO on inflammation in steatotic and non-steatotic LT from DBDs. Hepatic levels of MPO, edema, MDA, and nitrotyrosines. For A and B, six transplants per group in each measurement. *$p < 0.05$ versus Sham; $^{+}p < 0.05$ versus LT; $^{\#}p < 0.05$ versus BD+LT.

current study in LT from DBDs indicate the specificity of IL-6 and IL-10 to protect each type of the liver. Such differential effects of IL-6 and IL-10 are not surprising considering the huge amount of evidence concerning different signaling pathways underlying injuries of the type I/R in liver that are either steatotic or non-steatotic (62–65). In addition, the type of surgical procedure (warm I/R versus LT from DBDs) should be taken into account, since the pathogenic mechanisms underlying warm I/R and LT from DBDs are quite different (26, 66). In the same way, different ischemia times (60 min in warm I/R versus 4 h in LT from DBDs) and the presence or absence of BD, among other aspects, are known to distinctly affect the underlying signaling pathways of hepatic damage (67–69).

In the present study, hepatic IL-1β levels seem to be similar in LT groups of non-steatotic and steatotic grafts, while liver damage was higher in groups with steatotic grafts. Although these results might seem incongruous, it should be noted that IL-1β levels in liver tissue do not determine the contribution to liver injury and/or the vulnerability of steatotic livers subjected to transplantation. In the present study, the participation of IL-1β in the exacerbated liver damage observed in steatotic livers is demonstrated from the evidence that we next describe. First of all, the involvement of a mediator in liver damage is evidenced by pharmacologically modulating such mediator and verifying if the liver damage parameters are altered, as we have previously demonstrated in numerous research works from our group (48, 68, 70–72). In this sense, the present study investigated the role of IL-1β in the damaging effects induced by BD in both steatotic and non-steatotic liver grafts. Thus, treatment with an IL-1 receptor antagonist (BD+IL-1ra+LT) attenuated damage in both types of liver since when compared to the group without that intervention (BD+LT), all parameters for hepatic injury and inflammatory response were reduced. Thus, we observed that inhibition of IL-1β action reduced injury both in the presence and in the absence of steatosis, which means that IL-1β is involved in hepatic damage induced by BD and LT, in both types of grafts. In the case of steatotic grafts, inhibition of IL-1β resulted in a greater degree of reduction in liver damage and inflammation compared to the magnitude of reduction seen in non-steatotic livers. Then, our results show that IL-1β is responsible for the exacerbated damage observed in steatotic grafts when they are subjected to BD and LT, since when the action of this cytokine is inhibited, the higher liver damage recorded in the BD+LT group with steatotic grafts is absent. In the present study, the effect of the IL-1β antagonist in the LT groups without BD was not analyzed, since the investigation is

10.3389/fimmu.2023.1178909

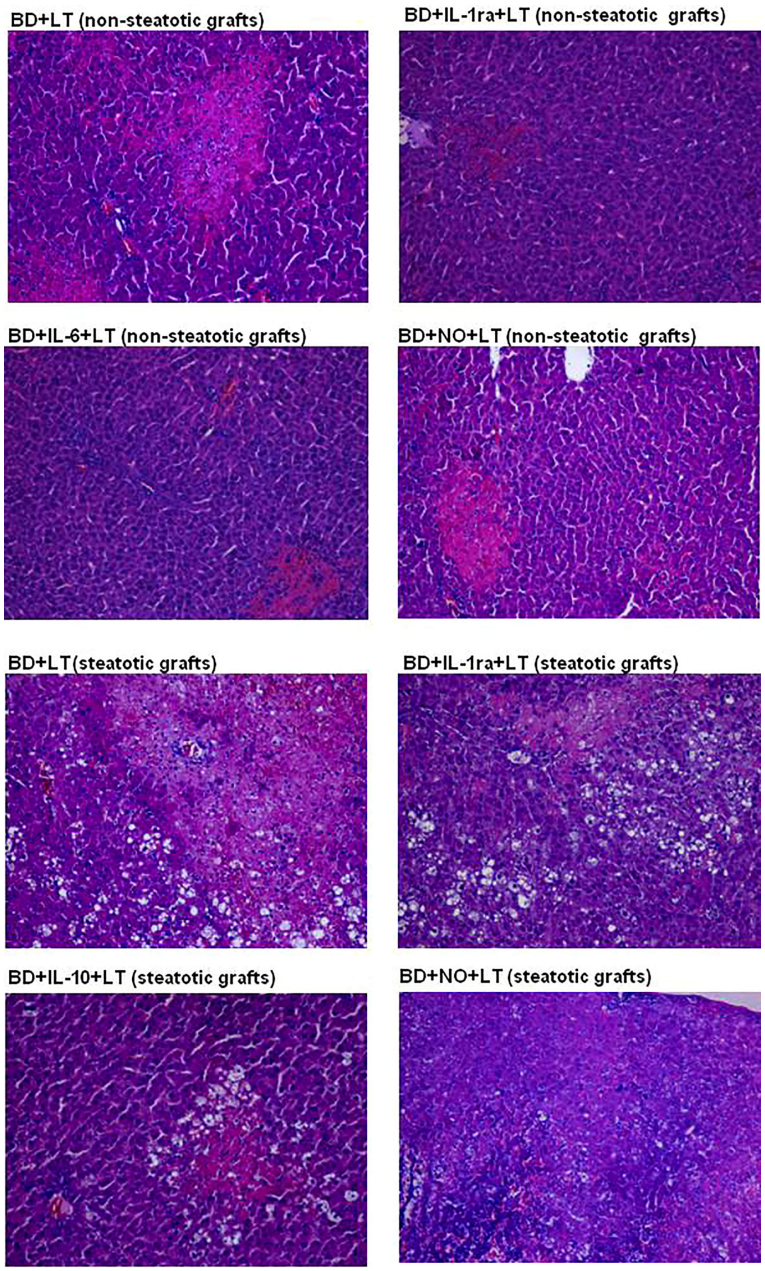

FIGURE 11
Representative photographs of histological changes in non-steatotic livers and steatotic LT from DBDs. In the BD+LT group, histological evaluation of non-steatotic livers showed moderate multifocal areas of coagulative necrosis and neutrophil infiltration, randomly distributed throughout the parenchyma, whereas the extent and the number of necrotic areas were reduced in the BD+IL-1ra+LT, BD+IL-6+LT, and BD+NO+LT groups (4x). Steatotic liver grafts from the BD+LT and BD+NO+LT groups showed extensive and confluent areas of coagulative necrosis, while the extent and the number of necrotic areas were reduced in the BD+IL-1ra+LT and BD+IL-10+LT groups (4x).

focused on the surgical context of BD+LT, which are the most approximate conditions to what is presented in clinical practice. Researching these two combined experimental settings could yield the best results, which are of translational interest. Secondly, in the context of liver damage associated with transplantation, it has been reported that equal levels of a mediator, for instance when administering NO or cortisol at the same dose, can cause different effects on hepatic injury in steatotic and non-steatotic livers (2, 48). In the present research, similarly to that occurring with IL-1β at 4 h after transplantation, supplying a NO donor at the same dose in both liver types led to different results: NO donor was beneficial in non-steatotic livers but resulted in detrimental effects in the presence of steatosis. Indeed, the steatotic livers show more vulnerability to the generation of peroxinitrites in the presence of NO donors than non-steatotic ones. Therefore, considering the above and the fact that steatotic livers are considered pathological (73), it is not surprising that at the same hepatic levels of IL-1β, the damaging effects of this cytokine may be more evident in steatotic livers, than in the case of normal livers. This is not unexpected owing to the widely documented differences that exist between

steatotic and non-steatotic livers, with respect to molecular mechanisms, and morphological and functional differences underlying I/R liver injury, which inevitably occurs when both types of grafts undergo transplantation (74, 75). Additionally, it is important to mention that in the surgical setting of LT and BD, signaling mechanisms downstream IL-1β involved different levels of cAMP depending on the type of liver, and this occurred even though both steatotic and non-steatotic livers have similar levels of IL-1β. Our results indicated that levels of cAMP were higher in experimental groups with steatotic livers than in those with non-steatotic ones submitted to LT and BD, and it was demonstrated (through an experiment involving inhibition of IL-1β action) that IL-1β was responsible for cAMP generation in such experimental conditions. Noticeably, hepatic levels of cAMP induced by IL-1β was in parallel with degree of liver damage observed in each type of graft, that is, higher cAMP levels in steatotic livers subjected to LT and BD, compared to the levels recorded in the homologous group with non-steatotic livers. This agrees with a previous study evaluating the role of cAMP in LT from donors without BD, which indicated that increases in cAMP observed in steatotic grafts were responsible for the vulnerability of steatotic livers to I/R and exacerbated damage (76). Finally, we also explored levels of IL-1β at earlier reperfusion times than 4 h in steatotic and non-steatotic livers. We found that IL-1β in liver increased as reperfusion occurs and such enhancement was more apparent in the presence of steatosis. After 1 and 2 h after LT, levels of IL-1β increased in livers with and without steatosis when undergoing LT and BD, but hepatic IL-1β was more elevated in steatotic livers than those recorded in respective analogous groups with non-steatotic livers. These results indicate that, unlike what occurred in non-steatotic livers, the damaging effects of IL-1β are more intense as early as 1 h in steatotic livers, thus reinforcing the conclusion that IL-1β contributes to the exacerbated damage shown by steatotic livers in the conditions evaluated in the present study.

We postulated that the mechanism of action of IL-6 or IL-10 in non-steatotic and steatotic livers, respectively, is the inhibition of IL-1β production, which, in turn, downregulates cAMP. Abolition of IL-1β was crucial to achieve benefits of IL-6 or IL-10 against liver injury. Several findings that support the existence of this signaling mechanism are further revealed. In non-steatotic livers undergoing LT and BD, we found that if IL-6 is inhibited (BD+anti-IL-6+LT), hepatic levels of IL-1β are increased only in non-steatotic livers and liver damage is exacerbated in this type of liver. All of this means that in LT and BD in non-steatotic livers, IL-6 reduces IL-1β, which is necessary to limit liver injury. If IL-6 is inhibited but the action of IL-1β is also inhibited, there is no aggravated liver damage. On the other hand, administration of exogenous IL-6 (BD+IL-6+LT group) reduced damage parameters and decreased hepatic IL-1β in non-steatotic liver. Benefits from IL-6 were abolished if we administered IL-1β. This demonstrates that IL-1β is a downstream mediator of IL-6 and its regulation is a fundamental part of the signaling mechanisms underlying beneficial effects of IL-6 in non-steatotic grafts subjected to LT and BD. In the case of steatotic livers subjected to LT and BD, suppression of IL-10 (BD+anti-IL-10 +LT) increased damage, inflammation, and IL-1β in liver. Such effects were not observed when both IL-10 and IL-1β effects were repressed. Therefore, in steatotic liver grafts from LT and BD, IL-10 decreases IL-1β levels, and this is required to restrain hepatic damage. When IL-10 is hindered, IL-1β increases and injury is impaired in steatotic livers. Provided that IL-10 is inhibited but also prevents IL-1β action, then intensified injury is absent in that type of liver. Treatment steatotic liver grafts with exogenous IL-10 reduced injury and inflammation and decreased IL-1β levels in that type of liver. These advantageous effects in steatotic livers were abolished if we administered IL-1β. Hereby, IL-1β is a downstream mediator for IL-10 and its regulation is crucial as it is part of the signaling pathway necessary to accomplish protection from IL-10 in steatotic grafts subjected to LT and BD. Last, we explore whether cAMP could be a mediator downstream IL-1β. In this sense, we observed that (a) cAMP levels increased in both steatotic and non-steatotic grafts from DBDs and transplanted, and (b) in conditions of pharmacological modulation of IL-1β, cAMP levels were not affected. These findings confirmed that, downstream of IL-6 in normal livers and IL-10 in steatotic livers, cAMP is a mediator of the deleterious effects of IL-β. Interestingly, hepatic cAMP levels reflected the different degrees of injury seen between steatotic and non-steatotic livers subjected to the same surgical conditions evaluated in the present study. Accordingly, previous reports described that cAMP affected the main mechanisms responsible for the vulnerability of steatotic livers to I/R damage (without BD), including oxidative stress, endothelial cell damage, and edema (45). Hence, in our hands, cAMP also appears to be related to the exacerbated damage suffered by livers with steatosis in LT and BD, although more experiments need to be performed to verify this.

The present investigation suggests that in LT of grafts from DBDs, the source of IL-6, IL-10, and IL-1β is the liver itself, without involving other organs as a source of these cytokines. Hepatic levels for these three cytokines were modified during the reperfusion in the recipient, and none of them suffered changes either in the donor with BD or during back table surgical procedures (before the implantation of liver grafts in recipients). In fact, our results indicated that after transplantation in recipients from DBDs, IL-6 and IL-10 in non-steatotic and steatotic livers, respectively, gradually diminished as reperfusion occurs. Contrary to this, IL-1β in such both liver types increased as reperfusion progressed. All of this demonstrated that IL-1β in non-steatotic and steatotic liver grafts is already being regulated by IL-6 and IL-10, respectively, at early reperfusion times. Then, during reperfusion in LT from DBDs as IL-6 or IL-10 decreases in each type of liver, the production of IL-1β also increases. Remarkably, unlike what occurred in non-steatotic livers, the damaging effects of IL-1β were more intense as early as 1 h in steatotic livers, since IL-1β levels are higher in this type of liver beginning reperfusion. As previously mentioned, this could be related to exacerbated damage shown by steatotic livers in the conditions evaluated in the present study.

Several investigations have found in murine and cell-based studies that IL-6 signaling for more than 24 h induces insulin resistance in adipose and hepatic tissue (77–79). Similarly, clinical and experimental studies have also shown that IL-10 is directly related to insulin action, *in vivo*, and that exogenous IL-10 could improve insulin action in skeletal muscle and liver (80–82). In our hands, treatment with either IL-6 or IL-10 did not induce changes

in plasma levels of glucose, insulin, or lipid profile parameters (including HDL, LDL, triglycerides, and cholesterol) from recipients transplanted after 4 h of reperfusion, when compared with animals without treatment (that is, BD+IL-6+LT and BD+IL-10+LT vs. BD+LT) with steatotic and non-steatotic liver grafts from DBDs (data not shown). Therefore, modulation of either IL-6 or IL-10 does not have effects on the metabolic profile of the recipients under the conditions evaluated in the present study, the early period of reperfusion. Such opposite results concerning literature reports (77–82) are not surprising considering the facts described below. One of the cited studies used a model of 3T3-L1 adipocytes or isolated human fat cells (79). It is widely known that experimental models based on isolated cell cultures do not reproduce the clinical setting of LT from DBDs (in which the response of a single cell type is not observed but rather, a response produced by the complex interrelationship of various cell types). Therefore, it is foreseeable that the results obtained in the study of a single isolated cell type will not be reproduced in the *in vivo* experimental conditions of our study. In another cited study, IL-6 was administered continuously in a mouse model without any liver injury, and biochemical features of insulin resistance were observed immediately after cessation of IL-6 supplementation for 5 to 7 days (78). In our experimental conditions, the administration of IL-6 was performed only twice, 24 h and 12 h before the induction of BD, which means that IL-6 would affect livers experiencing the detrimental effects of BD and I/R injury associated with transplantation. In this latter experimental setting, IL-6 had no effect on insulin resistance. All this points to the fact that the effect of IL-6 on insulin resistance and metabolic profile could depend on liver pathology as well as the different experimental conditions. This is not surprising due to the widely documented differences that exist between livers undergoing I/R and those that are not subjected to this type of damage, with respect to molecular signaling and functional differences (83, 84). Regarding IL-10, in a study with mice presenting severe hepatic steatosis and defective insulin signal transduction plus diabetes, animals were treated with two daily doses of an IL-10 inhibitor for 5 days. Upon such time, mice exhibited worsening of insulin signaling and the activation of gluconeogenic and lipidogenic pathways, suggesting that IL-10 exerts a protective role for liver insulin resistance associated with steatosis (82). Under the conditions evaluated in our study, the administration protocol to modulate the action of IL-10 was different and shorter, in addition to the fact that although animals with steatotic livers were used in some of our experimental groups, they did not present diabetes and instead were subjected to the injurious consequences of BD and cold ischemia. These marked differences in the experimental settings could explain why, in our investigation, IL-10 has no effect on insulin resistance at 4 h post-transplantation. On the other hand, insulin resistance and alterations in adipokines such as adiponectin and leptin might have a central role in liver metabolic damage after transplantation, as stated in a recent clinical study by Eshraghian et al. (85). Regulation of adipocytokines has been shown as a promising strategy for reducing I/R injury in steatotic livers, based on adipocytokines' effects on inflammation, steatosis, fibrosis, and molecular pathways of liver damage and regeneration (86). However, a role for adipokines and insulin resistance in pathogenesis of steatosis does not occur at least in the conditions evaluated in our study, since levels of glucose, insulin, and adiponectin were similar in plasma at 4 h of reperfusion in experimental groups BD+IL-6+LT, BD+IL-10+LT, BD+anti-IL-6 +LT, BD+anti-IL-10+LT, and BD+LT, with steatotic and non-steatotic liver grafts from DBDs (data not shown). Noticeable differences between the clinical study of Eshraghian et al. and ours might account to explain such results. We evaluated biochemical parameters at 4 h after transplantation, as usually performed in investigations evaluating injurious effects of hepatic I/R inherent with liver surgery; meanwhile, in the clinical study, alterations were evaluated at a mean time of 38 months after LT. Also, in our experimental model, all recipients of LT were lean animals without any pathology, whereas recipients in Eshraghian et al.'s research had diverse liver pathologies before undergoing transplantation.

The mechanisms through which IL-6 and IL-10 modulate the generation of IL-1β were not part of the objectives of the present study. On the other hand, the possibility that IL-6 or IL-10 influenced Kupffer cells and infiltrated recipient-derived macrophages after transplantation should not be discarded. In fact, according to data reported in the literature, IL-6 and IL-10 are strongly related to Kupffer cells' action (16, 87–89). It has been reported that IL-10 may regulate proinflammatory mediators' release in a liver perfusion model or in isolated Kupffer cells (89) and that IL-10 via Kupffer cells protected steatotic livers modulating the production of IL-1β in a mouse model of warm ischemia (16). Because of this relation between IL-6 and IL-10 and Kupffer cells in such surgical conditions, the involvement of the regulation of Kupffer cells by IL-6 and IL-10 in the experimental model presented in this research could not be discarded. Thus, elucidating the participation of Kupffer cells as a mediator through which IL-6 or IL-10 induces IL-1β production might deserve future intensive investigations.

Results presented in the present manuscript indicate that both IL-6 and IL-10, through the regulation of IL-1β, affect infiltration and accumulation of neutrophils. This conclusion was reached, since MPO levels were affected when the cytokines IL-6, IL-10, and IL-1β were pharmacologically modulated, either separately or in combination (depending on the type of livers in which they were shown to exert their action). Additionally, there are many reports in the literature indicating that IL-6 and/or IL-10 are capable of also modulating macrophages and chemokines (90–98), and therefore, the possibility that this is also happening under the conditions of the present study cannot be dismissed. IL-6 and IL-10 have been identified as important modulators of macrophage activity in the context of liver injury and disease (91–98). Under similar conditions of hepatic injury, IL-10 inhibited production of various CXC chemokines (90, 92), and in a rat model of orthotropic LT, IL-10 modulated CXCL2 chemokine or macrophage activity, thus affecting the early period after I/R (91). Regarding IL-6, it upregulated CXCL1 chemokine in conditions of injury in several tissues including liver (93, 94), and in experimental models of hepatic I/R injury, CXCL10 and IL-6 were strongly correlated (96). Also, IL-6 would be related to the activity and

ligands of CXCL2/CXCR2 chemokine in partial hepatectomy and I/R (95). Interestingly, a correlation between CXCL10 and IL-6 has been recently reported in human subjects after solid organ transplantation with BD donors (97). Thus, it would be valuable to explore issues related to chemokines and macrophages in future research that are currently outside the scope of this manuscript.

Other immune cells such as natural killer (NK) cells, dendritic cells (DCs), T lymphocytes (LT) CD4+ and CD+8, or Kupffer cells (KC) seem to have an important role in mechanisms underlying injurious postoperative outcomes in the setting of LT (99), and thus, a relationship between signaling pathways described in the present research (IL-6/IL-1b or IL-10/IL-1b) and such immune cells, in the context of LT from DBDs, should not be discarded. NK cells have been reported as modulators of I/R injury and, according to different authors, the infiltration of these immune cells into the liver exacerbates liver injury, promoting other inflammatory cells' infiltration in the graft (100). A relation has been established between NK cells and IL-6 or IL-10. IL-6 prevents liver inflammation via suppression of NK cells, since administration of IL-6 markedly attenuated the ability of NK cells to kill hepatocytes *in vitro*, which has been suggested to play an important role in the pathogenesis of hepatitis (101). In addition, IL-10 has been reported as an inhibitor of NK cells and their receptors, downregulating its cytotoxic activity in LT (100). Recently, compelling evidence has delineated the role of DCs in hepatic I/R injury and several results support that DCs modulate levels of IL-6 and IL-10 in liver submitted to ischemia injury (102, 103). T lymphocytes (CD4+) produce chemokines that amplify KC activation, which promote neutrophil recruitment and adherence into the liver sinusoids, aggravating IR injury (104). CD4+ T cells accumulate rapidly in mouse LT following cold storage, and in this sense, as early as at 1 h post-transplant, a massive infiltration of liver graft with CD4 T cells is found. In such conditions, CD4+ T cells express TIM-1 and modulation of this signaling mediator has resulted in the regulation of IL-6 and IL-10 production, and amelioration of cold hepatic ischemia-mediated LT inflammation and damage (105). After I/R injury, steatotic livers have showed increased infiltrating CD8+ cells in association with high levels of parameters of liver damage and proinflammatory cytokines (106). As occurring in the case of CD4+ cells, some reports have indicated that CD8+ cells may also regulate IL-6 and IL-10 in liver tissue (107, 108). Interestingly, induction of IL-6 expression in the liver prevented CD8+ T cell-mediated liver injury (109). All this constitutes interesting topics to be addressed in years to come, in order to better comprehend multiple complex interrelations between immune cells and inflammatory mediators that are established in liver grafts suffering from I/R inherent with LT and injurious effects of BD.

The data provided in this study determined that IL-6/IL-10 protects liver grafts from DBDs and, thus, hepatocytes, in an indirect way, if considering that the benefits of IL-6/IL-10 can only be achieved through the regulation of IL-1β. The mechanisms triggered downstream of the NO/IL-6/IL-1β pathway in non-steatotic livers and of the NO/IL-10/IL-1β pathway in steatotic ones resulted in beneficial effects such as reduction of endothelial damage, neutrophil accumulation, oxidative stress, and cellular edema. Surely, the attenuation of these cellular events protects the integrity of hepatocytes, and indeed, the detrimental effects of endothelial damage, neutrophil accumulation, and oxidative stress on hepatocytes are well known (62, 86, 110). In this sense, the reduction of such parameters was precisely associated with a decrease in graft damage parameters directly related to hepatocytes, such as ALT levels (released from hepatocytes) and damage score (evaluated directly in a liver tissue sample in which it is possible to observe the integrity or destruction of hepatocytes). Some studies have indicated that both IL-6 (in a rat model of partial LT) and IL-10 (in a rat model of hepatic I/R injury) have beneficial effects on hepatocytes, since they demonstrated that these cytokines promoted the proliferation of hepatocytes (111, 112). In these terms, there is the possibility that in the model of the present study (liver transplant with grafts from DBDs) IL-6 and/or IL-10 could also exert a direct action on the functionality and integrity of the hepatocyte. On the other hand, it is important to mention that to determine a direct hepatocyte response to IL-6 or IL-10 modulation, evaluation in an *in vitro* model is required, to isolate hepatocytes from the influence of non-parenchymal liver cells. Therefore, in the *in vivo* model used in the present investigation, it is not possible to conclude whether a cell type is being directly affected by IL-6 or IL-10, since the damage and inflammation parameters obtained from the LT from the DBD model are the result of the interaction of all cell types present in the liver. Although some aspects of I/R inherent to LT have been replicated *in vitro* to determine direct effects on hepatocytes (113–115), they are by no means the same conditions that occur when LT is performed in clinical practice. The great relevance of *in vivo* models is that they allow mimicking what occurs in clinical settings, where an interaction between different cell types occurs, and not the effects of a single cell type. Our study is an investigation of translational medical science, and in this field, what is sought is to reproduce as faithfully as possible in an experimental model what happens in clinical practice. This is extremely important so that in the short or medium term, the results can have an application in the clinical setting (116, 117) and, in that way, contribute to solving problems in LT from DBD that arises in our investigation.

Some studies in myocardial ischemia (24) and warm hepatic I/R (15) indicate that NO can induce IL-10 production, and in the setting of partial LT, NO has been shown to have the capacity to regulate generation of IL-6 (25). Moreover, I/R experimental models have also previously been used to demonstrate that NO inhibits the production of IL-1 (15), as is also the case when LPS induces hepatotoxicity (118). As data from the present research pointed to NO being upstream of IL-6 or IL-10, we investigated whether exogenous NO administration could confer protection against injury in LT from DBDs by stimulating IL-6 release in non-steatotic livers and IL-10 in steatotic ones. In our hands, in non-steatotic grafts from DBDs, exogenous NO increased IL-6, and this reduced IL-1β, thereby protecting against oxidative stress, inflammation, and damage. However, treatment with exogenous NO did not modify the levels of either IL-10 or IL-1β in steatotic

grafts from DBDs, but worsened oxidative stress, inflammation, and damage.

It is known that NO can act as an antioxidant, a vasodilator, and an antineutrophil, which means that this molecule has important potential to provide protection (48, 119). In contrast, it is also known that when combined with superoxide (O_2^-), the same NO molecule can form the detrimental $ONOO^-$ ion (120). If *in vivo* production of NO as well as O_2^- are at high levels, then $ONOO^-$ may be formed, with the well-known concomitant oxidative and cytotoxic effects (48, 121, 122). Antioxidant defenses in cells are reduced by $ONOO^-$, and it can also inactivate certain enzymes and in some proteins lead to nitration of tyrosine residues, which can have negative effects on different functions and also interfere with the process of signal transduction (123). Also, $ONOO^-$ promotes an inflammatory response in the liver, which includes, among other cellular events, the accumulation of neutrophils and cellular edema (124, 125). Interestingly, our results concerning nitrotyrosine hepatic levels indicate that $ONOO^-$ is potentially one of the most important reactive oxidants when we are considering steatotic liver grafts from DBDs. In agreement with this finding, we also found that when dealing with steatotic liver grafts obtained from DBDs, an increase in the levels of nitrotyrosine was also related to the negative effects that substances that are exogenous donors of NO had in terms of liver injury, inflammation, and levels of oxidative stress. This could partly explain why exogenous NO is harmful in the surgical setting of steatotic LT from DBDs. In contrast, in non-steatotic liver grafts from DBDs, exogenous NO (which was not associated with nitrotyrosine generation) protected against damage, oxidative stress, and inflammation. As previously mentioned, $ONOO^-$ is formed when the condition of high production of both NO and O_2^- occurs. In steatotic grafts from DBDs, these conditions come about when exogenous NO is administered, since these grafts generate reactive species intensely in LT from DBDs, and therefore, peroxynitrites are formed and liver damage is exacerbated. On the other hand, in the case of non-steatotic grafts from DBDs, since far fewer ROS are produced in LT from DBDs, when they are treated with exogenous NO, the conditions necessary to form $ONOO^-$ do not occur, and for this reason, no detrimental outcomes are observed. This hypothesis explains the differential effect of exogenous NO on the two types of grafts. Given such circumstances, it may be possible to develop some preventive strategies based on the use of NO donors for application in circumstances of non-steatotic grafts from DBDs used in LT; however, if steatosis is found to be present, then this same treatment would not be appropriate.

From our study, for the first time, we described signaling pathways underlying the I/R injury inherent to LT from DBDs that were specific depending on the presence or absence of steatosis in the liver graft. We showed that the fact that a liver is initially either steatotic or non-steatotic prior to graft collection may prove to be the determining factor for the endogenous signaling pathway. The fact that, in both types of liver grafts, we saw that proinflammatory and anti-inflammatory ILs were not well balanced as a result of BD induction could explain, at least partially, the detrimental effects induced by BD. Indeed, the results derived from the different pharmacological treatments indicate that the reduced ability to generate anti-inflammatory ILs (IL-6 in non-steatotic livers and IL-10 in steatotic ones) and the subsequent higher IL-1β levels in both types of liver grafts from DBDs were associated with the development of more severe liver injuries and inflammation, in both steatotic and non-steatotic LT from DBDs. Unfortunately, liver grafts from DBDs exhibit a decreased ability to endogenously generate such anti-inflammatory interleukins, as demonstrated by the results of the present study. This situation causes the grafts from DBDs to be unable to limit the high levels of IL-1β that were registered in both types of grafts, and consequently high levels of inflammation and damage occur.

The discovery of these mechanisms of action of IL-6 in non-steatotic livers and IL-10 in steatotic grafts allowed us to identify possible therapeutic targets whose effectiveness in reducing liver damage was evaluated in our research. Given such results and previous reports indicating that IL-1β is involved in the upregulation of reactive oxygen species (ROS) (15) and the production of inflammatory mediators (62, 126) observed in I/R liver injury, it could be useful to treat non-steatotic liver grafts with exogenous IL-6 or adopt a strategy based on supplementation with NO, and to treat steatotic ones with exogenous IL-10, with the purpose of limiting the inflammation and oxidative stress induced by IL-1β. Because of the results of the present research, the application of NO donors in steatotic liver grafts from DBDs would not be appropriate. Herein, we demonstrate a differential effect of NO supplementation depending on the type of liver graft from DBDs, since such a pharmacological strategy only protects non-steatotic grafts against damage through regulating the IL-6–IL-1β pathway, while in contrast, NO supplementation exacerbates oxidative stress, inflammation, and damage and does not affect the IL-10–IL-1β pathway in steatotic liver grafts.

In our view, it would be more appropriate to use pharmacological strategies with benefits in both types of livers (whether steatotic or non-steatotic), as there are no effective methods to distinguish between the presence and the absence of steatosis, or the degree of steatosis in the clinical context of DBDs (127). In such a case, given the preclinical results presented in the current study, the use of exogenous IL-6 or IL-10 and NO donors as therapeutic strategies may not be appropriate because of their specificity to only protect one type of graft and even NO donors can be prejudicial if steatosis is indeed present. Highlighting this type of disadvantage is extremely important for clinical surgical teams, because some studies have established that if a drug is useful in a model of hepatic I/R (whatever it may be), it could be used in all other settings involving liver injury from I/R (128–130). In this sense, the findings of the present study contribute to support the idea that, in the context of hepatic I/R, different therapeutic strategies have to be applied depending on each clinical context of I/R and dependently of the type of the liver (steatotic versus non-steatotic liver). Based on all of this, when performing LT, protection against the negative effects of BD may be provided by treatment

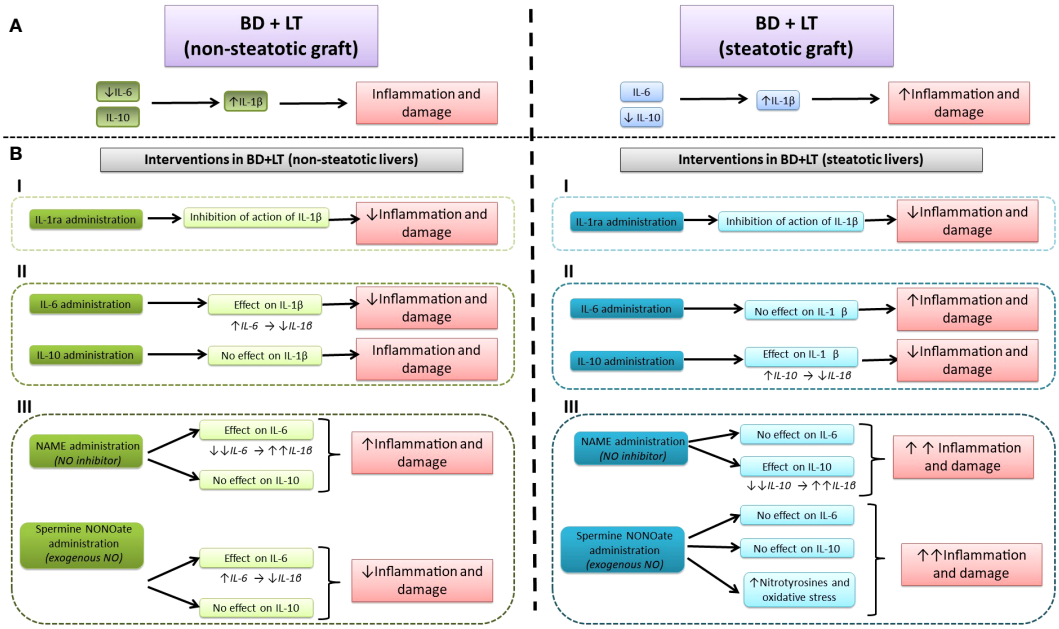

FIGURE 12
Signaling pathways highlighted by the current study. **(A)** Schematic representation of the role of interleukins in liver injury during transplantation with steatotic and non-steatotic grafts from DBDs. **(B)** Different pharmacological interventions: (I) effect of IL-1receptor antagonist, modulating the action of IL-1β; (II) effect of IL-6 and IL-10, modulating IL-1β levels; (III) effect of NO, modulating levels of IL-6, IL-10, and IL-1β.

adopting a strategy based on inhibiting the action of endogenous IL-1β, since such a strategy has been shown to be beneficial in liver grafts from DBDs both in the presence and in the absence of steatosis. The findings derived from the present investigation indicate that the administration of an IL-1β receptor antagonist would be an effective therapeutic strategy that potentially could be used in real clinical situations of LT from DBD. Since IL-1β inhibition has been shown to be equally effective in the presence or absence of steatosis, clinicians did not have to worry about knowing the degree of fatty infiltration that a liver graft that is going to undergo transplantation could have.

In conclusion, results from our research showed that the fact that a liver is initially either steatotic or non-steatotic prior to graft collection may prove to be the determining factor for the signaling pathway in livers undergoing LT from DBDs. This is the NO/IL-6/IL-1b pathway in non-steatotic livers, and the NO/IL-10/IL-1b pathway in steatotic ones (summarized in Figure 12). From this, the usefulness of a therapy based on inhibiting the effects of IL-1β (using an IL-1 receptor antagonist) was demonstrated, which was effective in protecting against damage in both types of graft. Findings from the current study might be of considerable clinical relevance and could make a great contribution to the field of developing effective and efficient strategies that result in a reduction of the incidence of complications after LT in the case of grafts obtained from deceased donors, whether steatosis is present or not. In addition to the above, the present research established that the time frame between the declaration of BD and organ retrieval provides an important window for protective intervention, thus avoiding possible side effects in the recipient. From all of the above, it is clear that the results from the present investigation are of scientific and clinical relevance. Undoubtedly, further research beyond the scope of the present study will be necessary to determine whether the benefits of these strategies demonstrated in experimental models could reach clinical practice.

Data availability statement

The raw data supporting the conclusions of this article will be made available by the authors, without undue reservation.

Ethics statement

All procedures were approved by the Laboratory Animal Care and Use Committee of the University of Barcelona and by the Generalitat de Catalunya (DAAM 9353). European Union regulations (Directive 86/609 EEC) for animal experiments were respected.

Author contributions

CP designed the study; CP, AC-R, and MM-C performed the groups of experiments, and biochemical and histological analyses; CP, AC-R, and MM-C contributed to data interpretation; AC-R,

CM-S, and AS-G gathered the related literature and prepared the figures; AC-R drafted the manuscript; AT reviewed the manuscript and aided in its writing; CP provided a critical appraisal of the manuscript, expertise, and review. All authors contributed to the article and approved the submitted version.

Funding

The Spanish Ministerio de Ciencia supported this research (PID2021-123123OB-100) as did the European Union (via the European Regional Development Fund "Una manera de hacer Europa").

Conflict of interest

The authors declare that the research was conducted in the absence of any commercial or financial relationships that could be construed as a potential conflict of interest.

Publisher's note

References

1. Rudge C, Matesanz R, Delmonico FL, Chapman J. International practices of organ donation. *Br J Anaesth* (2012) 108:i48–55. doi: 10.1093/bja/aer399

2. *Global Observatory on Donation and Transplantation* (2022). Available at: www.trasplant-observatory.org (Accessed June 20, 2022).

3. Jiménez-Castro MB, Gracia-Sancho J, Peralta C. Brain death and marginal grafts in liver transplantation. *Cell Death Dis* (2015) 6:6. doi: 10.1038/cddis.2015.147

4. Abouna GM. Organ shortage crisis: problems and possible solutions. *Transplant Proc* (2008) 40(1):34–8. doi: 10.1016/j.transproceed.2007.11.067

5. Vodkin I, Kuo A. Extended criteria donors in liver transplantation. *Clin Liver Dis* (2017) 21(2):289–301. doi: 10.1016/j.cld.2016.12.004

6. Álvarez-Mercado AI, Gulfo J, Romero Gómez M, Jiménez-Castro MB, Gracia-Sancho J, Peralta C. Use of steatotic grafts in liver transplantation: current status. *Liver Transpl* (2019) 25(5):771–86. doi: 10.1002/lt.25430

7. Steggerda JA, Bloom MB, Noureddin M, Brennan TV, Todo T, Nissen NN, et al. Higher thresholds for the utilization of steatotic allografts in liver transplantation: Analysis from a U.S. national database. *PloS One* (2020) 2:15. doi: 10.1371/journal.pone.0230995

8. Rogier J, Roullet S, Cornélis F, Biais M, Quinart A, Revel P, et al. Noninvasive assessment of macrovesicular liver steatosis in cadaveric donors based on computed tomography liver-to-spleen attenuation ratio. *Liver Transpl* (2015) 21(5). doi: 10.1002/lt.24105

9. Verran D, Kusyk T, Painter D, Fisher J, Koorey D, Strasser S, et al. Clinical experience gained from the use of 120 steatotic donor livers for orthotopic liver transplantation. *Liver Transpl* (2003) 9(5). doi: 10.1053/jlts.2003.50099

10. Gabrielli M, Moisan F, Vidal M, Duarte I, Jiménez M, Izquierdo G, et al. Steatotic livers. Can we use them in OLTX? Outcome data from a prospective baseline liver biopsy study. *Ann Hepatol* (2012) 11(6):891–98.

11. Núñez K, Thevenot P, Alfadhli A, Cohen A. Complement activation in liver transplantation: role of donor macrosteatosis and implications in delayed graft function. *Int J Mol Sci* (2018) 19(6). doi: 10.3390/ijms19061750

12. Purvis JW, Orandi BJ, Dhall D, McLeod C, Gutierrez Sanchez LH, Gray M, et al. Hepatic macrosteatosis in the US pediatric deceased liver donor population. *Pediatr Transplant* (2022) 26(1). doi: 10.1111/petr.14155

13. Song Z, Humar B, Gupta A, Maurizio E, Borgeaud N, Graf R, et al. Exogenous melatonin protects small-for-size liver grafts by promoting monocyte infiltration and releases interleukin-6. *J Pineal Res* (2018) 65(1). doi: 10.1111/jpi.12486

14. Camargo CAJr., Madden JF, Gao W, Selvan RS, Clavien PA. Interleukin-6 protects liver against warm ischemia/reperfusion injury and promotes hepatocyte proliferation in the rodent. *Hepatology* (1997) 26(6):1513–20. doi: 10.1002/hep.510260619

15. Serafin A, Roselló-Catafau J, Prats N, Gelpí E, Rodés J, Peralta C. Ischemic preconditioning affects interleukin release in fatty livers of rats undergoing ischemia/reperfusion. *Hepatology* (2004) 39(3):688–98. doi: 10.1002/hep.20089

16. Sutter AG, Palanisamy AP, Ellet JD, Schmidt MG, Schnellmann RG, Chavin KD. Interleukin-10 and Kupffer cells protect steatotic mice livers from ischemia-reperfusion injury. *Eur Cytokine Netw* (2014) 25(4):69–76. doi: 10.1684/ecn.2015.0359

17. Shirasugi N, Wakabayashi G, Shimazu M, Oshima A, Shito M, Kawachi S, et al. Up-regulation of oxygen-derived free radicals by interleukin-1 in hepatic ischemia/reperfusion injury. *Transplantation* (1997) 64(10):1398–403. doi: 10.1097/00007890-199711270-00004

18. Gottschall PE, Tatsuno I, Arimura A. Regulation of interleukin-6 (IL-6) secretion in primary cultured rat astrocytes: synergism of interleukin-1 (IL-1) and pituitary adenylate cyclase activating polypeptide (PACAP). *Brain Res* (1994) 637(1-2):197–203. doi: 10.1016/0006-8993(94)91233-5

19. Romero LI, Kakucska I, Lechan RM, Reichlin S. Interleukin-6 (IL-6) is secreted from the brain after intracerebroventricular injection of IL-1 beta in rats. *Am J Physiol* (1996) 270(3 Pt 2):R518–24. doi: 10.1152/ajpregu.1996.270.3.R518

20. Phillips L, Toledo AH, Lopez-Neblina F, Anaya-Prado R, Toledo-Pereyra LH. Nitric oxide mechanism of protection in ischemia and reperfusion injury. *J Invest Surg* (2009) 22(1):46–55. doi: 10.1080/08941930802709470

21. Anaya-Prado R, Toledo-Pereyra LH, Walsh J, Guo RF, Reuben J, Ward PA. Exogenous nitric oxide donor and related compounds protect against lung inflammatory response after hemorrhagic shock and resuscitation. *J Trauma* (2004) 57(5):980–8. doi: 10.1097/01.ta.0000135354.72494.8d

22. Hatano E, Bennett BL, Manning AM, Qian T, Lemasters JJ, Brenner DA. NF-kappaB stimulates inducible nitric oxide synthase to protect mouse hepatocytes from TNF-alpha- and Fas-mediated apoptosis. *Gastroenterology* (2001) 120(5):1251–62. doi: 10.1053/gast.2001.23239

23. Franco-Gou R, Roselló-Catafau J, Casillas-Ramirez A, Massip-Salcedo M, Rimola A, Calvo N, et al. How ischaemic preconditioning protects small liver grafts. *J Pathol* (2006) 208(1):62–73. doi: 10.1002/path.1859

24. Zingarelli B, Hake PW, Yang Z, O'Connor M, Denenberg A, Wong HR. Absence of inducible nitric oxide synthase modulates early reperfusion-induced NF-kappaB and AP-1 activation and enhances myocardial damage. *FASEB J* (2002) 16(3):327–42. doi: 10.1096/fj.01-0533com

25. Nagai K, Yagi S, Afify M, Bleilevens C, Uemoto S, Tolba RH. Impact of venous-systemic oxygen persufflation with nitric oxide gas on steatotic grafts after partial orthotopic liver transplantation in rats. *Transplantation* (2013) 95(1):78–84. doi: 10.1097/TP.0b013e318277e2d1

26. Jiménez-Castro MB, Negrete-Sánchez E, Casillas-Ramírez A, Gulfo J, Alvarez-Mercado AI, Cornide-Petronio ME, et al. The effect of cortisol in rat steatotic and non-steatotic liver transplantation from brain-dead donors. *Clin Sci* (2017) 131(7):733–46. doi: 10.1042/CS20160950

27. Sikalias N, Karatzas T, Alexiou K, Mountzalia L, Demonakou M, Kostakis ID, et al. Intermittent ischemic preconditioning protects against hepatic ischemia-reperfusion injury and extensive hepatectomy in steatotic rat liver. *J Invest Surg* (2018) 31(5):366–77. doi: 10.1080/08941939.2017.1334844

28. Güllüoğlu BM, Aktan AO, Yeğen C, Kurtel H, Yalin R. Endothelin release is augmented with captopril in rat ischemia-reperfusion injury of the liver. *Res Exp Med* (1996) 196(4):227–33. doi: 10.1007/BF02576845

29. Sikalias N, Terzopoulou M, Alexiou K, Mountzalia L, Kamparoudi P, Zacharioudaki A, et al. The effect of 30-minute ischemia on the levels of IL6, TNFα, NO, glutathione and lactic acid in the hepatic tissue of rats with hepatic steatosis. *Hellenic J Surg* (2019) 91:65–74. doi: 10.1007/s13126-019-0508-0

30. Portakal O, Inal-Erden M. Effects of pentoxifylline and coenzyme Q10 in hepatic ischemia/reperfusion injury. *Clin Biochem* (1999) 32(6):461–6. doi: 10.1016/s0009-9120(99)00041-7

31. Schmitz SM, Dohmeier H, Stoppe C, Alizai PH, Schipper S, Neumann UP, et al. Inhaled argon impedes hepatic regeneration after ischemia/reperfusion injury in rats. *Int J Mol Sci* (2020) 21(15):5457. doi: 10.3390/ijms21155457

32. Jiménez-Castro MB, Meroño N, Braz MM, Gracia-Sancho J, Martínez-Carreres L, Cornide-Petronio ME, et al. The effect of brain death in rat steatotic and non-steatotic liver transplantation with previous ischemic preconditioning. *J Hepatol* (2015) 62(1):83–91. doi: 10.1016/j.jhep.2014.08.026

33. Micó-Carnero M, Casillas-Ramírez A, Caballeria-Casals A, Rojano-Alfonso C, Sánchez-González A, Peralta C. Role of dietary nutritional treatment on hepatic and intestinal damage in transplantation with steatotic and non-steatotic liver grafts from brain dead donors. *Nutrients* (2021) 13(8):2554. doi: 10.3390/nu13082554

34. Van der Hoeven JA, Lindell SL, van Schilfgaarde R, Molema G, Ter Horst GJ, Southard JH, et al. Donor brain death reduces survival after transplantation in rat livers preserved for 20 hr. *Transplantation* (2001) 72(9):1632–6. doi: 10.1097/00007890-200111150-00016

35. Kandemir M, Yaşar NF, Özkurt M, Özyurt R, Bektur Aykanat NE, Erkasap N. The role of anakinra in the modulation of intestinal cell apoptosis and inflammatory response during ischemia/reperfusion. *Turk J Med Sci* (2021) 51(4):2177–84. doi: 10.3906/sag-2010-111

36. Toth B, Yokoyama Y, Schwacha MG, George RL, Rue LW3rd, Bland KI, et al. Insights into the role of interleukin-6 in the induction of hepatic injury after trauma-hemorrhagic shock. *J Appl Physiol* (1985) 97(6):2184–9. doi: 10.1152/japplphysiol.00499.2004

37. Tuna M, Erman T, Ildan F, Göçer AI, Tuna N, Polat S. Effect of neutralization of rat IL-6 bioactivity on collateral blood supply from retrograde flow via cortical anastomoses in the rat central nervous system. *Neurol Res* (2002) 24(4):405–8. doi: 10.1179/016164102101200104

38. Liu P, Xu B, Hock CE. Inhibition of nitric oxide synthesis by L-name exacerbates acute lung injury induced by hepatic ischemia-reperfusion. *Shock* (2001) 16(3):211–7. doi: 10.1097/00024382-200116030-00007

39. Selzner M, Clavien PA. Failure of regeneration of the steatotic rat liver: disruption at two different levels in the regeneration pathway. *Hepatology* (2000) 31 (1):35–42. doi: 10.1002/hep.510310108

40. Yagihashi A, Hirata K, Zou XM, Tsuruma T, Araya J, Yajima T, et al. Downregulation of cytokine-induced neutrophil chemoattractants and reduction of reperfusion injury in liver allograft by interleukin-10. *Transplant Proc* (2000) 32 (7):2302. doi: 10.1016/s0041-1345(00)01673-0

41. Zou XM, Hirata K, Nie G, Liang YW, Zhang JG, Qin HD, et al. Investigation of rhIL-10 inhibition of acute rejection after liver transplantation. *Transplant Proc* (2000) 32(7):2123–4. doi: 10.1016/s0041-1345(00)01598-0

42. Matsumoto S, Hara T, Mitsuyama K, Yamamoto M, Tsuruta O, Sata M, et al. Essential roles of IL-6 trans-signaling in colonic epithelial cells, induced by the IL-6/soluble-IL-6 receptor derived from lamina propria macrophages, on the development of colitis-associated premalignant cancer in a murine model. *J Immunol* (2010) 184 (3):1543–51. doi: 10.4049/jimmunol.0801217

43. Atreya R, Mudter J, Finotto S, Müllberg J, Jostock T, Wirtz S, et al. Blockade of interleukin 6 trans signaling suppresses T-cell resistance against apoptosis in chronic intestinal inflammation: evidence in crohn disease and experimental colitis *in vivo*. *Nat Med* (2000) 6(5):583–8. doi: 10.1038/75068

44. Ye M, Joosse ME, Liu L, Sun Y, Dong Y, Cai C, et al. Deletion of IL-6 exacerbates colitis and induces systemic inflammation in IL-10-deficient mice. *J Crohns Colitis* (2020) 14(6):831–40. doi: 10.1093/ecco-jcc/jjz176

45. Micó-Carnero M, Casillas-Ramírez A, Sánchez-González A, Rojano-Alfonso C, Peralta C. The role of neuregulin-1 in steatotic and non-steatotic liver transplantation from brain-dead donors. *Biomedicines* (2022) 10(5):978. doi: 10.3390/biomedicines10050978

46. Peralta C, Prats N, Xaus C, Gelpí E, Roselló-Catafau J. Protective effect of liver ischemic preconditioning on liver and lung injury induced by hepatic ischemia-reperfusion in the rat. *Hepatology* (1999) 30(6):1481–9. doi: 10.1002/hep.510300622

47. Serafin A, Roselló-Catafau J, Prats N, Xaus C, Gelpí E, Peralta C. Ischemic preconditioning increases the tolerance of Fatty liver to hepatic ischemia-reperfusion injury in the rat. *Am J Pathol* (2002) 161(2):587–601. doi: 10.1016/S0002-9440(10)64214-9

48. Carrasco-Chaumel E, Roselló-Catafau J, Bartrons R, Franco-Gou R, Xaus C, Casillas A, et al. Adenosine monophosphate-activated protein kinase and nitric oxide in rat steatotic liver transplantation. *J Hepatol* (2005) 43(6):997–1006. doi: 10.1016/j.jhep.2005.05.021

49. Cai LL, Xu HT, Wang QL, Zhang YQ, Chen W, Zheng DY, et al. EP4 activation ameliorates liver ischemia/reperfusion injury via ERK1/2-GSK3β-dependent MPTP inhibition. *Int J Mol Med* (2020) 45(6):1825–37. doi: 10.3892/ijmm.2020.4544

50. Franco-Gou R, Peralta C, Massip-Salcedo M, Xaus C, Serafín A, Roselló-Catafau J. Protection of reduced-size liver for transplantation. *Am J Transplant* (2004) 4 (9):1408–20. doi: 10.1111/j.1600-6143.2004.00532.x

51. Kleiner DE, Brunt EM, Van Natta M, Behling C, Contos MJ, Cummings OW, et al. Design and validation of a histological scoring system for nonalcoholic fatty liver disease. *Hepatology* (2005) 41(6):1313–21. doi: 10.1002/hep.20701

52. Wu Y, Liu Q, Wang Y, Li F, Chan LW, Wen Y, et al. Diagnostic efficiency on ultrasound shear wave elastography in evaluation of steatosis severity for non-alcoholic fatty liver disease: a rat model. *Eur J Med Res* (2023) 28(1):75. doi: 10.1186/s40001-023-01042-5

53. Huang S, Deng Z, Wang W, Liao G, Zhao Y, Zhong H, et al. CS27109, A selective thyroid hormone receptor-β Agonist alleviates metabolic-associated fatty liver disease in murine models. *Int J Endocrinol* (2023) 2023:4950597. doi: 10.1155/2023/4950597

54. Tatsumi K, Sasaki H, Fujita A, Doi A, Kanaya Y, Furuta H, et al. Effect of anti-oxidants, Ricetrienol and α-tocopherol, on adipocytokine abnormalities and fatty liver in Otsuka Long-Evans Tokushima Fatty diabetic rats. *J Diabetes Investig* (2011) 2 (3):186–92. doi: 10.1111/j.2040-1124.2010.00090.x

55. Abdulqader F, Yu L, Vickers MH, Firth EC, McGlashan SR. Voluntary physical activity in early life attenuates markers of fatty liver disease in adult male rats fed a high-fat diet. *Br J Nutr* (2023) 129(10):1667–76. doi: 10.1017/S0007114522002562

56. Riva G, Villanova M, Cima L, Ghimenton C, Bronzoni C, Colombari R, et al. Oil red O is a useful tool to assess donor liver steatosis on frozen sections during transplantation. *Transplant Proc* (2018) 50(10):3539–43. doi: 10.1016/j.transproceed.2018.06.013

57. Rittié L. Method for picrosirius red-polarization detection of collagen fibers in tissue sections. *Methods Mol Biol* (2017) 1627:395–407. doi: 10.1007/978-1-4939-7113-8_26

58. Sanches SC, Ramalho LN, Augusto MJ, da Silva DM, Ramalho FS. Nonalcoholic steatohepatitis: A search for factual animal models. *BioMed Res Int* (2015) 2015:574832. doi: 10.1155/2015/574832

59. Kucera O, Cervinkova Z. Experimental models of non-alcoholic fatty liver disease in rats. *World J Gastroenterol* (2014) 20(26):8364–76. doi: 10.3748/wjg.v20.i26.8364

60. Shirakawa F, Yamashita U, Chedid M, Mizel SB. Cyclic AMP–an intracellular second messenger for interleukin 1. *Proc Natl Acad Sci U.S.A.* (1988) 85(21):8201–5. doi: 10.1073/pnas.85.21.8201

61. Turunen JP, Mattila P, Renkonen R. cAMP mediates IL-1-induced lymphocyte penetration through endothelial monolayers. *J Immunol* (1990) 145(12):4192–7. doi: 10.4049/jimmunol.145.12.4192

62. Jiménez-Castro MB, Cornide-Petronio ME, Gracia-Sancho J, Peralta C. Inflammasome-mediated inflammation in liver ischemia-reperfusion injury. *Cells* (2019) 8(10):1131. doi: 10.3390/cells8101131

63. Jiménez-Castro MB, Cornide-Petronio ME, Gracia-Sancho J, Casillas-Ramírez A, Peralta C. Mitogen activated protein kinases in steatotic and non-steatotic livers submitted to ischemia-reperfusion. *Int J Mol Sci* (2019) 20(7):1785. doi: 10.3390/ijms20071785

64. Gehrau RC, Mas VR, Dumur CI, Suh JL, Sharma AK, Cathro HP, et al. Donor hepatic steatosis induce exacerbated ischemia-reperfusion injury through activation of innate immune response molecular pathways. *Transplantation* (2015) 99(12):2523–33. doi: 10.1097/TP.0000000000000857

65. Imarisio C, Alchera E, Bangalore Revanna C, Valente G, Follenzi A, Trisolini E, et al. Oxidative and ER stress-dependent ASK1 activation in steatotic hepatocytes and Kupffer cells sensitizes mice fatty liver to ischemia/reperfusion injury. *Free Radic Biol Med* (2017) 112:141–8. doi: 10.1016/j.freeradbiomed.2017.07.020

66. Cornide-Petronio ME, Bujaldon E, Mendes-Braz M, Avalos de León CG, Jiménez-Castro MB, Álvarez-Mercado AI, et al. The impact of cortisol in steatotic and non-steatotic liver surgery. *J Cell Mol Med* (2017) 21(10):2344–58. doi: 10.1111/jcmm.13156

67. Mendes-Braz M, Elias-Miró M, Jiménez-Castro MB, Casillas-Ramírez A, Ramalho FS, Peralta C. The current state of knowledge of hepatic ischemia-reperfusion injury based on its study in experimental models. *J BioMed Biotechnol* (2012) 2012:298657. doi: 10.1155/2012/298657

68. Álvarez-Mercado AI, Negrete-Sánchez E, Gulfo J, Ávalos de León CG, Casillas-Ramírez A, Cornide-Petronio ME, et al. EGF-GH axis in rat steatotic and non-steatotic liver transplantation from brain-dead donors. *Transplantation* (2019) 103(7):1349–59. doi: 10.1097/TP.0000000000002636

69. Zaouali MA, Padrissa-Altés S, Ben Mosbah I, Alfany-Fernandez I, Massip-Salcedo M, Casillas-Ramirez A, et al. Improved rat steatotic and nonsteatotic liver preservation by the addition of epidermal growth factor and insulin-like growth factor-I to University of Wisconsin solution. *Liver Transpl* (2010) 16(9):1098–111. doi: 10.1002/lt.22126

70. Cornide-Petronio ME, Negrete-Sánchez E, Mendes-Braz M, Casillas-Ramírez A, Bujaldon E, Meroño N, et al. The effect of high-mobility group box 1 in rat steatotic and nonsteatotic liver transplantation from donors after brain death. *Am J Transplant* (2016) 16(4):1148–59. doi: 10.1111/ajt.13560

71. Alfany-Fernandez I, Casillas-Ramirez A, Bintanel-Morcillo M, Brosnihan KB, Ferrario CM, Serafin A, et al. Therapeutic targets in liver transplantation: angiotensin II in nonsteatotic grafts and angiotensin-(1-7) in steatotic grafts. *Am J Transplant* (2009) 9(3):439–51. doi: 10.1111/j.1600-6143.2008.02521.x

72. Jiménez-Castro MB, Casillas-Ramírez A, Mendes-Braz M, Massip-Salcedo M, Gracia-Sancho J, Elias-Miró M, et al. Adiponectin and resistin protect steatotic livers undergoing transplantation. *J Hepatol* (2013) 59(6):1208–14. doi: 10.1016/j.jhep.2013.07.015

73. Linares I, Hamar M, Selzner N, Selzner M. Steatosis in liver transplantation: current limitations and future strategies. *Transplantation* (2019) 103(1):78–90. doi: 10.1097/TP.0000000000002466

74. Neri AA, Dontas IA, Iliopoulos DC, Karatzas T. Pathophysiological changes during ischemia-reperfusion injury in rodent hepatic steatosis. *In Vivo* (2020) 34 (3):953–64. doi: 10.21873/invivo.11863

75. Gracia-Sancho J, Casillas-Ramírez A, Peralta C. Molecular pathways in protecting the liver from ischaemia/reperfusion injury: a 2015 update. *Clin Sci* (2015) 129(4):345–62. doi: 10.1042/CS20150223

76. Jimenez-Castro MB, Casillas-Ramirez A, Massip-Salcedo M, Elias-Miro M, Serafin A, Rimola A, et al. Cyclic adenosine 3',5'-monophosphate in rat steatotic liver transplantation. *Liver Transpl* (2011) 17(9):1099–110. doi: 10.1002/lt.22359

77. Kistner TM, Pedersen BK, Lieberman DE. Interleukin 6 as an energy allocator in muscle tissue. *Nat Metab* (2022) 4(2):170–9. doi: 10.1038/s42255-022-00538-4

78. Klover PJ, Zimmers TA, Koniaris LG, Mooney RA. Chronic exposure to interleukin-6 causes hepatic insulin resistance in mice. *Diabetes* (2003) 52(11):2784–9. doi: 10.2337/diabetes.52.11.2784

79. Rotter V, Nagaev I, Smith U. Interleukin-6 (IL-6) induces insulin resistance in 3T3-L1 adipocytes and is, like IL-8 and tumor necrosis factor-alpha, overexpressed in human fat cells from insulin-resistant subjects. *J Biol Chem* (2003) 278(46):45777–84. doi: 10.1074/jbc.M301977200

80. Wan X, Zhu X, Wang H, Feng Y, Zhou W, Liu P, et al. PGC1α protects against hepatic steatosis and insulin resistance via enhancing IL10-mediated anti-inflammatory response. *FASEB J* (2020) 34(8):10751–61. doi: 10.1096/fj.201902476R

81. Straczkowski M, Kowalska I, Nikolajuk A, Krukowska A, Gorska M. Plasma interleukin-10 concentration is positively related to insulin sensitivity in young healthy individuals. *Diabetes Care* (2005) 28(8):2036–7. doi: 10.2337/diacare.28.8.2036

82. Cintra DE, Pauli JR, Araújo EP, Moraes JC, de Souza CT, Milanski M, et al. Interleukin-10 is a protective factor against diet-induced insulin resistance in liver. *J Hepatol* (2008) 48(4):628–37. doi: 10.1016/j.jhep.2007.12.017

83. Heydari M, Cornide-Petronio ME, Jiménez-Castro MB, Peralta C. Data on adiponectin from 2010 to 2020: therapeutic target and prognostic factor for liver diseases? *Int J Mol Sci* (2020) 21(15):5242. doi: 10.3390/ijms21155242

84. Álvarez-Mercado AI, Rojano-Alfonso C, Micó-Carnero M, Caballeria-Casals A, Peralta C, Casillas-Ramírez A. New insights into the role of autophagy in liver surgery in the setting of metabolic syndrome and related diseases. *Front Cell Dev Biol* (2021) 9:670273. doi: 10.3389/fcell.2021.670273

85. Eshraghian A, Nikeghbalian S, Shamsaeefar A, Kazemi K, Fattahi MR, Malek-Hosseini SA. Hepatic steatosis and liver fat contents in liver transplant recipients are associated with serum adipokines and insulin resistance. *Sci Rep* (2020) 10(1):12701. doi: 10.1038/s41598-020-69571-1

86. Jiménez-Castro MB, Casillas-Ramírez A, Negrete-Sánchez E, Avalos-de León CG, Gracia-Sancho J, Peralta C. Adipocytokines in steatotic liver surgery/transplantation. *Transplantation* (2019) 103(1):71–7. doi: 10.1097/TP.0000000000002098

87. Stienstra R, Saudale F, Duval C, Keshtkar S, Groener JE, Van Rooijen N, et al. Kupffer cells promote hepatic steatosis via interleukin-1beta-dependent suppression of peroxisome proliferator-activated receptor alpha activity. *Hepatology* (2010) 51(2):511–22. doi: 10.1002/hep.23337

88. Wen Y, Lambrecht J, Ju C, Tacke F. Hepatic macrophages in liver homeostasis and diseases-diversity, plasticity and therapeutic opportunities. *Cell Mol Immunol* (2021) 18(1):45–56. doi: 10.1038/s41423-020-00558-8

89. Yokoyama Y, Kitchens WC, Toth B, Schwacha MG, Rue LW3rd, Bland KI, et al. Role of IL-10 in regulating proinflammatory cytokine release by Kupffer cells following trauma-hemorrhage. *Am J Physiol Gastrointest Liver Physiol* (2004) 286(6):G942–6. doi: 10.1152/ajpgi.00502.2003

90. Kopydlowski KM, Salkowski CA, Cody MJ, Van Rooijen N, Major J, Hamilton TA, et al. Regulation of macrophage chemokine expression by lipopolysaccharide *in vitro* and *in vivo*. *J Immunol* (1999) 163(3):1537–44. doi: 10.4049/jimmunol.163.3.1537

91. Yang ZF, Ho DW, Ngai P, Lau CK, Zhao Y, Poon RT, et al. Antiinflammatory properties of IL-10 rescue small-for-size liver grafts. *Liver Transpl* (2007) 13(4):558–65. doi: 10.1002/lt.21094

92. Li X, Klintman D, Sato T, Hedlund G, Schramm R, Jeppsson B, et al. Interleukin-10 mediates the protective effect of Linomide by reducing CXC chemokine production in endotoxin-induced liver injury. *Br J Pharmacol* (2004) 143(7):865–71. doi: 10.1038/sj.bjp.0706015

93. Klein C, Wüstefeld T, Assmus U, Roskams T, Rose-John S, Müller M, et al. The IL-6-gp130-STAT3 pathway in hepatocytes triggers liver protection in T cell-mediated liver injury. *J Clin Invest* (2005) 115(4):860–9. doi: 10.1172/JCI23640

94. Ahuja N, Andres-Hernando A, Altmann C, Bhargava R, Bacalja J, Webb RG, et al. Circulating IL-6 mediates lung injury via CXCL1 production after acute kidney injury in mice. *Am J Physiol Renal Physiol* (2012). doi: 10.1152/ajprenal.00025.2012

95. Cheng N, Kim KH, Lau LF. Senescent hepatic stellate cells promote liver regeneration through IL-6 and ligands of CXCR2. *JCI Insight* (2022) 7(14):e158207. doi: 10.1172/jci.insight.158207

96. Zhai Y, Shen XD, Gao F, Zhao A, Freitas MC, Lassman C, et al. CXCL10 regulates liver innate immune response against ischemia and reperfusion injury. *Hepatology* (2008) 47(1):207–14. doi: 10.1002/hep.21986

97. Piemonti L, Sordi V, Pellegrini S, Scotti GM, Scavini M, Sioli V, et al. Circulating CXCL10 and IL-6 in solid organ donors after brain death predict graft outcomes. *Sci Rep* (2021) 11(1):6624. doi: 10.1038/s41598-021-86085-6

98. Schmidt-Arras D, Rose-John S. IL-6 pathway in the liver: From physiopathology to therapy. *J Hepatol* (2016) 64(6):1403–15. doi: 10.1016/j.jhep.2016.02.004

99. Li X, Li S, Wu B, Xu Q, Teng D, Yang T, et al. Landscape of immune cells heterogeneity in liver transplantation by single-cell RNA sequencing analysis. *Front Immunol* (2022) 13:890019. doi: 10.3389/fimmu.2022.890019

100. Huang M, Cai H, Han B, Xia Y, Kong X, Gu J. Natural killer cells in hepatic ischemia-reperfusion injury. *Front Immunol* (2022) 13:870038. doi: 10.3389/fimmu.2022.870038

101. Sun R, Tian Z, Kulkarni S, Gao B. IL-6 prevents T cell-mediated hepatitis via inhibition of NKT cells in CD4+ T cell- and STAT3-dependent manners. *J Immunol* (2004) 172(9):5648–55. doi: 10.4049/jimmunol.172.9.5648

102. Zhou CZ, Wang RF, Cheng DL, Zhu YJ, Cao Q, Lv WF. FLT3/FLT3L-mediated CD103+ dendritic cells alleviates hepatic ischemia-reperfusion injury in mice via activation of treg cells. *BioMed Pharmacother.* (2019) 118:109031. doi: 10.1016/j.biopha.2019.109031

103. Zhang M, Ueki S, Kimura S, Yoshida O, Castellaneta A, Ozaki KS, et al. Roles of dendritic cells in murine hepatic warm and liver transplantation-induced cold ischemia/reperfusion injury. *Hepatology* (2013) 57(4):1585–96. doi: 10.1002/hep.26129

104. Elias-Miró M, Jiménez-Castro MB, Peralta C. Ischemia-reperfusion injury associated with liver transplantation in 2011: past and future. *InTech* (2012). doi: 10.5772/28586

105. Zhang Y, Ji H, Shen X, Cai J, Gao F, Koenig KM, et al. Targeting TIM-1 on CD4 T cells depresses macrophage activation and overcomes ischemia-reperfusion injury in mouse orthotopic liver transplantation. *Am J Transplant* (2013) 13(1):56–66. doi: 10.1111/j.1600-6143.2012.04316.x

106. Kolachala VL, Palle S, Shen M, Feng A, Shayakhmetov D, Gupta NA. Loss of L-selectin-guided CD8+, but not CD4+, cells protects against ischemia reperfusion injury in a steatotic liver. *Hepatology* (2017) 66(4):1258–74. doi: 10.1002/hep.29276

107. Roh YS, Park S, Lim CW, Kim B. Depletion of foxp3+ Regulatory T cells promotes profibrogenic milieu of cholestasis-induced liver injury. *Dig Dis Sci* (2015) 60(7):2009–18. doi: 10.1007/s10620-014-3438-2

108. Rood JE, Canna SW, Weaver LK, Tobias JW, Behrens EM. IL-10 distinguishes a unique population of activated, effector-like CD8+ T cells in murine acute liver inflammation. *J Leukoc Biol* (2017) 101(4):1037–44. doi: 10.1189/jlb.3A0916-221RR

109. Cheng L, Wang J, Li X, Xing Q, Du P, Su L, et al. Interleukin-6 induces Gr-1+CD11b+ myeloid cells to suppress CD8+ T cell-mediated liver injury in mice. *PloS One* (2011) 6(3):e17631. doi: 10.1371/journal.pone.0017631

110. Peralta C, Jiménez-Castro MB, Gracia-Sancho J. Hepatic ischemia and reperfusion injury: effects on the liver sinusoidal milieu. *J Hepatol* (2013) 59(5):1094–106. doi: 10.1016/j.jhep.2013.06.017

111. Selzner N, Selzner M, Tian Y, Kadry Z, Clavien PA. Cold ischemia decreases liver regeneration after partial liver transplantation in the rat: A TNF-alpha/IL-6-dependent mechanism. *Hepatology* (2002) 36(4 Pt 1):812–8. doi: 10.1053/jhep.2002.35535

112. Dinant S, Veteläinen RL, Florquin S, van Vliet AK, van Gulik TM. IL-10 attenuates hepatic I/R injury and promotes hepatocyte proliferation. *J Surg Res* (2007) 141(2):176–82. doi: 10.1016/j.jss.2006.09.018

113. Ferrigno A, Berardo C, Di Pasqua LG, Siciliano V, Richelmi P, Nicoletti F, et al. Selective blockade of the metabotropic glutamate receptor mGluR5 protects mouse livers in *in vitro* and *ex vivo* models of ischemia reperfusion injury. *Int J Mol Sci* (2018) 19(2):314. doi: 10.3390/ijms19020314

114. Taneja C, Prescott L, Koneru B. Critical preservation injury in rat fatty liver is to hepatocytes, not sinusoidal lining cells. *Transplantation* (1998) 65(2):167–72. doi: 10.1097/00007890-199801270-00004

115. Alwadei N, Rashid M, Chandrashekar DV, Rahighi S, Totonchy J, Sharma A, et al. Generation and characterization of CYP2E1-overexpressing hepG2 cells to study the role of CYP2E1 in hepatic hypoxia-reoxygenation injury. *Int J Mol Sci* (2023) 24(9):8121. doi: 10.3390/ijms24098121

116. Baxi V, Edwards R, Montalto M, Saha S. Digital pathology and artificial intelligence in translational medicine and clinical practice. *Mod Pathol* (2022) 35(1):23–32. doi: 10.1038/s41379-021-00919-2

117. Spitaleri G, Farrero M. Translational medicine in brain stem death and heart transplantation. *Transplantation* (2020) 104(11):2258–9. doi: 10.1097/TP.0000000000003218

118. Kim YM, Talanian RV, Li J, Billiar TR. Nitric oxide prevents IL-1beta and IFN-gamma-inducing factor (IL-18) release from macrophages by inhibiting caspase-1 (IL-1beta-converting enzyme). *J Immunol* (1998) 161(8):4122–8. doi: 10.4049/jimmunol.161.8.4122

119. Moncada S, Erusalimsky JD. Does nitric oxide modulate mitochondrial energy generation and apoptosis? *Nat Rev Mol Cell Biol* (2002) 3(3):214–20. doi: 10.1038/nrm762

120. Beckman JS, Koppenol WH. Nitric oxide, superoxide, and peroxynitrite: the good, the bad, and ugly. *Am J Physiol* (1996) 271(5 Pt 1):C1424–37. doi: 10.1152/ajpcell.1996.271.5.C1424

121. Ferdinandy P, Schulz R. Nitric oxide, superoxide, and peroxynitrite in myocardial ischaemia-reperfusion injury and preconditioning. *Br J Pharmacol* (2003) 138(4):532–43. doi: 10.1038/sj.bjp.0705080

122. Stamler JS. Redox signaling: nitrosylation and related target interactions of nitric oxide. *Cell* (1994) 78(6):931–6. doi: 10.1016/0092-8674(94)90269-0

123. MacMillan-Crow LA, Crow JP, Thompson JA. Peroxynitrite-mediated inactivation of manganese superoxide dismutase involves nitration and oxidation of critical tyrosine residues. *Biochemistry* (1998) 37(6):1613–22. doi: 10.1021/bi971894b

124. Mazzon E, Serraino I, Li JH, Dugo L, Caputi AP, Zhang J, et al. GPI 6150, a poly (ADP-ribose) polymerase inhibitor, exhibits an anti-inflammatory effect in rat models of inflammation. *Eur J Pharmacol* (2001) 415(1):85–94. doi: 10.1016/s0014-2999(01)00809-3

125. Das S, Alhasson F, Dattaroy D, Pourhoseini S, Seth RK, Nagarkatti M, et al. NADPH oxidase-derived peroxynitrite drives inflammation in mice and human nonalcoholic steatohepatitis via TLR4-lipid raft recruitment. *Am J Pathol* (2015) 185(7):1944–57. doi: 10.1016/j.ajpath.2015.03.024

126. Shito M, Wakabayashi G, Ueda M, Shimazu M, Shirasugi N, Endo M, et al. Interleukin 1 receptor blockade reduces tumor necrosis factor production, tissue injury, and mortality after hepatic ischemia-reperfusion in the rat. *Transplantation* (1997) 63 (1):143–8. doi: 10.1097/00007890-199701150-00026

127. Tien C, Remulla D, Kwon Y, Emamaullee J. Contemporary strategies to assess and manage liver donor steatosis: a review. *Curr Opin Organ Transplant* (2021) 26 (5):474–81. doi: 10.1097/MOT.0000000000000893

128. Liu Y, Qin X, Lei Z, Chai H, Huang Z, Wu Z. Tetramethylpyrazine inhibits neutrophil extracellular traps formation and alleviates hepatic ischemia/reperfusion injury in rat liver transplantation. *Exp Cell Res* (2021) 406(1):112719. doi: 10.1016/j.yexcr.2021.112719

129. Liu YX, Jin LM, Zhou L, Xie HY, Jiang GP, Chen H, et al. Sirolimus attenuates reduced-size liver ischemia-reperfusion injury but impairs liver regeneration in rats. *Dig Dis Sci* (2010) 55(8):2255–62. doi: 10.1007/s10620-009-1002-2

130. Saavedra-Lopes M, Ramalho FS, Ramalho LN, Andrade-Silva A, Martinelli AL, Jordão AAJr, et al. The protective effect of CAPE on hepatic ischemia/reperfusion injury in rats. *J Surg Res* (2008) 150(2):271–7. doi: 10.1016/j.jss.2008.01.039

frontiers | Frontiers in Immunology

TYPE Original Research
PUBLISHED 20 September 2023
DOI 10.3389/fimmu.2023.1261666

OPEN ACCESS

EDITED BY
Diana Boraschi,
Chinese Academy of Science (CAS), China

REVIEWED BY
Paola Italiani,
National Research Council (CNR), Italy
Claudia Nold,
Hudson Institute of Medical Research, Australia

*CORRESPONDENCE
Philip Bufler
philip.bufler@charite.de

RECEIVED 19 July 2023
ACCEPTED 31 August 2023
PUBLISHED 20 September 2023

CITATION
Kröhn L, Azabdaftari A, Heuberger J, Hudert C, Zilbauer M, Breiderhoff T and Bufler P (2023) Modulation of intestinal IL-37 expression and its impact on the epithelial innate immune response and barrier integrity.
Front. Immunol. 14:1261666.
doi: 10.3389/fimmu.2023.1261666

Modulation of intestinal IL-37 expression and its impact on the epithelial innate immune response and barrier integrity

Laura Kröhn[1], Aline Azabdaftari[1,2], Julian Heuberger[3], Christian Hudert[1], Matthias Zilbauer[4], Tilman Breiderhoff[1] and Philip Bufler[1]*

[1]Department of Pediatric Gastroenterology, Nephrology and Metabolic Diseases, Charité Universitätsmedizin Berlin, Berlin, Germany, [2]Berlin Institute of Health at Charité - Universitätsmedizin Berlin, Berlin, Germany, [3]Department of Hepatology and Gastroenterology, Charité Universitätsmedizin Berlin, Berlin, Germany, [4]Wellcome Trust–Medical Research Council Stem Cell Institute, University of Cambridge, Cambridge, United Kingdom

Background and Aims: Intestinal epithelial cells separate the luminal flora from lamina propria immune cells and regulate innate immune responses in the gut. An imbalance of the mucosal immune response and disrupted intestinal barrier integrity contribute to the evolution of inflammatory bowel diseases. Interleukin (IL)-37 has broad anti- inflammatory activity and is expressed by the human intestinal epithelium. Mice ectopically expressing human IL-37 show reduced epithelial damage and inflammation after DSS-induced colitis. Here, we investigated the impact of IL-37 on the innate immune response and tight junction protein expression of mouse intestinal organoids and the modulation of *IL37* expression in human intestinal organoids.

Methods: Murine intestinal organoids were generated from IL-37tg and wildtype mice. Human ileal organoids were generated from healthy young donors.

Results: Expression of transgene IL-37 or recombinant IL-37 protein did not significantly reduce overall proinflammatory cytokine mRNA expression in murine intestinal organoids. However, higher *IL37* expression correlated with a reduced proinflammatory cytokine response in murine colonic organoids. *IL37* mRNA expression in human ileal organoids was modulated by proinflammatory cytokines showing an increased expression upon TNF-α-stimulation and decreased expression upon IFN-gamma stimulation. Transgene IL-37 expression did not rescue TNF-α-induced changes in morphology as well as ZO-1, occludin, claudin-2, and E-cadherin expression patterns of murine jejunal organoids.

Conclusions: We speculate that the anti-inflammatory activity of IL-37 in the intestine is mainly mediated by lamina propria immune cells protecting intestinal epithelial integrity.

KEYWORDS

innate immune response, inflammatory bowel disease, IL-37, intestinal organoid, intestinal barrier, tight junctions, cytokines

Introduction

The intestinal epithelium is the largest epithelial layer in the human body that is in contact with the environment (1). Intestinal epithelial cells (IEC) form the barrier between the intestinal luminal microbiome and the lamina propria immune cell compartment and mediate innate immune responses of the gut (2). Cytokines secreted by either resident or infiltrating immune cells modulate epithelial proliferation, apoptosis, and barrier function, and vice versa, epithelial cells themselves can initiate immune responses at the mucosal level (3). IEC express a variety of cytokine receptors and receptors to sense pathogens or pathogen-associated molecular patterns (2, 4, 5). Subsequent signaling pathways induce cytokine and chemokine secretion by IECs to recruit immune cells to the site of inflammation (2, 4–6) with destructive (7–12) or beneficial effects (13–15) on the intestinal epithelial barrier.

The functional crosstalk between IEC and immune cells via cytokines and chemokines is tightly balanced in the healthy gut (3). In contrast, an impaired gut barrier integrity and imbalance of the mucosal immune response can contribute to inflammatory bowel diseases (16–21). The imbalance of mucosal immune responses may be caused by an exaggerated immune activation or the loss of anti-inflammatory, protective immune mechanisms. As such, it has been shown that, i.e., the overproduction of interleukin (IL)-12 by macrophages (22), genetic variants of NOD2 overactivating NF-κB in monocytes (23), or alterations in TLR expression (20) are associated with Crohn's disease. On the other hand, reduced anti-inflammatory mechanisms such as disturbed TGF-ß signaling in inflammatory bowel disease (IBD) patients (24), reduced number of regulatory T cells in peripheral blood in patients with ulcerative colitis (25) or IL-10 or IL-10 receptor deficiency in pediatric patients with early-onset enterocolitis (26) are examples of a harmful, overactivated immune response in the gut.

IL-37, an anti-inflammatory member of the IL-1 family, is attributed to balancing the intestinal immune response, and a homozygous loss-of-function variant has been shown to be associated with infantile-onset IBD (27). IL-37 acts via two different pathways. Extracellular IL-37 binds to the IL-18 receptor 1 (IL-18RI) and a single IL-1R-related molecule (SIGIRR), forming the tripartite complex and suppressing MyD88-dependent proinflammatory signals (28, 29). Intracellular IL-37 interacts upon caspase-1 cleavage with Smad3, translocates to the nucleus, and reduces the production of proinflammatory cytokines (30, 31).

IL-37 reduces proinflammatory cytokine secretion in mouse macrophages, human monocytes, and epithelial cells upon stimulation with LPS or IL-1ß (30) and inhibits systemic inflammation in various murine disease models (30, 32–35). IL-37 also displays an anti-inflammatory role within the epithelium, as shown in experiments on T84 colonic carcinoma cells (36), human and murine intestinal organoids (37), and dextran sodium sulfate (DSS)-colitis mice (32). Studies even showed that IL-37 expression was increased in the human intestinal epithelium of IBD patients (38, 39).

Inflammation compromises the integrity of the gut barrier (16, 17, 40). Several proinflammatory cytokines were shown to regulate the expression of tight junction (TJ) proteins, leading to decreased transepithelial electrical resistance (TEER) and increased paracellular permeability (7–12), while anti-inflammatory cytokines protect the intestinal barrier integrity (13–15). The role of IL-37 on the intestinal epithelial proinflammatory response and the intestinal epithelial barrier is not well understood yet.

The aim of this study is to analyze the impact of transgene IL-37 (tgIL-37) on innate immune response and TJ protein expression in murine intestinal organoids and to investigate the regulation of *IL37* expression in human intestinal organoids.

Materials and methods

Chemicals and reagents

Reagents were purchased from Sigma-Aldrich GmbH (Munich, Germany) [ethylenediaminetetraacetic acid (EDTA), bovine serum albumin (BSA), sucrose, D-sorbitol], Thermo Fisher Scientific (Munich, Germany) [Dulbecco`s Phosphate - Buffered Solution (DPBS), Hank`s Balanced Salt Solution (HBSS)], Merck Life Science KGaA (Darmstadt, Germany) (Na_2HPO_4, KH_2PO_4, NaCl, KCl), or other manufacturers as indicated.

Generation of human organoids

Human intestinal forceps biopsies were taken during routine endoscopies from the terminal ileum of two patients without intestinal inflammation (boy, 16 years; girl, 16 years) at Charité -Universitätsmedizin Berlin and collected in HBSS. Patients and legal guardians gave written consent (EA/134/19).

After sampling, ileum biopsies were incubated in EDTA (2.5 mM), followed by vigorous pipetting to isolate crypts, and then Matrigel was added for organoid culture as described (41). Plates were incubated at 37°C and 7% CO_2. Organoid medium was prepared as described (Supplementary Table S1) and replaced every other day (41). Organoids were passaged every 10 to 14 days.

Generation of murine organoids, passage, and freezing

C57BL/6J mice expressing human IL-37 (IL-37tg) have been described previously (30). Age-matched mice from the congenic control line (WT) were used as controls. IL-37tg and WT mice were bred under specific pathogen-free conditions. Three 8– 14- week-old mice of each genotype were used for organoid generation.

Jejunal organoids from middle jejunal tissue and colonic organoids from distal colonic tissue were generated as previously described with modifications (42, 43). Gut segments were rinsed with ice-cold DPBS, opened longitudinally, cut into 10-mm pieces, and washed by vortexing several times until the supernatants became clear. Crypts were isolated as described (42) but with an incubation of 20 min for the jejunum and 90 min for the colon in small intestinal or colonic crypt isolation buffer (42). After incubation, biopsies were washed in DPBS. Crypts were then released by vigorously shaking the tissue segments in DPBS, and the supernatant was collected in 0.1% BSA/PBS and centrifuged at 300 ×*g* for 5 min at 4°C. Crypts were

diluted to 200 crypts per µl in Matrigel (Corning Limited-Life Sciences, Amsterdam, The Netherlands, 354230) and seeded as 20 µl domes in 48-well plates. Culture plates were incubated for 30 min at 37°C. The respective organoid culture medium (Supplementary Table S2) was then added. The medium was supplemented with Y-27632 (Merck Millipore) for the first 2 days. Organoid cultures were maintained at 37°C and 5% CO_2. The medium was changed every other day, and colonic organoids were passaged every 5–6 days and jejunal organoids every 4–5 days. A detailed description of organoid generation, passage, and freezing is described in the Supplementary material.

Stimulation of murine jejunal and colonic organoids

Jejunal and colonic organoids were thawed as previously described (42), cultured, and passaged at least once before experiments were performed. For experiments, only cultures from passages four to nine were chosen. Jejunal organoids were stimulated with TNF-α (Gibco, Thermo Fisher Scientific) and colonic organoids were stimulated with LPS (O55:B5, Sigma), as indicated in the figure legends.

Gene expression analysis

Organoids were harvested for mRNA isolation 4 h after stimulation. Culture medium was removed, and Matrigel domes were washed in DPBS. Organoids of four to five domes were resuspended in 1 ml of Trizol (Invitrogen, Carlsbad, CA, USA), incubated at room temperature for 10 min, and vortexed. mRNA was purified from the aqueous phase following the manufacturer's protocol, including DNAse digestion (GenElute™ Mammalian Total RNA Miniprep Kit, Sigma). Reverse transcription into cDNA was done using 1 µg of total RNA (Applied Biosystems, Carlsbad, CA, USA). Quantitative PCR (qPCR) was performed using the SYBR Green Master Mix (Applied Biosystems). Primer sequences are summarized in Table 1. Measurements were quantified using Quant Studio Design and Analysis software (Applied Biosystems). Gene expression was normalized to *Hprt* expression and untreated control condition.

Western blotting

For Western blotting, jejunal organoids were harvested 48 h after stimulation. Matrigel domes were dissolved by incubating for 30 min in organoid harvesting solution (Cultrex, R&D systems, Abingdon, UK), centrifuged, and washed in ice-cold DPBS. Pelleted organoids were resuspended in a lysis buffer containing protease inhibitors. The total protein amount was quantified using the bicinchoninic acid assay kit (Thermo Fisher). Each lane of any kD Mini-Protean TGX precast gel was loaded with 17 µg of protein samples and transferred to the PVDF membrane. After blocking (5% milk powder in Tris- buffered saline/0.05% Tween 20), the membrane was stained with mouse monoclonal antibodies against α-claudin-2 (Thermo Fisher; clone 12H12; 1:500), α-occludin (Thermo Fisher; mouse OC-3F10; 1:1,000), α-ZO-1 (Thermo Fisher; clone 1A12; 1:500), and α-actin (Santa Cruz, Biotechnology, Heidelberg, Germany; clone 1A4; 1:1,000). Densitometric analysis was performed with ImageJ, and signal densities were normalized to the signal density of actin.

Immunofluorescence

For immunofluorescence microscopy, jejunal organoids were harvested with organoid harvesting solution 48 h after stimulation. As previously described (44), 5- µm slides of paraffinized agarose domes containing organoids were generated. After rehydration, antigen retrieval was performed in boiling Tris-EDTA Tween buffer. Slides were incubated in 10% donkey serum/DPBS containing 0.3 % Triton X-100 and with primary antibodies (Supplementary Table S4) overnight at 4°C. The next day, slides were stained with secondary antibodies (α-rabbit Alexa488 or α-mouse Alexa647) (Invitrogen; donkey; 1:1,000) for 1 h at room temperature and counterstained with DAPI. Image acquisition was performed with ×25 glycerol immersion on a Zeiss confocal LSM980 NLO microscope with Airyscan, and images were analyzed using Zen software.

Statistical analysis

Results are expressed as the mean values with 1 standard deviation (SD). A paired Student's *t*-test was applied to compare treated versus untreated conditions in one experimental group. An unpaired Student's *t*-test was used for comparisons between organoids generated from WT and IL-37tg mice. For data that were not considered as normally distributed using the Shapiro–Wilk test, the corresponding nonparametric tests (Wilcoxon signed-rank test or Mann–Whitney *U* test) were performed. For correlation analysis, statistical significance was tested with Pearson´s correlation and the Student's two-tailed *t*-test. Outliers were defined by ROUT (Q = 1%) and Grubbs (alpha = 0.05) test. All tests were performed using GraphPad Prism software (version 9.3.1). A *p*-value of 0.05 or less was considered significant.

Results

Cytokine response and the expression of IL-37 and its receptor components in WT and tgIL-37 intestinal organoids

To corroborate whether *IL37* impacts the immune response of intestinal epithelial cells, we stimulated intestinal organoids generated from IL-37tg and WT mice with TNF-α and IL-1β, as well as LPS and flagellin. Murine jejunal organoids were most potently stimulated by TNF-α and colonic organoids by LPS, inducing the highest mRNA expression levels of *Cxcl1*, *Cxcl2*,

TABLE 1 Gene-specific primer sequences.

Gene	Forward primer	Reverse primer
Cxcl1	AGG CTT GCC TTG ACC CTG AA	CAG AAG CCA GCG TTC ACC AG
Cxcl2	CTG CCA AGG GTT GAC TTC AA	TTT TGA CCG CCC TTG AGA GT
Ccl20	GTG GGT TTC ACA AGA CAG ATG GC	CCA GTT CTG CTT TGG ATC AGC G
Tnf	GTG CCT ATG TCT CAG CCT CT	CTG ATG AGA GGG AGG CCAT T
Tlr4	AGC TTC TCC AAT TTT TCA GAA CTT C	TGA GAG GTG GTG TAA GCC ATG C
Tlr5	TGG ATG GAT GCT GAG TTC CC	TGG CCA TGA AGA TCA CAC CT
IL37	TCC TGG ACT CTG GGA ATC TC	AGA GGC TGA GCT CAA GGA TG
Sigirr	CAG TGG CTG AAA GAT GGT CTG G	AGT TGA GCA CCA GGA CAC TGG A
Il18r1	AGA GCT GAT CCA GGA CAC ATG G	TGG TGG ACA GAA AAC ACG CAG G
Tjp1	GTT GGT ACG GTG CCC TGA AAG A	GCT GAC AGG TAG GAC AGA CGA T
Ocln	GCA AGT TAA GGG ATC TGC AGA	TCT CCC ACC ATC CTC TTG AT
Cldn2	GTC ATC GCC CAT CAG AAG AT	AGG GAA CCA GTC TCC GTT C
Hprt	CCT AAG ATG AGC GCA AGT TGA A	ACA GGA CTA GAA CAC CTG CTA A

Ccl20, and *Tnf* within a 4-h stimulation period (Supplementary Figure S1; Figures 1A, B).

TgIL-37 expression was not associated with a significant change in proinflammatory cytokine mRNA expression in jejunal and colonic organoids before and after stimulation, despite a trend toward reduced *Cxcl1*, *Cxcl2*, and *Tnf* mRNA levels in colonic IL-37tg-derived organoids (Figures 1A, B).

Jejunal and colonic organoids generated from IL-37tg mice showed a trend toward higher *IL37* expression after stimulation with TNF-α and LPS, respectively (Figure 1C). Similarly, *IL37* expression was threefold induced by TNF-α in human ileal organoids but not by LPS or IL-1β, while IFN-gamma downregulated the expression of *IL37* (Figure 1D). *IL37* expression in human ileal organoids was gradually induced by TNF-α over a 24 -h period (Supplementary Figure S2).

Baseline *IL37* expression was higher in murine colonic (CT mean: 32.4) versus jejunal organoids (CT mean: 34.4) (Supplementary Table S5). In colonic organoids, higher *IL37* mRNA expression was associated with reduced *Cxcl2* and *Tnf* mRNA expression, as indicated by the significant correlation between *IL37*-ΔCt-values of stimulated IL-37tg-derived organoids and their relative *Cxcl2* and *Tnf* mRNA expression (Figure 1E).

The lack of correlation between *IL-37* expression and the inflammatory response of jejunal organoids could be due to differences in anti-inflammatory IL-37 signaling. We therefore analyzed the mRNA expression of IL-37 receptor components in jejunal and colonic organoids. *Il18r1* expression was eight times higher in WT colonic organoids compared to WT jejunal organoids before and 10 times higher after stimulation with TNF-α (Figure 1F). Baseline *Il18r1* mRNA expression was higher in IL-37tg-derived colonic organoids compared to WT-derived colonic organoids (Supplementary Figure S3). *Sigirr* is highly expressed in both jejunal and colonic organoids (CT mean: 25.2 and 26.2) (Figure 1G), and the expression was two times higher in WT jejunal organoids compared to WT colonic organoids before and after stimulation (Figure 1F). The relation of *Il18r1* and *Sigirr* mRNA expression between jejunal and colonic organoids was similar in IL-37tg organoids and WT organoids (Supplementary Figure S4).

RhIL-37 protein does not modulate the proinflammatory cytokine response in murine jejunal organoids

IL-37 has intra- and extracellular functionality (28, 30, 31, 45). In order to test the impact of extracellular IL-37 on proinflammatory cytokine expression in gut epithelial cells, we added rhIL-37 to jejunal organoids derived from WT mice (Figure 2). rhIL-37 did not modulate the mRNA expression of *Cxcl1*, *Cxcl2*, *Ccl20*, and *Tnf* in jejunal organoids after TNF-α treatment (Figure 2).

Morphologic changes of WT and IL-37tg-derived organoids after TNF-α treatment

Since *IL37* expression did not markedly alter the intestinal epithelial immune response (Figures 1A, B), we evaluated the impact of IL-37 on the morphology of organoids derived from WT and IL-37tg mice during inflammation. Under untreated conditions, the morphology of WT and IL-37tg-derived murine organoids was similar (Figure 3A). Jejunal organoids grew as buds and colonic organoids in a spherical shape (Figure 3A). After TNF-α treatment, jejunal WT and IL-37tg-derived organoids displayed spherical rounding (Figure 3B), while the gross morphology of colonic organoids remained similar after LPS treatment. The shape of organoids was similar in both genetic traits.

10.3389/fimmu.2023.1261666

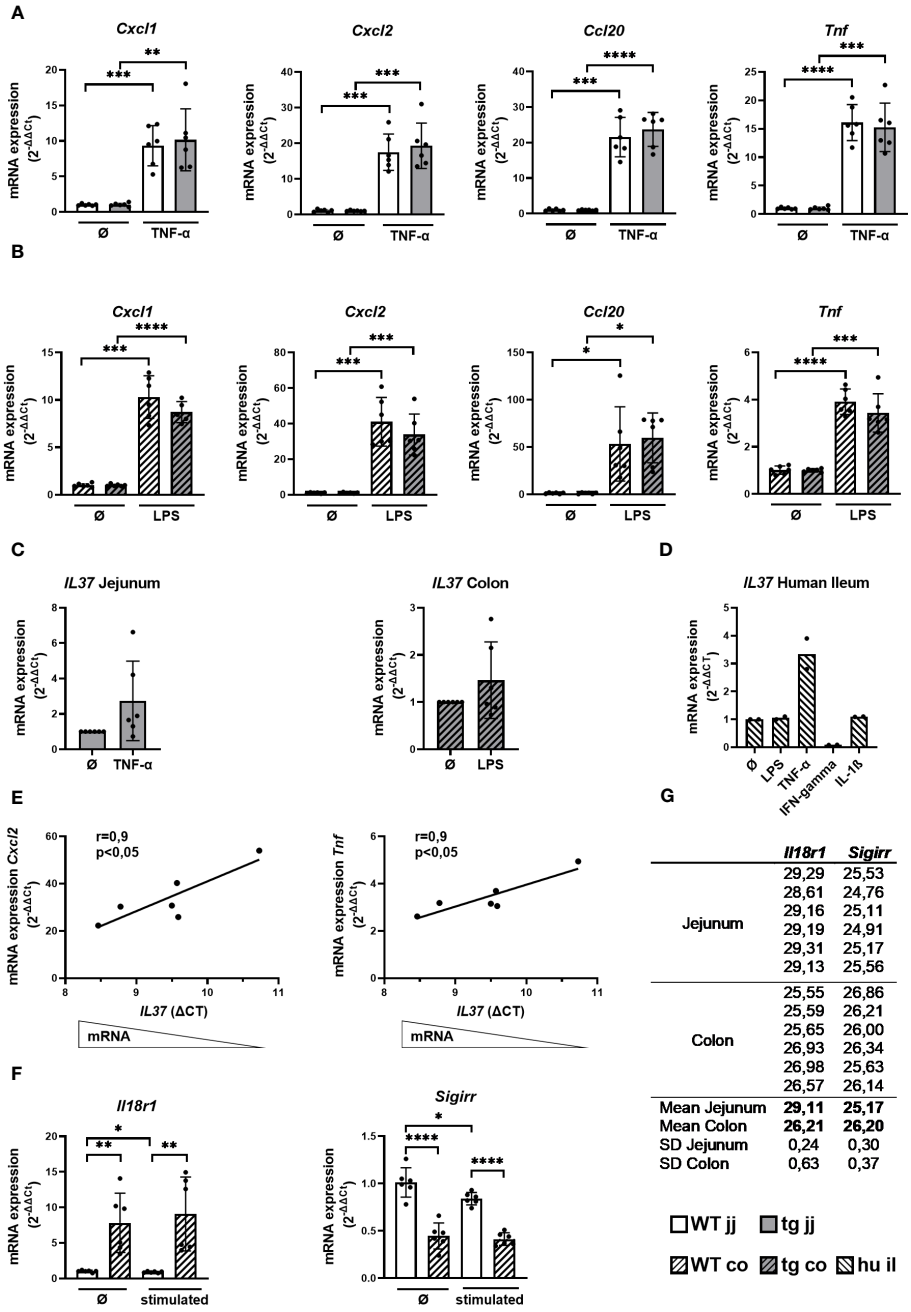

FIGURE 1
Cytokine response and the expression of IL-37 and its receptor components in WT and tgIL-37 intestinal organoids. Jejunal and colonic organoids derived from IL-37tg and WT mice were stimulated for 4 h with murine TNF-α (10 ng/ml) or LPS O55:B5 (1,000 ng/ml) (37) in culture medium. mRNA expression of cytokines in **(A)** jejunal and **(B)** colonic organoids was measured by qPCR and expressed as fold change relative to the mean of unstimulated organoids of the respective mouse ($2^{-\Delta\Delta CT}$). **(C)** Induction of *IL37* mRNA expression in stimulated IL-37tg-derived organoids was measured by qPCR and expressed as fold change relative to unstimulated organoids ($2^{-\Delta\Delta CT}$). **(D)** Human ileal organoids (il, n = 2, two donors) were stimulated for 24 h with LPS O55:B5 (1,000 ng/ml), human TNF-α (10 ng/ml), human IFN-gamma (20 ng/ml), and human IL-1ß (10 ng/ml) in the culture medium. mRNA expression of IL-37 was measured by qPCR and expressed as fold change relative to unstimulated organoids ($2^{-\Delta\Delta CT}$). **(E)** Correlation of cytokine mRNA expression relative to mean of unstimulated colonic organoids of the respective mouse ($2^{-\Delta\Delta CT}$) with *IL37*-ΔCT-values of stimulated colonic organoids derived from IL-37tg mice. **(F)** mRNA expression of *Il18r1* and *Sigirr* in jejunal and colonic WT organoids was measured by qPCR and expressed as fold change relative to mean of unstimulated jejunal organoids ($2^{-\Delta\Delta CT}$). **(G)** Mean CT-values of *Il18r1* and *Sigirr* qPCR duplicates in jejunal and colonic WT organoids. Each experiment was performed with organoid lines of two different mice and repeated three times (in total n = 6). Open bars: organoids derived from WT mice (WT); grey bars: organoids derived from IL-37tg mice (tg); no pattern: jejunal organoids (jj); striped pattern: colonic organoids (co). Each data point represents a single organoid line. Data are expressed as the mean with SD. *$p \leq 0.05$; **$p \leq 0.01$; ***$p \leq 0.001$; ****$p \leq 0.0001$.

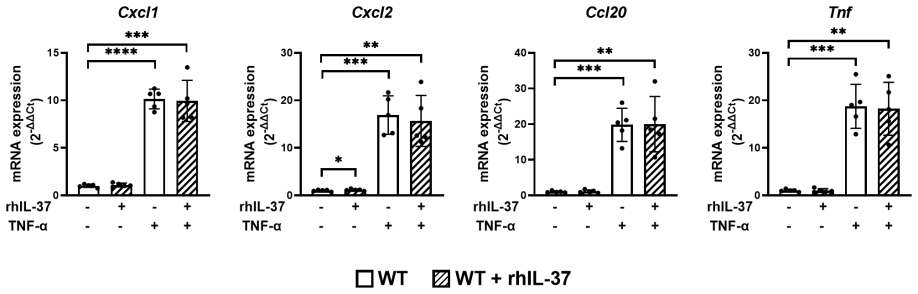

FIGURE 2
RhIL-37 protein does not modulate the proinflammatory cytokine response in murine jejunal organoids. Jejunal WT-derived organoids were stimulated for 4 h with TNF-α (10 ng/ml) with or without rhIL-37 (100 pg/ml; R&D systems). mRNA expression of cytokines was measured by qPCR and expressed as fold change relative to the mean of unstimulated organoids of the respective mouse ($2^{-\Delta\Delta CT}$). Open bars: organoids derived from WT mice (WT); striped: organoids treated with rhIL-37 (WT + rhIL-37). Each data point represents a single organoid line. Data are expressed as the mean with SD. *$p \leq 0.05$; **$p \leq 0.01$; ***$p \leq 0.001$; ****$p \leq 0.0001$.

Downregulation and disassembling of intestinal barrier proteins in murine organoids after treatment with inflammatory stimuli are not modulated by tgIL-37 expression

Spherical rounding of small intestinal organoids after TNF-α treatment can be caused by increased TJ permeability (46). Therefore, we analyzed ZO-1, occludin, and claudin-2 mRNA and protein expression in organoids derived from WT and IL-37tg mice before and after respective treatments. There was no significant difference in TJ protein expression between WT- and IL-37-tg-derived organoids on mRNA and protein levels before and after stimulation (Figures 4A, B, D). Changes in barrier protein expression and distribution, analyzed by immunofluorescence analysis, were similar in WT- and IL-37tg-derived organoids (Figure 4E).

On the mRNA level, *Tjp1* expression, encoding ZO-1, was unchanged after TNF-α treatment in jejunal organoids (Figure 4A) and colonic organoids (Figure 4B). Expression of *Ocln*, encoding occludin, was reduced by 8% in IL-37tg-derived jejunal organoids (Figure 4A), by 9% in WT-derived colonic organoids (Figure 4B), and by 8% in IL-37tg-derived colonic organoids (Figure 4B). Expression of *Cldn2*, encoding claudin-2, was reduced by 28% in WT-derived jejunal organoids (Figure 4A), by 32% in IL-37tg-derived jejunal organoids (Figure 4A), by 47% in WT- derived colonic organoids (Figure 4B), and by 40% in IL-37tg-derived colonic organoids (Figure 4B).

Western blot analysis (Figures 4C, D) showed a trend toward reduction of ZO-1 in IL-37tg-derived organoids after TNF-α treatment but not in WT organoids. Occludin was reduced by 35% in WT- and by 36% in IL-37tg-derived organoids, and claudin-2 was not significantly reduced by 43% in WT- and by 51% in IL-37tg-derived organoids. Claudin-2 baseline expression is highly varied between single organoid lines, independent of the genotype (Supplementary Figure S5).

In the immunofluorescence analysis (Figure 4E), ZO-1, occludin, and claudin-2 displayed a strong signal at the apical side of epithelial cells, indicating expression within the TJs. Additionally, occludin showed basolateral staining and claudin-2 an intracellular staining. E-cadherin was highly enriched at the basolateral side and at the lateral membranes, indicating expression within the adhering junctions. ZO-1, occludin, and claudin-2 expression patterns were largely disrupted by TNF-α treatment. E-cadherin staining was restricted to the basolateral side and less detectable at the lateral membranes and at the apical sides after TNF-α treatment. Other than ZO-1, occludin, and E-cadherin, claudin-2 was not expressed homogenously within the organoids but was predominately located within crypt domains (Supplementary Figure S6).

Discussion

In this study, we show that IL-37 does not modulate the gross cytokine response of murine intestinal organoids after immune stimulation with TNF-α or LPS by using tgIL-37 mice or treatment by rhIL37. However, we show that *IL37* expression is upregulated upon proinflammatory stimulation in murine and human organoids. More subtle analyses demonstrate a negative correlation between *IL37* expression and proinflammatory cytokine response in murine colonic organoids. IL-37 did not alter the TNF-dependent downregulation and structural alteration of TJ proteins in murine jejunal organoids.

There was no significant change in proinflammatory cytokine mRNA expression by IL-37tg jejunal or colonic organoids after TNF-α or LPS stimulation. In accordance with these results, we could also not observe differences in cytokine response after treatment with rhIL-37. This indicates that IL-37, expressed within the intestinal epithelium, does not grossly limit the immune response of IEC in an auto- or paracrine manner. Differences within the experimental approach might explain the contrasting results to the observation of Allaire and colleagues describing a downregulation of proinflammatory *Ccl20* and *Cxcl2* in flagellin- and IL-1ß-stimulated murine colonic organoids by treatment with rhIL-37 protein (37). Accordingly, Günaltay et al. showed that CRISPR/Cas knockdown of *IL37* increases the spontaneous chemokine expression in T84 IECs (36). We previously reported that hematopoietic-derived IL-37 from bone marrow transplantation is sufficient to ameliorate the severity of DSS-induced colitis in WT mice (32). This indicated the relevance of

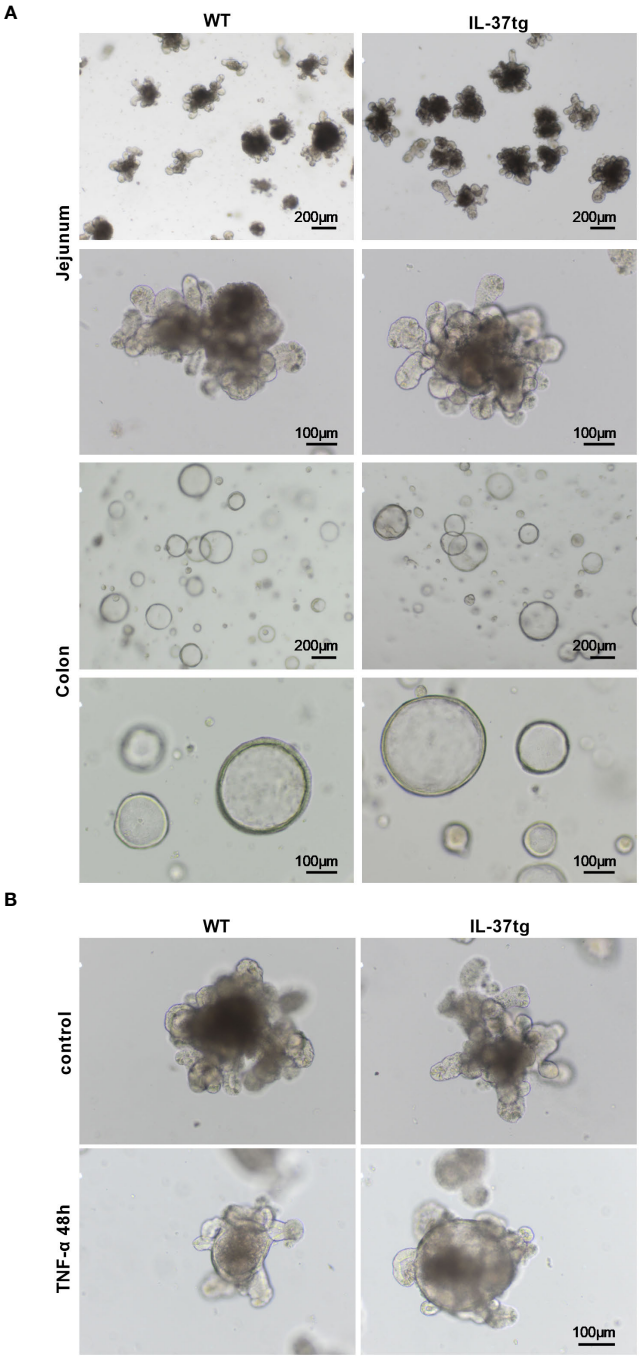

FIGURE 3
Morphologic changes of WT and IL-37tg-derived organoids after TNF-α treatment. **(A)** Representative light microscope images of murine jejunal and colonic organoids in extracellular matrix on days 3 to 4 under baseline conditions. **(B)** Representative light microscope images of jejunal organoids in extracellular matrix with or without 48 h TNF-α (10 ng/ml) stimulation. One representative picture out of six independent stimulation experiments is shown.

tgIL-37 expressed by immune cells to control mucosal inflammation. Since neither tgIL-37 nor rhIL-37 protein modulated the epithelial immune response in our organoid model, we speculate that predominantly extracellular IL-37, released from IECs at the site of tissue inflammation, contributes to the control of the immune response of intestinal mucosa-associated immune cells.

IL37 expression in IL-37tg mice is driven by a constitutively active CMV-promotor (30). However, like in healthy human tissue, baseline levels of IL-37 mRNA and protein are low in unstimulated IL-37tg mice, which is due to mRNA instability elements within the coding region of IL-37 (30, 47). *IL37* expression is also low in resting jejunal and colonic organoids generated from IL-37tg mice, but we were able to show a trend toward increased levels after stimulation. In human ileal organoids, only TNF-α but not LPS or IL-1ß induced *IL37* expression, while IFN-gamma reduced *IL37* expression. This is consistent with observations on T84 epithelial colon carcinoma cells (38). Upregulation of *IL37* by TNF-α is also in line with a high epithelial *IL37* expression in IBD correlating with higher disease

10.3389/fimmu.2023.1261666

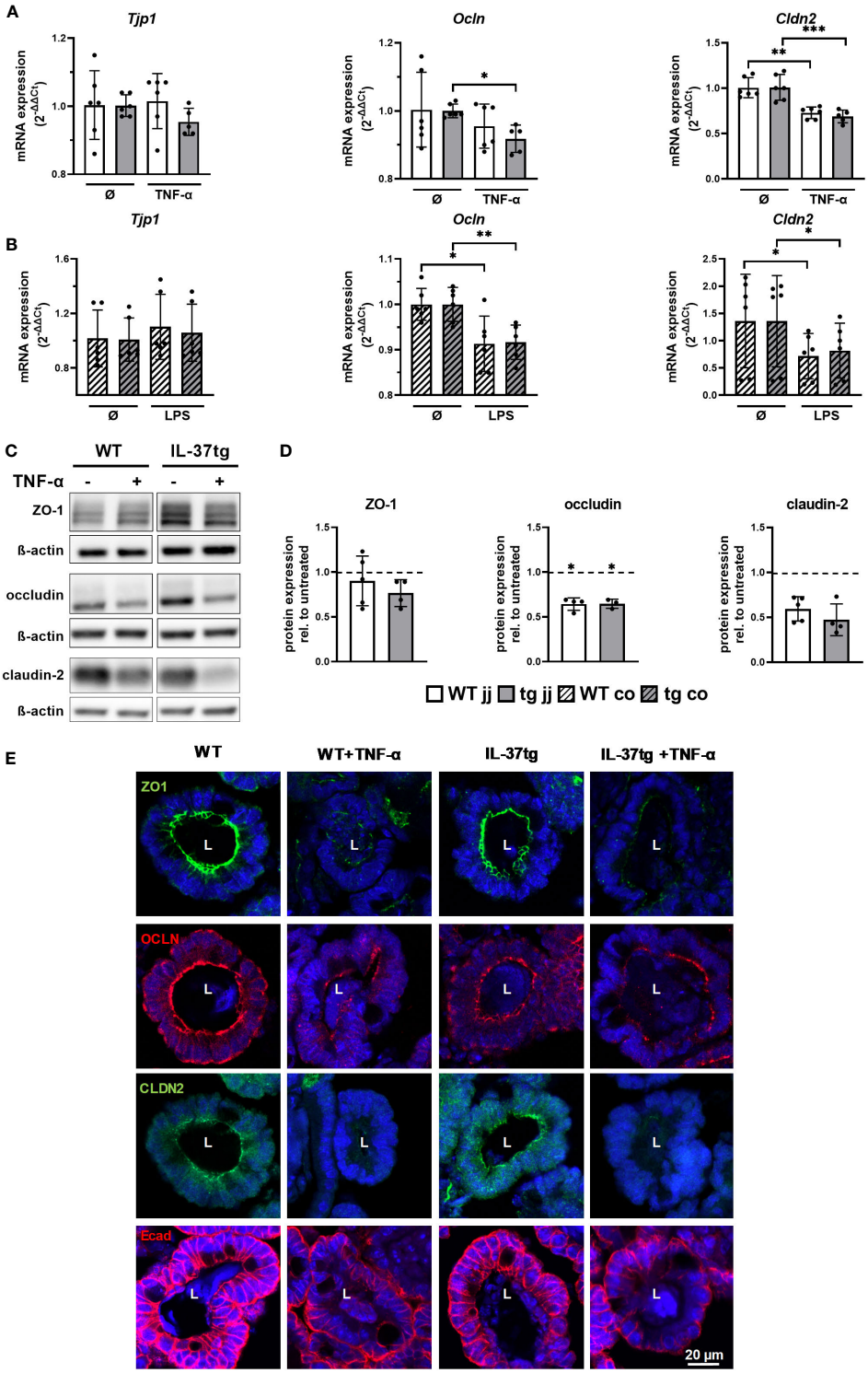

FIGURE 4
Downregulation and disassembling of intestinal barrier proteins in murine organoids after treatment with inflammatory stimuli is not modulated by tgIL-37 expression. Jejunal and colonic organoids were stimulated for 4 h with TNF-α (10 ng/ml) or LPS (1,000 ng/ml). mRNA expression of TJ proteins ZO-1 (*Tjp1*), occludin (*Ocln*), and claudin-2 (*Cldn2*) in **(A)** jejunal and **(B)** colonic organoids was measured by qPCR and expressed as fold change relative to mean of unstimulated organoids of the respective mouse ($2^{-\Delta\Delta CT}$). For Western blot and immunofluorescence analysis, jejunal organoids were stimulated for 48 h with TNF-α (10 ng/ml). **(C)** Representative Western blots of TJ proteins in jejunal WT- and IL-37tg-derived organoids. **(D)** Densitometric analysis of Western blots of TJ proteins in TNF-α-treated jejunal WT- and IL-37tg-derived organoids. Protein expression is represented as relative to untreated organoids (dotted line). Stars indicate the significance of downregulation after stimulation. **(E)** Representative immunofluorescence images of barrier proteins in WT- and IL-37tg-derived jejunal organoid crypt domains stained with ZO-1 (ZO1, green), occludin (OCLN, red), claudin-2 (CLDN2, green), and E-cadherin (Ecad, red). L, lumens. Open bars: organoids derived from WT mice (WT); closed bars: organoids derived from IL-37tg mice (tg); no pattern: jejunal organoids (jj); striped: colonic organoids (co). Each data point represents a single organoid line. Data are expressed as the mean with SD. *$p \leq 0.05$; **$p \leq 0.01$; ***$p \leq 0.001$.

activity (38, 48). In murine and human small intestinal organoids, there was only a minor inflammatory response to LPS, which might be caused by low expression of TLR4 in both and missing TLR4-associated accessory protein expression in human organoids [Supplementary Figure S1 and as previously shown (49)]. Insufficient immune stimulation could therefore explain the lack of *IL37* induction after LPS treatment in human ileal organoids. The induction of *IL37* by TNF-α in human ileal organoids was similar to that in murine jejunal organoids, corresponding to a high immune stimulation by TNF-α in murine and may be as well in human small intestinal organoids (Supplementary Figure S1).

Increasing levels of tgIL-37 mRNA, induced by proinflammatory signals, correlated with a lower *Cxcl2* and *Tnf* response in LPS-stimulated colonic organoids. This negative correlation was not observed in jejunal organoids after stimulation. Since SIGIRR is evenly expressed throughout the murine gut (50), as similarly seen in our jejunal and colonic organoids, we speculate that a higher expression of the IL-37 receptor component *Il18r1* (51–53) in colonic organoids sensitizes for autologous, anti-inflammatory IL-37 signaling. Indeed, polymorphisms in the IL18RI-IL18RAP locus are associated with adult and early-onset IBD (54–56), underlining the relevance of the IL-18RI for human disease activity to target both proinflammatory IL-18 and anti-inflammatory IL-37 immune pathways. In addition, tgIL-37 expression itself is associated with a markedly higher *Il18r1* expression in our IL-37tg colonic organoids, suggesting a regulatory effect of IL-37 on bona fide *Il18r1* expression (Supplementary Figure S3). Pretreatment with rhIL-37 was shown to induce SIGIRR expression in humans, LPS-stimulated PBMCs and M1 macrophages (45) indicating that IL-37 induces upregulation of its receptor components to increase its anti-inflammatory capacity.

TJ proteins claudin-2, ZO-1, or occludin are key determinants of epithelial integrity against mucosal inflammation in IBD (17, 18, 40, 57). The impact of TNF-α on epithelial barrier function was extensively studied in 2D cell culture models (10–12, 58). 3D organoid models are a good representation of the epithelial architecture, with a villi-like structure and composition of a variety of epithelial subtypes. However, studies of TJ proteins and IL-37 in organoids are scarce. In our model, TNF-α and LPS caused significant changes in TJ protein expression and morphology in jejunal and colonic organoids. Nevertheless, overall TJ protein expression and organoid morphology were similar between WT- and IL-37tg-derived organoids before and after stimulation. This indicates that tgIL-37 expression in IEC does not prevent the disturbance of TJ protein expression during inflammation.

In summary, our 3D intestinal organoid model enabled us to investigate the impact of IL-37 on IEC innate immune responses and intestinal barrier function, irrespective of epithelial immune cell activation. We show that *IL37* expression is induced in intestinal epithelial cells but has no major impact on modulating IEC innate immune responses itself and does not prevent murine intestinal organoids from altered barrier protein expression after stimulation. We conclude that the protective effect of IEC-derived IL-37 on the intestinal epithelial barrier in murine models of IBD and potentially the human gut is more mediated by downregulating the release of proinflammatory mediators from lamina propria immune cells than intestinal epithelial cells.

Data availability statement

The raw data supporting the conclusions of this article will be made available by the authors, without undue reservation.

Ethics statement

The studies involving humans were approved by Ethics committee Charité Universitätsmedizin Berlin. The studies were conducted in accordance with the local legislation and institutional requirements. Written informed consent for participation in this study was provided by the participants' legal guardians/next of kin. The animal study was approved by Landesamt für Gesundheit und Soziales Berlin. The study was conducted in accordance with the local legislation and institutional requirements.

Author contributions

LK: Conceptualization, Writing – review & editing, Data curation, Formal Analysis, Investigation, Methodology, Visualization, Writing – original draft. AA: Writing – original draft, Conceptualization, Data curation, Investigation, Methodology, Supervision, Writing – review & editing. JH: Methodology, Supervision, Writing – review & editing. CH: Writing – review & editing, Resources. MZ: Conceptualization, Resources, Methodology, Supervision, Writing – review & editing. TB: Project administration, Writing – original draft, Conceptualization, Investigation, Methodology, Supervision, Writing – review & editing. PB: Writing – review & editing, Writing – original draft, Data curation, Resources, Visualization, Conceptualization, Funding acquisition, Investigation, Methodology, Project administration, Supervision, Validation.

Funding

LK was supported by the Deutsche Forschungsgemeinschaft (DFG, German Research Foundation)-GRK 2318-318905415. AA was supported by the Deutsche Forschungsgemeinschaft (DFG-German Research Foundation, project number 501883972) and by the BIH-Charité Junior Clinician Scientist Program funded by Charité-Universitätsmedizin Berlin and the Berlin Institute of Health (BIH).

Acknowledgments

We thank Kerstin Sommer and Franziska Weiß for excellent technical support and Felix Heymann for assistance on the confocal microscope. Jörg-Dieter Schulzke is thanked for his continuing support. Charles A. Dinarello is thanked for his longstanding support and for providing IL-37tg mice. We thank the patients

and their families for contributing to our research. We acknowledge financial support from the Open Access Publication Fund of Charité – Universitätsmedizin Berlin and the German Research Foundation (DFG).

Conflict of interest

The authors declare that the research was conducted in the absence of any commercial or financial relationships that could be construed as a potential conflict of interest.

The author(s) declared that they were an editorial board member of Frontiers, at the time of submission. This had no impact on the peer review process and the final decision.

Publisher's note

Supplementary material

The Supplementary Material for this article can be found online at: https://www.frontiersin.org/articles/10.3389/fimmu.2023.1261666/full#supplementary-material

References

1. Peterson LW, Artis D. Intestinal epithelial cells: regulators of barrier function and immune homeostasis. *Nat Rev Immunol* (2014) 14:141–53. doi: 10.1038/nri3608

2. Maldonado-Contreras AL, McCormick BA. Intestinal epithelial cells and their role in innate mucosal immunity. *Cell Tissue Res* (2011) 343:5–12. doi: 10.1007/s00441-010-1082-5

3. Andrews C, McLean MH, Durum SK. Cytokine tuning of intestinal epithelial function. *Front Immunol* (2018) 9:1270. doi: 10.3389/fimmu.2018.01270

4. Bogunovic M, Davé SH, Tilstra JS, Chang DTW, Harpaz N, Xiong H, et al. Enteroendocrine cells express functional Toll-like receptors. *Am J Physiol-Gastrointest Liver Physiol* (2007) 292:G1770–83. doi: 10.1152/ajpgi.00249.2006

5. Vavricka SR, Musch MW, Chang JE, Nakagawa Y, Phanvijhitsiri K, Waypa TS, et al. hPepT1 transports muramyl dipeptide, activating NF-κB and stimulating IL-8 secretion in human colonic Caco2/bbe cells. *Gastroenterology* (2004) 127:1401–9. doi: 10.1053/j.gastro.2004.07.024

6. Jung HC, Eckmann L, Yang SK, Panja A, Fierer J, Morzycka-Wroblewska E, et al. A distinct array of proinflammatory cytokines is expressed in human colon epithelial cells in response to bacterial invasion. *J Clin Invest* (1995) 95:55–65. doi: 10.1172/JCI117676

7. Kinugasa T, Sakaguchi T, Gu X, Reinecker H-C. Claudins regulate the intestinal barrier in response to immune mediators. *Gastroenterology* (2000) 118:1001–11. doi: 10.1016/S0016-5085(00)70351-9

8. Tsai P-Y, Zhang B, He W-Q, Zha J-M, Odenwald MA, Singh G, et al. IL-22 upregulates epithelial claudin-2 to drive diarrhea and enteric pathogen clearance. *Cell Host Microbe* (2017) 21:671–681.e4. doi: 10.1016/j.chom.2017.05.009

9. Al-Sadi R, Ye D, Boivin M, Guo S, Hashimi M, Ereifej L, et al. Interleukin-6 modulation of intestinal epithelial tight junction permeability is mediated by JNK pathway activation of claudin-2 gene. *PloS One* (2014) 9:e85345. doi: 10.1371/journal.pone.0085345

10. Mankertz J, Amasheh M, Krug SM, Fromm A, Amasheh S, Hillenbrand B, et al. TNFα up-regulates claudin-2 expression in epithelial HT-29/B6 cells *via* phosphatidylinositol-3-kinase signaling. *Cell Tissue Res* (2009) 336:67–77. doi: 10.1007/s00441-009-0751-8

11. Fischer A, Gluth M, Pape U-F, Wiedenmann B, Theuring F, Baumgart DC. Adalimumab prevents barrier dysfunction and antagonizes distinct effects of TNF-α on tight junction proteins and signaling pathways in intestinal epithelial cells. *Am J Physiol-Gastrointest Liver Physiol* (2013) 304:G970–9. doi: 10.1152/ajpgi.00183.2012

12. Ma TY, Iwamoto GK, Hoa NT, Akotia V, Pedram A, Boivin MA, et al. TNF-α-induced increase in intestinal epithelial tight junction permeability requires NF-κB activation. *Am J Physiol-Gastrointest Liver Physiol* (2004) 286:G367–76. doi: 10.1152/ajpgi.00173.2003

13. Lorén V, Cabré E, Ojanguren I, Domènech E, Pedrosa E, García-Jaraquemada A, et al. Interleukin-10 Enhances the Intestinal Epithelial Barrier in the Presence of Corticosteroids through p38 MAPK Activity in Caco-2 Monolayers: A Possible Mechanism for Steroid Responsiveness in Ulcerative Colitis. *PloS One* (2015) 10: e0130921. doi: 10.1371/journal.pone.0130921

14. Zheng L, Kelly CJ, Battista KD, Schaefer R, Lanis JM, Alexeev EE, et al. Microbial-derived butyrate promotes epithelial barrier function through IL-10 receptor–dependent repression of claudin-2. *J Immunol* (2017) 199:2976–84. doi: 10.4049/jimmunol.1700105

15. Kominsky DJ, Campbell EL, Ehrentraut SF, Wilson KE, Kelly CJ, Glover LE, et al. IFN-γ–mediated induction of an apical IL-10 receptor on polarized intestinal epithelia. *J Immunol* (2014) 192:1267–76. doi: 10.4049/jimmunol.1301757

16. Salim SY, Söderholm JD. Importance of disrupted intestinal barrier in inflammatory bowel diseases. *Inflammation Bowel Dis* (2011) 17:362–81. doi: 10.1002/ibd.21403

17. Schmitz H, Barmeyer C, Fromm M, Runkel N, Foss HD, Bentzel CJ, et al. Altered tight junction structure contributes to the impaired epithelial barrier function in ulcerative colitis. *Gastroenterology* (1999) 116:301–9. doi: 10.1016/s0016-5085(99)70126-5

18. Xu P, Elamin E, Elizalde M, Bours PPHA, Pierik MJ, Masclee AAM, et al. Modulation of intestinal epithelial permeability by plasma from patients with crohn's disease in a three-dimensional cell culture model. *Sci Rep* (2019) 9:2030. doi: 10.1038/s41598-018-38322-8

19. Merlin D, Si-Tahar M, Sitaraman SV, Eastburn K, Williams I, Liu X, et al. Colonic epithelial hPepT1 expression occurs in inflammatory bowel disease: transport of bacterial peptides influences expression of MHC class 1 molecules. *Gastroenterology* (2001) 120:1666–79. doi: 10.1053/gast.2001.24845

20. Cario E, Podolsky DK. Differential alteration in intestinal epithelial cell expression of toll-like receptor 3 (TLR3) and TLR4 in inflammatory bowel disease. *Infect Immun* (2000) 68:7010–7. doi: 10.1128/IAI.68.12.7010-7017.2000

21. Bouma G, Strober W. The immunological and genetic basis of inflammatory bowel disease. *Nat Rev Immunol* (2003) 3:521–33. doi: 10.1038/nri1132

22. Liu Z, Colpaert S, D'Haens GR, Kasran A, de BM, Rutgeerts P, et al. Hyperexpression of CD40 ligand (CD154) in inflammatory bowel disease and its contribution to pathogenic cytokine production. *J Immunol* (1999) 163:4049–57. doi: 10.4049/jimmunol.163.7.4049

23. Hugot J-P, Chamaillard M, Zouali H, Lesage S, Cézard J-P, Belaiche J, et al. Association of NOD2 leucine-rich repeat variants with susceptibility to Crohn's disease. *Nature* (2001) 411:599–603. doi: 10.1038/35079107

24. Monteleone G, Kumberova A, Croft NM, McKenzie C, Steer HW, MacDonald TT. Blocking Smad7 restores TGF-β1 signaling in chronic inflammatory bowel disease. *J Clin Invest* (2001) 108:601–9. doi: 10.1172/JCI12821

25. Sun X, He S, Lv C, Sun X, Wang J, Zheng W, et al. Analysis of murine and human Treg subsets in inflammatory bowel disease. *Mol Med Rep* (2017) 16:2893–8. doi: 10.3892/mmr.2017.6912

26. Glocker E-O, Kotlarz D, Boztug K, Gertz EM, Schäffer AA, Noyan F, et al. Inflammatory bowel disease and mutations affecting the interleukin-10 receptor. *N Engl J Med* (2009) 361:2033–45. doi: 10.1056/NEJMoa0907206

27. Zhang ZZ, Zhang Y, He T, Sweeney CL, Baris S, Karakoc-Aydiner E, et al. Homozygous IL37 mutation associated with infantile inflammatory bowel disease. *Proc Natl Acad Sci* (2021) 118:e2009217118. doi: 10.1073/pnas.2009217118

28. Nold-Petry CA, Lo CY, Rudloff I, Elgass KD, Li S, Gantier MP, et al. IL-37 requires the receptors IL-18Rα and IL-1R8 (SIGIRR) to carry out its multifaceted anti-inflammatory program upon innate signal transduction. *Nat Immunol* (2015) 16:354–65. doi: 10.1038/ni.3103

29. Dinarello CA, Nold-Petry C, Nold M, Fujita M, Li S, Kim S, et al. Suppression of innate inflammation and immunity by interleukin family member interleukin-37. *Eur J Immunol* (2016) 46:1067–81. doi: 10.1002/eji.201545828

30. Nold MF, Nold-Petry CA, Zepp JA, Palmer BE, Bufler P, Dinarello CA. IL-37 is a fundamental inhibitor of innate immunity. *Nat Immunol* (2010) 11:1014–22. doi: 10.1038/ni.1944

31. Bulau A-M, Nold MF, Li S, Nold-Petry CA, Fink M, Mansell A, et al. Role of caspase-1 in nuclear translocation of IL-37, release of the cytokine, and IL-37 inhibition of innate immune responses. *Proc Natl Acad Sci* (2014) 111:2650–5. doi: 10.1073/pnas.1324140111

32. McNamee EN, Masterson JC, Jedlicka P, McManus M, Grenz A, Collins CB, et al. Interleukin 37 expression protects mice from colitis. *Proc Natl Acad Sci USA* (2011) 108:16711–6. doi: 10.1073/pnas.1111982108

33. Henry CJ, Casás-Selves M, Kim J, Zaberezhnyy V, Aghili L, Daniel AE, et al. Aging-associated inflammation promotes selection for adaptive oncogenic events in B cell progenitors. *J Clin Invest* (2015) 125:4666–80. doi: 10.1172/JCI83024

34. Coll-Miró M, Francos-Quijorna I, Santos-Nogueira E, Torres-Espin A, Bufler P, Dinarello CA, et al. Beneficial effects of IL-37 after spinal cord injury in mice. *Proc Natl Acad Sci USA* (2016) 113:1411–6. doi: 10.1073/pnas.1523212113

35. Ballak DB, van Diepen JA, Moschen AR, Jansen HJ, Hijmans A, Groenhof G-J, et al. IL-37 protects against obesity-induced inflammation and insulin resistance. *Nat Commun* (2014) 5:4711. doi: 10.1038/ncomms5711

36. Günaltay S, Ghiboub M, Hultgren O, Hörnquist EH. Reduced IL-37 production increases spontaneous chemokine expressions in colon epithelial cells. *Dig Dis Sci* (2017) 62:1204–15. doi: 10.1007/s10620-016-4422-9

37. Allaire JM, Poon A, Crowley SM, Han X, Sharafian Z, Moore N, et al. Interleukin-37 regulates innate immune signaling in human and mouse colonic organoids. *Sci Rep* (2021) 11:8206. doi: 10.1038/s41598-021-87592-2

38. Imaeda H, Takahashi K, Fujimoto T, Kasumi E, Ban H, Bamba S, et al. Epithelial expression of interleukin-37b in inflammatory bowel disease. *Clin Exp Immunol* (2013) 172:410–6. doi: 10.1111/cei.12061

39. Weidlich S, Bulau A-M, Schwerd T, Althans J, Kappler R, Koletzko S, et al. Intestinal expression of the anti-inflammatory interleukin-1 homologue IL-37 in pediatric inflammatory bowel disease. *J Pediatr Gastroenterol Nutr* (2014) 59:e18. doi: 10.1097/MPG.0000000000000387

40. Zeissig S, Bürgel N, Günzel D, Richter J, Mankertz J, Wahnschaffe U, et al. Changes in expression and distribution of claudin 2, 5 and 8 lead to discontinuous tight junctions and barrier dysfunction in active Crohn's disease. *Gut* (2007) 56:61–72. doi: 10.1136/gut.2006.094375

41. Sato T, Stange DE, Ferrante M, Vries RGJ, van Es JH, van den Brink S, et al. Long-term expansion of epithelial organoids from human colon, adenoma, adenocarcinoma, and barrett's epithelium. *Gastroenterology* (2011) 141:1762–72. doi: 10.1053/j.gastro.2011.07.050

42. Mizutani T, Clevers H. Primary intestinal epithelial organoid culture. In: Ordóñez-Morán P editor. *Intestinal stem cells: methods and protocols. Methods in molecular biology*. Springer US, New York (2020). p. 185–200. doi: 10.1007/978-1-0716-0747-3_11

43. Grinat J, Kosel F, Goveas N, Kranz A, Alexopoulou D, Rajewsky K, et al. Epigenetic modifier balances Mapk and Wnt signalling in differentiation of goblet and Paneth cells. *Life Sci Alliance* (2022) 5:e202101187. doi: 10.26508/lsa.202101187

44. Heuberger J, Trimpert J, Vladimirova D, Goosmann C, Lin M, Schmuck R, et al. Epithelial response to IFN-γ promotes SARS-CoV-2 infection. *EMBO Mol Med* (2021) 13:e13191. doi: 10.15252/emmm.202013191

45. Li S, Neff CP, Barber K, Hong J, Luo Y, Azam T, et al. Extracellular forms of IL-37 inhibit innate inflammation in *vitro* and in *vivo* but require the IL-1 family decoy receptor IL-1R8. *Proc Natl Acad Sci USA* (2015) 112:2497–502. doi: 10.1073/pnas.1424626112

46. Hahn S, Nam M-O, Noh JH, Lee DH, Han HW, Kim DH, et al. Organoid-based epithelial to mesenchymal transition (OEMT) model: from an intestinal fibrosis perspective. *Sci Rep* (2017) 7:4-6, 8. doi: 10.1038/s41598-017-02190-5

47. Bufler P, Gamboni-Robertson F, Azam T, Kim S-H, Dinarello CA. Interleukin-1 homologues IL-1F7b and IL-18 contain functional mRNA instability elements within the coding region responsive to lipopolysaccharide. *Biochem J* (2004) 381:503–10. doi: 10.1042/BJ20040217

48. Wang W, Dong K, Zhou L, Jiao G, Zhu C, Li W, et al. IL-37b gene transfer enhances the therapeutic efficacy of mesenchumal stromal cells in DSS-induced colitis mice. *Acta Pharmacol Sin* (2015) 36:1377–87. doi: 10.1038/aps.2015.51

49. Kayisoglu O, Weiss F, Niklas C, Pierotti I, Pompaiah M, Wallaschek N, et al. Location-specific cell identity rather than exposure to GI microbiota defines many innate immune signalling cascades in the gut epithelium. *Gut* (2021) 70:687–97. doi: 10.1136/gutjnl-2019-319919

50. Garlanda C, Riva F, Polentarutti N, Buracchi C, Sironi M, De Bortoli M, et al. Intestinal inflammation in mice deficient in Tir8, an inhibitory member of the IL-1 receptor family. *Proc Natl Acad Sci USA* (2004) 101:3522–6. doi: 10.1073/pnas.0308680101

51. Kumar S, Hanning CR, Brigham-Burke MR, Rieman DJ, Lehr R, Khandekar S, et al. Interleukin-1F7B (IL-1H4/IL-1F7) is processed by caspase-1 and mature IL-1F7B binds to the IL-18 receptor but does not induce IFN-γ production. *Cytokine* (2002) 18 (2):61–71. doi: 10.1006/cyto.2002.0873

52. Pan G, Risser P, Mao W, Baldwin DT, Zhong AW, Filvaroff E, et al. IL-1H, an interleukin-1-related protein that binds IL-18 receptor/IL-1Rrp. *Cytokine* (2001) 13 (1):1–7. doi: 10.1006/cyto.2000.0799

53. Bufler P, Azam T, Gamboni-Robertson F, Reznikov LL, Kumar S, Dinarello CA, et al. A complex of the IL-1 homologue IL-1F7b and IL-18-binding protein reduces IL-18 activity. *Proc Natl Acad Sci* (2002) 99:13723–8. doi: 10.1073/pnas.212519099

54. Imielinski M, Baldassano RN, Griffiths A, Russell RK, Annese V, Dubinsky M, et al. Common variants at five new loci associated with early-onset inflammatory bowel disease. *Nat Genet* (2009) 41:1335–40. doi: 10.1038/ng.489

55. Barrett JC, Hansoul S, Nicolae DL, Cho JH, Duerr RH, Rioux JD, et al. Genome-wide association defines more than 30 distinct susceptibility loci for Crohn's disease. *Nat Genet* (2008) 40:955–62. doi: 10.1038/ng.175

56. Hedl M, Zheng S, Abraham C. The IL18RAP region disease polymorphism decreases IL-18RAP/IL-18R1/IL-1R1 expression and signaling through innate receptor–initiated pathways. *J Immunol* (2014) 192:5924–32. doi: 10.4049/jimmunol.1302727

57. Heller F, Florian P, Bojarski C, Richter J, Christ M, Hillenbrand B, et al. Interleukin-13 is the key effector th2 cytokine in ulcerative colitis that affects epithelial tight junctions, apoptosis, and cell restitution. *Gastroenterology* (2005) 129:550–64. doi: 10.1053/j.gastro.2005.05.002

58. Bruewer M, Luegering A, Kucharzik T, Parkos CA, Madara JL, Hopkins AM, et al. Proinflammatory cytokines disrupt epithelial barrier function by apoptosis-independent mechanisms. *J Immunol* (2003) 171:6164–72. doi: 10.4049/jimmunol.171.11.6164

frontiers | Frontiers in Immunology

TYPE Original Research
PUBLISHED 23 October 2023
DOI 10.3389/fimmu.2023.1227268

OPEN ACCESS

EDITED BY
Annalisa Del Prete,
University of Brescia, Italy

REVIEWED BY
Simona Gabriela Bungau,
University of Oradea, Romania
Paola Italiani,
National Research Council (CNR), Italy

*CORRESPONDENCE
Giselle Pentón-Rol
gpentonrol2011@gmail.com

RECEIVED 23 May 2023
ACCEPTED 02 October 2023
PUBLISHED 23 October 2023

CITATION
Marín-Prida J, Rodríguez-Ulloa A, Besada V, Llopiz-Arzuaga A, Batista NV, Hernández-González I, Pavón-Fuentes N, Marciano Vieira ÉL, Falcón-Cama V, Acosta EF, Martínez-Donato G, Cervantes-Llanos M, Lingfeng D, González LJ, Fernández-Massó JR, Guillén-Nieto G, Pentón-Arias E, Amaral FA, Teixeira MM and Pentón-Rol G (2023) The effects of Phycocyanobilin on experimental arthritis involve the reduction in nociception and synovial neutrophil infiltration, inhibition of cytokine production, and modulation of the neuronal proteome.
Front. Immunol. 14:1227268.
doi: 10.3389/fimmu.2023.1227268

The effects of Phycocyanobilin on experimental arthritis involve the reduction in nociception and synovial neutrophil infiltration, inhibition of cytokine production, and modulation of the neuronal proteome

Javier Marín-Prida[1], Arielis Rodríguez-Ulloa[2], Vladimir Besada[2,3], Alexey Llopiz-Arzuaga[2,4], Nathália Vieira Batista[5], Ignacio Hernández-González[6], Nancy Pavón-Fuentes[7], Érica Leandro Marciano Vieira[8], Viviana Falcón-Cama[2,9], Emilio F. Acosta[10], Gillian Martínez-Donato[2], Majel Cervantes-Llanos[2], Dai Lingfeng[3], Luis J. González[2], Julio Raúl Fernández-Massó[2], Gerardo Guillén-Nieto[2,9], Eduardo Pentón-Arias[2,9], Flávio Almeida Amaral[5], Mauro Martins Teixeira[5] and Giselle Pentón-Rol[2,9]*

[1]Center for Research and Biological Evaluations, Institute of Pharmacy and Food, University of Havana, Havana, Cuba, [2]Division of Biomedical Research, Center for Genetic Engineering and Biotechnology, Havana, Cuba, [3]China-Cuba Biotechnology Joint Innovation Center (CCBJIC), Yongzhou Zhong Gu Biotechnology Co. Ltd, Yongzhou, China, [4]Department of Cellular Engineering and Biocatalysis , Institute of Biotechnology, National Autonomous University of Mexico (UNAM), Cuernavaca, Mexico, [5]Laboratory of Immunopharmacology, Department of Biochemistry and Immunology, Instituto de Ciências Biológicas, Universidade Federal de Minas Gerais, Belo Horizonte, Minas Gerais, Brazil, [6]Department of Non-Clinical Research, Isotopes Center, San José de Las Lajas, Mayabeque, Cuba, [7]Immunochemical Department, International Center for Neurological Restoration (CIREN), Havana, Cuba, [8]Translational Psychoneuroimmunology Group, School of Medicine, Federal University of Minas Gerais (UFMG), Belo Horizonte, Brazil, [9]Departments of Physiological or Morphological Sciences, Latin American School of Medicine (ELAM), Havana, Cuba, [10]Department of Characterization, Center for Advanced Studies of Cuba, Havana, Cuba

Introduction: The antinociceptive and pharmacological activities of C-Phycocyanin (C-PC) and Phycocyanobilin (PCB) in the context of inflammatory arthritis remain unexplored so far. In the present study, we aimed to assess the protective actions of these compounds in an experimental mice model that replicates key aspects of human rheumatoid arthritis.

Methods: Antigen-induced arthritis (AIA) was established by intradermal injection of methylated bovine serum albumin in C57BL/6 mice, and one hour before the antigen challenge, either C-PC (2, 4, or 8 mg/kg) or PCB (0.1 or 1 mg/kg) were administered intraperitoneally. Proteome profiling was also conducted on

glutamate-exposed SH-SY5Y neuronal cells to evaluate the PCB impact on this key signaling pathway associated with nociceptive neuronal sensitization.

Results and discussion: C-PC and PCB notably ameliorated hypernociception, synovial neutrophil infiltration, myeloperoxidase activity, and the periarticular cytokine concentration of IFN-γ, TNF-α, IL-17A, and IL-4 dose-dependently in AIA mice. In addition, 1 mg/kg PCB downregulated the gene expression for T-bet, RORγ, and IFN-γ in the popliteal lymph nodes, accompanied by a significant reduction in the pathological arthritic index of AIA mice. Noteworthy, neuronal proteome analysis revealed that PCB modulated biological processes such as pain, inflammation, and glutamatergic transmission, all of which are involved in arthritic pathology.

Conclusions: These findings demonstrate the remarkable efficacy of PCB in alleviating the nociception and inflammation in the AIA mice model and shed new light on mechanisms underlying the PCB modulation of the neuronal proteome. This research work opens a new avenue to explore the translational potential of PCB in developing a therapeutic strategy for inflammation and pain in rheumatoid arthritis.

KEYWORDS

Phycocyanobilin, rheumatoid arthritis, hypernociception, glutamatergic transmission, proteome, neutrophils, inflammation, C-Phycocyanin

1 Introduction

Rheumatoid arthritis (RA) stands as a persistent autoimmune disease, marked by widespread synovitis and, at times, by relentless bone deterioration (1). The ensuing joint abnormalities, which include rigidity and deformity, precipitate a distressing setback of mobility in RA-afflicted individuals and eventually lead to varying degrees of bone decomposition, harm to ligaments and tendons, and skeletal muscle weakening (2).

The initiation and extension of chronic RA inflammation involves both adaptive and innate immune cells. Neutrophils have been identified as the predominant leukocyte in the joints of individuals with active RA (3). Their role in the disease's pathogenesis includes tissue damage and the discharge of proinflammatory cytokines as well as an important crosstalk with other immune cells such as T cells and dendritic cells (DCs) (4–6). Animal models of arthritis have provided more direct evidence of neutrophil involvement in this disease. In the K/BxN mouse RA model, neutrophil depletion led to the complete reversion of the joint inflammation, showing no signs of swelling either in the forefeet or the ankle joints (7). Likewise, chemokines commonly found in rheumatoid synovial fluid drew neutrophils into the affected joints in an arthritis mice model induced by collagen, while the neutrophil depletion also completely prevented the disease development in this model (8).

Furthermore, impairment of the resolution of inflammation acquires a prominent role in perpetuating clinical dysfunction in chronic diseases such as RA. It has been noted that a persistent failure in neutrophil death is correlated with an increased severity of experimental arthritis in mice (9). Even when neutrophils die, their disposal is dependent on the expression of "eat-me" signals that trigger the engulfing activity of phagocytes, a process called efferocytosis, which may also fail during RA (10). Therefore, considering the diverse roles of neutrophils uncovered in the development of RA, it comes as no surprise that they have become crucial focal points for potential novel disease-modifying treatments.

The prevailing symptom of RA is pain, as confirmed by noteworthy data showing that 97% of individuals with early RA experience pain, and this serves as the primary cause for their initial consultation with healthcare practitioners (11). The onset of pain precedes the visible signs of RA (12, 13), leading to psychological affliction and disturbances in sleep patterns (14). Furthermore, pain emerges as a pivotal factor that influences crucial aspects of daily life. Even when the pain intensity is mild, it can significantly impede regular activities (15). The joint's synovium and capsule primarily house the peripheral afferent fibers stemming from the dorsal root ganglion (DRG). Within these regions, a considerable population of primary Aα and Aβ sensory neurons are engaged in mechanosensation, while Aδ and C fibers are responsible for nociception (16). Additionally, sensory periphery nerves are also distributed throughout the joint capsule, lateral area of the meniscus, subchondral bone, ligaments, tendon sheaths, and muscles. All these areas also contribute significantly to the emergence of arthritic pain by exposing their innervating nerves to sensitizing factors secondary to the arthritic progressive tissue

erosion (17). Notably, synovitis within the joint stands as a key pathophysiological mechanism of RA pain generation, directly engaging and sensitizing the afferent nerves of the periphery through a range of soluble mediators, including bradykinin, prostaglandins, cytokines, and the main excitatory neurotransmitter glutamate (18, 19).

Indeed, glutamatergic signaling in the joints has emerged as a major factor in the pathophysiology of arthritic pain. Numerous studies have consistently reported a significant increase in glutamate concentration in the synovial fluid of humans with RA (20, 21) and in animal models of this disease (22). In one study, a single intra-articular injection of a glutamate receptor antagonist successfully inhibited allodynia, a type of pain that arises from a typically non-painful stimulus, in rats with complete Freund's adjuvant-induced arthritis (23). The accumulation of glutamate in the arthritic joint is believed to originate from the peripheral dorsal root ganglion (DRG) nerve terminals due to a marked increase in the production of glutaminase, the primary glutamate synthetic enzyme in neurons (24). This excess glutamate is subsequently released into the extracellular space, leading to an autocrine or paracrine sensitization process. Additional evidence supporting this conclusion comes from studies showing that inhibiting glutaminase peripherally has potent analgesic effects in rats with carrageenan-induced paw inflammation (25).

In parallel to this peripheral sensitization, the mechanisms that regulate pain in the central nervous system are also critically dependent on the sensitization of neurons present in the dorsal horn of the spinal cord, which receive input from the DRG Aδ and C fibers. This central sensitization, caused by the hyperexcitability of spinal neurons, accompanied by a shortage or augmentation of descending inhibitory or facilitatory pathways, respectively, leads to the amplification of the receptive field and an increase in pain sensitivity (26). Distinctive phases occurring in this spinal sensitization of RA pain have been postulated. In the acute phase of the disease, this phenomenon is dictated by the enhanced release of glutamate from the DRG afferent presynaptic endings, which acts on its ionotropic (NMDA, AMPA, kainite) and metabotropic receptors present in the postsynaptic neurons of the spinal dorsal horn (27). In the long-lasting stage of RA, a marked influence of microglia and astrocyte activity on synaptic processing has been documented in diverse chronic models of this malady (28).

Based on these premises, it is reasonable to investigate how neurons respond to excitatory glutamatergic stimulation to predict the possible mediators of inflammatory pain processing. Proteomics studies have proven to be a valuable tool in identifying important cellular markers and pathways of neuronal responses and translatability at a mechanistic level (29). Among those extensively studied cellular models is the human SH-SY5Y neuronal cell line, known for its predictability in assessing neuronal glutamate receptors excitability (30) and responses to inflammatory stimuli such as lipopolysaccharide (31) or cytokines (32). Utilizing this model provides an appropriate experimental framework to detect distinct changes in proteomic profiles under glutamatergic stimulation, potentially leading to new mechanistic hypotheses.

The primary objective of RA therapy is to attain disease remission by easing its symptoms and enhancing the overall quality of life. RA treatment currently involves five main drug classes: pain relievers, non-steroidal anti-inflammatory drugs, glucocorticoids, biologic disease-modifying antirheumatic drugs (bDMARDs), and non-biologic or synthetic DMARDs (33). Despite their usefulness, these treatment approaches often come with undesirable side effects, and approximately 20-40% of patients with RA do not exhibit a positive clinical response to these therapies (34). As a result, there is a pressing need for innovative treatment alternatives to achieve this unmet need in RA treatments.

C-Phycocyanin (C-PC) is the main protein composing the phycobilisomes of *Spirulina platensis* microalgae. This phycobiliprotein is constituted by the α and β subunits, polypeptides with molecular weights of 17.6 and 18 kDa, respectively, which contain as a prosthetic group, a tetrapyrrolic ring structure named Phycocyanobilin (PCB) that is linked by thioether bonds to cysteines 84 (α chain), 82 and 153 (β chain) (35). This compound functions as the chromophore of the protein complex for energy transduction in the cyanobacteria´s phycobilisomes, and it is associated with the antioxidant (36) and immunomodulatory (37) activities of C-PC. The beneficial properties of *Spirulina platensis* extracts, the natural source of C-PC/PCB, have been studied in several animal models of arthritis (38). By exerting a combination of antioxidant, antiangiogenic, and anti-inflammatory actions, the raw preparations of *Spirulina platensis* have shown promising evidence for alleviating arthritic injuries (39–41). However, to the best of our knowledge, there is no previous report describing the antinociceptive and inflammopharmacological activities of PCB in the context of inflammatory arthritis.

Considering their properties, here we provide evidence that PCB, either administered in pure form or released *in vivo* from its prodrug, the biliprotein C-PC, has protective actions in an experimental setting that mimics several hallmarks of the human disease RA in mice, with emphasis on arthritis-associated nociception and inflammation. This hypothesis was demonstrated through observations that highlight this therapy's potential to effectively cope with functional, immunological, and pathological arthritic injuries. Furthermore, we aimed to assess the effects of PCB on glutamate-induced proteome changes in SH-SY5Y neurons, seeking novel mechanistic insights that may explain the counteractive actions of this molecule against arthritis nociception.

2 Materials and methods

2.1 Reagents

Sigma-Aldrich (St. Louis, USA) was the commercial supplier of the reagents for most experiments, except in those accordingly indicated. The raw material of *Spirulina platensis* was a kind gift from Genix (Labiofam, Havana, Cuba). The extraction of C-PC from this biomass followed the procedures already standardized and published by our group, which are confirmed by an aqueous two-phase separation

system (42). The final C-PC purity solution was higher than 4 (analytical grade) and this stock was kept refrigerated at 4°C during the duration of the experiments. The working dilutions of C-PC were prepared with sterile phosphate buffer saline (PBS) pH 7.4 immediately before its administration to mice. PCB was commercially obtained in powder (Cat. No. SC-396921, Santa Cruz Biotechnology, Inc., Dallas, USA), diluted with sterile PBS pH 7.4 at 5 mg/mL, and stocked in frozen aliquots (-20°C). Immediately before the administration, the PCB solutions (light-protected) were diluted from the stock according to the scheduled dose.

2.2 Laboratory mice

Male C57BL/6 mice (6-8 weeks old) provided by the Federal University of Minas Gerais (UFMG) (43), Belo Horizonte, Brazil, were maintained in the animal rooms of the Immunopharmacology Laboratory, Department of Biochemistry and Immunology at UFMG. Animals received standard food and filtered water *ad libitum* with temperature and humidity-controlled conditions. All procedures involving animal care and handling were approved by the UFMG ethics committee (CEUA UFMG:165/2009).

2.3 Antigen-induced arthritis in mice and treatment schedules

AIA was induced following a previously described procedure (43). Briefly, mice were intraperitoneally anesthetized with a mixture of 100 mg/kg of ketamine and 10 mg/kg of xylazine (44) and then immunized by an intradermal shot at the tail base of an emulsion containing 500 µg of methylated bovine serum albumin (mBSA; Sigma) and 100 µL of saline plus Freund's complete adjuvant (CFA; Sigma) at 1:1 ratio (v:v). After two weeks, the challenge with 10 µg of mBSA (in 10 µL sterile saline) was performed by injecting it intra-articularly in the right knee joint of anesthetized mice. At the appropriate time points, euthanasia of the mice was carried out as permitted according to Annex IV of Directive 2010/63/EU, with an anesthetic overdose (180 mg/kg of ketamine and 24 mg/kg of xylazine, intraperitoneally).

Three separate experiments and different outcome assessments were performed. In the first experiment, five groups of mice (n=5-6 each one) were separated at random and divided into groups composed of the control mice receiving an injection of 10 µL sterile saline in the same joint and mice with AIA treated intraperitoneally either with vehicle (PBS pH 7.4) or with C-PC at 2, 4, or 8 mg/kg one hour before the antigen challenge. In the second experiment, the same treatment schedule and route of administration were used, and the mice were allocated at random into four groups (n=6 each one) made up of, in addition to the control, the diseased animals treated with increasing doses of PCB (0.1 or 1 mg/kg), or with PBS pH 7.4 (defined as the vehicle). In the first two experiments, the hypernociception (a pain index measured in the affected right paw), the myeloperoxidase (MPO) activity, and the neutrophil infiltration in the affected knee cavity were determined following previously described procedures (45).

Finally, the third experiment used a similar design to the second. It included the control, the AIA + vehicle, and the AIA + PCB 1 mg/kg groups (n=4-6 each one) but the experiment aimed to perform a histopathological evaluation of the diseased knee.

2.4 Evaluation of hypernociception

An electronic pressure device equipped with a polypropylene tip (4.15 mm^2) transducer was utilized (Insight Instruments, Ribeirão Preto, Sao Paulo, Brazil). Prior to the study, mice were subjected to a 30-min room adaptation when housed in acrylic cages (12 x 10 x 17 cm high) with a wired floor. Mechanical stimulation was realized while the mice were completely calm, by applying a force with the transducer tip to the central field of the affected paw. Consequently, the bending of the femorotibial joint was produced, accompanied by the retraction of the stimulated paw. The device registered the force intensity when the paw retreat was completed, and the results were expressed as the change in withdrawal threshold (in grams) (46).

2.5 Determination of MPO activity and CXCL1 levels

The assessment of the MPO activity and the CXCL1 protein levels was performed in the periarticular tissue homogenate coming from the right knee joint and processed by Ultra-Turrax (Ika, Minas Gerais, Brazil). The MPO activity was evaluated as described (47), by the enzymatic reaction of 25 µL of sample in the presence of 25 µL of 3,3'-5,5'-tetramethylbenzidine (TMB) at 1.6 mM as the color reagent, followed by the spectrophotometric measurement of the reaction product at 450 nm. The absorbance values were interpolated in a standard curve made with a simultaneous assay on 5% casein peritoneal-induced neutrophils, and results were expressed as relative arbitrary units.

CXCL1 was measured by an ELISA kit as indicated by the supplier instructions manual (Duo-Set kits, R&D Systems, Minneapolis, MN, USA).

2.6 Intra-articular neutrophil quantification

The cavity of the right knee was cleansed with sterile PBS (two times with 5 µL), added to 90 µL sterile PBS, and stored on ice. The total quantity of leukocytes was immediately counted with a Neubauer chamber when the samples (10 µL) were stained with Turk's solution. The remaining samples were mounted on slides through a cytospin instrument (Shandon III; Thermo Shandon, Frankfurt, Germany). Differential leukocyte assessment in these slides was performed with a May-Grünwald-Giemsa staining following standard morphologic parameters (48).

2.7 Real-time PCR

Total RNA was extracted from popliteal lymph nodes (LNs) with TRIzol reagent (Invitrogen, Rockville, MD) (49). All qPCR assays were done in triplicate with gene-specific primers (Supplementary Table S1), which were used at 300 nM (OriGene Technologies, USA). The reaction products were detected with Fast SYBR Green PCR Master Mix in the Applied Biosystems 7900HT Fast Real-Time PCR System (Applied Biosystems, Foster City, CA, USA). Bi-distilled water was used as a negative control for all assays, either for the target or for the housekeeping genes. The results were calculated following the 2-ΔΔCt method (50).

2.8 Cytometric Bead Array

After careful dissection of the periarticular tissues, these were homogenized with Ultra-Turrax (Ika, Minas Gerais, Brazil) in the presence of a protease-inhibitor mix in PBS pH 7.4. Supernatants were obtained by centrifugation at 13,000g for 10 min at 4 °C and frozen-stored (-70 °C) until needed for the CBA assay. Four cytokines were evaluated (TNF-α, IFN-γ, IL-17A, and IL-4) following the kit's protocol (BD™ CBA Mouse Inflammation Kit, BD Biosciences, San Diego, CA), and quantified on a FACS Calibur flow cytometer (Becton Dickinson, San Jose, CA).

2.9 Histopathological analysis

The right knee joints were collected for histological evaluation. After the fixation step in 10% buffered formalin (pH 7.4), a 30-day decalcification phase was done by incubating the samples in 14% EDTA pH 7.2 at 20-25 °C prior to paraffin embedding, cutting in sections, and staining with 5 µM hematoxylin/eosin. A pathology specialist blindly analyzed two sections/knee joints with a light microscope and assigned a score to each of the following parameters: hyperplasia of the synovium, immune cell infiltration, and bone erosion. The arthritis index was calculated by summing the score of each of these parameters, ranging from 0 to 8, with a higher index indicating an increased injury (51). Representative images for each experimental group were taken with a microscope-coupled digital camera and processed with Image J software (National Institutes of Health, Bethesda, MD).

2.10 Isotopic labeling

The radioactive labeling was accomplished with ^{125}I using the Iodogen method (52). Briefly, an Iodogen coated 0.5 mL microtube (Eppendorf, USA) was placed in 1 M phosphate buffer (pH 7.0), using 37 MBq [^{125}I]-NaI (Isotop, Hungary) in 1 M NaOH and gently stirred for 5 min. Afterward, the labeling was done through the addition of 100 µg of C-PC dissolved in 100 µL of purified water. Then, the radiolabel was continued for an additional time of 20 min. The labeled C-PC was separated from the reaction medium in a Sephadex G25 column (GE Healthcare, USA) previously equilibrated in 1 M phosphate buffer (pH 7.0). Finally, the blue fractions with radiochemical purities of at least 90% were pooled and stored at 4°C until use. Blood samples (70 µL) were collected from the retro-orbital plexus by means of a heparinized capillary in anesthetized rats at 1, 15, and 30 min after the administration of 5 mg/kg C-PC. All samples were centrifuged at 10,000 rpm for 5 min. The 20µL plasma aliquot was added to 0.5 mL of 0.1% bovine serum albumin and 0.5 mL of 20% trichloroacetic acid. The insoluble material obtained by centrifugation at 10,000 rpm for 5 min (Eppendorf, Germany) was analyzed in a gamma counter (Berthold, Germany).

2.11 Biodistribution and pharmacokinetics of C-PC

Lewis rats were used to evaluate the biodistribution and pharmacokinetics of C-PC administered by four different routes: intraperitoneal (ip), intravenous (i.v.), intranasal (i.n), and oral. For the i.v. and i.n. routes, a unique dose of 1mg/kg was used. The samples were taken at 1, 4, 8, 12, and 24 h post-administration in the five rats of this subgroup. For the i.n. scheme, the samples were also collected at 1, 10, and 30 min after receiving the compound, in addition to long-time sampling at 1, 2, 4, and 24 h. In all experiments, tissue distribution was determined at 24 h by euthanasia under narcosis overdose. Percent of accumulated dose per sample was calculated with respect to 1 mL of standard dilution of administered dose measured in the same condition in a well-type scintillation counter calibrated for the energy of ^{125}I. Results are expressed as percent of uptake relative to total radioactivity dose (% D) or percent of uptake per mass of tissue (%D/g).

Pharmacokinetic analysis was carried out following the non-compartmental approach using Pkanalix (Monolix Suite 2021R2, Lixoft, France).

2.12 Cell culture and experimental groups

Human SH-SY5Y cells were maintained in culture DMEM/F12 medium supplemented with fetal bovine serum, penicillin, streptomycin, and L-glutamine. The study was divided into three groups, each one containing 4 x 10^6 SH-SY5Y cells: 1) non-treated cells (used as a control), 2) PCB plus Glutamate, and 3) Glutamate. After 24 h of pre-stimulation with 0.1 µM PCB, the medium was replaced with freshly prepared 0.01 µM PCB plus 60 µM Glutamate (group 2) or 60 µM Glutamate alone (group 3) for another day. Afterward, the medium was removed; cells were washed using cold PBS and processed to conduct proteomic expression analysis. Three biological replicates were used per group.

2.13 Differential protein expression

Proteins were extracted in 1.5% SDS/50 mM DTT with boiling for 10 minutes. Samples were filtered by FASP according to Wisniewski

(53) after the reaction of cysteines with iodoacetamide. Overnight Lysyl endopeptidase and 6 h Trypsin digestions were performed at 37 °C. Samples (1 µg) were analyzed in a Thermo Exploris 480 mass spectrometer via LC-ESI-MS/MS. A nanoLC Ultima 3000 coupled through a Pepmap column (75 µm x 150 mm) to the MS was used. Gradients of 80% acetonitrile in 0.1% formic acid were performed in 120 min at 300 nL/min flow rate. The mass spectrometer was operated in data-dependent analysis (DDA) mode with dynamic exclusion of 30 s and full-scan MS spectra (m/z 350–1650) with a resolution of 120,000 (m/z 200), followed by fragmentation of the most intense ions within 1 s cycle time with high energy collisional dissociation (HCD), normalized collision energy (NCE) of 30.0, and resolution of 15,000 (m/z 200) in MS/MS scans.

Identification of peptides and proteins was based on the match-between-runs procedure using MaxQuant software (v1.6.14.0) (54), considering oxidation (M), deamidation (NQ), and N-terminal acetylation as variable modifications. Alignment of chromatographic runs was allowed with a 20-min alignment window and a time matching of 5 min between runs. Filtering and quantification were performed in the Perseus computational platform (v1.614.0) (54). Student's t-test was employed to identify statistically significant changes (p-values lower than 0.05) in protein levels, after filtering for two valid values in each group.

2.14 Bioinformatics analysis

Differentially modulated proteins associated with inflammation, pain, arthritis, neurodegenerative diseases, and glutamatergic transmission were identified by a literature search in the Pubmed database (https://pubmed.ncbi.nlm.nih.gov/). To retrieve the information contained in Pubmed, the text mining tools Chilibot (chip literature robot) (http://www.chilibot.net/) and GeneCUP (https://genecup.org/) were used (55, 56). The data mining study was complemented with the information retrieved from the Diseases 2.0 database (https://diseases.jensenlab.org). Such a database provides confidence scores to disease-gene associations annotated using text mining and data integration tools (57). Diseases related to differentially modulated proteins were also retrieved from DisGeNET (https://www.disgenet.org/) and GAD_Disease databases by using the DAVID functional annotation tool (https://david.ncifcrf.gov/) (58, 59). Interactions among differentially modulated proteins were retrieved using the STRING database (http://string-db.org/) (60). In such analysis, all STRING interaction sources were selected and the confidence score was fixed at 0.4. The biological network of functional associations was visualized using Cytoscape software (v.3.5) (61).

2.15 Statistical analysis

The statistical analysis was carried out with the GraphPad Prism software version 9.5.1 (GraphPad Software Inc., CA, USA). All data was expressed as the mean ± standard error of the mean (S.E.M.). Data from the control and the AIA + vehicle groups obtained from different experiments were pooled for the statistical analysis of the hypernociception, the neutrophil quantification, and the MPO activity. The normality of the data was assessed, and when appropriate, it was analyzed by one-way ANOVA and Tukey's multiple comparisons test (parametric). Non-Gaussian measurements were analyzed by Kruskal-Wallis and Dunn's multiple comparisons tests (non-parametric). Differences between groups were considered statistically significant at $p<0.05$ (Supplementary Table S2).

3 Results

3.1 C-PC ameliorates AIA-induced injury

We started our study with the evaluation of C-PC in the AIA mice model, with the assumption that this biliprotein acts as a prodrug during its *in vivo* administration by releasing the pharmacologically active compound PCB into the body. The tetrapyrrole PCB is linked to the specific cysteine residues in C-PC through thioether linkages. Its unbinding could be by means of enzymatic activities as proteases in the form of short peptides or inclusive by the direct rupture of the thioether bond. Another form implies the acidic pH in the stomach, in which this chemical bond is unstable. Nevertheless, the PCB could be linked to another plasmatic protein (i.e., albumin) to facilitate its transport to target cells.

As observed in Figure 1A, the AIA mice that received the vehicle treatment presented a significantly increased nociception in comparison with the control group. The prophylactic administration of either of the three doses of C-PC (2, 4, or 8 mg/kg) was able to significantly reduce the hypernociception in AIA mice one day following the antigen challenge, in comparison with the AIA + vehicle (Figure 1A). AIA also produced a notable increase of neutrophil infiltration, as well as MPO activity in the periarticular tissue of vehicle-treated mice (Figures 1B, C). The treatment with C-PC at the three doses evaluated significantly curtailed the entrance and accumulation of neutrophils in the affected synovial cavity (Figure 1B) and the MPO activity (Figure 1C). In addition, C-PC significantly diminished the CXCL1 chemokine concentrations at all doses assessed with respect to the diseased animals that received the vehicle. (Figure 1D). It is noteworthy that a dose-response effect for the range of doses of C-PC evaluated was not observed.

3.2 Biodistribution and pharmacokinetics of C-PC

A radioactive assessment was conducted to determine the C-PC's biodistribution in various tissues. In the i.p., i.v., i.n., and oral routes, radioactivity was detected at levels representing less than 2% of the total administered dose. Conversely, as expected upon oral administration, the accumulation of C-PC was notably higher within the digestive tract, particularly in the large intestine (Figure 2). The pharmacokinetic analysis revealed that i.v. administration led to an exponential decline in plasma C-PC levels. This decay was characterized by an average clearance of 8.9 mL/h and a distribution volume at the stationary phase of 295 mL, which closely matched the body mass of the experimental subjects.

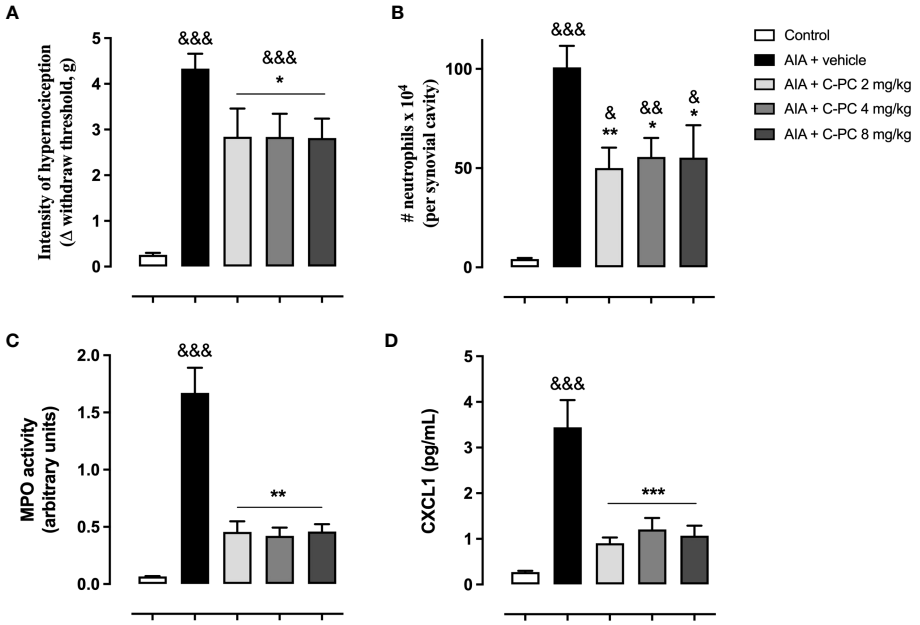

FIGURE 1
C-Phycocyanin reduces the hypernociception **(A)**, neutrophil infiltration **(B)**, MPO activity **(C)**, and CXCL1 levels **(D)** in AIA mice. Data are mean ± SEM of 5-11 mice/group. *p<0.05, **p<0.01, ***p<0.001, compared with vehicle-treated arthritic mice; $^{\&}$p<0.05, $^{\&\&}$p<0.01, $^{\&\&\&}$p <0.001, compared with control (ANOVA + Tukey's tests).

Elimination was nearly complete 24 h after i.v. administration, as indicated by an area under the curve of 22.7 h ⋆ μg/mL. Oral and i.n. administrations demonstrated similar trends in the plasmatic C-PC levels, with the maximum concentration reached at 1 and 4 h, respectively. However, the maximum concentration was much higher in the case of i.n. administration, reaching the value of 12.0 μg/mL, compared to the value of 6.8 μg/mL achieved by the oral route at these time points. Indeed, when comparing the areas under the curve, a clear increase was evident for the i.n. route with 226 h ⋆ μg/mL, whereas for the oral route, it was 77 h ⋆ μg/mL (Supplementary Figure S1).

3.3 Dose-response effects of PCB against hypernociception and neutrophil infiltration in mice with AIA

The prophylactic PCB treatment was effective in ameliorating the arthritis-induced hypernociception in mice following one day of antigen challenge, with respect to the AIA animals receiving the vehicle (Figure 3A). The quantification of the leucocyte infiltration into the inflamed knee revealed that the pretreatment with PCB significantly lessened the neutrophil agglomeration in the synovial space, showing a response associated with the used doses, when

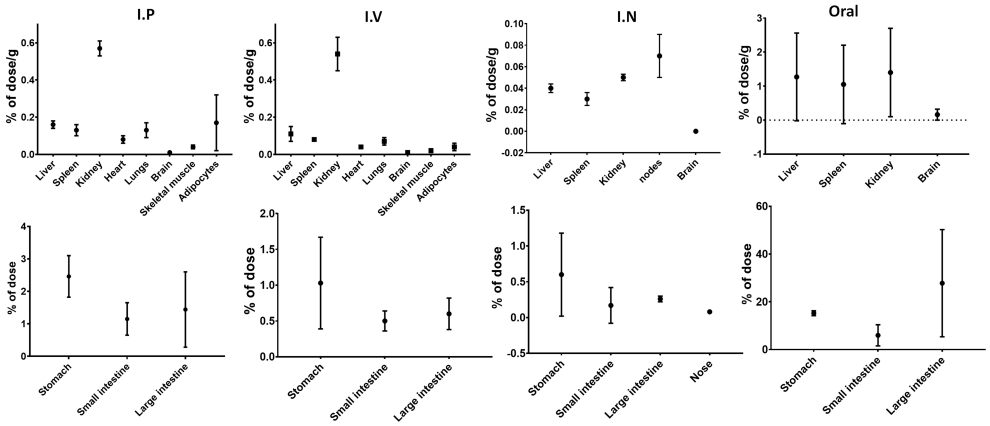

FIGURE 2
Distribution of C-PC after intraperitoneal (n=4), intravenous, nasal (n=2), and oral (n=2) administration in Lewis rats. Values expressed as %D/g of tissue or %D relative to total dose and standard deviation.

10.3389/fimmu.2023.1227268

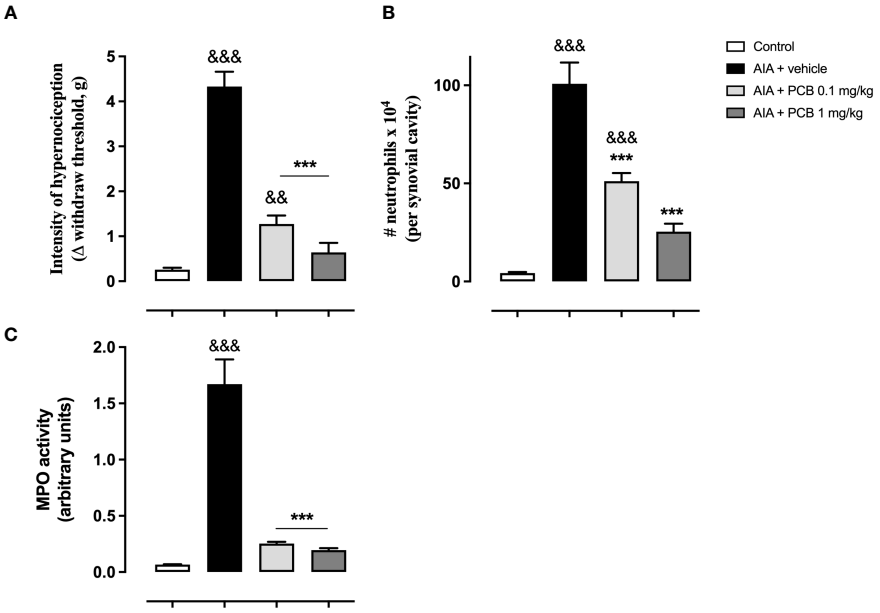

FIGURE 3
Phycocyanobilin ameliorates the hypernociception **(A)**, the neutrophil accumulation **(B)**, and the MPO activity **(C)** in mice with acute AIA. Data are mean ± SEM of 5-11 mice/group. ***p<0.001, compared with vehicle-treated arthritic mice; $^{\&\&}$p<0.01, $^{\&\&\&}$p <0.001, compared with control (ANOVA + Tukey's tests).

statistically contrasting with the vehicle AIA mice (Figure 3B). Similarly, PCB produced a decline in the MPO activity in relation to the AIA mice that were injected with vehicle solution. (Figure 3C). Importantly, this effect of PCB followed a dose-response behavior.

3.4 PCB effects on cytokine production and T cell markers expression in mice with AIA

On the other hand, a significant downregulation of PCB at 1 mg/kg on the transcriptional factors T-bet (Th1), RORγ (Th17), and the proinflammatory cytokine IFNγ was observed compared with the AIA + vehicle group, as determined by qPCR analysis of popliteal lymph nodes (Figure 4A). Likewise, PCB treatment dose-dependently restricted the expression of cytokines mediating a proinflammatory Th1 phenotype in periarticular tissue homogenate as assessed by CBA: IFN-γ with a significant difference and a clear trend towards a reduction for TNF-α when the AIA + PCB 1 mg/kg was compared with the AIA + vehicle (Figure 4B). Furthermore, a significant drop was also achieved with the treatment of 1 mg/kg PCB, the uppermost dose used, for the cytokine IL-17A (Figure 4B). Interestingly, treatment with both PCB amounts tested (0.1 and 1 mg/kg) produced a significant reduction of the cytokine IL-4, characteristic

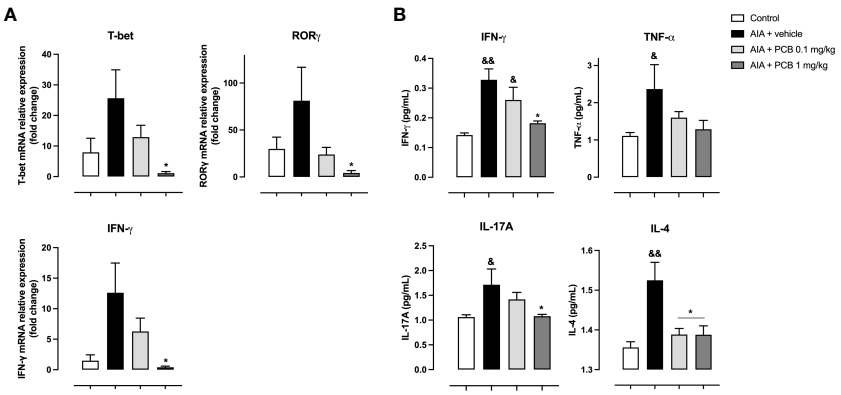

FIGURE 4
Effect of Phycocyanobilin on **(A)** mRNA levels by qPCR in popliteal lymph nodes, and **(B)** protein levels by Cytometric Bead Array (CBA) in the supernatant from periarticular tissues homogenates. Data are mean ± SEM of 5-6 mice/group. *p<0.05, compared with vehicle-treated arthritic mice; $^{\&}$p<0.05, $^{\&\&}$p<0.01, compared with control. ANOVA + Tukey tests for IFN-γ (mRNA and protein), T-bet, RORγ, and IL-4; Kruskal-Wallis + Dunn tests for TNF-α and IL-17A.

of a Th2 response, in AIA mice compared with diseased animals receiving the vehicle (Figure 4B).

3.5 PCB reduces the tissue damage in the lesioned joint of mice with AIA

Based on this encouraging evidence, we then decided to perform a histological assessment of the affected knees to confirm the protective activity of PCB on the tissue structure. The healthy control is shown in panel 5A (Figure 5A). On the contrary, those animals affected by the disease and receiving the vehicle treatment showed a rise of the arthritis index, with a distinctive synovial accumulation of polymorphonuclear cells (Figure 5B). This feature was counteracted by 1 mg/kg PCB, which dramatically reduced the leucocyte exudate in the joint space (Figure 5C) Accordingly, the arthritis index showed a significant reduction in diseased animals treated with PCB at 1 mg/kg compared with AIA + vehicle group (Figure 5D).

3.6 PCB regulates the proteome profile in glutamate-exposed SH-SY5Y neuronal cells

To identify the array of proteins under the regulation of PCB, we conducted quantitative proteomic analysis on SH-SY5Y neuronal cells. These cells were exposed to the excitatory neurotransmitter glutamate and subsequently treated with or without PCB over a 24-hour period. Out of a total of 4,511 identified proteins, 19 proteins displayed differential modulation in cells treated with PCB (Table 1, Figure 6, and Supplementary Table S3). An additional comparative study was performed to quantify the proteins modulated by either the PCB treatment or the glutamate injury independently by using non-treated SH-SY5Y cells as the control condition (Supplementary Table S4 and Supplementary Figure S2).

For a better understanding of putative cellular processes affected by PCB, the 19 differentially modulated proteins were classified using the information from disease databases and text mining tools (Supplementary Table S4). As shown in Figure 7, besides proteins related to neurodegenerative diseases, PCB treatment downregulates proteins involved in arthritis and pain. Furthermore, proteins that play a role in glutamatergic transmission and inflammation were also modulated in response to PCB treatment.

4 Discussion

The first-ever published observations regarding the beneficial actions of *Spirulina* extracts against arthritis were published in 2002

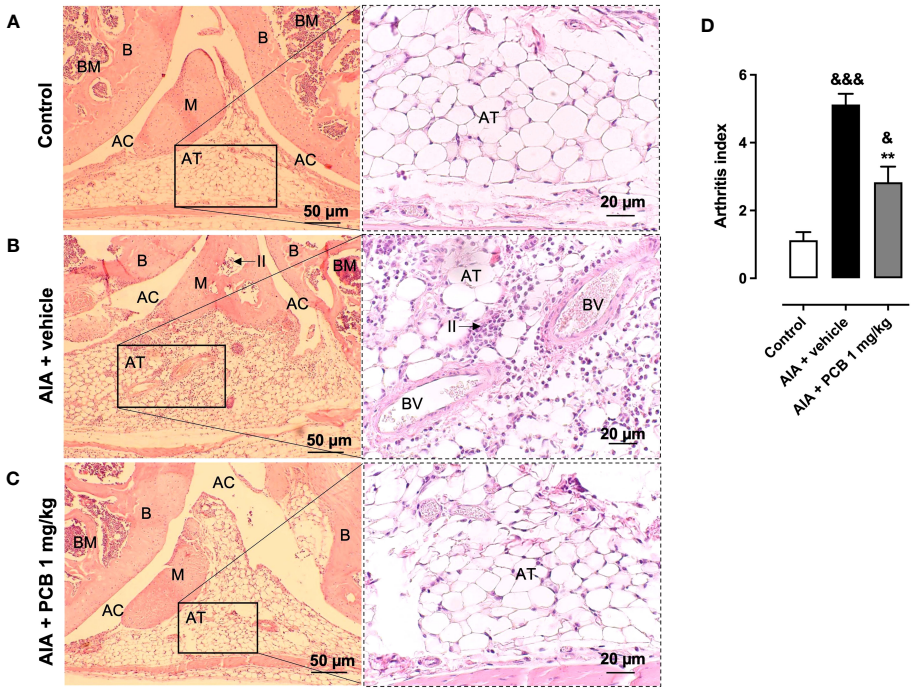

FIGURE 5
Histological assessment of PCB on the knee joint in AIA mice. Photographs are representative of **(A)** Control, **(B)** AIA + vehicle, and **(C)** AIA + 1 mg/kg PCB. **(D)** Quantitative evaluation of PCB effects on the arthritic index. The right panels are magnified 2.5 times the respective region in the left panel for **(A-C)**. Histopathological confirmation of the AIA-caused joint inflammation is evident on panels **(B)**, such as the occurrence of inflammatory infiltrate (II), indicated by arrows, in the adipose tissue (AT) and inside the meniscus (M). It is also observed in panels **(B)** an increase in blood vessels (BV) with their red blood cells inside the AT and the modification of tissue morphology when examining in relation to the other panels **(A, C)**. AT, Adipose Tissue; AC, Articular Cavity; B, Bone; BM, Bone Marrow; M, meniscus; and II, Inflammatory Infiltrate. Data are mean ± SEM of 4-6 mice/group. **p<0.01, compared with vehicle-treated arthritic mice; $^{\&}$p<0.05, $^{\&\&\&}$p <0.001, compared with control (ANOVA + Tukey's tests).

10.3389/fimmu.2023.1227268

TABLE 1 Differentially modulated proteins SH-SY5Y cells treated with PCB.

UniProt _ACC [a]	Description	Gene Symbol [b]	FC [c]	*p*-value [c]
PCB up-regulated proteins				
Q9C0D9	Ethanolaminephosphotransferase 1	EPT1	1.35	1.96
Q9NVG8	TBC1 domain family member 13	TBC1D13	1.27	1.49
Q9H9C1	Spermatogenesis-defective protein 39 homolog	VIPAS39	0.98	1.55
Q15528	Mediator of RNA polymerase II transcription subunit 22	MED22	0.83	3.77
Q8NBM4	Ubiquitin-associated domain-containing protein 2	UBAC2	0.69	1.36
Q9H9A5	CCR4-NOT transcription complex subunit 10	CNOT10	0.69	1.43
Q9NVR5	Protein kintoun	DNAAF2	0.65	1.61
Q9H900	Protein zwilch homolog	ZWILCH	0.64	2.08
Q9BUN8	Derlin-1	DERL1	0.60	1.42
Q9H490	Phosphatidylinositol glycan anchor biosynthesis class U protein	PIGU	0.60	1.76
PCB down-regulated proteins				
Q8N806	Putative E3 ubiquitin-protein ligase UBR7	UBR7	-0.59	1.54
Q9Y5X1	Sorting nexin;Sorting nexin-9	SNX9	-0.60	2.06
Q9H0V9	VIP36-like protein	LMAN2L	-0.64	1.39
Q92575	UBX domain-containing protein 4	UBXN4	-0.64	1.41
H0YLW0	Signal recognition particle 14	SRP14	-0.69	1.64
O75044	SLIT-ROBO Rho GTPase-activating protein 2	SRGAP2	-0.69	1.40
O43318	Mitogen-activated protein kinase kinase kinase 7	MAP3K7	-0.78	1.99
Q16637	Survival motor neuron protein	SMN1	-1.34	1.81
Q96FJ2	Dynein light chain 2, cytoplasmic	DYNLL2	-1.37	2.11

[a] Accession numbers in the UniProtKB database.
[b] Recommended gene name (official gene symbol) as provided by UniProtKB.
[c] Fold change (FC) and p-values of differentially modulated proteins according to quantification performed in Perseus computational platform (v1.614.0) [(–) downregulated].

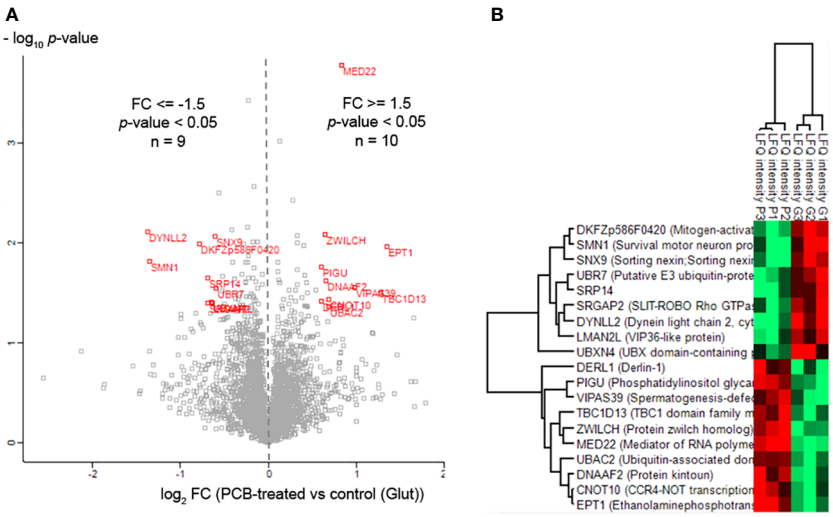

FIGURE 6
Proteomic profile modulated by PCB in SH-SY5Y cells. **(A)** Volcano plot of quantified proteins from SH-SY5Y cells after PCB treatment. Red points indicate those proteins that met the statistical significance cutoff (|FC| ≥ 1.5; *p*-value<0.05). **(B)** Hierarchical clustering of proteins differentially modulated by PCB treatment compared to cells subjected to Glutamate damage (three replicates per condition). Red and green colors mean upregulated and downregulated, respectively.

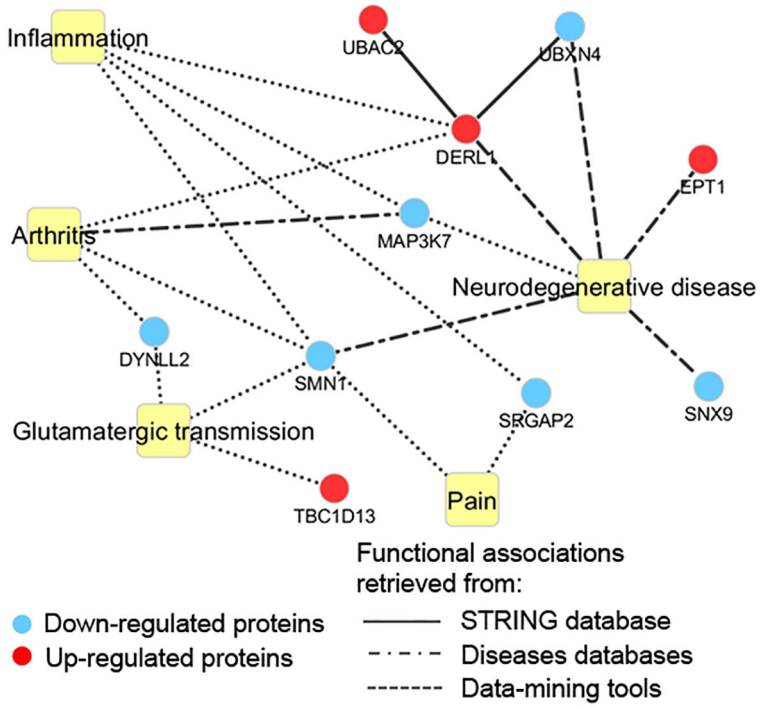

FIGURE 7
Functional terms associated with the proteomic profile modulated by PCB. Edges types are represented according to the data source.

by a Cuban group in a model of this disease in mice induced by zymosan (62). This group attributed the observed effect to C-PC, which constitutes around 15% of *Spirulina* dry biomass (63). Our group has studied the actions of C-PC in animal models of multiple sclerosis, such as the Experimental Autoimmune Encephalomyelitis, in which we have reported positive outcomes of this biliprotein, in a manner dependent on the dose, in the range of 2, 4, and 8 mg/kg, when administered intraperitoneally (64). Using the same experimental setting, we tested three PCB amounts (0.1, 0.5, and 1 mg/kg), and a dose-response positive activity was also obtained (65). Thus, previous observations have confirmed that PCB is the main responsible agent for the biological activities of C-PC (66), as demonstrated in different experimental scenarios such as ischemic stroke (66) and acute kidney damage (67). Following this reasoning, we first intended to evaluate if the administration of C-PC could alleviate AIA in mice. Then, we questioned whether the application of PCB may counteract the AIA-induced injury by assessing different outcomes: functional (hypernociception), immunological (neutrophils and cytokines), biochemical (MPO activity), gene expression, and histopathological. The doses of PCB used in the present study were calculated in function of the C-PC composition. As mentioned above, this biliprotein contains three PCBs attached. Although the lower PCB dose evaluated (0.1 mg/kg) is equivalent to 2 mg/kg C-PC, we highlight the fact that the higher PCB dose used in this study (1 mg/kg) is equivalent to a 2.5-fold increase of 8 mg/kg C-PC (higher evaluated dose). Since a dose-response effect was not observed with these C-PC administered amounts, we increased the PCB dose to better detect the dose dependence of its pharmacological activity against AIA.

Our observations confirmed a significant C-PC-promoted reduction of pain and joint inflammation in AIA mice. Reports of anti-arthritic properties of this compound have been demonstrated with other arthritis models. These anti-arthritic properties of the compound are attributed to its selective inhibitory property on COX-2, its efficacy in eliminating free radicals, and inhibiting lipid peroxidation (68). C-PC can prevent osteoarthritis by attenuating the oxidative stress in chondrocytes induced by H_2O_2 (69). Interestingly, a similar property has also been reported by our group for the PCB treatment inhibiting the H_2O_2 damage in PC12 cells (70). C-PC has been shown to act on fundamental processes such as inflammation, chondral degeneration, and oxidative stress in canine *in vitro* osteoarthritis (71). Our study evidenced that C-PC significantly reduced the alpha chemokine CXCL1 in the AIA model. CXCL1 has been shown to have neutrophil chemoattractant activity in inflamed tissue in arthritis following activation of the CXCR2 receptor (72). Notably, antagonism of this CXCR2 receptor has resulted in an inhibition of neutrophil migration strongly associated with reduced injury in rats experiencing AIA (73). In patients with RA, the rise of CXCL1 expression correlated with the accumulation of neutrophils (74). This evidence suggests that the inhibition of the CXCL1 expression could mediate the protective actions of C-PC in AIA mice, via the decreased infiltration of neutrophils to the injured joint tissue.

The biodistribution of C-PC following i.v., i.p., and i.n. administration exhibited notably low levels across all examined tissues. However, in the case of oral administration, significant levels of the radioactive-labeled product were detected along the entire digestive tract. Notwithstanding, at least 50% of the product

appears to be absorbed and redirected by blood flow. This result is consistent with the way that the molecule goes to its target sites. An important point to consider is that radiolabeling occurs mainly at the residues His and Tyr of the protein by nucleophilic aromatic substitution (75). This reaction is not possible in PCB due to the absence of aromatic carbon-hydrogens as part of its structure. However, PCB is released from C-PC after proteolysis (76), and it could reach the bloodstream and be transported throughout the body in solution given its stability (77) or attached to serum albumin (78), in a chemical association that appears to be mutually protective against oxidative damage, keeping the antioxidant activity and the chemical structure of this tetrapyrrole.

Furthermore, the pharmacokinetic results are in line with the significant chemical and biological disparities between the digestive tract and the nasal route. As mentioned above, oral administration of C-PC is followed by the degradation of its polypeptide moieties, resulting in the liberation of PCB. This tetrapyrrole has been identified as the active molecule accountable for the observed pharmacological effects of C-PC (67). Consequently, it becomes plausible that the radioactivity detected in plasma after oral administration comprises short peptides covalently linked to PCB. Supporting this observation are the clearance values of 5.6 mL/h following the i.n. administration and 21.0 mL/h for the oral route. Such elevated clearance values are indicative of compounds with lower molecular weights. Additionally, the potential shielding effect of the polypeptide moieties on the prosthetic group could explain the prolonged retention in plasma of the initially administered protein through the i.n. route. Taken together, the biodistribution and pharmacokinetics behavior of C-PC across different routes of administration contribute to understanding how this compound, and its derivative PCB, interacts with different tissues and how the body processes it. This essential data can also guide future dosing strategies and the design of drug delivery systems to ensure that the drug reaches its intended target. In this line of thinking, we can envision the application of nanotechnology for improving the controlled delivery of PCB toward targeted tissues. The nanotechnology-enabled PCB delivery systems, such as liposomes or nanoparticles, can enhance the bioavailability and stability of this tetrapyrrole, leading to prolonged therapeutic effects in RA (79).

RA is a pathology associated with impairment in the redox and immunological balances, and neutrophils are key mediators in both processes (80). In this study, we observed that both molecules, C-PC and PCB, limit the severity of AIA due to, at least in part, inhibiting the migration of neutrophils to the affected synovial cavity. In this context, neutrophils may directly damage knee structures, such as the bone and the cartilage, through the production of proteases and reactive oxygen species (ROS). Additionally, neutrophils could also dictate some inflammation processes either by antigen presentation or by the release of soluble factors, including prostaglandins, chemokines, cytokines, and leukotrienes (81). Dysregulated activation of neutrophils and their derived ROS production are implicated in tissue damage and destruction in RA (82).

The distinctive harm caused by RA to the cartilage and bone of the knee is associated with synovial exudate of immune cells and a disproportionate increase of proinflammatory factors such as TNF-α, IFN-γ, and IL-17A (83, 84). Our results demonstrated that a PCB-mediated effect was detected by qPCR on the T-bet (Th1 phenotype) and RORγ (Th17 phenotype) transcriptional factors expression, as well as IFN-γ cytokine in popliteal lymph nodes. At the protein level, PCB also reduced the concentration of the proinflammatory cytokines TNF-α, IFN-γ, and IL-17A in periarticular tissue.

IFN-γ and IL-17A are versatile cytokines widely involved in inflammatory diseases, mediating both immune activation and tolerance. In our study, a protective role of PCB in AIA mice was demonstrated, which could be associated with a reduction of both cytokines, critical components of the inflammatory damage induced by AIA (85).

These cytokines were measured in periarticular tissue homogenate, suggesting that a diverse set of immune cells, other than neutrophils, may also be locally involved in the AIA-induced acute synovial inflammation. Our observations point to an involvement of IL-17A-producing T cells, known as Th17 cells, in this pathological scenario. Accumulated evidence has shown the pivotal role of Th17 cells in diverse pathological conditions encompassing the immune system. These specialized cells have demonstrated their involvement in various autoimmune disease models (86). Notably, they have been linked to the progression of experimental autoimmune encephalomyelitis (EAE) (87), and collagen-induced arthritis (88). Furthermore, Th17 cells facilitate the recruitment of neutrophils in airways and in collagen-induced arthritis (89, 90), contributing to the perpetuation of the inflammatory milieu in arthritis. Moreover, Th17 plays a significant role in osteoclastogenesis, as it efficiently upregulates the expression of RANKL on osteoclast precursors (91, 92). This molecular modulation sets the stage for the induction of osteoclast formation and bone resorption, contributing to the pathogenesis of arthritis.

Th17 cells *in vitro* differentiation from naïve $CD4^+$ T subset is dependent on the cytokines TGF-β, IL-6, and IL-23 via induction of the transcription factor RORγ (93). We have previously demonstrated that PCB inhibits the proliferation of antigen-activated encephalitogenic $CD4^+$ T cells in rats and in 2D2 mice (56). This supports the results of the current study, in which we observed a downregulation effect of PCB on the Th17 master transcriptional factor RORγ in popliteal lymph nodes. Thus, PCB may inhibit the proliferation of naïve activated $CD4^+$ T precursor cells leading to a reduced number of differentiated Th17 in the periphery, which consequently will provoke their limited migration into the affected joint. In addition, it has been demonstrated an inductor activity of C-PC/PCB on the differentiation of regulatory T cells (Treg) (94). Treg inhibits the activity and differentiation of Th17 cells and favors the amelioration of experimental inflammatory arthritis (95, 96).

On the other hand, over the past few years, intriguing findings have advanced the insight of neutrophils from mere short-lived first responders of the innate immune system, towards active participants in adaptive immunity, particularly in chronic inflammatory disorders such as RA (97). In this newfound role, neutrophils serve as accomplices, not just bystanders of cells from the adaptive immune response such as T cells and DCs. The decisive role of neutrophils in guiding the trajectory of T-cell development,

orchestrated by DCs, towards Th17 cells, relies on potent factors present within their granule content, which include neutrophil elastase (98) and lactoferrin (99). Our data suggest that by inhibiting the neutrophil accumulation and activity in the inflamed joint, C-PC/PCB may indirectly curtail the Th17 cell development driven by the interaction between neutrophils and DCs.

Furthermore, a direct effect of PCB on the function of human monocyte-derived DCs has been reported. Pre-treatment of human DCs *in vitro* with PCB before stimulation with lipopolysaccharide led to a significant reduction in the supernatant levels of cytokines IL-12p70 and IL-23, accompanied by a reduced expression of costimulatory molecules CD83 and CD40 (100). When these lipopolysaccharide-stimulated DCs were treated with PCB and cocultured with allogeneic $CD4^+$ T cells, Basdeo et al. (2016) observed a significant decrease of more than 50% in the production of IFN-γ, which is characteristic of Th1 cell polarization, compared to the untreated control (89). This evidence suggests that PCB halts the maturation of DCs, leading to a drop in their production of polarizing cytokines, ultimately downregulating the adaptive inflammatory response. Thus, PCB may also prevent the development of synovial inflammation by directly inhibiting the professional antigen-presenting functions of DCs recruited into the affected synovium (101), along with the consequent reactivation of $CD4^+$ T cells (102).

It is noteworthy to mention our results indicating the decreasing effect of both PCB doses on the cytokine IL-4, a cytokine that is known for its anti-inflammatory properties, is produced by Th2 and Tc2 cells, but the action of IL-4 on other types of T cells, such as CD8+, Tregs, and Th9 T cells, has been also described. Furthermore, a versatile effect of IL-4 is known on B cells (103). The regulatory function of IL-4 on inflammation depending on the context of RA is known (104). Though this cytokine is frequently reported to mediate anti-inflammatory events, its proinflammatory actions have also been described as probably controlled by Th cells. This biphasic IL-4 activity could, therefore, restrain immunity when cellular components are involved, while fostering the humoral component of the immune response, in a context-specific manner (105). Interestingly, the IFN-γ/IL-4 ratio (106) could better express the Th1/Th2 balance that explains the effect of PCB on AIA.

In addition to the biological actions of PCB here observed, this organic molecule presents other advantages in relation to C-PC when considering its pharmaceutical development (1): it can be obtained either by chemical synthesis (107, 108) or by genetic engineering of its synthesizing enzymes in *E. coli* (109) (2), chemical products such as PCB avoid exhaustive bioequivalence studies because a well physicochemical characterization is enough to introduce it as therapeutic agents (3), PCB could be attached to protein drugs in combined therapies (4), PCB is more stable than C-PC under proteases attack, and (5) due to the small size of PCB (relative to C-PC), it may overpass many body compartments prohibited to large macromolecules, such as the blood-brain barrier. Because of all of the above, we decided to carry out our experiment with this tetrapyrrole to evaluate its effects as a possible treatment for RA.

In this study, we performed a proteomic profiling of glutamate-exposed SH-SY5Y neuronal cells as an *in vitro* model to evaluate the effects of PCB on one of the main excitatory signaling in nociception and neurodegeneration. The modulation of proteins related to biological processes such as inflammation, glutamatergic transmission, and pain were evaluated. Those associated with pathologies such as arthritis and neurodegenerative diseases were also considered. After the analysis, we found that only 19 proteins were differentially modulated in SH-SY5Y cells treated with both PCB and glutamate. It is worth noting that the concentration of glutamate used (60 μM) was relatively high (110, 111), which may be a limitation of the present study. However, the evidence obtained may have opened new insights regarding the PCB effects on neuronal excitatory states.

Through a protein network analysis, we identified that the proteins influenced by PCB treatment were interconnected with diseases and implicated in biological processes. One notable finding was the PCB downregulation of Mitogen-activated protein kinase 7 (MAP3K7) or a ubiquitin-dependent kinase of MKK and IKK (TAK1) (112). MAP3K7 is a serine/threonine kinase that integrates many biochemical signals. This protein is involved in numerous cellular processes such as proliferation, differentiation, transcriptional regulation, and development. As a part of the mechanism of this kinase, after activation by extracellular stimuli, it translocates to the nucleus and regulates gene expression by phosphorylating various transcription factors (113, 114). MAP3K7 has also been strongly implicated in many of the processes underlying the pathology of rheumatoid arthritis (115, 116) and neurodegenerative diseases (117) in which inflammation (118, 119) is implicated. The current findings suggest that MAP3K7 downregulation may also contribute to the PCB effects on the reduction of neuroinflammation-induced microglial dysfunction as was identified in our previous study. Furthermore, MAP3K7 plays a crucial role in pain signaling from various causes, including inflammation. Notably, the utilization of the MAP3K7 inhibitor takinib demonstrated its capacity to mitigate inflammatory, neuropathic, and primary pain, in animal models established through intraplantar administration of complete Freund's adjuvant, chronic constriction injury, and systemic introduction of catechol-O-methyltransferase, respectively (120). MAP3K7 inhibition was also able to diminish the expression of pain-associated mediators in synovial cells isolated from arthritis patients, suggesting its important role in managing peripheral sensitization in arthritis nociception (121). Therefore, by downregulating MAP3K7 expression, PCB may act on the amelioration of arthritis pain.

Neutrophils in the synovial fluid of patients with arthritis exhibit a reduced ability to suppress activated T cells, possibly related to changes in proteins involved in cell-cell contact and inflammation (122). Among the proteins involved in the interaction between neutrophils and T cells is Dynein light chain 2 (DYNLL2) (123), which regulates the dynein 1 function and subsequently the cargo and movement of vesicles and organelles through microtubules (124). This protein has also been documented to play a central role in the interaction of the NMDA receptor-associated scaffold complex and the enhancement of the synaptic

NMDA receptor activity (125). In our study, we identified a downregulation of the DYNLL2 protein in SH-SY5Y cells treated with PCB. One possible explanation could be associated with key elements in the mechanisms that underlie the protective effects of PCB, such as the reduction of oxidative stress through the inhibition of NADPH oxidase (42) and the amelioration of inflammation.

Another protein that displayed downregulation was the Survival Motor Neuron Protein 1 (SMN1), a constituent of a complex catalyzing the assembly of small nuclear ribonucleoproteins (snRNPs). The expression of this protein was associated with levels of inflammatory cytokines (IL-1β and TNF-α) in osteoarthritis (126). Thus, the limited expression of SMN1 induced by PCB may contribute to keeping the levels of these proinflammatory cytokines during arthritis under control, as a previously observed effect of PCB on these cytokines in a model of experimental autoimmune encephalomyelitis (65). On the other hand, PCB also induced a downmodulation of SLIT-ROBO Rho GTPase-activating protein 2 (SRGAP2) in SH-SY5Y cells treated with glutamate. This protein participates in neuronal morphogenesis and is also linked with neuronal migration during cerebral cortex development (127, 128). In this context, it has been reported that the elimination of endogenous expression of SRGAP2 promotes neurite growth in differentiated cells (129) and contributes to the restriction of osteoclastogenesis during arthritis-related inflammation (130).

Another modulated process was identified as mediated by Derlin-1 (DERL1), a protein that serves as a functional component of endoplasmic reticulum-associated degradation of misfolded proteins (131). Its disruption hampers neurite outgrowth and nervous system development, ultimately leading to brain atrophy (132). In our study, we observed an upregulation of the DERL1 in glutamate-exposed SH-SY5Y cells treated with PCB, which may impact functions related to the endoplasmic reticulum. One study reported that DERL1 colocalized with neurofibrillary tangles in the brain of patients with Alzheimer's disease and could play an important role in endoplasmic reticulum-associated neurodegeneration (133). Another protein that has been shown to interact with DERL1 is the mutated superoxide dismutase 1 (SOD1), which accumulates and misfolds in motor neurons in amyotrophic lateral sclerosis (134), another neurodegenerative disease, and the interaction with DERL1 is involved in the disease pathophysiology (135). Another DERL1 interacting protein is the NADPH oxidase subunit p22phox, and a previous report has shown that this interaction regulates the partner degradation of p22phox, with potential implications in the reactive oxygen species-producing capacity of this enzyme (136). This accumulated evidence suggests that PCB could potentiate the adequate functioning of endoplasmic reticulum quality control by upregulating DERL1, and thus preventing the associated cellular dysfunction (132). In this sense, it has been suggested that inhibitors of endoplasmic reticulum stress could mitigate chondrocyte damage and reduce arthritis degeneration (137).

Another interesting result of our study was the upregulation of the ethanolamine phosphotransferase 1 (EPT1) protein by PCB in SH-SY5Y cells. This enzyme transfers phosphoethanolamine from cytidine diphosphate-ethanolamine to lipid acceptors to form ethanolamine glycerophospholipids via the 'Kennedy' pathway (138). This kinase is part of the enzymes required to synthesize phosphatidylethanolamine within the myelin membrane (139). Studies in a patient with spastic paraplegia revealed hypomyelination and brain atrophy demonstrating its role in the myelination process and in maintaining normal phospholipid homeostasis (140). These studies are consistent with the reported effect of PCB on myelin in an animal model of experimental autoimmune encephalomyelitis (141).

5 Conclusion and future perspectives

In summary, the data presented in this study demonstrate that the preemptive administration of C-PC and PCB effectively mitigates mBSA-induced arthritic injuries in mice. This was achieved by limiting hypernociception and reducing neutrophil infiltration and MPO activity, all of which are closely linked to the inflammatory injury occurring in the knee during RA. Moreover, PCB exhibits the ability to modulate the local concentration of proinflammatory cytokines and the inflammatory infiltrate within the affected joint, thereby preserving the structural integrity of the tissue.

The evidence presented here regarding the biodistribution of C-PC opens an intriguing perspective when considering the future administration of its derivative PCB for RA. As follow-up research, exploring the oral route of PCB administration could potentially offer advantages such as improved patient compliance, reduced invasiveness, and enhanced systemic delivery.

The significance of glutamatergic signaling in joint-related pain in RA is well-known. In the context of this study, the integration of bioinformatics tools facilitated the *in vitro* assessment of PCB's impact on the neuronal proteome when subjected to glutamate excitation. This approach led to the identification of proteins associated with pivotal biological processes including pain, inflammation, and glutamatergic transmission, which hold substantial relevance for pathologies such as RA.

The findings from this investigation point toward a potential application of PCB as an innovative therapeutic approach for RA. Furthermore, the study provides insights into the potential mechanisms of action and therapeutic targets associated with the effects of PCB. Ultimately, these results offer promising avenues for further exploration and development of this novel treatment for RA and related conditions involving inflammatory pain.

Data availability statement

The original contributions presented in the study are included in the article/Supplementary Material. Further inquiries can be directed to the corresponding author.

Ethics statement

Ethical approval was not required for the studies on humans in accordance with the local legislation and institutional requirements because only commercially available established cell lines were used.

The animal study was approved by Federal University of Minas Gerais (UFMG) ethics committee (CEUA UFMG:165/2009). The study was conducted in accordance with the local legislation and institutional requirements.

Author contributions

JM-P: conceptualization, writing, formal analysis, investigation, and funding acquisition. AR-U: investigation (proteomic analysis) and writing. VB: investigation (proteomic analysis). AL-A: conceptualization, formal analysis and writing. NB: investigation (AIA model). IH-G: investigation (PK/BD studies). NP-F: investigation and funding acquisition. ÉMV: investigation and formal análisis (performance and analysis of flow cytometry). VF-C: investigation (microscopy analysis). EA: investigation (microscopy analysis). GM-D: investigation and project administration. MC-L: investigation (cell culture). DL: investigation (proteomic studies). LG: investigation (proteomic studies) and methodology. JF-M: investigation, formal analysis, and methodology. GG-N: methodology, project administration, and funding acquisition. EP-A: methodology and writing. FA: methodology and writing. MT: methodology, writing, and funding acquisition. GP-R: conceptualization, writing, original draft, project administration, methodology, and funding acquisition. All authors contributed to the article and approved the submitted version.

Funding

This work was partially supported by the Science without Borders Program of Brazil (Project No. 405878/2013-3).

Conflict of interest

Authors VB and DL were employed by the company Yongzhou Zhong Gu Biotechnology Co. Ltd.

The remaining authors declare that the research was conducted in the absence of any commercial or financial relationships that could be construed as a potential conflict of interest.

Publisher's note

Supplementary material

The Supplementary Material for this article can be found online at: https://www.frontiersin.org/articles/10.3389/fimmu.2023.1227268/full#supplementary-material

SUPPLEMENTARY TABLE 3
Proteomic profile regulated by PCB in SH-SY5Y cells.

SUPPLEMENTARY TABLE 4
Data sources of the functional terms associated with PCB-modulated proteins.

SUPPLEMENTARY FIGURE 1
Plasma concentration of C-PC after oral (squares), i.n. (circles) and i.v. (triangle) administrations at doses as described in the Material and Method section.

SUPPLEMENTARY FIGURE 2
(A) PCA analysis of protein cell extracts after PCB treatment versus control cells demonstrates how both groups are different; red and blue squares correspond to PCB-treated and non-treated replicates, respectively. **(B)** Volcano plot showing the proteins differentially modulated ($p<0.05$) after PCB treatment in comparison to control cells. **(C)** Hierarchical clustering of proteins differentially expressed by PCB treatment compared to control cells (three replicates per each condition). Up- and down-regulated genes are in blue and pink colors, respectively.

References

1. Minichiello E, Semerano L, Boissier M-C. Time trends in the incidence, prevalence, and severity of rheumatoid arthritis: A systematic literature review. *Joint Bone Spine* (2016) 83:625–30. doi: 10.1016/j.jbspin.2016.07.007

2. Coutant F, Miossec P. Evolving concepts of the pathogenesis of rheumatoid arthritis with focus on the early and late stages. *Curr Opin Rheumatol* (2020) 32:57–63. doi: 10.1097/BOR.0000000000000664

3. Kitsis E, Weissmann G. The role of the neutrophil in rheumatoid arthritis. *Clin Orthop Relat Res* (1991) 265:63–72.

4. Kasama T, Miwa Y, Isozaki T, Odai T, Adachi M, Kunkel S. Neutrophil-derived cytokines: potential therapeutic targets in inflammation. *Curr Drug Target -Inflammation Allergy* (2005) 4:273–9. doi: 10.2174/1568010054022114

5. Firestein GS. Immunologic mechanisms in the pathogenesis of rheumatoid arthritis. *JCR: J Clin Rheumatol* (2005) 11:S39–44. doi: 10.1097/01.rhu.0000166673.34461.33

6. Mantovani A, Cassatella MA, Costantini C, Jaillon S. Neutrophils in the activation and regulation of innate and adaptive immunity. *Nat Rev Immunol* (2011) 11:519–31. doi: 10.1038/nri3024

7. Wipke BT, Allen PM. Essential role of neutrophils in the initiation and progression of a murine model of rheumatoid arthritis. *J Immunol* (2001) 167:1601–8. doi: 10.4049/jimmunol.167.3.1601

8. Tanaka D, Kagari T, Doi H, Shimozato T. Essential role of neutrophils in anti-type II collagen antibody and lipopolysaccharide-induced arthritis. *Immunology* (2006) 119:195–202. doi: 10.1111/j.1365-2567.2006.02424.x

9. Cox JH, Starr AE, Kappelhoff R, Yan R, Roberts CR, Overall CM. Matrix metalloproteinase 8 deficiency in mice exacerbates inflammatory arthritis through delayed neutrophil apoptosis and reduced caspase 11 expression. *Arthritis Rheum* (2010) 62:3645–55. doi: 10.1002/art.27757

10. Singhal A, Kumar S. Neutrophil and remnant clearance in immunity and inflammation. *Immunology* (2022) 165:22–43. doi: 10.1111/imm.13423

11. Diederik DC, Kristien V der E, Veerle S, Donna P, Johan J, Rene W, et al. The perspective of patients with early rheumatoid arthritis on the journey from symptom onset until referral to a rheumatologist. *Rheumatol Adv Pract* (2019) 3:1–8. doi: 10.1093/rap/rkz035

12. Ebbinghaus M, Müller S, Segond von Banchet G, Eitner A, Wank I, Hess A, et al. Contribution of inflammation and bone destruction to pain in arthritis: A study in murine glucose-6-phosphate isomerase–induced arthritis. *Arthritis Rheumatol* (2019) 71:2016–26. doi: 10.1002/art.41051

13. Zheng L-X, Li K-X, Hong F-F, Yang S-L. Pain and bone damage in rheumatoid arthritis: role of leukotriene B4. *Clin Exp Rheumatol* (2019) 37:872–8.

14. Zaidel C, Musich S, Karl J, Kraemer S, Yeh CS. Psychosocial factors associated with sleep quality and duration among older adults with chronic pain. *Popul Health Manag* (2021) 24:101–9. doi: 10.1089/pop.2019.0165

15. Ahlstrand I, Björk M, Thyberg I, Falkmer T. Pain and difficulties performing valued life activities in women and men with rheumatoid arthritis. *Clin Rheumatol* (2015) 34:1353–62. doi: 10.1007/s10067-015-2874-5

16. Schaible H-G, Grubb BD. Afferent and spinal mechanisms of joint pain. *Pain* (1993) 55:5–54. doi: 10.1016/0304-3959(93)90183-P

17. Walsh DA, McWilliams DF. Pain in rheumatoid arthritis. *Curr Pain Headache Rep* (2012) 16:509–17. doi: 10.1007/s11916-012-0303-x

18. Boyden SD, Hossain IN, Wohlfahrt A, Lee YC. Non-inflammatory causes of pain in patients with rheumatoid arthritis. *Curr Rheumatol Rep* (2016) 18:30. doi: 10.1007/s11926-016-0581-0

19. Hinoi E, Yoneda Y. Possible involvement of glutamatergic signaling machineries in pathophysiology of rheumatoid arthritis. *J Pharmacol Sci* (2011) 116:248–56. doi: 10.1254/jphs.11R03CR

20. McNearney T, Speegle D, Lawand N, Lisse J, Westlund KN. Excitatory amino acid profiles of synovial fluid from patients with arthritis. *J Rheumatol* (2000) 27:739–45.

21. McNearney TA, Westlund KN. Excitatory amino acids display compartmental disparity between plasma and synovial fluid in clinical arthropathies. *Int J Clin Exp Pathol* (2013) 6:492–7.

22. Lawand NB, McNearney T, Westlund KN. Amino acid release into the knee joint: key role in nociception and inflammation. *Pain* (2000) 86:69–74. doi: 10.1016/S0304-3959(99)00311-5

23. Lam FF, Ng ES. Substance P and glutamate receptor antagonists improve the anti-arthritic actions of dexamethasone in rats. *Br J Pharmacol* (2010) 159:958–69. doi: 10.1111/j.1476-5381.2009.00586.x

24. Miller KE, Balbás JC, Benton RL, Lam TS, Edwards KM, Kriebel RM, et al. Glutaminase immunoreactivity and enzyme activity is increased in the rat dorsal root ganglion following peripheral inflammation. *Pain Res Treat* (2012) 2012:1–9. doi: 10.1155/2012/414697

25. Hoffman EM, Miller KE. Peripheral inhibition of glutaminase reduces carrageenan-induced Fos expression in the superficial dorsal horn of the rat. *Neurosci Lett* (2010) 472:157–60. doi: 10.1016/j.neulet.2010.01.066

26. Walsh DA, McWilliams DF. Mechanisms, impact and management of pain in rheumatoid arthritis. *Nat Rev Rheumatol* (2014) 10:581–92. doi: 10.1038/nrrheum.2014.64

27. Cao Y, Fan D, Yin Y. Pain mechanism in rheumatoid arthritis: from cytokines to central sensitization. *Mediators Inflammation* (2020) 2020:1–11. doi: 10.1155/2020/2076328

28. Schaible H, König C, Ebersberger A. Spinal pain processing in arthritis: Neuron and glia (inter)actions. *J Neurochem* (2023) 00:1–19. doi: 10.1111/jnc.15742

29. Schwaid AG, Krasowka-Zoladek A, Chi A, Cornella-Taracido I. Comparison of the rat and human dorsal root ganglion proteome. *Sci Rep* (2018) 8:13469. doi: 10.1038/s41598-018-31189-9

30. Qiu Q, Sun L, Wang XM, Lo AC, Wong KL, Gu P, et al. Propofol produces preventive analgesia *via* GluN2B-containing NMDA receptor/ERK1/2 signaling pathway in a rat model of inflammatory pain. *Mol Pain* (2017) 13:174480691773746. doi: 10.1177/1744806917737462

31. Zhang Q, Zhou L, Xie H, Zhang H, Gao X. HAGLR aggravates neuropathic pain and promotes inflammatory response and apoptosis of lipopolysaccharide-treated SH-SY5Y cells by sequestering miR-182–5p from ATAT1 and activating NLRP3 inflammasome. *Neurochem Int* (2021) 145:105001. doi: 10.1016/j.neuint.2021.105001

32. Imbesi C, Ettari R, Irrera N, Zappalà M, Pallio G, Bitto A, et al. Blunting neuroinflammation by targeting the immunoproteasome with novel amide derivatives. *Int J Mol Sci* (2023) 24:10732. doi: 10.3390/ijms241310732

33. George G, Shyni GL, Raghu KG. Current and novel therapeutic targets in the treatment of rheumatoid arthritis. *Inflammopharmacology* (2020) 28:1457–76. doi: 10.1007/s10787-020-00757-9

34. Prasad P, Verma S, Surbhi, Ganguly NK, Chaturvedi V, Mittal SA. Rheumatoid arthritis: advances in treatment strategies. *Mol Cell Biochem* (2023) 478:69–88. doi: 10.1007/s11010-022-04492-3

35. Cervantes-Llanos M, Lagumersindez-Denis N, Marín-Prida J, Pavón-Fuentes N, Falcon-Cama V, Piniella-Matamoros B, et al. Beneficial effects of oral administration of C-Phycocyanin and Phycocyanobilin in rodent models of experimental autoimmune encephalomyelitis. *Life Sci* (2018) 194:130–8. doi: 10.1016/j.lfs.2017.12.032

36. Patel A, Mishra S, Ghosh PK. Antioxidant potential of C-phycocyanin isolated from cyanobacterial species Lyngbya, Phormidium and Spirulina spp. *Indian J Biochem Biophys* (2006) 43:25–31.

37. Grover P, Bhatnagar A, Kumari N, Narayan Bhatt A, Kumar Nishad D, Purkayastha J. C-Phycocyanin-a novel protein from Spirulina platensis- *In vivo* toxicity, antioxidant and immunomodulatory studies. *Saudi J Biol Sci* (2021) 28:1853–9. doi: 10.1016/j.sjbs.2020.12.037

38. Wu Q, Liu L, Miron A, Klímová B, Wan D, Kuča K. The antioxidant, immunomodulatory, and anti-inflammatory activities of Spirulina: an overview. *Arch Toxicol* (2016) 90:1817–40. doi: 10.1007/s00204-016-1744-5

39. Kumar N, Singh S, Patro N, Patro I. Evaluation of protective efficacy of Spirulina platensis against collagen-induced arthritis in rats. *Inflammopharmacology* (2009) 17:181–90. doi: 10.1007/s10787-009-0004-1

40. Ali EAI, Barakat BM, Hassan R. Antioxidant and angiostatic effect of spirulina platensis suspension in complete freund's adjuvant-induced arthritis in rats. *PloS One* (2015) 10:e0121523. doi: 10.1371/journal.pone.0121523

41. Gutiérrez-Rebolledo GA, Galar-Martínez M, García-Rodríguez RV, Chamorro-Cevallos GA, Hernández-Reyes AG, Martínez-Galero E. Antioxidant effect of *spirulina (Arthrospira) maxima* on chronic inflammation induced by freund's complete adjuvant in rats. *J Med Food* (2015) 18:865–71. doi: 10.1089/jmf.2014.0117

42. Marín-Prida J, Liberato JL, Llópiz-Arzuaga A, Stringhetta-Padovani K, Pavón-Fuentes N, Leopoldino AM, et al. Novel Insights into the Molecular Mechanisms Involved in the Neuroprotective Effects of C-Phycocyanin against Brain Ischemia in Rats. *Curr Pharm Des* (2022) 28:1187–97. doi: 10.2174/1381612828666220506145542

43. Felix FB, Vago JP, Fernandes D de O, Martins DG, Moreira IZ, Gonçalves WA, et al. Biochanin A regulates key steps of inflammation resolution in a model of antigen-induced arthritis *via* GPR30/PKA-dependent mechanism. *Front Pharmacol* (2021) 12:662308. doi: 10.3389/fphar.2021.662308

44. Flecknell P. *Laboratory animal anaesthesia. 4th ed*. Boston: Elsevier (2016). doi: 10.1016/C2013-0-13494-0

45. Coelho FM, Pinho V, Amaral FA, Sachs D, Costa VV, Rodrigues DH, et al. The chemokine receptors CXCR1/CXCR2 modulate antigen-induced arthritis by regulating adhesion of neutrophils to the synovial microvasculature. *Arthritis Rheum* (2008) 58:2329–37. doi: 10.1002/art.23622

46. Sachs D, Coelho FM, Costa VV, Lopes F, Pinho V, Amaral FA, et al. Cooperative role of tumour necrosis factor-α, interleukin-1β and neutrophils in a novel behavioural model that concomitantly demonstrates articular inflammation and hypernociception in mice. *Br J Pharmacol* (2011) 162:72–83. doi: 10.1111/j.1476-5381.2010.00895.x

47. Barcelos LS, Talvani A, Teixeira AS, Vieira LQ, Cassali GD, Andrade SP, et al. Impaired inflammatory angiogenesis, but not leukocyte influx, in mice lacking TNFR1. *J Leukoc Biol* (2005) 78:352–8. doi: 10.1189/jlb.1104682

48. da Silveira KD, Coelho FM, Vieira AT, Sachs D, Barroso LC, Costa VV, et al. Anti-inflammatory effects of the activation of the angiotensin-(1–7) receptor, mas, in experimental models of arthritis. *J Immunol* (2010) 185:5569–76. doi: 10.4049/jimmunol.1000314

49. Garlet GP, Cardoso CRB, Campanelli AP, Ferreira BR, Avila-Campos MJ, Cunha FQ, et al. The dual role of p55 tumour necrosis factor-α receptor in *Actinobacillus actinomycetemcomitans* -induced experimental periodontitis: host protection and tissue destruction. *Clin Exp Immunol* (2006) 147:128–38. doi: 10.1111/j.1365-2249.2006.03260.x

50. Livak KJ, Schmittgen TD. Analysis of relative gene expression data using real-time quantitative PCR and the 2−ΔΔCT method. *Methods* (2001) 25:402–8. doi: 10.1006/meth.2001.1262

51. Williams AS, Richards PJ, Thomas E, Carty S, Nowell MA, Goodfellow RM, et al. Interferon-γ protects against the development of structural damage in experimental arthritis by regulating polymorphonuclear neutrophil influx into diseased joints. *Arthritis Rheum* (2007) 56:2244–54. doi: 10.1002/art.22732

52. Fraker PJ, Speck JC. Protein and cell membrane iodinations with a sparingly soluble chloroamide, 1,3,4,6-tetrachloro-3a,6a-diphenylglycoluril. *Biochem Biophys Res Commun* (1978) 80:849–57. doi: 10.1016/0006-291X(78)91322-0

53. Wiśniewski JR, Mann M. Consecutive proteolytic digestion in an enzyme reactor increases depth of proteomic and phosphoproteomic analysis. *Anal Chem* (2012) 84:2631–7. doi: 10.1021/ac300006b

54. Cox J, Hein MY, Luber CA, Paron I, Nagaraj N, Mann M. Accurate proteome-wide label-free quantification by delayed normalization and maximal peptide ratio extraction, termed maxLFQ. *Mol Cell Proteomics* (2014) 13:2513–26. doi: 10.1074/mcp.M113.031591

55. Chen H, Sharp BM. Content-rich biological network constructed by mining PubMed abstracts. *BMC Bioinf* (2004) 5:147. doi: 10.1186/1471-2105-5-147

56. Gunturkun MH, Flashner E, Wang T, Mulligan MK, Williams RW, Prins P, et al. GeneCup: mining PubMed and GWAS catalog for gene–keyword relationships. *G3 Genes|Genomes|Genetics* (2022) 12:1–9. doi: 10.1093/g3journal/jkac059

57. Grissa D, Junge A, Oprea TI, Jensen LJ. Diseases 2.0: a weekly updated database of disease–gene associations from text mining and data integration. *Database* (2022) 2022:1–8. doi: 10.1093/database/baac019

58. Huang DW, Sherman BT, Lempicki RA. Systematic and integrative analysis of large gene lists using DAVID bioinformatics resources. *Nat Protoc* (2009) 4:44–57. doi: 10.1038/nprot.2008.211

59. Sherman BT, Hao M, Qiu J, Jiao X, Baseler MW, Lane HC, et al. DAVID: a web server for functional enrichment analysis and functional annotation of gene lists (2021 update). *Nucleic Acids Res* (2022) 50:W216–21. doi: 10.1093/nar/gkac194

60. Szklarczyk D, Kirsch R, Koutrouli M, Nastou K, Mehryary F, Hachilif R, et al. The STRING database in 2023: protein–protein association networks and functional

enrichment analyses for any sequenced genome of interest. *Nucleic Acids Res* (2023) 51: D638–46. doi: 10.1093/nar/gkac1000

61. Shannon P, Markiel A, Ozier O, Baliga NS, Wang JT, Ramage D, et al. Cytoscape: A software environment for integrated models of biomolecular interaction networks. *Genome Res* (2003) 13:2498–504. doi: 10.1101/gr.1239303

62. Remirez D, González R, Merino N, Rodriguez S, Ancheta O. Inhibitory effects of Spirulina in zymosan-induced arthritis in mice. *Mediators Inflammation* (2002) 11:75–9. doi: 10.1080/09629350220131917

63. Padyana AK, Bhat VB, Madyastha KM, Rajashankar KR, Ramakumar S. Crystal structure of a light-harvesting protein C-phycocyanin from Spirulina platensis. *Biochem Biophys Res Commun* (2001) 282:893–8. doi: 10.1006/bbrc.2001.4663

64. Pentón-Rol G, Lagumersindez-Denis N, Muzio L, Bergami A, Furlan R, Fernández-Massó JR, et al. Comparative neuroregenerative effects of C-phycocyanin and IFN-beta in a model of multiple sclerosis in mice. *J Neuroimmune Pharmacol* (2016) 11:153–67. doi: 10.1007/s11481-015-9642-9

65. Marín-Prida J, Pavón-Fuentes N, Lagumersindez-Denis N, Camacho-Rodríguez H, García-Soca AM, Sarduy-Chávez R de la C, et al. Anti-inflammatory mechanisms and pharmacological actions of phycocyanobilin in a mouse model of experimental autoimmune encephalomyelitis: A therapeutic promise for multiple sclerosis. *Front Immunol* (2022) 13:1036200. doi: 10.3389/fimmu.2022.1036200

66. Pentón-Rol G, Marín-Prida J, McCarty MF. C-phycocyanin-derived phycocyanobilin as a potential nutraceutical approach for major neurodegenerative disorders and COVID-19- induced damage to the nervous system. *Curr Neuropharmacol* (2021) 19:2250–75. doi: 10.2174/1570159X19666210408123807

67. Garcia-Pliego E, Franco-Colin M, Rojas-Franco P, Blas-Valdivia V, Serrano-Contreras JI, Pentón-Rol G, et al. Phycocyanobilin is the molecule responsible for the nephroprotective action of phycocyanin in acute kidney injury caused by mercury. *Food Funct* (2021) 12:2985–94. doi: 10.1039/D0FO03294H

68. Reddy CM, Bhat VB, Kiranmai G, Reddy MN, Reddanna P, Madyastha KM. Selective inhibition of cyclooxygenase-2 by C-phycocyanin, a biliprotein from spirulina platensis. *Biochem Biophys Res Commun* (2000) 277:599–603. doi: 10.1006/bbrc.2000.3725

69. Young I-C, Chuang S-T, Hsu C-H, Sun Y-J, Lin F-H. C-phycocyanin alleviates osteoarthritic injury in chondrocytes stimulated with H 2 O 2 and compressive stress. *Int J Biol Macromol* (2016) 93:852–9. doi: 10.1016/j.ijbiomac.2016.09.051

70. Marín-Prida J, Pavón-Fuentes N, Llópiz-Arzuaga A, Fernández-Massó JR, Delgado-Roche L, Mendoza-Marí Y, et al. Phycocyanobilin promotes PC12 cell survival and modulates immune and inflammatory genes and oxidative stress markers in acute cerebral hypoperfusion in rats. *Toxicol Appl Pharmacol* (2013) 272:49–60. doi: 10.1016/j.taap.2013.05.021

71. Martinez SE, Chen Y, Ho EA, Martinez SA, Davies NM. Pharmacological effects of a C-phycocyanin-based multicomponent nutraceutical in an in-vitro canine chondrocyte model of osteoarthritis. *Can J Vet Res* (2015) 79:241–9.

72. Sawant KV, Poluri KM, Dutta AK, Sepuru KM, Troshkina A, Garofalo RP, et al. Chemokine CXCL1 mediated neutrophil recruitment: Role of glycosaminoglycan interactions. *Sci Rep* (2016) 6:33123. doi: 10.1038/srep33123

73. Barsante MM, Cunha TM, Allegretti M, Cattani F, Policani F, Bizzarri C, et al. Blockade of the chemokine receptor CXCR2 ameliorates adjuvant-induced arthritis in rats. *Br J Pharmacol* (2008) 153:992–1002. doi: 10.1038/sj.bjp.0707462

74. Hou S-M, Chen P-C, Lin C-M, Fang M-L, Chi M-C, Liu J-F. CXCL1 contributes to IL-6 expression in osteoarthritis and rheumatoid arthritis synovial fibroblasts by CXCR2, c-Raf, MAPK, and AP-1 pathway. *Arthritis Res Ther* (2020) 22:251. doi: 10.1186/s13075-020-02331-8

75. Hermanson GT. "The reactions of bioconjugation.,". In: *Bioconjugate techniques*. Academic Press (2013). p. 229–58. doi: 10.1016/B978-0-12-382239-0.00003-0

76. Minic SL, Stanic-vucinic D, Vesic J, Krstic M, Nikolic MR, Velickovic TC. Digestion by pepsin releases biologically active chromopeptides from C-phycocyanin, a blue-colored biliprotein of microalga *Spirulina*. *J Proteomics* (2016) 147:132–9. doi: 10.1016/j.jprot.2016.03.043

77. Shkolnikov Lozober H, Okun Z, Parvari G, Shpigelman A. The effect of storage and pasteurization (Thermal and high-pressure) conditions on the stability of phycocyanobilin and phycobiliproteins. *Antioxidants* (2023) 12:568. doi: 10.3390/antiox12030568

78. Radibratovic M, Minic S, Stanic-Vucinic D, Nikolic M, Milcic M, Cirkovic Velickovic T. Stabilization of human serum albumin by the binding of phycocyanobilin, a bioactive chromophore of blue-green alga spirulina: molecular dynamics and experimental study. *PloS One* (2016) 11:e0167973. doi: 10.1371/journal.pone.0167973

79. Radu A-F, Bungau SG. Nanomedical approaches in the realm of rheumatoid arthritis. *Ageing Res Rev* (2023) 87:101927. doi: 10.1016/j.arr.2023.101927

80. Fearon U, Hanlon MM, Wade SM, Fletcher JM. Altered metabolic pathways regulate synovial inflammation in rheumatoid arthritis. *Clin Exp Immunol* (2019) 197:170–80. doi: 10.1111/cei.13228

81. Chaney S, Vergara R, Qiryaqoz Z, Suggs K, Akkouch A. The involvement of neutrophils in the pathophysiology and treatment of osteoarthritis. *Biomedicines* (2022) 10:1604. doi: 10.3390/biomedicines10071604

82. Fresneda Alarcon M, McLaren Z, Wright HL. Neutrophils in the pathogenesis of rheumatoid arthritis and systemic lupus erythematosus: same foe different M.O. *Front Immunol* (2021) 12:649693. doi: 10.3389/fimmu.2021.649693

83. Doodes PD, Cao Y, Hamel KM, Wang Y, Rodeghero RL, Mikecz K, et al. IFN-γ Regulates the requirement for IL-17 in proteoglycan-induced arthritis. *J Immunol* (2010) 184:1552–9. doi: 10.4049/jimmunol.0902907

84. Roberts CA, Dickinson AK, Taams LS. The interplay between monocytes/macrophages and CD4+ T cell subsets in rheumatoid arthritis. *Front Immunol* (2015) 6:571. doi: 10.3389/fimmu.2015.00571

85. Pinto LG, Cunha TM, Vieira SM, Lemos HP, Verri WA, Cunha FQ, et al. IL-17 mediates articular hypernociception in antigen-induced arthritis in mice. *Pain* (2010) 148:247–56. doi: 10.1016/j.pain.2009.11.006

86. Ouyang W, Kolls JK, Zheng Y. The biological functions of T helper 17 cell effector cytokines in inflammation. *Immunity* (2008) 28:454–67. doi: 10.1016/j.immuni.2008.03.004

87. Liu R, Du S, Zhao L, Jain S, Sahay K, Rizvanov A, et al. Autoreactive lymphocytes in multiple sclerosis: Pathogenesis and treatment target. *Front Immunol* (2022) 13:996469. doi: 10.3389/fimmu.2022.996469

88. Murphy CA, Langrish CL, Chen Y, Blumenschein W, McClanahan T, Kastelein RA, et al. Divergent pro- and antiinflammatory roles for IL-23 and IL-12 in joint autoimmune inflammation. *J Exp Med* (2003) 198:1951–7. doi: 10.1084/jem.20030896

89. Laan M, Cui Z-H, Hoshino H, Loëtvall J, Sjoüstrand M, Gruenert DC, et al. Neutrophil recruitment by human IL-17 *via* C-X-C chemokine release in the airways. *J Immunol* (1999) 162:2347–52. doi: 10.4049/jimmunol.162.4.2347

90. Lubberts E, Joosten LAB, Oppers B, van den Bersselaar L, Coenen-de Roo CJJ, Kolls JK, et al. IL-1-independent role of IL-17 in synovial inflammation and joint destruction during collagen-induced arthritis. *J Immunol* (2001) 167:1004–13. doi: 10.4049/jimmunol.167.2.1004

91. Kotake S, Udagawa N, Takahashi N, Matsuzaki K, Itoh K, Ishiyama S, et al. IL-17 in synovial fluids from patients with rheumatoid arthritis is a potent stimulator of osteoclastogenesis. *J Clin Invest* (1999) 103:1345–52. doi: 10.1172/JCI5703

92. Lubberts E, van den Bersselaar L, Oppers-Walgreen B, Schwarzenberger P, Coenen-de Roo CJJ, Kolls JK, et al. IL-17 promotes bone erosion in murine collagen-induced arthritis through loss of the receptor activator of NF-κB ligand/osteoprotegerin balance. *J Immunol* (2003) 170:2655–62. doi: 10.4049/jimmunol.170.5.2655

93. Zhou L, Ivanov II, Spolski R, Min R, Shenderov K, Egawa T, et al. IL-6 programs TH-17 cell differentiation by promoting sequential engagement of the IL-21 and IL-23 pathways. *Nat Immunol* (2007) 8:967–74. doi: 10.1038/ni1488

94. Pentón-Rol G, Martínez-Sánchez G, Cervantes-Llanos M, Lagumersindez-Denis N, Acosta-Medina EF, Falcón-Cama V, et al. C-Phycocyanin ameliorates experimental autoimmune encephalomyelitis and induces regulatory T cells. *Int Immunopharmacol* (2011) 11:29–38. doi: 10.1016/j.intimp.2010.10.001

95. Yang S, Zhang X, Chen J, Dang J, Liang R, Zeng D, et al. Induced, but not natural, regulatory T cells retain phenotype and function following exposure to inflamed synovial fibroblasts. *Sci Adv* (2020) 6:1–13. doi: 10.1126/sciadv.abb0606

96. Langdon K, Haleagrahara N. Regulatory T-cell dynamics with abatacept treatment in rheumatoid arthritis. *Int Rev Immunol* (2018) 37:206–14. doi: 10.1080/08830185.2018.1465943

97. Hafkamp FMJ, Groot Kormelink T, de Jong EC. Targeting DCs for tolerance induction: don't lose sight of the neutrophils. *Front Immunol* (2021) 12:732992. doi: 10.3389/fimmu.2021.732992

98. Souwer Y, Groot Kormelink T, Taanman-Kueter EW, Muller FJ, van Capel TMM, Varga DV, et al. Human TH17 cell development requires processing of dendritic cell–derived CXCL8 by neutrophil elastase. *J Allergy Clin Immunol* (2018) 141:2286–2289.e5. doi: 10.1016/j.jaci.2018.01.003

99. de la Rosa G, Yang D, Tewary P, Varadhachary A, Oppenheim JJ. Lactoferrin acts as an alarmin to promote the recruitment and activation of APCs and antigen-specific immune responses. *J Immunol* (2008) 180:6868–76. doi: 10.4049/jimmunol.180.10.6868

100. Basdeo SA, Campbell NK, Sullivan LM, Flood B, Creagh EM, Mantle TJ, et al. Suppression of human alloreactive T cells by linear tetrapyrroles; relevance for transplantation. *Trans Res* (2016) 178:81–94.e2. doi: 10.1016/j.trsl.2016.07.011

101. Suwa Y, Nagafuchi Y, Yamada S, Fujio K. The role of dendritic cells and their immunometabolism in rheumatoid arthritis. *Front Immunol* (2023) 14:1161148. doi: 10.3389/fimmu.2023.1161148

102. Prendergast CT, Patakas A, Al-Khabouri S, McIntyre CL, McInnes IB, Brewer JM, et al. Visualising the interaction of CD4 T cells and DCs in the evolution of inflammatory arthritis. *Ann Rheum Dis* (2018) 77:579–88. doi: 10.1136/annrheumdis-2017-212279

103. Vitetta ES, Ohara J, Myers CD, Layton JE, Krammer PH, Paul WE. Serological, biochemical, and functional identity of B cell-stimulatory factor 1 and B cell differentiation factor for IgG1. *J Exp Med* (1985) 162:1726–31. doi: 10.1084/jem.162.5.1726

104. Iwaszko M, Biały S, Bogunia-Kubik K. Significance of interleukin (IL)-4 and IL-13 in inflammatory arthritis. *Cells* (2021) 10:3000. doi: 10.3390/cells10113000

105. Harada Y, Tanaka S, Motomura Y, Harada Y, Ohno S, Ohno S, et al. The 3′ Enhancer CNS2 is a critical regulator of interleukin-4-mediated humoral immunity in follicular helper T cells. *Immunity* (2012) 36:188–200. doi: 10.1016/j.immuni.2012.02.002

106. Kawashima M. Effect of treatment of rheumatoid arthritis with infliximab on IFN , IL4, T-bet, and GATA-3 expression: link with improvement of systemic inflammation and disease activity. *Ann Rheum Dis* (2004) 64:415–8. doi: 10.1136/ard.2004.022731

107. Gossauer A, Hinze RP. Synthesis of bile pigments. 7. An improved chemical synthesis of racemic phycocyanobilin dimethyl ester. *J Org Chem* (1978) 43:283–5. doi: 10.1021/jo00396a023

108. Bishop JE, Nagy JO, O'Connell JF, Rapoport H. Diastereoselective synthesis of phycocyanobilin-cysteine adducts. *J Am Chem Soc* (1991) 113:8024–35. doi: 10.1021/ja00021a032

109. Zhao X, Gao H, Wang Y, Wang Z, Zhou J. Efficient synthesis of phycocyanobilin by combinatorial metabolic engineering in *escherichia coli*. *ACS Synth Biol* (2022) 11:2089–97. doi: 10.1021/acssynbio.2c00016

110. Sun ZW, Zhang L, Zhu SJ, Chen WC, Mei B. Excitotoxicity effects of glutamate on human neuroblastoma SH-SY5Y cells *via* oxidative damage. *Neurosci Bull* (2010) 26:8–16. doi: 10.1007/s12264-010-0813-7

111. Gardón DP, Cervantes-Llanos M, Matamoros BP, Rodríguez HC, Tan C, Marín –Prida J, et al. Positive effects of Phycocyanobilin on gene expression in glutamate-induced excitotoxicity in SH-SY5Y cells and animal models of multiple sclerosis and cerebral ischemia. *Heliyon* (2022) 8:e09769. doi: 10.1016/j.heliyon.2022.e09769

112. Wang C, Deng L, Hong M, Akkaraju GR, Inoue J, Chen ZJ. TAK1 is a ubiquitin-dependent kinase of MKK and IKK. *Nature* (2001) 412:346–51. doi: 10.1038/35085597

113. Ninomiya-Tsuji J, Kishimoto K, Hiyama A, Inoue J, Cao Z, Matsumoto K. The kinase TAK1 can activate the NIK-IκB as well as the MAP kinase cascade in the IL-1 signalling pathway. *Nature* (1999) 398:252–6. doi: 10.1038/18465

114. Edlund S, Bu S, Schuster N, Aspenström P, Heuchel R, Heldin N-E, et al. Transforming growth factor-β1 (TGF-β)–induced apoptosis of prostate cancer cells involves smad7-dependent activation of p38 by TGF-β-activated kinase 1 and mitogen-activated protein kinase kinase 3. *Mol Biol Cell* (2003) 14:529–44. doi: 10.1091/mbc.02-03-0037

115. Panipinto PM, Singh AK, Shaikh FS, Siegel RJ, Chourasia M, Ahmed S. Takinib inhibits inflammation in human rheumatoid arthritis synovial fibroblasts by targeting the janus kinase-signal transducer and activator of transcription 3 (JAK/STAT3) pathway. *Int J Mol Sci* (2021) 22:12580. doi: 10.3390/ijms222212580

116. Clark A R. The p38 MAPK pathway in rheumatoid arthritis: A sideways look. *Open Rheumatol J* (2012) 6:209–19. doi: 10.2174/1874312901206010209

117. Iwamoto M, Nakamura Y, Takemura M, Hisaoka-Nakashima K, Morioka N. TLR4-TAK1-p38 MAPK pathway and HDAC6 regulate the expression of sigma-1 receptors in rat primary cultured microglia. *J Pharmacol Sci* (2020) 144:23–9. doi: 10.1016/j.jphs.2020.06.007

118. Mu N, Gu J, Huang T, Zhang C, Shu Z, Li M, et al. A novel NF-κB/YY1/microRNA-10a regulatory circuit in fibroblast-like synoviocytes regulates inflammation in rheumatoid arthritis. *Sci Rep* (2016) 6:20059. doi: 10.1038/srep20059

119. Khan D, Bedner P, Müller J, Lülsberg F, Henning L, Prinz M, et al. TGF-β Activated kinase 1 (TAK1) is activated in microglia after experimental epilepsy and contributes to epileptogenesis. *Mol Neurobiol* (2023) 60:3413–22. doi: 10.1007/s12035-023-03290-2

120. Scarneo S, Zhang X, Wang Y, Camacho-Domenech J, Ricano J, Hughes P, et al. Transforming growth factor-β-activated kinase 1 (TAK1) mediates chronic pain and cytokine production in mouse models of inflammatory, neuropathic, and primary pain. *J Pain* (2023) 24:1633–44. doi: 10.1016/j.jpain.2023.04.011

121. Uchida K, Takano S, Matsumoto T, Nagura N, Inoue G, Itakura M, et al. Transforming growth factor activating kinase 1 regulates extracellular matrix degrading enzymes and pain-related molecule expression following tumor necrosis factor-α stimulation of synovial cells: an in *vitro* study. *BMC Musculoskelet Disord* (2017) 18:283. doi: 10.1186/s12891-017-1648-4

122. Arve-Butler S, Mossberg A, Schmidt T, Welinder C, Yan H, Berthold E, et al. Neutrophils lose the capacity to suppress T cell proliferation upon migration towards inflamed joints in juvenile idiopathic arthritis. *Front Immunol* (2022) 12:795260. doi: 10.3389/fimmu.2021.795260

123. Suyama S, Kodaira-Hirano M, Otgon-Uul Z, Ueta Y, Nakata M, Yada T. Fasted/fed states regulate postsynaptic hub protein DYNLL2 and glutamatergic transmission in oxytocin neurons in the hypothalamic paraventricular nucleus. *Neuropeptides* (2016) 56:115–23. doi: 10.1016/j.npep.2015.08.008

124. Asante D, Stevenson NL, Stephens DJ. Subunit composition of the human cytoplasmic dynein-2 complex. *J Cell Sci* (2014) 127:4774–87. doi: 10.1242/jcs.159038

125. Moutin E, Raynaud F, Fagni L, Perroy J. GKAP-DLC2 interaction organizes postsynaptic scaffold complex to enhance synaptic NMDA receptor activity. *J Cell Sci* (2012) 125:2030–40. doi: 10.1242/jcs.098160

126. Cucchiarini M, Madry H, Terwilliger EF. Enhanced expression of the central survival of motor neuron (SMN) protein during the pathogenesis of osteoarthritis. *J Cell Mol Med* (2014) 18:115–24. doi: 10.1111/jcmm.12170

127. Guo S, Bao S. srGAP2 arginine methylation regulates cell migration and cell spreading through promoting dimerization. *J Biol Chem* (2010) 285:35133–41. doi: 10.1074/jbc.M110.153429

128. Fossati M, Pizzarelli R, Schmidt ER, Kupferman JV, Stroebel D, Polleux F, et al. SRGAP2 and its human-specific paralog co-regulate the development of excitatory and inhibitory synapses. *Neuron* (2016) 91:356–69. doi: 10.1016/j.neuron.2016.06.013

129. Ma Y, Mi Y-J, Dai Y-K, Fu H-L, Cui D-X, Jin W-L. The Inverse F-BAR Domain Protein srGAP2 Acts through srGAP3 to Modulate Neuronal Differentiation and Neurite Outgrowth of Mouse Neuroblastoma Cells. *PloS One* (2013) 8:e57865. doi: 10.1371/journal.pone.0057865

130. Shin B, Kupferman J, Schmidt E, Polleux F, Delany AM, Lee S. Rac1 inhibition *via* srgap2 restrains inflammatory osteoclastogenesis and limits the clastokine, SLIT3. *J Bone Mineral Res* (2020) 35:789–800. doi: 10.1002/jbmr.3945

131. Lilley BN, Ploegh HL. A membrane protein required for dislocation of misfolded proteins from the ER. *Nature* (2004) 429:834–40. doi: 10.1038/nature02592

132. Sugiyama T, Murao N, Kadowaki H, Nishitoh H. Chemical chaperones ameliorate neurodegenerative disorders in Derlin-1-deficient mice *via* improvement of cholesterol biosynthesis. *Sci Rep* (2022) 12:21840. doi: 10.1038/s41598-022-26370-0

133. Honjo Y, Ito H, Horibe T, Shimada H, Nakanishi A, Mori H, et al. Derlin-1-immunopositive inclusions in patients with Alzheimer's disease. *Neuroreport* (2012) 23:611–5. doi: 10.1097/WNR.0b013e3283552a75

134. Taiana M, Sassone J, Lauria G. Mutant SOD1 accumulation in sensory neurons does not associate with endoplasmic reticulum stress features: Implications for differential vulnerability of sensory and motor neurons to SOD1 toxicity. *Neurosci Lett* (2016) 627:107–14. doi: 10.1016/j.neulet.2016.05.057

135. Mori A, Yamashita S, Uchino K, Suga T, Ikeda T, Takamatsu K, et al. Derlin-1 overexpression ameliorates mutant SOD1-induced endoplasmic reticulum stress by reducing mutant SOD1 accumulation. *Neurochem Int* (2011) 58:344–53. doi: 10.1016/j.neuint.2010.12.010

136. Miyano K, Okamoto S, Kajikawa M, Kiyohara T, Kawai C, Yamauchi A, et al. Regulation of Derlin-1-mediated degradation of NADPH oxidase partner p22 by thiol modification. *Redox Biol* (2022) 56:102479. doi: 10.1016/j.redox.2022.102479

137. Lee S-Y, Wong P-F, Jamal J, Roebuck MM. Naturally-derived endoplasmic reticulum stress inhibitors for osteoarthritis? *Eur J Pharmacol* (2022) 922:174903. doi: 10.1016/j.ejphar.2022.174903

138. Wang Z, Yang M, Yang Y, He Y, Qian H. Structural basis for catalysis of human choline/ethanolamine phosphotransferase 1. *Nat Commun* (2023) 14:2529. doi: 10.1038/s41467-023-38290-2

139. Kunishita T, Vaswani KK, Morrow CR, Novak GP, Ledeen RW. Ethanolamine kinase activity in purified myelin of rat brain. *J Neurochem* (1987) 48:1–7. doi: 10.1111/j.1471-4159.1987.tb13119.x

140. Horibata Y, Elpeleg O, Eran A, Hirabayashi Y, Savitzki D, Tal G, et al. EPT1 (selenoprotein I) is critical for the neural development and maintenance of plasmalogen in humans. *J Lipid Res* (2018) 59:1015–26. doi: 10.1194/jlr.P081620

141. Pentón-Rol G, Marín-Prida J, Falcón-Cama V. C-phycocyanin and phycocyanobilin as remyelination therapies for enhancing recovery in multiple sclerosis and ischemic stroke: A preclinical perspective. *Behav Sci* (2018) 8:15. doi: 10.3390/bs8010015

frontiers | Frontiers in Immunology

TYPE Original Research
PUBLISHED 03 November 2022
DOI 10.3389/fimmu.2022.1036200

OPEN ACCESS

EDITED BY
Raffaella Bonecchi,
Humanitas University, Italy

REVIEWED BY
Hartmut Wekerle,
Max Planck Society, Germany
Javier Ochoa-Repáraz,
Boise State University, United States

*CORRESPONDENCE
Giselle Pentón-Rol
giselle.penton@cigb.edu.cu

SPECIALTY SECTION
This article was submitted to Cytokines and Soluble Mediators in Immunity, a section of the journal Frontiers in Immunology

RECEIVED 04 September 2022
ACCEPTED 19 October 2022
PUBLISHED 03 November 2022

CITATION
Marín-Prida J, Pavón-Fuentes N, Lagumersindez-Denis N, Camacho-Rodríguez H, García-Soca AM, Sarduy-Chávez RdlC, Vieira ÉLM, Carvalho-Tavares J, Falcón-Cama V, Fernández-Massó JR, Hernández-González I, Martínez-Donato G, Guillén-Nieto G, Pentón-Arias E, Teixeira MM and Pentón-Rol G (2022) Anti-inflammatory mechanisms and pharmacological actions of phycocyanobilin in a mouse model of experimental autoimmune encephalomyelitis: A therapeutic promise for multiple sclerosis. *Front. Immunol.* 13:1036200. doi: 10.3389/fimmu.2022.1036200

Anti-inflammatory mechanisms and pharmacological actions of phycocyanobilin in a mouse model of experimental autoimmune encephalomyelitis: A therapeutic promise for multiple sclerosis

Javier Marín-Prida[1], Nancy Pavón-Fuentes[2], Nielsen Lagumersindez-Denis[3], Hanlet Camacho-Rodríguez[4], Ana Margarita García-Soca[1], Rocío de la Caridad Sarduy-Chávez[1], Érica Leandro Marciano Vieira[5], Juliana Carvalho-Tavares[6], Viviana Falcón-Cama[4,7], Julio Raúl Fernández-Massó[4], Ignacio Hernández-González[8], Gillian Martínez-Donato[4], Gerardo Guillén-Nieto[4,7], Eduardo Pentón-Arias[4,7], Mauro Martins Teixeira[9] and Giselle Pentón-Rol[4,7]*

[1]Center for Research and Biological Evaluations, Institute of Pharmacy and Food, University of Havana, Havana, Cuba, [2]Immunochemical Department, International Center for Neurological Restoration (CIREN), Havana, Cuba, [3]Institute of Neuropathology, University Medical Center Göttingen, Göttingen, Germany, [4]Biomedical Research Department, Center for Genetic Engineering and Biotechnology, Havana, Cuba, [5]Translational Psychoneuroimmunology Group, School of Medicine, Federal University of Minas Gerais (UFMG), Belo Horizonte, Brazil, [6]Department of Physiology and Biophysics, Institute of Biological Sciences, Federal University of Minas Gerais (UFMG), Belo Horizonte, Minas Gerais, Brazil, [7]Latin American School of Medicine (ELAM), Havana, Cuba, [8]Isotopes Center, San José de Las Lajas, Mayabeque, Cuba, [9]Laboratory of Immunopharmacology, Department of Biochemistry and Immunology, Instituto de Ciências Biológicas, Universidade Federal de Minas Gerais, Belo Horizonte, Minas Gerais, Brazil

Cytokines, demyelination and neuroaxonal degeneration in the central nervous system are pivotal elements implicated in the pathogenesis of multiple sclerosis (MS) and its nonclinical model of experimental autoimmune encephalomyelitis (EAE). Phycocyanobilin (PCB), a chromophore of the biliprotein C-Phycocyanin (C-PC) from *Spirulina platensis*, has antioxidant, immunoregulatory and anti-inflammatory effects in this disease, and it could complement the effect of other Disease Modifying Treatments (DMT), such as Interferon-β (IFN-β). Here, our main goal was to evaluate the potential PCB benefits and its mechanisms of action to counteract the chronic EAE in mice. MOG_{35-55}-induced EAE was implemented in C57BL/6 female mice. Clinical signs, pro-inflammatory cytokines levels by ELISA, qPCR in the brain and immunohistochemistry using precursor/mature oligodendrocytes cells antibodies in the spinal cord, were assessed. PCB enhanced the neurological condition, and waned the brain

concentrations of IL-17A and IL-6, pro-inflammatory cytokines, in a dose-dependent manner. A down- or up-regulating activity of PCB at 1 mg/kg was identified in the brain on three (*LINGO1*, *NOTCH1*, and *TNF-α*), and five genes (*MAL*, *CXCL12*, *MOG*, *OLIG1*, and *NKX2-2*), respectively. Interestingly, a reduction of demyelination, active microglia/macrophages density, and axonal damage was detected along with an increase in oligodendrocyte precursor cells and mature oligodendrocytes, when assessed the spinal cords of EAE mice that took up PCB. The studies *in vitro* in rodent encephalitogenic T cells and *in vivo* in the EAE mouse model with the PCB/IFN-β combination, showed an enhanced positive effect of this combined therapy. Overall, these results demonstrate the anti-inflammatory activity and the protective properties of PCB on the myelin and support its use with IFN-β as an improved DMT combination for MS.

KEYWORDS

interferon-β, proinflammatory cytokines, remyelination, antioxidants, experimental autoimmune encephalomyelitis, multiple sclerosis, phycocyanobilin

Introduction

The discovery of neuroprotective molecules that can promote remyelination in animal models has currently generated expectations for the development of new drugs for multiple sclerosis (MS). This is a central nervous system (CNS) disease that comprises chronic autoimmune-related demyelination and neurodegeneration producing sensorimotor dysfunction with high prevalence in young adults (1). MS has been classified according to its clinical presentation in: relapsing-remitting (RRMS), secondary progressive (SPMS), primary progressive (PPMS), and progressive relapsing MS (PR). Eighty percent of the patients with MS express the RRMS form which in turn, after 10-20 years, progresses to the SPMS form (2). Few disease-modifying therapies (DMT) have been found for the treatment of the main clinical forms (RRMS and SPMP) and even fewer for PPMS (3). MS pathogenesis has been associated with two processes, i.e. one related to the inflammatory response induced by a dysfunction of the immune system and the other related to the neurodegenerative events. DMTs that have received authorization for clinical use are directed against targets of the immune system, having little or no direct impact on neuroglial injury processes (4). Therefore, the development of drugs targeting myelin protection and/or remyelination or the use of combined therapies are relevant strategies in the therapeutic arsenal of this disease.

In this context, Phycocyanobilin (PCB), a linear tetrapyrrolic chromophore of C-Phycocyanin (C-PC) from the cyanobacterium *Spirulina platensis* could be a therapeutic candidate for MS. Our group has previously shown the beneficial effects of C-PC and PCB in nonclinical models of neurological diseases, such as the experimental autoimmune encephalomyelitis (EAE) model of MS (5–7) as well as rodent models of cerebral ischemia (8–10). Their effects were mediated by a diverse antioxidant, immunomodulatory, anti-inflammatory and myelin-protective/remyelinating capabilities (11).

In MS, the disruption of the blood-brain barrier (BBB) enables the cerebral infiltration of autoreactive T cells, increasing the levels of proinflammatory cytokines. As consequence, the molecular and cellular cascade initiated produces the CNS immune self-attack, which is most prominent at the first phases of MS in which the activated microglia and infiltrating macrophages destroy oligodendrocytes (OD) and promote demyelination (12). Indeed, the chief pathological feature of MS is the axonal demyelination and damage, which interrupts or decelerates the propagation of the action potential through the axons (13). The reverse process is the remyelination in which oligodendrocyte precursor cells (OPC) create new myelin sheaths on axons of the CNS. In the remyelination process, the neuronal functional recovery is fostered by either endogenous, through boosting neuronal repair processes, or exogenous, through stimulating OPC, the cells that produce myelin in the CNS (14). The remyelination is a very effective process in normal people and even at the early stages of MS, however it fails in the chronic stage of the disease (15), showing the importance of developing myelin-targeted therapies.

Hence, the objectives of our study were to understand the molecular and cellular mechanisms induced by PCB on the EAE inflammatory response and on the myelin protection and/or remyelination, specifically its effect on the activation, migration

and differentiation of OPC. Furthermore, we investigated the potential benefit of the pharmacological combination of PCB with IFN-β (the first-ever approved DMT for MS) as a novel therapy for MS.

Material and methods

Reagents

The PCB (Cat. No. SC-396921, Santa Cruz Biotechnology, Inc., Dallas, USA) was solubilized with sterile PBS pH 7.4 at a concentration of 5 mg/mL. This stock solution was stored at -20 °C until use. When needed, a stock aliquot was diluted at the working concentration, preserved in dark, and immediately applied to the experiment. Unless otherwise indicated, every other reagent was acquired from Sigma-Aldrich (St. Louis, MO, USA) with its highest grade.

Animals

This study used female C57BL/6 mice (8-10 weeks old) provided by the Animal Care Facilities of the Federal University of Minas Gerais, Belo Horizonte, Brazil. The standard husbandry conditions included food and water ad libitum and a light/dark cycle of 12 h. All national and international regulations for the procedures involving mice were followed, and the animal ethics committee of the Federal University of Minas Gerais approved this study protocol (No. CEUA - 255/2015).

Establishment of EAE model

EAE was induced as previously described (16). Mice were subcutaneously (s.c.) injected with 0.1 mL emulsion, which contained 100 µg of murine MOG_{35-55} (CIGB, Havana, Cuba) diluted in 50 µL saline and 50 µL Freund's Complete Adjuvant (CFA), and supplemented with 4.0 mg/mL of *Mycobacterium tuberculosis* H37RA (Difco Laboratories, Detroit, MI, USA), followed by two intraperitoneal (i.p.) administrations (day 0 and day 2 after immunization) of 300 ng pertussis toxin diluted in 200 µL saline. Control mice were treated with saline instead of the emulsion following a similar procedure. The neurological dysfunction was scored daily in a double-blind way using a modified scale (17). The score of 0 denoted no clinical signs, 0.5: tail tone reduction distally, 1: complete flaccid tail, 1.5: tail paralysis and walking imbalance, 2: tail paralysis and hind limb frailty (unilateral), 2.5: tail paralysis and hind limb frailty (bilateral), 3: hind limb paralysis (bilateral), 3.5: hind limb paralysis (bilateral) of and fore limbs frailty, 4: paralysis of hind and fore limbs (bilateral), and 5 indicated death. The area under the curve (AUC), representing clinical severity, was analyzed.

Treatment schedules

Five experimental groups of mice were randomly distributed (n=6-7 per group). These included non-immunized animals (naïve), and EAE disease mice receiving the following i.p. treatments daily, once a day: sterile PBS (vehicle) or PCB at 0.1, 0.5, or 1 mg/kg, from day 0 until day 26 post-immunization. In follow-up experiments, animals (n = 9-10 each) received the vehicle or 1 mg/kg PCB daily by the oral route (intragastric gavage) once a day, or mouse 5000 U IFN-β (Cat. No. K00020, PBL, USA) subcutaneously (s.c.) every second day or the combination of both compounds. In these latest experiments, two schedules were assessed:

Prophylactic: PCB and IFN-β treatments were administered from day 0 of the induction to the end of the experiment (24 days)

Late therapeutic: PCB and IFN-β treatments were administered starting at 14 days post-induction until the end of the experiment (24 days)

Histological and immunohistochemistry analysis of the mice spinal cords

Humane euthanasia was performed at the end of the study (day 26), followed by the perfusion with ice-cold PBS, and the fixation of the dissected spinal cords by immersion in 4% paraformaldehyde. The examined region of the spinal cord was the lumbar part, which is frequently and rapidly affected in EAE (18), and contains motor neurons that innervate the hindlimb muscles (19). The tissue was embedded in paraffin, and between 9-10 serial sections of 1-3 µm thickness were cut at 100 µm intervals in the rostral to caudal direction, from paraffin blocks using a sliding microtome and used for staining. Demyelination was evaluated by staining with Luxol fast blue combined with periodic acid-Schiff (LFB-PAS). The inflammatory markers were assessed by immunohistochemistry (IHC) with the following primary antibodies for T cells and macrophages/activated microglia, respectively: anti-CD3 (1:150, Cat. No. C1597C01, DCS, Hamburg, Germany) and anti-Mac-3 (CD107b) (1:200, Cat. No. 553322, BD Bioscience, Franklin Lakes NJ, USA). Additionally, an anti-amyloid precursor protein (APP) (1:2000, Cat. No. MAB348, Chemicon, Temecula, CA, USA) was used for evaluating the axonal injury. Moreover, an anti-tubulin polymerization-promoting protein (TPPP/p25) (1:500, Cat. No. 92305, Abcam, Cambridge, UK) and an anti-Olig2 (1:300, Cat. No. 18953, IBL, Hamburg, Germany) were used for detecting mature OD and OPC, respectively. A streptavidin-biotin protocol

(biotinylated secondary antibodies and streptavidin conjugated to horseradish peroxidase) was performed to reveal the antigen-primary antibody binding with 3,3'-diaminobenzidine as the chromogen.

Morphometric analysis

The stained spinal cord sections were photographed by using a digital camera (Software Cell Sens Dimension v.1.7.1, DP71, Olympus, Germany) coupled with a light microscope (Olympus BX51, Germany). The Image J software (v. 1.46r, NIH, USA) was used for the measurement of the areas and the number of marked cells. The percentage of demyelinated area, as well as the densities of immunostained cells for each marker (CD3, Mac-3, TPPP/p25, Olig2 and APP) were determined in relation to the total area of the white matter, and expressed as % or # cells^{+}/mm^{2}, respectively.

Quantification of the brain levels of IL-17A, IL-6 and IL-10

After performing the animals' euthanasia once anesthetized on day 26 post-immunization, both mice's cerebral hemispheres were dissected and divided sagittally at 2.0 mm lateral from bregma. The cerebral tissue closest to the sagittal suture was mechanically homogenized (IKA Works Ultra-Turrax, USA) by mixing 100 mg of tissue in 1 mL of an ice-cold extraction solution (0.4 M NaCl, 0.05% Tween 20, 0.5% bovine serum albumin, 0.1 mM phenylmethylsulfonylfluoride, 0.1 mM benzetonium chloride, 10 mM EDTA and 20 KIU aprotinin, prepared in PBS pH 7.4). After centrifugation at 15,000 ×g for 10 min at 4°C, the supernatants were stored at −70°C until use. The assessment of IL-17A, IL-6, and IL-10 levels was accomplished with the adequate ELISA Kit (R&D Systems, Minneapolis, MN, USA), following the supplier's protocols.

Quantitative real-time PCR

The dissected cerebral tissues after concluding the study (day 26) were conserved in RNAlater (Ambion Inc., Applied Biosystems, Foster City, CA, USA), homogenized, and provided for RNA isolation by using TRIzol (Invitrogen, San Diego, CA, USA). The cDNA synthesis was performed with 1 µg of RNA (High-Capacity cDNA Archive Kit, Applied Biosystems, Foster City, CA, USA) and then used for Quantitative Real Time PCR (qPCR) in triplicate, in accordance with the Minimal Information for Publication of qPCR Experiments (MIQE) guidelines (20). The BLAST algorithm was implemented for designing the gene-specific primers (Supplementary Table 1), which were used at 300 nM (Metabion, Martinsried, Germany). The detection system consisted in the Fast SYBR Green PCR Master Mix and the Applied Biosystems 7900HT Fast Real-Time PCR System (Applied Biosystems, Foster City, CA, USA). Bi-distilled water, used as reaction control, did not generate any signal for either the target or the housekeeping genes. The 2-ΔΔCt method (21) implemented in the REST© software (22) was used for the analysis and quantification of the mRNA levels.

Measurement of Treg

The mice spleens were collected in HBSS under sterile conditions in a biosafety cabinet, minced with scissors, and passed through a steel mesh to homogenize the cell suspension containing red blood cells (RBCs). This was then subsequently lysed (9 parts of Milli-Q water and 1 part of sterile PBS 10X) and centrifuged (177× *g*, 10 min at 4°C). The resulting pellet was washed three times with ice-cold PBS 1X, and finally resuspended in RPMI-1640 medium supplemented with 10% fetal bovine serum (FBS) and 1% penicillin–streptomycin. The cell viability was assessed by the trypan blue technique and resulted above 95%. The single-cell suspensions were resuspended in the final concentration to 1 x 10^{7} cells/mL and marked for Fc receptor block (Innovex, NB309). After Fc block, the cells were co-incubated for 20 minutes at 4°C with cy-chrome (Cy), phycoerythrin (PE) or fluorescein isothiocyanate (FITC)-labeled antibodies that detect the cell surface markers CD4 or CD25, or with an anti-isotype control (eBioscience, and BD Pharmingen, San Diego, CA, USA). Thereafter, the cells were fixed with 2% formaldehyde, permeabilized and marked with a phycoerythrin (PE)-conjugated anti-Foxp3 monoclonal antibody by using the eBioscience™ Foxp3/Transcription Factor Staining Buffer Set (eBioscience, CA, USA). The appropriate controls (PE-labeled antibody and unstimulated cells) were incorporated in all assays. The signal acquisition was carried out with FACS CantoII (Becton & Dickinson, San Jose, CA, USA) above the 50 000 gated events on the lymphocytes population given the low frequency of positive events, and processed through the Diva® software (Becton & Dickinson, San Jose, CA, USA).

Analysis of the flow cytometry results

The analysis of the patterns and frequencies of CD4^{+} CD25^{high} T lymphocytes was performed with the FlowJo program (Tree Star, Ashland, OR, USA). Three different fluorochromes were used for each set of analyses, for example, anti-CD25-FITC, anti-Foxp3-PE, and anti-CD4-PE-Cy5.5 for Treg cells. The lymphocytes gate was selected, encompassing the upper right region of the dot-plot in which the double-positive cells for CD25-FITC and CD4-PE-Cy5 were present, and a new dot-plot was generated for selected the cells positive for Foxp3-

PE (23). The quadrant markers were always limited based on the negative populations, the isotype controls and the fluorescence minus one control (FMO).

Proliferation assay

The cell line ($T_{MBP\text{-}GFP}$) was cultured and stimulated as previously reported (24). This line was previously stablished following a technique in which rat $CD4^+$ T lymphocytes specifically reactive to myelin basic protein (MBP), were retrovirally engineered to produce green fluorescent protein (GFP) (25). $T_{MBP\text{-}GFP}$ cells (4 x 10^4 cells/well, 96-well plates) were co-cultured with irradiated rat thymocytes (5000 rad, 10^6 cells/well) in complete DMEM/1% rat serum with 10 µg/mL MBP, with either of the following experimental conditions: PCB alone at 50, 100 or 200 µg/mL, IFN-β alone at 10^3 U/mL, and the combination of 10^3 U/mL IFN-β + PCB at 50, 100 or 200 µg/mL. After 48 h of incubation, MTT (3-[4,5-dimethylthiazol-2-yl]-2,5-diphenyltetrazolium bromide) at 0.5 mg/mL was incorporated to the medium, and cultured for another 4 h. $CD4^+$ T cells from the spleen and lymphonodes of 2D2 mice were seeded at 2 x 10^5 cells/well in RPMI medium with 10% fetal calf serum (FCS) and co-stimulated with 2 µg/mL anti-CD3/anti-CD28 at 37°C, 5% CO_2. Purified $CD4^+$ T cells were incubated with 5 x 10^3 U/mL IFN-β alone, PCB alone at 10, 50 or 250 µg/mL or together with 5 x 10^3 U/mL IFN-β. Two days later, CD4+ T cells were split 1:2 by using the same medium containing IL-2 at 10 ng/mL of final concentration, and incubated again for one day. Then, the cells were cultured with MTT at 0.5 mg/mL (by adding to the medium) for additional 4 h. After that, the medium was discarded, the formazan crystals were dissolved in 150 µL/well of dimethyl sulfoxide (DMSO), and a microplate reader (Perkin Elmer, Victor 2) was used for measuring the absorbance at 570 nm.

Intracellular localization of PCB

$T_{MBP\text{-}GFP}$ cells (5 x 10^5 cells/well) were seeded in 12-well plates together with irradiated rat thymocytes (5000 rad, 1.25 x 10^7 cells/well) in complete DMEM/1% rat serum with 10 µg/mL MBP and 200 µg/µL PCB for 3 h. Immediately afterwards, the nuclear DNA of T cells was labeled with DAPI following a previously described procedure with minor changes (26). Briefly, T cells were collected in 15 mL tubes, centrifuged at 400 g, at room temperature for 3 min, washed with PBS 1X (0.5 mL) and fixed during 10 min at 4°C with 4% paraformaldehyde (0.5 mL). T cells were treated first with 0.2% Triton X-100 (0.5 mL) and later with 1 µg/mL DAPI (0.5 mL) at room temperature for 5 and 10 min, respectively, with three washes of PBS 1X (0.5 mL) between them and again after completing the DAPI staining. By using a cytospin device (800 rpm, 3 min), T cells were transferred to microscope slides and cover slips were mounted with Fluoromount-G. Images acquisition was performed with a confocal microscope (Leica) for DAPI (λex=359 nm, λem=461 nm) and PCB (λex=550 nm, λem=591-641 nm) fluorescence. The Fiji software was used for analysis (27).

Statistical analysis

The statistical analysis was carried out with the GraphPad Prism software 6.0 (GraphPad Inc., CA, USA). Data are expressed as the mean ± S.E.M. Kolmogorov-Smirnov normality test were applied to all data sets. One-way-ANOVA followed by Newman-Keuls tests, or Kruskal-Wallis followed by Dunn´s tests for multiple comparisons between three or more groups were used when appropriate. Statistical comparison for qPCR data was done with the REST© software. P values of $p<0.05$ (*), $p<0.01$ (**), and $p<0.001$ (***) were considered statistically significant.

Results

PCB delayed and attenuated the clinical signs progression of EAE mice

The daily motor behavior of EAE mice receiving the intraperitoneal (i.p.) administration of either the vehicle or PCB at different doses was evaluated from the day of immunization until the end of the study (Figure 1). Interestingly, on average, the EAE + vehicle group presented the onset of the disease on day 9.8 ± 1.14, with the first animal being sick on day 7 following the immunization (Figure 1A). In contrast, the treatment with PCB at 0.1, 0.5 and 1 mg/kg postponed the beginning of clinical symptoms, on average, until the days 13.57 ± 1.82, 15.57 ± 1.81 and 15.29 ± 1.92 post-induction, respectively. Notably, the delay of the disease onset was statistically significant when the 0.5 and 1 mg/kg doses of PCB were compared with the vehicle-treated EAE mice ($p<0.05$, Kruskal-Wallis + Dunn's multiple comparisons test, Supplementary Table 2). On the other hand, Figure 1B shows the quantification of the area under the curve of clinical progression, which represents the EAE neurological severity. EAE animals treated with the vehicle showed an area of 43.04 ± 10.65 (arbitrary units), while this parameter decreased to values of 25.46 ± 4.46, 24.14 ± 5.92 and 18.39 ± 4.55 for PCB at 0.1, 0.5 and 1 mg/kg, respectively. Statistically significant differences were observed between the EAE vehicle- and the EAE PCB-treated animals at the highest dose. This result indicates that the i.p. administration of PCB was able to retard the appearance of the disease's symptoms and to reduce the EAE neurological severity.

10.3389/fimmu.2022.1036200

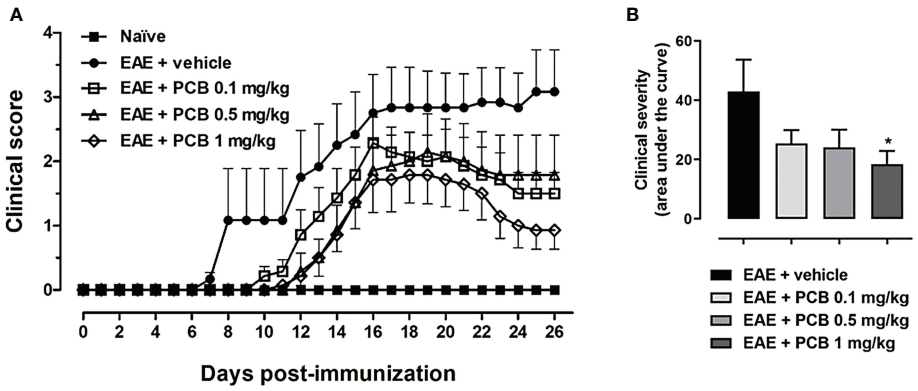

FIGURE 1
Effect of PCB in a murine model of chronic progressive EAE. **(A)** Daily clinical assessment of the mice. **(B)** Clinical severity determined by the area under the curve (in arbitrary units). MOG_{35-55} immunized mice received a daily i.p. injection of PBS (vehicle) or PCB at 0.1, 0.5 or 1 mg/kg, from day 0 until day 26 post-immunization. A numeric scale with the ascending graveness was used to score every day the clinical signs of the mice, ranging from 0 (no disease) to 5 (death). The naïve group (non-immunized animals) remained healthful during the entire study period (score 0). Data are expressed as the mean ± S.E.M (n=6-7 per group). The asterisk (*) is indicative of significant differences with vehicle-treated EAE mice (*p<0.05, ANOVA + Newman-Keuls tests).

PCB reduces pro-inflammatory cytokines in the brain of mice with EAE

To further investigate the impact of PCB treatment on the expression of IL-17A, IL-6 (pro-inflammatory), and IL-10 (anti-inflammatory/immunoregulatory) cytokines in the brain of mice with EAE, an ELISA protocol has been used (Figures 2A–C). EAE vehicle-treated mice showed significantly higher levels of all measured cytokines compared to healthy naïve animals. Animals with EAE that received 0.5 and 1 mg/kg PCB evidenced a significant decline in the levels of IL-17A and IL-6 pro-inflammatory cytokines compared to the vehicle-treated EAE mice. These results suggest an anti-inflammatory action of PCB against the EAE progression in mice brains.

PCB positively modulates the expression of genes related to remyelination/demyelination processes in mice brains

We evaluated the genes modulation in the brain of EAE animals treated with PCB at 0.1, 0.5 and 1 mg/kg (Figure 3). We observed an up-regulation of genes that could mediate myelin damage (*LINGO1*, *NOTCH1* and *TNF-α*), accompanied by the down-regulation of genes that may be involved in myelin preservation (*CXCL12*, *MAL*, *MOG*, *NKX2-2*, and *OLIG1*) in vehicle-treated EAE mice compared with naïve animals. In this ratio, a statistically significant difference was obtained for *TNF-α* (up), *CXCL12* (down) and *MOG* (down). The PCB-treated EAE animals at all doses, were compared to the EAE vehicle group. PCB at 0.1 mg/kg, regarding the genes that may influence the myelin destruction, only the *TNF-α* reversed its modulation (downward). On the contrary, all the myelin-favorable genes (except the *MAL* gene) inverted their modulation (upward), although no statistically significant differences were observed at this dose. When the sick mice received 0.5 mg/kg PCB, a similar modulation was detected in myelin-adverse genes. Finally, a dose-dependent effect of PCB was observed, which reached an inverse modulation for all genes studied at the highest dose of PCB (1 mg/kg). Moreover, a statistical difference was found for the *TNF-α* gene (down) and the *CXCL12* gene (up).

PCB reduces demyelination and neuroinflammation in the spinal cords of EAE mice

Several areas of demyelination (purple area) were observed in EAE animals treated with the vehicle, also present (in a lesser proportion) with the lowest dose of PCB 0.1 mg/kg (Figure 4A). In contrast, intact myelin (expressed as an intense blue area) was observed in healthy mice (image not shown). Demyelination in the spinal cord white matter was clearly ameliorated in the diseased animals treated with all doses of PCB, particularly those of 1 and 0.5 mg/kg (Figure 4A). These results express the dose-dependent effect of PCB in reducing demyelination. The quantification of the demyelinated areas resulted in a significant decrease in this parameter in the EAE animals treated with the highest doses of PCB, 0.5 and 1 mg/kg, compared to those treated with the vehicle. On the other hand, immunostaining for Mac-3, a microglial and macrophages marker, and for the T lymphocytes marker CD3,

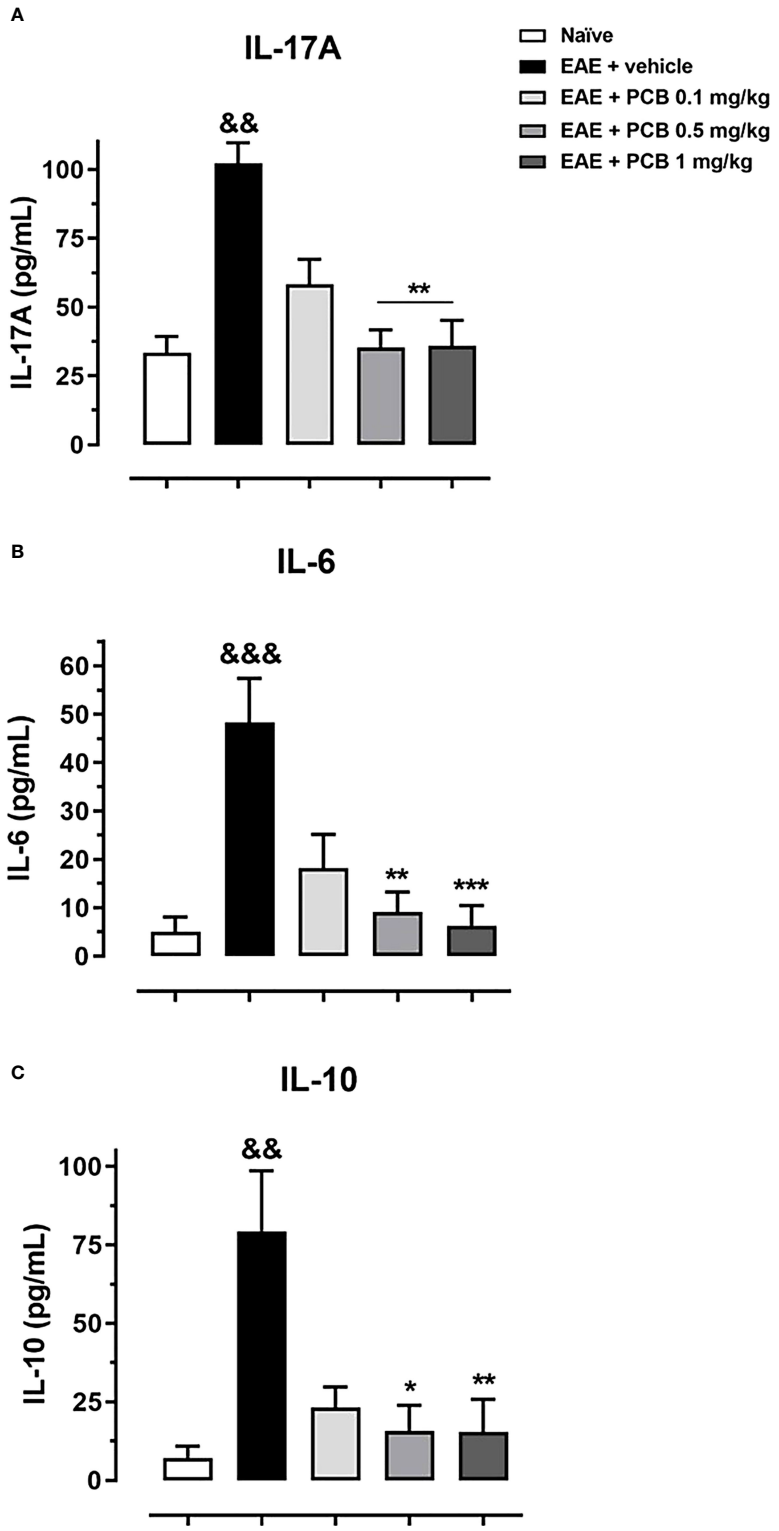

FIGURE 2
Evaluation of the PCB effect on the brain expression of cytokines in EAE mice. MOG_{35-55} immunized mice received a daily i.p. injection of PBS (vehicle) or PCB at 0.1, 0.5 or 1 mg/kg, from day 0 until day 26 post-immunization. At this moment, the protein levels of the cytokines **(A)** IL-17A, **(B)** IL-6, and **(C)** IL-10 were assessed by the respective ELISA commercial kits. Data are expressed as mean ± S.E.M. (n=6-7 per group). The ampersand (&) and asterisk (*) are indicative of significant differences with non-immunized naïve and vehicle-treated EAE mice, respectively (*p<0.05, **p<0.01, ***p<0.001; $^{\&\&}$p <0.01, $^{\&\&\&}$p <0.001, Kruskal-Wallis + Dunn's tests).

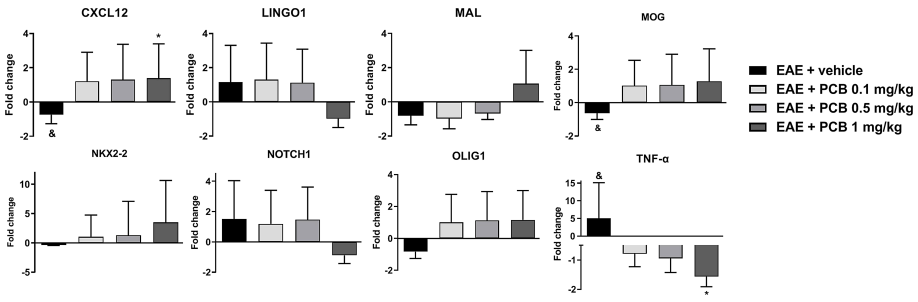

FIGURE 3
Effect of PCB on expression levels of demyelinating/remyelinating-related genes assessed by Real Time PCR in the brain of EAE mice. The panels show the mRNA levels of *CXCL12*, *LINGO1*, *MAL*, *MOG*, *NKX2-2*, *NOTCH1*, *OLIG1* and *TNF-α*. MOG_{35-55} immunized mice received a daily i.p. injection of PBS (vehicle) or PCB at 0.1, 0.5 or 1 mg/kg, from day 0 until day 26 post-immunization. Data are expressed as mean ± S.E.M. (n=4 per group). The ampersand (&) and asterisk (*) are indicative of significant differences with non-immunized naïve and vehicle-treated EAE mice, respectively (*p<0.05, $^{\&}$p<0.05, REST© software).

were also carried out. The results expressed a significant inhibitory effect of PCB on both markers (Figures 4B, C). Representative images show the high density of Mac-3 and CD3 expression (brown spots) in the EAE + vehicle, which is lower in the groups of EAE mice that received PCB. No immunostaining for Mac-3 or CD3 was detected in the spinal cords of healthy mice (image not shown). Statistical analyses confirmed a significant dose-dependent diminution of the densities of Mac-3 and CD3 in PCB-treated EAE animas at all doses compared to those receiving the vehicle.

PCB increases OPC, matured OD and reduces axonal damage in the spinal cords of EAE mice

OPC and mature OD identification in the white matter of spinal cords was performed using an anti-Olig2 antibody (Figure 5A) or an anti-TPPP/p25 (Figure 5B), respectively. IHC was also performed for the APP as a marker of axonal damage (Figure 5C). A dose-dependent effect of PCB on the levels of these three markers was found when compared to the EAE animals treated with the vehicle. PCB at the highest dose (1 mg/kg) showed a statistically significant increase of both oligodendrocyte markers (Olig2 and TPPP/p25). Furthermore, there was a statistically significant rise of Olig2 in both the lowest and the intermediate doses of PCB (0.1 and 0.5 mg/kg). Regarding TPPP/p25, there was also an increase of this marker in the EAE + PCB 0.5 mg/kg group, but not at the dose of 0.1 mg/kg of PCB. Moreover, PCB also showed a dose-dependent effect on the APP density. At the intermediate and the highest dose of PCB, this treatment significantly reduced APP levels. However, there was no difference in APP density between the EAE mice treated with lowest doses of PCB compared to those treated with the vehicle (Figure 5C).

"*In vitro*" and "*in vivo*" effects of PCB and its combination with IFN-β

The inhibitory effects of PCB and its combination with IFN-β was assessed in rat $T_{MBP\text{-}GFP}$ cells and in T cells isolated from the spleen of 2D2 mice. There was a clear trend that PCB alone was able to inhibit the proliferation of MBP-stimulated rat $T_{MBP\text{-}GFP}$ cells dose-dependently. However, when cultured with IFN-β alone at 10^3 U/mL, no anti-proliferative action of this drug was observed. Remarkably, the combination of both compounds showed a statistically significant effect and the dose-dependent inhibition of $T_{MBP\text{-}GFP}$ cell proliferation (Supplementary Figure 1). Furthermore, PCB also inhibited the proliferation of $CD4^+$ T cells isolated from 2D2 mice. The results showed a clear tendency to reduction in the proliferation of these activated $CD4^+$ T cells when treated with PCB alone at 10, 50 and 250 µg/mL (Supplementary Figure 2). However, this inhibitory effect was not evident with the treatment of 10^3 U/mL IFN-β alone, but it was significant when combined with 250 µg/mL PCB (Supplementary Figure 2). On the other hand, the intracellular localization analysis revealed that PCB was accumulated in the perinuclear region of $T_{MBP\text{-}GFP}$ cells (Supplementary Video 1).

In the next set of experiments, we evaluated the PCB/IFN-β combination in the mouse model of EAE. When the prophylactic regimen was implemented, two EAE-treated groups (PCB and the combination) showed a significant decrease in the clinical severity as evidenced by the area under the curve of disease progression with respect to the EAE + vehicle group. However, when the administration was in the therapeutic schedule, starting at day 14 post-immunization once the disease symptoms were already present, no differences in the neurological progression between groups were found (Figure 6). Accordingly, when the expression of some cytokines were assessed after concluding the prophylactic regimen, the EAE vehicle-treated mice showed significantly higher expression of

10.3389/fimmu.2022.1036200

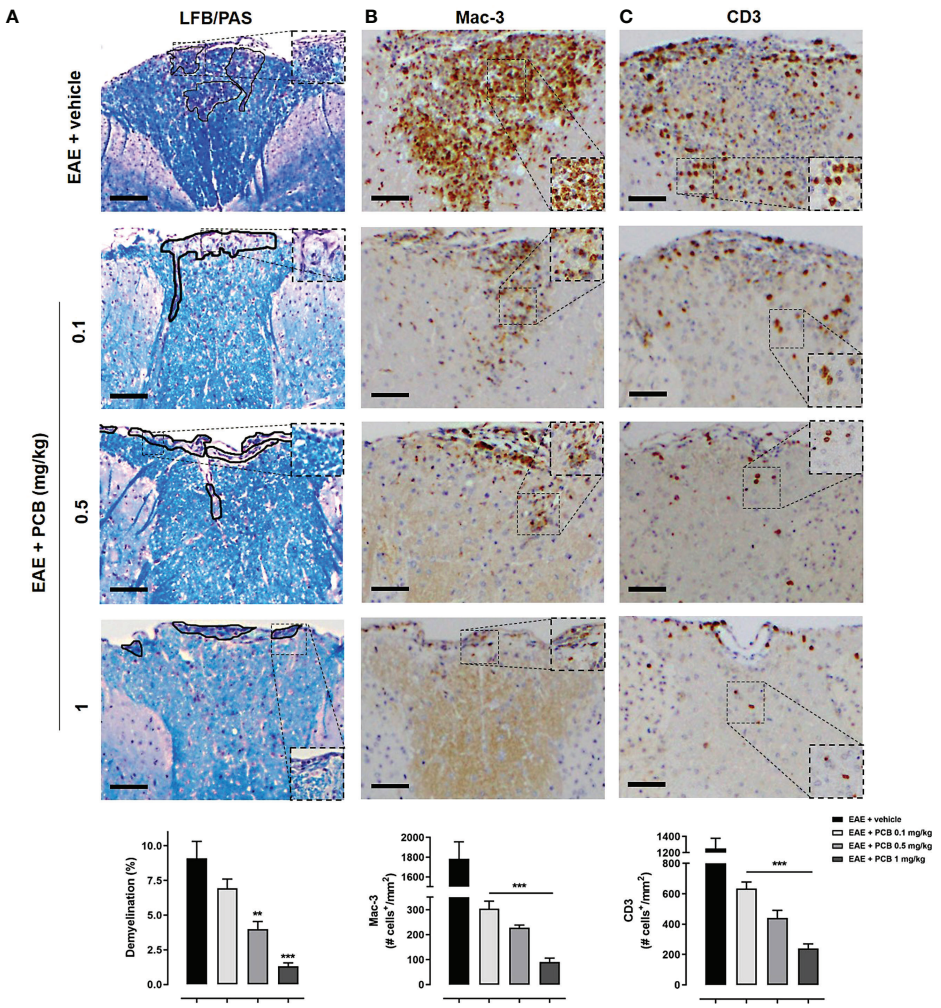

FIGURE 4
Histological and immunohistochemical assessment of the PCB effects on myelination and inflammation markers in spinal cords of EAE mice. The representative cross-sectional images and the respective morphometric evaluation per variable are shown in each panel. **(A)** Demyelination (LFB/PAS). **(B)** Macrophages/activated microglia (Mac-3). **(C)** T cells (CD3). MOG_{35-55} immunized mice received a daily i.p. injection of PBS (vehicle) or PCB at 0.1, 0.5 or 1 mg/kg, from day 0 until day 26 post-immunization. The areas marked with black pencil indicate demyelination. The percentage of demyelination and the cell densities (number of positive marked cells per mm^2) were calculated by dividing with total area of the white matter in transversal sections. Data are expressed as mean ± SEM (n=4-7 per group). The asterisks indicate statistically significant differences vs. EAE + vehicle group (**p<0.01, ***p<0.001, Kruskal-Wallis + Dunn's tests for LFB/PAS and Mac-3, ANOVA + Newman-Keuls tests for CD3). Bar: 50 µm.

IL-17A, IL-6, and IL-10 when compared to the naïve group (Figure 7A). On the contrary, the EAE mice treated with the PCB/IFN-β combination significantly reduced the brain expression levels of these cytokines compared with EAE vehicle-treated mice, reaching levels comparable to those of naïve animals (Figure 7A). The individual treatments also significantly reduced IL-10, and for IL-17A and IL-6, only IFN-β was evident to be significant, although a clear decreasing trend was detected with PCB alone (Figure 7A). Interestingly, a significant induction of Treg was found, as evidenced by the mean fluorescence intensity in the spleen of animals treated with the PCB/IFN-β combination (Figure 7B). Regarding the gene modulation in the brain, we found that *LINGO1* and *MAL* genes were up- or down-regulated, respectively, in the EAE vehicle-treated versus untreated animals (Figure 7C). For the *MAL* gene, an inverse modulation (upward) was obtained only for the EAE animals treated with the PCB/IFN-β combination, but not with the separate treatments, compared to EAE vehicle-treated group (Figure 7C). However, the *LINGO1* gene remained down-regulated with either the individual or the combined treatments (Figure 7C).

10.3389/fimmu.2022.1036200

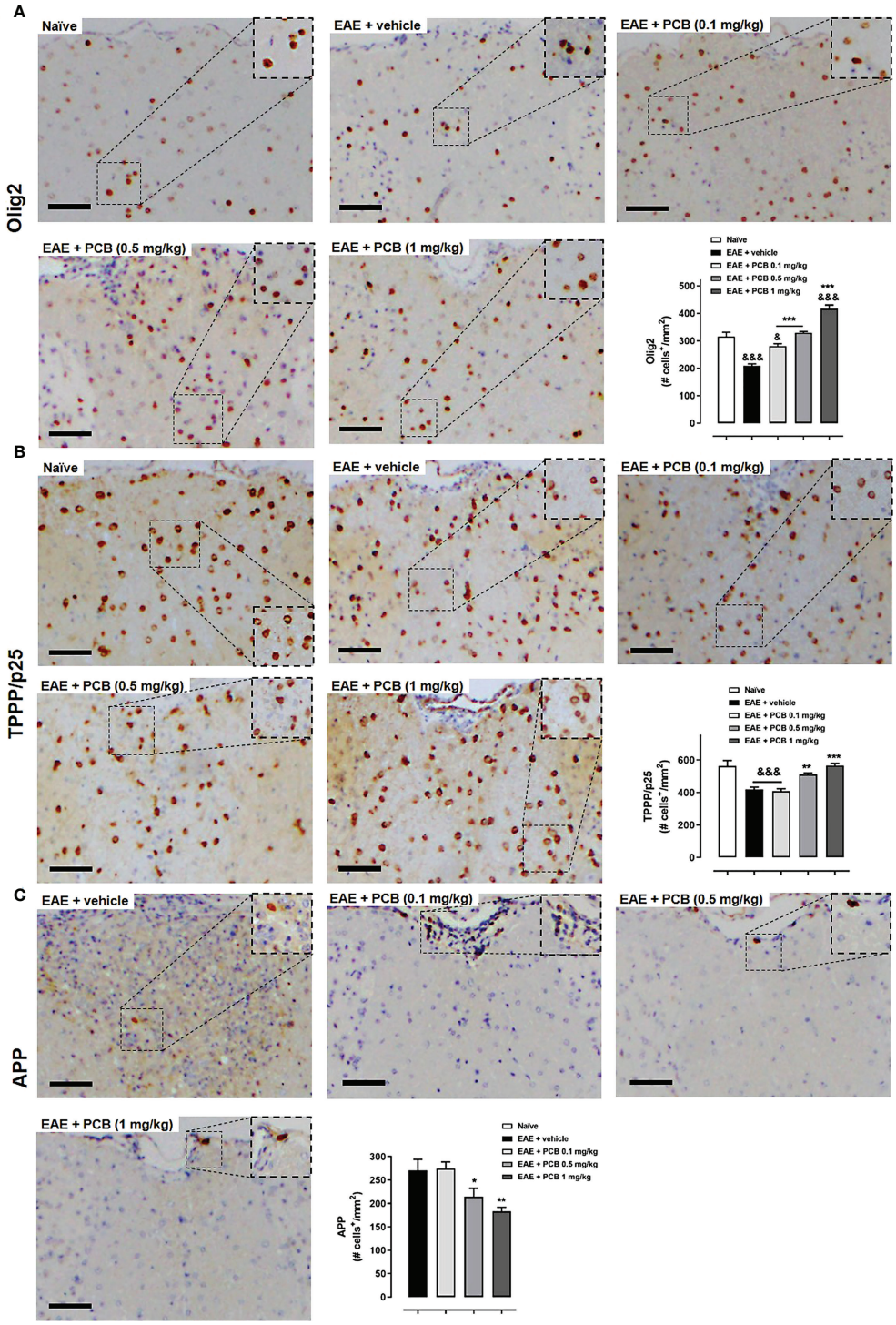

FIGURE 5
Immunohistochemical assessment of the PCB effects on oligodendrocyte and neuronal markers in spinal cords of EAE mice. The representative cross-sectional images and the respective morphometric evaluation per variable are shown in each panel. **(A)** Oligodendrocytes precursor cells (Olig2). **(B)** Mature oligodendrocytes (TPPP/p25). **(C)** Acute axonal damage (APP). MOG_{35-55} immunized mice received a daily i.p. injection of PBS (vehicle) or PCB at 0.1, 0.5 or 1 mg/kg, from day 0 until day 26 post-immunization. The cell densities (number of positive marked cells per mm^2) were calculated by dividing with total area of the white matter in transversal sections. Data are expressed as mean ± SEM (n=4-7 per group). The ampersand (&) and asterisk (*) are indicative of significant differences with non-immunized naïve and vehicle-treated EAE mice, respectively (*p<0.05, **p<0.01, ***p<0.001; $^{\&}$p<0.05, $^{\&\&\&}$p<0.001, ANOVA + Newman-Keuls tests). Bar: 50 µm.

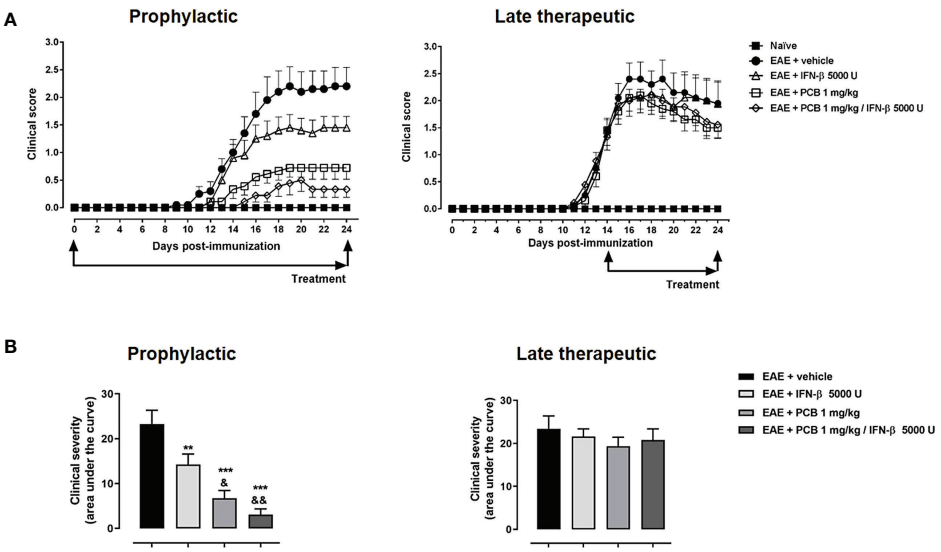

FIGURE 6
Effect of the treatment with the combination PCB/IFN-β and each compound individually on the clinical progression of EAE mice. **(A)** Daily clinical assessment of the mice. **(B)** Clinical severity determined by the area under the curve (in arbitrary units). MOG_{35-55} immunized mice were treated either with oral PCB at 1 mg/kg daily (once a day), with subcutaneous IFN-β at 5000 U every other day, or with their combination, initiating at day 0 (prophylactic schedule), or after the occurrence of the first disease symptoms at day 14 post-induction (late therapeutic schedule), lasting until day 24 post-immunization. A numeric scale with the ascending graveness was used to score every day the clinical signs of the mice, ranging from 0 (no disease) to 5 (death). The naïve group (non-immunized animals) remained healthful during the entire study period (score 0). Data are expressed as the mean ± S.E.M. (n=9-10 per group). The ampersand (&) and asterisk (*) are indicative of significant differences with IFN-β-treated or vehicle-treated EAE mice, respectively (**p<0.01, ***p<0.001, $^{\&}$p<0.05, $^{\&\&}$p<0.01, ANOVA + Newman-Keuls tests).

Discussion

In the present study, the outcomes and underlying mechanisms of the PCB administration were assessed in the EAE-MOG_{35-55} model of MS. We selected this model as appropriate for the PCB evaluation given the presence of both main components of the MS pathogenesis: immune dysfunction and neurodegeneration (5, 6, 11). Previously, we have reported that the anti-inflammatory and antioxidant properties of PCB and C-PC mediate their neuroprotective effects in animal models of cerebral ischemia (8–10). Such observations, therefore, suggest that these natural molecules might also curtail the pathogenesis of MS by acting on those pivotal deleterious processes.

Cytokines are mediators of both the innate and adaptive immunity (28). In this report, the administration of PCB in the MOG_{35-55} murine EAE model evidenced a significant dose-dependent reduction of cerebral expression of IL-17A and IL-6 in with respect to vehicle-treated EAE subjects. IL-17A and IL-6 are pro-inflammatory cytokines reported to play a key role in EAE (29). In this regard, several experimental models support the role of inflammatory cytokines in EAE; for example: anti-IL-17A antibodies cause a delay in disease progression in the EAE model (30), while the IL-17A blockade attenuates EAE (31), and mice either deficient of IL-17A or that received anti-IL-17A were protected from EAE establishment (32). In the same line, anti-IL-6 receptor monoclonal antibodies inhibited the development of EAE (33). Such evidence supports the positive impact of the cytokines reduction promoted by PCB in EAE. Moreover, we identified an increase in the IL-10 immunoregulatory cytokine in vehicle-treated EAE animals (similar to the IL-17A and IL-6 proinflammatory cytokines), which also decreased significantly with the PCB treatment. A possible explanation for this observation is that the immune system produces IL-10 as a negative feedback mechanism to maintain immune homeostasis from pro-inflammatory overreactions. Indeed, it has been shown that the IL-17 cytokine could also be produced not only by Th17 cells, but also by macrophages and T cells lacking either IL-10 or IL-10 receptor expression (34). The presence of recombinant IL-10 in the culture of these immune cells abrogates the production of IL-17, thus demonstrating the critical immune regulating role of IL-10 (34). Then, when the PCB treatment counteracts the overproduction of the pro-inflammatory cytokines (IL-17A and IL-6), the immunoregulatory component (IL-10) is also reduced as a balancing immune response.

Moreover, in our study, we inspected the dose-dependent outcome of PCB on the modulation of different genes related to the myelin physiology. We grouped them into genes whose products may injure the myelin in specific conditions (*LINGO1*,

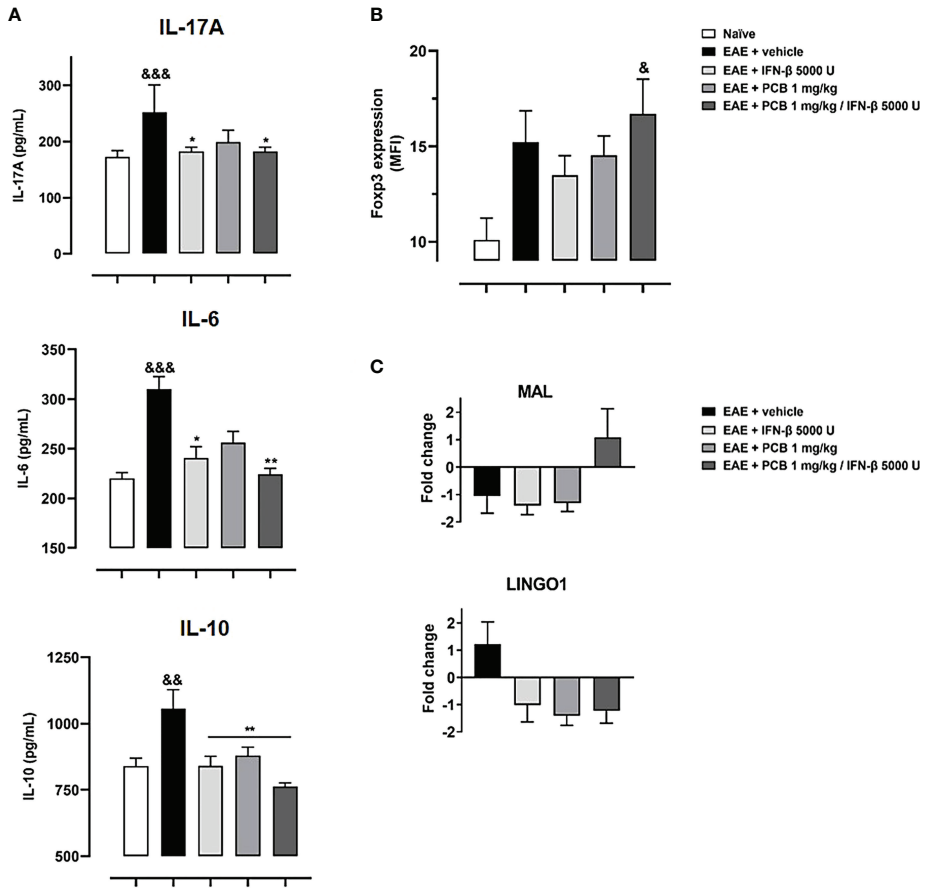

FIGURE 7
Effect of the treatment with the combination PCB/IFN-β and each compound individually on the cerebral expression of cytokines (protein levels) and of demyelinating/remyelinating-related genes (mRNA levels), as well as on the Treg levels in spleen of EAE mice. Panels show **(A)** the cytokines levels IL-17A, IL-6 and IL-10 from brain as assessed by ELISA, **(B)** Treg cells from mice spleen analyzed in the $CD4^+$ $CD25^{high}$ gate and expressed as Foxp3 Mean Fluorescence Intensity (MFI), **(C)** mRNA levels of *LINGO1* and *MAL* genes as assessed by quantitative Real Time PCR from the mice brain. MOG_{35-55} immunized mice were treated either with oral PCB at 1 mg/kg daily (once a day), with subcutaneous IFN-β at 5000 U every other day, or with their combination, initiating at day 0 (prophylactic schedule), or after the occurrence of the first disease symptoms at day 14 post-induction (late therapeutic schedule), lasting until day 24 post-immunization. Data are expressed as mean ± S.E.M. (n=4-7 per group). The ampersand (&) and asterisk (*) are indicative of significant differences in comparison to non-immunized naïve and to vehicle-treated EAE mice, respectively. (*p<0.05, **p<0.01, $^{\&}$p<0.05, $^{\&\&}$p<0.01, $^{\&\&\&}$p <0.001, Kruskal-Wallis + Dunn's tests when compared with EAE + vehicle group for IL-17A and IL-16, or according to ANOVA + Newman-Keuls tests for IL-10 and MFI of Fopx3).

NOTCH1, and *TNF-a*) and those that could preserve it or participate in the myelogenesis multi-step process (*CXCL12*, *MAL*, *MOG*, *NKX2-2*, *OLIG1*).

The TNF-α cytokine has been shown to be a pleiotropic cytokine. In the cuprizone model of demyelination, animals deficient in TNF-α showed a significant delay in remyelination along with a significant decline in the number of mature OD (35). In contrast, the treatment of cuprizone-fed mice with XPro1595, a specific inhibitor of soluble TNF-α able to enter into the CNS, promoted early remyelination and impeded motor behavior deterioration (36), which suggests the relevant role of this cytokine in MS remyelination failure. That being so, it was also confirmed that the selective inhibition of soluble TNF-α improves recovery in the EAE mice model (37). In our study in diseased EAE animals (vehicle-treated), the *TNF-α* gene was up-regulated, however, EAE animals treated with the three doses of PCB showed down-regulation of the *TNF-α* gene. This suggests that PCB may favor the remyelination process by limiting the expression of TNF-α.

On the other hand, both the *LINGO1* and the *NOTCH1* genes, were up-regulated in the vehicle- or the PCB (0.1 and 0.5 mg/kg)-treated EAE animals, but both genes were down-regulated by the highest dose of this compound (1 mg/kg). It has been shown that the loss of the LINGO1 function in EAE mice led to a neurological improvement (38), while in the cuprizone animal model, an anti-LINGO1 antibody improved remyelination and neurobehavioral performance (39). Furthermore, the intranasal delivery of siRNA-loaded chitosan

nanoparticles targeting LINGO1 was associated with signs of repair, neuroprotection, and remyelination in rats with ethidium bromide-triggered demyelination (40). On the other hand, by using the cuprizone animal model it was showed that inhibition of the *NOTCH1* gene expression by using an specific siRNA, accelerated remyelination mainly through increasing the mature OD in the brain lesions (41). In another study, with the aim of establishing whether NOTCH-JAGGED signaling regulated the rate of remyelination, young and adult animals were compared in the cuprizone model and no significant differences were found (42). Similarly, other authors have found that both NOTCH1 receptor and its ligand JAGGED1 were notably expressed in demyelinated areas of mice with EAE (43). Although the mechanistic role of LINGO1 and NOTCH1 in demyelination/remyelination processes in MS is yet to be fully elucidated, the available reports point to a deleterious action on the myelogenesis (44). Thus, the downregulation of these genes by PCB at the highest dose suggests a positive effect in promoting the formation of new myelin.

Furthermore, we identified the downregulation of the *CXCL12*, *MOG*, *NKX2-2*, *OLIG1* and *MAL* genes in the brain of sick EAE animals receiving the vehicle and an upregulation of the four first genes when those were treated with the three doses of PCB. The exception was found with the *MAL* gene in which its expression was increased only in the group EAE + PCB 1 mg/kg.

It has been observed that the lentivirus-mediated overexpression of CXCL12 in the *corpus callosum* with cuprizone-induced demyelination enhances OPC proliferation (45). Another study in which neonatal OPCs were isolated from rats showed that CXCL12 induces the activation of MEK/ERK and PI3K/AKT signaling in OPC promoting their migration (46). On the other hand, the primary physiological function of MOG, a protein exclusively present on the surface of myelin sheaths and OD processes, is not yet clearly established. However, its expression at the beginning of the myelination events and throughout the OD maturation process supports a likely involvement of this protein in the correct structural integrity of the myelin sheaths (47).

Other relevant protein in these aspects is NKX2-2, an important transcriptional factor for OPC differentiation. The expression of this gene has been detected in early CNS demyelinated lesions caused by ethidium bromide in rats, but not in old adult animals which have the slowest myelination speed. Thus, this evidence supports the notion that the abundance of NKX2-2 could accelerate remyelination in damaged CNS regions (48). In another study, by using *in situ* hybridization, immunofluorescence, and co-immunoprecipitation, it was demonstrated that the protein domains of NKX2-2 is critically present in OD differentiation (49). Similarly, another important mediator of myelin formation is OLIG1. It has been reported that when a neural progenitor cell (NPC) transplantation was performed in *OLIG1*$^{-/-}$ and *OLIG1*$^{+/+}$ mice infected with mouse hepatitis virus, only wild-type recipients exhibited extensive remyelination and differentiated preferentially in OPC (50). Previous reports have also suggested the potential involvement of OLIG1 in brain ischemia repair mechanisms when observed that its expression pattern was closely associated with endogenous remyelination (51). Besides these mediators, the MAL protein is predominantly expressed in OD, and it has been shown through genetic ablation procedures its relevant role in the axon-myelin interaction (52). Interestingly, a positive modulation of the *MAL* gene expression was also found in studies of our team using C-PC and PCB in animal models of MS (6) and cerebral ischemia (9), respectively. Therefore, the evidence shown above expresses the positive effects of PCB on these pro-myelinating genes and their potential involvement in myelin restoration in mice with EAE.

Accordingly, the LFB staining analysis of spinal cords revealed the presence of extensive demyelinated areas in mice of the EAE vehicle group, in agreement with previous reports (53, 54), as well as the significant increase of activated microglia, macrophages and T cells, supporting the inflammatory features involved in EAE (55, 56). In contrast, a significant reduction of CNS microglia/macrophages was observed in EAE animals that received any of the three PCB doses, and thus confirms its role in the action mechanisms for resisting this disease (57, 58). In the context of MS, activated microglia also contribute to neuronal and OD injury by acting as a paramount source of reactive oxygen species (ROS) (59). Indeed, microglial NADPH oxidase has been demonstrated to be one of the main sources of ROS in active MS lesions (60). The oxidative damage to lipids and DNA of the OPC, OD, and neurons, is closely associated with CNS demyelination and neurodegeneration (61). In this sense, PCB can inhibit the microglial NADPH oxidase (62). The inhibition of this enzyme is considerably beneficial in this context because it produces the superoxide anion radical which later reacts with nitric oxide favoring the rapid production of peroxynitrite, a key mediator of myelin and axon toxicity (63). PCB can also reduce oxidative damage by acting as a peroxynitrite scavenger (64). Therefore, the antioxidant activities of PCB may restore the redox balance in EAE mice and contribute to the myelin/axonal repair mechanisms.

Under pathological conditions, the activated microglia favors the infiltration of pro-inflammatory immune cells in the CNS by secreting matrix metalloproteinases (MMPs), mediators of BBB breakdown (65). Thus, the PCB treatment may prevent such events by limiting the rise in activated microglia. In addition, PCB can have a positive neuroaxonal effect by reducing the microglial secretion levels of pro-inflammatory cytokines, such as IFN-γ and TNF-α (66), and cytokines involved in the Th1 and Th17 response such as IL-12, IL-6 and IL-23 (67). The cytokines that mediate the inflammatory responses in MS and EAE may also directly impact on the myelinating capacity of OD (68). Indeed, IFN-γ and TNF-α act as pro-apoptotic inducers in human oligodendroglial cells, and furthermore, they potentiated the extent of cell death when co-incubated together (69).

In our study, an increase in OPC (identified by the Olig2 marker) and mature OD (evidenced by TPPP/p25) mediated the effects of PCB, suggesting the pro-myelination action of PCB, given that Olig2 functions as a transcription factor during the development of OD (70). Previously, it has been observed that the specific overexpression of Olig2 in OPC under demyelinating conditions promotes their migration to the CNS lesions and their differentiation into mature OD, which lead to an early remyelination process in lysophosphatidylcholine-intoxicated mice (71). Although this strongly suggests that PCB may induce the formation of new myelin in EAE mice, further evidence in this regard could be assessed in non-immunological demyelination models, such as the cuprizone or the lysophosphatidylcholine mice models.

The increase in the expression of Olig2 and TPPP/p25 caused by PCB indicates that this molecule favors the proliferative and migratory functions of OPC and their final differentiation into mature OD capable of myelinating the injured axons. The optimal expression of TPPP/p25 plays key physiological roles in the differentiation of OPC to mature myelinating OD (72). The TPPP/p25 protein is essential in the dynamics of the regeneration of the microtubule system during the elongation process previous to the myelin sheath structuring (73). These microtubules are essential for the structural stability and plasticity of myelinating OD. Furthermore, the evidence suggests that TPPP/p25 is also involved in the cellular metabolism, because its expression produces an increase in ATP levels (74). In MS patients, an increase in TPPP/p25 was detected in remyelinating lesions (73). OD that express TPPP/p25 extensively are able to form a compact myelin sheath that wraps the axon. The novel-formed myelin cover may physically curtail the direct action of immune cells and inflammatory molecules that mediate the damage to the axon, and it may also restore the trophic support to it (75).

Here, the axonal protecting activity of PCB was also evaluated, and its dose-dependent benefit at 0.5 and 1 mg/kg was demonstrated in animals with EAE. This could be related to the rapid restoration of the myelin trophic support that enables the survival and functionality of the axons. Therefore, it reduces axonal damage and the occurrence of intrinsic axonal defects that mediate physical and biochemical signals preventing myelination (76). The reduction of the abnormal accumulation of APP indicates that the axons are viable and rapid anterograde transport of APP occurs through them (77). The transported APP exerts trophic and synaptogenic roles, suggesting a restoration of the synapse (78), which is affected during demyelination (79).

On the other hand, *in vitro* studies in $T_{MBP\text{-}GFP}$ encephalitogenic cells, demonstrated that PCB (and its combination with IFN- β) was able to inhibit the proliferation of these cells. Similarly, in these cells, the perinuclear location of the PCB was identified using the confocal microscope.

IFN-β is a standard treatment for MS, but it comes with limitations (80). In order to surpass this, the combination of IFN-β with other compounds acting on targets from either the immune or the nervous systems can potentially be a better therapeutic strategy for MS than IFN-β alone (81, 82). Hence, certain studies show the effects of IFN-β when co-administered with other DMTs. For example, one study showed a synergistic effect of IFN-β and dimethyl fumarate in EAE (83). A second study showed that the addition of a 1α,25-dihydroxyvitamin D3 analog with IFN-β produced additional immunomodulatory effects for the prevention of EAE (84). A third study demonstrated that the IFN-β-secreting mesenchymal stem cells and minocycline combination considerably reduced the clinical deterioration of EAE (85). A fourth study reported that the combined therapy of high doses of methylprednisolone with IFN-β had a synergistic effect in EAE (86). Our group demonstrated with a microarray assay of the brain of EAE mice that C-PC modulated additional desirable biological processes compared to IFN-β (6). Following this line of reasoning, here we report the beneficial effects of the PCB/IFN-β combination in EAE, thus supporting its complementarity.

The efficacy of IFN-β was assessed in the setting of EAE while combined therapies have also been tested in the EAE model demonstrating their effects (85, 87). In our study, the combined therapy of PCB/IFN-β, was, therefore, evaluated in the animal model of EAE. PCB in the combined therapy was administered orally, the efficacy of which had been previously demonstrated by our group when it was applied individually at different doses to EAE mice (7). This aspect is relevant for the potential clinical translation since the Spirulin-derived PCB administered orally has been issued the US Food and Drug Administration category of Generally Recognized As Safe (GRAS) (88).

A superior clinical effect was identified here in EAE animals treated with the PCB/IFN-β combined therapy when both molecules are administered prophylactically. However, no beneficial effect was observed when both molecules were administered in a late therapeutic regimen, which then open the perspective of a further evaluation with higher doses of these compounds. In our study, we have identified that both IFN-β and PCB, and to a greater extent, the treatment using both molecules, reduced the cerebral expression of pro-inflammatory cytokines IL-17A and IL-6. Consistently, the effectiveness of IFN-β in the EAE model induced by rodent recombinant $MOG_{35\text{-}55}$ (independent of B cells) has been clearly related to the diminution of CNS pro-inflammatory cytokines (89). Another study also shows that the effectiveness of IFN- β is related to an inflammasome-dependent EAE model (90). Additionally, a greater induction of Treg in the spleen of the animals was achieved with the PCB/IFN-β combined therapy. A similar result on Treg was previously obtained by our group with the treatment of C-PC of peripheral blood mononuclear cells

isolated from patients with MS (5). Along these lines of evidence, Treg can promote the differentiation of OPC and, consequently, favor their remyelination capability in the injured CNS (91). Interestingly, the PCB/IFN-β combined treatment differentially modulated the cerebral expression of *MAL* (upregulation) and *LINGO1* (downregulation) genes, supporting the remyelinating advantage of this pharmacological combination. PCB adds to this combination its anti-inflammatory, antioxidant, and remyelinating capabilities as have been shown in rodent models of EAE, and in other models of neurodegenerative diseases (92).

Conclusion

There is an urgent need to identify MS drugs that target demyelination, which is a "gap" in the DMTs available thus far. PCB is well known for its neuroprotective and anti-inflammatory properties. In this study, we elucidated for the first time important clues of the mechanism by which PCB can promote remyelination in mice suffering EAE, comprising the stimulation of both the OPC and the mature OD. Moreover, PCB had also an advantageous impact on the reduction of axonal damage. On the other hand, the effect of PCB on the reduction of pro-inflammatory cytokines and its relationship with demyelination/remyelination processes is also highlighted in this study. Finally, the herein identification of the clinical superiority of the combination PCB/IFN-β, its associated reduction of pro-inflammatory cytokines and the increase of Treg, supports its potential application as a new feasible therapy for MS.

Data availability statement

The original analysis of this study is presented in Supplementary Table 2. Inquiries regarding data sharing can be requested from the corresponding author.

Ethics statement

The animal study was reviewed and approved by the institutional animal ethics committee of the Federal University of Minas Gerais, (CEUA - 255/2015), Belo Horizonte, Brazil.

Author contributions

JM-P, conceptualization, writing, formal analysis, investigation, and funding acquisition. NP-F, formal analysis, investigation, and funding acquisition. NL-D, conceptualization, formal analysis, and investigation. HC-R, investigation (performing qPCR). AG-S, investigation (imaging and morphometry). RS-C, investigation (imaging and morphometry). ELMV, investigation and formal analysis (performance and analysis of flow cytometry). JC-T, investigation (EAE model) and writing. VF-C, investigation (microscopy analysis). JF-M, investigation, formal analysis, and methodology. IH-G, investigation and writing. GM-D, investigation and project administration. GG-N, methodology, project administration, and funding acquisition. EP-A, methodology and writing. MMT, methodology, writing, and funding acquisition. GP-R, conceptualization, writing, original draft, project administration, methodology, and funding acquisition. All authors contributed to the article and approved the submitted version.

Funding

This work was partially supported by the Federal Ministry of Education and Research of Germany (BMBF) (Project number: 01DN18042) and the Science without Borders Program of Brazil (Project No. 405878/2013-3).

Acknowledgments

We would like to thank Prof. Naoto Kawakami and Dr. Isabel Bauer for their technical assistance and contribution to the grant from BMBF.

Conflict of interest

The authors declare that the research was conducted in the absence of any commercial or financial relationships that could be construed as a potential conflict of interest.

Publisher's note

Supplementary material

The Supplementary Material for this article can be found online at: https://www.frontiersin.org/articles/10.3389/fimmu.2022.1036200/full#supplementary-material

SUPPLEMENTARY FIGURE 1
Effects of the combination PCB + IFN-β on rat encephalitogenic $T_{MBP-GFP}$ cells. Effect on the proliferation: $T_{MBP-GFP}$ cells (4 x 10^4 cells/well) were cultured for 48 h in different treatment conditions in 96-well plate with the presence of irradiated rat thymocytes (5000 rad, 10^6 cells/well). Complete DMEM/1% rat serum with 10 µg/mL MBP was used. Immediately after, 0.5 mg/mL MTT was added to the medium and cultured for another 4 h. After medium removal, the resulting formazan was solubilized and its absorbance was measured at 570 nm. Data is presented as mean ± S.E.M. Ampersand (&) and asterisk (*) indicate significant differences in comparison to 10^3 U/mL IFN-β and control, respectively (**p<0.01, ***p<0.001 vs control; $^{\&}$p<0.05, $^{\&\&}$p <0.01 vs IFN-β, according to Kruskal-Wallis + Dunn's tests).

SUPPLEMENTARY FIGURE 2
Effects of the combination PCB + IFN-β on the proliferation of $CD4^+$ T cells from 2D2 mice. PCB was incubated with purified $CD4^+$ T cells at different concentrations in the presence of absence of 5 x 10^3 U/mL IFN-β. A seeding density of 2 x 10^5 cells/well was used for the co-stimulation of $CD4^+$ T cells with anti-CD3 and anti-CD28 at 2 µg/mL in 96-well plate. Two days later, $CD4^+$ T cells were incubated with IL-2 at 10 ng/mL for another 24 h. Then, MTT assay was performed and its cellular reduction was measured by the absorbance at 570 nm. Positive and negative controls indicate the absence of the drugs in the medium or no incubation with anti-CD3/anti-CD28/IL-2/drugs, respectively. Data is presented as mean ± S.E.M. Ampersand (&) and asterisk (*) indicate significant differences in comparison to 10^3 U/mL IFN-β and control, respectively (***p<0.001 vs control; $^{\&\&}$p <0.01 vs IFN-β, according to Kruskal-Wallis + Dunn's tests).

SUPPLEMENTARY VIDEO 1
$T_{MBP-GFP}$ cells (5 x 10^5 cells/well) were cultured in 12-well plate together with irradiated rat thymocytes (5000 rad, 1.25 x 10^7 cells/well) in complete DMEM/1% rat serum with 10 µg/mL MBP and 200 µg/µL PCB for 3 h. Immediately after, nuclear DNA was labeled with 1 µg/mL DAPI, the image was taken by confocal microscopy and analyzed by Fiji software. Blue and red colors indicate the presence of the cell nucleus and PCB, respectively, in two $T_{MBP-GFP}$ cells.

References

1. Imitola J, Chitnis T, Khoury SJ. Insights into the molecular pathogenesis of progression in multiple sclerosis: potential implications for future therapies. *Arch Neurol* (2006) 63(1):25–33. doi: 10.1001/archneur.63.1.25

2. Dutta R, Trapp BD. Relapsing and progressive forms of multiple sclerosis: insights from pathology. *Curr Opin Neurol* (2014) 27(3):271–8. doi: 10.1097/WCO.0000000000000094

3. Bross M, Hackett M, Bernitsas E. Approved and emerging disease modifying therapies on neurodegeneration in multiple sclerosis. *Int J Mol Sci* (2020) 21 (12):4312. doi: 10.3390/ijms21124312

4. Podbielska M, O'Keeffe J, Pokryszko-Dragan A. New insights into multiple sclerosis mechanisms: Lipids on the track to control inflammation and neurodegeneration. *Int J Mol Sci* (2021) 22(14):7319. doi: 10.3390/ijms22147319

5. Pentón-Rol G, Martínez-Sánchez G, Cervantes-Llanos M, Lagumersindez-Denis N, Acosta-Medina EF, Falcón-Cama V, et al. C-phycocyanin ameliorates experimental autoimmune encephalomyelitis and induces regulatory T cells. *Int Immunopharmacol* (2011) 11(1):29–38. doi: 10.1016/j.intimp.2010.10.001

6. Pentón-Rol G, Lagumersindez-Denis N, Muzio L, Bergami A, Furlan R, Fernández-Massó JR, et al. Comparative neuroregenerative effects of c-phycocyanin and IFN-beta in a model of multiple sclerosis in mice. *J Neuroimmune Pharmacol* (2016) 11:153–67. doi: 10.1007/s11481-015-9642-9

7. Cervantes-Llanos M, Lagumersindez-Denis N, Marín-Prida J, Pavón-Fuentes N, Falcon-Cama V, Piniella-Matamoros B, et al. Beneficial effects of oral administration of c-phycocyanin and phycocyanobilin in rodent models of experimental autoimmune encephalomyelitis. *Life Sci* (2018) 194:130–8. doi: 10.1016/j.lfs.2017.12.032

8. Pentón-Rol G, Marín-Prida J, Pardo-Andreu G, Martínez-Sánchez G, Acosta-Medina EF, Valdivia-Acosta A, et al. C-phycocyanin is neuroprotective against global cerebral ischemia/reperfusion injury in gerbils. *Brain Res Bull* (2011) 86(1-2):42–52. doi: 10.1016/j.brainresbull.2011.05.016

9. Marín-Prida J, Pavón-Fuentes N, Llópiz-Arzuaga A, Fernández-Massó JR, Delgado-Roche L, Mendoza-Marí Y, et al. Phycocyanobilin promotes PC12 cell survival and modulates immune and inflammatory genes and oxidative stress markers in acute cerebral hypoperfusion in rats. *Toxicol Appl Pharmacol* (2013) 272(1):49–60. doi: 10.1016/j.taap.2013.05.021

10. Pavón-Fuentes N, Marín-Prida J, Llópiz-Arzuaga A, Falcón-Cama V, Campos-Mojena R, Cervantes-Llanos M, et al. Phycocyanobilin reduces brain injury after endothelin-1- induced focal cerebral ischaemia. *Clin Exp Pharmacol Physiol* (2020) 47(3):383–92. doi: 10.1111/1440-1681.13214

11. Pentón-Rol G, Marín-Prida J, Falcón-Cama V. C-phycocyanin and phycocyanobilin as remyelination therapies for enhancing recovery in multiple sclerosis and ischemic stroke: A preclinical perspective. *Behav Sci (Basel)* (2018) 8 (1):15. doi: 10.3390/bs8010015

12. Luo C, Jian C, Liao Y, Huang Q, Wu Y, Liu X, et al. The role of microglia in multiple sclerosis. *Neuropsychiatr Dis Treat* (2017) 13:1661–7. doi: 10.2147/NDT.S140634

13. Steck AJ, Stalder AK, Renaud S. Anti-myelin-associated glycoprotein neuropathy. *Curr Opin Neurol* (2006) 19(5):458–63. doi: 10.1097/01.wco.0000245368.36576.0d

14. Kuehn BM. Scientists probe strategies to repair neuron damage in multiple sclerosis. *JAMA* (2011) 305(9):871–4. doi: 10.1001/jama.2011.208

15. Tanaka T, Yoshida S. Mechanisms of remyelination: recent insight from experimental models. *Biomol Concepts* (2014) 5(4):289–98. doi: 10.1515/bmc-2014-0015

16. Pinto BF, Ribeiro LNB, da Silva GBRF, Freitas CS, Kraemer L, Oliveira FMS, et al. Inhalation of dimethyl fumarate-encapsulated solid lipid nanoparticles attenuate clinical signs of experimental autoimmune encephalomyelitis and pulmonary inflammatory dysfunction in mice. *Clin Sci (Lond)* (2022) 136(1):81–101. doi: 10.1042/CS20210792

17. Kerfoot SM, Kubes P. Overlapping roles of p-selectin and Î ± 4 integrin to recruit leukocytes to the central nervous system in experimental autoimmune encephalomyelitis. *J Immunol* (2002) 169(2):1000–6. doi: 10.4049/jimmunol.169.2.1000

18. Pyka-Fosciak G, Stasiolek M, Litwin JA. Immunohistochemical analysis of spinal cord components in mouse model of experimental autoimmune encephalomyelitis. *Folia Histochem Cytobiol* (2018) 56(3):151–8. doi: 10.5603/FHC.a2018.0018

19. Sengul G, Watson C. Spinal cord. In: Watson C, Paxinos G, Puelles L, editors. *The mouse nervous system. chapter 13*. San Diego, CA: Academic Press (2012). p. 424–58. doi: 10.1016/B978-0-12-369497-3.10013-5

20. Bustin SA, Benes V, Garson JA, Hellemans J, Huggett J, Kubista M, et al. The MIQE guidelines: minimum information for publication of quantitative real-time PCR experiments. *Clin Chem* (2009) 55(4):611–22. doi: 10.1373/clinchem.2008.112797

21. Livak KJ, Schmittgen TD. Analysis of relative gene expression data using real-time quantitative PCR and the 2(−delta delta C(T)) method. *Methods* (2001) 25(4):402–8. doi: 10.1006/meth.2001.1262

22. Pfaffl MW, Horgan GW, Dempfle L. Relative expression software tool (REST©) for group-wise comparison and statistical analysis of relative expression results in real-time PCR. *Nucleic Acids Res* (2002) 30(9):e36. doi: 10.1093/nar/30.9.e36

23. Henríquez C, Morán G, Carrasco C, Sarmiento J, Barría M, Folch H, et al. Modulatory role of regulatory T cells in a murine model of severe equine asthma. *BMC Vet Res* (2017) 13(1):117. doi: 10.1186/s12917-017-1037-0

24. Kawakami N, Lassmann S, Li Z, Odoardi F, Ritter T, Ziemssen T, et al. The activation status of neuroantigen-specific T cells in the target organ determines the clinical outcome of autoimmune encephalomyelitis. *J Exp Med* (2004) 199(2):185–97. doi: 10.1084/jem.20031064

25. Flügel A, Willem M, Berkowicz T, Wekerle H. Gene transfer into CD4+ T lymphocytes: green fluorescent protein-engineered, encephalitogenic T cells illuminate brain autoimmune responses. *Nat Med* (1999) 5(7):843–7. doi: 10.1038/10567

26. Chazotte B. Labeling nuclear DNA using DAPI. *Cold Spring HarbProtoc* (2011). doi: 10.1101/pdb.prot5556

27. Schindelin J, Arganda-Carreras I, Frise E, Kaynig V, Longair M, Pietzsch T. Fiji: an open-source platform for biological-image analysis. *Nat Methods* (2012) 9 (7):676–82. doi: 10.1038/nmeth.2019

28. Szelényi J. Cytokines and the central nervous system. *Brain Res Bull* (2001) 54(4):329–38. doi: 10.1016/s0361-9230(01)00428-2

29. Harrington LE, Hatton RD, Mangan PR, Turner H, Murphy TL, Murphy KM, et al. Interleukin 17-producing CD4+ effector T cells develop *via* a lineage distinct from the T helper type 1 and 2 lineages. *Nat Immunol* (2005) 6(11):1123–32. doi: 10.1038/ni1254

30. Kap YS, Jagessar SA, van Driel N, Blezer E, Bauer J, van Meurs M, et al. Effects of early IL-17A neutralization on disease induction in a primate model of experimental autoimmune encephalomyelitis. *J Neuroimmune Pharmacol* (2011) 6 (3):341–53. doi: 10.1007/s11481-010-9238-3

31. Setiadi AF, Abbas AR, Jeet S, Wong K, Bischof A, Peng I, et al. IL-17A is associated with the breakdown of the blood-brain barrier in relapsing-remitting multiple sclerosis. *J Neuroimmunol* (2019) 332:147–54. doi: 10.1016/j.jneuroim.2019.04.011

32. McGinley AM, Sutton CE, Edwards SC, Leane CM, DeCourcey J, Teijeiro A, et al. Interleukin-17A serves a priming role in autoimmunity by recruiting IL-1β-Producing myeloid cells that promote pathogenic T cells. *Immunity* (2020) 52 (2):342–356.e6. doi: 10.1016/j.immuni.2020.01.002

33. Serada S, Fujimoto M, Mihara M, Koike N, Ohsugi Y, Nomura S, et al. IL-6 blockade inhibits the induction of myelin antigen-specific Th17 cells and Th1 cells in experimental autoimmune encephalomyelitis. *Proc Natl Acad Sci U S A* (2008) 105(26):9041–6. doi: 10.1073/pnas.0802218105

34. Gu Y, Yang J, Ouyang X, Liu W, Li H, Yang J, et al. Interleukin 10 suppresses Th17 cytokines secreted by macrophages and T cells. *Eur J Immunol* (2008) 38 (7):1807–13. doi: 10.1002/eji.200838331

35. Arnett HA, Mason J, Marino M, Suzuki K, Matsushima GK, Ting JP. TNF alpha promotes proliferation of oligodendrocyte progenitors and remyelination. *Nat Neurosci* (2001) 4(11):1116–22. doi: 10.1038/nn738

36. Karamita M, Barnum C, Möbius W, Tansey MG, Szymkowski DE, Lassmann H, et al. Therapeutic inhibition of soluble brain TNF promotes remyelination by increasing myelin phagocytosis by microglia. *JCI Insight* (2017) 2(8):e87455. doi: 10.1172/jci.insight.87455

37. Brambilla R, Ashbaugh JJ, Magliozzi R, Dellarole A, Karmally S, Szymkowski DE, et al. Inhibition of soluble tumour necrosis factor is therapeutic in experimental autoimmune encephalomyelitis and promotes axon preservation and remyelination. *Brain* (2011) 134(9):2736–54. doi: 10.1093/brain/awr199

38. Mi S, Hu B, Hahm K, Luo Y, Kam Hui ES, Yuan Q, et al. LINGO-1 antagonist promotes spinal cord remyelination and axonal integrity in MOG-induced experimental autoimmune encephalomyelitis. *Nat Med* (2007) 13 (10):1228–33. doi: 10.1038/nm1664

39. Moradbeygi K, Parviz M, Rezaeizadeh H, Zargaran A, Sahraian MA, Mehrabadi S, et al. Anti-LINGO-1 improved remyelination and neurobehavioral deficit in cuprizone-induced demyelination. *Iran J Basic Med Sci* (2021) 24(7):900–7. doi: 10.22038/ijbms.2021.53531.12043

40. Youssef AEH, Dief AE, El Azhary NM, Abdelmonsif DA, El-Fetiany OS. LINGO-1 siRNA nanoparticles promote central remyelination in ethidium bromide-induced demyelination in rats. *J Physiol Biochem* (2019) 75(1):89–99. doi: 10.1007/s13105-018-00660-6

41. Fan H, Zhao JG, Yan JQ, Du GQ, Fu QZ, Shi J. Effect of Notch1 gene on remyelination in multiple sclerosis in mouse models of acute demyelination. *J Cell Biochem* (2018) 119(11):9284–94. doi: 10.1002/jcb.27197

42. Stidworthy MF, Genoud S, Li WW, Leone DP, Mantei N, Suter U, et al. Notch1 and Jagged1 are expressed after CNS demyelination, but are not a major rate-determining factor during remyelination. *Brain* (2004) 127(9):1928–41. doi: 10.1093/brain/awh217

43. Seifert T, Bauer J, Weissert R, Fazekas F, Storch MK. Notch1 and its ligand Jagged1 are present in remyelination in a T-cell- and antibody-mediated model of inflammatory demyelination. *Acta Neuropathol* (2007) 113(2):195–203. doi: 10.1007/s00401-006-0170-9

44. Bove RM, Green AJ. Remyelinating pharmacotherapies in multiple sclerosis. *Neurotherapeutics* (2017) 14(4):894–904. doi: 10.1007/s13311-017-0577-0

45. Patel JR, Williams JL, Muccigrosso MM, Liu L, Sun T, Rubin JB, et al. Astrocyte TNFR2 is required for CXCL12-mediated regulation of oligodendrocyte progenitor proliferation and differentiation within the adult CNS. *Acta Neuropathol* (2012) 124:847–60. doi: 10.1007/s00401-012-1034-0

46. Tian Y, Yin H, Deng X, Tang B, Ren X, Jiang T. CXCL12 induces migration of oligodendrocyte precursor cells through the CXCR4 activated MEK/ERK and PI3K/AKT pathways. *Mol Med Rep* (2018) 18(5):4374–80. doi: 10.3892/mmr.2018.9444

47. Peschl P, Bradl M, Höftberger R, Berger T, Reindl M. Myelin oligodendrocyte glycoprotein: Deciphering a target in inflammatory demyelinating diseases. *Front Immunol* (2017) 8:529. doi: 10.3389/fimmu.2017.00529

48. Fancy SP, Zhao C, Franklin RJ. Increased expression of Nkx2.2 and Olig2 identifies reactive oligodendrocyte progenitor cells responding to demyelination in the adult CNS. *Mol Cell Neurosci* (2004) 27(3):247–54. doi: 10.1016/j.mcn.2004.06.015

49. Zhang C, Huang H, Chen Z, Zhang Z, Lu W, Qiu M. The transcription factor NKX2-2 regulates oligodendrocyte differentiation through domain-specific interactions with transcriptional corepressors. *J Biol Chem* (2020) 295(7):1879–88. doi: 10.1074/jbc.RA119.011163

50. Whitman LM, Blanc CA, Schaumburg CS, Rowitch DH, Lane TE. Olig1 function is required for remyelination potential of transplanted neural progenitor cells in a model of viral-induced demyelination. *Exp Neurol* (2012) 235(1):380–7. doi: 10.1016/j.expneurol.2012.03.003

51. Zhao H, Gao XY, Liu ZH, Lin JW, Wang SP, Wang DX, et al. Effects of the transcription factor Olig1 on the differentiation and remyelination of oligodendrocyte precursor cells after focal cerebral ischemia in rats. *Mol Med Rep* (2019) 20(5):4603–11. doi: 10.3892/mmr.2019.10713

52. Schaeren-Wiemers N, Bonnet A, Erb M, Erne B, Bartsch U, Kern F, et al. The raft-associated protein MAL is required for maintenance of proper axon–glia interactions in the central nervous system. *J Cell Biol* (2004) 166(5):731–42. doi: 10.1083/jcb.200406092

53. Jurynczyk M, Jurewicz A, Bielecki B, Raine C, Selmaj K. Overcoming failure to repair demyelination in EAE: gamma-secretase inhibition of notch signaling. *J Neurol Sci* (2008) 265(1-2):5–11. doi: 10.1016/j.jns.2007.09.007

54. Constantinescu C, Farooqi N, O'Brien K, Gran B. Experimental autoimmune encephalomyelitis (EAE) as a model for multiple sclerosis (MS). *Br J Pharmacol* (2011) 164(4):1079–106. doi: 10.1111/j.1476-5381.2011.01302.x

55. Rawji K, Wee V. The benefits and detriments of Macrophages/Microglia in models of multiple sclerosis. *Clin Dev Immuno* (2013) 2013:948976. doi: 10.1155/2013/948976

56. Gao H, Danzi M, Choi C, Taherian M, Dalby C, Ellman D, et al. Opposing functions of microglial and macrophagic TNFR2 in the pathogenesis of experimental autoimmune encephalomyelitis. *Cell Rep* (2017) 18(1):198–212. doi: 10.1016/j.celrep.2016.11.083

57. Kotter M, Zhao C, van Rooijen N, Franklin R. Macrophage-depletion induced impairment of experimental CNS remyelination is associated with a reduced oligodendrocyte progenitor cell response and altered growth factor expression. *Neurobiol Dis* (2005) 18(1):166–75. doi: 10.1016/j.nbd.2004.09.019

58. Neumann H, Kotter M, Franklin R. Debris clearance by microglia: an essential link between degeneration and regeneration. *Brain* (2009) 132(2):288–95. doi: 10.1093/brain/awn109

59. Simpson DSA, Oliver PL. ROS generation in microglia: Understanding oxidative stress and inflammation in neurodegenerative disease. *Antioxid (Basel)* (2020) 9(8):743. doi: 10.3390/antiox9080743

60. Fischer MT, Sharma R, Lim JL, Haider L, Frischer JM, Drexhage J, et al. NADPH oxidase expression in active multiple sclerosis lesions in relation to oxidative tissue damage and mitochondrial injury. *Brain* (2012) 135(3):886–99. doi: 10.1093/brain/aws012

61. Haider L, Fischer MT, Frischer JM, Bauer J, Höftberger R, Botond G. Oxidative damage in multiple sclerosis lesions. *Brain* (2011) 134(7):1914–24. doi: 10.1093/brain/awr128

62. McCarty MF, Barroso-Aranda J, Contreras F. Oral phycocyanobilin may diminish the pathogenicity of activated brain microglia in neurodegenerative disorders. *Med Hypotheses* (2009) 74(3):601–5. doi: 10.1016/j.mehy.2008.09.061

63. Haslund-Vinding J, McBean G, Jaquet V, Vilhardt F. NADPH oxidases in oxidant production by microglia: activating receptors, pharmacology and association with disease. *Br J Pharmacol* (2017) 174(12):1733–49. doi: 10.1111/bph.13425

64. Bhat VB, Madyastha KM. Scavenging of peroxynitrite by phycocyanin and phycocyanobilin from spirulina platensis: protection against oxidative damage to DNA. *BiochemBiophys Res Commun* (2001) 285(2):262–6. doi: 10.1006/bbrc.2001.5195

65. Mirshafiey A, Asghari B, Ghalamfarsa G, Jadidi-Niaragh F, Azizi G. The significance of matrix metalloproteinases in the immunopathogenesis and treatment of multiple sclerosis. *Sultan Qaboos Univ Med J* (2014) 14(1):e13–25. doi: 10.12816/0003332

66. Takeuchi H. Neurotoxicity by microglia: mechanisms and potential therapeutic strategy. *Clin Exp Neuroimmunol* (2010) 1(1):12–21. doi: 10.1111/j.1759-1961.2009.00001.x

67. Heppner F, Greter M, Marino D. Experimental autoimmune encephalomyelitis repressed by microglial paralysis. *Nat Med* (2005) 11(2):146–52. doi: 10.1038/nm1177

68. Schmitz T, Chew LJ. Cytokines and myelination in the central nervous system. *ScientificWorldJournal* (2008) 8:1119–47. doi: 10.1100/tsw.2008.140

69. Buntinx M, Moreels M, Vandenabeele F, Lambrichts I, Raus. J, Steels P, et al. Cytokine-induced cell death in human oligodendroglial cell lines: I. synergistic effects of IFN-gamma and TNF-alpha on apoptosis. *J Neurosci Res* (2004) 76 (6):834–45. doi: 10.1002/jnr.20118

70. Mei F, Wang H, Niu J, Wang L, He Y. Stage-specific deletion of Olig2 conveys opposing functions on differentiation and maturation of oligodendrocytes. *J Neurosci* (2013) 33(19):8454–62. doi: 10.1523/JNEUROSCI.2453-12.2013

71. Wegener A, Deboux C, Bachelin C, Frah M, Kerninon C, Seilhean D, et al. Gain of Olig2 function in oligodendrocyte progenitors promotes remyelination. *Brain* (2015) 138(1):120–35. doi: 10.1093/brain/awu375

72. Lehotzky A, Lau P, Tokési N, Muja N, Hudson LD, Ovádi J. Tubulin polymerization-promoting protein (TPPP/p25) is critical for oligodendrocyte differentiation. *Glia* (2010) 58(2):157–68. doi: 10.1002/glia.20909

73. Höftberger R, Fink S, Aboul-Enein F, Botond G, Olah J, Berki T, et al. Tubulin polymerization promoting protein (TPPP/p25) as a marker for oligodendroglial changes in multiple sclerosis. *Glia* (2010) 58(15):1847–57. doi: 10.1002/glia.21054

74. Ovádi J, Orosz F. An unstructured protein with destructive potential: TPPP/p25 in neurodegeneration. *Bioessays* (2009) 31(6):676–86. doi: 10.1002/bies.200900008

75. Podbielska M, Banik NL, Kurowska E, Hogan EL. Myelin recovery in multiple sclerosis: the challenge of remyelination. *Brain Sci* (2013) 3(3):1282–324. doi: 10.3390/brainsci3031282

76. Witte ME, Mahad DJ, Lassmann H, van Horssen J. Mitochondrial dysfunction contributes to neurodegeneration in multiple sclerosis. *Trends Mol Med* (2014) 20:179–87. doi: 10.1016/j.molmed.2013.11.007

77. Terwel D, Dewachter I, Van Leuven F. Axonal transport, tau protein, and neurodegeneration in alzheimer's disease. *Neuromol Med* (2002) 2:151–65. doi: 10.1385/NMM:2:2:151

78. Moya KL, Benowitz LI, Schneider GE, Allinquant B. The amyloid precursor protein is developmentally regulated and correlated with synaptogenesis. *Dev Biol* (1994) 161:597–603. doi: 10.1006/dbio.1994.1055

79. Dutta R, Chang A, Doud MK, Grahame JK, Ribaudo MV, Young EA, et al. Demyelinitation causes synaptic alterations in hippocampi from multiple sclerosis patients. *Ann Neurol* (2011) 69:445–54. doi: 10.1002/ana.22337

80. Plosker GL. Interferon-β-1b: a review of its use in multiple sclerosis. *CNS Drugs* (2011) 25(1):67–88. doi: 10.2165/11206430-000000000-00000

81. Ghasami K, Faraji F, Fazeli M, Ghazavi A, Mosayebi G. Interferon beta-1a and atorvastatin in the treatment of multiple sclerosis. *Iran J Immunol* (2016) 13 (1):16–26.

82. Faraji F, Hashemi M, Ghiasabadi A, Davoudian S, Talaie A, Ganji A, et al. Combination therapy with interferon beta-1a and sesame oil in multiple sclerosis. *Complement Ther Med* (2019) 45:275–9. doi: 10.1016/j.ctim.2019.04.010

83. Reick C, Ellrichmann G, Thöne J, Scannevin RH, Saft C, Linker RA, et al. Neuroprotective dimethyl fumarate synergizes with immunomodulatory interferon beta to provide enhanced axon protection in autoimmune neuroinflammation. *Exp Neurol* (2014) 257:50–6. doi: 10.1016/j.expneurol.2014.04.003

84. van Etten E, Gysemans C, Branisteanu DD, Verstuyf A, Bouillon R, Overbergh L, et al. Novel insights in the immune function of the vitamin d system: synergism with interferon-beta. *J Steroid Biochem Mol Biol* (2007) 103(3-5):546–51. doi: 10.1016/j.jsbmb.2006.12.094

85. Hou Y, Heon Ryu C, Jun JA, Kim SM, Jeong CH, Jeun SS. Interferon β-secreting mesenchymal stem cells combined with minocycline attenuate experimental autoimmune encephalomyelitis. *J Neuroimmunol* (2014) 274(1-2):20–7. doi: 10.1016/j.jneuroim.2014.06.001

86. Schmidt J, Stürzebecher S, Toyka KV, Gold R. Interferon-beta treatment of experimental autoimmune encephalomyelitis leads to rapid nonapoptotic termination of T cell infiltration. *J Neurosci Res* (2001) 65(1):59–67. doi: 10.1002/jnr.1128

87. Aizman E, Mor A, Chapman J, Assaf Y, Kloog Y. The combined treatment of copaxone and salirasib attenuates experimental autoimmune encephalomyelitis (EAE) in mice. *J Neuroimmunol* (2010) 229(1-2):192–203. doi: 10.1016/j.jneuroim.2010.08.022

88. Eriksen NT. Production of phycocyanin a pigment with applications in biology, biotechnology, foods and medicine. *Appl Microbiol Biotechnol* (2008) 80 (1):1–14. doi: 10.1007/s00253-008-1542-y

89. Agasing AM, Gawde S, Kumar G, Turner E, Axtell RC. B cell function impacts the efficacy of IFN-β therapy in EAE. *J Neuroimmunol* (2020) 338:577106. doi: 10.1016/j.jneuroim.2019.577106

90. Inoue M, Williams KL, Oliver T, Vandenabeele P, Rajan JV, Miao EA, et al. Interferon-β therapy against EAE is effective only when development of the disease depends on the NLRP3 inflammasome. *Sci Signal* (2012) 5(225):ra38. doi: 10.1126/scisignal.2002767

91. Dombrowski Y, O'Hagan T, Dittmer M, Penalva R, Mayoral SR, Bankhead P, et al. Regulatory T cells promote myelin regeneration in the central nervous system. *Nat Neurosci* (2017) 20(5):674–80. doi: 10.1038/nn.4528

92. Pentón-Rol G, Marín-Prida J, McCarty MF. C-phycocyanin-derived phycocyanobilin as a potential nutraceutical approach for major neurodegenerative disorders and COVID-19-induced damage to the nervous system. *Curr Neuropharmacol* (2021) 19:000–0. doi: 10.2174/1570159X19666210408123807

frontiers | Frontiers in Immunology

TYPE Original Research
PUBLISHED 26 September 2023
DOI 10.3389/fimmu.2023.1178172

OPEN ACCESS

EDITED BY
Lindsay B. Nicholson,
University of Bristol, United Kingdom

REVIEWED BY
Florence Apparailly,
INSERM U1183 Institut de Médecine Régénératrice et de Biothérapie (IRMB), France
Sahil Mahajan,
The Ohio State University, United States

*CORRESPONDENCE
Nassima Bekaddour
nassima_47@hotmail.fr
Jean-Philippe Herbeuval
jean-philippe.herbeuval@parisdescartes.fr

RECEIVED 02 March 2023
ACCEPTED 14 July 2023
PUBLISHED 26 September 2023

CITATION
Bekaddour N, Smith N, Beitz B, Llibre A, Dott T, Baudry A, Korganow A-S, Nisole S, Mouy R, Breton S, Bader-Meunier B, Duffy D, Terrier B, Schneider B, Quartier P, Rodero MP and Herbeuval J-P (2023) Targeting the chemokine receptor CXCR4 with histamine analog to reduce inflammation in juvenile arthritis. *Front. Immunol.* 14:1178172. doi: 10.3389/fimmu.2023.1178172

Targeting the chemokine receptor CXCR4 with histamine analog to reduce inflammation in juvenile arthritis

Nassima Bekaddour[1,2]*, Nikaïa Smith[3], Benoit Beitz[4], Alba Llibre[3], Tom Dott[4], Anne Baudry[5], Anne-Sophie Korganow[6,7,8], Sébastien Nisole[9], Richard Mouy[10], Sylvain Breton[10,11], Brigitte Bader-Meunier[10,12], Darragh Duffy[3], Benjamin Terrier[13], Benoit Schneider[5], Pierre Quartier[10,12], Mathieu P. Rodero[1,2] and Jean-Philippe Herbeuval[1,2]*

[1]Centre National de la Recherche Scientifique (CNRS) Unité Mixte de Recherche (UMR)-8601, Université Paris Cité, Paris, France, [2]Chemistry and Biology, Modeling and Immunology for Therapy (CBMIT), Paris, France, [3]Translational Immunology Unit, Institut Pasteur, Université Paris Cité, Paris, France, [4]BIOASTER, Lyon, France, [5]Institut National de la Santé et de la Recherche Médicale (INSERM) Unité Mixte de Recherche (UMR)-S1124, Team Stem Cells, Signaling and Prions, Université Paris Cité, Paris, France, [6]Institut National de la Santé et de la Recherche Médicale (INSERM) Unité Mixte de Recherche (UMR) - S1109, Faculté de Médecine, Fédération Hospitalo-Universitaire OMICARE, Fédération de Médecine Translationnelle de Strasbourg (FMTS), Université de Strasbourg, Strasbourg, France, [7]Department of Clinical Immunology and Internal Medicine, National Reference Center for Rare Autoimmune Diseases Centre National de Référence des maladies auto-immunes et systémiques rares de Strasbourg (RESO), Hôpitaux Universitaires de Strasbourg, Strasbourg, France, [8]Unité de Formation et de Recherche (UFR) Medicine, University of Strasbourg, Strasbourg, France, [9]Institut de Recherche en Infectiologie de Montpellier (IRIM), Université de Montpellier, Centre National de la Recherche Scientifique (CNRS) Unité Mixte de Recherche (UMR) 9004, Montpellier, France, [10]Paediatric Haematology-Immunology and Rheumatology Department, Centre de référence des rhumatismes inflammatoires et maladies auto-immunes systémiques rares de l'enfant (RAISE) Reference Centre for Rare Diseases, Hôpital Universitaire Necker, Assistance Publique-Hôpitaux de Paris, Paris, France, [11]Paediatric Radiology Department, Necker-Enfants Malades University Hospital, Paris, France, [12]Pediatric Immunology-Hematology and Rheumatology Unit, Laboratory of Immunogenetics of Pediatric Autoimmune Diseases, INSERM U1163, Necker-Enfants Malades Hospital, Assistance Publique - Hôpitaux de Paris (APHP), Imagine Institute, Université Paris Cité, Paris, France, [13]Department of Internal Medicine, National Referral Center for Rare Systemic Autoimmune Diseases, Assistance Publique Hôpitaux de Paris-Centre (APHP-CUP), Université de Paris, Paris, France

Introduction: Among immune cells, activated monocytes play a detrimental role in chronic and viral-induced inflammatory pathologies, particularly in Juvenile Idiopathic Arthritis (JIA), a childhood rheumatoid arthritis (RA) disease. The uncontrolled activation of monocytes and excessive production of inflammatory factors contribute to the damage of bone-cartilage joints. Despite the moderate beneficial effect of current therapies and clinical trials, there is still a need for alternative strategies targeting monocytes to treat RA.

Methods: To explore such an alternative strategy, we investigated the effects of targeting the CXCR4 receptor using the histamine analog clobenpropit (CB). Monocytes were isolated from the blood and synovial fluids of JIA patients to assess CB's impact on their production of key inflammatory cytokines. Additionally, we administered daily intraperitoneal CB treatment to arthritic mice to evaluate its effects on circulating inflammatory cytokine levels,

immune cell infiltrates, joints erosion, and bone resorption, as indicators of disease progression.

Results: Our findings demonstrated that CXCR4 targeting with CB significantly inhibited the spontaneous and induced-production of key inflammatory cytokines by monocytes isolated from JIA patients. Furthermore, CB treatment in a mouse model of collagen-induce arthritis resulted in a significant decrease in circulating inflammatory cytokine levels, immune cell infiltrates, joints erosion, and bone resorption, leading to a reduction in disease progression.

Discussion: In conclusion, targeting CXCR4 with the small amino compound CB shows promise as a therapeutic option for chronic and viral-induced inflammatory diseases, including RA. CB effectively regulated inflammatory cytokine production of monocytes, presenting a potential targeted approach with potential advantages over current therapies. These results warrant further research and clinical trials to explore the full therapeutic potential of targeting CXCR4 with CB-like molecules in the management of various inflammatory diseases.

KEYWORDS

monocytes, cytokines, arthritis, inflammation, treatment

Introduction

Rheumatoid arthritis (RA) is a long inflammatory condition that results to the aggressive synovial hyperplasia causing destruction of articular joints. Joint inflammation is characterized by proliferation of macrophage-like (1) and fibroblast-like synoviocytes to form a pannus, which invades and destroys the cartilage (2). Juvenile Idiopathic Arthritis (JIA) is a rare and complex form of RA affects children younger than 16 years old, characterized by a multifactorial disorder with heterogeneous manifestations that include all forms of chronic arthritis (3, 4). Over-production of TNF-α, IL-1β and IL-6 is strongly involved in most forms of JIA (5, 6). The release of such inflammatory factors by monocytes depends on several highly conserved families of pattern recognition receptors (PRR), one of them being the Toll-like receptor family (TLRs). The increase in circulating TNF-α levels in all forms of JIA argues for a major contribution of monocytes to disease progression (7). This is supported by the observation that monocytes for systemic JIA patients produced more inflammatory cytokines than monocytes from healthy donors in response to TLR4 and TLR8 stimulation (8). Current antirheumatic drugs, including corticosteroids and antibodies-based biotherapies, target inflammatory macrophages or macrophages secreted cytokines to reduce synovial inflammation. However, not all patients respond to antibody therapy and chronic application of glucocorticoids leads to severe side effects, highlighting the need for novel therapeutic strategies.

In the context of chronic and acute inflammatory diseases, the chemokine receptor CXCR4 could emerge a potential therapeutic target. We previously showed that histamine and the histamine analog clobenpropit (CB) through their engagement of CXCR4 exhibited a broad-spectrum inhibitory activity on the production of all subtypes of interferons (IFN) in TLR7-activated human plasmacytoid dendritic cells (pDCs) (9). Moreover, intranasal spray of CB resulted in drastic reduction of type I and III IFN secretions in broncho-alveolar lavages from Influenza A virus (IAV) infected mice (9). Of note, the anti-IFN activity of CB was not associated with histamine receptors but strictly dependent on CXCR4 (9). As CXCR4 is highly expressed by all immune cells, including monocytes and macrophages, we hypothesize that CB could also downmodulate monocyte-driven inflammation in rheumatoid arthritis.

In this study, we explored the potential of CB to decrease the production of proinflammatory cytokines by monocytes obtained from the blood and synovial fluids of individuals diagnosed with Juvenile Idiopathic Arthritis (JIA). In these monocytes, we evaluated both the spontaneous and induced cytokine production. Finally, we further probed *in vivo* whether CB treatment would attenuate inflammation and impair disease progression in a model of collagen-induced arthritic mice.

Results

CB down-regulates TNF-α, IL-1β, and IL-6 productions in TLR-7/8-activated monocytes

To first assess the potential anti-inflammatory properties of histamine and the histamine analog CB, we took advantage of the

monocyte-derived THP-1 NF-κB reporter cell line. Upon TLR7/8 activation by R848, the reporter gene SEAP is induced by activation of the NF-κB signaling pathway. We thus measured the production of SEAP by R848-activated THP-1 cells in the presence or absence of varying concentration of histamine (Figure 1A) or CB (Figure 1B) ranging from 1 to 100 μM. We showed that CB, and to a lesser extent histamine, reduced in a dose-dependent manner activation of NF-κB in THP-1 cells, without any obvious toxicity. In addition, CB treatment (20 μM) prevented the transcription of TNF-α, IL-1β and IL-6 encoding genes in R848-activated THP-1 cells (Figure 1C).

To extend our results obtained with THP-1 cell line, we next tested the ability of CB to control cytokine production in R848-stimulated human blood mononuclear cells (PBMCs) from healthy donors (HD). We first tested the overall effect of CB by measuring the concentrations of multiple cytokines (*i.e.* IL-1β, -6, -8, -10, TNF- α …), chemokines (*i.e.* CCL2, CCL3, CCL4, CCL5…), growth factors (*i.e.* EGF, FGF, VEGF…) and interferons (IFNα/β/γ) in the cell culture medium of R848-stimulated PBMCs with or without of CB (20 μM) (n=5) (Figure 1D). CB downmodulated the R848-induced production of chemokines, growth factors, IFN subtypes, and all proinflammatory cytokines, including TNF-α, IL-1β and IL-6 (Figures 1D, E). Mass Cytometry (CyTOF) analysis revealed that among PBMCs monocytes represented the main producers of TNF-α, IL-1β and IL-6 upon TLR7/8 stimulation by R848. CB treatment drastically reduced the production of those inflammatory factors by R848-activated monocytes (Figures 1F, G) (n=4). To better evaluated the effect of CB on the proinflammatory cytokines, we purified monocytes from the blood of HD. Accordingly, using a multiplex bead-based assay (Figure 1H) and intracellular flow cytometry staining of TNF-α and IL-1β, we showed in monocytes purified from HD that CB inhibited the production of TNF-α and IL-1β (IC_{50} = 2,8 μM and IC_{50} = 8 μM, respectively) with no observed toxicity (Figure 1I).

CB controls activation of monocytes from healthy individuals in a CXCR4-dependent manner

We next tested whether the anti-inflammatory properties of CB depend on CXCR4. In our initial approach, we employed the widely recognized CXCR4 antagonist AMD3100 to regulate the anti-inflammatory effects of CB on activated PBMCs. Cells were cultured with increased concentrations of AMD3100 in presence of CB (20μM) and R848 for 24h. The supernatants were transferred to reporter THP1-Dual cells allowing simultaneous quantification of the activity of IRF and NF-κB promoters. We showed that CB reduced activation of both IRF and NF-κB and that AMD3100 blocked the anti-inflammatory activity of CB in a concentration dependent manner (Figures 2A, B).

We further quantified TNF-α, IL-1β and IL-6 productions in R848-stimulated primary purified monocytes from HD in the presence of CB (20 μM) and increasing concentrations of AMD3100 (up to 50 μM) using flow cytometry. As expected, AMD3100 inhibited in a dose-dependent manner the ability of CB to reduce intracellular TNF-α, IL-1β and IL-6 levels in monocytes without noticeable toxicity (Figures 2C, D).

To firmly establish that CB immunoregulatory activity relates to CXCR4, the expression of CXCR4 was silenced in primary monocytes using small interfering RNA (siRNA). While the transfection of a siRNA control (siControl) had no impact on the CB-induced inhibition of pro-inflammatory cytokines, CB lost its ability to inhibit TNF-α, IL-1β and IL-6 intracellular productions in CXCR4-silenced human monocytes (siCXCR4) (Figures 2E, F). Taking into account the 95% transfection efficiency in monocytes, we checked that CXCR4 expression was strongly reduced in siCXCR4-transfected monocytes compared to siControl (Figures 2G, H). These overall data show that the immunoregulatory effects of CB strictly depends on CXCR4 engagement.

CB inhibits spontaneous proinflammatory cytokine production in JIA patients' monocytes

Our next attempt was to prob whether CB exerts an anti-inflammatory effect on immune cells isolated from JIA patients. Spontaneous inflammation is a well-known hallmark of JIA. While elevated levels of IL-6 are easily measurable in the plasma of RA patients (10), the detection of circulating TNF-α in these patients remains a challenge. Thus, to capture TNF-α in the plasma, we developed a TNF-α digital ELISA (Simoa) that detects TNF-α for concentrations as low as 1 fg/mL. Using this technology, we measured detectable levels of TNF-α in patients' plasma and found higher concentration of TNF-α in blood plasma from JIA patients than in HD (JIA patients' median = 3.4 pg/mL *vs.* HD' median = 1.07 pg/mL) (Figure 3A). To better capture the spontaneous inflammation in JIA patients, we conducted a gene expression analysis on a set of 579 markers associated with inflammation on purified monocytes of PBMC from HD and JAI patients. As compared to HD, the expression of 51 inflammatory genes significantly increased and 16 decreased in oligoJIA patients (Figure 3B). The results of the principal components analysis (PCA) revealed that monocytes in each group grouped together (Figure 3C). Pathway analysis using DAVID (11, 12) showed enrichment in the rheumatoid arthritis pathway (Figure 3D). Since JIA is primarily a joint-related inflammatory disease (13), this prompted us to examine the inflammatory status of synovial fluids. Using Simoa technology, we measured TNF-α concentrations between 3 and 26 pg/mL (median = 10.8 pg/mL) in synovial fluid (SF) from eighteen JIA patients' knees with active arthritis (Figure 3E). When comparing circulating levels of TNF-α in plasma and SF from six matched patients, higher levels of TNF-α were systematically measured in SF compared to blood plasma (Figure 3F).

We next assessed the effect of CB treatment on the spontaneous TNF-α production by human monocytes isolated from PBMCs (Figure 3G) and synovial fluid mononuclear cells (SFMCs) (Figure 3H) from JIA patients. CB treatment significantly decreased TNF-α levels in the culture medium of both SFMCs and PBMCs monocytes. We also showed that CB exerted a dose-

10.3389/fimmu.2023.1178172

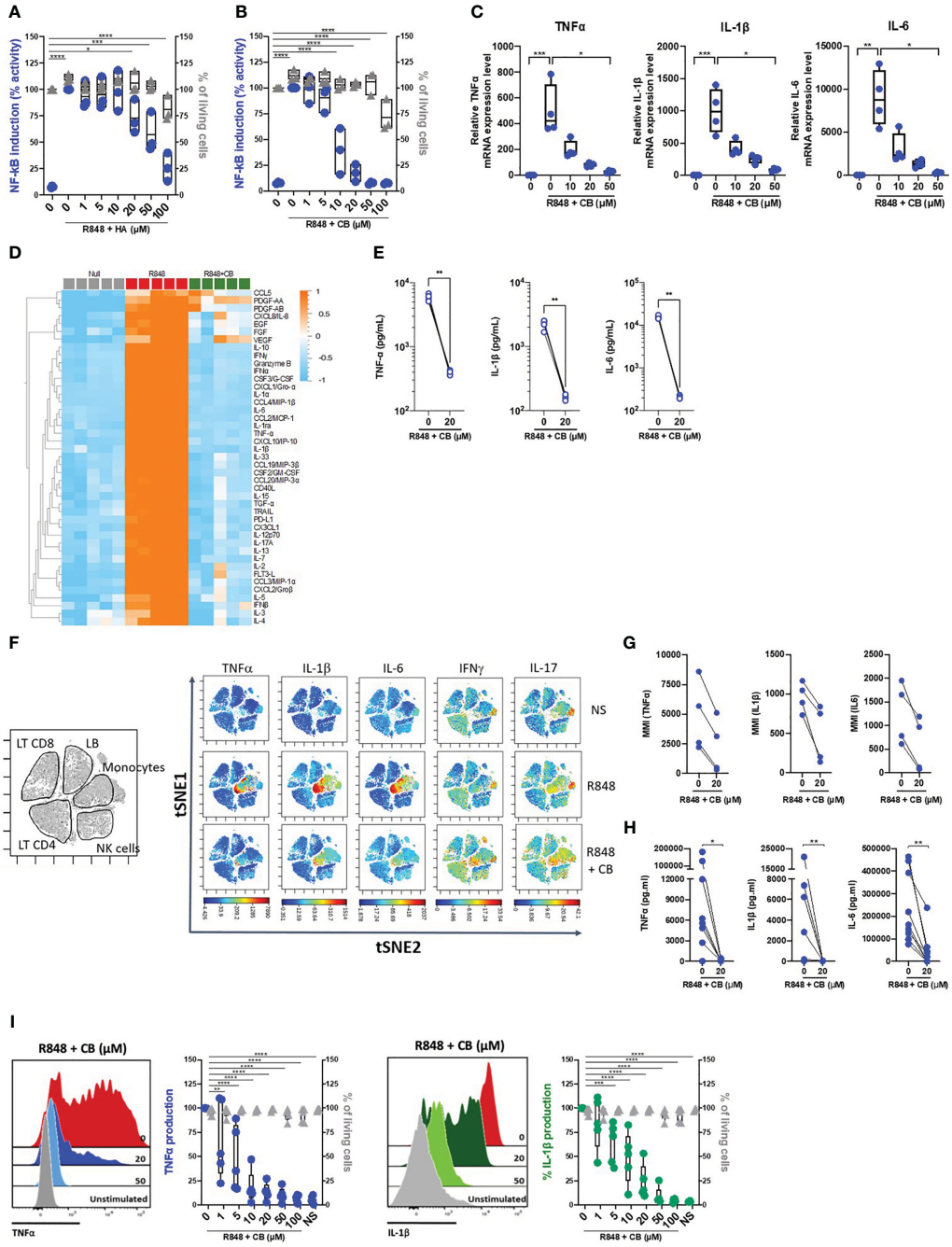

FIGURE 1
CB inhibited TLR-7/8-mediated TNF-α, IL-1β and IL-6 production by human monocytes. **(A, B)** THP1 NF-κB reporter cells were treated with increasing concentration of Histamine **(A)** or CB **(B)** ranging from 1 to 100 µM then stimulated with R848 (5 µg/ml) for 24 hours. NF-κB reporter activity was measured using QUANTI-Blue, a SEAP detection reagent. **(C)** mRNA levels of TNF-α, IL-1β and IL-6 from THP1-dual pre-incubated with increased doses of CB and stimulated overnight with R848 (5 µg/ml), were measured by RT-qPCR and normalized to RPL13A. Kruskal-Wallis with Dunn's multiple comparisons test. **(D-G)** PBMCs from healthy donors (HD) were preincubated with CB (20 µM) then stimulated with R848 (5 µg/mL) overnight. **(D, E)** Cytokine production was measured in the supernatant using a bead-based multiplexed immunoassay system Luminex. **(D)** Heatmap representation of statistically different cytokines ($P<0.05$) between the different conditions (Null, R848, R848+CB), ordered by hierarchical clustering. Up-regulated cytokines are shown in orange, and down-regulated in blue. P values were determined with the Kruskal-Wallis test. **(E)** Individual cytokines from the Luminex are represented. Mann-Whitney test. **(F)** PBMCs were analyzed by mass cytometry (CyTOF) and tSNE analysis were performed using CD56, CD3, CD11c, BDCA4, CD14, HLADR, CD123, CD4, CD8, and CD19 markers. Intracellular levels of TNF-α, IL-1β, IL-6, IFNγ, and IL-17were evaluated. **(G)** Mean Metal Intensity (MMI) of TNF-α, IL-1β, and IL-6 was evaluated on gated monocytes from four different donors. **(H)** Cytokine production was measured in the supernatants of purified monocytes from nine HD using the multiplex bead-based immunoassay LEGENDplex. Mann-Whitney test. **(I)** Purified monocytes from five HD were preincubated with increased doses of CB then stimulated with R848 during 5 h. Intracellular levels of TNF-α and IL-1β as well as viability were evaluated by flow cytometry. SSC-A, side scatter. FSC-A, forward scatter. 2-way ANOVA. All data are presented as median ± range. ****$P < 0.0001$, ***$P < 0.001$, **$P < 0.01$, *$P < 0.05$.

10.3389/fimmu.2023.1178172

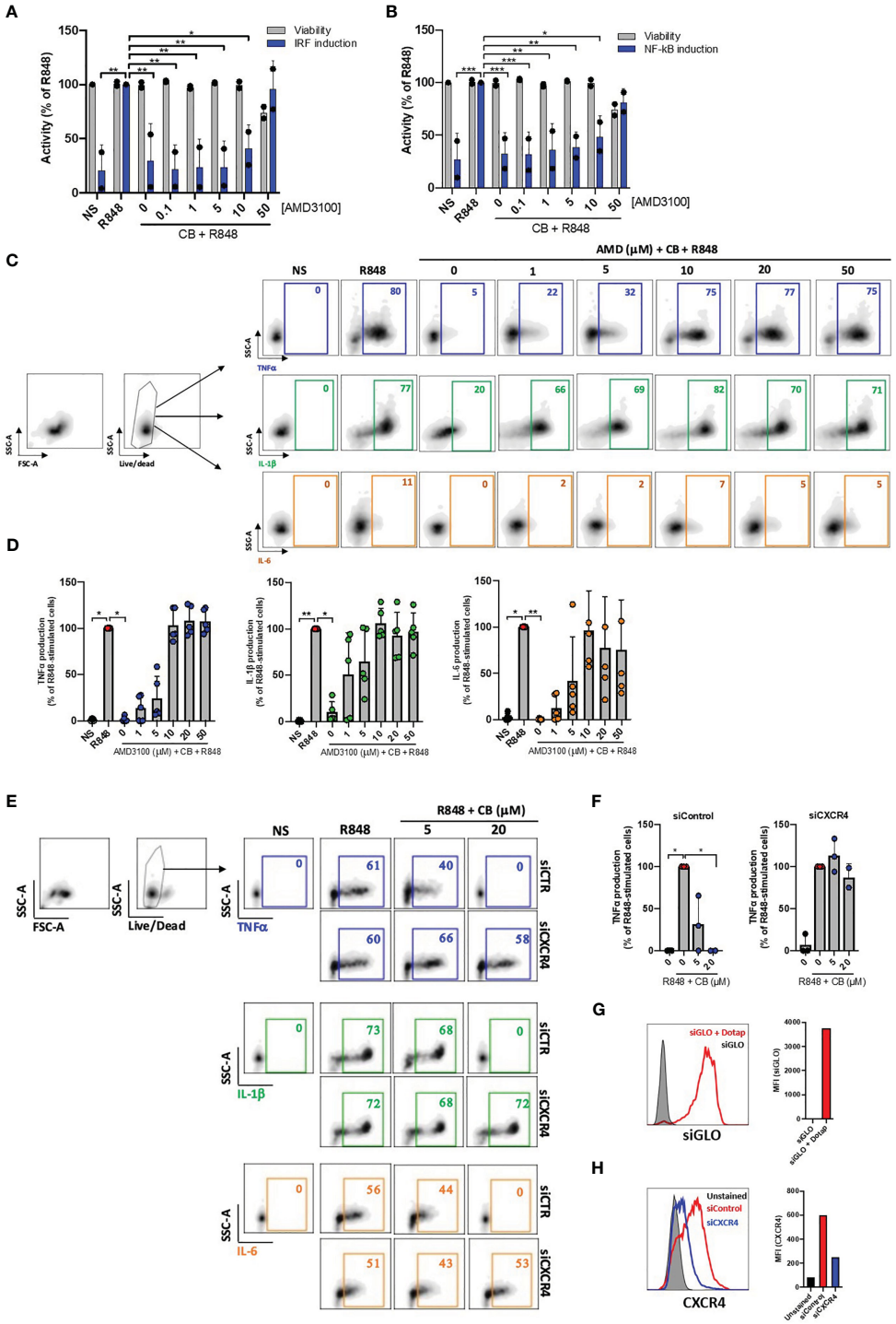

FIGURE 2
CB immunoregulatory activity on primary monocytes is CXCR4 dependent. **(A)** and **(B)** PBMCs from two healthy donors were cultured in presence of increased concentrations of AMD3100, then treated with CB (20 µM) and activated with R848 (5 µg/mL) for 24 hours. The level of **(A)** interferons and **(B)** inflammatory cytokines in the culture supernatants was measured using the reporter cell line THP1-dual. Two-way ANOVA with Dunnett's multiple comparisons test. **(C)** and **(D)** Isolated monocytes from five healthy donors were cultured in presence of increased concentrations of AMD3100, then treated with CB (20 µM) and activated with R848 (1 µg/mL) for 6 hours. Intracellular levels of TNF-α, IL-1β and IL-6 were evaluated by flow cytometry, **(C)** dot plot representation from a donor and **(D)** histogram representation from 5 donors. Friedman with Dunn's multiple comparisons test. **(E, F)** Monocytes were treated for 24 hours with CXCR4 siRNA (siCXCR4) or Control siRNA (siControl) at 160 nM. Cells were then pre-incubated with CB (20 µM) and stimulated with R848 (1µg/mL) for 6 hours. Intracellular levels of TNF-α, IL-1β and IL-6 were evaluated by flow cytometry: **(E)** dot plot representation from a donor and **(F)** histogram representation from 3 donors. Data shown as the median +/-s.d. Krustal-Wallis with Dunn's multiple comparisons test. **(G)** the efficiency of transfection with dotap on monocytes was evaluated with GLO siRNA in flow cytometry. **(H)** The expression of CXCR4 on monocytes treated with siControl and siCXCR4 was assessed by flow cytometry. **P < 0.01, *P < 0.05. NS, nonstimulated.

10.3389/fimmu.2023.1178172

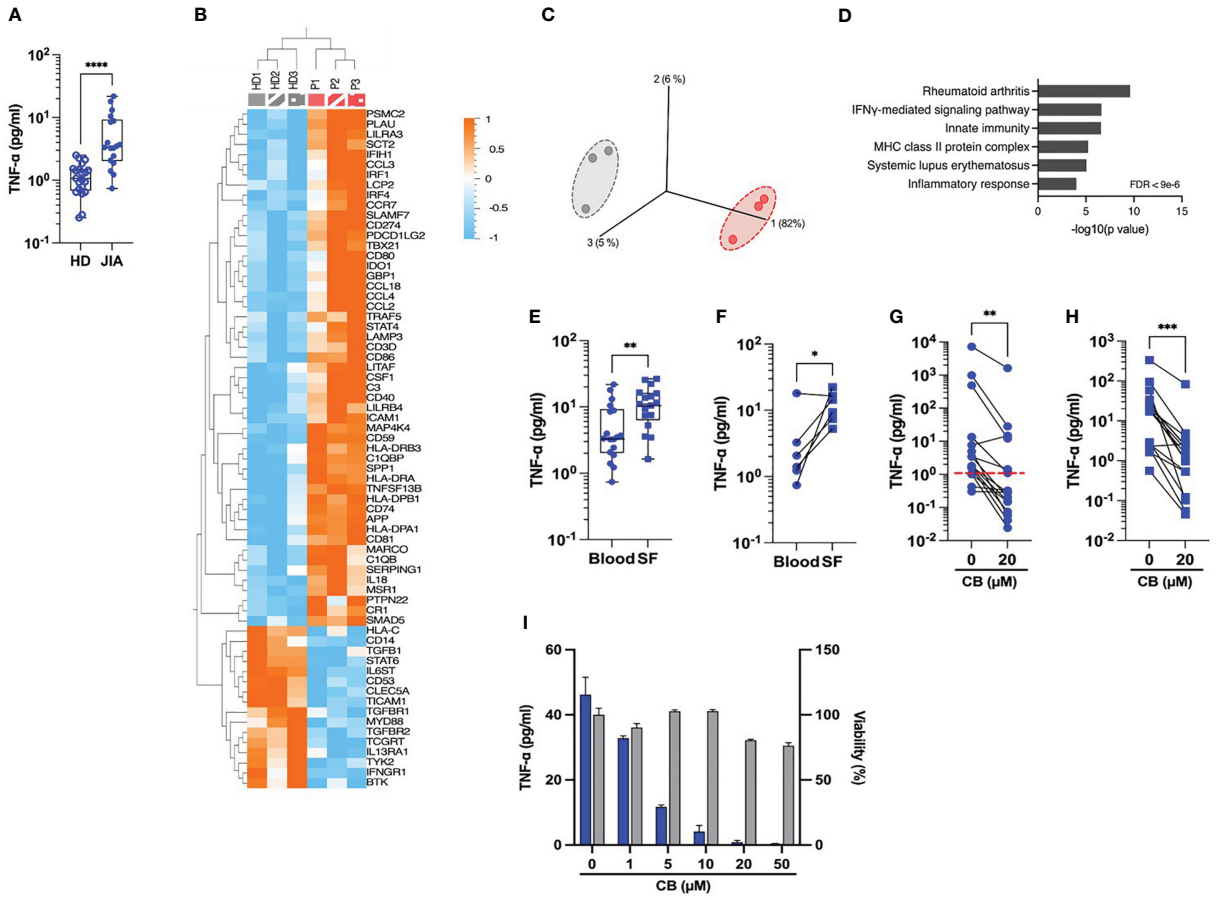

FIGURE 3
CB controls spontaneous inflammation in cells from JIA patients. **(A)** TNF-α was measured in the plasma of blood from HD and JIA patients by digital ELISA (Simoa). Box and whisker plots with median ± range. Mann-Whitney test. **(B)** Monocytes from blood from three healthy donors (HD) and three oligoJIA patients were isolated and total RNA extracted from the cells was isolated and subsequently analyzed using the NanoString nCounter system. Heat map illustrates the fold increase in mRNA expression levels of genes that exhibited significant differential expression between the two groups. ($P < 0.05$, fold change > 1.5). **(C)** PCA was performed based on genes from the array differentially expressed between the HD (gray) and the JIA patients (red). ($P < 0.05$, fold change > 1.5). **(D)** David pathway analysis was used for pathway enrichment analysis of differentially upregulated genes in JIA patients compared to the HD. **(E)** TNF-α was dosed in the plasma from blood or synovial fluids (SF) of JIA patients by Simoa. Mann-Whitney test. **(F)** TNF-α levels in paired plasma and SF from six different donors were dosed by Simoa. Wilcoxon test. TNF-α was measured in the supernatant of monocytes by digital ELISA (Simoa) purified from PBMCs of twenty JIA patients **(G)** or SFMCs of seventeen JIA patients **(H)**. Average baseline of HD is represented by the red dashed line. Mann-Whitney test. **(I)** Monocytes from one JIA patient were treated with various concentration of CB for 16h and TNF-α was measured in the supernatant by digital ELISA (Simoa). ****$P < 0.0001$, ***$P < 0.001$, **$P < 0.01$, *$P < 0.05$.

dependent anti-inflammatory effect in purified monocytes from SF of one patient without any significant toxicity (Figure 3I).

Altogether, these data provide evidence that CB inhibits the spontaneous production of inflammatory cytokines by blood and synovial human monocytes within an arthritic context.

CB attenuates R848-induced cytokine production in JIA patients' cells

We next evaluated whether CB would also inhibit cytokine production by stimulated immune cells from JIA patients. To this purpose, we first compared cytokine production by PBMCs from HD and JIA patients using the 45-plex bead-based immunoassay Luminex. We showed that PBMCs from three JIA patients out (P11, P16 and P28) of five secreted more cytokines than those of HD (Figure 4A). This result confirms that cells from JIA patients are hyperresponsive to TLR-7/8 stimulation (8). Furthermore, CB reduced R848-induced inflammatory cytokine production by HD PBMCs as well as inflammatory cytokine hypersecretion by cells from JIA patients, and most drastically CCL20, CCL2 and CCL3 (Figure 4B). As monocytes are the main producers of proinflammatory cytokines, we purified monocytes from blood patients' suffering from oligo articular (n=20), polyarticular (n=8) or systemic (n=5) JIA, or enthesitis-related arthritis (ERA) (n=3). For all subtypes of JIA, CB treatment drastically reduced levels of IL-1β and TNF-α and reduced level of IL-6 in the culture medium of R848-activated patients' monocytes (Figure 4C).

Finally, using purified SFMCs from JIA patients we showed that CB inhibited the production of the 40 soluble factors induced by R848 activation (Figure 4D). Overall data indicate that CB could

10.3389/fimmu.2023.1178172

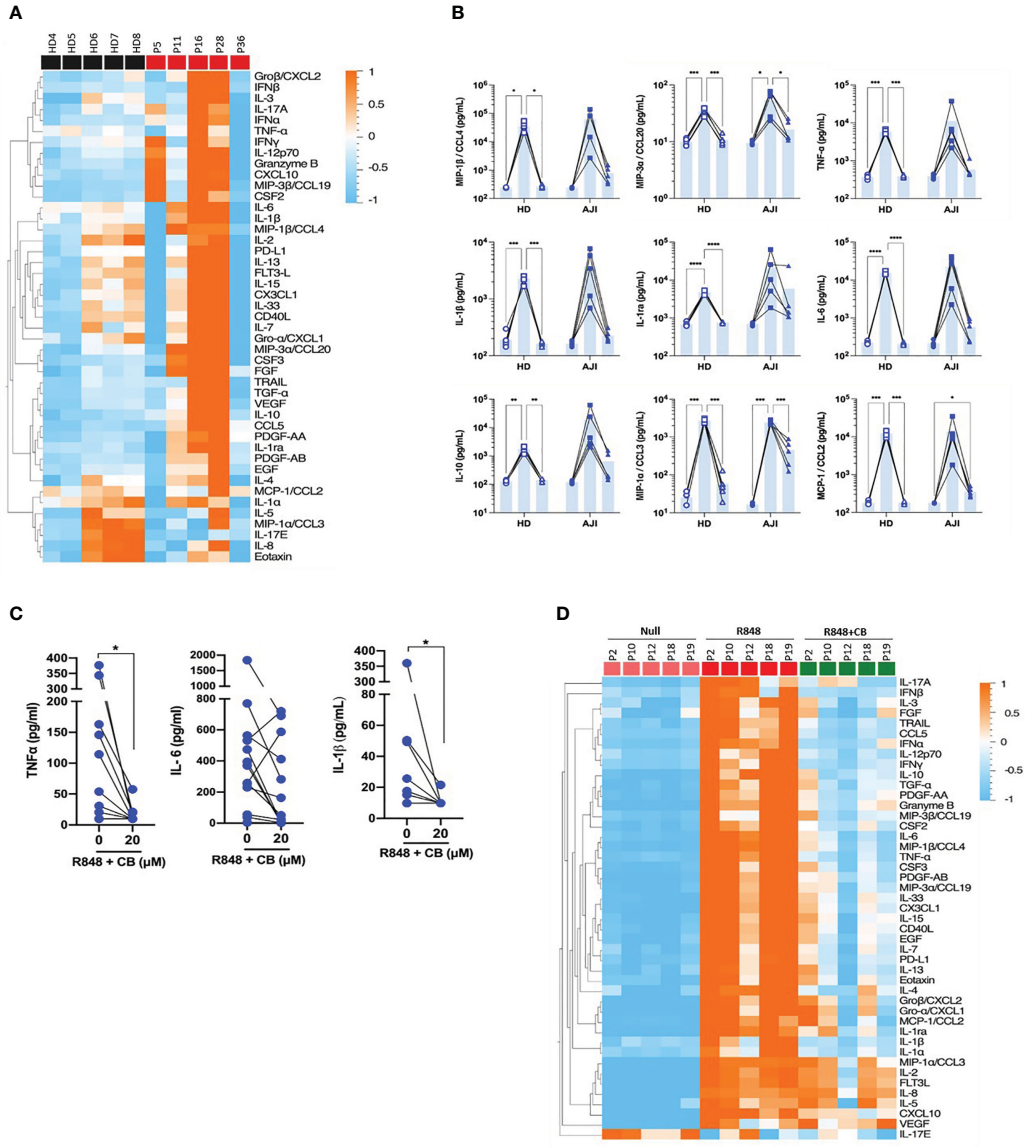

FIGURE 4
CB controls R848-induced inflammation in cells from JIA patients. **(A)** PBMCs from HD and JIA patients were incubated with R848 (5 μg/mL) for 16h. P2 P12 P18 and P19 patients are oligoJIA, P10 is an polyJIA. Cytokine production was measured in the supernatant using a bead-based multiplexed immunoassay system Luminex. Heatmap representation of statistically different cytokines (P<0.05) in PBMCs supernatant upon R848 stimulation between HD and JIA patients, ordered by hierarchical clustering. Mann-Whitney test. **(B)** PBMCs from HD and JIA patients were pre-incubated with CB at 20 μM and then stimulated with R848 (5 μg/mL) for 16h. Cytokine production was measured in the supernatant using a bead-based multiplexed immunoassay system Luminex. Individual cytokines are represented. Two-way RM ANOVA with Tukey *post hoc* correction. **(C)** Monocytes from JIA patients were pre-incubated with CB at 20 μM and then stimulated with R848 (5 μg/mL) for 16h. IL-6, IL-1β and TNF-α production was measured in the supernatant using the multiplex bead-based immunoassay LEGENDplex. Mann-Whitney test. **(D)** SFMCs were pre-incubated with CB at 20 μM and then stimulated with R848 (5 μg/mL) for 16h. P5 P11 and P28 patients are oligoJIA, P16 is a polyJIA and P36 an sJIA. Cytokine production was measured in the supernatant using a bead-based multiplexed immunoassay system Luminex. ****P < 0.0001, ***P < 0.001, **P < 0.01, *P < 0.05.

reduce hyper secretion of inflammatory cytokines observed in JIA patients during flares.

CB inhibits inflammatory cytokine and reduces disease progression in collagen-induced arthritis mouse model

The anti-inflammatory properties of CB in PBMCs, SFMCs and purified monocytes of JIA patients, suggest that CB represents a promising therapeutic option for arthritis. Consequently, we proceeded to evaluate the potential therapeutic impact of CB in DBA/1J mice, which serve as a mouse model for arthritis-like pathology known as collagen-induced arthritis (CIA) (14). CIA mice exhibit numerous clinical, histological, and immunological similarities to human RA (15). This includes symmetric joint involvement, synovitis, cartilage, and bone erosions. Several studies reported a major role of IL-1β in disease development in CIA mouse model (16), as well as a pathologic role of IL-6 in the effector phase of autoimmune arthritis by promoting bone destruction (17).

CIA mice were daily intraperitoneally injected with CB (at 3 mg/kg (mpK), 10 mpK, and 30 mpK) over a two-week period. As a reference drug, the corticosteroid prednisolone (15 mpK) was also injected in CIA mice. CB treatment did not exert any effect on mouse body weight whatever the dose tested overtime (Figure 5A), indicating no major toxicity of CB in treated mice. While CIA mice displayed elevated levels of circulating IL-1β and IL-6 two weeks after disease onset (Figure 5B), CB treatment resulted in a profound decrease of both cytokines (Figure 5B). Of note, the highest dose of CB (30 mpK) was as efficient as the referenced corticosteroid prednisolone.

Additionally, we conducted an investigation to assess the impact of CB treatment on the progression of the disease.The daily injection of CB attenuated the progression of the disease during the 14 days of treatment (Figure 5C). Mice treated with CB had thinner paws than mice treated with PBS (Figure 5D). In arthritic mice, the histological analysis of the tissue injury revealed severe cartilage damage (yellow arrow), bone remodeling (black arrow) and tissue infiltration by immune cells (green arrow) (Figure 5E). Daily CB treatment attenuated all these pathological markers (Figure 5E). To further characterize the effect of CB treatment, individual paws were scored, reflecting the severity of the disease. CB treatment drastically reduced the terminal paw score (Figure 5F), which was associated with reduced inflammation, cartilage damage, bone remodeling on limbs and pannus (Figures 5G, H).

Discussion

In this study, we reveal a broad-spectrum anti-inflammatory activity of the histamine analog CB. Our findings reveal a notable decrease in the production of key inflammatory cytokines when monocytes derived from the blood and synovial fluids of individuals with JIA are exposed to CB. This reduction is observed both in spontaneous and induced cytokine production. This immunomodulatory activity of CB strictly depends on the engagement of CXCR4 chemokine receptor. In addition, CB displays high efficiency *in vivo* to reduce inflammation and subsequent tissue damage in arthritic mice, leading to reduction of disease progression. In summary, our results strongly indicate that the targeting of CXCR4 using CB-like molecules holds great potential as a therapeutic approach for inflammatory diseases characterized by detrimental hyperactivation of monocytes.

The pro-inflammatory cytokines TNF-α and IL-6 are major contributors to JIA and RA (18, 19). The clinical benefits observed upon inhibiting TNF-α and IL-6 strongly support the hierarchical significance of these two pro-inflammatory factors among all the factors produced during JIA flares. While the TNF-α signature has been clearly identified in JIA patients (20), systemic TNF-α protein remains, however, difficult to detect and measure, notably because most classical ELISAs are not sensitive enough to detect TNF-α concentration below one pg/mL. To overcome this challenge, we developed an ultrasensitive digital TNF-α ELISA (Simoa) with attomolar sensitivity that permits to show that TNF-α concentration in plasma from JIA patients is six-fold higher than the one in healthy donors. Through Simoa experiments, we also measured that TNF-α concentration in synovial fluid JIA patients is higher in their synovial fluid than that in plasma. In most forms of RA, including JIA, blood monocytes are attracted to synovial fluids where they differentiate into inflammatory macrophages (1) and produce joint-degrading mediators. These immune cells emerge as being the major sources of TNF-α. Accordingly, we show that purified monocytes from JIA patients spontaneously produce more TNF-α than monocytes from healthy donors. As previously described by Cepika et al. (1), we also confirm that monocytes from JIA patients are hyperresponsive to TLR-7/8 activation compared to healthy individuals. Our study provides evidence that CB is a powerful inhibitor of pro-inflammatory cytokine and chemokine production in inflammatory monocytes derived from the blood or synovial fluid of individuals with Juvenile Idiopathic Arthritis (JIA). Interestingly, CB anti-inflammatory activity is not restricted to TNF-α and IL-6, as the inflammatory signature of JIA patients is largely toned down under CB exposure. These *ex vivo* results suggest that CB potentially reduces hypersecretion of cytokines and chemokines observed in JIA patients during flares. In RA animal models, IL-6 has been shown to promote osteoclast activation, synoviocyte proliferation, and recruitment to inflammatory areas, leading to the development of synovial pannus (17). In conjunction with IL-1β, IL-6 enhances the production of matrix metalloproteinases, thereby contributing to the degradation of joints and cartilage (21). In collagen-induced arthritis (CIA) mice, daily treatment of CB exhibits strong anti-inflammatory properties by blocking both IL-1β and IL-6 secretions. According to massive reduction of cartilage damage, bone remodeling, immune cell tissue infiltration and pannus CB treatment results in reduced disease progression and paw thickness in arthritic mice similarly to the referenced corticosteroid prednisolone. These *in vivo* experiments validate the concept of the immunomodulatory activity of CB observed *in vitro* and *ex vivo* on synovial monocytes from JIA patients.

In competition assays using the CXCR4 antagonist AMD3100 or siRNA-based experiments to down-regulate CXCR4 expression, we further demonstrated that CB anti-inflammatory activity on monocytes strictly depends on CXCR4. Beyond the impact of CXCR4 signaling on regulation of the IFN pathway (9), this result highlights that CXCR4 also represents a broad spectrum regulator of inflammation in various cell types, including pDC and monocytes. The concurrent anti-IFN and anti-inflammatory effects exerted by CXCR4 can have substantial clinical advantages, particularly considering the frequent presence and functional activity of type I interferons (IFNs) in RA (22). It is worth noting that a recent study has revealed significantly elevated levels of CXCR4 and its natural ligand, CXCL12, in both the serum and joint synovial fluids of individuals with active RA when compared to a control group (23). Furthermore, the expression levels of CXCR4 and CXCL12 in the active RA group were found to be higher compared to the group in remission (23). Higher accessibility to CXCR4 in RA patients makes targeting the CXCR4 anti-inflammatory pathway a particularly promising strategy for these pathologies.

For instance, drugs that target TNF-α, IL-6 and IL-1β cytokines or their receptors have shown beneficial effects in JIA patients (18).

10.3389/fimmu.2023.1178172

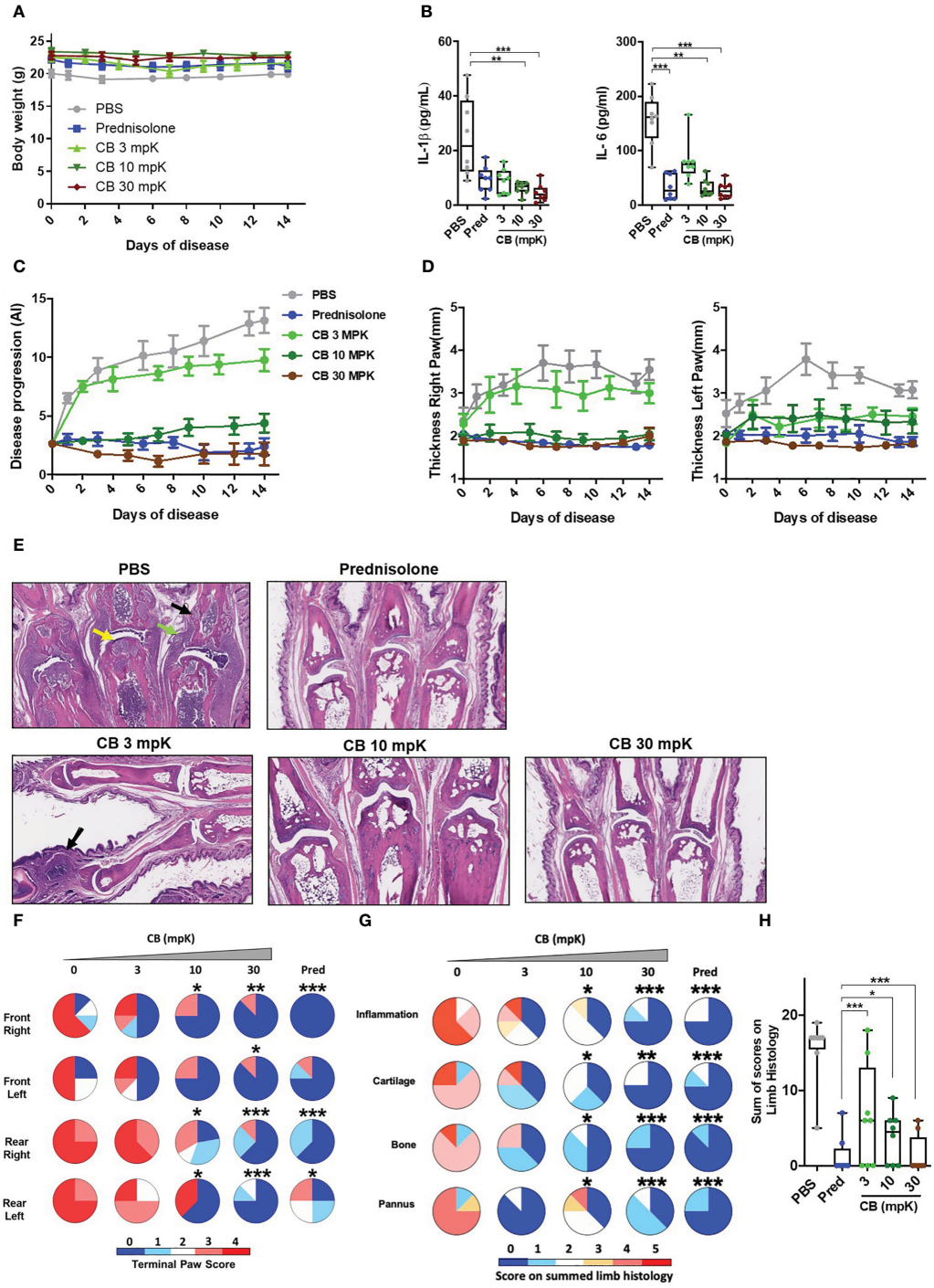

FIGURE 5
CB controls inflammation and disease onset in collagen induced arthritic mice. **(A)** The body weight of collagen induced arthritic mice treated with prednisolone (Pred, 15 mpK) or 3, 10, or 30 mpK of CB was measured every other day. **(B)** IL-1β and IL-6 were measured by ELISA in the serum after 2 weeks of treatment. Kruskal-Wallis test with Dunn's *post hoc* correction. **(C)** the progression of the disease was assessed according to several markers in the legs. **(D)** The thickness of the legs was measured. **(E)** Representative hematoxylin and eosin staining of paw sections from collagen induced arthritic mice treated with prednisolone (Pred, 15 mpK) or 3, 10, or 30 mpK of CB: joints with pannus and inflammation (green arrow), loss of articular cartilage (yellow arrow) and bone remodeling (black arrow). **(F)** Impact of the treatment was evaluated by a paw score, signs of arthritis in all paws according to a 0-4 scale of ascending severity, after 2 weeks of treatments. **(G)** Effects of the treatment on the scoring for inflammation, cartilage damage, bone remodeling, and pannus after 2 weeks of treatment. **(H)** Combined disease score after 2 weeks of treatment. Kruskal-Wallis test with Dunn's *post hoc* correction. All data are presented as median ± range, ***P < 0.001, **P < 0.01, *P < 0.05. *n* = 8 mice per group.

However, these treatments are often associated with highly heterogeneous responses across patients in terms of efficacy and treatment resistance. Consequently, it is not uncommon for a patient to change medication throughout the course of the disease. To some extent, this could be explained by the very high specificity of these treatments toward a single cytokine in a set of diseases characterized by a very broad inflammatory spectrum. By contrast to targeted therapies, corticosteroids have been used for decades to block overall pro-inflammation in RA patients, with, however, strong side-effects (24). In order to address these limitations, innovative approaches such as Janus kinase (JAK) inhibitors have emerged as promising strategies. These small molecules effectively inhibit the activity of JAK, and they have demonstrated reasonable success in treating the adult form of arthritis (25–27). Regarding strategies targeting JAK, our findings demonstrate that CB treatment effectively inhibits a broad range of cytokines *in vitro*, ex vivo, and *in vivo*.

In contrast, CB exerts its effects at an earlier stage compared to JAK inhibitors. Instead of directly targeting cytokine-mediated signaling, CB acts one step upstream by inhibiting the production of inflammatory cytokines. This approach may offer certain advantages in terms of therapy efficacy compared to JAK inhibitors. The significant suppression of disease progression observed in mice with RA following treatment with CB provides strong validation for the concept of targeting CXCR4 using CB-like molecules as a potential therapeutic strategy for arthritic conditions. Indeed, CB exhibits all the essential characteristics of a promising new drug for the treatment of rheumatoid arthritis (RA). It is a small molecule that has demonstrated an absence of side effects in *in vivo* preclinical models. CB specifically targets the widely expressed immune cell receptor CXCR4, and it exerts a broad anti-inflammatory effect by modulating cytokine production. These attributes collectively highlight CB as a potential candidate for RA therapy.

In summary, the minimal cytotoxicity of CB, coupled with its wide-ranging inhibitory effects on ex vivo production of inflammatory cytokines and its therapeutic efficacy demonstrated *in vivo*, indicates that the use of CB-like molecules to target CXCR4 could serve as a novel and promising therapeutic strategy for chronic inflammatory diseases, including rheumatoid arthritis.

Materials and methods

Blood samples isolation and culture of blood leukocytes

The blood samples obtained from donors in good health were sourced from "Etablissement Français du Sang" (agreement # 07/CABANEL/106), located in Paris, France. The use of materials from JIA patients was conducted with the approval of the Comité de Protection des Personnes (N° EudraCT: 2018-A01358-47) in France. The experimental procedures involving human blood adhered to the guidelines set by the European Union and the Declaration of Helsinki. Informed consent was obtained from all donors, including both healthy individuals and patients. Table 1 provides a summary of the clinical data pertaining to the JIA patients. *In vitro* experiments were conducted using human

TABLE 1 Clinical information of recruited patients.

Patients	Age	Gender	Disease	Treatment	TNF-α (pg.ml) - Blood			TNF-α (pg.ml) - SF		
					plasma	Null	CB	plasma	Null	CB
P1	18	F	oligoJIA	apranax	1,9	–	–	25,6	–	–
P1'	18	F	oligoJIA	apranax	0,7	–	–	22,3	–	–
P2	5	F	oligoJIA	ibuprofen		–	–	26,5	331,1	83,3
P3	5	F	oligoJIA	ibuprofen	18,1	–	–	16,4	2,6	0,5
P4	13	F	oligoJIA	naproxen		–	–	3,5	–	–
P5	10	F	oligoJIA ANA+	voltaren + inexium	2,4	1,7	0,3	11,1	–	–
P6	16	M	ERA	celecoxib	–	–	–	1,6	2,0	0,1
P7	17	M	polyJIA RF-	Tocilizumab	–	13,2	1,1	16,1	19,1	4,1
P8	15	F	polyJIA RF-	tocilizumab + abatacept	–	–	–	13,8	0,6	0,0
P9	5	F	polyJIA	tocilizumab + cortansyl	1,2	3,4	0,2	–	94,8	4,8
P9'	5	F	polyJIA	tocilizumab + cortansyl		1,0	0,0	9,3	–	–
P10	17	M	polyJIA RF-	methotrexate	–	–	–	11,6	2,9	0,1
P11	15	F	oligoJIA	untreated	1,4	4,9	0,1	5,3	2,3	2,6
P12	11	F	oligoJIA	untreated	–	–	–	7,5	18,9	2,0

(Continued)

10.3389/fimmu.2023.1178172

TABLE 1 Continued

Patients	Age	Gender	Disease	Treatment	TNF-α (pg.ml) - Blood			TNF-α (pg.ml) - SF		
					plasma	Null	CB	plasma	Null	CB
P13	15	M	oligoJIA	untreated	3,7	0,3	0,3	5,2	1,0	21,6
P14	16	F	oligoJIA	untreated	–	–	–	10,5	57,4	0,1
P15	5	F	oligoJIA ANA+	untreated	–	7,7	14,7	14,4	–	–
P16	17	M	polyJIA RF- ANA+	untreated	2,1	3,4	1,4	3,6	–	–
P16'	17	M	polyJIA RF- ANA+	untreated	–	–	–	7,4	–	–
P17	16	M	ERA	celecoxib	–	–	–	–	1,6	–
P18	11	F	oligoJIA ANA+	methotrexate + adalimumab	–	–	–	–	17,0	0,0
P18'	11	F	oligoJIA ANA+	methotrexate + adalimumab	–	–	–	–	17,9	1,5
P18"	11	F	oligoJIA ANA+	Methotrexate + Adalimumab	–	–	–	–	25,0	2,4
P19	18	F	oligoJIA	untreated	–	–	–	–	24,0	2,4
P20	16	F	oligoJIA	untreated	–	–	–	–	1,6	0,5
P21	12	F	oligoJIA	untreated	8,8	–	–	–	1,0	34,1
P22	14	M	ERA	Adalimumab	21,8	1,8	0,2	–	–	–
P23	17	F	oligoJIA	Infliximab + Methotrexate + prednisone	23,7	0,3	1,1	–	–	–
P24	13	M	polyJIA	Cortancyl + Arava		7201,1	1620,7	–	–	–
P24'	13	M	polyJIA	Cortancyl + Arava	8,5	1,6	0,0	–	–	–
P25	18	F	sJIA	Ruxolitinib + Prednisone	3,2	0,4	0,3	–	–	–
P26	18	F	oligoJIA	Methotrexate	13,2			–	–	–
P27	18	M	polyJIA RF- ANA+	Methotrexate + Cortancyl	0,0	1,0	0,1	–	–	–
P28	3	F	oligoJIA	untreated	3,3	1,7	0,1	–	–	–
P29	17	F	oligoJIA	untreated	10,5	–	–	–	–	–
P30	13	M	oligoJIA	untreated	4,0	–	–	–	–	–
P31	5	F	oligoJIA ANA+	untreated	3,3	–	–	–	–	–
P31'	5	F	oligoJIA ANA+	untreated	3,5	–	–	–	–	–
P31"	5	F	oligoJIA ANA+	untreated	3,3	–	–	–	–	–
P32	5	F	sJIA	anti-IL-1	–	2,2	6,3	–	–	–
P33	12	F	sJIA	Tocilizumab + Cortancyl + Methotrexate	–	27,9	980,3	–	–	–
P34	5	F	polyJIA RF-	Tocilizumab	–	13,5	1,1	–	–	–
P35	18	F	sJIA	Tocilizumab	–	0,0	1,3	–		
P36	16	M	sJIA	Tocilizumab + Cortancyl	–	12,1	486,9	–	–	–

SF, synovial fluid; oligoJIA, oligoarticular juvenile idiopathic arthritis; ERA, enthesitis-related arthritis; polyJIA, polyarticular juvenile idiopathic arthritis; sJIA, systemic juvenile idiopathic arthritis; RF, rheumatoid factor; ANA, antinuclear factor. The Null and CB columns correspond to TNF-α assay data by Simoa performed on supernatants of isolated monocytes from blood or synovial fluid of JIA patients. Null: untreated monocytes, CB: monocytes treated with 20 µM CB.

mononuclear cells obtained from peripheral blood or synovial fluid (SF) through centrifugation using density gradient medium (STEMCELL Technologies). Human monocytes were isolated by positive selection using Human CD14 microbeads (Miltenyi). SFMC (Synovial fluid mononuclear cells), PBMC (Peripheral blood mononuclear cells), and monocytes were cultured in RPMI 1640 medium (Invitrogen, Gaithersburg, MD) (R10) supplemented with 10% heat-inactivated fetal bovine serum and 1mM glutamine (Hyclone, Logan, UT). The JIA patients were identified as P1 to P36 (refer to Figure 2).

Cell stimulation

PBMCs were initially seeded at a concentration of 2.106 cells per milliliter (mL), while monocytes isolated from either PBMCs or

SFMCs were seeded at a concentration of 1.10^6 cells per mL. Prior to a 16-hour stimulation with the TLR-7/8 agonist Resiquimod – R848 at a concentration of 5 µg/mL or as specified, the cells were pre-treated for 1 hour with AMD3100 (Sigma-Aldrich) and/or clobenpropit (CB) (Sigma Aldrich) at a concentration of 20 µM (or other specified concentration). Subsequently, flow cytometry or mass cytometry techniques were employed to collect the cells, and supernatants were collected to detect cytokine levels. For intracellular staining, Brefeldin A (BFA) was added to the cells 30 minutes after stimulation and incubated for 5 hours.

THP1-dual cells (Invivogen) were seeded at a concentration of 1.106 cells per mL in RPMI 1640 (Invitrogen, Gaithersburg, MD) (R10) medium supplemented with 10% heat-inactivated fetal bovine serum, 2mM glutamine (Hyclone, Logan, UT), 25mM HEPES, and 1% Pen-Strep. Before a 24-hour stimulation with the TLR-7/8 agonist Resiquimod – R848 at a concentration of 5 µg/mL, the cells were pre-treated for 1 hour with clobenpropit (CB) (Sigma Aldrich) or Histamine at concentrations ranging from 1 to 100 µM. The activity of the NF-κB reporter was measured using QUANTI-Blue, a SEAP detection reagent, following the instructions provided by the supplier.

Mass cytometry

Peripheral blood mononuclear cells (PBMCs) obtained from healthy donors were stimulated with R848 in the presence of CB. Brefeldin A was added overnight to the culture. Following stimulation, PBMCs were treated with a mixture of surface antibodies and Rh isotopes in PBS for 20 minutes at room temperature. Both commercially available and custom-conjugated antibodies were used to create a panel for phenotypic and functional analysis. Two DNA interchelators, Rhodium isotope mass 103 and Iridium isotopes mass 191 & 193, were employed to determine cell viability and gate the singlet cells during analysis. Prior to analysis, each antibody was titrated using PBMCs. Subsequently, the cells were fixed with Fix-I solution (Maxpar Fix-I buffer; Fluidigm) for 15 minutes at room temperature. After fixation, the cells were incubated with anti-cytokine antibodies and Ir isotopes in Perm-S solution for 30 minutes at room temperature (Maxpar Perm-S buffer; Fluidigm). Before CyTOF acquisition, the cells underwent three washes with highly pure water and were resuspended in water at a maximum concentration of 500,000 cells/mL (Maxpar Water; Fluidigm). Data acquisition was performed using a CyTOF2 instrument (Fluidigm) and the analysis included data cleaning using FlowJo software and the application of the viSNE algorithm in Cytobank for the primary analysis. The table (Table 2) provides the details of antibodies coupled with the respective metals.

Flow cytometry

The cells underwent a PBS wash and were subsequently treated with a viability stain, Zombie Aqua (Biolegend), for 30 minutes at a temperature of 4°C. Following the wash, the cells were suspended in PBS containing 2% FCS and 2mM EDTA and stained with the extracellular mix, APC Vio770 anti CD14 (clone REA599) from Miltenyi Biotec, at a dilution of 1/100. For intracellular staining of TNF-α and IL-1β, an Inside Stain kit (Miltenyi Biotec) was utilized in accordance with the manufacturer's instructions. In brief, the cells were fixed with 250 µL of the Inside Fix solution for 20 minutes at room temperature (RT), then washed and stained with 100 µL of the Inside Perm solution containing PE anti TNF-α (clone cA2, Miltenyi Biotec) and APC anti-IL-1β (clone REA1172, Miltenyi Biotec) antibodies at a dilution of 1/50 for 30 minutes at RT. Data acquisition was carried out using a Canto II flow cytometer and analyzed using Diva software (BD Biosciences, San Jose, CA) and FlowJo software (Treestar, Ashland, OR).

CXCR4 knockout experiments

The experiment involved seeding monocytes at a density of 105 cells/100 µl in 96-well plates and placing them in an incubator at 37° C. Two types of siRNA, namely control siRNA (qiagen) and CXCR4 siRNA (SMARTPool, Dharmarcon), were diluted in DOTAP (1,2-dioleoyl-3-trimethylammonium-propane; Roche Applied Sciences). The mixture was gently combined and allowed to incubate at room temperature for 15 minutes. Following the incubation period, the mixture was added to the cultured cells, achieving a final concentration of 160 nM. The cells were then further incubated at 37°C for 24 hours prior to the addition of treatments and stimulation.

Cytokine detection

The supernatants underwent cytokine production testing through two different methods. The first method involved utilizing the LEGENDplex Antivirus Human panel bead assay (Biolegend, San Diego, USA) as per the manufacturer's instructions. Alternatively, a commercial Luminex multi-analyte assay (Biotechne, R&D systems) was also employed, following the provided instructions.

Simoa

A novel Simoa digital ELISA specific to TNF-α was developed by employing a Quanterix Homebrew Assay and incorporating two commercially available antibodies (28). Initially, the 28401 antibody (R&D) clone was utilized as a capture antibody following the coating of paramagnetic beads (0.3 mg/mL). The ab9635 polyclonal antibody (Abcam) was biotinylated (biotin/Ab ratio = 30:1) and employed as the detector. To establish the standard curve, recombinant TNF-α (R&D) was used after conducting cross-reactivity assessments. The limit of detection was determined by calculating the average value of all blank runs ± 3 standard deviations (SDs), resulting in a detection limit of 1 fg/mL.

TABLE 2 Antibodies for mass cytometry.

Targets	Metals	Clones	Suppliers	References
CD45	89Y	HI30	Fluidigm	3089003B
CD38	112Cd	HIT2	Life technologies	Q22150
HLA-DR	115 In	L243	Ozyme	BLE307651
IL-1β	141 Pr	8516	R & D Systems	MAB201-100
CD27	142 Nd	O323	Ozyme	BLE302802
CD123	143 Nd	6H6	Ozyme	BLE306002
CD4	145 Nd	RPA-T4	Ozyme	BLE300516
CD8	146 Nd	RPT-T8	Ozyme	BLE301018
CD86	148 Nd	FM95	Miltenyi	130-095-212
IL-17	151 Eu	CZ8-23G1	Miltenyi	130-095-212
CD304 (BDCA4)	152 Sm	AD5-17F6	Miltenyi	130-095-212
CD11C	153 Eu	Bu15	Ozyme	BLE337202
Il-6	154 Sm	MG2-13A5	Miltenyi	130-095-212
CD279 (PD-1)	156 Gd	PD1.3.1.3	Miltenyi	130-095-212
CD14	160 Gd	M5E2	Ozyme	BLE301810
IFNγ	161 Dy	45-15	Miltenyi	130-095-212
CD185 (CXCR5)	162 Dy	REA103	Miltenyi	130-095-212
CCR7 (CD197)	163 Dy	REA108	Miltenyi	130-095-212
IFN α2	165 Ho	3C5	R & D Systems	H00003440-M27
TNF-α	166 Er	cA2	Miltenyi	130-095-212
CD56	168 Er	HCD56	Ozyme	BLE318324
CD45RA	169 Tm	T6D11	Miltenyi	130-095-212
CD3	170 Er	BW264/56	Miltenyi	130-095-212
IgM	172 Yb	PJ2-22H3	Miltenyi	130-095-212
IgD	174 Yb	IgD26	Miltenyi	130-095-212
CXCL10	175 Lu	REA334	Miltenyi	130-095-212
CD19	176 Yb	LT19	Miltenyi	130-108-029
CD278 (ICOS)	198 Pt	REA183	Miltenyi	130-095-212
CD16	209 Bi	3G8	Fluidigm	3209002B

RNA isolation and real-time quantitative RT-PCR analyses

The THP1-Dual monocyte cells were cultured at a density of 1.6.106 cells/mL. Prior to a 24-hour stimulation with R848 at a concentration of 10 μg/mL, the cells were pre-treated with clobenpropit (CB) for 1 hour. To isolate the total RNA, an E.Z.N.A. kit (Omega Bio-Tek, USA) was used following the manufacturer's instructions. For the synthesis of first-strand cDNA, the Prime Script RT Master Mix kit (Takara Bio Europe, France) was employed. Quantitative real-time PCR was conducted at 60°C using the Takyon ROX SYBR MasterMix (Eurogentec, Belgium) in the CFX384 Touch Real-Time PCR Detection System (Bio-Rad, France). The RT-qPCR analyses utilized the primers provided in the list below:

RPL13A: forward primer, 5'-AACAGCTCATGAGGCTACGG-3'; reverse primer, 5'-TGGGTCTTGAGGACCTCTGT-3'

IL1B: forward primer, 5'-CCTGTCCTGCGTGTTGAAAGA-3'; reverse primer, 5'-GGGAACTGGGCAGACTCAAA-3'

IL6: forward primer, 5'-GACAGCCACTCACCTCTTCA-3'; reverse primer, 5'-CCTCTTTGCTGCTTTCACAC-3'

TNF-α: forward primer, 5'-CCTGCTGCACTTTGGAGTGA-3'; reverse primer, 5'-GAGGGTTTGCTACAACATGGG-3'

Nanostring gene expression analysis

Isolated monocytes from both control subjects and patients were used to extract total RNA. The extracted RNA was diluted to a concentration of 20 ng/µl using ribonuclease-free water. Subsequently, 100 ng (5 µl) of each sample was subjected to analysis utilizing the Human Immunology kit v2 and Nanostring Counter. To ensure accuracy, each sample underwent individual multiplexed reactions, consisting of eight negative probes and six serial concentrations of positive control probes. The resulting data was then imported into the nSolver analysis software (version 2.5) for quality assessment and data normalization, adhering to NanoString analysis guidelines. This normalization process involved the utilization of positive probes and housekeeping genes. Prior to hierarchical clustering using Qlucore Omics Explorer version 3.1, the mRNA expression levels were logarithmically transformed. For pathway analysis, the DAVID bioinformatics databank (https://david.ncifcrf.gov) was employed. Supplementary data includes the presented mRNA levels.

Mice

Washington Biotechnology, INC conducted animal experiments in a manner that ensured unbiased results. The animals were housed in a controlled environment with regulated temperature, humidity, and 12-hour light/dark cycles. They had access to food and water without restriction. The mouse experiments conducted by Washington Biotechnology, INC were reviewed and approved by the WBI Animal Care and Use Committee under the reference IACUC NO. 17 006. The experimental procedures followed the guidelines outlined in the "Guide for the Care and Use of Laboratory Animals" and adhered to ethical standards and regulations. On Day 0, the mice were weighed, and the thickness of their hind limbs was measured using a digital caliper. They were then subcutaneously injected with a 50 µL emulsion of collagen and Complete Freund's Adjuvant at the base of their tails. On Day 21, the mice were weighed again and received a subcutaneous injection of a 50 µL emulsion of collagen and Incomplete Freund's Adjuvant at the base of their tails. After this, the mice were divided into five groups, each consisting of eight mice. From Day 21 to Day 35, the first group received intraperitoneal injections of PBS. The second group was administered prednisolone (Sigma, P4153) orally via daily gavage at a dosage of 10 mL/kg, which had been dissolved in 3 mL of PBS to form a 1.5 mg/mL solution. The mice in groups 3, 4, and 5 were treated with CB. Briefly, CB was dissolved in PBS and administered daily through intraperitoneal injections at dosages of 3 mg/kg, 10 mg/kg, and 30 mg/kg respectively (groups 3 to 5). On Day 35, all mice were weighed, assessed for signs of arthritis, and their hind paw volumes were recorded. The mice were anesthetized and their blood was collected in pre-chilled EDTA tubes. The blood samples were processed to obtain plasma, which was then frozen and subsequently thawed at room temperature. The plasma samples were diluted 1:2 and analyzed using ELISA to measure levels of IL-1β (R&D Systems, Cat. MLB00C) and IL-6 (R&D Systems, Cat. M6000B). The limbs were individually removed and preserved in 10% neutral buffered formalin.

Histology on mice limbs

Formalin-fixed mouse paws were processed routinely, sectioned at approximately 8 microns, and stained with hematoxylin and eosin. Glass slides were evaluated using light microscopy by a board-certified veterinary pathologist. The severity of histologic findings was scored using the following scoring criteria as adapted from Crissman et al (29).

- Inflammation

0=Normal

1=Minimal infiltration of inflammatory cells in synovium and periarticular tissue of affected joints

2=Mild infiltration, if paws, restricted to affected joints

3=Moderate infiltration with moderate edema, if paws, restricted to affected joints

4=Marked infiltration affecting most areas with marked edema

5=Severe diffuse infiltration with severe edema

- Cartilage Damage

0=Normal

1=Minimal=minimal to mild loss of toluidine blue staining with no obvious chondrocyte loss or collagen disruption in affected joints

2=Mild=mild loss of toluidine blue staining with focal mild (superficial) chondrocyte loss and/or collagen disruption in affected joints

3=Moderate=moderate loss of toluidine blue staining with multifocal moderate (depth to middle zone) chondrocyte loss and/or collagen disruption in affected joints

4=Marked=marked loss of toluidine blue staining with multifocal marked (depth to deep zone) chondrocyte loss and/or collagen disruption in most joints

5=Severe =severe diffuse loss of toluidine blue staining with multifocal severe (depth to tide mark) chondrocyte loss and/or collagen disruption in all joints

- Bone Resorption

0=Normal

1=Minimal=small areas of resorption, not readily apparent on low magnification, rare osteoclasts in affected joints

2=Mild=more numerous areas of, not readily apparent on low magnification, osteoclasts more numerous in affected joints

3=Moderate=obvious resorption of medullary trabecular and cortical bone without full thickness defects in cortex, loss of some medullary trabeculae, lesion apparent on low magnification, osteoclasts more numerous in affected joints

4=Marked=Full thickness defects in cortical bone, often with distortion of profile of remaining cortical surface, marked loss of medullary bone, numerous osteoclasts, affects most joints

5=Severe=Full thickness defects in cortical bone and destruction of joint architecture of all joints

Statistics

Cellular data sets were analyzed by Mann-Whitney test to compare the group with CB treatment to the untreated group. Flow cytometry data were performed using FlowJo software.

Animal data are shown as median and min/max. Data sets were analyzed by ANOVA (Kruskal-Wallis) tests with Dunn's post-test for multiple comparisons with the different concentrations of CB and prednisolone treatment. Data analysis and graph preparation were performed using GraphPad Prism 8 software (GraphPad Software, San Diego, CA). Statistical significance was determined with a threshold of $p < 0.05$, indicating values below this threshold were considered statistically significant. Heatmaps were generated using Qlucore OMICS explore Version 3.5 (26) software.

Data availability statement

The data presented in the study are deposited in the Gene Expression Omnibus repository, accession number GSE243512.

Ethics statement

The blood from healthy donors was obtained from "Etablissement Français du Sang" (convention # 07/CABANEL/106), Paris, France. For JIA patients' material, the study was approved by the Comité de Protection des Personnes (N° EudraCT: 2018-A01358-47) in France. Written informed consent to participate in this study was provided by the participants' legal guardian/next of kin.

Author contributions

NB, NS, MR and J-PH conceived and designed the study. NB, NS, and J-PH had complete access to all the data generated in the study and assume full responsibility for the data's integrity and the accuracy of the data analysis. NB, NS, PQ, and MR contributed to writing the paper. BS and J-PH wrote the paper. NB, NS, BB, TD, AB and J-PH performed data analysis. RM, SB, BBM, BT and PQ were involved in the clinical study and sample collection. BB, AL, TD, AB, SN, and MR performed specific experiments and/or analysis. All authors participated in the review process of the manuscript and provided their final approval for the version that is intended for publication. All authors unanimously take responsibility for all aspects of the work, ensuring that any questions concerning the accuracy or integrity of any part of the research are thoroughly investigated and appropriately resolved.

Funding

This research was financially supported by the Agence National de la Recherche sur le SIDA et les Hépatites (ANRS) under the grant awarded to J-PH for conducting the experiments. NB received a fellowship (AAP 2017-166) for this work. NS is a recipient of the European Molecular Biology Organization (EMBO) Long-Term Fellowship (LT-834-2017) and the Pasteur-Roux-Cantarini Fellowship.

Acknowledgments

We express our gratitude to Stephanie Dupuy from the Common Service of Flux Cytometry (B2M) at Paris Descartes University for her invaluable assistance. Additionally, we extend our thanks to Fabrice Porcheray for his support in mass cytometry at BIOASTER Paris.

Conflict of interest

Author PQ reports personal fees from Abbvie, personal fees from BristolMyers Squibb, personal fees from Chugai-Roche, personal fees from Lily, personal fees from Novartis, personal fees from Novimmune, personal fees from sweedish orphan biovitrum, personal fees from Sanofi, outside the submitted work. Authors J-PH and NS have a patent WO2017216373A1 issued.

The remaining authors declare that the research was conducted in the absence of any commercial or financial relationships that could be construed as a potential conflict of interest.

The reviewer FA declared a shared parent affiliation with the author SN to the handling editor at the time of review.

Publisher's note

Supplementary material

The Supplementary Material for this article can be found online at: https://www.frontiersin.org/articles/10.3389/fimmu.2023.1178172/full#supplementary-material

References

1. Szekanecz Z, Koch AE. Macrophages and their products in rheumatoid arthritis. *Curr Opin Rheumatol* (2007) 19:289–95. doi: 10.1097/BOR.0b013e32805e87ae

2. Yeo L, Adlard N, Biehl M, Juarez M, Smallie T, Snow M, et al. Expression of chemokines CXCL4 and CXCL7 by synovial macrophages defines an early stage of

rheumatoid arthritis. *Ann Rheum Dis* (2016) 75:763–71. doi: 10.1136/annrheumdis-2014-206921

3. Petty RE, Southwood TR, Manners P, Baum J, Glass DN, Goldenberg J, et al. International League of Associations for Rheumatology classification of juvenile idiopathic arthritis: second revision, Edmonton, 2001. *J Rheumatol* (2004) 31:390–2.

4. Martini A, Lovell DJ. Juvenile idiopathic arthritis: state of the art and future perspectives. *Ann Rheum Dis* (2010) 69:1260–3. doi: 10.1136/ard.2010.133033

5. Ou L-S, See L-C, Wu C-J, Kao C-C, Lin Y-L, Huang J-L. Association between serum inflammatory cytokines and disease activity in juvenile idiopathic arthritis. *Clin Rheumatol* (2002) 21:52–6. doi: 10.1007/s100670200012

6. Möller B, Villiger PM. Inhibition of IL-1, IL-6, and TNF-α in immune-mediated inflammatory diseases. *Springer Semin Immun* (2006) 27:391. doi: 10.1007/s00281-006-0012-9

7. Mangge H, Kenzian H, Gallistl S, Neuwirth G, Liebmann P, Kaulfersch W, et al. Serum cytokines in juvenile rheumatoid arthritis. Correlation with conventional inflammation parameters and clinical subtypes. *Arthritis Rheum* (1995) 38:211–20. doi: 10.1002/art.1780380209

8. Cepika A-M, Banchereau R, Segura E, Ohouo M, Cantarel B, Goller K, et al. A multidimensional blood stimulation assay reveals immune alterations underlying systemic juvenile idiopathic arthritis. *J Exp Med* (2017) 214:3449–66. doi: 10.1084/jem.20170412

9. Smith N, Pietrancosta N, Davidson S, Dutrieux J, Chauveau L, Cutolo P, et al. Natural amines inhibit activation of human plasmacytoid dendritic cells through CXCR4 engagement. *Nat Commun* (2017) 8:14253. doi: 10.1038/ncomms14253

10. Gualtierotti R, Ingegnoli F, Griffini S, Grovetti E, Meroni PL, Cugno M. Prothrombotic biomarkers in patients with rheumatoid arthritis: the beneficial effect of IL-6 receptor blockade. *Clin Exp Rheumatol* (2016) 34:451–8.

11. Huang DW, Sherman BT, Lempicki RA. Systematic and integrative analysis of large gene lists using DAVID bioinformatics resources. *Nat Protoc* (2009) 4:44–57. doi: 10.1038/nprot.2008.211

12. Huang DW, Sherman BT, Lempicki RA. Bioinformatics enrichment tools: paths toward the comprehensive functional analysis of large gene lists. *Nucleic Acids Res* (2009) 37:1–13. doi: 10.1093/nar/gkn923

13. de Jager W, Hoppenreijs EPAH, Wulffraat NM, Wedderburn LR, Kuis W, Prakken BJ. Blood and synovial fluid cytokine signatures in patients with juvenile idiopathic arthritis: a cross-sectional study. *Ann Rheum Dis* (2007) 66:589–98. doi: 10.1136/ard.2006.061853

14. Pietrosimone KM, Jin M, Poston B, Liu P. Collagen-induced arthritis: A model for murine autoimmune arthritis. *Bio Protoc* (2015) 5. doi: 10.21769/bioprotoc.1626

15. Hegen M, Keith JC, Collins M, Nickerson-Nutter CL. Utility of animal models for identification of potential therapeutics for rheumatoid arthritis. *Ann Rheum Dis* (2008) 67:1505–15. doi: 10.1136/ard.2007.076430

16. Williams RO, Marinova-Mutafchieva L, Feldmann M, Maini RN. Evaluation of TNF-α and IL-1 blockade in collagen-induced arthritis and comparison with combined anti-TNF-α/anti-CD4 therapy. *J Immunol* (2000) 165:7240–5. doi: 10.4049/jimmunol.165.12.7240

17. Lipsky PE. Interleukin-6 and rheumatic diseases. *Arthritis Res Ther* (2006) 8 Suppl 2:S4. doi: 10.1186/ar1918

18. McInnes IB, Buckley CD, Isaacs JD. Cytokines in rheumatoid arthritis - shaping the immunological landscape. *Nat Rev Rheumatol* (2016) 12:63–8. doi: 10.1038/nrrheum.2015.171

19. Feldmann M, Brennan FM, Maini RN. Rheumatoid arthritis. *Cell* (1996) 85:307–10. doi: 10.1016/S0092-8674(00)81109-5

20. Prince FH, Dorai Raj AK, Otten MH, Cheung PP, Tymms KE, van Suijlekom-Smit LW, et al. TNF-alpha inhibitors for juvenile idiopathic arthritis. *Cochrane Database Syst Rev* (2018) 2018:CD008598. doi: 10.1002/14651858.CD008598.pub2

21. Wong PKK, Campbell IK, Egan PJ, Ernst M, Wicks IP. The role of the interleukin-6 family of cytokines in inflammatory arthritis and bone turnover. *Arthritis Rheum* (2003) 48:1177–89. doi: 10.1002/art.10943

22. Rönnblom L, Eloranta M-L. The interferon signature in autoimmune diseases. *Curr Opin Rheumatol* (2013) 25:248–53. doi: 10.1097/BOR.0b013e32835c7e32

23. Peng L, Zhu N, Mao J, Huang L, Yang Y, Zhou Z, et al. Expression levels of CXCR4 and CXCL12 in patients with rheumatoid arthritis and its correlation with disease activity. *Exp Ther Med* (2020) 20:1925–34. doi: 10.3892/etm.2020.8950

24. Hua C, Buttgereit F, Combe B. Glucocorticoids in rheumatoid arthritis: current status and future studies. *RMD Open* (2020) 6:e000536. doi: 10.1136/rmdopen-2017-000536

25. Fleischmann R, Mysler E, Hall S, Kivitz AJ, Moots RJ, Luo Z, et al. Efficacy and safety of tofacitinib monotherapy, tofacitinib with methotrexate, and adalimumab with methotrexate in patients with rheumatoid arthritis (ORAL Strategy): a phase 3b/4, double-blind, head-to-head, randomised controlled trial. *Lancet* (2017) 390:457–68. doi: 10.1016/S0140-6736(17)31618-5

26. Fleischmann R, Kremer J, Cush J, Schulze-Koops H, Connell CA, Bradley JD, et al. Placebo-controlled trial of tofacitinib monotherapy in rheumatoid arthritis. *N Engl J Med* (2012) 367:495–507. doi: 10.1056/NEJMoa1109071

27. Vieira M-C, Zwillich SH, Jansen JP, Smiechowski B, Spurden D, Wallenstein GV. Tofacitinib versus biologic treatments in patients with active rheumatoid arthritis who have had an inadequate response to tumor necrosis factor inhibitors: results from a network meta-analysis. *Clin Ther* (2016) 38:2628–2641.e5. doi: 10.1016/j.clinthera.2016.11.004

28. Wu D, Milutinovic MD, Walt DR. Single molecule array (Simoa) assay with optimal antibody pairs for cytokine detection in human serum samples. *Analyst* (2015) 140:6277–82. doi: 10.1039/c5an01238d

29. Crissman JW, Goodman DG, Hildebrandt PK, Maronpot RR, Prater DA, Riley JH, et al. Best practices guideline: toxicologic histopathology. *Toxicol Pathol* (2004) 32:126–31. doi: 10.1080/01926230490268756

frontiers | Frontiers in Immunology

TYPE Review
PUBLISHED 28 April 2023
DOI 10.3389/fimmu.2023.1162739

OPEN ACCESS

EDITED BY
Diana Boraschi,
Chinese Academy of Science (CAS), China

REVIEWED BY
Kamal Moudgil,
University of Maryland, United States
Eliane Piaggio,
Institut National de la Santé et de la Recherche Médicale (INSERM), France

*CORRESPONDENCE
Maria del Carmen Domínguez-Horta
mcarmen.dominguez@cigb.edu.cu

RECEIVED 09 February 2023
ACCEPTED 18 April 2023
PUBLISHED 28 April 2023

CITATION
Domínguez-Horta MdC, Serrano-Díaz A, Hernández-Cedeño M, Martínez-Donato G and Guillén-Nieto G (2023) A peptide derived from HSP60 reduces proinflammatory cytokines and soluble mediators: a therapeutic approach to inflammation.
Front. Immunol. 14:1162739.
doi: 10.3389/fimmu.2023.1162739

A peptide derived from HSP60 reduces proinflammatory cytokines and soluble mediators: a therapeutic approach to inflammation

Maria del Carmen Domínguez-Horta[1,2]*, Anabel Serrano-Díaz[1], Mabel Hernández-Cedeño[1], Gillian Martínez-Donato[3] and Gerardo Guillén-Nieto[2,3]

[1]Autoimmunity Project, Pharmaceutical Division,Center for Genetic Engineering and Biotechnology, Havana, Cuba, [2]Physiology Department, Latin American School of Medicine, Havana, Cuba, [3]Biomedical Research Division, Center for Genetic Engineering and Biotechnology, Havana, Cuba

Cytokines are secretion proteins that mediate and regulate immunity and inflammation. They are crucial in the progress of acute inflammatory diseases and autoimmunity. In fact, the inhibition of proinflammatory cytokines has been widely tested in the treatment of rheumatoid arthritis (RA). Some of these inhibitors have been used in the treatment of COVID-19 patients to improve survival rates. However, controlling the extent of inflammation with cytokine inhibitors is still a challenge because these molecules are redundant and pleiotropic. Here we review a novel therapeutic approach based on the use of the HSP60–derived Altered Peptide Ligand (APL) designed for RA and repositioned for the treatment of COVID-19 patients with hyperinflammation. HSP60 is a molecular chaperone found in all cells. It is involved in a wide diversity of cellular events including protein folding and trafficking. HSP60 concentration increases during cellular stress, for example inflammation. This protein has a dual role in immunity. Some HSP60-derived soluble epitopes induce inflammation, while others are immunoregulatory. Our HSP60-derived APL decreases the concentration of cytokines and induces the increase of FOXP3+ regulatory T cells (Treg) in various experimental systems. Furthermore, it decreases several cytokines and soluble mediators that are raised in RA, as well as decreases the excessive inflammatory response induced by SARS-CoV-2. This approach can be extended to other inflammatory diseases.

KEYWORDS

HSP60, APL, cytokines, inflammation, rheumatoid arthritis, CIGB-814/CIGB-258, COVID-19, Jusvinza

1 Introduction

Cytokines are molecules with relatively low molecular weights. These proteins are secreted by several immune cells (1, 2). Some cytokines are pro-inflammatory and others are anti-inflammatory. Consequently, they act mostly as regulators of immune and inflammatory responses (3–5).

Additionally, cytokines have important functions in a diversity of biological events including cell activation, differentiation, and proliferation (6, 7). Furthermore, cytokines play a crucial role in acute and chronic inflammation, and tumor progression, as well as in the onset and chronicity of autoimmune diseases (1, 6, 8).

The inhibition of proinflammatory cytokines has been used in the treatment of autoimmune diseases such as RA (9–11). Some of these drugs were repositioned in the management of COVID-19 patients (12, 13). However, controlling hyperinflammation with cytokine inhibitors is still a challenge, because these molecules are redundant and pleiotropic (14, 15). Likewise, these drugs are immunosuppressive and they can lead to the fall of the general condition of COVID-19 patients (16–18).

In this article, we focus on an original approach to the control of inflammation using an APL derived from HSP60. This therapeutic concept is focused on the induction of peripheral tolerance using a modified autoantigen implicated in RA pathogenesis. HSP60 was the autoantigen chosen for the APL design. Interestingly, this protein plays a dual role in immunity, i.e. certain soluble HSP60-derived epitopes induce inflammation and others are immunoregulatory (19–23).

The APL designed has anti-inflammatory properties and increases Treg in preclinical models of RA (24, 25). Clinical investigations in RA patients indicate that this molecule is safe and reduces inflammation (26–28).

Based on these results we decided to investigate whether this molecule could be useful in treating the hyperinflammation that distinguishes COVID-19 patients who are progressing to severe and critical conditions. The treatment with this peptide inhibited several cytokines and soluble mediators associated with hyperinflammation in COVID-19 patients (29, 30).

Given all these results, the anti-inflammatory effects of this molecule are assessed in other experimental models of inflammation.

2 HSP60, autoantigen selected for APL design

Among the autoantigens involved in RA pathogenesis, we selected HSP60 for the APL design. This selection was supported by the therapeutic potential of HSP60 for autoimmune diseases. We hypothesized that an APL derived from HSP60 would enhance these therapeutic effects.

HSP60 is extremely conserved in evolution (31, 32). This protein is classified as a chaperone and is located inside the mitochondria where, together with the co-chaperonin Hsp10, it assists in protein homeostasis (33, 34).

However, under certain physiological conditions, HSP60 is located in other cellular organelles and it can even appear in the extracellular space. At these sites, HSP60 participates in pathogenic events such as inflammation, autoimmunity and carcinogenesis (35, 36).

HSP60 has an interesting connection with innate and acquired immune response, which is related to its conservation through evolution and its chaperone function.

This molecule has been described as an innate signal for macrophages and dendritic cells. Macrophages in reaction to HSP60 produce pro-inflammatory molecules (37–39). HSP60 stimulates the maturation of dendritic cells (40).

This chaperone was identified as a dominant bacterial antigen during infections or vaccination. Both biological events are characterized by the secretion of antibodies to bacterial HSP60 (41). Moreover, autoantibodies to self-HSP60 are identified in several autoimmune diseases such as RA, lupus, inflammatory bowel disease and atherosclerosis (42–46).

Furthermore, autoantibodies against HSP60 are present in healthy subjects; for example, an Ig M iso-type autoantibody against HSP60 was identified within the blood of the umbilical cord of some newborns (47), and IgM and IgG autoantibodies against HSP60 were identified in healthy human beings (48).

On the other hand, epitopes derived from mycobacterial HSP65 that are identical to the HSP60 human peptide, induced cytotoxic T cell reactivity in healthy humans (20). Besides, T cells against HSP60 self-peptides were found in the blood of the umbilical cord of healthy neonates (39). These facts indicate that it is normal to find effector T cells to self-HSP60 from birth.

Cohen hypothesized that HSP may be included in the "immunological homunculus", which comprises several dominant antigens involved in an intricate biologic regulatory network (40).

Other authors have described that T cells to self-HSP60 are related to spontaneous remission in juvenile idiopathic arthritis (41, 42) and induce resistance to induction of experimental arthritis in Lewis rats (43–45). T cells against HSP60 that secreted IL-10 can be favorable in attenuating inflammation during autoimmune diseases and harmful in infections (42, 46, 47). In contrast, T cells vs HSP60 that produce proinflammatory cytokines can be damaging in autoimmune diseases and beneficial against pathogens (48).

Studies about HSP60 have progressively increased in recent years, mainly because of its potential as an approach for emerging therapeutic procedures in inflammatory diseases and severe chaperonopathies such as several kinds of cancer, as well as inflammatory and autoimmune diseases and neurodegenerative diseases (36, 49–52).

Particularly, since the regulatory effect of HSP60 on the immune response is well defined, several authors have proposed different approaches for its use in the treatment of autoimmune diseases (22, 23). Regardless of the potential risks of generating adverse inflammatory effects, diverse formulations of HSP60 and peptides derived from it, have been studied in experimental models without observing pathological autoimmunity (53).

Furthermore, reports show the use of the immunomodulatory properties of HSP60 and its peptides in clinical trials for

autoimmune diseases (54–57). However, none of these therapeutic candidates have become registered drugs.

We believe that there are key points in the success of the treatments based on peptides derived from HSP60 for their use in inflammation and the reduction of pro-inflammatory cytokines, i.e., the selection of a specific epitope, the biodistribution of this molecule and the frequency of its administration.

3 An APL designed from HSP60 as an inductor of peripheral tolerance

The identification of an epitope from HSP60 is a critical factor for induced peripheral tolerance as a possible treatment for autoimmune diseases.

The potential of the APLs as tolerance inductors has been previously reported (58–60). APLs are similar to the wild-type peptide but with one or two mutations in the essential interaction positions with the T-cell receptor (TCR) or with the HLA class II molecules that modify the pathways for the activation of T cells. These APL can modify the response of autoreactive T cells by several mechanisms (60–64).

In contrast with other authors, we selected the N-terminal sequence from human HSP60 (amino acids 90 to 109). This region is much conserved, it is 100% identical in humans, monkeys, fish, rats and mice, but the match is 50% with *Mycobacterium tuberculosis* (*Mt*). In this sequence, the Propred computer algorithm (65) predicted new epitopes that would be interacting directly with the HLA class II molecule associated with RA. Aspartic acid 18 was substituted by leucine (Figure 1). This mutation increased the affinity between APL and HLA class II molecules, according to the bioinformatic prediction (24).

Furthermore, potential binding motifs (cores) of this APL and its wild type peptide (E18-3), and the affinity of both to HLA class II alleles related with RA, were analyzed by the NetMHCIIpan platform (66, 67). This algorithm indicated that APL has two possible overlapping epitopes. A notable feature is that the replacement of Asp-18 in E18-3 with a Leu raises the affinity of APL to HLA class II. Predictions using NetMHCIIpan advise that the novel peptide binds to more RA related HLA class II molecules and has a better affinity than E18-3 (68).

This novel peptide was called APL-1 or CIGB-814 in preclinical and clinical studies in RA. This peptide was renamed CIGB-258 during clinical research in COVID-19 patients. Subsequently,

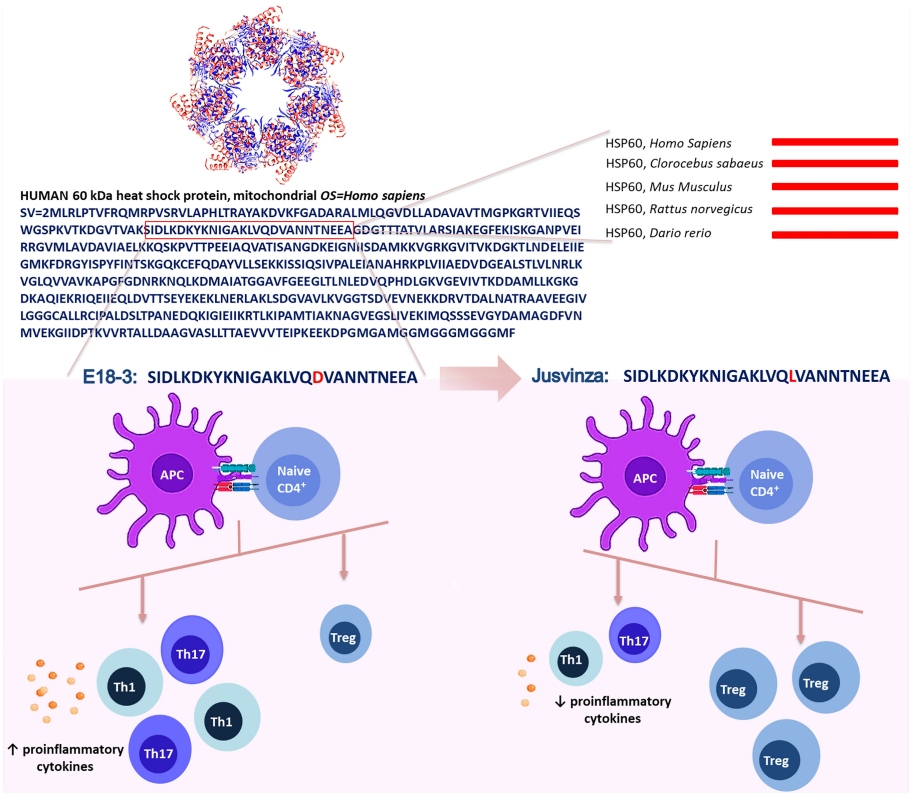

FIGURE 1
Jusvinza was designed from the N-terminal region of the human HSP60 (amino acids from 90 to 109). This sequence is 100% identical between humans, rats, mice, monkeys and Zebrafish (lines red). In this region, the aspartic acid-18 (red) involved in the interaction with the HLA class II molecule was substituted by leucine (red). This change increased the affinity between Jusvinza and HLA class II molecules. Jusvinza induces an increase of FOXP3+ regulatory T cells (Treg) and reduces proinflammatory cytokines. In contrast, the wild-type peptide did not induce Treg cells and increase proinflammatory cytokines.

CIGB-258 was granted Authorization for Emergency Use (AEU) by the Cuban Regulatory Authority for COVID-19 patients under the commercial name of Jusvinza.

4 Biodistribution and pharmacokinetics (PK) of Jusvinza

The biodistribution profile of a drug is essential in activating the molecular mechanisms that induced peripheral tolerance. Hence, depending on the organ where the drug is positioned, it may be able to interact with antigen-presenting cells (APC), T cells and cytokines that mediate the induction of tolerance.

The biodistribution of a peptide can be affected by the dose, as well as by the inoculation route. Jusvinza was mainly distributed in the stomach and small intestine, after being inoculated in Lewis rats. The levels of Jusvinza increased in lymph nodes (LNs) at 24 hours, compared to four hours postadministration. This peptide was likewise found in the liver, spleen, heart and lungs (Figure 2A). The biodistribution of Jusvinza was almost the same for the three routes studied (subcutaneous, intravenous and intradermal routes) (69). This biodistribution profile is interesting because the small intestine is specialized in the induction of tolerance (70).

In addition, the highest concentration of Jusvinza in the blood plasma of rats was found at 0.5 to 1 hour; and the half-life in the blood was calculated to be of six hours. These results agree with the PK profile identified in RA patients included in the Phase I Clinical Trial (27).

Recently, we have identified that Jusvinza binds only with apolipoprotein A-I (Apo-AI) and transthyretin in human plasma. The identification of these proteins were through affinity chromatography using as the matrix a pearl-shaped resin (ChemMatrix) - coupled to Jusvinza. The eluted proteins were accurately identified by mass spectrometry (nano ESI-MS). Apo-AI and transthyretin are involved in lipid metabolism, and changes in their conformation and concentration have been associated with diseases such as type II diabetes and atherosclerosis. These results agree with those of Cho et al, who demonstrated that Jusvinza enhanced HDL stability (71).

Future research is needed to elucidate the biological significance of the binding of Jusvinza to Apo-AI and transthyretin.

5 Jusvinza reduces inflammation and TNFα in two animal models for RA

The biological effect of Jusvinza was assessed in an experimental model in rats (72). Jusvinza has an epitope that could be bound to rat MHC class II molecules (RT1.BI); according to the MHC2PRED software (73). In this animal model, the disease is induced in rats

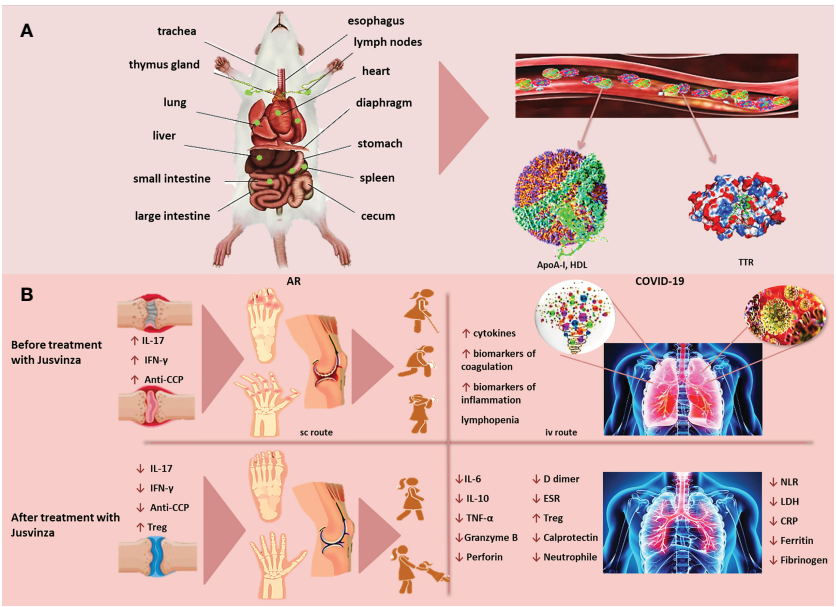

FIGURE 2
(A) Jusvinza is mainly distributed to the stomach and small intestine, as early as 4 hours post-administration. The concentration of Jusvinza increased in lymph nodes (LNs) at 24 hours post-administration. This peptide was also found in the liver, spleen, heart and lungs in Lewis rats. Jusvinza binds apolipoprotein A-I (Apo-AI) and transthyretin (TTR) in plasma. **(B)** Jusvinza reduces inflammation in animal models and RA patients. The processing and presentation of this APL by the antigen-presenting cells (APC) to the autoreactive T lymphocytes in the periphery could induce the expansion of Treg. These cells migrate to the swollen joints and attenuate autoreactive T cells responsible for arthritis pathogenesis. In addition, Jusvinza reduces TNFα, IL-17, interferon-gamma (IFN-γ), anti-CCP antibodies and neutrophil migration. Jusvinza reduces hyperinflammation in COVID-19 patients. Jusvinza can inhibit the activity of monocytes, macrographs and neutrophils. This inhibition may contribute to the decrease of IL-6, TNFa and IL-10, as well as the restoration of lymphocyte counts in patients. Additionally, this peptide can induce Treg. These activated cells migrate to inflamed sites and could cross-recognize the wild-type epitope from HSP60 expressed in the endothelial tissue and inhibit autoimmune damage induced during viral infection.

through immunization with *Mt* in incomplete Freund's adjuvant (AA). Jusvinza reduced the inflammation and pannus in these rats with arthritis.

However, the original epitope from HSP60 did not produce these therapeutic effects in rats. Besides, the treatment with Jusvinza significantly reduces TNFα levels in the spleen of treated animals compared to the placebo group. This clinical efficacy induced by Jusvinza was associated with an increase of Treg in the rats.

The AA model is characterized by the fact that immunization with *Mt* protects against subsequent attempts to induce this disease. This effect is due to the induction of Treg against a conserved epitope from HSP60 (aa from 256 to 270) and the secretion of regulatory cytokines (41, 74). These factors could favor the therapeutic effect of Jusvinza in the AA model. Hence, it was essential to assess the therapeutic effect of Jusvinza in another animal model, in which Treg cells are not induced against HSP60 in the course of the disease.

Consequently, the therapeutic effect of Jusvinza was evaluated in Collagen Induced Arthritis (CIA) in DBA/1 mice (75). Jusvinza monotherapy was able to reduce inflammation in these mice. The therapeutic effect was similar to mice inoculated with Jusvinza plus methotrexate (MTX) (25). Furthermore, pannus development was not detected in mice treated with Jusvinza. This indicates that the migration of macrophages and neutrophils did not take place in the joints of mice treated with this peptide.

These results were also linked to a decrease in TNFα levels. This cytokine is crucial for the onset and chronicity of RA. TNFα can stimulate proinflammatory cytokine production, increasing the expression of adhesion molecules and neutrophil activation, and enhancing antibody secretion by plasmatic cells (76–78).

Contrary to the effect in the spleen of AA rats treated with Jusvinza, Treg was not detected in CIA mice. Nevertheless, the treatment with Jusvinza plus MTX induced Treg in the spleen of CIA mice. The molecular mechanism of MTX is not associated with an induction of Treg in mice (79). But, the decrease of TNFα mediated by MTX can favor the induction of Treg by Jusvinza. The results suggest that MTX plus Jusvinza could have a molecular synergic effect in the CIA model.

Jusvinza reduced inflammation in AA and CIA models mediated by the expansion of Treg at the periphery. These cells could migrate to the swollen joints and decrease autoreactive T cell activity that perpetuates arthritis, blocking the production of proinflammatory cytokines and the consequent neutrophil migration.

6 Jusvinza induces Treg with suppression activity and reduces IL-17 secreted by Th17

Jusvinza induced Treg in draining lymph nodes and spleen from healthy BALB/c mice. At the same time, the wild-type epitope of HSP60 recruits more CD4+ FoxP3- T lymphocytes, showing that the mutation of the wild-type peptide was effective in inducing Treg and reinforces the beneficial potentials of Jusvinza for the management of RA patients (24).

In addition, experiments with peripheral blood mononuclear cells (PBMC) from RA patients indicate that Jusvinza induces Treg (24, 80). In contrast, the wild-type peptide did not induce Treg (24).

Furthermore, autologous cross-over experiments showed that Jusvinza-treatment had a significant effect in reducing IL-17 levels. Jusvinza can induce Tregs and its suppressive activity against antigen-specific T lymphocytes cells, whereas the activated T effector cells produce less IL-17 (68).

The change of sequence produced in Jusvinza could increase Treg in RA patients and specifically inhibit autoreactive T cells. Treatment with Jusvinza could help restore the healthy Th17/Treg balance for patients with RA and other autoimmune diseases.

7 Jusvinza reduces inflammation, proinflammatory cytokines and autoantibodies against cyclic citrullinated peptides (anti-CCP) in RA patients

The safety of Jusvinza was assessed in patients with RA, during an open phase I clinical trial. Twenty patients with moderately active RA were involved in this study. Three doses (1, 2.5 and 5 mg) of Jusvinza were evaluated by the subcutaneous route. This study included the restriction of the use of non-steroidal anti-inflammatory drugs, disease-modifying anti-rheumatic drugs and corticosteroids, as of four weeks before the start of the Jusvinza treatment. Clinical response in patients was assessed following the guidelines of the American College of Rheumatology and Disease Activity Score in 28 joints. Function and health-related quality of life, quantification of inflammatory biomarkers and radiographic changes in patients were also evaluated.

Jusvinza was well tolerated at all doses. The adverse effects detected were minor and reversible, essentially irritation at the inoculation site. Treatment with this peptide diminished disease activity and magnetic resonance imaging score in patients. This treatment enhanced the health-related quality of life of all patients included in the study. Moreover, Jusvinza significantly reduced IL-17 and interferon-gamma (IFN-γ) in patients (26).

RA is mediated by autoreactive T lymphocytes, with TH1 and TH17 phenotypes. However, antibodies against citrullinated self-proteins have a pathogenic role in this disease. Anti-CCP antibodies are related to a fast course of RA, primary erosive damage, increased inflammation and disability in patients (80).

Jusvinza induced a significant reduction of anti-CCP antibodies in patients (28). These results suggest that Jusvinza could inhibit B lymphocytes that produce these pathogenic antibodies.

Another explanation is related to the possible induction of Treg by Jusvinza in patients. This peptide increases Tregs in some experimental models (24, 25). Tregs have different mechanisms of action that may depend on cell contact, through which they can induce apoptosis on effector T cells and plasma cells secreting anti-CCP antibodies (81). Interestingly, Jusvinza decreased the viability of PBMC isolated from RA patients by inducing apoptosis (82).

Furthermore, Jusvinza might affect the citrullination process by decreasing IL-17. Interactions with viruses or bacteria that activate NETosis are the leading sources of protein citrullination in RA (83). NETosis is a type of regulated cell death dependent on the formation of neutrophil extracellular traps. Some studies describe that HSP60 disturbs the effector functions of neutrophils, i.e. HSP60 enhances the phagocytic activity of neutrophils (84); bacterial HSP GroEL from *Staphylococcus epidermidis* biofilms promoted ADN decondensation and induced NETosis (85); inflammatory cytokines can lead to NETosis in neutrophils from RA patients (86). Specifically, IL-17 has widespread inflammatory effects on the joints, inducing bone and cartilage erosions and promoting the migration of inflammatory molecules to the synovia (87). This cytokine plays an important role in the regulation of anti-citrullinated protein antibody secretion (88).

Jusvinza decreases IL-17 and soluble mediators as anti-CCP antibodies, and it can stimulate the activation of the suppressive activity of Tregs (24, 68) (Figure 2B). Therefore, all results confirm the beneficial effect of Jusvinza and its possible medical application in the reduction of inflammation in RA and other inflammatory diseases.

8 Jusvinza reduces cytokines involved in the "cytokine storm" and soluble mediators of inflammation in COVID-19 patients

The clinical spectrum of COVID-19 is very widespread and complex. Patients may range from asymptomatic cases to those showing a rapid progression toward acute respiratory distress syndrome (ARDS) and death (89). Patients progressing to severe stages present an exacerbated inflammatory response, evidenced by the increase in the serum concentration of inflammation biomarkers (90). A group of these patients progresses to cardiovascular collapse, multiple organ failure, and death. Under these conditions, the treatments used for inflammatory chronic diseases have been repositioned to reduce hyperinflammation in COVID-19 patients (91, 92).

The anti-inflammatory effects of Jusvinza in several experimental models of RA are associated with TNFα reduction and Treg induction. At the same time, the therapeutic effect and the reduction of IL-17, IFNγ and autoantibodies against citrullinated self-proteins in RA patients (24, 26, 28, 68, 80) were the rational bases in the proposal of this molecule for the management of hyperinflammation in COVID-19 patients. Consequently, the Cuban Regulatory Authority approved the exploratory use of this peptide for COVID-19 patients in critical and serious conditions.

Exploratory studies in COVID-19 patients revealed that this APL promotes clinical and radiological improvement linked to a decrease in systemic inflammation biomarkers and IL-6, TNFα and IL-10 (29, 93). The treatment with this peptide was granted the AEU by the Cuban Regulatory Authority for COVID-19 patients (94). After this AEU, Jusvinza was included in the Cuban guidelines for the management of COVID-19 patients with signs of hyperinflammation (95).

High levels of IL-6, associated with disease severity, have been widely described in COVID-19 patients (96, 97). IL-6 is considered one of the most important cytokines in infections, along with IL-1 and TNF-α (98). Jusvinza reduced IL-6 levels linked to the clinical improvement of patients (29).

TNF-α stimulates an ongoing inflammatory response associated with autoimmune diseases (99, 100). TNF-α is a pro-inflammatory cytokine that can support T cell apoptosis by interacting with its receptor (101, 102). This cytokine is essential in the pathogenesis of lung fibrosis and SARS-CoV-2 infection (103). Interestingly, TNF-α is significantly reduced with Jusvinza therapy (29).

On the other hand, critically ill COVID-19 patients display an increase of IL-10 related to a worsening of this disease (104). IL-10 is a cytokine with many pleiotropic properties in immunoregulation and inflammation (105). The coronaviruses have intricate mechanisms that use the immunoregulatory function of IL-10 for immune evasion, helping virus replication (106). An association between a high concentration of IL-10 with the fall and functional exhaustion of CD8+ and CD4+T cells has been found in COVID-19 patients (107), indicating that this cytokine plays a key role in SARS-CoV-2 pathogenesis. The Jusvinza treatment led to IL-10 reduction after 96 hours of therapy. This reduction was associated with the clinical improvement of patients (29). IL-10 is secreted by macrophages, monocytes and T cells. However, T cells can not contribute to the high concentration of IL-10 because these patients are characterized by a marked lymphopenia, typical of COVID-19. Jusvinza diminishes monocyte and macrophage counts under cell stress (82). This is possibly the mechanism through which IL-10 is reduced in COVID-19 patients treated with Jusvinza. Besides, the reduction of IL-6 and TNF-α could downregulate IL-10.

Furthermore, high concentrations of calprotectin (S100A8/A9) are associated with negative clinical results in COVID-19 patients (108). Jusvinza reduces calprotectin in sera from COVID-19 patients and this reduction was correlated with the contraction in neutrophil count. These results are interesting because calprotectin is also increased in patients with chronic inflammatory diseases, inducing cytokine production (109).

Lymphopenia, with significantly reduced numbers of T lymphocytes, has been described in severe COVID-19 patients. This lymphopenia is related to the functional activities of cytotoxic T lymphocytes in COVID-19. Natural killer cells, total T cells, as well as CD8+ T cells, are lower in patients showing severe disease than in healthy persons (110).

Likewise, Granzyme B and perforin are increased in CD8+ T cells in severely ill patients (111). Both proteins decreased in the serum 96 hours after the treatment with Jusvinza. This reduction was related to the stabilization of lymphocyte and neutrophil counts in the patients (29).

Additionally, Tregs are significantly reduced in severely ill COVID-19 patients (112, 113). Jusvinza induces Tregs in seriously ill COVID-19 patients (29). Gammazza et al. identified an epitope from HSP60 that is common with the SARS-CoV-2 replicase polyprotein 1ab. These authors suggested that post-

translational modifications during metabolic stress produced by hypertension and diabetes could disturb HSP60 localization and induce an endothelial injury (114). The beneficial result of Jusvinza in COVID-19 patients could be facilitated by the induction of Treg. These cells migrate to inflamed tissues and could cross-recognize the wild-type peptide from HSP60. This new "cross-talk" could induce regulatory mechanisms that would reduce autoimmune damage in the endothelium produced by viral infection. Moreover, Jusvinza could inhibit the activity of neutrophils, monocytes and macrographs. This inhibition may influence the decrease of several proinflammatory cytokines and soluble mediators of inflammation, as well as the increase of lymphocyte counts (Figure 2B). All these effects could resolve exacerbated inflammation and contribute to a positive outcome for the patients.

These results are the premise for the evaluation of the anti-inflammatory effect of Jusvinza in other experimental models of inflammation.

9 Anti-inflammatory activity of Jusvinza against acute toxicity induced by carboxy methyl lysine in Zebrafish

High levels of inflammatory cytokines have characterized severe stages of COVID-19 (113), autoimmune diseases and inflammatory chronic diseases (115). The non-enzymatic glycation of proteins and carbohydrates induces some glycation end products, related to hyperinflammation (116). The glycation of high-density lipoproteins (HDL) is associated with the dysfunctional activity of this lipoprotein (117), which could enhance inflammation. Glycated HDL were found to be toxic in different human cells (118, 119), and in Zebrafish and its embryos, producing reactive oxygen species and showing a slower development rate (120).

Zebrafish (*Danio rerio*) is a routinely used model to assess the toxicity of advanced glycation end products (120) and to evaluate the anti-inflammatory effect of therapeutic candidates.

Recently, Cho et al. studied the therapeutic effect of Jusvinza against inflammation induced by N-"-carboxymethyl lysine (CML) in Zebrafish embryos and adults (71). High concentrations of CML have been identified in the serum of patients with diabetes mellitus and atherosclerosis (121, 122). These patients also showed extremely high inflammatory cytokines, such as IL-1 and TNFα, indicating that a high CML concentration is linked to a pro-inflammatory condition (123). CML produced an important glycation and aggregation of HDL that disturbs the structure and function of HDL, which is linked to a reduction in apolipoprotein A-I stability (118).

Microinjection of CML in Zebrafish embryos produces high embryonic death rates, where survival is of only 18% of the fish showing developmental defects. However, Jusvinza co-injection induces a significant increase in survival and normal development of the fish. Furthermore, an intraperitoneal inoculation of CML in adult Zebrafish produced acute paralysis, sudden death, and affected its swimming capacity through hyperinflammation. But, a co-inoculation of Jusvinza caused a quicker recovery of swimming capacity and a higher survivable rate. Interestingly, the group treated only with CML showed a survival rate of 49%, while the group treated with CML and inoculated with Jusvinza had a survival rate of 97%, with a significant decrease in liver inflammation.

On the other hand, these authors compared the efficacy of Jusvinza, Infliximab (Remsima®), and Tocilizumab (Actemra®) in the model of the acute death of Zebrafish induced by CML. The results showed that the Jusvinza group had a quicker recovery and swimming capacity, with a higher survivable rate than the Remsima® group (71).

10 Conclusions and perspectives

This review describes an important translational research outcome; from the design of an APL for the induction of tolerance in RA, followed by its assessment in experimental models, and finally the treatment of the inflammation that characterizes RA and COVID-19 patients.

The anti-inflammatory effect of Jusvinza constitutes an attractive therapeutic approach for an extensive variety of diseases, characterized by inflammation and high levels of proinflammatory cytokines, such as autoimmune diseases, COVID-19, atherosclerosis, diabetes and neurodegenerative diseases.

Author contributions

Conceptualization: MdCD-H; Writing – original draft: MdCD-H, AS-D, and MH-C; Writing – review & editing: MdCD-H, AS-D, MH-C, GM-D, and GG-N. All authors contributed to the article and approved the submitted version.

Acknowledgments

We are grateful to Dr Miriam Ribas and Professor Eduardo Pentón for their assistance with the English style and grammar corrections and manuscript copy-editing services.

Conflict of interest

The authors declare that the research was conducted in the absence of any commercial or financial relationships that could be construed as a potential conflict of interest.

Publisher's note

References

1. Stow JL, Murray RZ. Intracellular trafficking and secretion of inflammatory cytokines. *Cytokine Growth Factor Rev* (2013) 24:227–39. doi: 10.1016/j.cytogfr.2013.04.001

2. Gulati K, Guhathakurta S, Joshi J, Rai N, Ray A. Cytokines and their role in health and disease: a brief overview. *MOJ Immunol* (2016) 4:1–9. doi: 10.15406/moji.2016.04.00121

3. Rodrigues G, Bottaro G, Gobbe M, Maschio-Signorini LB, Pires de Campos DA. Proinflammatory and anti-inflammatory cytokines mediated by NF-κB factor as prognostic markers in mammary tumors. *Mediators Inflamm* (2016) 2016:10. doi: 10.1155/2016/9512743

4. Azizi G, Mirshafiey A. The potential role of proinflammatory and antiinflammatory cytokines in Alzheimer disease pathogenesis. *Immunopharmacol Immunotoxicol* (2012) 34:881–95. doi: 10.3109/08923973.2012.705292

5. Souza K, Gurgul-Convey E, Elsner M, Lenzen S. Interaction between pro-inflammatory and anti-inflammatory cytokines in insulin-producing cells. *J Endocrinol* (2008) 197:139–50. doi: 10.1677/JOE-07-0638

6. Dinarello CA. Historical insights into cytokines. *Eur J Immunol* (2007) 37(Suppl. 1):S34–45. doi: 10.1002/eji.200737772

7. Lacy P, Stow JL. Cytokine release from innate immune cells: association with diverse membrane trafficking pathways. *Blood* (2011) 118:9–18. doi: 10.1182/blood-2010-08-265892

8. O'Shea JJ, Ma A, Lipsky P. Cytokines and autoimmunity. *Nat Rev Immunol* (2002) 2:37–45. doi: 10.1038/nri702

9. Li P, Zheng Y, Chen X. Drugs for autoimmune inflammatory diseases: from small molecule compounds to anti-TNF biologics. *Front Pharmacol* (2017) 8:460. doi: 10.3389/fphar.2017.00460

10. Lai Y, Dong C. Therapeutic antibodies that target inflammatory cytokines in autoimmune diseases. *Int Immunol* (2016) 28(4):181–8. doi: 10.1093/intimm/dxv063

11. Findeisen KE, Sewell J, Ostor AJK. Biological therapies for rheumatoid arthritis: an overview for the clinician. *Biologics* (2021) 15:343–52. doi: 10.2147/BTT.S252575

12. Sanghai N, Shafiq K, Tranmer GK. Drug discovery by drug repurposing: combating COVID-19 in the 21st century. *Mini Rev Med Chem* (2021) 21:3–9. doi: 10.2174/1389557520999200824103803

13. Yousefi H, Mashouri L, Okpechi SC, Alahari N, Alahari SK, Yousefi H, et al. Repurposing existing drugs for the treatment of COVID-19/SARS-CoV-2 infection: a review describing drug mechanisms of action. *Biochem Pharmacol* (2021) 183:114296. doi: 10.1016/j.bcp.2020.114296

14. Moraga I, Spangler J, Mendoza JL, Garcia KC. Multifarious determinants of cytokine receptor signaling specificity. *Adv Immunol* (2014) 121:1–39. doi: 10.1016/B978-0-12-800100-4.00001-5

15. Ozaki K, Leonard WJ. Cytokine and cytokine receptor. pleiotropy and redundancy. *J Biol Chem* (2002) 277(33):29355–8. doi: 10.1074/jbc.R200003200

16. Capraa R, De Rossia N, Mattiolib F, Romanelli G, Scarpazza C, Sormani MP, et al. Impact of low dose tocilizumab on mortality rate in patients with COVID-19 related pneumonia. *Eur J Internal Med* (2020) 76:31–5. doi: 10.1016/j.ejim.2020.05.009

17. Peterson D, Damsky W, King B. The use of janus kinase inhibitors in the time of SARS-CoV-2. *J Am Acad Dermatol* (2020) 82(6):e223–6. doi: 10.1016/j.jaad.2020.03.099

18. Gatti M, Turrini E, Raschi E, Sestili P, Fimognari C. Janus kinase inhibitors and coronavirus disease (COVID)-19: rationale clinical evidence and safety issues. *Pharmaceuticals* (2021) 14(8):738. doi: 10.3390/ph14080738

19. Cohen-Sfady M, Nussbaum G, Pevsner-Fischer M, Mor F, Carmi P, Zanin-Zhorov A, et al. Heat shock protein 60 activates b cells via the TLR4-MyD88 pathway. *J Immunol* (2005) 175(6):3594–602. doi: 10.4049/jimmunol.175.6.3594

20. Munk ME, Schoel B, Modrow S, Karr RW, Young RA, Kaufmann SH, et al. T Lymphocytes from healthy individuals with specificity to self-epitopes shared by the mycobacterial and human 65-kilodalton heat shock protein. *J Immunol* (1989) 143 (9):2844–9.

21. Prakken BJ, Roord S, Ronaghy A, Wauben M, Albani S, van Eden W. Heat shock protein 60 and adjuvant arthritis: a model for T cell regulation in human arthritis. *Springer Semin Immunopathol* (2003) 25:47–63. doi: 10.1007/s00281-003-0128-7

22. Cohen IR, Quintana FJ, Mimran A. T Regs in T cell vaccination: exploring the regulation of regulation. *J Clin Invest* (2004) 114:1227–32. doi: 10.1172/JCI23396

23. van Eden W, van der Zee R, Prakken B. Heat-shock proteins induce T-cell regulation of chronic inflammation. *Nat Rev Immunol* (2005) 5:318–30. doi: 10.1038/nri1593

24. Dominguez MC, Lorenzo N, Barberá A, Darrasse-Jeze G, López N, Hernández MV, et al. An altered peptide ligand corresponding to a novel epitope from heat-shock protein 60 induces regulatory T cells and suppresses pathogenic response in an animal model of adjuvant induced athritis. *Autoimmunity* (2011) 44(6):471–82. doi: 10.3109/08916934.2010.550590

25. Lorenzo N, Altruda F, Silengo L, Dominguez MC. APL-1, an altered peptide ligand derived from heat-shock protein, alone or combined with methotrexate attenuates murine collagen induced arthritis. *Clin Exp Med* (2017) 17:209–16. doi: 10.1007/s10238-016-0412-7

26. Prada D, Gómez J, Lorenzo N, Corrales O, López A, González E, et al. Phase I clinical trial with a novel altered peptide ligand derived from human heat-shock protein 60 for treatment of rheumatoid arthritis: safety, pharmacokinetics and preliminary therapeutic effects. *J Clin Trials* (2018) 8:1. doi: 10.4172/2167-0870.1000339

27. Cabrales-Rico A, Ramos Y, Besada V, Domínguez MC, Lorenzo N, García O, et al. Development and validation of a bioanalytical method based on LC–MS/MS analysis for the quantitation of CIGB-814 peptide in plasma from rheumatoid arthritis patients. *J Pharm BioMed Anal* (2017) 143:130–40. doi: 10.1016/j.jpba.2017.05.030

28. Corrales O, Hernández L, Prada D, Gómez J, Reyes Y, Lopez AM, et al. CIGB-814, an altered peptide ligand derived from human heat-shock protein 60, decreases anti-cyclic citrullinated peptides antibodies in patients with rheumatoid arthritis. *Clin Rheumatol* (2019) 38:955–60. doi: 10.1007/s10067-018-4360-3

29. Hernández-Cedeño M, Venegas-Rodríguez R, Peña-Ruiz R, Bequet-Romero M, Santana-Sanchez R, Penton-Arias E, et al. CIGB-258, a peptide derived from human heat-shock protein 60, decreases hyperinflammation in COVID-19 patients. *Cell Stress Chaperones* (2021) 26(3):515–25. doi: 10.1007/s12192-021-01197-2

30. Baldomero JE, Del Río A, del Rosario L, Venegas R, Hernández M, Serrano A, et al. Early treatment with a peptide derived from the human heat-shock 60 protein avoids progression to severe stages of COVID-19. *J Biotechnol BioMed* (2021) 4(4):196–210. doi: 10.26502/jbb.2642-91280045

31. Gupta RS. Evolution of the chaperonin families (Hsp60, Hsp10 and tcp- 1) of proteins and the origin of eukaryotic cells. *Mol Microbiol* (1995) 15:1–11. doi: 10.1111/j.1365-2958.1995.tb02216.x

32. Marino Gammazza A, Bucchieri F, Grimaldi LME, Benigno A, Conway de Macario E, Macario AJL, et al. The molecular anatomy of human Hsp60 and its similarity with that of bacterial orthologs and acetylcholine receptor reveal a potential pathogenetic role of anti-chaperonin immunity in myasthenia gravis. *Cell Mol Neurobiol* (2012) 32:943–47. doi: 10.1007/s10571-011-9789-8

33. Richardson A, Landry SJ, Georgopoulos C. The ins and outs of a molecular chaperone machine. *Trends Biochem Sci* (1998) 23:138–43. doi: 10.1016/s0968-0004(98)01193-1

34. Vilasi S, Bulone D, Caruso-Bavisotto C, Campanella C, Marino-Gammazza A, San Biagio PL, et al. Chaperonin of group I: oligomeric spectrum and biochemical and biological implications. *Front Mol Biosci* (2018) 4:99. doi: 10.3389/fmolb.2017.00099

35. Macario AJL, Conway de Macario E. Molecular mechanisms in chaperonopathies: clues to understanding the histopathological abnormalities and developing novel therapies. *J Pathol* (2020) 250:9–18. doi: 10.1002/path.5349

36. Hoter A, Rizk S, Naim HY. The multiple roles and therapeutic potential of molecular chaperones in prostate cancer. *Cancers* (2019) 11(8):1194. doi: 10.3390/cancers11081194

37. Osterloh A, Kalinke U, Weiss S, Fleischer B, Breloer M. Synergistic and differential modulation of immuneresponses by Hsp60 and lipopolysaccharide. *J Biol Chem* (2007) 282:4669–80. doi: 10.1074/jbc.M608666200

38. Vabulas RM, Ahmad-Nejad P, da Costa C, Miethke T, Kirschning CJ, Häcker H, et al. Endocytosed HSP60s use toll-like receptor2 (TLR2) and TLR4 to activate the toll/interleukin-1 receptor signaling pathway in innate immune cells. *J Biol Chem* (2001) 276:31332–39. doi: 10.1074/jbc.M103217200

39. Lehnardt S, Schott E, Trimbuch T, Laubisch D, Krueger C, Wulczyn G, et al. A vicious cycle involving release of heat shock protein 60 from injured cells and activation of toll-like receptor 4 mediates neurodegeneration in the CNS. *J Neurosci* (2008) 8 (10):2320–31. doi: 10.1523/JNEUROSCI.4760-07.2008

40. Cohen IR, Young DB. Autoimmunity, microbial immunity and the immunological homunculus. *Immunol Today* (1991) 12:105–10. doi: 10.1016/0167-5699(91)90093-9

41. Kaufmann SH. Immunity to bacteria. *Curr Opin Immunol* (1989) 2:353–59. doi: 10.1016/0952-7915(89)90141-6

42. De Kleer IM, Kamphuis SM, Rijkers GT, Scholtens L, Gordon G, De Jager W, et al. The spontaneous remission of juvenile idiopathic arthritisis characterized by CD30+Tcells directed to human heat-shock protein 60 capable of producing the regulatory cytokine interleukin-10. *Arthritis Rheumatol* (2003) 48:2001–10. doi: 10.1002/art.11174

43. Anderton SM, van der Zee R, Prakken B, Noordzij A, van Eden W. Activation of T cells recognizing self 60-kD heat shock protein can protect against experimental arthritis. *J Exp Med* (1995) 181:943–52. doi: 10.1084/jem.181.3.943

44. Quintana FJ, Hagedorn PH, Elizur G, Merbl Y, Domany E, Cohen IR. Functional immunomics: microarray analysis of IgG autoantibody repertoires predicts the future response of mice to induced diabetes. *Proc Natl Acad Sci U.S.A* (2004) 101(Suppl.2):14615–21. doi: 10.1073/pnas.0404848101

45. Paul GA, van Kooten PJ, van Eden W, van der Zee R. Highly autoproliferative T cells specific for 60-kDa heat shock protein produce IL-4/IL-10 and IFN γ and are protective in adjuvant arthritis. *J Immunol* (2000) 165:7270–7. doi: 10.4049/jimmunol.165.12.7270

46. Xu Q, Willeit J, Marosi M, Kleindienst R, Oberhollenzer F, Kiechl S, et al. Association of serum antibodies to heat-shock protein 65 with carotid atherosclerosis. *Lancet* (1993) 341(8840):255–9. doi: 10.1016/0140-6736(93)92613-x

47. Merbl Y, Zucker-Toledano M, Quintana FJ, Cohen IR. Newborn humans manifest autoantibodies to defined self molecules detected by antigen microarray informatics. *J Clin Invest* (2007) 117(3):712–8. doi: 10.1172/JCI29943

48. Lang A, Benke D, Eitner F, Engel D, Ehrlich S, Breloer M, et al. Heat shock protein 60 is released inimmune-mediated glomerulonephritis and aggravates disease: *in vivo* evidence for an immunologic danger signal. *J Am Soc Nephrol* (2005) 16(2):383–91. doi: 10.1681/ASN.2004040276

49. Marino Gammazza A, Rizzo M, Citarrella R, Rappa F, Campanella C, Bucchieri F, et al. Elevated blood Hsp60, its structural similarities and cross-reactivity with thyroid molecules, and its presence on the plasma membrane of oncocytes point to the chaperonin as an immunopathogenic factor in hashimoto's thyroiditis. *Cell Stress Chaperones* (2014) 19:343–53. doi: 10.1007/s12192-013-0460-9

50. Meng Q, Li BX, Xiao X. Toward developing chemical modulators of hsp60 as potential therapeutics. *Front Mol Biosci* (2018) 5:35. doi: 10.3389/fmolb.2018.00035

51. Basset CA, Rappa F, Lentini VL, Barone R, Pitruzzella A, Unti E, et al. Hsp27 and Hsp60 in human submandibular salivary gland: quantitative patterns in healthy and cancerous tissues with potential implications for differential diagnosis and carcinogenesis. *Acta Histochem* (2021) 123:151771. doi: 10.1016/j.acthis.2021.151771

52. Santha M, Durham HD, Vigh L, Prodromou C. Editorial: the role of heat shock proteins in neuroprotection. *Front Pharmacol* (2020) 11:1227. doi: 10.3389/fphar.2020.01227

53. Prakken BJ, van der Zee R, Anderton SM, van Kooten PJ, Kuis W, Van Eden W. Peptide-induced nasal tolerance for a mycobacterial heat shock protein 60 T cell epitope in rats suppresses both adjuvant arthritis and nonmicrobially induced experimental arthritis. *Proc Natl Acad Sci USA* (1997) 94:3284–9. doi: 10.1073/pnas.94.7.3284

54. Huurman VA, Decochez K, Mathieu C, Cohen IR, Roep BO. Therapy with the hsp60 peptide DiaPep277^{TM} in c-peptide positive type 1 diabetes patients. *Diabetes Metab Res Rev* (2007) 23:269–75. doi: 10.1002/dmrr.691

55. Raz I, Avron A, Tamir M, Metzger M, Symer L, Eldor R, et al. Treatment of new-onset type 1 diabetes with peptide DiaPep277 is safe and associated with preserved beta-cell function: extension of a randomized, double-blind, phase II trial. *Diabetes Metab Res Rev* (2007) 23:292–8. doi: 10.1002/dmrr.712

56. Koffeman EC, Genovese M, Amox D, Keogh E, Santana E, Matteson EL, et al. Epitope-specific immunotherapy of rheumatoid arthritis: clinical responsiveness occurs with immune deviation and relies on the expression of a cluster of molecules associated with T cell tolerance in a double-blind, placebo-controlled, pilot phase II trial. *Arthritis Rheumatol* (2009) 60:3207–16. doi: 10.1002/art.24916

57. Kirkham B, Chaabo K, Hall C, Garrood T, Mant T, Allen E, et al. Safety and patient response as indicated by biomarker changes to binding immunoglobulin protein in the phase I/IIA RAGULA clinical trial in rheumatoid arthritis. *Rheumatology* (2016) 55:1993–2000. doi: 10.1093/rheumatology/kew287

58. Alleva DG, Gaur A, Jin L, Wegmann D, Gottlieb PA, Pahuja A, et al. Immunological characterization and therapeutic activity of an altered-peptide ligand, NBI-6024, based on the immunodominant type 1 diabetes autoantigen insulin b-chain (9–23) peptide. *Diabetes* (2002) 51:2126–34. doi: 10.2337/diabetes.51.7.2126

59. Aruna BV, Sela M, Mozes E. Suppression of myasthenogenic responses of a T cell line by a dual altered peptide ligand by induction of CD4+CD25+ regulatory cells. *PNAS* (2005) 102:10285–90. doi: 10.1073/pnas.0504578102

60. Zhao J, Li R, He J, Shi J, Long L, Li Z. Mucosal administration of an altered CII263-272 peptide inhibits collagen-induced arthritis by suppression of Th1/Th17 cells and expansion of regulatory T cells. *Rheumatol Int* (2008) 29:9–16. doi: 10.1007/s00296-008-0634-4

61. Katsara M, Deraos G, Tselios T, Matsoukas J, Apostolopoulos V. Design of novel cyclic altered peptide ligands of myelin basic protein MBP83-99 that modulate immune responses in SJL/J mice. *J Med Chem* (2008) 51:3971–8. doi: 10.1021/jm8000554

62. De Magistris M, Alexander J, Coggeshall M, Altman A, Gaeta FC, Grey HM, et al. Antigen analog-major complex histocompatibility complexes act as antagonist of the T cell receptor. *Cell* (1992) 68(4):625 –34. doi: 10.1016/0092-8674(92)90139-4

63. Evavold BD, Allen PM. Separation of IL-4 production from Th cell proliferation by an altered T cell ligand. *Science* (1991) 252:1308–10. doi: 10.1126/science.1833816

64. Paas-Rozner M, Sela M, Mozes E. A dual altered peptide ligand down-regulates myasthenogenic T cell responses by up-regulating CD25- and CTLA-4-expressing CD4 + T cells. *Proc Natl Acad Sci U.S.A.* (2003) 100:6676–81. doi: 10.1073/pnas.1131898100

65. Singh H, Raghava GPS. ProPred: prediction of HLA-DR binding sites. *Bioinformatics* (2001) . 17:1236–7. doi: 10.1093/bioinformatics/17.12.1236

66. Dimitrov I, Garnev P, Flower DR, Doytchinova I. MHC class II binding prediction-a little help from a friend. *J BioMed Biotechnol* (2010) 2010:705821. doi: 10.1155/2010/705821

67. Lin HH, Zhang GL, Tongchusak S, Reinherz EL, Brusic V. Evaluation of MHC-II peptide binding prediction servers: applications for vaccine research. *BMC Bioinf* (2008) . 1(12):S22–32. doi: 10.1186/1471-2105-9-S12-S22

68. Barberá A, Lorenzo N, van Kooten P, van Roon J, de Jager W, Prada D, et al. APL-1, an altered peptide ligand derived from human heat-shock protein 60, induces selective activation of nTreg which suppress CD4+ effector T cells from rheumatoid arthritis patients. *Cell Stress Chaperones* (2016) 21:735–44. doi: 10.1016/j.intimp.2013.10.010

69. Domínguez MC, Cabrales A, Lorenzo N, Padrón G, González LJ. Biodistribution and pharmacokinetic profiles of an altered peptide ligand derived from heat-shock proteins 60 in Lewis rats. *Cell Stress Chaperones* (2020) . 25(1):133–40. doi: 10.1007/s12192-019-01054-3

70. Steimle A, Frick J. Molecular mechanisms of induction of tolerant and tolerogenic intestinal dendritic cells in mice. *J Immunol Res* (2016) 2016:12. doi: 10.1155/2016/1958650

71. Cho KH, Kim JE, Nam HS, Kang DJ, Na HJ. Anti-inflammatory activity of CIGB-258 against acute toxicity of carboxymethyllysine in paralyzed zebrafish via enhancement of high-density lipoproteins stability and functionality. *Int J Mol Sci* (2022) 23(17):10130. doi: 10.3390/ijms231710130

72. Ulmansky R, Cohen CJ, Szafer F, Moallem E, Fridlender ZG, Kashi Y, et al. Resistance to adjuvant arthritis is due to protective antibodies against heat shock protein surface epitopes and the induction of IL-10 secretion. *J Immunol* (2002) 168:6463–9. doi: 10.4049/jimmunol.168.12.6463

73. Lata S, Bhasin M, Raghava GP. Application of machine learning techniques in predicting MHC binders. *Methods Mol Biol* (2007) 409:201–15. doi: 10.1007/978-1-60327-118-9_14

74. Van Eden W, van der Zee R, Paul AG, Prakken BJ, Wendling U, Anderton SM, et al. Do heat shock proteins control the balance of T cell regulation in inflammatory diseases? *Immunol Today* (1998) 19:303–7. doi: 10.1016/s0167-5699(98)01283-3

75. Reche PA, Glutting JP, Zhang H, Reinherz EL. Enhancement to the RANKPEP resource for the prediction of peptide biding to MHC molecules using profiles. *Immunogenetics* (2004) 56(6):405–19. doi: 10.1007/s00251-004-0709-7

76. Scott DL, Kingsley GH. Tumor necrosis factors inhibitors for rheumatoid arthritis. *N Engl J Med* (2006) . 355:704–12. doi: 10.1056/NEJMct055183

77. Choy EH, Panayi GS. Cytokine pathways and joint inflammation in rheumatoid arthritis. *N Engl J Med* (2001) 344:904–16. doi: 10.1056/NEJM200103223441207

78. Carpentier I, Coormaert B, Beyaert R. Function and regulation of tumor necrosis factor type 2. *Curr Med Chem* (2004) 11:2205–12. doi: 10.2174/0929867043364694

79. Montesinos MC, Takedachi M, Thompson LF, Wilder TF, Fernández P, Cronstein BN. The anti-inflammatory mechanism of methotrexate depends on extracellular conversion of adenine nucleotides to adenosine by ecto-5'-nucleotidase: findings in a study of ecto-5'-nucleotidase gene-deficient mice. *Arthritis Rheumatol* (2007) 56:1440–5. doi: 10.1002/art.22643

80. Domínguez MC, Lorenzo N, Barberá A, Padrón G, Torres AM, Hernández MV, et al. Therapeutic effect of two altered peptide ligands derived from the human heat shock protein 60 in experimental models of rheumatoid arthritis. *Biotecnología Aplicada* (2013) 30:153–6.

81. Wang P, Zheng SG. Regulatory T cells and b cells: implication on autoimmune diseases. *Int J Clin Exp Pathol* (2013) 6:2668–74.

82. Barberá A, Lorenzo N, Garrido G, Mazola Y, Falcón V, Torres AM, et al. APL-1, an altered peptide ligand derived from human heat-shock protein 60, selectively induces apoptosis in activated CD4+ CD25+ T cells from peripheral blood of rheumatoid arthritis patients. *Int Immunopharmacol* (2013) 17:1075–83. doi: 10.1016/j.intimp.2013.10.010

83. Konig MF, Andrade F. A critical reappraisal of neutrophil extracellular traps and NETosis mimics based on differential requirements for protein citrullination. *Front Immunol* (2016) 7:461. doi: 10.3389/fimmu.2016.00461

84. Osterloh A, Geisinger F, Piédavent M, Fleischer B, Brattig N, Breloer M. Heat shock protein 60 (HSP60) stimulates neutrophil effector functions. *J Leukoc Biol* (2009) 86:423–34. doi: 10.1189/jlb.0109011

85. Dapunt U, Gaida MM, Meyle E, Prior B, Hänsch GM. Activation of phagocytic cells by staphylococcus epidermidis biofilms: effects of extracellular matrix proteins and the bacterial stress protein GroEL on netosis and MRP-14 release. *Pathog Dis* (2016) 74 (5):ftw035. doi: 10.1093/femspd/ftw035

86. Khandpur R, Carmona-Rivera C, Vivekanandan-Giri A, Gizinski A, Yalavarthi S, Knight JS. NETs are a source of citrullinated autoantigens and stimulate inflammatory responses in rheumatoid arthritis. *Sci Transl Med* (2013) 5 (178):178ra40. doi: 10.1126/scitranslmed.3005580

87. Maddur MS, Miossec P, Kaveri SV, Bayry J. Th17 cells: biology pathogenesis of autoimmune, inflammatory diseases and therapeutic strategies. *Am J Pathol* (2012) 181:8–18. doi: 10.1016/j.ajpath.2012.03.044

88. Modi S, Soejima M, Levesque MC. The effect of targeted rheumatoid arthritis therapies on anti-citrullinated protein autoantibody levels and b cell responses. *Clin Exp Immunol* (2013) 173:8–17. doi: 10.1111/cei.12114

89. Wiersinga WJ, Rhodes A, Cheng AC, Peacock SJ, Prescott HC. Pathophysiology, transmission, diagnosis, and treatment of coronavirus disease 2019 (COVID-19): a review. *JAMA* (2020) 324(8):782–93. doi: 10.1001/jama.2020.12839

90. Xu Z, Shi L, Wang Y, Zhang J, Huang L, Zhang C, et al. Pathological findings of COVID-19 associated with acute respiratory distress syndrome. *Lancet Respir Med* (2020) 8:420–2. doi: 10.1016/S2213-2600(20)30076-X

91. REMAP-CAP Investigators, Gordon AC, Mouncey PR, Al-Beidh F, Rowan KM, Nichol AD, et al. Interleukin-6 receptor antagonists in critically ill patients with COVID-19. *N Engl J Med* (2021) 384(16):1491–502. doi: 10.1056/NEJMoa2100433

92. Guimaraes PO, Quirk D, Furtado RH, Maia LN, Saraiva JF, Antunes MO, et al. Tofacitinib in patients hospitalized with COVID-19 pneumonia. *N Engl J Med* (2021) 385(5):406–15. doi: 10.1056/NEJMoa2101643

93. Domínguez-Horta MC, Venegas-Rodríguez R, Guillén-Nieto G, Martínez-Donato G, Hernández-Cedeño M, Bequet-Romero M, et al. CIGB-258, péptido inhibidor de la hiperinflamación en pacientes con COVID-19. *Anales la Academia Cienc Cuba* (2022) 12(1):e1072.

94. Centro para el Control Estatal de Medicamentos(CECMED). *Jusvinza, emergency use authorization for the treatment of patients with COVID-19 (Autorizo de uso de emergencia a jusvinza, para el tratamiento de pacientes con COVID-19)* (2020). Available at: https://www.cecmed.cu/covid-19/aprobaciones/jusvinza-cigb-258-1 (Accessed August 10, 2020).

95. Centro Nacional de Información de Ciencias Médicas. *Protocolo de actuación nacional para la COVID-19* (2020). Biblioteca Médica Nacional. Available at: http://files.sld.cu/bmn/files/2020/08/bibliodir-agosto-2020.pdf (Accessed August 30, 2020).

96. Mehta P, McAuley D, Brown M, Sanchez E, Tattersall R, Manson J, et al. COVID-19: consider cytokine storm syndromes and immunosuppression. *Lancet* (2020) 395(10229):1033–4. doi: 10.1016/S0140-6736(20)30628-0

97. Li G, Fan Y, Lai Y, Han T, Li Z, Zhou P, et al. Coronavirus infections and immune responses. *J Med Virol* (2020) 92(4):424–32. doi: 10.1002/jmv.25685

98. Dienz O, Rincon M. The effects of IL-6 on CD4 T cell responses. *Clin Immunol* (2009) 130:27–33. doi: 10.1016/j.clim.2008.08.018

99. Choy E. Understanding the dynamics: pathways involved in the pathogenesis of rheumatoid arthritis. *Rheumatology* (2012) 51(5):v3–11. doi: 10.1093/rheumatology/kes113

100. Zhao Z, He S, Yu X, Lai X, Tang S, Mariya M EA, et al. Analysis and experimental validation of rheumatoid arthritis innate immunity gene CYFIP2 and pan-cancer. *Front Immunol* (2022) 13:954848. doi: 10.3389/fimmu.2022.954848

101. Gupta S, Bi R, Kim C, Chiplunkar S, Yel L, Gollapudi S. Role of NF-κB signaling pathway in increased tumor necrosis factor-α-Induced apoptosis of lymphocytes in aged humans. *Cell Death Differ* (2005) 12(2):177–83. doi: 10.1038/sj.cdd.4401557

102. Gupta S, Su H, Agrawal S, Gollapudi S. Molecular changes associated with increased TNF-α-induced apoptotis in naïve (TN) and central memory (TCM) CD8+ T cells in aged humans. *Immun Ageing* (2018) 15:2. doi: 10.1186/s12979-017-0109-0

103. Yang Z, Wang S, Li Q, Yuming L, Maoti W, Hongsheng G, et al. Determining SARS sub-clinical infection: a longitudinal seroepidemiological study in recovered SARS patients and controls after an outbreak in a general hospital. *Scand J Infect Dis* (2009) 41(6):507–10. doi: 10.1080/00365540902919384

104. Huang C, Wang Y, Li X, Ren L, Zhao J, Hu Y, et al. Clinical features of patients infected with 2019 novel coronavirus in wuhan, China. *Lancet* (2020) 395:497–506. doi: 10.1016/S0140-6736(20)30183-5

105. Rojas JM, Avia M, Martín V, Sevilla N. IL-10: a multifunctional cytokine in viral infections. *J Immunol Res* (2017) 2017:6104054. doi: 10.1155/2017/6104054

106. Perlman S, Dandekar AA. Immunopathogenesis of coronavirus infections: implications for SARS. *Nat Rev Immunol* (2005) 5(12):917–27. doi: 10.1038/nri1732

107. Diao B, Wang C, Tan Y, Chen X, Liu Y, Ning L, et al. Reduction and functional exhaustion of T cells in patients with coronavirus disease 2019 (COVID-19). *Front Immunol* (2020) 1:827(11). doi: 10.3389/fimmu.2020.00827

108. Chen L, Long X, Xu Q, Tan J, Wang G, Cao Y, et al. Elevated serum levels of S100A8/A9 and HMGB1 at hospital admission are correlated with inferior clinical outcomes in COVID-19 patients. *Cell Mol Immunol* (2020) 17:992–4. doi: 10.1038/s41423-020-0492-x

109. Wang S, Song R, Wang Z, Jing Z, Wang S, Ma J. S100A8/A9 in inflammation. *Front Immunol* (2018) 9:1298. doi: 10.3389/fimmu.2018.01298

110. Zheng M, Gao Y, Wang G, Song G, Liu S, Sun D, et al. Functional exhaustion of antiviral lymphocytes in COVID-19 patients. *Cell Mol Immunol* (2020) 17:533–5. doi: 10.1038/s41423-020-0402-2

111. Zheng HY, Zhang M, Yang CX, Zhang N, Wang XC, Yang XP, et al. Elevated exhaustion levels and reduced functional diversity of T cells in peripheral blood may predict severe progression in COVID-19 patients. *Cell Mol Immunol* (2020) 17:541–3. doi: 10.1038/s41423-020-0401-3

112. Wang W, Su B, Pang L, Qiao L, Feng Y, Ouyang Y, et al. High-dimensional immune profiling by mass cytometry revealed immunosuppression and dysfunction of immunity in COVID-19 patients. *Cell Mol Immunol* (2020) 17:650–2. doi: 10.1038/s41423-020-0447-2

113. Qin C, Zhou L, Hu Z, Zhang S, Yang S, Tao Y, et al. Dysregulation of immune response in patients with COVID-19 in wuhan, China. *Clin Infect Dis* (2020) 71 (15):762–8. doi: 10.1093/cid/ciaa248

114. Gammazza AM, Légaré S, Lo Bosco G, Fucarino A, Angileri F, de Macario EC, et al. Human molecular chaperones share with SARS-CoV-2 antigenic epitopes potentially capable of eliciting autoimmunity against endothelial cells: possible role of molecular mimicry in COVID-19. *Cell Stress Chaperones* (2020) 25:737–41. doi: 10.1007/s12192-020-01148-3

115. Hunter CA, Jones SA. IL-6 as a keystone cytokine in health and disease. *Nat Immunol* (2015) 16:448–57. doi: 10.1038/ni.3153

116. Sellegounder D, Zafari P, Rajabinejad M, Taghadosi M, Kapahi P. Advanced glycation end products (AGEs) and its receptor, RAGE, modulate age-dependent COVID-19 morbidity and mortality. a review and hypothesis. *Int Immunopharmacol* (2021) 98:107806. doi: 10.1016/j.intimp.2021.107806

117. Farbstein D, Levy AP. HDL dysfunction in diabetes: causes and possible treatments. *Expert Rev Cardiovasc Ther* (2012) 10:353–61. doi: 10.1586/erc.11.182

118. Park KH, Jang W, Kim KY, Kim JR, Cho KH. Fructated apolipoprotein a-I showed severe structural modification and loss of beneficial functions in lipid-free and lipid-bound state with acceleration of atherosclerosis and senescence. *Biochem Biophys Res Commun* (2010) 392:295–300. doi: 10.1016/j.bbrc.2009.12.179

119. Park KH, Shin DG, Cho KH. Dysfunctional lipoproteins from young smokers exacerbate cellular senescence and atherogenesis with smaller particle size and severe oxidation and glycation. *Toxicol Sci* (2014) 140:16–25. doi: 10.1093/toxsci/kfu076

120. Park KH, Cho KH. A zebrafish model for the rapid evaluation of pro-oxidative and inflammatory death by lipopolysaccharide, oxidized low-density lipoproteins, and glycated high-density lipoproteins. *Fish Shellfish Immunol* (2011) 31:904–10. doi: 10.1016/j.fsi.2011.08.006

121. Bucala R, Makita Z, Vega G, Grundy S, Koschinsky T, Cerami A, et al. Modification of low density lipoprotein by advanced glycation end products contributes to the dyslipidemia of diabetes and renal insufficiency. *Proc Natl Acad Sci USA* (1994) 91:9441–5. doi: 10.1073/pnas.91.20.9441

122. Basta G, Schmidt AM, De Caterina R. Advanced glycation end products and vascular inflammation: implications for accelerated atherosclerosis in diabetes. *Cardiovasc Res* (2004) 63:582–92. doi: 10.1016/j.cardiores.2004.05.001

123. Devaraj S, Dasu MR, Rockwood J, Winter W, Griffen SC, Jialal I. Increased toll-like receptor (TLR) 2 and TLR4 expression in monocytes from patients with type 1 diabetes: further evidence of a proinflammatory state. *J Clin Endocrinol Metab* (2008) 93:578–3. doi: 10.1210/jc.2007-2185

frontiers | Frontiers in Immunology

TYPE Original Research
PUBLISHED 17 August 2022
DOI 10.3389/fimmu.2022.974188

OPEN ACCESS

EDITED BY
Diana Boraschi,
Shenzhen Institute of Advanced Technology (SIAT), Chinese Academy of Science (CAS), China

REVIEWED BY
Cosima T Baldari,
University of Siena, Italy
Luciana D'apice,
National Research Council (CNR), Italy

*CORRESPONDENCE
Tania Carmenate
carmenate@cim.sld.cu

†Deceased

SPECIALTY SECTION
This article was submitted to Cytokines and Soluble Mediators in Immunity, a section of the journal Frontiers in Immunology

RECEIVED 20 June 2022
ACCEPTED 27 July 2022
PUBLISHED 17 August 2022

CITATION
Carmenate T, Montalvo G, Lozada SL, Rodriguez Y, Ortiz Y, Díaz C, Avellanet J, Kim J, Surh CD, Graça L and León K (2022) The antitumor effect induced by an IL-2 'no-alpha' mutein depends on changes in the CD8+ T lymphocyte/Treg cell balance. *Front. Immunol.* 13:974188. doi: 10.3389/fimmu.2022.974188

The antitumor effect induced by an IL-2 'no-alpha' mutein depends on changes in the CD8$^+$ T lymphocyte/Treg cell balance

Tania Carmenate[1]*, Galia Montalvo[1], Sum Lai Lozada[1], Yaretnis Rodriguez[1], Yaquelin Ortiz[1], Claudia Díaz[1], Janet Avellanet[1], Juhee Kim[2], Charles D. Surh[2†], Luis Graça[3] and Kalet León[1]

[1]Immune Regulation Department, Centro de Inmunología Molecular, Havana, Cuba, [2]Division of Integrative Biosciences and Biotechnology, Pohang University of Science 12 and Technology (POSTECH), Pohang, South Korea, [3]Instituto de Medicina Molecular, Faculdade de Medici na da Universidade de Lisboa, Lisbon, Portugal

High doses of interleukin-2 (IL-2) have been used for the treatment of melanoma and renal cell carcinoma, but this therapy has limited efficacy, with a ~15% response rate. Remarkably, 7%–9% of patients achieve complete or long-lasting responses. Many patients treated with IL-2 experienced an expansion of regulatory T cells (Tregs), specifically the expansion of ICOS$^+$ highly suppressive Tregs, which correlate with worse clinical outcomes. This partial efficacy together with the high toxicity associated with the therapy has limited the use of IL-2-based therapy. Taking into account the understanding of IL-2 structure, signaling, and *in vivo* functions, some efforts to improve the cytokine properties are currently under study. In previous work, we described an IL-2 mutein with higher antitumor activity and less toxicity than wtIL-2. Mutein was *in silico* designed for losing the binding capacity to CD25 and for preferential stimulation of effector cells CD8$^+$ and NK cells but not Tregs. Mutein induces a higher anti-metastatic effect than wtIL-2, but the extent of the *in vivo* antitumor activity was still unexplored. In this work, it is shown that mutein induces a strong antitumor effect on four primary tumor models, being effective even in those models where wtIL-2 does not work. Furthermore, mutein can change the *in vivo* balance between Tregs and T CD8$^+$ memory/activated cells toward immune activation, in both healthy and tumor-bearing mice. This change reaches the tumor microenvironment and seems to be the major explanation for mutein efficacy *in vivo*.

KEYWORDS

IL-2 mutein, treg, cancer therapy, CD8$^+$ T cells, TME

Abbreviations: Foxp3, forkhead box P3 transcription factor; γ_c, common γ-chain; IL-2R, IL-2 receptor; IU, international units; Tregs, regulatory T cells; wtIL-2, wild-type human IL-2.

Introduction

IL-2 is a cytokine with a pivotal role in the control of immune system homeostasis, acting on both effector and regulatory lymphocytes (1). The IL-2 binds to the multimeric IL-2 receptor (IL-2R) expressed on different lymphocyte subsets and induces lymphocyte survival, proliferation, and activation. The heterotrimeric IL-2R is composed of three subunits: IL-2Rα (CD25), IL-2R β (CD122), and IL-2Rγc (CD132). The IL-2Rβ and IL-2Rγc chains are responsible for signaling and together form the dimeric intermediate affinity receptor (KD ~ 1 nM) highly expressed on memory phenotype (MP) $CD8^+CD44^{hi}$ and NK cells (2). The α-chain (CD25) is expressed constitutively on $CD4^+Foxp3^+$Tregs (3) and transiently on activated $CD4^+$ and $CD8^+$ T cells (4) and together with IL-2Rβand IL-2Rγc forms the high-affinity IL-2R (KD ~ 1 pM) (5, 6).

Based on its immune-stimulatory activity, IL-2 has been used in the treatment of advanced melanoma and renal cell carcinoma, but its high toxicity precludes its extended use (7). Nevertheless, it is notable that 15%–30% of treated patients experienced clinical improvements including long-lasting responses (8). However, some patients became unresponsive to the therapy, probably associated with the expansion of the highly suppressive $ICOS^+$Tregs (9, 10). As IL-2-based therapy has not reached the expectancy, improving the IL-2 therapeutic index is still an active and important topic. Among other examples are the immunocytokine format for directing IL-2 to the tumor cells (11, 12), IL-2 fusion with the IgG-Fc region to increase the molecule half-life (13), or increasing the half-life and changing molecular properties with site-directed pegylation that has been assayed (14). Moreover, the design and evaluation of different muteins seem to be reasonable to increase therapy efficacy (15, 16). One of the ideas is to change the IL-2 distribution among different lymphocyte populations, based on the differential expression of IL-2Rαβγc or IL-2Rβγc. We previously described a mutein, named no-alpha, with a severe decrease in affinity to CD25 (16). No-alpha mutein behaves as an agonist with higher antitumor activity but lower toxicity than wtIL-2. In the present work, we extended the demonstration of the antitumor capacity of no-alpha mutein to four primary tumor models and survival induction in two spontaneous metastases models. Mutein was originally designed to induce preferentially $CD8^+$ and NK *in vivo* expansion and activation, but this issue remained to be fully demonstrated *in vivo*. Here we demonstrate that mutein can change the $CD8^+$MP/Treg balance *in vivo* in both healthy and tumor-bearing mice. This change toward immunity reaches the tumor microenvironment, and it is mainly due to the specific increment in $CD8^+$ T-cell proliferation without any important change in Treg accumulation or activation.

Methods

Mice

Seven- to eight-week-old female C57BL/6 and BALB/c mice were obtained from The National Center for Laboratory Animal Breeding (Havana, Cuba), Animal Resources Centre, IBS Pohang Institute of Basic Science (Pohang, Korea), or Instituto Gulbenkian de Ciencia (Oeiras, Portugal). Food and water were administered *ad libitum*. The experiments were performed according to the International Guidelines for the Care and Use of Laboratory Animals, using standardized procedures of the three institutes.

Production and purification of hIL-2 no-alpha mutein from insoluble material

The hIL-2 no-alpha mutein was produced in *Escherichia coli*, and the isolation of inclusion bodies and purification of the protein were performed as previously described (16). Briefly, the frozen pellets were suspended in 10 mM of Tris and 1 mM of EDTA (pH 8) (TE) and sonicated using an ultrasonic cell disrupter (IKA, Wilmington, NC, USA). The insoluble material was harvested by centrifugation (18,000 ×*g*) and washed successively with 4 M of urea-TE and 1% Triton X-100–TE using an Ultra Turrax T8 homogenizer. For further purification, aGE AKTA explorer system was used; the protein was extracted with 6 M of guanidinium hydrochloride–TE at 0.1 g/ml (wet weight), and renaturation was carried out by dialysis. For further purification, protein was applied to a reverse-phase C4 column (Vydac). In this final chromatography, the recombinant polypeptides were purified using an H_2O–acetonitrile–trifluoroacetic acid system, with a linear gradient (30%–85% of acetonitrile) and 0.6 ml/min flow. Finally, the proteins were dialyzed against 10 mM of acetate (pH 4), filtered through 0.2-μm filters, and stored at 4°C. The molecule was tested for low endotoxin levels, and the biological activity was evaluated using the CTLL-2 cell proliferation assay.

In vivo effect on T-cell populations

Healthy mice were treated with wtIL-2 (20,000 or 40,000 international units (IU)) or no-alpha mutein (200 or 400 IU) for 6 days twice a day. After the treatments, the spleens were harvested, and the cell suspension was obtained, stained, and analyzed by flow cytometry. For assessing BrdU incorporation, mice were fed with BrdU in the water 3 days before sacrifice. The BrdU staining was performed with the specific kit from BD Biosciences (San Jose, CA, USA) following the fabricant instructions.

Antibodies and flow cytometry

All fluorochrome-conjugated mAbs used for flow cytometry measurement were from Thermo Fisher (Waltham, MA, USA) unless otherwise stated: fluorescein isothiocyanate (FITC) or BV-conjugated anti-CD3 (145-2C11), PE or APC-conjugated anti-CD4 (L3T4), PB or FITC-conjugated anti-Foxp3 (NRRF-30), PE-Cy7-conjugated anti-CD25(3C7), APC-Cy7-conjugated anti-CD8 (eBio H35-17.2), BV605 or APC anti-CD44 (IM7), PE-conjugated anti-CD122(5H4), and APC-conjugated anti-CD45(30-F11). Intracellular Foxp3 staining sets were purchased from eBioscience (San Diego, CA, USA). Live/dead fixable near IR dye from Thermo Fisher Scientific was used for dead cell discrimination. Samples were measured using a flow cytometer Gallios (Beckman Coulter, Brea, CA, USA) or LSR Fortessa (Becton Dickinson, Franklin Lakes, NJ, USA) and analyzed using Kaluza software or FlowJo software (TreeStar, Inc., San Carlos, CA, USA).

Tumor challenges and treatments

Mouse transplantable tumor cell lines used melanoma MB16, colon CT26, mammary tumor 4T1, lung carcinoma 3LL-D122, and lung carcinoma TC1 cells maintained in Dulbecco's modified Eagle medium (DMEM) F12 (GIBCO, Grand Island, NY, USA) supplemented with 10% heat-inactivated fetal bovine serum, 2 mM of L-glutamine, 50 U/ml of penicillin, 50 µg/ml of streptomycin. All cells were maintained at 37°C under a humidified 5% CO_2 atmosphere. Tumor cells were harvested using trypsin/EDTA and resuspended in phosphate-buffered saline (PBS) for *in vivo* experiments. All the tumor cells were inoculated in the right flank s.c., except the 4T1 cells that were inoculated in the mammary gland and the 3LL-D122 cells that were inoculated in the footpad. For the 3LL-D122 spontaneous metastasis model, the primary tumors were eliminated by surgery when they reached a diameter of 9 mm. Treatments consisted of two cycles of five daily i.p. injections of PBS, wtIL-2 (30,000 IU), or no-alpha mutein (300 IU) twice a day, and the cycle was repeated after one resting week. Tumor size was assessed using a microcaliper every 3 days, and the tumor volume was calculated using the following formula: $(\text{width}^2 \times \text{length})/2$. For the spontaneous metastases models with 3LL-D122 and 4T1 cells, the mouse survival was also monitored periodically for 80 days. For tumor-infiltrating lymphocyte evaluation, tumors were mechanically dissociated. First, the tumors were cut into small pieces and then meshed through a 70-µm cell strainer using a syringe plunger. The obtained cell suspensions were centrifuged, stained, and analyzed by flow cytometry.

Data and statistical analysis

For statistical analysis, the Graph Pad Prism 4.0 software was used. For comparison of the CD8/Treg ratios, and BrdU incorporation levels in healthy mice parametric ANOVA followed by Tukey's multiple comparison test were applied. In the antitumor assays, a two-way ANOVA followed by Bonferroni's test was applied for comparison of the tumor curves; for survival analysis, the log-rank test was used. In the case of CD8/Treg ratio in tumor-bearing mice, the Kruskal–Wallis test followed by Dunn's test for multiple comparisons was used.

Results

IL-2 no-alpha mutein is able to modify the $CD8^+$MP/Treg balance in healthy mice

The IL-2-derived no-alpha mutein was previously characterized by its capacity to stimulate *in vitro* cells with different forms of IL-2R. To evaluate the effect of the IL-2 no-alpha mutein on $CD8^+$MP and Treg balance *in vivo*, B6 mice were treated with both molecules, and the accumulation and proliferation of both populations on the spleens of treated mice were measured. Mice were treated with 20,000 IU of wtIL-2 or 200 IU of mutein, and the selected doses expressed as protein mass correspond to 20 µg of wtIL-2 and 20 µg of no-alpha mutein and are equivalent for cells expressing the IL-2Rβγc, for which the two molecules induce similar levels of proliferation *in vitro* (16). Figure 1A shows representative results obtained in the experiments. As expected, the mice treated with mutein showed higher percentages of $CD8^+$MP cells, reaching 38.8%, and the wtIL-2 induced a lower accumulation level of 15.25% still above the value of 10.7% in the control group. On the contrary, the wtIL-2 was the only molecule able to increase the percentage of Tregs among the $CD4^+$ T lymphocytes, reaching approximately 15% in comparison with the typical 10% observed in the control group and the group treated with mutein. To test the overall impact on the balance effector/regulatory cell, mice were treated with two different doses of each molecule: 20,000 or 40,000 IU for wtIL-2 and 200 or 400 IU for mutein. Total $CD8^+CD44^{hi}CD122^+$ T cells and $CD4^+CD25^+Foxp3^+$ cells on the spleens were quantified. The mice treated with mutein showed a higher $CD8^+$MP/Treg ratio than the mice treated with wtIL-2 in both dose levels. The results show that regardless of the dose, mutein is always able to expand $CD8^+$MP T cells preferentially (Figure 1B). To define if the observed accumulation was related to an increment in proliferation, the incorporation of BrdU by the cells in treated mice was measured. Figure 1C shows representative histograms, and Figures 1D, E

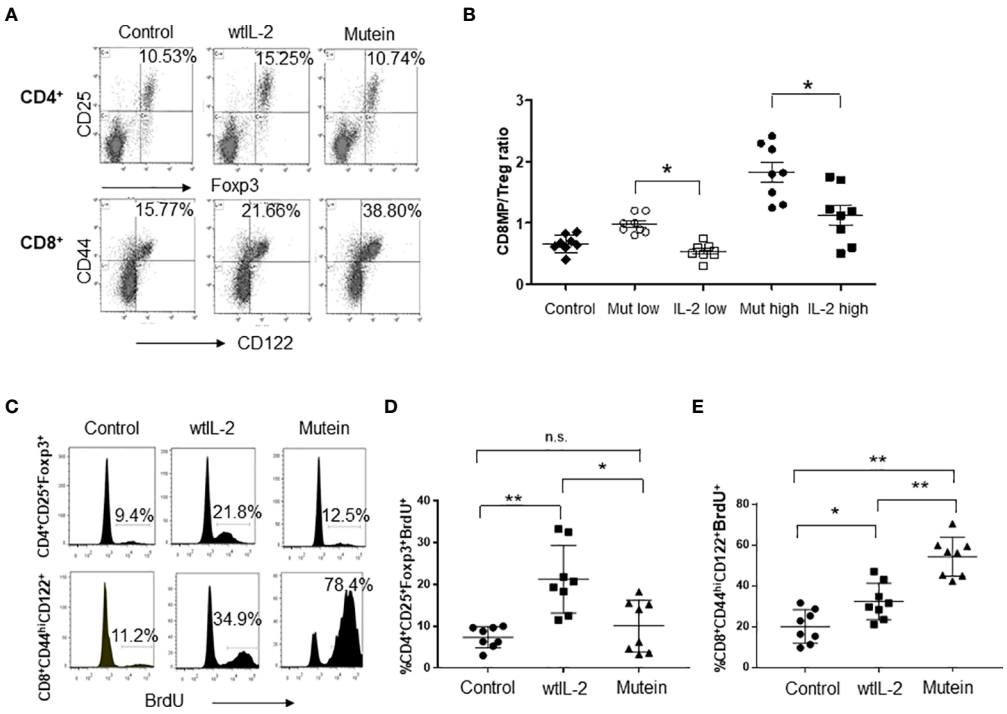

FIGURE 1
No-alpha mutein induces accumulation and proliferation of CD8$^+$MP cells but not Tregs. Mice were treated i.p. with 20,000 IU of wtIL-2 or 200 IU of mutein during a week, and the percentages and numbers of CD8$^+$MP and Tregs on the spleens of treated mice were determined. **(A)** Representative dot plots. **(B)** CD8$^+$MP/Treg cell ratio measured on mice treated with two different doses of wtIL-2 and no-alpha mutein: low doses, 20,000 IU of wtIL-2 or 200 IU of mutein; high doses 40,000 IU of wtIL-2 or 400 IU of mutein. The experiment was performed three times; representative data are presented, n = 8 per treatment, p < 0.05, Bonferroni test. For BrdU incorporation, mice were treated with 20,000 IU of wtIL-2 or 200 IU of mutein and fed with BrdU in the water for the last 3 days of treatments. **(C)** Representative histograms of BrdU incorporation. **(D, E)** Cumulative data from two independent experiments, n = 8, Tukey's test was used for multiple comparisons ($p < 0.001$ **; $p < 0.05$ *). n.s., non significant.

show cumulative data from two independent experiments. Mutein induced an outstanding increment on BrdU$^+$ CD8$^+$MP cells, in a range from 40% to almost 80% of CD8$^+$MP cells in the S phase of the cell cycle. The wtIL-2, on the contrary, induced a higher accumulation of Tregs, with an increment in the percentages of BrdU positive Tregs, in a range from 11% to 32% being statistically different from the average level observed in the control group 7.4% (Figure 1D).

IL-2 no-alpha mutein reduces primary tumor growth and is able to modify the CD8/Treg balance in tumor-bearing mice

It was previously demonstrated that no-alpha mutein induces an important anti-metastatic effect in the MB16 and 3LL-D122 experimental metastasis tumor models (16). Now we extended the study of the antitumor activity to other models with tumor cell lines from different origins. In the models for primary tumor growth studied (CT26, MB16, TC1, and 4T1), mutein was able to delay tumor growth (Figure 2A). The most important finding was that in two models (MB16 and 4T1) in which the wtIL-2 did not show any effect, mutein was highly effective in delaying the primary tumor growth, and the difference between mutein and the wtIL-2 was statistically significant for both tumor models ($p < 0.05$*, $p < 0.001$**).

Next, we evaluated the capacity of the IL-2 mutein to change the balance of CD8$^+$MP/Tregs in tumor-bearing mice. Although different tumors induce different suppressive mechanisms (17), we have previously studied that all the tumors used in the present work expand Tregs on mouse spleens above the normal levels, even when other suppressive populations can also be expanded. We focused on the balance of CD8/Tregs because of the well-known function of IL-2 stimulating these populations. Furthermore, the results confirm our hypothesis about the mechanism of action of mutein.

We evaluated the accumulation of CD8$^+$MP and Tregs on the spleens of tumor-bearing mice treated with IL-2 or mutein on day 21 after tumor implant. First, we selected the MB16

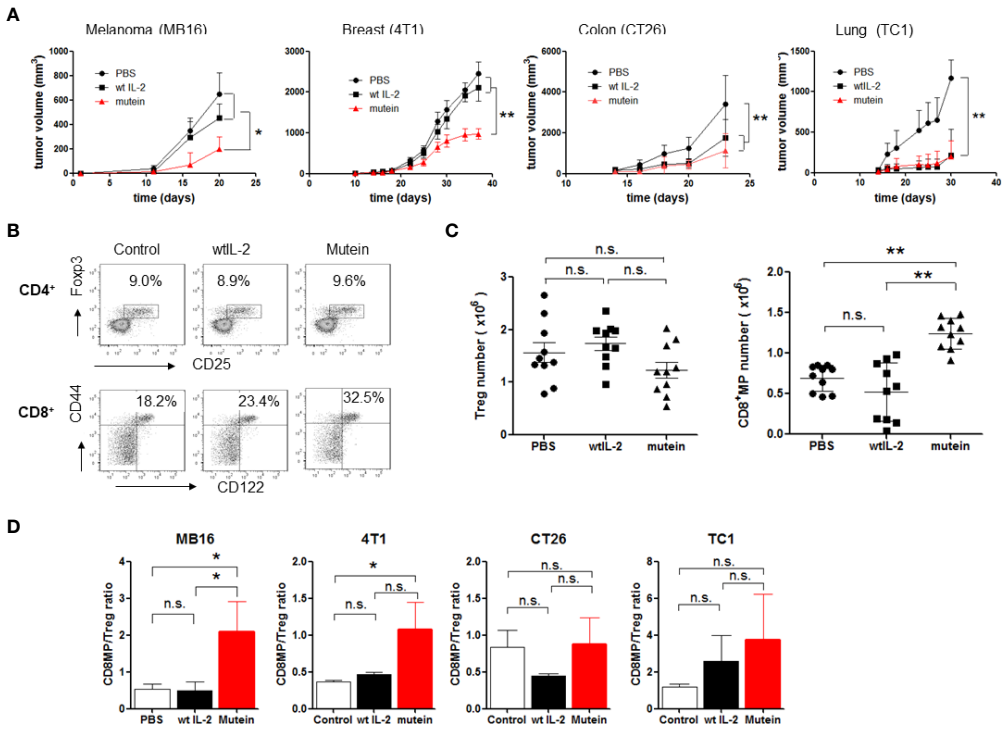

FIGURE 2
No-alpha mutein induces a potent antitumor effect in four different tumor models and is able to change CD8$^+$MP/Treg balance in tumor-bearing mice in the spleens. Mice were inoculated with tumor cells and received 300 IU of mutein or 30,000 IU wtIL-2, twice a day, for 2 weeks separated by a resting week. MB16, CT26, and TC-1 cells were inoculated s.c. on the right flank; 4T1 cells were inoculated on mammary glands. **(A)** Tumor growth curves. **(B)** Representative dot plots from spleen of MB16-bearing mice. **(C)** CD8$^+$MP and Treg number from spleens of MB16-bearing mice. **(D)** CD8$^+$MP/Treg ratios on spleens of mice inoculated with the different tumor cell lines. Cumulative data from three experiments, n = 9 per treatment. Statistical differences in tumor growth were determined by two-way ANOVA test, using GraphPad software ($p < 0.001$ **; $p < 0.05$ *). n.s., non significant.

tumor model because it is one of the tumor models where mutein showed a higher antitumor effect than the wtIL-2. Figure 2B shows representative results of CD8$^+$MP and Treg measurement on melanoma-bearing mice treated with the different molecules, and Figure 2C shows cumulative data of cell number. There were no statistical differences in Tregs number among the groups treated with wtIL-2, mutein, or PBS as control. However, the percentage and number of CD8$^+$MP cells increased notably in the mice treated with no-alpha mutein, reaching 32% of CD8$^+$ cells and more than 1×10^6 cells, while the mice treated with the wtIL-2 only showed a discreet increase in the percentages reaching 23% of CD8$^+$MP cells close to the value of the control group (18%); nevertheless, the number of activated CD8$^+$ cells was similar for the group treated with the wtIL-2 and the control group. The increment on CD8$^+$MP cells but not in Tregs results in a change in the CD8$^+$MP/Treg balance toward immune activation (Figure 2D). This change on CD8$^+$MP/Treg balance was also observed for the 4T1 model and, to a less extent, not statistically different for CT26 and TC1 models. Interestingly, the two models where mutein induced the highest effect on primary tumor growth (MB16 and 4T1) were those with statistical differences in the CD8$^+$MP/Tregs ratio between the groups treated with mutein and the wtIL-2.

IL-2 no-alpha mutein increases the survival of tumor-bearing mice and changes the CD8$^+$/Treg balance in the tumor microenvironment

No-alpha mutein effect on survival of tumor-bearing mice was also tested. The experimental tumor models 4T1 and 3LL-D122 were selected due to their capacity for inducing spontaneous metastases. Mice were treated with 30,000 IU of wtIL-2 or 300 IU of mutein; these doses are equivalent in the ability to stimulate effector cells, both CD8$^+$ activated and NK cells expressing the dimeric IL-2 receptor (βγc). Similar to the traditional treatment used in humans, the molecules were administered twice a day for 5 days, and the same treatments were repeated a week apart (Figure 3A). In both cases, the mice treated with mutein showed a higher survival ratio than the mice treated with the wtIL-2 ($p <$

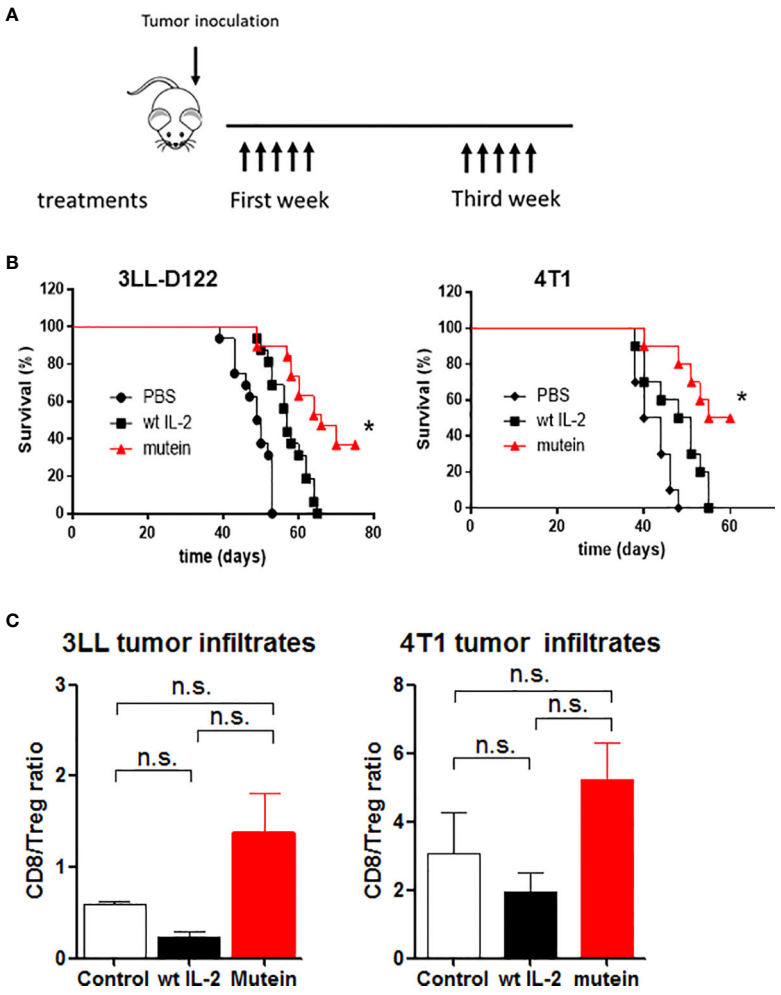

FIGURE 3
No-alpha mutein induces higher survival than wtIL-2 and induces changes in the tumor microenvironment. Mice were inoculated with 4T1 cells in the mammary gland or with 3LL-D122 on the foot pad; in the case of 3LL-D122, the primary tumors were eliminated by surgery when the control reached 9 mm; mice were treated with 30,000 IU wtIL-2 and 300 IU of no-alpha mutein or phosphate-buffered saline (PBS), and survival was observed. **(A)** Treatment schedule. **(B)** 3LL-D122 and 4T1 survival curves from spontaneous metastasis development. Survival curves were compared by log-rank test. **(C)** For tumor infiltrate measurement, mice were sacrificed when tumors reached 5–6 mm diameter and analyzed by flow cytometry. The graph represents the ratio between percentages of $CD8^+$T lymphocytes and Treg referred to as total $CD45^+$ cells.
n.s., non significant. *p< 0.05.

0.05), and both groups showed better survival than the control group treated with PBS (Figure 3B).

To study if the effect on immune balance reaches the tumor microenvironment, mice inoculated with 4T1 and 3LLD-122 cells were treated as described above. After the primary tumors were 6–7 mm in diameter, the mice were sacrificed, and the tumors were collected and analyzed by flow cytometry. TILs were evaluated as percentages of $CD8^+$ or $CD4^+CD25^+Foxp3^+$ T lymphocytes from the total number of $CD45^+$ cells, and the ratio between percentages is shown (Figure 3C). The tumors treated with mutein showed a higher level of $CD8^+$T lymphocytes than the tumors treated with the wtIL-2, inducing a desired increment in the balance $CD8^+$/Tregs in the tumor microenvironment.

Discussion

IL-2 is a pleiotropic cytokine with a central role in the control of the immune response (1). Due to its effect on both effector and regulatory T cells, IL-2 has been evaluated as a therapeutic tool in a wide range of diseases related to cancer and autoimmunity (8, 18). After several years of using high-dose IL-2 therapy for cancer treatment, many approaches are under study aiming to improve the therapeutic index of the cytokine.

We have previously described the design and evaluation of an IL-2 mutein with a reduced binding capacity to the alpha chain of the IL-2R, named 'no-alpha mutein'; mutein shows a higher anti-metastatic effect and less toxicity than wtIL-2, opening the

opportunity to a better IL-2-based tumor therapy (16). Now the evaluation of the antitumor effect of mutein was expanded to other tumor cell lines and experimental settings. Mutein showed a strong effect in delaying primary tumor growth and inducing a better survival ratio in the models of spontaneous metastases induced by 4T1 and 3LL-D122 cell lines. Moreover, the effect on activated $CD8^+$MP cells vs Tregs balance in the spleens was measured in healthy and tumor-bearing mice. Mutein was able to increase $CD8^+$MP/Treg ratio in both settings, validating the hypothesis that it is enough to eliminate the interaction of the IL-2 molecule with the receptor alpha chain to achieve a preferential expansion of IL-2Rβγc-expressing cells. The effect of mutein was also measured in the tumor microenvironment of 4T1 and 3LL-D12 models, and a change in the $CD8^+$/Treg balance was found.

The selection of the appropriate dose to compare the *in vivo* effect was an important choice. Usually, the IL-2 dose used in humans corresponds to 600,000 IU/kg, and it is considered a high dose treatment; in most tumor experiments in mice, an equivalent dose of 30,000 IU is used, corresponding with 1–3 µg of wtIL-2 per dose. For mutein, as well as for the wtIL-2, the biological activity is determined in the cell proliferation assay for the CTLL-2 cell line expressing the IL-2Rαβγc. As mutein only binds to the dimeric receptor, more molecules are needed to achieve the same level of CTLL-2 proliferation. We considered the 100-fold difference in the affinity of the IL-2Rαβγc vs the IL-2Rβγc and chose 300 IU as the equivalent dose for mutein; this dose corresponds with 10 to 30 µg of mutein depending on the specific activity of the production batch. Mutein has shown lower toxicity than wtIL-2; consequently, it is possible to use 30 µg or higher doses without inducing severe toxic effects on treated mice.

When the selected doses were evaluated *in vivo*, the activated $CD8^+CD44^{hi}CD122^+$T cells accumulated to higher levels in the healthy mice treated with mutein than in the mice treated with wtIL-2. To study the $CD8^+$MP/Treg ratio in healthy mice, two dose levels were evaluated; mutein showed a significant change toward immune activation rather than suppressive condition. Taking into account the $CD8^+$ preferential expansion demonstrated *in vivo*, we can speculate that when different lymphocyte populations are present and compete for the cytokine, mutein is captured preferentially by the $CD8^+$ cells, which express a high level of the dimeric βγc IL-2R form.

In this work, we explored how general could be the advantage of no-alpha mutein over wtIL-2 and used several tumor models regardless of whether Treg expansion is the main suppressive mechanism or not. We demonstrated that in the models with higher Treg expansion, such as MB16 and 4T1, the differences in the antitumor activity between mutein and the wtIL-2 were higher as well as the changes induced on $CD8^+$MP/Treg ratio. Consequently, mutein should be advantageous in the treatment of those cancer diseases where the Treg expansion is relevant; in these settings, we expect better efficacy and lower percentages of non-responder patients due to lower levels of $ICOS^+$Treg proliferation. A phase I clinical trial evaluating mutein safety is already in progress.

Expansion of Tregs in lymphoid organs and the tumor microenvironment is one of the tumor mechanisms to escape from immune surveillance (19). In humans, Treg increment is related to worse outcomes in many tumor diseases, and the expansion of ICOS-positive Tregs is related to IL-2 therapy unresponsiveness (9). Several examples are attempting to target Tregs in order to achieve significant antitumor responses; antibodies against CTLA-4, GITR, CXCR4, ICOS, and CD25 have been used for this purpose (20–24), although the restricted expression of the target molecules on Tregs can be sometimes questioned. Vargas *et al.* provided an elegant demonstration of specific $CD25^+$ expression on Tregs in both mice and human tumor infiltrates. They demonstrated that increasing the CD25 mAb PC-61 affinity to activating FcγRs was sufficient to specifically deplete Tregs in the tumor microenvironment and to improve the antitumor effect of mAb alone or in combination with PD-1 mAb (25). Another outstanding finding was the induction of systemic antitumor response after intratumor Treg depletion with a mAb targeting CTLA-4 molecule, underscoring the relevance of Tregs as immunosuppressive mechanisms in tumor settings (22). Also, there is the work from Cheung *et al.*, which improved the old concept of the ONTAK molecule, with the production of a second-generation IL-2 diphtheria toxin fusion protein with higher activity and better formulation than the previous one, and the demonstration of Treg depletion in spleens and LN together with a potent antitumor activity (26).

In the present work, not Treg depletion but changes in the balance of CD8/Tregs were achieved, treating the mice with no-alpha mutein. The goal was to abolish Treg expansion mediated by IL-2 while conserving the immunostimulatory properties of the cytokine-activating effector cells. Recently a similar idea was accomplished through a different approach (14). Charych *et al.* developed a modified IL-2, with a site-directed PEG attachment on the alpha surface of the molecule; the modified IL-2 (NKTR-214) also increased the $CD8^+$/Tregs ratio and has a higher half-life, which could be an advantage for treatment schedule but also a problem considering the toxic effects associated with the IL-2 molecule. NKTR-214 shows a potent antitumor effect both alone and in combination with a PD-1 mAb. Also, the first phase I clinical trial was conducted by assaying safety and dose regimen for the NKTR-214 molecule; moderate responses were observed together with several adverse events associated with the treatment. Levin *et al.* also described an IL-2 mutein with agonistic properties (15); H-9 has an increased affinity for the β chain of IL-2R, and although it conserves the capacity to induce Treg proliferation, also induced an outstanding effect on $CD8^+$ cells and induces higher antitumor activity than wtIL-2.

In conclusion, our results extend previous studies from our group and other laboratories showing that IL-2 muteins can lead to an antitumor effect *in vivo* by expanding effector $CD8^+$ T cells while restricting the expansion of Treg cells. The benefit of this approach for cancer treatment will now be assessed under clinical trials that have been already initiated.

Data availability statement

The raw data supporting the conclusions of this article will be made available by the authors, without undue reservation.

Ethics statement

This study was reviewed and approved by Ethic Committees for laboratory animal care and use at the CIM, Havana; Postech, Korea and at the IMM, Lisbon.

Author contributions

TC, GM, YO designed and performed *in vivo* antitumor experiments. TC, JK, JA, YO, design and performed *in vivo* experiments for lymphocytes changes. CD, JA, TC, performed tumor microenvironment measurements. SLL, YR purified wtIL-2 and IL-2 mutein. TC wrote the document, CHDS, LG and KL design experiments, generated ideas and discuss the experiment designs and results. All authors contributed to the article and approved the submitted version.

Funding

The research was supported by Cuban Academy of Science and by the Cuban government. The authors also acknowledge the financial help received from Professor Charles D'Surh, and Professor Luis Graça.

Conflict of interest

The authors declare that the research was conducted in the absence of any commercial or financial relationships that could be construed as a potential conflict of interest.

Publisher's note

References

1. Boyman O, Sprent J. The role of interleukin-2 during homeostasis and activation of the immune system. *Nat Rev Immunol* (2012) 12(3):180–90. doi: 10.1038/nri3156

2. Zhang X, Sun S, Hwang I, Tough DF and Sprent J. Potent and selective stimulation of memory-phenotype $CD8^+$ T cells *in vivo* by IL-15. *J Immunol* (1998) 8(5):591–9. doi: 10.1016/s1074-7613(00)80564-6

3. Thomas R, Malek TR, Yu A, Zhu L, Matsutani T, Adeegbe D. Bayer AL.IL-2 family of cytokines in T regulatory cell development and homeostasis. *J Clin.Immunol* (2008) 28(6):635–9. doi: 10.1007/s10875-008-9235-y

4. Cantrel D, Smith K. Transient expression of interleukin-2 receptors. *J Exp Med* (1983) 158:1895–911. doi: 10.1084/jem.158.6.1895

5. Robb RJ, Greene WC, Rusk CM. Low and high affinity cellular receptors for interleukin 2. implications for the level of tac antigen. *J Exp Med* (1984) 160 (4):1126–46. doi: 10.1084/jem.160.4.1126

6. Taniguchi T, Minami Y. The IL-2/IL-2 receptor system: a current overview. *Cell* (1993) .73(1):5–8. doi: 10.1016/0092-8674(93)90152-g

7. Siegel JP, Puri RJ. Interleukin-2 toxicity. *J Clin Oncol* (1991) 9(4):694–704. doi: 10.1200/JCO.1991.9.4.694

8. Rosenberg SA. IL-2: the first effective immunotherapy for human cancer. *J Immunol* (2014) .192(12):5451–8. doi: 10.4049/jimmunol.1490019

9. Ahmadzadeh M, Rosenberg SA. IL-2 administration increases $CD4^+$ CD25hi $Foxp3^+$ regulatory T cells in cancer patients. *Blood* (2006) 107(6):2409–14. doi: 10.1182/blood-2005-06-2399

10. Sim GC, Martin-Orozco N, Jin L, Yang Y, Wu S, Washington E, et al. IL-2 therapy promotes suppressive $ICOS^+$Treg expansion in melanoma patients. *J Clin.Immunol* (2014) 124(1):99–110. doi: 10.1172/JCI46266

11. Gillies SD, Lan Y, Williams S, Carr F, Forman S, Raubitschek A, et al. An anti-CD20–IL-2 immunocytokine is highly efficacious in a SCID mouse model of established human b lymphoma. *Blood* (2005) 105(10):3972–8. doi: 10.1182/blood-2004-09-3533

12. Klein C, Waldhauer I, Nicolini VG, Freimoser-Grundschober A, Nayak T, Vugts DJ, et al. Cergutuzumabamunaleukin (CEA-IL2v), a CEA-targeted IL-2 variant-based immunocytokine for combination cancer immunotherapy: Overcoming limitations of aldesleukin and conventional IL-2-based immunocytokines. *Oncoimmunol.* (2017) .6(3):e1277306. doi: 10.1080/2162402X.2016.1277306

13. Vazquez-Lombardi R, Loetsch C, Zinkl D, Jackson J, Schofield P, Deenick EK, et al. Potent antitumour activity of interleukin-2-Fc fusion proteins requires fc-mediated depletion of regulatory T-cells. *Nat Commun* (2017) 8(1):1–12. doi: 10.1038/ncomms15373

14. Charych DN, Hoch U, Langowski JL, Lee SR, Addepalli MK, Kirk PB, et al. NKTR-214, an engineered cytokine with biased IL2 receptor binding, increased tumor exposure, and marked efficacy in mouse tumor models. *Clin Canc. Res* (2016) 22(3):680–90. doi: 10.1158/1078-0432.CCR-15-1631

15. Levin AM, Bates DL, Ring AM, Krieg C, Lin JT, Su L, et al. Exploiting a natural conformational switch to engineer an interleukin-2 'superkine. *Nature.* (2012) 484(7395):529–33. doi: 10.1038/nature10975

16. Carmenate T, Pacios A, Enamorado M, Moreno E, Garcia-Martínez K, Fuente D, et al. Human IL-2 mutein with higher antitumor efficacy than wild type IL-2. *J Immunol* (2013) 190(12):6230–8. doi: 10.4049/jimmunol.1201895

17. Mosely SIS, Prime JE, Sainson RCA, Koopmann JO, Wang DYQ, Greenawalt DM, et al. Rational selection of syngeneic preclinical tumor models for immunotherapeutic drug discovery. *Cancer Immunol Res* (2017) 5(1):29–41. doi: 10.1158/2326-6066.CIR-16-0114

18. Pol JG, Caudana P, Paillet J, Piaggio E, Kroemer G. Effects of interleukin-2 in immunostimulation and immunosuppression. *J Exp Med* (2020) 217(1): e20191247. doi: 10.1084/jem.20191247

19. Serrels A, Lund T, Serrels B, Byron A, McPherson RC, von Kriegsheim A, et al. Nuclear FAK controls chemokine transcription, tregs, and evasion of anti-tumor immunity. *Cell*. (2015) 163(1):160–73. doi: 10.1016/j.cell.2015.09.001

20. Mahne AE, Mauze S, Joyce-Shaikh B, Xia J, Bowman EP, Beebe AM, et al. Dual roles for regulatory T-cell depletion and costimulatory signaling in agonistic GITR targeting for tumor immunotherapy. *Cancer Res* (2017) 77(5):1108–18. doi: 10.1158/0008-5472

21. Mo L, Chen Q, Zhang X, Shi X, Wei L, Zheng D, et al. Depletion of regulatory T cells by anti-ICOS antibody enhances anti-tumor immunity of tumor cell vaccine in prostate cancer. *Vaccine* (2017) 35(43):5932–8. doi: 10.1016/j.vaccine.2017.08.093

22. Marabelle A, Kohrt H, Levy R. Intratumoral anti-CTLA-4 therapy: enhancing efficacy while avoiding toxicity. *Clin Cancer Res* (2013) . 19(19):5261–3. doi: 10.1158/1078-0432

23. Kim JH, Kim BS, Lee SK. Regulatory T cells in tumor microenvironment and approach for anticancer immunotherapy. *Immune Netw*. (2020) . 20(1):e4. doi: 10.4110/in.2020.20.e4

24. Sugiyama D, Nishikawa H, Maeda Y, Nishioka M, Tanemura A, Katayama I, et al. Anti-CCR4 mAb selectively depletes effector-type FoxP3$^+$ CD4$^+$ regulatory T cells, evoking antitumor immune responses in humans. *Proc Natl Acad Sci* (2013) 110(44):17945–50. doi: 10.1073/pnas.1316796110

25. Arce Vargas F, Furness AJS, Solomon I, Joshi K, Mekkaoui L, Lesko MH, et al. Fc-optimized anti-CD25 depletes tumor-infiltrating regulatory T cells and synergizes with PD-1 blockade to eradicate established tumors. *Immunity*. (2017) . 46(4):577–86. doi: 10.1016/j.immuni.2017.03.013

26. Cheung LS, Fu J, Kumar P, Kumar A, Urbanowski ME, Ihms EA, et al. Second-generation IL-2 receptor-targeted diphtheria fusion toxin exhibits antitumor activity and synergy with anti–PD-1 in melanoma. *Proc Natl Acad Sci* (2019) 116(8):3100–5. doi: 10.1073/pnas.1815087116

frontiers | Frontiers in Immunology

TYPE Original Research
PUBLISHED 14 February 2023
DOI 10.3389/fimmu.2023.1050113

OPEN ACCESS

EDITED BY
Marita Troye Blomberg,
Stockholm University, Sweden

REVIEWED BY
Giselle Penton-Rol,
Center for Genetic Engineering and Biotechnology (CIGB), Cuba
Wen Zhang,
Tongji University, China

*CORRESPONDENCE
Giusi Barra
g.barra@icb.cnr.it
Carmela Gallo
carmen.gallo@icb.cnr.it
Angelo Fontana
afontana@icb.cnr.it
angelo.fontana@unina.it

†These authors have contributed equally to this work

SPECIALTY SECTION
This article was submitted to Vaccines and Molecular Therapeutics, a section of the journal Frontiers in Immunology

RECEIVED 21 September 2022
ACCEPTED 27 January 2023
PUBLISHED 14 February 2023

CITATION
Barra G, Gallo C, Carbone D, Ziaco M, Dell'Isola M, Affuso M, Manzo E, Nuzzo G, Fioretto L, D'Ippolito G, De Palma R and Fontana A (2023) The immunoregulatory effect of the TREM2-agonist Sulfavant A in human allogeneic mixed lymphocyte reaction.
Front. Immunol. 14:1050113.
doi: 10.3389/fimmu.2023.1050113

The immunoregulatory effect of the TREM2-agonist Sulfavant A in human allogeneic mixed lymphocyte reaction

Giusi Barra[1*†], Carmela Gallo[1*†], Dalila Carbone[1], Marcello Ziaco[1], Mario Dell'Isola[2], Mario Affuso[2], Emiliano Manzo[1], Genoveffa Nuzzo[1], Laura Fioretto[1], Giuliana D'Ippolito[1], Raffaele De Palma[3] and Angelo Fontana[1,2*]

[1]Bio–Organic Chemistry Unit, Institute of Biomolecular Chemistry, Consiglio Nazionale delle Ricerche, Pozzuoli, Italy, [2]Laboratory of Bio-Organic Chemistry and Chemical Biology, Department of Biology, University of Naples "Federico II", Napoli, Italy, [3]Department of Internal Medicine, University of Genova, Genova, Italy

Introduction: Sulfavant A (SULF A) is a synthetic derivative of naturally occurring sulfolipids. The molecule triggers TREM2-related maturation of dendritic cells (DCs) and has shown promising adjuvant activity in a cancer vaccine model.

Methods: the immunomodulatory activity of SULF A is tested in an allogeneic mixed lymphocyte reaction (MLR) assay based on monocyte-derived dendritic cells and naïve T lymphocytes from human donors. Flow cytometry multiparametric analyses and ELISA assays were performed to characterize the immune populations, T cell proliferation, and to quantify key cytokines.

Results: Supplementation of 10 μg/mL SULF A to the co-cultures induced DCs to expose the costimulatory molecules ICOSL and OX40L and to reduce release of the pro-inflammatory cytokine IL-12. After 7 days of SULF A treatment, T lymphocytes proliferated more and showed increased IL-4 synthesis along with downregulation of Th1 signals such as IFNγ, T-bet and CXCR3. Consistent with these findings, naïve T cells polarized toward a regulatory phenotype with up-regulation of FOXP3 expression and IL-10 synthesis. Flow cytometry analysis also supported the priming of a CD127-/CD4+/CD25+ subpopulation positive for ICOS, the inhibitory molecule CTLA-4, and the activation marker CD69.

Discussion: These results prove that SULF A can modulate DC-T cell synapse and stimulate lymphocyte proliferation and activation. In the hyperresponsive and uncontrolled context of the allogeneic MLR, the effect is associated to differentiation of regulatory T cell subsets and dampening of inflammatory signals.

KEYWORDS

small molecule, drug discovery, dendritic cells, immunoregulation, vaccine adjuvant, cancer immunotherapy, homeostasis, inflammation

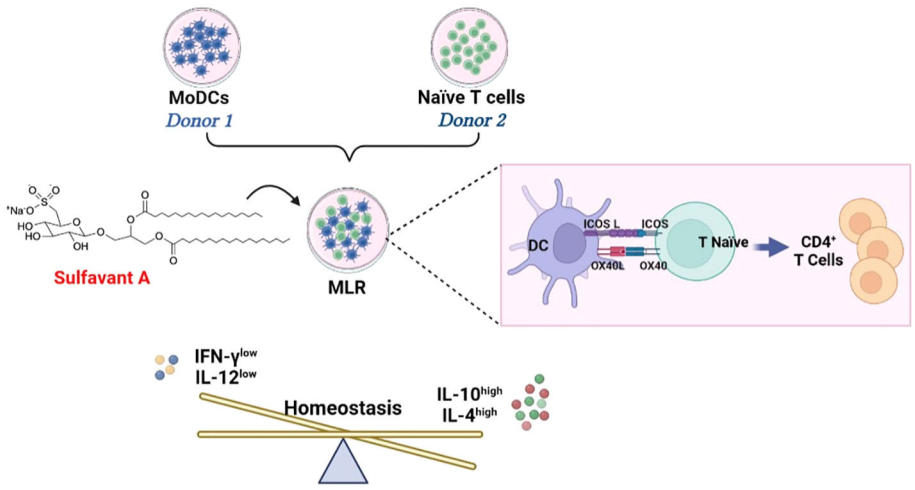

GRAPHICAL ABSTRACT

Introduction

Dendritic cells (DCs) are innate immune cells which uniquely trigger naïve T cell activation and differentiation by providing T-cell-receptor ligands and co-stimulatory molecules (1). The interaction between DC and T cell, named the immune synapse, has a great functional plasticity that allows to modulate the activation of immunogenic or tolerogenic response (2) (3). The exchange of signals and the microenvironment established during the immune synapse helps to control the magnitude, type, and efficacy of the immune response (1). However, the mechanisms by which DCs are able to transduce the environmental stimuli and prime an effective T cell response are the result of inhibitory and stimulatory signals that are only partly understood. These signals are neither consequential nor accessory but are all part of a finely regulated bidirectional process orchestrating the dialogue between DCs and T cells. Notably, in the absence of an adequate apposition of effector and accessory molecules, T cells become anergic (1) (4). In this context, a great interest has recently arisen for new drugs capable of triggering and controlling activation and proliferation of T cells by modulating the immune synapse (5).

The mixed lymphocyte reaction (MLR) constitutes an effective tool to test activation, inhibition, or functional alteration of proliferating T cells in a model of immune microenvironment. In the classical allogeneic MLR experiments, T cells and monocyte derived DCs (MoDCs) from distinct individuals are co-cultured. The allogeneic forms of major histocompatibility complex (MHC) molecules on MoDCs stimulate proliferation and activation of T cells more strongly than conventional exposure to antigens. The technique provides a model for the study of the immune synapse (6) and, over the time, the assay has been widely employed for the preclinical tests of immunomodulatory molecules with applications in immune-oncology, autoimmunity, inflammation, vaccine development (7) (8).

Sulfavant A (SULF A) is a synthetic sulfolipid derived from naturally occurring sulfoquinovosides that are essential components of the chloroplast membranes in the photosynthetic organisms (9). The molecule primes an unconventional maturation of MoDCs through a toll like receptor (TLR)-independent mechanism leading to up-regulation of the costimulatory and MHC molecules along with hypoproduction of cytokines (10) (11) (12) (13). The molecule has been proposed as a vaccine adjuvant (EU Patent n. EP3007725B1) and despite the divergence from the inflammatory mechanisms of conventional adjuvants, retains the ability to activate immune protection in an experimental model of a prophylactic vaccine against melanoma in B16F10 mice (11). Very recently, we showed that SULF A can bind the triggering receptor expressed on myeloid cells (TREM2) which helps explain the unusual mechanism of action of the sulfolipid and the ability to trigger *in vitro* the differentiation of a homeostasis-inducing DC subpopulation that we named *homeDC* (14).

In the current study, we investigate the effect of SULF A in an experimental model of allogeneic MLR with MoDCs isolated from a human donor that were co-cultured with naïve T cells of another individual at 1:10 ratio. The sulfolipid was tested at a concentration of 10 μg/mL that corresponds to the active dose used in previous experiments to stimulate *in vitro* DC maturation (10). The aim of the study was to evaluate whether SULF A affects T cell activation and proliferation in the context of allogeneic MLR, as well as to gain more insight into the effects of SULF A on adaptive immunity and the mechanisms of immune homeostasis.

Abbreviations: CTLA-4, Cytotoxic T-Lymphocyte Antigen 4; CXCR3, C-X-C Motif Chemokine Receptor 3; DC, dendritic cell; FoxP3, fork head box Protein 3; GATA 3, GATA 3 Binding Protein 3; ICOS, Inducible T Cell Costimulator; ICOSL, Inducible T Cell Costimulator Ligand; IFNγ, Interferon Gamma; IL-, interleukin; MoDC, monocyte derived dendritic cells; MLR, mixed lymphocytes reaction; OX40, Tumor necrosis factor receptor superfamily member 4; OX40-L, Tumor necrosis factor receptor superfamily member 4 ligand; RORγT, retinoid orphan receptor gamma T; T-bet, T-box transcription factor TBX21; TGFβ, trasforming growth factor β; TNFa, Tumor necrosis factor alpha; TLR, Toll-Like Receptor; TREM2, Triggering Receptor Expressed on Myeloid Cells 2.

Materials and methods

Isolation and culture of human primary cells

Monocyte-derived dendritic cells (MoDCs) were differentiated from human peripheral blood of healthy volunteers collected from Umberto I Hospital of Nocera Inferiore, Salerno (Italy). No identifying information on the donors was retained.

After density gradient isolation of Peripheral blood mononuclear cells (PBMCs) by routine Ficoll (Ficoll Paque Plus, GE Healthcare, USA), monocytes were separated by CD14 microBeads (Miltenyi Biotec, Auburn, CA, USA). Cell purity was verified by flow cytometer (FACS) analysis using human monoclonal antibodies: CD3 Percp (SK7) (Becton Dickinson), CD14 Vioblue (REA599), and CD45 FITC (REA747) (Miltenyi Biotech, Auburn, CA, USA). The CD14+/CD3-/CD45+ cells had always a purity higher than 98%. Monocytes were cultured for 6 days in RPMI medium supplemented with 10% FBS and 1% pen/strep in the presence of IL-4 (5 ng/mL) and GM-CSF (100 ng/mL) to obtain immature dendritic cells (iMoDCs). On day 6, iMoDCs were harvested, centrifuged (10 min, 300 g) and stained with CD3 Percp (SK7) (Becton Dickinson), CD14 Vioblue (REA599), CD11c FITC (REA618), CD80 PE (2D10), CD83 APC (REA714), antibodies (Miltenyi Biotec, Auburn, CA, USA) to verify cells differentiation by flow cytometry. The CD3-/CD14-/CD83-/CD80low/CD11c+ population was always higher than 95%. Naïve T cells were obtained from different buffy coats. After PBMCs separation, cells were isolated by naïve pan T cells isolation kit (Miltenyi Biotec, Auburn, CA, USA) according to manufacturer instructions. The purity of the population was verified by FACS using the human monoclonal antibodies CD3 Percp (SK7) (Becton Dickinson), CD45RA FITC (REA562), CD45RO PE(REA611), and CCR7 PeVio770 (REA108) (Miltenyi Biotec, Auburn, CA, USA). The CD3+/CD45RA+/CD45RO-/CCR7+ population had always a purity higher than 96%.

Allogeneic mixed lymphocyte reaction assay

MoDCs (stimulators) and naïve CD3+ T lymphocytes (responders) deriving from six different donors were cultured in a ratio of 1:10 (10.000 stimulators:100.000 responders) in round-bottomed 96-well plates with RPMI medium completed with 10% human AB serum in the presence of 10 µg/mL SULF A in PBS (MLR +SULF A). The concentration of SULF A used was established on the basis of previous dose-response experiments (10) (14). Untreated co-cultures were used as control (MLR). For the analysis of MoDCs, co-cultures were harvested and analyzed by flow cytometry after 48h. The analysis was carried out by antibody staining with CD86 PEVio 615 (REA968), CD11c FITC (REA618), CD14 Vioblue (REA599), (Miltenyi Biotec, Auburn, CA, USA) ICOSL APC (2D3), and OX40L PE (11C3.1) (Sony Biotechnology). For the analysis of T cells, co-cultures were analyzed by flow cytometry after 7 days. Functional surface markers were stained by anti CD3 Percp (SK7) (Becton Dickinson), CD4 PEVio 615 (REA623) or PE (SK3) (Becton Dickinson), CD8 APCvio770 (REA734), CD25 FITC (REA570) or PE (REA570), CD127 PEvio615 (MB15-18C9), CTLA-4 PEvio770 (REA1003), CD69 APCVIO770 (REA824), (Miltenyi Biotech) OX40 FITC (ACT35), ICOS Alexa fluor 700 (C398.4A) (Biolegend). For detection of intracellular cytokines, cells were treated for 6 hours at 37°C with 10 ng/mL phorbol 12-myristate 13-acetate (PMA), 500 ng/mL ionomycin, and 10 µg/mL brefeldin A (BFA) (Sigma Aldrich, Milan, Italy) and then stained with, IL-4 APC (BD4-8) (Sony Biotechnologies), IFNγ Vioblue (REA600), TNFα APC (REA656) and IL-17 PE (CZ8-23G) (Miltenyi Biotech, Auburn, CA, USA).

Lymphocyte proliferation assay

T cell proliferation was analyzed by flow cytometry using Cell Trace™ CFSE Cell Proliferation Kit (Thermo Fisher, Waltham, MA, USA). Naïve T cells (at least $2x10^6$) were suspended in PBS 5% AB serum and labeled with 5uM carboxyfluorescein succinimidyl ester (CFSE). Cells were washed 3 times with 5% AB serum in PBS, suspended in the co-culture medium again and an aliquot was immediately acquired by flow cytometry to set the initial fluorescence (time zero). After addition to stimulators MoDCs, dilution of the CFSE signal was measured every day to establish the experimental conditions for cell number and proliferation rate. The 7-day endpoint was selected because T cells showed a consistent proliferation rate and their number in the well did not exceed 1,5 $x10^6$/mL. CFSE dilution was recorded by flow cytometry as loss of fluorescence within 7 days from the addition of 10 µg/mL of SULF A (MLR+SULF A). Untreated co-cultures were used as blank (MLR) whereas co-cultures with 1 µg/mL phytohemagglutinin (PHA) were used as a positive control of proliferation. Gating strategies are shown in Supplementary Figure 1. The CFSE is reported as percentage of CFSE negative cells.

Flow cytometry

Flow cytometry was performed by FACSAriaTM (BD Bioscience) or MACSQUANT 16® Analyzer (Miltenyi Biotec). For surface staining, cells were washed in PBS and stained with Viobility™ 405/520 Fixable Dye (Miltenyi Biotec, Auburn, CA, USA) for live cell discrimination. After washing in the staining buffer (SB) (2% FBS and 0.1% sodium azide in PBS), cells were incubated at 4°C with the mixture of antibodies and isotype controls according to incubation time and quantity suggested by the manufacturers. After two additional washes, cells were acquired for the FACS analysis. For the detection of intracellular cytokines, surface markers of live cells were stained as described above. Cells were then fixed and permeabilized by BD Cytofix/Cytoperm™ kit (BD Bioscience, Frankin Lake, NJ, USA) and incubated at 4°C for 20 minutes. After two washes in BD Perm/Wash™ buffer (diluted 1:10), cells were stained with the different intracellular antibodies, according to manufacturer instructions. Cells were washed in BD Perm/Wash™ and suspended in SB for the analysis. Flow cytometry was performed on 5000 events for each population of interest according to the instrument recommendations. Isotypic and FMO controls were performed to exclude nonspecific fluorescence and set the plot axis position. Control in FITC channel and back gating strategies were used to exclude cell autofluorescence.

Real-time PCR

Total RNA was isolated using Trizol Reagent (Thermo Fisher, Waltham, MA, USA) according to manufacturer instructions. RNA quantity and purity were measured by a NanoDrop 2000 spectrophotometer (Thermo Fisher Scientific). Sample purity was checked at A260/A280 ratio between 1.80 and 2.00. Gene expression was measured by RT-qPCR by using validated primers for *T-bet, RORγT, GATA3, FOXP3, IL-10, IL-21* and *TGFβ* after 7 days from addition of SULF A to MLR test. 18S Ribosomal RNA (rRNA) was used as a housekeeping gene to normalize sample-to-sample systematic variation in RT-qPCR. ΔCt method was used to calculate the relative gene expression.

ELISA

IL-12p70, TNFα, and IL-10 were measured in the supernatants of the co-cultures at 48h and 7 days using commercially available kits (Thermo Fisher Scientific, Waltham, MA, USA) following the manufacturer instructions. Each sample was tested in duplicate and the colorimetric reaction (absorbance at 450 nm) was quantified by EZ Read 2000 (Biochrom Ltd, Harvard bioscience) spectrophotometer. Absorbance was converted to pg/mL according to the standard curve generated with a five-parameter logistic curve fit.

Statistical analysis

Gates between 0.5 and 1% positive events were set for isotype controls in flow cytometry. Flow Jo v10 (BD Biosciences) or MACS Quantify (Miltenyi Biotec) software were used for the measurements. Statistical analysis between the mean values for two groups were performed by non-parametric (two-sample) T test. The paired version of the test was used when replicates were matched in the two conditions. A *P* value less than 0.05 was considered statistically significant. Graphics were drawn by GraphPad Prism 8 (GraphPad Software, San Diego California, USA).

Results

Effect of SULF A on T cell proliferation in the MLR assay

DCs are potent inducers of lymphocytes activation in allogeneic MLR. The expression of high levels of MHC and the exposition of costimulatory molecules, make them particularly suitable to elicit a strong T cell response (6). Starting from this assumption, we used the MLR model to study the effect of SULF A on naïve T lymphocytes proliferation. The MLR condition led to proliferation of about 40% of T CD3+ population after 7 days. The addition of SULF A to the co-cultures was associated to a further increase of 20%, overall reaching a mean proliferation of 60% (Figures 1A–E). In order to investigate whether this activation concerned T helper or cytotoxic T cells, we analysed CFSE dilution in T CD4+ and TCD8+ subsets according to the gate strategy reported in Supplementary Figure 1. The T CD4+ subset showed a basal proliferation of 30% reaching 50% when SULF A was added to the co-culture (Figures 1F-J). Slight changes were registered for the T CD8+ subset for which the baseline proliferation of 10% increased by only 5% with the addition of the sulfolipid (Figures 1K–O). Minor differences of proliferation were observed among the three compartments when naïve T cells were cultured in the presence of antiCD3/antiCD28 beads used as stimulus (not shown).

DC phenotype in the MLR assay after addition of SULF A

To better understand the effect of SULF A on T cell response developing in the MLR context, we decided to study cytokine production along with DC phenotype. After 48 h from the treatment with SULF A, we observed that IL-12, a prototypic proinflammatory cytokine, was significantly reduced. The levels of IL-10, the main cytokine involved in the down-regulation of inflammatory processes, increased but did not reach formal statistical significance (P =0.0625) (Figures 2A–B); no change was detectable for the TNFα production (Supplementary Figure 2). According to the gating strategy described in Supplementary Figure 3, flow cytometry showed upregulation of the surface expression of the OX40L and ICOSL of DCs after SULF A addition to the co-cultures (Figures 2C–D). OX40L and ICOSL belong to the group of costimulatory molecules which are not constitutively expressed by resting DCs but are secondary exposed on the cell surface especially in the course of tolerogenic or regulatory immune response (1) (15) (16). The binding of OX40L with OX40 promotes T cells autocrine production of IL-4 and Th2 polarization (16). Molecules able to induce OX40L upregulation on DCs are of interest for clinical treatments of atopic dermatitis and asthma (17) (18). ICOSL is mainly involved in follicular T cells polarization, adaptive tolerance, and the maintenance of effector/regulatory T cells balance (19) (20). In experimental models of allergic encephalomyelitis (EAE) and autoimmune type 1 diabetes, blockade of ICOS/ICOSL is associated to severe worsening of the diseases (21).

Gene and protein expression by CD4$^+$ T cells in the presence of SULF A

In order to characterize priming of naïve CD4+ T cell, we considered the effect of SULF A on the hallmarks of Th1 and Th2 response in co-cultures at day 7. SULF A significantly downregulated the gene expression of the transcription factor *T-bet* (Figure 3A) and surface expression of CXCR3 marker (Figure 3B), while gating analysis of flow cytometry data (Supplementary Figure 4) revealed a consistent reduction of the intracellular level of IFNγ (Figure 3C) but no change of TNFα (P=0.062) (Figure 3D). In agreement with the down-regulated production of IL-12 at 48h, these data supported the attenuation of Th1 differentiation by SULF A. Pro-inflammatory markers related to Th17 response, such as IL-17 (Supplementary Figure 4) or the transcription factor *RORγT* (Supplementary Figure 5A), as well as the pleiotropic cytokine *TGFβ*

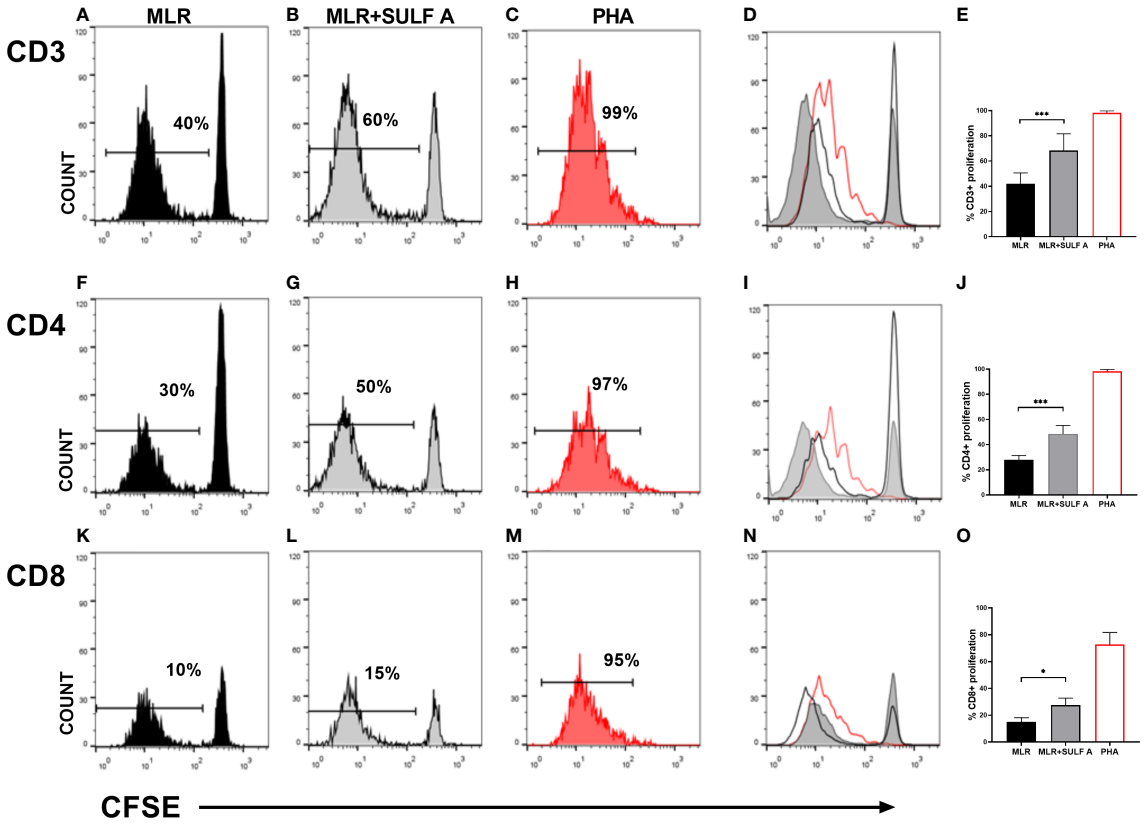

FIGURE 1
T cells proliferation induced by SULF A. Naïve T cells proliferation was assessed by CFSE dilution after 7 days of co-culture. The analysis was performed on 5000 live/T CD3+ cells. Histogram plots relative to one representative experiment are shown for CD3+ panels **(A–D)**, for CD4+ panels **(F–I)** and for T CD8+ panels **(K-N)**. Numbers in the plots indicate the percentage of proliferating cells. Panels **(D)** (T CD3+), **(I)** (T CD4+), **(N)** (T CD8+) show the overlay of the three experimental conditions for each subset. The bar graphs **(E, J, O)** represent the mean of 6 experiments. Gate strategy is reported in Supplementary Figure 1. MLR = untreated cocultures; MLR+SULF A = cocultures treated with 10 *μg*/mL SULF A; PHA= cocultures treated with 1 μg/mL phytohemagglutinin (positive control). Statistical analysis was performed by one-way Anova non parametric test. *$P < 0.05$; ***$P < 0.001$.

(Supplementary Figure 5) were unaffected in the allogeneic MLR and were unresponsive to SULF A addition. On the other hand, the sulfolipid increased the expression of the transcription factor *GATA3* (Figure 3E) and significantly increased the intracellular production of IL-4 (Figure 3F), both signature of type 2 immunity. Expression of *IL-21*, also implicated in the development of humoral responses, responses was found up-regulated (Supplementary Figure 5C) IL-4 is as multifunctional, immunoregulatory cytokine mostly associated with the suppression of pro-inflammatory signals, the dampening of the excessive immune response, and the stimulation of tissue repair and homeostasis (22).

T cell differentiation in the MLR assay after addition of SULF A

After 7 days, the co-cultures treated with SULF A showed a high expression of the transcription factor *FOXP3* fork head box Protein 3 (FoxP3) (Figure 4A) and a significant increase of IL-10 synthesis (Figures 4B–C). In these samples, flow cytometry gating of T cells (Supplementary Figure 6) revealed a consistent expansion of CD127-/CD4+/CD25+ subpopulation after addition of SULF A (Figure 4D-J). CD127 is a marker typically expressed on effector T cells, instead T CD4+ cells negative or low-level expressing this marker but positive for CD25 are generally associated to immunoregulation (23). In this population, SULF A also up-regulated the immune checkpoint receptor CTLA-4 (Figure 4K), and the inducible T-cell costimulatory receptor ICOS (Figure 4L). While CTLA-4 is constitutively expressed on FOXP3+/CD25+/CD4+Treg cells and is up-regulated in conventional T cells only after activation, ICOS is an indicator of T cell-mediated immune response. Notably, the initiation of the ICOS pathway is triggered by binding to ICOSL whose exposure is significantly increased on the DC surface 48h after the addition of SULF A to the MLR. According to these results, this population matched with the portion of proliferating T cells and were fully positive for the early activation marker CD69 (Figure 4M).

Discussion

DCs are key players in activation and control of the immune response by presentation of the antigen to T cells in the context of

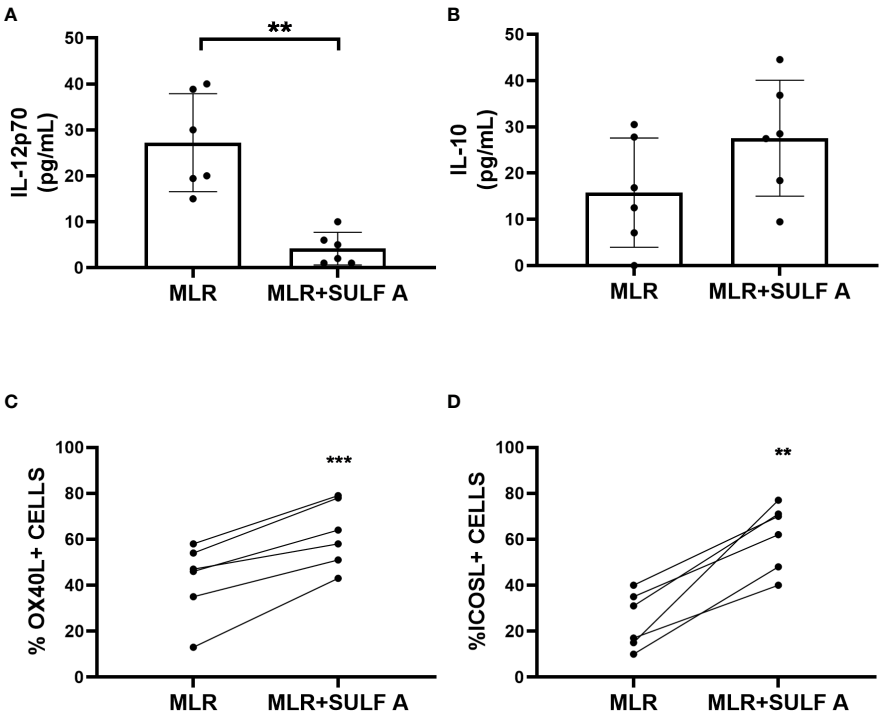

FIGURE 2
Response of cultured MoDCs with naïve T lymphocytes 48h after addition of SULF A. **(A–B)** Levels of cytokines IL-12 and IL-10 in supernatants measured by ELISA assay; **(C–D)** Surface expression of the costimulatory molecules OXO40L and ICOSL of live CD11c+/CD3- DCs measured by FACS. The gating strategy used for these markers is reported in Supplementary Figure 3. MLR= untreated co-cultures; MLR+SULF A= co-cultures treated with 10 μg/mL SULF A. Statistical analysis (n = 6) was performed by paired non parametric two tailed T test. *$P < 0.05$; ***$P < 0.001$.

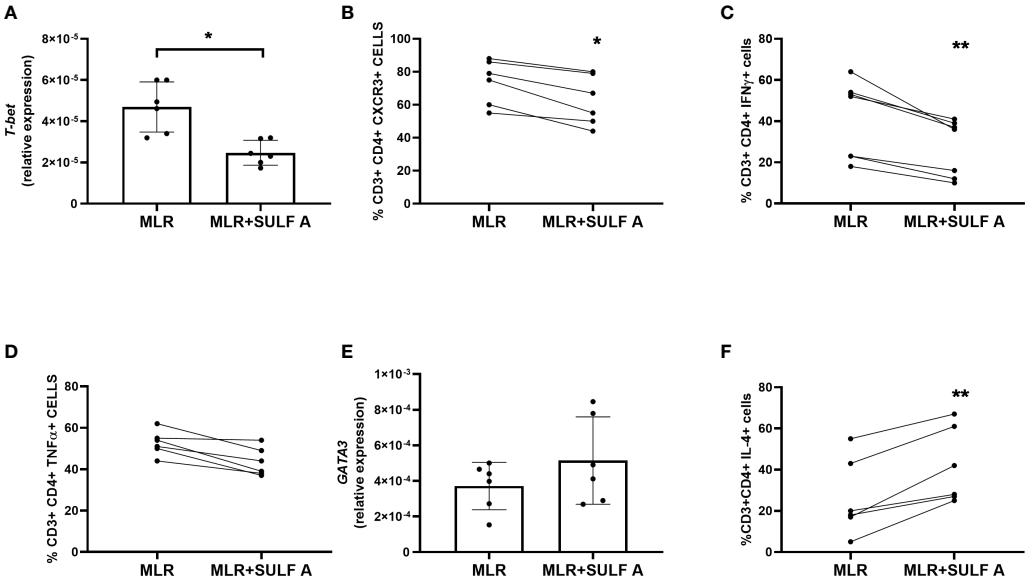

FIGURE 3
Effect of SULF A on Th1 and Th2 markers in the allogeneic MLR experiment. **(A)** RNA Expression of the transcription factor *T-bet* measured by qPCR after 7 day from the addition of SULF A to the co-cultures; **(B–D)** Surface expression of CXCR3, intracellular levels of IFNγ and TNFα measured by FACS; **(E)** RNA expression of the transcription factor GATA-3 measured by qPCR; **(F)** Intracellular level of IL-4 measured by FACS. All qPCR results (mean ± s.d) were normalized to 18S mRNA and analyzed by ΔCt method. Flow cytometry was performed on live CD3+/CD4+ cells (5000 events acquired) according to the gating strategy reported in Supplementary Figure 4. The intracellular cytokines were detected after a treatment of 6 hours with PMA, ionomycin and BFA. MLR = untreated co-cultures; MLR+SULF A = co-cultures treated with 10 $\mu g/mL$ SULF **(A)** Statistical analysis (n = 6) was performed by paired non parametric Two-tailed T-test. *$P < 0.05$; **$P < 0.01$.

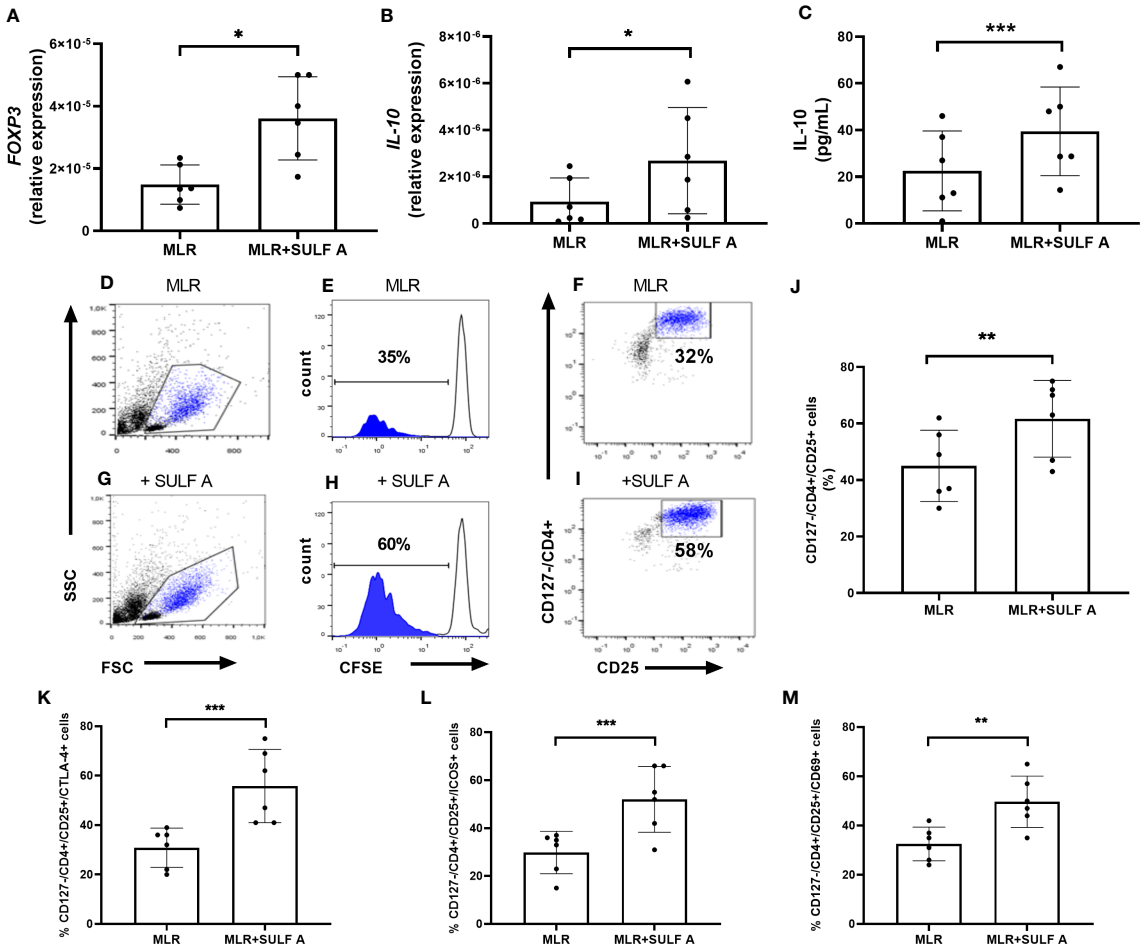

FIGURE 4
SULF A-dependent expansion of T cells in the allogeneic MLR experiment. RNA Expression of *FOXP3* **(A)** and IL-10 **(B)** measured by qPCR. Results were normalized to 18S mRNA and analyzed by ΔCt method. Values on y-axis represent the relative expression of mRNA levels compared to control. **(C)** IL-10 concentration in the MLR supernatants measured by ELISA assay. **(D–I)** Representative flow cytometry analysis of proliferating and CFSE-negative populations corresponding to the CD127-/CD4+/CD25+ subset. Analysis gated 5000 live cells. **(J)** SULF A-dependent expansion of CD127-/CD4+/CD25 + T cells (mean ± s.d) on 6 different experiments. The analysis was carried out acquiring 5000 live cells according to the gate strategy reported in Supplementary Figure 5; **(K-M)** Levels of cells positive for CTLA-4, ICOS and CD69 measured by flow cytomtery within CD127-/CD4+/CD25+ population. MLR = untreated co-cultures; MLR+SULF A = co-cultures treated with 10 *μg*/mL SULF **(A)** Statistical analysis was performed by paired non parametric two tailed T test. *$P < 0.05$; **$P < 0.01$; ***$P < 0.001$.

major histocompatibility (MHC) molecules and delivery of additional input in the form of costimulatory surface ligands and cytokines (1) (4). The bidirectional DC-T cell synapse is a cornerstone of adaptive immunity and has been the subject of many studies although the DC response has received less attention than T cell activation and differentiation (24). The effective tuning of the immune synapse requires combination of stimulatory and inhibitory signals to provide adequate protection and prevent aberrant response leading to pathological progression. One of the best-known examples of these mechanisms is the interaction of the costimulatory molecule CD28 and the inhibitory counterpart CTLA-4 along with their ligands CD80 and CD86 (25) (26).

SULF A is a small organic molecule suitable for pharmaceutical applications due to the property of triggering an unconventional maturation of DCs and initiating an effective immune response *in vivo* (11) (14). In this study we showed that SULF A can modulate DC-T cell synapse in the context of the allogeneic MLR. According to the previous reports (14), addition of SULF A to MLR determined DC maturation after 48h with increased expression of the costimulatory molecules ICOSL and OX40L in conjunction with down-regulation of cytokine IL-12 and up-regulation of IL-10. This condition led to additional T cell proliferation and, although T CD4+ and T CD8+ subsets were both promoted, it was skewed towards T CD4+ proliferation. The whole CD4+ T cell subset also expressed high levels of *GATA3*, the main transcription factor involved in Th2 polarization (27), along with increased IL-4 production and down-regulated levels of IFNγ and CXCR3 in comparison to control. In addition to the upregulation of *FOXP3* of the CD4+ T cells, gated analysis on the proliferating subset also indicated the selection of a CD127-CD4+CD25+CD69+ population by SULF A. This finding correlates with the release of high level of IL-10 and up-regulation of ICOS and CTLA-4 expression, and suggested the priming of

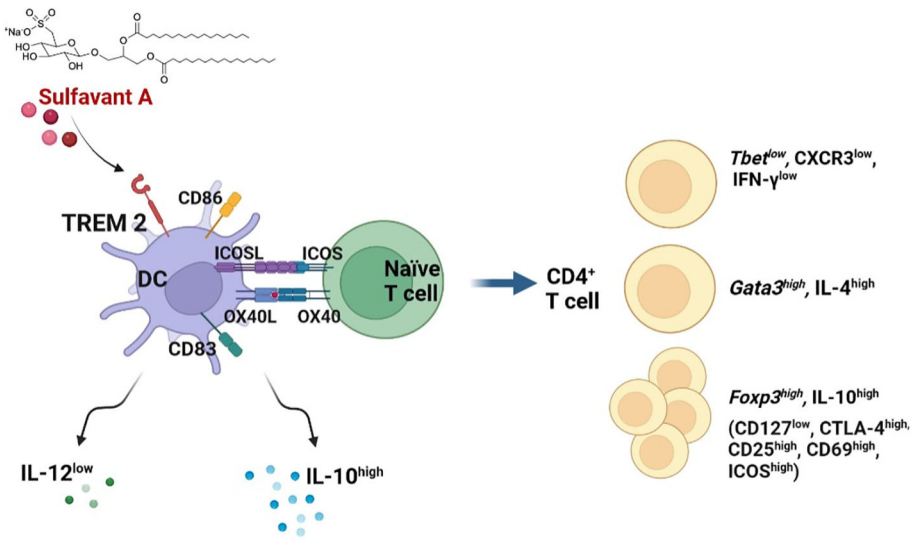

FIGURE 5
Graphic representation of the proposed mechanism of action of SULF A in MLR. After activation of DCs by TREM2, SULF A affects the stimulatory and inhibitory signalling of immune synapse. The glycolipid induces homeostasis restoration by promoting the release of IL-10, reduction of IL-12 and exposure of OX40L and ICOSL on DC membranes. The overall response is a robust T cell stimulation associated to a regulatory mechanism aimed at restoring homeostasis after the allogeneic immune reaction (image created with Biorender.com).

regulatory subpopulations functionally committed to maintain immune tolerance (23) (28). Moreover, ICOS is an activation marker that cooperates to maximize and sustain CD4+ and CD8+ T cell responses (29) but ICOS+ Tregs have stronger abilities of suppression and survival than ICOS- Tregs (30) (31) (32). It is worth noting that this response of the T cell compartment after 7 days was coherent with the early differentiation of tolerogenic DCs at 48h (Figure 5).

SULF A binds to TREM2, an immune receptor of the immunoglobulin superfamily, more effectively than other ligands so far reported. We put forward that the engagement of TREM2 correlates with the maturation of DCs committed to maintain homeostasis (14). The selection of this DC subset can also contribute to the regulatory response observed in the allogeneic MLR after the addition of the sulfolipid. This hypothesis agrees with the immunomodulatory properties of TREM2 that acts as a homeostasis effector in the central nervous system (33) and antagonizes the pro-inflammatory pathways originating from TLRs in DCs (34). The role of TREM2 in the immune response is still debated and could vary in relation to tissue- or organ-specific factors. However, recent studies on T CD8 + cancer infiltration indicate that the deficiency of tumor associated macrophages (TAMs) positive for TREM2 is associated with a stronger cytotoxic T cell activity and a higher responsivity to anti PD-1 immunotherapy (35) (36). In tumor microenvironment, TREM2 expressed on TAMs is also directly involved in *FOXP3* Treg cells recruitment and T CD8+ suppression, and Colonna et al., reported that anti-TREM2 mAB treatment could reduce the infiltration of immunosuppressive macrophages and expand the presence of cells expressing immunostimulatory molecules (36) (37) (38).

In conclusion, our results suggest that the immunomodulatory sulfolipid SULF A promotes a regulatory response in allogeneic MLR. Notably, the molecule triggers a negative modulation of the immune synapse by expression of co-inhibitory molecules on DCs and T cells, along with the release of cytokines, such as IL-4 and IL-10, favoring the dampening of inflammation. In the hyperresponsive and inflammatory context of the allogeneic MLR, the overall outcome is a tolerogenic effect that is likely aimed to restoration of homeostasis. However, it is possible that SULF A could elicit inhibitory or stimulatory immune responses in a context-dependent manner. This hypothesis may explain the effective activation of antigen-induced immune protection that SULF A has shown *in vivo* (11) and agrees with recent findings on the different modulation of immune cells by TREM2 and PRRs in relation to different microenvironments and physiopathological disorders (39) (40).

Data availability statement

The original contributions presented in the study are included in the article/Supplementary Material. Further inquiries can be directed to the corresponding authors.

Author contributions

GB and CG prepared and performed the experiments. DC, MA, MD supported the experimental work and analysis; GB, MA, DC, MD collected the data. GB and CG analyzed the results. GB performed the statistical analysis. EM, LF, MZ prepared SULF A; GN and Gd'I carried out the chemical analysis. RP contributed to the interpretation of the results and, together AF, conceived the study. AF planned the experiments, analyzed the results and, together with GB, drafted the manuscript. All authors contributed to the article and approved the submitted version.

Funding

This research was supported by the project "Antitumor Drugs and Vaccines from the Sea (ADViSE)" (CUP B43D18000240007–SURF 17061BP000000011; PG/2018/0494374) funded by POR Campania FESR 2014–2020 "Technology Platform for Therapeutic Strategies against Cancer" Action 1.1.2 and 1.2.2. and by the project "Development of therapeutic agents for COVID and LONG COVID from natural small molecules" (n. 15, PG/2022/370426 of 18/07/2022) funded by POR FESR CAMPANIA 2014-2020 -"Implementation of research and development services for the fight against Covid-19", DD n. 19/2022. AF also acknowledges the support of the project "Implementation of new immunomodulatory small molecules for the prophylaxis and treatment of severe symptoms of COVID-19 (IMO4CoV)", Ident. n. FISR2020IP_04530, funded by Fondo Integrativo Speciale per la Ricerca (FISR) 2020.

Acknowledgments

Authors are grateful to Dr. Carmine Oricchio and Dr. Caterina Del Gaudio of Presidio Ospedaliero Umberto I of Nocera Inferiore, Salerno (Italy) for providing the human blood samples. We acknowledge BioSEArch SRL for the permission to use Sulfavant A. The authors also thank Dr. Lucio Caso for the technical support.

Conflict of interest

The authors declare that the research was conducted in the absence of any commercial or financial relationships that could be construed as a potential conflict of interest.

Publisher's note

Supplementary material

The Supplementary Material for this article can be found online at: https://www.frontiersin.org/articles/10.3389/fimmu.2023.1050113/full#supplementary-material

References

1. Sallusto F, Lanzavecchia A. The instructive role of dendritic cells on T-cell responses. *Arthritis Res* (2002) 4(Suppl 3):S127–32. doi: 10.1186/ar567

2. Eisenbarth SC. Dendritic cell subsets in T cell programming: Location dictates function. *Nat Rev Immunol* (2019) 19:89–103. doi: 10.1038/s41577-018-0088-1

3. Hilligan KL, Ronchese F. Antigen presentation by dendritic cells and their instruction of CD4+ T helper cell responses. *Cell Mol Immunol* (2020) 17:587–99. doi: 10.1038/s41423-020-0465-0

4. Sallusto F, Lanzavecchia A. Efficient presentation of soluble antigen by cultured human dendritic cells is maintained by granulocyte/macrophage colony-stimulating factor plus interleukin 4 and downregulated by tumor necrosis factor alpha. *J Exp Med* (1994) 179:1109–18. doi: 10.1084/jem.179.4.1109

5. Gallo C, Barra G, Saponaro M, Manzo E, Fioretto L, Ziaco M, et al. A new bioassay platform design for the discovery of small molecules with anticancer immunotherapeutic activity. *Mar Drugs* (2020) 18:604. doi: 10.3390/md18120604

6. Tourkova IL, Yurkovetsky ZR, Shurin MR, Shurin GV. Mechanisms of dendritic cell-induced T cell proliferation in the primary MLR assay. *Immunol Lett* (2001) 78:75–82. doi: 10.1016/S0165-2478(01)00235-8

7. Kwon M, Choi YJ, Sa M, Park S-H, Shin E-C. Two-round mixed lymphocyte reaction for evaluation of the functional activities of anti-PD-1 and immunomodulators. *Immune Netw* (2018) 18(6):e45. doi: 10.4110/in.2018.18.e45

8. Emerson RO, Mathew JM, Konieczna IM, Robins HS, Leventhal JR. Defining the alloreactive T cell repertoire using high-throughput sequencing of mixed lymphocyte reaction culture. *PloS One* (2014) 9:1–7. doi: 10.1371/journal.pone.0111943

9. Manzo E, Fioretto L, Pagano D, Nuzzo G, Gallo C, De Palma R, et al. Chemical synthesis of marine-derived sulfoglycolipids, a new class of molecular adjuvants. *Mar Drugs* (2017) 15:288. doi: 10.3390/md15090288

10. Manzo E, Gallo C, Fioretto L, Nuzzo G, Barra G, Pagano D, et al. Diasteroselective colloidal self-assembly affects the immunological response of the molecular adjuvant sulfavant. *ACS Omega.* (2019) 4:7807–14. doi: 10.1021/acsomega.8b03304

11. Manzo E, Cutignano A, Pagano D, Gallo C, Barra G, Nuzzo G, et al. A new marine-derived sulfoglycolipid triggers dendritic cell activation and immune adjuvant response. *Sci Rep* (2017) 7:6286. doi: 10.1038/s41598-017-05969-8

12. Fioretto L, Ziaco M, Gallo C, Nuzzo G, d'Ippolito G, Lupetti P, et al. Direct evidence of the impact of aqueous self-assembly on biological behavior of amphiphilic molecules: The case study of molecular immunomodulators sulfavants. *J Colloid Interface Sci* (2022) 611:129–36. doi: 10.1016/j.jcis.2021.12.054

13. Manzo E, Fioretto L, Gallo C, Ziaco M, Nuzzo G, D'Ippolito G, et al. Preparation, supramolecular aggregation and immunological activity of the bona fide vaccine adjuvant sulfavant s. *Mar Drugs* (2020) 18(9):451. doi: 10.3390/md18090451

14. Gallo C, Manzo E, Barra G, Fioretto L, Ziaco M, Nuzzo G, et al. Sulfavant a as the first synthetic TREM2 ligand discloses a homeostatic response of dendritic cells after receptor engagement. *Cell Mol Life Sci* (2022) 79:369. doi: 10.1007/s00018-022-04297-z

15. Hoffmann C, Noel F, Grandclaudon M, Massenet-Regad L, Michea P, Sirven P, et al. PD-L1 and ICOSL discriminate human secretory and helper dendritic cells in cancer, allergy and autoimmunity. *Nat Commun* (2022) 13:1983. doi: 10.1038/s41467-022-29516-w

16. Ito T, Wang Y-H, Duramad O, Hori T, Delespesse GJ, Watanabe N, et al. TSLP-activated dendritic cells induce an inflammatory T helper type 2 cell response through OX40 ligand. *J Exp Med* (2005) 202:1213–23. doi: 10.1084/jem.20051135

17. Kaisar MMM, Ritter M, del Fresno C, Jónasdóttir HS, van der Ham AJ, Pelgrom LR, et al. Dectin-1/2–induced autocrine PGE 2 signaling licenses dendritic cells to prime Th2 responses. *PloS Biol* (2018) 16:1–28. doi: 10.1371/journal.pbio.2005504

18. Jember AG, Zuberi R, Liu FT, Croft M. Development of allergic inflammation in a murine model of asthma is dependent on the costimulatory receptor OX40. *J Exp Med* (2001) 193:387–92. doi: 10.1084/jem.193.3.387

19. Li DY, Xiong XZ. ICOS+ tregs: A functional subset of tregs in immune diseases. *Front Immunol* (2020) 11. doi: 10.3389/fimmu.2020.02104

20. Yamazaki S, Inaba K, Tarbell KV, Steinman RM. Dendritic cells expand antigen-specific Foxp3+CD25+CD4+ regulatory T cells including suppressors of alloreactivity. *Immunol Rev* (2006) 212:314–29. doi: 10.1111/j.0105-2896.2006.00422.x

21. Rottman JB, Smith T, Tonra JR, Ganley K, Bloom T, Silva R, et al. The costimulatory molecule ICOS plays an important role in the immunopathogenesis of EAE. *Nat Immunol* (2001) 2:605–11. doi: 10.1038/89750

22. Heeb LEM, Egholm C, Boyman O. Evolution and function of interleukin-4 receptor signaling in adaptive immunity and neutrophils. *Genes Immun [Internet].* (2020) 21:143–9. doi: 10.1038/s41435-020-0095-7

23. Yu N, Li X, Song W, Li D, Yu D, Zeng X, et al. CD4(+)CD25 (+)CD127 (low/-) T cells: a more specific treg population in human peripheral blood. *Inflammation* (2012) 35:1773–80. doi: 10.1007/s10753-012-9496-8

24. Tai Y, Wang Q, Korner H, Zhang L, Wei W. Molecular mechanisms of T cells activation by dendritic cells in autoimmune diseases. *Front Pharmacol* (2018) 9:642. doi: 10.3389/fphar.2018.00642

25. Oyewole-Said D, Konduri V, Vazquez-Perez J, Weldon SA, Levitt JM, Decker WK. Beyond T-cells: Functional characterization of CTLA-4 expression in immune and non-immune cell types. *Front Immunol* (2020) 11:608024. doi: 10.3389/fimmu.2020.608024

26. Seidel JA, Otsuka A, Kabashima K. Anti-PD-1 and anti-CTLA-4 therapies in cancer: Mechanisms of action, efficacy, and limitations. *Front Oncol* (2018) 8:86. doi: 10.3389/fonc.2018.00086

27. Zhu J, Yamane H, Cote-Sierra J, Guo L, Paul WE. GATA-3 promotes Th2 responses through three different mechanisms: Induction of Th2 cytokine production, selective growth of Th2 cells and inhibition of Th1 cell-specific factors. *Cell Res* (2006) 16:3–10. doi: 10.1038/sj.cr.7310002

28. Yu L, Yang F, Zhang F, Guo D, Li L, Wang X, et al. CD69 enhances immunosuppressive function of regulatory T-cells and attenuates colitis by prompting IL-10 production. *Cell Death Dis [Internet]*. (2018) 9:905. doi: 10.1038/s41419-018-0927-9

29. Tahiliani V, Hutchinson TE, Abboud G, Croft M, Salek-Ardakani S. OX40 cooperates with ICOS to amplify follicular Th cell development and germinal center reactions during infection. *J Immunol* (2017) 198:218–28. doi: 10.4049/jimmunol.1601356

30. Chen Q, Mo L, Cai X, Wei L, Xie Z, Li H, et al. ICOS signal facilitates Foxp3 transcription to favor suppressive function of regulatory T cells. *Int J Med Sci* (2018) 15:666–73. doi: 10.7150/ijms.23940

31. Busse M, Krech M, Meyer-Bahlburg A, Hennig C, Hansen G. ICOS mediates the generation and function of CD4 + CD25 + Foxp3 + regulatory T cells conveying respiratory tolerance. *J Immunol* (2012) 189:1975–82. doi: 10.4049/jimmunol.1103581

32. Herman AE, Freeman GJ, Mathis D, Benoist C. CD4+CD25+ T regulatory cells dependent on ICOS promote regulation of effector cells in the prediabetic lesion. *J Exp Med* (2004) 199:1479–89. doi: 10.1084/jem.20040179

33. Painter MM, Atagi Y, Liu C-C, Rademakers R, Xu H, Fryer JD, et al. TREM2 in CNS homeostasis and neurodegenerative disease. *Mol Neurodegener* (2015) 10:43. doi: 10.1186/s13024-015-0040-9

34. Deczkowska A, Weiner A, Amit I. The physiology, pathology, and potential therapeutic applications of the TREM2 signaling pathway. *Cell* (2020) 181:1207–17. doi: 10.1016/j.cell.2020.05.003

35. Katzenelenbogen Y, Sheban F, Yalin A, Yofe I, Svetlichnyy D, Jaitin DA, et al. Coupled scRNA-seq and intracellular protein activity reveal an immunosuppressive role of TREM2 in cancer. *Cell* (2020) 182:872–885.e19. doi: 10.1016/j.cell.2020.06.032

36. Molgora M, Esaulova E, Vermi W, Hou J, Chen Y, Luo J, et al. TREM2 modulation remodels the tumor myeloid landscape enhancing anti-PD-1 immunotherapy. *Cell* (2020) 182:886–900.e17. doi: 10.1016/j.cell.2020.07.013

37. Zhou L, Wang M, Guo H, Hou J, Zhang Y, Li M, et al. Integrated analysis highlights the immunosuppressive role of TREM2(+) macrophages in hepatocellular carcinoma. *Front Immunol* (2022) 13:848367. doi: 10.3389/fimmu.2022.848367

38. Zhang H, Liu Z, Wen H, Guo Y, Xu F, Zhu Q, et al. Immunosuppressive TREM2 (+) macrophages are associated with undesirable prognosis and responses to anti-PD-1 immunotherapy in non-small cell lung cancer. *Cancer Immunol Immunother* (2022) 71 (10):2511–22. doi: 10.1007/s00262-022-03173-w

39. Qiu H, Shao Z, Wen X, Jiang J, Ma Q, Wang Y, et al. TREM2: Keeping pace with immune checkpoint inhibitors in cancer immunotherapy. *Front Immunol* (2021) 12:716710. doi: 10.3389/fimmu.2021.716710

40. Man SM, Jenkins BJ. Context-dependent functions of pattern recognition receptors in cancer. *Nat Rev Cancer*. (2022) 22:397–413. doi: 10.1038/s41568-022-00462-5

Frontiers in Immunology

Explores novel approaches and diagnoses to treat immune disorders.

The official journal of the International Union of Immunological Societies (IUIS) and the most cited in its field, leading the way for research across basic, translational and clinical immunology.

Discover the latest Research Topics

See more →

Frontiers

Avenue du Tribunal-Fédéral 34
1005 Lausanne, Switzerland
frontiersin.org

Contact us

+41 (0)21 510 17 00
frontiersin.org/about/contact